ELSEVIER

Talanta 48 (1999) 1–7

Talanta

Studies on 2-(2-thiazolylazo)-5-diethylaminophenol as a precolumn derivatizing reagent in the separation of platinum group metals by high performance liquid chromatography

Hong Wang, Hua-Shan Zhang *, Jie-Ke Cheng

Department of Chemistry, Wuhan University, Wuhan 430072, People's Republic of China

Received 23 June 1997; received in revised form 29 October 1997; accepted 30 October 1997

Abstract

Five platinum group metals, Pt(II), Ir(IV), Ru(III), Rh(III) and Os(IV) have been separated by high performance liquid chromatography (HPLC) using 2-(2-thiazolylazo)-5-diethylaminophenol (TADAP) as a precolumn derivatizing reagent. The whole analysis was completed on a C_{18} column in 23 min at 574 nm, with the mobile phase of methanol–water (69.5:30.5, v:v) containing 4 mmol l^{-1} tetrabutylammonium bromide (TBA Br) and 10 mmol l^{-1} pH6.0 acetate buffer. The detection limits ($S/N = 3$) of Pt(II), Ir(IV), Ru(III), Rh(III) and Os(IV) were 0.39, 9.74, 1.64, 0.29 and 1.29 ng ml^{-1}, respectively. This method was rapid, sensitive and simple.

Keywords: Reversed-phase high performance liquid chromatography (RP-HPLC); Platinum group metal; 2-(2-thiazolylazo)-5-diethylaminophenol (TADAP)

1. Introduction

The reversed-phase HPLC (RP-HPLC) spectrophotometric technique has been proved to be an effective tool for the separation and determination of trace amount platinum group metal ions. The method usually involves complex formation of noble metals with suitable derivatizing reagents. Many kinds of developing reagents have been used as complexing agents, such as bipyridyl [1], diethyl dithiocarbamate [2,3], acetylacetone [4], 8-hydroquinolines [5] and heterocyclic azos [6–8]. There are *S*, *N* chelating atoms in the molecules of thiazolylazo reagents, which can react with platinum metals to form colored thermodynamically stable complexes according to the Lewis acid–base concept. Therefore, their applications in HPLC are focused mainly on the separation of platinum metals. Os, Rh and Ru were separated as 4-(2-thiazolylazo) resorcinol (TAR) complexes [9,10]. 1-(2-Thiazolylazo)-2-naphenol (TAN) was used in the HPLC determination of Pd and Rh [11]. The separation of Ru, Rh and Pd was obtained by 2-(2-thiazolylazo)-5-diethylaminophenol (TADAP) [12]. The 4-(2-benzothiazolylazo) resocinol (BTAR) chelates of Ru, Rh

* Corresponding author. e-mail: lotus@wip.whcnc.ac.cn

0039-9140/99/$ - see front matter
PII S0039-9140(97)00360-3

Table 1
Spectrophotometric properties of TADAP (R) metal chelates

Chelate	Pt–R	Ir–R	Ru–R	Rh–R	Os–R	Pd–R
ε_{max} (nm)	574	573	595	581	590	574
$\varepsilon_{max} \times 10^{-4}$ (l mol^{-1} cm^{-1})	3.15	1.73	4.14	5.36	1.67	3.26
$\varepsilon_{574} \times 10^{-4}$ (l mol^{-1} cm^{-1})	3.15	1.73	3.16	5.15	1.37	3.26

and Os were separated on a C_{18} column, [13]. Recently, a new reagent, 2-(6-methyl-2-benzothiazolylazo)-5-diethylaminophenol (MBTAE) was synthesized and used as a derivatizing reagent in HPLC separation [14,15]. After the separation of Pt, Rh, Pd and Os [14], five noble metals Ru, Rh(Ir), Pd, Os and Pt were determined within about 40 min [15], which is the most thus far. In order to find a rapid, simple and conventional method for separating noble metals as much as possible, a common reagent, TADAP, was used in this study and its chelates of five platinum group metals, Pt, Ir, Ru, Rh and Os were eluted in 23 min with the mobile phase of methanol–water (69.5:30.5, v:v) containing 4 mmol l^{-1} tetrabutylammonium bromide (TBA Br) and 10 mmol l^{-1} pH 6.0 acetate buffer at 574 nm on a C_{18} column. The detection limits (S/N = 3) were 0.39, 9.74, 1.64, 0.29 and 1.29 ng ml^{-1}, respectively. The proposed method gave a rapid, sensitive and simple method for the simultaneous determination of multi-platinum group metals by HPLC.

2. Experimental

2.1. Apparatus

An LC-10 HPLC apparatus (Japan Analytical) with an ODS column (5 μm, 150 × 4.6 mm i.d.; Beijing Analytical Instrument Factory) and an S-3702 UV-VIS detector (AIC, Japan) was used.

2.2. Reagents

Stock solutions of Ir(IV), Ru(III), Rh(III) and Os(IV) in 1 mol l^{-1} hydrochloric acid were prepared from analytical-reagent grade $(NH_4)_2IrCl_6$, $RuCl_3$, $RhCl_3$ and $(NH_4)_2OsCl_6$, respectively. Pt(II) standard solution was prepared from K_2PtCl_6 (AR) standard solution by reduction with sodium sulphite.

Buffer solutions were adjusted to the required pH with 1 mol l^{-1} acetic acid and 1 mol l^{-1} sodium acetate solution using the acidimer. Tetrabutylammonium bromide was purchased from the Medical Company of Beijing. A 0.05% solution of TADAP (synthesized in our lab) in absolute ethanol was used and other reagents were used as purchased. Doubly distilled water was used for all solution preparation.

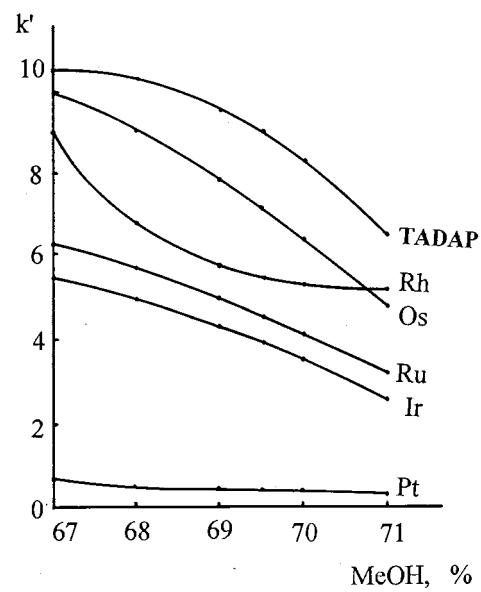

Fig. 1. Effect of methanol concentration on k' mobile phase: methanol–water in different ratios, 4 mmol l^{-1} TBA Br and 10 mmol l^{-1} pH 6.0 acetate buffer; column, C_{18} (5 μm, 150 × 4.6 mm i.d.); detection wavelength, 574 nm; flow rate, 1.0 ml min^{-1}; injection, 20 μl; detector sensitivity, 0.02 AUFS.

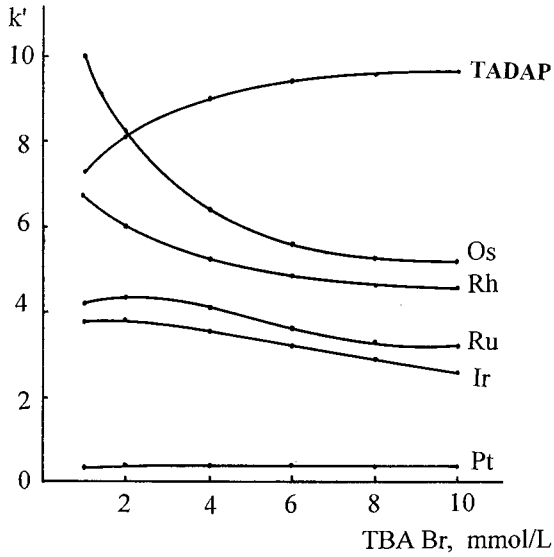

Fig. 2. Effect of TBABr concentration on k' mobile phase: methanol–water = 60.5:30.5 (v:v), 10 mmol l^{-1} pH 6.0 acetate buffer, TBA Br with different concentrations; other conditions as shown in Fig. 1.

2.3. Procedure

Acetate buffer (5.0 ml of 1 mol l^{-1}, pH 5.0) and TADAP solution (5 ml, 0.05%) were transferred into an aqueous solution containing 3, 30, 10, 5 and 28.5 μg of Pt, Ir, Ru, Rh and Os, respectively. The mixture was heated in a water bath at 80–85°C for 1 h, after which 10 ml of 95% alcohol was added immediately. After having cooled to room temperature, the solution was diluted to 25.00 ml with water. A 20 μl aliquot of this solution was injected into the chromatographic column for analysis.

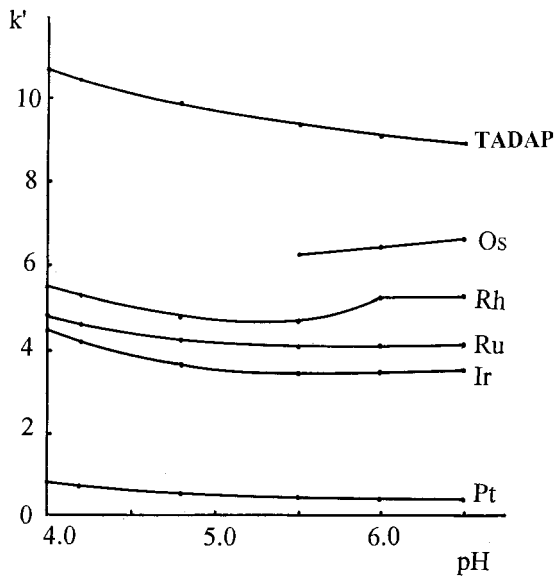

Fig. 3. Effect of pH on k' mobile phase: methanol:water = 60.5:30.5 (v:v), 4 mmol l^{-1} TBA Br, 10 mmol l^{-1} acetate buffer with different pHs; other conditions as shown in Fig. 1.

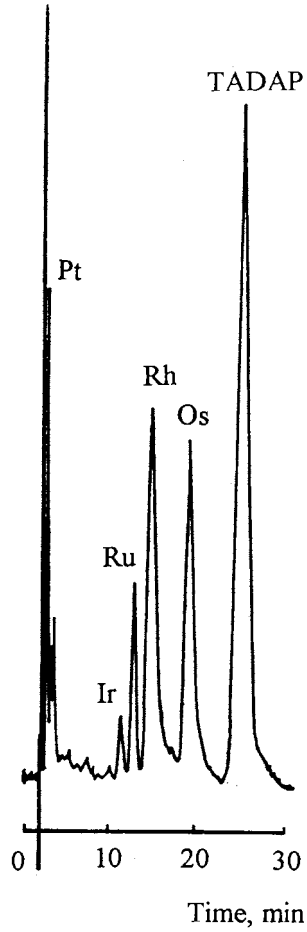

Fig. 4. Separation of Pt–, Ir–, Ru–, Rh– and Os–TADAP chelates by HPLC mobile phase: methanol:water = 60.5:30.5 (v:v), 4 mmol l^{-1} TBA Br, 10 mmol l^{-1} pH 6.0 acetate buffer; other conditions as shown in Fig. 1.

For HPLC analysis, the ODS column was pre-equilibrated with the mobile phase for 30 min. The complexes were eluted at a flow-rate of 1.0

Table 2
Regression equation, calibration range and detection limit of metal ions

Metal chelate	Regression equation[a]	r	Calibtation range (ng ml^{-1})	Detection limit (ng ml^{-1}; S/N = 3)
Pt–R	$y = 4.198 \times 10^3 + 1.943 \times 10^5 x$	0.9933	8–800	0.37
Ir–R	$y = -1.180 \times 10^2 + 1.618 \times 10^4 x$	0.9989	80–2000	9.74
Ru–R	$y = 1.771 \times 10^3 + 8.595 \times 10^4 x$	0.9940	12–800	1.64
Rh–R	$y = -5.187 \times 10^3 + 6.282 \times 10^5 x$	0.9983	4–800	0.29
Os–R	$y = -4.510 \times 10^2 + 9.050 \times 10^4 x$	0.9995	57–1140	1.29

[a] x, Concentration of the metal ion (μg ml^{-1}); y, peak area of the corresponding chelate (arbitrary unit).

ml min^{-1} and detected at 574 nm. The detector sensitivity was set at 0.02 absorbance unit for full scale deflection (AUFS). The peak areas were measured for quantitative calculations.

3. Results and discussion

3.1. Spectrophotometric properties

In a weak acidic solution, platinum group metal ions can form stable and colored chelates in the present of TADAP (the absorption data are given in Table 1). The maximum absorption wavelengths of these chelates were in the range 573–595 nm, with 574 nm being used in this experiment.

3.2. Chromatographic separation

In the literature cited above, methanol–water or acetonitrile–water comprised the basic composition of the mobile phase. The methanol–water system was chosen by test (the effect of the methanol content on the capacity factors (k') is shown in Fig. 1). The k' value of each chelate fell rapidly with increased methanol content and the change patterns of the retention times of these chelates were remarkably different. This even caused the alteration of the elution order of the chelates. Therefore, it was much more difficult to select a suitable methanol content for a good separation. When the methanol content was below 68.0%, the TADAP peak affected that of Os–TADAP. If the methanol content above 70.0%, the peaks of Rh–TADAP and Os–TADAP interfered with each other. In the methanol content range of 68.5–69.0%, Rh and Ru overlapped. The separation could only be obtained in a narrow range of methanol content. The ratio of methanol to water was set at 69.5:30.5 (v:v) for further studies.

The retention times of these chelates were long and the peak shapes poor, except for Pt–TADAP in the mobile phase of methanol–water (69.5:30.5, v:v) containing acetate buffer only. With the addition of the ion-interaction reagent, TBA Br, the elution rates of most of these chelates were accelerated, while that of Pt–TADAP was almost unchangeable (Fig. 2). It could be concluded, based on the ion-interaction model proposed by Bidlingmeyer [16,17], that the chelates of Ir–, Ru–, Rh– and Os–TADAP were positively-charged. The effect of TBA Br could also be interpreted by the ion-interaction model (4 mmol l^{-1} of TBA Br was available in this experiment).

Table 3
Tolerance limits of foreign ions (μg)

Metal ion	Amount of foreign ion (μg)											
	Cr(III)	Cr(VI)	Mn(II)	Pd(II)	Hg(II)	Pb(II)	Fe(III)	Ni(II)	Cu(II)	Zn(II)	Co(II)	V(V)
Pt	160	160	160	160	160	160	20	20	40	160	20	0.2
Ir	160	160	160	160	160	160	5	5	40	160	0.2	20
Ru	160	160	160	160	160	160	20	20	40	160	0.2	40
Rh	160	160	160	160	160	160	20	20	40	160	20	40
Os	160	160	160	160	160	160	20	20	40	160	20	40

Table 4
Comparison of thiazolylazo reagents used in the determination of platinum group metals by HPLC

Derivatizing reagent	Noble metal determined	Mobile phase	Detection limit (ng ml^{-1}; S/N = 3)	Reference
TAR	Os, Rh, Ru	Acetonitrile–water, TBA Br, buffer	—	[9]
	Os, Rh, Ru	Methanol–water, TBA Br, acetate buffer	5–17	[10]
TAN	Pd, Rh	Actonitrile–water, acetate buffer	50, 19 ng[a]	[11]
TADAP	Pd, Rh, Ru	Methanol–water, buffer, cetyltrimethylammonium bromide	1000, 200, 300	[12]
BTAR	Ru, Rh, Os	Methanol–water, TBA Br, buffer	3.7–108	[13]
MBTAE	Pt, Rh, Pd, Os	Methanol–n-butanol–water, TBA Br, ethylenediamine diacetic acid diethyl acetate, acetate buffer	1.5, 0.54, 0.6, 1.0	[14]
	Ru, Rh(Ir), Pd, Os, Pt	Methanol–water, malic acid, acetate buffer	1.77, 0.057 (0.47), 0.17, 0.89, 0.55[b]	[15]
TADAP	Pt, Ir, Ru, Rh, Os	Methanol–water, TBA Br, acetate buffer	0.37, 9.74, 1.64, 0.29, 1.29	This paper

[a] The determination limit.
[b] S/N = 2.

The acidity of the mobile phase was controlled by acetate buffer solution. The acidity and concentration of the buffer had a complicated influence in the chromatographic system, which would affect not only the solubilities and dissociations of the chelates, but also the effect of TBA^+. In order to separate these chelates well, the effect of acetate buffer was investigated. With pH < 5.5, the Os–TADAP peak could not be detected (Fig. 3). Within the range 5–20 mmol l^{-1}, the buffer concentration had no obvious effect on the retention times of the chelates (in this experiment, 10 mmol l^{-1} of pH 6.0 acetate buffer was used).

3.3. Calibration

Under optimum conditions, separation of the TADAP chelates of Pt, Ir, Ru, Rh and Os was achieved with the mobile phase of methanol–water (69.5:30.5, v:v) containing 4 mmol l^{-1} TBA Br and 10 mmol l^{-1} pH 6.0 acetate buffer (Fig. 4). It was interesting to note that the elution sequence was related to the valencies of the metal ions, except in the case of Ir. Ions having the same valences showed an elution sequence consistent with their positions in the periodic table. The whole analysis was fulfilled in 23 min, with detection limits (S/N = 3) of 0.39, 9.74, 1.64, 0.29 and 1.29 ng ml^{-1}, respectively. The regression equations, calibration ranges and detection limits of these metal ions are listed in Table 2.

3.4. Interference

In order to examine the selectivity of the proposed method, the interference of foriegn ions was investigated. Under the precolumn derivatization conditions, Ni, Co, Fe, V, Cu and Pd reacted with TADAP to form colored chelates. Cu could not be eluted, V interfered with the determination of Pt and Co interfered with Ir and Ru. The peaks of Fe and Ni could be separated with the elements determined. Eight folds of Pd were allowed. When 5.0 ml of 0.05% TADAP was used, with the amounts of Pt, Ir, Ru, Rh and Os being 3, 20, 10, 5 and 14 μg in 25 ml respectively, the allowance of the foreign ions was obtained by the experiment (see Table 3). This was expressed as the maximum amount to be determined within an error of ± 5%.

4. Conclusion

A comparison of the proposed method with others using thiazolylazo reagents in the determination of the platinum group metals by HPLC is given in Table 4. This method appears to be more

sensitive, convenient and rapid, providing a simple method for the determination of a multi-noble metal by HPLC.

Acknowledgements

This research was supported by the National Natural Science Foundation of China.

References

[1] S.J. Valenty, P.E. Behnken, Anal. Chem. 50 (1978) 834.
[2] B.J. Mueller, R.J. Lovett, Anal. Chem. 59 (1987) 1405.
[3] B.J. Mueller, R.J. Lovett, Anal. Chem. 57 (1985) 2693.
[4] R.C. Gurira, P.W. Carr, J. Chromatogr. Sci. 20 (1982) 461.
[5] B. Wenclawiak, F. Bickmann, Bunseki Kagaku 33 (1984) E67.
[6] H.S. Zhang, W.Y. Mou, J.K. Cheng, Talanta 41 (1994) 1459.
[7] N. Uehara, Y. Annoh, T. Shimizu, Y. Shijo, Anal. Sci. 5 (1989) 111.
[8] Y.S. Nikitin, N.B. Morozova, S.N. Lanin, T.A. Bal'shova, V.M. Ivanov, E.M. Basova, Talanta 34 (1987) 223.
[9] E.M. Basova, T.A. Bol'shova, E.N. Shapovalova, V.M. Ivanov, Zh. Anal. Khim. 45 (1990) 1947.
[10] Q. Liu, H. Zhang, J. Cheng, Talanta 38 (1991) 669.
[11] N.A. Baketova, E.M. Basova, V.M. Ivanov, T.A. Bol'shova, Zh. Anal. Khim. 45 (1990) 2178.
[12] E.N. Shapovalova, I.V. Mishenina, E.M. Bosova, T.A. Bol'shova, O.A. Shpigun, Zh. Anal. Khim. 46 (1991) 1503.
[13] H.S. Zhang, Z.D. Shi, J.K. Cheng, J. Wuhan Univ. (Nat. Sci. Ed.) 80 (1993) 18.
[14] Q. Liu, J. Liu, Y. Tong, J. Cheng, Anal. Chim. Acta 269 (1992) 223.
[15] Q. Liu, Y. Wang, J. Liu, J. Cheng, Anal. Sci. 9 (1993) 523.
[16] B.A. Bidlingmeyer, S.N. Deming, W.P. Price Jr., B. Sachok, M. Petrusek, J. Chromatogr. 186 (1979) 419.
[17] B.A. Bidlingmeyer, J. Chromatogr. Sci. 18 (1980) 525.

ELSEVIER

Talanta 48 (1999) 9–13

Talanta

A new sensitive reagent for identifying and determining Cu^{2+}

DongLan Ma *, Dongsheng Xia, FengLing Cui, JianPing Li, Yulu Wang

Department of Chemistry, Henan Normal University, Xin Xiang, Henan, 453002, People's Republic of China

Received 3 October 1997; received in revised form 7 January 1998; accepted 13 January 1998

Abstract

The synthesis of the new long-chain saturated fatty hydrocarbon substituting group compound, *N*-undecyl-*N'*-(sodium *p*-aminobenzenesulfonate)-thiourea (UPT) is described. According to the studies on its analytical performance, it is found that this reagent can be used to identify Cu^{2+} (PD 6.3) and determine microamounts of copper ($\varepsilon_{300.4\ nm} = 2.39 \times 10^5$ l mol^{-1}cm^{-1}) in aqueous solution. Both of their sensitivities and selectivity's are better than other common methods [1–3].These new methods are simple and convenient and can provide satisfactory results on samples.

Keywords: Copper; Spectrophotometry; *N*-undecyl-*N'*-(sodium *p*-aminobenzenesulfonate)-thiourea

1. Introduction

Copper is a necessary element in the human body. Microamount copper takes part in oxidization inside the human body and is relative to some illness' of the body [4,5], so, it is important to determine and identify microamount of copper. Typically, there are four categories of organic reagents to determine microamount of copper: the most sensitive reagents of every category are as follows: azo reagent, 2-(5-bromo-2-pyridylazo)-5-diethylaminophenol ($\varepsilon_{530.4\ nm} = 1.5 \times 10^5$ l mol^{-1} cm^{-1}) [6]; sulfocompound, 1-phenyl-3-thiobenzoyl-thioisothiocyanic acid ($\varepsilon_{360.4\ nm} = 1.27 \times 10^5$ l mol^{-1}cm^{-1}) [7]; ionic associate reagent, ethyl ester of Eosin ($\varepsilon_{610\ nm} = 9.4 \times 10^4$ l mol^{-1}cm^{-1}) [8]; porphyrin derivative reagent, α, β, γ, δ–tetra-(4-dimethylaminophenyl)-porphyrin ($\varepsilon_{433\ nm} = 3.9 \times 10^6$ l mol^{-1}cm^{-1}) [9]. In the four categories of reagents, porphyrin derivative reagents have excellent sensitivity, but their selectivity's are not good [10,11]. The new reagent (UPT) has not only very good sensitivity ($\varepsilon_{300.4\ nm} = 2.39 \times 10^5$ l mol^{-1}cm^{-1}) but also good selectivity (interfering ions: only Fe^{3+} and Au^{3+}) .In an organic spectrophotometric reagent, saturated fatty hydrocarbon substituting groups often decrease its water solubility and are not contributory to improving its sensitivity, so, saturated fatty hydrocarbon substituting groups are generally not inserted in the compound. In the new compound (UPT), there is not only a long-chain saturated fatty hydrocarbon substituting group but also a water-soluble sulfonate group. The water-soluble sulfonate group was inserted in the compound

* Corresponding author.

0039-9140/99/$ - see front matter
PII S0039-9140(98)00033-2

(UPT) to improve its water-solubility. The long-chain saturated fatty hydrocarbon substituting group and the water-soluble sulfonate group can act as surface active agents to improve the agent's sensitivity. Experimental data have indicated that these compounds have excellent analytical characteristics [12]. The new long-chain saturated fatty hydrocarbon substituting group compound (UPT) was also synthesized and studied. Their optimum conditions are studied. The applications of the reagent to identify and determine various samples are also investigated.

2. Experimental

2.1. Instruments

PE-240 element analyser (USA). SP3-300 IR spectrophotometer (PYE-Unicam company, UK). PERKIN-ELMER LAMBDA 17UV/VIS spectrophotometer.Varian VXR300 spectrometer. 53W UV/VIS spectrophotometer (Shanghai Optical Instruments Factory, Shanghai).

2.2. Reagents

All chemicals are analytical grade reagents.

2.2.1. Identification

The concentration of UPT is 0.05%. The aqueous solution of usual anions and cations are 10 mg ml^{-1}.

2.2.2. Determination

Standard copper(II) solution is 1 mg ml^{-1}. Working copper(II) solution is 10 μg ml^{-1}. UPT solution is 10^{-3} mol l^{-1}.

2.3. Preparation of UPT

p-Hydrazino-phenylsulfoacid (4.7 g) [13] was put into a 100 ml, three-necked flask, and 3% NaOH was dropped in to dissolve *p*-hydrazino-phenylsulfoacid and make the solution's value. The system was heated in a water bath at 85–90°C and stirred. Then 7.66 g undecyl-isothiocyanate [14] and 26 ml alcohol were added. After 4–5 h, the reaction was ended. The product was condensed and recrystallized with water and alcohol to give white powder with a yield of 79%. Element analysis: calculated (%), C 51.6, H 7.09, N 9.93; found (%), C 51.78, H 7.09, N 9.77; IR: 1135,1045 (C═S); 1228, 1170, 1135 (NH—CS—NH); 1228, 1170 (C_6H_4—SO_3). UV (solvent:H_2O): $\lambda = 246.4$ nm ($\varepsilon = 4.55 \times 10^4$ l mol^{-1} cm^{-1}).H′-NMR (δ) [ppm]: 1.232(3H, t, CH_3), 3.387 (2H, q, CH_2), 6.556–7.432 (4H, m, ArH), 9.627 (H, s, NH).

3. The application in analytical chemistry

3.1. Chemical properties

No characteristic phenomena were observed in either acid or alkaline media when UPT is mixed with usual anions and cations except Cu^{2+}, Ag^{+}, Ni^{2+} and Hg^{2+}, which can react with UPT to give distinct phenomena in certain media. Especially Cu^{2+} showed high sensitivity and selectivity. Their optimum conditions are studied.

3.2. Identification of Cu^{2+}

Procedure: In a centrifugal tube, one drop of Cu^{2+} stock solution was treated with one drop of

Table 1
The sensitivities of Cu^{2+}

Sensitivities ions	Limit of identification	Concentration limit	PD[a]
Cu^{2+}	0.014	0.46	6.3

[a] PD, 6–1 mg–1 gv (*v* is the volume of ion solution (ml), *m* is the limit of identification).

Table 2
Identification for synthetic samples

No.	Solution state	Phenomenon	Result	Components in solution
A	Yellow turbid. Sol.	Blue	Cu^{2+} [b]	K^+, Na^+, Ca^{2+}, Ag^+,Cu^{2+},SCN^-,Al^{3+},Fe^{3+}, Hg^{2+}, NO^{3-}, SO_4^{2-}, CO_3^{2-}, PO_4^{3-}, F^-, Cl^-,Br^-, I^-,VO_3^-,WO_4^{2-}, $B_4O_7^{2-}$, MoO_4^{2-}
B	Blue turbid sol.	a	Cu^{2+} [c]	Mg^{2+}, Ag^+, Ba^{2+}, Cr^{3+}, Bi^{3+},Pb^{2+}, NO_2^-, S^{2-}, WO_4^{2-}, AsO_4^{3-}, $C_2O_4^{2-}$
C	Brown turbid sol.	Blue	Cu^{2+} [b]	Cu^{2+}, Sr^{2+}, Mn^{2+}, Sn^{2+}, Sb^{3+}, SiO_3^{2-}, CO_3^{2-}, SO_3^{2-}, AsO_4^{3-}
D	Colorless sol.		Cu^{2+} [c]	Sn^{4+}, Al^{3+},Ca^{2+},K^+, Mg^{2+}, S_2 O_3^{2-} $F-$, $Cl-$,$Br-$, MoO_4^{2-}

a No distinct phenomenon taking place.
[b] Existence of the ion in the sample.
[c] Non-existence of the ion in the sample.

0.05 mol^{-1} HCl solution and two drops of UPT. When the tube was shaken, a blue colour appeared, which indicated the presence of Cu^{2+}.

4. Result and discussion

Effects of media: Usual acids and alkalis (H_2SO_4, HNO_3, HCl, CH_3COOH, $(NH_4)_2SO_4$, NaOH, NH_3H_2O) of different concentration were used as media in which the ions reacted with UPT. According to experiments, the optimum media and concentration for identification of Cu^{2+} is 0.05 mol^{-1} HCl.

Dosage test of UPT: One drop of stock solution of metal ion was treated with acidified according to the method described above. UPT solution was added drop by drop to reveal it thoroughly. It was finally shown that UPT dosage was two drops.

Interference of coexitent ion: There is only S^{2-} interfering tested ions: (K^+, Na^+, NH_4^+, Mg^{2+}, Ca^{2+}, Sr^{2+}, Ba^{2+}, Cr^{3+}, Al^{3+}, Fe^{2+}, Fe^{3+}, Sb^{3+}, Zn^{2+}, Mn^{2+}, Co^{2+}, Ni^{2+}, Ag^+, Pb^{2+}, Hg^{2+}, Cd^{2+}, Sn^{2+}, Sn^{4+}, NO_2^-, NO_3^-, SO_3^{2-}, SO_4^{2-}, $S_2O_3^{2-}$, CO_3^{2-}, PO_4^{3-}, F^-, Cl^-, Br^-, I^-, S^{2-}, SCN^-, VO_3^-, WO_4^{2-}, AsO_4^{3-}, AsO_3^{3-}, $B_4O_7^{2-}$, MoO_4^{2-}, $C_2O_4^{2-}$, TiO_3^{2-}).

Elimination of interference: Interference of S^{2-} could be eliminated by acidifying the sample with HNO_3, and then heating the solution to vaporise the excess nitric acid.

The sensitivities of Cu^{2+}: Table 1.

The application to the sample: The results with UPT as an identification reagent were correspondent with components of samples. See Tables 2 and 3.

4.1. Determination of Cu^{2+}

4.1.1. Procedure

Take a known volume of copper solution in a 25 ml standard flask, add 2 ml CH_3COONa—CH_3COOH buffer solution (pH 5.4) and 3 ml UPT solution, dilute to about 20 ml with distilled water, heat in 100°C boiling water bath for 13 min, remove, cool to room temperature in water, dilute to mark with distilled water and mix thoroughly. Measure the absorbance at 300.4 nm against a reagent blank prepared similarly without copper.

Spectra of absorbance: The maximum absorbance of UPT solution is at 246.4 nm. The complex Cu-UPT's is at 300.4 nm. At 300.4 nm, the UPT's absorbance is very low and does not interfere with the complex's.

Media: Several buffer solutions (CH_3COONa—CH_3COOH, Na_2HPO_4—KH_2PO_4, $Na_2B_4O_7$—KH_2PO_4) were tested. There is less interference of

Table 3
Identification for standard samples

Sample	Medium	Phenomenon	Result
Positive mud	HCl	Blue	Cu[a]
Mineral	HCl	Blue	Cu[a]
Hair	HCl	Blue	Cu[a]
Deposit of hydrographic net	HCl	Blue	Cu[a]
Wheat skin	HCl	Blue	Cu[a]

[a] Existence of the ion in the sample.

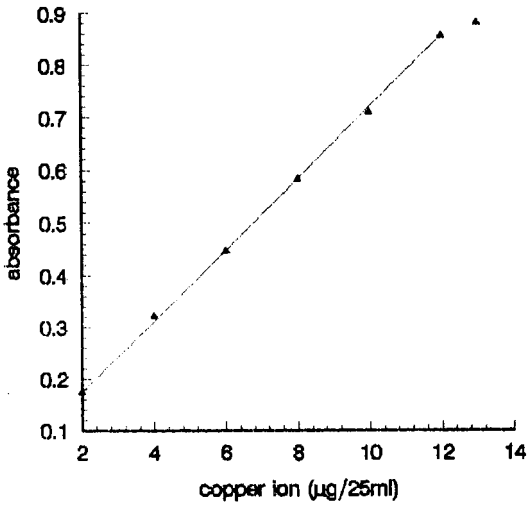

Fig. 1. Calibration curve. Saturation method: $\varepsilon_{300.4\ nm} = 2.39 \times 10^5$ l mol^{-1}cm^{-1}; slop method: $\varepsilon_{300.4\ nm} = 1.09 \times 10^5$ l mol^{-1}cm^{-1}.

different ions and higher sensitivity in CH_3COONa—CH_3COOH buffer solution than in others. CH_3COONa—CH_3COOH buffer solution is recommended.

Effect of pH value: At the range of pH 5.0–5.8, the complex's absorbance is maximum and constant. pH 5.4 is recommended.

Dosage of UPT (10^{-3} mol l^{-1}): The complex's maximum and constant absorbance is obtained when the dosage of UPT is >2.5 ml. Three milliliters is recommended.

The reaction temperature and time: At low temperature, UPT's color reaction is very slow. Less time was needed when the reaction is at 100°C. The complex's maximum absorbance is obtained when it is heated over 13 min. After 13 min, the complex is stable for at least 6 h.

The molar ratio of complex: The composition of the complex was established by Job's method of continuous-variation and the molar-ratio method, and found to be 1:3 (Cu:UPT).

The interference of coexistent ion: Interfering ions are Fe^{3+} and Au^{3+} (tested ions: K^+, Na^+, NH_4^+, Mg^{2+}, Ca^{2+}, Sr^{2+}, Ba^{2+}, Cr^{3+}, Al^{3+}, Fe^{2+}, Fe^{3+}, Sb^{3+}, Zn^{2+}, Mn^{2+}, Co^{2+}, Ni^{2+}, Ag^+, Pb^{2+}, Hg^{2+}, Cd^{2+}, Sn^{2+}, Sn^{4+}, Ru^{3+}, Rh^{3+}, Os^4, Y^{3+}, Cu^{2+}, NO_2^-, NO_3^-, SO_3^{2-}, SO_4^{2-}, $S_2O_3^{2-}$, CO_3^{2-}, PO_4^{3-}, F^-, Cl^-, Br^-, I^-, S^{2-}, SCN^-, VO_3^-, WO_4^{2-}, AsO_4^{3-}, AsO_3^{3-}, $B_4O_7^{2-}$, MoO_4^{2-}, $C_2O_4^{2-}$, CH_3COO^-, TiO_3^{2-}).

Elimination of interference: Interference of Fe^{3+} (or Au^{3+}) could be eliminated by masking with NaF (or separating in advance).

Working curve: The calibration graph was linear in the range 2–12 g of copper(II) in a volume of 25 ml. Its molar absorptivity is 2.39×10^5 l mol^{-1} cm^{-1} (Fig. 1).

Application: The results with UPT as an identification reagent showed a good agreement with the samples' actual value. Table 4.

5. Conclusion

The long-chain saturated fatty hydrocarbon substituting group compound (UPT) has good analytical characteristics and is an excellent organic spectrophotometric reagent. It can be applied in analysis and have value in application and theory.

Table 4
Determination of copper's content of samples

Sample	Standard content (μg g^{-1})	Found content (μg g^{-1})	Average found (μg g^{-1})	Relative standard deviation (%)
Aluminium alloy	180.0	173.92, 174.47, 174.13, 174.23	174.19	0.14
Dry pig liver	75.63	76.01, 75.77, 75.89, 75.81	75.87	0.15
Wheat skin	15.854	16.930, 15.879, 15.875, 16.076	16.19	0.31

References

[1] B. Jewsbury, Analyst 78 (1953) 363.
[2] R.W. Geiger, E.B. Sandell, Anal. Chim. Acta 8 (1953) 197.
[3] Z. Holzecher, L. Divis, M. Kval, Hand Book of Organic Reagents in Inorganic Analysis, Ellis Horwood, 1976, p. 146.
[4] J.K. Cheng, Microamount Anal. 1 (1986) 90.
[5] Y.Z. Hong, Si Chuan Da Xue Xue Bao, 25 (1988) 378.
[6] Y. Sun, X.C. Han, Phys. Test. Chem. Anal. 4 (1987) 221.
[7] S.Q.R. Ilyas, A.P. Joshi, Mikrochim. Acta 2 (1980) 263.
[8] T. Sakai, N. Ohno, L.P.A. Damovich, Zh. Anal. Khim. 29 (1974) 1905.
[9] X.Q. Mao, F.L. Tang, Chem. Agent 9 (1987) 334.
[10] K. Aomura, Anal. Chim. Acta 14 (1975) 53.
[11] H. Ishii, Talanta 24 (1977) 417.
[12] D.L. Ma, L. Zhang, Lab. Anal. 2 (1996) 43–46.
[13] Z.L. Li, X.F. Huang, Synthesis and Application of Organic Reagents, Hunan Science Publishing House, Changsha, China.
[14] A.F. Bckay, D.L. Garamaise, R. Gandry, H.A. Baker, G.Y. Paris, et al., J. Am. Chem. Soc. 81 (1995) 4328–4335.

ELSEVIER

Talanta 48 (1999) 15–21

Talanta

Room temperature phosphorescence of 1-naphtalenacetamide included in β-cyclodextrin in presence of 1,3-dibromopropane

A. Muñoz de la Peña [a,*], M.C. Mahedero [a], A. Espinosa-Mansilla [a], A. Bautista Sánchez [a], M. Reta [b]

[a] *Department of Analytical Chemistry, University of Extremadura, Avda Elvas s/n, E-06071 Badajoz, Spain*
[b] *Department of Chemistry, University National of Rio Cuarto, Rio Cuarto, Argentina*

Received 3 November 1997; received in revised form 23 February 1998; accepted 27 February 1998

Abstract

The spectral characteristics of the inclusion of 1-naphthalenacetamide in β-cyclodextrin have been studied by luminescence methods. The addition of bromoalcohols or bromoalkanes produces a decrease of the fluorescence of the inclusion complex, giving rise to a new band corresponding to phosphorescence emission. The emission intensity is much higher in the presence of bromoalkanes than in the presence of bromoalcohols. The deoxygenation of the solutions is achieved by flowing nitrogen, by the addition of sodium sulphite and by a combination of both methods, which results in the most effective approach. The phosphorescence emission is produced in the turbid suspension formed in the presence of the bromoalkane. The formation of microcrystals seems necessary to obtain phosphorescence emission from the ternary system.

Keywords: Room temperature phosphorescence; 1-Naphthalenacetamide; β-Cyclodextrin; 1,3-Dibromopropane

1. Introduction

Fluid solution room temperature phosphorescence emission (RTP) has usually been obtained in organized media that are heterogeneous at a microscopic level [1]. Among those proposed have been micellar media [2–4] and molecular compounds capable of forming inclusion complexes [5,6]. Among the usual organized media forming inclusion complexes are cyclodextrins (CDs) [5] and azaparacyclophanes [6]. In cyclodextrins, some of the systems described include molecules possessing a heavy-atom in its structure, as halonaphthalenes [5,7,8] or 6-bromo-2-naphtol [9]. More commonly, the presence of an external heavy atom is necessary to obtain phosphorescence emission. The heavy-atom increases the rate of the intersystem-crossing process and populates

* Corresponding author. Tel: +34 24 289378; fax: +34 24 2893752; e-mail: arsenio@unex.es

0039-9140/99/$ - see front matter
PII S0039-9140(98)00105-2

the triplet state. The first heavy-atom containing species proposed for fluid solution RTP in CDs was 1,2-dibromoethane by Cline Love [10–12].

Hamai proposed 2-bromoethanol and 2,3-dibromopropanol, in the presence of β-cyclodextrin, to obtain RTP from acenaphthene [13]. In all the mentioned cases, a previous deoxygenation of the solutions by passing a stream of nitrogen was performed. Later on, Muñoz de la Peña et al. observed RTP from acenaphthene in β-CD, in the presence of 2-bromoethanol [14], and of 1-naphthyl-oxy-acetic acid and 1-naphthylacetic acid, in the presence of 2-bromoethanol and 2,3-dibromopropanol [15], by using sodium sulphite as chemical deoxygenant, in a similar manner to the method proposed for micellar systems [16].

In this paper, an extension of previous studies on the RTP emission from pesticides that are naphthalene derivatives has been performed. For the present study, 1-naphthaleneacetamide (NAAM) has been selected. NAAM is a phytohormone used to influence the growing of plants. One of the main objectives and need of analysis of this compound is in the control of agricultural products for human consumption.

The phosphorescence characteristics of NAAM were studied in rigid ethanolic solutions at low temperature, with 17 other plant growth regulators [17]. Later on, a study was performed at room temperature, using filter paper as the solid substrate, and compared with low temperature [18]. In the presence of 1.0 M sodium iodide as the external heavy atom species, the phosphorescence signal was 10.5 times higher than in the absence of sodium iodide [19]. The RTP signal was used for the determination of NAAM in the presence of several pesticides [20].

In this work, the use of two bromoalcohols, 2-bromoethanol and 2,3-dibromopropanol, and two bromoalkanes, 1,2-dibromoethane and 1,3-dibromopropane (1,3-DBP), as the source of external heavy atoms, are investigated. The RTP emission of NAAM induced in β-CD solutions is characterized. The advantages of the deoxygenation of the solutions by passing nitrogen, by adding sodium sulphite or by both is also investigated.

2. Instrumentation

Fluorescence and phosphorescence measurements were made on an SLM Aminco Bowman luminescence spectrometer, equipped with two xenon lamps, a 150 W continuous wavelength and a 7 W pulsed, interfaced with a PC 386 microcomputer. Data acquisition and data analysis were performed by use of the AB2 software version 2.0, running under OS/2. Solutions were excited at 282 nm, the maximum excitation wavelength of 1-naphthaleneacetamide. Fluorescence measurements were made with excitation and emission band widths of 4 nm. The phosphorescence measurements were performed using typically delay time and gate time values of 1.0 and 5.0 ms, respectively. The slits were maintained at 8 nm for excitation and emission. All measurements were performed at 20.0 ± 0.1°C by use of a thermostatic cell holder and a Selecta model Frigiterm thermostatic bath.

For the deoxygenation of the samples, two procedures were used. In the first one, sodium sulphite was added to the solutions to have a final 0.06 M concentration, and the phosphorescence signal was monitored until a constant value was reached. In the second one, nitrogen was passed in an anaerobic cell during 10 min, measuring the phosphorescence immediately. In some of the experiments, sodium sulphite was added to those solutions at which nitrogen gas was already passed.

3. Reagents

All the experiments were realized using analytical grade chemicals. Purified LC-grade water (Millipore Milli-Q system) was used. 1-Naphthaleneacetamide (96%) was obtained from Chem service (West Chester, PA) and used as received. A 1×10^{-4} M stock solution in water was prepared. β-CD was obtained from Cyclolab (Budapest) and used as received. A stock 1.25×10^{-2} M β-CD was prepared. 2-Bromoethanol (95%), 2,3-dibromopropanol (96%) and 1,2-dibromoethane (99%) were obtained from Aldrich and 1,3-dibromopropane (98%) from Sigma. Anhy-

drous sodium sulphite (> 98%) was obtained from Merck. Sodium sulphite solutions were prepared daily and kept in tightly stoppered containers.

4. Results and discussion

4.1. Obtention of RTP in the presence of 1,3-DBP

Previously, fluid solution RTP emission has been obtained for 1-naphthylacetic acid and for 1-naphthyl-oxy-acetic acid in the presence of 2-bromoethanol and 2,3-dibromopropanol [15]. Two bromoalkanes, 1,2-dibromoethane [21] and 1,2-dibromopropane [22] have been also reported for the observation of RTP emission from 1-naphthylacetic acid in β-CD. In preliminary studies, 2-bromoethanol, 2,3-dibromopropanol, 1,2-dibromoethane and 1,3-dibromopropane were evaluated for RTP from NAAM. Under optimum conditions of measurements, the best results were found when using 1,3-dibromopropane. For the experimental conditions used, the RTP emission observed in the presence of 1,2-dibromoethane was approximately half that obtained with 1,3-dibromopropane. The RTP signal obtained in the presence of the bromoalcohols was significantly lower than in the presence of the bromoalkanes. Consequently, 1,3-dibromopropane (1,3-DPB) was selected as the optimum source of external heavy atoms perturbed in our system.

The excitation spectrum of 1×10^{-5} M NAAM in water shows a maximum at 282 nm, while the emission spectrum shows maxima at 325 and 338 nm. A small increment in the emission intensity and a small bathochromic shift of about 1 nm are produced in the presence of β-CD. The effect of adding 1,3-DBP on the fluorescence of NAAM was investigated in the absence of β-CD and in the presence of 1×10^{-2} M β-CD. The results obtained are presented in Fig. 1. It can be concluded that the fluorescence of NAAM decreases as the concentration of 1,3-DBP in the medium increases and that the maximum effect is observed for concentrations of 1,3-DBP lower than 1%. It is also evident that the action of 1,3-DBP on the fluorescence emission is much pronounced in the presence of β-CD than in the absence, which indicates a greater interaction of the bromoalkane with NAAM inside the CD cavity when the inclusion complex is formed.

RTP emission has been obtained from NAAM in aqueous solutions of β-CD, in the presence of 1,3-DBP, previous deoxygenation of the solutions. To perform the deoxygenation, two procedures were evaluated. In the first one, the deoxygenation was effected by adding sodium sulphite to the solutions to attain a chemical disappearance of the dissolved oxygen. Also, the classical bubbling of a stream of nitrogen gas through the solution was performed. The RTP measurements indicated that a combination of both procedures gave the best results. Upon de-aeration of NAAM solutions containing both β-CD and 1,3-DBP, a new emission appears at longer wavelength regions than the fluorescence with bands at 483 and 520 nm. In Fig. 2, the RTP spectra of NAAM in 1×10^{-2} M β-CD in the absence and presence of 1% 1,3-DBP are shown. Sodium sulphite in concentration 0.04 M was added, the solution was stirred for 2 min to favor the formation of the inclusion compound, and nitrogen gas was passed through the solution

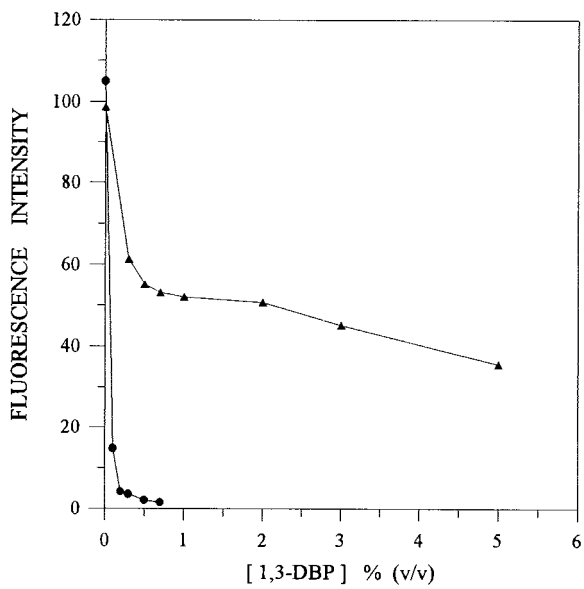

Fig. 1. Effect of 1,3-DBP on the fluorescence intensity of NAAM in the absence (▲), and the presence (●) of β-CD. [NAAM] = 1×10^{-5} M, [β-CD] = 1×10^{-2} M, $\lambda_{ex} = 282$ nm, $\lambda_{em} = 325$ nm.

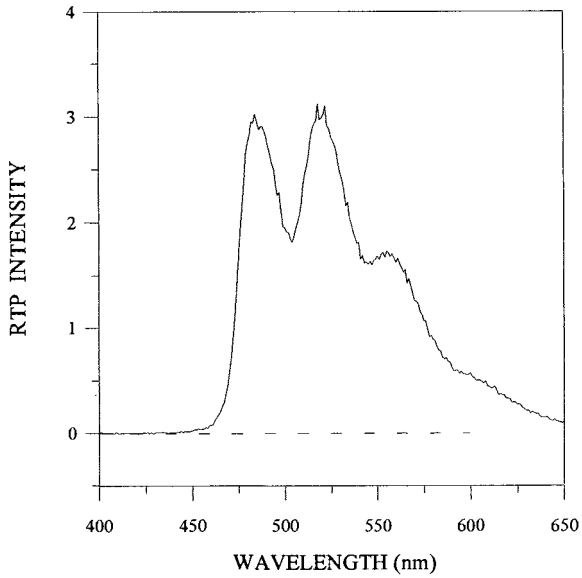

Fig. 2. RTP spectra of the complex β-CD:NAAM in the absence (---) and presence (—) of 1% (v/v) 1,3-DBP. [NAAM] = 5×10^{-5} M, [β-CD] = 1×10^{-2} M, [Na_2SO_3] = 0.04 M, λ_{ex} = 282 nm.

for 10 min to complete the deoxygenation process. In the described conditions, the solution became turbid. This is in agreement with other authors who reported on the RTP from several compounds in the presence of bromoalkanes [10,11,21,22,25]. In the absence of the bromoalkane, no phosphorescence signal appeared. In contrast, an appreciable RTP emission was evident in the presence of 1,3-DBP.

4.2. Kinetics of the reaction: optimization of chemical variables

The phosphorescence emission signal was not obtained instantly but developed with time. In Fig. 3, the results obtained when monitoring the RTP emission with time at the optimum wavelengths are represented. An enhancement of the phosphorescence signal is observed during the first 40 s and the RTP emission remained constant during the next 60 s, diminishing after this time. For the rest of the experiments, the RTP emission was measured after 1 min of preparation. Before taking the measurements, the solution was stirred for 2 min to form the inclusion complex.

The concentration of sodium sulphite was optimized by monitoring the phosphorescence emission from NAAM in the presence of various concentrations of this compound. In Fig. 4, the results obtained, when the solution was stirred for 2 min and nitrogen was passed for 10 min before taking the measurements, are shown. It can be observed that the phosphorescence emission increased when the sodium sulphite concentration in the medium increased until a sodium sulphite concentration of 0.06 M. For concentrations of sodium sulphite higher than 0.06 M, the RTP emission remains constant. The phosphorescence obtained in the presence of sodium sulphite is about twice the signal obtained by only passing nitrogen through the solution.

For a 0.06 M sodium sulphite concentration, the time required for complete deoxygenation by passing nitrogen was studied. The phosphorescence emission increased as the time of nitrogen purging increased. For deoxygenation times longer than 8 min, a maximum constant signal is obtained. The RTP intensity obtained in the presence of sodium sulphite alone is around three times lower than in the case of nitrogen purging

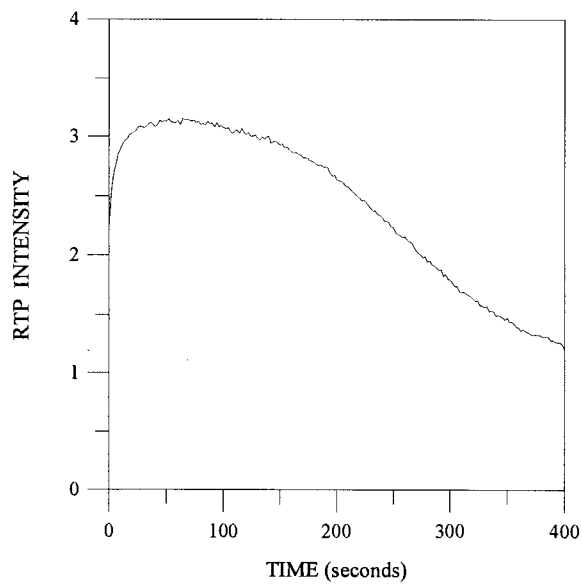

Fig. 3. Evolution of the RTP signal with the time. [NAAM] = 5×10^{-5} M, [β-CD] = 1×10^{-2} M, [Na_2SO_3] = 0.04 M, 1,3-DBP 1% (v/v), λ_{ex} = 282 nm, λ_{em} = 483 nm.

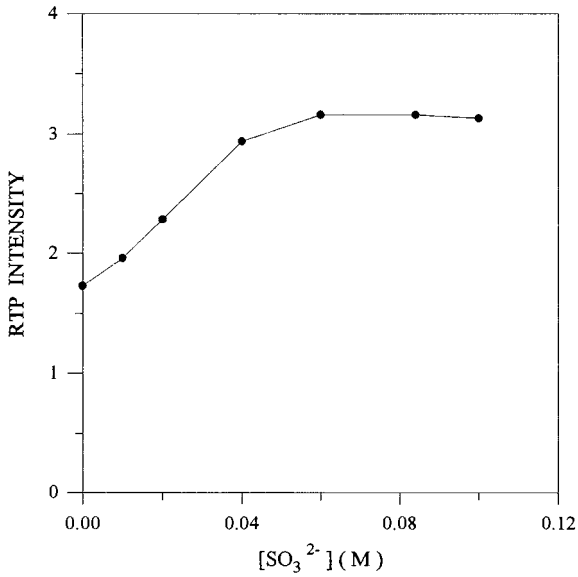

Fig. 4. Influence of sodium sulphite content on the RTP emission. [NAAM] = 5×10^{-5} M, [β-CD] = 1×10^{-2} M, 1,3-DBP 1% (v/v), Nitrogen purging during 10 min, $\lambda_{ex} = 282$ nm.

for more than 8 min. For further experiments, a deoxygenation time of 10 min was selected. These experiments demonstrate that a combination of both sodium sulphite and nitrogen passing is more effective for deoxygenation of the samples than only the bubbling of nitrogen through the solution or only the addition of sodium sulphite.

For these conditions, the influence of the 1,3-DBP content on the RTP signal was investigated. The results obtained are represented in Fig. 5. The phosphorescence emission is only obtained in the presence of the bromoalkane giving the maximum intensity for percentages of 1,3-DBP between 0.3 and 0.5%. For 1,3-DBP contents higher than 0.5%, the RTP signal slightly decreased. For further experiments, a 0.4% 1,3-DBP content was selected as optimum.

The concentration of β-CD in the medium also influenced the RTP emission. In the absence of the cyclodextrin, no phosphorescence is obtained. The RTP increased as the cyclodextrin concentration increased, reaching a constant level for cyclodextrin concentrations higher than 1×10^{-2} M. A 1×10^{-2} M β-CD is selected as optimum as this concentration is close to the limit of solubility of the cyclodextrin.

Under the optima operating conditions selected, the calibration graph obtained by plotting the RTP intensity versus NAAM concentration was linear in the range 0.46–4.62 μg ml^{-1}, with a Pearson's correlation coefficient of 0.996. A detection limit of 0.39 μg ml^{-1} was determined, according to the Long and Winefordner criterium [23], following a method of estimation using the data set of calibration [24]. For a series of ten measurements on a solution containing 3.2 μg ml^{-1} of NAAM, the relative standard deviation obtained was 2.3%.

4.3. Microscopic study and molecular modelling

Jin et al. [25] performed studies on the RTP of several polycyclic aromatic hydrocarbon and nitrogen heterocyclic compounds, included in β-CD. In all cases, the authors found that the RTP signals were intense only when turbidity or precipitates appeared in the system. Among the sources of heavy atoms assayed, the highest RTP signals were obtained with bromoalkanes and cyclohexane.

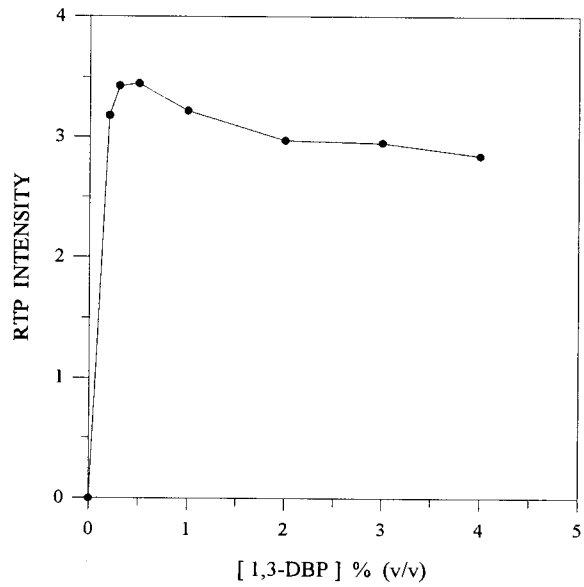

Fig. 5. Influence of 1,3-DBP content on the RTP emission. [NAAM] = 5×10^{-5} M, [β-CD] = 1×10^{-2} M, [Na_2SO_3] = 0.06 M, Nitrogen purging during 10 min, $\lambda_{ex} = 282$ nm, $\lambda_{em} = 483$ nm.

Weinberger and Cline Love [26] also reported the obtention of intense RTP from several polycyclic aromatic hydrocarbons by a related approach, in which the analytes formed microcrystalline or colloidal suspensions in aqueous solutions.

In a similar manner to these reports, in our system, a significant effect is produced when turbidity appears, resulting in an intensification of the RTP, and stabilization of the triplet state. This effect explains the differences obtained when the phosphorescence emission produced in the presence of bromoalcohols (transparent solutions) is compared with the phosphorescence emission in the presence of bromoalkanes (turbid solutions).

To measure the characteristics of the precipitate, a study was performed by optical microscopy. For that study, a solution containing 1.4 μg ml^{-1} of NAAM, in presence of 1×10^{-2} M β-CD, 0.4% 1,3-DBP and 0.06 M Na_2SO_3 was prepared and once homogeinized, a small sample was deposited by the aid of a capillary tube in a porta and introduced into the microscope. The results obtained allowed us to conclude that the precipitate suspended in the solution was composed of microcrystals with a size of the order of the micrometres.

With the object of characterizing the inclusion complexes formed between β-CD, NAAM and 1,3-DBP, a molecular modelling simulation has been performed using the Corey–Pauling–Kolton molecular model based in the Van der Waals radii. From the model, it was evident that in the interior of the cyclodextrin cavity there was enough space for the inclusion of both NAAM and 1,3-DBP forming a ternary complex. This study is in agreement with the spectroscopic evidences already discussed for the system. The designation of the phosphorescence emission to a ternary association has been suggested by various authors [5,10,11]. This is an analogous case to those reported in the literature respect to the observation of RTP from several compounds included in β-CD in the presence of haloalkanes [10,11,21,22,25,27–31]. In those cases, similar to ours, reproducible results were obtained by the authors, in spite of the observed turbidity.

5. Conclusions

With respect to the system under study, it can be concluded that the evidence indicates the formation of a ternary complex composed of the bromoalkane, the cyclodextrin and NAAM. In addition, it can be concluded that, because a bromoalkane excess exists in dispersion in the aqueous solution of the CD, a suspension is formed in our experimental conditions. In this way, the cyclodextrin and the molecules included in its cavity are forming microcrystals, producing the observed turbidity.

It is evident that the formation of the inclusion complex of NAAM is an important factor causing a rigid microenvironment for the system, with the heavy atom very close to the NAAM molecules, leading to an effective spin-orbit coupling and favouring the RTP emission. At the same time, the microcrystals formation further stabilize the triplet state producing an increase in the phosphorescence emission.

Acknowledgements

The authors acknowledge the D.G.E.S. of the Ministry of Education and Culture of Spain (Project PB95-1141) for financial support of this work. A. Bautista Sánchez acknowledges a fellowship from the Consejería de Educación y Juventud-Junta de Extremadura.

References

[1] T. Vo-Dihn, Room Temperature Phosphorescence for Chemical Analysis, Wiley, New York, 1984.
[2] L.J. Cline Love, M. Skrilec, J.G. Habarta, Anal. Chem. 52 (1980) 754.
[3] A. Sanz-Medel, P.L. Martínez García, M.E. Díaz García, Anal. Chem. 59 (1987) 774.
[4] G. Ramis Ramos, I.M. Khasawneh, M.C. García Alvarez-Coque, J.D. Winefordner, Anal. Chim. Acta 212 (1988) 235.
[5] N.J. Turro, J.D. Bolt, Y. Kuroda, I. Tabushi, Photochem. Photobiol. 35 (1982) 69.
[6] H. Kim, S.R. Crouch y, M.J. Zabik, Anal. Chem. 61 (1989) 2475.

[7] N.J. Turro, T. Okubo, C.-J. Chung, J. Am. Chem. Soc. 104 (1982) 1789.
[8] N.J. Turro, G.S. Cox, X. Li, Photochem. Photobiol. 37 (1983) 149.
[9] S. Hamai, J. Phys. Chem. 99 (1995) 12109.
[10] S. Scypinski, L.J. Cline Love, Anal. Chem. 56 (1984) 322.
[11] S. Scypinski, L.J. Cline Love, Anal. Chem. 56 (1984) 331.
[12] L.J. Cline Love, M.L. Grayeski, J. Noroski, R. Weinberger, Anal. Chim. Acta. 170 (1985) 3.
[13] S. Hamai, J. Am. Chem. Soc. 111 (1989) 3954.
[14] A. Muñoz de la Peña, I. Durán-Merás, F. Salinas, I.M. Warner, T.T. Ndou, Anal. Chim. Acta 255 (1991) 351.
[15] A. Muñoz de la Peña, F. Salinas, M.J. Gómez, M. Sánchez Peña, I. Durán-Merás, Talanta 40 (1993) 1657.
[16] M.E. Díaz García, A. Sanz-Medel, Anal. Chem. 58 (1986) 1436.
[17] L.B. Sanders, J.D. Winefordner, J. Agr. Food. Chem. 20 (1972) 166.
[18] J.J. Aaron, E.M. Kaleel, J.D. Winefordner, Agr. Food Chem. 27 (1979) 1233.
[19] J.J. Aaron, J.D. Winefordner, Analysis 7 (1979) 168.
[20] F.B. Asafu-Adjaye, S.Y. Su, Anal. Chem. 58 (1986) 539.
[21] S. Zhang, C. Liu, Y. Bu, Fenxi Huaxue 16 (1988) 495.
[22] S. Zhang, C. Liu, Y. Bu, Fenxi Huaxue 16 (1988) 682.
[23] G.L. Long, J.D. Winefordner, Anal. Chem. 55 (1983) 713A.
[24] L. Cuadros Rodríguez, A.M. García Campaña, C. Jimenez Linares, M. Roman Ceba, Anal. Lett. 26 (1993) 1243.
[25] W. Jin, Y. Wei, A. Xu, C. Liu, Spectrochim. Acta 50A (1994) 1769.
[26] R. Weinberger, L.J. Cline Love, Appl. Spectrosc. 39 (1985) 516.
[27] Y.S. Wei, W.J. Jin, R.H. Zhu, G.W. Xing, C.S. Liu, S.S. Zhang, B.L. Zhou, Spectrochim. Acta 52A (1996) 683.
[28] C.G. Gao, Y.S. Wei, W.J. Jin, C.S. Liu, Fenxi Huaxue 24 (1996) 1015.
[29] H.R. Zhang, Y.S. Wei, W.J. Jin, C.S. Liu, Fenxi Huaxue 24 (1996) 1253.
[30] Y.S. Wei, C.S. Liu, S.S. Zhang, Fenxi Huaxue 19 (1991) 533.
[31] S.M. Shuang, K.C. Feng, C.S. Liu, S.S. Zhang, Fenxi Huaxue 19 (1991) 1265.

ELSEVIER

Talanta 48 (1999) 23–38

Talanta

pH-ISEs with an expanded measuring range based on calix[4]arenes: specific features of the behaviour and description of the electrode response

V.V. Egorov *, Yu.V. Sin'kevich

Institute for Physico-Chemical Problems of the Belarusian State University, 14, Leningradskaya Str., 220080 Minsk, Belarus

Received 30 December 1997; received in revised form 19 May 1998; accepted 22 May 1998

Abstract

This article contains a description of pH-ISEs with plasticised PVC membranes that contain calix[4]arene or *p*-tertbutylcalix[4]arene as an ionophore and tetradecylammonum nitrate taken in a subequivalent amount relative to calyxarene as an ionic additive. It has been discovered that real ISEs have an extraordinarily wide measuring range which is about 1.5–2 pH units wider then the measuring range of tridecylamine-based ISEs under the same conditions. Just as in the case of amine-type neutral carriers-based pH-ISEs, the upper detection limit depends on the concentration and lipophilicity of anions and the lower limit, on the concentration and lipophilicity of cations present in the sample solution. A simple quantitative description of the electrode response and the detection limits of such ISEs is suggested which is based on inclusion of extraction equilibria at the membrane/solution interface for two limiting cases: complete dissociation and strong association of ions in the membrane. Interface equilibria constants that occur in the acid and alkali media are estimated experimentally in model extraction systems. Characteristics of the ISEs calculated with use of the estimated constants agree satisfactorily with those measured experimentally. Probable reasons of the expansion of the measuring range of the ISEs considered in comparison with ISEs based on amine-type neutral carriers are discussed.

Keywords: pH-electrodes; Calix[4]arenes; Detection limits; Ion association

1. Introduction

Ionophores-based pH-electrodes described in [1] for the first time attract researchers' attention, primarily, because of their low membrane resistance in comparison with glass electrodes. This allows their miniaturization, which is especially important for medical and biological research. Such electrodes can also have other applications, for example, in the food industry, where the use of glass electrodes is sometimes dangerous because of their brittleness, or in fluoride-containing acid solutions, where the lifetime of a glass electrode is limited.

Until recently, in membranes of these ISEs, basic compounds were used, such as various amines and their derivatives (amides, phenoxazi-

* Corresponding author. Tel.: +375 172 264700; fax: +375 172 264126.

0039-9140/99/$ - see front matter
PII S0039-9140(98)00207-0

nes, etc.) [2–22]. In [23,24] it has been shown that highly lipophilic pH indicators used in optical sensors can be efficient as neutral carriers of H^+-electrodes. Recently, extensive studies of pH-electrodes with aminated polyvinylchloride membranes have been carried out, in which the modified polymer functions as an ionophore [22,25–30].

Theoretical aspects of operation of ionophores-based pH-ISEs are discussed in some articles. Simon [9] with his team has shown for the first time at a qualitative level that in the acid region, disturbance of the electrode function is caused by protonation of the ionophore in the membrane as a result of extraction of the acid from the sample solution, while in the alkali region the interfering effect of metal cations is exhibited. It should be noted that the position of the response range (dynamic interval) of such electrodes depends on basicity of the ionophore. Egorov et al. [15] suggested a quantitative model that described the boundary potential of such ISEs with account of extraction equilibria at the membrane/solution interface with the assumption of strong ion association in the membrane. In this model the diffusion potential inside the membrane was neglected. Buck et al. [29] suggested a theory which described the electrode response of aminated PVC membranes with fixed sites, from which it followed that the ratio of ion mobilities in the membrane can be important. Finally, with the assumption of complete ion dissociation, Bakker et al. [19] obtained simple quantitative relations which described the electrode response and detection limits of such ISEs. In particular, it follows from these relations that the measuring range depends on the salt background, the solvation ability of the plasticizer and the neutral carrier/liquid ion exchanger ratio in the membrane and can only be shifted but cannot be expanded by choosing the basicity of the ionophore.

Quite recently, while seeking solvation additives capable of changing the membrane selectivity, we have noticed that introduction of the acidic compounds *p*-tertbutylcalix[4]arene or 3-nonyloxyphenol into the anion-exchange membrane was accompanied by the appearance of a pH-function [31]. In this case, the measuring range of the ISE based on *p*-tertbutylcalix[4]arene was unexpectedly wide (approximately, 1.5–2 pH units wider than that of the tridecylamine-based pH-ISE under the same conditions). In the present work new experimental data on the operation of such type of ISEs are presented, reasons for expanding the dynamic interval are discussed and quantitative relations which describe the behaviour of such ISEs are suggested with account of extraction equilibria at the membrane/solution interface.

2. Experimental

2.1. Reagents

Calix[4]arene (I) and *p*-tertbutylcalix[4]arene (II) were synthesized at the Department of Organic Chemistry of the Belarusian State University, following the procedures developed in [32,33], respectively. 3-Nonyloxyphenol (III) was produced at our laboratory by alkylation of resorcin by nonyl bromide and purified by vacuum distillation. Palmitic acid (IV) of reagent grade was recrystallized from ethanol. Tetradecylammonium nitrate (V) and tetradecylammonium picrate were produced at our laboratory with the method of anion exchange from tetradecylammonium iodide which was synthesized by exhaustive ammonia alkylation by decyl iodide in acetonitrile [34] and cleared from amines, following [35]. Potassium salt of 1,2,3-trinonyloxybenzenesulfonic acid (VI) was synthesized by alkylation of pyrogallol by nonyl bromide, followed by sulfonation and cleared from impurities, according to [36]. Tridecylamine (VII) was produced by the treatment of a chloroform solution of tridecylamine hydrochloride with aqueous alkali solution, followed by evaporation of the solvent. The formulas of the electro-active substances I–VII are presented in Fig. 1. The membrane plasticizers *o*-nitrophenyloctyl ether (*o*-NPOE), dibytylphthalate (DBP) and trihexylphosphate (THP) (all of reagent grade) were cleared from acid impurities with the extraction procedure [37]. Polyvinylchloride C-7059 was used as a polymeric membrane matrix and newly distilled cyclohexanone was used for dissolution of the PVC. Reagents of analytical

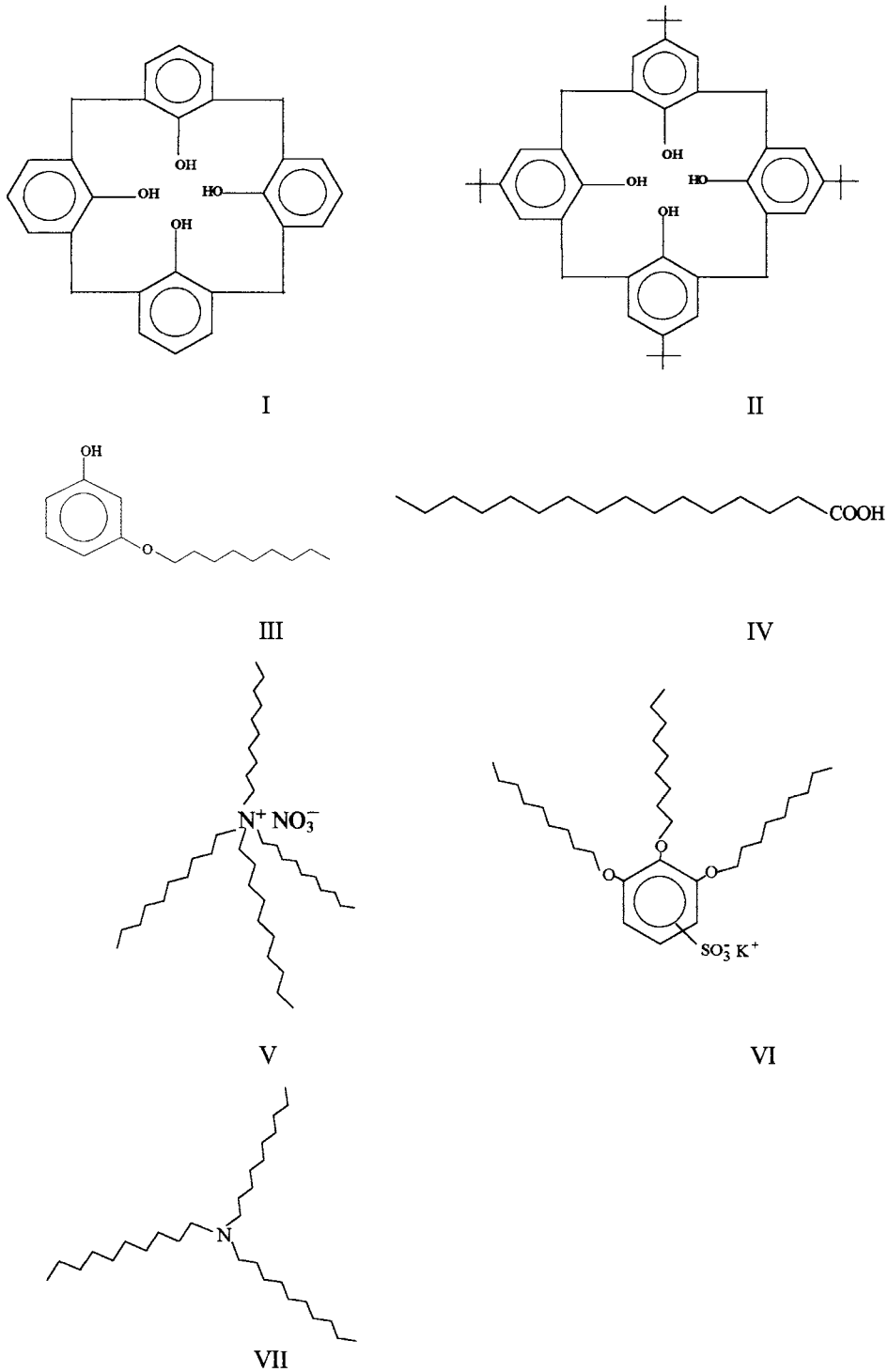

Fig. 1. The formulas of electrode-active substances used in this work.

grade and higher were used for preparation of aqueous solutions. Organic solvents (chloroform and toluene) were of analytical grade.

2.2. Production of ISE membranes and potentiometric measurements

The ISE membranes were produced by conventional methods [38]. The mass plasticizer/polymer ratio was 2:1 in all membranes. The concentration of ionophores (I)–(IV) was 3×10^{-2} M, and the concentration of ionic additive (V) was 3×10^{-3} M. Concentrations of (VI) and (VII) constituted 1×10^{-2} and 2×10^{-2} M, respectively. Universal buffer mixtures prepared by adding the necessary amount of 0.2 M solution of sodium hydroxide to the mixture of boric, acetic and phosphoric acids, 0.04 M each [39], containing, in addition, 0.1 M NaCl, were used as an inner reference solution. For membranes that contained (I)–(III) and (VII) as ionophores, we used buffer solutions with pH 8, and for (IV)-based membranes, solutions with pH 5. Before potentiometric measurements, the electrodes were soaked in the respective buffer solutions that did not contain NaCl. The potentiometric measurements were made at 293 ± 1 K with the cell:

Ag, AgCl| KCl, Sat ¦ Sample solution| Membrane| Reference solution| AgCl, Ag

An I-130 digital ionometer was used as a millivoltmeter. E.m.f. was measured in 10 times-diluted solutions of the universal buffer mixture that were prepared on the respective electrolyte background. The pH values were controlled with a glass ESL-43-07 electrode.

2.3. Estimation of interphase equilibria constants

2.3.1. Estimation of equilibrium constants K'_{ex} of the process illustrated in Eq. (8)

Since plasticizers used have a density closed to unity and high viscosity, which hinders clear phase separation in their extraction systems with water, for estimation of K'_{ex} of the process described by Eq. (8) (see later here), we used the model water–toluene system. This change of the solvent seems admissible in this case, since, just as toluene, the plasticizers used do not exhibit properties of Lewis acids, and therefore are not capable of anions solvation. Moreover, the free energy of solvation of the molecular calixarene form LH which is formed in the process illustrated in Eq. (8) also should not depend strongly on the solvent nature as calixarenes are able to form intramolecular hydrogen bonds. However, it should be noted that unlike calixarenes, for (III) and (IV) capable of forming hydrogen bonds with plasticizer molecules that exhibit properties of Lewis bases, the solvent effect may be more important. The constants K'_{ex} were estimated for different acids as follows. First, K'_{ex} was determined for picric acid. To do this, we prepared a toluene solution which contained 1×10^{-2} M ionophore (I)–(IV) and 1×10^{-3} M tetradecylammonium picrate. Ten millilitres of the prepared solution was placed into test tubes with ground-in plugs and shaken with 10 ml of the water phase, varying pH. After equilibrium had been attained, the phases were separated and picrate-ion concentration in the water phase was determined spectrophotometrically with an SF-26 instrument at $\lambda = 410$ and 430 nm, and equilibrious concentrations of the other components in the organic phase were calculated from the mass balance equations. For picric acid the constants K'_{ex} were calculated from the equation:

$$(K'_{ex})_{Hpic} = \frac{\bar{C}_{LH} \cdot \bar{C}_{R+Pic-}}{\bar{C}_{R+L-} \cdot a_{H+} \cdot C_{Pic-}}$$

where, in accordance with Eq. (8), $\bar{C}_{LH} = \bar{C}_L^{tot} - C_{Pic-}$, $\bar{C}_{R+Pic-} = \bar{C}_R^{tot} - C_{Pic-}$, $\bar{C}_{R+L-} = C_{Pic-}$, $\bar{C}_L^{tot}$, and $\bar{C}_R^{tot}$ are the initial concentrations of ionophore and tetradecylammonium picrate in the organic phase.

Then, exchange constants of picrate for various anions were determined. To this end, the toluene phase prepared just as in the previous case, was shaken with aqueous solutions containing the interesting ion X^- (Cl^- 1 M, Br^- 1M, NO_3^- 0.1 M, SCN^- 0.01 M, ClO_4^- 0.01 M) and having pH at which displacement of picrate ions into the water phase does not take place in the absence of ions X^-. For (I), (II) and (IV) these pH were 4, and 7 for (III). The concentration of picrate ion in

Table 1
The ion exchange constants of Pic^- for anion X^- in different systems

Anion	The organic solvent			
	Toluene	I (1×10^{-2} M) in toluene	III (1×10^{-2} M) in toluene	IV (1×10^{-2} M) in toluene–DBP mixture 9:1
Cl^-	7.08×10^{-9}	9.03×10^{-9}	7.16×10^{-7}	1.03×10^{-7}
Br^-	1.78×10^{-7}	1.73×10^{-7}	2.94×10^{-6}	5.32×10^{-7}
NO_3^-	1.26×10^{-6}	8.31×10^{-7}	9.43×10^{-6}	1.56×10^{-6}
SCN^-	1.00×10^{-4}	9.40×10^{-5}	6.07×10^{-4}	2.19×10^{-4}
ClO_4^-	1.41×10^{-3}	7.29×10^{-4}	9.71×10^{-4}	5.04×10^{-4}

The ion exchanger is tetradecylammonium picrate (1×10^{-3} M) solution.

the water phase was determined with spectrophotometric methods, concentrations of the other components were determined from the mass balance, and exchange constants were calculated from the equation:

$$K_{\mathrm{Pic}^-,\mathrm{X}^-}=\frac{C^2_{\mathrm{Pic}^-}}{(C_{\mathrm{X}^-}-C_{\mathrm{Pic}^-})\cdot(\bar{C}^{\mathrm{tot}}_{\mathrm{R}}-C_{\mathrm{Pic}^-})}$$

Experimental exchange constants $K_{\mathrm{Pic}^-,\mathrm{X}^-}$, are given in Table 1. Subsequently, the equilibrium constants of the process illustrated in Eq. (8) for different ions were calculated from the equation:

$$(K'_{\mathrm{ex}})_{\mathrm{HX}}=(K'_{\mathrm{ex}})_{\mathrm{HPic}}\cdot K_{\mathrm{Pic}^-,\mathrm{X}^-}$$

Obtained K'_{ex} values are given in Table 2.

2.3.2. Estimation of equilibrium constants $K'_{H,Y}$ of process Eq. (6)

Since as a result of the process illustrated in Eq. (6) polarity of the components in the organic phase greatly changes (the molecular form of the ionophore LH is transformed into the ion associate Y^+L^-), the equilibrium constant of this process should depend substantially on the solvent nature. In this case the DBP–chloroform mixture (2:1) was chosen as a solvent modeling the PVC membrane plasticized by DBP. However, any attempts to experimentally determine the ion exchange constants of hydrogen ion for alkaline metal cations ($K'_{\mathrm{H,Y}}$) for ionophores (I) and (II) failed because of close experimental and blank (without ionophore in the organic phase) signals. In the case of (III) and (IV), stable emulsions were observed which were not destroyed under centrifugation, which also prevented estimation of $K'_{\mathrm{H,Y}}$ for metal cations. Therefore, we estimated $K'_{\mathrm{H,Y}}$ for the tetraethylammonium cation. To this end, we experimentally determined the extraction constant of the tetraethylammonium picrate ion pairs by the DBP–chloroform mixture. Tetraethylammonium chloride and sodium picrate of variable concentrations were introduced into the water phase adjusted to pH 12 and shaken with an equal volume of the organic phase. After phases separation, the concentration of the picrate ion in the water phase was determined spectrophotometrically and the extraction constant was calculated from the formula:

$$K_{\mathrm{Y}^+\mathrm{Pic}^-}=\frac{C^0_{\mathrm{Pic}}-C_{\mathrm{Pic}^-}}{C_{\mathrm{Pic}^-}\cdot(C^0_{\mathrm{Y}^+}+C_{\mathrm{Pic}^-}-C^0_{\mathrm{Pic}^-})}$$

where $C^0_{\mathrm{Pic}^-}$, $C^0_{\mathrm{Y}^+}$ are the initial concentration of picrate ion and tetraethylammonium cation in the water phase; C_{Pic^-} is the picrate concentration measured after extraction. The calculated value of $K_{\mathrm{Y}^+\mathrm{Pic}^-}$ was 3×10^2 M^{-1}.

It can be easily shown that the interphase equilibrium constants considered are related by:

$$K'_{\mathrm{H,Y}}=\frac{K_{\mathrm{Y}^+\mathrm{Pic}^-}}{(K'_{\mathrm{ex}})_{\mathrm{HPic}}}\cdot\frac{(k_{\mathrm{ass}})_{\mathrm{Y}^+\mathrm{L}^-}\cdot(k_{\mathrm{ass}})_{\mathrm{R}^+\mathrm{Pic}^-}}{(k_{\mathrm{ass}})_{\mathrm{Y}^+\mathrm{Pic}^-}\cdot(k_{\mathrm{ass}})_{\mathrm{R}^+\mathrm{L}^-}},$$

where $K'_{\mathrm{H,Y}}$ and $(K'_{\mathrm{ex}})_{\mathrm{HPic}}$ are the equilibrium constants of processes illustrated in Eqs. (6) and (8), respectively; $K_{\mathrm{Y}^+\mathrm{Pic}^-}$ is the extraction constant for tetraethylammonium picrate; k_{ass} are ion association constants for the respective ion pairs. Since in this case both R^+ and Y^- are quaternary ammonium cations, it can be expected that

Table 2
The equilibrium constants of the process illustrated in Eq. (8) for different carriers

Anion	The organic phase			
	I in toluene	II in toluene	III in toluene	IV in toluene–DBP mixture 9:1
Cl^-	3.86×10^2	2.68×10^3	1.77×10^7	1.79×10^3
Br^-	7.41×10^3	5.14×10^4	7.28×10^7	9.26×10^3
NO_3^-	3.55×10^4	2.47×10^5	2.33×10^8	2.71×10^4
SCN^-	4.02×10^6	2.79×10^7	1.50×10^{10}	3.81×10^6
ClO_4^-	3.11×10^7	2.17×10^8	2.40×10^{10}	8.77×10^6
Pic^-	4.24×10^{10}	2.97×10^{11}	2.47×10^{13}	1.74×10^{10}

The concentration of $R^+...L^-$ in organic phase is 1×10^{-3} M, the concentration of LH is 1×10^{-2} M.

the factor expressed by the ion association constants will be close to unity. Then,

$$K'_{H,Y} \approx \frac{K_{Y+Pic-}}{(K'_{ex})_{HPic}}$$

3. Theory

3.1. Basic assumptions

In order to simplify the formalism that describes the electrode response and to obtain rather simple expressions for characterization of the main parameters of ISEs as a function of the membrane composition, the solution studied and interphase and intramembrane equilibria constants, we made the following assumptions:

1. The change in the boundary potential at the membrane/solution interface is controlling for changes in the e.m.f. The boundary potential at the membrane/inner reference solution interface is assumed constant. Inside the membrane the diffusion potential can be neglected.
2. The ratio of activities of the components in the contacting layers of the membrane and solution are determined by extraction equilibria constants. It should be noted that the activities of the components in the contacting membrane layer that is in contact with the sample solution can be greatly different from their activities in the bulk of the membrane. While the activities of the components in the contacting layer of the solution are assumed to be equal to their activities in the bulk of the solution.
3. The activity coefficients of all membranes components are assumed constant. This makes it possible to use concentrations instead of activities, therefore simple electroneutrality and mass balance relations can be used for quantitative description of the composition of the contacting membrane layer.

The assumptions made above are not strictly justified but they are conventionally used in development of rather simple models for description of the electrode response in various systems [40–43].

Moreover, to simplify the formalism and to obtain rather simple final results from which direct conclusions can be made, we considered only two limiting cases (a) all ion components are fully dissociated and (b) ion components are ideally associated into ion pairs.

3.2. A model of the potential-forming reaction

When the membrane which initially contained calixarene HL and tetradecylammonium nitrate $R^+NO_3^-$ is soaked in a buffer solution with pH close to a neutral one, an equilibrium is established between the membrane and solution:

$$\overline{LH} + \overline{R_4^+NO_3^-} \rightleftharpoons \overline{R^+L^-} + H^+ + NO_3^- \qquad (1)$$

This equilibrium is substantially shifted rightwards and as a result, tetradecylammonium nitrate salt is almost completely destroyed and in the membrane the salt occurs which is formed by quaternary ammonium cation with the calixarenate ion R^+L^- and the molecular form of calixarene LH (since calixarene is taken in an excessive amount relative to tetradecylammonium nitrate).

For a membrane of this type, the potential-forming reaction can be expressed as calixarenate ion-stimulated hydrogen ion transfer from water to the membrane:

$$H^+ + \overline{L^+} \rightleftharpoons \overline{LH}. \quad (2)$$

In this case the calixarenate ion L^- can be considered as a charged carrier for hydrogen ions.

Within the above assumptions, the electrode function is described by the equation:

$$E = E^0 + \frac{RT}{F} \ln \frac{a_{H^+}}{\bar{C}_{H^+}}. \quad (3)$$

In this case, constancy of the concentration of hydrogen ions generated in the membrane following the reaction:

$$\overline{LH} \overset{K_a}{\rightleftharpoons} \bar{L}^- + \bar{H}^+ \quad (4)$$

is a condition of linearity of the electrode function. In this reaction K_a is the calixarene dissociation constant in the membrane. It is evident that this condition is satisfied, if the ratio of the molecular to anion calixarene forms in the membrane ($\bar{C}_{LH}/\bar{C}_{L^-}$) is constant. This constancy is attained due to introduction of the lipophilic quaternary ammonium cations R^+, forming salt with the calixarenate ion, into the membrane and excess of the molecular calixarene form.

Both in alkali and acid media, constancy of the ratio $\bar{C}_{LH}/\bar{C}_{L^-}$ can be disturbed in the membrane layer contacting with the sample solution. In an alkali medium, the hydrogen ion can be exchanged for the cation present in the solution:

$$\overline{LH} + Y^+ \overset{K_{H,Y}}{\rightleftharpoons} \bar{L}^- + \bar{Y}^+ + H^+ \quad (5)$$

(in the case of complete dissociation), or:

$$\overline{LH} + Y^+ \overset{K_{H,Y}}{\rightleftharpoons} \overline{L^- ... Y^+} + H^+ \quad (6)$$

(in the case of strong ion association in the membrane).

In an acid medium, the calixarenate ion can be transformed into the molecular form as a result of extraction of the acid from the solution to the contacting membrane layer:

$$\overline{L^-} + H^+ + X^- \overset{K_{ex}}{\rightleftharpoons} \overline{LH} + \overline{X^-} \quad (7)$$

(in the case of complete dissociation), or:

$$\overline{R^+ .... L^-} + H^+ + X^- \overset{K'_{ex}}{\rightleftharpoons} \overline{LH} + \overline{R^+ ... X^-} \quad (8)$$

(in the case of strong ion association in the membrane).

3.3. Quantitative description of the electrode response

In accordance with Eqs. (3) and (4), for such type of membranes, in the general case, the electrode response is described by the equation:

$$E = E^0 + \frac{RT}{F} \ln \frac{a_{H^+} \cdot \bar{C}_{L^-}}{K_a \cdot \bar{C}_{LH}}, \quad (9)$$

where $\bar{C}_{L^-}$, $\bar{C}_{LH}$ are the equilibrium concentration of the respective calixarene forms in the membrane layer contacting with the sample solution.

3.3.1. The case of complete dissociation

In the region of moderate pH, in which the effect of extraction processes illustrated in Eqs. (5) and (7) on concentrations of the components in the contacting membrane layer can be neglected, the relations are valid:

$$\bar{C}_{L^-} = \bar{C}_R^{tot}, \quad (10)$$

$$\bar{C}_{LH} = \bar{C}_L^{tot} - \bar{C}_R^{tot}, \quad (11)$$

where $\bar{C}_R^{tot}$ is the total ion exchanger concentration in the membrane and $\bar{C}_L^{tot}$ is the total calixarene concentration. In this case it is assumed that the contribution of dissociation products of the molecular calixarene form LH to the ion concentration in the membrane can be neglected. Then, Eq. (9) takes the form

$$E = E^0 + \frac{RT}{F} \ln \frac{a_{H^+} \cdot \bar{C}_R^{tot}}{K_a \cdot (\bar{C}_L^{tot} - \bar{C}_R^{tot})}, \quad (12)$$

i.e. the theoretical Nerstian relation E-pH holds.

In the region of high pH, where the ion exchange process illustrated in Eq. (5) takes place, the concentration of the molecular form of calixarene LH in the contacting membrane layer is described by equation:

$$\bar{C}_{LH} = \frac{\bar{C}_{Y^+} \cdot \bar{C}_{L^-} \cdot a_{H^+}}{a_{Y^+} \cdot K_{H,Y}} \quad (13)$$

In the limiting case, in which hydrogen ions are almost completely exchanged for cations Y^+, the relations are valid:

$$\bar{C}_{L^-} = \bar{C}_L^{tot}, \quad (14)$$

$$\bar{C}_{Y^+} = \bar{C}_L^{tot} - \bar{C}_R^{tot}. \quad (15)$$

Substituting Eqs. (14) and (15) into Eq. (13) and subsequently into Eq. (9), we obtain:

$$E = E^0 + \frac{RT}{F} \ln \frac{K_{H,Y} \cdot a_{Y^+}}{(\bar{C}_L^{tot} - \bar{C}_R^{tot}) \cdot K_a}. \quad (16)$$

In this case the electrode response is determined only by the activity of the ions Y^+ in the solution. If measurements are made on the fixed background of the foreign ion Y^+, $E = \text{const}$.

Comparison of Eqs. (16) and (12) shows that in this case the interfering effect of the foreign ions is described by Nikolsky's equation, in which the selectivity coefficient is determined by the exchange constant and, in addition, depends on the concentration of the ionic additive:

$$K_{ij}^{Pot} = \frac{K_{H,Y}}{\bar{C}_R^{tot}}. \quad (17)$$

Calculating the lower detection limit for hydrogen ions, following IUPAC recommendations [44] as an intersection point of extrapolated linear sections of the electrode response described by Eq. (12) and Eq. (16), we obtain:

$$a_{H^+}(LDL) = \frac{K_{H,Y}}{\bar{C}_R^{tot}} \cdot a_{Y^+}. \quad (18)$$

In the region of low pH, where acid is extracted from the sample solution, following Eq. (7), the concentration of calixarenate ion L^- in the contacting membrane layer is described by the equation:

$$\bar{C}_{L^-} = \frac{\bar{C}_{LH} \cdot \bar{C}_{X^-}}{K_{ex} \cdot a_{H^+} \cdot a_{X^-}}. \quad (19)$$

In the limiting case, in which the equilibrium of the process illustrated in Eq. (7) is substantially shifted rightwards so that almost the entire calixarene is displaced from the salt with the ion exchanger and transformed into the molecular form, the following relations are valid:

$$\bar{C}_{LH} = \bar{C}_L^{tot}, \quad (20)$$

$$\bar{C}_{X^-} = \bar{C}_R^{tot}. \quad (21)$$

Substituting Eqs. (20) and (21) into Eq. (19) and subsequently into Eq. (9) we obtain the equation which describes the electrode response in strongly acid solutions:

$$E = E^0 + \frac{RT}{F} \ln \frac{\bar{C}_R^{tot}}{K_{ex} \cdot K_a \cdot a_{X^-}}. \quad (22)$$

In this case the potential is independent of pH and is a function of the activity of anions in the solution. If measurements are made on the constant background of the anions X^-, $E = \text{const}$.

Similar to LDL, the upper detection limit can be calculated as the intersection point of extrapolated linear sections of the electrode function described by Eqs. (12) and (22), hence:

$$a_{H^+}(UDL) = \frac{\bar{C}_L^{tot} - \bar{C}_R^{tot}}{K_{ex} \cdot a_{X^-}}. \quad (23)$$

3.3.2. The case of strong ion association in the membrane

In the region of moderate pH, where the effect of extraction processes illustrated in Eqs. (6) and (8) on concentration of the components in the contacting membrane layer can be neglected, just as in the case when complete dissociation of the compounds in the membrane takes place, the concentration of molecular calixarene form $\bar{C}_{LH}$ is described by Eq. (11) and the concentration of ion associate of calixarene with the ion exchanger is equal to the total ion exchanger concentration in the membrane:

$$\bar{C}_{R^+L^-} = \bar{C}_R^{tot}. \quad (24)$$

In this case it is assumed that the part of free ions in the membrane is negligibly small in comparison with the part of ion associates and can be neglected in the mass balance equations. Then the concentration of free calixarenate anion is described by the equation

$$\bar{C}_{L^-} = \sqrt{\frac{\bar{C}_R^{tot}}{(k_{ass})_{R^+L^-}}}, \quad (25)$$

where $(k_{ass})_{R^+L^-}$ is the association constant for ions R^+ and L^-, and the electrode response equation has the form:

$$E = E^0 + \frac{RT}{F} \ln \frac{a_{H^+} \cdot \sqrt{\bar{C}_R^{tot}}}{K_a \cdot \sqrt{(k_{ass})_{R^+L^-}} \cdot (\bar{C}_L^{tot} - \bar{C}_R^{tot})}, \quad (26)$$

i.e. theoretical Nernstian relation E-pH holds.

In the region of high pH, where ion exchange process illustrated in Eq. (6) takes place, the equilibrium concentration of the ion associate, which is formed by the foreign ion Y^+ with the calixarenate ion L^-, is described by the equation:

$$\bar{C}_{Y^+L^-} = \frac{K'_{H,Y} \cdot \bar{C}_{LH} \cdot a_{Y^+}}{a_{H^+}}. \quad (27)$$

In this case the mass balance equation for calixarene has the form:

$$\bar{C}_{LH} = \bar{C}_L^{tot} - \bar{C}_R^{tot} - \bar{C}_{Y^+L^-} \quad (28)$$

Substitution of Eq. (28) into Eq. (27) gives:

$$\bar{C}_{Y^+L^-} = \frac{K'_{H,Y} \cdot (\bar{C}_L^{tot} - \bar{C}_R^{tot}) \cdot a_{Y^+}}{a_{H^+} + K'_{H,Y} \cdot a_{Y^+}}. \quad (29)$$

It can be easily shown that in the present case the free calixarenate ion concentration is described by the equation:

$$\bar{C}_{L^-} = \sqrt{\frac{\bar{C}_{R^+L^-}}{(k_{ass})_{R^+L^-}} + \frac{\bar{C}_{Y^+L^-}}{(k_{ass})_{Y^+L^-}}}, \quad (30)$$

where $(k_{ass})_{R^+L^-}$, $(k_{ass})_{Y^+L^-}$ are the respective association constants.

Since the ion associate R^+L^- does not participate in the exchange process Eq. (6), its equilibrium concentration is described by Eq. (24). Substituting Eqs. (24) and (29) into Eq. (30), we find the equilibrium concentration of the free calixarenate ion $\bar{C}_{L^-}$. Further, calculating the concentration $\bar{C}_{LH}$ of the molecular form of calixarene from mass balance Eq. (28) and substituting the resultant $\bar{C}_{L^-}$ and $\bar{C}_{LH}$ into Eq. (9), we can calculate the electrode response.

In the limiting case, where the exchange of hydrogen ions for cations Y^+ occurs almost completely, relations:

$$\bar{C}_{Y^+L^-} = \bar{C}_L^{tot} - \bar{C}_R^{tot}, \quad (31)$$

$$\bar{C}_{L^-} = \sqrt{\frac{\bar{C}_R^{tot}}{(k_{ass})_{R^+L^-}} + \frac{(\bar{C}_L^{tot} - \bar{C}_R^{tot})}{(k_{ass})_{Y^+L^-}}}, \quad (32)$$

are valid, and the equilibrium concentration of the molecular calixarene form is very low and calculated from the exchange equilibrium:

$$\bar{C}_{LH} = \frac{(\bar{C}_L^{tot} - \bar{C}_R^{tot}) \cdot a_{H^+}}{K'_{H,Y} \cdot a_{Y^+}}. \quad (33)$$

Substitution of Eqs. (32) and (33) into Eq. (9) gives:

$$E = E^0 + \frac{RT}{F} \ln \frac{a_{Y^+} K'_{HY} \cdot \sqrt{\frac{\bar{C}_R^{tot}}{(k_{ass})_{R^+L^-}} + \frac{(\bar{C}_L^{tot} - \bar{C}_R^{tot})}{(k_{ass})_{Y^+L^-}}}}{K_a \cdot (\bar{C}_L^{tot} - \bar{C}_R^{tot})} \quad (34)$$

In this case, the potential is independent of pH and is a function of the activity of the cation Y^+ in the solution studied. The expression for the selectivity coefficient:

$$K_{ij}^{Pot} = K'_{H,Y} \cdot \sqrt{\frac{(k_{ass})_{R^+L^-}}{(k_{ass})_{Y^+L^-}} \cdot \left(\frac{\bar{C}_L^{tot} - \bar{C}_R^{tot}}{\bar{C}_R^{tot}} \right) + 1} \quad (35)$$

follows from a comparison of Eq. (34) and Eq. (26). It follows from Eq. (35) that in this case the selectivity coefficient depends on the constant of the exchange process, the membrane composition and the ratio of the constants of association of the calixarenate ion with the cation exchanger R^+ and the interfering cation Y^+.

In this case, the lower detection limit for hydrogen ions calculated as the intersection point of extrapolated linear sections of the electrode function that are described by Eqs. (26) and (34), is expressed by the equation:

$$a_{H^+}(\mathrm{LDL}) = a_{Y^+} \cdot K'_{H,Y} \cdot \sqrt{\frac{(k_{ass})_{R^+L^-}}{(k_{ass})_{Y^+L^-}} \cdot \left(\frac{\bar{C}_L^{tot} - \bar{C}_R^{tot}}{\bar{C}_R^{tot}} \right) + 1} \quad (36)$$

Or, in view of the fact that:

$$K'_{H,Y} = \frac{k_{Y^+}}{k_{H^+}} \cdot K_a \cdot (k_{ass})_{Y^+L^-}, \quad (37)$$

where k_{Y^+}, k_{H^+} are so-called individual distribution coefficients of the respective ions introduced by Eisenman [45] and K_a is the acid dissociation

constant for calixarene in the membrane, we obtain:

$$a_{H^+}(\mathrm{LDL}) = a_{Y^+} \cdot K_a \cdot \frac{k_{Y^+}}{k_{H^+}} \cdot (k_{ass})_{Y^+L^-} \sqrt{\frac{(k_{ass})_{R^+L^-}}{(k_{ass})_{Y^+L^-}} \cdot \left(\frac{\bar{C}_L^{tot} - \bar{C}_R^{tot}}{\bar{C}_R^{tot}}\right) + 1}. \quad (38)$$

Eq. (38) describes LDL as a function of acidity of calixarene LH, lipophilicity and activity of the foreign ion Y^+, of the membrane composition and of the ratio of ion association constants.

In the region of low pH, where acid is extracted from the solution studied following Eq. (8), the concentration R^+L^- in the contacting membrane layer is described by equation:

$$\bar{C}_{R^+L^-} = \frac{\bar{C}_{R^+X^-} \cdot \bar{C}_{LH}}{K'_{ex} \cdot a_{H^+} \cdot a_{X^-}}. \quad (39)$$

Proceeding from the mass balance conditions for ion exchanger and calixarene, we obtain, respectively:

$$\bar{C}_{R^+X^-} = \bar{C}_R^{tot} - \bar{C}_{R^+L^-}, \quad (40)$$

$$\bar{C}_{LH} = \bar{C}_L^{tot} - \bar{C}_{R^+L^-}. \quad (41)$$

Substituting Eqs. (40) and (41) into Eq. (39), we obtain the quadratic equation for $\bar{C}_{R^+L^-}$, whose solution gives:

$$\bar{C}_{R^+L^-} = \frac{\bar{C}_R^{tot} + \bar{C}_L^{tot} + K'_{ex} \cdot a_{H^+} \cdot a_{X^-}}{+\sqrt{(\bar{C}_R^{tot} + \bar{C}_L^{tot} + K'_{ex} \cdot a_{H^+} \cdot a_{X^-})^2 - 4 \cdot \bar{C}_R^{tot} \cdot \bar{C}_L^{tot}}2} \quad (42)$$

Further, calculating the free calixarenate ion concentration from:

$$\bar{C}_{L^-} = \frac{\bar{C}_{R^+L^-}}{\bar{C}_{R^+} \cdot (k_{ass})_{R^+L^-}} \quad (43)$$

where $\bar{C}_{R^+}$ is described by the equation:

$$\bar{C}_{R^+} = \sqrt{\frac{\bar{C}_{R^+L^-}}{(k_{ass})_{R^+L^-}} + \frac{\bar{C}_R^{tot} - \bar{C}_{R^+L^-}}{(k_{ass})_{R^+X^-}}} \quad (44)$$

and finding the concentration of the molecular calixarene form from Eq. (41) and substituting the obtained values into Eq. (9), we can calculate the electrode response.

In the limiting case, when equilibrium of process Eq. (8) is substantially shifted rightwards, the relation is valid:

$$\bar{C}_{R^+X^-} = \bar{C}_R^{tot}. \quad (45)$$

In this case, the concentration of the molecular calixarene concentration is described by Eq. (20), and the concentration of the ion associate R^+L^- is very low and can be calculated from the equilibrium constant of process illustrated in Eq. (8) as:

$$\bar{C}_{R^+L^-} = \frac{\bar{C}_R^{tot} \cdot \bar{C}_L^{tot}}{K'_{ex} \cdot a_{H^+} \cdot a_{X^-}}. \quad (46)$$

In this case the concentration of the free ion L^- is described by Eq. (43) and the concentration of the cation R^+ is determined by the expression:

$$\bar{C}_{R^+} = \sqrt{\frac{\bar{C}_R^{tot}}{(k_{ass})_{R^+X^-}}}. \quad (47)$$

The substitution of Eqs. (46) and (47) into Eq. (43) gives:

$$\bar{C}_{L^-} \frac{\bar{C}_L^{tot} \cdot \sqrt{\bar{C}_R^{tot} \cdot (k_{ass})_{R^+X^-}}}{K'_{ex} \cdot (k_{ass})_{R^+L^-} \cdot a_{H^+} \cdot a_{X^-}}. \quad (48)$$

Substituting Eqs. (48) and (20) into Eq. (9), we obtain the equation which describes the electrode response:

$$E = E^0 + \frac{RT}{F} \ln \frac{\sqrt{\bar{C}_R^{tot} \cdot (k_{ass})_{R^+X^-}}}{K_a \cdot K'_{ex} \cdot (k_{ass})_{R^+L^-} \cdot a_{X^-}}. \quad (49)$$

In this case the potential is independent of pH and is a function of the activity of the anion X^- in the solution studied. Calculating the upper detection limit for hydrogen ions as the intersection point of extrapolated linear sections of the electrode function, described by Eqs. (26) and (49), we obtain:

$$a_{H^+}(\mathrm{UDL}) = \frac{(\bar{C}_L^{tot} - \bar{C}_R^{tot}) \cdot \sqrt{(k_{ass})_{R^+X^-}}}{K'_{ex} \cdot \sqrt{(k_{ass})_{R^+L^-} \cdot a_{X^-}}} \quad (50)$$

Or, in view of the fact that:

$$K'_{ex} = \frac{1}{K_a} \cdot k_{H^+} \cdot k_{X^-} \cdot \frac{(k_{ass})_{R^+X^-}}{(k_{ass})_{R^+L^-}}, \quad (51)$$

where k_{H^+}, k_{X^-} are individual distribution coefficients, we obtain the equation which describes UDL as a function of acidity of calixarene LH,

lipophilicity and activity of the anion X^-, the membrane composition and the ratio of ion association constants:

$$a_{H^+}(\mathrm{UDL}) = \frac{K_a \cdot (\bar{C}_L^{tot} - \bar{C}_P^{\tau o \tau}) \cdot \sqrt{(k_{ass})_{R+L-}}}{k_{H^+} \cdot k_{X^-} \cdot \sqrt{(k_{ass})_{R+X-}} \cdot a_{X^-}}. \quad (52)$$

4. Results and discussion

Fig. 2 is comparison of electrode functions of calix[4]arene, *p*-tertbutylcalix[4]arene and tridecylamine-based ISEs in standard conditions (on the background of 0.2 M NaCl). As can be seen, the electrodes based on both calixarenes have a measuring range of about the same width which exceeds the measuring range of the tridecylamine-based ISE by about 1.5–2 pH units.

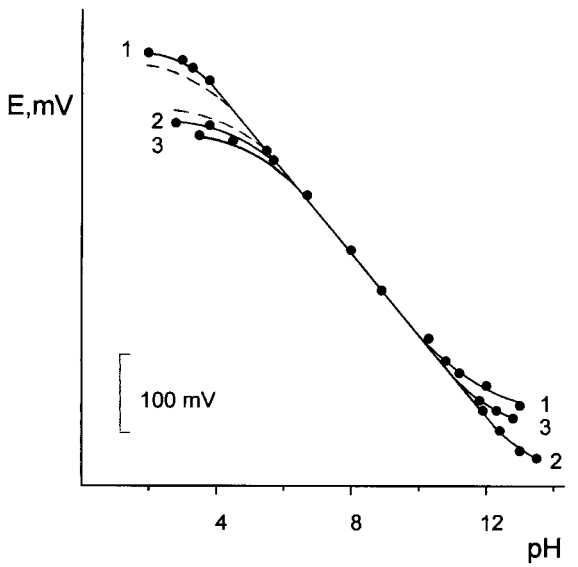

Fig. 2. The effect of the nature of neutral carriers on the electrode response of pH-ISEs in universal buffer solutions on the background of NaCl 0.2 M: experimental (-●-) and calculated (---). All the membranes contain PVC and *o*-nitrophenyloctyl ether (1:2). The electrode-active substances are (1) I and V, (2) II and V, (3) VII and VI, the concentrations of electrode-active substances here and later are given in Section 2. To calculate the electrode response according to Eqs. (9) and (41)–(44), the following assumptions were made: $(K_{ass})_{R+L-} = (k_{ass})_{R+X-}$, the values K'_{ex} are equal to those experimentally obtained in water–toluene system: 3.86×10^2 for I and 2.68×10^3 for II, respectively.

While the measuring range for the considered electrodes is defined as the activity range between the upper and lower detection limits, as was done by Bakker [19] for neutral carrier-based pH electrodes, for the case of complete dissociation we obtain from Eqs. (18) and (23):

$$\Delta\mathrm{pH} = \log\frac{a_{H^+(\mathrm{UDL})}}{a_{H^+(\mathrm{LDL})}} = \log\frac{\bar{C}_R^{tot} \cdot (\bar{C}_L^{tot} - \bar{C}_R^{tot})}{K_{H,Y} \cdot K_{ex} \cdot a_{Y^+} \cdot a_{X^-}}. \quad (53)$$

Or, in view of the fact that:

$$K_{H,Y} \cdot K_{ex} = \frac{\bar{C}_{Y^+} \cdot \bar{C}_{X^-}}{a_{Y^+} \cdot a_{X^-}} \equiv K_{X,Y}, \quad (54)$$

we obtain the equation which coincides with Bakker's equation for membranes based on neutral carriers of amine nature [19]:

$$\Delta\mathrm{pH} = \log\frac{\bar{C}_R^{tot} \cdot (\bar{C}_L^{tot} - \bar{C}_R^{tot})}{K_{X,Y} \cdot a_{Y^+} \cdot a_{X^-}}. \quad (55)$$

It follows from Eq. (55) that with the assumption of complete ion dissociation in the membrane, differences in the measuring ranges between calixarene- and tridecylamine-based membranes should be determined only by quantitative differences in the membrane composition. After appropriate calculations (membrane compositions are given in Section 2), we obtain that all the three membranes should have approximately the same measuring range (for the amine-containing membranes, ΔpH is about 0.1 pH units wider than it is for the calixarene-containing membranes). But the real situation is quite different. Thus, the model which assumes complete ion dissociation in the membrane fails to explain the differences observed.

For the case of strong association, the measuring range is determined in a similar way from Eqs. (38) and (52) as:

$$\Delta\mathrm{pH} = \log\frac{\bar{C}_L^{tot} - \bar{C}_R^{tot}}{K_{X,Y} \cdot a_{Y^+} \cdot a_{X^-}} - \frac{1}{2}\left[\log(k_{ass})_{R+X-} + \log(k_{ass})_{Y+L-} + \log\left(\frac{\bar{C}_L^{tot} - \bar{C}_R^{tot}}{\bar{C}_R^{tot}} + \frac{(k_{ass})_{Y+L-}}{(k_{ass})_{R+L-}}\right)\right] \quad (56)$$

A similar expression can also be obtained for amine-type neutral carriers-based membranes which contain salt of the protonated amine cation LH^+ with the lipophilic anion R^- and the free amine L [46]:

$$\Delta pH = \log\frac{\bar{C}_L^{tot} - \bar{C}_R^{tot}}{K_{X,Y}\cdot a_{Y^+}\cdot a_{X^-}} - \frac{1}{2}\left[\log(k_{ass})_{LH^+X^-} + \frac{1}{2}\log(k_{ass})_{Y^+R^-} + \frac{1}{2}\log\left(\frac{\bar{C}_l^{tot} - \bar{C}_R^{tot}}{\bar{C}_R^{tot}} + \frac{(k_{ass})_{LH^+X^-}}{(k_{ass})_{LH^+R^-}}\right)\right]. \quad (57)$$

The form of Eqs. (56) and (57) is practically the same. However, association constants which are present in them are assigned to different compounds and can be substantially different in value. Therefore, even if the other (concentration and solvation) conditions are equal, ion association effects can bring about differences in the measuring range for the electrodes based on calixarenes and amines. Pairwise comparison of the association constants which enter into Eqs. (56) and (57) allows the following conclusions.

1. If R^+ is the quaternary ammonium cation and LH^+ is the protonated tertiary amine cation, then $(k_{ass})_{R^+X^-} \ll (k_{ass})_{LH^+X^-}$ This conclusion is based on the known fact that even in nitrobenzene, association constants for quaternary ammonium salts are lower by about three orders of magnitude than association constants for amine salts [47]. Moreover, in media with a lower dielectric constant, this difference should be even larger.
2. If L^- is a calixarenate ion and R^- is tetraphenylborate, it is most likely that $(k_{ass})_{Y^+L^-} > (k_{ass})_{Y^+R^-}$.The quantitative aspect of this inequality is uncertain, though it is most likely that the difference in the association constants is not very large, since, as can be judged from operation of H-selective membranes based on calixarenes, in the region of high pH, the calixarenate ion is not likely to have any substantial abilities to form complexes with metal cations. If R is the lipophilic sulfonic acid anion, then, it is most likely that $(k_{ass})_{Y^+L^-} < (k_{ass})_{Y^+R^-}$
3. Quaternary ammonium salts have extraordinarily low association constants [47]. Therefore the relation $\frac{(k_{ass})_{Y^+L^-}}{(k_{ass})_{R^+L^-}}$ should be much more than unity (except for the case, where Y^+ is the quaternary ammonium cation). On the other hand, in media with a moderate dielectric constant association constants of tetraphenylborate and chloride with quaternary ammonium cations differ by two orders of magnitude [48]. As shown in [49], in the case of the salts of tertiary amines dependence of the association constant on the nature of the anion is even stronger than in the case of quaternary ammonium salts. Thus, the ratio $\frac{(k_{ass})_{LH^+X^-}}{(k_{ass})_{LH^+R^-}}$ should also be much higher than unity. It is difficult to evaluate these ratios, however, it can be expected that even though $\frac{(k_{ass})_{Y^+L^-}}{(k_{ass})_{R^+L^-}} > \frac{(k_{ass})_{LH^+X^-}}{(k_{ass})_{LH^+R^-}}$, this difference is not too large.

Thus, the experimentally observed difference in the measuring range of ISEs based on calixarenes in comparison with amine-based ISEs is probably caused, primarily, by the difference in the association constant of the quaternary ammonium cation R^+ and the tertiary amine cation LH^+ with the background anion X^-.

The observed displacement of the measuring range of the calix[4]arene-based ISEs into the region of low pH in comparison with *p*-tertbutylcalix[4]arene-based ISEs agree with Eqs. (38) and (52), since, according to the theory of the effect of substituents in the benzene ring [50], calix[4]arene is a stronger acid in comparison with *p*-tertbutylcalix[4]arene.

Fig. 3 is an illustration of the effect of nature and concentration of the background anion X^- on the electrode response in the region of low pH. The experimental curves *E*-pH satisfactorily agree with those theoretically calculated according to Eqs. (9) and (41)–(44) with the K'_{ex} experimentally determined in the model system water-toluene with the assumption of equality of the association constants $(k_{ass})_{R^+L^-}$ and $(k_{ass})_{R^+X^-}$ in the membrane.

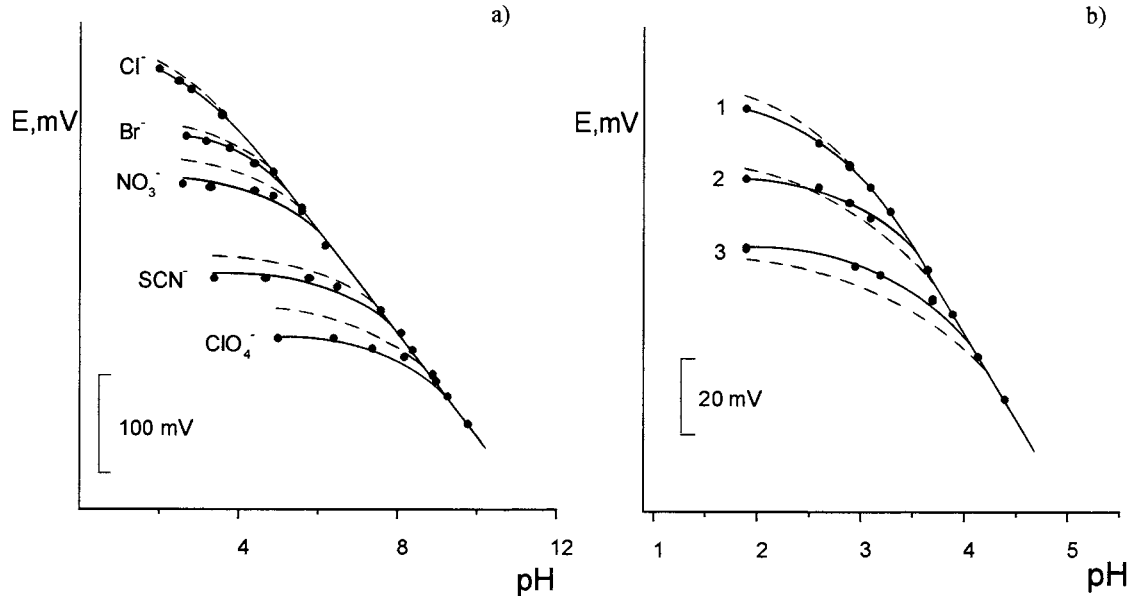

Fig. 3. The effect of the nature of the background electrolyte (a) and its concentration (b) on the electrode response of pH-ISEs based on (I) and (V) at low pH region: experimental (-●-) and calculated (---). (a) The background concentration is 0.02 M; the background electrolytes are indicated in the figure; the plasticizer is *o*-nitrophenyloctyl ether. (b) The background electrolyte is NaCl (1) 0.02 M, (2) 0.07 M, (3) 0.2 M; the plasticizer is dibutylphthalate. To calculate the electrode response according to Eqs. (9) and (41)–(44), the following assumptions were made: $(K_{ass})_{R+L^-} = (k_{ass})_{R+X^-}$, the values K'_{ex} are equal to those experimentally obtained in water–toluene system: 3.86×10^2 for Cl^-, 7.41×10^3 for Br^-, 3.55×10^4 for NO_3^-, 4.02×10^6 for SCN^-, 3.11×10^7 for ClO_4^-.

Fig. 4 illustrates the effect of the nature and concentration of the background cation Y^+ on the operation of ISEs in the region of high pH. In solutions containing the tetraethylammonium cation, for which the exchange constant $K'_{H,Y}$ is estimated in the model system (Section 2), the experimental curves *E*-pH agree well with the theoretical curves calculated from Eqs. (9), (24) and (28)–(30) with the assumption of $(k_{ass})_{R+L^-} = (k_{ass})_{Y+L^-}$.

Fig. 5 illustrates the effect of the plasticizer nature on the measuring range of ISEs. One can see that use of *o*-nitrophenyloctyl ether instead of dibytylphthalate is accompanied by noticeable expansion of the measuring range, while in the case of THP used as a plasticizer, the measuring range becomes substantially narrower, especially, from the region of high pH. The effect of *o*-nitrophenyloctyl ether can be explained qualitatively by the action of two factors: solvation and ion association. As it was indicated by Bakker et al. [19], plasticizers with ester functions can coordinate interfering metal cations, whereas *o*-NPOE lacks such functions. On the other hand, the high dielectric constant of *o*-NPOE can also play its role which results in a decrease in association constants and their leveling, which, in accordance with Eq. (56), should be accompanied by expansion of the measuring range. In the case of THP, the solvation factor is evidently controlling. This plasticizer which has high basicity [51] is capable of effective solvation of metal cations, which results in an increase in $K'_{H,Y}$ and, according to Eq. (36), in an increase in LDL.

It is interesting to compare characteristics of ISEs based on calixarenes and different compounds which provide for the operation of ISEs, following a similar mechanism. In Fig. 6 one can see the electrode functions of ISEs based on 3-nonyloxyphenol and palmitic acid. It can be seen

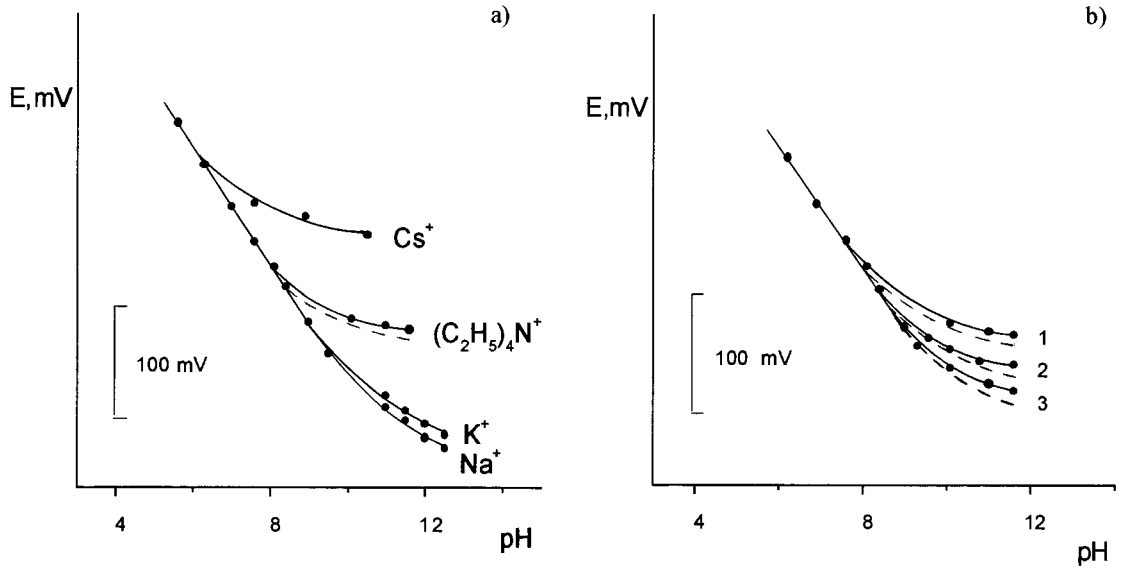

Fig. 4. The effect of the nature of the bakground electrolyte (a) and its concentration (b) on the electrode response of pH-ISEs at high pH region: experimental (-●-) and calculated (---).The electrode-active substances are I and V. (a) The background electrolytes are (1) NaCl (0.2 M), (2) KCl (0.2 M), (3) $(C_2H_5)_4NCl$ (0.02 M), (4) CsCl (0.02 M). (b) The background electrolyte is $(C_2H_5)_4NCl$: (1) 0.02 M, (2) 0.007 M, (3) 0.002 M. To calculate the electrode response according to Eqs. (9), (24) and (28)–(30), the following assumptions were made: $(k_{ass})_{R+L-} = (k_{ass})_{Y+L-}$, $K'_{H,Y} = 7.08 \times 10^{-9}$ (this value was estimated as described in experimental for the extraction system water–(DBP–chloroform mixture 2:1).

that these compounds actually provide for the pH response in a certain pH range, but for them the measuring range is much narrower than it is in the case of calixarenes used as ionophores.

In the case of 3-nonyloxyphenol, the measuring range is narrowed mainly at the cost of the upper detection limit (UDL). This can be explained by the solvation effect which is caused by participation of 3-nonyloxyphenol in anion solvation. In particular, this effect is exhibited in substantial levelling the exchange constants of picrate ion for hydrophylic anions in the presence of 3-nonyloxyphenol in the toluene phase, in comparison with exchange constants in pure toluene (Table 1). For example, for chloride ions, in the presence of 3-nonyloxyphenol the exchange constant becomes larger by two orders of magnitude. It is interesting to note that the presence of calixarenes in the toluene phase has almost no effect on the anion exchange constants, which indicates low solvation ability of calixarenes in relation to anions and is probably caused by formation of intramolecular hydrogen bonds. In view of the fact that the effect of leveling the exchange constants observed in the presence of 3-nonyloxyphenol is of a different nature (since the picrate ion is also solvated), it should be expected that the rate of increase of k_{X-} will be even higher, which is confirmed indirectly by the data of Table 2. In view of the structure of calixarenes, it can be suggested reasonably that values of K_a and, consequently, K'_{ex} (Eq. (51)) for them should be comparable with the respective values for 3-nonyloxyphenol. Meanwhile, it is experimentally found that K'_{ex} for hydrophylic anions in the presence of 3-nonyloxyphenol (Table 2) are higher by four to five orders of magnitude than they are in the presence of calixarenes. As a result, UDL decreases accordingly.

In the case of ISEs based on palmitic acid, two factors should be taken into consideration. First, the solvation ability of the molecular acid form in relation to anions, which should lead to a decrease in UDL, in a way similar to the case of

3-nonyloxyphenol. Second, the complexing ability of palmitic acid anion in relation to metal cations, which should be accompanied by an increase in $(k_{ass})_{Y+L-}$ and, according to Eq. (38) will lead to growth of LDL. These two factors result in substantial narrowing of the measuring range.

5. Conclusion

The model of strong ion association in the membrane which is considered in the present work is certainly abstraction, and in real membranes, especially those containing plasticizers with a high dielectric constant, the part of free ions can be appreciable [52]. Nevertheless, it is useful, since consideration of this model allows at least qualitative interpretation of experimentally observed differences in the width of the measuring range for ISEs based on amines and calixarenes. Moreover, it can be expected that correlations between association constants and measuring ranges of such ISEs that follow from Eqs. (38), (52) and (56) should be preserved, at least qualitatively (as a trend) in markedly dissociated systems too, in which the free ions concentration cannot be neglected in the mass balance equations.

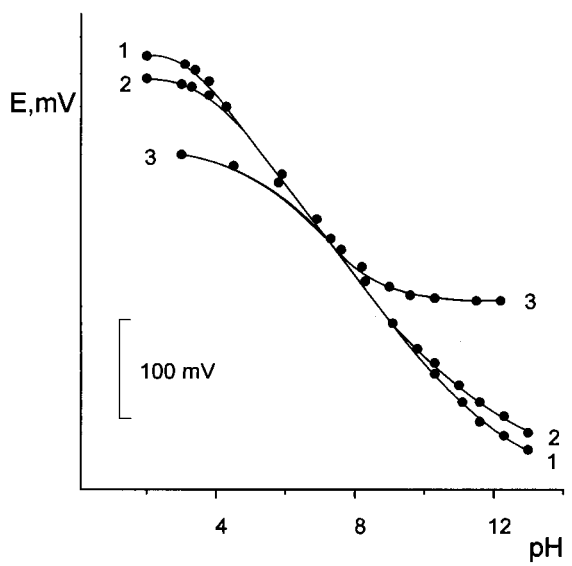

Fig. 5. The effect of the nature of the plasticiser on the operation range of pH-ISEs in universal buffer solutions. The background electrolyte is NaCl 0.2 M. The plasticizers are: (1) *o*-nitrophenyloctyl ether, (2) dibutylphthalate, (3) trihexylphosphate. The electrode-active substances are I and V.

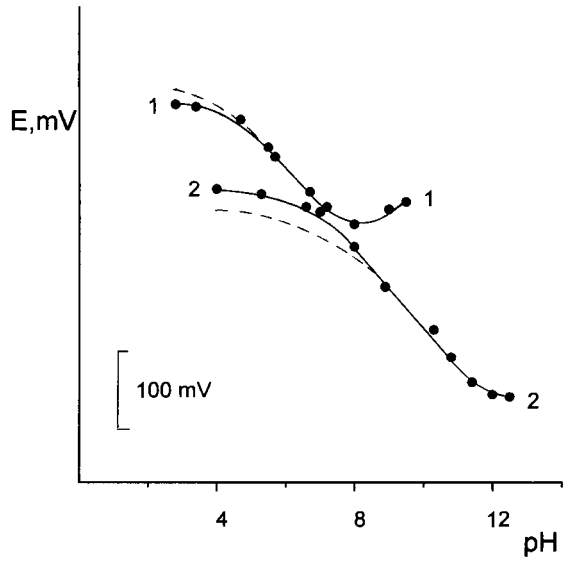

Fig. 6. The electrode response of pH-ISEs based on IV and V (1) and III and V (2) in universal buffer solutions on the background of NaCl 0.2 M: experimental (-●-) and calculated (---). The plasticizers are (1) dibutylphthalate and (2) *o*-nitrophenyloctyl ether. To calculate the electrode response according to Eqs. (9) and (41)–(44), the following assumptions were made: $(k_{ass})_{R+L-} = (k_{ass})_{R+X-}$, the values K'_{ex} are equal to those experimentally obtained in water–toluene and water–(toluene–DBP 9:1) systems: 1.77×10^7 for III and 1.79×10^3 for IV, respectively.

The results of the present study suggest, in particular, that the wide measuring range that can be attained for pH-ISEs based on calixarenes is caused by a favorable combination of the following factors:

- a rather low ability of quaternary ammonium ions (for example, in comparison with protonated amine cations) to associate with background anions;
- a low solvation ability of molecular calixarene forms in relation to background anions;
- a low complexing ability of calixarenate ions in relation to cations.

The measuring range is also expanded as the dielectric constant increases and the solvation ability of the plasticizer decreases.

References

[1] R.L. Coon, N.C.J. Lai, J.P. Kampine, J. Appl. Physiol. 40 (1976) 625.
[2] D. Erne, D. Ammann, W. Simon, Chimia 33 (1979) 88.
[3] P. Schulthess, Y. Shijo, H.V. Pham, E. Pretsch, D. Ammann, W. Simon, Anal. Chim. Acta 131 (1981) 111.
[4] D. Ammann, F. Lanter, R.A. Steiner, P. Schulthess, Y. Shijo, W. Simon, Anal. Chem. 53 (1981) 2267.
[5] D. Erne, K.V. Schenker, D. Ammann, E. Pretsch, W. Simon, Chimia 35 (1981) 178.
[6] P. Anker, D. Ammann, W. Simon, Microchim. Acta 1 (1983) 237.
[7] C. Hongbo, E.H. Hansen, J. Růžička, Anal. Chim. Acta 169 (1985) 209.
[8] V.V. Egorov, Ya.F. Lushchik, G.L. Starabinets, V.A. Shevtsova, Vestsi AN BSSR, Ser, Khim. Nauk, 4 (1985) 50.
[9] U. Oesch, Z. Brzŏzka, A. Xu, B. Rusterholz, G. Suter, H.V. Pham, D.H. Welti, D. Ammann, E. Pretsch, W. Simon, Anal. Chem. 58 (1986) 2285.
[10] G.L. Starobinets, V.V. Egorov, Ya.F. Lushehik, Zh. Anal. Khim. 41 (1986) 1030.
[11] U. Oesch, Z. Brzŏzka, A. Xu, W. Simon, Med. Biol. Eng. Comput. 25 (1987) 414.
[12] H.-L. Wu, R.-Q. Yu, Talanta 34 (1987) 577.
[13] P. Chao, D. Ammann, U. Oesch, W. Simon, F. Lang, Pflügers Arch. 411 (1988) 216.
[14] V.V. Egorov, Ya.F. Lushchik, Elektrokhim. 24 (1988) 983.
[15] V.V. Egorov, Ya.F. Lushchik, Talanta 37 (1990) 461.
[16] L.T. Jin, Z.L. Shi, J.N. Ye, J.G. Qian, V.Z. Fang, Anal. Chim. Acta 244 (1991) 165.
[17] R. Yuan, Y.Y. Chai, R.Q. Yu, Analyst 117 (1992) 1891.
[18] T.J. Cardwell, R.W. Cattrall, L.W. Deddy, K.A. Murphy, Aust. J. Chem. 45 (1992) 435.
[19] E. Bakker, A. Xu, E. Pretsch, Anal. Chim. Acta 295 (1994) 253.
[20] V.V. Egorov, Ya.F. Lushchik, V.A. Novash, Zh. Anal. Khim. 49 (1994) 620.
[21] K.N. Mikhel'son, O.V. Mukhacheva, V.M. Lutov, V.Ya. Semenii, A.N. Khutsishvili, USSR Author Sert., 1326977 IB, 1987, 28.
[22] E. Lindner, V.V. Cosofret, R.P. Kusy, R.P. Buck, T. Rosatzin, U. Shaller, W. Simon, J. Jeney, K. Toth, E. Pungor, Talanta 40 (1993) 957.
[23] V.V. Cosofret, T.M. Nahir, E. Lindner, R.P. Buck, Electroanal. Chem. Interfacial Electrochem. 327 (1992) 137.
[24] T.M. Nahir, R.P. Buck, Helv. Chim. Acta 76 (1993) 407.
[25] S.C. Ma, N.A. Chaniotakis, M.E. Meyerhoff, Anal. Chem. 60 (1988) 2293.
[26] S.C. Ma, M.E. Meyerhoff, Mikrochim. Acta 1 (1990) 197.
[27] V.V. Cosofret, E. Lindner, R.P. Buck, R.P. Kusy, J.Q. Whitley, J. Electroanal. Chem. 345 (1993) 169.
[28] E. Lindner, T. Rosatzin, J. Jeney, V.V. Cosofret, W. Simon, R.P. Buck, J. Electroanal. Chem. 352 (1993) 309.
[29] R.P. Buck, V.V. Cosofret, E. Lindner, Anal. Chim. Acta 282 (1993) 273.
[30] V.V. Cosofret, E. Lindner, R.P. Buck, R.P. Kusy, J.Q. Whitley, Electroanalysis 5 (1993) 725.
[31] V.V. Egorov, Ya.F. Lushchik, T.A. Ovsjannikova, O.G. Kulinkovich, I.V. Astapovich, Zh. Anal. Khim. 52 (1997) 292.
[32] J.D. Loon, A. Arduini, W. Verboom, R. Ungaro, G.J. Hummel, S. Harkema, D.N. Reinhoudt, Tetrahedron Lett. 30 (1989) 2681.
[33] C.D. Gutche, L. Lin, Tetrahedron 42 (1986) 1663.
[34] Veigand-Hilgetag, The Methods of the Experiment in Organic Chemistry, Khimia, Moscow, 1968.
[35] G.L. Starobinets, E.M. Rakhman'ko, S.M. Lestchev, T.V. Tsyplenkova, USSR Author Sert., 702003, IB, 1979, 45.
[36] Ya.F. Lushchik, Some Regularities of the Functioning and Analytical Application of Cation-Selective Electrodes Based on Lipophilic Sulphonic Acids and their Compositions with Neutral Carriers, Kand. Diss., Minsk, 1988.
[37] T.M. Alkhazishili, N.V. Astakhova, V.V. Egorov, Z.F. Kirpichnikova, L.V. Koleshko, E.M. Rakhman'ko, G.L. Starobinets, Yu.M. Tarasova, A.N. Khutsishvili, USSR Author Sert., 1310401, IB, 1987, 18.
[38] K. Cammann, Das Arbeiten mit Ionenselektiven Elektroden, Springer, Berlin, 1979.
[39] Yu.Y. Lur'e, A Handbook on Analytical Chemistry, Khimiya, Moscow, 1979.
[40] W.E. Morf, The Principles of ISEs and of Membrane Transport, Academia Kiado, Budapest, 1981.
[41] U. Schaller, E. Bakker, U.E. Spichiger, E. Pretsch, Anal. Chem. 66 (1994) 391.
[42] E. Bakker, M. Nägele, U. Schaller, E. Pretsch, Electroanalysis 7 (1995) 817.
[43] E. Bakker, R.K. Meruva, E. Pretsch, M.E. Meyerhoff, Anal. Chem. 66 (1994) 3021.
[44] R.P. Buck, E. Lindner, Pure Appl. Chem. 66 (1994) 2527.
[45] J. Sandblom, G. Eisenman, J.L. Walker, J. Phys. Chem. 71 (1967) 3862.
[46] V.V. Egorov, Ya.F. Lushchik, Yu.V. Sin'kevich, Elektrokhimia 34 (1998) 1480.
[47] C.R. Witschonke, C.A. Kraus, J. Am. Chem. Soc. 69 (1947) 2472.
[48] V.V. Egorov, N.D. Borisenko, E.M. Rakhman'ko, Y.F. Lushchic, S.S. Kacharskii, Talanta 44 (1997) 1735.
[49] E.M. Rakman'ko, Physico-Chemical foundations of application of extraction by lipophilic quaternary ammonium salts in analysis, Doct. Diss., Minsk, 1994.
[50] C.K. Ingold, Structure and Mechanism in Organic Chemistry, Cornell University Press, London, 1969.
[51] V. Gutmann, Coordination Chemistry in Non-Aqueous Solutions, Springer, New York, 1968.
[52] R.D. Armstrong, G. Horvai, Electrochim. Acta 35 (1990) 1.

ELSEVIER

Talanta 48 (1999) 39–47

Talanta

Determination of platinum and ruthenium in Pt and Pt–Ru catalysts with carbon support by direct and derivative spectrophotometry

Maria Balcerzak *, Elżbieta Święcicka, Elżbieta Balukiewicz

Department of Analytical Chemistry, Warsaw University of Technology, Noakowskiego 3, 00-664 Warsaw, Poland

Received 2 March 1998; received in revised form 13 May 1998; accepted 22 May 1998

Abstract

Platinum and ruthenium in carbon supported Pt and Pt–Ru catalysts were determined by direct and derivative spectrophotometric methods. Complexes of platinum and ruthenium with $SnCl_3^-$ ligands (tin(II) chloride in HCl) were used to determine both metals in solutions obtained after digestion of the samples of the catalysts. Platinum in the Pt/C catalyst can be determined in solutions obtained by digestion of the samples in aqua regia. Derivative spectrophotometry was used to determine both metals in the presence of each other in solutions obtained after digestion of samples of the Pt–Ru/C catalyst in the mixture of $HCl + HNO_3$ (6:1). The first derivative at 377 nm ('zero-crossing' point of ruthenium) and the second-derivative values at 495 nm ('zero-crossing' point of platinum) were used to estimate the concentration of platinum and ruthenium, respectively.

Keywords: Noble metals analysis; Platinum; Ruthenium; Derivative spectrophotometry

1. Introduction

Catalysts of the platinum group metals have been widely used in various chemical processes. The excellent chemisorption, selective activity towards reactants and resistance to oxidation at high temperature make them very effective catalysts, e.g. in ammonia oxidation, petroleum reforming, Fischer–Tropsch synthesis and the pharmaceutical industry. Platinum, palladium and rhodium are widely used as components of automotive catalysts. They reduce the emission of nitrogen oxides, carbon monoxide and hydrocarbons into the environment. Platinum metals show an excellent performance in many catalytic combustion processes used for obtaining more controllable energy with minimal release of pollutants into the environment [1,2]. These processes involve a reaction of fuel with oxygen absorbed on the catalyst. The combination of two or three platinum metals usually shows significantly higher catalytic activity as compared with a single metal. An active catalyst is usually distributed over a

* Corresponding author. Tel.: +48 22 6607471; fax: +48 22 6282741; e-mail: mbal@ch.pw.edu.pl

0039-9140/99/$ - see front matter
PII S0039-9140(98)00212-4

large surface area and a thermally stable support (e.g. alumina, carbon, SnO_2 or V_2O_5).

Recently, platinum and ruthenium have been applied in fuel cells as effective catalysts, e.g. in the electro-oxidation reaction: $MeOH + H_2O \rightarrow CO_2 + 6H^+ + 6e$. Catalysts, in the form of metal black, dispersed on the surface of the support, can be prepared by chemical reduction of the appropriate salt solutions. Pt–Ru bimetallic catalysts supported on activated carbon provide a significant increase in the efficiency of the anodic reaction of methanol oxidation as compared with single Pt catalysts [3–6]. Ruthenium increases the amount of OH_{ads} or O_{ads} species, which enhance the catalytic activity of platinum to oxidize methanol at higher potentials. It is supposed that ruthenium exists on the surface of the catalysts in the form of a hydrous oxide. The increased activity of Pt at lower potentials is probably connected with the enhanced number of active sites in the presence of ruthenium.

Other metals and compounds, e.g. Sn, ZrO_2 and Nb_2O_5 have also been used to enhance the catalytic activity of platinum. They help to maintain the catalytic properties of the active components, but usually have little or no catalytic activity of their own.

The purpose of this work was to develop methods for the determination of platinum (ca. 20%) and ruthenium (ca. 3%) in carbon supported Pt and Pt–Ru catalysts used in the electro-oxidation of methanol. The spectrophotometric measurements employ complexes of platinum and ruthenium with $SnCl_3^-$ ligands. The application of derivative spectrophotometry allowed the determination of platinum and ruthenium in the same solutions without separation of the metals. The separation step is usually necessary prior to the determination of the noble metals by most analytical techniques [7]. Methods of the determination of a particular metal in a mixture are of special interest. They usually enable the carrying out the determination in a shorter time and enhance the precision of the results.

Derivative spectrophotometric methods based on mathematical processing of overlapping absorption spectra enable one to isolate an individual signal of a particular element from the mixture. Interfering effects can be eliminated by selection of a suitable derivative order and the wavelength value. The derivative spectra can be easily calculated with the aid of appropriate software. Theoretical and instrumental aspects of the derivative spectrophotometric technique are discussed in detail [8].

2. Experimental

2.1. Apparatus and reagents

The absorbance was measured and the absorption spectra were recorded using a Hitachi U-3300 spectrophotometer (Japan) with 1-cm cells. Derivative spectra were calculated using the GRAMS/386 program (Galactic Industries) and the Savitzky–Golay algorithm.

The ruthenium standard solution (1 mg ml^{-1} Ru) was prepared by fusion of 100.0 mg powdered ruthenium in a silver crucible with 1 g sodium peroxide. The temperature was gradually increased to a dark red glow (ca. 450°C) and maintained for 10 min. The sample was allowed to cool, dissolved in water, and acidified with conc. HCl. The mixture was heated and the coagulated AgCl was filtered and washed with 0.1 M HCl. The filtrate was diluted to 100.0 ml with 1 M HCl.

The platinum standard solution (1.0 mg ml^{-1} Pt) was prepared by dissolving 100.0 mg platinum (99.99%) in 16 ml aqua regia. The solution obtained was evaporated almost to dryness. Conc. HCl (3 ml) was added and the solution was evaporated once again. The residue was dissolved in 1 M HCl and the solution obtained was diluted to 100.0 ml with 1 M HCl.

Tin(II) chloride was used as a 1 M solution in 2 M HCl.

2.2. Procedures

2.2.1. Determination of platinum in the Pt/C catalysts

An accurate weight (in the range of 2–20 mg) of the Pt/C catalyst was placed in a quartz crucible. Carbon was removed from the sample by

carefully burning it (on the gas burner). The residue was dissolved in 4 ml aqua regia. The solution obtained was evaporated almost to dryness. Conc. HCl (3 ml) was added and the solution was evaporated almost to dryness once again. The residue was dissolved in 2 M HCl. The solution obtained was transferred into a 25-ml volumetric flask (a 1/5 volume of the solution obtained was used for the determination in the samples above 5 mg). $SnCl_2$ (1.25 ml 1 M) was added and the solution was made up to the mark with 2 M HCl. The absorbance of the solution was measured at 402 nm against the blank. The concentration of platinum was calculated using the appropriate regression equation.

2.2.2. Determination of platinum and ruthenium in the Pt–Ru/C catalysts

An accurate weight (in the range of 2–20 mg) of the Pt–Ru/C catalyst was placed in a 25-ml beaker. The sample was treated with 3.5 ml $HCl + HNO_3$ (6:1) and heated on a hot plate for ca. 2 h. Carbon was separated from the sample by filtering it. The filtered solution was evaporated almost to dryness. Conc. HCl (3 ml) was added and the evaporation repeated. The residue was dissolved in 5 M HCl and transferred into a 25-ml volumetric flask (again a 1/5 volume of the solution obtained was used for the determination in the samples above 5 mg). $SnCl_2$ (1.25 ml) was added and the solution was diluted up to the mark with 5 M HCl. The solution was heated at 90 ± 1°C for 45 min. The sample was cooled to room temperature. The spectrum of the solution was recorded in the range 300–700 nm against the blank at the following instrumental parameters: interpoint distance 0.2 nm, slit 1 nm, scan speed 120 nm min^{-1}.

The first derivative absorption spectrum was calculated (with 75 points and a second degree polynomial). The value of the first derivative was measured at 377 nm. The concentration of platinum was calculated using an appropriate regression equation.

The second derivative spectrum was calculated (with 75 points and a second degree polynomial, by consecutive calculation from the first derivative values). The value of the second derivative was measured at 495 nm. The concentration of ruthenium was calculated using the appropriate regression equation.

3. Results and Discussion

3.1. Digestion procedures

Two digestion procedures for Pt/C and Pt–Ru/C catalysts were examined. In the first one the samples examined were subjected to preliminary burning in order to remove carbon before dissolution of platinum and ruthenium. The process of burning should be carried out very carefully because of possible losses of the metals which can escape from the samples with the tiny carbon particles. The oxidation of carbon in an oven with a controlled temperature was also carried out to check the reproducibility of the burning conditions.

The residue was treated with hot aqua regia to convert platinum and ruthenium into soluble chloride complexes. Nitroso complexes of platinum and ruthenium, which can be formed during the dissolution of metals in aqua regia, can be decomposed by evaporation of the solutions with hydrochloric acid. In this study the excess of nitric acid was removed from the samples before the determination of the metals by double evaporation with hydrochloric acid.

In the second digestion procedure the samples of the catalysts were directly treated with aqua regia in the presence of carbon. The carbon was separated by filtration after 2 h heating of the mixture on a hot plate. Small samples are convenient for the dissolution of the samples in acids due to the high volume of the activated carbon. Platinum and ruthenium were determined in the filtrate after removal of the excess of nitric acid.

Instead of aqua regia a mixture of $HCl + HNO_3$ (6:1) was used for the quantitative digestion of the samples of Pt–Ru catalysts, in order to reduce the amount of nitric acid used. According to the literature [9] losses of ruthenium may occur

during heating of the samples in HNO_3 medium, due to the oxidation to RuO_4. The volatilization of ruthenium can be enhanced by high nitric acid concentration, high temperature and prolonged heating. The mixture of $HCl + HNO_3$ (6:1) was applied previously for digestion of a Pt–Ru(4) alloy [10]. No losses of ruthenium were observed.

3.2. Determination of platinum in the Pt/C catalyst

In chloride solutions platinum, as well as the other noble metals, reacts with $SnCl_3^-$ ligands with the formation of an anionic, yellow complex [11–14]. The complex is formed at room temperature immediately after mixing up the reagents. The experiments carried out in this study showed that platinum was quantitatively converted into the complex in 0.8–6.0 M hydrochloric acid and 0.02–0.5 M $SnCl_2$. A solution of 2 M HCl and 0.05 M $SnCl_2$ was considered as the optimum for the formation of the complex. Nitric acid should be removed from the solutions before the reaction of platinum with tin(II) chloride.

The molar absorptivity of the complex at $\lambda_{max} = 402$ nm is 8.3×10^3 l mol^{-1} cm^{-1} (Fig. 1a curves 1 and 2). Beer's law is obeyed up to 35 μg Pt ml^{-1}. The regression equation is $y = 0.041c - 0.0016$, where y is the absorbance measured and c is the concentration of platinum (μg ml^{-1}). The correlation coefficient $R^2 = 0.9948$. The precision and accuracy of the determination of platinum with tin(II) chloride are shown in Table 1. The R.S.D. is 0.5–1.1%.

Platinum in the solution obtained after digestion of the Pt/C catalyst was determined after conversion into the above complex. The obtained results show good agreement independently of the digestion procedure used (Table 2). Platinum (16.7%) was determined when the carbon was separated (by burning on the gas burner or in the oven (R.S.D. 0.9 and 0.5%, respectively)) prior to the dissolution of the samples in aqua regia. Platinum at 16.8% (R.S.D. 1.1%) and 16.6% (R.S.D. 1.0%) was determined after treatment of the samples with aqua regia or with the mixture of $HCl + HNO_3$ (6:1) followed by separation of carbon by filtration.

The accuracy of the determination of platinum in the catalyst was examined by analyzing samples with known amounts of platinum (100 and 250 μg Pt in the form of a chloride complex) added to the samples before the digestion step. Quantitative recovery of platinum was observed for all digestion procedures used. The quick removal of carbon by burning on the gas burner substantially shortens the time of analysis. This procedure was chosen as the optimum for digestion of the Pt/C catalyst.

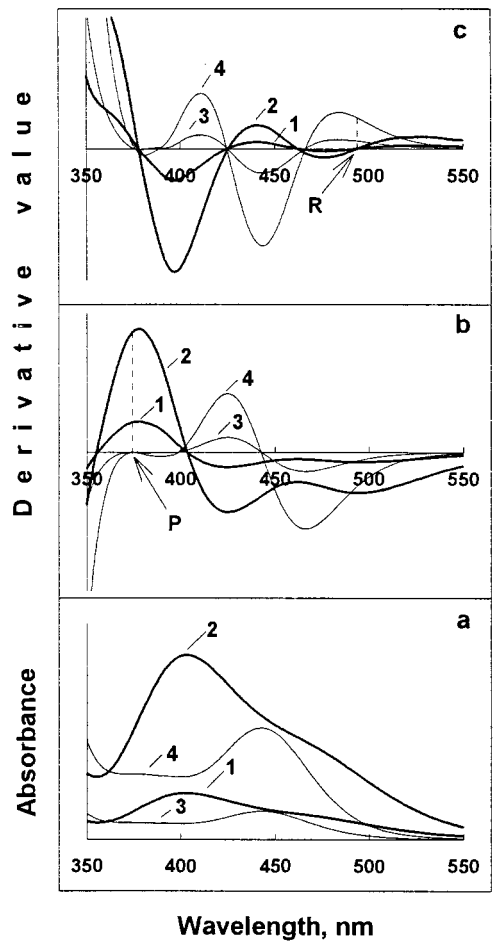

Fig. 1. Direct (a) and derivative (first-order (b) and second-order (c)) spectra of the complexes of platinum (6 and 24 μg Pt ml^{-1}, curves 1 and 2, respectively) and ruthenium (6 and 24 μg Ru ml^{-1}, curves 3 and 4, respectively) with tin(II) chloride.

Table 1
Statistical evaluation of the results of the determination of platinum in the form of the complex with tin(II) chloride by direct spectrophotometry

Platinum (μg)		S.D. (μg)	R.S.D. (%)	Confidence limits[b] (μg)
Added	Found[a]			
200.0	200.1	2.20	1.1	200 ± 2
400.0	402.4	2.89	0.7	402 ± 3
800.0	801.9	3.49	0.5	802 ± 4

[a] $n = 6$.
[b] $\alpha = 0.05$.

3.3. Determination of platinum and ruthenium in the Pt–Ru/C catalyst

Ruthenium reacts with tin(II) chloride in hydrochloric acid with the formation of an anionic complex with $SnCl_3^-$ ligands [11,12,15]. Quantitative conversion of ruthenium into the complex takes place in the medium 5 M HCl and 0.05 M $SnCl_2$ after 45 min heating at 90 ± 1°C [13]. The molar absorptivity of the complex at $\lambda_{max} = 445$ nm is 2.7×10^3 l mol^{-1} cm^{-1} (Fig. 1 curves 3 and 4). Platinum is also quantitatively converted into a complex with $SnCl_3^-$ groups under the same conditions as for ruthenium. No changes in the spectrum of the platinum complex were observed when heating the solution. However, the determination of platinum and ruthenium in the presence of each other by direct spectrophotometry is not possible because the spectra of the complexes examined overlap in the whole wavelength range of interest (Fig. 1a).

The experiments have shown that the signals of both metals can be resolved by applying derivative spectrophotometry. The GRAMS/386 program from Galactic Industries and the Savitzky–Golay algorithm [16] were used to calculate the derivative spectra. The derivative spectra obtained from the zeroth-order spectra of the complexes of platinum and ruthenium with tin(II) chloride are shown in Fig. 1b and c. Satisfactory smoothed spectra were obtained when a second degree polynomial and 75 points were used for the calculation.

It was found that platinum could be determined in the presence of ruthenium by first-derivative spectrophotometry (Fig. 1b curves 1 and 2). The first derivative spectrum of ruthenium crosses the zero line at 377 nm (Fig. 1b curves 3 and 4, point P) independently of the ruthenium concentration. The value of the signal for platinum corresponding to the 'zero-crossing' point of ruthenium can be a basis for the determination of platinum. This value depends only on the platinum concentration in the solutions examined. The calibration curve for the determination of platinum at 377 nm is linear up to 28 μg ml^{-1}. The regression equation is $y = 1.88 \times 10^{-4}c - 1.08 \times 10^{-5}$ ($R^2 = 0.9999$). The sensitivity of the method, calculated as $s_{y/x}/m$, where $s_{y/x}$ and m are the average deviation from the regression line and the slope of the calibration curve, respectively, equals to 0.07 μg Pt ml^{-1}.

The consecutive calculation of the second derivative spectra enables one to isolate the signal of ruthenium from the mixture with platinum. The second-derivative spectrum of platinum crosses the zero line at $\lambda = 495$ nm (Fig. 1c curves 1 and 2, point R) independently of the platinum concentration. The value of the second derivative of ruthenium at the 'zero-crossing' point of platinum corresponds only to the concentration of ruthenium in the solution examined. The linear concentration range for the determination of ruthenium at 495 nm by the second-derivative spectrophotometry is up to 35 μg ml^{-1}. The regression equation is $y = 4.75 \times 10^{-7}c - 3.85 \times 10^{-8}$ ($R^2 = 0.9998$). The sensitivity of the method ($s_{y/x}/m$) amounts to 0.13 μg Ru ml^{-1}.

Derivative spectra of mixtures containing various amounts of platinum and ruthenium are

Table 2
The results of the determination of platinum in a Pt/C catalyst by direct spectrophotometry

Sample weight (mg)	Platinum added (μg)	Platinum found (μg)	Platinum content (%)
Preliminary burning of the carbon on the gas burner			
3.3		556	16.9
3.8		638	16.8
4.3		717	16.7
9.8		1630	16.6
2.4	100	502	16.8
3.9	250	896	16.6
$\bar{x} = 16.7\%$, $s = 0.15\%$, R.S.D. $= 0.9\%$, $\mu = 16.7 \pm 0.2\%$ ($\alpha = 0.05\%$)			
Preliminary burning of the carbon in the oven			
16.0	2669	16.7	
16.0		2683	16.8
17.2		2880	16.7
17.7		2944	16.6
16.6	100	2866	16.7
17.3	250	3118	16.6
$\bar{x} = 16.7\%$, $s = 0.08\%$, R.S.D. $= 0.5\%$, $\mu = 16.7 \pm 0.1\%$ ($\alpha = 0.05\%$)			
Direct digestion in aqua regia			
3.5		586	16.7
5.9		983	16.7
9.1		1515	16.6
12.5		2084	16.7
7.9	100	1431	16.8
2.1	250	609	17.1
$\bar{x} = 16.8\%$, $s = 0.18\%$, R.S.D. $= 1.1\%$, $\mu = 16.8 \pm 0.2\%$ ($\alpha = 0.05\%$)			
Direct digestion in $HCl + HNO_3$ (6:1)			
4.2		692	16.5
4.6		763	16.6
4.6		765	16.6
5.4		898	16.6
1.9	100	420	16.8
6.4	250	1295	16.3
$\bar{x} = 16.6\%$, $s = 0.17\%$, R.S.D. $= 1.0\%$, $\mu = 16.6 \pm 0.2\%$ ($\alpha = 0.05\%$)			

shown in Fig. 2. The R.S.D. of the results obtained for the concentration of both metals in the synthetic mixtures do not exceed 1.5 and 3.3% for platinum and ruthenium, respectively (Table 3).

Platinum and ruthenium in the Pt–Ru/C catalyst were determined by the methods developed. More reproducible and higher results for the content of ruthenium (3.4%, R.S.D. 4.4%) were obtained when the samples examined were digested by direct treatment with a mixture of acids $HCl + HNO_3$ (6:1) in the presence of carbon (Table 4). Losses of ruthenium (ca. 80–90%) were observed when the preliminary separation of carbon by burning was applied. These losses may be due to the conversion of ruthenium at high temperature into ruthenium dioxide which, in contrast to the hydrous form, is insoluble in acid [7]. Partial oxidation of ruthenium at higher temperature into a volatile tetroxide is also possible. Quantitative recovery of platinum was observed when the samples were treated with acids in the presence of carbon (Table 5). Platinum at 22.3% (R.S.D. 1.5%) and 22.2% (R.S.D. 0.9%) were determined after direct digestion of the samples in aqua regia and in the mixture $HCl + HNO_3$ (6:1), respectively.

The accuracy of the determination of both metals was evaluated by analyzing samples of the

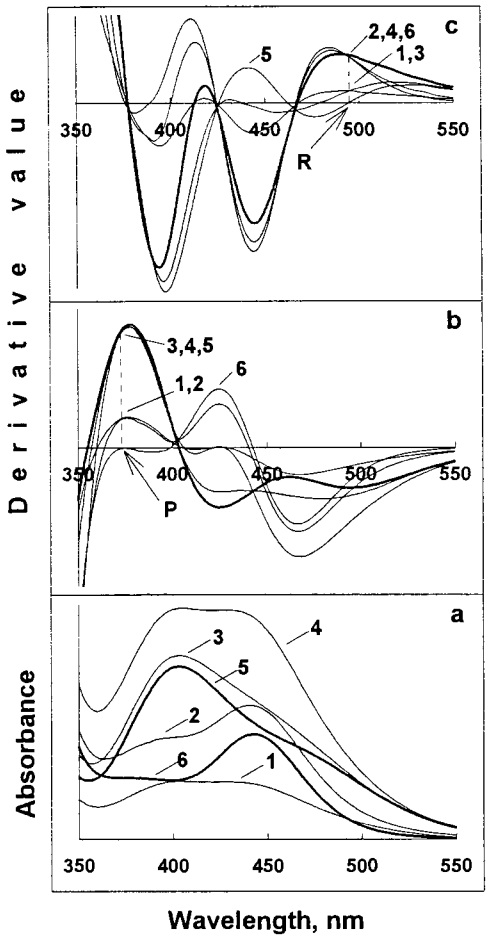

Fig. 2. Direct (a), first-order (b) and second-order (c) derivative spectra of mixtures of platinum and ruthenium complexes with tin(II) chloride: 6 μg Pt ml^{-1} + 6 μg Ru ml^{-1} and 24 μg Ru ml^{-1}, curves 1 and 2, respectively; 24 μg Pt ml^{-1} + 6 μg Ru ml^{-1} and 24 μg Ru ml^{-1}, curves 3 and 4, respectively; 24 μg Pt ml^{-1} (curve 5) and 24 μg Ru ml^{-1} (curve 6).

catalyst to which known amounts of ruthenium (100 and 500 μg) and platinum (100, 250 and 1898 μg) were added. Both metals, in the form of chloride complexes, were introduced to the samples before the digestion step. The results obtained (Tables 4 and 5) confirm the quantitative recovery of both metals from the catalyst samples examined.

4. Conclusions

Platinum and ruthenium in Pt and Pt–Ru catalysts with carbon support can be determined by spectrophotometric and derivative spectrophotometric methods. The complexes of both metals with tin(II) chloride can be used for the determination.

Platinum in the Pt/C catalyst can be determined directly in the solutions obtained after digestion of the samples in aqua regia and the transformation of platinum into a complex with $SnCl_3^-$ ligands. Carbon can be eliminated by burning prior to the treatment of the samples with aqua regia.

Platinum and ruthenium in the Pt–Ru/C catalyst can be determined in the same solutions by numerical calculation of the first- and second-order derivative spectra, respectively. The mixture $HCl + HNO_3$ (6:1) was chosen for the digestion of the samples of the Pt–Ru/C catalyst. Losses of ruthenium were observed when the burning step was applied for removing the carbon. Carbon can be separated from the samples by filtration after dissolution of both metals.

Table 3
Statistical evaluation of the results of the determination of platinum and ruthenium in synthetic mixtures by first- and second-order derivative spectrophotometry

Pt+Ru added (μg)	Pt+Ru determined[a] (μg)	S.D. Pt/Ru (μg)	R.S.D. Pt/Ru (%)	Confidence limits[b] Pt/Ru (μg)
150.0+150.0	149.3+150.6	1.27/1.42	0.9/0.9	149 ± 1/151 ± 2
150.0+600.0	149.8+611.0	3.64/4.26	1.5/0.7	150 ± 4/611 ± 5
600.0+150.0	581.2+153.5	1.07/5.12	0.2/3.3	581 ± 1/154 ± 5
600.0+600.0	580.0+609.3	3.54/4.87	0.6/0.8	580 ± 4/609 ± 5

[a] $n = 6$.
[b] $\alpha = 0.05$.

Table 4
The results of the determination of ruthenium in a Pt–Ru/C catalyst by second derivative spectrophotometry

Sample weight (mg)	Ruthenium added (μg)	Ruthenium found (μg)	Ruthenium content (%)
Direct digestion in aqua regia			
14.7		413	2.8
21.7		603	2.8
11.5		329	2.9
14.8		418	2.8
10.1		284	2.8
11.1		362	3.3
23.9	500	1260	3.2
13.1	500	886	3.0
$\bar{x} = 3.0\%$, $s = 0.21\%$, R.S.D. = 7.0%, $\mu = 3 \pm 0.2\%$ ($\alpha = 0.05\%$)			
Direct digestion in $HCl + HNO_3$ (6:1)			
10.2		365	3.6
7.4		264	3.6
8.5		296	3.5
9.5		325	3.4
2.6		86	3.3
2.1		69	3.3
2.1	100	168	3.2
2.6	100	187	3.3
$\bar{x} = 3.4\%$, $s = 0.15\%$, R.S.D. = 4.4%, $\mu = 3.4 \pm 0.1\%$ ($\alpha = 0.05\%$)			

Table 5
The results of the determination of platinum in a Pt–Ru/C catalyst by first derivative spectrophotometry

Sample weight (mg)	Platinum added (μg)	Platinum found (μg)	Platinum content (%)
Direct digestion in aqua regia			
14.7		3231	22.0
21.7		4705	21.7
11.5		2566	22.3
14.8		3301	22.3
23.9		5393	22.0
13.1		2946	22.6
10.1	1898	4118	22.6
11.1	1898	4402	22.5
$\bar{x} = 22.3\%$, $s = 0.33\%$, R.S.D. = 1.5%, $\mu = 22.3 \pm 0.3\%$ ($\alpha = 0.05\%$)			
Direct digestion in $HCl + HNO_3$ (6:1)			
10.2		2294	22.5
7.4		1650	22.3
8.5		1905	22.4
9.5		2088	22.0
2.1		671	22.1
2.6		711	22.2
2.6	100	465	22.0
2.1	250	578	22.0
$\bar{x} = 22.2\%$, $s = 0.20\%$, R.S.D. = 0.9%, $\mu = 22.2 \pm 0.2\%$ ($\alpha = 0.05\%$)			

Acknowledgements

The authors wish to thank Professor Jan Przyłuski of the Warsaw University of Technology for providing the samples of the catalysts for analysis. The work was supported by the State Committee for Scientific Research (Project No. 3 T09A 042 08 sponsored 1995–1997).

References

[1] G.W. Cordonna, M. Kosanovich, E.R. Becker, Plat. Met. Rev. 33 (1989) 46.
[2] F.R. Hartley, Chemistry of the Platinum Group Metals, Elsevier, Amsterdam, 1991, pp. 60–74.
[3] A. Hamnett, G.L. Troughton, Chem. Ind. (London) 13 (1992) 480.
[4] M. Uchida, Y. Aoyama, M. Tanabe, N. Yanagihara, N. Eda, A. Ohta, J. Electrochem. Soc. 142 (1995) 2572.
[5] A.S. Aricò, Z. Połtarzewski, H. Kim, A. Morana, G. Giordano, V. Antonucci, J. Power Sources 55 (1995) 159.
[6] B.R. Rauche, F.R. McLarnon, E.J. Cairns, J. Electrochem. Soc. 142 (1995) 1073.
[7] J.C. Van Loon, R.R. Barefoot, Determination of the Precious Metals, Wiley, Chichester, 1991.
[8] G. Talsky, Derivative Spectrophotometry, VCH, Weinheim, 1994.
[9] T. Sato, J. Radioanal. Nucl. Chem. 129 (1989) 77.
[10] Z. Marczenko, M. Balcerzak, Chem. Anal. (Warsaw) 24 (1979) 867.
[11] F.J. Young, R.D. Gillard, G. Wilkinson, J. Chem. Soc. (1964) 5176.
[12] M. Balcerzak, Analusis 22 (1994) 353.
[13] O.I. Milner, G.F. Shipman, Anal. Chem. 27 (1955) 1476.
[14] S.S. Berman, E.C. Goodhue, Can. J. Chem. 37 (1959) 370.
[15] M. Balcerźak, W. Woźniak, Microchem. J. 37 (1988) 326.
[16] A. Savitzky, M.J.E. Golay, Anal. Chem. 36 (1964) 1627.

.

ELSEVIER

Talanta 48 (1999) 49–55

Talanta

Separation and preconcentration of metal ions and their estimation in vitamin, steel and milk samples using *o*-vanillin-immobilized silica gel

B.S. Garg, R.K. Sharma *, J.S. Bist, N. Bhojak, Sachin Mittal

Department of Chemistry, University of Delhi, Delhi-110007, India

Received 20 January 1998; received in revised form 28 May 1998; accepted 8 June 1998

Abstract

o-Vanillin-immobilized silica gel has been used for the adsorption and estimation of copper, cobalt, iron and zinc by both batch and column techniques. Metal ions were quantitatively retained on the column packed with immobilized silica gel in the pH range 4.0–6.0 for Cu, 5.0–6.0 for Co, 4.5–6.0 for Fe and 6.0–8.0 for Zn. The distribution coefficient D determined for each metal was as follows (ml g^{-1}): Fe, 5.4×10^2; Cu, 4.9×10^2; Zn, 4.4×10^2; Co, 3.8×10^2. Methods have been developed to estimate zinc, copper and cobalt in milk, steel and vitamin samples, respectively.

Keywords: *o*-Vanillin; Immobilized silica gel; Metal ions; Solid phase extraction; Milk; Steel; Vitamin

1. Introduction

Many methods have been developed for the preconcentration of trace metals from various samples. These include coprecipitation, electrodeposition, liquid–liquid extraction, solid–liquid extraction and filter papers impregnated with chelating agent. However, the solid phase extraction approach has gained rapid acceptance because of its amenability to automation and the availability of a wide variety of sorbent phases.

Chelating solid phases can be tailor-made for selective trace metal analysis with applications in both solid phase extraction and liquid chromatography [1,2]. Appropriate chelating reagents can be chemically bonded to or otherwise immobilized on to support matrices, thus providing complexing or chelating solid phases. Many materials such as dithiocarbamate cellulose [3], styrene–divinylbenzene matrix functionalised with iminodiacetic acid [4–6], dimethylglyoxalbis(4-phenyl-3-thiosemicarbazone) [7], 8-quinolinol [8,9] and 2-(2-(5-chloropyridylazo)-5-dimethylamino)-phenol [8] and silica gel functionalised with 1-propanethiol [10,11], didecylaminoethyl-β-tridecylammonium iodide [12], *N*-propyl-*N*′-(1-(2-thiobenzothiazole)-2,2′,2″-trichloroethyl) urea [13], diethyldithio-carbamate [14], poly(*N*-chloranil-*N*,*N*,*N*′,*N*′-tetramethylethylene diammonium di-sulfosalicylate)

* Corresponding author. Tel.: +91 11 7256250; fax: +91 11 7257336; e-mail: dchem1@del2.vsnl.net.in

0039-9140/99/$ - see front matter
PII S0039-9140(98)00223-9

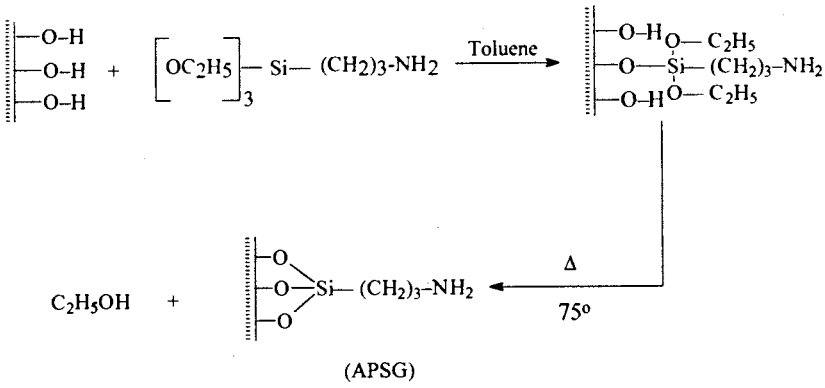

Scheme 1.

[15], amidoxime group [16], 1-nitroso-2-naphthol [17], *o*-phenanthroline [18], 2,2′-bipyridine [18], 3-hydroxy-2-methyl-1,4-naphthoquinone [19] and 2-pyridinecarboxaldehyde phenylhydrazone [20,21] have been used as chelating solid supports. Among these, silica based chelating resins are most commonly used since immobilization reactions on silica are relatively simple, especially when compared to immobilization involving organic polymers. Silica based chelating resins shows fast metal ion-exchange kinetics, the lack of which precludes the use of many organic polymer-based chelating resins [22–26]. Silica has good mechanical strength and swelling stability required for its use in solid phase extraction [27,28].

o-Vanillin and its derivatives are of considerable interest due to their widespread applications in biological [29–31] and analytical fields [32,33]. Goel et al. [34] and other workers [35–38] have demonstrated the strong chelation behaviour of *o*-vanillin with various transition metal ions.

Considering the strong binding behaviour of *o*-vanillin with Fe, Co, Zn, Cu, we have designed and synthesized a silica based *o*-vanillin complexing agent. The batch and column adsorption of various transition metals and its application in the estimation of metal ions in various samples is described.

2. Experimental

2.1. Apparatus

A digital (ECIL model) pH meter 5651A and a Shimadzu AA-640-13 atomic absorption spectrophotometer were used. A glass tube of 100 mm length and 7 mm i.d. was used as a chromatographic column.

2.2. Materials and solvents

o-Vanillin (Fluka) and 3-aminopropyltriethoxy silane (Fluka) were used as obtained. Column chromatographic silica gel (G.S. Chemicals, India), 60–120 mesh was activated by heating it in an oven for 12 h at 200°C before using.

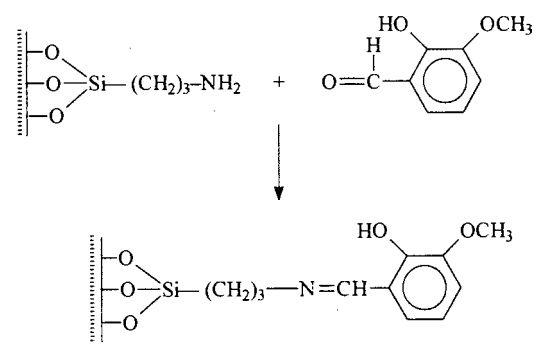

Scheme 2.

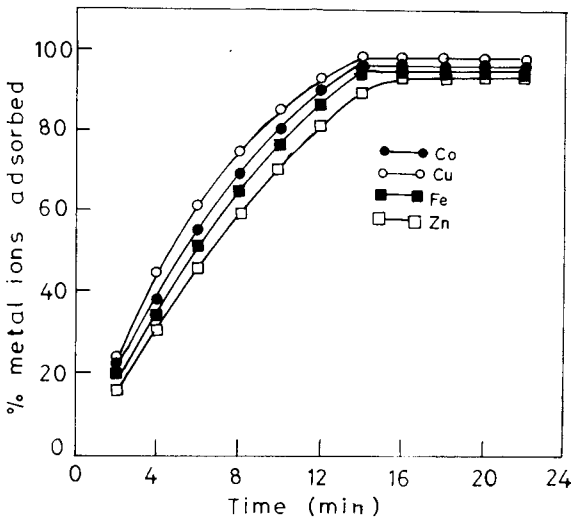

Fig. 1. Plot of percentage metal adsorbed vs. time.

Organic solvents were dried using the methods described in the literature [39]. All metal salts used were of AR grade and double distilled water has been used throughout the study. pH in the range 3.5–6.0 was maintained by acetate buffers by mixing the required volumes of 0.2 M acetic acid and sodium acetate. pH below 3.5 was maintained by HCl, whilst pH above 6.0 was maintained by NaOH solution.

2.3. Preparation of immobilized silica gel

Preparation of the immobilized silica gel was carried out as reported by Kubota et al. [40]. Immobilization of *o*-vanillin on the silica gel was performed in two steps.

2.3.1. Step I

Activated silica gel (50 g) was suspended in 200 ml 10% (v/v) 3-aminopropyltriethoxy silane in dry toluene. The mixture was refluxed for 12 h in a nitrogen atmosphere with constant stirring. The resulting aminopropyl silica gel (APSG) was filtered, washed consecutively with toluene, ethanol and acetone and then heated at 75°C for 10 h in a vacuum line (Scheme 1).

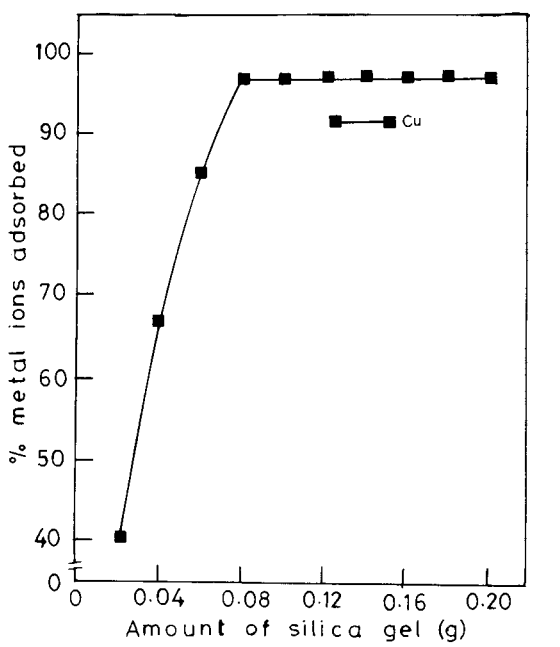

Fig. 2. Plot of percentage metal adsorbed vs. amount of silica gel.

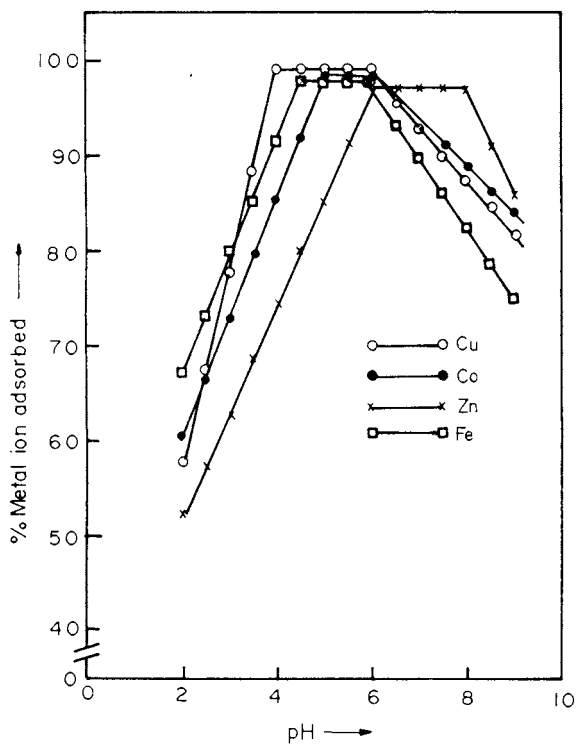

Fig. 3. Plot of percentage metal adsorbed vs. pH.

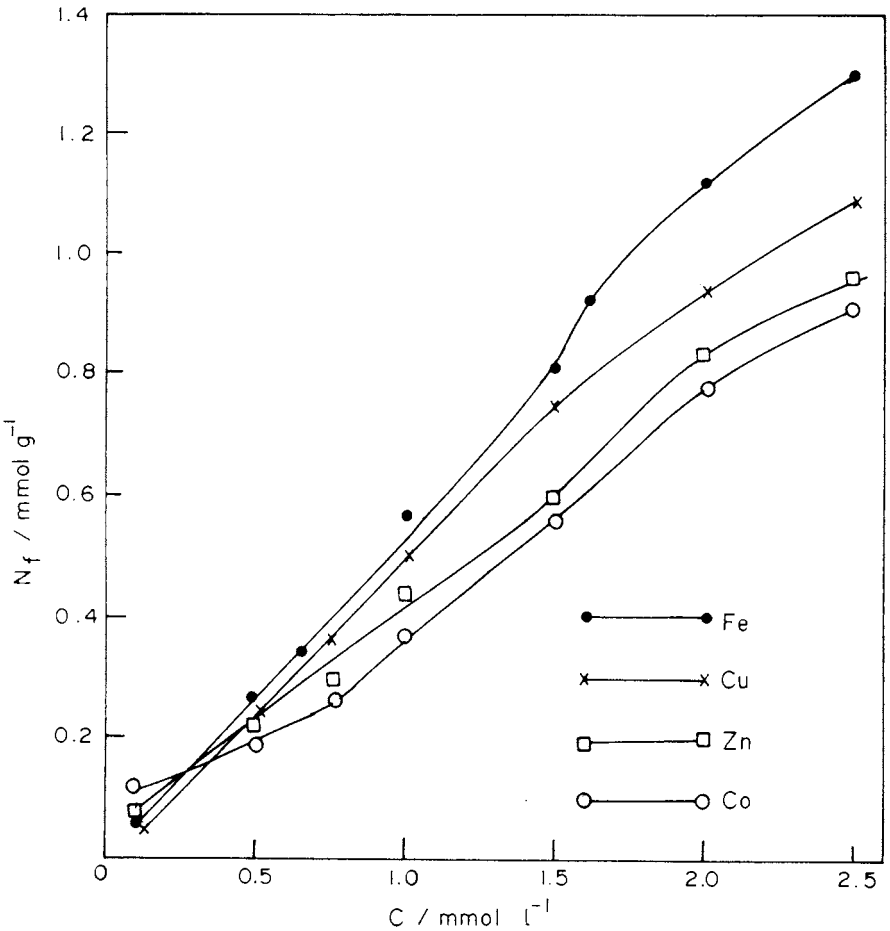

Fig. 4. Adsorption isotherm of metal ions at 25°C. pH: Co, 5.0; Cu, 5.0; Fe, 5.0; Zn, 6.0. Amount of buffer 5.0 ml.

2.3.2. Step II

The APSG (10 g) was reacted with *o*-vanillin (10 g) in anhydrous diethylether with constant stirring. The mixture was filtered, washed and the immobilized silica gel so obtained was heated at 55°C for 8 h in a vacuum line (Scheme 2).

The infrared spectrum confirmed the occurrence of coupling reaction. The band at 1640 cm^{-1} is due to the C–N stretching frequency of the imino group.

2.4. Procedure

2.4.1. Batch experiment

Immobilized silica gel was equilibrated with a suitable amount of metal ion solution for a fixed period of time and the unreacted metal ion was determined in the supernatant by atomic absorption spectroscopy (MS).

2.4.2. Column experiment

For the column experiment, the immobilized silica gel was packed in the glass column and individual metal ion solutions at a definite pH (between 4.0–8.0) were percolated at a flow rate of 2 ml min^{-1}. The metal ions were then eluted from the column using 0.1 N HNO_3 and determined by AAS. Each metal experiment was carried out in triplicate in order to determine the precision of the method.

2.4.3. Optimization of adsorption time

The time required for the solid liquid system to

Table 1
Preconcentration and recovery of metal ions

Ion	Concentration of metal ions (mg l^{-1})	pH	Recovery (mg l^{-1})	Recovery (%)	S.D.
Fe	5	5.0	4.93	98.6	0.48
Cu	5	5.0	4.94	98.8	0.56
Zn	5	6.0	4.94	98.8	0.54
Co	5	5.0	4.93	98.6	0.57

Number of experiments, 3; eluent volume, 15 ml.

Table 2
Determination of Cu in steel samples A and B

Sample	Certified composition (%)	Cu taken (%)	Cu found (%)	Recovery (%)	S.D.
A	Cu = 0.22, Mn = 0.74, C = 0.24, Si = 0.31, Cr = 1.17, Mo = 0.51	0.22	0.215	99	0.69
B	Si = 0.06, Zn = 0.045, Al = 7.50, Cu = 0.04, Mn = 0.24	0.04	0.039	97	0.02

Number of experiments, 3; pH, 5.0.

attain the equilibrium condition was determined by placing 10 ml the solution of metal ions (10 mg l^{-1}) maintained at the required pH in various conical flasks and shaking with 0.08 g modified silica gel. The supernatant from each flask was separated off at different time intervals and the metal ions were determined by AAS. The amount of metal ions adsorbed by the solid phase was determined by the equation:

$$N_f = (x - y)/z \quad (1)$$

where x is the initial amount of metal ions (in mmol l^{-1}), y is the amount of metal ions in the supernatant (in mmol l^{-1}), z is the mass of the modified silica gel (g) and N_f is the amount of metal ions adsorbed per g of modified silica gel.

3. Results and discussion

3.1. Optimization of adsorption time

The time taken for the adsorption of the metal ion and the attainment of the equilibrium condition by the immobilized silica gel is of considerable importance. The time taken for the system to reach equilibrium is found to be about 14 min in the case of Cu, Co, Fe(II) and 16 min for Zn (Fig. 1).

3.2. Effect of amount of modified silica gel

The percentage retention of metal ions on modified silica gel was determined by batch experiment by using different amounts of silica gel. A metal ions solution (10 ml, 10 mg l^{-1}) was maintained at the required pH and diluted to 20 ml and was stirred with different amounts of modified silica gel (between 0.02–0.20 g). The supernatant was removed and the amount of metal ions in it was determined by AAS. The percentage retention of metal ions on the modified silica gel was best when 0.08 g modified silica gel was used. Fig. 2 is representative of all the metals studied though showing only Cu. The percentage recovery for Fe and Co is 98.6% and for Zn is 98.8% when 0.08 g modified silica gel was used.

3.3. Effect of pH

The metal solutions were adjusted to a fixed pH (between 2.0–9.0) and passed through a column at a flow rate of 2 ml min^{-1}. Then the metal ions were eluted from the column and their determination by AAS gave the percentage recoveries of the eluted metal ions at various pH. The pH range studied was between 2.0 and 9.0. Fig. 3 shows the effect of pH on the retention of metal ions on the

Table 3
Determination of Zn in milk samples

Sample	Amount of Zn present (μg g^{-1})	Amount of Zn found (μg g^{-1})	Recovery (%)	S.D.
A	56	52.5	92.8	0.70
B	57	53	92.9	0.56
C	60	55	91.6	0.98

Number of experiments, 3; pH, 6.0.

Table 4
Determination of Co in vitamins

Sample	Co present (mg l^{-1})	Co found (mg l^{-1})	Recovery (%)	S.D.
A	22	20.0	90.9	0.60
B	23	20.8	90.4	0.97
C	21	19.1	90.9	0.70

Number of experiments, 3; pH, 5.0.

immobilized silica gel. Cu has been quantitatively retained in the pH range of 4.0–6.0. In case of Fe, the pH range was found to be 4.5–6.0. Zn shows maximum adsorption in the pH range of 6.0–8.0 while for Co, this pH range is 5.0–6.0.

3.4. Effect of flow rate

The dependency of uptake of the transition metal ions on the flow rate was studied for Cu, Co, Fe and Zn at the pH of maximum complexation, the solution flow rate being varied from 0.5 to 5.0 ml min^{-1}. Adsorption was quantitative and reproducible in the range. The flow rate was maintained at 2 ml min^{-1} throughout the experiment.

3.5. Adsorption isotherms

The adsorption isotherms were determined using the batch technique at 25°C. Solutions of metal ions in the concentration range 2×10^{-5}–2.5×10^{-3} mol l^{-1} were maintained at the required pH (pH 5.0 for Cu, Co and Fe and 6.0 for Zn) with 5 ml buffer and shaken for 45 min with the modified silica gel. The metal ions in the supernatant were determined by AAS and the amount of metal adsorbed was calculated using Eq. (1). The distribution coefficient, D, is defined as $D = N_f/C$, where N_f is expressed in mmol g^{-1}, and C is in mmol ml^{-1}. The average values of D calculated for each metal (ml g^{-1}) in the concentration range 2×10^{-5}–2.5×10^{-3} mol l^{-1}, are found to be: Fe, 5.4×10^2; Cu, 4.9×10^2; Zn, 4.4×10^2; Co, 3.8×10^2 (Fig. 4).

3.6. Effect of temperature

Adsorption of metal ions is found to be affected by the change in temperature. The equilibrium constant for complexation decreases as the temperature is lowered. It was found that adsorption increases with increase in temperature up to 35°C but remained constant after that.

3.7. Effect of electrolytes

Various electrolytes such as sodium chloride, potassium nitrate and potassium chloride caused no improvement in adsorption.

3.8. Preconcentration and recovery of metal ions

The results of preconcentration and recovery of metal ions using the column method are shown in Table 1. It can be seen that in each instance, the recovery is almost 98%. The volume of eluent was 15 ml in every case.

3.9. Determination of Cu in Steel, Zn in milk samples and Co in vitamins

Steel, milk and vitamin samples were prepared as described previously [19]. Recovery data for Cu in steel solutions is given in Table 2. The recovery was found to be 97–99%. Table 3 shows that Zn in milk samples is quantitatively recovered by the immobilized silica gel. Recovery is 92% and thus the separation is quite effective. Co in vitamin samples can by determined by using the immobilized silica gel with a recovery of 90% (Table 4).

4. Conclusion

In conclusions, using a new type of vanillin immobilized silica gel, Fe, Cu, Co and Zn can be readily determined. This solid phase extraction method shows fast metal ion-exchange kinetics and high sorption efficiency. The proposed method is widely applicable for the measurement of trace Cu, Co and Zn in a variety of samples such as steel, milk and vitamins.

Acknowledgements

JSB and NB are thankful to the University Grants Commission (UGC), India and SM is thankful to the Council of Scientific and Industrial Research (CSIR), India for financial assistance.

References

[1] R.K. Sharma, Microchem. J. 51 (1995) 289.
[2] R.K. Sharma, Analyst 126 (1995) 2203.
[3] S. Imai, M. Muroi, R. Matsushita, Anal. Chim. Acta 113 (1980) 139.
[4] R. Bonoforti, R. Ferraorli, Anal. Chim. Acta 162 (1984) 33.
[5] A.J. Paulson, Anal. Chem. 58 (1986) 183.
[6] P. Pakalns, Anal. Chim. Acta 120 (1980) 289.
[7] S. Hoshi, H. Fujuiyama, K. Nakamura, Talanta 41 (1994) 503.
[8] A.N. Masi, R.A. Olsina, Talanta 40 (1993) 931.
[9] L. Elci, M. Soylak, M. Dogan, Fresenius' J. Anal. Chem. 342 (1992) 175.
[10] U. Koklu, S. Akman, O. Gocer, G. Domer, Anal. Lett. 28 (1995) 357.
[11] S. Akman, H. Ince, U. Koklu, Anal. Sci. 7 (1991) 799.
[12] O.A. Zaporozhets, O.Y. Nadzhafora, A.I. Zubenko, V.V. Sukhan, Talanta 41 (1994) 2067.
[13] N.A. D'yachenko, A.K. Trofimchuk, V.V. Sukhan, J. Anal. Chem. 50 (1995) 772.
[14] S. Rio Segada, B. Perez-Cid, C. Bendicho, Fresenius' J. Anal. Chem. 351 (1995) 798.
[15] B.B. Prasad, A. Kumar, S. Sundd, React. Polym. 23 (1994) 229.
[16] I.N. Voloschik, M.L. Litvina, B.A. Rudenko, J. Chromatogr. A 671 (1994) 51.
[17] I.M. Maksimova, E.l. Morosanova, Zh. Anal. Khim. 49 (1994) 602.
[18] Y.J. Park, K.H. Jung, K.K. Park, T.Y. Eom, J. Colloid. Interface Sci. 160 (1993) 324.
[19] B.S. Garg, J.S. Bist, R.K. Sharma, N. Bhojak, Talanta 43 (1996) 2093.
[20] S. Watanesk, A.A. Schilt, Talanta 33 (1986) 895.
[21] N. Simonzadeh, A.A. Schilt, Talanta 35 (1988) 187.
[22] R.E. Sturgeon, S.S. Berman, S.N. Willie, J.A.H. Desauinier, Anal. Chem. 53 (1981) 2337.
[23] F. Vernon, H. Eccles, Anal. Chim. Acta 63 (1972) 403.
[24] D.E. Leyden, in: D.E. Leyden, W.T. Collins (Eds.), Silylated Surfaces, Gordoin and Breach, New York, 1980, p. 321.
[25] T. Seshadri, A. Kuttrup, Fresenius' Z. Anal. Chem. 296 (1979) 247.
[26] D.E. Leyden, G.H. Luttrell, Anal. Chem. 47 (1975) 1612.
[27] R. Van Grieken, Anal. Chim. Acta 143 (1982) 3.
[28] P. Sulthivaiyakit, A. Kettrup, Anal. Chim. Acta 169 (1985) 331.
[29] W. Kazuko, O. Toshihiro, S. Yasuhiko, Mutat. Res. 218 (1989) 105.
[30] S. Takahashi, T. Mutso, A. Yutaka, Biochem. Biophys. Res. Commun. 162 (1989) 1376.
[31] K. Watanabe, O. Kazu, L. Ohta, T. Toshihiro, Mutat. Res. 243 (1990) 273.
[32] D.P. Goel, K.C. Trikha, R.P. Singh, Proc. Indian Acad. Sci. 68 (1968) 82.
[33] D.P. Goel, K.C. Trikha, R.P. Singh, Indian J. Appl. Chem. 32 (1969) 62.
[34] D.P. Goel, K.C. Trikha, R.P. Singh, Indian J. Chem. 6 (1968) 662.
[35] S. Sengupta, N.R. Bannerjee, J. Electrochem. Soc. India 38 (1989) 101.
[36] S. Sengupta, N.R. Bannerjee, Croat. Chem. Acta 62 (1989) 471.
[37] S.S. Kulkarni, M.L. Narwade, Acta Cienc. Indica Chem. 16 (1990) 245.
[38] J.G. Jones, J.B. Poole, J.C. Tomkinson, R.J.P. Williams, J. Chem. Soc. (1958) 2001
[39] Vogel's Textbook of Practical Organic Chemistry, 4th ed., Longman, London, 1978, p. 264.
[40] L.T. Kubota, J.C. Moreia, Y. Gushikem, Analyst 114 (1989) 1385.

ELSEVIER

Talanta 48 (1999) 57–62

Talanta

Separation and determination of fluoride in plant samples

H.B. Li *, X.R. Xu

State Key Laboratory of Environmental Aquatic Chemistry, Research Center for Eco-Environmental Sciences, Chinese Academy of Sciences, P.O. Box 2871, Beijing 100085, People's Republic of China

Received 2 February 1998; received in revised form 1 June 1998; accepted 8 June 1998

Abstract

A simple and rapid separation method is described for the determination of fluoride in plant samples. Fluoride is separated by distillation in the presence of H_2SO_4 and H_2O_2 in a dry air steam. The variables that influence the distillation quantitation were optimized. The fluorides separated were subsequently determined by a spectrophotometric method of the La(III)–F^-–alizarin complexone system. The precision of the procedure was significant, and the RSD was 3.7%. The accuracy of the method was statistically satisfactory, and the recovery was from 95.9 to 104.4%.

Keywords: Fluoride; Separation; Distillation; Determination; Plant sample

1. Introduction

The effect of fluoride on human beings has a dual role as an essential trace element and at high levels as a toxic substance. Therefore, fluoride has received much attention with regard to medicine, pharmacy, public health and environmental protection. It is important and necessary to determine fluoride of plants because fluoride is known to affect various types of plants and, thus, both man and animals are susceptible to poisoning by fluoride-contaminated food or feedstuffs.

Fluoride determination can sometimes be carried out in the presence of matrix compounds and by adding, if necessary, a complexing agent. Generally, however, fluoride must be separated to avoid interference. The separation methods for plant samples are mainly distillation after mineralization in an alkaline medium [1,2], and diffusion, either with or without ashing [3,4]. The distillation is time-consuming and the volume of the distilled fraction is too large. Diffusion allows the separation of a large number of samples at the same time. However, it also takes a long time when only a few samples need to be handled.

In this paper, a simple and rapid method to separate fluoride from plant samples is developed.

* Corresponding author. E-mail: xuxr@mail.rcees.ac.cn

0039-9140/99/$ - see front matter
PII S0039-9140(98)00225-2

2. Experimental

2.1. Apparatus

A 721 spectrophotometer (Shanghai No.3 Analytical Instrument Factory) was used.

2.2. Reagents

NaF, H_2SO_4, H_2O_2, NaOH and HCl were all commercially available (made in China) and were used without any further purification except where it is stated. All reagents were puprapure or analytical pure grade. Deionized water was used throughout. Concentrated H_2SO_4 was heated till sulfur trioxide white smoke was produced in order to get rid of fluoride. The standard sodium fluoride solution was 1000 μg ml^{-1}. A stock solution of the fluoride ion (1000 μg ml^{-1}) was prepared by dissolving 0.2210 g sodium fluoride, maintained under well-dried conditions, in 100 ml water and stored in a polyethylene bottle. The working solution was prepared by suitable dilution of the stock solution with water.

2.3. Procedure

The plant samples were put into a round-bottom flask. The apparatus was installed as shown in Fig. 1. NaOH solution was added preliminarily into the gas-washing bottle in order to get rid of the fluoride in the air. NaOH solution was added in advance to the collector. Phenolphthalein was added as an indicator if determined by spectrophotometry. The operating process used the following steps: The tap to fill the separating funnel with water was turned on. Then the piston of the separating funnel was turned on to add water to the glass bottle so that the air was forced out. The air entered the round-bottom flask through the gas-washing bottle. Carrying with HF and SiF_4, it arrived at the collector. H_2SO_4 was added by the sample-adding apparatus. Then H_2O_2 was dripped into the round-bottom flask by

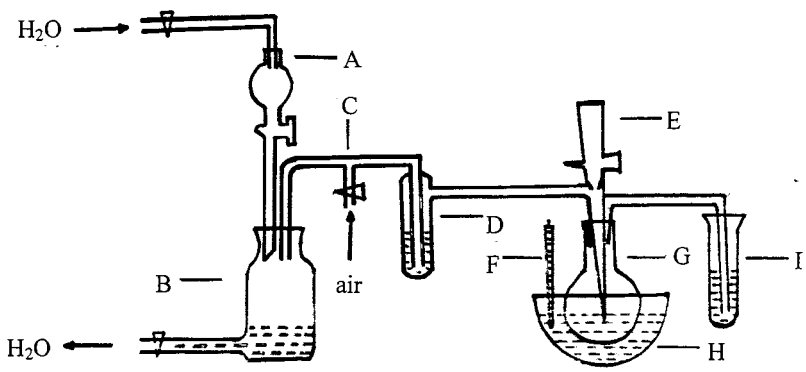

Fig. 1. Separating apparatus: (A) separating funnel; (B) glass bottle; (C) three-way pipe; (D) gas-washing bottle; (E) sample-adding apparatus; (F) thermometer; (G) round-bottom flask; (H) oil bath; (I) collector.

Table 1
Results of collecting fractions of tea

Temperature (°C)	Time (min)				Total value (μg g^{-1})
	10	20	30	40	
150	108.6	17.5	7.0	—[a]	134.0
160	143.3	10.8	—	—	154.2
170	176.5	—	—	—	176.5
180	178.0	—	—	—	178.0

[a] Nothing was detected.

Table 2
The precision of the method for mulberry leaf samples

Sample No.	1	2	3	4	5	6	7	8	9	10	X	SD	RSD (%)
F found (μg g^{-1})	31.2	28.5	30.5	32.5	29.8	30.1	30.9	29.5	32.0	31.5	30.7	1.1	3.7

Table 3
The recovery of the method for mulberry leaf samples

Sample No.	1	2	3	4	5	6	7	8	9	10
Mass (mg)	348.2	461.3	401.8	362.1	487.3	422.8	367.9	413.4	390.6	403.4
F found (μg)	12.1	12.5	11.3	11.9	12.7	12.9	11.8	11.4	12.6	12.4
F added (μg)	12.0	12.0	12.0	12.0	12.0	24.0	24.0	24.0	24.0	24.0
F found (μg)	23.6	24.3	23.8	24.0	24.6	36.8	36.0	35.2	36.9	36.1
Recovery (%)	95.9	98.4	104.4	100.8	99.2	99.2	101.7	98.2	102.4	97.6

the sample-adding apparatus. The temperature of the glycerin bath was controlled with an adjustable transformer. If the air was supplied by a pump and an electrothermal cap was used, the operation process was simpler and easier.

Dried plant samples (0.3–0.5 g) (such as tea leaves, tobacco leaves, and mulberry leaves) were placed into the distillation bottle and linked to every part as shown in Fig. 1. Concentrated H_2SO_4 (5 ml) was added at 110°C and 8 ml 30% H_2O_2 solution was added dropwise. The samples were distilled at 175–180°C for 10 min. Then the distillation was continued for 5 min after 2 ml 30% H_2O_2 was added dropwise. The flow rate of the carrier gas was 0.4 l min^{-1}. The Time to add concentrated H_2SO_4 and H_2O_2 was 10 min followed by distillation at 175–180°C for 15 min. Therefore, it took about 25–30 min to process a sample.

The effect of the separation was studied by a spectrophotometric method of the La(III)–F^-–alizarin complexone system. The process was carried out according to Ref. [5].

3. Results and discussion

There were many factors affecting the separation. Here only the concentrations of H_2SO_4 and H_2O_2, the heating temperature and time were studied. Other factors, such as the flow rate of the carrier gas, 0.4 l min^{-1}, the volume of the round-bottom flask, 100 ml, the distance from the top of the tube to the bottom of the flask, 0.5 cm, were kept constant.

3.1. Effect of H_2SO_4 concentration

Under the conditions of the addition of 10 ml 30% H_2O_2, and heating for 20 min at 180°C, for 0.3–0.5 g dried tea samples, no effect was seen on the separation when the volume of concentrated H_2SO_4 was from 3 to 6 ml. However, when the volume of concentrated H_2SO_4 was less than 5 ml, white precipitation was produced in the digested solution. If the volume of concentrated H_2SO_4 was 5 ml or more, then no white precipitation was produced and the digested solution was clear. The white precipitation may be $CaSO_4$. When the volume of concentrated H_2SO_4 was more than 5 ml, the precipitation could be turned into soluble $Ca(HSO_4)_2$. Consequently, 5 ml concentrated H_2SO_4 was chosen. It was noted that less acid fog was produced if the drop rate of H_2SO_4 to H_2O_2 was controlled properly.

3.2. Effect of H_2O_2 concentration

Under the conditions of the addition of 5 ml concentrated H_2SO_4, and heating for 20 min at 180°C, for 0.3–0.5 g dried tea samples, the effect of separation was almost constant when the volume of 30% H_2O_2 was more than 8 ml. If the differences

Table 4
Results of the determination of fluorine in tea leaves

Sample No.	Fuding						Mingshan 23					
	1	2	3	4	5	Mean	1	2	3	4	5	Mean
Tender leaves (μg g^{-1})	282.3	302.5	312.7	316.7	269.8	297.0	235.6	219.1	198.9	222.6	197.6	214.8
Older leaves (μg g^{-1})	986.7	998.3	1021.1	1044.5	976.6	1005.4	943.5	911.3	893.0	927.2	889.2	912.8

in plant samples were considered, the volume of 30% H_2O_2 in later experiments should be 10 ml to ensure complete digestion. Furthermore, surplus H_2O_2 decomposed to H_2O and O_2, which had no effect on the determination of fluoride. So H_2O_2 could be added in excess.

3.3. Effect of temperature and time

Under the conditions of the addition of 5 ml concentrated H_2SO_4 and 10 ml 30% H_2O_2, for 0.3–0.5 g dried samples, the results for the collected fraction of tea are shown in Table 1. From the data in Table 1, it can be seen that the separation was complete when heated for 10 min at 170°C considering the difference between the parallel samples. Therefore, the heating temperature was controlled at 175–180°C. Considering the diluting effect of collecting at different sections, the heating time should be 10–15 min.

3.4. Blank and absorption

The blank value was found to be almost zero by doing five experiments. Additionally, the second-order water absorption experiment was carried out using 95 μg F^- (five times). That is, two gas-washing bottles were used in tandem and the second bottle absorbed the gas from the first bottle. There was no fluoride detected in the second bottle. Thus, it could be seen that the fluoride compounds can be absorbed completely by first-order water absorption. Because there was little H_2SO_4 acid fog produced in the experiment, the absorption solution containing NaOH was used.

3.5. Precision of the method

Under the above optimum conditions, for 0.3–0.5 g mulberry leaves, the precision of the method was determined and the results are shown in Table 2. The RSD was 3.7%.

3.6. Recovery

The recovery of the method was determined with mulberry leaf samples and the results are shown in Table 3. The recovery was 95.9–104.4%.

3.7. Determination of fluorine in tea leaf

Two kinds of tea leaves produced from two location were processed by the separation method developed. The fluorides separated were determined by spectrophotometry. One sample was of older leaves and tender leaves of Fuding Tea produced on the purple soil of Zheyin Mountain. The other sample was tea from Mingshan 23 produced on the yellow soil of Mingshan county. The tea leaves sample was a gift from Professor Yao in the Department of Chemistry in Sichuan Normal University. The results are shown in Table 4.

The ratio of fluorine in older and tender leaves of Fuding was 3.4:1, and that of Mingshan 4.2:1. The difference in fluorine between the older and tender leaves among the different soils, locations and types was large. Furthermore, fluorine was higher in the older leaves than in the tender because of enrichment of the leaves from the fluorine in the air.

Tea is a popular drink in China. The above results suggest that tea made from the tender leaves should be taken in areas containing high fluorine, and should be drunk less, to prevent chronic poisoning owing to the surplus fluorine absorbed. In areas of low fluorine, tea made of the older leaves, which contain more fluorine, should be taken, thus removing the need to add fluorine to the water to prevent disease from lack of fluorine.

4. Conclusions

A simple and rapid method to separate the fluoride from plant samples has been established. It combines wet digestion (H_2SO_4 and H_2O_2 were used) with distillation using air as the carrier gas. The volume of collected liquid is several millilitres. The procedure to handle a sample takes only 25–30 min. The proposed method is simpler and more rapid than distillation after mineralization in an alkaline medium. Diffusion allows separation of a large number of samples at the same time. However, the proposed method is more

rapid than diffusion when only a few samples need to be handled. That is, diffusion is adopted when a lot of samples need to be handled and the proposed method is adopted when only a few samples need to be handled.

Acknowledgements

The support of the National Natural Science Foundation of China is greatly appreciated.

References

[1] H.H. Willard, O.B. Winter, Ind. Eng. Chem. Anal. Ed. 5 (1933) 7.
[2] J.K. Wilkeysn, Anal. Chem. 47 (1975) 2053.
[3] M. Nedeljkovic, B. Antonijevic, V. Matovic, Analyst (London) 116 (1991) 477.
[4] B. Culik, Anal. Chim. Acta 189 (1986) 329.
[5] Scientific Research Cooperation Group of Analytical Methods for Environmental Pollution, Analytical Methods for Environmental Pollution, vol. 1, 2nd ed., Inorganic Analysis, Science Press, Beijing, 1987, pp. 331–337 (in Chinese).

ELSEVIER

Talanta 48 (1999) 63–69

Talanta

Direct determination of cadmium in calcium drug samples using electrothermal atomic absorption spectrometry with a metal tube atomizer and thiourea as a matrix modifier

Shamim Ahsan [a,*], Satoshi Kaneco [a], Kiyohisa Ohta [a], Takayuki Mizuno [a], Yoko Taniguchi [b]

[a] *Department of Chemistry for Materials, Faculty of Engineering, Mie University, Tsu, Mie 514-8507, Japan*
[b] *Mie Industrial Research Institute, 3845, Takachaya-komori-cho, Tsu, Mie 514-0008, Japan*

Received 25 February 1998; received in revised form 1 June 1998; accepted 8 June 1998

Abstract

A laboratory constructed molybdenum tube atomizer was used for direct determination of trace cadmium in drug samples by the electrothermal atomic absorption spectrometric (ETAAS) method. An ultrasonic agitation method for a solution including the sample powder was used. A calibration curve was constructed with a cadmium standard solution including matrix. To eliminate interference from other matrix elements, a chemical modifier thiourea, was used. The detection limit were 17 pg ml^{-1} (3 S/N), and the RSD of the direct analysis was 5–17%. The results for cadmium in the four drug samples analysed by the direct ETAAS method matched well with those obtained with nitric acid digested samples. The recovery of added cadmium was 103–106%. An accurate method is elaborated for the determination of cadmium in drug samples by direct ETAAS techniques. The merits of this method are rapid calibration, simplicity, fast analysis, and low cost.

Keywords: Cadmium; Direct atomization; Drug sample; Electrothermal atomization; Molybdenum tube atomizer

1. Introduction

The toxic effects of small amounts of cadmium, an ubiquitous and biologically non-essential element in biological and environmental samples have been known for many years [1]. Cadmium accumulates in the human body and has a long biological half-life (average 30 years). A tolerable weekly intake of 0.4–0.5 mg of cadmium per adult (60 kg) has been defined in the FAO/WHO Codex Alimentarius [2]. Drugs containing cadmium also have associated risks of serious health hazard on continued use at low dosage. Therefore, from the public health point of view, it is necessary to develop some rapid and simple method for the determination of cadmium at low levels in human consumable products such as drugs.

* Corresponding author. Tel.: +81 59 2319427; fax: +81 59 2319427/9442/9471; e-mail: na60236@cc.mie-u.ac.jp

0039-9140/99/$ - see front matter
PII S0039-9140(98)00226-4

Generally cadmium is analyzed by different common techniques such as: flame atomic absorption spectrometry [3], atomic fluorescence spectrometry [4], neutron activation analysis [5], inductively coupled plasma-atomic emission spectrometry [6], X-ray fluorescence (XRF) and potentiometric stripping analysis (PSA) [7]. However, one of the most sensitive techniques for cadmium determination is considered to be electrothermal atomization atomic absorption spectrometry (ETAAS). Some unique properties of ETAAS suggest the appropriateness of this technique for direct elemental analysis of solid samples [8]. Other notable features of solid sampling by ETAAS are: substantially minimized risk of contamination and/or loss of analyse, improve detection limit, lower blank zero, and the submilligram sample size offers the possibility of microheterogeneity measurements. One review of the literature [9] recognizes ETAAS as the preferred method for solid sample analysis. Until now numerous studies [8,10–20] have been conducted for the determination of cadmium by ETAAS using a graphite furnace. In recent years interest in the use of metal tube atomizers has increased compared to graphite and carbon atomizers. So far, this type of atomizer has demonstrated superior performance and better sensitivity. However, very little information has been reported on its application. Only a few studies reported on accurate direct determination of cadmium in biological materials by ETAAS using a metal tube atomizer [21,22]. The influence of additives on cadmium appears to be complex and varies depending upon the type and quantity of the matrix introduced. Thiourea has been successfully used as a modifier for cadmium determination in biological samples [23].

Direct atomic absorption spectrometry analysis of solids has the important advantages of not requiring any decomposition, separation, and/or concentration processes and also encompasses other benefits: time-saving, no contamination from chemicals, and reduced loss of volatile elements. To date no information is available on the direct determination of cadmium in calcium drug samples by ETAAS using a metal tube atomizer. This has prompted the pursuit of research to develop a rapid analytical methodology.

The present study was initiated with the objective of investigating the efficiency of the ETAAS method using a molybdenum tube atomizer and thiourea as the matrix modifier to determine cadmium in calcium drug samples.

2. Experimental

2.1. Apparatus and measurements

A molybdenum tube atomizer (20×1.8 mm i.d., wall thickness 0.05 mm), made from high purity molybdenum sheet (99.5% purity, from Rembar) was used for direct atomization of the sample. The samples were injected by glass micropipette through a 0.3-mm diameter hole at the mid point of the tube.

All experiments were carried out using a Nippon Jarrell-Ash 0.5-m Ebert-type monochromator atomic absorption spectrometer equipped with an R943 photomultiplier tube (Hamamatsu Photonics), a fast response amplifier, a storage oscilloscope (Iwatsu MS-5021) and a microcomputer (SORD M223). A cadmium hollow cathode lamp (Hamamatsu Photonics) was used at the cadmium resonance line of 228.8 nm. The molecular background absorption was checked with a deuterium lamp (Original Hanau D200F). A step down transformer and a transformer (Yamabishi voltslider, S-130-30, capacity 3 kVA) supplied electric power for heating the atomizer. In order to collimate the light beam and eliminate radiation from the atomizer surface, two pinholes were set in the front and at the rear end of the atomizer. An optical pyrometer (Chino Works) and a microcomputer program were used to calibrate the atomizer temperature against the photodiode voltage. Grinding of the drug samples to different particle sizes was carried out using an agate mortar and a filter (Nippon Rikagaku Kikai, ISO 38). An optical microscope (Kenko, KL-1200) was used to determine the particle size of ground powder drug samples. A Mettler H20 semimicro analytical balance (sensitivity ± 0.01 mg) was used for weighing the samples and chemicals. Before injection into the atomizer sample homogenization was carried out using an ultrasonic

washing apparatus (UT-4, 26 KHZ, Kokusai Electric) for all the powdered drug samples. Ultrapure water was prepared using an ADVENTEC ultrapure water system CW-102.

The baseline was measured by heating without a sample. The time constant is 4 ms. The atomic absorption signal was evaluated from the peak height. The absorption signal from the amplifier and the atomizer temperature signal from the photodiode were monitored with a storage oscilloscope and fed simultaneously to a microcomputer.

2.2. Reagents and chemicals

All reagents and chemicals used were of analytical grade or spectroscopic purity.

A standard cadmium solution (3 ng ml^{-1}, 0.001 M nitric acid) was prepared from $Cd(NO_3)_2$ in 0.1 M nitric acid (Wako, Japan). Standard stock solutions of the matrix elements $CaHPO_4.2H_2O$ (Kanto, Japan) and $CaCO_3$ (Nacalai Tesque, Japan) were prepared by dissolving in utrapure water. Thiourea solution (5 mg ml^{-1}) was prepared by diluting in pure water. Working standard solutions of appropriate concentrations for this analytical study were prepared by dilution of stock standard solutions with pure water immediately before use. H_2O_2 (30%) and 0.05 M nitric acid were used for acid digestion.

2.3. Procedures

For the determination of cadmium in the calcium drug samples, a 1 μl aliquot of standard solution containing 3 ng ml^{-1} cadmium and a matrix element containing 20 mg ml^{-1} $CaHPO_4.2H_2O$ and $CaCO_3$ were pipetted into the molybdenum tube atomizer to prepare the calibration curve. A portion (1 μl) of matrix modifier thiourea (5 mg ml^{-1}) was injected into the tube after drying at 100°C for 20 s which follows the atomization steps as mentioned in Table 1. The atomization temperature corresponds to a heating rate of 3.4°C ms^{-1}.

2.3.1. Wet digestion and direct atomization

An accurately weighed (5 g) drug sample with 3 ml hydrogen peroxide (30%) and 1 ml (0.05 M) nitric acid was digested in a Uni-seal decomposition vessel and heated at 120°C for 3 h in an electric oven. The acid-digested sample diluted to 10 ml with pure distilled water after cooling. Alternatively, the powdered drug samples were ground to a very fine mesh and filtered to an average particle size of 3 μm for direct atomization. A portion (0.2 g) of the filtered samples were transferred into a 10 ml volumetric flask and diluted to the desired volume with pure distilled water. Immediately before the sample injection ultrasonic agitation (5 min) was employed to homogenize the samples.

3. Results and discussion

To increase the sensitivity for some metals and also to protect the atomizer from oxidation by traces of oxygen in the argon it has been reported [24–26] that there is a need for the addition of hydrogen to the purge gas in the ETAAS method. Suzuki [23] studied the effect of hydrogen including the optimal purge gas flow rate for cadmium atomization in a molybdenum tube atomizer. A sharper and highest peak absorption was observed at a flow rate for argon of 480 ml min^{-1} added to H_2 at 20 ml min^{-1}. Due to the high volatility of cadmium some difficulties are encountered for its determination by ETAAS, thus restricting the use of a high pyrolysis temperature and the production of concomitant background signals. This refers to the use of a matrix modifier. It has been reported that thiourea reacts with many elements to form a complex and, upon

Table 1
Experimental conditions of direct atomization-atomic absorption spectrometry of cadmium in the drug sample

Element	Cadmium
Argon (ml min^{-1})	48
Hydrogen (ml min^{-1})	20
Drying (°C for 20 s)	100
Ashing (°C for 20 s)	300
Atomization (°C for 3 s)	2100
Calibration range (ng ml^{-1})	0–3

Analytical line 228.8 nm.

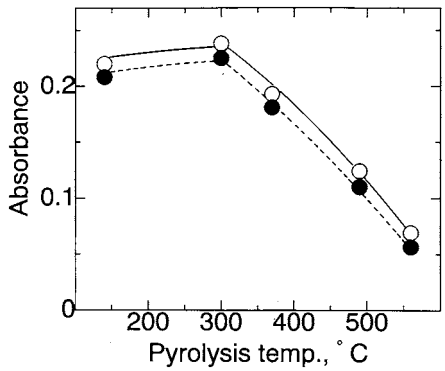

Fig. 1. Effect of the pyrolysis temperature on the atomic absorption signal of the drug matrix in cadmium with and without thiourea modifier. O, without thiourea; O, with thiourea (cadmium 3 pg).

heating the complex, the mixture mainly decomposes to make the metal sulfide [24]. The sulphide formation in atomizing process serves to eliminate the interference of the matrix elements, since the sulfide is generally more volatile and dissociative than the oxide concerned, thus atomizing easily. Therefore, thiourea was selected as the chemical modifier for this determination. In the case of the molybdenum tube atomizer the absorption profile of cadmium was characterized by a sharper and narrower peak with an increase in the heating rate [24,27–29]. Hence, the optimal atomization temperature for the cadmium measurements was 2100°C (heating rate 3.4°C ms^{-1}).

3.1. Influence of pyrolysis temperature

The pyrolysis temperature for elemental analysis in a specific matrix may vary considerably with the type of instrument, atomization cell, analyse sample, and other factors [9]. Using a metal tube atomizer, one of the earlier studies [23] has applied a pyrolysis temperature of 300°C for cadmium determination in a biological sample. Nevertheless, the influence of pyrolysis temperature on the calcium drug sample A having a particle size 3 μm was investigated using a molybdenum tube atomizer with and without the matrix modifier. Fig. 1 shows the effect of the pyrolysis temperature on the absorption of cadmium. The curve trends are more or less stable in the temperature range 140–300°C, but absorbance gradually decreased thereafter. Significant lowering of the absorbance was observed after 370°C and at $>$ 560°C the absorbance diminished. The best absorption peak was obtained at 300°C, which agrees with the earlier pyrolysis temperature used for cadmium determination. In the range $<$ 300°C, the absorbance of cadmium with and without thiourea was lower. This phenomena is presumably related to the higher melting point of the sulfide (CdS 1750°C) [30]. At 300°C the major part of the sample matrix in the presence of thiourea seems to be transformed to sulphide. In the molybdenum tube atomizer the temperature at which cadmium appeared in the presence of thiourea was 650°C. The melting point of cadmium nitrate is 350°C [30] and at around 300°C the sulphide appears to be more stable.

Consequently, 300°C was selected as the optimal pyrolysis temperature for the determination of cadmium in the calcium drug samples.

3.2. Particle size effect measurement

The particle size distribution of the sample has been shown to be an important parameter in influencing the quality of the results in the direct analysis of solids by ETAAS [31–37]. The accuracy and precision of the measurement can be affected either by inadequate homogeneity or poor sample representation, and/or incomplete recovery of the matrix during the atomization process. An investigation was, therefore, conducted to assess the effect of three different average particle sizes 30 ± 2, 15 ± 1, and 3 ± 1 μm of drug sample A, respectively. With the variation in particle size significant changes in absorption were observed. Absorption gradually increased with smaller particle size together with a decrease in RSD (Table 2). These phenomena may be due to good dispersion and homogeneity of relatively small sized powders in the sample solution. RSDs with larger size are probably due to the variation in the number of the particles. Hence, an average particle size of 3 μm has been used for the determination of trace cadmium in the drug samples.

Table 2
Effect of the particle size of the calcium drug on cadmium absorbance and RSD of the absorbance

Sample	Average particle size (μm)	Absorbance	RSD of absorbance (%)
A	3 ± 1	0.230	9.67
	15 ± 1	0.193	17.3
	30 ± 2	0.148	22.6

$n = 5$.

3.3. Application of ultrasonic agitation

For the stabilization of the sample suspension a variety of techniques have been successfully applied. Of these, ultrasonic homogenization is no doubt the most efficient approach applicable for sample stabilization and homogeneity. The effect of ultrasonic agitation on a solution of drug powder sample A with a 3 μm average particle size was studied. The results are shown in Fig. 2. At zero agitation the sample was manually stirred for 2–3 s. The peak absorption increased for up to a 5 min agitation time and became a plateau at more than 5 min agitation time and also the RSD calculated from five repeated measurements was good after a 5 min agitation time. From this result, an agitation time of 5 min was selected for the calcium drug samples.

3.4. Characteristic mass, detection limit, and reproducibility

A reasonably good accuracy and precision of measurement are a prerequisite of any analytical techniques [8]. Therefore, the detection limit, characteristic mass, and reproducibility were investigated. In this determination the absolute characteristic mass (gave an integrated absorbance of 0.0044) of cadmium by the atomizer was 50 fg and the detection limit was 17 fg (3 S/N, corresponding to 17 pg ml^{-1}, 10 μl injected), which were computed from the lower linear portion of the calibration curve of the drug sample and deviation of the baseline for blank firings. These values are better than the characteristic mass (28 pg) and detection limit (20 pg ml^{-1}) obtained for direct determination of water by an AAS-atom trapping technique [38], 140 pg ml^{-1} obtained from biological tissue using Zeeman-effect background corrected AAS [16], 150 pg ml^{-1} obtained from a blood sample by GFAAS [18], and those with ICP-AES (2 ng ml^{-1}) and ICP-MS (0.2 ng ml^{-1}) [39] under normal conditions. The better sensitivity observed with a molybdenum tube atomizer is presumably due to the nonporosity of the wall of the atomizer [40], lack of formation of the carbide [41], and also may have been attributed due to narrower diameter of the tube.

The reproducibility of cadmium together with the matrix elements AAS signal by the use of a molybdenum tube atomizer was investigated. An RSD of 5% was obtained for cadmium at 3 ng ml^{-1} (1μl, corresponding to 3 pg cadmium) and the matrix element for 10 measurements. The SD of the blank measurement was 0.002.

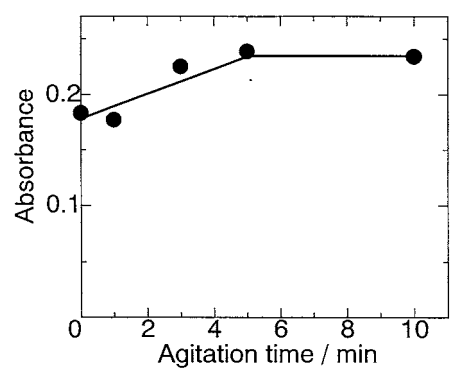

Fig. 2. Effect of the ultrasonic agitation time on a solution of sample A powder.

Table 3
Determination of cadmium in the calcium drug samples

Sample	Particle size (μm)	Added (ng g^{-1})	Concentration of cadmium		
			Direct analysis (ng g^{-1})	Recovery (%)	Nitric acid digestion (ng g^{-1})
A	3	0	51.0 ± 5.0 (10.0)	—	49.0 ± 3.0 (6.0)
B	3	0	8.31 ± 1.40 (17.0)		8.1 ± 0.8 (10.0)
		30	40.0 ± 3.0 (7.5)		—
C	3	0	96.0 ± 14.0 (15.0)	106	97.5 ± 7.0 (7.0)
		30	127 ± 12 (9.5)	103	—
D	3	0	40.0 ± 2.0 (5.0)		41.0 ± 1.6 (4.0)
		30	71.0 ± 3.0 (4.0)	103	—

$n \geq 5$.
Percent RSD in parenthesis.

3.5. Analysis of cadmium in drug samples

The present method was applied to the determination of trace amounts of cadmium in calcium drug samples with an average particle size of 3 μm. The optimum analytical conditions used in this method is presented in Table 1. For accurate determination of cadmium the finely meshed (3μm average particle size) and the acid digested calcium drug samples were dissolved in pure water to an appropriate volume. Thiourea was used to eliminate interference from other matrixes. A linear calibration graph was constructed from 3 ng ml^{-1} cadmium and 20 mg ml^{-1} standard matrix solutions. The content of cadmium present in the drug samples is presented in Table 3. The results of direct atomization with a 3 μm average particle size sample were found to be in good agreement with those of the acid digested method. The RSD for five replicate analyses of the direct sampling ranges from 5 to 17%, which is reasonable for the direct atomization technique. Using a deuterium lamp as the light source, insignificant background absorption signals were observed for all the drug samples. In order to compare the test results from both the direct and wet digestion methods by statistical interpretation the Student's *t*-test was performed, which shows no significant difference. The recovery of spiked-cadmium in the drug samples B, C, and D was in the range 103–106%. This suggests excellent recovery of cadmium.

4. Conclusions

Direct determination of solid samples employing a laboratory constructed molybdenum tube atomizer by ETAAS was demonstrated to be a feasible approach in the analysis of calcium drug samples. For the determination of cadmium in the drug sample thiourea served as an efficient modifier to remove interference. More over, the use of a molybdenum tube atomizer together with an argon–hydrogen atmosphere gave the benefit of higher sensitivity and a longer lifetime for the metal tube (more than 5000 firings) compared to 200–250 firings for a graphite furnace [42]. Hence, a low cost conventional method has been developed which is capable of measuring trace level cadmium in drug samples with good accuracy.

Acknowledgements

This research was supported by the Ministry of Education and Culture of Japan.

References

[1] J.L. Domingo, Toxicol. Environ. Health 42 (1994) 123.
[2] L.T. Avigdor, Swiss Food 78 (1987) 13.
[3] I. Kojima, S. Kondo, J. Anal. At. Spectrom. 8 (1993) 115.
[4] L. Ebdon, P. Goodall, S.J. Hill, P.B. Stockwell, K.C. Thompson, J. Anal. At. Spectrom. 8 (1993) 723.
[5] S. Landsberger, S. Larson, D. Wu, Anal. Chem. 65 (1993) 1506.
[6] M.C. Valdés-Hevia, Y. Temprano, M.R. Fernández de la Campa, A. Sanz-Medel, J. Anal. At. Spectrom. 9 (1994) 231.
[7] S.M. Pyle, et al., Environ. Sci. Technol. 30 (1996) 204.
[8] J. Štupar, K. Dolinšek, Spectrochim. Acta B 51 (1996) 665–683.
[9] F.J. Langmyhr, G. Wibetoe, Prog. Anal. At. Spectrosc. 8 (1985) 207.
[10] G. Strübel, V.R. Glinder, K.H. Grobecker, K. Jarrar, Fresenius' Z. J. Anal. Chem. 337 (1990) 316.
[11] F. Dolinšek, J. Štupar, V. Vrščaj, J. Anal. At. Spectrom. 6 (1991) 653.
[12] J.Y. Cabon, A.L. Bihan, J. Anal. At. Spectrom. 7 (1992) 383.
[13] C.R. Lan, Analyst 118 (1993) 189.
[14] H. Chuang, H. Shang-Da, Spectrochim. Acta B 49 (1994) 283–288.
[15] L.C. Robles, A.J. Aller, Talanta 42 (1995) 1731.
[16] B. Sures, H. Taraschewski, C. Haug, Anal. Chimi. Acta 311 (1995) 135.
[17] G.V. Dalen, J. Anal. Atom. Spectrom. 11 (1996) 1087.
[18] J.K. Sysalová, Biol. Trace Elem. Res. 56 (1997) 321.
[19] P. Viñas, I. López-Garcia, M. Lanzón, M. Hernandez-Cordoba, J. Agric. Food Chem. 45 (1997) 3952.
[20] J.P. Snell, S. Sandberg, W. Frech, J. Anal. Atom. Spectrom. 12 (1997) 491.
[21] K. Ohta, W. Aoki, T. Mizuno, Talanta 35 (1988) 831.
[22] K. Ohta, W. Aoki, T. Mizuno, Mirochim. Acta 1 (1990) 81–86.
[23] M. Suzuki, K. Ohta, Anal. Chem. 54 (1982) 1686.
[24] M. Suzuki, K. Ohta, Prog. Anal. Atom. Spectrosc. 6 (1983) 49.
[25] W. Frech, A. Cedergren, Anal. Chim. Acta (1976) 82–83.
[26] M.W. Routh, Anal. Chem. 52 (1980) 182.
[27] K. Ohta, S.Y. Su, T. Mizuno, Anal. Lett. 20 (1987) 1399.
[28] K. Ohta, S. Itoh, T. Mizuno, Talanta 38 (1991) 325.
[29] K. Ohta, T. Sugiyama, T. Mizuno, Analyst 115 (1990) 279.
[30] D.R. Lide, (Ed.), Handbook of Chemistry and Physics, 72nd ed., CRC Press, Boston, MA, 1991, pp. 4–47.
[31] K.W. Jackson, A.P. Newman, Analyst 108 (1983) 261.
[32] M.W. Hinds, K.W. Jackson, A.P. Newman, Analyst 110 (1985) 947.
[33] S.C. Stephen, J.M. Ottaway, D. Littlejohn, Fresenius' Z. Anal. Chem. 328 (1987) 346.
[34] C.W. Fuller, R.C. Hutton, B. Preston, Analyst 106 (1981) 913.
[35] V. Majidim, J.A. Holcombe, Spectrochim. Acta B 45 (1990) 753.
[36] N.J. Miller-Ihli, Fresenius' Z. Anal Chem. 337 (1990) 271.
[37] T. Nakamura, T. Kusata, H. Matsumoto, J. Sato, Anal. Biochem. 226 (1995) 256.
[38] H. Sun, L. Yang, D. Zhang, J. Sun, Talanta 44 (1997) 1979.
[39] L.H.J. Lajunen, Spectrochemical Analysis by Atomic Absorption and Emission, Royal Society of Chemistry, Cambridge, 1992, pp. 231.
[40] Y. Zheng, R. Woodriff, J.A. Nicholas, Anal. Chem. 56 (1984) 1388.
[41] D.A. Katskov, A.M. Shtepan, I.L. Grinshtein, A.A. Pupyshev, Spectrochim. Acta B 47 (1992) 1023.
[42] M. Bettinelli, U. Baroni, F. Fontana, P. Poisetti, Analyst 110 (1985) 19.

ELSEVIER

Talanta 48 (1999) 71–79

Talanta

Titrations in non-aqueous media: potentiometric investigation of symmetrical and unsymmetrical tetra-aryl porphyrins with 4-nitrophenyl and 4-aminophenyl substituents in nitrobenzene solvent

Necla Gündüz, Turgut Gündüz *, Mustafa Hayvalı

Department of Chemistry, Faculty of Science, University of Ankara, Ankara, Turkey

Received 7 July 1997; received in revised form 26 May 1998; accepted 9 June 1998

Abstract

The basicity of the symmetrical and unsymmetrical tetraphenylporphyrins, namely 5,10,15,20-tetraphenylporphyrin (I) (references), 5-(4-nitrophenyl)-10,15,20-triphenylporphyrin (II), a mixture of 5,10-bis(4-nitrophenyl)-15,20-diphenylporphyrin and 5,15-bis(4-nitrophenyl)-10,20-diphenylporphyrin (III), 5,10,15-tris(4-nitrophenyl)-20-phenylporphyrin (IV), 5,10,15,20-tetrakis(4-nitrophenyl)porphyrin (V), 5-(4-aminophenyl)-10,15,20-triphenylporphyrin (VI), a mixture of 5,10-bis(4-aminophenyl)-15,20-diphenylporphyrin and 5,15-bis(4-aminophenyl)-10,20-diphenylporphyrin (VII), 5,10,15-tris(4-aminophenyl)-20-phenylporphyrin (VIII) and 5,10,15,20-tetrakis(4-aminophenyl)porphyrin (IX), was investigated potentiometrically in nitrobenzene solvent. This investigation showed that these compounds are basic rather than acidic. Although they can not be titrated even with tetrabuthylammonium hydroxide, they can easily be titrated with perchloric acid to give well shaped and stoichiometric end-points. In addition they all undergo two proton reactions per porphyrin molecule. However, compounds VI, VII, VIII and IX each shows a second end-point to give three, four, five and six proton reactions, respectively, per porphyrin molecule. Half neutralization potentials (measures of their basicity) of these compounds are: I = 368, II = 409, III = 432, IV = 461, V = 520, VI = 340, VII = 302, VIII = 238 and IX = 225 mV versus Ag/AgCl in methanol. These potentials clearly indicate that, if *para*-hydrogen with respect to the porphyrin core of tetraphenylporphyrin (I) is replaced with an acidifying nitro group (II, III, IV and V) the basicity of I decreases. This decrease is approximately proportional to the number of nitro groups. Each nitro group decreases the half neutralization potential by about 35 mV. On the other hand, if *para*-hydrogen indicated above is replaced with a basifying amino group (VI, VII, VIII and IX) the basicity increases. This increase is also approximately proportional to the number of amino groups. Each amino group increases the half neutralization potential by about 36.7 mV. The values 35 and 36.7 mV indicate that in nitrobenzene solvent the electron releasing power of an amino group to the porphyrin system is a little stronger than the electron withdrawing power of a nitro group from the porphyrin system. All these observations reveal that the nitrogen atoms at the core

* Corresponding author. Tel.: +90 312 2126720, ext. 1281; fax: +90 312 2232395.

PII S0039-9140(98)00222-7

of the porphyrin molecules are strongly influenced by changes at the periphery of the molecules, which is a very good indication that the substituted phenyl groups and the cores of the porphyrins are nearly in the same plane.

Keywords: Potentiometry; Titrimetry; Porphyrins; Non-aqueous media

1. Introduction

Porphyrins are very important natural and synthetic compounds. Naturally occurring porphyrins play a vital role in the maintenance of the animal and plant bodies [1], because they constitute the basis of the respiratory systems. Haemoglobins, cytochromes and chlorophylls are the best known porphyrin pigments [2,3]. Heamoglobins and cytochromes contain iron(II) ion and chlorophylls contain magnesium ion [4–6]. Another naturally occurring porphyrin is vitamin B12, which contains cobalt(II) ion [7].

Synthetic porphyrins are numerous. These compounds also form complexes with cations like their naturally occurring congeners [8]. Such porphyrins are used for diverse industrial and scientific purposes, e.g. for protection of paints against ultraviolet light, as colouring pigments in paints, especially in automobile paints, as ingredients in plastics, for the identification of carcinogenic tissues in the human body [9] and ^{57}Co porphyrin complexes are used in chemotherapy [9].

Synthetic porphyrins have also recently been tested for the conversion of solar energy into electrical energy [10]. Although the various properties of synthetic poprhyrins have been well studied, no reports except one [11] of their basicities in non-aqueous media have appeared so far. This study was aimed at further investigations of such properties of porphyrins, because, such studies can provide valuable knowledge about the structure of the porphyrins. In order to do this, nine symmetrical or unsymmetrical 5,10,15,20-tetraaryl porphyrins having 4-nitrophenyl and 4-amino-phenyl substituents were synthesized, namely 5,10,15,20-tetraphenylporphyrin (I) (reference), 5-(4-nitrophenyl)-10,15,20-triphenylporphyrin (II), a mixture of 5,10-bis(4-nitrophenyl)-15,20-diphenylporphyrin and 5,15-bis(4-nitrophenyl)-10,20-diphenylporphyrin (III), 5,10,15-tris(4-nitrophenyl)-20-phenylporphyrin (IV), 5,10,15,20-tetrakis(4-nitrophenyl)porphyrin (V), 5-(4-aminophenyl)-10,15,20-triphenylporphyrin (VI), a mixture of 5,10-bis(4-aminophenyl)-15,20-diphenylporphyrin and 5,15-bis(4-aminophenyl)-10,20-diphenylporphyrin (VII), 5,10,15-tris(4-aminophenyl)-20-phenylporphyrin (VIII) and 5,10,15,20-tetrakis(4-aminophenyl)porphyrin (IX). Their structures are shown in Fig. 1.

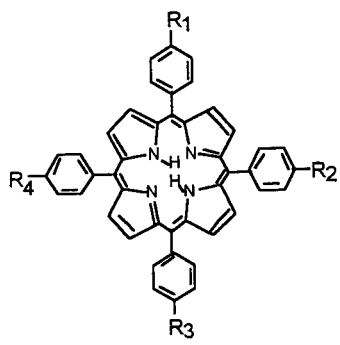

No	R_1	R_2	R_3	R_4
I	H	H	H	H
II	NO_2	H	H	H
III	NO_2	NO_2	H	H
	NO_2	H	NO_2	H
IV	NO_2	NO_2	NO_2	H
V	NO_2	NO_2	NO_2	NO_2
VI	NH_2	H	H	H
VII	NH_2	NH_2	H	H
	NH_2	H	NH_2	H
VIII	NH_2	NH_2	NH_2	H
IX	NH_2	NH_2	NH_2	NH_2

Fig. 1. Structure of 4-substituted phenyl symmetrical and unsymmetrical porphyrins.

These porphyrins were obtained from pyrrole and benzaldehyde or pyrrole and para-substituted benzaldehydes in dry dichloromethane or propionic acid as solvent [12–17]. The raw materials were purified by column chromatographic techniques. Compounds obtained chromatographically were examined for purity and found to be sufficiently pure to investigate their basicity in non-aqueous media. Solubility studies of these compounds showed that they are sufficiently soluble in nitrobenzene to carry out the planned basicity investigations.

2. Experimental

2.1. Apparatus

A Chemtrix model 60A potentiometer equipped with a combined glass electrode and a modified Ag/AgCl electrode was used for potentiometric titrations. The Ag/AgCl was modified by emptying out the aqueous KCl solution and replacing it with a saturated solution of KCl in dry methanol. All titrations were carried out in a specially designed cell which is illustrated in Ref. [11].

The cell was connected to a water circulating thermostat, which kept the temperature of the cell and its contents at 25 ± 1°C. The cell had a capacity of approximately 50 ml and was connected to the combined glass electrode via inlet A to a thin tipped semi-micro burette via inlet B and to a nitrogen cylinder via inlet C. The semi-micro burette enabled the titrant solution to be read within 0.01 ml.

Infrared absorbtion spectra were obtained from a Mattson 1000-FTIR spectrometer in KBr discs and are reported in cm^{-1} units. Proton (400 MHz) NMR spectra were recorded with a Bruker DPX FT-NMR spectrometer (Me_4Si as internal standard); elemental analyses were carried out on a LECO CHNS-9323, in TÜBITAK-SAGE; UV–Vis spectra were recorded by UNICAM UV2-100 series spectrometers.

2.2. Chemicals

Nitrobenzene (Merck 98% pure) was used after purification. Purification was done as follows: approximately 50 g dry phosphorous pentoxide (P_2O_5) was added to 0.5 l nitrobenzene in a well stoppered round bottomed flask and was left for 5 days in the dark and then was distilled over phosphorous pentoxide under vacuum. Nitrobenzene boiling at 78°C was collected in a well dried, dark coloured, ground glass stoppered bottle . Nitrobenzene purified in this manner was tested for a potentiometric working range. To 20 ml nitrobenzene was added 0.1 ml 0.02 M perchloric acid in nitrobenzene and the positive mV limit, measured by the potentiometer described above, was found to be $+980$ mV. Secondly to 20 ml nitrobenzene was added 0.1 ml 0.02 M tetrabutylammonium hydroxide in 2-propanol and its negative mV limit was found to be -780 mV. Nitrobenzene purified in this way has shown a greater potentiometric working range than nitrobenzene purified by previous methods [18]. Because of this wide working range for nitrobenzene reached in this way, the half neutralization potentials of 5,10,15,20-tetraphenylporphyrin, 5,10,15,20-tetrakis(4-nitrophenyl)porphyrin and 5,10,15,20-tetrakis(4-aminophenyl)porphyrin were found to be higher than the previous ones [11].

Dichloromethane (Merck 99% purity) was used after purification. It was first shaken with concentrated sulphuric acid until it became colourless, then the sulphuric acid layer was separated using a separating funnel. The dichloromethane layer was shaken first with a 5% Na_2CO_3 solution and then shaken vigorously with distilled water and subsequently dried with CaH_2 and distilled at normal pressure. The constant-boiling distillate was placed in a dark-coloured glass-stoppered flask and was kept over molecular sieves (4 Å) in the dark.

Chloroform (Merck 99% purity) was used after purification. It was first shaken vigorously with distilled water and the chloroform layer was separated using a separating funnel. The chloroform was then dried with $CaCl_2$ and distilled in a tall distillation column.

Pyrrole (Merck, 99% purity) was purified by distillation under high vacuum over zinc dust. Benzaldehyde (Merck 98% purity) was used after distillation under vacuum. Tetrabutylammonium

hydroxide was purchased from Merck as a 0.01 M stock solution in 2-propanol and was diluted to 0.02 M with 2-propanol. The solution was diluted as described previously [19]. Perchloric acid was purchased from Merck (70% purity) and 0.02 M solution in nitrobenzene was prepared as described previously [20]. Silica gel (Merck 230–400 mesh) was used after activation at 150°C. 4-Nitrobenzaldehyde (Fluka puriss grade) was used as received. Boron trifluoride ethyl etherate complex (Fluka) 48% solution in diethyl ether and used as received.

5,10,15,20-Tetraphenylporphyrin (I) was prepared by the method of Lindsey and co-workers [12–14]. IR (KBr, cm^{-1}) 3317 (ν_{NH}), 1597 ($\nu_{C=C}$) 978. ^1H NMR ($CDCl_3$); δ ppm, 8.89 (s, 8H, β pyrrole), 8.26 (d, 8H, $J=5.8$ Hz, *ortho*-phenyl) 7.80 (m, 12H, *meta*/*para*-phenyl), −2.94 (s, 2H, pyrrole NH), vis. (λ_{max}, CH_2Cl_2); ($\log \epsilon$) 418 (6.39); 514 (5.02); 550 (4.68); 590 (4.54); 646 (4.49). Anal. Calcd. for $C_{44}H_30N_4$: C, 85.96; H, 4.92; N, 9.12%. Found: C, 85.64; H, 4.82; N, 8.96%.

5-(4-Nitrophenyl)-10,15,20-triphenyl porphyrin (II) was prepared by the method given in Ref. [21]. IR (KBr, cm^{-1}) 3317 (ν_{NH}), 1597, 1520 ($\nu_{NO_2\ asym.}$) 1473, 1350 ($\nu_{NO_2\ sym.}$), 972. ^1H NMR ($CDCl_3$); δ ppm, 8.92 (d, 2H, $J=4.8$ Hz, β pyrrole), 8.89 (s, 4H, β pyrrole), 8.76 (d, 2H, $J=4.8$ Hz, β pyrrole), 8.66 (d, 2H, $J=8.4$ Hz, nitrophenyl), 8.42 (d, 2H, $J=8.4$ Hz, nitrophenyl), 8.24 (d, 6H, $J=8.7$ Hz, *ortho*-phenyl), 7.80 (m, 9H, *meta*/*para*-phenyl), −2.79 (s, 2H, pyrrole NH), vis. (λ_{max}, CH_2Cl_2); ($\log \epsilon$) 418 (6.26); 514 (5.18); 552 (4.98); 590 (4.89); 644 (4.81). Anal. Calcd. for $C_{44}H_{29}N_5O_2$: C, 80.10; H, 4.43; N, 10.62%. Found: C, 80.39; H, 4.10; N, 10.42%.

5,10 + 5,15-Bis(4-nitrophenyl)-15,20-diphenyl-porphyrin (III) was prepared by the method given in Ref. [21]. IR (KBr, cm^{-1}) 3317 (ν_{NH}), 1597, 1520 ($\nu_{NO_2\ asym.}$) 1466, 1350 ($\nu_{NO_2\ sym.}$), 972. ^1H NMR ($CDCl_3$); δ ppm, 8.94 (d, 2H, $J=4.6$ Hz, β pyrrole), 8.90 (s, 2H, β pyrrole), 8.81 (s, 2H, β pyrrole), 8.77 (d, 2H, $J=4.7$ Hz, β pyrrole, 8.66 (d, 4H, $J=8.2$, Hz nitrophenyl), 8.41 (d, 4H, $J=8.2$ Hz, nitrophenyl), 8.24 (d, 4H, $J=6.7$ Hz, *ortho*-phenyl), 7.81 (m, 6H, *meta*/*para*-phenyl), −2.73 (s, 2H, pyrrole NH), vis. (λ_{max}, CH_2Cl_2); ($\log \epsilon$) 420 (6.33); 516 (5.24); 552 (5.04); 590 (4.93); 646 (4.85). Anal. Calcd. for $C_{44}H_{28}N_6O_4.H_2O$: C, 73.11; H, 4.19; N, 11.63%. Found: C, 73.35; H, 4.41; N, 11.54%.

5,10,15-tris(4-Nitrophenyl)-20-phenylporphyrin (IV) was prepared by the method given in Ref. [21]. IR (KBr, cm^{-1}) 3317 (ν_{NH}), 1597, 1520 (ν_{NO_2} asym.) 1473, 1350 ($\nu_{NO_2\ sym.}$), 964. ^1H NMR ($CDCl_3$); δ ppm, 8.94 (d, 2H, $J=4.8$ Hz, β pyrrole), 8.92 (s, 4H, β pyrrole), 8.79 (d, 2H, $J=4.8$ Hz β pyrrole), 8.68 (d, 6H, $J=8.4$ Hz, nitrophenyl), 8.42 (d, 6H, $J=8.4$ Hz, nitrophenyl), 8.22 (d, 2H, $J=6.5$ Hz, *ortho*-phenyl), 7.82 (m, 3H, *meta*/*para*-phenyl), −2.76 (s, 2H, pyrrole NH), vis. (λ_{max}, CH_2Cl_2); ($\log \epsilon$) 422 (6.15); 516 (5.15); 552 (4.97); 594 (4.88); 646 (4.80). Anal. Calcd. for $C_{44}H_{27}N_7O_6$: C, 70.47; H, 3.63; N, 13.08%. Found: C, 70.89; H, 3.45; N, 12.55%.

5,10,15,20-tetrakis-(4-Nitrophenyl)porphyrin (V) was prepared by the method of Bettelheim et al. [16]. IR (KBr, cm^{-1}) 3309 (ν_{NH}), 1589, 1520 ($\nu_{NO_2\ asym.}$), 1342 ($\nu_{NO_2\ sym.}$), 972. ^1H NMR (DMSO); δ ppm, 8.90 (s, 8H, β pyrrole), 8.69 (d, 8H, $J=7.31$ Hz, nitrophenyl), 8.52 (d, 8H, $J=$ 6.8 Hz, nitrophenyl), −2.89 (s, 2H, pyrrole NH), vis. (λ_{max}, CH_2Cl_2); ($\log \epsilon$) 424 (6.22); 518 (5.12); 558 (5.05); 594 (4.90); 652 (4.81). Anal. Calcd. for $C_{44}H_{26}N_8O_8$: C, 66.48; H, 3.30; N, 14.11%. Found: C, 66.63; H, 3.44; N, 13.73%.

5-(4-Aminophenyl)-10,15,20-triphenylporphyrin (VI) was prepared by the method given in Ref. [21]. IR (KBr, cm^{-1}) 3464, 3371 (ν_{NH_2}), 3317 (ν_{NH} pyrrole), 1612 ($\nu_{C=C,C=N}$), 1512 ($\nu_{NH_2\ bent}$), 972. ^1H NMR ($CDCl_3$); δ ppm, 8.96 (d, 2H, $J=4.7$ Hz, β pyrrole), 8.85 (m, 6H, β pyrrole), 8.24 (d, 6H, $J=7.3$ Hz, *ortho*-phenyl), 8.02 (d, 2H, $J=8.1$ Hz, aminophenyl), 7.78 (m, 9H, *meta*/*para*-phenyl), 7.07 (d, 2H, $J=8.1$ Hz, aminophenyl), 4.00 (s, 2H, NH_2), −2.70 (s, 2H, pyrrole NH), vis. (λ_{max}, CH_2Cl_2); ($\log \epsilon$) 420 (6.44); 516 (5.27); 554 (5.11); 592 (4.98); 648 (4.94). Anal. Calcd. for $C_{44}H_{31}N_5$: C, 83.91; H, 4.96; N, 11.13%. Found: C, 83.81; H, 5.24; N, 11.56%.

5,10 + 5,15-Bis(4-aminophenyl)-15,20-diphenylporphyrin (VII) was prepared by the method given in Ref. [21]. IR (KBr, cm^{-1}) 3448, 3371 (ν_{NH_2}), 3325 ($\nu_{NH\ pyrrole}$), 1612 ($\nu_{C=C,C=N}$), 1512 ($\nu_{NH_2\ bent}$), 964. ^1H NMR ($CDCl_3$); δ ppm, 8.90 (m, 8H, β pyrrole), 8.24 (d, 4H, $J = 7.0$ Hz, *ortho*-phenyl), 8.02 (d, 4H, $J = 8.0$ Hz, aminophenyl), 7.78 (m, 6H, *meta*/*para*-phenyl), 7.07 (d, 4H, $J = 7.9$ Hz, aminophenyl), 4.02 (s, 4H, NH_2), −2.67 (s, 2H, pyrrole NH), vis. (λ_{max}, CH_2Cl_2); (log ∈) 424 (6.46); 518 (5.30); 556 (5.18); 594 (5.00); 650 (5.04). Anal. Calcd. for $C_{44}H_{32}N_6$: C, 81.95; H, 5.01; N, 13.04%. Found: C, 82.20; H, 5.41; N, 12.55%.

5,10,15-tris(4-Aminophenyl)-20-phenylporphyrin (VIII) was prepared by the method given in Ref. [21]. IR (KBr, cm^{-1}) 3448, 3371 (ν_{NH_2}), 3325 ($\nu_{NH\ pyrrole}$), 1612 ($\nu_{C=C,C=N}$), 1512 ($\nu_{NH_2\ bent}$), 964. ^1H NMR ($CDCl_3$); δ ppm, 8.94 (s, 6H, β pyrrole), 8.84 (d, 2H, $J = 4.7$ Hz, β pyrrole), 8.24 (d, 2H, $J = 5.7$ Hz, *ortho*-phenyl), 8.02 (d, 6H, $J = 7.07$ Hz, aminophenyl), (d, 6H, $J = 7.07$ Hz, aminophenyl), 7.77 (d, 3H, J = 7.0 Hz, *meta*/*para*-phenyl) 7.07 (d, 6H, $J = 7.73$ Hz, aminophenyl),), 4.01 (s, 6H, NH_2), −2.66 (s, 2H, pyrrole NH), vis. (λ_{max}, CH_2Cl_2); (log ∈) 424 (6.46); 518 (5.30); 556 (5.18); 594 (5.00); 650 (5.04). Anal. Calcd. for $C_{44}H_{33}N_7$: C, 80.09; H, 5.04; N, 14.87%. Found: C, 79.78; H, 5.19; N, 14.33%.

meso-tetrakis-(4-Aminophenyl)porphyrin(IX) was prepared by the method of Bettelheim et al [16]. IR (KBr, cm^{-1}) 3440, 3363 (ν_{NH_2}), 3325 (ν_{NH} pyrrole), 1612 ($\nu_{C=C,C=N}$), 1512 ($\nu_{NH_2\ bent}$), 964. ^1H NMR ($CDCl_3$ + DMSO); δ ppm, 8.84 (s, 8H, β pyrrole), 7.84 (d, 8H, $J = 8.33$ Hz, aminophenyl), 7.00 (d, 8H, $J = 8.1$ Hz, aminophenyl), 4.85 (s, 8H, NH_2), −2.70 (s, 2H, pyrrole NH), vis. (λ_{max}, CH_2Cl_2); (log ∈) 426 (6.46); 520 (5.22); 560 (5.19); 596 (4.95); 654 (5.00). Anal. Calcd. for $C_{44}H_{34}N_8$: C, 78.30; H, 5.08; N, 16.61%. Found: C, 78.55; H, 5.22; N, 16.13%.

3. Results and discussion

Solutions (1×10^{-3} M) of nine symmetrical and unsymmetrical tetra(4-substituted-phenyl) porphyrins in nitrobenzene were first titrated potentiometrically with a 0.02 M solution of tetrabutylammonium hydroxide in isobutanol, but no end-points or meaningfull titration curves in nitrobenzene or even in pyridine were observed. This indicates that these compounds are not sufficiently acidic to be titrated even with one of the strongest non-aqueous bases. This odd behaviour can probably be explained with the very strong resonance in the core or centre of the porphyrins. As a result of strong resonance, the core of a porphyrin becomes rich in negative charge. Such negative charges envelope perfectly the protons on the *N*-21 and *N*-23 nitrogens and negatively charged OH^- ion can not penetrate into this electron trough, and react with a proton. As a result of this obstruction, neutralization reaction between tetrabutylammonium hyroxide and porphyrin cannot occur.

On the other hand the titration of these compounds with perchloric acid (0.02 M) gave very well defined and stoichiometric end-points. Each porphyrin molecule given above undergoes a two-proton reaction and gives one end-point. This indicates that negatively charged core attracts two protons eagerly at the same time. This means that porphyrin molecules have a very extensive resonance system. As a result of this extensive resonance, a positive charge in the core (centre) of the porphyrin molecule is very effectively dissipated throughout the molecule. The titration curves of the nitrophenyl porphyrins II, III, IV and V are given in Fig. 2. As is easily seen from the figure, the potential jumps of these compounds at the end-points are very large. They range from 250–350 mV. Such potential jumps for a non-aqueous medium are considered to be excellent. The half neutralization potentials of these compounds with respect to the reference (5,10,15,20,-tetraphenylporphyrin) are given in Table 1.

Differences of the half-neutralization potentials of the nitrotetraphenylporphyrins from the half-neutralization potential of the reference (tetraphenylporphyrin) versus the number of nitro group are given in Fig. 3 (upper part of the graph). As is easily seen from the figure each nitro group entering into the tetraphenylporphyrin

Table 1
Half-neutralization potentials of symmetrical and unsymmetrical porphyrins titrated potentiometrically with perchloric acid in nitrobenzene solvent at room temperature

Compound	Number	hnp (mV)	Δhnp (mV)
5,10,15,20-Tetraphenylporphyrin (references)	I	368	00
5-(4-Nitrophenyl)-10,15,20-triphenylporphyrin	II	409	+41*
5,10+5,15-Bis(4-nitrophenyl)-15,20-diphenylporphyrin	III	432	+64
5,10,15-Tris(4-nitrophenyl)-20-phenylporphyrin	IV	461	+93
5,10,15,20-Tetrakis(4-nitrophenyl)porphyrin	V	520	+152
5-(4-aminophenyl)-10,15,20-triphenylporphyrin	VI	340	−28**
5,10+5,15-Bis(4-aminophenyl)-15,20-diphenylporphyrin	VII	302	−66
5,10,15-Tris(4-aminophenyl)-20-phenylporphyrin	VIII	238	−130
5,10,15,20-Tetrakis(4-aminophenyl)porphyrin	IX	225	−143

hnp, Half neutralization potential.
+, Decrease in basicity or increase in acidity; −, increase in basicity or decrease in acidity.
* Arithmetic mean of the potential increase per nitro group is 35 mV, calculated from the sum of the potential increase divided by the sum of the number of the nitro groups.
** Arithmetic mean of the potential decrease per amino group is 36.7 mV, calculated from the sum of the potential decrease divided by the sum of the number of the amino groups.

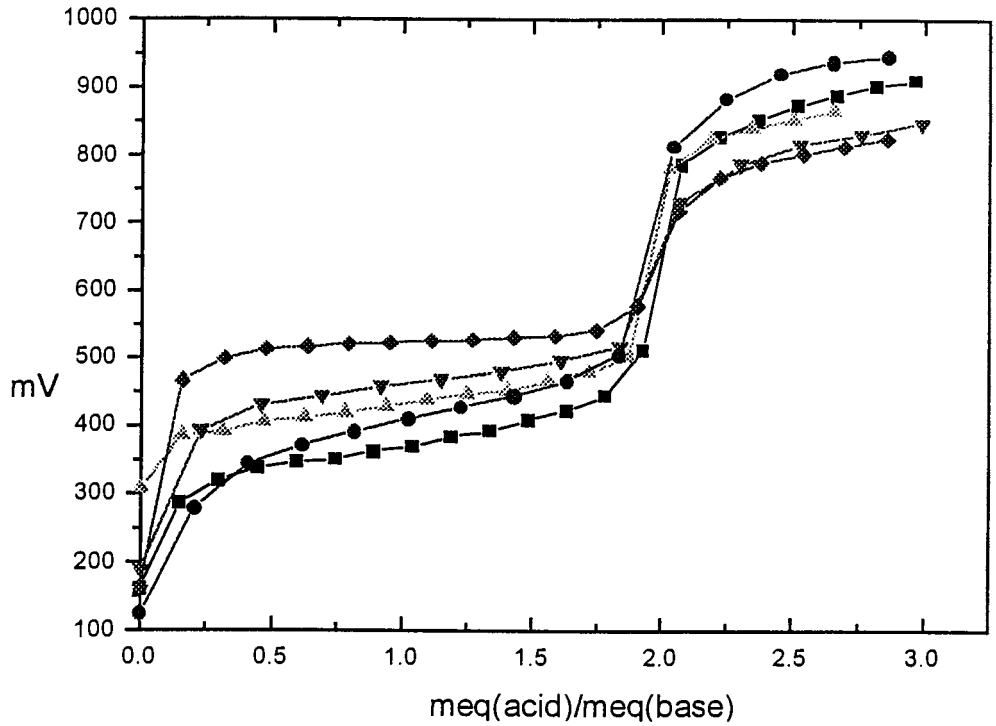

Fig. 2. Titration curves of the nitrophenyl porphyrin solutions (0.001 M) with perchloric acid (0.02 M) in nitrobenzene solvent. (■) Tetraphenylporphyrin; (●) 5-(4-nitrophenyl)-10,15,20-triphenylporphyrin; (▲) 5,10 + 5,15-bis-(4-nitrophenyl)-15,20-diphenylporphyrin; (▼) 5,10,15-tris-(4-nitrophenyl)-20-phenylporphyrin; and (◆) 5,10,15,20-tetrakis-(4-nitrophenyl)porphyrin.

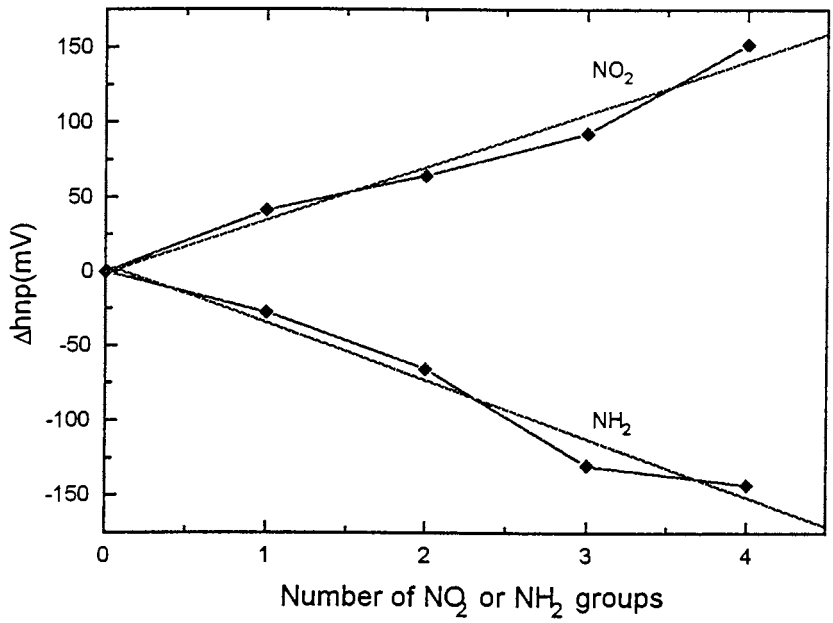

Fig. 3. The increase of the half neutralization potentials of the nitrophenyl porphyrins (upper part of the graph) and the decrease of the half neutralization potentials of the aminoporphyrins (lower part of the graph) with respect to 5,10,15,20-tetraphenylporphyrin (reference) determined by using perchloric acid as titrant in nitrobenzene solvent at room temperature. Concentrations of the reactions are perchloric acid solution 0.02 M and porphyrins 0.001 M.

molecule at the periphery decreases the basicity of the molecule approximately linearly. The mean of these decreases is 35 (a linear regression slope = 35.6 mV supports this strongly). This means that nitrobenzene rings attached to the porphyrin core participate strongly in the resonance of the porphyrin core. This strongly supports our previous findings [11].

Closer investigation of the titration curves (Fig. 2.) shows that the titration curve of 5,10,15,20-tetrakis(4-nitrophenyl)porphyrin (V) is approximately a horizontal straight line in the buffer region. This means that the half-neutralized solution of this compound can be used for calibration of a potentiometer at least for titrations to be carried out in nitrobenzene solvent.

All the results obtained indicate that phenyl groups attached to the porphyrin molecule participate in the resonance of the nitrotetraphenyl porphyrin molecule. Otherwise minor changes in the phenyl group would not affect the basicity of the core of the porphyrins. This results shows that the substituted phenyl groups and the cores of the porphyrins are nearly in the same plane, in contrast to the conclusions of Gottwald and Ullman [22] and Burke et al. [23] who considered that the phenyl groups are either perpendicular or at least oblique to the plane of the porphyrin.

Titration curves of the amino porphyrins (VI, VII, VIII and IX) together with the titration curve of the reference (I) are given in Fig. 4. As is easily seen from titration curves all the amino porphyrins give two end-points. The mole ratio of acids to porphyrin at these points are 2:1 and varying from 3:1 to 6:1, for the first and second end-points, respectively.

The first end-point belongs to the neutralization reaction of the nitrogen atoms at the core of porphyrins with the perchloric acid. The second end-point belongs to the neutralization reaction of the nitrogen atom or atoms found to be at the periphery of the porphyrin molecule, because all the amine groups at the periphery of the molecule are equivalent. Rigorous investigation of Fig. 3. shows that there is a good correlations between

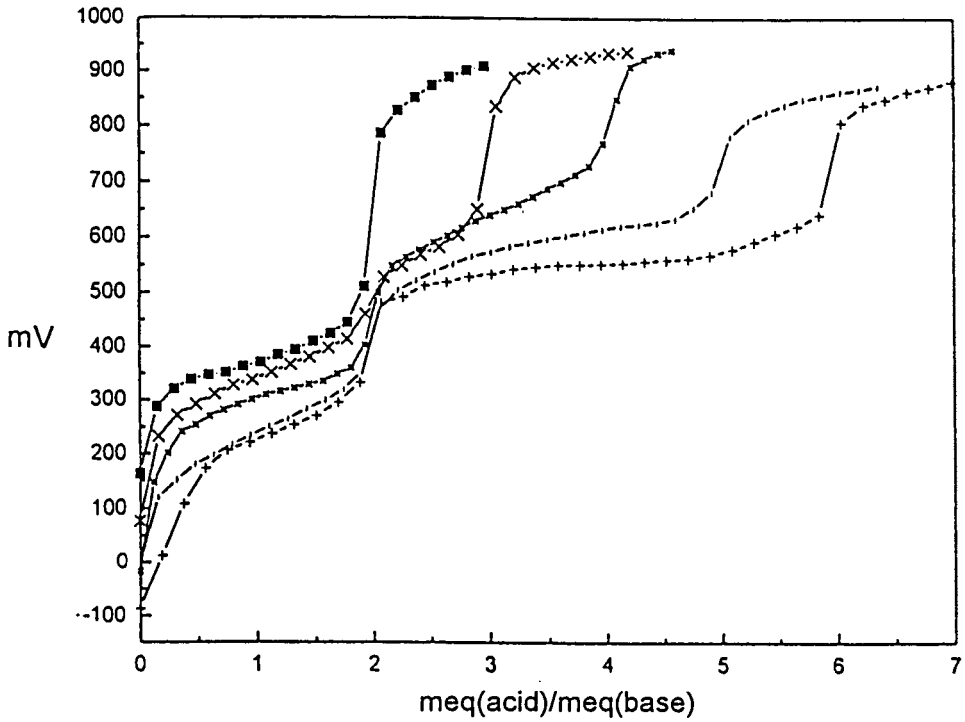

Fig. 4. Titration curves of the aminophenyl porphyrin solutions (0.001 M) with perchloric acid (0.02 M) in nitrobenzene solvent. (■) Tetraphenylporphyrin; (X) 5-(4-aminophenyl)-10,15,20-triphenylporphyrin; (∗) 5,10 + 5,15-bis-(4-aminophenyl)-15,20-diphenylporphyrin; (|) 5,10,15-tris-(4-aminophenyl)-20-phenylporphyrin; and (+) 5,10,15,20-tetrakis-(4-aminophenyl)porphyrin.

the number of amino groups and the basicity increase of the aminophenyl porphyrins.

Each amino group increases the half neutralization potential of the porphyrin molecule by about 36.7 mV, the slope of the linear regression, 38.8 mV, supports this value strongly.

Data obtained from the titration curves are shown in Table 1.

Another interesting conclusion that can be drawn from the potential decrease and increase in values given for nitro and aminophenyl porphyrins is that the basifying power of an amino group is slightly greater than the acidifying power of a nitro group. We believe that this is an important property observed in this laboratory.

4. Conclusions

From the potentiometric titration of nine symmetric and unsymmetric nitrophenyl and aminophenyl porphyrins in nitrobenzene, the following conclusions can be drawn. Two of the four nitrogen atoms in the core of the porphyrin molecule (symmetrical and unsymmetrical) are very basic in character. They can be titrated with perchloric acid to give a single well shaped endpoint in nitrobenzene solvent. The basicities of the porphyrin are very sensitive to changes at the periphery. For example, while one nitro group at the periphery decreases the half neutralization potential by, on average, 35 mV, two nitro groups decreases the half neutralization potential by very nearly twice as much as does one nitro group, etc. This means that the basicity decrease of the tetraphenylporphyrin is proportional to the number of nitro groups. On the other hand one amine group increases the half neutralization potential of the tetraphenylporphyrin by about 36.7 mV, on average. This also means that the basicity decrease of the tetraphenylporphyrin is proportional to the number of amine groups. These examples

show that the electron releasing power of the amine group is greater than the electron withdrawing power of nitro group, at least in the porphyrin molecules. This is a new observation that the effect of the amine group is stronger than the effect of the nitro group in the reverse direction. All these observations show that porphyrins are very sensitive to changes at the periphery. Above all, the present study has shown that symmetrical and unsymmetrical aminophenylporphyrins can undergo from two up to six proton cations to give stable ions with two, three, four, five or six positive charges in nitrobenzene solvent. We believe that this is an unusual observation for non-aqueous media.

References

[1] L.R. Milgrom, J. Chem. Soc. Perkin Trans. 1 (1986) 1483.
[2] R.G. Little, J. Heterocycl. Chem. 18 (1981) 129.
[3] T. Mashiko, J.C. Marchon, D.T. Musser, C.A. Reed, J. Am. Chem. Soc. 101 (1979) 3653.
[4] J. Almog, J.E. Baldwin, M.J. Crossley, et al., Tetrahedron 37 (1981) 3589.
[5] V. Thanabal, V. Krishnan, J. Am. Chem. Soc. 104 (1982) 3643.
[6] J.L. Sessler, S.J. Weghorn, T. Morishima, M. Rosingana, V. Lynch, J. Halpern, J. Am. Chem. Soc. 114 (1992) 8306.
[7] M.K. Geno, J. Halpern, J. Am. Chem. Soc. 109 (1987) 1238.
[8] A.D. Adler, F.R. Longo, J. Inorg. Nucl. Chem. 32 (1970) 2443.
[9] N. Datta-Gupta, T.J. Bardos, J. Heterocycl. Chem. 3 (1966) 495.
[10] L.R. Milgrom, N. Mofidi, J. Chem. Soc. Perkin Trans. 2 (1989) 301.
[11] T. Gündüz, N. Gündüz, M. Hayvalý, Anal. Chim. Acta 278 (1993) 243.
[12] A.D. Adler, F.R. Longo, J.D. Finarelli, J. Org. Chem. 23 (1967) 476.
[13] J.S. Lindsey, I.C. Schreiman, H.C. Hsu, P.C. Kearney, A.M. Marguerettaz, J. Org. Chem. 52 (1987) 827.
[14] J.S. Lindsey, R.W. Wagner, J. Org. Chem. 54 (1989) 828.
[15] J.S. Lindsey, D.C. Mauzerall, J. Am. Chem. Soc. 104 (1982) 4498.
[16] A. Bettelheim, B.A. White, S.A. Raybuck, R.W. Murray, Inorg. Chem. 26 (1987) 1009.
[17] J.P. Collman, R.R. Gagne, C.A. Reed, T.R. Halbert, G. Lang, W.T. Robinson, J. Am. Chem. Soc. 97 (1975) 1427.
[18] E. Kiliç, T. Gündüz, Analyst 111 (1986) 949.
[19] T. Gündüz, N. Gündüz, E. Kiliç, F. Köseoğlu, S.G. Öztaş, Analyst 113 (1988) 715.
[20] T. Gündüz, N. Gündüz, E. Kiliç, A. Kenar, G. Çetinel, Analyst 111 (1986) 1099.
[21] W.J. Kruper Jr., T.A. Chamberlin, M.K. Kochanny, J. Org. Chem. 54 (1989) 2753.
[22] L.K. Gottwald, E.F. Ullman, Tetrahedron Lett. 63 (1969) 3071.
[23] J.M. Burke, J.R. Kincaid, T.G. spiro, J. Am. Chem. Soc. 100 (1978) 6077.

ELSEVIER

Talanta 48 (1999) 81–89

Talanta

Critical assessment of the parameters that affect the selection of coating compounds for piezoelectric quartz crystal microbalances

M. Teresa S.R. Gomes *, Armando C. Duarte, João A.B.P. Oliveira

Department of Chemistry, University of Aveiro, 3810 Aveiro, Portugal

Received 30 January 1998; received in revised form 19 May 1998; accepted 9 June 1998

Abstract

The selection of the compound to be used as a coating for a piezoelectric quartz crystal is of utmost importance in the development of a chemical sensor. The relevant parameters to be evaluated (stability, sensitivity, reversibility, response time, reproducibility, and selectivity), and the main variables affecting the results and influencing the choice of coatings are discussed and illustrated with experiments performed during the evaluation of coatings to detect carbon dioxide. © 1999 Elsevier Science B.V. All rights reserved.

Keywords: Quartz crystal microbalance; Piezoelectric quartz crystal; Coating

1. Introduction

Whenever the interaction between the analyte and the crystal electrodes does not result in a significant mass change, a coating must be applied. The interaction between the coating and the analyte may just involve an absorption process, or chemical interactions may take place, which can be described by adsorption, chemisorption or coordination chemistry. A stronger interaction is associated with better selectivity, although reversibility is poorer [1].

Often, the mechanism of the interaction between the coating and analyte is unknown [2], and coating selection has been largely empirical [3]. Sensitivity, response time, and reversibility need to be evaluated by the observation of the results obtained from tests conduced under specific experimental conditions.

Coating selection generally relies upon comparison of frequency decreases obtained by the interaction between the different coatings and the analyte. However, it is not unusual to see in the literature comparisons between ratios of the observed frequency decrease and coating amount, obtained from single experiments with each coating. Without a coating procedure capable of assuring reproducibility, these observations have limited value. Temperature and flow rate are among the other parameters that can influence the results.

* Corresponding author. Tel.: +351 34 370722; fax: +351 34 370084; e-mail: mtgomes@dq.ua.pt

PII S0039-9140(98)00218-5

Although the choice of coating is one of the most important steps in the development of a sensor, the basic parameters that sustain the choice are usually allied to a high variability or obtained after unavoidable assumptions. The main characteristics influencing the performance of the sensor, as well as the basic assumptions, will be reviewed and critically discussed. Contributions to this discussion can be found dispersed in the literature, but different issues, some reported here for the first time, are illustrated with examples obtained during the choice of coating for a quartz crystal to detect CO_2.

2. Experimental

2.1. Apparatus

The crystals were coated on one side with a commercial air-brush (Badger 200), in front of which rotated a plate with orifices to hold the crystal upright. After coating, the crystal was introduced into a glass cell through which a constant nitrogen flow of 50 cm^3 min^{-1}, controlled with a variable area flowmeter (Cole Parmer), was maintained. Both the spraying device and the glass cell are described elsewhere [4].

In all the experiments, CO_2 was injected, through an Omnifit (ref. 3301) septum injector, into the nitrogen flow, before the crystal cell. The syringes were SGE (Scientific Glass Engineering) gas tight, with a valve.

The piezoelectric crystals were 9 MHz (SIWARD), the frequency was monitored with a universal counter board (Keithley MetraByte), and the data were stored in ASCII file format.

The images of the surface of the crystal were obtained with an Jenaphot 2000 (Zeiss) optical microscope, coupled to an Quantimet 500 (Leica) image analyser.

2.2. Reagents

1,2-Diaminoethane (Fluka 03550), diethylenetriamine (Riedel de Häen 15918) and triethylenetetramine (Merck 814392) were dissolved in acetone (Merck 14). *N*,*N*,*N*″,*N*″-tetrakis (2-hydroxyethyl) ethylenediamine (THEED) (Fluka 87600) and tetramethylammonium fluoride tetrahydrate (TMAF) (Aldrich 10,721-2) were dissolved in ethanol (Merck 11727). Nitrogen was R grade and carbon dioxide was N45, both from ArLíquido.

3. Sensor performance characteristics dependent on the coating

3.1. Stability

The coating must not evaporate and must be stable in the working environment when free of analyte.

Often, the coating compound is dissolved in a volatile solvent, before the coating application, and complete evaporation of the solvent must be accomplished before experiments can be performed. Generally, a frequency stabilisation, after a sudden rise, as shown in Fig. 1, is a good indication of the complete evaporation of the solvent.

However, apparent anomalies, to the best of our knowledge, reported here for the first time, were observed with a coating of THEED. As Fig. 2 shows, there is a frequency decrease, after the initial frequency rise, of the coated crystal under the nitrogen flow. In a series of 24 amines, this behaviour was observed just with THEED, which was the most viscous amine tested. Fig. 3 shows the microscopic images of two different regions of a crystal electrode (central and peripheral zones), obtained, along with the time, after spraying with a solution of 1% THEED in absolute ethanol. Between observations, the crystal was kept in a cell under a constant nitrogen flow of 50 cm^3 min^{-1}. The first microscopic images (Fig. 3a) show the distribution of small drops of the coating on the crystal. These drops became less pronounced with time and, as Fig. 3b shows, holes are formed at an intermediate stage. Fig. 4 shows the microscopic image of the same peripheral zone of the electrode of the coated crystal, 8 days after application of the coating, and it is clear that no drops could be distinguished on the crystal surface. The changes observed on the crystal sur-

face were mainly attributed to the effect of nitrogen on the crystal, as no significant changes on the crystal surface could be seen on a crystal, coated in a similar way but kept in the absence of nitrogen flow, even 7 h after application of the coating.

Changes in the shape of the spray droplets, including the appearance of hollow forms, during the drying process have been reported, and two stage evaporation is a common process [5]. The first period of drying is characterised by a constant evaporation rate, until a critical point is reached where saturated conditions are no longer maintained, and the dried shell increases with time, causing a decrease in the rate of evaporation. This is termed the falling rate period or second period of drying [5].

The two different stages with different evaporation rates could explain the two periods of frequency increase that could be seen in Fig. 2. The frequency decreasing period, in between, must be related to coating migration, until the formation of an uniform film from the initial droplet distribution, passing through the hollow forms and drying shell formation. In fact, Glassford [6,7] stated that the frequency shift is proportional to the ratio of the kinetic energy of the deposit to that of the bare crystal. Since the velocity in a liquid deposit decreases with distance from the crystal surface, the mean velocity of the droplet, and hence its kinetic energy and induced quartz crystal microbalance (QCM) response, will be less than for the uniformly distributed material.

3.2. Sensitivity

Sensitivity must be evaluated comparing the responses of different coated crystals for the same analyte concentration. Fig. 5 shows the frequency decrease observed when 5 cm^3 CO_2 were injected

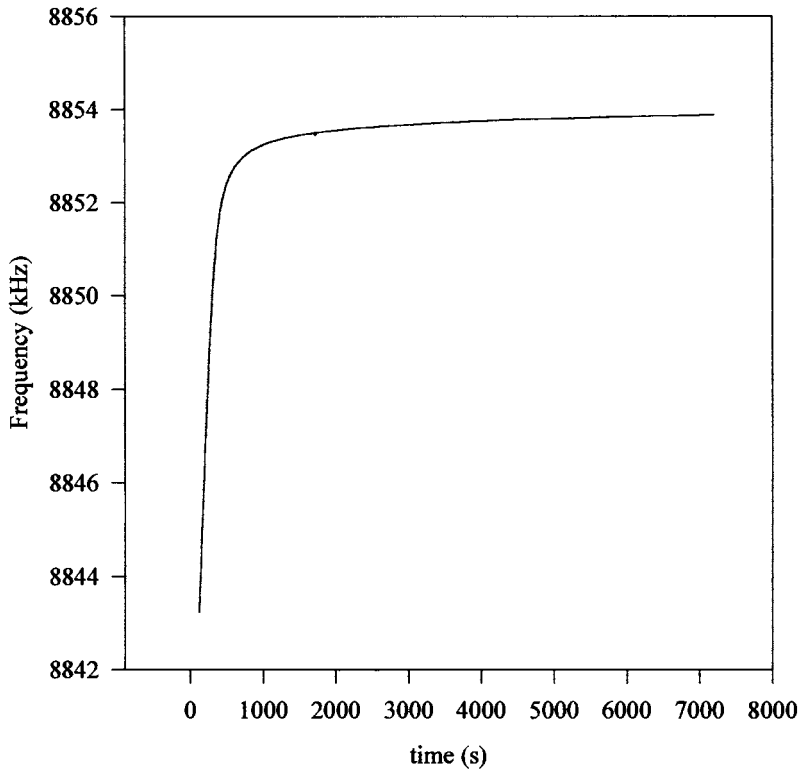

Fig. 1. Frequency of a crystal (uncoated crystal frequency = 8862.294 kHz) recorded at 2.5°C, after spraying with a solution of 1% (v/v) 1,2-diaminoethane in acetone.

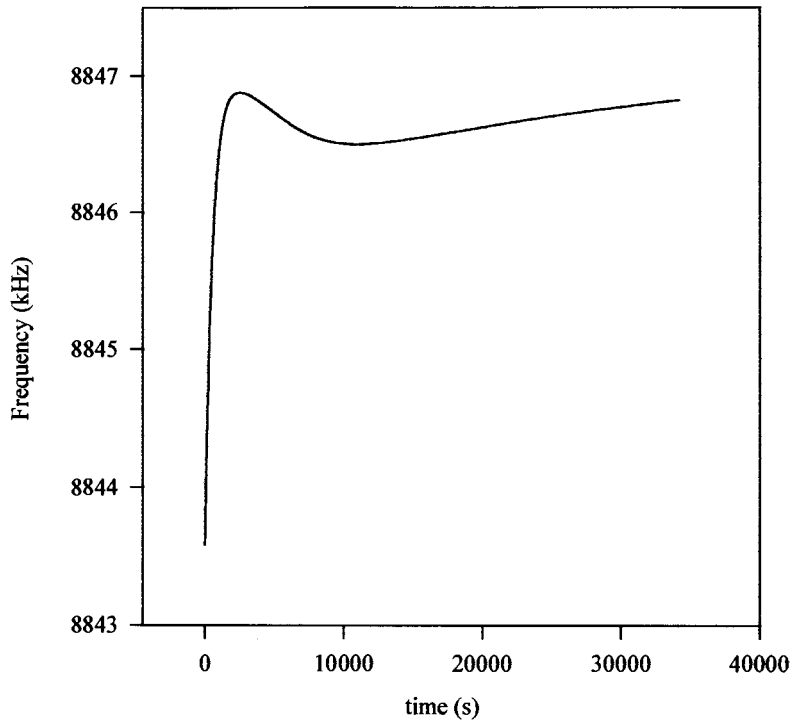

Fig. 2. Frequency of a crystal (uncoated crystal frequency = 8865.778 kHz) recorded after spraying with a solution of 1% (w/v) THEED in ethanol.

over crystals coated with various amounts of diethylenetriamine and triethylenetetramine. The spray coating allows enough reproducibility to compare sensitivities of different coated crystals and, as shown, the responses to CO_2 correlate with the amount of coating for both coated crystals. The crystal coated with triethylenetetramine shows, for the same quantity of CO_2, a greater frequency decrease than the one coated with diethylenetriamine, as the number of amino groups in a molecule of the former is greater than in the latter.

However, sensitivity is closely influenced by coating stability, and, for experiments where coating migration takes place, it changes with time.

Sensitivity variations with time were observed during experiments in which a crystal coated with THEED was kept under a nitrogen flow, and a sequence of injections of CO_2 were performed into the nitrogen stream that reached the coated crystal. After coating, both the time elapsed and the frequency of the crystal have been recorded. Then, 5 cm^3 CO_2 have been injected, and the corresponding signal measured. After complete recover from the interaction with CO_2, the frequency of the crystal could be measured again, and the process repeated several times. For these experiments, sensitivity was defined as the frequency decrease due to the CO_2 injection (Hz), divided by the frequency change induced in the crystal by the THEED coating (Hz). Fig. 6 shows both the sensitivity variations with time, and the frequency changes of a crystal coated with THEED. This limited long term stability does not necessarily invalidate the use of the coated crystal for quantitative work, as, for limited periods, the sensitivity of the coated crystal, especially if coated a long time ago, can be constant [8].

Even if constant stability and sensitivity with time can be assured, as in the previously reported experiments involving crystals coated with TMAF for CO_2 monitoring [9], sensitivity comparisons

between different coatings is not a straightforward task. Several instrumental variations can influence the observed frequency shifts due to the interaction between the coating and the analyte, as no calibration of the experimental apparatus is possible. Besides, reproducible results can only be obtained if the coating application can be reproduced, which is highly dependent on the coating method used [4], and can not be guaranteed with syringe, dropping, or smearing applications.

Comparison of the responses obtained by the interaction of a known quantity of analyte with crystals of different coatings are often made with a single coated crystal for each coating compound, although replicates are generally obtained after repeated contact between the same coated crystal and the analyte. This procedure obviously does not show the possible variation due to the coating application processes which would probably invalidate any future comparisons. Besides, even if a reproducible method to coat the crystal is used, reproducibility can, in principle, only be

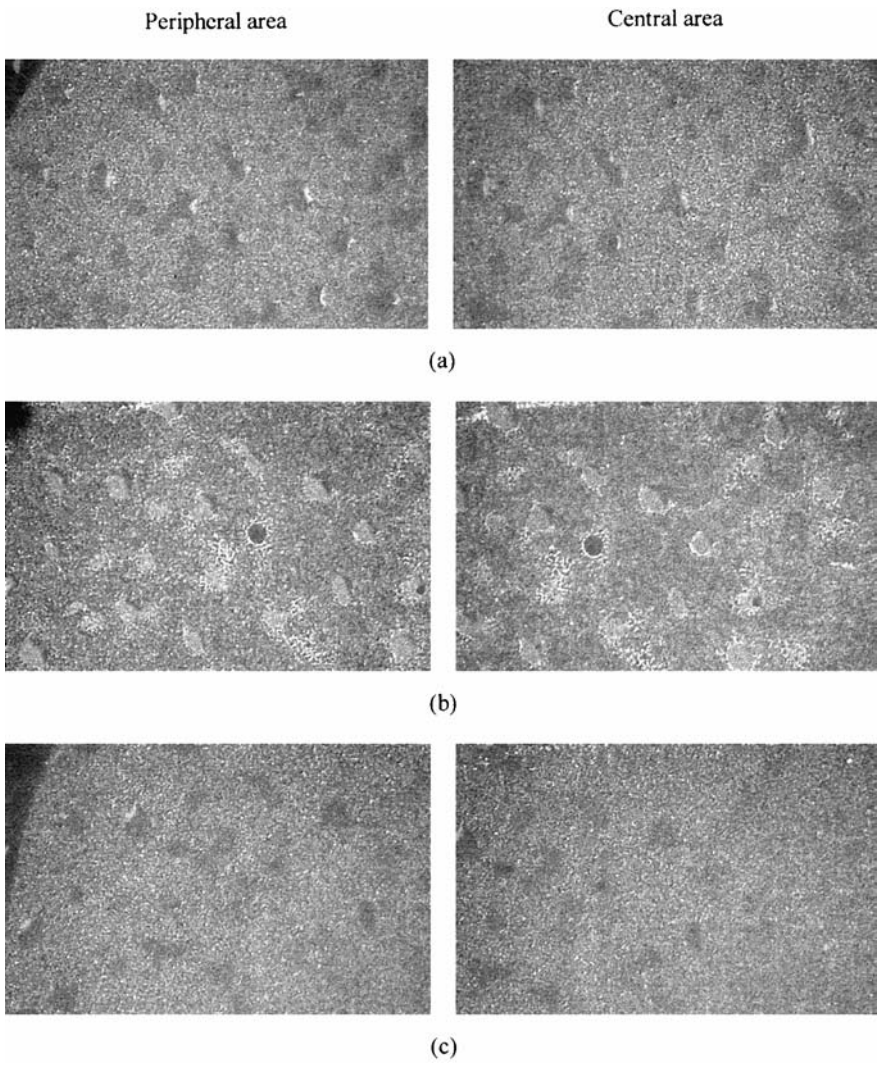

Fig. 3. Microscopic images (magnification $\times 54$) of the central and peripheral areas of the electrodes of a crystal coated with THEED kept under a nitrogen flow of 50 cm^3 min^{-1} for: (a) 10, (b) 20, and (c) 158 min.

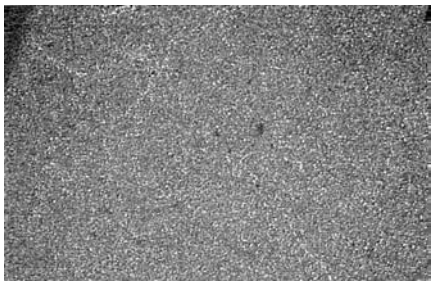

Fig. 4. Microscopic image (magnification × 54) of the same peripheral area of the electrodes of the same crystal as in Fig. 3 kept under nitrogen for 8 days.

assured for coating compounds with similar physical properties. It is also known that, for instance, in cases where adsorption is the phenomenon responsible for the interaction between the coating and the analyte, the frequency shifts, observed after contact of the coated crystal with a known quantity of analyte, increase with the amount of coating just until saturation of the surface of the crystal. Therefore, the function that can describe the responses of each coated crystal to a known amount of analyte, versus coating amount, needs to be known.

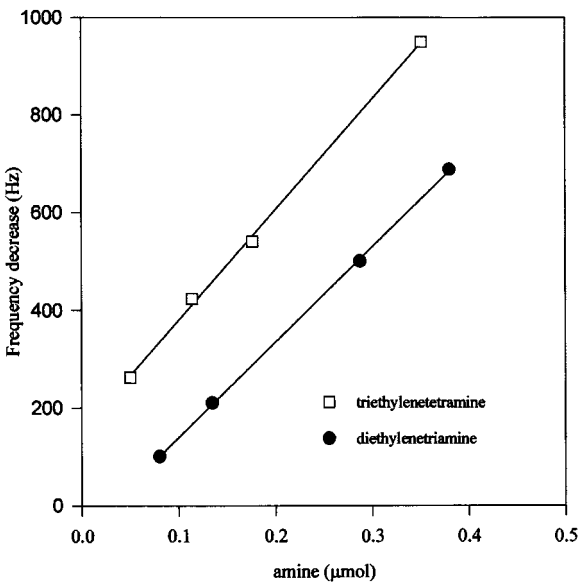

Fig. 5. Frequency decrease of crystals coated with different amounts of triethylenetriamine and diethylenediamine, with injections of 5 cm^3 CO_2.

The sensitivities of crystals, coated with different compounds, are often represented as a function of the amount of coating, which for most coating application methods is unknown. The amount of coating is then calculated by the Sauerbrey equation, which is only valid for rigid thin films, and does not include any parameters related to the different film properties.

Sensitivity is highly dependent on temperature, and, as Fig. 7 shows, decreases with it, for an exothermic adsorption process. The magnitude of the frequency shifts also depends on the flow rate, as can be seen in Fig. 8, and on the cell design [10].

3.3. Reversibility

Reversibility depends on the energy involved in the interaction between the coating and the analyte. As far as selectivity is concerned, specific chemical reactions or chemisorption are preferred. However, the analytes are then strongly and often irreversibly bonded, So, for reversibility, weaker adsorptive interactions are preferred. Obviously, the conflicting requirements lead to a compromise solution.

Fig. 9 shows the frequency signal observed for two crystals, one coated with diethylenetriamine, and the other with THEED, when 5 cm^3 CO_2 were injected into the nitrogen flow of 50 cm^3 min^{-1}. The amount of coating was not the same on both crystals. The amounts of coating, that allowed the observation of comparable frequency decreases for both crystals, were chosen. In spite of the observed frequency decrease, the slow recovery of the crystal coated with diethylenetriamine impairs its use as a sensor. In fact, under the same circumstances, the crystal coated with diethylenetriamine does not recover from a frequency decrease of 82 Hz in 70 min, while a crystal coated with THEED shows complete recover, after a signal of 93 Hz, in 185 s.

As Fig. 10 shows, an increase in temperature increases the rate of desorption, although, as mentioned above, for exothermic processes, the observed responses are smaller. There are, however, some other situations reported, in which the observed frequency shifts do not arise just as a

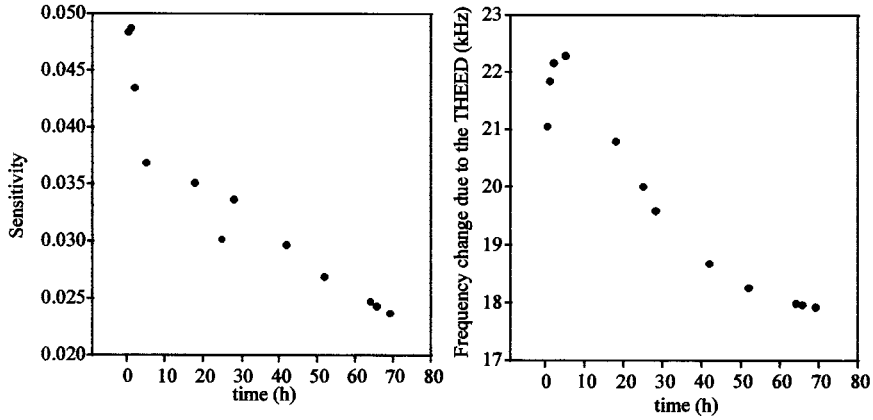

Fig. 6. Sensitivity to CO_2 and frequency of a crystal coated with THEED, under a nitrogen flow of 50 cm^3 min^{-1}, at a constant temperature of 44.0°C.

response to mass changes, but where phase changes take place, as a result of the interaction between the coating and the analyte [9], and where temperature effects are more complex.

An increase in the flow rate generally decreases the recovery time, although it can also increase coating volatility and affect sensitivity. Some situations, where the recovery processes require special treatment, show no effect for the flow rate on the crystal recovery. Crystals with mercury amalgamated onto gold electrodes, that require a temperature around 170°C to clean them [11], are a well known example.

3.4. Response time

Sensitivity and response time are also contradictory requirements. If the interaction phenomenon is ruled by penetration and diffusion of a gas, long response times are expected.

Flow rate affects the magnitude of the response, as is shown in Fig. 8, and, therefore, response time is flow dependent. As temperature also affects the frequency shift, which decreases with increasing temperature for an exothermic process, such as the interaction between THEED and CO_2, a variation in response time is expected after temperature changes.

3.5. Reproducibility

Reproducibility is mainly dependent on the coating application and stability, as well as on sample introduction, and measurement technique.

Sample introduction can give rise to pressure and flow variations, and can influence the fre-

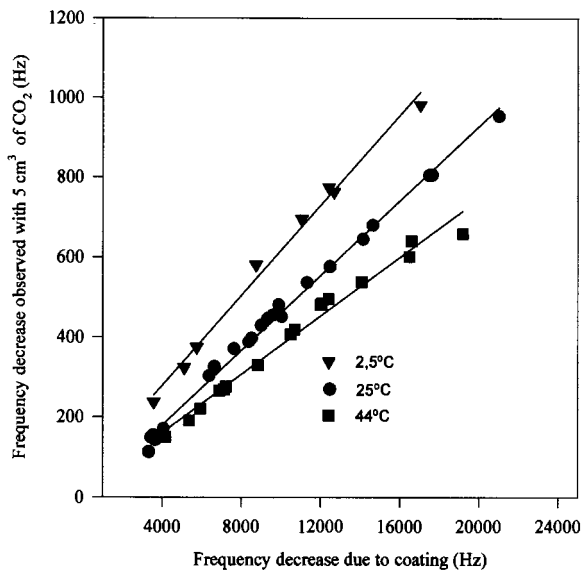

Fig. 7. Observed frequency decreases when 5 cm^3 CO_2 were injected over crystals coated with THEED, kept at a controlled temperature.

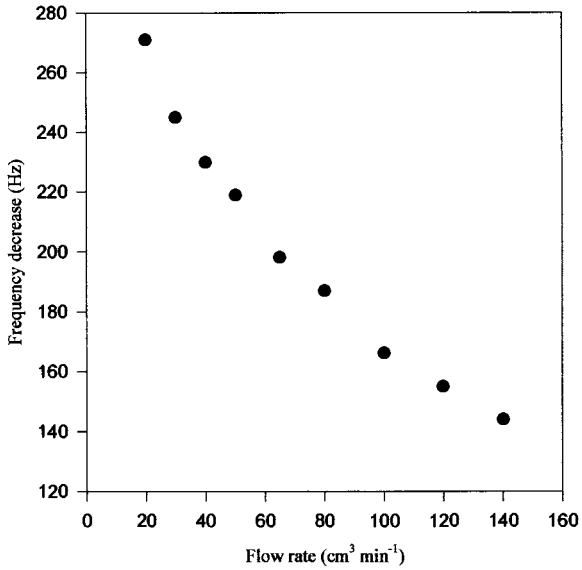

Fig. 8. Frequency decrease of a crystal coated, on one side, with THEED, after an injection of 3.0 cm^3 CO_2 at different nitrogen flows.

quency measured. Stockbridge [12] showed that, with the admission of a gas, the frequency of a crystal would increase linearly with the pressure, due to the effects of hydrostatic pressure on the elastic moduli of quartz, and would decrease linearly with the half power of the pressure, due to the shear impedance of the gas. Besides, the viscosity of most liquids can change over several orders of magnitude in the range of pressures of interest for most applications [13], and an increase in the frequency of the coated crystal is generally observed with the sample introduction in FIA experiments [14]. A positive pulse observed when CO_2 was injected into the nitrogen flow is shown in Fig. 11. It can be seen that the pressure pulse is effectively separated from the signal, with the insertion of a 264 cm long coil, between the injecting port and the crystal cell.

3.6. Selectivity

Selectivity is often limited on these sensors, and tests for suspected interferences need to be performed. The tests should be run for the maximum expected content of each compound, and if an interference is confirmed, physical or chemical traps must be added to the methodology. As an example, it can be said that THEED is at least 10 times more sensitive to SO_2 than to CO_2. However, the SO_2 interference was successfully eliminated, and the crystal could be used to determine CO_2 in wine, if a drop of H_2O_2 was added to 10 cm^3 of the sample [14].

4. Concluding remarks

The performance of a QCM is totally dependent on the coating of the crystal. In spite of the major importance of the choice of the coating material, this selection is subjected to enormous experimental variability and unavoidable assumptions. However, every day, new coatings are proposed to solve old or new analytical problems, and a careful investigation of the parameters to be taken into account in coating selection and, most of all, honest consideration of the variations and assumptions that influence the results are needed.

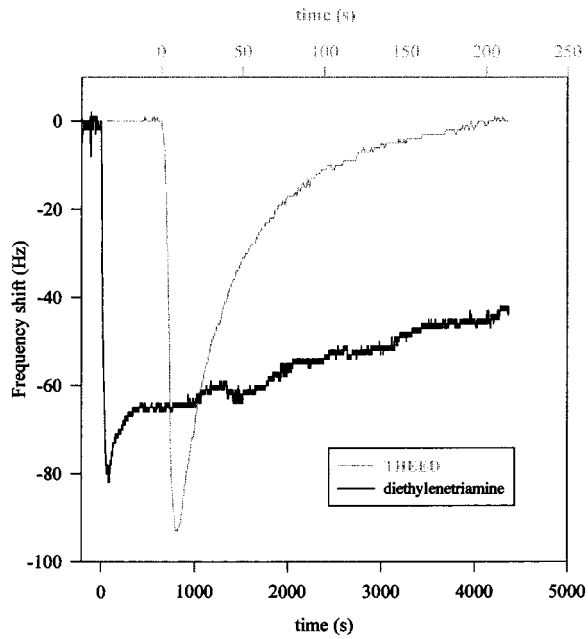

Fig. 9. The shape of the frequency signals observed when 5 cm^3 CO_2 were injected over two crystals coated with diethylenetriamine and THEED, respectively.

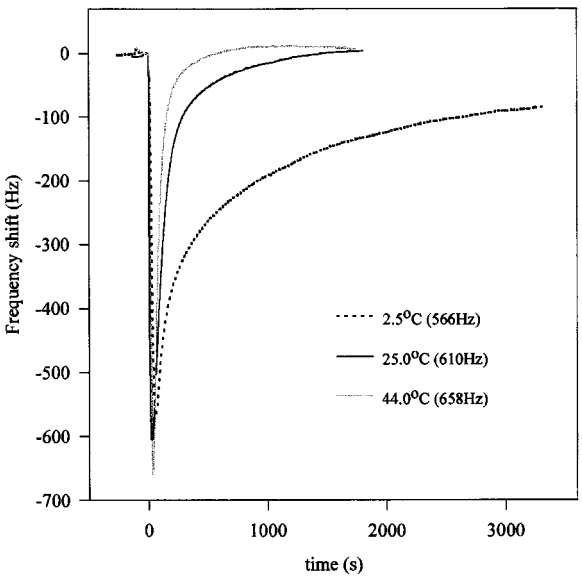

Fig. 10. Frequency changes observed during the complete process of adsorption/desorption for crystals coated with THEED, at several temperatures.

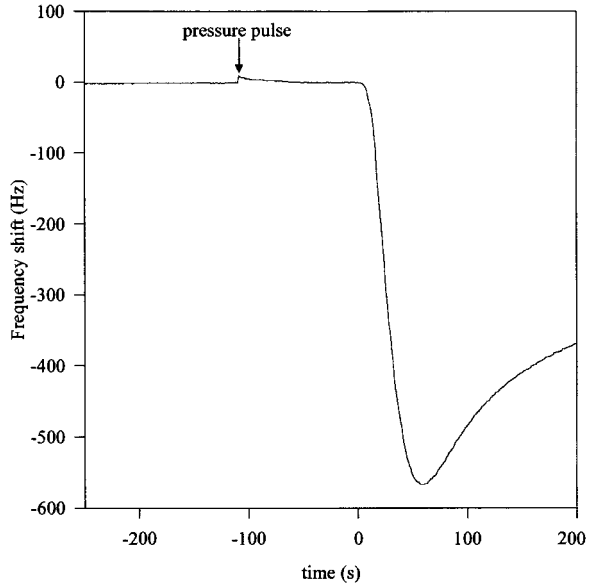

Fig. 11. The pressure pulse observed during the injection of 5 cm^3 CO_2. Time zero was assigned to the beginning of the frequency decrease signal.

Stability is not influenced just by the vapour pressure of the coating compound, but also by the coating methodology used and by the viscosity of the applied layer. Experimental parameters such as temperature, flow, and sample introduction need to be carefully controlled, as they affect the frequency of the crystal itself, as well as the interaction between the coating and the analyte.

Ultimately, the best coating depends on the specific application, and, for CO_2, we have found that crystals coated with THEED were more sensitive than the ones with TMAF, although the coating was more stable for the latter [9]. We can recommend crystals coated with TMAF for analysis where quantification is necessary, and longer stability if calibration is demanded, and THEED for detection of trace amounts.

References

[1] M.S. Nieuwenhuizen, A.W. Barendsz, Sens. Actuators 11 (1987) 45.
[2] O.S. Milanko, S.A. Milinkovic, L.V. Rajakovic, Anal. Chim. Acta 269 (1992) 289.
[3] A.R. Katritzky, R.J. Offerman, Crit. Rev. Anal. Chem. 21 (1989) 83.
[4] M.T. Gomes, A.C. Duarte, J.P. Oliveira, Anal. Chim. Acta 300 (1995) 329.
[5] K. Masters, Spray Drying Handbook, Wiley, New York, 1979.
[6] A.P.M. Glassford, J. Vac. Sci. Technol. 15 (1978) 1836.
[7] A.P.M. Glassford, Application of the quartz crystal microbalance to space system contamination studies, in: C. Lu, A.W. Czanderna (Eds.), Applications of Piezoelectric Quartz Crystal Microbalances, chap. 9, Elsevier, Amsterdam, 1984.
[8] M.T. Gomes, A.C. Duarte, J.P. Oliveira, Sens. Actuators B 26 (1995) 191.
[9] M.T.S.R. Gomes, T.A. Rocha, A.C. Duarte, J.A.B.P. Oliveira, Anal. Chim. Acta 335 (1996) 235.
[10] M. Trojanowicz, T.K. vel Krawczyk, Sens. Actuators B 9 (1992) 33.
[11] A.A. Suleiman, G.G. Guilbault, Anal. Chem. 56 (1984) 2964.
[12] C.D. Stockbridge, in: K.H. Behnrdt (Ed.), Vacuum Microbalance Techniques, vol.5, Plenum, New York, 1966, pp. 147–191.
[13] V. Tsionsky, E. Gileadi, Langmuir 10 (1994) 2830.
[14] M.T. Gomes, A.C. Duarte, J.P. Oliveira, Anal. Chim. Acta 327 (1996) 95.

ELSEVIER

Talanta 48 (1999) 91–102

Talanta

Determination of ion exchange equilibrium constants of strongly acidic resins with alkaline-earth metals by means of the potentiometric titrations technique

Gregorio Borge *, Gorka Arana, Luis A. Fernández, Juan M. Madariaga

Kimika Analitikoaren Departamentua, Euskal Herriko Unibertsitatea (UPV/EHU), 644 P.K., E-48080 Bilbao, Spain

Received 9 March 1998; received in revised form 28 May 1998; accepted 9 June 1998

Abstract

A recently developed methodology for the determination of ion exchange equilibrium constants has been applied to ion exchange systems of 1:2 stoichiometry. Potentiometric titrations with variable ionic strength were carried out. Ionic medium titrations were performed for the estimation of the liquid junction potential. The modified Bromley's methodology and the Wilson model were used for the estimation of the activity coefficients of the species in the aqueous and resin phase, respectively. A modification of the Henderson equation is used for the estimation of liquid junction potentials in the mixtures including 1:2 electrolytes. Equilibrium constants for the H^+/M^{2+} (M = Mg, Ca, Sr and Ba) exchange systems in the strongly acidic resins Dowex CM-15 and Dowex C650 were studied.

Keywords: Ion exchange equilibrium constants; Potentiometry; Ionic strength; Methods of calculation

1. Introduction

Determination of ion exchange equilibrium constants is usually performed by means of two experimental methodologies: the batch method and the column method. Both can be considered as expensive methodologies, since the amount of chemicals needed is large and the time necessary for reaching equilibrium and for the subsequent analysis is long.

Our workgroup has recently presented a new methodology for the determination of ion exchange equilibrium constants based on the potentiometric titrations technique [1]. It was applied to the determination of thermodynamic equilibrium constants for ion exchange systems of 1:1 stoichiometry: equilibria between the proton form of the resin and the alkaline metals for strong acidic resins were studied at 25°C. Potentiometric titrations gave faster results and saved a great amount of chemicals, since many experimental data can be obtained with one experiment.

The main problem arising from the application of potentiometric titrations to the determination of ion exchange equilibrium constants is that the

* Corresponding author. Tel.: +34 9 44647700, ext. 2397; fax: +34 9 44648500; e-mail: qapbobrg@lg.ehu.es

0039-9140/99/$ - see front matter
PII S0039-9140(98)00219-7

so called constant ionic medium methodology cannot be applied, since strong electrolytes commonly used as ionic media are not inert for non highly selective ion exchangers. This means that the activity coefficients of the species in solution will change during the titration and that the estimation of the liquid junction potential cannot be performed by making use of the approximation of Biedermann [2–4]. The applied methodology relates the emf value measured in these potentiometric titrations with variable ionic strength to the activity of the species in the solution by means of the following equation:

$$E = E^0 + g \log \{H^+\} + E_j \quad (1)$$

where E^0 is the standard potential of the electrochemical cell and the liquid junction term E_j is estimated using the modification of the Henderson equation recently developed by our workgroup [5]:

$$E_j = -g \frac{\sum_i (z_i/|z_i|)\lambda_i(\{i\}_2 - \{i\}_1)}{\sum_i |z_i|\lambda_i(\{i\}_2 - \{i\}_1)} \log \frac{\sum_i |z_i|\lambda_i\{i\}_2}{\sum_i |z_i|\lambda_i\{i\}_1} \quad (2)$$

Subscripts '1' and '2' in Eq. (2) refer to the reference electrode and test solutions, respectively, of the corresponding electrochemical cell. It has been experimentally proved that Eq. (2) is useful for estimating the liquid junction potential in mixtures of electrolytes of 1:1 stoichiometry [1,5]. The stoichiometry of the electrolytes is important for the estimation of the ionic conductivities (λ_i), since conductivity (which was estimated in this case by means of the extended Falkenhagen equation [6,7]) depends directly on the stoichiometry of the electrolytes in solution. On the other hand, the estimation of the liquid junction potential by means of Eq. (2) requires knowledge of the activity and concentration of all ionic species in solution. Because of this, mass-balances of the ion exchange equilibria have to be solved at the same time as Eq. (1), in order to obtain the value of the proton concentration from the emf experimental value. Equations used for the estimation of λ_i are in Appendix A.

Activities are used in Eqs. (1) and (2) and, thus, the estimation of the activity coefficients has to be performed. The activity coefficients of the species in the aqueous phase are estimated using the modified Bromley's methodology (MBM) [8–10], which can be used in the molar concentration scale:

$$\log \gamma_M = -\frac{A(z_M)^2 I^{1/2}}{1 + I^{1/2}} + \sum_X \left(\dot{B}_{MX} \frac{(|z_M| + |z_X|)^2}{4} [X] \right) \quad (3)$$

where

$$\dot{B}_{MX} = \frac{(0.06 + 0.6B_{MX})|z_M z_X|}{\left[1 + \frac{1.5}{|z_M z_X|} I\right]^2} + B_{MX} \quad (4)$$

Eqs. (1)–(4) relate the emf value experimentally obtained to the concentrations and activity coefficients of the species in the aqueous phase. The determination of the thermodynamic equilibrium constants requires a knowledge of the concentrations and the activity coefficients of the species in the resin phase. Concentrations in this phase can be related to those in the aqueous phase by means of the mass-balance equations of the system. On the other hand, the activity coefficients can be estimated using the so called Wilson model [11,12], which proposes the following dependence of the activity coefficient on the concentration:

$$\ln f_H = 1 - \ln(\overline{x_H} + \overline{x_M}\lambda_{HM}) - \left(\frac{\overline{x_H}}{\overline{x_H} + \overline{x_M}\lambda_{HM}} + \frac{\overline{x_M}\lambda_{MH}}{\overline{x_H}\lambda_{MH} + \overline{x_M}} \right) \quad (5)$$

$$\ln f_H = 1 - \ln(\overline{x_H}\lambda_{MH} + \overline{x_M}) - \left(\frac{\overline{x_H}\lambda_{HM}}{\overline{x_H} + \overline{x_M}\lambda_{HM}} + \frac{\overline{x_M}}{\overline{x_H}\lambda_{MH} + \overline{x_M}} \right) \quad (6)$$

In the present study, this methodology is extended to ion exchange systems with 1:2 stoichiometry. The ion exchange equilibrium constants of two non selective cationic resins, Dowex CM-15 and Dowex C650, are determined for the system H^+/M^{2+} (M = Mg, Ca, Sr and Ba). The suitability of Eq. (2) for ion exchange systems of 1:2 stoichiometry was previously studied by carrying out the corresponding ionic medium potentiometric titrations.

2. Experimental

2.1. Resins

Dowex CM-15 (macroporous, 15% DVB) and Dowex C650 (monoporous, 10% DVB) are strongly acidic resins with sulphonate as the active group. Both were washed with water and treated with HCl (Normasolv, 35%) to excess in order to ensure the proton form. The resins were finally washed with water and kept completely swollen. The swollen resin was weighed after air drying for the experimental work.

Characterization of the resins was performed following the methods described elsewhere for the determination of the densities in the proton form [13] and the water content [14]. The exchange capacity (q_{max}) was determined by means of a batch methodology and by potentiometric titrations, adding known amounts of alkaline hydroxide solutions. The results are given in Table 1.

2.2. Ionic medium potentiometric titrations

Potentiometric titrations were carried out by measuring the emf of the following electrochemical cell:

$$\mathrm{Ag|AgCl|MCl_2}\ 0.1\ \underset{(3)}{\mathrm{M}},\ \mathrm{AgCl\ sat.}\|\underset{(1)}{\mathrm{MCl_2}}\ 0.1\ \mathrm{M}\|\underset{(2)}{\text{test solution}}|\mathrm{G.E.} \quad (7)$$

Double junction reference electrodes Ag|AgCl (Metrohm 6.0726.100) and glass electrodes (Metrohm 6.0101.000) were used. Two kind of test solutions were used.

2.2.1. HCl solutions

Deionized MilliQ water (75 cm^3) were titrated with 0.4 mol dm^{-3} HCl (Fluka, p.a.) solutions. These titrations were performed for M = Mg, Ca, Sr and Ba. Thus, the only difference between titrations was the composition of the bridge solution and the internal solution in the reference electrode. The bridge solutions were prepared from $MgCl_2$ (Fluka, BioChemika Mikroselect), $CaCl_2 \cdot 2H_2O$ (Fluka, BioChemika Mikroselect), $SrCl_2 \cdot 6H_2O$ (Fluka, Chemika puriss., p.a. ACS), and $BaCl_2 \cdot 2H_2O$ (Fluka, Chemika puriss., p.a., ACS). All solutions were prepared in MilliQ water. The internal solutions were prepared adding AgCl to aliquots of the corresponding bridge solution.

2.2.2. Mixtures of HCl and $MgCl_2$

MilliQ water was titrated with two solutions of 0.4 mol dm^{-3} HCl and 0.4 mol dm^{-3} $MgCl_2$. The solutions were added from independent burettes following different addition phases during each titration. HCl only was added in the first phase, whereas further phases included simultaneous addition of both HCl and $MgCl_2$. The final solutions obtained in the titrations were 0.02 mol dm^{-3} in HCl and 0.01 mol dm^{-3} in $MgCl_2$, approximately. In this case $MgCl_2$ was the electrolyte in the reference electrode.

Titrations were carried out using an automated system developed in this laboratory [15]. The electrochemical cell was inserted in a thermostatic bath at 25.0 ± 0.1°C. The signals from the electrodes, preamplified by an operational amplifier in order to get an adequate electric signal, were measured by a Hewlett-Packard HP-EI326B voltmeter incorporated into a VXI data acquisition system connected to the computer. The voltmeter

Table 1
Characteristics of the resins

	Dowex CM-15	Dowex C650
q_{max} (mmol g^{-1})	3.43 ± 0.07	3.46 ± 0.05
Water content (%)	28.1 ± 0.9	28.6 ± 1.0
Dry resin density $\rho^{a}_{A,d}$ (g cm^{-3})	0.620 ± 0.005	0.739 ± 0.006
Swollen resin density $\rho^{b}_{A,s}$ (g cm^{-3})	0.562 ± 0.003	0.552 ± 0.002
Density of the volume change of the solution ρ^{c}_{B} (g cm^{-3})	1.29 ± 0.02	1.31 ± 0.02

[a] $\rho_{A,d}$ = g dry resin per cm^3 dry resin.
[b] $\rho_{A,s}$ = g dry resin per cm^3 swollen resin.
[c] ρ_B = g dry resin per (cm^3 water and resin-cm^3 water added).

has a resolution of 5 1/2 digits within the measurement range ± 1 V, and it was programmed to perform 100 real measurements in 1 s with a theoretical precision of ± 15 μV. The mean of these measurements is calculated, and when the S.D. of the emf (i.e. the mean of the obtained means) over a pre-set period of time (about 6 min) was less than 0.04 mV, an instruction for a new addition was given by the computer to the burette. Addition of the titrants was performed using Metrohm 665 automatic burettes connected to the computer via a RS-232C interface. Each titration took around 24 h, and all of them were carried out at least twice.

2.3. Ion exchange potentiometric titrations

The same electrochemical cell in the same experimental set-up was used. In this case, the test solution was a known amount of resin in the proton form, between 0.10 and 0.80 g, in 75 cm^3 of MilliQ water, which was titrated with 0.2 mol dm^{-3} MCl_2 solutions. The titrations were performed for M = Mg, Ca, Sr and Ba. Each titration took around 40 h and all of them were carried out at least three times. The metal in the reference electrodes and in the titrant solutions was the same in every case and all metal solutions were prepared from the chemicals described above. All the metal solutions in this study were standardized following the usual titrimetric methods [16].

3. Results and data treatment

3.1. Ionic medium potentiometric titrations

Fig. 1 shows the results of one titration for $CaCl_2$ and $BaCl_2$ solutions in the reference electrode. Similar curves were obtained for the other titrations of H_2O with HCl using $MgCl_2$ or $SrCl_2$ solutions in the reference electrode, and for the titrations of H_2O with HCl and $MgCl_2$. The validity of the model for the liquid junction term in Eq. (2) was tested by checking the nernstian behaviour of the system. This kind of verifying calculations have been used by Fiol et al. [17].

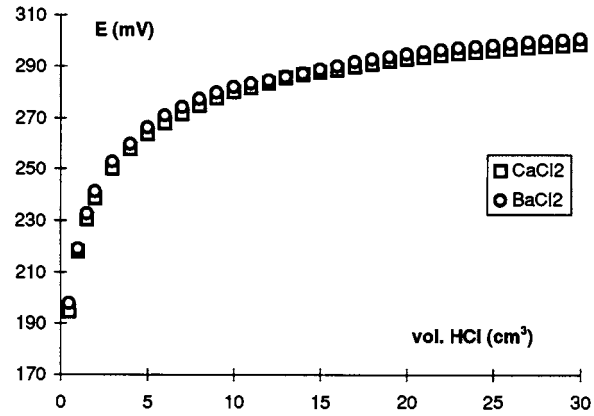

Fig. 1. Titrations of H_2O with HCl for reference electrodes containing solutions of $CaCl_2$ and $BaCl_2$.

Checking of the nernstian behaviour of the system is performed by rearranging the terms in Eq. (1):

$$E - E_j = E^0 + g \log \{H^+\} \quad (8)$$

The variable $(E - E_j)$ can be calculated using Eq. (2), since the concentration of all the ionic species in solution and all the necessary parameters for the Bromley and Falkenhagen models are known. The plot $(E - E_j)$ versus $\log \{H^+\}$ should give a straight line whose ordinate is the standard potential of the electrochemical cell and whose slope should be 59.16 mV. Eq. (A2) in Appendix A is used for the titrations with HCl only. The corresponding plots obtained from a titration for each system are presented in Fig. 2.

On the other hand, Eqs. (A3), (A4) and (A5) in Appendix A are applied to the titrations with mixtures of HCl and $MgCl_2$ in order to estimate the conductivity of the ions. Fig. 3 shows the plots of Eq. (8) for two titrations of this kind.

Table 2 presents the results of the linear correlations for a titration in each case. Taking into account that most of the titrations showed a nernstian behaviour and that the Sr and Ba systems showed very slight deviations from the value $g = 59.16$ mV, the model was taken as valid for the estimation of the liquid junction potentials in this kind of systems.

Table 3 contains the values of the proton concentrations and activities and of the liquid junction potential for some points of a titration with

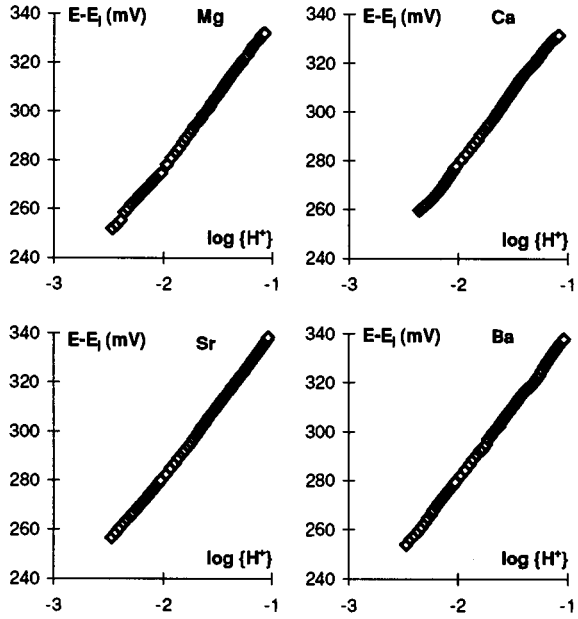

Fig. 2. Test of the nernstian behaviour of the titrations of H_2O with HCl for reference electrodes containing solutions of MCl_2 (M = Mg, Ca, Sr and Ba).

$CaCl_2$ solution in the reference electrode, in order to show the concentration interval in which the proposed model can be applied. As can be seen, the liquid junction potential value is high and cannot be considered negligible. The interval of proton concentration is that used in the ion exchange potentiometric titrations.

3.2. Ion exchange potentiometric titrations

As an example, Fig. 4 shows the profiles of two of the titrations obtained for the H^+–Sr^{2+} ion exchange system in Dowex C650. The same kind of plots were obtained for the other systems in the study.

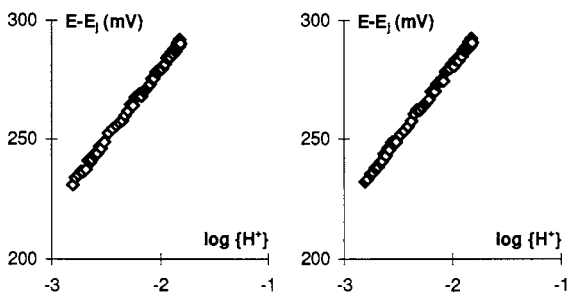

Fig. 3. Test of the nernstian behaviour of the titrations of H_2O with HCl and $MgCl_2$.

The mathematical treatment of these titrations was performed following the methodology previously reported [1]. This included the correction of the solution volume using the densities $\rho_{A,d}$, $\rho_{A,s}$ and ρ_B of the resin (see the definitions in Table 1). The activity coefficients of the species in the aqueous phase were estimated directly in the molar concentration scale by means of the MBM. The B_{MX} values used in this study are 0.121 ($MgCl_2$), 0.101 ($CaCl_2$), 0.089 ($SrCl_2$), and 0.066 ($BaCl_2$) [9]. Values are given in $dm^3\ mol^{-1}$. The activity coefficients of the species in the resin phase were estimated using the Wilson model following Eqs. (5) and (6). The interaction parameters λ_{HM} and λ_{MH} are estimated together with the thermodynamic equilibrium constants, since no information about these systems has been found in the literature.

In this case, the mass-balance equations of the whole system can be written as follows:

$$\text{proton: } q_{max}g_{res} + h_0v_0 = q_Hg_{res} + [H^+]v_{tot} \quad (9)$$

$$\text{metal: } c_{MCl_2}v = q_Mg_{res} + [M^{2+}]v_{tot} \quad (10)$$

$$\text{resin: } q_{max} = q_H + 2q_M \quad (11)$$

$$\text{chloride: } 2c_{MCl_2}v + h_0v_0 = [Cl^-]v_{tot} \quad (12)$$

where v is the volume of the titrant added, v_0 is the initial volume in aqueous phase (corrected with the values of the densities), v_{tot} is the total volume and q_i is the number of moles of the i species in the resin phase per g. h_0 Is the initial concentration of protons in solution. Eqs. (9)–(12) can be rearranged and $[Cl^-]$, $[M^{2+}]$, q_H and q_M can be expressed as a function of the proton concentration. The other quantities are known, except h_0.

The liquid junction potential in Eq. (1) was estimated using Eq. (2). Estimation of the ionic conductivities in Eq. (2) was performed using Eqs. (A3), (A4) and (A5) proposed in Appendix A. The activity coefficients in Eqs. (2), (A3), (A4) and (A5) were estimated using the MBM.

On the other hand, the slightly acidic emf value (between 60 and 130 mV) obtained in the initial points of the titrations was interpreted proposing

Table 2
Results of the correlation of Eq. (8)

Reference solution	Titrant	g (mV)	E^0 (mV)	r
$MgCl_2$	HCl	59.1 ± 0.2	395.7 ± 0.4	0.99947
$CaCl_2$	HCl	59.3 ± 0.1	396.6 ± 0.2	0.99974
$SrCl_2$	HCl	58.94 ± 0.09	398.5 ± 0.1	0.99991
$BaCl_2$	HCl	58.8 ± 0.3	397.9 ± 0.4	0.99919
$MgCl_2$	$HCl + MgCl_2$	59.3 ± 0.3	398.2 ± 0.8	0.99790

an initial proton concentration (h_0) for each system [1]. In this case, the h_0 value was obtained from Eqs. (1) and (2) considering the initial solution of each titration as a very dilute one. In this situation, the activity coefficients of the species are equal to unity and the conductivities are the limiting ones found in Ref. [18]. Thus, Eqs. (1) and (2) can be rearranged and the following expression is obtained:

$$\log h_0 = \frac{\dfrac{E-E^0}{g} + \dfrac{\lambda^0_M\gamma^{ref}_M - 2\lambda^0_{Cl}\gamma^{ref}_{Cl}}{2\lambda^0_M\gamma^{ref}_M + 2\lambda^0_{Cl}\gamma^{ref}_{Cl}} \times \log \dfrac{\lambda^0_H + \lambda^0_{Cl}}{2[MCl_2]_{ref}(\lambda^0_M\gamma^{ref}_M + \lambda^0_{Cl}\gamma^{ref}_{Cl})}}{1 - \dfrac{\lambda^0_M\gamma^{ref}_M - 2\lambda^0_{Cl}\gamma^{ref}_{Cl}}{2\lambda^0_M\gamma^{ref}_M + 2\lambda^0_{Cl}\gamma^{ref}_{Cl}}} \quad (13)$$

where E is the experimental emf value of the first point in each titration (no MCl_2 is added yet) and the term 'ref' referres to the bridge solution in the reference electrode.

3.2.1. Calculation of the ion exchange equilibrium constant

There is no available program to perform the mathematical treatment of these data. Because of this, an iterative method had to be developed for taking into account the variation of the ionic strength in the estimation of the liquid junction potential and the activity coefficients. The Nlreg program (P.H. Sherrod, Nonlinear Regression Analysis Program, Nashville, 1991–1995), which permits the resolution of iterative calculations, was used in order to perform the calculations.

The equilibrium in the titration cell and the corresponding ion exchange equilibrium constant are:

$$2\overline{RH} + M^+ \rightleftharpoons \overline{R_2M} + 2H^+ \quad (14)$$

$${}^0K^M_H = \frac{[H^+]^2(\gamma_H)^2(\overline{x_M})(f_M)}{(\overline{x_H})^2(f_M)^2[M^{2+}](\gamma_M)} \quad (15)$$

The molar fractions in the resin phase, the metal concentration in the aqueous phase, and the activity coefficients in both the aqueous and resin phases can be expressed as a function of $[H^+]$ and h_0, using the mass-balance equations and the expressions of the activity coefficients previously reported. Therefore, all the variables in Eq. (15) can be expressed as a function of $[H^+]$ and the unknown parameters ${}^0K^M_H$, E^0, λ_{HM} and λ_{MH}.

As it can be seen, the dependence of ${}^0K^M_H$ with the proton concentration is complicate, since the mass-balance equations and expressions for the activity coefficients have to be considered. Because of this, the following iterative method is proposed. The terms in Eq. (15) are rearranged as follows:

$$y = {}^0K^M_H(\overline{x_H})^2(f_H)^2[M^{2+}](\gamma_M) - [H^+]^2(\gamma_H)^2(\overline{x_M})(f_M) = 0 \quad (16)$$

Initial values of the unknown parameters of the system are given in the input, so the roots of Eq. (16) can be solved, and the values of $[H^+]$ are obtained for these initial values of the parameters.

Once the proton concentration is known, the emf value of the aqueous solution is estimated following Eqs. (1) and (2) and using the parameters

Table 3
Values of liquid junction potential and proton concentrations and activities throughout a titration with $CaCl_2$ in the reference electrode

v (HCl) (cm^3)	E (mV)	10^2 [H^+] (mol dm^{-3})	10^2 {H^+} (mol dm^{-3})	E_j (mV)
0.50	200.26	0.272	0.257	−52.7
2.00	238.69	1.07	0.964	−38.9
5.00	264.22	2.57	2.22	−34.6
10.00	281.536	4.83	4.04	−34.1
15.00	288.456	6.85	5.62	−34.7
20.00	293.02	8.65	7.01	−35.6
25.00	294.88	10.3	8.25	−36.4

Emf data were obtained with S.D.s lower than ±0.04 mV.

values initially proposed. The emf value calculated, $E_{calc,i}$, is then compared with the emf experimental value, and the sum of squared absolute errors in the potential is calculated:

$$U_{abs} + \sum_{i+1}^{N_p} (E_{calci,i} - E_{exp,i})^2 \quad (17)$$

where N_p is the number of experimental points.

The capacity of the Nlreg program is used to try different values of the unknown parameters in order to obtain the minimum U_{abs} value. The calculation is repeated until this minimum value is obtained. The values of the parameters used in this case are taken as the valid ones.

The parameters were calculated taking into account all the valid titrations for each system. Results of the fits (values of the thermodynamic equilibrium constant, the Wilson parameters and the statistical results) for Dowex CM-15 and Dowex C650 are shown in Table 4. Values of E^0 are not shown since they varied for each titration. As an example, Fig. 5 shows the distribution of errors for the system H^+–Ca^{2+} in Dowex C650. This kind of distributions were obtained for all the systems in the study.

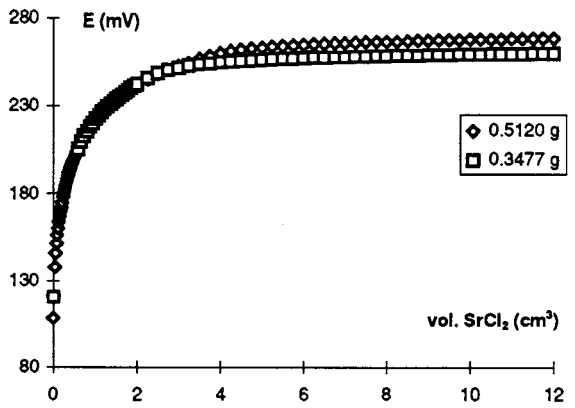

Fig. 4. Potentiometric titrations obtained for the H^+–Sr^{2+} system in Dowex C650. The legend indicates the resin weight in the proton form.

4. Discussion

A method previously reported [1] for the determination of thermodynamic equilibrium constants of ion exchange systems of 1:1 stoichiometry has been applied to 1:2 systems. The method is based on the potentiometric titrations technique without constant ionic strength.

The use of a variable ionic strength during the titrations is necessary since the ion exchangers studied are not highly selective resins. The consequent variation of the activity coefficients is considered using the MBM. On the other hand, the estimation of the liquid junction potential has been performed using a slightly modified model of that previously used [1,5], since it is based on the estimation of the ionic conductivities of the ions in solution, which depends on the stoichiometry of the electrolytes. These changes have been established based on experimental potentiometric titrations without ion exchanger, but unfortunately it has not been possible to apply the model here obtained to the emf data obtained from the potentiometric titrations with constant ionic

Table 4
Thermodynamic equilibrium constants and Wilson parameters for the H^+–M^{2+} ion exchange system in Dowex CM-15 and Dowex C650

Resin	M^{2+}	${}^0K_H^M$	λ_{MH}	λ_{MH}	N_p	σ_{TOT}^a
Dowex CM-15	Mg^{2+}	0.16 ± 0.01	0.53 ± 0.02	0.02 ± 0.02	110	0.37
	Ca^{2+}	2.1 ± 0.2	0.3 ± 0.1	0.5 ± 0.2	99	0.62
	Sr^{2+}	2.7 ± 0.2	0.2 ± 0.1	0.6 ± 0.1	119	0.56
	Ba^{2+}	3.5 ± 0.4	2.0 ± 0.3	1.0 ± 0.1	55	0.56
Dowex C650	Mg^{2+}	0.36 ± 0.07	0.6 ± 0.08	0.3 ± 0.1	66	0.61
	Ca^{2+}	0.37 ± 0.07	0.27 ± 0.04	0.6 ± 0.1	110	0.27
	Sr^{2+}	3.8 ± 0.3	0.8 ± 0.2	0.15 ± 0.07	110	0.58
	Ba^{2+}	5.6 ± 0.6	0.7 ± 0.2	0.1 ± 0.1	110	0.64

[a] $\sigma_{TOT} = \sqrt{\frac{U_{abs}}{N_p} - N_k}$; $U_{abs} = \sum_{i=1}^{N_p} (E_{calc,i} - E_{exp,i})^2$.

strength, since 1:2 strong electrolytes are rarely used as ionic medium.

The selectivity of the ion exchangers is usually represented by means of the equilibrium quotient of the systems defined as

$$K_H^M = {}^0K_H^M \frac{(f_H)^2}{f_M} = \frac{[H^+]^2(\gamma_H)^2(\overline{x_M})}{(\overline{x_H})^2[M^{2+}](\gamma_M)} \quad (18)$$

In this study, the equilibrium quotient of the systems cannot be directly obtained from the experimental results, since the whole mathematical treatment has to be performed in order to know the concentrations in each phase. Nevertheless, the equilibrium quotient values have been calculated from the values of the thermodynamic equilibrium constants and the Wilson parameters shown in Table 4. Fig. 6 shows the plots of the calculated equilibrium quotients for the H^+–M^{2+} ion exchange equilibria in Dowex CM-15 and Dowex C650 versus the metal molar fraction in the resin. The variation of the equilibrium quotient with the metal concentration in the resin phase shows that the selectivity depends on the composition and the activity coefficients of the species, since these are the variables present in Eq. (18). In general, the selectivity in these systems increases with the ionic radius of the ion exchanged.

Table 5 presents the values found in the literature for the Wilson parameters for H^+–M^{2+} systems in strongly acidic cation resins with sulphonate as the active group. The number of parameters is small for performing comparisons with the results obtained here. The Wilson parameters obtained in this study do not show clear trends, therefore the relationships between the values of the Wilson parameters and the ions in this study cannot be ascertained.

Application of the potentiometric titrations technique has allowed the fast determination of the thermodynamic equilibrium constants of eight ion exchange systems. Chemicals and time have been saved, but it should be stressed that this determination is based on the simplicity of the mass-balance equations of the system. Further

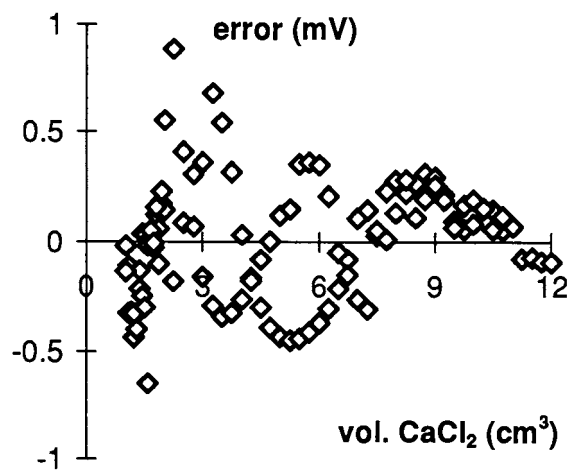

Fig. 5. Error distribution for titrations of Dowex C650 in the proton form with $CaCl_2$.

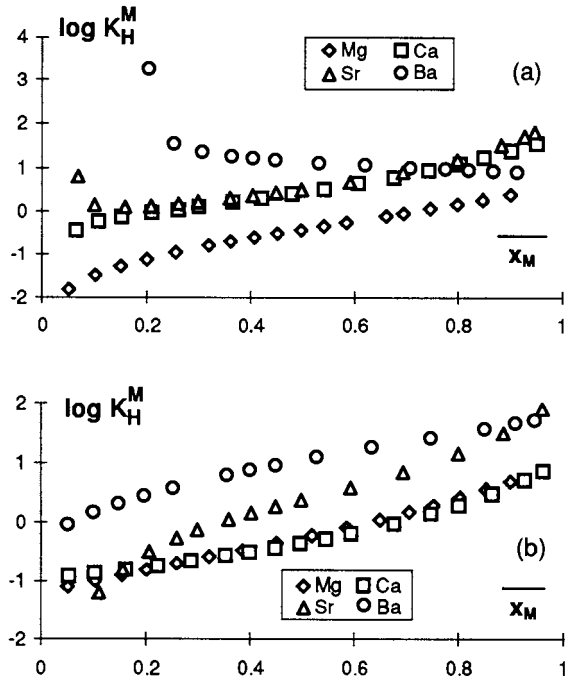

Fig. 6. Equilibrium quotient vs. metal concentration in the resin phase for $H^+ - M^{2+}$ equilibria in Dowex CM-15 (a) and Dowex C650 (b).

Table 5
Values of the Wilson parameters for strongly acidic sulphonate resins

Resin	System	λ_{ij}	λ_{ji}	Reference
Lewatit SP120	H–Mg	13.41	0.0034	[21]
Dowex HCR-3	H–Ca	2.52	0.397	[11]

complication of the aqueous phase under study (i.e. complexation equilibria of the metal) would probably require a robust calculation program for solving the mass-balance equations.

5. List of Symbols

A	0.5115 at 25°C
a	parameter of the extended Falkenhagen equation
B, B_1, B_2	parameters of the extended Falkenhagen equation
B_{MX}	interaction parameter of the MBM
$\dot{B}_{MX}$	intermediate term in the MBM
c_{MCl_2}	concentration of the titrant solution
E	emf value of the electrochemical cell
E^0	standard potential of the electrochemical cell
E_{calc}	calculated emf value
E_{exp}	experimental emf value
E_j	liquid junction potential
f_i	activity coefficient of i in the resin phase
g	59.16 mV
G.E.	glass electrode
g_{res}	resin weight
h_0	initial concentration of protons
$\{i\}$	activity of i species
$[i]$	concentration of i species
I	ionic strength
K_H^M	equilibrium quotient
${}^0K_H^M$	ion exchange thermodynamic equilibrium constant between H^+ and M^+
N_k	number of parameters
N_p	number of points per g resin
q	$= (\lvert z_M z_X \rvert (\lambda_M^0 + \lambda_X^0)) / ((\lvert z_M \rvert + \lvert z_X \rvert)(\lvert z_X \rvert \lambda_M^0 + \lvert z_M \rvert \lambda_X^0))$
q_i	mol Ri per g resin
q_{max}	ion exchange capacity of the resin
r	correlation coefficient
U_{abs}	sum of squared absolute errors
v	volume of titrant added
v_0	initial volume of titration
v_{tot}	total volume of titration
x_i	molar fraction of i in the resin phase
y	function of the constant equilibrium
z_i	charge of i
γ_i	activity coefficient of i in the aqueous phase
$\gamma^{ref,i}$	activity coefficient of i in the reference electrode solution
λ_i	molar conductivity of i
$\lambda^{0,i}$	limit conductivity of i

λ_{ij}	Wilson parameter between i and j in the resin phase
Λ	conductivity of a solution
Λ^0	limiting conductivity of an electrolyte
$\rho_{A,d}$	dry resin density
$\rho_{A,s}$	swollen resin density
ρ_B	solution volume change density
σ_{TOT}	S.D. of the fit

Acknowledgements

This research was supported by the European Union (project LIFE 94/E/A121/E/01409/PVA). GB is grateful for the Scholarship granted to him by the Basque Government.

Appendix A. Estimation of the ionic conductivities λ_i

Eq. (2) has been proved for 1:1 electrolytes [1,5]. Due to the different stoichiometry of the electrolytes used in this study, the model for the ionic conductivities in Eq. (2) has to be reproposed. The model is based on the extended Falkenhagen equation for the conductivity of a pure electrolyte [6,7], applied to 1:2 electrolytes:

$$\Lambda = \left[\Lambda^0 - \frac{B_2\sqrt{\{MX_2\}}}{1 + B\mathbf{a}\sqrt{\{MX_2\}}}\right] \left[1 + \frac{B_1\sqrt{\{MX_2\}}}{1 + B\mathbf{a}\sqrt{\{MX_2\}}} \frac{e^{(1-\sqrt{q})B\mathbf{a}\sqrt{\{MX_2\}}} - 1}{(1-\sqrt{q})B\mathbf{a}\sqrt{\{MX_2\}}}\right] \quad \text{(A1)}$$

where $\{MX_2\}$ is the activity of the electrolyte MX_2 on the molar scale. The values of the parameters B and B_2 are 0.570 $l^{1/2}$ $mol^{-1/2}$ $Å^{-1}$ and 157.5 $l^{1/2}$ s cm^2 $mol^{-3/2}$ for 1:2 electrolytes [18]. Values of B_1 in $l^{1/2}$ $mol^{-1/2}$ are -0.691 for $MgCl_2$, -0.7014 for $CaCl_2$ and $SrCl_2$, and -0.707 for $BaCl_2$ [19]. The values of the **a** parameters used in this study are 5.2 Å for $MgCl_2$, 5.0 Å for $CaCl_2$, 4.2 Å for $BaCl_2$ [20], and 4.6 Å for $SrCl_2$ [21]. The applicable range of the extended Falkenhagen equation can cover up to 5.0 mol dm^{-3} concentration in the best case.

Division of Eq. (A1) into two terms corresponding to each ion is based on the suggestions by Robinson and Stokes [18]. These authors suggested the division of the conductivity into two ionic contributions using the simpler Onsager's equation. This can be accomplished using the limiting conductivity of the ion instead of that of the electrolyte and by division of the terms expressed as a sum of different contributions of both ions. The following equations are proposed for the ionic conductivity of individual ions:

$$\lambda_M = \left[\lambda_M^0 - \frac{\frac{2}{3}B_2\sqrt{\{MX_2\}}}{1 + B\mathbf{a}\sqrt{\{MX_2\}}}\right] \left[1 + \frac{B_1\sqrt{\{MX_2\}}}{1 + B\mathbf{a}\sqrt{\{MX_2\}}} \frac{e^{(1-\sqrt{q})B\mathbf{a}\sqrt{\{MX_2\}}} - 1}{(1-\sqrt{q})B\mathbf{a}\sqrt{\{MX_2\}}}\right]$$

$$\lambda_X = \left[\lambda_X^0 - \frac{\frac{1}{3}B_2\sqrt{\{MX_2\}}}{1 + B\mathbf{a}\sqrt{\{MX_2\}}}\right] \left[1 + \frac{B_1\sqrt{\{MX_2\}}}{1 + B\mathbf{a}\sqrt{\{MX_2\}}} \frac{e^{(1-\sqrt{q})B\mathbf{a}\sqrt{\{MX_2\}}} - 1}{(1-\sqrt{q})B\mathbf{a}\sqrt{\{MX_2\}}}\right] \quad \text{(A2)}$$

The values of the ionic limiting conductivities used in this study are 349.81 (H^+), 53.05 (Mg^{2+}), 59.50 (Ca^{2+}), 59.45 (Sr^{2+}), 63.63 (Ba^{2+}), and 76.35 (Cl^-) [18]. The values are given in S cm^2 mol^{-1}.

Eq. (2) allows the estimation of the liquid junction potential of any pure electrolyte solution if all the parameters for the estimation of the activity coefficients by the MBM, and for the estimation of ionic conductivities by the extended Falkenhagen equation are known. The situation is more complicated if electrolyte mixtures are considered: modelling the conductivity of a mixture of electrolytes (with a minimum of three ions) is difficult due to the lack of selectivity of the technique. For example, the division of the extended Falkenhagen equation expressed in Eq. (A2) is not applicable to electrolyte

mixtures, since the specific counterion corresponding to the ion under study is not known.

In this study, the model proposed for ionic conductivities of ions in a mixture of 1:1 electrolytes is adapted to the presence of 1:2 electrolytes and was tested empirically. The model can be easily explained for a mixture of HCl and $MgCl_2$: the mixture can be considered as a sum of the two initial pure electrolyte solutions, HCl and $MgCl_2$, and the conductivity of the ions in these initial solutions can be expressed by means of Eq. (A2). These equations are rewritten taking into account the activity of the ions instead of that of the electrolyte, so the conductivity of the ions are related to their own concentrations and activity coefficients.

In the case of the proton, the conductivity λ_H is due to the initial HCl solution, since the other solution does not contain protons. Therefore, the parameter **a** used in the equation of λ_H is that corresponding to HCl. The same criterium is used for the magnesium, so the conductivities of H^+ and Mg^{2+} in the mixture will be:

$$\lambda_H = \left[\lambda^0_H - \frac{\frac{1}{2}B_2\sqrt{\{H^+\}}}{1+B\mathbf{a}_{HCl}\sqrt{\{H^+\}}}\right] \times \left[1+\frac{B_1\sqrt{\{H^+\}}}{1+B\mathbf{a}_{HCl}\sqrt{\{H^+\}}} \frac{e^{(1-\sqrt{q})B\mathbf{a}_{HCl}\sqrt{\{H^+\}}}-1}{(1-\sqrt{q})B\mathbf{a}_{HCl}\sqrt{\{H^+\}}}\right] \quad \text{(A3)}$$

$$\lambda_{Mg} = \left[\lambda^0_{Mg} - \frac{\frac{2}{3}B_{2_{MgCl_2}}\sqrt{\{Mg^{2+}\}}}{1+B_{MgCl_2}\mathbf{a}_{MgCl_2}\sqrt{\{Mg^{2+}\}}}\right] \times \left[1+\frac{B_{1_{MgCl_2}}\sqrt{\{Mg^{2+}\}}}{1+B_{MgCl_2}\mathbf{a}_{MgCl_2}\sqrt{\{Mg^{2+}\}}} \frac{e^{(1-\sqrt{q})B_{MgCl_2}\mathbf{a}_{MgCl_2}\sqrt{\{Mg^{2+}\}}}-1}{(1-\sqrt{q})B_{MgCl_2}\mathbf{a}_{MgCl_2}\sqrt{\{Mg^{2+}\}}}\right] \quad \text{(A4)}$$

The contribution of the chloride in each of the initial solutions is estimated in the same way, but the conductivity of the chloride in the mixture is taken as the sum of the contributions of both initial solutions multiplied by the fraction of chloride of each initial solution in the mixture. Eq. (A5) is therefore proposed.

$$\lambda_{Cl} = \frac{[H^+]}{[H^+]+2[Mg^{2+}]} \times \left[\lambda^0_{Cl} - \frac{\frac{1}{2}B_{2_{HCl}}\sqrt{\{Cl^-\}}}{1+B\mathbf{a}_{HCl}\sqrt{\{Cl^-\}}}\right] \times \left[1+\frac{B_{1_{HCl}}\sqrt{\{Cl^-\}}}{1+B_{HCl}\mathbf{a}_{HCl}\sqrt{\{Cl^-\}}} \frac{e^{(1-\sqrt{q})B_{HCl}\mathbf{a}_{HCl}\sqrt{\{Cl^-\}}}-1}{(1-\sqrt{q})B_{HCl}\mathbf{a}_{HCl}\sqrt{\{Cl^-\}}}\right] + \frac{2[Mg^{2+}]}{[H^+]+2[Mg^{2+}]} \times \left[\lambda^0_{Cl} - \frac{\frac{1}{3}B_{2_{MgCl_2}}\sqrt{\{Cl^-\}}}{1+B_{MgCl_2}\mathbf{a}_{MgCl_2}\sqrt{\{Cl^-\}}}\right] \times \left[1+\frac{B_{1_{MgCl_2}}\sqrt{\{Cl^-\}}}{1+B_{MgCl_2}\mathbf{a}_{MgCl_2}\sqrt{\{Cl^-\}}} \frac{e^{(1-\sqrt{q})B_{MgCl_2}\mathbf{a}_{MgCl_2}\sqrt{\{Cl^-\}}}-1}{(1-\sqrt{q})B_{MgCl_2}\mathbf{a}_{MgCl_2}\sqrt{\{Cl^-\}}}\right] \quad \text{(A5)}$$

References

[1] G. Borge, J.M. Madariaga, Talanta 45 (1997) 463.
[2] G. Biedermann, L.G. Sillén, Arkiv Kemi 5 (1953) 425.
[3] F.J.C. Rossotti and H. Rossotti, The Determination of Stability Constants and Other Equilibrium Constants in Solution, McGraw-Hill, New York, 1961, pp. 145–150.
[4] G.T. Hefter, Anal. Chem. 54 (1982) 2518.
[5] G. Borge, L.A. Fernández, J. M Madariaga, J. Electroanal. Chem. 440 (1997) 183.
[6] H. Falkenhagen, M. Leist, G. Kelbg, Ann. Phys. 6 (1952) 51.
[7] A. De Diego, A. Usobiaga, J.M. Madariaga, J. Electroanal. Chem. 430 (1997) 263.
[8] L.A. Bromley, AIChE J. 19 (1973) 313.
[9] G. Borge, R. Castaño, M.P. Carril, M.S. Corbillón, J.M. Madariaga, Fluid Phase Equilib. 121 (1996) 85.
[10] G. Borge, N. Etxebarria, L.A. Fernández, M.A. Olazabal, J.M. Madariaga, Fluid Phase Equilib. 121 (1996) 99.
[11] M.A. Mehablia, D.C. Shallcross, G.W. Stevens, Chem. Eng. Sci. 49 (1994) 2277.
[12] M.A. Mehablia, D.C. Shallcross, G.W. Stevens, Extr. Ion Exchange. 14 (1996) 309.
[13] M. Marhol, Ion Exchangers in Analytical Chemistry, Their Properties and Use in Inorganic Chemistry, Elsevier, Amsterdam, 1982, p. 34.
[14] M. Iborra, C. Fité, J. Tejero, J.F. Cunnill, J.F. Izquierdo, React. Polym. 21 (1993) 65.

[15] R. Cazallas, L.A. Fernández, N. Etxebarria, J.M. Madariaga, Lab. Robot. Autom. 5 (1993) 161.
[16] G.H. Jeffery, J. Bassett, J. Mendham, R.C. Denney, Vogel's Textbook of Quantitative Chemical Analysis, 5th ed., Longman, Harlow, 1989, p. 329.
[17] S. Fiol, F. Arce, X.L. Arnesto, G. Penedo, M. Sastre de Vicente, Fresenius'. J. Anal. Chem. 343 (1992) 469.
[18] R.A. Robinson, R.H. Stokes, Electrolyte Solutions, Butterworths, London, 1965.
[19] G. Vázquez, R. Méndez, R. Blázquez, An. Quím. A 81 (1985) 135.
[20] M. Postler, Collect. Czech. Chem. Commun. 35 (1970) 2244.
[21] G. Borge, PhD thesis, University of the Basque Country (Bilbao), 1996.

ELSEVIER

Talanta 48 (1999) 103–107

Talanta

Sensitive flow injection colorimetry of nitrite by catalytic coupling of *N*-phenyl-*p*-phenylenediamine with *N*,*N*-dimethylaniline

Ryoichi Kadowaki [a], Shigenori Nakano [a,*], Takuji Kawashima [b]

[a] *Chemical Institute, Faculty of Education, Tottori University, Koyama-cho, Tottori 680-0945, Japan*
[b] *Laboratory of Analytical Chemistry, Department of Chemistry, University of Tsukuba, Tsukuba 305-8571, Japan*

Received 26 March 1998; received in revised form 8 June 1998; accepted 9 June 1998

Abstract

A rapid, sensitive and selective flow-injection colorimetry method is proposed for the determination of trace amounts of nitrite. It is based on the nitrite's catalytic effect on the oxidative coupling of *N*-phenyl-*p*-phenylenediamine with *N*,*N*-dimethylaniline to produce a green dye ($\lambda_{max} = 735$ nm) in the presence of bromate. The change in absorbances of the dye were monitored in continuos flow mode. Linear calibration curves were obtained for the nitrite concentration range 2.0–100 ng ml^{-1}. The proposed method had a low detection limit (0.6 ng ml^{-1}) and high sample throughput (approximately 30 samples h^{-1}). The RSD for 10 and 50 ng ml^{-1} nitrite were 2.4 and 1.3% ($n = 10$), respectively. The method has been successfully applied to the determination of nitrite in river water samples.

Keywords: Nitrite determination; Catalytic analysis; Flow injection analysis; *N*-phenyl-*p*-phenylenediamine; *N*,*N*-dimethylaniline; Bromate

1. Introduction

Nitrite is toxic in animals and humans, and serves as a reactant with amines or amides to form toxic nitroso compounds [1]. It exists in nature as a result of the incomplete oxidation of ammonia or reduction of nitrate. The use of nitrate and/or ammonium salts as fertilizers in agriculture has increased the nitrite concentration in surface and subsurface water. The presence of nitrite in natural water gives an indication of pollution and eutrophication. Nitrite is also used as a food preservative. Thus the determination of trace amounts of nitrite is of importance, particularly in the fields of environmental and food chemistry.

Many methods for determining nitrite by photometric, fluorimetric and chemiluninescent detection have been reported using batchwise and flow-injection procedures [2–18]. Some methods are based on the stoichiometric reactions of nitrite

* Corresponding author. Fax: +81 857 315109; e-mail: nakano@fed.tottori-u.ac.jp

0039-9140/99/$ - see front matter
PII S0039-9140(98)00227-6

with organic compounds such as rhodamine 6G, L-tyrosine and 4-nitroaniline [2–11]. The kinetic-based methods are attractive for the determination of nitrite at trace levels. Several kinetic methods have recently been reported for nitrite determination based on its promoting, accelerating or catalytic action on indicator reactions [2,12–20]. Although these methods have a high sensitivity, they suffer from some interfering ions.

The color formation of *N*-phenyl-*p*-phenylenediamine (PPDA) with *N*,*N*-dimethylaniline (DMA) in the presence of an oxidant has already been used as an indicator reaction for the sensitive catalytic determination of vanadium [21], iron [22] and copper [23]. The present authors found that this coloration is also catalyzed by trace amounts of nitrite in the presence of bromate. This paper describes a colorimetric flow-injection determination of nitrite based on its catalysis of the reaction. Under optimum conditions, nitrite in the range 2–100 ng ml^{-1} can easily be determined with a sampling frequency of about 30 h^{-1} and an RSD of 2.4% at the 10 ng ml^{-1} level ($n = 10$). The selectivity of the method is satisfactory EDTA is used as a masking agent for interfering ions.

2. Experimental

2.1. Reagents

All chemicals used were of analytical-reagent grade and all solutions were prepared with deionized water obtained from a Milli-Q purification system (Millipore).

A standard nitrite solution (1.0 mg ml^{-1}) was prepared from sodium nitrite (Wako Junyaku) dried at 105°C. The working standard solutions were prepared daily by diluting the standard solution with water.

PPDA, from Aldrich, was used as received. A 2.0×10^{-4} mol l^{-1} PPDA solution containing 1.0×10^{-3} mol l^{-1} EDTA (Dojindo Laboratories) and 0.5% (w/v) polyoxyethylene(20) sorbitan monooleate (Tween 80, Kanto Kagaku) was prepared in 5.0×10^{-4} mol l^{-1} sulfuric acid. A 5.0×10^{-3} mol l^{-1} DMA (Wako Junyaku) solution was prepared by dissolving appropriate amounts of the compound in 0.02 mol l^{-1} sulfuric acid. A 0.5 mol l^{-1} sodium bromate solution was prepared.

2.2. Apparatus

Fig. 1 shows the flow-injection manifold for the determination of nitrite. It consisted of the following components: two double-plunger micropumps (Tokyo Rika PS-3.2W), a sixway injection valve (Sanuki Kogyo SVM-6M2) with a loop, a circulating thermostated bath (Toyo LH-l000C), a spectrophotometer (Japan Spectroscopic UVIDEC-320) with a 10-mm micro flow-cell (20 μl) and a recorder (Hitachi 056). All connecting lines and the reaction coil were made from 0.5 mm i.d. Teflon tubing.

A Hitachi U-2000A double-beam spectrophotometer with 10-mm cells was used for the measurement of the absorption spectra. A Toa model HM-5S pH meter was also used.

2.3. Procedure

Carrier (R1, water) and reagent solutions (R2, bromate; R3, DMA and sulfuric acid; and R4, PPDA, Tween 80 and EDTA) were injected into the reaction coil at a flow rate of 0.8 ml min^{-1} (Fig. 1). A 188 μl sample solution containing less than 100 ng ml^{-1} nitrite was injected into the carrier stream by a loop-valve injector (S), and

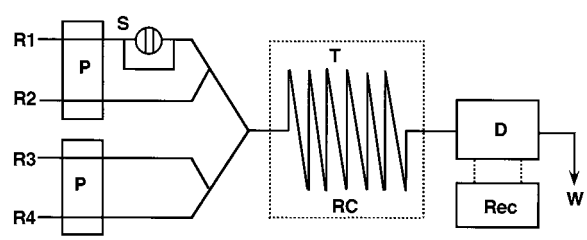

Fig. 1. Flow-injection manifold for the determination of nitrite. R1, carrier (H_2O); R2, $NaBrO_3$ (0.5 mol l^{-1}); R3, DMA (5.0×10^{-3} mol l^{-1})–H_2SO_4 (0.02 mol l^{-1}); R4, PPDA (2.0×10^{-4} mol l^{-1})–Tween 80 (0.5% (w/v))–EDTA (1.0×10^{-3} mol l^{-1}); P, micropump (0.8 ml min^{-1}); S, sample injector (188 μl); T, thermostated bath (55°C); RC, reaction coil (10 m); D, detector (735 nm); Rec, recorder; W, waste (pH 2.2).

then mixed in the reagent solutions. The nitrite-catalyzed reaction occurred in the reaction coil (RC, 10 m) submerged in the thermostated bath (T) at 55.0 ± 0.1°C. The absorbance of the product was measured at 735 nm.

3. Results and discussion

In the presence of bromate, PPDA couples with DMA to form a green dye which has an absorption maximum at 735 nm and is thought to be *N*-diphenylamine-*N*′,*N*′-dimethyl-*p*-benzoquinone diimine-*N*′-ium as described previously [21]. This color formation is catalyzed by trace amounts of nitrite. The process may be due to the reduction of nitrite to nitric oxide and then cycling back to nitrite [2]. The change in the absorbance of the green dye at 735 nm was continuously monitored throughout this study.

3.1. Effect of flow-injection and chemical variables

The flow-injection and chemical variables were optimized by using the manifold shown in Fig. 1 and a standard solution of 50 ng ml^{-1} nitrite. Owing to the increase in the reaction time, lower flow rates and longer reaction coils gave higher heights for the baseline and peak due to the uncatalyzed and catalyzed reactions. Since the higher values of the baseline provided poorer stability, the flow rate of each stream and reaction coil length were fixed at 0.8 ml min^{-1} and 10 m, respectively. An increase in sample size increased the height and width of the peaks; a 188-μl sample solution was introduced into the flow-line to achieve good sample throughput. Fig. 2 shows the effect of the reaction temperature on the uncatalyzed and catalyzed reactions. Raising the temperature increased the height of the baseline and peak. Having regard for the satiability of the baseline, the reaction coil was heated at 55°C.

Fig. 3 shows the effect of pH on the rates of uncatalyzed and catalyzed reaction in the range 1.7–3.4. Both the baseline and peak are higher at lower pH. Taking into account the baseline stability, the pH of the reaction mixture in the reaction

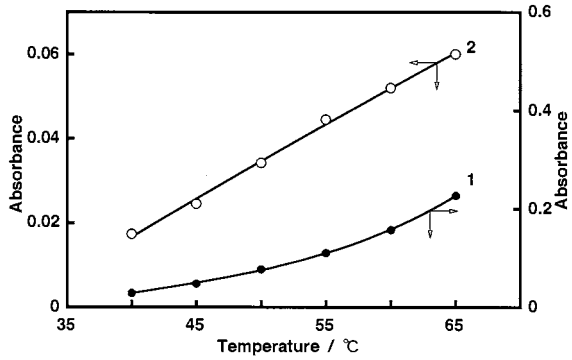

Fig. 2. Effect of the reaction temperature on the uncatalyzed (1) and catalyzed (2) reactions. Conditions as in Fig. 1 except for the temperature. Concentration of NO_2^-, 50 ng ml^{-1}.

coil was adjusted to ca. 2.2 by adding sulfuric acid to reservoir R3.

The effects of PPDA, DMA and bromate concentrations were studied. Tween 80 which did not affect the catalytic effect of nitrite was used for the dissolution of PPDA because of its poor solubility in water. Furthermore, the surfactant suppressed the adsorption of the dye on the inner surface of the tubing [24]. An increase in the PPDA concentration caused an increase in the rate of uncatalyzed and catalyzed reactions. The peak height was almost constant at concentrations above 1.0×10^{-4} mol l^{-1}; the height of the baseline began to level off at 0.5×10^{-4} mol l^{-1} PPDA. The concentration of PPDA used for the procedure was 2.0×10^{-4} mol l^{-1}. With an in-

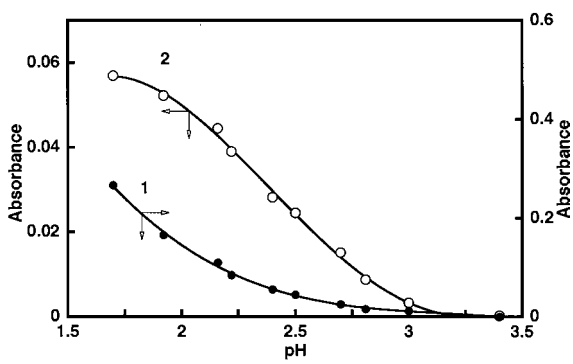

Fig. 3. Effect of pH on the uncatalyzed (1) and catalyzed (2) reactions. Conditions as in Fig. 1 except for pH. Concentration of NO_2^-, 50 ng ml^{-1}.

crease in the DMA and bromate concentrations, the rates for the catalyzed and uncatalyzed reactions also increased. Taking into account the height of the baseline and the sensitivity, DMA and bromate concentrations were chosen to be 5.0×10^{-3} and 0.5 mol l^{-1}, respectively.

3.2. Calibration graph

The calibration graphs for nitrite were prepared according to the recommended procedure. The relationship between peak height and nitrite concentration was linear from 2.0 to 100 ng ml^{-1}. The detection limit for a signal-to-noise ratio of 2 was 0.6 ng ml^{-1}. The reproducibility was satisfactory; the RSD for ten determinations of 10 and 50 ng ml^{-1} nitrite were 2.4 and 1.3%, respectively. The sample throughput was about 30 h^{-1}.

3.3. Effect of diverse ions

As reported previously [21–23], vanadium, iron and copper catalyzed the indicator reaction and their interference with the determination of nitrite should be eliminated. EDTA was chosen as a masking agent because of its small influence on the nitrite-catalyzed reaction. The effect of EDTA concentration up to 1.5×10^{-3} mol l^{-1} was examined in the presence of 100 ng ml^{-1} vanadium(V); at concentrations above 0.2×10^{-3} mol l^{-1}, EDTA effectively suppressed the catalytic effect of vanadium(V). Therefore the EDTA concentration was fixed at 1.0×10^{-3} mol l^{-1}; 500 ng ml^{-1} of vanadium(V) and iron(III), and 1000 ng ml^{-1} of copper(II) did not cause interference.

The effect of other diverse ions on the determination of 50 ng ml^{-1} nitrite was studied in the presence of EDTA. The results are summarized in Table 1; an error of $\pm 5\%$ is considered as acceptable. Most ions in the table can be tolerated at concentrations of 1000 ng ml^{-1}. Although 100 ng ml^{-1} of chromium(VI) and iron(II) gave positive errors, they did not interfere at concentrations below 50 ng ml^{-1}. The levels of these ions normally present in natural water samples is tolerable.

Table 1
Tolerance limits for diverse ions in the determination of 50 ng ml^{-1} nitrite

Tolerance limit (ng ml^{-1})	Ion added
100 000	K(I), Na(I), NH_4^+, BO_3^{3-}, Cl^-, ClO_4^-, NO_3^-, PO_4^{3-}, $P_2O_7^{4-}$, citrate, tartrate
10 000	As(V), Ca(II), Ce(III), Cr(III), Mn(II), Se(IV), W(VI), F^-, oxalate
5000	Al(III), Cd(II), Co(II), Mg(II), Ni(II)
1000	Ag(I), Ce(IV), Cu(II), Hg(II), Mo(VI), Pb(II), Zn(II), Br^-
500	Fe(III), V(V), I^-
50	Cr(VI), Fe(II)

3.4. Application

The proposed method was applied to the determination of nitrite in river water samples. Freshly collected samples were filtered through a 0.45-μm Millipore filter and kept at 4°C after the addition of a few drops of chloroform. Determinations of nitrite in the filtrates were carried out by using the recommended procedure with calibration curves and standard addition methods. The filtrates were also analyzed by a reference method using the

Table 2
Determination of nitrite in river water samples

Sample[a]	Nitrite in sample[b] (ng ml^{-1})		
	Present method		Reference method[c]
	(I)[d]	(II)[e]	
Engoji-gawa	17.2 ± 0.1	17.4 ± 0.1	18
Kyufukuro-gawa	39.7 ± 0.2	40.4 ± 0.6	44
Ohro-gawa	50.6 ± 0.5	52.3 ± 1.1	54
Sendai-gawa	7.6 ± 0.2	7.7 ± 0.1	LD[f]
Shiomi-gawa	9.7 ± 0.1	9.3 ± 0.1	LD
Tenjin-gawa	56.7 ± 0.4	58.7 ± 0.2	61

[a] Collected at Tottori Prefecture, Japan.
[b] Average of three determinations.
[c] Photometric method using sufanilamide and *N*-(1-naphthyl)ethylenediamine.
[d] Working curve method.
[e] Standard addition method.
[f] Lower detection limit.

reaction of sulfanilamide with *N*-(1-naphthyl)ethylenediamine [25]. Table 2 shows the analytical values obtained by the proposed and reference methods. These values are consistent with each other.

In conclusion, a combination of the nitrite-catalyzed reaction with a flow-injection technique allowed the simple, rapid and precise determination of nitrite at ng ml^{-1} levels. This flow-injection method is suitable for routine water analysis.

References

[1] I.A. Wolff, A.E. Wasserman, Science 177 (1972) 15.
[2] J.B. Fox, CRC Crit. Rev. Anal. Chem. 15 (1985) 283.
[3] M. Nakamura, T. Mazuka, M. Yamashita, Anal. Chem. 56 (1984) 2242.
[4] S. Flamerz, W.A. Bashir, Analyst 110 (1985) 1513.
[5] F. Shirato, Y. Okajima, C. Maekoya, Y. Takata, Bunseki Kagaku 38 (1989) 413.
[6] A.R. Thorton, J. Pfab, R.C. Massey, Analyst 114 (1989) 747.
[7] R.S. Braman, S.A. Hendrix, Anal. Chem. 61 (1989) 2715.
[8] S. Kartikeyan, T.P. Rao, C.S.P. Iyer, A.D. Damodaran, Mikrochim. Acta 111 (1993) 193.
[9] N. Jie, J. Yang, F. Meng, Talanta 40 (1993) 1009.
[10] A. Chaurasia, K.K. Verma, Talanta 41 (1994) 1275.
[11] S. Diallo, P. Bastard, P. Prognon, C. Dauphin, M. Hamon, Talanta 43 (1996) 359.
[12] M. Jiang, F. Jiang, J. Duan, X. Tang, Z. Zhao, Anal. Chim. Acta 234 (1990) 403.
[13] T. Okutami, A. Sakuragawa, S. Kamikura, M. Shimura, S. Azuchi, Anal. Sci. 7 (1991) 793.
[14] J.M. Calatayud, C.M. Hernandez, Microchem. J. 43 (1991) 143.
[15] R. Montes, J.J. Laserna, Anal. Sci. 7 (1991) 467.
[16] A.A. Ensafi, M. Samimifar, Talanta 40 (1993) 1375.
[17] A. Afkhami, A.A. Mogharnesband, Anal. Lett. 27 (1994) 991.
[18] A.A. Ensafi, M. Keyvanfard, Anal. Lett. 27 (1994) 169.
[19] A.A. Mohamed, M.F. El-shahat, T. Fukasawa, M. Iwatsuki, Analyst 121 (1996) 89.
[20] A. Afkhami, F. Jalali, Microchem. J. 57 (1997) 224.
[21] S. Nakano, E. Kasahara, M. Tanaka, T. Kawashima, Chem. Lett. (1981) 597.
[22] S. Nakano, M. Odzu, M. Tanaka, T. Kawashima, Mikrochim. Acta 1 (1983) 403.
[23] S. Nakano, M. Tanaka, M. Fushihara, T. Kawashima, Mikrochim. Acta 1 (1983) 457.
[24] S. Nakano, K. Tujii, T. Kawashima, Talanta 42 (1995) 1051.
[25] JIS K0102, Testing Methods for Industrial Wastewater, Japanese Industrial Standards Committee, Tokyo, 1986.

ELSEVIER

Talanta 48 (1999) 109–118

Talanta

Detection of artefacts and peak identification in reversed-phase HPLC of metallothioneins by electrospray mass spectrometry

Hubert Chassaigne, Ryszard Łobiński *

Laboratoire de Chimie Bio-Inorganique et Environnement, CNRS EP132, Hélioparc, 2, av. Pr. Angot, 64000 Pau, France

Received 10 April 1998; received in revised form 5 June 1998; accepted 9 June 1998

Abstract

The use of ion-spray mass spectrometry rendered it possible to characterize the signals obtained during studies of the polymorphism of metallothionein (MT) by reversed-phase (RP) HPLC in terms of the molecular mass. Artefact signals due to incomplete metallation, exchange of metals with the impurities of the column stationary phase and cross-contamination of the preparations purified by size-exclusion and anion-exchange chromatography may be present. On the other hand, some signals in RP HPLC with UV detection considered to belong to a single species were found to be composed of several complexes eluting precisely at the same time. On-line electrospray mass spectrometry was used to systematize the knowledge of the MT isoforms and subisoforms by attributing to each of the eluting peaks the molecular mass of the form involved and can be used to compare the results obtained for the different groups.

Keywords: Electrospray mass spectrometry; Reversed-phase HPLC; Metallothioneins; Isoforms

1. Introduction

Metallothioneins (MTs) are a group of non-enzymatic low molecular mass (6–7 kDa), metal binding proteins which are resistant to thermocoagulation and acid precipitation [1]. The interest in the determination and characterization of mammalian metallothioneins (isolated from liver, kidney and brain samples) is due to their potential roles in homeostatic control, metabolism and detoxification of a number of trace metals (Zn, Cu, Cd and Hg) [2]. Metallothioneins induced by cadmium are also thought to be involved in the development of the resistance of human tumor cells to anti-cancer drugs [3].

Mammalian metallothioneins exist as isoforms that are the product of genetic polymorphism characteristic of MT genes in animals and humans and, consequently, they draw attention for studies of metal-mediated gene expression mechanisms

* Corresponding author. Tel.: +33 5 59806885; fax: +33 5 59801292; e-mail: Ryszard.Lobinski@univ-pau.fr

0039-9140/99/$ - see front matter
PII S0039-9140(98)00220-3

[4]. This polymorphism occurs during the evolution of a species and consists of the variation of the primary structure of a metallothionein by the substitution of 1–15 amino acids. Isoforms with minor differences such as one amino acid residue were detected as subgroups of the two major isoforms and are termed subisoforms [5]. Whereas sequences of the major isoforms have been decoded [6], the difficulties in the separation and identification of the minor subisoforms are responsible for the lack of literature data regarding their identity.

To date, characterization of MT polymorphism by reversed-phase (RP) HPLC has been based on the retention time and on the intensity of the UV absorption which has led to speculative, confusing and often contradictory data because of the virtual impossibility of knowing what species was detected. Indeed, the use of apparently identical analytical techniques and operating conditions (column, mobile phase) does not seem to give similar results for samples of the same origin [7–9]. Not only do the chromatograms show different morphologies but also differ in the number of peaks observed. The likely reason for this is the presence of ghost peaks in the chromatograms, possibly coming from products of oxidation (i.e. dimers or polymerized products), from different conformations, or from different metal composition (metalloforms). The absence of standards of sufficient and documented purity makes the unambiguous identification of an MT-species in an HPLC eluate impossible without tedious isolation and off-line sequencing. Capillary zone electrophoresis apparently offers a higher resolution [10,11] but again the spectrophotometric detection does not allow the identification of the eluted species.

The objective of this study was to investigate the signals observed during the analysis of metallothioneins by RP HPLC with UV detection by on-line pneumatically assisted electrospray (ion-spray) mass spectrometry (MS). Electrospray MS in the infusion mode was proposed to characterize the MT-2 isoform [12,13].

2. Experimental

2.1. Apparatus

HPLC was performed using an ABI 140C microbore syringe pump, an ABI model 112A injection module and an ABI model 785A absorbance detector equipped with a microbore cell (Applied Biosystems, Foster City, CA). Electrospray MS experiments were performed using a PE-SCIEX API 300 ion-spray triple-quadrupole mass spectrometer (Thornhill, ON). BioToolBox software was used for the calculation of molecular masses and deconvoluting of protein mass spectra.

2.2. Standards and solutions

Liquid chromatography grade methanol (Sigma-Aldrich) and Milli-Q (Millipore, Bedford, MA) water were used to prepare the buffer solutions. The buffer solution was prepared by dissolving 5 mmol l^{-1} ammonium acetate in water (or in 50% methanol) and adjusting the pH to 6.0 with acetic acid. The buffers were sparged with helium to remove dissolved oxygen and thus attain a non-oxydizing environment. This is an important consideration in light of the observed susceptibility of MTs to oxidise during isolation [14].

Metallothionein preparations MT-1 (94H9504) and MT-2 (34H95161) from rabbit liver was purchased from Sigma-Aldrich (Saint Quentin Fallavier, France). The preparations contained 6.0% Cd, 0.6% Zn and 0.5% Cu for MT-1, and 5.3% Cd, 0.7% Zn and 0.5% Cu for MT-2, as found by independent ICP MS analysis. Batch-to-batch variation can be significant; the preparations should be checked for purity and fully characterized prior to their use as standards [15].

The stock MT solution (1 mg ml^{-1}) was prepared by dissolving 1 mg metallothionein in 1 ml water. Working solutions were prepared by the dilution of the stock solution with water or buffer as required. The stock solution was kept in a fridge at 4°C in the dark.

2.3. Chromatographic conditions

Separations were carried out using a Vydac C_8 150 mm × 1 mm × 5 μm column. The optimized elution program included a preconcentration step of 2 min at 100% buffer A followed by the linear gradient elution up to 60% buffer B within 48 min. Buffer A was 5 mM acetate buffer in water (pH 6.0) and buffer B was 5 mM acetate buffer in 50% methanol–water (pH 6.0). The injection volume was 5 μl. The pump flow was set at 40 μl min^{-1} which corresponded to a pressure of 4.5 MPa. The solutions were degassed by sparging with helium.

2.4. Electrospray MS conditions

The column effluent at 40 μl min^{-1} was introduced via a fused silica capillary (100 μm i.d.) that was inserted into the ion-spray needle held at 4400 V (ion-spray voltage). The orifice potential was set to 60 V. The mass spectrometer was calibrated on the basis of known masses in the range 30–3000 amu, such that the mass deviation was <0.1 amu. The mass spectrometer was operated with a resolution such that the valleys between peaks differing by 1 m/z unit was less than 20% of the peak maximum and the peak width at half-height was <0.8 amu. Limited range mass spectra of 1250–1450 and 1600–1800 were acquired for the Cd_4–MT and Cd_7–MT complexes using a 0.5 Da step size and a dwell time of 1 ms resulting in a scan time of about 0.8 s.

3. Results and discussion

3.1. Optimization of chromatographic conditions

Since the MT-1 and MT-2 preparations are pure in terms of SEC and anion-exchange chromatography an orthogonal separation mechanism—RP chromatography—was optimized. The separation of MT isoforms is most frequently carried out by RP chromatography between a non-polar stationary phase (usually a covalently bound C_8 or C_{18} linear hydrocarbon), and a relatively polar mobile phase. RP HPLC seems to be superior to SEC and ion-exchange, because the packing material for RP chromatography is principally free of ligands for metals [15]. Since hydrophobicity of a polypeptide primarily dictates its retention in RP chromatography, gradual elution of individual MT isoforms of a mixture is achieved by decreasing the polarity of the mobile phase by the addition of methanol or acetonitrile. Isolation of MT isoforms by RP HPLC is reviewed in Refs. [14,16]. Wide-bore (4–5 mm) 15–25 cm long columns are the most frequently used. The narrow-bore and microbore columns are expected to gain in significance soon because of their higher sensitivity and resolution. UV detection has so far been used in the majority of studies. A microbore column was chosen to assure the compatibility of the separation flow rate with those tolerated by the electrospray source.

Neutral buffers are usually used [14]. They allow the preservation of the native peptide conformation and of the original metal composition of the MT molecule. The UV absorbance per mass unit is higher, separation faster, less organic solvent is required and higher recoveries ($>90\%$) are obtained in comparison with acidic buffer systems. Acetonitrile, *n*-propanol and methanol are the most common organic modifiers. The latter was chosen because it offers the best ionization conditions in an electrospray source. Methanol was reported to allow the separation of MT-2 and MT-1 on a C_8 reversed-phase column with a linear gradient to 30% methanol with a neutral buffer [15].

3.2. RP HPLC of MT-2

Fig. 1 shows a chromatogram obtained for MT-2 under conditions similar to those of Van Beek and Baars [15] with UV and ESI MS detection. It shows a sharp peak eluting at ca. 22% methanol preceded by several small signals. However, the mass spectrum taken at the peak apex (Fig. 2a) indicates that this major peak (peak 4) is not chromatographically pure. Actually, it is composed of signals of several species in the molecular mass region of 6700–7000 Da. Note that in contrast to the poorly defined Cd_7–MT-2 envelope in the infusion mass spectrum taken at pH 7 (not

shown), the mass spectrum obtained on-line is relatively well resolved and allows one to determine precisely the molecular masses of the eluting Cd_7 complexes.

Table 1 summarizes the molecular masses of the rabbit liver MT isoforms calculated on the basis of the sequences reported in the literature [17]. On this basis, molecular masses of the Cd_7 complexes of these isoforms that are actually subject to the separation in Fig. 1 (at pH 7.0) were calculated using the formula: $M(Cd_7\text{–MT}) = M(\text{apo–MT}) + 7M_{Cd} - 14M_H$ [13]. It is surprising that none of the molecular masses found in the mass spectrum of the major peak corresponds to any of the MT-2 isoforms reported in the literature; the differences reaching several mass units. The association of peaks in Fig. 2a with apo-MTs on the basis of the similarity of the intensity pattern (the

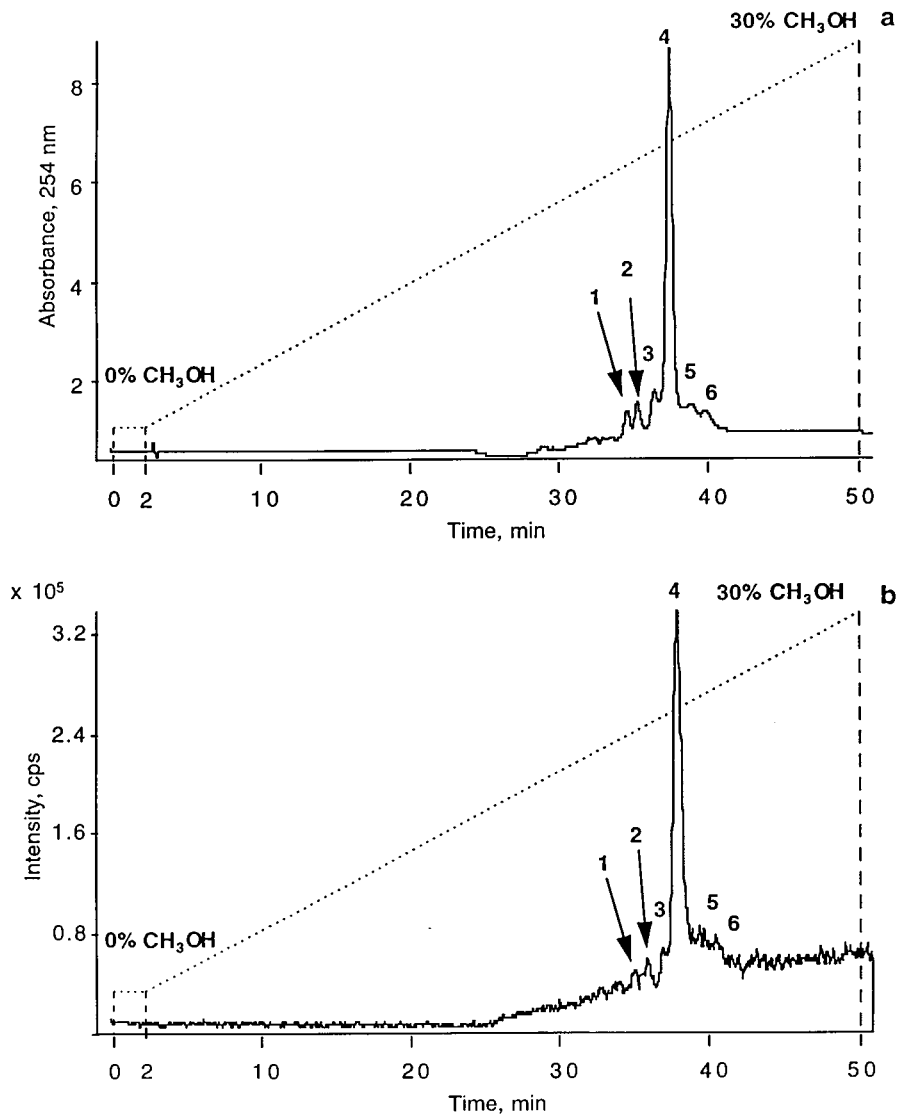

Fig. 1. Separation of MT-2 putative isoforms by RP HPLC using methanol as the mobile phase at pH 7 (1 μg injected): a, UV detection at 254 nm; b, IS MS detection in the TIC mode. The dotted line indicates the gradient used.

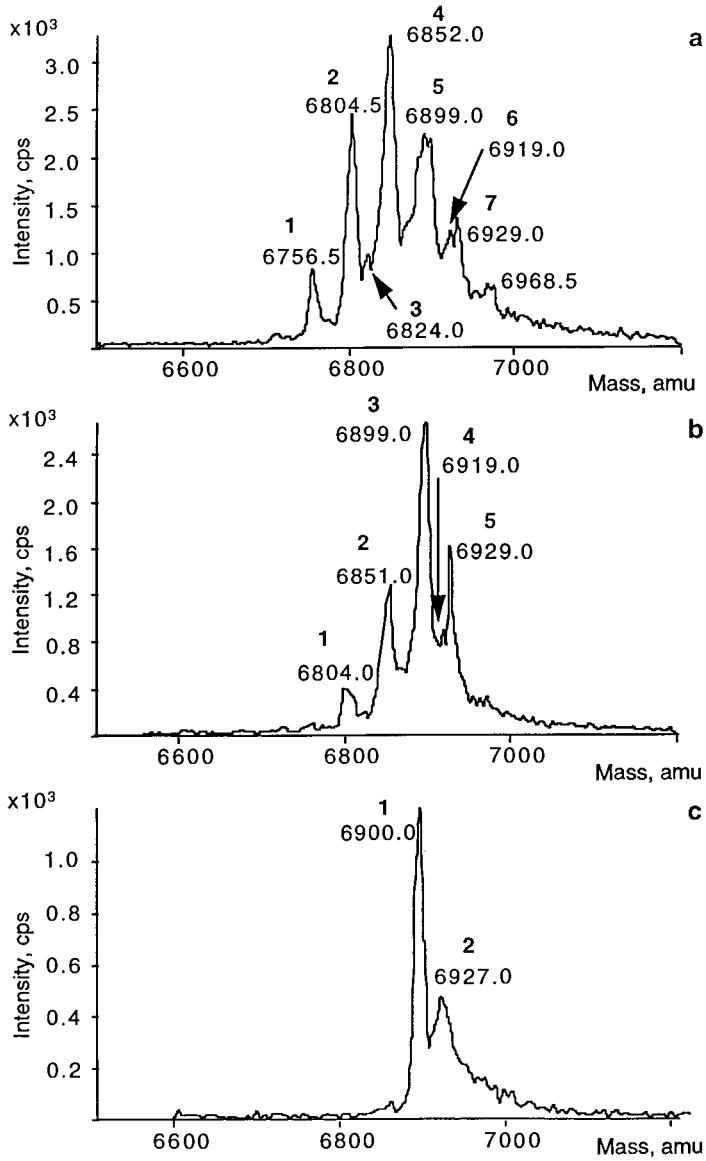

Fig. 2. Snapshots (reconstructed mass spectrum) obtained for the major peak in the chromatogram. a, Mobile phase at pH 7: (1) Cd_4Zn_3–MT-2a, (2) Cd_5Zn_2–MT-2a, (3) Cd_5Zn_2–MT-2c, (4) Cd_6Zn–MT-2a, (5) Cd_7–MT-2a, (6) Cd_7–MT-2b, (7) Cd_7-MT-2c; b, mobile phase at pH 6: (1) Cd_5Zn_2–MT-2a, (2) Cd_6Zn–MT-2a, (3) Cd_7–MT-2a, (4) Cd_7–MT-2b, (5) Cd_7–MT-2c; and c, mobile phase at pH 5: (1) Cd_7–MT-2a, (2) Cd_7–MT-2c.

dominating MT-2a isoform) of the forms well known in the literature [12,13,18] is not straightforward either. In the spectrum in Fig. 2a the peak tentatively associated with the MT-2a isoform 6899 Da is not the most intense. It is preceded by several intense signals of unknown origin that, because of the lower masses, are not likely to be attributed to adducts with solvent molecules. The difference in molecular mass below 100 Da is also too small to consider fragment ions resulting from the loss of *N*-acetylated Met and Asp residues from the amino acid terminal of

the protein. This is not likely to be a fragmentation attributed to the electrospray process since the intensities of these peaks do not vary with their charge states. Further this fragmentation should be greatly reduced in spectra of metallated proteins if these are ESI artefacts which is not the case [13]. The difference between the $M_{\text{MT-2a}}$ of 6899 and $M = 6852$ of the major peak which is also too low to be attributed to the loss of a Cd atom but matches perfectly the replacement of one Cd atom by one Zn atom to produce a compound Cd_6Zn–MT-2a. This difference is reproduced in the other peaks to the left of the major peak to correspond to the compounds Cd_5Zn_2–MT-2a and Cd_4Zn_3–MT-2a. These potential artefact peaks were further studied in detail by varying the pH of the mobile phase (and thus the electrospray ionization).

A decrease of pH of the mobile phase to pH 6 leads to an improved mass spectrometric purity of the Cd_7–MT-2 peaks and to a decrease in the intensities of the peaks with lower molecular masses that confirms the above evoked hypothesis of the presence of the mixed Cd–Zn complexes (Fig. 2b). The three reported isoforms: Cd_7–MT-2a–c can be clearly seen with molecular masses perfectly matching those calculated on the basis of apo–MTs (Table 1) whereas the mixed Cd–Zn complexes are apparently destroyed at this pH. At pH 5 (Fig. 2c) only peaks corresponding to those seen in the apo–MT-2 spectrum remain with similar intensities (the Cd_7–MT peak is composed only of the two major isoforms of Cd_7–MT-2a and Cd_7–MT-2c) whereas the peaks of the Zn-containing species have disappeared completely. The decrease in pH does not significantly affect the retention time of the major MT peak. At pH 6 the morphology of the chromatogram is identical; but the major peak (total ion current (TIC) mode) is more intense due to more favourable IS ionization conditions. At pH 5, in addition to a peak at 37 min a peak at 45 min also appears of which the MS snapshot reproduces the pattern of Cd_4–MT-2 found by infusion ESI MS. At pH 4 the peak of Cd_7 disappears. The latter results from the loss of cadmium from the β-domain. The peak of Cd_4–MT-2 gives an MS snapshot identical with the mass spectrum of Cd_4–MT-2b acquired in the infusion mode.

Table 1
Molecular masses of the rabbit liver metallothionein isoforms calculated on the basis of the sequences

Isoform	Molecular mass (Da)	
	Apo–MT	Cd_7–MT[a]
MT-2a	6125.32	6898.05
MT-2b	6146.33	6919.06
MT-2c	6155.34	6928.07
MT-2d	6215.43	6988.16
MT-2e	6241.55	7014.28
MT-1a	6145.35	6918.08

[a] $M(Cd_7\text{–MT}) = M(\text{apo–MT}) + 7M_{Cd} - 14M_H$.

The results discussed above show that signals obtained in UV are far from being spectrally pure. Moreover, replacement of Cd by Zn does not change the hydrophobicity of the complex and they will elute at the same time. Electrospray MS is at present the only technique that can study the stoichiometry of these complexes in HPLC effluents. The hypothesis of the presence of mixed complexes is much more probable than those assuming that electrospray ionization at higher pH may create artefacts, or that several conformers of similar hydrophobicities coelute and a decrease in pH simplifies the number of species present.

Fig. 3 shows mass spectra of the minor signals present in the chromatogram of MT-2 from rabbit liver. It can be seen that, despite relatively poor abundance these spectra are of sufficient quality to allow the determination of the molecular masses of the eluting species. The mass spectrometric purity of these signals is relatively good and a major peak can usually be distinguished. No match in terms of the metallocomplex could be found for peak 1 which represents a species having a $M = 6864.5 \pm 0.5$ Da. Peak 2 contains two species for which identification at this level can be only speculative. Peak 3 contains the fourth sequenced isoform of MT-2, MT-2d with a molecular mass of 6989 ± 1 Da, and a peak that can be tentatively assigned to the MT-1a isoform ($M = 6918 \pm 2$ Da) that can be considered to be an impurity of the MT-2 preparation. The two small signals (5 and 6) after the major peak

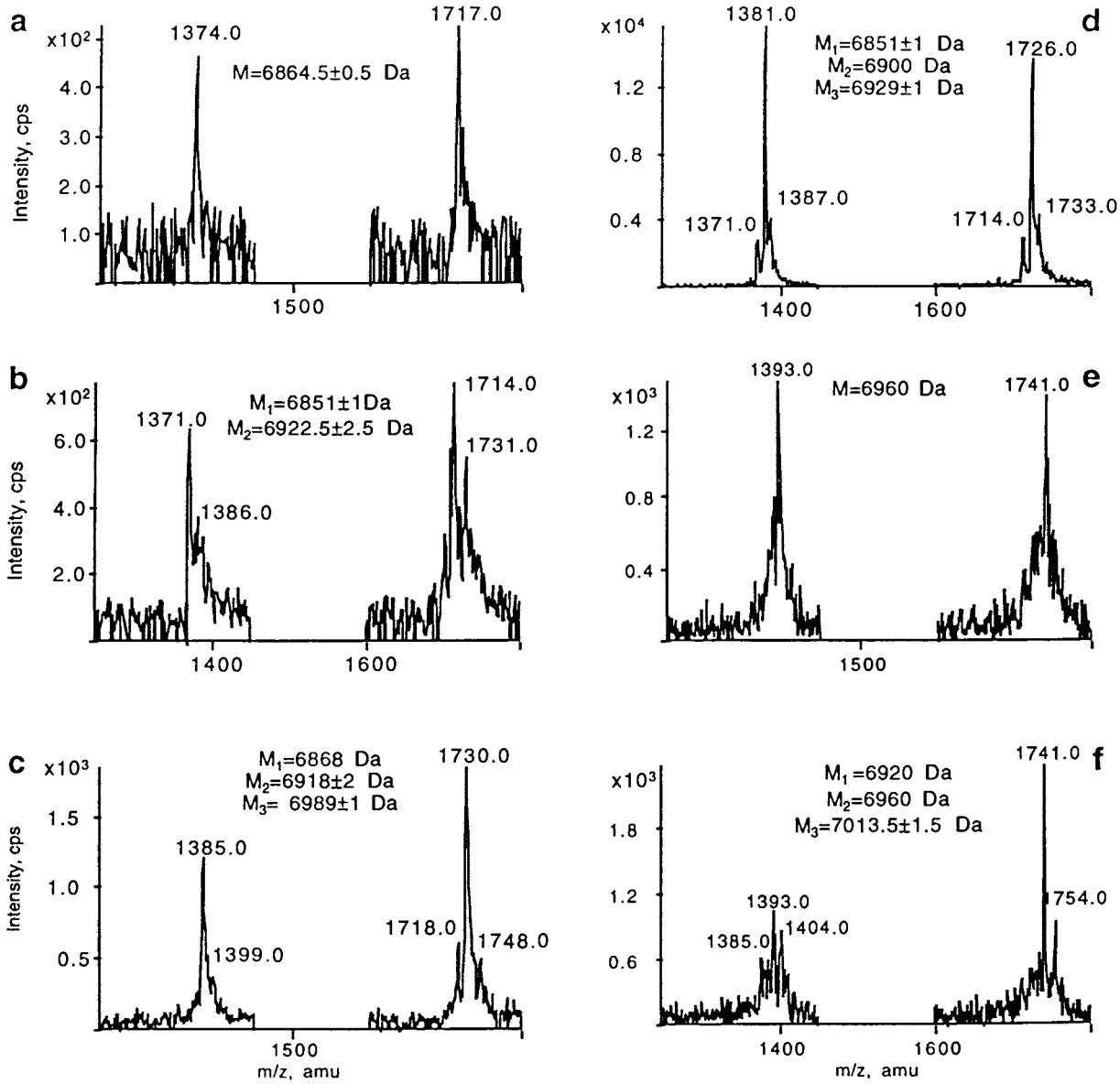

Fig. 3. Snapshots of the peaks present in the chromatogram of the MT-2 rabbit liver preparation with methanol as the mobile phase at pH 6 (1 μg injected): a, peak 1; b, peak 2; c, peak 3; d, peak 4; e, peak 5; and f, peak 6.

correspond to a compound with a molecular mass of 6960 Da (not identified). Peak 6 which is not pure in terms of mass spectrometry contains the isoform MT-2e ($M = 7013.5 \pm 1.5$ Da).

The results shown in Figs. 1–3 also show that the separation of the individual MT-2 isoforms as Cd_7 complexes is hardly possible by RP chromatography with methanol as the mobile phase. The results obtained with UV detection should therefore be treated with caution for the possibility of different artefacts. This chromatography, however, allows the acquisition of well resolved mass spectra of the fully metallated forms which is impossible in the direct mode.

3.3. RP HPLC of MT-1

A chromatogram of the MT-1 preparation, obtained under similar conditions to that of MT-2 and shown in Fig. 4a and b, is more complex than that of MT-2 and shows several major peaks (two of them, peaks 5 and 6, are not baseline resolved). The morphology of the chromatogram with UV detection is identical to that of a TIC chromatogram. The complex morphology of the MT-1 preparation observed with a methanolic mobile phase is in contrast to that of Van Beek [15] who apparently observed a single peak attributed to MT-1. The mass spectra taken at the apex of each of the peaks are shown in Fig. 5. Some of them show complex mass spectra and in many of them it is impossible to identify the prevailing form. Note that for some isoforms the molecular masses

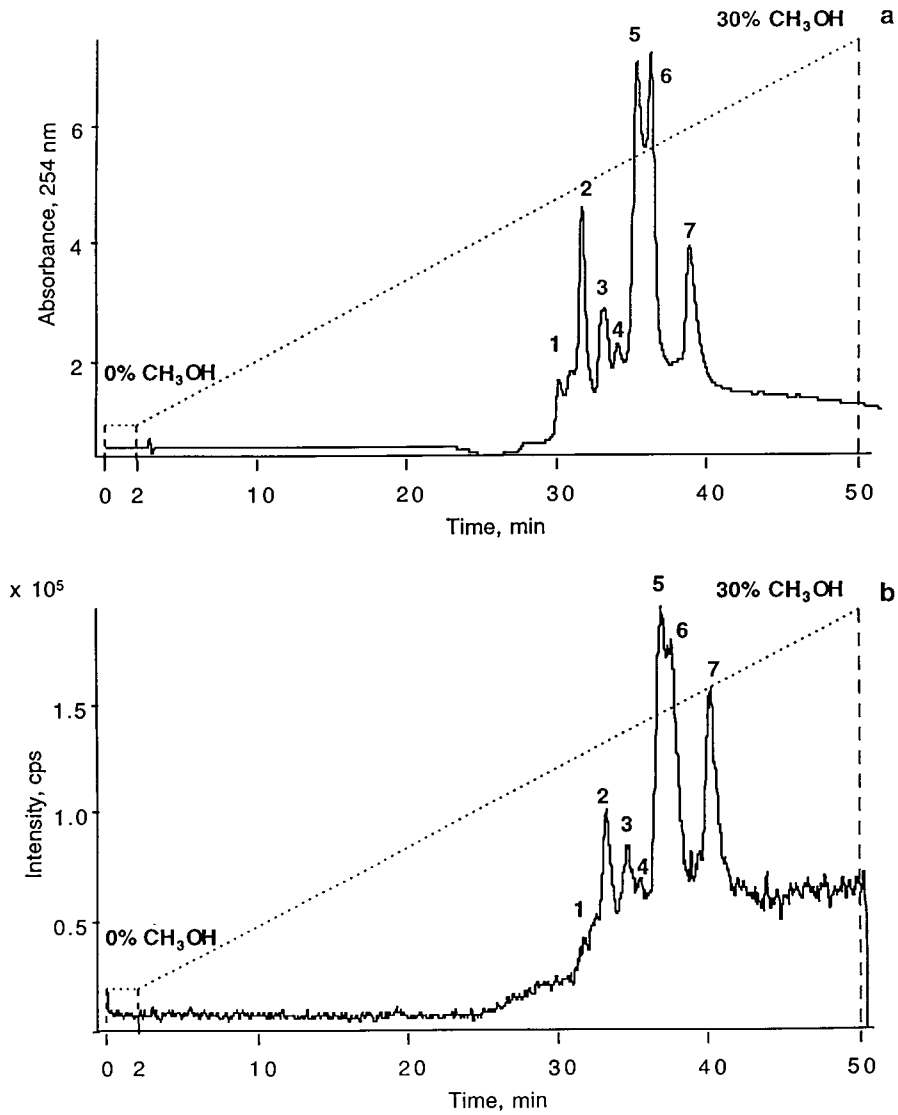

Fig. 4. Separation of MT-1 putative isoforms by RP HPLC using methanol as the mobile phase at pH 6 (1 μg injected): a, UV detection at 254 nm; b, IS MS detection in the TIC mode. The dotted line indicates the gradient used.

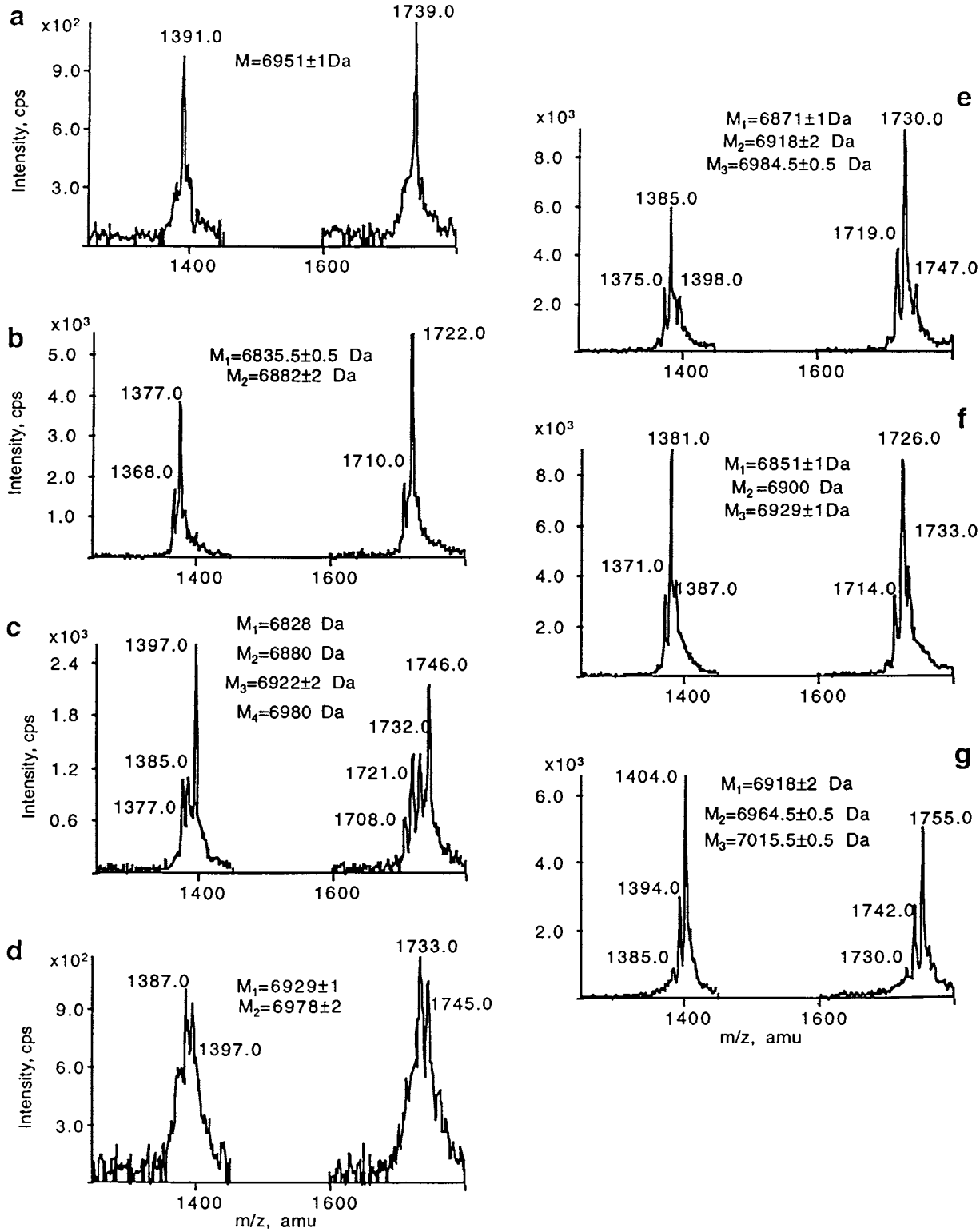

Fig. 5. Mass spectrometric snapshots of the peaks present in the chromatogram in Fig. 4: a, peak 1; b, peak 2; c, peak 3; d, peak 4; e, peak 5; f, peak 6; and g, peak 7.

of an MT-1 species and an MT-2 species are very close and the choice can be based only on taking into account the preliminary separation on an anion-exchange column.

The determination of molecular masses of the eluting compounds can shed some light on the discussion regarding the order of elution (value of the capacity factor k') of metallated MT-2 and MT-1 complexes. This order was found reversed (in comparison to anion-exchange) and this is explained by the higher hydrophobicity of MT-2a compared to MT-1a (based on the primary sequences reported by Kimura [17]). Fig. 5 corroborates the earlier observation that the form MT-1a ($M = 6918 \pm 2$ Da, peak 5) actually elutes before MT-2a ($M = 6900$ Da, peak 6) which claims to reconsider the validity of the extension of the rule that the capacity factors (k') of peptides can be calculated as a sum of the constituting amino acids to metallothioneins [9]. This rule developed for less than 20 amino acids may indeed have its limitations for longer polypeptide chains of which the chromatographic behaviour also depends, apparently, on their conformation. Moreover, the use of a methanolic mobile phase does not allow one to separate MT-1a and MT-2a. What is separated, in the literature, as MT-1 from MT-2 is probably a mixture of other dominant MT-1 isoforms ($M = 7015.5 \pm 0.5$ Da, peak 7) which elute well after MT-2. No discussion is possible on the dependence of hydrophobicity on the sequence because the sequences of the subisoforms eluting as peak 7 are apparently not known. Peak 4 contains the isoform known as MT-2c which has a molecular mass of 6929 ± 1 Da. The three first eluting compounds (peaks 1–3) for which no matches were found may be complexes with metals other than Cd (e.g. Cu).

4. Conclusions

Ion-spray detection in RP chromatography offers the possibility of precise determination of the molecular mass of the eluting isoforms of metallothioneins and should allow the systematization of the knowledge based so far on the results obtained with UV detection. The isoforms sequenced in the literature could be identified but the number of isoforms actually present in the MT preparations seems to be larger. Even the peaks that appear pure in an HPLC UV chromatogram usually contain more than one signal. Running chromatography at different pH with the simultaneous monitoring of the eluting peaks is recommended to avoid the misinterpretation of the chromatographic snapshots because of artefacts due to the presence of the mixed metallocomplexes.

References

[1] M.J. Stillman, Coord. Chem. Rev. 144 (1995) 461–511.
[2] J.F. Riordan, B.L. Valee (Eds.), Metallobiochemistry Part B. Metallothioneins and Related Molecules, Methods in Enzymology, vol. 205, Academic Press, New York, 1991.
[3] T. He, D. Fabris, C. Fenselau, Proc. 45th ASMS Conf. on Mass Spectrometry and Allied Topics, Palm Springs, CA, 1997.
[4] D.H. Hamer, in: K.T. Suzuki, N. Imura, M. Kimura (Eds.), Metallothionein III: Biological Roles and Medical Implications, Birkhäuser, Boston, MA, 1993.
[5] K.T. Suzuki, in: M.J. Stillman, C.F. Shaw, K.T. Suzuki (Eds.), Metallothioneins Synthesis, Structure and Properties of Metallothioneins, Phytochelatins and Metalthiolate Complexes, VCH, New York, 1992.
[6] J.H.R. Kägi, in: K.T. Suzuki, N. Imura, M. Kimura (Eds.), Metallothionein III: Biological Roles and Medical Implications, Birkhäuser, Boston, MA, 1993.
[7] S. Klauser, J.H.R. Kägi, K.J. Wilson, Biochem. J. 209 (1983) 71–80.
[8] M.P. Richards, N.C. Steele, J. Chromatogr. 402 (1987) 243–256.
[9] G. Bordin, F. Cordeiro Raposo, A.R. Rodriguez, Can. J. Chem. 72 (1994) 1238–1245.
[10] M.P. Richards, J.H. Beattie, J. Capillary Electrophor. 1 (1994) 196–207.
[11] V. Virtanen, G. Bordin, A.R. Rodriguez, J. Chromatogr. A 734 (1996) 391.
[12] K.A. High, B.A. Methven, J.W. McLaren, et al., Fresenius' J. Anal. Chem. 351 (1995) 393–402.
[13] X.L. Yu, M. Wojciechowski, C. Fenselau, Anal. Chem. 65 (1993) 1355–1359.
[14] M.P. Richards, Methods Enzymol. 205 (1991) 217–238.
[15] H. Van Beek, A.J. Baars, J. Chromatogr. 442 (1988) 345–352.
[16] R. Lobinski, H. Chassaigne, J. Szpunar, J. Talanta 46 (1998) 271–289.
[17] M. Kimura, N. Otaki, M. Imano, in: J.H.R. Kägi, M. Nordberg (Eds.), Metallothionein, Birkhäuser, Basel, 1979.
[18] H. Chassaigne, R. Lobinski, Fresenius' J. Anal. Chem. 361 (1998) 267–273.

ELSEVIER

Talanta 48 (1999) 119–126

Talanta

Binding of polyanions by biogenic amines. III[1]. Formation and stability of protonated spermidine and spermine complexes with carboxylic ligands

Alessandro De Robertis [a], Concetta De Stefano [a], Antonio Gianguzza [b], Silvio Sammartano [a,*]

[a] *Dipartimento di Chimica Inorganica, Chimica Analitica e Chimica Fisica dell'Università, Salita Sperone 31, I-98166 Messina (Vill. S. Agata), Italy*

[b] *Dipartimento di Chimica Inorganica dell'Università, Via Archirafi 26, I-90123, Palermo, Italy*

Received 14 April 1998; received in revised form 6 June 1998; accepted 9 June 1998

Abstract

The formation and stability of protonated spermidine and spermine–carboxylic ligand complexes (seven systems) were studied potentiometrically (H^+-glass electrode). ALH_r species are formed (A = spermidine, spermine, L^{z-} = acetate, malonate, 1,2,3-propanetricarboxylate, 1,2,3,4-butanetetracarboxylate; $r = 1...m+n-1$, where m and n are the maximum degree of protonation of the amine and of the carboxylic ligand, respectively), and their stability is a function of charges involved in the formation reaction. For the equilibrium $H_iA^{i+} + H_jL^{(j-z)} = ALH_{i+j}^{(i+j-z)}$ the linear relationship $\log K_{ij} = 0.46\ \zeta$ ($\zeta = |i(z-j)|$) was found. By means of this simple equation a mean free energy value can be obtained per salt bridge (n), namely $-\Delta G° = 5.25 \pm 0.15$ kJ mol^{-1} n^{-1}. Species formed by the highest charged ligands are quite stable ($K > 10^3$ mol^{-1} dm^3) and potentially play an important role in the speciation of biofluids, as shown by speciation diagrams and simulated experiments.

Keywords: Biogenic amines; Carboxylic ligands; Anion coordination chemistry; Formation constants; Potentiometry; Speciation of biological fluids

1. Introduction

Amines are present in biofluids in quite high concentrations. In terms of aminogroups we have 1–2, 0.1–0.05, 15–30, 0.2–0.3 mmol dm^{-3} in urine, blood, sperm and sweat, respectively [1]. Among these amines, diamines (putrescine and cadaverine), triamine (spermidine) and tetramine (spermine), play an essential role in some important biochemical processes (e.g. the stabilization of DNA and RNA). From the coordination chemistry point of view, the most interesting characteristic of biogenic amines regards their high positive charge in physiological pH conditions

* Corresponding author. Tel.: +39 90 393659; fax: +39 90 392827; e-mail: sammartano@chem.unime.it

[1] Parts I and II of this series: [3,4].

0039-9140/99/$ - see front matter
PII S0039-9140(98)00221-5

(pH is 6.1 for urine and 7.4 for blood, etc.), i.e. they are fully protonated, whilst other amines, such as ethylenediamine, diethylenetriamine, etc. (general formula $C_{(2n-2)}N_n$ $N_{(5n-2)}$), in the neutral-fairly alkaline pH range are partially deprotonated. This means, in turn, that bio-polyammonium cations exhibit high ability to interact with polyanions. Carboxylic ligands are also present in biofluids, and in terms of carboxylic groups we have 3–5, 2–4 and >20 mmol dm^{-3} in urine, blood and sperm, respectively [1], and in the physiological pH range they are fully deprotonated. Therefore, the interaction of this class of ligands with biogenic amines represents both a good model for studying polyamine–polyanion complexes and an interesting real system whose speciation must be investigated.

Recently we reported quantitative data on the formation of polyammonium cations–polyanions complexes [2–4], including several systems containing ligands of biological interest. In these studies, we found that ALH_r complexes (A = amine; L = polyanion; $r = 1...m+n-1$, m and n = maximum degree of protonation of amine and polyanion) are quite stable, and their stability, according to the electrostatic nature of the bond(s), is a linear function of the charges involved in the formation reaction.

As a further step in our studies on the complexation ability of polyammonium cations, we report in this paper quantitative data relative to the systems amine (spermidine (spd), spermine (sper))-carboxylic ligands (acetate (ac), malonate (mal), 1,2,3-propanetri-carboxylate (tca) and 1,2,3,4-butanetetracarboxylate (btc)), in aqueous solution, at 25°C, using the potentiometric (H^+-glass electrode) technique.

2. Experimental

2.1. Materials

Spermidine trihydrochloride and spermine tetrahydrochloride (Aldrich or Sigma) were used without further purification and their purity, checked alkalimetrically, was always $>99.5\%$. All polyanions considered in this work (Fluka) were used without further purification. The purity of all the ligands, checked by potentiometric titrations, was always $>99.5\%$. Standard solutions of NaOH and HCl were prepared by diluting concentrated Fluka ampoules and were standardised against potassium biphthalate and sodium carbonate, respectively. Grade A glassware and twice distilled water were used for all solutions.

2.2. Apparatus

The free hydrogen ion concentration was measured using two potentiometric titrators with appropriate software for fully computerized titrations. The two different equipment consist of (a) an Amel 337 potentiometer coupled with a Metrohm glass saturated calomel electrode mod. 6.0232.100 and (b) a Metrohm 654 potentiometer coupled with a combination Ross type electrode 8102. The titrant was delivered by a Metrohm Dosimat 665 dispenser. The titration program allows the evaluation of equilibrium potential values and determines the amount of titrant based on the actual buffering properties on the titrated solution, so that there is a difference in pH values of 0.05–0.08 between two successive readings; the e.m.f. was considered to be stable when the variation was <0.1 mV within 5 min.

2.3. Procedure

Twenty five millilitres of the solution containing the polyanion and the amine hydrochloride under study were titrated with standard NaOH up to 80–90% neutralisation. Titrations were performed without adding background salt in order to minimize the interference of Na^+ (which forms complexes with polyanions) and Cl^- (which forms complexes with amines Section 3). Concentrations used in the experiments were $C_{amine} = 5–20$ mmol dm^{-3} and $C_{anion} = 2.5–40$ mmol dm^{-3} (lower concentrations for higher charged polyanions). A separate titration of HCl at about the same ionic strength (adjusted with NaCl) as the sample under study, was carried out to determine the standard electrode potential

E^0. The reliability of pH-metric measurements in the alkaline range was checked by calculating pK_w values. A stream of purified and presaturated N_2 was bubbled through all solutions in order to exclude the presence of CO_2 and O_2.

2.4. Calculations

The computer program ESAB2M [5] was used to calculate the purity of the reagents and to refine all the parameters related to the calibration of the electrode system. The computer programs BSTAC [6] and STACO [7] were used to calculate the formation constants. The ionic strength dependence of formation constants was taken into account by using the Debye–Hückel type equation [7–9]

$$\log \beta = \log {}^{T}\beta - z^* \sqrt{I}/(2 + 3\sqrt{I}) + CI + DI^{3/2} \quad (1)$$

where β = formation constants; ${}^{T}\beta$ = formation constant at zero ionic strength; $C = c_0 p^* + c_1 z^*$; $D = d_1 z^*$; $p^* = \Sigma p_{reactants} - \Sigma p_{products}$; $z^* = \Sigma z^2_{reactants} - \Sigma z^2_{products}$; p and z are the stoichiometric coefficients and the charges, respectively. For the calculations performed in this work we used the values of $c_0 = 0.10$, $c_1 = 0.23$ and $d_1 = -0.1$ [9]. Computer programs STACO and BSTAC are able to perform calculations in non-constant ionic strength. Distribution diagrams were obtained by the computer program ES4ECI [6].

3. Results

3.1. Protonation constants

Protonation constants of carboxylic ligands have been already reported together with Na^+ weak complex formation constants [10–12], and the relative values are given in Table 1. Protonation constants of spermidine and spermine are reported in Table 2, together with Cl^- weak complex formation constants (unpublished data from these laboratories). Since Na^+ and Cl^- complexes seriously interfere with the formation of amine–carboxylic anion complexes, we worked in the absence of background salt. Nevertheless, small concentrations of sodium and chloride ions are present in solution arising from titrant NaOH and amine hydrochloride, and the interactions of these ions are taken into account in the calculations.

Table 1
Protonation constants of some organic anions[a] and formation constants of Na^+complexes at $I = 0$ mol dm^{-3} and $T = 25$°C

p	q	log β^{b}_{pq}			
		ac^-	mal^{2-}	tca^{3-}	btc^{4-}
0	1	4.74	5.70	6.49	7.18
0	2		8.56	11.41	13.01
0	3			15.09	17.54
0	4				20.92
1	0	−0.2	0.91	1.40	1.82
1	1		5.66	7.31	8.67
1	2			11.56	13.94
1	3				17.76
2	0			1.98	3.45
2	1			6.96	9.31
3	0				3.30

[a] ac^- = acetate [10]; mal^{2-} = malonate [10]; tca^{3-} = tricarballylate [11]; btc^{4-} = butanetetracarboxylate [12].
[b] Log β_{pq} refers to the reaction: $pNa^+ + L^{z-} + qH^+ = Na_pLH_q^{(j+p-z)}$.

Table 2
Protonation and chloride complex formation constants of spermidine and spermine in aqueous solution, at 25°C and $I = 0$ mol dm^{-3}

p	q	log β^{a}_{pq}	
		spd[b]	sper[b]
0	1	10.85	10.70
0	2	20.52	20.40
0	3	28.50	28.72
0	4	—	35.94
1	1	10.65	10.58
1	2	21.19	21.09
1	3	29.51	29.87
1	4	—	37.47
2	3	30.28	30.29
2	4	—	38.69

[a] Log β_{pq} refers to the reaction $pCl^- + A^0 + qH^+ = ACl_pH_q^{(q-p)}$.
[b] Unpublished results from these laboratories.

Table 3
Formation constants of protonated spermidine–organic polyanions at $T = 25$°C and $I = 0$ mol dm^{-3}

p	q	r[a]	log $\beta \pm 3s$[b]	Reaction	log K
$L = ac^-$					
1	1	1	11.84 ± 0.10	$HA^+ + L^- = ALH^0$	1.0
1	1	2	21.77 ± 0.07	$H_2A^{2+} + L^- = ALH_2^+$	1.2
1	1	3	30.07 ± 0.08	$H_3A^{3+} + L^- = ALH_3^{2+}$	1.6
$L = mal^{2-}$					
1	1	1	11.69 ± 0.09	$HA^+ + L^{2-} = ALH^-$	0.8
1	1	2	22.25 ± 0.03	$H_2A^{2+} + L^{2-} = ALH_2^0$	1.7
1	1	3	31.41 ± 0.02	$H_3A^{3+} + L^{2-} = ALH_3^+$	2.9
1	1	4	35.67 ± 0.03	$H_3A^{3+} + HL^- = ALH_4^{2+}$	1.5
$L = tca^{3-}$					
1	1	1	11.9 ± 0.2	$HA^+ + L^{3-} = ALH^{2-}$	1.0
1	1	2	22.95 ± 0.04	$H_2A^{2+} + L^{3-} = ALH_2^-$	2.4
1	1	3	32.47 ± 0.02	$H_3A^{3+} + L^{3-} = ALH_3^0$	4.0
1	1	4	37.60 ± 0.02	$H_3A^{3+} + HL^{2-} = ALH_4^+$	2.6
1	1	5	41.0 ± 0.1	$H_3A^{3+} + H_2L^- = ALH_5^{2+}$	1.1
$L = btc^{4-}$					
1	1	1	12.9 ± 0.3	$HA^+ + L^{4-} = ALH^{3-}$	2.0
1	1	2	24.04 ± 0.04	$H_2A^{2+} + L^{4-} = ALH_2^{2-}$	3.5
1	1	3	33.90 ± 0.03	$H_3A^{3+} + L^{4-} = ALH_3^-$	5.4
1	1	4	39.76 ± 0.04	$H_3A^{3+} + HL^{3-} = ALH_4^0$	4.1
1	1	5	44.24 ± 0.03	$H_3A^{3+} + H_2L^{2-} = ALH_5^+$	2.7
1	1	6	47.52 ± 0.06	$H_3A^{3+} + H_3L^- = ALH_6^{2+}$	1.5

[a] Indexes refer to the reaction $p(\text{spd}) + qL^{z-} + rH^+ = (\text{spd})_pL_qH_r^{(r-qz)}$.
[b] uncertainties expressed as $\geq 95\%$ confidence interval.

3.2. Amine–carboxylic ligand complexes

The analysis of potentiometric data showed that in all the investigated systems ALH_r complexes are formed with $r = 1, 2 \ldots n + m - 1$ (n and m = maximum protonation degree of amines and carboxylic ligands, respectively). In Tables 3 and 4, we report the formation constants of spermidine and spermine–carboxylate complexes, respectively, both as overall formation constants and partial formation constants, according to the reaction ($r = i + j$):

$$H_iA^{i+} + H_jL^{(z-j)-} = ALH_r^{(r-z)} \ (\log K_{ij}) \qquad (2)$$

As expected, the most stable species are those relative to the reaction

$$H_nA^{n+} + L^{z-} = ALH_n^{(n-z)} \ (\log K_{n0}) \qquad (3)$$

In Fig. 1 we report log K_{n0} versus $|z|$, for both spermidine and spermine complexes. As can be seen, quite a good linear fit, with zero intercept, is obtained:

$$\log K_{n0} = a_n \ |z| \qquad (4)$$

with $a_3 = 1.41 \pm 0.09$ and $a_4 = 1.82 \pm 0.05$, for the two amines, respectively (mean deviation in log K_{n0}, $\varepsilon = 0.13$ and 0.10 for spermidine and spermine complexes). Besides, note that $a_3 \sim \frac{3}{4}a_4$, i.e. positive and negative charges have approximately the same influence on the stability of these complexes. By considering all log K_{ij} values of Tables 3 and 4 (weighing heavier the values relative to the most important species Section 4), we found the simple general equation

$$\log K_{ij} = 0.46 \ (\pm 0.02) \ \zeta \qquad (5)$$

where $\zeta = i(z - j)$. Also in this case the fit is very good (mean deviation in log K_{n0}, $\varepsilon = 0.12$), as can be seen in Fig. 2.

Table 4
Formation constants of protonated spermine–organic polyanions at $T = 25$°C and $I = 0$ mol dm^{-3}

p	q	r[a]	log $\beta \pm 3s$[b]	Reaction	log K
$L = mal^{2-}$					
1	1	1	11.95 ± 0.11	$HA^+ + L^{2-} = ALH^-$	1.2
1	1	2	22.67 ± 0.02	$H_2A^{2+} + L^{2-} = ALH_2^0$	2.3
1	1	3	31.79 ± 0.02	$H_3A^{3+} + L^{2-} = ALH_3^+$	3.1
1	1	4	39.64 ± 0.02	$H_4A^{4+} + L^{2-} = ALH_4^{2+}$	3.7
1	1	5	43.37 ± 0.03	$H_4A^{4+} + HL^- = ALH_5^{3+}$	1.7
$L = tca^{3-}$					
1	1	1	12.61 ± 0.04	$HA^+ + L^{3-} = ALH^{2-}$	1.9
1	1	2	23.44 ± 0.02	$H_2A^{2+} + L^{3-} = ALH_2^-$	3.0
1	1	3	32.98 ± 0.02	$H_3A^{3+} + L^{3-} = ALH_3^0$	4.3
1	1	4	41.45 ± 0.01	$H_4A^{4+} + L^{3-} = ALH_4^+$	5.5
1	1	5	46.25 ± 0.01	$H_4A^{4+} + HL^{2-} = ALH_5^{2+}$	3.8
1	1	6	49.82 ± 0.02	$H_4A^{4+} + H_2L^- = ALH_6^{3+}$	2.5
$L = btc^{4-}$					
1	1	1	13.02 ± 0.08	$HA^+ + L^{4-} = ALH^{3-}$	2.3
1	1	2	24.22 ± 0.04	$H_2A^{2+} + L^{4-} = ALH_2^{2-}$	3.8
1	1	3	34.17 ± 0.03	$H_3A^{3+} + L^{4-} = ALH_3^-$	5.4
1	1	4	43.04 ± 0.03	$H_4A^{4+} + L^{4-} = ALH_4^0$	7.1
1	1	5	48.54 ± 0.01	$H_4A^{4+} + HL^{3-} = ALH_5^+$	5.4
1	1	6	52.74 ± 0.01	$H_4A^{4+} + H_2L^{2-} = ALH_6^{2+}$	3.8
1	1	7	55.81 ± 0.02	$H_4A^{4+} + H_3L^- = ALH_7^{3+}$	2.3

[a] Indexes refer to the reaction $p(sper) + qL^{z-} + rH^+ = (sper)_pL_qH_r^{(r-qz)}$.
[b] Uncertainties expressed as $\geq 95\%$ confidence interval.

As regards spermine–carboxylic ligand systems, some species are also formed with the stoichiometric coefficient of the polyanion > 1: $(sper)(mal)_2H_4^0$ ($ALH_4^{2+} + L^{2-} = AL_2H_4^0$; log $K = 2.3$); $(sper)(tca)_2H_4^{2-}$ ($ALH_4^+ + L^{3-} = AL_2H_4^{2-}$; log $K = 1.6$) and $(sper)(tca)_2H_6^0$ ($ALH_5^{2+} + HL^{2-} = AL_2H_6^0$; log $K = 1.7$). Also for these species the stability follows the trend shown by Eq. (5) (log $K = 0.51\ \zeta$).

In Figs. 3 and 4 the speciation diagrams for two systems, are reported. For the system H^+-sper-tca^{3-} the most important species is $(sper)(tca)H_4^+$ which shows a maximum formation percentage in the range 6.5–7.2. In the system H^+-spd-btc^{4-}

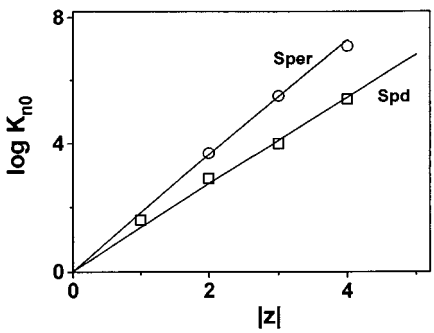

Fig. 1. Log K_{n0} (Eq. (3)) versus anion charge for spermidine and spermine complexes with carboxylic ligands, at 25°C and $I = 0$ mol dm^{-3}.

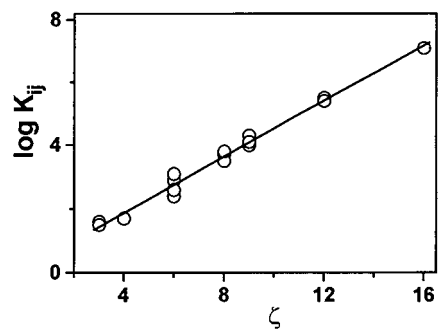

Fig. 2. Log K_{ij} (Eq. (2)) versus ζ for spermidine and spermine complexes with carboxylic ligands, at 25°C and $I = 0$ mol dm^{-3}.

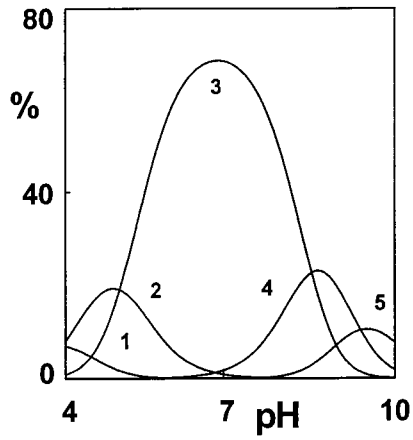

Fig. 3. Speciation diagram for the system H^+-sper-tca at 25°C (percentages calculated with respect to sper). $C_{Na} = C_{Cl} = 0.1$ mol dm^{-3}; $C_{sper} = 0.5$ mmol dm^{-3}; $C_{tca} = 5$ mmol dm^{-3}. Species: (1) ALH_6^{3+} (2) ALH_5^{2+} (3) ALH_4^{+} (4) ALH_3^{0} (5) ALH_2^{-}. Species with formation percentages < 5% were ignored.

the major species is $(spd)(btc)H_3^-$ with a maximum formation percentage in the pH range 7–7.7. By considering the formation of the other minor species for both systems, we have a broader pH range ($\sim$4.5–9) where the formation of amine–carboxylate complexes is highly significant.

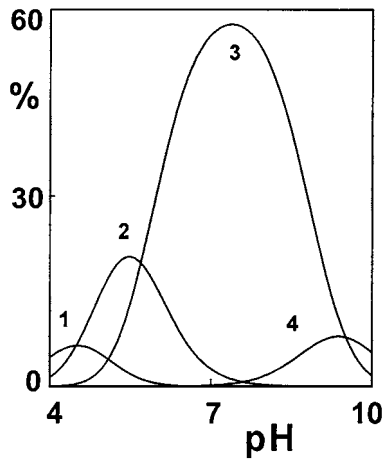

Fig. 4. Speciation diagram for the system H^+-spd-btc at 25°C (percentages calculated with respect to spd). $C_{Na} = C_{Cl} = 0.1$ mol dm^{-3}; $C_{spd} = 0.5$ mmol dm^{-3}; $C_{btc} = 5$ mmol dm^{-3}. Species: (1) ALH_5^{+} (2) ALH_4^{0} (3) ALH_3^{-} (4) ALH_2^{2-}. Species with formation percentages < 5% were ignored.

4. Discussion

4.1. The stability of amine carboxylate complexes

The stability of spermidine and spermine–polycarboxylic ligand complexes is quite relevant and follows a simple trend determined by the charges involved in the formation reaction. By considering the crude approximation $n = \zeta/2$ (n is the number of possible salt bridges) we have, from Eq. (5), a mean free energy value

$$-\Delta G^\circ = 5.25 \pm 0.15 \text{ kJ mol}^{-1}\, n^{-1} \quad (6)$$

This value is significantly lower than that of putrescine and cadaverine complexes of carboxylic ligands [4] ($-\Delta G^\circ = 6.5$ kJ mol^{-1} n^{-1}), and may account for the higher charge dispersion in tri- and tetra- amines than in diamines. An useful comparison can be made between protonated amines and alkaline earth metal complexes [10–12] of carboxylic ligands. The stability of Ca^{2+}-carboxylate complexes [10–12] can be expressed by an equation very similar to Eq. (5):

$$\log K(\text{CaL}) = 0.60\ \zeta \quad (5a)$$

(with $\zeta = 2z$), or

$$-\Delta G^\circ = 6.8 \text{ kJ mol}^{-1}\, n^{-1} \quad (6a)$$

A similar behaviour is shown by Mg^{2+} complexes. Therefore one can affirm, on a quantitative basis, that the stability of alkaline earth and amine-carboxylic ligand complexes is comparable, (in particular as concerns diamines). If we consider that, in the physiological pH range, biogenic polyamines are fully protonated, this leads to possible competition between ammonium and alkaline earth cations.

4.2. Medium effects

As one can see in Tables 1 and 2, carboxylic ligands form Na^+ complexes, and protonated amines form Cl^- complexes whose stability rapidly increases with the increase in charge. The formation of these complexes strongly interferes with the formation of amine carboxylic ligand complexes. In Fig. 5 we report Σ% (sum of

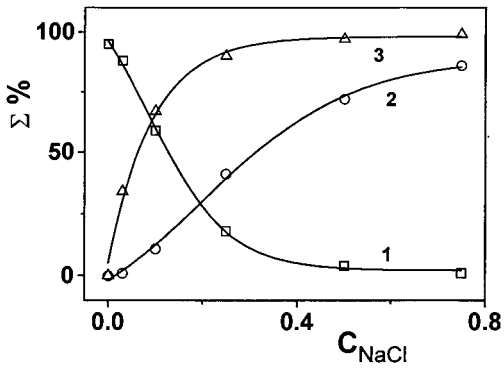

Fig. 5. Sum of formation percentages versus NaCl concentration in the system H-spd-btc, at pH = 7.5. $C_{spd} = 0.5$, $C_{btc} = 5$ mmol dm^{-3}. Species: (1) spd-btc-H (2) spd-H-Cl (3) btc-Na-H.

percentages of Na^+, Cl^- and amine–carboxylate complexes) versus NaCl concentration. As can be seen, increasing concentrations of NaCl lead to the formation of high percentages of Na^+ and Cl^- complexes with a decrease in percentages of amine–carboxylate species. At $I = 0.15$ mol dm^{-3} (the ionic strength of blood) this decrease is of $\sim 40\%$, and at $I > 0.6$ mol dm^{-3} the percentage of amine–carboxylate species becomes negligible. At constant ionic strength (or NaCl concentration; we consider mainly this salt because it is the principal component of most natural fluids) the concentration of reactants plays an important role, as shown in Fig. 6, where Σ% is reported

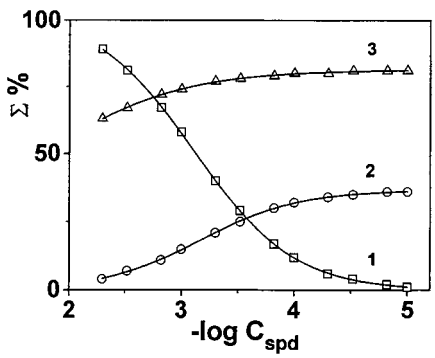

Fig. 6. Sum of formation percentages versus $-\log C_{spd}$ in the system H-spd-btc, at pH = 7. $C_{NaCl} = 0.1$ mol dm^{-3}. 1. Mixed spd-btc species; 2. protonated spd chloride species; 3. sodium btc species.

Table 5
Percentage of diamines and triamines complexed by carboxylic ligands[a], at different pH values, at 25°C

pH	% Diamines	% Triamines
6	8.9	11.5
7	10.2	12.6
8	10.4	11.1

[a] $C_{diam} = 2.1$, $C_{triam} = 0.6$, $C_{dicarbox} = 3.5$, $C_{tricarbox} = 1.0$ mmol dm^{-3}; $I = 0.1$ (NaCl) mol dm^{-3}.

versus $-\log$(amine concentration), with constant C_{amine}/C_{carbox} ratio. It is interesting to note that even at $C_{amine} < 0.1$ mol dm^{-3}, the percentage of amine–carboxylic ligand complexes is small but significant ($C_{spd} = 0.1$ mmol dm^{-3}, Σ% (spd–btc complexes) = 12).

4.3. Relevance of protonated amine–carboxylic ligand complexes

The real role of these complexes in the speciation of biological fluids can be studied by computer simulation. As an example, we considered a system containing di- and triamines, di- and tricarboxylic ligands and NaCl. Rough mean values (by taking into account different biofluids) were used for the concentrations of amines and carboxylic ligands, together with average equilibrium constants (this work and [3]). In Table 5 we report the results of this simulation at different pH values. As can be seen, the percentage of amines complexed by carboxylic ligands is significant in the whole pH range of biofluids. This is a very simple simulated experiment, which does not take into account the different composition of different biofluids, and the presence of other interfering components, but it is indicative of the importance of considering these species.

4.4. Comparison with analogous systems

Several protonated open-chain amine–polyanion complexes have been studied in these laboratories [2–4] and recently the investigations over the six-year period 1991–1996 have been summarised in a short review [13]. In all these

investigations we found a similar stability for similar complexes (same charges in the reactants). This is in agreement with the non-covalent nature of the bond. The stability of some polyazacycloalkane–polyanion complexes has also been reported [14]. We have taken into account the stability of the complexes formed by these cyclic amines with the carboxylic ligands [15–17] and, by correcting $\log K$ values to zero ionic strength [2], we obtained $\log K$ 0.51 ± 0.04 ζ and $-\Delta G^\circ = 5.8 \pm 0.5$ kJ $mol^{-1} n^{-1}$, which is in very good agreement with the value found here Eq. (6).

4.5. Final remarks

The findings of this work can be summarised as follows:

1. The stability of protonated spermine and spermidine–carboxylic ligand complexes, ALH_r, is very similar to that of similar species [2–4,13] of other open chain amines, and also to that of some polyazacycloalkanes [14–17].
2. Stability constants, and therefore ΔG° values, can be expressed by simple linear relationships, Eqs. (4) and (5), and a mean free energy value per salt bridge has been found, which can be used as a prediction tool (Figs. 1 and 2).
3. The possible competition between protonated bioamines and alkaline earth cations has been demonstrated on a quantitative basis, Eqs. (6) and (6a).
4. Medium and concentration effects, quantitatively reported in Figs. 5 and 6 are very important in the determination of the real speciation of biofluids. The relevance of the complexes formed by biopolyammonium cation–carboxylic anion complexes is shown in Table 5.

Acknowledgements

We thank MURST and CNR for financial support.

References

[1] C. Lentner (Ed.), Documenta Geigy Scientific Tables, 8th edn., Ciba-Geigy Limited, Basel, 1981.
[2] A. De Robertis, C. De Stefano, O. Giuffrè, S. Sammartano, J. Chem. Soc., Faraday Trans. 92 (1996) 4219.
[3] A. De Robertis, C. De Stefano, A. Gianguzza, S. Sammartano, Talanta 46 (1998) 1085.
[4] C. De Stefano, A. Gianguzza, R. Maniaci, D. Piazzese, S. Sammartano, Talanta 46 (1998) 1079.
[5] C. De Stefano, P. Princi, C. Rigano, S. Sammartano, Ann. Chim. (Rome) 77 (1987) 643.
[6] C. De Stefano, P. Mineo, C. Rigano, S. Sammartano, Ann. Chim. (Rome) 83 (1993) 243.
[7] C. De Stefano, C. Foti, O. Giuffrè, P. Mineo, C. Rigano, S. Sammartano, Ann. Chim. (Rome) 86 (1996) 257.
[8] P.G. Daniele, A. De Robertis, C. De Stefano, S. Sammartano, Miscellany of scientific papers offered to Enric Casassas, S. Alegret, J.J. Arias, D. Barceló, J. Casal, J. Router (Eds.), Universitat Autonoma de Barcelona, Barcelona, Spain, 1991.
[9] A. Casale, P.G. Daniele, A. De Robertis, S. Sammartano, Ann. Chim. (Rome) 78 (1988) 249.
[10] P.G. Daniele, A. De Robertis, C. De Stefano, S. Sammartano, C. Rigano, J. Chem. Soc., Dalton Trans. 2353 (1985); P.G. Daniele, C. De Stefano, E. Prenesti, S. Sammartano, Curr. Top. Solut. Chem. 1 (1994) 95.
[11] C. De Stefano, C. Foti, A. Gianguzza, Talanta 41 (1994) 1715.
[12] A. De Robertis, C. Foti, A. Gianguzza, Ann. Chim. (Rome) 83 (1993) 485.
[13] P.G. Daniele, E. Prenesti, A. De Robertis, C. De Stefano, C. Foti, O. Giuffré, S. Sammartano, Ann. Chim. (Rome) 87 (1997) 415; see also errata corrige, ibidem 88 (1998) 447.
[14] A. Bianchi, M. Micheloni, P. Paoletti, Coord. Chem. Rev. 110 (1991) 17.
[15] B. Dietric, M.W. Hosseini, J.M. Lehn, R.B. Sessions, J. Am. Chem. Soc. 103 (1981) 1282.
[16] E. Kimura, A. Sakonaka, T. Yatsunami, M. Kodama, J. Am. Chem. Soc. 103 (1981) 3041.
[17] M.W. Hosseini, J.M. Lehn, Helv. Chim. Acta 69 (1986) 587.

ELSEVIER

Talanta 48 (1999) 127–134

Talanta

Simple and rapid enzymatic assay of ornithine decarboxylase activity

Lassina Badolo *, Valérie Berlaimont, Marianne Helson-Cambier, Michel Hanocq, Jacques Dubois

Laboratory of Bioanalytical Chemistry, Toxicology and Applied Physical Chemistry, Institute of Pharmacy, Université Libre de Bruxelles, Campus de la Plaine, Bld. du Triomphe CP 205/1, 1050 Brussels, Belgium

Received 22 May 1998; received in revised form 11 June 1998; accepted 12 June 1998

Abstract

Since the induction of putrescine synthesis by ornithine decarboxylase (ODC) is observed in many pathological and physiological processes, a useful and simple method to assay this enzyme activity should be an interesting tool to quantify the biological importance of its induction. An enzymatic method to assay ODC is reported here. This method is based on the reaction between putrescine and soya diamine oxidase. The reaction releases H_2O_2, which is measured by a colorimetric method. The validation of this method showed good accuracy ($98 \pm 5\%$ of recovery). High precision and reproducibility were obtained. A linearity with a correlation coefficient of 0.999 in the range of 2.5–25 nmol was obtained. This method is also rugged and specific. The application of the assay of ODC activity showed that it is useful as a rapid and simple tool for assaying ODC activity in vitro. Comparison with the HPLC determination of ODC activity shows strong correlation along with the high accuracy of the two methods.

Keywords: Putrescine; Ornithine decarboxylase; Enzymatic assay; Soya amine oxidase; Validation

1. Introduction

Natural polyamines (putrescine, spermidine and spermine) were found to be essential for cell proliferation and differentiation in normal and neoplastic tissue [1,2]. The growing importance of these amines in different biological processes explains the effort to quantify these compounds in different media including seminal plasma, urine, serum and plasma [3–5].

The intracellular level of polyamines is strictly regulated by a series of synthesis and retroconversion enzymes [6]. Ornithine decarboxylase (ODC, EC 4.1.1.17), the first enzyme in polyamine biosynthesis, is one of the most regulated enzymes known [7]. It is induced by many kinds of stimuli, and its suppression by specific inhibitors or mutation inhibits cellular growth and transformation. Therefore ODC has been identified as a potential

* Corresponding author. Tel.: +32 2 6505219; fax: +32 2 6505187; e-mail: blassina@hotmail.com

0039-9140/99/$ - see front matter
PII S0039-9140(98)00228-8

target in the chemotherapy of cancer and parasitic diseases [8].

This enzyme splits ornithine into putrescine and CO_2. It is the lead into the polyamine pathway and in mammalian cells, governs the rate of synthesis of polyamine.

Regarding the role of ODC, many molecules are synthesised to inhibit its activity. This activity was, until now, determined by using labelled ornithine ([^{14}C]ornithine releases putrescine and [^{14}C]O_2 which is assayed with a scintillator) [9,10] or HPLC assays [11].

The methods used to assay polyamine in biological samples can be divided into two broad categories, the chromatographic and the enzymatic ones. Chromatographic methods [12,13] are widely used in polyamine studies as they allow the separation and measurement of different types of polyamines with excellent resolution and good specificity. However the laborious pre-treatment of the samples and the long analysis times make these methods time consuming and unsuitable for routine use.

Some enzymatic determination of total polyamines or higher polyamines (spermine and spermidine) based on the ability of amine oxidases to catalyse the oxidation of polyamines have been described [3,4,14]. Fagerström et al. [15] have developed a chemiluminescence-based system for the determination of polyamines in biological samples. Although this method has the advantage of relative simplicity, it requires an initial extraction step on silica gel. Furthermore the value measured represents the total amount of polyamines (putrescine + spermidine + spermine).

The goal of this study was to develop a rapid and simple spectrophotometric method to assay ODC activity in vitro. This method which requires no initial purification of polyamines from the samples, provides a direct measurement of the putrescine in term of the quantity of H_2O_2 generated by reaction with soybean amine oxidase and would be suitable as the basis for routine screening for assaying this polyamine in ODC test. Endogenous polyamines are eliminated by dialysing the ODC proteins. This method was validated and used to measure ODC activity.

2. Materials and methods

2.1. Materials

Horse radish peroxidase type II, *Escherichia coli* ODC and diaminohexane were from Sigma, USA; 4-aminoantipyrin and tris-(hydroxymethyl)-aminomethane were from Aldrich, Germany; phenol was from Merck, Germany; putrescine, 5″-pyridoxal phosphate and ornithine monohydrochloride were from Fluka-Chemika; P388D1 mouse lymphoid neoplasm cells were from ATCC CCL-46, USA. An Ultrasphere C_{18} column (250 × 4.6 mm i.d., 5 μm particle size) from Beckman (Berkeley, CA) was used for the HPLC assay of putrescine.

2.2. Methods

2.2.1. Purification of soybean amine oxidase (EC 1.4.3.6)

The soybean amine oxidase (SAO) was purified as described by Nikolov et al. [16]. Briefly soybean (glycine max) seeds were germinated at room temperature for 7 days in the dark. The seedlings were blended in an equal volume of water. The macerate was filtered and the supernatant fractionated by different concentrations of ammonium sulphate. The precipitates were dissolved in a minimum of phosphate buffer (pH 7.8) and applied to a Sephacryl S-200 column eluted with the buffer solution. Fractions were collected and the most active ones were pooled and desalted by Sephadex G-25. The final purification factor was 165 with an activity of 4.4 U mg^{-1} of stable lyophilised extract (1 U releases 1 μmol h^{-1} H_2O_2). The solid enzyme was stored at -25°C.

2.3. Enzymatic assay of putrescine

Putrescine was measured by a colorimetric quantification of the H_2O_2 released after its oxidation by SAO. The assay was performed, according to the method of Emerson [17] adapted for the microplate (96 wells) assay and absorbances were read with an iEMS reader/dispenser MF. Each well contained 230 μl reaction mixture composed of: 50 μmol buffer Tris pH 9.5, 50 μg phenol, 40

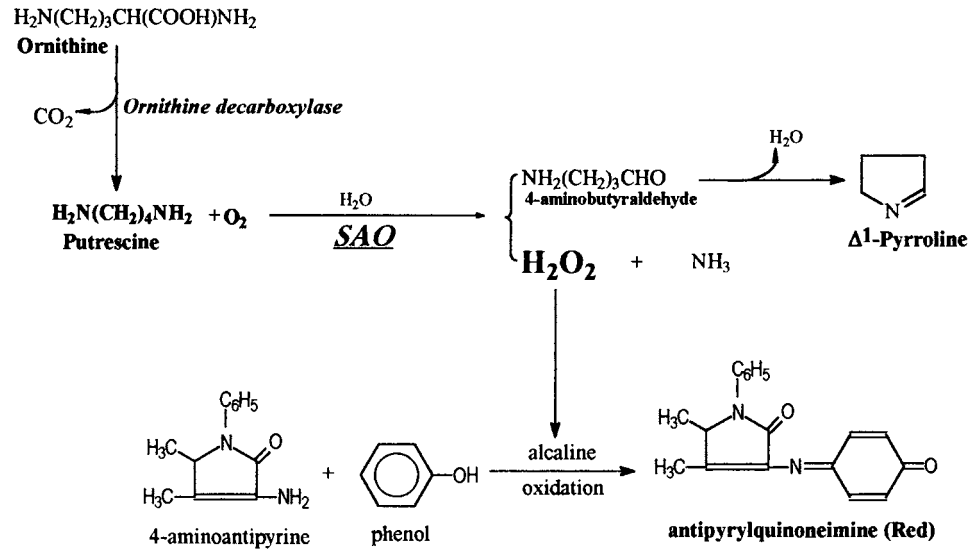

Fig. 1. Chemistry of the enzymatic assay of ODC activity.

μg 4-aminoantipyrin, 0.11 U SAO, 3.5 U horseradish peroxidase and different amounts of putrescine (from 2.5 to 50 nmol). 30 μg P388D1 cells crude extract protein were added to spiked samples to simulate a biological medium. The reaction starts by addition of the substrate. The oxidation of 1 mol putrescine by SAO generated 1 mol H_2O_2 which reacts with 4-aminoantipyrin and phenol by the means of horse radish peroxidase to yield a coloured complex that absorbs at 492 nm (reference: 690 nm).

The absorbance was determined every 10 min. The assay was stopped at the end of the oxidation reaction, indicated by the end of the change in absorbances (3 h in the range of concentrations used). The results were analysed by the Biolise software system (version 3.6 Kinetic TechGen International).

2.4. Ornithine decarboxylase assay

E. coli ornithine decarboxylase (0.222 mg) (4.8 mU–1 U releases 1 μmol CO_2 min^{-1} from ornithine) in 100 μl buffer (20 mM sodium phosphate, 0.2 mM EDTA and 0.1 mM 5″-pyridoxal phosphate, pH 7.4) were incubated at 37°C for 5 min, then 50 μl water were added and further incubated for 15 min. Ornithine (50 μl, 5 mM) were added and the reaction allowed to proceed for 30–90 min. The test was ended by heating the mixture at 90°C for 1 min to denature the ODC protein. The mixture (25 μl) was directly used for the putrescine assay.

The chemistry of the enzymatic determination of ODC activity is described in Fig. 1.

The ODC activity was also determined by using a previously described HPLC method [11]. The test was performed as for the enzymatic determination, but it was ended by addition of 1 ml $HClO_4$ (6% v/v). The assay was done after the derivatization of putrescine as benzoyl–putrescine.

2.5. Validation

The validation procedures were based on the European guidelines for analytical methods validation [18]. The protocol was established to determine simultaneously the linearity, the accuracy and the precision. The test was done on 5 different days (1 day = 1 group). The standard assays were carried out in parallel with the biological ones; this latter medium was obtained by spiking putrescine with P388D1 cells crude extract which

Table 1
Linearity

	Standard ($n=20$)	Spiked samples ($n=20$)	t(0.01,18) Comparison between standard and sample
Slope ± S.D. (AU nmol^{-1})	0.0165 ± 0.0002	0.0159 ± 0.0001	2.56 (NS)
Intercept ± S.D. (AU)	0.023 ± 0.003	0.025 ± 0.002	0.77 (NS)
Correlation	0.999	0.999	
t(0.01, 18) Comparison of intercept to 0	7.6 (S)	13.3 (S)	

S and NS are, respectively, significant and not significant in terms of statistics according to the Student two way test, $t(0.01, 18) = 2.88$.

was previously dialysed to eliminate endogenous polyamines.

The test was performed by assaying putrescine at five different concentrations, each carried out in quadruplicate. The precision was determined by assaying three concentrations each carried out eight times within a day for 5 different days.

The ruggedness was determined within a day. Each of the values was the absorbance of wells prepared independently.

The blank corresponds in each case to the same mixture of reagent as the sample, excluding the substrate, for the method described. The substrate (putrescine) is replaced by an equivalent volume of water or P388D1 crude extract depending on the standard or the sample tests.

3. Results

3.1. Linearity and specificity

The regression parameters of the relationship between the absorbances resulting from the enzyme reaction and various amounts of putrescine are summarised in Table 1. The linearity was determined in a range 2.5–25.0 nmol putrescine for $n = 20$. The Cochran test showed a within-assay homoscedasticity ($C_{obs} = 0.57 < C(0.05, 4, 4) = 0.63$). A significant slope with a linear relation was also calculated by the F test ($F_{obs} = 17683 \gg F(0.05, 1, 18) = 4.35$).

The correlation coefficient obtained with the standard solution and the biological samples was 0.999 for both. The intercepts obtained with the standard and the spiked samples were statistically different from zero. Putrescine in a biological media was thus determined by using a standard curve as reference. When the standard curve was compared to the sample one, both the intercepts and the slopes were not statistically different. The biological medium did not interfere with the measurement and, thus, allows this method to be useful for the routine determination of ODC activity in polyamine free biological media.

The specificity of this method was proved in biological media, as the blank absorbances were negligible. The substrate specificity for SAO was also tested and it was found that the enzyme was able to oxidise putrescine, spermidine and propanediamine (results not shown). Spermine, benzylamine and 1,6-hexanediamine were negligibly attacked. Ornithine and glutamine were not oxidised [16,19]. Therefore this method is useful for the measurement of putrescine in the absence of the other polyamines in a medium. This is particularly the case when testing the activity of ODC.

3.2. Recoveries, precision and reproducibility

The recoveries were evaluated on the basis of the parameters of the standard linear regression of the sample for four different amounts of putrescine (2.5, 5, 12.5 and 25 nmol) (Table 2). The mean of the recovery values was 98 ± 5% with a confidence interval from 95.6 to 100.2%.

The homoscedasticity was verified by the Cochran test at a level of 0.01.

Table 2
Accuracy: recoveries of spiked samples vs. the standard

$\overline{xi}$ (nmol putrescine)	$\overline{yi} \pm$ S.D. (Abs U)	$\overline{Yi} \pm$ S.D. (%)
2.5	$0.0620 \pm 0.00.$	95 ± 6
5.0	0.106 ± 0.006	101 ± 7
12.5	0.228 ± 0.004	99 ± 2
25.0	0.421 ± 0.006	96 ± 1

The recoveries are calculated by introducing the data of the spiked samples in the formula of the standard linear regression. The formula used is: $Yi = [(yi - a)/b]*100/xi$ where a and b are the intercept and the slope of the standard plot, respectively. For each value of putrescine $n = 5$.

In comparison to the within-assays errors, the between-assays errors were not statistically different ($F_{obs} = 1.43 < F(0.05, 3, 16) = 3.24$); this is tantamount to saying that the between-assays differences were not significant.

The reliability was determined using three different amounts of putrescine (5, 12.5 and 25 nmol), the precision of the assay was evaluated by assaying eight times in one assay (within-assay) and the reproducibility in five consecutive assays (between-assay). The results in Table 3 show good precision and reproducibility for each amount of putrescine.

3.3. Ruggedness

The ruggedness was determined by changing the enzyme SAO concentration, the total protein concentration and the pH of the medium. These parameters were chosen in order to reflect the practical difficulties encountered to control them closely.

Table 3
Precision and reproducibility

Parameters	Putrescine (nmol) ($n = 40$)		
	5.0	12.5	25.0
k	5	5	5
Mean (Abs AU)	0.0976	0.2274	0.417
CV reproducibility (%) ($n = 40$)	2.2	3.0	2.5
CV precision (%) ($n = 8$)	0.07	0.12	0.05

The reliability is determined by using three different concentrations of putrescine, each carried out eight times in a day ($n = 8$). This experiment is repeated for 5 days ($k = 5$).

The results summarised in Table 4 show that neither the enzyme concentration nor the total protein amount in the media changed the absorbances obtained. However, the pH of the medium is very important (when going from 9.5 to 10) to maintain the enzyme activity at the same level.

At fixed pH the absorbances were independent of the SAO activity or the protein content in the test. At pH 9.0 the absorbances were not statistically different from those at pH 9.5, however increasing the pH from 9.5 to 10 raised the absorbances and gave a significant difference ($t_{obs} = 22.6 \gg t_{calc} = 2.36$) between the results.

The absorbances of the blank at pH 9 and 10 were similar, suggesting that the difference observed was not due to the instability of the reagents.

3.4. Detection and quantification limits

These limits were based on the absorbances of the intercept considered as a blank obtained through the validation process for the biological samples. The detection limit was equal to three times the S.D. of the blanks and the quantification limit, 10 times the S.D.-blank. The detection and quantification limits were 377 pmol and 1.26 nmol, respectively.

3.5. Application to the assay of ODC and comparison of enzymatic and HPLC results

Fig. 2 shows that putrescine was determined with good precision in the ODC assay by both techniques (HPLC and enzymatic). The correlation between the two methods is high and the mean of the recoveries of enzymatic determination versus HPLC is $105 \pm 7\%$.

4. Discussion

The validation results of the enzymatic assay of putrescine showed that this method is an efficient analytical tool to determine ODC activity. Good

Table 4
Ruggedness

	Parameters studied			
	SAO activity (U)	Proteins (μg)	AU	Mean ± S.D. (AU)
Control	($n = 5$) (pH 9.5)	0.11	30	0.228 ± 0.004
Samples ($n = 4$) (pH 9.0)	0.088	40	0.231	
	0.088	20	0.232	
	0.132	40	0.233	0.231 ± 0.002
	0.132	20	0.229	$t_{obs} = 1.38$
Samples ($n = 4$) (pH 10.0)	0.132	40	0.310	
	0.132	20	0.314	
	0.088	40	0.300	0.310 ± 0.007
	0.088	20	0.315	$t_{obs} = 22.6$

Blanks absorbances ($n = 4$) were 0.027 ± 0.001; 0.029 ± 0.003 AU at pH 9 and 10 respectiveley. Absorbances obtained in each pH are compared to those obtained with controls using the t-test. t_{calc} (0.05, 7) = 2.37. The amount of putrescine for each test was 12.5 nmol.

linear correlation (0.999) together with high intra-assay and inter-assay precision ensure its success for assaying putrescine with good accuracy (mean of 98%). The absence of a difference between the standard results and the biological ones makes this method useful for testing ODC activity in polyamine-free biological media, and so the extensive purification of SAO and ODC enzymes is not necessarily required. This conclusion is in accordance with the ruggedness results, which show that putrescine determinations are independent of the total amount of protein and the activity of SAO. However the pH of the medium should be strictly controlled as it influences the absorbances obtained.

Beside the HPLC method thin-layer chromatography, gas chromatography, and radioimmunoassays were also used to measure polyamines in biological media [20–22].

The thin-layer chromatography , while sensitive, has the disadvantage of being time-consuming and it generates side products which have to be discarded by pre-chromatography on silica gel columns.

The gas chromatography spectrometry technique utilising deuterated analogues of polyamines as internal standards is sensitive, but requires extensive sample clean-up procedures. Moreover the high cost of the instrument precludes its use in many laboratories.

A radioimmunoassay involving the use of anti-spermine cross-reacting with spermidine and pure anti-spermidine antibodies was also described [22,23]. This method could be a useful tool for clinical application due to its sensitivity and simplicity, but up to the present no anti-putrescine antibody has been described.

The methods used to measure polyamines were generally developed as clinical tools for the assay of polyamine in different biological samples (urine, blood, seminal fluid, etc.).

Until now the conventional method used to test ODC activity has been the determination of $[^{14}C]O_2$ [10]. This method is useful for ODC assays both in vitro and in vivo. Although easy to use, this labelling method requires special equipment (a scintillator) and expensive labelled products. Besides the labelling assay of ODC, our method is particularly adapted to assay ODC activity in vitro. This enzyme is becoming more and more implicated in different biological signals making it the target of growing interest for understanding many biological processes. These include cell proliferation, central nervous disorders [24] and toxic pollution by heavy metals [25]. Our method is a good alternative to the above mentioned methods for micromolar assays when putrescine is the only polyamine in the medium.

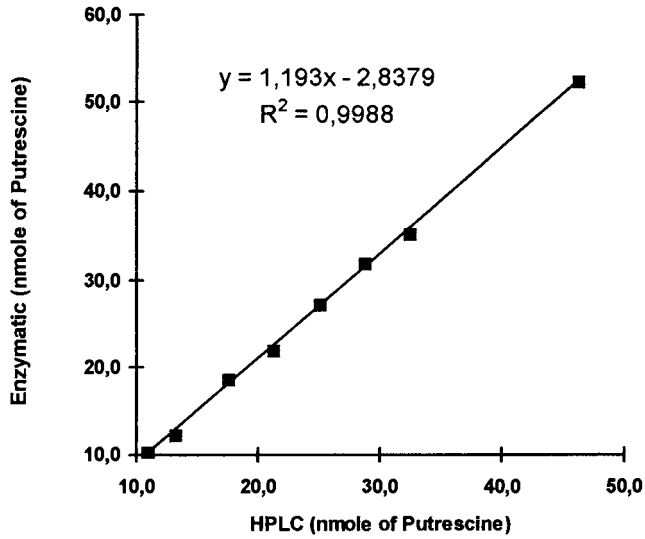

Fig. 2. Comparison between the HPLC and enzymatic determination of ODC activity. The test is performed in both cases by incubating the ODC with 5 mM of ornithine for eight incubation times (from 30 to 90 min) and the amount of putrescine formed is assayed by HPLC and enzymatic methods. The results are the mean of two and three replicates for the enzymatic and HPLC methods, respectively. The assays are performed as described in Section 2.2.

When compared to the HPLC method (Fig. 2)—the most usual for separating and assaying polyamines—for testing the ODC activity, our method offers considerable convenience, in avoiding derivatization, and multiple extractions. Furthermore multiple samples may be analysed in parallel. Even without automated equipment 96 samples may readily be assayed by spectrometry in one batch to yield results within 5 h of ODC reaction instead of more than 48 h with HPLC. The enzymatic method is accurate as HPLC as it shows high linear correlation and good recoveries for different concentrations of putrescine. This comparison suggests that the enzymatic assay could validly replace the HPLC one in the range of putrescine concentration used.

However one has to bear in mind that the SAO might interfere with the tested compound; this fact must be taken into account to avoid any erroneous conclusions. This enzymatic method affords a rapid, simple and cheap tool for testing ODC activity, the most important enzyme of the polyamine biosynthesis. This approach could be extended to other synthesis enzymes (spermidine synthase and spermine synthase) and then applied to the test, in vitro, of new inhibitors of polyamine biosynthesis.

Acknowledgements

This work was supported by a grant from the Burkina Faso Scholarship Service.

References

[1] C.W. Tabor, H. Tabor, Annu. Rev. Biochem. 45 (1976) 285–306.
[2] A.E. Pegg, Biochem. J. 234 (1986) 249–262.
[3] C. Fernandez, R.M. Sharrard, N. Monks, C.L.R. Barrett, Clin. Chim. Acta 227 (1994) 201–208.
[4] S. Kubota, M. Okada, K. Imahori, N. Ohsawa, Cancer Res. 43 (1983) 2363–2367.
[5] K. Maruta, R. Teradaira, N. Watanabe, et al., Clin. Chem. 35 (8) (1989) 1694–1696.
[6] A.E. Pegg, Cancer Res. 48 (1988) 759–774.
[7] S. Huyashi, Y. Murakami, Biochem. J. 306 (1995) 1–10.
[8] A.E. Pegg, L.M. Shantz, C.S. Coleman, J. Cel. Biochem. Suppl. 22 (1995) 132–138.
[9] O. Ruiz, D.O. Alonzo-Garrido, G. Buldain, R.B. Frydman, Biochem. Biophys. Acta 873 (1986) 53–61.

[10] J. Jänne, H.G. Williams-Ashman, J. Biol. Chem. 246 (1971) 1725–1732.
[11] E. Schenkel, V. Berlaimont, J. Dubois, M. Helson-Cambier, M. Hanocq, J. Chromatogr. B 668 (1995) 189–197.
[12] N. Seiler, Methods Enzymol. 94 (1983) 3.
[13] D.H. Russell, J.D. Ellingson, T.P. Davis, J. Chrom. 273 (1983) 263–274.
[14] R. Stevanato, B. Mondovi, S. Sabatini, A. Rigo, Anal. Chim. Acta 237 (1990) 391–397.
[15] R. Fagerström, P. Seppanen, J. Janne, Clin. Chim. Acta 143 (1984) 45–50.
[16] I. Nikolov, V. Pavlov, I. Minkov, D. Danijanov, Experimentia 46 (1990) 765–767.
[17] E. Emerson, J. Org. Chem. 8 (1943) 346–356.
[18] J. Caporal-Gauthier, J.M. Nivet, P. Algranti, et al., S.T.P. Pharma Prat. 2 (4) (1992) 205–239.
[19] M. Okada, S. Kawashima, K. Imahori, J. Biochem. 86 (1979) 97–104.
[20] S.H. Weltlaufer, L.H. Weinstein, J. Chromatogr. 441 (1988) 361–366.
[21] X.C. Jiang, Biomed. Chromatogr. 4 (1990) 73–77.
[22] I. Garthwaite, A.D. Stead, C.C. Rider, Biochem. Soc. Trans. 17 (1989) 1056–1057.
[23] D. Bartos, R.A. Campbell, F. Bartos, D.P. Grettie, Cancer Res. 35 (1975) 2056–2060.
[24] L. Badolo, J. Dubois, M. Helson-Cambier, M. Hanocq, Eur. J. Pharmacol. 342 (2-3) (1998) R1–R2.
[25] M.Z. Hauschild, Ecotoxicol. Environ. Saf. 26 (2) (1993) 228–247.

ELSEVIER

Talanta 48 (1999) 135–141

Talanta

Potentiometric flow titration of iron(II) and chromium(VI) based on flow rate ratio of a titrant to a sample

Hideyuki Katsumata, Norio Teshima, Makoto Kurihara, Takuji Kawashima *

Laboratory of Analytical Chemistry, Department of Chemistry, University of Tsukuba, Tsukuba 305-8571, Japan

Received 24 March 1998; received in revised form 11 June 1998; accepted 15 June 1998

Abstract

A new potentiometric flow titration has been proposed based on the relationship of the flow rates between titrant and sample solutions. A sample solution is pumped at a constant flow rate. The flow rate of the titrant solution is gradually increased at regular time intervals and a flow rate for the titrant solution in the vicinity of the equivalence point is obtained. The concentration of the sample is calculated by C_S (mol l^{-1}) = (R_T (ml min^{-1}) × C_T (mol l^{-1}))/R_S (ml min^{-1}), where C_S, C_T, R_S, and R_T denote the unknown sample concentration, titrant concentration in the reservoir, the flow rate of the sample solution which is a constant rate, and the flow rate of the titrant solution at an inflection point, respectively. The potentiometric flow titration of iron(II) with cerium(IV) and of chromium(VI) with iron(II) has been presented. The titration time of the proposed method is about 10 min per sample. An R.S.D. of the method is 0.77% for seven determinations of 1×10^{-3} mol l^{-1} iron(II). Similarly, the flow titration of chromium(VI) with iron(II) is carried out over the range 1×10^{-4}–1×10^{-3} mol l^{-1} chromium(VI) and is successfully applied to the determination of chromium in high carbon ferrochromium.

Keywords: Potentiometric flow titration; Flow rate ratio; Iron(II); Cerium(IV); Chromium(VI)

1. Introduction

In titrimetric analysis, we would measure the volume of a substance of known concentration which is required just to react with an analyte in a sample solution. Many redox reactions are considerably more complex than acid–base ones and are usually slow, although the applications are versatile in analytical chemistry. A promising approach directed towards more rapid throughput is the application of the flow injection technique to titrimetric analysis [1].

Before flow injection analysis (FIA) was proposed, Blaedel et al. [2] reported continuous flow titration in which the flow rate of the titrant was changed to find suitable end-point. In this method, a manual titration curve is needed to determine the end-point potential band under particular conditions prior to analysis. Then, the flow rate of a titrant was controlled and kept at the recorder potential in the end-point band and

* Corresponding author. Tel.: +81 298 536521; fax: +81 298 536503; e-mail: kawashima@staff.chem.tsukuba.ac.jp

0039-9140/99/$ - see front matter
PII S0039-9140(98)00231-8

reached the steady state potential. The values of the pumping rate were read out as counts per 7.5 s. Since the pumping rate is not read out in ml min^{-1}, it is necessary to calibrate the pumping rate versus the concentration of a standard solution. Fleet et al. [3] proposed a gradient titration principle: the flow rates of the sample and the titrant streams were kept constant, the concentration of the titrant being increased in the form of a gradient. The resulting mixture of the titrant and the sample, forming a continuous stream, was monitored by an ion-selective electrode which thus indicated the end-point of the titration. Ruzicka et al. [4] introduced an FIA to titrimetric analysis in 1977. They used peak width as a measure of the determination; the sample concentration was determined by comparing the peak width of a sample solution with that of a standard solution. It had been possible to obtain highly reproducible concentration gradients within a sample zone injected into the moving stream. Astrom [5] reported a titrimetric method for the determinations of strong bases such as sodium hydroxide and potassium hydroxide using peak height as a measure of the determination. In this case, an acid–base mixture had a linear pH response when titrated with a strong base. There are general remarks about these continuous flow titrations given by Abicht [6] and Toth et al. [7,8]. Imato et al. [9–16] reported FIA titration using the reaction of buffer solution with a sample solution. These methods can be applicable to acid–base, chelatometric and redox titrations. Their characteristic features were pH, metal ion and potential buffers for acid–base, chelatometric and redox titrations, respectively. For example, an ORP electrode and a stream of an Fe(III)/Fe(II) potential buffer solution containing bromide ion were used and a large transient potential change due to bromine generated by an oxidation reaction between bromide and chromium(VI) in the presence of iron(II) was monitored [16]. However, the methods described above require a calibration graph prepared by using a series of standard sample solutions. Therefore, it is worthwhile to develop a new flow titration method without a calibration graph from the viewpoint of analytical chemistry. This paper describes the potentiometric flow titration of iron(lI) with cerium(IV) and chromium(VI) with iron(II) based on the measurements of the flow rate ratio of a titrant to a sample solution in the vicinity of the end-point. One of the methods is successfully applied to the determination of chromium in high carbon ferrochromium issued by The Japan Iron and Steel Federation.

2. Principle

The conventional titrimetric method is that the sample concentration is determined by the volume ratio between the titrant and the sample required throughout the titration. The proposed method is based on the measurement of the ratio between the flow rates of analyte and titrant solutions in place of the ratio of both solution volumes. That is, a sample solution is pumped at a constant flow rate and the potential values of the sample solution are monitored, and then the flow rate of titrant solution is increased at regular time intervals. The potential change is recorded at each flow rate and a differential point at the end-point is calculated. The flow rate of titrant at the end-point is obtained as the inflection point from the differential curve. When the flow rate (ml min^{-1}) of the titrant solution at the equivalence point is obtained, the concentration of the sample is calculated by Eq. (1):

$$C_S\ (\text{mol}\ l^{-1}) = \frac{R_T\ (\text{ml}\ \text{min}^{-1}) \times C_T\ (\text{mol}\ l^{-1})}{R_S\ (\text{ml}\ \text{min}^{-1})} \quad (1)$$

where C_S, C_T, R_S, and R_T denote the unknown sample concentration, the titrant concentration in the reservoir, the flow rate of the sample solution which is a constant rate, and the flow rate of the titrant solution at an inflection point, respectively.

3. Experimental

3.1. Reagents

All of the reagents used were of analytical grade. The water used to prepare the solutions

was purified with a Milli-Q PLUS water system (Millipore).

Stock solutions of iron(II), cerium(IV) and chromium(VI) (1×10^{-2} mol l^{-1}) were prepared and standardized as described previously [17–20]. Working solutions of the metal ions were prepared by suitable dilution with 5×10^{-3} mol l^{-1} sulfuric acid.

3.2. Apparatus

A schematic flow diagram for the determination of iron(II) and/or chromium(VI) is shown in Fig. 1. Two double-plunger micro pumps (Sanuki Kogyo, DMX-2000) were used to propel the sample and titrant solutions. The flow lines were made from Teflon tubing (0.5 mm i.d.). The potential change was monitored with a pH/mV meter (Denki Kagaku Keiki (DKK), PHL-20) equipped with a flow-through type platinum ORP and silver/silver chloride reference electrodes (DKK, Model FLC-11), and traced on a recorder (Chino, EB 22005). The pH of the sample and titrant solution were measured with a pH/mV meter (Shibata Kagaku, PH-810).

3.3. Procedure for the flow titration of iron(II) with cerium(IV)

The pH of the iron(II) and cerium(IV) solutions was adjusted to ca. 0 by adding the proper amounts of 10 mol l^{-1} sulfuric acid. In the flow system (Fig. 1), a sample solution of iron(II) in reservoir S was pumped at a flow rate of 0.500 ± 0.002 ml min^{-1} and the potential values of the solution were monitored. A titrant solution of cerium(IV) was pumped from reservoir R and the flow rate of the cerium(IV) solution was increased manually by turning a counter dial on the pump. A rapid increase in the flow rate of the titrant (e.g. 0.4–0.5 ml min^{-1}) was carried out in the regions of the start and the end of the titration and the flow rate was slowly increased by 0.01 ml min^{-1} at 1 min intervals in the vicinity of the equivalence point. The redox reaction of iron(II) with cerium(IV) proceeded in the reaction coil (RC, 2 m long) at room temperature. The flow rate of the titrant at the end-point was obtained as an inflection point from the differential curve calculated from the titration curve.

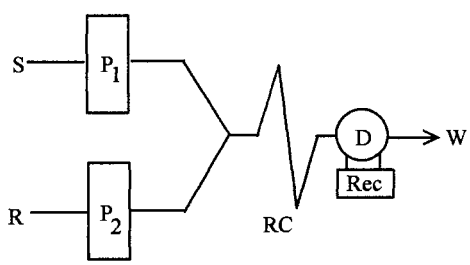

Fig. 1. Flow diagram of the flow titration of iron(II) with cerium(IV) and of chromium(VI) with iron(II). S, sample solution; R, titrant solution. The symbols P, RC, D, Rec and W denote pump, reaction coil (2 m), pH/mV meter equipped with an ORP electrode, recorder, and waste, respectively.

3.4. Procedure for the flow titration of chromium(VI) with iron(II)

The procedure was the same as described in Section 3.3, except for the change in the flow rate of the iron(II) solution (titrant). The flow rate of the iron(II) solution was increased rapidly in the regions of the start and end of the titration and slowly increased by 0.01 ml min^{-1} at 1.5 min intervals in the vicinity of the equivalence point.

4. Results and discussion

4.1. The calibration and precision of the flow rates of the sample and titrant solutions

The calibration of the flow rates was carried out at about 0.2, 0.5, 1, 1.5 and 2 ml min^{-1} as follows. Water in the reservoirs was pumped for 10 min and the outflow water was collected in a weighing bottle and the mass of collected water was measured each time. The mass of water was converted to the flow rate (ml min^{-1}) at room temperature. A linear relationship was obtained between the flow rates (ml min^{-1}) and the counter numbers (rpm) of the pumps over the range 0–2 ml min^{-1}. The precision of the flow rates of the sample and titrant solutions at 0.520 and 0.486 ml min^{-1} was 0.49% ($n = 5$) and 0.52% ($n = 5$), respectively.

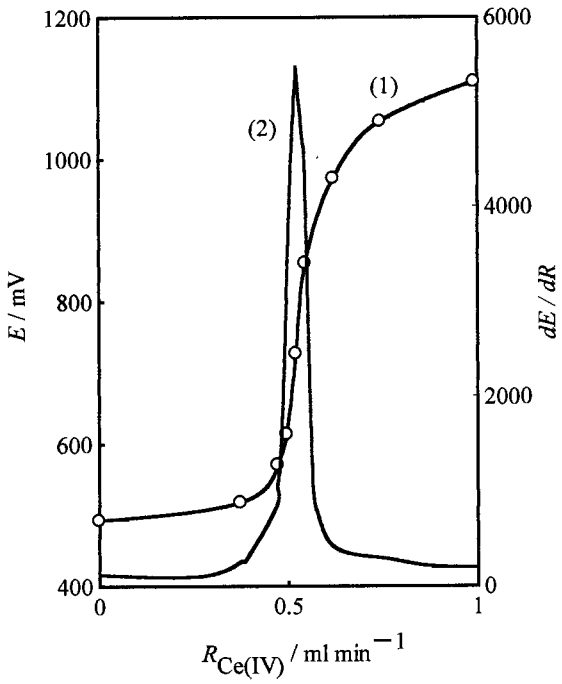

Fig. 2. Titration curves for iron(II) with cerium(IV). (1), titration curve; (2), differential curve. Conditions as in the text.

4.2. Potentiometric flow titration of iron(II) with cerium(IV)

4.2.1. Titration curves of iron(II) with cerium(IV)

When the flow rate of cerium(IV) solution was stepwise increased at 0.01 ml min^{-1} min^{-1}, the titration curve of iron(II) with cerium(IV) was obtained in ca. 50 min. From a practical point of view, only the data in the vicinity of the equivalence point is needed. Thus, the flow rate of the cerium(IV) solution was increased rapidly in the regions of the start and end of the titration and slowly increased at a flow rate of 0.01 ml min^{-1} min^{-1} in the vicinity of the equivalence point. The results are shown in Fig. 2. An analytical time of ca. 10 min was sufficient to perform this titration with good precision. An analytical time of ca. 10 min was chosen for the procedure.

4.2.2. Effect of variables

The optimum conditions were examined by pumping 1×10^{-3} mol l^{-1} cerium(IV) and 1×10^{-3} mol l^{-1} iron(II) solutions in reservoirs R and S, respectively. All measurements were carried out at room temperature.

The effect of the waiting time before changing the flow rate of the cerium(IV) solution (R) was examined over the range 1–2 min in the vicinity of the equivalence point. The potential break increased with increasing waiting time. Taking into consideration the rapid analytical time, a waiting time of 1 min was selected for the procedure.

The effect of the flow rate of the iron(II) solution (S) was examined over the range 0.500–1.00 ml min^{-1}. The end-point appeared beyond the equivalence point with increasing the flow rate. The relative errors of the analytical values were 0.26, 0.71, and 1.47% for 0.500, 0.750, and 1.00 ml min^{-1}, respectively, because the redox reaction could not proceed completely before the solution reached the detector. Hence, a 0.500 ml min^{-1} iron(II) flow rate was selected for the procedure.

4.2.3. Determination of iron(II)

The flow titration of iron(II) was carried out over the range 5×10^{-4} -2×10^{-3} mol l^{-1} at a constant concentration of cerium(IV) (1×10^{-3} mol l^{-1}). The reproducibility of the method was satisfactory with an R.S.D. of 0.77% for seven determinations of 1×10^{-3} mol l^{-1} iron(II) and the recovery of iron(II) was 100–101%.

4.3. Potentiometric flow titration of chromium(VI) with iron(II)

4.3.1. Titration curves of chromium(VI) with iron(II)

The titration of chromium(VI) with iron(II) was carried out by varying the analytical time. When the flow rate of the iron(II) solution was increased rapidly at the start and end regions of the titration and slowly increased (0.01 ml min^{-1} per 1.5 min) in the vicinity of the equivalence point, an analytical time of ca. 12 min was sufficient for the titration and the precision was satisfactory. The titration curves of chromi-

um(VI) with iron(II) and the differential curves obtained from the titration curves are shown in Fig. 3.

4.3.2. Effect of variables

The optimum conditions were examined by pumping chromium(VI) (3.33×10^{-4} mol l^{-1}) and iron(II) (1×10^{-3} mol l^{-1}) solutions in reservoirs S and R, respectively. All measurements were performed at room temperature.

The effect of the waiting time before changing the flow rate of the iron(II) solution was examined over the range 1–2 min. Although the potential break was observed at the equivalence point for each waiting time, the reproducibility of the method was poorer at a waiting time of less than 1 min. Thus, a waiting time of 1.5 min was selected for the procedure.

The effect of the flow rate of the chromium(VI) solution in the vicinity of the equivalence point was examined over the range 0.500–1.00 ml min^{-1}. At a 1.00 ml min^{-1} flow rate for the chromium(VI) solution, the potential values continued to decrease from the start region of the titration to the equivalence point, because the redox reaction could not proceed completely before the solution reached the detector. The relative errors of the analytical results were 0.60, 0.85, and 1.50% for 0.500, 0.750, and 1.00 ml min^{-1}, respectively. Thus, a 0.500 ml min^{-1} flow rate for the chromium(VI) solution was selected for the procedure.

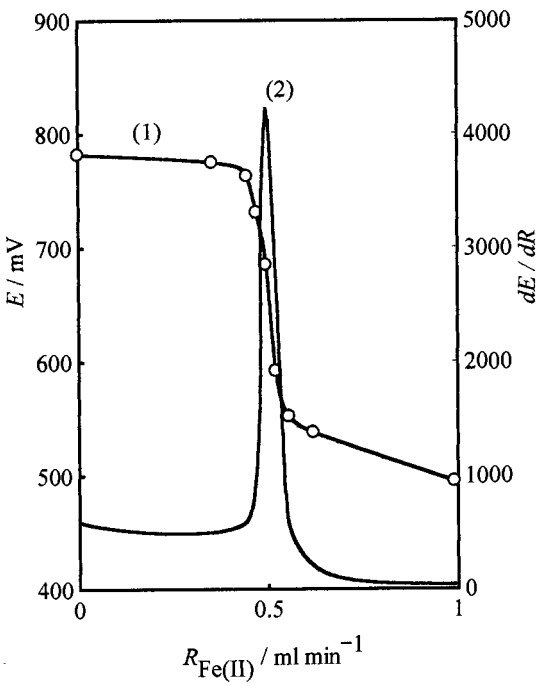

Fig. 3. Titration curves for chromium(VI) with iron(II). (1), titration curve; (2), differential curve. Conditions as in the text.

4.3.3. Determination of chromium(VI)

The flow titration of chromium(VI) was performed over the range 1×10^{-4}–1×10^{-3} mol l^{-1}. The reproducibility of the method was satisfactory with an R.S.D. of 0.84% for seven determinations of 3.33×10^{-4} mol l^{-1} chromium(VI) and the recovery of chromium(VI) was 99–101%.

4.3.4. Interferences

The effect of diverse ions on the titration of 3.33×10^{-4} mol l^{-1} chromium(VI) with iron(II) was examined (Table 1). The following compounds and ions have no influence: NaCl, KNO_3, Mg(II) and Ca(II) (0.1 mol l^{-1}); Cr(III), Mn(II), Fe(III), Ni(II), Cu(II), Co(II), and Zn(II) (1×10^{-3} mol l^{-1}). Vanadium(V) and vanadium(IV) caused serious interference in the flow titration of chromium(VI) with iron(II). The end-point of chromium(VI) could not be detected from the titration curves in the presence of 1×10^{-4} mol l^{-1} vanadium(V) or 1×10^{-4} mol l^{-1} vanadium(IV). The tolerance limits of vanadium(V) and vanadium(IV) were 1×10^{-5} mol l^{-1}, respectively.

4.3.5. Application to ore sample

The proposed method described in Section 3.4 was applied to the determination of chromium in high carbon ferrochromium issued by The Japan Iron and Steel Federation. The digestion of this material was carried out by alkali fusion [21]. The digested solution was diluted 60 times with water before measurement. The results obtained by the proposed method are given in Table 2. The analytical results are in good agreement with the certified value.

Table 1
Effect of diverse ions on the titration of 3.33×10^{-4} mol l^{-1} Cr(VI) with Fe(II)[a]

Ion or salt	Concentration Cr(VI)		Ion or salt	Concentration Cr(VI)	
	Added (mol l^{-1})	Found (10^{-4} mol l^{-1})		Added (mol l^{-1})	Found (10^{-4} mol l^{-1}
NaCl	0.1	3.32	V(IV)	1×10^{-4}	—[b]
KNO_3	0.1	3.33		1×10^{-5}	3.37
Mg(II)	0.1	3.33	Mn(II)	1×10^{-3}	3.33
Ca(II)	0.1	3.32	Fe(III)	1×10^{-3}	3.31
Al(III)	1×10^{-3}	2.28	Ni(II)	1×10^{-3}	3.33
	1×10^{-4}	3.35	Cu(II)	1×10^{-3}	3.35
Cr(III)	1×10^{-3}	3.34	Co(II)	1×10^{-3}	3.33
V(V)	1×10^{-4}	—[b]	Zn(II)	1×10^{-3}	3.33
	1×10^{-5}	3.28			

[a] A $\pm$ 2% error was considered to be tolerable.
[b] A potential break was not obtainable.

5. Conclusions

A new potentiometric flow titration has been developed based on the relationship between the flow rates of the sample and titrant solutions. The flow rate of the titrant solution at the end-point was obtained from the differential curve of the titration curve: differentiation of the titration can be easily calculated. The sample concentration is calculated from the ratio of the flow rates of the titrant and the sample solution. Note that the proposed method needs no calibration curve prepared by using a series of standard solutions. The titration of iron(II) with cerium(IV) and of chromium(VI) with iron(II) has been presented. The analytical time of the proposed method was 10–12 min. The proposed method was successfully applied to the determination of chromium in high carbon ferrochromium with good reproducibility.

Table 2
Determination of chromium in high carbon ferrochromium[a]

Found (% (m/m))	Certified value (% (m/m))
56.2 ± 0.1 ($n = 3$)	56.15 ± 0.134

[a] The digested solution was diluted 60 times with water before measurement.

Acknowledgements

We gratefully acknowledge the financial support of this study by a Grant-in-Aid for Scientific Research No. 09640715 and No. 0264 (NT) from the Ministry of Education, Science, Sports and Culture.

References

[1] J. Ruzicka, E.H. Hansen, Flow Injection Analysis, Wiley, New York, 1988.
[2] W.J. Blaedel, R.H. Laessig, Anal. Chem. 36 (1964) 1617.
[3] B. Fleet, A.Y.W. Ho, Anal. Chem. 46 (1974) 9.
[4] J. Ruzicka, E.H. Hansen, H. Mosbaek, Anal. Chim. Acta 92 (1977) 235.
[5] O. Astrom, Anal. Chim. Acta 88 (1977) 17.
[6] S.M. Abicht, Anal. Chim. Acta 114 (1980) 247.
[7] K. Toth, G. Nagy, Z. Feher, G. Horvai, E. Pungor, Anal. Chim. Acta 114 (1980) 45.
[8] Z. Feher, G. Nagy, I. Slezsak, K. Toth, E. Pungor, Anal. Chim. Acta 273 (1993) 521.
[9] N. Ishibashi, T. Imato, K. Tsukiji, Anal. Chim. Acta 190 (1986) 185.
[10] H. Ohura, T. Imato, S. Yamasaki, N. Ishibashi, Anal. Sci. 3 (1987) 453.
[11] N. Ishibashi, T. Imato, Anal. Chim. Acta 214 (1988) 349.
[12] T. Imato, A. Katafuchi, T. Hamazoe, J. Yagi, K. Takahara, N. Ishibashi, Anal. Sci. 5 (1989) 777.
[13] H. Ohura, T. Imato, Y. Asano, S. Yamasaki, N. Ishibashi, Anal. Sci. 6 (1990) 541.
[14] N. Ishibashi, T. Imato, S. Yamasaki, H. Ohura, Anal. Chim. Acta 261 (1992) 405.

[15] T. Imato, K. Ishii, N. Ishibashi, Anal. Sci. 8 (1992) 631.
[16] H. Ohura, T. Imato, S. Yamasaki, N. Ishibashi, Buseki Kagaku 43 (1994) 31.
[17] H. Itabashi, K. Umetsu, K. Satoh, T. Kawashima, Anal. Sci. 6 (1990) 721.
[18] K. Umetsu, H. Itabashi, K. Satoh, T. Kawashima, Anal. Sci. 7 (1991) 115.
[19] N. Teshima, T. Kawashima, Bull. Chem. Soc. Jpn. 69 (1996) 1975.
[20] H. Katsumata, N. Teshima, T. Kawashima, Anal. Sci. 13 (1997) 825.
[21] JIS G 1313, Methods for Chemical Analysis of Ferrochromium, Japanese Industrial Standards Committee, Tokyo, 1989.

ELSEVIER

Talanta 48 (1999) 143–150

Talanta

Decomposition mechanism of an artemisinin-type compound via hemin-electrocatalysis

Hong-Yuan Chen [a,*], Yang Chen [a], Shi-Min Zhu [a], Ning-Sheng Bian [a], Feng Shan [b], Ying Li [b]

[a] *Department of Chemistry, The State Key Laboratory of Coordination Chemistry, Nanjing University, Nanjing 210093, China*
[b] *Shanghai Institute of Materia Medica, Chinese Academy of Sciences, Shanghai 200031, China*

Received 22 October 1997; received in revised form 8 June 1998; accepted 15 June 1998

Abstract

The interaction between a typical derivative of artemisinin and hemin was investigated by electrochemical and spectroelectrochemical methods. This derivative can be reduced via hemin-catalysis at the glassy carbon electrode, the cathodic overpotential is decreased by ca. 650 mV. A HPLC method for separating the products of the catalytic reaction was established. They were identified either in H_2O–CH_3CN solution or in tetrahydrofuran, respectively. The structures of these products show that the hemin-catalyzed decomposition of an artemisinin-type compound on the glassy carbon or reticulated vitreous carbon electrode can be achieved by both electrochemical reduction and rearrangement. The conclusion that the reaction of artemisinin with hemin is a critical step in the antimalarial mechanism of artemisinin can be drawn.

Keywords: Artemisinin derivative; Hemin; Decomposition mechanism; HPLC; UV-spectroelectrochemistry

1. Introduction

Malaria is one of the most widespread infectious diseases in the world. Every year about 500 million people are infected by it, and over 2.7 million infected people die, most of them are children [1]. Because of the rapidly developing resistance of the malaria parasite *Plasmodium falciparum* to currently used alkaloidal drugs such as quinine and chloroquine, new non-alkaloidal artemisinin-type antimalarial drugs have become increasingly important. Artemisinin (or qinghaosu, Fig. 1a) is a sesquiterpene endoperoxide extracted from a Chinese herbal remedy *Artemisia annua* L. Structurally artemisinin is entirely different from all previous antimalarial drugs. Its unconventional structure and novel mode of action give make it particularly effective against drug-resistant *P. falciparum* and cerebral malaria [2].

The antimalarial activity of artemisinin is closely related to its endoperoxide bridge. The absence of this moiety leads to complete antimalarial inertness [3,4]. Further studies showed that the antimalarial action of artemisinin appears to involve two steps [5–7]. First, the endoperoxide

* Corresponding author. Tel.: +86 25 3353198; fax: +86 25 3317761; e-mail: HYChen@nju.edu.cn

0039-9140/99/$ - see front matter
PII S0039-9140(98)00230-6

moiety of artemisinin interacts with intraparasitic heme to generate unstable free radical intermediates; then the resulting free radical, or a further rearranged radical or electrophile alkylates specific malaria proteins to poison the malaria parasite. In this process the first step is a key one. Zhang et al. [8] demonstrated that the cleavage of the endoperoxide bridge was caused by intraparasitic hemin via a catalytic reduction. However, up to now the detailed reaction process has not been reported. In this study we used electrochemical and spectroelectrochemical methods and HPLC to further investigate the reaction process through the interaction of artemisinin derivative $QCOC_6H_5$ (Fig. 1c) with hemin. The reason to choose $QCOC_6H_5$ is that artemisinin and its common derivatives, such as dihydroartemisinin (Fig. 1b) and artemether, almost do not possess UV–visible absorption or fluorescent chromophores or functional groups for determination [9]. $QCOC_6H_5$ is promising in that it gives a lot of information on its reduced products during the reaction process from its strong UV absorbent group $-COC_6H_5$. In addition, $QCOC_6H_5$ itself is a potent antimalarial agent [10] and the reaction situation of the artemisinin derivative with hemin will also give verification of the emerging antimalarial mechanism.

2. Experimental

2.1. Materials

Compound $QCOC_6H_5$ was synthesized according to the literature [10]. Its H_2O–CH_3CN solution was prepared by dissolving the compound in acetonitrile, then diluting to the desired concentration containing 50% acetonitrile (v/v) with pH 6.47 phosphate buffer. Its tetrahydrofuran (THF) solution was prepared by directly dissolving the compound in THF containing 0.10 M $LiClO_4$ as supporting electrolyte. Acetonitrile is HPLC reagent grade (Shanghai Ludu). The preparation of the phosphate buffer was by mixing seven portions of 0.0667 M KH_2PO_4 with three portions of 0.0667 M Na_2HPO_4. Hemin (purchased from Shanghai Institute of Biochemistry, Academia Sinica, Shanghai) solution was made immediately prior to each experiment by dissolving hemin in several drops of 0.25 M NaOH, diluting this solution with phosphate buffer, and then bringing it to pH 7.0–7.5 with 0.20 M HCl. All other chemicals are of analytical reagent grade. Deionized-distilled water was used to prepare all aqueous solutions.

Compounds **2** and **3** (Fig. 1d and e) were prepared according to the literature [11]. Their characteristic values are listed as follows: Compound **2**: m.p. 160–163°C (petroleum ether–ethyl acetate); $[\alpha]_D = +20.35°$ (c, 0.74, CH_3Cl); IR (KBr, cm^{-1}): 1750, 1720, 1592; ^1H NMR(400 MHz, $CDCl_3$): δ 0.91(6H, t), 2.08 (3H, s), 3.93 (1H, m), 4.30 (1H, m), 6.08 (1H, d, $J = 9.5$ Hz), 6.30 (1H, s), 7.26–7.56 (3H, m), 8.03–8.12 (2H, m); Anal. Calc. for $C_{22}H_{28}O_6$: C 68.02, H 7.26. Found: C 67.82, H 7.30%. Compound **3**: m.p. 97–98°C (petroleum ether–ethyl acetate); $(\alpha)_D = -56.86°$ (c, 0.28, CH_3Cl); IR (KBr, cm^{-1}): 3527, 1713, 1280, 1013, 818, 714; ^1H NMR (300 MHz, $CDCl_3$): δ 0.91 (3H, d, $J = 6.3$ Hz), 1.04 (3H, d, $J = 7.1$ Hz), 1.55 (3H, s), 2.75 (1H, m), 3.52 (1H, m), 5.33 (1H, s), 5.98 (1H, d, $J = 6.9$ Hz), 7.43 (2H, t), 7.56 (1H, t), 8.08 (2H, d, $J = 7.1$ Hz); Anal. Calcd. for $C_{22}H_{28}O_6$: C 68.02, H 7.26. Found: C 67.74, H 7.30%.

2.2. Methods

2.2.1. Cyclic voltammetry (CV)

A model BAS-100B electrochemical analyzer (BAS, USA) was used for CV measurements at room temperature. A three-electrode cell with a glassy carbon (GC) working electrode (3.0 mm diameter), a platinum wire auxiliary electrode and an Ag/AgCl reference electrode with saturated KCl was employed. The glassy carbon electrode was polished with γ-Al_2O_3 (10 μm grit size) and cleaned by an ultrasonic wave washer before the experiments. All solutions were deaerated with pure nitrogen. An atmosphere of nitrogen was maintained over the test solution

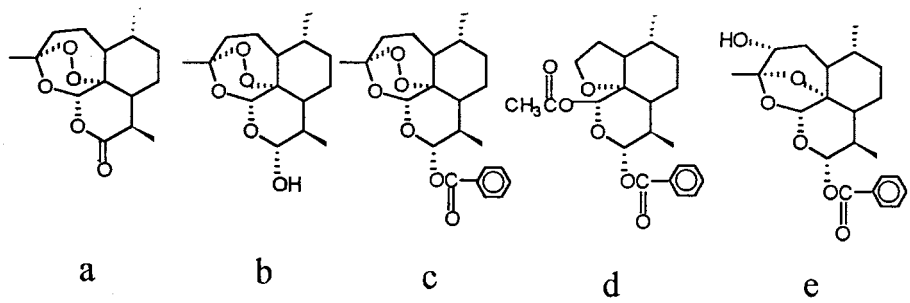

Fig. 1. Structures of (a) artemisinin, (b) dihydroartemisinin, (c) $QCOC_6H_5$, (d) compound **2** and (e) compound **3**.

and ohmic drop compensation was applied in every experiment.

2.2.2. High performance liquid chromatography (HPLC) analysis

A Varian 5060 LC system with a UV-100 variable-wavelength detector (Varian, USA) was used for the LC experiments. Separation was accomplished using a Alltech C18 absorbsphere HS column (150×4.6 mm i.d., 5 μm particles) (Alltech, USA). The mobile phase was phosphate buffer–acetonitrile (35:65 v/v) at a flow rate of 1.0 ml min^{-1}. The column temperature was kept at 35°C. The detection wavelength was 235 nm.

The bulk electrolysis of $QCOC_6H_5$ was also performed with a model BAS-100B. The electrodes are the same as that in the CV experiment. Electrolysis potential was controlled at -0.70 V.

2.2.3. UV-spectroelectrochemistry (SEC)

In the SEC experiments, the cell container is made of quartz (thickness 2.0 mm) and its working volume with the three-electrode system inserted is 560 μl. A reticulated vitreous carbon (RVC) (Pfrizer, USA) made by cutting it into slices was used as the working electrode (transparency 37%). The reference electrode and auxiliary electrode were Ag/AgCl and a platinum wire, respectively. The UV absorption spectra were recorded on a model UV-240 spectrophotometer (Shimazu, Japan). The applied voltage was controlled by a potentiostat (XJP-821B, Jiangsu Electroanalytic Instrument Factory). In every experiment, a new RVC slice was used in case it was blunt or contaminated.

3. Results and discussion

3.1. The reduction of $QCOC_6H_5$

The cyclic voltammogram of $QCOC_6H_5$ is shown in Fig. 2a. Only one cathodic peak at -1.18 V but no anodic one was observed. It means that the reduction of $QCOC_6H_5$ is entirely irreversible. The fact that dihydroartemisinin (shown in Fig. 1b) also displays only one cathodic peak near -1.0 V in same experimental conditions suggests that the cathodic peak of $QCOC_6H_5$ (at -1.18 V) is caused by the reduction of its peroxide group, rather than its carbonyl bond. The cathodic peak current decreased with the numbers of cyclic scan and then reached

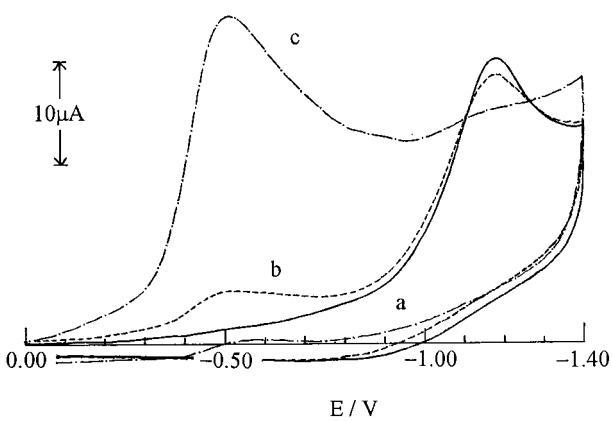

Fig. 2. Cyclic voltammogram in pH 6.47 phosphate buffer containing 50% acetonitrile (v/v). Scan rate: 100 mV s^{-1}. (a) $1.85-10^{-3}$ M $QCOC_6H_5$, (b) and (c) 1.85×10^{-3} M $QCOC_6H_5$ in the presence of 1.0×10^{-7} and 1.0×10^{-5} M hemin, respectively.

actually a stable value. Experimental results showed that the peak currents linearly increase with the scan rates in the range of $50 \sim 1200$ mV s^{-1}. This suggests that the reduction of $QCOC_6H_5$ is an adsorption-controlled electrode process. The pH of solution nearly has no effect on the cathodic peak potential. However, with the increasing ratio of aprotic solvent CH_3CN in CH_3CN–H_2O, the peak at -1.18 V elongates and becomes ill-defined, and till this peak disappears in CH_3CN medium. It would be concluded that the overall reaction depends upon the proton contribution. Controlled-potential electrolysis at -1.30 V for $QCOC_6H_5$ shows that its reduction is a two-electron process. From the facts mentioned above, the electrode processes may be outlined as follows:

$$Q(-O-O-)COC_6H_5 \xrightarrow{2e,\ slow}$$

$$Q(-O-O-)COC_6H_5 \xrightarrow{protonation,\ fast} \text{Reduction Products}$$

3.2. The reduction of hemin

A well-defined cyclic voltammogram of hemin with a cathodic peak at -0.36 V and an anodic peak at -0.28 V was obtained under the same experimental conditions carried out for $QCOC_6H_5$. The experimental result that the peak currents are linear with the scan rates in the range from 50 to 1200 mV indicated that the reduction of hemin is attributed to a surface-adsorption electrode process.

3.3. Hemin-catalyzed reduction of $QCOC_6H_5$

When hemin was gradually added to the phosphate buffer solution containing 1.85×10^{-3} M $QCOC_6H_5$, a new cathodic peak appeared at ca. -0.53 V (Fig. 2b). The peak current increased with the concentration of hemin, while the original peak current of $QCOC_6H_5$ decreased. When the concentration of hemin reached 1.0×10^{-5} M, the peak of $QCOC_6H_5$ completely disappeared (Fig. 2c). Fixing the concentration of hemin at 1.0×10^{-4} M and varying the concentration of $QCOC_6H_5$ from 1.0×10^{-4} to 2.0×10^{-3} M, the cathodic peak current increased linearly with the concentration of $QCOC_6H_5$. Considering the peak potential of species, it was revealed that $QCOC_6H_5$ was catalytically reduced by hemin with a reduction of cathodic overpotential for ca. 650 mV.

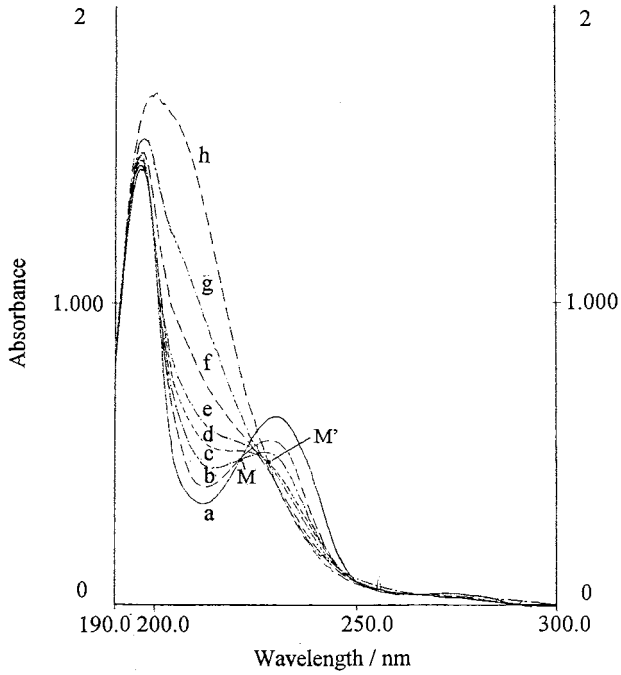

Fig. 3. Absorption spectra of 2.68×10^{-4} M $QCOC_6H_5$. Other solution conditions as in Fig. 2a. Applied potential: -1.40 V vs. Ag/AgCl. Electrolysis time (min): (a) 0, (b) 1, (c) 2, (d) 3, (e) 6, (f) 9, (g) 14 and (h) 19.

3.4. UV-SEC of interaction between $QCOC_6H_5$ and hemin

The UV-spectra of $QCOC_6H_5$ at various electrolysis times are shown in Fig. 3. The adsorption peak at 197 nm increased and the peak at 230 nm decreased with increasing electrolysis time. It is of interest to note that the peak at 197 nm slightly shifts towards the long wavelength and the peak at 230 nm slightly shifts towards the short wavelength. At last (see curve h, electrolysis for 19 min), the peak of 197 nm shifts to 200 nm, and the peak of 230 nm disappears. No well-defined isobestic point was observed. It could be found that the 'isobestic point' seems to be moved from

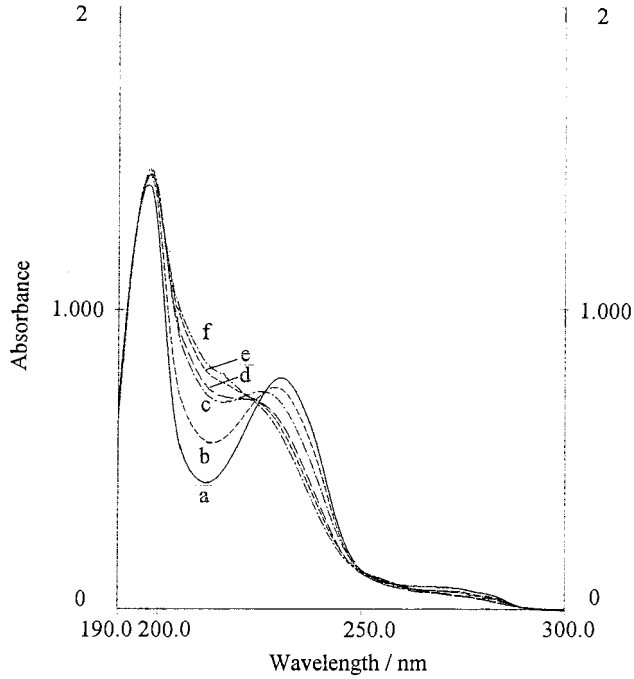

Fig. 4. Absorption spectra of 2.68×10^{-4} M $QCOC_6H_5$ in the presence of 3.20×10^{-5} M hemin. Other solution conditions as in Fig. 2a. Applied potential: -0.68 V vs. Ag/AgCl. Electrolysis time (min): (a) 0, (b) 2, (c) 6, (d) 10, (e) 17 and (f) 25.

M to M' (a trace of 'isobestic point' M can be observed). Obviously, the structures of the products have a great deal of different chromophore moieties from that of $QCOC_6H_5$. Fig. 4 is the plot of UV-spectra of $QCOC_6H_5$ versus electrolysis time at -0.68 V in the presence of hemin. No obvious variation in the shape of the curve was observed between Fig. 4 and Fig. 3, except the relatively clear 'isobestic point' (area). But the increase in the peak at 197 nm and the decrease in the peak at 230 nm in Fig. 4 are much slower than those in Fig. 3. This reveals that hemin can catalyze the reduction (decomposition) of $QCOC_6H_5$ at a more positive potential of -0.68 V, leading to a reduction of cathodic overpotential of ca. 650 mV. The result further verifies the conclusion derived from CV.

3.5. HPLC separation and determination of reduced products of $QCOC_6H_5$ via hemin catalysis

In order to determine the products from the reaction between $QCOC_6H_5$ and hemin, the $QCOC_6H_5$ solutions containing hemin were electrolyzed at -0.70 V potential (versus Ag/AgCl) for about an hour. $QCOC_6H_5$ can not be reduced at this potential in the absence of hemin, but can be reduced via catalysis in the presence of hemin. The chromatograms of the electrolyzed solution are shown in Fig. 5a. Besides the peak with $t_R = 8.29$ obtained from the unelectrolyzed $QCOC_6H_5$ (Fig. 5d), a series of new peaks appear with $t_R = 4.06$, 5.49 and 6.69 min, respectively. In order to identify the electrolyzed products of $QCOC_6H_5$, compounds **2** and **3** were used as standard samples, which are the homologous products of the pyrolysis and metabolism of artemisinin [12–14] and also from the chemical reaction of $QCOC_6H_5$ with $FeSO_4$ [11]. From Fig. 5a, compared to Fig. 5b and c, it was found that compound **2** is a product and compound **3** is not. Other unknown products are the peaks with $t_R =$ 4.06 and 6.69.

The chromatograms of a mixed solution using aprotic solvent THF to replace H_2O–CH_3CN are

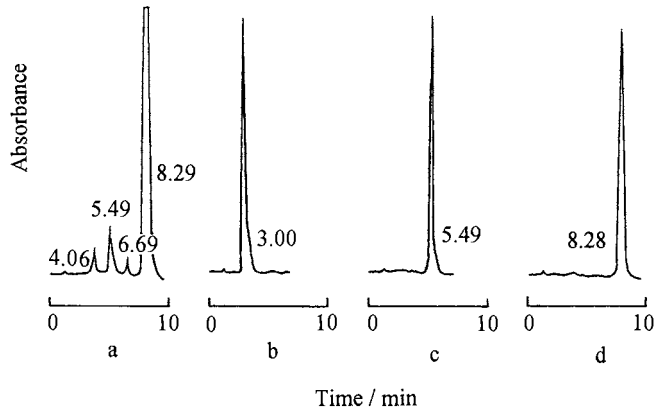

Fig. 5. HPLC chromatograms in pH 6.47 phosphate buffer containing 50% acetonitrile (v/v) for: (a) 2.10×10^{-3} M $QCOC_6H_5$ in the presence of 7.50×10^{-4} M hemin after about 60 min electrolysis, (b) compound **3**, (c) compound **2** and (d) $QCOC_6H_5$. Electrolysis potential: -0.70 V vs. Ag/AgCl.

shown in Fig. 6a. In comparing Fig. 6a with Fig. 6b and c, it is easily found that compound **3** with $t_R = 2.95$ and compound **2** with $t_R = 5.42$ are the products. In addition, there are still two unknown products with $t_R = 4.01$ and 4.47.

The peaks with $t_R = 4.06$ in Fig. 5a and with $t_R = 4.01$ in Fig. 6a seem to be formed from an identical substance by electrolysis. The slight difference of both retention times was probably caused the different solvent, similar to the difference of retention time for compound **2** and that of $QCOC_6H_5$ in Fig. 5a and Fig. 6a.

3.6. The mechanism of decomposition of $QCOC_6H_5$ and the antimalarial action

In the presence of hemin the original cathodic peak of $QCOC_6H_5$ at -1.18 V disappeared and a new cathodic peak appeared at -0.53 V, which separated the cathodic peak of hemin by 0.13 V. The cathodic overpotential of $QCOC_6H_5$ is decreased by ca. 650 mV. The reduction of $QCOC_6H_5$ is achieved with the aid of hemin. Firstly, hemin coordinated with $QCOC_6H_5$ to produce a complex compound and the compound adsorbed onto the electrode surface. Then, this compound was reduced and decomposed fast to hemin and the reduction product(s) of $QCOC_6H_5$. Because hemin can be regenerated via the decomposition reaction, a great cathodic peak current arose at ca. -0.53 V, even though at a very low concentration of hemin, meanwhile the original cathodic peak of $QCOC_6H_5$ disappeared.

Compounds **2** and **3** produced from the catalytic reaction are the isomerization products of $QCOC_6H_5$. It shows that the decomposition of $QCOC_6H_5$ also includes a rearrangement process besides the electrochemical reduction process. From these results and the structures of isomerization products of $QCOC_6H_5$, we are able to propose the whole processes of the decomposition mechanism of $QCOC_6H_5$ via hemin electrocatalysis at the GC electrode as shown as in Scheme 1.

In this scheme, the decomposition of the intermediate hemin(II)·$QCOC_6H_5$* is supposed to be achived by further reduction into the final form $QCOC_6H_5$ (red) and by inner electron exchange into isomerization products. The formation mechanism of the isomerization products **2** and **3** can be expressed as follows: Fenton-type cleavage of the peroxide bridge in intermediate hemin(II)·$QCOC_6H_5$* firstly produces **4** and **6**; the radical intermediate **4** may undergo β-scission into the primary carbon-centered radical **5** which then forms product **2**. Intermolecular hydrogen abstraction from C-4 in another radical **6** gives **7,** **8** and ultimately **3** if, in the proton solution (H_2O–CH_3CN), **8** via subsequent protonation

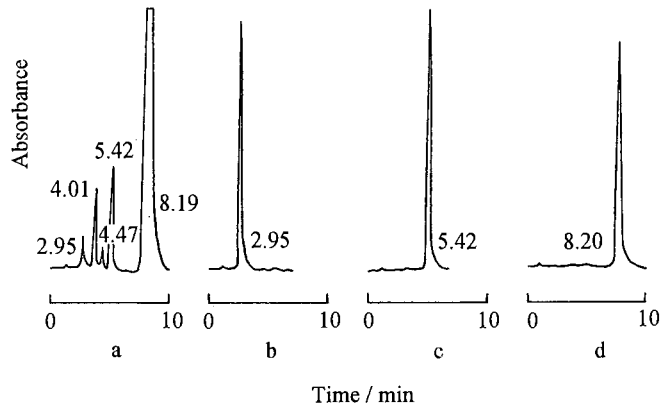

Fig. 6. HPLC chromatograms in THF containing 0.10 M $LiClO_4$ for: (a) 2.10×10^{-3} M $QCOC_6H_5$ in the presence of 7.50×10^{-4} M hemin after about 60 min electrolysis, (b) compound **3**, (c) compound **2** and (d) $QCOC_6H_5$. Electrolysis potential: -0.70 V vs. Ag/AgCl.

leads to other products. Collateral evidence for the suggested mechanism is that Fe^{2+} or hemin–$PhCH_3SH$ or hemin–*N*-acetyl cysteine can act with artemisinin to generate similar compounds **2** and **3** via a single electron exchange pathway in the chemical reaction[15,16].

The antimalarial action of artemisinin may be mediated by the hemin-catalyzed reduction of

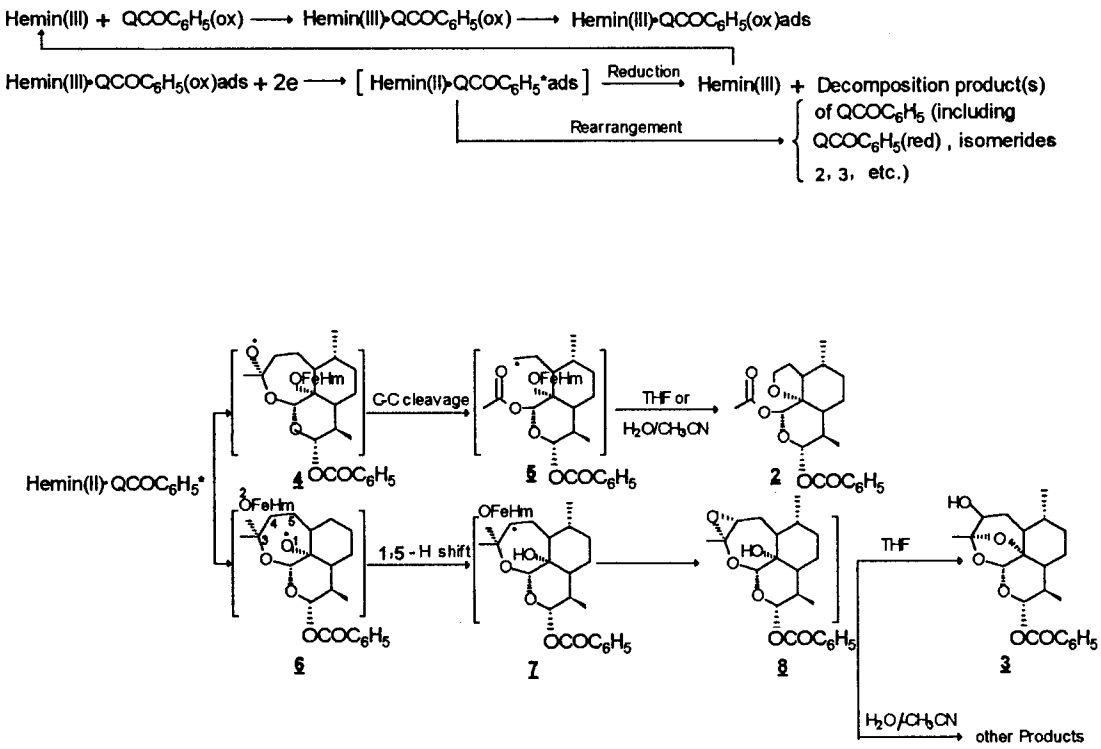

Scheme 1.

artemisinin into cytotoxic radical intermediates [17,18]. Here we found that the decomposition of an artemisinin derivative by hemin-catalysis on the GC electrode included not only electrochemical reduction but also rearrangement. Since these products, having lost a peroxide group, appear in the rearrangement process, the intermediates which poison the malaria parasite by alkylating its specific proteins were also probably produced via a rearrangement reaction. Thus, the rearrangement reaction may be an important step in the antimalarial process.

In summary, from the above studies, we found that $QCOC_6H_5$, a potent antimalarial derivative of artemisinin, can be reduced by hemin-catalysis. In the reduction process the appearance of a new cathodic peak and the disappearance of the original cathodic peak was observed, which is similar to the hemin-catalyzed reduction of its parent artemisinin [8]. Such a similarity further supports current views that the antimalarial action of artemisinin may initiate the interaction with the intraparasitic hemin, also showing that $QCOC_6H_5$ and artemisinin probably share a common mode of action. Two products from the electrocatalytic reaction, and the homologues of metabolism of artemisinin as well, were found and identified. The structures of these products imply that the hemin-catalyzed decomposition of artemisinin-type compounds on the GC electrode comprises two pathways: electrochemical reduction and rearrangement. These results are helpful in understanding the antimalarial mechanism of artemisinin-type compounds at the molecular level.

Acknowledgements

This work was supported by the National Natural Science Foundation of China (29775010) and the Research Laboratory of Electroanalytic Chemistry, Changchun Institute of Applied Chemistry.

References

[1] World Health Organization, The World Health Report 1996—Fighting Disease, Fostering Development, WHO, Geneva, Switzerland, 1996.
[2] Qinghaosu Antimalaria Coordinating Research Group, Chin. Med. J. 92 (1979) 811.
[3] Qinghaosu Cooperative Research Group on Qinghaosu and its Derivatives as antimalarials, J. Trad. Chin. Med. 2 (1982) 3.
[4] Qinghaosu Cooperative Research Group on Qinghaosu and its Derivatives as antimalarials, J. Trad. Chin. Med. 2 (1982) 17.
[5] S.R. Meshnick, C.W. Jefford, G.H. Posner, M.A. Avery, W. Peters, Parasitol. Today 12 (1996) 79.
[6] J.N. Cumming, P. Ploypradith, G.H. Posner, Adv. Pharmacol. 37 (1997) 253.
[7] S.R. Meshnick, T.E. Taylor, S. Kamchonwongpaisan, Microbiol. Rev. 60 (1996) 301.
[8] F. Zhang, D.K. Grosser Jr., S.R. Meshnick, Biochem. Phamacol. 43 (1992) 1805.
[9] G. Edward, Trans. R. Soc. Trop. Hyg. 88 (Suppl.) (1994) 37.
[10] Y. Li, P.L. Yu, Y.X. Chen, et al., Acta Pharm. Sin. 16 (1981) 434.
[11] W.M. Wu, Z.J. Yao, Y.L. Wu, K. Jiang, Y.F. Wang, H.B. Chen, F. Shan, Y. Li, J. Chem. Soc. Chem. Commun. 18 (1996) 2213.
[12] A.J. Lin, D.L. Klayman, J.M. Hoch, J.V. Silverton, C.F. George, J. Org. Chem. 50 (1985) 4504.
[13] V. Leskovac, A.D. Theoharides, Comp. Biochem. Physiol. 99C (1991) 391.
[14] I.S. Lee, H.N. Elsohly, E.M. Croom, C.D. Hufford, J. Nat. Prod. 52 (1989) 337.
[15] G.H. Posner, J.N. Cumming, P. Ploypradith, H.O. Chang, J. Am. Chem. Soc. 117 (1995) 5885.
[16] R.K. Haynes, S.C. Vonwiller, Tetrahedron Lett. 37 (1996) 253.
[17] S.R. Meshnick, Y.Z. Yong, V. Lima, F. Kuyers, S. Kamchonwongpaisan, Y. Yuthavong, Antimicrob. Agents Chemother. 37 (1993) 1108.
[18] W. Asawamahasakda, I. Ittarat, Y.M. Pu, H. Ziffer, S.R. Meshnick, Antimicrob. Agents Chemother. 38 (1994) 1854.

ELSEVIER

Talanta 48 (1999) 151–162

Talanta

Solubility and thermal stability of some amino–mellitate compounds

Roberta Curini [a], Alessandro De Robertis [b,*], Claudia Foti [b], Stefano Materazzi [a], Maria Antonietta Orrù [a]

[a] *Dipartimento di Chimica, Università "La Sapienza", Piazzale A. Moro, I-00100 Rome, Italy*
[b] *Dipartimento di Chimica Inorganica, Chimica Analitica e Chimica Fisica dell'Università, Salita Sperone 31, I-98166 Messina (Vill. S. Agata), Italy*

Received 23 February 1997; received in revised form 9 June 1998; accepted 17 June 1998

Abstract

By reaction between the anion of mellitic acid (benzenehexacarboxylic acid) and some protonated linear polyamines (diethylenetriamine, triethylenetetramine, tetraethylene–pentamine, pentaethylenehexamine, spermidine, and spermine), fairly insoluble complexes have been obtained, with the general formula $(amine)_x(mellitate)H_6$ (diethylenetriamine and spermidine, $x=1$; triethylenetetramine and spermine, $x=0.75$; tetraethylenepentamine, $x=0.6$ and 0.8; pentaethylenehexamine, $x=0.5$). K_{s0} values for these complexes have been determined at $I=0$ mol dm^{-3} and $T=25°C$ ($\log K_{s0}$ ranges between -48.2 and -56.6). The solubility has been studied as a function of pH and of ionic strength. The thermal analysis, performed using air or argon flow, showed that all the solids behave in a similar way. In the range 20–120°C the loss of hydration water occurs, and in the range 150–350°C the first step of non oxidative decomposition takes place, with complete decomposition at 650°C in air flow, whilst in argon flow the decomposition is still incomplete at 900°C. Preliminary results of a parallel diffractometric study are also reported.

Keywords: Amino–mellitate complexes; Solubility; Thermal analysis; Anion coordination chemistry

1. Introduction

Anion coordination chemistry, which studies the interactions of the anions with cationic organic ligands constitutes the minority of all the thermodynamic data on the formation of complex species reported in classical compilations [1–5]. Papers on the interactions between inorganic and organic anions with macrocyclic amines [6–12] and with open chain amines [13–16] have been published.

Anion coordination chemistry and its applications are also the subject of some quite interesting reviews [17–20]. Recently, literature data concerning the formation of ligand–ligand complexes between linear polyamines and anions of organic and inorganic acids have been reviewed [21], iden-

* Corresponding author. Tel.: +39 90 391354; fax: +39 90 392827; e-mail: derobertis@chem.unime.it

0039-9140/99/$ - see front matter
PII S0039-9140(98)00232-X

tifying regularities between the complex formation constant values and the charges involved in the formation reactions, for the different classes of ligands. The stability of these kind of complexes varies, in terms of formation constants, from approximately 1 to 10^{10} mol^{-1} dm^3, as a function of the charges of the reactants involved in the formation reaction [21]. When the anion is benzenehexacarboxylic acid (hexacharged anion), only the formation constants with protonated diethanolamine and ethylenediamine were determined [14], since, for polyamines with higher charges, precipitation occurs, even in dilute solutions.

No thermal stability data has been reported until now for insoluble anion coordination compounds. A study of the characteristics of these solid compounds (stoichiometry, solubility, and thermal stability) is reported in this paper. The solid complexes obtained in the reaction of benzenehexacarboxylic acid (mellitic acid, H_6mlt) with diethylenetriamine (dien), triethylenetetramine (trien), tetraethylenepentamine (tetren), pentaethylenehexamine (penten), spermidine (spd), and spermine (sper), were considered. Solubility data were determined at 25°C.

2. Experimental

2.1. Materials and instrumentation

The solution of H_6mlt was prepared from purum product (Fluka) as purchased, since its purity, checked alkalimetrically, was always $\geq 99.2\%$. The solutions of polyamines were prepared from the analytical grade product (Fluka), after purification by transformation into the corresponding hydrochlorides [22]. Analytical grade Fluka reagent was used for the preparation of tetramethylammonium hydroxide (Me_4NOH) solution, then standardized against potassium biphthalate (Fluka puriss). The $AgNO_3$ solution was prepared from C. Erba RP reagent and potentiometrically titrated with standard NaCl, prepared by weighing of C. Erba RP reagent, previously dried in a oven at 110°C. NaOH and $HClO_4$ standard solutions were prepared by diluting concentrates from C. Erba ampoules. The $NaClO_4$ (C. Erba RP) standard solution was prepared by weighing after vacuum-drying. All solutions were prepared with double distilled water, and grade A glassware was used.

A Beckman DU50 single beam spectrophotometer was used for the measurements of the mlt concentration and a Metrohm model 654, coupled with a silver and double junction Ag/AgCl electrode, was used for chloride potentiometric titrations. Amine concentration measurements were carried out with a Dionex HPLC model DX500, equipped with a Dionex Ionpac CG10 guard column. Detection was performed by integrated pulsed amperometry with a gold working electrode and a combined pH-Ag/AgCl reference electrode (Dionex model ED40). For the post column reaction a Dionex reagent delivery module was used. Thermoanalytical data were obtained by a Perkin-Elmer TGA7: the scan rate was 10°C min^{-1}, the operational atmosphere was air or argon (HPLC reagent grade) at a flow rate of 100 ml min^{-1}. The thermobalance was coupled with a 1760X Perkin-Elmer FTIR spectrometer, to obtain the IR spectra of the TG evolved gas: the decomposition vapours or gases were flushed, by means of a heater transfer line, to the IR gas cell.

2.2. Preparation of the precipitates

The precipitates were prepared by mixing known volumes of standard H_6mlt and polyamine hydrochlorides, in the quantities reported below, in suitable vials and in a total volume of 50 ml. Lower and higher analytical concentrations of H_6mlt ranged between 4 and 15 mmol dm^{-3}, and those of polyamines between 4 and 20 mmol dm^{-3}, selected to have the ratio mmol polyamine:mmol H_6mlt ranging between 0.3 and 3.0, and the molar fraction of H_6mlt (mf) ranging between 0.23 and 0.75. For every amine–mellitate system 8–12 tests were carried out. The vials were shaken at $T = 25 \pm 1$°C for 24 h; preliminary tests established that longer stirring times were unnecessary. The saturated solutions were separate by filtration and the solids, collected in gooch crucibles, were washed with water and acetone, and vacuum-dried. Further experimental details are reported in a previous paper [23].

A wide range of reagent concentrations were chosen in order to verify the possibility of obtaining different precipitation stoichiometries as a function of the relative concentrations of mlt and polyamines.

2.3. Analysis of the solutions and of the precipitates

The mellitate concentration was determined by spectrophotometric UV measurement ($\lambda = 293$ nm, $\varepsilon = 687 \pm 1$), after suitable dilution and alkalinization (pH 13, Me_4NOH), in order to ensure that mlt was neither protonated nor complexed with polyamine. Preliminary tests established a linear calibration graph for mlt concentrations up to 3 mmol dm^{-3}, and that polyamines and Me_4NOH do not interfere with the measurements.

Polyamine concentrations were determined by HPLC (De Robertis and De Stefano, work in progress) after separation from mlt, by elution of the initial alkalinized solution (0.1 mol dm^{-3} Me_4NOH) through a strong anionic exchange resin in OH^- form. The neutral amine was collected and then analysed by HPLC (amperometric detector) using a mixture of 2.0 mol dm^{-3} $NaClO_4$ (60–85%), 0.1 mol dm^{-3} $HClO_4$ (5–10%) and acetonitrile (5%) as the mobile phase. Measurement reproducibility was established for polyamine concentrations up to 0.5 mmol dm^{-3}, according to the polyamine analyzed; at least three analyses were carried out for each sample. Preliminary separation was necessary since significant and variable quantities of amine form protonated complex species with mlt at the acidic elution pH of HPLC. Chloride concentrations in the solutions after precipitation were also determined: in each test, within experimental error, we found no variation in concentration and therefore we have concluded that the precipitates were all chloride-free. Proton concentration after precipitation was calculated as six times the analytical concentrations of mlt after precipitation, plus n times (n = maximum degree of protonation in the polyamines) the initial analytical concentrations of polyamine. To confirm the precipitation ratios, and to calculate the number of molecules of water of crystallisation that were present in the solid, elemental analysis of the precipitates was carried out.

2.4. Calculations

All the calculations were performed by appropriate computer programs (ES4ECI [24] for calculating free concentrations and distribution diagrams; TDA for the extrapolation to zero ionic strength of K_{s0} [25]). The dependence on ionic strength of the solubility products was taken into account by using the semiempirical Debye–Hückel type equation (Eq. (1)), widely used both for complexes in solution [26–30] and for solubility products [23]:

$$pK_{s0} = p^{T}K_{s0} - z^{*}I^{1/2}/(2 + 3I^{1/2}) + CI + DI^{3/2} \quad (1)$$

where pK_{s0} is the solubility product at I ionic strength, $p^{T}K_{s0}$ is the solubility product at infinite dilution, and

$$C = p^{*}c_0 + z^{*}c_1; \quad D = z^{*}d_1;$$

in which

$$z^{*} = \sum (\text{charges})^2_{\text{reactants}} - \sum (\text{charges})^2_{\text{products}}$$

$$p^{*} = \sum (\text{mol})_{\text{reactants}} - \sum (\text{mol})_{\text{products}}$$

The values used for the empirical parameters are [27]: $c_0 = -d_1 = 0.1$ and $c_1 = 0.23$; therefore Eq. (1) becomes:

$$pK_{s0} = p^{T}K_{s0} - z^{*}[I^{1/2}/(2 + 3I^{1/2}) - 0.23I + 0.1I^{3/2}] + 0.1p^{*}I \quad (1a)$$

In this study we used Eq. (1a), since the ionic strength values in our experiments are included in a limited range of values, and this did not allow accurate estimation of C and D. Concentrations and equilibrium parameters are given in the molar scale.

3. Results

3.1. Protonation, simple and mixed ligand complexes

The protonation constants of polyamines and of mellitic acid (dien (Ref. [30]) log $K_1^H = 9.80$, log $K_2^H = 8.74$, log $K_3^H = 3.66$; spd (Ref. [31]): log $K_1^H = 10.85$, log $K_2^H = 9.67$, log $K_3^H = 7.98$; trien (Ref. [32]): log $K_1^H = 9.67$, log $K_2^H = 8.87$, log $K_3^H = 6.12$, log $K_4^H = 2.38$; sper (Ref. [31]): log $K_1^H = 10.70$, log $K_2^H = 9.70$, log $K_3^H = 8.32$, log $K_4^H = 7.22$; tetren (Ref. [32]): log $K_1^H = 9.83$, log $K_2^H = 9.01$, log $K_3^H = 7.73$, log $K_4^H = 3.90$, log $K_5^H = 1.88$; penten (Ref. [33]): log $K_1^H = 9.89$, log $K_2^H = 9.06$, log $K_3^H = 8.08$, log $K_4^H = 5.82$, log $K_5^H = 3.08$, log $K_6^H = 1.60$; mlt (Ref. [34]): log $K_1^H = 7.85$, log $K_2^H = 6.45$, log $K_3^H = 5.09$, log $K_4^H = 3.47$, log $K_5^H = 2.14$, log $K_6^H = 0.92$) have already been studied. Amines (A) also form weak species with the chloride ion, whose stability is linearly dependent on the charge of the polyammonium cation [33], according to the equation:

$$\log K_{ij} = 1.37(i-1) - 0.78(i-1)j^{-1} \quad (2)$$

reaction $AH_i^{i+} + jCl^- = AH_iCl_j^{(i-j)+}$

The formation constants of mixed proton–mellitate–amine complexes (not experimentally determinable owing to precipitation) were calculated (according to Ref. [21] using the equation:

$$\log K_{ij} = -2.3 + 1.42z_{cat} + 1.095z_{an} - 0.45\Delta z \quad (3)$$

reaction $AH_i^{i+} + H_jmlt^{(z-j)-}$

$= A(mlt)H_{(i+j)}^{(z-i-j)-}$

(z_{cat} and z_{an} is the charge of the cation and anion, respectively; $\Delta z = |z_{cat} + z_{an}|$), and are reported in Table 1. In the pH range considered for the formation of insoluble complexes, soluble mixed species with $i < 6$ can be neglected.

3.2. Precipitates

3.2.1. System dien–mlt–H

Table 2 shows, for each trial, the initial concentrations of the reactants and those determined after precipitation, as the mmol of mlt and dien in the precipitates. As we can see, the ratio R ($R =$ mmol dien:mmol mlt in the precipitate) is always approximately equal to one (1.01 ± 0.02). We can, therefore, conclude that the formula of the precipitates is (dien)(mlt)H_6. Elemental analysis (Table 3) confirms this formula and allows us to conclude that the solid is tetrahydrate, i.e. (dien)(mlt)$H_6.4H_2O$. By considering the ratio C:N in the empirical formula $C_{16}O_{12}H_{19}N_3$ we can also affirm that the precipitation occurs between the triprotonated form of the amine and of the mellitate. Let us indicate the solubility product of the generic compound $A_i(mlt)H_6$ as

$$K_{s0} = [A]^i[mlt][H]^6 \quad (4)$$

or

$$pK_{s0} = ipA + p(mlt) + 6pH \quad (4a)$$

($pX = -\log[X]$). In order to calculate the solubility products of (dien)(mlt)H_6, the free concentration of the species must be computed. Starting from the analytical concentrations of all the species (mlt, dien, Cl^-, H^+) after precipitation and from the formation constants of all the complexes present in the solution, we were able to calculate for any trial, by means of the ES4ECI computer program [24], the free concentrations of the species, and therefore the pK_{s0} at the ionic strength and pH values of the solutions. Table 2 shows the values of pK_{s0} and p^TK_{s0} obtained for all the trials, together with their mean values $\pm 3 \times$ S.D. Fig. 1 shows the curve calculated by means of Eq. (1), (——), and the experimental values (○) of the

Table 1
Overall formation constants of mixed complexes $A(mlt)H_i$, expressed as $\log \beta_{11i}^a$

i	A = dies	Spd	trien	sper	tetren	penten
6	46.8	52.9	49.1	—	—	—
7	48.8	54.7	52.6	61.5	58.4	—
8	49.3	55.2	54.5	63.4	58.9	61.5
9	—	—	55.1	64.0	60.8	65.0
10	—	—	—	—	61.4	67.0
11	—	—	—	—	—	67.5

Calculated according Ref. [21], at $I = 0$ mol dm^{-3} and $T = 25$°C.

[a] β_{11i} referring to reaction $A^0 + mlt^{6-} + iH^+ = A(mlt)H_i^{(i-6)+}$.

Table 2
Analytical details and results in the system dien–mlt–H

No.	Reactants[a]		r[b]	mf[c]	After precipitation[a]		
	H_6mlt	dien			mlt	dien	H^+
1	4.99	6.02	1.21	0.45	0.72	1.82	22.43
2	5.99	5.02	0.84	0.54	1.52	0.41	24.18
3	9.98	11.97	1.20	0.45	1.75	3.62	46.45
4	6.96	19.95	2.86	0.26	0.63	13.55	63.67
5	12.01	3.99	0.33	0.75	8.51	0.37	63.05
6	6.00	14.04	2.34	0.30	0.72	8.79	46.44
7	9.98	11.97	1.20	0.45	1.65	3.52	45.83
	Precipitate (mmol)			Solubility details			
	mlt	dien	R[d]	I[e]	pH	pK_{s0}	p^TK_{s0}
1	0.213	0.210	0.99	0.022	1.85	48.29	50.62
2	0.223	0.231	1.03	0.018	1.79	48.06	50.23
3	0.411	0.417	1.01	0.043	1.56	47.65	50.64
4	0.316	0.319	1.01	0.084	1.69	47.17	50.64
5	0.175	0.181	1.03	0.031	1.66	48.28	50.91
6	0.264	0.262	0.99	0.059	1.76	47.35	50.54
7	0.416	0.422	1.01	0.043	1.55	47.68	50.69

$p^TK_{s0} = 50.6 \pm 0.1$[f]

[a] Concentration, in mmol dm^{-3}; [b] ratio dien:H_6mlt; [c] ratio H_6mlt:(H_6mlt + dien); [d] ratio dien:mlt; [e] ionic strength, in mol dm^{-3}; [f] ± 3 times S.D.

dependence of solubility products on ionic strength; as we can see, the values are very similar.

3.2.2. System spd–mlt–H

For this system we also obtained as the precipitation ratio $R = 1.00 \pm 0.01$, namely (spd)(mlt)H_6. Elemental analysis values are shown in Table 3. These allowed us to calculate that the solid is three-hydrate. The thermodynamic solubility product, calculated as above reported, is $p^TK_{s0} = 56.6 \pm 0.1$.

3.2.3. System trien–mlt–H

We found, for this system, a precipitation ratio $R = 0.75 \pm 0.02$, corresponding to the compound having the empirical formula $(trien)_3(mlt)_4H_{24}$. We have preferred, in writing the empirical formula, to use the divided index (i.e. $(trien)_{0.75}(mlt)H_6$), in order to underline the fraction of tetraprotonated polyamine bound for each $H_3(mlt)^{3-}$. The elemental analysis confirms this stoichiometry (Table 3) and, in addition, shows that $(trien)_{0.75}(mlt)H_6$ cystrallizes with 1.5 water molecules. The solubility product $p^TK_{s0} = 48.4 \pm 0.1$.

3.2.4. System sper–mlt–H

We followed the same procedure as for the previous trials and always obtained a ratio for the precipitates of $R = 0.75 \pm 0.04$. This value indicates the formation of the species $(sper)_{0.75}(mlt)H_6$. A typical result of the elemental analysis is shown in Table 3. This result allowed us to confirm the stoichiometry of precipitation and is in agreement with the presence in the elementary cell of 5 molecules of water of crystallisation. As for the solubility product, we calculated $p^TK_{s0} = 54.9 \pm 0.1$.

3.2.5. System tetren–mlt–H

The results of analysis indicate the formation of two different kinds of precipitates, whose composition is a function of mf, as shown in Fig. 2.

Table 3
Empirical formula and elemental analysis of precipitates[a]

Species	C%	H%	N%	O%
(dien)(mlt)H_6.4H_2O	37.11 (37.14)	5.29 (5.26)	8.14 (8.19)	49.46 (49.48)
(spd)(mlt)H_6.3H_2O	42.08 (42.15)	5.77 (5.77)	7.72 (7.76)	44.43 (44.32)
$(trien)_{0.75}$(mlt)H_6.1.5H_2O	41.31 (41.38)	4.99 (4.74)	8.51 (8.77)	45.19 (45.11)
$(sper)_{0.75}$(mlt)H_6.5H_2O	40.03 (40.10)	6.26 (6.13)	7.28 (7.20)	46.42 (46.57)
$(tetren)_{0.6}$(mlt)H_6.2.4H_2O	40.46 (40.44)	4.74 (4.97)	8.39 (8.42)	46.04 (46.17)
$(tetren)_{0.8}$(mlt)H_6.4H_2O	38.72 (39.07)	5.62 (5.77)	9.91 (9.90)	45.43 (45.26)
$(penten)_{0.5}$(mlt)H_6.2H_2O	41.24 (41.27)	4.68 (4.85)	8.57 (8.50)	45.51 (45.31)

[a] Theoretical values in parenthesis.

Precipitate type 1, formed at mf > 0.6 (5 trials), has $R = 0.60 \pm 0.01$, and corresponds to the compound $(tetren)_{0.6}$(mlt)H_6, and type 2, formed at mf < 0.4 (6 trials), have $R = 0.80 \pm 0.01$, and corresponds to the compound $(tetren)_{0.8}$(mlt)H_6. The composition of two different precipitates is consistent with the molar fraction of H_6mlt of the starting solutions, i.e. smaller molar fraction of mlt corresponds to a compound having a lower mlt content, and vice versa. For the two kinds of precipitates, the elemental analysis results are shown in Table 3. In this case too, we were able to calculate the number of water of crystallisation molecules, which are 2.4 for type 1 precipitates and 4 for type 2. We also calculated the $p^T K_{s0}$ of the two solids: these are 48.8 ± 0.3 and 55.3 ± 0.4 for precipitates type 1 and 2, respectively.

3.2.6. System penten–mlt–H

The results obtained indicated the formation of only one type of precipitate having $R = 0.49 \pm 0.01$ and corresponding to the species $(penten)_{0.5}$(mlt)H_6. The composition was confirmed by elemental analysis (Table 3). The solid analysed crystallises with 2 molecules of water. Other samples crystallise with 3 and 3.5 molecules of water per molecule of $(penten)_{0.5}$(mlt)H_6. We think this to be due to the fact that the water is bound very weakly, as confirmed by thermogravimetric analysis (see Section 3.4), in which loss of weight was noticeable after first heating. The thermodynamic solubility product $p^T K_{s0} = 48.2 \pm 0.3$.

3.3. Dependence of solubility on pH and ionic strength

The solubility of proton–amine–mellitate mixed complexes strongly depend on the proton and NaCl concentrations. The effect of pH (Fig. 3) is simply due to the formation of soluble species for pH < 2 (full protonated mellitate and small percentages of $A(mlt)H_i$ species with $i > 6$) and for pH > 3.5 (deprotonation of mellitate and amine). The effect of NaCl concentration (Fig. 4) is due to the formation of both Na^+–mellitate and Cl^-–protonated amine complexes.

3.4. Thermal analysis

When oxygen or air is the operational atmosphere, the thermogravimetric curve (TG) and its

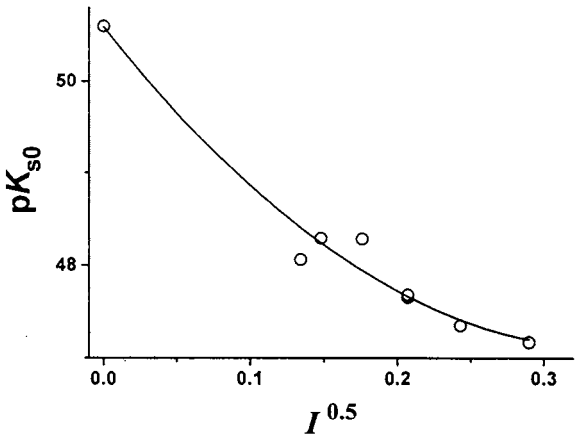

Fig. 1. Dependence of pK_{s0} values of (dien)(mlt)H_6 on ionic strength. Full line: Eq. (1); (o) experimental values.

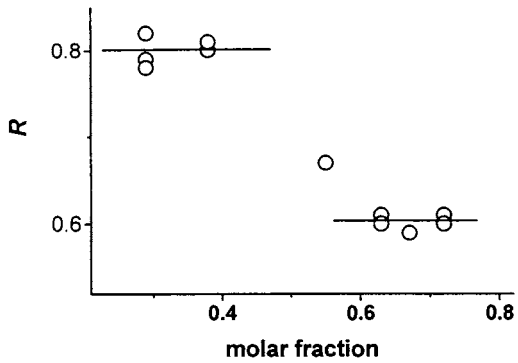

Fig. 2. R values (R = mmol tetren:mmol mlt), as a function of molar fraction of mlt, in the system tetren–mlt–H.

first derivative (DTG) show, for (dien)(mlt)H_6, five main processes (Fig. 5A). For the sake of simplicity, we refer to 2 molecules of (dien)(mlt)H_6. The first TG step, in the range 20–120°C, is the loss of 8 hydration water molecules (weight loss: theor. 13.93%, exper. 13.73%), followed, in the range 150–350°C, by a subsequent release of water (9 molecules; weight loss: theor. 15.66%, exper. 16.34) and of carbon dioxide (3 molecules; weight loss: theor. 12.77%, exper. 12.56). The FTIR spectra of the TG evolved gas (Fig. 6) prove that water, and then water and carbon dioxide are released. By comparing the TG curves (Fig. 5) when the flow is oxygen (A) or argon (B), it can be clearly seen that in the range 20–350°C there are no differences between the curves; this confirms that release of carbon dioxide is not due to an oxidation process. The subsequent processes (over 350°C) show different profiles with oxygen or argon flow. With oxygen flow, between 330 and 510°C, a process having a derivative maximum of 450°C can be noted, corresponding to the loss of 2 anhydridic fragments (–CO–O–CO–) and all the fragments containing N (weight loss: theor.: 33.28%, exper.: 33.27%). The final oxidation process (weight loss: theor. 24.36%, exper. 24.10%) ends at 630°C. When the flow is Ar, the two processes with derivative maxima at 450 and 580°C recorded with oxygen (or air) flow become a single broad process, with derivative maximum at 500°C, but at 900°C thermal decomposition is not yet complete.

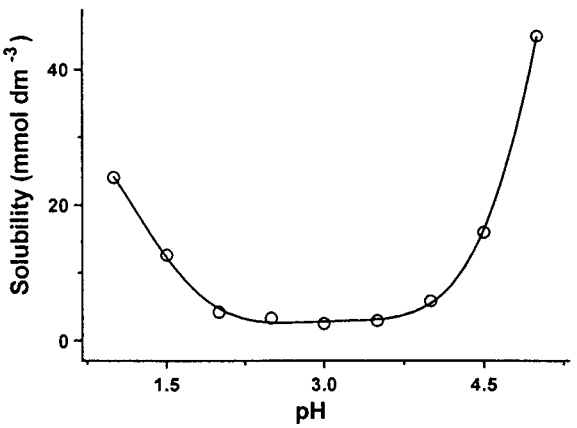

Fig. 3. Solubility (mmol dm^{-3}) of (dien)(mlt)H_6 in 0.6 mol dm^{-3} NaCl, plus a strong acid or base, as a function of pH.

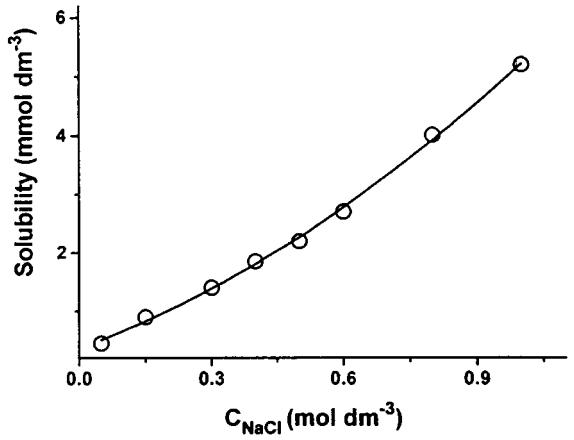

Fig. 4. Solubility (mmol dm^{-3}) of (dien)(mlt)H_6 at pH 3, as a function of analytical concentration of NaCl (C_{NaCl}).

Very similar behaviour is shown by (spd)(mlt)H_6 with respect to (dien)(mlt)H_6. In the temperature range 20–130°C (oxygen flow) we observe the first TG process, related to the loss (we consider 2 molecules of (spd)(mlt)H_6) of 6 hydration water molecules. Subsequently the thermogravimetric curve indicates two superimposed processes due to the loss of 9 water molecules and then 3 carbon dioxide molecules; this process finishes at 310°C. The TG-FTIR spectra of the evolved gas confirm the water–water–carbon dioxide release in the temperature range 20–310°C. In the last 310–650°C range, can be noted

two processes, exactly as described for the (dien)(mlt)H_6 compound. The differences between the theoretical and experimental values for weight loss are always $< 1\%$. The argon operational atmosphere confirms the presence of only one broad process above 350°C with respect to the two well defined processes previously described when the flow was oxygen. The TG processes, when the operational flow is air or oxygen, are similar.

On heating $(trien)_{0.75}(mlt)H_6$, a thermal profile with three main processes is observed in the range 20–350°C. The first process (we refer to the molecule with integer indexes, i.e. $(trien)_3(mlt)_4H_{24}$), complete at 120°C, is the release of 6 hydration water molecules. Two further processes, the first corresponding to the loss of 12 water and then 2 carbon dioxide molecules, the second corresponding to the loss of 6 water and 4 carbon dioxide molecules, can be seen from the DTG curve, although they partially overlap. The reaction mechanism and the radicals involved are exactly the same as those reported for (dien)(mlt)H_6. These processes are exhausted at 310°C. The same TG profiles with oxygen, air or argon flow in this temperature range, prove that the processes are not oxidation. These processes

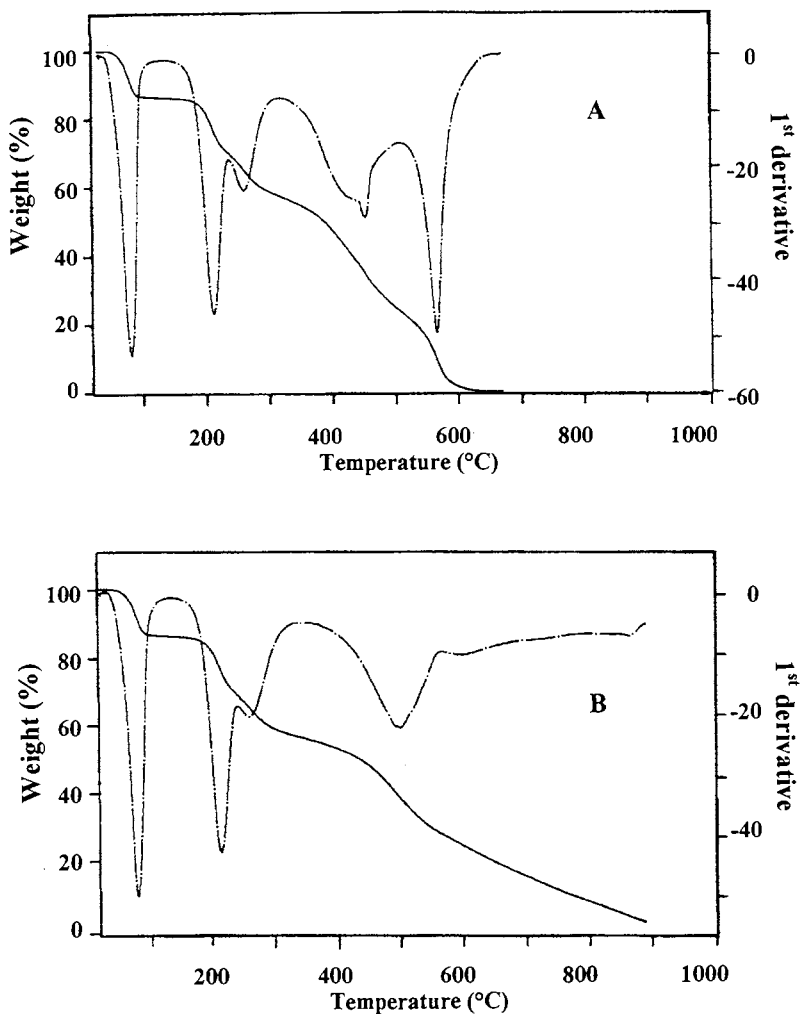

Fig. 5. Thermogravimetric curve (TG, full line) and 1st derivative (DTG, dotted line) of (dien)(mlt)H_6. A, oxygen flow; B, argon flow. Scanning rate: 10°C min^{-1}; gas flow: 100 ml min^{-1}.

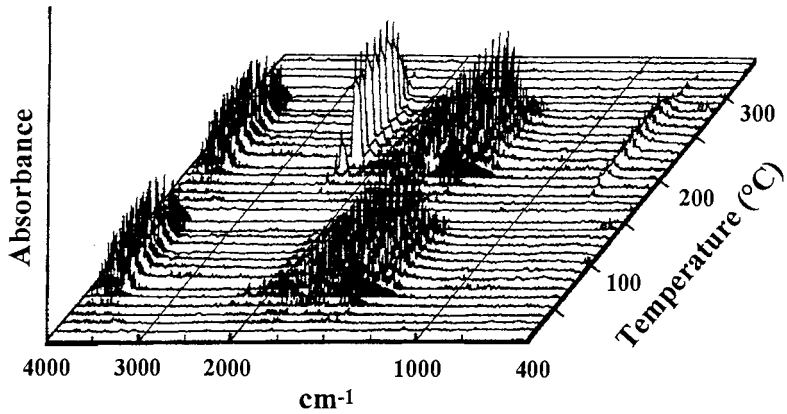

Fig. 6. Stacked plot of the IR spectra of the evolved gas, for the first releasing process (air flow) of (dien)(mlt)H_6.4H_2O.

give the same TG-FTIR spectra obtained for (dien)(mlt)H_6. The differences between the theoretical and experimental values in weight loss are always $< 1\%$. Over 350°C (oxygen flow) two more overlapping processes can be noted, the first being the release of 4 anhydridic and 3 N-containing fragments, and the second being total degradation, which is complete at 620°C.

The thermal behaviour of $(sper)_{0.75}(mlt)H_6$ (we refer to the formula $(sper)_3(mlt)_4H_{24}$, with integer indexes), using air or oxygen flow, initially shows a well defined weight loss corresponding to the loss of 20 molecules of hydration water which is complete at about 150°C. Subsequently, we observe a further two partially overlapping processes involving the loss of 18 molecules of water and 6 of carbon dioxide. The process is complete at about 300°C and it occurs without oxidation (there is an analogous result if the flow is Ar). Above this temperature two superimposed processes (oxygen flow) are noticeable, the first due to the loss of anhydridic and N-containing fragments, the second to the complete oxidation of the carbonaceous residue. The whole process is complete at 650°C. The differences between the theoretical and experimental values in weight loss are always $< 1\%$. If the operational atmosphere is Ar, decomposition occurs at a higher temperature with a broad peak.

The two different precipitates obtained from the reaction between H_6L and tetren ((tetren)$_{0.6}$(mlt)H_6, (type 1); (tetren)$_{0.8}$(mlt)H_6, (type 2)) have different TG profiles. Precipitate type 1, i.e. $(tetren)_3(mlt)_5H_{30}$, loses (oxygen flow) 12 molecules of water of crystallisation in two superimposed phases starting from room temperature and ending at 135°C. It follows other partially superimposed processes. The loss of 22.5 molecules of H_2O and 7.5 of carbon dioxide takes place between 135 and 315°C and is followed by the usual demolition in an air or oxygen environment completed in two phases: the first between 315 and 510°C, the second between the latter temperature and 600°C. The same TG analysis performed in argon flow confirms non-oxidative decomposition between room temperature and 315°C. At 600°C there is still a residue of 34%. In the case of the type 2 precipitate, (tetren)$_{0.8}$(mlt)H_6, i.e. $(tetren)_4(mlt)_5H_{30}$ TG analysis, when oxygen or argon flows were used, two different kinds of decomposition were confirmed. As regards the temperatures and the products of decomposition (oxygen flow) between room temperature and 135°C the loss of 20 water molecules can be observed, and between the latter temperature and 310°C there is a further loss of 25 molecules of water and 7 of carbon dioxide. Oxidative decomposition follows in two separate, partially overlapping phases: the first occurs between 310 and 530°C, the second is complete at 620°C.

The TG curve of $(penten)_{0.5}(mlt)H_6$ is the sample, when the flow is oxygen or air, shows five main and not well defined processes, which can be explained in terms of their similarity to the com-

pounds already discussed, and with the help of DTG. If we consider (penten)(mlt)$_2$H$_{12}$, the first process, which starts at room temperature, involves the release of 4 hydration water molecules and is complete at about 130°C. Two processes in the range 130–300°C follow, the first due to the release of 3.5 water molecules, the second to the release of water (5.5 molecules) and carbon dioxide (3 molecules). These are followed by the loss, in the range 300–530°C, of anhydridic and N-containing fragments. Finally, total degradation of the compound is complete at 650°C. The differences between the theoretical and experimental values in weight loss are always $< 1.5\%$. A comparison with the TG profile when argon flow is used, shows that also in this case processes up to 300°C are not oxidative, while those at higher temperatures occur only with oxidation.

3.5. Diffractometric analysis

The diffractometric analysis (Bruno and De Robertis, work in progress) shows (Fig. 7) that only 3 oxygen (O2, O8 and O12) belonging to the carboxylic groups of the mellitic acid bear hydrogens. These hydrogens are involved in very strong hydrogen bonds that occur among symmetry related mellitic anions (the O···O distances range from 2.466(3) up to 2.476(3) Å while the O–H···O angles vary from 161.9 to 174.1°). The amine is for charge balance in its fully protonated form, with the terminal nitrogens (N1 and N3) bonded to 3 hydrogens (–(NH_3^+)) and with the central nitrogen (N2) bonded to 2 hydrogens (–(NH_2^+)–). Also, aminic hydrogens are involved in strong hydrogen bonds which occur among the protonated amine, water molecules, and deprotonated mellitic acid, thus making a very complicated frame ((N···O) hydrogen bond distances vary from 2.674(4) to 2.970(4) Å). Water molecules interact with each other (O···O range from 2.719(4) up to 2.975(5) Å), as above with the amine and with the mellitic acid (O···O varies from 2.760(4) to 2.956(4) Å). All hydrogens except those belonging to the water molecules (for which an ideal geometry has been used) have been located from Fourier difference maps and then positioned during subsequent least squares cycles in calculated position.

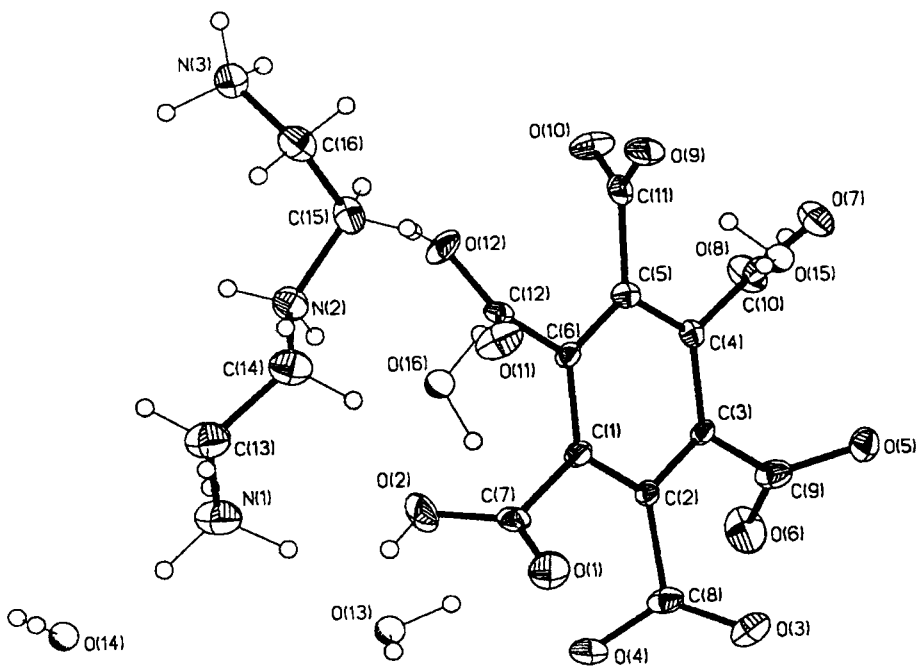

Fig. 7. Structure of the elementary unit of (dien)(mlt)H_6.4H_2O.

Table 4
Solubility products (± 3 S.D.) at $I = 0$ mol dm^{-3} and $T = 25$°C

Formula	$pK_{s0} \pm 3$ S.D	Formula	$pK_{s0} \pm 3$ S.D.
(Dien)(mlt)H_6	50.6 ± 0.1	(Spd)(mlt)H_6	56.6 ± 0.1
$(Trien)_{0.75}$(mlt)H_6	48.4 ± 0.1	$(Sper)_{0.75}$(mlt)H_6	54.9 ± 0.1
$(Tetren)_{0.6}$(mlt)H_6	48.8 ± 0.3	$(Tetren)_{0.8}$(mlt)H_6	55.3 ± 0.4
$(Penten)_{0.5}$(mlt)H_6	48.2 ± 0.3		

4. Discussion

The results concerning the solubility of the compounds are grouped in Table 4. For all the amines considered, the precipitation reactions took place between the three-deprotonated form of the mellitic acid (H_3mlt^{3-}) and the fully protonated amines. We have confirmed this assumption by X-ray diffractometry. If we consider that the pH of the solutions after precipitation varies between 1.4 and 2.0 (average value 1.7 ± 0.1) and that at pH 1.5 we have maximum $H(mlt)^{5-}$ formation whereas maximum H_3mlt^{3-} formation occurs at pH 4.2, we could conclude that the precipitation stoichiometry is independent of pH, but depends on the possibility of a suitable crystalline organisation. Only in the case in which the amine is tetren, does the formation of an other type of precipitate with different stoichiometry occur; this species is formed (Fig. 2) when trials are undertaken using a large excess of amine concentration with respect to the mellitic acid. Also in this case the acidity of the solutions has no influence on the type of precipitate. In fact, in the formation of precipitate with $R = 0.60$ the pH varies between 1.5 and 1.7, and in the case of $R = 0.80$ the variation in pH is between 1.6 and 1.8.

Precipitates in which the amines have the same type of structure, i.e. aminic groups intercalated with ethylenic ones (dien, trien, tetren, and penten), have practically the same solubility products. Precipitates in which the amines are spd and sper (these amines have longer aliphatic chains between the aminic groups) are slightly more insoluble than those in which the amines are dien and trien, respectively.

The number of molecules of water of crystallisation present in the various precipitates varies considerably, without any apparent correlation with their composition.

From the comparative analysis of the TG curves we were able to draw the following conclusions. The number of molecules of water of crystallisation, previously calculated by elemental analysis, was confirmed. Dehydration occurs for all the precipitates up to 150°C, but with a different course: in the case of (dien)(mlt)H_6 water loss is well defined, while for (penten)$(mlt)_2H_{12}$ the loss starts at room temperature and continues gradually up to completion; for the other compounds with intermediate aminic groups, the behaviour is proportional. Between 150 and 350°C, all the precipitates obtained from the reaction between AH_n^{n+} (n = maximum degree of protonation of amine) and H_3mlt^{3-}, denote the loss of 4.5 molecules of water and 1.5 molecules of carbon dioxide for each unit of A_i(mlt)H_6 (i.e. $AH_3^{3+} + H_3mlt^{3-}$). $(Tetren)_{0.8}$(mlt)H_6 (precipitate type 2) obtained between (tetren)H_5^{5+} and H_2mlt^{4-}, which loses 5 molecules of water and 1.4 of carbon dioxide, is the exception to this rule. Between 350 and 500°C, when the flow is oxygen (or air), we observe a total loss of N – containing residuals and a partial loss of anhydridic fragments. The course of the DTG curve, in this range of temperatures, is the same for all the homologous amines. The compounds obtained with spd and sper, and with tetren type 2 differ. Complete decomposition takes place between 500 and 650°C. When nitrogen or argon are used as the operational atmospheres, the TG spectra up to 350°C of all the precipitates are the same as those obtained for oxygen or air flow. Over this temperature, the profiles are different (at 650°C there is about 30% of residuals for all the samples) and total decomposition of the mixture occurs at about 900°C.

Acknowledgements

We thank CNR and MURST for financial support, Professor S. Sammartano for helpful discussions, and Professor G. Bruno for the preliminary results of the parallel crystallographic investigations.

References

[1] L.G. Sillèn, A.E. Martell, Stability Constants of Metal Ion Complexes, Spececial Publication 17, Chemical Society, London, 1964.

[2] L.G. Sillèn, A. E. Martell, Stability Constants of Metal Ion Complexes, Supplement Special Publication 25, Chemical Society, London, 1971.

[3] E. Högfeldt, Stability Constants of Metal Ion Complexes: Inorganic Ligands, Pergamon, Oxford, 1982.

[4] D.D Perrin, Stability Constants of Metal Ion Complexes. Organic Ligands, Pergamon, Oxford, 1979.

[5] R.M. Smith, A.E. Martell, Critical Stability Constants, vol.1 (1974), vol. 2 (1975), vol. 3 (1977), vol. 4 (1976), vol. 5 (1982), vol.6 (1989), Plenum, New York.

[6] A. Bianchi, M. Micheloni, P. Paoletti, Coord. Chem. Rev. 110 (1991) 17.

[7] R.M. Izatt, K. Pawlak, J.S. Bradshaw, R.L. Bruening, Chem. Rev. 95 (1995) 2529.

[8] B. Dietrich, M.W. Hosseni, J.M. Lehn, R.B. Sessions, J. Am. Chem. Soc. 103 (1981) 1282.

[9] A. Bianchi, M. Micheloni, P. Orioli, P. Paoletti, S. Mangani, Inorg. Chim. Acta 146 (1988) 153.

[10] F. Peter, M. Gross, M.W. Hosseini, J.M. Lehn, R.B. Sessions, J. Chem. Soc. Commun. 1067 (1981).

[11] E. Garcia-Espãna, M. Micheloni, P. Paoletti, A. Bianchi, Inorg. Chim. Acta 102 (1985) L9.

[12] A. Bencini, A. Bianchi, E. Garcia-Espãna, et al., Inorg. Chem. 26 (1987) 3902.

[13] P.G. Daniele, A. De Robertis, C. De Stefano, D. Gastaldi, S. Sammartano, Ann. Chim. (Rome) 83 (1993) 575.

[14] A. De Robertis, C. De Stefano, C. Foti, O. Giuffrè and S. Sammartano, J. Chem. Res. (S) 60 (1996).

[15] C. De Stefano, C. Foti, O. Giuffrè, P. Mineo, C. Rigano, S. Sammartano, Ann. Chim. (Rome) 86 (1996) 257.

[16] A. De Robertis, C. De Stefano, O. Giuffrè, S. Sammartano, J. Chem. Soc. Faraday Trans. 92 (1996) 4219.

[17] H.E. Katz, in: J.L. Atwood, J.E.D. Davies, D.D. MacNicol (Eds.), Inclusion Compounds, vol. 4, Oxford University Press, Oxford, 1991.

[18] C. Seel, A. Galán, J. de Mendoza, Top. Curr. Chem. 175 (1995) 101.

[19] B. Dietrich, Pure Appl. Chem. 65 (1993) 1457.

[20] A. Bianchi, K. Bowman-James, E. García-España (Eds.), Supramolecular Chemistry of Anion, Wiley, New York, 1997.

[21] P.G. Daniele, E. Prenesti, A. De Robertis, et al., Ann. Chim. (Rome) 87 (1997) 415 see also errata corrige, ibidem, 88 (1998) 447.

[22] D.D Perrin, W.L.F. Armorego, D.R. Perrin, Purification of Laboratory Chemicals, Pergamon, Oxford, 1966.

[23] A. De Robertis, A. Gianguzza, S. Sammartano, Talanta 42 (1995) 1651.

[24] C. De Stefano, P. Mineo, C. Rigano, S. Sammartano, Ann. Chim. (Rome) 83 (1993) 243.

[25] C. De Stefano, S. Sammartano, P. Mineo, C. Rigano, in: A. Gianguzza, E. Pellizzetti, S. Sammartano (Eds.), Marine Chemistry—An Environmental Analytical Chemistry Approach, Kluwer, Amsterdam, 1997.

[26] P.G. Daniele, A. De Robertis, C. De Stefano, S. Sammartano, C. Rigano, J. Chem. Soc. Dalton Trans. 2353 (1985).

[27] P.G. Daniele, A. De Robertis, C. De Stefano, S. Sammartano, in: S. Alegret, J.J. Arias, D. Barcelò, J. Casal, G. Rauret (Eds.), Miscellany of Scientific Papers offered to Enric Casassas, Bellaterra, Universitat Autonoma de Barcelona, 1991.

[28] A. Casale, P.G. Daniele, A. De Robertis, S. Sammartano, Ann. Chim. (Rome) 78 (1988) 249.

[29] A. Casale, P.G. Daniele, C. De Stefano, S. Sammartano, Talanta 36 (1989) 903.

[30] A. De Robertis, C. De Stefano, G. Patané, Termochim. Acta 209 (1992) 7.

[31] C. De Stefano, C. Foti, A. Gianguzza, O. Giuffrè, S. Sammartano, J. Chem Soc. Faraday Trans. 92 (1996) 1511.

[32] A. De Robertis, C. De Stefano, G. Patané, S. Sammartano, J. Solution Chem. 22 (1993) 927.

[33] A. Casale, C. Foti, S. Sammartano, G. Signorino, Ann. Chim. (Rome) 88 (1998) 55.

[34] A. De Robertis, C. De Stefano, C. Foti, Ann. Chim. (Rome) 86 (1996) 155.

ELSEVIER

Talanta 48 (1999) 163–171

Talanta

Extraction photometric determination of yperite by phthaleins

Emil Halámek, Zbyněk Kobliha *

Department of Chemistry, Military University, 682 03 Vyškov, Czech Republic

Received 10 December 1997; received in revised form 12 June 1998; accepted 17 June 1998

Abstract

Extraction spectrophotometric determination of sulfidic yperite, based on the reaction with four phthaleins, was developed. The method is technically simpler than the determination of yperites with reagent T-135 (alkaline-aqueous ethanolic thymolphthalein solution) because it does not require heating at 80°C, cooling and acidification of the reaction mixture. Selection of the appropriate phthalein, and particularly optimization of the reagent composition and extraction of the coloured reaction product in chloroform, markedly increased the selectivity of the determination of yperites (HD, HN-3). The reaction is performed in a medium of increased polarity due to the low content of alcohol which enables the reaction to proceed at temperatures of 5–20°C without any marked loss of sensitivity. Using ^{1}H and ^{13}C NMR spectroscopy, the reaction products of HD and *o*-cresolphthalein were identified and an ionic mechanism for the reaction of HD with phthaleins is suggested.

Keywords: Spectrophotometric determination; Yperite; Phthaleins

1. Introduction

Bis(2-chloroethyl) sulfide (1,1′-thiobis(2-chloroethane), sulfidic yperite, H, HD-GAS) represents one of the oldest war poisons. In the recent decades both the most common yperites (sulfur mustard and nitrogen mustard) have been somewhat rehabilitated as cytostatic and antipsoriatic drugs. Yperite is a cell poison severely affecting the organism. According to its characteristic and predominating effects on the skin it belongs to the class of the so-called blistering agents. As a war gas, yperite (in German Schwefel-Lost (S-Lost) or Gelbkreuz (yellow cross)) was used for the first time in Belgium [1] in 1917.

For the detection and determination of yperite many physical [2–4] and physicochemical [5–10] methods have been developed. Beside more demanding experimental techniques, yperite has been detected and determined by colorimetric [11–15] and spectrophotometric [16–18] methods.

The most frequently used method for the determination of yperites is the one suggested by Telicin [19]. The method is based on the reaction of yperite with alkali metal salts of thymolphthalein which are deeply blue-coloured. Acidification converts the excess alkaline salt of thymolphthalein into its colourless form and the solution remains yellow or orange-coloured, de-

* Corresponding author. E-mail: kobliha@vvs-pv.cz

0039-9140/99/$ - see front matter
PII S0039-9140(98)00235-5

pending on the concentration of yperite. The reaction product was identified by IR spectrophotometry in acidic medium as an ester of thymolphthalein and thiodiglycol [19]. The method requires heating the reaction mixture at 80°C for 20 min, cooling and acidification with acetic acid.

To lower the detection limit from 1 to 0.5 μg ml^{-1}, extraction of the reaction product into toluene or benzene is recommended [20]. The method of detection and determination of bis(2-chloroethyl) sulfide and alkyl-bis(2-chloroethyl)-amines (nitrogen mustards, HN-1, 2, 3 GAS) by phthalein is correctly considered as a group reaction of alkyl halides. The determination is interfered with by chlorpicrin, ethyl bromoacetate, bromoacetone, 1,2-dichloroethane and other alkyl halides [21].

Assuming the ionic mechanism of the alkylation reaction between the alkaline form of phthaleins and thiranium or aziridinium ions, formed from the mustards in a polar medium, we decided to check this reaction with four selected phthaleins. The aim was to find a method which, with the same sensitivity, would be substantially simpler, i.e. would not require prolonged heating or pH adjustment, and would be more selective, detecting only the most reactive alkyl halides to which the mustards undoubtedly belong. On the basis of preliminary experiments we performed further extraction spectrophotometric studies with 1-naphtholphthalein (I), *p*-xylenolphthalein (II), *o*-cresolphthalein (III) and thymolphthalein (IV) in order to find the optimum reaction conditions and compare the procedure with the hitherto used [19] detection and determination of yperite with alkaline aqueous-methanolic solution of thymolphthalein (reagent T-135).

2. Experimental

2.1. Chemicals and apparatus

Bis(2-chloroethyl) sulfide (97.6%), tris(2-chloroethyl)ammonium chloride (99.2%), 2-chloroethyldimethylammonium chloride (98.3%), bromobenzyl cyanide (93.0%) and chlorpicrin (97.3%) were prepared in the Army Factory VOZ 072, Zemianské Kostolany, Slovak Republic. *o*-Cresolphthalein was purchased from Aldrich, USA; *p*-xylenolphthalein from Fluka, Switzerland; 1-naphtholphthalein, thymolphthalein, 1,2-dichloroethane and the other chemicals used were Merck (Germany) products of analytical purity. Chloroform for extraction was thrice shaken with redistilled water, distilled as an azeotropic mixture at 60°C and stored in a dark-glass bottle.

Spectrophotometric measurements were performed on a single beam UV–visible spectrophotometer SPEKOL 11 (Zeiss, Jena, Germany), ^{1}H NMR (500.13 MHz) and ^{13}C NMR (125.76 MHz) spectra were taken on a Bruker Avance DRX 500 spectrometer using tetramethylsilane as the internal standard.

2.2. Experimental procedures

In order to determine the relationship $A = f(\lambda)$, 5 mM solutions of phthalein were prepared by dissolving the appropriate amount of the compound in methanol (5 ml), adding 0.1 M aqueous

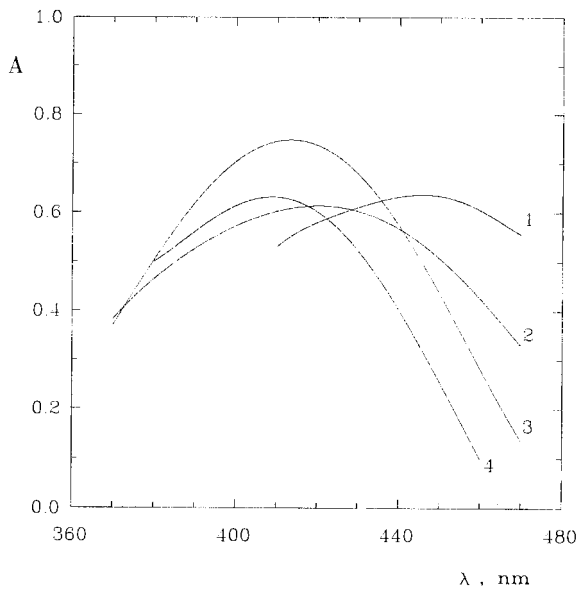

Fig. 1. Absorption curve of sulfidic yperite ($C_{HD} = 75$ μM) with 1-naphtholphthalein (1), thymolphthalein (2), *p*-xylenolphthalein (3) and *o*-cresolphthalein (4); $C_{Ph} = 5$ mM, extraction with chloroform.

Table 1
Parameters of extraction spectrophotometric determination of HD with 1-naphtholphthalein (I), *p*-xylenolphthalein (II), *o*-cresolphthalein (III), thymolphthalein (IV) and reagent T-135

Parameter[a]	Phthalein				T-135
	I	II	III	IV	
λ_{max} (nm)	446	415	410	420	445
C_{Ph} (mM)	1	10	5	5	15
V_{MeOH}/V (%)	10	20	12,5	30	78[b]
C_{NaOH} (mM)	5	10	10	50	114[c]
k (l mol^{-1})	2170	4050	5730	4010	11 740
S.D.$_k$ (l mol^{-1})	21	38	37	39	51
r	0.998	0.998	0.999	0.998	0.999
q	0.036	0.028	0.033	−0.011	0.002
S.D.$_{y/x}$	0.0007	0.0004	0.0006	0.0004	0.0002
L_D (μg ml^{-1})	3.7	2.3	1.65	3.25	0.4
L_Q (μg ml^{-1})	6.5	4.5	3.15	8.45	0.9

Reaction time 20 min, temperature 20°C (80°C for T-135).
[a] λ_{max}, Absorbance maximum; C_{Ph}, phthalein concentration; V_{MeOH}/V, methanol content; C_{NaOH}, concentration of sodium hydroxide in the reagent; k calibration curve slope ($A = k.c+q$); S.D.$_k$, S.D. of calibration curve slope; q, shift on the y axis; r, correlation coefficient; S.D.$_{y/x}$, S.D. estimate for the calibration straight line points; L_D, detection limit; L_Q, determination limit.
[b] In ethanol.
[c] Potassium hydroxide.

solution of sodium hydroxide (2.5 ml) and making up to 25 ml with water. A is the absorbance and λ is the wavelength.

The phthalein solution (2 ml) was pipetted into a test tube with a ground stopper and a methanolic solution of yperite ($C_{HD} = 3$ mM; 50 μl) was added via a micropipette. C_{HD} is the concentration of yperite. The mixture was allowed to stand at 20°C for 20 min and then shaken with chloroform (2 ml) for 2 min. After removal of the aqueous layer by suction, the absorbance of the organic phase was measured in a glass cell, $l = 1$ cm, against pure chloroform.

The kinetics of the reaction of yperite with phthaleins were measured from 0 to 25 min at 2.5 min intervals. The chloroform extracts were measured at the absorption maxima (λ_{max}, nm) for 1-naphtholphthalein (446), *p*-xylenolphthalein (415), *o*-cresolphthalein (410) and thymolphthalein (420).

The relationship $A = f(C_{Ph})$ was followed for phthalein concentrations $C_{Ph} = 0.5$–10 mM.

The effect of the methanol content in the reaction mixture was studied in the following way. Solutions of the phthaleins I ($C_{Ph} = 1$ mM), II ($C_{Ph} = 10$ mM), III, IV ($C_{Ph} = 5$ mM) were prepared by dissolving the appropriate amount of the phthalein in 2.5–17.5 ml methanol (in 2.5 ml steps), adding aqueous 0.1 M NaOH (5 ml) and making up with water to 50 ml. The absorbance of the extracts was read at λ_{max}.

To determine the relationship $A = f(C_{NaOH})$ the appropriate amount of the phthalein was dissolved in methanol (C_{Ph}, mM; V_{MeOH}, ml): I (1; 10), II (10; 20), III (5; 12.5) and IV (5; 30). To the solution of the phthalein an aqueous NaOH solution was pipetted so that its concentration in the mixture, after making up with water to 100 ml, was 2.5–100 mM in 2.5 mM steps. The absorbance of the coloured extract obtained in the manner described was read at λ_{max}.

To measure the calibration relationship $A = f(C_{HD})$ we prepared the following solutions of the phthaleins (C_{Ph} in mM; V_{MeOH}/V in %; C_{NaOH} in mM): I (1; 10; 5), II (10; 20; 10), III (5; 12.5; 10) and IV (5; 30; 50) which were then made up to 100 ml.

The phthalein solution (2 ml) was pipetted into test tubes and then a methanolic solution of yperite (10 to 100 μl; $C_{HD} = 5$ mM) was added in 10

μl steps by means of a micropipette. After mixing, the solution was set aside at 20°C for 20 min and then extracted with chloroform (2 ml) by shaking for 2 min. After removal of the aqueous phase by suction, absorbance of the organic extract was measured at λ_{max}.

The effect of temperature was studied by evaluating the calibration of the HD–*o*-cresolphthalein method at 5, 10, and 15°C.

Products of the reaction of *o*-cresolphthalein with HD were determined as follows. A solution of *o*-cresolphthalein (1.4542 g) in methanol (105 ml) was mixed with 0.1 M NaOH (84 ml) and the mixture was made up with water to 840 ml. To the solution obtained was added dropwise a solution of HD (1.2218 g) in methanol (25 ml) under stirring. After standing for 20 min, the product was extracted with three portions (20 ml each) of chloroform, the extract was dried over anhydrous $CaSO_4$, the solvent was evaporated in vacuo and the remaining product was dried over solid KOH in a desiccator.

The number of products in the reaction mixture was preliminarily estimated by TLC on the plates DC Alufolien, Kieselgel 60 F_{254} (Merck) in chloroform–methanol (100:5 v/v); spots were detected under a UV lamp at 254 nm. The products were than separated by chromatography on a 4×25 cm column of silica gel (Kieselgel 40–60) in chloroform–methanol (100:5 v/v). The solvent was evaporated in vacuo from the individual fractions on a rotatory evaporator. For the NMR measurements, the residues, after evaporation, were dissolved in $CDCl_3$ or DMSO-D_6.

3. Results and discussion

The dependence $A = f(\lambda)$ for chloroform extracts of the reaction products of HD with phthaleins is depicted in Fig. 1; the λ_{max} values are given in Table 1. The kinetics of the reaction with the phthaleins studied is shown in Fig. 2. After 20 min at 20°C the extracts exhibit constant absorbance values.

We also studied the dependence $A = f(C_{Ph})$. The optimum concentrations of the phthaleins, C_{Ph}, are given in Table 1.

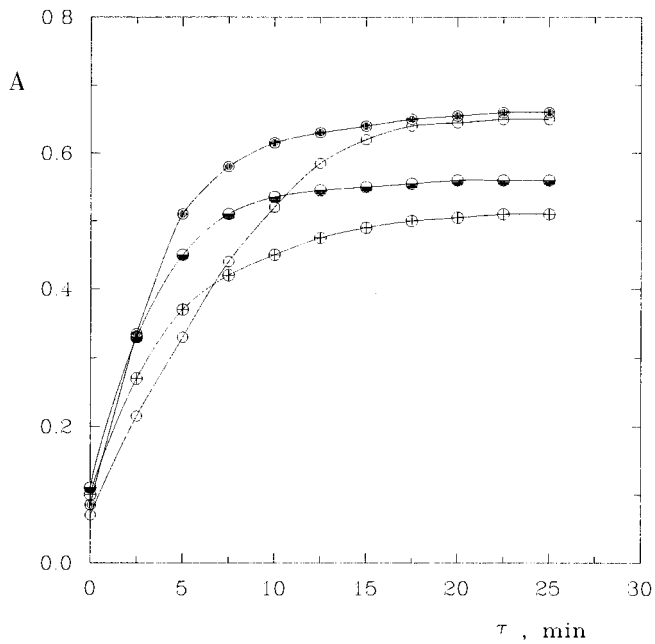

Fig. 2. Kinetics of reaction of sulfidic yperite ($C_{HD} = 75$ μM) with 1-naphtholphthalein, A_{446} (●); thymolphthalein, A_{420} (○); *p*-xylenolphthalein, A_{415} (◒); and *o*-cresolphthalein, A_{410} (⊕). $C_{Ph} = 5$ mM, temperature 20°C, extraction with chloroform.

A necessary condition for the reaction of yperite with phthaleins is the presence of hydroxide ions in the reaction medium that converts the indicator into its quinoid form and also influences the hydrolysis of yperite. For hydrolysis of yperite in a homogeneous polar medium, Price and Wakefield [22] suggested a reaction scheme involving an intermediate sulfonium or thiranium cation with a strongly polar S^+–C bond which is the bearer of its high reactivity. The thiranium cation has been detected by Groenewold et al. [23]. However, the formation of thiranium ions and its rate depend only on the polarity and temperature of the medium. The rate of formation of the thiranium intermediate is the rate-determining step [24]. The alkaline medium removes the hydrogen ions formed and therefore somewhat accelerates the hydrolysis of thiranium ions and shifts this concurrent reaction in favour of the hydroxy derivative. On the basis of these facts we determined the optimum concentration of sodium hydroxide in the solution of the reagent (Table 1). The optimum concentrations of hydroxide ions found closely correspond with the optimized concentrations of the indicators. It was shown that for the preparation of the reagent such an amount of hydroxide is necessary as to convert the phthalein into its quinoid form. A further increase in hydroxide ion concentration has a negative effect because it accelerates hydrolysis of the thiranium cation.

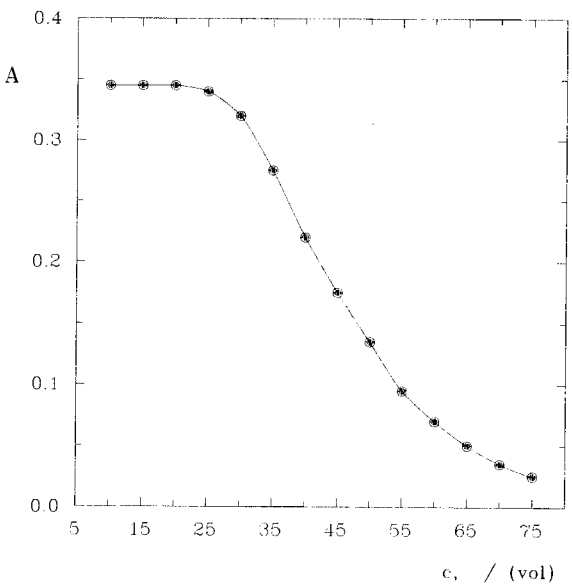

Fig. 3. Dependence of the absorbance of the reaction product from sulfidic yperite ($C_{HD} = 75$ μM) on the methanol content in reagent T-135; A_{445}, temperature 20°C, reaction time 20 min.

According to the hitherto used procedure, the spectrophotometric determination of yperite was performed with reagent T-135 containing 78% (by volume) of ethanol [19]. This high alcohol content decreases considerably the polarity of the medium and thus slows down the formation of the thiranium cation that reacts with the alkaline form of the phthalein. The effect of the polarity of the reaction medium in the reaction with reagent T-135 was followed using a variable content of methanol at constant phthalein concentration and at 20°C (Fig. 3). We found that increasing the alcohol content decreases markedly the formation of the ester of thymolphthalein with 1-(2-chloroethyl)thiranium chloride. The optimum methanol content in the reagent used in our modified spectrophotometric determination of HD is given in Table 1.

We investigated the reaction products of HD with *o*-cresolphthalein using column chromatography on silica gel. In addition to yperite and *o*-cresolphthalein, we isolated three reaction products, V, VI and VII (Scheme 1) that were identified by ^{1}H NMR and ^{13}C NMR spectroscopy. Characteristic chemical shifts of the chosen functional groups are presented below (Ar = aryl):

^{1}H NMR spectrum (ppm):

product V—2.06 (CH_3–Ar); 2.91 (–CH_2–S); 3.65 (–CH_2–Cl); 4.14 (–CH_2–O–CO–Ar); 6.32 (Ar–OH); 6.0–7.0 (C_6H_4)OH(CH_3);

product VI—3.78 (–CH_2–O–Ar); not found (Ar–OH); 7.6–7.9 (C_6H_4)COOH;

product VII—3.78 (–CH_2–O–Ar); 4.14 (–CH_2–O–CO–Ar); 6.82 (Ar–OH).

^{13}C NMR spectrum (ppm):

product V—32.8, 34.0 (–CH_2–S–CH_2–); 43.1 (–CH_2–Cl); 63.3 (–CH_2–O–CO–Ar);

product VI—43.1 (–CH_2–Cl); 61.04 (–CH_2–O–Ar);

product VII—31.33, 36.08 (–CH_2–S–CH_2–); 60.06 (–CH_2–O–Ar); 68.13(–CH_2–O–CO–Ar).

The molar ratios 1:1 of the phthalein to the reaction products of yperite (V and VI) and 2:1 (VII) were calculated from the rate of the integral intensity signals of the aromatic and alifatic pro-

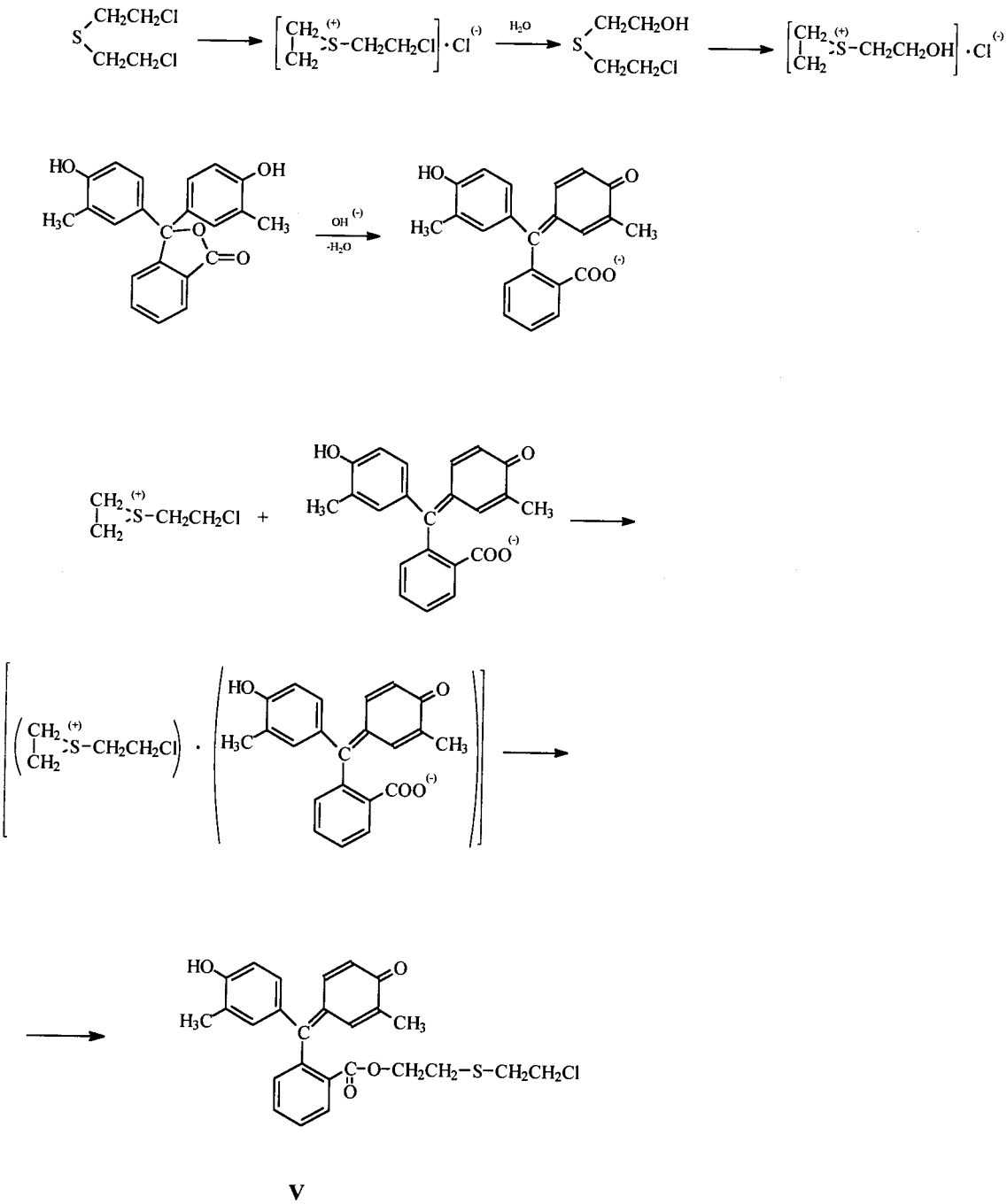

Scheme 1.

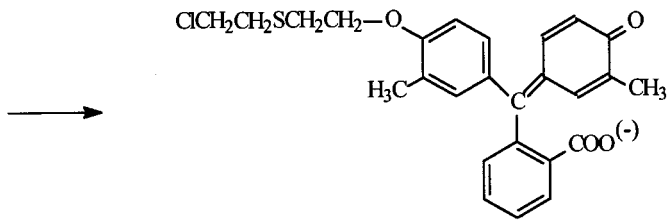

VI

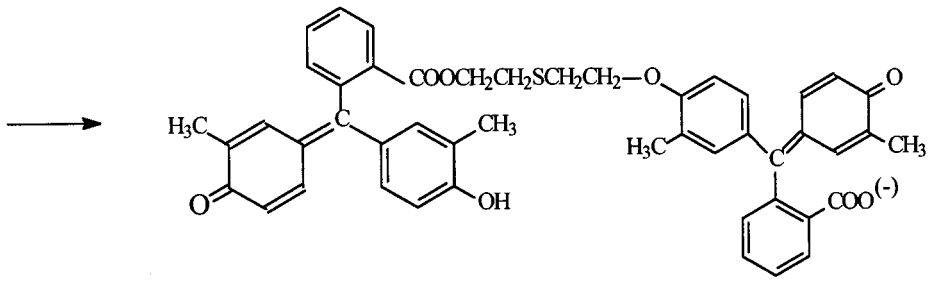

VII

Fig. 1. (*Continued*)

tons. On the basis of the NMR results, we suggest the ionic mechanism of the reaction of yperite with phthaleins according Scheme 1.

The parameters of the extraction photometric determination of HD with the phthaleins studied are given in Table 1. All the determinations obey the Lambert–Beer law in the HD concentration range 25–250 μM. The highest detection limit ($L_D = 1.65$ μg ml^{-1}) and determination limit ($L_Q = 3.15$ μg ml^{-1}), as calculated according to Ref. [25], were found for the extraction photometric determination with *o*-cresolphthalein. The accuracy of the method [26] was tested by means of a *t*-test at the confidence level $\acute{\alpha} = 0.05$.

The extraction spectrophotometric determination of HD with *o*-cresolphthalein was performed at 5, 10 and 15°C and the pertinent parameters are listed in Table 2. The method allows sulfidic yperite to be determined even at 5°C at concentrations as low as 8.5 μg ml^{-1}.

The determination of tris(2-chloroethyl)amine (nitrogen mustard, HN-3) was also studied. The extraction spectrophotometric method allows detection and determination of HN-3 in concentrations 0.8 and 1.5 μg ml^{-1}, respectively, whereas for the existing method using reagent T-135 the respective values are 0.6 and 0.8 μg ml^{-1}.

Table 2
Parameters of extraction spectrophotometric determination of HD with *o*-cresolphthalein at different temperaturesreaction time 20 min, measured at 410 nm)

Parameter	Temperature (°C)		
	5	10	15
k (l mol^{-1})	2470	3180	4730
S.D.$_k$ (l mol^{-1})	41	38	39
q	0.036	0.035	0.033
r	0.994	0.996	0.997
S.D.$_{y/x}$	0.0002	0.0003	0.0004
L_D (μg ml^{-1})	4.75	3.3	2.1
L_Q (μg ml^{-1})	8.5	7.5	5.5

Table 3
Comparison of detection limits for HD (HN-3), selected alkyl halides and chlorpicrin in detection by reagent T-135 and by the extraction spectrophotometric method using *o*−cresolphthalein

Analyte	Method			
	L_D (mg ml^{-1})		ß	
	T-135	Extraction	T-135	Extraction
HD	0.0004	0.0016	—	—
Tris(2-chloroethyl)amine (HN-3)	0.0006	0.0008	—	—
2-Chloroethyldimethylamine	0.005	0.24	13	150
Bromobenzyl cyanide	0.013	0.21	33	131
1,2-Dichloroethane	1.88	24.57	4700	15356
Chlorpicrin	>300	>300	187 500	750 000

The interference effect ß is expressed as the ratio of the detection limit of the interfering compound and the detection limit for HD.

The determination of yperite with reagent T-135 is not a selective reaction. A similar reaction also proceeds with other alkyl halides [21]. We evaluated and compared the selectivity of the determination of HD with reagent T-135 and by the extraction spectrophotometric method using *o*-cresolphthalein. Concentrations of selected alkyl halides interfering with the determination of HD are given in Table 3. Chlorpicrin at a concentration of 300 mg ml^{-1} does not interfere in either of the methods studied.

The modified method is more selective in the determination of yperites (HD and HN-3). It is markedly simpler because, in contrast to the method employing reagent T-135, it does not require heating at 80°C, cooling and acidification of the reaction mixture. In particular, this determination of yperites (HD, HN-3) is more selective. These results were achieved by selection of a more suitable phthalein and especially by the optimization of the reagent composition in combination with extraction. The reaction is carried out in a medium of increased polarity due to the lower alcohol content which makes it possible to perform the reaction at temperatures of 5–20°C without a significant decrease in sensitivity. Thanks to its general dependability, simple execution, satisfactory sensitivity and higher selectivity, this method of extraction spectrophotometric determination of yperites can be recommended for automated analysis of a large number of samples as a substitute for the hitherto used photocolorimetric methods of detection with reagent T-135.

References

[1] J. Meyer, Der Gaskampf und die chemischen Kampfstoffe, von S. Hirzel, Leipzig, 1926, p. 51.
[2] A.J. Caffrey, J.D. Cole, R.J. Gehrke, R.C. Greenwood, IEEE Trans. Nucl. Sci. 39 (1992) 1422.
[3] P. Bach, J.L. Ma, D. Froment, J.C. Jaureguy, Nucl. Instrum. Methods Phys. Res. B 79 (1993) 605.
[4] J.W. Grate, S.L. Rose-Pehrson, D.L. Venezky, M. Klusty, H. Wohltjen, Anal. Chem. 65 (1993) 1868.
[5] P.A. D'Agostino, C.J. Porter, Rapid Commun. Mass Spectr. 6 (1992) 717.
[6] R.B. Black, R.J. Clarke, D.B. Cooper, R.W. Read, D. Utley, J. Chromatogr. 637 (1993) 71.
[7] M. Kokko, J. Chromatogr. 630 (1993) 231.
[8] C.D. Raghuveeran, R.C. Malhotra, R.S. Dangi, J. Liq. Chromatogr. 16 (1993) 1615.
[9] W. Vycudilik, Forensic Sci. Int. 28 (1985) 131.
[10] S. Munavalli, M. Pannella, J. Chromatogr. 437 (1988) 423.
[11] V. Grignard, G. Rivat, Ann. Chim. Phys. 15 (1921) 5.
[12] G.A. Shröter, Angew. Chem. 49 (1936) 164.
[13] M. Obermiller, Angew. Chem. 49 (1936) 162.
[14] V. Kratochvíl, J. Martinek, Chem. Zvesti 23 (1969) 382.
[15] F.M. Issa, H.Z. Youssef, R.M. Issa, Egypt. J. Chem. 18 (1975) 257.
[16] J. Epstein, Anal. Chem. 19 (1947) 272.
[17] E.G. Trams, Anal. Chem. 30 (1958) 256.
[18] J.H. Mason, J. Chem. Soc. 151 (1952) 146.

[19] J. Matoušek, I. Tomeček, Analyse synthetischer Gifte, Militärverlag, Berlin, 1965.
[20] J. Matoušek, I. Tomeček, J. Souček, Cesk. Farm. 30 (1981) 11.
[21] S. Franke, Lehrbuch der Militärchemie, vol. 2, Militärverlag, Berlin, 1977, p. 326.
[22] C.C. Prince, L.B. Wakefield, J. Org. Chem. 12 (1947) 232.
[23] G.S. Groenewold, J.C. Ingram, A.D. Appelhans, J.E. Delmore, D.A. Dahl, Environ. Sci. Technol. 29 (1995) 2107.
[24] V.N. Aleksandrov, V.I. Emelyanov, Otravlyayushchie veshchestva, Voennoe izdatelstvo, Moscow, 1990, p. 131.
[25] Computer program ADSTAT, version 1.2, Trilobyte, Prague, 1991.
[26] J.A. Dean, Analytical Chemistry Handbook, McGraw-Hill, New York, 1995, p. 20.1.

ELSEVIER

Talanta 48 (1999) 173–179

Talanta

Determination of low molecular weight organic acids in soil solution by HPLC

Patrick A.W. van Hees [a,*], Johan Dahlén [b], Ulla S. Lundström [a], Hans Borén [a], Bert Allard [b]

[a] *Deptartment of Chemistry and Process Technology, Mid Sweden University, 851 70 Sundsvall, Sweden*
[b] *Department of Water and Environmental Studies, University of Linköping, 581 83 Linköping, Sweden*

Received 14 November 1997; received in revised form 30 April 1998; accepted 18 June 1998

Abstract

An HPLC method employing an ion exclusion column was developed for the determination of low molecular weight organic acids in soil solution. The method includes extensive sample pretreatment using ultrafiltration and cation exchange. The method showed linear calibration graphs ($r > 0.99$) and the limits of detection in the range 0.1–26 μM. The recovery of eleven added acids ranged from 89 to 102%. Soil solutions of five horizons of a podzolised soil were analysed. The results showed that these compounds made up 1–3% of the dissolved organic carbon and 0–14% of the acidity. Identification of the major acids was also carried out by capillary zone electrophoresis.

Keywords: HPLC; Organic acids; Soil solution; Capillary zone electrophoresis

1. Introduction

Low molecular weight (LMW) organic acids are produced during degradation of organic material in soils, e.g. example litter and dead roots by fungi and bacteria [1]. Furthermore, exudates from different fungi and the roots of a number of plants may contain acids of this kind [2,3]. These acids may also participate in polymerisation reactions [4]. A number of different aliphatic acids have been found in forest soils, e.g. oxalic, citric, formic, acetic, malic, lactic, and fumaric acids [1,5,6]. The total content of these acids is estimated to account for 2–10% of the total dissolved organic carbon (DOC) in spodosols (e.g. podzols) [1,6].

Many low molecular weight acids have high stability constants with different metal ions [7]. It has been found that up to 37% of the Al in the soil solution of an O-horizon of a podzolised soil was bound to these compounds [5]. Due to their complexing ability they are believed to be involved in the translocation of Al and Fe in the podzolisation process [8], and can also enhance the weathering of primary minerals [9]. In addition their role as possible Al detoxifiers in forest soils has been discussed [7].

* Corresponding author. Tel.: +46 60 148493; fax: +46 60 148802; e-mail: Hees@kep.mh.se

0039-9140/99/$ - see front matter
PII S0039-9140(98)00236-7

Different HPLC techniques have been used for the separation of aliphatic acids in soil and litter extracts/solutions. For example, ion exchange chromatography (IEC) has been employed in some cases [6,10,11]. This technique has low limits of detection, but, for example, unsuitable capacity factors may cause problems [10]. Ion exclusion HPLC columns in combination with UV detection have also been used [1,7,12]. Although this type of column offers good selectivity, the determination can be interfered by unretained substances which cause a large void peak with tailing. Capillary electrophoresis and gas chromatography are two other techniques that successfully have been applied to similar samples [13,14].

The aim of this study has been to develop an HPLC method for the qualitative and quantitative determination of low molecular weight organic acids in the soil solution. To ensure the identification of the acids capillary electrophoresis was employed.

2. Experimental

2.1. Site

A sediment soil was sampled at Hyytiälä Forestry Field Station in Finland, (61°48'N, 24°19'E) for the determination of LMW acids. The site was forested with Norway spruce (*Picea abies)* and Scots pine (*Pinus sylvestris)* about 100 years old. The field layer consisted of *Vaccinium myrtillus* and moss. The soil was podzolised and the soil horizons had a thickness of about: O:10 cm, E:15 cm and B: 40 cm.

2.2. Instruments

A Beckman J2-21 centrifuge (Beckman, Spinco Division, Palo Alto, CA) was used for preparing the soil solution. DOC in the soil solutions was determined using a Shimadzu 5000 (Shimadzu, Osaka, Japan). The HPLC system (Shimadzu LC-10, Shimadzu, Osaka, Japan) featured a diode array detector. Detection was performed at 210 nm. A column oven (Pharmacia HPLC column oven 2155, Pharmacia, Uppsala, Sweden) was also mounted. Data acquisition was performed using the Class VP 5.0 (Shimadzu) computer program. A Supelcogel C610-H (Supelco, Richmond, PA, USA) ion exclusion column (300 × 7.8 mm) was employed for separation of the small organic acids. Ultrafiltration was carried out using a stirred cell Amicon 8050 with Diaflo YM-1 filters (cut-off size 1000 Da) (Amicon, Beverly, MA). Capillary zone electrophoresis (CZE) analysis was performed on a Quanta 4000 (Waters, Milford, MA). Titration was performed employing an ABU900 Autoburette system controlled by a TIM900 Titration Manager (Radiometer, Copenhagen, Denmark).

2.3. Chemicals

All organic acids (present in their acid form or as Na/K salts) were of analytical reagent grade with the exception of lithium lactate (GR). All acids were obtained from Aldrich (Steinheim, Germany) and Merck (Darmstadt, Germany). Phosphoric acid (85%) (AR) was purchased from Aldrich. The Bio-Rex cation exchange resin was bought from Bio-Rad (Hercules, CA). 1,2,4-Benzenetricarboxylic acid was obtained from Janssen (Beerse, Belgium), tetradecyltrimethylammonium bromide (TTAB) from Sigma (Labkemi, Stockholm, Sweden) and octanesulfonate from Fluka (Buchs, Switzerland). The water used was ion exchanged and run through a Milli-Q system (Millipore, Bedford, MA).

2.4. Soil solutions

The centrifugation drainage technique and sampling procedure described by Giesler and Lundström [15] were used to obtain the soil solutions. When sampling the mor (O-horizon), the upper organic soil was removed and divided into two layers. The green parts were removed. The B1 and B2 samples were taken at 0–5 and 5–10 cm depth in the illuvial horizon, respectively. The soil samples were centrifuged for 30 min at a speed of 14000 rpm. After centrifugation the collected centrifugates were filtered through a 0.45 μm filter (Millex-HV, Millipore) and the pH was then determined. The soil solution was finally transferred

to 10 ml polypropylene tubes and stored in a freezer until further analysis.

2.5. Sample preparation and HPLC analysis

A stirred ultrafiltration cell (model 8050, Amicon) equipped with a Diaflo YM-1 filter was used for removing interfering compounds. The device was pressurised by N_2 gas at a pressure of 3–3.5 bar, and the filtrate was collected in a tube surrounded by ice. The sample (10 ml) was filtered twice and the filters were changed between the two runs. Before use the ultra filters were immersed for at least 1 h in firstly 0.1 M NaOH, secondly 5% (w/w) NaCl, and finally rinsed twice in Milli-Q water. This cleaning procedure was needed to ensure the removal of, especially, lactic acid which otherwise could contaminate the sample. A blank was run and no interfering peaks were found.

The sample was then acidified by means of 0.5 M H_2SO_4 to pH $\sim$ 3, and run through a cation exchanger (0.4 ml Bio-Rex 70, 200–400 mesh) in the H^+ form. The first 1 ml of eluate after the pH change was discarded and then a sample of approximately 4 ml was collected. The sample was immediately run on the HPLC column.

The mobile phase consisted of 0.2% (v/v) H_3PO_4 and the flow rate was 0.5 ml min^{-1}. The injection volume was 50 μl. First one run was carried out with a column oven temperature of 30°C. A second run was then performed at 60°C when citric, shikimic and lactic acids were determined. This procedure was required due to the overlapping of lactic and shikimic acids at 30°C and the appearance of a ghost peak interfering the determination of citric acid. The acids were calibrated using standards which had been treated in the same way.

2.6. CZE analysis

CZE analysis was carried out according to [16] and was performed on a Quanta 4000. An 82-cm (74-cm to detector) fused-silica capillary (J&W Scientific, Folsom, CA) with an i. d. of 75 μm and a carrier electrolyte consisting of 5 mM 1,2,4-benzenetricarboxylic acid with 0.5 mM TTAB (pH 8) were used. TTAB was added to reverse the electroosmotic flow. Injection was performed by electrokinetic injection at -5 kV for 45 s or by hydrostatic injection at 100 mm for 30 s, and the applied separation voltage was -15 kV. The analytes were detected by indirect UV detection at 254 nm. Octanesulfonate, which acts as a terminating electrolyte, was added to the samples to final concentrations of 70 μM to achieve an isotachophoretic steady state during the sample introduction.

2.7. Titrations of soil solution

The sample was first acidified to pH < 2.5 and run through a cation exchanger. It was then bubbled with N_2 for 15 min and titrated by means of 0.01 M NaOH. The evaluation was made using the procedure outlined by Molvæsmyr and Lund [17] based on the Gran extrapolation giving the concentrations of strong (SA) and weak acids (WA).

3. Results and discussion

3.1. Calibration and performance

A satisfactory separation of a wide range of acids could be achieved (Table 1). The performance of the HPLC method was evaluated with regard to limits of detection, calibration and recoveries of standard additions. Citric, shikimic and lactic acids were determined at 60°C, all other acids at 30°C. The results are presented in Table 1. Succinic acid was also tested and it was found that this acid had very similar retention times to shikimic acid, both at 30 and 60°C. However, succinic acid could not be found in the samples when running CZE.

All calibration graphs were linear and had a correlation coefficient $r > 0.99$. Two or three replicates were run and each standard was injected twice. In the case of fumaric, shikimic and oxalic acids lower concentrations of the standards were used due to its high UV-absorbance. Recovery studies were performed by standard addition of all acids to three samples of the E-horizon.

Table 1
Calibration of organic acids

Acid	Concentration (μM)	Replicates (n)	Corrolation coefficient (r)	LOD (μM)	Recovery ($n = 3$) (standard addition 100 μM)[a] (%)	Retention time (min)
Acetic	50, 250, 500	3	0.994	23.9	93 ± 8	21.42
Citric	50, 250, 500	2	1.000	3.1	99 ± 5	12.04[b]
Formic	50, 250, 500	3	0.998	16.0	95 ± 7	19.98
Fumaric	5, 25, 50	2	0.992	0.1	102 ± 3	24.25
Lactic	50, 250, 500	2	0.995	7.1	97 ± 6	17.95[b]
Malic	50, 250, 500	3	0.998	6.1	105 ± 7	14.67
Malonic	50, 250, 500	3	0.996	8.1	100 ± 7	15.36
Oxalic	50, 250, 500	3	0.998	0.4	89 ± 15	10.09
	5, 10, 25	2	0.993			
Propionic	50, 250, 500	3	0.998	25.7	98 ± 8	26.00
Shikimic	5, 10, 25	2	0.994	0.2	101 ± 3	16.94[b]
Tartaric	50, 250, 500	3	0.993	4.0	100 ± 7	13.25

Confidence limits (95%) of standard addition to sample.
[a] In the case of fumaric and shikimic acids 10μM; [b] determined at 60°C, all other acids at 30°C.

Table 2
HPLC determinations and titration data of the soil solutions from Hyytiälä

	O1	O2	E	B1	B2
pH	3.76	3. 53	3. 83	4. 85	5.99
Acetic acid (μM)	174+28	67+42	—	—	—
Citric acid (μM)	80+6	27+7	19+6	—	—
Fumaric acid (μM)	2.4+5	1.3+6	1.3+5	1.1+6	—
Lactic acid (μM)	27+41	n.d.	n.d.	n.d.	n.d.
Oxalic acid (μM)	7.2+2	4. 5+3	4.1+3	8.5+3	tr.
Shikimic acid (μM)	21.4+2	5.1+2	1.6+2	1.7+2	1.3+2
DOC (mM)	32.33	22.08	4.94	3.13	1.02
%LMW acids of DOC	3.3	1.6	3.1	1.2	0.9
WA(tot)[a] (meq l^{-1})	3.44	2.22	0.96	0.42	0.37
%LMW acids (meq l^{-1}) of WA(tot)	14.0	7.5	7.7	5.0	0.3

Data is given for pH, concentrations+confidence limits(95%), DOC, and total WA (WA(tot)) content.
n.d., Not detectable, area of peak smaller than intercept of calibration equation or below LOD; tr., traces, peak identified but not integrated.
[a] In the case of O1 SA is included.

Good recovery values were obtained for all acids. The poorer value for oxalic acid can partly be explained by the larger variance and the fact that this acid elutes close to the void peak. A correct determination of this acid might be difficult when analysing samples with very high DOC levels (>1000 ppm). The limits of detection (LOD), calculated as the concentration corresponding to three times the background noise, were in the range 0.1–26 μM. The values were in accordance with the UV absorbance of the different acids, resulting in better limits of detection for the acids with higher absorbance. The repeatability for natural samples was checked by performing duplicate analyses for two samples (see below), and was estimated as the pooled S.D. for the replicates. The deviation was in the range 0.03–1.40 μM for the commonly detected acids (citric, shikimic, oxalic and fumaric acids). The variance for acids found in natural samples was not significantly greater than for standards as evaluated by *F*-tests [18].

3.2. Application and identification

Soil solutions from five soil layers were analysed for LMW organic acids, SA and WA content using the methods described above (Table 2). A comparison of a chromatogram before and after the sample clean-up procedure is shown in Fig. 1. The acids were identified by comparing retention times and where possible, due to the void peak, UV spectra. In the case of oxalic, citric and fumaric acids these were also confirmed by standard additions.

In order to obtain an independent identification of the organic acids, some of the samples were also analysed by CZE. Identification was made by retention time and by spiking the samples with a small amount of organic acid stock solution. By this procedure citric, fumaric, lactic, oxalic, acetic and shikimic acids were tentatively identified in the CZE electropherograms. Although the analysis was performed on a qualitative basis it could be established that the concentrations determined by the HPLC application were of the same order of magnitude as compared to the CZE analysis. An electropherogram of the O2 horizon solution is showed in Fig. 2.

Two replicates of the O1 and E horizons including pretreatment and HPLC analysis were made, but single analyses were carried out for the other samples. Each sample was injected twice on the HPLC column. Several different acids were identified, of which all have been reported earlier [1,5,19]. Shikimic acid and traces of oxalic acid

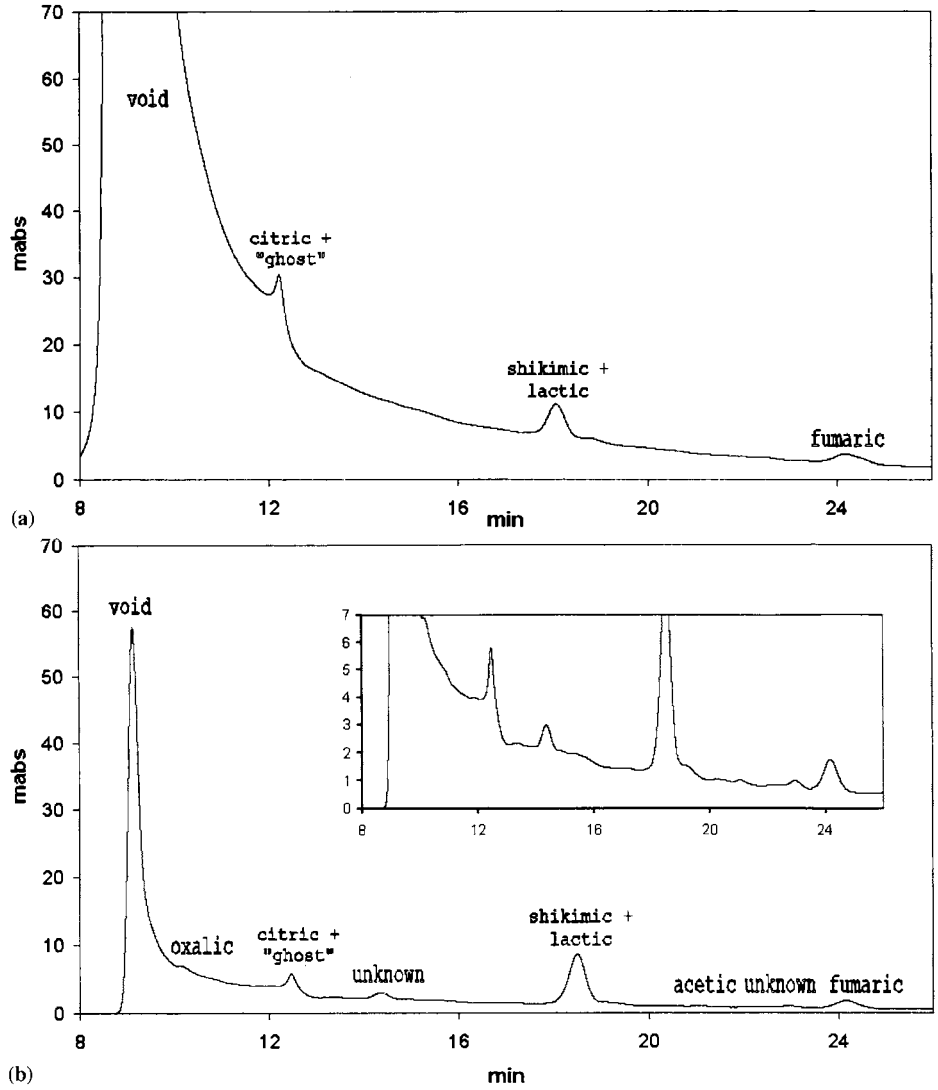

Fig. 1. HPLC chromatogram (run at 30°C) of an O2 soil solution before (a) and after pretreatment (b). The insert picture in (b) shows an enlargement of the chromatogram.

were found in all horizons. Citric and fumaric acids were also observed in most samples. As would have been expected the concentrations decrease in the deeper soil layers. A small increase of oxalic and shikimic acids was however observed in the B1 horizon.

Concerning the acidity, the fraction of the LMW organic acids made up 0.3–14.0% of the WA(tot). SA was only found in O1, and was included in the WA(tot) value because experiments showed that for citric and oxalic acids the carboxyl group with the lowest pK_a was not included in the WA(tot) measurement. The percentage of LMW acids decreases through the soil profile. Regarding the DOC, LMW acids made up 0.9–3.3%. Also the fraction of the DOC consisting of LMW acids generally decreased in the deeper horizons.

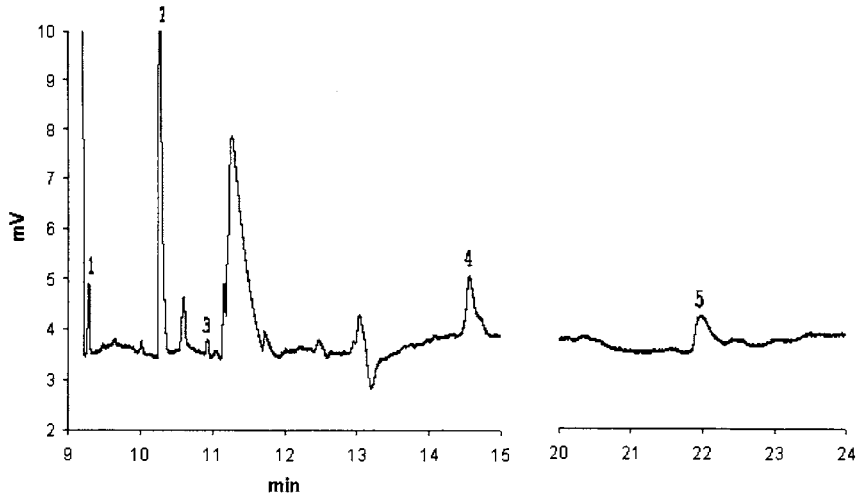

Fig. 2. CZE electropherogram of an O2 soil solution after pretreatment. Electrokinetic injection. Peaks: 1, oxalic; 2, citric; 3, fumaric; 4, acetic; 5, shikimic acids.

Acknowledgements

This study was financially supported by the Swedish Natural Science Research Council (NFR). The authors would like to thank A.-M. van Hees, M. Nyström and V. Stigsson for assistance. Dr H. Ilvesniemi is acknowledged for providing facilities for the field work and L. Backman for soil sampling.

References

[1] T.R. Fox, N.B. Comerford, Soil Sci. Soc. Am. J 54 (1990) 1139.
[2] L. Ström, T. Olsson, G. Tyler, Plant Soil 167 (1994) 239.
[3] T. Wickman, Weathering assessment and nutrient availability in coniferous forests, PhD dissertation, Royal Institute of Technology, Stockholm, 1996.
[4] A.A. Pohlman, J.G. McColl, Soil Sci. Soc. Am. J. 53 (1989) 686.
[5] P.A.W. van Hees, A.-M.T. Andersson, U.S. Lundstöm, Chemosphere 33 (1996) 1951.
[6] A.J. Krzyszowska, M.J. Blaylock, G.F. Vance, M.B. David, Soil Sci. Soc. Am. J. 60 (1996) 1565.
[7] N.V. Hue, G.R. Craddock, F. Adams, Soil Sci. Soc. Am. J. 50 (1986) 28.
[8] U.S. Lundström, N. van Breemen, A.G. Jongmans, Eur. J. Soil Sci. 46 (1995) 489.
[9] U. Lundström, L.-O. Öhman, J. Soil Sci. 41 (1990) 359.
[10] R. Baziramakenga, R.R. Simard, G.D. Leroux, Soil Biol. Biochem. 27 (1995) 349.
[11] Y. Shen, L. Ström, J.-Å. Jönsson, G. Tyler, Soil. Biol. Biochem. 28 (1996) 1163.
[12] A.A. Pohlman, J.G. McColl, Soil Sci. Soc. Am. J. 52 (1988) 265.
[13] O. Devêvre, J. Garbaye, B. Botton, Mycol. Res. 100 (1996) 1367.
[14] A.M. Szmigielska, K.C.J. Van Rees, G. Cieslinski, P.M. Huang, Commun. Soil Sci. Plant Anal. 28 (1997) 99.
[15] R. Giesler, U.S. Lundström, Soil Sci. Am. J. 57 (1993) 1283.
[16] J. Dahlén, S. Bertilsson, C. Pettersson, Environ. Int. 22 (1996) 501.
[17] K. Molvæsmyr, W. Lund, Water Res. 17 (1983) 303.
[18] J.C. Miller, J.N. Miller, Statistics for Analytical Chemistry, 3rd ed., Ellis Horwood, Chichester, 1993, p. 60.
[19] J.G. McColl, A.A. Pohlman, J.M. Jersak, S.C. Tam, R.R. Northup, Organics and metal solubility in California forest soils, in: S.P. Gessel et al. (Eds.), Sustained Productivity of Forest Soils, Proc. 7th North American Forest Soils Conf., Vancouver, 24–28 July 1990. Faculty of Forestry Publication, University of British Columbia, 1990, pp. 178–195.

ELSEVIER

Talanta 48 (1999) 181–187

Talanta

Synthesis and complexation behavior of *N*-(1-naphthylmethyl)-1,4,7,10, 13-pentaoxa-16-azacyclooctadecane

Kanji Kubo [a,*], Ryoichi Ishige [b], Junko Kubo [b], Tadamitsu Sakurai [b]

[a] *Institute of Advanced Material Study, 86, Kyushu University, Kasuga-koen, Kasuga, Fukuoka, 816-8580, Japan*
[b] *Department of Applied Chemistry, Faculty of Engineering, Kanagawa University, Kanagawa-ku, Yokohama, 221-0802, Japan*

Received 30 March 1998; received in revised form 18 June 1998; accepted 18 June 1998

Abstract

A fluorescent photoinduced electron transfer (PET) sensor (**3**) that consists of 1-aza-18-crown-6 and a 1-naphthyl pendant shows a fluorescent increase with bivalent metal ions and a fluorescent decrease with monovalent metal ions. ^{1}H and ^{13}C NMR analyses of this 1:1 complexation behavior revealed that Ba^{2+} strongly coordinates with the azacrown nitrogen to cause a dramatic decrease in the intramolecular charge-transfer character. In addition, it was suggested that not only the metal ion-dependent coordinated structure of the resulting complex but also the interaction between the thiocyanate anion and the naphthyl group play a role in controlling the extent of the emission-intensity increase and decrease that was observed in the presence of a given metal salt.

Keywords: Fluorescence photoinduced electron transfer sensor; Bivalent metal ions; Monovalent metal ions

1. Introduction

As an approach to the manipulation of intramolecular electron transfer dynamics, photoresponsive supramolecular systems are of great significance, particularly for their potential application to nanoscale devices for a cation sensor and switch [1,2]. There are extensive investigations into the characterization of fluoroionophores including crown ether, calixarene, and cyclodextrin derivatives with naphthalene, umbelliferone, anthracene, or pyrene fluorophore [3–12]. Recently, it was found that the azacrown ethers act as electron donors in a typical exciplex-forming system that involves an appropriate electron acceptor [13,14]. The addition of metal salts enhanced the fluorescence emission intensity of *N*-(1-pyrenylmethyl) - 1,4,7,10,13 - pentaoxa - 16 - azacycloocta - decane (**1**) and *N*,*N*′-bis(1-naphthylmethyl)-1,4,10,13-tetraoxa-7,16-diazacyclooctadecane (**2**) [15–17], while the presence of metal salts exerted a strong effect on the ratio of the monomer versus excimer emission intensity of *N*,*N*′-bis(1-pyrenyl-

* Corresponding author. Tel.: +81 92 5837807; fax: +81 92 5837810; e-mail: kubo-k@cm.kyushu-u.ac.jp

0039-9140/99/$ - see front matter
PII S0039-9140(98)00229-X

methyl)-1,4,10,13-tetraoxa-7,16-diazacyclooctadecane [17–19]. Thus, it is interesting to investigate the complex formation with metal salts using fluorescence spectroscopy. We now report the fluorescence behavior of the azacrown ether (**3**) with a naphthyl pendant in the presence of metal salts.

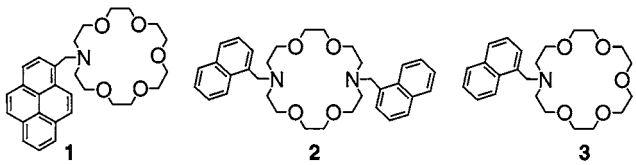

1 **2** **3**

2. Experimental

Elemental analyses were performed on a Perkin-Elmer PE2400 series II CHNS/O analyzer. Melting points were obtained with a Yanagimoto micro melting point apparatus and were uncorrected. NMR spectra were measured on a JEOL JNM-500 model spectrometer in $CDCl_3$; the chemical shifts were expressd by a δ unit using tetramethylsilane as an internal standard. IR spectra were recorded on a Hitachi model 270-30 infrared spectrophotometer. Fluorescence spectra were measured with a Hitachi model F-4500 spectrofluorimeter. The stationary phase for the column chromatography was Merck and the eluant was a mixture of methanol, ethyl acetate, chloroform, and hexane.

2.1. Synthesis of N-(1-naphthylmethyl)-1,4,7,10, 13-pentaoxa-16-azacyclooctadecane (3)

A tetrahydrofuran solution (10 cm^3) of 1-aza-18-crown-6 (1,4,7,10,13-pentaoxa-16-azacyclooctadecane (0.13 g, 0.50 mmol), triethylamine (0.5 cm^3, 3.6 mmol), 1-chloromethylnaphthalene (0.27 g, 1.52 mmol) was refluxed for 12 h. The mixture was then diluted with 1.0 M NH_3 (10 cm^3) and extracted with ethyl acetate. The solvent was evaporated and the residue was purified by column chromatography over silica gel (70–230 mesh, Merck) using hexane and ethyl acetate (1:1 v/v) as the eluent. The analytically pure sample showed the following physical and spectroscopic properties:

N-(1-naphthylmethyl)-1,4,7,10,13-pentaoxa-16-azacyclooctadecane (**3**): ^{1}H NMR $\delta = 2.86$ (4H, t, $J = 5.8$ Hz), 3.59-3.71 (20H, m), 4.09 (2H, s), 7.39 (1H, dd, $J = 7.6$, 8.2 Hz), 7.44–7.50 (3H, m), 7.74 (1H, d, $J = 7.6$ Hz), 7.82 (1H, dd, $J = 7.6$, 9.5 Hz), 8.34 (1H, d, $J = 8.2$ Hz). ^{13}C NMR $\delta = 54.3$ (2C), 58.7, 70.1 (2C), 70.4 (2C), 70.8 (2C), 70.9 (2C), 70.9 (2C), 124.8, 125.2, 125.5, 125.6, 127.2, 127.7, 128.3, 132.5, 133.8, 135.4. IR (NaCl) ν 792, 1116, 1247, 1293, 1350, 1452, 1596, 2860 cm^{-1}. Anal. Calc. for $C_{23}H_{33}N_1O_5$: C, 68.46; H, 8.24; N, 3.47. Found; C, 68.38; H, 8.51; N, 3.37%.

2.2. Determination of association constants (K)

The titrations were conducted by adding a crown-ether solution (2.0×10^{-5} M for **3** in methanol) progressively containing excess metal salts, using a 0.25 cm^3 syringe, to a cuvette containing 2.0 cm^3 of the crown-ether solution (2.0×10^{-5} M for **3** in methanol). The solutions were homogenized by ultrasonic waves for 3 min. The spectrum was recorded after each addition, as shown in Fig. 3. The added equivalents of the cation were then plotted against the emission-intensity change at 333 nm (excited at 280 nm). Even though the solvent takes part in the association interaction, the solvent concentration is virtually unaffected. Therefore, we express the interaction of metal salts in terms of the equilibrium [17,20]:

$$CE + M \rightleftharpoons CE \cdot M \tag{1}$$

Also, K should be expressed as follows:

$$K = [CE \cdot M]/[CE][M] = [CE \cdot M]/([CE_0] - [CE \cdot M])([M_0] - [CE \cdot M]) \tag{2}$$

$$[CE \cdot M] = a[CE_0] = (I - I_0[CE_0])/(I_{CE \cdot M} - I_0) \tag{3}$$

From Eqs. (2) and (3), the following equation can be derived:

$$[M_0] = a/K(1 - a) + a[CE_0], \tag{4}$$

where $[CE_0]$ and $[M_0]$ are the initial concentrations of the crown ether and the metal salt, I and I_0 are the observed emission intensities of the crown ethers in the presence and in the absence of

the metal ion and $I_{CE \cdot M}$ is the observed emission intensity of the complex of the crown ether and the metal ion.

A self-written nonlinear curve-fitting computer program (Eq. (4)) was used to fit the experimental titration curves [17,20]. The association constants were determined from the emission-intensity changes at 333 nm using the equation as given in Table 1.

3. Result and discussion

The naphtalene-functionalized azacrown ether (**3**) was prepared by the *N*-alkylation of 1-aza-18-crown-6 with 1-chloromethylnaphthalene in THF-triethylamine (95% yield). The structure and purity of **3** were ascertained by ^{1}H NMR spectroscopy and elemental analysis (Scheme 1).

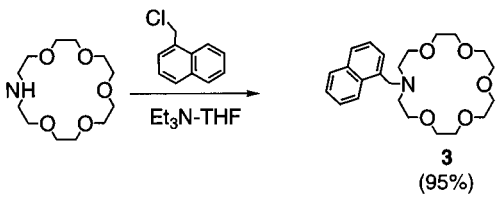

Scheme 1.

Fig. 1 illustrates the fluorescence spectral behavior of **2** (2.0×10^{-5} M, 1 M = 1 mol dm^{-3}) and **3** (4.0×10^{-5} M) in methanol at room temperature. Fluoroionophores **2** and **3** (when excited at 280 nm) gave a broad emission band with a maximum at 474 nm in addition to monomer emission (335 nm). The formation of an intramolecular exciplex should be responsible for the appearance of the former emission band. The latter emission-band intensities of **2** and **3** were reduced to approximately 1/440 and 1/30 that of the 1-methylnaphthalene (4.0×10^{-5} M), respectively, accompanied by the occurrence of exciplex fluorescence. This indicates that the quenching of the excited naphthalene chromophore by the azacrown unit proceeds by a mechanism similar to that for the classical naphthalene–aliphatic amine system [13,14]. The larger quenching of **2** means that the two intramolecular nitrogen aroms and naphthalene rings participate in intramolecular electron transfer in the excited state.

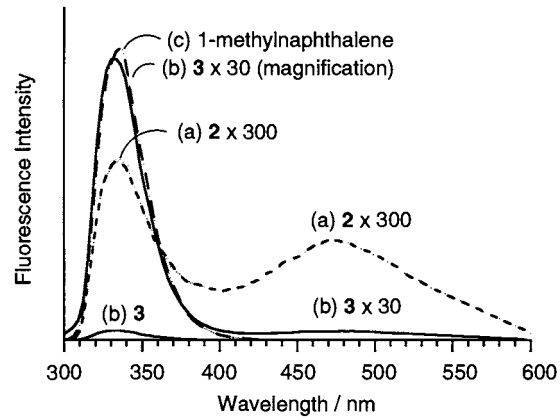

Fig. 1. Fluorescence spectra of (a) **2** (2.0×10^{-5} M), (b) **3** (4.0×10^{-5} M), and (c) 1-methylnaphthalene (4.0×10^{-5} M) in methanol at room temperature.

Fig. 2 illustrates the fluorescence spectral behavior of **3** (2.0×10^{-5} M) in methanol at room temperature. A dramatic change in the emission intensity of **3** (I_3) was observed upon the addition of various amounts of metal cations (Li^+, Na^+, K^+, Rb^+, Cs^+, Ca^{2+}, Ba^{2+}, Zn^{2+}, and Mg^{2+}) and NH_4^+. When the metal salts were added (20 molar equivalent), the relative emission intensity ratio ($I_{complex}/I_3$), being used as a measure of the molecular recognition sensing, changed from 0.4 to 4.5 depending on the nature of metal cations as shown in Fig. 3.

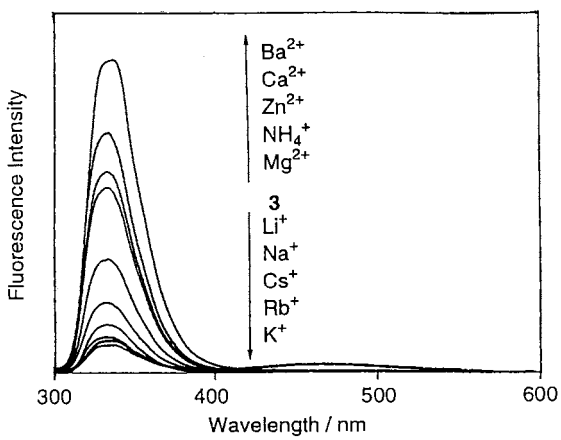

Fig. 2. Fluorescence spectra of **3** (2.0×10^{-5} M) with and without various metal cations (4.0×10^{-4} M) in methanol, as excited at 280 nm.

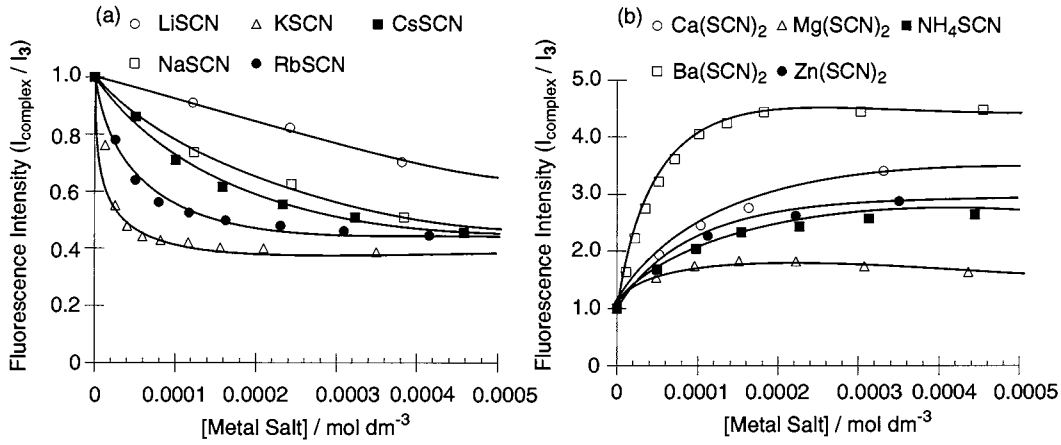

Fig. 3. Dependence of fluorescence intensities of **3** (2.0×10^{-5} M) at 333 nm on the concentration of various metal cations (added as thiocyanate salts) in methanol.

Clearly, the emission intensity changes with an increase in the metal ion concentration. Interestingly, the intensity ratio ($I_{complex}/I_3$) was different among bound metal ions and was decreased in the following order: Ba^{2+} (4.5) > Ca^{2+} (3.4) > Zn^{2+} (2.9) > NH_4^+ (2.6) > Mg^{2+} (1.6) > Li^+ (0.70) > Na^+ (0.51) > Cs^+ (0.48) > Rb^+ (0.45) > K^+ (0.38). It is clearly seen from Fig. 3 that the emission intensity increased along with an increase in the concentration of the bivalent metal ions and ammonium ion, except for alkali metal ions. The observed enhancement indicates the inhibition of exciplex formation by complexation with a metal salt. Furthermore, it is noteworthy that the **3**–alkali thiocyanate complex exhibited a decrease in its monomer emission intensity relative to that of **3** itself. This suggests that the observed quenching is due to the presence of thiocyanate ion. A similar quenching by the thiocyanate anion was explained based on the photoinduced electron transfer from this anion to the naphthalene chromophore [21]. From the relative emission-intensity ratio ($I_{complex}/I_3$), one can estimate the size and the valence of metal ions that were incorporated into the host cavity.

Metal-ion concentration dependence of the emission intensity (Fig. 3) allowed us to determine K by the non-linear curve-fitting method (Table 1) [17,20].

Table 1
Association constants (M^{-1}) of **1**, **2**, and **3** for metal salts in methanol and methanol–chloroform (9:1 v/v)

Metal salts	**1**	**2**		**3**
	CH_3OH:$CHCl_3$ (9:1 v/v)	CH_3OH:$CHCl_3$ (9:1 v/v)	CH_3OH	CH_3OH
LiSCN	48 ± 3		27 ± 5	2400 ± 310
NaSCN	1010 ± 60		123 ± 9	3890 ± 300
KSCN	56 200 ± 2470	2800 ± 140	1850 ± 320	98 200 ± 10 500
RbSCN	15 100 ± 780		305 ± 26	51 400 ± 4500
CsSCN	4630 ± 280		97 ± 30	6260 ± 750
NH_4SCN	2530 ± 80		1490 ± 165	15 800 ± 1300
$Zn(SCN)_2$	158 ± 14		126 ± 13	1330 ± 120
$Mg(SCN)_2$	513 ± 19		3240 ± 200	29 600 ± 1700
$Ca(SCN)_2$	847 ± 74		61 ± 4	7100 ± 700
$Ba(SCN)_2$	22 300 ± 400		710 ± 114	51 300 ± 19 600

The azacrown (**3**) showed the following cation selectivity: K: $Zn^{2+} < Li^{+} < Na^{+} < Cs^{+} < Ca^{2+} < NH_4^{+} < Mg^{2+} < Ba^{2+} < Rb^{+} < K^{+}$. This selectivity order is distinct from that for **1** (K: $Li^{+} < Zn^{2+} < Mg^{2+} < Ca^{2+} < Na^{+} < NH_4^{+} < Cs^{+} < Rb^{+} < Ba^{2+} < K^{+}$) [16 – 18] and **2** ($K$: $Li^{+} < Ca^{2+} < Cs^{+} < Na^{+} < Zn^{2+} < Rb^{+} < Ba^{2+} < NH_4^{+} < K^{+} < Mg^{2+}$)[15]. The order of K values for K^{+} is **2** < **1** < **3**, indicating that the two naphthalene rings and one pyrene ring inhibit the complexation with metal ions to some extent [4,15–18]. Comparison of the selectivity order for **1**–**3** confirms that the size and electronic property of the aromatic pendants attached to the azacrown nitrogen atoms may control the selectivity of the host toward metal cations in a delicate manner. In spite of the small association constant for **3** in methanol, the emission intensity of this host was greatly enhanced in the presence of metal salts, establishing that **3** has a high fluorescence switch-on ability for complexation with various metal ions.

Binding interactions of the host (**3**) with alkali metal and bivalent metal ions were examined using ^{1}H NMR spectroscopy. When alkali metal salts were added, each resonance peak was shifted to downfield or upfield depending on the nature of added metal cations (Fig. 4b and c), while the addition of bivalent metal ions decreased the original-signal intensities with an increase in new-signal intensities (Fig. 4d and e).

These spectral changes confirm that the exchange rates are different between the alkali metal and bivalent metal ions. The gradual upfield shift of the proton signal in the azacrown unit with added KSCN (Fig. 4b and c) shows that the exchange process between the free host and its potassium complex is rapid as compared to the NMR time scale: time-averaged NMR shifts are observed depending upon the guest concentrations. On the other hand, the original (free host, **3**) signal intensities decreased and the intensities of new signals (of the corresponding complex **3**–$Ba(SCN)_2$) appearing at 3.79, 4.45 and 8.24 ppm increased as the $Ba(SCN)_2$ concentration was increased (Fig. 4d and e). Thus, the exchange process for this complex is slow enough even at room temperature, compared with the NMR time scale, to give new signal corresponding to the barium complex (**3**– $Ba(SCN)_2$). The difference in exchange rate between KSCN and $Ba(SCN)_2$

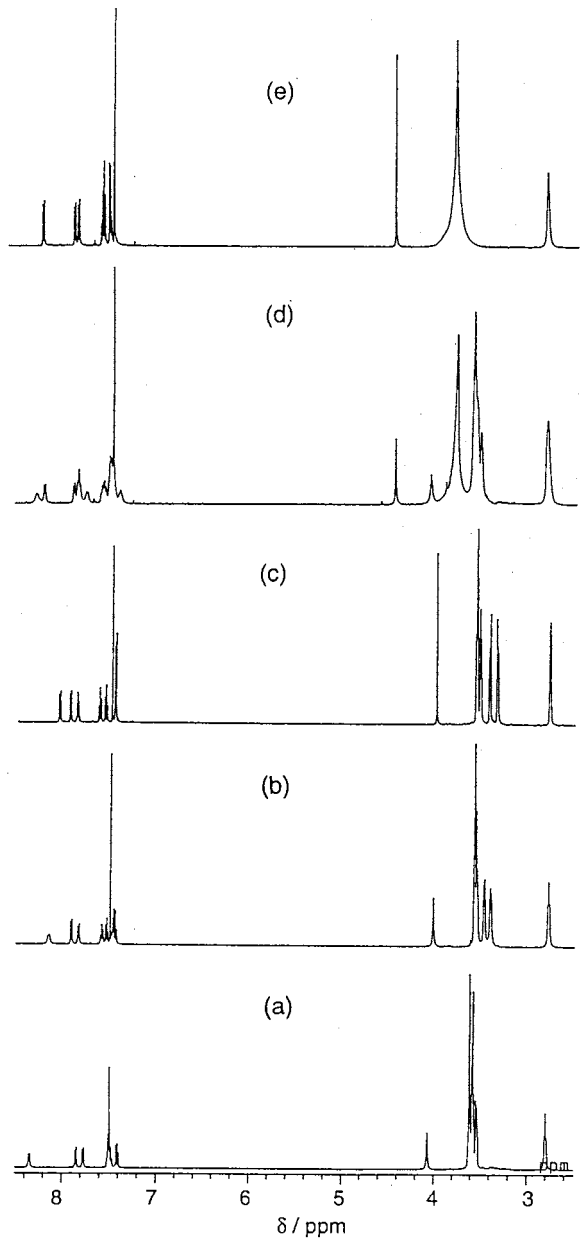

Fig. 4. ^{1}H NMR spectral changes of **3** (1.0×10^{-2} M) with KSCN and $Ba(SCN)_2$ in CD_3CN–$CDCl_3$ (1:1 v/v) at 298 K. Concentration of metal salts: (a) 0, (b) [KSCN] = 0.5×10^{-2}, (c) [KSCN] = 1.0×10^{-2}, (d) [$Ba(SCN)_2$] = 0.5×10^{-2}, and (e) [$Ba(SCN)_2$] = 1.0×10^{-2} M.

should be responsible for a large difference in the relative emission-intensity ratio for these metal ions (Fig. 3).

Further detailed information on the cation binding behavior for **3** was obtained by $^{1}H/^{13}C$ NMR spectroscopy. The chemical (δ) and induced ($\Delta\delta$) shifts of the selected proton and carbon signals of the host (**3**) with and without metal cations are summarized in Table 2. Interestingly, Ba^{2+} produced an even more remarkable chemical-shift change for the methylene carbon signal.

Table 2
Changes of ^{1}H NMR and ^{13}C NMR chemical shifts of **3** (1.0×10^{-2} M) with various metal salts (1.0×10^{-2} M) in CD_3CN–$CDCl_3$ (1:1 v/v)

	Naphthylmethyl group		
	Naphthyl group	–CH_2–	
	H-8	H	C
3	8.36	4.07	58.8
LiSCN	8.22 (−0.14)	4.08 (+0.01)	56.3 (−2.5)
NaSCN	8.10 (−0.26)	4.01 (−0.06)	57.0 (−1.8)
KSCN	8.06 (−0.30)	3.99 (−0.08)	57.5 (−0.7)
RbSCN	8.16 (−0.20)	4.01 (−0.06)	57.8 (−1.0)
CsSCN	8.26 (−0.10)	4.05 (−0.02)	57.6 (−1.2)
NH_4SCN	8.12 (−0.24)	4.06 (−0.01)	56.6 (−2.2)
$Zn(SCN)_2$	8.19 (−0.17)	4.86 (+0.79)	54.5 (−4.3)
$Mg(SCN)_2$	8.20 (−0.16)	4.87 (+0.80)	54.5 (−4.3)
$Ca(SCN)_2$	8.44 (+0.08)	4.60 (+0.53)	50.5 (−8.3)
$Ba(SCN)_2$	8.24 (−0.12)	4.45 (+0.38)	49.7 (−9.1)

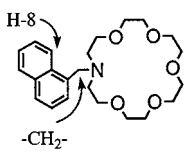

The magnitude of the metal ion-induced shift for this carbon signal decreased in the following order: $Ba(SCN)_2$ (−9.1) > $Ca(SCN)_2$ (−8.3) > $Zn(SCN)_2$ (−4.3) > $Mg(SCN)_2$ (−4.0) > LiSCN (−2.5) > NH_4SCN (−2.2) > NaSCN (−1.8) > CsSCN (−1.2) > RbSCN (−1.0) > KSCN (−0.7), clearly demonstrating that the nitrogen atom in the azacrown ether has a propensity to strongly coordinate with cations. The presence of bivalent metal salts induced a dramatic downfield shift ($\Delta\delta = 0.80$ for $Mg(SCN)_2$, 0.79 for $Zn(SCN)_2$, 0.53 for $Ca(SCN)_2$, and 0.38 for $Ba(SCN)_2$) of the methylene proton signal of the 1-naphthylmethyl group. These downfield shifts may be due to the strong interaction of the cations with the azacrown nitrogen. On the other hand, NaSCN, KSCN, RbSCN and CsSCN caused distinct upfield shifts of the H-8 and methylene proton signal of the 1-naphthylmethyl group. These upfield shifts must be due to shielding effects by thiocyanate anion. The interaction between the thiocyanate anion and the naphthalene ring may be responsible for a large difference in the relative emission-intensity ratio for metal salts.

4. Conclusions

The conclusion are: (1) the fluorescence quenching of the host itself occurs by intramoleculer electron transfer between the naphthyl group and the nitrogen atom in the crown ring, and the bivalent cation binding to the host azacrown results in an emision-intensity enhancement; (2) the metal cation-induced emission-intensity enhancement originates from the affinity of the nitrogen atom in the azacrown ether for cations; (3) the alkali metal salts induced fluorescence quenching is explained by intramoleculer photoinduced electron transfer from the thiocyanate anion to the naphthyl group; and (4) the azacrown ether having a 1-naphthyl pendant may be utilized as a new fluorescent sensor for metal cations and counter anions.

References

[1] J.-M. Lehn, Angew. Chem. Int. Ed. Engl. 27 (1988) 89.
[2] J.-M. Lehn (Ed.), Supramolecular Chemistry, VCH, Weinheim, 1995.
[3] H.G. Löhr, F. Vögtle, Acc. Chem. Res. 18 (1985) 65.
[4] A.P. de Silva, S.A. de Silva, J. Chem. Soc. Chem. Commun. (1986) 1709.
[5] I. Aoki, H. Kawabata, K. Nakashima, S. Shinkai, J. Chem. Soc. Chem. Commun. (1991) 1771.

[6] R.A. Bissell, A.P. Silva, H.Q.N. Gunaratne, P.L.M. Lynch, G.E.M. Maguire, K.R.A.S. Sandanayake, Chem. Soc. Rev. 21 (1992) 187.
[7] S. Alihodzic, M. Zinic, B. Klaic, et al., Tetrahedron Lett. 34 (1993) 8345.
[8] L. Fabrizzi, A. Poggi, Chem. Soc. Rev. 24 (1995) 197.
[9] A.P. de Silva, H.Q.N. Gunaratne, T. Gunnlaugsson, et al., Pure Appl. Chem. 48 (1996) 1443.
[10] G.E. Collins, L.-S. Choi, Chem. Commun. (1997) 1135.
[11] J.H.R. Tucker, H.-B. Laurent, P. Marsau, S. W. Riley, J.-P. Desvergne, Chem. Commun. (1997) 1165.
[12] K. Kubo, E. Yamamoto, T. Sakurai, Heterocycles 45 (1997) 1457.
[13] N.K. Petrovch, A.I. Shushin, E.L. Frankevich, Chem. Phy. Lett. 82 (1981) 339.
[14] N.K. Petrov, V.N. Borisenko, M.V. Alfimov, T. Fiebig, H. Staerk, J. Phy. Chem. 100 (1996) 6368.
[15] K. Kubo, R. Ishige, N. Kato, E. Yamamoto, T. Sakurai, Heterocycles 45 (1997) 2365.
[16] K. Kubo, T. Sakurai, Rep. Inst. Adv. Mater. Study Kyushu Univ. 10 (1996) 85.
[17] K. Kubo, N. Kato, T. Sakurai, Bull. Chem. Soc. Jpn. 70 (1997) 3041.
[18] K. Kubo, T. Sakurai, Chem. Lett. (1996) 959.
[19] K. Kubo, N. Kato, T. Sakurai, Acta Cryst. 53C (1997) 132.
[20] A. Mori, K. Kubo, H. Takeshita, Coord. Chem. Rev. 148 (1996) 71.
[21] S. Iwata, K. Tanaka, J. Chem. Soc. Chem. Commun. (1995) 1491.

ELSEVIER

Talanta 48 (1999) 189–199

Talanta

Kinetics and mechanism of amitraz hydrolysis in aqueous media by HPLC and GC-MS

E. Corta, A. Bakkali, L.A. Berrueta, B. Gallo *, F. Vicente

Department of Analytical Chemistry, Faculty of Sciences, University of the Basque Country, P.O. Box 644, 48080 Bibao, Spain

Received 9 March 1997; received in revised form 22 June 1998; accepted 23 June 1998

Abstract

Degradation processes of amitraz in aqueous media have been studied by spectrophotometry, HPLC and GC-MS. Amitraz undergoes hydrolysis reactions at any pH, but towards the acidic pH range hydrolysis proceeds at a faster rate. Depending on the pH value, different products of the hydrolysis have been identified. The main degradation products are 2,4-dimethylaniline at very acidic pH values (pH < 3), *N*-(2,4-dimethylphenyl)-*N′*-methylformamidine and 2,4-dimethylphenylformamide at less acidic media (pH 3–6) and 2,4-dimethylphenylformamide at basic pH. The mechanisms of the different hydrolysis processes have been elucidated.

Keywords: Amitraz; Hydrolysis; Kinetics; HPLC

1. Introduction

Amitraz (IUPAC name: *N*-methylbis(2,4-xylyliminomethyl)amine and development code BTS 27419) is a non-systemic acaricide and insecticide, with contact and respiratory action. Its mode of action probably involves an interaction with octopamine receptors in the nervous system of the ticks causing an increase in nervous activity. Amitraz is used to control all stages of tetranychid and eriophyid mites, pear suckers, scale insects, mealybugs, whitefly, aphids and eggs and first instar larvae of lepidoptera on pome fruit, citrus fruit, cotton, stone fruit, bush fruit, strawberries, hops, cucurbits, aubergines, capsicums, tomatoes, ornamentals and some crops. It is also used as an animal ectoparasiticide to control ticks, mites and lice on cattle, dogs, goats, pigs and sheep [1,2]. Additionally, amitraz is often used against varroasis disease, caused by the mite *Varroa jacobsoni* and affects *Apis Mellifera*. Amitraz shows a high activity against *V. jacobsoni*, and low toxicity for bees [3].

The degradation of amitraz in several fruit crops and soil has been studied and more than 95% of the residue left on the crop and soil samples can be accounted for as compounds amitraz, *N*-(2,4-dimethylphenyl)-*N′*-methylformamidine (BTS 27271) and 2,4-dimethylphenylformamide (BTS 27919). BTS 27271 and BTS 27919 arise from amitraz by a hydrolysis process [4].

* Corresponding author. Tel.: +34 94 4647700; fax: +34 94 4648500; e-mail: qapgaheb@lg.ehu.es

0039-9140/99/$ - see front matter
PII S0039-9140(98)00237-9

When added to honey, amitraz was fully degraded over a period of 2–4 weeks, depending on the honey type and the honey pH, and the degradation products that were found mainly are BTS 27919, BTS 27271 and 2,4-dimethylaniline (BTS 24868) [5,6]. Among them, BTS 24868 and BTS 27271 retain toxic activity [7]. Spanish laws define amitraz residues as the sum of amitraz and BTS 27271 and specify different maximum residue levels (LMR) depending on the type of food from 0.02 to 1 mg kg^{-1}.

Amitraz determinations are based on hydrolytic conversion of both amitraz and its degradation products to 2,4-dimethylaniline [8] and subsequent determination by HPLC [9] or GC [10–12].

The purpose of this research was to study amitraz degradation and the kinetics of the hydrolysis reaction in aqueous media, this information being relevant to evaluate the toxicity of amitraz residues in some crops. The hydrolysis of amitraz into buffers at different pH values and into acetonitrile–buffer environments has been examined and the reaction rate constants and half-life times calculated, hydrolysis products being identified by HPLC and CG-MS. Following these results, a new hydrolysis mechanism has been proposed.

A partial hydrolysis study in aqueous media has been recently reported by Pierpoint et al. [13] in which the kinetics of amitraz hydrolysis in relation to pH, as well as the effects of the hydrolysis of cosolvent and metal ions have been studied. Our study provides new data on this subject and proposes a novel hydrolysis mechanism controlled by pH.

2. Experimental

2.1. Reagents and chemicals

The compounds studied, amitraz, BTS 27919, BTS 24868 and BTS 27271 hydrochloride salt (ZK 049844), were kindly supplied by Schering Agrochemicals. The stock standard solutions of these compounds were prepared in acetonitrile (amitraz is not stable in methanol) at a concentration of 1000 μg ml^{-1} and were stored at 4°C in the dark.

Acetonitrile (Romil, Harvehill, UK) was of HPLC grade. The water used in all experiments was purified on a Milli-Q system from Millipore (Bedford, MA). Sodium acetate, acetic acid, phosphoric acid, sodium hydrogen and dihydrogen phosphates, sodium carbonate, sodium hydrogen carbonate and sodium hydroxide were of analytical quality from Merck (Darmsdt, Germany). The aqueous buffers were: 0.05 M HCl (pH 1.3), 0.05 M H_3PO_4–NaH_2PO_4 (pH 2–3), 0.1 M HAc–NaAc (pH 4–5), 0.1 M NaH_2PO_4–Na_2HPO_4 (pH 6–8) and 0.1 M $NaHC0_3$–Na_2CO_3 (pH 10).

The test hydrolysis solutions were prepared by dilution of the amitraz stock solution with the appropriate aqueous buffer. At pH 3.0 amitraz is soluble in water since it is positively charged ($pK_a = 4.2$ [1]) but at pH > 3.0 the addition of acetonitrile was necessary in order to solubilize amitraz. The pH values tabulated are measured after the addition of acetonitrile as apparent pH. The effect of the cosolvent on the rate and the product profile is negligible until 50% of the cosolvent [13].

To study the hydrolysis of amitraz at pH values in which hydrolysis is very fast, UV–Vis spectrophotometry was used. The change of the absorbance of 20 μg l^{-1} amitraz solutions in 0.05 M aqueous buffer with time at a fixed wavelength (285 nm) and 25°C was measured. For the cases in which the hydrolysis is slow enough, HPLC with spectrophotometric detection was used and the variation of peak area or concentration of 20 μg l^{-1} amitraz solution in 0.1 M acetonitrile–buffer (40:60 v/v) at 25°C against the hydrolysis time was measured.

2.2. Instrumentation

A Shimadzu UV-260 spectrophotometer was used for all the spectrophotometric measurements. The absorbance was measured at a fixed wavelength (285 nm) as a function of time.

HPLC was used to measure the amitraz peak area decrease as a function of time. The chromatographic system consisted of two HPLC pumps (LKB, Barcelona, Spain) 2150, a high pressure mixer LKB 2152-400, an HPLC controller LKB 2152, a Rheodyne (Cotati, USA)

7125 sample injector with a loop of 50 μl and a Waters (Barcelona, Spain) 484 UV–Vis detector. A Waters Nova-Pack C18 column (15 cm × 3.9 mm i.d., 4 μm) was used. The effluent was monitored at 210 nm. The elution was performed under binary gradient conditions. Pump A: acetonitrile–0.01 M TEA (pH 6.1 with 0.75 M H_3PO_4) (90:10 v/v) and pump B: acetonitrile–0.01 M TEA (pH 6.1 with 0.75 M H_3PO_4) (30:70 v/v). The gradient profile was 0 min., 100% B; 1.5 min., 100% B, 15 min., 0% B. The flow-rate was 1 ml min^{-1}.

GC-MS was used to confirm the identity of the degradation products. A Hewlett-Packard (Palo Alto, CA) series II 5890 gas chromatograph coupled to a Hewlett-Packard Engine 5989B mass spectrometer in the electronic impact mode was used. The capillary column used was an HP-5 (Crosslinked 5% PH ME siloxane) 30 m × 0.32 mm × 0.25 mm film thickness. A 1 μl volume of the hydrolysis solution was chromatographed under the following conditions: injector temperature was 250°C; the initial column temperature (40°C) was held for 1.50 min., then increased to 150°C at 40°C min^{-1} and held for 1 min, then elevated to 250°C at 30°C min^{-1} and held for 2 min. The carrier was helium and the pressure in the column head was 100 kPa. In the spectrometer the source and quadrupole temperature were kept at 250 and 100°C.

3. Results and discussion

In Fig. 1, variation of the absorption spectra versus time for two solutions of amitraz buffered at pH 2.1 and 10.7 (with 40% acetonitrile) is shown. Study of absorption spectra reveals two different behaviours as regards to pH. At pHs around 2.0, the peak of absorption for amitraz

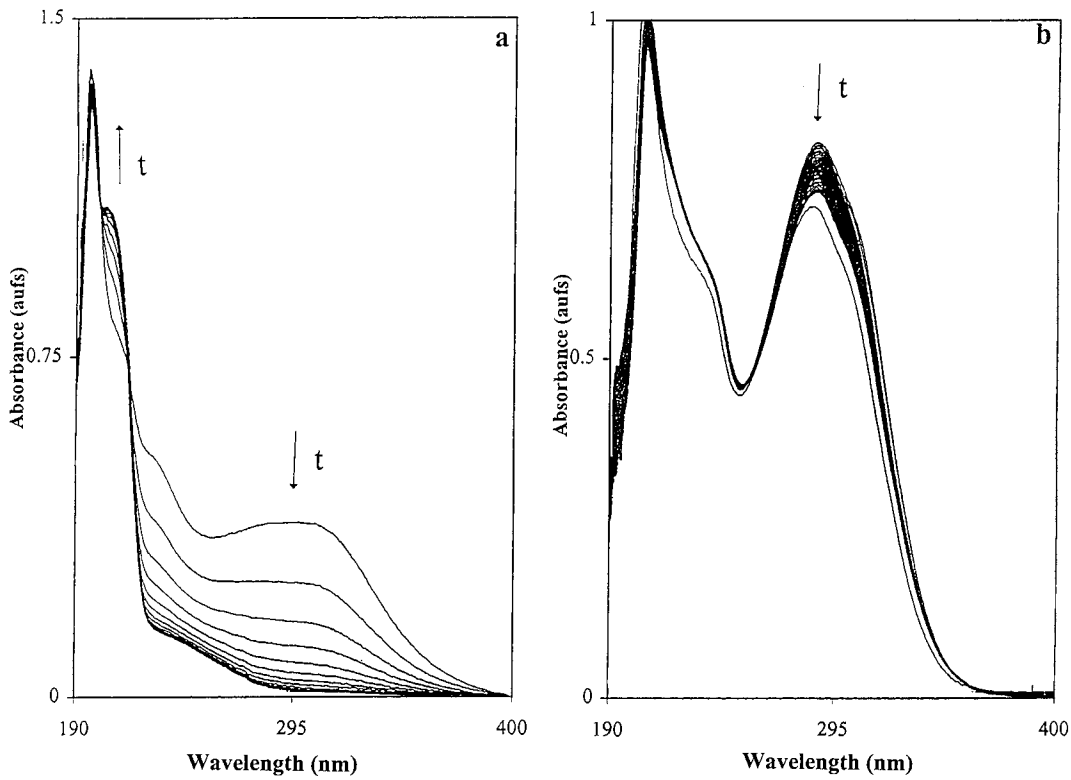

Fig. 1. Variation of the absorption spectra with hydrolysis time at room temperature for an amitraz solution of 10 μg ml^{-1} in (a) buffer of pH 2.1 (each cycle 2 min) and (b) buffer of pH 10.7 with 40% acetonitrile (each cycle 30 min).

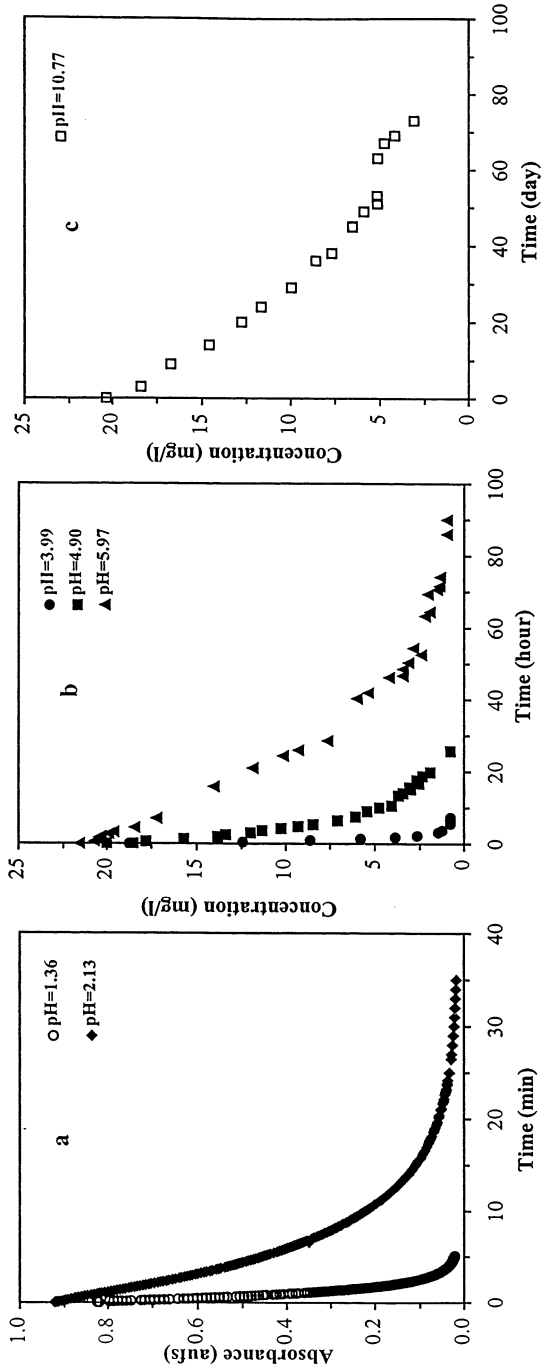

Fig. 2. (a) Variation of the absorbance at 285 nm vs. time for a 20 μg ml^{-1} amitraz solution in 0.05 M buffer at 25°C and different pH values: (○) 1.36 and (◆) 2.13. (b), (c) Variation of the concentration of amitraz vs. time, for a 20 μg ml^{-1} amitraz solution in acetonitrile–0.1 M buffer (40:60 v/v) at 25°C and different pH values: (●) 3.99, (■) 4.90, (▲) 5.97 and (□) 10.77.

Table 1
Apparent reaction rate constants (k) and half-life time values for the hydrolysis of amitraz at different pH media

Apparent pH	k (min^{-1})	$t_{1/2}$ (min)
1.36	0.868 ± 0.003	0.798 ± 0.003
2.13	0.1437 ± 0.0004	4.82 ± 0.01
3.99	0.0103 ± 0.0009	67 ± 6
4.90	0.00190 ± 0.00005	361 ± 9
5.97	0.00063 ± 0.00001	1108 ± 17
10.77	$(1.7 \pm 0.1) \times 10^{-5}$	$(43 \pm 3) \times 10^{3}$

appears at 195 nm with a shoulder at 299 nm and the spectra show a decrease in the band at 299 nm with time, whereas one shoulder appears at 203 nm. Over this pH, two absorption peaks are evident at 200 and 285 nm and a decrease of the intensity of the peak at 285 nm is also observed.

Variations observed in the absorption spectra suggest that amitraz suffers hydrolysis processes in acid and basic media as has been reported by other authors [1,13]. In order to study these processes in depth, spectrophotometry was used for the pH values in which the hydrolysis is very fast and HPLC with spectrophotometric detection for the cases in which the slow rate of the hydrolysis process allows for it. In the first case, the absorbance was measured at a fixed wavelength (285 nm) as a function of the hydrolysis time (Fig. 2a). When HPLC measurements were performed, a decrease of the amitraz peak area with hydrolysis time appeared (Fig. 2b and c). Using both techniques, the apparent reaction rate constant and the amitraz half-life time were calculated at each pH value (Table 1). The $\ln (A_0/A)$ for spectrophotometry and $\ln (C_0/C)$ for HPLC as a function of hydrolysis times were represented, being explained by a first order kinetic.

Under the HPLC separation conditions, amitraz showed a peak at retention time 15.5 min. When hydrolyzed solutions obtained at the various essayed pHs were injected, a different number of peaks were obtained. Retention times for these peaks were 1.46, 2.47, 3.38, 4.31 and 7.88 min which belong to amitraz hydrolysis products (Fig. 3). The peaks at 2.47, 3.38 and 4.31 min are the most abundant and persistent and were identified as BTS 27271, BTS 27919 and BTS 24868, respectively, by the injection of standard solutions and

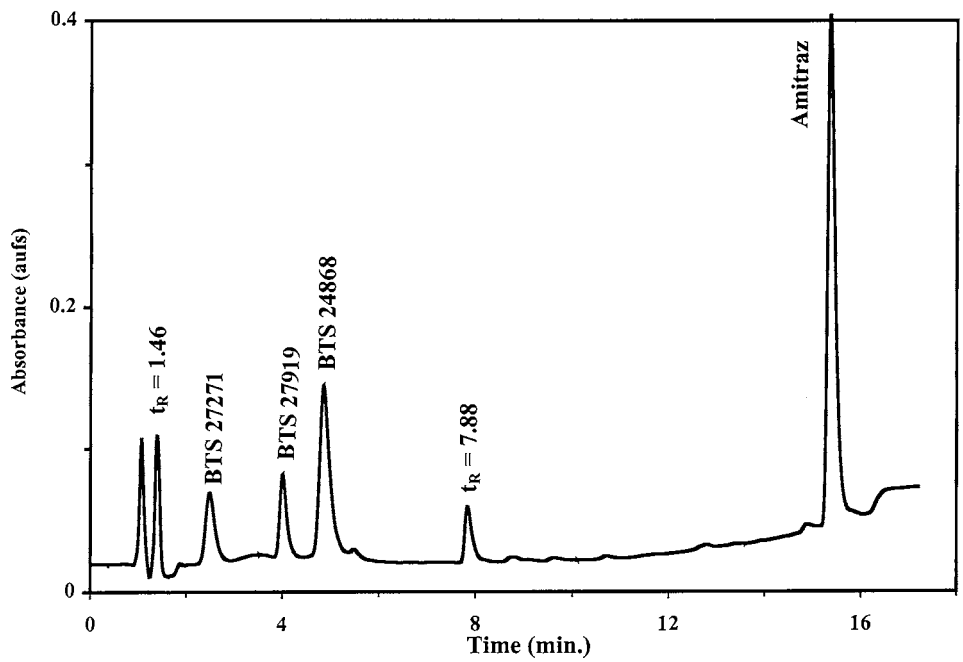

Fig. 3. HPLC chromatogram of amitraz hydrolysis solution at pH 1.36 after 1 min, (hydrolysis not completed).

Table 2
Retention times of the degradation products and percentage against total peak area for each degradation product peak at different pH values

Apparent pH	Retention time of peaks (min)					
	1.46	2.47 (BTS27271)	3.38 (BTS27919)	4.31 (BTS24868)	7.88[a]	15.50 (Amitraz)
1.3	20	16	13	51	N.D.	N.D.
2.0	14	26	21	39	N.D.	N.D.
3.0	6	36	28	30	N.D.	N.D.
3.9	3	52	39	6	N.D.	N.D.
4.9	N.D.	50	49	1	N.D.	N.D.
6.2	N.D.	47	51	2	N.D.	N.D.
8.2	N.D.	N.D.	81	5	N.D.	14
10.2	N.D.	N.D.	67	23	N.D.	10

[a] Peak corresponding to an intermediate product of the hydrolysis.

comparison of the retention times. Additionally, identity was confirmed by injection of the hydrolyzed samples in the GC-MS equipment. Amitraz and its degradation products give peaks at retention times of 15.55, 4.53, 6.39 and 6.73 min, respectively (Fig. 4). These peaks were identified as the BTS 24868 ($t_R = 4.53$ min), BTS 27919 ($t_R = 6.39$ min), and BTS 27271 ($t_R = 6.73$ min) by comparison of the retention times and mass spectra with those of standard solutions (Fig. 4). Pierpoint et al. [13] did not detect the formamidine BTS 27171.

In Table 2 the retention times of the products of hydrolysis and its percentage against total peak area for each degradation peak at different pH values are shown. This percentage has been calculated at acidic pH values just when the quantity of amitraz becomes null (less than 3 hydrolysis days), and at basic pH when the amitraz concentration is lower than 15% (60–70 hydrolysis days). The main degradation products, different depending on the pH value, are: BTS 24868 at pH < 3, BTS 27271 and BTS 27919 at less acidic media (pH 3–6) and BTS 27919 at basic pH. This suggests at least, three different hydrolysis reactions.

Fig. 5 aims to explain the nature of the reaction proceeding at pH < 3 where BTS 24868 is the main degradation product. This figure shows the evolution of the HPLC peak areas of the degradation products as a function of hydrolysis time for an amitraz solution at pH 1.41. While the amitraz peak disappears (a few minutes), five new peaks become evident. One of them is a transitory peak of the reaction ($t_R = 7.88$ min), which shows only in the first moments of the hydrolysis in very acidic media, whereas the other four ($t_R = 1.46$ min, BTS 24868, BTS 27919 and BTS 27171) are the final products.

In view of these results, two reaction mechanisms could be proposed (mechanism 1 and mechanism 2 of reaction 1, Fig. 6). The difference between the two mechanisms is the way in which the aniline BTS 24868 is generated: from formamide BTS 27919 and/or formamidine BTS 27171 (mechanism 1) or from the amitraz (mechanism 2).

To check if BTS 24868 is generated from formamide BTS 27919 and/or formamidine BTS 27171, the stability of the standard solutions of BTS 27919 and BTS 27271 at acidic pH and room temperature have been studied. After only 5 days at pH < 2 a BTS 27919 instability has been observed with a reaction half-life of 2–3 days at pH 1.4. This hydrolysis reaction derives from aniline BTS 24868 as a reaction product (reaction 4 of Fig. 6). On the other hand BTS 27271 is stable in acidic pHs for at least 5 days.

In conclusion, the quick formation of aniline BTS 24868 (less than 1 h) in hydrolysis of amitraz observed in Fig. 5, implies, necessarily, the formation of the aniline directly from amitraz (mechanism 2) and not from formamide BTS 27919 (much slower) or from formamidine BTS 27271

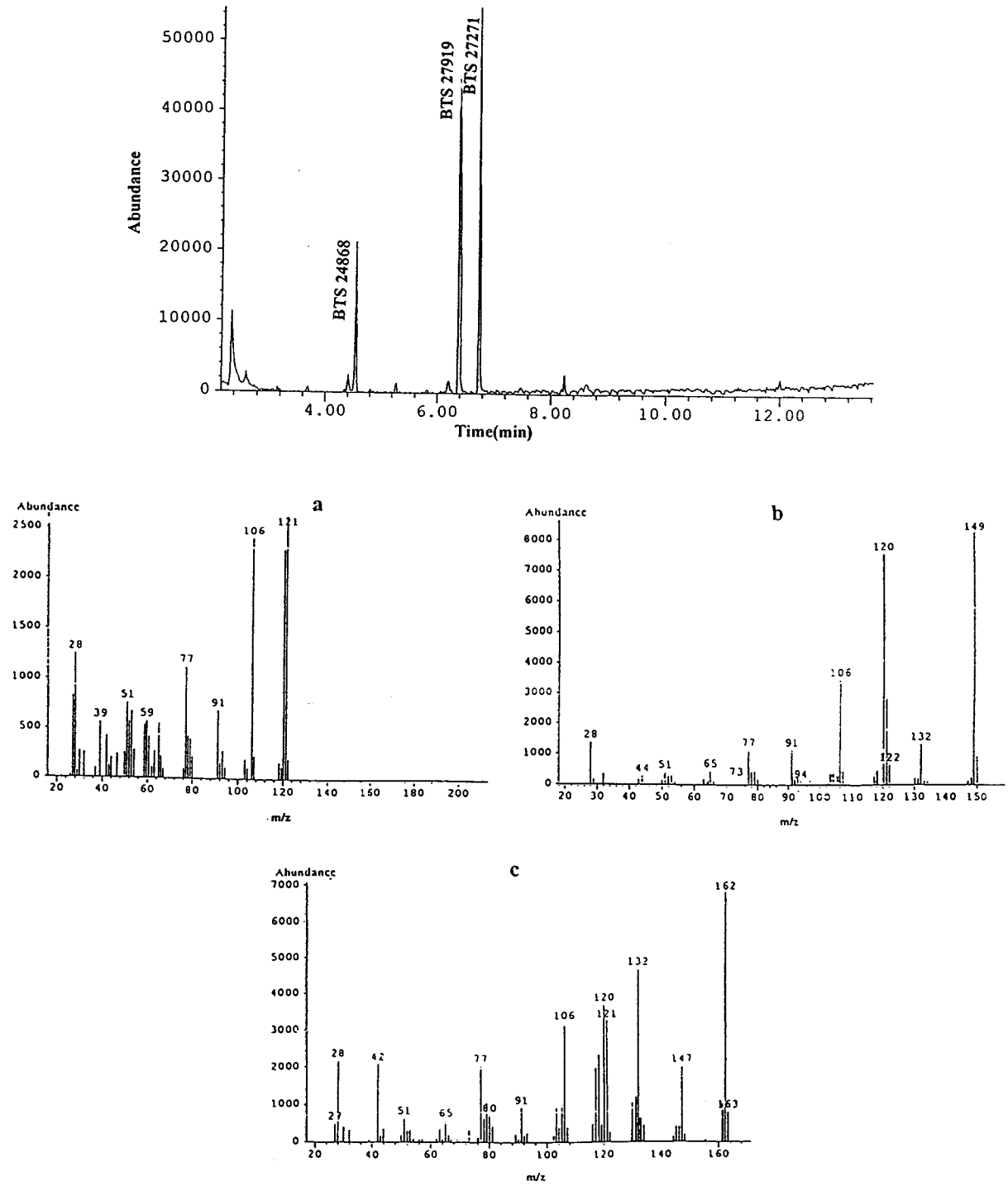

Fig. 4. CG-MS chromatogram corresponding to a 100 μg ml^{-1} amitraz solution at pH 3.0 after total hydrolysis and mass spectra corresponding to (a) BTS 24868, (b) BTS 27919 and (c) BTS 27271.

(stable at acid pHs). This reaction is also confirmed by the presence of the transitory peak at 7.88 min, that could not be identified, but it is probably an intermediate compound of this reaction (mechanism 2 of reaction 1, Fig. 6). As shown in Table 2, mechanism 2 only happens at acid pH and is the main hydrolysis process at $pH < 3$. This quick detection of aniline BTS 24868 in very acid media has not been described by Pierpoint et al. [13]. Besides, the formation of the aniline from formamide BTS 27919 can be observed in Fig. 5, but only after 2 or 3 h from the start of the hydrolysis, when the peak of the formamide starts to decrease slowly and that of the aniline increases slowly (reaction 4, Fig. 6).

At pHs between 3 and 6, formamide BTS 27919 and formamidine BTS 27271 are the main products and appear in equivalent quantities, this suggest a second reaction (reaction 2 of Fig. 6) that would be predominant at pHs between 3 and 6.

In basic media, a third reaction happens leading to formamide BTS 27919 as the most important degradation product (reaction 3 of Fig. 6) although, significant quantities of BTS 24868 reappear. This BTS 24868 (Table 2) is now from the BTS 27919 degradation (reaction 4 of Fig. 6) and not directly from amitraz as happened at very acidic pH values. Reaction 4 takes place more slowly at basic pH than at acid media ($t_{1/2} = 2–3$ days at pH 1.4), as established by Pierpoint et al. [13] who calculated the half-life time of BTS 27919 at pH 9.12 as 300 days.

4. Conclusions

Amitraz is unstable in the whole pH range,

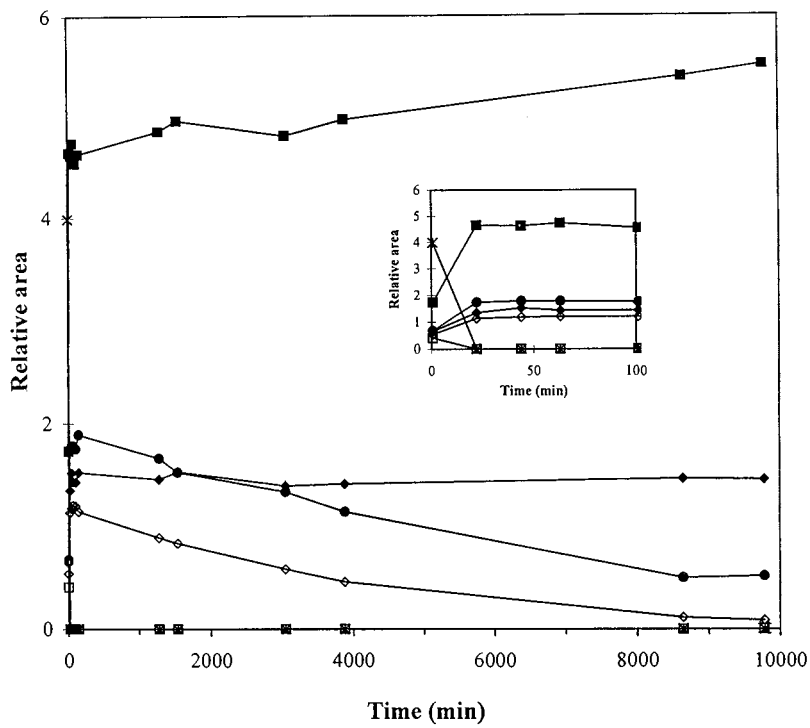

Fig. 5. Evolution of the HPLC peak areas of the degradation products as a function of the hydrolysis time at pH 1.41. (●) $t_R = 1.46$ min, (◆) BTS 27171, (◇) BTS 27919, (■) BTS 24868, (□) $t_R = 7.88$ min and (∗) amitraz.

REACTION 1 (main reaction at pH < 3)

Mechanism 1

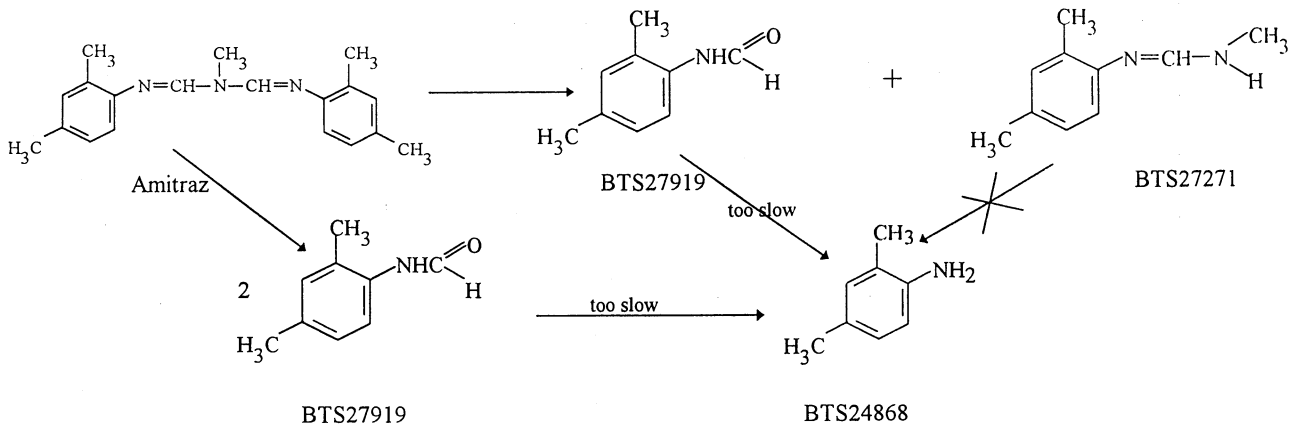

Mechanism 2

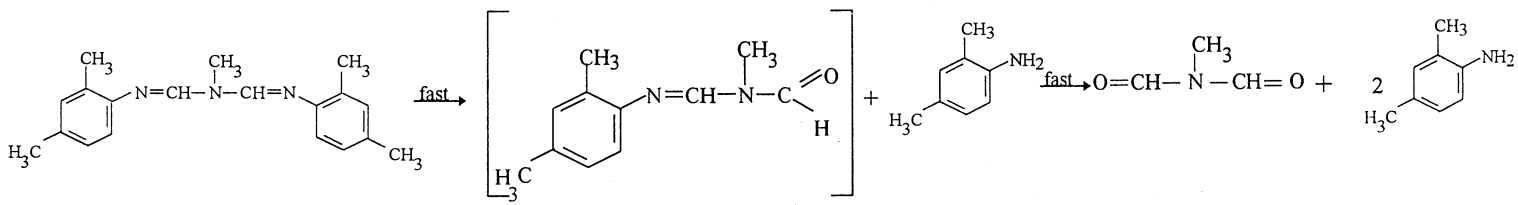

Fig. 6. Reactions proposed for the degradation of amitraz in aqueous media.

REACTION 2 (main reaction at 3 < pH< 6)

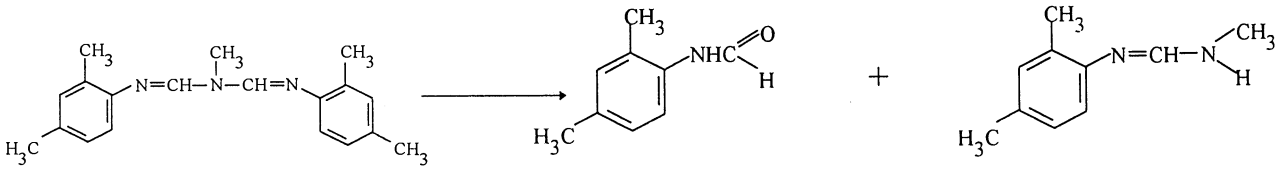

REACTION 3 (main reaction at basic pH)

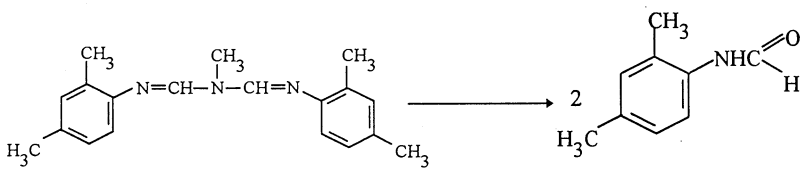

REACTION 4

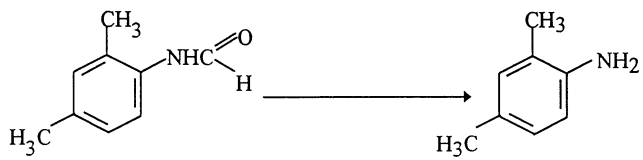

(b) BTS27919 BTS24868

Fig. 6. (*Continued*)

undergoing faster hydrolysis at acidic pH values (at $pH < 2$ the degradation is almost instantaneous). The nature of the degradation products depends on the pH. At very acidic pHs the main degradation product is the compound BTS 24868, at less acidic pHs the main products are BTS 27271 and BTS 27919 and at basic pH BTS 27919 is the principal hydrolysis compound. The identified degradation products could be found as amitraz residues in food and surface waters samples. Some of these residues have toxicological importance, as in the case of BTS 27271 and BTS 24868.

Acknowledgements

The authors wish to thank to the Ministerio de Educación y Ciencia for a FPI grant. These studies were supported by the Universidad del País Vasco/Euskal Herriko Unibertsitatea (Project No. EA145/93) and the Comisión Interministerial de Ciencia y Tecnología (Project No. ALI95-0451). The standards were kindly provided by Schering Agrochemicals.

References

[1] C. Tolim, The Pesticide Manual, vol. 1, 10th ed., The British Crop Protection Council and Royal Society of Chemistry, UK, 1994, p. 35.
[2] B. Tudek, J. Gajewska, M. Szczypka, I. Rahden-Staron, T. Szymczyk, Mutat. Res. 204 (1988) 585.
[3] R. Cozzani, M. Di Pietrogiacomo, Ind. Aliment. 18 (1989) 608.
[4] E. Hornish Rex, M.A. Clasby, J.L. Nappier, J.M. Nappier, A.G. Hoffman, J. Agric. Food Chem. 32 (1984) 1219.
[5] S. Bogdanov, V. Kilchenmann, A. Imdorf, Mitt. Sekt. Bienen 3 (1988) 1.
[6] J.J. Jimenez, J.L. Bernal, M.J. Del Nozal, L. Toribio, J. High Resolut. Chromatogr. 20 (1997) 81.
[7] C.O. Knowles, A.K. Gayen, J. Econom. Entomol. 76 (1982) 410.
[8] M.A. Fernandez-Muiño, M.T. Muniategui, J.F. Huidobro, J. Simal-Lozano, J. Food Prot. 58 (1995) 449.
[9] L. Serpe, G. Oliviero, A. Begliomini, Ind. Aliment. 28 (1989) 1173.
[10] M. Lodesani, A. Pellacani, S. Bergomi, E. Carpana, T. Rabitti, P. Lasagni, Apidologie 23 (1992) 257.
[11] M.B. Taccheo, M. De Paoli, C. Spessotto, Pest. Sci. 23 (1988) 59.
[12] K. Ameno, C. Fuke, S. Ameno, T. Kiriu, T. Shinohara, I. Ijiri, J. Anal. Toxicol. 15 (1991) 116.
[13] A.C. Pierpoint, C.J. Hapeman, A. Torrents, J. Agric. Chem. 45 (1997) 1937.

ELSEVIER

Talanta 48 (1999) 201–208

Talanta

Simultaneous detection of three drugs labeled by cationic metal complexes at a nafion-loaded carbon paste electrode

Anne-Line Bordes, Bernd Schöllhorn, Benoît Limoges, Chantal Degrand *

Equipe Electrosynthèse et Electroanalyse Bioorganique, SEESIB (UMR 6504 CNRS), Université Blaise Pascal de Clermont-Ferrand, 24 Avenue des Landais, 63177 Aubière, France

Received 9 April 1997; received in revised form 19 June 1998; accepted 23 June 1998

Abstract

The synthesis of the pentaammine ruthenium(II) complex of *N*-isonicotinoyl–nortriptyline (NORPy-Ru^{2+}) was performed and its electrochemical properties at a nafion-loaded carbon paste electrode were examined. The anodic oxidation of the positively charged labeled antidepressant proceeded at -0.06 V (versus Ag/AgCl, 0.05 M Cl^-). A detection limit of 0.075 μM (S/N = 3) was achieved at physiological pH by square-wave voltammetry after a 5-min preconcentration step, with a linear response over the range 0.075–5.0 μM. With a view to a future triple-analyte immunoassay, the detection of NORPy-Ru^{2+} was also examined in the presence of two labeled antiepileptics previously synthesised, i.e. phenytoin labeled by a ferroceneammonium salt (oxidation potential at 0.26 V) and phenobarbital labeled by a cobaltocenium salt (reduction potential at -1.05 V). The simultaneous detection of the three labeled drugs proceeded with analytical performances similar to those corresponding to the separate accumulation of each tracer. However it was observed that the pentaammine ruthenium(II) complexes of pyridine and its derivatives were not stable in the presence of serum, which does not allow for their use as redox cationic labels in a multi-analyte immunoassay to be envisaged.

Keywords: Ruthenium(II) complex; Nortriptyline; Antiepileptics; Multi-analyte immunoassay

1. Introduction

Multi-analyte immunoassays, in which several analytes are measured simultaneously in a single assay, present several advantages such as reduction of analysis time, work simplification, decrease in sample volume, and lowering of the overall cost per test [1,2]. One of the two major approaches developed to date involves the use of more than one label [3]. Dual-analyte immunoassays have been reported with the simulta-

* Corresponding author. Tel.: +33 4 73407159; fax: +33 4 73274443; e-mail: degrand@cicsun.univ-bpclermont.fr

0039-9140/99/$ - see front matter
PII S0039-9140(98)00238-0

neous use of two radiolabels [4], or two fluorescent [5], enzyme [6], spin [7] or metal–ion [8] labels. Examples with more than two labels are rare and have appeared only recently [9,10] using either a combination of lanthanide chelate labels and their time-resolved fluorescence detection [9], or several IR-active organometallic labels [10]. The main limitation to this approach is the simultaneous detection of different labels in the final step procedure, because it is difficult to find a combination of labels which can be detected distinctly and with similar sensitivities using a single technique. Moreover, it is often necessary to separate the free labeled antigens from the antibody-bound labeled antigens; only dual-analyte immunoassays based on two spin labels [7] and two fluorescent labels [5] avoided this step.

Our group has recently developed an analytical technique that combines competitive homogeneous immunoassay with electrochemical detection using a nafion-modified electrode and an antigen covalently attached to a positively charged redox label [11–14]. This technique allows multi-analyte assays to be carried out and it was possible to simultaneously detect submicromolar concentrations of two antiepileptic drugs, i.e. phenobarbital (PB) and phenytoin (5,5-diphenylhydantoin, DPH) at a nafion-loaded carbon paste electrode (CPE) [15]. PB and DPH were labeled by a cobaltocenium salt (Cc^+) and a ferroceneammonium salt (N^+Fc), respectively [16], and the standard redox potentials of PB-Cc^+ and DPH-N^+Fc were -1.05 and 0.26 V, respectively. A square wave voltammetric (SWV) detection limit of ca. 0.2 μM was reached for each labeled drug after a 5-min accumulation step [15]. The anionic perfluorosulfonated polymer nafion was able to selectively preconcentrate the cationic labeled drugs and therefore to enhance the sensitivity of the detection method. Since the immunoassay was conducted in homogeneous media, it was not necessary to separate the two free labeled drugs from the two antibody-bound labeled drugs, which provided an important advantage compared with other multi-analyte immunoassay formats. However the moderate reproducibility of the data allowed only semi-quantitative assays (positive/negative test) for clinical serum samples to be envisaged.

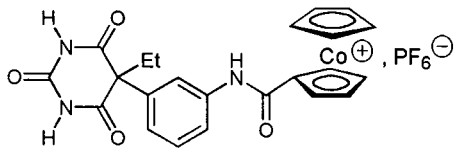

PB-Cc$^+$

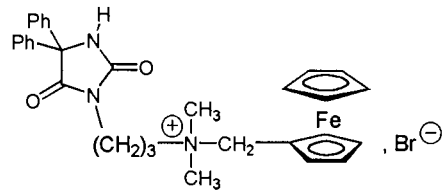

DPH-N$^+$Fc

In this paper we explore the possibility of using the cationic pentaammine complex $(Ru(NH_3)_5(Py))^{2+}$ (Py = pyridyl) as another positively charged redox label with a view to a future triple-analyte immunoassay using a nafion-loaded CPE. A third labeled drug was synthesised starting from the hydrochloride of isonicotinic acid chloride. In the first step, the acid chloride was covalently linked to the antidepressant nortriptyline. We thus obtained the pyridyl ligand *N*-isonicotinoyl-nortriptyline (NORPy) which was then bound to a pentaammine ruthenium(II) complex. The accumulation and SWV detection of the resulting $(Ru^{II}(NH_3)_5(NORPy))^{2+}$ complex (NORPy-Ru^{2+}) within nafion were examined in the absence and in the presence of the two labeled drugs PB-Cc^+ and DPH-N^+Fc. Several studies have addressed the redox and electrocatalytic properties of $(Ru^{II}(NH_3)_5(PyH))^{2+}$ or $(Ru^{II}(NH_3)_5(PyX))^{2+}$ (PyX = substituted pyridine) in nafion [17–23]. They have shown that the reversible oxidation of the complexes proceeds at ca. 0 V, versus SCE, i.e. in a potential range quite distinct from the potential range of the cobaltocenium or ferroceneammonium salt.

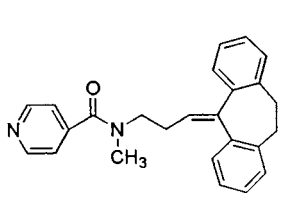

NORPy

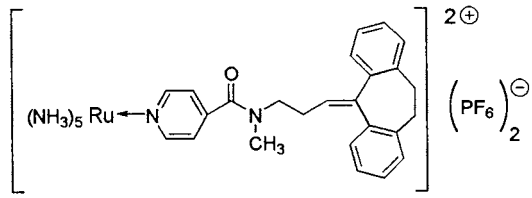

NORPy-Ru^{2+}

2. Experimental

2.1. Starting materials and reagents

Chloropentaammine ruthenium(III)dichloride was obtained from Johnson Matthey, and nortriptyline hydrochloride (99%) and rabbit normal serum (RNS) were purchased from Sigma. PB-Cc^+ [16], DPH-N^+Fc [16] and ($Ru^{II}(NH_3)_5$(PyH)) $(PF_6)_2$ [24] were prepared as described in the references cited.

Phosphate buffer (4.35 mM NaH_2PO_4, 15.1 mM Na_2HPO_4, and 50 mM NaCl, pH 7.4) containing 1% ethanol was used in all experiments unless stated otherwise. Stock solutions of each labeled drug in pure ethanol were stored at 0–4°C. All reagents were of analytical grade and water was deionized and doubly distilled.

2.2. General

NMR spectra were recorded on a Bruker AC 400 spectrometer. Infrared spectra were obtained with a Nicolet Impact 400 FT spectrometer. Elemental analyses and mass spectra were performed by the Centre National de la Recherche Scientifique (CNRS) at Vernaison. Preparative column chromatography was performed on silica gel (Merck 60 mesh). The air and water sensitive reactions were carried out under an argon atmosphere in purified solvents and were monitored by thin layer chromatography (TLC) (silica gel on aluminium foil, Merck 1.05554).

2.3. Synthesis of the labeled nortriptyline

2.3.1. Synthesis of NORPy

The hydrochloride of nortriptyline was treated with aqueous 1 M NaOH solution. After vigorous stirring for 30 min the product was extracted several times with ether. The organic phase was dried over $MgSO_4$. Evaporation of the ether gave the free base of nortriptyline as a white powder in a 97% yield.

Triethylamine (5.31 g, 53 mmol) and isonicotinic acid chloride (1.99 g, 11 mmol) were added under an argon atmosphere to a solution of nortriptyline (2.15 g, 8.2 mmol) in dried THF (120 ml). The mixture was stirred for 24 h at room temperature. The reaction was monitored by TLC. The less soluble acid chloride was dissolved completely in the course of the reaction. The hydrochloride of triethylamine generated formed a white precipitate. After 24 h the mixture was filtered over celite. The filtrate was concentrated by evaporation of THF in a vacuum and diethyl ether (140 ml) was added. The mixture was extracted four times with water (50 ml, pH 7). After drying of the organic phase over $MgSO_4$ the solvents were evaporated and the crude white solid product NORPy was collected in a 52% yield (1.57 g). Recrystallisation from acetone (12.5 ml) afforded the pure product NORPy (1.02 g, 34% yield) with a melting point of 123–124°C. ^{1}H NMR (400 MHz, acetone-d_6): δ_{ppm} 8.64 (d, 1H, J 5.9 Hz, py C–H), 8.50 (d, 1H, *J* 5.9 Hz, py C–H), 7.33–6.98 (m, 10H, phenyl and py C–H), 5.96 (t, 0.4H, *J* 7.4 Hz, –CH=isomer A), 5.65 (t, 0.6H, *J* 7.8 Hz, –CH=isomer B), 3.73–3.59 (m, 1H), 3.35 (t, 2H, *J* 7.0 Hz, N–CH_2), 3.32–3.15 (m, 2H), 3.00–2.70 (m, 5H), 2.52–2.42 (mc, 0.4H, *J* 6.7Hz, –CH_2–CH=isomer A), 2.36 (mc, 0.6H, *J* 6.7Hz, –CH_2–CH=isomer B). ^{13}C NMR (400 MHz, acetone-d_6): δ_{ppm}168.5/168.2, 150.1/150.0, 145.3/144.7, 144.3, 141.2, 140.8, 140.0, 139.6, 139.4, 136.9, 130.1/130.0, 128.5, 128.23, 128.17, 128.07, 128.0, 127.7/127.6, 127.3/127.2, 126.0/125.9, 121.1, 121.0, 50.3/46.6, 36.5/31.9, 33.5/31.7, 28.5/27.3. IR (KBr): *v* 3425 (w, large), 3061 (w), 3032

Table 1
Elemental analysis for $(Ru^{II}(NH_3)_5(NORPy))(PF_6)_2$

	C	H	N	F	P	Ru
Calcd. for $C_{25}H_{39}N_{70}F_{12}P_2Ru$	35.55	4.65	11.61	26.99	7.33	11.97
Ratio relative to C	1	0.131	0.327	0.759	0.206	0.337
Found	27.08	3.60	8.38	20.74	—	8.83
Ratio relative to C	1	0.133	0.309	0.766	—	0.326

(w), 2980 (w), 2951 (w), 2925 (m), 2366 (m), 2336 (m), 1627 (s), 1592 (m), 1546 (m), 1498 (m), 1484 (m), 1443 (m), 1400 (s), 1273 (m), 1100 (m), 834 (m), 782 (m), 768 (m) cm^{-1}. MS (EI, 70 eV): m/z (relative intensity) 368 (9, (M^+)), 178 (8), 165 (5), 151 (4), 140 (7), 128 (4), 117 (7), 115 (8), 106 (100), 91 (17), 79 (5), 77 (55), 51 (25), 44 (6), 42 (11), 28 (3). *Anal.* Calc. for $C_{25}H_{24}N_{20}$ (368.48): C, 81.49; H, 6.57; N, 7.60. Found: C, 81.27; H, 6.79; N, 7.40%.

2.3.2. Synthesis of (N-isonicotinoyl-nortriptyline) pentaammine ruthenium(II) bis(hexafluorophosphate) (NORPy-Ru^{2+})

The synthesis of $(Ru^{II}(NH_3)_5(NORPy))(PF_6)_2$ was carried out by applying the procedure of Ford et al. [24] for the unsubstituted pyridine complex.pThe whole reaction was carried out in the dark. Trifluoroacetic acid (40 μl) was added to a mixture of Ag_2O (59 mg, 0.25 mmol) and bidistilled water (1.2 ml). After 30 min at room temperature chloropentaammine ruthenium(III)dichloride (79 mg, 0.27 mmol) was added. The precipitated silver chloride was filtered off. The filtrate, containing an aqueous solution of chloropentaammine ruthenium(III)bis(trifluoroacetate) was sent over an activated zinc amalgam column (diameter 1.5 cm, length 8 cm). The solution of the resulting aquapentaammine ruthenium(II)bis(trifluoroacetate) was slowly added to a stirred solution of NORPy (2.04 g, 5.54 mmol) in distilled acetone (50 ml) at room temperature and under an argon atmosphere. During the reaction the color of the solution turned red. After 90 min the solution was concentrated by evaporation of the solvents under reduced pressure. The precipitated NORPy was separated by filtration. After adding bidistilled water (100 ml) the filtrate was extracted four times with diethyl ether (50 ml). The purity of the aqueous phase was confirmed by TLC. The product NORPy-Ru^{2+} was precipitated by adding potassium hexafluorophosphate. The very fine orange powder had to be filtered over celite and dissolved in methanol. The product NORPy-Ru^{2+} (1.73 g) was finally obtained as an orange solid by evaporation of the methanol under reduced pressure. Decomposition occured above 120°C. ^1H NMR (400 MHz, acetone-d_6): δ_{ppm} 8.87 (d, 1H, J 5.9 Hz, py C–H), 8.79 (d, 1H, J 5.9 Hz, py C–H), 7.35–7.03 (m, 10H, phenyl and py C–H), 5.95 (t, 0.6H, J 7.4 Hz, –CH=isomer A), 5.66 (t, 0.4H, J 7.4 Hz, –CH=isomer B), 3.66 (mc, 1H), 3.45 (mc, 1H), 3.42-3.24 (m, 2H), 3.17 (mc, 2H), 3.00–2.75 (m, > 12H), 2.60 (s, large, 6H), 2.54–2.39 (mc, 2H). MS (ELECTROSPRAY$^+$, CH_3CN– H_2O, 80 V, 50°C): m/z 277.5 $((M-2\times PF_6)^{2+}/2)$, 252.2 $((M-2\times PF_6-3\times NH_3)^{2+}/2)$, 243.4 $((M-2\times PF_6-4\times NH_3)^{2+}/2)$. ^{13}C NMR (400 MHz, DMSO-D_6): δ_{ppm} 168.6/168.1, 157.0, 144.4, 143.3, 140.7, 140.3, 139.4, 139.0, 138.3, 138.1, 136.6, 130.0, 128.2, 127.8, 127.3, 126.1, 125.8, 121.3, 121.2, 49.8/46.5, 36.7/32.3, 33.1/31.3, 28.2/27.1. IR (KBr): ν 3638 (w), 3359 (m, large), 3066 (w), 3011 (w), 2930 (w), 1618 (s), 1511 (w), 1491 (m), 1450 (m), 1416 (m), 1368 (w), 1283 (m), 1202 (s), 1089 (s), 846 (s), 809 (m), 780 (m), 559 (s), 473 (s) cm^{-1}.

The experimental values of the elemental analysis in Table 1 are without exception lower than the calculated percentages. Nevertheless all the elemental ratios are in agreement with the proposed formula. The observed presence of more than 10% Si lead to the conclusion that silica had been partially dissolved in methanol during the filtration over celite.

Table 2
Separate accumulation (5 min) of each labeled drug at a nafion-loaded CPE in phosphate buffer solutions (pH 7.4) containing 1% ethanol

Labeled drug	E_{pa}	Detection limit (μM)	Linear range (μM)	Sensitivity (A M^{-1})	Reference
PB-Cc^{+}	−1.05	0.05	0.1–3.0	20	[15]
DPH-N^{+}Fc	0.26[a]	0.025[b]	0.05–1.0[b]	50[b]	[15]
NORPy-Ru^{2+}	−0.06	0.075	0.075–5.0	6	This study

[a] 10% Ethanol; [b] 4% ethanol.

2.4. Electrochemical instrumentation and detection

An EG&G PAR 273 potentiostat interfaced to a IBM XT 286 computer system with PAR 270 software was used for SWV. The selected parameters were given by Limoges et al. [11] ($E_{sw} = 50$ mV, $f = 100$ Hz, $\delta E = 2$ mV). The electrochemical experiments were carried out at a controlled temperature (25°C) in a one-compartment glass cell with a working volume of 1 ml. The working electrode was a nafion-loaded CPE prepared as described in Ref. [13]. Graphite powder (125 mg) of average diameter 100 μm (Johnson Matthey, ref. 730181) was mixed with 500 μl of Aldrich nafion solution, 120 μl of an ethanol solution contaning LiOH (0.14 M), 80 μl 1-octanol and 3 ml ethanol. After the slurry was sonicated for 15 min, the solvent was removed under vacuum, silicon oil (104 mg) was added to the residue and thorough mixing was accomplished using a mortar and pestle. A plastic tip with an i.d. of 3 mm was filled with the modified carbon paste, which was then pressed into the holder. An Ag/AgCl (50 mM NaCl) electrode was used as the reference and a Pt wire as the counter electrode. For the accumulation and detection procedures, the rotating nafion-loaded CPE was exposed to the solution at 600 rpm under an open electrical circuit for 5 min. It was followed by a voltage scan in the positive direction (−1.3–0.6 V). Between each measurement, a small amount of paste was pushed out of the tip and cut with a razor blade, and then the resulting new electrode was polished on a Teflon sheet [13].

The electrochemical study was carried out in non-deaerated phosphate buffer (pH 7.4) containing 1% EtOH unless stated otherwise and in absence of light when the Ru(II) complexes were involved. The photodegradation of the NORPy-Ru^{2+} ion was confirmed by a rapid decrease of the voltammetric currents when the electrochemical cell was not carefully protected from light. Conversely, the Ru(II) tracer solutions were observed to be stable for 8 h in the dark, in the 22–37°C temperature range, even in the presence of oxygen.

3. Results and discussion

Table 2 indicates the anodic peak potential values E_{pa} obtained in the case of each labeled drug at a nafion-loaded CPE by square wave voltammetry under the following conditions. The accumulation proceeded for 5 min at a rotating electrode (600 rpm) under open circuit and it was followed by a voltage scan in the positive direction (−1.3–+0.6 V) with a view to the simultaneous detection of the three drugs. One of the advantages of the oxidation scan procedure was that it avoided the need to deaerate the buffer solution, because dioxygen was irreversibly reduced to hydrogen peroxide at the beginning of the scan, as shown previously [13]. The data given in Table 2 indicate that more than 0.3 V separates the anodic peaks of DPH-N^{+}Fc and NORPy-Ru^{2+}. Therefore the two peaks did not overlap when the simultaneous SWV detection of the three labeled drugs was carried out (Fig. 1).

The SWV calibration plot of NORPy-Ru^{2+} at a nafion-loaded CPE was obtained and the corresponding electroanalytical data, i.e. detection limit (S/N = 3), linear range and sensitivity, were compared with those of PB-Cc^{+} and DPH-N^{+}Fc separately accumulated under similar conditions

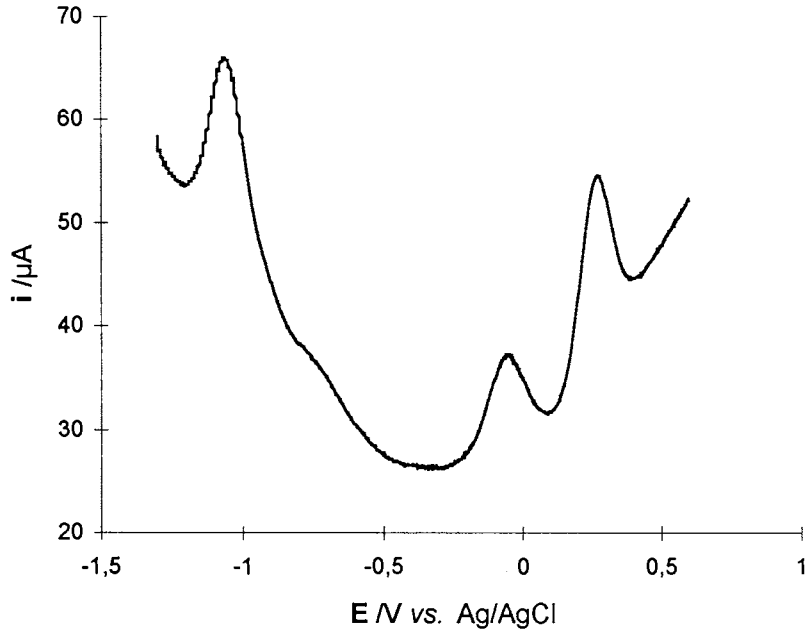

Fig. 1. SWV curve for PB-Cc$^+$ (1 µM; $E_{pa} = -1.05$ V), NORPy-Ru^{2+} (1.25 µM; $E_p = -0.06$ V) and DPH-N$^+$Fc (1 µM; $E_p = 0.26$ V) at a nafion-loaded CPE in phosphate buffer (pH 7.4) containing 1% ethanol. Preconcentration time 5 min at 600 rpm.

(Table 2). The best sensitivity was achieved with DPH-N$^+$Fc in a phosphate buffer containing 4% ethanol. It was previously observed [14,15] that the ethanol content interfered with the accumulation of cationic labeled drugs in a complex manner. In the case of DPH-N$^+$Fc and PB-Cc$^+$ the maximum anodic peak current (i_{pa}) values were reached with ethanol contents of 4 and 1%, respectively [15]. The following experiments were conducted at a constant 1% ethanol content, which led to similar sensitivities for the three labeled drugs, after separate or simultaneous accumulation, as shown in Fig. 1 and Table 3. This Table indicates that the SWV detection does not differ significantly, whatever the mode of accumulation. It also indicates rather high values (11–26%) for the R.S.D., which confirms the moderate reproducibility of the experimental data, as already emphasized in Section 1.

The possible interference of the serum on the SWV detection of the novel labeled drug was examined with the aim of performing a triple-analyte immunoassay in clinical serum samples. The effect of RNS on the peak current of PB-Cc$^+$ and DPH-N$^+$Fc was previously studied in detail [15]. Fig. 2 shows the influence of increasing amounts of RNS on the relative current response of NORPy-Ru^{2+} after 1 h of incubation (curve A). A dramatic decrease is observed even at very low serum contents, since the decrease reaches ca. 80% of the initial peak current with as low as 1% RNS. This unexpected result suggests that the Ru^{2+} $(NH_3)_5$(Py) label is not adapted to immunoassay, owing to non-specific interactions between the labeled drug and the serum proteins and/or the instability of the tracer in a seric medium. It was previously shown [14] that serum proteins associate to some extent with labeled drugs by non-specific interactions and that the resulting bulky complexes cannot accumulate within nafion, which leads to a decrease of the current response. However this decrease remains moderate with hydrophilic cationic labels. For instance if the PB-Cc$^+$ and DPH-N$^+$Fc labeled drugs are considered, the decrease reaches in each case ca. 20% of the initial peak current in the presence of 1% RNS, [15]. Clearly, non-specific interactions cannot account exclusively for the steep decrease

Table 3
SWV peak current values of the labeled drugs after accumulation (5 min) at a nafion-loaded CPE in phosphate buffer (pH 7.4) containing 1% ethanol

Labeled drug	C° (μM)	Separate accumulation		Simultaneous accumulation	
		i_{pa} (μA)	R.S.D.[a] (%)	i_{pa} (μA)	R.S.D.[b] (%)
PB-Cc^+	1	20.0 ± 4.2	21	19.4 ± 3.7	19
DPH-N^+Fc	1	17.5 ± 4.5	26	14.9 ± 1.6	11
NORPy-Ru^{2+}	1.25	8.5 ± 2	23	7.1 ± 1.7	24

[a] Nine measurements; [b] four mesurements.

of curve A in Fig. 2, and so the stability of the $Ru^{2+}(NH_3)_5(Py)$ label in seric media appears questionable. The effect of RNS on the accumulation and detection of the more hydrophilic unsubstituted $Ru(NH_3)_5(PyH)^{2+}$ ion was examined in order to throw light on this. Curve B of Fig. 2 shows that the current response decreases linearly with increasing amounts of RNS, to reach 60% of its initial value in the presence of 5% RNS incubated for 1 h. The current response became lower when the incubation period was prolonged, as shown in Fig. 3 (curve A) and it was as low as 15% of its initial value after 4 h of incubation. These results are consistent with a slow degradation of the $Ru(NH_3)_5(PyH)^{2+}$ complex in a seric medium, since non-specific interactions are in equilibrium in less than 1 h, as previously observed [25] and confirmed with DPH-N^+Fc (curve B, Fig. 3).

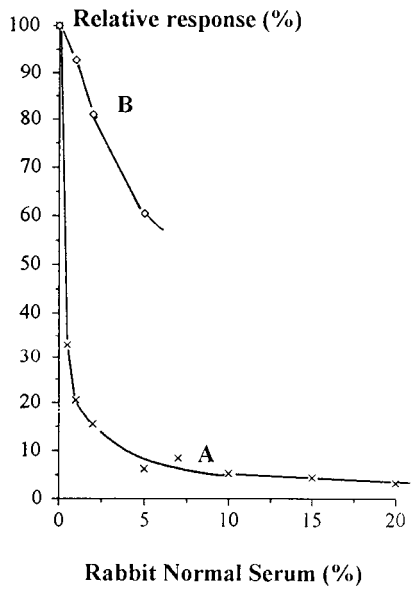

Fig. 2. Effect of RNS on the SWV peak current of (A) NORPy-Ru^{2+} (1.25 μM) and (B) $Ru(NH_3)_5(PyH)^{2+}$ (1.25 μM) in phosphate buffer (pH 7.4) containing 1% ethanol, after 1 h of incubation at 37°C. Preconcentration time 5 min at 600 rpm.

4. Conclusions

The simultaneous detection of three cationic labeled drugs at micromolar concentrations was

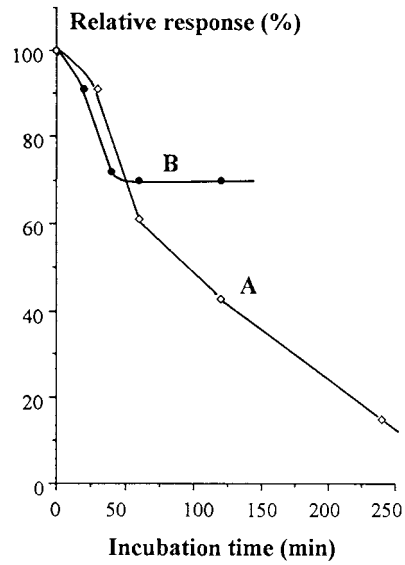

Fig. 3. Effect of the incubation time at 37°C on the SWV peak current of (A) $Ru(NH_3)_5(PyH)^{2+}$ (1.25 μM) and (B) DPH-N^+Fc (1 μM) in phosphate buffer (pH 7.4) containing 1% ethanol and 5% RNS. Preconcentration time 5 min at 600 rpm.

successfully performed at a nafion-loaded CPE, owing to their distinct redox potentials. No significant cross interferences between the tracers were observed, which is a major advantage with a view to multi-detections. However triple-analyte immunoassay cannot be envisaged with pentaammine ruthenium(II) complexes of pyridine derivatives, owing to their instability in the presence of serum.

References

[1] L.J. Kricka, Clin. Chem. 38 (1992) 327.
[2] J.P. Yvert, J.F. Delagneau, Ann. Biol. Clin. 51 (1993) 43.
[3] L.J. Kricka, in: E.P. Diamandis, T. K. Christopoulos (Eds.), Immunoassay, Academic Press, New York, 1996, pp. 389.
[4] S. Gutcho, L. Mansbach, Clin. Chem. 23 (1977) 1609.
[5] K.J. Dean, S.G. Thompson, J.F. Burd, R.T. Buckler, Clin. Chem. 26 (1983) 1051.
[6] T. Porstmann, E. Nugel, P. Henklein, H. Doepel, J. Immunol. Methods 158 (1995) 95.
[7] H. Sayo, M. Hosokawa, Chem. Pharm. Bull. 33 (1985) 2866.
[8] F.J. Hayes, H.B. Halsall, W.R. Heineman, Anal. Chem. 66 (1994) 1860.
[9] Y.Y. Xu, K. Pettersson, K. Blomberg, I. Hemmilä, H. Mikola, T. Lövgren, Clin. Chem. 38 (1992) 2038.
[10] A. Varenne, Thèse de l'Université Paris VI, 1994.
[11] B. Limoges, C. Degrand, P. Brossier, R.L. Blankespoor, Anal. Chem. 65 (1993) 1054.
[12] A. Le Gal La Salle, B. Limoges, J.Y. Anizon, C. Degrand, J. Electroanal. Chem. 350 (1993) 329.
[13] S. Rapicault, B. Limoges, C. Degrand, Anal. Chem. 68 (1996) 930.
[14] B. Limoges, C. Degrand, P. Brossier, J. Electroanal. Chem. 402 (1996) 175.
[15] A.L. Bordes, B. Limoges, P. Brossier, C. Degrand, Anal. Chim. Acta 356 (1997) 195.
[16] A.L. Bordes, B. Schöllhorn, B. Limoges, C. Degrand, Appl. Organomet. Chem. 12 (1998) 59.
[17] H.Y. Liu, F.C. Anson, J. Electroanal. Chem. 184 (1985) 411.
[18] C.M. Lieber, N.S. Lewis, J. Am. Chem. Soc. 107 (1985) 7190.
[19] M.Y. Tsou, F.C. Anson, J. Phys. Chem. 89 (1985) 3818.
[20] C.M. Lieber, M.H. Schmidt, N.S. Lewis, J. Am. Chem. Soc. 108 (1986) 6103.
[21] M.H. Schmidt, N.S. Lewis, J. Phys. Chem. 92 (1988) 2018.
[22] H. Van Rysnyk, B.J. Hinds III, B.L. Simmons, D.S. Solomon, J. Electrochem. Soc. 139 (1992) 3098.
[23] E. Sabatini, F.C. Anson, J. Electroanal. Chem. 386 (1995) 111.
[24] P.C. Ford, DE F.P. Rudd, R. Gaunder, H. Taube, J. Am. Chem. Soc. 90 (1968) 1187.
[25] B. Limoges, Thèse de l'Université Blaise Pascal de Clermont-Ferrand, 1993.

ELSEVIER

Talanta 48 (1999) 209–217

Talanta

Determination of lasalocid with sensitized terbium(III) luminescence detection

M.P. Aguilar-Caballos *, A. Gómez-Hens, D. Pérez-Bendito

Department of Analytical Chemistry, Faculty of Sciences, University of Córdoba, E-14004 Córdoba, Spain

Received 6 March 1998; received in revised form 23 June 1998; accepted 26 June 1998

Abstract

The luminescence of the lasalocid-terbium(III) system in the presence of Triton X-100 and trioctylphosphine oxide has been studied by obtaining kinetic and equilibrium measurements and using the stopped-flow mixing technique. The initial rate and luminescence signal of this system are directly proportional to the lasalocid concentration, which allows one to develop very simple, fast, automatic methods for the determination of this analyte. Kinetic and equilibrium data can be obtained in only 0.1 and 10 s, respectively. The calibration graphs were linear over the range 0.004–5.0 μg ml^{-1} (kinetic method) and 0.01–5.0 μg ml^{-1} (equilibrium method) and the detection limits achieved were 1 and 3 ng ml^{-1}, respectively, equivalent to 2 and 6 ng g^{-1} lasalocid in a chicken liver sample, which are similar to those afforded by the chromatographic methods described for this determination. The relative standard deviation of both methods was close to 2%. The analytical recoveries obtained by applying the kinetic and equilibrium methods to drinking water, poultry feed and chicken liver samples ranged from 95.6 to 102.1% and from 95.9 to 104.9%, respectively.

Keywords: Lasalocid; Lanthanide-sensitized luminiscence; Kinetic and equilibrium methods; Stopped-flow technique; Samples analysis

1. Introduction

Lasalocid is a carboxylic polyether antibiotic used in veterinary practice as an antiprotozoal agent for the prevention of coccidiosis in poultry and, also, as a growth promoter when added at sub-therapeutic levels to improve the efficiency of feed conversion. Together with other compounds such as salinomycin, narasin and monensin, lasalocid belongs to the group of ionophore antibiotics, which show special structural properties. Thus, they form complexes with monovalent and divalent cations and are capable of acting as carriers of these ions across biological membranes [1]. These properties have given also rise to the development of ion-selective electrodes based on these compounds [2,3].

The interest in the control of lasalocid in poultry and animal tissues justifies the numerous chromatographic methods reported. Although thin layer [4–6] and gas chromatography [7,8] have

* Corresponding author. Tel.: +34 957 218614; fax: +34 957 218606.

0039-9140/99/$ - see front matter
PII S0039-9140(98)00240-9

been used, most of these methods are based on the use of liquid chromatography with fluorimetric detection, either by measuring the intrinsic fluorescence of lasalocid [8–13] or by using a derivatization reaction with 1-(bromoacetyl) pyrene [14,15] or 9-anthryldiazomethane [16]. The lowest detection limit of these methods was 5 ng g^{-1} [13], which is ten-times higher than that obtained by using liquid-chromatography-electrospray mass spectrometry [17].

As known, chromatography is the best way to achieve the simultaneous determination of two or more analytes, such as mixtures of lasalocid with other ionophore antibiotics [14–16], or to determine a single analyte in a complex sample, such as lasalocid in animal tissue samples [8–13]. Although all these methods require a previous clean-up step in order to remove the most part of the sample matrix, the chromatographic separation is also required to avoid the interference of the remaining sample matrix in the intrinsic fluorescence of lasalocid. However, the use of chromatography can be avoided by developing a selective method which allows the chemical and/or spectral discrimination of the analytical signal as alternative to the physical separation of the analyte from the remaining sample matrix. Thus, this paper reports a non-chromatographic luminescence method for the determination of lasalocid in different samples. With the aim of obtaining adequate sensitivity and selectivity levels, instead of measuring the intrinsic fluorescence of lasalocid, which can be interfered by other components of the sample matrix, its luminescent complex with terbium(III) in the presence of a surfactant (Triton X-100) and a synergistic agent (trioctylphosphine oxide, TOPO) has been studied for the first time. Lanthanide chelates show large Stokes shifts and narrow and intense emission bands, as a result of the intramolecular energy transfer process from the ligand to the central ion, which avoids or minimizes selectivity limitations of photoluminescent methods. This study has been carried out by using stopped-flow mixing technique, which allows the automation of the measurement step and the simple adaptation of the method to routine analysis. Although this technique is generally used together with the kinetic methodology, both kinetic and equilibrium measurements have been obtained, as the equilibrium of the system is rapidly reached, with the aim of comparing the analytical features of both methodologies.

2. Experimental

2.1. Instrumentation

An SLM-Aminco (Urbana IL) Model 8100 photon-counting spectrofluorimeter, equipped with a 450 W continuous xenon arc source and a R928 photomultiplier tube, was used. The instrument was furnished with an SLM-Aminco Milliflow stopped-flow module, which was fitted with an observation cell of 0.2 cm path length and controlled by the associated electronics, the computer and a pneumatic syringe drive system. The solutions in the stopped-flow module were kept at a constant temperature of 25°C by circulating water form a thermostated tank.

2.2. Reagents

All chemicals used were of analytical-reagent grade. A stock solution (1 mg ml^{-1}) of sodium lasalocid (Sigma) was prepared in ethanol and stored at 4°C for up to 2 months. Working solutions (20 μg ml^{-1}) were made weekly by suitable dilution in distilled water. A 10^{-2} M terbium(III) solution was made by dissolving an appropriate amount of terbium(III) nitrate pentahydrate (Aldrich) in distilled water. A 3×10^{-3} M solution of TOPO (Sigma) was prepared in 80% of ethanol. An 1% Triton X-100 aqueous solution and an ammonium acetate buffer solution (0.2 M, pH 6.2) were also used.

2.3. Procedure

A solution containing terbium(III) (9×10^{-4} M), TOPO (4.2×10^{-5} M), Triton X-100 (0.05%) and ammonium acetate buffer (3×10^{-2} M, pH 6.2) was used to fill one of the two 10 ml reservoir syringes of the stopped-flow module. The other syringe was filled with a solution containing lasa-

locid standard solution, in the range 0.004–5.0 μg ml^{-1} (kinetic method) or 0.010–5.0 μg ml^{-1} (equilibrium method), Triton X-100 (0.05%) and the same buffer concentration. After the two 2 ml drive syringes had been filled, 0.04 ml of each solution was mixed at a flow-rate of 20 ml s^{-1} in the mixing chamber in each run. The variation of the luminescence intensity with time throughout the reaction was monitored at λ_{ex} 318 nm and λ_{em} 545 nm up to a constant signal was reached (ca. 10 s), in order to obtain kinetic and equilibrium measurements. All measurements were carried out at 25°C and by using the direct fluorescence mode. Kinetic data were obtained by applying the initial rate method to the values acquired from the detector, which were processed by the microcomputer, furnished with a linear regression program for application of this kinetic method. The initial rate was determined in $\sim$0.1 s. Each sample was assayed in triplicate and the blank signal was found to be negligible.

2.4. Determination of lasalocid in real samples

Lasalocid was determined in three different samples, namely drinking water, poultry feed and chicken liver samples, which were spiked with appropriate amounts of the analyte. The drinking water sample did not require any pretreatment, so that an appropriate amount of sample was treated as described above. The poultry feed sample (0.5–1 g) was digested with ethanol (25 ml) and 36% hydrochloric acid (0.5 ml) for 20 min in an ultrasonic bath at 40°C. The solution was filtered and diluted to 100 ml with ethanol. An appropriate volume (1 ml) of this solution was treated as described above. The chicken liver sample was treated similarly to the poultry feed sample but, after the solution was filtered, it was diluted to 100 ml with distilled water and passed through a C_{18} cartridge where the analyte was retained. Finally, lasalocid was eluted with 1 ml of 70% ethanol solution and treated as described above.

3. Results and discussion

Although lasalocid (Fig. 1) shows intrinsic fluorescence (λ_{ex} 310 nm, λ_{em} 420 nm), its intensity is not very high and its emission band can be interfered by species present in the sample matrix. Thus, as indicated above, the aim of this study was to develop a selective method for the determination of this compound which avoids its chromatographic separation [8–13]. Taking into account the capability of lasalocid to form very stable complexes [2] and the special features of lanthanide chelates in the presence of surfactants and synergistic ligands [18], a systematic study of the behaviour of lasalocid was carried out. An intense luminescence signal with the terbium(III)-TOPO-Triton X-100 system was found at the characteristic emission bands of terbium(III) (490, 545 and 580 nm), as Fig. 2 shows, where the excitation and emission spectra of this system are compared with those obtained for lasalocid alone. As can be seen, the lanthanide complex shows a luminescence signal about 6-fold higher than that of lasalocid. According to the reaction of terbium(III) with other compounds such as *p*-aminobenzoic acid [19] and salicylic acid [20], it can be suggested that the main functional group of lasalocid responsible for the complex formation with terbium(III) is the aromatic carboxylic acid.

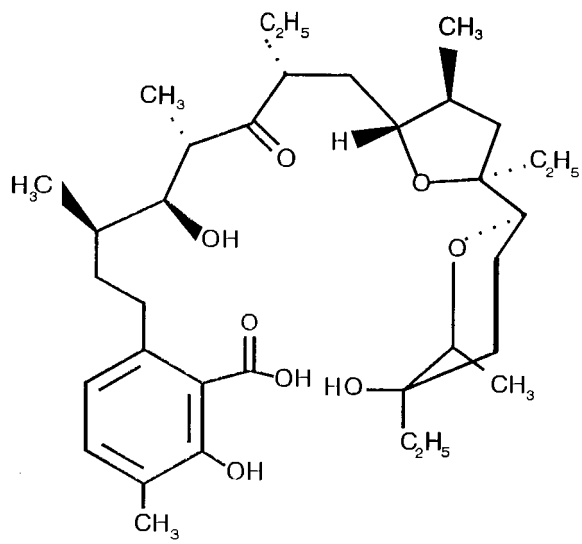

Fig. 1. Chemical formula of lasalocid.

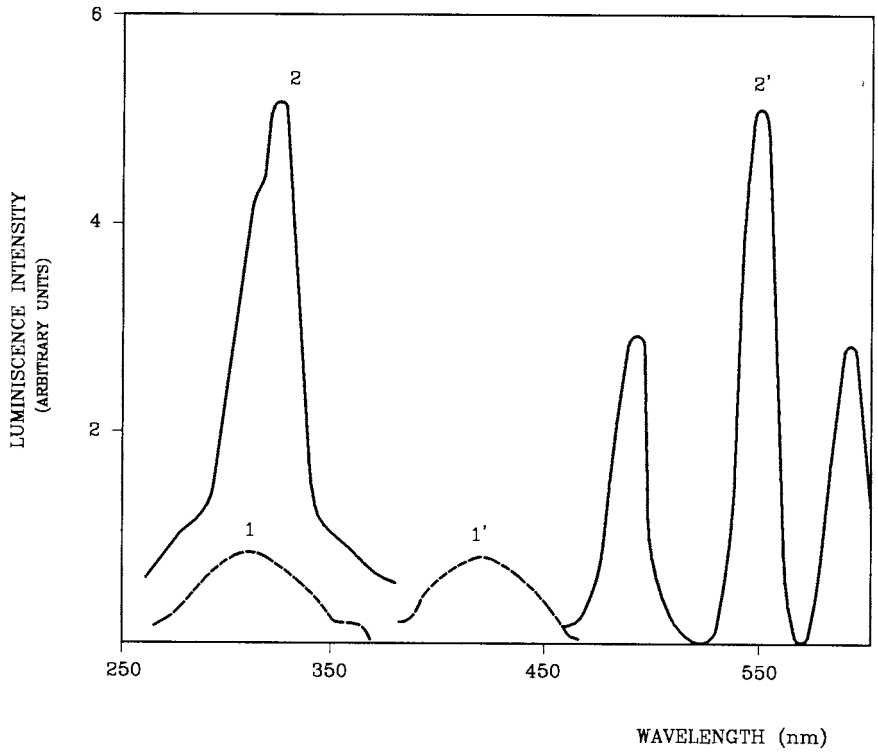

Fig. 2. Excitation (1,2) and emission (1′,2′) spectra of lasalocid (1,1′) and lasalocid-terbium(III)-TOPO-Triton X-100 system (2,2′). [Lasalocid], 1 μg ml^{-1}; [terbium(III)], 10^{-3} M; [TOPO], 4.2×10^{-5} M; [Triton X-100], 0.05%.

In addition to TOPO, other synergestic ligands such as EDTA and 1,10-phenanthroline were assayed but EDTA did not increase the luminescence of the lasalocid chelate and the signal obtained in the presence of 1,10-phenanthroline was lower than that obtained with TOPO. With regard to the surfactants assayed, any luminescence signal was obtained in the presence of a cationic surfactant such as cetyltrimethylammonium bromide, while an anionic surfactant, such as sodium dodecyl sulfate, increased the blank signal at the same value than that of the lasalocid chelate. However, the luminescence of the chelate notably increased in the presence of Triton X-100, a non-ionic surfactant, as can be seen in Fig. 2. Under these conditions, the maximum of the excitation band of the system was 318 nm, which suggests an interaction between lasalocid and this surfactant. Other non-ionic surfactants such as Tween-20 and Tween-40 also caused a positive effect on the system but the luminescence signal obtained was about a 50% lower than that obtained with Triton X-100.

Fig. 3 shows the kinetic curves obtained by using stopped-flow mixing technique for the lasalocid-terbium(III) chelate in the absence or presence of Triton X-100 and TOPO, where the positive effect of the surfactant and the synergistic ligand in the initial rate and luminescence signal is evident. The initial rate can be measured in only 0.1 s and the equilibrium signal is reached in about 10 s, so that both parameters can be used for the rapid determination of lasalocid. The kinetic behaviour of this system was very dependent on the distribution of the reactants between the two syringes of the stopped-flow module. The best results were obtained when terbium(III) and TOPO were placed in one syringe, lasalocid in the other and Triton X-100 and the buffer solution in both syringes, so that the micelle concentration and the pH in the mixing chamber were the same as in the syringes. However, while the static lu-

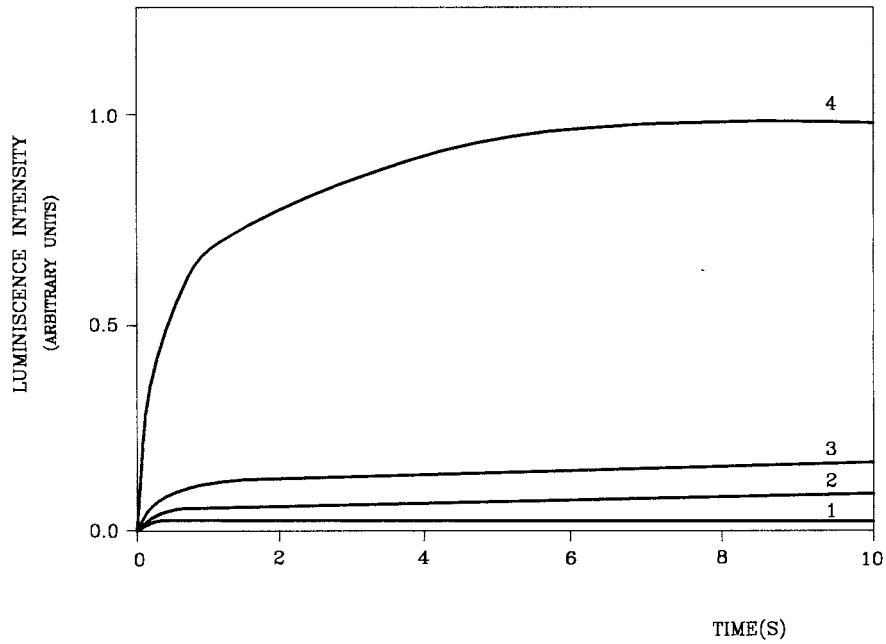

Fig. 3. Kinetic curves obtained for the lasalocid-terbium(III) system alone (1), and in the presence of TOPO (2), Triton X-100 (3) and TOPO and Triton X-100 (4). [Lasalocid], 0.2 μg ml^{-1}; [terbium(III)], 10^{-3} M; [TOPO], 4.2×10^{-5} M; [Triton X-100], 0.05%.

minescent signal obtained by placing TOPO together with lasalocid was the same than that obtained when this ligand was placed together with terbium(III), the rate of formation of the chelate was so high that the time constant of the instrument used did not afford its measurement.

3.1. Effect of variables

The variables affecting the system were optimized by the univariate method and by using kinetic and equilibrium measurements. All concentrations given are initial concentrations in the syringes (twice the actual concentrations in the reaction mixture at time zero after mixing). Each result was the mean of three measurements.

The study of the effect of the pH on the system was carried out by adjusting the pH value of each solution in the syringes, which allowed the same value to be obtained in the mixing chamber as checked in the wastes. Fig. 4(A) shows the variation of the initial rate and equilibrium signal with this variable where can be seen that the optimum pH range is 5.8–6.8 and 5.5–7.5, respectively. Three buffer solutions (hexamine, imidazole and ammonium acetate) were assayed to adjust the pH. An ammonium acetate buffer of pH 6.2 was chosen because the other two buffers slightly decreased both measurement parameters. The optimum concentration range of that buffer was $2.1–4.2 \times 10^{-2}$ M. As described above, the presence of Triton X-100 in the system is essential to obtain the luminescence signal. The initial rate and the equilibrium signal were constant and independent of the concentration of this surfactant in the range 0.02–0.08 and 0.02–0.06%, respectively. As the critical micelle concentration of this surfactant is 0.018%, these results show that the positive effect of Triton X-100 can be mainly ascribed to the formation of the micelles, which shield the chelate and favour the intramolecular energy transfer process. However, as indicated above, this surfactant could also enter into the coordination sphere of the terbium(III) chelate, which would justify the slight red shift observed in the excitation spectrum of this system.

Fig. 4(B) shows the effect of terbium(III) concentration on the initial rate and luminescence

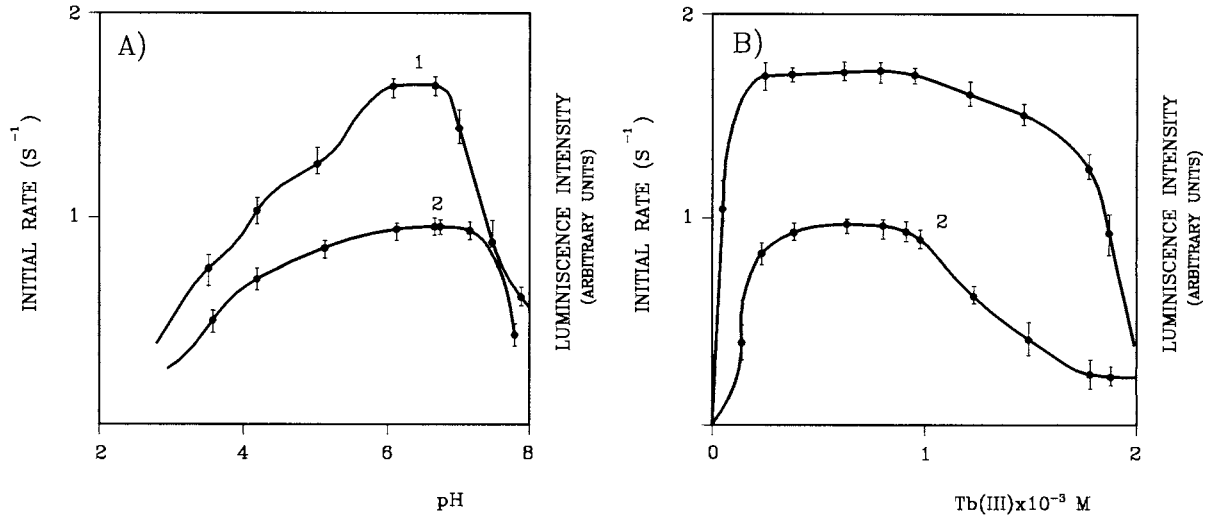

Fig. 4. Effect of pH (A) and terbium(III) concentration (B) on the initial rate (1) and luminescence intensity (2) of the lasalocid system. [Lasalocid], 0.2 μg ml^{-1}; [TOPO], 4.2×10^{-5} M; [Triton X-100], 0.05%.

signal, where it can be seen that the optimum concentration range is 2×10^{-4}–10^{-3} M. Although a higher terbium(III) concentration decreased both parameters, its effect was more marked in the luminescence signal. The study of the TOPO concentration in the system showed a constant and positive effect of this synergistic ligand on both the initial rate and equilibrium signal in the range 1.6–5×10^{-5} M. As organic solvents are known to alter and eventually destroy surfactant micelles and lasalocid and TOPO are dissolved in ethanol, the effect of this solvent on the system was studied, finding that both the initial rate and equilibrium signal are not affected by the presence of ethanol up to a concentration of 7%. The temperature has no effect on the initial-rate and equilibrium signal over the range 15–30°C, so that a temperature of 25°C was selected to carry out all the experiments.

3.2. Features of the method

Kinetic and equilibrium measurements were made from the luminescence intensity-time curves obtained at λ_{ex} 318 nm and λ_{em} 545 nm from solutions prepared under the above-described optimum conditions and containing different lasalocid concentrations. The initial rate was measured in ca. 0.1 s and the equilibrium signal in ca. 10 s. Table 1 summarizes the features of the calibration graphs of both methods. The wide linear ranges obtained required using two different instrumental sensitivities. The correlation coefficients suggest very good calibration linearity.

The detection limit obtained, calculated according to IUPAC recommendations [21] was 1 ng ml^{-1}, based on initial-rate measurements, and 3 ng ml^{-1}, based on equilibrium measurements. Similar detection limit values were obtained in the presence of a sample of chicken liver spiked with lasalocid and treated as described in Section 2.4. Taking into account this treatment, the detection limits referred to the sample were 2 and 6 ng g^{-1} by using kinetic and equilibrium measurements, respectively. The precision was determined by calculating the relative standard deviation ($n = 11$) at two analyte concentrations, namely 0.02 and 1.2 μg ml^{-1}. The results obtained were 2.1 and 1.9% (kinetic method) and 2.2 and 2.0% (equilibrium method).

The selectivity of the lasalocid determination was studied by assaying several compounds used in veterinary practice (Table 2). The maximum concentration tested for each potential interferent

Table 1
Quantitative performance of the kinetic and equilibrium methods

Method	Linear range (μg ml^{-1})	Slope ± SD[a]	Intercept ± SD	r[b]
Kinetic	0.004–1.8	9.7 ± 0.3	(3.0 ± 0.2) × 10^{-3}	0.998
	1.8–5.0	0.85 ± 0.03	(8.0 ± 0.1) × 10^{-3}	0.997
Equilibrium	0.01–1.8	5.1 ± 0.3	(7.1 ± 1) × 10^{-3}	0.998
	1.8–5.0	0.32 ± 0.03	0.3 ± 0.07	0.996

[a] Kinetic method (s^{-1} μg^{-1} ml), equillibrium method (μg^{-1} ml).
[b] Correlation coefficient, $n = 10$.

was 100-fold that of the analyte. None of the compounds assayed was found to interfere at the same concentration level of lasalocid and the selectivity was very similar for both kinetic and equilibrium methods. The most important interference was caused by carbadox, which shows an intense fluorescence emission at 492 nm, but its use has been prohibited following reports of carcinogenicity.

As can be seen, although the kinetic method allows a lower detection limit to be obtained, both methods show very similar features and are suitable for the determination of low lasalocid concentrations.

3.3. Applications

The proposed kinetic and equilibrium methods were applied to the analysis of drinking water, poultry feed and chicken liver samples. Although lasalocid is generally determined in the latter two samples, a drinking water sample was also analyzed taking into account that the treatment to the poultry at present is preferably given in the drinking water instead of the feed. Different amounts of lasalocid were added to each sample in order to carry out the recovery study. The drinking water sample was directly analysed while the other two samples required the treatment described in Section 2.4. With regard to the chicken liver sample, which required a previous clean-up treatment involving the use of a C_{18} cartridge, the composition and amount of the eluent necessary to attain the complete separation of lasalocid from the column was studied. The results obtained showed that 1 ml of 70% ethanol allowed lasalocid to be completely eluted. Table 3 lists the analytical recoveries obtained, which ranged from 95.6 to 102.1% and from 95.9 to 104.9% by the kinetic and equilibrium method, respectively. These results show that both methods are adequate for the determination of lasalocid in these samples.

Table 2
Effect of foreign substances over the determination of 0.2 μg ml^{-1} of lasalocid

Compound	Maximum concentration tolerated (μg ml^{-1})	
	K[a]	E[a]
Tylosin	20[b]	20
Amikacin	20	20
Ampicillin	20	20
Spyramicin	20	18
Tetracycline	20	18
Sulphaquinoxaline	20	18
Monensin	18	18
Vancomycin	16	20
Carbadox	4	2

[a] K, kinetic method; E, equilibrium method.
[b] Maximum concentration tested.

4. Conclusions

Based on the results obtained, the luminescent system of lasalocid with terbium(III) in the presence of Triton X-100 and TOPO can be used with analytical purposes and is a valid alternative to existing chromatographic methods for the determination of lasalocid. Although the analysis of complex samples such as chicken liver requires the

Table 3
Recovery of lasalocid added to real samples

Sample	Lasalocid concentration[a]				
	Added	Found[b]		Recovery (%)	
		K[c]	E[c]	K[c]	E[c]
Drinking water	10	9.8 ± 0.2	10.2 ± 0.4	95.6	102.4
	20	20.3 ± 0.4	19.8 ± 0.3	97.8	99.0
	40	40.1 ± 0.3	38.4 ± 0.6	102.1	95.9
Poultry feed	75	75.1 ± 0.7	74 ± 2	100.1	98.7
	100	99 ± 2	104 ± 5	99.2	103.7
	125	126 ± 1	125 ± 4	100.9	100.2
Chicken liver	20	19.1 ± 0.4	21.0 ± 0.6	95.6	104.9
	30	29.3 ± 0.2	29.5 ± 0.4	97.8	98.2
	40	40.8 ± 0.5	40.2 ± 0.8	102.1	100.6

[a] Drinking water and chicken liver (ng g^{-1}); poultry feed (μg g^{-1}).
[b] Average of three determinations.
[c] K, kinetic method; E, equilibrium method.

previous separation of the most part of the sample matrix, which is also a general prerequisite for the chromatographic determination, the formation of the luminescent chelate allows the selective determination of lasalocid avoiding its physical separation from the remaining components of the sample matrix. After the previous treatment, the use of stopped-flow mixing technique allows the manipulations involved in the determination step to be reduced and kinetic and/or equilibrium measurements are obtained shortly after mixing. Hence, this approach can be adapted to the routine determination of lasalocid in a simpler way than a chromatographic method.

As described elsewhere [22,23], some methods based on the formation of lanthanide chelates and the use of stopped-flow mixing technique attain the adequate selectivity by combining the special spectral features of these chelates with kinetic measurements. However, the results obtained from this study show that only the formation of the lasalocid-terbium(III) chelate is enough to obtain the adequate selectivity and both dynamic and static measurements can be indistinctly used for the rapid and automatic determination of lasalocid.

Acknowledgements

The authors are grateful to the DGICyT (Dirección General Interministerial de Ciencia y Tecnología) for financial support (Grant No. PB96-0984).

References

[1] B.C. Pressman, Annu. Rev. Biochem. 45 (1976) 501.
[2] K. Suzuki, K. Tohda, Trends Anal. Chem. 12 (1993) 287.
[3] K. Suzuki, K Tohda, H. Aruga, M. Masuzoe, H. Iroue, T. Shirai, Anal. Chem. 60 (1988) 1714.
[4] P.J. Owles, Analyst 109 (1984) 1331.
[5] H. Asukabe, H. Yoneyama, Y. Mori, K. Harada, M. Suzuki, H. Oka, J. Chromatogr. 396 (1987) 261.
[6] P.A. Vanderkop, J.D. Mac Neil, J. Chromatogr. 580 (1990) 386.
[7] G. Weiss, M. Kaykaty, B. Miwa, J. Agric. Food Chem. 31 (1983) 78.
[8] D.R. Newkirk, C.J. Barnes, J. Assoc. Off. Anal. Chem. 72 (1989) 581.
[9] M. Kaykaty, G. Weiss, J. Agric. Food Chem. 31 (1983) 81.
[10] G. Weiss, N.R. Felicito, M. Kaykaty, G. Chen, A. Caruso, E. Hargroves, C. Crowley, A. MacDonald, J. Agric. Food Chem. 31 (1983) 75.
[11] L.R. Frank, C.J. Barnes, J. Assoc. Off. Anal. Chem. 72 (1989) 584.

[12] S. Horii, K. Miyahara, C. Momma, J. Liq. Chromatogr. 13 (1990) 1411.
[13] G.C. Gerhardt, C.D.C. Salisbury, H.M. Campbell, Food Addit. Contam. 12 (1997) 731.
[14] H. Asukabe, H. Murata, K. Harada, M. Suzuki, H. Oka, Y. Ikai, J. Chromatogr. 657 (1993) 349.
[15] H. Asukabe, H. Murata, K.I. Harada, M. Suzuki, H. Oka, Y. Ikai, J. Agric. Food Chem. 42 (1994) 112.
[16] E.E. Martínez, W. Shimoda, J. Assoc. Off. Anal. Chem. 69 (1986) 637.
[17] W.J. Blanchflower, D.G. Kennedy, Analyst 120 (1995) 1129.
[18] Y.Y. Xu, I.A. Hemmilä, T.N.E. Lövgren, Analyst 117 (1992) 1061.
[19] S. Panadero, A. Gómez-Hens, D. Pérez-Bendito, Talanta 45 (1998) 829.
[20] S. Panadero, A. Gómez-Hens, D. Pérez-Bendito, Anal. Chim. Acta 329 (1996) 135.
[21] G.L. Long, J.D. Winefordner, Anal. Chem. 55 (1983) 712A.
[22] S. Panadero, A. Gómez-Hens, D. Pérez-Bendito, Analyst 120 (1995) 125.
[23] B. Sendra, S. Panadero, A. Gómez-Hens, Anal. Chim. Acta 355 (1997) 145.

ELSEVIER

Talanta 48 (1999) 219–224

Talanta

Spectrophotometric determination of copper(II) at low μg l^{-1} levels using cation-exchange microcolumn in flow-injection

İbrahim Işıldak *, Adem Asan, Müberra Andaç

Ondokuz Mayıs University, Faculty of Education, Department of Chemistry, 55100 Samsun, Turkey

Received 2 April 1998; received in revised form 25 June 1998; accepted 26 June 1998

Abstract

A simple spectrophotometric flow-injection method is reported for the highly sensitive and fast determination of copper(II). The method is based on the formation of coloured Cu(II)-(4-methylpiperidinedithiocarbamate)$_2$ complex when the copper solutions are introduced into a tertiary reagent stream containing 4-methylpiperidinedithiocarbamate. The coloured complex is then selectively monitored at 435 nm. To increase interactions between copper(II) and colour forming reagent and preconcentrate of copper(II), a microcolumn containing strong cation exchange resins was placed between injection manifold and spectrophotometer. The system required no mixing chamber and allowed a sample throughput >60 sample h^{-1}. The calibration graph was linear in the range 5–100 μg l^{-1}. The detection limit was <0.5 μg l^{-1} for 20 μl injection volume of copper(II) ion solution. The developed method was applied to environmental, copper processing water, and ore samples.

Keywords: Flow-injection photometric method; Copper(II) determination; 4-Methylpiperidine-dithiocarbamate; Microcolumn

1. Introduction

Copper is known as one of the main toxic elements in the environment. Several methods such as atomic absorption spectrometry (AAS) [1], inductively coupled plasma-mass spectrometry (ICP-MS) [2], and ion selective electrode (ISE) [3] have been developed to determine the copper(II) ions in solutions depending on its concentration. However, some of them suffer from either sensitivity or selectivity, and also analyses are time consuming.

The determination of metal ions in flow-injection systems have received a growing amount of attention in recent years since its simplicity, speed and versatility which allows the method to be used in conjunction with a variety of detection systems such as spectrophotometry [4], ISE [5], AAS [6], and ICP-MS [7].

Copper(II) has been selectively determined in flow-injection systems by forming coloured com-

* Corresponding author. Tel.: +90 362 4450118; fax: +90 362 4450300; e-mail: oandac@ihlas.net.tr

0039-9140/99/$ - see front matter
PII S0039-9140(98)00241-0

plexes with chelating agents which often show a strong absorption at a characteristic wavelength. Dithiocarbamates are the most frequently reported complexing agents due to the strong chelating ability of the sulphur groups and their ability to form nearly insoluble metal salts with all metals except alkali and alkaline earth metals. Most of the copper chelates of dithiocarbamates were insufficiently soluble even at trace levels for aqueous solutions which it makes difficult the on-line determination in flow-injection systems. In an earlier work [8], a water-soluble copper chelate formed with diethanoldithiocarbamate as a colour forming reagent was utilised for direct spectrophotometric determination of copper(II) ion in the mg l^{-1} range using an aqueous carrier solution. A highly sensitive method for the direct spectrophotometric determination is required due to lower concentrations of copper(II) ions present in most river, sea and copper processing solutions.

The possibility of on-line preconcentration by inclusion of solid sorbents such as chelating agents or ion exchange resins in flow through microcolumns can provide an improvement in sensitivity and selectivity [9]. The presence of alkyl group in dithiocarbamate does not significantly alter its complexing ability, but it can determine other physical properties of the complex such as solubility and absorbtivity. Choosing the methylpiperidine derivative of dithiocarbamate as the colour developing reagent can offer a greatest sensitivity of the alkyl dithiocarbamate derivatives due to the presence of a chromophore.

In this communication, a flow-injection method being capable of determining copper(II) ions in the low μg l^{-1} ranges by incorporating a strong cation exchange microcolumn in flow-line for on-line preconcentration, and a tertiary solvent system to have direct determination of Cu(II) using 4-methylpiperidinedithiocarbamate as a colour developing reagent is described.

2. Experimental

2.1. Reagents and samples

All chemicals were of analytical reagent grade and deionized water was used throughout. A copper stock solution (ca. 63 mg l^{-1}) was prepared from $Cu(NO_3)_2 \cdot 3\ H_2O$ (E.Merck). Copper working standard solutions were prepared daily by several dilutions of the stock standard solution with 0.001 mol l^{-1} nitric acid or deionized water. During the determination of copper in real samples, copper working standard solutions were prepared by several dilution of fresh standard stock solution with deionized water only. Interference studies were carried out by using the chloride or nitrate salts of the metal cations.

4-Methylpiperidinedithiocarbamic acid potassium salt (K-MPDC) was synthesised according to the method described previously [10].

The M-(4-MPDC)$_n$ complexes were prepared by mixing equal volumes of 0.001 mol l^{-1} standard solutions of each metal in 0.001 mol l^{-1} nitric acid with 0.01 mol l^{-1} (K-MPDC) in deionized water [10]. The precipitates were filtered, washed with deionized water and ethanol and dried at 100–110°C. When required, the solutions of M-(4-MPDC)$_n$ complexes were prepared in chloroform.

Reagent carrier solution was composed of (K-MPDC) in chloroform 10%, ethylalcohol 80% and 0.1 mol l^{-1} acetate buffer solution 10%, pH 4.2.

The cation exchange resin used was the sodium form of A650 W (100–200 mesh) from BioRad Labs.

2.2. Apparatus

A high pressure liquid chromatography pump furnished with stainless-steel tubing was used to propel the samples and reagent solutions. Samples (20 μl) were injected into the carrier stream by a Rhodyne injection valve provided with a loop.

The absorbance of the coloured complex formed was measured with a Perkin Elmer series 3 UV visible spectrophotometer equipped with a flow-through microcell and connected to a strip chart recorder.

The cation exchange resin column (25–2 mm i.d.) was machined in a perspect block and was connected to the outlet of the injection value with the shortest possible length (5 cm × 0.8 mm i.d.) of polyethylene tubing. The resin was held inside

the column by plugging the two ends with discs of porous polyethylene held in by O-rings.

UV-visible spectra of M-(4-MPDC)$_n$ complexes were taken using a UV-visible spectrophotometer (GBC Cintra 20, Australia).

2.3. Procedure

The FI system used is simple and shown schematically in Fig. 1. The sample (S) injected into the reagent carrier solution (RCS), soon loads the column filled with the cation-exchange resin. 4-MPDC in the carrier solution interacts with metal ions retained in the microcolumn (MC), and then elutes by coloured complex forming. The interacted zone containing coloured complex is carried toward the flow-through spectrophotometric detector cell (SD) in which the Cu-(4-MPDC)$_2$ complex is selectively monitored at 435 nm and recorded continuously on the chart recorder (R).

For the determination of copper(II) in sea and river water samples, 50 ml of undiluted river and sea water samples in Nalgene plastics were filtered over a 0.45 μm filter from Millipore (Milford, MA), and then 20 μl of each filtered water sample was used as in the procedure described above. For the determination of copper(II) in copper ore samples; 1 g of a powdered copper ore sample was weighed in a glass beaker and dissolved in concentrated $HNO_3 + HCl$ mixture by heating on a mechanical heater. The cooled solution was filtered and diluted with deionized water then proceeded as described above.

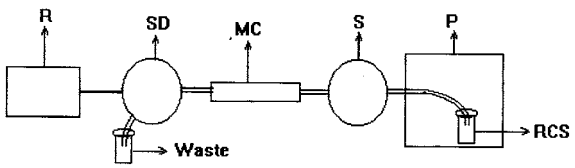

Fig. 1. Schematic diagram of the flow-injection system used for spectrophotometric determination of copper (II). RCS, reagent carrier solution (4-MPDC) in 80% ethanol, 10% chloroform + 10% 0.1 M acetic acid-acetate buffer in water (pH, 4.2). P, HPLC pump; S, Rhodyne sample injection valve; MC, microcolumn; SD, spectrophotometric detector; R, recorder.

2.4. Spectrophotometric studies

Metal ions react with 4-MPDC in aqueous medium to form several complexes with different stoichiometry. These complexes are slightly soluble in aqueous medium but fairly soluble in chloroform. Absorption spectra those correspond to solutions of 10–100 mg l^{-1} of metal complexes were taken in chloroform. There are absorbance maximums at 254 and 274 nm for all metal complexes, although Cu-(4-MPDC)$_2$ complex has an absorbance maximum at 435 nm. But Fe(II), Ni(II), Mn(II) and Cr(III)-(4-MPDC)$_n$ complexes also show negligible absorption at this wavelength. So this phenomenon can specifically be used for the determination of copper(II) ion in solutions.

2.5. Cation-exchange resin microcolumn

The cation exchange resin microcolumn has been employed in FIA for on-line preconcentration and a fast interaction of metal ions with 4-MPDC in the carrier solution to develop coloured complexes. A strongly cation-exchange resin was selected because metal ions are strongly bound by the resin so that a low amount of the resin can be used. Higher amounts of the resin minimised the use of higher flow-rates due to an increase of hydrodynamic pressure. On the other hand, both the retention time in the cation exchange microcolumn, and the residence time in the tubing in the flow-path determine the sampling time. At a flow-rate of 0.8 ml min^{-1}, a throughput of 60 sample analyses per hour was achieved for samples with concentrations ranging from 5 to 500 μg l^{-1} at a 20 μl injection volume.

It was ensured that all connections in the flow path had a tight fit. This was necessary to prevent leakage, which could occur because of the increased hydrodynamic pressure caused by inserting the column in the analytical path.

A mixing coil was inserted instead of the cation-exchange resin microcolumn in the analytical path. But peak shape and sensitivity for copper(II) was poorer and lower, respectively, for all concentration levels studied.

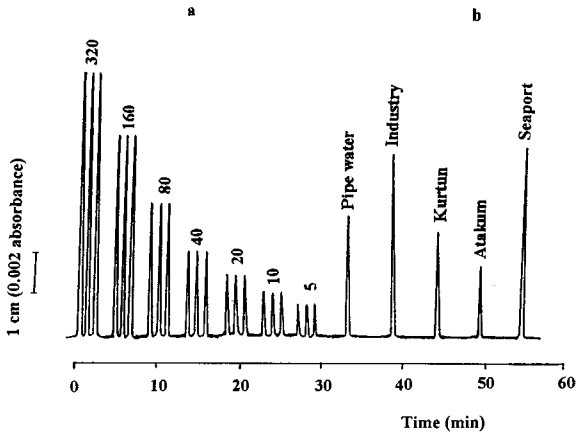

Fig. 2. Recorder outputs obtained with cation-exchange microcolumn in the flow-injection system. (a) Standard solution of Cu(II) (5–320 μg l^{-1}) injected. (b) Real sample solutions (for concentrations see Table 2). Figures above the peaks indicate concentrations in μg l^{-1}.

3. Results and discussion

The specific absorbance maximum of the Cu-$(4MPDC)_2$ complex at 435 nm can be applied for the selective determination of copper(II) in the flow-injection system shown in Fig. 1. The Cu-$(4MPDC)_2$ complex was found to be insufficiently soluble even at trace levels for aqueous solutions to be used directly. For the direct spectrophotometric determination of Cu(II), chloroform which dissolves the Cu-$(4MPDC)_2$ complex must be used as a reagent carrier solvent But this can reduce the life time of components of the system. Therefore, a tertiary solvent system (ethylalcohol–chloroform–acetate buffer solution in ratio 80:10:10) has been developed as a reagent carrier solution. The introduction of copper(II) ion in solution into the reagent carrier solution from the injection valve produces a positive response on the chart recorder, which was free from background absorption from the reagent as illustrated in Fig. 2(a).

Fig. 2(a) indicates that the flow signals for copper(II) ion show good reproducibility. The responses to 20 μl injection volumes of 5–100 μg l^{-1} solutions of copper(II) ions were linear. The relative standard deviation for 10 injections of samples containing 30 μg l^{-1} copper(II) was 0.85%. Under optimised solutions the detection limit was $\sim$0.5 μg l^{-1} for a 20 μl injection volume.

For rapid and sensitive continuous spectrophotometric analyses of copper(II) ion in solutions the use of the cation exchange microcolumn for on-line preconcentration is satisfactory, providing low ranges to be determined (μg l^{-1}). Such a high sensitivity is well suited to the determination of copper(II) in sea, river, and copper processing water samples.

3.1. Effect of concentration of 4-MPDC

The effect of concentration of 4-MPDC in the reagent carrier solution on the peak height was examined in the FI system using 0.63 and 3.2 mg l^{-1} copper(II) solutions. The concentration of 4-MPDC was varied over the range 0.1–1% (w/v), at pH 4.2 and a flow rate of 0.8 ml min^{-1}. For each concentration level of copper(II) ion, peaks were maximal at a concentration of 0.5% (w/v). Therefore, a concentration of 0.5% (w/v) of 4-MPDC as colour developing reagent in the carrier solution was chosen.

3.2. Effect of flow-rate

The flow-rate of reagent carrier solution was varied from 0.5 to 1.5 ml min^{-1}. The peak height decreased with increasing flow-rate (Fig. 3). Taking into consideration of the stability of the pump, peak shape and sampling time, the flow-rate of the reagent carrier solution was adjusted to 0.8 ml min^{-1}.

3.3. Effect of pH

Using 4-MPDC (0.5% (w/v)) in acetate buffer (as 10% (v/v) in the reagent carrier solution) system the effect of the pH was examined over the range 3.2–5.2. The peak height decreased with increasing pH (Fig. 4). Only at higher concentrations of Cu(II) in standard sample solution, the peak height decreased with increasing the pH. As the peak height was not strongly affected by the change of pH at lower concentrations of Cu(II). The pH of the acetate buffer system was fixed to 4.2 throughout the study.

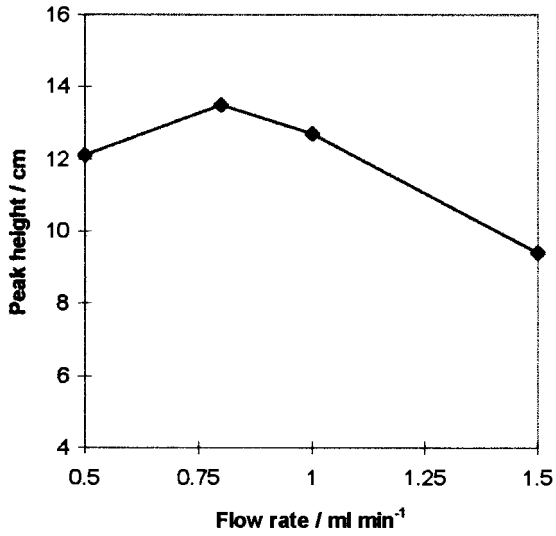

Fig. 3. Effect of flow-rate of reagent carrier solution on the peak height, 3.2 mg l^{-1} of Cu(II), 4-MPDC 0.5% (w/v).

3.4. Effect of foreign ions

The effects of some likely interfering ions were examined. Table 1 summarizes the tolerance limits of interfering ions on the determination of 50 μg l^{-1} copper(II). Most of the ions examined did not interfere with the copper(II) concentrations up to at least 500-fold excesses. But cobalt(II) and Ni(II) at the amounts of 700 μg l^{-1}, and iron(II) at the amounts of 900 μg l^{-1} gave positive interference. They did not interfere at amounts < 500 and 700 μg l^{-1}, respectively.

Table 1
Tolerance limits of foreign ions on the determination of 50 μg l^{-1} copper(II) ion

Tolerance limit (μg l^{-1})	Ion added
Over 100 000	Na(I), K(I), Ca(II), Mg(II), NO_3-, PO_4^{3-}, SO_4^{2-}, Cl^-, CO_3^{2-}, Br^-
10 000	Zn(II), Pb(II), Sn(II), Cd(II)
5000	Hg(II), Mn(II), Fe(III), Cr(VI), Cr(III)
500	Co(II), Ni(II), Fe(II)

The levels of this metal ions normally presented in sea and river water samples, and copper processing solutions were tolerable.

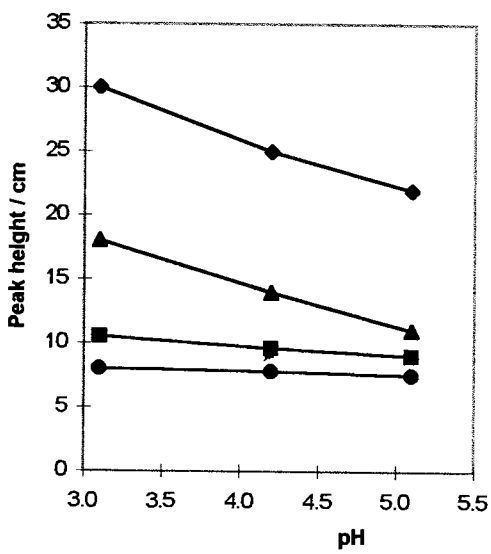

Fig. 4. Effect of pH on the peak height. Flow-rate: 0.8 ml min^{-1}; 4-MPDC 0.5% (w/v). (1) 6.4 mg l^{-1}; (2) 3.2 mg l^{-1}; (3) 1.6 mg l^{-1}; (4) 0.8 mg l^{-1}.

3.5. Applications

To evaluate the applicability of the proposed flow-injection method, it was applied to the determination of copper(II) in river and sea water samples, and copper processing solutions. The samples collected from different sources were filtered and directly injected into the flow line. Both calibration curve and standard addition methods were carried out. The values obtained from the calibration curve and the standard addition methods are in good agreement with each other. Examples of recorded output for different water samples and copper processing solutions are shown in Fig. 2(b). The results are summarised in Table 2.

The proposed method was also applied to the analysis of copper(II) in solutions obtained conventionally from ore samples. For the copper rich ore sample the results obtained are in good agreement with the certified values (Table 2). However, for the ore sample processed to waste in which iron(II) is present in significant amounts severe interference was produced.

Table 2
Determination of copper(II) in water, copper processing solution and ore samples

Sample[a]	Copper(II) in sample[b] (μg l^{-1})		
	Found[c]	Found[d]	Certified[e]
Seashore water			
Seaport	83.00 (0.15)		
Atakum	38.10 (0.08)	37.65 (0.06)	
Baruthane	44.78 (0.12)		
Organized industry	78.25 (0.12)	77.50 (0.08)	
River water			
Selyeri	59.85 (0.08)		
Kurtun	55.12 (0.08)	54.55(0.06)	
Copper processing solution			
Pipe water	54.00 (0.04)	53.70 (0.03)	
Storage water	60.05 (0.04)	59.65 (0.03)	
Ore samples[f]			
Copper rich ore	24.44 (0.32)	—	24.16 (0.20)
Copper ore processed to waste 'Iron(II) rich ore'	20.67 (0.55)	18.50 (0.40)	2.10 (0.20)

[a] Samples were collected at Samsun, Turkey.
[b] Values in parenthesis are the relative standard deviations for $n = 5$.
[c] Calibration curve method.
[d] Standard addition method.
[e] Provided by copper processing factory body.
[f] Values indicated as % (w/w).

References

[1] Analytical Methods for Atomic Absorption Spectrometry, Perkin-Elmer, 1976.
[2] K.E. Jarvis, A.L. Gray, R.S. Houk, Handbook of Inductively Coupled Plasma Mass Spectrometry, Blackie, Glasgow, 1992.
[3] K. Minoura, K. Fukushima, Chikyu Kagaku 22 (1988) 47.
[4] S. Nakano, K. Nakaso, K. Noguchi, T. Kawashima, Talanta 44 (1997) 765.
[5] Yu.A. Zolotov, L.K. Shpigun, I. Ya. Kolotyrkina, E.A. Novikov, O.V. Bazanova, Anal. Chim. Acta 200 (1987) 21.
[6] E.B. Milosavljevic, J. Ruzýcka, E.H. Hansen, Anal. Chim. Acta 169 (1985) 321.
[7] K.K. Falkner, J.M. Edmond, Anal. Chem. 62 (1990) 1477.
[8] R.M. Smith, T.G. Hurdley, Anal. Chim. Acta 166 (1984) 271.
[9] J. Haginaka, Trends Anal. Chem. 10 (1991) 17.
[10] B. Batı, H. Cesur, H. Batı, M. Özdemir, Turk. J. Chem. 19 (1995) 66.

ELSEVIER

Talanta 48 (1999) 225–229

Talanta

Short Communication

Chemiluminescence flow system for the determination of ammonium ion

Wei Qin [a,b], Zhujun Zhang [a,*], Baoxin Li [a], Youyuan Peng [a]

[a] *Department of Chemistry, Shaanxi Normal University, Xi'an 710062, People's Republic of China*
[b] *Department of Chemistry, Nanjing University, Nanjing 210008, People's Republic of China*

Received 2 April 1998; received in revised form 30 June 1998; accepted 10 July 1998

Abstract

A novel chemiluminescence (CL) system for ammonium ion combined with flow-injection analysis is presented in this paper. It is based on the CL reaction between luminol, immobilized electrostatically on an anion-exchange column, and chlorine electrochemically generated on-line via a platinum electrode from hydrochloric acid in a coulometric cell. Ammonium ion reacts with chlorine and decreases the observed CL intensity. The system responds linearly to ammonium ion concentration in the range 1.0–100 μM, and the detection limit is 0.4 μM. A complete analysis, including sampling and washing, could be performed in 1 min with a relative standard deviation of $< 6.0\%$. The system is stable for over 500 determinations and has been applied successfully to the determination of ammonium ion in rainwater samples.

Keywords: Chemiluminescence; Flow-injection analysis; Ammonium ion

1. Introduction

Flow injection chemiluminescence (CL) analysis has received much attention in various fields for its high sensitivity, rapidity, simplicity and feasibility. However, a limitation to widespread application of this technique is the requirement to prepare large quantities of analytical reagents and continuously deliver them into the reaction zones. This is undesirable not only for operational convenience and the simplicity of detection device, but also for the cost, environment and resource considerations [1]. An effective approach to solve this problem is to employ CL reagents in immobilized or solid-state format. So far these solid-state CL flow injection systems have been extensively investigated [2–6]. In these systems, analytes are detected by the CL reactions either with the immobilized reagents directly or with the dissolved reagents which are released from the immobilized substrates or the solid-state forms by some appropriate eluents.

For the continuing development of such solid-state CL flow injection systems, this paper reports

* Corresponding author. Fax: +86 29 5308748.

0039-9140/99/$ - see front matter
PII S0039-9140(98)00246-X

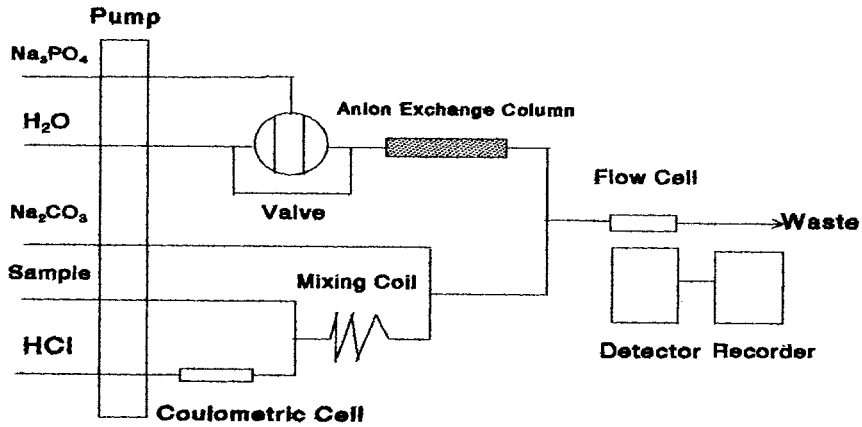

Fig. 1. Schematic diagram of the flow system for the determination of ammonium ion.

a new CL system for the determination of ammonium ion based on the inhibition of ammonium ion in the CL reaction between luminol and chlorine [7]. In this system, not only was luminol immobilized on an anion exchange column, but also a coulometric cell with platinum electrodes was introduced into the flow line for on-line electrochemical generation of the unstable and toxic analytical reagent chlorine from hydrochloric acid. By passing sodium phosphate through the column with immobilized luminol, luminol is eluted from the resin and then mixes and reacts with chlorine under basic conditions to produce a CL signal. Ammonium ion is detected by the decreased CL intensity from the reaction with chlorine. The proposed method offers advantages of simplicity, rapidity and high sensitivity for the determination of ammonium ion.

2. Experimental

2.1. Apparatus

The flow system employed in this work is shown in Fig. 1. A peristaltic pump delivered all flow streams at a flow rate (per tube) of 3.5 ml min^{-1}. PTFE tubing (1.0 mm i.d.) was used to connect all components in the flow system. The stream of 0.15 M hydrochloric acid was passed through the coulometric cell for on-line electrogeneration of chlorine and then mixed and reacted with the sample stream in a mixing coil (1.0 mm i.d.) of 25 cm length to form nitrogen trichloride, thus reducing the chlorine. Before reaching a spiral flow cell (200 μl), the resulting stream merged with the stream of 0.3 M sodium carbonate and that of luminol which was eluted by the injection of 2×10^{-3} mol dm^{-3} sodium phosphate solution through the column with immobilized reagent, prepared as described before [5], via a six-way injection valve.

The coulometric cell was made of a mini glass column (30 × 3 mm i.d.), which contained a set of two platinum electrodes with an area of 2×10 mm and a distance of 1 mm between them. The constant coulometric current was supplied by a KLT-1 coulometer (Jiangsu Electroanalytical Instrument Plant, China).

The CL emission was transduced to an electric signal by a Hamamatsu R456 photomultiplier tubed placed close to the flow cell and recorded with an XWT-204 recorder (Shanghai Dahua Instrument and Meter Plant, China).

Absorbance monitoring was done using a UV-spectrophotometer Model-752 (Shanghai Third Analytical Instrument Plant, China).

2.2. Reagents

All the reagents were of analytical grade; doubly distilled water was used for the preparation of

Table 1
Characteristics of eluents for the determination of ammonium ion[a]

Type of CL intensity	Relative CL intensity						
	Na_3PO_4	Na_2SO_4	Na_2CO_3	$NaNO_3$	NaCl	NaAc	NaOH
I	270	155	105	75	60	45	40
II	138	90	53	38	44	23	28
III	132	65	52	37	16	22	12

[a]The concentration of each eluent was 2×10^{-3} M. (I): CL intensity in the absence of ammonium ion; (II): CL intensity in the presence of 6 μM ammonium ion; (III): decreased CL intensity.

solutions. A stock solution of ammonium ion (0.01 M) was prepared by dissolving 0.5349 g of ammonium chloride in 1000 ml bidistilled water. Standard test solutions were prepared by appropriate dilution of the stock solution. A 0.25 mol dm^{-3} luminol solution was prepared by dissolving 4.43 g of luminol in 100 ml of 0.5 mol dm^{-3} NaOH solution. D201 anion exchange resin purchased from Nankai University was used for immobilization of luminol.

2.3. Procedures

Reagents and samples were pumped at a constant speed until a stable baseline was recorded. Then 0.15 ml of eluent containing 2×10^{-3} M sodium phosphate was injected into the carrier stream and luminol was released quantitatively. The concentration of ammonium ion was quantified by the CL intensity.

3. Results and discussion

3.1. Selection of eluent

The immobilized luminol can be eluted from the resin by various anions injected through the anion exchange column. The characteristics of some eluents including NaCl, $NaNO_3$, NaAc, NaOH, Na_2SO_4, Na_2CO_3 and Na_3PO_4 were evaluated and the results are shown in Table 1. It can be seen that sodium phosphate was the best eluent with the highest CL intensity and decreased CL intensity. Therefore, sodium phosphate was used as eluent for subsequent work.

3.2. Effect of eluent concentration

The release of luminol was controlled by the concentration of sodium phosphate injected. The eluent concentration was varied in order to maximize the CL signal. As shown in Fig. 2, increasing the eluent concentration gives increasing CL intensity. Considering a compromise between high CL intensity and long lifetime of the column, 2×10^{-3} M sodium phosphate was chosen as optimum. In this case, the amount of luminol released was 6.5×10^{-8} mol measured by UV-vis absorbance and the column with immobilized luminol could be used over 500 times.

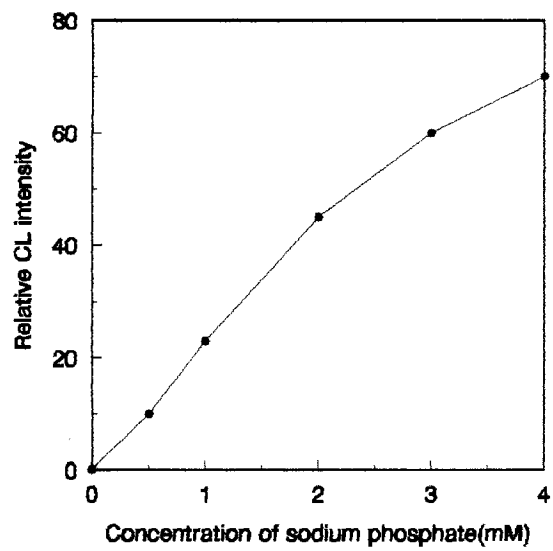

Fig. 2. Effect of eluent concentration on CL intensity.

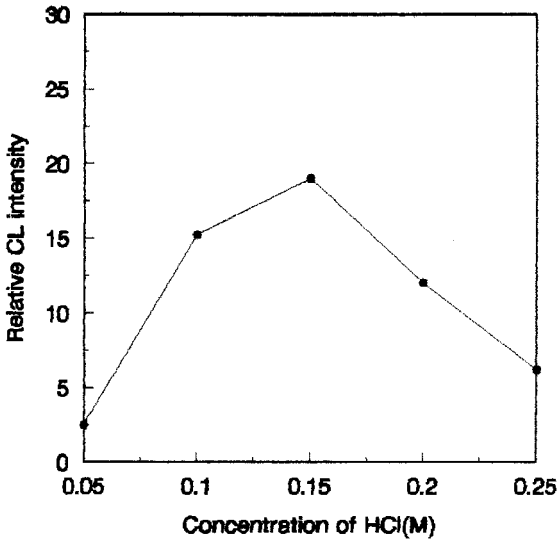

Fig. 3. Effect of HCl concentration on CL intensity.

3.3. Effect of hydrochloric acid concentration

To prevent the oxidation of H_2O to oxygen at the anode platinum electrode, hydrochloric acid was employed as the electrolyte for the efficient on-line generation of chlorine. The effect of hydrochloric acid concentration was examined and the results are shown in Fig. 3. It can be seen that maximum CL intensity could be obtained at 0.15 M of HCl concentration; lower or higher than this value would cause a decrease of coulometric efficiency due to the oxidation of H_2O or that of platinum electrode itself. Hence 0.15 M of hydrochloric acid was employed in subsequent experiments.

3.4. Effect of length of mixing coil

For the efficient reaction between chlorine and ammonium ion, a mixing coil was added after the merging point of the chlorine and sample streams and its length was tested from 5 to 60 cm. It was found that a suitable length leading to a high CL intensity and an effective inhibiting effect was 25 cm; longer lengths decreased the CL intensity due to the instability of dilution chlorine, while shorter lengths caused incomplete reduction of chlorine thus decreasing the suppression by ammonium ion.

3.5. Effect of sodium carbonate concentration

Due to the nature of the luminol reaction, which is more favored in basic conditions, sodium carbonate was introduced into the manifold by a flow line to mix with the downstream containing hydrochloric acid and to create the carbonate buffer suitable for the CL reaction. The effect of sodium carbonate concentration on CL intensity was investigated for the range 0.1–1.0 M. Sodium carbonate (0.3 M) was found to be optimum for higher CL intensity and better reproducibility. In this case, the pH at the mixing point was ~ 10.2.

3.6. Performance of the system for ammonium ion measurements

Since ammonium ion is measured by the decreased CL intensity from the oxidation reaction with the CL reagent chlorine, it is obvious that small amounts of ammonium ion can be detected linearly by small amounts of chlorine, and vice versa. Therefore, the linear range of the system is determined by the amount of chlorine electrochemically generated in the coulometric cell, and is in turn determined by the constant coulometric current values employed. In this system, 0.02 and 0.10 mA of currents were chosen for the determination of ammonium ion over the range 1.0–10 μM and the range 10–100 μM, respectively; the corresponding regression equations were $I = 24.5–2.0[NH_4^+]$ (μM) with a correlation coefficient 0.997 and $I = 38.2–2.5[NH_4^+]$ (10 μM) with a correlation coefficient 0.996. Increasing the current value can widen the linear range, but unfortunately may produce a large amount of gaseous hydrogen in the coulometric cell, which would cause a poor reproducibility. At a flow rate of 3.5 ml min^{-1}, a complete analysis for the determination of ammonium ion could be performed in 1 min including sampling and washing. The detection limit was 0.4 μM (3σ) and the relative standard deviation was $< 6.0\%$ for 4 μM ammonium ion ($n = 7$).

Table 2
Results of analysis of ammonium ion in rainwater

Sample	Proposed method[a] (μM)	Recovery (%)	Spectrophotometry[a] (μM)
Rainwater 1	45 (±4.8%)	92	49 (±6.5%)
Rainwater 2	15 (±5.5%)	105	12 (±8.3%)
Rainwater 3	22 (±5.0%)	96	24 (±7.5%)
Rainwater 4	64 (±4.2%)	106	60 (±5.5%)

[a] Average of four measurements (±RSD).

3.7. Interferences

The influences of foreign species were investigated by analyzing a standard solution of 4 μM ammonium ion to which increasing amounts of interfering species were added. The tolerable limit of a foreign species was taken as a relative error $\not> 5\%$. The tolerated ratio of foreign ions to 4 μM ammonium ion was >1000 for Na^+, K^+, Cl^-, Br^-, $H_2PO_4^-$, SO_4^{2-}, NO_3^- and HCO_3^-, 100 for Ca^{2+} and Mg^{2+}, and 10 for Al^{3+} and Zn^{2+}, respectively. Equal amounts of reducing substances such as Fe^{2+}, S^{2-} and SO_3^{2-}, which could destroy the chlorine, or those of transition metal cations such as Fe^{3+}, Mn^{2+}, Ni^{2+}, and Cu^{2+}, which might affect the mechanism of luminol–chlorine reaction [8], interfered with the determination of 4 μM ammonium ion. However, these interferences can be eliminated by a distillation step, which is described below.

3.8. Sample analysis

An appropriate volume of rainwater samples collected on different days was poured into a 500 ml flask, then 15 ml of 0.01 M borate was added, the solution adjusted to pH 9.5 with 6 N NaOH and diluted to 250 ml with bidistilled water. The flask was connected to the distillation system. Then 25 ml of 0.04 N H_2SO_4 was added to a 250 ml absorption bottle; the lower end of the condenser pipe should be immersed in the absorption liquid. The solution was heated until ~ 100 ml of distillate was collected. The pH of the distillate was then neutralized and the resulting distillate was diluted to 150 ml with bidistilled water. The concentration of ammonium ion was determined by the present system and the results are given in Table 2, which agree well with those obtained by indophenol spectrophotometry [9].

Acknowledgements

This study was supported by the National Natural Science Foundation of China (No. 39730160).

References

[1] A. Kuniyoshi, K. Hatta, T. Suzuki, A. Masuda, M. Yamada, Anal. Lett. 29 (1996) 673.
[2] W. Qin, Z.J. Zhang, C.J. Zhang, Anal. Chim. Acta 361 (1998) 201.
[3] T.A. Nieman, Mikrochim. Acta, III (1988) 239.
[4] P. van Zoonen, D.A. Kamminga, C. Gooijer, N.H. Velthorst, R.W. Frei, Anal. Chim. Acta 174 (1985) 151.
[5] W. Qin, Z.J. Zhang, S.N. Liu, Anal. Lett. 30 (1997) 11.
[6] W. Qin, Z.J. Zhang, C.J. Zhang, Analyst 122 (1997) 685.
[7] D.F. Marino, J.D. Ingle Jr, Anal. Chem. 53 (1981) 455.
[8] P.R. Kraus, S.R. Crouch, Anal. Lett. 20 (1987) 183.
[9] W.T. Bolleter, C.J. Bushman, P.W. Tidwell, Anal. Chem. 33 (1961) 592.

ELSEVIER

Talanta 48 (1999) 231–233

Talanta

Letter to the Editors

Evaluation of the Procedure for Alkaline Digestion Solvent Estimation for Methyl Mercury Artifact Formation

Lian Liang *, Steve Lazoff

Cebam Analytical, Inc., 3927 Aurora Avenue North, Seattle, WA 98103, USA

Received 27 October 1997; accepted 13 November 1997

Dear sir:

The technique of aqueous phase ethylation, carbon or Tenax trap collection, followed by isothermal GC separation, and atomic fluorescence detection has been extensively used for determination of methyl mercury in a variety of environmental samples [1,2]. Since the matrix interferences on ethylation reaction are very severe, to minimize the interferences, several procedures including distillation [3,4], alkaline digestion/solvent extraction [5], and solvent extraction after $KBr/H_2SO_4/Cu$ leaching [6,7] were used for isolation of methyl mercury from sediment samples. Recent publications have demonstrated the formation of significant artifactual methyl mercury in the distillation procedure [8,9]. In response to questions of colleagues on whether the alkaline digestion/solvent extraction makes significant artifacts, this letter presents results showing that methyl mercury artifact formation is much less significant when sediment samples are prepared using alkaline digestion/solvent extraction.

The procedure of alkaline digestion/solvent extraction was evaluated for methyl mercury artifact formation by analyzing sediment samples spiked with large amounts of Hg^{2+} and unspiked prior to using the entire alkaline digestion/solvent extraction procedure. Analysis followed by aqueous phase ethylation, Tenax trap precollection, isothermal GC separation, and atomic fluorescence detection. The difference in methyl mercury concentrations between the spiked and unspiked samples was considered to be artifactual methyl mercury. The percent ratio of percent artifactual methyl mercury to percent methyl mercury found in unspiked samples was considered as percent error.

Four bog type sediment samples from Duluth and Portland were used, two lake sediments (#1, #3), and two river sediments (#2, #4). Sample #1 was spiked at five different levels between 5 and 62 μg g^{-1}. Percent methyl mercury artifact is presented relative to Hg^{2+} spike added. The other samples were spiked at one higher level only. The results are shown in Table 1. It was found that the methyl mercury artifacts increased linearly with increasing spiked Hg^{2+} concentration within spiked levels of 5–20 μg g^{-1}. Methyl mercury artifacts were observed for each sample, ranging from 0.001 to 0.002% of the total Hg (spiked plus unspiked) concentra-

* Corresponding author. Tel.: +1 206 6329097; fax: +1 206 6322417: e-mail: Cebam@wolfenet.com

PII S0039-9140(97)00418-9

Table 1
Experimental results of evaluating the procedure of alkaline digestion/solvent extraction for methyl mercury artifact formation

Sample I.D.	Sample size (wet) (g)	Spiked with Hg^{2+} (ng g^{-1})	THg (ng g^{-1})	MeHg found as Hg (ng g^{-1})	MeHg artifact as Hg (ng g^{-1})	% MeHg	% MeHg artifact	% Error
#1			307	1.01		0.33		
#1 spike A	0.936	5342	5649	1.10	0.09		0.0017	0.52
#1 spike B	0.978	10 224	10 531	1.23	0.22		0.0022	0.67
#1 spike C	0.984	20 325	20 632	1.42	0.41		0.0020	0.61
#1 spike D	0.959	41 710	42 017	1.76	0.73		0.0017	0.52
#1 spike E	0.965	62 176	62 483	1.91	0.90		0.0014	0.42
#2			90.3	0.22		0.24		
#2 spike	0.968	41 322	41 412	0.91	0.69		0.0017	0.71
#3			212	0.46		0.22		
#3 spike	0.972	41 152	41 364	1.21	0.75		0.0018	0.82
#4			333	1.34		0.40		
#4 spike	0.991	40 362	41,552	2.13	0.79		0.0020	0.50

tion. The artifactual methyl mercury ratios are small compared to the ratios found in the unspiked sediment samples of 0.22–0.40%. Artifact formation by the alkaline digestion/solvent extraction procedure is thus found to be insignificant for these sediment samples. In fact, the percent error caused by artifacts may be even much smaller than those listed in Table 1 due to the equilibrium between concurrent methylation and demethylation processes [10]. Samples containing Hg^{2+} as high as the spiked samples would also contain higher levels of methyl mercury. Therefore, artifact methyl mercury as a percent of true methyl mercury would be even lower than that found in this study.

It should be pointed out that previous research has demonstrated that the use of low-quality ethylation reagent (sodium tetraethyl borate, $NaBEt_4$) could result in the formation of artifactual methyl mercury during the ethylation reaction when large amounts of Hg^{2+} are present [3]. Thus, new batches of $NaBEt_4$ should be checked for artifact formation prior to use.

References

[1] N.S. Bloom, Can. J. Fish. Aquat. Sci. 46 (1989) 1131.
[2] L. Liang, M. Horvat, N.S. Bloom, Talanta 41 (3) (1994) 371.
[3] M. Horvat, N.S. Bloom, L. Liang, Anal. Chim. Acta 281 (1993) 135.
[4] M. Horvat, L. Liang, N.S. Bloom, Anal. Chim. Acta 282 (1993) 153.
[5] L. Liang, M. Horvat, E. Cernichiari, B. Gelein, S. Balogh, Talanta 43 (1996).
[6] A. Alli, R. Jaffe, R. Jones, J. High Resolut. Chromatr. 17 (1994) 745.
[7] A. Furutani, J.W.M. Rudd, Appl. Environ. Microbiol. 40 (1980) 770.
[8] H. Hintelmann, R. Falter, G. Iigen, R.D. Evans, Fresenius J. Anal. Chem. 358 (1997) 363.
[9] N.S. Bloom, J.A. Colman, L. Barber, Fresenius J. Anal. Chem. 358 (1997) 371.
[10] P.J. Craig, P.D. Bartlett, Nature (London) 275 (1978) 635.

ELSEVIER

Talanta 48 (1999) 243–246

Talanta

Author Index

Volume 47 (1998)

Note: Author Index of Volume 47 included here due to omission in Vol. 47 No. 5

PII S0039-9140(98)00342-7

Note: Author Index of Volume 47 included here due to omission in Vol. 47 No. 5

Note: Author Index of Volume 47 included here due to omission in Vol. 47 No. 5

Note: Author Index of Volume 47 included here due to omission in Vol. 47 No. 5

ELSEVIER

Talanta 48 (1999) 247–251

Talanta

Subject Index

Volume 47 (1998)

Note: Subject Index of Volume 47 included here due to omission in Vol. 47 No. 5

PII S0039-9140(98)00343-9

.

ELSEVIER

Talanta 48 (1999) 255

Talanta

Editorial

Aims and scope

The editors are very pleased to announce that Talanta has been experiencing an increase in the number of papers submitted to the journal. This steady increase in submissions will require the journal to become more strict in its editorial policy and to reject papers that do not closely fit the journal's aims and scope. To this effect, authors are encouraged to carefully read the aims and scope of the journal, and to consider the following criteria before submitting a paper to Talanta.

Talanta provides a forum for fundamental studies and original research papers dealing with all branches of pure and applied analytical chemistry. Classical analytical techniques such as volumetric titrations, UV-visible spectrophotometry (including derivative spectrophotometry), fluorimetry, polarography and related pulsed voltammetric techniques, and so forth, are considered as routine analytical methods, and manuscripts dealing with these methods should be submitted for publication in Talanta only if substantial improvement over existing official or standard procedures is clearly demonstrated. New reagents should demonstrate clear advantages, and their presentation should be comprehensive, rather that generating a series of similar papers.

Solvent extraction methods are well established, and new methods should demonstrate improvements in waste generation, non-hazardous material substitutes, and ease of use (automation).

Application of an original method to real matrices is encouraged, provided that it is properly validated following recommendations of official institutions. The developed method should especially comprise information on selectivity, sensitivity, detection limits, accuracy, reliability and speciation capabilities (e.g. in the case of trace metal analysis). Proper statistical treatment of the data should be provided.

Application of classical analytical approaches such as polarography, voltammetry (pulsed), UV-visible spectrophotometry (and derivative), and fluorimetry to relatively simple matrices having no major interference, such as drug formulations or reconstituted samples, are discouraged unless considerable improvements over other methods in the literature (time saving, accuracy, precision, cleaner chemistry, automation) are highlighted.

Papers dealing with analytical data such as stability constants, pK_a values, etc. should be published in more specific journals, unless novel analytical methodology is demonstrated, or important analytical data are provided which could be useful in the development of analytical procedures.

Gary D. Christian
Jean-Michel Kauffmann
Editors-in-Chief
April, 1998.

PII S0039-9140(98)00239-2

ELSEVIER

Talanta 48 (1999) 257–267

Talanta

Review

Membrane filtration studies of aquatic humic substances and their metal species: a concise overview. Part 2. Evaluation of conditional stability constants by using ultrafiltration

T.I. Nifant'eva [a,*], V.M. Shkinev [a], B.Ya. Spivakov [a], P. Burba [b]

[a] *Vernadsky Institute of Geochemistry and Analytical Chemistry, Russian Academy of Sciences, 117975 Moscow, Russia*
[b] *Institute of Spectrochemistry and Applied Spectroscopy, 44139 Dortmund, Germany*

Received 22 January 1998; received in revised form 19 May 1998; accepted 23 July 1998

Abstract

The assessment of conditional stability constants of aquatic humic substance (HS) metal complexes is overviewed with special emphasis on the application of ultrafiltration methods. Fundamentals and limitations of stability functions in the case of macromolecular and polydisperse metal–HS species in aquatic environments are critically discussed. The review summarizes the advantages and application of ultrafiltration for metal–HS complexation studies, discusses the comparibility and reliability of stability constants. The potential of ultrafiltration procedures for characterizing the lability of metal–HS species is also stressed. © 1999 Elsevier Science B.V. All rights reserved.

Keywords: Humic substances; Metal complexes; Stability constants; Ultrafiltration

1. Introduction

In aquatic environments humic substances (HS) contribute the major part to the refractory organic carbon dissolved there [1]. Generally, HS consist of complex mixtures of related organic polyelectrolytes of varying molecular size, (sub)structures and functionalities hardly separable even by high-performance separation procedures [2]. In our preceding paper we reported on the size fractionation of aquatic HS and their metal species by means of sequential-stage ultrafiltration (UF) processes stressing their analytical capabilities and limitations [3]. The present report summarizes the application of UF to metal–HS complexation studies.

The necessity to incorporate the contribution of HS in chemical modeling of natural aquatic systems has been well recognized [4]. Particularly, the toxicity, bioavailability, transport processes and hydrogeochemical cycles of metals depend on the nature and the thermodynamic stability of their complexes formed. In the case of heavy metals their complexes with humic substances (HS) are the main class of their species in natural waters

* Corresponding author. Fax: +7 095 9382054; e-mail: concentr@glas.apc.org

0039-9140/99/$ - see front matter
PII S0039-9140(98)00249-5

[5]. Such modeling requires reliable stability constants (K) of metal–HS complexes (or metal–fulvic acid (FA) and metal–humic acid (HA) complexes in the case of subdivided HS) for input as parameters. However, the progress in quantifying metal–HS interactions has been troublesome up to now. The physical and chemical heterogeneity of such substances, the variety of polymeric effects inherent to the system hamper the thermodynamic description of the complexation reactions. A comprehensive thermodynamic model for metal–HS interactions has to take into account that: (i) K decreases with metal loading because HS include many coordinating sites of different nature and the strongest sites are saturated first; (ii) K decreases with metal loading because attractive, negative charge of HS is compensated by the bound metal; (iii) the formation of metal ion bridges and compensation of charge influence the changes in conformation of polymeric molecule and result in intra- or intermolecular condensation, which may cause a decrease in the number of sites available to form complexes. The same effects should be taken into account while concerning the K dependence on pH and ionic strength. Thus, it is evident that the K values obtained from one set of parameters can not be applied to another set of experimental conditions.

Due to the absence of a model completely describing the K dependence on different factors the possibility of measurement of conditional stability constants in natural water is of practical interest. This means that the analytical method used for this purpose should be applicable to the study of metal speciation even at low concentrations. A variety of methods (e.g. potentiometric titration with ISE, voltammetry, ion exchange, spectrofluorometry, gel filtration chromatography, dialysis, ultrafiltration) are conventionally used for the assessment of conditional stability constants of metal–HS complexes overviewed in Table 1 [6–50]. According to various environmental studies, UF methods are merely limited by the detection limits of the applied determination method (e.g. atomic spectrometry) [51]. Potentiometric methods, which are probably the most used method for metal–HS complexation studies (see Table 1), suffer from the lack of sensitivity

Table 1
Analytical methods used for the assessment of stability constants of metal–humic substances (HS), metal–humic acid (HA) and metal–fulvic acid (FA) complexes

Metal	Ligand	Source	Reference
Potentiometric titration with ion-selective electrodes			
Cd(II)	HA	Soil	[6]
	FA	River, soil	[7,8]
	HS	Aquatic	[9]
Ca(II)	FA	River	[10]
		Peat, Armadale, Laurentian	[11]
		Lake	[12]
Cu(II)	HA	Soil	[6]
	FA	Soil	[13,14]
		Lake, river, peat	[14,8]
		Sewage sludge	[15]
		Sea	[16]
	HS	Lake	[17]
		Swamp	[18]
		Estuarine	[19]
Mg(II)	FA	Soil	[13]
Pb(II)	HA	Lake, river	[20]
		Soil	[6]
	FA	Lake, river	[20]
		Sewage sludge	[21]
			[8]
Voltammetric techniques			
1. Anodic stripping voltammetry			
Cu(II)	HA	Peat	[22]
		Lake	[23]
	FA	Soil	[24]
		Lake	[23]
		Sewage sludge	[21]
			[8]
	HS	Sea	[25,26]
		Swamp	[27]
		Sewage sludge	[28]
Cd(II)	FA		[8]
		Sewage sludge	[21]
	HS	Sewage sludge	[28]
Pb(II)	FA		[8]
		Sewage sludge	[21]
	HS	Sea	[29]
Zn(II)	HS	Sea	[30,31]
2. Cathodic stripping voltammetry			
Cu(II)	HS	Sea	[32]
Co(II)	HS	Sea	[33]
Zn(II)	HS	Sea	[31]
3. Differential pulse polarography			
Co(II)	HA	Aldrich	[34]
Ni(II)	HA	Aldrich	[34]
Eu(III)	HA	Aldrich	[34]

Table 1 (*Continued*)

Metal	Ligand	Source	Reference
III. Ion exchange			
Cu(II)	FA	Surface waters	[35]
	HS	River, swamp, soil	[36]
Co(II)	HA	Aldrich	[34]
	FA	Armadale	[37]
Zn(II)	FA	Armadale	[37]
		Surface waters	[35]
	HS	River, swamp, soil	[36]
Ni(II)	HA	Aldrich	[34]
	FA	Surface waters	[35]
	HS	River, swamp, soil	[36]
Cd(II)	FA	Ground water	[38]
		Surface waters	[35]
	HS	River, swamp, soil	[36]
Eu(III)	HA	Aldrich	[34]
	FA	Armadale	[37]
	FA	Bersbo	[39]
U(VI)	HA	Soil	[40]
IV. Spectrofluorimetry			
Co(II)	FA	Soil, river	[41]
Ni(II)	FA	Soil, river	[41]
Cu(II)	FA	Soil	[24]
	HS	River, swamp, sea	[42]
Eu(III)	HS	Swamp	[27]
		River	[43]
Cm(III)	HA	Aldrich	[44]
V. Gel filtration chromatography			
Ca(II)	FA	Peat	[45]
	HS	Lake, sea, soil	[45]
Cd(II)	FA	Peat	[45]
	HS	Lake, sea, soil	[45]
Co(II)	FA	Peat	[45]
	HS	Lake, sea	[45]
Cu(II)	FA	Peat	[45]
	HA	Peat	[45]
	HS	Lake, river, sea	[45]
Hg(II)	FA	Peat	[45]
	HS	Lake, river, sea	[45]
Mg(II)	FA	Peat	[45]
	HS	Lake, sea	[45]
Mn(II)	FA	Peat	[45]
	HS	Lake, sea	[45]
Ni(II)	FA	Peat	[45]
	HS	Lake, sea	[45]
Am(III)	FA	Ground water	[46]
	HA	Aldrich	[46]
VI. Dialysis			
Co(II)	HA	Aldrich	[34]
		Peat	[47]
Cd(II)	FA		[8]
		Sewage sludges	[21]
	HS	Sewage sludges	[28]
Cu(II)	FA		[8]
		Sewage sludges	[21]
	HS	Sewage sludges	[28]
Ni(II)	HA	Aldrich	[34]
Pb(II)	FA		[8]
		Sewage sludges	[21]
Sn(II)	HA	Aldrich	[34]
Eu(III)	HA	Aldrich	[34]
VII. Ultrafiltration			
Ca(II)	FA	Peat, Armadale, Laurentian	[11]
Co(II)	HS	Oxic waters	[48]
Cu(II)	HS	Oxic waters	[48]
		Swamp	[27]
Cd(II)	FA	Ground water	[38]
	HS	Swamp	[27]
	HS	Aquatic	[49]
Ni(II)	HS	Oxic waters	[48]
Mn(II)	HS	Oxic waters	[48]
Zn(II)	HA	Lake	[3]
	HS	Swamp	[27]
	HS	Oxic waters	[48]
Eu(III)	FA	Aquatic	[39,50]
	HA	Aldrich	[51]
Th(IV)	FA	Aquatic	[50]
U(VI)	FA	Aquatic	[50]

and could not be applied to the measurements in natural waters [52–54]. The limitation of voltammetric methods, which are among the most sensitive and theoretically advanced, is their usefulness for only some elements, while UF is applicable to a wide range of different elements [52,54]. Compared to other separation techniques used for K determinations, an important advantage of UF is that this method takes not so long time as dialysis and does not disturb the complexation equilibria like ion-exchange chromatography [54].

2. Complexation models for metal–HS species

The various complexation models applied to describing metal–HS interactions can be classified as discrete ligand models [55–57] and continuous multiligand models [19,56,58–60]. In the discrete ligand approach only a few ligands or binding

sites are required to fit experimental data. On the other hand, in the continuous distribution approach it is assumed that a large number of heterogeneous ligands with a range of binding affinities are involved in metal binding characterized by a continuous distribution (e.g. Gaussian) of the stability constants. There are several modifications of the discrete model, considering the polymer molecule, e.g. as separate microphase or rigid sphere [55,61,62]. In such refined models electrostatic (surface) complexation is also considered and contributions due to ionic strength effects may be incorporated. The comparison of different types of models is given elsewhere [4,58,63,64]. It should be noted that though the continuous models have several distinct advantages, the literature survey indicates that the most popular is still the discrete model. This model has been applied in the UF stability constant determinations.

The discrete model offers different kinds of approaches which enable the explanation of complexation of metal ions by fulvic and humic acids. 1:1 stoichiometry is usually assumed for metal–ligand complexes and Scatchard method [65,66] of K calculation is widely used for single and rather often also for two-site models. Buffle et al. [20] have observed the failure in many cases by applying the Scatchard method to describe the metal complexation producing the suggestion for the formation of both 1:1 and 1:2 metal–ligand complexes.

3. Metal–humic substance complexation studies by ultrafiltration

The literature survey shows that in the studies of the stability constant determinations carried out by UF methods only the 1:1 stoichiometry model has been applied. The overall stability constant (more correctly overall complex formation function [39] or average equilibrium function [52]) is defined as

$$K = \frac{\sum_i [\mathrm{ML}_i]}{M \sum_i [\mathrm{L}_i]} = \frac{M_\mathrm{b}}{M \cdot L} \quad (1)$$

Where $M_\mathrm{b} = \Sigma_i ML_i$ is the total concentration of the metal bound to all the active sites, M is the free metal concentration, $L = \Sigma L_i$ is the total ligand concentration.

Marinsky and Ephraim [55,67] incorporated to this equation also the term concerning the metal concentration correction due to separate phase effects.

Let us assume that the UF retention R of both the ligand and complex by the membrane are complete ($R_L = 1$, $R_{ML} = 1$), whereas the free metal ions pass through the membrane ($R_M = 0$). The free metal concentration in Eq. (1) is thus accepted to be equal to the total metal concentration in the filtrate. Furthermore, M_b is the total concentration in the cell, which can be obtained from the difference between the total metal concentration in the sample and the free metal ion concentration. This kind of approach has been usually applied in different studies [11,27,38,39,49,68–70]. However, the retention of 100% ($R = 1$) is seldom obtained in actual practice. This is probably due to the polydispersity in the dimension of the membrane pores. Moreover, the molecular weight cutoff limits depend very strongly on the configuration and charge of the compounds which are depending on the pH, ionic strength and other conditions of the solution [71]. The values of R_M for divalent and trivalent cations have also been found to be greater than zero [52,39,68,71] and the values vary, e.g. with pH, ionic strength and the nature of inorganic anions present. Thus, the assumption that the UF retentions of both the ligand and the complex over the membrane may sometimes result in systematically wrong values of K.

A more refined method proposed by Buffle [52] permits the determination of complexation data in the case when $R_M > 0$ and $R_L < 1$. Eq. (1) has been applied to the cell solution:

$$K = \frac{M_\mathrm{b}^c}{M^c \cdot L^c} = \frac{\alpha^c - 1}{L^c} \quad (2)$$

where superscript c denotes the concentration in the UF cell, $\alpha = M_\mathrm{t}/M$ is the ratio of the total metal concentration to its free concentration.

The retention coefficient R_x of each species x is defined as

$$R_x = 1 - \frac{x^f}{x^c} \quad (3)$$

where $x = M$, L or ML, superscripts f and c denote the concentration in the filtrate and in the UF cell, respectively.

Combination of Eq. (2) with Eq. (3) for M and L and with mass balance equation for M and L for both cell and filtrate solutions leads to

$$\frac{M_t^f}{M_t^c} = \frac{R_{ML} - R_M}{\alpha^c} + (1 - R_{ML}) \quad (4)$$

At a low ratio of $[ML]^c/L^c$ the conformation and size of the ligand are only slightly changed by the presence of bound M, so that R_{ML}, which is not always easily measurable, can be now replaced by R_L. Thus, α^c from Eq. (4) and then K from Eq. (2) can be calculated by simply measuring the total metal and ligand concentrations both in the cell and in the filtrate, and separate measuring R_M and R_L. It was found that the maximum range in which α^c can be precisely measured is $1.2 < \alpha^c < 50$ [52]. This range is more narrow than the range obtained by potentiometry or voltammetry that was considered as a drawback of this method. However, the main pitfall of this approach is probably the fact that by describing metal–HS interactions the values of R_M are obtained for metal retention in the absence of ligand. If R_M increases, for example, with increasing of pH, as it was the case with for Zn [71], Eu [39,70] and Sr [70], it may be due to the formation of hydroxocomplexes of the metal ions and their adsorption on the membrane or walls of the cell, to the formation of colloid particles, etc. However, in the presence of natural organic ligand the competitive reactions of the complexation may decrease the importance of this process and thus decrease the real R_M values.

Besides the estimation of the overall stability constant, the approach for describing metal–HS interactions may be based on the calculation of the stability constants for each acidic site of the polymer molecule:

$$\beta_i = \frac{ML_i}{M \cdot L_i} \quad (5)$$

If inter-site interactions are not taken into account, the relation between K and β_i can be expressed [39,49] as

$$K = \frac{\sum_i \beta_i \alpha_i Ab_i}{\sum_i \alpha_i Ab_i} \quad (6)$$

where α_i is the degree of ionization of site i, and Ab_i is the abundance of the site i. For example, for well characterized Bersbo fulvic acid, five acidic sites with varying pK values and corresponding abundances are: $pK_1 = 1.70$, $Ab_1 = 0.20$; $pK_2 = 3.3$, $Ab_2 = 0.25$; $pK_3 = 5.0$, $Ab_3 = 0.30$; $pK_4 = 6.50$, $Ab_4 = 0.20$; $pK_5 = 7.0$, $Ab_5 = 0.05$ [72]. α_i values can be computed at each pH. Initial guesses for the β_i are made with the aid of reported values obtained of the complex formation constant for the reaction between the envisaged functionality of each site and the metal ion. After the UF determinations of the overall stability constants, the values of β_i may be obtained by iterative matrix manipulations. The results of such experiment was obtained for Eu [39] and Cd [38] complexes with fulvic acids by Ephraim et al.

However, as it was mentioned above, the Scatchard method is the most widely used for the determination of stability constants for different binding sites. But in this case only two or maximum three sites can be considered. The Scatchard parameter is defined [62] as:

$$v = \frac{M_b}{L} \quad (7)$$

Then Eq. (8)

$$\frac{v}{M} = \beta_i n - \beta_i v \quad (8)$$

is employed where n is the number of binding sites per molecule. A plot of v/M versus v yields a straight line with a negative slope equal to the β_i. The Scatchard plots usually show two linear parts: (1) a linear part with a large slope at low free metal concentrations, which is attributed to the strong binding sites on the polymer molecule and (2) a linear part exhibiting little slope at high

free metal ion concentration, attributed to binding at weaker sites. This kind of method was applied by Tuschall and Brezonik for the UF determination of β_1 and β_2 for Cu–HS complexes [27]. Langmuir plots were applied by Caceci [68] to calculate β_2 for Eu complexes with HA after UF separation.

Thus, different complexation models and methods of calculations have been applied to the results of UF investigation of metal–HS complexation. It should be noted, however, that all the obtained parameters (constants, binding site concentrations) should be regarded as no more than mathematical curve-fitting parameters without any chemical meaning. Their principal utility is their ability to accurately predict overall metal complexation by humic substances within the experimental conditions.

John et al. [49] demonstrated a good example of the possibilities of UF as a method of characterizing metal–humic substance interactions. Combination of the size fractionation data of HS and Cd with UF stability constant calculations make it possible to obtain fractional K for each fraction of HS, having M_w in the range $500–10^3$, $10^3–10^4$ and $>10^4$. It was found that the binding strength of the second UF fraction ($10^3–10^4$) is about ten times higher than for two other fractions.

4. Comparability and reliability of stability constants.

For the critical evaluation of the complexation data obtained from the UF method, their comparison with the results of other analytical techniques should be made. The problem, which is often encountered while comparing the literature data, is the variety of methods for determining the L concentration in Eq. (1) and thus the value and unity of the obtained stability constants. The most simple way is to express the ligand concentration in gram of HS per liter, or gram of total organic carbon per liter (the carbon content of humic matter is $\sim 50\%$). However, HS concentration (g l^{-1}) is usually multiplied by the total hydrogen capacity (eq g^{-1}), which is obtained by the potentiometric titration in aqueous or non-aqueous media. The obtained value should be multiplied by the degree of dissociation at a particular pH. For rigorous calculation at high metal loading the concentration of bound metal should also be subtracted to obtain free carboxylate concentration.

The other approach by estimating L values in Eq. (1) is based on the determination of complexation capacity (CC) of HS, which is the total maximum concentration of bound metal (mol) per gram of carbon or per gram of HS and is obtained from the results of metal titration of HS. CC appears for various reasons to be lower than the hydrogen capacity [1] and the calculated K values may be higher than those obtained from the previously described approach. It should be noted also that CC depends not only on the initial degree of dissociation but also on the nature of metal ion. For example, it was shown, that CC value for Cu(II) was higher than that for several other metals [27,73]. This deflection was attributed for the existence of binding sites specific for the Cu(II) ion [73]. In determining CC of HS under natural conditions the attention should be paid to the fact that some of binding sites could be occupied by the metal ions initially present in water.

Sometimes for HS with known average molecular mass M_w the ligand concentration is expressed in mol l^{-1}. For example, John et al. [49] defined average molecular weight 750 for the HS-fraction having M_w in the range of $500–10^3$, 5×10^3 for the HS-fraction having M_w in the range $10^3–10^4$ and 2×10^4 for the HS-fraction $>10^4$. An interesting result was obtained when the calculated K values were converted to per weight basis. The order of K in this case was changed for the two weak fractions. It should be underlined, however, that the nominal molecular weight obtained from UF separations may not fully correspond to the actual molecular weight of the original HS-fraction. The cut-off characteristics of membranes are given for filtration of spherical compounds, while the structure and properties of humic molecules are quite different. This can result in a retention of HS molecules which molecular weight is considerably smaller than the cut-off value of the respective membrane [49].

It is also remarkable that in the case of stability constant calculations by using of the Scatchard plots the method of expressing L concentration does not affect the K values. However, the main problem, which is encountered in stability constants data analysis, is that the rigorous comparison can be done only for the data obtained under the same experimental conditions: ionic strength of the solution, pH (or more correctly degree of ionization of polymer molecule) and metal loading. If the fulfilment of all of these criteria is not possible, such a comparison may be rather rough or ambiguous.

As the nature and properties of HS differ significantly, depending on various factors such as origin (river or sea water, soils, etc.) and methods of isolation and purification, the most desirable is the comparison of K values generated with different analytical methods only for those obtained from the same sample of HS. Tuschall and Brezonic [27] compared β_1 and β_2 values for Cu complexes of HS obtained by UF, anodic stripping voltammetry (ASV), ion-selective electrode (ISE), fluorescence spectroscopy (FS) and differential spectroscopy using a competing ligand (CLDS). The investigation was performed with two swamp water samples at single pH value of 6.25, constant ionic strength and different metal loading. From the titration data obtained Scatchard plots were constructed. The UF method yielded results comparable with those obtained by ISE, CLDS and FS. The stability constants based on ASV titration were considerably lower than other. This was explained by the fact that the metal complexes of HS were reduced at the mercury electrode under the experimental conditions.

A comparison of K- and β-values obtained by UF, ISE and ion-exchange (IE) methods in Cd–FA complexation studies was made by Ephraim and Hao [38]. The investigation was performed in the pH range of 3–8, at two ionic strength values and different FA concentrations. The obtained stability constants were in the order: IE > UF > ISE. For example, at pH 6 the values for $\log K$ were 4.8, 3.3 and 2.7, respectively. This corresponds the variance of the previously discussed results, when UF and ISE yielded similar values for stability constants. The observed deflection may be due to the fact that ISE measurements in [38] were made under considerably higher metal loading than in UF experiments, where a trace amount of ^{115}Cd was used, and thus the effect of decreasing K with increasing metal loading is observed. However, a comparison of K values for Ca–FA complexes obtained from UF and ISE studies [11] under the equal metal loading reveals the same order for stability constants (IE, UF > ISE). Most probably, the above discussed stability constant values for Cu–HS complexes of UF method obtained by Tuschall and Brezonic [27] probably have a small error due to the fact that the measurements were performed with natural water samples and atomic absorption spectrometry (AAS). In this case the AAS measured not only the free Cu ion concentration, as in ISE method, but also the concentration of Cu present in inorganic complexes and in complexes of small organic ligands. Thus, taking this into account, it is possible that the K values obtained by UF studies may also have larger values then those obtained by ISE measurements.

A comparison of K- and β-values obtained by UF and IE methods in Eu–FA complexation studies was made by Ephraim [39]. The investigation was performed in the pH range of 3–8, at single ionic strength value for two FA concentrations. The obtained stability constants were in the order: IE > UF. Unexpected results were obtained for the dependence between the pH and stability constants. While the IE method showed a typical growth for $\log K$ values with increasing pH, $\log K_{Eu}$ obtained from the UF experiments were insensitive to changes in the pH of the system. The same effect was observed by Caceci [51] when studying Eu–HA interaction by UF. This phenomenon was explained by possible fragmentation of HS molecules by Eu ions into low-molecular-weight complexes which pass through the membrane [39]. This behavior seems to be unique for the Eu–HS interaction (normal $\log K$ dependences on pH were obtained by UF for Cd [38,49], Sr [70] and Ca [11]) which becomes detectable only by the UF experiments.

When considering different UF techniques, the survey of literature shows that K determinations

are usually performed by using the 'batch' method [52,11,39,38,68]. In order to minimize as much as possible the perturbation of the medium due to the separation step, only a small fraction of the original solution is filtrated ($\not> 10\%$). A special UF cell was designed to minimize the surface area of the membrane in order to avoid both significant losses due to adsorption effects and contamination from the membrane surface [52]. The comparison of mathematical models for the 'batch' and two 'continuous flow' UF methods used for the measurements of complexation properties of HS is given elsewhere [74]. A continuous flow UF method was applied by Tuschall and Brezonic for K determination of Zn, Cu, Cd complexes of HS [27]. A comparison of their results for Zn–HA interaction with those assessed by Buffle and Staub [52] using batch UF, shows good agreement of K values obtained at the same metal loading.

5. Lability of metal–HS species studied by UF

Metal–HS species are preferably considered as macromolular complexes which can be more or less characterized by thermodynamic stability functions. In the case of dissolved HS naturally occurring in aquatic environments it has to be realized, however, that these substances and their metal species are constituents of a complex and dynamic colloid system [75] which can hardly be described by thermodynamic functions. The reactivity of such colloidal HS–metal species can be better characterized by kinetic methods, for instance by assessing the 'availability' of the metal fractions bound to HS. Ligand exchange reactions of immobilized and dissolved EDTA-type chelators have been shown to be an efficient method for the specification of labile and inert metal species in aquatic HS samples [76].

Performing a time-controlled EDTA exchange of metal–HS species in a conventional UF cell their reaction kinetics can be studied by stepwise short filtration (1–2 min) of the EDTA-metal complexes formed [76]. The results of such exchange reactions between original metal species (e.g. Al, Fe, Mn, Zn) in a HS-rich bog water and dissolved EDTA is shown in Fig. 1, compared to an analogous EDTA exchange of artificial metal loadings of the same HS. As can be seen, the natural Al and Fe species in this HS sample (VM6-UF) gently pre-concentrated by preparative UF are only partially available to EDTA, even after reaction periods of 3 days. On the other hand, equivalent artificial metal loadings of the same HS (VM6-XAD8) pre-isolated as practically metal-free humic sample by conventional sorption onto XAD8 [1] are much more reactive towards EDTA. Such significant lability differences between natural and artificial metal–HS species are well comparable to those previously obtained by ion exchange methods [77].

Just recently, exchange reactions of metal isotopes (e.g. ^{53}Cr(III), ^{65}Cu(II)) complexed with HS, which were assessed by UF and isotope dilution analysis (IDA) using inductively coupled plasma-mass spectrometry (ICP-MS), have been shown to be a promising procedure for the evaluation of their lability [78]. Accordingly, Cr(III) species in aquatic HS were exhibited to be practically exchange-inert, in contrary to the studied Cu(II) species being very labile towards isotope exchange.

6. Conclusions

According to the literature studies discussed above the conclusion can be drawn that UF has been established as an efficient and reliable technique for the evaluation of metal–HS stability functions. Its main advantages are: (i) the possibility of measuring stability constants in waters under nature-like conditions hardly altering the original equilibria of the system to be studied, and (ii) its applicability to a wide range of metals. It is worth to mention that the most promising advantage of this technique namely based on the combination of molecular-size fractionation of metal–HS species by sequential-stage UF [3] and simultaneous determination of their conditional stability constants in the obtained fractions is still unexploited. It would be also interesting to compare the conditional stability constants K determined for metal complexes in size-classified HS

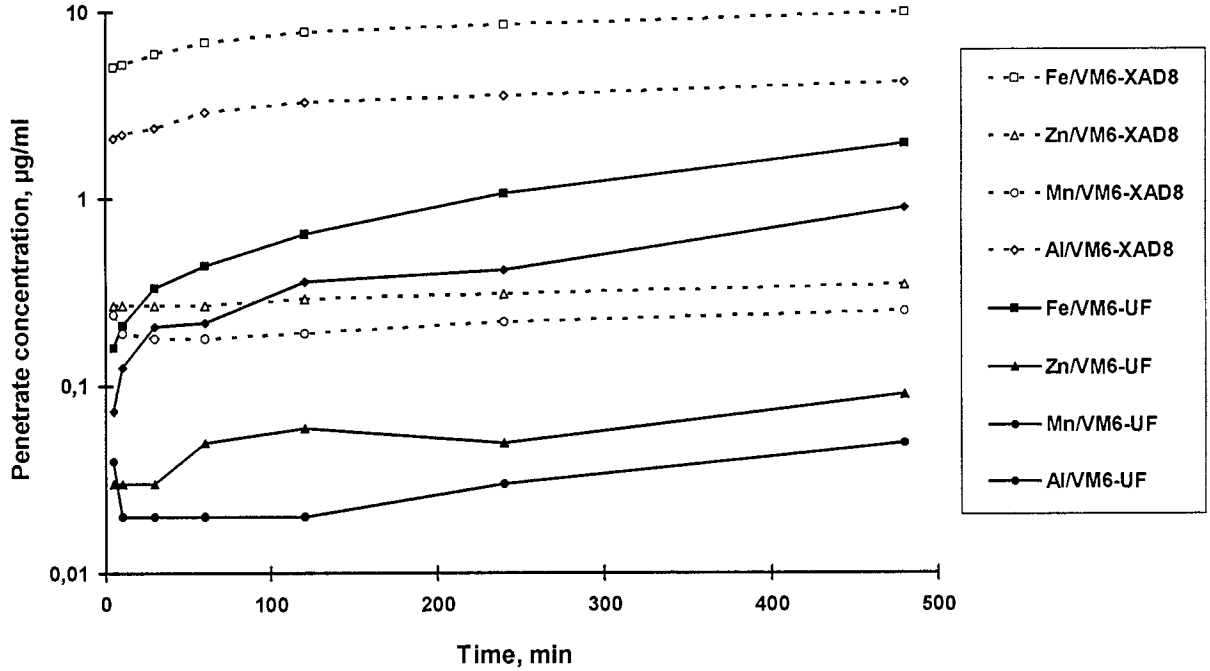

Fig. 1. Ligand exchange between metal–HS species and EDTA as a function of time characterized by time-controlled UF (HS: VM6-UF and -XAD8 from Venner Moor, Münster, Germany; 200 ml sample, 1.0 mg ml^{-1} HS, pH 5.0, 1.2 µmol ml^{-1} EDTA; UF: 1 kDa as nominal cut-off; total metal concentrations: 5.1 µg ml^{-1} Al, 14.5 µg ml^{-1} Fe, 0.32 µg ml^{-1} Mn and 0.44 µg ml^{-1} Zn, pH 5.0) (according to [76]).

fractions by using such online UF technique with those estimated by conventional titrimetric procedures. Taking into account the polydisperse character of HS the existence of several fractions of HS molecules with different complexation abilities seems to be reasonable. For this purpose complexation models taking into consideration the uneven distribution of binding sites in HS mixtures are needed. It has to be kept in mind, however, that, besides such thermodynamic functions, for a more refined characterization of metal–HS species in aquatic environments detailed informations on their kinetic stability are required, too.

Acknowledgements

The financial support from the Russian Foundation of Basic Research and the Deutsche Forschungsgemeinschaft (DFG-ROSIG, Bonn, Germany) is gratefully acknowledged.

References

[1] G. Aiken, D. McKnight, R.L. Wershaw (Eds.), Humic Substances in Soil, Sediment and Water, Wiley, New York, 1985.
[2] F.H. Frimmel, Chromatographic characterization of the acid-soluble part of humic substances, in: G. Matthess, F.H. Frimmel, P. Hirsch, H.D. Schulz, E. Usdowski (Eds.), Progress in Hydrogeochemistry, Springer, Berlin, 1992, pp. 24–28.
[3] P. Burba, P. Aster, T. Nifant'eva, V. Shkinev, B. Ya. Spivakov, Talanta 45 (1998) 977.
[4] J. Buffle, Complexation Reactions in Aquatic Systems: An Analytical Approach, Ellis Horwood, Chichester, 1988.
[5] J. Allard, H. Boren, A. Grimvall (Eds.), Humic Substances in the Aquatic and Terrestrial Environment, Springer, Berlin, 1991.
[6] S.Y. Choi, H. Moon, S. Jun, K.H. Chung, Bull. Korean. Chem. Soc. 15 (1994) 581.
[7] R.A. Saar, J.H. Weber, Can. J. Chem. 57 (1979) 1263.
[8] A. Castetbon, M. Corrales, M. Astruc, M. Dotin, J.M. Sterrit, J.N. Lester, Environ. Technol. Lett. 7 (1986) 495.
[9] J.J. Alberts, J.P. Giesy, Conditional stability constants of trace metals and naturally occurring humic materials:

application in equilibrium models and verification with field data, in: R.F. Christman, E.T. Gjessing (Eds.), Aquatic and Terrestrial Humic Materials, Ann Arbor, MI, 1983, pp. 333–348.
[10] N. Paxeus, M. Wedborg, Calcium binding to an aquatic fulvic acid, in: B. Allard, H. Boren, A. Grimvall (Eds.), Humic Substances in the Aquatic and Terrestrial Environment, Springer, Berlin, 1991, pp. 287–296.
[11] A.S. Mathuthu, J.H. Ephraim, Talanta 40 (1993) 521.
[12] B.A. Dempsey, C.R. O'Melia, Proton and calcium complexation of four fulvic acid fractions, in: R.F. Christman, E.T. Gjessing (Eds.), Aquatic and Terrestrial Humic Materials, Ann Arbor, MI, 1983, pp. 239–273.
[13] C.H. Langford, D.S. Gamble, A.W. Underdown, S. Lee, Interaction of metal ions with a well characterized fulvic acid, in: R.F. Christman, E.T. Gjessing (Eds.), Aquatic and Terrestrial Humic Materials, Ann Arbor, MI, 1983, pp. 219–237.
[14] J. Buffle, P. Deladoey, F.L. Greter, W. Haerdi, Anal. Chim. Acta 116 (1980) 274.
[15] G. Sposito, Environ. Sci. Technol. 15 (1981) 396.
[16] H.M.V.M. Soares, M.T.S.D. Vasconcelos, Anal. Chim. Acta 293 (1994) 261.
[17] W. Verwej, H. De Haan, T. De Boer, J. Voerman, Freshwater Biol. 21 (1989) 427.
[18] J.R. Tuschall, P.L. Brezonik, Anal. Chim. Acta 149 (1983) 45.
[19] M.S. Shuman, J.B. Collins, P.J. Fitzgerald, D.L. Olson, Distribution of stability constants and dissociation rate constants among binding sites of estuarine copper-organic complexes: rotated disk electrode studies and an affinity spectrum analysis of ion-selective electrode and photometric data, in: R.F. Christman, E.T. Gjessing (Eds.), Aquatic and Terrestrial Humic Materials, Ann Arbor, MI, 1983, pp. 349–370.
[20] J. Buffle, F.L. Greter, W. Haerdi, Anal. Chem. 49 (1977) 216.
[21] R.M. Sterritt, J.N. Lester, Water Res. 19 (1984) 1149.
[22] M. Fukushima, K. Hasebe, M. Taga, Anal. Chim. Acta 270 (1992) 153.
[23] M.S. Shuman, J.L. Cromer, Environ. Sci. Technol. 13 (1979) 543.
[24] J.H. Weber, Metal speciation studies in the presence of humic materials, in: R.F. Christman, E.T. Gjessing (Eds.), Aquatic and Terrestrial Humic Materials, Ann Arbor, MI, 1983, pp. 315–331.
[25] G. Scarano, E. Bramanti, A. Zirino, Anal. Chim. Acta 264 (1992) 153.
[26] K.H. Coale, K.W. Brunland, Limnol. Oceanogr. 33 (1988) 1084.
[27] J.R. Tuschall, P.L. Brezonik, Complexation of heavy metals by aquatic humus. A comparative study of five analytical methods, in: R.F. Christman, E.T. Gjessing (Eds.), Aquatic and Terrestrial Humic Materials, Ann Arbor, MI, 1983, pp. 275–294.
[28] J. Baron, M. Legret, M. Astruc, Environ. Technol. 11 (1990) 151.
[29] G. Capodaglio, K.H. Coale, K.W. Bruland, Mar. Chem. 29 (1990) 221.
[30] K.W. Bruland, Limnol. Oceanogr. 34 (1989) 269.
[31] J.R. Donat, K.W. Bruland, Mar. Chem. 28 (1990) 301.
[32] C.M.G. van den Berg, J.R. Donat, Anal. Chim. Acta 257 (1992) 281.
[33] H. Zhang, C.M.G. van den Berg, R. Wollast, Mar. Chem. 28 (1990) 285.
[34] P. Warwick, J. Bennett, L. Riley, D. Zhu, A. Hall, G.M. Williams, Comm. Eur. Communities (Rep.), 1994, 70.
[35] D.T. Hawath, M.R. Pitluck, B.D. Pollard, J. Liq. Chromatogr. 10 (1987) 2877.
[36] P. Burba, Fresenius J. Anal. Chem. 348 (1994) 301.
[37] J.H. Ephraim, J.A. Marinsky, S.J. Cramer, Talanta 36 (1989) 437.
[38] J.H. Ephraim, X. Hao, Sci. Total Environ. 81/82 (1989) 625.
[39] J.H. Ephraim, Sci. Total Environ. 108 (1991) 261.
[40] Z. Tao, J. Du, Radiochim. Acta 64 (1994) 225.
[41] R.A. Saar, J.H. Weber, Anal. Chem. 52 (1980) 2095.
[42] D.K. Ryan, J.H. Weber, Environ. Sci. Technol. 16 (1982) 866.
[43] W. Susetyo, J.C. Dobbs, L.A. Carreira, L.V. Azarraga, D.M. Grim, Anal. Chem. 62 (1990) 1215.
[44] V. Moulin, J. Tits, C. Moulin, P. Decembox, P. Mauchien, O. de Ruty, Radiochim. Acta 58–59 (1992) 121.
[45] R.F.C. Mantoura, A. Dickson, J.P. Riley, Estuar. Coastal Mar. Sci. 6 (1978) 387.
[46] V.M. Moulin, M.S. Caceci, M.J. Theyssier, Complexation behaviour of humic substances from granitic groundwater towards Am(III), in: B. Allard, H. Boren, A. Grimvall (Eds.), Humic Substances in the Aquatic and Terrestrial Environment, Springer, Berlin, 1991, pp. 305–313.
[47] L.R. van Loon, S. Granacher, H. Harduf, Anal. Chim. Acta 268 (1992) 235.
[48] J. Lee, Water Res. 17 (1983) 501.
[49] J. John, B. Salbu, E.T. Gjessing, H.E. Bjornstad, Water Res. 22 (1988) 1381.
[50] M. Norden, Y. Albinsson, J.H. Ephraim, B. Allard, A comparative study of europium, thorium and uranium binding to aquatic fulvic acid, in Mater. Res. Soc. Symp. Proc. 249, Scientific Basis for Nuclear Waste Management XVI. 1993, pp. 759–764.
[51] J. Buffle, D. Perret, M. Newman, The use of filtration and ultrafiltration for size fractionation of aquatic particles, in: J. Buffle, H.P. van Leeuwen (Eds.), Environmental Particles, Lewis Publishers, USA, 1992, pp. 171–229.
[52] J. Buffle, C. Staub, Anal. Chem. 56 (1984) 2837.
[53] T.A. Neubecker, H.E. Allen, Water Res. 17 (1983) 1.
[54] R.A. Saar, J.H. Weber, Environ. Sci. Technol. 16 (1982) 510A.
[55] J.A. Marinsky, J. Ephraim, Environ. Sci. Technol. 20 (1986) 349.
[56] J.P. Giesy, J.J. Alberts, D.W. Evans, Env. Toxicol. Chem. 5 (1986) 139.

[57] J. Buffle, R.S. Altman, M. Filella, Anal. Chim. Acta 232 (1990) 225.
[58] E.M. Perdue, C.R. Lytle, Environ. Sci. Technol. 17 (1983) 654.
[59] D.S. Gamble, A.W. Underdown, C.H. Langford, Anal. Chem. 52 (1980) 1901.
[60] J.C.M. de Wit, W.H. van Riemsdijk, M.M. Nederlof, D.G. Kinnibwigh, L.K. Koopal, Anal. Chim. Acta 232 (1990) 189.
[61] E. Tipping, Anal. Proceedings 30 (1993) 186.
[62] W.E. Falck, The incorporation of natural organic mattercation interaction into the speciation code PHREEQE, in: B. Allard, H. Boren, A. Grimvall (Eds.), Humic Substances in the Aquatic and Terrestrial Environment, Springer, Berlin, 1991, pp. 277–285.
[63] J. Buffle, Circulation of metals in the environment, in: H Sigel (Ed.), Metal Ions in Biological Systems, Cpt 6, Marcel Dekker, New York, 1984.
[64] D.A. Dzombak, W. Fish, F.M.M. Morel, Environ. Sci. Technol. 20 (1986) 669.
[65] G. Scatchard, J.S. Coleman, A.L. Shen, J. Am. Chem. Soc. 79 (1957) 12.
[66] I.H. Scheinberg, Science 215 (1982) 312.
[67] J. Ephraim, S. Alegret, A. Mathuthu, M. Bicking, R.L. Malcom, J.A. Marinsky, Environ. Sci. Technol. 20 (1986) 354.
[68] M.S. Caceci, Radiochim. Acta 39 (1985) 51.
[69] J.H. Ephraim, J.A. Marinsky, Anal. Chim. Acta 232 (1990) 171.
[70] M. Norden, J. Ephraim, B. Allard, Interaction of strontium and europium with an aquatic fulvic acid studied by ultrafiltration and ion exchange techniques, in: B. Allard, H. Boren, A. Grimvall (Eds.), Humic Substances in the Aquatic and Terrestrial Environment, Springer, Berlin, 1991, pp. 297–303.
[71] C. Staub, J. Buffle, W. Haerdi, Anal. Chem. 56 (1984) 2843.
[72] J.H. Ephraim, H. Boren, C. Pettersson, I. Arsenie, B. Allard, Environ. Sci. Technol. 23 (1989) 287.
[73] B.T. Hart, Environ. Technol. Lett. 2 (1981) 95.
[74] J.H. Gamble, M.I. Haniff, R.H. Zienius, Anal. Chem. 58 (1986) 732.
[75] J. Buffle, G.G. Leppard, Environ. Sci. Technol. 29 (1995) 2169.
[76] B. Aster, A. von Bohlen, P. Burba, Spectrochim. Acta B 52 (1997) 1009.
[77] P. Burba, J. Rocha, D. Klockow, Fresenius J. Anal. Chem. 349 (1994) 800.
[78] W. Marx, Diplom-thesis, University of Mainz, Germany, 1997.

ELSEVIER

Talanta 48 (1999) 269–275

Talanta

Selective measurement of chromium(VI) by fluorescence quenching of ruthenium

Taha M.A. Razek [1,a], Scott Spear [a], Saad S.M. Hassan [b], Mark A. Arnold [a,*]

[a] *Department of Chemistry and Optical Science and Technology Center, 230 Iowa Advanced Technology Laboratory, University of Iowa, Iowa, IA 52242 USA*

[b] *Chemistry Department, Faculty of Science, Ain-Shams University, Cairo, Egypt*

Received 27 March 1998; accepted 15 June 1998

Abstract

A flow injection method is described for the selective measurement of chromium(VI) in aqueous solutions. This method is based on the dynamic quenching of ruthenium(II) fluorescence. The detection limit is 0.43 ppm and 40 samples can be analyzed per hour. Selectivity is demonstrated over ferrous, nickel, cupric and zinc cations and no effect is observed from sulfate, chloride, borate and phosphate. Some interference quenching was measured for cyanide and nitrate, but the method is more responsive to chromium(VI) by factors of 10.2 and 82, respectively. The effects of solution pH, carrier stream flow rate and ruthenium concentration are demonstrated. Results indicate the method is suitable for measuring chromium(VI) in effluents from electroplating baths.

Keywords: Chromium(VI); Fluorescence quenching; Electroplating baths

1. Introduction

Chromium is an important element in environmental science and water pollution control. Natural levels of chromium in unpolluted water are below 2 ppb and its toxicity effects demand a maximum permissible chromium level of 50 ppb in drinking water [1]. Of its various oxidation states, chromium(VI) poses the greatest risk to human health because of its known actions of toxicity, its high solubility in aqueous solutions and its relatively rapid mobility in soil and solid wastes. Chromium(VI) is known to damage exposed skin, irritate mucous membranes, produce pulmonary sensitivity, create dental erosion, cause loss of weight, induce renal damage, and target the respiratory tract and skin [2–4]. In addition, experimental evidence links chromium(VI) with various types of cancer [5].

Environmental chromium(VI) is generated largely by metal cleaning processes, surface finishing and metal coating processes, ink pigments, dye manufacture and chromate water treatment

* Corresponding author. Tel.: +319 3351368; fax: +319 3531115; e-mail: mark-arnold@uiowa.edu

[1] On leave from Department of Natural and Biological Sciences, Institute of Environmental Studies and Research, Ain-Shams University, Cairo, Egypt.

0039-9140/99/$ - see front matter
PII S0039-9140(98)00245-8

[6]. Effluents from these processes must be monitored to ensure proper chromium removal prior to releasing these effluents into the environment.

Many analytical methods are available for measuring chromium in water samples. General methods include gravimetry, titrimetry [7], colorimetry [8], potentiometry [9], spectrophotometry [10–14], fluorometry [15–17], chemiluminescence spectrometry [18,19], chromatography [20], and solid-phase spectrophotometry coupled with anion exchange membrane for preconcentration [21]. Although, the lowest detection limits are provided by graphite-furnace atomic absorption spectrometry [22], this technique is not well suited for field applications. Flow injection methods coupled with ion exchange [23], co-precipitation or extraction pre-concentration steps have been proposed for field applications.

This work evaluates the use of dynamic quenching of a ruthenium dye for chromium(VI) measurements. Ruthenium dyes are well known reagents for measuring oxygen in gaseous and aqueous media [24–27]. These measurements are based on dynamic quenching of ruthenium fluorescence by oxygen. In the presence of ambient oxygen ruthenium fluorescence quenching can be detected in the presence of chromium(VI) and this quenching can be used to measure chromium(VI) at sub-ppm concentrations.

2. Experimental work

2.1. Apparatus

All fluorescence measurements were made with an SLM-Aminco SPF 500 C spectrofluorometer equipped with a 250 watt xenon arc lamp for excitation. Ruthenium fluorescence was measured by setting the excitation monochrometer to 450 nm with a 1.0 nm slit width and the emission monochrometer to 610 nm with a 7.5 nm slit width.

2.2. Chemicals and reagents

Hypophosphorous acid 50% was purchased from Aldrich (Mikwaukee, WI). Methanol (GR grade) was obtained from EM Science (Gibbstown, NJ). Ethanol (dehydrated, 200 proof) was obtained from Pharmco (Brookfield, CT). 4,7 Diphenyl 1,10 phenanthroline (dpp) was used as received from Lancaster (Windham, NH). Potassium petachlororuthenate monohydrate III ($K_2(RuCl_5.H_2O)$) was purchased from Alpha (Ward Hill, MA). Phosphoric Acid 85%, KH_2PO_4, and Na_2HPO_4 were purchased from Fisher Scientific (Fairlawn, NJ).

All standard solutions were prepared with analytical grade materials used as received. Buffer solutions were prepared according to Christian and Purdy [28]. Ruthenium II tris 4,7-diphenyl 1,10 phenanthroline was made according to the published procedure by Lin et al. [29]. All ruthenium standard solutions were prepared by dissolving the dried ruthenium II tris 4,7-diphenyl 1,10 phenanthroline powder in a minimum amount of ethanol and then diluting to mark with distilled-deionized water. Chromium standard solutions were made by dissolving dried potassium dichromate in distilled-deionized water.

2.3. Procedures

Dynamic quenching of ruthenium by chromium(VI) was initially characterized by adding the appropriate materials to a disposable polymethylmethacrylate cuvette and measuring the resulting solution fluorescence in the SLM-Aminco fluorimeter. In general, batch measurements of this type were carried out in aqueous solutions of the ruthenium reagent with different amounts of Cr(VI).

The flow injection manifold was constructed according to the schematic diagram presented in Fig. 1. A Harvard model 44/1 syringe pump was used to flow equal volumes of the buffered ruthenium reagent and the carrier buffer through the system. The sample was carried from a six-port injector loop (Upchurch, model V 450) to a mixing-tee where it was mixed with the ruthenium reagent. These two solutions were allowed to mix for 60–100 s as they proceed to the fluorometer for detection. A micro-flow through quartz fluorescence cell was used for detection. The sample loop of the injection port was made to hold 1.0 ml of solution.

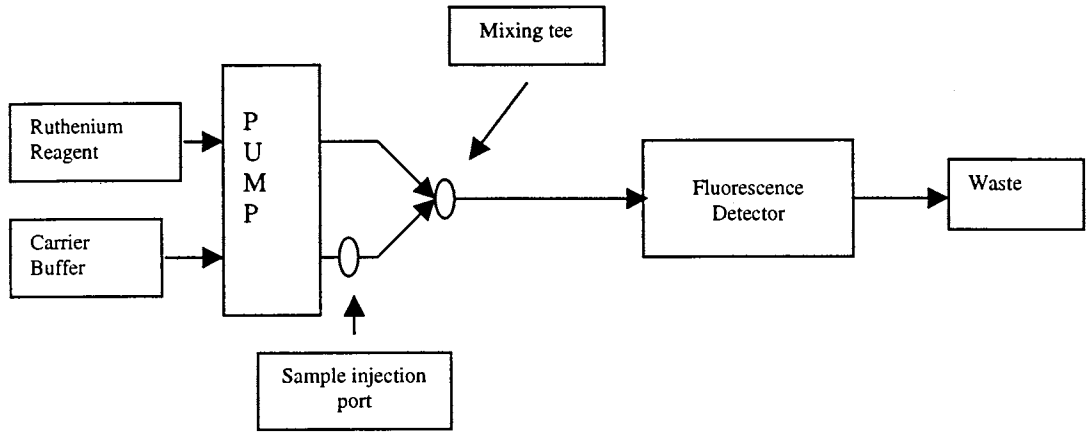

Fig. 1. Flow injection manifold for the determination of chromium(VI) by ruthenium fluorescence quenching.

The response to chromium(VI) was measured as the decrease in luminescence according to the well known Stern–Volmer relationship ($I_0/I = 1 + K_{SV}$ [Q]). In this expression, I_0 and I correspond to the fluorescence intensity in the absence and presence of the quenching agent, K_{SV} corresponds to the Stern–Volmer constant and [Q] denotes the concentration of the quenching agent. In the FIA experiments, I_0 was taken as the mean intensity measured for the carrier buffer just before the sample was injected and I was taken as the peak fluorescence signal following sample injection.

3. Results and discussions

Chromium(VI) quenches the fluorescence of ruthenium in a linear Stern–Volmer manner. A plot of $(I_0/I - 1)$ versus chromium(VI) concentration is linear over a chromium concentration range from 3 to 28 ppm. Least squares regression analysis of these data gives a slope of 3.6 ($\pm$0.1) ppm^{-1}, y-intercept of -3.7 ($\pm$2.0) and r-square of 0.9956.

The effect of ruthenium concentration on the extent of fluorescence quenching was established by using the FIA system and comparing responses observed for a series of chromium(VI) solutions ranging in concentration from 0.25 to 5.0 ppm. At all chromium concentrations tested, the extent of fluorescence quenching increased as the ruthenium concentration increased from 5 to 50 μM. These findings indicate greater sensitivity can be obtained with higher levels of ruthenium. Unless indicated otherwise, the ruthenium concentration was set at 15 μM in order to conserve reagent.

The effect of carrier buffer flow rate was examined over a range of flow rates from 2 to 7 ml min^{-1}. The degree of fluorescence quenching was recorded for a series of chromium concentrations with a fixed ruthenium level of 15 μM. The results are shown in Fig. 2 where the magnitude of fluorescence quenching is plotted versus solution flow rate. The measurement is relatively independent of flow rate at values below 3.0 ml min^{-1}. The magnitude of the signal drops significantly at faster flow rates corresponding to insufficient mixing times before detection. The flow rate was set at 2.0 ml min^{-1} unless specified otherwise.

In an attempt to identify the ideal pH for the measurement, the effect of solution pH on the excitation and emission spectra of ruthenium was established. Fig. 3 shows the results of this experiment where the excitation and emission spectra are superimposed for the different pHs tested. The greatest excitation and emission intensities were observed when the solution pH was 2.9 and 3.6. Luminescence falls sharply at pH values below 2.9 and above 9.9. The emission intensity is relatively insensitive to pH over the broad range from 6.5 to 9.0.

The observations described above, motivated an experiment to establish the degree of chromium based fluorescence quenching of ruthenium at pHs between 6.5 and 9.0. This experiment was carried out with the FIA configuration where the magnitude of response was recorded for a series of chromium concentrations with different pHs for the sample and carrier buffer. The results are summarized in Fig. 4 where pH 8.0 is optimal over this tested pH range.

A Stern–Volmer plot and typical time trace are provided in Fig. 5 for the FIA system operating at pH 8.0. In this experiment, the carrier flow rate was 2.0 ml min^{-1} and the ruthenium concentration was 15 μM. The Stern–Volmer plot is linear over the tested concentration from 5 to 60 ppm. This line is characterized by a slope of 0.049 ($\pm$0.001) ppm^{-1}, a y-intercept of 0.02 ($\pm$0.02) and an r-square of 0.9991. The corresponding estimated limit of detection ($S/N = 3$) is 1.22 ($\pm$ 0.02) ppm.

We also examined the Stern–Volmer plot for data collected with the FIA system operating at pH 3.0. Again, the flow rate was 2 ml min^{-1}, but the ruthenium concentration was increased to 50 μM in this experiment in order to enhance the measurement sensitivity. The resulting Stern–Volmer plot and a typical time trace are presented in Fig. 6. The response to chromium is more

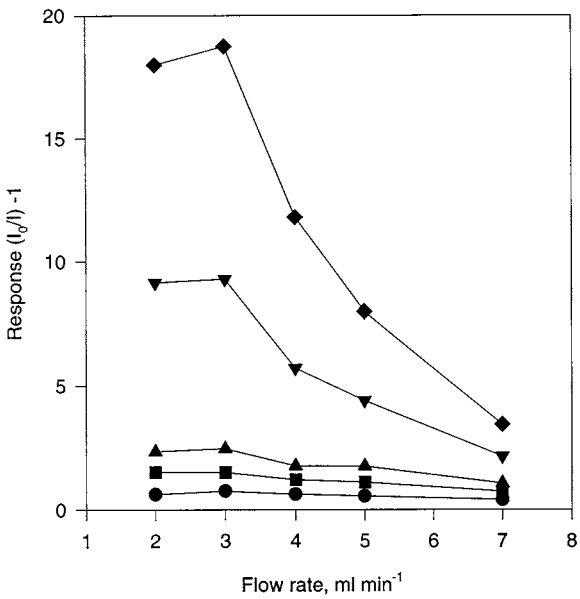

Fig. 2. Effect of carrier stream flow rate on the magnitude of fluorescence quenching measured for chromium concentrations of 20 (circle), 25 (square), 30 (up-triangle), 40 down-triangle, and 50 (diamond) ppm.

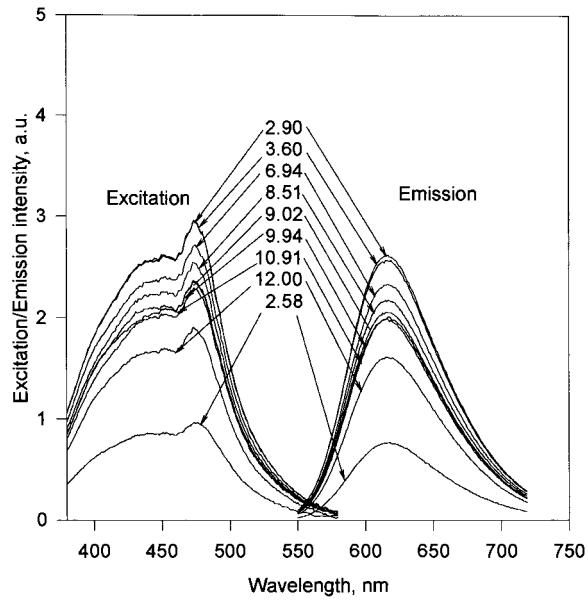

Fig. 3. Excitation and emission spectra for ruthenium II tris 4,7-diphenyl 1,10 phenanthroline at the indicated pH values.

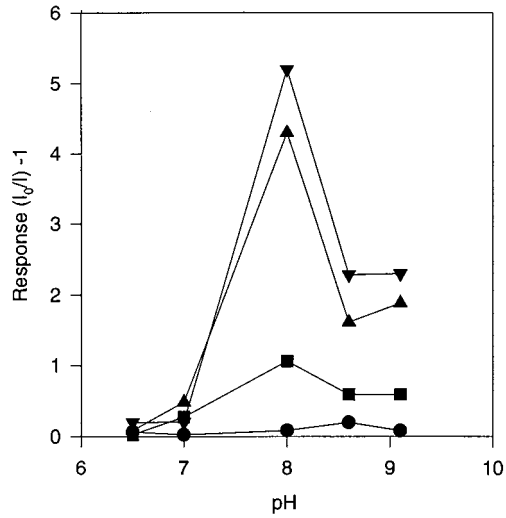

Fig. 4. Effect of carrier buffer pH on the magnitude of response to 10 (circles), 30 (square), 50 (up-triangle) and 60 (down-triangle) ppm of chromium.

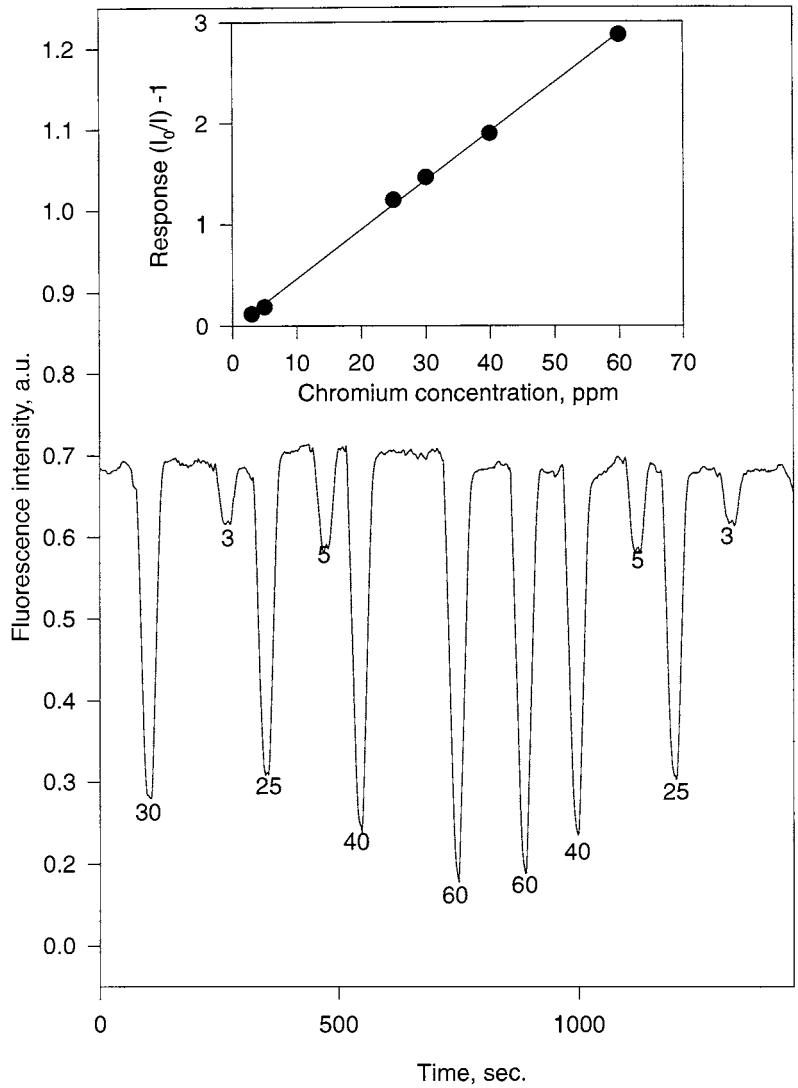

Fig. 5. Fluorescence intensity time trace for the indicated concentrations of chromium when the FIA system operates at pH 8.0. Inset shows the corresponding Stern–Volmer plot.

sensitive under these conditions. Linear regression analysis indicates a slope of 0.29 ($\pm$ 0.02) ppm^{-1}, a y-intercept of 0.21 ($\pm$ 0.04), and an r-square of 0.9795 over the tested chromium concentration range (0.1–5 ppm). The computed limit of detection is 0.43 ($\pm$ 0.027) ppm under these conditions.

Selectivity for chromium(VI) was investigated by monitoring the response observed after injecting samples with high concentrations of potential interfering cations and anions. The list of tested cations includes nickel(II), copper(II), zinc(II), and iron(II). These cations represent the most likely interferences in effluents from common electroplating baths. Each cation was tested by injecting a 1000 ppm solution of the cation prepared with the chloride salt. No fluorescence quenching was observed from any of these cations. The tested anions include cyanide, sulfate, nitrate, chloride, borate, and phosphate. Again, these anions were tested at 1000 ppm concentrations from

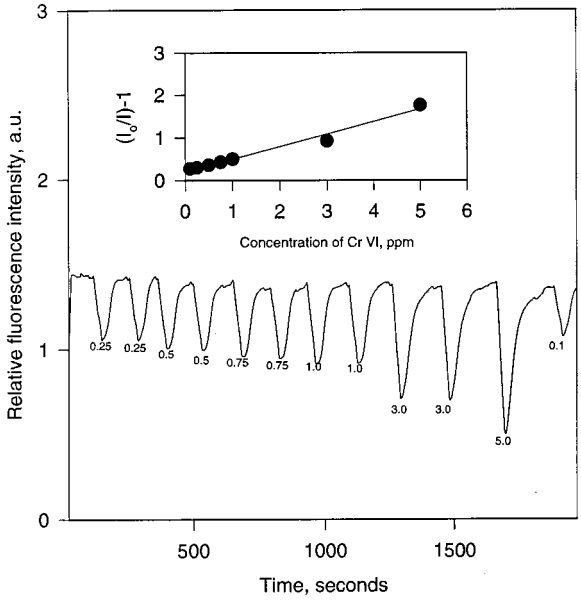

Fig. 6. Fluorescence intensity time trace for FIA system operating at pH 3.0 and 50 μM ruthenium. The corresponding Stern–Volmer plot is provided at the inset.

solution prepared with the sodium salt. No response was observed for sulfate, chloride, borate and phosphate. Significant quenching was observed, however, for both cyanide and nitrate. The relative magnitude of these interfering responses compared to chromium(VI) was established by interpolating from the corresponding chromium Stern–Volmer plot. This analysis shows that 1000 ppm nitrate gives the same response as 98 ppm chromium and 1000 ppm cyanide gives the same response as 12.2 ppm chromium. These values correspond to selectivity ratios of 10.2 and 82, respectively, relative to chromium(VI). Finally, no response was observed from a single solution composed of a mixture of nickel, copper, zinc, iron, sulfate, chloride, borate, and phosphate.

4. Conclusion

Chromium(VI) can be measured selectively by the proposed FIA system based on ruthenium fluorescence quenching. This method is suitable for on-site measurements of environmental samples. The method provides sufficient selectivity over interferences prevalent in the metal finishing industry e.g. electroplating. Finally, the method does not require a sample pretreatment step to remove iron and copper which are the primary interferences of in the 1,5 dipheylcarbazide method [30].

References

[1] F. Richard, A. Bourg, Aqueous chemistry of chromium, a review, Water Resour. 25 (1991) 807.
[2] M. Sittig, Priority Toxic Pollutants, Health Impacts and Allowable Limits, Noyes Data Corporation, 1980, p. 158.
[3] C.R. Brunner, Hazardous Air Emissions from Incineration, Chapman and Hall, London, 1985.
[4] S.A. Katz, H. Salem, The Biological and Environmental Chemistry of Chromium, VCH Publishers, New York, 1994.
[5] International Agency for Research on Cancer IARC, International Agency for Research on Cancer Monographs on the Evaluation of the Carcinogenic Risks to Humans, Vol. 49, Chromium, Nickel, and Welding, IARC publications, 1990.
[6] W.J. Cooper, Chem. Water Reuse 1 (1981) 265.
[7] N.H. Furman, F.J. Welcher, W.W. Scott, Standard Methods of Chemical Analysis V1, Van Nostrand, 1962.
[8] C.C. Luke, Anal. Chem. 30 (1958) 359.
[9] S.S.M. Hassan, M.N. Abbas, G.A.E. Moustafa, Talanta 43 (1996) 797–804.
[10] H. Wang, J. Pan, Q. Xu, Fenxi Huaxue 24 (1996) 195.
[11] M.A. Zayed, B.N. Barsoum, A.E. Hassan, Microchem. J. 54 (1996) 72.
[12] J.B. Raj, Acta Cienc. Indica 21 (1995) 134.
[13] N. Balasubramanian, V. Maheswari, J. AOAC Int. 79 (1996) 989.
[14] V. Maheswari, N. Balasubramanian, Chem. Anal. (Warsaw) 41 (1996) 569.
[15] N. Jie, J. Jiang, Analyst 116 (1991) 395.
[16] N. Jie, J. Yang, J. Guo, Anal. Lett. 25 (1992) 1447.
[17] Z. Zhang, Y. Mao, Y. Tang, Y. Fang, Fenxi Huaxue 24 (1996) 1109.
[18] Z. Holzbecher, L. Kabrt, J. Jansta, Call. Czech. Chem. Comm. 47 (1982) 1606.
[19] H. Zhang, X. Yang, L. Wu, Fuxi Huaxua 23 (1995) 1148.
[20] E.J. Arar, J.O. Pfaff, J. Chromatogr. 546 (1991) 335.
[21] V. Ososkov, B. Kebbekus, D. Chbro, Anal. Lett. 29 (1996) 1829.
[22] N. Miller-Ihli, Chromium, in: M. Stoeppler (Ed.), Hazardous Metals in the Environment, Elsevier, Amsterdam, 1992, p. 373.

[23] J.L. Nowicki, K.S. Johonson, K.H. Coale, V.A. Elord, S.H. Lieberman, Anal. Chem. 66 (1994) 2732.
[24] H. Chuang, M.A. Arnold, Anal. Chem. 69 (1997) 1899.
[25] W. Xu, R.C. Mc Donough, B. Langsdorf, J.N. Demas, B.A. DeGraff, Anal. Chem. 66 (1994) 4133.
[26] P. Hartmann, J.P. Leiner, M.E. Lippisch, Anal. Chem. 67 (1995) 88.
[27] I. Klimant, O.S. Wolfbeis, Anal. Chem. 67 (1995) 3160.
[28] G.D. Christian, W.C. Purdy, J. Electroanal. Chem. 3 (1962) 363.
[29] C.-T. Lin, W. Bottcher, M. Chou, N.J. Sutin, J. Am. Chem. Soc. 98 (1976) 6536.
[30] A.E. Greenberg, L.S. Clesceri, A.D. Eaton, Standard Methods for the Examination of Water and Wastewater, American Public Health Association, 18th edn., 1992, pp. 3/59–60.

ELSEVIER

Talanta 48 (1999) 277–282

Talanta

Determination of trace chromium(VI) and molybdenum(VI) in natural and bottled mineral waters using long pathlength absorbance spectroscopy (LPAS)

Wensheng Yao, Robert H. Byrne *

University of South Florida, Department of Marine Science, St. Petersburg, FL 33701 USA

Received 8 May 1998; accepted 16 June 1998

Abstract

A liquid core waveguide (LCW) has been used to extend the sensitivity of conventional absorbance spectroscopy for chromium(VI) and molybdenum(VI). Analysis of Cr(VI) and Mo(VI) concentrations in water samples with a 5.0 m pathlength LCW made of Teflon AF-2400 provides 0.2 and 0.6 nM detection limits, respectively. No preconcentration is required in this analysis. The proposed procedures were applied to the determination of chromium(VI) and molybdenum(VI) in natural waters and commercial drinking water. The analytical apparatus is very simple and robust and is amenable to miniaturization and autonomous operation.

Keywords: Chromium; Molybdenum; Liquid core waveguide; Long pathlength absorbance spectroscopy

1. Introduction

Chromium and molybdenum are essential nutrients for life which, in excess, can cause metabolic disturbances [1]. Both elements exist in nature in variable oxidation states. In natural environments, the most stable oxidation states of chromium are Cr(VI) and Cr(III). Cr(VI) is considered much more toxic than Cr(III). Even though thermodynamic calculations show that Cr(VI) should predominate in oxic conditions, Cr(III) coexists due to the slow kinetics of Cr(III) oxidation. Cr(III) has a strong tendency to adsorb onto surfaces while Cr(VI) (as CrO_4^{2-}) has a high mobility in natural waters [2]. The most abundant species of molybdenum in oxic aquatic environments, molybdate (MoO_4^{2-}), also has a generally high mobility. In anoxic environments, Mo(VI) is reduced to lower oxidation state sulfides and oxides [3].

Although the concentration of molybdenum in seawater is relatively high (~ 0.1 μM), the concentrations of chromium and molybdenum in most natural waters are very low. Consequently, most procedures reported for chromium and molybdenum analysis of natural waters include preconcentration and/or a separation step prior to

* Corresponding author. Tel.: +727 5531508; fax: +727 5531189; e-mail: byrne@seas.marine.usf.edu

0039-9140/99/$ - see front matter
PII S0039-9140(98)00243-4

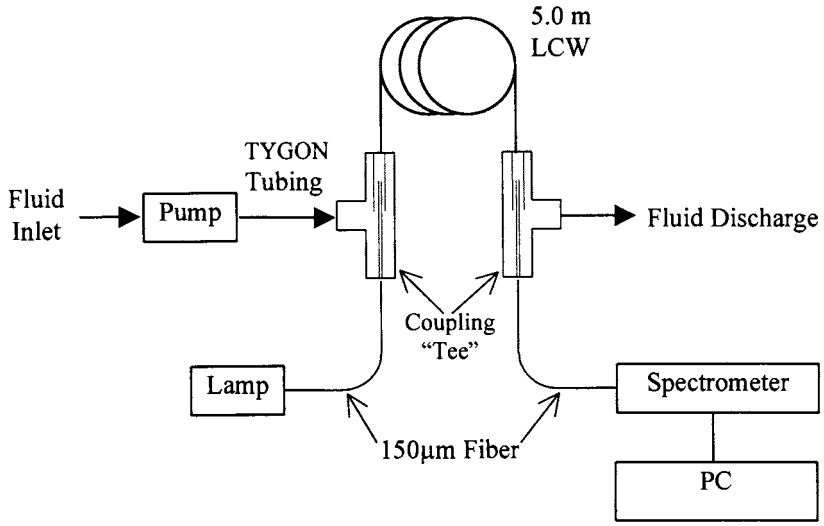

Fig. 1. Overview of the LPAS experimental setup.

detection [4–9] via spectrophotometry or atomic spectroscopy techniques. The one method currently available for direct determination of Mo in natural waters at nanomolar levels is catalytic adsorption polarography [10]. Compared to most analytical techniques, spectrophotometric analysis is inexpensive and easy to perform. Although spectrophotometric analysis also has the advantage of being species specific (eg. Cr^{3+} versus CrO_4^{2-}), relatively poor sensitivity (i.e. detection limits on the order of 20–50 nM) has greatly limited the direct application of spectrophotometry for analysis of Cr and Mo in natural waters.

The inherent sensitivity of colorimetric Cr(VI) and Mo(VI) analysis is limited principally by optical pathlength. Liquid core waveguides (LCW) provide long optical pathlengths by constraining light propagation within a liquid medium which has a higher refractive index (R.I.) than the surrounding solid tubing [11]. An amorphous fluoropolymer form of Teflon designated AF-2400 (Dupont), has an R.I. of ~ 1.29 and many of the desirable chemical properties of Teflon [12,13]. An LCW constructed of Teflon AF-2400 with a water core provides total internal reflection for light rays intersecting the water/tubing interface at 19° or less. We have recently used a Teflon AF-2400 LCW to lower the detection limit of colorimetric Fe(II), nitrite and nitrate analysis [14,15] by more than an order of magnitude. In the work described here, we apply long pathlength absorbance spectroscopy (LPAS) to the colorimetric determination of Cr(VI) and Mo(VI) at nanomolar concentrations. The methods outlined in this work are simple and sensitive.

Many colorimetric reagents have been proposed for spectrophotometric determination of chromium(VI) and molybdenum(VI) [16]. One widely used colorimetric reagent for chromium(VI) is diphenycarbazide. The molar extinction coefficient of the colored product formed through procedures using diphenycarbazide is 4.2×10^4 at 546 nm [17]. Deguchi et al. [18] proposed a method involving bromopyrogallol red–Zephiramine for colorimetric analysis of molybdate. The molar absorptivity of the colored complex in this case is 5.6×10^4 near 630 nm [18]. Our 5.0 m LPAS analyses for Cr(VI) and Mo(VI), utilizing species with molar absorptions in the order of 5×10^4, provide absorbances in the order of 0.025 at one nM levels of Cr(VI) and Mo(VI).

2. Experimental

2.1. Apparatus

The compact experimental setup for LPAS analysis of Cr(VI) and Mo(VI) is shown in Fig. 1. The heart of the setup is a Teflon AF-2400 LCW (Biogeneral), with an inner diameter equal to 560 μm and an outer diameter equal to 800 μm. A 5.0 m length of LCW was coiled and placed in a 10 cm diameter chamber to prevent introduction of ambient light into the LCW. A custom 'T' was designed to interface the LCW to an optical fiber (Polymicro Technologies, 150 μm core diameter) and standard 5 mm ID TYGON tubing (Fig. 1). This 'T' allows insertion of the optical fiber in the Teflon AF-2400 tubing. Sample solutions enter and exit the LCW through an annular gap between the fiber and tubing. A palm-sized CCD array spectrometer (Ocean Optics S2000) and fiber-coupled tungsten halogen lamp (Ocean Optics LS-1) provide spectral absorbance measurements. Continuous sampling is achieved with a peristaltic pump (Rainin, model RP-1) at a flow rate of ~ 2 cm^3 min^{-1}. In order to avoid formation of bubbles in the system, the pump is active only during periods of sample introduction. Bubbles inadvertently introduced to the system are, however, easily flushed out by continuous pumping of sample.

2.2. Reagents

All solutions were prepared with distilled water purified in a Milli-Q system (Millipore Super Q, 18 MΩ) and were stored in PTFE bottles. All reagents were analytical-reagent grade unless otherwise noted and were used without further purification.

Cr(VI) was analyzed using the diphenycarbazide method [16]. A 25% diphenylcarbazide solution was prepared by dissolving 0.25 g of the reagent in 100 ml of acetone. H_2SO_4, diluted 1:1 with Milli-Q water, was prepared from trace-metal grade sulfuric acid. A Cr(VI) stock standard solution (1 mM) was prepared from $K_2Cr_2O_7$. Serial dilutions of the stock solution with Milli-Q water and seawater were used to construct calibration curves.

Mo(VI) was analyzed using the bromopyrogallol red–Zephiramine method [18]. The three reagents used on this analysis were 0.003% (w/v) bromopyrogallol red (BPR), 0.01 M Zephiramine (benzyldimethyltetradecylammonium chloride), and 5 M HCl (trace-metal grade). A Mo(VI) stock standard solution (1 mM) was prepared from Na_2MoO_4.

2.3. Procedures

2.3.1. Cr(VI) analysis

H_2SO_4 1:1 (0.2 ml) and diphenylcarbazide reagent (0.2 ml) were added to 25 ml of each sample and the resulting solution was mixed thoroughly. Absorbance at 546 nm ($_{546}A$) was used for the determination of Cr(VI) concentrations. Absorbances were referenced to a non-absorbing wavelength (700 nm) in order to compensate for baseline drift.

2.3.2. Mo(VI) analysis

Sample solutions (25 ml) were combined with 0.5 ml of 5 M HCl, 0.1 ml of 0.01 M Zephiramine and 0.1 ml of 0.003% BPR, and mixed thoroughly. Absorbances at 630 nm ($_{630}A$) were measured after allowing 20 min for color development. Absorbances were referenced to a non-absorbing wavelength (700 nm) to compensate for baseline drift.

All sample absorbances (A) were obtained as ratios of transmitted light intensity ($A = \log I_0/I$) using samples with (I) and without (I_0) reagents.

3. Results and discussion

3.1. Chromium(VI) analysis

Fig. 2 shows LPAS absorbance response ($_{546}A$) as a function of Cr(VI) concentration. The simple analytical apparatus shown in Fig. 1 produced a linear absorbance response for Cr(VI) concentrations between 0 and 30 nM. The seawater used to construct the Fig. 2 calibration curve had been subjected to a Fe(II) co-precipitation [19] in order to remove trace amounts of Cr(VI) as well as Cr(III). Standard curves in water and seawater

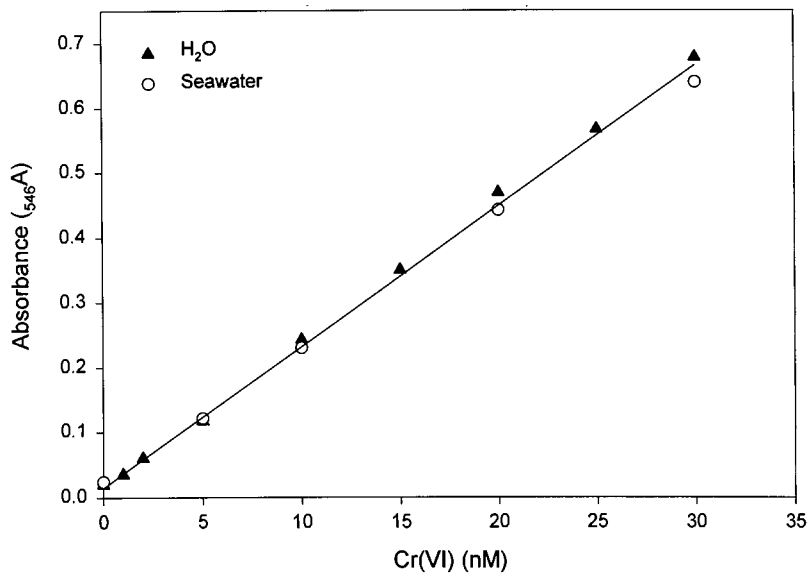

Fig. 2. Cr(VI) standard curves (0 to 30 nM) for Milli-Q water and seawater using a 5.0 m LPAS system.

are identical (Fig. 2) indicating that there are no significant ionic strength effects and no specific ion effects from the major components of seawater. The colored-complex molar adsorptivity obtained using the 5.0 m pathlength (4.4×10^4) is in good agreement with the value (4.2×10^4) determined with conventional 10 cm spectrophotometric cells [17]. The Cr(VI) detection limit, defined as three times the standard deviation of the measurement blank (Milli-Q water + reagents), was 0.2 nanomolar. The relative standard deviation for five measurements of 5.0 nM Cr(VI) was 2%.

Reagent absorbance is often negligible for colorimetric analysis at micromolar concentration levels. LPAS analysis is, however, capable of detecting absorbance contributions from species which have very low concentrations or molar absorptivities. In order to perform accurate analysis at nanomolar levels, the inherent contribution of reagent absorbances must be rigorously evaluated. Our analyses, resulting in an absorbance intercept of only 0.020 (Fig. 2), demonstrate that reagent absorbance contributions in LPAS Cr(VI) analyses are very small.

The diphenycarbazide method is highly specific for chromium(VI). Interference in the determination of chromium is produced only when Fe, V, Mo, Cu, or Hg are present in much higher concentrations [16]. None of these elements, except Mo, is present in substantially higher concentrations than chromium in most natural waters. Our analyses indicated that molybdenum(VI) concentrations on the order of ~ 0.1 μM produced no interference in the determination of 5 nM chromium(VI).

3.2. Mo(VI) analysis

Fig. 3 shows the calibration curve for Mo(VI) in Milli-Q water for concentrations between 0 and 30 nM. No calibration curve was obtained for Mo(VI) in seawater because of the relatively high (~ 0.1 μM) Mo(VI) concentrations in seawater. However, major components of seawater (such as Ca^{2+}, Mg^{2+}, Sr^{2+}, SO_4^{2-}, Br^-) have been shown not to interfere with Mo(VI) analysis [18].

The detection limit for Mo(VI), defined as three times the standard deviation of the measurement blank (Milli-Q water + reagents), was 0.6 nM. The relative standard deviation for five measurements of 5.0 nM Mo(VI) was 6%. The higher detection limit of Mo(VI), relative to that of Cr(VI), is due to a relatively high reagent absorbance at 630 nm and, additionally, the poorer

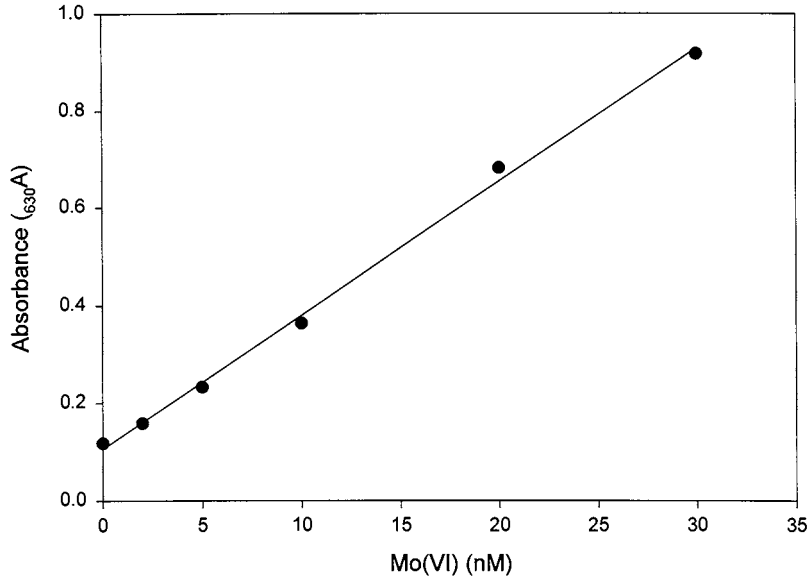

Fig. 3. Mo(VI) standard curve (0 to 30 nM) for Milli-Q water using a 5.0 m LPAS system.

precision of Mo(VI) analysis. In Mo(VI) analysis the reagent absorbance spectrum is not completely separated from that of the Mo–BPR complex, resulting in the relatively large intercept in Fig. 3 (0.110). In addition, we observed that the Mo–BPR complex adsorbs to the LCW tubing to some extent, causing absorbance ($_{630}A$) to increase continuously as a sample solution is pumped through LCW. This contributes to the poorer analytical precision for Mo(VI) relative to Cr(VI), which does not exhibit this behavior. In our work, absorbances ($_{630}A$) were recorded after the sample solution had been pumped for 3 min. Following this procedure, the Mo–BPR complex molar adsorptivity obtained with the 5.0 m pathlength is 5.5×10^4. This is in good agreement with the value, 5.6×10^4, determined with conventional 10 cm spectrophotometric cells [18]. Mo–BPR complex adhering to LCW walls can be easily removed by flushing the LCW with 1.0 M HCl. Since Milli-Q water is insufficient for this purpose, LPAS systems should be cleaned with HCl between each Mo(VI) analysis.

Many kinds of ions have been shown not to interfere with the determination of Mo(VI). However, antimony(III), iron(III), tin(IV), zirconium(IV), hafnium(IV), vanadium(V), chromium(VI) and tungsten(VI) begin to interfere with Mo(VI) analysis when their concentrations are comparable to that of Mo(VI) [18]. Many of these elements are highly reactive and are unlikely to be present at concentrations comparable to Mo(VI) in most natural waters. Exceptions might include chromium(VI) and vanadium(V). The interference of these elements can be masked with 1% (w/v) ascorbic acid plus 0.05 M EDTA [18]. Our analysis indicated that 5 nM Cr(VI) has a negligible effect on the determination of 5 nM Mo(VI), while 50 nM Cr(VI) decreases the signal of 5 nM Mo(VI) by $\sim 11\%$.

3.3. Application

The LPAS analysis described above was used to determine concentrations of Cr(VI) and Mo(VI) in a variety of natural samples (Table 1). Surface seawater, collected in Gulf of Mexico, showed a Cr(VI) concentration equal to 3.6 nM. Typical Cr(VI) concentrations in surface seawater obtained by AAS analysis after preconcentration are between 3.0 and 4.0 nM [20]. The Mo(VI) concentration in seawater was determined after five-fold dilution with Milli-Q water. A Mo(VI) concentration of 98 nM was obtained using the calibration

Table 1
LPAS determination of Cr(VI) and Mo(VI) in natural waters

Sample	Cr(VI)	Mo(VI)
Surface seawater (Gulf of Mexico)	3.6 nM	98 nM[a]
Rain water	<0.2 nM	<0.5 nM
Spring waters (bottled)[b]		
Brand #1	<0.2, <0.2	40.0, 39.2
#2	14.4, 15.0	41.4, 43.5
#3	1.6, 1.5	5.2, 6.8
#4	8.7, 10.1	6.0, 5.7
#5	10.3, 9.8	260[a], 273[a]

[a] Measured after dilution.
[b] Concentration (nM) measured in two different bottles.

curve constructed in Milli-Q water (Fig. 3). This value is comparable to the typical Mo(VI) concentration of seawater (~ 107 nM) obtained by AAS analysis [21].

The concentrations of Cr(VI) and Mo(VI) in rain waters were below the detection limits. Cr(VI) and Mo(VI) levels differed significantly in various brands of bottled spring waters. Cr(VI) concentrations ranged from below the detection limit to as much as 15 nM. These concentrations can be viewed in the context of a 2 μM maximum contaminant level for current drinking water standards [22]. Mo(VI) concentrations in the bottled spring waters ranged from 5.2 to 273 nM. The agreement between Cr(VI) and Mo(VI) concentrations in different bottles of the same brand of water is generally excellent.

4. Conclusions

One of the most significant advantages of LPAS analysis is its substantial simplicity and amenability to miniaturization and autonomous analysis. The sample size requirement for LPAS analysis obtained using a liquid core waveguide is very low. The internal volume of a 5.0 m LCW (560 μm ID) is ~1.2 cm^3. The techniques presented in this work increase the sensitivity of conventional colorimetric Cr(VI) and Mo(VI) analysis by approximately two orders of magnitude without preconcentration. LPAS analysis can be used for routine monitoring of harmful chemical species in drinking waters.

Acknowledgements

This work was supported by the Office of Naval Research under contract # N00014-96-1-5011.

References

[1] J.J.R. Fraústro da Silva, R.J.P. Williams, The Biological Chemistry of the Elements, Clarendon Press, Oxford, 1993, p. 541.
[2] F.C. Richard, A.C.M. Bourg. Wat. Res. 25 (1991) 807.
[3] K.K. Bertine, K.K. Turekian, Geochim. Cosmochim. Acta 37 (1973) 1415.
[4] J.F. Pankow, G.E. Janauer, Anal. Chim. Acta 69 (1974) 97.
[5] R.E. Cranston, J.W. Murray, Anal. Chim. Acta 99 (1978) 275.
[6] G.L. Ou-Yang, J.F. Jen, Anal. Chim. Acta 279 (1993) 329.
[7] K. Wrobel, K. Wrobel, P.L. Lopez-de-Alba, L. Lopez-Martinez, Talanta 44 (1997) 2129.
[8] J.C. de Andrade, R.E. Bruns, S. de Paula Eiras, Analyst 118 (1993) 213.
[9] S. Hoshi, K. Konuma, K. Sugawara, M. Uto, K. Akatsuka, Talanta 44 (1997) 1473.
[10] B. Magyar, S. Wunderli, Mikrochim. Acta (Wien) 3 (1985) 223.
[11] L. Wei, K. Fujiwara, K. Fuwa, Anal. Chem. 55 (1983) 951.
[12] W.H. Buck, P.R. Resnick, Dupont Technical Product Information, 1993.
[13] R. Altkon, I. Koev, R.P. Van Duyne, M. Litorja, Appl. Optics 36 (1997) 8992.
[14] R.D. Waterbury, W. Yao, R.H. Byrne, Anal. Chim. Acta 357 (1997) 99.
[15] W. Yao, R.H. Byrne, R.D. Waterbury, Environ. Sci. Tech. (1998) submitted.
[16] Z. Marczenko, Spectrophotometric Determination of Elements, JWS, New York, 1976.
[17] T.L. Allen, Anal. Chem. 30 (1958) 447.
[18] M. Deguchi, M. Iizuka, M. Yashiki, Jpn Analyst 23 (1974) 760.
[19] R.E. Cranston, J.W. Murray, Anal. Chim. Acta 99 (1978) 275.
[20] J.W. Murray, B. Spell, B. Paul, in: C.S. Wong, E. Boyle, K.W. Bruland, J.D. Burton, E.D. Goldberg (Eds.), Trace Metals in Sea Water, Plenum, New York, 1983, pp. 643–669.
[21] R.W. Collier, Limnol. Oceanogr. 30 (1985) 1351.
[22] F.W. Pontius, J. Am. Water Works Assoc. 90 (1998) 38.

ELSEVIER

Talanta 48 (1999) 283–292

Talanta

Simultaneous spectrophotometric determination of Fe and Ni with xylenol orange using principal component analysis and artificial neural networks in some industrial samples

M. Kompany-Zareh [a], A. Massoumi [a,*], Sh. Pezeshk-Zadeh [b]

[a] *Department of Chemistry, Shahid Beheshti University, Evin, Tehran 19839, Iran*
[b] *Department of Chemistry, Islamic Azad University, Tehran, Iran*

Received 26 February 1998; received in revised form 10 June 1998; accepted 17 June 1998

Abstract

Artificial neural networks (ANNs) are among the most popular techniques for nonlinear multivariate calibration in complicated mixtures using spectrophotometric data. In this study, Fe and Ni were simultaneously determined in aqueous medium with xylenol orange (XO) at pH 4.0. In this way, after reducing the number of spectral data using principal component analysis (PCA), an artificial neural network consisting of three layers of nodes was trained by applying a back-propagation learning rule. Sigmoid transfer functions were used in the hidden and output layers to facilitate nonlinear calibration. Adjustable experimental and network parameters were optimized, 30 calibration and 20 prediction samples were prepared over the concentration ranges of 0–400 μg l^{-1} Fe and 0–300 μg l^{-1} Ni. The resulting R.S.E. of prediction (S.E.P.) of 3.8 and 4.7% for Fe and Ni were obtained, respectively. The method has been applied to the spectrophotometric determination of Fe and Ni in synthetic samples, some Ni alloys, and some industrial waste waters.

Keywords: Fe; Ni; Artificial neural networks; Xylenol orange

1. Introduction

The various multivariate calibration methods that exist today differ in the mathematical form of the model and the way in which the model equations are solved. Most models rely on the property that the contributions of the measurement variables to the result are additive. Multiple linear regression (MLR), principal component regression (PCR), and partial least-squares regression (PLS) fall into this category.

Nonlinear calibration models are required if interactions between the different components in the sample have to be accounted for. Sometimes this is accomplished by extending the measurement vector with quadratic and cross-terms of the measurements [1] and followed by the application

* Corresponding author. Tel.: +98 21 2401765; fax: +98 21 2403041; e-mail: a-massoumi@cc.sbu.ac.ir

0039-9140/99/$ - see front matter
PII S0039-9140(98)00233-1

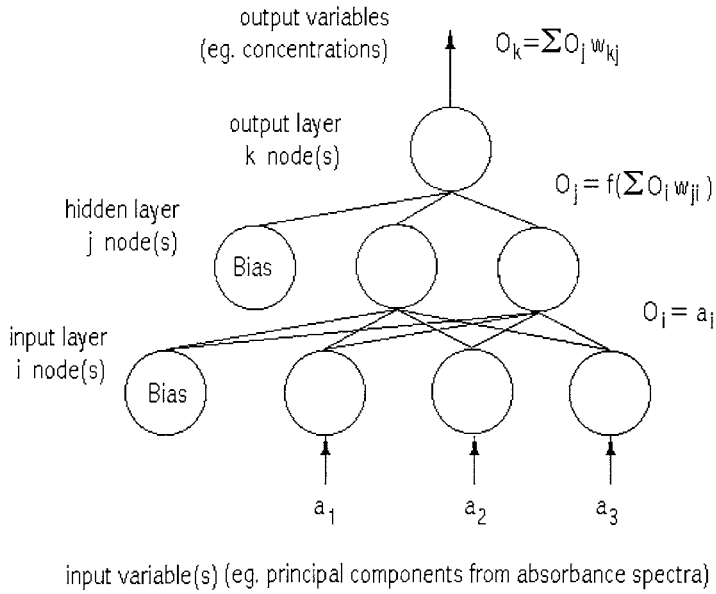

Fig. 1. (a) Schematic representation of a three-layer artificial neural network. Each circle is a node.

of a linear method to the extended measurement data. If the measurement vector is large and no a priori knowledge about the interaction terms which are important is available, this approach drowns in the large number of input data. Artificial neural networks (ANNs) are particularly suited as calibration models in this situation [2].

The aim in this study was the simultaneous determination of Fe and Ni in some complex mixtures using xylenol orange (XO), which is a popular reagent in spectrophotometric determination of different metal ions such as Ni and Fe [3–9]. In most cases the metal chelates formed by this ligand have ML-type composition (or M_2L_2), but as XO behaves as a polybasic ligand with two coordinate sites, the composition of the resulting chelates are usually complicated [6], particularly in the case of the Fe cation in acidic solution [10]. Interaction between the species and, as a result, spectral nonlinearity in the system containing XO is probable. Therefore a nonlinear calibration model such as principal component–artificial neural networks (PC-ANN) [11] could be used for the calibrations. This calibration method consists of principal component analysis (PCA) which is a statistical method for reducing the number of data without loss of any valuable information [12] and artificial neural networks (ANN) which have generated widespread interest and popularity for nonlinear calibration in the past few years [11,13,14].

On the other hand, it is reported that the difference between λ_{max} of Fe(II)–XO (at about 530 nm) and Ni–XO (570 nm) complexes is more than that of Fe(III)–XO (550 nm) and Ni–XO [6]. On that basis, we selected Fe(II)–XO as a suitable system for study and decided to reduce all Fe(III) ions to Fe(II), although there is not much quantitative information about the stability and stoichiometry of Fe(II)–XO complex in the literature.

In this way, the simultaneous determination of Fe(II) and Ni(II) in the presence of a limited excess of reagent, using nonlinear multivariate calibration with PC-ANN, were carried out and gave satisfactory results. The same procedure was suitable for the simultaneous and satisfactory determination of Fe and Ni in nichrome and chromel alloys, and some waste water samples.

Table 1
Artificial neural network specifications and parameters

Parameter	Simulated data
Input nodes	Variable (see text)
Hidden nodes	Variable (see text)
Output nodes	2
Learning rate	0.2
Momentum	0.5
Gain	1.0
Input layer transfer function	Sigmoid
Hidden layer transfer function	Sigmoid
Output layer transfer function	Sigmoid
Maximum number of iterations	25 000
Optimum number of iterations	5000

2. Theory

2.1. ANNs

The fundamental processing element of an artificial neural network is a node (Fig. 1). Each node has a series of weighted inputs, w_i, which may be either external signals or the output from other nodes. In our application, the external input signals are principal components calculated from absorbance values, A_i, measured at I wavelengths in a spectrum. The sum of the weighted inputs is transformed with a linear or nonlinear transfer function. A popular nonlinear transformation function is the sigmoid function [15]:

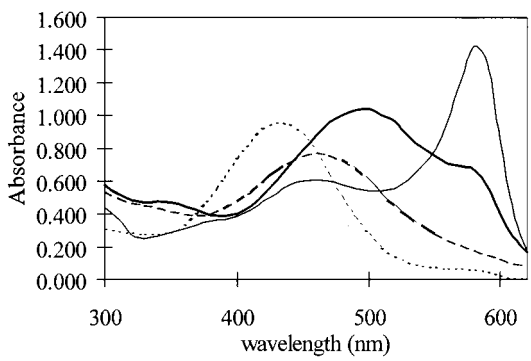

Fig. 2. Absorption spectra of XO and the XO complexes of Fe(II) and Ni(II) and their mixture at pH ~ 6.0: (···) $C_{XO} = 1.0$ mmol l^{-1}; (- - -) $C_{Fe} = 5.00$ μmol l^{-1}; (——) $C_{Ni} = 5.00$ μmol l^{-1}; (——) $C_{Tot} = 10.00$ μmol l^{-1}.

$$f(x) = \frac{1}{1 + e^{(-x/\theta)}} \quad (1)$$

The function has an output in the range from 0 to 1, where x is the weighted sum of the inputs and θ is the gain. The gain serves to modify the shape of the sigmoid curve.

It has been claimed that an arbitrary nonlinear mapping of input domains to output domains can be achieved by using three layers in an artificial neural network [16]. In this paper, also, a feed-forward network was constructed by using three layers of nodes: an input layer, a hidden layer, and an output layer, as shown in Fig. 1. The input nodes transfer the weighted input signals to the nodes in the hidden layer. A connection between node i in the input layer and node j in the hidden layer is represented by a weighting factor w_{ji}. These weights are adjusted during the learning process. Each layer also has one bias input, as shown in Fig. 1, to accommodate nonzero offsets in the data. The value of the bias input is always set to 1.0. A term is included in the vector of weights to connect the bias to the corresponding layer. This weight is also automatically adjusted during the training process. The number of hidden nodes is an adjustable parameter and determines the complexity of the neural network. The output of each hidden node is a sigmoid function of the sum of that node's weighted inputs. The gain, θ, in the sigmoid function is also an adjustable parameter. The outputs from each node in the hidden layer are sent to each node in the output layer. For our calibration applications, two output nodes were used in the output layer, having two outputs equal to the scaled concentration of the components of interest. The concentration values were scaled to lie in the range from 0.0 to 1.0 by adding an offset and multiplying by a constant. Scaled outputs are necessary to accommodate the bounded range of the sigmoid output function (0.0–1.0) when it is used for the output nodes. During the learning procedure, a series of input patterns (e.g. principal components from spectra) with their corresponding expected output values (e.g., scaled concentrations) are presented to the network in an iterative fashion while the weights are adjusted. The training process is terminated when the desired level of precision is

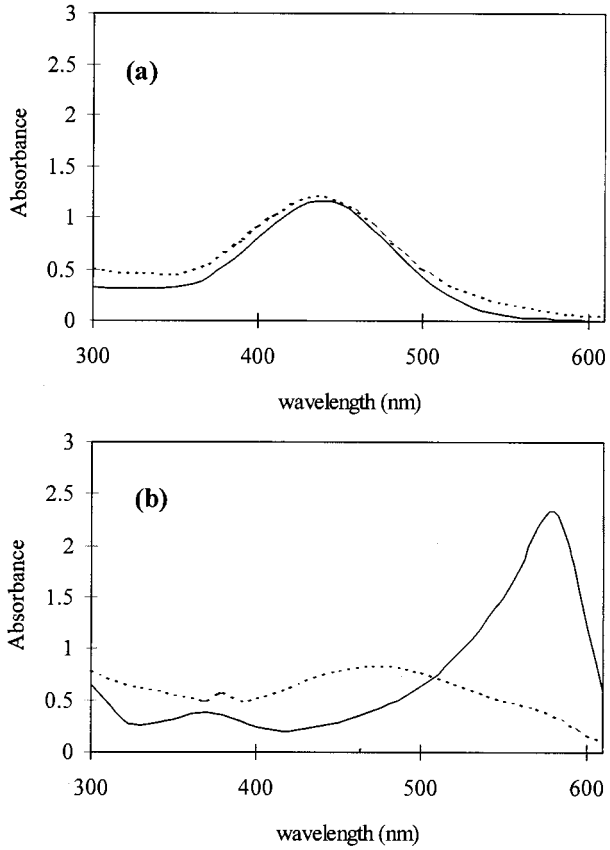

Fig. 3. Effect of pH on the absorption spectra of the XO complexes of Fe(II) and Ni(II): $C_{XO} = 1.2$ mmol l^{-1}; $C_{Fe} = C_{Ni} = 5.00$ μmol l^{-1}.

achieved between the expected output and the actual output. In this work, the error in the expected output is back-propagated through the network by using the generalized delta rule to determine the adjustments to the weights [15]. When the output transfer function is sigmoid, the output layer error term is given by:

$$\delta_{pk} = (t_{pk} - o_{pk}) o_{pk} (1 - o_{pk}) \quad (2)$$

where δ_{pk} is the error term for observation p at output node k, t_{pk} is the expected output for observation p, and o_{pk} is the actual node output. The term $o_{pk}(1\text{-}o_{pk})$ is the derivative of the sigmoid function. The error term at the node j of the hidden layer that uses a sigmoid transfer function is:

$$\delta_{pj} = o_{pj}(1 - o_{pj}) \sum_{k=1}^{K} \delta_{pk} w_{kj} \quad (3)$$

The error terms from the output and hidden layers are back-propagated through the network by making adjustments to the weights of their respective layers. Weight adjustments, or delta weights, are calculated according to [15]:

$$\Delta w_{ji}(n) = \eta \delta_{pj} o_{pj} + \alpha \Delta w_{ji}(n-1) \quad (4)$$

where Δw_{ji} is the change in the weight between node j in the hidden layer and node i in the input layer. In Eq. (4), η is the learning rate, δ_{pj} is the error term for observation p at node j of the hidden layer, o_{pj} is the observed output for node i of the input layer for observation p, and α is the momentum. The terms n and $n-1$ refer to the present iteration and the previous iteration, re-

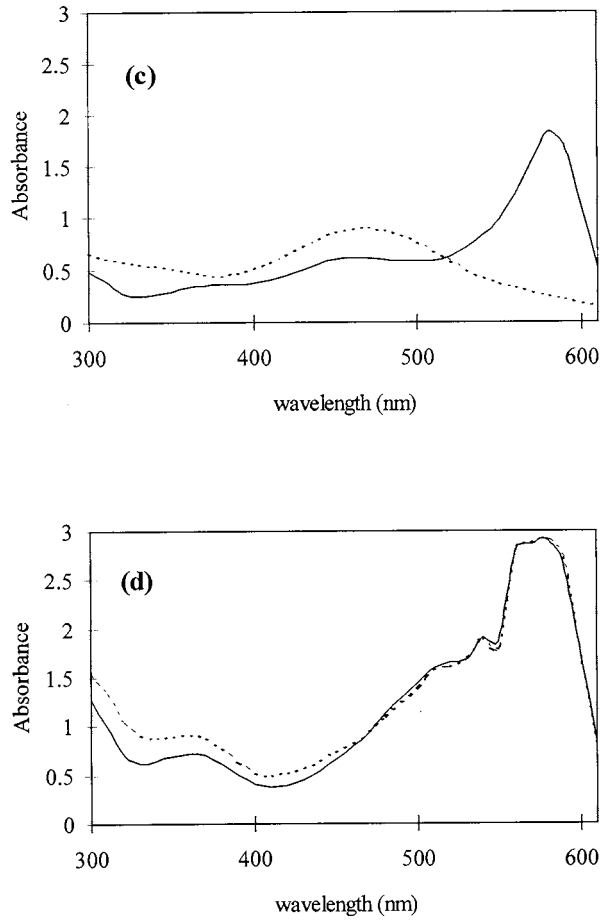

Fig. 3. (*Continued*)

spectively. The presentation of the entire set of p training observations is repeated when the number of iterations, n, exceeds p. An equation similar to Eq. (4) is used to adjust the weights connecting the hidden layer of nodes in the output layer.

Prior to the start of training, all of the weights in the network are set to random values and the learning rate and the momentum are initialized. When the learning rate is set too high, a local minimum may be encountered during the descent down the error surface. If it is set too low, the rate of learning can be too slow. To help resolve this dichotomy, Rumelhart et al. [15] suggested the use of a momentum term that would act to reinforce the general trends in the changes in the weights, filter out high frequency fluctuations, and increase the speed of lower learning rates.

ANN have been observed to give stable behavior for subtle perturbations and random noise in the input signals compared to other nonlinear methods. This behavior is attributed to the signal-averaging effect of the summations and the bounded output domain of the sigmoid transfer function. In addition, ANN have been observed to be fault tolerant due to the automatic incorporation of the redundant nodes.

2.2. PCA

The back-propagation training algorithm for ANN belongs to a class of function minimization technique called the steepest descent methods [13].

These methods for function minimization perform poorly, especially when the input variables are highly correlated. In order to address the above deficiencies experiments have been begun with orthogonal transformations of the input variables using singular value decomposition (Eq. (5)) of training set spectra (**Y**) to give q columns of orthogonal input variables, or principal components, in the matrix, $\mathbf{Y}^* \equiv \mathbf{U}_q$:

$$\mathbf{Y} = \mathbf{U}_q \mathbf{S}_q \mathbf{V}_q^T \quad (5)$$

The columns in **U** associated with very small singular values are not included in $\mathbf{U}_q$. These new variables are used instead of the original variables. Validation spectra or unknown sample spectra, $\mathbf{y}_m$, are projected into the space spanned by the row basis vectors $\mathbf{V}_q$ to give the new transformed variables, $\mathbf{y}_m^*$:

$$\mathbf{y}_m^* = \mathbf{y}_m \mathbf{V}_q \mathbf{S}_q^{-1} \quad (6)$$

When principal components (input variables) having significant information for the calibration problem are pruned, a large increase in the S.E. of calibration (S.E.C.) can be observed. The addition of insignificant orthogonal variables to the calibration model, on the other hand, results in an increase in the S.E. of prediction (S.E.P.). The selection of the optimum number of orthogonal input variables is necessary and will be discussed in the next sections.

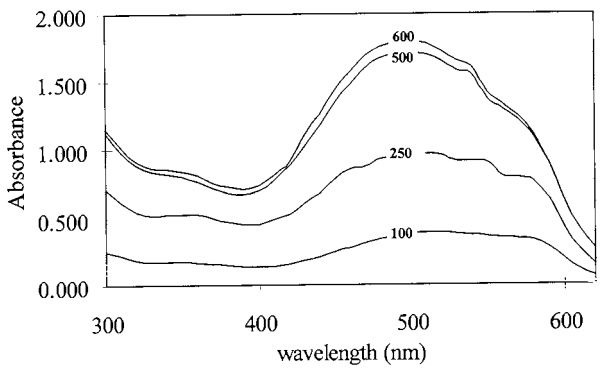

Fig. 4. Effect of XO concentration on the absorption spectra of the XO complexes of Fe(III) and Ni(II): $C_{Fe} = C_{Ni} = 5.00$ μmol l^{-1}; C_{XO} is 100, 250, 500, and 600 times C_{Fe}.

3. Experimental

3.1. Chemicals

Stock solutions of Fe(III) and Ni(II) containing 100 μg l^{-1} of each metal were standardized gravimetrically or by EDTA titration. Xylenol orange (XO) was supplied by Merck, Darmstadt. Aqueous stock solutions (10 mmol l^{-1}) were used. Hydroxylammonium chloride and buffer solutions were also obtained from Merck, Darmstadt. All other chemicals used were of analytical grade quality and bidistilled water from a silica apparatus was used.

3.2. Instruments, software, and conditions

A Milton Roy 3000 spectrophotometer with 10 mm quartz cells was employed. A digital pH-meter, Metrohm 691, with a combined glass calomel electrode 6.0202.100 was used. A back-propagation neural network having three layers was created with a Visual-Basic software package written in our laboratory. The specifications for the network created for the calibrations are listed in Table 1. They were found to be optimal for fast learning with low prediction errors. The concentration of the components were uniformly distributed over the range from 0.00 to 5.11 μmol l^{-1} and from 0.00 to 7.16 μmol l^{-1} for Ni and Fe, respectively. In each set of experiments, 30 calibration standards and 20 test standards were prepared. The UV–visible spectra of the mixtures were obtained over the wavelength range 300–620 nm in increments of 10 nm. PCA calculations on the spectra obtained for the estimation of network input variables were performed using a MATLAB version 4.2a software package, based on the factor analysis methods [12].

3.3. Procedure

To the mixture of metal nitrates 0.5 ml 10% (w/v) hydroxylammonium chloride was added and after 10 min of slight shaking, successively 4.0 ml of acetic acid–acetate buffer (pH 4) and 2.5 ml 10 mmol l^{-1} XO was also added. The pH was

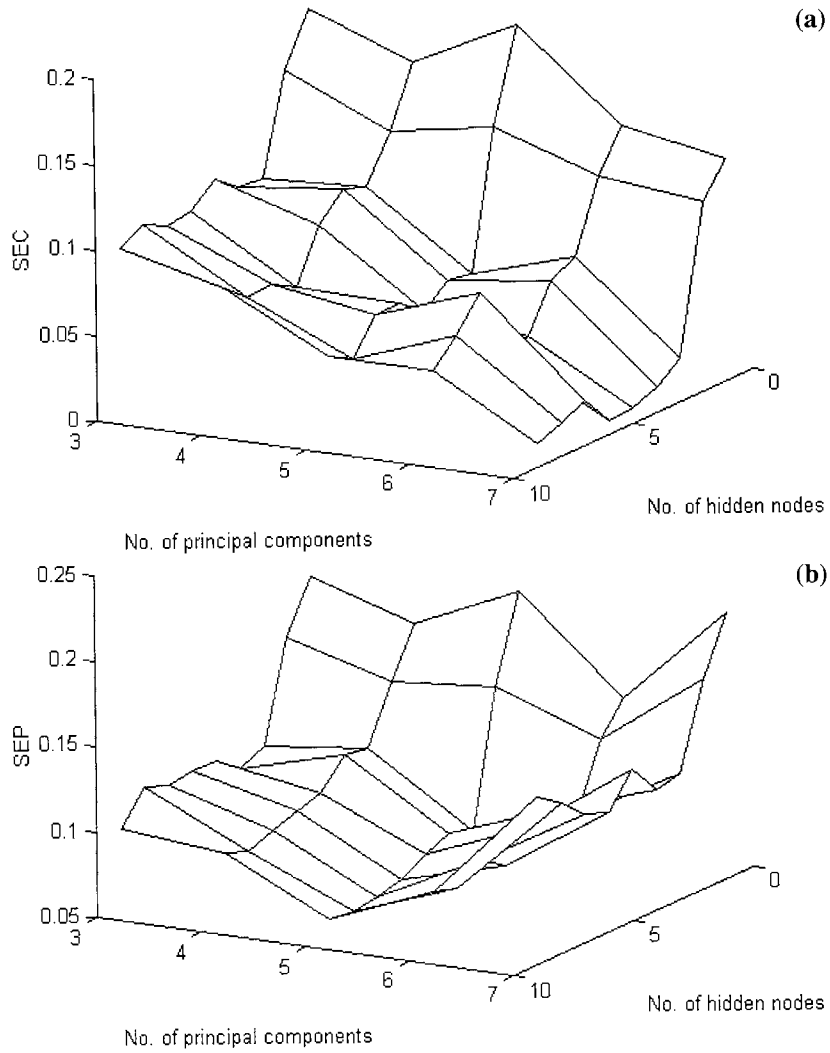

Fig. 5. Plots of S.E.C. (a) and S.E.P. (b) as functions of the number of applied principal components and the number of hidden layers. The minimum in the S.E.P. surface is when the number of applied principal components and hidden layers are 5 and 8, respectively.

adjusted to 4.0 by adding some drops of 0.1 mol l^{-1} NaOH. The solution was heated on a boiling water bath for 20 min, cooled with water to room temperature, and transferred to a 10.0 ml volumetric flask and made up to the mark with water. The spectra was measured 10 min after making up. To mask interfering ions such as Al(III), Zr(IV), and Ti(IV), 0.5 ml 0.4% (w/v) F^- was added to the prepared solutions 5 min after the development of Fe(II)–XO and Ni(II)–XO chelates. The spectra was measured 3 min after addition of F^-.

3.4. Alloy samples

Accurately weighted amounts of approximately 0.1 g of metal was treated with 10 ml 13 mol l^{-1} HNO_3 and evaporated to near dryness three times. The solution was transferred into a 1000 ml calibrated flask and made up to the mark with

distilled water. The volume required to obtain Fe and Ni concentrations within the range of calibration graph on dilution to 10 ml was prepared and the process was continued as described above.

4. Results and discussion

The absorbance spectra of the Fe–XO and Ni–XO complexes, and a mixture of both complexes and the corresponding reagent blank are shown in Fig. 2. It is obvious that the linearly summing the spectra of the solutions containing the Ni and Fe complexes results in an spectrum different from that of the solution containing both metal complexes. Therefore, a nonlinear calibration model is necessary.

Table 2
Estimated and actual concentrations of Fe(II) and Ni(II) in synthetic and real mixtures.

Samples	Ni (μg l^{-1})		Fe (μg l^{-1})	
	Actual	Found	Actual	Found
Synthetic				
1	0	7	0	−2
2	188	183	276	259
3	88	91	357	371
4	123	117	357	358
5	247	243	112	115
6	64	71	179	186
7	152	160	237	232
8	188	183	357	352
9	266	269	51	63
10	183	185	180	187
11	149	146	22	8
12	16	11	295	280
13	239	247	10	8
14	116	107	226	213
15	15	24	61	51
Real[a]				
Nichrome	310	297 ± 12	80	83 ± 6
Chromel	290	301 ± 14	100	100 ± 5
Waste water (I)[b]	210	215 ± 6	250	246 ± 7
Waste water (II)[b]	50	45 ± 8	380	384 ± 8

[a] Found values format is: average ± S.D.
[b] Actual values for waste water samples are the reported values from flame atomic absorption spectrometry.

4.1. Optimization of experimental variables

The absorbance of the solution of XO–metal complexes decreases gradually with the time of standing at most wavelengths. About 10% of the intensity was diminished within the first 2 h, and about 2% within an additional 2 h. So, the measurements of spectra were made 10 min after preparation of the solutions. To obtain the total concentration of Fe in solution, probable Fe(III) was reduced quantitatively to Fe(II) over 10 min using hydroxylammonium chloride, and before the addition of the ligand, because the reduction takes place slowly after the formation of the Fe(III)–XO complex. The effect of pH on the absorbance spectra of each metal complex was studied over the pH range 2–8. As shown in Fig. 3, the maximum selectivity, and better sensitivity for Ni and Fe occurs approximately at pH 4. Therefore pH 4 was chosen as the optimum working pH. The ionic strength of the solution studied was adjusted with sodium nitrate. It was found that an increase in ionic strength had no considerable effect on the complexes spectra, even when the concentration of the salt was 4.0 mol l^{-1}. The influence of XO concentration on the spectra of the solution containing both Fe and Ni and the corresponding blank solution was studied. It is illustrated in Fig. 4 that the difference between the absorption spectrum of the solution containing both metal complexes and that of the corresponding reagent blank solution increases with an increase in XO concentration. The concentration of both metals at this stage of the study is about 5.00 μmol l^{-1} and considerable changes in differences between the XO complexes and the blank (ligand) spectra are obtained until the reagent to Fe molar ratio is about 500 ([XO] = 2.5 mmol l^{-1}). Therefore 2.5 mmol l^{-1} was selected as the optimum XO concentration for the study.

4.2. Optimization of networks variables and number of factors

A learning rate of 0.2 was found to work well with the spectroscopic data sets. If the learning rate was set too high, the network became unstable and divergent. The presence of such diver-

gent behavior increased with the size of the network (e.g. the number of hidden layers). As various learning rates were being investigated, momentum values were also varied in the hopes of finding a ratio for the relative combination of the two parameters that would give the most rapid optimization of the network. A momentum of 0.5 was found to work well with the data.

The most versatile transfer function that can be used to model a variety of relationship is the sigmoid type [17]. In our nonlinear system, also, sigmoid hidden and output layers functions were found to be optimum for calculations. The gain for the sigmoid functions was set to 1.0 which resulted in subtle improvements in the network performance, i.e. lower prediction errors.

The proper number of nodes in the hidden layer and principal components, or nodes, in the input layer were determined simultaneously by training ANN with different number of nodes in the hidden and output layers, and then, comparing the prediction errors from an independent test set for each network. Fig. 5 shows two plots of the S.E.C. and the S.E.P. as a function of number of nodes in the hidden layer and principal components in the input layer. The values for S.E.C. and S.E.P. are the root mean squared errors for the calibration set and the test set, respectively. As illustrated in Fig. 5b, a minimum in S.E.P. occurred when eight and five nodes were used in the hidden and input layers, respectively. For this data set we believe that networks with fewer than eight nodes in the hidden layer do not have sufficient complexity to model the data precisely, while networks with more than nine nodes are unnecessarily complex, thereby propagating too much random noise through the net to the output nodes. Fig. 5b also shows that introduction of more than five principal components in the calculations causes an increase in S.E.P. These principal components are physically not significant and are associated entirely with experimental noise, although they result in a decrease in S.E.C. (Fig. 5a).

In the optimized experimental and network conditions obtained, the resulting relative S.E.P. for Fe and Ni in the validation samples (20 samples) were 3.5 and 4.2%, respectively [18]. According to the Wilcoxon signed rank test method [19] at the significance level of 95% ($P = 0.05$), there is no evidence for the systematic difference between the estimated and actual values of concentrations.

Continued training beyond 5000 iterations frequently resulted in a slight increase in S.E.P. as the learning iteration increased while S.E.C. leveled off or continued to decrease slightly. We believe this behavior is due to overfitting, where the network begins to model random noise specific to the calibration data.

4.3. Interferences

The interference effect of several anions were studied, along with that of the corresponding sodium salts. Chloride, nitrate, and sulfate anions did not interfere. Large amounts of phosphate, tartrate, and citrate reduced the absorbance considerably. EDTA which could form stable complexes with Ni(II) and Fe(II) decreased the absorbance.

Among the different cations tested Ca(II), Mg(II), Na(I), K(I), Cd(II), Pb(II), Tl(II), and Zn(II) did not interfere. The interference effect of Al(III), Zr(IV), and Ti(IV) were eliminated by the addition of a 0.4% solution of F^-, and that of V(IV) and Cr(III) were eliminated by changing their concentrations in the calibration steps, in addition to the concentrations of the analytes.

4.4. Synthetic samples

The results of the prediction of the concentrations of Fe(II) and Ni(II) in the synthetic samples, containing different concentrations of some interfering cations and F^- as a masking agent, are summarized in Table 2. The resulting relative S.E.P. for Fe and Ni in this case were 3.8 and 4.7%, respectively. The calculated relative error values in this case is higher than that of 20 without interference validation samples, which are 3.5 and 4.2% for Fe and Ni, respectively. This is due to the presence of interferences in the synthetic samples.

4.5. Alloy samples

For the simultaneous evaluation of Ni and Fe contents in nichrome and chromel alloys, using the proposed method, a set of 17 calibration solutions, eight validation (prediction) solutions, and eight alloy test solutions were used. The spectral interference effect of Cr(III) was eliminated by changing its concentration in the calibration and validation samples, in addition to the concentration of Fe and Ni ions. The results obtained for alloy samples are shown in Table 2.

4.6. Waste water samples

The proposed method was also applied to the determination of Ni and Fe in two industrial waste water samples. The results of the determinations, using the proposed method, was compared with the results obtained by FAAS (five measurements: mean $\pm$ S.D.). The results are shown in Table 2 and shows good agreement between the two methods.

5. Conclusion

On the whole, this study indicates that even when a completely nonlinear response is present, ANN may be capable of giving a satisfactory performance for spectroscopic calibration in real samples.

References

[1] M. Bos, Anal. Chim. Acta 166 (1984) 261.
[2] M. Bos, A. Bos, W.E. van der Linden, Analyst 118 (1993) 323.
[3] M. Otomo, Anal. Chem. 36 (1963) 809.
[4] M. Otomo, Anal. Chem. 36 (1963) 137.
[5] W.J. de Wet, G.B. Bohrens, Anal. Chem. 40 (1968) 200.
[6] K.L. Cheng, CRC-Handbook of Organic Analytical Reagents, 2nd printing, CRC Press, Boca Raton, FL, 1990.
[7] H. Nishida, T. Nishida, T. Segawa, Bunseki Kagaku 28 (6) (1979) 379.
[8] C. Zhang, M. Xu, J. Wang, Diandu Yu Huanbao 14 (6) (1994) 25.
[9] E. Zheng, Yejin Fenxi 9 (6) (1989) 54.
[10] T. Vesiene, Z. Baciuliene, Liet. TSR Makslu Akad. Darb. Ser. B 2 (1985) 34.
[11] P.J. Gemperline, J.R. Long, V.G. Gregoriou, Anal. Chem. 63 (1991) 2313.
[12] E.R. Malinowski, Factor Analysis in Chemistry, 2nd ed., Wiley, New York, 1991.
[13] P.J. Gemperline, Chemom. Intell. Lab. Syst. 15 (1992) 115.
[14] J.R. Long, V.G. Gregoriou, P.J. Gemperline, Anal. Chem. 62 (1990) 1791.
[15] D.E. Rumelhart, J.L. McClelland, the PDP Research Group, Parallel Distributed Processing: Exploration in the Microstructure of Cognition, Part 1, MIT Press, Cambridge, MA, 1986.
[16] R.P. Lippman, IEEE ASSP Mag. 4 (1987) 4.
[17] W.R. Hruschka, K.H. Norris, Appl. Spectrosc. 36 (1982) 261.
[18] M. Otto, W. Wegscheider, Anal. Chem. 57 (1985) 63.
[19] J.C. Miller, J.N. Miller, Statistics for Analytical Chemistry, 2nd ed., Ellis Horwood, Chichester, UK, 1988.

ELSEVIER

Talanta 48 (1999) 293–303

Talanta

Reactivity of NASICON with water and interpretation of the detection limit of a NASICON based Na^+ ion selective electrode

F. Mauvy, E. Siebert *, P. Fabry

Laboratoire d'Electrochimie et de Physicochimie des Matériaux et des Interfaces[1], *ENSEEG, 1130 Rue de la Piscine, BP 75, 38402 Saint Martin d'Hères cedex, France*

Received 2 April 1997; received in revised form 12 June 1998; accepted 17 June 1998

Abstract

The leaching of Na^+ ions from NASICON of composition $Na_3Zr_2Si_2PO_{12}$ to the aqueous solution was evidenced. The origin of the Na^+ leaching was studied using Na^+ concentration and pH measurements as well as solution and X-ray analyses. The Na^+ released was mainly attributed to the dissolution of a second phase, predominantly amorphous. The rate of Na^+ release was found to be dependent on the inverse of the square of the particle size. It is proposed that it is controlled by diffusion within the particle. An effective diffusion coefficient was deduced to be of the order of 5×10^{-10} cm^2 s^{-1}. The nature of the detection limit of the NASICON based Na^+ ion selective electrodes is discussed.

Keywords: NASICON; Ion selective electrode; Detection limit

1. Introduction

Since the work of Hong and Goodenough [1,2], a NASICON of formula $Na_3Zr_2Si_2PO_{12}$, has been proposed for many electrochemical devices, e.g. batteries and electrochemical sensors. NASICON stands for 'Na Super Ionic Conductor'. It consists of ZrO_6 octaedra linked by corners to $(Si,P)O_4$ tetrahedra. This rigid oxide network forms a three dimensional lattice of intersecting conduction channels in which are localized the Na^+ ions. For migration, the Na^+ ions must pass through 'bottlenecks' well adjusted to the size of the Na^+ ions. This material was proposed as the sensitive membrane for the analysis of Na^+ ions in solutions [3–5]. Compared to commercially available glass electrodes, the main advantages of NASICON based ion selective electrodes (ISE) are low impedance, robustness and better selectivity with regard of H^+, Li^+ and K^+ ions, due to the well calibrated size of the conduction sites [6]. However, the detection limit is only of the order of 10^{-4} M, that is almost ten times higher than that of glass membranes at pH 8. It is generally ac-

* Corresponding author: Tel.: +33 476826573; fax: +33 476826670; e-mail: Elisabeth.Siebert@lepmi.inpg.fr

[1] Laboratory INPG, associated to CNRS UMR 5630, and to University J. Fourier, Grenoble.

0039-9140/99/$ - see front matter
PII S0039-9140(98)00234-3

cepted that the detection limit of ISEs is governed by the solubility of the membrane or leaching out of the active ion originating from ionic exchange or dissolution. It can also be due to proton interference, as seen in silica glass membranes. Recently, the detection limit of carrier-based ISEs was related to the extraction of the inner electrolyte leading to a net flux of ions from the inner filling solution to the sample solution [7]. In the case of NASICON, the proton interference is lower than in glass electrodes and transmembrane electrolyte diffusion cannot occur. The origin of the detection limit is still not well understood.

In the 1980s, NASICON was reported to be insensitive to degradation by moisture and stable in water, contrary to β alumina [8,9]. About 10 years ago, Ahmad et al. [10] had revised this point and showed that all NASICON, irrespective of their mode of preparation, react with water to some extent. According to these authors, the materials prepared by a ball-milling process were found to react faster than those prepared by gel processing. An exchange of sodium for hydronium ions in acid aqueous solutions was also shown on NASICON, at room temperature [11]. The results from these authors indicate that NASICON strongly prefers Na^+ ions relative to H_3O^+ ions. Impedance studies performed on NASICON demonstrate that the NASICON–aqueous NaCl interface changes as a function of time [12], whereas the interface between NASICON and polyethylene oxide based ionic polymer is very stable [12,13]. This would suggest that NASICON reacts with water. Previous studies of the stability of such material in water [5] have shown that Na^+ ions were released from the NASICON. Two phenomena were proposed: (i) a solubility product effect, and/or (ii) sodium exchange by the proton.

The purpose of this study was to examine further the behavior of NASICON in contact with water in order to identify the origin of the Na^+ leaching and to interpret the detection limit in NASICON based ISE. Solutions of suspended NASICON powder were studied as a function of the purity of the sample. The kinetics of Na^+ leaching was evaluated as a function of the size of the particle. The results are discussed in terms of ionic exchange or dissolution. They were analysed with respect to the detection limits previously determined [5].

2. Experimental

2.1. Materials and procedure

NASICON of composition $Na_3Zr_2Si_2PO_{12}$ was prepared by the sol-gel process as previously described [5]. The starting materials were $Si(OC_2H_5)_4$ (VENTRON), $Zr(OC_3H_7)_4$ (VENTRON), NaOH (R.P. PROLABO) and $NH_4H_2PO_4$ (R.P. NORMAPUR). The sol-gel powder was calcined at 1000°C in air. It is well known that sintered NASICON may show the presence of second phases. The purity of the samples was checked by X-ray diffraction (XRD). Single phase NASICON powders as determined from XRD were tested. NASICON powders containing different amounts of monoclinic zirconia as the second phase were also tested for comparison.

The diameter of the particles was measured with a particle size analyzer (Cilas 1064) based on light scattering. Scanning electron microscopy was also performed to confirm the particle size and to determine the morphology of the particle. A typical example of the particle size distribution of the NASICON powder suspension is given in Fig. 1. The average diameter of the particles and the S.D. were deduced from this histogram. Three mean sizes of particle were tested i.e. 10, 30 and 160 μm.

A weighed amount of NASICON powder was suspended in distilled water and placed in a thermostated cell. Argon (U) was bubbled through the suspension to minimize the effects due to CO_2. The experiments were performed in pure distilled water or with 0.1 M $BaCl_2$ as the supporting electrolyte. The solution was stirred magnetically. The Na^+ concentration and pH of the suspension were measured as a function of time. At the end of the experiment, the solution was separated from the powder by filtration for ICP-AES analyses. The NASICON residual powder was analysed by X-ray diffraction.

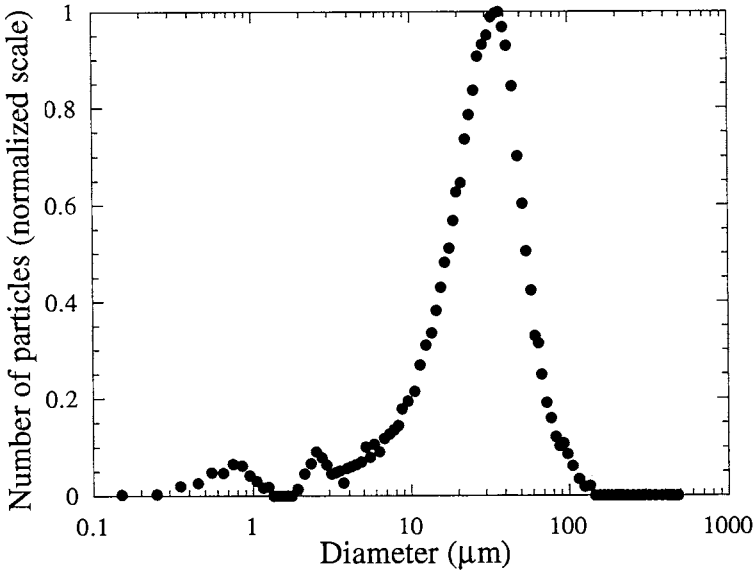

Fig. 1. Particle size distribution of a typical NASICON suspension.

2.2. Na^+ concentration and pH measurements

The pH measurements were performed at 25°C with a pH glass electrode (Radiometer Analytical). Contamination by CO_2 was clearly evident in some experimental results, after 1 h of equilibration time. To clarify this point, the pH of a solution of 10^{-3} M KOH was measured under argon as a function of time. It was found to be constant and it began to decrease after 1 h. For this reason, only the results obtained at a time less than 1 h have been taken into account.

The change with time of the sodium activity of the suspension was measured with a Na^+ ion selective electrode (Ingold or Radiometer Analytical). The electrode was calibrated in aqueous solutions containing fixed amounts of sodium chloride, for different pH over the range 9–11, corresponding to the pH measured in this study. Over this range, the proton interference of the glass electrode is very low [5].

2.3. Solution and X-ray analyses

The ICP-AES analyses were performed by the Science and Surface Company (Charbonnieres, France). The Na and P concentrations in the solution were determined with a precision of 5%.

X-ray diffraction were carried out at room temperature, with a Siemens D500 diffractometer $\theta/2\theta$ using Cu Kα radiation, step scanning at 0.02° intervals of 2θ.

2.4. Calibration curve

The Na^+ ISE was assembled as depicted in Ref. [5]. A liquid internal reference system was used. It can be represented by the following electrochemical chain:

Ag/AgCl/NaCl 0.1 M, pH 8/NASICON

The internal solution was made from Tris 8 electrolyte purchased from Radiometer Analytical. The sample solutions were also made from Tris 8 electrolyte. A saturated calomel electrode (SCE) was used as the external reference electrode. To avoid any K^+ contamination from SCE, a double junction was used.

3. Results and discussion

3.1. Reactivity with water

The pH of a solution of suspended NASICON

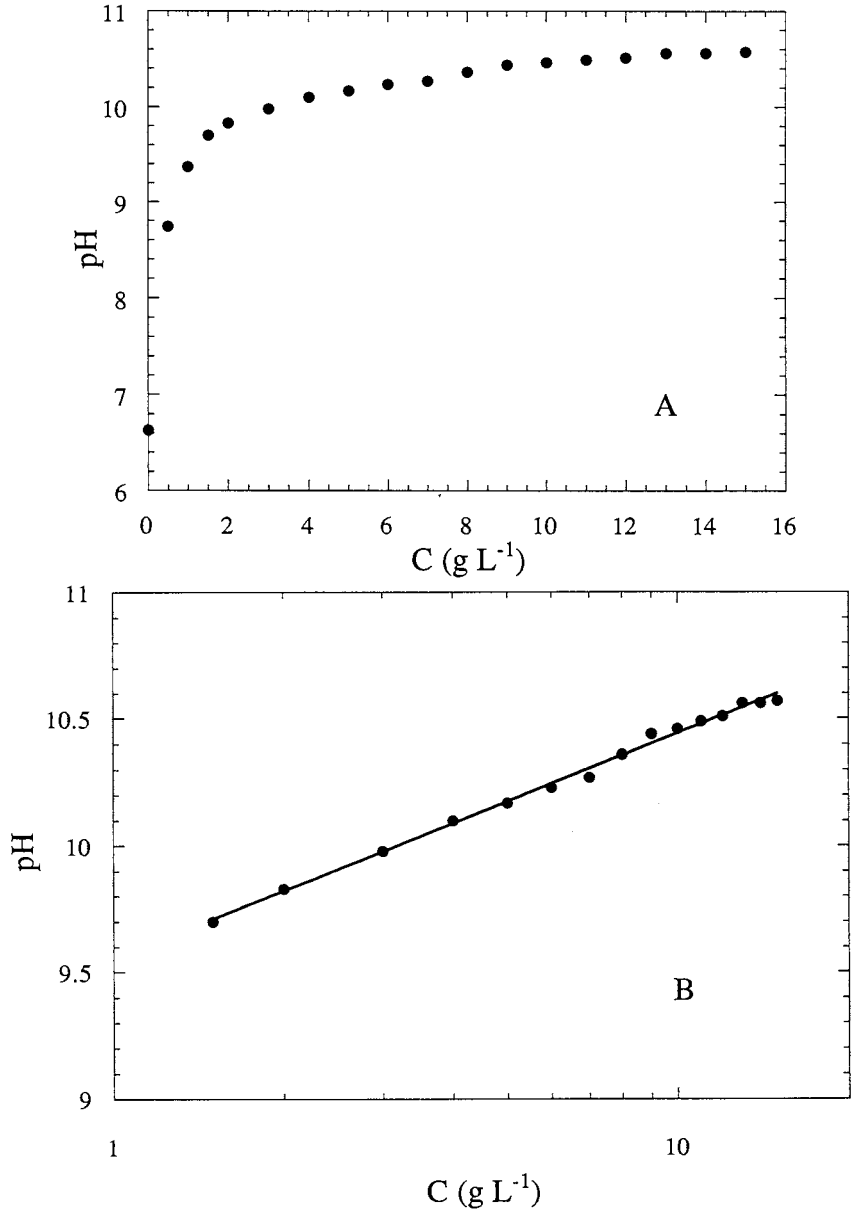

Fig. 2. (A) pH vs. the amount of NASICON powder suspended in distilled water (linear scale). The pH was measured after 15 min. (B) pH versus the amount of NASICON powder suspended in distilled water (logarithmic scale in the basic domain). The pH was measured after 15 min.

powder as a function of the amount of NASICON powder is shown in Fig. 2. As shown by Ahmad et al. [10], the pH of water increases in contact with NASICON. For small amounts of NASICON in the suspension, the pH increases as a function of NASICON concentration. For NASICON concentrations higher than 1 g l^{-1}, the pH increases slightly. As seen from the pH versus

log C_{Na} plot, the variation of OH^- concentration is proportional to the amount of NASICON powder. This may indicate that the reaction between NASICON and water is total. The pH for 1 g of powder is higher than that reported by Ahmad et al. [10] for NASICON of the same composition. The pH 7 reported by these authors could be due to stronger contamination by CO_2 because their experiments were not performed under argon.

Typical variations as a function of time of the sodium concentration and pH of a solution of suspended NASICON powder (1 g l^{-1}) are shown in Fig. 3 and Fig. 4, respectively. As seen from Fig. 3, Na^+ ions are leached from the NASICON when in contact with water. The amount of Na^+ ions released into the solution and the pH vary in the same way and reach steady state values. Table 1 summarizes the Na^+ concentration and pH values reached in the steady state, for NASICON powder of composition $Na_3Zr_2Si_2PO_{12}$ in pure water and with a supporting electrolyte. No significant influence due to the presence of $BaCl_2$ as the supporting electrolyte is observed. Three experiments performed on the same powder in distilled water show that there is some dispersion of the Na^+ concentration in the steady state. The pH is almost equal to 10.8. As proposed for glass [14–17], it was first suggested that NASICON reacts with water by ion exchange between the hydronium ions from the water and sodium ions in NASICON [5]. The results in Table 1 would indicate that 10% of the sodium contained in NASICON should be exchanged and that the exchange constant should be high. A rough estimation from the concentration of Na^+ and H_3O^+ in the solution and molar fraction in the solid would lead to a value of 10^6 for the exchange constant. This does not agree with the results of Komorowski et al. [18] who found that NASICON strongly prefers Na^+ ions relative to H_3O^+: the proton exchange is partial in 0.2 M HCl, indicating a low value for the exchange constant. Moreover, the pH resulting from the Na^+–H_3O^+ exchange should be one unit higher than that obtained experimentally. To confirm this result, NASICON powder was separated from the solution and suspended again in distilled water. The Na^+ concentration and pH of the suspension are shown in Fig. 3Fig. Fig. 4. The amount of Na^+ released in the solution decreases significantly (about 5–10 times). This confirms that the Na^+ released during the first stage cannot be attributed to ionic exchange equilibrium. It also indicates that Na^+ leaching does not result from a solubility product.

The amount of Na^+ released was studied as a function of the NASICON material. Three types of NASICON powders from three different samples of identical basic composition were tested. The corresponding XRD patterns are shown in Fig. 5. The powder, P1 showed the presence of the NASICON phase. It was indexed on a rhomboedral cell with $a = 9.06$ Å and $c = 22.97$ Å. It was free of zirconia. The second one, P2, showed small amount of monoclinic zirconia in addition to NASICON. The last one, P3, showed large amount of monoclinic zirconia and the presence of a third phase which was identified as Na_3PO_4 from the diffraction peak at $2\theta = 20.7$ which is one of the most intense peaks expected for this compound.

The Na^+ concentration and pH measured for these three types of NASICON powders are summarized in Table 2. The amount of Na^+ released is highly dependent on the presence of secondary phases in the sample. The Na^+ concentration increases as the amount of zirconia in the sample increases. This result agrees with the difference of reactivity observed by Ahmad et al. [10] as a function of the mode of preparation of NASICON. Their NASICON was prepared by a ball-milling process and contained zirconia in addition to NASICON which is more reactive than those prepared by a gel route which is free of zirconia.

The XRD patterns of the powder after reaction with water were also measured. No change in the patterns was observed for the powder containing a small amount of zirconia. The cell parameters remained the same. On the powder P3, the peak attributed to Na_3PO_4 was found to disappear completly after reaction with water.

Analyses of the solution demonstrated that there was a significant loss of phosphorus from the NASICON powder (Fig. 6). The phosphorus concentration in the solution was found to be of

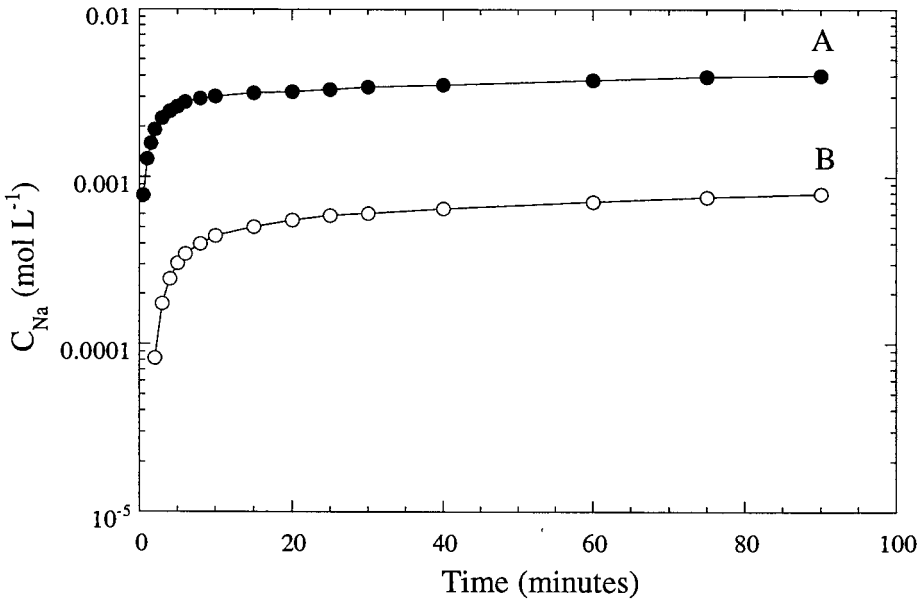

Fig. 3. Plot of C_{Na} vs. time for suspended NASICON in distilled water: (A) fresh NASICON powder, (B) NASICON powder separated from the solution and suspended again (1 g of NASICON powder was suspended in 100 ml of solution).

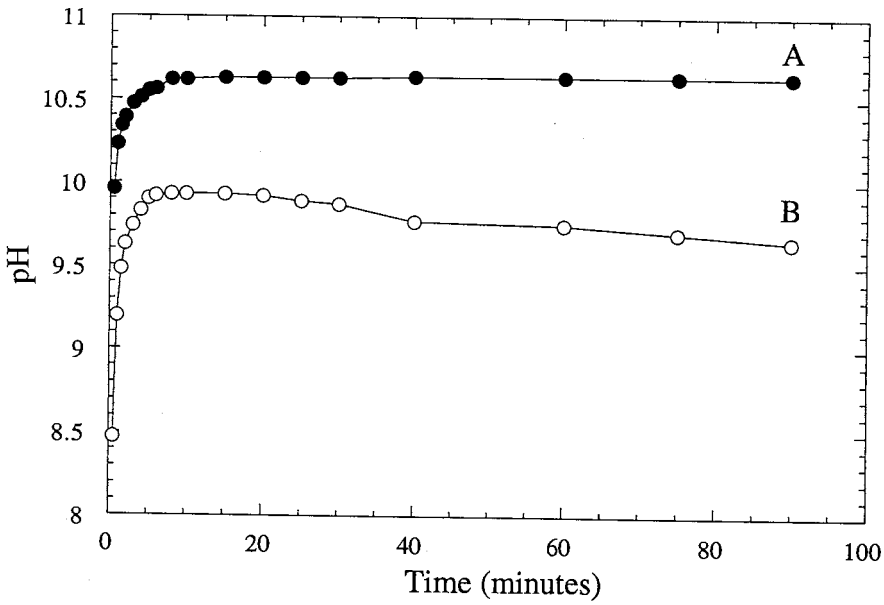

Fig. 4. Plot of pH vs. time for suspended NASICON in distilled water: (A) fresh NASICON powder, (B) NASICON powder separated from the solution and suspended again (1 g of NASICON powder was suspended in 100 ml of solution).

the order of 6×10^{-3} M and almost three times lower than the Na^+ concentration. This is the same ratio as the stoichiometry in NASICON or Na_3PO_4. Komorowski et al. [18] have also shown by ICP analyses that there is a loss of phosphorus and no loss of zirconium in the first stage of their ion exchange experiments in 0.2 M HCl solutions. The P concentration for 1 g of NASICON in 100

Table 1
Na^+ concentration and pH at steady state for a solution of suspended NASICON of composition $Na_3Zr_2Si_2PO_{12}$

Electrolyte	C_{Na+} (M)	pH
0.1 M BaCl2	7×10^{-3}	>10
H_2O	6×10^{-3}	10.8
H_2O	8×10^{-4}	10.9
H_2O	3×10^{-3}	10.7

NASICON (1 g) for 100 ml of solution.

Table 2
Na^+ concentration and pH at steady state for solutions of suspended NASICON

NASICON	ZrO_2	M (g)	C_{Na+} (M)	pH
P1	No	1.5	3×10^{-3}	10.6
P2	Small	1	4×10^{-3}	10.8
P3	High	0.5	1.6×10^{-2}	>11.1

M (g) of NASICON powder in 100 ml of solution. The NASICON powder contained different amounts of zirconia.

ml of solution, deduced from their experiments is equal to 6×10^{-4} M. This value is in agreement with the concentration of Na^+ released by NASICON powder free of zirconia (Table 2).

It can therefore be proposed that the Na^+ released is mainly due to the dissolution of a phase rich in phosphorus which is not easily seen by XRD. This phase would always be present, to some extent, in the sample and be predominantly amorphous. It was identified in samples containing large amounts of impurities as Na_3PO_4. From the results in Table 2, it can be deduced that there is almost 1.2 wt.% Na_3PO_4 in sintered NASICON which appears as a pure NASICON phase by XRD. To confirm this point, the pH expected from the dissolution of this Na_3PO_4 has been calculated. The values of Na^+ concentrations in Table 2 allows the calculation of the phosphate concentrations. From these last values, if it is assumed that PO_4^{3-} is a strong base ($pK_a = 12.4$) the pH deduced are, respectively, equal to 11, 11.1 and 11.7 and of the order of what we measured.

The kinetics of Na^+ released was studied as a function of the size of the particle. As seen from Fig. 7, the rate of Na^+ release was found to increase with decreasing particle size. The fraction of Na^+ released into the solution at time t, $F(t)$,

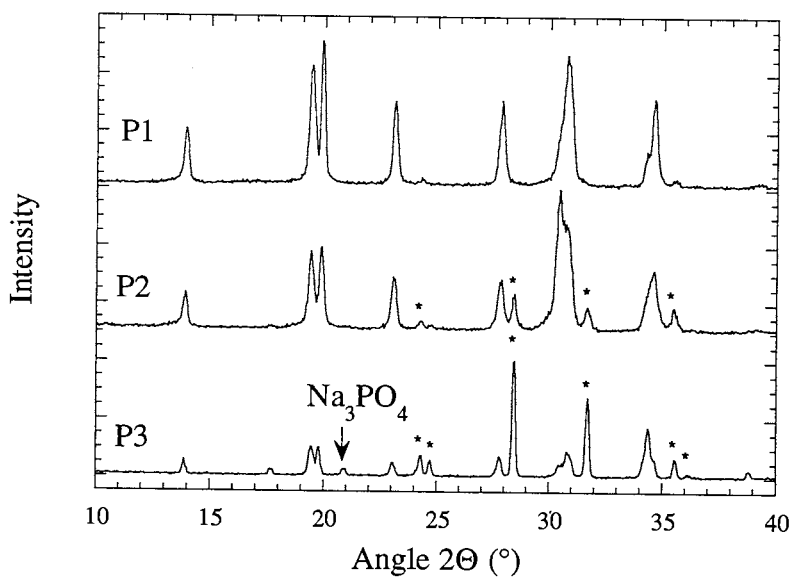

Fig. 5. XRD patterns of the three types of NASICON powders. P1, NASICON; P2, NASICON with monoclinic ZrO_2; P3, NASICON with monoclinic ZrO_2 and Na_3PO_4. The stars indicate monoclinic ZrO_2.

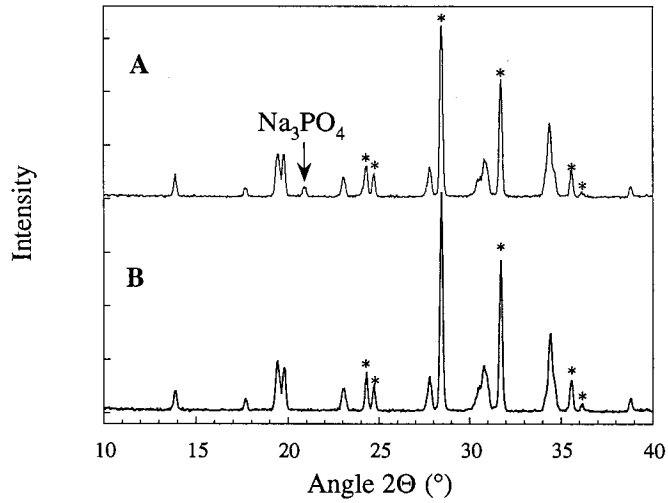

Fig. 6. XRD patterns of the NASICON powder P3 before (A) and after (B) reaction with distilled water.

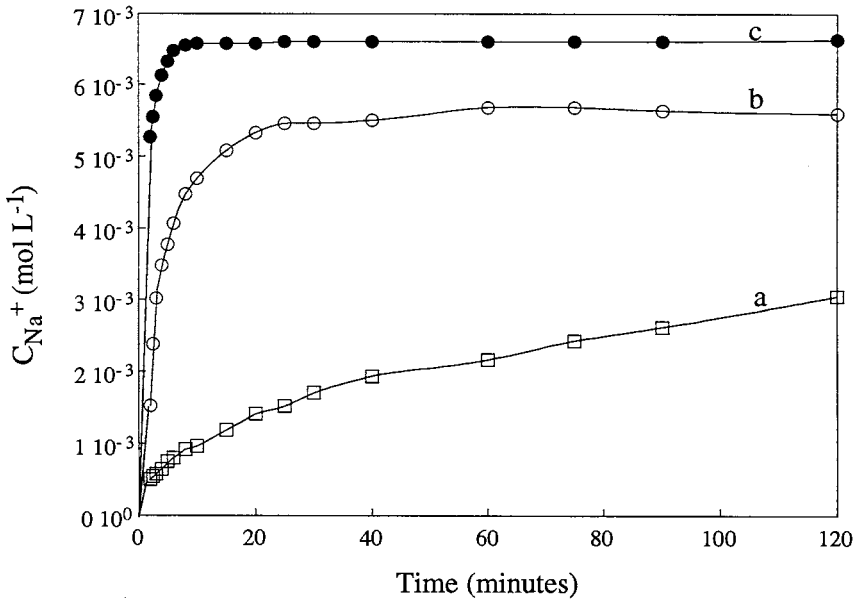

Fig. 7. Plot of C_{Na} vs. time for NASICON suspension as a function of the particle size: (a) 160, (b) 30, and (c) 10 μm.

is defined as:

$$F(t) = \frac{C_{Na}(\infty) - C_{Na}(t)}{C_{Na}(\infty)} \quad (1)$$

where $C_{Na}(\infty)$ is the Na^+ amount released after infinite time and $C_{Na}(t)$ is the amount released at time t. It was identified by the classical equation:

$$F(t) = \frac{6}{\pi^2} \sum_{n=1}^{\infty} \frac{1}{n^2} \exp(-n^2 Bt) \quad (2)$$

which describes the radial diffusion in a homogeneous sphere for a uniform initial distribution of a diffusing substance and with a concentration constant at the surface [19]. The results are reported

Table 3
B values and interdiffusion coefficients D deduced from fitting to Eq. (2)

Particule size (μm)	B (min^{-1})	D ($cm^2\ s^{-1}$)	Correlation coefficient
30	0.17	6.5×10^{-10}	0.999
30	0.12	4.6×10^{-10}	0.997
10	0.55	2×10^{-10}	0.999
160	0.006	6.5×10^{-10}	0.999

in Table 3. Good correlations were obtained indicating that Eq. (2) can be used to describe the process of release. This may suggest that the dissolution reaction is a diffusion-controlled process. The transport of cations in the intergranular region of the NASICON sample may be proposed. The mathematical description of this problem is complex because of the real geometry. However our results indicate that the Na^+ leaching seems to behave as if it was fixed by the diffusion in a hypothetical homogeneous medium, and that the amorphous soluble phase is dispersed homogeneously in the NASICON membrane. An effective diffusion coefficient D_{eff} which takes into account the complexity of the geometry can be deduced from the coefficient B according to the equation:

$$B = \frac{\pi^2 D_{eff}}{r^2} \quad (3)$$

where D_{eff} is the effective diffusion coefficient and r the radius of the particle. The results are reported in Table 3. A $D_{eff} = 5\times10^{-10}$ $cm^2\ s^{-1}$ is so obtained.

3.2. Interpretation of the detection limit

A typical calibration curve for a Na^+ ISE based on NASICON is shown in Fig. 8. As expected the potentiometric response follows the Nernst equation at high Na^+ concentration and a plateau at a low Na^+ level is observed. According to the I.U.P.A.C. recommendations [20], the detection limit is defined as the concentration at the point of intersection of the extrapolated linear midrange and final low concentration level segments of the calibration plot. The detection limit of the NASICON based ISE has been measured previously [5,21] in Tris buffered solution (pH 8), for different sintering temperatures and membrane porosities. The results are summarized in Table 4. For high density samples ($>90\%$), the detection limit is constant and always of the order of 10^{-4} M. For samples of lower density (85%), the detection limit increases. This point was also observed for screen printed layers of low density for which the detection limit is around 5×10^{-3} M [22]. It was also obtained with other compositions of NASICON. For example with the $Li_{1.3}Al_{0.3}Ti_{1.7}(PO_4)_3$ membrane [21], the Li^+ detection limit is about 10^{-4} M for a 93% densified membrane and this value increases to 10^{-3} M when the membrane is only 85% densified.

The study of the Na^+ released in solution versus time has shown that this amount is not governed by a solubility product. As a result the detection limit cannot be explained by the solubility of the membrane as is the case for silver halide electrodes [23]. The detection limit is also not fixed by the proton interference as proposed in Na^+ sensitive glass electrodes [24]. In fact, if we assume that the detection limit corresponds to the H_3O^+ response, it depends on the potentiometric selectivity coefficient, $K^{POT}_{Na,H}$, according to the equation:

$$E = E^o + \frac{RT}{F}\ln\left(a_{Na} + K^{POT}_{Na,H}\times a_H\right) \quad (4)$$

where a_{Na} and a_H are the activities of the sodium and hydronium ions in solution. R, T and F have their classical meaning. The results reported in Ref. [5] show that $K^{POT}_{Na,H}$ depends on the sintering temperature: $K^{POT}_{Na,H} = 5$ for a membrane sintered at 1200°C and in the range 50–80 for a membrane sintered at 1000°C. As the pH of the sample solution is around 8 and the detection limit is nearly the same for the NASICON membrane sintered at 1000 and 1200°C (Table 4), we can conclude that

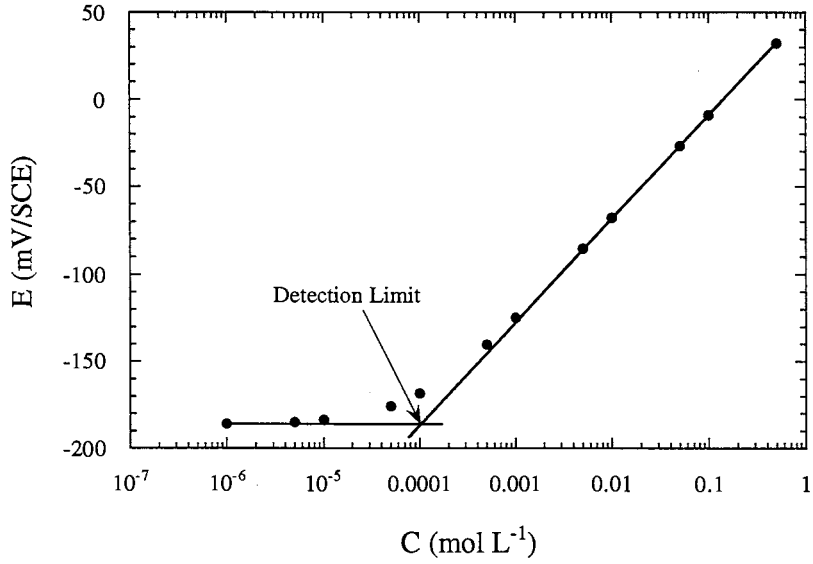

Fig. 8. Example of a calibration curve. The detection limit is 10^{-4} M.

the detection limit is not fixed by the proton interference.

From the present results for NASICON powder, we propose that the detection limit may be linked to the Na^+ amount released in aqueous solution, originating from the dissolution of a second phase dispersed in the sample and identified as Na_3PO_4. From the weight of the NASICON pellet (≈ 0.5 g) in the ISE and the values of Table 2, it shows that the expected amount of Na^+ in solution is about 10^{-3} M. Such a value is about ten times higher than the detection limit. To explain this difference, it could be proposed that the steady state concentration is not reached because the surface area of exchange exposed to the solution is much less important for the NASICON pellet than for the powder. To verify this point, we have calculated the time necessary to reach a Na^+ concentration equal to 10% of the steady state expected value. According to previous results, the Na^+ release is governed by a diffusion process with an effective diffusion coefficient almost equal to 5×10^{-10} cm^2 s^{-1}. The amount of Na^+ released for a sample of thickness L during the first stage of the response is given by the following equation established for the diffusion in a plane sheet [19]:

$$\frac{M_t}{M_\infty} = \frac{2}{L} \times \left(\frac{D_{\text{eff}} \times t}{\pi} \right)^{0.5} \quad (5)$$

where M_t and M_∞ are the amount of the diffusing substance at time t and infinity, respectively. L is the thickness of the pellet which is assumed to be highly densified and D_{eff} is the effective diffusion coefficient of the substance. The time necessary to reach a steady state for a sample of 3 mm thickness is almost equal to 16 days; that is longer than the time of the experiment. It can therefore be concluded that the detection limit does not correspond to the Na^+ concentration in the bulk of the solution due to the dissolution of Na_3PO_4.

The previous oversimplified model does not take into account the porosity of the sample and assumes that the stirring of the solution is ideal.

Table 4
Detection limit in mol l^{-1} vs. sintering temperature and relative density

Sintering temperature (°C)	Density (%)		
	85	90	99
1000			10^{-4}
1150		2.7×10^{-4}	10^{-4}
1200	3×10^{-4}	1.5×10^{-4}	1.5×10^{-4}

Due to the porosity, the exchange surface is greater and the concentration at the NASICON solution interface may be greater than that expected from Eq. (5). It may be suggested that the detection limit corresponds to the activity of the Na^+ released in the pores. As expected from this interpretation, the density of the NASICON membrane greatly influences the detection limit and so, the higher the porosity, the higher the detection limit.

4. Conclusion

NASICON of composition $Na_3Zr_2Si_2PO_{12}$ reacts with water. The dissolution of an amorphous phase dispersed in the material is proposed to be responsible for the Na^+ released. This phase is identified as Na_3PO_4 in materials with large amount of secondary phases. The kinetics of Na^+ leaching is controlled by a diffusion process. Accordingly, the detection limit of the NASICON based ISE may be proposed to be related to the activity of the Na^+ released in the pores of the membrane. In agreement with this interpretation, the densification of the sample greatly influences the detection limit: the higher the density, the lower the detection limit.

References

[1] H.Y.P. Hong, Mater. Res. Bull. 11 (1976) 173.
[2] J.B. Goodenough, H.Y.P. Hong, J.A. Kafalas, Mater. Res. Bull. 11 (1976) 203.
[3] J. Engell, S. Mortensen, Radiometer Int. Patent WO 84/01829, 1984.
[4] P. Fabry, J.P. Gros, J.F. Million-Brodaz, M. Kleitz, Sens. Actuators 15 (1988) 38.
[5] A. Caneiro, P. Fabry, H. Khireddine, E. Siebert, Anal. Chem. 63 (1991) 2550.
[6] H. Khireddine, P. Fabry, A. Caneiro, B. Bochu, Sens. Actuators B40 (1997) 223.
[7] S. Mathison, E. Bakker, Anal. Chem. 70 (1998) 303.
[8] J.J. Auborn, D.W. Johnson, Solid State Ion. 5 (1981) 315.
[9] G.R. Miller, B.J. Mc Entire, T.D. Hadnagy, J.R. Rasmussen, R.S. Gordon, A.V. Virkar, in: P. Vashista, J.N. Mundy, G.K. Shenoy (Eds.), Fast Ion Transport in the Solid, Elsevier, Amsterdam, 1979, p. 83.
[10] A. Ahmad, T.A. Wheat, A.K. Kuriakose, J.D. Canaday, A.G. Mcdonald, Solid State Ion. 24 (1987) 89.
[11] J. Gulens, B.W. Hildebrandt, J.D. Canaday, A.K. Kurriakose, T.A. Wheat, A. Ahmad, Solid State Ion. 35 (1989) 45.
[12] C. Gondran, PhD thesis in Electrochemistry, I.N.P. Grenoble, 1994.
[13] C. Gondran, F. Albert, E. Siebert, Solid State Ion. 84 (1996) 131.
[14] A. Wikby, J. Electroanal. Chem. 33 (1971) 145.
[15] B.C. Bunker, G.W. Arnold, D.E. Day, P.J. Bray, J. Non-Cryst. Solids 87 (1986) 226.
[16] R.H. Doresmus, J. Non-Cryst. Solids 19 (1975) 137.
[17] F.G.K. Baucke, J. Non-Cryst. Solids 19 (1975) 75.
[18] P.G. Komorowski, S.A. Argyropoulos, R.G.V. Hanock, et al., Solid State Ion. 48 (1991) 295.
[19] J.M. Vergnaud, Liquid Transport Processes in Polymeric Materials. Modelling and Industrial Applications, Prentice-Hall, Englewood Ciffs, NJ, 1991.
[20] R.P. Buck, E. Lindner, Pure Appl. Chem. 66 (1994) 2527.
[21] M. Cretin, P. Fabry, Anal. Chim. Acta 354 (1997) 291.
[22] N. Poignet, PhD thesis in Electrochemistry, I.N.P. Grenoble, 1997.
[23] W.E. Morf, The principle of Ion-Selective Electrodes and Membranes Transport, Elsevier, Amsterdam, 1981, pp. 165–210.
[24] C.M. Huang, Y.C. Jean, K.L. Cheng, F.C. Chang, J. Electrochem. Soc. 142 (1995) L175.

ELSEVIER

Talanta 48 (1999) 305–320

Talanta

Diode lasers in analytical chemistry

Totaro Imasaka *

Department of Chemical Science and Technology, Faculty of Engineering, Kyushu University, Hakozaki, Fukuoka 812, Japan

Received 2 June 1998; received in revised form 27 June 1998; accepted 29 June 1998

Abstract

In this review article, I report the structure and characteristics of a diode laser and the figure of merits in the application to analytical spectroscopy. This diode laser is currently used in absorption-based and fluorescence-based spectrometries. Due to their ultra-high detectability, single atoms and molecules can be detected in the extreme case. Moreover, selectivity is improved by time-resolved spectrometry and also by a combination with separation techniques such as chromatography. Second harmonic generation is employed to extend the laser wavelength, in order to expand the analytical application. Finally, limitations of the diode laser are pointed out, and the problem, which should be solved in the near future, is also described.

Keywords: Diode laser; Spectroscopy; Chromatography

1. Introduction

A laser is used in the detection of even single atoms and molecules, because of its good monochromaticity and good beam focusing capability. A laser is, however, expensive and has some difficulties in operation and maintenance. Therefore, a laser is used only in specific fields of practical application. In 1962, 2 years later from the invention of a Ruby laser, a diode laser was reported by Nathan et al. [1]. An infrared laser made of Pb salts (e.g. $Pb_{1-x}Sn_xSe$ or $Pb_{1-x}Sn_xTe$) has been developed for use in atmospheric monitoring of the environmental pollutants, but it requires liquid helium in its operation. Thus it has not been widely used in practical applications.

Recently, many types of diode lasers emitting in the near-infrared or far-red region are developed for use in a bar-code reader, a compact disk, and a laser printer. At present, such a diode laser can be conveniently used, similarly to a light-emitting diode, thus allowing the use in practical applications. Due to low cost, compactness, tunability, stable output power, long lifetime, and easy operation and maintenance, it has been used successfully in analytical spectroscopy. Various types of analytes, which have an absorption band in the near-infrared region, are measured by absorption-based spectrometry such as conventional absorption spectrometry, photoacoustic spectrometry, and thermal lens spectrometry.

* Tel.: +81 92 6423563; fax: 81 92 6325209; e-mail: imasaka@cstf.kyushu-u.ac.jp

0039-9140/99/$ - see front matter
PII S0039-9140(98)00244-6

Fluorescence spectrometry is more advantageous, because of low or negligible background signal. Detectability can be substantially improved by best use of good monochromaticity and good beam focusing capability of the laser. However, near-infrared fluorometry has seldom been studied, therefore a new protocol for analytical procedure should be investigated, e.g. development of labelling reagents and dye-labelled antibody for immunoassay. In practical trace analysis, the sample contains many chemical species, and then a separation technique such as high-performance liquid chromatography and capillary electrophoresis is suggested to be combined.

A diode laser is also employed successfully in atomic spectrometry, because of fine tunability of the diode laser. The emitting wavelength of the hollow cathode lamp is fixed, and it is difficult to measure the background signal. A frequency-modulation technique, which can easily be accomplished in diode laser spectrometry, allows background subtraction and thus provides better detectability. Doppler-free measurements have already been performed. Unfortunately, only several electronic transitions of atoms are available in the near-infrared region. Then, the sample is discharged to form metastable atoms or ions and is measured by optogalvanic spectrometry. The detectability can be further improved by using a plasma current modulation technique. For further expansion of the application field, it is possible to convert the laser wavelength into the ultraviolet region by harmonic generation.

Diode laser spectrometry, however, has several disadvantages as well, i.e. low pulse energy and limited tunability of the laser and a poor labelling efficiency for the dye emitting in the near-infrared region. Thus, further studies of diode laser spectrometry is required for its practical use in analytical spectroscopy.

2. Structure and characteristics of diode laser

2.1. Structure and wavelength

When positive and negative potentials are applied to p-type and n-type semiconductors forming clad layers, electrons and holes are injected into the boundary. Due to a population inversion, strong stimulated emission occurs in the active channel of the waveguide. The emission wavelength depends on the band gas of the semiconductor, which is affected by the composition of the materials used. Table 1 shows the emitting wavelengths of the diode lasers commercially available. The wavelengths are restricted in the near-infrared and far-red regions. Recently, diode lasers emitting in the yellow, green, and blue regions have been developed. They are, however, not commercialized yet, probably due to a short lifetime of the device.

2.2. Frequency tuning and mode hopping

A diode laser is usually operated in a single transverse mode except for a high-power devise frequently used as a pump source for a solid-state laser. The cavity length of the diode laser is several hundreds of microns and the separation of the longitudinal mode is 0.1–1 nm. Thus it is possible to measure the spectrum of the longitudinal modes even by using a low-resolution monochromator. A diode laser operated in a single longitudinal mode is also commercially available. A distributed-feedback diode laser has been developed, in which a periodical structure is constructed in the semiconductor to fix the emitting wavelength determined by its periodicity. The wavelength of the diode laser can be slightly tuned by changing the cavity length, which is accomplished by changing the temperature and/or the injection current of the diode. The spectral bandwidth is very narrow, which is in the order of several megahertz or less. However, it should be careful about mode hopping in the

Table 1
Composition of the semiconductor material and emitting wavelength of laser

Composition	Emitting wavelength (nm)
AlGaInP	630, 670, 680, 690
AlGaAs	780, 830
InGaAs	980
InGaAsP	1310, 1480, 1550

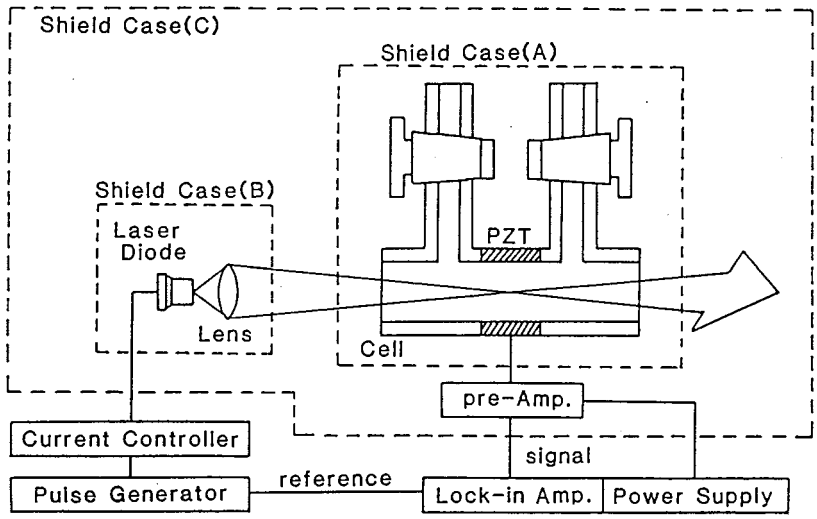

Fig. 1. Experimental apparatus for diode-laser-based photoacoustic spectrometry.

operation. The emitting wavelength of the specific longitudinal mode can be shifted only a limited extent. The output power decreases, and a different longitudinal mode appears and can be tuned in the slightly different region. The overall tuning range is wide (e.g. > 30 nm), but the tuning range of the single longitudinal mode is limited (e.g. < 1 nm). The polarization of the output beam is parallel to the direction of the hetero-junction, and the polarization ratio is usually several hundred.

2.3. Output characteristics

Due to a narrow channel of the waveguide, the laser beam diverges with an angle of 10–20° by diffraction. Then, it is necessary to collimate the beam using a lens with a large numerical aperture such as a microscope objective or a non-spherical plastic lens designed for this purpose. The output power of the small-frame single-mode diode laser is typically 3–40 mW, though a large-frame multimode laser exceeding 10 W is already commercialized. The laser power is usually monitored by an integrated photodiode whose output is used for feedback control of the laser power. It is possible to stabilize the output power to a noise level $< 0.001\%$. The response of the laser diode is very fast, and it is possible to operate at a repetition rate of several gigahertz. The pulsewidth can be reduced to several tens of picoseconds or less. The lifetime of the diode laser depends on the condition used. The value is estimated to be 10^3 h^{-1} for a device used for general measurements and 2.4×10^4 h^{-1} for data communications. When a diode laser is deteriorated, a bright spot disappears and the spectral bandwidth becomes broad. Thus it is easily recognized by looking at the projected pattern on a white paper with the naked eye.

3. Molecular spectrometry

3.1. Absorption-based spectrometry

The first study of near-infrared diode laser spectrometry was published in 1983; to my knowledge, the spectrometric work was reported earlier than the spectroscopic work [2]. Since no analytical sample, which is fluorescent in the near-infrared region, was known, the first experiment was performed by absorption-based spectrometry. Phosphorus, which is known as an environmental pollutant, was measured by the molybdenum blue method, in which a complex of molybdenum and phosphorus having an absorption band at 800 nm was measured by photoacoustic spectrometry with a diode laser emitting at 818 nm (5 mW) using an instrument shown in Fig. 1. In this preliminary

work, this method was neither sensitive nor practical. In fact, the diode laser was destroyed in several minutes, since it should be operated above the specification given by the manufacturer. Otherwise, no signal was observed even for the sample with an absorbance of unity. On the other hand, a significantly better result was obtained based on conventional absorption spectrometry using a light-emitting diode [3].

3.1.1. Absorption spectrometry

As described, the output power of the diode laser can be regulated, and the noise level is greatly reduced. Then, a straightforward application of a diode laser to absorption spectrometry provides a simple and sensitive means for trace analysis [4] and has been applied to flow injection analysis [5] and slab-gel electrophoresis [6]. Direct and indirect absorption schemes are employed for monitoring effluents in capillary electrophoresis [7,8]. A long capillary cell is useful for enhancing the detectability by a factor of ten [9,10]. The detectability can be improved by measuring intracavity absorption, providing a minimum absorbance of 10^{-4} for a condensed phase sample [11]. This approach is further used for detection of the analyte in column liquid chromatography [12]. The approach based on absorption spectrometry is used for monitoring gases (e.g. NH_3 and NO_2) in the atmosphere [13–17]. The minimum detectable pressure of pure NO_2 is 0.1 μbar with 2 m absorption path-length, corresponding to an absorbance of 10^{-6} [17]. The moisture is also measured by this method [13,18]. A frequency modulation technique greatly improves the detectability especially for the sample in the gas phase, since it has a very narrow spectral feature. Water vapor is monitored using a 2.5 mW distributed-feedback diode laser emitting at 1.3 μm [19]. A minimum detectable absorption of 5×10^{-7} is achieved. Similarly, sensitive and fast detection of NO_2 is accomplished by measuring the phase shift in high-frequency heterodyne spectrometry [20]. A minimum NO_2 absorption of 10^{-6} is measured with an effective bandwidth of 6 Hz.

3.1.2. Photoacoustic spectrometry

Since the detectability in conventional absorption spectrometry is determined by the stability of the light source, it is difficult to improve the detectability by increasing the output power of the laser. Thus the spectrometric methods measuring the heat generated by absorption of laser radiation have been suggested to be employed. A possible approach is photoacoustic spectrometry, as described [2]. Phosphate ions are concentrated on a membrane filter as molybdophosphate-*n*-dodecyltrimethylammonium bromide and are measured by placing it in a solid-phase photoacoustic cell [21]. The detection limit of PO_4^{3-} is reported to be 3 ng ml^{-1}. Photoacoustic spectrometry is also used for trace-gas monitoring [22]. The detection limit reported for ammonia is 24 ppt ($S/N = 3$). Solid suspended particles (carbon) are measured by photoacoustic spectrometry [23].

3.1.3. Thermal lens spectrometry

Another approach for absorption-based spectrometry might be thermal lens spectrometry. When phosphorus is measured directly in the aqueous phase based on the heteropolyblue method, the detection limits are 3.3 and 1 ppb in the single and dual beam experiments, respectively. When the sample is measured after solvent extraction into 2-butanol, the detection limits are improved to 0.3 ppb for both the methods, which corresponds to an absorbance of 2×10^{-4} [24]. Iron (II) is also determined with 2-nitroso-5-diethylaminophenol [25]. A cross-beam experiment is performed using a high-power diode-array laser [26]. In order to simplify the analytical instrument, optical fibers are used for light introduction and transmission in the measurement [27].

3.2. Fluorescence spectrometry

Photothermal diode laser spectrometry is useful for sensitive detection of the analyte absorbing the near-infrared emission. However, it requires a high-power laser source to improve the detectability; the detection limit is similar to that of absorption spectrometry when a 1 mW laser is used as a light source, though it strongly depends on the experimental conditions used, e.g. solvent, tem-

perature, etc. On the other hand, the analyte can be measured at ultratrace levels by fluorometry using a low-power laser source with an output power of several milliwatts. Thus fluorometry is more advantageous in trace analysis. However, no fluorescent molecule having an absorption band in the near-infrared region was known, except polymethine dyes currently used as laser dyes which are strongly fluorescent in the near-infrared region (600–1000 nm); see Fig. 2 for the chemical structures of the polymethine dyes. Therefore, diode laser fluorometry was first applied to polymethine dyes [28]. It was pointed out that the detection limit (8×10^{-12} M) was two orders of magnitude better than the value obtained by a conventional fluorometer. The high detectability is partly due to a low blank signal arising from the fact that very few organic compounds are fluorescent in the near-infrared region.

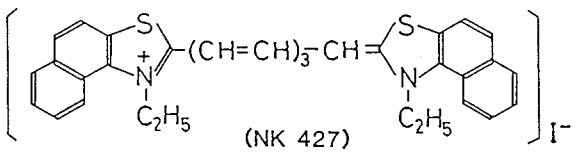

(NK 427)

3,3′-diethyl-2,2′-(4,5,4′,5′-dibenzo) thiatricarbocyanine iodide

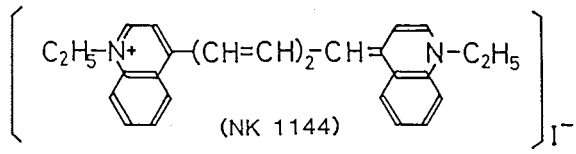

(NK 1144)

1,1′-diethyl-4,4′-quinodicarbocyanine iodide

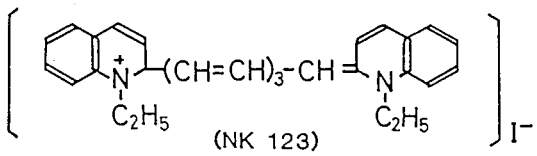

(NK 123)

1,1′-diethyl-2,2′-quinodicarbocyanine iodide

Fig. 2. Chemical structures of polymethine dyes.

3.2.1. Detectability

Due to a good beam focusing capability of the laser, a small detector with a nanoliter or picoliter volume can be constructed. A small number of molecules, e.g. 8000, has been detected [29,30]. In order to remove unwanted fluorescence from cell walls, a liquid jet is used as a flowing cell [31,32]. The detection limit is reported to be 3000 molecules. This value is inferior to the work using an argon ion laser by over three orders of magnitude, which is partly due to lower photomultiplier photocathode and fluorescent dye quantum efficiencies. Recently, single molecules are detected by observing photon bursts using an avalanche photodiode with a higher quantum efficiency [33]. It is noted that a diode laser is already integrated in a commercial fluorescence spectrometer and is used for practical works [34–36].

3.2.2. Fluorescent dyes and their applications

Most analytical samples are nonfluorescent in the near-infrared region, therefore diode laser fluorometry cannot be applied directly. Thus it is necessary to develop an analytical procedure to measure the analyte using a near-infrared dye. The first analytical work demonstrated is ion-pair solvent extraction of a negatively-charged surfactant with a positively-charged near-infrared dye to an organic phase and succeeding measurement of the fluorescence intensity by diode laser fluorometry [28,37]. Such an experiment is also carried out using a far-red diode laser [38]. By making a survey of research, fluorescence of indocyanine green, a water-soluble near-infrared dye, was found to be quenched by hydrogen peroxide (H_2O_2) in the presence of a transition metal which acts as a catalyst; the experiment was successful only when the water used in the experiment was purified by a distiller made of metal and was unsuccessful when purified further by passing the water through an ion exchange column and by doubly-distilling with a distiller made of glass, indicating that impurity metal is essential in this protocol (see the reference for details) [39]. This approach is combined with the following enzymatic assay producing hydrogen peroxide:

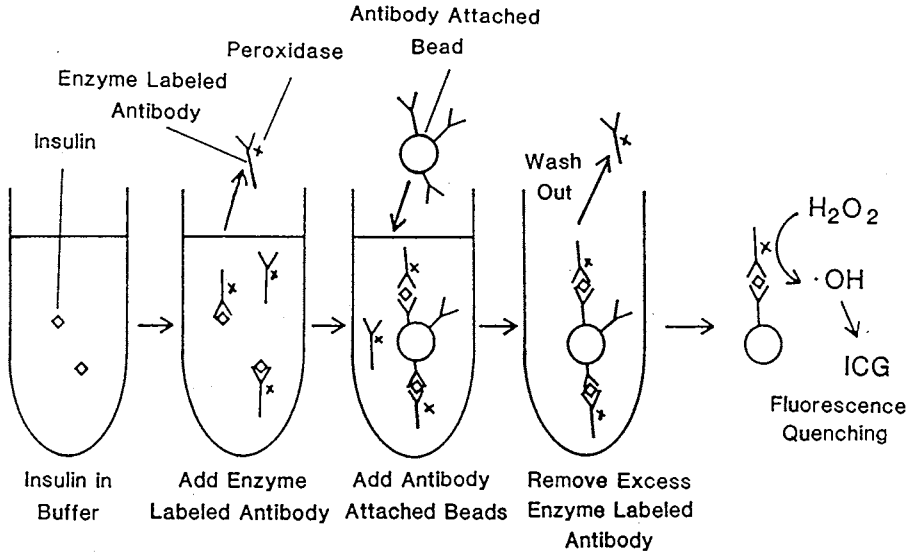

Fig. 3. Procedure for enzyme-linked immunoassay of insulin using indocyanine green (ICG).

$$\text{xanthine} + O_2 + H_2O \xrightarrow{\text{xanthine oxidase}} \text{uric acid} + H_2O_2 \quad (1)$$

A calibration graph for xanthine is constructed in the range from 5×10^{-5} to 5×10^{-7} M. This analytical system is further combined with enzyme immunoassay of insulin by the scheme shown in Fig. 3 [40]. The detection limit reported is 10 μunit ml^{-1}.

It is possible to use different types of fluorescent dyes when a diode laser emitting at 670 or 630 nm is used. For example, rhodamine, oxazine, and thiazine dyes (see Fig. 4 for their chemical structures) can be used for labelling protein molecules using a bifunctional reagent such as water-soluble carbodiimide [41]. Some of the dyes are already used in practical applications. For example, methylene blue is employed for the determination of ethanol using dehydrogenase. This protocol has been used in diode laser fluorometry [42]. Protein is also measured based on a fluorescence immunoassay [43–45]. For example, a near-infrared dye is derivatized with an isothiocyanate functional group and is conjugated to goat anti-human immunoglobulins. After purification by column chromatography, the conjugate is used in an immunoassay to detect human immunoglobulins [43]. Solutions of human immunoglobulin with concentrations as low as 10^{-10} M have been measured with a minimum of interference [45].

The fluorescence nature of the dye is changed, when it is bound on the surface of protein. Thus the binding constant of the near-infrared dye to bovine serum albumin is evaluated by fluorescence spectrometry [46]. Fluorescence characteristics are changed, depending on concentrations of DNA [47,48], O_2 [49], and pH of the solution [50], and diode laser fluorometry is used for monitoring these species. Fig. 5 shows a schematic illustration of PVC-bound Oxazine 750 dye, which is employed as a sensor reversibly responsive to potassium ion concentration in the range from 10^{-3} to 10^{-1} M [51]. The selectivity coefficient for sodium ion is reported to be 2×10^{-3}. Native fluorescence of chlorophyll (685 or 730 nm) is directly measured using a diode laser emitting at 635 nm for the purposes of plant physiology and stress detection [52].

3.2.3. Time-resolved fluorometry

The response of the diode laser is very fast, and then short highly-repetitive pulses can be generated. This is desirable for the application to time-resolved fluorometry, especially in time-correlated

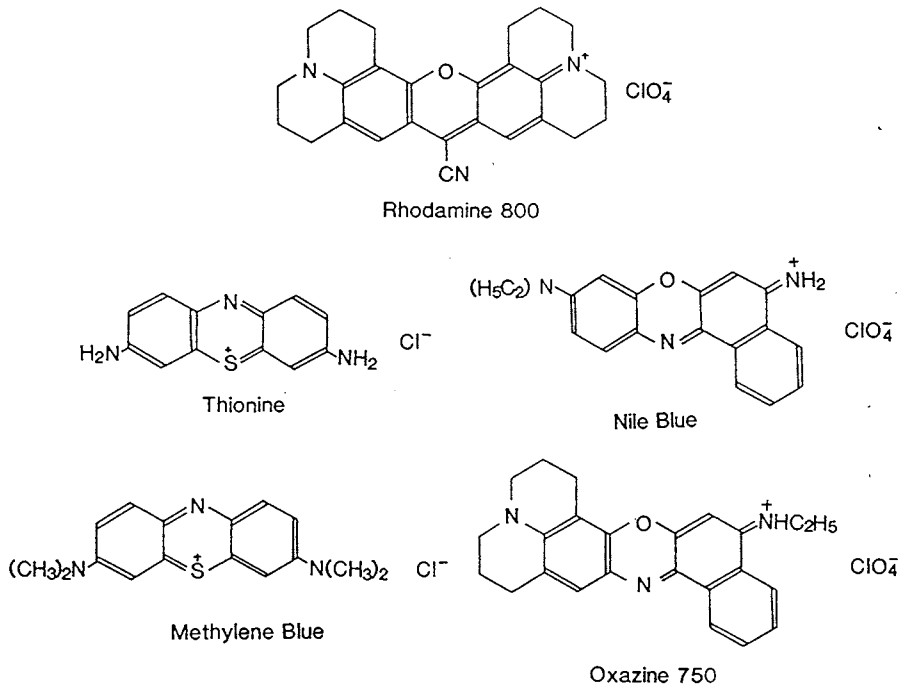

Fig. 4. Chemical structures of far-red dyes.

photon counting. Such an instrument is first applied to lifetime measurements of the polymethine dyes dissolved in various solvents, and the observed value is correlated with the polarity of the solvent [53]. In order to improve the time resolution, a single-photon avalanche photodiode is used for fluorescence detection, and the time resolution is improved to 275 ps [54]. This analytical instrument is used for dynamic lifetime measurements in DNA sequencing. An avalanche photodiode is also useful to improve the detectability, and the fluorescent bursts of individual antibody molecules labelled with single dye molecules are detected and identified by characteristics fluorescence lifetimes of the dyes [55]. The tumor marker mucine is detected in neat human serum by single-molecule events. Phase fluorometry is also demonstrated using a continuously-modulated laser diode [56].

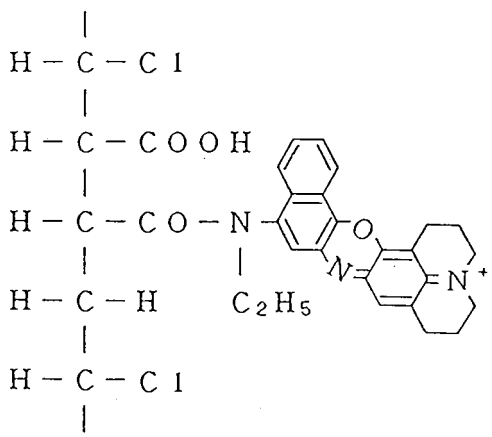

Fig. 5. Structure of optical fiber sensor for potassium ion.

3.2.4. Combination with separation technique

Diode laser spectrometry is very sensitive but has limited selectivity, which is attributed to poor tunability of the diode laser. Thus additional selectivity is needed, e.g. by a combination with a separation technique such as chromatography. The first study is the separation of near-infrared dyes by ion-pair liquid chromatography [57]. Similar work is performed for aluminum phthalocyanine photosensitizers giving strong fluorescence in

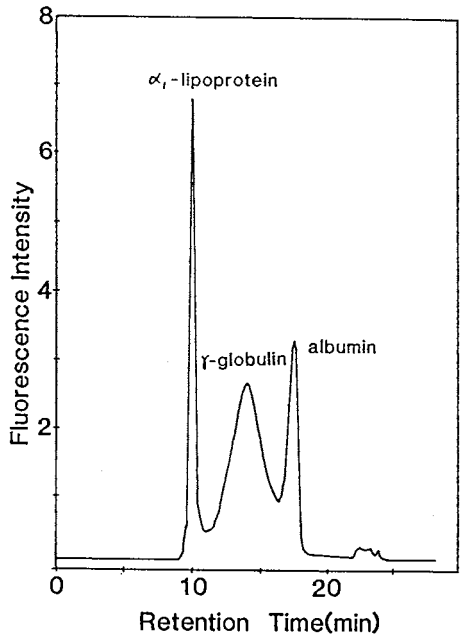

Fig. 6. Chromatogram for protein in human serum measured by diode laser fluorometry.

the far-red region [58]. A chromatogram of protein contained in human serum is shown in Fig. 6, in which indocyanine green is used as a labelling reagent [59]. This reagent becomes fluorescent when physically bound on protein, and then protein is detected as a signal enhancement of the fluorescence. Indocyanine green is also used as a marker in clinical research to measure hepatic blood flow and cardiac output. Then, diode laser fluorometry is used for the quantitation of indocyanine green in plasma [60]. A far-red dye such as Oxazine 750 is covalently bound with amino groups of protein and is detected after separation by liquid chromatography [41]. Similarly, Nile blue is combined with phenylacetic acid in plasma through an amino linkage in the presence of 2-chloro-1-methylpyridinium iodide (carboxylic acid activator) and triethylamine (base catalyst). The limit of derivatization of phenylacetic acid is reported to be 10^{-9} M in phosphate-buffered saline [61]. As shown in Fig. 7, various types of dyes have already been synthesized for labelling biological molecules and some of them are already commercially available. Amino acid, thiols, and carboxylic acids are labelled with far-red dyes and are measured by liquid chromatography. The detection limits are 10^{-12} M levels (several tens of amol) for labelled compounds and 10^{-9}–10^{-8} M levels for the analyte, the latter of which is limited by the reactivity of the labelling reagent [62–65]. Indirect fluorometry is applied to the sample having no absorption band in the near-infrared and far-red regions [65,66]. Limits of detection for *n*-alkyl alcohols are in the order of 10^{-8} mol injected. The application of diode laser fluorometry to liquid chromatography is reviewed elsewhere [67,68].

The dimension of the liquid chromatograph detector is typically 1 mm i.d., 10 mm long. An incoherent light source such as a xenon arc lamp can be focused efficiently into this volume. The output power of the light passed through a monochromator is several milliwatts, when the slit width is adjusted to give a spectral bandwidth of 10–30 nm. Thus diode laser fluorometry is advantageous, when it is applied to the detector whose volume should be reduced to nanoliter levels. Recently, capillary electrophoresis and capillary micellar electrokinetic chromatography have been developed for better separation of the sample. However, these analytical methods require a narrow (ca. 50 μm) capillary for sample separation and a detector with a nanoliter or picoliter volume. Otherwise, a chromatogram would be severely degraded. Thus laser fluorometry is advantageous in such separation techniques. At the time of the first preliminary study, no labelling reagent was available. Then, the reagent having a succinimidylester group to react with an amino group was synthesized from a far-red dye, i.e. Azur B, which was combined with mercaptoacetic acid using a bifunctional reagent and succeeding to *N*-(e-maleimidocaproyloxy)succinimide (EMCS) to bind with an amino group. Unfortunately, no purified reagent was obtained, probably due to poor skill in organic synthesis. However, the researcher tried to react amino acids with a trace amount of labelling reagent suspected to be present in the final solution. The electropherogram obtained is shown in Fig. 8 [69]. Labelled arginine and glycine are clearly observed, though

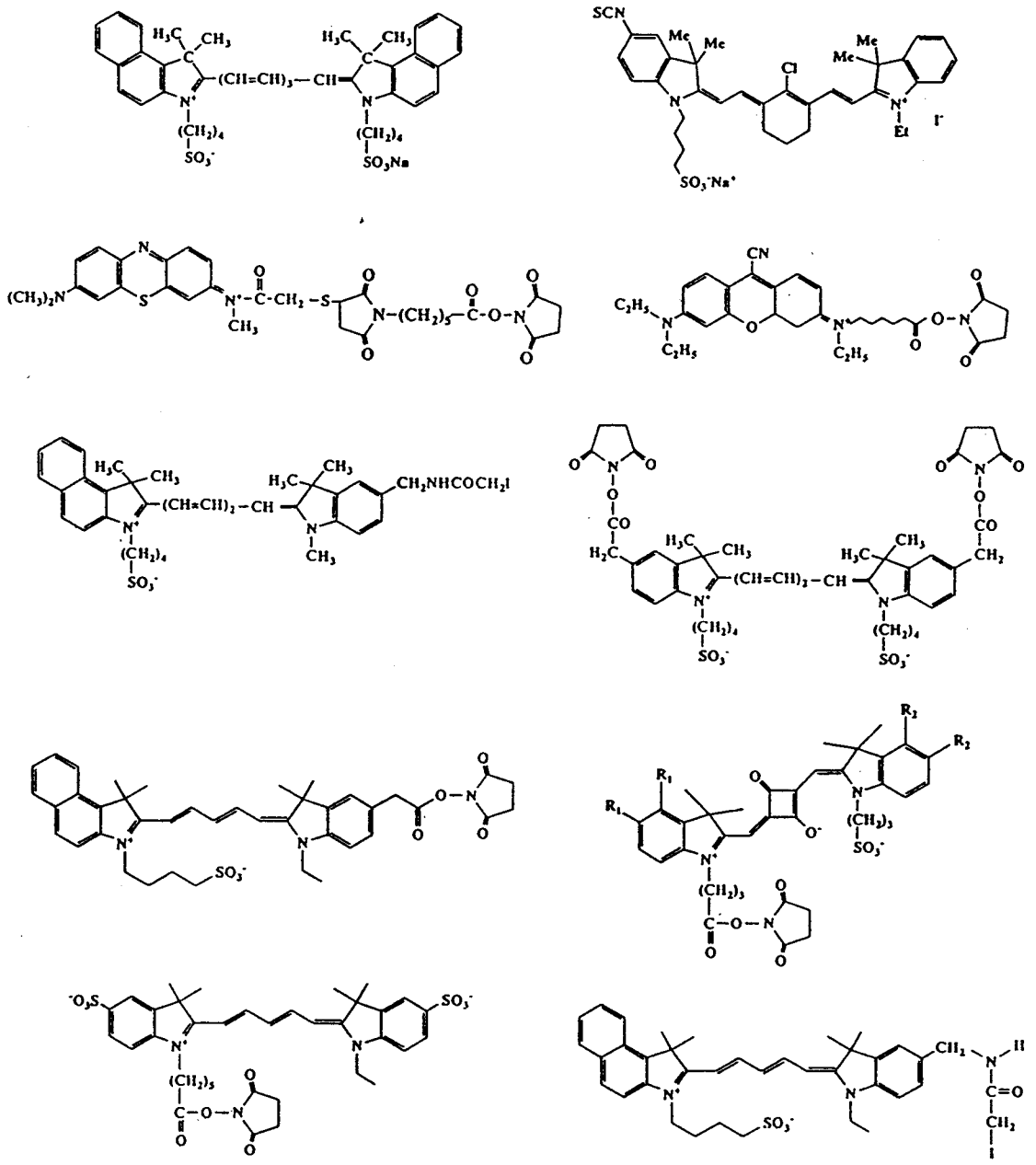

Fig. 7. Labeling reagents developed for near-infrared and far-red fluorometry.

a very large peak, probably arising from side reaction products, appears.

Many labelling reagents have been developed and commercialized until now. For example, a compound of 9-cyano-*N*,*N*,*N*′-triethyl-*N*′-triethyl-*N*′-(5′-succinimidyloxycarbonylpentyl) pyronine is synthesized and used for labelling amino acids. The detection limit of the labelled amino acids are reported to be subattomole levels (800 zmol for glycine) [70]. This labelling reagent is also used for labelling protein [71]. In more sophisticated works, a detection limit of 5×10^{-11} M (0.1

amol) is achieved for labelled glycine [72]. Due to limited reactivity of the succinimidyl ester functionality, the analytes are, however, derivatized at a concentration of 10^{-6} M in aqueous solutions. An oligonucleotide labelled with a far-red dye, named Cy5, is synthesized and used for DNA sequencing [73]. The detection limit achieved with a 2.5 mW far-red diode laser is about 10^{-10} M. Diode laser spectrometry is also applied to DNA oligonucleotides developed on the gel plate for DNA sequencing [74]. A specific DNA fragment is recognized by a hybridization reaction with a DNA fluorescent probe and is detected after separation by free-solution capillary electrophoresis [75]. In order to enhance the detectability, a photomultiplier is replaced with an avalanche photodiode [76]. Time-resolved laser fluorometry is used for sample detection in capillary electrophoresis [77].

Many analytical samples have no functional group for derivatization. In this case, it is suggested to use indirect spectrometry. Flavin adenine dinucleotide and deoxyadenosine monophosphate are measured by micellar electrokinetic chromatography using methylene blue as a visualizing reagent [78]. The response mechanism is illustrated in Fig. 9 [79]. The fluorophore is replaced with the analyte on the surface of the micelle, and the fluorescence intensity decreases. Thus the analyte is detected as a negative peak from the baseline level. Aromatic amines and nitrocompounds are also separated and detected indirectly at millimolar levels [79]. The application of diode laser fluorometry to capillary electrophoresis and micellar electrokinetic chromatography is reviewed elsewhere [80].

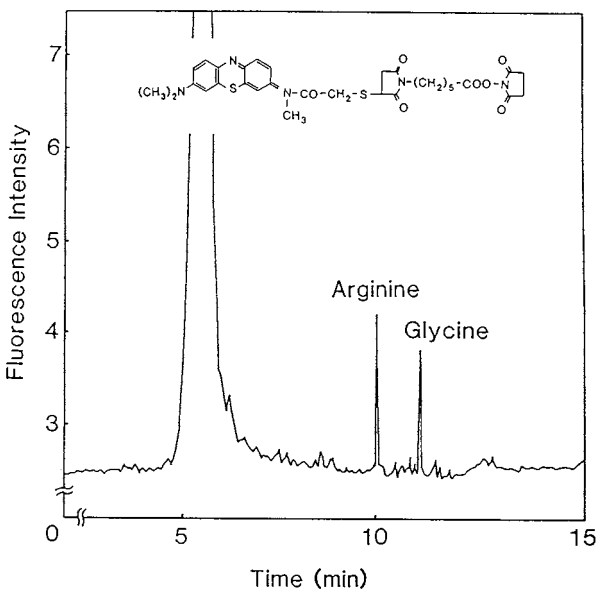

Fig. 8. Electropherogram of amino acids measured by diode laser fluorometry. The chemical structure of the labeling dye is shown in the figure.

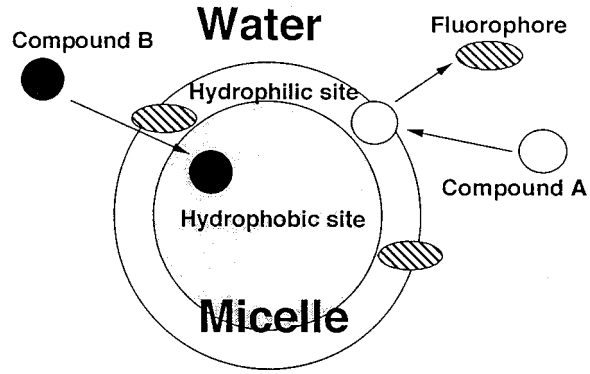

Fig. 9. Schematic illustration for the mechanism of indirect sample detection using Oxazine 750 as visualizing reagent.

3.3. Other spectrometric methods

Several other diode laser spectrometries have been reported. Some of them are based on the detection of refractive index change [81–84]. Good beam pointing stability and stable output power of the diode laser are preferential in this application. Refractive index change can generally be used for detection of the analyte whose refractive index is different from the solvent. This approach is used for the detection of polymers in size-exclusion chromatography. The detection limit is reported to be 4×10^{-9} RIU. The mass detection limit is 540 pg (1.1 fmol), which corresponds to 0.9 ppm or 2.4 nM injected [85]. This approach is also employed for measurements of low-nanogram quantities of carbohydrates [86]. A new type of approach, hologram-based refractive index detector, is applied to capillary electrophoresis [87].

Polarimetry is useful for the measurement of optically-active substances and is applied to enantiomeric determination after separation by liquid chromatography [88,89]. The detection limit is in the 0.02–10 mg ml^{-1} range. Magneto-optical rotation is also employed as a universal on-line detector in liquid chromatography [90,91].

It is well known that a laser is essential in Raman spectrometry. However, high capital, operation, and maintenance costs restrict its wide applications. In addition, background fluorescence, which decreases with increasing the wavelength of the laser source, should be carefully minimized. Though a Nd: YAG laser emitting at 1.06 μm is sometimes used to reduce the background, all the detectors are insensitive in the spectral region above 1 μm. A diode laser is used as a light source in Raman spectrometry and is combined with a monochromator equipped with a charge-coupled device sensitive in the near-infrared region [92,93]. This approach reduces the background fluorescence and improves the detectability, and allows instantaneous spectrometric measurements. Surface-enhanced Raman spectrometry is also demonstrated using a diode laser [94].

Analytical applications of a diode laser to molecular spectrometry are reviewed elsewhere [95–103].

4. Atomic spectrometry

In conventional atomic spectrometry, a hollow cathode lamp is employed, because of a simple structure and a narrow spectral linewidth. The emitting wavelength is determined by the electronic transition of the element filled in the lamp, which is exactly identical to the absorbing wavelength of the element to be measured. The linewidth is several hundred megahertz, which is determined by the temperature and pressure of the gas filled in the lamp. Since the emitting wavelength is fixed, and, as a result, it is difficult to subtract the background signal by recording the absorption spectrum. A diode laser has significantly higher light intensity, narrower linewidth, more stable output power, and smaller dimension. Thus, the diode laser has preferred characteristics for application to atomic spectrometry. Moreover, the tunability of the diode laser provides an opportunity for frequency modulation spectrometry, allowing background subtraction and thus detection of the analyte at lower concentrations. The narrow linewidth of the laser opens the possibility for Doppler-free spectrometry, providing better spectral selectivity.

4.1. Absorption spectrometry

The first application of a near-infrared diode laser to atomic spectroscopy was, to my knowledge, reported in 1983. This paper is entitled 'Laser spectroscopy on a shoestring' [104]. A single-mode AlGaAs diode laser emitting at 794.7 nm is used for spectral measurements of Rb (D_1; $5^2S_{1/2}-5^2P_{1/2}$ transition) in an atomic beam, and the isotope shift between ^{87}Rb and ^{85}Rb is reported to be 81.4 ± 5.0 MHz. The detection limit of the Rb vapor measured in the graphite furnace is reported to be 2.1 pg [105]. Diode laser spectrometry is also applied to the evaluation of the absolute density of Rb in a reservoir cell and in a flame [106]. The determination of the isotope ratios of Ba by laser-enhanced-ionization Doppler-free two-photon ($791 + 821$ nm) laser spectroscopy [107], observation of quantum beat echoes in the Cs vapor (D_1 transition; wavelength is not specified) [108], and high-resolution saturated-absorption optical-heterodyne detection spectrometry of Ca (657 nm) [109] are reported.

4.2. Optogalvanic and other spectrometries

The number of atomic transitions in the near-infrared region is very limited, which makes the practical application of a diode laser to atomic spectrometry difficult. The transition from a metastable level, however, frequently occurs in the near-infrared region. Thus the sample is discharged to form metastable atoms (or ions) and the transition to a higher energy level is measured by monitoring the electric current of the discharge. This spectrometric technique is called optogalvanic spectrometry. A diode laser is employed for detections of noble gases and ac-

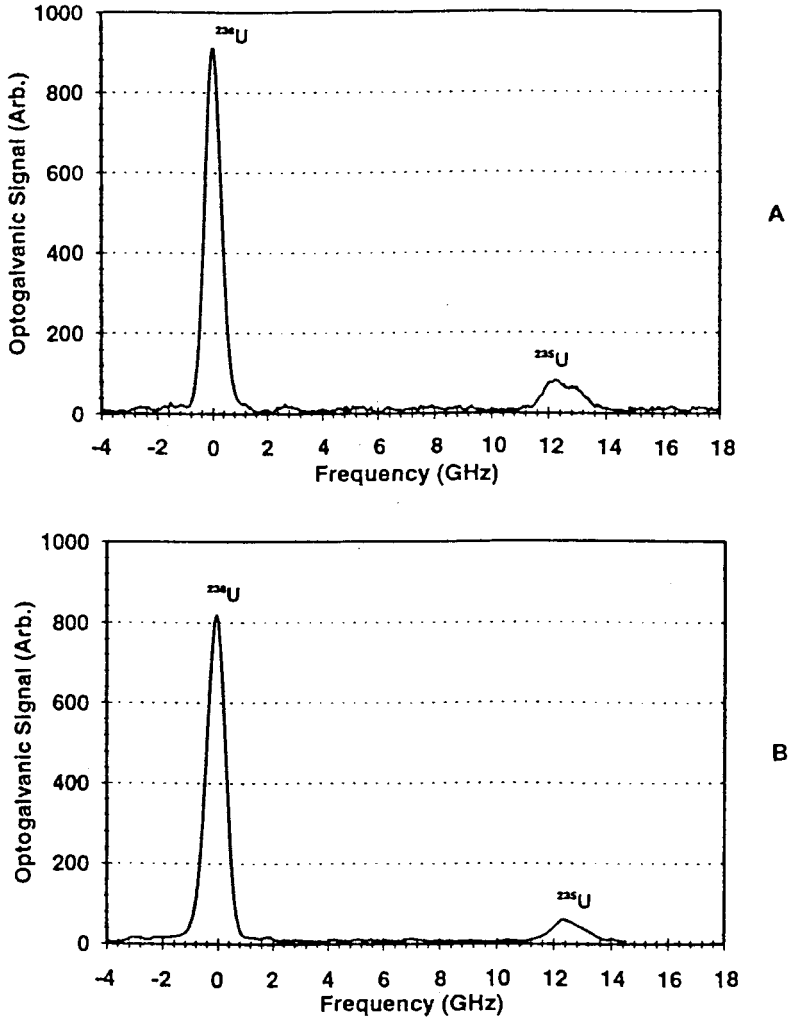

Fig. 10. Optogalvanic spectra recorded for enriched uranium sample. Exciting source; (A) Ti: sapphire laser (B) diode laser: emitting wavelength: 776.19 nm.

tinide atoms [110–112]. Fig. 10 shows the optogalvanic spectra for an enriched uranium sample (9.97% ^{235}U) [112]. The isotope peaks are clearly resolved, and the isotope ratio can readily be determined. Frequency change of plasma wave in low-pressure discharges, which arises from ion density variation by resonant laser excitation, is used for sensitive and selective detection of the impurities in the plasma [113] and is also applied to the detector for gas chromatography [114]. Chlorine atoms occurred by discharges of chlorinated hydrocarbons in oil and chlorophenols in plant extracts and are measured based on atomic absorption spectrometry using wavelength-modulated laser diodes and current-modulated plasmas [115]. Absorbances as low as 10^{-7} are measured, and the detection limit for tetrachlorophenol in a plant extract is found to be ca. 30 ng ml^{-1}. A diode laser (754 nm) is also used in the initial optical transition of La, which is followed by two-color resonance ionization [116].

The construction of the diode lasers with and without an external cavity consisting of a grating and their operation characteristics are reported

elsewhere [117,118], which may be useful as introductory references for the researchers who wish to start diode-laser-induced atomic spectrometry. The reader may also refer to the review papers published elsewhere [118–120].

5. Use of second harmonic emission

Though the tunable range of the diode laser is limited, it can be extended by second harmonic generation. The first analytical study of the frequency-doubled diode laser is the application to an optical fiber sensor for oxygen [121].

Now, frequency-doubled diode lasers are commercially available and have been used as light sources in fluorometry combined with capillary electrophoresis and micellar electrokinetic chromatography. Polycyclic aromatic hydrocarbons are directly measured [122,123], and amino acids are determined after labelling with a coumarin succinimidylester having an absorption band at 437 nm [69]. The output power is limited to 0.05–0.1 mW, but the amount detection limit is reported to be comparable to those obtained by the chromatograph detector using a conventional laser source. Recently, the laser power has been enhanced to 0.5 mW using a KTP waveguide [124], which is larger than the optimum output power (0.3 mW) determined by photobleaching of the labelling dye. The blue output beam (424 nm) is suitable for excitation of naphthalene-2,3-dicarboxaldehyde (NDA). Various amino acids in body fluids are labelled and measured, and the detection limits are reported to be 0.9 amol.

Second harmonic emission of the diode laser is also used in atomic spectrometry. A frequency-doubled external-cavity-diode-laser source emitting at 394 nm is employed for measurements of Al vapor density by atomic absorption spectrometry and is suggested to be used for monitoring the elements in physical vapor deposition processes [125]. Second harmonic emission is generated in a diode laser device itself. The output power is picowatt levels, but it is sufficient for application to atomic absorption spectrometry [126] and also to molecular fluorescence spectrometry [127]. A fluorophore of 8-hydroxy-1,3,6-pyrenetrisulfonic acid can be detected at 10^{-6} M levels and is used as a pH indicator in neutralization titration.

6. Future works

A diode laser has various advantages as a light source in spectrometry. However, it also has disadvantages: (1) the pulse energy is generally small, which arises from a small active volume of the diode laser. Thus it is difficult to use in multiphoton ionization spectrometry: (2) the tunable range of the diode laser is very limited, which originates from a lack of efficient semiconductor materials emitting in the visible and ultraviolet regions. Several approaches are proposed to solve these problems. For example, a multi-mode high-power diode laser is used as a pump source for a solid-state laser such as an Nd: YAG laser. Due to a large active volume of the solid-state laser, a large pulse energy can be generated. A frequency-multiplied Nd: YAG laser is used as a pump source for an optical parametric oscillator. By frequency doubling and mixing of the output, the spectral region can, in theory, be covered from the ultraviolet to the infrared using a single optical system. A similar laser system will be constructed using a high-power continuous-wave Nd:YAG laser pumped by a high-power diode laser. Such a widely tunable laser might be developed in the near future and will be used practically in the studies of high-resolution spectrometry of atoms and molecules at trace levels. The dimension of the laser system can be substantially reduced and may be conveniently used in analytical spectroscopy.

The above high-performance laser system can be used in various applications, but the system is rather complicated, increasing the cost of the analytical instrument. Thus the development of a simpler and more straightforward approach has been suggested, in which diode laser spectrometry can be used in routine works, e.g. in biological assay. Diode laser fluorometry is very sensitive, and a labelled biological molecule can be detected at 10^{-12} M levels. However, the analyte molecule should be labelled at concentrations of 10^{-6}–10^{-7} M, due to poor reactivity of the reagent.

Generally, a near-infrared dye has a large conjugated bond, and, as a result, a large molecular size. Thus the reactive site is sometimes surrounded by a chromophore group, reducing the reactivity of the reagent. Moreover, most near-infrared and far-red dyes are photosensitive and are easily decomposed under strong irradiation of the light. Unfortunately, many decomposition products occur, making the assignment of the peaks difficult in chromatography and electrophoresis. Thus development of a new labelling reagent giving a high labelling efficiency, a long storage lifetime, and no side-reaction product is desirable for practical trace analysis.

Due to limited tunability of the diode laser, it has been suggested to use it for specific purposes. The sizes and the power consumption rates of the diode laser and the avalanche photodiode are very small. Moreover, the electricity for a high-voltage power supply and the amount of solvent used in capillary electrophoresis are small. Therefore, capillary electrophoresis combined with diode laser/avalanche photodiode spectrometry may be advantageously used in the field works.

I am convinced that diode laser spectrometry will be widely used in routine works probably in the next 10 years. For successful works, analytical chemists are requested to do cooperative works with organic chemists and biochemists. In such cooperative works, analytical chemists will be able to have opportunities for further successes in the development of diode laser spectrometry to open a new frontier in advanced technologies.

References

[1] M.I. Nathan, W.P. Dumke, G. Burns, F.H. Dill Jr, G. Lasher, Appl. Phys. Lett. 1 (1962) 62.
[2] Y. Kawabata, T. Kamikubo, T. Imasaka, N. Ishibashi, Anal. Chem. 55 (1983) 1419.
[3] T. Imasaka, T. Kamikubo, Y. Kawabata, N. Ishibashi, Anal. Chim. Acta 153 (1983) 261.
[4] M. Soylak, U. Sahin, A. Ülgen, L. Elci, M. Gogan, Anal. Sci. 13 (1997) 287.
[5] M.K. Carroll, J.F. Tyson, Appl. Spectrosc. 48 (1994) 276.
[6] T. Imasaka, T. Fuchigami, N. Ishibashi, Anal. Sci. 7 (1991) 491.
[7] W. Tong, E.S. Yeung, J. Chromatogr. 718 (1995) 177.
[8] S.J. Williams, E.T. Bergström, D.M. Goodall, H. Kawazumi, K.P. Evans, J. Chromatogr. 636 (1993) 39.
[9] T. Korenaga, F. Sun, Anal. Chim. 318 (1996) 195.
[10] T. Korenaga, F. Sun, Talanta 43 (1996) 1471.
[11] E. Unger, G. Patonay, Anal. Chem. 61 (1989) 1425.
[12] A.J.G. Mank, O. Larsen, H. Lingeman, C. Gooijer, U.A.Th. Brinkman, N.H. Velthorst, Anal. Chim. Acta 323 (1996) 1.
[13] M. Ohtsu, H. Kotani, H. Tagawa, Jpn J. Appl. Phys. 22 (1983) 1553.
[14] K. Chan, H. Ito, H. Inaba, Appl. Opt. 22 (1983) 3802.
[15] D.M. Bruce, D.T. Cassidy, Appl. Opt. 29 (1990) 1327.
[16] D.M. Sonnenfroh, M.G. Allen, Appl. Opt. 35 (1996) 4053.
[17] L. Gianfrani, G. Gagliardi, G. Pesce, A. Sasso, Appl. Phys. B 64 (1997) 487.
[18] R.S. Inman, J.J.F. McAndrew, Anal. Chem. 66 (1994) 2471.
[19] C.B. Carlisle, D.E. Cooper, Appl. Phys. Lett. 56 (1990) 805.
[20] W. Lenth, M. Gehrtz, Appl. Phys. Lett. 47 (1985) 1263.
[21] J. Shida, H. Takahashi, K. Oikawa, Talanta 41 (1994) 1861.
[22] M. Fehér, Y. Jiang, J.P. Maier, A. Miklós, Appl. Opt. 33 (1994) 1655.
[23] K. Kato, Bunseki Kagaku 43 (1994) 317.
[24] K. Nakanishi, T. Imasaka, N. Ishibashi, Anal. Chem. 57 (1985) 1219.
[25] T. Imasaka, K. Sakaki, N. Ishibashi, Anal. Chim. Acta 243 (1991) 109.
[26] A.C. Forteza, C.T. Más, J.M.E. Ripoll, V.C. Martín, G. Ramis-Ramos, Anal. Chim. Acta 282 (1993) 613.
[27] D. Rojas, R.J. Silva, R.E. Russo, Rev. Sci. Instrum. 63 (1992) 2989.
[28] T. Imasaka, A. Yoshitake, N. Ishibashi, Anal. Chem. 56 (1984) 1077.
[29] Y. Kawabata, T. Imasaka, N. Ishibashi, Talanta 33 (1986) 281.
[30] A.P. Larson, H. Ahlberg, S. Folestad, Appl. Opt. 32 (1993) 794.
[31] P.A. Johnson, T.E. Barber, B.W. Smith, J.D. Winefordner, Anal. Chem. 61 (1989) 861.
[32] S.J. Lehotay, P.A. Johnson, T.E. Barber, J.D. Winefordner, Appl. Spectrosc. 44 (1990) 1577.
[33] S.A. Soper, B.L. Legendre Jr, Appl. Spectrosc. 52 (1998) 1.
[34] J. Hicks, D. Andrews-Wilberforce, G. Patonay, Anal. Instrum. 19 (1990) 29.
[35] C. Wersig, W. Finke, E. Händler, H.P. Josel, E. Schmidt, SPIE 1885 (1993) 389.
[36] J.W. Silzel, R.J. Obremski, SPIE 1885 (1993) 439.
[37] M.A. Roberson, D. Andrews-Wilerforce, D.C. Norris, G. Patonay, Anal. Lett. 23 (1990) 719.
[38] T. Imasaka, H. Nakagawa, N. Ishibashi, Anal. Sci. 6 (1990) 765.
[39] T. Imasaka, T. Okazaki, N. Ishibashi, Anal. Chim. Acta 208 (1988) 325.

[40] T. Imasaka, H. Nakagawa, T. Okazaki, N. Ishibashi, Anal. Chem. 62 (1990) 2404.
[41] T. Imasaka, A. Tsukamoto, N. Ishibashi, Anal. Chem. 61 (1989) 2285.
[42] T. Imasaka, T. Higashijima, N. Ishibashi, Anal. Chim. Acta 251 (1991) 191.
[43] A.E. Boyer, M. Lipowska, J.M. Zen, G. Patonay, V.C.W. Tsang, Anal. Lett. 25 (1992) 415.
[44] R.J. Williams, N. Narayanan, G.A. Casay, M. Lipowska, L. Strekowski, G. Patonay, J.M. Peralta, V.C.W. Tsang, Anal. Chem. 66 (1994) 3102.
[45] R.J. Williams, J.M. Peralta, V.C.W. Tsang, N. Narayanan, G.A. Casay, M. Lipowska, L. Strekowski, G. Patonay, Appl. Spectrosc. 51 (1997) 836.
[46] A.J. Sophianopoulos, J. Lipowski, N. Narayanan, G. Patonay, Appl. Spectrosc. 51 (1997) 1511.
[47] T. Fuchigami, T. Imasaka, N. Ishibashi, Proceedings ICAS Kyushu Post Conference, 1991, 5.
[48] T. Imasaka, Anal. Sci. 9 (1993) 329.
[49] W. Xu, K.A. Kneas, J.N. Demas, B.A. DeGraff, Anal. Chem. 68 (1996) 2605.
[50] J.M. Zen, G. Patonay, Anal. Chem. 63 (1991) 2934.
[51] Y. Kawabata, K. Yasunaga, T. Imasaka, N. Ishibashi, Anal. Sci. (supplement) 7 (1991) 1465.
[52] P. Mazzinghi, Rev. Sci. Instrum. 67 (1996) 3737.
[53] T. Imasaka, A. Yoshitake, K. Hirata, Y. Kawabata, N. Ishibashi, Anal. Chem. 57 (1985) 947.
[54] B.L. Legendre Jr, D.C. Williams, S.A. Soper, R. Erdmann, U. Ortmann, J. Enderlein, Rev. Sci. Instrum. 67 (1996) 3984.
[55] M. Sauer, C. Zander, R. Müller, B. Ullrich, K.H. Drexhage, S. Kaul, J. Wolfrum, Appl. Phys. B 65 (1997) 427.
[56] R.B. Thompson, J.K. Frisoli, J.R. Lakowicz, Anal. Chem. 64 (1992) 2075.
[57] K. Sauda, T. Imasaka, N. Ishibashi, Anal. Chim. Acta 187 (1986) 353.
[58] A.J.G. Mank, C. Gooijer, H. Lingeman, N.H. Velthorst, U.A.Th. Brinkman, Anal. Chim. Acta 290 (1994) 103.
[59] K. Sauda, T. Imasaka, N. Ishibashi, Anal. Chem. 58 (1986) 2649.
[60] M. Gui, S. Nagaraj, S.V. Rahavendran, H.T. Karnes, Anal. Chim. Acta 342 (1997) 145.
[61] S.V. Rahavendran, H.T. Karnes, Anal. Chem. 69 (1997) 3022.
[62] A.J.G. Mank, H.T.C. van der Laan, H. Lingeman, C. Gooijer, U.A.Th. Brinkman, N.H. Velthorst, Anal. Chem. 67 (1995) 1742.
[63] A.J.G. Mank, E.J. Molenaar, H. Lingeman, C. Gooijer, U.A.Th. Brinkman, N.H. Velthorst, Anal. Chem. 65 (1993) 2197.
[64] A.J.G. Mank, M.C. Beekman, N.H. Velthorst, U.A.Th. Brinkman, H. Lingeman, C. Gooijer, Anal. Chim. Acta 315 (1995) 209.
[65] S.J. Lehotay, A.M. Pless, J.D. Winefordner, Anal. Sci. 7 (1991) 863.
[66] H. Kawazumi, H. Nishimura, T. Ogawa, J. Liq. Chromatogr. 15 (1992) 2233.
[67] A.J.G. Mank, H. Lingeman, C. Gooijer, Trends Anal. Chem. 11 (1992) 210.
[68] A.J.G. Mank, H. Lingeman, C. Gooijer, Trends Anal. Chem. 15 (1996) 1.
[69] T. Higashijima, T. Fuchigami, T. Imasaka, N. Ishibashi, Anal. Chem. 64 (1992) 711.
[70] T. Fuchigami, T. Imasaka, Anal. Chim. Acta 282 (1993) 209.
[71] T. Fuchigami, T. Imasaka, M. Shiga, Proc. SPIE 1885 (1993) 435.
[72] A.J.G. Mank, E.S. Yeung, J. Chromatogr. A 708 (1995) 309.
[73] F.T.A. Chen, A. Tusak, S. Pentoney Jr, K. Konrad, C. Lew, E. Koh, J. Sternberg, J. Chromatogr. A 652 (1993) 355.
[74] L.R. Middendorf, J.C. Bruce, R.C. Bruce, R.D. Eckles, S.C. Roemer, G.D. Sloniker, SPIE 1885 (1993) 423.
[75] T. Kaneta, T. Okamoto, T. Imasaka, Anal. Sci. 12 (1996) 875.
[76] H. Kawazumi, J.M. Song, T. Inoue, T. Ogawa, Anal. Sci. 11 (1995) 587.
[77] J.M. Song, H. Kawazumi, T. Inoue, T. Ogawa, J. Chromatogr. A 727 (1996) 330.
[78] T. Fuchigami, T. Imasaka, Anal. Chim. Acta 291 (1994) 183.
[79] T. Kaneta, T. Imasaka, Anal. Chem. 67 (1995) 829.
[80] T. Kaneta, T. Imasaka, J. Spectrosc. Soc. Jpn. 44 (1995) 21.
[81] J. Pawliszyn, Anal. Chem. 58 (1986) 3207.
[82] J. Pawliszyn, Rev. Sci. Instrum. 58 (1987) 245.
[83] J. Pawliszyn, Anal. Chem. 60 (1988) 2796.
[84] D.O. Hancock, R.E. Synovec, Anal. Chem. 60 (1988) 2812.
[85] D.O. Hancock, R.E. Synovec, Anal. Chem. 60 (1988) 1915.
[86] D.O. Hancock, R.E. Synovec, J. Chromatogr. 464 (1989) 83.
[87] B. Krattiger, G.J.M. Bruin, A.E. Bruno, Anal. Chem. 66 (1994) 1.
[88] D.K. Lloyd, D.M. Goodall, H. Scrivener, Anal. Chem. 61 (1989) 1238.
[89] Z. Wu, D.M. Goodall, D.K. Lloyd, P.R. Massey, K.C. Sandy, J. Chromatogr. 513 (1990) 209.
[90] H. Kawazumi, H. Nishimura, Y. Otsubo, T. Ogawa, Talanta 38 (1991) 965.
[91] H. Kawazumi, Y. Otsubo, T. Ogawa, Eng. Sci. Rep. (Kyushu University) 13 (1991) 171.
[92] Y. Wang, R.L. McGreery, Anal. Chem. 61 (1989) 2647.
[93] J.M. Williamson, R.J. Bowling, R.L. McCreery, Appl. Spectrosc. 43 (1989) 372.
[94] S.M. Angel, M.L. Myrick, Anal. Chem. 61 (1989) 1648.
[95] T. Imasaka, N. Ishibashi, Am. Biotechnol. Lab. 6 (1988) 34.
[96] T. Imasaka, N. Ishibashi, Anal. Chem. 62 (1990) 363A.
[97] T. Imasaka, N. Ishibashi, Prog. Quantum Electron. 14 (1990) 131.
[98] T. Imasaka, Appl. Fluoresc. Technol. 2 (1990) 1.

[99] T. Imasaka, Anal. Sci. 9 (1993) 329.
[100] T. Imasaka, Spectrochim. Acta Rev. 15 (1993) 329.
[101] T. Kaneta, T. Imasaka, J. Spectrosc. Soc. Jpn 44 (1995) 21.
[102] T. Imasaka, Bunseki (1996) 420.
[103] T. Imasaka, Adv. Liq. Chromatogr. (1996) 123.
[104] J.C. Camparo, C.M. Klimcak, Am. J. Phys. 51 (1983) 1077.
[105] P.A. Johnson, J.A. Vera, B.W. Smith, J.D. Winefordner, Spectrosc. Lett. 21 (1988) 607.
[106] T.E. Barber, P.E. Walters, J.D. Winefordner, N. Omenetto, Appl. Spectrosc. 45 (1991) 524.
[107] J. Lawrenz, A. Obrebski, K. Niemax, Anal. Chem. 59 (1987) 1232.
[108] T. Mishina, M. Tanigawa, Y. Fukuda, T. Hashi, Optics Comm. 62 (1987) 166.
[109] A.S. Zibrov, R.W. Fox, R. Ellingsen, C.S. Weimer, V.L. Velichansky, G.M. Tino, L. Hollberg, Appl. Phys. B 59 (1994) 327.
[110] T. Gustavsson, H. Martin, Rev. Sci. Instrum. 57 (1986) 1132.
[111] R.J. Lipert, S.C. Lee, M.C. Edelson, Appl. Spectrosc. 46 (1992) 1307.
[112] C.M. Barshick, R.W. Shaw, J.P. Young, J.M. Ramsey, Anal. Chem. 66 (1994) 4154.
[113] J. Franzke, D. Veza, K. Niemax, Inst. Phys. Conf. Ser. No. 128, Section 9 (1992) 343.
[114] J. Franzke, A.V. Irmer, D. Veza, K. Niemax, Proc. Reson. Ioniz. Spectrosc. (1994) 277.
[115] A. Zybin, K. Niemax, Anal. Chem. 69 (1997) 755.
[116] R.W. Shaw, J.P. Young, D.H. Smith, Anal. Chem. 61 (1989) 695.
[117] L. Ricci, M. Weidemüller, T. Esslinger, A. Hemmerich, C. Zimmermann, V. Vuletic, W. König, T.W. Hänsch, Optics Comm. 117 (1995) 541.
[118] J. Lawrenz, K. Niemax, Spectrochim. Acta 44B (1989) 155.
[119] R. Hergenröder, K. Niemax, Spectrochim. Acta 43B (1988) 1443.
[120] K. Niemax, A. Zybin, C.S.P.H. Groll, Anal. Chem. 68 (1996) 351A.
[121] T. Okazaki, T. Imasaka, N. Ishibashi, Anal. Chim. Acta 209 (1988) 327.
[122] T. Imasaka, K. Nishitani, N. Ishibashi, Analyst 116 (1991) 1407.
[123] T. Kaneta, T. Yamashita, T. Imasaka, Anal. Chim. Acta 299 (1994) 371.
[124] M. Jansson, J. Roeraade, F. Laurell, Anal. Chem. 65 (1993) 2766.
[125] W. Wang, M.M. Fejer, R.H. Hammond, M.R. Beasley, C.H. Ahn, M.L. Bortz, T. Day, Appl. Phys. Lett. 68 (1996) 729.
[126] K. Sakurai, N. Yamada, Opt. Lett. 14 (1989) 233.
[127] T. Imasaka, T. Hiraiwa, N. Ishibashi, Mikrochim. Acta 2 (1989) 225.

ELSEVIER

Talanta 48 (1999) 321–331

Talanta

Alcohol sensing membrane based on immobilized ruthenium(II) complex in carboxylated PVC and surface covalently bonded alcohol oxidase

Rebecca Choi Wan Lau [1], Martin Ming Fat Choi *, Jianzhong Lu

Department of Chemistry, Hong Kong Baptist University, Kowloon Tong, Hong Kong, People's Republic of China

Received 15 April 1998; received in revised form 9 July 1998; accepted 10 July 1998

Abstract

Alcohol sensing membranes coated on overhead transparency films for the continuous monitoring of ethanol, propanol and butanol are presented. Alcohol oxidation catalyzed by alcohol oxidase in conjunction with the fluorescence quenching reaction of oxygen-sensitive dye ion-pair, tris(4,7-diphenyl-1,10-phenanthroline) ruthenium(II) didodecylsulphate was chosen for the determination. Alcohol oxidase was immobilized covalently on a plasticized carboxylated poly(vinyl chloride) membrane and the oxygen-sensitive dye ion-pair was entrapped in the same membrane. The sensing membrane relates oxygen consumption, as a result of enzymatic oxidation, to alcohol concentration. Measurements have been performed in air-saturated alcohol standard solutions of pH 7.0. Storage stability, reproducibility and the effect of pH on sensing membrane performance have been studied in detail. The alcohol sensing membrane proposed here is simple to prepare and has a fairly rapid response time of < 1 min. It has been successfully applied to the determination of the ethanol contents in various spirits.

Keywords: Ruthenium(II) didodecylsulphate; Alcohol oxidation; Carboxylated PVC

1. Introduction

The rapid and accurate determination of alcohol is receiving attention in fermentation, quality control of beverages and blood analysis. Traditionally, alcohol is determined by gas chromatography and distillation methods [1,2], combined with subsequent measurements of density and refractometry. However, these methods either require distillation of the sample or extensive reagent preparation. In recent years, intensive works have been performed on the development of optical sensors. They have been accepted as advantageous because they can be miniaturized, are cheap to be manufactured and quite safe. Two kinds of optical alcohol sensor device have been developed over the past decade. Only a few sen-

* Corresponding author. Tel.: +852 2339 7839; fax: +852 2339 7348; e-mail:mfchoi@net1.hkbu.edu.hk

[1] Present address: Department of Chemistry, The Hong Kong University of Science & Technology, Clear Water Bay, Kowloon, Hong Kong.

0039-9140/99/$ - see front matter
PII S0039-9140(98)00248-3

Table 1
Compositions of M_1 to M_4 oxygen-sensitive optode membrane

Membrane	Weight of polymer (mg)	Weight of TBP (mg)	Weight of $Ru(dpp)_3(DS)_2$ (mg)	Emission peak maximum (nm)	Relative fluorescence intensity
M_1	83	83	1.3	593.7	8.2
M_2	83	166	1.3	593.2	5.7
M_3	83	249	1.3	592.6	3.8
M_4	83	332	1.3	592.0	3.1

Table 2
Compositions of M_5 to M_{10} oxygen-sensitive optode membrane

Membrane	Weight of polymer (mg)	Weight of TBP (mg)	Weight of $Ru(dpp)_3(DS)_2$ (mg)	Relative fluorescence intensity
M_5	83	332	2.6	1.8
M_6	83	332	3.9	2.7
M_7	83	332	5.2	3.2
M_8	83	332	6.5	2.4
M_9	83	332	7.8	1.6
M_{10}	83	332	9.1	0.7

sors, upon exposure to alcohol, show fluorescence enhancement of fluorescein derivatives [3] and malachite green [4] or fluorescence quenching of polyaromatic-substitute 1,3-oxazoles, thiazoles [5] and *p*-*N*,*N*-dioctylamino-4′-trifluoroacetylstilbene [6]. In most cases the recognition process is based on the enzymatic recognition of alcohol. The transduction is performed by optically detecting changes in the reduced form of nicotinamide adenine dinucleotide (NADH) concentration, the production of hydrogen peroxide or the consumption of oxygen (O_2) [7–11]. Other enzyme-based amperometric alcohol senosrs based on alcohol oxidase have already been described in detail [12,13]. The sensitivity and limit of detection of the electrochemical sensors are far better than the newly developed optical ones. However, optical sensors can offer some advantages over electrochemical sensors such as immunity to electromagnetic interference, possibility of remote and in situ monitoring and ease of fabricating a multi-component detecting system [14]. Considerable research effort will continue to expend in developing biosensors and chemosensors based on optical methods. Wolfbeis and Posch [15] have mentioned the entrapment of alcohol oxidase and tris(2,2′-bipyridyl) ruthenium(II) dichloride into silica gel for fibre optic sensing of ethanol. Although these existing sensors for the determination of alcohol have been successfully realized, there is still a demand for a fast-responsive, mass-produced and light-emitting diode (LED) compatible alcohol sensor.

Recently, Koncki et al. [16] have successfully immobilized an enzyme and a pH-sensitive dye in a polymeric membrane for detection of urea. Borrowing this novel idea, we fabricated sensing membranes based on the immobilization of alcohol oxidase and tris(4,7-diphenyl-1,10-phenanthroline) ruthenium(II) didodecylsulphate ($Ru(dpp)_3(DS)_2$) onto carboxylated poly(vinyl chloride) (PVC-COOH). Dissolved O_2 optodes were first fabricated by immobilizing the dye ion-pair in plasticized PVC-COOH optode membranes coated on overhead transparency films. Alcohol sensing membrane was subsequently constructed by using a simple and well-known 1-ethyl-3-(3-dimethylaminopropyl) carbodiimide condensation reaction and immobilizing alcohol oxidase on the same PVC–COOH matrix.

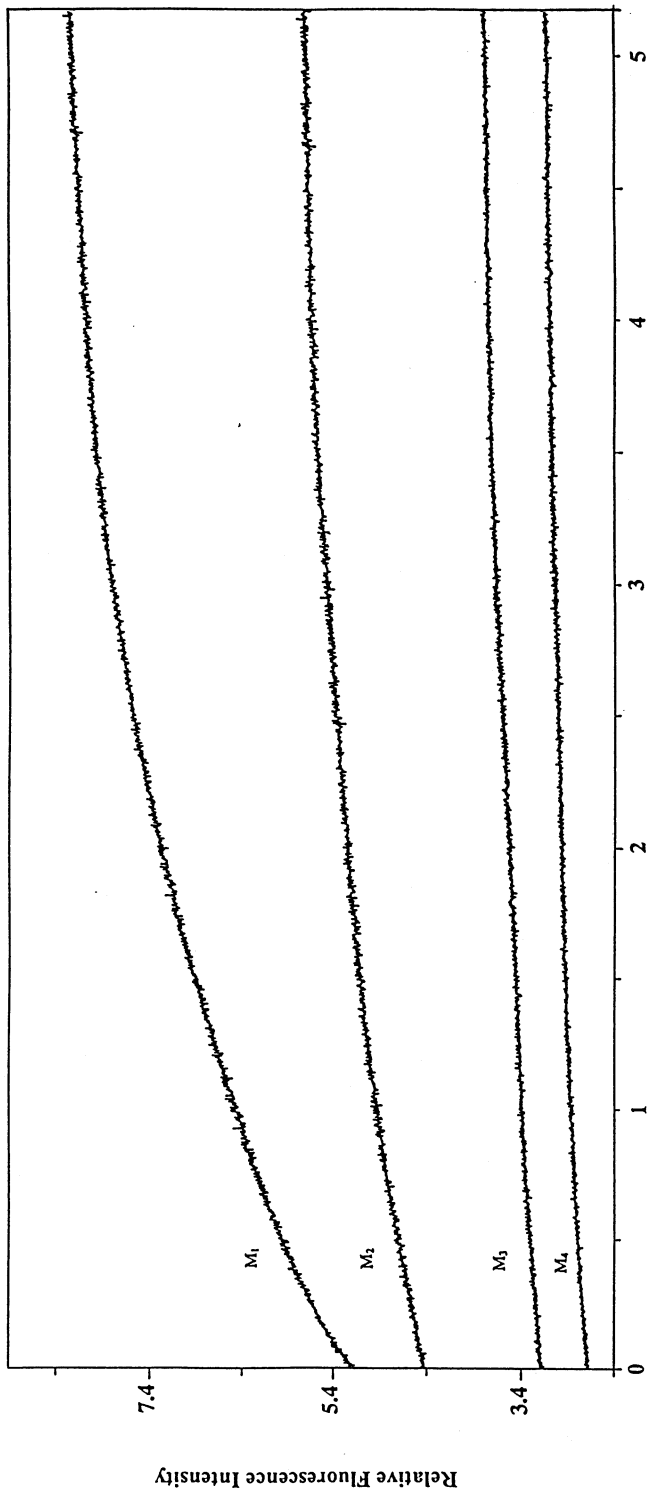

Fig. 1. Observed relative fluorescence intensity versus time curves for M_1–M_4 optode membranes while immersed in air-saturated 50 mM phosphate buffer solution at pH 7.0 and 20°C. The plasticizer content is $M_1 = 83$; $M_2 = 166$; $M_3 = 249$; $M_4 = 332$ mg.

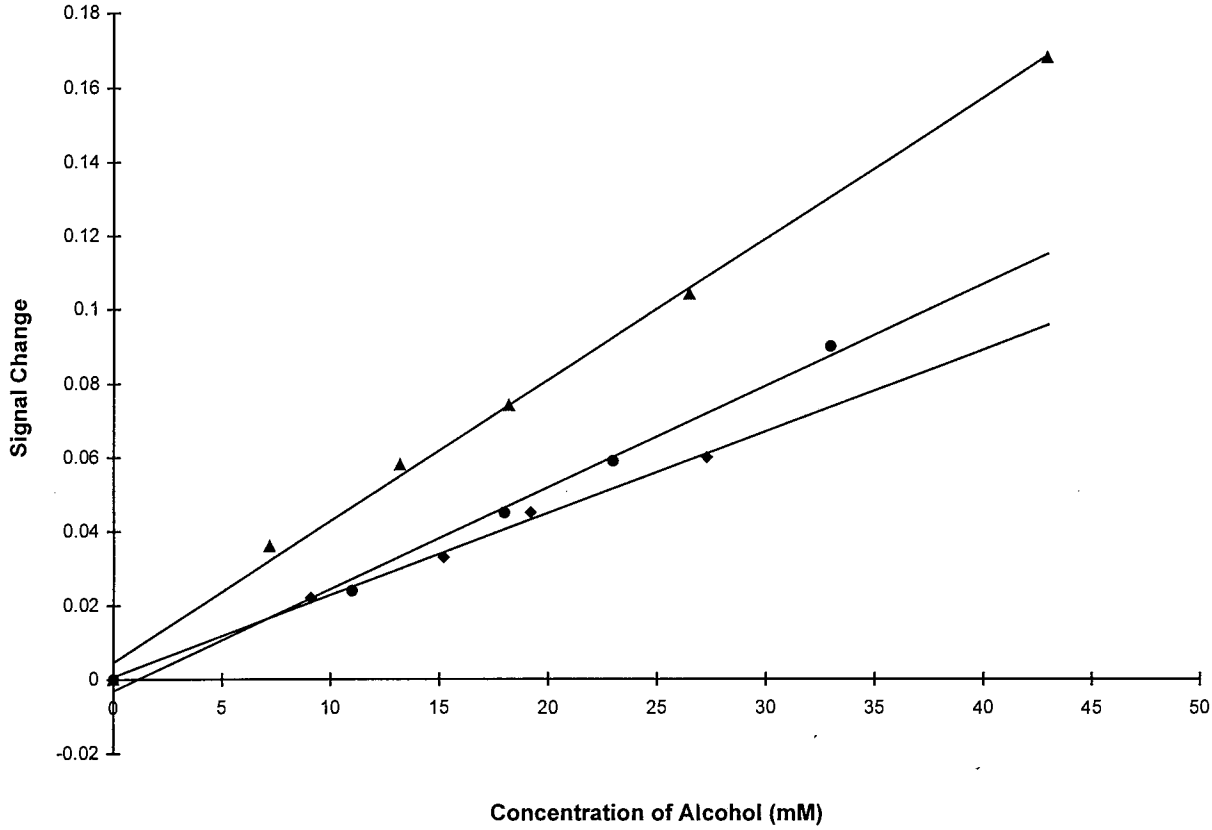

Fig. 2. Calibration curves for various alcohols. (▲): Ethanol; (●): propanol; (◆): butanol. Buffer concentration: 50 mM phosphate; pH: 7.0; temperature: 20°C.

	Slope*	y-intercept*	r^2
Ethanol	0.0038 ± 0.000064	0.0047 ± 0.0016	0.9971
Propanol	0.0027 ± 0.000038	0.0030 ± 0.0009	0.9940
Butanol	0.0022 ± 0.00014	0.0008 ± 0.0026	0.9961

* 95% confidence limit.

The sensing membrane presented here has three advantages. First, in the past these optode membranes were usually coated on glass or quartz solid supports which are easily broken if they are handle carelessly. The cutting of the glass material into different shapes and sizes is also inconvenient. Presently, we make use of overhead transparencies as our solid support for the mass production of the optode membranes. The use of overhead foils has been recently adapted in the industry for mass production of optode membranes [17]. The transparency is inexpensive, light, strong, water-proof and also has no visible light absorption. It can easily be cut into different shapes and sizes using scissors or a scalpel and be fixed to any sensor heads. Second, using a high-brightness blue LED, combined with a miniature photodiode detection system, the present PVC-based sensing membrane will have the potential for a low-cost, high-performance, simple and

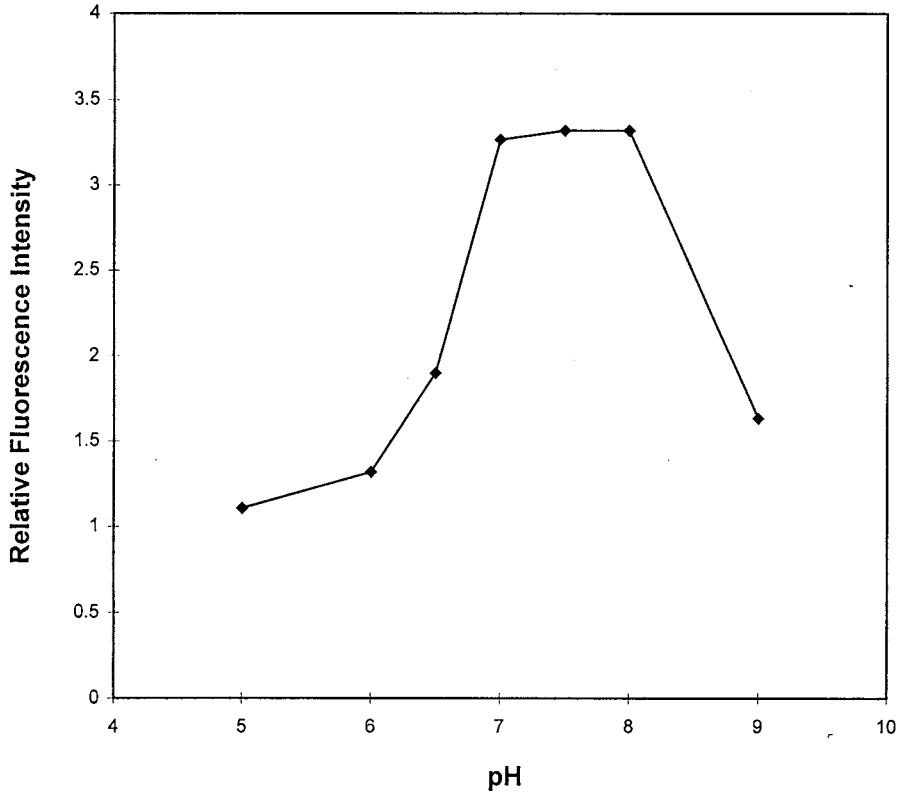

Fig. 3. Effect of pH on the response of the alcohol sensing membrane to 42.6 mM ethanol buffer solutions. Buffer concentration: 50 mM phosphate; temperature: 20°C.

portable alcohol sensor for use in many fields from quality control of beverages to on-line fermentation monitoring. Third, this sensing membrane shows a fast forward and reverse response time by using a highly active and extremely thin enzyme layer deposited on an oxygen-sensitive optode membrane.

2. Experimental

2.1. Chemicals and reagents

Alcohol oxidase (from Hansenula species) with a specific activity of 11 U mg^{-1} solid from Sigma (St. Louis, MO), was covalently immobilized on the oxygen-sensitive membrane via the coupling reagent 1-ethyl-3-(3-dimethylaminopropyl) carbodiimide (EDC) from Sigma. High relative molecular mass carboxylated poly(vinyl chloride) (PVC-COOH), plasticizer tri-*n*-butyl phosphate (TBP), tetrahydrofuran (THF) and various kinds of alcohols were purchased from Aldrich Chemical (Milwaukee). Dithiothreitol, sodium dihydrogen phosphate, disodium hydrogen phosphate and trisodium phosphate were obtained from Fluka Chemical (Buchs, Switzerland).

Tris(4,7-diphenyl-1,10-phenanthroline) ruthenium(II) didodecylsulphate dye ion-pair [Ru-$(dpp)_3(DS)_2$] was synthesized according to a modified procedure reported in the literature [18]. Standard solutions (0.1 M) of various alcohols were prepared by adding appropriate volumes of alcohols in phosphate buffers (50 mM). A series of standard solutions were then prepared by successive dilutions with buffer solutions.

2.2. Instrumentation

Fluorescence spectra were recorded using a spectrofluorometer, consisting of a lamp power supply (model LPS-220), a xenon lamp (model A1010), and a photomultiplier detection system (model 710), from Photon Technology International (London, Ontario, Canada). A Hewlett-Packard model 5890 Series II gas chromatograph equipped with a flame ionization detector and a HP-20M (Carbowax 20M) column was used to determine the ethanol contents of various spirits.

2.3. Preparation of dissolved oxygen-sensitive optode membrane

A cocktail of polymer solution was prepared by dissolving 5.2 mg of dye ion-pair, 332 mg of TBP and 83 mg of PVC-COOH powder in 2 ml of THF. An aliquot of 0.2 ml of this solution was applied to a dust-free transparency which was fixed in a spin-on device. A membrane of approximately 4 μm thickness was then coated onto the transparency and dried in ambient air before use. The size of the membrane was 36 mm in diameter.

2.4. Assembly of the alcohol sensing membrane

A freshly prepared solution containing 1 mg of EDC and 1 mg of alcohol oxidase per 0.2 ml of water was deposited on the surface of a O_2-sensitive membrane and left overnight at room temperature. Before use, the membrane was put in a phosphate buffer (pH 7.0, buffer concentration 50 mM) for at least 2 h in order to condition it and to remove unbound enzyme.

2.5. Procedures

A membrane coated on a transparency film was fitted into a quartz cuvette well covered with a polytetrafluoroethylene lid and then placed in the cuvette holder of the spectrofluorometer. About 3.5 ml of various test solutions were injected into the cuvette using a syringe. A color filter with 530 nm cut-on wavelength (L.O.T.-Oriel, Leatherhead, Surrey, UK) was used to remove the scattered light from the excitation source. In order to perform the continuous measurements, the old solution was pumped out and the fresh solution was injected instantly. Fluorescence measurements were taken under batch conditions.

3. Results and discussion

3.1. Fabrication of dissolved oxygen-sensitive membrane

Highly lipophilic $Ru(dpp)_3(DS)_2$ was prepared in 88.4% yield, starting from ruthenium (III) trichloride hydrate, according to the reported procedure [18]. The compound in its solid form is extremely stable and can be stored in the dark for a long period of time without any deterioration.

The oxygen-sensitive membrane is a thin layer of $Ru(dpp)_3(DS)_2$ dye ion-pair immobilized in the plasticized PVC-COOH. Compared with that in acetonitrile, the emission spectra of $Ru(dpp)_3(DS)_2$ immobilized on the PVC-COOH are blue-shifted from 614 to 592 nm. The shift of emission peak maximum is caused by the change of the micro-environment surrounding the $Ru(dpp)_3(DS)_2$ dye ion-pair. The fluorescence excitation and emission spectra characteristic of $Ru(dpp)_3(DS)_2$ immobilized on PVC–COOH matrix coated on a transparency film or a quartz solid support is very similar. However, the transparency film is cheaper and is easy to cut into different shapes and sizes. Furthermore, prolong-used optode membranes coated on transparency films can be simply disposed and replaced with new ones once their sensing performances deteriorate. The storage of packs of optode membranes is very convenient and they are light and portable. As a result, we decided to mass-produce all our sensing membranes coated on overhead transparency films as the solid support material.

The fluorescence of the dye ion-pair strongly and fully reversibly quenched by molecular O_2. The effects of the ingredients on the optode membrane were investigated in more detail. It can be found that, with increasing plasticizer content, a reduction in the fluorescence intensity of $Ru(dpp)_3(DS)_2$ fluorophore can be noted due to the decrease in concentration of fluorophore in

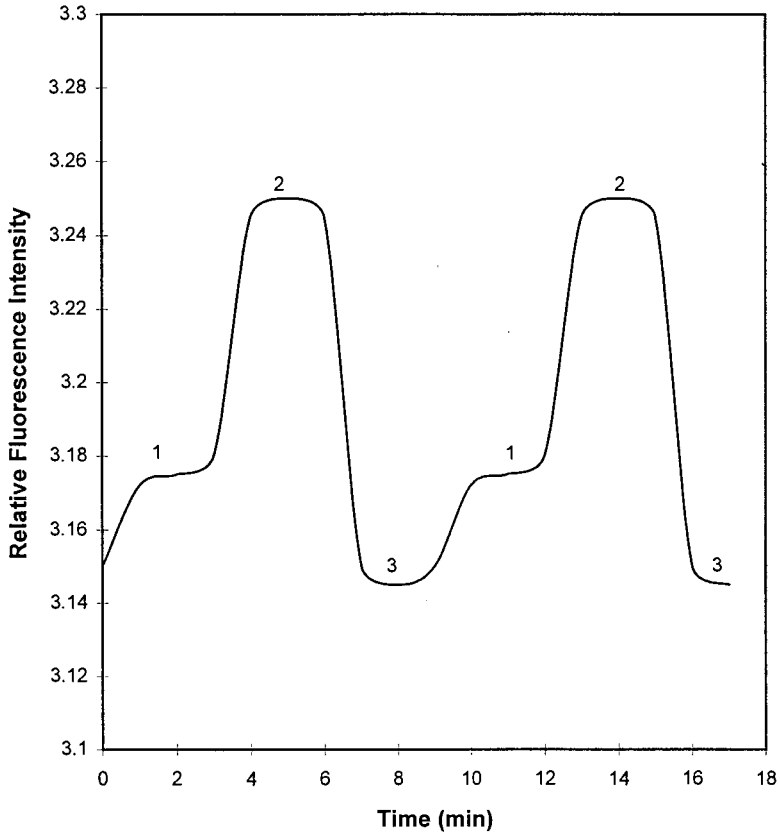

Fig. 4. Typical time–response curve of the alcohol sensing membrane for the determination of ethanol solutions. (1) 7.2 mM ethanol; (2) 26.5 mM ethanol; (3) 50 mM phosphate buffer solution at pH 7.0 and 20°C.

the membrane. For membranes M_1 to M_4 (Table 1), with increasing contact time of the membranes with the buffer solutions, it can be observed that the fluorescence intensities gradually increase but the increments gradually slow down (Fig. 1). The duration for membranes M_1 to M_4 reaching 95% of final fluorescence intensity were 4, 3.5, 2.5 and 1.5 h, respectively. It is possible that plasticized PVC membranes undergo substantial water uptake when immersed in aqueous solutions. Plasticizers and water can form a micro-emulsion on the surface of the bulk membrane and this provides a large interfacial area for the uptake of the ion-pair indicator from the bulk to the surface of the membrane. With increasing plasticizer content, the rate of surface adsorption of the indicator increases which constitutes a faster speed in reaching the plateau of the fluorescence intensity shown in Fig. 1. This observation has been fully explained by Mohr and Wolfbeis [19]. We further studied the effect of the contact time of the optode membrane on the fluorescence intensity of $Ru(dpp)_3(DS)_2$. After the membranes were soaked in the buffer solution for 4 h, the fluorescence intensities of four kinds of membranes all tended to be constant, and kept unchanged overnight. A compromise must be made between the contact time and the fluorescence intensity. For convenience, membrane M_4 was used in all further studies. The fluorescence intensity of membrane M_4 was smaller than that of other membranes; however, it is strong enough for the present work. In addition, higher level of plasticizer content in the film increases markedly the sensitivity of the film towards oxygen as explained by Mills and Thomas [20]. The effect of the plasticizer content

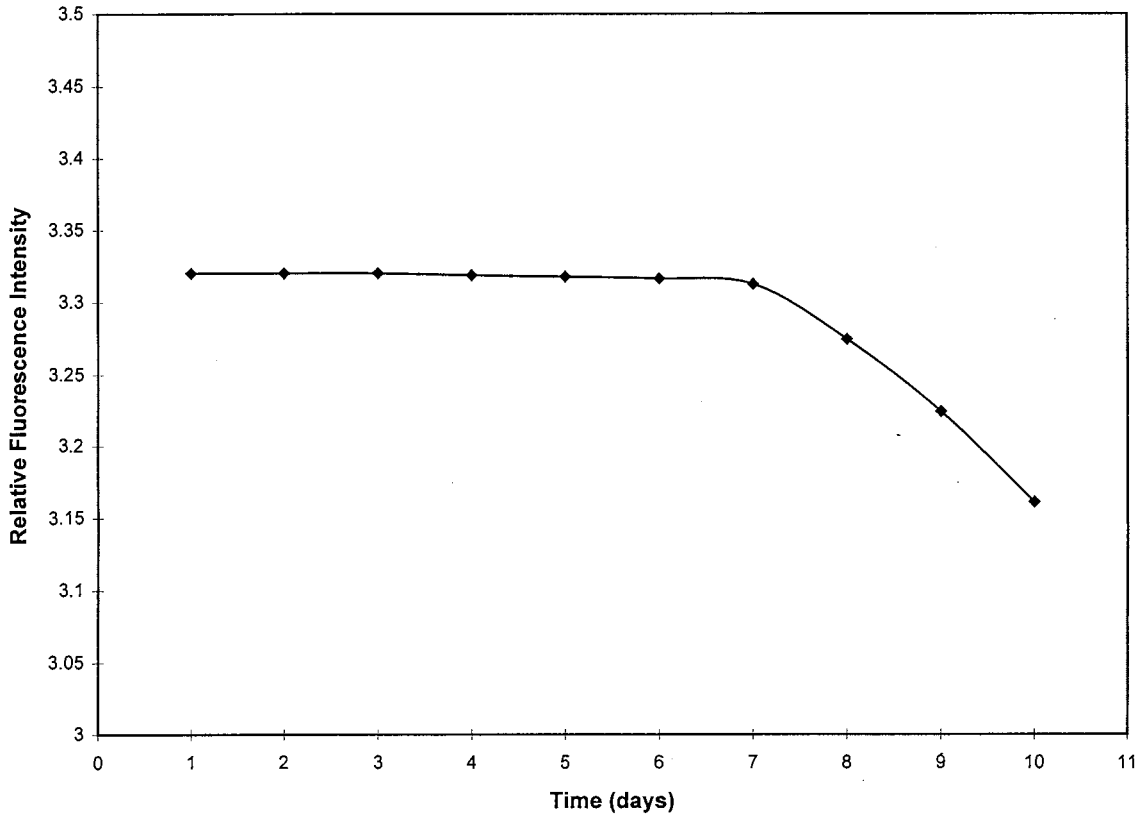

Fig. 5. Operational stabilities of the alcohol sensing membrane for the determination of 42.6 mM ethanol in 50 mM phosphate buffer solution at pH 7.0 and 20°C.

on the fluorescence spectrum has also been studied. It was found that no obvious spectral change occurred except that emission peak maxima were slightly blue-shifted with increasing plasticizer content.

The $Ru(dpp)_3(DS)_2$ concentration has a greater effect on the fluorescence intensity (Table 2). The fluorescence intensity reached a maximum when the amount of $Ru(dpp)_3(DS)_2$ was at 5.2 mg. At higher concentrations of O_2 indicator, the fluorescence intensities significantly decreased which strongly suggests that high content of $Ru(dpp)_3(DS)_2$ can cause self-quenching. Thus, $Ru(dpp)_3(DS)_2$ content was controlled at 5.2 mg throughout these experiments.

The 90% forward and reverse response can be reached within 20 s. Immobilized $Ru(dpp)_3(DS)_2$ is photostable. A linear graph was obtained when I_o/I was plotted against $[O_2]$ using Stern–Volmer equation; I_o is the fluorescence intensity recorded in a 100% N_2-saturated buffer solution as a function of $[O_2]$. The regression equation is $I_o/I = 0.0218\,[O_2] + 0.9912$ ($r^2 = 0.994$). The linear range was up to 80% O_2-saturated buffer solution. The limit of detection, which is based on three times the standard deviation at zero dissolved O_2 concentration, was determined to be 17.6 μM. Although the sensitivity and limit of detection of the O_2-sensitive optode membrane is not as good as those described in the literature [21], it is a good substrate for the subsequent alcohol oxidase immobilization and it will be described in the following section.

3.2. Analytical features of the alcohol sensing layer

In order to make an O_2 transducer in conjunction with an alcohol sensing layer, alcohol oxidase

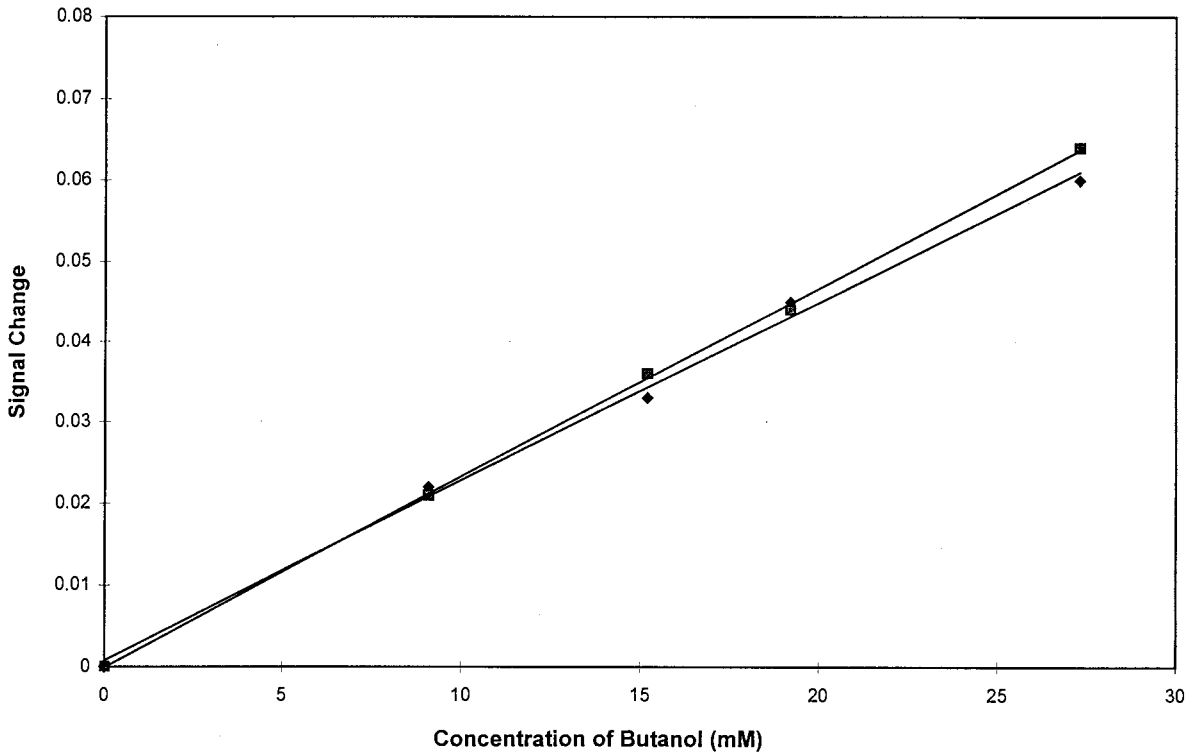

Fig. 6. Reproducibility of two sets of the alcohol sensing membranes for the determination of butanol in 50 mM phosphate buffer solution at pH 7.0 and 20°C.

Set no.	Slope*	y-intercept*	r^2
1	0.0023 ± 0.00014	0.00009 ± 0.0026	0.9995
2	0.0022 ± 0.00014	0.0008 ± 0.0026	0.9961

* 95% confidence limit.

is immobilized on PVC-COOH using a simple EDC condensation reaction. The enzyme immobilization procedures are very simple and proceed smoothly under mild conditions. The resulting enzyme membranes show good activity and possess high stability, mechanical resistance and flexibility.

The enzyme is specific for lower primary alcohols, according to the equation

$$RCH_2OH + O_2 \xrightarrow[\text{oxidase}]{\text{alcohol}} RCHO + H_2O$$

In this study we attempted to show the substrate selectivity of this enzyme from an organism, Hansenula species. As shown in Fig. 2, ethanol is indeed the best substrate for the Hansenula enzyme, the order of reactivity being ethanol > propanol > butanol. The limits of detection were calculated to be 4.0, 7.5 and 6.0 mM for ethanol, propanol and butanol, respectively. But the response to iso-propanol, iso-butanol and *tert*-butanol was low and the response to methanol was inconsistent.

The dependence of enzymatic activity on the pH of the phosphate buffer (50 mM) was investigated over the pH range 5.0–9.0 (Fig. 3). In this experiment, 42.6 mM ethanol were dissolved in the phosphate buffer solutions. It can be found that the optimum pH is 7.0–8.0. When the working temperatures were raised to 30°C or above, the response to ethanol decreased markedly and it

Table 3
Results of the determination of ethanol contents in various commercial spirits

Sample[a]	Ethanol concentration (%, v/v)			
	Found[b]	Reported	GC[b]	Dilution factor
Gienfiddich	44.3 ± 1.8	43	43.29 ± 1.20	300
Herbs liquor	46.5 ± 0.6	48	47.70 ± 0.52	300
Kiu Kiang Chiew	30.6 ± 2.3	NR	31.52 ± 0.32	200

Using the null hypothesis and *t*-test, there are no significant difference at 95% confidence level between the methods [22].
[a] Manufacturers: GIenfiddich, Scotland; Herbs Liquor, Thailand, Kiu Kiang Chiew, People's Republic of China.
[b] Average of three measurements.
NR, Not reported.

is probable that higher temperature caused the enzyme inactive.

Response time and reversibility of an alcohol sensing membrane was demonstrated by applying the membrane to two different ethanol concentration solutions alternatively (Fig. 4). It can be noted that the full-steady state is achieved within 1 min, which represents a fairly rapid response alcohol sensing system. The alcohol sensing membrane can be renewed easily by washing it with phosphate buffer. The standard deviation for ten replicate measurements of a 10 mM ethanol solution was 5%.

The storage stability of the immobilized alcohol oxidase is quite good as shown in Fig. 5. When the membrane with the immobilized alcohol oxidase was stored in a 10 mM dithiothreitol solution, i.e. an antioxidant which can prevent the sulphydryl group (–SH) of the enzymes from being oxidized, the enzyme membrane was stable for 7 days.

The reproducibility of the enzymatic membrane fabrication was examined by performing calibrations of butanol with two sets of the enzyme membrane. The relative fluorescence intensities are found to be reproducible (Fig. 6).

3.3. Sample analysis

Three commercial spirits were analyzed for their ethanol contents. The procedure involved dilution of spirits with the working buffer (dilution factor is 200–300) and three repetitive determinations. The concentrations of the diluted sample solutions were calculated from the calibration graph. The results compare favorably with those obtained by gas chromatography (GC) as shown in Table 3. The statistical study for the two methods also demonstrated that there were no significant differences between them at 95% confidence level [22].

4. Conclusion

The alcohol sensing membrane presented here is based on the use of inexpensive overhead transparencies as the solid support, alcohol oxidase as the recognition of alcohols and $Ru(dpp)_3(DS)_2$ dye ion-pair as the O_2 indicator, and compatible with LED devices. Therefore, it is ideally suited for mass production of the alcohol sensing membranes. Aside from its specific utility in this alcohol sensing schemes, the method for immobilizing enzyme on PVC–COOH is a very simple procedure for the construction of enzyme bulk optode membranes. A thin enzyme layer in conjunction with a sensitive indicating system results in a transparent film which has a fast response time. The results indicate the potential for a mass-produced and high performance alcohol sensing membrane for use in a wide range of continuous alcohol monitoring.

Acknowledgements

The authors express their appreciation to HKUST for the use of FAB-MS, ^1H NMR and

gas chromatograph. Financial support from HKBU (Project Nos. FRG/96-97/II-54 and FRG/96-97/II-62) is gratefully acknowledged.

References

[1] K. Helrich, Official Methods of Analysis of the Association of Official Analytical Chemists, 15th edn., Association of Official Analytical Chemists, Arlington, Virginia, 1990, Vol. 2, p. 739.
[2] F.L. Hart, M.J. Fisher, Modern Food Analysis, Springer, New York, 1971.
[3] H.-H. Zeng, K.-M. Wang, D. Li, R.-Q. Yu, Talanta 41 (1994) 969.
[4] D.N. Simon, R. Czolk, H.J. Ache, Thin Solid Films 260 (1995) 107.
[5] G. Orellana, A.M. Gomez-Carneros, C. de Dios, A.A. Garcia-Martinez, M.C. Moreno-Bondi, Anal. Chem. 67 (1995) 2231.
[6] G.J. Mohr, U.E. Spichiger-Keller, Anal. Chim. Acta 351 (1997) 189.
[7] B.S. Walters, T.J. Nielsen, M.A. Arnold, Talanta 35 (1988) 151.
[8] N.W. Cornell, R.L. Veech, Anal. Biochem. 132 (1983) 418.
[9] F. Lazaro, M.D. Luque de Castro, M. Valcarcel, Anal. Chem. 59 (1987) 1859.
[10] X. Xie, A.A. Suleiman, G.G. Guilbault, Z. Yang, Z. Sun, Anal. Chim. Acta 266 (1992) 325.
[11] R.W. Marshall, T.D. Gibson, Anal. Chim. Acta 266 (1992) 309.
[12] K. Mitsubayashi, K. Yokoyama, T. Takeuchi, I. Karube, Anal. Chem. 66 (1994) 3297.
[13] A.R. Vijayakumar, E. Csöregi, A. Heller, L. Gorton, Anal. Chim. Acta 327 (1996) 223.
[14] M.A. Arnold, Anal. Chem. 64 (1992) 1015A.
[15] O.S. Wolfbeis, H.E. Posch, Fresenius, Z. Anal. Chem. 332 (1988) 255.
[16] R. Koncki, G.J. Mohr, O.S. Wolfbeis, Biosens. Bioelectron. 10 (1995) 653.
[17] M.J.P. Leiner, Sensors Actuators B 29 (1995) 169.
[18] I. Klimant, O.S. Wolfbeis, Anal. Chem. 67 (1995) 3160.
[19] G.J. Mohr, O.S. Wolfbeis, Analyst 121 (1996) 1489.
[20] A. Mills, M. Thomas, Analyst 122 (1997) 63.
[21] C. McDonagh, B.D. MacCraith, A.K. McEvoy, Anal. Chem. 70 (1998) 45.
[22] J.C. Miller, J.N. Miller, Statistics for Analytical Chemistry, 3rd edn, Ellis Horwood, Chichester, 1993, pp. 55–58.

ELSEVIER

Talanta 48 (1999) 333–339

Talanta

Comparison of microwave-assisted extraction of triazines from soils using water and organic solvents as the extractants

Guohua Xiong, Baoying Tang, Xiaoqing He, Mingqiao Zhao, Ziping Zhang, Zhanxia Zhang *

Department of Chemistry, Zhongshan University, Guangzhou 510275, People's Republic of China

Received 4 March 1998; received in revised form 13 July 1998; accepted 15 July 1998

Abstract

Microwave-assisted extraction (MAE) for the separation of atrazine, simazine and prometryne from synthetic soil samples, using water and some organic solvents as the extractants, was studied in detail. The effects of the soil matrix, the soil moisture and the pH of the aqueous extraction system on the MAE efficiency were also studied. It was found that the three triazines could be efficiently extracted under the conditions of 100% magnetron power output (600 W), the first grade of pressure (from 0.1 MPa to 0.5 MPa), 30 ml solvent and 4 min microwave heating with water or organic solvents, except for prometryne with dichloromethane solvent for 1–4 g sandy loam sample. This interesting result was explained by triazines' solubility in water, their sorption properties in soils and the ability of the solvent to absorb microwave energy. Finally, evaluation of the extraction efficiency, as well as the treatment and determination of MAE extracts, suggested that water, as a cheap, safe and environmentally friendly solvent, can be a good alternative to organic solvents, used as the extractants for MAE of triazines from soils.

Keywords: Microwave-assisted extraction (MAE); Soil; Atrazine; Simazine; Prometryne; Water; Organic solvent

1. Introduction

Triazines, important herbicides used in agriculture worldwide, are ubiquitous environmental pollutants in soils and waters. Thus their rapid determinations are of much concern. Recently, Dean et al. [1] have written a good review on the sample preparation and chromatographic determination of triazines. Generally, liquid–solid extraction (LSE) methods, typically the Soxhlet extraction coupled with chromatographic techniques, are performed for the determination of triazines in soil samples. However, these sample-preparation procedures are time-consuming and need a large amount of organic solvents. Durand et al. [2,3] reported that the isolation of chlorotriazines and their degradation products from soil

* Corresponding author. Fax: +86 20 84189173; e-mail: stdp18@zsu.edu.cn

0039-9140/99/$ - see front matter
PII S0039-9140(98)00250-1

Table 1
Physical and thermodynamic properties of several solvents

Solvent	Permittivity[a], ε	Heat of vaporisation[a], ΔH_v (kJ mol^{-1})	Radiation time (s) required to reach 0.5 MPa[b]	Temperature (°C) responding to 0.5 MPa at gas–liquid equilibrium[c]
Methanol	32.63 (25°C)	37.567	29	112.0
Acetone	20.70 (25°C)	31.972	59	112.6
Dichloromethane	9.08 (20°C)	31.683	172	93.6
n-Hexane	1.89 (20°C)	31.912	—[d]	130.9
Acetone-*n*-hexane (1:1, v/v)	—	—	84	—
Water	78.30 (25°C)	46.021	69	151.1

[a] Cited from [14].
[b] Detected in the MK-1 pressure automatically controlled sample-dissolving system; solvent volume, 30ml; microwave power output, 600 W.
[c] Calculated according to Antoine equation $\log p = A - B/(t + C)$; p, mm Hg; t, °C. The temperatures of acetone, dichloromethane and *n*-hexane exceeded the suitable ranges of Antoine equation.
[d] Can not be detected—after microwave radiation for 3 min, the pressure in the extraction vessel did not increase obviously.

samples, with methanol or methanol–water (90:10), using Soxhlet extraction, needed 12 h.

In recent years, microwave-assisted extraction (MAE) has been developed for the extraction of a variety of toxic organic contaminants, such as PAHs, PCBs, phenols and pesticides from soils, sediments and other solid matrices [4–11]. Compared with traditional LSE methods, the sample-preparation time and the solvent amount are immensely reduced, without decreasing the extraction efficiencies of the target analyses.

It is interesting to note that water sometimes plays an important role in MAE, e.g. the sample moisture could affect the recovery of target analyte [6,9], water may be added into a non-polar organic extractant such as toluene, to help it absorb the microwave energy [10] and some aqueous solution may be substituted for organic solvents for the extraction of some organic compounds [11,12]. Stout et al. [11] reported a MAE of imidazolinone herbicides in soil at the ppb level with 0.1 M NH_4OAc /NH_4OH as the extractant. Steinheimer [12] reported a method for extracting atrazine and its principal degradation products from agricultural soil at 95–98°C by microwave heating, in which five extractions, with water followed by diluted hydrochloric acid as the extractants, were performed. In our previous work [13], the MAE of atrazine from soil using pure water as the extractant was studied in detail. Only a 4 min extraction at a pressure from 0.1 MPa to 0.5 MPa was required and the extract could be directly detected by an enzyme-linked immunosorbent assay (ELISA) using an EnviroGard Triazine QuantiTube test kit (Millipore, USA).

In this paper, three triazine herbicides, namely atrazine, simazine and prometryne, were selected to investigate the MAE of triazines from soils. Water and some organic solvents were used as extractants. These were studied in detail and compared with each other. The extracts were detected by capillary GC with a nitrogen–phosphorus selective detector (NPD). The main aim of this paper was to further demonstrate the possibility of using water to replace currently used organic solvents as the extractant for MAE of triazines from soils.

2. Experimental

2.1. Reagents and solvents

The stock solutions of atrazine (GSBG23040-92), simazine (GSBG23077-94) and prometryne (GSBG23082-94) were national standard solution of China, 100 μg ml^{-1} in acetone.

Table 2
Triazines recoveries by MAE using different solvents[a] ($n = 3$)

Solvent	Atrazine		Simazine		Prometryne	
	Rec%	RSD%	Rec%	RSD%	Rec%	RSD%
Methanol	99.8	5.4	100.4	6.8	97.6	3.7
Acetone-*n*-hexane (1:1, v/v)	90.4	3.6	92.7	5.0	86.3	7.2
Dichloromethane	87.7	8.1	89.2	3.8	38.5	4.5
Water	90.8	5.7	88.5	7.4	87.6	6.6

[a] 1 g synthetic sandy loam containing 2 μg g^{-1} atrazine, simazine and prometryne, respectively; 30 ml solvent; magnetron power output at 100% (600 W); pressure at the first stage (0.1–0.5 MPa); microwave heating for 4 min.

Methanol, ethanol, acetone, acetonitrile, hexane and dichloromethane were of analytical grade, purchased from Guangzhou Chemical Reagents, China. They were redistilled in a glass distillator before use. Water used as solvent was double distilled.

2.2. Soil preparation

2.2.1. Triazine-free soils

To prepare triazine-free soils, a sandy loam and a clay were each collected from the agricultural lands in Guangzhou, China. No triazine herbicides had been used previously in the agricultural lands. The collected soil samples were air-dried, pulverised and sieved through a 60 mesh sieve. In order to remove the possible triazines and other organic contaminants,100 g of each of the soil samples was immersed in 200 ml dichloromethane for 24 h. After repeating this clean-up procedure twice, the treated soil was spread out on a tray and air-dried for 4 h in a fume hood, to remove as much dichloromethane as possible.

Bentonite and florisil used as the triazine-free matrices were of chemical-reagent grade, purchased from Guangzhou Chemical Reagents. They were also cleaned up with dichloromethane, in the same way as the agricultural soils described above.

2.2.2. Soil standards (references)

The soil standards containing 2 μg g^{-1} atrazine, simazine and prometryne, respectively, were prepared by spiking the three triazines into each of triazine-free soils prepared above. To ensure that the triazine was well distributed, a reasonable amount of acetone was added to moisten the soil and careful agitation was performed. An air-drying procedure was then followed. These standards were prepared 10–14 days prior to soil analysis.

2.3. MAE procedure and extracts treatment

A 600 W microwave sample preparation system (Model MK-1, Xin-Ke Institute of Applied Microwave Technology, Shanghai, China) was used for MAE. The extraction conditions can be optimised by adjusting the three parameters, namely the magnetron power output, the heating time and the pressure in the air-tight digestion vessel. The pressure is controlled by a specially designed optical fibre sensor. There are eight separate grades for pressure selection, and pressures as high as 4 MPa can be attained. The volume of the PTFE lined digestion vessel is ≈ 60 ml. The turntable can hold nine vessels.

All MAEs were performed using the MK-1 microwave sample preparation unit. A 1–4 g portion of soil was accurately weighed and transferred into the PTFE liner of the sample vessel, to which the studied solvent was added. The vessels were then placed symmetrically on the microwave turntable. The extraction was carried out at the first pressure grade for a few minutes at 100% magnetron power output when the pressure went from 0.1 MPa to 0.5 MPa and then remained at 0.5 MPa. Upon completion, the vessels were cooled to room temperature. After cooling, the supernatant was carefully decanted and the soil

Table 3
Effect of pH on triazines recoveries by MAE for aqueous extraction system[a] ($n = 3$)

Acid or basic matter added in water	pH of aqueous solution	Atrazine		Simazine		Prometryne	
		Rec%	RSD%	Rec%	RSD%	Rec%	RSD%
NaOH	12.1	80.2	5.9	79.6	4.2	85.5	5.2
NH_3–NH_4CI	9.8	86.5	4.8	84.7	2.5	90.7	6.4
HAc–NaAc	4.7	90.1	6.3	86.5	3.6	83.6	3.4
HCI	1.8	83.3	8.2	73.8	3.9	80.4	5.7
—	7.0	90.8	5.7	88.5	7.4	87.6	6.6

[a] Other MAE conditions were the same as Table 2.

was rinsed with some solvents. The combined solutions (i.e. the supernatant and the rinsing solution) were centrifuged for 15 min at 4000 rpm, to separate the fine particulate. The supernatant was then evaporated to dryness in a rotary evaporator. Finally, 500 μl *n*-hexane was added to dissolve the residue.

2.4. GC-NPD procedure

A HP 6890 GC (Hewlett-Packard, USA), equipped with an NPD, was used for analysis of the extracts. A 30 m × 0.25 mm i.d. × 0.25 μm HP-5MS fused-silica capillary column, coated (chemically bonded) with 5% biphenyl and 95% dimethylpolysiloxane (Hewlett-Packard, US) was employed. An aliquot of 1 μl of the treated extract, was used for each of GC-NPD analyses. Nitrogen was used as both the carrier gas, at a flow-rate of 50 cm s^{-1}, and the make-up gas, at 30 ml min^{-1}. The temperatures of the injector and detector were maintained at 260 and 280°C, respectively. The column was programmed from 150 to 220°C at 5°C min^{-1}.

3. Results and discussion

3.1. Behaviours of organic solvents and water in MAE

Methanol, acetone and dichloromethane are all good solvents used in traditional extraction of triazines. For MAE, the solvent used as the extractant requires with proper permittivity (∈) to receive the microwave energy and transform it into thermal energy. The selected physical and thermodynamic properties of methanol, dichloromethane, acetone and *n*-hexane were presented in Table 1. The required microwave radiation time for each of the solvents to reach a pressure of 0.5 MPa in the air-tight vessel in MK-1 microwave unit was recorded and also presented. Water used as the MAE solvent was also studied and compared with the organic solvents. It was shown that the pressure increase was in the order: methanol > acetone > water ≫ dichloromethane. For *n*-hexane, no detectable pressure increase was observed. The rate of pressure increase seemed to relate to the solvent's ability to absorb the microwave energy, its specific heat and its heat of vaporisation. Water showed quite a rapid increase of pressure, in spite of its great heat of vaporisation, because it is a strongly polar compound that can efficiently absorb the microwave energy. For the MK- 1 microwave unit, the temperature of the extraction system was mainly decided by the pressure control and the extractant's properties. It can not be observed directly but can be calculated by Antoine equation [14] through the data of pressure in a proper range. It is obvious that different solvents show a different increase in temperature, with the same increase in pressure in the air-tight vessel in the MK- 1 microwave unit.

3.2. Triazines recoveries by MAE

A 1–4 g portion of synthetic soil sample (sandy loam) was used to examine the triazines recoveries

Table 4
Effect of soil moisture on triazines recoveries by MAE with dichloromethane solvent[a] ($n = 3$)

Soil moisture %	Atrazine		Simazine		Prometryne	
	Rec%	RSD%	Rec%	RSD%	Rec%	RSD%
0	87.7	8.1	89.2	3.8	38.5	4.5
5	89.3	6.5	90.7	8.5	54.8	6.3
10	91.5	7.7	91.6	4.2	78.0	4.7
15	93.7	5.4	93.3	4.9	85.5	3.7

[a] Other MAE conditions were as the same as Table 2.

by MAE. The magnetron power output of the microwave unit was set at 100% (600 W). The pressure control was selected at the first stage (from 0.1 MPa to 0.5 MPa). Methanol, acetone-*n*-hexane (1:1, v/v), dichloromethane and water were studied as the MAE solvents. Experimental results showed that 30 ml solvent and 4 min microwave heating offered a quite efficient extraction for atrazine, simazine and prometryne with water or organic solvents, except for prometryne with dichloromethane solvent. It was found that sample weight in the range of 1–4 g did not markedly affect triazines recoveries. Considering the sampling variability for real-word samples, a 4 g portion of soil sample is desirable. Methanol provided the highest recovery for the three triazines. It was surprising that water was about as efficient as the organic solvents for MAE of triazines, and the recovery of prometryne by MAE with dichloromethane solvent was very low.

To explain the results, a literature study was performed on triazines solubility and their sorption properties in soils. Triazines have some polarity in their molecular structures. The solubility of atrazine, simazine and prometryne in water is 33, 5, and 48 ppm, respectively, at 20–25°C. Otherwise, triazines can be strongly sorbed in soils. In general, prometryne can be sorbed in soils more strongly than atrazine and simazine [15]. It was found that triazines sorption in soils was mainly correlated to the organic content, the clay content, the cationic exchanging capacity, the pH and the specific surface area of the soil [15,16]. Generally, the higher the soil's organic content and clay content, the stronger the triazines were sorbed. Donerty et al. [16] reported that the correlation coefficients of prometryne's sorption correlated to the organic content, the cationic exchanging capacity and the specific surface area of the soil, were 0.98, 0.95 and 0.92, respectively. Recently, Koskinen et al. [17] developed a method to research the sorption–desorption of atrazine in field-moist soils using supercritical CO_2 extraction technique. In their work, it was found that the sorption coefficient was also correlated to the soil moisture. But the correlation seemed very complicated and was different for each different soil sample studied. Therefore, the MAE results can be explained in three aspects: triazines solubility, their sorption in soils and the solvent's ability to absorb the microwave energy. Water can efficiently absorb the microwave energy and transform it into thermal energy. When the pressure was up to 0.5 MPa, the temperature of the water solvent in the air-tight MAE system would go to ≈ 150°C (Table 1). The permittivity (polarity) of water decreases with increasing temperature [18], which could increase the solubility of triazines in water (e.g. the permittivity of water at 200°C is about the same as methanol at 25°C). Moreover, water is a polar solvent which can strongly interact with the polar surface of soil under the MAE conditions and weaken, and even break, the triazine–soil bones. Therefore, triazines desorption from soil would become easier. Because dichloromethane has less polarity and less ability to absorb microwave energy, it can not interact strongly with the inorganic polar matter in soils, and the required microwave radiation time to reach a pressure of 0.5 MPa in the air-tight vessel in MK-1 microwave unit for dichloromethane, was as long as ≈ 170 s (Table 1). It is not difficult

Table 5
The effect of soil matrices on triazines recoveries by MAE[a] ($n = 3$)

Soil matrix	Solvent	Atrazine		Simazine		Prometryne	
		Rec%	RSD%	Rec%	RSD%	Rec%	RSD%
Clay	Methanol	100.2	6.3	100.6	4.8	98.2	4.9
	Acetone-*n*-hexane (1:1, v/v)	95.4	3.6	96.3	4.3	92.5	5.5
	Dichloromethane	89.3	3.3	91.1	7.2	54.3	5.4
	Water	92.7	5.2	90.6	4.1	89.4	3.5
Bentonite	Methanol	101.3	4.2	100.8	5.6	99.8	3.8
	Acetone-*n*-hexane (1:1, v/v)	98.9	2.8	99.5	5.4	98.6	4.9
	Dichloromethane	94.4	5.9	95.3	4.7	90.3	3.8
	Water	95.3	2.5	94.5	4.3	95.1	6.2
Florisil	Methanol	100.7	3.5	100.2	6.1	99.5	4.8
	Acetone-*n*-hexane (1:1, v/v)	99.2	6.9	99.8	3.7	99.1	5.7
	Dichloromethane	94.1	6.8	94.9	3.8	91.0	7.5
	Water	96.0	3.2	96.7	2.6	94.4	6.8

The recoveries of triazines by MAE from sandy loam were presented in Table 2.
[a] Other MAE conditions were the same as Table 2.

to understand that prometryne, because it has the greatest solubility both in water and in the three triazines, and it has the strongest sorption in soil, can be easily extracted by MAE with water or methanol or acetone-*n*-hexane (1:1, v/v) as the extractant, but can not be efficiently extracted with dichloromethane Table 2.

3.3. Effect of pH on MAE for aqueous extraction system

To examine the effect of pH on MAE of triazines from soils, the aqueous solutions used as the extractants were adjusted to different pH with NaOH, NH_3–NH_4CI, HAcNaAc and HCI, respectively. The results are given in Table 3. It can be seen that the recoveries of triazines were reasonably good within the pH range of 4.7–9.8. Evidently, water is an optimum solvent for MAE of triazines from soils.

3.4. Effect of soil moisture on MAE with organic solvents

To examine the effect of soil moisture on the recoveries of triazines by MAE, soils with different degrees of moisture and different types of organic solvents were used for investigation. It was found that there was no marked effect of soil moisture on triazines recoveries when using methanol or acetone-*n*-hexane (1:1, v/v) as the extractants. But the triazines recoveries would be significantly improved, in the presence of moisture in soil, when using dichloromethane solvent, especially for prometryne. As shown in Table 4, the higher the moisture content, in the range of 0–15%, the higher the recoveries of triazines. this may be explained by water's ability to help the extraction system absorb the microwave energy and enhance the desorption of triazines from soils.

3.5. Effects of soil matrices on MAE for both aqueous and organic extraction systems

To examine the effect of soil matrices on the recoveries of triazines by MAE, four synthetic soil samples, namely sandy loam (organic carbon content $\approx 1\%$), clay (organic carbon content $\approx 0.05\%$), bentonite and florisil were employed and studied. It was found that soil matrices can affect the triazines recoveries by MAE for both aqueous and organic extraction systems. It was shown in Table 5 that the organic content was a more significant factor than the clay content, for triazines recoveries by MAE. The recovery decreased in the presence of organism in soil.

3.6. Evaluation of the treatment and determination of the MAE extracts for both aqueous and organic extraction systems

For organic extraction systems, the MAE extracts could be easily concentrated with a rotary evaporator or cleaned up before determination, or directly sent to GC or HPLC analysis if the analyte concentration was high enough and the extraction solution was pure enough. In comparison, the treatment procedure for aqueous extraction solution was somewhat time-consuming. Moreover, aqueous solution can not be directly injected into a common GC column. However, the aqueous solution of triazines can be easily detected by reversed-phase HPLC. In addition, according to our previous research [13], the aqueous solution of a single triazine was especially suitable for detection by ELISA, using a commercial ELISA kit (Millipore, USA) which offers a direct, rapid, cheap and sensitive determination. Besides the above-mentioned, the most important advantages of using water as the MAE solvent are it's friendliness to the environment and the low cost.

4. Conclusion

Methanol and acetone-*n*-hexane (1:1, v/v) are the best organic solvents for extracting atrazine, simazine and prometryne from soils by MAE. Water solvent is about as efficient as the organic solvents. Since water is a strongly polar compound, it can interact strongly with the polar matter in soils to enhance the desorption of triazines from soils. Moreover, water can receive the microwave energy efficiently to transform it into thermal energy to increase the solubility of triazines. Water is a very cheap, safe and environmentally-friendly solvent. Although the treatment procedure of aqueous extraction solution is somewhat time-consuming and aqueous solution can not be directly analysed by GC, the aqueous MAE solution of triazine can be easily detected by HPLC or ELISA and be detected by GC after evaporation to dryness and transfer into organic medium with a little organic solvent. It is hoped that it might replace the currently used organic solvents for extracting triazines from soils by MAE.

References

[1] J.R. Dean, G. Wade, I.J. Barnabas, J. Chromatogr. 733 (1996) 295.
[2] G. Durand, D. Barcelo, Anal. Chim. Acta 243 (1991) 259.
[3] G. Durand, R. Forteza, D. Barcelo, Chromatographia 28 (1989) 597.
[4] K. Ganzler, A. Salgo, K. Valko, J. Chromatogr. 371 (1986) 299.
[5] K. Ganzler, I. Szinai, A. Salgo, J. Chromatogr. 520 (1990) 257.
[6] V. Lopez-Avila, R. Yong, W.F. Bechet, Anal. Chem. 66 (1994) 1097.
[7] I.J. Barnabas, J.R. Dean, I.A. Fowlis, S.P. Owen, Analyst 120 (1995) 1897.
[8] B. Lalere, J. Szpunar, H. Budzinski, P. Garrigues, O.F.X. Donard, Analyst 120 (1995) 2665.
[9] F.E. Onuska, K.A. Terry, Chromatographia 36 (1993) 191.
[10] A. Pastor, E. Vazquez, R. Ciscar, M. de la Guardia, Anal. Chim. Acta 344 (1997) 241.
[11] S.J. Stout, A.R. daCunha, D.G. Allardice, Anal. Chem. 68 (1996) 653.
[12] T.R. Steinheimer, J. Agric. Food Chem. 41 (1993) 588.
[13] G. Xiong, J. Liang, S. Zou, Z. Zhang, Anal. Chim. Acta (in press).
[14] J.A. Dean, Lange's Handbook of Chemistry, 13th ed., McGraw-Hill, New York, 1985, pp. 10–28.
[15] Shaoquan Su, An Introduction to Herbicides (Chinese), Science Press, Beijing, 1989, pp. 208.
[16] P.J. Donerty, G.F. Warren, Weed Res. 9 (1969) 20.
[17] W.C. Koskinen, E.A. Rochette, Intern. J. Environ. Anal. Chem. 65 (1996) 223.
[18] Y. Yang, S. Blwadt, S.B. Hawthorne, D.J. Miller, Anal. Chem. 67 (1995) 4571.

ELSEVIER

Talanta 48 (1999) 341–346

Talanta

Polarographic determination of cyanide as contaminant in pralidoxime mesylate formulations

Paulo C. do Nascimento *, Denise Bohrer, Leandro M. de Carvalho

Department of Chemistry, Federal University of Santa Maria, RS 97111 970, Brazil

Received 2 April 1998; received in revised form 14 July 1998; accepted 15 July 1998

Abstract

A method for the polarographic determination of cyanide as contaminant in pralidoxime mesylate (PM) formulations was developed. The volatile cyanide formed in the formulations was stabilized as tetracyanonickelate (TCN) anion complex after reaction with ammoniacal Ni(II) solution. The stable TCN anion complex ($K_{stb} = 10^{31}$) was determined by anodic stripping voltammetry at the hanging mercury drop electrode (HMDE). The polarographic signal was proportional to the cyanide concentration and the high concentration of PM did not interfere. The linear range of calibration was from 1.2 to 16 μg cyanide with $r = 0.998$. The RSD was 1.3% ($n = 5$) for 2.4 μg cyanide and a detection limit of 0.8 μg cyanide was calculated. The proposed method is adequate as a quality control of PM formulations.

Keywords: Cyanide determination; Polarography; Pralidoxime formulations

1. Introduction

Certain oxime formulations as pralidoxime mesylate (PM) have therapeutic value as an antidote to poisoning from organophosphate agricultural chemicals, chemical warfare agents, and drugs acting as cholinesterase inhibitors. It is typically formulated as a concentrated solution (ca. 25 mg ml^{-1}) in ampules for intravenous administration or as a powder (ca. 200 mg) in a closed flask to prepare the injectable dose with 10 ml of physiological solution.

* Corresponding author. E-mail: npaulo@quimica.ufsm.br

0039-9140/99/$ - see front matter
PII S0039-9140(98)00252-5

(1) (2) (3) (4)

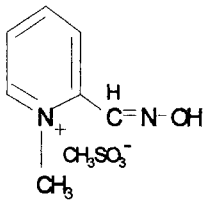

Pralidoxime mesylate

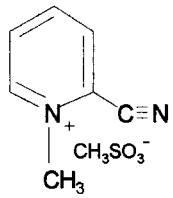

2-cyano -1- methylpyridinium mesylate

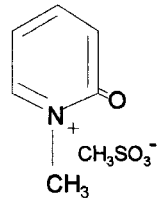

1- methylpyridone

HCN

The stability and storage life of pralidoxime formulations have been extensively studied [1–8] and its decomposition route also includes (in pH > 4) among organic degradation products (2) and (3), hydrogen cyanide (4). It seems possible that the cyanide present in pralidoxime formulations remains dissolved in the aqueous phase of the closed ampules and consequently it can be delivered to the patients.

Although many methods for the determination of cyanide have been described in the literature there are three problems [9] in its direct application to the pralidoxime formulations; the high concentration of pralidoxime in the injectable dose, the decomposition products which interfere directly with the method and lastly the conditions used in the analytical method that can cause a change in the cyanide concentration. To partially overcome these difficulties many methods use gas dialysis in conjunction with flow-systems to separate the analyte from the matrix through a desorption–reabsorption step in the dialysis units. However, such methods are time consuming and the sensitivity is limited, in some extension, on the low efficiencies (typically 10–15%) of the gas transfer in the dialysis units [10–14].

Free cyanide ions can be determined by polarography, in several alkaline supporting electrolytes, due to its signal obtained from the mercury oxidation on the dropping electrode. In these electrolytes, the cyanide is relatively stable in its non-volatile form (CN^-) although it is partially liberated during the bubbling process to obtain deaerated solutions or in the storage of the samples. Alternatively, cyanide can be determined by polarography in a very stable form, as the tetracyanonickelate (TCN) anion complex. It is formed instantaneously due the reaction of Ni^{2+} ions in ammoniacal solutions with cyanide,

$$[Ni(NH_3)_6]^{2+} + 4CN^- \rightarrow [Ni(CN)_4]^{2-} + 6NH_3,$$

and has a high cumulative stability constant of formation ($\sim 10^{22}$–10^{31}) [15] to keep the cyanide in a stable condition for the polarographic analysis. Even limited amounts of cyanide ions cause a complete formation of the TCN anions and this reaction was already used as basis of procedures for the determination of nickel by spectrophotometry [16] and cyanide by spectrophotometry [17], polarography and atomic absorption spectrophotometry [18].

Polarographic analysis of Ni(II) ions shows in many electrolytes an irreversible behavior associated with the reduction of the Ni(II) ions. The half-wave potentials lie in the range of -1200 to -800 mV (versus Ag/AgCl) [19] as it can also be observed in ammoniacal media ($E_{1/2} = -900$ mV versus Ag/AgCl). The addition of cyanide ions to a polarographic cell that contains ammoniacal Ni(II) solution produces a splitting in the Ni(II) signal into two peaks. While the peak by -900 mV decreases, the peak by -450 mV increases proportionally to the cyanide concentration [20]. Some other ligands such as rhodanid [21], azide [22,23], albumin [24], pilocarpine [25] can improve the reversibility of the Ni(II) reaction on the mercury electrode and also produce an anticipation on its reduction wave to more positive potentials giving the so-called catalytic nickel prewaves [26–31]. This effect can be assigned to a ligand-catalytic effect and it is related to the ability of

the ligand to act as a bridge in the electrical double layer facilitating the transfer of electrons in the electrode reaction [26].

In this work we describe a fast and simple polarographic method based on the formation of the TCN anion complex, to assay cyanide as contaminant in pralidoxime mesylate formulations. The high concentration of pralidoxime in the polarographic cell (ca. 10 g l^{-1}) or its decomposition products have not interfered and previous dilutions of the sample or gas dialysis steps were not necessary.

2. Experimental

2.1. Instrumentation

Differential pulse-polarographic measurements (DPP) were made on a Metrohm 646 VA processor/ 675 VA sample changer and polarograms were recorded, in the DME (dropping mercury electrode) mode between -1000 and -100 mV with the instrument settings: drop time, 600 ms; scan rate, 10 mV s^{-1}; pulse amplitude, -50 mV; pulse duration, 40 ms. At the HMDE (hanging mercury drop electrode) mode measurements, polarograms were recorded between -800 and -100 mV and a pre-concentration time of 180 s at -800 mV was used. All potentials quoted were measured against an Ag/AgCl, KCl 3 mol l^{-1} reference electrode and the polarographic cell volume was 20 ml.

2.2. Reagents and solutions

All the chemicals used were of analytical grade. Dilutions were made with deionized water, which was further purified on a MilliQ high-purity water device (Molsheim, France).

Pralidoxime solutions were prepared by the dissolution of the pralidoxime mesylate (Rhodia Farma, São Paulo, Brazil) in 10 ml of an (pH 9) ammoniacal 8×10^{-4} mol l^{-1} $NiCl_2$ solution in 0.1 mol l^{-1} NH_3-NH_4Cl.

Standard cyanide solutions were prepared prior to use by dilution of a stock standard sodium cyanide solution (0.1 mol l^{-1} in 0.1 mol l^{-1} NaOH), standardized according to the method of Archer [32].

Electrolyte solution was 10 ml of an ammoniacal 10^{-3} mol l^{-1} KCl solution pH 10 buffered with NaOH 10^{-3} mol l^{-1}. Deaerated electrolytes were obtained by sparging for 10 min with nitrogen.

2.3. Analytical procedure

In the analysis, 10 ml of the ammoniacal Ni(II) solution (8×10^{-4} mol l^{-1} $NiCl_2$ in 0.1 mol l^{-1} NH_3-NH_4Cl) was injected through the rubber stopper of the flask containing 0.2 g of PM and the flask shaken to the complete dissolution of the sample. The flask was opened and the solution directly introduced in the polarographic cell that contains 10 ml of a deaerated electrolyte solution.

3. Results and discussion

3.1. Polarographic determination of cyanide in presence of pralidoxime mesylate

The cyanide determination as TCN anion complex, in its more sensitive form, was done in the HMDE mode, by anodic stripping voltammetry. The Ni(II) ions as TCN anion complex were reduced on the mercury electrode at -800 mV and the anodic stripping was done, after 180 s of preconcentration time, as indicated by the equations:

$$Ni(CN_4)^{2-} + 2e^- \rightarrow Ni(Hg) + 4CN^- \quad \text{(reduction)}$$

$$Ni(Hg) + 4CN^- \rightarrow Ni(CN)_4^{2-} + 2e^- \quad \text{(stripping)}$$

Without cyanide ions in the polarographic cell no peaks were observed in the anodic stripping after preconcentration at -800 mV.

Preconcentration times in the range of 0–240 s (at time intervals of 30 s) were tested relative to the peak height obtained in the analysis of 2.4 μg of cyanide as TCN anion complex. Up to 180 s increases on the peak height were not observed probably due to the low solubility of the nickel [33] on the mercury electrode (4.8×10^{-5} % w/w).

The peak height by -450 mV obtained by the stripping was cyanide concentration proportional

and large amounts of PM have not interfered. Fig. 1 shows the polarographic peaks obtained by the addition of successive amounts of cyanide to a polarographic cell that contains 0.2 g of PM dissolved in the electrolyte and ammoniacal Ni(II) solution.

Under these conditions, the peak height was related to the cyanide concentration according to the calibration function; $y = 11.3 \times -2.1$ ($r = 0.998$), where y is the observed current (in nA) and x is the cyanide amount (in μg) present in the polarographic cell. The relative standard deviation was 1.3% for five measurements of 2.4 μg cyanide and a linear dynamic range was observed from 1.2 to 16 μg cyanide. The detection limit for the method was 0.8 μg cyanide (40 μg l^{-1} cyanide in the polarographic cell), calculated from the standard deviation ($n = 3$) of the noise of the equipment at −450 mV. The lowest cyanide amount determined in the presence of 0.2 g of PM was 1.2 μg (0.0006% of CN^- relative to the PM).

Without ammoniacal Ni(II) ions in polarographic cell, the cyanide liberated from the PM formulations could not be determined due to the loss of volatile cyanide and due to the sensitivity required, considering that the anodic stripping could be not used.

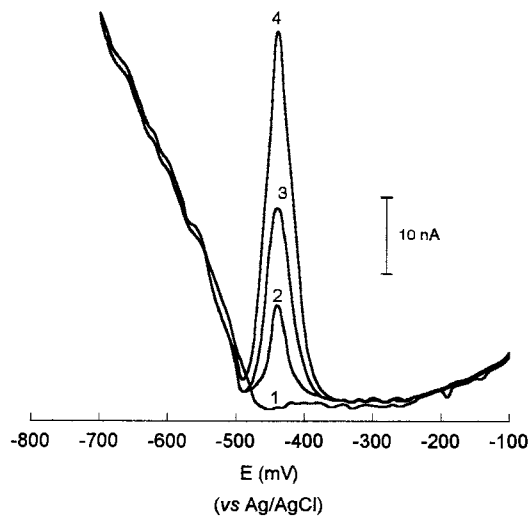

Fig. 1. Polarograms of cyanide as TCN anion complex in presence of 0.2 g of PM obtained at the HMDE mode. Curves (1) 0 μg CN^-; (2) 1.2 μg CN^-; (3) 2.4 μg CN^-; (4) 4.8 μg CN^-.

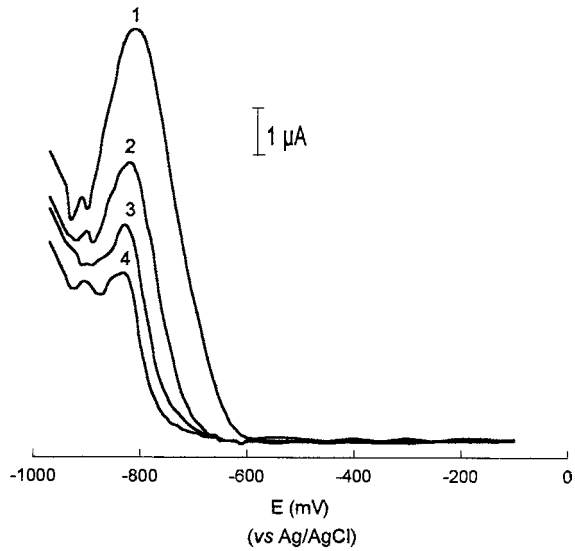

Fig. 2. Polarograms of PM solutions (10 g l^{-1}) submitted to 80°C heating periods. Curves (1) 0 min; (2) 30 min; (3) 60 min; (4) 120 min. Polarograms recorded at DME mode at 20°C.

3.2. Polarographic behavior of pralidoxime mesylate in presence of ammoniacal Ni(II) solution

Pralidoxime mesylate, in alkaline electrolytes, showed a polarographic peak by −850 mV but, it cannot be used to quantify pralidoxime in the presence of Ni(II) ions, since both peaks are relatively broad as observed in irreversible electrode processes. Fig. 2 shows polarograms of PM obtained after different time intervals at 80°C to accelerate its decomposition. Besides cyanide, organic degradation products are formed and the degradation pathway [4,34] of PM in pH > 4 produces cyanide as result of a hydroxyl-ion catalyzed dehydration to 2-cyano-1-methylpyridinium mesylate that is subsequently hydrolyzed to 1-methylpyridone and cyanide. Although the degradation products produce no polarographic peaks between −850 and −200 mV, the peak by −850 mV could be used to follow the progressive degradation of PM. While the peaks by −850 mV obtained in the presence of PM and Ni(II) ions decreases (see Fig. 2) the peaks by −450 mV increases (see Fig. 1) proportionally to the cyanide concentration. It can be also observed in Fig. 1

Table 1
Polarographic determination of cyanide and recovery experiments in the presence of 0.2 g of pralidoxime mesylate

CN^- added (μg)	Elapsed time before the measurements (min)	Temperature (°C)	CN^- found[b] (μg)	Recovery (%)
0	0	20	nd	—
0	15	20	nd	—
0	30	20	nd	—
0	60	20	nd	—
0	120	20	nd	—
0	2d[a]	20	3.24	—
0	60	80	13.90	—
1.2	0	20	$1.19 \pm 1.5\%$	99.8
2.4	0	20	$2.41 \pm 1.3\%$	100.2
4.8	0	20	$4.78 \pm 1.2\%$	99.7

[a] d: day.
[b] Values calculated from the calibration function ($n = 5$).

the high current values in the potential region < 0.5 V probably due to the high concentration of the PM and Ni(II) excess in the polarographic cell.

3.3. Polarographic determination of cyanide as degradation product of pralidoxime mesylate

To test if the proposed method was producing cyanide as a result of the alkaline conditions [3,34–36], PM samples (0.2 g) were each dissolved in 10 ml of the ammoniacal Ni(II) solution (pH 10) and they were left for various time intervals, before the measurements. Polarograms were recorded twice, one of them was used to estimate the degradation of the PM (with the electrode operating at the DME mode) and the other to determine the cyanide amounts (with the electrode operating at the HMDE mode). One sample was also submitted to heating in alkaline conditions and additionally some samples of PM were spiked with cyanide to the recovery experiments. The cyanide measurements were always conducted by transferring the solutions (i.e. PM dissolved in 10 ml of Ni(II) ammoniacal solution on its own flasks) to the polarographic cell with 10 ml of the deaerated electrolyte. Table 1 shows the results of the cyanide determination by the proposed method. The values were calculated from the calibration function.

Cyanide was not detected in PM formulations after a period of 120 min at 20°C. By heating the solution to 80°C for 60 min, a cyanide amount of 0.007% was produced from 0.2 g of a PM formulation. These results indicated that the method was adequate to determine the cyanide formed by the degradation of PM formulations. Therefore, due to the stability of the TCN anion complex and also due to the good sensitivity of the polarographic method, low concentrations of cyanide can be detected in the PM formulations.

4. Conclusion

The cyanide analysis in PM formulations by the proposed method is rapid, sensitive and allows its determination at trace levels without gas transfer steps in dialysis units and dilutions of the samples.

References

[1] E.M. May, J.E. Pearse, Anal. Proc. 20 (1983) 179.
[2] R.J. Barkman, J. Mond. Pharm. (1963) 53.
[3] R. Barkman, B. Edgren, A. Sundwall, J. Pharm. Pharmacol. 15 (1963) 671.
[4] R.I. Ellin, J. Am. Chem. Soc. 80 (1958) 6588.
[5] R.I. Ellin, J. Pharm. Sci. 71 (1982) 1057.
[6] R.I. Ellin, J.S. Carlese, A.A. Kondritzer, J. Pharm. Sci. 51 (1962) 141.
[7] G. Spoljaric, Z. Lazarevic, R. Bonevski, Acta Pharm. Jugosl. 32 (1982) 185.
[8] A.W. Boecke, Pharm. Weekbl. 113 (1978) 713.
[9] L.S. Bark, H.G. Higson, Analyst 88 (1963) 751.
[10] W.E. van der Linden, Anal. Chim. Acta 151 (1983) 359.

[11] J.S. Canham, G. Gordon, G.E. Pacey, Anal. Chim. Acta 209 (1988) 157.
[12] D. Utley, Analyst 115 (1990) 1239.
[13] J.A. Nóbrega, M.D. Capelato, R. Gama, J. Braz. Chem. Soc. 5 (1994) 91.
[14] M.T. Oms, A. Cerdà, A. Cladera, V. Cerdà, R. Fortaleza, Anal. Chim. Acta 318 (1996) 251.
[15] G.H. Kelsall, J. Electrochem. Soc. 138 (1991) 108.
[16] M.W. Scoggings, Anal. Chem. 42 (1970) 301.
[17] M.W. Scoggings, Anal. Chem. 44 (1972) 1294.
[18] P.C. do Nascimento, G. Schwedt, Anal. Chim. Acta 283 (1993) 755.
[19] R. Neeb, Inverse Polarographie und Voltammetrie, Verlag Chemie, Weinhein, 1969, p. 212.
[20] P.C. do Nascimento, D. Bohrer, L.M. Carvalho, Analyst 123 (1998) 1151.
[21] M. van Sway, R.S. Deelders, Nature 191 (1961) 241.
[22] A.J. Moteo, E.R. Gonzales, L.A. Avaca, Can. J. Chem. 64 (1986) 413.
[23] F.C. Anson, Acc. Chem. Res. 8 (1975) 400.
[24] A.S. Perez, J.E.F. de Frutos, Anal. Chim. Acta 317 (1995) 319.
[25] J.M.L. Fonseca, D. Fojón, Anal. Chim. Acta 230 (1990) 97.
[26] H.B. Mark Jr, C.N. Reilley, Anal. Chem. 35 (1963) 195.
[27] H.B. Mark Jr, C.N. Reilley, J. Electroanal. Chem. 4 (1962) 189.
[28] H.B. Mark Jr, Anal. Chem. 36 (1964) 940.
[29] H.B. Mark Jr, J. Electroanal. Chem. 7 (1964) 276.
[30] J.M.L. Fonseca, D. Fojón, Anal. Chim. Acta 230 (1990) 97.
[31] C. Giovedi, R. Tokoro, J. Braz. Chem. Soc. 8 (1997) 187.
[32] E.E. Archer, Analyst 83 (1958) 571.
[33] I.E. Krasnova, A.J. Zebreva, Elektrochimja 2 (1966) 230.
[34] P. Fyhr, A. Brodin, L. Ernerot, J. Lindquist, J. Pharm. Sci. 75 (1986) 608.
[35] D. Utley, J. Chromatogr. 265 (1983) 311.
[36] D. Utley, J. Chromatogr. 396 (1987) 237.

ELSEVIER

Talanta 48 (1999) 347–353

Talanta

Modification of iodometric determination of total and reactive sulfide in environmental samples

Zenon Pawlak [a,*], Agnieszka S. Pawlak [b]

[a] *State Health Laboratories, Utah Department of Health, 46 North Medical Drive, Salt Lake City, UT 84113, USA*
[b] *Department of Surgery, University of Texas Health Science Center, 6431 Fannin, Suite 4.268, Houston, TX 77030, USA*

Received 9 December 1997; received in revised form 15 July 1998; accepted 21 July 1998

Abstract

In iodometric determination of sulfide two reactions are taking place when alkaline solution is added to HCl acid–iodine. The main oxidation reaction (1), $H_2S + I_2 = 2HI + S$; and side reaction of sulfide (2), $S^{-2} + 4I_2 + 8OH^- = SO_4^{2-} + 8I^- + 4H_2O$. Preference of reaction (2) over (1) is dependent on pH increasing to >7. When sulfide solution of pH 9 was mixed with HCl acid–iodine, the recovery exceeded 120%, but the recovery of a solution with a pH of 13 exceeded 200%. To eliminate the side reaction in iodometric titration, the sulfide solution must be acidic when it is mixed with HCl–iodine. To avoid the side reaction (2), the pH of sulfide solutions were adjusted with acetic acid to pH 5.5, mixed with HCl–iodine solution and then titrated with standard thiosulfate with precision and accuracy $< \pm 3\%$.

Keywords: Reactive sulfide; Sulfide side reaction error; pH of mixing sulfide–iodine

1. Introduction

Sulfide concentrations in water and waste water solutions are analytically determined as total sulfide or as reactive sulfide concentrations [1–6]. The total sulfide measurements may be performed on samples prepared by precipitating sulfide in forms of ZnS or CdS [7]. The reactive sulfide analysis is based on the measurement of the amount of hydrogen sulfide released upon contact with aqueous acid (pH 2) in a closed system and then captured in weak alkaline NaOH (≈ 0.25 N). For reactive sulfide extraction processes NaOH solutions will absorb hydrogen sulfide, but in the presence of OH^- ions will cause a divergence in iodometric sulfide determinations [8]. The differences between total sulfide and reactive sulfide is in method of extraction, not in method of sulfide analysis.

Alternative absorption reagents for hydrogen sulfide have been studied, such as: a solution of diluted 0.015 N sodium hydroxide + 30% ethanol [9]; and 0.1 N sodium hydroxide + 1% triethanolamine + 0.1 M EDTA [10].

Useful quantitative tests for measuring sulfide include titrometric, colorimetric, potentiometric, coulometric and ion-selective electrode methods

* Corresponding author. Tel.: +1 801 584 8400; fax: +1 801 584 8486; e-mail: ZPawlak@doh.state.UT.US

0039-9140/99/$ - see front matter
PII S0039-9140(98)00253-7

[3,11,16]. The most common titrometric method is the iodine oxidation technique, which is designated for hazardous samples containing more than 1 mg l^{-1} of sulfide. The methylene blue method of colorimetric determination is based on the reaction of sulfide, ferric chloride, and dimethyl-*p*-phenylenediamine; which results in the formation of methylene blue. The methylene blue method is used for samples of low sulfide concentrations between 0.1 and 20 mg l^{-1}. The potentiometric method, utilizing silver/silver sulfide electrode in titration of dissolved sulfide, is applicable for contamination >0.03 mg l^{-1}.

Many contradictions appear in the literature regarding the accuracy of the iodometric determination of hydrogen sulfide. The iodometric method of determination of hydrogen sulfide and sulfides utilizes the following reaction (reaction 1):

$$H_2S + J_2 = 2HJ + S \quad (1)$$

which takes place in an acidic medium.

According to the procedure [13], for reasonably satisfactory results, the sulfide solution must be diluted with DI water to a low concentration of about 0.01 mol l^{-1}. The sulfide solution should be added to the excess of acidified iodine solution, not conversely.

Hence, if alkaline solutions (pH 9–13) containing sulfide are added to HCl acid–iodine, there is a very high risk that part of the sulfide will be oxidized to sulfate (reaction 2) [6,8,12]:

$$S^{-2} + 4I_2 + 8OH^- = SO_4^{2-} + 8I^- + 4H_2O \quad (2)$$

The purpose of our study was to evaluate the pH resulting from the mixing of sulfide solutions in pH range 9–13 with HCl acid–iodine solutions, and the impact of various conditions on the accuracy of the results of iodometric determination of sulfide. We are going to prove in our experiment that by adjusting the pH of alkaline sulfide solutions with acetic acid, an accuracy of $\pm 3\%$ is achieved. To obtain quality data, the solution of sulfide must be brought to an acidic range of pH 5–6, mixed with HCl acid–iodine solution, then the excess of iodine must be back titrated with thiosulfate until the blue, starch-iodide color disappears.

2. Materials and methods

2.1. Stock solution

Sulfide reference solutions were prepared from $Na_2S \cdot 9H_2O$ in 1l DI (deionized) water, which were standardized using 0.025 N iodine solution and 0.025 N sodium thiosulfate solutions. Sulfide reference solutions contained 6.9 and 16.1 mmol l^{-1}. These standards are unstable and should be prepared weekly, and refrigerated when not used.

2.2. Working solution

The amounts of 10, 20, 40 and 80 ml of reference sodium sulfide solution were diluted to 1000 ml volume in DI water or 0.25 N sodium hydroxide solution. A total of 100 ml of the working solution was titrated with thiosulfate using author's procedure, standard procedure, non-standard procedure or EPA 9030 method.

2.3. Methods of titration

2.3.1. Author's procedure

A total of 100 ml of sulfide (working solution) in 0.25 N NaOH solution (pH 13) was added to a flask containing 1.5 ml of glacial acetic acid and 15 ml of DI water. Case study A: The buffered sulfide solution of pH 5.5 was added to the mixture of 8 ml 6 N HCl + excess of 0.025 N iodine + 15 ml of DI water and then titrated with thiosulfate with starch acting as the indicator.

2.3.2. Standard procedure

Case study C: 100 ml of sodium sulfide (working solution) in 0.25 N NaOH solution (pH 13) was added to the mixture of 8 ml 6 N HCl, 15 ml of DI water, and excess of 0.025 N iodine solution, and then titrated with thiosulfate solution, using starch as the indicator. Case study B: Samples of sodium sulfide dissolved in DI water, resulting in pH 9.2–10.5, were analyzed.

2.3.3. Non-standard procedure

Case study D: 100 ml of sodium sulfide (working solution) in 0.25 N NaOH solution (pH 13) was added to the mixture of excess 0.025 N iodine

solution and 15 ml of DI water, acidified with 8 ml 6 N HCl and then titrated with thiosulfate solution, using starch as indicator.

2.3.4. EPA Method 9030 (sulfide determination) and 7.3.4 interim guidance for reactive sulfide (extraction procedure)

'Test method to determine hydrogen sulfide released from wastes', SW-846, chapter 7, section 7.3.4.2, provides a procedure to release hydrogen sulfide upon contact with an aqueous acid. The trapping solution of 0.25 N NaOH solution is quantified for content of sulfide by method 9030. For reactive sulfide concentration, part 7.2.3 in method 9030 is substituted as follows: 'The trapping solution must be brought to pH of 2 before proceeding with iodometric titration' (see section 7.3.4.2 part 7.7 in test methods SW-846). A 100 ml aliquot of sulfide in 0.25 N NaOH solution was used for the determination of sulfide by iodometry.

Case study E (reactive sulfide, SW-846, chapter 7, section 7.3.4.2 extraction, and EPA 9030 determination procedure): The amount of 1, 2, 4, and 8 ml of sodium sulfide (stock solution) were extracted and titrated according to the SW-846 chapter 7 and EPA 9030 procedures. A 100 ml of trapping solution in a 0.25 N NaOH solution was adjusted to pH 2 with HCl, the sulfide solution was added to the mixture of excess 0.025 N iodine solution, 2 ml 6 N HCl and 20 ml DI water, then titrated with thiosulfate solution. If the sulfide solution was brought to pH 2 using HCl, part of the sulfide was relased to the air as hydrogen sulfide.

Case study F (total sulfide, EPA method 9030): Sulfide was precipitated as ZnS (using five drops 2 N zinc acetate per 100 ml sample and a few drops of NaOH solution to produce a pH >10), filtered out, with precipitate returned to the original bottle, then 100 ml of DI water was added, resulting in a solution with pH of 10.5. The sulfide solution was subsequently mixed with HCl acid–iodine solution, resulting in a solution with a pH 10.5 and titrated with thiosulfate solution (EPA method 9030).

Sulfide samples were investigated at different pH conditions for six cases; A, B, C, D, E and F (Table 1). Calculations of sulfide concentration were made: 1 ml of 0.0250 N iodine reacts with 0.4 mg sulfide. The results for the six cases studied are shown in Table 1 and Fig. 1.

3. Results and discussion

One of the critical points of iodometric titration of sulfide is ignoring the pH value of sulfide solutions in the mixing process with the HCl acid–iodine mixture. Most methods found in the literature [1,6,8,13] recommend that the sulfide solution, which has pH over 7, be added to an acidified iodine solution, and not the reverse. However, some current standard iodometric methods [2,3,5] for titration of precipitated ZnS ignore this principle and recommended adding iodine first, and acidifying next. An error may occur due to the side oxidation of sulfide to sulfate, because the sulfide solutions usually are weakly alkaline. Mixing an alkaline sulfide solution with an HCl acid–iodine solution causes the side reaction (2) to take place to a considerable extent. Analyzing sulfide solutions with pH of about 9 and above during the mixing procedure, serves as the basis for these experiments. Also, the EPA 9030 method describing the use of HCl acid to bring the alkaline sulfide solution (pH of 13) to a pH of 2 must be changed, because of the hydrogen sulfide that is released.

Table 1 shows the results of titration of sulfide solutions using author's method, standard procedure (method approved), non-standard procedure, and the EPA 9030 method of iodometric titration. The content of sulfide was measured iodometrically for samples of sulfide in solutions of pH's 9.2–10.5, pH 13, and also precipitated as total sulfide in form of ZnS.

In Case study A it was found, that decreasing the pH of the sulfide solution from 13 to 5.5 before mixing with HCl acid–iodine, can improve sulfide analysis. Neutralization of hydroxide ions in sulfide solution by acetic acid showed no release of hydrogen sulfide, but treatment with hydrochloric acid of pH 2 (EPA method 9030), causes a release of hydrogen sulfide. An important step in eliminating the error resulting from side

Table 1
Iodometric determination of sulfide in alkaline samples

Sample status (titration procedure)	Set # 1			Set # 2		
Case study	Standard solution (μmol l^{-1})	Recovery[a]		Standard solution (μmol l^{-1})	Recovery[a]	
		(μmol l^{-1})	(%R)		(μmol l^{-1})	(%R)
(A) Standard solution in 0.25 N sodium hydroxide, treated with acetic acid, pH 5.5 (this procedure)	6.9	7.0	101	16.1	16.3	101
	13.8	13.7	99	32.3	32.3	100
	27.7	27.4	99	64.5	63.9	99
	55.4	55.4	100	129.0	129.0	100
Average (%D)[b]		±2.5			±2.3	
(B) In DI water, pH 9.2–10.5 (standard procedure)	6.9	8.3	120	16.1	18.4	114
	13.8	15.7	114	32.3	36.5	113
	27.7	32.4	117	64.5	68.5	106
	55.4	58.2	105	129.0	131.6	102
Average (%D)		±6.8			±3.2	
(C) In 0.25 N sodium hydroxide solution, pH 13 (standard procedure)	6.9	16.1	234	16.1	32.4	201
	13.8	29.0	210	32.3	56.8	176
	27.7	49.9	180	64.5	93.5	145
	55.4	87.0	157	129.0	160.0	124
Average (%D)		±8.4			±4.8	
(D) In 0.25 N sodium hydroxide solution, pH 13 (non-standard procedure)	6.9	18.3	265	16.1	39.0	242
	13.8	34.5	250	32.3	71.1	220
	27.7	63.7	230	64.5	118.7	184
	55.4	108.0	195	129.0	188.3	146
Average (%D)		±5.3			±4.3	
(E) Reactive sulfide in 0.25 N NaOH, treated with HCl, pH 2. (EPA 9030 procedure)	6.9	6.0	87	16.1	13.8	86
	13.8	11.9	86	32.3	27.1	84
	27.7	23.6	85	64.5	54.2	84
	55.4	47.6	86	129.0	109.7	85
Average (%D)		±3.5			±2.2	
(F) Total sulfide precipitated ZnS, solution pH 10.5 (EPA 9030 procedure)	6.9	7.6	110	16.1	17.4	108
	13.8	14.8	107	32.3	34.2	106
	27.7	28.8	104	64.5	66.4	103
	55.4	55.4	100	129.0	127.7	99
Average (%D)		±2.6			±2.2	

[a] Recovery or accuracy (%R) is expressed as a ratio: B/A; C/A; D/A; E/A and F/A × 100%.
[b] Precision (%D) is the 'relative percent difference' between duplicate test results, (%D) = (difference/average value) × 100%, the mean of 2–4 duplicates.

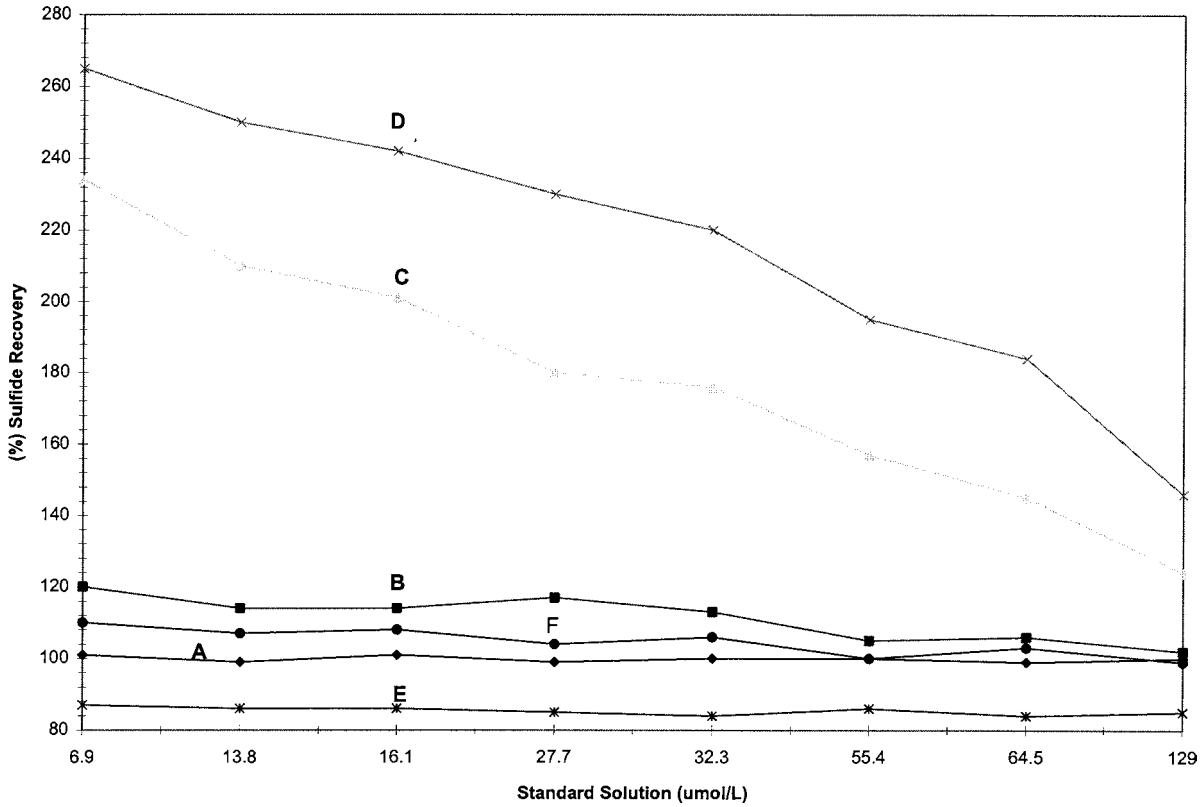

Fig. 1. Influence of pH on sulfide solutions in mixing process with HCl acid–iodine in iodometric titration with thiosulfate: Reactive sulfide solution (pH 13) treated with HCl to pH 2, followed by HCl acid–iodine (curve E); sulfide solution (pH 13) treated with acetic acid to pH 5.5 and than HCl acid–iodine (curve A); total sulfide precipitated as ZnS, treated with HCl acid–iodine (curve F); sulfide solution (pH 9.2–10.5) treated with HCl acid–iodine solution (curve B); sulfide solution (pH 13) treated with HCl acid–iodine (curve C); sulfide solution (pH 13) treated with iodine and then HCl solution (curve D).

reaction (2) is to change the pH from pH 13 to 5.5 by using acetic acid (as shown in this work). The obtained recoveries of sulfide were in range 99–101% and precision $< \pm 3\%$. The above experiments have confirmed that slight modifications in the methods may produce great differences in the results.

The standard solution of sodium sulfide in DI water resulted in pH 9.2–10.5 in the measured range of concentrations. In Case study B (Table 1), mixing a weakly alkaline sulfide with HCl acid–iodine solution using standard titration procedure (Std-Titr-Proc) resulted in side reaction (2). However, the 120% recovery of this technique is not quite sufficient for ordinary analytical work. Experiments have shown that the precision were from ± 3.2 to $\pm 6.8\%$ and recoveries from 120 to 102%.

In Case study C, sulfide in a high alkaline solution (pH 13) was added to an excess of HCl acid–iodine solution and back titrated with thiosulfate (Std-Titr-Proc). In the mixing process, sulfide was oxidized by reaction (1) and partially by reaction (2). It was found that the recoveries were in range of 234–124% for low and high standard sulfide solutions, respectively. The results have poor precision, $\pm 8.4\%$ in the lower range of the sulfide concentration. During the mixing process, the pH value of the solution changed slowly and unevenly, resulting in partial oxidation of sulfide to sulfate.

In Case study D, a high alkaline sulfide solution (pH 13) was added to an excess of non-acidified iodine solution, then 8 ml of 6 N HCl was added (Non-Std-Titr-Proc). The observed recoveries of sulfide were in the range of 265–146% for low and high standard solutions, respectively These results can be explained by the occurrence of reaction (2). Comparison of reaction (2) with reaction (1) shows that 1 mol of sulfide in alkaline solution uses 4 mol of iodine, compared to 1 mol in the acid solution. The reaction between sulfide and iodine in an alkaline solution is a kinetic process and is dependant on the concentrations of hydroxide ions and the concentration of oxidizer [14]. Considering Case study D, where sulfide in 0.25 N NaOH solution was mixed with excess of iodine solution first and then acidified, we found reaction (2) occurred to a higher extent for lower concentrations of sulfide in the sample. Reaction (2) is quite extensive in alkaline solutions with much stronger oxidants than iodine [8]. However, reaction (2) should be avoided and eliminated in sulfide determination. The way to eliminate the side reaction is to neutralize the hydroxide ions by bringing the sulfide solution into an acidic range with acetic acid and then mixing with HCl acid–iodine solution.

Results for the reactive sulfide test are shown for Case study E in Table 1. 100 ml samples were acidified with HCl to pH 2, mixed with HCl acid–iodine and titrated with thiosulfate. Our recoveries of sulfide were 84–87% and passed 50% of the EPA method requirements. It may be concluded that strong hydrochloric acid causes the release of hydrogen sulfide, therefore resulting in lower values.

Results of determination of total sulfide are shown for Case study F in Table 1. The recoveries were in the range of 110–99%, higher recoveries in low ranges of concentrations are related to the partial oxidation of sulfide to sulfate.

In Fig. 1 the percentage recovery of sulfide is plotted against standard concentrations of sulfide for six cases. The graph shows iodometric results of: Reactive sulfide solution (pH 13) treated with HCl to pH 2 and than HCl acid–iodine (curve E); sulfide solution (pH 13) treated with acetic acid to pH 5.5 and than HCl acid–iodine (curve A); total sulfide precipitated as ZnS, treated with HCl acid –iodine (curve F); sulfide solution (pH 9.2–10.5) treated with HCl acid–iodine solution (curve B); sulfide solution (pH 13) treated with HCl acid–iodine (curve C); sulfide solution (pH 13) treated with iodine and then HCl solution (curve D).

Fig. 1 illustrates the dependence of recovery of the sulfide reaction over the concentration range 6.9–129 μmol l^{-1}. In the studied concentration range (Case study C and D) sulfides showed high recoveries in the beginning, then decreased in the range of interest. As ratio [sulfide]/[iodine] increases with sulfide concentration, the sulfate formation (side reaction 2), decreases. Only under similar conditions, with pH constant, and [iodide] $\gg$ [sulfide] is the recoverable total sulfur in the form of sulfate [14]. In our experiment, excess of [iodide] was only 3 $\times$ higher than [sulfide], but it should be a 10- to 20-fold excess.

The kinetics of the oxidation of hydrogen sulfide and hydrosulfide ion to sulfur and sulfate in aqueous solution by hydrogen peroxide was investigated more than the same reaction with iodine [14,15]. Hydrogen peroxide is recommended for the treatment of odors due to the generation of hydrogen sulfide in municipal sewage treatment systems, in concrete sewer lines, and in other anaerobic environments where organic matter and sulfides are present.

With pH 8 and above, the predominant product of oxidation is sulfate, and 10-fold excess of oxidizing agent is required for the reaction to go to high yield or completion. The results are summarized in Table 2.

In alkaline solution, in presence of hydrogen peroxide, under the pseudo first-order rate constant k_{obsd} (rate $= k_{obsd}$ $[S^{2-}]_T$, $k_{obsd} = k_c$ $[H_2$

Table 2
Sulfate yield for some oxidants in alkaline media

Oxidizing agent	E° (V)	pH	% SO_4^{2-}
Hydrogen peroxide [14]	1.77	8.5	99
Potassium permanganate [[8](a)]	0.59	13.5	97
Sodium hypochlorite [[8](a)]	0.89	13.5	69
Iodine (this work)	0.54	13	<50

$O_2][H^+]$), sulfate was the only product observed [14]. The reaction of hydrogen sulfide and hydrogen peroxide has been studied kinetically, at pH 8.1, 25°C, $\mu = 0.4$, the overall rate constant (k_c) for the formation of sulfate, $k_c = 2.61\ min^{-1.}$ and only 0.021 at pH 5.05 [14].

4. Conclusions

On the basis of experimental results, the following conclusions can be drawn:

1. When alkaline sulfide solution is mixed with HCl acid–iodine solution, there is a high risk that besides the main reaction (1), the side reaction (2) will also influence our results, giving poor accuracy especially for low sulfide content.
2. It was found that adjusting the pH of alkaline sulfide samples to pH 5.5 with acetic acid before mixing with HCl acid–iodine solution, gave results with precision and accuracy $< \pm 3$ in sulfide determination (Case study A). When alkaline sulfide solution was brought to a pH of 2 with HCl (EPA 9030 method) part of the sulfide was released as hydrogen sulfide (Case study F).
3. The very high variation of side reaction (2) observed in Case study C (where sulfide solutions a pH of 13 were mixed with HCl acid–iodine to give recoveries of 234–124%), indicates of importance of pH in iodometric determination of sulfide.

Acknowledgements

The authors thank Don Gentry for helpful discussions.

References

[1] United States Environmental Protection Agency, Test Methods for Evaluating Solid Waste: Physical and Chemical Methods, 3rd ed., SW–846, United States Environmental Protection Agency, Washington DC, 1986, Methods 9030, and chapter 7 section 7.3.4.2.
[2] National Institute for Occupational Safety and Health, NIOSH Manual and Analytical Methods, National Institute for Occupational Safety and Health, Cincinnati, OH, 1977, Method No. S.4.
[3] American Public Health Association, Standard Methods for the Examination of Water and Wastewater, 19th ed., American Public Health Association, Washington DC, 1995, pp. 4–122, pp. 4–131.
[4] M.W. Skougstad, M.J. Fishman, L.C. Friedman, D.E. Erdmann, S.S. Dunkan, (Eds.), Methods for Determination of Inorganic Substances in Water and Fluvial Sediments: Techniques of Water-Resources Investigations of the United States Geological Survey, Book 5, 1979, pp. 619–620.
[5] F.J. Wechler (Ed.), Standard Methods of Chemical Analysis, 6th ed., vol. 2, part B, Van Norstrand, 1962, pp. 2484–2488.
[6] I.M. Kolthoff, B. Belcher,V.A. Stenger, G. Matsuyama, in: Volumetric Analysis, vol. 3, Interscience Publishers, 1957, pp. 291–292.
[7] W.L. Bamesberger, D.F. Adams, Environ. Sci. Technol. 47 (1969) 258–261.
[8] O. Bethage, Anal. Chimica Acta (a) 9 (1953) 129–139; ibid., (b) 10 (1954) 113–116.
[9] L.P. Van DenBerge, A. Devreese, M. Vanhoorne, Am. Ind. Hyg. Assoc. J. 46 (1985) 693–695.
[10] J.T. Purdham, L. Yongyi, Am. Ind. Hyg. Assoc. J. 51 (1990) 269–272.
[11] I.M. Kolthoff, P.J. Elving, E.B. Sandell, in: Treatise on Analytical Chemistry, vol. 7, part 2, Interscience Publishers, New York-London, 1961, pp. 75–79.
[12] I.M.Z. Kolthoff, Anal. Chem. 60 (1921) 448–457.
[13] G.H. Jeffry, J. Baset, J. Mandham, R.C. Denney, in: Vogel's Textbook of Quantitative Chemical Analysis, 5th ed., Longman Scientific and Technical, New York, 1989 pp. 398–399.
[14] M.R. Hoffmann, Environ. Sci. Technol. 11 (1977) 61–66.
[15] Y.G. Adewuyl, G.R. Carmichael, Environ. Sci. Technol. 21 (1987) 170–177.
[16] D.T. Pierce, M.S. Applebee, C. Lacher, J. Bessie, J. Environ. Sci. Technol. 32 (1998) 1734–1737.

ELSEVIER

Talanta 48 (1999) 355–362

Talanta

Differential pulse polarographic determination of tin in alloys and environmental samples after preconcentration with the ion pair of 2-nitroso-1-naphthol-4-sulfonic acid and tetradecyldimethylbenzylammonium chloride onto microcrystalline naphthalene or by column method

Mohammad Ali Taher [a,*], Bal Krishan Puri [b]

[a] *Department of Chemistry, Shahid Bahonar University of Kerman, Kerman, Iran*
[b] *Department of Chemistry, Indian Institute of Technology Delhi, Hauzkhas, New Delhi 110016, India*

Received 24 March 1998; received in revised form 20 July 1998; accepted 21 July 1998

Abstract

A highly selective, sensitive, rapid and economical differential pulse polarographic method has been developed for the determination of trace amount of tin in various standard alloys and environmental samples after adsorption of its 2-nitroso-1-naphthol-4-sulfonic acid-tetradecyldimethylbenzylammonium chloride on microcrystalline naphthalene in the pH range of 8.7–10.6. After filtration, the solid mass is shaken with 8–10 ml of 3.5 M hydrochloric acid and tin is determined by differential pulse polarography (DPP). Tin can alternatively be quantitatively adsorbed on 2-nitroso-1-naphthol-4-sulfonic acid-tetradecyldimethylbenzylammonium-naphthalene adsorbent packed in a column and determined similarly. The detection limit is 0.15 μg ml^{-1} (signal to noise ratio = 2) and the linearity is maintained in the concentration range 0.5–220 μg ml^{-1} with a correlation coefficient of 0.9995 and relative standard deviation of ±0.88%. Characterization of the electroactive process included an examination of the degree of reversibility. Various parameters such as the effect of pH, volume of aqueous phase and interference of a number of metal ions on the determination of tin has been studied in detail to optimize the conditions for determination in standard alloys and environmental samples.

Keywords: Differential pulse polarography; Tin determination; Standard alloys; Environmental samples; 2-Nitroso-1-naphthol-4 sulfonic acid; Tetradecyldimethylbenzylammonium chloride; Microcrystalline naphthalene

1. Introduction

The reagent 2-nitroso-1-naphthol-4-sulfonic acid (nitroso-*S* salt) was introduced by Hoffman [1] for the qualitative and later by Wise and Brandt [2] for the quantitative determination of

* Corresponding author. Tel.: +98 341 237001-9; fax: +98 341 232142; e-mail: taher@arg3.uk.ac.ir

0039-9140/99/$ - see front matter
PII S0039-9140(98)00254-9

cobalt. This reagent reacts with many metal ions of form water-soluble, colored chelate complex and has been applied widely in the liquid–liquid extraction spectrophotometric determination of metals in materials [3]. The most common techniques available for the pre-concentration of metals from aqueous samples are solvent extraction, and column methods using various adsorbents such as thiol cotton [4], activated carbon [5], adsorption resins [6,7], green tea leaves [8], chelating resins [9], cellulose [10], and polythioether [11]. Although some of these adsorbents are fairly effective but their methods of preparation are lengthy, and also involve rigid conditions. Solvent extraction is a simple and convenient technique for separating and concentrating metal ions, but it can not be applied directly to metal ions, which form stable complexes with the chelating agents only at elevated temperature. This difficulty can be overcome by using naphthalene as the extractant [12] for thermally stable metal chelates [13]. Solid–liquid separation after adsorption of metal chelates on microcrystalline naphthalene is more rapid and convenient, and can be applied to many types of metal complexes [14–16]. The preconcentration of this metal ion is also possible by passing their aqueous solutions over nitroso-*S*-TDBA-naphthalene adsorbent taken in a column. The microcrystalline naphthalene is rapid but the column method gives a better preconcentration factor [17–19].

In the literature, attention has been paid to the direct polarographic determination of metals after extraction of their metal complexes into organic solvents [20–24]. Unfortunately, electro-chemical methods for the direct determination of reducible substances require that the solvent used should have a fairly high dielectric constant in order to obtain well defined polarograms. Therefore, the organic phases after extraction have to be mixed with a suitable solvent of high dielectric constant to obtain well defined polarograms [25,26]. The main disadvantages of this method are that sensitivity is lost and the preconcentration factor is considerably lowered. Hence, the aim of preconcentration and direct determination of a metal is lost. For the direct determination of metal ions after extraction of their metal complexes into molten naphthalene, and dissolution of the product in an organic solvent such as dimethylformamide [27], an inert gas normally N_2 or H_2 has to be passed for at least 10–15 min to remove dissolved oxygen, again making the method more time consuming and less reproducible owing to the partial evaporation of the organic solvent.

In the present paper, we have developed a simple, rapid and economical method for the direct differential pulse polarographic determination of tin after adsorption of its nitroso-*S*-tetradecyldimethylbenzylammonium (TDBA) complex onto microcrystalline naphthalene, and subsequent desorption by 10 ml of 3.5 M hydrochloric acid. After desorption of the metal complex with HCl onto microcrystalline naphthalene method, there is no need to remove naphthalene, and HCl itself acts as a supporting electrolyte. The dissolved O_2 may be removed by $NaBH_4$ solution which provide additional NaCl in the reaction of $NaBH_4$ with HCl which can also acts as a supporting electrolyte and control the pH of the medium at the same time. The reagent Nitroso-*S* selected is very cheap, easily accessible and does not interfere in the polarography estimation of this metal ion. Most of the problems with above mentioned polarographic methods are solved by this method. The various parameters have been evaluated. The method is found to be highly selective, rapid, economical and fairly sensitive, the developed procedure has been used for determination of trace amount of tin in various standard alloys and environmental samples.

2. Experimental

2.1. Apparatus and reagents

Polarograms were recorded with an Elico CL-90 three electrodes polarography. It was outfitted with a model LR-108 X-Y recorder. Cyclic voltammograms were recorded with a cyclic voltammeter (model CV-27) outfitted with a X-Y-T recorder. All atomic absorption measurements were made using an atomic absorption spectrometer (Varian AA model 475). The glass column used for the preconcentration was 60 mm long

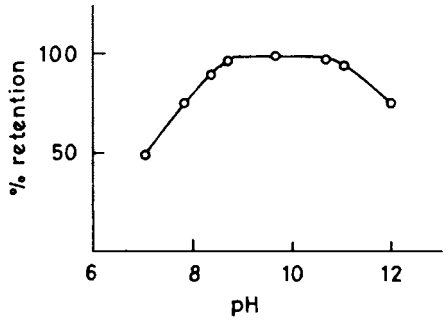

Fig. 1. Effect of pH of adsorption of tin complex: tin, 15 μg in 10 ml final solution [8 ml 3.5 M HCl and 2 ml 0.002% (v/v) Triton X-100]; reference, reagent blank. Instrumental setting: scan rate, 12 mV s^{-1}; X = Y = 100 mV cm^{-1}; sensitivity, 0.1 μA V^{-1}; drop time, 0.5 s.

and had an i.d. of 7 mm. It was plugged with polypropylene fibers and filled with the adsorbent to a height of 1.0–1.2 cm after slightly pressing/compacting with a flat glass rod.

An Elico pH meter was employed for pH measurements. Tin chloride solution was prepared by dissolving in a few ml of concentrated HCl by heating on a hot plate. After cooling, the solution was diluted with doubly distilled water and standardized by established method [28]. A 1% solution of tetradecyldimethylbenzylammonium-4-sulfonic acid (nitroso-*S*) was prepared using distilled

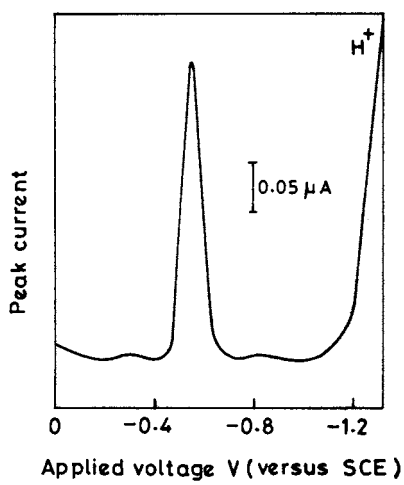

Fig. 2. A typical differential pulse polarogram of tin. Conditions and instrumental setting same as in Fig. 1.

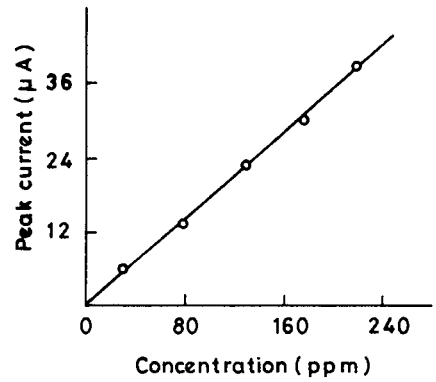

Fig. 3. Calibration curve for tin. Conditions and instrumental setting same as in Fig. 2.

water. A 20% solution of naphthalene was prepared in acetone. A 4% solution of $NaBH_4$ was prepared in 0.2 M NaOH solution. Solutions of alkali metal salts (1%) and various metal salts (0.1%) were used for studying the interference of

Table 1
Effect of foreign salts and ions

Salt or ion	Tolerance limit (mg)
$CH_3COONa.3H_2O$, KNO_3	1 g
NH_4SO_4	250
NaF	200
NH_4Br	150
KSCN	90
KI, NaCl	70
K_2CO_3, sodium oxalate	50
Sodium potassium tartrate, trisodium citrate	40
Na_2 EDTA	100 μg
Zn(II), Mo(VI)	45
Mn(II)	40
Cr(VI), Se(VI)	15
Ti(VI), Ga(II), Al(III)	18
U(VI), V(V), Te(IV)	3
Bi(III)	2.5
Fe(III)	50 μg, 1.5[a]
Rh(III), Ru(III), Cd(II)	1.7
Pd(II), Os(VIII)	1.3
Co(II), Ni(II), Cu(II), Pb(II)	0.7
Cr(VI), Sb(III)	0.5
Tl(I)	0.2

Tin was taken, 15 μg, in all tests.
[a] After masking with 2 ml of 5% triethanolamine solution.

Table 2
Analysis of tin in standard alloys

Sample	Composition %	Concentration %	
		Certified value	Found*+
NIST SRM 629 Zinc alloy	Fe 0.017, Al 5.15 Mg 0.094, Cr 0.0008 Mn 0.0017, Ni 0.0075 Si 0.078, Cu 1.50 Pb 0.0135, Cd 0.0155	0.012	0.011 ± 0.001[a]
NIST SRM 94C Zn-base die casting alloy	Ni 0.006, Mn 0.014 Fe 0.018, Mg 0.042 Al 4.13, Cu 1.01, Pb 0.006 Cd 0.002	0.006	0.006 ± 0.0008[b]
NIST SRM 627 Zn-base alloy CE	Mg 0.030, Fe 0.023 Cr 0.0038, Mn 0.014 Ni 0.0029, Si 0.021 Al 3.88, Cu 0.132, Pb 0.0083 Cd 0.005	0.0042	0.0040 ± 0.0004[b]
NIST SRM 627 Zn-base alloy E	Mg 0.094, Fe 0.17, Cr 0.0008; Mn 0.017, Ni 0.0075, Si 0.078 Al 5.15, Cu 0.50, Pb 0.0135 Cd 0.015	0.012	0.011 ± 0.002[a]
NKK 916 Al Alloy	Si 0.41, Fe 0.54, Mn 0.011 Mg 0.10, Cr 0.05, Ni 0.06 Zn 0.30, Ti 0.10, V 0.02 Zr 0.05, Bi 0.03, B 0.0006 Co 0.03, Sb 0.01, Pb 0.04 Cd 0.27	0.05	0.052 ± 0.004[a]

A 2 ml volume of 5% triethanolamine solution was added as masking reagent.
[a] Microcrystalline naphthalene method was applied.
[b] Column method was applied.
* Average of five determinations, $\pm$ SD.
+ Standard addition method was applied.
NIST SRM, National Institute of Standards and Technology, Standard ReferenceMaterials.
NKK, Nippon Keikinzoku kogyo.

anions and cations, respectively. Buffer solution of pH ≈ 10 was prepared by mixing of 0.5 M ammonia and 0.5 M ammonium acetate solutions in appropriate ratio.

2.2. Preparation of nitroso-S-TDBA-naphthalene adsorbent

A solution of naphthalene was prepared by dissolving 20 g naphthalene in 40 ml of acetone on a hot-plate stirrer at ≈ 35°C. It was transferred to a beaker containing 1500 ml of distilled water and 0.9 g (0.0028 mol) of nitroso-*S* salt in a fast stream with continuous stirring at room temperature. $TDBA^+ Cl^-$ (1.2 g, 0.0031 mol) was dissolved in 500 ml of distilled water by warming on a hot plate. It was mixed with the above solution (naphthalene-acetone-nitroso-*S* salt in water). The yellow naphthalene material co-precipitated with TDBA and nitroso-*S* was stirred for about 2 h and then allowed to stand for another 2 h at room temperature. The supernatant solution was decanted off and the residue washed twice with distilled water. The adsorbent

Table 3
Analysis of tin in environmental samples

Sample	Amount found by present method* ($\mu g\ g^{-1}$)	Amount found by AAS^{+*} ($\mu g\ g^{-1}$)
Fly ash near Indraprastha, (IP) power station, New Delhi, India	5.26 ± 0.03	5.25 ± 0.06
Soil near Wazirpur industrial area, New Delhi, India	13.45 ± 0.06	13.48 ± 0.08
Sediment of Yamuna river near Wazirpur industrial waste disposal point, New Delhi, India	2.45 ± 0.04	2.44 ± 0.05
Industrial effluents from electroplating and ceramic industry, Wazirpur industrial area, New Delhi, India	$310 \pm 4\ \mu g\ ml^{-1}$	$312 \pm 3\ \mu g\ ml^{-1}$

A 2 ml volume of 5% triethanolamine solution was added as masking reagent.
* Average of five determinations, $\pm$ SD.
$^{+}$ After preconcentration by column method.

in the form of slurry was stored in a brown bottle for subsequent use.

2.3. General procedure onto microcrystalline naphthalene

An aliquot of tin solution (containing 5–2200 μg) was placed in a 100 ml of an Erlenmeyer flask with tightly fitting stopper. Then 1 ml of 0.1% of the reagent (nitroso-*S*) was added to it and the mixture was diluted to 30–40 ml with water. The pH was adjusted to ≈ 10 with 2 ml of the buffer, then, 2 ml of 1% TDBA solution was added. The solution was mixed well and allowed to stand for a few seconds. Then, 2 ml of a 20% solution of napthalene in acetone was added to it, shaking continuously. The solid mass so formed, consisting of naphthalene and metal complex was separated by filtration on a Whatman filter paper (No. 1041). The residue was shaken vigorously with 8 ml of 3.5 M hydrochloric acid and transferred to the polarographic cell. After the addition of 2 ml of 0.002% (v/v) Triton X-100 solution, the differential pulse polarogram was recorded.

2.4. General procedure by column method

An aliquot of tin solution containing 5–2200 μg of tin was taken in 25 ml beaker. The pH of this solution was adjusted to 10 with the addition of 2 ml of a buffer solution and diluted it to ≈ 15 ml with distilled water. The column loaded with the adsorbent nitroso-*S*-TDBA-naphthalene was conditioned to pH 10 with 2–3 ml of buffer and then the metal solution was passed through the column at a flow rate of 1 ml min^{-1}. The packing was washed with a small volume of water. Desorption of metal was carried out by passing 8 ml of 3.5 M of HCl at a flow rate of 1 ml min^{-1} and the solution was transferred to the polarogaphic cell. After the addition of 2 ml of 0.002% (v/v) Triton X-100 solution, the differential pulse polarogram was recorded.

3. Results and discussion

3.1. Reversibility of tin reduction process

In the present work, the differential pulse polarograms for tin, in HCl-Triton X-100 medium as supporting electrolyte, show half peak widths of 61 ± 3 mV, in both normal and reverse scan modes. Plots of the applied potential versus log $[i/(i_d - i)]$ from d.c. polarogram has slope of -41 ± 3 mV ($r = 0.999$, and $N = 5$, where r is the correlation coefficient and N is the number of data points). The cyclic voltammogram of tin reveals that tin gives cathodic and anodic peaks with ΔE_p -7513 mV and the ratio of cathodic peak current (I_{pc}) and anodic peak current (I_{pa}) is found to be 1.8. Hence, all these studies clearly

establish the quasi-reversibility of tin reduction process under these conditions [29,30].

3.2. Retention characteristics of nitroso-S-TDBA-naphthalene

The TDBA chloride is water soluble well known quaternary ammonium salt widely used as a counter ion in anionic metal complexes in the solvent extraction of metals. The reagent 2-nitroso-1-naphthol-4-sulfonic acid has one sulfonic acid group capable of dissociation and thus it can form ion pairs (nitroso-*S*:TDBA = 1:1) with quaternary ammonium cations as follows:

$$C_{10}H_5(OH)(NO)-SO_3^- + (R)_4N^+ \rightleftharpoons [C_{10}H_5(OH)(NO)-SO_3]^-[R_4N]^+ \quad (1)$$

The ion pair formed between the anionic nitroso-*S* and cationic $TDBA^+$ is easily co-precipitated with microcrystalline naphthalene. The ion-pair reaction between nitroso-*S* and several well known quaternary ammonium salts was therefore tried to develop new adsorbents. Preliminary results indicated that only $TDBA^+$ and cetyltrimethylammonium ($CTMA^+$) can form an ion-pair with nitroso-*S*. In the present study $TDBA^+$ as the counter ion has been selected, since it is relatively cheaper than $CTMA^+$ and has excellent retention characteristics of metal ions.

3.3. Reaction conditions

The reaction conditions were investigated with 15 μg of tin. Adsorption were carried out at different pH, keeping other variables constant. It was found that the tin complex was quantitatively adsorbed on naphthalene in the pH range 8.7–10.6 (Fig. 1). Addition of 0.5–10 ml of buffer did not have any effect on the adsorption, therefore, 2.0 ml of the ammonium acetate buffer was used in all the subsequent experiments. The reagent concentration was also varied. It was found that adsorption was quantitative for 0.7–4.0 ml of 0.1% reagent. Consequently, 2.0 ml of reagent solution was used in subsequent studies. Various amounts of naphthalene was added to the sample solution, keeping other variables constant, it was observed that the peak height remained constant with the addition of 0.8–3.5 ml of 20% naphthalene solution. Therefore, 2 ml of 20% naphthalene solution was used in subsequent studies. The effect of shaking time on the adsorption indicated that the peak height remained constant over the range of 0.5–7.0 min. Therefore, 1 min of shaking time was recommended in the present work.

While in the case of column method, the flow rate was varied from 0.5 to 8 ml min^{-1}, it was found that a flow rate of 0.5–5.0 ml min^{-1} did not affect adsorption. A flow rate of 1 ml min^{-1} was recommended in all experiments.

The volume of the aqueous phase was varied in the range of 10–700 ml under the optimum conditions, keeping other variables constant. It was observed that the signal height was almost constant up to 200 ml (preconcentration factor of 20). However, for convenience, all the experiments were carried out with 40 ml of the aqueous phase.

Whereas, in the case of column method, peak height was almost constant up to an aqueous phase volume of 600 ml. Therefore, a preconcentration factor of 60 can be achieved by the column.

Preliminary observations indicated that tin complex was desorbed completely with 8–10 ml of 3.0–4.0 M hydrochloric acid. Therefore, 8–10 ml of 3.5 M hydrochloric acid was used in the present work.

3.4. Retention capacity of the adsorbent

The retention capacity of adsorbent was determined by a batch method. The experiment was performed by taking 500 μg of tin, 2 ml of the buffer (pH ≈ 10) and 40 ml of water in a beaker. This solution was transferred into a separatory funnel and then a suitable amount of the adsorbent nitroso-*S*-TDBA-naphthalene added to it. The separatory funnel was vigorously shaken on a mechanical shaker for 5 min. The solid mass was separated by filtration and tin was determined from the filtrate by AAS. The solid mass on the filter paper was dried in an oven, kept in a dessicator, and then weighed to know the mass of

the adsorbent. The maximum amount of tin retained was 6.5 mg g^{-1} of nitroso-*S*-salt, the adsorbent. It was also noted that the retention capacity depends on the amount of TDBA and nitroso-*S* supported on naphthalene. From the stoichiometry in Eq. (1), the molar ratio of nitroso-*S* and $TDBA^+$ is 1:1. From the observations on the preparation of the adsorbent, it was found that the use of nitroso-*S* (0.9 g ≈ 0.0028 M), $TDBA^+$ (1.2 g ≈ 0.0031 M) and 20 g of naphthalene were enough for the complete retention of the metal ions.

3.5. Calibration

A typical polarogram for tin is given in Fig. 2. A calibration graph for the determination of tin was prepared according to the general procedure under the optimum conditions developed above from its differential pulse polarogram with different concentration. The detection limit was 0.15 μg ml^{-1} (signal to noise ratio = 2) and this was linear over the concentration range 0.5–220 μg ml^{-1} (Fig. 3) with a correlation coefficient of 0.9995 and a relative standard deviation of ± 0.88%.

3.6. Effect of foreign ions

Various salts and metal ions were added individually to a solution containing 15 μg of tin and the general procedure was applied. The tolerance limit (error < 3%) is given in Table 1. Among the salts examined, most did not interfere at the g–mg level, only EDTA interfered seriously due to the higher formation constant of tin–EDTA complexes than the nitroso-*S*. Among the metal ions studied, many did not interfere even at the milligram level. Thus the method is highly selective without the use of masking agents. The proposed procedure has therefore been applied to the determination of tin in alloys and environmental samples without any prior separations.

3.7. Determination of tin in standard alloys

The proposed method has been applied to the determination of tin in National Institute of Standards and Technology, Standard Reference Materials NIST SRM 629 zinc alloy, NIST SRM 94C Zn-base die casting alloys, NIST SRM 627 Zn-base alloy CE, NIST SRM 627 Zn-base alloy E and in Nippon Keikinzoku Kogyo (NKK) 916 Al alloy.

An appropriate amount sample of the standard alloy was completely dissolved in ≈20 ml of hydrochloric acid (1 + 1) by heating on a water-bath and then 2 ml of 30% hydrogen peroxide was added to the solution. The excess of peroxide was decomposed by heating the solution on a water-bath. the solution was cooled and filtered if needed, and the filtrate was diluted to 100 ml with double distilled water in a calibrated flask, 50–100 ml of this solution was taken, and tin was determined by the general procedure (Table 2).

3.8. Analysis of tin in environmental samples

3.8.1. Solid environmental samples

Solid environmental samples were dried in an oven at 200°C for 2 h. A 1.0–10.0 g part of each of the samples were decomposed with 5.0–6.0 M HCl [31], then 3–5 ml of 30% hydrogen peroxide was added to it. The mixture was heated in a hot plate to almost dryness. The residue was then dissolved in 10 ml of l M HCl, diluted with 10 ml of distilled water and filtered if needed. Finally, the solution was made up to 100 ml with distilled water in a calibrated volumetric flask. An aliquot of each solution (40–100 ml) was taken individually and analyzed by the general procedure after masking iron(III) with triethanolamine solution. The results are given in Table 3.

3.8.2. Liquid environmental samples

A liquid volume of 100–1000 ml of environmental sample was taken and 5 ml of concentrated HNO_3 was added to it. The solution was heated to almost dryness on a hot plate. The residue was dissolved in 5 ml of l M HCl and finally, the solution was made up to 100 ml with distilled water in a calibrated volumetric flask [32]. An aliquot of this sample solution (40–100 ml) was taken individualy and analyzed by the general procedure after iron(III) was masked with triethanolamine. The result is given in Table 3.

4. Conclusions

It is difficult to obtain a well defined polarogram in the traditional analysis for metals after extraction of their complexes into an organic solvent owing to the low dielectric constant of the organic phase. Sensitivity is lost if it is mixed with another solvent of high dielectric constant. Another major disadvantage is the removal of dissolved oxygen, which is a tedious and time consuming process. Moreover, the reproducibility of the method is effected by the partial evaporation of organic solvent. The reported method has solved most of these problems and has been successfully tested for the determination of tin in various environmental samples and standard alloys. The determination of tin by a cyclic voltammetric technique using a gold amalgamated electrode after adsorption of tin complex onto microcrystalline naphthalene or column method can be possible, but the sensitivity and reproducibility of this method are relatively low. Column methods improve the preconcentration but are time consuming.

References

[1] O. Hoffman, Chem. Ber. 18 (1885) 46.
[2] W.M. Wise, W.W. Brandt, Anal. Chem. 26 (1954) 693.
[3] A.K. De, R.A. Chalmers, S.M. Khopkar, Solvent Extraction of Metals, Van Nostrand, London, 1970.
[4] M.Q. Yu, G.Q. Liu, Q. Jin, Talanta 30 (1983) 265.
[5] B.M. Vanderborght, R.E. Vangrieken, Anal. Chem. 40 (1977) 311.
[6] L. Elci, Anal. Lett. 26 (5) (1993) 1025.
[7] M. Soylak, L. Elci, Int. J. Environ. Anal. Chem. 66 (1) (1997) 51.
[8] K. Kimura, H. Yamashita, J. Komada, Bunseki Kagaku 35 (1986) 400.
[9] D.G. Biecher, Anal. Chem. 37 (1965) 1054.
[10] P. Burba, P.G. Willmer, Talanta 30 (1983) 381.
[11] A.S. Khan, A. Chow, Talanta 33 (1986) 182.
[12] A. Wasey, R.K. Bansal, B.K. Puri, A.L.J. Rao, Talanta 31 (1984) 205.
[13] M. Satake, G. Kano, S. Usami, B.K. Puri, Indian J. Chem. 27A (1988) 265.
[14] M. Satake, M.C. Mehra, Microchem. J. 27 (1982) 182.
[15] M. Satake, Y. Matsumura, M.C. Mehra, Mikrochim. Acta 1 (1980) 455.
[16] J.L. Lin, M. Satake, B.K. Puri, Analyst 110 (1985) 1351.
[17] M.A. Taher, B.K. Puri, Analyst 120 (1995) 1589.
[18] M.A. Taher, B.K. Puri, Ann. Chim. (Rome) 85 (1995) 183.
[19] M.A. Taher, B.K. Puri, Talanta 43 (1996) 247.
[20] Y. Nagaosa, N. Sato, Buseki Kagaku 36 (1984) 877.
[21] T. Odshima, Y. Kawate, H. Ishii, Bunseki Kagaku 37 (1988) 439.
[22] Y. Nagaosa, T. Sona, Anal. Lett. 17 (1984) 243.
[23] Y. Nagaosa, Anal. Chim. Acta 115 (1980) 81.
[24] Y. Nagaosa, K. Kobayshi, Talanta 31 (1984) 593.
[25] T. Fujinaga, Y. Nagaosa, Chem. Lett. 6 (1987) 587.
[26] A.M. Bond, Modern Polarogaraphic Methods in Analytical Chemistry, Marcel Dekker, New York, 1980, p. 250.
[27] B.K. Puri, M. Gantam, T. Funginaga, Bull. Chem. Soc. Jpn. 52 (1979) 3415.
[28] A.I. Vogel, A text book of Quantitative Inorganic Analysis, 4th ed., Longman, London, 1978.
[29] A.M. Bond, Modern Polarographic Methods in Analytical Chemistry, Marcel Dekker, New York, 1980.
[30] J. Heyrovsky, J. Kuta, Principles of Polarography, Publishing House of the Czechoslovak Academy of Sciences, Prague, 1966.
[31] P.D. Goulden, Environmental Pollution Analysis, Heydrn, London, 1978.
[32] S. Usami, S. Yamada, B.K. Puri, M. Satake, Mikrochim. Acta 1 (1989) 263.

ELSEVIER

Talanta 48 (1999) 363–367

Talanta

A novel biosensor for specific determination of hydrogen peroxide: catalase enzyme electrode based on dissolved oxygen probe

Sinan Akgöl, Erhan Dinçkaya *

Department of Biochemistry, Faculty of Science, Ege University, 35100 Bornova-Izmir, Turkey

Received 9 April 1998; received in revised form 16 July 1998; accepted 21 July 1998

Abstract

A biosensor for the specific determination of hydrogen peroxide was developed using catalase (EC 1.11.1.6) in combination with a dissolved oxygen probe. Catalase was immobilized with gelatin by means of glutaraldehyde and fixed on a pretreated teflon membrane served as enzyme electrode. The electrode response was maximum when 50 mM phosphate buffer was used at pH 7.0 and at 35°C. The biosensor response depends linearly on hydrogen peroxide concentration between 1.0×10^{-5} and 3.0×10^{-3} M with a response time of 30 s. The sensor is stable for >3 months so in this period >400 assays can be performed.

Keywords: Catalase; Hydrogen peroxide; Biosensor; Catalase electrode; Catalase immobilization

1. Introduction

Hydrogen peroxide is an important industrial material, being used for waste water treatment, sterilization and as a source of oxygen. Determination of hydrogen peroxide is also very important in the food industry; e.g. it is added as antibacterial agent to milk and has to be removed by catalase addition before milk microbiologically transformed into cheese. In addition to this the detection of hydrogen peroxide plays and important role in the electrochemistry of many enzyme based amperometric biosensors [1,2]. This is not only because hydrogen peroxide is itself an important analyte in many areas, including industry, clinical laboratory and the environment, but also because many of the oxidases frequently used to realize amperometric sensors for biologically important substrates have hydrogen peroxide as an end product [3].

Hydrogen peroxide has been determined by spectrophotometric [4,5], enzymatic [6], thermooptic [7], and chemiluminescence [8,9]. These techniques can suffer from various interferences and can also be time-consuming, with many requiring expensive reagents.

The aim of the present study is to develop a relatively inexpensive and simple procedure to determine hydrogen peroxide concentration.

* Corresponding author. Fax: +90 232 3881036; e-mail: Erbchem@fenfak.ege.edu.tr

0039-9140/99/$ - see front matter
PII S0039-9140(98)00255-0

The amount of oxygen produced which was in proportion to hydrogen peroxide concentration, was determined by YSI 54 A model oxygenmeter according to the reaction shown below;

$$H_2O_2 \xrightarrow{\text{Catalase}} 1/2O_2 + H_2O$$

For the preparation of catalase electrode, catalase was immobilized on the surface of the YSI 5739 model oxygen probe. The enzyme was immobilized directly on the gas permeable membrane of a dissolved oxygen probe by copolymerization with gelatin, using the bifunctional agent glutaraldehyde.

2. Experimental

2.1. Chemicals

Catalase (EC 1.11.1.6) (from bovine liver), 225 bloom calf skin gelatin and glutaraldehyde were obtained from Sigma, St. Louis, MO. All other chemicals were purchased from E. Merck, Darmstadt, FRG.

2.2. Apparatus

YSI 5739 model dissolved oxygen (DO) probes based on amperometric consist of Au (cathode), Ag-AgCl (anode), half-saturated KCl (electrolyte) and a teflon membrane (0.001 in. thick FEP teflon membrane) which is selective for oxygen. DO probes were connected to a YSI 54 A model oxygenmeter (YSI, Yellow Springs, Ohio). Ultrathermostat (Colora, FRG) were also used.

2.3. Electrode preparation

The membrane (teflon membrane) of DO probe was pretreated with a 0.5% lauryl sulphate solution in 50 mM phosphate buffer (pH 7.5). Catalase (3.33 mg catalase ml^{-1} (9324.2 IU ml^{-1})) and 225 bloom gelatin (33.3 mg ml^{-1}) were mixed at 38°C in distilled water. The mixed solution (200 μl) was spread over the DO probe membrane (1.13 cm^2) and allowed to dry at 4°C for 2 h. Finally it was immersed in 2.5% glutaraldehyde in 50 mM phosphate buffer (pH 7.5) for 3 min. The enzyme electrode contained 0.59 mg catalase cm^{-2} (1650.3 IU cm^{-2}) and 5.9 mg cm^{-2} gelatin.

2.4. Measurements of oxygen production by enzyme electrode

These were carried out at 35°C and varying hydrogen peroxide concentrations in steady-state condition. All the measurements were carried out using a thermostatic cell [10,11]. In the steady-state method, addition of hydrogen peroxide caused a rapid current increase due to hydrogen peroxide destruction in the enzyme layer, which reached a steady-state, within 30 s and dissolved oxygen was recorded by oxygen meter.

3. Results and discussion

3.1. Enzyme electrode optimization

3.1.1. Effect of pH

The pH dependence of the electrode signal was investigated and a pH of 7.0 was found to be optimum.

3.1.2. Effect of buffer system

The electrode response was examined in different working buffers, such as phosphate, Tris–HCl and HEPES buffers at 50 mM. The electrode response was highest with phosphate buffer and hence phosphate buffer was chosen as the working buffer.

3.1.3. Effect of buffer concentrations

Phosphate buffer at varying concentrations (25, 50 and 100 mM) was tested for maximum electrode response. For 25 and 50 mM, the same electrode response was found. However, in the case of increasing the buffer concentration to 100 mM, the electrode response decreased $\sim 10\%$, in comparison with 25 and 50 mM. This can be explained in terms of the increasing effects of the ionic strength on enzymatic activity as negative. As the buffer capacity of 50 mM buffer concentration was higher than the 25 mM one, it was preferred. Therefore, 50 mM phosphate buffer was used in all measurements throughout this work.

3.1.4. Effect of temperature

The effect of varying temperature (25–45°C) on the response was examined (Fig. 1). The highest electrode responses were observed between 30–35°C. As a result of the effect of temperature on enzymatic activity, electrode responses decreased below and above these temperatures. Consequently, 35°C was selected as the working temperature.

3.1.5. Effect of the amount of the enzyme

The enzymatic activity of the bioactive membrane layer depended upon the amount of enzyme (Fig. 2). Below 82.5 IU cm^{-2} (2.95×10^{-2} mg catalase cm^{-2}) catalase activity value, the electrode response decreased as a result of decreased enzymatic activity and above this value, no increase of sensitivity was observed due to limited diffusion of substrates into extremely cross-linked membrane layer. However, for the longer life time of the electrode, enzymatic activity was chosen as 1650.3 IU cm^{-2} (0.59 mg catalase cm^{-2}).

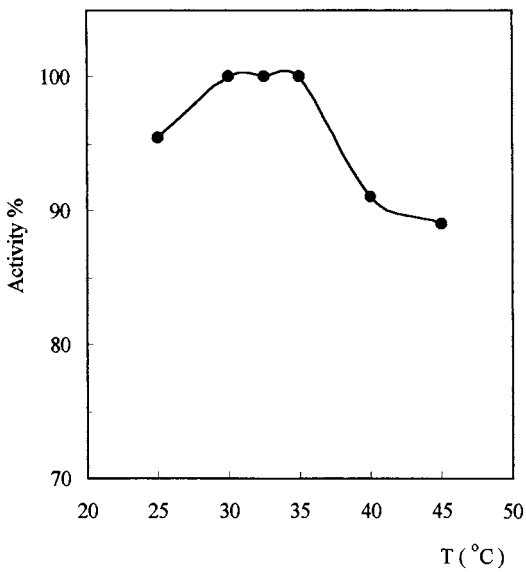

Fig. 1. Effect of temperature on the catalase biosensor. The amount of catalase and gelatin were kept constant as 0.59 mg catalase cm^{-2} (1650.3×10^{-3} IU cm^{-2}) and 5.9 mg gelatin cm^{-2}, respectively. Hydrogen peroxide concentration was 0.6 mM. Working conditions: phosphate buffer; pH: 7.0, 50 mM, 35°C.

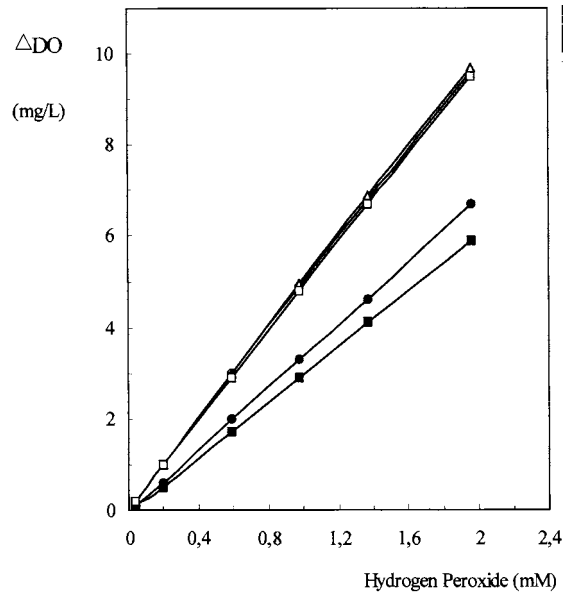

Fig. 2. Effect of enzyme amount on electrode response. Bioactive membrane layers of catalase enzyme electrodes contain fixed concentration of gelatin (5.9 mg cm^{-2}) and varying levels of catalase activity. The amount of catalase;-■-, 2.95×10^{-4} mg catalase cm^{-2} (82.5×10^{-2} IU cm^{-2}); -●-, 0.59×10^{-3} mg catalase cm^{-2} (1650.3×10^{-3} cm^{-2}); -○-, 2.95×10^{-2} mg catalase cm^{-2} (82.5 IU cm^{-2}); -△-, 0.59 mg catalase cm^{-2} (1650.3 IU cm^{-2}); -□-, 11.8 mg catalase cm^{-2} (33005.8 IU cm^{-2}).

3.1.6. Effect of amount of gelatin

The effect of varying amount of gelatin (5.9 mg cm^{-2}, 11.8 mg cm^{-2}, 17.7 mg cm^{-2}) on electrode response was investigated. Increasing the gelatin amount 2-fold and 3-fold in bioactive membrane layer has caused a decrease in the electrode response ~ 7 and 14%, respectively. High amounts of gelatin thicken the membrane layer which increases the diffusion barrier. Depending on this fact, electrode responses decrease. For the preparation of the membrane 5.9 mg gelatin amount was preferred as both obtaining high electrode responses and the practical preparation of the bioactive membrane layer.

3.2. Analytical characteristics

3.2.1. Linear range

Catalase enzyme electrode response depends linearly on hydrogen peroxide concentration be-

tween 1.0×10^{-5}–3.0×10^{-3} M with response time 30 s.

3.2.2. Accuracy

Hydrogen peroxide standard solutions (0.59 mM) prepared by dilution of a 9.79 M stock solution. The biosensors when tested for its accuracy on 18 standard solutions ($n = 18$) of hydrogen peroxide containing equal amounts of hydrogen peroxide gave $\pm 4.20 \times 10^{-3}$ standard deviation (SD) and 0.71% variation coefficient (CV) as mean value for the assayed samples of hydrogen peroxide.

3.2.3. Stability

The stability of the enzyme electrode was assessed by its storage and operational efficiency. In order to determine the biosensor storage stability, only five measurements were done for a 3 month period. The biosensor was not used except this purpose. The enzyme electrode was stored at 4°C in a flask which contains the some amount of distilled water. The water provides a moisture medium therefore the dryness of the gelatin–catalase layer is prevented. All measurements were carried out in the phosphate buffer (pH 7.0, 50 mM) at 35°C. After the storage period, it was determined that the retained activity of the enzyme electrode is $>90\%$ of its starting activity (Fig. 3).

On the other hand, another catalase enzyme electrode which has same properties was used for the determination of operational stability of the electrode. Five measurements were done per day during a 3 month period. All measurements were carried out in the phosphate buffer (pH 7.0, 50 mM) at 35°C. During the experimental period >400 assays were carried out using the same electrode.

The results obtained for this biosensor were compared with those of earlier catalase sensors and it was found that the new method is rapid, uses conventional apparatus and its economical in its use of enzyme. The advantage as compared with the catalase electrode described by Dajun [12] lies in expanding of the linear range from 1.0×10^{-5}–1.0×10^{-3} hydrogen peroxide to 1.0×10^{-5}–3.0×10^{-3}. For the catalase sensor described by Li [13], the response time is 5 min. In addition to these, for the bacteria based biosensor of hydrogen peroxide developed by Tai [14] life time has been reported to be 65 days. For the organic phase biosensors of hydrogen peroxide described by Wang [15], relative standard deviations are 1.6–1.9%. For the biosensor of hydrogen peroxide developed by Dajun [12] the variation coefficient is 6.1%. On the other hand, the response time and life time of our sensor are 30 s and at least 3 months, respectively. At the reproducibility studies, standard deviation and variation coefficient of our sensor are $\pm 4.20 \times 10^{-3}$ and 0.71%, respectively. However, >400 assays can be performed during 3 months with the sensor based on catalase immobilized in gelatin, thus indicating clear superiority of this method over the earlier ones.

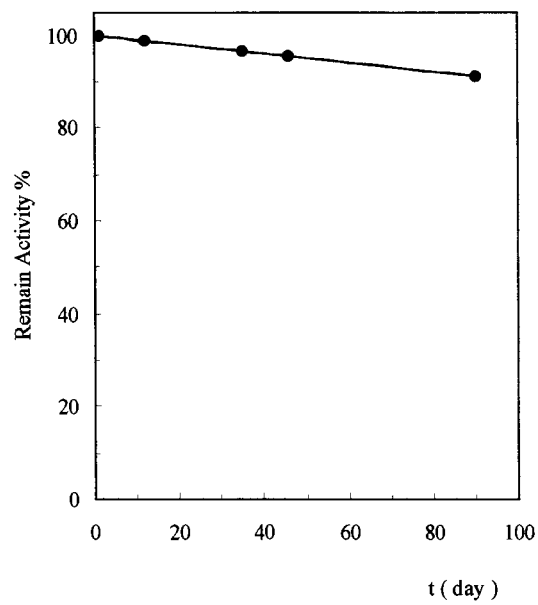

Fig. 3. The storage stability of catalase electrode. The amount of catalase and gelatin were kept constant as 0.59 mg catalase cm^{-2} (1650.3×10^{-3} IU cm^{-2}) and 5.9 mg gelatin cm^{-2}, respectively. Hydrogen peroxide concentration was 0.04 mM. Working conditions: phosphate buffer; pH: 7.0, 50 mM, 35°C.

References

[1] M. Cosgrove, G.J. Moddy, J.D.R. Thomas, Analyst 113 (1988) 1811.
[2] A. Ciucu, V. Magearu, C. Luca, Anal. Lett. 18 (B3) (1985) 299.
[3] I.C. Popescu, G. Zetterberg, L. Gorton, Biosens. Bioelectr. 10 (1995) 443.
[4] F. Wang, Y.Z. Wu, S.S. Shang, Y.X. Ci, Fresenius J. Anal. Chem. 344 (1992) 556.
[5] H. Afsar, B. Demirata, Fresenius J. Anal. Chem. 347 (1993) 460.
[6] G. Demmano, E. Selegny, J.C. Vincent, Eur. J. Biochem. 238 (1996) 735.
[7] X.Z. Wu, H. Shindoh, T. Hobo, Anal. Chim. Acta 299 (1995) 33.
[8] F. Preuschoff, U. Spohn, D. Janasek, E. Weber, Biosens. Bioelectr. 9 (1994) 543.
[9] D. Price, P.J. Worsfold, R.F.C. Mantourna, Anal. Chim. Acta 298 (1994) 121.
[10] E. Dinckaya, A. Telefoncu, Ind. J. Biochem. Biophys. 30 (1993) 282.
[11] E. Dinçkaya, A. Telefoncu, Turk. J. Chem. 18 (1994) 1.
[12] C. Dajun, W. Xiaqin, Z. Zukin, Sensors Actuators B 13–14 (1993) 554.
[13] J.Z. Li, Z.J. Zhang, L. Li, Talanta 41 (1994) 1999.
[14] G.V. Tai, M.L. Wen, C.Y. Wang, Microchem. J. 53 (1996) 152.
[15] J. Wang, G. Rivas, J. Liu, Anal. Lett. 28 (1995) 2287.

ELSEVIER

Talanta 48 (1999) 369–375

Talanta

Colour reaction of chromium (VI) with *N*,*N*-diethyl-1,4-phenylenediame in the presence of ethanol and cyclohexyldiamine tetraacetic acid as well as its application in the species analysis of chromium

Minghao Zhang [a,*], Quanru Zhang [a], Zheng Fang [a], Zhenchun Lei [b]

[a] *Department of Chemistry, Central South University of Technology, Changsha 410083, People's Republic of China*
[b] *Central Laboratory of Analysis, Shuikoushan Mine Work Bureau, Shuikoushan 421513, People's Republic of China*

Received 14 January 1998; received in revised form 21 July 1998; accepted 22 July 1998

Abstract

A simple, rapid and precise spectrophotometric method for the determination of Chromium (III and IV) has been developed. The reaction of Cr(VI) with *N*,*N*-diethyl-1,4-phenylenediamine is almost complete in a twinkling, which yields a red product with a wavelength of maximum absorption at 530 nm. Beer's Law is obeyed in the Cr concentration range of 0–2.0 μg ml^{-1}. The molar absorptivity is 5.0×10^4 l mol^{-1} cm^{-1}, limit of detection 0.002 μg ml^{-1} and relative SD = 1.13% for 5.04 μg Cr. The colouring rate and absorbance are not noticeably affected by temperature from 2 to 45°C. The amounts of Cr(VI) and Cr(III) were measured by determining Cr(VI) first under the condition of masking Cr(III) by cyclohexyldiamine tetraacetic acid, and then the total amount by oxidation of Cr(III). The method was applied to the analyses of some industrial waste waters containing Cr with satisfactory results.

Keywords: Chromium; *N*,*N*-diethyl-1,4-phenylene diamine spectrophotometry; Cyclohexyldiamine tetraacetic acid

1. Introduction

There is little conclusive evidence of the toxic effects of Cr(III) so far. In most cases, Cr(III) is even considered to be an essential element in nutrition [1]. Contrarily, Cr(VI) is a carcinogen. Because of the unique biochemical roles of chromium [2–4], the species analysis of the chromium ions is very important not only in environmental, clinical and biological research, but also in the control of industrial waste water. Usually, Cr(III) and Cr(VI) interfere with each other in the species analysis. Hence, a two-stage analysis is carried out by using chromatographic [5–13], solvent extraction [14–17], precipitation [18], volatility [19] and electrochemical separations [20,21]. Unfortunately, the results obtained

* Corresponding author. Fax: +86 731 8879672; e-mail: x-hgs@csut.edu.cn

0039-9140/99/$ - see front matter
PII S0039-9140(98)00256-2

have an unacceptable precision, a few of the good analytical methods are very time-consuming and some of the instruments are more complicated.

In this paper, a new method for the species analysis of chromium will be reported, based on the colour reaction of Cr(VI) with *N*,*N*-diethyl-1,4-phenylenediamine sulphate (TSS) [22] in the presence of ethanol. The individual amount of Cr(VI) is measured, first under the condition of masking Cr(III) by cyclohexyldiamine tetraacetic acid (CyDTA), then the total Cr after the oxidation of Cr(III) into Cr(VI), and then the Cr(III) is obtained from the difference. It has the principal advantages of rapid colouring at room temperature, apparent independence of the colouring rate and absorbance from temperature, simple and convenient procedure, better stability and selectivity, wide linear range, higher sensitivity and good reproducibility

2. Experimental

2.1. Apparatus

A spectrophotometer (Model 72G, Shanghai Analytical Instrument Factory) with stoppered comparison cell of 1 cm (or 0.5 cm) optical path and a pH meter (Model 25, Shanghai Kanchuan Metals Factory) were used.

2.2. Reagents

Ethanol, 0.1% $AgNO_3$ solution, and 25% $(NH_4)_2S_2O_8$ solution.

HAc–NaAc buffer solution, pH 3.8 (25°C): 32 g anhydrous sodium acetate was dissolved in a small amount of water, pH was adjusted to 3.8 with glacial acetic acid ($\approx$ 134 ml) and diluted to 1000 ml with ethanol.

0.40% CyDTA solution: 2.0 g CyDTA was dissolved in 50 ml of 4% NaOH solution, and the resulting solution was diluted to 500 ml with ethanol.

TSS ethanol solution: A mixture of 4.25 g TSS and 10 ml of 1:1 H_2SO_4 was dissolved in ethanol and diluted to 250 ml with ethanol. The solution was stable in a light-proof bottle placed in a refrigerator for up to 9 months.

The mixed standard solution of equimolar Cr(III) and Cr(VI): 2.8289 g primary standard $K_2Cr_2O_7$ was dissolved in a small amount of water, acidified with two drops of sulphuric acid, and diluted to 1000 ml. The concentration of the Cr(VI) stock solution was 1 g l^{-1}. The stock solution of 1 g Cr(III) l^{-1} was prepared by reducing Cr(VI) with H_2O_2. The mixed standard solution should be prepared daily [23] by 100 times subsequent dilution of the stock solutions.

Redistilled water was used, other reagents except chromium salts were of analytical grade.

2.3. Method for determination

Determination of Cr(VI): The standard or sample solution containing $\approx$10 μg Cr(VI) to be measured and 8.0 ml HAc–NaAc buffer solution was added into 25 ml comparison tubes, then 0.5 ml CyDTA solution was added to each one. After shaking up the mixture, 1.5 ml TSS ethanol solution was added. It was diluted to the mark with water and shaken up again. The absorbance at 530 nm wavelength was measured against the reagent blank prepared in the same manner, in order to obtain the amount of Cr(VI).

Determination of the total amount of Cr: A known volume of standard of sample solution containing total Cr of $\approx$10 μg, 10 ml water, 4 drops 0.1% $AgNO_3$ solution and 1 ml 25% $(NH_4)_2S_2O_8$ solution, were added to 50 ml flasks, to oxidize Cr(III) into Cr(VI). The solution was boiled and vaporized to almost dry and then transformed quantitatively into 25 ml comparison tubes with HAc–NaAc buffer solution and water. The absorbance was measured in the same manner as mentioned above, in order to obtain the total amount of Cr.

3. Results

3.1. Absorption Spectra

The wavelength of maximum absorbance for the chromophore product was 530 nm. The relative molar absorption coefficient is 5.0×10^4 l $mol^{-1} \cdot cm^{-1}$. Pure TSS had no absorption peak in the wavelength range of 400–600 nm.

3.2. Effect of acidity

The experimental results showed that, at pH 3.0–4.6, the absorbance is at a maximum and fundamentally invariable. Hence, HAc–NaAc buffer solution pH 3.8, was selected to control the colouring acidity, considering the intrinsic acidic or basic property of a sample.

3.3. Effect of reagent amounts

HAc–NaAc buffer solution: The experiment showed that >6.0 ml of the buffer solution was suitable and 8.0 ml was recommended.

TSS solution: The maximum and stable absorbance occurred when 1.0–2.5 ml TSS solution was added under the selected conditions. Therefore, 1.5 ml was selected.

CyDTA solution: CyDTA was used as a masking agent of Cr(III) and some other ions coexisting with Cr(VI). The experiment showed that under the selected conditions Cr(III) did not interfere with determining Cr(VI) and the masking to the other interfering ions was also very effective, when the amount of CyDTA was ≥ 0.20 ml. Therefore, 0.5 ml CyDTA solution was recommended. However, the amount of CyDTA used should be properly increased, if the amount of Cr(III) and the other ions is greater.

Ethanol: The effect of ethanol on the stability of the colouring product is shown in Table 1. The stable time of absorbance lasted for ≈ 20 min in the non-ethanol medium. The more ethanol present, the more the colour compound stabilized. The absorbance lasted for >69 min and the sensitivity increased by $\approx 10\%$ when the ethanol concentration was $\geq 30\%$. However, a kind of white precipitation emerged when the volume ratio was $\geq 57\%$. Therefore, the volume ratio of 31% was chosen, but the amount of ethanol used could be somewhat decreased according to practical conditions.

3.4. Effects of temperature and time

The experiment showed that the colouring rate and absorbance were virtually unaffected by temperature between 2 and 45°C, and that the absorbance reached maximun value, almost in an instant, after the beginning of the colour reaction. It's stable time was long, as shown in Table 1.

3.5. Analytical characteristics

Beer's Law was obeyed over Cr concentration range of 0–2.0 μg ml^{-1}. The linear equation fixed was $A = 0.009 + 0.464C$ (A, absorbance; C, Cr concentration) and the correlation coefficient 0.998. The limit of detection was 0.002 μg ml^{-1}.

3.6. Interferences

Forty-six diverse substances were added individually to the test solution to examine their influence. Under the condition of the pre-oxidation of Cr(III), the valence states or existing forms of some coexisting substances were changed. As a result, their interferences with the determination of Cr(VI) and the total Cr might be different.

Interferences with determining Cr(VI): Such ions as NO_3^-, SO_4^{2-}, Ac^-, $C_2O_4^{2-}$, HPO_4^{2-}, $H_2PO_4^-$, AsO_3^{3-}, CyDTA anion, K^+, Na^+, NH_4^+, Mn^{2+}, Ca^{2+}, Mg^{2+}, Ba^{2+}, and Fe^{2+} were not of influence. The tolerance limits (error 5%) of the other interference substances are listed in Table 2. MnO_4^- and ClO^- (or HClO, or Cl_2) have an influence on the determination. However, they may be eliminated [24,25].

Table 1
The effect of ethanol on stability of the colouring product

Used amount of ethanol (ml)	Absorbance	Stable time[a] of absorbance (min)
0	0.340	20
2.0	0.364	36
4.0	0.376	49
6.0	0.384	60
8.0	0.385	69
10.0	0.385	73
12.0	0.384	76
14.0	0.385	78
14.5	0.384	80
15.0	Precipitation emerges	—
16.0	Precipitation emerges	—

[a] The absorbance decreased very slowly over the stable time.

Table 2
The tolerance limits of the substances interference with the determination of 0.4 μg ml^{-1} of chromium (25 ml) with TSS under selected conditions

Determination of Cr(VI)		Determination of total Cr	
Substance added	Amount tolerated (μg ml^{-1}, 25 ml)	Substance added	Amount tolerated (μg· ml^{-1}, 25 ml)
Sb(III)	200	Bi(III)	82
Bi(III)	82	Pb(IV) Pb(II) As(V) As(III)	64
Pb(IV)As(V)	64	Mo(VI)Ni(II)	48
Mo(VI) Ni(II)	48	Zn(II) Hg(II) Co(II) Ag(I)	40
Zn(II) Hg(II) Co(II) Ag(I)	40	W(VI) Al(III) Mg(II) Sb(V) Sb(III)	34
W(VI) Al(III) Mg(II) Sb(V)	34	Sn(IV) Sn(II) Fe(III) Fe(II) Cu(II)	16
Pb(II)	24	$NHCl_2$	14
Sn(IV) Fe(III) Cu(II)	16	NH_2Cl	11.9
Cr(III)	9.2	NCl_3	11.2
Cd(II)SO_3^{2-}	8.0	Cd(II)	8.0
NO_2^-	7.6	ClO^-	7.1
ClO_3^-	5.5	ClO_2^-	5.0
Sn(II)	5.2	ClO_3^-	3.8
ClO_2^-	1.9	V(V)	1.7
V(V)	1.7		
$NHCl_2$	0.7		
NH_2Cl	0.5		
NCl_3	0.3		

Interferences with determining total Cr: NO_3^-, NO_2^-, SO_4^{2-}, SO_3^{2-}, Ac^-, $C_2O_4^{2-}$, HPO_4^{2-}, $H_2PO_4^-$, CyDTA anion, K^+, Na^+, NH_4^+, Ca^{2+}, Mg^{2+}, and Ba^{2+} ions did not influence the measurement of total Cr. The tolerance limits (error 5%) of the other interference substances are also listed in Table 2.Mn^{2+} had an influence, because it was oxidized into MnO_4^-. The influence could be eliminated as stated above.

3.7. Applications

The method (I) had been applied to the species analysis of the chromium ions in industrial waste water. The results are shown in Table 3.

4. Discussion

The pattern of the absorption spectrum and the maximum absorption wavelength in the absence of ethanol, were basically the same as in the presence of it, but with a slight decrease in peak factor. The same pattern showed that the ratio of Cr(III):TSS in the colour complexes in medium with or without ethanol, does not vary. This was found to be 1:3, by spectrophotometry. The reason for the difference in the intensity of the maximum wavelength might be the difference of the potentials of the Cr(VI)/Cr(III) electrode pair [26] in the water–ethanol and water solvents. The former was measured as 1.39 V and the latter as 1.32 V. The difference favours the reduction of Cr(VI). In addition, Cr(III) can completely complex with TSS at 50°C and in 56 min, to form the same colouring product as Cr(VI).

It is found that $3.0 > pH > 4.6$ is not suitable for colouring acidity, because, to provide a pair of coordinate electrons from TSS is difficult at $pH < 3.0$, while the oxidition ability of Cr(VI) will decrease greatly at $pH > 4.6$.

In general, the complex, whose ligand is CyDTA, is the more stable among the complexes, which consist of a metal ion and various common

Table 3
The analytical results of Cr(III), Cr(VI) and the total Cr in some industrial waste water (μg l^{-1})

Sources of water samples	Item measured	Parallel measurements with method I								Average of method I	RSD (%)	Average of II[c]
a												
	Total Cr	341	337	338	333	332	339	337	330	336	1.13	334
	Cr(VI)	239	233	230	234	237	238	229	234	234	1.55	230
	Cr(III)	102	104	108	99	95	101	108	96			
b	Total Cr	172	176	170	169	173	171	168	174	172	1.57	171
	Cr(VI)	116	120	121	119	119	116	121	123	119	2.08	116
	Cr(III)	56	56	49	50	54	55	47	51			

[a] The waste water discharged by the chromium shop in Hunan Ferro-alloy Plant.
[b] The waste water discharged by the manganese and chromium salt shop in Hunan Chemicals Plant
[c] A reference method [24] using diphenylamine urea as a colouring reagent.

aminocarboxylic acids [27]. The experiment showed that, among six common aminocarboxylic acids EDTA, CyDTA, DTPA, EGTA, HEDTA, and NTA, CyDTA is the best masking agent for Cr(III). It can mask Cr(III) completely and does not decrease the sensitivity.

At room temperature (25°C) and in the water–ethanol mixture, the stability constants of Cr(III)–CyDTA and Cr(III)–TSS were determined experimentally to be $10^{27.3}$ and $10^{32.9}$, respectively. The calculation showed that CyDTA does not interfere with the colour reaction between Cr(III) and TSS under the selected conditions, which was also experimentally supported. However, in the medium without ethanol, the cumulation constant was found to be $10^{31.8}$. It accords fundamentally with the stable time of the colour complex.

As is well known, the composition of solvent will influence the stability of a complex. Because the mechanism is considerably complicated, there has been little extensive research in this area, although it is often mentioned in many literatures. In our opinion, the main reason for the increase of the stability of the colour complex in the ethanol–water is as follows:

The nitrogen atom of TSS, that has a lone electron pair, could take part in the following resonance [28]

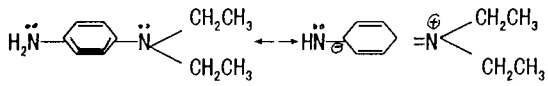

(A) (B)

In HAc–NaAc buffer (pH 3.8) medium, B would accept H^+ prior to A to form

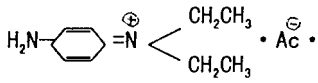

Therefore, the co-ordinate ability of B is weaker than A. Because the polarity of ethanol solvent is lower than water, A and B exist easy in ethanol and water, respectively, according to the theory of similarity compatibility, i.e. ethanol–water mixed solvent is more favourable to the colour reaction than water. Hence, the colour complex in ethanol–water mixture is more stable than in water. Ethanol does not have a great influence on the colouring rate. The rates are all very fast, regardless of whether or not the medium contains ethanol. The halftimes of the former and the latter were determined to be < 200 s and ≈ 300 s, respectively, by comparison to the maximum absorption of the colouring solution containing 10 μg Cr under the studied conditions (24°C). The reason may be that most of the new-born (non-hydrous) Cr(III) reduced from Cr(VI) could react directly with TSS, and the Cr(III) solvated in the mixed solvent also has higher activity in the colouring co-ordination reaction than in pure water, since the primary solvation shell of Cr(III) contains ethanol and acetate [29,30]. In particular, the introduction of acetate ion can decrease the charge of the complex ion, weaken Cr(III)-ligand bond in the solvated metal ion and make the bond easily break. Therefore, the rate of the substitution reaction, i.e. the colour reaction, increases greatly.

5. Conclusion

The colour reaction of Cr(VI) with TSS in the presence of ethanol and CyDTA, provides a simple and rapid spectrophotometric approach for determining total Cr and the species analysis of Cr(III) and Cr(VI). The method has very wide linear range, excellent selectivity, reproducibility and colour stability. The molar absorptivity is 5.0×10^4 l mol^{-1} cm^{-1}, limit of detection 0.002 μg ml^{-1} and relative SD 1.13% for 5.04 μg Cr. The colouring is almost instantaneous and both the rate of the reaction and the absorbance are independent of temperature in the range of 2–45°C.

References

[1] K. Schwartz, W. Mertz, Arch. Biochem. Biophys. 85 (1959) 292.
[2] F. Borguet, R. Cornelis, N. Lameire, Biol. Trace Elem. Res. 26 (1990) 499.
[3] H. Salem, S.A. Katz, Sci. Total Environ. 86 (1989) 59.
[4] K.M. Jop, K.L. Dickson, P.B. Dorn, T.F. Parkertun, J.H. Ridgers, Environ. Toxicol. Chem. 6 (1987) 697.

[5] H.G. Beere, P. Jones, Anal. Chim. Acta 293 (3) (1994) 237.
[6] K.W. Edgell, J.E. Longbottom, R.J. Joyce, J. AOAC Int. 77 (4) (1994) 994.
[7] J. Lu, X. Zhang, B. Zhang, W. Qin, Z. Zhang, Gaodeng Xuexiao Huaxue Xuebao. 14 (6) (1993) 771.
[8] J. Posta, H. Berndt, S.K. Luo, G. Schaldach, Anal. Chem. 65 (19) (1993) 2590.
[9] C.M. Andrle, J.A.C. Broekaert, J Fresenius, Anal. Chem. 346 (6–9) (1993) 653.
[10] J.F. Jen, G.L. Ou-Yang, C.S. Chem, S.M. Yang, Analyst 118 (10) (1993) 1281.
[11] R. Milacic, J. Stupar, Analyst 119 (1994) 627.
[12] R.K. Mugo, K.J. Orians, Anal. Chim. Acta 271 (1) (1992) 1.
[13] J.F. Pankow, D.P. Leta, J.W. Lin, S.E. Out, W.P. Shum, G.E. Januuer, Sci. Total Environ. 7 (1977) 17.
[14] E. Beceiro-Gonzalez, J. Barciela-Garcia, P. Bermejo-Barrera, A. Bermejo-Barrera, Fresenius J. Anal. Chem. 344 (7–8) (1992) 301.
[15] E. Becerio-Gonzalez, P. Bermejo-Barrera, A. Bermejo-Barrera, J. Barciela-Garcia, C. Barciela-Alonso, J. Anal. At. Spectrom. 8 (4) (1993) 649.
[16] A.R. Chakraborty, R.K. Mishra, Chem. Speciat. Bioavailab. 4 (4) (1992) 131.
[17] R. Nusko, K.G. Heumann, Anal. Chim. Acta 286 (3) (1994) 283.
[18] Y.S. Kim, S.J. Park, J.M. Choi, Bull. Korean Chem. Soc. 14 (3) (1993) 330.
[19] W.S. Fung, W.C. Sham, Analyst 119 (5) (1994) 1029.
[20] J.C. Vidal, J.M. Sanz, J.R. Castillo, Fresenius J. Anal. Chem. 344 (6) (1992) 234.
[21] R.M. Issa, B.A. Abdel-Nabey, H. Dadek, Electrochim. Acta. 13 (1968) 1827.
[22] S. Liang, in: B. Chen (Ed.), Higher Organic Chemistry, Higer Education Press, Beijing, 1993, pp. 230–233.
[23] A.G. Cox, C.W. Mcleod, Mikrochim. Acta 109 (1–4) (1992) 161.
[24] S. Lin, Chemical Analysis of Metallurgy, Metallurgical Industry Press, Beijing, 1980, pp. 140–148.
[25] J. Yin, P. Shen, Oxides of halogen, in: Inorganic Chemistry, People Education Press, Shanghai, 1978, pp. 56–59.
[26] K.R. O'Halloran, Ph.D. Thesis, University of Queensland (1990).
[27] Z. Zhao, D. Lu, Stability constants of the complexes of aminocarboxylic acids, in: Analytical Chemistry, The People's Education Press, Beijing, 1990, p. 211, 563.
[28] D. Cheng, Organic Structure Analysis, Press of Science and Technology, Beijing, 1993, pp. 186–197.
[29] S. Zhu, The Simple and Clear Study Course of Coordination Chemisty, Tianjin Press of Science and Technology, Tianjin, 1994, pp. 142–157.
[30] J. Burgess, Metal Ions in Solution, Wiley, New York, 1978, p. 107.

ELSEVIER

Talanta 48 (1999) 377–384

Talanta

Application of the effects of solvent and dissolved oxygen on the determination of benzo[*a*]pyrene by constant-wavelength synchronous spectrofluorimetry in smoke-flavouring

M.S. García Falcón, S. González Amigo, M.A. Lage Yusty *, B. Laffon Lage, J. Simal Lozano

Department of Analytical Chemistry, Nutrition and Bromatology, Area of Nutrition and Bromatology, Faculty of Pharmacy, University of Santiago de Compostela, 15706 Santiago de Compostela, Spain

Received 19 February 1998; received in revised form 12 June 1998; accepted 27 July 1998

Abstract

This work studies the effects of solvent and of dissolved oxygen in the determination of benzo[*a*]pyrene (B*a*P) by constant-wavelength synchronous spectrofluorimetry in smoke-flavour agents, as confirmation and quantification techniques. The wavelength of the most intense peak at the optimum excitation–emission wavelength interval (20 or 110 nm in most of nine solvents) varied by up to 5 nm, and the detection and quantification limits by a factor of up to 30. The best quantification limit was obtained with DMSO (0.09 μg l^{-1}). The deoxygenation of the analyte solution decreased detection and quantification limits, by a variable factor (8–1.13 in the case of *n*-hexane and DMSO, respectively).

Keywords: Spectrofluorimetry; Benzo[*a*]pyrene; Dissolved oxygen; Smoke-flavour agents

1. Introduction

Polycyclic aromatic hydrocarbons (PAHs) are noted for their environmental persistence and ubiquity, some are suspected carcinogens and/or mutagens, necessitating monitoring of PAH levels in diverse matrices (e.g. sediments, biota, and foodstuffs). Often, benzo[*a*]pyrene (B*a*P) is sought as an indicator of the presence of other PAHs, for example in drinking water [1], smoked food and smoked-flavour agents [2].

Analysis of PAHs or B*a*P in foods and smoked-flavour agents is problematic owing to the inherent complexity of these matrices, and the low analyte levels to be detected. To overcome these problems, selective analytical techniques with very low detection limits must be used, such as UV absorption spectrophotometry or spectrofluorimetry, the latter being 10–1000 times more sensitive than the former. For highly complex matrices, however, these techniques are not usually suffi-

* Corresponding author. Tel.: +34 981 594626; fax: +34 981 594912; e-mail: mlagey@usc.es

0039-9140/99/$ - see front matter
PII S0039-9140(98)00261-6

ciently selective, and so are used in combination with liquid chromatography to clean up the samples. In the case of spectrofluorimetry, adequate selectivity, with no loss in sensitivity, can be obtained by using synchronous excitation. This technique first developed by Lloyd [3], increases selectivity while maintaining sensitivity, and reduces experimental errors; it is rapid, simple and particularly adequate as a method for routine monitoring of organic pollutants, and it has been used by various investigators for PAH analysis [4–12].

The validity of any qualitative or quantitative analytical method that employs fluorimetry is highly dependent on the solvent used [13,14], which should comply with a series of requirements. It must have high purity, be transparent at the excitation and emission wavelengths and be free of interfering Raman or Rayleigh bands [7–9], and, preferably be inexpensive and non-toxic, have high extractive capacity, and enhance the fluorescence of the analyte, and maintain it stable in solution.

The PAHs, especially B*a*P, are photosensitized oxidation by dissolved oxygen [15–17]. Furthermore, the high efficiency of oxygen as a quencher of excited states means that it can also interfere with analysis by reducing fluorescence intensity.

In this work, we have studied the effects of more commonly used solvents [18–22] and dissolved oxygen on the determination of B*a*P by constant-wavelength synchronous spectrofluorimetry in smoked-flavour agents and its possible use as confirmation and quantification technique.

2. Experimental

2.1. Apparatus

All spectrofluorimetric measurements were performed in a Perkin-Elmer LS-50 luminescence spectrometer equipped with a xenon lamp, Monk-Gillieson monochromators and 1 cm quartz cuvettes with teflon stoppers. Spectral data acquisition and processing were carried out by means of the program Fluorescence Data Manager (v. 2.5 and 3.5) on a PC (with 4 RAM) serially interfaced (RS232C) to the LS-50.

2.2. Reagents and standards

B*a*P was supplied by Aldrich. Residue analysis grade *n*-hexane, organic trace analysis grade dichloromethane (DCM), analysis grade dimethylsulfoxide (DMSO) and acetone were purchased from Merck, HPLC grade methanol and acetonitrile (ACN) were from Scharlau, analysis grade benzene, chloroform and toluene were from Normasolv, and nitrogen (SEO N-45) was from the Sociedad Española de Oxígeno.

Stock solutions containing 100 mg l^{-1} of B*a*P were prepared in *n*-hexane and were stored at 4°C in glass vials wrapped in aluminium foil to avoid possible light degradation. B*a*P standards (0.5, 1, 2, 4, and 8 μg l^{-1}) were prepared by transferring small aliquots of this stock solution into volumetric flasks, evaporating the hexane under a nitrogen stream, and diluting the residue with the solvent to be studied.

Table 1
Optimum excitation–emission wavelength intervals ($\Delta\lambda$) for synchronous spectrofluorimetric analysis of B*a*P in nine solvents, the peak wavelength for the most intense signal is also given

Solvent	$\Delta\lambda$ (nm)	Peak wavelength (nm)
n-Hexane	20	384
	110	295
Toluene	20	387.5
	100	301.5
Benzene	20	387.5
	110	298.5
Chloroform	20	387.5
	110	298.5
Methanol	25	380.5
	110	295.5
Dichloromethane	20	387
	110	298
Acetone	20	385
Acetonitrile	20	386
	100	297
Dimethylsulfoxide	20	389
	110	299

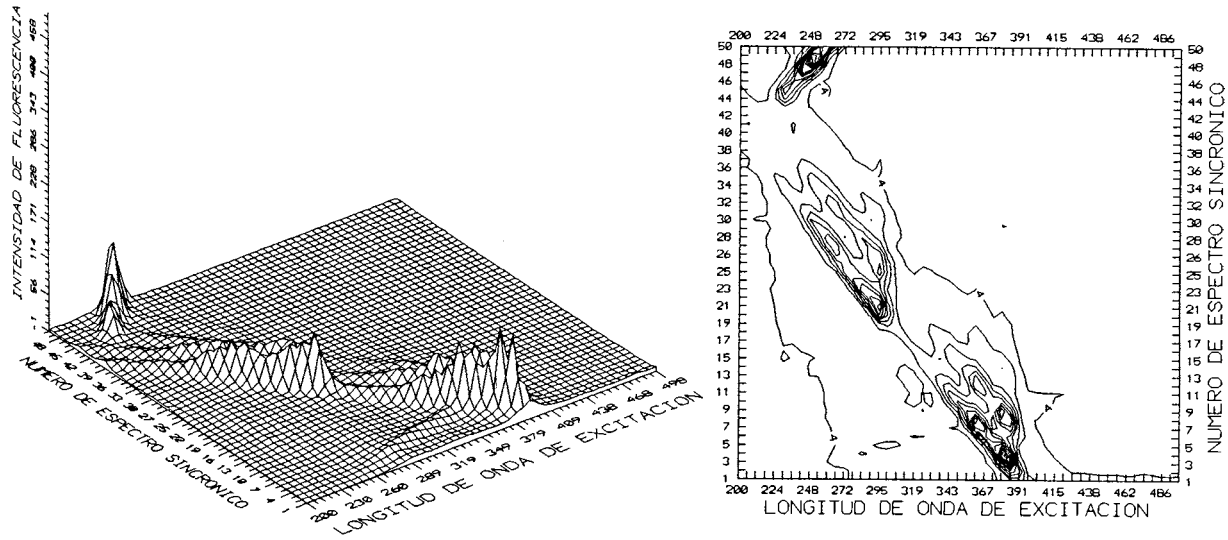

Fig. 1. Three-dimensional and contour plots of synchronous fluorescence spectra of B*a*P in *n*-Hexane (excitation and emission slits: 5 nm; scan speed: 240 nm min^{-1}).

2.3. Procedure

2.3.1. Effect of the solvent

Fifty synchronous scans of each of the nine solvents, and also of 8 μg l^{-1} solutions of B*a*P in each solvent, were recorded between 200 and 500 nm the fluorescence range of PAHs. In successive scans, the wavelength interval between the excitation and emission monochromators ($\Delta\lambda$) was increased by 5 nm, starting from 10 nm for the first scan [$\Delta\lambda = 10 + 5(n-1)$ nm; n = scan number]. The excitation and emission slit-widths were both sets at 5 nm; the scan speed was 240 nm min^{-1}.

The optimum value of $\Delta\lambda$ for the analysis of B*a*P in each solvent was selected by comparing solvent and analyte spectra displayed in three dimensions and as contour maps; in both cases, these were obtained using the commercial graphics program, Surfer, in conjunction with a program written in-house in Turbo BASIC [23,24].

Having determined the optimum value of $\Delta\lambda$ for each solvent, the standard solutions were analyzed in triplicate.

2.3.2. Effect of dissolved oxygen

For each concentration of B*a*P in each of the nine solvents, the sample was transferred to the quartz cuvette and nitrogen was bubbled through it at 50 ml min^{-1} for 2 min. Then, the cuvette was closed and the synchronous fluorescence spectrum of the B*a*P was recorded at the optimum $\Delta\lambda$ determined above. Analyses were carried out in triplicate.

2.3.3. Sample analyses

These studies have been applied to real samples (water-soluble smoke). Extraction of B*a*P from water-soluble smoke and subsequent clean-up of the extracts were carried out as described by Laffon et al. [25].

The *n*-hexane extract (5 ml) untreated and deoxygenated with nitrogen, were recorded between 200 and 500 nm at a scan speed of 240 nm min^{-1} and with excitation and emission slits-widths both set to 5 nm. The excitation–emission wavelength difference was 20 nm.

The *n*-hexane extract was evaporated, re-dissolved in DMSO (5 ml) and then, recorded under the same conditions.

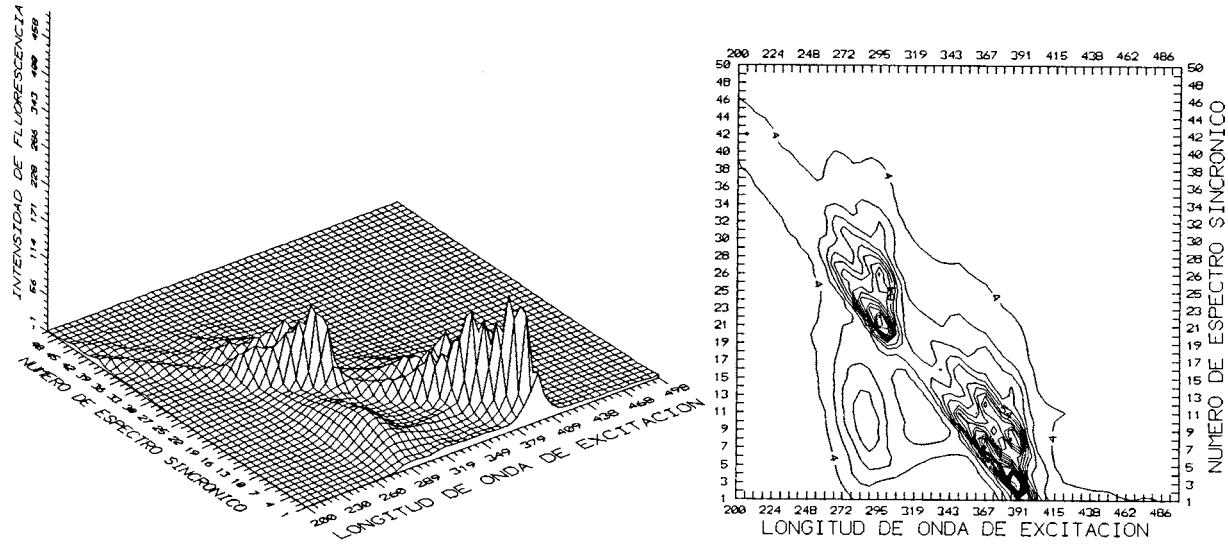

Fig. 2. Three-dimensional and contour plots of synchronous fluorescence spectra of B*a*P in DMSO (excitation and emission slits: 5 nm; scan speed: 240 nm min^{-1}).

3. Results and discussion

3.1. Effect of the solvent

First, the 3-dimensional and contour plots of the spectra of each solvent studied were obtained [24]. The optimum excitation–emission wavelength interval for synchronous spectrofluorimetric analysis of B*a*P in each solvent ($\Delta\lambda$), together with the wavelength at which the most intense analyte peak appeared, is given in Table 1.

The 3-dimensional and contour plots were very useful for the sensible choice of optimum $\Delta\lambda$ for the analysis of B*a*P in each solvent (i.e. figures in *n*-hexane and DMSO, Figs. 1 and 2). In most of the solvents studied, a suitably intense, well resolved peak was obtained with a $\Delta\lambda$ of either 20 or 110 nm. Exceptions were methanol ($\Delta\lambda = 25$ or 110 nm), toluene (20 or 100 nm) and acetone (20 nm, acetone is opaque in UV region). The wavelength of the most intense peak also varied according to the solvent, ranging from 384 to 389 nm for $\Delta\lambda = 20$ nm, and from 295 to 299 nm for $\Delta\lambda = 110$ nm, in *n*-hexane and in DMSO, respectively.

None of the solvents produced peaks that interfered with the signal for B*a*P at the optimum $\Delta\lambda$, the suitability of DCM, *n*-hexane and methanol for spectrofluorimetric analysis of PAHs has been studied previously, [24]. Calibration lines were constructed by regressing mean peak-height above the baseline on standard concentration for each solvent. Table 2 lists the regression and correlation coefficients for the calibration lines at each value of $\Delta\lambda$. Table 3 gives the corresponding detection limits (DL) and quantification limits (QL), which were calculated following the guidelines laid down by the ACS Subcommittee on Environmental Analytical Chemistry [26] as the concentration corresponding to the mean blank signal plus 3 and 10 SD's, respectively. The lowest DL and QL were obtained for DMSO at $\Delta\lambda =$ 110 nm.

3.2. Effect of dissolved oxygen

The necessary time for complete deoxygenation of the solutions was evaluated by making short scans during deoxygenation. At a nitrogen flow rate of 50 ml min^{-1}, there was no appreciable increase in the fluorescence intensity of the selected peak for times longer than 2 min. The possibility that the solution had been concentrated through evaporation of the solvent was

Table 2
Regression and correlation coefficients for the calibration lines obtained for B*a*P determination in nine solvents by synchronous spectrofluorimetry at the indicated values of $\Delta\lambda$

Solvent	$\Delta\lambda$ (nm)	Calibration line[a] range: 0.5–8 μg l^{-1}		*r*	Calibration line[b] range: 0.5–8 μg l^{-1}		*r*
		I = Ax + B			I = Ax + B		
		A	B		A	B	
n-Hexane	20	3.79	0.219	0.9999	29.2	0.967	0.9999
	110	4.08	−0.342	0.9999	32.1	−0.707	0.9999
Toluene	20	6.40	−1.251	0.9998	16.4	1.201	0.9999
	100	5.06	−0.043	0.9999			
Benzene	20	10.6	0.152	0.9999	25.71	2.127	0.9997
	110	10.2	−0.645	0.9999			
Chloroform	20	8.48	−0.577	0.9999	18.01	−1.730	0.9996
	110	9.29	−0.395	0.9999	19.92	−2.665	0.9993
Methanol	25	9.11	−0.432	0.9997	28.19	−0.333	0.9999
	110	10.8	−0.096	0.9996	34.61	−1.402	0.9999
Dichloromethane	20	8.55	0.910	0.9990	19.02	0.262	0.9990
	110	10.1	0.913	0.9998	19.96	2.535	0.9996
Acetone	20	6.24	0.189	0.9999	24.12	−1.007	0.9999
Acetonitrile	20	7.07	−0.236	0.9998	24.72	−0.849	0.9999
	110	8.77	0.098	0.9997	30.70	−0.869	0.9999
Dimethylsulfoxide	20	21.59	0.079	0.9999	23.56	0.067	0.9999
	110	22.85	−0.455	0.9999	26.81	−0.561	0.9999

[a] Untreated solution.
[b] Deoxygenated solution.

ruled out by comparing the scan for each solution with that for the same solution after it had been fully deoxygenated and then allowed to re-oxygenate. There were no appreciable differences between the intensities of the peaks in these scans.

The data for the calibration lines obtained with deoxygenated solvents are listed in Table 2. This table lists too the different slopes of the calibration lines, an increase of the slope implies a greater sensibility of the analyte. The greatest slopes were obtained with deoxygenated solvents. DL and QL for B*a*P in each solvent (Table 3), were calculated, as above. Table 2 does not include these data for the standard solutions in benzene and toluene for $\Delta\lambda$ of 110 and 100 nm, respectively, since interfering peaks due to unknown impurities appeared in the corresponding spectra of the deoxygenated solutions. For these solutions, the lowest DL and QL were obtained using acetone, acetonitrile or *n*-hexane.

3.3. Quantification and confirmation of BaP in water soluble liquid smoke

Although the fluorescence excitation maximum for BaP in *n*-hexane was obtained with 110 nm interval, the interferences of the samples were less evident in the peak obtained with a 20 nm interval, and so this peak was used for quantification.

Quantification of the B*a*P was performed by measurement of the peak-height above the baseline between 377 and 392 nm of the direct spectrum in *n*-hexane (deoxygenated) solution obtained with $\Delta\lambda = 20$ nm and with the calibration line.

Table 3
Detection limits (DL) and quantification limits (QL) for B*a*P determination in nine solvents by synchronous spectrofluorimetry at the indicated values of $\Delta\lambda$

Solvent	$\Delta\lambda$ (nm)	Dl[a] (μg l^{-1})	Ql[a] (μg l^{-1})	DL[b] (μg l^{-1})	QL[b] (μg l^{-1})	QL[a]/QL[b]
n-Hexane	20	0.20	0.65	0.03	0.08	8.10
	110	0.07	0.23	0.009	0.03	7.67
Toluene	20	0.14	0.49	0.066	0.22	2.23
	100	0.78	1.99			
Benzene	20	0.04	0.17	0.04	0.14	1.21
	110	0.03	0.13			
Chloroform	20	0.12	0.38	0.061	0.18	2.11
	110	0.13	0.44	0.060	0.20	2.20
Methanol	25	0.043	0.14	0.014	0.05	2.80
	110	0.044	0.17	0.013	0.05	3.40
Dichloromethane	20	0.053	0.18	0.02	0.08	2.25
	110	0.086	0.29	0.04	0.15	1.93
Acetone	20	0.032	0.12	0.008	0.03	4.00
Acetonitrile	20	0.039	0.16	0.01	0.05	3.20
	110	0.058	0.19	0.02	0.05	3.80
Dimethylsulfoxide	20	0.027	0.09	0.02	0.08	1.13
	110	0.03	0.12	0.02	0.10	1.20

[a] Untreated solution.
[b] Deoxygenated solution.

The concentration (in μg kg^{-1}) of B*a*P in the water-soluble liquid smoke was obtained by multiplying its concentration (μg l^{-1}) in the hexane eluate by a factor of 2.5 [25].

It was noted that the effect quenching of dissolved oxygen was also dependent on the solvent used to dissolve the analyte: improvements in DL could also be obtained by evaporating the hexane and dissolving the extract in DMSO, as was reflected in the finding that deoxygenation of this DMSO solution increased B*a*P fluorescence by a mean factor of 1.13, whereas a roughly 8.10 (Table 2) increase usually following deoxygenation of the corresponding hexane solution. This difference and the fact that the fluorescence excitation maximum of B*a*P shifts to 389 nm in DMSO (Table 1) were used to confirm the identity of the analyte (Fig. 3)

The B*a*P contents of the water-soluble smoke in μg kg^{-1} are listed in Table 4. These results indicate little differences with the results obtained by second derivative [25]; this was possibly because the obvious interferences observed in the peak obtained with the direct spectrum due to background absorption were effectively eliminated by taking the second derivative.

4. Conclusions

1. Change in the solvent. The sensitivity of B*a*P determination by constant-wavelength synchronous spectrofluorimetry depends on the solvent used: the lowest DL and QL are obtained with DMSO, and the highest with *n*-hexane.
2. The effects of oxygen quenching on the sensitivity of B*a*P determination by this technique also depend on the solvent, these effects are smaller in benzene or DMSO and greatest in *n*-hexane, for which roughly 8-fold improvements in DL and QL can be obtained by deoxygenation.

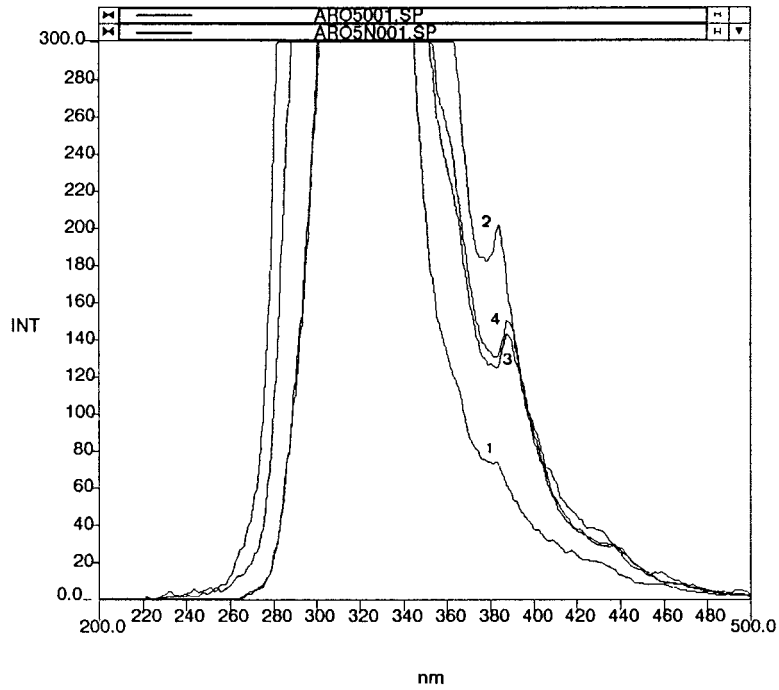

Fig. 3. Synchronous spectra of sample 5 in: *n*-hexane (1); *n*-hexane deoxygenated (2); DMSO (3) and DMSO deoxygenated (4).

3. The possibility of obtaining low DL and QL with synchronous spectrofluorimetric analysis by deoxygenating this solvent, together with the transparency in the UV/Vis range of hexane (see ref. [21]), lead us to recommend *n*-hexane as solvent for synchronous spectrofluorimetric analysis of B*a*P.
4. The use of *n*-hexane and deoxygenation improve the application of constant-wavelength synchronous spectrofluorimetry to the analysis of B*a*P in real sample.

Table 4
Content of B*a*P (μg kg^{-1}) in water-soluble smoke

Sample	B*a*P (μg kg^{-1})
1	ND
2	ND
3	6.22
4	ND
5	1.92
6	0.67
7	7.32
8	ND
9	ND
10	0.27
11	ND
12	0.47

ND = 0.19 μg kg^{-1}.

Acknowledgements

The authors thank the Consellería de Educación y Ordenación Universitaria of the Xunta de Galicia (N.W. Spain), for the concession of bursary to M.S. García-Falcón.

References

[1] World Health Organization (WHO), Guidelines for drinking-water quality, Vol. 2, World Health Organization, Geneva, 1984.
[2] Council of the European Communities, Directive 88/388/EEC, Off. J. Eur. Communities L 184 (1988) 61.

[3] J.B.F. Lloyd, Nature (London) 64 (1971) 231.
[4] T. Vo-Dinh, R.B. Gammage, A.R. Hawthorne, J.H. Thorngate, Environ. Sci. Technol. 12 (1978) 1297.
[5] T. Vo-Dinh, Anal. Chem. 50 (1978) 396.
[6] J.C. Andre, M. Bouchy, M.L. Viriot, Anal. Chim. Acta 105 (1979) 297.
[7] E.L. Inman, J.D. Winefordner, Anal. Chim. Acta 138 (1982) 245.
[8] E.L. Inman, J.D. Winefordner, Anal. Chem. 54 (1982) 2018.
[9] J.C. André, A. Bouchy, J.Y. Jezequel, Anal. Chim. Acta 185 (1986) 91.
[10] P.H. Baudot, M.L. Viriot, J.C. Andre, J.Y. Jezequel, M. Lafontaine, Analusis 19 (1991) 85.
[11] C.M. Byron, T.C. Werner, J. Chromatog. Educ. 68 (1991) 43.
[12] M.S. García Falcón, S. González Amigo, M.A. Lage Yusty, M.J. López de Alda Villaizán, J. Simal Lozano, Talanta 43 (1996) 659.
[13] W.E. Acree, S.A. Tucker, L.A. Cretella, et al., Appl. Spectrosc. 44 (1990) 951.
[14] M. Tachibana, K. Koshiishi, M. Kurusawa, Anal. Chim. Acta 215 (1988) 347.
[15] J.A. Lebo, J.L. Zajicek, T.R. Schwartz, L.M. Smith, M.P. Beasley, Pestic. Ind. Chem. Residues 74 (1991) 538.
[16] K. Takatsuki, S. Suzuki, N. Sato, I. Ushizawa, J. Assoc. Off. Anal. Chem. 68 (1985) 945.
[17] D. Thomas, A. Ronald, Environ. Sci. Technol. 19 (1985) 1004.
[18] S.R. Wild, K.C. Jones, Chemosphere 23 (1991) 243.
[19] R.F. Mothershead, R.C. Hale, Mar. Environ. Res. 33 (1992) 145.
[20] E. Sandell, R. Levinen, A. Kiviranta, Polycycl. Aromat. Compd. (Suppl. 3) (1993) 415.
[21] K.B. Larsson, H. Pyysalo, S. Marketta, Z Lebensm, Unters. Forsch. 187 (1988) 546.
[22] S.N. Al-yakoob, T. Saeed, H. Al-Hashash, Environ. Int. 20 (1994) 221.
[23] M.J. López de Alda Villaizán, M. Simal Gándara, J. Simal Lozano, M.A. Lage Yusty, M.S. García Falcón, Libro de Ponencias y Comunicaciones del V Congreso Farmaceutico de Alimentación, Consell de Colegis Farmacéutics de Catalunya and Vocalía Nacional de Alimentación del Consejo General de Colegios Oficiales Farmacéuticos de España (Ed.), Platja d'Aro, Girona, Spain, 1994, p. 113.
[24] M.J. López de Alda Villaizán, M.E. Alvarez Piñeiro, M.S. García Falcón, M.A. Lage Yusty, J. Simal Lozano, Analusis 22 (1994) 495.
[25] B. Laffon Lage, M.S. García Falcón, S. González Amigo, M.A. Lage Yusty, J. Simal Lozano, Food Addit. Contam. 14 (5) (1997) 469.
[26] American Chemical Society (ACS) Subcommittee on Environmental Analytical Chemistry, Anal. Chem. 52 (1980) 2241.

ELSEVIER

Talanta 48 (1999) 385–392

Talanta

Quantitative measurements of ammonium, hydrogenophosphate and Cu(II) by diffuse reflectance spectrometry

A. Ghauch [a,*], J. Rima [b], A. Charef [a], J. Suptil [a], C. Fachinger [a], M. Martin-Bouyer [a]

[a] *Université de Savoie, ESIGEC LCIE Campus Scientifique, Savoie Technolac 73376 le bourget du lac-cedex, France*
[b] *Université libanaise, Faculté des Sciences (II) Fanar, Laboratoire de spectroscopie moléculaire, Jedeidet el Metn BP 90656, Lebanon*

Received 16 March 1998; received in revised form 13 July 1998; accepted 27 July 1998

Abstract

Diffuse reflectance spectrometry is shown to be useful for the quantitative determination of small amounts of pollutants. The relation between sample concentration and reflectance is described by the Kubelka–Munk equation. The experiments were performed with a laboratory constructed diode array spectrophotometer. We can obtain the quantitative reflectance values of different precipitates like ammonium with Nessler's reagent, hydrogenophosphate with silver nitrate and a complex such as Cu(II) with dithiooxamide 'rubeanic acid' by forming a spot colour on filter paper. We have obtained for each reagent a calibration curve by plotting the relative intensity of reflectance versus the log of the mol $(dm^3)^{-1}$ concentration. The linearity was obtained for Cu(II) from 8×10^{-4} to 2.5×10^{-2} mol l^{-1} with $r^2 = 0.9838$ and from 10^{-3} to 10^{-1} mol l^{-1} for polyphosphate with $r^2 = 0.9975$ and from 5×10^{-4} to 5×10^{-2} mol l^{-1} for ammonium with $r^2 = 0.9889$. We can consider that for a direct measurement of the intensity of reflectance, it is possible to perform quantitative spot-test analysis.

Keywords: Phosphate; Ammonium; Copper(II); Reflectance

1. Introduction

It has been found that when drops of solution come into contact with a suitable reagent on filter paper coloured reaction products are produced on the surface of the paper, producing distinct flecks or rings within a circle wetted by water. This local accumulation accompanying spot reaction on filter paper is very important because it enhances the discernibility of coloured reaction products, especially if they are insoluble in aqueous media, or when coloured water-soluble reaction products are adsorbed on filter paper [1]. Furthermore, the degree of colour spot was found to be proportional to the concentration of the test analyte. The limit of detection can be observed when a visible colour appears on filter paper or on a spot plate [1].

* Corresponding author. Tel.: +33 479 758844; fax +33 479 758843; e-mail: Antoine.Ghauch@procyon.Univ.savoie.fr

0039-9140/99/$ - see front matter
PII S0039-9140(98)00260-4

The optical sensing of chemical species is based on their interaction with light. Absorption, emission and reflection are the three common optical techniques employed for measurement. In this work, we are interested in reflectance spectrometry. The precision of reflectance spectrometry measurements cannot be better than 10% as mentioned by Kealey [2], and then quantitative results have often been considered unreliable. Nevertheless, the development of new techniques with optical fibres [3] or reflectance spheres has changed the situation for the better [4–6].

If transmittance spectroscopy is considered a quantitative and reproducible analysis, the reflectance spectroscopy is considered qualitative and non-reproducible due to the effect of the inhomogeneous media [7]. Wendlandt and Hetch [8] discussed the difference between specular reflection and diffuse reflection and these phenomena are important in quantitative analysis. Specular reflection or mirror reflection is defined by Fresnel equations and occurs from smooth surfaces. Diffuse reflection results by penetration of the incident radiation into the interior of the solid substrate, and multiple scattering occurs after partial absorption at the boundaries of individual particles or fibres of the solid matrix. Ideal diffuse reflection takes place when the angular distribution of the reflected radiation is independent of the incidence angle of radiation source [9]. Thus, it is interesting to show that the reflectance signal is related to the analyte concentration on the support [2–7].

In absorption analysis, a diminution of the power of the radiation is noted when it passes through the sample. The decrease in the light intensity is determined by the number of absorbing species in the light path, and is related to the concentration, C, of the absorbing species through the Beer–Lambert equation: $A = \log I_0/I = \varepsilon l C$ (1). Where A is the optical density, l is the length of the light path and ε is the molar absorptivity, which is characteristic of the analyte substance at a given wavelength.

In reflectance analysis, the optical density for reflectance measurements is $A_R = -\log T_R$ where $T_R = I/I_0$ is the reflecting power, I_0 being the intensity of incident radiant energy and I the intensity of that which reflected by the medium. T_R varies between 0 and 1 and its equal to 1 when the reflectance signal is set to the incident, condition which be accomplished with compressed $BaSO_4$, MgO, or KBr powder [2–10].

The most widely used model is the Kubelka–Munk theory. Here, a thick semi-infinite scattering layer is assumed and reflectance, T_R, is related to the concentration, C, of the absorbing species on the scattering layer through the molar absorptivity, ε, and the scattering coefficient s, as follows: $F(T_R) = (1 - T_R)^2/2 \quad T_R = k/s$ (2) where $k = \varepsilon C$. Taking the logarithm of the remission function gives $\log F(T_R) = \log k - l \log s$ (3). Thus, if $\log F(T_R)$ is plotted against the wavelength or wave number for a sample, the curve should correspond to the real absorption spectrum of the compound determined by transmission measurements, except for a displacement by $-\log s$ in the ordinate direction [8].

Then, the remission function given in eq 3 can be written: $F(T_R) = \text{Cte. } C$ (4). Where C is the molar concentration and it has been assumed that $k = 2.303\varepsilon C$, where ε is the molar extinction coefficient and T_R is the fraction of incident light reflected by a sample [8].

A linear relation between T_R and the sample concentration is found by the application of Kubelka–Munk equation for high and moderate concentration but a distinct deviation from linearity is observed for low sample concentration [11].

For quantitative purposes, many different calibrations plots can be proposed to empirically fit T_R to the concentration through linear relationships. Some examples of these plots are: (a) $\log (T_R - T'_R)$ versus 1/C; (b) $[(1 - T_R)^2/(2\ T_R)]$ versus $\log C$, and (c) $(T_R - T'_R)$ versus $[C/(1 - C)]$, where T_R is the reflectance of the sample and T'_R is the reflectance of the support used which gives good straight lines [8,10–15].

If we consider I_R the reflectance intensity of the matrix plus analyte/reagent/product and I'_R the reflectance intensity of the matrix, and if we neglect scattering losses, I'_R will always be greater than I_R. A linearity can be also obtained if we plot: $(I'_R - I_R)$ versus $\log C$ (eq 4).

Many works can be cited which evaluate quantitative analysis by reflectance spectrometry. Rei-

necke et al. [11] utilised the exact value for the absolute reflectance of KBr powder to detect a low concentration of dioctyl phtalate. Narayanaswamy et al [16] studied properties of redox media equilibrium of some quinonoid indicators when they are immobilised by adsorption on XAD-2, synthetic copolymer, by reflectometry measurement. Tubino et al [4] reported the detection of some metals Ni(II), Fe(II), and Cr(VI) using a Labsphere reflectance accessory adapted to a UV-Visible spectrophotometer. Oliveira et al. [17] investigated reflectance spectrometry in determination of carbon monoxide in his colour reaction with immobilised palladium(II) on paper. Nakano et al. [18] studied the detection of hydrogen chloride using the intensity of reflected light, which is proportional to the degree of colour obtained by contacting it with pH paper.

In this study, a quantitative analysis carried out by measuring the reflectance of the colour developed in complexation reactions occurring on filter paper surfaces. We did not measure the transmission because filter paper is not transparent and comparison would not be informative. A home-built reflectometer was used for measurements. A linear relationship for calibration curves was achieved by plotting $(I'_R - I_R)$ versus log analyte concentration mol $(dm^3)^{-1}$. The results encourage the application of reflectance measurements in quantitative spot analysis, in spite of procedural difficulties.

2. Experimental section

2.1. Reagents

All the chemicals were analytical-reagent grade and used without further purification. Whatman No. 1 filter paper was employed as a solid substrate, and distilled water was used throughout. Copper(II) sulfate, di-sodium hydrogenophosphate, ammonium sulfate, silver nitrate, were obtained from Prolabo. Dithiooxamide 98% (rubeanic acid), Nessler's reagent, were acquired from Aldrich. Whatman No. 1 filter paper was purchased from Whatman International. Buffer solutions were purchased from Reagecon.

2.2. Instrumentation

2.2.1. Schematic block diagram

The basic concept of this system is simple (Fig. 1). Light from 12 W halogen source is passed through two lenses and guided to the region where it interacts with a chemical transducer, which placed into the sample compartment. This interaction with the colour spot results in a variation of the optical signal, and the varied light, which is encoded with chemical information is collected into the detection system. A laboratory-constructed sample holder was used. The angle of incident exciting light is slightly less than 45° in order to get more diffuse reflection and less specular component. A 40 mm^2 circular window limited the exposed paper area.

2.2.2. Spectrograph and detector system

After the reflected light passed through the lens of spectrograph, a mirror directed the light beam through a 200-μm entrance slit. The slit width controlled the wavelength resolution at the detector, about 4.7 nm as configured. A smaller slit would give finer resolution (unnecessary in this application). A similar mirror directed the light beam coming from the first one onto a diffraction grating. This grating made by Jobin-Yvon has a groove spacing of 200 lines mm^{-1}. The diffraction grating spread the light beam across wavelength from 200 to 800 nm. A third mirror directed the beam to the diode array detector made by Hamamatsu model S 3901-512 Channels. The detector was calibrated for wavelengths by measuring the output from a low-pressure mercury vapour lamp, which contained a narrow-band mercury emission line at 253.7 nm. The lamp was removed after calibration. After initial calibration, cheeks showed no drift in the position of this 253.7-nm line. We note that for other lines of the spectrum of the lamp, correction is made automatically.

2.2.3. Computer control and data processing system

A 486 DX-33 computer controlled all measurement functions. Instrument control software was developed at our laboratory, using the Microsoft

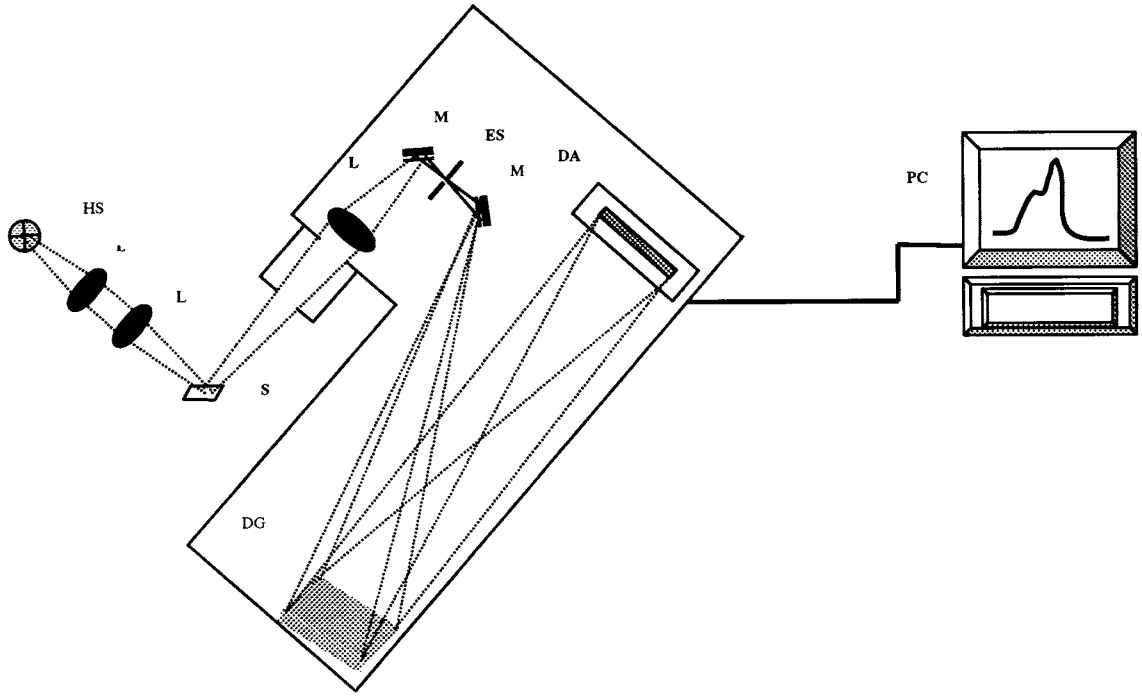

Fig. 1. Instrumentation system for reflectance measurements: HS, halogen source; L, lenses; S, sample; M, mirrors; ES, entrance slit; DG, diffraction grating; DA, diode array; PC, computer control and data processing system.

QuickBasic language. Communication with the diode-array driver and detector used a data translation LAB PC from National Instrument 12-bit analogue and digital I/O board.

The advantage of a diode-array detector over the traditional motor driven scanning monochromator and photomultiplier tube is that the entire spectrum can be collected rapidly (35 ms). We can create references of spectra for some pollutants for qualitative measurements and after which a quantitative procedure will be accomplished by considering the optical density of the significant pollutant at a specific absorption band.

2.3. Sample preparation

Different stocks solutions were prepared as following.

2.3.1. Copper

A stock solution 5×10^{-2} M was prepared in distilled water from solid $CuSO_4$, $5H_2O$ and diluted several times in order to create a calibration curve. (8×10^{-4}, 1×10^{-3}, 2.5×10^{-3}, 5×10^{-3}, 8×10^{-3}, 10^{-2} and 2.5×10^{-2} M). Rubeanic acid, which is the ligand agent, was prepared to give 0.5% in 96% ethanolic solution.

2.3.2. Phosphate

A stock solution 10^{-1} M was prepared in distilled water from solid Na_2HPO_4, 12 H_2O and diluted several times in order to construct a calibration curve. (10^{-3}, 5×10^{-3}, 10^{-2}, and 5×10^{-2} M. The reacting agent is a 0.5 M solution of $AgNO_3$ prepared in distilled water with other dilutions.

2.3.3. Ammonium

A stock solution 5×10^{-2} M was prepared in distilled water from solid $(NH_4)_2SO_4$ and diluted several times in order to create a calibration curve, (5×10^{-4}, 10^{-3}, 4×10^{-3}, 8×10^{-3}, 10^{-2}, and 5×10^{-2} M). The reacting solution is the Nessler's reagent.

Filter paper was cut into 1-cm discs. We did not consider the modification of the intrinsic reflectance of the filter paper because we were interested by the intensity of radiant energy, which reflected, by the media. Whatman No. 1 filter paper transmittance measurements were taken. The results have shown that the filter paper is not transparent with the used exciting light. So we can neglect its transmittance. The same results were obtained after carrying out the spot test reactions. All solutions were spotted with appropriate reagents V_r, using 10 μl Hamilton microsyringe. For all measurements, the reagent solutions were spotted and subsequently, the analytes were added on the centre of each disc. The blank was performed by spotting batches of filter paper discs with the proper quantities of analyte V_a followed by the appropriate volume of distilled water V_w used for each test. Thus, each type of sample had its own blank (I'_R) and the total intensity measured for analyte (I_R), was subtracted from the blank.($I'_R - I_R$).

All measurements were performed in a dark chamber in order to reduce background noise from ambient light. The reflectance spectrum ranged from 350 up to 800 nm and the reflectance values were taken at 650 nm for phosphate, at 533 nm for ammonium complex and at 665 nm for the copper complex.

3. Results and discussion

To obtain the calibration curve of the Cu(II), the blank was performed by spotting $V_a = 2$ μl and $V_w = 2$ μl. In order to have the reflectance of the sample, V_w was replaced by $V_r = 2$ μl of rubeanic acid, the complex reagent. Before spotting solutions on the surface of the matrix, Whatman No. 1 filter paper were soak with standard pH solution from pH 4 to 10. Reactions of copper(II) complexation were carrying out. A positive reponse is indicated by appearance of an intense green colour on the surface of the paper. We note that it is no effect of pH on the reaction of complexation between rubeanic acid and copper(II). The calibration curve carrying out at pH 7 is presented in Fig. 2.

The copper(II)–rubeanic acid complex has a maximum I_R at 665 nm. All intensity reflectance values were taken after 4 min, the drying time of filter paper. The linear dynamic range LDR was found from to be 5×10^{-4} to 2.5×10^{-2} mol l^{-1}. The sensitivity of the method was noted $D = 10$ PPM [18]. The threshold of measure found in this work is 5.4×10^{-4} M which is equivalent to 34 PPM if we plot the intersection of the curve with the abscissa for $y = 1312.9\ x - 965.1$ where $x =$ log (10^4 [Cu(II)])/mol l^{-1}). This threshold is greater than the background and close to the limit of detection (LOD).

This threshold is higher than the limit of detection LOD found in literature because the green colour in not very discernible at low concentration where plot was non linear. Also, at concentrations greater than 2.5×10^{-2} mol l^{-1}, the spot test develops an intense green colour and the intensity value of reflectance is reduced because of absorption.

The interference's for copper(II) are those found in the 'Analyse qualitative minérale' [19]. Nickel gives an intense violet spot; cobalt develops a brown colour. In the presence of these two cations, we can discern the coloration of copper(II) in the centre of the filter paper surrounded by the circles of cobalt and nickel. These phenomena were due to the difference in the diffusion of cations or small particles migrate farther than

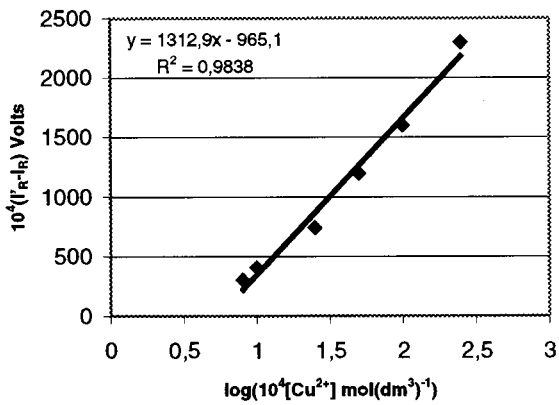

Fig. 2. Calibration curve for copper. Formation of a green interior complex on batch of filter paper. Reflectance intensities were taken at 665 nm. The correlation coefficient is $r^2 = 0.9838$.

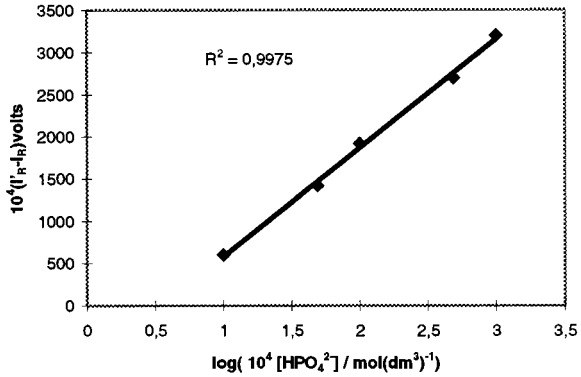

Fig. 3. Calibration curve for HPO_4^{2-}. Formation of a yellow precipitate turned to black on the batch of filter paper. Reflectance intensities were taken at 650 nm. The correlation coefficient is $r^2 = 0.9975$.

large ones. Silver and mercury also interfere at high concentration [18].

To obtain the calibration curve of hydrogenophosphate, the blank was performed by spotting $V_a = 2$ μl and $V_w = 2$ μl. In order to have the reflectance of the sample, V_w was replaced by $V_r = 2$ μl of 0.5 M silver nitrate the complex reagent. A positive reponse is indicated by the appearance of yellow colour on the surface of the paper. This colour subsequently disappeared and changed to black in presence of excess of silver nitrate and illumination with white light. The calibration curve is presented in Fig. 3.

The precipitate $Ag_2HPO_4\downarrow$ has a yellow colour, but it is not stable and the intensity of black colour developed is proportional to the yellow, which represented the amount of hydrogenophosphate. We note that the more the disc filter paper is illuminated in the same measurement, the more the intensity of the reflectance decreases. We can explain that by the formation of the metal oxide or the metal itself by a photochemical reaction induced by the incident light. We have derived a calibration curve with different concentrations of silver nitrate: 0.1; 0.25; 0.5 M and we have obtained the best linearity with the 0.5 M solution at 650 nm. All measurements were taken after one minute of illumination because at 30 s, paper humidity is higher and this decrease the signal (Fig. 6) and for more than 1 min, we risk loss time and precipitate stability. Fig. 4 illustrate the reflectance spectrum of $Ag_2HPO_4\downarrow$ with the reflectance intensity I_R plotted versus the wavelength.

The calibration curve shows a LDR for hydrogenophosphate from 10^{-3} to 10^{-1} M. The threshold of measure found in this work is 3.5×10^{-4} M. which equivalent to 33 PPM if we consider the intersection of the curve of Fig. 4 with the abscissa for $y = 1285.3\ x - 698.55$ where $x = \log\ (10^4\ [HPO_4^{2-}]/\text{mol}\ l^{-1})$.

Another test based on the reduction of ammonium phosphomolybdate gave a sensitivity $D = 10$ PPM for phosphoric anions [18]. AsO_4^{3-} and SiO_3^{2-} give the same reaction. A large number of oxidants also gave analogous reaction.

To obtain the calibration curve of ammonium, the blank was performed by spotting $V_a = 2$ μl and $V_w = 3$ μl. In order to have the reflectance of the sample, V_w was replaced by $V_r = 3$ μl of Nessler's reagent. A positive response was indicated by the appearance of yellow colour on the surface of the paper. The degree of colour is proportional to the concentration of ammonium spotted on the paper. The calibration curve is presented on Fig. 5.

The calibration curve shows a LDR for ammonium from 5×10^{-4} to 5×10^{-2} M. The threshold of measure found in this work is 1.02×10^{-4} M. which is equivalent to 3.67 PPM if we

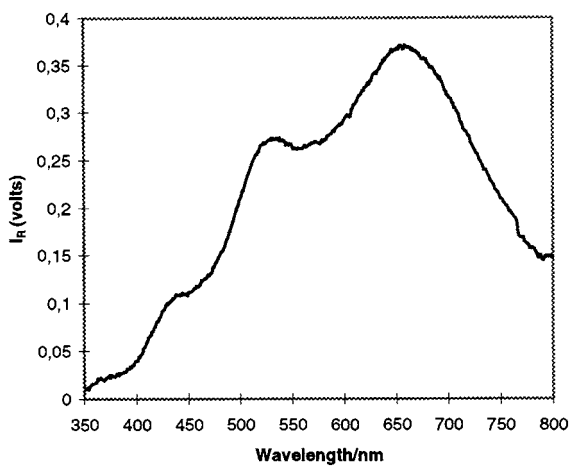

Fig. 4. Reflectance spectrum: formation of $Ag_2HPO_4\downarrow$ precipitate on filter paper. I_R values were taken after 1 min of illumination of substrate in the sample holder of the system.

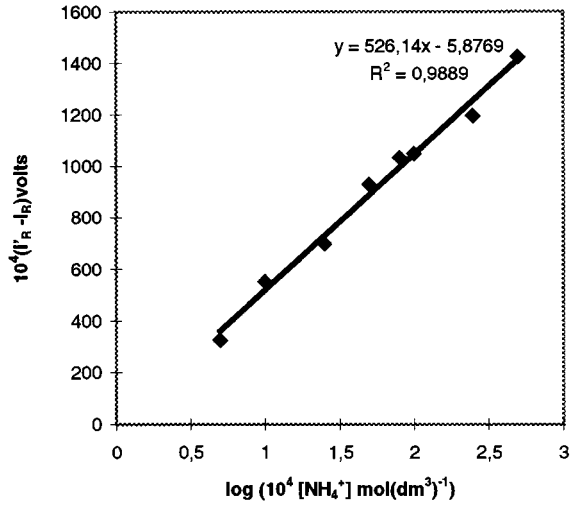

Fig. 5. Calibration curve for Ammonium. Formation of a yellow–orange coloured precipitate $NH_2Hg_2I_3\downarrow$ on filter paper. Reflectance intensities were taken at 533 nm. The correlation coefficient is $r^2 = 0.9889$.

consider the intersection of the curve of Fig. 5 with the abscissa for $y = 526.14 \quad x - 5.8769$ where $x = \log\ (10^4\ [NH_4^+]/\text{mol}\ l^{-1})$. All I_R values were taken 60 s after deposition of analyte on filter paper. This was found to be the best time to take measurements because we obtained the best linearity and we could reduce the time of analysis even through the complex formed

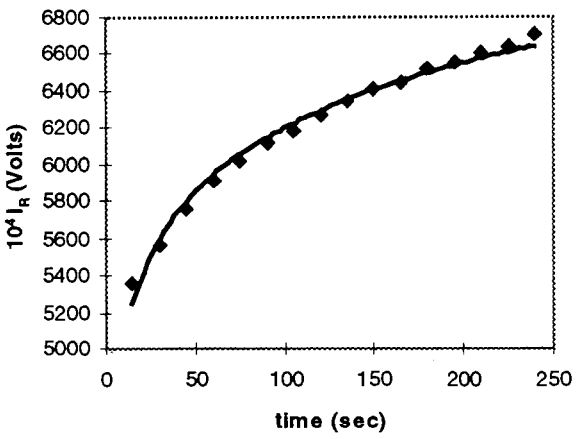

Fig. 6. Variation of reflectance intensity of filter paper spotted with analyte solution versus time (s). $[NH_4^+] = 5.10^{-2}$ M.

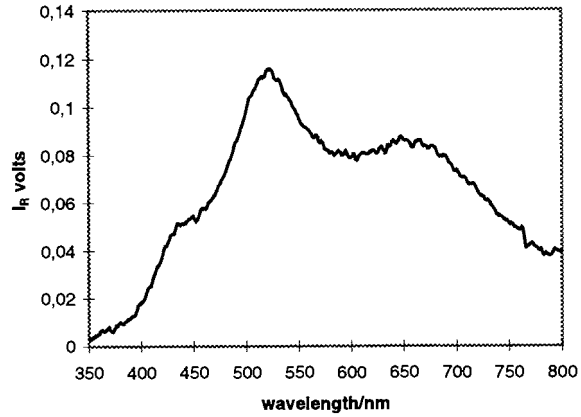

Fig. 7. Reflectance spectrum of ammonium-Nessler's reagent complex $NH_2Hg_2I_3\downarrow$ was taken at 533 nm. $[NH_4^+] = 5 \times 10^{-2}$ M.

did not degrade with time. Fig. 6 shows the increase of reflectance intensity. The intensity of reflectance of filter paper is dependent of the properties of this one. In fact, the more the humidity of the filter paper is high, the more the reflectance intensity decreases. This is due to the effect of water molecules, which is trapped into the fibre of cellulose, and then the paper absorbed a part of energy and reflected the diffuse one.

All measurements of reflectance are realised at 533 nm. The reflectance spectrum of the complex ammonium-Nessler's reagent $NH_2Hg_2I_3\downarrow$ is represented in Fig. 7.

Various methods were used in order to determine the amount of ammonia such as absorbance spectrophotometry based on Nessler's reagent or indophenol blue [20], fluorimetry [21], or from the change of pH or conductance [22], caused by the hydrolysis of ammonia in the acceptor solution. This principle has already been used in clinical analysis for ammonia, not only in flow systems but also in a spot test with dry thin film [23,24].

All our results show that diffuse reflectance spectrometry can be considered a quantitative method for analysis in the visible region of the spectrum. However, this type of spot test, in which inorganic and organic reagents can be

used, is obviously limited to reactions which do not require either strong heating or evaporation, or a highly alkaline or acidic reaction theatre, since filter paper or solid matrix is attacked in such instances [1]. Using an optimised treatment of digitised spectra can eliminate problems of interference. This work has been made in our laboratory in order to eliminate interference came from the different constituents of water by the UV-Vis absorption spectra [25].

To obtain a good linearity in our measurements, we have chosen a portable sample holder, which can be removed and replaced at the same position. The incident light should be fixed on the same spot of the filter paper, which represented 40 mm^2 of surface. We should also have a good uniformity for all colour spots on matrix. This was accomplished by using a 10 μl Hamilton microsyringe in order to develop equal coloured areas at the centre of matrix.

4. Conclusion

The results show that the appropriate use of the reflectance spectrometry leads to satisfying quantitative measurements. To ensure satisfactory results, some conditions must be respected, such as uniform spot test colour, good reflectance holder (metallic support or gelatine matrix), analyte solution will not reacted with the matrix and a short distance between sample and detector. This work shows the potential reflectance diffuse spectrometry for a quantitative analysis. Our system can be accomplished by using fibre optical device or reflectance microsphere [4]. One of the main goals in this work is to build a routine reflectometer apparatus in order to control water pollution. The possibility of automation can be envisaged, improving the quality and performance rate of the results for quantitative analytical purposes.

Acknowledgements

The future work in reflectance studies will be sponsored by CRAFT European project number BRST-CT 97-5143, the authors thank the European community for the next financial support.

References

[1] Feigl, V. Anger, Spot Tests in Inorganic Analysis, 6th ed. Elsevier, Amsterdam, 1972.
[2] D. Kealey, Talanta 19 (1972) 1563.
[3] R. Narayanaswamy, Analyst 118 (1993) 317.
[4] M. Tubino, A. Vitorino Rossi, M. E.A. de Magalhaes, Anal. Lett. 30 (2) (1997) 271–282.
[5] H.G. Hecht, Appl. Spec. 37 (1983) 348.
[6] M.A. Mauri, R.A. Allston, T.J. Casey, N.T. Spellman, K.A.Willis, Appl. Spec. 37 (1983) 269.
[7] R. Narayanaswamy, F. Sevilla III, Mikrochim. Acta I (1989) 293.
[8] W.W. Wendlandt, H.G. Hecht, Reflectance spectroscopy, in: Chemical Analysis, vol. 21, Interscience, New York, 1966.
[9] Körtum, G. Reflectance Spectroscopy, Springer-Verlag, New York, 1969.
[10] W.W. Wendlandt (Ed.), Modern Aspects of Reflectance Spectroscopy, Plenum press, New York, 1968.
[11] D. Reinecke, A. Jensen, F. Fister, U. Scherman, Anal. Chem. 60 (1988) 1221.
[12] F. Gurm, T.E. Wigghtman, Appl. Optics 16 (1977) 2775.
[13] S.B. Savvin, L.M. Trutneva, O.P. Shoeva, Z. Anal. Khim. 48 (1993) 502.
[14] D Kealey, Talanta 21 (1974) 475.
[15] D Kealey, Talanta 23 (1976) 715.
[16] R. Narayanaswamy, F. Sevilla III, Anal. Chim. Acta, 189 (1986) 365.
[17] W.A. Oliviera, P.R. Saliba, J. Braz. Chem. Soc. 5 (1994) 39.
[18] N. Nakano, A. Yamamoto, Y. Kobayashi, K. Nagashima, Analyst 118 (1993) 1539.
[19] E. Wenger, D. Monnier, Y. Rusconi. Analyse Quantitative Minérale. Genève, Suisse 1955.
[20] J. Ruzika, E.H. Hansen, Flow Injection Analysis, Wiley, New York, 1981, p. 79.
[21] T. Aoki, S. Uemura, M. Munemori, Anal. Chem. 55 (1983) 1620.
[22] R.M. Carlson, Anal. Chem. 50 (1978) 1528.
[23] M.W. Sundburg, R.W. Becker, T.W. Esders, J. Figueras, C.T. Goodhue, Clin. Chem. 29 (1983) 645.
[24] J. Toffaletti, N. Blosser, T. Hall, S. Smith, D. Tompkins, Clin. Chem. 29 (1983) 684.
[25] E. Naffrechoux. Application des propriétés d'absorption UV des eaux et des effluents à la réalisation d'une station de mesure de la pollution, PhD Thesis, University of Savoie, France, 1990.

ELSEVIER

Talanta 48 (1999) 393–402

Talanta

Equilibrium studies of mercury(II) complexes with penicillamine

H. Kõszegi-Szalai *, T.L Paál

National Institute of Pharmacy, Budapest, Hungary

Received 24 March 1998; received in revised form 14 July 1998; accepted 27 July 1998

Abstract

The complex-formation equilibria of mercury(II) with penicillamine have been investigated in acidic and neutral conditions. A liquid–liquid extraction method using dithizone as auxiliary ligand was applied for the determination of the stability constants of three differently protonated 1:2 metal/ligand complexes formed at $pH < 3$. Evidence has been found by potentiometry and confirmed by Raman spectroscopy for the existence of 1:3 metal/ligand complex besides 1:1 and 1:2 species at $pH > 4$. The stability constants of $HgL_3H_3^-$ and HgL_2H^- complexes as well as the macroscopic protonation constants of the ligand were determined from pH-metric data. The binding sites in the complexes with a special regard to the possible role of $-COO^-$ and $-NH_2$ groups in the coordination have been discussed.

Keywords: Mercury(II); Penicillamine; Stability constants

1. Introduction

Penicillamine (*d*-3,3-dimethylcysteine) is a chelating agent which facilitates the elimination of certain heavy metal ions, including copper, lead and mercury from the organism by the formation of stable soluble complexes that are readily excreted by the kidney [1]. Mercurimetric assays for various penicilline compounds and penicillamine itself are based on the high stability of mercury(II)-penicillamine complexes as well [2].

Complexes of Hg^{2+} with penicillamine and the chemically very similar L-cysteine have been investigated by several authors [3–6] applying pH-metric methods exclusively.

Although Sugiura and Tanaka [5] have previously emphasized that the evaluation of pH-metric data could not be carried out by the usual methods in this case, the determined stability constant of the Hg^{2+}–penicillamine 1:1 complex was only an approximate one ($\lg\beta_1 = 16.4$). Doornbos and Faber [7] raised first general doubts about the sole application of a pH-metric method for the determination of these stability constants. They pointed out that, due to the very high stability of these Hg(II)–sulfhydryl ligand complexes, there is no real competition between protons and mercury(II) ions.

In a polarographic study [8] on Hg(II)–cysteine complexes the stoichiometry of complex species was supposed to be 1:2, 2:2 and 3:2 without explaining why the formation of 2:2 Hg–cysteine

* Corresponding author. Tel.: +36 1 3171488; fax: +36 1 318 1167; e-mail: tpaal@ogyi.hu

0039-9140/99/$ - see front matter
PII S0039-9140(98)00258-6

complex instead of 1:1 one was assumed. The stability constant $\beta_2 = 39.4$ was published for Hg (cysteine)$_2$ complex by Van Der Linden and Beers [9], who used a direct potentiometric method measuring Hg^{2+} activity with a mercury indicator electrode.

The complexation of Hg(II) by glutathione, cysteine and penicillamine was studied by Cheesman et al. [10] under excess ligand conditions by ^{13}C NMR spectroscopy. Formation of Hg(thiol)$_3$ complexes was concluded by them from the chemical shift data and similar findings were also reported by us [2] for penicillamine in an earlier paper.

A liquid–liquid distribution method followed by radiometric determination of the concentrations of labelled Hg(II) both in the aqueous and organic phases was applied and stability constants $\lg\beta_2 = 40.0$ for Hg(HL)$_2$ and $\lg\beta_2 = 42.7$ for HgL_2 were determined by Stary et al. [11] studying Hg(II)–cysteine equilibria. In spite of the several papers published on Hg–thiol ligand complexes, no stability constants for Hg(II) penicillamine 1:2 complexes have been published yet.

Moreover, although most of the authors agreed that the deprotonated sulfhydryl groups are the predominant binding sites in Hg(LH)$_2$ complexes (L-cysteine, penicillamine), there is still no agreement in the possible role of amino and carboxyl groups in the coordination [10,12,13].

The aim of the present work was to gain a better understanding of Hg(II)–penicillamine complex formation equilibria, to find a simple but accurate liquid–liquid extraction method for the determination of the differently protonated, extremely stable 1:2 complexes and to provide evidence for the existence of Hg(penicillamine)$_3$ complexes in slightly acidic and neutral solutions as well as to accumulate data on their stability by pH metric and Raman spectroscopic methods.

2. Experimental section

2.1. Materials

Penicillamine was purchased from Sigma. Mercuric perchlorate standard solutions were made by dissolving mercuric oxide yellow (Merck) in perchloric acid of known concentration. Dithizone solutions in CCl_4 were freshly diluted from a stock solution specially purified [14]. All the reagents used were of analytical grade.

2.2. Methods and instruments

During the pH-metric titrations e.m.f. were measured with an OP-208 Precision Digital pH meter (Radelkis, Hungary) using an OP-7183 glass electrode (Radelkis) and double liquid junction Ag/AgCl reference electrode (OP-0871P). NaCl (0.5M) saturated with AgCl as inner and $NaClO_4$ (0.5M) as outer junction electrolytes were applied.

During mercurimetric titrations at constant pH e.m.f were measured using an additional digital pH meter and an additional pair of electrodes including a platinum wire electrode (OP 6123) and another double junction reference electrode (OP-0871P).

All e.m.f. measurements were carried out at 25 ± 0.1°C in a water-jacketed titration cell and a continuous stream of oxygen-free nitrogen was passed over the solutions.

For spechtrophotometric measurements in the liquid–liquid extraction studies a Perkin-Elmer Lambda UV/VIS spectrophotometer was used.Raman spectra were recorded on a Cary model 82 laser Raman spectrophotometer with Spectra-physics model 164 argon ion laser (514.5 nm).

2.3. Symbols

Hg_T, L_T, D_T, Br_T^- represent the total concentrations of mercury(II), penicillamine, dithizone and bromide, respectively. I, ionic strength; L, penicillamine; L^{2-}, penicillamine deprotonated at its sulphydryl, amino and carboxyl groups; LH^-: penicillamine with ionised carboxyl group and protonated amino or sulphydryl groups; LH_2, penicillamine with protonated sulphydryl and amino groups and ionised carboxyl group; LH_3^+, fully protonated penicillamine

$$K_1 = \frac{[LH^-]}{[L^{2-}][H^+]}, \quad K_2 = \frac{[LH_2]}{[L^-][H^+]},$$

$$K_3 = \frac{[LH_3^+]}{[LH_2][H^+]}$$

the successive macroscopic protonation constants of penicillamine

$\bar{z}$ is the average number of protons ionized from protonated penicillamine due to complex formation with a mercury(II) ion; [], the actual concentration of the species indicated in the parenthesis; $[]_{org}$ and $[]_{aq}$, the actual concentrations in the organic and aqueous phases, respectively.

$$\beta_{2ext} = \frac{[Hg(DH)_2]_{org}[H^+]_{aq}^2}{[Hg^{2+}]_{aq}[DH_2]_{org}^2}$$

the extraction stability constant of Hg(II)–dithizone complex

$\lg\beta_1$, 9.00; $\lg\beta_2$, 17.10; $\lg\beta_3$, 19.40; $\lg\beta_4$, 21.00: the logarithms of the stability constants of $HgBr^+$, $HgBr_2$, $HgBr_3^-$ and $HgBr_4^{2-}$ complexes, respectively. *P* represents the level of probability for the confidence limits indicated; *n*, the number of measured values used for the calculation of the constant.

$$\beta_{xyz} = \frac{[Hg_xL_yH_z]}{[Hg^{2+}]^x[L^{2-}]^y[H^+]^z}$$

the stability constants of mercury(II)–penicillamine complexes.

2.4. Measurements

2.4.1. Potentiometric measurements

In order to maintain a constant ionic strength throughout the titrations the ionic strength of all solutions including the titrants was adjusted to $I = 0.5$ M with $NaClO_4$.

For the determination of macroscopic protonation constants of penicillamine the mixture of 20.0 ml of 0.1 M $HClO_4$ and 10.0 ml of 6×10^{-2} M penicillamine was titrated with standardised, carbonate-free 0.1 M NaOH, measuring the pH of the solution.

For the determination of protonation constant K_3 more precisely 30.0 ml solution (0.5 M $HClO_4$ and 0.1 M penicillamine) was titrated with 0.5 M NaOH.

For studying Hg(II)–penicillamine complex formation equilibria Calvin-titrations [15] and titrations with Hg^{2+} at constant pH values were carried out.

2.4.1.1. Calvin titrations. The mixture of 5.0 ml of 0.1 M penicillamine solution, 10.0 ml of 0.1 M $HClO_4$ and 5.0 ml of 0.5 M $NaClO_4$ solution was titrated with 0.1 M NaOH. The same titration in the presence of 1.0 ml of 0.05 M $Hg(ClO_4)_2$ containing 0.05 M free $HClO_4$ was also carried out. Titrations of 2.0, 4.0 and 8.0 ml of 0.1 M penicillamine with 0.1 M NaOH in the absence of mercury(II) and in the presence of 2.0, 8.0 and 0.4 ml of 0.05 M $Hg(ClO_4)_2$, respectively, in the initial volumes of 20.0 ml were also made.

2.4.1.2. Titrations with Hg^{2+} at constant pH values. The pH of 30.0 ml 6.6×10^{-2} M penicillamine solution was adjusted to the required initial value ranging from 2.0–8.5 with 0.1 M NaOH or 0.1 M $HClO_4$ first, and these solutions were titrated with 0.05 M $Hg(ClO_4)_2$ solution adjusting the pH of the solution with 0.1 M NaOH, after each portion of 0.05 M Hg $(ClO_4)_2$ solution, to the initial value.

Mercurimetric titrations were carried out the same way as titrations with Hg^{2+} at constant pH, but e.m.f-s between the platinum wire and the additional double junction reference electrodes were also recorded.

2.4.2. Liquid/liquid extraction measurements

For the determination of both the extraction stability constant (β_{2ext}) of the $Hg(HD)_2$ complex and the stability constants of Hg(II)–penicillamine complexes the equal volumes of aqueous solutions of known concentrations (Hg_T, Br_T^-, or L_T, $[H^+]$) and dithizone solutions in CCl_4 (D_T) were intensively shaken for 1 min at 25 ± 0.2°C.

The actual concentrations of the free dithizone in the organic phase $[H_2D]_{org}$ were measured spectrophotometrically at the wavelength of 620 nm. The concentrations of the solutions are shown in Table 1.

Table 1
The concentrations (mol dm^{-3}) of the solutions during the liquid/liquid extraction measurements for the determination of the extraction stability constant of $Hg(HD)_2$ complex (Part A) and of the stability constants of HgL_2H_2, $HgL_2H_3^+$ and $HgL_2H_4^{2+}$ complexes (Part B)

Part A

$Hg_T \times 10^6$	$Br_T^- \times 10^2$	$[H^+] \times 10^2$	$D_T \times 10^5$	$[H_2D]_{org} \times 10^5$	$Hg_T \times 10^5$	$Br_T^- \times 10^2$	$[H^+] \times 10^2$	$D_T \times 10^5$	$[H_2D]_{org} \times 10^5$
2.50	15.0	20.0	1.72	1.35	5.00	15.0	20.0	1.72	1.12
2.50	45.6	2.00	2.02	1.62	5.00	9.00	20.0	1.72	0.874
2.50	15.0	20.0	1.75	1.36	6.50	41.7	2.00	2.02	1.07
3.00	28.2	20.0	1.75	1.55	7.50	40.8	2.00	2.02	0.964
4.00	44.2	2.00	2.02	1.39	7.50	18.0	20.0	1.80	1.13
5.00	43.2	2.00	2.02	1.26	7.50	25.5	20.0	1.80	1.42
5.00	27.0	20.0	1.72	1.48	7.50	12.0	20.0	1.80	0.840
5.00	21.0	20.0	1.72	1.33	7.50	6.00	20.0	1.80	0.552

Part B

$Hg_T \times 10^5$	$L_T \times 10^3$	$[H^+] \times 10^2$	$D_T \times 10^5$	$[H_2D]_{org} \times 10^5$	$Hg_T \times 10^5$	$L_T \times 10^3$	$[H^+] \times 10^2$	$D_T \times 10^5$	$[H_2D]_{org} \times 10^5$
0.250	2.54	1.90	2.84	2.54	1.25	2.90	4.77	2.81	1.79
0.500	1.87	1.90	2.84	2.12	1.25	3.48	4.72	2.81	1.92
0.500	3.41	1.90	2.84	2.35	1.25	4.65	4.63	2.81	2.11
0.750	1.19	19.9	1.20	0.65	1.25	1.07	9.90	2.97	1.16
0.750	2.38	19.8	1.20	0.86	1.25	2.14	9.81	2.97	1.59
0.750	3.57	19.7	1.20	1.01	1.25	3.20	9.72	2.97	1.86
1.25	1.08	2.43	2.43	0.95	1.25	3.74	9.67	2.97	2.03
1.25	2.15	2.36	2.43	1.37	1.25	4.27	9.62	2.97	2.12
1.25	2.69	2.33	2.43	1.52	1.25	1.47	19.9	2.28	1.01
1.25	3.23	2.29	2.43	1.66	1.25	2.94	19.7	2.28	1.39
1.25	1.19	0.949	2.35	1.09	1.25	5.88	19.5	2.28	1.82
1.25	2.38	0.901	2.35	1.49	1.25	0.95	0.0562	2.29	0.96
1.25	2.97	0.878	2.35	1.64	1.25	1.91	0.0562	2.29	1.43
1.25	3.56	0.856	2.35	1.77	1.25	2.38	0.0562	2.29	1.46
1.25	4.16	0.834	2.35	1.85	1.25	2.86	0.0562	2.29	1.66
1.25	1.16	4.91	2.81	0.80	1.25	3.81	0.0562	2.29	1.82
1.25	2.32	4.82	2.81	1.61					

2.4.3. Raman spectroscopic measurements

Raman spectra of penicillamine solutions ($L_T = 0.6$, pH 7.1) and of solutions ($L_T = 1.0$ M, Hg_T: 0.2 M, pH 7.10) were recorded and Raman scattering intensities of SH stretching vibration at 2570 cm^{-1} and CH stretching vibration at 2940 cm^{-1} were measured.

3. Equations and calculations

(a) Determination of protonation constants K_1 and K_2 of penicillamine ($12 > pH > 5$)

$$L_T = L^{2-} + HL^- + H_2L \quad (1)$$

From the law of electroneutrality

$$Na_T^+ + [H^+] - [OH^-] - ClO_{4T}^- = 2[L^{2-}] + [HL^-] \quad (2)$$

Dividing Eq. (1) by Eq. (2) and denoting with C the left hand side of Eq. (3), which comprises the measured data:

$$C = \frac{L_T}{Na_T^+ + [H^+] - [OH^-] - ClO_{4T}} = \frac{[L^{2-}] + K_1[H^+][L^{2-}] + K_1K_2[H^+]^2[L^{2-}]}{2[L^{2-}] + K_1[H^+][L^{2-}]} \quad (3)$$

After rearrangement of Eq. (3)

$$\frac{2C-1}{(1-C)[H^+]} = K_1 + K_1K_2\frac{[H^+]}{1-C} \quad (4)$$

Protonation constants K_1 and K_2 as well as their standard deviations were gained by linear regression from Eq. (4).

(b) K_3 of penicillamine was calculated from the pH-metric data ($3.5 > pH > 0.7$) with the formula:

$$K_3 = \frac{L_T}{(ClO_{4T}^- - Na_T^+ - [H^+])[H^+]} - \frac{1}{[H^+]} \quad (5)$$

(c) Determination of extraction stability constant of $Hg(HD)_2$ complex

$$Hg_T = [Hg^{2+}]_{aq} + [HgBr^+]_{aq} + [HgBr_2]_{aq} + [HgBr_3^-]_{aq} + [HgBr_4^{2-}]_{aq} + [Hg(HD)_2]_{org} \quad (6)$$

$$D_T = [H_2D]_{org} + 2[Hg(HD)_2]_{org} \quad (7)$$

Using the definitions of stability constants and combining Eq. (6), and Eq. (7)

$$\beta_{2ext} = \frac{\alpha_{Br}(D_T - [H_2D]_{org})[H^+]^2}{[H_2D]_{org}^2(2Hg_T - D_T + [H_2D]_{org})} \quad (8)$$

where

$$\alpha_{Br} = 1 + \beta_1Br_T^- + \beta_2(Br_T^-)^2 + \beta_3(Br_T^-)^3 + \beta_4(Br_T^-)^4, \quad \text{since} \quad Br_T >> Hg_T \quad (9)$$

(d) Determination of stability constants β_{122}, β_{123}, β_{124} from liquid/liquid extraction studies

$$Hg_T = [Hg^{2+}]_{aq} + [Hg(HD)_2]_{org} + [HgL_2H_2]_{aq} + [HgL_2H_3]_{aq} + [HgL_2H_4]_{aq} \quad (10)$$

$$D_T = [H_2D]_{org} + 2[Hg(HD)_2]_{org} \quad (11)$$

After combination of Eq. (10) and Eq. (11), using the definitions of stability constants and taking into account that $L_T >> Hg_T$.

$$\frac{2Hg_T\beta_{2ext}[H_2D]_{org}^2}{D_T - [H_2D]_{org}[H^+]_{aq}^2} - \frac{\beta_{2ex}[H_2D]_{org}^2}{[H^+]_{aq}^2} - 1 = \frac{\beta_{122}L_T^2[H^+]_{aq}^2}{\alpha_H^2} + \frac{\beta_{123}L_T^2[H^+]_{aq}^3}{\alpha_H^2} + \frac{\beta_{124}L_T^2[H^+]_{aq}^4}{\alpha_H^2} \quad (12)$$

where

$$\alpha_H = 1 + K_1[H^+] + K_1K_2[H^+]^2 + K_1K_2K_3[H^+]^3$$

As the left hand side of Eq. (12) comprises measured data, β_{122}, β_{123}, β_{124} can be calculated by three variables multiple linear regression.

(e) For determination of β_{121}, and β_{133} from pH metric measurements ($4 < pH < 6.3$) there were two computer iteration methods used. In one version values of $[L^{2-}]$ were gained with assumed β_{121} and β_{133} from Eq. (13) first and values of $\bar{z}$ were calculated from Eq. (14). After comparing of $\bar{z}$ calculated and obtained from the measurements data by Eq. (15) β_{121} and β_{133} were refined until the best curve fitting was obtained.

$$\frac{L_T - [L^{2-}]\alpha_H}{Hg_T} = \frac{2\beta_{122}[H^+] + 2\beta_{121} + 3\beta_{133}[H^+]^2[L^{2-}]}{\beta_{122}[H^+] + \beta_{121} + \beta_{133}[H^+]^2[L^{2-}]} \quad (13)$$

$$\bar{z} = \frac{2\beta_{122}[H^+] + 3\beta_{121} + 3\beta_{133}[H^+]^2[L^{2-}]}{\beta_{122}[H^+] + \beta_{121} + \beta_{133}[H^+]^2[L^{2-}]} \quad (14)$$

$$\bar{z} = \frac{V_{NaOH}C_{NaOH} - V_{Hg}C_{HClO_4}}{V_{Hg}C_{Hg}} \quad (15)$$

where

- V_{NaOH} and C_{NaOH} are the volumes (ml) and concentration (M) of NaOH standard solutions used to restore the initial pH of L solutions after adding V_{Hg} ml of $Hg(ClO_4)_2$ standard solution to them.
- C_{Hg} and C_{HClO_4} are the Hg(II) and free $HClO_4$ concentrations (M) of $Hg(ClO_4)_2$ standard solutions.

The other version of computation was made by the use of the nonlinear least squares program PSEQUAD [16].

(f) Evaluation of Raman spectroscopic measurements.

From the ratios of the Raman scattering inten-

sities of SH and CH streching vibrations at 2570 and 2940 cm^{-1}, respectively, the average number of penicillamine molecules bound to one Hg(II) ion through their sulphydryl groups was calculated by Eq. (16).

$$\bar{n} = \frac{L_{T1}}{Hg_T}\left(1 - \frac{q_1}{q}\right) \quad (16)$$

where L_{T1} represents the total concentration of the ligand in the solutions containing mercury(II) (Hg_T); q_1, the ratio of the intensities of SH and CH vibrations specified above for the solutions of ligand containing Hg(II) (L_{T1}, Hg_T); q, the ratio of the intensities of SH and CH vibrations in the solutions of penicillamine that do not contain Hg(II) and the pH of which is equal to that of the solution with L_{T1} and Hg_T.

4. Results and discussion

Macroscopic protonation constants determined in the present work (Table 2) are in good agreement with the literature data [3,4,17].

Similarly, the water-carbon tetrachloride extraction stability constant of Hg–dithizone 1:2 complex re-determined by us at 25 ± 0.2°C ($I =$ 0.5 $NaClO_4$) using bromide ions as auxiliary ligands in the aqueous phase is in accordance with the value of $\lg\beta_{2ext} = 26.85 \pm 0.25$ published by Breant [18], who applied I^- ions in her measurements. The extraction stability constant $\log \beta_{2ext} = 26.53 \pm 0.05$ ($P = 0.95$, $n = 16$) and protonation constants determined in the present study were used in the calculations of stability constants of Hg(II)–penicillamine complexes.

Mercurimetric titration curves of penicillamine at different constant pH values suggested, as expected, quantitative formation of 1:2 and 1:1 Hg–penicillamine complexes at metal ligand ratios of 1:2 and 1:1, respectively, even at very low pH (see Fig. 1).

Table 2
Macroscopic protonation constants of penicillamine

Constant	log K	log confidence limits ($P = 0.95$)	n
K_1	10.42	0.01	78
K_2	7.88	0.01	78
K_3	1.90	0.02	65

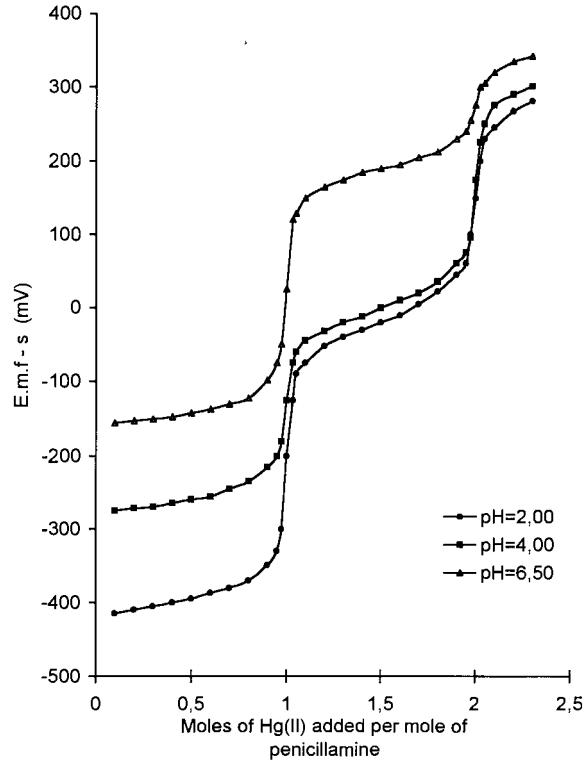

Fig. 1. Potentiometric titration curves of penicillamine titrated with $Hg(ClO_4)_2$ at constant pH (platinum wire indicator electrode).

The average numbers of protons splitting off the ligand(s) due to complexation with a mercury(II)-ion /$\bar{z}$/ calculated from pH-metric data (Fig. 2) were not lower than 2.0 under pH 6.8.

This supports the doubts of Doornbos et Faber [7] surrounding the applicability of the sole pH-metric method for the determination of stability constants of these complexes. However, these $\bar{z}$ values provide some information on the possible binding sites involved in complex formation. The $\bar{z} = 2.0$ found at 1:1 Hg_T: L_T ratio in the pH range 3.0–6.5 refers to the coordination involving both sulphydryl and amino groups in the 1:1 complex, since both of them are protonated in the free ligand within this pH range.

$\bar{z} = 2.0$ found at pH even as low as 2.0, at which $\sim 44\%$ of the carboxyl groups of the free

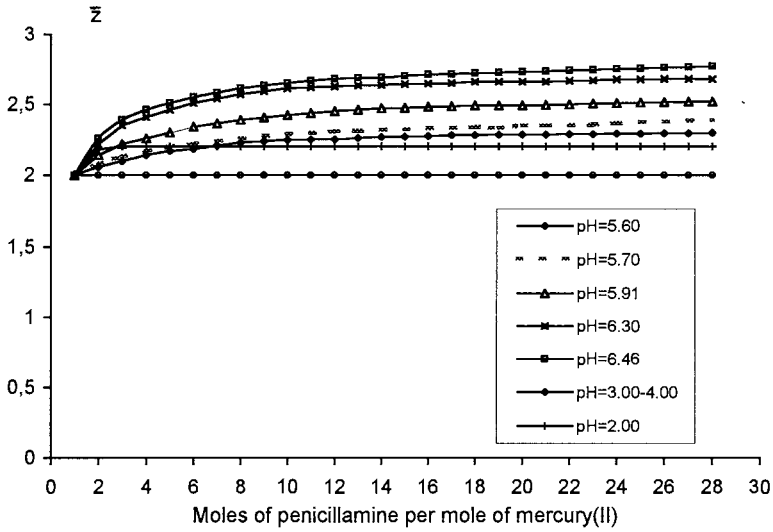

Fig. 2. The average number of protons ionized from penicillamine due to complexation with a Hg(II) ion ($\bar{z}$) as a function of L_T/Hg_T.

ligands are protonated, indicates, however, that the latter probably do not take part in the coordination, and their protonation constant in the 1:1 complex does not differ significantly from K_3 of the free ligand.

The same $\bar{z} = 2.0$ values at Hg_T: L_T ratios of 1:2–30 in the pH range 3.0–4.0 seem to be in agreement again with the theory of the previous authors [7–11] who supposed that two –SH groups were involved through proton ionisation in 1:2 Hg–cysteine complex formation leaving the two ammonium groups non-coordinated.

Values of $\bar{z} > 2.0$ at pH 2.0 at Hg_T: L_T ratios of 1:2–30 do not allow us to decide whether additional partial coordination of carboxylate groups in HgL_2 complex occurs or the observed $\bar{z} = 2.2$ values are the consequence of the slightly increased acid dissociation of carboxyl groups in the 1:2 complex compared to that of the free ligand. Due to the quantitative complex formation stability constants of complexes formed under pH 4.0 can not be calculated from pH-metric data. For this purpose a liquid–liquid extraction method was developed.

This method, similar to that of Stary and Kratzer [11] used for studying Hg(II)–cysteine equilibria, was based on the competition of dithizone and the SH-ligand. In our experiments, however, the distribution of Hg(II) between the organic phase containing dithizone and the aqueous phase containing penicillamine was not followed by radiometry, using labelled Hg(II), but it was calculated from Hg_T, L_T, D_T and $[H_2D]_{org}$ data measured spectrophotometrically.

Under the conditions of the liquid/liquid extraction measurements the formation of 1:1 Hg–penicillamine complexes cannot be expected as $L_T >> Hg_T$. However, due to the pH range applied ($0.70 < pH < 3.25$), the protonation of the carboxyl groups of the 1:2 metal/ligand complexes, i.e. the formation of $HgL_2H_3^+$ and $HgL_2H_4^{2+}$ complexes besides HgL_2H_2 species had to be assumed.

The determined stability constants of the differently protonated HgL_2 complexes (Fig. 3) are shown in Table 3.

For the stability of the relevant $HgL_2H_3^+$ and $HgL_2H_4^{2+}$ complexes with the related ligand cysteine there are no data available in the literature. However, the values of $\beta_2 = [HgL_2H_2]/[Hg^{2+}][LH^-]^2$ for the ligand of cysteine determined by Van der Linden and Beers [9] and Stary and Kratzer [11], respectively, can be compared to our β_{122} taking into account that $\beta_{122} = \beta_2 \cdot K_1^2$.

The stability constants for Hg(cysteine)$_2$ com-

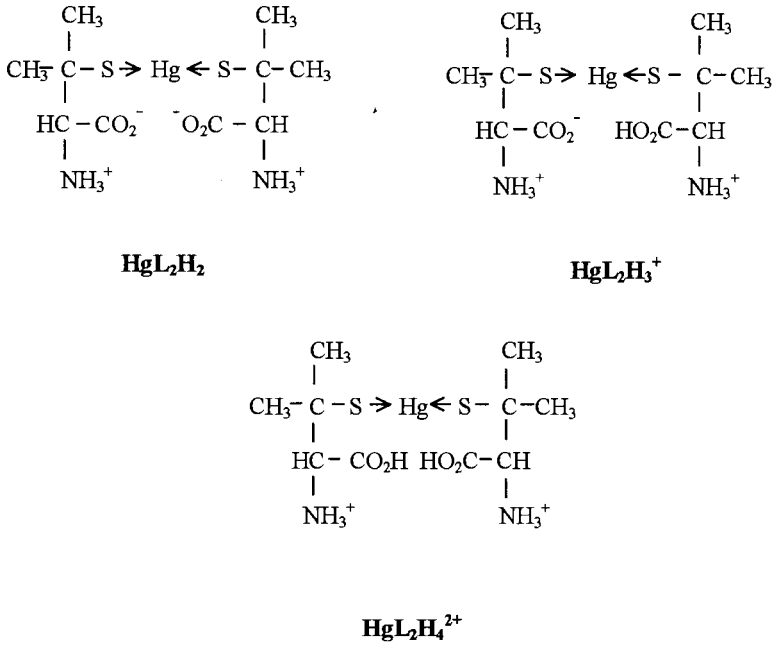

Fig. 3. The structures of the HgL_2H_2, $HgL_2H_3^+$ and $HgL_2H_4^{2+}$ complexes.

plexes (Table 3) are of similar magnitude, although in accordance with the differences in the protonation constants of the two ligands they are to some extent higher than the value of β_{122} for penicillamine.

The ratio of β_{123} and β_{122} i.e. the protonation constant of one of the $-COO^-$ groups in the HgL_2 complex is 97.7. This value is very similar to the K_3 of the free ligand ($\lg K_3 = 1.90$). Although the ratio of β_{124} and β_{123} i.e. the protonation constant of the other $-COO^-$ group in the HgL_2H^+ complex is significantly lower ($\beta_{124}/\beta_{123} = 28.2$), even this increased acidity of the second carboxyl group can not be regarded as an evidence for its bonding to the mercury(II). The difference of 0.54 between the logarithms of protonation constants of the two $-COO^-$ groups in the 1:2 complex practically corresponds to the value of 0.6, which is statistically expected for the consecutive equilibria of this type.

Thus our results seem to reaffirm the theory of non-coordinated carboxylates, and the formation of linear 1:2 complexes with two coordinated sulphydryl groups at pH values < 4.0.

The values of $\bar{z}$ varying between 2.00–2.80 in the pH range of 4.00–6.70 ($L_T > Hg_T$) could only be explained by the formation of additional complex species compared to those encountered in the evaluation of liquid/liquid extraction results.

The pH-metric data were fitted against several models assuming Hg–L complexes of different stoichiometry and structure including mixed ligand complexes with L and OH^- as well.

The best curve fitting was obtained by the model comprising the additional formation of

Table 3
Stability constants of the HgL_2H_2, $HgL_2H_3^+$ and $HgL_2H_4^{2+}$ complexes

Constant	log β	log confidence limits ($P = 0.95$)	n
β_{122}	59.03 (60.4[a], 61.0[b])	0.02	33
β_{123}	61.02	0.02	33
β_{124}	62.47	0.04	33

[a] β_{122} for Hg(cysteine)$_2$ complex calculated from β_2 published by Van der Linden and Beers [9].
[b] β_{122} for Hg(cysteine)$_2$ complex calculated from β_2 published by Stary and Kratzer [11].

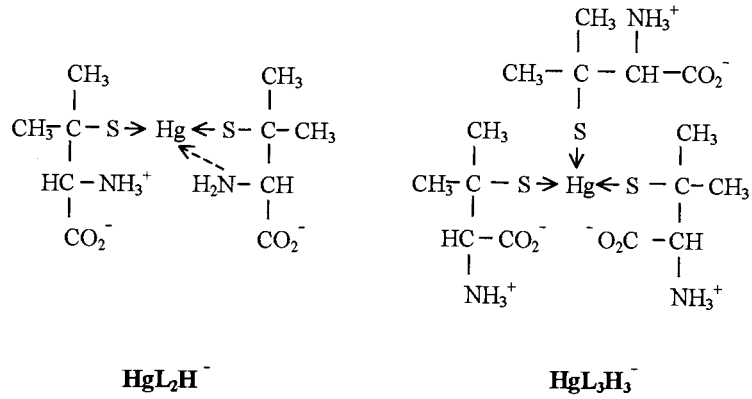

Fig. 4. The structures of the HgL_2H^- and $HgL_3H_3^-$ complexes.

Table 4
Stability constants of the HgL_2H^- and $HgL_3H_3^-$ complexes

Constant	log β	log confidence limits ($P = 0.95$)	n
β_{121}	52.03	0.02	40
β_{133}	72.43	0.01	40

HgL_2H^- and $HgL_3H_3^-$ complexes besides HgL_2H_2 (see Fig. 4). The stability constants of HgL_2H^- and $HgL_3H_3^-$ are shown in Table 4.

In the complex HgL_2H^- both the additional coordination of an $-NH_2$ group and the increased acid dissociation of one of the ammonium groups of HgL_2H_2 complex without its coordination can be assumed. Significantly increased acidity of the ammonium group ($pK = 7.00$) in the HgL_2H_2 complex compared to that of the free ligand seems to support the first, the strong tendency of Hg(II) to form linear S–Hg–S type complexes instead of trigonal planar ones is backing up the second idea.

Equilibrium studies indicating the formation of $HgL_3H_3^-$ complex have not been published yet.

From ^{13}C NMR spectra versus pH data in alkaline medium (pH 9.5–11.5) the stability constants of $K_{f3} = [HgL_3]/[HgL_2][L]$, $K_{f3H} = [HgL_3H]/[HgL_2][HL]$, and $K_{f3H_2} = [HgL_3H_2]/[HgL_2H][HL]$ were determined by Cheesman et al. [10]. Converting β_{133} determined in the present work to K_{f3H3} by the formula:

$$K_{f3H_3} = [HgL_3H_3]/[HgL_2H_2][HL] = \frac{\beta_{133}}{\beta_{122}K_1}$$

to make it comparable to the published constants $\lg K_{f3} = 3.59 \pm 0.35$, $\lg K_{f3H} = 3.35 \pm 0.29$ and $\lg K_{f3}H_2 = 3.11 \pm 0.25$ of Cheesman et al. our

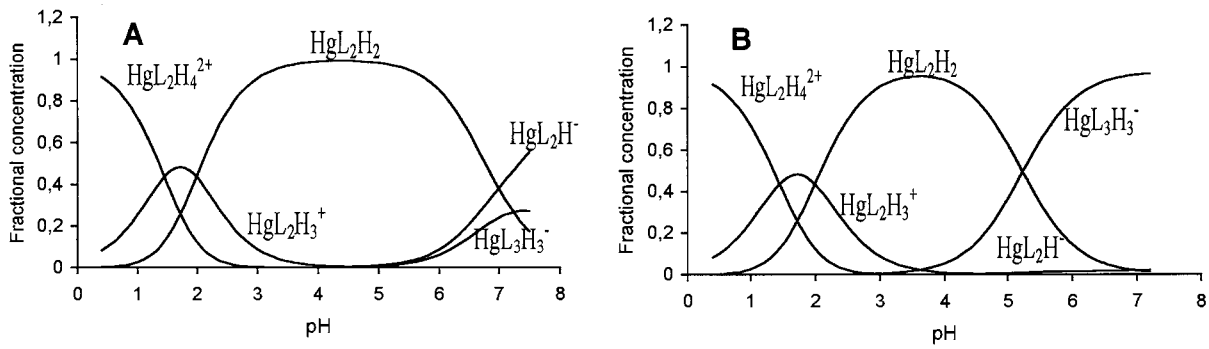

Fig. 5. pH dependence of species distributions at non-complexed ligand concentrations of 5×10^{-3} M (A) and 0.4 M (B).

value of $\lg K_{f3}H_3 = 2.98 \pm 0.06$ was in very good agreement with Cheesman's constants.

Species distributions calculated with the determined stability constants (Fig. 5) show that in solutions with $L_T = 1.0$ M, $Hg_T = 0.2$ M, pH 7.0, $\sim 97\%$ of the total Hg(II) is present in 1:3 Hg/ligand complex.

From the Raman spectra of these solutions and from those of penicillamine solutions without Hg(II) $q = 0.61 \pm 0.05$ and $q_1 = 0.235 \pm 0.03$ were gained. For the average number of ligands coordinated to Hg(II) via their deprotonated –SH groups $\bar{n} = 3.07$ was found by Eq. (16). This value provides strong evidence for the formation of 1:3 complexes under conditions of $L_T/Hg_T > 2$ and pH > 4.

Acknowledgements

The authors are grateful to Professor K. Burger, who provided helpful advice and discussions. Professor I. Nagypál and Gy. Jalsovszky are thanked for assistance with computation and Raman spectra.

References

[1] Martindale, The Extra Pharmacopoeia, 3rd edn, Royal Pharmaceutical Society, London, 1996, pp. 989–992.
[2] H. Köszegi-Szalai, T.L. Paal, E. Fazekas-Juhász, Acta Pharm. Hung. 55 (1985) 266.
[3] E.J. Kuchinkas, Y. Rosen, Arch. Biochem. Biophys. 97 (1962) 370–372.
[4] G.R. Lenz, A.E. Martell, Biochemistry 3 (6) (1964) 745–750.
[5] Y. Sugiura, H. Tanaka, Chem. Pharm. Bull. 18 (4) (1970) 693–701.
[6] M.M. Shoukry, M. Mohamed, Egypt. J. Chem. 28 (5) (1986) 443–445.
[7] D.A. Doornbos, J.S. Faber, Pharm. Weekblad 99 (1964) 289.
[8] W. Stricks, I.M. Kolthoff, J. Am. Chem. Soc. 75 (1953) 5673.
[9] W.E. Van der Linden, C. Beers, Anal. Chim. Acta 68 (1973) 143–154.
[10] B.V. Cheesman, A.P. Arnold, D.L. Rabenstein, J. Am. Chem. Soc. 110 (1988) 6659–6664.
[11] J. Stary, K. Kratzer, J. Radioanal. Nucl. Chem. Lett. 126 (1) (1988) 69–75.
[12] O.N. Loginova, B.I. Peshchevitskii, M.A. Fedotov, Izv. Sib. Otd. Akad. Nauk SSSR. Ser. Khim. Nauk 1 (1987) 61–64.
[13] E.S. Gruff, S.A. Koch, J. Am. Chem. Soc. 112 (3) (1990) 1245–1247.
[14] J.F. Duncan, F.G. Thomas, J. Inorg. Nucl. Chem. 4 (1957) 376.
[15] M. Calvin, N. Melchior, J. Am. Chem. Soc. 70 (1948) 3270.
[16] L. Zékány, I. Nagypál, PSEQUAD: A comprehensive program for the calculation of potentiometric and spectrophotometric equilibrium data using analytical derivatives, Cpt 8, in: D. Leggett (Ed.), Computational Methods for the Determination of Stability Constants, Plenum Press, New York, 1985.
[17] D.D. Perrin, I.G. Sayce, J. Chem. Soc. A (1968) 53–57.
[18] M. Breant, Bull. Soc. Chim. France, 948 (1956).

ELSEVIER

Talanta 48 (1999) 403–407

Talanta

Acid volatile sulfide determination in sediments using elemental analyzer with thermal conductivity detector

Haidi D. Fiedler [a,*], Roser Rubio [b], Gemma Rauret [b], Isidre Casals [c]

[a] *Departamento de Química, Universidade Federal de Santa Catarina, Florianópolis, Santa Catarina 88040-900, Brazil*
[b] *Departament de Química Analítica, Universitat de Barcelona, Avda Diagonal 647, 08028 Barcelona, Spain*
[c] *Serveis Científico Tècnics, Universitat de Barcelona, C. Martí Franquès s/n, 08028 Barcelona, Spain*

Received 8 May 1998; received in revised form 27 July 1998; accepted 27 July 1998

Abstract

A method for the determination of acid volatile sulfides (AVS) in sediments, using a common elemental analyzer with thermal conductivity detector, is proposed. The method uses a mixture of Sn and V_2O_5 for pyrolysis and combustion to determine total sulfur (TS), and non volatile sulfur (NVS), after an acidic attack. AVS is calculated as the difference between TS and NVS. The method for TS is validated by analyzing a certified reference material. The recovery in the determination of acid volatile sulfide is determined by spiking a river sediment with ZnS. The method is accurate and gives a good reproducibility, recovering 97.7–99.6% of the sulfur in the 0–3% total sulfur content, with SD of $\approx 0.015\%$.

Keywords: Acid volatile sulfide; Sulfur; Elemental analyzer; Thermal conductivity detector; Polluted sediments

1. Introduction

The sulfur cycle in the environment is complex due to the wide variety of naturally-occurring forms and oxidation states [1]. Sulfur-containing minerals are precipitated and accumulate under different physico–chemical conditions and through several pathways, in marine, lacustrine and riverine sediments. In unpolluted aquatic sediments, sulfur species are found in association with iron [2], iron sulfide, usually present in the form of pyrite (FeS_2), or mackinawite (FeS), which is the most common metal sulfide in sediments. In reducing conditions and in the presence of organic matter, sulfates are reduced to dissolved sulfide and this may lead to the deposition of insoluble metal sulfides, such as lead and cadmium. The acid volatile sulfides (AVS) can be considered as a measure of mobilizable sulfides, mainly iron monosulfide [3]. The relationship AVS/free metal ion has been used as an indicator of sediment quality [4] since, as long as excess AVS is present, metal ions are present as insoluble sulfides [5]. The complex environmental redox variations influence the transformation of sulfides

* Corresponding author. Fax: +55 48 3319987; e-mail: fiedler@reitoria.ufsc.br

0039-9140/99/$ - see front matter
PII S0039-9140(98)00257-4

and can promote the mobility of elements such as Hg, Zn, Pb, Cu, and Cd and increase the acidity [3,6,7].

Industrial processes, such as processing of coal, ores and other minerals, can contribute to the presence of sulfides in waters. The presence of pyrite (isometric structure) and marcasite (orthorombic structure) contributes to acid drainage [8,9], which can contaminate soils and sediments and damage groundwaters. Oil industries [10], domestic effluents and the lack of sufficient wastewater treatment plants, can lead to high sulfide concentrations in sediments. Thus, the determination of sulfide and total sulfur (TS) is important, not only for knowledge of the sulfur cycle, but also for the identification of trace elements in the aquatic environment. The AVS fraction should be routinely analyzed in sediments. Accordingly, reliable analytical methods for sulfide monitoring should be easily available, providing good sensitivity, reproducibility and accuracy and automatic methods for continuous monitoring are necessary.

Methods described for the determination of AVS in sediments use acidification at high temperature, followed by trapping of the resulting hydrogen sulfide by precipitation with metal solutions [11]. Final measurements are normally carried out by colorimetry [12], potentiometry using ion-selective electrode [13], or a chromatographic system [2]. Although analysis using standard induction-furnace methods, coupled with infrared detectors, is well established, for TS determination, it is not always available in all laboratories. Nevertheless, there is no method available for AVS and sulfur determination in sediments that permits the analysis of a large number of samples per day, with good precision and accuracy.

This paper describes a new method for the determination of AVS and TS in sediments, using a common 'elemental analyzer with thermal conductivity detector' (EA/TCD). The proposed method is able to process small samples and provides low detection limits and good precision. The method uses fewer reagents and less manipulation of the sample than other methods [2,11–13].

2. Experimental

This paper deals only with the determination of TS and AVS in dry sediments. Detailed methods for sampling, sample storage and pretreatment, which are important in the analysis of anoxic sediments, have been described elsewhere [14]

2.1. Sampling and sample treatment

2.1.1. Certified reference material

Lake sediment LKSD, from the Geological Survey of Canada, Canada Centre for Mineral and Energy Technology (CANMET), was utilized; total sulfur certified, 0.99%.

Besides the LKSD certified reference material, samples of sediment collected from the River Besòs (Catalonia, Spain) were analyzed. The Besòs basin is one of the most polluted areas in Catalonia [15], mainly owing to the high discharge of industrial and domestic effluents and the lack of sufficient wastewater treatment plants. Sediment was collected at a depth of 10–15 cm and placed in polyethylene containers. The sediment was left to settle for 2 weeks and the supernatant water was removed. After drying, the < 63 μm particle size fraction was retained after sieving and bottled in dark glass containers.

2.2. Instrumentation and apparatus

A Carlo Erba Model EA 1108 elemental analyzer, equipped with a flash combustion furnace, a Porapak PQS chromatographic column and a thermal conductivity detector, was used for S determination. Samples were weighed using a micro-balance model Micro M2P (Sartorius, Göttingen, Germany) and Sn capsules. Homogenization of samples was achieved using a ball-bearing grinder Spex Mixer/Mill (Spex Industries, Metuchen, NJ).

2.3. Reagents

Sulfanilamide, zinc sulfide, vanadium pentoxide, metallic tin, calcium oxide and magnesium oxide were of analytical grade. Doubly de-ionized water, 18.3 Mohm cm resistivity, obtained from a

Culligan Ultrapure-GS system, was used to prepare the standard solutions and reagents.

2.4. Procedures

The elemental analyzer was calibrated with sulfanylamide and zinc sulfide. For each sample of sediment, two aliquots were analyzed: aliquot 1 to determine TS and aliquot 2 to determine non volatile sulfur (NVS). For each aliquot, 1 g of sediment was weighed.

The scheme followed for the determination of TS and NVS is shown in Fig. 1. For NVS determination, the acidic attack was conducted overnight with continuous stirring at 60°C.

For determination of TS and NVS, 11–13 mg of the homogenized solid mixture from aliquot 1 and 19–20 mg of the homogenized solid mixture from aliquot 2 were weighed in tin capsules and introduced into the elemental analyzer.

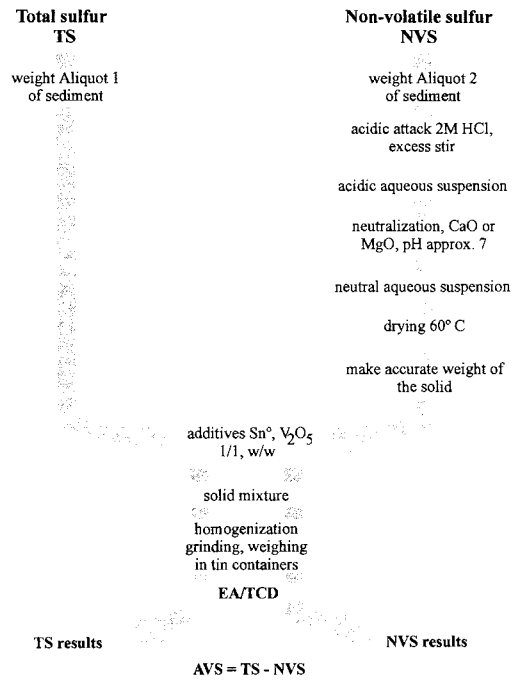

Fig. 1. Steps followed to analyze TS and NVS in a sediment sample. The AVS content in the sample is calculated as the difference between these experimental results.

3. Results and discussion

It is well known that V_2O_5 acts as an oxidizing agent, in addition to the amount of oxygen supplied to the oven of the elemental analyzer and assures the completion of the combustion at 1020°C. Thus, in order to improve pyrolysis and combustion, a mixture of Sn and V_2O_5, in a 1/1 w/w ratio, was added to each aliquot of sample (for TS determination) and to each solid residue after acidification (for NVS determination), before grinding the mixture. In this oxygen-rich atmosphere, the powdered Sn yields SnO_2 and the exothermic reaction heats the sample in the oven and facilitates the pyrolysis of sulfates and the oxidation of metal sulfides to SO_2 and metal oxides.

After establishing the optimum working conditions, the method was validated by determining the total sulfur content of the certified reference material LKSD4, which had 0.99% sulfur. A mean value of TS = 0.98%, with SD = 0.006%, was calculated from eight independent determinations. Clearly, the method shows an excellent agreement with the certified value for LKSD4.

Aliquots of the river sediment, without added ZnS and spiked with different known amounts of ZnS, were analyzed in order to determine the recovery of TS. The aliquots were treated following the scheme in Fig. 1, ensuring a homogeneous mixture of the spike and the sample. From the results shown in Table 1, it can be concluded that a good level of recovery of total sulfur is obtained in all cases (between 97.7 and 99.6%). As shown by the SD, individual determinations (eight samples) show good repeatability. A linear regression of the total sulfur (TS%) versus added sulfide (AVS), shows a correlation coefficient of 0.9993 and yields Eq. (1)

$$TS\% = 1.8832 + 0.9461 \times AVS \quad (1)$$

which in turn allows us to estimate calculated values for the spiked ZnS, agreeing with a difference $\leq 0.024\%$ with the added sulfide (values included in Table 1 for comparative purposes). Since each of the values in Table 1 correspond to the mean value of eight independent determinations, the SDs are strongly indicative that the

Table 1
Recovery and determination of acid volatile sulfides in ZnS-spiked river sediment[a]

Sample	Added ZnS (%)	Total sulfur, theoretical (%)	Total sulfur, recovered (%)	Standard deviation (s)	Yield (TS) (%)
1	0	—	1.888	0.015	—
2	0.107 (0.105)[b]	1.995	1.983	0.013	99.4
3	0.248 (0.259)[b]	2.136	2.128	0.013	99.6
4	0.493 (0.469)[b]	2.381	2.327	0.009	97.7
5	0.955 (0.965)[b]	2.843	2.796	0.014	98.3

[a] Each value is the mean of eight independent determinations using EA-TCD.[b] Calculated from the linear correlation between total sulfur (TS) and added sulfide, see text.

Table 2
Percentages of TS, NVS and AVS determined in sediment samples[a]

River sediment				LSKD-4 sediment
Sample A		Sample B		
Aliquot 1	Aliquot 2	Aliquot 1′	Aliquot 2′	
%TS	%NVS	%TS	%NVS	%TS
1.888	1.855	1.888	1.853	0.980
(*s*: 0.015)	(*s*: 0.003)	(*s*: 0.015)	(*s*: 0.009)	(*s*: 0.006)
%AVS: 0.033		%AVS: 0.035		Certified value: 0.99%

[a] TS, NVS and AVS correspond to total sulfur, non volatile sulfur and acid volatile sulfide, respectively. Each value is the mean of eight independent determinations using EA-TCD and *s* corresponds to the standard deviation.

procedure shows good repeatability and demonstrates also the goodness of the analytical pathway. Clearly, for samples with AVS contents such as those of the spiked samples, the proposed method behaves appropriately.

A lower limit of detection could be established by analysis of the top oxic layer of the river sediment, where the AVS content is virtually nil (0.02–0.03%) [14]. Thus, the contents of TS, NVS and AVS were determined in the river sediment and the results are reported in Table 2. Results obtained with LKSD4 are included for comparison purposes. Two samples (A and B) of the river sediment were analysed for TS and for determining NVS and eight replicates of each were carried out. The values obtained for both TS and NVS are rather similar and in all cases a good level of reproducibility is observed. Clearly, the determined value of 0.034% represents, most probably, the lower limit of detection with this method., since SD of the TS determination is $\approx 0.015\%$. If we permit ourselves to mimic instrumentational language, we could say that we are close to the lowest detectable signal-to-noise ratio.

The proposed method shows a good reproducibility and recovers $98.7 \pm 1.0\%$ of the total sulfur, in the 0–3% total sulfur content. Thus, the proposed TS and NVS (and hence AVS) determination by the EA-TCD method is revealed as a useful analytical technique for sulfur determination in polluted and unpolluted sediment samples.

Finally, a lower limit of detection can be established at $\approx 0.03\%$ and we believe that although the method was standardized for sediments, it should be valuable for a variety of materials such as soils, coal, sludges and other geochemical samples. This technique may seem time-consuming at first sight, but its main advantage is that once all the steps are assembled in series, up to fifty samples per day can be analyzed with good results.

Acknowledgements

H. Fiedler thanks CNPq (Conselho Nacional de Desenvolvimento Científico e Tecnológico) and CAPES (Coordenação de Aperfeiçoamento de Pessoal de Ensino Superior), Brazil.

References

[1] A.J.B. Zehnder, S.H. Zinder, in: O. Hutzinger (Ed.), Handbook of Environmental Chemistry, Vol. 1, part A: The Natural Environment and the Biogeochemical Cycles, Springer–Verlag, Berlin, 1980.
[2] G.A. Cutter, T.J. Oatts, Anal. Chem. 59 (1987) 717.
[3] U. Förstner, in: W. Salomons, W.M. Stigliani (Eds.), Biogeodynamics of Pollutants in Soils and Sediments, Springer, Berlin, 1995.
[4] E.N. Leonard, V.R. Mattson, D.A. Benoit, R.A. Hoke, G.T. Ankley, Hydrobiologia 271 (1993) 87.
[5] D.M. Di Toro, J.D. Mahony, D.J. Hansen, et al., Environ.Toxicol.Chem. 9 (1990) 1487.
[6] W. Stumm, J. Morgan, Aquatic Chemistry, 2nd ed., Wiley-Interscience, New York, 1981.
[7] A.C.M. Bourg, J.P.G. Loch, in: W. Salomons, W.M. Stigliani (Eds.), Biogeodynamics of Pollutants in Soils and Sediments, Springer, Berlin, 1995.
[8] W. Stumm, J. Morgan, Aquatic Chemistry: An Introduction Emphasizing Chemical Equilibria in Natural Waters, Wiley, New York, 1970, p. 153.
[9] J.A. Solari, H.D. Fiedler, C.L. Schneider, Fuel 68 (1989) 536.
[10] K.A. Kvenvolden, J.B. Rapp, F.D. Hostettler, J.L. Morton, J.D. King, G.E. Claypool, Science 234 (1986) 1231.
[11] W. Wuncheng, J.M. Barcelona, J. Environ. Int. 9 (1983) 129.
[12] W. Davison, J.P. Lishman, Analyst 108 (1983) 1235.
[13] L. Giani, L. Eden, H. Gebhardt, Z. Pflanzenernaehr. Bodenkd. 149 (1986) 354.
[14] H.D. Fiedler, J.F. López-Sánchez, R. Rubio, et al., Analyst 119 (1994) 1109.
[15] G. Rauret, R. Rubio, J.F. López-Sánchez, E. Casassas, Water Res. 22 (1988) 449.

ELSEVIER

Talanta 48 (1999) 409–413

Talanta

Cloud-point preconcentration of fulvic and humic acids

Robert L. Revia *, George A. Makharadze

Department of Chemistry, Tbilisi State University, Chavchavadze Ave. 3, Tbilisi, 380028, Georgia

Received 1 April 1998; received in revised form 24 July 1998; accepted 28 July 1998

Abstract

The cloud-point extraction technique was used for preconcentration of fulvic and humic acids. The effect of the acidity of solution, the equilibration temperature and time, the amount of added surfactant (Triton X-100) and the time of centrifugation on the recovery were examined. The recoveries of fulvic and humic acids achieved under optimised conditions were 82% and 96%, respectively.

Keywords: Fulvic acid; Humic acid; Cloud-point extraction; Triton X-100

1. Introduction

Humic substances are present in natural waters in low concentration [1,2]. Therefore, preconcentration is required for their determination. Currently, the following techniques are used for these purposes: chromatographic methods using the XAD-2 and XAD-8, DEAE-cellulose, Duolite A-7 and activated charcoal. Despite many advantages, these methods are labour intensive, time consuming and expensive [3–6]. Consequently, an elaboration of rapid and simple methods of concentration of humic substances remains relevant. On the other hand, the property of aqueous micellar solutions of non-ionic surfactants undergoing a phase separation (cloud-point phenomenon) upon alteration of the conditions (temperature, pressure, additives, etc.), has been successfully used in many fields of analytical chemistry [7–11]. In fact, this unique behaviour of aqueous surfactant micellar systems can be employed for the preconcentration of analytes before their determination by HPLC [12–15]. The advantages of cloud-point extraction are based on the use of chromatographic extraction mechanism for liquid–liquid extraction processes. This attaches to the system more flexibility (multiplicity of variables). The methodology is simple since one needs only to heat the solution above cloud-point temperature. It is economically profitable due to low costs of chemicals and inexpensive equipments. The surfactant-rich phase obtained is compatible with hydroorganic mobile phases used in HPLC, what facilitates further determination of the analytes. The preconcentration factors obtained in many cases are similar to those of other preconcentration techniques. Cloud-point extraction procedure is a more rapid compared with solid phase extraction and not so labour intensive.

* Corresponding author. Fax: +995 32 221965; e-mail: faculty@tsu.ge

0039-9140/99/$ - see front matter
PII S0039-9140(98)00262-8

The aim of this work was the use of the cloud-point extraction technique for the preconcentration of humic substances from aqueous matrix. The extraction conditions were optimised by variation of experimental parameters.

2. Experimental

2.1. Sample preparation

The fulvic (FA) and humic (HA) acids were isolated from water of the river Mtkvari (Georgia). The water sample was enriched by freezing-out [16]. The sample obtained was acidified with concentrated hydrochloric acid to pH 2.0. The HA was coagulated from the solution on a water bath at 60°C. After the coagulation of the HA, the solution was centrifuged for 10 min at 8000 rpm and passed through a membrane filter (Sinpor N6, Prague, Czech Republic). For the purification of the FA from some organic impurities, the charcoal (BAU, Russia) was used [6]. Finally, the FA sample was passed through a cation-exchanger (KU-2, Russia). The HA precipitate was washed with distilled water, which was acidified with hydrochloric acid and then with distilled water. The obtained samples of the HA and FA were dried under the vacuum. Then, model solutions of HA and FA with a concentration of 0.03 mg ml^{-1} were prepared. In the pH studies, the required acidity was adjusted by the addition of hydrochloric acid or sodium hydroxide.

2.2. Equipment and procedure

The aliquot (10 ml) of the model solution containing Triton X-100 was pipetted into a test tube which then was placed into a thermostated water bath. The phase separation was completed by centrifugation at 3000 rpm. The centrifuge was placed in a thermostated oven at an appropriate temperature. In these experiments, the sample acidity, equilibration temperature and time, time of centrifugation and surfactant concentration were varied in order to study their effect on the efficiency of cloud-point extraction.

After the two phases had been separated, aliquot of bulk aqueous phase (7 ml) was carefully taken by syringe and analysed photoelectrocolourimetrically using the photoelectrocolourimeter KFK-2 (Russia). The measurements were performed at 364 nm. One centimetre path-length quartz cells were used. In all cases, the absorbance was measured against the reference solution which contained all the reagents present in the test solution, except for the analyte. The surfactant-rich phase was analysed using the HPLC. It should be noted, that the volume of the surfactant-rich phase obtained varied depending on the experimental conditions. In all cases 50 μl of the surfactant-rich phase was collected by microsyringe and 10 μl was injected into the chromatographic system. Chromatographic analysis was realised with microcolumn liquid chromatograph 'Milichrom-1' (Nauchpribor, Oryol, Russia) with UV detector. Detection was achieved at 230 nm. The chromatographic column (100×2 mm i.d.) was packed with Separon-C_{18} (Lachema, Brno, Czech Republic). The particle diameter was 5 μm. Separation was performed in isocratic conditions with mobile phase flow-rate 50 μl min^{-1}. The eluent was a mixture of n-propanol and 15 mM tetrabutylammonium hydroxide in 0.05 M Na_2HPO_4 (25:75). The mobile phase pH was adjusted to the value of 4.0 with phosphoric acid. The time equivalent of the void volume was determined by injection of 5 μl methanol and measuring the time from injection to changing detector signal. (The capacity factors for the FA and HA were 0.13, 0.89, 0.62, 4.68, 22.11 and 0.04, 0.19, 0.71, 2.62, respectively.) It should be noted that under given chromatographic conditions, Triton X-100 is retained on the stationary phase and does not overlap with the peaks of the analytes. In order to remove Triton X-100 remaining in the stationary phase after the analytes have been eluted, the chromatographic column was treated after each injection by a mixture of methanol–water in a ratio 90:10 (v/v). When the HA samples were analysed, the 20 μl of concentrated (20 M) sodium hydroxide solution was added to surfactant-rich phase in order to dissolve precipitated HA.

For both, the bulk aqueous and surfactant-rich phases calibration curves were made. It should be noted that calibration curves were made for each experiment separately. (In pH studies they were plotted for each value of pH, because the optical density of FA and HA solutions significantly depends on acidity [6]).

The calculations of the distribution coefficients, the recovery and concentration factors were performed according to Frankewich and Hinze [12]. All the reported results are the average of triplicate measurements.

Triton X-100 was obtained from Rohm & Haas. All other chemicals were of analytical grade from different sources.

3. Results

The results obtained show that the partitioning of FA and HA between bulk aqueous and surfactant-rich phases significantly depends on the acidity of a solution. The distribution coefficient increased as the pH of the solution decreased (Fig. 1). This fact probably can be explained by the transformation of FA and HA from the ionic to the molecular form with the reduction of acidity in the solution. These neutral forms of humic substances interact more strongly with micellar

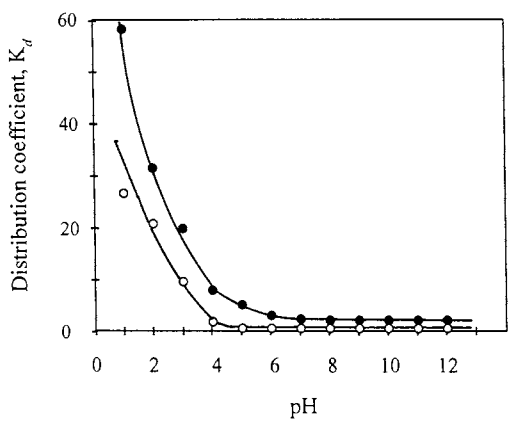

Fig. 1. Dependence of distribution coefficient of FA (○) and HA (●) on pH of extraction mixture. Conditions: equilibration temperature = 80°C; equilibration time = 5 min; time of centrifugation = 5 min; concentration of Triton X-100 = 3% (wt.).

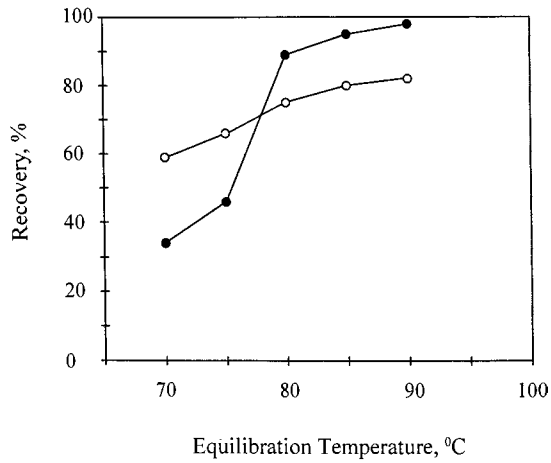

Fig. 2. Effect of variation of the equilibration temperature on the recovery of FA (○) and HA (●) from model solution. Conditions: pH = 1.0; equilibration time = 5 min; time of centrifugation = 5 min; concentration of Triton X-100 = 3% (wt.).

aggregates of non-ionic surfactant than their ionic forms. As a result, the amount of extracted analyte and distribution coefficient increase with decreasing pH. Thus, when the pH of a solution is reduced to the value which is in the area of FA pK value (pK 4.15 (G.A. Makharadze, R.L. Revia, unpublished research)), the distribution coefficient begins to increase. So, the less FA and HA are dissociated, the higher the recovery.

The effect of equilibration temperature on the recovery of the FA and HA is shown in Fig. 2. As one can see, the recovery increases with an increase of the equilibration temperature. In order to make sure that it is not a result of the degradation of humic molecules at high temperatures, the FA and HA solutions containing the same amount of the surfactant were heated to 90°C. The solutions were cooled and the separated phases were mixed. Then the effect of equilibration temperature on the extraction was investigated under the same conditions as in Fig. 2. The results obtained were exactly the same as in Fig. 2. Simultaneously, an increase of equilibration temperature is accompanied by a reduction of the volume of surfactant-rich phase. It is known, that in aqueous solutions, non-ionic surfactants are present in a hydrated state. As the temperature is increased, the hydrogen bonds are disrupted and

dehydration occurs [17]. The higher the temperature the more degree of dehydration. As a result, the higher the temperature the lower the amount of water in a surfactant-rich phase and consequently the smaller is the volume of this phase. Thus, the preconcentration factor, as well as the recovery increase with increasing of equilibration temperature. Thus, in this experiment (Fig. 2), the preconcentration factor is increased from 4.6 at 70°C to 13.5 at 90°C.

As for the time of equilibration, a time longer than 10 min does not result any significant improvement of recovery of the investigated substances (Fig. 3).

The dependence of the recovery of FA and HA on the time of centrifugation is shown in Fig. 4. One can see that the recovery initially increases rapidly but then remains practically unaffected. At the same time, with increasing the time of centrifugation the volume of the surfactant-rich phase changes very slightly. According to this data a centrifugation time of 10 min was selected.

The effect on the recovery of surfactant concentration was also investigated. In these studies, the concentration of Triton X-100 was increased from 1% to 10% (wt.). The results obtained show that an increase of surfactant concentration causes a slight increase of recovery for FA (Fig. 5). It is also possible to improve recovery by multistep extraction. Thus, for example, the recovery for FA was increased from 82% to 92% by triple cloud-point extraction (conditions as in Fig. 5, concentration of Triton X-100—4% wt.). Unfortunately, in both cases the preconcentration factor was significantly diminished due to the increase of the volume of the surfactant-rich phase.

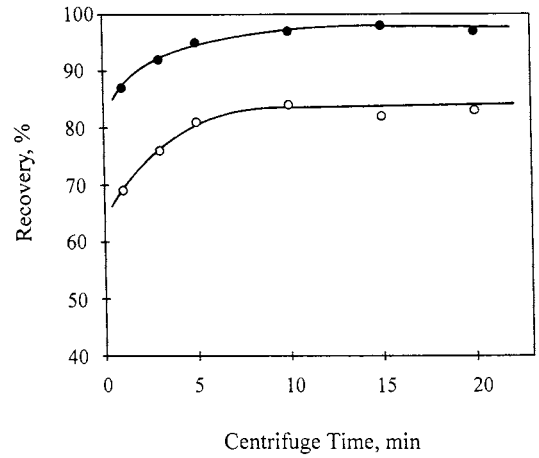

Fig. 4. Dependence of the extraction efficiency of FA (○) and HA (●) on the time of centrifugation. Conditions: pH = 1.0; equilibration temperature = 85°C; equilibration time = 10 min; concentration of Triton X-100 = 3% (wt.).

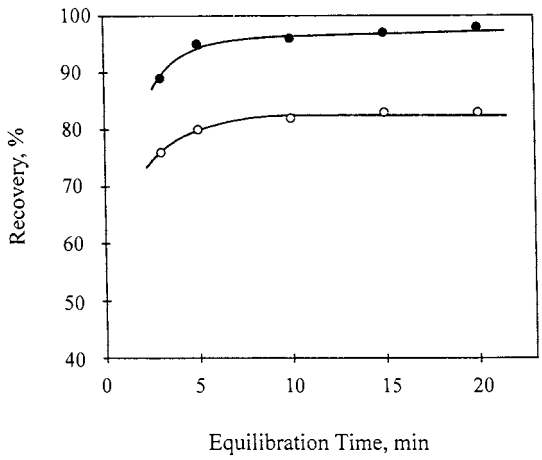

Fig. 3. Dependence of the extraction efficiency of FA (○) and HA (●) on the time of equilibration. Conditions: pH = 1.0; equilibration temperature = 85°C; time of centrifugation = 5 min; concentration of Triton X-100 = 3% (wt.).

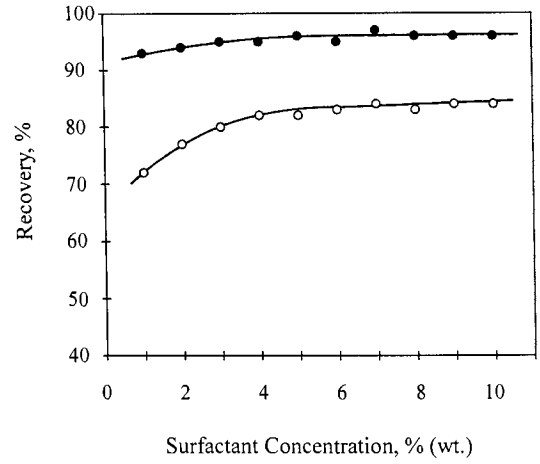

Fig. 5. Variation of the extraction efficiency of FA (○) and HA (●) as a function of the surfactant concentration (wt.%). Conditions: pH = 1.0; equilibration temperature = 85°C; equilibration time = 10 min; time of centrifugation = 10 min.

The degree of extraction of FA and HA achieved at optimised conditions (conditions as in Fig. 5, concentration of Triton X-100—4% wt.) were 82% and 96%, respectively, the preconcentration factor was 13.5. The reproducibility of the extraction of FA and HA in optimised conditions expressed as relative standard deviations was 2.84% and 7.69%, respectively.

From the results obtained can be concluded that cloud-point extraction can be used for the preconcentration of microquantities of humic substances from an aqueous matrix in order of their further determination by HPLC. This technique is simple, rapid and inexpensive. It could be successfully developed and used as an alternative technique to other techniques for the preconcentration of humic substances from natural waters. If one takes into account the wide range of the currently available non-ionic surfactants and the variety of the properties of their aqueous solutions, it is possible to obtain more desirable cloud-point extraction conditions and to obtain a higher recovery and increased concentration factors for humic substances.

References

[1] J.A. Leenheer, in: L.A. Baker (Ed.), Environmental Chemistry of Lakes and Reservoirs, Advances in Chemistry Series N237, American Chemical Society, 1994, p. 196.
[2] G.A. Makharadze, G.M. Varshal, G.D. Supatashvili, Gidrokhimicheskie materialy (Hydrochem. Mater. Russ.) 106 (1989) 22.
[3] G.R. Aiken, in: F.H. Frimmel, R.F. Christman (Ed.), Humic Substances and Their Role in the Environment, Wiley, Chichester, 1988, pp. 15–28.
[4] R.L. Malcolm, in: B. Allard, H. Boren, A. Grimvall (Ed.), Humic Substances in the Aquatic and Terrestrial Environment, Lecture Notes in Earth Sciences, vol. 33, 1991, pp. 9–36.
[5] M.-H. Sorouradin, M. Hiraide, Y.-S. Kim, H. Kawaguchi, Anal. Chim. Acta 281 (1993) 191.
[6] G.M. Varshal, T.K. Veljukhanova, I.S. Sirotkina, R.D. Jartseva, Gidrokhimicheskie materialy (Hydrochem. Mater. Russ.) 59 (1973) 143.
[7] W.L. Hinze, E. Pramauro, Crit. Rev. Anal. Chem. 24 (1993) 133.
[8] G.L. McIntire, Crit. Rev. Anal. Chem. 21 (1990) 257.
[9] L. Buhai, M. Rigan, Talanta 37 (1990) 885.
[10] H. Watanabe, T. Kamidate, S. Kawamorita, K. Haraguchi, M. Miyajima, Anal. Sci. 3 (1987) 433.
[11] B.R. Ganong, J.P. Delmore, Anal. Biochem. 193 (1991) 35.
[12] R.P. Frankewich, W.L. Hinze, Anal. Chem. 66 (1994) 944.
[13] B. Moreno Cordero, J.L. Pérez Pavón, C. Garcia Pinto, M.E. Fernandez Laespada, Talanta 40 (1993) 1703.
[14] C. Garcia Pinto, J.L. Pérez Pavón, B. Moreno Cordero, Anal. Chem. 67 (1995) 2606.
[15] T. Saitoh, W.L. Hinze, Anal. Chem. 63 (1991) 2520.
[16] I.S. Sirotkina, N.S. Zagudaeva, G.M. Varshal, Gidrokhimicheskie materialy (Hydrochem. Mater. Russ.) 53 (1972) 147.
[17] I.A. Gritskova, R.M. Panich, S.S. Voiutski, Uspekhi Khimii (Russ. Chem. Rev.) 1965 (1989) 11.

ELSEVIER

Talanta 48 (1999) 415–423

Talanta

Determination of methylamphetamine and related compounds in human urine by high performance liquid chromatography/electrospray/mass spectrometry

Ming-Ren S. Fuh *, Kaun-Tung Lu

P.O. Box 86–72, Department of Chemistry, Soochow University, Taipei, Taiwan, ROC

Received 31 March 1998; received in revised form 31 July 1998; accepted 31 July 1998

Abstract

A study of liquid chromatography/electrospray/mass spectrometry (LC/ES/MS) for the determination of methylamphetamine and related compounds (amphetamine, ephedrine, phenylpropanolamine) in human urine was undertaken. We assessed the effect of collision induced dissociation (CID) spectra generated by varying exit voltage of capillary and skimmer. The responses of ES/MS in different mobile phase and the effects of mobile phase modifier were examined. An isocratic LC method using methanol/water (80/20) and acetic acid (0.001%) as a modifier to separate these compounds was developed. Microporous ultrafiltration technique was employed to pre-treat urine sample prior to LC/ES/MS analysis. Good recoveries for methylamphetamine and amphetamine were determined as well as linearity, detection limit and precision associated with this method were determined. Drug spiked urine samples and urine samples of methylamphetamine addicts were successfully measured by this newly developed method.

Keywords: Methylamphetamine; Human urine; Liquid chromatography; Electrospray; Mass spectrometry

1. Introduction

The abuse of amphetamine and methylamphetamine is a serious problem in Taiwan. Determining amphetamine and related compounds in human urine sample is thus an important task. Gas chromatography/mass spectrometry (GC/MS) has been extensively employed for the determination of amphetamine and related compounds in biological fluids [1–5]. An extraction procedure is often required to transfer the analyte from aqueous biological fluid to organic solvent for GC/MS measurement.

Several high performance liquid chromatography (HPLC) methods, utilizing fluorescence derivatization or photodiode array detector, have been developed to analyze amphetamine in biological fluids [6–10]. Radioimmunoassay and enzymeimmunoassay are often used to screen urine or biological samples [11]. However, faulty results are often obtained due to the poor specificity of

* Corresponding author. Tel.: + 886 2 28819471; fax: + 886 2 28811053; e-mail: msfuh@mbm1.scu.edu.tw

0039-9140/99/$ - see front matter
PII S0039-9140(98)00264-1

these tests [12]. The extraction procedure required for GC and GC/MS methods was eliminated in some of these methods since analysis of aqueous sample is possible by HPLC directly. However, these methods are quantitative and not qualitative owing to the lack of structural information.

HPLC/electrospray/MS (HPLC/ES/MS) has emerged as an effective and useful analytical technique. ES ionization produces ions at atmospheric pressure and relatively low temperature which minimizes thermal decomposition of labile compound. Furthermore, an aqueous sample can be analyzed with little or no sample preparation. Although ES is a soft ionization technique, structural information can be obtained by collision-induced-dissociation (CID). HPLC/ES/MS has proved to be sensitive and accurate for the analysis of environmental pollutants, biopolymers, drugs, organometals and so on [13–19]. This study evaluates the effectiveness of LC/ES/MS in analyzing methylamphetamine, amphetamine, ephedrine, and phenylpropanolamine in human urine sample.

2. Experimental

2.1. Chemical

HPLC grade acetonitrile, methanol (Malinckrodt Baker, Paris, KY, USA) and water (HPLC grade, Labscan, Dublin, Ireland) were used throughout the experiment. Amphetamine, ephedrine and phenylpropanolamine were purchased from Sigma (St. Louis, MO, USA). Methylamphetamine was obtained from Radian International LLC (Austin, TX, USA). Formic acid and propionic acid were from Aldrich (Milwaukee, WI, USA). Acetic acid was purchased from Nacalai Tesque (Kyoto, Japan).

2.2. Mass spectrometric analysis

A HP-5989B mass spectrometer equipped with a HP-59987A electrospray interface (Hewlett Packard, Palo Alto, CA, USA) was used. Heated nitrogen gas (350°C, 12.5 l min^{-1}) evaporated solvent from the spray chamber. Compressed nitrogen (80 psi) was used for nebulization. The cylinder electrode in the spray chamber was set at -4000 V. The end plate and capillary entrance voltage were set at -3500 and -6000 V. The voltage of skimmer 1, lens 1, skimmer 2, lens 2 and lens 3 were set at 31.0, -1.0, 10.2, 12.4 and -86 V, respectively.

Mass spectra collected in scan mode were obtained by scanning from 10 to 170 m/z in 0.5 s. Nine scans were averaged with a step size 0.1 over the measured mass range. HP Chemstation analysis package (G1034C, version C.03.00) was utilized to determined the molecular mass.

2.3. Instrumentation

A syringe pump (model 22, Harvard Apparatus, Natick, MA, USA) was employed for flow infusion experiments. A HP1050 four solvent gradient pump (Hewlett Packard, Palo Alto, CA, USA) was used for LC and flow injection analysis. An Intersil ODS-80A (3.2×250 mm, 5 μm, Vercotech, Taipei, Taiwan) with an on-line filter was used for chromatographic separation throughout the analysis.

2.4. Urine sample preparation

Microporous ultrafiltration system was employed for sample pre-treatment prior to LC/ES/MS measurement. The sample solution (200 μl) was placed in a microconcentrator system with a 3000 Da molecular weight cut-off filter (Microcon-3, Amicon, Beverly, MA, USA) and centrifuged (4°C) for approximately 3 h at $10000 \times g$. The clear supernatant was separated and subjected to LC/ES/MS analysis.

2.5. Standard solution

Standard solution (0.01 M) of each amine (amphetamine, methylamphetamine, ephedrine, phenylpropanolamine) was prepared in HPLC grade water. These stock solutions were then further diluted to yield the appropriate working solutions. All solutions were stored at 4°C in the dark.

3. Results and discussion

3.1. Mass spectra

In general, ES is a soft ionization technique with little fragmentation of molecule. However, an increase in the exit voltage of capillary (CapEx-V) between the electrospray probe and quadrupole may induce molecular fragmentation. This work investigate the effect of CapEx-V on fragmentation of amphetamine and related compounds. Most of the CID fragment ions detected were identified on the basis of cleavages of various groups from the molecule as shown in Fig. 1. The acceleration voltage increases with an increasing molecular ion $[M+H]^+$ fragmentation. Although molecule fragmentation enhances the structural information of chemical compound, it decreases the abundance of protonated molecular ion $[M+H]^+$ often used for quantitative analysis in selective ion mode (SIM), thus, the sensitivity of assay. For both methylamphetamine and amphetamine, the characteristic fragment ions are $[M+H]^+$ and $[C_6H_5CH_2CHCH_3]^+$ at 119 m/z, and $[C_6H_5CH_2]^+$ at 91 m/z. For phenylpropanolamine and ephedrine, $[M+H]^+$ and one fragmentation ion $[M+H-H_2O]^+$ were observed. Fig. 1 depicts the mass spectra of these compounds.

We have decided to set CapEx-V at 100 V for the rest of this study. Sufficient and stable molecular and fragment ions which could be used for qualitative identification and quantitative analysis are produced at this potential. At lower potential, little fragment ions were produced for structure identification. Insufficient molecular ions were detected for sensitive quantitative measurement at higher potential.

3.2. Electrospray response in different mobile phase compositions

It has been reported that the composition of mobile phase has significant effect on ion intensity during ES/MS analysis [20]. Our preliminary LC results suggested that these compounds could be separated by using acetonitrile/water (70/30; v/v) or methanol/water (80/20; v/v) as a mobile phase. The experiment was therefore conducted by infusing 1 μM of each test chemical in either methanol/water or acetonitrile/water solution into the ESP interface at a flow rate of 200 μl min^{-1}. The results indicate that methanol/water mixture caused slightly higher $[M+H]^+$ abundance compared to acetonitrile/water mixture. This might attribute to that acetonitrile is an aprotic solvent which does not protonate the analyte sufficiently; thus, decrease ES/MS response.

3.3. Effect of mobile phase additive on electrospray response

Adding organic additives to enhance the chromatographic separation of basic compounds has been reported [21,22]. However, competition of the mobile phase additives with sample ionization resulting in a higher background is known [23,24]. Therefore, HPLC chromatographic separation and ionization efficiency of ES/MS must be compromised.

We examined the effects of various compositions of three additives (formic acid, acetic acid and propinic acid) in methanol/water (80:20) on ES/MS analysis. A concentration of 1 μM of each chemicals in various solution was infused into the ES interface at a flow rate of 200 μl min^{-1}. The results are summarized in Fig. 2. The addition of a small amount of acid (0.001%) enhanced the intensities of $[M+H]^+$ of all compounds while formic acid induced the most significant enhancement. The extent to which the intensities of $[M+H]^+$ of these compounds was decreased when adding 0.01% of acid; furthermore, the $[M+H]^+$ intensity of amphetamine was lower even in the absence of acid. By increasing the acid content to 0.1%, we found that the intensity of $[M+H]^+$ of these compounds, except phenylpropanolamine, was lower than that in the absence of added acid.

3.4. LC/ES/MS analysis

Although the addition of small amount of formic acid has greater enhancement on ES/MS response, unacceptable chromatographic separation make it unsuitable for this study. Therefore, methanol/water (80/20; v/v) with 0.001% (v/v)

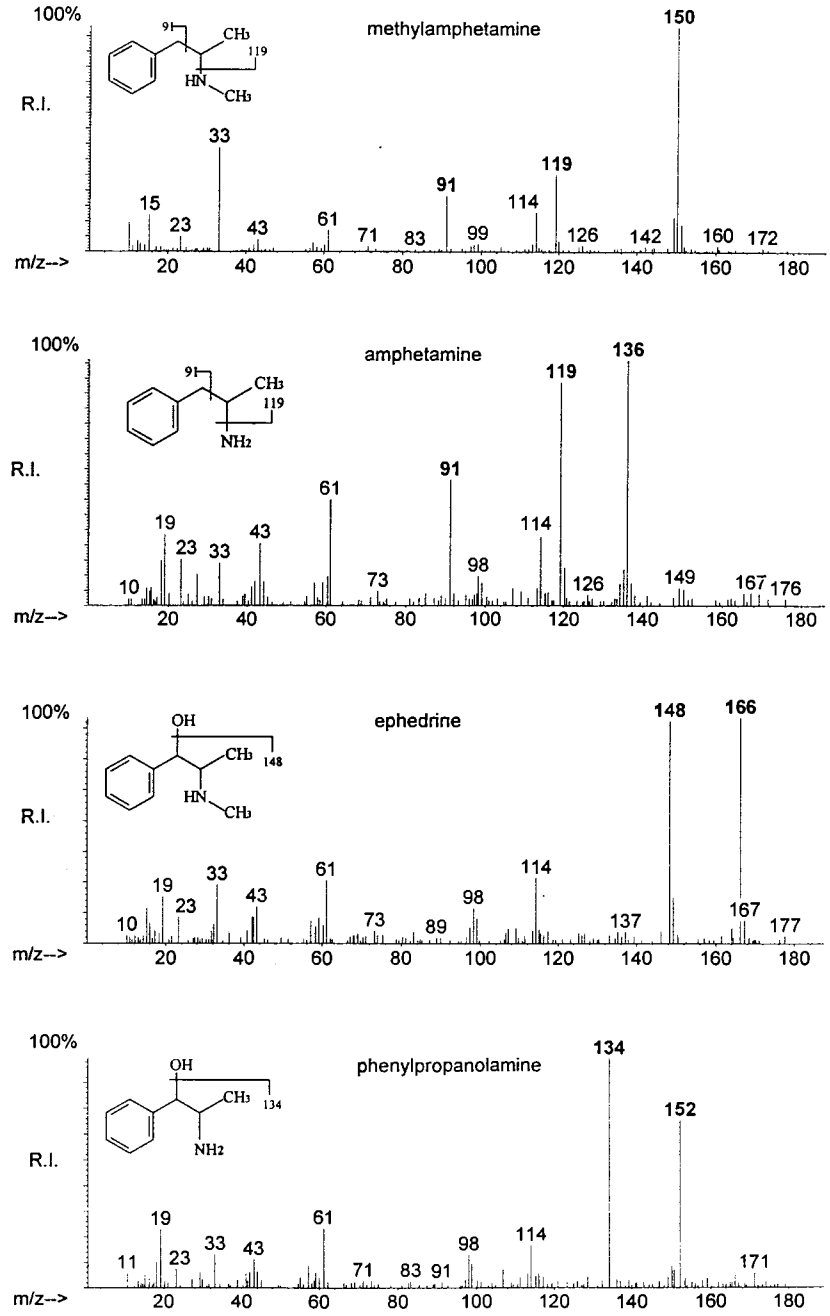

Fig. 1. Mass spectra of methylamphetamine and related compounds. CapEx-V was set at 100 V. The compound was dissolved in methanol. R.I., relative intensity.

acetic acid added solvent was used as a mobile phase for LC separation. Although the presence of small amount of acetic acid decreased the sensitivity of detection, it improved the separation greatly. Fig. 3 presents the extracted ion trace of spiked water sample. There are two major com-

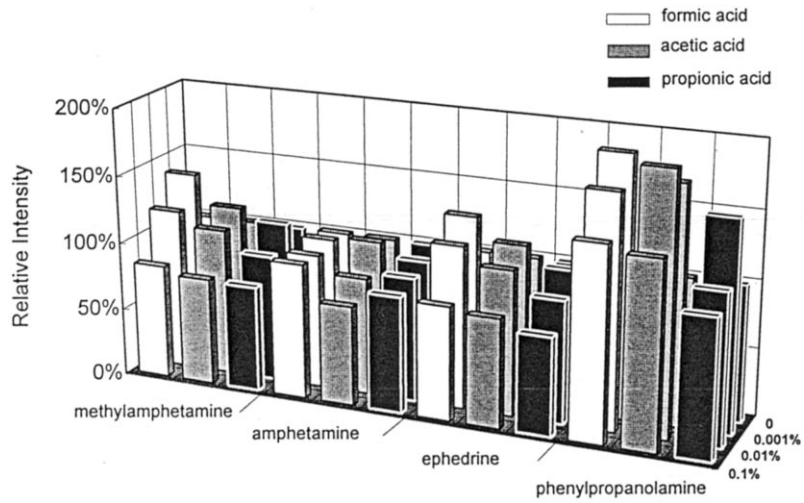

Fig. 2. Effects of additives on the electrospray intensity for methylamphetamine and related compounds.

mon fragmented ions ($m/z = 119$ and 91; as shown in Fig. 3(c) and (d)) observed for amphetamine and methylamphetamine; therefore, three ions ($m/z = M + 1$, 119 and 91) could be used to identify these two compounds. This is frequently required for drug analysis. Although overlaps occur between ephedrine and amphetamine peaks, these two compounds can be differentiated by different molecular ions.

3.5. Linearity and detection limit

Linearity range of each compound was evaluated by injecting standards (100, 250, 500, 750 and 1000 ng ml^{-1}) into LC/ES/MS for analysis; the results are summarized in Table 1. The calibration curve of each compound was constructed by measuring the masses of selective ions (amphetamine, $m/z = 136$, 119, 91; methylamphetamine, $m/z = 150$, 119, 91; ephedrine, $m/z = 166$, 148; phenylpropanolamine, $m/z = 152$, 134). Good linearity of each compound was observed throughout the concentration range examined. In addition, the detection limit of each compound was estimated and summarized in Table 1.

3.6. Precision

The precision of this newly developed LC/ES/MS method was assessed by replicating the analysis of amphetamine or methylamphetamine spiked samples. For amphetamine, the inter-day precision showed a coefficient of variation (CV) of 0.8–5.9% while the CV of intra-day precision was 0.5–3.8%. For methylamphetamine, the inter-day and intra-day CVs ranged from 0.6 to 6.4% and from 1.9 to 6.3%, respectively. Details of precision study are summarized in Table 2.

3.7. Urine sample pretreatment

Microporous ultrafiltration technique which utilizes semi-permeable membrane to separate species by molecular size was used to filter proteins and other residues in urine sample. This is to prolong the life of LC column and minimize interference from urine. In this study, a 3000 Da cut-off microporous membrane was utilized. Molecules with molecular weight greater than 3000 will be retained by porous membrane.

The recovery of microporous ultrafiltration procedure was examined and the results are sum-

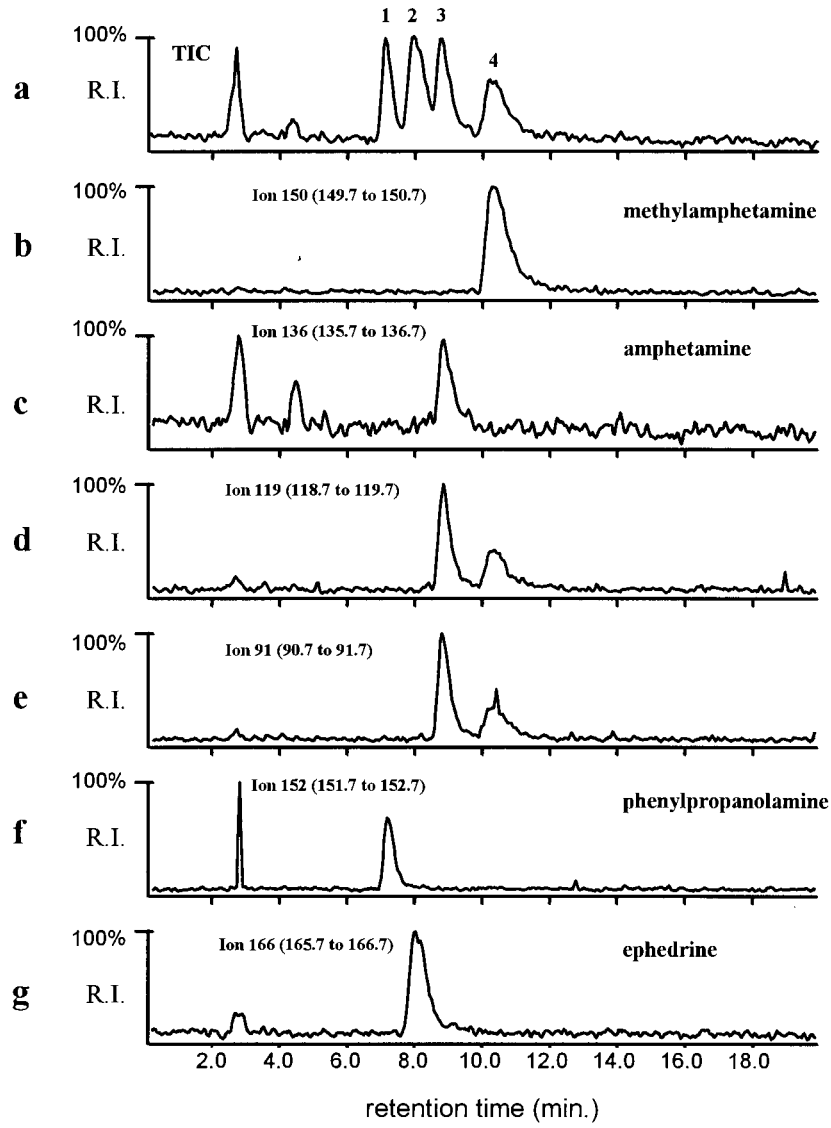

Fig. 3. LC/ES/MS reconstructed total ion current (TIC) and SIM chromatograms of a spiked water sample. The concentration of each compound was 1 μM. (a) 1, phenylpropanolamine; 2, ephedrine; 3, amphetamine; 4, methylamphetamine. (b)–(g) Extracted ion profile. Injection volume, 20 μl; flow rate, 0.5 ml min^{-1}. R.I. relative intensity.

marized in Table 3. We have found that pre-treating microporous membrane with water would greatly improve the recoveries. Good recoveries ranged from 87 to 96% for amphetamine and methylamphetamine were determined. In addition, the chemical structure of these two compounds remained intact.

3.8. Determination of methylamphetamine in human urine

Fig. 4 summarizes the LC/ES/MS results of drug-free urine and methylamphetamine spiked urine. For urine blank ultrafiltrate, there were some residues eluted between 2 and 6 min; how-

Table 1
Detection limits and calibration data for amphetamine and related compounds from 100 to 1000 ng ml^{-1}

Compound	Calibration equation[a]	r^2	D.L.[b]
Amphetamine	$Y = 30\,250X + 28\,575$	0.996	27
Methyl-amphetamine	$Y = 18\,497X + 70\,617$	0.998	14
Ephedrine	$Y = 19\,845X + 580\,715$	0.996	17
Phenyl-propanolamine	$Y = 11\,633X + 143\,179$	0.999	15

[a] 20 μl injection. Calibration curve was obtained by plotting peak area (Y) versus concentration, ng ml^{-1} (X).
[b] Detection limit, ng ml^{-1}. Three times S/N ratio.

Table 2
Inter-day and intra-day precision study

Added conc. (ng ml^{-1})	Measured conc. (ng ml^{-1})			
	Intra-day[a]		Inter-day[a]	
	Amp[c]	mAmp[d]	Amp[c]	mAmp
100				
Mean	106	95	102	93
SD	4	6	6	6
CV (%)	3.8	6.3	5.9	6.4
250				
Mean	247	247	249	252
SD	1	5	11	6
CV (%)	0.5	2.0	4.4	2.4
500				
Mean	511	514	517	517
SD	14	10	8	5
CV (%)	2.7	1.9	1.6	1.0
750				
Mean	764	749	750	737
SD	18	34	12	10
CV (%)	2.3	4.5	1.6	1.4
1000				
Mean	984	995	991	1002
SD	11	23	8	6
CV (%)	1.1	2.3	0.8	0.6

[a] Mean and SD represent three different samples for each concentration.
[b] Inter-day reproducibility was determined from three different runs over a 1-week period.
[c] Amphetamine.
[d] Methylamphetamine.

ever, nothing was measured after 7 min. The delay of methylamphetamine elution in urine sample might be attributed to secondary effect caused by protein in urine sample. However, it dose not appear to affect the analytical results. By extracting chromatogram for selected ions ($m/z = 150$, 119 and 91), one can specify the presence of methylamphetamine. The application of this newly developed method was demonstrated by examining drug spiked urine samples and methylamphetamine addicts' urine samples; the results were summarized in Table 4. Adequate agreement between theoretical and measured values was determined.

Table 3
Recovery of microporous ultrafiltration

Added conc. (ng ml^{-1})	Sample	Recovery[a] (%)	Recovery[b] (%)
Amphetamine			
125	1		91 ± 3
	2		93 ± 2
	3		91 ± 3
250	1	77 ± 2	91 ± 3
	2	75 ± 3	91 ± 1
	3		93 ± 2
500	1	73 ± 2	93 ± 3
	2	75 ± 3	93 ± 2
	3		95 ± 2
1000	1	75 ± 2	90 ± 3
	2	71 ± 2	89 ± 1
	3		89 ± 2
Methylamphetamine			
125	1		94 ± 2
	2		94 ± 3
	3		87 ± 2
250	1		91 ± 3
	2		89 ± 3
	3		89 ± 2
500	1		90 ± 3
	2		91 ± 2
	3		92 ± 2
1000	1		90 ± 2
	2		88 ± 2
	3		87 ± 2

[a] Mean $\pm$SD represent three measurements. Microporous ultrafiltration (Mirocon-3) used as received.
[b] Mean $\pm$SD represent three measurements. 200 μl of HPLC grade water was filtered by Microcon-3 as described in Section 2 first. Methylamphetamine or amphetamine spiked samples were pretreated subsequently.

4. Conclusion

This study presents a LC/ES/MS method to determine amphetamine, methylamphetamine, ephedrine and phenylpropanolamine in human urine. Urine sample was pretreated with microporous ultrafiltration membrane to remove proteins and other large molecules to enhance the detection sensitivity and prolong the life of LC column. Adequate LC separation was achieved by utilizing an C_{18} column and a mobile phase containing methanol/water (80/20) with 0.001% acetic acid.

Structural information of analyte molecules can be obtained with proper adjustment of the capillary exit voltage. Three-ion combination SIM analysis which is often required for most of drug monitoring program was utilized to identify amphetamine and methylamphetamine. However, only two ions were observed for ephedrine and phenylpropanolamine owing to the lack of fragmentation of these molecules. Good linear correlation and low detection limit were achieved by SIM. In addition, good inter-day and intra-day precisions were determined. The application of this newly developed method was demonstrated by analyzing drug addicts' urine samples. Currently, we are evaluating the feasibility of using various LC columns to enhance separation and of using atmospheric chemical ionization/MS (APCI/MS) for the determination of these compounds.

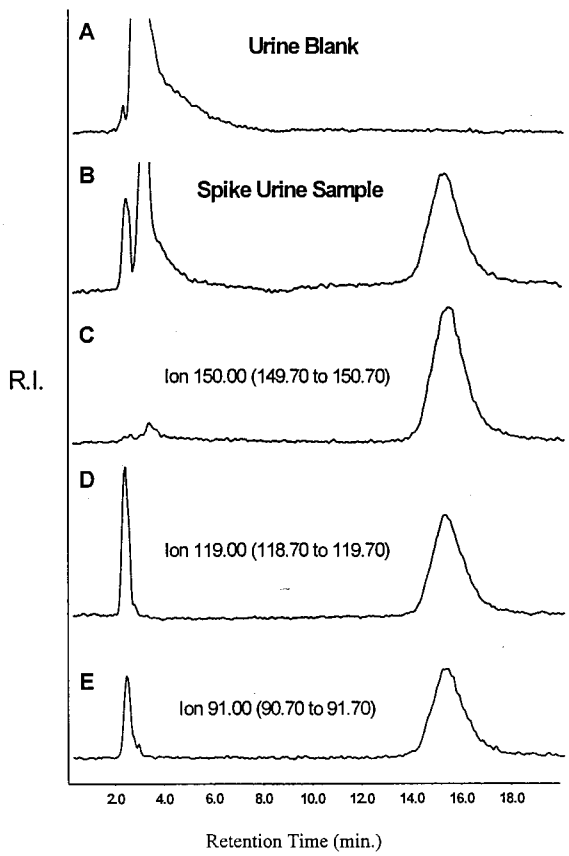

Fig. 4. LC/ES/MS reconstructed TIC and SIM chromatograms of a methylamphetamine (500 ng ml^{-1}) spiked urine and a drug-free urine. (a) TIC of drug-free urine, (b) TIC of spiked urine, (c)–(e) extracted ion profiles of spiked urine sample. Injection volume, 20 μl; flow rate, 0.5 ml min^{-1}. R.I. relative intensity.

Table 4
LC/ES/MS analysis results of drug spiked and drug addict's urine samples

Sample	Measured[a] (ng ml^{-1})
Amphetamine spiked	
250	247 ± 8
250	262 ± 5
500	514 ± 7
500	511 ± 9
750	764 ± 10
750	743 ± 8
Methylamphetamine spiked	
250	258 ± 11
250	251 ± 7
500	514 ± 9
500	508 ± 6
750	738 ± 10
750	749 ± 8
Drug addicts sample[b]	
i (262 ± 4)	259 ± 11
ii (540 ± 6)	528 ± 12
iii (518 ± 6)	503 ± 12

[a] Mean $\pm$SD represent three measurements.
[b] These samples were previously determined by GC/MS. Mean $\pm$SD represent three measurements.

Acknowledgements

We thank Dr. Wynn Pan of National Yang-Ming University and Dr. Dong-Linag Lin of Investigation Bureau, Ministry of Justice for helpful

suggestions. This work was supported by the National Science Council of Taiwan.

References

[1] C.R. Clark, J. Deruiter, F.T. Noggle, J. Chromatogr. Sci. 30 (1992) 399.
[2] H.P. Sievert, Chirality 6 (1994) 295.
[3] H.J. Leis, W. Windischhofer, R. Wintersteiger, Biol. Mass Spectrom. 23 (1994) 637.
[4] P. Ellerbe, T. Long, M.J. Welch, J. Anal. Toxicol. 17 (1993) 165.
[5] H. Gjerde, I. Hasvold, G. Pettersen, A.S. Christophersen, J. Anal. Toxicol. 17 (1993) 65.
[6] T.K. Wang, M.S. Fuh, J. Chromatogr. B 686 (1996) 285.
[7] M.S. Fuh, T.K. Wang, W.H.T. Pan, J. Liq. Chromatogr. Relat. Technol. 20 (1997) 1605.
[8] P.C. Falco, C.M. Legua, R.H. Hernandez, A.S. Cabeza, J. Chromatogr. B 663 (1995) 235.
[9] F.X. Zhou, I.S. Krull, Chromatographia 35 (1993) 153.
[10] J.F. Bowyer, P. Clausing, G.D. Newport, J. Chromatogr. B 666 (1995) 241.
[11] S.A. Eremin, A.B. Smirnov, G. Gallacher, D.A. Smith, D.L. Colbert, Analyst 118 (1993) 1325.
[12] A.M. Roda, C. Gioacchini, C.M. Baraldini, J. Chromatogr. B 665 (1995) 281.
[13] J.B. Fenn, M. Mann, C.K. Meng, S.F. Wong, C.M. Whitehouse, Science 246 (1989) 64.
[14] M.H. Allen, B.I. Shushan, LC-GC 11 (1993) 112.
[15] W.M.A. Nissen, J.V.D. Greff, Liquid Chromatography Mass Spectrometry, Principle and Application, Chromatographic Science, vol. 58, Marcel Dekker, New York, 1992.
[16] R.D. Voyksner, Environ. Sci. Technol. 28 (1994) 118A.
[17] J.F. Garcia, D. Barcelo, J. High Resolut. Chromatogr. 16 (1993) 633.
[18] H. Owabuchi, E. Kitazawa, N. Kobayashi, H. Watanabe, M. Kanai, K. Nakamura, Biol. Mass Spectrom. 23 (1994) 540.
[19] R.P. Gibb, H. Cockerhman, G.A. Goldfogel, G.M. Lawson, V.A. Raisys, J. Forensic Sci. 38 (1993) 124.
[20] R.F. Straub, R.D. Voyksner, J. Chromatogr. 647 (1993) 167.
[21] J.A. Ballantine, D.E. Games, P.S. Slater, Rapid Commun. Mass Spectrom. 9 (1995) 1403.
[22] M. Greig, R.H. Griffey, Rapid Commun. Mass Spectrom. 9 (1995) 97.
[23] A.P. Bruins, T.R. Covey, J.D. Henion, Anal. Chem. 59 (1987) 2642.
[24] M.G. Ikonomou, A.T. Blades, P. Kebarle, Anal. Chem. 62 (1990) 957.

ELSEVIER

Talanta 48 (1999) 425–436

Talanta

Studies of spline wavelet least square in processing electrochemical signals

Xiaoping Zheng, Jinyuan Mo *, Tianyao Xie

Department of Chemistry, Zhongshan University, Guangzhou, 510275, PR China

Received 29 January 1998; received in revised form 30 July 1998; accepted 3 August 1998

Abstract

The application of spline wavelet least square (SWLS) in analytical chemistry signals is presented in this paper. As a new technique in signal processing, to extract useful signals from high noise, the influences of different parameters on the results of processing is discussed in details. If the suitable parameters are selected, useful signals can be filtered from the noise of $S/N = 0.5$. The relative error of peak current is less than 3.0%, and that of peak potential is less than 10%. Comparison of this method with wavelet multifrequency channel decomposition (WMCD) and spline least square (SLS) has also been made and it indicates that SWLS can solve some problems in WMCD and SLS. The experimental results are also satisfactory.

Keywords: Spline wavelet; Least square; Signal processing

1. Introduction

A large number of experimental data is obtained through analytical apparatus. These data are often given as the form of graph, curve or numbers. With the rapid development of the application of computer science in analytical chemistry, the processing of signals is gradually changing from analogue signals to digital signals. The conversion between analogue and digital signal are achieved through A/D and D/A conversion. The processing of digital signal (discrete data) has becoming more and more important in analytical chemistry. The signal obtained through apparatus often has random noise, especially when the concentration of the reagent is very low, the noise is so high that it often submerges the useful signals. So, on one hand, those signals should be filtered to remove the random noise; on the other hand, those discrete data should be serialized for the purpose of further analysis. In order to solve these problems, a useful chemometrics method called curve fitting is often used. The principle of this method is to choose or construct a new function $f(x)$, using it to approximate the original signal points, achieving the purpose of removing noise and serialization of the discrete data. There are many curve fitting methods, including interpolation, spline smoothing, spline least square [1] and many kinds of regression methods [2]. As a simple curve fitting method,

* Corresponding author. Fax: +86 20 84187564; e-mail: cedc1s@zsulink.zsu.edu.cn

0039-9140/99/$ - see front matter
PII S0039-9140(98)00266-5

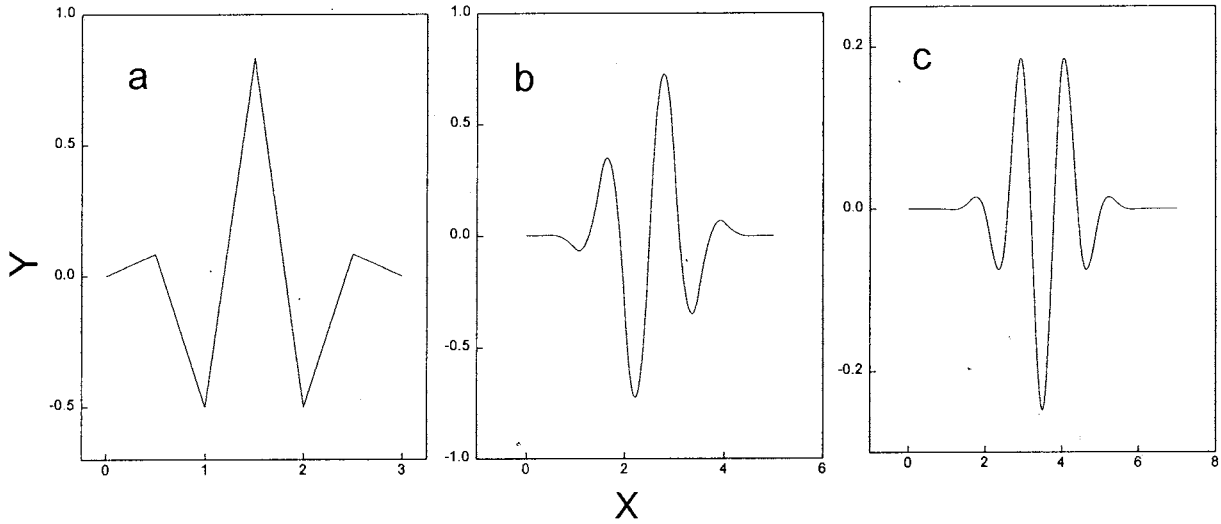

Fig. 1. Different mth-order spline wavelet. (a) $\psi_2(x)$; (b) $\psi_3(x)$; (c) $\psi_4(x)$.

Interpolation has been applied in processing electroanalytical signals [3]. But it can't process signals having random noise. Because the new function produced through interpolation passes the original data points entirely, it remains all the errors of the original data, and can only be used in processing smoothed curve. The principle of spline smoothing is based on the thinking of 'integration difference.' The mathematics procedure is very simple and can be applied in many kinds of signals. But the result is not very ideal, useful signals can only be filtered from the noise of $S/N = 10$ [4]. So it is not suitable for processing signals with high noise. The principle of producing new function of the regression methods and spline least square are all least square. The thinking of least square is to make the sum square of errors between the new function and the original data points to be minimum. That's, to try to meet the trend of the original signals. Regression method includes linear regression and nonlinear regression. They have been used widely in analytical chemistry [5–7]. However, those methods have a common shortcoming, the regression equation is determined according to the trend of the original data; so it is difficult for some complex systems to use regression methods. Spline least square is a better method than regression methods. Spline function is used in this method. It can achieve the purpose of removing random noise and serialization of the discrete data. However, for high noise signals, the peak current of the processed curve is much lower than that of the theoretical curve [8].

Wavelet analysis is a hot topic recently. It is a new signal processing technique. It's the milestone in the developing history of Fourier transform. It conquers the difficulties of those old filtration in choosing window function, objective function and transfer matrix. It can extract useful signals from high random noise without knowing any information about the original signals. Many works about the wavelet multifrequency channel decomposition (WMCD) have been done [9–18], such as the couple application of spline wavelet and Fourier transform in processing analytical chemistry signals, spline wavelet multifiltering analysis, etc. But there are still some shortcomings in WMCD. As for those signals whose value of starting point or ending point is not equal to zero, this point of the processed curve will drop suddenly to zero. The processed curve will stray from the theoretical curve. Another problem is that the processing result of WMCD is connected with the shape of the curve, so it is not suitable for processing some kinds of signals.

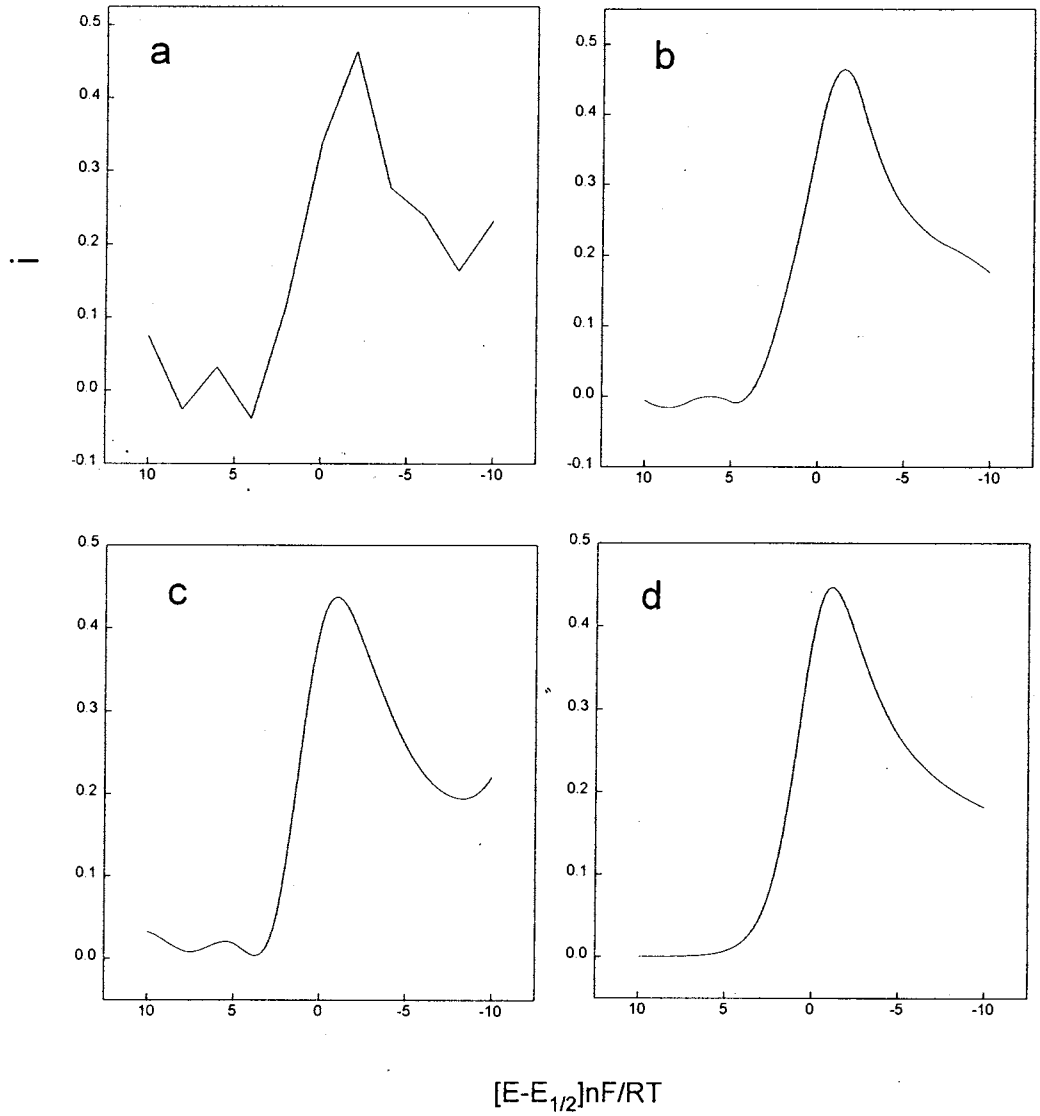

Fig. 2. Effect of different mth-order spline wavelet (m); $S/N = 0.5$, $h = 5$, $k = 1000$. (a) $m = 2$; (b) $m = 3$; (c) $m = 4$; (d) theoretical curve.

Up to date, all the works of wavelet transform in processing signals are mainly based on the principle of Mallat's decomposition algorithm. The original signals are decomposed to high frequency signals and low frequency signals, then filter the high frequency noise. There are no reports about the application of wavelet function in curve fitting. Spline wavelet has explicit expression, which can be considered for applying in curve fitting. So, researches on spline wavelet least square (SWLS) has been made. It indicates that the denoising results of this method is fairly good, useful signals can be filtered from the noise of $S/N = 0.5$. It is effective in processing many complex nonlinear systems. It is significant that it also can solve the above-mentioned problems in WMCD. Comparison of SWLS with another filtration method spline least square (SLS) has

Table 1
The relative errors of peak current and peak potential with 2nd-order spline wavelet and $0.5 \leq S/N \leq 100$

S/N scope	h							
	3		4		5		6	
	I_p (%)	E_p (%)	I_p (%)	E_p (%)	I_p (%)	E_p (%)	I_p (%)	E_p (%)
100	−8.042	−12.326	−2.201	7.865	4.162	10.712	1.786	10.713
80	−8.001	−12.322	−2.242	7.869	4.205	10.713	1.782	10.715
60	−8.042	−12.324	−2.221	7.862	4.183	10.713	1.783	10.716
40	−7.998	−12.324	−2.178	7.862	4.285	10.714	1.783	10.712
20	−8.006	−12.327	−2.028	7.863	4.256	10.716	1.788	10.715
10	−8.019	−12.328	−2.257	7.864	4.376	10.718	1.682	10.716
5	−7.796	−12.328	−2.105	7.864	4.156	10.718	1.750	10.716
2	−8.537	−12.330	−2.302	7.868	5.156	10.716	2.268	10.718
1	−8.612	−12.334	−3.245	7.871	5.271	10.712	2.178	10.724
0.8	−8.656	−12.338	−3.305	7.874	5.302	10.716	2.078	10.725
0.5	−8.458	−12.339	−3.346	7.878	5.752	10.723	2.681	10.852

also been made. The results indicate that SWLS can be used more widely in signal processing. It can process some special-shaped curve. This method enlarges the application of spline wavelet in signal processing and shows the advantages of spline wavelet in processing signals.

2. Theory

The principle of least square has been widely used in chemometrics. For a series discrete data points (x_i, y_i) on a certain district $[a, b]$

$$a = x_0 < x_1 < x_2 < \cdots < x_{k-1} < x_k = b,$$

a new function $g = f(x)$ should be found to make

$$\sum_{i=1}^{k} [f(x_i) - y_i]^2 P_i \tag{1}$$

minimum, where P_i is called weight coefficient. The value of it is assumed to be one in this text.

$g = f(x)$ may be chosen as triangle functions, spline functions and others. In this paper, we chose spline wavelet function $\{\varphi_i(x)\}_{i=1}^{n}$ to fit the above-mentioned data $\{(x_i, y_i)\}_{i=1}^{k}$. Under the condition $k \gg n$, $f(x)$ can be expressed as follows:

$$f(x) = \sum_{i=1}^{n} c_i \varphi_i \tag{2}$$

where $\varphi_i(x)$ is spline wavelet function, n is the number of the spline wavelet function used in curve fitting. The expression of $\varphi_i(x)$ can be seen in Eq. (3):

$$\varphi_i(x) = \psi_m \left(\frac{x - x_{(i-1/2)}}{h} \right), \quad i = 1, 2, ..., n \tag{3}$$

where h is the distance between two $\varphi_i(x)$, m is the different order of spline wavelet function. Fig. 1 shows the different order spline wavelet ($m = 2, 3, 4$).

Now, we can see, if the coefficients c_i in Eq. (2) are known, the new function $f(x)$ will be easily constructed. So the main problem is how to get the value of c_i. The calculation of c_i is based on the principle of least square.

Eq. (1) can be regarded as the function of the coefficients c_i, that's

$$I(c_1, c_2, ..., c_n) = \sum_{\text{vol}}^{k} [f(x_i) - y_i]^2 \tag{4}$$

In order to know the minimum value of Eq. (4), the partial derivatives are set to zero,

$$\frac{\partial I}{\partial c_i} = 0, \quad i = 1, 2, ..., n \tag{5}$$

From Eq. (5), the following linear equations can be obtained,

Table 2
The relative errors of peak current and peak potential with 3rd-order spline wavelet and $0.5 \leq S/N \leq 100$

S/N scope	h							
	3		4		5		6	
	I_p (%)	E_p (%)	I_p (%)	E_p (%)	I_p (%)	E_p (%)	I_p (%)	E_p (%)
100	−0.909	3.572	1.585	4.286	1.411	4.256	−7.192	10.071
80	−0.886	3.571	1.550	4.283	1.427	4.253	−7.207	10.071
60	−0.882	3.578	1.590	4.281	1.393	4.257	−7.206	10.075
40	−0.912	3.578	1.547	4.301	1.484	4.304	−7.250	10.085
20	−0.942	3.583	1.499	4.322	1.493	4.312	−7.246	10.088
10	−0.953	3.642	1.585	4.328	1.475	4.322	−7.530	10.125
5	−1.125	3.759	1.815	5.331	1.277	5.548	−7.504	10.248
2	−1.400	8.786	1.855	7.524	1.717	7.321	−8.000	11.453
1	−1.521	11.786	1.884	8.527	2.416	8.352	−8.415	12.354
0.8	4.756	11.884	2.429	8.214	2.740	8.714	−8.986	12.547
0.5	4.870	11.964	2.476	9.524	2.863	9.440	−10.217	12.984

Table 3
The relative errors of peak current and peak potential with 4th-order spline wavelet and $0.5 \leq S/N \leq 100$

S/N scope	h							
	3		4		5		6	
	I_p (%)	E_p (%)	I_p (%)	E_p (%)	I_p (%)	E_p (%)	I_p (%)	E_p (%)
100	0.589	3.571	−1.749	10.714	−3.676	11.286	0.207	10.214
80	0.560	3.573	−1.748	10.714	−3.679	11.289	0.217	10.215
60	0.592	3.581	−1.752	10.721	−3.752	11.304	0.224	10.324
40	0.601	3.580	−1.764	10.721	−3.752	11.302	0.238	10.325
20	0.895	3.582	−1.985	10.722	−3.755	11.331	0.251	10.714
10	1.123	3.687	−2.015	10.727	−3.862	11.286	0.283	10.214
5	1.568	3.752	−2.153	10.729	−3.844	11.625	0.283	10.351
2	1.752	3.854	−2.187	10.735	−4.326	11.819	0.528	10.357
1	2.854	4.254	−4.231	10.654	−5.093	11.809	2.193	10.359
0.8	4.562	5.326	−6.793	10.928	−5.359	12.143	2.735	11.054
0.5	9.212	7.216	−7.456	11.028	−6.342	12.542	4.156	11.257

$$\sum_{j=1}^{n} \langle \varphi_i, \varphi_j \rangle c_j = \langle \varphi_i, y \rangle, \quad i = 1, 2, ..., n \tag{6}$$

where, $\langle \varphi_i, \varphi_j \rangle = \Sigma_{v=1}^{k} \varphi_i(x_v)\varphi_j(x_v)$

$$\langle \varphi_i, y \rangle = \sum_{v=1}^{k} \varphi_i(x_v) y_v \tag{7}$$

The format of matrix is: $AC = F$.

Using Eqs. (3) and (6), the value of A and F in the matrix can be calculated and c_i will be obtained easily. Then, the new function $f(x)$ can be constructed through $f(x) = \Sigma_{i=1}^{n} c_j \varphi_j$. As for signal processing, $f(x)$ will be the useful signals extracted from the original data points with high noise. As for mathematical processing, $f(x)$ is the fitting function of the above discrete data, we can obtain any values of y (or x) if the value of x (or y) is known.

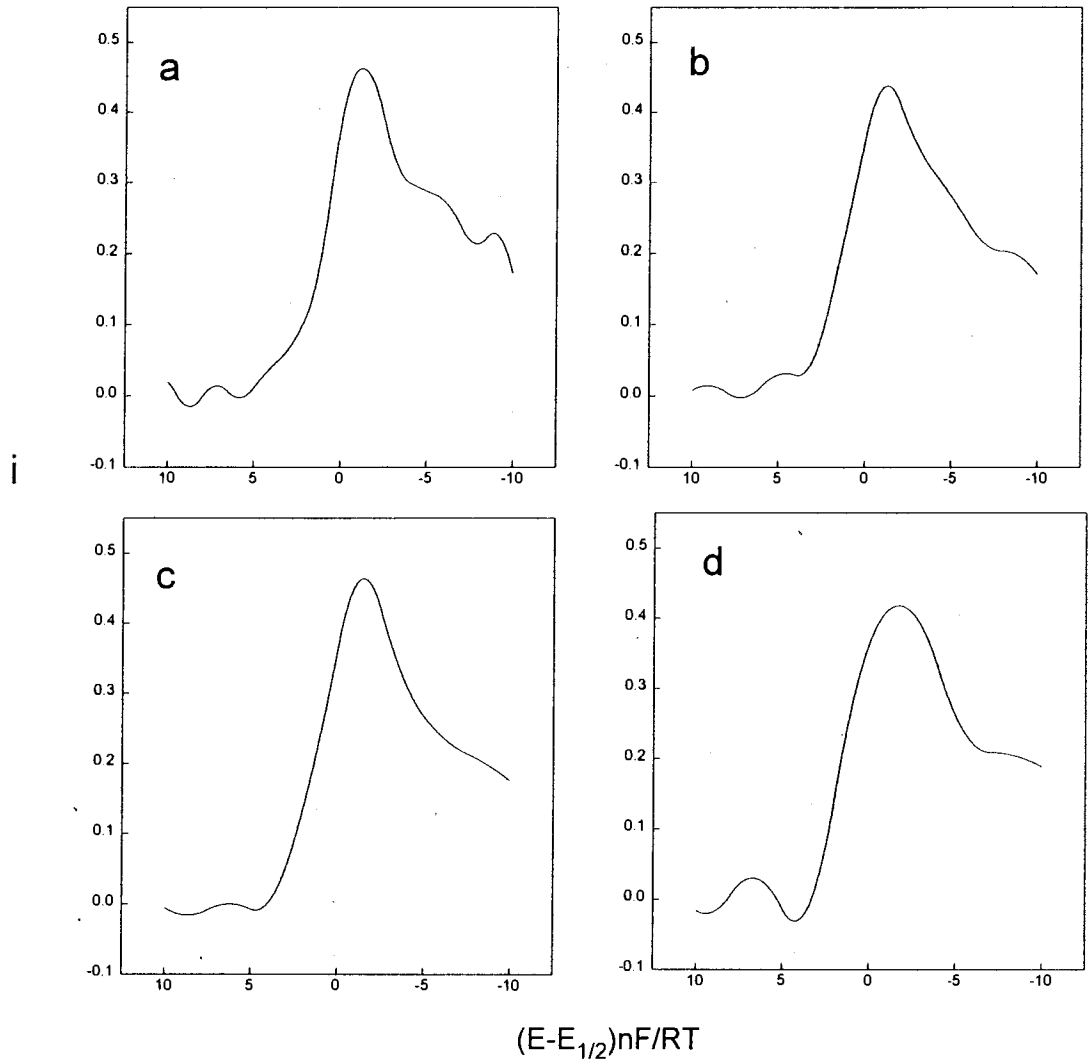

Fig. 3. Effect of different distance between spline wavelet (h); $S/N = 0.5$, $m = 3$, $k = 1000$. (a) $h = 3$; (b) $h = 4$; (c) $h = 5$; (d) $h = 6$.

3. Experimental

3.1. Chemicals

A standard solution of 0.1 mol l^{-1} HCHO was prepared with de-ionized water. The stock solution was diluted, when necessary, to prepare samples. Girard's reagent T was 0.005 and 0.1 mol l^{-1} NH_4Cl–NH_3 buffer solution was used as electrolyte.

3.2. Instrumentation and procedures

The differential pulse stripping voltammetry (DPSV) was carried out on BAS-100 (Bioanalytical Systems, West Lafayette, IN) equipped with three electrode system. The working electrode was hanging mercury electrode. The reference electrode and auxiliary electrode were Ag/AgCl electrode and saturated calomel electrode respectively. The scanning potential was of the

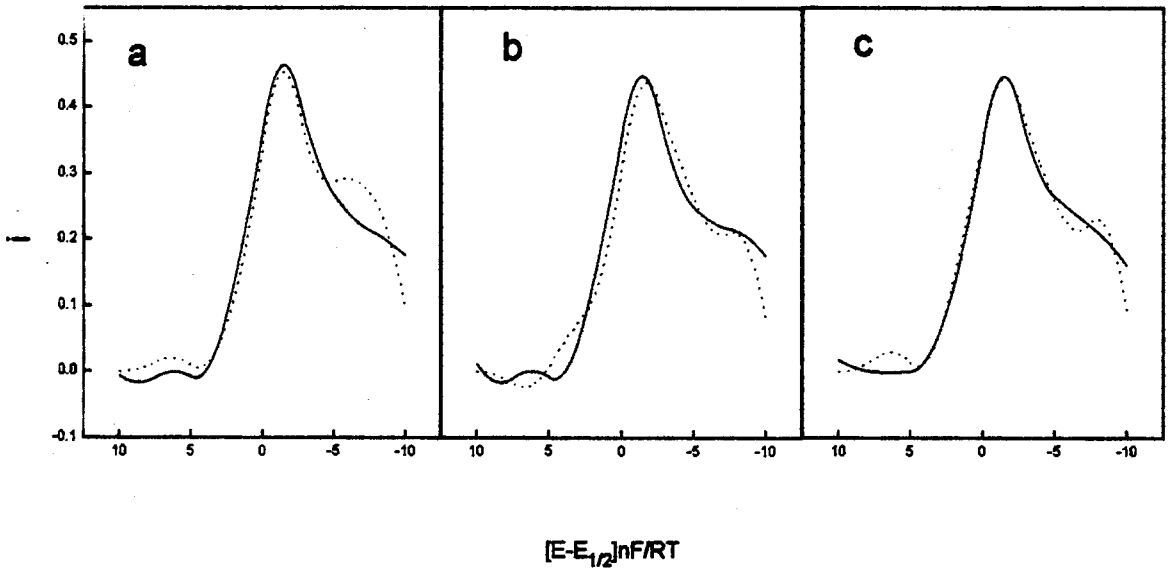

Fig. 4. Processing results of SWLS and WMCD, three times processing results of the same theoretical curve (——): processing result of SWLS; (· · ·): processing result of WMCD.

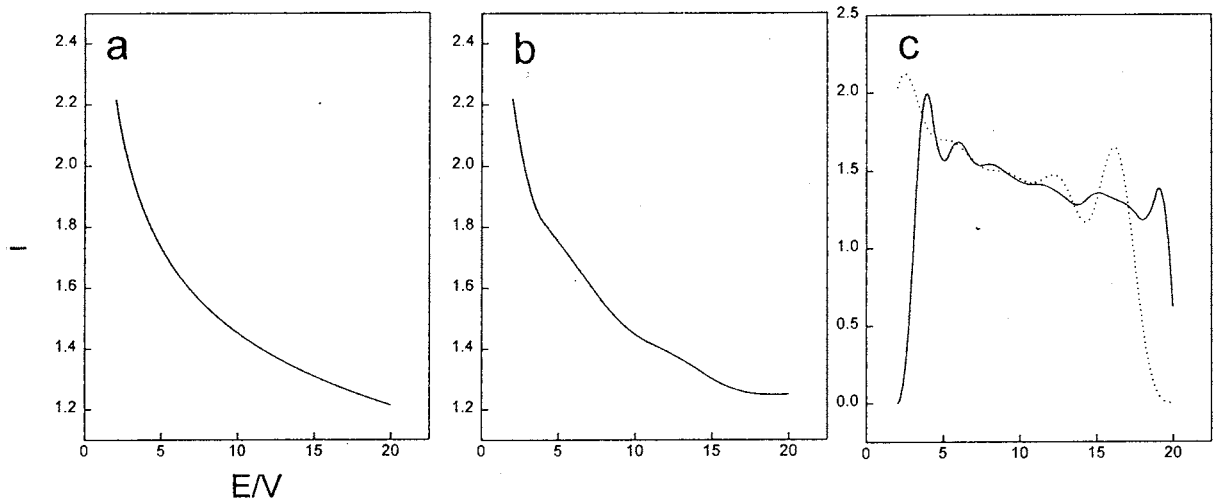

Fig. 5. Processing results of SWLS, WMCD and SLS. (a) The theoretical curve; (b) processing result of SWLS; (c) (——) processing result of WMCD; (· · ·) processing result of SLS.

range from -1.0 to -1.5 V; pulse amplitude $\Delta E = 50$ mV; pulse width, 50 ms; sampling width, 17 ms; pulse period, 10 s; deposit time, 200 ms; sensitivity, $1e-7(A/V)$. Solutions were de-aerated with high-purified nitrogen.

The experimental data were transferred from the BAS-100 to the IBM-PC computer for processing.

4. Results and discussion

The spline wavelet least square (SWLS) of the discrete signals is applied in analytical chemistry to extract the useful information (peak height, peak potential and peak shape) from the high noise signals. The effect of different parameters, the different mth-order spline wavelet basis m, the

Table 4
The relative errors of peak current (I_p (%)) and peak potential (E_p (%)) with 3rd-order spline, $h=2$ and $0.5 \leq S/N \leq 100$

S/N	100	80	60	40	20	10	5	2	1	0.8	0.5
I_p (%)	−2.518	−2.553	−2.551	−2.637	−2.685	−2.764	−2.950	3.067	−3.599	4.206	4.650
E_p (%)	6.071	6.071	6.071	6.071	6.071	6.071	6.286	7.644	8.762	9.566	10.762

distance between the spline wavelet basis h and the signal-to-noise ratio S/N, has been discussed in details. Our laboratory-written software package of SWLS algorithm in True Basic is used to select the optimum values of m, h and S/N and to process the signals with high frequency noise. Simulating signals shown in Fig. 2(d) is studied. It stands for a kind of typical voltammetry curve in electroanalytical chemistry. Random noise is added to this theoretical curve, then spline wavelet least square is used to process the simulating signals. In order to compare the results obtained by SWLS procedures, the relative errors between the theoretical and processed peak current (I_p%), the relative errors between the theoretical and processed peak potential (E_p%) are calculated and listed in Tables 1–3. Comparison of SWLS with WMCD and SLS has also been made in order to show the advantages of SWLS. Then the voltammetric signals with large noise are processed to show the implementation of a SWLS application in an actual analysis system according to the conditions discussed.

4.1. Data processing of simulating signal

4.1.1. Effect of different mth-order spline wavelet basis (m)

If $S/N=0.5$, the distance between spline wavelet used in curve fitting $h=5$, the numbers of sampling points $k=1000$ are fixed. The value of m changes from 2 to 4. The processed results are shown in Fig. 2. From the figures, only for $m=3$, the processed curve is similar to the theoretical curve and the errors are also very small, as can be seen in Table 2. So, $m=3$ is chosen to be the optimum value.

4.1.2. Effect of different distance between spline wavelet basis used in curve fitting (h)

h is a very important parameter in SWLS. It decides the number of spline wavelet basis used in curve fitting (n), the larger h is, the smaller n is. If h is not chosen correctly, the processed curve will be over-processed or under-processed. As for the curve in Fig. 2(d), if $S/N=0.5$, $m=3$ and $k=1000$ are fixed, the distance between spline wavelet basis, h, ranges from 3 to 6, the processed results are shown in Fig. 3. From the figures, only for $h=5$, the processed curve is similar to the theoretical curve. When h is smaller than 5, there are still many fluctuations on the processed curve, that means the noise is not removed entirely. When h is larger than 5, the peak currents of the processed curve are smaller than the theoretical curve. So, we choose $h=5$ as the optimum value.

4.1.3. Effect of different S/N

The practical significance of the noise in analytical chemistry is expressed by S/N which is commonly used to estimate the detectability of a given method. The lower the S/N is, the less useful information the signal include. If $m=3$, $h=5$, $k=1000$ are fixed, S/N varies from 100 to 0.5, the processed results are listed in Table 2. From the table, even if S/N decreases to 0.5, the results exhibit a better reduction of the high noise.

4.1.4. The results of I_p% and E_p%

The influence of different m, h, and S/N on I_p% and E_p% are illustrated in Tables 1–3. From the tables, satisfactory results of $I_p\% < 3\%$ and $E_p\% < 10\%$ (if S/N 0.5) can be obtained if the third-order spline wavelet basis is selected while distance between spline wavelet $h=5$.

According to the results discussed in details above, we came to the conclusion that the third-

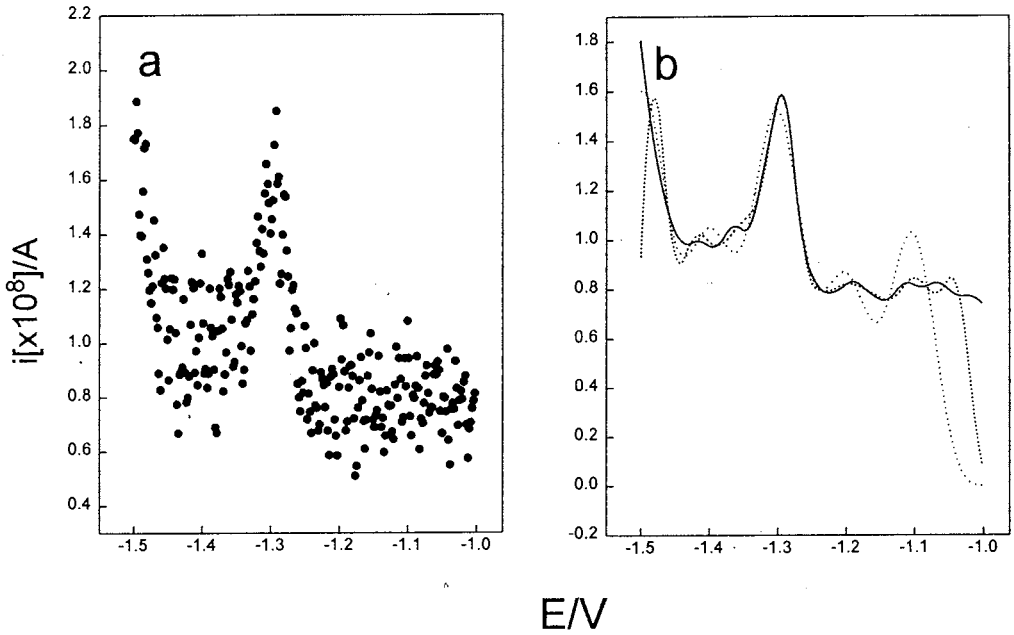

Fig. 6. Experimental results of WMCD and SWLS. (a) Experimental data of [HCHO] = 5×10^{-8} mol l^{-1}; (b) (——) processing result of SWLS; (– – –) processing result of WMCD; (· · ·) processing result of SLS.

order spline wavelet basis and distance between spline wavelet $h = 5$ are optimal values. They can be used in both quantitative and qualitative analysis.

4.2. Comparison of SWLS with WMCD

WMCD is also a very useful filtration method. It can extract useful signal from high noise, even if S/N decreases to 0.3. It can give the signal representation of the frequency domain distribution state in the time domain since it has the property of time frequency domain localization. But there are still some problems that can't be solved by this method. When it processes those signals whose value of starting point or ending point is not equal to zero, that side of the processed curve will drop suddenly to zero. This phenomenon is caused by the characteristic of spline function. Another problem is its not being suitable for filtering some special-shaped curve. During the research on SWLS, we found it can solve these problems existing in WMCD. Comparison of these two methods indicates that spline wavelet least square is better than WMCD in the following aspects.

When SWLS is used to process those signals whose value of starting point or ending point is not equal to zero, this side of processed curve will not drop suddenly to zero (see the dotted line in Fig. 4(a)–(c)). Three different random noises ($S/N =$ 0.5) are added to the theoretical curve in Fig. 2(d), then those curves are processed with WMCD and SWLS respectively. The results could be seen in Fig. 4. It shows clearly that the results obtained from SWLS are better than those from WMCD; the processed curve is more similar to the theoretical curve. The processing errors X^2 of the whole curve are calculated as the following equation:

$$X^2 = \sum_{i=1}^{n} (y_i - y_i^*)^2 \tag{8}$$

where y_i is the value of ith point of the theoretical curve, y_i^* is the value of ith point of the processed curve. The X^2 of the curve processed by WMCD is 0.8390, and X^2 of the curve processed by SWLS is 0.7046 (all the values of X^2 are average values of three determinations).

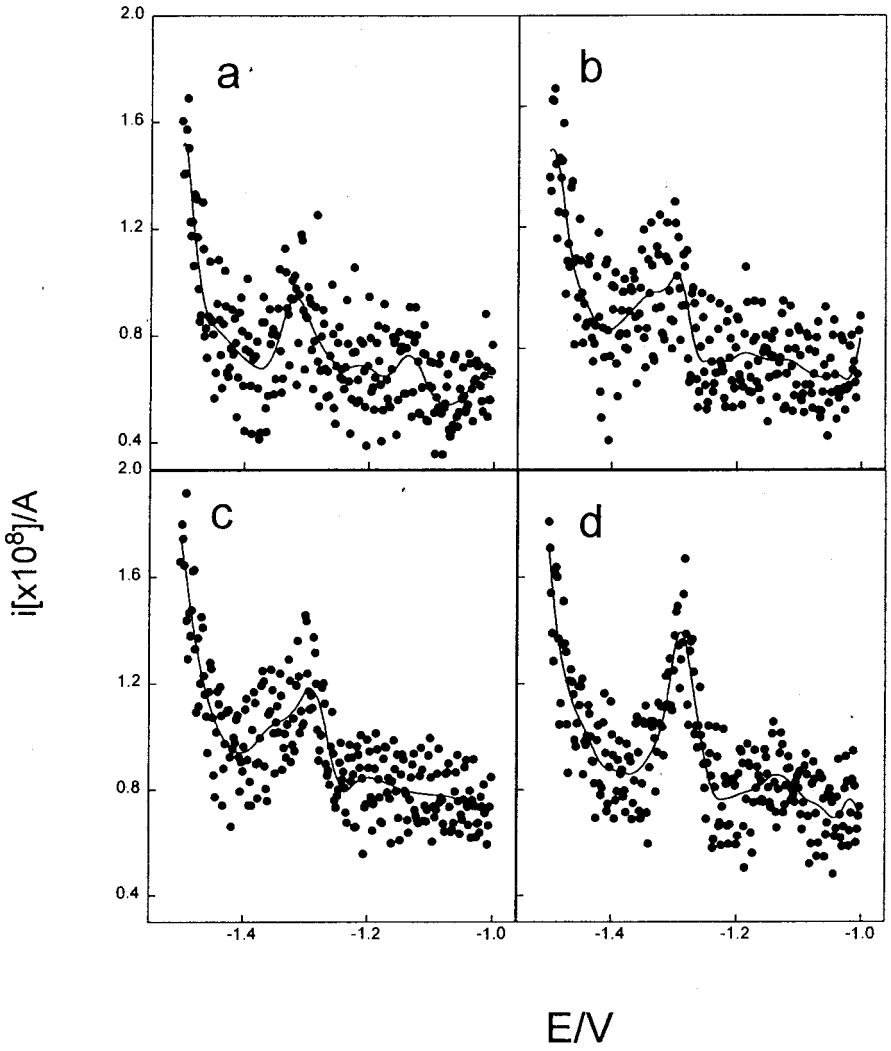

Fig. 7. Experimental results of SWLS with different concentration of HCHO, (· · ·) original data; (——) processed curve; (a) 1×10^{-8} mol l^{-1}; (b) 2×10^{-8} mol l^{-1}; (c) 3×10^{-8} mol l^{-1}; (d) 4×10^{-8} mol l^{-1}.

SWLS is suitable for special-shaped curves. The shapes of signals that collected in analytical experiments are not always a peak-shaped curve. Sometimes we need to process a kind of signal that shown in Fig. 5(a). It stands for the current versus time curve at a stair in step voltammetry. The solid line in Fig. 5(c) shows the processed results of WMCD ($S/N = 1$), the curve is distorted seriously contrast to the theoretical curve; two sides of it all drop to zero. The processing result of WMCD on such curve is not ideal, useful signals can only be filtered from $S/N = 10$. While SWLS can get much better result, it can extract useful signal from high noise of $S/N = 1$ and the processed curve (see Fig. 5(b)) is sill similar to the theoretical curve.

There is no limitation of number of sampling points in SWLS. The number of sampling points in WMCD must be 2^n (n is an integer) according to its algorithm. This causes difficulties in the practical experiments that often can't meet this demand. While in SWLS, the number of the

Table 5
Regression data of SWLS, WMCD and SLS in processing experimental data

	Regression data	Slope	Intercept	Standard deviation of slope	Standard deviation of intercept	R
SWLS	$y = 7.21 \times 10^{-10} + 0.169x$	0.169	7.21×10^{-10}	6.16×10^{-3}	2.04×10^{-10}	0.9980
WMCD	$y = 7.52 \times 10^{-10} + 0.162x$	0.162	7.52×10^{-10}	9.72×10^{-3}	3.23×10^{-10}	0.9946
SLS	$y = 7.40 \times 10^{-10} + 0.149x$	0.149	7.40×10^{-10}	7.07×10^{-2}	5.66×10^{-10}	0.9806

sampling points hasn't such limitation, it could be any number, and needn't be 2^n.

The algorithm of SWLS is simpler and quicker. According to Mallat's decomposition algorithm, the signals processed by WMCD must be decomposed many times. As for those high noise signals, they will be decomposed from truncation frequency $l = 10$ to $l = 3$, that means seven times filtering. While in SWLS, the signals will be processed only one time, even if $S/N = 0.5$. So its algorithm is simpler and quicker.

4.3. Comparison of SWLS with SLS

Spline least square (SLS) has been used in processing voltammetric signals [8], to remove random noise and serialize the discrete data. It can get useful signals from the noise of $S/N = 0.5$. So we can say, it is also a very useful signal processing technique. The principle of its processing signals is the same as that of SWLS and their algorithm are also very similar. During the research, we still found some shortcomings of SLS.

The relative errors of I_p% and E_p% of SLS are always larger than that of SWLS. The third-order spline and distance between spline $h = 2$ are chosen as the optimum value according to the paper [8], S/N ranges from 100 to 0.5, SLS is used to process the theoretical curve shown in Fig. 2(d). Then the relative errors of I_p% and E_p% are calculated and listed in Table 4. Comparing the data in Table 4 with the data in Table 2, we can see the values of error in Table 4 are all higher than those in Table 2 ($h = 5$). That indicate that the processed curves of SWLS are more similar to the theoretical curve than the processed curve of SLS.

In order to see if SLS is suitable for processing some curves with special shape, we use it to process the theoretical curve shown in Fig. 5(a) ($S/N = 1.0$). The processing result is shown in Fig. 5(c) (the dot line). From the figure, we can see the processed curve is distorted seriously, one side of it drops to zero and there's still many fluctuations on the curve. That indicates that SLS is also not suitable for processing such kind of curve, while using SWLS can get satisfactory result (see Fig. 5(b)).

Comparison of SWLS with two other filtration: WMCD and SLS has been made. From the above discussion, we can reach the conclusion that SWLS can be applied more widely in signals processing. It can process some special-shaped curve without any correction. It can solve some problems existing in WMCD and SLS. Its algorithm is very simple and quick.

4.4. Experimental results

Girard's reagent T can react with HCHO as the following equation:

$$\underset{\text{A}}{\text{HCHO}} + \text{Cl}^- \text{Me}_3\text{N} + \underset{\text{Girard's T}}{\text{CH}_2\text{CONHNH}_2}$$
$$\rightarrow \text{Cl}^- \text{Me}_3\text{N} + \text{CH}_2\text{CON}\underset{\text{B}}{\text{H}}\text{NH}{=}\text{CH}_2 + \text{H}_2\text{O}$$

the product of reaction B is electroactive, it can be used to determine HCHO.

The determination of HCHO was carried out on BAS 100 with differential pulse stripping voltammetry (DPSV) on the above-mentioned conditions. When the concentration of HCHO is

5×10^{-8} mol l^{-1}, the original data could be seen in Fig. 6(a). In order to compare the filtering results of WMCD, SLS and SWLS, the original data was processed by the three methods respectively and the results were shown in Fig. 6(b). The filtering parameters of WMCD are based on the results in paper [9]; that of SLS are the third-order spline and $h=2$. The third-order spline wavelet and $h=5$ are chosen as the optimum value of SLS. From the figures, we could see that the processed result of SWLS was better than that of WMCD and SLS. The two sides of the curve processed by WMCD (the dash line in Fig. 6(b)) all dropped to zero. One side of the curve processed by SLS (the dot line in Fig. 6(b)) also dropped to zero, while this phenomenon didn't happen to the curve processed by SWLS. The peak current of the curve processed by SLS was lower than the peak current of the curve processed by SWLS. It was clearly that the solid line in Fig. 6(b) was more similar to the practical curve.

Then, a series of different concentration HCHO were determined, the original data (see black dot in Fig. 7) were processed by SWLS, WMCD and SLS respectively. The solid lines in Fig. 7 were the processed results of SWLS. Because the value of the peak current was too small, all of them in Figs. 6 and 7 were multiplied by 10^8. The concentrations of HCHO in Fig. 7(a)–(d) were 1, 2, 3 and 4×10^{-8} mol l^{-1}, respectively. Then calibrations of peak current versus concentration were plotted. The regression data were listed in Table 5. Apparently, SWLS had the best results among these three methods.

From Figs. 6 and 7 and the regression data, it is clearly that SWLS can get very satisfactory results in processing experimental data. It can not only filter the random noise, but also can get very good linearity relationship that proved the accuracy of SWLS in processing signals.

Acknowledgements

This work was supported by the National Natural Science Foundation of China and the Natural Science Foundation of Guangdong Province.

References

[1] Y.S. Li, D.X. Qi, Spline Methods, Science, 1979.
[2] R.Q. Yu, Introduction of Chemometrics, Hunan Education, Hunan, 1990.
[3] J.Y. Mo, T.Y. Xie, R.J. Zhang, P.X. Cai, Chin. J. Anal. Chem. (in Chinese) 21 (1993) 416.
[4] T.Y. Xie, J.Y. Mo, Finxi Shiyanshi (in Chinese) 12 (1993) 41.
[5] J.H. Liu, Chin. J. Anal. Chem. (in Chinese) 23 (1995) 922.
[6] J.H. Liu, Finxi Shiyanshi (in Chinese) 15 (1996) 15.
[7] D.L. Zhang, Chin. J. Anal. Chem. (in Chinese) 23 (1995) 1390.
[8] T.Y. Xie, J.Y. Mo, Acta Chim. Sinica (in Chinese) 53 (1995) 274.
[9] L.J. Bao, J.Y. Mo, Anal. Chem. 69 (1997) 3053.
[10] X.Y. Zou, J.Y. Mo, Anal. Chim. Acta 340 (1997) 115.
[11] X.Y. Zou, J.Y. Mo, Chin. Sci. Bull. 42 (1997) 640.
[12] X.Q. Lu, J.Y. Mo, Analyst 121 (1996) 1019.
[13] X.Q. Lu, J.Y. Mo, Chem. J. Chin. Univ. (in Chinese) 17 (1996) 1522.
[14] L.J. Bao, J.Y. Mo, Z.Y. Tang, Acta Chim. Sinica (in Chinese) 55 (1997) 907.
[15] L. Yan, J.Y. Mo, Chin. Sci. Bull. (in Chinese) 40 (1995) 1567.
[16] W. Liu, J.H. Xiong, H. Wang, et al., Chem. J. Chin. Univ. (in Chinese) 6 (1997) 860.
[17] B. Walczak, B. Bogaert, D.L. Massart, Anal. Chem. 68 (1996) 1742.
[18] J.B. Zheng, H.B. Zhong, H.Q. Zhang, Chin. J. Anal. Chem. (in Chinese) 26 (1998) 25.

ELSEVIER

Talanta 48 (1999) 437–449

Talanta

High performance liquid chromatographic determination of *N*-nitrosoamines by pre-column fluorescence derivatization with acridone-*N*-acetyl chloride

Jinmao You [a], Xinjun Fan [a], Wenjian Lao [a], Qingyu Ou [a,*], Qingcun Zhu [b]

[a] *Lanzhou Institute of Chemical Physics, Chinese Academy of Science, Lanzhou, 730000, PR China*
[b] *Department of Chemistry, Qufu Normal University, Qufu, Shandong, 273165, PR China*

Received 30 March 1998; received in revised form 30 July 1998; accepted 3 August 1998

Abstract

A sensitive high performance liquid chromatographic method for the determination of *N*-nitrosoamines with pre-column fluorescence derivatization has been developed. *N*-nitrosoamines are first changed into secondary amines using denitrosation reagent, then react with acridone-*N*-acetyl chloride (ARC-Cl) to produce corresponding secondary amine derivatives, which exhibit a strong fluorescence. Maximum emission for ARC derivatives is 430 nm (λ_{ex} 404 nm). The labelled derivatives are very stable, less than 4% decomposition occurs after heating at 40°C for 24 h. Fluorescence intensities of derivatives are higher in neutral and alkaline than in acidic solutions. This method, in conjunction with a multi-gradient program, offers a baseline resolution of the ARC derivatives from a linear acetonitrile gradient. Separation is carried out on a reverse phase C_{18} column. Derivatization and chromatographic conditions are optimized. The relative standard deviation ($n = 6$) at an analytical concentration of 10 pmol of each *N*-nitroamine is less than 4.5%. The detection limits at the fmol level. The method described is also suitable for analysis of other amino compounds in different biological samples.

Keywords: Column liquid chromatography; *N*-nitroso compounds; Fluorescence derivatization; Acridone-*N*-acetyl chloride (ARC-Cl); Denitrosation

1. Introduction

N-Nitrosoamines existed widely in environment or food. The carcinogenicity of *N*-nitrosoamines was first discovered in 1956 by Magee and Barnes [1]. Most of them are known to be potent carcinogens in animals [2]. The determination of *N*-nitrosoamines by LC is of great pharmacological and analytical importance. *N*-Nitrosoamines are formed in air, water, soil and even in the human body when the appropriate amines and nitrile precursors are present by Eq. (1).

$$RR'NH + HONO \rightarrow RR'N{-}N{=}O + H_2O \quad (1)$$

There has been a great deal of concern as to the extent of their occurrence in the environment [3]. It has been estimated that the existed levels for the volatile *N*-nitrosamines in man as low as 5–10 μg

* Corresponding author.

0039-9140/99/$ - see front matter
PII S0039-9140(98)00265-3

kg^{-1} (ppb) [4]. For this reason, minimum detection limits of at least 10 ppb are generally accepted as an essential prerequisite for the determination of this class of compounds in environmental samples. Several existing LC analytical methods, which provide sensitivity at the ppb level, have been reported for the determination of *N*-nitrosoamines [5–7]. In addition, a common method of the acid-catalyzed denitrosation of *N*-nitroso compounds in refluxing 1,2-dichloroethane and subsequent detection of the liberated nitric oxide via its chemiluminescence reaction with ozone was also demonstrated by Gough and Woollam [8] and Downes et al. [9]. This method for direct determination of *N*-nitoso functional group needs a tedious treating procedure, resulting in impractically long analysis times.

Many of *N*-nitrosoamines do not show absorption in UV region, in order to increase detection sensitivity and improve selectivity, general methods employ derivatization agents. High performance liquid chromatographic separation of *N*-nitrosoamines by pre-column derivatization [10,11] or post-column derivatization [12,13] have also been described. However, the sensitivities of these methods described for determination of *N*-nitroso compounds are unsatisfactory. A more practically sensitive method is the acid-catalyzed denitrosation of *N*-nitroso compounds in refluxing 1,2-dichloroethane and subsequent detection of liberated secondary amines via fluorescence derivatization. At present, 4-(2-phthalimidyl)-benzoyl chloride (PIB-Cl) has been used as a fluorescence derivatization reagent for the determination of *N*-nitrosoamines [14]. The PIB-Cl method offers greater sensitivity, but is not appropriate to aromatic amines. At the same time, more interfering peaks are observed with standing of derivatized solution, this is probably due to the fact that PIB-Cl derivatives lead to decomposition during analysis.

With the developing of current techniques for separation of amino compounds by LC or CE, derivatization is of crucial importance. The determination of amino compounds using new fluorescence reagents by reversed-phase liquid chromatography (RP-LC) with pre-column or post-column derivatization is still an active field. An ideal reagent should fulfill several requirements [15]. First, it should be stable and give rapid reaction in high yields at low temperature and the reaction products should be sufficiently stable. Excess reagent or by-products from the reaction should not disturb the separation. Further, the reagent should be selective for the target analysis. The reagent should contain or produce a strong UV absorption or high fluorescence intensity. In addition, the reagent should be inexpensive or be easily prepared. The derivatives must be of a good solubility so as to reduce analysis times.

For this purpose, we synthesized acridone-*N*-acetylchloride (ARC-Cl) by means of microwave irradiation, which used as pre-column fluorescence derivatization agent for the sensitive determination of *N*-nitrosoamines. ARC itself is of high fluorescence. However, this property is not a limiting factor. Provided the conditions of elution and composition of mobile phase, the disturbance of ARC itself on separation can be eliminated. In contrast to PIB derivatives, the solubilities of ARC derivatives are greater than that of PIB derivatives. By comparison the molecular structure with PIB, the fluorescence intensity of ARC is also higher than that of PIB because it contains a nitrogen atom providing a pair of lone electron. The π-conjugated system of molecule is dramatically extended and results in a strong fluorescence emission. The pre-column derivatization developed in experiment does not require solvent extraction steps to remove excess derivatization agent prior to chromatography. So this process decreases the errors in operation.

This paper discusses the evaluation of a more practical method designed as a conversion of *N*-nitrosoamines into corresponding secondary amines. It was found that the adding of appropriate amount of *N*,*N*-dimethyl aniline in denitrosation solution could accelerate the reaction rate of denitrosation by decreasing the nitric oxide concentration because *N*,*N*-dimethyl aniline reacts more easily with liberated nitric oxide resulting in a major yield of *p*-nitroso-*N*,*N*-dimethyl aniline, which does not disturb the fluorescence detection. The denitrosation for *N*-nitroso compounds was easily completed under the mild conditions. This

process would reduce the whole of analysis time because the analyzed solute molecule discarded a nitroso functional group. The LC separation of corresponding secondary amine derivatives was performed on a Spherisorb C_{18} column with acetonitrile as eluent by gradient elution at a flow of 1.0 ml min^{-1}. In addition, the spectral and chromatographic behaviors of the ARC derivatives were also investigated.

2. Experimental

2.1. Apparatus

A model 655 liquid chromatograph equipped with an 650-10S fluorescence spectrophotometer (Hitachi), a Rheodyne 7125 injection valve (USA), a 655 proportioning valve and a 644-61 integrator (Hitachi) were used in experiments. Fluorescence excitation and emission spectra were obtained on 650-10S fluorescence spectrophotometer (Hitachi). Excitation and emission bandwidths were both set at 10 nm. *N*-nitrosoamine derivatives were separated on a 200 × 4.6 mm, 5 μm Spherisorb column (Dalian Institute of Chemical Physics, Chinese Academy of Sciences). A paratherm U_2 electronic isothermal water-bath (Germany) was used to control column temperature. Galanz WP 750B microwave oven, 2450 MHz (China, Shanghai) was used to synthesize acridone-*N*-acetic acid. All mobile phases were treated ultrasonically for 15 min to remove gas bubbles prior to use. UV absorption curves were recorded on a 330-ultraviolet-visible spectrophotometer (Hitachi). Detection was carried out at a fluorescence detector (excitation 404 nm, emission 435 nm).

2.2. Reagents

All reagents were obtained from commercial sources and were reagent grade or better, unless noted below. The organic solvent used for liquid chromatography was LC grade acetonitrile (Jining). Doubly distilled water was used and boiled to remove carbon dioxide before use. All solvents were filtered with a 0.45 μm filtration disk. Chemicals used include triethylamine, boric acid, ammonium dihydrogenorthophosphate were all purchased from Jinan (Shandong). Ammonium dihydrogenorthosphate stock solution (2.67 M), used for preparation of LC eluent, was adjusted to pH 6.5 with ammonia solution. Borate buffer was prepared from 200 mM boric acid solution adjusted to pH 8.5 with 4 M sodium hydroxide solution prepared from sodium hydroxide pellets. Triethylamine stock solution (0.36 M) was also adjusted to pH 6.5 with hydrochloride acid (2.0 M) for preparation of LC eluent. Redistilled *N*,*N*-dimethyl aniline was diluted with acetonitrile to give a final concentration of 2.0 M. The *N*-nitrosoamines were synthesized by reaction of corresponding secondary amines with nitrites in an acidic medium according to previous method [10], These compounds were dissolved in purified acetonitrile and the stock solution (1.0×10^{-4} M) was diluted before use.

Quenching reagent was acetonitrile–water–acetic acid (20:3:2 v/v). The denitrosation reagent was prepared by diluting 10 ml of 48% m/m aqueous hydrobromic acid to give a final volume of 100 ml with acetic anhydride.

2.3. Synthesis of acridone-N-acetic acid

Acridone 4.00 g was dissolved in DMF (7 ml), then ethyl bromoacetate (5 ml) and potassium hydroxide (4.0 g) were added, the mixture under microwave irradiation for 18 s at 525 W, then mixture was extracted by 15 ml of 4 M potassium hydroxide solution. The pH of extracted solution was adjusted to 2.0 with 2 M hydrochloric acid, the precipitation was removed and washed with 10% methanol (20 ml × 3). The rough product was recrystallized from toluene and acetic acid (95:5) to afford a yellow crystal. yield 3.6 g (60%), m.p. 249–252°C. Found, C 74.61, H 4.86, N 6.20; calculated, C 74.66, H 4.88, N 6.22; IR (KBr), 3000–2500 (–COOH), 1720 (C=O), 1530 (ph), 1235, 743; MS, *m*/*z*: 239(M^+), 240(M + 1), 214(M–COOH); 152 (M–NCH_2COOH); ^1H NMR, 2.75 (–CH_2–COOH), 4.58(–*N*–CH_2–), 7.08–8.06 (ph).

2.4. Preparation of ARC-Cl acetonitrile solution

0.1905 g acridone-*N*-acetic acid, was added to a 10 ml of volumetric flask, then 3.0 ml thionyl chloride redistilled was added and followed by shaking for about 30 s to ensure good mixing, then heated for 40 min in a water-bath at 80°C. The solvent was evaporated by blowing with N_2. the dry sample was redissolved by addition of acetonitrile to 50 ml in a 50-ml volumetric flask as a 16 mM of ARC-Cl stock solutions for preparation of *N*-nitrosoamine derivatives. Unless stated otherwise, the concentration of derivatization agent used was 16 mM. All stock solutions, except the borate buffer, were stored in a refrigerator at 4°C.

2.5. Derivatization procedure

Appropriate amount of sample solution (about 50 μl, containing each of *N*-nitrosoamine 50–100 pmol) was added in a centrifuge tube. A 30 μl of *N*,*N*-dimethyl aniline acetonitrile solution was added to ensure a good mixing, then added 50 μl of aliquot of denitrosation reagent and heated for 4 min in a isothermal water-bath at 30°C. After removal of the solvent by a blowing of N_2 to dryness, the dry sample was redissolved by addition of 30 μl of pure acetonitrile and 50 μl of borate buffer (pH 8.5, 0.2 M), then adding 50 μl of ARC-Cl acetonitrile solution. The centrifuge tube agitated and the derivatization allowed for a reaction time of 30–60 s for ARC derivatization. Finally, the reaction was stopped by adding 50 μl of quenching reagent and the mixture was used directly for analysis.

2.6. Chromatographic conditions

Separation of the ARC derivatives was carried out using a binary gradient. Eluent A was 20 mM ammonium dihydrogenorthophosphate + 9 mM triethylamine (pH 6.5)–methanol (95:5) and B was acetonitrile–water (75:25). The flow rate was constant at 1.0 ml min^{-1} and the column temperature was kept at 35°C. The fluorescence emission wavelength at 430 nm (excitation at 404 nm). Unless stated otherwise, the gradient for separation of corresponding derivatives was shown in Table 1.

2.7. Determination of fluorescence quantum efficiencies

Dimethylamine derivative (3.0 μM) was dissolved in various solvent system. The fluorescence emission spectra were recorded with an excitation wavelength of 404 nm for ARC-derivative in a 1 cm quartz cell on an 650-10S spectrofluorimeter. Detection of fluorescence efficiencies were accomplished by comparison with acridone-*N*-acetic acid, as standards ($\phi_{fl'} = 1.0$), respectively. The ϕ_{fl} value for a given derivative was calculated according to the equation:

$$\frac{\phi_{fl}}{\phi_{fl'}} = \frac{I_f(1 - 10^{-A'})}{I_{f'}(1 - 10^{-A})}$$

where ϕ_{fl} and $\phi_{fl'}$ are the fluorescence quantum efficiencies for the given derivatives and the standard. A and A' are the absorbency of the derivatives and the standard solutions (determined by UV). I_f and $I_{f'}$ are the areas under the emission curves of the derivative and the standard, respectively. Quantum efficiencies were measured in 100%, 50% acetonitrile and 50% methanol solutions, respectively.

Table 1
Chromatographic gradient conditions

Time (min)	A (%)	B (%)
0	82	18
10	77	23
14	77	23
25	45	55
35	45	55
40	1	99
45	1	99

Eluent A, 20 mM ammonium dihydrogenortho-phosphate + 9 mM triethylamine–methanol (95:5); eluent B, acetonitrile–water (75:25); flow rate, 1.0 ml min^{-1}.

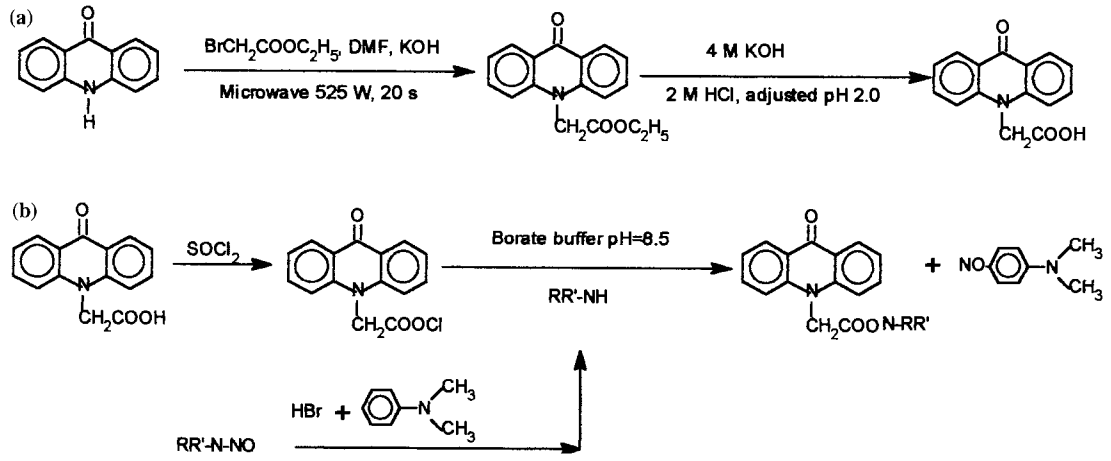

Fig. 1. The synthesis and derivatization processes.

3. Results and discussion

3.1. Enhanced reaction efficiency by microwave irradiation

Recently, interest has been growing in applying microwave heating for preparation of organic and biological samples [16–18]. Microwave irradiation perturbs molecules into dipole rotation without causing rearrangement of their structures. The energy absorbed by polar substances stimulates dipole rotation of molecules. If the molecules are water, friction caused by dipole rotation of water molecule generate heat after microwave irradiation. If the polar organic molecules dissolved in non-polar solutes, in *n*-hexane for example, the irradiated molecules would act as a stirring bar and accelerates the rate of the reactions. In our experiment, ARC could not be synthesized using the method of conventional heating. By means of microwave irradiation, ARC was easily prepared by this unique technology. A systematic study of suitable reaction condition to find an appropriate input power for the complete reaction without overheating is highly desirable. Four different input powers were chosen, and the reaction times were carried out within 20–25 s to find the optimal condition for synthesis of derivatization agent. It is found that an input power of 525 W is very suitable for the synthesis of ARC. The synthesis and derivatization reaction processes are shown in Fig. 1(a) and (b), respectively.

3.2. Stability of derivatives

The stabilities of ARC derivatives at room temperature (25°C) were investigated by analyzing standards containing 10 pmol of each *N*-nitrosoamine. The derivatives were stored at 5°C at room temperature in darkness as well as in daylight for a period of two weeks, during which time they were analyzed four times. As expected, daylight had no effect on stability. All the derivatives were stable during this time. The relative standard deviations for normalized peak areas varying between 1.0 and 3.0% for ARC derivatives. Derivatization solution was mixed with solvent (CH_3OH/CH_3CN/water = 5:30:65, containing 20 mM ammonium dihydrogenortho-phosphate + 9 mM triethylamine pH 6.5) and were kept at constant temperature in a water-bath at 40°C for three days, during which time they were analyzed three times. The extent of decomposition was determined from the ratio of the peak height for the derivatives before and after heating. The derivatives exhibited less than 4% decomposition. These results show that the stabilities of ARC derivatives are incomparably superior to that of PIB derivatives and enough to allow further analysis of derivatized samples at least 24 h at room temperature.

3.3. Optimization for denitrosation reaction

It was known that *N*-nitrosoamines undergo cleavage at the N–NO bond in the presence of a hydrogen bromide–acetic acid mixture, resulting in the formation of the corresponding secondary amines and the liberation of nitric oxide. If being a *N*-nitrosoaromatic amine, the liberated nitric oxide reacts immediately with corresponding liberated aromatic secondary amine to form *p*-nitroaromatic secondary amine. It was found, in experiment, that the *N*,*N*-dimethyl aniline was added to reaction system, resulting in a major yield of *p*-nitrosadimethlaniline. In other words, the nitroso groups of *N*-nitrosoaromatic amines would transfer from *N*-nitrosoaromatic amine to *N*,*N*-dimethyl aniline molecule, which accelerates the reaction rate by decreasing the nitric oxide concentration in reaction by intermolecular reaction. It was also found that a excess of approximately 10^3 mol of *N*,*N*-dimethyl aniline per mol of *N*-nitroso compound would give a completely diversion for all liberated nitroso groups, which would reduced the whole of analysis time because the analyzed solute molecule discarded a nitroso functional group. At the same time, *p*-nitroso-*N*,*N*-dimethyl aniline formed did not disturb the separation using a fluorescence detection.

According to Drescher and Frank [19], the denitrosation of *N*-nitroso compounds in dilute dichloromethane solution occurs rapidly at ambient temperature. The yield of denitrosation products is essentially independent of hydrogen bromide concentration provided, a minimum excess of approximately 10^3 mol of hydrogen bromide per mol of *N*-nitroso compound will give a completely reaction. On the basis of our experiments, it is also found that this is a true except for *N*-nitrosopyrrolidine. The denitrosation of *N*-nitrosopyrrolidine is completed in 1.5 h under the above conditions. However, further study indicated, under the presence of *N*,*N*-dimethyl aniline, that the reaction time can also be reduced to about 4 min when the reaction temperature is kept at 30°C.

3.4. Fluorescence properties of derivatives

The maximum emission wavelength of corresponding dimethylamine derivative is 430 nm (λ_{ex} 404 nm) for ARC. The effect of solvent on the fluorescence spectra and intensity of representative ARC-dimethylamine derivative is shown in Table 2. As can be seen from Table 2, the fluorescence intensities in pure acetonitrile is 21% stronger than that in methanol. The emission wavelength in acetonitrile–water is shorter than that in methanol–water (except 100% acetonitrile). In acetonitrile–water solutions causes a red shift of emission wavelength with decrease of acetonitrile concentration and a decrease in fluorescence intensity. There is a 15.6% difference for ARC in the fluorescence intensity between 50% of acetonitrile solution and 50% methanol solution. Derivatives show a little change in fluorescence quantum efficiencies with increasing of solvent polarity. The ϕ_{fl} value for ARC-derivative changes from 0.698 to 0.541 in going from 100 to 50% acetonitrile and from 0.573 to 0.532 in going from 100 to 50% methanol.

3.5. Effects of pH and temperature on fluorescence intensity

ARC itself contains a carboxylic group, the fluorescence emission intensity in 50% acetonitrile solution changes with the changing of pH. It can be seen that the fluorescence emission intensity of ARC is greater in basic solution than in acidic solution. The fluorescence emission intensity retain constant at $pH < 3$, because ARC itself is not dissociated in this range. In addition, the fluorescence emission intensity is also retained constant at $pH > 8.5$, because it has been dissociated completely in this range. It can be seen that the fluorescence emission intensity of derivatization agent gradually increase with increasing pH in the range of 3.0–8.5. The result is shown in Fig. 2.

The fluorescence intensity of ARC in non-aqueous solvent was investigated using a varying temperature. The curves were depicted in 15°C increments from 15 to 75°C. Emission spectra

Table 2
Effect of solvent polarity on the fluorescence property of representative ARC-dimethylamine derivative (pH adjusted to 6.5 with buffer)

Solvent v/v %	Maximum wavelength		Relative intensity $n=5$	ϕ_{fl}
	Ex.	Em.		
CH_3CN/H_2O				
100		430	1.20	0.698[a]
90+10		430	1.19	
80+20		430	1.18	
70+30		429	1.15	
60+40		429	1.13	
50+50	404	430	1.11[b]	0.541[a]
40+60		431	1.04	
30+70		432	0.99	
20+80		432	0.98	
10+90		435	0.96	
CH_3OH/H_2O				
100		447	100[c]	0.573[a]
90+10		445	0.99	
80+20		435	0.98	
70+30		435	0.98	
60+40		435	0.97	
50+50	404	435	0.96[b]	0.532[a]
40+60		435	0.95	
30+70		433	0.94	
20+80		433	0.94	
10+90		433	0.93	

[a] Relative $\phi_{fl'}=1.0$ in acetonitrile.
[b] Difference in fluorescence intensity, $(1.11-0.96)/0.96=15.6\%$.
[c] Relative fluorescence intensities of ARC as 100% in pure methanol.

were collected using an excitation wavelength chosen on the basis of the maximum intensity in the excitation spectra. Fig. 3 shows typical spectra, which exhibits different fluorescence intensity in *n*-pentanol solvent at temperatures ranging from 15 to 75°C. It can be seen that the emission intensities decrease with increase temperature possibly due to the hydrogen bonding between the ARC and solvent. It is known that the viscosity of the medium surrounding the fluorescence probe has a direct correlation between the fluorescence measurements and the bulk viscosity. This type of correlation will be used to estimate the microviscosity afforded in different organic solvent at different temperature. Details will be reported later. By experiments, it can be seen that ARC is thermally stable and exhibited no significant decomposition over the temperature ranges investigated. A kinetic analysis of fluorescence intensity can be lead to a linear correlation between $\ln I_{em}$ and $1/T$, which shows in Fig. 4. The slope of the working curves yield emission stabilization energy of 26.18 kJ mol^{-1} for ARC.

3.6. Optimization of reaction conditions for derivatization

In developing the ARC for determination of *N*-nitrosoamines, it was important to assess the effect of ARC concentrations and reaction time for derivatized fluorescence signals. For this experiment, a solution of 10 pmol dimethylamine was prepared, which was interfused with ARC-Cl at a concentration range from 0 to 16 mM, and

dissolved in borate buffer (pH 8.5). Unless stated otherwise, the other conditions as described in the experimental section. It was found that fluorescence signals for dimethylamine derivative increases with the varying of derivatization agent concentrations from 0 to 8 mM. The fluorescence intensity kept constant when the concentration of derivatization agent is over 8 mM. The effect of reaction time on fluorescence intensity for dimethylamine was also investigated, and the results shown that the fluorescence intensity for analytes steadily increased from 30 to 60 s and kept a constant after 60 s. It was indicated that the speed of derivatization of ARC-Cl was faster than that of PIB-Cl.

Acetonitrile was used as the reaction co-solvent in preference to acetone as it avoided the problem of precipitation of the derivatives of hydrophobic *N*-nitrosoamines. In preliminary studies, borate, phosphate and bicarbonate buffers were investigated for use in the derivatization. Both borate and bicarbonate were satisfactory, but phosphate proved unacceptable as it produced a large interfering peaks. Derivatization of secondary amines was carried out in borate buffer at pH 8.5 for

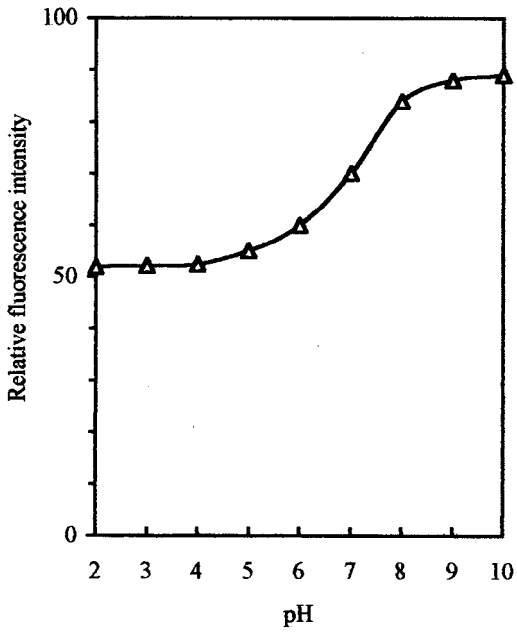

Fig. 2. Effect of pH on ARC itself fluorescence intensity.

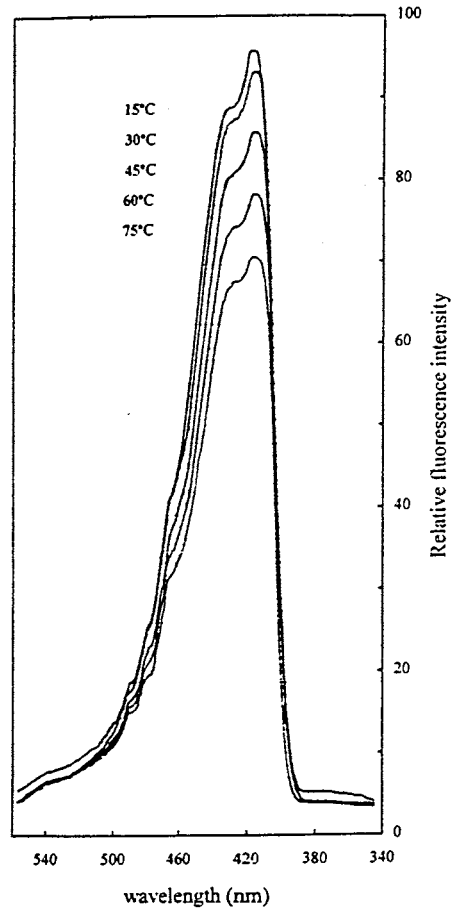

Fig. 3. Fluorescence spectra of ARC at different temperature in *n*-pentanol solvent.

times from 30 to 60 s for ARC. The use of acetonitrile as co-solvent evidently causes derivatization of secondary amines to proceed more slowly than in acetone, but adjustment of the pH of the borate buffer to 8.5–9.0 gave a complete derivatization during this time. The reaction rate was compared with relative peak heights of liberated secondary amines at various intervals by derivatization with ARC. The effect of derivatization time on peak heights was shown in Fig. 5.

Additionally, *N*,*N*-dimethyl aniline was added into the denitrosation solution to be profitable for the diversion of *N*-nitroso groups because it not only accelerates the reaction rate but also eliminates the disturbance of released nitric oxide. On

the other hand, *N*,*N*-dimethyl aniline itself dose not disturb the separation using a fluorescence detection. In addition, excess derivatization reagent will change into ARC-OH, which does not disturb on the separation of other derivatives as it was eluted firstly.

3.7. Effect of triethylamine concentration on retention

The effect of triethylamine concentration on the retention value of ARC derivatives is investigated. The result shows that the k' values of solutes decrease with increasing triethylamine content, peak spreading is reduced and column efficiency improved. It is probably due to the fact that these variations derive from interaction of the solutes with residual silanol groups on the silica surface [20,21]. The nitrogen in triethylamine can easily form coordinate bond with the oxygen of residual hydroxyls on the surface of stationary phase, thus the residual acidic sites on the surface decrease with the amount of triethylamine added. This process can efficiently reduce non-specific sorption of solutes. Several mobile phases were tested for this analytical separation. The use of chromatographic eluent containing triethylamine gave a good reproducibility in the qualitative and the quantitative analysis of derivatives. The pH (in the range of 5–7) does not influence the retention of ARC-OH, which is easily separated from other derivatives by adjusting the composition of eluent A, In order to achieve the efficient derivatization, 16 mM of derivatization reagent is adopted for *N*-nitroso compounds derivatized in our experiments. Optimum separation is obtained by addition of 9 mM triethylamine in the mobile phase A.

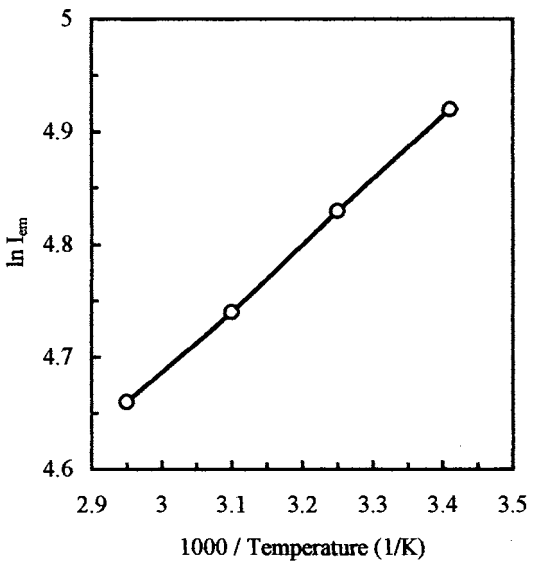

Fig. 4. Effect of the temperature (1/K) on the fluorescence intensity (ln I_{em}) of ARC in *n*-pentanol solvent.

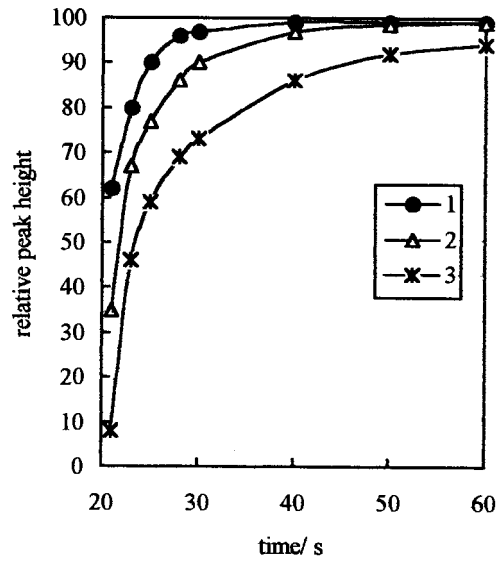

Fig. 5. Reaction rates of ARC-Cl with dimethylamine (100 pmol), diethylamine (100 pmol) and pyrrolidine (100 pmol). Reaction system: borate buffer (pH 8.5) containing 0.1 μM *N*,*N*-dimethyl aniline. 1, dimethylamine; 2, diethylamine; 3, pyrrolidine.

3.8. LC separation of derivatives

The separation of a denitrosated mixture of *N*-nitrosoamines or *N*-nitrosoaromatic amines was carried out using a reverse phase Spherisorb-C_{18} column. When eluent A was 20 mM ammonium dihydrogenorthophosphate + 9 mM triethylamine–methanol (90:10), it is found that *N*-nitrosodimethylamine, *N*-nitrosopyrrolidine and *N*-nitrosoethylamine derivatives were constantly found to be not offered baseline resolu-

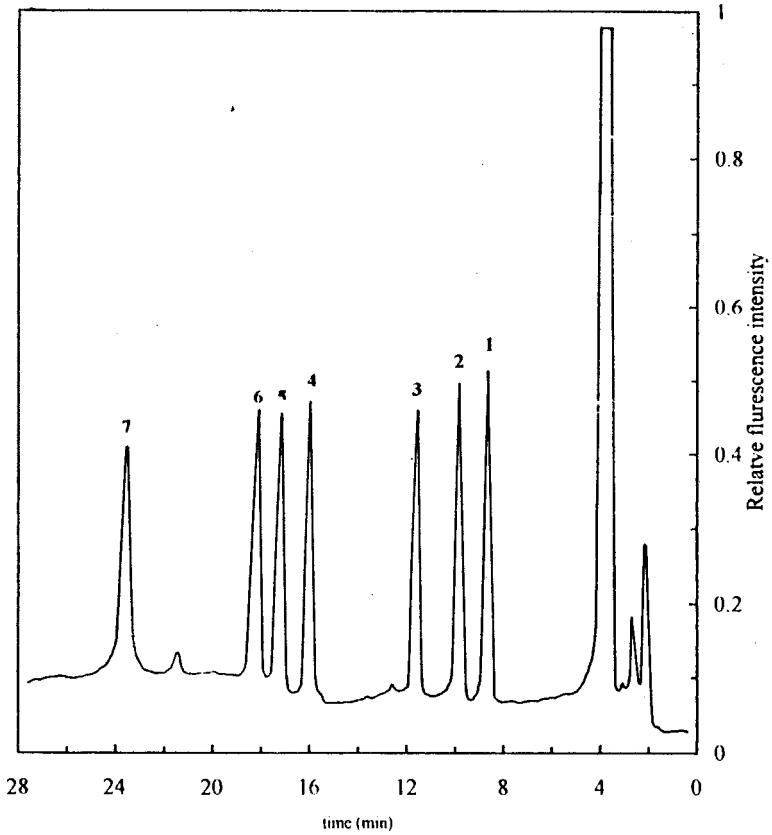

Fig. 6. Chromatogram of a 10 pmol standard derivatives detected by fluorescence (excitation wavelength 404 nm, emission 430 nm). Chromatographic conditions: column 200 × 4.6 mm Spherisorb 5 μm; eluent A: 20 mM ammonium dihydrogenorthophosphate + 9 mM triethylamine–methanol (95:5%); eluent B: acetonitrile–water (75:25%); flow rate, 1.0 ml min^{-1}; column temperature, 35°C; gradient as Table 1. 1, *N*-nitrosodimethylamine; 2, *N*-nitrosopyrrolidine; 3, *N*-nitrosodiethylamine; 4, *N*-nitrosopiperidyl; 5, *N*-nitrosodipropylamine; 6, *N*-nitrosomethylphenylamine; 7, *N*-nitrosodibutylamine.

tion. However, that is easily separated by varying the composition of mobile phase. When eluent A was 20 mM ammonium dihydrogenorthophosphate + 9 mM triethylamine–methanol (95:5), these derivatives mentioned as above were found to be offered a satisfactory baseline resolution as shown Fig. 6.

3.9. Analysis of N-nitrosoamines in soil

For the analysis of *N*-nitrosoamines in soil, 100 g samples were weighed out and transferred to a volumetric flask and was mixed with a 50-ml portion of dichloromethane for 20 min. The samples were then filtered to remove insoluble particulate matter. After the filtrate was transferred to a 100-ml volumetric flask, the solution was treated with 20 g of anhydrous sodium sulfate. The dried extracts were then concentrated to a final volume of 10 ml under a stream of dry nitrogen at 30°C. For the denitrosation reaction, the concentrated extracts were transferred to 50-ml test tubes and brought to a total volume of 20 ml with fresh methylene chloride. A 0.5 ml of *N*,*N*-dimethyl aniline acetonitrile solution was added to ensure a good mixing, after immediately the adding of 1.0 ml of denitrosation reagent solution, the mixture was heated for 4 min in a isothermal water-bath at 30°C. After removal of the solvent by a blowing of N_2 to dryness, the sample was redissolved

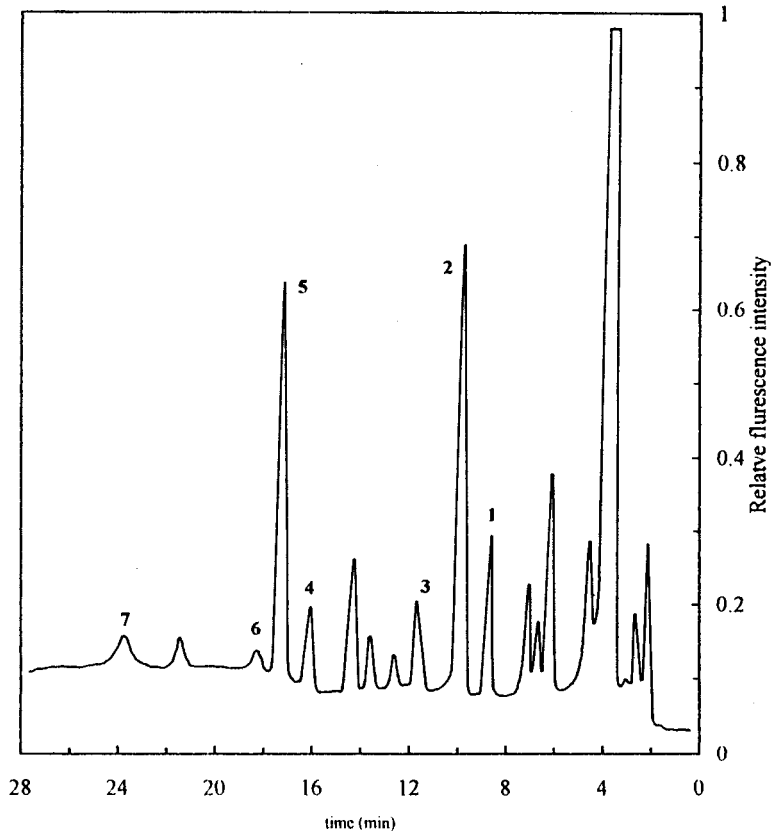

Fig. 7. Chromatographic separation of derivatized secondary amines from soil. Chromatographic conditions: column 200 × 4.6 mm Spherisorb 5 μm; eluent A: 20 mM ammonium dihydrogenorthophosphate + 9 mM triethylamine–methanol (95:5%); eluent B: acetonitrile–water (75:25%); flow rate, 1.0 ml min^{-1}; column temperature, 35°C; gradient as Table 1. 1, *N*-nitrosodimethylamine; 2, *N*-nitrosopyrrolidine; 3, *N*-nitrosodiethylamine; 4, *N*-nitrosopiperidyl; 5, *N*-nitrosodipropylamine; 6, *N*-nitrosomethylphenylamine; 7, *N*-nitrosodibutylamine.

by addition of 0.5 ml of pure acetonitrile. Derivatization was carried out as previously described. The separation of *N*-nitrosoamines in soil was shown in Fig. 7.

4. Linearity of derivatives

The linearities of the *N*-nitrosoamine derivatives were established by the analysis of six different concentrations of corresponding standards, over a 100-fold range. These standards gave on-column injection amounts ranging from 1.0 to 100 pmol for *N*-nitrosodimethylamine, *N*-nitrosopyrrolidine, *N*-nitrosodiethylamine, *N*-nitrosodipropylamine and *N*-nitrosopiperidyl; and from 2.0 to 200 pmol for *N*-nitrosomethylphenylamine and *N*-nitroso dibutylamine. All of the derivatives were found to give a linear response with the correlation coefficients for peak heights greater than 0.998, and listed in Table 3.

4.1. Detection limits and sensitivity

The sensitivity are depend upon the size of column. Narrow or microbore columns give a further increase in sensitivity especially when baseline subtraction is used. The representative

Table 3
Regression analysis of calibration graphs and other quantitative data for ARC derivatives

Compound	Linear range injected amount pmol	Calibration graph[a]	Correlation coefficient	RSD%[b] ($n=6$)	Detection limit[c] (fmol)
N-nitrosodimethylamine	1.0–100	$y=0.2028+0.1408x$	0.9986	4.2	24
N-nitrosopyrrolidine	1.0–100	$y=0.0342+0.1327x$	0.9992	4.0	30
N-nitrosodiethylamine	1.0–100	$y=0.0517+0.1185x$	0.9990	4.3	46
N-nitrosopiperidine	1.0–100	$y=0.0485+0.0995x$	0.9994	4.1	50
N-nitrosodipropylamine	1.0–100	$y=0.0199+0.0860x$	0.9995	4.2	64
N-nitrosomethylphenylamine	2.0–200	$y=0.0257+0.0752x$	0.9987	4.5	117
N-nitrosodibutylamine	2.0–200	$y=0.0114+0.0609x$	0.9988	4.3	128

[a] y in cm, x in pmol injected amount.
[b] Relative standard deviation for 10 pmol of each ARC derivatives
[c] $S/N=3$.

derivatives of 10 pmol of *N*-nitrosodimethylamine and *N*-nitrosodiethylamine are investigated. Their peak heights corresponding ARC derivatives are 3.0 times as high as PIB derivatives. Detection limit is depend upon different detector. The detection limit, defined as thrice the size of the background noise for *N*-nitroso compounds is 24–128 fmol for ARC. Under the same operational conditions, PIB give a corresponding detection limit of 65–335 fmol. The low detection limit is directly attributable to the removal of impurities present in the reagents and blank water. These impurities can be eliminated by purifying the reagent and will give a further increase in sensitivity. The detection limits ($S/N=3$) were calculated from peak heights and also listed in Table 3.

5. Conclusions

In contrast to derivatization agent PIB, the derivatives of ARC exhibits a high solubility and a large molar absorptivity in derivatized solution which makes it more sensitive than PIB derivatives. ARC derivatives are detected at levels of 2.6 times lower than PIB derivatives. In comparison PIB with ARC, PIB is unstable and exists more interfering peaks with standing of the derivatized solution. At the same time, aromatic amines give no fluorescent products for PIB under the proposed derivatization conditions, which makes its application to be limited in analysis. The present work has shown that ARC is a highly sensitive and effective derivatization reagent. Complete derivatization took less than 1 min at room temperature, and its derivatives are stable for at least 24 h in neutral solution. Corresponding hydrolysates of ARC does not interfere with the LC analysis by adjusting the composition of mobile phase. Derivatization yield of close to 100% was achieved for derivatized compounds. These characteristics make it to be an attractive derivatization agent.

References

[1] P.N. Magee, J. Barnes, J. Cancer 10 (1956) 114.
[2] H.H. Xu, *N*-nitroso Compounds in the Environment, Science Press, Beijing, 1988.
[3] I.A. Wolff, A.E. Wasserman, Science 177 (1972) 15.
[4] G.S. Drescher, C.W. Frank, Anal. Chem. 50 (1978) 2118.
[5] H.J. Issaq, J.H. Meconnell, D.E. Weiss, J. Liq. Chromatogr. 9 (1986) 1783.
[6] H.J. Issag, M. Glennon, D.E. Weiss, C.N. Chmany, J.E. Saavedra, J. Liq. Chromatogr. 9 (1986) 2763.
[7] H.J. Issaq, I.Z. Atamna, N.M. Schultg, G.M. Muschik, J.E. Saavedra, J. Liq. Chromatogr. 12 (1989) 771.
[8] T.A. Gough, C.J. Woolam, in: Environmental *N*-nitroso compounds Analysis and Formation, IARC Scientific. No. 14, IARC, Lyon, 1976, p. 85.
[9] M.J. Downes, M.W. Edwards, T.S. Elsely, C.L. Walters, Analyst (London) 101 (1976) 742.
[10] Q.H. Wan, C.G. Fu, Cepu 4 (1986) 238.
[11] Z. Wang, C.G. Fu, H.D. Xu, J. Chromatogr. 589 (1992) 349.
[12] S.H. Lee, L.R. Field, J. Chromatogr. 386 (1987) 137.
[13] M. Righezza, M.H. Murello, A.M. Siouffi, J. Chromatogr. 410 (1987) 145.
[14] M.H. Zheng, C.G. Fu, H.D. Xu, Anlyst 118 (1993) 269.
[15] H. Wan, P.E. Andersson, A. Engstom, L.G. Blomberg, J. Chromatogr. A 704 (1995) 179.
[16] S.-T. Chen, S.-T. Chiou, Y.-H. Chu, H.-T. Wang, Int. J. Pept. Protein Res. 30 (1987) 572.
[17] S.-H. Chio, K.-T. Wang, J. Chromatogr. 448 (1988) 404.
[18] S.-H. Chio, K.-T. Wang, J. Chromatogr. Biomed. Appl. 491 (1989) 424.
[19] G.S. Drescher, C.W. Frank, Anal. Chem. 50 (1987) 2118.
[20] M.T. Hearn, B. Grego, J. Chromatogr. 255 (1983) 125.
[21] M.T. Hearn, B. Grego, J. Chromatogr. 266 (1983) 75.

ELSEVIER

Talanta 48 (1999) 451–459

Talanta

Headspace solid phase microextraction (HSSPME) for the determination of volatile and semivolatile pollutants in soils

Maria Llompart [a,*], Ken Li [b], Merv Fingas [b]

[a] *Departamento de Quimica Analitica Nutricion y Bromatologia, Facultad de Quimica, Universidad de Santiago de Compostela, E-15706 Santiago de Compostela, Spain*

[b] *Emergencies Science Division, Environment Canada, Environmental Technology Centre, 3439 River Road, Ottawa, ON, Canada*

Received 3 April 1998; received in revised form 10 July 1998; accepted 3 August 1998

Abstract

We have investigated the use of headspace solid phase microextraction (HSSPME) as a sample concentration and preparation technique for the analysis of volatile and semivolatile pollutants in soil samples. Soil samples were suspended in solvent and the SPME fibre suspended in the headspace above the slurry. Finally, the fibre was desorbed in the Gas Chromatograph (GC) injection port and the analysis of the samples was carried out. Since the transfer of contaminants from the soil to the SPME fibre involves four separate phases (soil-solvent-headspace and fibre coating), parameters affecting the distribution of the analytes were investigated. Using a well-aged artificially spiked garden soil, different solvents (both organic and aqueous) were used to enhance the release of the contaminants from the solid matrix to the headspace. It was found that simple addition of water is adequate for the purpose of analysing the target volatile organic chemicals (VOCs) in soil. The addition of 1 ml of water to 1 g of soil yielded maximum response. Without water addition, the target VOCs were almost not released from the matrix and a poor response was observed. The effect of headspace volume on response as well as the addition of salt were also investigated. Comparison studies between conventional static headspace (HS) at high temperature (95°C) and the new technology HSSPME at room temperature ($\sim$ 20°C) were performed. The results obtained with both techniques were in good agreement. HSSPME precision and linearity were found to be better than automated headspace method and HSSPME also produced a significant enhancement in response. The detection and quantification limits for the target VOCs in soils were in the sub-ng g^{-1} level. Finally, we tried to extend the applicability of the method to the analysis of semivolatiles. For these studies, two natural soils contaminated with diesel fuel and wood preservative, as well as a standard urban dust contaminated with polyaromatic hydrocarbons (PAHs) were tested. Discrimination in the response for the heaviest compounds studied was clearly observed, due to the poor partition in the headspace and to the slow kinetics of all the processes involved in HSSPME.

Keywords: Solid phase microextraction; Headspace; VOC; Soil analysis

* Corresponding author. Tel./fax: + 34 981 547141; e-mail: qblvrlgb@usc.es

0039-9140/99/$ - see front matter
PII S0039-9140(98)00263-X

1. Introduction

A recent advance in sample preparation for trace analysis is solid phase microextraction (SPME) technology. In this solvent-free extraction technique, developed in 1989 by Pawliszyn [1–5], the analytes are adsorbed directly from an aqueous [3] or gaseous phase [6] onto a fused-silica fibre coated with a polymeric phase. Hence sampling, extraction and concentration are accomplished in a single step. The entire assembly is mounted in a modified syringe needle which, after exposure to the sampling media (water or air), is inserted into the heated injection port of a GC. The analytes are desorbed in the GC injector and analysis of the samples is carried out. Separation and detection then proceed in the usual manner. The SPME fibre can also be suspended in the headspace above the aqueous or solid sample (headspace solid phase microextraction (HSSPME)), which eliminates interference problems because the fibre is not in contact with the sample [7,8]. SPME has become very popular in the last 2 or 3 years, especially in environmental analysis [9–14].

Environmental contamination with volatile organic chemicals (VOCs) associated with fuel/petroleum usage is widespread in the world. Spills during transport and leaking storage tanks are the main sources of contamination to soils, ground water and air. Other sources of petroleum product contamination are heating oil tanks, refineries, aboveground tanks, terminals, pipelines, or accidental spills from other sources. These compounds have gained prominence in environmental pollution control over the past decade as a result of increased environmental and health concerns and the introduction of new regulations. The most commonly used protocols for the analysis of VOCs in water are static headspace (HS) or purge-and-trap techniques (PAT). These techniques have also been applied to the analysis of soils and sediments [15].

In this paper we present the development of a HSSPME method to extract volatile organic compounds (VOCs) from soil matrices. Model VOCs include toluene, *ortho*-, *meta*- and *para*-xylene, chlorobenzene, 1,2-, 1,3- and 1,4-dichlorobenzene. Soil samples were suspended in solvent and the SPME fibre suspended in the headspace above the slurry. Finally the fibre was desorbed in the GC injection port and the analysis of the samples was carried out. Different parameters affecting the distribution of the analytes between the different phases were investigated. The HSSPME method at room temperature (~ 20°C) was compared with conventional automated HS sampling at high temperature (95°C). Due to the lack of adequate reference soil material of VOC, a typical urban soil was spiked with a mixture of target compounds and aged for several months to simulate real soil samples. Conventional HS results were compared to the HSSPME results and found to be in good agreement. The proposed method offered significant advantage in terms of linearity, precision and detection limits. Although this method shown to be well suited for VOC analysis, compounds of low volatility partition poorly into HS and are generally not amenable to headspace type of analysis. The limitation of the HSSPME method developed in this work for the analysis of semivolatiles was studied through three naturally contaminated samples: one with hydrocarbons and another two with PAHs.

2. Experimental

2.1. Instrumentation

Static headspace analysis was performed using a Hewlett Packard HP19395A headspace sampler and a HP5890 Series II gas chromatograph equipped with a 5970 mass selective detector (MSD). Experimental parameters of the HS sampler were as follows: equilibration time, 30 min (nominal); bath temperature, 95°C; sample loop, 3 ml; valve/loop temperature, 110°C; valve operation sequence of pressurisation, 10 s; venting and filling of loop, 5 s; and injection 15 s. The carrier gas was helium at 80 ml min^{-1}; and the auxiliary pressure of 1.5 bar. Normal HS was run using a constant heating time accessory on the headspace sampler, consisted of a sample magazine and the controlling pneumatics which dropped one vial at a time into the heated carousel as the previous

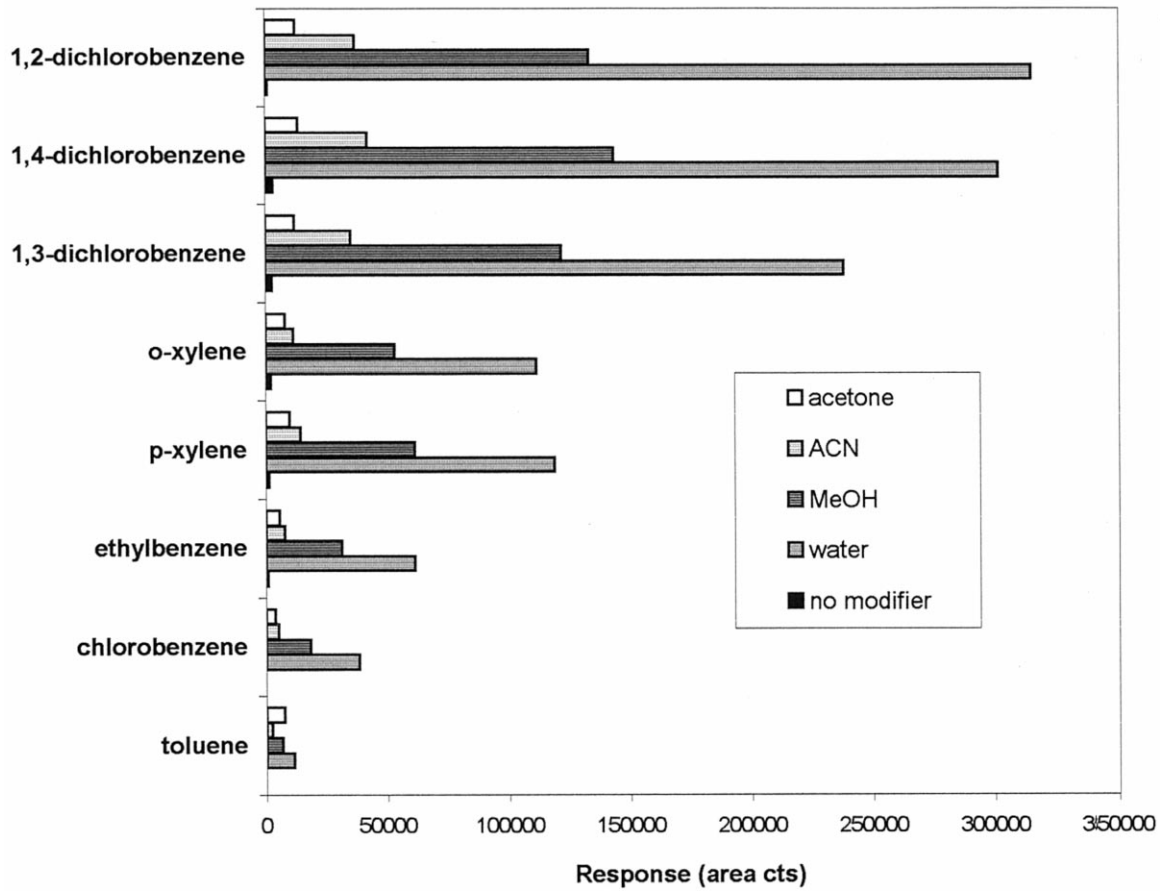

Fig. 1. Effect on the response after the addition of different polar solvents to the soil.

sample was being analysed, such that each sample vial was equilibrated for the time equivalent to one GC run (heating up and cooling down; nominally 30 min).

A manual SPME holder was used with a 100-μm polydimethylsiloxane fibre assembly (Supelco, Mississauga, ON). The analysis was performed on the above system with the headspace transfer line detached from the injection port. GC conditions were the same in normal HS and in HSSPME analysis, and were as follows: inlet temperature, 225°C; inlet mode, split operation with split ratio 1:10 (splitless operation in SPME); split vent flow, 60 ml min^{-1}; oven temperature, 40°C hold 5 min, rate 7.5°C min^{-1} to final temperature 200°C; column, 30-m SPB-1, 0.53 mm i.d., 1.5-μm film, column flow, 7.5 ml min^{-1} nominal; linear velocity, 40 cm s^{-1} at 100°C. An open-split interface was used to limit the flow to the MSD to 0.7 ml min^{-1}. The MSD was operated in SIM mode.

For PAHs analysis another GC/MSD system similar to the one above was employed with a 30-m DB-5 GC column (0.25 mm i.d., 0.25 μm film). GC temperature program was: oven temperature, 80°C hold 1 min, rate 15°C min^{-1} to final temperature 300°C. The injector temperature was 260°C and the capillary interface temperature was 300°C. The MSD was operated in selected ion monitoring mode with two or three monitored ions per compound. Both systems were controlled by a HPChem station (DOS series).

For total hydrocarbon analysis, a 5890 GC equipped with flame ionisation detector (FID) was used. A 30-m DB-5 GC column (0.25 mm

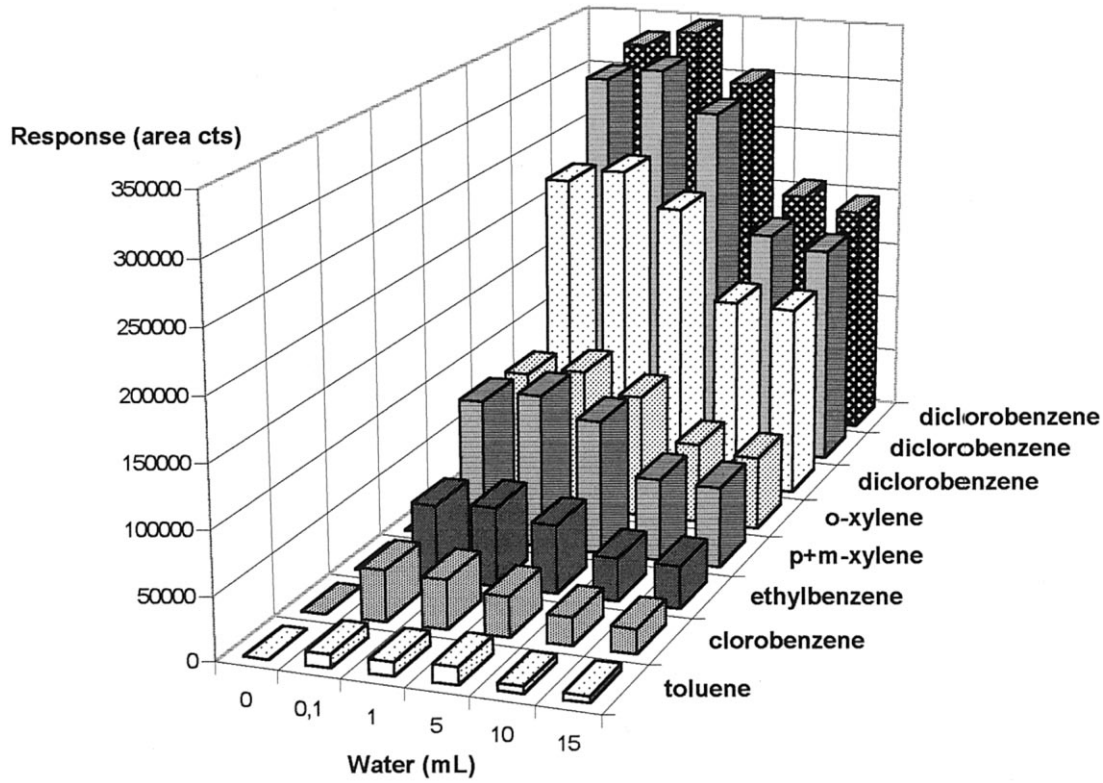

Fig. 2. Effect on the response after the addition of different amounts of water to the soil.

i.d., 0.25 μm film) was used. Oven temperature was 50°C for 1 min and heated to 310°C at the rate of 15°C min^{-1}. Injector and detector temperature were 280 and 310°C, respectively. The GC column flow was nominally 1 ml min^{-1}.

2.2. Reagents and chemicals

A ten-components VOC standard of 2000 μg ml^{-1} of each of the target analytes was obtained from HP (part no. 8500-6080). The target analytes were benzene, toluene, chlorobenzene, ethylbenzene, *p*-, *m*-, *o*-xylene, 1,2-, 1,3- and 1,4-dichlorobenzene. The standard was diluted ten times in methanol to give a spiking solution of 200 μg ml^{-1}.

All the solvents (analytical grade) were purchased from Caledon (Belleville, ON, Canada).

For the study of volatiles, experiments were performed in a sandy-loam sub-surface soil collected from a garden in an urban area in Ottawa. This soil consists of 48.4% sand, 32.3% silt and 13.3% clay with 2.0% organic carbon. After removing twigs and extraneous material it was dried in an oven at 90°C for 4 h and then homogenised by crushing in a mortar and screened to a particle size of 200 μm. This soil did not contain any of the VOCs studied in this work. About 100 g was weighed out in a jar, to which the VOC standard mixture dissolved in 100 ml of methanol was added to give a soil concentration of 2 μg g^{-1} of each of the VOC target compounds. The slurry was allowed to stand, loosely covered to protect it from dust, and stirred occasionally until the methanol completely evaporated (approximately 2 days). The soil was then capped and kept in a desiccator. The final VOC content of this soil was not known due to evaporation loss during preparation and storage (approximately 18 months). Benzene has not been included in this study be-

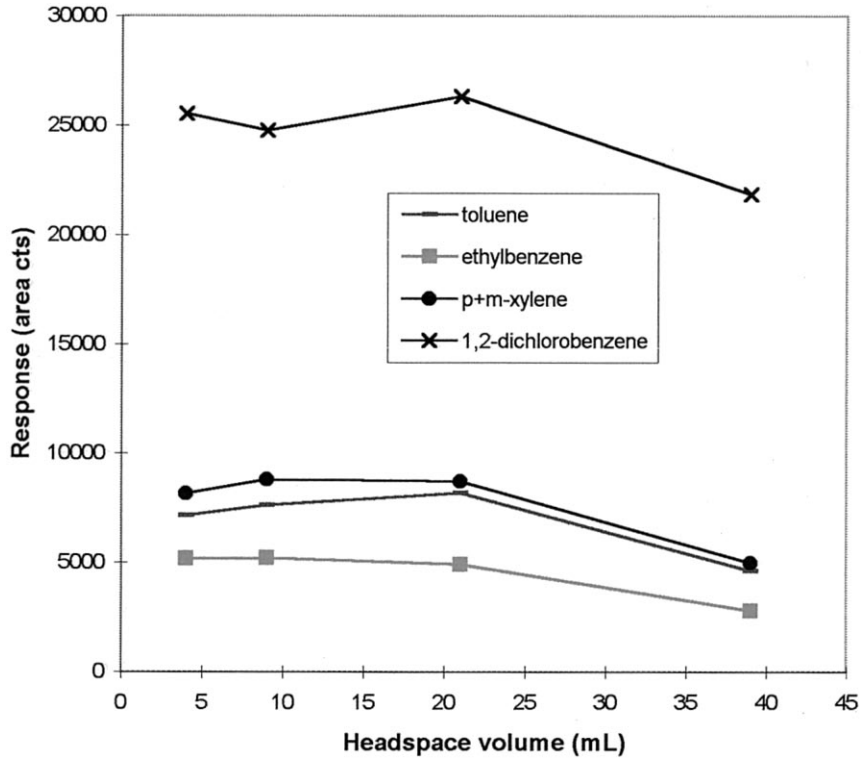

Fig. 3. Effect on the response with the headspace volume.

cause due to its high volatility, it was not detected in the aged soil. Soils spiked in this manner, and aged for a long period of time, resembled a real sample more than the common technique of spiking one spot in the soil matrix just before analysis, because the target analytes were in more intimate contact with the soil particles, and thus maximising analyte/matrix interaction.

Table 1
HSSPME detection and quantification limits for the target VOCs

	Detection limit (ng g^{-1})	Quantification limit (ng g^{-1})
Toluene	0.23	0.78
Chlorobenzene	0.15	0.49
Ethylbenzene	0.08	0.27
p+*m*-Xylene	0.05	0.16
o-Xylene	0.07	0.23
1,3-Dichlorobenzene	0.14	0.47
1,4-Dichlorobenzene	0.13	0.42
1,2-Dichlorobenzene	0.15	0.49

For calibration studies a standard addition protocol was used. Different levels of VOCs were added to the spiked soil. A 1-g soil aliquot was added into a 20-ml vial and spiked with a 100-μl of MeOH containing the VOCs. After capping, the vials were tumbled for 0.5 h and allowed to equilibrate at room temperature for 24 h before sampling and analysis.

For the analysis of semivolatiles three real samples were used: (i) a soil contaminated with diesel fuel from a gas process plant, in which we analysed the total hydrocarbon content; (ii) a wood preservative contaminated soil (SRS103-100) purchased from Fisher Scientific (Fair Lawn, NJ) for the analysis of PAHs; and (iii) an urban dust (SRM 1649) purchased from NIST (Gaithersburg, MD) for the analysis of PAHs.

Table 2
HSSPME versus HS: linear correlation coefficients and ratio of responses (HSSPME/HS)

	Correlation coefficients		Ratio of responses (HSSPME/HS)
	HSSPME	HS	
Toluene	0.9993	0.9971	2
Chlorobenzene	0.9999	0.9981	2
Ethylbenzene	0.9992	0.9987	3
p+*m*-Xylene	0.9989	0.9996	10
o-Xylene	0.9999	0.9998	7
1,3-Dichlorobenzene	0.9997	0.9991	8
1,4-Dichlorobenzene	0.9993	0.9975	7
1,2-Dichlorobenzene	0.9991	0.9973	7

2.3. Conventional HS sampling

HS sampling and analysis was performed following the method proposed by Voice and Kolb [15]. Two grams of soil were introduced into a 22-ml HS-vial. Three millilitres of water were added to each vial and then the vial was placed in the HS bath at 95°C for 0.5 h before analysis.

2.4. HSSPME sampling

Different amounts of water or organic solvents were added into 1 g soil in a 22-ml HS-vial, to promoted the release of volatiles. A 1-cm stir bar was placed in each vial, which was sealed with an aluminium cap with a Teflon-lined septum. The SPME fibre was suspended in the HS for 30 min. The water–soil mixture was stirred during the sampling time to promote faster equilibrium. Once sampling was complete, the fibre was immediately inserted into the GC injector port for desorption. A desorption time of 3 min at 260°C was enough for quantitative desorption of all the analytes studied and no carry over was observed.

3. Results and discussion

The fibre exposure time required for equilibrium between phases was not studied since it is a matrix dependant parameter. However, we found equilibrium was reached after 30 min. Further exposure up to 1 h did not show any increase in the response.

3.1. Optimisation of HSSPME conditions

The degree of partitioning of VOCs between the soil and the HS is generally very low. To promote the release of volatiles, water can be added to the soil [7,16]. The effect of adding water as well as organic polar solvents to the sample matrix was studied. Fig. 1 shows the responses obtained after adding 100 μl of different solvents to 1 g of sample. As can be seen, there was an increase in the response in all cases. The highest results, however, were obtained using water, which produced a 100-fold increment to the signal obtained without the addition of solvent.

Different mechanisms are involved in the desorption of volatiles from the soil into the headspace when a polar solvent is used. One of them is the displacement of the analytes from the active sites in the soil. The active sites are usually polar functional groups that have more affinity for polar compounds than for less polar ones. The polar compounds added to the soil will substitute, at least in part, the VOCs on these active sites and, in consequence, the VOCs will be released into the headspace. Another mechanism involved is the competition between the matrix and the solvent for the analytes. Part of the analytes can be desorbed from the soil into the solvent by solvation, and then from the solvent into the headspace.

The quantity of water added to 1 g of soil was investigated next. The experiments were carried out with the addition of water between 0 and 15 ml. The results are shown in Fig. 2. This plot

Table 3
Concentration of VOCs (ng g^{-1}) found in the well-aged spiked soil by HSSPME and by HS

	HSSPME		HS	
	Mean (ng g^{-1})[a]	RSD (%)	Mean (ng g^{-1})[a]	RSD (%)
Toluene	33.1	10.0	22.7	12.8
Chlorobenzene	79.0	2.2	52.8	8.9
Ethylbenzene	64.7	4.0	61.3	7.0
p+*m*-Xylene	104.6	4.2	95.0	10.0
o-Xylene	75.9	5.6	75.7	8.9
1,3-Dichlorobenzene	583.9	2.1	628.5	6.2
1,4-Dichlorobenzene	651.8	3.9	747.2	11.5
1,2-Dichlorobenzene	807.2	4.2	881.1	8.2

[a] $n = 3$.

exhibits a maximum response for 1 ml of water added to the system. However, the responses obtained between 100 μl and 5 ml were not significantly different. When the amount of water added was 5 ml or more, the responses decreased. The results clearly demonstrate that the addition of water to the samples is necessary to release the VOCs into the gas phase. The fact that the responses were practically not dependent on the amount of water between 100 μl and 5 ml for a 1-g sample size has a significant practical advantage, because in real soil samples, the moisture content can be very different, and is often not known. The results of this study indicate that the HSSPME method proposed for the target VOCs is not sensitive to the moisture level of the soil. For subsequent studies, the amount of water added to 1 g of soil was set at 1 ml.

The effect of the addition of salt to the samples was also studied. One gram of KCl was added to each vial and HSSPME was performed in the same manner. In contrast to other authors [7], no increase in the response was observed after the addition of salt. The addition of salt to aqueous samples is frequently used to enhance the sensitivity of headspace analysis of polar compounds; for non-polar compounds this effect is expected to be insignificant [17,18]. The analytes studied in this paper have very low polarity and, consequently no significant enhancement in sensitivity should be expected after the addition of salt.

The effect of the headspace volume on extraction efficiency was investigated next. A set of experiments was performed using 1 g of soil and 1 ml of water in different size vials, with a headspace volume of 4, 9, 21 and 39 ml. The results obtained for toluene, ethylbenzene, *p*-xylene and 1,2-dichlorobenzene are shown in Fig. 3. The responses obtained were similar for headspace volumes between 4 and 21 ml. The ability to work with bigger HS volume without decreasing the response of the method has an important practical advantage; if the fibre is situated further from the stirred soil/water mixture there is a lesser tendency for soil particles to stick on the fibre, which results in a cleaner operation. It also removes the constraint of using a particular size container. For a headspace volume of approximately 40 ml the response was lower, between 54 and 82% of the response obtained with the other three headspace volumes.

3.2. Repeatability, reproducibility, detection limit and quantification limit

A series of five consecutive extractions were performed on different aliquots of soil in order to evaluate the repeatability of the HSSPME method. The precision of the HSSPME method was very good and the relative standard deviations (%RSD) were between 1 and 5% for all the compounds.

Table 4
MSD Response obtained for PAHs in urban dust (SRM1649) after HSSPME at 20 and 100°C (The reference concentration values are also given)

	Reference value (μg g^{-1})	Response (area cts)	
		20°C	100°C
Phenanthrene	4.5	2170	1714626
Fluoranthene	7.1	1641	1146076
Pyrene	6.6	nd	62831
Benzo(a)anthracene	2.6	nd	150455
Chrysene	3.6	nd	53840
Benzo(b,k)fluoranthene	8.2	nd	12027
Benzo(a)pyrene	2.9	nd	7623
Benzo(g,h,i)perylene	4.5	nd	801
Indeno(1,2,3-cd)pyrene	3.3	nd	674

nd, not detected.

Another series of five extractions of the same soil were performed in different days to evaluate the reproducibility of the method. The precision was also very good and the %RSD were between 3 and 6% for all the compounds, with the exception of toluene (RSD = 10%).

The detection and quantification limits (signal-to-noise ratio = 3 and 10, respectively) were also determinated and are reported in Table 1. Detection and quantification limits for all the target VOCs were in the sub-ng g^{-1} level.

3.3. Linearity study and validation of the method: conventional HS versus HSSPME

Calibration studies for both techniques, HS and HSSPME, were performed. To accommodate for possible matrix effects and the incomplete transfer of analytes to the HS, a standard addition protocol was performed on the well-aged spiked soil. A five-level calibration study was carried out with the addition of each target analyte between 0 and 2 μg g^{-1}. One gram of soil was spiked with a 100-μl of MeOH containing the analytes. After capping, the vials were tumbled for 0.5 h and allowed to equilibrate at room temperature for 24 h before sampling and analysis. Both techniques gave linear calibration curves for all the target analytes, and the regression coefficients obtained for each compound are shown in Table 2. HSSPME was found to have better linearity than conventional HS, with correlation coefficients in 0.999 or greater for all the compounds. The concentration of analytes found in the soil with HSSPME and conventional HS are shown in Table 3. Statistical tests showed that the two techniques gave equivalent results for all the analytes with the exception of chlorobenzene and toluene. For these compounds HSSPME gave higher results than HS. The precision obtained with HSSPME was also better than conventional HS (Table 3). The sensitivity of both techniques was also compared. The responses obtained with HSSPME method were between two and 11 times higher than those with the HS method (Table 2).

3.4. Application of the method to less volatile compounds

For soil samples, the application of SPME is limited to sampling the headspace over the soil or soil water mixture to avoid the contact between the fibre and the soil. We tried to extend the application of the HSSPME method proposed in this paper to the analysis of semivolatiles. The possibility of analysing semivolatile compounds in solid samples at room temperature is largely limited by the poor release of these compounds into the vapour phase. For these studies three naturally contaminated samples, one with diesel and the other two with PAHs, were tested. Discrimination in the responses obtained was observed in

both cases for the high boiling compounds, due to their low partition into the headspace and to the slow kinetics that these compounds have at room temperature. After 30 min sampling, the system is still far away from equilibrium. In the diesel soil sample, the characteristic diesel hump around C14–C20 was only barely detectable in the chromatogram when compared to that from conventional solvent extraction. In the wood preservative soil and in the urban dust, both contaminated with PAHs, it was only possible to identify PAHs smaller than four rings.

For quantitative analysis of semivolatiles in soils it is necessary to promote the partition of the compounds into the headspace and speed up the mass transfer process. One of the possibilities is to heat the soil-water slurry. In fact, increasing the temperature from 20 to 100°C and sampling for the same time (30 min), all the PAHs in the soil could be identified. In the urban dust, which concentration in PAHs is much more lower than in the wood preservative soil, all the PAHs contained could be detected, but the responses for benzo(g,h,i)perylene and indeno(1,2,3-cd)pyrene were very low. Table 4 shows the MSD responses obtained for this certified reference material after HSSPME at 20 and 100°C. The certified concentration values are also given. Even at 100°C the discrimination in the responses with the size of the PAH is very significant. Further research in the application of HSSPME for the analysis of semivolatiles in soils is being performed.

4. Conclusions

HSSPME at room temperature ($\sim$20°C) has been shown to be a very suitable methodology for the quantitative determination of VOCs in soil samples. The addition of water to the soil is required to release the volatiles into the gas phase. The enhancement in the sensitivity over conventional HS at 95°C is significant. The technique offers good performance in terms of precision (RSD $\sim$ 5%) and linearity, and because of simplicity and low equipment cost, is well suited for the rapid quantification of residual volatiles in landfill or spill samples. For semivolatile compounds in the mid-boiling range, the HSSPME proposed method did not perform well, due to the poor partition of these compounds into the headspace and to the slow kinetics of all the process involved in HSSPME that these compounds have at room temperature. At higher temperature, an adequate screening analysis of a soil sample contaminated with PAHs could be done, but still very low response for the six-ring analytes was obtained. Further studies are being performed to extend the application of HSSPME to the quantitative analysis of semivolatiles.

References

[1] J. Pawliszyn, Solid Phase Microextraction. Theory and Practice, Wiley-VHC, New York, 1997.
[2] C.L. Arthur, J. Pawliszyn, Anal. Chem. 62 (1990) 2145.
[3] C.L. Arthur, L.M. Killan, S. Motlagh, M. Lim, D.W. Potter, J. Pawliszyn, Environ. Sci. Technol. 26 (1992) 979.
[4] A.A. Boyd-Boland, M. Chai, Y.Z. Luo, Z. Zhang, M.J. Yang, J. Pawliszyn, T. Gorecki, Environ. Sci. Technol. 28 (1994) 569A.
[5] Z. Zhang, M.J. Yang, J. Pawliszyn, Anal. Chem. 66 (1994) 844A.
[6] M. Chai, J. Pawliszyn, J. Environ. Sci. Technol. 29 (1995) 693.
[7] Z. Zhang, J. Pawliszyn, J. High Resolut. Chromatog. 16 (1993) 689.
[8] J. Czerwinsky, B. Zygmunt, J. Namiesnik, Fresenius J. Anal. Chem. 356 (1996) 80.
[9] K.D. Buchholz, J. Pawliszyn, J. Anal. Chem. 66 (1994) 160.
[10] A.A. Boyd-Boland, S. Magdic, J. Pawliszyn, Analyst 121 (1996) 929.
[11] H. Lakso, W.F. Ng, Anal. Chem. 69 (1997) 1866.
[12] T.K. Choudhury, K.O. Gerhardt, T.P. Mawhinney, Environ. Sci. Technol. 30 (1996) 3259.
[13] B.L. Wittkamp, S.B. Hawthorne, D.C. Tilotta, Anal. Chem. 69 (1997) 1204.
[14] J. Poerschmann, Z. Zhang, F.-D. Kopinke, J. Pawliszyn, J. Anal. Chem. 69 (1997) 597.
[15] T.C. Voice, B. Kolb, Environ. Sci. Technol. 27 (1993) 709.
[16] Z. Zhang, J. Pawliszyn, Anal. Chem. 67 (1995) 34.
[17] B. Kolb, L.S. Ettre, Static Headspace-Gas Chromatography. Theory and Practice, Wiley-VHC, New York, 1997.
[18] Z.E. Penton, in: P.R. Brown, E. Grushka (Eds.), Advances in Chromatography, vol. 37, Chapter 5, Marcel Dekker, New York, 1997.

ELSEVIER

Talanta 48 (1999) 461–467

Talanta

Evaluation of luminol–H_2O_2–KIO_4 chemiluminescence system and its application to hydrogen peroxide, glucose and ascorbic acid assays

Yanxiu Zhou [a,*], Tsutomu Nagaoka [a], Feng Li [b], Guoyi Zhu [b]

[a] *Department of Applied Chemistry, Faculty of Engineering, Yamaguchi University, 2557 Tokiwadai, Ube, 755-8611, Japan*
[b] *Changchun Institute of Applied Chemistry, Chinese Academy of Sciences, National Analytical Research Center of Electrochemistry and Spectroscopy, Changchun, 130022, PR China*

Received 19 May 1998; received in revised form 3 August 1998; accepted 4 August 1998

Abstract

A novel chemiluminescence (CL) system was evaluated for the determination of hydrogen peroxide, glucose and ascorbic acid based on hydrogen peroxide, which has a catalytic–cooxidative effect on the oxidation of luminol by KIO_4. Hydrogen peroxide can be directly determined by luminol–KIO_4–H_2O_2 CL system. The detection limit was 3.0×10^{-8} mol l^{-1} and the calibration graph was linear over the range of 2.0×10^{-7}–6.0×10^{-4} mol l^{-1}. The relative standard deviation of H_2O_2 was 1.1% for 2.0×10^{-6} mol l^{-1} ($N = 11$). Glucose was indirectly determined through measuring the H_2O_2 generated by the oxidation of glucose in the presence of glucose oxidase at pH 7.6. The present method provides a source for H_2O_2, which, in turn, coupled with the luminol–KIO_4–H_2O_2 CL reaction system. The CL was linearly correlated with glucose concentration of 0.6–110 μg ml^{-1}. The relative standard deviation was 2.1% for 10 μg ml^{-1} ($N = 11$). Detection limit of glucose was 0.08 μg ml^{-1}. Ascorbic acid was also indirectly determined by the suppression of luminol–KIO_4–H_2O_2 CL system. The calibration curve was linear over the range of 1.0×10^{-7}–1.0×10^{-5} mol l^{-1} of ascorbic acid. The relative standard deviation was 1.0% for 8.0×10^{-7} mol l^{-1} ($N = 11$). Detection limit of ascorbic acid was 6.0×10^{-8} mol l^{-1}. These proposed methods have been applied to determine glucose, ascorbic acid in tablets and injection.

Keywords: Chemiluminescence; Hydrogen peroxide; Glucose; Ascorbic acid

1. Introduction

Hydrogen peroxide (H_2O_2) and potassium periodate (KIO_4) were two kinds of oxidants normally used to oxidize luminol (5-amino-2,3-dihydro-1,4-phthalazine dione) in a aqueous alkali solution to give a characteristic blue luminescence. Numerous workers have investigated the use of luminol–H_2O_2 [1–3] for determination of organic and inorganic species. Unfortunately, problems often arise with H_2O_2 due to it is not stable

* Corresponding author. Tel.: +81 836 359928; fax: +81 836 359933; e-mail: yzhou@po.cc.yamaguchi-u.ac.jp

0039-9140/99/$ - see front matter
PII S0039-9140(98)00267-7

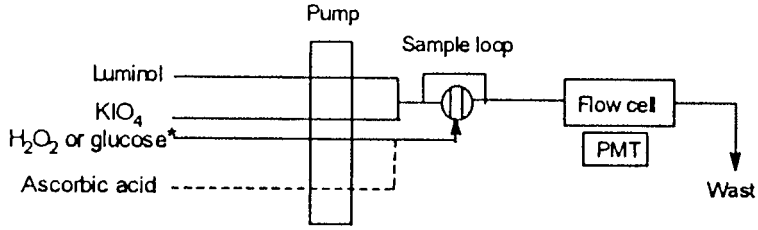

Fig. 1. Schematic diagram of the reaction manifold used for the FIA-CL determination of hydrogen peroxide, glucose and AA. Dot lines (- - -) will work when AA is determined. * When determination of AA, only H_2O_2 passes through this line.

especially for operation in flow injection analysis (FIA) systems. KIO_4 was very stable, a low baseline with a narrow signal peak could be obtained. Furthermore, it did not generate bubbles in the tubes of the FIA system. From these reasons, luminol–KIO_4 chemiluminescence (CL) system has attracted more attention recently and is of analytical interest for the determination of species such as Co(II) [4], Mn(II) [4,5] and Fe(II) [5]. In this work, a novel flow injection methods with CL detection for the sensitive determination of H_2O_2 by using luminol–H_2O_2–KIO_4 system was proposed and also applied to determine glucose and ascorbic acid (AA) in tablets and injection.

2. Experimental

2.1. Reagents

Luminol was purchased from Merck–Schuchardt. Potassium periodate was obtained from Beijing Center Chemicals. The other reagents were all A.R. grades. Reagent solutions were made with doubly distilled water from a quartz apparatus. Stock solutions of luminol were prepared in 0.1 mol l^{-1} KOH solution, then adjusted to 0.01 mol l^{-1} and stored at 4°C. A stock solution of 60 U ml^{-1} glucose oxidase (GOD) and aqueous glucose standards were prepared by diluting a stock solution containing 1 mg ml^{-1} glucose. A 0.1 mol l^{-1} NaOH–Na_2CO_3 solution was used to control the pH for the determination of H_2O_2 and AA. A 0.5 mol l^{-1} Na_2HPO_4-NaH_2PO_4 buffer was used to determinate of glucose. A stock solution containing 1.0×10^{-2} mol l^{-1} AA, 4.0×10^{-3} mol l^{-1} H_2O_2, 2.7×10^{-3} mol l^{-1} KIO_4 and 1.0×10^{-2} mol l^{-1} ethylene diamine tetraacetic acid (EDTA) was used in this experiments.

2.2. Apparatus and procedure

The FIA system for H_2O_2 detection was illustrated in Fig. 1. It employed an eight-channel peristaltic pump and a microprocessor-controlled poly(tetrafluoroethylene) rotary injection valve. All manifold tubing was poly (tetrafluoroethylene) (0.8-mm i.d.) except for the standard peristaltic pump tubing (poly (vinyl chloride)(PVC)). Luminol and KIO_4 working solutions were mixed. Then a 30-μl sample was injected into the mixed solution and driven through the flow cell. A transparent spiral tube with 12-cm length and 1.08 mm i.d. was employed as the CL flow cell in this system. Light intensity was measured with a R212UH photomultiplier. All the experiments were performed at room temperature at a flow rate of 2.1 ml min^{-1} for each pathway.

2.3. Assay procedure for glucose

To a 10-ml volumetric flask were successively added: standard solution of glucose, 2 ml 0.5 mol l^{-1} Na_2HPO_4–NaH_2PO_4 buffer (pH 7.6), 2.5 ml stock solution of GOD, and 1 ml 1×10^{-2} mol l^{-1} EDTA and then diluted to 10 ml, the mixture was allowed to stand at 30°C for 30 min, and was then cooled in ice bath water to stop the enzymatic reaction. The other procedures were the same as above.

Luminescence studies of luminol–H_2O_2–KIO_4 were undertaken with a RF-5000 spectropho-

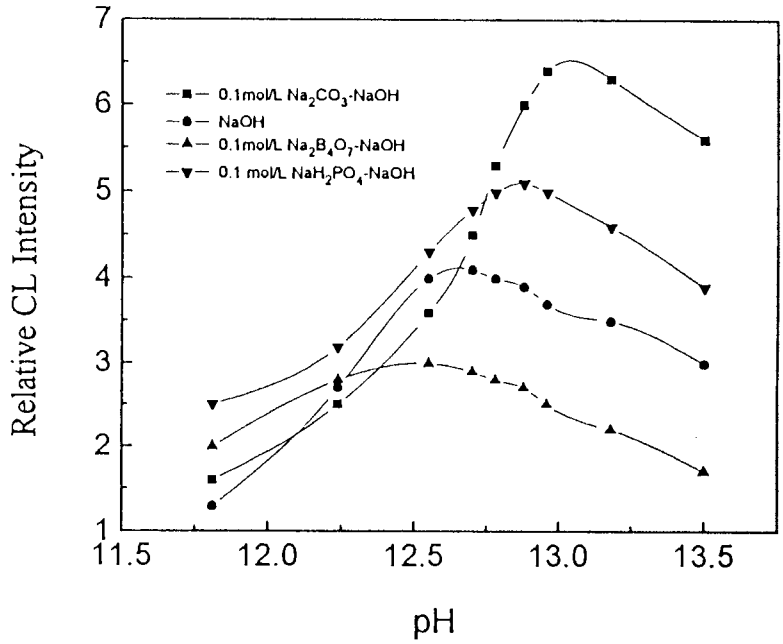

Fig. 2. Effect of pH on the CL intensity from 1×10^{-5} mol l^{-1} H_2O_2 in the presence of 1.5×10^{-4} mol l^{-1} luminol and 2.7×10^{-3} mol l^{-1} KIO_4.

tofluorometer (Shimadzu, Japan). The RF-5000 spectrophotofluorometer was also used to obtain the spectrum of excitation and emission.

3. Results and discussion

3.1. Procedure for evaluation of luminol–H_2O_2–KIO_4 CL system

A series of experiments were carried out to establish the optimum conditions for the system used. The parameters optimized included flow rate, pH and the concentration of luminol, KIO_4 and EDTA.

3.1.1. Flow rate

The influence of flow rate for the luminol–H_2O_2–KIO_4 system was investigated. Although the signal increased with increasing the flow rate, the maximum emission intensity was highly dependent on the rate of mixing of sample and reagents. Since the pump can not adjust the flow rates independently for eight channels and the signal did not vary significantly from 1.75 to 2.8 ml min^{-1}, the 2.1 ml min^{-1} was chosen as the optimum flow rate.

3.1.2. pH

Four kinds of media, 0.1 mol l^{-1} Na_2CO_3–NaOH, NaOH, 0.1 mol l^{-1} $Na_2B_4O_7$–NaOH and 0.1 mol l^{-1} NaH_2PO_4–NaOH were chosen to obtain the optimum condition for determination of H_2O_2. Light emission did not vary significantly for pH ranging from 12.96 to 13.18 when a 0.1 mol l^{-1} Na_2CO_3–NaOH was used (Fig. 2). The optimal pH for CL reaction was at pH 13 and the 0.1 mol l^{-1} NaOH–Na_2CO_3 was used to control the pH. Even though 0.1 mol l^{-1} NaOH could used only to control the pH of the solution around 13, Na_2CO_3 has been found to have an effective promotion for this CL system. Thus 0.1 mol l^{-1} NaOH–Na_2CO_3 was used to control the pH.

3.1.3. Optimization of reagents

The concentrations of luminol, KIO_4 and EDTA were all optimized for the FIA–CL sys-

tem. The concentration of each reagent varied independently.

3.1.4. Luminol concentration

The intensity of light catalyzed by 1×10^{-5} mol l^{-1} H_2O_2 as a function of luminol concentration showed that the reaction was most efficient at 1.0×10^{-4}–2.0×10^{-4} mol l^{-1} luminol (Fig. 3).

3.1.4.1. Potassium periodate concentration. Fig. 4 shows a plot of CL intensity as a function of KIO_4 concentration. At low concentrations, light emission was proportional to KIO_4 concentration. Further increasing concentration would decrease the light emission. So the reaction was most efficient when KIO_4 concentration was between 2.6×10^{-3} and 3.0×10^{-3} mol l^{-1}.

3.1.4.2. EDTA concentration. The luminol–KIO_4 and luminol–H_2O_2 CL reactions were well known. The luminol–KIO_4 CL reaction was not only catalyzed by H_2O_2, but also by some metal ions [5,6]. The addition of EDTA would greatly reduce the luminescence of the reaction because of the rapid complex formation of EDTA with metal ions that catalyze the luminol–KIO_4–H_2O_2 reaction [7]. Therefore, the addition of

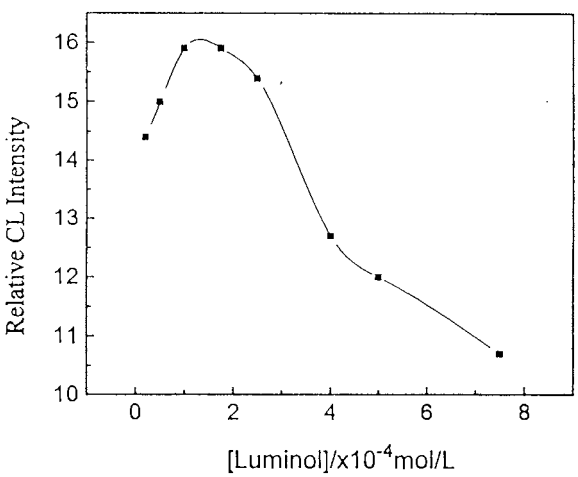

Fig. 3. Effect of luminol concentration on the CL intensity, from 1×10^{-5} mol l^{-1} H_2O_2 in the presence of 2.7×10^{-3} mol l^{-1} KIO_4 in 0.1 mol l^{-1} Na_2CO_3–NaOH buffer solution, pH 13.0.

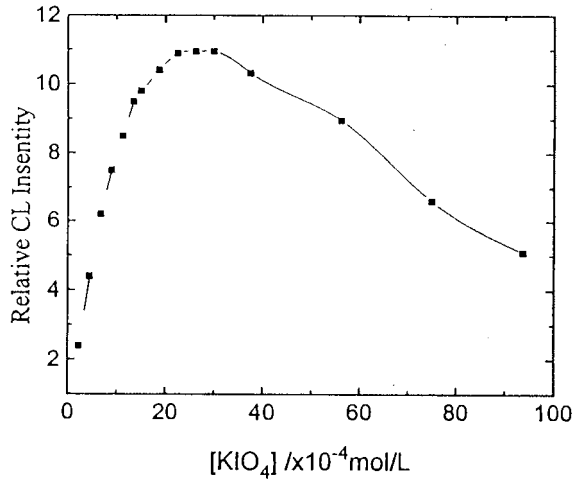

Fig. 4. Effect of KIO_4 concentration on the CL intensity from 1.0×10^{-5} mol l^{-1} H_2O_2 in the presence of 1.5×10^{-4} mol l^{-1} luminol in 0.1 mol l^{-1} Na_2CO_3–NaOH buffer solution, pH 13.0.

EDTA to mask foreign ions would improve the selectivity of the determination of H_2O_2 with the proposed method. No noticeable decrease in light emission was found for a concentration of EDTA lower than 2.0×10^{-3} mol l^{-1}. However, when the EDTA concentration was higher than 2.0×10^{-3} mol l^{-1}, a substantial decrease in light emission was observed. Hence, 1.0×10^{-3} mol l^{-1} EDTA was chosen for masking metal ions.

3.1.5. Interference studies

The interference of foreign ions on the determination of H_2O_2 (2.0×10^{-6} mol l^{-1}) in the luminol–KIO_4–H_2O_2 CL system was also studied. 1000-fold excesses of Na^+, F^-, Cl^-, Br^- and NO_3^- did not interfere in light-producing reaction in catalyzed with 2.0×10^{-6} mol l^{-1} H_2O_2. The H_2O_2 peak can not be affected in the presence of 4.0×10^{-4} mol l^{-1} Mg^{2+}, 2.0×10^{-4} mol l^{-1} Cu^{2+}, Ca^{2+}, 1.6×10^{-4} mol l^{-1} Mn^{2+}, 1.2×10^{-4} mol l^{-1} Ni^{2+}, Zn^{2+}, 1.0×10^{-4} mol l^{-1} Cd^{2+}, 4.0×10^{-5} mol l^{-1} Fe^{2+}, Fe^{3+}, 2.0×10^{-5} mol l^{-1} Pb^{2+}, 8×10^{-5} mol l^{-1} Cr^{3+} and 1.0×10^{-6} mol l^{-1} Co^{2+}. The effectiveness was expressed as the recovery for beyond $100 \pm 5\%$.

3.1.6. CL kinetic property and analytical parameters

With all of the above established conditions, the CL intensity reached the maximum value in only 1 s, and the half peak width was 1.6 s when 1×10^{-5} mol l^{-1} H_2O_2 was injected.

Various concentrations of H_2O_2 were measured under these experimental conditions. The calibration curve was linear in the H_2O_2 concentration of range 2.0×10^{-7}–6.0×10^{-4} mol l^{-1}, and the relative standard deviation was 1.1% for 2.0×10^{-6} mol l^{-1} ($N = 11$, repeatability was measured with standard solutions).

3.1.7. A possible mechanism of H_2O_2–KIO_4–luminol CL system

The luminescence spectra were very similar except for the differences of intensity. The maximum wavelengths were all at 427 nm. Though H_2O_2 had high a catalytic–cooxidative effect on the CL reaction of the luminol–KIO_4, it did not change the mechanism of the luminol–KIO_4 CL reaction as the excitation and emission spectra of luminol–KIO_4, luminol–H_2O_2 and luminol–KIO_4–H_2O_2 CL systems were also very similar.

3.2. Determination of glucose

The determination of hydrogen peroxide (H_2O_2) was very important in biological and clinical application. A brief study was made to see the feasibility of utilizing the glucose–glucose oxidase reaction coupled with the luminol–KIO_4–H_2O_2 CL reaction system as a means of determining glucose. Hydrogen peroxide was produced and then determined by its catalytic–cooxidative effect on the luminol–KIO_4 CL reaction.

3.2.1. Enzyme reaction

The appropriate conditions for the enzymatic reaction were studied as following.

3.2.1.1. Incubation time and the amount of enzyme. The effect of the incubation time and the amount of enzyme on the enzymatic reaction were investigated. A test solution containing 10 μg ml^{-1} glucose was allowed to react with several concentrations of GOD. The results showed that a concentration of 5 U ml^{-1} was the least minimum for the enzymatic reaction and an excess of GOD up to 15 U ml^{-1} did not influence CL intensity. As shown in Fig. 5, the lower amounts of the enzyme, the more incubation time. As for 15 U ml^{-1} GOD, CL intensity did not change during a period of up to 30 min. The results suggested that H_2O_2 be produced quantitatively for at least 30 min for the amount of GOD lower than 5 U ml^{-1}.

3.2.1.2. Incubation temperature. The enzymatic reaction was carried out with incubation at various temperatures, and then the CL intensity was measured. A maximum CL intensity was observed in the range 20–50°C. Therefore, the enzymatic reaction was carried out for 30 min at 30°C.

3.2.2. CL kinetic property and analytical parameters

The calibration graph for glucose standard solution was obtained under the optimum conditions. The calibration curve was linear over the range 0.6–110 μg ml^{-1} of glucose and the relative standard deviation was 2.1% for 10 μg ml^{-1} ($N = 11$). Repeatability was measured with stan-

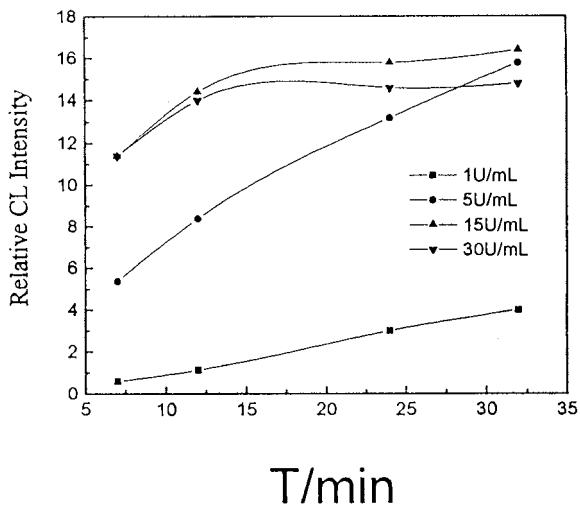

Fig. 5. Relationship between the rate of transformation and the amount of enzyme, [luminol] = 1.5×10^{-4} mol l^{-1}, [KIO_4] = 2.7×10^{-3} mol l^{-1}, [H_2O_2] = 1.0×10^{-5} mol l^{-1}, 0.1 mol l^{-1} Na_2CO_3–NaOH solution, pH 13.0, 15 U ml^{-1} GOD.

Table 1
Determination results of AA in Vitamin C tablets and injection

Sample	Nominal content	Present method	Iodimetry
Vitamin C tablet (mg tablet^{-1})	100	97.9	98.1
	50	48.8	48.7
Vitamin C injection (g ml^{-1})	0.1	0.098	0.099
	0.125	0.124	0.124

dard solutions and detection limit of glucose was 0.08 μg ml^{-1}.

3.3. Determination of AA in vitamin C and injection

The determination of AA in vitamins and natural products was of great importance. Owing to the wide use of AA in canned fruits, vegetables, animal foods and drugs, and because of its significance in human physiology, there are numerous conventional methods for and reviews on the determination of AA [3,8–10]. AA interfered strongly in the luminol–KIO_4–H_2O_2 CL system when determining H_2O_2, then caused a remarkable suppression of this CL system in a quantitative way (see the following reaction). So an assay for ascorbic based on the CL reaction of luminol–KIO_4 with inhibition of H_2O_2 was established to evaluate the luminol–KIO_4–H_2O_2 CL system:

$$AA + H_2O_2 \rightarrow \text{dehydroascorbic acid (DHAA)} + 2H_2O$$

3.3.1. Interference studies

This method has been used to determine the content of AA in tablets and injection, so the interference existing in tablets and injection on the determination of AA was studied. When the concentration of glucose, sucrose, lactic acid and citrate was 1 mmol l^{-1}, fructose, tartaric acid and sodium benzoate was 0.1 mmol l^{-1}, they did not interfere the reaction.

3.3.2. CL kinetic property and analytical parameters

With all of the above established conditions, the CL signal was suppressed about 35% when 4×10^{-6} mol l^{-1} AA was injected, and 68% when the concentration of AA was 8×10^{-6} mol l^{-1}. The concentration of H_2O_2 was 4×10^{-5} mol l^{-1} in this CL system.

The calibration graph for AA standard solution was obtained under the optimum conditions. The calibration curve was linear over the range 1.0×10^{-7}–1.0×10^{-5} mol l^{-1} of AA. The relative standard deviation was 1.0% for 8.0×10^{-7} mol l^{-1} ($N = 11$). Detection limit of AA was 6.0×10^{-8} mol l^{-1}.

3.3.3. Sample analysis

The proposed method was applied only to the determination of AA in pure vitamin tablets and injection. The AA was determined by this FIA–CL system and later by iodimetry [11], as shown in Table 1. The results obtained by the methods were in good agreement with those obtained by iodimetry.

4. Conclusion

The results presented here demonstrated the feasibility of using luminol–KIO_4–H_2O_2 CL system for the rapid, simple, sensitive and universal detection of H_2O_2, glucose and AA with offering good reproducibility by a very small amount of sample. A unique feature of the method was that this CL system gave a low baseline. Clearly, This CL system was excellent for the determination of H_2O_2 and would also applicable to some substrate that yields hydrogen peroxide when undergoing enzyme catalysis or reacting with hydrogen peroxide in a quantitative way and caused a suppression of this CL system.

Acknowledgements

The authors gratefully acknowledge the financial support of this work from Daqing Water Supply, China. Furthermore, Y.Z. would like to express her grateful acknowledge to Japan Society for the Promotion of Science for a postdoctoral fellowship.

References

[1] J.R. Lu, S.H. Jia, J. Chin. Chem. Acta 42 (6) (1984) 562.
[2] R. Escobar, Q.X. Lin, A. Guiraum, F.F. Delarosa, Analyst 118 (1993) 643.
[3] J.M. Kim, Y.L. Huang, R.D. Schmid, Anal. Lett. 23 (12) (1990) 2173.
[4] Q. Lin, A. Guiraum, R. Escobar, Anal. Chim. Acta 283 (1993) 379.
[5] Y.X. Zhou, G.Y. Zhu, Talanta 44 (1977) 2041.
[6] Y.X. Zhou, F. Li, G.Y. Zhu, J. Sun, J. Lei, Chin. J. Anal. Chem. 25 (3) (1977) 334.
[7] R.E. Hamm, J. Am. Chem. Soc. 75 (1953) 5670.
[8] W.P. Yang, B.L. Li, Z.J. Zhang, G.H. Tian, Chin. J. Anal. Chem. 24 (5) (1996) 579.
[9] A.A. Alwarthan, Analyst 118 (1993) 637.
[10] C.Q. Zhu, L. Wang, J.L. Wu, Chin. J. Anal. Lab. 15 (1) (1996) 49.
[11] The Pharmacopoeia Committee of Health Department of People's Republic of China, Pharmacopoeia of People's Republic of China, Chemical Industry Press, People's Health Press, Beijing, 1990, p. 644.

ELSEVIER

Talanta 48 (1999) 469–475

Talanta

Simultaneous determination of naproxen, salicylic acid and acetylsalicylic acid by spectrofluorimetry using partial least-squares (PLS) multivariate calibration[1]

Alberto Navalón, Rosario Blanc, Monsalud del Olmo, José Luis Vilchez *

Department of Analytical Chemistry, University of Granada, E-18071, Granada, Spain

Received 25 February 1998; received in revised form 6 August 1998; accepted 7 August 1998

Abstract

Determination of naproxen, salicylic acid and acetylsalicylic acid has been carried out in mixtures of up to three components by recording emission fluorescence spectra between 300 and 520 nm with an excitation wavelength of 290 nm. The excitation–emission spectra of these compounds are strongly overlapped, which does not permit their direct determination without previous separation by conventional methodologies. Here, a method is proposed for the determination of these chemicals by the use of a full-spectrum multivariate calibration method, partial least-squares (PLS). The experimental calibration matrix was designed with 18 samples. The concentrations were varied between 0.1 and 1.0 μg ml^{-1} for naproxen, 0.5 and 5.0 μg ml^{-1} for salicylic acid and from 2.0 to 12.0 μg ml^{-1} for acetylsalicylic acid. The cross-validation method was used to select the number of factors. To check the accuracy of the proposed method, the optimized model, obtained using PLS-1, was applied to the determination of these compounds in pharmaceuticals and human serum samples previously spiked with different amounts of each chemical.

Keywords: Spectrofluorimetry; Naproxen; Salicylic acid; Acetylsalicylic acid

1. Introduction

Naproxen, [(+)-2-(6-methoxy-α-methyl-2-naphthaleneacetic acid] (NAP) is widely used as an active ingredient in pharmaceutical compounds. This non-steroidal anti-inflammatory drug is mainly used clinically as an alternative to aspirin or in conjunction with salicilates because of its better absorption following oral administration and fewer adverse effects. In plasma or serum, NAP is the predominant species [1].

Several chromatographic [2,3], spectrophotometric [4], mass fragmentographic [5] and spectrofluorimetric [6] methods have been proposed for the determination of unchanged NAP in pharmaceuticals and serum. Spectrofluorimetric methods, based on the intrinsic fluorescence of NAP in 1% acetic acid–chloroform solution, are particularly sensitive.

* Corresponding author. Tel.: +34 58 243326; fax: +34 58 243328; e-mail: jvilchez@goliat.ugr.es

[1] This article is dedicated to the memory of Professor A. Arrebola-Ramírez of the University of Granada, Spain.

0039-9140/99/$ - see front matter
PII S0039-9140(98)00268-9

The simultaneous determination of salicylic acid (SA) and acetylsalicylic acid (ASA) in pharmaceuticals and biological fluids have been extensively studied by using a wide variety of analytical techniques, such as gas–liquid chromatography (GLC) [7], thin-layer chromatography (TLC) [8] and high-performance liquid chromatography (HPLC) [9,10].

For a long time ASA was not thought to be fluorescent and was spectrofluorimetrically measured in aqueous solution by conversion to salicylic acid. However, Miles [11] and Schenk [12] found that ASA shows fluorescence in 1% acetic acid–chloroform solvent. Although the fluorescence maxima of ASA and SA are sufficiently resolved in this solvent mixture, the much higher quantum efficiency of SA and the presence of a large excess of one component (especially SA) in the mixtures inevitably lead to spectral overlaps. To solve this problem, the simultaneous determination of these chemicals has been accomplished by second-derivative synchronous fluorescence spectroscopy [13].

Recently, second-derivative synchronous fluorescence spectroscopy has also been applied to the determination of naproxen and salicylic acid in human serum previous extraction with 1% acetic acid–chloroform [14], because conventional fluorescence spectrometry is not suitable for the determination of serum naproxen in patients simultaneously receiving salicylates.

Taking into account that naproxen, salicylic acid and acetylsalicylic acid present fluorescence in 1% acetic acid–chloroform solvent, a chemometric model based on the application of a partial least-squares (PLS) method is proposed for determining them in ternary, binary and one-component mixtures. The application of multivariate calibration techniques has resulted in improved applicability, precision and accuracy in multicomponent spectral analysis, even in those cases where there is considerable overlap of spectral features [15–17]. The results obtained show that direct fluorometric analysis with a multivariate calibration technique can be an alternative and fast method for the simultaneous determination of these chemicals in different media.

2. Experimental

2.1. Apparatus and software

All spectrofluorimetric measurements were performed using a Perkin–Elmer LS-50 luminescence spectrometer, equipped with a xenon discharge lamp (20 kW), Monk–Gillieson monochromators, a Quantic Rhodamine 101 counter to correct the excitation spectra, a Gated photomultiplier and a Braun Melsungen Thermomix 1441 thermostat.

The LS-50 spectrometer was interfaced with a Mitac MPC 3000F-386 microcomputer supplied with FL Data Manager Software (Perkin–Elmer) for spectral acquisition and subsequent manipulation of spectra.

The GRAMS-386 level I Version 1.0 software package, with PLS plus Version 2.1 G applications software [18] was used for the statistical processing of data and the applications of PLS methods.

2.2. Reagents

Spectroscopic grade chloroform (Merck) was used to prepare a 1% v/v solution of acetic acid (Merck) in chloroform. Henceforth this mixture will be referred as 'mixed solvent'.

Stock standard solutions of NAP (Sigma), SA (Sigma) and ASA (Sigma) containing 10.0, 20.0 and 100.0 mg l^{-1} respectively were prepared by exact weighing of the reagents and dissolution in the mixed solvent. Working standard solutions were obtained by appropriate dilution with the mixed solvent. The stock standard solutions of NAP, SA and ASA were stable for at least 1 month at room temperature.

2.3. Sample treatment

2.3.1. Pharmaceutical formulations

For Aspirina (Bayer) and Naproxin (Roche SA), ten tablets of each pharmaceutical formulation were weighed individually for obtain the average weight. The tablets were powdered and mixed and 1 mg of this mixture was extracted

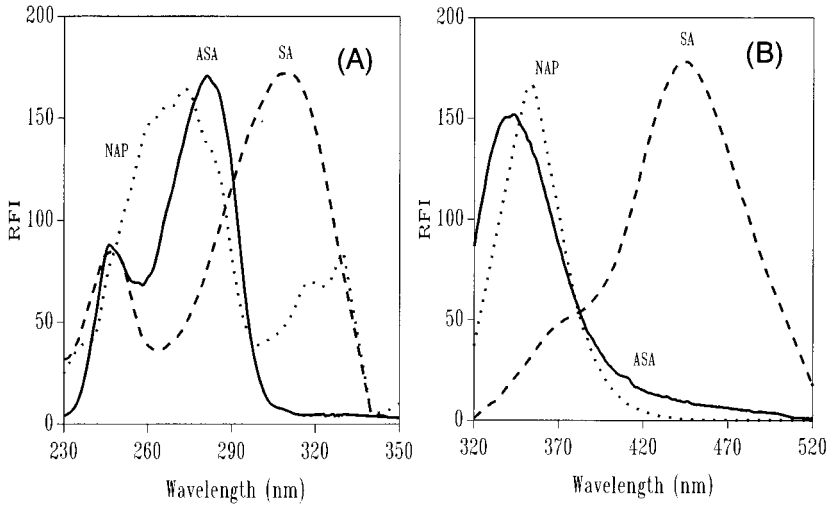

Fig. 1. Excitation (a) and emission (b) spectra of NAP (•••), SA (- - -) and ASA (——) in 1% acetic acid–chloroform solvent.

with 100 ml of the mixed solvent by sonication for 15 min and was filtered through fibre glass. Aliquots of this solution were diluted to 10 ml with the mixed solvent.

Spectral acquisition and calculation were performed in the same manner as in Section 2.4.

Table 1
Concentration data (μg ml^{-1}) for the different mixtures used in the calibration set

Standard	NAP	SA	ASA
1	0.36	2.16	3.24
2	0.30	1.92	6.48
3	0.12	1.44	10.80
4	0.36	1.92	4.32
5	0.18	1.44	9.72
6	0.48	1.68	5.40
7	0.42	1.44	8.10
8	0.30	1.08	10.80
9	0.48	1.44	7.02
10	0.60	1.68	3.78
11	0.72	1.32	4.32
12	0.84	0.84	5.94
13	0.78	0.60	7.02
14	0.90	0.60	5.94
15	0.96	0.60	6.48
16	0.30	—	—
17	—	1.68	—
18	—	—	10.80

2.3.2. Human serum samples

A total of 1.25 ml of human serum containing 10–100 μg ml^{-1} of NAP and 10–100 μg ml^{-1} of SA (these concentrations are typical for NAP and SA levels in serum during the first 12 h from a typical subject following an oral dosage of 650 mg of Aspirin [19] and 500 mg of NAP[1]) were diluted to 50 ml with deionized water and the pH was fixed between 2 and 3 with HCl 0.5 M. One mililitre of this solution was mixed with 4 ml of mixed solvent. The mixture was sonicated for 5 min and centrifuged for 10 min at $1500 \times g$. NAP and SA were determined in the organic layer, as described in Section 2.4.

2.4. Analytical procedure

An aliquot of the sample containing up to 1.0 μg ml^{-1} for NAP, and/or up to 2.5 μg ml^{-1} for SA and/or up to 12.0 μg ml^{-1} for ASA was

Table 2
Statistical parameters obtained for the PLS-1 model

Component	Factors	RMSD	R^2
NAP	5	0.012654	0.998
SA	3	0.024358	0.998
ASA	3	0.091378	0.999

Table 3
Determination of NAP, SA and ASA in synthetic mixtures

NAP			SA			ASA		
Added (μg ml^{-1})	Found (μg ml^{-1})	Rec. (%)	Added (μg ml^{-1})	Found (μg ml^{-1})	Rec. (%)	Added (μg ml^{-1})	Found (μg ml^{-1})	Rec. (%)
0.48	0.48	100.00	2.40	2.36	98.33	2.16	2.00	92.59
0.48	0.46	95.83	0.96	0.96	100.00	8.64	8.87	102.66
0.72	0.71	98.61	0.96	0.96	100.00	6.48	6.48	100.00
0.42	0.41	97.62	2.64	2.42	91.67	4.32	4.02	93.06
0.48	0.46	95.83	2.16	2.07	95.83	2.16	1.97	91.20
0.60	0.58	96.67	1.80	1.72	95.56	3.24	2.95	91.05
0.30	0.28	93.33	1.08	1.03	95.37	11.88	11.30	95.12
0.60	0.57	95.00	0.60	0.59	98.33	5.40	5.36	99.26
0.84	0.81	96.43	0.96	0.91	94.79	7.56	7.11	94.05
—	—	—	1.20	1.20	100.00	2.16	2.37	109.72
—	—	—	2.40	2.23	92.92	6.48	5.97	92.13
0.24	0.26	108.33	—	—	—	9.72	10.49	107.92
0.96	1.06	110.42	—	—	—	5.40	5.57	103.15
0.72	0.74	102.78	0.72	0.72	100.00	—	—	—
0.12	0.11	91.67	1.44	1.47	102.08	—	—	—
0.96	1.06	110.42	—	—	—	—	—	—
—	—	—	0.72	0.75	104.17	—	—	—
—	—	—	—	—	—	2.76	3.03	109.78

diluted to 10 ml with the mixed solvent. The emission spectra were recorded at 20.0 ± 0.5°C between 300 and 520 nm, maintaining the excitation wavelength at 290 nm. Both excitation and emission slit-widths were 4 nm and the scan rate of the emission monochromator was 240 nm min^{-1}. The optimized calibration model for the PLS-1 method was applied to spectra of the samples to calculate the concentration of each chemical in the mixture.

3. Results and discussion

3.1. Selection of the spectral features

Naproxen, salicylic acid and acetylsalicylic acid show native fluorescence in 1% acetic acid–chloroform solution, but the mixture presents a difficult resolution problem because of the spectral overlap of these compounds, which is most apparent with naproxen and acetylsalicylic acid. Fig. 1 shows the excitation (a) and emission (b) spectra of each compound in 1% acetic acid–chloroform solvent. In this solvent mixture, the excitation and emission wavelengths are 273/353 nm for naproxen, 310/444 nm for salicylic acid and 282/341 nm for acetylsalicylic acid, respectively.

Emission spectra of NAP and ASA are closely overlapped, whereas the emission spectrum of SA is clearly defined at higher wavelengths. Therefore it is difficult to find a common emission wavelength to record the excitation spectra of them without losing sensitivity. However, in the excitation spectra of NAP, ASA and SA a common wavelength interval at 275–300 nm appears, in which all three show significant fluorescent signals. For this reason, a 290 nm excitation wavelength was fixed to record the emission fluorescence spectra of the mixture. The spectral region between 300 and 520 nm containing 441 wavelength values (with 0.5 nm intervals) was selected for recording the emission spectra.

Table 4
Determination of NAP and ASA in pharmaceutical formulations

Pharmaceutical formulation	Reference method ± S.D.[a] (g)		Proposed method ± S.D.[a] (g)	
	NAP	ASA	NAP	ASA
Aspirina	—	0.398 ± 0.012	—	0.402 ± 0.019
Naproxin	0.497 ± 0.015	—	0.502 ± 0.011	—

[a] Standard deviation for nine independent determinations.

3.2. Calibration and selection of the number of factors

A training set of 18 standard samples was taken from different ternary and individual mixtures (Table 1). To choose the calibration samples, the concentrations of the constituents to be determined were randomly selected in order to span all dimensions.

The PLS model was developed in the PLS-1 mode. In order to select the number of factors, a cross-validation method, leaving out one sample at a time, was used [20]. Given the set of 18 calibration spectra, the PLS-1 calibration on 17 calibration spectra was performed and, using this calibration, the concentration of the compounds in the sample left out during calibration was predicted. This process was repeated 18 times until each calibration sample had been left out once. The concentration of each sample was then predicted and compared with the known concentration of the reference sample and the prediction error sum of squares (PRESS) was calculated. The PRESS was calculated in the same manner each time a new factor was added to the PLS-1 model.

$$\mathrm{PRESS} = \sum_{i=1}^{m} (\hat{c}_i - c_i)^2$$

In this equation, m is the total number of calibration samples, $\hat{c}_i$ represents the estimated concentration and c_i the reference concentration for the ith sample left out of the calibration during cross-validation.

To select the optimum number of factors, the criterion of Haaland and Thomas [20,21] was used. The maximum number of factors used to determine the optimum PRESS was selected as ten (half the number of standards plus one). The F-statistic was used to make the significance determination.

As the difference between the minimum PRESS and other PRESS values becomes smaller, the probability that each additional factor is significant also decreases. Haaland and Thomas empirically determined that an F-ratio probability of 0.75 is a good choice. We selected as the optimum the number of factors for the first PRESS value whose F-ratio probability drops below 0.75. It was found that the optimum number of factors for the PLS-1 algorithm was five for NAP and three for SA and ASA by applying mean-centered pre-processing algorithms to the spectra.

3.3. Statistical parameters

The values of the root mean square error of cross-validation (RMSECV), which is an estimate of the absolute error of prediction by cross-validation for each component in the calibration matrix and the squared correlation coefficients (R^2), obtained when plots of actual versus predicted concentration were constructed, are summarized in Table 2.

These statistical parameters have been obtained by applying mean-centered pre-processing algorithms to the data set. Mean-centering is traditionally applied in PLS models [15,22] and involves the subtraction of the variable mean from the individual variable values. This process was found to be worthwhile in order to optimize the model. With raw data, the statistical parameters obtained for naproxen and salicylic acid are slightly better; in the case of acetylsalicylic acid, which shows the higher value for RMSD with the

Table 5
Simultaneous determination of NAP and SA in human serum

Sample	Spiked[a] (μg ml^{-1})		Found[b] (μg ml^{-1})		Recovery (%)	
	NAP	SA	NAP	SA	NAP	SA
Serum 1	38.4	90.8	37.9 ± 0.7	94.1 ± 4.1	98.7	103.6
	104.0	108.0	103.3 ± 0.3	107.6 ± 0.1	99.3	99.6
	48.0	104.0	46.5 ± 2.1	99.2 ± 4.5	96.9	95.4
Serum 2	38.4	90.8	37.9 ± 0.7	94.1 ± 4.1	98.7	103.6
	104.0	108.0	103.3 ± 0.3	107.6 ± 0.1	99.3	99.6
	48.0	104.0	46.5 ± 2.1	99.2 ± 4.5	96.9	95.4
Serum 3	38.4	90.8	37.9 ± 0.7	94.1 ± 4.1	98.7	103.6
	104.0	108.0	103.3 ± 0.3	107.6 ± 0.1	99.3	99.6
	48.0	104.0	46.5 ± 2.1	99.2 ± 4.5	96.9	95.4

[a] Refers to original samples.
[b] Mean value ± standard deviation for five determinations.

optimized model, increases markedly its value when raw data are used.

3.4. Synthetic mixtures

The optimized PLS-1 model allows the determination of NAP, SA and ASA in mixtures of up to three components selected in the same concentration ranges used in the calibration set. The synthetic mixtures were made from the stock standard solutions. Table 3 summarizes the composition of artificial mixtures, the predicted concentration values and the recovery obtained. The results obtained are satisfactory for most of the mixtures tested.

3.5. Applications of the method

3.5.1. Pharmaceuticals formulations

The proposed method was applied to commercial NAP and ASA formulations of The Spanish Pharmacopeia, Naproxin and Aspirina. Samples were treated and analyzed as described under Section 2. HPLC was used as reference method for the determination of ASA in Aspirina [23] and naproxene in Naproxin [24]. The results obtained, summarized in Table 4, show good agreement between the obtained values by the reference and PLS methods.

3.5.2. Human serum samples

The proposed method was also applied to determination of NAP and SA in human serum samples previously spiked with these chemicals. Samples were treated and analyzed as described under Section 2. Table 5 shows that satisfactory recovery values were obtained for the samples assayed.

4. Conclusions

The simultaneous fluorometric determination of naproxen, salicylic acid and acetylsalicylic acid mixtures seems feasible using fluorescence emission spectra and spectral data treatment with partial least squares (PLS-1). Only one model is necessary to determine these chemicals in ternary or binary mixtures and to perform individual determination of them in pharmaceutical formulations and human serum previosly extracted with 1% acetic acid–chloroform.

Acknowledgements

This work was supported by the Spanish Interministerial Commission of Science and Technology (CICYT) (Project No. PB96-1404).

References

[1] M.V. Calvo, J.M. Lanao, A. Dominguez-Gil, Int. J. Pharm. 38 (1987) 117.
[2] S.H. Wan, S.B. Martin, J. Chromatogr. 170 (1979) 473.
[3] S. Wanwimolruk, J. Liq. Chromatogr. 13 (1990) 1611.
[4] M.S. Mahrous, M.M. Abdel-khalek, M.E. Abdel-hamid, J. Assoc. Off. Anal. Chem. 68 (1985) 535.
[5] N.E. Larsen, K. Marinelli, J. Chromatogr. 222 (1981) 482.
[6] M. Anttila, J. Pharm. Sci. 66 (1977) 433.
[7] L.J. Walter, D.F. Biggs, R.T. Coutts, J. Pharm. Sci. 63 (1974) 1754.
[8] J.C. Morrison, J.M. Orr, J. Pharm. Sci. 55 (1966) 936.
[9] G.W. Peng, M.A.F. Gadala, V. Smith, A. Peng, W.L. Chiou, J. Pharm. Sci. 67 (1978) 710.
[10] I. Bekersky, H.G. Boxenbaum, M.H. Whiston, C.V. Puglisi, R. Pocelinko, S.A. Kaplan, Anal. Lett. 10 (1977) 539.
[11] C.I. Miles, G.H. Schenk, Anal. Chem. 42 (1970) 656.
[12] G.H. Schenk, F.H. Boyer, C.I. Miles, D.R. Wirz, Anal. Chem. 44 (1972) 1593.
[13] D.G. Konstantianos, P.C. Ioannou, C.E. Efstahiou, Analyst 116 (1991) 373.
[14] D.G. Konstantianos, P.C. Ioannou, Analyst 121 (1996) 909.
[15] M. del Olmo, C. Díez, A. Molina, I. de Orbe, J.L. Vílchez, Anal. Chim. Acta 335 (1996) 23.
[16] A. Espinosa-Mansilla, F. Salinas, M. del Olmo, I. de Orbe, Appl. Spectr. 50 (1996) 449.
[17] A. Muñoz de la Peña, I. Durán-Meras, M.D. Moreno, F. Salinas, M. Martínez-Galera, Fresenius J. Anal. Chem. 351 (1995) 571.
[18] GRAMS-386 Software Package, Version 1.0 and Add-on Application PLS plus Version 2.1 G, Galactic Industries, Salem, NH.
[19] E.N. Amick, W.D. Mason, Anal. Lett. 12 (1979) 629.
[20] D.M. Haaland, E.V. Thomas, Anal. Chem. 60 (1988) 1193.
[21] D.M. Haaland, E.V. Thomas, Anal. Chem. 60 (1988) 1202.
[22] P. McLaurin, P.J. Worsfold, P. Norman, M. Crane, Analyst 118 (1993) 617.
[23] D.P. Venema, P.C.H. Hollman, K.P.L.T.M. Janssen, M.B. Katan, J. Agric. Food Chem. 44 (1996) 1762.
[24] I. Panderi, M. Paissi-Poulou, Analyst 119 (1994) 697.

ELSEVIER

Talanta 48 (1999) 477–484

Talanta

On-line high-performance liquid-chromatographic separation and cold vapor atomic absorption spectrometric determination of methylmercury and inorganic mercury

S. Río-Segade, C. Bendicho *

Departamento de Química Analítica y Alimentaria, Area Química Analítica, Universidad de Vigo, Facultad de Ciencias (Química), As Lagoas-Marcosende s/n, 36200 Vigo, Spain

Received 13 March 1998; received in revised form 4 August 1998; accepted 7 August 1998

Abstract

A reversed-phase high-performance liquid chromatography (HPLC) method with cold vapor atomic absorption spectrometry (CV-AAS) detection is developed for mercury speciation. In this paper, the efficiency of tetrabutylammonium bromide reagent and sodium chloride in a methanol–water mixture as mobile phase is evaluated for HPLC separation of methylmercury and inorganic mercury coupled with on-line CV-AAS determination. Both mercury species are separated on a reversed-phase C_{18} column. Several parameters (e.g. composition and flow-rate of mobile phase) are investigated for the optimization of HPLC separations. CV-AAS technique parameters are also studied for their effect on sensitivity (sodium borohydride and sodium hydroxide concentrations in the reducing agent, reducing agent flow-rate, length of the reduction coil and nitrogen flow-rate). Quantitative recoveries for both inorganic mercury and methylmercury are obtained from a spiked natural water sample.

Keywords: Cold vapor atomic absorption spectrometry; High-performance liquid chromatography; Inorganic mercury; Methylmercury

1. Introduction

The toxicity of metals, their environmental mobility and tendency to be accumulated in living systems are strictly correlated with their chemical forms. Usually, knowledge of the total concentration gives only poor information about the potential risk.

Mercury is found throughout the ecosystem in trace amounts: in soil, air, water and living organisms. During recent years, particular concern has been raised about the presence of mercury species in aquatic food chains, which has long been recognised as a major environmental pollution issue and health hazard for humans. It is well known that inorganic mercury is converted by aquatic organisms into methylmercury, which can be easily bioaccumulated and shows significant biomagnification [1]. Since organomercury com-

* Corresponding author. Tel.: +34 986 812281; fax: +34 986 812382; e-mail: bendicho@uvigo.es

0039-9140/99/$ - see front matter
PII S0039-9140(98)00269-0

pounds such as methylmercury are much more toxic to man than inorganic mercury [2], speciation of the chemical forms is required.

The most reliable approaches today to tackle the problem of element speciation are hybrid analytical techniques resulting from the coupling of a powerful chromatographic separation technique with a specific detector.

The most widely used technique for the speciation of mercury involves gas chromatography (GC) with detection by atomic emission spectrometry (AES) [3,4], atomic absorption spectrometry (AAS) [5,6], atomic fluorescence spectrometry (AFS) [7] or inductively coupled plasma mass spectrometry (ICP-MS) [8]. Recently, mercury compounds (inorganic and organic mercury) have been separated by high-performance liquid chromatography (HPLC) and detected by microwave induced plasma atomic emission spectrometry (MIP-AES) [9], AFS [10] or ICP-MS [11,12]. Although these detection methods have unique analytical capabilities, their high instrumental and running costs make it difficult to use these methods for detection with GC or HPLC.

In general, cold vapor atomic absorption spectrometry (CV-AAS) has the advantages of its high sensitivity, absence of spectral interferences, relatively low operation costs, simplicity, speed and ready acceptance of liquid samples. The combination HPLC-CV-AAS has been reported for the speciation of mercury compounds [13–22].

Palmisano et al. [13] evaluated the efficiency of cysteine complexation to HPLC separation of inorganic mercury and methylmercury accomplished with on-line oxidation of mercury complexes and CV-AAS determination. The detection limits ($S/N = 2$) were 0.5 and 0.8 ng for inorganic mercury and methylmercury, respectively. Sarzanini et al. [14] used these cysteinato complexes for the ion-exchange separation of mercury species and subsequent determination by CV-AAS. Inorganic mercury, methylmercury and ethylmercury detection limits ($S/N = 3$) were 1, 5 and 2 ng, respectively. Sarzanini et al. [15] and Falter et al. [16,17] developed a HPLC-CV-AAS method based on formation of pyrrolidine dithiocarbamate complexes. The detection limits ($S/N = 3$) reported for inorganic mercury, methylmercury, ethylmercury and phenylmercury were 0.8, 10, 5 and 30 ng, respectively, when the Sarzanini method was used. Falter et al. achieved detection limits better than Sarzanini (80 pg for methylmercury, ethylmercury and phenylmercury and 90 pg for inorganic mercury) because they quantitatively destroyed the complexing compounds by ultraviolet (UV) irradiation before CV-AAS determination. In conclusion, the best detection limits, using complexing agents, are achieved when mercury complexes are destroyed by oxidation or UV irradiation.

Other authors used bromide [18] or chloride [19] for HPLC separation of mercury species. The detection limit obtained for dimethylmercury and diethylmercury was 30 ppb (3 ng) [19], $S/N = 3$, when UV irradiation was used. On-line oxidation of inorganic mercury, ethylmercury and methylmercury yielded detection limits ($S/N = 3$) of 9.4, 12.4 and 8.5 ng, respectively [18].

Aizpun et al. developed a HPLC-CV-AAS method for speciation of inorganic mercury and methylmercury using vesicular mobile phase [20]. The detection limits were 1 and 1.6 ng for methylmercury and inorganic mercury, respectively. Some workers [14–16,18,21,22] also carried out preconcentration procedures in order to achieve lower detection limits.

It has been shown [23–25] that quaternary ammonium halide salts are effective extractants for mercury compounds, both inorganic mercury and organomercury forming extractable anionic complexes in the presence of halide ions. The mechanism of extraction was explained by Tajima et al. [26] who first applied the scheme shown in the following equations to analyse Hg(II) halides in the presence of counterions such as tetra-n-butylammonium halides:

$$Hg^{2+} + 4X^- = HgX_4^{2-}$$

$$2R_4N^+ + HgX_4^{2-} = (R_4N)_2HgX_4$$

$$[2R_4NX + HgX_2 = (R_4N)_2HgX_4]$$

or:

$$R'HgX + X^- = R'HgX_2^-$$

$$R_4N^+ + R'HgX_2^- = (R_4N)R'HgX_2$$

$[R_4NX + R'HgX = (R_4N)R'HgX_2]$

Ion-pair HPLC with tetra-n-alkylammonium bromides was shown to be effective for the separation of mercury species [27] using UV and direct current argon plasma (DCP) or ICP-MS [12] as specific element detection. ICP-MS still has high instrumental costs. UV detection was sensitive for inorganic mercury determination. The methylmercury and inorganic mercury UV detection limits, defined as twice S/N ratio, were 8 and 0.8 ng, respectively. Using DCP detection, high detection limits were obtained (175 ng for methylmercury) due to the noise background and low atomization efficiency.

So far, reduction of mercury species present in the form of ion-pairs in a mobile phase has not been reported. In order to improve the detection limit for both mercury species, the effect of the mobile phase composition and flow-rate as well as CV-AAS parameters on CV generation from methylmercury and inorganic mercury as ion-pairs is studied and the HPLC-CV-AAS coupling is characterized.

2. Experimental

2.1. Instrumentation

The chromatographic system consisted of a Waters model 501 HPLC pump with an attached sample injection valve equipped with a 100 μl loop. The analytical reversed-phase column was Novapak C_{18} (150 × 3.9 mm i.d.; 4 μm) coupled with a Novapak C_{18} guard column (20 × 3.9 mm i.d.; 4 μm) obtained from Waters. The interfacing of HPLC to CV-AAS was accomplished by directly connecting tygon tubing (400 × 0.95 mm i.d.).

A Perkin-Elmer atomic absorption spectrometer model 2380 equipped with a quartz cell (160 mm length, 7 mm i.d., with quartz windows) and a flow injection (FI) system were used. A mercury hollow-cathode lamp operated at 6 mA was used as radiation source. The mercury resonance line at 253.7 nm and a slit width of 0.7 nm were used for measurements.

The FI system consisted of a Gilson four-channel peristaltic pump model Minipuls 3, a Perkin-Elmer membrane gas–liquid separator, a four-way injection valve (Reodyne) and a flowmeter (25–180 ml min^{-1} nitrogen; Fisher and Porter). Tygon tubings of different internal diameters were used for carrying the solutions.

2.2. Reagents

All chemicals used were of analytical-reagent grade. An inorganic mercury stock standard solution (1000 mg l^{-1}; Panreac, Barcelona, Spain) was used. A methylmercury stock standard solution (100 mg l^{-1}; Riedel de Haën, Seelze, Germany) was prepared by dissolving the appropriate amount of the solid in methanol (Panreac). This standard contained 2% (m/m) methanol and 1% (m/m) hydrochloric acid (Carlo Erba, Milan, Italy). Working mercury standard solutions of both compounds investigated were freshly prepared daily by appropriately diluting the stock standard solutions with 60% (v/v) methanol. The mobile phase was prepared by dissolving the appropriate amount of tetrabutylammonium bromide (TBABr; Aldrich, Madrid, Spain) and sodium chloride (Panreac) in a mixture of methanol and water. The mobile phase was filtered through membrane filters (0.45 μm; Gelman Sciences) just before use. Sodium borohydride was prepared by dissolving the solid (Merck, Hohenbrunn, Germany) in sodium hydroxide (Panreac). This solution was prepared fresh daily.

2.3. Procedure

A precolumn was placed before the analytical column in order to extend its lifetime. The method was based on the HPLC separation of inorganic mercury and methylmercury using 60% (v/v)–methanol–0.01 M tetrabutylammonium bromide–0.025 M sodium chloride (0.9 ml min^{-1}) followed by CV-AAS detection. The sample solutions were introduced into the injection loop (100 μl) and both mercury compounds were separated. The column effluent was mixed on-line with a stream of 0.01% (m/v) sodium borohydride

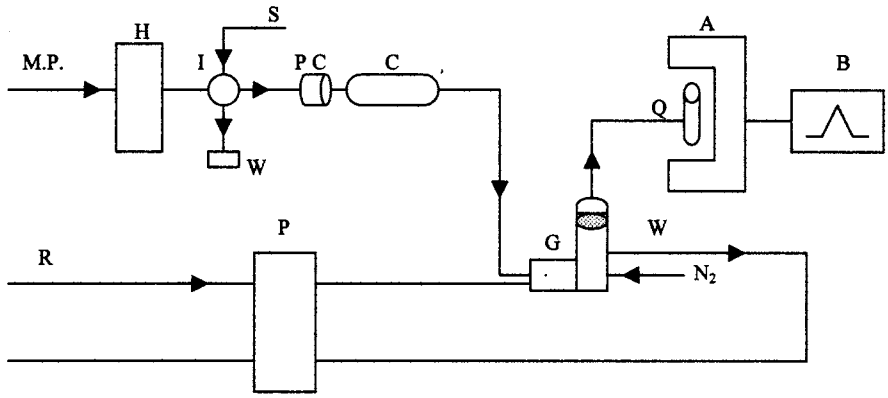

Fig. 1. HPLC-CV-AAS coupling diagram. MP, mobile phase; H, HPLC pump; I, injection valve; S, sample; W, waste; PC, precolumn; C, column; R, reducing agent; P, peristaltic pump; G, gas–liquid separator; Q, quartz cell; A, atomic absorption spectrometer; B, register.

solution (flow-rate 1 ml min^{-1}) and led into the gas–liquid separator by a continuous stream of nitrogen (flow-rate 65 ml min^{-1}). The mercury vapor was then passed into the quartz cell where the atomic absorption of mercury was measured at 253.7 nm. A schematic diagram of the system is shown in Fig. 1.

Parameters affecting chromatographic resolution, such as mobile phase composition and flow-rate, were examined using CV-AAS. After the chromatographic resolution was optimized, parameters influencing CV detection, such as the mixing of the column effluent with a hydrochloric acid solution through a mixing coil, sodium borohydride and sodium hydroxide concentrations, reducing agent flow-rate, length of the reduction coil and nitrogen flow-rate, were studied and optimized.

3. Results and discussion

3.1. Effect of chromatographic parameters on resolution

A number of experimental factors were investigated such as mobile phase composition (methanol, tetrabutylammonium bromide and sodium chloride concentrations) and flow-rate. The chromatographic conditions were optimized in respect to resolution, sensitivity, peak symmetry and separation time. All separations were performed at room temperature under isocratic conditions.

The effect of the methanol concentration was optimized. When the concentration of methanol in 0.01 M tetrabutylammonium bromide and 0.15 M sodium chloride was changed from 40 to 60% (v/v) (1.2 ml min^{-1}), the logarithm of capacity factors (k') decreased linearly (Fig. 2) as was commonly found for reversed-phase systems. This effect was more accentuated for inorganic mercury. However, when the methanol concentration was below 60% (v/v), two peaks were encountered

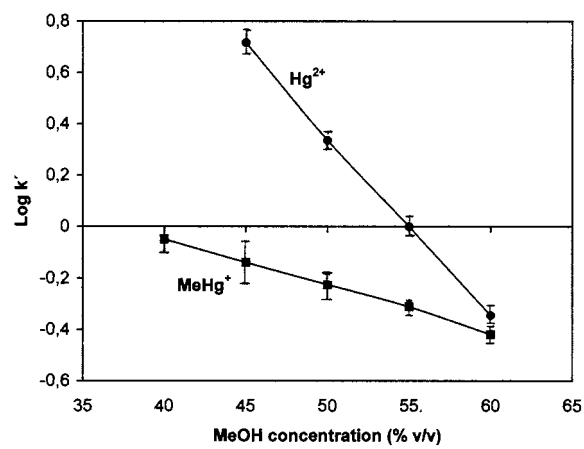

Fig. 2. Effect of the methanol concentration on the capacity factor for Hg^{2+} and $MeHg^{+}$.

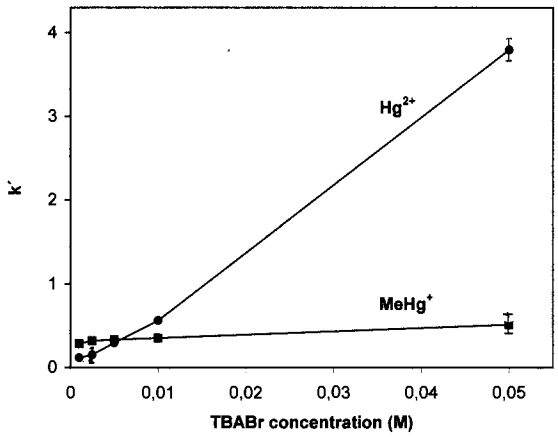

Fig. 3. Effect of the tetrabutylammonium bromide concentration on the capacity factor for Hg^{2+} and $MeHg^{+}$.

for inorganic mercury. Therefore, 60% (v/v) methanol was chosen although the chromatographic separation was worse. Ho and Uden [27] did no report anything about the appearance of two peaks for inorganic mercury.

Different concentrations (0.001–0.05 M) of tetrabutylammonium bromide in the mobile phase were also investigated. The results (Fig. 3) showed significant variations especially for k' corresponding to inorganic mercury. This behaviour can be attributed to the higher stability constant for $HgCl_4^{2-}$, which indicates that it requires a greater amount of ion-pair reagent for completing ion-pair formation. The increase in the retention time of inorganic mercury on addition of higher tetrabutylammonium bromide concentrations means that its retention is greatly dependent on the ion-pair reagent concentration. The concentration selected for further studies was 0.01 M due to the broading of peak shapes found at higher ion-pair reagent concentrations than 0.01 M.

Another parameter studied was the sodium chloride concentration in the eluent. The effect of the sodium chloride concentration on the capacity factors of inorganic mercury and methylmercury can be observed in Fig. 4. Inorganic mercury formed charged complexes with the chloride ion, $HgCl_4^{2-}$. An increase of sodium chloride concentration should promote the $HgCl_4^{2-}$ formation. The capacity factor of inorganic mercury decreased by the greater solubility of $HgCl_4^{2-}$ in the mobile phase. The formation of singly charged chloride complexes of methylmercury caused little change on its capacity factor as the sodium chloride concentration was increased. When the concentration of sodium chloride was changed from 0 to 0.1 M, the retention times of inorganic mercury decreased sharply and more symmetrical and sharper peak shapes for both species were achieved; 0.025 M sodium chloride was found optimal for HPLC. When using shorter analytical columns than Ho and Uden [27] as those used in this work, lower sodium chloride concentrations were needed in order to achieve good separations.

The mobile phase flow-rate should be fast enough to avoid broading and non-reproducible peak shapes, but not too fast to separate both inorganic mercury and methylmercury with sufficient resolution (1.76). The optimum flow-rate was 0.9 ml min^{-1} (Fig. 5).

The sensitivity for both mercury species was dependent on the mobile phase composition. When methanol or sodium chloride concentrations were increased the absorbance signal of both species increased. Tetrabutylammonium bromide concentrations higher than 0.005 M caused the absorbance to decrease. A decrease in the mobile phase flow-rate had also negative effect on sensitivity. As consequence, the mercury sensitivity is limited by both composition and flow-rate of mobile phase required for HPLC separation. The

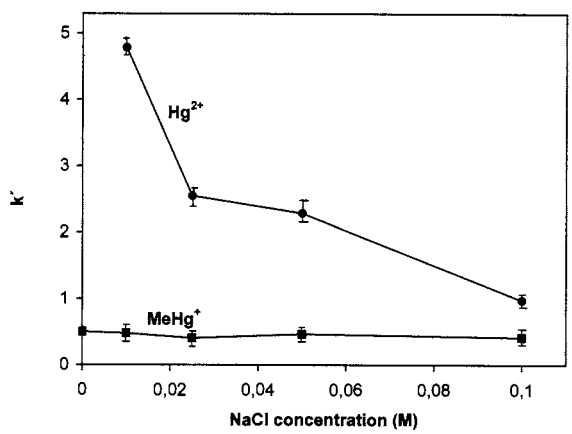

Fig. 4. Effect of the sodium chloride concentration on the capacity factor for Hg^{2+} and $MeHg^{+}$.

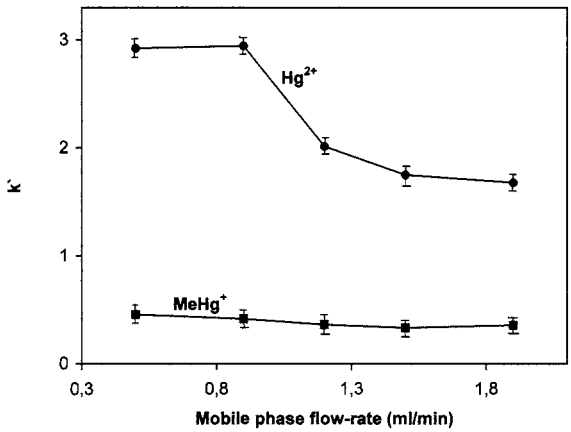

Fig. 5. Effect of the mobile phase flow-rate on the capacity factor for Hg^{2+} and $MeHg^{+}$.

dead time of the chromatographic system was 1.8 min.

3.2. Effect of cold vapor technique parameters on sensitivity

In order to perform CV-AAS determinations, several variables were optimized to obtain maximum sensitivity for inorganic mercury and methylmercury. The effect of the mixing of the column eluent with a hydrochloric acid solution through a mixing coil before reduction was examined. Inorganic mercury and methylmercury standard solutions (60 μg l^{-1}) were injected (500 μl) in a 60% (v/v) methanol–0.01 M tetrabutylammonium bromide–0.025 M sodium chloride stream (0.9 ml min^{-1}) without separation column, and then they were mixed with a reducing agent. The absorbance of both species decreased slightly with increasing 0.25% (m/m) hydrochloric acid flow-rate from 0 to 2.4 ml min^{-1} and with increasing the mixing coil length due to a possible dispersion effect. When the concentration of hydrochloric acid at 1 ml min^{-1} was changed from 0 to 3% (m/m), a maximum absorbance signal was observed in the concentration range of 0–0.50% (m/m) and 0.25–0.50% (m/m) for inorganic mercury and methylmercury, respectively. Therefore, the hydrochloric acid concentration (0.25%, m/m) used in the previous studies was in the optimum range. From these studies we can conclude that the premixing of the column eluent with a hydrochloric acid solution before reduction step should be eliminated because a decrease in the absorbance was produced.

The sodium borohydride concentration in the reducing agent is critical in the determination of mercury by CV generation. The maximum absorbance signals of inorganic mercury were related with low concentrations of sodium borohydride (0.01–0.10%, m/v) and a virtually constant response was observed for methylmercury in the concentration range from 0.01 to 0.75% (m/v). In order to avoid any possible matrix interference, the sodium borohydride concentration used was as low as possible. A 0.01% (m/v) sodium borohydride concentration was chosen as optimum.

The effect of the concentration of sodium hydroxide in the reducing agent was also optimized. When the concentration of sodium hydroxide in 0.01% (m/v) sodium borohydride solution was changed from 0.03 to 5% (m/v), the inorganic mercury absorbance increased in the range of the sodium hydroxide concentration 0.03–1% (m/v). A steady-state absorbance signal was observed at concentrations higher than 1% (m/v). When methylmercury was injected, a virtually constant absorbance was observed in the concentration range from 0.03 to 5% (m/v). A concentration of 1% (m/v) was used.

It was observed that for both species the absorbance increased with increasing reductor flow-rate from 0.2 to 1.1 ml min^{-1}. The optimum range was 1.1–1.4 ml min^{-1} and 1.1–2 ml min^{-1} for inorganic mercury and methylmercury, respectively.

Maximum absorbance was obtained for both mercury species when the reduction reaction was carried out directly in the chemifold and the nitrogen flow-rate was 65 ml min^{-1}. A summary of the optimum operating conditions is given in Table 1.

3.3. Analytical figures of merit

A typical chromatogram for a solution containing inorganic mercury and methylmercury is

Table 1
Optimized chromatographic and CV-AAS parameters

HPLC parameters	
Pump	Isocratic
Column	Novapak C_{18} (150 × 3.9 mm i.d.; 4 μm)
Mobile phase composition	60% (v/v) MeOH–0.01 M TBABr–0.025 M NaCl
Mobile phase flow-rate	0.9 ml min^{-1}
Sample loop	100 μl
CV-AAS parameters	
Reducing agent	0.01% (w/v) $NaBH_4$ in 1% (w/v) NaOH
Reducing agent flow-rate	1 ml min^{-1}
Nitrogen flow-rate	65 ml min^{-1}

shown in Fig. 6. As can be seen, both species were fully resolved and the separation was complete in less than 12 min.

Calibration was performed with a series of inorganic mercury and methylmercury standards. The sensitivity (m) was the slope value obtained by least squares regression analysis of the calibration curves for peak height measurements. It was expressed as the average value of three determinations ± standard deviation. The sensitivities were 0.340 ± 0.010 and 0.331 ± 0.004 l mg^{-1} for inorganic mercury and methylmercury, respectively.

The detection limit was defined as three times the standard deviation from ten replicate determinations of a blank divided by sensitivity (3σ m^{-1}). The detection limits for inorganic mercury and methylmercury were 1.13 and 1.32 ng, respectively. The detection limits were similar to other HPLC-CV-AAS methods without preconcentration. HPLC-CV-AAS yielded better detection limits than HPLC-UV and HPLC-DCP-AES [27] for methylmercury using similar chromatographic parameters. On the other hand, detection limits for both mercury species were very close when using CV-AAS unlike methods that use same HPLC separation mode but different detector.

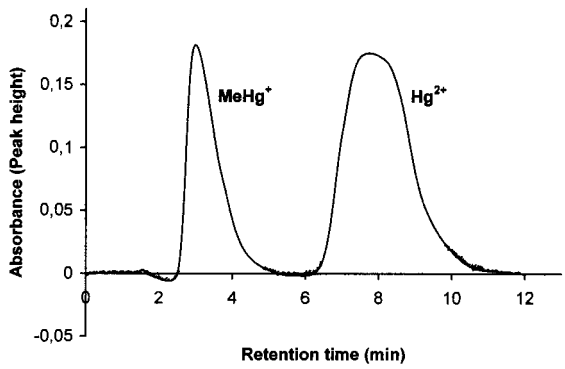

Fig. 6. Chromatogram showing separation of $MeHg^+$ (50 ng) and Hg^{2+} (50 ng) under optimized conditions.

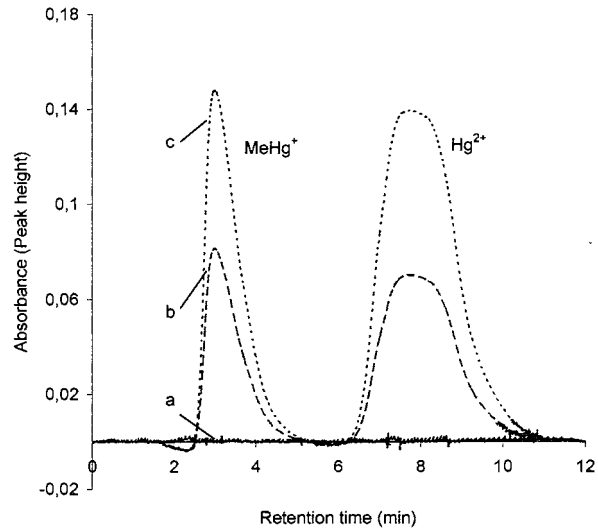

Fig. 7. Chromatograms of (a) an unspiked natural water sample, (b) a natural water sample spiked with $MeHg^+$ and Hg^{2+} (20 ng each) and (c) a natural water sample spiked with $MgHg^+$ and Hg^{2+} (40 ng each).

The precision of the method was determined by ten successive injections of inorganic mercury (50 ng) and methylmercury (50 ng). The relative standard deviations (R.S.D.) of the absorbance measurements (peak height) were 5.55 and 4.28% for inorganic mercury and methylmercury, respectively.

3.4. Determination of inorganic mercury and methylmercury in a spiked natural water

The proposed method was applied to the determination of inorganic mercury and methylmercury in river water (Miño river, Spain) (Fig. 7). The sample solution was filtered through a mem-

brane filter (0.45 μm) just before use. The results obtained for both species were below the detection limits. In order to evaluate the proposed method, the sample was spiked with concentrations between 20 and 80 ng of each mercury compound analysed. Recoveries of inorganic mercury and methylmercury were in the range of 93.97–100% and 97.88–103.6%, respectively. A study of interferences was not performed because the typical ions present in river water samples did not cause interferences in the methylmercury and inorganic mercury determination.

4. Conclusions

A good separation of inorganic mercury and methylmercury was achieved using 60% (v/v) methanol–0.01 M tetrabutylammonium bromide–0.025 M sodium chloride as mobile phase. Parameters affecting CV-AAS sensitivity were optimized for inorganic mercury and methylmercury using mobile phase as carrier solution (sodium borohydride and sodium hydroxide concentrations in the reducing agent, reducing agent flow-rate, length of the reduction coil and nitrogen flow-rate). CV generation was efficient for both inorganic mercury and methylmercury in the mobile phase. Ion-pair HPLC coupled to CV-AAS yielded similar detection limit for inorganic mercury in comparison with UV detection. Detection limit for methylmercury was improved eighth times in comparison with UV detection. Similar detection limits were obtained for both mercury species (1.13 and 1.32 ng for inorganic mercury and methylmercury, respectively). Precision expressed as R.S.D. was 5.5 and 4.3% for inorganic and methyl mercury, respectively. Recoveries for both mercury species from a spiked natural water sample were quantitative.

Acknowledgements

This work was financially supported by the Spanish Education and Culture Ministry (DGES) and by the Galicia Goverment (Xunta de Galicia) in the framework of the projects PB95-0727 and XUGA 38301B96, respectively. A predoctoral grant financially supported by the Xunta de Galicia is also gratefully acknowledged.

References

[1] T. Suzuki, N. Imura, T. Clarkson, Advances in Mercury Toxicology. Plenum Press, New York, 1991.
[2] M. Hempel, Y.K. Chau, B.J. Dutka, R. McInnis, K.K. Kwan, D. Liu, Analyst 120 (1995) 721.
[3] J.P. Snell, W. Frech, Y. Thomassen, Analyst 121 (1996) 1055.
[4] M.S. Jimenez, R.E. Sturgeon, J. Anal. Atom. Spectrom. 12 (1997) 597.
[5] H. Emteborg, H.W. Sinemus, B. Radziuk, D.C. Baxter, W. Frech, Spectrochim. Acta 51B (1996) 829.
[6] C.M. Tseng, A. de Diego, F.M. Martin, D. Amouroux, O.F.X. Donard, J. Anal. Atom. Spectrom. 12 (1997) 743.
[7] D.W. Bryce, A. Izquierdo, M.D. Luque de Castro, Anal. Chem. 69 (1997) 844.
[8] H. Hintelmann, R.D. Evans, Fresenius J. Anal. Chem. 358 (1997) 378.
[9] J.M. Costa, F. Lunzer, R. Pereiro, A. Sanz-Medel, N. Bordel, J. Anal. Atom. Spectrom. 10 (1995) 1019.
[10] R. Falter, G. Ilgen, Fresenius J. Anal. Chem. 358 (1997) 407.
[11] C.C. Wan, C.S. Chen, S.J. Jiang, J. Anal. Atom. Spectrom. 12 (1997) 683.
[12] C.F. Harrington, T. Catterick, J. Anal. Atom. Spectrom. 12 (1997) 1053.
[13] F. Palmisano, P.G. Zambonin, N. Cardellicchio, Fresenius J. Anal. Chem. 346 (1993) 648.
[14] C. Sarzanini, G. Sacchero, M. Aceto, O. Abollino, E. Mentasti, Anal. Chim. Acta 284 (1994) 661.
[15] C. Sarzanini, G. Sacchero, M. Aceto, O. Abollino, E. Mentasti, J. Chromatogr. 626 (1992) 151.
[16] R. Falter, H.F. Scholer, Fresenius J. Anal. Chem. 353 (1995) 34.
[17] R. Falter, H.F. Scholer, J. Chromatogr. A 675 (1994) 253.
[18] J.C.G. Wu, Spectrosc. Lett. 24 (1991) 681.
[19] R. Falter, H.F. Scholer, Fresenius J. Anal. Chem. 348 (1994) 253.
[20] B. Aizpun, M.L. Fernandez, E. Blanco, A. Sanz-Medel, J. Anal. Atom. Spectrom. 9 (1994) 1279.
[21] R. Eiden, R. Falter, B. Agustin-Castro, H.F. Scholer, Fresenius J. Anal. Chem. 357 (1997) 439.
[22] E. Munaf, H. Haraguchi, D. Ishii, Anal. Chim. Acta 235 (1990) 399.
[23] F.L. Moore, Environ. Sci. Technol. 6 (1972) 525.
[24] Y. Talmi, V.E. Norvell, Anal. Chim. Acta 85 (1976) 203.
[25] F.L. Moore, Environ. Lett. 10 (1975) 77.
[26] K. Tajima, M. Nakamura, S. Takagi, F. Kai, Y. Osajima, J. Liquid Chromatogr. 9 (1986) 1021.
[27] Y.S. Ho, P.C. Uden, J. Chromatogr. A 688 (1994) 107.

ELSEVIER

Talanta 48 (1999) 485–490

Talanta

Experimental study of kinematic focusing. Comparison of electroinjection and sequential injection determination of copper

Victor P. Andreev [a,*], Natalia B. Ilyina [a], David A. Holman [b], Louis D. Scampavia [b], Gary D. Christian [b]

[a] *Institute for Analytical Instrumentation, Russian Academy of Sciences, 26 pr. Rigsky, St. Petersburg, 198103, Russian Federation*
[b] *Department of Chemistry, Box 351700, University of Washington, Seattle, WA 98195-1700, USA*

Received 1 April 1998; received in revised form 3 August 1998; accepted 7 August 1998

Abstract

The recently predicted phenomenon of kinematic focusing was studied experimentally using copper ions and EDTA as reactants. Kinematic focusing occurs, in electroinjection analysis, when the detected reaction product moves at the same rate as the reagent present in excess. Thus, reaction product accumulates without dispersion at the front of the excess reagent. Cu-EDTA^{2-} complex was observed at 254 nm to form an exceptionally sharp peak as the front of the EDTA zone passed by the detector. The concentrating effect of kinematic focusing was quantified by electroinjection of premixed Cu-EDTA^{2-}. Sensitivity was compared to that of sequential injection analysis using a 1 cm optical pathlength. Sensitivity was highest in the electroinjection mode, in spite of its 120 μm capillary pathlength, due to kinematic focusing.

Keywords: Electroinjection; Sequential injection; Kinematic focusing

1. Introduction

In 1993, capillary zone electrophoresis (CZE) was used in a novel way to perform reagent chemistry [1,2]. Sample and reagent have opposite directions of electrokinetic movement for many reagent chemistries. In this case, sample and reagent zones merge and react when injected electrophoretically from opposite ends of a capillary. The product peak is then detected photometrically near the middle of the capillary. Use of CZE in this way to perform reagent chemistry was termed electroinjection analysis (EIA), by analogy to its predecessor, flow injection analysis. EIA takes advantage of the fact that analyte and reagent are often oppositely charged. But it is even possible by this method to mix reactants with the same charge when their electrophoretic mobilities are different. The only limitation is that the reactant that is injected in the opposite direction of the electroosmotic flow must have electrophoretic mobility of the opposite sign and it must be

* Corresponding author. Tel.: +7 7812 2517038.

0039-9140/99/$ - see front matter
PII S0039-9140(98)00270-7

higher than the electroosmotic mobility of the buffer [3].

Mixing without mechanical dispersion is the key to EIA sensitivity. EIA is unusual in that it does not resort to flow dispersion or turbulence to mix reactants. Instead, reactant molecules encounter each other because they are pulled through solution rather than being carried by solution. One cannot say that reactant solutions are mixed, and dilution factors due to convective mixing do not apply. Instead, the total volume of solution which contains the reaction product is determined by the difference between velocity of product and velocity of excess reagent. As an example of enhanced sensitivity, the detection limit of chromium(VI) in water was 2 ppb [3]. Sensitivity of EIA is highest when the said velocity difference happens to be at or near zero. This is the phenomenon of kinematic focusing that was found for copper and EDTA as reactants [4].

The objective of the present paper is the further experimental study of kinematic focusing using the copper as analyte and EDTA as excess reagent. The concentrating effect of kinematic focusing was quantified by comparing EIA peak height to those of premixed reactants injected in the same system. EIA with kinematic focusing was also compared to sequential injection analysis (SIA), which is based on laminar flow convective mixing [5]. Detection limits of EIA, SIA, and electroinjection of premixed product are compared here.

2. Theory

The mathematical model of EIA was developed [3], for the case where the initial concentration of reagent, c_{R0}, was much higher than the initial concentration of sample, c_{10}, and the characteristic time of chemical reaction, $t_c = k_0^{-1} = (k + C_{R0})^{-1}$ was much smaller than the characteristic diffusion time, $t_D = \min\{l_S^2/D_S, l_R^2/D_R\}$, where k_+ is the direct reaction rate; l_S, and l_R are the initial lengths of sample and reagent zones; and D_S, and D_R are the diffusion coefficients of sample and reagent molecules. The reverse reaction rate does not appear because it was considered to be zero. With these assumptions, the set of diffusion–migration–reaction equations describing sample, reagent, and product zone evolution was solved analytically. The maximum values of product concentration, c_{2max}, were determined by the following simple and exact formulae:

$$c_{2max} = c_{10}\left|\frac{v_1 - v_R}{v_R - v_2}\right|\left[1 - \exp\left(-k_0\frac{l_S}{v_1 - v_R}\right)\right]$$

$$\text{if} \quad v_2 \neq v_R \quad \text{and} \quad \frac{l_S}{l_R} < \left|\frac{v_1 - v_R}{v_R - v_2}\right| \tag{1}$$

$$c_{2max} = c_{10}\left|\frac{v_1 - v_R}{v_R - v_2}\right| \times \left[1 - \exp\left(-k_0\frac{l_S|v_R - v_2|}{|v_1 - v_R|(v_1 - v_R)}\right)\right]$$

$$\text{if} \quad v_2 \neq v_R \quad \text{and} \quad \frac{l_S}{l_R} < \left|\frac{v_1 - v_R}{v_R - v_2}\right| \tag{2}$$

$$c_{2max} = C_{10}k_0\frac{l_S}{v_1 - v_2} \qquad \text{if} \quad v_2 = v_R \tag{3}$$

where $v_1 = (\mu_{ep1} + \mu_{osm})E$, $v_R = (\mu_{epR} + \mu_{osm})E$, $v_2 = (\mu_{ep2} + \mu_{osm})E$ are the velocities of sample, reagent and product zones; μ_{ep1}, μ_{epR}, μ_{ep2} are the corresponding electrophoretical mobilities; μ_{osm} is the electroosmotic mobility of the buffer; E is the electric field strength.

For fast chemical reactions, reaction is much faster than the interaction of sample and reagent zones. So the exponents in Eqs. (1) and (2) are practically equal to zero, and the product peak maximum is determined by the kinematic focusing factor:

$$f_2 = \left|\frac{v_1 - v_R}{v_R - v_2}\right| = \left|\frac{\mu_{ep1} - \mu_{epR}}{\mu_{epR} - \mu_{ep2}}\right| \tag{4}$$

If product and reagent electrophoretic mobilities are close then the denominator in Eq. (4) is small, and the product peak will be sharp. For the case of equal μ_{epR} and μ_{ep2}, the product peak will be higher for longer zone interaction times $t_{int} = l_S/(v_1 - v_R)$ when compared to the characteristic chemical reaction time $t_c = k_0^{-1}$. As seen, Eq. (3) is the limiting case for Eq. (2).

Reaction product will be sharply concentrated at the reagent front when conditions are satisfied for kinematic focusing. Two critical conditions

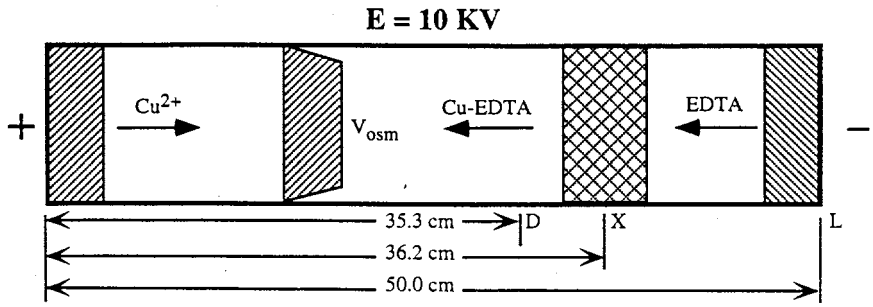

Fig. 1. Schematic representation of EIA determination of copper. E is the electric field strength, L is the length of the capillary, D is the position of the detector, x is the point at which sample and reagent meet, v_{osm} is the electroosmotic mobility of the buffer.

are (i) reaction is fast compared to the zone interaction time, and (ii) the product and excess reagent migration rates are identical or nearly so. Generally, reagent concentration is in excess, so unreacted analyte cannot penetrate beyond the immediate front of the reagent zone if reaction is fast. If this condition is satisfied, then kinematic focusing occurs at the front of the reagent zone when the reagent velocity is virtually the same as that of the product. In that case, reagent molecules at the front of the zone continue to migrate at the same velocity even after being converted to product; and product accumulates like a moving sheet without dispersion.

Experimentally, Cu(II) and Cu-EDTA complex absorb at 254 nm, so their velocities in the capillary were determined separately from the EIA experiment. Reagent (EDTA) does not absorb at this wavelength, so its velocity was calculated from the elapsed time at which the Cu-EDTA complex was detected, t_a. This situation is illustrated in Fig. 1 and is described by:

$$\frac{x}{v_{Cu}}+\frac{(x-D)}{v_{Cu\text{-}EDTA}}=t_a \qquad \frac{x}{v_{Cu}}=\frac{(L-x)}{v_{EDTA}} \tag{5}$$

where x is the unknown meeting point of sample and reagent; D is the position of the detector; v_{Cu}, v_{EDTA} are the known velocities of sample and complex, and v_{EDTA} is the unknown velocity of the reagent. These equations can be easily solved to obtain the values of x and v_{EDTA}:

$$x=\frac{(t_a v_{Cu} v_{Cu\text{-}EDTA}+D v_{Cu})}{(v_{Cu}+v_{Cu\text{-}EDTA})} \tag{6}$$

$$v_{EDTA}=\frac{v_{Cu}(L-x)}{x} \tag{7}$$

3. Experimental

3.1. Equipment

3.1.1. EIA and CZE apparatus

We constructed a capillary electrophoresis system, described previously [2], to perform EIA. It was capable of injecting sample and reagent simultaneously and electrokinetically from the opposite ends of the capillary. Absorbance was measured at $\lambda = 254$ nm through fused silica capillaries (120 μm i.d., 380 μm o.d.) with a total length of 50 cm. The detector was placed 35.3 cm from the anode end of the capillary. At the beginning of each day, capillaries were conditioned with 0.1 M NaOH for 5 min, then rinsed with water and running buffer for no less than 5 min.

3.1.2. SIA apparatus

The SIA instrument was a FIAlab 3000 model (Alitea Instruments USA) including a stepper motor syringe pump and six-port rotary selection valve. Absorbance was measured in a flow through cell having 1 cm pathlength in a Hewlett Packard 8452A Diode Array Spectrophotometer.

3.1.3. Chemicals

All chemicals used were of analytical reagent grade.

The capillary in EIA experiments was filled with the acetate buffer (pH 4.8, 10 mM). The

buffer was prepared as follows: 5 ml of 0.1 M NaOH was neutralized with acetic acid to pH 4.8 and diluted to a final volume of 50 ml. The same buffer was used as carrier in SIA experiments.

A standard solution of EDTA was prepared as follows: 16.8 g of EDTA sodium salt was dissolved in 0.5 l of distilled water to obtain a 0.1 M solution. This was diluted 100-fold with the running buffer before use.

Stock solution of Cu(II): 0.25 g of $CuSO_4.5H_2O$ was dissolved in 100 ml of distilled water (approximately 0.01 M solution) and the concentration of Cu(II) was checked complexometrically. This stock solution was diluted with running buffer before use.

3.2. Procedure

3.2.1. EIA procedure

The capillary was filled with acetate buffer (10 mM, pH 4.8). Sample and reagent were injected simultaneously and electrokinetically from the anode and cathode ends of the capillary, respectively. Copper moved electrophoretically in the same direction as the electroosmotic flow for an injection time of 10 s. The injection voltage and working voltage were the same and equal to 10 kV. The total analysis time was 2.5 min.

For the working conditions, pH 4.8 and $E = 20$ kV m^{-1}, the velocities of Cu(II) and Cu-EDTA species were measured in separate CZE experiments.

3.2.2. CZE procedure

Sample and reagent from the EIA experiments (at double the concentrations) were premixed and then injected electrokinetically from the cathode end of the capillary filled with the acetate buffer (10 mM, pH 4.8). The injection time was 10 s, and injection and working voltages were 10 kV. The time from injection until detection of the product peak was 3.5 min.

3.2.3. SIA procedure

Sample volume, reagent volume, and flow rate parameters were optimized for SIA determinations. The best results were obtained with the following experimental parameters: 0.1 ml sample volume, 0.04 ml reagent volume, 2 ml min^{-1} sample and reagent aspiration rate, 0.3 ml min^{-1} injection flow rate.

4. Results and discussion

Fig. 2(A)–(C) present the typical peak shapes for EIA determination of Cu(II) by reaction with EDTA for three values of Cu(II) concentration: 1×10^{-5}, 3×10^{-5} and 5×10^{-5} M. As shown, the peaks for the lowest concentration of Cu(II) were reproducible and significantly higher than the noise level.

Fig. 3(A) presents EIA results for 0.1 mM Cu(II) using 1 mM EDTA. For comparison, Fig. 3(B) presents CZE of Cu-EDTA complex premixed using the same concentrations of Cu(II) and EDTA as in Fig. 3(A). The EIA peak height was about three times higher than in the CZE case. All the experimental conditions were the same except for the means of mixing. So the 3-fold gain in product concentration at the detection point was likely due to kinematic focusing.

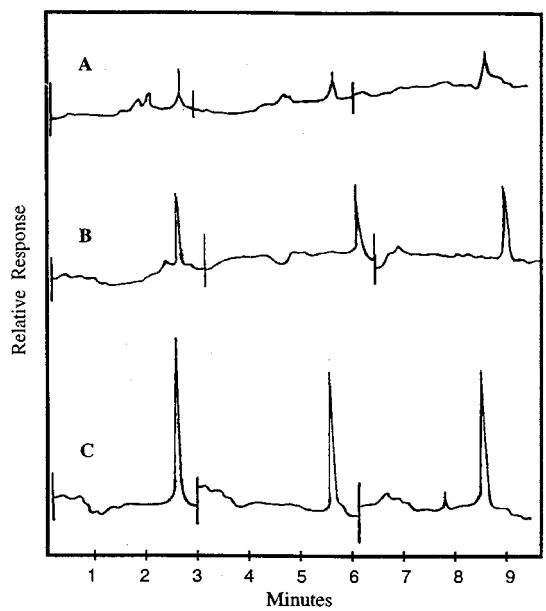

Fig. 2. Typical peak shapes for EIA determination of copper. Copper concentration. (A) 1×10^{-5} M, (B) 3×10^{-5} M, (C) 5×10^{-5} M.

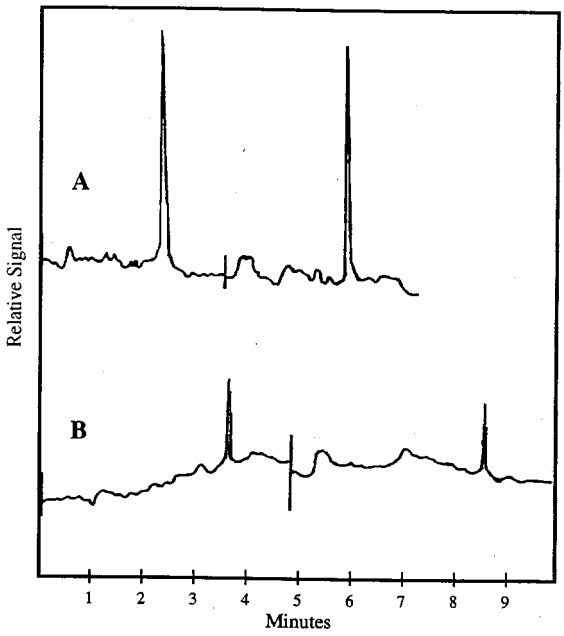

Fig. 3. Comparison of EIA determination of copper (A) and CZE of preformed Cu-EDTA complex (B). Copper concentration 1×10^{-4} M in both cases.

Several experimental parameters were needed to estimate the effect of kinematic focusing by Eq. (2). These were the sample and reagent zone lengths injected during 10 s, and reactant migration rates. Migration rates of reactants were measured in separate CZE experiments as $v_{Cu} = 15.8$ cm min^{-1}, and $v_{Cu\text{-}EDTA} = 4.2$ cm min^{-1}. According to Eqs. (6) and (7) the coordinate of the meeting point of sample and reagent was $x = 36.2$ cm and the velocity of EDTA was $v_{EDTA} = 6.05$ cm min^{-1}. So the velocities of product and reactant were close enough to concentrate the product by kinematic focusing. Reactant zone lengths were: $l_S = 2.6$ cm, $l_R = 1$ cm.

With the above parameters we can state that

$$\frac{l_S}{l_R} < \left| \frac{(v_1 - v_2)}{(v_R - v_2)} \right|$$

The time of zone interaction

$$\left| \frac{l_S(v_R - v_2)}{(v_1 - v_2)(v_1 - v_R)} \right|$$

was equal to 2.5 s. However, to calculate the product peak maximum by Eq. (2), one must know k_0. Unfortunately, it was not possible with our equipment to measure the characteristic chemical reaction time for Cu-EDTA complex formation. We were only able to calculated it based on our results and the mathematical model. The effect of kinematic focusing was diminished by a relatively slow reaction, comparable to the zone interaction time. For an instantaneous reaction, the gain in peak height, estimated by the kinematic focusing factor (Eq. (4)), would have been $f = 5.26$ for our experimental velocities. The observed 3-fold gain implies that the bracketed expression in Eq. (2) must have been equal to 0.57, giving a characteristic reaction time of $k_0^{-1} = 3$ s.

Fig. 4 compares the dependence of the product peak heights versus sample concentration for EIA and CZE modes. It can be seen that peaks for the EIA case were always higher and the gain was larger for the case of smaller sample concentration, when the condition $c_{10} \ll c_{R0}$ was better satisfied.

Fig. 5 presents the product peak shapes produced by the SIA mode of analysis for sample

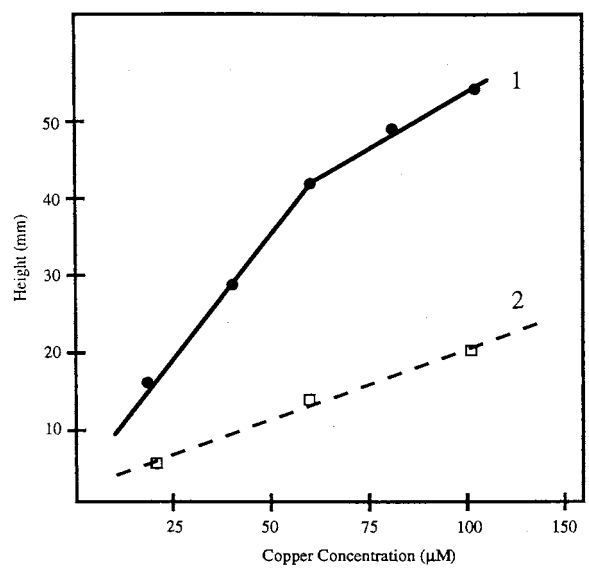

Fig. 4. Product peak height versus sample concentration: 1) EIA mode; 2) CZE mode.

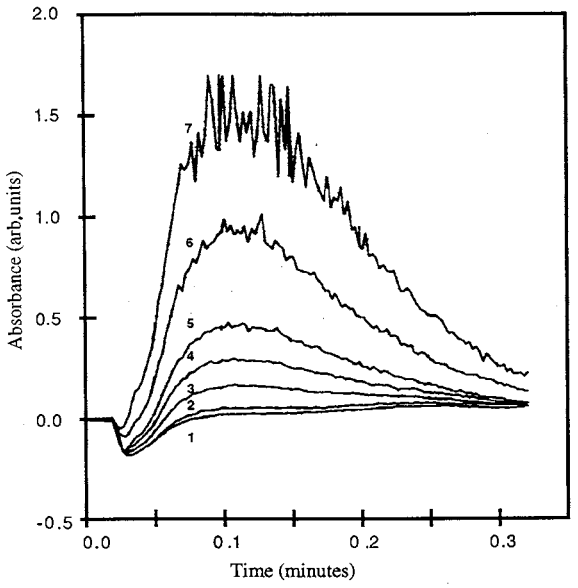

Fig. 5. Typical peak shapes for SIA determination of copper. Copper concentration: (1) blank; (2) 1×10^{-5} M; (3) 5×10^{-5} M; (4) 10×10^{-5} M; (5) 25×10^{-5} M; (6) 50×10^{-5} M; (7) 100×10^{-5} M.

concentrations varying from 1×10^{-5} to 1×10^{-3} M. As can be seen, the product peak for the lowest concentration was practically at the detection limit.

Fig. 6 presents the dependence of product peak amplitude versus sample concentration for the SIA case. By comparison of Figs. 2 and 4–6, the sensitivity was noticeably higher for EIA. While evaluating these results, it is important to remember that the optical path length was equal to 1 cm in the SIA case and 0.012 cm in the EIA case. The local product concentration during the EIA experiment was, therefore, about 80 times higher than that of the SIA experiment. Increased concentration of product was due to kinematic focusing, and the absence of a convective dilution factor.

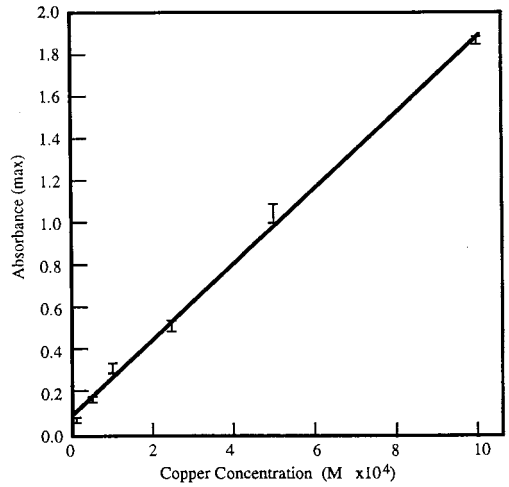

Fig. 6. Product peak amplitude versus sample concentration for SIA mode. The mean of the series of five experiments and the intervals of confidence ($P = 0.95$) are shown for each of the six copper concentration values.

Acknowledgements

This material is based upon work supported by the U.S. Civilian Research and Development Foundation under Award No. RC1-183.

References

[1] V.P. Andreev, Patent of Russian Federation No. 2075070, July 19, 1993.
[2] V.P. Andreev, A.G. Kamenev, N.S. Popov, Talanta 43 (1996) 909.
[3] V.P. Andreev, N.B. Ilyina, E.V. Lebedeva, A.G. Kamenev, N.S. Popov, J. Chromatogr. A 772 (1997) 115.
[4] V.P. Andreev, N.B. Ilyina, Nauchnoye priborostroenie (in Russian) 7 (1997) 100.
[5] T. Gübeli, G.D. Christian, J. Ruzicka, Anal. Chem. 63 (1991) 2407.

ELSEVIER

Talanta 48 (1999) 491–494

Talanta

Short communication

Catalytic hydrogen evolution in the presence of methylthiohydantoin–glycine and cobalt(II) ion: a study by cathodic stripping voltammetry at a hanging mercury drop electrode

Florinel Gabriel Bănică [a,*], Nicolae Spătaru [b]

[a] *Norwegian University of Science and Technology, Department of Chemistry (Rosenborg), N-7034 Trondheim, Norway*
[b] *Institute of Physical Chemistry, Roumanian Academy, Spl. Independenţei 202, Bucharest, Romania*

Received 19 March 1998; received in revised form 16 July 1998; accepted 27 July 1998

Abstract

The carbon–sulfur bond in methylthiohydantoin–glycine (MTH–Gly) is broken during the deposition on the mercury electrode at potentials around −0.1 V versus SCE, giving mercury sulfide which is detected by the characteristic cathodic peak at −0.7 V. If cobalt (II) is also present, the product of the deposition step is a mixture of mercury and cobalt sulfides. During the cathodic scan, the last one is reduced to a transient Co(0) species that catalyses the reduction of hydrogen ion to the hydrogen molecule by a mechanism alike to that emphasized for the Co(II)-sulfide ion system (F.G. Bănică, N. Spătaru, T. Spătaru, Electroanalysis 9 (1997) 1341). This electrode process induces a cathodic peak at −1.4 V that enables the determination of MTH–Gly down to 10^{-7} M in the borax buffer at pH 8.5. The possible extension of this method to other classes of organic sulfur compounds is briefly discussed.

Keywords: Catalytic hydrogen current; Thiohydantoin derivatives; Cathodic stripping voltammetry; Amino acids

1. Introduction

Thiohydantoin derivatives of amino acids are the final products of the Edman reaction, one of the common methods for sequencing of peptides [1,2]. A detailed investigation of cathodic stripping voltammetry (CSV) of various compounds in this class was performed by Moreira et al. [3]. The emerging analytical method is based on the formation of a mercury or copper compound during the accumulation on the mercury electrode. The analytical response results from the reduction of the metal ion in this compound while the cathodic scan is performed. Long before, the electroanalytical chemistry of some thiohydantoins was ap-

* Corresponding author. Tel.: +47 73596957; fax: +47 73596255; e-mail: f.banica@chembio.ntnu.no

0039-9140/99/$ - see front matter
PII S0039-9140(98)00259-8

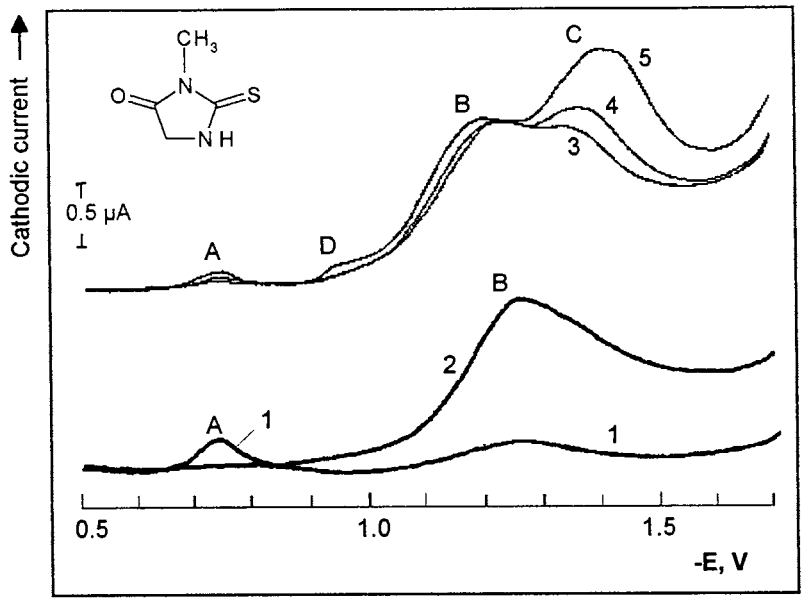

Fig. 1. Cathodic stripping voltammograms in the MTH–Gly-Co(II) system. E_d, −0.1 V (curve sections between −0.1 and −0.5 V were omitted for simplicity). Co(II) (mM): *1*, 0; *2–5*, 0.1. MTH–Gly (μM): *2*, 0; *1*, *3–5*, 0.5. Deposition time (min): *1*, 2, *5*, 5; *3*, 2; *4*, 3.

proached by investigating the catalytic hydrogen evolution on the dropping mercury electrode under the typical conditions for the polarographic Brdička wave [4].

The above findings prompted us to investigate the CSV of thiohydantoin derivatives in the presence of Co(II) as a continuation of our previous research on CSV of hydrogen sulfide anion in the presence of Co(II) [5]. That resulted in the detection of the catalytic hydrogen evolution in the potential range that is typical for the Brdička wave [6] after the accumulation of sulfide ion at a potential less negative than −0.6 V versus SCE.

2. Experimental

Methylthiohydantoin–glycine (MTH–Gly, 3-methyl-2-thioxo-imidazolidin-4-one (Sigma), inset to Fig. 1) was used in this preliminary investigation. The background electrolyte was a borax buffer (0.05 M, pH 8.5). The accumulation potential and time were −0.1 V and 1 min, respectively, if not stated otherwise. The accumulation was performed with stirring on a fresh mercury drop. After 30 s rest interval, the cathodic linear scan occurred with a scan rate of 4 V min^{-1}. All potentials refer to the SCE. Other experimental details were reported elsewhere [5].

3. Results and discussion

In the absence of Co(II) the CS voltammogram displays only one peak at −0.7 V (labeled by A in Fig. 1, curve 1) due to mercury reduction in the accumulated product. Since this peak lies at the same potential than that produced by sulfide ion [5], it is reasonable to assume that MTH–Gly decomposes during the accumulation and the final product is mercury sulfide. Mercury ion in this compound is afterwards reduced in the range of the peak A. Actually, the splitting of the carbon–sulfur double bond on the positively charged mercury electrode is well substantiated as, for example, in the case of thioamides (ref. [7] and references therein). The hump on curve 1 in Fig. 1 at about −1.25 V is also evident on the voltam-

mogram recorded for the background electrolyte alone and is, consequently, ascribed to double layer effects.

The effect of Co(II) is shown in Fig. 1, curves 3–5, that demonstrates the occurrence of the new peak C (at about −1.4 V) in addition to the peak B due to Co(II) reduction. Curve 2 in Fig. 1 proves that the peak C does not occur in the absence of MTH–Gly even if Co(II) is present. The small shoulder D on curve 5 in this figure is alike to the cobalt prewave evidenced by DC polarography in the presence hydrogen sulfide ion [8]. This is an additional proof for the formation of mercury sulfide during the deposition step. Peak C current rises with the increase in Co(II) concentration (Fig. 2). At the same time, the peak A current decreases with the increase in Co(II) concentration in the same way as it happens in the case of sulfide ion peak [5].

As shown in Fig. 1, curves 3–5, the peak C current increases with the deposition time proving that this peak is due to a product of the deposition step. The change of the deposition potential (E_d) from 0.0 V towards more negative values produces a steadily decreases of the peak C current till the zero value for $E_d \leq -0.4$ V. The same trend is exhibited by the peak A. This behavior is opposite to that of the sulfide ion. Sulfide ion is efficiently accumulated at potentials as negative as −0.6 V and the peak C current decrease when E_d shifts towards a more positive value [5]. This essential distinction between MTH–Gly and sulfide ion arises from the difference in the accumulation mechanism. Thus, in the case of sulfide ion, the accumulated product is a positively charged Co(II)-sulfide complex, which forms in the bulk of the solution [5]. Conversely, in the case of MTH–Gly, the first step should be the splitting of the carbon–sulfur bond. Bond breaking is stimulated by the interaction of sulfur atom in MTH–Gly with the mercury ion produced by the anodic reaction of mercury electrode at electrode potentials more positive than −0.4 V. Therefore, the final product is mercury sulfide that is accumulated on the electrode surface. Taking into account the depression of the peak A in the presence of Co(II), it results that mercury is partially substituted by this ion. Consequently, a mixture of cobalt and mercury sulfides are formed during the accumulation step.

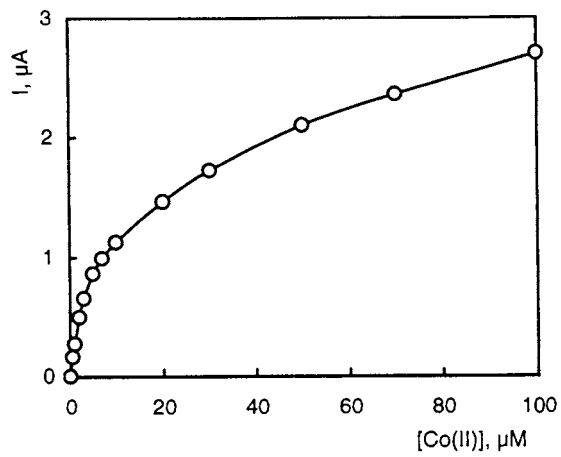

Fig. 2. Effect of Co(II) concentration on peak C current (peak potential, −1.4 V). MTH–Gly, 10 μM.

Except for the effect of E_d, the peak C shows the same characteristics than the analogous peak produced by sulfide ion under similar conditions. Therefore, it is assigned to the catalytic hydrogen evolution by the mechanism formulated in ref. [5]. The key step in this mechanism is the reduction of Co(II) in cobalt sulfide to a transient Co(0) species. This is able to bind a proton and convert it into a hydride ion by an intramolecular electron transfer. Hydride ion reaction with a proton donor leads subsequently to the formation of the hydrogen molecule. Simultaneously, Co(II) sulfide is regenerated by the intramolecular electron transfer and enter a new catalytic cycle. The cycle is interrupted by the decomposition of the intermediate Co(0) species. The peak shape of the voltammetric pattern is evidently due to the gradual depletion of adsorbed Co(II) sulfide via the decay of the transient Co(0) species.

As an alternative interpretation, it may be inferred that hydrogen evolution in the range of the peak C is catalyzed by a Co(II)-complex. However, this assumption is contradicted by polarographic data available in literature. Thus, it was demonstrated that monothiohydantoins (a class to whom MTH–Gly also belongs) cannot catalyze the hydrogen evolution on the dropping mercury electrode in the presence of Co(II) [4]. Only

2,4-dithiohydantoins showed this property [4]. Moreover, sulfide ion does not induce a polarographic catalytic hydrogen wave in the potential range of the peak C in a Co(II)-containing borate buffer [8]. Consequently, peak C cannot be assigned to the catalysis by a Co(II)-MTH–Gly complex nor to the effect of Co(II) sulfide in the colloidal state.

Peak C current is directly proportional to MTH–Gly concentration up to 10 μM. The proper selection of the deposition time leads to the occurrence of a linear response within various concentration limits. Concentrations as low as 10^{-7} M can be detected after 5 min of accumulation. The relative standard deviation for five runs at 5×10^{-7} M was of 7%. As in the case of sulfide ion [5] the separation of peaks B and C is highly improved by recording the derivative voltammogram. The use of DP voltammetry instead of linear scan voltammetry does not improve the sensitivity but brings about some distortions of the curve probably due to the tensammetric response. This is not surprising as the advantages of linear scan voltammetry as compared to DP voltammetry in the case of adsorptive stripping analysis were already pointed out [9]. It is worth noting that the method described here belongs to the class of indirect stripping voltammetry, according to the nomenclature suggested by Fogg [10].

Additional experiments with thiourea instead of MTH–Gly produced analogous voltammetric patterns. Consequently, it is possible to assert that the method described in this paper could be employed not only for the determination of thiohydantoin derivatives but also for other classes of sulfur compounds. The single prerequisite is that the carbon–sulfur bond is sufficiently labile as to get broken during the deposition on the mercury electrode. Moreover, the difference in the strength of the carbon–sulfur bond could afford to discriminate between different compounds by the proper selection of E_d.

References

[1] L. Stryer, Biochemistry, W.H. Freeman, New York, 1995, p. 55.
[2] P.D. Bailey, An Introduction to Peptide Chemistry, Wiley, Chichester, 1990, p. 89.
[3] J.C. Moreira, R.D. Miller, A.G. Fogg, Electroanalysis 3 (1991) 385.
[4] P. Zuman, M. Kuik, Collect. Czech. Chem. Commun. 24 (1959) 3861.
[5] F.G. Bănică, N. Spătaru, T. Spătaru, Electroanalysis 9 (1997) 1341.
[6] A. Căluşaru, J. Electroanal. Chem. 15 (1967) 269.
[7] F.G. Bănică, M. Florea, E. Diacu, Electroanalysis 2 (1990) 43.
[8] D. Marin, C. Teijeiro, Can. J. Chem. 66 (1988) 2335.
[9] J. Wang, in: A.J. Bard (Ed.), Electroanalytical Chemistry, vol. 16, Marcel Dekker, New York, 1989, p. 1.
[10] A.G. Fogg, Analyt. Proc. 31 (1994) 313.

ELSEVIER

Talanta 48 (1999) 495–498

Talanta

Erratum

Erratum to "Spectrophotometric method for determination parts per million levels of cyclohexylamine in water" [Talanta 47 (1998) 421–437] ☆

A.G. Kumbhar, S.V. Narasimhan *, P.K. Mathur

Water and Steam Chemistry Laboratory (WSCL), Chemistry Group, BARC, Indira Gandhi Centre for Atomic Research Campus, Kalpakkam, Tamil Nadu, 603 102, India

The Publisher regrets that Tables 3 and 5 and Figs. 2 and 6 of this article were printed incorrectly. The correct versions follow:

Table 3
Proton peak positions of adduct ^{1}H-NMR spectrum and their attributes to respective carbon atoms

Peak position (ppm)	No. of proton integral	Proton attributed to carbon
1.26, 1.30, 1.35, 1.40, 1.44, 1.49	5.2	C3 and C5 CHA proton (four Nos)
1.69, 1.74, 1.82	3.5	C2 and C6 CHA protons (four Nos)
1.85, 2.13	2.2	C4 CHA protons (two Nos)
3.57	1.0	C1 CHA proton (one No.)
5.90	0.97	C3 NQS OH proton (one No.)
6.69	0.92	C2 NQS OH proton (one No.)
7.5–8.2	4.04	C5, C6, C7, C8 NQS proton (four Nos)

* Corresponding author. Tel.: +91-4114-40397; fax: +91-4114-40360.

☆ PII of original article: S0039-9140(98)00152-0.

PII S0039-9140(98)00367-1

Table 5
Heteronuclear (HETCOR) NSM spectrum (^{1}H and ^{13}C) of adduct

^{1}H peaks				^{13}C Peaks	
ppm	Integral area	Expected No. of H	Group	PPM	No. of carbons
Aldyl part of the adduct					
1.49					
1.44					
1.40					
1.35	5.2				
1.30					
1.26		8	C2, C3, C4, C5 and C6	32.15	2C
				25.29	1C
1.85				24.79	2C
1.82	3.47				
1.74					
1.69					
2.13	2.2	2			
3.57	1.01	1	C1	52.99	1C
Aryl part of the adduct					
5.90	0.97		C3	99.39	1C
7.83					
7.79					
7.69				133.97	
7.66	3.04			131.74	4C
7.62				128.85	
7.61		4	C5, C6, C7, C8	121.80	
7.57					
7.53					
8.12	1.0				
8.13					
6.69	0.92	1	C2	99.39	1C
			C1	176.05	1C
			C9	131.21	1C
			C10	130.81	1C
			C4	119.51	1C

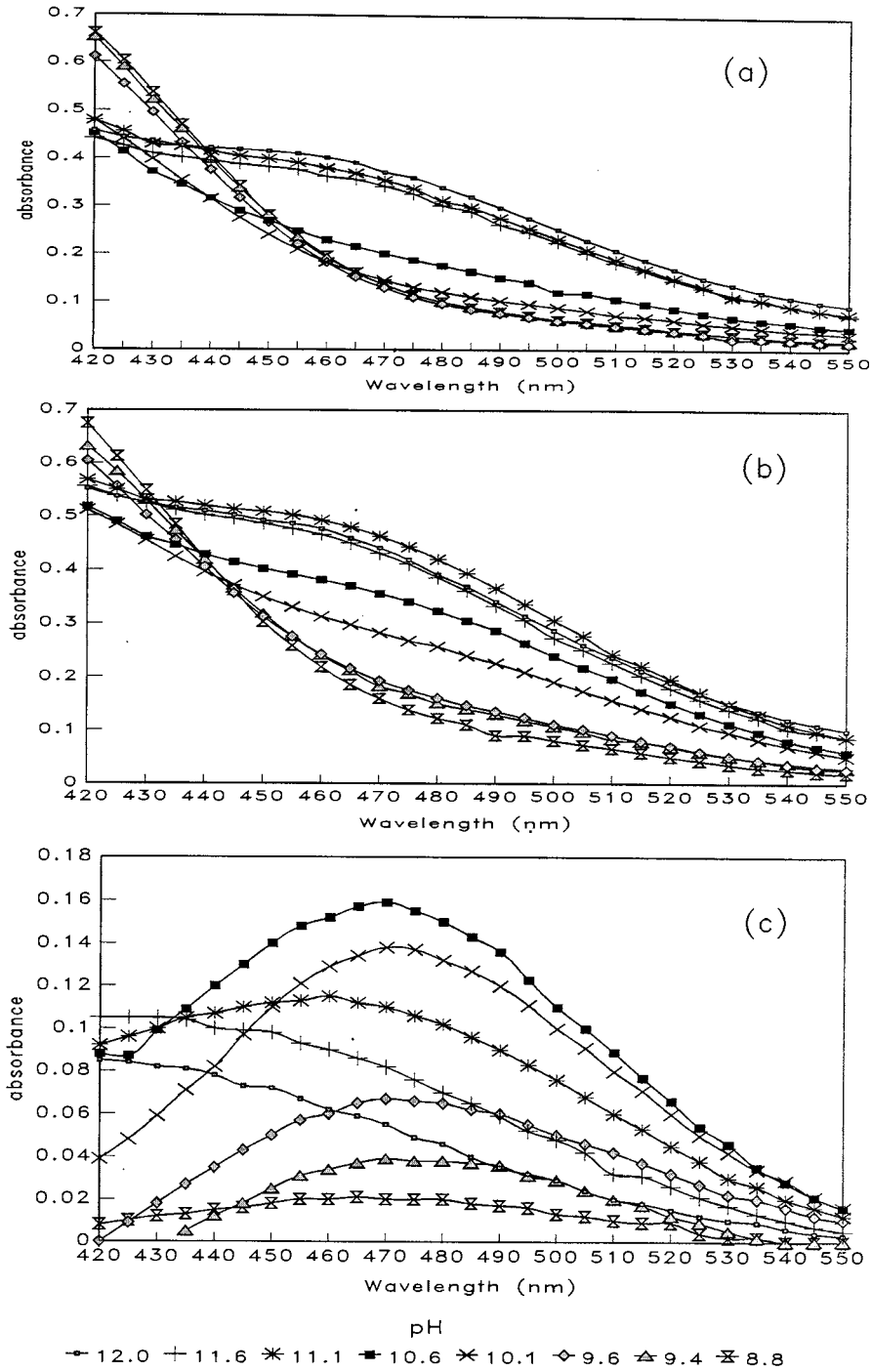

Fig. 2. (a) UV–vis spectra of reagent blank solution vs. DM water at various pH values, Path length: 1 cm, NQS (0.6%): 0.5 ml. (b) UV–vis spectra of 5 ppm CHA-NQS adduct vs. DM water at various pH values. Path length: 1 cm, NQS (0.6%): 0.5 ml. Final CHA concentration: 5 ppm. (c) UV–vis spectra of CHA-NQS adduct vs. reagent blank at various pH values. Path length: 1 cm, NQS (0.6%): 0.5 ml. Final CHA concentration: 5 ppm.

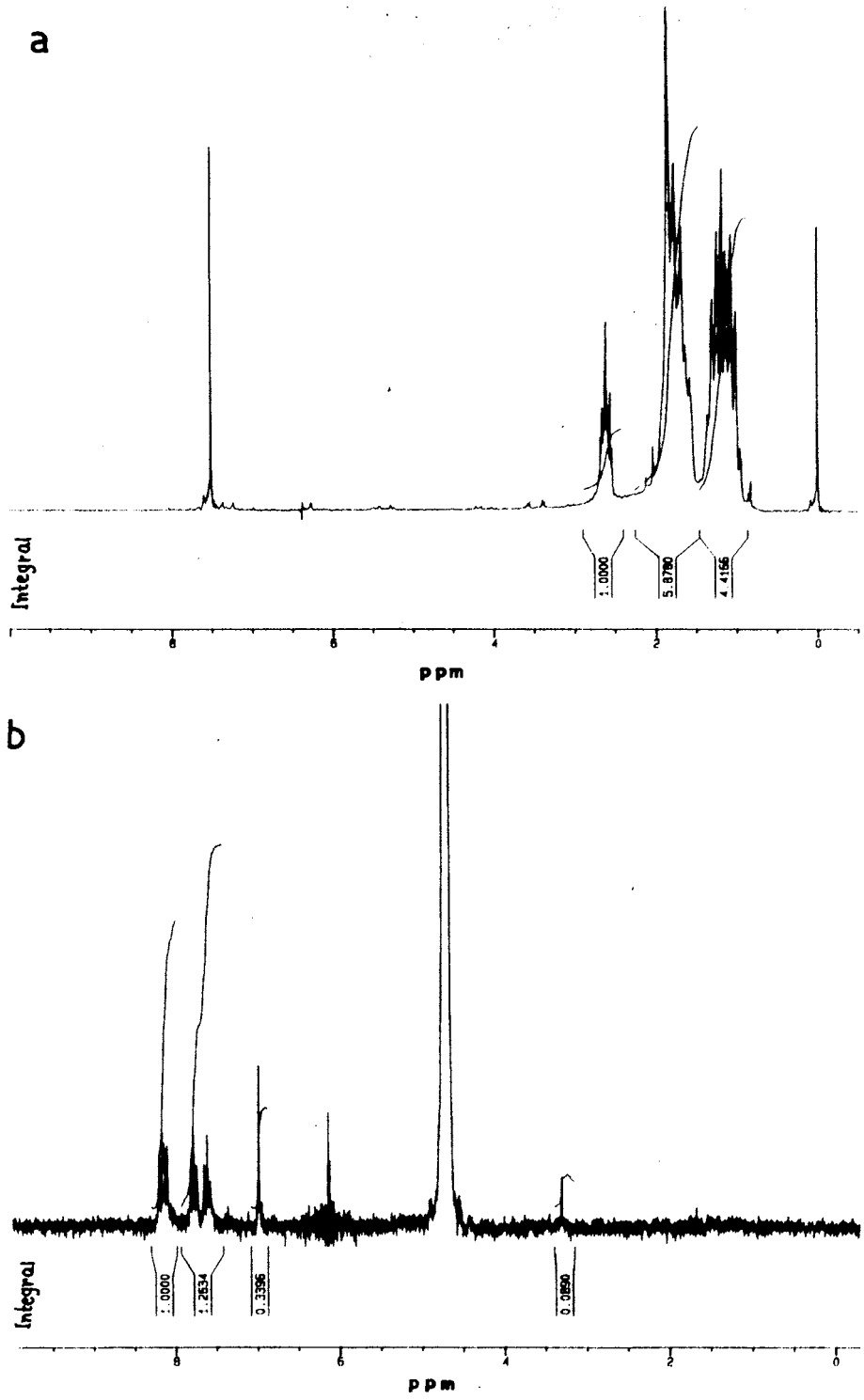

Fig. 6. ^{1}H-NMR spectra of (a) CHA, (b) NQS.

ELSEVIER

Talanta 48 (1999) 499

Talanta

Editorial

Aims and scope

The editors are very pleased to announce that Talanta has been experiencing an increase in the number of papers submitted to the journal. This steady increase in submissions will require the journal to become more strict in its editorial policy and to reject papers that do not closely fit the journal's aims and scope. To this effect, authors are encouraged to carefully read the aims and scope of the journal, and to consider the following criteria before submitting a paper to Talanta.

Talanta provides a forum for fundamental studies and original research papers dealing with all branches of pure and applied analytical chemistry. Classical analytical techniques such as volumetric titrations, UV-visible spectrophotometry (including derivative spectrophotometry), fluorimetry, polarography and related pulsed voltammetric techniques, and so forth, are considered as routine analytical methods, and manuscripts dealing with these methods should be submitted for publication in Talanta only if substantial improvement over existing official or standard procedures is clearly demonstrated. New reagents should demonstrate clear advantages, and their presentation should be comprehensive, rather that generating a series of similar papers.

Solvent extraction methods are well established, and new methods should demonstrate improvements in waste generation, non-hazardous material substitutes, and ease of use (automation).

Application of an original method to real matrices is encouraged, provided that it is properly validated following recommendations of official institutions. The developed method should especially comprise information on selectivity, sensitivity, detection limits, accuracy, reliability and speciation capabilities (e.g. in the case of trace metal analysis). Proper statistical treatment of the data should be provided.

Application of classical analytical approaches such as polarography, voltammetry (pulsed), UV-visible spectrophotometry (and derivative), and fluorimetry to relatively simple matrices having no major interference, such as drug formulations or reconstituted samples, are discouraged unless considerable improvements over other methods in the literature (time saving, accuracy, precision, cleaner chemistry, automation) are highlighted.

Papers dealing with analytical data such as stability constants, pK_a values, etc. should be published in more specific journals, unless novel analytical methodology is demonstrated, or important analytical data are provided which could be useful in the development of analytical procedures.

Gary D. Christian
Jean-Michel Kauffmann
Editors-in-Chief
April, 1998.

PII S0039-9140(98)00239-2

ELSEVIER

Talanta 48 (1999) 501–509

Talanta

Advantages and limitations of thermal lens spectrometry over conventional spectrophotometry for absorbance measurements

J. Georges *

Laboratoire des Sciences Analytiques, UMR 5619, Bât. 308, Université Claude Bernard-Lyon 1, 69622 Villeurbanne Cedex, France

Received 6 April 1998; received in revised form 18 June 1998; accepted 1 July 1998

Abstract

This review considers the advantages and the limitations that thermal lens spectrometry has over conventional spectrophotometry for the measurement of optical absorption in specific applications. The photothermal method is characterized by its intrinsic sensitivity resulting from the indirect nature of the measurement and amplified by physical and thermo-optical parameters which are not effective in absorbance measurements. Other advantages include a weak dependence on light scattering and the complementary nature of photothermal spectra with respect to absorption and emission spectra for speciation studies at very low concentrations. The main drawbacks are the convective noise, the background absorbance and the complexity of the experimental set-up, especially when differential or wavelength scanning measurements are required.

Keywords: Thermal lens spectrometry; Advantages; Drawbacks

1. Introduction

Thermal lens spectrometry (TLS) belongs to a class of thermo-optical methods which rely on the measurement of heat generated from non radiative relaxation processes following absorption of optical radiation [1–4]. In such a method, the absorbing sample is excited using a pump laser having a radial Gaussian intensity profile. Non radiative decay of excited states results in local heating and the formation of a transverse refractive index gradient which behaves as a diverging lens. The thermal lens (TL) is detected by its effect on the propagation of a probe beam tuned to a wavelength not absorbed by the sample. The far-field change in probe beam power is related to the amount of energy absorbed by the analyte and to its concentration and/or absorbance.

Since the discovery of the thermal lens effect, both theoretical and experimental works have been carried out and the thermal lens technique has been extensively reviewed. Instrumental developments, including single-beam, dual-beam, colinear and transverse configurations, differential measurements, multiwavelength and tunable in-

* Tel.: +33 4 78949510; fax: +33 4 72431078; e-mail: j.georges@cpe.fr

0039-9140/99/$ - see front matter
PII S0039-9140(98)00242-2

struments, have been described [5]. Theoretical models have been put forward using either cw-laser or pulsed-laser excitation and mathematical expressions of the signal have been derived [6–15]. Photothermal spectroscopy is often considered as an indirect way for measuring optical absorption because the method measures an effect produced by optical absorption. The indirect nature of the measurement has resulted in a variety of applications which have been developed simultaneously with experimental and theoretical studies. These applications include chemical analysis of low-absorption samples [16–22], the determination of fluorescence quantum yields and fundamental studies allowed by the direct observation of radiationless deactivation processes [23,24].

Although thermal lens spectrometry has a wide range of potential applications, the method has not become a popular method for routine chemical analysis. This is probably because of the lack of cheap, easy-to-operate tunable lasers in the UV and the visible with good beam quality. However, these instrumental and economical constraints should be overcome in peculiar applications where the technique could compete very favorably with transmission measurements. The aim of this review was to outline the potential advantages and the limitations of thermal lens spectrometry and those applications where the technique can be a more powerful analytical method than conventional absorption techniques.

2. Sensitivity: intrinsic enhancement and limitations

The thermal lens effect is monitored as the far-field change in probe beam spot size, by sampling the laser power that passes through a pinhole. The thermal lens signal is expressed as the relative power change:

$$S = \frac{\Phi_o - \Phi}{\Phi_o} \quad (1)$$

where Φ_o and Φ are the transmitted power before and after the formation of the thermal lens, respectively. The signal resulting from an optimum position of the probe and excitation beam waists against the sample cell, using mode-mismatched excitation and probe beams and eliminating non-linear terms, has been defined as:

$$S = 2.3\ A\frac{P}{\lambda_p\, k}\frac{dn}{dT} = 2.3AE_{cw} \quad (2)$$

for cw-laser excitation [10,13], and

$$S \approx 2.3\ A\frac{4\ Q}{3\lambda_p\ \rho\ C_p\ \omega_{exc}^2}\frac{dn}{dT} = 2.3AE_p \quad (3)$$

for pulsed-laser excitation [11,15], assuming that the excitation and probe beam waists are equal. A is the decadic absorbance, P (W) is the radiant power, Q (J) is the pulse energy, λ_p (cm) is the wavelength of the probe beam, ω_{exc} (cm) is the minimum radius of the excitation beam into the sample cell and ρ (g cm^{-3}), C_p (J g^{-1} K^{-1}), k (W cm^{-1} K^{-1}) and dn/dT (K^{-1}) are the density, the heat capacity, the thermal conductivity and the refractive index gradient of the medium, respectively. In the above equations, it is assumed that the heat yield is unity, i.e. the analyte is not luminescent and all the absorbed power is dissipated in the form of heat in a time shorter than the time scale of the measurement.

In order to see how the thermal lens method can enhance absorbance measurements, the transmission signal measured in conventional absorption spectrophotometry,

$$T = \frac{\Phi}{\Phi_o} = 10^{-A} \quad (4)$$

where Φ_o and Φ are the incident and transmitted radiant power, respectively, can be expressed in a form similar to that of Eq. (1):

$$\frac{\Delta\Phi}{\Phi_o} = 1 - T = (1 - 10^{-A}) \approx 2.3A \quad (5)$$

For the same absorbance, the thermal lens signal will be increased by a factor, E_{cw} or E_p, called the enhancement factor [25], which depends on the solvent and on the experimental set-up.

The sensitivity of the photothermal method can be enhanced by increasing the excitation power in cw-TLS or the excitation irradiance in pulsed-TLS, and by using solvents with good thermo-optical properties, i.e. solvents with high refractive index gradient and low density, thermal conduc-

Table 1
Pysical parameters of various solvents and theoretical enhancement factors, E_{cw} and E_p as defined in Eqs. (2) and (3), respectively.

Solvent	ρ (g cm^{-3})	$10^4 \times k$ (W cm^{-1} K^{-1})	C_p (J g^{-1} K^{-1})	$10^4 \times dn/dT$ (K^{-1})	E_{cw}	E_p
Water (10°C)	0.9997	57.9	4.192	−0.392	11	0.8
Water (20°C)	0.9982	59.7	4.182	−0.877	23	1.8
Water (30°C)	0.9956	61.3	4.179	−1.184	31	2.4
Ethanol	0.79	16.7	2.42	−3.9	370	17
n-Pentane	0.63	11.3	2.29	−5.5	770	32
CCl_4	1.59	10.3	0.86	−5.8	890	36
Air	0.00117	2.61	1.01	−0.0088	5	63
CO_2 (atm.)	0.00179	1.66	0.84	−0.0138	13	77
CO_2 (sc)	0.468	16	90	−800	79000	160

Parameters for water as a function of temperature were obtained from [26]; parameters for other media are from [12,16]; parameters for supercritical CO_2 were estimated from [27]. In sc CO_2, a 100-fold sensitivity increase, relative to the same measurement in carbon tetrachloride, has been achieved using cw-laser excitation. Enhancements factors were calculated for $\lambda_p = 632.8$ nm, $P = 100$ mW, $Q = 100$ μJ and $\omega_{exc} = 50$ μm.

tivity and heat capacity (Table 1). With both cw- and pulsed-laser excitation, water is a poor solvent while organic solvents induce larger enhancement factors. In gas, pulsed-laser excitation provides greater sensitivities than does cw-laser excitation thanks to very low densities. Because the thermal expansion of a fluid diverges near its critical point and the resulting change in refractive index with temperature tends to infinity, supercritical CO_2 is expected to be a very efficient medium for thermal lensing. Since the thermal conductivity and the density of supercritical CO_2 are similar to those of organic solvents, then the intrinsic sensitivity of the TL method should be very attractive for detection in supercritical fluid chromatography. In contrast to that observed in gas at atmospheric pressure, cw-laser excitation is expected to be more efficient than pulsed-laser excitation because ρ and C_p increase faster than k.

The pulsed-laser TL signal is inversely proportional to the square of the excitation beam waist while the cw-laser TL signal is independent of the beam size. However, in a colinear dual-beam experimental set-up, the size of the excitation beam into the sample cannot be decreased without bounds not only because of geometrical and optical constraints in beam alignment and sample positioning, but also because this would invalidate the assumption that the beam size remains approximately constant into the sample [28,29]. In fact, the beam size restriction is valid for both the excitation and probe beams and the sample cell should be short compared to the shorter one of the two confocal distances. These constraints can produce some limitations comparatively to conventional spectrophotometry because the sensitivity of the thermal lens method is therefore not always proportional to the sample pathlength.

Other limitations that can partly cancel the intrinsic sensitivity of the photothermal method and increase the limit of detection are the noise and the background absorbance. Besides the usual sources of noise encountered in performing optical measurements with laser light sources, i.e. pointing noise, flicker noise and shot noise [30,31], another source of background noise which is associated with the photothermal effect is the convective noise [32,33]. Convection occurs when too much heat is deposited into the sample. Sample heating induces convective movements of the solution in the thermal lens region, thus producing local variations of the temperature and deformations of the refractive index gradient. It results that the probe beam can undergo deformations of the intensity profile and direction changes, which degrades the measurements when the far-field power change of the probe beam is sampled behind a pinhole. Thermal convection increases linearly with the signal and decreases when the thermal lens effect decreases, which is important when blank and limits of detection (LODs) are determined. However, the convective noise can

seriously degrade LODs when high excitation power or energy and solvents with high background absorbances are used. The convective noise depends on the viscosity and the density of the solvent and generally increases with solvents of better thermo-optical properties [34]. It results that the difference between LODs obtained in water and other solvents decreases, mainly at large values of the blank absorbance.

Increase the excitation power or energy to improve the sensitivity of the TL method not only increases the convective noise, but also can produce nonlinear absorption effects such as multiphoton absorption [35] and optical saturation or optical bleaching [36–39]. These effects can arise when using continuous excitation sources with moderate power or pulsed excitation sources with very low energy, depending on the degree of focusing of the excitation beam into the sample. Optical saturation or bleaching will limit the amount of energy or power absorbed by the sample and therefore decrease the sensitivity, while multiphoton absorption will enhance the photothermal signal.

Another effect that cannot be ignored in thermal lens spectrometry is sample matrix. Matrix effects have been first reported by Phillips et al. [40] and then more extensively studied by Franko and Tran [41] in aqueous solutions. In water, the addition of electrolytes always results in an enhancement of the thermal lens signal, while in ethanol the signal can be decreased upon addition of the same electrolytes [42]. The reason for signal variation is due to changes in the thermo-optical parameters of the solvent, especially the refractive index gradient dn/dT. For example, the thermo-optical properties of water are improved by 35% upon the addition of 1 M NaI where the only contribution of dn/dT is $\sim 27\%$. The salt effect depends on the electrolyte and the influence of the anion is more important than that of the cation. Also, the effect depends on the mode of operation of the excitation laser [42] because of a different contribution of the individual factors such as density, thermal conductivity and heat capacity on the cw- and pulsed-laser thermal lens signal.

3. Measurements in samples with high background absorbance

TLS and related photothermal method have been shown to be very sensitive spectroscopic techniques for measuring absorbances as low as 10^{-7} [16,43]. However, the method has been mainly applied to situations where the experimental background does not limit the measurement. The high sensitivity may not be useful in analytical applications where the background absorbance is significant. Background absorbance can be due to the solvent or to the presence of impurities or concomitants, such as free ligands in coloured reactions. Not only the background absorbance increases the convective noise, but subsequently decreases the dynamic reserve of the method [44], i.e. its ability to detect small signal changes in the presence of a large background signal. Applications to the analysis of aluminum [45] and terbium [46] through complexation with highly absorbing ligands have shown the limits of the thermal lens method. Like in conventional spectrophotometry, the intrinsic dynamic reserve is not better than $\sim 1 \times 10^3$.

A lot of methods including differential measurements and wavelength discrimination have been developed [5,11] in order to minimize or eliminate the background signal, but improvements in dynamic reserve have been only moderate. The first differential thermal lens spectrometer has been introduced by Dovichi and Harris [47] in a single beam experiment. The technique uses two cells, one cell containing the blank and the second cell filled with the analyte. Both cells are positioned along the beam axis on either side of the waist of the laser beam. The differential response results from the antisymmetric dependence of the thermal lens effect on the position of the thermal lens relative to the beam waist. The diverging lens has a converging or diverging effect when positioned before or after the waist, respectively. In this manner, the background signal is optically substracted from that of the sample. Pang and Morris [48] extended the use of single-beam differential arrangement to the detection of eluents in liquid chromatography using a split solvent flow and a reference column con-

nected to the reference cell. The system allowed efficient solvent absorbance compensation and increased the signal-to-noise ratio. Berthoud and Delorme [49] developed a differential arrangement using a dual-beam configuration with matched focus positions for the separate pump and probe beams. This instrument which allowed compensation of 95–98% of the background signal was applied to the recording of photothermal spectra of Nd^{3+} and Pr^{3+} at low concentration levels and to the analysis of Nd^{3+} in $HClO_4$ solution with a detection limit of 5×10^{-6} M. A similar differential experiment has also been described by Erskine and Bobbitt [50]. In their set-up, the pump and probe beams were not colinear but were crossed at an oblique angle, thus decreasing interferences between both beams while allowing an optimum interaction length inside the cells. Moreover, the excitation beam was split into two excitation beams which were separately focused into either detection cells, minimizing the effects of pointing variations on the excitation beams. Spatial separation of the pump and probe beams eliminates the need to remove the pump beams before the detection system and decreases the noise originating from the interaction of the laser beams. This sytem was characterized by a dynamic reserve of 2.5×10^5, which is about two orders of magnitude better than that obtained by conventional spectrophotometry. However, differential arrangements are difficult to build owing to the complexity of beam alignment and sample cell positioning and errors can originate from difference in laser power at the two cells.

4. Measurements in light-scattering samples

The presence of light-scattering materials can introduce significant errors in absorbance measurements by conventional spectrophotometry. In this method, the analytical signal is derived from the amount of light not transmitted through the sample, and transmission or absorbance are defined according to Eq. (4) where Φ is the power transmitted by the sample in the absence of scattering. Any factor which contributes to the loss of transmitted light will decrease the transmission and increase the true absorbance. In the presence of scattering, the measured transmission, T', will result from the attenuation of light by both analyte absorption and sample scattering [11]:

$$T' = T_a\, T_s = \frac{\Phi}{\Phi_o}\,\frac{(\Phi_o - \Phi_s)}{\Phi_o} \tag{6}$$

where Φ_s is the scattered power. Then, the absorbance measured in the presence of scattering can be expressed as:

$$A' = -\log T' = -\log\left[(\Phi - s\,\Phi)/\Phi_o\right] \tag{7}$$

where $s = \Phi_s/\Phi_o$ is the degree of scattering [51].

In thermal lens spectrometry, light scattering may affect the signal magnitude not only through attenuation of the probe beam in a manner similar to that observed in a transmission method, but also through attenuation of the excitation beam resulting in a loss of power absorbed by the analyte.

4.1. Effect on the probe beam

As expressed in Eq. (1), the thermal lens signal is measured as the relative change in probe beam power before and after the formation of the thermal lens. As Φ_o and Φ are measured on the same sample cell and are temporally separated, both measurements are equally affected by scattering losses and Eq. (1) may be written as [51]:

$$S = \frac{(\Phi_o - s\Phi_o) - (\Phi - s\Phi)}{\Phi_o - s\Phi_o} = \frac{\Phi_o - \Phi}{\Phi_o} \tag{8}$$

Eq. (8) shows that scattering results in no effect on the measured thermal lens signal, provided that the scattered power is small with respect to the incident power and the spatial profile of the probe beam is not changed. When necessary, it is possible to correct the optical perturbations created on the probe beam by optically inhomogeneous samples by using a phase-conjugate thermal lens spectrometer [52].

4.2. Effect on the absorbed power

Light scattering may affect the strength of the thermal lens by reducing the power available to sample absorption. In the presence of scattering,

the optical power absorbed by the analyte, P_a, can be written as [11]:

$$P_a = P\frac{\alpha}{\alpha_s + \alpha}[1 - 10^{-(\alpha_s + \alpha)\ell}] \quad (9)$$

where ℓ(cm) is the optical pathlength, α (cm^{-1}) is the absorption coefficient and α_s (cm^{-1}) is the scattering coefficient [53]. Since the photothermal signal is proportional to the amount of energy absorbed, it is possible to evaluate the effect of scattering on the amplitude of the photothermal signal and to make a theoretical comparison with absorbance taken as $A' = (\alpha_s + \alpha)\ell$. The results obtained for $\alpha = 0.01$ cm^{-1} and α_s up to 0.1 cm^{-1} (Fig. 1) show that scattering has a small influence on the amount of energy absorbed in comparison to changes produced on absorbance.

Thermal lens spectrometry has been experimentally compared to conventional absorbance measurements on samples with substantial light-scattering properties [51]. While deviations from the expected values in excess of more than two orders of magnitude were observed in transmission measurements, the tl method provided absorbance values which were quite accurate and almost independent of the scattering coefficient (Table 2). Power and Langford [54] measured optical absorbance in untreated natural waters,

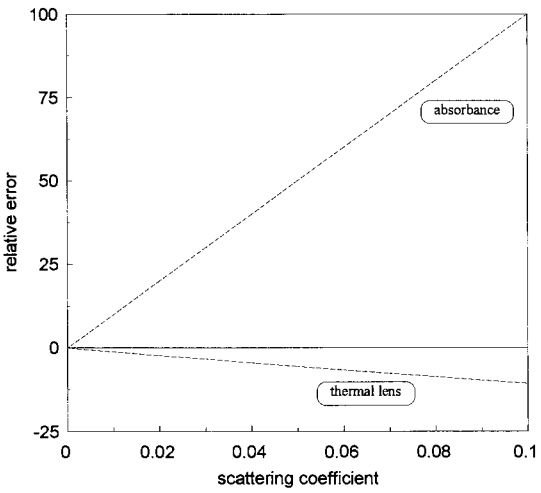

Fig. 1. Relative errors in absorbance and thermal lens signal as a function of the scattering coefficient, calculated for $\alpha = 0.01$ cm^{-1} and $\ell = 1$ cm.

Table 2
Comparison of absorbances obtained by conventional spectrophotometry and thermal lens spectrometry under conditions of light scattering (from [51])

True absorbance	Turbidity number	Measured absorbance	
		Spectrophotometry	TLS
0.002	0.0	0.002	0.0029
	0.5	0.007	0.0030
	2.0	0.020	0.0027
	10.0	0.063	0.0027
	50.0	0.308	0.0030
0.02	0.0	0.020	0.022
	0.5	0.031	0.022
	2.0	0.036	0.022
	10.0	0.086	0.022
	50.0	0.324	0.022
0.1	0	0.104	0.095
	0.5	0.121	0.092
	2.0	0.109	0.086
	10.0	0.170	0.086
	50.0	0.396	0.082

yielding valuable information on the composition of humic acids. The method was able to distinguish true sample absorption from light scattering for $\alpha_s\ell$ values < 0.15, and a detection limit of 20 $\mu g\ l^{-1}$ has been obtained for Armadale fulvic acid. Thermal lens spectrometry has been applied to kinetic speciation studies of metal ions in the presence of colloidal ligands [55]. These experiments have shown that, while light scattering by nonabsorbing particles causes no interferences in TLS, homodisperse colloids which absorb at the pump laser wavelength increase the noise. The TL method has allowed the determination of pesticides in water including small latex particles. The technique was better than conventional spectrophotometry by a factor of about 20 in terms of LOD [56].

In highly scattering samples, the absorbed power is no longer a simple function of the optical pathlength and the scattering coefficient [11]. Because of scattering, the optical path through the sample is increased, which may result in an increase of the absorbed power. However, this effect is partly cancelled by the fact that energy is

absorbed over a greater volume than that defined by the excitation beam in the absence of scattering and the scattered light does not contribute appreciably to the photothermal signal [57].

5. Applications to speciation and chemical equilibria

The knowledge of migration mechanisms of lanthanides and actinides in ground waters requires the determination of the concentration, the oxidation state and the speciation of these species [58]. It is well known that the absorption transitions of rare earth ions are characterized by narrow bands in the uv and visible range with very weak intensities. As no chemical treatment or enrichment processes can be performed prior to the analysis, sensitive and selective methods are needed for spectral measurements. Moreover, the decay of excited rare earth ions involves different radiative and non radiative relaxation processes depending on the oxidation state, the medium and possibly on the excitation wavelength. Since the photothermal signal results from heat generated through radiationless relaxation processes, the photothermal spectrum does not necessarily coincide with the absorption spectrum [59]. Therefore, not only the method can be more sensitive than conventional absorption, but also the photothermal spectrum can give information which are complementary to those available from absorption and emission spectra. However, precise measurements require to account for changes in excitation irradiance and in waist position while scanning the laser wavelength.

The thermal lens method has allowed the study of the absorption spectrum of U(VI) depending on its chemical form at concentrations (4×10^{-6} M) which are inaccessible to conventional spectrophotometry [60]. Variations of the photothermal spectral features due to complexation by carbonate ions have been observed for Nd(III) and Pr(III) at concentrations as low as 2×10^{-5} M [49,61]. A fully automated thermal lens apparatus including two dye lasers controlled by a microcomputer with constant excitation power for spectrum scanning has been developed for detection and speciation of actinides [62]. Photothermal spectra of plutonium at different oxidation states were obtained for concentrations as low as 3×10^{-7} M and the limit of detection at constant wavelength was in the range $4–8 \times 10^{-8}$ M. In order to collect spectral data in hot groundwaters for nuclear waste applications, the photothermal spectrum of Nd^{3+} in water has been recorded as a function of the temperature [26]. Thanks to the temperature dependence of the refractive index gradient [63], the sensitivity of the method at 90°C was about twice greater than that at 25°C, while the absorptivity was decreased by $\sim 20\%$.

The superiority of the thermal lens technique over conventional absorption measurements for low concentrations and/or weakly absorbing species has been demonstrated in the kinetic determination of the rate constant of the photochemical nucleophilic aromatic substitution of 1,2-dimethoxy-4-nitrobenzene [64]. In addition to advantages such as accuracy and precision, the technique has allowed kinetic studies with reagents whose concentrations were about 100 times lower than those required by conventional kinetic methods.

In some cases, the intrinsic sensitivity of TLS can be further amplified by the fact that the physical quantity producing the thermal lens signal can vary differently from absorbance. It is well known that chemical effects where an analyte gives rise to products with different spectral features generally induce non-linear dependence of absorbance versus concentration and deviations from Beer's law [31]. These effects, including pH- or concentration-dependent equilibria and formation of aggregates, are commonly studied by conventional spectrophotometry. However, when the absorption spectra of species involved in the equilibrium are not completely resolved and when one species is fluorescent, the thermal lens method can be more sensitive than absorption to monitor the reaction. Considering an analyte in equilibrium between a nonfluorescent form, A, and a fluorescent form, B, with concentrations C_a and C_b, respectively, and with molar absorptivities ε_a and ε_b at the specified wavelength. Assuming that each component separately obeys Beer's law, the total absorbance of the solution is the sum of individual absorbances:

$$A_t = (\varepsilon_a C_a + \varepsilon_b C_b)\ell \quad (10)$$

Unless $\varepsilon_a = \varepsilon_b$, the plot of A_t versus the analytical concentration of the analyte is not linear and deviation of the plot with respect to Beer's law can be used to determine the equilibrium constant.

In thermal lens spectrometry, the signal is proportional to the energy absorbed by the solution and therefore to the absorbance, but is ultimately determined by the amount of energy actually released as heat [65]:

$$S \propto (1 - 10^{-A_t})\left[\frac{A_a}{A_t} + \frac{A_b}{A_t}\left(1 - \Phi_f \frac{\bar{\nu}_f}{\nu_{exc}}\right)\right] \quad (11)$$

where Φ_f is the fluorescence quantum yield of B, ν_{exc} and $\bar{\nu}_f$ are the excitation frequency and the average fluorescence frequency of B, respectively. It results that when the absorbance of the solution varies, the amount of heat released varies differently because the contribution of one species (B) is weighted by the term $(1 - \Phi_f \bar{\nu}_f / \nu_{exc})$ which accounts for the fraction of energy released as radiant energy. Thermal lens spectrometry has been applied to the investigation of dimerization equilibria of rhodamine 6G in aqueous solutions [66]. As shown in Fig. 2, deviations of the thermal lens signal with respect to the signal expected for a pure monomeric solution were much greater than variations of absorbance with respect to Beer's law. The experiments have allowed the determination of the dimerization constant of the dye which was far more precise than the values previously derived from absorption measurements.

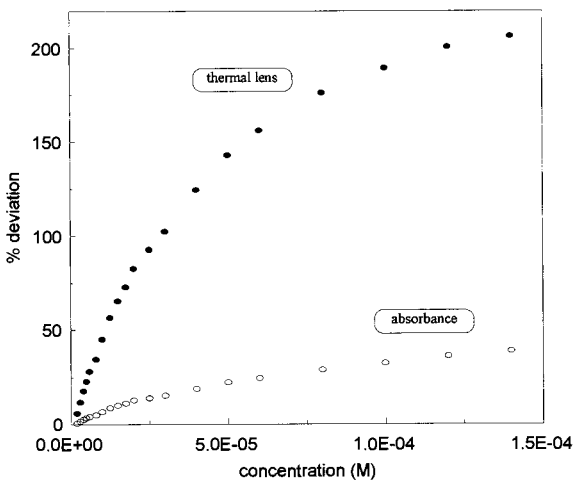

Fig. 2. Observed deviations of the thermal lens signal and absorbance as a function of concentration for rhodamine 6G in water at 488 nm, comparatively to signals calculated for a pure monomeric solution.

References

[1] H.L. Fang, R.L. Swofford, The thermal lens in absorption spectroscopy, in: D.S. Kliger (Ed.), Ultrasensitive Laser Spectroscopy, Academic Press, New York, 1983.
[2] J.M. Harris, N.J. Dovichi, Anal. Chem. 52 (1980) 695A.
[3] J.M. Harris, Thermal lens effect, in: E.H. Piepmeier (Ed.), Analytical Applications of Lasers, Wiley-Interscience, New York, 1986.
[4] J. Georges, J.M. Mermet, Analusis 16 (1988) 203.
[5] M. Franko, C.D. Tran, Rev. Sci. Instrum. 67 (1996) 1.
[6] C. Hu, J.R. Whinnery, Appl. Opt. 12 (1973) 72.
[7] S.J. Sheldon, L.V. Knight, J.M. Thorne, Appl. Opt. 21 (1982) 1663.
[8] C.A. Carter, J.M. Harris, Appl. Opt. 23 (1984) 476.
[9] T. Berthoud, N. Delorme, P. Mauchien, Anal. Chem. 57 (1985) 1216.
[10] J. Shen, R.D. Lowe, R.D. Snook, Chem. Phys. 165 (1992) 385.
[11] S.E. Bialkowski, Photothermal spectroscopy methods for chemical analysis, in: J.D. Winefordner (Ed.), Chemical Analysis, vol. 134, Wiley, New York, 1996.
[12] K. Mori, T. Imasaka, N. Ishibashi, Anal. Chem. 54 (1982) 2034.
[13] J. Georges, Talanta 41 (1994) 2015.
[14] M. Fischer, J. Georges, Anal. Chim. Acta 322 (1996) 117.
[15] R. Brennetot, J. Georges, Spectrochim. Acta 54A (1998) 111.
[16] N.J. Dovichi, CRC Crit. Rev. Anal. Chem. 17 (1987) 357.
[17] S.E. Bialkowski, Spectroscopy 1 (1986) 26.
[18] M.D. Morris, K. Peck, Anal. Chem. 58 (1986) 811A.
[19] A. Berthod, Spectrochim. Acta Rev. 13 (1990) 11.
[20] G. Ramis-Ramos, Anal. Chim. Acta 283 (1993) 623.
[21] R.D. Snook, R.D. Lowe, Analyst 120 (1995) 2051.
[22] Y. Martin-Biosca, M.C. Garcia-Alvarez-Coque, G. Ramis-Ramos, Trends Anal. Chem. 16 (1997) 342.
[23] S.E. Braslavsky, G.E. Heibel, Chem. Rev. 92 (1992) 1381.
[24] J. Georges, Spectrochim. Acta Rev. 15 (1993) 39.
[25] N.J. Dovichi, J.M. Harris, Anal. Chem. 51 (1979) 728.
[26] J.D. Spear, R.J. Silva, G.L. Klunder, R.E. Russo, Appl. Spectrosc. 47 (1993) 1580.
[27] R.A. Leach, J.M. Harris, Anal. Chem. 56 (1984) 1481.
[28] C.A. Carter, J.M. Harris, Appl. Spectrosc. 37 (1983) 166.
[29] S.E. Bialkowski, Anal. Chem. 58 (1986) 1706.
[30] S.R. Erskine, D.R. Bobbitt, Appl. Spectrosc. 42 (1988) 331.

[31] J.D. Ingle Jr, S.R. Crouch, Spectrochemical Analysis, Prentice-Hall, Englewood Cliffs New Jersey, 1988.
[32] C.E. Buffet, M.D. Morris, Appl. Spectrosc. 37 (1983) 455.
[33] E.F. Simo Alfonso, M.A. Rius Revert, M.C. Garcia Alvarez-Coque, G. Ramis-Ramos, Appl. Spectrosc. 44 (1990) 1501.
[34] Y. Martin Biosca, M.J. Medina Hernandez, M.C. Garcia-Alvarez-Coque, G. Ramis-Ramos, Anal. Chim. Acta 296 (1994) 285.
[35] A.J. Twarowski, D.S. Kliger, Chem. Phys. 20 (1977) 253.
[36] G. Ramis-Ramos, J.J. Baeza-Baeza, E.F. Simo Alfonso, Anal. Chim. Acta 296 (1994) 107.
[37] Y. Martin Biosca, E.F. Simo Alfonso, J.S. Esteve Romero, J.J. Baeza Baeza, G. Ramis-Ramos, Anal. Chim. Acta 307 (1995) 145.
[38] A. Chartier, S.E. Bialkowski, Anal. Chem. 67 (1995) 2672.
[39] R. Brennetot, J. Georges, Spectrochim. Acta A, in press.
[40] C.M. Phillips, S.R. Crouch, G.E. Leroi, Anal. Chem. 58 (1986) 1710.
[41] M. Franko, C.D. Tran, J. Phys. Chem. 95 (1991) 6688.
[42] M. Fischer, J. Georges, Anal. Chim. Acta 334 (1996) 337.
[43] T.D. Harris, A.M. Williams, Proc. SPIE-Int. Soc. Opt. Eng. 426 (1983) 105.
[44] S. Mho, E.S. Yeung, Anal. Chem. 57 (1985) 2253.
[45] R.D. Lowe, R.D. Snook, Anal. Chim. Acta 250 (1991) 95.
[46] A. Chartier, C.G. Fox, J. Georges, Analyst 118 (1993) 157.
[47] N.J. Dovichi, J.M. Harris, Anal. Chem. 52 (1980) 2338.
[48] T.J. Pang, M.D. Morris, Anal. Chem. 57 (1985) 2153.
[49] T. Berthoud, N. Delorme, Appl. Spectrosc. 41 (1987) 15.
[50] S.R. Erskine, D.R. Bobbitt, Appl. Spectrosc. 43 (1989) 668.
[51] J.B. Thorne, D.R. Bobbitt, Appl. Spectrosc. 47 (1993) 360.
[52] D.M. Plumb, J.M. Harris, Appl. Spectrosc. 46 (1992) 1346.
[53] Z.A. Yasa, W.B. Jackson, N.M. Amer, Appl. Opt. 21 (1982) 21.
[54] J.F. Power, C.H. Langford, Anal. Chem. 60 (1988) 842.
[55] D.W. Gutzman, C.H. Langford, Anal. Chim. Acta 283 (1993) 773.
[56] Q.E. Khuen, W. Faubel, H.J. Hache, Fresenius J. Anal. Chem. 348 (1994) 533.
[57] J.D. Spear, R.E. Russo, R.J. Silva, Appl. Opt. 29 (1990) 4225.
[58] N. Omenetto, Appl. Phys. B 46 (1988) 209.
[59] T. Sawada, S. Oda, H. Shimizu, H. Kamada, Anal. Chem. 51 (1979) 688.
[60] N. Omenetto, P. Cavalli, G. Rossi, G. Bidoglio, G.C. Turk, J. Anal. At. Spectrosc. 2 (1987) 579.
[61] G. Bidoglio, G. Tanet, P. Cavalli, N. Omenetto, Inorg. Chim. Acta 140 (1987) 293.
[62] C. Moulin, N. Delorme, T. Berthoud, P. Mauchien, Radiochim. Acta 44/45 (1988) 103.
[63] M. Franko, C.D. Tran, Anal. Chem. 61 (1989) 1660; Chem. Phys. Lett. 158 (1989) 51.
[64] M. Franko, C.D. Tran, Rev. Sci. Instrum. 62 (1991) 2438.
[65] J. Georges, Spectrochim. Acta 51A (1995) 985.
[66] M. Fischer, J. Georges, Spectrochim. Acta 53A (1997) 1419.

ELSEVIER

Talanta 48 (1999) 511–516

Talanta

Spectrophotometric determination of lead in biological samples with dibromo-*p*-methyl-methylsulfonazo

Zaijun Li [a,*], Zhenzhong Zhu [a], Yepu Chen [a], Chung-Gin Hsu [b], Jiaomai Pan [b]

[a] *Department of Chemical Engineering, Wuxi University of Light Industry, Wuxi 214036, People's Republic of China*
[b] *Department of Chemistry, East China Normal University, Shanghai 200062, People's Republic of China*

Received 8 April 1998; received in revised form 30 June 1998; accepted 10 July 1998

Abstract

A new highly sensitive and selective chromogenic reagent, dibromo-*p*-methyl-methylsulfonazo (DBM-MSA), was studied for determination of lead. In 0.24 mol l^{-1} phosphoric acid medium, which greatly increases the selectivity, lead reacts with DBM-MSA to form a 1:2 blue complex which has a sensitive absorption peak at 642 nm. Under the optimal conditions, Beer's law was obeyed over the range 0–0.6 μg ml^{-1} Pb(II). The molar absorptivity and Sandell's sensitivity are 1.02×10^5 l mol^{-1} cm^{-1} and 0.00203 μg cm^{-2}, respectively. The limit of quantification, limit of detection and relative standard deviations were found to be 7.30 and 2.21 ng ml^{-1} and 1.1%, respectively. It is found that, except for Ca(II) and Ba(II), all foreign ions studied do not interfere with the determination. The interference caused by Ca(II) and Ba(II) can be easily eliminated by prior extraction with potassium iodide-methylisobutylketone. The method has been applied to the determination of lead in some biological samples with satisfactory results.

Keywords: Spectrophotometry; Lead determination; Dibromo-*p*-methyl-methylsulfonazo; Biological samples

1. Introduction

The determination of lead is becoming increasingly important. However, the number of reagents available for the spectrophotometric determination of lead is relatively small. The main reagents are dithiazone [1,2], diethyldithio-carbamate [3,4], 4-(2-pyridilazo)resorcinol [5], diphenylcarbazone [6], Arsenazo III [7], 2-(2-thiazolylazo)-*p*-cresol [8], and porphyrin compounds [9,10]. Although each chromogenic system has its advantages and disadvantages with respect to sensitivity, selectivity and rapidity due to using different chromogenic reagents, most of them require extraction using an organic solvent, surfactants or even fierce toxic cyanide as a masking agent to increasing the sensitivity or selectivity (see Table 1).

Dibromo-*p*-methyl-methylsulfonazo (DBM-MSA) (**1**), an asymmetric bisazo derivative of chromotropic acid with one *o*-sulfonic functional group, synthesized in this laboratory [11], has been used for the spectrophotometric determination of barium [12] and strontium [13]. It was

* Corresponding author. Fax: +86 510 5865424; e-mail: cheng@wxuli.edu.cn

0039-9140/99/$ - see front matter
PII S0039-9140(98)00247-1

Table 1
Review of some spectrophotometric methods for the determination of lead

Reagent	Phase	λ_{max} (nm)	$\epsilon \times 10^4$	Remarks	Reference
Dithizone	CCl_4	520	2.5	Light sensitive Hg, Zn, Cu, Fe interfere	[2]
Diethyldithio-carbamate	CCl_4	435	1.3		[4]
4-(2-Pyridilazo)	Aqueous	520	4.3	Ag, Cd, Co, Cu, Hg, Ni, Zn interfere	[5]
resorcinol					
Diphenylcarbazone	Aqueous pH = 9.0–10.4	525	7.2		[6]
Arsenazo III	Aqueous pH = 2.5–4.5	660	3	Fe, Al, Cu, Th, Ti, U interfere	[7]
2-(2-Thiazolylazo)	Aqueous	650	2.07	Cu, Ni, Co, Zn, Fe, Cd interfere	[8]
-*p*-cresol	pH = 9.0–10.0				
Porphyrin compounds	Aqueous pH = 10.4	479	22	Cu, Zn, Ni, Hg, Fe, Mn, Cd, Ca, Mg interfere	[10]

found that DBM-MSA also gave a sensitive reaction with lead in acidic medium. In this paper, we develop a spectrophotometric method for lead determination with DBM-MSA in phosphoric acid medium, as well as applying it to the determination of lead in some biological samples.

This method is one of the most convenient and efficient methods for the determination of lead at the present time.

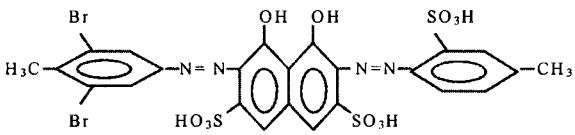

(I)

2. Experimental

2.1. Synthesis of DBM-MSA

2.1.1. p-Methylphenylamine-2-sulfonic acid

p-Methylphenylamine (50 g) and concentrated H_2SO_4 (50 g) were added to a three-necked flask, heated on an oil bath at 210–220°C for 2 h, then cooled to crystallize. Activated carbon was added and the mixture re-crystallized with water. *p*-Methylphenylamine-2-sulfonic acid was obtained with a productive rate of 68.6%.

2.1.2. 2,6-Dibromo-p-methylphenylamine

p-Methylphenylamine (2.0 g) was dissolved in 25 ml of 1:1 HCl, and 2 ml of bromine (premixed with 5 ml of acetic acid) added with a dropping funnel while stirring, maintaining the reaction temperature below 40°C. After stirring for 3 h, the precipitate was filtered, washed with water and dried at 80°C. 2.6-Dibromo-*p*-methylphenylamine was obtained with a productive rate of 88%.

2.1.3. p-Methylsulfonazo

p-Methylphenylamine-2-sulfonic acid (4.0 g) was dissolved in 30 ml of 1 mol l^{-1} NaOH, and 2.0 g $NaNO_2$ were added and mixed well. The mixture was then added dropwise to 20 ml of 1:1 cold HCl to diazotize, and the reaction temperature was maintained below 5°C. Chromotropic acid (8.0 g) was dissolved in 50 ml of 40% (W/W) NaAc solution, keeping the temperature below 5°C, dropped into the above diazotized solution and left to stand overnight. The mixture was then acidified to pH 1 with concentrated HCl, left to stand for 4 h, and the precipitate filtered, washed with 50 ml of 1:1 HCl and dried. *p*-Methylsulfonazo was obtained with a productive rate of 85.7%.

2.1.4. Dibromo-p-methyl-methylsulfonazo

Dibromo-*p*-methylphenylamine (1.1 g) was dissolved in 15 ml of 1:1 HCl, drops of $NaNO_2$ solution (0.4 g of $NaNO_2$ in 3 ml of H_2O) added and the temperature maintained below 5°C. LiOH (5.0 g) was dissolved in 20 ml of H_2O and 2.0 g of *p*-methylsulfonazo added, controlling the temperature below 5°C, the above diazotized solution added dropwise and the mixture left to stand for 4–5 h. After filtering, 20 ml of concentrated HCl were added in the aqueous phase to precipitate DBM-MSA and the mixture was left to stand for 4 h, then the precipitate was filtered, washed with 50 ml of 1:1 HCl and dried under the infrared lamp. The crude product (DBM-MSA) was obtained with a productive rate of 42.4%.

2.1.5. Purification of DBM-MSA

Crude DBM-MSA (1 g) was dissolved in 100 ml H_2O and extracted with 100 ml of *n*-butanol several times. The organic phase was discarded and all the aqueous phase mixed. Concentrated HCl (10 ml) was added along with 100 ml of *n*-butanol for extraction, then the aqueous phase was discarded. This was followed by addition of 25 ml of 1 mol l^{-1} NaOH to the organic phase to twice perform back-extraction. Concentrated HCl (20 ml) was added to the aqueous phase, stood overnight, filtered and dried under the infrared lamp.

The purity of DBM-MSA was checked by paper chromatography using a mixture of 5% sodium citrate and 25% ammonia (5 + 2) as an eluent. A single blue band existed to confirm that DBM-MSA was pure. Thermogravimetry analysis showed that DBM-MSA contained two molecules of water and the result of elemental analysis corresponded with the composition of DBM-MSA.

2.2. Apparatus

Absorption spectra and absorbance were recorded and measured with a Beckman DU-7HS spectrophotometer, using a 2.0 cm cell.

2.3. Reagents

Unless otherwise stated, all reagents used were of analytical grade and all solutions were prepared with distilled, deionized water.

2.3.1. Standard lead solution

A standard lead solution was prepared by dissolving lead oxide (specpure) in 2 mol l^{-1} HNO_3, evaporating the solution to remove the excess acid, and diluting with (1 + 100) HNO_3 to a given volume. The working standard solution (10 μg ml^{-1}) was prepared by diluting the standard lead solution with water.

2.3.2. Dibromo-p-methyl-methylsulfonazo

A 0.05% solution was prepared by dissolving 125 mg of DBM-MSA in 250 ml water. DBM-MSA was synthesized as previously described in Ref. [11].

2.3.3. Phosphoric acid

A 3 mol l^{-1} solution was prepared by diluting concentrated H_3PO_4 with water.

2.4. Procedure

A solution containing less than 15 μg of lead was transferred into a 25 ml calibrated flask. 2 milliliters of 3.0 mol l^{-1} H_3PO_4 and 5.0 ml of 0.05% DBM-MSA solution was added successively, the solution was diluted to the mark with water and mixed well. The absorbance at 642 nm in a 2 cm cell was measured versus the reagent blank.

3. Results and discussion

3.1. Absorption spectra

Absorption spectra of DBM-MSA at various acidities are shown in Fig. 1. It can be found that the reagent absorption is greatly influenced by acidity. At 642 nm, which is the maximum absorption peak of the Pb–DBM-MSA complex, the absorbance of the reagent first decreased gradually (pH = 13 ~ 4) and then increased slightly

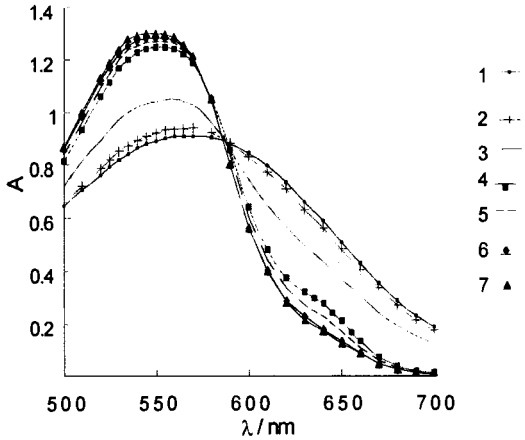

Fig. 1. Effect of pH on the absorbance of DBM-MSA. (1) pH l3, (2) pH 7.2, (3) pH 6.8, (4) pH 0.5, (5) pH 1.

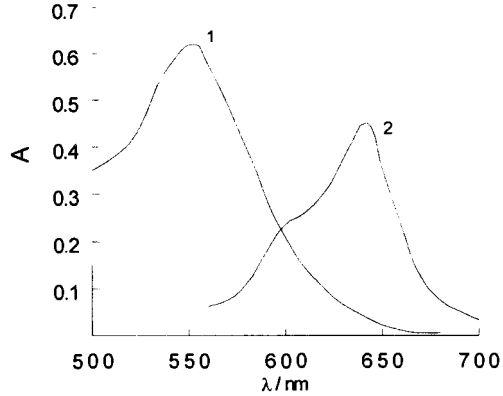

Fig. 3. Absorption spectra of the Pb(II)–DBM-MSA complex and DBM-MSA. 1.1 ml of 10 μg ml^{-1} Pb(II) + 5.0 ml of 0.05% DBM-MSA + 2.0 ml of 3.0 mol l^{-1} H_3PO_4. (1) Reagent against water and (2) complex against reagent blank.

($pH \leq 1$). The influence of the pH on the absorbance of the Pb(II)–DBM-MSA complex is shown in Fig. 2. At $pH \leq 3$, the complex absorbance remained almost constant and at a maximum. We controlled the final pH by adding 2 ml of 3 mol l^{-1} H_3PO_4 to the 25 ml calibrated flask (pH about 1.4) in order to keep the color reaction reproducible, constant and sensitive.

The absorption spectra of lead with DBM-MSA complex is shown in Fig. 3. The maximum absorption of DBM-MSA was 554 nm, whereas the Pb–DBM-MSA complex gave absorption peaks at 642 nm. Therefore, a wavelength of 642 nm was chosen for the spectrophotometric measurement of lead complex against reagent blank.

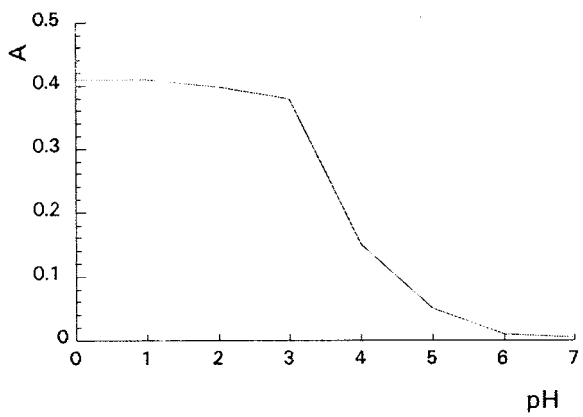

Fig. 2. Effect of pH on the absorbance of DBM-MSA complex. 1 ml of 10 μg ml^{-1} Pb(II) + 5.0 ml of 0.05% DBM-MSA. $\lambda = 642$ nm.

3.2. Effect of reaction media

The absorbances of the Pb(II)–DBM-MSA complex were almost unchanged when H_2SO_4, HCl, HNO_3 and H_3PO_4 were chosen as the reaction media. Owing to the fact that H_3PO_4 can combine iron and increase the method's selectivity, we chose H_3PO_4 as the reaction medium.

In 25 ml of solution, the presence of 1.0–5.0 ml of 3.0 mol l^{-1} H_3PO_4 gave a maximum and constant absorbance. An excess of H_3PO_4, over 5.0 ml, could cause the absorbance to decrease. An optimum amount of 2.0 ml of 3.0 mol l^{-1} H_3PO_4 is recommended, which corresponds to 0.24 mol l^{-1} H_3PO_4 in the final solution.

3.3. Effect of amounts of DBM-MSA

With the increase of the volume of 0.05% DBM-MSA, the absorbance increased rapidly, followed by remaining almost at a maximum and unchanged; after that it dropped slowly. In 25 ml of solution, the optimum volume of 0.05% DBM-MSA was 3.0–7.0 ml. Thus, an addition of 5.0 ml of 0.05% DBM-MSA is recommended.

3.4. Characteristics of the complex

The color complex could be formed immediately at 0–20°C. The absorbance of the complex could stabilize for at least 12 h under 20°C. The composition ratio of the Pb(II)–DBM-MSA complex obtained using Job's method of continuous variation and the slope-ratio method was 1:2 (Pb(II):DBM-MSA).

3.5. Analytical characteristics

The calibration graph was constructed according to the usual procedure (see Section 2.4). Beer's law was obeyed over the range 0–0.6 μg ml^{-1} Pb(II). The molar absorptivity and Sandell's sensitivity were calculated from the slope of the calibration graph to be 1.02×10^5 l mol^{-1} cm^{-1} and 0.00203 μg cm^{-2}, respectively. The limit of detection as defined by IUPAC [14] and the limit of quantitation [15,16] were found to be 2.21 and 7.30 ng ml^{-1}, respectively. Ten replicate analyses of a test solution containing 10 μg of lead by the procedure gave a relative standard deviation of 1.1%. According to the procedure, another calibration graph, constructed on various lead concentrations plus 300 mg Ca(II) with potassium iodide-methylisobutylketone (KI-MIBK) for extraction and determination [17], were almost the same as that discussed. This indicates that the extraction has no effect on the results.

3.6. Effect of foreign ions

Under the optimum conditions, the effects of various foreign ions on the determination of 10 μg Pb(II) were examined separately. With a relative error of less than $\pm 5\%$, the tolerance limits for various foreign ions are listed in Table 2.

It is found that, except for Ca(II) and Ba(II), all the foreign ions studied do not interfere with the determination. The interference caused by Ca(II) and Ba(II) can be easily reduced by prior extraction with KI-MIBK from 0.002 to 400 and 200 mg, respectively.

3.7. Sample analysis

The proposed method was applied to the determination of Pb(II) in a biological sample. Prior to the determination, the samples were pretreated in the following way.

We weighed out 3.0–5.0 g of the sample, dried it in an electric furnace at 550–600°C and ashed it in a muffle furnace. After that, the ash was dissolved with 5 ml of 0.1 mol l^{-1} HNO_3 and the solution transferred to a 60 ml separating funnel. We added 1 ml of 25% (W/W) KI, 2.5 ml of 6 mol l^{-1} HCl and diluted to 25 ml with water. The solution was extracted with 10 ml of MIBK and the aqueous solution transferred to another 60 ml separating funnel. The aqueous solution was re-extracted with 10 ml of MIBK, the aqueous layer discarded and the organic phase washed with 5 ml of water. The organic phase was merged, then back-extracted with 1 ml of 2 mol l^{-1} NaOH and 9 ml of water. The aqueous phase was transferred into a 25 ml calibrated flask, and then 1.0 ml of

Table 2
Effect of foreign ions

Foreign ions	Amout added (mg)	Pb(II)	Recovery (%)
K(I)	100.0	10.0	100
Na(I)	100.0	10.0	100
NH_4(I)	100.0	10.0	100
F^-	100.0	10.0	100
Cl^-	100.0	10.0	100
PO_4^{3-}	100.0	10.0	100
NO_3^-	100.0	10.0	100
SO_4^{2-}	100.0	9.9	99
Ag(I)	20.0	10.0	100
Ni(II)	20.0	10.1	101
Al(III)	10.0	10.0	100
Cr(III)	10.0	10.1	101
Cu(II)	10.0	10.2	102
Fe(III)	10.0	10.1	101
Zn(II)	10.0	10.0	100
Mn(II)	2.0	10.1	101
Hg(II)	1.5	10.1	101
Mo(VI)	1.0	10.1	101
Cd(II)	0.5	10.0	100
Mg(II)	0.5	10.4	104
Ti(IV)	0.2	10.3	103
Ba(II)	0.002	10.5	105
Ca(II)	0.002	10.5	105

Table 3
Determination of Pb(II) in biological samples

Samples	Found by the proposed method (μg g^{-1})[a]	Found by atomic absorption spectroscopy (μg g^{-1})[a]
Malt extract	0.32 ± 0.004 $F = 1.78$, $t =$ 0.04	0.31 ± 0.03
Pearl	1.02 ± 0.014 $F = 1.15$, $t =$ 0.01	1.03 ± 0.015
Rice	0.31 ± 0.004 $F = 1.56$, $t =$ 0.15	0.34 ± 0.005
Hops	0.46 ± 0.008 $F = 1.56$, $t =$ P0.05	0.44 ± 0.010

[a] $X \pm St/n^{1/2}$ ($n = 5$); the t- and F-values refer to comparison of the proposed method with the atomic absorption spectroscopy method. Theoretical values at 95% confidence limits: $F = 6.39$, $t = 2.78$.

2.0 mol l^{-1} HCl, 2.0 ml of 3.0 mol l^{-1} H_3PO_4 and 5.0 ml 0.05% DBM-MSA were added, and the solution diluted to the mark with water. The absorbance was measured at 642 nm in a 2 cm cell against the correspondent blank. The results are good agreement with those for lead found by atomic absorption spectroscopy (see Table 3).

In order to check the accuracy of the proposed method, a study was carried out on various amounts of lead for extraction and determination. The relative difference between the absorbances obtained with and without extraction did not exceed $\pm 0.5\%$ and the extraction recovery ranged from 99.5 to 99.9%.

3.8. Conclusions

First, the proposed method is very simple and rapid. The chromogenic reaction completed immediately and the formed complex was stable for at least 12 h at 0–20°C. The reaction medium, 0.24 mol l^{-1} H_3PO_4, is more simple than that of other methods [1–10].

Second, the proposed method is sensitive. Its molar absorptivity was much better than that in Refs. [1–8] and comparable with the latest results reported in Refs. [9,10].

Third, the proposed method has very high selectivity. Its selectivity is much better than that of any other regents reported for the determination of lead. Nearly all the anions and most of the cations cannot interfere with the chromogenic reaction. The interference by Ca(II) and Ba(II) can be easily reduced by extraction with KI-MIBK.

So, the proposed method can be used routinely for the determination of lead in biological materials, alloys and other samples.

References

[1] Z. Marczenko, Spectrophotometric Determination of Elements, Wiley, New York, 1973.
[2] J. Pan, Y. Chen, H. Yan, Chromagenic Reagents and their Applications in Spectrophotometric Analysis, Shanghai Science and Technology Press, Shanghai, 1981, p. 283
[3] J.F. Tertoolen, D.A. Detmar, C. Buijze, Z. Anal. Chem. 167 (1959) 401.
[4] L.C. Willemsons, Handbook of Lead Chemicals, Project LC-116, 1nternational Lead Zinc Research Organisation, New York, 1986
[5] R.M. Dagnall, T.S. West, P. Young, Talanta 12 (1965) 583.
[6] N. Trinder, Analyst 91 (1966) 587.
[7] M. Xiao, Lihua jianyan Huaxue Fence 24 (1988) 130.
[8] S.L.C. Ferreira, M.G.M. Andrade, I.P. Lobo, A.C.S. Costa, Anal. Lett. 24 (1991) 1675.
[9] H. Liu, B. Wu, Y. Qu, Lihua Jianyan Huaxue Fence 22 (1986) 118, 184, 251
[10] J. Pan, Z. Li, C.-G. Hsu, Fenxi ShiYanShi 13 (1994) 29.
[11] Y. Liu, J. Pan, C.-G. Hsu, Huaxue ShiJi 18 (1996) 1.
[12] J. Pan, Y. Liu, C.-G. Hsu, Fenxi ShiYanShi 15 (1996) 30.
[13] Y. Liu, J. Pan, C.-G. Hsu, Lihua Jianyan Huaxue Fence 32 (1996) 9.
[14] G.L. Long, J.D. Wineforder, Anal. Chem. 55 (1983) 712A.
[15] G.L. Long, J.D. Wineforder, Anal. Chem. 52 (1980) 2242.
[16] J. Medinilla, F. Ales, F.G. Sanchez, Talanta 33 (1986) 329.
[17] C.L. Luke, Anal. Chim. Acta 39 (1967) 447.

ELSEVIER

Talanta 48 (1999) 517–525

Talanta

Determination of rare earth impurities in high purity gadolinium oxide by inductively coupled plasma mass spectrometry after 2-ethylhexylhydrogen-ethylhexy phosphonate extraction chromatographic separation

Xinde Cao [a,b,*], Ming Yin [a], Bing Li [a]

[a] *Institute of Rock and Mineral Analysis, Chinese Academy of Geological Sciences, Beijing 100037, People's Republic of China*
[b] *Department of Chemistry, University of Science and Technology of China, Hefei 230026, People's Republic of China*

Received 9 March 1998; received in revised form 6 July 1998; accepted 15 July 1998

Abstract

A method was developed for the determination of rare earth impurities in high purity Gd_2O_3 by inductively coupled plasma mass spectrometry (ICP-MS). The matrix suppression effect of Gd_2O_3 on signals of rare earth impurities was compensated for by Re internal standardization. The spectra overlap interferences from GdH, GdO, $GdOH_n$ ($n=1-3$) on Tb, Tm, Yb and Lu were eliminated by 2-thylhexylhydrogen-2-ethylhexy phosphonate (EHEHP) extraction chromatographic separation. The detection limits for REEs were 0.005–0.017 ng ml^{-1} in solution and 0.002–0.05 μg g^{-1} in solid. Recoveries of spiked sample for REEs were from 88 to 121% with the precision of 1.0–7.5% RSD. Determination of trace REEs in two Gd_2O_3 samples were performed. The method can be applied to analysis of 99.99–99.9999% high purity Gd_2O_3.

Keywords: Inductively coupled plasma mass spectrometry; High purity Gd_2O_3; Rare earth impurity; Extraction chromatographic separation

1. Introduction

With the development of applications of high purity rare earth element (REE) products in many industrial fields such as the semiconductor, high temperature superconductor and optoelectronics areas, the demand for purity analysis of REE products is increasing. As a result, it is critically important to be able to accurately determine trace levels of REE impurities in high purity REE products. Traditionally, X-ray fluorescence (XRF) [1], neutron activation analysis (NAA) [2] and inductively coupled plasma emission spectrometry (ICP-AES) [3] have been used for REE estimation. However, these methods are only effective for the analysis of 99–99.99% purity of REE products but not adequate for REE products with purity of superior to 99.99% in terms of sensitivity, analysis time and data interpretation.

* Corresponding author. Fax: +86 551 3631760; e-mail: Wang Cheng@bbs.ustc.edu.cn

0039-9140/99/$ - see front matter
PII S0039-9140(98)00251-3

As a result of its inherent, low detection limits, simple spectra, wide dynamic range and multi-element determination capability, inductively coupled plasma mass spectrometry has been applied to determine REEs in some fields. Many reports are available on REE determination using ICP-MS, mainly in geochemical fields [4]. In recent years, there have been a few papers published for REE purity estimation by ICP-MS [5–9]. The major problems encountered in the application of the technique to the determination of trace REEs in high purity REE products are the matrix suppression effect and the spectra overlap interferences originated from matrix-induced polyatomic ions. The matrix suppression effect could be compensated for by internal standardization [10,11]. The spectra interferences from the single element matrix with multi-isotopes are so complicated that some REEs could not be determined directly by ICP-MS. For industrial high-purity REE products, the concentration difference between matrix and REE impurities can be up to 10^6 or more. Large differences in concentration cause serious interference problems. Such interferences could be eliminated by solvent extraction [9] or using ETV-ICP-MS [5] and IC-ICP-MS [6]. In case of high-purity Gd_2O_3, polyatomic ions from Gd matrix with O and H cover a wide range of masses, leading to the failure in direct determination of Tb, Tm, Yb and Lu by ICP-MS.

Several papers were reported for REE impurities in high-purity Gd_2O_3. Liu et al. [12] determined nine REE impurities in high-purity Gd_2O_3 by ICP-MS based on Re internal standardization, but no data for Tb, Tm, Yb and Lu were given due to the spectra overlap interferences from matrix induced polyatomic ions. Kawabata et al. [6] used ion chromatorgraphy to separate individual REE in order of elution time before sample introduction into ICP. Thus ICP-MS analysis could be carried out sequentially for each REE. In this case, interferences from polyatomic ions were virtually eliminated, but a high concentration of organic eluent and buffer agents might provoke a carbon deposition at a sampling orifice of the ICP-MS system or cause clogging of the ICP torch, resulting in a drift in sensitivity of the instrument. Takaku et al. [13] utilized a high-resolution mass spectrometer for the direct determination of trace levels of REE impurities in high-purity Gd_2O_3. In their work, doubly charged ions were used for the determination of Tb, Tm, Yb and Lu in order to avoid spectra overlap from matrix induced polyatomic ions. However, the sensitivities for these elements were not high enough because the production ratio of doubly to singly charged ions is usually low.

In this work, (EHEHP) extraction chromatography was used to separate Tb, Tm, Yb and Lu from Gd_2O_3 matrix before their determination by ICP-MS and other then REE impurities free from spectra overlap interferences were directly determined by ICP-MS with Re as an internal standard.

2. Experimental

2.1. Instrument and reagents

VG Plasma Quad ICP-MS (VG Elemental, Winsford, Cheshire, UK) was used in this work. The operating conditions used in this work are presented in Table 1. A model 501 constant-temperature water bath (Shanghi, China) was used to control the temperature at 50 ± 1°C in the course of chromatographic separation. A glass column ($\varnothing 20 \times 850$ mm) with constant temperature jacket was used for chromatographic separation.

A 12-channel peristaltic pump (GILSON, France) was adopted to introduce solutions to the column at a constant speed. (EHEHP) resin was available from Yuelong Metal Company of Shanghai. Deionized water purified further by distillation was used throughout. All acids were of supra-pure grade (Beijing Chemical Plant). A 1 μg ml^{-1} mixed REE standard solution (2% (v/v) HNO_3) was prepared from 1 mg ml^{-1} individual stock solutions (Center of National Standard Material, China). High-purity Gd_2O_3 samples were supplied by the Beijing General Institute for non-ferrous metals.

Table 1
The operation parameters for plasma quard ICP-MS

Inductively coupled plasma		Measurement conditions	
Forward power	1250 W	Sample uptake	1.0 ml min^{-1}
Reflected power	<5 W	MCA channels	2048
Coolant gas flow rate	15 l min^{-1}	Dwell time	250 μs
Auxiliary gas flow rate	0.5 l min^{-1}	Sweeps	120
Nebulizer gas flow rate	0.80 l min^{-1}		
Interface		Spectrometer	
Sampling depth	10 mm	Chamber vacuum	$2.0–3.0\times10^{-4}$ Pa
Diameter of sampling cone (Ni)	1.0 mm	Resolution (5% peak height)	0.6–0.7 amu
Diameter of skimmer cone (Ni)	0.7 mm	Ion lens system	optimized by ^{115}In

2.2. Sample preparation

2.2.1. Sample preparation for direct ICP-MS analysis

A powdered Gd_2O_3 sample (10 mg) was decomposed with 4 ml of 6.2% HNO_3. The solution was transferred into a 10 ml volumetric flask, added by 1 μg Re internal standard and diluted to volume with water. The sample solution was for direct ICP-MS analysis.

2.2.2. Sample preparation for chromatographic separation

A powdered Gd_2O_3 (10 mg) sample was decomposed with 2 ml of 50% HCl and evaporated to dryness. The dried residue was dissolved by heating with 10 ml of 1% HCl and cooled for chromatographic separation.

2.2.3. Column preparation

A total of 100 g of (EHEHP) resin was soaked in 50% HCl for 12 h and then loaded into the glass column. The resin was washed with 50% HCl until total removal of Fe^{3+} was achieved. After washing to pH 4–5 with water, the resin was preconditioned with 1% HCl.

2.2.4. Chromatographic separation

The sample solution for chromatographic separation above was loaded quantitatively into the column at a flow rate of 0.3 ml min^{-1}. After rinsing the top of the column with 10 ml of 1% HCl, 250 ml of 5.8% HCl were used to wash off La, Ce Pr, Nd, Sm, Eu and most of matrix Gd. Then, Tb (also Dy) was eluted with 70 ml of 17% HCl and collected in a 200 ml beaker. Another 150 ml of 17% HCl were used to remove Ho and Er from the column. Then, 150 ml of 50% HCl were passed through the column. This fraction containing Tm, Yb and Lu was collected in another 200 ml beaker. The tow fractions containing Tb and Tm, Yb, Lu were evaporated to near dryness on a hot plate and the residues were dissolved with 4 ml of 6.2% HNO_3 and transferred into a 10 ml flask, respectively. Re internal standard (1 μg) was added to each flask and diluted to the volume for determinations of Tb, Tm, Yb and Lu by ICP-MS.

In order to avoid contamination, it is necessary to purify deionized water, to treat glassware with care and to process in a clean atmosphere.

2.3. ICP-MP determination

Higher abundant isotopes of the analytes were selected along with consideration of isotropes free from isobaric and polyatomic ion interferences. The limit of detection (LOD) is defined as the corresponding concentration values of three times of the standard deviation (3σ) in ten determinations of 2% HNO_3 blank solution, and the limit of quantitation (LOQ) defined as the corresponding concentration values of ten times the standard deviation (10σ) and with consideration of dilution factors of the samples. The LOD and LOQ values for REEs are shown in Table 2.

Re was used as an internal standard to correct instrumental drift and signal suppression effect. The instrument software automatically performs blank subtraction, calibration and calculation of analyte concentrations of synthetic standards and unknown samples.

3. Results and discussion

3.1. Spectra overlap interferences originated from Matrix Gd

Many investigations have been reported on spectroscopic interferences in determination of REEs by ICP-MS [14,15]. The results suggest that there exist few interferences from background and very low background noise is observed in the mass range of REEs. It has been proven that the main interferences in the analysis of high-purity REE products come from the spectra overlap due to the matrix induced polyatomic ions [16]. Gd has seven isotopes and polyatomic ions from Gd matrix cover a wide range of masses from 168 to 78 m/z, which make no isotopes available for Tm, Yb and Lu. Also ^{158}GdH overlaps with ^{159}Tb (mono-isotope element), making the direct determination of Tb impossible. The spectra interferences originated from matrix Gd and their interference factors are shown in Table 3.

Table 2
Isotopes, detection limits, quantitation limits of the analytes

Element	Isotope (abundance%)	LOD (ng ml^{-1}) (3σ, $n=10$)	LOQ (μg g^{-1}) (10σ, $n=10$)
Y	89 (100)	0.009	0.03
La	139 (99.9)	0.007	0.02
Ce	140 (88.5)	0.015	0.05
Pr	141 (100)	0.009	0.03
Nd	146 (17.2)	0.017	0.05
Sm	147 (15.0)	0.013	0.04
Eu	153 (52.2)	0.006	0.02
Tb	159 (100)	0.006	0.02
Dy	163 (24.9)	0.011	0.03
Ho	165 (100)	0.005	0.02
Er	166 (33.6)	0.008	0.03
Tm	169 (100)	0.005	0.02
Yb	172 (21.9)	0.009	0.03
Lu	175 (97.4)	0.006	0.02

As can be seen clearly in Table 3, the levels of interference coefficients (GdX^+/Gd^+) for different polyatomic ions increase in order of $GdOH_3^+$, GdH^+, $GdOH_2^+$, $GdOH^+$ and GdO^+. The inference from GdO^+ is the most serious with a interference coefficient (GdO^+/Gd^+) of 9×10^{-3}. In the case of high-purity REE product analysis the concentration of matrix is usually up to 1 mg ml^{-1}. So the interference even for GdH^+ (with interference coefficient of 7×10^{-5}) can not be neglected. In order to determine Tb, Tm, Yb and Lu, matrix separation procedure should be considered.

3.2. Matrix suppression effect and internal standardization

Matrix suppression effect is another main problem in high-purity REE product analysis. Much research [17–19] has been carried out on matrix effect in ICP-MS analysis. Generally, moderate amounts (0.1–1%) of matrix ion can change analyte signals significantly. Drift of analyte sensitivity and calibration curves can limit both accuracy and precision. In this work, a sample dilution factor of 1000 (1 mg ml^{-1} of GD_2O_3) was used for direct determination of REE impurities, and analyte signal declines of 15–30% for most individual REEs were observed. Internal standardization has been proposed as a possible remedy for matrix effect and instrumental drift [7]. In this study, Re were used as internal standards to effectively compensate the matrix effect and instrumental drift.

3.3. Conditions of extraction chromatographic separation

3.3.1. Gradient elution chromatrography

In order to separate Tb, Tm, Yb, and Lu from matrix of Gd_2O_3 effectively, gradient elution was performed and gradient elution curves were made by chromatographic separation of a synthetic sample. Terbium (with single isotope ^{159}Tb) is next to gadolinium in atomic number and suffers from a spectra overlap interference of $^{158}GdH^+$.

Table 3
The spectra overlap interferences originated from matrix Gd and their interference factors

Matrix (abundance%)	Interfering species			Interfered isotopes (abundance%)	Interference coefficient	Unavailable element
	MH^+	MO^+	MOH_n^+			
^{154}Gd (2.2)		$^{154}GdO^+$		^{170}Er (15.0)	9×10^{-3} (GdO^+/Gd^+)	
^{155}Gd (14.8)		$^{155}GdO^+$	$^{154}GdOH^+$	^{171}Yb (14.3)		
^{156}Gd (20.5)		$^{156}GdO^+$	$^{155}GdOH^+$	^{172}Yb (21.9)	2×10^{-3} ($GdOH^+/Gd^+$)	
			$^{154}GdOH_z^+$			
^{157}Gd (15.7)		$^{157}GdO^+$	$^{156}GdOH^+$	^{173}Yb (16.2)	7×10^{-5} ($GdOH_2^+/Gd^+$)	Yb
			$^{155}GdOH_2^+$			
			$^{154}GdOH_3^+$			
^{158}Gd (24.8)	$^{158}GdH^+$			^{159}Tb (100)	7×10^{-5} (GdH^+/Gd^+)	Tb
		$^{158}GdO^+$	$^{157}GdOH^+$	^{174}Yb (31.8)		
			$^{156}GdOH_3^+$			Lu
			$^{156}GdOH_3^+$	^{175}Lu (97.4)		
^{160}Gd (21.7)	$^{160}GdH^+$			^{161}Dy (18.9)		
		$^{160}GdO^+$		^{176}Lu (2.6)		
				^{176}Yb (2.6)		
			$^{160}GDOH_3^+$		9×10^{-6} ($GdOH_3^+Gd^+$)	

In practice, it is not necessary to separate Tb from Gd completely because of very low interference coefficient for GdH^+. A total of 250 ml of 5.8% HCl removed a large portion of the Gd matrix from column. Then 220 ml of 17% HCl passed through the column to recover Tb and washed out a small portion of Gd remaining on the column. In Tb fraction the concentration of Gd was <100 mg ml^{-1} and the interference from $^{158}GdH^+$ on ^{159}Tb could be neglected. At this time, Tm, Yb and Lu still remained on the column. Finally, 150 ml of 50% HCl were used to collect Tm, Yb and Lu. In fractions of Tm, Yb and Lu, the concentration of Gd was <10 ng ml^{-1} and the interference from polyatomic ions on Tm, Yb and Lu were negligible. Fig. 1 illustrates the gradient elution chromatographic curves of REEs.

3.3.2. Flow rate of elution on chromatographic separation

Three flow rates of elution of 1.0–1.1, 1.3–1.4 and 1.6–1.7 ml min^{-1} were tested. The results show that the flow rate of elution slightly influences the position and shape of analyte peaks but significantly influences the amount of Gd remaining in Tb fraction and Tm, Yb and Lu fraction. The more Gd remains in the fractions if the flow rate of elution is higher. To avoid Gd remaining in the fractions as low as possible, flow rate of 1.0–1.1 ml min^{-1} was selected in this work.

3.3.3. Matrix separation efficiency and column blank

Fig. 2 illustrates the spectra (130–180 m/z) from high-purity Gd_2O_3 sample solutions before and after chromatographic separation. The spectra in Fig. 2(a) is from direct determination of 1 mg ml^{-1} of high purity Gd_2O_3 sample solution. A series of strong peaks from Gd matrix appear at 152–160 m/z. The peaks from polyatomic ions can be seen clearly at 159 m/z ($^{158}GdH^+$) and from 168 to 178 m/z, making no isotopes available for Tb, Tm, Yb and Lu. The spectra in Fig. 2(b) is from Tb fraction after chromatographic separation. There are weaker peaks from Gd matrix appearing at 152–160 m/z and a small peak at 159 m/z is contributed to Tb in

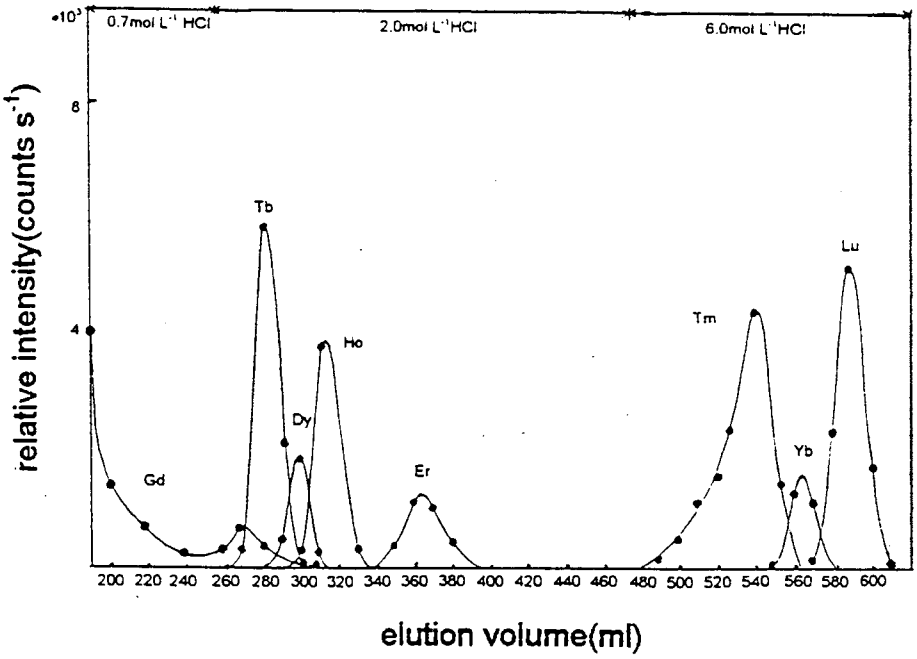

Fig. 1. The gradient elution curve of rare earth impurities in high-purity Gd_2O_3.

the original sample. The spectra in Fig. 2(c) is from Tm, Yb and Lu fraction after chromatographic separation. The peaks from Gd matrix are very small and no peaks are visible form 168–178 m/z. Repeated tests showed that a high separation efficiency and a good reproducibility were obtained.

Column blank levels for Tb, Tm, Yb and Lu were as low as that obtained from 2% HNO_3 solution. But for light REEs, especially for La

Table 4
The recovery of spiked samples for REEs

Element	Added (ng ml^{-1})	Found (ng ml^{-1})	Recovery (%)	RSD[a] (%)
Y	10	10.8	108	3.1
La	10	9.4	94	2.5
Ce	10	9.3	93	1.8
Pr	10	9.6	96	3.4
Nd	10	10.4	104	7.5
Sm	10	10.2	103	6.0
Eu	10	9.4	94	2.8
Tb[b]	10	12.1	121	3.2
Dy	10	9.1	91	3.7
Ho	10	8.8	88	4.1
Er	10	10.6	106	3.9
Tm[b]	10	9.1	91	1.0
Yb[b]	10	11.0	110	2.7
Lu[b]	10	9.3	93	3.2

[a] The relative standard deviation of three replicates.
[b] After extraction chromatographic separation.

Table 5
The results (μg g^{-1}) of sample analysis by ICP-MS

Samples	Y	La	Ce	Pr	Nd	Sm	Eu	Tb	Dy	Ho	Er	Tm	Yb	Lu	ΣREE
BD940819	0.551	0.27	0.53	0.10	0.25	0.09	<0.03	3.15	0.46	<0.02	<0.09	<0.03	<0.08	<0.03	5.36
FA940905	3.26	0.17	0.45	0.14	0.30	1.82	1.81	2.76	0.08	<0.02	0.11	0.26	1.54	1.70	14.30

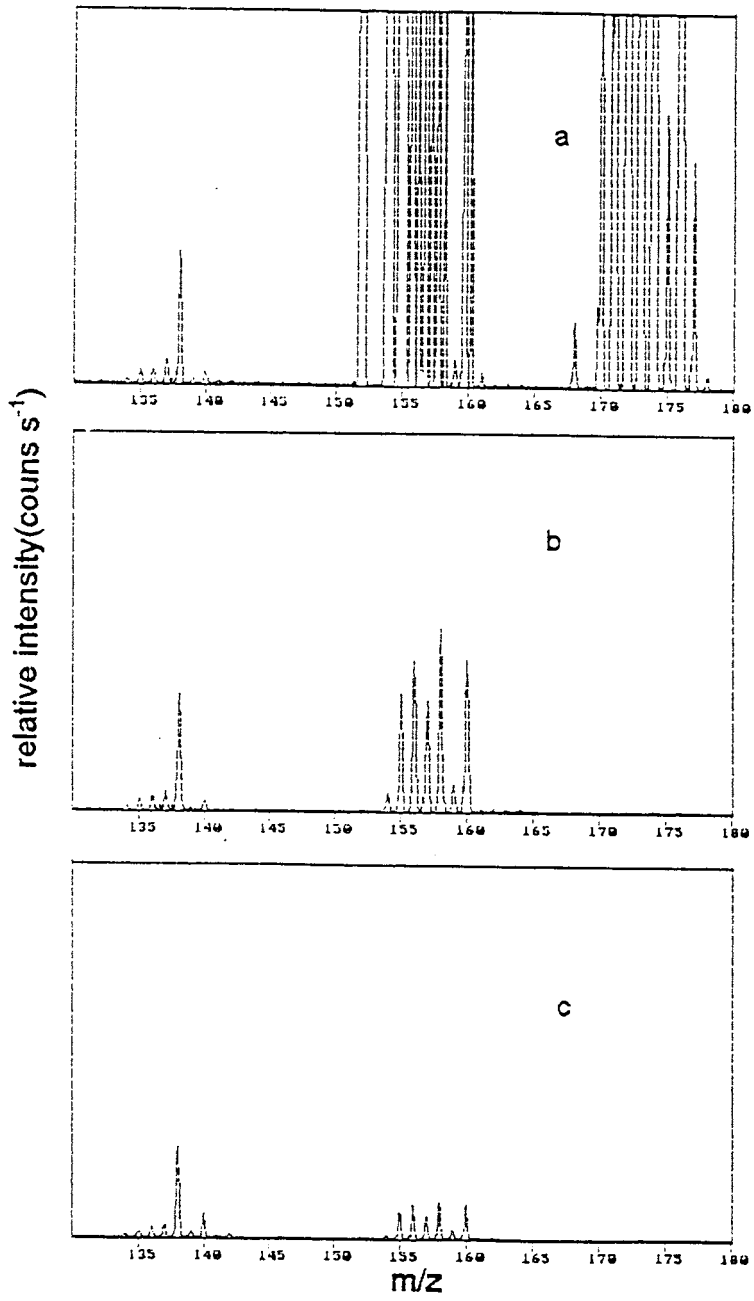

Fig. 2. The mass spectra of high-purity Gd_2O_3 solution with the mass ranging 130–180 m/z; (a) before separation; (b) Tb-collected elution after separation; (c) Tm, Yb and Lu collected solution after separation.

and Ce, considerable column blank levels were observed, which is liable to variation in separate runs. That is the main reason why the light REEs were determined by ICP-MS directly.

3.4. Accuracy and precision of spiked samples

Owing to the lack of certified gadolinium oxide standard materials, the validity of the method was

verified by separation and analysis of a spiked sample. The recoveries and precision for replicates were given in Table 4. The results suggested that the recoveries and precision for REE impurities are satisfactory.

3.5. Sample analysis

Two high-purity Gd_2O_3 samples were analyzed. The concentration for Y and 13 REE impurities in the two samples were summarized in Table 5. The total REE impurities in BD940819 and FA940905 are 5.36 and 14.30 μg g^{-1}, respectively.

4. Conclusion

The combination of extraction chromatography with high performance ICP-MS provides an effective, rapid, precise and reliable technique for the determination of Y and 13 REEs in high-purity gadolinium oxide. Spectra overlap interferences from matrix-induced polyatomic ions on Tb, Tm, Yb and Lu were effectively eliminated by (EHEHP) extraction chromatographic separation and Y and 13 trace REE impurities were determined by ICP-MS. Re was used as an internal standard to effectively compensate for the analyte signal suppression effect and instrumental drift. The proposed method is especially useful when small amounts of expensive samples are to be processed and Gd_2O_3 samples with purity of 99.99–99.9999% are required to be analyzed.

Acknowledgements

This work was supported by the Chinese National Natural Science Foundation (No. 29475190)

References

[1] C.R. Lalonde, J.I. Dalton, Can. J. Spectrosc. 26 (1982) 163.
[2] E.S. Gladney, N.W. Bower, Geostand. Newsl. 9 (1985) 261.
[3] J.G. Crock, F.E. Lichte, Anal. Chem. 54 (1982) 1329.
[4] K.E. Jarvis, J. Anal. At. Spectrom. 4 (1989) 563.
[5] N. Shitaba, M. Fudagawa, M. Kubota, Anal. Chem. 63 (1991) 636.
[6] K. Kawabata, Y. Kishi, O. Kawagchi, et al., Anal. Chem. 63 (1991) 2137.
[7] M. Yin, B. Li, T.F. Fu, Chin. J. Anal. Sci. 11 (1995) 13.
[8] V.K. Panday, J.S. Becker, Fresenius. J. Anal. Chem. 352 (1995) 327.
[9] B. Li, Y. Zhang, M. Yin, Analyst 122 (1997) 543.
[10] V. Balaram, K.V. Anjaiah, M.R.P. Reddy, Analyst 120 (1995) 1401.
[11] T.F. Fu, M. Yin, Chin. J. Anal. Chem. 6 (1991) 167.
[12] X.S. Liu, S.Q. Cai, F.F. Liu, et al., Chin. J. Anal. Chem. 4 (1997) 431.
[13] Y. Takaku, K. Masuda, T. Takahagchi, et al., J. Anal. At. Spectrom. 8 (6) (1993) 687.
[14] E.H. Evans, J.J. Giglio, J. Anal. At. Spectrom. 8 (1993) 1.
[15] K.E. Jarvis, A.L. Gray, E. McCurdy, J. Anal. At. Spectrom. 4 (1989) 743.
[16] M. Yin, B. Li, Chin. J. Rock Miner. Anal. 13 (1993) 781.
[17] C. Vandecasteele, H. Vanhoe, R. dams, J. Anal. Spectrom. 8 (1993) 781.
[18] M.A. Vaughan, G. Horlick, Appl. Spectrosc. 4 (1986) 434.
[19] D. Beauchemin, J.W. McLaren, S.S. Berman, Spectrochim. Acta. 42B (3) (1987) 467.

ELSEVIER

Talanta 48 (1999) 527–535

Talanta

Uptake and extraction chromatographic separation of mercury(II) by triisobutylphosphine sulfide (TIBPS) sorbed on silica gel and decontamination of mercury containing effluent

Rashmi Singh, A.R. Khwaja, Bina Gupta, S.N. Tandon *

Department of Chemistry, University of Roorkee, Roorkee-247 667, India

Received 16 March 1998; received in revised form 6 August 1998; accepted 7 August 1998

Abstract

Batch experiments on the uptake of (Hg(II)) from nitric acid medium by coated inert support have been conducted. The effect of different variables like equilibration time, concentration of acid, metal ion and extractant has been studied. Binary separations of Hg(II) from other metal ions have been carried out. Experiments to evaluate the recycling capacity of the columns reveal a practically insignificant change in the extraction efficiency of the extractant. The practical utility of the columns has been demonstrated by decontaminating mercury containing waste effluent.

Keywords: Mercury(II); Triisobutylphosphine sulfide; Chromatographic separation; Decontamination

1. Introduction

Mercury is a serious pollutant of the biosphere and it has to be removed before it is converted into extremely toxic alkylmercury. Different adsorbents have been used for its removal from wastewater. The desorption of mercury from some of these adsorbents may not be necessarily convenient. Recently, reversed phase columns are finding applications for the treatment of metal loaded waste [1–7]. The alkyl phosphines marketed by Cytec are becoming popular as metal ion extractants owing to their poor aqueous solubility, good hydrolytic stability and selectivity. The inherent advantages make these extractants attractive alternatives for use as stationary phases for the separation of metal ions [8–10]. The selectivity of triisobutylphosphine sulfide (TIBPS) for (Hg(II)) is by now well established [11–13] and it may be important to explore this extractant for the separation and removal of Hg(II) from waste effluents by extraction chromatography.

* Corresponding author. Fax: +91 1332 73560; e-mail: chemt@rurkiu.ernet.in

0039-9140/99/$ - see front matter
PII S0039-9140(98)00275-6

2. Experimental

2.1. Materials and equipments

The radioisotopes ^{51}Cr, ^{54}Mn, ^{58}Co, ^{57}Fe, ^{65}Zn and ^{203}Hg, used for the distribution studies, were obtained from Board of Radiation and Isotope Technology, Mumbai, India. TIBPS was received as a gift sample from Cytec, Canada. It was purified by the method suggested by the supplier [14] and the purity was checked by melting point and gas chromatography. All other chemicals used were of analytical grade.

A well-type NaI(Tl) scintillation counter was used for the measurement of gamma activity of radioisotopes. Inductively coupled plasma atomic emission spectrometry (ICP–AES) (8440 PLASMA LABTAM, Australia) and atomic absorption spectrometry (Perkin Elmer 3100, USA) were used for obtaining the distribution data of Ni(II), Cu(II), Cd(II) and Pb(II) and checking the yield in separations. For the determination of mercury in separation studies, a hydride generator was appended with the instrument.

2.2. Methodology

Silica gel for column chromatography was silanized by following the procedure cited elsewhere [15]. Dry silanized silica gel was slurried with toluene solution of varying amounts of TIBPS (0.020–1.0 g TIBPS per gram of silanized silica gel). Toluene was then evaporated by gentle stirring. At different steps, care was taken to avoid vigorous mixing so that there is no change in the particle size of the support.

To check the homogeneity of impregnated silica gel (ISG), varying amounts (10–300 mg) of the impregnated inert support were immersed in 1.0 ml of labelled mercury solution (1.0×10^{-4} M) in 0.10 M HNO_3; while for the kinetics study, ~ 25 mg of ISG was taken, keeping the aqueous phase the same. The mixture was equilibrated on a water bath at 25 ± 0.1°C. The batch experiments for loading on ISG were carried out by using labelled Hg(II) (1.0×10^{-5}–0.10 M) solution in 0.10 M HNO_3. Experiments were also carried out at varying concentrations of TIBPS (0.020–1.0 g of extractant per gram of inert support) adsorbed on silica gel using labelled Hg(II) solution (1.0×10^{-4} M) in 0.010 M HNO_3. The distribution ratio (D) values were calculated by using the expression.

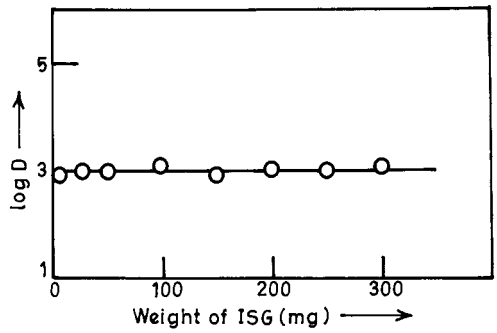

Fig. 1. Uptake of Hg(II) on varying amounts of ISG. Conditions: $[Hg(II)] = 1.0 \times 10^{-4}$ M; $[HNO_3] = 0.10$ M; $[TIBPS]_S =$ 1g per gram of ISG.

$$D = [(A_i - A_f)/A_f](V/M) \text{ ml g}^{-1}$$

where A_i and A_f are the activities of the tracers in initial and final solutions, V is the volume of the solution taken in a particular experiment and M is the amount of the impregnated inert support. In all the above experiments, the solution was centrifuged and a suitable aliquot of the aqueous phase was radioassayed. In cases where radioisotopes were not used, the concentrations were measured.

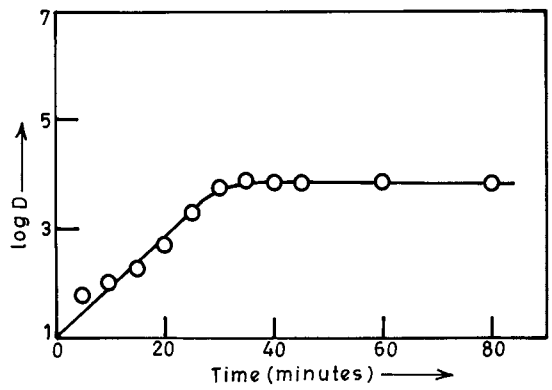

Fig. 2. Effect of equilibration time on the uptake of Hg(II) on ISG. Conditions: $[Hg(II)] = 1.0 \times 10^{-4}$ M; $[HNO_3] = 0.10$ M; $[TIBPS]_S = 1$g per gram of ISG.

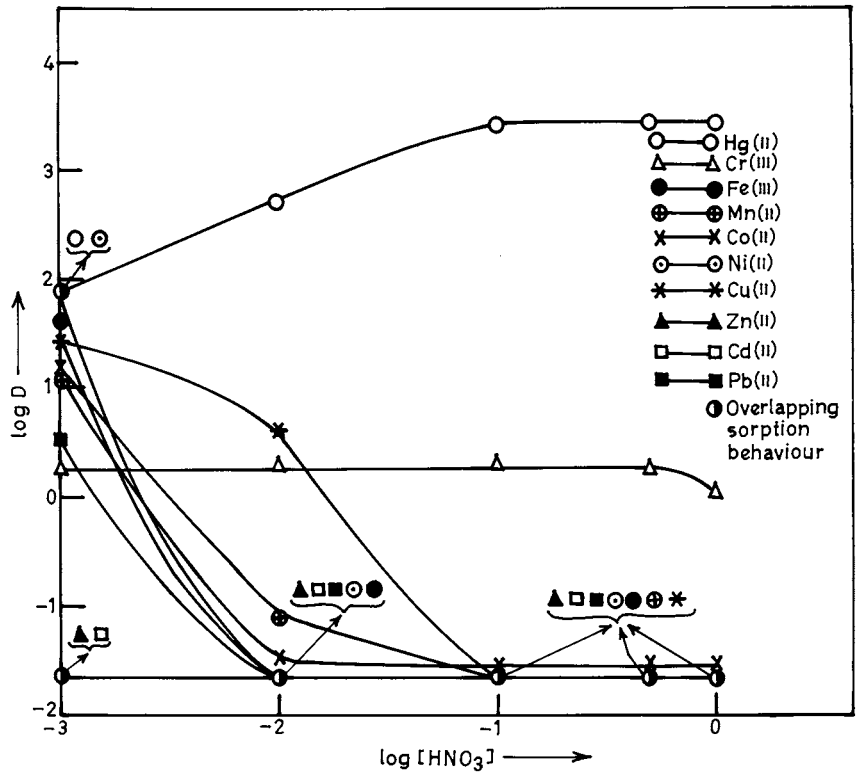

Fig. 3. Effect of concentration of nitric acid on uptake of metal ions on ISG. Conditions: [metal ion] = 1.0×10^{-4} M; $[TIBPS]_S = 1$ g per gram of ISG.

The retention behaviour of the various metal ions at different acidities was determined by adding about 25 mg of ISG to 1.0 ml solution of the metal ion (1.0×10^{-4} M) in varying concentrations (1.0×10^{-3}–1.0 M) of HNO_3. For column studies, the impregnated inert support (~ 1 g) was left overnight in the required concentration of the acid and then transferred to a glass column of 1 cm internal diameter. The flow rate of the column was adjusted to 0.5 ml min^{-1}. For separations, the column was loaded with a mixture containing equimolar (1.0×10^{-4} M) quantities of the metal ions which were eluted with appropriate eluants. Equal fractions of the eluants with respect to volume were collected and assayed by ICP–AES. The results reported are the average of a minimum of two determinations. The column was regenerated by washing it with water until the eluant was almost neutral. It was then preconditioned with the required concentration of the acid. The recycling capacity of the TIBPS loaded silica gel column was checked up to ten cycles.

A 50 ml sample of the paper and pulp industry effluent was boiled with 5 ml HNO_3, cooled, filtered and made up to a known volume [16]. The commercial sodium hydroxide sample was dissolved in a known volume of distilled water. Prior to feeding it on the column, suitable aliquots of the above solutions were adjusted to pH ~ 1.

3. Results and discussion

The homogeneity of ISG was checked in batch experiments by taking different amounts of impregnated inert support in 1.0 ml of labelled solution of Hg(II) in 0.10 M HNO_3. The log D values plotted against different amounts of support gives a straight line parallel to the x axis

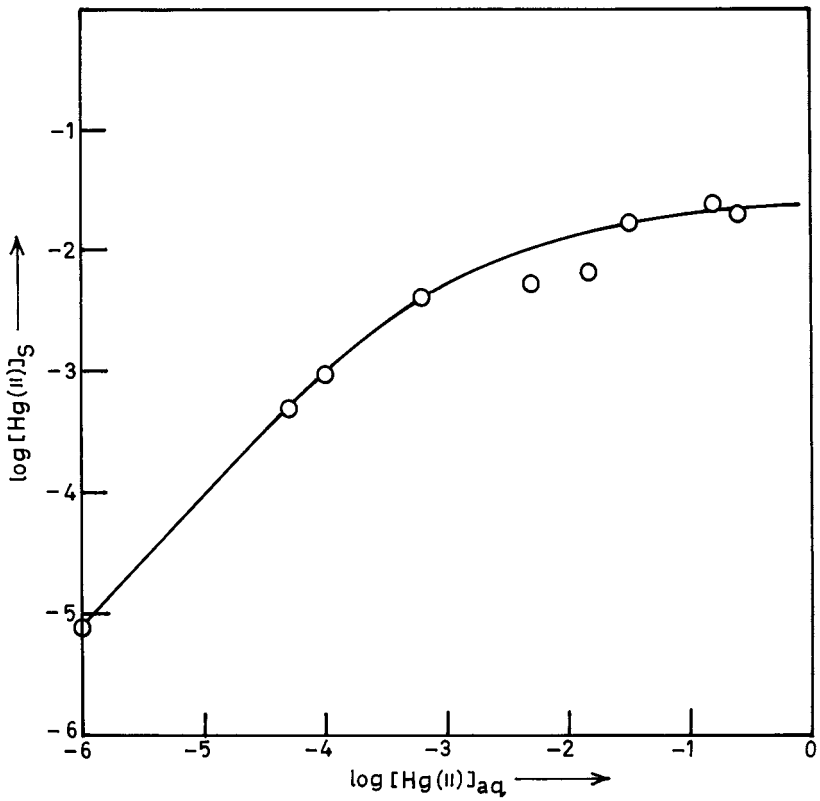

Fig. 4. Loading curve of Hg(II) on ISG from nitric acid medium. Conditions: $[HNO_3] = 0.10$ M; $[TIBPS]_S = 1$g per gram of ISG.

which shows a certain kind of ideal behaviour of the solid phase (Fig. 1). The values are within $\pm 5\%$ of the mean value. The findings ascertain that the loaded material is fairly homogeneous. The homogeneity was checked for each batch of the coated material.

The results of the kinetics of uptake of Hg(II) on ISG from 0.10 M HNO_3 at 25 ± 0.1°C, conducted by batch experiments, are shown in Fig. 2. From the plot of log D versus time it is apparent that it takes 35 min to attain equilibrium. For other experiments, the inert support was equilibrated for a period of 40 min to ensure complete equilibration.

3.1. Uptake behaviour

The batch studies for the adsorption behaviour of Hg(II) and other metal ions such as Cr(III), Fe(III), Mn(II), Co(II), Ni(II), Cu(II), Zn(II), Cd(II) and Pb(II) from 1.0×10^{-3} to 1.0 M HNO_3 on ISG are presented in Fig. 3. With the increase in the concentration of nitric acid, an increase in the D value of Hg(II) is observed and limiting value is attained at 0.10 M HNO_3. The retention of Fe(III), Mn(II), Co(II), Ni(II) and Pb(II) is negligible up to 0.010 M HNO_3 and then it shoots up with a decrease in acid concentration. The D value of Cu(II) decreases with increasing acid concentration up to 0.10 M HNO_3 and then assumes a constant low value. The uptake of Cr(III) remains the same throughout the studied range of acid molarity, except at 1.0 M HNO_3 where a slight decrease in D value is observed. Zn(II) and Cd(II) show negligible uptake in the entire studied range of acid molarity. The trends of uptake behaviour of different metal ions are similar to the liquid–liquid extraction behaviour of these metal ions in TIBPS [12].

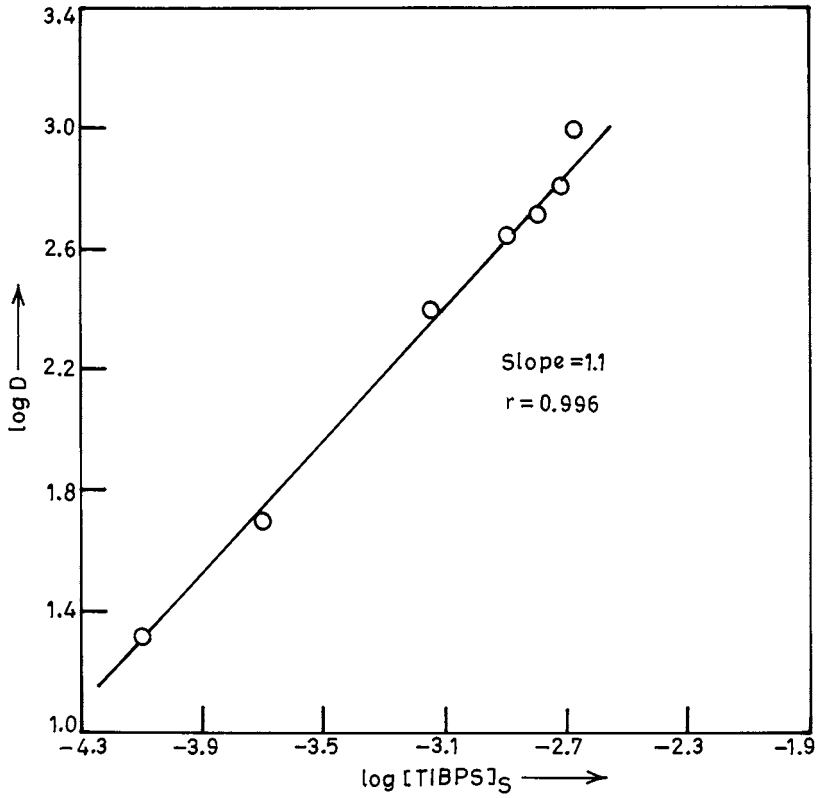

Fig. 5. Effect of concentration of TIBPS sorbed on silica gel on the uptake of Hg(II). Conditions: $[Hg(II)] = 1.0 \times 10^{-4}$ M; $[HNO_3] = 0.010$ M.

3.2. Effect of concentration of the metal ion

The results of batch experiments of partitioning of different concentrations (1.0×10^{-5}–0.10 M) of Hg(II) on ISG from 0.10 M HNO_3 are shown in Fig. 4. The concentration of Hg(II) on impregnated inert support increases linearly with the increase in its concentration in the range 1×10^{-5}–1×10^{-3} M. This suggests that the distribution is independent of the concentration and the partitioning metal species remains the same in this concentration range. However, as the inert support gets saturated, the mercury concentration on the coated material tends to assume a constant value. From the plot, it can be concluded that the loaded extractant molecules can hold the metal ion to about one-tenth of its molar concentration. The metal loaded on the support is much smaller than the value observed earlier in the liquid–liquid extraction experiments [12]. This tends to suggest that all the extractant molecules coated on the support are not easily accessible for binding the metal ion.

3.3. Effect of extractant concentration

To establish the nature of species formed during the extraction chromatography, uptake of Hg(II) from 0.010 M HNO_3 on silica gel loaded with different amounts of TIBPS (0.020–1.0 g sorbed per gram of inert support) was studied under batch conditions. Fig. 5 shows the plot of $\log D$ versus $\log [TIBPS]_S$ (where $[TIBPS]_S =$ weight of TIBPS per kg of impregnated inert support/molecular weight of TIBPS). There is an increase in the extraction with the increase in the concentration of the extractant coated on the inert support. The log–log plot gives a straight

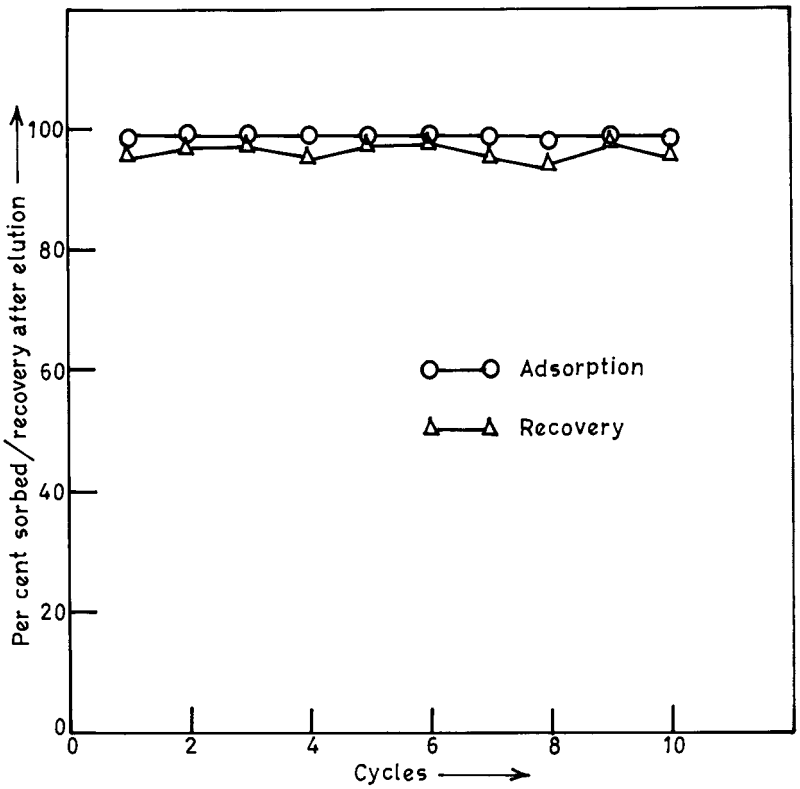

Fig. 6. Variation in the sorption or recovery of Hg(II) in successive cycles employing ISG. Conditions: $[Hg(II)] = 1.0 \times 10^{-4}$ M; $[HNO_3] = 0.10$ M; $[TIBPS]_S = 1$ g per gram of ISG. [Stripping agent] = 0.010 M sodium thiosulfate.

line with a slope around one, suggesting the metal to extractant ratio to be 1:1, and the extracting species could be proposed as $Hg(NO_3)_2 \cdot TIBPS$. This is similar to the species proposed previously [12].

3.4. Equilibrium treatment

The equilibrium constant (K) for the reaction

$$(Hg^{2+})_{aq} + (2NO_3^-)_{aq} + (TIBPS)_S \rightleftarrows [Hg(NO_3)_2 \cdot TIBPS]_S \quad (1)$$

is represented by

$$K = \frac{[Hg(NO_3)_2 \cdot TIBPS]_S}{[Hg^{2+}]_{aq}[NO_3^-]^2_{aq}[TIBPS]_S} \quad (2)$$

Assuming that $[Hg(NO_3)_2 \cdot TIBPS]_S$ is the only extracting species and the metal ions in the aqueous phase predominantly exist as Hg^{2+}, the distribution ratio is given by

$$D = \frac{[Hg(NO_3)_2 \cdot TIBPS]_S}{[Hg^{2+}]_{aq}} \quad (3)$$

and under conditions where $[NO_3^-]$ remains constant, Eq. (2) simplifies to

$$\log K = \log D - \log [TIBPS]_S \quad (4)$$

The equilibrium constant (K), as calculated using Eq. (4), is equal to 3.8×10^5.

3.5. Behaviour of different eluting agents

For the recovery of Hg(II) from the column, 5% NH_4Cl in 1:10 NH_3, 0.010 M sodium thiosulfate and DL-pencillamine, which form strong complexes with Hg(II), were tried. Sharp elution peaks are observed in the case of DL-pencillamine and 0.010 M sodium thiosulfate, whereas with 5% NH_4Cl in 1:10 NH_3, the peaks are broad and a larger volume of the eluant is required for the

Table 1
Separation conditions and recovery of Hg(II) from other metal ions employing ISG columns

Sl. no.	Metal ions	Eluant	Recovery (%)	Separation factor (β)
1	Cr(III)–Hg(II)	0.10 M HNO_3–0.010 M sodium thiosulfate	98–99	4.9×10^3
2	Fe(III)–Hg(II)	0.10 M HNO_3–0.010 M sodium thiosulfate	95–99	3.2×10^3
3	Mn(II)–Hg(II)	0.10 M HNO_3–0.010 M sodium thiosulfate	98–99	3.2×10^3
4	Co(II)–Hg(II)	0.10 M HNO_3–0.010 M sodium thiosulfate	97–98	3.2×10^3
5	Ni(II)–Hg(II)	0.10 M HNO_3–0.010 M sodium thiosulfate	90–98	9.8×10^2
6	Cu(II)–Hg(II)	0.10 M HNO_3–0.010 M sodium thiosulfate	95–99	4.9×10^3
7	Zn(II)–Hg(II)	0.10 M HNO_3–0.010 M sodium thiosulfate	96–97	3.2×10^3
8	Cd(II)–Hg(II)	0.10 M HNO_3–0.010 M sodium thiosulfate	98–99	3.2×10^3
9	Pb (II)–Hg(II)	0.10 M HNO_3–0.010 M sodium thiosulfate	97–99	4.8×10^3

Conditions: [metal ion] = 1.0×10^{-4}–1.0×10^{-4} M (1:1); [extractant] = 1 g per gram of ISG; [aqueous phase] = 0.10 M HNO_3.

complete elution of mercury. Because of cost constraints, 0.010 M sodium thiosulfate solution was preferred over DL-pencillamine.

3.6. Effect of temperature

The effect of temperature on uptake of Hg(II) was studied under batch conditions by equilibrating the loaded inert support with an aqueous phase containing 1.0×10^{-4} M labelled mercury solution in 0.010 M HNO_3. A plot of $1/T$ versus $\log D$ shows a linear increase in the uptake with the increase in temperature. Using a van't Hoff type equation, the ΔH value as calculated from the slope is 11.43 kJ mol^{-1}. This indicates the reaction to be endothermic.

3.7. Regeneration of column for repeated use

Experiments were conducted to check the regeneration power of the column for repeated use by adsorbing Hg(II) from 0.10 M HNO_3. The loaded Hg(II) on columns was washed with 0.010 M sodium thiosulfate solution. The column was regenerated by washing it with water until the eluant was almost neutral. Thereafter, it was preconditioned with the required concentration of the acid for subsequent use. The adsorption–elution cycle was checked for ten cycles. The results shown in Fig. 6 reveal a practically insignificant change in the efficiency of the column for the removal of Hg(II) for at least ten cycles.

3.8. Separations

The data on adsorption of the various metal ions at different acid concentrations reveal that Hg(II) can be conveniently separated from Cr(III), Fe(III), Mn(II), Co(II), Ni(II), Cu(II), Zn(II), Pb(II) and Cd(II) on the column at 0.10 M HNO_3. Hg(II) is strongly retained on the column, whereas Cr(III), Fe(III), Mn(II), Co(II), Ni(II), Cu(II), Zn(II), Pb(II) and Cd(II) get eluted at this molarity of acid. The loaded Hg(II) is eluted by washing the column with 0.010 M sodium thiosulfate solution. The conditions of separation and percentage recovery of the metal ions are summarized in Table 1. A representative elution curve of Hg(II)–Cd(II) separation is shown in Fig. 7.

3.9. Decontamination of waste effluent

The black liquor generated in the paper and pulp industry is discharged into the waste streams after treatment, but some small scale industries discharge the black liquor as such without any treatment, thus adding to the mercury pollution load. The results on the decontamination of the waste effluent from mercury are shown in Table 2. Hg(II) is quantitatively retained on the column and subsequently recovered from the columns by washing it with 0.010 M sodium thiosulfate solution. The recovery in all cases is $>95\%$. Because of the selectivity of the extractant for Hg(II), these columns do not get unnecessarily loaded with other metal ions present in the waste.

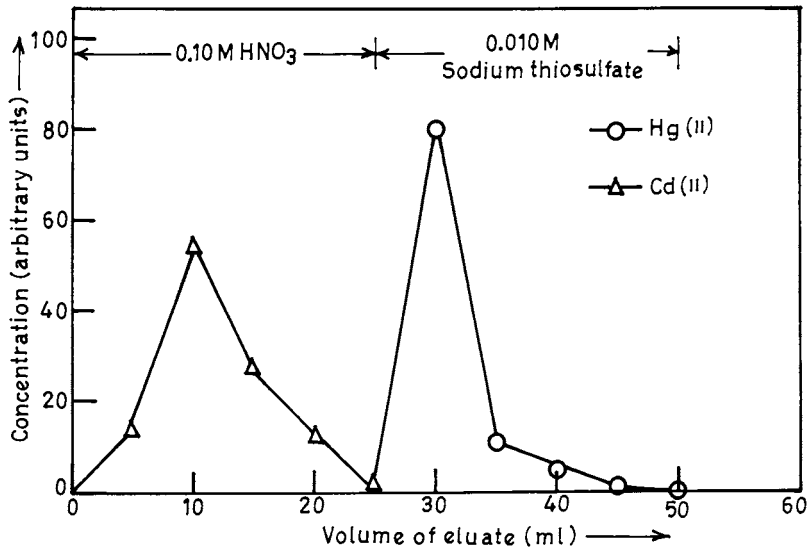

Fig. 7. Elution curves of Hg(II) and Cd(II) on ISG.

Table 2
Removal of mercury from waste effluent employing ISG columns

Sl. no	Sample	Concentration before loading on the column (ppm)[a]	Concentration of Hg(II) in the aqueous phase after adsorption (ppm)[b]	Recovery of mercury from the column(%)
1	WW 1	0.89	<0.001	97 ± 2*
2	WW 2	0.75	<0.001	96 ± 3*
3	BL 1	0.97	<0.001	97 ± 2*
4	BL 2	0.45	<0.001	96 ± 3*
5	BL 3	1.32	<0.001	97 ± 2*
6	BL 4	1.30	<0.001	96 ± 2*

WW 1, wastewater of Gambhir Paper Mills, Saharanpur, India; WW 2, wastewater of Star Paper Mills, Saharanpur, India); BL 1, black liquor of Gambhir Paper Mills, Saharanpur, India; BL 2, black liquor of Star Paper Mills, Saharanpur, India; BL 3, black liquor of Shreyans Paper, Ahmedgarh, India; BL 4, black liquor of Ruchika Paper Mills, Shimla, India.
[a] Based on five replicate runs, the coefficient of variance (v) was within ± 2%.
[b] Based on the detection limit of ICP–AES.
*Standard deviation based on five runs.

4. Conclusions

The results presented in this paper clearly indicate the potential of TIBPS loaded columns for the removal of mercury from wastewater. Invariably, sharp elution curves are obtained by using a simple eluting agent. The results of regeneration show a good recycling capacity. Furthermore, the selectivity of TIBPS for Hg(II) avoids unnecessary loading of the column with other metal ions encountered in the effluents.

Acknowledgements

Thanks are due to Cytec, Canada, for providing TIBPS. Financial support of Society for Participatory Research in Asia (PRIA), Council of

Scientific and Industrial Research (CSIR) and All India Council of Technical Education (AICTE), New Delhi, India, is gratefully acknowledged.

References

[1] J.H. Barnes, C. Bates, F.R. Hartley, Hydrometallurgy 10 (1983) 205.
[2] Y. Cheng, H. Chang, Z. Yan, Mo Xexue Yu Jishu 84 (4) (1988) 24.
[3] P. Bathstone, S. Bompadry, G. Fava, G. Gobbi, Talanta 30 (1984) 15.
[4] J.N. Mathur, M.S. Murali, R.H. Iyer, A. Ramanujam, P.S. Dhami, V. Gopalkrishnan, L.P. Badheka, A. Banerji, Nucl. Technol. 109 (1995) 216.
[5] V. Gopalkrishnan, P.S. Dhami, A. Ramanujam, M.V.B. Krishna, M.S. Murali, J.N. Mathur, R.H. Iyer, A.K. Bauri, A. Banerji, J. Radioanal. Nucl. Chem. 191 (2) (1995) 279.
[6] G.J. Lumetta, D.W. Wester, J.R. Morrey, M.J. Wagner, Solvent Extr. Ion Exch. 11 (1993) 663.
[7] G.S. Barney, R.G. Covan, Proceedings of the American Chemical Society National Meeting, San Francisco, CA, 1992.
[8] K.S. Panesar, O.V. Singh, S.N. Tandon, Talanta 41 (8) (1994) 1341.
[9] S.K. Yadav, Ph.D. Thesis, University of Roorkee, Roorkee, India, 1993.
[10] A.Saily, S.N. Tandon, J. Liq. Chrom. Rel. Techol. 21 (3) (1998) 407.
[11] Y. Baba, Y. Umezaki, K. Inoue, Solvent Extr. Ion. Exch. 4 (1) (1986) 15.
[12] R. Singh, S.N. Tandon, Talanta 44 (1997) 843.
[13] M.L.P. Reddy, A.D. Damodaran, M.C.S. Reddy, Radiochim. Acta 76 (1997) 109.
[14] W.A. Rickelton, Cyanex 471X, American Cyanamid Company, Technical Brochure, SPT-015, 1985.
[15] T. Braun, G. Ghersini (Eds.), Extraction Chromatography, Elsevier, Amsterdam, 1975, pp. 50–51.
[16] APHA, AWWA, WPCF, Standard Methods for the Examination of Water and Wastewater, APHA Publication, Washington, DC, 1985, p. 148.

ELSEVIER

Talanta 48 (1999) 537–549

Talanta

Determination of cadmium in hair and blood by tungsten coil electrothermal atomic absorption spectrometry with chemical modifiers

Carlos G. Bruhn [a,*], José Y. Neira [a], Gonzalo D. Valenzuela [a], Joaquim A. Nóbrega [b]

[a] *Departamento de Análisis Instrumental, Facultad de Farmacia, Universidad de Concepción, P.O. Box 237, Concepción, Chile*
[b] *Departamento de Química, Universidade Federal de Sao Carlos, Caixa Postal 676, 13565-905 Sao Carlos, SP, Brazil*

Received 18 March 1998; received in revised form 10 August 1998; accepted 10 August 1998

Abstract

Three chemical modifiers ($(NH_4)_2HPO_4$, $NH_4H_2PO_4$, and Pd as $Pd(NO_3)_2$) were evaluated for the determination of Cd in acid-digested solutions of hair and blood using electrothermal atomic absorption spectrometry in a tungsten coil atomizer (TCA). All modifiers caused some thermal stabilization of Cd when compared to the behavior observed in nitric acid medium. The best effects were observed in 15 μg ml^{-1} Pd medium; the characteristic mass of Cd was 0.3 pg and the method detection limits were 0.009 μg g^{-1} in hair and 0.2 μg l^{-1} in blood. In addition to a slight thermal stabilization effect, Pd also increased the sensitivity for Cd by ca. 40% and the tungsten coil lifetime by 20% (i.e. from 300 to 360 heating cycles), reduced background signals, and eliminated condensed phase interferences caused by concomitants. The accuracy (3.2% as mean relative error in the Pd modifier) was checked for the determination of Cd in acid-digested solutions of certified reference materials of human hair and blood and by recoveries of Cd in spiked hair and blood samples by both TCA and a graphite furnace procedure. All results obtained in chemical modifiers are in agreement at a 95% confidence level.

Keywords: Chemical modifiers; Tungsten coil electrothermal atomizer; Cadmium; Hair; Blood

1. Introduction

Electrically heated tungsten wires have been used as atomization sources for trace element determinations in electrothermal atomic absorption spectrophotometry (ETAAS) since the early 1970s, when Williams and Piepmeier [1] proposed a rigidly wound filament from commercially available light bulbs for this purpose. The subsequent reports of these and other authors [2–10] dealt with the improvement of instrumental parameters and optimization of element determination. Nevertheless, the lack of commercial spectrometers with fast data processing limited their practical applications. Almost 16 years after Piepmeier's pioneering work, Berndt and Schaldach [11] proposed the use of inexpensive low-power tungsten

* Corresponding author. Fax: +56 41 231903; e-mail: cbruhn@udec.cl

0039-9140/99/$ - see front matter
PII S0039-9140(98)00276-8

coils (150 W) as electrothermal atomizers. This simple system was satisfactorily used for the determination of trace levels of arsenium, antimony and tin in pure gold [12], alkaline and alkaline-earth elements in ammonium paratungstate [13], cadmium in biological and botanical materials [14], barium in waters [15], cadmium, cobalt, chromium, lead, manganese, and nickel in waters, soft drinks and wines [16,17], chromium in river waters [18], lead in residual waters [19], in blood [20–23], in paints [22] and in hair [23].

The main obstacle to the dissemination of this atomizer is the occurrence of matrix interferences. These interferences were avoided by a matrix separation procedure [19] or using a matrix matching approach [20]. Despite the feasibility of these procedures and their easy implementation with commercially available systems, as is the case of matrix separation and preconcentration steps, sample manipulation is somewhat increased.

A more conventional approach to overcome these interferences could be the use of chemical modifiers, as routinely applied in ETAAS with graphite atomizers. The main difficulty for adopting this strategy is the lack of systematic studies related to the performance of chemical modifiers in metallic atomizers. The search for suitable chemical modifiers cannot only be based on the available background information and the extensive studies using graphite atomizers. Considering that the tungsten coil atomizer (TCA) is an essentially non-isothermal atomizer, normally heated in a reductive gas mixture ($Ar–H_2$), it should be thought of in a different way. Additionally, the fast generation of an atomic cloud, i.e. ten-fold faster than in ETAAS with a graphite atomizer, and its short residence time [16], lead to a transient absorption signal which can be measured in spectrometers with fast data processing. The residence time of free atoms in the optical beam is sufficiently short to reduce the effectiveness of recombination reactions as an atom sink. Recently, it was demonstrated that the interference caused by alkaline and alkaline-earth elements in the atomization of Pb in the TCA occurs in the condensed phase [23].

In this previous work it was also pointed out that most published studies related to chemical modifiers were carried out by a Japanese group and involved the use of thiourea, sulfur and ammonium thiocyanate [23]. So far, there are essentially three studies employing chemical modifiers in the TCA. In one of them, EDTA was used to reduce alkaline and alkaline-earth interferences in the determination of Ba in waters [15]. In the other, a $NH_4H_2PO_4$ + Triton X-100 + HNO_3 mixture was used to dilute the blood before Pb determination [21]. Recently, a more complete study was published evaluating the use of $(NH_4)_2HPO_4$, $NH_4H_2PO_4$, and Pd as $Pd(NO_3)_2$ as chemical modifiers in the determination of Pb in acid-digested solutions of hair and blood [23]. It was showed that Pd incremented the sensitivity, improved the background signal correction, caused a thermal stabilization of the analyte, and augmented the coil lifetime by 20%, probably owing to condensed phase effects.

Table 1
Thermal programs for Cd with the tungsten coil atomizer

Step	Time (s)	Voltage (V)/temp. (°C)	Read
(A) In 0.2% v/v HNO_3			
1	40	0.5/250	
2	10	0	
3	0.2	0	Yes
4	1	10.0/1670	
5	2	11.0/1700	
6	20	0	
(B) In phosphate chemical modifier[a] + 0.2% v/v HNO_3			
1	45	0.5/250	
2	10	0.6/300	
3	10	0.7/330	
4	10	0	
5	0.2	0	Yes
6	1	11.0/1700	
7	2	13.0/1850	
8	20	0	
(C) In 15 μg ml^{-1} Pd (as $Pd(NO_3)_2$) + 0.2% v/v HNO_3			
1	40	0.5/250	
2	10	0.6/300	
3	10	0.7/330	
4	10	0	
5	0.2	0	Yes
6	1	12.0/1800	
7	2	13.0/1850	
8	20	0	

[a] 0.33 mg ml^{-1} $(NH_4)_2HPO_4$ or 0.29 mg ml^{-1} $NH_4H_2PO_4$.

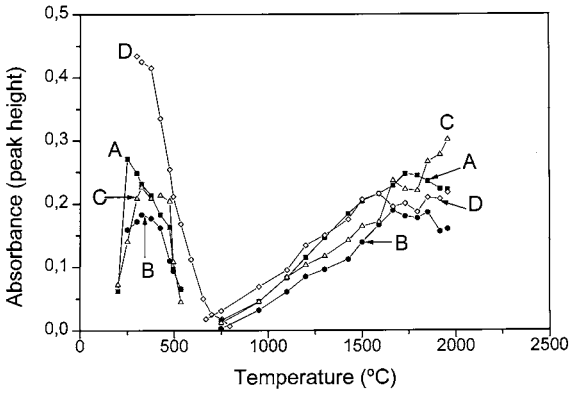

Fig. 1. Pyrolysis and atomization curves for Cd reference solutions (3.0 μg l^{-1}). All solutions prepared in 0.2% v/v HNO_3, (A) no modifier; (B) 1.32 mg ml^{-1} $(NH_4)_2HPO_4$; (C) 1.15 mg ml^{-1} $NH_4H_2PO_4$, and (D) 15 μg ml^{-1} Pd (as $Pd(NO_3)_2$).

Based on the performance of Pd as a modifier and the interferences observed in the determination of Cd in biological materials using the TCA [14], we decided to critically evaluate the use of Pd in the determination of Cd in hair and blood. To extend the knowledge in this area, the use of phosphates was also evaluated. However, elucidation of the mechanisms by which these modifiers appear to affect the atomization behavior of Cd in the TCA is beyond the scope of this work. The developed procedure was applied for Cd determination in acid-digested solutions of hair and blood. These matrices were chosen to assess the performance of the TCA considering both its complexity and its relevance in toxicological studies of short-term and long-term exposition [24]. Because of the ease with which samples can be collected, transported, stored and analyzed, hair analysis could be valuable in screening individuals and populations for exposure to Cd [25]. However, the clinical perspectives of Cd determination in hair and blood are not the aim of the present work.

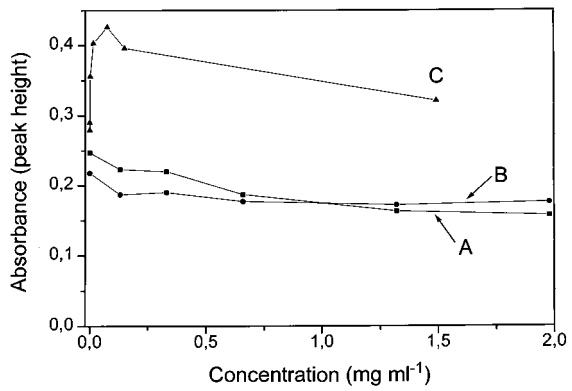

Fig. 2. Effect of the concentration of the chemical modifier (A) $(NH_4)_2HPO_4$; (B) $NH_4H_2PO_4$; and (C) Pd (as $Pd(NO_3)_2$).

Table 2
Interference effects[a] on 1.5 μg l^{-1} Cd absorbance with 15 μg ml^{-1} Pd and without chemical modifier by various co-existing ions in the tungsten coil atomizer

Interferent	Without Pd			With Pd		
	N1	N2	N3	N1	N2	N3
Cu^{2+} [b]	110	105	102	–	–	–
Mg^{2+} [b]	107	100	95	99	99	97
Zn^{2+} [b]	102	124	116	96	97	101
Fe^{3+} [b]	103	102	101	–	–	–
Na^{+} [c]	87	107	91	103	101	100
K^{+} [c]	100	99	102	–	–	–
Ca^{2+} [c]	98	96	100	–	–	–
Cl^{+} [c]	104	151	145	103	104	103
S (as SO_4^{2-})[c]	100	108	122	103	104	103
P (as PO_4^{3-})[c]	81	54	62	102	84	64

[a] Expressed with respect to Cd peak height absorbance in 0.2% v/v HNO_3 normalized to 100%.
[b] Interferent concentrations: N1 = 1 mg l^{-1}; N2 = 5 mg l^{-1}; N3 = 10 mg l^{-1}.
[c] Interferent concentrations: N1 = 1 mg l^{-1}; N2 = 10 mg l^{-1}; N3 = 100 mg l^{-1}.

2. Experimental

2.1. Apparatus

A Perkin–Elmer (PE) model 1100 atomic absorption spectrometer (Überlingen, Germany) with deuterium arc background correction equipped with a TCA [11] was used. The background corrected peak height absorbance was measured at the 228.8 nm Cd resonance line and lamp current and slit-width setting corresponded to the manufacturer's recommendations. Other equipment details (i.e. TCA power supply and computer control interface; graphite furnace and

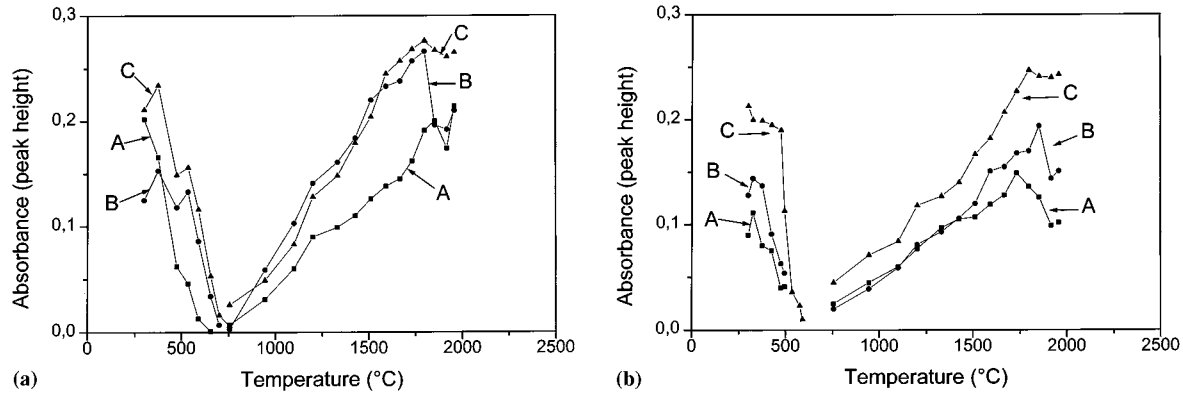

Fig. 3. Pyrolysis and atomization curves for 1.5 μg l^{-1} Cd (spike) in acid-digested solutions of (a) hair and (b) blood. All solutions prepared in 0.2% v/v HNO_3: (A) no modifier; (B) 0.33 mg ml^{-1} $(NH_4)_2HPO_4$; and (C) 15 μg ml^{-1} Pd (as $Pd(NO_3)_2$).

autosampler used to check for method accuracy; microwave digestion system and rotors used to digest samples and evaporate the digests) were as described elsewhere [23]. Aliquots of 10 μl of the solutions were delivered into the coil using a Transferpette (Brand). Table 1 shows the voltage–time heating programs established for Cd in each chemical modifier after optimizing the dry, pyrolysis and atomization steps. The graphite furnace (HGA-700) was used with pyrolytic graphite-coated graphite tubes (Part No. B3001254) and pyrolytic graphite platforms (Part No. B3001256), and the heating conditions (temperature/ramp time/hold time/gas flow) for the determination of Cd in solution digests of hair and blood were as follows: dry 1, 90°C/5 s/5 s/300 ml min^{-1}; dry 2, 130°C/5 s/25 s/300 ml min^{-1}; pyrolysis, 800°C/20 s/30 s/300 ml min^{-1}; atomize, 1200°C/0 s/5 s/0 ml min^{-1}; clean, 2300°C/1 s/3 s/300 ml min^{-1}; cool, 20°C/1 s/10 s/300 ml min^{-1}. Sample aliquots of 10 μl were applied with the PE model AS-70 autosampler.

2.2. Reagents, materials and samples

All reagents, gases, ultrapure (u.p.) water, the cleaning of glass and plastic materials, and the chemical modifier stock solutions were as described elsewhere [23]. Cadmium stock solution (1000 μg ml^{-1}) was prepared from Titrisol concentrate (Merck, Darmstadt, Germany) and reference solutions (0, 0.5, 1.0, 1.5, 2.0, 3.0 and 4.0 μg l^{-1}) were prepared daily by stepwise dilution and made up in 0.2% v/v HNO_3. Cadmium reference solutions were prepared in the following chemical modifiers with optimized concentrations: (a) 0.29 mg ml^{-1} $NH_4H_2PO_4$ + 0.2% v/v HNO_3; (b) 0.33 mg ml^{-1} $(NH_4)_2HPO_4$ + 0.2% v/v HNO_3; and (c) 15 μg ml^{-1} Pd (as $Pd(NO_3)_2$) + 0.2% v/v HNO_3. Reference materials of human hair (BCR-397) (Community Bureau of Reference (BCR), Belgium), GBW-09101 and GBW07601 (National Research Centre for Certified Reference Materials (NRCCRM), China) and lyophilized blood (CRM-195, BCR) with certified Cd concentrations were used to validate the atomization system with the chemical modifiers in study for Cd determination in human hair and blood. Argon–hydrogen (90:10) in ETAAS with the TCA and extra-pure argon (99.998%) in ETAAS with a graphite furnace were used as the purge gas throughout.

The chemical modifier used for the graphite furnace determination of Cd was a solution containing 2.88 mg ml^{-1} $NH_4H_2PO_4$ + 0.2% v/v HNO_3 applied in 10 μl aliquots.

The optimization studies of thermal program conditions were performed in human hair and blood samples obtained from two volunteers (males and non-smokers). The hair sample was collected, cleaned and prepared in powdered form following the procedure described by Bruhn et al. [26]. Blood (10 ml) was collected by venipuncture with disposable syringe and stainless-steel needle,

Table 3
Calibration graphs[a] for Cd in 0.2% v/v HNO_3 and chemical modifiers obtained with the tungsten coil atomizer[b]

Solution	Calibration range (μg l^{-1})	Slope ± s	Intercept ± s	Standard error[c]	Correlation coefficient
0.2% v/v HNO_3	0–3.0	0.0967 ± 0.0023	0.0009 ± 0.0045	0.004(6)	0.9989
0.33 mg ml^{-1} $(NH_4)_2HPO_4$ + 0.2% v/v HNO_3	0–3.0	0.0862 ± 0.0012	0.0033 ± 0.0022	0.003(7)	0.9995
0.29 mg ml^{-1} $NH_4H_2PO_4$ + 0.2% v/v HNO_3	0–3.0	0.0521 ± 0.0001	0.0048 ± 0.0057	0.008(6)	0.9985
15 μg ml^{-1} Pd + 0.2% v/v HNO_3	0–2.5	0.1373 ± 0.0037	0.0009 ± 0.0045	0.004(6)	0.9989

[a] Linear regression ($A = mC + b$) representative of $n = 6$ for each data point.
[b] Obtained with an eight-step thermal program.
[c] Number of data points in parentheses.

and was transferred into a pre-cleaned polypropylene tube (serum tube No. 46.390.001 with polypropylene cap, Sarstedt), mixed slowly for few minutes with an anticoagulant (Na_2EDTA, 18.6 mg) and stored at 4°C until analysis. Five pre-cleaned tubes containing the anticoagulant were filled with 10 ml u.p. water, stirred in a vortex for 30 s, stored for 48 h at 4°C, and thereafter these solutions were analyzed for Cd by the proposed methodology, and the levels found in all of them were below the limit of detection.

A portion of the hair sample (100 mg) was weighed into the Milestone TFM vessel, 2 ml of concentrated HNO_3 and 0.5 ml of H_2O_2 were added, and digestion was according to manufacturer's suggested program. The solution digest in the same vessel was placed in the MCR-6-E rotor and evaporated in the microwave system using a six-step evaporation program (36 min) developed in this laboratory. The residue was dissolved in 3 ml 7% v/v HNO_3, transferred into a 10 ml volumetric flask and diluted with u.p. water.

Although for blood the digestion step may not be essential [21], preliminary experiments performed in this laboratory for Cd determination in 1 + 1 diluted blood with a chemical modifier solution (0.73 mg ml^{-1} $(NH_4)_2HPO_4$ + 0.25% v/v Triton X-100 + 0.2% v/v HNO_3) were unsatisfactory because the tungsten coil became distorted and brittle after few sample aliquots were subjected to the heating program. A similar effect was reported earlier by Krug et al. [20] in experiments for blood Pb determination in 1 + 9 diluted blood (pretreated with Triton X-100) by ETAAS with a TCA using the same coil, attributed to the formation of tungsten carbide at high temperatures affecting the coil properties. Hence, in this work, blood samples (0.5–1.0 ml) were digested with 4 ml HNO_3 + 1 ml H_2O_2 under pressure and evaporated in the microwave system, following the same procedure and conditions used for hair. For blood with Cd levels < 1.0 μg l^{-1}, up to 2.5 ml aliquot was used. Blank solutions of the acid digestion were prepared likewise throughout.

2.3. Procedure

The alignment of the TCA in the spectrophotometer's radiation beam, the coil conditioning, the absorbance measurement and time were as described previously [23]. Real-time temperature measurement in this atomizer is difficult due to the high temperature gradient existing around the coil, as well as because of the high heating rate. Earlier, a large temperature gradient (600–750°C) was established in this atomizer between vapor temperature (measured spectroscopically by the two-line atomic absorption method) and coil surface temperatures (measured 0.3 mm above the coil with a thermocouple), and was attributed to the 0.3-mm gap above the coil surface and to heat losses in the volume above the coil [16]. However, the temperature of the coil itself is important, in particular during the pyrolysis step [18]. Thus, in this work, the coil temperature was estimated by voltamperometric measurements, considering the

Table 4
Analytical figures of merit obtained for Cd in 0.2% v/v HNO_3 and chemical modifiers[a] with the tungsten coil atomizer

	Cd			
	HNO_3 0.2% v/v	$(NH_4)_2HPO_4$ 0.33 mg ml^{-1}	$NH_4H_2PO_4$ 0.29 mg ml^{-1}	Pd (as $Pd(NO_3)_2$) 15 μg ml^{-1}
Reciprocal sensitivity (μg l^{-1})	0.05	0.05	0.08	0.03
Characteristic mass (pg)	0.5	0.5	0.8	0.3
Linear working range (μg l^{-1})	0–3.0	0–3.0	0–3.0	0–2.5
Within-run reproducibility (RSD%)	3.6	4.0	5.7	5.5
Detection limit[b] (μg l^{-1})	0.1	0.09	0.1	0.05

[a] Solutions of $(NH_4)_2HPO_4$, $NH_4H_2PO_4$, and Pd, respectively, prepared in 0.2% v/v HNO_3.
[b] 10 μl aliquot.

electric current and voltage measured in the voltage range between 0.3 and 15.0 V, the electric resistance of the coil (obtained by Ohm's law) and the calculated resistivity. The temperature was estimated by interpolation of the resistivity in known and tabulated resistivity/temperature values for tungsten in the literature [27]. The mean uncertainty of this temperature estimates in the range 130–1960°C, obtained from triplicate voltamperometric measurements made at 0.1 V intervals in the 0.3–3.0 V range, and at 0.5 intervals between 3.0 and 15.0 V, is 6.2% (2.6–13%). The accuracy of these temperatures was confirmed by visual observation of the melting point (m.p.) of pure salts deposited on the coil surface [28] (i.e. $(NH_4)_2HPO_4$ (m.p. = 155°C), $NH_4H_2PO_4$ (m.p. = 190°C), $NaNO_2$ (m.p. = 271°C), $NaNO_3$ (m.p. = 307°C), $KClO_3$ (m.p. = 368°C), $K_2Cr_2O_7$ (m.p. = 398°C), CuCl (m.p. = 422°C), $CuCl_2$ (m.p. = 630°C), NaCl (m.p. = 801°C) and Na_2SO_4 (m.p. = 884°C)) and heated at selected voltages corresponding to their approximate melting points obtained from the literature [27]. The dry and atomization voltage–time conditions for Cd were studied in 0.2% v/v HNO_3 and in the phosphate chemical modifier solutions: 1.15 mg ml^{-1} $NH_4H_2PO_4$ + 0.2% v/v HNO_3 and 1.32 mg ml^{-1} $(NH_4)_2HPO_4$ + 0.2% v/v HNO_3 using a six-step thermal program including dry, 'cool-down', cool (to enable the Read function of the spectrometer to be triggered), atomization, clean and cool steps. After the optimum dry and atomization voltage–time conditions had been established, a study of the concentration effect of both phosphate modifiers on Cd sensitivity was carried out in the range 0–2.88 mg ml^{-1} ($NH_4H_2PO_4$) and 0–3.30 mg ml^{-1} ($(NH_4)_2HPO_4$) to verify the optimum phosphate concentrations. Thereafter, an eight-step thermal program was applied to include a second dry and a pyrolysis steps; solutions of digested hair and blood samples (prepared in PTFE bomb) were diluted (1 + 1) with u.p. water, added with a 1.5 μg l^{-1} Cd spike without and with both phosphate chemical modifiers, and used to determine the pyrolysis and atomization voltage–time conditions for Cd. The pyrolysis curves for Cd with phosphate modifiers in each sample matrix were obtained by varying the pyrolysis voltage, while keeping the atomization voltage constant at 10.0 V in 0.2% v/v HNO_3, and 11.0 V in $NH_4H_2PO_4$ (0–1.15 mg ml^{-1}) + 0.2% v/v HNO_3 and in $(NH_4)_2HPO_4$ (0–1.32 mg ml^{-1}) + 0.2% v/v HNO_3. In the hair study, the concentration effect of both phosphates was also assessed. Having established the optimum pyrolysis voltages, the atomization curves were obtained for each phosphate modifier and sample matrix. At this stage, Pd was also included as a chemical modifier, and the pyrolysis and atomization curves were obtained for Cd in 15 μg ml^{-1} Pd + 0.2% v/v HNO_3, using the eight-step thermal program. Under the optimized pyrolysis and atomization conditions, Pd concentration as a chemical modifier for Cd was optimized in the range 0.15–1500 μg ml^{-1}.

Table 5
Determination of Cd in certified reference materials of human hair and blood without and with three chemical modifiers by electrothermal atomic absorption spectrometry with a tungsten coil atomizer

Certified reference material	Certified concentration	HNO_3 0.2% v/v	$(NH_4)_2HPO_4$ 0.33 mg ml^{-1}	$NH_4H_2PO_4$ 0.29 mg ml^{-1}	Pd 15 μg ml^{-1}	ETAAS[c]
Cd (μg g^{-1})[a](n)[b]						
BCR CRM 397 (human hair)	0.521 ± 0.026	0.592 ± 0.080(3)	0.526 ± 0.012(3)	0.523 ± 0.012(3)	0.524 ± 0.009(3)	0.531 ± 0.045(3)
GBW-09101 (human hair)	0.095 ± 0.012	0.106 ± 0.015(3)	0.103 ± 0.021(3)	0.096 ± 0.003(3)	0.093 ± 0.008(3)	0.095 ± 0.007(3)
GBW-07601 (human hair)	0.11 ± 0.02	0.12 ± 0.01(3)	0.12 ± 0.01(3)	0.12 ± 0.02(3)	0.12 ± 0.01(3)	0.12 ± 0.05(3)
Cd (μg l^{-1})(n)[b]						
BCR CRM 195 (blood)	5.37 ± 0.24	5.60 ± 1.24(3)	5.47 ± 0.24(3)	5.63 ± 0.80(3)	5.43 ± 0.51(3)	5.49 ± 0.62(3)

[a]Mean ± standard deviation (95% confidence level) based on dry weight (hair).
[b]Number of independent determinations.
[c]Electrothermal atomic absorption spectrometry with a graphite furnace.

Interference effects of cations and anions according to the concentrations present in digest solutions of human hair and blood, considering both the sample amount digested and the final solution volume, were assessed for Cd in aqueous reference solutions, without and with 15 μg ml^{-1} Pd. For cations, the effects of Na^+, K^+, Ca^{2+}, Cu^{2+}, Mg^{2+}, Fe^{3+} and Zn^{2+} as nitrates in 0.2% v/v HNO_3 were studied at three concentrations in the range 1.0–100 mg l^{-1} plus 1.5 μg l^{-1} Cd. The anions studied likewise corresponded to Cl^- (as NH_4Cl and NaCl), SO_4^{2-} (as $(NH_4)_2SO_4$ and Na_2SO_4) and PO_4^{3-} (as $NH_4H_2PO_4$ and NaH_2PO_4). In each instance, the absorption magnitude, peak shape and background absorption were compared with those of Cd without interferents both in aqueous standards and in 15 μg ml^{-1} Pd as a modifier. This study was performed with the optimized thermal programs for Cd in 0.2% v/v HNO_3 and in 15 μg ml^{-1} Pd + 0.2% v/v HNO_3 using 10 μl injections.

The analytical performance of the system was assessed for Cd in each chemical modifier by systematic evaluation of the linear working range, characteristic mass (m_o), the repeatability, and detection limit ($3s_{blank}$/slope). The calibration curve was obtained under optimized thermal conditions. Also, precision and accuracy were estimated by the determination of Cd in CRMs of hair and blood, by recoveries of Cd from spiked human hair and blood, and by comparison with the results obtained by ETAAS with a graphite furnace under stabilized temperature platform furnace conditions.

3. Results and discussion

In graphite furnace atomizers, regardless of their design and method of atomization, integrated absorbance is used for quantification because this measurement mode is less affected by matrix composition and atomizer heating rate. The situation is different in the TCA where the signal duration is very short (0.2 s) [16] and its shape is highly dependent on the heating rate (20–30 K ms^{-1}). As was shown recently by Krakovská and Pulis [29,30], in electrothermal atomization in a tungsten tube atomizer with heating rates in the 5–20 K ms^{-1} range (ten-fold higher than in a graphite tube atomizer), the absorbance peak can be evaluated on the basis of the height or the integrated area. In fact, better detection limits and relative standard deviation

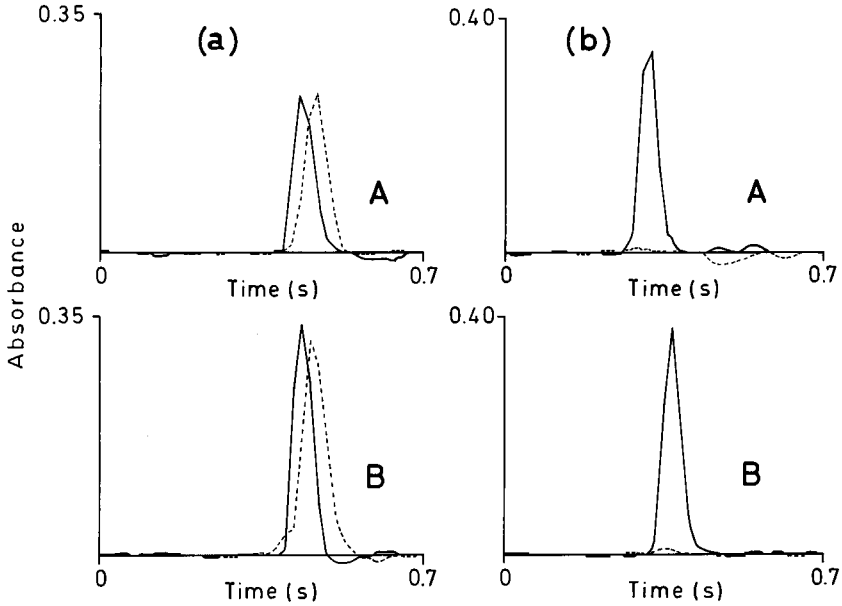

Fig. 4. Atomic (——) and background (- - -) signals for acid-digested solutions of (a) blood and (b) human hair: (A) without modifier and (B) with 15 μg ml^{-1} Pd (as $Pd(NO_3)_2$) as chemical modifier.

values are obtained for Cd, Co and V with or without chemical modifiers, with peak height evaluation [29]. The short-time absorption signals in the TCA are relatively small, measured in integrated absorbance, in contrast to graphite furnace atomic absorption spectrometry because of the larger residence time of the latter, and this measurement mode caused a large loss in sensitivity in the TCA (i.e. by a factor of 15–35). Therefore, quantification using peak height absorbance was much easier and was the measurement mode applied in the TCA.

3.1. Study of $(NH_4)_2HPO_4$ as chemical modifier

It can be seen in Fig. 1 (curve B) that hydrogenphosphate caused a thermal stabilization of Cd in the TCA. In a 0.2% v/v HNO_3 medium (Fig. 1, curve A), the maximum pyrolysis temperature without Cd losses was 250°C, and in a 1.32 mg ml^{-1} $(NH_4)_2HPO_4$ medium, the maximum pyrolysis temperature was 380°C. However, in spite of this beneficial effect, the absorbance signal measured in this later medium was 35% lower than in nitric acid solution. Considering that this decrease in sensitivity is not caused by Cd losses, this effect can be correlated to negative interferences promoted by hydrogenphosphate in Cd atomization. The optimal atomization temperatures were 1670 and 1730°C, in nitric acid and in hydrogenphosphate media (Fig. 1), respectively.

The effect of the chemical modifier concentration on the Cd absorbance was also evaluated (Fig. 2, curve A). There is a continuous decrease in absorbance up to 1.32 mg ml^{-1} $(NH_4)_2HPO_4$. Higher concentrations led to a less pronounced signal decrease. A concentration of 0.33 mg ml^{-1} $(NH_4)_2HPO_4$ was selected and used thereafter.

Taking into account these data, the heating program shown in Table 1 was used for further investigations. A cool-down step was implemented after pyrolysis since it caused a slight improvement in the sensitivity; however, the effect is less pronounced than that previously observed for Pb [23].

The supposed interference effect caused by hydrogenphosphate was evaluated with solutions containing from 1 to 100 mg l^{-1} P (as PO_4^{3-}) and expressed relative to Cd absorbance without the interferent (normalized to 100%). Data in Table 2

Table 6
Determination of Cd[a] in human blood and hair by atomic absorption spectrometry with the tungsten coil atomizer (TCA) and by electrothermal atomic absorption spectrometry with a graphite furnace (ETAAS)

Sample	Blood[b]		Hair[c]	
	TCA	ETAAS	TCA	ETAAS
Worker	1.9 ± 0.6	1.9 ± 0.1	0.06 ± 0.02	0.05 ± 0.03
Student	<0.2	<0.3	0.08 ± 0.03	0.05 ± 0.03
Recovery study (%)[d]	98 ± 7	101 ± 5	101 ± 6	101 ± 2

[a] 95% confidence interval in triplicate independent determinations.
[b] Concentration of Cd in $\mu g\ l^{-1}$.
[c] Concentration of Cd in $\mu g\ g^{-1}$ based on dry weight.
[d] $0.08 \pm 0.03\ \mu g\ g^{-1}$ Cd (hair); $<0.2\ \mu g\ l^{-1}$ Cd (blood); $1.5\ \mu g\ l^{-1}$ Cd addition in final solution.

show a negative effect caused by ammonium hydrogenphosphate on Cd atomization. The same study was performed with sodium hydrogenphosphate on Cd and the effect was also negative but less pronounced (e.g. $<20\%$ drop in Cd signal), and noticeable at 10 and 100 mg l^{-1} P; it was corrected by addition of 15 $\mu g\ ml^{-1}$ Pd (as $Pd(NO_3)_2$). The negative interferences of 1 mg l^{-1} P as ammonium hydrogenphosphate in 1.5 $\mu g\ l^{-1}$ Cd was also corrected by adding 15 $\mu g\ ml^{-1}$ Pd (as $Pd(NO_3)_2$). However, Pd only decreased the interference in 10 mg l^{-1} P medium and had no effect on 100 mg l^{-1} P interference. The effect of higher concentration of Pd was not evaluated since as it will be shown later; this would cause a reduction in the Cd absorbance signal.

For a better understanding of this interference process, 5 μl aliquots of Cd and P (as ammonium hydrogenphosphate) solutions were introduced in opposite ends of the tungsten coil, and the heating cycle was implemented. Previously, it was established that there was no mixture of both solutions during the dry step. Since the interference levels were similar to those observed when analyte and interferent were physically mixed onto the tungsten coil, it can be concluded that the interference is occurring in the gaseous phase because it manifests itself even without physical mixing in the condensed phase.

This behavior confirms that despite a slight thermal stabilization effect, ammonium hydrogenphosphate cannot probably be recommended as a chemical modifier for Cd atomization in the TCA.

To obtain a more complete evaluation, ammonium hydrogenphosphate was added to acid-digested solutions of hair and blood, and pyrolysis and atomization curves were obtained (Fig. 3). In acid-digested solutions of hair (Fig. 3a), the pyrolysis curve again shows an improvement in thermal stability and a loss in sensitivity for temperatures lower than 420°C when compared to Cd in nitric acid medium. At higher temperatures, the sensitivity is better in phosphate medium owing to the thermal stabilization effect. On the other hand, the atomization curve in hydrogenphosphate led to higher absorbance signals than those obtained in nitric acid or in dihydrogenphosphate media. Different results were generated in acid-digested solutions of blood (Fig. 3b). In these cases, the sensitivity obtained in hydrogenphosphate medium in the pyrolysis and atomization curves was better than that attained in nitric acid medium at all temperatures applied. The phosphates present in the blood matrix complicate the interpretation of these results, but certainly it is related to the enhancement effect observed.

The calibration graph and figures of merit for Cd in hydrogenphosphate medium are shown in Tables 3 and 4, respectively. Data obtained reflected the previous results and the negative interference effect is evidenced by the slope of the analytical curve when compared to that obtained in nitric acid medium, i.e. sensitivity losses of 11% (Table 3). The analytical figures of merit obtained experimentally are comparable to those generated in nitric acid medium, and slightly better than

those obtained in dihydrogenphosphate medium (Table 4). Despite phosphate interference, accurate results were obtained for Cd determination in acid-digested solutions of hair and blood in certified reference materials at a 95% confidence level (Table 5). Since the addition of the chemical modifier did not correct interference effects, the quantification was performed adopting the standard additions method. Considering the obtained results with all CRMs (Table 5), the mean relative error is 5.1% and the mean relative standard deviation (RSD%) is 8.9%.

Overall, ammonium hydrogenphosphate was useful for allowing the application of a higher temperature during the pyrolysis step (380°C), but the accuracy was attained when employing the standard additions method.

3.2. Study of $NH_4H_2PO_4$ as chemical modifier

The influence of dihydrogenphosphate on Cd atomization in the TCA is similar to that previously observed with hydrogenphosphate. As discussed, the main effect seems to be negative interference and all previous comments remain valid. The negative interference effect is different from that observed in a graphite atomizer, in which a sensitivity gain was obtained when using dihydrogenphosphate as modifier in the determination of Cd in urine [31].

In 1.15 mg ml^{-1} dihydrogenphosphate medium, pyrolysis and atomization curves (Fig. 1, curve C) presented higher absorbance than those obtained in hydrogenphosphate medium, but again the absorbances were significantly lower than those obtained in nitric acid medium. The pyrolysis curve indicates a thermal stabilization of Cd from 300 to 480°C.

Regarding the chemical modifier concentration effect, the decrease in absorbance signal in dihydrogenphosphate medium was less pronounced than that observed in hydrogenphosphate (Fig. 2, curve B), i.e. the Cd absorbance signal obtained in 1.73 mg ml^{-1} solution is only 10% lower than that obtained in 0.29 mg ml^{-1} medium. This latter concentration was used thereafter in all measurements, unless otherwise mentioned.

Related to the pyrolysis and atomization curves in acid-digested solutions of hair and blood, the behavior is similar to that observed in hydrogenphosphate medium and only this modifier is shown in Fig. 3 to avoid curve overlap.

The calibration graph and figures of merit are shown in Tables 3 and 4, respectively. As previously mentioned, the negative effect can be observed when comparing the slopes of the calibration curves in dihydrogenphosphate and in nitric acid media, i.e. there is a 46% loss in sensitivity owing to this depressive effect. As shown in Table 5, the standard additions method provided accurate results for CRMs at a 95% confidence level. Considering the obtained results with all CRMs (Table 5), the mean relative error is 3.8% and the mean RSD% is 9.1%.

3.3. Study of Pd (as $Pd(NO_3)_2$) as chemical modifier

In a recent work, beneficial effects caused by Pd as a chemical modifier in the determination of Pb in acid-digested solutions of hair and blood using the TCA [23] were demonstrated. It was shown that Pd caused a thermal stabilization of Pb, enhanced Pb absorbance, eliminated condensed phase interferences, reduced background signals, and improved tungsten coil lifetime by up to 20% [23]. Considering that both Cd and Pb are volatile elements, it is expected that the positive effects caused by Pd on Pb atomization in the TCA could also be observed for Cd. However, previous experimental studies showed that hydrogen present in the purge gas (i.e. 10% v/v) was essential for Pb atomization, and it was not necessary for Cd atomization in the TCA [14,16,20]. This indicates that mechanisms of atomization are different and, thus, the action of Pd can also be changed.

According to our expectations, the sensitivity obtained for Cd in 15 μg ml^{-1} Pd medium was ca. 40% better than that obtained without Pd (Fig. 1, pyrolysis curve D), but Cd thermal stabilization was not pronounced, i.e. the maximum pyrolysis temperature without Cd losses is 330°C. Thus, the use of Pd as chemical modifier could not be effective for thermal volatilization of con-

comitants during the pyrolysis step without Cd losses.

The optimum Pd concentration was established as 15 μg ml^{-1} (Fig. 2). Using this modifier concentration and the heating program shown in Table 1, the effect of Pd on concomitant interferences in Cd atomization was evaluated (Table 2). Palladium effects were not evaluated in solutions containing from 1 to 10 mg l^{-1} Cu^{2+}, Fe^{3+}, or K^+ and 1 to 100 mg l^{-1} Ca^{2+} because interferences were not observed in all these media ($< 5\%$ as a mean). Except for phosphate (as ammonium dihydrogenphosphate) and chloride (as sodium salt), Pd was effective for eliminating interferences caused by Mg^{2+}, Zn^{2+}, Na^+, Cl^- (as ammonium salt), SO_4^{2-} (as ammonium and sodium salts) and PO_4^{3-} (as sodium salt). Without Pd, the volatilization of NH_4Cl probably reduced losses of Cd as chloride and this led to a signal enhancement in 10 and 100 mg l^{-1} Cl^- (Table 2). Nevertheless, minor Cd losses (e.g. a signal decrease of 18%) became apparent in 100 mg l^{-1} Cl^- as NaCl, most likely due to the lower volatility of the latter, and were reduced to 13% but not eliminated in Pd modifier. Phosphate (as $Na_2H_2PO_4$) led to a signal decrease of 16 and 17% in 10 and 100 mg l^{-1} PO_4^{3-}, respectively, and this effect was eliminated in Pd medium. According to an experiment performed with introduction of individual solutions of Cd and the studied ions in opposite ends of the tungsten coil without mixing, most of these interference processes apparently occur in the condensed phase. As mentioned before, phosphate interference (as $NH_4H_2PO_4$) on Cd seemed to occur in the gaseous phase, which is different from the effect observed on Pb atomization [23]. Thus, even without complete understanding of the Pd action to suppress interferences on Cd atomization, it can be supposed that it was effective for correcting condensed phase interferences and it had no clear effect to avoid gaseous phase interferences.

Using acid-digested solutions of hair and blood (Fig. 3), it was established that the maximum pyrolysis temperatures are 330 and 250°C in media with 15 μg ml^{-1} Pd and without Pd, respectively. The recommended atomization temperature for blood-digested samples in Pd medium is 1850°C, which is 180°C higher than the optimum atomization temperature in nitric acid medium.

The thermal program shown in Table 1 was used for establishing the calibration graph (Table 3) and evaluating the figures of merit (Table 4). The slope obtained in Pd medium is 42% higher than that found in nitric acid medium which results in the best overall sensitivity (characteristic mass, 0.3 pg; instrumental detection limit, 0.05 μg l^{-1}, as shown in Table 4). The method detection limits ($3s_{blank}$/slope) for Cd, using Pd as a chemical modifier, were 0.009 μg g^{-1} in hair and 0.2 μg l^{-1} in blood, considering subsamples of 100 mg and 2.5 ml, respectively. The attained sensitivity is suitable for the determination of Cd in acid-digested solutions of hair and blood. Data shown in Table 5 were obtained applying the standard additions method and results obtained without chemical modifier (in nitric acid medium), although adequate in two CRMs of hair low in Cd, are not quite satisfactory in hair and blood with relatively high Cd levels. Without modifier, the mean relative error was 9.6% and the mean uncertainty was 14.5% (8.3–22.1%); both figures were considered relatively high. The results obtained with chemical modifiers in all CRMs are in agreement with certified concentrations and with values determined by ETAAS in a graphite tube with a platform at a 95% confidence level. In the obtained results using Pd modifier in all CRMs (Table 5), the mean relative error is 3.2% and the mean RSD% is 7.0%, which are satisfactory for triplicate determinations. These figures are better than those attained without and with the other modifiers evaluated, which again shows the better performance of the Pd modifier. Another alternative for Cd quantitation is the use of a calibration curve with matrix-matched standards prepared in cadmium-spiked blood. However, this approach was not attempted in this work. Representative atomic and background signals for Cd in acid-digested solutions of human hair and blood with and without Pd as modifier are shown in Fig. 4. Results obtained with Pd as chemical modifier for occupationally exposed (worker) and non-exposed (student) individuals in blood and hair samples show low Cd levels and are in good agreement

with graphite furnace data at a 95% confidence level (Table 6). When Cd was added to blood and hair samples low in Cd content before digestion to make a final concentration of 1.5 μg l^{-1} Cd after dilution, the mean recoveries by TCA were 98 ± 7% ($n = 3$) and 101 ± 6% ($n = 3$), respectively, and were comparable with the results obtained by graphite furnace with a platform.

All positive effects caused by Pd on Pb atomization in the TCA [23] were also observed for Cd in this same atomizer.

4. Conclusion

All chemical modifiers evaluated, i.e. $(NH_4)_2HPO_4$, $NH_4H_2PO_4$, and Pd (as $Pd(NO_3)_2$), caused some thermal stabilization on Cd atomization in the TCA and rendered better accuracy and precision than without modifier use. However, negative interferences caused by phosphates prevent their use as a chemical modifier for Cd in the TCA. On the other hand, Pd as modifier, in addition to overcoming condensed phase interferences and stabilizing Cd thermally, also improved the tungsten coil lifetime by up to 20% (i.e. from 300 to 360 heating cycles) and reduced background signals. Palladium action is not fully understood but its analytical applicability was clearly demonstrated by Cd determination in acid-digested solutions of hair and blood. None of the modifiers studied eliminated the need for the standard additions method in Cd quantitation. Alternatively, the matrix matching approach could also be adopted.

Acknowledgements

We are grateful to Fondo Nacional de Desarrollo Científico y Tecnológico (FONDECYT) (research grant No 1960664) and to Dirección de Investigación of the Universidad de Concepción, Concepción, Chile (DIUC research grant No 94.71.11-1) for financial support; to Dr H. Berndt for providing the TCA unit through the agreement of co-operation between the Institute für Spektrochemie und angewandte Spektroskopie (ISAS) Dortmund, Germany, and the Facultad de Farmacia, Universidad de Concepción; and to Centro EULA-Chile of the Universidad de Concepción for allowing the use of their PE-1100B atomic absorption spectrophotometer with HGA-700 graphite furnace and AS-70 autosampler. The authors acknowledge the assistance of Mr Victor H. Campos in sample preparation and Cd determination by ETAAS with a graphite furnace.

References

[1] M. Williams, E.H. Piepmeier, Anal. Chem. 44 (1972) 1342.
[2] J.E. Cantle, T.S. West, Talanta 20 (1973) 459.
[3] M.P. Newton, J.V. Chauvin, D.G. Davis, Anal. Lett. 6 (1973) 89.
[4] M.P. Newton, D.G. Davis, Anal. Lett. 6 (1973) 923.
[5] J.V. Chauvin, M.P. Newton, D.G. Davis, Anal. Chim. Acta 65 (1973) 291.
[6] W. Lund, B.V. Larsen, Anal. Chim. Acta 70 (1974) 299.
[7] W. Lund, B.V. Larsen, Anal. Chim. Acta 72 (1974) 57.
[8] R.D. Reid, E.H. Piepmeier, Anal. Chem. 48 (1976) 338.
[9] V.B. Atnashev, V.N. Muzgin, Yu.B. Atnashev, Zh. Anal. Khim. 37 (1982) 1590.
[10] Yu.B. Atnashev, V.E. Korepanov, V.N. Muzgin, Zh. Prikl. Spektrosk. 42 (1985) 537.
[11] H. Berndt, G. Schaldach, J. Anal. At. Spectrom. 3 (1988) 709.
[12] E. Ivanova, I. Havesov, H. Berndt, G. Schaldach, Fresenius J. Anal. Chem. 336 (1990) 320.
[13] E. Ivanova, I. Havesov, H. Berndt, G. Schaldach, J. Anal. Chem. 336 (1990) 484.
[14] M.F. Giné, J.A. Nóbrega, F.J. Krug, V.A. Sass, B.F. Reis, H. Berndt, J. Anal. At. Spectrom. 8 (1993) 243.
[15] M.M. Silva, R.B. Silva, F.J. Krug, J.A. Nóbrega, H. Berndt, J. Anal. At. Spectrom. 9 (1994) 861.
[16] C.G. Bruhn, F.E. Ambiado, H.J. Cid, R. Woerner, J. Tapia, R. Garcia, Anal. Chim. Acta 306 (1995) 183.
[17] C.G. Bruhn, F.E. Ambiado, H.J. Cid, R. Woerner, J. Tapia, R. Garcia, Quim. Anal. 15 (1996) 191.
[18] M. Knochen, E. Saritsky, I. Dol, Quim. Anal. 15 (1996) 184.
[19] M.M. Silva, F.J. Krug, P.V. Oliveira, J.A. Nóbrega, B.F. Reis, D. Penteado, Spectrochim. Acta Part B 51 (1996) 1925.
[20] F.J. Krug, M.M. Silva, P.V. Oliveira, J.A. Nóbrega, Spectrochim. Acta 50 (1995) 1469.
[21] P.J. Parsons, H. Qiao, K.M. Aldous, E. Mills, W. Slavin, Spectrochim. Acta 50 (1995) 1475.
[22] C.L. Sanford, S.E. Thomas, B.T. Jones, Appl. Spectrosc. 50 (1996) 174.
[23] C.G. Bruhn, J.Y. Neira, G.D. Valenzuela, J.A. Nóbrega, J. Anal. At. Spectrom. 13 (1998) 29.

[24] D.L. Tsalev, Atomic Absorption Spectrometry in Occupational and Environmental Health Practice: Progress in Analytical Methodology, Vol. 3, CRC Press, Boca Raton, FL, 1995.
[25] A. Chatt, S.A. Katz, Hair Analysis. Applications in the Biomedical and Environmental Sciences, VCH Publishers, New York, 1988.
[26] C.G. Bruhn, A.A. Rodríguez, C. Barrios, V.H. Jaramillo, J. Becerra, U. González, N.T. Gras, O. Reyes, S. Salud, J. Anal. At. Spectrom. 9 (1994) 531.
[27] D.R. Lide (Ed.), CRC Handbook of Chemistry and Physics, 71st edn., CRC Press, Boca Raton, FL, 1990–1991, pp. 10–283.
[28] S. Nakamura, Y. Kobayashi, M. Kubota, Spectrochim. Acta Part B 48 (1986) 817.
[29] E. Krakovská, P. Pulis, Spectrochim. Acta 51 (1996) 1271.
[30] E. Krakovská, Spectrochim. Acta 52 (1997) 1327.
[31] C.F. Bruhn, G.A. Navarrete, Anal. Chim. Acta 130 (1981) 209.

ELSEVIER

Talanta 48 (1999) 551–557

Talanta

Optical chromatography
Size determination by eluting particles

Jun Makihara, Takashi Kaneta, Totaro Imasaka *

Department of Chemical Science and Technology, Faculty of Engineering, Kyushu University, Hakozaki, Fukuoka 812, Japan

Received 13 April 1998; received in revised form 10 August 1998; accepted 11 August 1998

Abstract

A new method for the determination of particle size was developed using optical chromatography. After separating polystyrene particles, the laser power was gradually reduced, permitting the elution of small to large particles. Particle size was calculated from the laser power when the particle was eluted with a medium flow. This approach is more accurate than the technique previously reported because there is no need to determine the position of the beam waist. Advantages of the new approach are discussed theoretically and experimentally. The precision in size determination was improved by a factor of 3.3, i.e. the standard deviation in the measurement was reduced from 10 to 3% for 1 μm beads by replacing optical chromatography with the present method.

Keywords: Laser; Radiation pressure; Optical chromatography

1. Introduction

Ashkin recently reported an optical technique which uses laser radiation pressure and which can be used for the control and manipulation of micrometer-sized particles [1]. The technique is based on the transfer of momentum between particles and the laser beam [2] and allows one to manipulate a particle without destruction or contact, suggesting that it would be useful in the field of biomedical and biological sciences. The manipulation technique, which is called laser trapping, laser manipulation, optical tweezers, or laser levitation, has been applied to polymer particles [1,3] and intact living cells, such as red blood cells [4], human sperm [5], phytoplankton [6], virus and bacteria [7], and DNA molecules [8].

Optical chromatography is a new method for the separation of particles using a radiation force and medium flow [9]. In this method, a laser beam is focused into a solution which contains particles counter-flowing coaxially in a capillary. The particle is kept at an equilibrium position, where the radiation force is identical to the force induced by the liquid flow. Consequently, the particles are separated as a function of size, as shown in Fig. 1. We have previously applied optical chromatography to the separation of polystyrene beads [9], human erythrocyte cells [10], and immunoassays [11]. In optical chromatography, the particle size is determined by determining the distance from

* Corresponding author. Tel.: +81 92 6423563; fax: +81 92 6325209; e-mail: imasaka@cstf.kyushu-u.ac.jp

0039-9140/99/$ - see front matter
PII S0039-9140(98)00272-0

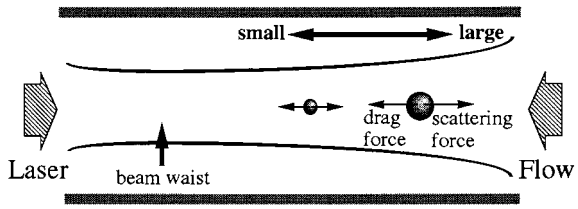

Fig. 1. Schematic diagram of optical chromatography.

the beam waist to the retained position of the particle. However, it is difficult to accurately determine the position of the beam waist. In this study, a new approach for the accurate determination of particle size is demonstrated which does not require measuring the position of the beam waist. A schematic illustration of the approach is shown in Fig. 2. In Fig. 2a, the particles stop at different equilibrium positions depending on their sizes. In this situation, larger particles are located further from the beam waist. When the laser power is reduced gradually, the smallest particles approach the beam waist. Further reduction of the laser power results in the elution of the particles (Fig. 2b). After the smallest particles are completely eluted, the next particles are eluted in turn (Fig. 2c). As a result, the particle size can be determined by the laser output when the particle elutes. In this paper, advantages in the proposed method are discussed theoretically and experimentally and compared with a technique which has been reported previously [10].

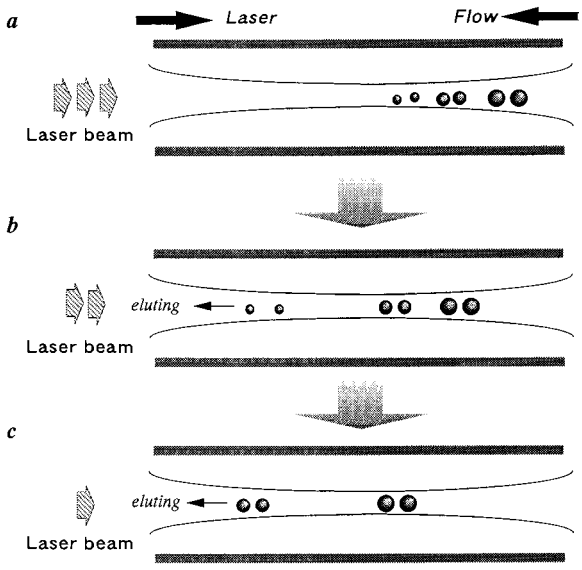

Fig. 2. Principle of size determination: (a) separation of particles, (b) elution of the smallest particles by decreasing the laser output power gradually, (c) elution of subsequent particles.

2. Theory

In general, radiation pressure applied to microspheres can be expressed by two forces. The first is the radial force, a gradient force, and the second is the axial force, a scattering force. A fundamental equation was derived in a previous paper [10], defining one-dimensional motion, i.e. referring to only a drag force induced by a medium flow and the scattering force based on a ray-optics model. The force applied for a microsphere is calculated as

$$F = 2\frac{n_1 P}{c}\left(\frac{a}{\omega}\right)^2 Q_s - 6\pi\eta a u \tag{1}$$

and, ω, the radius of the beam, can be expressed by the following equation.

$$\omega^2(z) = \omega_0^2\left\{1 + \left(\frac{z}{z_c}\right)^2\right\} \tag{2}$$

The particle stops when the drag force is equal to the scattering force in Eq. (1). Therefore, the retention distance, z, can be expressed by

$$z = z_c\sqrt{\frac{n_1 P Q_s a}{3\pi\eta c u \omega_0^2} - 1} \tag{3}$$

When the laser output power is gradually decreased, the particle approaches the beam waist as predicted by Eq. (3). In optical chromatography, the maximum radiation pressure is observed at the beam waist, and therefore the particles at the beam waist are the smallest which are retained. Thus, the particle which stops at the beam waist would be eluted by decreasing the laser power. By substituting $Z = 0$ in Eq. (3), the following equation is obtained.

$$a_0 = \frac{3\pi\eta c\omega_0^2}{n_1 Q_s}\frac{u}{P} \tag{4}$$

where a_0 is the minimum particle size to be retained at the beam waist. As noted in Eq. (4), the minimum particle size depends on the laser power and flow rate.

Dispersion of particles will cause the underestimation of particle size in this technique, because the dispersed particle may pass through the beam waist for the case where particles are retained near the beam waist. It is assumed that the dispersion of particles in optical chromatography is caused by Brownian motion of the particle and by instrument fluctuations, induced by variations in laser power and flow rate. Based on a preliminary theoretical calculation, the effect of Brownian motion was negligible compared with that caused by instrument fluctuations. Thus, it is assumed that only instrument fluctuation induced by variations in laser power, ΔP, and in flow rate, Δu, is a major factor in dispersion of the particles. The variation of the force applied to a particle, dF, is then given by

$$dF = \left(\frac{\partial F}{\partial \zeta}\right)\Delta\zeta + \left(\frac{\partial F}{\partial P}\right)\Delta P + \left(\frac{\partial F}{\partial u}\right)\Delta u \tag{5}$$

where ζ is defined as z/z_c and z_c is the confocal distance. When the particle is stopped at the equilibrium position, dF is equal to zero. From Eqs. (1), (2) and (5), the dispersion of the particle position, $\Delta\zeta$, is calculated by

$$\Delta\zeta = \frac{1+\zeta^2}{2\zeta}\left(\frac{\Delta P}{P} - \frac{\Delta u}{u}\right) = \frac{1+\zeta^2}{2\zeta}\, v \tag{6}$$

where v indicates instrument fluctuation, and is denoted as

$$v = \left(\frac{\Delta P}{P} - \frac{\Delta u}{u}\right) \tag{7}$$

From Eq. (6), the dispersion of the particle position, $\Delta\zeta$, is a function of ζ and v. The relationship between ζ and $\Delta\zeta$, calculated by Eq. (6), is shown in Fig. 3. (The solid lines are calculated by assuming that instrument fluctuation is 1, 5 and 10%, respectively, and a dashed line represents $\zeta = \Delta\zeta$. The intersecting point of the solid and dashed lines indicates the size of the particle to be eluted due to particle dispersion, since the particle passes through the beam waist when $\zeta \leq \Delta\zeta$). For example, if the instrument fluctuation is 1%, $\Delta\zeta$ is equal to ζ at $\zeta = 0.75$. Thus, one of the particles to be retained at $\zeta = 0.75$ is dispersed to the beam waist and then eluted. This results in an underestimation of the size measurement. As noted in Fig. 3, the relative error by the particle size determined using this technique becomes larger with increasing instrument fluctuation. However, the relative error, which is due to instrument fluctuation, is independent of the particle size. The parameter, ζ' is defined as the retention distance for ζ when the particle elutes, i.e. $\zeta' = \Delta\zeta$. Substituting $\zeta = \zeta'$ and $\Delta\zeta = \zeta'$, the following equation can be derived

$$\zeta' = \sqrt{\frac{v}{2-v}} \tag{8}$$

Consequently, particle size is determined by the following equation.

$$a_0 = \frac{3\pi\eta u c\omega_0^2}{n_1 P Q_s}(1+\zeta'^2) = \frac{3\pi\eta u c\omega_0^2}{n_1 P Q_s}\left(\frac{2}{2-v}\right) \tag{9}$$

Thus, the relative error in the determination of particle size can be calculated from Eq. (9). For example, when v is equal to 5%, the particle size is the underestimated by 2.4%, which is independent of size.

Table 1 shows a theoretical comparison between the current technique, now in general use, and the new approach described here. First, it is unnecessary to measure the position of the beam waist in the new approach because the particle size is determined by observing the elution of particles. Second, selectivity is theoretically better since the particle position is in the vicinity of the

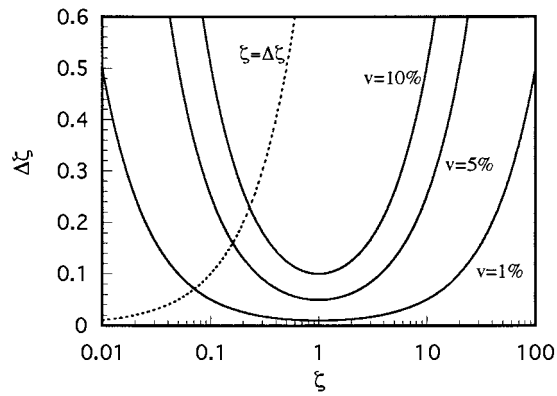

Fig. 3. Relationship between $\Delta\zeta$ and ζ.

Table 1
Theoretical comparison between the current technique and the new approach

	Current technique	New approach
Measurement of beam waist position	Necessary	Not necessary
Selectivity and accuracy	Not good	Good
Inaccuracy occurring from instabilities in laser output power and flow rate	Not sensitive	Sensitive
Dynamic range	Wide	Narrow
Measurement	Image detector	Photo detector

beam waist [10]. In addition, accuracy can be improved by a higher degree of selectivity and a reduction in the error associated with the need to measure the beam waist position. Third, it can be confirmed theoretically that this method is sensitive to instabilities in the laser output power and flow rate. Fourth, the dynamic range is narrower since resolution is lower for large particles which are eluted at the lowest laser output power. However, adjustments in the radius of the beam waist and the flow rate can change the dynamic range. Finally, for purposes of detection, it is possible to use a conventional photodetector such as a photomultiplier tube and diode detector, rather than an image sensor.

3. Experimental

3.1. Apparatus

A schematic diagram of the experimental apparatus used in this study was shown in previous papers [10,11]. An argon ion laser (GLG3200, Nippon Electric, Tokyo, Japan) emitting at 514.5 nm was focused by a lens (focal length, 50 mm). The fluctuation of laser power is controlled within $\pm 0.5\%$ using a feedback circuit and the resolution attained is 10 mW. The ends of a fused silica capillary (GL Science, Tokyo, Japan; 200 μm i.d., 375 μm o.d.) were immersed into reservoirs containing a buffer solution. The sample solution was introduced by gravity using a siphon method. The flow rate of the medium was adjusted to ca. 0.18 mm s^{-1} by adjusting the levels of the buffer solution. The motion of samples was observed by a video system coupled with a charge-coupled-device camera. The experimental apparatus and the operation conditions have been described in detail in a previous paper [10].

3.2. Procedure

Three types of polystyrene latex beads with different diameters (0.997, 3.03 and 10.5 μm; refractive index, 1.59) were obtained from Polyscience (Warrington, PA). The particles were suspended in water (refractive index, 1.59; viscosity, 1×10^{-3} Pa s) and treated for 15 min in an ultrasonic agitator to avoid possible coagulation between the beads. The suspension was then introduced sequentially from the inlet side of the capillary to a quartz cell using a siphon method. The sample was dispersed appropriately for retention of a single bead, in order to prevent the possibility of measuring condensed beads. After a single bead was stopped, the laser power was decreased gradually until it was eluted. The laser power, at which the beads were eluted, was recorded. In addition, a size separation of two types of beads (0.997 and 3.03 μm) was attempted.

4. Results and discussion

Particle radius, a, is proportional to the value of u/P as noted in Eq. (2). Thus, particle radii were calculated using the flow rate and the laser power when the particles were eluted. The histogram of the particle diameter calculated by Eq. (2) is shown in Fig. 4. The measurement was carried out at a constant flow rate of approximately 0.18 mm s^{-1}. As shown in Fig. 4, experi-

mentally determined particle diameters are distributed over a range. The distribution is caused by several sources, including instrument fluctuation as described in Section 2, errors in measurement, and the original deviation in the size of the samples.

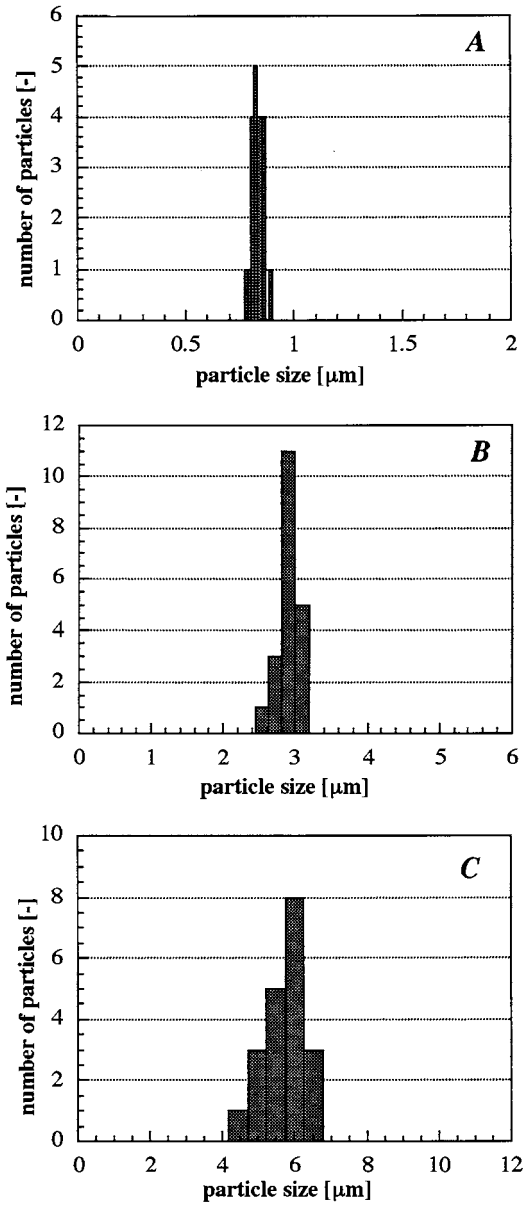

Fig. 4. Histogram showing the values for particle diameter versus the number of eluting particles. The values for particle diameter were calculated using Eq. (2). Instrument fluctuation is not taken into consideration, i.e. Eq. (7) is not used. For each determination, only one particle was retained and then eluted to avoid the problem of coagulation of particles.

Table 2
Comparison of certified and experimental values

Particle size (μm) (R.S.D. (%))	
Certified	Experimental
0.997(1.9)	0.931(3.4)
3.03(1.4)	2.91(4.9)
10.5(12.8)	5.65(9.5)

The mean particle diameters obtained from the data sheet and those obtained in this study are listed in Table 2. The discrepancy between certified and experimental values is noted for 0.997 and 3.03 μm. This may be caused by the laser which is not operated in an exact single transverse mode. This problem can be solved by calibration based on the certified value of a standard particle. It should be noted that the diameter for a 10.5 μm particle is much smaller than the certified value. Such a discrepancy may arise from invalid approximation for calculating the Q_s value in Eq. (2). In Table 2, Q_s is constant at 0.129 in the calculation of particle diameters as reported previously [10]. However, this value is valid only when the beam diameter is much smaller than the particle diameter. In this study, the diameter of the beam waist is 18.82 μm, so that the approximation described is not reasonable for a 10.5 μm particle. Thus, it is necessary to increase the beam radius of the beam waist by altering the focusing condition in order to measure a larger particle.

The relative standard deviations (R.S.D.s) of the diameters determined by the present approach were compared with the certified values provided by the manufactures. The results are also shown in Table 2. The values are several-fold larger than those expected from the data sheet provided with the polystyrene latex spheres. However, the S.D. of the particle diameter determined by the present technique is several percent, which is much smaller than ca. 10% obtained by current optical chromatography. Thus, the present approach is more accurate than the current technique as predicted by the theoretical study.

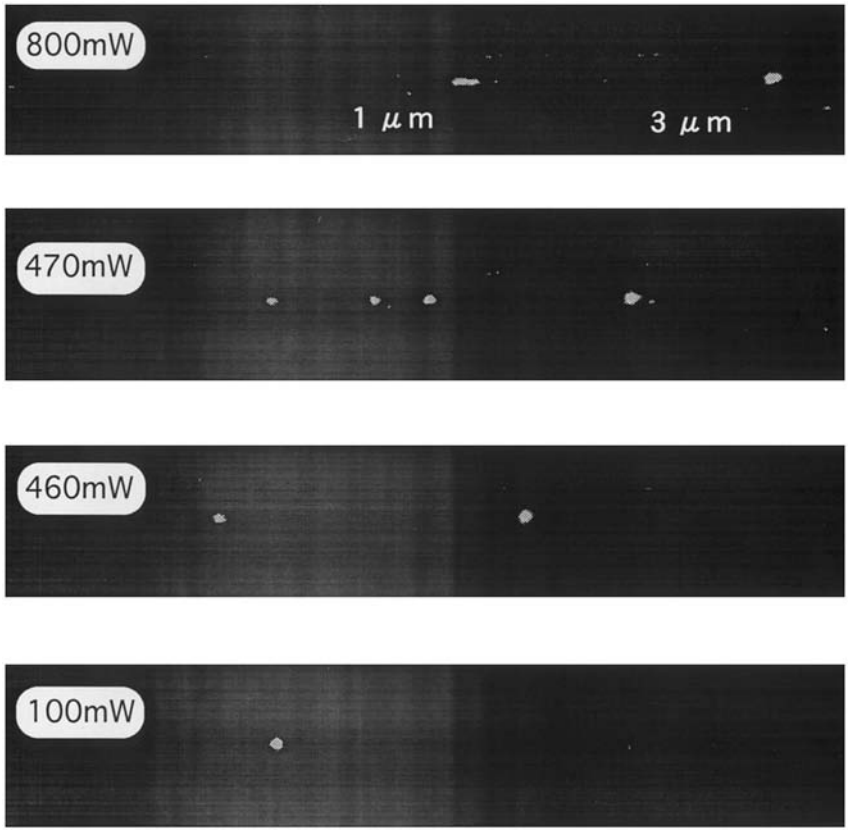

Fig. 5. Photograph of two types of beads separated using optical chromatography. In this case, three 1 μm beads and one 3 μm bead were separated.

The present method was applied to the determination of the particle sizes for a mixed sample. Fig. 5 shows a photograph of the particles eluted by decreasing the laser power. Two types of the beads, 1 and 3 μm in diameter, were separated at 800 mW of laser power using optical chromatography. In this case, three 1 μm beads and one 3 μm bead were separated. Decreasing the laser power resulted in movement of the particle to the beam waist followed by eluting of the particles. When the laser output was adjusted to 470 mW, two 1 μm beads were eluted. After passing the beam waist, each particle was accelerated by the liquid flow, so that the beads were separated. In addition, one residual 1 μm bead was eluted by decreasing the laser power to 460 mW. One 3 μm bead approached the beam waist as the laser power was decreased, and then eluted at 100 mW.

The resolution in the particle size measurement remains limited, as is shown in Table 2. This can be attributed to fluctuations in laser power, beam waist size, and flow rate of the pump system. In this study, the laser power is decreased in order to realize particle elution, but the beam quality, i.e. the beam waist size, can be changed when the laser power is changed. This results in inaccuracy in the particle size measurement. A possible solution to this problem is to use a laser beam attenuator to alter the laser power or to use a more sophisticated laser, e.g. a diode-laser-pumped Nd:YAG laser, in which the beam focusing parameter is unchanged even when the laser power is changed. It is also possible to change the flow rate of the solution rather than the laser power, although a high-precision flowing system is required to accomplish this. Thus, better preci-

sion in instrumentation will provide more reliable results.

The present approach has several advantages over other methods, such as the classical light scattering technique which is well known as a method with high precision. For example, the number of particles required for the measurement is very small and even a single particle can be measured after collection by a radiation force. Therefore, the present technique can be applied to individual biological cells. In addition, this method can be applied to a mixed sample without combining it with any other separation techniques. In addition, the particles can be collected as a function of size, if necessary. It is well known that the multi-angle laser light scattering (MALLS) technique is capable of precise and accurate measurements of particle sizes. However, the result obtained by MALLS represents only the average value in the case of a mixed sample. Therefore, this technique must be combined with a separation technique such as field flow fractionation [12].

5. Conclusion

Compared with the current technique in optical chromatography, a new approach is as follows.

1. By decreasing the personal error and separating the sample around the beam waist at which selectivity is highest, accuracy can be improved.
2. The dynamic range is narrower because resolution is lower when the particle elutes at smaller laser output power and because samples larger than the beam waist diameter cannot be evaluated.
3. It is possible to use a photo detector, instead of an image sensor; for example, the light scattered by the sample particle can be directly measured.

6. Nomenclature

a	particle diameter
c	rate of the light
n_1	refractive index of liquid
P	laser output
Q_s	conversion efficiency
u	flow rate
v	variation induced by changes of laser output power and flow rate (%)
z	retention distance of particle
z_c	confocal distance

Greek letters

η	viscosity of liquid
λ	wavelength
ω	radius of beam
ω_0	radius of beam waist
ζ	z/z_c

Acknowledgements

This research is supported by Grants-in-Aid for Scientific Research from the Ministry of Education of Japan. We thank Dr Michael R. Shortreed for helpful discussions.

References

[1] A. Ashkin, Phys. Rev. Lett. 24 (1970) 156.
[2] N.B. Tudor, J.S. Miriam, A.C. Harry, C.S. Gary, C.S. Carleton, C.M. John, Appl. Opt. 26 (1987) 5311.
[3] A. Ashkin, J.M. Dziedzic, J.E. Bjorkholm, S. Chi, Opt. Lett. 11 (1986) 288.
[4] P.J.H. Bronkhorst, G.J. Streekstra, J. Grimbergen, E.J. Nijhof, J.J. Sixma, G.J. Brakenhoff, Biophys. J. 69 (1995) 1666.
[5] K. Karsten, S. Lars, L. Yagang, S. Greg, P. Pasqualle, T. Yona, W.B. Michael, J.T. Bruce, Cell. Mol. Biol. 42 (1996) 501.
[6] G.J. Sonek, Y. Liu, R.H. Iturriaga, Appl. Opt. 34 (1995) 7731.
[7] A. Ashkin, J.M. Dziedzic, Science 235 (1987) 1517.
[8] D.W. Michelle, Y. Hong, L. Robert, G. Jeff, M.B. Steven, Biophys. J. 72 (1997) 1335.
[9] T. Imasaka, Y. Kawabata, T. Kaneta, Y. Ishidzu, Anal. Chem. 67 (1995) 1763.
[10] T. Kaneta, Y. Ishidzu, N. Mishima, T. Imasaka, Anal. Chem. 69 (1997) 2701.
[11] T. Hatano, T. Kaneta, T. Imasaka, Anal. Chem. 69 (1997) 2711.
[12] H. Thielking, D. Roessner, W.M. Kulicke, Anal. Chem. 67 (1995) 3229.

ELSEVIER

Talanta 48 (1999) 559–569

Talanta

Extraction of sodium and potassium picrates with 16-crown-5 into various diluents. Elucidation of fundamental equilibria determining the extraction selectivity for Na^+ over K^+

Yasuyuki Takeda *, Chihiro Takagi, Shinichiro Nakai, Kiyokazu Endo, Shoichi Katsuta

Department of Chemistry, Faculty of Science, Chiba University, Yayoi-cho, Inage-ku, Chiba 263-8522, Japan

Received 8 May 1998; received in revised form 10 August 1998; accepted 11 August 1998

Abstract

The constants of the overall extraction equilibrium (K_{ex}), the partition for various diluents having low dielectric constants ($K_{D,MLA}$), the aqueous ion-pair formation (K_{MLA}), and the dimer formation in CCl_4 of 16-crown-5 (16C5)–alkali metal (Na, K) picrate 1:1:1 complexes were determined at 25°C; the distribution constants of 16C5 were also measured at 25°C. The log K_{MLA} of Na and K are 4.14 ± 0.19 and 3.05 ± 0.28, respectively. The partition behavior of 16C5 and its 1:1:1 complexes with the alkalimetal picrates can be explained by regular solution theory, except for $CHCl_3$; the molar volumes and solubility parameters of 16C5 and the 1:1:1 complexes were determined. The magnitude of K_{ex} largely depends on that of K_{MLA}. For every diluent, 16C5 always shows Na^+ extraction-selectivity over K^+. The K_{MLA} value most contributes to the extraction selectivity of 16C5 for Na^+ over for K^+ among the three fundamental equilibrium constants, the aqueous 1:1 complex-formation constant of 16C5 with the alkali metal ion, K_{MLA}, and $K_{D,MLA}$. Furthermore, correct contributions of a methylene group to distribution constants of organic compounds between diluents of low dielectric constants and water were determined by the distribution constants of 16C5 and 15-crown-5; the additivity of the contributions of functional groups to the partition constant of a crown ether was verified.

Keywords: Solvent extraction; Selectivity; Fundamental equilibria; Ion-pair formation constant in water; Distribution behavior; Solvent effects; Regular solution theory; Molar volume; Solubility parameter; Additivity; Methylene group contribution; 16-Crown-6; Alkali metal picrates

1. Introduction

Although the selectivity of 16-crown-5 (16C5) for Na^+ over for K^+ is low in water, 16C5 shows high Na^+ extraction-selectivity over K^+ between

* Corresponding author. Fax: +81 43 2902874; e-mail: takeda@scichem.c.chiba-u.ac.jp

0039-9140/99/$ - see front matter
PII S0039-9140(98)00273-2

benzene and water [1]. The Na^+ extraction-selectivity of 16C5 over K^+ varies with the diluent [1,2]. The Na^+ extraction-selectivity has been qualitatively explained by the appropriate cavity size and the favorable orientation of the donor oxygen atoms of 16C5. But the change in the Na^+ extraction-selectivity with the diluent cannot be interpreted by the size–fit concept and the conformation of the donor oxygen atoms. In order to quantitatively clarify the enhanced selectivity and the change in the extraction-selectivity from the standpoint of equilibrium, it is necessary to analyze the overall extraction equilibrium between water and a diluent of low dielectric constant by the four fundamental equilibria; partition of 16C5, complex formation of 16C5 with an alkali metal ion in water, ion-pair formation of the 16C5 complex with an anion in water, and partition of the ion-pair 16C5 complex. The partition constant of the ion-pair 16C5 complex provides information on solute–solvent interaction of the electroneutral complex. The solvent dependence of the Na^+ extraction-selectivity of 16C5 over K^+ reflects the variation with the diluent of the difference in interaction with the diluent of the ion-pair 16C5 complex between Na^+ and K^+. In most cases, overall extraction constants for sodium and potassium picrates and partition constants of 16C5 can be measured. The 1:1 complex-formation constants of 16C5 with Na^+ and K^+ in water have been determined [3]. It is difficult to measure the ion-pair formation constants in water and the partition constants of 16C5–sodium and 16C5–potassium salt 1:1:1 complexes because stabilities in water of the 16C5–metal ion complexes and the ion-pair 1:1:1 complexes are low [3] and not so high, respectively. The method of determining the ion-pair formation constant in water of a crown ether–metal ion complex with an anion has been established [4–8]. In this study, according to the method, the ion-pair formation constants in water of 16C5–sodium and 16C5–potassium picrate 1:1:1 complexes were determined by solvent extraction at 25°C. By means of the ion-pair formation constants in water, the partition constants of the 1:1:1 complexes were calculated from the other two fundamental equilibrium constants and the overall extraction constants. The fundamental equilibria which govern the Na^+ extraction-selectivity of 16C5 over K^+ were completely elucidated.

Another principle object of this study is to obtain the correct contribution of a methylene group to a distribution constant of an organic compound between a diluent of low dielectric constant and water. Generally, the methylene group contribution has been determined from the slope of a straight line given by plots of ion-pair extraction constants of tetraalkylammonium salts against the number of carbon atoms of the tetraalkylammonium ion. However, the methylene group contribution thus determined is an apparent one because the overall ion-pair extraction process comprises one ionic reaction process; namely, an ion-association process of the cation with the anion in water. Consequently, 16C5 was chosen because of the electroneutrality and the extra methylene group compared with 15-crown-5 (15C5).

2. Experimental

2.1. Materials

16C5 was synthesized by the method of Ouchi et al. [2], and purified by distillation under vacuum. All the organic solvents were analytical grade. 1,2-Dichloroethane (1,2-DCE) was purified by distillation. All the other solvents were used as received. They were washed three times with deionized water prior to use. Picric acid and alkali metal hydroxides were analytical grade. The solvent parameters are presented in Table 1.

2.2. Distribution constants of 16C5

The experiments were similar to those described in the previous paper [4]. Extractions were conducted at 25 ± 0.2°C. The concentration range of 16C5 was from 8.8×10^{-6} to 4.0×10^{-3} M (1 M = 1 mol dm^{-3}). The distribution constants of 16C5 are summarized in Table 2.

2.3. Extraction of alkali metal picrates with 16C5

The experimental procedures were almost the same as those described in the previous paper [4]. Extractions were performed in the pH 10.5–12.2 region at 25 ± 0.2°C. Concentration ranges of 16C5, NaOH, KOH, and picric acid were 1.7×10^{-5} to 3.1×10^{-2}, $(3.1–3.6) \times 10^{-2}$, $(2.2–4.3) \times 10^{-2}$ and $(2.0–4.1) \times 10^{-3}$ M, respectively. In order to keep the ionic strength in the aqueous phase as constant as possible, the sum of the initial total electrolyte concentrations was held at between 2×10^{-2} and 5×10^{-2} M throughout the extraction experiments. In blank experiments, there was no extraction in the absence of 16C5.

3. Theory and results

When an aqueous phase of an alkali metal picrate (MA) and an organic phase of a crown ether (L) are equilibrated, the equilibrium constants are defined as

Table 1
Solvent parameters at 25°C

No.	Solvent[a]	δ[b]	V[c]	ϵ_r[d]
1	DCM	9.7	63.9	8.93
2	CF	9.3	80.7	4.81[e]
3	CTC	8.6	97.1	2.24[e]
4	1,1-DCE	9.1	85	10.0[f]
5	1,2-DCE	9.8	79.4	10.36
6	CBu	8.4	104	7.39[e]
7	BZ	9.16	89.4	2.275
8	TE	8.93	106.9	2.379
9	*m*X	8.80	123.5	2.4
10	CB	9.5	102.1	5.62
11	BB	9.87	105	5.40
12	*o*-DCB	10.0	112.8	9.93
13	Water	17.55[g]	18.1	

[a] DCM, dichloromethane; CF, chloroform; CTC, carbon tetrachloride; 1,1-DCE, 1,1-dichloroethane; 1,2-DCE, 1,2-dichloroethane; CBu, chlorobutane; BZ, benzene; TE, toluene; *m*X, *m*-xylene; CB, chlorobenzene; BB, bromobenzene; *o*-DCB, *o*-dichlorobenzene.
[b] Solubility parameter ($cal^{1/2}$ $cm^{-3/2}$) (Ref. [9,34]).
[c] Molar volume (cm^3 mol^{-1}) (Ref. [35]) (density).
[d] Ref. [36].
[e] 20°C.
[f] 18°C.
[g] Ref. [37].

$$K_{ex} = [MLA]_o/[M^+][L]_o[A^-] \quad (1)$$

$$K_{D,L} = [L]_o/[L] \quad (2)$$

$$K_{ML} = [ML^+]/[M^+][L] \quad (3)$$

$$K_{MLA} = [MLA]/[ML^+][A^-] \quad (4)$$

$$K_{D,MLA} = [MLA]_o/[MLA] \quad (5)$$

$$K_{MA} = [MA]/[M^+][A^-] \quad (6)$$

$$K_2 = [(MLA)_2]_o/[MLA]_o^2 \quad (7)$$

where the subscript 'o' and the lack of subscript designate the organic and the aqueous phase, respectively. The dissociation of MLA into ML^+ and A^- in the organic phases is neglected because of the low dielectric constants (ϵ_r) of the diluents used in this study. The overall extraction equilibrium constant (K_{ex}) can be written as

$$K_{ex} = K_{D,L}^{-1} K_{ML} K_{MLA} K_{D,MLA} \quad (8)$$

where $K_{MLA}K_{D,MLA} = [MLA]_o/[ML^+][A^-] = K_{ex,ip}$.

Under very basic conditions (pH > 11), mass balances are as follows;

$$[M]_t = [M^+] + [ML^+] + [MA] + [MLA] + [MLA]_o + 2[(MLA)_2]_o \quad (9)$$

$$[L]_t = [L] + [L]_o + [ML^+] + [MLA] + [MLA]_o + 2[(MLA)_2]_o \quad (10)$$

$$[HA]_t = [A^-] + [MA] + [MLA] + [MLA]_o + 2[(MLA)_2]_o \quad (11)$$

the subscript 't' denoting the total concentration. Eqs. (12)–(14) are derived from Eqs. (9)–(11);

$$a([L]_o[A^-])^2[M^+]^2 + \{1 + K_{MA}[A^-] + (b + c[A^-])[L]_o\}[M^+] - [M]_t = 0 \quad (12)$$

$$a([M^+][A^-])^2[L]_o^2 + \{d + (b + c[A^-])[M^+]\}[L]_o - [L]_t = 0 \quad (13)$$

$$a([M^+][L]_o)^2[A^-]^2 + \{1 + (K_{MA} + c[L]_o)[M^+]\}[A^-] - [HA]_t = 0 \quad (14)$$

Table 2
Distribution constants for 16C5 and 1:1:1 16C5–alkali metal picrate complexes at 25°C

No.	Solvent	$K^{a}_{D,L}$	log $K_{D,L}$	log $K_{D,MLA}$	
				Na	K
1	DCM	$(1.22 \pm 0.03) \times 10$	1.086	0.93	1.43
2	CF	$(2.83 \pm 0.04) \times 10$	1.452	0.77	1.11
3	CTC	$(2.53 \pm 0.08) \times 10^{-1}$	−0.597	−1.54	
4	1,1-DCE	1.39 ± 0.02	0.143		
5	1,2-DCE	2.11 ± 0.02	0.324	0.62	0.87
6	CBu	$(1.65 \pm 0.04) \times 10^{-1}$	−0.783	−0.90	−1.09
7	BZ	$(3.97 \pm 0.04) \times 10^{-1}$ [b]	−0.401	−0.54	−0.90
8	TE	$(2.54 \pm 0.06) \times 10^{-1}$	−0.595	−0.69	−1.18
9	*m*X	$(1.61 \pm 0.01) \times 10^{-1}$	−0.793	−0.96	−1.46
10	CB	$(5.52 \pm 0.13) \times 10^{-1}$	−0.26	−0.01	−0.12
11	BB	1.03 ± 0.02	0.0128	−0.03	0.08
12	*o*-DCB	1.07 ± 0.01	0.0294	0.15	0.24

For abbreviations, see footnote to Table 1.
[a] Each value is the average of 14–22 measurements. The uncertainties are the standard deviations.
[b] Ref. [1].

where $a = 2K_2K_{ex}^2$, $b = K_{D,L}^{-1}K_{ML}$, $c = K_{D,L}^{-1}K_{ML}K_{MLA} + K_{ex}$, and $d = 1 + K_{D,L}^{-1}$.

The distribution ratio (D) of the alkali metal is represented by

$$D = ([MLA]_o + 2[(MLA)_2]_o) / ([M^+] + [MA] + [ML^+] + [MLA]) \quad (15)$$

When $[M^+] \gg [MA] + [ML^+] + [MLA]$ and $[MLA]_o \gg 2[(MLA)_2]_o$, Eq. (15) is transformed into

$$D = K_{ex}[L]_o[A^-] \quad (16)$$

As a first approximation, the $[L]_o$ and $[A^-]$ values of Eq. (16) are calculated from Eqs. (17) and (18), respectively:

$$[L]_o = ([L]_t - [MLA]_o)/(d + b[M^+]) \quad (17)$$

$$[A^-] = [HA]_t - [MLA]_o \quad (18)$$

where $[M^+]$ (first approximate value) $= [M]_t - [MLA]_o$. Plots of $\log(D/[A^-])$ versus $\log [L]_o$ always give a straight line with a slope of 1 in every case, indicating the formation of a 1:1 complex of 16C5 with the alkali metal ion and the validity of the above assumptions. The first approximate K_{ex} value for each system was determined based on these assumptions.

The distribution constant ($K_{D,L}$) of the crown ether is estimated by Eq. (19), derived from the regular solution theory [9]:

$$RT \ln K_{D,L}/(\delta_w - \delta_o) = V_L(\delta_w - 2\delta_L) + V_L\delta'_o \quad (19)$$

where $\delta'_o = \delta_o + RT(1/V_o - 1/V_w)/(\delta_w - \delta_o)$; δ_w, δ_o, and δ_L refer to the solubility parameters of water, the organic solvent, and the crown ether, respectively; V_L, V_o, and V_w designate the molar volumes of the crown ether, the organic solvent, and water, respectively. The distribution constant ($K_{D,MLA}$) of an ion-pair complex MLA is estimated by

$$RT \ln K_{D,MLA}/(\delta_w - \delta_o) = V_{MLA}(\delta_w - 2\delta_{MLA}) + V_{MLA}\delta'_o \quad (20)$$

V_{MLA} and δ_{MLA} being the molar volume and solubility parameter of MLA, respectively. Combining Eqs. (19) and (20) leads to

$$\log K_{D,MLA} = \{V_{MLA}(\delta_w + \delta'_o - 2\delta_{MLA}) / V_L(\delta_w + \delta'_o - 2\delta_L)\} \log K_{D,L} \quad (21)$$

Eq. (22) is obtained by adding $\log K_{MLA}$ to both sides of Eq. (21),

$$\log K_{ex,ip} = \{V_{MLA}(\delta_w + \delta'_o - 2\delta_{MLA}) / V_L(\delta_w + \delta'_o - 2\delta_L)\} \log K_{D,L} + \log K_{MLA} \quad (22)$$

When the δ values of L and MLA are nearly equal, Eq. (22) leads to

$$\log K_{ex,ip} = (V_{MLA}/V_L) \log K_{D,L} + \log K_{MLA} \quad (23)$$

Plots of the first approximate $\log K_{ex,ip}$ values versus $\log K_{D,L}$ values show a good linear relationship for the respective alkali metals except for chloroform (CF). The first approximate values of $\log K_{MLA}$ were determined from the intercepts of the $\log K_{ex,ip}$ versus $\log K_{D,L}$ plots. The second approximate $[A^-]$ value was calculated from Eq. (24) by using the first approximate values of $[M^+]$, $[L]_o$, and K_{MLA},

$$[A^-] = ([HA]_t - [MLA]_o)/\{(1 + (K_{MA} + e[L]_o)[M^+]\} \quad (24)$$

where $e = K_{D,L}^{-1} K_{ML} K_{MLA}$. The actual $[M^+]$, $[L]_o$, $[A^-]$, K_{MLA}, and K_{ex} values were calculated from Eqs. (1), (8) and (23)–(26) by a successive approximation method,

$$[M^+] = ([M]_t - [MLA]_o) / \{1 + b[L]_o + (K_{MA} + e[L]_o)[A^-]\} \quad (25)$$

$$[L]_o = ([L]_t - [MLA]_o)/\{d + (b + e[A^-])[M^+]\} \quad (26)$$

The $\log K_{ex}$ and $\log K_{MLA}$ values are summarized in Tables 3 and 4, respectively. The plots of the actual $\log K_{ex,ip}$ values versus $\log K_{D,L}$ values in Figs. 1 and 2 also show a good linear relationship for the respective alkali metals except for CF. The correlation coefficients for the Na and K systems are 0.964 and 0.966, respectively.

When $[M^+] \gg [MA] + [ML^+] + [MLA]$ and $2[(MLA)_2]_o \gg [MLA]_o$, Eq. (15) is transformed into

$$D = 2K_2 K_{ex}^2 [M^+][L]_o^2 [A^-]^2 \quad (27)$$

As a first approximation, the $[M^+]$, $[A^-]$, and $[L]_o$ values of Eq. (27) were calculated from Eqs. (28)–(30), respectively;

Table 3
Extraction equilibrium constants for 1:1:1 16C5–alkali metal picrate complexes at 25°C

No.	Solvent	$\log K_{ex}^a$		$\log K_{ex,ip}$	
		Na	K	Na	K
1	DCM	4.76 ± 0.01	3.79 ± 0.01	5.07	4.48
2	CF	4.24 ± 0.01	3.11 ± 0.01	4.91	4.16
3	CTC	3.98 ± 0.01		2.60	
4	1,1-DCE				
5	1,2-DCE	5.21 ± 0.01	3.99 ± 0.01	4.76	3.92
6	CBu	4.80 ± 0.01	3.14 ± 0.01	3.24	1.96
7	BZ	4.78 ± 0.01	2.95 ± 0.02	3.60	2.15
8	TE	4.82 ± 0.01	2.86 ± 0.01	3.45	1.87
9	*m*X	4.75 ± 0.01	2.78 ± 0.01	3.18	1.59
10	CB	5.17 ± 0.01	3.59 ± 0.02	4.13	2.93
11	BB	4.88 ± 0.01	3.52 ± 0.02	4.11	3.13
12	*o*-DCB	5.04 ± 0.01	3.66 ± 0.01	4.29	3.29

The uncertainties are the standard deviations. For abbreviations, see footnote to Table 1.
[a] Each value is the average of 10–16 measurements.

$$[M^+] = [M]_t - 2[(MLA)_2]_o \quad (28)$$

$$e[M^+](1 + K_{MA}[M^+])[A^-]^2 + \{(d + b[M^+])(1 + K_{MA}[M^+]) + e[M^+]([L]_t - [HA]_t)\}[A^-] - \{[HA]_t - 2[(MLA)_2]_o\}(d + b[M^+]) = 0 \quad (29)$$

$$[L]_o = \{[L]_t - 2[(MLA)_2]_o\} / \{d + (b + e[A^-])[M^+]\} \quad (30)$$

Table 4
Fundamental equilibrium constants in water at 25°C

	M	
	Na	K
$\log K_{MA}^a$	1.38	1.64
L = 16C5		
$\log K_{MLA}$	4.14 ± 0.19	3.05 ± 0.28
$\log K_{ML}^b$	0.78	0.40
L = 15C5		
$\log K_{MLA}^c$	4.43	3.27
$\log K_{ML}^d$	0.70	0.74

[a] Ref. [38].
[b] Ref. [3].
[c] Ref. [8].
[d] Ref. [39].

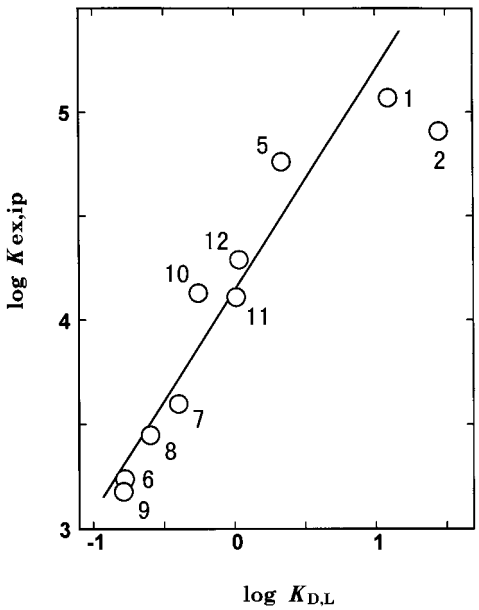

Fig. 1. Plots of actual log $K_{ex,ip}$ values versus log $K_{D,L}$ values for 16C5–sodium picrate system. The numbers correspond to those in Table 1.

Plots of $\log(D/[M^+][A^-]^2)$ versus $\log [L]_o$ in Fig. 3 give a straight line with a slope of 2. This shows that the dimer $(Na(16C5)A)_2$ is formed in the carbon tetrachloride under these experimental conditions. The first approximate K_2 value was calculated from Eqs. (1), (31) and (7),

$$[M]_{o,t} = [MLA]_o + 2[(MLA)_2]_o \quad (31)$$

where $[M]_{o,t}$ denotes the total concentration of the alkali metal in the organic phase. The actual log K_2 value was calculated to be 3.75 ± 0.04 from Eqs. (1), (7), (12)–(14) and (31) by a successive approximation method. The extra methylene group causes the dimer stability in CCl_4 to be lower for 16C5 than for 15C5 ($\log K_2 = 4.05$ [10]).

4. Discussion

Plots of $RT \ln K_{D,L}/(\delta_w - \delta_o)$ against δ'_o for 16C5 in Fig. 4 give a linear relationship except for CF (the correlation coefficient, $r = 0.901$). The additional methylene group causes the correlation coefficient of 16C5 to be higher than that of 15C5 (0.869) [4]; namely, the specific interaction of 16C5 with some of the diluents is weaker than that of 15C5. CF shows a very large positive deviation due to the hydrogen bond between 16C5 and CF. The V and δ values of 16C5 are obtained from the slope and the intercept to be 204 ± 31 and 11.9 ± 0.1, respectively. The V_L is greater for 16C5 than for 15C5 (Table 5). Although the standard deviation is relatively large, the difference (15 $cm^3\ mol^{-1}$) in V_L between 16C5 and 15C5 is nearly equal to the molar volume contribution of a methylene group (16.1 $cm^3\ mol^{-1}$) [11]. The experimental V_L value of 16C5 is almost identical with the calculated one (196 $cm^3\ mol^{-1}$) from molar volume group contributions [11]. The log $K_{D,L}$ is always 0.31–0.61 larger for 16C5 than for 15C5 (Eq. (32) and Table 6). The higher lipophilicity of 16C5 is attributed to the greater V_L and the smaller δ_L value of 16C5 compared with 15C5 (Eq. (19)).

Contributions of a methylene group (π_{CH_2}) and an ether oxygen atom (π_O) to log $K_{D,L}$ at 25°C can be estimated from log $K_{D,L}$ values of 16C5 and 15C5 by the following equations:

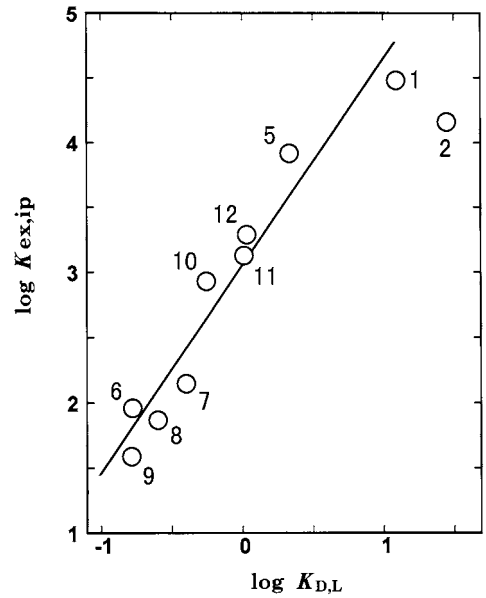

Fig. 2. Plots of actual log $K_{ex,ip}$ values versus log $K_{D,L}$ values for 16C5–potassium picrate system. The numbers correspond to those in Table 1.

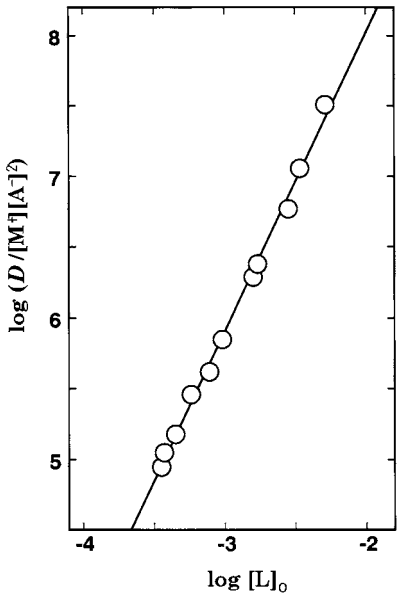

Fig. 3. Plots of $\log(D/[M^+][A^-]^2)$ versus $\log[L]_o$ for the 16C5–sodium picrate–CCl_4 system.

$$\pi_{CH_2} = \log K_{D,16C5} - \log K_{D,15C5} \quad (32)$$

$$\pi_O = (\log K_{D,L} - \pi_{CH_2} \times a) \div b \quad (33)$$

where a and b denote the number of methylene groups and ether oxygen atoms, respectively. The contribution of a benzo group ($\pi_{C_6H_4}$) to $\log K_{D,L}$ at 25°C can be calculated from the $\log K_{D,L}$ of B18C6 by the equation $\pi_{C_6H_4} = \log K_{D,B18C6} - \pi_{CH_2} \times 10 - \pi_O \times 6$. The π_{CH_2}, π_O, and $\pi_{C_6H_4}$ values are listed in Table 6, along with experimental $\log K_{D,L}$ values of crown ethers at 25°C and those estimated from the empirical parameters. The experimental $\log K_{D,L}$ for 18C6/chlorobutane (CBu), bromobenzene (BB), *o*-dichlorobenzene (*o*-DCB) and DB18C6/1,2-DCE systems are 0.51–0.58 smaller than the calculated ones. But experimental and calculated $\log K_{D,L}$ values of another system are equal within an error of −0.38 to 0.44. The additivity of the contribution of a functional group to the $\log K_{D,L}$ of a crown ether is verified.

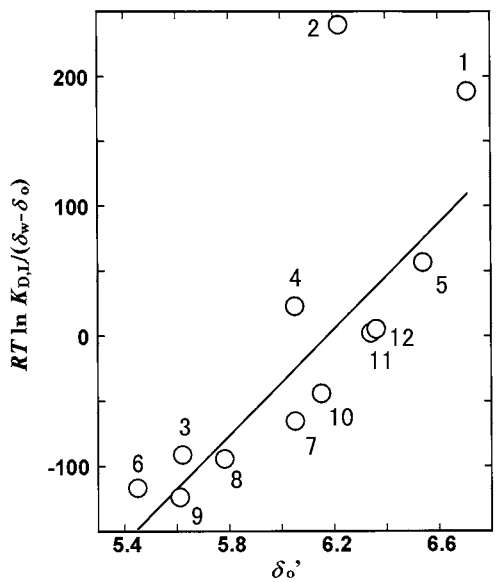

Fig. 4. Plots of $RT \ln K_{D,L}/(\delta_w - \delta_o)$ versus δ'_o for 16C5. The numbers correspond to those in Table 1.

Table 5
Molar volumes and solubility parameters for 16C5, 15C5, and their 1:1:1 complexes with alkali metal picrates at 25°C

	L	MLA	
		Na	K
L = 16C5			
V (cm^3 mol^{-1})	204 ± 31	242 ± 29	356 ± 52
δ (cal$^{1/2}$ cm$^{-3/2}$)	11.9 ± 0.1	11.9 ± 0.1	11.9 ± 0.1
L = 15C5 [8]			
V (cm^3 mol^{-1})	189	210	374
δ (cal$^{1/2}$ cm$^{-3/2}$)	12.0	12.0	12.0

The overall ion-pair extraction constant is the product of an ion-pair formation constant in water of a cation with an anion and a distribution constant of the resulting electroneutral ion pair. In general, the larger the size of organic cation or anion is, the greater the ion-pair formation constant in water is [26,27]. The π_{CH_2} values determined in this study are always smaller than those from the slopes of straight lines given by plots of 1:1 ion-pair extraction constants against the number of carbon atoms of cations or anions [28–31]; for example, tetraalkylammonium ions (cations): CF 0.59 [32] and 0.58 [27], benzene (BZ) 0.49 [33]; alkylsulfonate ions (anions) [26]: dichloromethane (DCM) 0.55 (PR), CF 0.61 (PR) and 0.66 (MG), carbon tetrachloride (CTC) 0.69 (EV), 1,2-DCE

Table 6
π_{CH_2}, π_O, $\pi_{C_6H_4}$, and log $K_{D,L}$ values at 25°C

No.	Solvent	π_{CH_2}	π_O	$\pi_{C_6H_4}$	log $K_{D,L}$									
					12C4		B15C5		18C6		DB18C6		DB24C8	
					Expt.	Calc.	Expt.	Calc.	Expt.	Calc.	Expt.	Calc.	Expt.	Calc.
1	DCM	0.44	−0.76	2.63		0.48		2.36	0.60 [7,17]	0.72		4.22		4.46
2	CF	0.53	−0.88	2.54	0.90 [12]	0.73		2.39	0.79 [18] 0.80[17]	1.09	3.90 [22]	4.04		4.40
3	CTC	0.61	−1.46			−0.96				−1.45				
4	1,1-DCE	0.54	−1.15	2.99		−0.28		1.56		−0.42		3.40		3.26
5	1,2-DCE	0.31	−0.61	2.60		0.04	1.93 [15]	2.02	0.03 [7] 0.05 [19]	0.06	3.5 [23]	4.01		4.04
6	CBu	0.42	−1.07	2.64		−0.92		0.64	−1.93 [7]	−1.39		2.22		1.76
7	BZ	0.41	−0.97	2.72	−0.82 [13]	−0.61	1.30 [16]	1.15	−1.27 [7] −1.20 [20] −1.24 [21] −1.15 [17]	−0.91	2.90 [24]	2.90	3.04 [25]	2.60
8	TE	0.55	−1.33	3.12	−1.19 [14]	−0.92		0.87	−1.59 [7] −1.62 [17]	−1.38		2.65		2.20
9	*m*X	0.58	−1.42	3.09		−1.05		0.63	−1.95 [7] −1.80 [17]	−1.57		2.30		1.78
10	CB	0.49	−1.13	3.03		−0.60		1.30	−1.07 [7] −0.90 [17]	−0.90		3.21		2.91
11	BB	0.46	−1.01	2.59		−0.36		1.22	−1.12 [7]	−0.54		2.80		2.62
12	*o*-DCB	0.53	−1.15	2.87		−0.36		1.36	−1.13 [7]	−0.55		3.08		2.90

For abbreviations, see footnote to Table 1.

0.46 (MG), BZ 0.62 (MG) and 0.64 (EV), toluene (TE) 0.62 (MG) and 0.67 (EV), chlorobenzene (CB) 0.59 (MG) and 0.57 (EV), *o*-DCB 0.70 (MG) (where PR, MG, and EV refer to para rosaniline, malachite green, and ethyl violet, respectively, and they are counter cationic dyes). This is attributed to the positive contribution of a methylene group for the ion-pair formation constant to the overall ion-pair extraction constant. A more accurate estimate of unknown $\log K_{D,L}$ values of crown ethers at 25°C requires the actual π_{CH_2} values determined in this study and the other empirical parameters calculated by using the actual π_{CH_2} values.

The π_{CH_2}-value sequence for the diluents except for CF is similar to that of the $\pi_{C_6H_4}$-value, but almost the reverse of the π_O-value sequence. The ether oxygen atom is hydrophilic, while both the methylene and benzo groups are lipophilic. The hydrophilicity of the ether oxygen atom is caused by hydrogen bonding between the ether oxygen atom and water. The π_O value varies most with the diluent. The benzo group is much more lipophilic than the methylene group. The $\pi_{C_6H_4}$ value is roughly six times larger than the π_{CH_2} value, except for CF and 1,2-DCE.

The $\log K_{D,MLA}$ values for 16C5 calculated by Eq. (8) are listed in Table 2. The plots of $RT \ln K_{D,MLA}/(\delta_w - \delta_o)$ against δ'_o for Na and K in Figs. 5 and 6, respectively, show a linear relationship except for CF. The abnormal behavior of CF due to hydrogen bonding is also observed for both the MLA complexes. Except for CF, the correlation coefficients (r) for Na and K are 0.950 and 0.938, respectively. The size-fitted Na(16C5)A complex follows the regular solution theory better than the size-misfitted K(16C5)A one. The M(16C5)A complex obeys the regular solution theory better than the corresponding M(15C5)A one ($r(Na) = 0.921$, $r(K) = 0.880$) [8]. 16C5 shields the central alkali metal ion more effectively than does 15C5 because of the larger size of 16C5 compared with 15C5. Except for CF, the V and δ values for the M(16C5)A complex were determined from the slope and the intercept, respectively. They are summarized in Table 5. The δ values of 16C5 and the M(16C5)A complexes are identical. The validity of Eq. (23) is verified.

Both the $V_{M(16C5)A}$ values are, as expected, larger than V_{16C5} value; the $V_{M(16C5)A}$ is much smaller for the size-matched Na^+ ion than for the size-mismatched larger K^+ ion. The same is true for 15C5 (Table 5). The V_{NaLA} of 16C5 is larger than that of 15C5; the V_{KLA} of 16C5 is comparable to that of 15C5. For the same crown ether, the smaller the V_{MLA} value is, the larger is the K_{MLA} value (Tables 4 and 5). There exists an intimate relation between the magnitude of V_{MLA} and that of K_{MLA} in case the conformations of MLA complexes of the same crown ether are similar. The K_{MLA} is much greater than the corresponding K_{MA}. The order of the K_{MLA} value ($Na > K$) is the reverse of that of the K_{MA} value ($Na < K$). The stronger hydration of Na^+ is responsible for the smaller K_{MA} value of Na^+ compared with K^+. Upon complexation, the water molecules bound to the size-fitted Na^+ ion are liberated more effectively compared with the size-misfitted larger K^+ ion; the influence of water molecules on the interaction between the cation in the cavity and the picrate ion is drastically reduced. The extra methylene group decreases the K_{MLA} values of the respective alkali metals from 15C5 to 16C5.

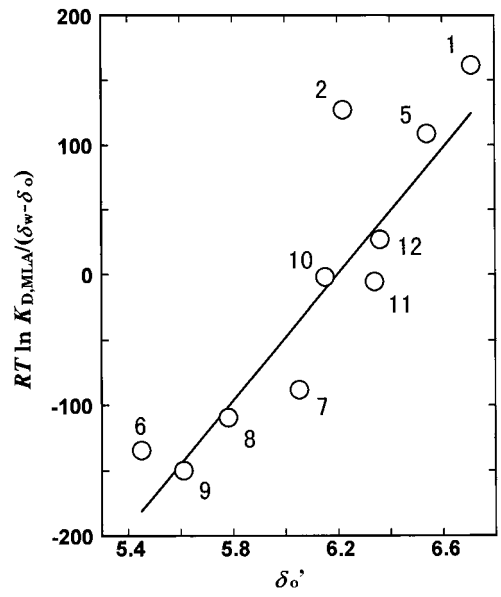

Fig. 5. Plots of $RT \ln K_{D,MLA}/(\delta_w - \delta_o)$ versus δ'_o for a 16C5–sodium picrate complex. The numbers correspond to those in Table 1.

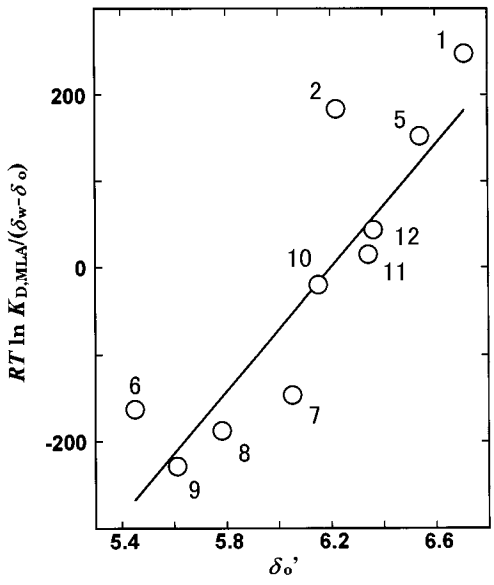

Fig. 6. Plots of $RT \ln K_{D,MLA}/(\delta_w - \delta_o)$ versus δ'_o for a 16C5–potassium picrate complex. The numbers correspond to those in Table 1.

For DCM, 1,2-DCE, BB, and *o*-DCB, the $\log K_{D,M(16C5)A}$ is greater for K than for Na. The reverse is found for all the other diluents. Eq. (34) is derived from Eq. (20),

$$RT \ln(K_{D,KLA}/K_{D,NaLA}) = (\delta_w - \delta_o)(V_{KLA} - V_{NaLA})(\delta_w + \delta'_o - 2\delta_{MLA}) \quad (34)$$

where $\delta_{MLA} = \delta_{NaLA} = \delta_{KLA}$ and L is 16C5. Signs of $\delta_w - \delta_o$ and $V_{KLA} - V_{NaLA}$ values are both positive. For DCM, 1,2-DCE, BB, and *o*-DCB, the $\delta_w + \delta'_o - 2\delta_{MLA}$ values of Eq. (34) are positive, resulting in the larger $K_{D,M(16C5)A}$ values of K compared with Na. For the other diluents, the values of $\delta_w + \delta'_o - 2\delta_{MLA}$ are all negative, leading to the smaller $K_{D,M(16C5)A}$ values of K compared with Na. The K_D-value orders of 16C5, Na(16C5)A, and K(16C5)A for the diluents are almost the same. Eqs. (19) and (20) show that the closer to the δ_L or the δ_{MLA} the δ_o is and the smaller the V_o, the greater the $K_{D,L}$ or the $K_{D,MLA}$ is. Although the δ_o value of DCM is not so close to the δ_{16C5} and $\delta_{M(16C5)A}$ values as the δ_o values of *o*-DCB, BB, and 1,2-DCE, 16C5 and its MLA complexes are most distributed into DCM among all the diluents. This is completely due to the smallest V_o of DCM. The δ_o value of *m*-xylene (*m*X) is closer to the δ_{16C5} and $\delta_{M(16C5)A}$ values compared with CBu, but 16C5 and its MLA complexes least distributed into *m*X of all the diluents. This is caused by the largest V_o of *m*X.

The $K_{M(16C5)A}$ is much the greatest among all the underlying equilibrium constants, i.e. $K_{D,L}$, K_{ML}, K_{MLA}, and $K_{D,MLA}$. For the same diluent, the signs of $\log K_{D,16C5}$ and $\log K_{D,M(16C5)A}$ are identical except for the Na(16C5)A–BB system, but the $K_{D,Na(16C5)A}$ and the $\log K_{D,16C5}$ are nearly equal to zero. Eq. (8) shows that the $\log K_{D,16C5}$ and the $\log K_{D,M(16C5)A}$ cancel each other. Thus, the magnitude of the $\log K_{ex}$ is determined mainly by that of the $\log K_{MLA}$. Plots of $\log K_{ex}$ and $\log K_{D,MLA}$ for representative diluents, $\log K_{MLA}$ and $\log K_{ML}$ versus crystal ionic radii of Na and K, are given in Fig. 7. From Table 3, 16C5 always shows higher extractability for Na than for K. The K_{MLA} most contributes to the extraction selectivity of 16C5 for Na over for K among the

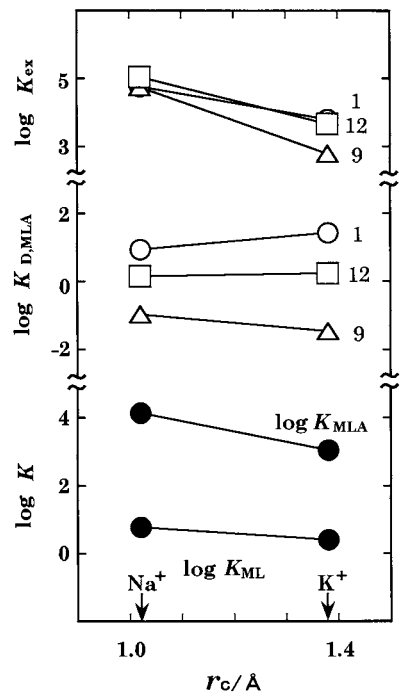

Fig. 7. Plots of $\log K_{ex}$, $\log K_{D,MLA}$, $\log K_{MLA}$, and $\log K_{ML}$ versus crystal ionic radii (r_c) of Na and K. The numbers correspond to those in Table 1.

three fundamental equilibrium constants (K_{ML}, K_{MLA}, and $K_{D,MLA}$). A similar tendency is observed for 15C5 [8]. The difference in $\log K_{MLA}$ between Na and K for 16C5 is nearly equal to that for 15C5. A favorable contribution of the K_{ML} to the Na extraction-selectivity is observed for 16C5, but is not at all for 15C5 (Table 4). The most favorable contribution of the $K_{D,MLA}$ to the Na extraction-selectivity of 16C5 is observed for *m*X and TE, while the most unfavorable contribution for DCM. This is responsible for the fact that 16C5 shows the highest Na extraction-selectivity over K for *m*X and TE and the lowest for DCM because the formation processes in water of the complex ion ML^+ and the ion pair MLA are common to every overall extraction system.

The higher Na extraction selectivity of 16C5 over K compared with 15C5 is observed only for CF, 1,2-DCE, and *o*-DCB; the reverse is true for BZ, TE, *m*X, CB, and BB; for DCM and CBu, the difference in $\log K_{ex}$ between Na and K for 16C5 is nearly equal to that for 15C5. The $\log K_{D,NaLA} - \log K_{D,KLA}$ value of 16C5 for CF and 1,2-DCE is greater than and, for *o*-DCB, is nearly equal to that of 15C5, making an additional contribution to the higher Na extraction-selectivity of 16C5 over K compared with 15C5. The $\log K_{D,NaLA} - \log K_{D,KLA}$ value of 16C5 for the other diluents is smaller than that of 15C5, which cancels the more favorable contribution of the K_{ML} to the Na extraction-selectivity of 16C5 compared with 15C5, resulting in the higher Na extraction-selectivity of 15C5 over K compared with 16C5, or the comparable Na extraction-selectivity of 15C5 to that of 16C5.

References

[1] Y. Takeda, T. Kimura, Y. Kudo, H. Matsuda, Y. Inoue, T. Hakushi, Bull. Chem. Soc. Jpn. 62 (1989) 2885.
[2] M. Ouchi, Y. Inoue, H. Sakamoto, A. Yamahira, M. Yoshinaga, T. Hakushi, J. Org. Chem. 48 (1983) 3168.
[3] Y. Takeda, T. Kimura, J. Incl. Phenom. 11 (1991) 159.
[4] Y. Takeda, C. Takagi, Bull. Chem. Soc. Jpn. 67 (1994) 56.
[5] Y. Takeda, H. Sato, S. Sato, J. Solution Chem. 21 (1992) 1069.
[6] Y. Takeda, A. Kawarabayashi, K. Takahashi, Y. Kudo, Bull. Chem. Soc. Jpn. 68 (1995) 1309.
[7] Y. Takeda, A. Kawarabayashi, K. Endo, T. Yahata, Y. Kudo, S. Katsuta, Anal. Sci. 14 (1998) 215.
[8] Y. Takeda, S. Hatai, H. Hayakawa, Y. Ono, T. Yahata, K. Endo, S. Katsuta, Talanta (1998) in press.
[9] J.H. Hildebrand, R.T. Scott, The Solubility of Nonelectrolytes, 3rd ed., Dover, New York, 1964.
[10] Y. Takeda, C. Takagi, J. Incl. Phenom. 17 (1994) 93.
[11] A.F.M. Barton, Handbook of Solubility Parameters and Other Cohesion Parameters, 2nd ed., CRC Press, Boca Raton, FL, 1991.
[12] Y. Hasegawa, H. Tanabe, S. Yoshida, Bull. Chem. Soc. Jpn. 58 (1985) 3649.
[13] Y. Takeda, Bull. Chem. Soc. Jpn. 53 (1980) 2393.
[14] R.M. Izatt, R.L. Bruening, G.A. Clark, J.D. Lamb, J.J. Christensen, Sep. Sci. Technol. 22 (1987) 661.
[15] M. Yamauchi, T. Imato, M. Katahira, Y. Inudo, N. Ishibashi, Anal. Chim. Acta 169 (1985) 59.
[16] Y. Takeda, Y. Wada, S. Fujiwara, Bull. Chem. Soc. Jpn. 54 (1981) 3727.
[17] H. Noguchi, Nippon Kagaku Kaishi 1990, 939.
[18] Y. Takeda, A. Tanaka, Bull. Chem. Soc. Jpn. 59 (1986) 733.
[19] A.G. Gaikwad, H. Noguchi, M. Yoshio, Anal. Sci. 3 (1987) 217.
[20] Y. Takeda, H. Kato, Bull. Chem. Soc. Jpn. 52 (1979) 1027.
[21] T. Iwachido, A. Sadakane, K. Toei, Bull. Chem. Soc. Jpn. 51 (1978) 629.
[22] T. Sekine, H. Wakabayashi, Y. Hasegawa, Bull. Chem. Soc. Jpn. 51 (1978) 645.
[23] H. Noguchi, H. Nakamura, M. Nagamatsu, M. Yoshio, Bull. Chem. Soc. Jpn. 55 (1982) 156.
[24] A. Sadakane, T. Iwachido, K. Toei, Bull. Chem. Soc. Jpn. 48 (1975) 60.
[25] Y. Takeda, Bull. Chem. Soc. Jpn. 52 (1979) 2501.
[26] S. Motomizu, A. Fujiwara, K. Toei, Bunseki Kagaku 32 (1983) 91.
[27] Y. Takeda, N. Ikeo, N. Sakata, Talanta 38 (1991) 1325.
[28] N.J. Harris, T. Higuchi, J.H. Rytting, J. Phys. Chem. 77 (1973) 2694.
[29] K. Gustavii, Acta Pharm. Suecica 4 (1967) 233.
[30] R. Modin, G. Schill, Acta Pharm. Suecica 4 (1967) 301.
[31] K.C. Yeh, W.I. Higuchi, J. Pharm. Sci. 61 (1972) 1649.
[32] S. Motomizu, S. Hamada, K. Toei, Bunseki Kagaku 32 (1983) 648.
[33] Y. Takeda, Y. Matsumoto, Bull. Chem. Soc. Jpn. 60 (1987) 2313.
[34] A.F.M. Barton, Chem. Rev. 75 (1975) 731.
[35] D.R. Lide, Handbook of Chemistry and Physics, 75th ed., CRC Press, Boca Raton, FL, 1994–1995.
[36] J.A. Riddick, W.B. Bunger, Organic Solvents, 3rd ed., Wiley-Interscience, New York, 1970.
[37] T. Wakahayashi, S. Oki, T. Omori, N. Suzuki, J. Inorg. Nucl. Chem. 26 (1964) 2255.
[38] T. Iwachido, Bull. Chem. Soc. Jpn. 45 (1972) 432.
[39] R.M. Izatt, R.E. Terry, B.L. Haymore, L.D. Hansen, N.K. Dalley, A.G. Avondet, J.J. Christensen, J. Am. Chem. Soc. 98 (1976) 7620.

ELSEVIER

Talanta 48 (1999) 571–577

Talanta

Chemiluminescence determination of sulfite in sugar and sulfur dioxide in air using Tris(2,2′-bipyridyl)ruthenium(II)-permanganate system

Hui Meng, Fengwu Wu, Zhike He *, Yun'e Zeng

Department of Chemistry, Wuhan University, Wuhan 430072, PR China

Received 19 May 1998; received in revised form 10 August 1998; accepted 11 August 1998

Abstract

A chemiluminescence (CL) detection for the determination of sulfite using the reaction of $Ru(bipy)_3^{2+}$ (bipy = 2,2′-bipyridyl) -SO_3^{2-}-$KMnO_4$ is described. The concentration of sulfite is proportional to the CL intensity from 5.0×10^{-8} to 1.25×10^{-4} mol l^{-1}. The limit of detection is 2.5×10^{-8} mol l^{-1} and the relative standard deviation is 4.9% for the 2×10^{-5} mol l^{-1} sulfite solution in six repeated measurements. This method has been successfully applied to the determination of sulfite in sugar and sulfur dioxide in air by using triethanolamine (TEA) as the absorbent material.

Keywords: Chemiluminescence; Sulfite; Triethanolamine; Air

1. Introduction

The determination of sulfite and sulfur dioxide are very important because of their use as food preservatives to prevent oxidation and bacterial growth and reducing agents in bleaching, as well as their potential toxicity as pollutants in the atmosphere. Many methods are available for their determination such as spectrophotometry [1,2], potentiometry [3,4], coulometry [5], gas chromatographic chemiluminence (CL) [6], HPLC fluorescence [7] and ion chromatography [8], but each has some drawback such as lack of sensitivity, selectivity, or simplicity. CL has been used for the determination of sulfite because of its high sensitivity and simplicity. The CL produced by sulfite was as follows: Sulfite can be oxidized by copper(II) [9] in alkaline solution, and reacts with chemiluminescent reagent luminol [10]. In acidic solution it was oxidized by potassium permanganate [11] or cerium(IV) sulfate [12]. The light emission intensity can be enhanced by the presence of some compounds, e.g. riboflavin for the reactions with permanganate [13,14] and cerium(IV) sulfate [15], flavin mononucleotide for the reaction with permanganate [16], 3-cyclohexylaminopropanesulphonic acid (CAPS) for the reaction with permanganate [14,17] and cerium(IV) sulfate [18], steroids for the reaction with potas-

* Corresponding author. Tel: +86 27 85805111; fax: +86 27 85803024; e-mail: wproject@public.wh.hb.cn

0039-9140/99/$ - see front matter
PII S0039-9140(98)00277-X

sium bromate [19] and sodium cyclamate for the reaction with cerium(IV) sulfate [20].

$Ru(bipy)_3^{2+}$ is an extremely versatile base reactant for a variety of electrogenerated CL processes [21,22], and has also recently become a useful CL reagent. It can be applied to determine 6-mercaptopurine [23] in alkaline medium, and to oxalic or tartaric acids etc. [24,25] in sulfuric medium with much higher sensitivity (the detection limit of oxalic acid is 2.7×10^{-8} mol l^{-1} [24]). It has been shown that $Ru(bipy)_3^{2+}$ is the luminophor in the above system [24] and it has been used in the sulfite–permanganate CL system to increase the sensitivity.

This paper describes the CL properties of the reaction between potassium permanganate and sulfite, in which the emission intensity is greatly enhanced by the presence of $Ru(bipy)_3^{2+}$ and a surfactant. The investigation was extended to the determination of sulfite in sugar. The concentration of sulfite is proportional to the CL intensity from 5.0×10^{-8} to 1.25×10^{-4} mol l^{-1}. The limit of detection is 2.5×10^{-8} mol l^{-1} and the relative standard deviation is 4.9% for the 2×10^{-5} mol l^{-1} sulfite solution in six repeated measurements. Triethanolamine (TEA) solution is a well-known sulfur dioxide absorbent [2,26]. We have used TEA solution to collect sulfur dioxide in air and determined the contents in air successfully.

2. Experimental

2.1. Apparatus

An LKB 1251 luminometer with a Dispenser SVD and a Dispenser controller DC (Pharmacia LKB Biotechnology AB, Sweden) and an Epson LX-800 printer (Seiko Epson, Japan) were used.

2.2. Reagents

All solutions were prepared from analytical-reagent grade materials in doubly distilled water.

A 1.0×10^{-2} mol l^{-1} stock solution of sulfite was prepared daily by dissolving 0.630 g of sodium sulfite in water and diluting with water to 500 ml.

The stock $Ru(bipy)_3^{2+}$ solutions were standardized by dissolving a weighed amount of $Ru(bipy)_3Br_2$ (prepared in our laboratory [23]) in water and diluting to volume. The concentration was 4.48×10^{-3} g ml^{-1}.

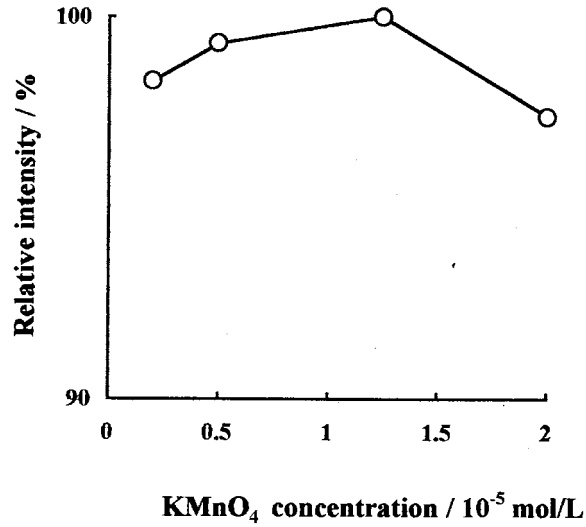

Fig. 1. Effect of $KMnO_4$ concentration in 2.5×10^{-3} mol l^{-1} sulfuric acid on the emission intensity from 8.0×10^{-6} mol l^{-1} sulfite in the presence of 1.12×10^{-5} g ml^{-1} $Ru(bipy)_3^{2+}$ and 5.0×10^{-4} mol l^{-1} SDBS.

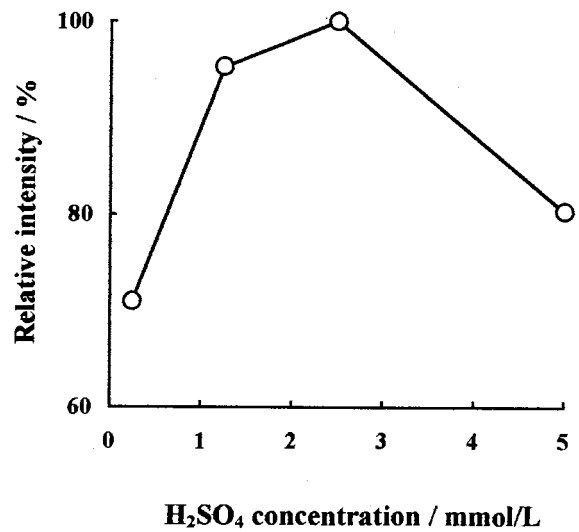

Fig. 2. Effect of H_2SO_4 concentration on the emission intensity from 8.0×10^{-6} mol l^{-1} sulfite at 1.25×10^{-5} mol l^{-1} $KMnO_4$ in the presence of 1.12×10^{-5} g ml^{-1} $Ru(bipy)_3^{2+}$ and 5.0×10^{-4} mol l^{-1} SDBS.

Table 1
Effect of different sensitizers

Sensitizer	Water	SDBS	Tween-20	Tween-40	Tween-80	Triton X-100	TPB	CPB	CTAB
Intensity (mV)	3.8	406	11.2	13.3	6.6	8.5	6.6	7.0	8.4

Potassium permanganate stock solutions were prepared by dissolving a weighed amount of $KMnO_4$ in water and adding a certain volume of 1.0 mol l^{-1} H_2SO_4 and diluting to volume. Working solutions were prepared by dilution of the stock solution with 1.0 mol l^{-1} H_2SO_4 and water.

The 2.0% solutions of Tween-20, Tween-40, Tween-80, and Triton X-100 were prepared by dissolving 2.0 g of each in water and diluting with water to 100 ml each.

The 1.0×10^{-2} mol l^{-1} solutions of sodium dodecyl benzene sulfonate (SDBS), tetradecyl pyridine bromide (TPB), cetyl pyridine bromide (CPB), cetyl trimethyl ammonium bromide (CTAB) were prepared by dissolving 0.348, 0.356, 0.384, 0.364 g, respectively in water and diluting with water to 100 ml.

A 1.0% stock solution of triethanolamine (TEA) was prepared by dissolving 1.0 g of TEA in water and diluting with water to 100 ml.

2.3. Procedure

A 0.2 ml portion of 4.48×10^{-5} g ml^{-1} $Ru(bipy)_3^{2+}$ and 0.2 ml 2×10^{-3} mol $^{-1}$ SDBS and 0.2 ml sodium sulfite solution were mixed, in this order, in sample cuvettes and then transferred into the measuring chamber at a constant temperature of 25°C. After pressing the start button, 0.2 ml of 5×10^{-5} mol l^{-1} $KMnO_4$ (1×10^{-2} mol l^{-1} H_2SO_4) was injected automatically and the peak height was recorded. The reagent blank (mV) was recorded using the same procedure, except that the sodium sulfite was replaced by doubly distilled water.

A calibration graph of emission intensity [I (mV)] versus the sulfite concentration [C (mol l^{-1})] were prepared to determine the sulfite content of the samples. A standard sample solution was included for every five samples.

2.4. Determination of sulfite in sugar

A sample solution of sugar was prepared by dissolving 3.42 g of sugar in water and diluting with water to 50 ml. Then 5.0 ml of the sample solution was transferred into a calibrated flask of 10 ml and diluted with water. The final solutions should contain $1 \times 10^{-6} - 5 \times 10^{-5}$ mol l^{-1} of sulfite. We then proceeded as with pure aqueous sulfite solutions.

2.5. Determination of sulfur dioxide in air

We transferred 10 ml of 0.1% TEA into the flasks of the air sampling apparatus and air, e.g. from outside room, was pumped through the flask for 2 h with a flow rate of 1.0 l min^{-1}. Any loss of solution due to evaporation was restored by adding 0.1% TEA solution after the termination

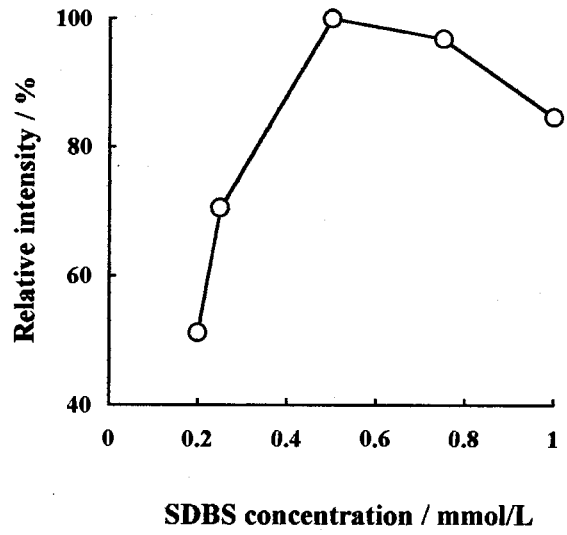

Fig. 3. Effect of SDBS concentration on the emission intensity from 8.0×10^{-6} mol l^{-1} sulfite at 1.25×10^{-5} mol l^{-1} $KMnO_4$ in the presence of 1.12×10^{-5} g ml^{-1} $Ru(bipy)_3^{2+}$ and 2.5×10^{-3} mol l^{-1} sulfuric acid.

Table 2
The regression results of the calibration graph of sulfite in water solution and TEA solution.

Solution	Range of concentraton (mol l^{-1})	n	a	b	r
Water	$5.0\times10^{-8}-1.25\times10^{-6}$	4	5.348	3.133×10^{7}	0.9998
	$1.25\times10^{-6}-2\times10^{-5}$	4	−29.07	5.9×10^{7}	0.9997
	$2\times10^{-5}-1.25\times10^{-4}$	5	767.4	1.791×10^{7}	0.9999
TEA	$1\times10^{-7}-2.5\times10^{-6}$	5	4.337	1.818×10^{7}	0.9995
	$2.5\times10^{-6}-1.25\times10^{-5}$	4	−71.1	4.916×10^{7}	0.9999

$I=a+b*C$ (I, mV units; C, mol l^{-1} units)

of sampling. The standard solutions were prepared using a 0.1% TEA solution. Spiked samples were prepared by mixing equal volume of the standard and sample solutions. We then proceeded as with pure aqueous sulfite solutions.

3. Results and discussion

3.1. The stability of the sulfite standard solution

The sulfite solutions of same concentration were prepared every day and preserved for determination. Seven solutions prepared in 1 week were measured. The intensity decreased along with time increases. The decrease of intensity of the solution prepared 1 day before was not more than 10% compared to the solution prepared freshly. It was obvious that the oxygen content of the solution affects the stability of sulfite solution. Therefore, the sulfite solution was prepared daily.

3.2. Effect of the concentration of $Ru(bipy)_3^{2+}$

The emission intensity increases with increasing concentration of $Ru(bipy)_3^{2+}$. The increase is less at low SO_3^{2-} concentration, but large at high SO_3^{2-} concentration. The background has less change. In order to get a wide linear range, 1.12×10^{-5} g ml^{-1} of $Ru(bipy)_3^{2+}$ was used in this study.

3.3. Effect of the concentration of $KMnO_4$ and sulfuric acid

The effect of the concentration of $KMnO_4$ in 2.5×10^{-3} mol l^{-1} sulfuric acid is shown in Fig. 1. The optimum concentration for the oxidant is 1.25×10^{-5} mol l^{-1} when 8×10^{-6} mol l^{-1} sulfite, 5×10^{-4} mol l^{-1} SDBS and 1.12×10^{-5} g ml^{-1} $Ru(bipy)_3^{2+}$ were used. $KMnO_4$ is a strong oxidant in sulfuric acid solution, and the CL intensity was effected by the concentration of the acid (see Fig. 2). The optimum concentration of sulfuric acid was 2.5×10^{-3} mol l^{-1}.

Table 3
Comparison of the dynamic linear range for sulfite afforded by the proposed CL method and other reported methods

Method	Dynamic linear range (mol l^{-1})	Reference
Spectrophotometry	$1.5\times10^{-5}-3.1\times10^{-4}$	[1]
	$7.8\times10^{-6}-1.3\times10^{-4}$	[2]
Potentiometry	$3.9\times10^{-4}-7.8\times10^{-3}$	[3]
	$5\times10^{-6}-0.1$	[4]
Coulometry	$2.3\times10^{-7}-3.9\times10^{-4}$	[5]
GC-CL	$3.1\times10^{-6}-1.6\times10^{-4}$	[6]
HPLC-FLUOR	$5\times10^{-6}-1\times10^{-3}$	[7]
Ion chromatography	$7.8\times10^{-6}-1.6\times10^{-3}$	[8]
Proposed CL method	$5.0\times10^{-8}-1.25\times10^{-4}$	

Table 4
Determination of sulfite in sugar

Sugar solution contents ($\times 10^{-6}$ mol l^{-1})	Added ($\times 10^{-6}$ mol l^{-1})	Found ($\times 10^{-6}$ mol l^{-1})	Recovery (%)
6.13 ± 0.14	5.0	10.81 ± 0.09	93.6
		10.83 ± 0.09	94.0
		10.69 ± 0.09	91.2
	10.0	15.22 ± 0.15	90.9
		15.49 ± 0.15	93.6
		15.12 ± 0.15	89.9

Table 5
Determination of sulfur dioxide in air

Air solution contents ($\times 10^{-6}$ mol l^{-1})	Added ($\times 10^{-6}$ mol l^{-1})	Found ($\times 10^{-6}$ mol l^{-1})	Recovery (%)
1.97 ± 0.12	2.0	1.94 ± 0.08	97.8
		1.88 ± 0.08	94.7
		1.90 ± 0.08	95.7
	6.0	4.20 ± 0.16	105.4
		3.77 ± 0.16	94.6
		3.88 ± 0.16	97.4

3.4. Effect of sensitizers

Eight kinds of sensitizers were investigated in our study. They were SDBS, Tween-20, Tween-40, Tween-80, Triton X-100, TPB, CPB, CTAB. At least two concentrations of the surfactants were tested. The enhancement of SDBS was much higher than that of the rest of surfactants in each condition. The value in Table 1 was obtained in one concentration condition. The effect of concentration of SDBS in the system is shown in Fig. 3. The optimum concentration for SDBS is 5×10^{-4} mol l^{-1}.

3.5. Effect of mixing order of reagents.

The emission intensity is effected by the mixing order of the reagents. It was shown that the emission intensity is the greatest when $Ru(bipy)_3^{2+}$ and SDBS were put into the cuvette at first, and then sulfite just before the cuvette was put into the chamber, and $KMnO_4$ was injected immediately. The major effect is caused by the oxidant [23].

3.6. Calibration and detection limit

Under the recommended conditions, the calibration graph was stepwise linear over the range $5.0 \times 10^{-8} - 1.25 \times 10^{-4}$ mol l^{-1} sulfite. The regression results of the calibration graph was listed in Table 2. The detection limit is 2.5×10^{-8} mol l^{-1} ($DL = 3s/r$), and the relative standard deviation (RSD) is 4.9% for the 2×10^{-5} mol l^{-1} sulfite solution ($n = 6$).

3.7. Comparison with other methods

Under the optimum conditions, the proposed method allows for the determination of sulfite with one to four orders of magnitude higher sensitivity than other reported methods based on various analytical techniques (see Table 3).

3.8. Effect of foreign ions

Various compounds commonly used in laboratory were tested from high to low concentration. It was shown that the CL intensity was

almost unchanged for the determination of 5×10^{-5} mol l^{-1} sulfite when they are present in the system. The list of ions and solvents is as follows: 2000-fold Na^+; 1000-fold K^+; 500-fold Ca^{2+}; 200-fold PO_4^{3-}; Ac^-; 100-fold sucrose; 10-fold Mn^{2+}; Al^{3+}; $C_2O_4^{2-}$; 1 mg ml^{-1} NH_4NO_3; 1 mol l^{-1} F^-; 0.001 mol l^{-1} Cu^{2+}; 0.001 mol l^{-1} EDTA; 0.5% methanol; ethanol; acetonitrile.

3.9. Determination of sulfite in sugar and sulfur dioxide in air

The method was applied to the determination of sulfite in sugar. Standard solutions of pure aqueous sulfite were used for the calibration line to determine the sample solutions of sugar with this method, because 100-fold sucrose has no effect on the determination of 5×10^{-5} mol l^{-1} sulfite. The recoveries were good enough for practical use. The determination results are listed in Table 4. The sulfite content in sugar is 22.7 mg kg^{-1}.

Several absorbing solutions have been investigated for the sampling of sulfur dioxide in the air (e.g. NaOH, Na_2CO_3, NaOH + citric acid etc.), but they are not suitable for this chemiluminescence system.

A TEA solution is a well-known, completely absorbing reagent for SO_2 [26]. It prevents the air oxidation of SO_3^{2-} formed from SO_2 absorbed by it. Previously, a $HgCl_2$•NaCl solution was used to collect SO_2 stably, however, this method required that the $HgCl_2$ solution must be saved after use because it is toxic.

A TEA solution with a higher concentration severely reduced the CL intensity of the sulfite–permanganate solution. A 0.1% TEA solution has less emission itself, and a smaller effect on the CL intensity. Therefore, sulfur dioxide can be sampled if air is purged through a 0.1% TEA absorbing solution. Further, the slope of the calibration graph is constant for a given TEA solution.

The calibration graph was stepwise linear from 1×10^{-7} to 1.25×10^{-5} mol l^{-1} of sulfite in the 0.1% TEA solution. The regression results of the calibration graph were listed in Table 2. It was used for analytical measurements of the air samples. The recoveries were good enough for practical use, and all of the determination results are listed in Table 5. The sulfur dioxide content in air is 10.5 μg m^{-3}.

In conclusion, the CL reaction of $Ru(bipy)_3^{2+}$-SO_3^{2-}-$KMnO_4$ can be satisfactorily applied to sensitive and reproducible determination of sulfite in sugar and sulfur dioxide in air. Our reported method is simple and easy. It has high sensitivity and wide linear range compared with other methods described in the introduction.

Acknowledgements

The authors thank the Chinese Natural Science Foundation and The Hubei Provincial Natural Science Foundation for financial support.

References

[1] L.G. Decnop-Weever, J.C. Kraak, Anal. Chim. Acta 337 (1997) 125.
[2] M. Pandurangappa, N. Balasubramanian, Analysis 24 (1996) 225.
[3] C.-Y. Chiou, T.-C. Chou, Electroanalysis 8 (1996) 1179.
[4] I. Ibrahim, Y. Cemal, B. Humeyra, Analyst 121 (1996) 1873.
[5] N. Ekkad, C.O. Huber, Anal. Chim. Acta 332 (1996) 155.
[6] A. Lavigne-Delcroix, D. Tusseau, M. Proix, Sci. Aliments 16 (1996) 267.
[7] J. Rethmeier, A. Rabenstein, M. Langer, U. Fischer, J. Chromatogr. 760 (1997) 295.
[8] E. Ruiz, M.I. Santillana, M. De Alba, M.T. Nieto, S. Garcia-Castellano, J. Liq. Chromatogr. 17 (1994) 447.
[9] J.M. Lin, T. Hobo, Anal. Chim. Acta 323 (1996) 69.
[10] Y.L. Huang, J.M. Kim, R.D. Schmid, Anal. Chim. Acta 266 (1992) 317.
[11] F. Meixner, W. Jaeschke, Fresenius' Z. Anal. Chem. 317 (1984) 343.
[12] K. Takeuchi, T. Ibusuki, Anal. Chim. Acta 174 (1985) 359.
[13] M. Yamada, T. Nakada, S. Suzuki, Anal. Chim. Acta 147 (1983) 401.
[14] S.A. Al-Tamrah, A. Townshend, A.R. Wheatley, Analyst 112 (1987) 883.
[15] J.L. Burguera, M. Burguera, Anal. Chim. Acta 214 (1988) 429.
[16] M. Kato, M. Yamada, S. Suzuki, Anal. Chem. 56 (1984) 2529.
[17] D.A. Paulls, A. Townshend, Analyst 121 (1996) 831.

[18] I.I. Koukli, E.G. Sarantonis, A.C. Calokerinos, Analyst 113 (1988) 603.
[19] A.B. Syropoulos, E.G. Sarantonis, A.C. Calokerinos, Anal. Chim. Acta 239 (1990) 195.
[20] I.M. Psarellis, E.G. Sarantonis, A.C. Calokerinos, Anal. Chim. Acta 272 (1993) 265.
[21] A. Juris, V. Balzani, F. Barigelletti, S. Campagna, P. Belser, A. Ven Zelewsky, Coord. Chem. Rev. 84 (1988) 85.
[22] H.S. White, A.J. Bard, J. Am. Chem. Soc. 104 (1982) 6891.
[23] Z.K. He, X.L. Liu, Q.Y. Luo, X.M. Yu, Y.E. Zeng, Anal. Sci. 11 (1995) 415.
[24] Z.K. He, H. Gao, L.J. Yuan, Q.Y. Luo, Y.E. Zeng, Analyst 122 (1997) 1343.
[25] Z.K. He, R.M. Ma, Q.Y. Luo, X.M. Yu, Y.E. Zeng, Acta Chim. Sin. 54 (1996) 1003.
[26] T. Korenaga, in: Development of a Passive Sampler for Sulfur Oxide Monitoring in China, The University of Tokushima, Japan, March 1996, pp. 53–54.

ELSEVIER

Talanta 48 (1999) 579–584

Talanta

Sorption behaviour of lanthanum(III), neodymium(III), terbium(III), thorium(IV) and uranium(VI) on Amberlite XAD-4 resin functionalized with bicine ligands

Kapil Dev, Rita Pathak, G.N. Rao *

Department of Chemistry, Indian Institute of Technology Delhi, Hauz Khas, New Delhi 110 016, India

Received 26 February 1998; received in revised form 10 August 1998; accepted 13 August 1998

Abstract

The complexing properties (capacity, pH effect, breakthrough curve) of a chelating resin, containing bicine ligands, were investigated for La(III), Nd(III), Tb(III), Th(IV) and U(VI). Trace amounts of these metal ions were quantitatively retained on the resin and recovered by eluting with 1 M hydrochloric acid. The capacity of the resin for La(III), Nd(III), Tb(III), Th(IV) and U(VI) was found to be 0.35, 0.40, 0.42, 0.25 and 0.38 mmol g^{-1}, respectively. Separation of U(VI) and Th(IV) from Ni(II), Zn(II), Co(II) and Cu(II) in a synthetic solution was carried out.

Keywords: Sorption behaviour; Bicine ligands; Chelation; Complexing

1. Introduction

Chelating resins are frequently used in analytical chemistry for preconcentration of metal ions and their separation from interfering constituents prior to their determination by an instrumental method. A number of chelating resins have been prepared by incorporating different functional groups (e.g. ethylenediamine tetraacetic acid [1], iminodiacetic acid [2–4], 8-hydroxyquinoline [5], etc.) and their analytical properties investigated.

The metal binding capacity, the metal binding strength and selectivity are important characteristics of a chelating resin. A high capacity is usually an advantage, as small amounts of chelating resin are sufficient to concentrate metal ions from a large sample volume, whereas strong metal binding can be disadvantageous in the elution step [6]. The selectivity of chelating resin is often related to that of the monomeric compound corresponding to the functional group. In our earlier communication, we have reported the synthesis of a polystyrenedivinylbenzene (XAD-4) based chelating resin containing bicine (*n*,*n*-bis(2-hydroxyethyl) glycine) groups and its analytical properties for some transition metal ions [7]. The resin has shown greater selectivity for some metal ions than that attainable with strongly binding resin containing aminopolycarboxylic acid groups. These studies are now extended to the

* Corresponding author. Fax: +91 11 6862037.

0039-9140/99/$ - see front matter
PII S0039-9140(98)00274-4

sorption behaviour of La(III), Nd(III), Tb(III), Th(IV) and U(VI).

Rare earth elements (REEs), uranium and thorium are important elements not only in industrial applications but also in energy and environmental problems. Trivalent REEs and thorium are chelated by resins such as chelex-100 [8], but this chelating resin also has an affinity for alkali and alkaline earth elements, which limits the concentration factor achievable, necessitating additional separation steps [9,10]. Myazaki and Barnes applied a poly(dithiocarbamate) chelating resin for concentration of some REEs and thorium, but the elution is tedious and requires resin digestion with strong mineral acids for quantitative elution [11]. Horvath and Barnes prepared a carboxymethylated polyethylenimine–polymethylene polyphenylene isocyanate chelating ion-exchange resin and applied it for concentration of transition metals, rare earths, uranium and thorium [12]. Masi and Olsina immobilized 8-quinolinol on Amberlite XAD-4, and used it for preconcentration of some REEs and subsequent determination by X-ray fluorescence [13].

In this paper, we report sorption behaviour of a XAD-4–bicine resin for thorium and uranium. XAD-4–Bicine resin shows higher selectivity for these elements and their separation from some transition metal ions (Ni(II), Zn(II), Co(II) and Cu(II)) is feasible on the resin columns.

2. Experimental

2.1. Reagents

Polystyrene divinylbenezene resin (Amberlite XAD-4) and bicine were obtained from Fluka (Buchs, Switzerland). The stock metal ion solutions were prepared by dissolving the following metal salts: La(III)/$La(NO_3)_3 \cdot 6H_2O$, U(VI)/$UO_2 \cdot 6H_2O$, Th(IV)/$Th(NO_3)_4 \cdot 4H_2O$, Nd(III)/$NdCl_3 \cdot 6H_2O$ and Tb(III)/$TbCl_3 \cdot 6H_2O$ (99.9% purity, BDH, India). The following buffers were used to control the pH of the solutions: hydrochloric acid–glycine (pH 1–3), sodium acetate–acetic acid (pH 3–6), ammonium acetate–ammonia (pH 6–8), and ammonium chloride–ammonia (pH 8–9).

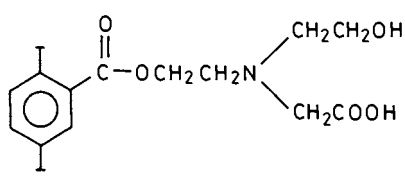

Fig. 1. XAD-4–Bicine resin.

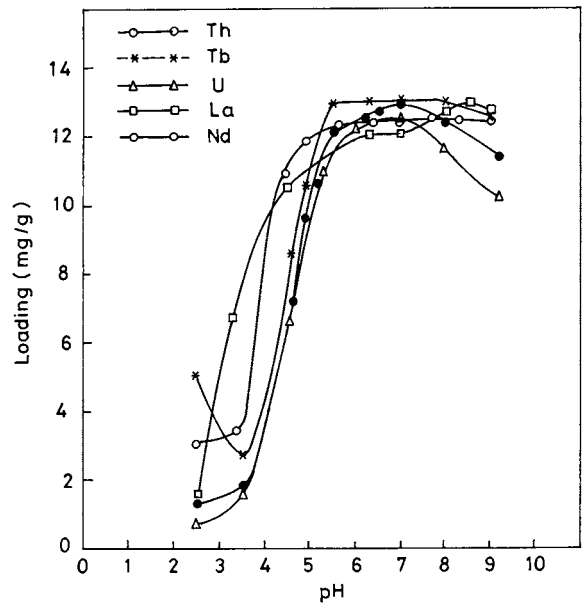

Fig. 2. Effect of pH on metal sorption with bicine resin.

2.2. Instrumentation

A digital visible spectrophotometer (Perkin–Elmer, Lambda 3B), A sequential inductively coupled plasma spectrometry–Auger electron spectrometry (ICP–AES) spectrometer (Perkin–Elmer, P-40) and an ECIL (Hyderabad, India) AA 4139 flame atomic absorption spectrometry (FAAS) spectrometer for determining metal concentrations, an Elico (Hyderabad, India) digital pH-meter (LI-120) for pH measurements and a mechanical shaker with incubator (Scientific, New Delhi, India) having a speed of 200 strokes min^{-1} was used for carrying out equilibrium studies.

Table 1
Metal uptake capacities

Metal ion	Optimum pH	Capacity (S.D.) (mmol g^{-1} resin)	CPPI resin[a]	Poly(dithiocarbamate) resin[b]
La(III)	6.15	0.35(0.02)		0.20
Nd(III)	7.58	0.40(0.01)		0.27
Tb(III)	7.52	0.42(0.01)		0.17
Th(IV)	6.95	0.25(0.02)	0.64	0.32
U(VI)	7.64	0.38(0.01)	0.33	

[a] From Ref. [12].
[b] From Ref. [11].

2.3. Preparation of XAD-4–bicine resin

Preparation and characterization of XAD-4–bicine resin (Fig. 1) has been described in a previous paper [7].

2.4. Optimum pH of metal ion uptake

The optimum pH of metal ion uptake was determined by batch equilibrium techniques. Excess metal ion (50 ml, 50 μg ml^{-1}) was shaken with 100 mg of resin for 1 h. The pH of the metal ion solution was adjusted prior to equilibration over a range of 2–9 with buffer solutions. After the equilibration, the sorbed metal ions were eluted with 1 M hydrochloric acid. The concentration of the metal ions in the solution was determined spectrophotometrically using Alizarin Red-S [14] as the colorimetric reagent for La(III), Nd(III) and Tb(III), Thoron [15] for Th(IV), and dibenzoylmethane [16] for U(VI).

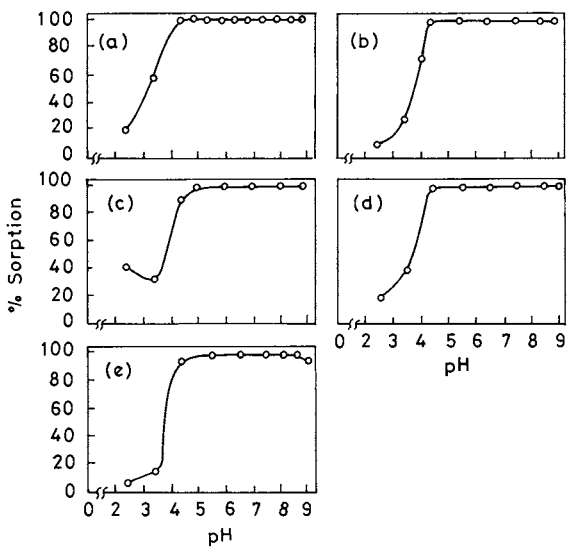

Fig. 3. pH dependence of the uptake of trace metals: (a) La(III), (b) Nd(III), (c) Tb(III), (d) Th(IV), (e) U(VI).

2.5. Resin capacity

The capacity of the resin was determined by shaking the excess metal ions (50 ml, 100 μg ml^{-1}) with 50 mg resin for 6 h at optimum sorption pH. The resin was filtered off and the concentration of the sorbed metal ion was determined spectrophotometrically after eluting it with 1 M hydrochloric acid.

2.6. pH dependence of trace metal ion uptake

A 50 ml volume of a buffered solution containing 5 μg ml^{-1} of metal ion was shaken with 100 mg of resin for 1 h in a glass stoppered bottle. The resin was filtered off and the concentration of the sorbed metal ions was determined after eluting with 1 M HCl (10 ml) and diluting the resultant sample solution to 50 ml with distilled water.

2.7. Equilibrium time

To determine the time of equilibrium for the metal under investigation, the metal ion solution (50 ml, 10 μg ml^{-1}) at a constant pH was sampled in six bottles. These bottles were removed from the shaker at regular intervals of time and the concentration of the sorbed metal ions was determined. The duplicate values agreed with a precision of $\pm 2\%$.

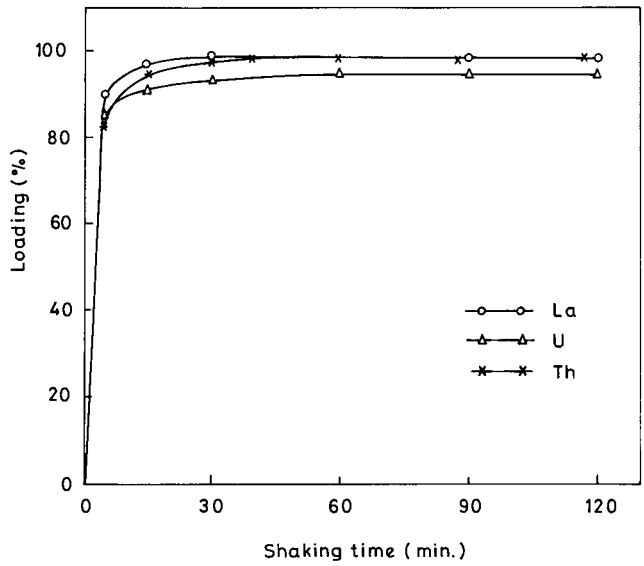

Fig. 4. Rate of uptake of metal ions.

2.8. Effect of diverse ions

Standard solutions of U(VI) and Th(IV) (50 ml, 10 μg ml^{-1}) containing 100, 500, 1000 and 1500 μg ml^{-1} of Cu(II), Ni(II), Pb(II), Cd(II), Zn(II), Hg(II), Mn(II), Fe(III) and Cr(III); 40000 and 50000 μg ml^{-1} of Na(I), K(I), Ca(II) and Mg(II); 40000 and 50000 μg ml^{-1} of Cl^-, NO_3^-, CH_3COO^- and SO_4^{2-} were analysed. The eluate was checked for U(VI) and Th(IV) by ICP–AES and transition metal ions by FAAS.

Table 2
Effect of diverse ions

Tolerance limit [ion]/[Th(IV)] or [U(VI)][a]	Diverse ion
>5000	Cl^-, NO_3^-, SO_4^{2-}, CH_3COO^-
>4000	Na(I), K(I), Ca(II), Mg(II)
100	Cu(II), Ni(II), Co(II), Zn(II) Cd(II), Cr(III)
50	Fe(III), Pb(II)

[a] Performed at pH 4.5 (amount of Th(IV) or U(VI) taken, 10 μg ml^{-1}).

2.9. Concentration and separation of metal ions

The batch equilibration technique was used to concentrate the trace metal ions. A sample solution (500 ml) containing 0.1 μg ml^{-1} metal ions was adjusted at optimum pH of sorption with a buffer solution and shaken with 100 mg of resin for 10 min. Sorbed metal ions were eluted with 1 M HCl (10 ml) and the concentration of the metal ions in the eluent was determined spectrophotometrically.

Separation of uranium and thorium from various transition metal ions was carried out on the XAD-4–bicine resin. A 50 ml solution containing uranium or thorium (20 μg ml^{-1}) and another

Table 3
Preconcentration of metal ion (amount of metal ion taken, 0.1 μg ml^{-1})

Metal	Sample volume (ml)	Metal found[a] (μg ml^{-1})
La(III)	500	4.86
Nd(III)	500	4.76
Tb(III)	500	4.95
Th(IV)	500	4.92
U(VI)	500	4.90

[a] Values agreed with a precision of ±1%.

Table 4
Separation of U(VI) from other metal ions performed at pH 4.5 (amount of U(VI) taken, 20 μg ml^{-1})

Metal ion	Amount of metal added (μg ml^{-1})	Amount of U(VI) found[a] (μg ml^{-1})	Metal ion found[a] (μg ml^{-1})
Ni(II)	10	19.8	9.92
Co(II)	10	19.5	9.94
Zn(II)	10	20.0	9.89
Cu(II)	10	19.4	9.76

[a] Values agree with a precision of ±1%.

Table 5
Separation of Th(IV) from other metal ions performed at pH 4.5 (amount of Th(IV) taken, 20 μg ml^{-1}) with the batch method

Metal ion	Amount of metal added (μg ml^{-1})	Amount of Th(IV) found[a] (μg ml^{-1})	Metal ion found[a] (μg ml^{-1})
Ni(II)	10	19.7	9.89
Zn(II)	10	20.1	10.02
Co(II)	10	19.6	9.92
Cu(II)	10	19.6	9.97

[a] Values agreed within ±1%.

metal ion was shaken with 100 mg of resin at pH 4.5. Uranium or thorium retained on the resin was eluted with 1 M hydrochloric acid (10 ml). The concentration of nickel, cobalt, zinc or copper was determined in the effluent by AAS.

3. Results and discussion

In a preliminary experiment, the sorption behaviour of La, Nd, Tb, Th, and U on XAD-4–bicine resin at different pH values was examined by the batch method and the results are presented in Fig. 2. Sorption begins in every case at pH 3–3.5 and a limiting value is attained near pH 6. A slight decrease in the sorption in observed beyond pH for most of the metal ions.

The capacity of the resin is an important factor to determine how much resin is required to quantitatively remove a specific metal ion from the solution. The capacity of each metal ion is reported in Table 1 along with the standard deviation (S.D.).

The theoretical value of the capacity should be equivalent to the ligand loading which is 0.44 mmol g^{-1} of resin for XAD-4–bicine resin (calculated from the nitrogen content). The lower values could be due to the rigidity of the polymeric matrix and the inability of all bicine groups participating in chelation due to steric restriction.

The pH dependence of trace metal ion uptake was carried out to determine if the uptake of trace quantities of the metal ion is possible at pH values other than the optimum pH for chelation. The results are shown in Fig. 3. The complete sorption for the trace metal ions is in the region of pH 4.5–9 for La(III), 4.5–9 for Nd(III), 5–9 for Tb(III), 4.5–9 for Th(IV) and 4.5–8.5 for U(VI).

A special feature in these breakthrough curves is the complete sorption of these metal ions in the pH range 4.5–5. This should enable their separation from many transition metal ions, which are not retained at all in this pH region [7].

Interaction of the resin with the metal ion is sufficiently rapid, allowing the resin to also be used in a packed column. Fig. 4 shows the rate of uptake of La(III), Th(IV) and U(VI) determined at optimum pH of sorption. More than 90% of the metal ion is extracted within 5 min of its interaction with the resin. A similar behaviour is observed for other metal ions.

The effect of diverse ions on the sorption of U(VI) and Th(IV) by XAD-4–bicine resin was investigated and results are shown in Table 2. The

tolerance limit is the maximum ratio of the concentration of diverse ion to that of U(VI) or Th(IV) at which the concentration of diverse ion in the eluate (1 M HCl) is negligible and the concentration of U(VI) or Th(IV) is the same as taken initially.

The resin has shown a high tolerance limit for alkali and alkaline earth metals. This is particularly useful for the analysis of U(VI) and Th(IV) in natural samples; for example, sea water, which contains large amount of alkali and alkaline earth metals.

Preconcentration of the metal ions on the resin was carried out and the results are shown in Table 3. Metal ions could be enriched up to 50 times with XAD-4–bicine resin. The chelated metal ions can be eluted from the XAD-4–bicine with dilute acids and the resin can be used repeatedly. In contrast, metals can be recovered effectively from the poly(dithiocarbamate) resin generally after the digestion of the resin [11]. The separation of trace amounts of uranium in the presence of diverse metal ions was carried out by the batch method (Table 4). Uranium is separable from nickel, copper, cobalt and zinc as they are not retained on the resin at pH 4.5. Similarly, separation of thorium was carried out from binary mixtures containing copper, nickel, cobalt or zinc (Table 5).

4. Conclusion

XAD-4–Bicine resin has a good potential for enrichment of trace amounts of La, Nd, Tb, Th and U from large sample volumes. The resin can be applied over a wide pH range (4.5–9) for collection of trace metals. The resin shows selectivity for these metal ions over some transition metal ions and permits their separation from the latter. The capacity of the resin is sufficiently high to preconcentrate more than one metal ion simultaneously.

Acknowledgements

The authors thank BRNS (Bhabha Atomic Research Centre, India) for financial assistance.

References

[1] E.M. Moyers, J.S. Fritz, Anal. Chem. 49 (1977) 418.
[2] M. Marhol, K.L. Cheng, Talanta 21 (1974) 751.
[3] S. Tomoshige, M. Hirai, H. Ueshima, Anal. Chim. Acta 115 (1980) 285.
[4] P. Figura, B. McDuffie, Anal. Chem. 1977 (1950) 49.
[5] W.M. Landing, C. Haraldsson, N. Paxeus, Anal. Chem. 58 (1986) 3031.
[6] S. Blain, P. Appriov, H. Handel, Analyst 116 (1991) 815.
[7] K. Dev, G.N. Rao, Talanta 42 (1995) 591.
[8] Bulletin 2020, Bio-Rad Laboratories Product Information, Richmond, CA, USA, 1976.
[9] S.S. Berman, J.W. McLaren, S.N. Willie, Anal. Chem. 52 (1980) 488.
[10] R.E. Sturgeon, S.S. Berman, J.A.H. Desavniers, A.P. Mykytivk, J.W. McLaren, D.S. Russell, Anal. Chem. 52 (1980) 1585.
[11] A. Myazaki, R.M. Barnes, Anal. Chem. 53 (1981) 299.
[12] Zs. Horvath, R.M. Barnes, Anal. Chem. 58 (1986) 1352.
[13] A.N. Masi, R.A. Olsina, Talanta 40 (1993) 931.
[14] R.W. Rinehart, Anal. Chem. 26 (1954) 1820.
[15] A. Mayer, G. Bradshaw, Analyst 77 (1952) 154.
[16] J.H. Yoe, F. Will III, R.A. Black, Anal. Chem. 25 (1953) 1200.

ELSEVIER

Talanta 48 (1999) 585–593

Talanta

Moisture induced solid phase degradation of L-ascorbic acid Part 1: a kinetic study using tristimulus colorimetry and a quantitative HPLC assay

Anthony B. Shephard [a], Steven C. Nichols [b], Alan Braithwaite [a,*]

[a] *Department of Chemistry and Physics, The Nottingham Trent University, Clifton Lane, Nottingham NG11 8NS, UK*
[b] *Rhône-Poulenc Rorer, Respiratory Technology, London Road, Holmes Chapel CW4 8BE, London, UK*

Received 3 March 1997; received in revised form 24 August 1998; accepted 25 August 1998

Abstract

L-Ascorbic acid was found to degrade in the solid phase with discoloration under the influence of moisture in proportion to the moisture content. This degradation pattern was different to that in solution and followed zero order kinetics. The exclusion of air reduced the rate of reaction suggesting the degradation may proceed via an oxidative route but no evidence was found for the presence of dehydroascorbic acid. A method was developed for the determination of dehydroascorbic acid using an automated precolumn reduction reaction with DL-dithiothreitol. The degradation was found to be zero order and activation energy was been measured at 37.57 kJ mol^{-1} by high performance liquid chromotography (HPLC) assay and 33.30 kJ mol^{-1} by tristimulus colorimetry, resulting in a 12.8% difference between the two methods. Tristimulus colorimetry was more sensitive to the onset of degradation than HPLC assay, but it is non-specific. The purpose of this study was to obtain kinetic data on the rate of degradation of L-ascorbic acid alone under the influence of moisture and air and to identify whether tristimulus colorimetry could be used as a rapid and non-destructive means of monitoring for the degradation of L-ascorbic acid in the solid phase. Further studies to determine the degradation pathway and to identify the degradation products are to be reported in subsequent papers.

Keywords: HPLC; Tristimulus colorimetry; Solid phase degradation; Ascorbic acid

1. Introduction

L-Ascorbic acid degrades in the solid phase under the influence of moisture [1,2]. De Ritter et al. studied the effect of silica gel on the stability of L-ascorbic acid [3]. They found that the loss of L-ascorbic acid was directly proportional to the amount of unbound moisture.

In solution, the first degradation step of L-ascorbic acid is dehydroascorbic acid. This reaction is reversible and by reducing dehydroascorbic

* Corresponding author. Tel.: +44-115-9418418; fax: +44-115-9486636; e-mail: alan.braithwaite@ntu.ac.uk.

0039-9140/99/$ - see front matter
PII: S0039-9140(98)00280-X

acid to L-ascorbic acid, the total amount of L-ascorbic acid can be determined. The dehydroascorbic acid can then irreversibly degrade to 2,3-diketogulonic acid which further degrades to produce a range of furan type products, ketoacids and carboxylic acids [4–8]. In the solid phase, degradation is characterized by the formation of a brown discoloration of unknown composition. The degree of discoloration is directly dependent upon the amount of moisture present.

Dehydroascorbic acid is difficult to quantify due to its instability and it is poorly retained in reverse-phase high performance liquid chromatography (HPLC) due to its highly polar character. Furthermore, a detector wavelength of 210 nm must be used due to the lack of conjugated chromophoric groups with the added problem of interference from other compounds. Therefore, HPLC assays have been developed which measure dehydroascorbic acid indirectly after reduction. The L-ascorbic acid content of the sample is first measured directly, the sample is then reduced using a mild reducing agent and the sample re-assayed for L-ascorbic acid. Any increase in the L-ascorbic acid content is due to dehydroascorbic acid [9–16]. Various reagents have been used for the reduction of dehydroascorbic acid to L-ascorbic acid. Nagy and Degrell [9], Ziegler et al. [11], Kim [12], Sapers et al. [14] and Okamura [16] used DL-dithiothreitol. Graham and Annette [15] and Nyyssönen et al. [10] used DL-homocysteine and Dhariwal et al. [13] used 2,3-dimercapto-1-propanol. The sample reduction procedures either involved a lengthy manual step prior to chromatography or a post-column reaction [11]. The work described in this paper was supported by an automated reduction reaction using an automated precolumn sample preparation system. The method was validated for optimization of reaction conditions, linearity, precision, sample reproducibility and limit of detection.

Vemuri et al. [17] have used tristimulus colorimetry to measure the colour stability of L-ascorbic acid tablets but did not confirm their findings with an assay for L-ascorbic acid. In this study, use was made of tristimulus colorimetry to monitor the extent of discoloration and results compared to those obtained by the quantitative high performance liquid chromatography (HPLC) of L-ascorbic acid.

2. Experimental

2.1. Sample preparation

The effect of moisture on the stability of L-ascorbic acid was investigated at levels between 0 and 10% v/w moisture. Samples of L-ascorbic acid, 10 g, were triturated with de-ionized water to produce samples with moisture levels of 0.5, 1, 2, 5 and 10% v/w. A 10 g sample containing no added moisture was used as a control. The samples were placed in Pierce Reactivials and sealed with a Teflon coated septum and screw cap. Samples with 5 and 10% v/w moisture were also placed on storage under an atmosphere of nitrogen to exclude oxygen. The samples were placed on storage at 50°C and additional samples containing 5% v/w moisture were stored at 15, 30 and 60°C, respectively. The samples were analyzed when prepared again after 7, 14, 28 and 42 days storage. After removal from storage, the samples were allowed to equilibriate to ambient temperature and ~ 500 mg were rapidly sampled into small sample vials, sealed and analyzed immediately to prevent changes in moisture content. The bulk material was returned to storage. Those stored under nitrogen were sampled under nitrogen into sample tubes flushed with nitrogen. The reaction vials were thoroughly purged with nitrogen before being replaced on storage.

2.2. Analysis

Samples were analyzed for total ascorbic acid (the sum of the oxidized and reduced forms of L-ascorbic acid, i.e. dehydroascorbic acid and L-ascorbic acid), L-ascorbic acid and colour change using tristimulus colorimetry.

Reagents: L-ascorbic acid, metaphosphoric acid (1% w/v aqueous), trifluoroacetic acid (0.1% v/v aqueous, pH 2.7), bromine solution (3% v/v

aqueous), tri-sodium orthophosphate, dodecahydrate, sodium dihydrogen orthophosphate, dihydrate, DL-dithiothreitol.

All reagents were purchased from Fisher Scientific UK, Loughborough.

2.2.1. Reducing reagent

The precolumn reducing reagent was prepared [11] by dissolving 1.135 g trisodium orthophosphate dodecahydrate, 0.665 g sodium dihydrogen orthophosphate dihydrate and 15 mg DL-dithiothreitol in 50 ml deionized water to produce a solution buffered at pH 7.6.

2.2.2. Equipment

Hewlett Packard HP1090M HPLC with diode array detection and ChemStation fitted with the Hewlett Packard micro oven and controller, part numbers 79848-66901 and 79848-66902.

Lichrospher 100 RP C18e (25 × 0.46 cm, 5 μm) column (Merck)

2.2.3. Procedure for precolumn sample preparation

A 2.5 ml aliquot of reagent solution was drawn into a heated capillary tube followed by a 5 ml aliquot of sample solution and finally another 2.5 ml aliquot of reagent solution. Once in the heated capillary tube, the solutions were mixed together by cycling backwards and forwards ten times. After heating for 1 min, the entire volume was injected onto the chromatographic column. The method was validated for optimization of reaction conditions, linearity, precision, sample reproducibility and limit of detection.

2.2.4. Assay for total L-ascorbic acid and dehydroascorbic acid

Approximately 100 mg of each sample was accurately weighed into a series of 100 ml volumetric flasks and dissolved in 1% w/v aqueous metaphosphoric acid solution to produce 1 mg ml^{-1} sample solutions. These solutions were diluted five-fold with 1% w/v aqueous metaphosphoric acid solution to produce 0.2 mg ml^{-1} L-ascorbic acid solutions for quantitative analysis. A 10 ml aliquot of each of the 0.2 mg ml^{-1} solutions was chromatographed isocratically in duplicate using reverse-phase HPLC with UV detection at 245 nm. The sample solutions were assayed initially for total L-ascorbic acid (dehydroascorbic acid and L-ascorbic acid) using the automated precolumn sample preparation system and then for L-ascorbic acid only against an external standard solution of 0.2 mg ml^{-1} L-ascorbic acid in 1% w/v aqueous metaphosphoric acid solution.

Once prepared, the L-ascorbic acid standard solution is stable for at least 12 h at room temperature with 99.95% w/w still remaining. The standard solid L-ascorbic acid can be stored at room temperature and is best replaced with fresh material after 12 months.

Chromatography was achieved on a Lichrospher 100 RP 18e, 25 × 0.46 cm, 5 μm column at 40°C using a mobile phase of 0.1% v/v aqueous solution of trifluoroacetic acid, pH 2.7, at a flow rate of 1.5 ml min^{-1}. Detection was carried out at 245 nm and the run time totalled 4 min.

2.2.5. Assay for L-ascorbic acid

Chromatography conditions were identical to those used for total L-ascorbic acid except the automated precolumn sample preparation system was bypassed and 5 ml aliquots of the same sample and standard solutions were chromatographed. Using a mobile phase of 0.1% v/v aqueous solution of trifluoroacetic acid, pH 2.7, the dissociation of L-ascorbic acid was completely suppressed and maximum column retention was obtained without the use of ion-pair reagents. A retention time of ~1.0 and 2.2 min was obtained for DL-dithiothreitol and L-ascorbic acid, respectively with the L-ascorbic acid eluting as a sharp symmetrical peak (Fig. 1).

2.3. Colour (tristimulus colorimetry)

Tristimulus colorimetry was used in the reflectance mode and colour measurements taken using the $L^*a^*b^*$ scale [17].

2.3.1. Reagents/apparatus

Trivector Tristimulus colorimeter, model CL6000, fitted with reflectance head, sample cup, diameter 10 mm and 10 mm deep.

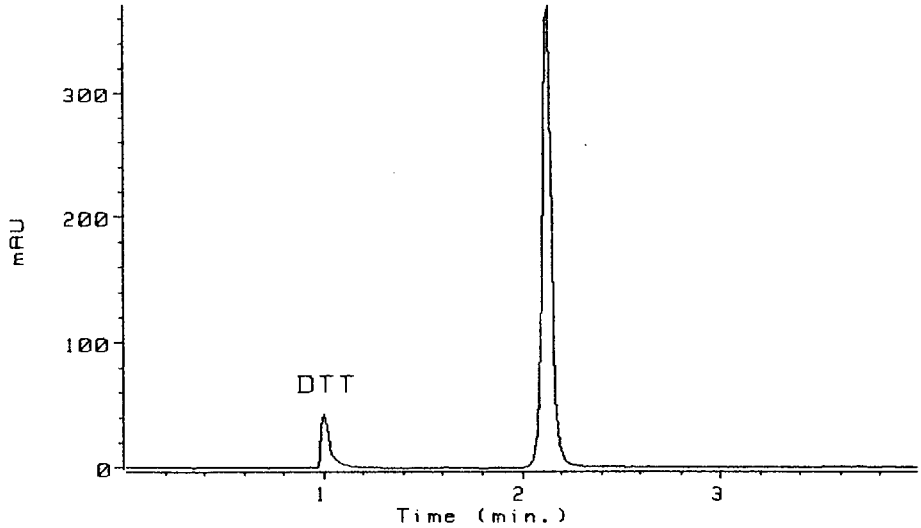

Fig. 1. Typical sample chromatogram for total L-ascorbic acid on a Lichrospher 100RP 18e column and 0.1% v/v aqueous solution of trifluoroacetic acid, isocratic.

2.3.2. Colour measurement

Approximately 100 mg of each sample was pressed into a sample cup and colour readings were taken using the reflectance head. Four readings were taken from each sample by rotating the cup through 90° between each reading. The mean of four values was recorded. The readings were recorded as $L^*a^*b^*$ values and calculated as colour differences ΔE^*ab. The visual appearance and colour of each sample was also noted.

3. Results and discussion

3.1. Assay for L-ascorbic acid and dehydroascorbic acid

In order to determine the recovery of the reaction, a 50 ml aliquot of a 0.2 mg ml^{-1} standard L-ascorbic acid solution in 1% w/v metaphosphoric acid was mixed with 0.5 ml of bromine solution, 3% v/v aqueous. The addition of the bromine solution caused partial oxidation of the L-ascorbic acid solution to dehydroascorbic acid with $\sim 74\%$ w/w L-ascorbic acid remaining.

An unoxidized aliquot of the standard solution was retained as a control solution. The solutions were assayed for both L-ascorbic acid only and for total L-ascorbic acid using the DL-dithiothreitol reagent to reduce the dehydroascorbic acid formed on oxidation back to L-ascorbic acid. Fixing the reaction temperature at 50°C, a temperature >45°C is required for complete conversion within 1 min [11]. The reaction time and number of mixes were optimized. After mixing for ten cycles, a reaction time of 60 s was found to give a mean recovery of 98.7% (Fig. 2). Statistical analysis for $n=6$ gave a relative SD of 0.57%, range 98.2–99.2%; see Ziegler et al. [11] who obtained a range 95–99%, and a mean of 96.7% working with a post-column derivation.

The reaction time, temperature and number of mixes were optimized by reacting replicate aliquots of the solution of L-ascorbic acid partially oxidized with bromine solution. Unacceptably low recoveries were obtained with six mixing cycles. After mixing for ten cycles, a reaction time of 60 s at 50°C was found to give a recovery of 98.7% (Table 1). There was no advantage in using a higher reaction temperature, i.e. 60°C where a similar recovery to that at 50°C was recorded.

Precision of the procedure using the precolumn derivatisation unit was measured using both unoxidized and the bromine oxidized L-ascorbic acid

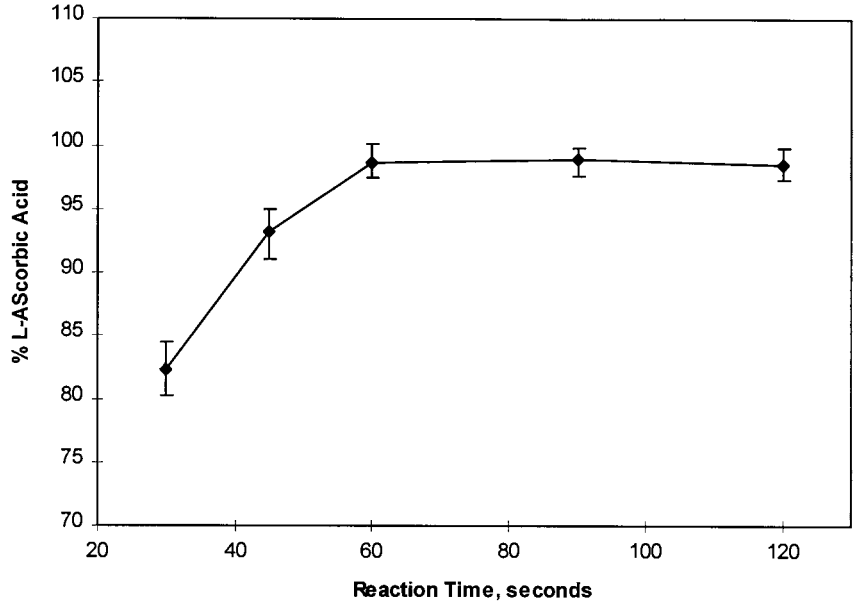

Fig. 2. Conversion of dehydroascorbic acid to L-ascorbic acid at 50°C and ten mixing cycles after reduction with dithiothreitol.

solution. The repeatability of injection was determined using six replicate injections of standard L-ascorbic acid solution, 0.2 mg ml^{-1} concentration. Relative standard deviation (RSD) was 0.10% when a standard unoxidized solution was chromatographed via the automated precolumn sample preparation system, 0.23% bypassing the system and 0.57% when the partially oxidized standard solution was chromatographed via the system. Assaying aliquots of dehydroascorbic acid and L-ascorbic acid solutions, 0.2 mg ml^{-1} in 1% w/v aqueous metaphosphoric acid gave a RSD of 2.31 and 1.05%, respectively.

Table 1
Optimization of reaction conditions for the reduction of dehydroascorbic acid with dithiothreitol using the Hewlett Packard precolumn reaction system

Reaction parameters (mixing cycles/time, s/temperature, °C)	Recovery (% w/w)
6/30/50	81.07
6/120/50	85.88
10/30/50	95.20
10/60/50	98.73
10/120/50	97.21
10/60/60	98.74

Linearity was demonstrated by reacting aliquots of dehydroascorbic acid solution in 1% w/v aqueous metaphosphoric acid, equivalent to 0–0.5 mg ml^{-1}, using the automated precolumn sample preparation system. The resulting calibration graph was linear between 1.5 and 0.5 mg ml^{-1} using diode array detection with a correlation coefficient of 0.9982. The limit of detection, taken as that solution concentration which produced a sample peak height which was three times baseline noise, was determined at 500 ng/ml and the absolute limit 5 ng. The linearity range and limit of detection for L-ascorbic acid only was identical to that of dehydroascorbic acid with a correlation coefficient of 0.9997. After $\sim$1000 injections, the performance of the column was undiminished with respect to peak tailing and resolution.

3.1.1. Sample analysis

Samples were freshly prepared and analyzed in small batches for total L-ascorbic acid in order to minimize the loss of dehydroascorbic acid as it is unstable in solution for extended periods of time.

Variation in assay results for both total L-ascorbic acid and L-ascorbic acid only were al-

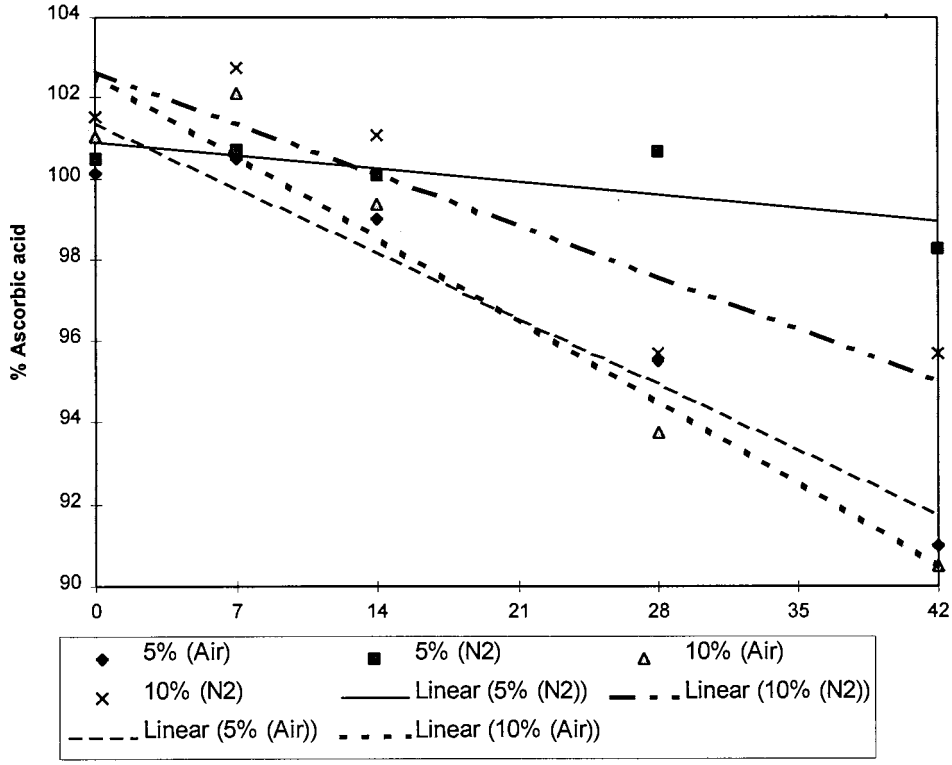

Fig. 3. Effect on stability of excluding air from moist L-ascorbic acid.

most without exception within $\pm 1\%$ of each other and were not consistently higher for total L-ascorbic acid. Due to the close agreement between the two assays (mean of duplicate injections of duplicate weights) and the inconsistent higher L-ascorbic acid assay, it was concluded there was no evidence for the presence of dehydroascorbic acid (Table 2). No dehydroascorbic acid was detected in the standard L-ascorbic acid reference material.

The presence of air and moisture was found to accelerate the degradation of L-ascorbic acid as assayed by HPLC (Fig. 3). Furthermore, the rate of degradation also increased with increasing moisture content and elevated temperatures (Fig. 4), as shown by the slopes of the plots, HPLC assay (Table 3).

From the slopes of the plots of total L-ascorbic acid against time, the rate constant, k, for each condition was calculated (Table 3). Since the plots were linear, the order of reaction was of zero order. A plot of ln k against $1/T$ for the 5% v/w moisture samples stored at 15, 30, 50 and 60°C gave a straight line plot, $R^2 = 0.9652$, and the activation energy was calculated at 37.57 kJ mol^{-1}.

3.2. Colour (tristimulus colorimetry)

Colour differences, ΔE^*ab for the sample were calculated and plotted against time to obtain rate constants (Table 2). Rate constants compared to quantitative HPLC assay were consistently higher, possibly due to interferences from side reactions producing other coloured compounds. A plot of ln k against $1/T$ for the 5% v/w moisture stressed samples stored at 15, 30, 50 and 60°C gave a straight line plot, $R^2 = 0.9992$, and the activation energy was calculated at 33.30 kJ mol^{-1}. This value was slightly lower than that obtained by quantitative HPLC assay.

Table 2
Mean of duplicate assay results for total L-ascorbic acid and L-ascorbic acid only (AA) for moisture stressed L-ascorbic acid stored at 50°C

Days storage	0% moisture (air excluded)		1% moisture (air present)		2% moisture (air present)		5% moisture (air present)		5% moisture (N_2 atmosphere)		10% moisture (air present)		10% moisture (N_2 atmosphere)	
	Total	AA	Total	AA	Total	AA	Total	AA	Total	AA	Total	AA	Total	AA
7	100.65	100.36	100.97	101.06	100.91	100.61	100.46	99.62	100.70	101.63	101.10	100.94	100.73	100.57
14	99.81	100.11	99.48	100.71	100.33	101.14	99.00	98.90	101.08	101.41	99.36	100.03	100.08	101.01
28	99.38	100.62	97.29	99.56	97.56	96.87	95.52	96.60	101.65	99.21	93.77	91.85	95.70	96.76
42	100.70	100.28	96.50	97.57	95.00	94.00	90.99	90.10	96.28	96.11	81.02	80.00	95.68	95.52

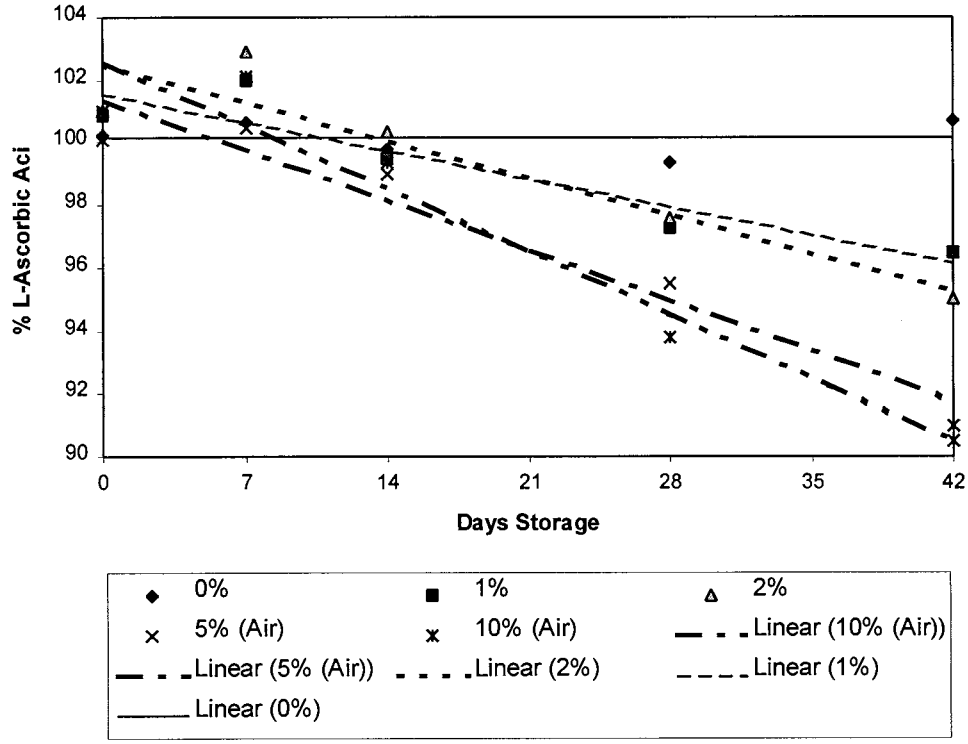

Fig. 4. Effect of moisture on the stability of L-ascorbic acid at 50°C.

3.2.1. Appearance of samples

Samples were visually assessed for colour and rated using a numerical scale from 1 to 5 (Table 3). The control sample, $< 0.1\%$ w/w moisture, remained unchanged throughout the study. The 5% v/w sample stored at 15°C and under nitrogen discoloured the least with the others turning a brown or dark brown colour with time. Again, this demonstrates the importance of excluding oxygen (and air) from L-ascorbic acid on storage. The sample stored at 60°C rapidly discoloured and turned a very dark brown colour after 14 days and further darkening was difficult to quantify visually.

4. Conclusion

L-ascorbic acid was found to degrade in the solid phase in the presence of moisture alone, the rate of degradation being reduced if air was excluded. The degradation was found to cause severe discoloration, the rate of which could be monitored by both tristimulus colorimetry and HPLC albeit with somewhat different results, tristimulus colorimetry consistantly producing higher values. This was believed to be due to HPLC being specific for L-ascorbic acid whereas tristimulus colorimetry measured the total degradation leading to discoloration. The reaction was found to be of zero-order. Rate constants and the activation energy were determined for L-ascorbic acid stressed with moisture by quantitative HPLC and tristimulus colorimetry and were found to compare favourably with values quoted by other workers [17,18]. Tristimulus colorimetry was found to be more sensitive to the onset of degradation, as shown by discoloration of the samples, than HPLC assay. Slightly discolored samples did not assay significantly lower than undegraded standard L-ascorbic acid. Severely discolored samples had the appearance of carbon but still as-

Table 3
Reaction constant, k (five points per plot, two repetitions) for moisture stressed L-ascorbic acid and visual assessment of sample colour change[a]

Storage condition (moisture, % v/w, temperature)	Technique/rate		Storage time (days)			
	HPLC/day (R^2)	$L^*a^*b^*$/day (R^2)	7	14	28	42
0%, 50°C	–	–	1	1	1	1
1%, 50°C	0.1141 (0.8705)	0.5768 (0.6881)	2	3	4	5
–	0.1556 (0.8700)	0.6684 (0.6508)	2	3	4	5
5%, under air, 50°C	0.2281 (0.9421)	0.6412 (0.6685)	3	3	4	5
5%, under N_2, 50°C	0.0659 (0.9568)	0.2994 (0.8518)	2	3	3	3
10%, under air, 50°C	0.4694 (0.8523)	0.6869 (0.6202)	3	4	5	5
10%, under N_2, 50°C	0.1584 (0.8254)	0.5541 (0.6799)	2	3	3	4
5%, 15°C	0.0298 (0.8706)	0.1290 (0.5886)	2	2	2	3
5%, 30°C	0.0524 (0.9231)	0.2725 (0.9768)	2	3	3	4
5%, 50°C	0.2281 (0.9421)	0.6412 (0.6685)	2	3	4	5
5%, 60°C	0.3238 (0.9863)	0.9387 (0.7505)	4	5	5	5

[a] Key: 1, white; 2, pale straw; 3, yellow; 4, brown; 5, dark brown.

sayed at 80% L-ascorbic acid. Tristimulus colorimetry was not as successful in differentiating between these severely discolored samples and HPLC assay was the preferred mode of assay for these samples.

The exclusion of air reduced the rate of reaction, inferring that degradation occurred via an oxidative route although no conclusive evidence was found for the presence of dehydroascorbic acid. It is conceivable that dehydroascorbic acid is formed but rapidly degrades even further as soon as it is formed.

By excluding air and moisture from L-ascorbic acid solid dose formulations on storage, the shelf-life of the product would be extended and the appearance of the product improved.

An automated and rapid precolumn reduction reaction was developed for the determination of total L-ascorbic acid (L-ascorbic acid and dehydroascorbic acid). A reaction time of only 60 s at 50°C was required for the reduction of dehydroascorbic acid to L-ascorbic acid.

References

[1] S.H. Lee, T.P. Labuza, J. Food Sci. 40 (2) (1975) 370–373.
[2] B.M. Laing, D.L. Schlüter, T.P. Labuza, J. Food Sci. 43 (5) (1978) 1440–1443.
[3] E. De Ritter, L. Magid, M. Osadca, S.H. Rubin, J. Pharm. Sci. 59 (2) (1970) 229–232.
[4] P. Finholt, R.B. Paulssen, I. Alsos, T. Higuchi, J. Pharm. Sci. 54 (1) (1965) 124–128.
[5] J.H. Tatum, P.E. Shaw, R.E. Berry, J. Agr. Food Chem. 17 (1969) 38–40.
[6] I.M. Coggiola, Nature 200 (1963) 954–955.
[7] L. Löwendahl, G. Petersson, Anal. Biochem. 72 (1976) 623–628.
[8] K. Niemelä, J. Chromatogr. 399 (1987) 235–243.
[9] E. Nagy, I. Degrell, J. Chromatogr. (Biomed. Appar.) 497 (1989) 276–281.
[10] K. Nyyssönen, S. Pikkarainen, M.T. Parviainen, K. Heinonen, I. Monenen, J. Liq. Chromatogr. 11 (8) (1988) 1717–1728.
[11] S.J. Ziegler, B. Meier, O. Sticher, J. Chromatogr. 391 (1987) 419–426.
[12] H-J. Kim, Assoc. Anal. Chem. 72 (4) (1989) 681–686.
[13] K.R. Dhariwal, P.W. Washko, M. Levine, Anal. Biochem. 189 (1990) 18–23.
[14] G.M. Sapers, F.W. Douglas, M.A. Ziolkowski, R.L. Miller, K.B. Hicks, J. Chromatogr. 503 (1990) 431–436.
[15] W.D. Graham, D. Annette, J. Chromatogr. 594 (1992) 187–194.
[16] M. Okamura, Clin. Chim. Acta. 103 (1980) 259.
[17] S. Vemuri, C. Taracatac, R. Skluzacek, Drug Dev. Ind. Pharm. 11 (1) (1985) 207–222.
[18] M.R. Blaugh, D. Chakravarty, J.L. Lach, Drug Stand. 26 (1958) 199.

ELSEVIER

Talanta 48 (1999) 595–606

Talanta

Moisture induced solid phase degradation of L-ascorbic acid part 2, separation and characterization of the major degradation products

Anthony B. Shephard [a], Steven C. Nichols [b], Alan Braithwaite [a,*]

[a] *Department of Chemistry and Physics, The Nottingham Trent University, Clifton Lane, Nottingham NG11 8NS, UK*
[b] *Rhône-Poulenc Rorer, Respiratory Technology, London Road, Holmes Chapel CW4 8BE, UK*

Received 6 January 1998; received in revised form 24 August 1998; accepted 25 August 1998

Abstract

The influence of moisture in the presence and absence of air on the solid state degradation of L-ascorbic acid has been investigated previously [1]. Reaction kinetics were studied using tristimulus colorimetry and a quantitative high performance liquid chromatographic assay for both total L-ascorbic acid and dehydroascorbic acid. The degradation gave rise to a discolouration of the samples, the most severely degraded samples were almost black in appearance although over 68% w/w of the L-ascorbic acid remained. The samples were analyzed for the presence of carbonyl compounds, furan related compounds, compounds responsible for the discolouration and evolution of carbon dioxide. No 2,4-dinitrophenylhydrazine (2,4-DNP) derivatives of carbonyl compounds or furan related compounds were detected by HPLC. An HPLC screening procedure was developed which was used to monitor for compounds responsible for the discolouration, at least eight unknown compounds were resolved and a relative response factor of 5.47 was assigned to them with respect to L-ascorbic acid at 280 nm. One mole of carbon dioxide was evolved per mole of L-ascorbic acid. This paper describes the investigation into the identity of the degradation products.

Keywords: Ascorbic acid; HPLC; Analysis; Solid phase degradation

1. Introduction

L-Ascorbic acid degrades in the solid phase under the influence of moisture [1–3]. De Ritter and co-workers studied the effect of silica gel on the stability of L-ascorbic acid [4]. They found that the loss of L-ascorbic acid was directly proportional to the amount of unbound moisture. The degradation is believed to follow a different pathway to that in solution and manifests itself as a discolouration from white to a dark brown colour. The degree of discolouration being directly dependent upon the amount of moisture present [1]. The appearance of this discolouration occurs before any noticeable decrease in purity as

* Corresponding author. Tel.: +44-115-941-8418; fax: +44-115-948-6636; e-mail: Alan.Braithwaite@ntu.ac.uk.

0039-9140/99/$ - see front matter
PII: S0039-9140(98)00279-3

measured by chemical or chromatographic means. A chromatographic method was developed to detect both the early stages of solid state degradation, as shown by a light brown discolouration, and for gross degradation as shown by an extremely dark brown discolouration.

Previous workers [5,6] have shown the effect of tablet lubricant and glidants on the stability of L-ascorbic acid in the solid phase but did not investigate the route of the degradation process or products formed. In solution the first degradation stage of L-ascorbic acid is the formation of dehydroascorbic acid. Von Euler and Hasselquist found that by heating L-ascorbic acid with 1 M sodium hydroxide solution at 100°C under an atmosphere of nitrogen the lactone ring opened [7]. By heating L-ascorbic acid solutions at different pH values below 5.5 under anaerobic conditions Finholt and co-workers demonstrated that carbon dioxide, furfural and xylose were formed [8]. It is feasible that carbon dioxide and other volatile compounds may be evolved during solid phase degradation.

The isolation of ten furan type compounds, two lactones, three acids and 3-hydroxy-2-pyrone was reported by Tatum, Shaw and Berry when L-ascorbic acid was heated in aqueous solution [9]. Coggiola found 2,5-dihydro-2-furoic acid to be a product of the anaerobic degradation of L-ascorbic acid in aqueous solution at 100°C [10]. In order to determine whether furan type compounds are a product of the solid phase degradation of L-ascorbic acid a HPLC screening process was developed for this investigation capable of resolving furan and related compounds that have previously been identified as degradation products of solution chemistry. Löwendahl and Petersson have investigated the degradation pathway of L-ascorbic acid in neutral and alkaline aqueous solution [11] and found that dehydroascorbic acid converts to 2-(threo-1, 2, 3-trihydroxy-propyl) tartronic acid. Niemelä [12] used GC/MS to detect over 50 compounds, of which 32 carboxylic acids could be identified during oxidative and non-oxidative alkali-catalysed degradation. Deutsch et al. [13] used GC-MS to determine the products and routes of the oxidation of L-ascorbic acid in aqueous solution using different oxidants. They found different oxidation conditions lead to different oxidation products.

Unknown polyketone compounds are suspected to be responsible for the brown discolouration found in degraded L-ascorbic acid. In addition aldehydes such as furfural and ketones such as 2,3-diketogulonic acid are known degradation products. The use of an acidic solution of 2,4-dinitrophenylhydrazine (2,4-DNP) as the derivatizing agent for carbonyl groups is well known [14,15]. The resulting 2,4-dinitrophenylhydrazones can be separated by reverse-phase HPLC using either methanol/water [16,17] or acetonitrile/water gradients [18–21]. Using this reagent successful separations of aliphatic C_1–C_{12} aldehydes [16,17,19–25,27], C_3–C_{11} ketones [16,17,22–27] and ketoacids [18,22,28,29] containing one or two oxo groups have been described.

The purpose of this study was to monitor any degradation products formed during storage. A further paper, to be published at a later date will describe the isolation and identification of the degradation products responsible for the brown discolouration and their chemical characterization.

2. Experimental

2.1. Methods

2.1.1. Sample preparation

The sample preparation was described previously [1]. Samples were solid L-ascorbic acid containing various moisture levels ranging from 0 to 10% w/w stored at temperatures of 15, 30, 50 and 60°C for 0, 7, 14, 28 and 42 days.

2.1.2. Analysis

Samples were analyzed for potential L-ascorbic acid degradation products i.e. carbonyl compounds; furan related compounds; coloured compounds; evolution of gases/volatile compounds.

2.2. Reagents

L-ascorbic acid, metaphosphoric acid, trifluoroacetic acid (TFA) solution (0.1% v/v

aqueous, pH 2.7), acetonitrile, 2,4-DNP, ethanol, 2-propanol, dehydroascorbic acid (DHAA). All reagents except DHAA were of analytical grade and purchased from Fisher Scientific UK, Loughborough, England. DHAA was obtained from Sigma-Aldrich, Poole, England.

2.3. Equipment

Hewlett Packard HP1090M HPLC with diode array detection and ChemStation. Lichrospher 100 RP C18e (25 × 0.46 cm, 5 μm) column (Merck). Hewlett Packard 5890 GC fitted with a Carbowax 20M WCOT capillary column (30 m × 0.22 mm, 0.15 μm film) and a HP Ultra 1 FSOT (12 m × 0.2 mm, thick film) and FID detector for the determination of volatile compounds.

Carlo Erba HRGC Mega 2 fitted with a GS-Q megabore fused silica column (30 m × 0.53 mm, thick film) and thermal conductivity detector for the determination of carbon dioxide.

2.3.1. Carbonyl compounds

Any carbonyl compounds formed during the degradation of L-ascorbic acid were converted into their 2,4-dinitrophenylhydrazones and were separated by reverse-phase HPLC using a water-acetonitrile gradient.

2.4. Derivatizing reagent/conditions

The reagent was prepared as a solution of 5 g 2,4-DNP in 60 ml metaphosphoric acid, 85%, and 40 ml ethanol. Initially the reagent was prepared as a solution of 5 g 2,4-DNP in 60 ml orthophosphoric acid, 85%, and 40 ml ethanol [30] but metaphosphoric acid was substituted for orthophosphoric acid after a study was found to increase the stability of L-ascorbic acid during the derivatization.

Reaction time and conditions initially investigated were those used for the determination of L-ascorbic acid by reaction with 2,4-DNP [31] where any L-ascorbic acid is oxidized to DHAA and then reacted at 37°C for 3 h with 2,4-DNP to form the osazone. The method described in this paper was developed not to oxidize the L-ascorbic acid to DHAA during the reaction yet still react with any carbonyl compounds present. Using solid phase degraded samples of L-ascorbic acid it was found that reaction conditions of heating at 50°C for 3 h were required for complete derivatization of potential degradation products as measured by conversion yields. The method was optimized to prevent the degradation of L-ascorbic acid during the derivatization step. The stabil-

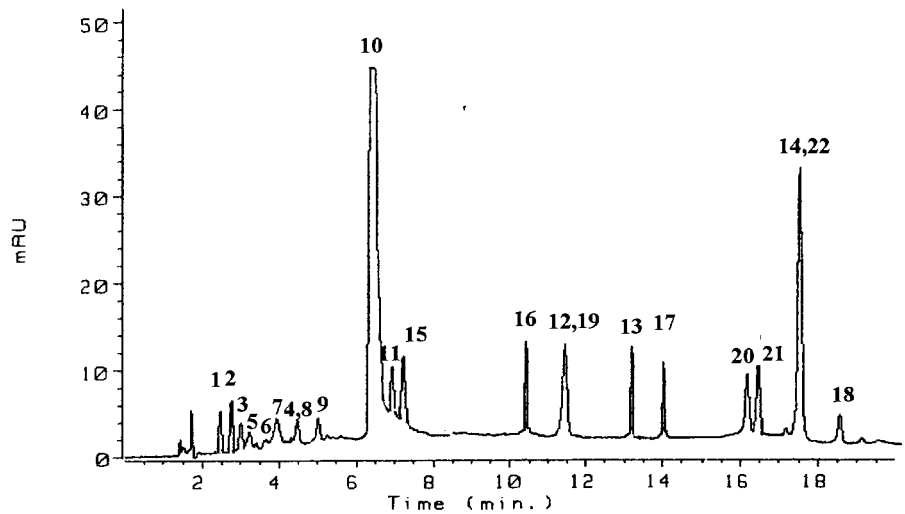

Fig. 1. Carbonyl standards mixture derivatized with 2,4-DNP: peak 1, threonic acid; 2, oxalic acid; 3 and 4, tartaric acid; 5, glyceric acid; 6, 2-ketogulonic acid; 7, glycolic acid; 8, formic acid; 9, acetic acid; 10, reagent; 11–14, glyoxilic acid; 15–18, glyoxal; 19, glyceraldehyde; 20, 2(5H)-furanone; 21, 2-furfural; 22, 2,3-diketogulonic acid.

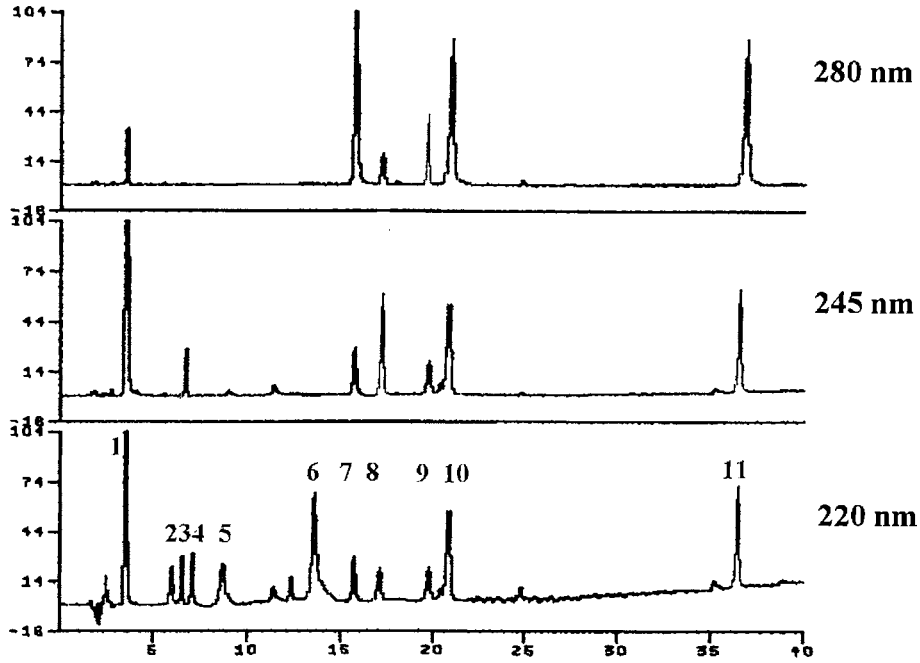

Fig. 2. Mixed furans and furan-type compounds at 280, 245, and 220 nm detector wavelength. Peaks: 1, L-ascorbic acid; 2, 2 (5H) furanone; 3, 2,5-dihydrofuran; 4, 2,3-dihydrofuran; 5, γ-butyrolactone; 6, furfuryl alcohol; 7, furfural; 8, 2-furoic acid; 9, furoin; 10, 2-acetylfuran; 11, furil.

ity of L-ascorbic acid under these reaction conditions was therefore studied by reacting 50 mg samples of pure L-ascorbic acid for 1, 2 and 3 h at 50°C to obtain the shortest practical reaction time. Samples were weighed into a series of Pierce Reactivials and dissolved in 5 ml 1% w/v aqueous metaphosphoric acid solution. The reagent, 1 ml, was added and the solutions mixed. The vials were then heated to the prescribed temperatures and times after which they were removed and sufficient acetonitrile added to dissolve any precipitate. The contents of the vials were quantitatively transferred to 25 ml volumetric flasks and the volume adjusted to 25 ml with the addition of water and mixed well. Reaction solutions were quantified for remaining L-ascorbic acid against an external standard using conditions described in Paper 1.

The stabilizing effect of metaphosphoric acid was also investigated to determine whether the reaction could be stabilized better at 50°C. Metaphosphoric acid is known to stabilize L-ascorbic acid in solution [32]. The stability of L-ascorbic acid in 2,4-DNP reagent solutions made with 5% w/v 2,4-DNP in metaphosphoric and orthophosphoric acid/solvent mixtures was investigated. All reactions were conducted at 50°C for 3 h.

2.5. Sample preparation/derivatization

The sample, 50 mg, was weighed into a Pierce Reactivial and dissolved in 1% w/v aqueous metaphosphoric acid solution, 10 ml, the reagent added, 1 ml, and mixed thoroughly. The vial was heated at 50°C for 3 h then cooled to room temperature. Any precipitate was dissolved by the addition of the minimum volume of acetonitrile, typically 10 ml, and the solution quantitatively transferred to a 25 ml volumetric flask then diluted to volume with deionized water and thoroughly mixed. A 5 μl aliquot was chromatographed on a Lichrospher RP 100 18e, 25 × 0.46 cm, 5μm column at 40°C using linear

Table 1
Stability of L-ascorbic acid, % w/w, reacted with 2,4-DNP reagent made with orthophosphoric acid

Reaction time (h)	37°C	50°C
1	99.8	98.7
2	99.6	98.2
3	98.0	97.7

Table 2
Comparison of stability of L-ascorbic acid after reaction for 3 h at 50°C with different 2,4-DNP reagent formulations

Reagent	L-ascorbic acid remaining (%) $n = 4$
6:4 orthophosphoric acid (85%)/ethanol	97.0
6:4 orthophosphoric acid (85%)/acetonitrile	95.9
6:4 metaphosphoric acid (50%)/ethanol	99.1
6:4 metaphosphoric acid (50%)/acetonitrile	98.1

gradient elution over 20 min from 24% v/v acetonitrile to 64% v/v acetonitrile acidified with 0.1% v/v aqueous solution of trifluoroacetic acid, pH 2.7, at a flow rate of 1.5 ml min^{-1}. Detection was carried out at 245 and 350 nm and the run time was 20 min.

In preliminary experiments the chromatographic system was optimized by using a standard mixture of potential carbonyl degradation products of L-ascorbic acid derivatized with 2,4-DNP reagent. A typical mixed standard chromatogram is shown in Fig. 1. The method was validated for reaction time, linearity, recovery of DHAA and limits of detection and quantification.

The reaction time was studied using a freshly prepared solution of DHAA. A 3 ml aliquot of a stock solution of DHAA equivalent to 1.5 mg was pipetted into a series of Pierce Reactivials and diluted with 10 ml of a 1% w/v aqueous metaphosphoric acid solution. The reagent, 1 ml, was added and the vials stoppered and heated at 50°C for pre-determined times. After reacting each vial was cooled and taken through the sample procedure. Aliquots from each flask were chromatographed in duplicate using the conditions previously described. The level of DHAA osazone was determined by assaying against an external standard solution of authentic material equivalent to a 100% conversion of 1.5 mg DHAA.

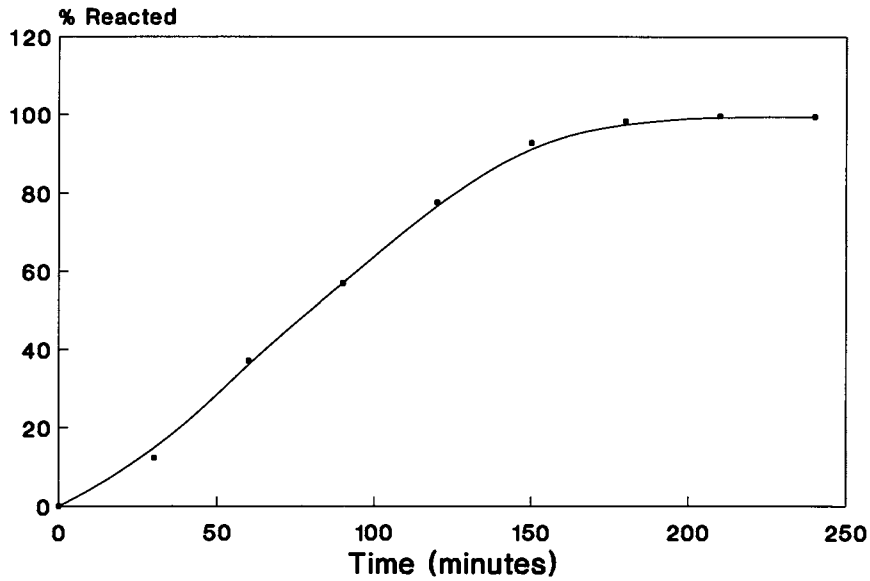

Fig. 3. Reaction time for reaction at 50°C of 2,4-DNP reagent with DHAA.

A calibration graph was constructed between 0 to 0.2 mg ml^{-1} DHAA by reacting, at 50°C for 3 h, a series of DHAA solutions with the reagent using the procedure described above. Duplicate injections of each solution were chromatographed and mean areas plotted against concentration.

Precision of the derivatization procedure was measured by taking six replicate aliquots of DHAA solution equivalent to 1.5 mg DHAA through the procedure and calculating the relative standard deviation of the osazone peak area.

Recovery of DHAA from L-ascorbic acid was determined by spiking six replicate 10 ml aliquots of L-ascorbic acid solution, equivalent to 50 mg L-ascorbic acid, with a DHAA solution equivalent to 1 mg DHAA. The spiked solutions were taken through the sample preparation procedure and recoveries calculated against a standard solution of DHAA equivalent to 1 mg DHAA taken through the same procedure.

The limit of detection (LOD) is defined as the smallest signal that can be confidently judged to be due to the analyte and not noise, typically this is taken as a signal to noise ratio of 3:1. The LOD was determined by taking low concentrations (0–0.02 mg ml^{-1}) of DHAA through the sample preparation procedure and then chromatographing the resultant solutions. The peak height due to the DHAA osazone was measured and compared against the background noise. Similarly the limit of quantification (LOQ) is defined as the smallest signal that can be measured with acceptable accuracy, typically this is taken as a signal to noise ratio of 10:1. The LOQ was determined alongside the LOD using the same solutions.

2.5.1. Furan related compounds

Approximately 100 mg of each sample was accurately weighed into a series of 100 ml volumetric flasks and dissolved in 1% w/v aqueous metaphosphoric acid solution to produce 1 mg ml^{-1} sample solutions. A 5 μl aliquot of each solution was chromatographed on a Lichrospher RP 100 18e, 25 × 0.46 cm, 5μm column at 40°C using linear gradient elution over 40 min from 0% v/v acetonitrile to 40% v/v acetonitrile acidified with 0.1% v/v aqueous solution of trifluoroacetic acid, pH 2.7, at a flow rate of 1.0 ml min^{-1}. Detection was carried out at 220, 245 and 280 nm and the run time was 40 min.

The gradient was optimized by using a standard mixture of potential furan and furan type degradation products of L-ascorbic acid. The detection limit was found to be 0.02 μg ml^{-1} for furfural at 280 nm. Fig. 2 illustrates a standard chromatogram with L-ascorbic acid at a concentration of 1 mg ml^{-1}.

2.5.2. Coloured compounds

Approximately 50 mg sample was accurately weighed into a 10 ml volumetric flask and dissolved in 10 ml 1% w/v metaphosphoric acid. A 10 μl aliquot was chromatographed on a Lichrospher RP 100 18e, 25 × 0.46 cm, 5μm column at 40°C using linear gradient elution over 5 min from 0% v/v 2-propanol to 40% v/v 2-propanol, aqueous at a flow rate of 1.0 ml min^{-1}. Detection was carried out at 245 and 280 nm and the run time was 15 min.

These conditions were developed using a severely degraded sample of L-ascorbic acid i.e. one with 10% w/w moisture stored at 60°C for 42 days. This sample was extremely dark brown in colour yet still assayed at 80% w/w L-ascorbic acid. This sample was dissolved in 1% w/v metaphosphoric acid at a concentration of 0.5 mg ml^{-1} and chromatographed. A solvent optimization software program, Hipac G, was used to resolve the mixture using reverse phase C8 and C18 stationary phases. Linear gradient elution using both neutral and acidic mobile phases containing water as mobile phase 'A' and methanol, 2-propanol, acetonitrile or tetrahydrofuran as mobile phase 'B' were studied. Two different gradient elutions were made per solvent system, typically one from 0% 'B' to 100% 'B' over 60 min and a quicker gradient using the same solvents. The software then used peak retention times to optimize the solvent composition to resolve the greatest number of peaks.

2.5.3. Evolution of gases/volatile compounds

Samples of L-ascorbic acid were triturated with water to produce samples at 5% v/w water. The samples were placed in Pierce Reactivials and each vial sealed with a PTFE septum and screw

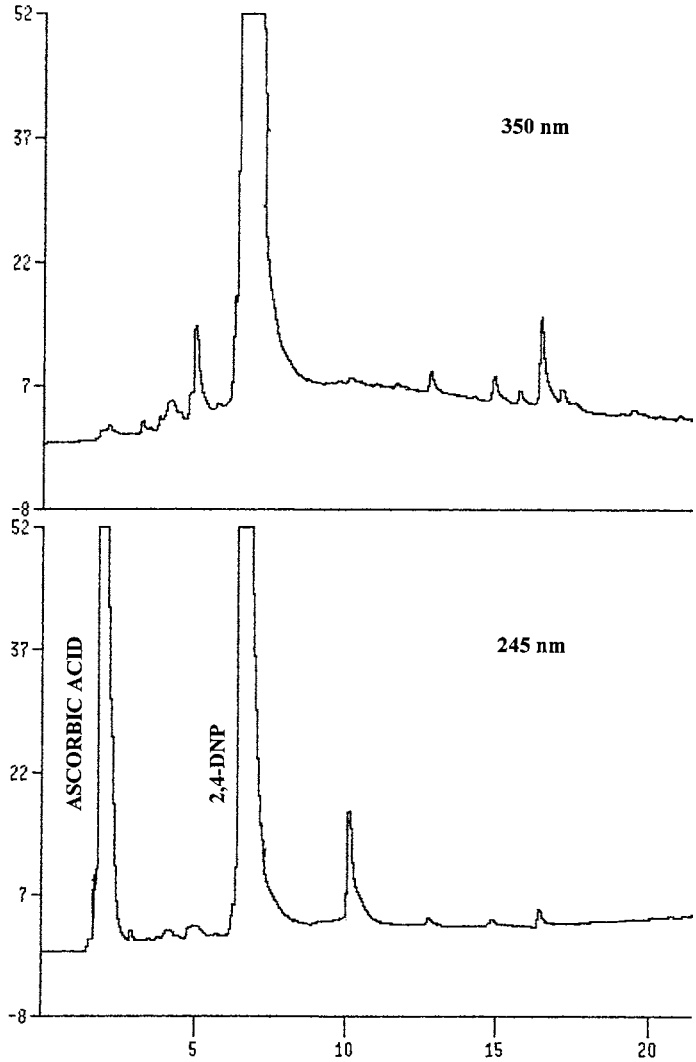

Fig. 4. Typical sample chromatogram after reaction with 2,4-DNP reagent at 50°C for 3 h.

cap. The vials were weighed and placed on storage at 60°C for 42 days. After removal from storage and equilibriation to room temperature the vials were connected to a manometer and the volume of gas produced on storage measured. A 100 μl aliquot of the head space above the samples was sampled using a gas syringe and chromatographed on a GS-Q, 30 m × 0.538 mm column at 30°C with a thermal conductivity detector at 200°C. After release of pressure the vials were re-weighed in order to determine the weight loss on storage. A calibration graph was constructed for carbon dioxide and found to be linear over the range 0.045–4.5 μmol.

3. Results and discussion

3.1. Carbonyl compounds

When reacted with the reagent made with orthophosphoric acid the L-ascorbic acid was found to be stable for up to 2 h at 37°C, Table 1.

The use of metaphosphoric acid instead of orthophosphoric acid and an alternative solvent, acetonitrile, was studied in order to increase the stability of the L-ascorbic acid during the derivatization procedure, Table 2.

Greatest stability was achieved using metaphosphoric acid mixtures and the reagent imparting greatest stability, the metaphosphoric acid (50%)/ethanol mixture, was adopted. The reaction time for conversion of DHAA to the osazone was found to be 180 min, the mean percentage conversion, $n = 4$, was plotted against time, Fig. 3.

After 180 min 99.5% conversion had occured and no increase was observed between 180 to 240 min.

Linearity was demonstrated by reacting aliquots of DHAA solution in 1% w/v aqueous metaphosphoric acid (0–0.2 mg ml^{-1}, equivalent to 0–10% w/w in the sample). The resulting calibration graph was linear with a correlation coefficient of 0.9992.

The limit of detection was determined at 0.01 mg ml^{-1}, equivalent to 0.05% w/w in a sample. After ≈ 100 injections the performance of the column was unchanged with respect to peak tailing and resolution.

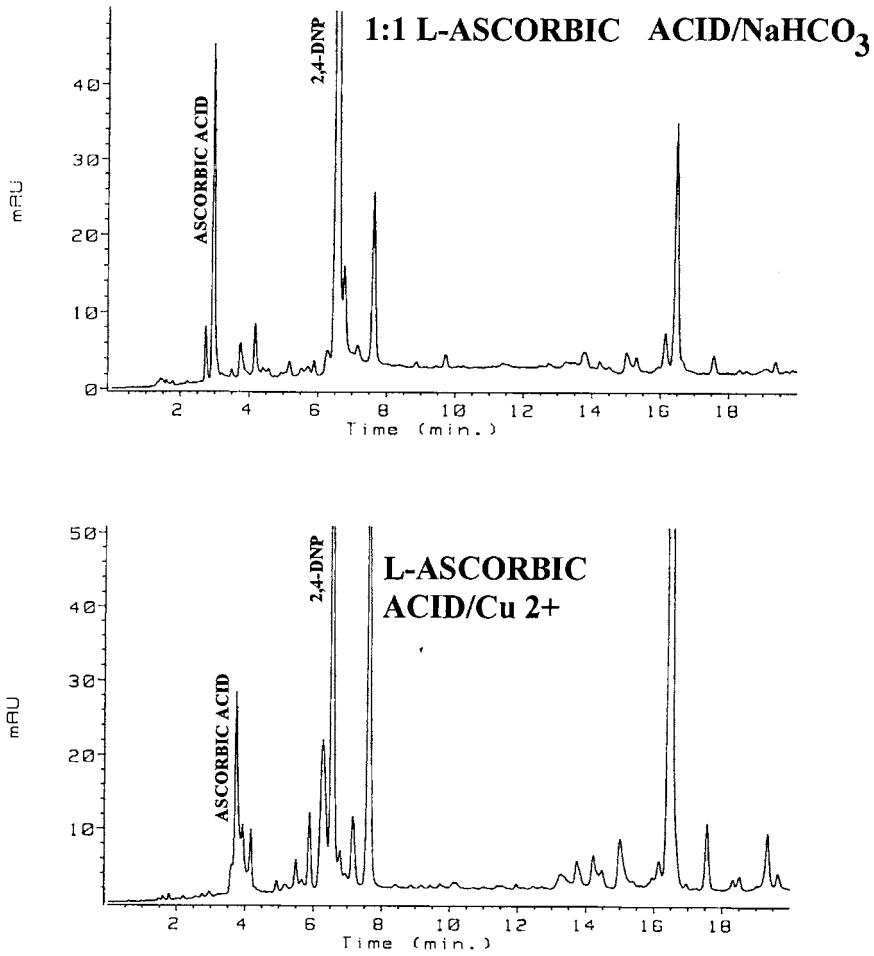

Fig. 5. Chromatogram at 350 nm of degraded L-ascorbic acid formulations reacted with 2,4-DNP at 50°C.

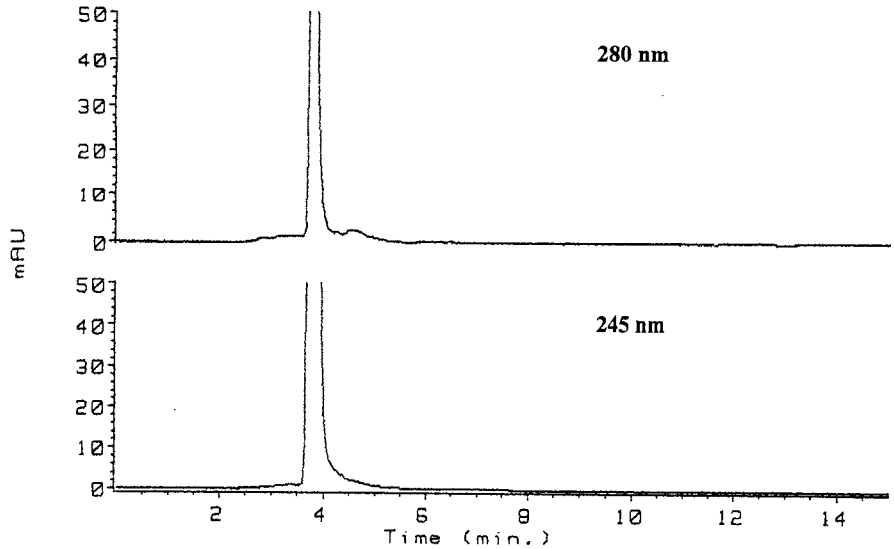

Fig. 6. Chromatogram of a visually degraded sample after storage at 60°C for 42 days. Chromatographed on a furan related compounds HPLC screen.

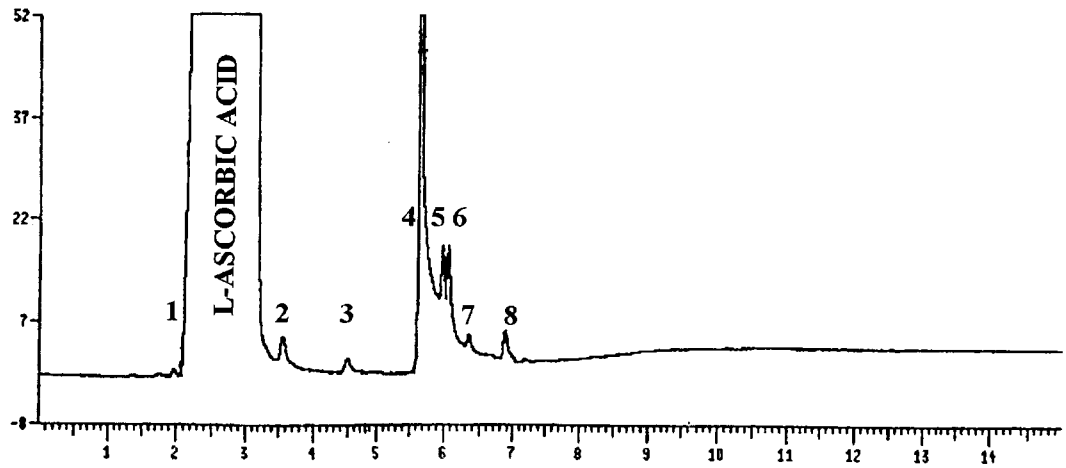

Fig. 7. Chromatogram of a visually degraded sample L-ascorbic acid with 5% v/w moisture stored at 60°C for 42 days.

3.2. Sample analysis

No extra peaks were observed in the chromatograms for any sample at all time points (0, 7, 14, 28 and 42 days). There was no evidence of any compounds being formed which would derivatize with 2,4-DNP for any sample. All the chromatograms were similar for all samples and conditions at all time points, Fig. 4. Peaks additional to L-ascorbic acid and 2,4-DNP are due to impurities in the 2,4-DNP reagent. The marked contrast between the chromatogram in Fig. 4 and that of L-ascorbic acid formulated with a molar equivalent of sodium hydrogen carbonate and also with 1000 ppm copper^{II} ions and exposed to high humidity and temperature (40°C/75% RH) for 28 days, see Fig. 5.

3.2.1. Furan related compounds

No additional peaks were observed in the chromatograms for any sample and any time point (0, 7, 14, 28 and 42 days). The first 15 min run time are expanded to illustrate the absence of any furan related compounds in a visually degraded sample, Fig. 6.

3.2.2. Coloured compounds

Eight different degradation products were detected in the most severely degraded samples, 42 days at 60°C, Fig. 7. The possibility that other degradation peaks may lie under the broad L-ascorbic acid peak was discounted after a 3-dimensional plot found no peaks coeluting that absorbed between 280 and 300 nm. A minor peak eluted prior to the main L-ascorbic acid peak and the other components within eight min run time. Samples that were visually only slightly discoloured exhibited the peak (4) eluting at 5.5 min and the two peaks eluting on its downslope (5, 6). This chromatographic system could be used as an early indicator of the onset of degradation.

The UV spectra of the first four peaks were similar with a λ_{max} of ≈ 275 nm and a shoulder at 350 nm and additional absorbance to 600 nm, Figs. 8 and 9.

The UV spectrum of peak 5 was similar to that of peaks 3 and 4. Peak 6 also exhibited a λ_{max} at 275 nm but was characterized by a secondary absorbance at 360 nm. Peak 7 had a λ_{max} at 300 nm and peak 8 at 360 nm with a secondary absorbance at 280 nm. In general the longer the peak retention time the longer the wavelength of the peak λ_{max}, presumably due to increasing conjugation.

The level of coloured degradants for the samples stored for 42 days at 50 and 60°C, expressed as a percentage of the total peak area, are given in Table 3. The effect of the presence of moisture upon the formation of the coloured degradation compounds can clearly be seen. There is an absence of all peaks in the sample with no moisture present and a steady increase in levels with increasing moisture content. The influence of temperature is also illustrated with the 5% moisture samples stored at 50 and 60°C. The total coloured impurities, expressed as a percentage of the total peak area, correlate closely with the HPLC assay results for L-ascorbic acid. A relative response factor of 5.47, with respect to L-ascorbic acid at 280 nm, was calculated for the coloured compounds using a known weight of the purified main coloured compound. This response factor was applied to all the eight peaks detected by this chromatographic screening. The coloured impurity peak levels, after multiplying by the relative response factor of 5.47, are presented alongside the HPLC assay values, Table 3.

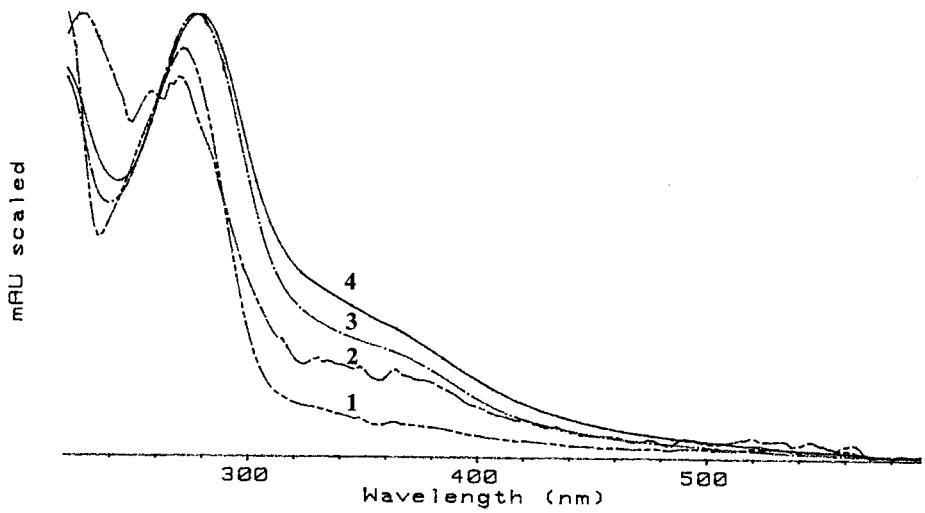

Fig. 8. UV spectra of coloured degradation products (peaks 1–4).

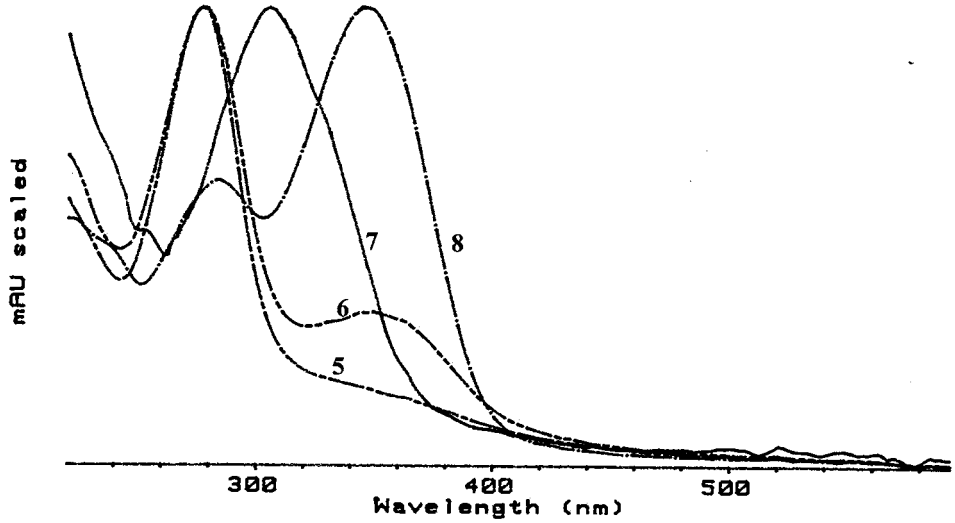

Fig. 9. UV spectra of coloured degradation products (peaks 5–8).

3.2.3. Evolution of gases/volatile compounds

There was an absence of volatile components in the samples when chromatographed on the HP Ultra 1 and Carbowax 20M columns with FID detection. Carbon dioxide was detected by GC with thermal conductivity detection. The volume of the gas evolved during degradation of the sample with 5% moisture stored at 60°C for 42 days was equivalent to 1 mole/mole starting material (L-ascorbic acid). The complex procedure to identify these degradation compounds is the subject of a following paper [33].

4. Conclusion

The solid state degradation of L-ascorbic acid under the influence of moisture produced discolouration of the samples. The samples failed to form derivatives with 2,4-DNP indicating the absence of carbonyl compounds although solid samples of L-ascorbic acid formulated with sodium hydrogen carbonate and copper ions stored similarly did produce carbonyl degradation products. Furans and furan related compounds were undetected using a HPLC screening procedure developed for the detection of these compounds. This is in contrast to heat degradaded solutions of L-ascorbic acid which degrade to furans which are detected on the HPLC screen.

Coloured compounds were detected using a water/2-propanol based reverse phase HPLC system and using this system early signs of degradation could be detected. The UV spectra of the compounds suggested they eluted in order of increasing conjugation. The shoulder in the UV spectrum at 350 nm and further absorbance down to 600 nm would also indicate that the compounds are highly conjugated systems.

Carbon dioxide was evolved during the degradation equivalent to a 1:1 molar ratio which may suggest the degradation products could be based around a five carbon ring compound.

This work demonstrates that degradation of L-ascorbic acid in the solid state is different to that in solution as furans were not detected or other volatile compounds produced. Carbon dioxide was evolved during the solid state degradation but may be in stoichiometrically different proportions to that produced when degraded in solution.

Table 3
Comparison of levels of coloured compounds and assay of L-ascorbic acid

Peak number (see Fig. 7)	Moisture (% v/w)/storage temperature					
	0% 50°C	1% 50°C	2% 50°C	5% 50°C	10% 50°C	5% 60°C
1			0.03	0.02		0.08
2			0.06	0.32	0.50	0.57
3						0.24
4		2.40	4.55	11.59	17.11	29.47
5		0.10	0.12	0.17	0.05	1.46
6		0.10	0.15	0.49	0.59	2.38
7				0.02	0.02	0.15
8				0.04	0.10	0.64
Total (%)		2.60	4.91	12.65	18.37	34.99
HPLC Assay % w/w, $n=4$	101.37	98.68	97.27	93.97	80.44	67.65

References

[1] A.B. Shephard, S.C. Nichols, A. Braithwaite, Talanta 48 (3) (1999) 585.
[2] S.H. Lee, T.P. Labuza, J. Food Sci. 40 (2) (1975) 370–373.
[3] B.M. Laing, D.L. Schlüter, T.P. Labuza, J. Food Sci. 43 (5) (1978) 1440–1443.
[4] E. De Ritter, L. Magid, M. Osadca, S.H. Rubin, J. Pharm. Sci. 59 (2) (1970) 229–232.
[5] S.A. Botha, J.L. Du Preez, A.P. Lötter, Drug Dev. Ind. Pharm. 12 (6) (1986) 811–827.
[6] R.B. Wortz, J. Pharm. Sci. 56 (9) (1967) 1169–1173.
[7] H. von Euler, H. Hasselquist, Arkiv Kemi 4 (1952) 169.
[8] P. Finholt, R.B. Paulssen, I. Alsos, T. Higuchi, J. Pharm. Sci. 54 (1) (1965) 124–128.
[9] J.H. Tatum, P.E. Shaw, R.E. Berry, J. Agr. Food Chem. 17 (1969) 38–40.
[10] I.M. Coggiola, Nature 200 (1963) 954–955.
[11] L. Löwendahl, G. Petersson, Anal. Biochem. 72 (1976) 623–628.
[12] K. Niemelä, J. Chromatogr. 399 (1987) 235–243.
[13] J.C. Deutsch, C.R. Santhosh-Kumar, K.L. Hassell, J.F. Kolhouse, Anal. Chem. 66 (3) (1994) 345–350.
[14] R.H Brandenberger, H. Brandenberger, in: K. Blau, G. King (Eds.), Handbook of Derivatives for Chromatography, Heydon, London, 1985, p. 248.
[15] E. Grosjean, D. Grosjean, Int. J. Environ. Anal. Chem. 61 (1) (1996) 47.
[16] K.I. Nakamura, M. Asami, S. Orita, K. Kawada, J. Chromatogr. 168 (1979) 221–225.
[17] G. Vigh, Z. Varga-Puchony, J. Hlavay, M. Petro-Turecza, I. Szarfold-Szalma, J. Chromatogr. 193 (1980) 432–435.
[18] B.S. Buslig, J. Chromatogr. 247 (1982) 193–195.
[19] P.R. Demko, J. Chromatogr. 179 (1979) 361–365.
[20] B. Reindl, H.J. Stan, J. Chromatogr. 235 (1982) 481–483.
[21] S. Selim, J. Chromatogr. 136 (1977) 271–275.
[22] G.A. Byrne, J. Chromatogr. 20 (1965) 528–532.
[23] J.M. Brummer, T.J. Muller-Penning, J. Chromatogr. 27 (1967) 290.
[24] E. Denti, M.P. Luboz, J. Chromatogr. 18 (1965) 325–330.
[25] A. Jart, A.J. Bigler, J. Chromatogr. 23 (1966) 261–263.
[26] L.J. Papa, L.P. Turner, J. Chromatogr. Sci. 10 (1972) 747–750.
[27] Y. Hoshika, Y. Jakata, J. Chromatogr. 120 (1976) 379–382.
[28] B.C. Hemming, C.J. Gubler, Anal. Chem. 92 (1979) 31–35.
[29] H. Terada, T. Hayashi, S. Kawai, T. Ohno, J. Chromatogr. 130 (1977) 281–283.
[30] Vogel's Textbook of Practical Organic Chemistry, 5th ed., Longman Scientific and Technical, 1966, p 1257.
[31] R. Strobecker, H.M. Henning, Vitamin Assay,Verlag Chemie, GMBH, Weinheim/Bergstr, 1966, p. 242–247.
[32] A. Fujita, D. Iwatake, Biochem. Z. 277 (1935) 293.
[33] A.B. Shephard, S.C. Nichols, A. Braithwaite, Talanta 48 (3) (1999) 607.

ELSEVIER

Talanta 48 (1999) 607–622

Talanta

Moisture induced solid phase degradation of L-ascorbic acid part 3, structural characterisation of the degradation products

Anthony B. Shephard [a], Steven C. Nichols [b], Alan Braithwaite [a,*]

[a] *Department of Chemistry and Physics, Nottingham Trent University, Clifton Lane, Nottingham NG11 8NS, UK*
[b] *Rhône-Poulenc Rorer, Respiratory Technology, London Road, Holmes Chapel CW4 8BE, UK*

Received 3 March 1997; received in revised form 11 September 1997; accepted 2 September 1998

Abstract

The influence of moisture on the solid phase degradation of L-ascorbic acid and the chemical characteristics of the degradation products have been investigated previously [Shephard et al. (1998) (in press)]. Moisture induced degradation in the solid phase leads to severe discolouration. This paper describes the isolation of the compounds responsible for the discolouration and their partial chemical identification. Eight different degradation compounds were found to be present in a severely discoloured sample [Shepherd et al. (1998) (in press)]. Three of the compounds were present at levels above 1% of the total chromatography peak area with the major degradation peak present at 29% in a sample with 5% v/w moisture present when stored at 60°C for 42 days. The major impurity was isolated and was found to exhibit a λ_{max} at 280 nm with further absorbance to 600 nm. This material was pyrolysed at 300, 500, and 600°C. Amongst the volatile pyrolysates tentatively identified were furfural, 2-furancarboxylic acid, 1-(2-furanyl)-ethanone, tetrahydrofuran and 1-(2-furanyl)-1-propanone along with some aromatic compounds such as benzene and phenol. The periodate consumption of the major impurity was examined and the products of the reaction investigated. Estimation of hydroxyl and carbonyl group content by acetyl group determination of the acetate and reduced acetate showed that for every five repeating units there was one hydroxyl group and for every four repeating units there was one carbonyl group. Elemental analysis gave 46.26% carbon, 5.42% hydrogen and 48.32% oxygen giving an empirical formula of CH_2O.

Keywords: Ascorbic acid; Solid phase; Degradation; Pyrolysis

1. Introduction

L-Ascorbic acid degrades in the solid phase under the influence of moisture [1–4]. De Ritter and co-workers studied the effect of silica gel on the stability of L-ascorbic acid [5]. They found that the loss of L-ascorbic acid was directly proportional to the amount of unbound moisture. The degradation is believed to follow a different pathway to that in solution and manifests itself as a discolouration from white to a dark brown

* Corresponding author. Tel.: +44-115-9418418; fax: +44-115-9486636; e-mail: alan.braithwaite@ntu.ac.uk.

0039-9140/99/$ - see front matter
PII: S0039-9140(98)00278-1

colour. The degree of discolouration being directly dependent upon the amount of moisture present [1]. The appearance of this discolouration occurs before any noticeable decrease in purity as measured by chemical or chromatographic means. A chromatographic method was developed to detect both the early stages of solid state degradation, as shown by a light brown discolouration, and for gross degradation as shown by an extremely dark brown discolouration. The isolation of ten furan type compounds, two lactones, three acids and 3-hydroxy-2-pyrone was reported by Tatum, Shaw and Berry [6] when L-ascorbic acid was heated in aqueous solution. Coggiola [7] found 2,5-dihydro-2-furoic acid to be a product of the anaerobic degradation of L-ascorbic acid in aqueous solution at 100°C.

The solid phase degradation of L-ascorbic acid under the influence of moisture has been reported [1,2]. The degradation was monitored by quantitative HPLC for the remaining L-ascorbic acid and also by tristimulus colourimetry for change in colour. No evidence was found for the presence of carbonyl compounds or furan related compounds. Carbon dioxide was evolved during the degradation with the evolution of 1 mol per mol L-ascorbic acid. A reverse phase HPLC screening procedure resolved up to eight different compounds that could be responsible for the discolouration of degraded samples. The major degradation compound resolved by the screening was present at 29% w/w. This degradation product was isolated and chemical and elemental analyses were performed.

Periodate consumption was measured in order to determine the ease at which the degradation product is oxidised and to estimate the number of hydroxyl groups present per moiety. The hydroxyl group content was estimated, first by acetylating the free hydroxy groups and then determining the acetate content by the Kuhn–Roth method. This method involves refluxing the acetate with chromic acid followed by distillation of the free acetic acid. Titration of the acid with dilute aqueous sodium hydroxide solution using phenolphthalein indicator enables the acetate content to be calculated. The carbonyl content was similarly determined after first reducing the carbonyl groups to hydroxyl, the difference between the two values is a measure of the carbonyl content. Pyrolysis at 300, 500, and 600°C followed by gas chromatography of the pyrolysates was used to gain an insight into the backbone structure of the compound.

This paper describes the isolation of the degradation products responsible for the discolouration and their chemical characterisation. Possible structures and a degradation pathway is proposed.

2. Experimental

2.1. Isolation of coloured degradation compound

The preparation of solid state degraded samples of L-ascorbic acid has previously been described [1]. The sample exhibiting the most extensive degradation, that with 5% v/w moisture stored at 60°C for 42 days, was chosen for the isolation of the major coloured degradation compound. Undegraded L-ascorbic acid was extracted from the coloured product by repeated washing with water. The aqueous extract was chromatographed to confirm the absence of L-ascorbic acid. The coloured product was dried under vacuum overnight at 50°C. Yield was 1.7 g from 10.0 g starting material.

2.2. Analysis

The isolated coloured compound was subjected to the following analyses:

1. periodate consumption;
2. estimation of hydroxyl and carbonyl group content;
3. pyrolysis at 300, 500, and 600°C;

Table 1
Hydroxyl and carbonyl content of degradation product

Sample	Acetyl, % w/w	Hydroxyl unit^{-1}	Carbonyl unit^{-1}
Reduced	25.48	0.43	0.24
Unreduced	10.99	0.19	–

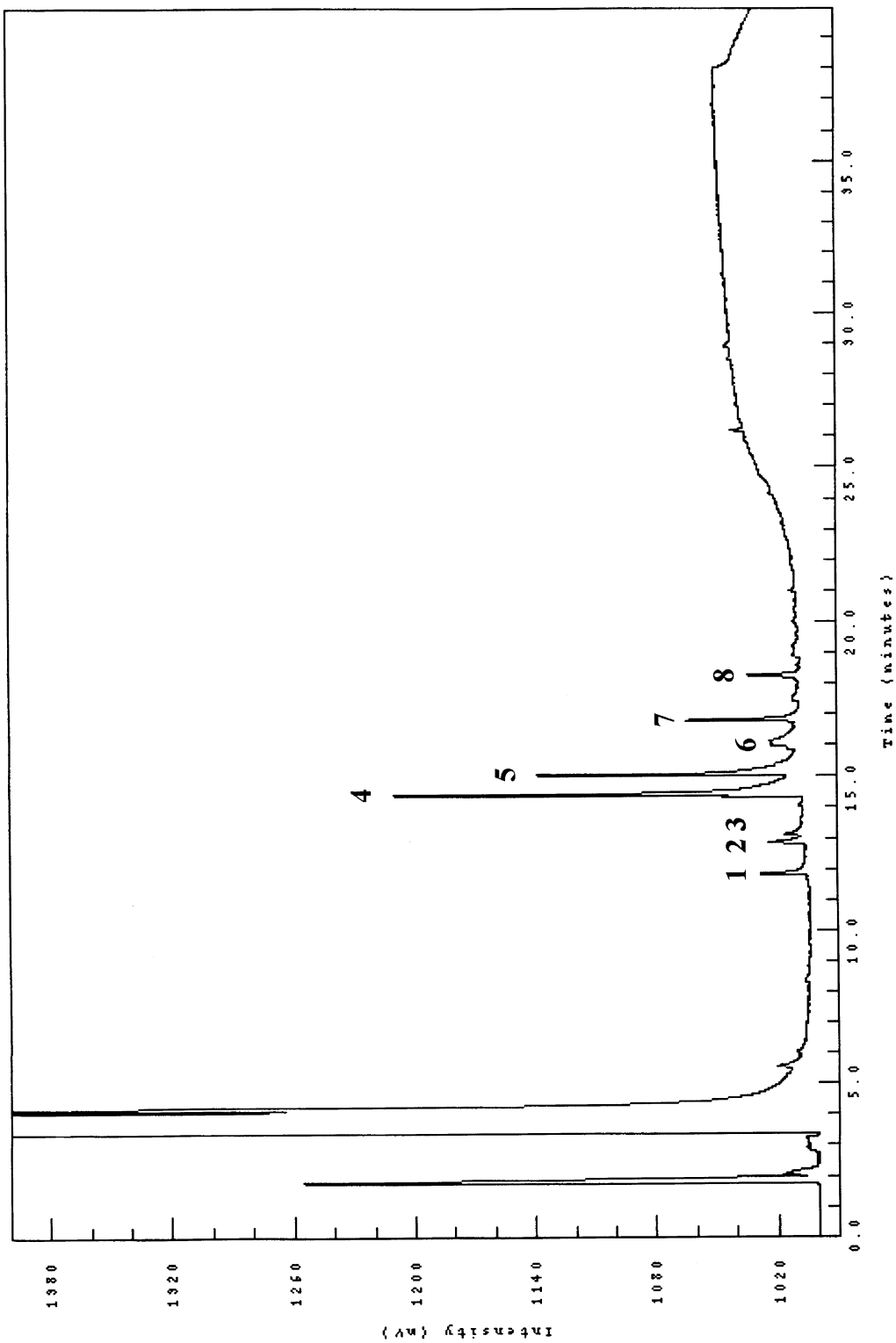

Fig. 1. Chromatogram of pyrolysate in dry trap.

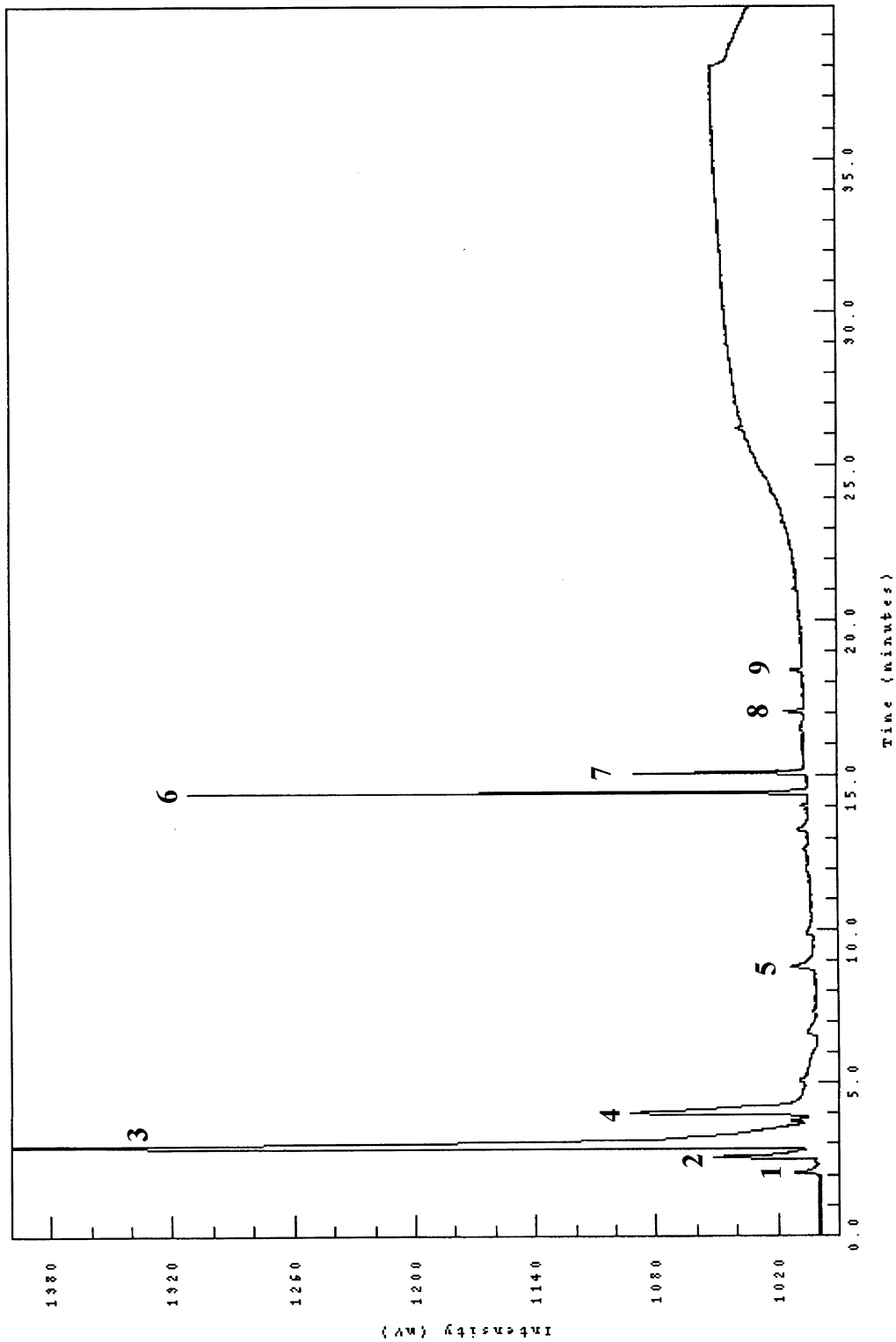

Fig. 2. Chromatogram of pyrolysate in water trap.

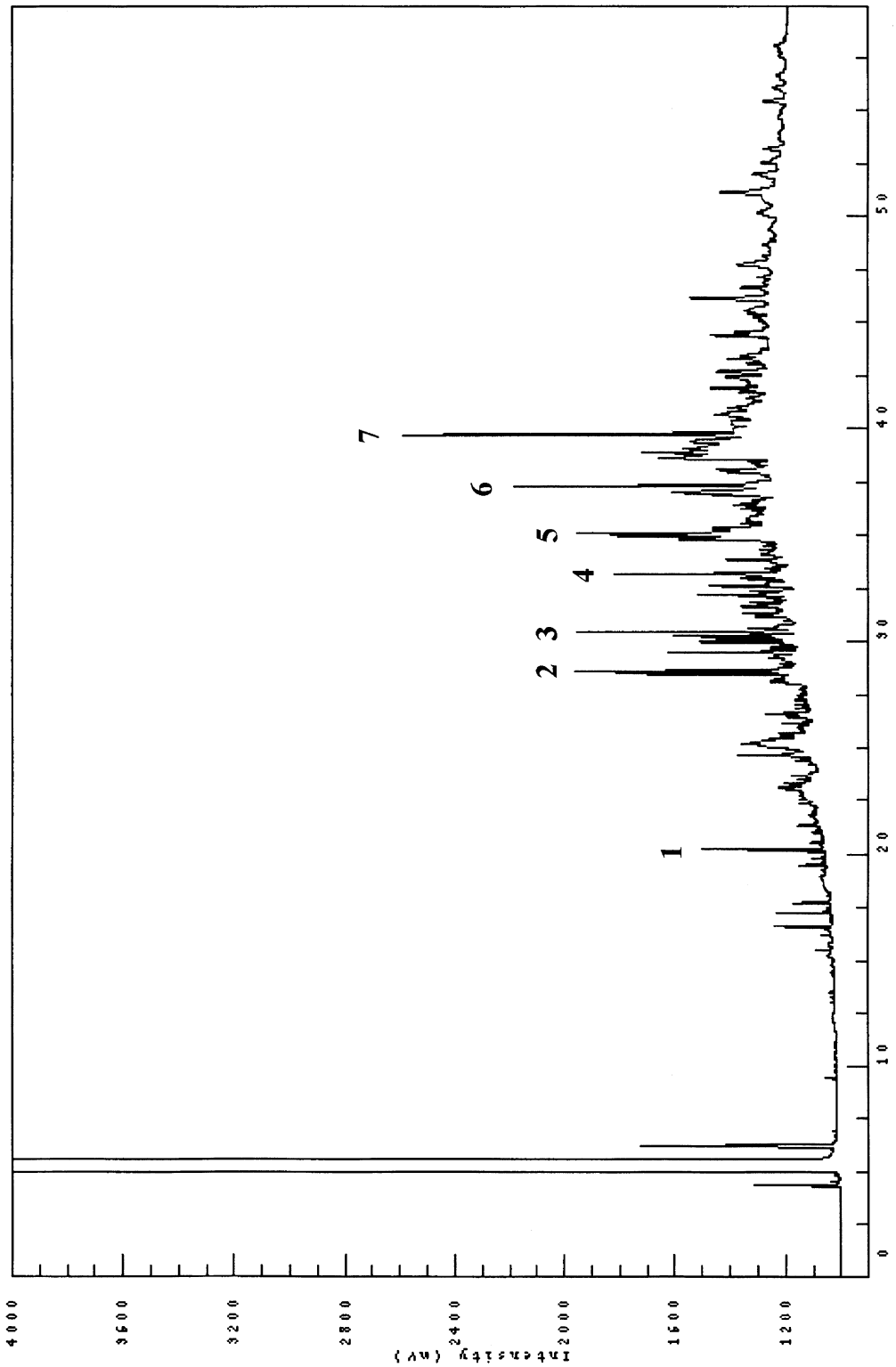

Fig. 3. Chromatogram of condensate from pyrolysis.

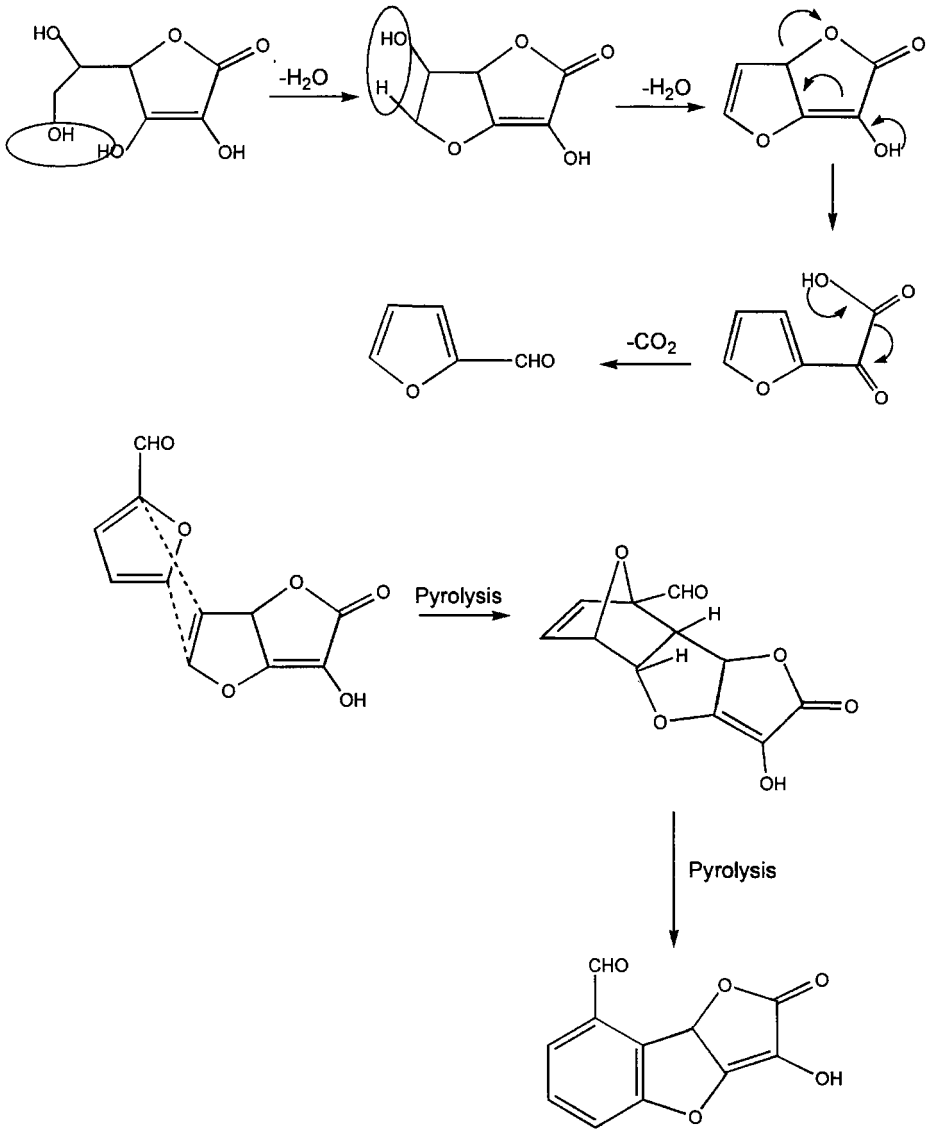

Fig. 4. Possible reaction scheme for formation of six membered aromatic rings.

4. further methods of analysis, e.g. IR, NMR and DSC.

2.3. Reagents

Sodium periodate
Sodium arsenite
Dichloromethane
2-Propanol
Ethanol
Deionised water
Chloroform
Chromic acid, saturated solution
Sodium hydroxide solution, aqueous, 0.01 and 0.02 M
Acetic anhydride
Pyridine
Sodium borohydride
Formaldehyde
Formic acid

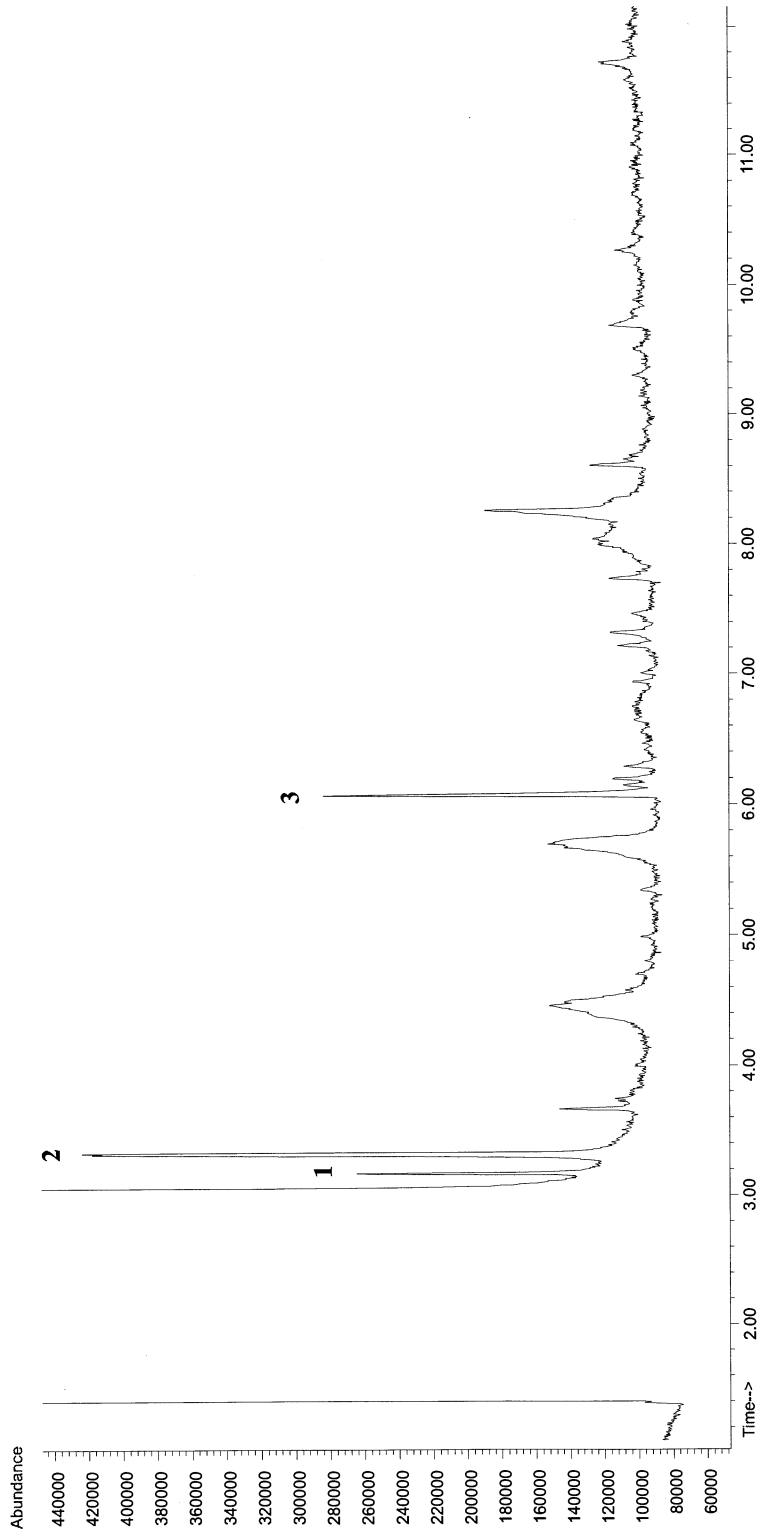

Fig. 5. Chromatogram after pyrolysis at 600°C, water trap.

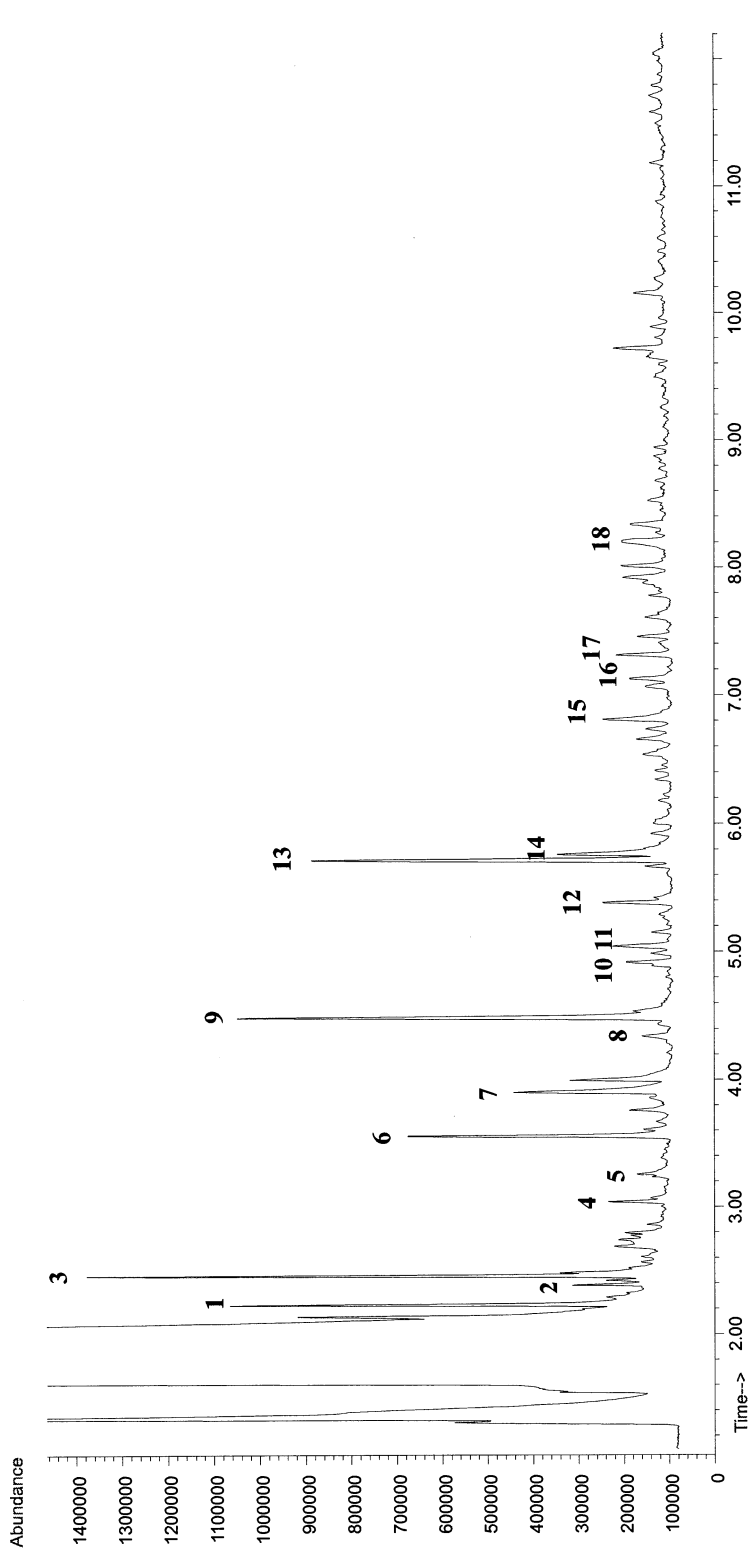

Fig. 6. Chromatogram after pyrolysis at 600°C, dichloromethane trap.

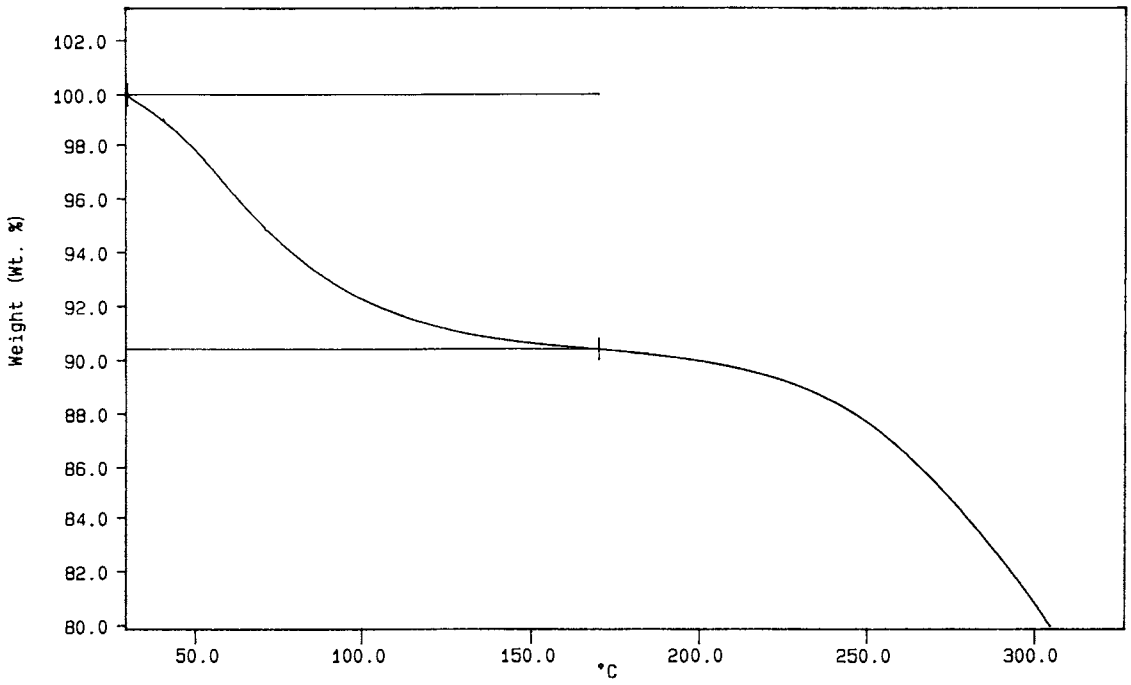

Fig. 7. TGA thermogram of coloured degradation product.

All reagents were of analytical grade and purchased from Fisher Scientific UK, Loughborough.

2.4. Equipment

Perkin Elmer DSC7 differential scanning calorimeter.
Shimadzu GC-17A with AOC-1400 autosampler and AOC-17 autoinjector fitted with a Carbowax 20M WCOT (25 m × 0.22 mm, 0.15 μm film) or HP1 WCOT (30 m × 0.53 mm × 0.365 μm film) for analysis of products after pyrolysis at 300 and 500°C.
Hewlett Packard HP 6890 with HP 5973 MSD fitted with a HP 5MS WCOT (30 m × 0.25 mm × 0.25 μm film) for analysis of products after pyrolysis at 600°C.
Carlo Erba CHNS-O EA 1108 Elemental Analyser.
Perkin Elmer FT-IR, model PE System 2000 FTIR.
Metrohm 684 KF Coulometer Karl Fischer instrument.
Bruker AMX 500 NMR spectrometer.
Pyrola-9 pyrolyser.

2.5. Periodate consumption

The sample (35 mg) was accurately weighed into a 200 ml volumetric flask and suspended in ethanol (80 ml). Water (80 ml) was added and the mixture left to stand at room temperature overnight. An aqueous solution of sodium periodate (0.5 M, 40 ml) was added and the volume adjusted with ethanol to 200 ml. A blank reaction was performed omitting the sample. The periodate content was determined initially and at intervals for up to 7 days titrating a 10 ml aliquot against sodium arsenite solution (0.05 M). Any free acid liberated was determined by titrating a 20 ml aliquot against 0.01 M NaOH with phenolphthalein as indicator. An aliquot of sample and blank solution was chromatographed by GC and formaldehyde and formic acid levels determined.

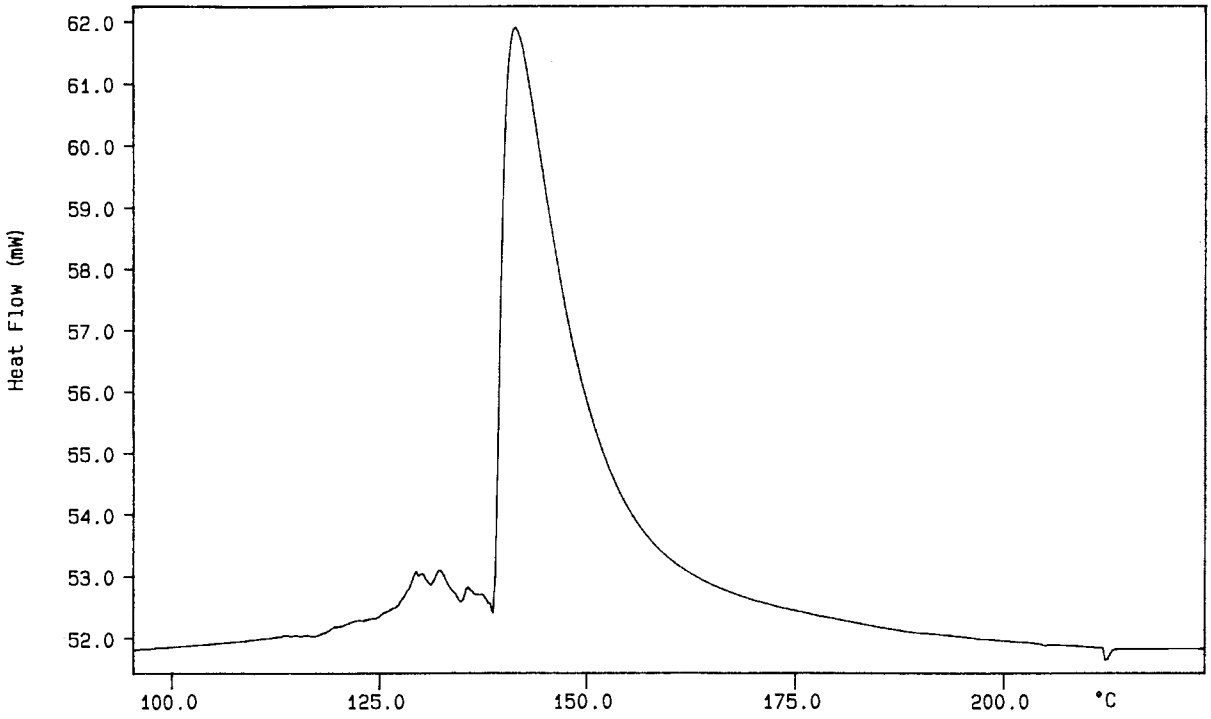

Fig. 8. DSC thermogram of coloured degradation product.

2.6. Estimation of hydroxyl and carbonyl group content

The hydroxyl group content was evaluated by acetylating the sample then determining the acetyl group of the acetate product by the Kuhn–Roth method. The sample (50 mg) was dissolved in an equimolar mixture of acetic anhydride in pyridine (6 ml) and reacted for 30 days at 25°C. The reaction was quenched by the addition of water (200 ml) and extracted with chloroform (3×15 ml). The chloroform extract was washed with water (3×20 ml) and dried over anhydrous sodium sulfate. Evaporation yielded the acetate which was quantified using the Kuhn–Roth method.

The carbonyl group content was determined by the same method but first reducing any carbonyl group present by hydrogenation. The sample (50 mg) was dissolved in 50% aqueous ethanol (30 ml) and the solution adjusted to pH 8–9 by the addition of pyridine (3 ml). Sodium borohydride was added (200 mg) and the mixture reacted for 18 h at room temperature. The mixture was evaporated to dryness and the residue suspended in water, separated by centrifugation and dried. Acetylation of the reduced compound was carried out as per the estimation of the hydroxyl group. The difference between acetyl groups before and after reduction correspond to the number of carbonyl groups present.

2.7. Pyrolysis at 300, 500 and 600°C

A 200 mg sample was pyrolysed at 300 and 500°C for 30 min under a stream of nitrogen using a Perkin Elmer DSC7 differential calorimeter. Any volatile compounds evolved were trapped in a series of three traps; an empty tube cooled in dry ice/2-propanol followed by a cold water trap (2 ml) and finally an ice cold dichloromethane trap (2 ml). The weight loss at each temperature was recorded. After pyrolysis the volume of water condensed in the empty tube was measured and

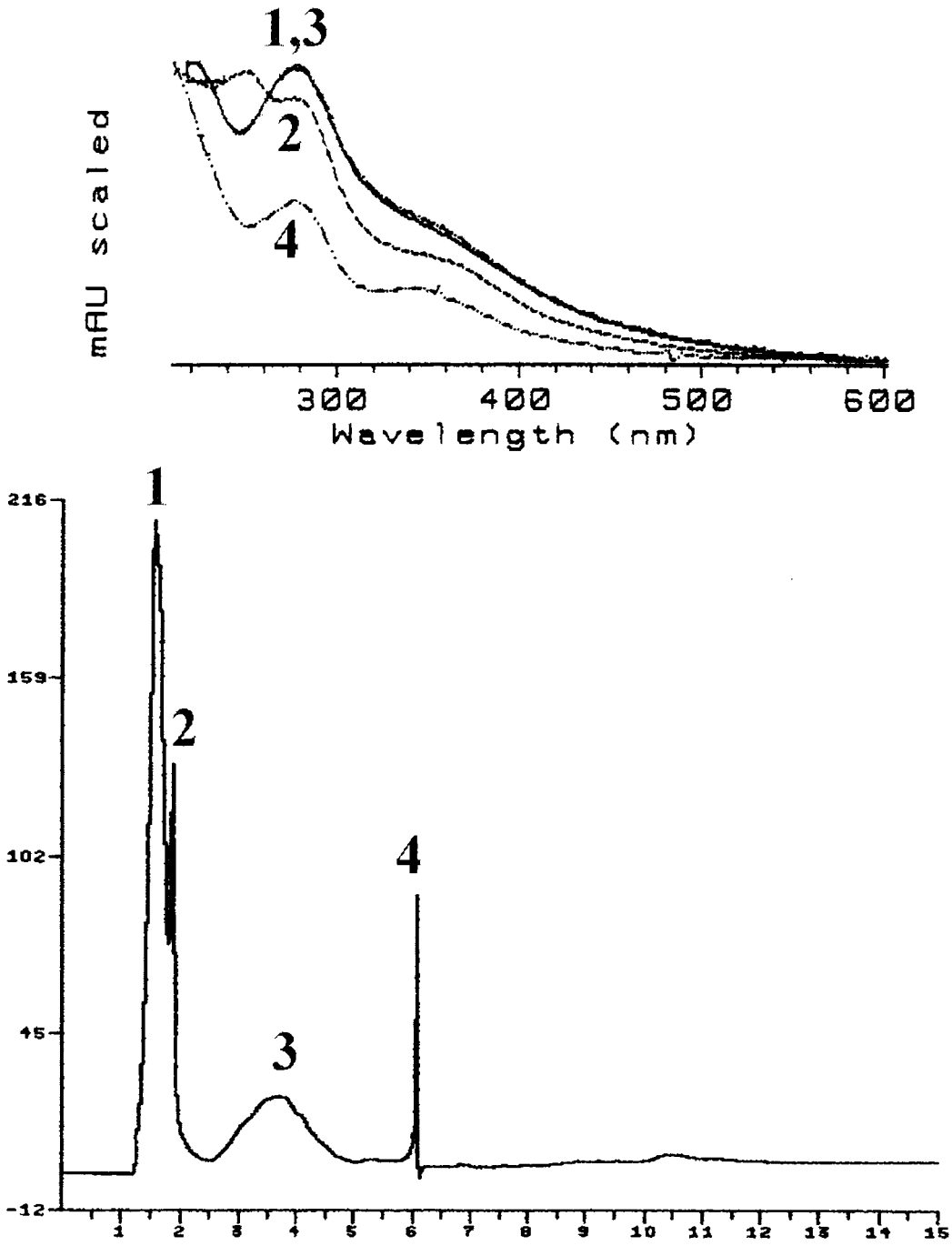

Fig. 9. Chromatogram of coloured degradation product after base hydrolysis.

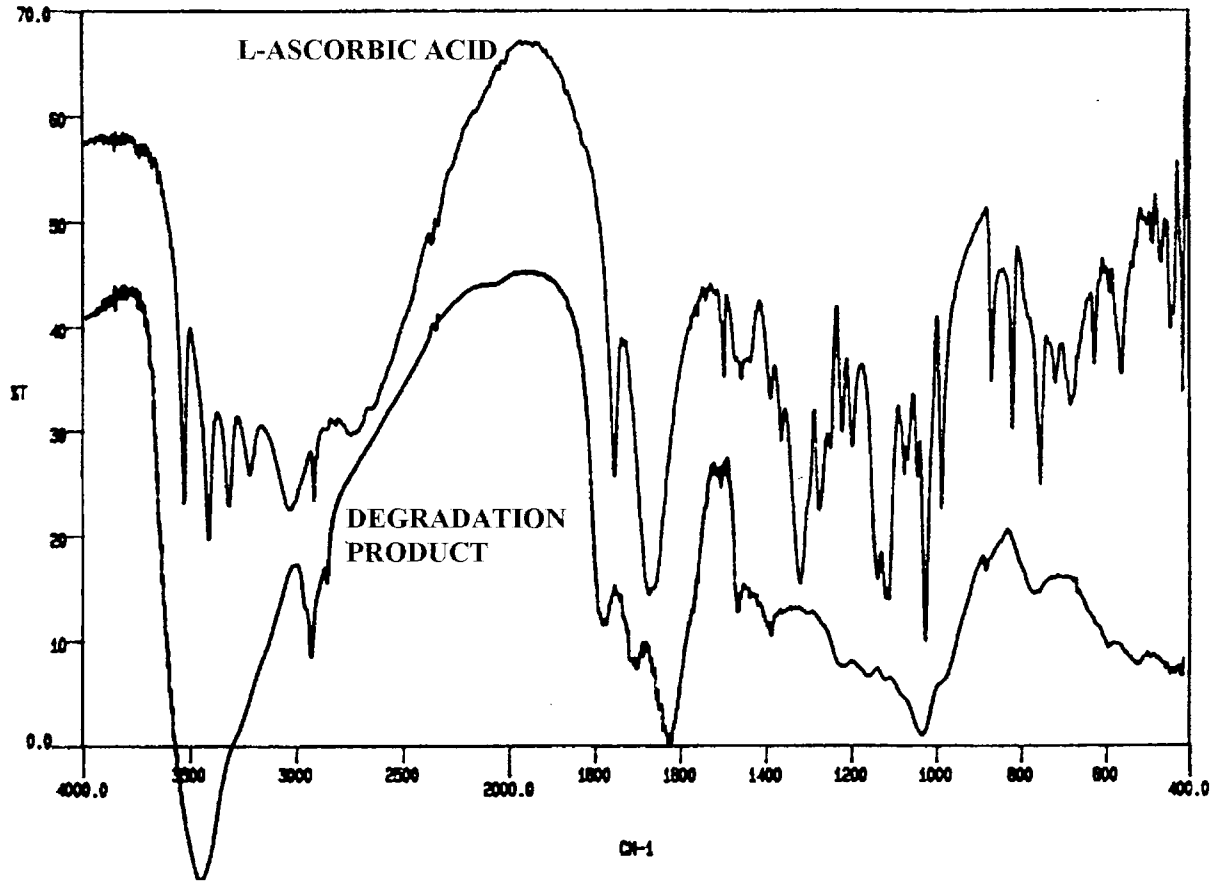

Fig. 10. Infra-red spectra of L-ascorbic acid and it's coloured degradation product.

the volume adjusted to 2 ml with water before chromatography. Chromatography of the pyrolysates was achieved on a Carbowax 20M WCOT column with a temperature ramp from 50 to 250°C at 10°C min^{-1}, helium carrier gas at 0.7 ml min^{-1}, injector/detector at 250°C.

Pyrolysis at 600°C was carried out on 10 mg samples using a Pyrola-9 pyrolyzer heating from 150 to 600°C in 2 s in a helium gas flow at 40 ml min^{-1}. Any volatile pyrolysates were trapped directly in either 1 ml water or 1 ml dichloromethane.

2.8. Further methods of analysis

1. Determination of the carbon, hydrogen and oxygen content using a Carlo Erba elemental analyser.
2. Measurement of pH of a 1% w/v suspension in carbon dioxide free water.
3. Thermal analysis including TGA in order to determine the type of weight loss and DSC to monitor for any transitions occurring during heating.
4. Acid and base hydrolysis followed by HPLC analysis using the chromatographic screening procedure described in [2].
5. Infra-red spectrum obtained as a KBr disk.
6. Moisture determination using a coulometric Karl Fischer instrument.
7. Attempts were made to obtain ^{1}H and ^{13}C nuclear magnetic resonance spectra in both DMSO and NaOD (solvents in which the solid was most soluble).

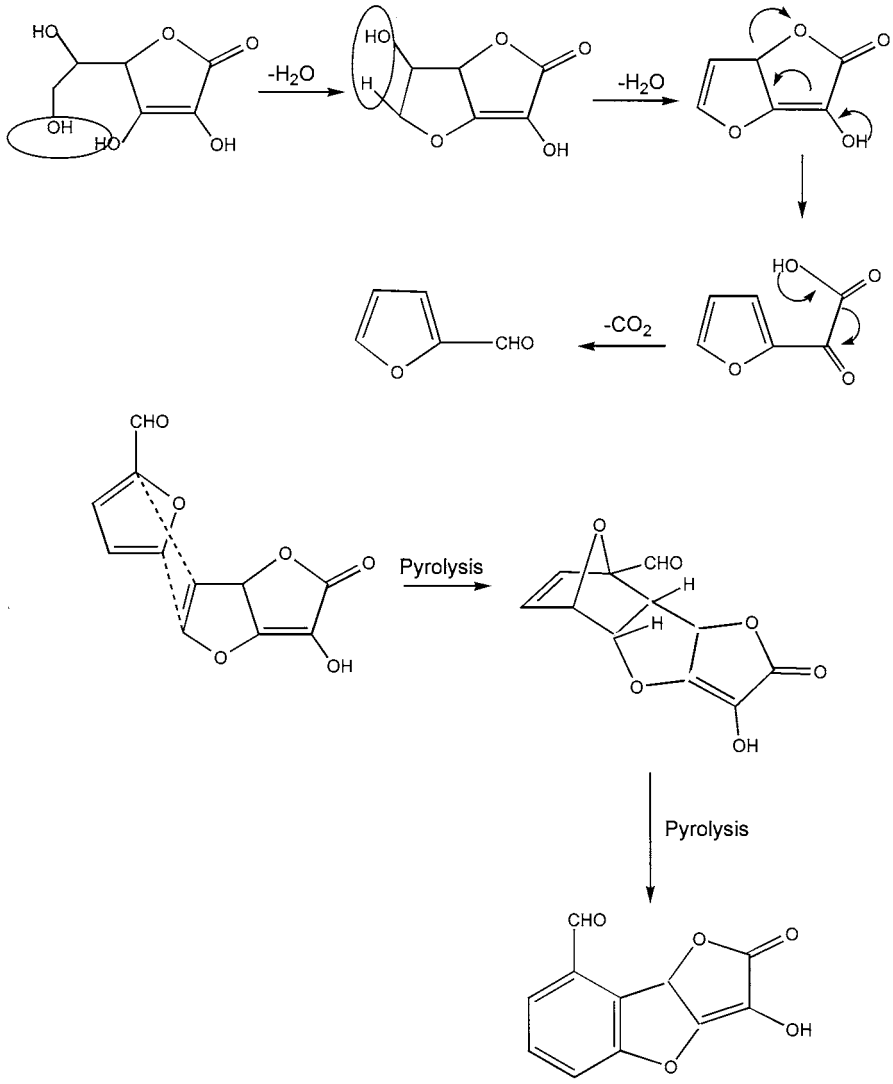

Fig. 11. Possible Diels–Alder product of L-ascorbic acid and 2,3-diketogulonic acid.

3. Results

3.1. Periodate consumption

Periodate consumption was observed to increase slowly for 22 h followed by a rapid accelleratory period then a gradual uptake to 166 h, periodate consumption was still occurring beyond 166 h. The initial slow consumption was possibly caused by the slow dissolution followed by reaction of the material as the initial suspension slowly dissolved followed by rapid oxidation of the dissolved material. Titration against 0.01 M NaOH solution consumed 2.0 ml more than a blank reaction solution. Gas chromatography failed to detect any formaldehyde or formic acid in the sample solution. The absence of these compounds suggests that any alcohol groups present are not on adjacent carbon atoms or primary alcohols.

3.2. Estimation of hydroxyl and carbonyl group content

Carbonyl group content was calculated assuming complete conversion of any carbonyl groups to hydroxyl groups, Table 1.

3.3. Pyrolysis at 300, 500 and 600°C

The weight loss was 30.34% w/w at 300°C and almost doubled to 59.02% w/w at 500°C, 200 μl of water condensed in the first dry condensing trap at 300°C and 100 μl at 500°C. GC of the pyrolysates at both temperatures were very similar with a higher concentration of components found in the 500°C traps. The dry trap gave eight peaks due to the condensate eluting between 12.0 and 19.0 min, Fig. 1. The two major peaks (peaks 4 and 5) had retention times of 14.4 and 15.1 min, respectively. In total the water trap condensate contained nine components of which two were major analytes (peaks 3 and 6) eluting at 2.9 and 14.4 min, Fig. 2. The dichloromethane trap contained no additional peaks to those present in a blank injection of dichloromethane solvent. Much more volatile material condensed on the inside of the DSC pan heater. This condensate was dissolved in a mixture of 1:1 methanol/dichloromethane (2 ml). Chromatography showed seven major higher boiling components not present in the three pyrolysate traps, Fig. 3, none of which could be identified.

GC-MS (EI) of the main peaks in the dry trap (Fig. 1) identified peak 1 as 2-furancarboxylic acid; peak 4 as 1,1′-(1-methyl-1,2-ethenediyl)bis-benzene; peak 5 as 2-phenyl-2,3-dihydroindene; and peak 8 as 1-methyl-2-(2-phenylethenyl) benzene. Other peaks were not identified. The first three peaks in the water trap (Fig. 2) were due to the solvent; peak 4 was identified as 2,3-dimethylbutane; peak 5 as 3-methylpentane; peak 6 as 1-(2-furanyl)-ethanone; peak 7 as 2-furancarboxaldehyde;and peak 8 as 1-(2-furanyl)-1-propanone.

The presence of furan related compounds in the pyrolysates can be accounted for by dehydration and decarboxylation giving rise to 2-furancarboxaldehyde [8]. Once formed the 2-furancarboxaldehyde could react as a conjugated diene and undergo a Diels–Alder reaction involving the 1,4-addition of an unsaturated furan (dienophile) to a conjugated diene. This reaction between two furan compounds would form an oxo-bridged six membered ring, which upon pyrolysis would eliminate water to produce a benzene ring, Fig. 4.

GC-MS (EI) of the products of pyrolysis at 600°C identified many furan related and aromatic compounds in both the water and dichloromethane traps, Figs. 5 and 6. Three peaks were identified in the water trap as formic and acetic acids and 2(5)-furanone, peaks 1–3, respectively. In the dichloromethane trap 18 compounds were identified as follows : (1) tetrahydrofuran; (2) *cis*-2-butenal; (3) benzene; (4) vinylfuran; (5) 2,3-dihydro-3-methyl-3-furan; (6) toluene; (7) cyclobutanol; (8) 3-penten-2-ol; (9) furfural; (10) ethylbenzene; (11) *p*-xylene; (12) styrene; (13) 2-acetylfuran; (14) 2(5)-furanone; (15) phenol; (16) benzofuran; (17) 1-(2-furanyl)-1-propanone; (18) ethylfuroate.

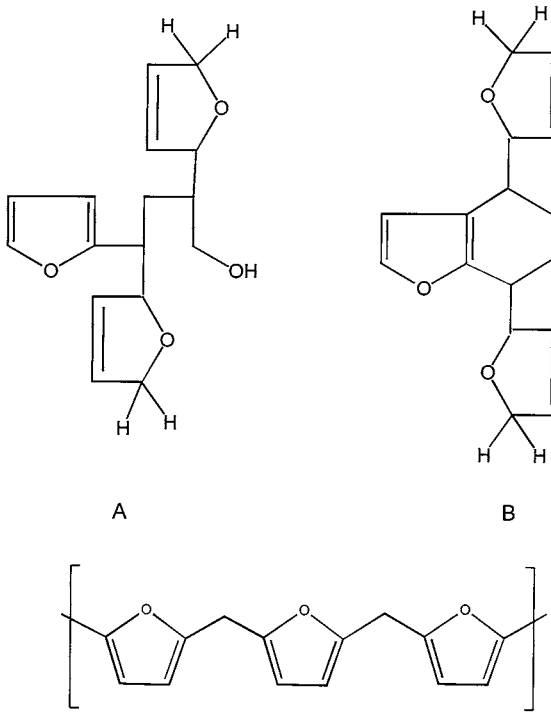

Fig. 12. Possible furan polymeric units.

3.4. Further analysis of the main coloured degradation product

Elemental analysis of the isolated main coloured degradation product gave 46.26% carbon, 5.42% hydrogen and 48.32% oxygen (by difference to 100%), empirical formula CH_2O. Moisture was determined at 2.61% w/w.

The pH of a 1% w/v aqueous suspension was found to be 2.78, identical to that for L-ascorbic acid.

^1H and ^{13}C NMR were inconclusive due to lack of signal, presumably due to the poor solubility in the solvents. ^1H NMR in dimethylsulfoxide gave very weak quartets at 6.7 and 8.0 ppm which could be due to a heterocyclic aromatic ring.

Thermal analysis by TGA showed a steady loss between 30 and 150°C with a plateau to 200°C (total loss 9.60%) followed by a rapid loss, presumably due to decarboxylation, Fig. 7.

DSC analysis gave one major endotherm at 137.9–195.8°C with a maximum at 141.5°C, $\Delta H = 135.41$ J g^{-1}. Small endothermic events were observed prior to the major endotherm between 121.4 and 136.4°C with a maximum at 129.5°C, $\Delta H = 3.60$ J g^{-1}, Fig. 8.

When dissolved in 0.2M NaOH solution and chromatographed, four peaks eluted which were poorly resolved. All peaks had similar spectra (λ_{max} at 280 nm with a shoulder at 340 nm), Fig. 9. Two were major peaks with 53.0 and 37.3% of the total area and the other two were minor peaks (7.1 and 2.6%). After isolating these components by semi-preparative HPLC and re-chromatographing, using the same HPLC system as above, each individual component eluted at the same retention time indicating that inter-conversion to the same compound may have taken place.

The infra-red spectrum, Fig. 10, shows a strong broad band at 3428 cm^{-1} which may be due to O–H stretch. Noticeably absent are the four bands between 3220 and 3525 cm^{-1} which are present in L-ascorbic acid and caused by the high frequency hydrogen bonded O–H stretching bands on C-5 and C-6. A sharper band at 2924 cm^{-1} is assigned to C–H stretch of alkyl groups. The region between 1800 and 1600 cm^{-1} is different from that in L-ascorbic acid with the strong absorption at 1754 cm^{-1} in L-ascorbic acid attributed to C=O stretching of the lactone ring now conjugated with C=C stretching vibration. The fingerprint region in the coloured degradation product is ill defined compared to L-ascorbic acid. The absence of detail may be attributed to loss of the hydroxy group on C-2 of L-ascorbic acid which gives rise to the strong, sharp band at 1320 cm^{-1} and 1275 cm^{-1} and the absence of a strong band at 1140 cm^{-1} may be due to loss of C-5 O stretch.

No dehydroascorbic acid was found during the solid phase degradation of L-ascorbic acid [2]. Due to the chemical instability of dehydroascorbic acid it may have been formed and immediately ring opened to give 2,3-diketogulonic acid (2,3-DKGA) which then reacted as a diene with L-ascorbic acid, Fig. 11. This would account for the apparent absence of dehydroascorbic acid.

4. Conclusion

From the chemical and spectral information obtained from this work it is suggested that the coloured degradation product is possibly polymeric and the structure made up of units of polymeric furan related compounds, Fig. 12, polymerised with the Diels–Alder product in Fig. 11. Structures A and B arise from electrophilic attack at α and β positions, respectively.

Moisture alone has been identified as a primary source of degradation of L-ascorbic acid in the solid phase [1]. Means of stabilising solid L-ascorbic acid formulations against the effect of moisture are required. Use of anhydrous or dried tablet excipients would minimise the effect of moisture or if this is not practical then encapsulating L-ascorbic acid in a hydrophobic shell may overcome the problem.

References

[1] A.B. Shephard, S.C. Nichols, A. Braithwaite, Talanta 48 (3) (1999) 585.
[2] A.B. Shephard, S.C. Nichols, A. Braithwaite, Talanta 48 (3) (1999) 595.

[3] S.H. Lee, T.P. Labuza, J. Food Sci. 40 (2) (1975) 370–373.
[4] B.M. Laing, D.L. Schlüter, T.P. Labuza, J. Food Sci. 43 (5) (1978) 1440–1443.
[5] E. De Ritter, L. Magid, M. Osadca, S.H. Rubin, J. Pharm. Sci. 59 (2) (1970) 229–232.
[6] J.H. Tatum, P.E. Shaw, R.E. Berry, J. Agr. Food Chem. 17 (1969) 38–40.
[7] I.M. Coggiola, Nature 200 (1963) 954–955.
[8] F.E. Huelina, Food Res. 18 (1953) 633.

ELSEVIER

Talanta 48 (1999) 623–631

Talanta

Non-extractive derivative spectrophotometric determination of cobalt in neutral micellar medium

Har Bhajan Singh [a,*], Narinder Kumar Agnihotri [b], Vinay Kumar Singh [c]

[a] *Department of Chemistry, University of Delhi, Delhi 110007, India*
[b] *Department of Chemistry, Motilal Nehru College, University of Delhi, Benito Juarez Road, Delhi 110021, India*
[c] *Department of Chemistry, Sri Aurobindo College, University of Delhi, Malviya Nagar, Delhi 110017, India*

Received 05 March 1998; received in revised form 14 August 1998; accepted 24 August 1998

Abstract

A sensitive derivative spectrophotometric method using 1-nitroso-2-naphthol has been developed for determination of trace amounts of cobalt in the presence of a neutral surfactant. Photometric parameters, viz., λ_{max}, molar absorption coefficient and analytical sensitivity of the complex formed in micellar media are 420 nm, 3.18×10^4 l mol^{-1} cm^{-1} and 2.05 ng ml^{-1}, respectively. Beer's law holds from 0.20 to 3.0 μg ml^{-1} of the analyte concentration. The method has a high sensitivity with a detection limit of 1.68 ng ml^{-1}. A selective determination of cobalt in presence of copper(II) or iron(III) using derivative spectral profiles and without any masking or pre-separation is also reported. Samples of drugs and standard alloys analysed by the proposed method yielded results comparable to those obtained using recommended procedures.

Keywords: 1-Nitroso-2-naphthol; Neutral surfactant; Micellar medium; Peak height; Trough depth; Cross-over point; Triton X-100.

1. Introduction

Cobalt is an important element, not only for industry but for biological systems as well. It is an essential micro nutrient for all living systems. It is present in vitamin B_{12} which is involved in the production of RBC and prevention of pernicious anemia. However, in larger amounts it is toxic and causes pulmonary disorders, dermatitis, nausea and vomiting [1]. As the difference between toxic and essential concentration levels of cobalt is quite narrow, its analysis in diverse matrices besides development of reliable analytical procedures for its determination at micro-levels is highly desirable.

Analytical chemistry of cobalt has developed considerably in recent years. Sensitive instrumental techniques other than spectrophotometry [2–7] such as spectrofluorimetry [8], x-ray fluorescence spectrometry [9], neutron activation analysis [10] and atomic absorption spectrometry [11] are reported for the analysis of cobalt in complex ma-

* Corresponding author. Tel.: +91-11-725-7794 & 725-6538; fax: +91-11-725-6541.

0039-9140/99/$ - see front matter
PII: S0039-9140(98)00286-0

trices. Though a number of photometric reagents, such as PAN [2], PAR [3], TAR [4], 5-Cl-PADAB [5], 5-Br-PADAB [6] are known for its determination, those containing nitroso group are generally selective and sensitive [7]. However, most of the determination procedures not only involve tedious and cumbersome extraction steps but also require pre-separation especially when ions of Cu, Fe, and Ni are present in large quantities [7]. Derivative spectrophotometric methods [12–14], though more selective, suffer from serious interferences when cations of iron, copper or nickel are present and no masking agent is used [13,14].

In the present communication, micelles [15] and derivatization of absorption spectra [16] have been made use of to develop a simple, inexpensive and selective method for trace analysis of cobalt. Impact of varying parameters such as pH, concentration of surfactant, the metal ion and the reagent on the absorbance of the cobalt complex have been studied. A method of selective determination in presence of copper(II) or iron(III) without any pre-separation is also proposed. The developed procedure has been applied for the determination of cobalt in samples of vitamin B_{12} and standard alloys.

2. Experimental

2.1. Instruments

A Shimadzu UV-260 recording spectrophotometer with 10 mm matched silica cells and ECIL digital pH meter were used for spectral and pH measurements respectively. First order derivative spectra were recorded with $\Delta\lambda = 2$ nm. The atomic absorption data were recorded at 240.7 nm on a Shimadzu spectrometer (AA-640-13) using air-acetylene flame.

2.2. Chemicals

An aqueous solution of cobalt(II) sulphate heptahydrate (0.01 M w.r.t. cobalt) was prepared and standardized volumetrically against EDTA. Working solutions were then prepared by diluting the standard solution. A solution of 1-nitroso-2-naphthol (4.0×10^{-4} M) was prepared by stirring 6.927 mg of the compound in 4.0 ml Triton X-100 at 60°C and diluting the resulting solution with water to 100 ml. All other chemicals used were of analytical grade.

2.3. Procedure

2.3.1. Determination of optimum experimental variables

Two sets of solutions, one with cobalt ions (4×10^{-5} M) and another without cobalt ions, and each containing 2.0×10^{-4} M ligand and 2.0% m/v Triton X-100 were prepared in the pH range 1.0–9.0 to study the effect of varying H^+ ion concentration.

Effect of changing the ligand and the metal ion concentrations on the absorbance of the resultant complex has been studied by preparing two sets of solutions, one containing increasing amount of the ligand (4.0×10^{-6}–2.0×10^{-4} M) and a fixed amount of cobalt ions (4.72×10^{-1} μg ml^{-1}) and the other containing increasing amount of cobalt ions (2.36×10^{-1}–2.36 μg ml^{-1}) and a fixed amount of the ligand (2.0×10^{-4} M), under optimal experimental conditions.

2.3.2. Determination of cobalt in pharmaceutical and standard samples

Appropriate amount of the sample, 1-nitroso-2-naphthol and Triton X-100 were taken to give a final concentration of 0.20–3.00 μg ml^{-1} cobalt, 2.0×10^{-4} M ligand and 2.0% (m/v) surfactant, unless stated otherwise. Absorbance spectra recorded against water and calibration curves in normal (at 420 nm) and first order derivative (at 440 and 570 nm) modes were prepared by measuring absorbance/derivative amplitude versus metal ion concentration. A trough depth at 440 nm in presence of Cu(II), and at 570 nm in presence of Fe(III) has been utilized to determine the concentration of cobalt using linear regression equations obtained with standard cobalt solutions. Cobalt content of the standard and sample solutions were also determined spectrometrically at 240.7 nm.

3. Results and discussion

3.1. Effect of experimental variables

Absorbance spectra of the ligand and its cobalt complex were recorded in the range 300-650 nm taking water as reference. The complex has two maxima at 420 and 315 nm and shows batho-hyperchromic shift with increase in pH. The absorbance at 420 nm is higher than at 315 nm and it also remains constant in the pH range 3.0–5.2. Subsequent studies were carried out at pH 3.8.

A neutral surfactant, Triton X-100, was selected for micelle media formation as it dissolves both the ligand and the complex more readily and enhances absorbance more than the cationic surfactants, cetylpyridinium chloride and cetyltrimethylammonium bromide or the anionic surfactant, sodium laurylsulphate. Varying the amount of Triton X-100 (0.0–4.0% m/v), showed an increase in absorbance at λ_{max} of the complex up to 1.75% m/v; a slight decrease was observed above 2.25% m/v. Subsequent studies were carried out at 2.0% m/v of Triton X-100 as maximum absorbance was observed in the concentration range 1.75–2.25% (m/v).

Absorbance values were corrected for the absorption of uncomplexed ligand and the corrected values plotted against the ligand concentration. There is a sharp increase in the absorbance with increase in the ligand-to-metal ratio up to 2 and this remains practically constant up to 15. Therefore, concentration of the reagent has been kept within the aforesaid limits, wherever possible.

3.2. Calibration graphs and analytical parameters

Absorption spectra of the solutions containing increasing amount of the analyte and fixed amounts of 1-nitroso-2-naphthol are shown in Fig. 1(a). Linear regression of absorbance, $[A]$ at λ_{max} of the complex on the metal ion concentration ($\mu g\ ml^{-1}$), $[C]$ shows following relationship with residue square of 0.9995.

$$[A] = 3.847 \times 10^{-1}[C] + 4.643 \times 10^{-1} \quad (1)$$

Use of corrected absorbance, $[A]_C$ (Eq. (2)) showed a better linear fit (Eq. (3)) with a residue square of 0.9997.

$$[A]_C = [A] - [V_L - R \times V_M]\left|\frac{[A]}{[V_L]}\right|_{\text{Ligand blank}} \quad (2)$$

$$[A]_C = 5.039 \times 10^{-1}[C] - 4.606 \times 10^{-3} \quad (3)$$

Where $[A]$ denote the value of the absorbance at λ_{max} of the complex, V_L and V_M are the molar volume of the ligand and the metal ion (both are equimolar) and R, the stoichiometry of the complex.

First derivative spectra of the above solutions containing increasing metal ion concentrations shows troughs at 329, 440, and 570 nm and a cross-over point at 420 nm, corresponding to λ_{max} of the complex while the ligand shows a trough at 405 nm (Fig. 1b). Trough depth, $[TD]$ measured from the base line of the ligand is found proportional to the metal ion concentration at these wavelengths. Measurement of derivative amplitudes at 329, 440 and 570 nm are recommended for quantitative work as evidenced by a good linear fit with a residue square of 0.998, 0.997 and 0.996, respectively (Eqs. (4)–(6)).

$$[TD]_{329\ nm} = 4.847[C] - 2.967 \times 10^{-1} \quad (4)$$

$$[TD]_{440\ nm} = 6.779[C] + 4.533 \times 10^{-1} \quad (5)$$

$$[TD]_{570\ nm} = 2.564[C] + 2.466 \times 10^{-1} \quad (6)$$

A linear calibration graph was obtained by plotting the absorbance at λ_{max} for concentration of cobalt in the range 0.20–3.00 $\mu g\ ml^{-1}$. The relative standard deviation for six determinations of 0.20 and 0.80 $\mu g\ ml^{-1}$ of the metal ion were 1.7 and 0.22%, respectively.

Analytical sensitivity, $S_A(=S_s/m$, where S_s is the standard deviation of the analytical signal at any particular analyte concentration and m, slope of calibration curve), limit of detection, C_L ($k=3$), limit of quantification, C_Q ($k=10$) and other characteristics of the cobalt complex in normal and derivative modes, as defined by IUPAC are reported in the Table 1.

3.3. Composition and conditional stability constant

Metal-to-ligand ratio in the complex, formed under optimum conditions as determined by Job's method of continuous variations, is found to be 1:3.

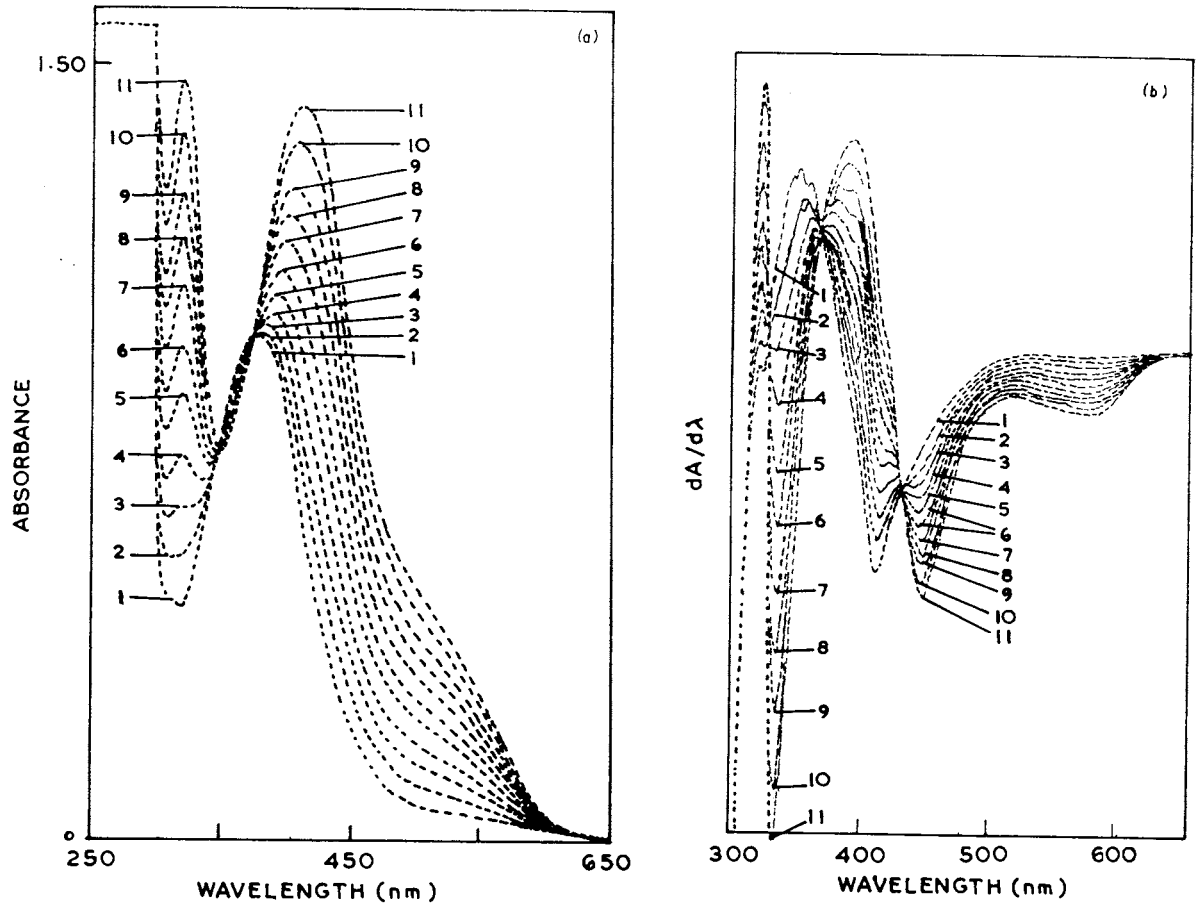

Fig. 1. (1) 1-Nitroso-2-naphthol, 2.0×10^{-4} M + Triton X-100, 2.0% (m/v); (2–11) contain increasing cobalt concentration from 2.36×10^{-1} to 2.36 μg ml^{-1} and each containing the ligand, 2.0×10^{-4} M + Triton X-100, 2.0% (m/v). (a) Normal mode, (b) First order derivative mode.

Conditional stability constant (k') [17] of the complex, taking due care of the existing metal ion-auxiliary ligand equilibria, has been calculated from the absorbance values and the concentration of the species present. The average of eight values of k' is found to be 6.02×10^{12} l^3 mol^{-3} with covariance of 10.23%.

3.4. Effect of foreign ions

A systematic study was made of the effect of the presence of diverse ions on the photometric determination of 0.80 μg ml^{-1} of cobalt ions using 1-nitroso-2-naphthol in normal as well as derivative modes; the results are given in Table 2. The cations of Cu and Fe interfere seriously while those of Cr, Mn, and V interfere moderately. Except EDTA, that masked the complexation reaction, no other anion interfered. Using derivative modes, interference due to the presence of cations of Cu, Fe, Cr, Mn, and V could be overcome.

3.5. Determination of cobalt in presence of Cu(II) or Fe(III) using derivative spectrophotometry

The selectivity of the method is significantly enhanced by recording derivative spectra in which closely over-lapped absorption peaks due to the complexes of cobalt, copper, and iron with 1-nitroso-2-naphthol get resolved into separate peaks, troughs and cross-over points.

Table 1
Analytical characteristics of the cobalt complex in neutral micellar medium, (Triton X-100) in normal and first order derivative spectrophotometric mode

Sr.	Photometric parameters[a]	Normal mode 420 nm	First order derivative mode 329 nm	440 nm	570 nm
1.	ε, 1 mol^{-1} cm^{-1}	3.18×10^4	–	–	–
2.	S, ng cm^{-2}	1.85	–	–	–
3.	$S_A(=S_s/m)$, ng ml^{-1}	2.05	1.18	0.56	1.34
4.	$C_{L(n=25,\ k=3)}$, ng ml^{-1}	6.16	3.55	1.68	4.02
5.	$C_{Q(n=25,\ k=10)}$, ng ml^{-1}	20.5	11.8	5.63	13.4
6.	Linear dynamic, range, ng ml^{-1}	$20.5–3.00\times10^3$	$11.8–3.00\times10^3$	$5.63–3.00\times10^3$	$13.4–3.00^3$
7.	RSD% ($n=6$)	0.22	3.66	0.18	0.29

[a] S, Sandell's sensitivity; S_A, analytical sensitivity; C_L, detection limit; C_Q, limit of quantification.

Table 2
Effect of diverse ions on the photometric determination of cobalt (0.80 μg ml^{-1}) with 1-nitroso-2-naphthol in micellar medium

Diverse ions	Amount added (μg)	% Error	Diverse ions (μg)	Amount added	% Error
Cations:					
Cr(III)	1000	−0.48	Fe(III)	100	1.91
Fe(II)	200	1.41	VO(II)	100	1.03
Ca(II)	1000	0.92	Mg(II)	1000	1.30
Pb(II)	600	1.74	Mn(II)	100	1.43
Cu(II)	100	−1.30	Zn(II)	800	1.81
Cd(II)	800	1.15	Hg(II)	600	1.55
Ni(II)	150	01.71	Tl(I)	800	1.08
Anions:					
Chloride	5000	−0.46	Bromide	6000	1.70
Iodide	4000	1.45	Thiocyanate	1000	−0.25
Ascorbate	1000	1.26	Tartrate	1000	−0.61
Citrate	4000	0.29	Oxalate	600	1.03
EDTA	100	−1.83	Borate	5000	−1.91
Acetate	7000	0.46	Fluoride	3000	2.01

Complexes with Cu(II) and Fe(III) with 1-nitroso-2-naphthol in neutral micellar medium show peaks at 405 and 410 nm, respectively (Fig. 2a). In first derivative mode Cu(II) complex shows a cross-over point (no change in the value of derivative amplitude on varying Cu(II) ion concentration) at 440 nm, a peak at 480 nm and two troughs at 422 and 512 nm. A zero point at 570 nm and troughs at 630 and 422 nm are observed in the absorption spectrum of Fe(III) complex in first order derivative mode (Fig. 2b). The cobalt content of the sample containing large amounts of Cu(II) ions can be determined by measuring derivative amplitude(trough depth) at 440 nm (the cross-over point of copper complex). The zero point of iron(III) complex at 570 nm is utilized to determine cobalt in presence of iron without any prior separation. Besides, measurements of trough depth of iron complex at 630 nm, the zero point of the cobalt complex, can be used to determine former in presence of the later.

3.6. Comparison

A comparative evaluation of the proposed method with some of the reported ones for the determination of cobalt is given in Table 3. It is evident that the former has distinct advantages

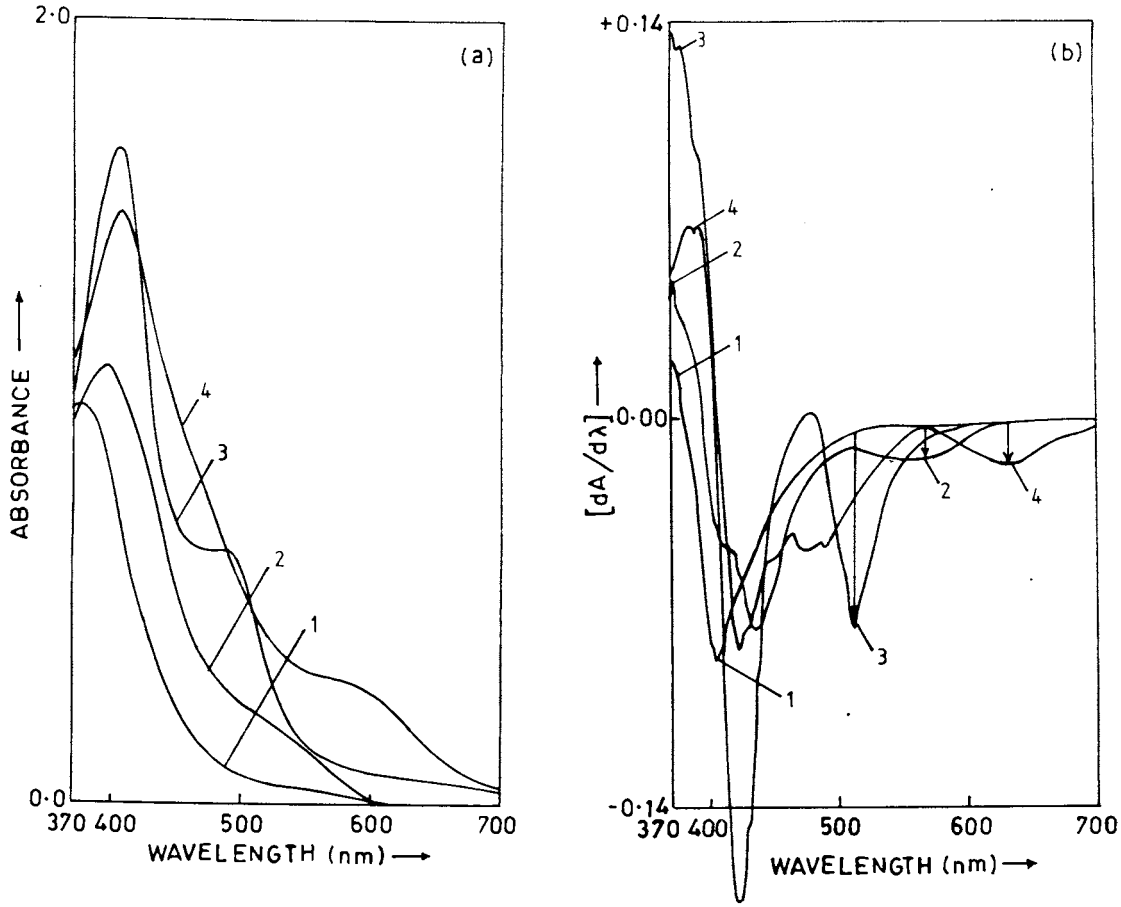

Fig. 2. Each containing 1-nitroso-2-naphthol, 2.0×10^{-4} M + Triton X-100, 2.0% (m/v); (1) no metal ion;(2) cobalt 0.50 μg ml^{-1}; (3) copper(II) 10.0 μg ml^{-1}; (4) iron(III), 10.0 μg ml^{-1}. (a) Normal mode, (b) First order derivative mode.

over the later in term of lower detection limit (1.68 ng ml^{-1}) and broader determination range ($5.63–3.00 \times 10^3$ ng ml^{-1}).

4. Analytical applications

The accuracy and applicability of the proposed method was evaluated by its application for the determination of cobalt in various pharmaceutical formulations and samples of standard alloys.

A sample, each of injectable Neurobion (Merck, India) and Sioneuron (Albert David Ltd., India) was digested with nitric acid in a covered beaker. The residue of the sample was leached with dilute sulphuric acid and diluted to the mark in a calibrated flask. Working solutions were prepared by taking an appropriate amount of the sample and its cobalt content determined by proposed method and by AAS (Table 4).

The method was also applied to the determination of cobalt in standard samples of a aluminum alloy (NKK, 920) and Japanese stainless steel (JSS, 653-7). A 0.1–0.5 g sample was dissolved in about 15 ml 1 + 1 hydrochloric acid by heating on a water-bath and 4–5 ml of 30% v/v hydrogen peroxide added. After digesting the solution for a 1/2 h it was cooled, filtered if necessary, and diluted to 100 ml. The cobalt content of the sample solution was read from the calibration graph prepared by measuring derivative amplitude at 440 nm (cross-over point of the copper(II)

Table 3
Comparative evaluation of various photometric reagents for the determination of cobalt

Reagent	Medium/solvent	λ_{max} (nm)	Molar absorptivity ($1\ mol^{-1}\ cm^{-1}$) $\times 10^4$	Linear range ($\mu g\ ml^{-1}$)	Reference
1-(2-Pyridylazo)-2-naphthol	Aqueous (TX–100[d])	620	1.9	0.4–3.2	[2]
4-(2-Pyridylazo)resorcinol	$CHCl_3$	520	6.4	–	[3]
4-(2-Thiazolyazo)resorcinol	Aqueous	510	6.0	0.2–2.0	[4]
4-(5-Chloro-2-pyridylazo)-1,3-diaminobenzen	Aqueous	570	11.3	0.02–0.5	[5]
4-(5-Bromo-2-pyridylazo)-1,3-diaminobenzen	Aqueous	575	11.6	0.034–0.504	[6]
2,2′-Dipyridyl-2-benzothiazolylhydrazone	Aqueous	530	2.5	2.7–58.9[b](0.007)[a]	[12]
2,2'–Dipyridyl–2–benzothiazolylhydrazone	$CHCl_3$	504	3.43	0.8–17.2[b]	[12]
2-Pyridyl-3′-sulphophenylmethanone 2-(5-nitro)pyridylhydrazone	Aqueous	496	5.69	0.05–1.0 (0.003)[a]	[13]
3-(4-Phenyl-2-pyridinyl)-5-phenyl-1,2,4-triazine + picric acid	1,2-dichloroethane	–	–	0.0072–0.50	[14]
1-Nitroso-2-naphthol	$CHCl_3$	410	–	0.004–0.020	[18]
1-Phenyl-4-phenylamino-1,2,4-triazolium Chloride + thiocyanate	1,2-dichloroethane	626	0.126	1.0–6.0	[19]
Bis(triphenyltetrazolium) + Thiocyanate	Propylene carbonate	631	0.108	0.25–20	[20]
Protriptylinium + thiocyanate	Acetone + $CHCl_3$	342	0.52	0.0–6.3	[21]
Phenanthraquinone monothiosemicarbazone	Water–methanol	550	1.24	0.8–4.0	[22]
3-Hydroxy-2-methyl-1,4-naphthoquinone 4-oxime	Naphthalene/DMF	430	2.09	0.12–1.8	[23]
1-Hydroxy-2-carboxyanthraquinone	Ethanol–water	494.5	–	0.75–4.5	[24]
Sodium diethyldithiocarbamate	Aqueous (CTAB[f])	324	2.17	0.0377 ± 0.0082[a]	[25]
Sodium diethyldithiocarbamate	CCl_4	322	2.33	0.0475 ± 0.0024[a]	[25]
Bis(2,4,4-trimethyl phentyl) phosphinic acid	Benzene	635	0.03	0.295–2.36[c]	[26]
Diethyl thiocarbamate	Aqueous (ADS[e])	322	2.22	0.0493 ± 0.0018[a]	[27]
2-Nitroso-1-naphthol-4-sulphonic acid	DMF	620	–	0.2–12	[28]
Disodium 1-nitroso-2-naphthol-3,6-disulphonate	DMF/$CHCl_3$	–	1.33	0.84–1.44	[29]
N-Hydroxy-N,N-diphenyl benzamidine	Toluene	405	0.70	0.10–12	[30]
2-(2-Benzothiazolyazo)-2-p-cresol	Aqueous (TX–100[d])	615	1.62	0.08–1.06(10)[a]	[31]
1-Nitroso-2-naphthol	Aqueous (TX–100[d])	420	3.18	0.0056–3.00 (1.68×10^{-3})[a]	Present work

[a] Detection limit.
[b] Units μg.
[c] Units mg.
[d] Triton X–100.
[e] ADS–ammoniumdodecylsulphate.
[f] CTAB–hexadecyltrimethylammonium bromide.

Table 4
Quantitative determination of cobalt in Pharmaceutical samples

Sample	Certified value (ppm)	Cobalt found[a]	
		Proposed method (RSD%)	AAS method (RSD%)
Neurobion (Inj.) Merck, India	21.74	21.700 ± 0.068 (0.31)	21.708 ± 0.056 (0.26)
Sioneuron (Inj.) Albert David Ltd., India	10.86	10.840 ± 0.059 (0.54)	10.837 ± 0.050 (0.46)

[a] Mean value of six determinations ± standard deviation.

Table 5
Determination of cobalt in standard reference materials

Sample	Composition (%)	Cobalt content		
		Certified value (%)	Proposed method[a]	AAS method[a]
Aluminum alloy, (NKK, 920)	Si 0.780, Fe 0.720, Zn 0.030, Mn 0.200, Mg 0.460, Co 0.100, Cr 0.270, Ni 0.290, Ga 0.050, Ti 0.015, Sn 0.200, Pb 0.100, V 0.150, Bi 0.060, Cu 0.710, Sb 0.010, Ca 0.030	0.100	0.1010 ± 0.0028	0.1003 ± 0.0034
Stainless steel, (JSS, 653-7)	C 0.068, Si 0.630, Cu 0.030, Ni 13.91, Mn 1.72, Co 0.350, Cr 22.53, N 0.0276	0.350	0.3511 ± 0.0039	0.3518 ± 0.0042

[a] Mean value of six determinations ± standard deviation.

complex) and 570 nm (zero point of the iron(III) complex). The results of quantitative estimation, certified values and those obtained using AAS are summarized in Table 5.

5. Conclusion

A simple, economical, sensitive and selective derivative spectrophotometric method for determination of cobalt in aqueous phase has been developed. Compared to the direct (4.00 ng ml^{-1}) [18] and derivative spectrophotometric methods (2.2 ng ml^{-1}), [14] the proposed method is more sensitive (1.68 ng ml^{-1}), selective and simpler because it neither requires extraction nor masking of diverse ions. Cobalt can even be determined in the presence of Cu(II), Fe(III) or Ni(II). Compared with other sensitive methods such as, AAS [11] (5 μg g^{-1}) electrothermal atomic absorption spectrometry (0.012 μg g^{-1}) [32], the present method is not only more sensitive but also cheaper and less complicated in terms of assay procedure and equipment used. The reported method has been successfully tested for the determination of cobalt in various pharmaceutical formulations and standard alloys.

Acknowledgements

The authors are grateful to the Ministry of Defence, Government of India, New Delhi, for providing financial assistance through their Grants-in-Aid Scheme.

References

[1] M. Barborik, J. Dusik, Brit. Heart J. 34 (1972) 113.
[2] H. Watanabe, Talanta 21 (1974) 295.
[3] M. Siroki, L. Maric, Z. Stefanac, M.J. Herak, Anal. Chim. Acta 75 (1975) 101.
[4] A.I. Busev, Z.I. Nemtseva, V.M. Ivanov, Zh. Anal. Khim. 24 (1969) 1376.
[5] S. Shibata, M. Furukawa, Y. Ishigugo, S. Sasaki, Anal. Chim. Acta 55 (1971) 231.
[6] E. Kiss, Anal. Chim. Acta 66 (1973) 385.
[7] K. Tôei, S. Motomizu, Analyst 101 (1976) 497.
[8] S. Stieg, T.A. Nieman, Anal. Chem. 49 (1977) 1322.
[9] B. Armitage, H. Zeitlin, Anal. Chem. Acta 53 (1971) 47.
[10] B. Maziere, J. Gros, D. Comar, J. Radioanal.Chem. 24 (1975) 707.
[11] J.S. Barros, Analyst 114 (1989) 369.
[12] R.B. Singh, T. Odashima, H. Ishii, Analyst 109 (1984) 43.
[13] T. Odashima, T. Kikuchi, W. Ohtani, H. Ishii, Analyst 111 (1986) 1383.
[14] M.I. Toral, P. Richter, L. Silva, Talanta 40 (1993) 1405.
[15] G.L. McIntire, Crit. Rev. Anal. Chem. 21 (1990) 257.
[16] F.S. Rojas, C.B. Ojeda, J.M.C. Pavon, Talanta 35 (1988) 753.
[17] A. Ringbom, J. Chem. Educ. 35 (1958) 282.
[18] E. Kentner, H. Zeitlin, Anal. Chim. Acta 49 (1970) 587.
[19] C. Calzolari, L. Favretto, Analyst 93 (1968) 494.
[20] M.C. Mehra, D. LeBlanc, Microchem. J. 24 (1979) 435.
[21] D.T. Burns, P. Hanprasopwattana, Anal. Chim. Acta 115 (1980) 389.
[22] R.K. Sharma, Sahadev, S.K. Sindhwani, Analyst 112 (1987) 1771.
[23] R.K. Sharma, S.K. Sindhwani, Talanta 35 (1988) 661.
[24] J.A. Murillo, J.M. Lemus, A.M. de la Pena, F. Salinas, Analyst 113 (1988) 1439.
[25] M.P. San Andres, M.L. Marina, S. Vera, Talanta 41 (1994) 179.
[26] B.R. Reddy, P.V.R. Bhaskara Sarma, Talanta 41 (1994) 1335.
[27] M.P. San Andres, M.L. Marina, S. Vera, Analyst 120 (1995) 255.
[28] M.A. Taher, B.K. Puri, Analyst 120 (1995) 1589.
[29] B.K. Puri, S. Balani, Talanta 42 (1995) 337.
[30] B.S. Chandravanshi, G. Asgedom, Chem. Anal. (Warsaw) 40 (1995) 225.
[31] M.S. Carvalho, I.C.S. Fraga, K.C.L. Neto, E.Q.S. Filho, Talanta 43 (1996) 1675.
[32] K. Akatsuka, I. Atsuya, Anal. Chem. 61 (1989) 216.

ELSEVIER

Talanta 48 (1999) 633–641

Talanta

The solubility of toluene in aqueous salt solutions

Simon R. Poulson *, Rebecca R. Harrington, James I. Drever

Department of Geology and Geophysics, University of Wyoming, Laramie, WY 82071-3006, USA

Received 8 June 1998; accepted 24 August 1998

Abstract

The solubility of toluene has been measured in distilled water, and in various inorganic salt solutions. Values of the Setschenow constant, K_S, which quantify toluene solubility versus salt concentration, have been determined for each salt. Values of K_S are compared to the activity of water for the salt solutions. Data from this study, consistent with earlier data, suggests that the effects of salts upon toluene solubility are non-additive. This contrasts the additive behavior of inorganic salts upon the solubility of nonpolar organic compounds, such as benzene and naphthalene, reported in the literature. Specific interaction between slightly polar toluene and ions in solution is suggested as a possible explanation for the non-additive effect of salts on the solubility of toluene. © 1999 Published by Elsevier Science B.V. All rights reserved.

Keywords: Setschenow constant; Toluene solubility; Salt concentration; Non-additive

1. Introduction

The solubility of aromatic hydrocarbons, such as toluene, in water, and the decrease in solubility in aqueous salt solutions is an important factor controlling the behavior of hydrocarbons in a variety of environments. Waterflood recovery of mobile, separate-phase hydrocarbons in the subsurface is a well established technique, using a well injection-and-recovery methodology. It was initially developed as a secondary recovery process to increase petroleum production efficiency [1], but has also been applied as a remedial technology at sites contaminated with a nonaqueous phase liquid [2,3]. Brines of various compositions may be used during waterflood recovery, as salinity influences the wettability of an organic liquid phase [4], and hence affects the efficiency of organic phase recovery [5,6]. Salinity can also affect the adsorption behavior of organic compounds onto natural organic matter [7], and hence will affect the mobility of organic compounds in the subsurface. For example, sorption coefficients of pyrene onto organic matter are 15% higher in a 0.34 molal NaCl solution compared to distilled water [8], i.e. pyrene is more strongly adsorbed onto organic matter in the presence of NaCl. Lastly, the solubility of hydrocarbons in salt solutions also has implications for petroleum migration [9]. Toluene is an important compound to consider as it is a significant, and very soluble,

* Corresponding author. Tel.: +1-702-784-6050; fax: +1-702-784-1833; e-mail: simonp@reno.rmci.net.

0039-9140/99/$ - see front matter
PII: S0039-9140(98)00292-6

component of both gasoline and petroleum, and is also an important industrial chemical in common use worldwide.

The solubility of neutral, nonpolar organic compounds in salt solutions has long been known to decrease in salt solutions of most inorganic ionic species, an effect commonly known as 'salting-out', although salts of large, organic cations can increase solubilities (known as 'salting-in'). An empirical relationship between the solubility of an organic compound and the salt concentration has long been recognized [10], where:

$$\log(C_0/C_{\text{salt}}) = S*K_S \quad (1)$$

where C_0 is the solubility of the organic compound in distilled water, C_{salt} is the solubility of the organic compound in the salt solution, S is the salt concentration, and K_S is the salting, or Setschenow, constant. The units of K_S are discussed in a later section. The major effect of inorganic salts in solution upon organic compound solubility is the formation of hydration shells around the ionic species, which effectively reduces the availability of free water to dissolve the inorganic compound. As the size and strength of ionic hydration shells are dependent upon the salt composition, values of K_S are also dependent upon the salt composition. Hence, it might be expected that there would be a correlation between the activity of water (i.e. the availability of free water to dissolve an organic compound) and the value of K_S. However, values of K_S are also dependent upon the molar volume of the organic compound [11], and upon the magnitude of any possible interaction between the organic compound and the dissolved salts. In the case of nonpolar organic compounds, such as benzene [12] and naphthalene [13,14], where there is no specific interaction between the organic compound and the dissolved salts, the effect of a mixture of salts is a simple summation of the effects of the contributions from the individual salts present:

$$K_S = \sum K_S^i * S_i \quad (2)$$

where K_S^i is the Setschenow constant for salt i, and S_i is the concentration of salt i in the salt mixture.

This study has measured the solubility of toluene in various aqueous salt solutions, by direct equilibration of liquid toluene with an aqueous solution, followed by direct analysis of the toluene concentration in solution by UV spectrophotometry. Calculation of the activity of water in salt solutions has also been performed, in order to investigate a possible correlation between the value of K_S and the activity of water.

2. Experimental methods

Each salt under investigation was prepared at three different concentrations, using distilled, deionized water and ACS grade reagents. Ten gram aliquots of salt solution (or distilled deionized water) were transferred into glass centrifuge tubes with PTFE-lined screw caps. All experiments were performed in triplicate. Approximately 0.4 g of pure ACS grade toluene was then added to each centrifuge tube, and the samples were mechanically agitated for 3 days. Samples were then centrifuged at approximately 2000 rpm for 8 min, to separate liquid toluene ($\rho = 0.87$ g/cm^3) from the aqueous solution. The underlying salt solution was sampled by passing a first, outer pipette through the lens of toluene, and then sampling the salt solution from the bottom of the centrifuge tube with a second, inner pipette.

Toluene concentrations in the salt solutions were measured by UV-visible spectrophotometry at a wavelength of 261.3 nm, using a Shimadzu UV160U dual beam UV-VIS scanning spectrophotometer (Shimadzu, Columbia, MD). Solutions were measured in a quartz cuvette with a PTFE stopper, with minimal headspace. Analytical standards were prepared daily from a stock solution of toluene dissolved in methanol. Triplicate analyses of each experiment indicated analytical reproducibilities with a typical standard deviation of 1.5%, with a maximum standard deviation of 3.4%. Linear regression of experimental data to determine values of K_S had values of $R^2 > 0.99$ for all salts except CsBr, which had a value of $R^2 = 0.97$. All experiments were performed at 23°C. The majority of previous studies have been conducted at 25°C, but other studies

[15,16] indicate that toluene solubility has little dependence upon temperature over the range of 20–25°C.

Additional salts were investigated, but experimental problems precluded quantification of the effect of these salts. These salts included $Ca(NO_3)_2$, KI, and CsI, which all interfered at the wavelength used to measure toluene concentrations, and Na_2SO_4 and CsCl, which resulted in emulsification of toluene, and prevented accurate measurement of toluene concentrations.

Activities of water in 1 molal salt solutions were calculated using the program PHRQPITZ [17]. Calculation of water activity for a CsBr solution was not possible as the appropriate Pitzer constants are not available for Cs^+, so the value for CsBr is taken from the literature [18].

3. Units of K_S

The units of K_S are dependent upon concentration in two ways, and need to be addressed in order to compare solubilities determined by different experimental studies. Firstly, inspection of Eq. (1) indicates that the K_S has units of 1/(salt concentration), where salt concentration may be molal (mol/kg water) or molar (mol/l solution). This distinction is not always clearly delineated, and has a small but significant effect upon the numerical value of K_S, depending upon solution density. For example, a 1 molal solution of $BaCl_2$ (17.2 wt.% $BaCl_2$), has a density of 1.169 g/cm^3 [18], and therefore is equivalent to a 0.967 molar solution of $BaCl_2$. Hence, K_S (l/mol) $= 0.034 * K_S$ (kg/mol). Secondly, the dimension of K_S will depend upon the dimension used to measure toluene solubility, with the two common units being mg toluene/l solution, and mg toluene/kg solution. At 25°C in distilled water, these values (i.e. C_0) are essentially identical, since $\rho_{water} = 0.997$ g/cm^3 at 25°C [19], i.e. a concentration of x mg/l $= 0.003 * x$ mg/kg (ignoring the effect of the dissolved toluene on solution density). However, in concentrated salt solutions, there is a significant difference in the numerical values of mg/l and mg/kg, again depending upon solution density. For example, a concentration of y mg/l toluene (i.e. C_{salt}) in a 1 molal $BaCl_2$ solution, is the same as a concentration of $0.85 * y$ mg/kg. Hence, K_S (C_0 and C_{salt} as mg/kg) $= K_S$ (C_0 and C_{salt} as mg/l) $- 0.07$, for $BaCl_2$.

Toluene solubility has been measured in this study as mg/l, as have most previous studies of toluene solubility in salt solutions. A number of studies [9,15,20] have reported solubilities as mg/kg. However, all of these studies sampled experimental solutions volumetrically, so it is assumed that these concentrations should have been reported as mg/l. Hence, no correction has been applied to these studies. Salt solutions were prepared in this study as molal solutions, and values of K_S in units of kg/mol are reported in Table 2. Values of K_S (kg/mol) are converted to values of K_S (l/mol) using compiled solution densities [18], and are reported in Tables 2 and 3. A solution density for CsBr is not available [18], so a solution density for CsCl was used instead.

4. Results

4.1. The solubility of toluene in distilled water

The solubility of toluene in distilled water was determined in this study to be 562.9 ± 9.6 mg/l. A comparison with values determined in other studies investigating the effect of salts on toluene solubility, and the various experimental methods used, is presented in Table 1. Table 1 demonstrates that a wide range of values for toluene solubility have been measured, ranging from 487 [21] to 588 ppm [22], with the value determined by this study falling within this range. A more exhaustive compilation of experimental studies that have measured the solubility of toluene in distilled water is available [23], with over 70 measurements performed since the first determination [24]. Quoted solubilities show a total range of 265 to 1581 mg/l, although the majority of values (the 10th to 90th percentile) lie in the range of 470 to 670 mg/l. While the value determined by this study comfortably lies within the range determined by previous studies, it is clear that there is no accurate, consensus value for the solubility of toluene in distilled water.

Table 1
Comparison of toluene solubility in distilled water, and experimental methods of studies investigating toluene solubility in salt solutions[a]

Study	Toluene solubility in distilled water	Experimental method
This study	562.9 ± 9.6 mg/l	Equilibration with liquid toluene, aqueous concn. by UV spectrophotometry
Desnoyers and Ichhaporia (1969) [22]	588 mg/l	Equilibration with liquid toluene, aqueous concn. by refractive index
Brown and Wasik (1974) [26]	566 ± 11 mg/kg	Vapor-aqueous phase experiments, with GC analysis, extrapolated liquid solubility calculations
Mackay and Shiu (1975) [28]	519.5 ± 9.6 mg/l	Vapor-aqueous phase experiments, with GC analysis, extrapolated liquid solubility calculations
Sada et al. (1975) [21]	487.3[b] mg/l	Volumetric titration using an organic dye as an end-point indicator
Sutton and Calder (1975) [20]	534.8 ± 4.9 mg/kg	Equilibration with liquid toluene via vapor phase, aqueous concn. by hexane extraction, evaporation/concentration, then GC
Price (1976) [9]	544.0 ± 15.0 mg/kg	Equilibration with liquid toluene, aqueous concn. by GC
Rossi and Thomas (1981) [15]	506.7 ± 6.1 mg/kg	Equilibration with liquid toluene, aqueous concentration by solid phase extraction, then GC
Sanemasa et al. (1984) [11]	521 mg/l	Equilibration with reduced toluene vapor pressure, aqueous concentration by chloroform extraction then UV spectrophotometry, followed by extrapolation
Keeley et al. (1988) [27]	580 ± 3 mg/l	Equilibration with liquid toluene, aqueous concn. by GC of equilibrated vapor

[a] Majority of experimental studies conducted at, or close to, 25°C.
[b] Converted from ml toluene/l, using $\rho_{toluene} = 0.865$.

4.2. The solubility of toluene in salt solutions

The results of the solubility experiments, including five salts that have not been studied before (KBr, $KHCO_3$, CsBr, $MgCl_2$, and $MgSO_4$), are listed in Table 2, and plotted in Fig. 1 as $\log(C_0/C_{salt})$ versus salt concentration, after Eq. (1). Values of K_S (l/mol), ranging from 0.050 (for CsBr) to 0.596 (for K_2SO_4), are determined by linear least-squares fit to the data in Fig. 1, and are also listed in Table 2. K_S values determined by this study are compared with K_S values compiled from the literature in Table 3. Comparison with previous studies is difficult, due to the limited quantity of data present in the literature, with only two previous studies of any great extent [11,21]. NaCl has been the most frequently studied (6 determinations of K_S), but there are only 5 other salts that have been measured more than once (NaBr, Na_2SO_4, KCl, K_2SO_4, $CaCl_2$, and $BaCl_2$). Values of K_S determined by this study tend to be slightly lower than previous measurements (e.g. NaCl, KCl, K_2SO_4, and $CaCl_2$), but some measurements are higher than previous values (e.g. $BaCl_2$), whereas the measurement for NaBr falls between two previous determinations.

In general, the trends in values of the Setschenow constants measured in this study are consistent with what might be expected, using a model where smaller, more highly charged ions will bind waters of hydration more tightly, hence reducing the availability of free water to dissolve toluene. Assuming that common ions have the same effect on K_S (l/mol), the effect of $Na > K > Cs$, as indicated by the bromide salts (K_S decreases from 0.180 to 0.150 to 0.050, for NaBr, KBr, then CsBr), and confirmed by the chloride salts (K_S decreases from 0.202 to 0.188, for NaCl and KCl). Similarly, the effect of $Cl > Br$, as demonstrated by both the Na salts (K_S decreases from 0.202 to 0.180, for NaCl and NaBr) and the K salts (K_S decreases from 0.188 to 0.150, for KCl and KBr). However, the alkaline earth chloride salts show an inconsistent pattern, in that the effect of $Mg > Ca$, as expected (K_S decreases from 0.354 to 0.289, for $MgCl_2$ and $CaCl_2$), but the value of K_S for

Table 2
Experimental results of toulene solubility in various aqueous salt solutions [a,b,c]

Salt	Salt concentration (molal)	Toulene solubility (mg/l)	K_S (kg/mol)	K_S (l/mol)	Water activity coefficient for 1 molal salt solution
Distilled water	–	562.9	–	–	–
NaCl	1.00	347.9	0.198	0.202	0.976
	2.00	216.2			
	3.00	144.4			
NaBr	0.53	445.0	0.176	0.180	0.966
	1.11	353.8			
	1.77	273.8			
KCl	0.50	445.6	0.182	0.188	0.968
	1.00	363.4			
	1.50	300.0			
KBr	0.50	476.7	0.147	0.150	0.968
	1.00	398.8			
	1.50	339.7			
$KHCO_3$	0.50	421.5	0.223	0.231	0.968
	1.00	320.6			
	1.50	262.5			
K_2SO_4	0.20	428.5	0.570	0.596	0.965
	0.40	324.6			
	0.60	257.3			
CsBr	0.50	519.9	0.048	0.050	0.97
	1.00	506.1			
	1.50	472.7			
$MgCl_2$	0.45	391.0	0.341	0.354	0.942
	0.90	278.5			
	1.35	194.4			
$MgSO_4$	0.50	351.0	0.425	0.428	0.981
	1.00	213.9			
	1.50	129.8			
$CaCl_2$	0.48	394.4	0.282	0.289	0.945
	0.97	283.9			
	1.45	220.3			
$BaCl_2$	0.48	352.1	0.462	0.478	0.951
	0.72	269.2			
	0.97	199.3			

[a] Water activity coefficients for 1 molal salt solutions are calculated using PHRQPITZ [17].
[b] Conversion of K_S from kg/mol to l/mol is discussed in text.
[c] A value for CsBr could not be calculated as the appropriate parameters for Cs^+ are not available, so the value for CsBr is taken from reference [18].

$BaCl_2$ (0.478) is greater than either $MgCl_2$ or $CaCl_2$. Similar trends were observed for Na versus K [11,21], and for Cl versus Br [11]. However, a value of K_S for $CaCl_2 > BaCl_2$ has been measured [21], in contrast to this study, but this study [21] also measured a value of K_S for $K_2SO_4 > Na_2SO_4$, which is the reverse of what might be expected.

5. Discussion and conclusions

Comparison of K_S values measured in this study to previous determinations shows only moderate agreement. This may not be surprising in light of apparent uncertainties in various experimental and analytical methods. There does not

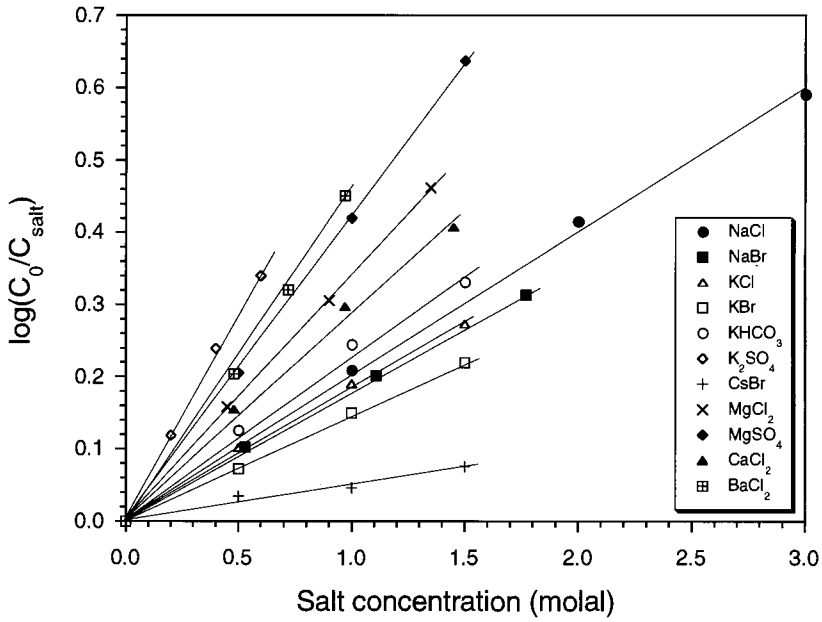

Fig. 1. Variation of toluene solubility (expressed as C_0/C_{salt}, where C_0 = toluene solubility in distilled water, and C_{salt} = toluene solubility in salt solution) versus salt concentration for various inorganic salts.

appear to be an accurate consensus value for the solubility of toluene in distilled water, which should be a more straightforward determination compared to the measurement of toluene solubility in salt solutions. However, comparison of just the 10 studies listed in Table 1 indicates a range of measurements for toluene solubility in distilled water from 487 to 588 ppm, and this range becomes much wider when considering the multitude of other studies which have measured toluene solubility (see earlier section). Clearly, measurement of toluene solubility in distilled water is an important factor in determining values of K_S. As an example, $\log(C_0/C_{salt})$ versus NaCl concentration is plotted in Fig. 2, using the value of C_0 measured in this study (563 mg/l), but also using values of C_0 of 543 and 583 mg/l (i.e. $\pm$ 20 ppm) with the same values of toluene solubility in NaCl solutions listed in Table 1. Interestingly, values of R^2 for the linear regressions are essentially identical in Fig. 2, indicating that the value of R^2 is not very sensitive to the exact value of C_0, but the value of K_S varies significantly, depending on the choice of C_0 ($K_S = 0.193$, 0.198, or 0.202 kg/mol, for $C_0 = 543$, 563, and 583 mg/l, respectively). As discussed earlier, a consensus value for the solubility of toluene in distilled water is not available, so this remains a factor of considerable uncertainty for measurements of K_S.

Values of the activity of water for 1 molal salt solutions, calculated using PHRQPITZ [17], are listed in Table 2, and plotted against values of K_S in Fig. 3. For a simple model of solution of a single organic compound in a variety of salt solutions, it might be expected that there would be a negative correlation between the value of K_S, and the activity of water in the salt solution. However, Fig. 3 clearly demonstrates that there is no significant correlation between water activity and value of K_S for toluene for the salts investigated by this study. Consideration of the number of water molecules bound in ionic hydration spheres, and hence the effect upon the effective concentration of bulk water in solution, could potentially predict values of K_S. This model does indeed qualitatively predict trends in values of K_S, e.g. a number of studies indicate a decrease in solvation numbers from Na to K to Cs, and also from Cl to Br [25]. As solvation numbers decrease, the amount of water tied up in hydration spheres decreases,

Table 3
Compilation of K_S values for toluene in various aqueous salt solutions

Salt	K_S (l/mol)	Ref.
LiCl	0.191	Sada et al. (1975) [21]
Li_2SO_4	0.593	Sada et al. (1975) [21]
NaF	0.336	Sanemasa et al. (1984) [11]
NaCl	0.202	This study
	0.205	Mackay and Shiu (1975) [28]
	0.267	Sada et al. (1975) [21]
	0.195[a]	Price (1976) [9]
	0.242	Sanemasa et al. (1984) [11]
	0.201[b]	Keeley et al. (1988) [27]
NaBr	0.180	This study
	0.113	Desnoyers and Ichhaporia (1969) [22]
	0.190	Sanemasa et al. (1984) [11]
NaSCN	0.066	Sanemasa et al. (1984) [11]
$NaNO_3$	0.154	Sanemasa et al. (1984) [11]
$NaClO_4$	0.139	Sanemasa et al. (1984) [11]
Na_2SO_4	0.650	Sada et al. (1975) [21]
	0.684	Sanemasa et al. (1984) [11]
KCl	0.188	This study
	0.205	Sada et al. (1975) [21]
	0.214	Sanemasa et al. (1984) [11]
KBr	0.150	This study
$KHCO_3$	0.231	This study
K_2SO_4	0.596	This study
	0.674	Sada et al. (1975) [21]
CsBr	0.050	This study
NH_4Cl	0.055	Sada et al. (1975) [21]
$(NH_4)_2SO_4$	0.415	Sada et al. (1975) [21]
$MgCl_2$	0.354	This study
$MgSO_4$	0.428	This study
$CaCl_2$	0.289	This study
	0.401	Sada et al. (1975) [21]
$BaCl_2$	0.478	This study
	0.278	Sada et al. (1975) [21]
	0.414	Sanemasa et al. (1984) [11]
$CuSO_4$	0.580	Sada et al. (1975) [21]
$ZnSO_4$	0.517	Sada et al. (1975) [21]
Natural sea water	0.083[c]	Rossi and Thomas (1981) [15]
Artificial sea water	0.154[c]	Brown and Wasik (1974) [26]
	0.149[c]	Sutton and Calder (1975) [20]
	0.131[c]	Price (1976) [9]

[a] Calculated from solubility data.
[b] Units of K_S unclear-K_S given in terms of ionic strength, but definition of ionic strength (i.e. in terms of molal or molar) not provided.
[c] Value = log ($C_0/C_{seawater}$), where C_0 = toluene solubility in distilled water, and $C_{seawater}$ = toluene solubility in seawater

and the concentration of water available to dissolve toluene increases. Hence, values of K_S are predicted to decrease from Na to K to Cs, and also from Cl to Br, which is observed experimentally. However, quantification of this model may be impossible due to the difficulty in assigning solvation numbers to each ion. Widely varying solvation numbers have been measured by different experimental methods [25], and solvation numbers may well be dependent upon salt concentration.

Consideration of the results of this study, and a previous study [21], suggests that the effects of salts on toluene solubility are not additive, in contrast to the results for benzene [12] and naphthalene [13,14]. If individual ion effects are additive, they will also be conservative, such that if two salts have a common anion, the difference in K_S values between salts of cation A versus cation B should be independent of the identity of the common anion. Similarly, in the case of salts with a common cation, the difference in K_S values between salts of anion X versus anion Y should be independent of the identity of the common cation. In this study:

$$\text{Na-K: } K_S(\text{NaCl})\text{-}K_S(\text{KCl}) = 0.014 \neq K_S(\text{NaBr})\text{-}K_S(\text{KBr}) = 0.030$$

$$\text{Cl-Br: } K_S(\text{NaCl})\text{-}K_S(\text{NaBr}) = 0.022 \neq K_S(\text{KCl})\text{-}K_S(\text{KBr}) = 0.038$$

Similarly, there are many additional examples for toluene [21], including:

$$\text{Na} - \text{K:}$$

$$K_S(\text{NaCl}) - K_S(\text{KCl}) = 0.062$$

$$\neq 0.5*[K_S(\text{K}_2\text{SO}_4) - K_S(K_2\text{SO}_4)] = -0.012$$

$$\text{SO}_4 - 2*\text{Cl:}$$

$$K_S(\text{Na}_2\text{SO}_4) - 2*[K_S(\text{NaCl})] = 0.116$$

$$\neq K_S([\text{NH}_4]_2\text{SO}_4) - 2*[K_S(\text{NH}_4\text{Cl})] = 0.305$$

This contrasts with data for benzene [12], for example:

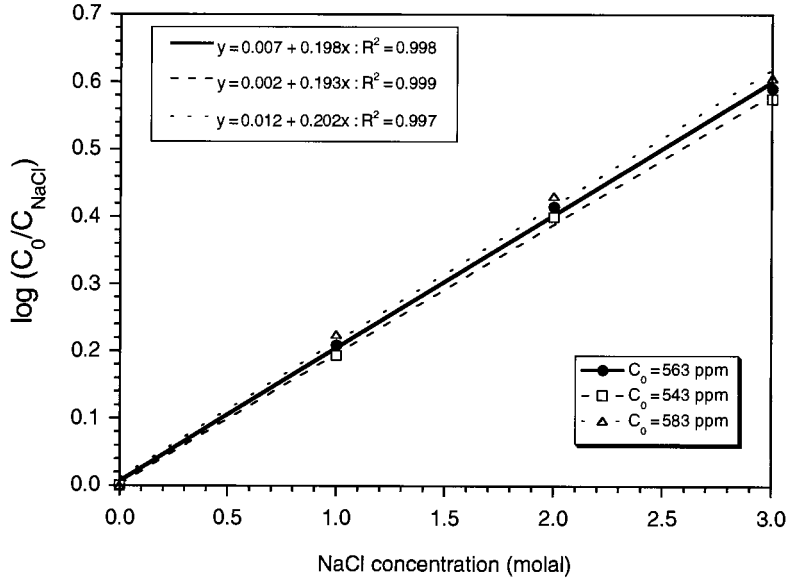

Fig. 2. Example of dependence of K_S value upon C_0 (toluene solubility in distilled water).

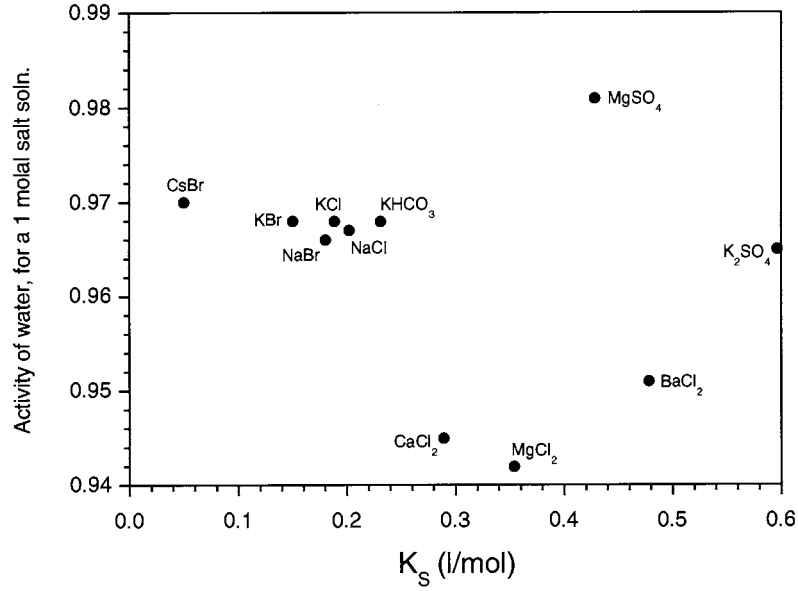

Fig. 3. Variation of activity of water for a 1 molal salt solution versus salting-out coefficient, K_S.

Na – K:

$$K_S(\text{NaCl}) - K_S(\text{KCl}) = 0.029$$

$$\approx K_S(\text{NaBr}) - K_S(\text{KBr}) = 0.026$$

Cl – Br:

$$K_S(\text{NaCl}) - K_S(\text{NaBr}) = 0.040$$

$$\approx K_S(\text{KCl}) - K_S(\text{KBr}) = 0.047$$

Similarly, direct experimental measurements of the solubility of naphthalene demonstrates addi-

tive behavior for binary mixtures of NaCl with either $MgCl_2$, Na_2SO_4, CsBr, $CaCl_2$, and KBr [13], and also artificial and natural sea water [14], although mixtures of NaCl with organic salts ($(n\text{-}C_4H_9)_4NBr$, $(CH_3)_4NBr$, and $C_4H_9SO_3Na$) were non-additive [13].

A possible explanation for the non-additive behavior observed for toluene in salt solutions compared to the additive behavior observed for benzene and naphthalene in inorganic salt solutions may be the slightly polar nature of toluene (dipole moment of 0.45 debyes: [19]) versus the non-polar nature of benzene and naphthalene. The slightly polar nature of toluene suggests that specific electrostatic interaction between toluene and ions in solution is possible, whereas similar interaction between non-polar benzene and naphthalene with ions in solution is unlikely. The exact mechanism whereby specific interaction between the organic compound and ions in solution is responsible for non-additive salt behavior is unclear, but is consistent with the observation that naphthalene exhibits non-additive behavior for mixtures of NaCl with organic salts [13]. In this case, specific interaction between naphthalene and the organic salts may be covalent, rather than electrostatic, in nature.

Acknowledgements

This study has been funded by an award from NSF-Environmental Geochemistry and Biogeochemistry (grant # EAR-9631735), with additional funding from the NSF-EPSCoR Biogeochemistry cluster award to the University of Wyoming (grant # OSR-9550477).

References

[1] G.P. Willhite, Waterflooding Society Petrol Engineers; Textbook Series, vol. 3, Society Petrol Engineers, Richardson, TX, 1986, p. 326.
[2] T. Sale, D. Applegate, Ground Water 35 (1997) 418.
[3] J.I. Gerhard, B.H. Kueper, G.R. Hecox, Ground Water 36 (1998) 283.
[4] G.J. Hirasaki, Soc. Petr. Eng. Form. Eval. 6 (1991) 217.
[5] H.O. Yildiz, N.R. Morrow, J. Petr. Sci. Eng. 14 (1996) 159.
[6] G.Q. Tang, N.R. Morrow, Soc. Petr. Eng. Res. Eng. 12 (1997) 269.
[7] R.P. Schwarzenbach, P.M. Gschwend, D.M. Imboden, Environmental Organic Chemistry, Wiley, New York, 1993, p. 681.
[8] S.W. Karickhoff, D.S. Brown, T.A. Scott, Water Res. 13 (1979) 241.
[9] L.C. Price, Am. Assoc. Pet. Geol. Bull. 60 (1976) 213.
[10] J. Setschenow, Z. Phys. Chem. Vierter Band 1 (1889) 117.
[11] I. Sanemasa, S. Arakawa, M. Araki, T. Deguchi, Bull. Chem. Soc. Japan 57 (1984) 1539.
[12] W.F. McDevit, F.A. Long, J. Am. Chem. Soc. 74 (1952) 1773.
[13] J.E. Gordon, R.L. Thorne, J. Phys. Chem. 71 (1967) 4390.
[14] J.E. Gordon, R.L. Thorne, Geochim. Cosmochim. Acta 31 (1967) 2433.
[15] S.S. Rossi, W.H. Thomas, Environ. Sci. Technol. 15 (1981) 715.
[16] D.G. Shaw (Ed.), Solubility Data Series. Volume 37, Hydrocarbons with water, seawater. Part 1: Hydrocarbons C_5 to C_7, Pergamon Press, New York, 1989, pp. 369–431.
[17] L.N. Plummer, D.L. Parkhurst, G.W. Fleming, S.A. Dunkle, U.S. Geological Survey; Reston; VA, Water Res. Inv. Rep. (1988) 88–4153.
[18] I.D. Zaytsev, G.G. Aseyev (Ed.), Properties of Aqueous Solutions of Electrolytes (M.A. Lazarev, V.R. Sorochenko, Trans.), CRC Press, Boca Raton, FL, 1992, p. 1773.
[19] J.A. Dean (Ed.), Lange's Handbook of Chemistry, 13th ed., McGraw-Hill, New York 1985, p. 1792.
[20] C. Sutton, J.A. Calder, J. Chem. Eng. Data 20 (1975) 320.
[21] E. Sada, S. Kito, Y. Ito, J. Chem. Eng. Data 20 (1975) 373.
[22] J.E. Desnoyers, F.M. Ichhaporia, Can. J. Chem. 47 (1969) 4639.
[23] D. Mackay, W.Y. Shiu, K.C. Ma, Illustrated Handbook of Physical-Chemical Properties and Environmental Fate for Organic Chemicals, Monoaromatic hydrocarbons, chlorobenzenes, and PCBs, vol. 1, Lewis Publishers, Boca Raton, FL, 1992, p. 697.
[24] H. Fühner, Chem. Ber. 57 (1924) 510.
[25] Y. Marcus, Ion Solvation, Wiley, New York, 1985, p. 306.
[26] R.L. Brown, S.P. Wasik, J. Res. Nat. Bur. Stds. (A. Phys. Chem.) 78A (1974) 453.
[27] D.F. Keeley, M.A. Hoffpauir, J.R. Meriwether, J. Chem. Eng. Data 33 (1988) 87.
[28] D. Mackay, W.Y. Shiu, Can. J. Chem. Eng. 53 (1975) 239.

ELSEVIER

Talanta 48 (1999) 643–648

Talanta

Piezoelectric detection of ion pairs between sulphonate and catecholamines for flow injection analysis of pharmaceutical preparations

Zhihong Mo [a,*], Xiaohui Long [a], Minjuan Zhang [b]

[a] *College of Chemistry and Chemical Engineering, Chongqing University, Chongqing 400044, China*
[b] *Qinghai Provincal Institute of Drug Control, Xining 810001, China*

Received 25 February 1998; received in revised form 21 August 1998; accepted 26 August 1998

Abstract

Fundamentals of ion-pair flow injection with piezoelectric detection were investigated experimentally and theoretically for the adsorption of dodecyl phenylsulfonate and interfacial ion-pair formation with epinephrine and L-dopa on silver electrode of quartz crystal microbalance. The influences of sulfonate concentration and operating parameters on the frequency response were demonstrated and provided the possibility for the discriminating determination of mixtures. The selected system of ion-pair flow injection with piezoelectric detection was applied to the determination of epinephrine and L-dopa. Calibration curves were linear in ranges 4.00–850 and 3.50–730 μg ml^{-1}, with detection limits of 1.22 and 1.05 μg ml^{-1} and sampling frequencies of 120 samples h^{-1}, for epinephrine and L-dopa, respectively. The method has been satisfactorily applied to the determination of catecholamines in pharmaceutical preparations.

Keywords: Ion-pair; Piezoelectric detection; Flow injection; Catecholamines

Ion-pair formation using surfactants has been widely applied in high-performance liquid chromatography and flow injection analysis. Since the initial work of Karlberg and Thelander on the determination of caffeine in acetylsalicylic acid preparations [1], a number of ion-pair formations with automated flow injection solvent extraction to drug evaluation have appeared [2]. However, solvent extraction required separation of ion-pair from carrier costs the method incorporation of a segmenter and consumption of organic solvent, and hereby the applicability is greatly limited.

Recently, a new method, ion-pairing flow injection with piezoelectric detection, without liquid–liquid extraction and phase separation, has been developed and applied to determinations of several pharmaceuticals [3,4]. This method has been based on in situ mass sensing of the adsorption of a surfactant on a piezoelectric crystal surface, and performed detection of ion-pair formation simultaneously with desorption of the surfactant on the crystal surface. In this paper, the fundamental

* Corresponding author.. E-mail: zhihmo@cqu.edu.cn.

0039-9140/99/$ - see front matter
PII: S0039-9140(98)00287-2

considerations for the surface adsorption, interfacial ion-pair formation and flow injection analysis with piezoelectric detection were treated theoretically and verified experimentally, and the determination of epinephrine and L-dopa in pharmaceutical preparations was satisfactorily carried out by the developed system.

Catecholamines in pharmaceutical preparations are present in relatively large amounts, and increasing efforts have been directed towards the development of simple and reliable analytical methods. Several procedures have been reported including titrimetric, spectrophotometric, fluorimetric, chromatographic and flow injection techniques [5–10].

1. Experimental

1.1. Reagents

A sodium dodecyl phenylsulfonate (SDPS) solution (0.02 M) was prepared in water and from this dilute carrier solutions were prepared. A hydrochloric acid solution (0.10 M) was prepared to adjust the pH of carrier solutions checked by a pH meter. Stock solutions (2 mg ml^{-1}) of epinephrine and L-dopa were prepared from the Sigma product in 0.01 M hydrochloride acid and stored frozen in dark bottles before use. From these, more dilute working solutions were prepared as required. All chemicals were of analytical grade. Ion exchange-distilled water was used throughout.

1.2. Apparatus

The flow injection system was the same as described previously [3], and a similar flow-through detector of small cell volume (25 μl) was used with a 10 MHz AT-cut piezoelectric crystal plated with silver electrodes. A laboratory-made TTL–IC oscillator [11] was connected to the crystal electrodes and the oscillating frequency was monitored with a SS7200 universal counter (SJZ No.4 Electronic Factory, China). An LP-2A speed modulation pump and a V-16A four-way multifunctional automatic valve fitted with a 50 μl by-pass coil (Xintong Scientific Instrument, China) were used. Flow lines were of PTFE tubing (0.8 mm i.d.).

2. Results and discussion

2.1. Adsorption of sodium dodecyl phenylsulfonate on electrode

Solutions of SDPS in the range 0–0.012 M were passing through the flow cell at various flow-rates of 0.1, 1.0, and 5.0 ml min^{-1}. The frequency was found to decrease significantly and became stable in a time proportional to the concentration of SDPS (C_S) and the inverse of flow-rate. As more SDPS presented in water, the frequency shift with respect to water (ΔF) increased linearly at lower SDPS concentration and slowed down to a limit and subsequently decreased, as shown in Fig. 1. In comparison among cases at different flow-rates, the limited frequency shift was almost constant, but the linear slope increased with the increase of the flow-rate and nearly unchanged at high flow-rates (>5.0 ml min^{-1}).

It has been known that the oscillating frequency is changed with viscoelastic and electric properties of the solution contacting with the

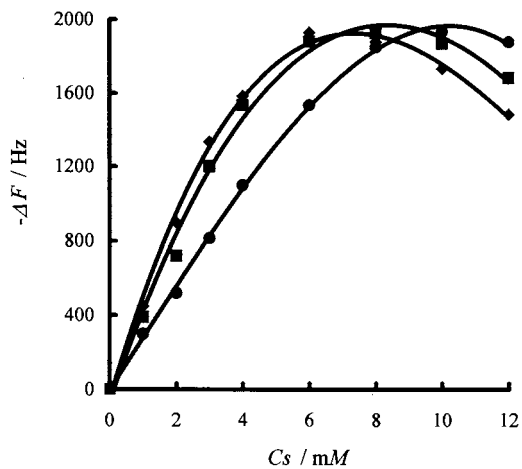

Fig. 1. Relationship of frequency shift (ΔF) with SDPS concentration (C_S) at various flow-rates: (●) 0.1; (■) 1.0; (◆) 5.0 ml min^{-1}.

electrode [11–13]. In the experiments, the density and viscosity were slightly changed with dilute surfactant solutions, and the frequency was nearly irrelevant to the conductivity of solutions by modulating the capacitor in series with the crystal [11]. Consequently, the frequency shift was caused predominantly by the small mass change of the electrode surface due to the adsorption of SDPS. According to the Sauerbrey equation, the frequency shift is linearly related to the surface concentration of adsorbates because the thin adsorption layer can be treated as being rigid [13]. Hence, curves in Fig. 1 directly demonstrate the relationship of the surface concentration (Γ) with the bulk concentration of SDPS. It can be imagined from those curves that the adsorption is based on the interaction of the electrode with hydrophobic groups of free surfactant molecules and reduced by the formation of micelle among surfactant molecules at high surfactant concentrations. The linear regime of $\Delta F - C_R$ curves can be described by the following equations:

$$\Delta F = -a\Gamma \quad \Gamma = KC_S \tag{1}$$

where $a = 0.226$ Hz cm^2 ng^{-1} for a 10 MHz crystal, K is an adsorption constant of the surfactant influenced by the flow-rate.

2.2. Response to injection of epinephrine and L-dopa

Sharp peaks occurred on the graph of the frequency versus time, responded to injections of epinephrine and L-dopa, as shown in Fig. 2. Injections were of relatively small volume and distributed completely in the long mixing coil in order to avoid the effect of bulk properties of injections on the frequency response. Accordingly, the peak corresponds to the change of surface SDPS concentration ($\Delta\Gamma$), which should be caused by both interfacial and homogeneous ion-pair formations between epinephrine or L-dopa and SDPS on the surface and in the bulk, and may also caused by distribution of SDPS in the mixing coil. The latter, however, was found to be much smaller by injection of a blank solution. It illustrated that the desorption by the decrease of bulk SDPS was too slow to keep pace with the

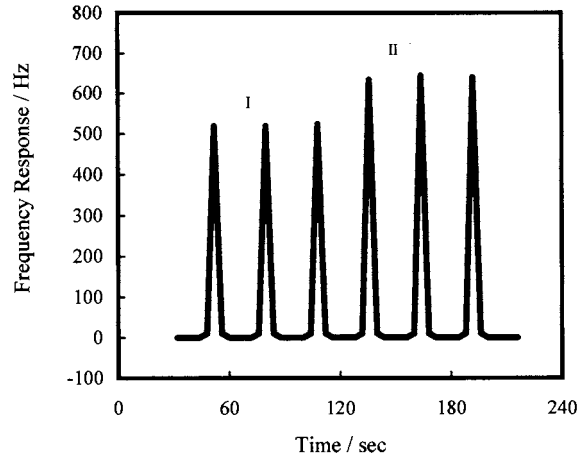

Fig. 2. FIA response of frequency versus time to injection of epinephrine (I) and L-dopa (II) using SDPS as carrier. Injection concentration, 300 μg ml^{-1}; concentration of SDPS, 0.004 M; flow-rate, 2.0 ml min^{-1}; and length of mixing coil, 250 mm.

injection band. Hence, in the linear adsorption regime of SDPS, the frequency response to an injection of catecholamine, nearly the peak height (f_p) for a sharp peak, can be obtained as follows:

$$f_p = -a\Delta\Gamma$$

$$\Delta\Gamma = -k_f t K C_I C_S [1 - kTC_S(D-1)/D]/D \tag{2}$$

where k, T, k_f and t are rate constants and reaction times for the homogeneous and interfacial ion-pair formation, respectively; C_I is the injection concentration; and D is the distribution degree in the mixing coil. In the experiments, $D \gg 1$, then

$$f_p = AC_I, \quad A = ak_f t K C_S (1 - kTC_S)/D \tag{3}$$

Hereby, the peak height is proportional to the injection concentration and can be applied to the determination of catecholamine concentration with an ascertained flow injection system using a fixed solution of SDPS as a carrier. As can be seen in Fig. 2, the frequency response to injection of L-dopa is more sensitive than that of epinephrine. According to Eq. (3), it implies that the rate constant for interfacial ion-pair formation of L-dopa is greater than that of epinephrine.

2.3. Effect of concentration of sodium dodecyl phenylsulfonate solution

The effect of the concentration of SDPS on the peak height is shown in Fig. 3. A flow-rate of 2.0 ml min^{-1} and an injection concentration of 300 μg ml^{-1} were fixed in experiments. The peak height was found to increase before achieving a maximum and subsequently decrease with higher surfactant concentrations. As can be seen, the maximum peak height and the corresponding concentration of L-dopa were larger and lower than those of epinephrine, respectively.

According to Eq. (3),

$$\partial f_p/\partial C_S = ak_f tKC_E C_S(1 - 2kTC_S)/D \quad (4)$$

It can be derived out by Eqs. (3) and (4) that the peak height achieves the maximum, $f_{pm} = ak_f tKC_E/4kTD$, at the corresponding concentration, called frequency-limited concentration, $C_k = 1/2kT$, and decreases to zero at $2C_k$. Here, the frequency-limited concentration of SDPS is only governed by the rate constant and reaction time for the homogeneous ion-pair formation in the mixing coil, unaffected by the concentration of injection and other factors. Once the experimental is fixed, the concentration, C_k, is only proportional to the inverse of rate constant, k, depended on the substance forming the ion-pair. It is implied that the value of C_k could be applied to the discriminating determination of mixtures.

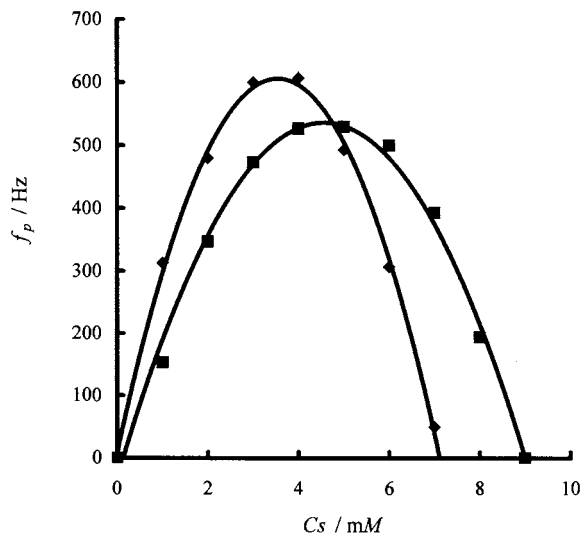

Fig. 3. Effect of SDPS concentration (C_S) on peak height (f_p) for injection of epinephrine (■) and L-dopa (◆). Injection concentration, 300 μg ml^{-1}; flow-rate, 2.0 ml min^{-1}; and length of mixing coil, 250 mm.

The peak height was found to change slightly with the change of the carrier pH in the range of 3–7. However, it decreased and increased sharply with lower carrier pH as pH < 3, using 2.00 mM and 6.00 mM surfactant carrier, respectively. The reason is that the concentration of free SDPS anion, C_S, decreases in strong acidic medium. Consequently, the carrier pH influences the peak height by way of the effect of C_S on the response.

2.4. Effect of operating parameters

As has been derived from Eq. (3), the peak height is relevant to the distribution degree (D) and reaction times (t and T), following $\partial f_p/\partial t > 0$, $\partial f_p/\partial T < 0$ and $\partial f_p/\partial D < 0$ when $kTC_S < 1$. In experiments, those affecting factors were controlled by three operating parameters, volumes of the mixing coil and injection (V and V_i) and the flow-rate (u). Actually, the relations of those affecting factors with the operating parameters are difficult to describe quantitatively. Qualitatively, the increase in u leads to shorter t and T, the increase in V leads to longer T and higher D and the increases in V_i leads to lower D.

The peak height was found to increase with faster flow-rates in the range of 0.5–1.5 ml min^{-1}, which indicates that the increase of peak height caused by shorter T is greater than the decrease by shorter t. When the flow-rate increased over 1.5 ml min^{-1}, the peak height was found to decrease, which indicates that the increase by shorter T is less than the decrease by shorter t. In addition, slower flow-rates below 0.1 ml min^{-1} resulted in wider peak widths as the re-adsorption of SDPS in the carrier was slowed down.

With lower volume (length) of mixing coil, the peak was found to be higher and sharper. But the frequency tended to irregularly changed with the injection concentration of catecholamines as the length of mixing coil was less than 250 mm (V = 125 μl) at 50 μl of the injection volume. With the

Table 1
Determination of epinephrine and L-dopa in pharmaceutical preparations

Sample[a]	Nominal value (mg ml^{-1})	Added (mg ml^{-1})	Titrimetric method found[b] (mg ml^{-1})	FIA method found[b] (mg ml^{-1})	Recovery (%)
Epinephrine ampoules	1.0		0.98 ± 0.003	0.976 ± 0.003	
		0.500		0.497 ± 0.002	99.4
Epinephrine ampoules	0.50		0.47 ± 0.005	0.485 ± 0.001	
		0.500		0.498 ± 0.002	99.6
Epinephrine tablets[c]	10.0		9.83 ± 0.008	9.92 ± 0.03	
		5.00		5.02 ± 0.03	100.4
L-dopa tablets[c]	10.0		9.92 ± 0.005	9.91 ± 0.02	
		5.00		5.01 ± 0.02	100.2

[a] Supplied by three Chinese manufactures.
[b] Average of five determinations ± SD.
[c] Prepared by dissolving the tablet in 25 ml of distilled water.

increase of injection volume, the peak height was found to increase. However, when the injection volume was larger than 50 μl at 125 μl of the mixing coil volume, the peak height was not in a linear relation to the injection concentration of catecholamines. It implies that the distribution degree should be large enough to assure that the frequency response is not influenced by the bulk properties of injections, as mentioned above.

2.5. Calibration graph and reproducibility

As seen above, the ion-pairing flow injection system was selected as SDPS concentration of 4.00 mM, a flow-rate of 2.0 ml min^{-1}, a mixing coil of 250mm and a injection volume of 50 μl. With correlation coefficient greater than 0.9995, linear calibration graphs of the peak height relative to the blank (water) versus the concentration were obtained for epinephrine in the range 4.00–850 μg ml^{-1} with a slope of 1.75 ± 0.01 Hz ml μg^{-1}, and for L-dopa in the range 3.50–730 μg ml^{-1} with a slope of 2.03 ± 0.01 Hz ml μg^{-1}. The SDs for injections of blank and 300 μg ml^{-1} epinephrine and L-dopa (10 replicates) were 0.71, 1.26, 0.97 Hz, respectively. The detection limits (3 × noise) were 1.22 μg ml^{-1} for epinephrine and 1.05 μg ml^{-1} for L-dopa. The relative SDs (10 replicates) were 0.24 and 0.16% for 300 μg ml^{-1} epinephrine and L-dopa, respectively. The sampling rate was about 120 samples h^{-1}.

2.6. Interference

The influence of foreign compounds that commonly company epinephrine and L-dopa in pharmaceutical preparations was studied by preparing solutions containing 300 μg ml^{-1} the catecholamine and increasing concentrations of the potential interferents up to 5 mg ml^{-1} or by adding an amount to give an error of ± 3%. The errors were determined by comparison with the peak heights given by a solution of analyte containing no foreign substances. 5 mg ml^{-1} of glucose, lactose, sucrose, asparate, citrate and tartrate were tolerated in the maximum amounts tested and 0.3 mg ml^{-1} of antipyrine, berberine, pilocarpine and sparteine hydrochloride were also tolerated in the determination of 300 μg ml^{-1} epinephrine and L-dopa.

2.7. Analysis of pharmaceutical preparations

The proposed method was satisfactorily applied to the determination of epinephrine and L-dopa in pharmaceutical preparations. Commercially available formulations were analyzed and the results obtained are summarized in Table 1. As can be

seen, for all formulations the assay results were in good agreement with values obtained by the non-aqueous titrimetric method [14]. The recoveries obtained by adding epinephrine or L-dopa to each pharmaceutical formulation are also given in Table 1.

3. Conclusions

Based on in situ monitoring of the surface concentration of the adsorbed surfactant, ion-pair flow injection with piezoelectric detection eliminates the requirement for separation between the free surfactant and ion-pair, resulting in the present simple and fast approach utilizing ion association. The sampling frequency, accuracy and precision superior to those given for conventional methods are improved by using a detector of small cell volume, and the sensitivity is also enhanced by the greater volume ratio of injection to detection cell. Moreover, the selectivity could be realized by the frequency-limited concentration of SDPS. Development would be in advance on gradient ion-pair flow injection with piezoelectric detection for the multicomponent analysis in pharmaceuticals.

References

[1] B. Karlberg, S. Thelander, Anal. Chim. Acta 98 (1978) 1.
[2] M. Valcarcel, M.D. Luque de Castro, J. Chromatogr. 393 (1987) 3.
[3] Z. Mo, M. Zhang, M. Li, Z. Xia, Anal. Lett. 30 (1997) 663.
[4] Z. Mo, J. Luo, M. Li, Analyst 122 (1997) 111.
[5] L.J. Bryan, S.R.O. Donnell, J. Chromatogr. 487 (1989) 29.
[6] M.P. Llavero, S. Rubio, A. Gomez-Hens, D. Perez-Bendito, Anal. Chim. Acta 229 (1990) 27.
[7] A. Kojlo, J. Martinez-Calatayud, J. Pharm. Biomed. Anal. 8 (1990) 663.
[8] T. Perez-Ruiz, C. Martinez-Lozano, V. Tomas, O. Val, Analyst 116 (1991) 857.
[9] T. Perez-Ruiz, C. Martinez-Lozano, V. Tomas, O. Val, Talanta 40 (1993) 1625.
[10] F.B. Salem, Anal. Lett. 26 (1993) 1959.
[11] S. Yao, Z. Mo, Anal. Chim. Acta 193 (1987) 97.
[12] S. Yao, L. Nie, Chin. J. Anal. Chem. 24 (1996) 234.
[13] M. Thompson, A.L. Kipling, W.C. Duncan-Hewitt, L.V. Rajakov, B.A. Cavic-Vlasak, Analyst 116 (1991) 881.
[14] Chinese Pharmacopoeia, part II, Chemical Industry Press and People Hygiene Press, Beijing, 1995, pp. 402.

ELSEVIER

Talanta 48 (1999) 649–657

Talanta

Design of Schiff base complexes of Co(II) for the preparation of iodide-selective polymeric membrane electrodes

Ruo Yuan *, You-Qun Song, Ya-Qin Chai, Shao-Xi Xia, Qiao-Yun Zhong, Bing Yi, Min Ying, Guo-Li Shen, Ru-Qin Yu

Institute of Chemometrics and Chemical Sensing Technology, Chemistry and Chemical Engineering College, Hunan University, Changsha 410082, China

Received 10 April 1998; received in revised form 24 August 1998; accepted 26 August 1998

Abstract

The response characteristics of some iodide-selective solvent polymeric membrane electrodes based on with *N*,*N*′-bis(salicylaldehyde-*n*-octyl) diimine cobalt(II) (Co(II)SAODI) which is a more lipophilic substitute for a previously reported iodide-carrier are described. The electrode doped with Co(II)SAODI into a plasticized poly(vinyl chloride) membrane exhibits an anti-Hofmeister selectivity pattern with high selectivity toward iodide, long lifetime and small interference from H^+. Quartz crystal microgravimetric measurements and ac impedance experiments show that the excellent selectivity for iodide is related to the unique interaction between the carriers and iodide and steric effect associated with the structure of the Schiff base ligands.

Keywords: Potentiometry; Iodide-selective electrode; Schiff base complexes

1. Introduction

Study on the anti-Hofmeister sensing materials with high selectivity for given anions is an expeditiously expanding domain in chemical sensors. Membranes based on ion exchangers such as lipophilic quaternary ammonium or phosphonium salts exhibit the classical Hofmeister behavior in which the membrane selectivity is mainly dominated by the free energy of hydration of ions involved [1,2]. Recently, electrodes using plasticized poly(vinyl chloride) (PVC) membranes doped with organometallic species and metal–ligand complexes including organotin species [3], organomercury [4,5], derivatives of vitamin B_{12} [6,7], Mn(IV) [8,9], Co(III) [10,11], Sn(IV) [12,13], Mo(V) [14] porphyrin complexes, Co(II) phthalocyanine derivatives [15] and electropolymerized Co(II) porphyrin derivative films [16] demonstrated potentiometric anion-selectivity sequences which are remarkably different from the Hofmeister pattern. These deviations are caused by the direct interaction between the central metal of the

* Corresponding author. Tel.: +86-731-8822661; Fax: +86-731-8824487; e-mail: ryuan@mail.hunu.edu.cn.

0039-9140/99/$ - see front matter
PII: S0039-9140(98)00289-6

membrane active components and analyte anion and steric effect associated with the structure of the ligand.

Schiff base complexes Co(II) can reversibly coordinate oxygen and have been extensively studied as 'model compounds' to simulate natural oxygen carriers containing a transition metal [17,18]. Recent studies showed that solvent polymeric membranes incorporating some Schiff base complexes of Co(II) as carrier exhibited considerable selectivity for iodide [19]. In this paper, the more lipophilic Schiff base complexes of Co(II) synthesized in our laboratory were incorporated into plasticized PVC membranes with 2-nitrophenyloctyl ester (*o*-NPOE) as a plasticizer to prepare electrodes with substantial improvement in selectivity toward iodide ion, long lifetime and small interference from hydrogen ion.

2. Experimental section

2.1. Reagents

Bis(2-naphtholaldehyde)ethylenediiminecobalt(II) (Co(II)napen) and bis(2-naphtholaldehyde)phenyldiiminecobalt(II) (Co(II)napophen) were prepared as reported in [20]. Bis(salicylaldehyde)ethylenediiminecobalt(II) (Co(II)salen) were prepared as described in [21–23]. The *o*-NPOE was synthesized as described by Honing [24]. The synthesis of hexadecyltrioctylammonium iodide (HTOAI) was described in [25]. PVC powder of chromatographic grade was a product of Shanghai Chemical. Redistilled deionized water and analytical grade reagents were used throughout.

2.2. Synthesis of *N,N′-bis(salicylaldehyde-n-octyl)diiminecobalt(II)*

The crude product of *N*-salicylaldehyde-*n*-octylimine (SAOI) was prepared as follows. To a solution of 3.0 g (22 mmol) salicylaldehyde in 50 ml boiling anhydrous ethanol add 2.8 g (22 mmol) *n*-octylamine. The reaction mixture was stirred and heated with reflux for 2 h and left the solution to cool to room temperature. The solvent was then removed under vacuum to leave the crude product as oil.

The Co(II)SAODI complex was prepared as follows. A warm solution of 0.91 g (4.3 mmol) $Co(CH_3COO)_2 \cdot 2H_2O$ in 25 ml of methanol was added to an ethanol solution (40 ml) of 2.0g (8.6 mmol) SAOI. The mixture was stirred and heated with reflux for 6 h in an atmosphere of nitrogen, then cooled to 0°C and allowed to stand for 12 h. The dark solid precipitate was filtered under suction, washed with anhydrous ethanol and dried in room temperature. (yield, 67%; melting point 67–69°C). Analysis: found C, 68.24; H, 8.83; N, 5.77; O, 6.82. Calculations for Co(II)SAODI: C, 68.88; H, 8.47; N, 5.35; O, 6.11. The structure of the Co(II)SAODI was identified by infrared (KBr) (Heraeus, C-H-N-O-S-Rapid Element Analyzer, Germany) and mass spectrometry(GC-17 A-QP-5000 System, Shimadzu, Japan) (see Fig. 1).

2.3. Membrane preparation

The iodide-selective solvent polymeric membrane incorporating Co(II)SAODI was prepared and assembled according to the method of Thomas and co-workers [26,27]. The membrane composition was optimized by using an orthogonal experimental design with the electrode linear response range and slope for iodide ion as the object function for optimization. The optimum composition obtained was 2.5% (w/w) ionophore, 65.5% (w/w) *o*-NPOE, and 32.0% (w/w) PVC. 25 mg Co(II)SAODI, 655 mg *o*-NPOE and 320 mg PVC were dissolved in 4 ml of freshly distilled THF and cast in 5 cm diameter glass rings on a glass plate. After drying (usually 48 h), individual membrane (0.8 cm diameter) was cut from this larger piece and mounted in electrode body for testing. The electrode membrane prepared was a thickness of 0.2 cm and a direct current resistance of 117.3 ± 0.3 kΩ (average of six determination). The other membranes containing membrane active component were prepared according to the similar to the method described above except for slight difference of the amount of composition.

2.4. Apparatus

Potentiometric and pH measurements were made with a model 901 microprocessor ion ana-

lyzer (Orion, Cambridge, MA, USA) and a Model PH-3C pH/mV meter (Rex Instrument Factory, Shanghai, China). The cells used for all mV measurements were of the following type: Hg; Hg_2Cl_2, KCl (satd.)/$NaNO_3$ (3 M)/sample solution//membrane//$NaNO_3$ M, pH 5.6 buffer/AgCl, Ag. The pH 5.6 buffer used was 1.0 M in citrate and 1.0 M in KCl. The external reference electrode was a double-junction saturated calomel electrode. Before use, the electrodes were preconditioned by soaking overnight in a Britton–Robinson buffer (B–R buffer) solution with pH 6. The B–R buffer solutions for testing the electrode function consisted of boric acid, acetic acid, and orthophosphoric acid (10 mM each), adjusted to various pH values with 1 M sodium hydroxide.

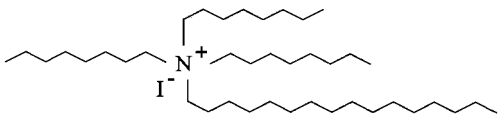

(I)

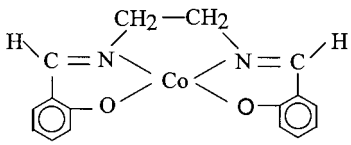

(II)

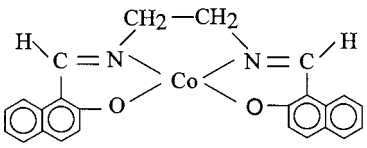

(III)

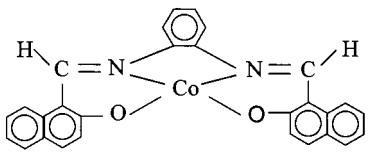

(IV)

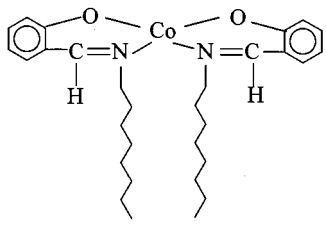

(V)

Fig. 1. Strutures of the carriers used to prepare solvent polymeric membrane electrodes [I, HTOAI; II, Co(II)salen; III, Co(II)napen; IV, Co(II) napophen; V, Co(II)SAODI].

2.5. Determination of emf response and selectivity of the electrodes

The emf measurements were carried out at 20°C by immersing the membrane electrode and the reference electrode into a glass beaker containing about 20 ml of the sample solution. Anion-selectivity coefficients, $\log K^{pot}_{I,X}$ were determined by separate solution method in a background electrolyte of pH 6.00 B–R buffer solution. The single-ion activities were calculated by using the extended Debye–Huckel equation.

2.6. Quartz crystal microgravimetric measurement

The measurement of the frequency shifts of chloroform phases were performed with a model CNN 3165 high resolution counter (Sump, Taiwan). The chloroform solutions containing 0.01 M Co(II)SAODI and the pure chloroform solutions were separately shaken with pH 6.0 B–R buffer solutions containing different concentrations of iodide over the range from 1×10^{-5} to 1×10^{-1} for 30 min and the organic phases were treated with 3% H_2O_2 in 1 M H_2SO_4 solution. The gold-coated quartz crystal was AT-cut with a fundamental resonance frequency of ≈ 8.5 MHz and used to absorb I_2 in the chloroform for 15 min to record the frequency shifts ΔF_1, ΔF_2, respectively. The chloroform phase containing 0.01 M Co(II)napophen was treated with the B–R buffer solutions containing different concentrations of I^- in the same manner as mentioned above to obtain the frequency shifts ΔF_3.

2.7. Ac impedance experiments

The ac impedance of the solvent polymeric membrane, plasticized with *o*-NPOE and containing 2.7 mmol of Co(II)SAODI, was measured with the PAR M368-2 system (EG&G Princeton

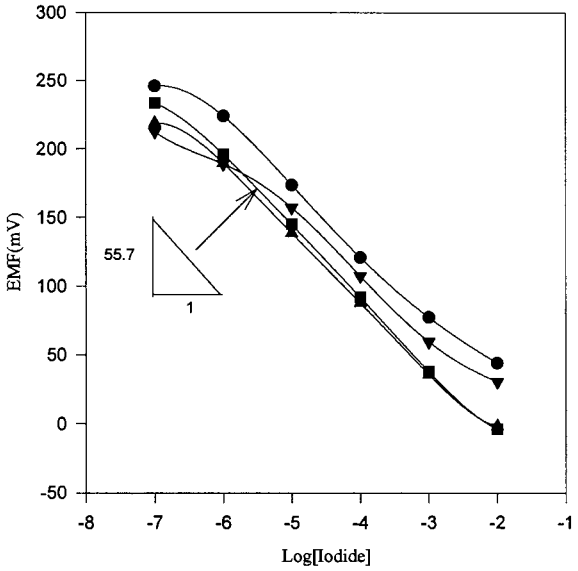

Fig. 2. Effect of the pH on the potentiometric response curves of the membrane electrode doped with Co(II)SAODI. The pH values of the B–R buffer were (●) 4.00; (■) 6.00; (▲) 8.00; (▼) 10.00.

Applied Research, Princeton, NJ) in pH 6.0 B–R buffer solution containing different concentrations of iodide. The working electrode was a Ag/AgCl foil with 0.5 cm^2 area. A Pt foil 0.5 cm^2 area and a saturated calomel electrode as a counter electrode and a reference electrode, respectively. The frequency range and ac amplitude used were 10^{-2}–10^5 Hz and 15 mV, respectively (at 18°C).

3. Results and discussion

3.1. Emf response characteristics and selectivity of electrodes based on Schiff base complexes of cobalt(II)

Three different buffers, B–R buffer at pH 4.00, 6.00, and 8.00, 10^{-2} M Tris–HCl, pH 7.00 and 10^{-2} M NaH_2PO_4–NaOH, pH 7.00, were used to study the effect of the pH on the response of the electrodes doped with Co(II)SAODI to iodide. Fig. 2 shows the results obtained when the electrode was immersed into the B–R buffer solutions with different pH values. The B–R buffer solutions with pH 4.00–8.00 were suitable buffers for the determination of iodide, and at pH 6.00, the analytical signal of the electrode presented better slopes and detection limits for iodide. The detection limits of the electrode deteriorate when the 10^{-2} M Tris–HCl, pH 7.00, or the 10^{-2} M NaH_2PO_4–NaOH, pH 7.00 buffers were used. Theses detection limits were 3.2×10^{-5} and 1.4×10^{-5} I^-.

As shown in Fig. 2, the electrode incorporating Co(II)SAODI exhibited a near-Nanstian potentiometric response for 2.3×10^{-2}–8.4×10^{-7} M I^- with a detection limit of 4.7×10^{-7} M and a slope of 55.7 ± 0.2 mV/pI^- (20°C) in the B–R buffer, pH 6.00. The time required for the electrode to 90% response was < 40 s which is similar to that observed with a classical ion exchanger membrane electrode. The dc resistance of the electrode membrane was 117.3 ± 0.2 kΩ (average of six determination). The SD of the electrode potential reading over a period of 24 h in the B–R buffer with pH 6.0 containing 10^{-3} M KI was 0.3 mV ($n = 144$) and the potential readings for the electrode dipped alternately into stirred solutions of 10^{-3} and 10^{-4} M KI demonstrated a SD of 0.4 mV over 4 h ($n = 12$). After contact of the electrode with flowing tap water for 4 months, no detectable loss of performance characteristics was observed. The electrode containing Co(II)napophen and Co(II)napen separately showed the rather poor potentiometric response properties (see Fig. 3). These detection limits are 6.2×10^{-4} and 2.7×10^{-4} M KI, respectively, and the slopes are 38.5 ± 0.3, 42.4 ± 0.2 mV/pI^-, respectively.

The potentiometric selectivity coefficients toward a series of anions presented for the solvent polymeric membranes containing different carriers are shown in Figs. 5 and 6. The electrode doped with Co(II)SAODI, for instance, showed a selectivity sequence of anions in the following order: iodide $\gg$ nitrite $\sim$ thiocyanate $>$ perchlorate $\sim$ periodate $>$ bromide $>$ nitrate $>$ chloride $>$ sulfate. It is clear that this anion-selectivity pattern deviates from that of the Hofmeister pattern found with HTOAI-based membrane.

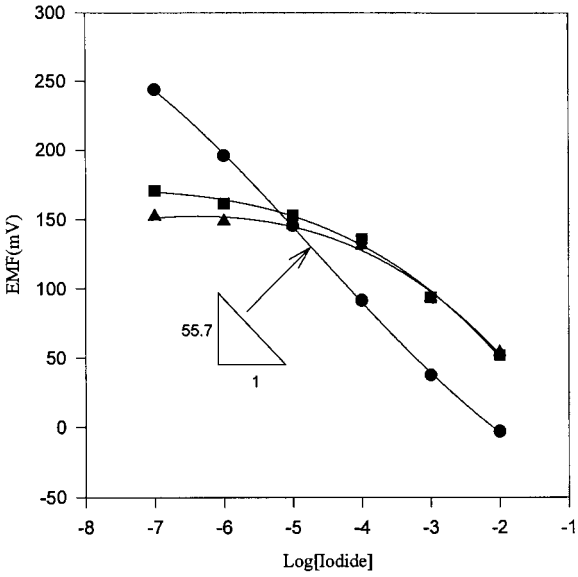

Fig. 3. Potentiometric response curves of Schiff base complexes of Co(II); (●) Co(II)SAODI; (■) Co(II)napen; and (▲) Co(II)napophen in B–R buffer with pH 6.00.

3.2. Mechanism of iodide response and selectivity

As mentioned earlier, the values of $K^{pot}_{I,SCN}$ of the PVC-based membranes containing Co(III) porphyrins as ionophores and electropolymerized [Co(*o*-NH_2)TPP] films were 1.3 [8], 5.6 [10] and 2.0×10^3 [16]. Although the selectivity coefficient between I^- and other halides (Br^- and Cl^-) of the electrode doped with metalloporphyrin complexes [10] is similar to that of the electrode incorporating Co(II)SAODI, It was noticeable that the values of the $K^{pot}_{I,SCN}$ and K^{pot}_{I,ClO_4} of the membrane containing the Co(II)SAODI were 6.3×10^{-4}, and 3.2×10^{-4}, respectively which are much less than those of membrane electrode based on metalloporphyrin complexes [10]. The unique potentiometric selectivity toward iodide must be related to the special interaction between Schiff base complexes of Co(II)SAODI and iodide ion. The Co(II) Schiff base complexes in the organic phase can serve as a coordinating site for iodide ion to form five-coordination [28,29] and the Fig. 4 demonstrates the possible response mechanism. As shown in Figs. 5 and 6, the electrode doped with Co(II)SAODI exhibited higher potentiometric selectivity toward iodide ion than that containing Co(II)salen, since Co(II)SAODI possesses stronger lipophilicity and steric structure of the ligand. The potentiometric response characteristics of the electrodes incorporating different carriers deteriorated in the following order: Co(II)SAODI > Co(II)napen > Co(II)napophen (see Figs. 2 and 3). Indeed, the equatorial plane of the Schiff base complexes of Co increases with increasing conjugation of the complexes, and the complexes containing naphthyl ridicals with the stronger conjugation than that containing phenyl radicals decreased the π electron density in the vicinity of the Co atom and weaken the interaction between the complexes and iodide [29,30]. The potentiometric response characteristics to ward iodide observed by the electrodes doped with different carriers were in fair agreement with the rule above (see Figs. 1 and 3). Figs. 5 and 6 also show that the values of the anion-selective coefficients of the electrodes doped with different ionophores determined by separate solution method (SSM) is better than that by mixed solu-

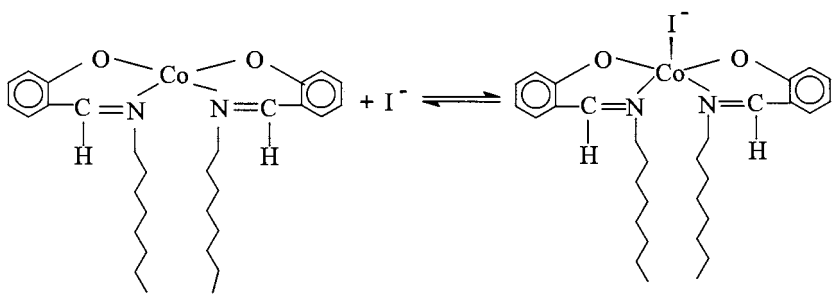

Fig. 4. Suggested coordination scheme of Co(II)SAODI with iodide.

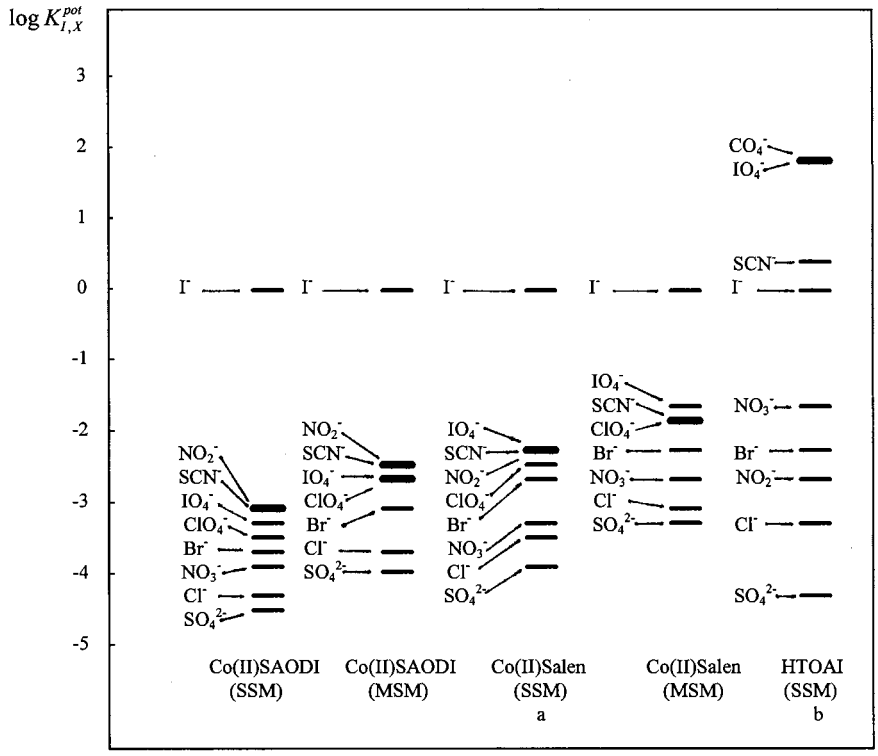

Fig. 5. Comparison of the selective coefficients, log $K^{pot}_{I,X}$ for the solvent polymeric membrane containing different active components. The present data were determined by the separate solution method (SSM) and the mixed solution method (MSM—the interferent concentration was kept at the level of 10^{-2} M), respectively. [a]From [19]. [b]HTOAI membrane was prepared with 63 wt.% *o*-NPOE, 32 wt.% PVC and 5 wt.% HTOAI.

tion method (MSM, the interferent concentration was kept at the level of 10^{-2} M), and the $\Delta\log K^{pot}_{I,X}$ obtained by the both methods is 0.2–1.

The effect of pH on the potentiometric response characteristics of the electrode incorporating Co(II)SAODI with a higher lipophilicity is small compared with electrode containing Co(II)salen (see Fig. 2 and [19]), when the pH values of the buffer solution are $8.00 > pH > 4.00$. In the solution with $pH > 8.00$, the potentiometric response properties of the electrode slightly deteriorated and the observation can be explained by hydroxide-coordinated central metal interference.

In order to identify the potentiometric response results obtained and further prove that the Co(II) Schiff base complexes is important for inducing iodide selectivity, the quartz crystal microgravimetric measurements and the ac impedance experiments were undertaken. The quartz crystal microgravimetric measurements were performed to confirm the existence of I_2 yielded from the oxidation of I^- which was transferred from aqueous phase into organic phase, by the deliberative addition of hydrogen peroxide as oxidizer. As shown in Fig. 7, the frequency shifts ΔF which were related to the interactions of the 10^{-2} M Co(II)SAODI in chloroform with the aqueous solutions containing I^- remarkably increased with increasing the concentrations of I^- in the aqueous solutions, and in the systems of carrier-free chloroform treated with the aqueous solutions containing different concentrations of I^-, no significant increase of ΔF was observed. The values of ΔF which were corresponded to the system of 10^{-2} M Co(II)napophen in chloroform treated with the aqueous solutions containing I^- is smaller than those of ΔF. The results obtained above indirectly proved that the transfer of I^-

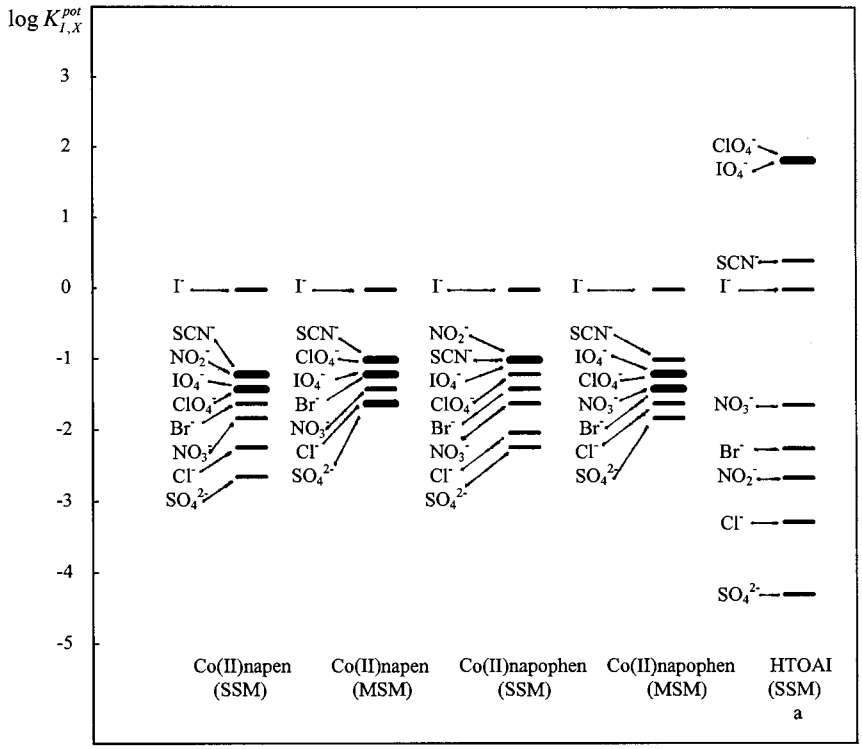

Fig. 6. Comparison of the selective coefficients, log $K_{I,X}^{pot}$ for the solvent polymeric membrane containing different active components. The present data were determined by the separate solution method (SSM) and the mixed solution method (MSM, the interferent concentration was kept at the level of 10^{-2} M), respectively. [a]HTOAI membrane was prepared with 63 wt.% *o*-NPOE, 32 wt.% PVC and 5 wt.% HTOAI.

across water/organic interface was taken up by Co(II) Schiff base complexes in the membrane phase.

The ac impedance of a solvent polymeric membrane containing 2.7 mmol of Co(II)SAODI conditioned in pH 6.00 B–R buffer solution containing 10^{-4} KI M were illustrated in Fig. 8. A well-resolved buck and surface impedance at high frequency region in addition to Warburg impedance at low frequency region were observed. The buck resistance decreased with increasing the concentration of KI: 50.2 kΩ cm in 10^{-6} M KI; 42.4 kΩ cm in 10^{-5} M KI; 38.2 kΩ cm in 10^{-4} M KI; and 35.7 kΩ cm in 10^{-3} M KI. It was evident that Co(II)SAODI could dominate iodide ion across the solvent polymeric membrane and the transfer process is diffusion controlled.

3.3. Preliminary application

The electrode doped with Co(II)SAODI was applied to the determination of iodide in drug preparations. A sample of 20–25 mg of iophendylatum was burned in an oxygen bomb with 15 ml of 5% H_2O_2 and 4.0 ml of 0.5 M NaOH as the absorbate. The absorbate was heated, acidified with H_2SO_4, and diluted with water. The sample solution obtained above was determinated by potentiometric titration method with 0.00500 M Ag_2SO_4 as the titrant and the membrane electrode containing Co(II)SAODI as the indicating electrode. Fig. 9 shows the E–V curve for this type of titration using a sample solution containing 20 mg of iophendylatum. The results obtained was 30.77 ± 0.34 (w/w)% in iodide ($n = 6$), which was

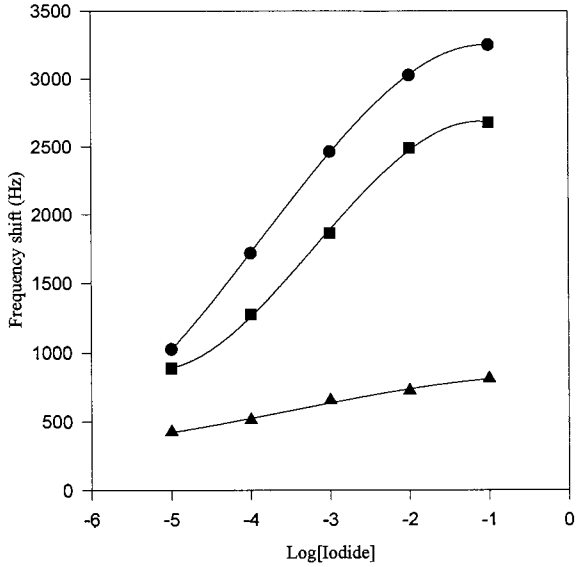

Fig. 7. Frequency shift values in different chloroform phases as a function of the concentration of iodide ion in B–R buffer (pH 6.00): (●) chloroform containing 10^{-2} M Co(II)SAODI; (■) chloroform containing 0.01 M Co(II)napophen; and (▲) carrier-free chloroform.

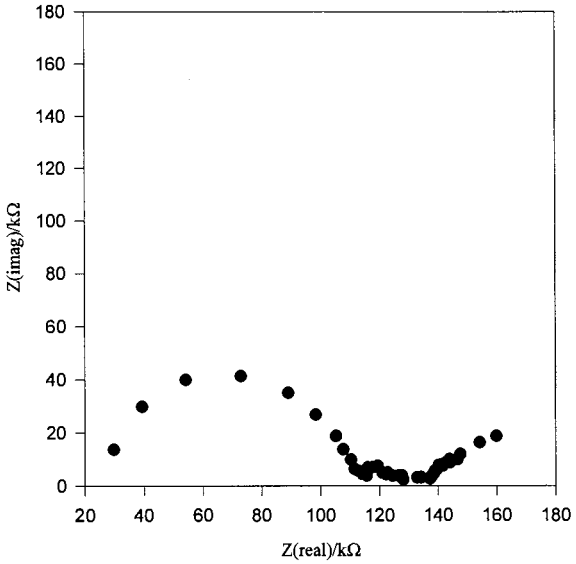

Fig. 8. Impedance plots of a membrane doped with 2.4 mmol Co(II)SAODI with *o*-NPOE as plasticizer immersed in B–R buffer containing 10^{-3} M KI (pH 6.00) (frequency, 1×10^5–1×10^{-2} Hz; ac amplitude, 15 mV; and temperature, 18°C).

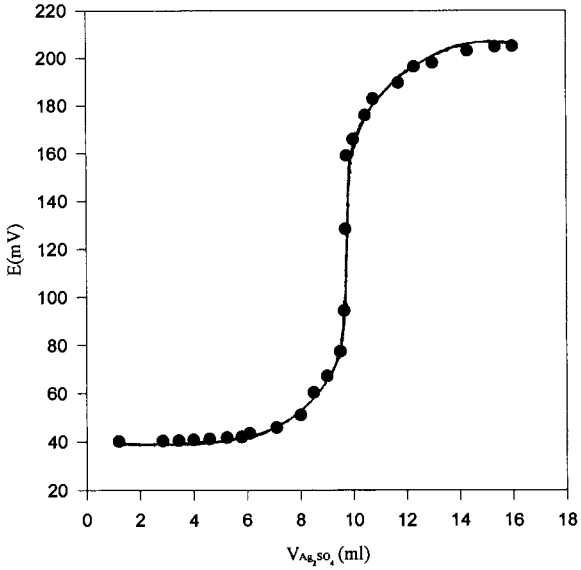

Fig. 9. E–V curve for titration of I^- in a sample solution with Ag_2SO_4.

in fair coincidence with the results [30.46 ± 0.27 (w/w)% in iodide, $n = 6$] given by precipitation method [31].

Acknowledgements

This work was supported by the National Natural Science Foundation of China and Chinese National Education committee Foundation for overseas student in addition to Natural Science Foundation of Hunan Province, China.

References

[1] K. Sollner, G.M. Shean, J. Am. Chem. Soc. 86 (1964) 1910.
[2] U. Wuthier, H.V. Pham, R. Zund, et al., Anal. Chem. 56 (1984) 535.
[3] U. Wuthier, H.V. Pham, E. Pretsch, et al., Helv. Chim. Acta 68 (1985) 1822.
[4] M.E. Meyerhoff, D.M. Pranitis, Anal. Chim. Acta 217 (1989) 123.
[5] R. Yuan, S.-Q. Lin, G.-L. Shen, D-Y. Tian, R.-Q. Yu, Acta Chim. Sini. 54 (1996) 516.
[6] P. Schulthess, D. Ammann, B. Krautler, C. Caderas, R. Stepanek, W. Simon, Anal. Chem. 57 (1985) 1397.

[7] R. Stepanek, B. Krautler, P. Schulthess, B. Lindemann, D. Ammann, W. Simon, Anal. Chim. Acta 182 (1986) 83.
[8] D. Ammann, M. Huser, B. Krautler, et al., Helv. Chim. Acta 69 (1986) 849.
[9] N.A. Chaniotakis, A.M. Chasser, M.E. Meyerhoff, J.T. Groves, Anal. Chem. 60 (1988) 185.
[10] A. Hodinar, A. Jyo, Chem. Lett. 198 (1988) 993.
[11] A. Hodinar, A. Jyo, Anal. Chem. 61 (1989) 1169.
[12] Q. Chang, M.E. Meyerhoff, Anal. Chim. Acta 186 (1986) 81.
[13] N.A. Chaniotakis, S.B. Park, E.M. Meyerhoff, Anal. Chem. 61 (1989) 566.
[14] H. Abe, E. Kokufuta, Bull. Chem. Soc. Jpn. 63 (1990) 1360.
[15] J.-Z. Li, X.-C. Wu, R. Yuan, H.-G. Yu, R.-Q. Yu, Analyst 119 (1994) 1363.
[16] S. Daunert, S. Wallace, A. Florido, G. Bachas, Anal. Chem. 63 (1991) 1676.
[17] E.I. Ochiai, J. Chem. Educ. 50 (1973) 443.
[18] T.G. Appleton, J. Chem. Educ. 54 (1977) 443.
[19] R. Yuan, Y.-Q. Chai, D. Liu, D. Gao, J.-Z. Li, R.Q. Yu, Anal. Chem. 65 (1993) 2572.
[20] H. Dai, J. Li, Z.-J. Han, H.-W. Chen, J. Inorg. Chem. China 4 (1988) 61.
[21] R.H. Bailes, M. Calvin, J. Am. Chem. Soc. 68 (1947) 1886.
[22] R. Deiasi, S.L. Holt, B. Post, Inorg. Chem. 10 (1971) 1498.
[23] B.T. Chen, Experimental Manual of Inorganic Chemistry, Beijing Normal University Press, Beijing, 1984.
[24] E. C. Horning, Organic Syntheses, collection vol. III, Wiley, New York, 1955, pp. 140.
[25] R.-Q. Yu, S.-S. Huang, Talanta 30 (1983) 427.
[26] G.J. Moody, R.B. Oke, J.D.R. Thomas, Analyst 95 (1970) 910.
[27] A. Graggs, G.J. Moody, J.D.R. Thomas, J. Chem. Educ. 51 (1974) 514.
[28] J.H. Burness, J.G. Dillard, L.T. Taylor, Syn. React. Inorg. Metal-Org. Chem. 6 (1976) 165.
[29] J.H. Burness, J.G. Dillard, L.T. Taylor, J. Am. Chem. Soc. 97 (1975) 6080.
[30] A.B.P. Lever, H.B. Gray, Acc. Chem. Res. 11 (1978) 348.
[31] Pharmacopoeia Committee of the Ministry of Health of China (Eds.), Chinese Pharmacopoeia, vol. 2, Chinese Health Press, Beijing, 1990.

ELSEVIER

Talanta 48 (1999) 659–667

Talanta

Flow injection turbidimetric determination of thiamine in pharmaceutical formulations using silicotungstic acid as precipitant reagent

Cícero Oliveira Costa-Neto [b], Airton Vicente Pereira [a], Clezio Aniceto [a], Orlando Fatibello-Filho [a,*]

[a] *Departamento de Química, Grupo de Química Analítica, Centro de Ciências Exatas e de Tecnologia, Universidade Federal de São Carlos, Caixa Postal, 676, CEP 13.560-970, São Carlos, Brazil*

[b] *Instituto de Química de São Carlos, Universidade de São Paulo, Caixa Postal 369, CEP 13.560-970, São Carlos, Brazil*

Received 11 June 1998; received in revised form 20 August 1998; accepted 26 August 1998

Abstract

A simple flow injection system is proposed for the determination of thiamine in pharmaceutical formulations. The determination is based on the precipitation reaction of thiamine with silicotungstic acid in acidic medium to form a thiamine silicotungstate suspension that is measured at 420 nm. Adding 0.05% (w/v) poly(ethyleneglycol) in the carrier solution (0.5 mol l^{-1} hydrochloric acid), an improvement in the sensitivity, repeatability and baseline stability of the flow injection system was obtained. The calibration graph was linear in the thiamine concentration range from 5.0×10^{-5} to 3.0×10^{-4} mol l^{-1} with a detection limit of 1.0×10^{-5} mol l^{-1}. The relative standard deviations for ten successive measurements of 1.0×10^{-4} mol l^{-1} and 2.5×10^{-4} mol l^{-1} thiamine were less than 1% and an analytical frequency of 90 h^{-1} was obtained.

Keywords: Thiamine; Flow injection; Turbidimetry; Silicotungstic acid; Pharmaceutical formulations

1. Introduction

Thiamine (Vitamin B_1) is a white crystalline powder, hygroscopic and with a nutlike taste used clinically in the treatment or prevention of beriberi [1]. Thiamine is administrated as the hydrochloride or nitrate, alone and in multivitamin preparations.

Several analytical methods have been developed for the determination of thiamine in a variety of samples [2]. Bioassay and microbiological procedures are tedious and time-consuming [3,4] while chemical methods are more accurate and rapid.

The official AOAC [5] method for determining thiamine is carried out by spectrofluorimetry after oxidation with potassium hexacyanoferrate(III) in alkaline medium to produce thiocrome, a compound with a blue fluorescence. Nevertheless, the thiocrome procedure requires a skilled technician,

* Corresponding author. E-mail: bello@dq.ufscar.br.

0039-9140/99/$ - see front matter
PII: S0039-9140(98)00293-8

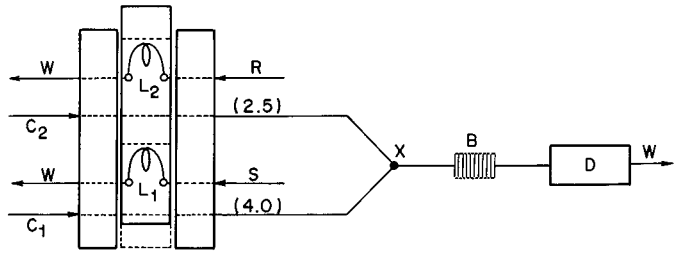

Fig. 1. Diagram of the FI system with merging zones used for thiamine determination. The peristaltic pump is not shown and broken line in the central bar of the manual injector shows the injection position. C_1, sample carrier solution (0.5 mol l^{-1} HCl containing 0.05% (w/v) poly(ethyleneglycol), flowing at 4.0 ml min^{-1}; C_2, reagent carrier solution (0.5 mol l^{-1} HCl containing 0.05% (w/v) poly(ethyleneglycol), flowing at 2.5 ml min^{-1}; *S*, sample or reference solution in 0.5 mol l^{-1} HCl containing 0.05% (w/v) poly(ethyleneglycol); *R*, reagent solution (5.0×10^{-4} mol l^{-1} silicotungstic acid in 0.5 mol l^{-1} HCl containing 0.05% (w/v) poly(ethyleneglycol); L_1, sample loop (50 cm; 250 μl); L_2, reagent loop (20 cm; 100 μl); *X*, confluence point; *B*, coiled reactor (100 cm) in a water-bath at 25°C, D, spectrophotometric cell at 420 nm and W, waste.

since the analytical steps such as oxidation of thiamine, solvent extraction and centrifugation must be performed under subdued light because both thiamine and thiocrome are light sensitive. Other procedures for the determination of this vitamin use spectrophotometry [6,7], potentiometry [8], HPLC [9–11] and polarography [12–14].

The thiocrome method was adapted in a flow injection (FI) procedure with fluorescence [15] and chemiluminescence [16] measurements.

Krug et al. [17] were the first to report on the use of turbidimetry in flow injection system for determining sulphate by monitoring the barium sulphate suspension. In spite of the routine use of flow injection systems with turbidimetric detection for the determination of inorganic species in plants and waters [18], applications to pharmaceutical products are limited. Martínez-Calatayud [19,20] has exploited the ion-association principle for turbidimetric determination of drugs in flow injection systems.

Thiamine has been determined gravimetrically by precipitation with silicotungstic acid as recommended by British Pharmacopoeia [21]. The precipitate is insoluble in water and its molecular formula was described as $[C_{12}H_{17}N_4OS]_2[Si(W_3O_{10})]_4$. However, this gravimetric procedure is tedious, once it involves several time-consuming steps such as digestion, filtration, heating to dryness and weighing.

This paper describes a flow injection turbidimetric procedure for the determination of thiamine in pharmaceutical preparations. The proposed method is based on the precipitation of thiamine with silicotungstic acid in acid medium to form a precipitate in suspension (thiamine silicotungstate) that is determined turbidimetrically at 420 nm. The method is extremely sensitive owing to the low solubility and colloidal form of the precipitate produced. The addition of 0.05% (w/v) poly(ethyleneglycol) as colloidal protector in all solutions increases both sensitivity and reproducibility and additionally it causes a reduction in washing time.

2. Experimental

2.1. Apparatus

The flow injection diagram is shown in Fig. 1. A Femto (São Paulo, Brazil) Model 432 spectrophotometer equipped with a glass flow-cell (optical path 1.0 cm) was used to measure the absorbance at 420 nm and peak heights were recorded on a Cole Parmer (Chicago, IL, USA) Model 1202-0000 x-t recorder. The solutions were pumped by a twelve-channel Ismatec (Zurich, Switzerland) Model RS 232 peristaltic pump supplied with Tygon pump tubing. Polyethylene tubing (0.8 mm id.) was used to assemble the manifold. Sample and reagent solutions were injected into the carrier streams using a laboratory-built three piece manual commutator [22] made of

Perspex, with two fixed bars and a sliding central bar.

Differential pulse polarographic measurements were performed with a Multi-Function Routine Radelkis (Budapest, Hungary) Model OH-107 polarograph.

2.2. Reagents and solutions

All reagents were of analytical-reagent grade and the solutions were prepared with water from a Millipore (Bedford, MA, USA) Milli-Q system (model UV Plus Ultra-Low Organics Water).

A 5.0×10^{-3} mol l^{-1} thiamine stock solution was prepared by dissolving 0.1686 g of thiamine hydrochloride (Sigma, St. Louis, USA) in 100 ml calibrated flask with 0.5 mol l^{-1} HCl. Reference solutions were prepared by proper dilution of the stock solution with 0.5 mol l^{-1} HCl containing 0.05% (w/v) poly(ethyleneglycol). All solutions were prepared just before injections into the FI system and were protected from light.

A 1.0×10^{-2} mol l^{-1} silicotungstic acid stock solution was prepared by dissolving 1.4392g of the solid (Merck) in 50 ml calibrated flask 0.5 mol l^{-1} HCl containing 0.05% (w/v) poly(ethyleneglycol) as colloidal protector. Reagent solutions were prepared by proper dilution of the stock solution with the same HCl solution.

2.3. Sample preparation

Ten tablets were ground to a fine powder using a mortar and pestle. An accurately weighed amount of the resulting powder of 25–100 mg was transferred to a 100 ml beaker containing 25 ml of 0.5 mol l^{-1} HCl containing 0.05% (w/v) poly(ethyleneglycol) and was stirred for 10 min. The suspension was filtered through a Whatman no. 1 filter paper and the solid was washed twice with the same HCl solution. The filtered solution was collected in a 100 ml calibrated flask and the volume was made up with 0.5 mol l^{-1} HCl solution containing 0.05% (w/v) poly(ethyleneglycol).

An aliquot of thiamine injection (ampoule) was transferred to a 100 ml calibrated flask and diluted to volume with 0.5 mol l^{-1} HCl solution containing 0.05% (w/v) poly(ethyleneglycol).

2.4. Polarographic procedure

A DC polarographic method proposed by Lingane and Davies [13] was adapted to a differential pulse polarographic mode using multiple standard additions method for thiamine determination in pharmaceutical formulations. All differential pulse polarograms of thiamine were obtained in 0.1 mol l^{-1} KCl solution using a saturated calomel electrode as reference. The potential was scanned from 0 to -1.70 V and peak currents were measured at peak potential (E_p) of -1.25 V.

2.5. Flow diagram

The flow injection merging zones diagram is shown in Fig. 1. When the central bar of the injector was moved to the injection position, sample (L_1, 250 μl) and reagent (L_2, 100 μl; 5.0×10^{-4} mol l^{-1} silicotungstic acid) were injected simultaneously as individual zones into the 0.5 mol l^{-1} HCl containing 0.05% (w/v) poly(ethyleneglycol) carrier streams (C_1 and C_2; flowing at 4.0 and 2.5 ml min^{-1}, respectively) and merged at confluence point x. The thiamine silicotungstate suspension formed in the reaction coil B (0.8 mm id, 100 cm) was transported by this carrier to the detector flow-cell (D) and the absorbance was monitored at 420 nm.

3. Results and discussion

3.1. Preliminary studies

The flow system characteristics were initially evaluated using a coloured compound (0.01% (w/v) potassium hexacyanoferrate (III)) as reagent solution (R) and 0.5 mol l^{-1} HCl instead of the sample solution (S) in the flow system diagram showed in Fig. 1. A systematic study then was made maintaining the flow rate of the sample solution in 4.0 ml min^{-1} and varying the flow rate of the reagent solution in the range from 1.7 to 5.1 ml min^{-1}. After that, the flow rate of the reagent solution was fixed in 4.0 ml min^{-1} and the flow rate of sample solution (0.5 mol l^{-1} HCl) was changed in the range 1.7–5.1 ml min^{-1}. Fig.

2 shows the best synchronicity obtained for a sample solution flow rate of 4.0 ml min^{-1} and reagent solution flow rate of 2.5 ml min^{-1}. An additional study of the effect of total flow-rate varying from 5.4 to 8.4 ml min^{-1}, maintaining constant the flow rate ratio, showed that the total flow-rate did not cause any effect in the analytical response. Therefore, a flow rate of 4.0 ml min^{-1} and 2.5 ml min^{-1} were selected for sample and reagent carrier solutions, respectively.

3.2. Nucleation study

During nucleation, ions in solution come together randomly and form small aggregates. Particle growth involves the addition of more ions to the primary nucleus to form a crystal. Nucleation proceeds faster than particle growth in a highly supersaturated solution, resulting in a suspension of tiny particles or a colloid [23]. On the other hand, in several FI systems involving turbidimetric detection, nucleation is a slow process that require several FI strategies to be performed [18]. Thus, the effect of carrier solution concentrations

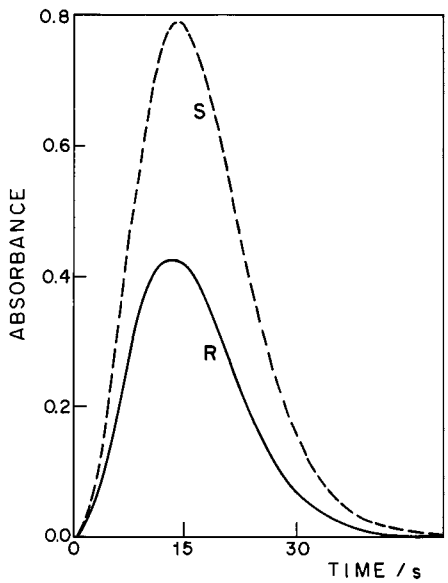

Fig. 2. Synchronicity study. *S*, sample (0.5 mol l^{-1} HCl), flowing at 4.0 ml min^{-1} and R, reagent solution (0.01% (w/v) potassium hexacyanoferrate(III)), flowing at 2.5.ml min^{-1}. The others variables were as described in Fig. 1.

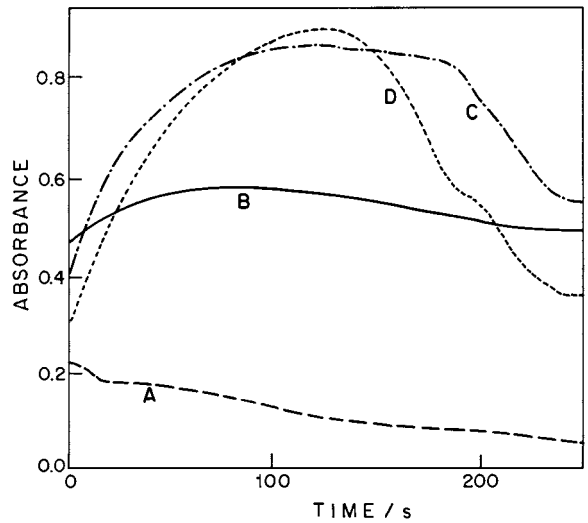

Fig. 3. Effect of silicotungstic acid concentration (*A*, 1.0×10^{-4}, *B*, 5.0×10^{-4}, *C*, 1.0×10^{-3} and *D*, 1.0×10^{-2} mol l^{-1}) on the nucleation rate of thiamine silicotungstate. The peristaltic pump was stopped at the maximum analytical signal ($t = 0$ s) and the others variables were as described in Fig. 1.

(HCl) and reagent concentration (silicotungstic acid) on the nucleation rate was also studied using the flow injection system depicted in Fig. 1. The effect of HCl concentration (carrier solution) varying from 0.25 to 1.5 mol l^{-1} on the analytical signal was studied using a 5.0×10^{-4} mol l^{-1} silicotungstic acid and thiamine in the concentrations of 5.0×10^{-5}, 1.0×10^{-4} and 2.0×10^{-4} mol l^{-1}. This study was carried out by introducing sample and reagent into the HCl carrier streams and after attaining the maximum analytical signal, the pump was stopped and the signal variation was measured until the steady state was achieved. The maximum analytical signal was attained in the 0.5 mol l^{-1} HCl. Consequently, this concentration was selected for this work.

Fig. 3 shows the effect of silicotungstic acid (reagent) concentration in the concentrations of (A): 1.0×10^{-4}, (B): 5.0×10^{-4}, (C): 1.0×10^{-3}, and (D) 1.0×10^{-2} mol l^{-1} on the nucleation rate of thiamine silicotungstate ($[C_{12}H_{17}N_4OS]_2[Si(W_3O_{10})]_4$). The peristaltic pump was stopped at the maximum analytical signal ($t = 0$ s) and the signal was recorded during 250 s. As it can be seen from this figure, the

lowest absorbance signal was obtained in 1.0×10^{-4} mol l^{-1} silicotungstic acid concentration (curve A) and the highest absorbance signal was attained in the 5.0×10^{-4} mol l^{-1} silicotungstic acid concentration (curve B). Also, at this concentration the absorbance signal was maintained practically constant during that interval of time, indicating a good dispersion and/or uniformity of the colloids in the sample zone. Therefore, this concentration was selected for this work. In the experimental conditions adopted, the nucleation rate of thiamine silicotungstate was rapid as expected owing to the low solubility of this compound. On the other hand, the precipitate produced is essentially in colloidal form, and no problem was observed such as blockage of the conduits or accumulation of precipitate in the flow-through cell, as commonly observed in previous flow injection turbidimetric procedures [18].

3.3. Influence of manifold parameters

The merging zones configuration was chosen because very small volumes of reagent (silicotungstic acid) is consumed in each injection and provides good repeatability, baseline stability and lower washing time. An asymmetrical merging zones flow system similar to that proposed by Bergamin et al [24] was developed in order to diminish the sample dilution at point x (Fig. 1), leading thus to higher sensitivity. The manifold parameters was conveniently determined by using a diluted yellow solution (potassium hexacyanoferrate(III)) in the study of the synchronization of the sample and reagent zones to each variation in the flow rate of the sample or reagent carrier stream. In order to check these preliminary results, additional experiments were carried out. The flow rates of the sample and reagent carrier streams were optimized in the flow rate range from 1.7 to 5.1 ml min^{-1} with L_1 and L_2 loop volumes of 250 μl and 125 μl, respectively, by an univariate approach. In this experiment, 1.0×10^{-3} mol l^{-1} silicotungstic acid and three different concentrations of thiamine (1.0×10^{-4}, 2.0×10^{-4} and 3.0×10^{-4} mol l^{-1}) were injected into the 0.5 mol l^{-1} HCl carrier streams. A 4.0 and 2.5 ml min^{-1} flow rates were selected to sample and reagent carrier stream, respectively as a compromise between sensitivity and sample throughput rate. A higher flow rate of the sample carrier stream was found to give the best sensitivity probably due to lower dispersion of the sample zone.

The effect of the sample and reagent injection volumes injected was studied by varying the volumes of L_1 and L_2 loops between 62.5–500 μl and 25–125 μl, respectively. The absorbance increased with increasing volumes up to 250 μl for sample and 100 μl for reagent, above which it remained practically constant. Therefore, 250 and 100 μl volumes were chosen to the sample and reagent, respectively.

The effect of the reactor coil length (B) was investigated in the range from 50–200 cm at constant flow rates. In this study, thiamine reference solutions in the concentration range from 1.0×10^{-4} to 4.0×10^{-4} mol ml^{-1} were used. The peak heights increased with the increases of the reaction coil up to 100 cm, above which a slight decrease was observed probably due to the dispersion of the sample zone. A 100 cm reaction coil was chosen in all further experiments.

3.4. Effect of the acidity

The effect of the HCl concentration used as carrier was tested in the concentration range from 0.25 to 1.5 mol l^{-1}. For each HCl concentration, thiamine reference solutions in the range from 1.0×10^{-4} to 3.0×10^{-4} mol ml^{-1} were injected in triplicate. The absorbance signal increased with increases in HCl concentration up to 0.5 mol l^{-1}, above which it remained constant (Fig. 4). The same results were found in the previous studies. A 0.5 mol l^{-1} HCl solution was selected in all further experiments.

3.5. Effect of colloid protectors

Colloid protectors have been used in previous flow injection turbidimetric procedures [18] as stabilisers of suspensions and to avoid adherence of the precipitate in the inner walls of the tubes and/or coils. The effect of colloid protectors poly(ethyleneglycol), ethyleneglycol, poly(vinylalcohol) and agar–agar on the sensitivity and washing time was studied in three different concentra-

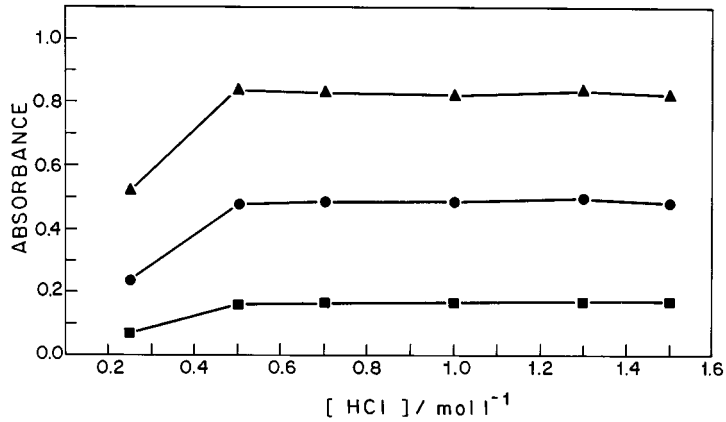

Fig. 4. Effect of HCl concentration used as carrier solutions on the analytical response for thiamine solutions in the concentrations of: (■) 1.0×10^{-4}, (●) 2.0×10^{-4} and (▲) 3.0×10^{-4} mol l^{-1}. Others variables were as described in Fig. 1.

Table 1
Effect of colloidal protector in the analytical signals of FI procedure[a]

Colloidal protector	Without	Absorbance % (w/v)		
		0.010	0.025	0.050
Poly(ethyleneglycol)	0.482 ± 0.009	0.550 ± 0.019	0.628 ± 0.005	0.667 ± 0.009
Ethyleneglycol	0.481 ± 0.012	0.583 ± 0.010	0.601 ± 0.004	0.610 ± 0.004
Poly(vinylalcohol)	0.485 ± 0.010	0.248 ± 0.006	0.174 ± 0.003	0.119 ± 0.005
Agar–agar	0.478 ± 0.008	0.154 ± 0.003	0.116 ± 0.003	0.112 ± 0.003

[a] Confidence level of 95% ($n = 5$).

tions (0.010, 0.025 and 0.050% w/v) of each compound added to all solutions (HCl carrier, sample and reagent) (Table 1). The sensitivity decreased continuously with increases in colloid protector concentration when agar–agar and poly(vinylalcohol) were used, probably due a decrease of nucleation sites and also an increase of the induction period. On the other hand, a slight increase was obtained with ethyleneglycol solution. However, a continuous increase in the sensitivity with increasing poly(ethyleneglycol) concentration up to 0.050% (w/v) was observed. In addition, better repeatability and lower washing time was obtained indicating a more uniform nucleation in the presence of this substance. Thus, 0.050% (w/v) poly(ethyleneglycol) was used in all solutions in the further experiments.

3.6. Effect of the reagent concentration

The effect of the silicotungstic acid concentration was studied in the concentration range from 1.0×10^{-4} to 1.0×10^{-2} mol l^{-1} for a 4.0×10^{-4} mol l^{-1} thiamine reference solution. Fig. 5 shows that the sensitivity increased with increases in silicotungstic acid concentration up to 5.0×10^{-4} mol l^{-1} and in higher concentration the signal gradually decreased followed by irreproducible results. This loss in the sensitivity is probably due to a variation in the size and number of precipitate particles for concentrations of silicotungstic acid higher than 5.0×10^{-4} mol l^{-1}. Therefore, 5.0×10^{-4} mol l^{-1} silicotungstic acid was chosen for further experiments.

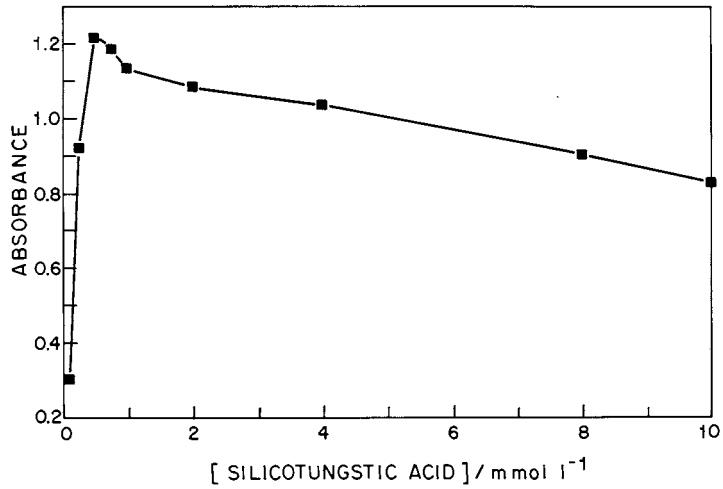

Fig. 5. Effect of the silicotungstic acid concentration used as reagent on the analytical response in the concentration range of 1.0×10^{-4} to 1.0×10^{-2} mol l^{-1} for 4.0×10^{-4} mol l^{-1} thiamine. Others variables were as described in Fig. 1.

3.7. Interference and recovery studies

The potential interference of excipients, salts and other vitamins which are commonly used in pharmaceutical preparations was evaluated. In this study, three known concentrations (1.5×10^{-5}, 1.5×10^{-4} and 1.5×10^{-3} mol l^{-1}) of these substances were injected in the flow system together a 1.5×10^{-4} mol l^{-1} thiamine reference solution. No interference in the flow injection procedure was observed for lactose, sucrose, starch, glycerol, saccharin, glucose, ascorbic acid, copper sulphate, manganese sulphate, magnesium sulphate, zinc sulphate, ferrous sulphate, vitamin A, vitamin E, cianocobalamine and pyridoxine hydrochloride. The presence of riboflavin (vitamin B_2) caused an increase in the peak height on the thiamine determination at 420 nm. This interference was removed by displacing the wavelength to 520 nm or by injecting a 0.5 mol l^{-1} HCl solution instead of reagent solution, in order to obtain the absorbance of the colour sample containing riboflavin, which is typically yellow.

Table 2
Recoveries from commercial samples spiked with three different amounts of thiamine

Sample	Thiamine(mg l^{-1})		Recovery (%)
	Added	Found	
Benerva	26.8	26.2	97.8
	40.4	39.2	97.0
	66.2	65.0	98.2
Doxal	26.8	27.0	100.7
	40.4	39.6	98.0
	66.2	67.2	101.5
Citineurin Ampoule	26.8	25.8	96.3
	40.4	38.8	96.0
	66.2	68.2	103.0

Recoveries from commercial samples spiked with three different amounts of thiamine are presented in Table 2. In this study, 1.5×10^{-5}, 1.5×10^{-4} and 1.5×10^{-3} mol l^{-1} of thiamine were added to each sample. Recoveries between 96.0 to 103.0% of thiamine from samples of three pharmaceutical formulations were obtained using the FI – turbidimetric procedure. This is good evidence of the accuracy of the proposed procedure.

3.8. Temperature effect

The study of temperature in the range from 15 to 45°C on the analytical response was investigated. The best temperature found was 25°C, thus this temperature was used in the further experiments.

Table 3
Comparison of results obtained by polarographic and proposed FI method for thiamine determination[a,b,c]

Sample	Label value	Polarographic	FI-method	Relative error (%)		C.V. (%)
	mg/tablets ou mg/ampoule			Re_1	Re_2	
Citoneurim ampoule	100	102.3 ± 0.8	104.6 ± 0.7	+4.6	+2.2	0.4
Benerva	300	296.4 ± 1.1	297.6 ± 0.4	−0.8	+0.4	0.2
Doxal	30	30.6 ± 0.6	29.5 ± 0.6	−1.7	−3.6	0.5
Citoneurim Tablets	100	102.2 ± 1.7	103.6 ± 0.5	+3.6	+1.4	0.4
Cristália	50	49.2 ± 0.6	49.8 ± 0.4	−0.4	+1.2	0.9

[a] Confidence level of 95% ($n = 4$).
[b] Re_1, FI-method versus label value.
[c] Re_2, FI-method versus polarographic procedure.

3.9. Calibration graph and applications

The proposed flow injection system under the optimized conditions was applied to determine thiamine in commercial pharmaceutical formulations. The results of the analysis of thiamine in commercial formulations are presented in Table 3. As it can be seen, close agreement between the determination of thiamine by the proposed flow injection procedure and the differential pulse polarography method ($r_1 = 0.9990$) were obtained for all samples. In addition, it also agreed with those declared on the labels ($r_2 = 0.9992$) confirming the accuracy of the flow injection turbidimetric method. The calibration graph for thiamine was linear in the concentration range from 5.0×10^{-5} to 3.0×10^{-4} mol l^{-1} with a detection limit of 1.0×10^{-5} mol l^{-1}. The regression equation was $Y = -0.02 + 3177.38$ C; $r = 0.9998$, where Y is the absorbance and C the concentration of thiamine in mol l^{-1}. The relative standard deviations for ten successive measurements of 1.0×10^{-4} mol l^{-1} and 2.5×10^{-4} mol l^{-1} thiamine were $< 1\%$, and 90 measurements h^{-1} were obtained.

4. Conclusion

The flow injection merging zones procedure developed in this work allows the determination of thiamine in several pharmaceuticals products using silicotungstic acid as precipitant reagent. The proposed method is accurate, precise, economical and presented an analytical frequency of 90 h^{-1}. The addition of 0.05% (w/v) poly(ethyleneglycol) in all solutions provided an increase in both sensitivity and repeatability and also reduced the washing time.

Acknowledgements

Financial support from FAPESP (Fundação de Amparo à Pesquisa do Estado de São Paulo, Processes 91/2637-5 and 92/2637-5), PADCT/CNPq (Process 62.0060/91-3) and also the scholarships granted by CAPES to C.O. C-N and by CNPq to A.V.P and C.A are gratefully acknowledged.

References

[1] A.G. Goodman, T.W. Rall, A.S. Nies, The Pharmacological Basis of Therapeutics, 8th ed., McGraw-Hill, New York, 1992, pp.1530.
[2] R. Strohecker, H.M. Henning, Análisis de Vitaminas, Paz Montalvo, Madrid, 1967, pp. 80.
[3] A.J. Kozik, J. Biochem. Biophys. Meth. 28 (1994) 147.
[4] C. Herve, P. Beyne, E. Delacoux, J. Chrom. Biomed. Appl. 653 (1994) 217.
[5] AOAC, Official Methods of Analysis, 40th ed., Arlington, 1984, pp. 836.
[6] A.F. Danet, J. Martínez-Calatayud, Talanta 41 (1994) 2147.
[7] D. Gupta, D.E. Cadwallader, J. Pharm. Sci. 57 (1968) 112.
[8] A. Campiglio, Analyst 119 (1994) 2209.

[9] United States Pharmacopeia XXIII, US Pharmacopeial Convention, Rockville, MD, 1995, pp.1530.
[10] P. Wimalasiri, R.B.H. Wills, J. Chromatogr. 318 (1985) 412.
[11] M. Kimura, Y. Itokawa, J. Chromatogr. 332 (1985) 181.
[12] T. Vergara, D. Marín, J. Vera, Anal. Chim. Acta 120 (1980) 347.
[13] J.J. Lingane, O.L. Davies, J. Biol. Chem. 137 (1941) 567.
[14] J.P. Hart, Electroanalysis of Biologically Important Compounds, Ellis Horwood Limited, New York, 1990, pp.165.
[15] N.Q. Jie, J.H. Yang, Z.G. Zhan, Anal. Lett. 26 (1993) 2283.
[16] N. Grekas, A.C. Calokerinos, Talanta 37 (1990) 1043.
[17] F.J. Krug, H. Bergamin-Filho, E.A.G. Zagatto, S.S. Jorgensen, Analyst 102 (1977) 503.
[18] S.M.B. Brienza, F.J. Krug, J.A. Gomes-Neto, A.R.A. Nogueira, E.A.G. Zagatto, J. Flow Injection Anal. 10 (1993) 187.
[19] J. Martínez-Calatayud, P. Campins Falcó, A. Sanchez Sampedro, Analyst 112 (1987) 87.
[20] J. Martínez-Calatayud, C.P. Martinez, Anal. Lett. 23 (1990) 1371.
[21] British Pharmacopoeia, HMSO, London, 1958, pp. 49.
[22] A.V. Pereira, C. Aniceto, O. Fatibello-Filho, Analyst 123 (1998) 1011.
[23] G.A. Walton, The formation and properties of precipitates, 2nd ed. Huntington, New York, 1979.
[24] H. Bergamin-Filho, E.A.G. Zagatto, F.J. Krug, B.F. Reis, Anal. Chim. Acta 101 (1978) 17.

ELSEVIER

Talanta 48 (1999) 669–673

Talanta

Determination of sulfate ion by potentiometric back-titration using sodium tetrakis (4-fluorophenyl) borate as a titrant and a titrant-sensitive electrode

Takashi Masadome [a,*], Yasukazu Asano [b]

[a] *Department of Chemical Science and Engineering, Ariake National College of Technology, Omuta, Fukuoka 836-8585, Japan*
[b] *Laboratory of Chemistry, Department of General Education, Ariake National College of Technology, Omuta, Fukuoka 836-8585, Japan*

Received 27 June 1998; received in revised form 24 August 1998; accepted 26 August 1998

Abstract

A potentiometric back-titration method for the determination of sulfate ions using a plasticized poly(vinyl chloride) membrane electrode sensitive to a titrant is described. The method is based on ion association between the excess of 2-aminoperimidinium added to the sulfate ion in the sample and sodium tetrakis (4-fluorophenyl) borate (FPB) in the titrant. The titration end-point was detected as a sharp potential change due to an increase in the concentration of the free FPB at the equivalence point. The end-point was detected even in the presence of a 20-fold excess of common cations and anions relative to the concentration of the sulfate ion within $\sim 2\%$ of titration error. A linear relationship between the concentration of the sulfate ion and the end-point volume of the titrant exists in the sulfate ion concentration range from 2×10^{-4} to 3×10^{-3} mol l^{-1} using 10^{-2} mol l^{-1} FPB solutions as the titrant. The present method could be applied to determine sulfate ions in sea water.

Keywords: Potentiometric back-titration; Sulfate ion; 2-Aminoperimidinium bromide; Sodium tetrakis (4-fluorophenyl) borate; Plasticized poly (vinyl chloride) membrane; Sea water

1. Introduction

The determination of sulfate ions is very important in mineralogy, biochemistry and environmental samples. As a result, urgent needs have increased for simple and sensitive analytical methods for the detection and measurement of sulfate ions in environmental water. Conventional methods such as nephelometric and spectrophotometric methods for the determination of sulfate ions require laborious procedures [1–5]. Recently, ion chromatography (IC) has often been used in the determination of sulfate ion. However, the durability of the ion exchange column is limited and IC is not cost-effective. Furthermore, the problem for the determination of sulfate ions in saline water by the IC method has been indicated

* Corresponding author. Fax: +81-944-531361; e-mail: masadome@chemical.ce.ariake-nct.ac.jp.

0039-9140/99/$ - see front matter
PII: S0039-9140(98)00290-2

by Singh et al. [6]. The ion-selective electrode (ISE) method is very promising, however, so far, no highly selective and sensitive sulfate-ISEs have developed [7,8].

A potentiometric titration method could be used successfully for the determination of sulfate ions using barium chloride as a titrant and a barium ISE as an indicator electrode [9–11]. However, the life time of ISE is limited as the titration should be performed in the mixture of alcohol with water. Recently, Vytras et al. [12] reported the new potentiometric titration method for the determination of sulfate ions and applied the method to the determination of organic sulfur. Their method is based on precipitation with barium chloride followed by potentiometric back-titration of the excess of barium ion in the presence of polyethylene glycol with tetraphenylborate using simple coated-wire type plasticized poly(vinyl chloride) (PVC) membrane ISE. Kataoka et al. [13] reported direct potentiometric titration of sulfate ion using 2-aminoperimidinium (Ap) solution as a titrant and Ap-ISE as an indicator electrode. However, it is troublesome to use the ISE because the ISE is a liquid membrane type. Furthermore, the potential change at the end-point is not sharp because of its relatively high solubility product of Ap-sulfate. It is supposed that Ap tends to form an ion association with a hydrophobic anion such as tetraphenylborate derivatives rather than a sulfate ion because Ap has relatively hydrophobic properties. Therefore, potentiometric back-titration of the excess of Ap salt added to the sulfate ion using tetraphenylborate derivatives as titrants and tetraphenylborate derivatives-ISE as indicator electrodes will be a promising method for the determination of sulfate ions.

In the previous short communication [14], we reported the potentiometric determination of sulfate ions by the back-titration method described above, using our tetraphenylborate-ISE [15–18] as the indicator electrode. Among the titrants examined, a solution of sodium tetrakis (4-fluorophenyl) borate was found to be superior. In the present paper, we will report further details of our potentiometric back-titration method for the determination of sulfate ions, i.e. the effect of coexisting ions on the determination of sulfate ions and the application of the present method to real water samples.

2. Experimental

2.1. Chemicals

Poly (vinyl chloride) (PVC) (degree of polymerization, 1100) and *o*-nitrophenyl octyl ether (*o*-NPOE) were obtained from Wako Pure Chemicals, Osaka, Japan and Dojindo Laboratories, Kumamoto, Japan, respectively and were used without further purification. 2-aminoperimidinium (Ap) bromide and sodium tetrakis (4-fluorophenyl) borate (FPB) were also obtained from Dojindo Laboratories. Sodium tetrakis(3,5-bis(trifluoromethyl)phenyl) borate (TFPB) dihydrate for preparation of Ap-ISE membrane was obtained from Dojindo Laboratories. All other reagents were of guaranteed grade.

2.2. Fabrication of indicator electrodes sensitive to FPB and Ap ions

The sensing membrane of a FPB-selective plasticized PVC membrane electrode was prepared as follows. *o*-NPOE (1.0 g) and PVC powder (0.4 g) were dissolved in tetrahydrofuran (THF). The resulting solution was poured onto a flat-bottomed glass dish. The THF was evaporated under standing at room temperature for 48 h to obtain a mother membrane. The thickness of the resulting PVC membrane is ~ 0.2 mm. A disk of 0.6 cm diameter was cut from the mother membrane and glued to the membrane housing of a DKK (Denki Kagaku Keiki, Tokyo, Japan) electrode body with a THF solution of PVC as an adhesive. A solution of 5×10^{-3} mol l^{-1} NaCl and 5×10^{-3} mol l^{-1} sodium dodecylsulfate (NaDS) and an Ag–AgCl electrode were used as an inner solution and an inner reference electrode, respectively, for fabrication of the electrode based on a FPB-selective plasticized PVC membrane without an added ion-exchanger. We obtained the most stable potential when NaDS/NaCl solution was used as an inner solution. Therefore, we used this solution as an

inner solution. The electrodes were conditioned by immersing them into a 1.0×10^{-3} mol l^{-1} FPB solution for 2–3 days. The FPB-ISE was then used as the indicator electrode for back-titration of the sulfate ion by titration with the FPB solution. An Ap-ISE based on TFPB as a cationic exchanger was also prepared. The membrane was composed of *o*-NPOE (1.0 g), PVC (0.4 g) and TFPB (0.009 g). A solution of 1×10^{-2} mol l^{-1} NaCl and an Ag–AgCl electrode were used as an inner solution and an inner reference electrode, respectively. The Ap-ISE was also conditioned by immersing it into a 1.0×10^{-2} mol l^{-1} Ap solution for 2–3 days. The Ap-ISE was then used as the indicator electrode for direct titration of the sulfate ion by titration with an Ap solution.

2.3. Standard procedure of potentiometric back-titration

20 ml of an appropriate concentration of sodium sulfate solution was placed in a beaker along with 20 ml of 1.0×10^{-2} mol l^{-1} Ap solution and both were mixed for ~ 15 min. An indicator electrode and a reference electrode (DKK type 4083) were then placed into the mixed solution of Ap and sodium sulfate. The reference electrode used is a double junction type Ag/ AgCl reference electrode with 3 mol l^{-1} potassium chloride as the inner filling solution and 1 mol l^{-1} lithium acetate as the outer filling solution. The mixed solution of Ap and sodium sulfate was then titrated with the 1.0×10^{-2} mol l^{-1} FPB solution while it was stirred. The potential of the indicator electrode relative to the reference electrode was measured with an ion-meter (DKK IOL-40). The stable potential was read after the addition of an appropriate volume of the titrant. The end-point was determined by the tangential method [19].

3. Results and discussion

3.1. Measurable concentration range of the present method

Fig. 1 shows the potentiometric back-titration curves for titration of excess Ap added to the sulfate ion in the sample solution with FPB using a FPB-ISE. The magnitude of the potential change at the end-point for the back-titration of the sulfate ion is smaller than that for a titration of Ap with FPB using a FPB-ISE [14]. The end-point volumes obtained by the potentiometric back-titration curves shown in Fig. 1 were compared with theoretical end-point volumes. The theoretical end-point volume was obtained by assuming a 2.3:1 reaction [4,13] between Ap and the sulfate ion and a 1:1 reaction between Ap and FPB. The end-point volumes obtained by potentiometric back-titration curves agreed with the theoretical end-point volumes within an error less than $\sim 2\%$. This means that the reaction between

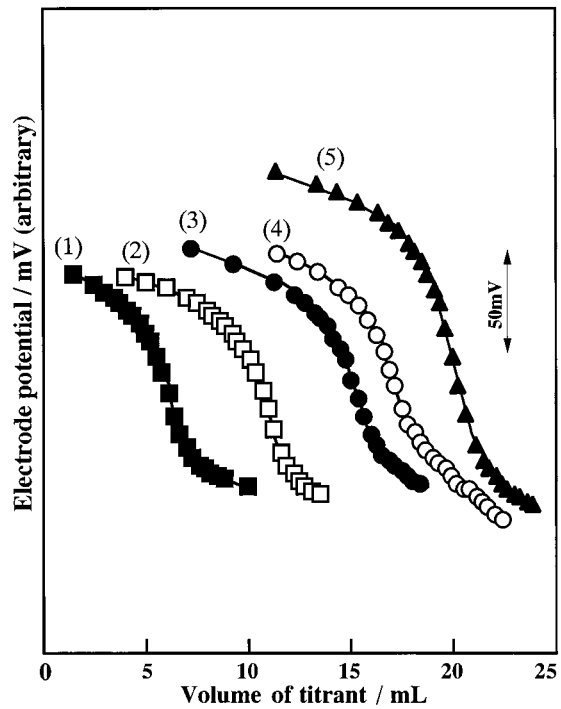

Fig. 1. Potentiometric titration curves for back-titration of sulfate ion with FPB solutions by using FPB-sensitive electrode as an indicator electrode. Sample: 20 ml of sulfate solution and 20 ml of 1.0×10^{-2} mol l^{-1} 2-aminoperimidinium (Ap) solution. (1) 3×10^{-3} mol l^{-1} Na_2SO_4; (2) 2×10^{-3} mol l^{-1} Na_2SO_4; (3) 1×10^{-3} mol l^{-1} Na_2SO_4; (4) 6×10^{-4} mol l^{-1} Na_2SO_4; (5) 0 mol l^{-1} Na_2SO_4. Titrant: 1.0×10^{-2} mol l^{-1} sodium tetrakis (4-fluorophenyl) borate (FPB); Electrode: FPB-sensitive electrode based on a plasticized PVC membrane.

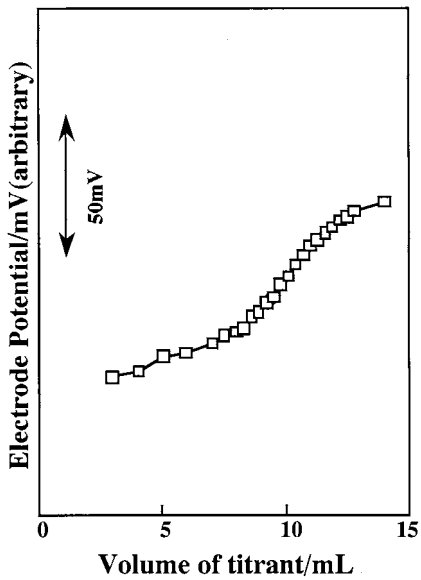

Fig. 2. Potentiometric titration curve for the direct titration of sulfate ion using 2-aminoperimidinium (Ap)-sensitive electrode as an indicator electrode and Ap solution as a titrant, respectively. Sample: 40 ml of 1×10^{-3} mol l^{-1} Na_2SO_4. Titrant: 1.0×10^{-2} mol l^{-1} Ap. Electrode: sodium tetrakis(3,5-bis(trifluoromethyl)phenyl) borate based Ap-sensitive PVC membrane electrode.

Ap and sulfate ion is stoicheiometric. The calibration graph between the end-point volume of the titrants and the concentration of sulfate ion was linear over the range from 2×10^{-4} to 3×10^{-3} mol l^{-1}. The graph equation is $y = -4603.33x + 20.17$; $r = 1.000$ ($n = 8$) where y is the end-point volume and x the concentration of the sulfate ion. The relative standard deviation of the end-point volume for the three times sulfate ions were titrated was less than $\sim 1.0\%$ for 6×10^{-4} mol l^{-1} and 1×10^{-3} mol l^{-1}, respectively.

3.2. A comparison of the present method with the direct titration method

Fig. 2 shows a direct titration curve of a sulfate ion (10^{-3} mol l^{-1}) using an Ap solution as a titrant and a Ap-ISE as an indicator electrode. From Figs. 1 and 2, we found that the magnitude of the potential change at the end-point for direct titration of the sulfate ion was only 10 mV and much smaller than that for the back-titration of the sulfate ion shown in curve 3 of Fig. 1. The precision of the potentiometric titration method depends on the slope of the line before and after the end-point. The potential change at the end-point for direct titration of the sulfate ion is not sufficiently large to obtain a precise end-point. These results mean that the solubility product of Ap-sulfate is relatively high and Ap tends to form ion association with hydrophobic anions such as FPB rather than a sulfate ion because Ap has relatively hydrophobic properties. From this result, we concluded that the back-titration method is better than the direct titration method for the determination of sulfate ions.

3.3. Effect of diverse ions on the determination of the sulfate ion

Real samples such as sea waters often contain cations and anions of relatively high concentration. Furthermore, Ap reacts with the high concentration anions such as NO_3^- and F^- ions to form precipitations of the Ap-anion [4]. Therefore, the effect of diverse ions in the sample solution on the titration of sulfate ion with FPB as the titrant was examined. Table 1 shows the effect of diverse ions on the determination of 6×10^{-4} mol l^{-1} sulfate ion. The magnitude of the potential jump at the end-point for the sulfate ion containing a coexisting ion (the potential jump, ~ 25 mV ml^{-1}) is lower than that for sulfate ions (the potential jump, 30 mV ml^{-1}). However, the end-point was detected even in the presence of a 20-fold excess in Cl^-, Br^-, NO_3^-, CH_3COO^-, F^-, Ca^{2+}, Mg^{2+}, Na^+ ions relative to the concentration of sulfate ions within $\sim 2\%$ of titration error.

3.4. Application of the present method to determination of sulfate ion in sea water

Table 2 shows the results of the recovery test of sulfate ions added to sea water. For all of the sample examined in this work, the recovery of the sulfate ion was satisfactory. This result shows that the present method can be applied to determine sulfate ions in sea water.

Table 1
Effect of coexisting salts (at 1.2×10^{-2} M level) on the potentiometric titration of 6×10^{-4} M sulfate ion

Coexisting salts	End-point (ml)	Relative error of end-point volume (%)[a]	Sensitivity (mV ml^{-1})
None	16.97	–	30.6
NaCl	16.65	−1.89	25.5
NaF	17.02	+0.29	25.0
CH_3COONa	16.70	−1.59	25.4
NaBr	17.02	+0.29	23.7
$NaNO_3$	17.05	+0.47	26.9
$MgCl_2$	16.69	−1.65	25.8
KCl	16.75	−1.30	26.0
$CaCl_2$	16.56	−2.42	23.4

[a] Relative error of end-point volume (%) was defined as {[(end-point volume for mixed solution of sulfate ion with coexisting salts)−(end-point volume for sulfate ion)]/(end-point volume for sulfate ion)}×100.

Table 2
The recovery tests of sulfate ions added to water samples

Sample	Added (mol l^{-1})	Found (mol $l)^{-1}$	Recovered (%)
Sea water (40-fold dilution)	3.0×10^{-4}	3.1×10^{-4}	103.3
	4.0×10^{-4}	4.3×10^{-4}	107.5

4. Conclusion

The present method allows for the simple and selective determination of sulfate ions by using the potentiometic back-titration method using a hydrophobic tetraphenylborate derivative (FPB) as a titrant and a plasticized PVC membrane electrode sensitive to the FPB as an indicator electrode. The present method is a useful alternative for the determination of sulfate ions in natural water. It is particularly suited for measurements in saline samples such as sea water due to ion chromatography of samples of this type [6] being difficult.

References

[1] R.J. Bertholacini, J.E. Barney, Anal Chem 29 (1957) 281.
[2] I. Iwasaki, S. Utsumi, T. Tarutani, T. Ozawa, Bull Chem Soc Jpn 30 (1957) 847.
[3] O. Kondo, H. Miyata, K. Toei, Anal Chim Acta 134 (1982) 353.
[4] W.I. Stephen, Anal Chim Acta 50 (1970) 413.
[5] K. Aihara, M. Kaneko, H. Wada, Taikiosengakkaishi 13 (1978) 223.
[6] R.P. Singh, E.R. Pambid, N.M. Abbas, Anal Chem 63 (1991) 1897.
[7] T. Kojima, K. Nakagawa, Y. Shigetomi, Anal Sci 10 (1994) 939.
[8] S. Nishizawa, P. Bühlmann, K.P. Xiao, Y. Umezawa, Anal Chim Acta 358 (1998) 35.
[9] A.M.Y. Jaber, G.J. Moody, J.D.R. Thomas, Analyst 101 (1976) 179.
[10] M. Gueggi, E. Pretsch, W. Simon, Anal Chim Acta 91 (1977) 107.
[11] W. Simon, F. Bongardt, O. Dinten, T. Kleiner, M.W. Laubli, E. Pretsch, F. Vogtle, Anal Chem 57 (1985) 2756.
[12] J. Kalous, D. Brazdova, K. Vytras, Anal Chim Acta 283 (1993) 645.
[13] T. Sakuhara, M. Kataoka, T. Kambara, Denki Kagaku 51 (1983) 905.
[14] T. Masadome, Y. Asano, Fresenius J Anal Chem (in press).
[15] N. Ishibashi, T. Masadome, T. Imato, Anal Sci 2 (1986) 487.
[16] T. Masadome, T. Imato, N. Ishibashi, Anal Sci 3 (1987) 121.
[17] T. Masadome, T. Imato, N. Ishibashi, Bunseki Kagaku 36 (1987) 508.
[18] T. Masadome, Doctoral Dissertation, Kyushu University, Fukuoka, Japan, 1993.
[19] J.G. Dick, Analytical Chemistry, chapter 5; McGraw-Hill, New York, 1973.

ELSEVIER

Talanta 48 (1999) 675–684

Talanta

Wet effluent parallel plate diffusion denuder coupled capillary ion chromatograph for the determination of atmospheric trace gases

C. Bradley Boring, Simon K. Poruthoor, Purnendu K. Dasgupta *

Department of Chemistry and Biochemistry, Texas Technical University, Lubbock, TX 79409-1061, USA

Received 8 July 1998; received in revised form 25 August 1998; accepted 26 August 1998

Abstract

We describe an inexpensive, compact parallel plate diffusion denuder coupled capillary IC system for the determination of soluble ionogenic atmospheric trace gases. The active sampling area (0.6×10 cm) of the denuder is formed in a novel manner by thermally bonding silica gel particles to the surface of Plexiglas plates. The effluent liquid from the parallel plate diffusion denuder is collected and preconcentrated on a capillary preconcentrator column before analysis using a capillary ion chromatograph. Using SO_2 as the test gas, collection efficiency is essentially quantitative at air sampling rates up to 500 ml min^{-1}. The system provides a limit of detection (LOD) of 1.6 parts per trillion for SO_2 for a 10 min sampling period.

Keywords: Denuder; Effluent; Trace gases

1. Introduction

The determination of trace concentrations of atmospheric pollutant gases and aerosol particles has become increasingly important due to their adverse health effects. Diffusion based sampling systems are commonly used to separate gas phase analytes from concomitantly present aerosol particles, allowing the accurate determination of both species. The principles of diffusion based sampling systems have been reviewed [1,2].

Wet effluent diffusion denuders provide the desired characteristics of diffusion based sampling devices: a continuously renewed sampling surface and an easily changed scrubbing solution for sampling a variety of gases. With a diffusion denuder of closely spaced parallel plate construction, high gas collection efficiencies are also achieved with a minimum of particle loss [3]. Wet effluent denuders utilize an easily wettable sampling surface to continuously introduce a collection liquid that flows down the active surfaces of the denuder. Soluble gases of interest present in the sampled air stream diffuse to the walls and are absorbed by the flowing liquid. The liquid containing the collected analyte is then aspirated from the base of

* Corresponding author. Fax: +1-806-742-1289; e-mail: sandyd@ttu.edu.

0039-9140/99/$ - see front matter
PII: S0039-9140(98)00285-9

the denuder and analyzed using continuous or semi-continuous liquid phase analyzers. The diffusion coefficient of even the smallest aerosol particles is much smaller than that of a gas molecule and the aerosol is therefore efficiently transmitted through the denuder. If desired, the aerosol can then be collected and analyzed, free from the interference of gases. Wet effluent diffusion denuders (WEDDs) thus provide a simple, versatile, and easily automated air sampling strategy for a number of trace atmospheric gases that can be collected into a liquid scrubber.

We have previously demonstrated the near real time analysis of atmospheric trace level gases with a variety of wet effluent denuder designs [3–6]. The most efficient of these designs was based on a parallel plate geometry [3]. The design used two glass plates (50 × 300 mm active area) in which a central channel is formed by placing a 3 mm thick spacer between the edges of the plates. A silica-rich soft glass layer was formed on the surface of the glass plates to form a highly wettable soluble gas scrubbing surface. Aqueous hydrogen peroxide was pumped down the wettable plates to collect soluble gases of interest. Using this parallel plate design, quantitative gas collection efficiency was possible with air sampling rates up to 10 l min^{-1}. Coupled to a standard ion chromatograph (IC), limits of detection in the sub parts per trillion (ppt) concentration range were observed for SO_2, HONO, and HNO_3 using an 8 min sample time. Further, low particle losses enabled the accurate determination of aerosols following gas collection with the parallel plate WEDD [7,8].

For the simultaneous determination of several gases, it is convenient to separate the corresponding liquid phase analytes chromatographically before detection. Gases that form characteristic ions in solution can be easily determined by coupling the WEDD to an ion chromatograph (IC). Detector response in IC is related to the analyte concentration, similar to many other liquid phase separation systems that rely on flow through detectors. Typically, the aqueous analytes in the denuder effluent are therefore preconcentrated prior to separation and subsequent detection. Furthermore, air sampling flow rates are maintained as high as possible (while preferably maintaining quantitative collection efficiency) to increase the analyte concentration in the WEDD effluent. If WEDDs can be coupled to analytical systems with improved mass sensitivities, several potential advantages can accrue: miniaturization of the WEDD would be possible where liquid and air flow rates will both be lower relative to the larger scale devices, without a decrease in the analyte concentration in the effluent. Lower liquid flow rates would result in lower reagent consumption and hence, longer unattended operation

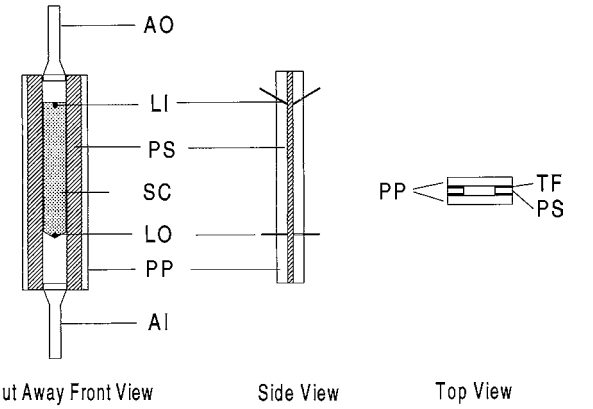

Fig. 1. Design of the parallel plate diffusion denuder. AI, air inlet; PP, Plexiglas plate; LO, liquid outlet; SC, silica coating; PS, Plexiglas spacer; LI, liquid inlet; AO, air outlet; TF, Teflon film.

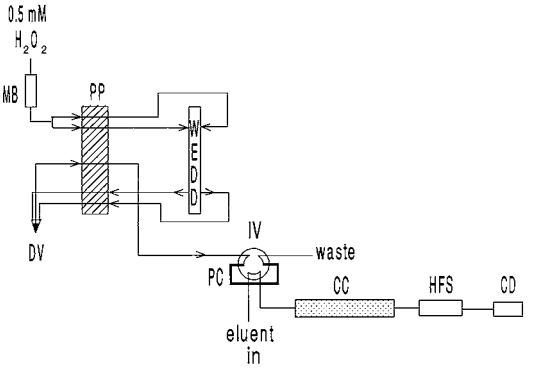

Fig. 2. Schematic of the liquid phase analytical system. MB, mixed bed ion exchange column; PP, peristaltic pump; WEDD, parallel plate wet effluent diffusion denuder; DV, degassing vial; IV, six port injection valve; PC, capillary preconcentrator column; CC, separation column; HFS, hollow fiber chemical suppressor; CD, conductivity detector.

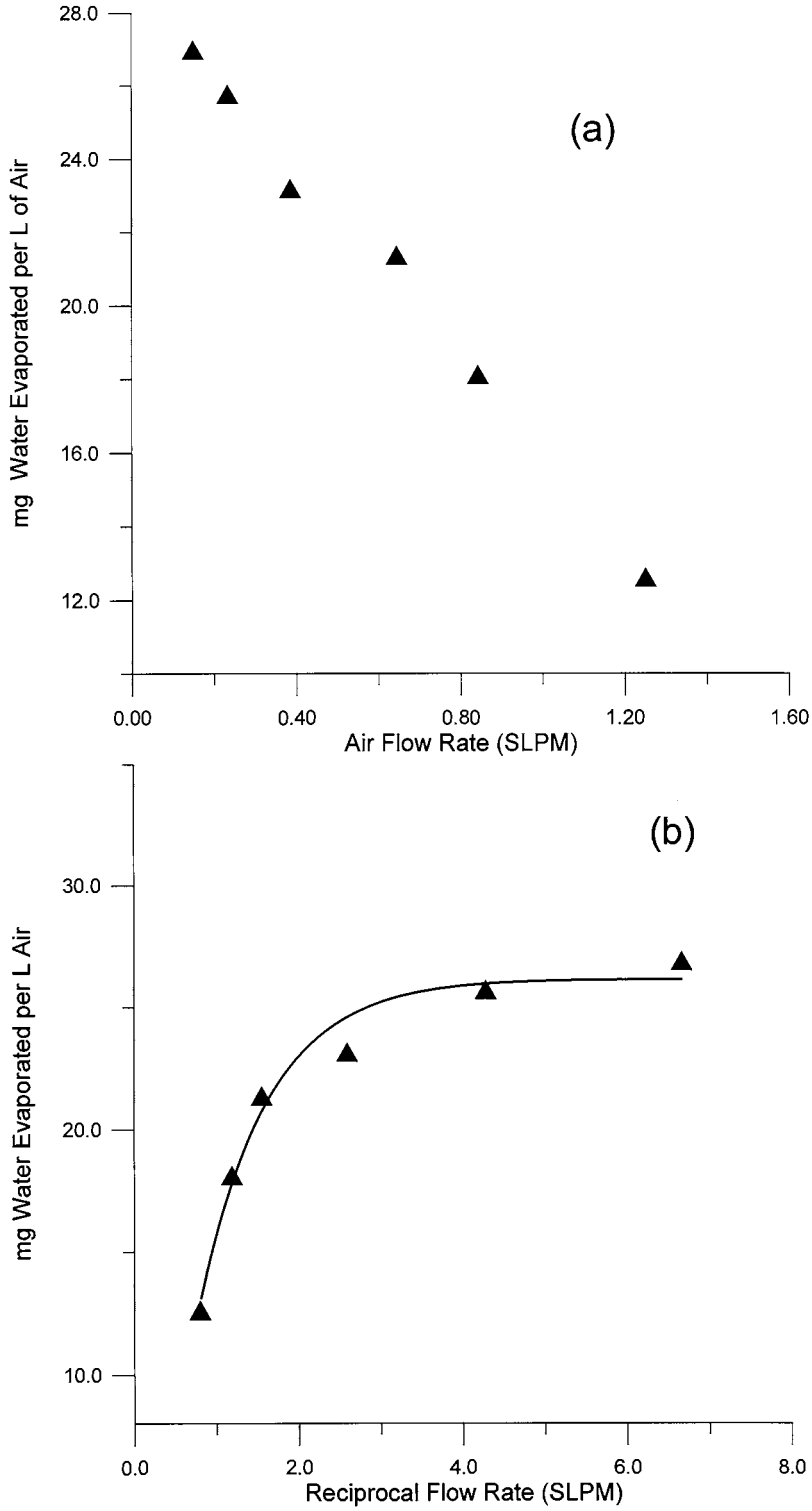

Fig. 3. (a) Evaporation loss per unit volume of air as a function of air flow rate; (b) evaporation loss per unit volume of air plotted as a function of the reciprocal air flow rate; the solid line represents the best fit line according to Eq. (1).

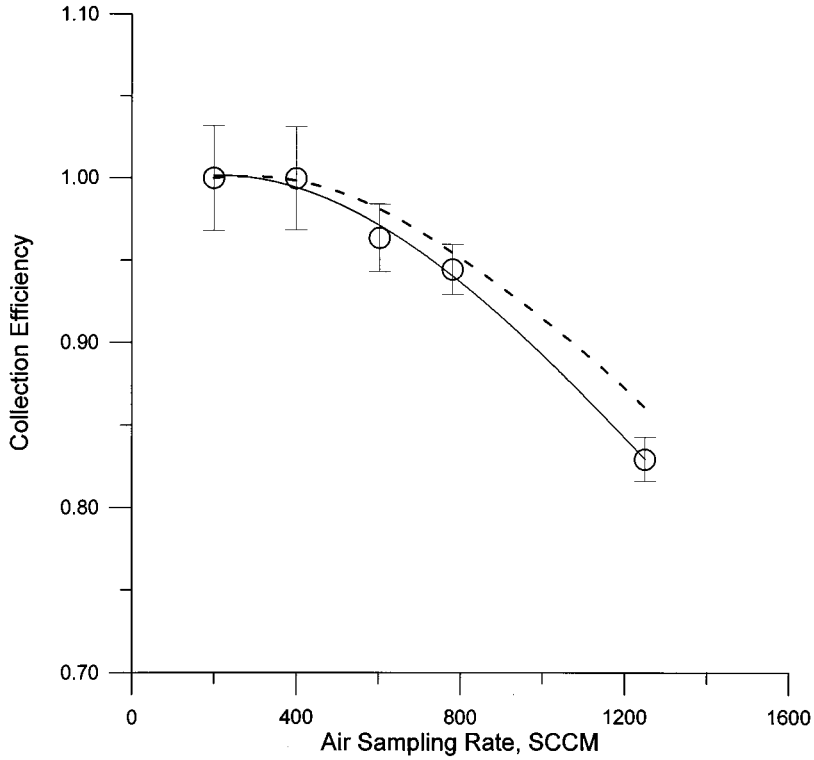

Fig. 4. Collection efficiency of the parallel plate diffusion denuder. The dashed line represents the computed theoretical efficiency and the solid line represents the best fit to the experimental data.

times. Lower air sampling rates will permit the use of small, battery powered air pumps that would greatly facilitate portability and field use.

Recently, we described a portable capillary ion chromatograph with suppressed conductometric detection for anion analysis [9]. The concentration Limits of detection (LODs) were comparable to standard bench-top IC systems but the mass LODs were better by >2 orders of magnitude. The development of this capillary ion chromatograph led us to investigate the possibility of performing trace gas analysis with a miniaturized parallel plate denuder coupled to this system. Compared to previous work, the fabrication of the denuder is simpler and faster and an order of magnitude less sample flow rate is necessary to achieve parts per trillion level LODs. The design and performance of this instrument is reported in this paper.

2. Experimental

2.1. Thermally bonded silica coated wet effluent diffusion denuder

Two Plexiglas plates ($22 \times 175 \times 3$ mm thick) were washed thoroughly with methanol followed by water and then allowed to dry. The plates were next covered with Teflon tape. The Teflon tape was then removed by a scalpel blade from the areas intended to constitute the wetted region. Silica particles (Aldrich), screened to give a size range of ~ 74–127 μm, were used to coat the Plexiglas plates. An aluminum block was machined to internally contain a heating element; this assembly provided a hot surface for thermally bonding the silica particles to the Plexiglas plates. The filtered silica particles were placed on the aluminum block, heated to ~ 250°C, for 10–15 min for preheating. One of the Plexiglas plates,

with the intended wettable area face down, was then placed on top of the heated silica particles and the aluminum block. A drill press, equipped with a flat aluminum plate, was used to press down the Plexiglas plate on the silica particles. Within a period of ~ 45 s, the silica particles get imbedded into the semi-molten surface of the Plexiglas. This plate is removed and the procedure is repeated with the other plate. After cooling, the coated regions were rinsed with a high velocity water stream to remove the loosely held particles. The entire procedure was then repeated until the silica coating appeared to be uniform over the exposed area of the plates. Two to three repeats are generally sufficient. Thermal bonding of the silica particles to the Plexiglas according to the above procedure may result in slight deformation of the plates. Such deformations can be removed by placing the treated Plexiglas plate on top of a flat aluminum plate and placing in an oven at 135°C for 30 min.

The design of the parallel plate WEDD is shown in Fig. 1. The denuder was constructed using 3 mm thick Plexiglas plates. Fully assembled, the shell of the PPDD measured $2.2 \times 17.5 \times 0.75$ cm. The silica coated region SC was 0.6×10 cm long. The silica coated region has a tapered V-shape at the bottom to facilitate liquid effluent collection. At the top and bottom of the silica coated region, holes were drilled to provide a liquid inlet LI and a liquid outlet LO. Stainless steel tubing (23 gauge) was push fit into these holes and epoxied in place. A 1.5 mm thick Plexiglas spacer PS, covered with Teflon film TF, was used to separate the two Plexiglas plates. The Teflon coated spacer completely covers the untreated edges of the plates and provides an inert surface for sampled gases entering the denuder. Spring-loaded clamps were placed all around the outer edges of the Plexiglas plates to seal the assembly. Air inlet tube AI and air outlet tube AO were made by thermally deforming Teflon tubing (4.6 mm i.d., 5 mm o.d.) to fit into the spacing between the Plexiglas plates. The air inlet/outlet tubes were roughened with sandpaper on the outside and epoxy adhesive was applied around it and on to the WEDD body to prevent any air leakage around these joints. The application of the adhesive also provides the desired rigidity to the inlet/outlet connections. Approximately 4 cm was left uncoated between the silica coating and the edge of the air inlet tubing to establish a laminar flow profile [1] before the sampled air comes into contact with the wetted area.

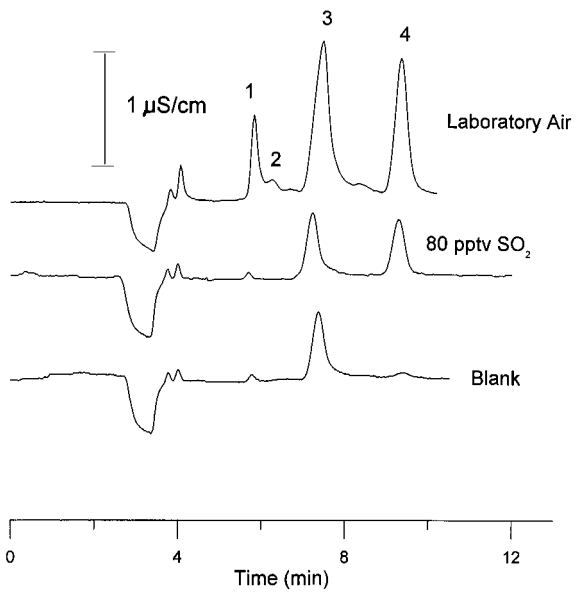

Fig. 5. Chromatogram resulting from sampling blank air and 80 pptv SO_2 (both at 500 SCCM) and laboratory air (250 sccm). Peak identities: 1, chloride; 2, nitrite; 3, carbonate; 4, sulfate.

2.2. Gas phase calibration system

The gas phase portion of the analytical system was tested with different concentrations of SO_2 as a test analyte. The basic arrangement has been described earlier [5]. Briefly, house air was cleaned and dried with a series of columns containing silica gel, activated charcoal, and soda lime. Sulfur dioxide standards were generated with a wafer type permeation device constructed in-house and maintained at 30°C. The device was gravimetrically calibrated and found to emit at a rate of 24 ng SO_2 min^{-1}. Mass flow controllers (FC-280, Tylan General, San Diego, CA) were used to provide necessary dilution and flow control.

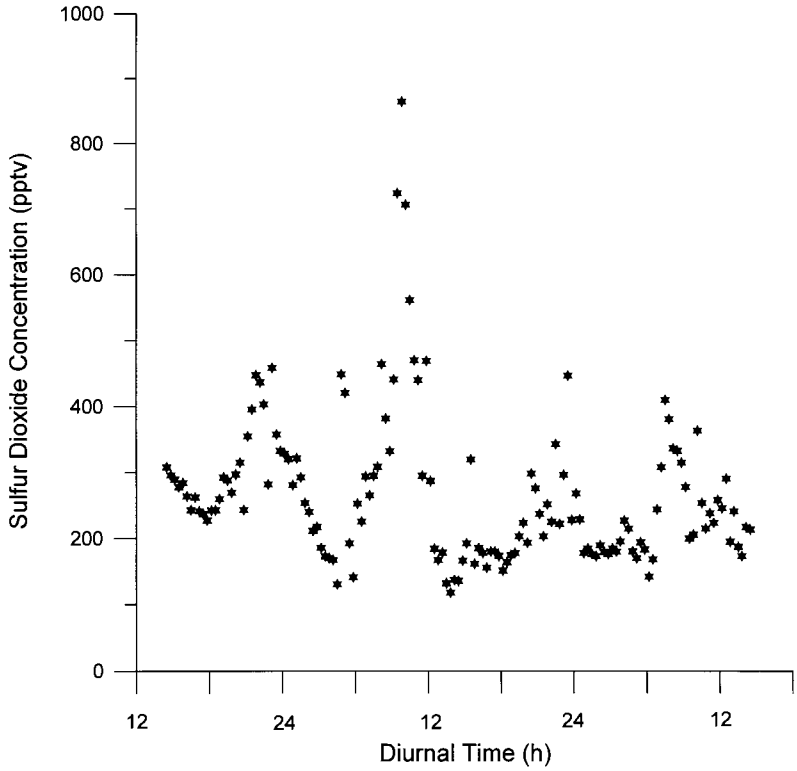

Fig. 6. Ambient air levels of SO_2 in Lubbock, TX over a 48 h period beginning Julian Day 119, 1998.

2.3. Liquid phase analytical system

The liquid phase portion of the instrument is shown in Fig. 2. Hydrogen peroxide (0.5 mM) is aspirated though a mixed bed deionizing column MB (Amberlite MB-1, Sigma, St. Louis, MO) to remove any ionic impurities present in the flow stream. The H_2O_2 is then pumped to the liquid inlet ports of the WEDD using an eight-channel peristaltic pump PP (Minipuls 2, Gilson Medical Electronics, six channels are used in this work). The liquid effluent from the denuder is aspirated by two other channels of the same pump and sent to a degassing vial DV (holdup volume ≤ 75 μl). The resulting liquid effluent, free from air bubbles, is pumped at a flow rate of 17 μl min^{-1} through a capillary preconcentration column PC (vide infra). A six port injection valve IV (Cheminert model C3-1006EH, Valco, Houston, TX), shown schematically in Fig. 2, allows the preconcentrator column to be switched from the load to the inject position and vice-versa. All data reported were obtained using a 10 min load/10 min inject cycle.

A previously described capillary scale suppressed conductometric IC [10] was used for separating, identifying and quantifying the sampled gas constituents. Briefly, this instrument consists of a syringe pump (Model 50300, Kloehn, Reno, NV) equipped with a 500 μl glass syringe (Kloehn), a pressure sensor (Model SP-70-A3000, Senso-Metrics, Simi Valley, CA; provided with home-built electronics), the previously mentioned electrically actuated 6 port injection valve IV, an 180 μm i.d., 35 cm long packed capillary analytical column (CC), a hollow fiber chemical suppressor [10], and a conductivity detector cell [9] connected to a Model ED40 electrochemical detector (Dionex, Sunnyvale, CA). Data acquisition was accomplished by an 80486 based PC via AI-450 software and an advanced computer interface, both from Dionex.

Capillary columns were packed in-house with AS-11 HC (high capacity) packing material from Dionex using a capillary version of the proprietary packing technique provided by Dionex. The preconcentration column consisted approximately of a 1.5 cm length of a 250 μm i.d., 350 μm o.d. packed capillary column. The exit frit for the precolumn was constructed as follows: ~1 cm of the packing material was first removed from a 2.5 cm long packed capillary column. A small piece of a glass fiber filter (Whatman, type GF/A) was then inserted against the packing and held in place by a 50 μm i.d., 150 μm o.d. fused silica capillary that was pushed inside the larger bore capillary. The nested capillary assembly were then secured with epoxy adhesive into place. The preconcentrator column PC was connected to the injection valve in such a manner that the flow direction through PC remained the same in both the load and inject modes. Separations were performed using a 25 mM NaOH eluent hydroxide at a flow rate of 2.2 μl min^{-1}. The retention time of sulfate was ~10 min under these conditions. A 3.5 mM solution of sulfuric acid flowing at ≤0.25 ml min^{-1} functioned as suppressor regenerant and resulted in a suppressed conductance of ~1.8 μS cm^{-1}.

Sodium hydroxide eluents were prepared from a 50% NaOH stock solution (J.T. Baker). Hydrogen peroxide was prepared from a 30% stock solution (Mallinckrodt). Distilled deionized water with a specific resistivity of ≥18 MΩ cm^{-1} was used to prepare all solutions. Analytical reagent grade chemicals were used throughout. Soda-lime traps were used to protect all solutions from CO_2 intrusion.

2.4. Determination of collection efficiency

The system was initially calibrated by preconcentrating different volumes (known flow rate passed through the preconcentrator column for different periods) of a 100 μg l^{-1} sulfate standard. The collection efficiency for gaseous SO_2 as a function of the air sampling rate was then determined by: (a) translating the observed response resulting from a given preconcentration period to an equivalent amount of sulfate with the help of the above calibration; (b) accounting for the total denuder effluent liquid volume during that period (because of evaporation losses, the effluent liquid flow rate from the WEDD is less than the input liquid flow rate; the WEDD liquid output was therefore gravimetrically measured); and (c) comparing the number of moles of sulfate in the WEDD effluent from (a) and (b) above, to the number of moles of gaseous SO_2 that was sampled through the system.

3. Results and discussion

3.1. Thermally bonded WEDD

The ability to prepare an easily wettable surface is critical for fabricating WEDDs. Although several methods have been developed for chemically bonding silica particles to glass plates [3–5], we found that thermally bonding silica gel particles onto the surface of Plexiglas plates is a simple, viable option for preparing a highly wettable sampling surface. It does not require high temperature ovens, fragile glass components and caustic chemicals can be avoided. The procedure is conceptually similar to imbedding porous glass particles on the interior walls of a PTFE tube as described by Gnanasekaran and Mottola [11] by a thermal process and results in a easy to fabricate and robust device.

3.2. Considerations on injection strategies

The success of any diffusion denuder based analysis approach depends on the ability of a denuder to collect the gaseous analyte of interest, preferably quantitatively. For a WEDD, it is further desirable to concentrate the analytes in the liquid effluent before separation and detection is performed. In a continuously operating WEDD, both the efficient uptake of the gaseous analyte by the denuder liquid and the subsequent concentration of the analytes in the effluent on a preconcentration column are important. The concentration of the analyte in the denuder effluent is maximized by minimizing the WEDD liquid flow rate. The input effluent flow rate down each plate of

the PPDD was 15 μl min^{-1}. The effective thickness of the liquid film in the absence of air flow was determined by injecting a KCl solution at the top of the denuder and measuring its mean residence time with a miniature bifilar wire conductivity detector [12] placed immediately at the exit of the WEDD. From a knowledge of the liquid flow rate, and the total active area of the denuder, the maximum film thickness was computed to be ~70 μm. A small film thickness is critical to achieve a good concentration factor for the gaseous analyte while minimizing sample carryover between successive determinations. Washout times with the present system were sufficiently small as to permit a new steady state signal to be fully established after one load/injection cycle following a step change in gas concentration at the denuder inlet.

A significant portion of the denuder input liquid evaporates during air sampling. The experimentally observed evaporation loss of water per liter (μl l^{-1}) of sampled air as a function of air flow rate is shown in Fig. 3(a). Theoretically, a maximum loss of 31 μl l^{-1} of sampled air (at 30 °C) would occur assuming the inlet air is completely dry and the air exiting the denuder is completely saturated with water. Experimentally, the evaporation loss was 87% of its maximum theoretical value (27 μl l^{-1}) at an air flow rate of 0.150 standard liters per minute (SLPM), and dropped to 41% of the maximum theoretical limit (12.7 μl l^{-1}) at an air flow rate of 1.250 SLPM. At high air flow rates, the equilibration of the air flowing through the denuder with the liquid surface becomes the primary factor governing evaporation. The expression for determining the theoretical amount of water evaporated at a specific air flow rate is the same type of equation used for determining the collection efficiency of denuders [3]:

$$1 - aW = be^{-c/Q} \quad (1)$$

where a, b, and c are constants, Q is the volumetric flow rate, and W is the amount of water evaporated per liter of air. Fig. 3(b) shows W plotted against the reciprocal air flow rate with the solid line representing the best fit to Eq. (1) ($a = 0.0381$, $b = 1.305$, $c = 1.182$). Under the maximum air flow rate tested with this denuder (1.25 SLPM), no dry spots developed over the active sampling surface of the PPDD using a liquid flow rate of 15 μl min^{-1} down each plate.

The liquid aspiration rate and the liquid influent flow rates in to the WEDD were maintained the same, 15 μl min^{-1} per plate. Due to the evaporation losses during air sampling, the aspiration rate is greater than the actual effluent flow rate at the bottom of the denuder. This causes air bubbles to be present in the effluent stream. The operating pressure of the capillary ion chromatograph was ~500 psi at a flow rate of 2.2 μl min^{-1}. This pressure was not sufficient to dissolve air bubbles present in the WEDD effluent. Under the circumstances, there are two alternatives to inject a bubble-free sample into the IC. The first alternative is to pump the entire denuder effluent through the precolumn followed by washing with degassed deionized water for a period of time to remove any bubbles trapped on the precolumn. The second alternative is the use of a degassing vial between the denuder exit and the precolumn. The degassing vial acts as a gravity based air separator-bubble free liquid aspirated from the bottom can be loaded onto the preconcentrator column. In the present work, the degassing vial alternative was chosen. Also, the six-port injector used in the present work permitted the use of only one preconcentrator column. Therefore the system was so configured as to apply aspiration to the degassing vial at a greater flow rate when the valve is in the inject position to empty it rapidly and minimize sample carryover. Eight port injector valves are commercially available that would allow the loading of one preconcentrator column while the other one is washed/chromatographed. Such an arrangement will benefit more from the first degassing alternative.

3.3. Preconcentration column

In a previous paper [9], the preconcentration of analytes using a 10 cm long packed capillary preconcentrator column was demonstrated. While analyte preconcentration using such a column was feasible in the present application, several im-

provements were desired. Firstly, the preconcentration column was sufficiently long so that the maximum flow rates through this column achievable by a peristaltic pump were much smaller than desired. Secondly, a carbonate peak that is always present in air samples and peaks from other impurities present in the H_2O_2 solution put through the WEDD interfered with the determination of low level analyte peaks. The presently developed preconcentrator column provided solutions to these two problems. A 1.5 cm long packed capillary column with a cross sectional area (250 μm i.d.) nearly twice as large as that of the separation column (180 μm i.d.) provided sufficient capacity for typical ambient air applications. This precolumn permitted flow rates up to 18 μl min^{-1} with a peristaltic pump relative to ~ 3 μl min^{-1} obtained with the precolumn used. In addition, passing the aqueous H_2O_2 through a mixed bed ion exchanger before the WEDD was found to remove ionic impurities that interfered with the chromatographic determination of the analytes. In the absence of H_2O_2 in the WEDD liquid, SO_2 is oxidized partially to sulfate resulting in both sulfite and sulfate peaks from sampling SO_2. Using dilute H_2O_2 results only in sulfate which improves and simplifies quantitation. There is no significant oxidation of collected nitrite to nitrate by H_2O_2.

3.4. Collection efficiency

The collection efficiency f for a parallel plate diffusion denuder is given by [5,13]

$$f = 1 - 0.91e^{-3.77\alpha^{DL/Q}} \quad (2)$$

where D is the diffusion coefficient of the gas (0.13 cm^2 s^{-1} for SO_2 [14]), L is the length of the tube, and Q is the volumetric flow rate. For a parallel plate denuder, the parameter α is given by:

$$\alpha = 2b/a \quad (3)$$

where a and b are the short and long dimensions of the active cross section of the denuder, respectively [13].

The collection efficiency for the parallel plate WEDD is shown graphically in Fig. 4 for low to sub-ppbv levels of SO_2. The solid line shows the collection efficiency for the WEDD whereas the dashed line shows the theoretical collection efficiency. Error bars represent ± 1 SD ($n = 3$). Collection efficiency is essentially unity up to ~ 500 cm^3 min^{-1} (SCCM) air sampling rate and drops to $\sim 83\%$ collection efficiency at 1250 SCCM. The theoretical collection efficiency for the WEDD at 1250 SCCM is $\sim 85\%$. This difference is well within the uncertainty of the diffusion coefficient value of SO_2 used for the calculations. In terms of diffusion coefficients for various gases, the diffusion coefficient for SO_2 is on the low end among those of common inorganic gases of interest and other soluble ionogenic gases such as HONO, HCl, HNO_3, etc. would be expected to be collected at least as efficiently as SO_2.

3.5. Response linearity and detection limits

An air sampling rate of 500 SCCM was chosen to evaluate the WEDD such that the collection efficiency is still essentially quantitative. The response linearity was studied over a SO_2 concentration range 20–2000 pptv. Higher concentrations of SO_2 result in nonlinear responses in the present detection system unless the sampling period or the sampling rate is reduced. However, the ambient SO_2 levels at our location are low and this range is adequate for ambient measurements, without reducing the sampling period. The linear r^2 value of the sulfate peak height vs. the sampled SO_2 concentration was 0.9980 for the entire concentration range. The relative standard deviation (RSD) was $\leq 3.2\%$ over this concentration range for each concentration sampled. Based on the uncertainty of the blank and the slope of the calibration plot, the limit of detection was determined to be 1.6 pptv ($S/N = 3$). Fig. 5 shows a chromatogram resulting from the sampling of clean air and ~ 80 pptv SO_2.

3.6. Ambient air studies

Laboratory air and ambient Lubbock air were sampled to evaluate system performance. A chromatogram resulting from sampling laboratory air is shown in Fig. 5. The system was operated at an

air sampling rate of 250 SCCM, to deliberately limit the response. The SO_2 concentration in this sample was determined to be ~ 400 pptv; this demonstrates the excellent SO_2 response even at low air sampling rates. In addition the sample also shows the presence of ~ 30 pptv HCl and ~ 2 pptv HONO.

Sulfur dioxide concentrations in Lubbock, TX were studied over a 48 h period where the WEDD was allowed to operate continuously for this time period without any user intervention. The results are shown in Fig. 6. These results correlate well with previously measured ambient SO_2 levels at this location [3].

In conclusion, a compact, inexpensive air sampling system has been developed capable of measuring down to low parts per trillion levels of SO_2 and similar other gases. The entire instrument can easily be transported into the field for analysis. Not only can this system be adapted for the simultaneous analysis of a number of gases, it can be easily automated and operate continuously for prolonged periods without any user intervention.

Acknowledgements

This research was supported by the US Environmental Protection Agency through STAR Grant R82-5344-01-0. However, the manuscript has not been reviewed by the agency and no endorsements should be inferred. Auxiliary support from Dionex Corporation is also acknowledged.

References

[1] P.K. Dasgupta, ACS Adv. Chem. Ser. 232 (1993) 41–90.
[2] Y.-S. Cheng, Air Sampling Instruments, 8th ed., Cohen, American Conference of Governmental Industrial Hygienists, Cincinnati, OH, 1995.
[3] P.K. Simon, P.K. Dasgupta, Anal. Chem. 65 (1993) 1134–1139.
[4] P.K. Simon, P.K. Dasgupta, Z. Vecera, Anal. Chem. 63 (1991) 1237–1242.
[5] Z. Vecera, P.K. Dasgupta, Anal. Chem. 63 (1991) 2210–2216.
[6] P.K. Dasgupta, L. Ni, P.K. Simon, D.C. Hindes, Anal. Chem. 69 (1997) 5018–5023.
[7] P.K. Simon, P.K. Dasgupta, Anal. Chem. 67 (1995) 71–78.
[8] P.K. Simon, P.K. Dasgupta, Environ. Sci. Technol. 29 (1995) 1534–1541.
[9] C.B. Boring, P.K. Dasgupta, A. Sjögren, J. Chromatogr. A 804 (1998) 45–54.
[10] A. Sjögren, C.B. Boring, P.K. Dasgupta, J.N. Alexander, Anal. Chem. 69 (1997) 1385–1391.
[11] R. Gnanasekaran, H.A. Mottola, Anal. Chem. 57 (1985) 1005–1009.
[12] S. Kar, P.K. Dasgupta, H. Liu, H. Hwang, Anal. Chem. 66 (1994) 2537–2543.
[13] F. De Santis, Anal. Chem. 66 (1994) 3503–3504.
[14] B.R. Fish, J.L. Durham, Environ. Lett. 2 (1971) 13–21.

ELSEVIER

Talanta 48 (1999) 685–693

Talanta

Kinetic study on the acidic hydrolysis of lorazepam by a zero-crossing first-order derivative UV-spectrophotometric technique

H.A. Archontaki [a,*], K. Atamian [a], I.E. Panderi [b], E.E. Gikas [b]

[a] *Laboratory of Analytical Chemistry, Department of Chemistry, University of Athens, Panepistimiopolis 157 71, Athens, Greece*
[b] *Division of Pharmaceutical Chemistry, Department of Pharmacy, University of Athens, Panepistimiopolis 157 71, Athens, Greece*

Received 6 January 1998; received in revised form 29 July 1998; accepted 27 August 1998

Abstract

A zero-crossing first-order derivative UV-spectrophotometric technique for monitoring the main degradation product, 6-chloro-4-(2-chlorophenyl)-2-quinazoline carboxaldehyde, was developed to study the acidic hydrolysis of lorazepam in hydrochloric acid solutions of 0.1 M. Due to the complete overlap of the spectral bands of the parent drug and the hydrolysis product (the range between their spectral maxima was only 3 nm), the graphical methods of derivative spectrophotometry were not efficient. The relative standard deviation of the proposed technique was less than 2.4% and the detection limit was 6.6×10^{-8} M. Accelerated studies at higher temperatures have been employed that enable rapid prediction of the long-term stability of this drug. Pseudo-first order reaction kinetics was observed. Kinetic parameters, k_{obs} and $t_{1/2}$, were calculated, which were similar to those estimated by an HPLC method developed in our laboratory.

Keywords: Zero-crossing technique; First-order derivative spectrophotometry; Acidic hydrolysis of lorazepam; 6-chloro-4-(2-chlorophenyl)-2-quinazoline carboxaldehyde

1. Introduction

The group of 1,4-benzodiazepines [1] is widely used in the treatment of nervous diseases such as anxiety, insomnia and epileptic convulsions because of the wide variety of their properties attributed to the complicated benzodiazepinic structure. Due to the therapeutic interest that these compounds present, research on their chemical stability as well as determination in pharmaceutical preparations and biological samples is needed for a better understanding of their physico-chemical, pharmacotherapeutic and toxicological behaviour.

Lorazepam [2], 7-chloro-5-(2-chlorophenyl)-3-hyroxy-2,3-dihydro-1H-1,4-benzodiazepin-2-one, I, is a minor tranquiliser and belongs to the above

* Corresponding author. Tel. +30-01-7274319/7274575; fax: +30-01-7231608; e-mail: archontaki@dc.uoa.gr.

0039-9140/99/$ - see front matter
PII: S0039-9140(98)00288-4

category, particularly to the oxazepam group of 1,4-benzodiazepin-2-one compounds, having a hydroxyl substituent at the 3-position of the diazepinic ring [3]. It is quite stable at room temperature in powder and solid dispersions, while it is hydrolysed in the presence of moisture to great extent following first-order reaction kinetics [4]. Stability of lorazepam at pH 7 (phosphate buffer) has been studied by a high-performance liquid chromatographic (HPLC) method, where experimental data were evaluated by an analog-hybrid computer simulation [5]. Another stability study on lorazepam in solid dosage form has been performed by HPLC [6], where both natural and accelerated degradation of this drug was examined. Hydrolysis of lorazepam and other 1,4 benzodiazepines in very acidic solutions (4 and 6 M HCl, respectively) has been also studied, resulted in the formation of the corresponding benzophenones [7,8]. Nevertheless, nothing clear and conclusive has been reported for its hydrolysis in acidic solutions in the pH region close to that of gastric fluid. For this purpose we decided to explore the hydrolysis process of lorazepam in such hydrochloric acid aqueous solutions.

In a previous paper [9] hydrolysis of lorazepam in aqueous acidic solutions using a reversed-phase HPLC method was investigated. In that study, 6-chloro-4-(2-chlorophenyl)-2-quinazoline carboxaldehyde, the main degradation product of lorazepam, has been isolated and fully identified. Kinetic measurements which carried out in 1.0, 0.1 and 0.01 M HCl solutions and at various temperatures led us to the conclusion that lorazepam degrades following first-order kinetics.

The aim of the present study was to complete the previous investigation with an insight into the versatility that derivative UV-spectrophotometry could show in such kinetic studies. Therefore, in this paper we report on the kinetic studies of acidic hydrolysis of lorazepam in 0.1 M HCl aqueous solutions using a zero-crossing first-order derivative UV-spectrophotometric technique. Calculations have been based on measurements of the main degradation product, II, at 231.6 nm, where lorazepam exhibits no contribution. Our results correlate well with those of the HPLC method developed in our laboratory [9]. The novelty of this research lies in the use of a zero-crossing derivative methodology for monitoring the product II. Zero-crossing derivative techniques have been proved very helpful in the quantitative analysis of several mixtures [10–17].

This work has been conducted in order to demonstrate the successful application of derivative spectrophotometry to the kinetic study on the decomposition of lorazepam and to propose this technique as a simple, versatile, environment protecting and inexpensive method in routine practical analytical work.

2. Experimental

2.1. Materials

Lorazepam, ($C_{15}H_{10}Cl_2N_2O_2$, M.W. = 321.17), of pharmaceutical purity grade was provided by Minerva Hellas A.E., Athens, Greece. 6-Chloro-4-(2-chlorophenyl)-2-quinazoline carboxaldehyde ($C_{15}H_8Cl_2N_2O$, M.W. = 303.15), was isolated in crystals by heating 0.4 g of I in 100ml of 0.1 M hydrochloric acid solution to 95°C for 6 h. All other reagents were of analytical grade and distilled deionised water was used for the preparation of solutions.

Stock methanolic solution of lorazepam, I, 6.1×10^{-4} M was prepared by dissolving the compound in methanol. This solution was stored in the dark at 4°C and was found to be stable for at least four weeks.

Stock standard solution of 6-chloro-4-(2-chlorophenyl)-2-quinazoline carboxaldehyde, II, 6.1×10^{-4} M was also prepared in methanol, stored at -10°C and used within 2 days of its preparation.

Working standard solutions of I and II were prepared daily in the ranges 3.0×10^{-6}–1.8×10^{-5} and 3.0×10^{-6}–2.1×10^{-5} M, in 0.1 M HCl, respectively and used for the construction of the corresponding calibration curves. Mixed working standard solutions of I and II were also prepared for the recovery studies in the following way: i) standard solutions of II in the ranges 3.0×10^{-6}–1.2×10^{-5} and 3.0×10^{-6}–$1.5 \times$

10^{-5} M containing constant concentration of I 1.2×10^{-5} and 6.1×10^{-6} M, respectively; ii) standard solutions of I in the ranges 3.0×10^{-6}–1.8×10^{-5} and 3.0×10^{-6}–1.2×10^{-5} M containing a constant concentration of II 6.1×10^{-6} and 9.2×10^{-6} M, respectively. All these solutions were analysed immediately after preparation.

2.2. Method

All spectrophotometric measurements were performed on a Hitachi (Tokyo, Japan) double beam UV/Vis spectrophotometer (Model U-2000). Operational parameters were as follows: scan mode, WL; data mode, ABS; with user baseline; start wavelength, 250 nm; stop wavelength, 220 nm; scan speed, 10 nm min^{-1} and medium response. In the first-order derivative mode a sensitivity of 1 was applied (a parameter that is related to the smoothing of the spectra required in every case).

A Heto water-bath was used for the accelerated kinetic studies.

2.3. Measurement procedure

Prepared working and mixed standard solutions of I and II were transferred into $1 \times 1 \times 4$ cm quartz cells and measured against a blank solution consisted of HCl 0.1 M. Zero-order derivative spectra were taken and then first-order derivative spectra were recorded over the wavelength range 220–250 nm. The first-derivative values at 231.6 and 234.6 nm were measured for the determination of the main degradation product of lorazepam and lorazepam (signals D_1) and calibration curves were constructed.

2.4. Kinetic investigation

The procedure followed for the kinetic study was similar to that described previously [18]. Hydrolysis was carried out in 0.1 M HCl solutions at elevated temperature. Duration of the kinetic experiments was 420, 300, 265 and 155 min at 53, 55, 58 and 60°C, respectively.

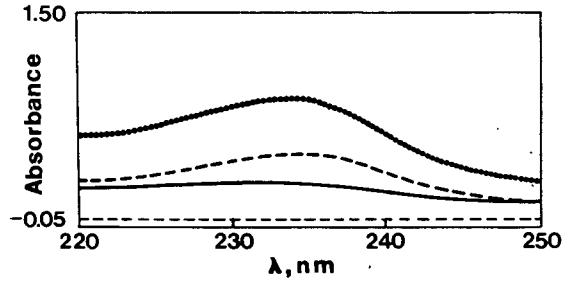

Fig. 1. Zero-order absorbance spectra of I (solid line), II (broken line) and a mixture of both (dotted line) in concentrations of 1.2×10^{-5} M each in 0.1 M HCl.

Treatment of the kinetic data was carried out using MINSQ software (version 4.03, MicroMath Scientific Software, Salt Lake City, UT, USA).

3. Results

3.1. Spectral characteristics

Fig. 1 shows zero-order absorption spectra of equal concentration (1.2×10^{-5} M) acidic aqueous solutions of lorazepam, 6-chloro-4-(2-chlorophenyl)-2-quinazoline carboxaldehyde and a mixture of both with peaks at 231.9, 234.7 and 233.7 nm, respectively. Fig. 2 presents their first-order derivative spectra with zero-crossing wavelength points of I at 231.6 nm and of II at 234.6 nm. Fig. 3 shows the fourth-order derivative spectra of I and II.

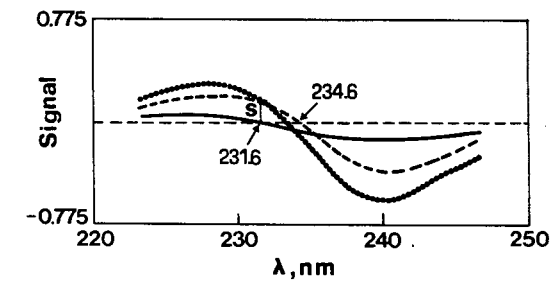

Fig. 2. First-order derivative spectra of I (solid line), II (broken line) and a mixture of both (dotted line) in concentrations of 1.2×10^{-5} M each in 0.1 M HCl. Zero-crossing wavelength points of I at 231.6 nm and of II at 234.6 nm are also indicated. *S* is the signal measured.

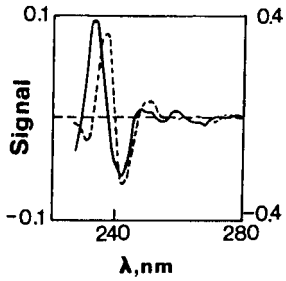

Fig. 3. Fourth-order derivative spectra of I (solid line) and II (broken line) in concentrations of 1.2×10^{-5} M each in 0.1 M HCl.

3.2. Performance characteristics

Under the experimental conditions described above, linear relationship between the selected derivative signals D_1 (231.6 nm) and concentration of II, was observed as shown in Table 1. Linearity was also observed with D_1 (234.6 nm) in the concentration range of $(0.3–1.8) \times 10^{-5}$ M and the equation obtained through regression analysis of data was: D_1 (234.6 nm) $= (-0.004 \pm 0.004) + (8486 \pm 356)$ C_I, $r = 0.997$, where standards of six different concentrations were used for the construction of this calibration curve. Preparing and measuring the standards of the same concentration of II and I three times each, relative standard deviation (RSD) was calculated and found less than 2.4 and 3% respectively, in the whole concentration range. To assess applicability of the proposed zero-crossing first-order derivative spectrophotometric technique to stability studies of lorazepam, an extent interference study between I and II was conducted. Mixed standard solutions were prepared, where the concentration of either I or II remained constant and the other was varied. Results of this investigation corresponding to measurements of D_1 (231.6 nm) are included in Tables 1 and 2. However, percentage recovery of I relying on measurements of D_1(234.6 nm) was not satisfactory, increasing as the concentration of the co-existing II increased (Table 3).

Detection limit (DL) and quantitation limit (QL) are defined as the concentrations that give a

Table 2
Spectroscopic determination and recovery of the degradation product II when (a) increasing amounts of II were added to a constant concentration of I and (b) increasing amounts of I were added to a constant concentration of II; measurements were based on the quantity D_1 (261.3 nm)

	Concentration of I, $\times 10^5$ M	Concentration of II, $\times 10^5$ M	% Recovery of II	Mean % recovery ± S.D.
		0.3	95.2	
		0.6	100.0	
(a)	0.6	0.9	100.0	98 ± 3
		1.2	96.6	
		1.5	98.6	
		0.3	100.0	
(a)	1.2	0.6	108.5	105 ± 4
		0.9	104.6	
		1.2	106.4	
(b)	0.3		97.6	
	0.6		97.6	
	0.9	0.6	95.2	99 ± 3
	1.2		102.3	
	1.5		101.2	
(b)	0.3		102.3	
	0.6	0.9	100.0	102 ± 1
	0.9		103.1	
	1.2		101.0	

Table 1
Analytical parameters of the calibration curves of 6-chloro-4-(2-chlorophenyl)-2-quinazoline carboxaldehyde (II) (a) in the absence and (b) in the presence of lorazepam (I) in 0.1 M aqueous HCl solutions; measurements were based on the signal of the first-derivative spectrum at 231.6 nm

Mode	Concentration range of II, $\times 10^5$ M	Concentration of I, $\times 10^5$ M	Selected wavelength, nm	Regression equation [b]		
				Intercept, $a \pm$ S.D.[a]	Slope, $b \pm$ S.D.[a]	$r(n)$[c]
(a) D_1	0.3–2.1	–	231.6	-0.007 ± 0.003	15012 ± 197	0.9996 (7)
(b) D_1	0.3–1.5	0.6	231.6	-0.007 ± 0.003	15100 ± 310	0.9994(5)
(b) D_1	0.3–1.2	1.2	231.6	-0.004 ± 0.002	15467 ± 216	0.9998 (4)

[a] S.D. are the standard deviations of the intercept and slope values [19].
[b] $D_1 = a + bc$, where c is the concentration in M.
[c] r is the correlation coefficient and n is the number of points in each calibration curve; each point is the mean of three experimental measurements.

Table 3
Recovery of lorazepam in the presence of increasing amounts of its main degradation product II; measurements were based on the quantity D_1 (234.6 nm)

Concentration of I, $\times 10^5$ M	Concentration of II, $\times 10^5$ M	% Recovery of I	Mean % recovery $\pm$ S.D.
	0.3	109.1	
	0.6	120.0	
0.6	0.9	130.9	131 ± 17
	1.2	141.8	
	1.5	152.7	

signal equal to $b + 3S_b$ and $b + 10S_b$, respectively, where b is the signal of the blank and S_b is its standard deviation [19,20]. S_b was estimated as half of the peak-to-peak noise in the blank signal. In the zero-crossing technique, with D_1 (231.6 nm), DL was found equal to 6.6×10^{-8} and QL equal to 8.6×10^{-7} M.

3.3. Kinetic investigation

Accelerated kinetic measurements were performed under the experimental conditions described earlier. Values of apparent reaction rate constant, k_{obs}, were estimated after treatment of the results by a non-linear parametric method (MINSQ). The mathematical model used was $Y = p(1 - e^{-k_{obs}t})$, applied to first and pseudo-first order reaction kinetics; where Y was the signal of II, e.g. D_1(231.6 nm), measured at time t and p is a constant factor for given experimental parameters. Fig. 4 shows a representative fit of this model applied to a set of experimental data. Goodness-of-fit statistics is expressed mainly by the square root of the coefficient of determination which was equal to 0.996, 0.998, 0.998 and 0.998 for the accelerated studies at 53, 55, 58 and 60°C, respectively.

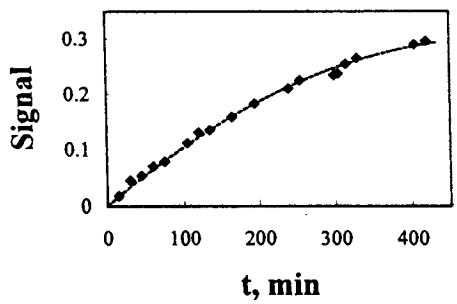

Fig. 4. Plot of the experimental points (◆) of the first-order derivative signal S, measured at 231.6 nm, versus time during an accelerated kinetic study of 2.4×10^{-4} M of lorazepam in 0.1 M HCl at 53°C. The MINSQ, least squares parameter estimation fit, is shown with the broken line (the model given followed first-order reaction kinetics).

Resulting values of k_{obs} along with calculated values of $t_{1/2}$, are given in Table 4. In the same table, results of a reversed-phase HPLC method, developed in our laboratory for comparison, are also presented.

4. Discussion

4.1. Mechanism

Before proceeding with the kinetic study, some clarification on the mechanism of acidic hydrolysis of lorazepam was necessary under the conditions used. The main degradation product (II) was isolated, identified by MS, IR, ^{1}H- and ^{13}C-NMR and proved to be 6-chloro-4-(2-chlorophenyl)-2-quinazoline carboxaldehyde [9]. This product could disproportionate and be oxidized or reduced to form the corresponding quinazoline carboxylic acid or quinazoline alcohol, respectively [2]. Only under much more rigorous acidic conditions (e.g. HCl 4.0 M) lorazepam degraded to (2-amino-5-chlorophenyl)(2-chlorophenyl)methanone which was also isolated and identified. Such a behaviour does not follow the general scheme of hydrolysis of 7-chloro-1,4-benzodiazepin-2-ones [21–26]. It is rather related to

Table 4
Results of kinetic study on lorazepam derived by the zero-crossing first-order derivative technique, D_1 (231.6 nm), compared with those obtained by a reversed-phase HPLC method [9]

C_{HCl}, M	θ, °C	Derivative method		HPLC method	
		$k_{obs} \times 10^3$, min^{-1}	$t_{1/2}$, min	$k_{obs} \times 10^3$, min^{-1}	$t_{1/2}$, min
0.1	53	2.2 ± 0.1	315	–	–
	55	3.3 ± 0.1	210	4.5 ± 0.1	154
	58	4.4 ± 0.1	158	6.1 ± 0.1	114
	60	6.0 ± 0.1	116	7.8 ± 0.1	89

oxazepam, 7-chloro-5-phenyl-3-hydroxy-2,3-dihydro-1H-1,4-benzodiazepin-2-one, reported in the literature [27–30] probably because of the common hydroxy-group in the 3-position of the diazepinic ring.

4.2. Spectrophotometric method

Due to the complete overlap of the spectral bands of compound I and II shown clearly in Fig. 1, conventional UV spectrophotometry cannot be used for their individual determination in binary mixtures. The distance between the spectral maxima of I (231.9 nm) and II (234.7 nm) is very short, barely 3 nm. As a consequence even the graphical methods of derivative spectrophotometry were not efficient. In Fig. 3 the fourth-order derivative spectra of I and II are presented, where a strong overlap between them still exists. However, graphical measurements (peak-to-peak or peak-to-baseline) often fail on the basis of systematic errors, unlike the zero-crossing measurements. The latter are measurements of absolute value of the total derivative spectrum at an abscissa value corresponding to the zero-crossing wavelengths of the derivative spectra of the individual components. Measurements made at the zero-crossing of the derivative spectrum of one of the two components would be a function only of the concentration of the other component.

Zero-crossing methodology was therefore applied to the first-order derivative spectra of I and II as shown in Fig. 2 to overcome the difficulty of the overlapping spectra. Working with both zero-crossing points, at 231.6 nm for lorazepam and at 234.6 nm for its degradation product, linear calibration curves were obtained with pure compounds as presented in Table 1 and mentioned in the results section. During the interference investigation of I or II from the presence of the other compound, determination of II in mixtures of I and II was possible, measuring at the zero-crossing point of 231.6 nm, as becomes clear from the corresponding percentage recoveries in Table 2. However, determination of I in the presence of II, measuring at the zero-crossing point of 234.6 nm was not feasible, as presented in Table 3. It may be due to its very low signal and the drift of the position of the other band.

Zero-crossing methodology is ideal in terms of systematic error, but it is more sensitive, compared with graphical measurements, to small drifts of the interfering band. As a result it is important to verify the exact position of the zero-crossing point frequently during the experiments. This was carried out systematically in our chemical system. However, this may be the cause of the relatively high standard deviation in the percentage recovery revealed in Table 2.

4.3. Evaluation of the zero-crossing technique

As shown in Table 1 there is a linear relationship between the signal of the first-derivative spectrum of II at the zero-crossing point of 231.6 nm in the absence and in the presence of I. Moreover, the corresponding regression equations present an intercept value essentially equal to zero and slopes that are statistically identical. These results were based on the application of t-test for a confidence

interval of 95% [19]. In addition to these, the mean percentage recovery of II in the presence of I is very close to 100% as it is obvious in Table 2.

From the above statistical evaluation of the derivative method, based on the results given in the appropriate section, its good linearity and reproducibility better than 3% for a confidence interval of 95% was demonstrated. Thus, it was concluded that the zero-crossing technique could be used for the kinetic study on the degradation of lorazepam to its main product II, monitoring the 6-chloro-4-(2-chlorophenyl)-2-quinazoline carboxaldehyde (II) and not lorazepam itself.

4.4. Kinetic investigation

From the good fit of the experimental points to the drawn curves (see Fig. 4 as an example) it was obvious that hydrolysis of lorazepam followed pseudo first-order reaction kinetics. This was in agreement with the results of the HPLC method developed in our laboratory and other information from the literature [4,5]. It should be pointed out here that the above statement may hold for lorazepam but when kinetics of degradation product II is examined, it should be treated carefully. In the examined case and during the experimental time of the derivative approach, lorazepam was degraded essentially to II. However, if the experiment lasts longer or in different acidic conditions, where II produces III in measurable quantities, then kinetics of degradation product II is not first-order any more and becomes more complex [9].

The results of the kinetic investigation of lorazepam by the zero-crossing technique are summarised in Table 4 along with those of the HPLC method [9]. The observed differences can be justified considering the presence of product III in late times. This product was not detected by the UV approach but it was measured by the HPLC method and probably affected the kinetics of degradation product II.

Since the reaction under study is not clearly a first-order reaction, activation energy was not calculated. However, k_{obs} and $t_{1/2}$ at 37°C can be estimated. This can give a good idea of the probability of degradation of lorazepam in the stomach fluid, where that $k_{obs}^{37} = 5.2 \times 10^{-4}$ min^{-1} and $t_{1/2}^{37} = 22$ h. Acidic hydrolysis of this drug may therefore occur in the stomach to a certain extent.

5. Conclusions

The zero-crossing first-order derivative spectrophotometric technique described in this work is a reliable, simple, inexpensive and fast method, developed for the kinetic study of lorazepam, monitoring its main degradation product. The low DL of II found in this approach and the fact that product II has been reported as the degradation product of lorazepam in its stability studies in solid dosage forms [2,5,6], may prove it useful as a stability indicating technique, as well.

Acknowledgements

The authors thank Minerva Hellas, greek pharmaceutical company for providing pharmaceutical purity grade lorazepam. They also thank Dr V. Roussis and Dr D. Argyropoulos for their assistance in the MS and NMR facilities, respectively. The main author expresses her gratitude to Dr M. Kondylis for his helpful comments.

References

[1] G.A. Archer, L.H. Sternbach, Chem. Rev. 68 (1968) 747.
[2] J.G. Rutgers, C.M. Sheaver, Anal. Prof. Drug Substances 9 (1980) 397.
[3] G.A. Neville, H.D. Beckstead, H.F. Shurvell, Can. J. Appl. Spectrosc. 37 (1992) 18.
[4] N. Udupa, S.V. Tatwawadi, K.D. Gode, Indian Drugs 23 (1986) 294.
[5] V. Kmetec, A. Mrhar, R. Karba, F. Kozjek, Int. J. Pharm. 21 (1984) 211.
[6] P.C. Dabas, H. Erguven, C.N. Carducci, Drug Dev. Ind. Pharm. 14 (1988) 133.
[7] E. Roets, J. Hoogmartens, J. Chromatogr. 194 (1980) 262.
[8] A. Morales-Rubio, J.V. Julian-Ortiz, A. Salvador, M. De la Guardia, Microchem. J. 49 (1994) 12.
[9] I.E. Panderi, H.A. Archontaki, E.E. Gikas, M. Parissi-Poulou, J. Liq. Chrom. Rel. Technol. 21 (1998) 1973.
[10] T.C. O'Haver, G.L. Green, Anal. Chem. 48 (1976) 312.
[11] T.C. O'Haver, Clin. Chem. 25 (1979) 1548.

[12] M. Mariaud, P. Dubois, P. Levillain, Analyst 113 (1988) 929.
[13] B. Morelli, J. Pharm. Sci. 77 (1988) 615.
[14] B. Morelli, J. Pharm. Sci. 79 (1990) 261.
[15] I. Panderi, M. Parissi-Poulou, J. Pharm. Biomed. Anal. 12 (1994) 151.
[16] A.F.M. El Walily, S.F. Belal, E.A. Heaba, A. El Kersh, J. Pharm. Biomed. Anal. 13 (1995) 851.
[17] J.J. Berzas, J. Rodriguez, G. Castaneda, Analyst 122 (1997) 41.
[18] H. Archontaki, Analyst 120 (1995) 2627.
[19] J.C. Miller, J.N. Miller, Statistics for Analytical Chemistry, Wiley, NY, 1984, Chapters 2–4.
[20] J.D. Ingle, Jr., S.R. Crouch, Spectrochemical Analysis, Prentice-Hall, NJ, 1988, Chapters 5 and 6.
[21] W.W. Han, G.J. Yakatan, D.D. Maness, J. Pharm. Sci. 65 (1976) 1198.
[22] W.W. Han, G.J. Yakatan, D.D. Maness, J. Pharm. Sci. 66 (1977) 573.
[23] W.W. Han, G.J. Yakatan, D.D. Maness, J. Pharm. Sci. 66 (1977) 795.
[24] T.J. Broxton, T. Ryan, S.R. Morrison, Aust. J. Chem. 37 (1984) 1895.
[25] T.J. Broxton, S.R. Morrison, Aust. J. Chem. 38 (1985) 1037.
[26] M.E. Moro, J. Novillo-Fertrell, M.M. Velazquez, L.J. Rodriguez, J. Pharm. Sci. 80 (1991) 459.
[27] S.C. Bell, S.J. Childress, J. Org. Chem. 29 (1964) 506.
[28] W. Sadee, E. Van der Kleijn, J. Pharm. Sci. 60 (1971) 135.
[29] J.A. Goldsmith, H.A. Jenkins, J. Grant, W.F. Smyth, Anal. Chim. Acta 66 (1973) 427.
[30] V.D. Reif, N.J. Deangelis, J. Pharm. Sci. 72 (1983) 1330.

ELSEVIER

Talanta 48 (1999) 695–703

Talanta

Atomization of Al in a tungsten coil electrothermal atomic absorption spectrophotometer

Pedro O. Luccas [a], Joaquim A. Nóbrega [a,*], Pedro V. Oliveira [a], Francisco J. Krug [b]

[a] *Departamento de Química, Universidade Federal de São Carlos, Caixa Postal 676, CEP 13565-905, São Carlos, SP, Brazil*
[b] *Centro de Energia Nuclear na Agricultura, Universidade de São Paulo, Caixa Postal 96, CEP 13400-970, Piracicaba, SP, Brazil*

Received 10 March 1998; received in revised form 31 August 1998; accepted 2 September 1998

Abstract

Electrothermal atomic absorption spectrophotometry of Al in a tungsten coil atomizer was evaluated and applied for its determination in hemodialysis fluid. The system was mounted on a Varian Spectra AA-40 spectrophotometer with continuum background correction and all measurements, in peak height absorbance, were done at 309.3 nm. The purge gas was a mixture of 90% Ar plus 10% H_2. Observation height, gas flow, drying, pyrolysis and atomization steps were optimized. The heating program was carried out by employing a heating cycle in four steps: dry, pyrolysis, atomization and clean. The determination of Al in hemodialysis solutions was performed by using a matrix-matching procedure. Al in hemodialysis solutions was determined by TCA and by electrothermal atomization with a graphite tube atomizer. There is no differences between results obtained by both methods at a confidence level of 95%. The characteristic mass of Al by using the TCA was 39 pg and the detection limit was 2.0 μg l^{-1}.

Keywords: Electrothermal atomic absorption spectrophotometry; Tungsten coil atomizer; Aluminum; Hemodialysis solution

1. Introduction

Investigations during the last ten years indicated that tungsten coil (150 W) can be used in some applications for determination of low concentrations of elements. This simple atomizer is characterized by its low power consumption, the coil geometry which allows homogeneous distribution of the samples, the typical heating rates of up to 30 K ms^{-1}, and the use of cooling systems is not necessary. This high heating rate is reached due to the low mass and low specific heat of the tungsten coil. The coil mass is about 100 mg and the specific heat is 0.133 J g^{-1} K^{-1}, both parameters are lower than those of a typical graphite tube and since the heating rate is inversely proportional to the mass and the specific heat, high heating rates can be attained. These data were properly showed by Krakovska [1] referring to tungsten tubes.

* Corresponding author. Tel. +55-16-2608208; fax: +55 16-2608350; e-mail: djan@zaz.com.br.

0039-9140/99/$ - see front matter
PII: S0039-9140(98)00294-X

The first studies with a tungsten coil atomizer were reported during the 1970's by Piepmeier and Williams [2], by Newton et al. [3], and by Lund and Larsen [4]. All these works emphasized the simplicity and low cost of this atomizer, but the occurrence of interferences and the difficulty to measure fast transient signals were also showed.

The tungsten coil atomizer proposal was revisited by Berndt and Schaldach [5] in the 1980's and it was applied for As, Sb and Sn determination in pure gold [6], alkaline and alkaline earth metals in ammonium paratungstate [7], Cd in biological and botanical materials [8], Ba in waters [9], Pb in blood [10–12] and paints [12], Cd, Co, Cr, Mn and Ni in water, soft drinks and wines [13,14], Cr in river water [15], Pb in waste water [16] and Cd and Pb in water [17]. However, its analytical applicability still need to be fully evaluated for different matrices and analytes. The tungsten coil atomizer is a low-cost device that can be heated even by a battery as recently showed by Sanford et al., [12]. These authors proposed a portable system with an estimated cost lower than $6000 including the notebook computer. This type of device could find specific applications to solve practical analytical problems demanded by the society, such as the determination of lead in blood of children [10–12].

The determination of trace concentrations of Al in clinical samples is important due to the physiological role of this element [18]. The European Committee established that diluted hemodialysis solutions should not contain Al concentrations higher than 10 μg l^{-1} [19]. The difficulty of determination of Al in hemodialysis solutions is evidenced by the high level of dispersion observed in the results obtained from different laboratories for the same sample [20]. Ideally the technique chosen should present a lower detection limit and should not be affected by the elevated concentration of alkalines, alkaline earths, and chloride ions in the matrix. In addition, depending on the clinical aspects involved, this solution also contains significant concentrations of glucose [21]. Previous developed procedures employed differential pulse voltammetry [22], flame atomic absorption spectrometry coupled to a flow injection system (FIA-FAAS) [23], inductively coupled plasma atomic emission spectrometry (ICP-AES) [24] and electrothermal graphite furnace atomic absorption spectrometry (ETAAS) [25,26]. Each one of these spectrochemical techniques present advantages and disadvantages for this analytical task. For FAAS, a previous step is necessary for matrix separation and analyte concentration owing to the high emission of the matrix components and the poor detection limit of this technique. The emission by matrix components and the presence of organic compounds also require a preliminary treatment of the sample before introduction in ICP's. Thus, the most straightforward technique to Al determination in hemodialysis solutions is ETAAS. Recently, Schlemmer [27] presented a discussion about the use of this technique for complex samples. Taking into account the technological achievements in this area, it is now possible to make direct analytical measurements in samples such as serum and seawater. The avoidance of sample pretreatment is important for trace metal analysis to circumvent contamination.

The performance of the electrothermal atomization technique with a tungsten tube atomizer was evaluated for determination of Al in biological materials [28]. The addition of hydrogen in the purge gas composition was effective for Al atomization.

The aim of this research was to evaluate the electrothermal atomization of Al in a tungsten coil atomizer. A procedure for Al determination in hemodialysis solutions was developed.

2. Experimental

2.1. Apparatus

A Varian Spectra AA-40 atomic absorption spectrophotometer, coupled with a Varian DS-15 Data Station, was used for experiments with the tungsten coil atomizer. An Al hollow cathode lamp and a deuterium source from the same manufacturer were used for measurements of atomic and background signals, respectively. The absorbance signal based on peak height was measured at 309.3 nm Al resonance line. All signals were detected with a time constant of 50 ms.

Table 1
Tungsten coil furnace heating program: pyrolysis and atomization curves

Step	Voltage (V)	Temp (°C)	Time (s)	Gas flow rate (l min^{-1})	Read
Dry	0.80	410	40	1.00	No
Pyrolysis	x[a]	525–1670	2.0	1.00	No
Atomization	y[b]	1670–2300	1.0	1.00	Yes

[a] x varied from 1.00 to 7.00 V.
[b] y varied from 7.00 to 15.00 V.

The tungsten coil (Osram 150 W) atomizer was fixed in two brass electrodes supported by a Teflon® fitting, which was inserted into a 10 cm flow-through cell mounted in a Perspex base. The whole assembly replaced the Varian GTA-96 graphite furnace as described by Silva et al., [9]. Sample aliquots of 10 μl were automatically delivered into the coil by means of the Varian GTA-96 autosampler. The tungsten coil was heated by a programmable power supply with a voltage feedback circuit (Anacom Equipament and Systems, São Bernardo do Campo, SP, Brazil). This power supply was interfaced with the DS 15 Data Station, thereby enabling the tungsten coil furnace operation to be started by pushing the start GTA command. A 90% v/v argon plus 10% v/v hydrogen mixture was used as protective gas.

A VarianAA-800 atomic absorption spectrophotometer equipped with Zeeman background correction and pyrolytically coated graphite atomizer was used for comparison of Al results in hemodialysis solutions.

2.2. Reagents and reference solutions

All solutions were prepared from analytical reagents and Milli-Q water (Millipore, MA) was used throughout, unless otherwise mentioned. Concentrate acids were distilled in quartz sub boiling stills (Kürner Analysentechnik, Germany).

Aluminium stock solution was prepared by dilution of Titrissol (Merck) in water. Analytical reference solutions (20–160 μg l^{-1}) of Al were prepared by appropriate dilutions of this stock. Reference solutions were prepared in two media: the first series in 0.014 mol l^{-1} HNO_3 and the other by adding Al known concentrations to an Al-free hemodialysis sample. The effect of concomitants were investigated by preparing solutions containing 200 μg l^{-1} of Al^{3+} and up to 3500 mg l^{-1} of Na^+ (NaCl), K^+ (KCl), Ca^{2+} ($CaCO_3$) or Mg^{2+} (MgO) in 0.014 mol l^{-1} of HNO_3 (Johnson Matthey Chemicals). Effects caused by acetate and glucose were evaluated by preparing solutions containing up to 2500 and 15 000 mg l^{-1} of each one of these compounds, both from Merck. In some experiments a 5% w/v of sodium tungstate (Merck) solution was used to recover the coil surface.

Hemodialysis solutions were collected during a hemodialysis session and were kept in polyethylene flasks. Sample storage was shorter than 1 week.

All polyethylene and glass flasks utilized in this work were cleaned in 50% v/v nitric acid solution during at least 24 h, followed by washing with distilled-deionized water.

2.3. Procedure

The tungsten coil was positioned just below the radiation beam, i.e. the beam passed over the upper side of the coil without any physical obstruction. Thus, the noise due to coil emission was not noticeable and a maximum analytical signal-to-noise ratio was obtained.

A 10 μl volume of Al reference solution (200 μg l^{-1}) was delivered into the tungsten coil. This volume and concentration were maintained constant during the electrothermal Al studies: pyrolysis and atomization curves, effect of acid concentration, effect of purge gas flow rate and composition, and effect of concomitants.

Table 2
Tungsten coil furnace heating program for Al determination in hemodialysis solutions

Step	Voltage (V)	Temp (°C)	Time (s)	Gas flow rate (l min^{-1})	Read
Dry	0.80	410	40	1.00	No
Pyrolysis	3.0	1075	20	1.00	No
Atomization	14.00	2230	1.0	1.00	Yes
Cooling	0	–	5.0	1.00	No
Clean	14.00	2230	1.0	1.00	No

The pyrolysis and atomization curves were obtained in nitric and hydrochloric acids. The heating program is shown in the Table 1. The pyrolysis curve was obtained applying 14.00 V in the atomization step. For obtaining the atomization curve, the pyrolysis voltage was kept at 3.00 V. The flow rate of 90% v/v argon plus 10% v/v hydrogen gas mixture was kept constant at 1.00 l min^{-1}.

In another experiment, the effect of flow rate of purge gas mixture was investigated from 0.40 to 1.40 l min^{-1} using the heating program presented in Table 2. The gas flow rate was varied using a Omel rotameter (São Paulo, SP, Brazil) calibrated by the supplier with a gas mixture containing 90% v/v Ar plus 10% v/v H_2

The effect of purge gas composition was evaluated during each step of the program. This procedure was implemented by changing the gas mixture by pure argon. The flow rate was kept at 1.00 l min^{-1}.

The sample pretreatment was done in the autosampler cup. By using a micropipet (Finnpipette), an aliquot of 900 μl of hemodialysis solution was transferred to the polyethylene autosampler cup (Varian GTA-96) containing 100 μl of 0.14 mol l^{-1} of nitric acid. The resulting solution was mixed by pumping the micropipet several times in the autosampler cup. Afterwards 10 μl of this solution was automatically delivered onto the tungsten coil atomizer by autosampler action.

The tungsten coil heating program used for evaluating the sample preparation procedure and Al determinations in hemodialysis solutions is shown in Table 2. The tungsten coil surface temperature was determined by measuring the electric current associated to each applied voltage. These data and the knowledge of the tungsten coil mass, density, length, and diameter allowed the calculation of the resistivity. The relation of the resistivity and temperature for tungsten materials can be easily found in the literature [29].

For comparison of results was adopted a graphite furnace procedure. Standard additions method was adopted for quantification. Analytical reference solutions containing 10 and 20 μg l^{-1} were prepared by dilution of the Al stock solution in 0.14 mol l^{-1} nitric acid. Al concentrations of 0, 10 and 20 μg l^{-1} were added to the samples by the autosampler. The wavelength selected was 396.2 nm and the results were based on peak area absorbance.

As chemical modifier it was used a solution containing 0.8% m/v $Mg(NO_3)_2$ in 1.1 mol l^{-1} HNO_3 according to [30]. The experiments were run without a platform with the heating program showed in Table 3.

Table 3
Graphite furnace heating program

Step	Temp (°C)	Time (s)	Gas flow rate (l min^{-1})	Read
1	95	5.00	3.0	No
2	95	40.0	3.0	No
3	120	20.0	3.0	No
4	500	10.0	3.0	No
5	500	20.0	3.0	No
6	1400	20.0	3.0	No
7	1400	20.0	3.0	No
8	1400	2.0	0.0	No
9	2500	0.6	0.0	Yes
10	2500	3.0	0.0	Yes
11	2500	2.0	3.0	No

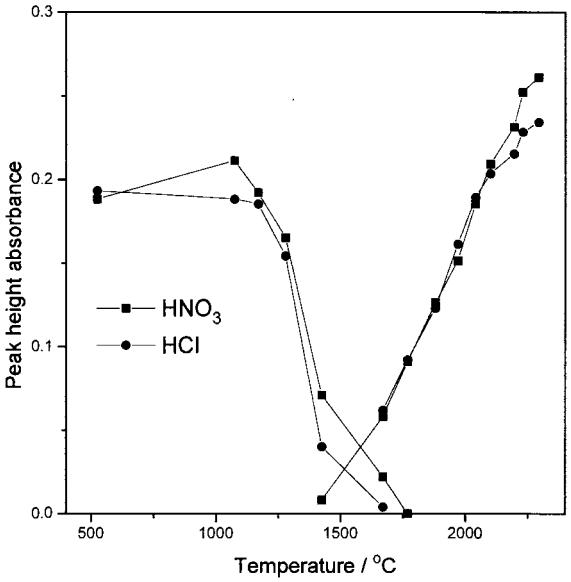

Fig. 1. Pyrolysis and atomization curves for Al solutions in hydrochloric and nitric acids.

3. Results and discussion

3.1. Pyrolysis and atomization curves

Although the maximum gas phase temperature occurred in the center of the tungsten atomizer, a baseline noise increase was verified when Al was measured at this point, most probably due to thermal expansion and emissivity of tungsten coil [29]. The sensitivity was slightly decreased when measurements were made with the tungsten coil positioned ca. 1 mm below the radiation beam. This observation height was adopted in all experiments to decrease the baseline noise.

The tungsten coil was heated using a three-step program (Table 1). The pyrolysis and atomization voltages were adjusted using the conventional double curves procedure, for 200 μg l^{-1} of Al in 0.014 mol l^{-1} of nitric and hydrochloric acids (Fig. 1). It can be seen that, either nitric or hydrochloric acids, up to 1070°C can be employed in the pyrolysis step without losses of analyte. The optimum atomization temperature was 2300°C, this temperature is smaller than that generally used for Al atomization in graphite atomizers (2400–2600°C). This slightly lower temperature for atomization could be an indication that in the tungsten coil atomizer the Al atomization mechanism is more influenced by chemical processes, such as reduction reactions, promoted by hydrogen than by thermal processes. These aspects will be discussed later.

3.2. Effect of flow rate and purge gas composition

Al atomization was strongly affected when the flow rate of the 90% v/v of argon plus 10% v/v of hydrogen gas mixture was varied from 0.40 to 1.40 l min^{-1}. The effect of the purge gas flow rate can be seen in the Fig. 2. The sensitivity increased at higher flow rates and as a compromise between signal magnitude and gas consumption all further experiments were carried out at 1.00 l min^{-1}. This is completely different of the stopped-flow condition using in ETAAS with a graphite furnace, but it should be mentioned that the so called purge gas in this technique should be seen as an atomization gas in the TCA, i.e. the atomization efficiency is critically dependent on the hydrogen present in the gas, which is also important to increase the tungsten coil lifetime.

The hydrogen contained in the purge gas probably acted in the reduction of Al oxides and this effect overcame the dilution of the atomic cloud. It could be supposed that the atomization efficiency could be improved by using higher concentrations of hydrogen in the gas mixture and flow

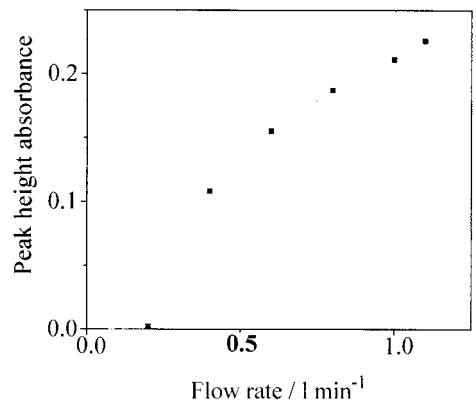

Fig. 2. Effect of the purge gas flow rate (90% Ar + 10% H_2 v/v).

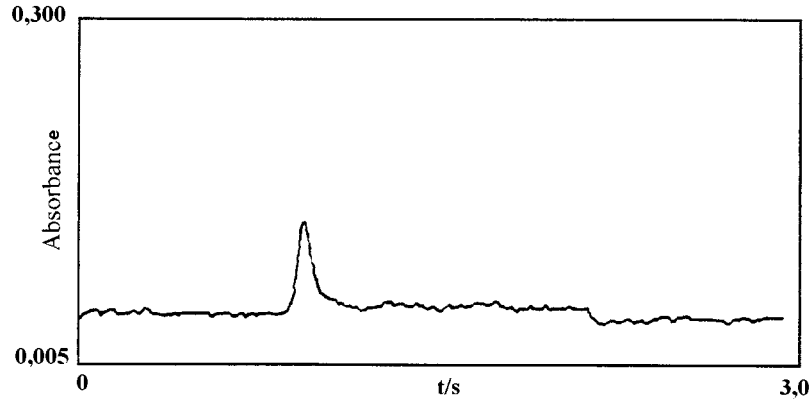

Fig. 3. Aluminum AA signal in the TCA: hemodialysis spiked-sample containing 93.7 μg l^{-1} Al^{3+}.

rates, also the hydrogen avoided tungsten oxidation in high temperatures. Ohta et al., [28] showed that up to 20% of hydrogen in the gas mixture caused a signal increment in the Al atomization in a tungsten tube atomizer. Above this amount of hydrogen, the peak height of the Al signal decreased and in pure hydrogen the Al signal became very small.

As previously related, atomization of barium [9] and lead [10] in tungsten coil atomizer was also strongly dependent on hydrogen in the purge gas composition.

Research done by Sychra et al., [31,32] regarding to the Al atomization mechanism in a tungsten tube atomizer showed strong dependence of atomization efficiency with hydrogen presence in the purge gas. They showed that Al could react with hydrogen of purge gas to form compounds with low dissociation energy.

In our study, no atom formation was observed in experiments carried out with pure argon during all steps of heating program or using only pure argon during the atomization step, thereby, confirming that hydrogen plays a decisive role in the atomization of Al.

3.3. Effect of concomitants

The interference studies were performed using peak height absorbance values because the sensitivity for peak area measurements is very low. Krakovska [33] showed that it is better to work with peak height absorbance than with peak area absorbance in the electrothermal atomization with a tungsten tube atomizer. According to this author, the best sensitivity in peak height is most probably caused by the fast rate of generation of free atoms under almost isothermal conditions and fast removal of the atoms from the atomizer. In tungsten coil, the residence time is shorter because the heating rate is faster. The shape of the transient absorption signals of 200 μg l^{-1} Al solution obtained without or with 100 mg l^{-1} of sodium in 0.014 mol l^{-1} of nitric acid did not change, but the peak height decreased in the presence of sodium. A typical aluminum atomic absorption signal obtained in the TCA is shown in the Fig. 3. The residence time of the signal is ca. 200 ms, which is ten-fold lower than typical graphite furnace signals.

Atomization of Al from solutions containing 200 μg l^{-1} of Al was negligibly affected by nitric or hydrochloric acids ranging from 0.014 to 1.4 mol l^{-1}. The lifetime of the tungsten coil was 200 and 20 heating cycles in the 0.014 and 1.4 mol l^{-1} media, respectively. The end of the tungsten coil lifetime was indicated by sudden loss of repeatability or by coil breakage.

The interference study was carried out considering the concomitants normally found in hemodialysis solutions (Na^+, K^+, Ca^{2+}, Mg^{2+}, acetate and glucose). All these concomitants acted as interferents in the Al atomization (Figs. 4 and 5). As expected, the atomic absorption signal for Al

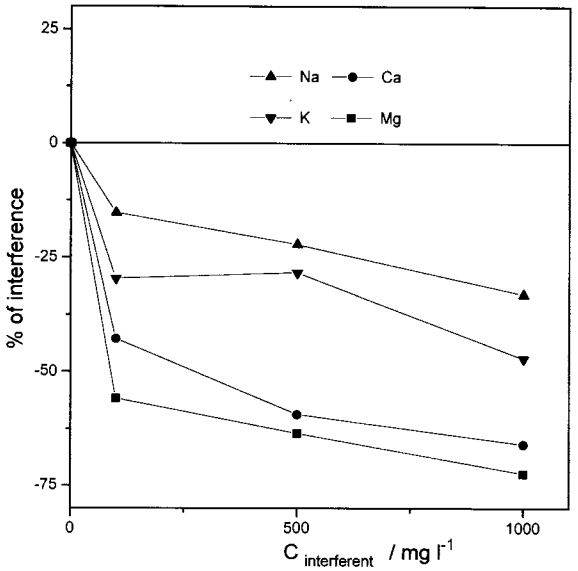

Fig. 4. Effect of inorganic concomitants on Al atomization.

was depressed in the presence of high concentrations of these concomitants. The effects were more intense for Ca and Mg. These effects could be related to H_2 consumption by alkaline-earth oxides and consequently a depletion in the availability of the reductor for Al formation.

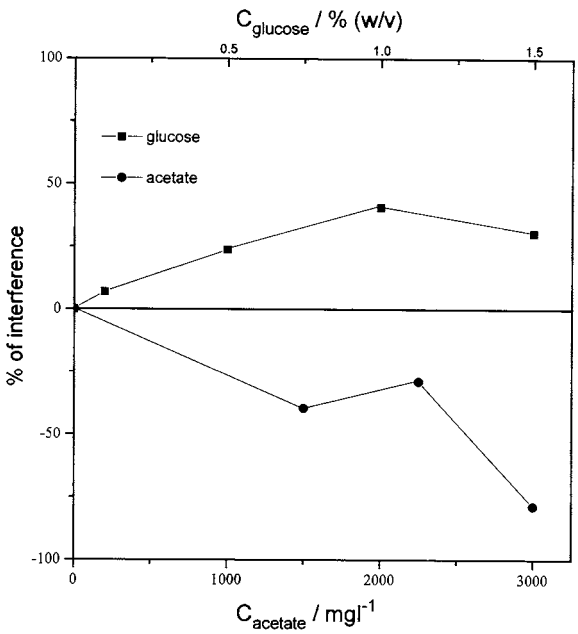

Fig. 5. Effect of organic concomitants on Al atomization.

The effect caused by organic concomitants present in hemodialysis solution is shown in the Fig. 5. The worst effect observed was caused by the action of glucose on tungsten coil surface. According to physical data [29], glucose is melted at 150°C and dehydrated at 200°C, followed by a thermal decomposition at about 300°C. The residues of carbon form a brittle tungsten specie with a melting point 800°C lower than the metallic tungsten. The formation of tungsten carbides was previously emphasized by [34] and X-ray diffraction data showed the action of carbon compounds as reductors in the tungsten surface in thermogravimetric experiments [35]. For solutions containing 1.5 mg l^{-1} of glucose, the lifetime of the tungsten coil was about 15 heating cycles and the precision was completely deteriorated (RSD > 25%). To avoid these effects some alternative procedures were investigated, such as the use of a longer pyrolysis step, the addition of a cleaning step in the heating program, and the use of tungstate to recover the surface after each heating cycle. This idea comes from one industrial method for tungsten production by reduction with hydrogen:

$$WO_4^{2-} + H^+ + \text{heat} \rightarrow WO_3.2H_2O + \text{heat} \rightarrow WO_3 + H_2 + \text{heat} \rightarrow W_{(s)}$$

This latter alternative was effective to avoid carbide accumulation, but the precision obtained for a solution containing 200 μg l^{-1} of Al in 0.014 mol l^{-1} HNO_3 was unsatisfactory (rsd = 21%, $n = 10$) probably due to surface changes caused by successive cycles of tungsten carbide formation and tungsten redeposition.

The best experimental approach to circumvent the destruction of the tungsten coil by glucose was the implementation of a cleaning procedure after atomization (Table 2). The cleaning procedure was implemented in two steps. In the first one, named as cool step, the tungsten coil was cooled at room temperature and the gases residues previously formed were purged by the gas flow. After, a 14.00 V was applied during 1.0 s to remove solid residues that remained on the tungsten surface. It was empirically observed that the cleaning proce-

Table 4
Addition–recovery of aluminum (mean ± SD) in hemodialysis solutions ($n = 5$)

Al added (μg l^{-1})	Al recovered (μg l^{-1})	% Recovery
20	20 ± 1.5	100
40	38.9 ± 1.2	97.4
60	56.3 ± 0.7	93.7
80	77.7 ± 0.9	97.1

Table 5
Mean values and SDs ($n = 4$) for Al determination in hemodialysis solutions by tungsten coil and by graphite furnace procedures

Sample	Tungsten coil (μg l^{-1})	Graphite furnace (μg l^{-1})
1	7.2 ± 0.5	7.2 ± 0.1
2	8.8 ± 2.2	9.2 ± 0.2
3	12.5 ± 3.8	12.4 ± 0.5
4	9.0 ± 1.1	7.8 ± 1.3

dure in two steps was more effective than the use of a longer atomization step. The power supply employed cannot apply voltages higher than 15.00 V.

On the other hand, the interference caused by organic and inorganic concomitants are still significant and they were not decreased by using a longer pyrolysis step. No losses of Al occurred even when 40 s pyrolysis step at 3.00 V (1100°C) was implemented, but this was not effective for eliminating interference. At this point, two alternatives could be investigated to avoid or correct interference: the employment of chemical modifiers or the adoption of a matrix matching procedure.

In spite of the 43% loss in sensitivity when comparing analytical curves obtained in nitric acid or in hemodialysis solution media, the matrix matching procedure seems to be more attractive considering possible contamination caused by the chemical modifier solution. As previously described, a hemodialysis sample solution without Al was used for preparing the analytical reference solutions.

3.4. Al Determination in hemodialysis solutions

Al reference solutions prepared in presence of hemodyalysis solution concomitants provided a linear analytical curve with a correlation coefficient of 0.9998. The linear coefficient and the slope were 0.0006164 and 0.0007914, respectively. The linear dynamic range for Al reference solutions was 20–160 μg l^{-1}. The detection limit ($3s_{blank}$/slope) was 2.0 μg Al l^{-1} and the characteristic mass was 39.6 pg. The characteristic masses obtained in a graphite tube and in a tungsten tube were 11.8 and 9.7 pg Al, respectively [36].

An addition–recovery experiment was performed to evaluate the accuracy of the TCA procedure. According to data showed in Table 4 the recoveries values varied from 93.7 to 100 for Al concentrations added varying from 20 to 80 μg l^{-1}.

The results for Al determination in four hemodyalysis solutions by employing the proposed procedure are presented in Table 5. Data were compared with those obtained by graphite furnace electrothermal atomic absorption spectrophotometry and at a 95% confidence level no statistical difference was observed between both procedures.

In spite of the 3-fold higher characteristic mass and ten-fold higher standard deviations observed for TCA when compared to GFAAS, the procedure proposed could be considered a simple alternative to allow a fast and permanent screening of hospital units in development countries where the use of expensive analytical instrumentation is not easily available. The relevance of this constant monitoring was demonstrated by Nosti et al., showing that the Al level in sera and dialysis waters were lower in hospitals with frequent control [37].

Acknowledgements

The fellowships received by P.O.L. and P.V.O. from Coordenadoria de Aperfeiçoamento de Pessoal de Nível Superior (CAPES) and Conselho Nacional de Desenvolvimento Científico e Tecno-

lógico (CNPq), respectively, and the researchships of J.A.N. and F.J.K. from CNPq are gratefully thanked. We also thank the PADCT-QEQ.01 (62.0585/94.3) and FAPESP (95/5782.7) for financial support. We also would like to thank Konrad Kamner (Osram, Germany) for kindly supplying the tungsten coils.

References

[1] E. Krakovska, J. Anal. At. Spectrom. 5 (1990) 205.
[2] E.H. Piepmeier, M. Williams, Anal. Chem. 44 (1972) 1342.
[3] M.P. Newton, J.V. Chauvin, D.G. Davis, Anal. Lett. 6 (1973) 89.
[4] W. Lund, B.V. Larsen, Anal. Chim. Acta 70 (1974) 311.
[5] H. Berndt, G. Schaldach, J. Anal. At. Spectrom. 3 (1988) 709.
[6] E. Ivanova, I. Havesov, H. Berndt, G. Schaldach, Fresenius J. Anal. Chem. 336 (1990) 320.
[7] E. Ivanova, I. Havesov, H. Berndt, G. Schaldach, Fresenius J. Anal. Chem. 336 (1990) 484.
[8] M.F.R. Giné, J.A. Nóbrega, F.J. Krug, V.A. Sass, B.F. Reis, H. Berndt, J. Anal. At. Spectrom. 8 (1993) 243.
[9] M.M. Silva, R.B. Silva, F.J. Krug, J.A. Nóbrega, H. Berndt, J. Anal. At. Spectrom 9 (1994) 861.
[10] F.J. Krug, M.M. Silva, P.V. Oliveira, J.A. Nóbrega, Spectrochim. Acta Part B 50 (1995) 1469.
[11] P.J. Parsons, H. Qiao, K.M. Aldous, E. Mills, W. Slavin, Spectrochim. Acta Part B 50 (1995) 1475.
[12] C.L. Sanford, S.E. Thomas, B.T. Jones, Appl. Spectrosc. 50 (1996) 174.
[13] C.G. Bruhn, F.E. Ambiado, H.J. Cid, R. Woerner, J. Tapia, R. Garcia, Anal. Chim. Acta 306 (1995) 183.
[14] C.G. Bruhn, F.E. Ambiado, H.J. Cid, R. Woerner, J. Tapia, R. Garcia, Química Anal. 15 (1996) 191.
[15] M. Knochen, E. Saritsky, I. Dol, Química Anal. 15 (1996) 184.
[16] M.M. Silva, F.J. Krug, P.V. Oliveira, J.A. Nóbrega, B.F. Reis, D. Penteado, Spectrochim Acta Part B 51 (1996) 1925.
[17] P. Ostrega, E. Bulska, A. Hulanicki, Chem. Anal. 38 (1993) 779.
[18] R. Massey, D. Taylor, Aluminium in Food and the Environment, The Royal Society of Chemistry, Cambridge, 1988.
[19] European Commission, Off. J. Eur. Commun. 23-7-1986, C/184/16, 1986.
[20] M.R. Pereiro-Garcia, A. López-Garcia, M.E. Diaz-Garcia, A. Sanz-Medel, J. Anal. At. Spectrom. 5 (1990) 15.
[21] S. Draibe, M. Cendoroglo, M.E.F. Carvalho, H.A.B. Ajzen, Ciência Hoje 18 (1994) 42.
[22] M.E. Carrera, V. Rodriguez, M.I. Toral, P. Richter, Anal. Lett. 26 (1993) 2575.
[23] P. Hernandez, L. Hernandez, J. Losada, Frezenius Z. Anal. Chem. 325 (1986) 300.
[24] F.E. Lichte, S. Hopper, T.W. Osborn, Anal. Chem. 52 (1980) 120.
[25] J.M. Gayón, J.P. Parajón, A. Sanz-Medel, C.S. Fellows, J. Anal. At. Spectrom. 7 (1992) 742.
[26] M. Aceto, O. Abollino, C. Sarzanini, E. Mentasti, F. Mariconti, At. Spectrosc. 15 (1994) 237.
[27] G. Schlemmer, At. Spectrosc. 17 (1996) 15.
[28] K. Ohta, M. Yokoyama, S. Itoh, T. Mizuno, Anal. Chim. Acta 291 (1994) 115.
[29] R.C. Weast (Ed.), Handbook of Chemistry and Physics, 66th ed., CRC Press, Boca Raton, 1985.
[30] S. Ericson, Varian Instruments at Work (AA-109), 1993.
[31] V. Sychra, D. Kolihová, O. Vyskocilová, R. Hlavac, Anal. Chim. Acta 105 (1979) 263.
[32] O. Vyskocilová, V. Sychra, D. Kolihová, Anal. Chim. Acta 105 (1979) 271.
[33] E. Krakovská, Spectrochim. Acta Part B 52 (1997) 1327.
[34] J. Komarek, M. Gamoczy, Collect. Czech. Chem. Commun. 56 (1991) 764.
[35] D.M. Santos, P.O. Luccas, E.T.G. Cavalheiro, J.A. Nóbrega, Accepted for presentation at the 5th Rio Symposium on Atomic Spectrometry. (Mexico, October 4–10, 1998).
[36] V. Sychra, J. Dolezal, R. Hlavác, L. Petros, O. Vyskocilová, D. Kolihová, P. Puschel, J. Anal. At. Spectrom. 6 (1991) 521.
[37] P. Nosti, M.D. Zapatero, M.L. Calvo, A. García de Jalón, J. Escanero, Prevention of Al exposure in hemodialysis patients, in: J. Nève, P. Chappuis, M. Lamand (Eds), Therapeutic Uses of Trace Elements, Plenum Press, New York, 1996.

ELSEVIER

Talanta 48 (1999) 705–710

Talanta

Cesium-ion selective electrodes based on calix[4]arene dibenzocrown ethers

Jong Seung Kim [a], Akira Ohki [b,*], Rina Ueki [b], Tomoko Ishizuka [b], Tomohiro Shimotashiro [b], Shigeru Maeda [b]

[a] *Department of Chemistry, Konyang University, Nonsan, 320-800, South Korea*
[b] *Department of Applied Chemistry and Chemical Engineering, Faculty of Engineering, Kagoshima University, 1-21-40 Korimoto, Kagoshima 890-0065, Japan*

Received 28 May 1998; received in revised form 26 August 1998; accepted 2 September 1998

Abstract

Four calix[4]arene dibenzocrown ether compounds have been prepared and evaluated as Cs^+-selective ligands in solvent polymeric membrane electrodes. The ionophores include 25,27-bis(1-propyloxy)calix[4]arene dibenzocrown-6 **1**, 25,27-bis(1-alkyloxy)calix[4]arene dibenzocrown-7s **2** and **3**, and 25,27-bis(1-propyloxy)calix[4]arene dibenzocrown-8 **4**. For an ion-selective electrode (ISE) based on **1**, the linear response concentration range is 1×10^{-1} to 1×10^{-6} M of Cs^+. Potentiometric selectivities of ISEs based on **1-4** for Cs^+ over other alkali metal cations, alkaline earth metal cations, and NH_4^+ have been assessed. For **1**-ISE, a remarkably high Cs^+/Na^+ selectivity was observed, the selectivity coefficient ($K^{Pot}_{Cs,Na}$) being ca. 10^{-5}. As the size of crown ether ring is enlarged from crown-6 (**1**) to crown-7 (**2** and **3**) to crown-8 (**4**), the Cs^+ selectivity over other alkali metal cations, such as Na^+ and K^+, is reduced successively. Effects of membrane composition and pH in the aqueous solution upon the electrode properties are also discussed.

Keywords: Calix[4]arene dibenzocrown ethers; Electrode; Cesium-selective ionophore; Poly(vinyl chloride) membrane

1. Introduction

There have been many studies about ion-selective electrodes (ISEs) for alkali metal cations, such as Na^+ and K^+ [1]. However, relatively a little attention has been paid to the development of Cs^+-selective electrodes. In early studies, Cs^+-ISEs based on ion-exchangers, tetraphenylborate and its derivatives, were reported [2–4]. A Cs^+-ISE based on the natural ionophore, valinomycin, was reported [5].

Some synthetic macrocycles have been employed in Cs^+-ISEs. Dibenzo-18-crown-6, which is essentially selective to K^+, was used for a Cs^+-ISE when the K^+ activity was relatively low [6]. Kimura et al. prepared a biscrown ether which showed selectivity for Cs^+ [7]. Use of another biscrown ether in a Cs^+-ISE was also reported [8]. Cadogan et al. examined a Cs^+-ISE based on

* Corresponding author. Fax: +81-99-2858339; e-mail: ohki@apc.eng.kagoshima-u.ac.jp.

0039-9140/99/$ - see front matter
PII: S0039-9140(98)00291-4

a calix[6]arene hexaester for which the selectivity coefficients for Cs^+ relative to Na^+ (log $K^{Pot}_{Cs,Na}$) were -3.6 to -3.9 [9]. Bocchi et al. have reported that a calix[4]arene crown ether compound, for which a polyether bridge connects the two phenolic oxygen within the molecule, exhibits a high Cs^+/Na^+ selectivity (log $K^{Pot}_{Cs,Na} = -4.46$) in an ISE [10]. Also, Cs^+-selective chemically modified field effect transistors were prepared by use of calix[4]arene crown-6 derivatives [11].

Asfari et al. have reported that the incorporation of an *o*-phenylene group in the polyether ring within a calix[4]arene crown-6 compound greatly enhances the lipophilicity and the selectivity for Cs^+ relative to other alkali metal cations in a liquid membrane transport system [12,13]. We have prepared calix[4]arene dibenzocrown ethers in which two *o*-phenylene groups are involved in the polyether ring [14,15]. In this study, we have prepared solvent polymeric membrane ISEs from the four calix[4]arene dibenzocrown compounds **1**-**4** (Fig. 1) as Cs^+-selective ionophores and examined the potentiometric selectivities for Cs^+ relative to other alkali metal cations, alkaline earth metal cations, and NH_4^+. A newly prepared calix[4]arene dibenzocrown-6 **1** provides a Cs^+/Na^+ selectivity which is higher than those so far reported in Cs^+-ISEs. Therefore, we have examined the Cs^+-ISE based on **1** in detail. Also, the effect of the structure of ionophore, such as the size of the polyether ring, upon the selectivity is evaluated.

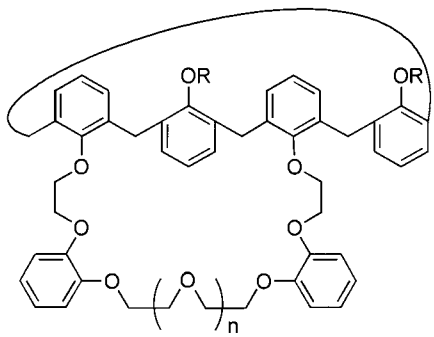

	n	R
1	0	C_3H_7
2	1	C_3H_7
3	1	C_8H_{17}
4	2	C_3H_7

Fig. 1. Structures of calix[4]arene dibenzocrown compounds.

2. Experimental

*2.1. Synthesis of 25,27-Bis(1-propyloxy) calix[4]arene dibenzocrown-6, 1,3-alternate (**1**)*

25,27-Bis(1-propyloxy)calix[4]arene [16], (1.0 g, 2.0 mmol) was dissolved in 50 ml of acetonitrile and an excess of Cs_2CO_3 (1.62 g, 5.0 mmol) and 1,2-bis[2-(2-mesyloxyethyloxy)phenoxy]ethane (1.03 g, 2.1 mmol) were added to the solution under N_2. The reaction mixture was refluxed for 24 h. Then acetonitrile was removed in vacuo and the residue was extracted with 100 ml of methylene chloride and 50 ml of 10% aqueous HCl solution. The organic layer was separated and washed twice with water. After the organic layer was separated and dried over anhydrous magnesium sulfate, the solvent was removed in vacuo to give a brownish oil. Filtration column chromatography with ethyl acetate-hexane (1:6) as eluent provided pure 1,3-alternate calix[4]arene dibenzocrown-6 as a white solid in over 90% yield. Mp 229–232°C. IR (KBr pellet, cm^{-1}); 3068 (Ar-H), 1501, 1451, 1254, 1196. ^1H NMR (400 MHz, $CDCl_3$) d 7.12-6.55 (m, 20H, Ar–*H*), 4.37 (t, 4H), 3.75 (s, 8H, $ArCH_2Ar$), 3.65–3.32 (m, 12H), 1.25–1.16 (m, 4H, $OCH_2CH_2CH_3$), 0.65 (t, 6H, CH_3). ^{13}C NMR ($CDCl_3$): ppm 157.5, 156.7 152.0, 149.7, 134.8, 134.7, 130.3, 129.9, 124.7, 123.3, 123.0, 122.8, 122.3, 115.9, 72.7, 71.0, 69.0, 68.0, 38.7, 23.3, 10.7. FAB MS m/z (M^+) calculated 806.21, found 806.11. Elemental analysis calculated for $C_{52}H_{54}O_8$: C, 77.41; H, 6.69. Found: C, 77.30; H, 6.71.

*2.2. Synthesis of 25,27-Bis(1-propyloxy) calix[4]arene dibenzocrown-8, 1,3-alternate (**4**)*

The synthetic method for **4** is the same as that of **1** except for use of 1,8-bis[2-(2-mesyloxyethy-

loxy)phenoxy]-3,5-dioxaoctane (1.21 g, 2.1 mmol) as the starting material. Mp 184–186°C. IR (KBr pellet, cm^{-1}): 3065 (Ar-H), 1590, 1505, 1451, 1251, 1197, 1127, 1042, 926. ^1H NMR ($CDCl_3$) d 7.10–6.54 (m, 20H, Ar–*H*), 4.20 (t, 4H), 4.08 (t, 4H), 3.90 (m, 4H), 3.87 (t, 4H), 3.76 (t, 4H), 3.71 (s, 8H, ArC*H*$_2$Ar), 3.41 (t, 4H, OC*H*$_2$CH$_2$CH$_3$), 1.45–1.38 (m, 4H, OCH$_2$C*H*$_2$CH$_3$), 0.78 (t, 6H, OCH$_2$CH$_2$C*H*$_3$). Elemental analysis calculated for $C_{56}H_{62}O_{10}$: C, 75.15; H 6.98. Found: C, 75.20; H, 6.99.

2.3. Other chemicals

Calix[4]arene dibenzocrown-7 compounds **2** [15] and **3** [17] were prepared by the reported methods. Poly(vinyl chloride) (PVC) with an average polymerization degree of 1100, dioctyl sebacate, and dibenzyl ether were purchased from Wako Pure Chemical Industries (Osaka, Japan). *o*-Nitrophenyl octyl ether (NPOE), *o*-nitrophenyl phenyl ether (NPPE), and potassium tetrakis(*p*-chlorophenyl)borate (KTpClPB) were obtained from Dojindo Laboratories (Kumamoto, Japan). Metal chlorides including CsCl and tetrahydrofuran (THF) were reagent-grade chemicals. Deionized water was prepared by passing distilled water through an Organo G-10 cartridge.

2.4. Preparation of PVC membranes

A typical PVC membrane was prepared as follows. PVC (50 mg), NPOE (100 mg), the ionophore (6.0 mg), and KTpClPB (2.0 mg) were dissolved in 1.5 ml of THF. An aliquot of the THF solution was poured onto a porous polytetrafluoroethylene (PTFE) membrane attached to a PVC tube and the solvent was allowed to evaporate for 15–20 min. Addition of the THF solution and evaporation were repeated eight or nine times. The resulting PVC tube with the coated PTFE membrane was fixed on a Denki Kagaku Keiki (DKK, Tokyo, Japan) number 7900 electrode body. An internal filling solution of 0.1 M CsCl was added to the electrode. The electrode was conditioned by soaking it in a 0.1 M CsCl solution for 12 h before use.

2.5. Measurements

Potentiometric measurements with a membrane electrode were carried out at 24–25°C with a voltage meter (DKK PHL-40 pH meter), a double junction Ag–AgCl reference electrode (DKK number 4083), and a magnetic stirrer to agitate the sample solution. The electrode cell was Ag–AgCl/0.1 M CsCl/PVC membrane/sample solution/0.1 M NH_4NO_3/3 M KCl/Ag–AgCl. Single ion activities were obtained as described in a previous paper [18]. The selectivity coefficients ($K^{Pot}_{Cs,M}$) for Cs^+ over other metal cations were determined by the fixed interference method [19]. The constant background concentrations of interfering ions were 5 mM for Rb^+, 10 mM for K^+ and NH_4^+, and 0.5 M for other cations.

3. Results and discussion

3.1. Response of ISEs based on calix[4]arene dibenzocrown compounds

Compounds **1–4** were incorporated as ionophores into solvent polymeric membranes in which PVC was the polymer and NPOE was the membrane solvent. For ISEs prepared from these membranes, the response to the change of Cs^+ activity was measured (Fig. 2). A Nernstian response or near Nernstian response (average slope = 58.5 mV decade^{-1}) was obtained for all of those ISEs in the range of 1×10^{-1} to 1×10^{-6} M for **1**, 1×10^{-1} to 3×10^{-6} for **3**, and 1×10^{-1} to 1×10^{-5} for **2** and **4**. It is found that calix[4]arene dibenzocrown-6 **1** is superior to the other calix[4]arene dibenzocrown compounds which have larger polyether rings in terms of the linear response range.

3.2. Potentiometric selectivities of calix[4]arene dibenzocrown compounds

For the solvent polymeric membranes based on **1–4**, potentiometric selectivities for Cs^+ relative to other alkali metal cations, alkaline earth metal cations, and NH_4^+ were determined by the fixed interference method [19]. The selectivity coeffi-

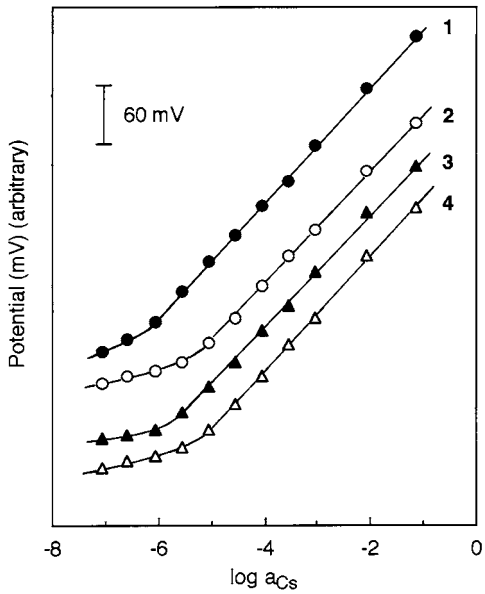

Fig. 2. Potentiometric responses of ISEs based on **1**–**4** to the change of Cs^+ activity. Aqueous solution of CsCl contained 0.01 M LiCl as a supporting electrolyte. In the membrane of ISE, the ionophore content was 6 wt% to the membrane solvent NPOE; while KTpClPB (53 mol% to the ionophore) was added.

cients expressed as log $K^{Pot}_{Cs,M}$ are presented in Fig. 3. The ISEs based on those ionophores exhibit a selectivity for Cs^+ over all of other cations tested.

Compound **1**, which is a calix[4]arene dibenzocrown-6, exhibits a quite high Cs^+ selectivity relative to Na^+ (log $K^{Pot}_{Cs,Na} = -4.88$). This selectivity is superior to those for a calix[6]arene hexaester [9] and for a calix[4]arene crown-6 compound without phenylene groups in the polyether ring [10]. Thus it is found that the incorporation of phenylene groups into the polyether ring of a calix[4]arene crown ether compound enhances the Cs^+/Na^+ selectivity.

Compared with **2**, which has a dibenzocrown-7 ring, the log $K^{Pot}_{Cs,M}$ values noted for **1** when M = Na^+ and K^+ are more negative by 0.39 and 0.46, respectively. Further enlargement in the size of dibenzocrown ether ring to dibenzocrown-8 produces a further decrease in the selectivities for Cs^+ relative to Na^+ and K^+. However, for Cs^+/Li^+ selectivity, ionophore **2** which possesses a dibenzocrown-7 ring is somewhat superior to **1**.

Compound **3**, with R = octyl in place of the propyl group in **2**, gives a Cs^+ selectivity similar to that for **2**. It is anticipated that the attachment of a long alkyl group on the phenolic oxygen in calix[4]arene crown compounds would not affect the selectivity.

3.3. Effect of membrane composition and pH

Since it was observed that **1** is an excellent ionophore in Cs^+-ISEs, solvent membrane electrodes based on **1** were evaluated more fully. Table 1 shows the effect of membrane solvent upon the Cs^+ selectivity in a **1**-ISE. Usually, the selectivity is better when a polar membrane solvent, such as NPOE (dielectric constant $\varepsilon = 24$), is used than that for less polar solvents, such as dioctyl sebacate ($\varepsilon = 4$) and dibenzyl ether ($\varepsilon = 4$), for polymeric membrane ISEs using neutral carriers [10,20]. However, sometimes solvents of low polarity work better than polar solvents [21]. When **1** is used in the Cs^+-ISE, polar membrane solvents, such as NPOE and NPPE, are somewhat preferable to low polar solvents.

In Fig. 4 is shown effect of the content of **1** in the membrane upon the Cs^+ selectivity. As the ionophore content increases, the Cs^+ selectivities over Na^+ and K^+ are enhanced, and the both selectivities become almost constant above 6 wt% of ionophore content. The effect of the KTpClPB content in the membrane was also examined (Fig. 5). As the content of KTpClPB increases, the Cs^+ selectivities over Na^+ and K^+ decrease. The Cs^+/K^+ selectivity becomes almost constant below 50 mol% of KTpClPB; whereas the Cs^+/Na^+ selectivity increases somewhat below 50 mol% of KTpClPB, reaching a log $K^{Pot}_{Cs,Na}$ value of -5.06 at 8.0 mol% of KTpClPB. When the lipophilic salt was not incorporated in the membrane, the electrode did not gave a stable response. The presence of KTpClPB in the membrane is needed in order to maintain the conductivity of membrane. However, it is anticipated that when KTpClPB is present in excess, free KTpClPB which is not accompanying the ionophore acts as an ion-exchanger and reduces the Cs^+ selectivity.

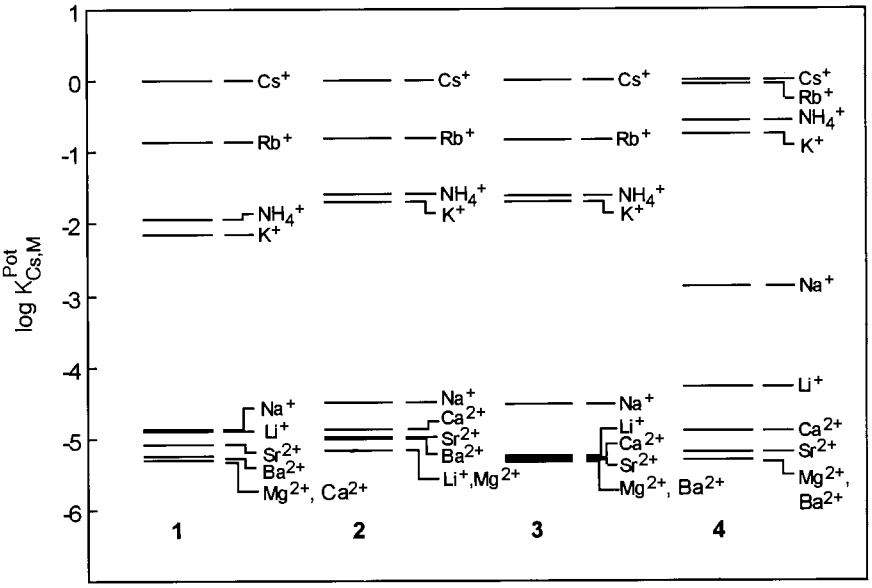

Fig. 3. Selectivity coefficients expressed as log $K^{Pot}_{Cs,M}$ of ISEs based on **1-4** for Cs^+ over other cations. The membrane conditions were the same as those in Fig. 2.

Measurement of the pH dependence of the electrode response was performed for **1**-ISE. The pH of the sample solutions was adjusted by use of 1.0 M NaOH and 1.0 M HCl. The emf remained constant in the pH range of 3–10 in the CsCl concentration range 10^{-3} to 10^{-5} M (Fig. 6).

4. Conclusion

An ISE based on newly prepared calix[4]arene dibenzocrown-6 **1** exhibits a high Cs^+ selectivity over other alkali metal cations and alkaline earth metal cations. Especially it showed an excellent log $K^{Pot}_{Cs,Na}$ value of -4.9 to -5.1 which is superior to those so far reported. Radioactive cesium with a long half-life is present in nuclear fuel reprocessing wastes which are usually high salinity media mainly with $NaNO_3$ [13]. Thus, calix[4]arene dibenzocrown-6 compounds, which have high Cs^+/Na^+ selectivities, may offer a new possibility for practical sensing and separation of Cs^+ in such radioactive wastes.

Table 1
Effect of membrane solvent in **1**-ISE[a]

Membrane solvent	log $K^{Pot}_{Cs,Na}$	log $K^{pot}_{Cs,K}$
NPOE	−4.88	−2.16
NPPE	−4.68	−1.95
Dioctyl sebacate	−4.25	−1.82
Dibenzyl ether	−4.21	−1.75

[a] The membrane conditions were the same as those in Fig. 2 except that the membrane solvent was varied.

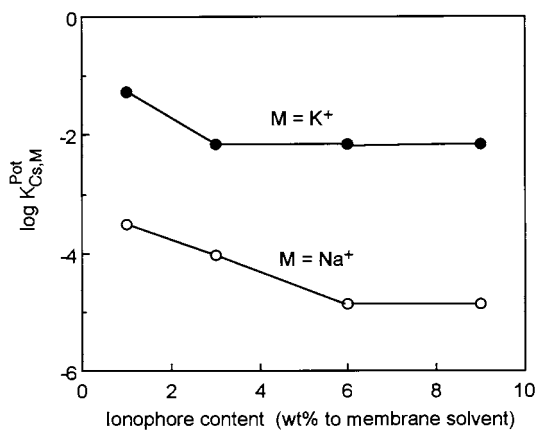

Fig. 4. Effect of the content of ionophore in the membrane upon the Cs^+ selectivity for **1**-ISE. The membrane conditions were the same as those in Fig. 2 except that various ionophore contents were used.

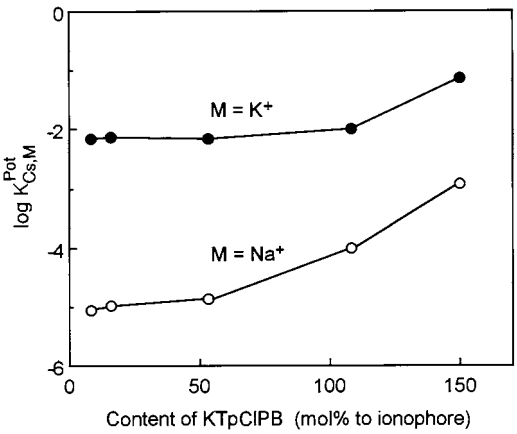

Fig. 5. Effect of the content of KTpClPB in the membrane upon the Cs^+ selectivity for **1**-ISE. The membrane conditions were the same as those in Fig. 2 except that various KTpClPB contents were used.

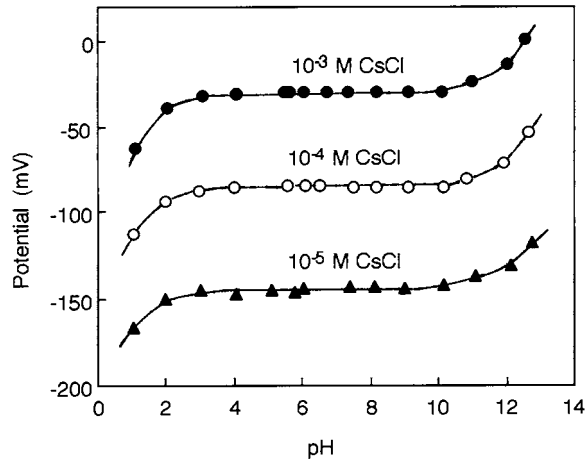

Fig. 6. Dependence of electrode response for **1**-ISE upon the pH of sample solutions at three different CsCl concentrations. The membrane conditions were the same as those in Fig. 2.

References

[1] Y. Umezawa, CRC Handbook of Ion-Selective Electrodes, CRC Press, Boca Raton, FL, 1990.
[2] R. Scholer, W. Simon, Helv. Chim. Acta 55 (1972) 1801.
[3] E. W. Baumann, Anal. Chem. 48 (1976) 548.
[4] C.J. Coetzee, A.J. Basson, Anal. Chim. Acta 92 (1977) 399.
[5] R.F. Cosgrove, A.E. Beezer, Anal. Chim. Acta 105 (1979) 77.
[6] B. Rieckemann, F. Umland, Z. Frezenius's, Anal. Chem. 323 (1986) 241.
[7] K. Kimura, H. Tamura, T. Shono, J. Electroanal. Chem. 105 (1979) 335.
[8] K.W. Fung, K.H. Wong, J. Electroanal. Chem. 111 (1980) 359.
[9] A. Cadogan, D. Diamond, M.R. Smyth, G. Svehla, M.A. McKervey, E.M. Seward, S.J. Harris, Analyst 115 (1990) 1207.
[10] C. Bocchi, M. Careri, A. Casnati, G. Mori, Anal. Chem. 67 (1995) 4234.
[11] R.J.W. Lugtenberg, Z. Brzozka, A. Casnati, R. Ungaro, J.F.J. Engberson, D.N. Reinhoudt, Anal. Chim. Acta 310 (1995) 263.
[12] Z. Asfari, C. Bressot, J. Vicens, et al., Anal. Chem. 67 (1995) 3133.
[13] C. Hill, J.-F. Dozol, V. Lamare, et al., J. Incl. Phenom. Mol. Rec. Chem. 19 (1994) 399.
[14] J.S. Kim, M.H. Cho, I.Y. Yu, et al., Bull. Korean Chem. Soc. 18 (1997) 677.
[15] J.S. Kim, A. Ohki, M.H. Cho, et al., Bull. Korean Chem. Soc. 18 (1997) 1014.
[16] A. Casnati, A. Pochini, R. Ungaro, et al., J. Am. Chem. Soc. 117 (1995) 2767.
[17] J.S. Kim, I.Y. Yu, J.H. Pang, J.K. Kim, Y.I. Lee, K.W. Lee, W.-Z Oh, Microchem. J. 58 (1998) 225.
[18] A. Ohki, J.-P. Lu, R.A. Bartsch, Anal. Chem. 66 (1994) 651.
[19] Recommendation for Nomenclature of Ion-Selective Electrodes, Pure Appl. Chem. 48 (1976) 127.
[20] A. Ohki, S. Maeda, J.P. Lu, R.A. Bartsch, Anal. Chem. 66 (1994) 1743.
[21] K. Kimura, T. Miura, M. Matsuo, T. Shono, Anal. Chem. 62 (1990) 1510.

ELSEVIER

Talanta 48 (1999) 711–718

Talanta

Analysis of haloacetic acid mixtures by HPLC using an electrochemical detector coated with a surfactant-nafion film

Hermes Carrero, James F. Rusling *

Department of Chemistry, University of Connecticut, U-60 Storrs, CT 06269-3060, USA

Received 22 June 1998; received in revised form 2 September 1998; accepted 9 September 1998

Abstract

High pressure liquid chromatography (HPLC) using an electrochemical (EC) detector electrode of pyrolytic graphite coated with a film of ionomer Nafion and the water-insoluble surfactant didodecyldimethylammonium bromide (DDAB) was used to achieve separation and detection of all six bromo- and chloro-acetic acids. The Nafion-DDAB film preconcentrates the acid anions facilitating their electrochemical detection by direct reduction at −1.2 V versus SCE. Detection limits were poorer than the EPA-approved GC-ECD method, but HPLC-EC avoids the derivatization necessary for GC. The HPLC-EC method also detected tribromoacetic acid, which has not been determined simultaneously with other halogenated acids by reported chromatographic methods. The HPLC-EC method using a Nafion-DDAB-coated detector electrode gave comparable results to GC-ECD for the determination of TCA in drinking water.

Keywords: High pressure liquid chromatography; Electrochemical detection; Derivatization; Drinking water

Haloacetic acids (HAAs) are found in industrial wastes and as byproducts of water chlorination [1–5] They are highly soluble in water and toxic to humans [3], plants and algae [6]. Monochloro- (MCA), dichloro- (DCA) and trichloroacetic (TCA) acids are produced during water chlorination. The presence of bromide ions may lead to monobromo- (MBA), dibromo- (DBA), and tribromoacetic (TBA), bromochloroacetic, bromodichloroacetic, and dibromochloroacetic acids [7,8].

Analysis of HAAs can be done by gas chromatography with electron capture detection (GC-ECD), which is the standard method of the U. S. Environmental Protection Agency (EPA) [9]. This method involves several extractions with organic solvent and chemical derivitization, and detection limits are in the low ppb range. Extraction previous to GC analysis is not efficient for TBA [8], which is a strong acid and remains in the acidic aqueous phase. Analysis of this acid must be done with another technique.

* Tel. +1-860-4864909; fax: +1-860-4862981; e-mail: jrusling@nucleus.chem.uconn.edu.

0039-9140/99/$ - see front matter
PII: S0039-9140(98)00295-1

New strategies to avoid extraction and derivatization in HAA analyses are desirable to increase simplicity and economize analysis time. Alternative methods based on high performance liquid chromatography (HPLC) have been proposed [4,10,11]. These procedures do not require extraction or derivatization, and a conventional reversed-phase C_{18} column can be used. However, UV detection at the wavelengths required (210 nm or lower) is subject to interferences in natural samples.

Reverse-phase ion pair chromatography has been applied to separation of HAAs [10]. The method employed Spherisorb C_{18} columns and indirect UV detection, with a mobile phase containing an ultraviolet-absorbing ion. The separation is effective for six acids but TBA was not studied and TCA has a long retention time.

Analysis of HAAs by ion chromatography with conductivity detection [4] had detection limits of 5 to 130 μg/l, still far above that of the GC-ECD technique. Good separation was obtained for all the acids studied except MCA and MBA which elute together. TBA was not determined in the analysis.

Electrodes coated with functional films designed to improve amperometric detection [12] of HAAs could make routine analysis of these compounds by HPLC feasible. We recently used films of the sulfonate ionomer Nafion and water-insoluble double-chain cationic surfactants for incorporation of various proteins. Such films enabled direct, reversible electrochemical studies of redox proteins [13] and impedance detection of antibody–antigen binding [14]. Electrochemical properties of these films are related to the self-organization of the surfactant molecules as bilayers in hydrophilic pockets and on the surface of the porous Nafion films.

Films of surfactant didodecyldimethyl ammonium bromide without Nafion act as ion exchangers [15], incorporating anions and blocking cations from entry. For example, DDAB films on electrodes preconcentrated metallophthalocyanine tetrasulfonates ($MPcTS4^-$) from solution by ion exchange to make stable films with electrocatalytic properties [16]. Also, trichloroacetic acid was preconcentrated 4-fold into DDAB films from 0.1 M KBr solutions [17].

The use of films in amperometric HPLC detectors requires mechanically stability, good mass and charge transport, permselectivity for the analyte and a linear, stable response. Simple DDAB films had all of these properties except good mechanical stability under hydrodynamic conditions [18]. However, film stability could be improved by making composites of DDAB with Nafion [13]. In this paper, we explore the use of Nafion-DDAB films on carbon electrodes for the electrochemical detection of HAAs following separation by HPLC.

1. Experimental

1.1. Chemicals

Monobromoacetic acid (99%) and trichloroacetic acid were from Janssen, Monochloroacetic acid (99 + %) and dichloroacetic acid were from Sigma, tribromoacetic acid (99%), dibromoacetic acid and 2,2-dichloropropionic acid (2,2-DCPA) were from Aldrich. Gas chromatography grade 1-propanol was from Burdick and Jackson, and distilled 'Baker analyzed' pentane was from Baker. Sulfuric acid (99.999%), sodium hydroxide (99.99%), sodium bromide (99 + %) were from Aldrich and 'Baker analyzed' glacial acetic acid was from Baker. Nafion was a 5% solution in ethanol from Aldrich. Didodecyldimethylammonium bromide (DDAB, 99 + %) was from Eastman Kodak. Water was purified with a Sybron-Barnstead Nanopure system to a specific resistance ≥ 16 MΩ cm. All other chemicals were reagent grade.

1.2. Apparatus and procedures

A BAS-100B/W electrochemical analyzer (Bioanalytical Systems) was used for voltammetric studies. A gas-tight, three-electrode water-jacketed cell was used. The working electrode was a 4.5 mm diameter pyrolytic graphite (PG) disk (HPG-99, Union Carbide) coated with a Nafion-DDAB film. A platinum wire counter electrode and a saturated calomel reference electrode (SCE) were used. The temperature was controlled at

25°C and the solutions were kept oxygen-free by bubbling nitrogen prior to voltammetry in solutions containing the analyte, 50 mM NaBr and acetate buffer (0.1 M acetic acid adjusted to pH 5.5 with NaOH). NaBr helps stabilize DDAB in its lamellar phase [15].

The HPLC system consisted of a Spectra Physics SP8810 isocratic pump combined with a BAS liquid chromatography CC-4 electrochemical detector cell. The applied potential and the response recorder was supplied by a BAS electrochemical analyzer similar to that used in voltammetric studies. The acids were separated on reversed-phase Econosphere (Alltech Corp.) 3μm C_{18} silica column, 80 mm long × 4.6mm i.d.. Detection was performed in the BAS CC-4 thin-layer flow cell which contained the coated PG working electrode, a stainless steel auxiliary electrode block and a Ag–AgCl reference electrode. The three electrodes were isolated from each other by a 127 μm-thick TG-5M cell gasket. The mobile phase was acetate buffer (pH 5.5) containing 50 mM NaBr.Elimination of oxygen from the mobile phase improved S/N. To assure oxygen removal from the HPLC mobile phase, a 1 l, three neck, round-bottomed flask was used as mobile phase reservoir. The flask hosted a mobile phase carrier tube, a helium input line, and a condenser, sealed from outside air. The degassing process was performed by bubbling, stirring and heating the mobile phase at 40°C. Then the solution was pumped through the system and allowed to equilibrate at room temperature. All tubing lines were stainless steel and PEEK to avoid entry of oxygen. Quantification was based on calibration curves made with standards treated under identical conditions as the samples.The gas chromatography system was a Hewlett-Packard 5890A with electron capture detection (ECD). The system contained two columns, DB-1701 and DB-5, 30 m × 0.32 mm (i.d.), that provided parallel information about the sample. The HAAs were separated following a temperature program, started by holding the temperature at 60°C for 0.5 min, and then increasing at a rate of 4°C/min up to a final value of 125°C with a equilibration time of 1.00 min. The quantification was based on the analyte relative response (RRa) to 2,2-dichloropropionic acid which was used as internal standard, using calibration curves of RRa versus concentration.

1.3. Film preparation

Electrodes were prepared by sealing pyrolytic graphite (PG) disks of 4.5 mm diameter into Plexiglas blocks for HPLC detection, or into polypropylene tubes for voltammetry. Prior to coating, the PG electrodes were polished with 400-grit SiC paper and then successively polished with 0.3 and 0.05 μm alumina on billiard cloth using a metallographic polishing wheel [19]. Finally the electrodes were polished without alumina on a clean, wet billiard cloth. The coating procedure first deposited 10 μl of Nafion 0.1% v/v in ethanol onto polished electrodes. Once the ethanol was evaporated, 10 μl of a 10 mM aqueous DDAB vesicle dispersion were spread onto the Nafion coated PG [13]. Aqueous DDAB dispersions were sonicated for 24 h to obtain the vesicles. The films were dried and stored in a closed container.

1.4. Sample preparation

Drinking water samples were prepared by using two analyte preconcentration methods, direct evaporation and solid phase extraction (SPE). Procedures were adapted from Reimann and coworkers [5] for samples to be analyzed by HPLC-EC:

1. Evaporation method: 20 ml of water sample were placed into a small petri dish, 2.0 ml aqueous sodium bicarbonate (500 mg/l) was added, and the solution evaporated at 60°C to a volume of 2 ml.
2. SPE method: Sep-Pak, Accell QMA (Millipore) cartridges were equilibrated by injecting 5 ml of NaCl solution (10%), followed by a 20 ml of water sample injected by a syringe pump at 1 ml/min. Following this, 3 ml distilled water were injected to wash out remaining impurities. The acids were recovered from the cartridge by eluting with 2 ml of 12.5 μl/ml sulfuric acid.

Similar procedures with the following modifications were used in sample preparation for GC:

1. Evaporation method. 10 μl of aqueous 1 mg/l DCPA was added to the sample as the internal standard. The sample was evaporated to dryness, and the residue redissolved in 1.0 ml of 1-propanol containing 25 μl concentrated sulfuric acid. The solution was transferred to a 10 ml glass vial, sealed and heated to 70°C for 2 h to esterify the HAAs. After cooling, 1.0 ml of pentane and 10 ml of aqueous solution of NaCl (10%) were added. The pentane phase, which extracted the esters, was analyzed by GC-ECD.
2. SPE method. Sep-Pak cartridges were conditioned with 5 ml of aqueous NaCl (10%). 20 ml of water sample spiked with 10 μl of the internal standard 2,2-dichloropropionic acid (DCPA, stock 1 mg/l solution) were passed through the cartridge at 1 ml/min. With the acids trapped in the anion exchanger, 3 ml of 1-propanol were added to wash out remaining impurities. To elute the acids, 2 ml of acidified 1-propanol solution containing 12.5 μg/ml concentrated sulfuric acid was pumped through the cartridge. The eluted solution collected in a 10 ml glass-vial was acidified with 190 μl concentrated sulfuric acid, sealed and heated at 70°C during 2 h to esterify the HAAs. The resulting solution was diluted with 18 ml of NaCl (20%) and the esters extracted with 1 ml of pentane. The pentane phase was washed with additional 9 ml of sodium chloride and analyzed by GC.

2. Results

2.1. Voltammetry

Cyclic voltammetry at PG electrodes in pH 5.5 buffer with no analyte present showed that the negative electrode potential window is extended to about −1.35 V versus SCE for electrodes coated with Nafion-DDAB films [20]. This is about 100 mV more negative than for bare PG.

Voltammetry of TCA shows (Fig. 1) a well-defined irreversible reduction peak at −1.1 V versus SCE on Nafion-DDAB-coated PG electrodes. On bare PG, there is no clearly identifiable peak for TCA, although a broad, small, ill-defined current rise is observed near −1.2 V. Although a larger, more negative peak is also observed on the bare electrode, it is similar to that found in the background. The second peak found for TCA is similar to that observed in the background buffer without TCA. Thus, Nafion-DDAB electrodes gave a clear, analytically useful peak for TCA, while bare PG did not.

The other chlorinated acetic acids also showed favorable positive shifts in reduction peak potentials on Nafion-DDAB-coated electrodes. Shifts in reduction potentials of the three bromoacetic acids on the Nafion-DDAB electrodes were less significant. Nevertheless, all reduction potentials were within the working window of the Nafion-DDAB electrodes (Table 1), and the peak currents were generally larger compared to bare PG electrodes [20].

Voltammetric results indicated that the best potential to afford simultaneous detection of all the acids was about −1.2 V. A potential more negative than that decreased the signal-to-noise ratio.

2.2. HPLC-EC of standards

Under continuous flow of mobile phase through the detector containing the Nafion-DDAB electrode, peaks for multiple injections of TCA decreased for the first 30 min, then stabilized

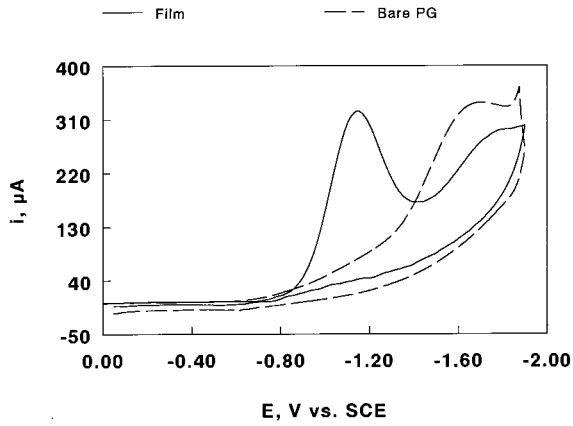

Fig. 1. Cyclic voltammograms of 1 mM TCA in pH 5.5 buffer + 50 mM NaBr at 0.1 V/s.

Table 1
Estimated detection limits for determination of haloacetic acids by chromatographic methods[a]

Acid	HPLC-EC[c] ($-E_p$, V/SCE)[d]	Detection limit, μg/l			
		Ion-pair [10]	Ion exclusion [4]	Ion exchange [4]	GC-EDC [9]
MCA	10000 (1.0)	2000	70	8	0.1
DCA	4000 (1.4)	10000	8	16	0.09
TCA	120 (1.1)	N.D.[b]	5	80	0.06
MBA	480 (1.2)	8000	85	21	0.08
DBA	160 (1.2)	15000	90	30	0.05
TBA	350 (1.1)	N.D.[b]	N.D.[b]	N.D.[b]	N.D.[b]

[a] Method headings given with references in superscripts.
[b] N.D., not detected.
[c] This work.
[d] Peak potential on Nafion-DDAB-PG from CV at 100 mV/s.

and gave reproducible responses for more than 7 h. Fig. 2 shows a typical response pattern for TCA over 3.5 h.

Fig. 3 compares two chromatograms of the same sample containing four HAAs detected on a Nafion-DDAB-coated PG detector electrode and on bare PG. Clearly, detection on the coated electrode shows a more stable baseline and improved signal-to-noise compared to bare PG.

The C_{18} 3μ column separated the six acids in less than 7 min. Fig. 4 a shows a chromatogram using the Nafion-DDAB coated detector for a solution containing the six standard acids for an injection volume of 10 μl. Fig. 4 b shows the separation of a more dilute sample at higher sensitivity and injection volume 100 μl. Skelly [11] found that that the retention time of the anions on a reversed phase column depends on the ionic strength of the mobile phase. Surface active sites on the stationary phase may play an important role in this type of separation.

Table 1 compares detection limits for the six HAAs studied by the HPLC-EC method with several alternatives. Detection limits were estimated as three times the average noise based on

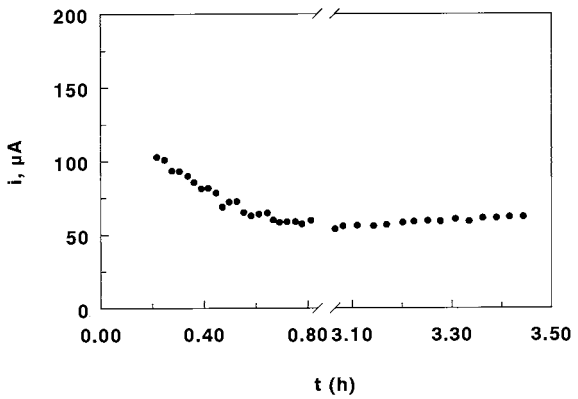

Fig. 2. Typical variation in peak current response of the Nafion-DDAB detector upon multiple injections of 5 mM TCA as a function of time in a continuous flow system (no column). Mobile phase: acetate buffer, pH 5.5 + 50 mM NaBr. Detector: PG electrode coated with Nafion-DDAB film at $E_{app} = -1.2$ V versus SCE; flow rate 0.8 ml/min.

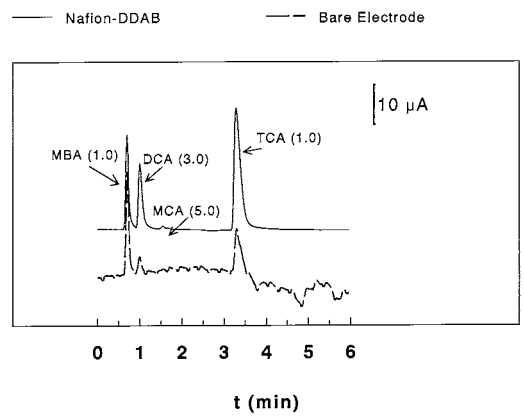

Fig. 3. HPLC with EC detection on bare and Nafion-DDAB-coated detector PG electrodes for mixture of MBA, DCA, MCA, and TCA with millimolar concentrations in parentheses, injection: 10 μl. Flow rate 0.8 ml/min; $E_{app} = -1.2$ V versus SCE.

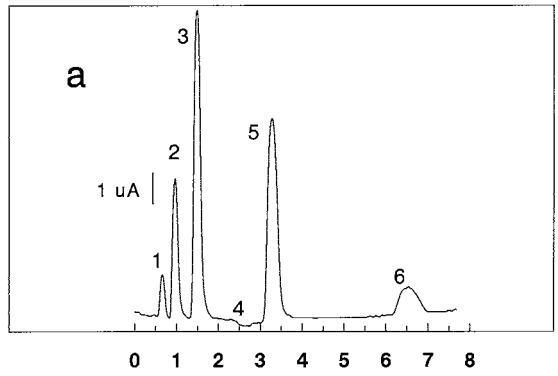

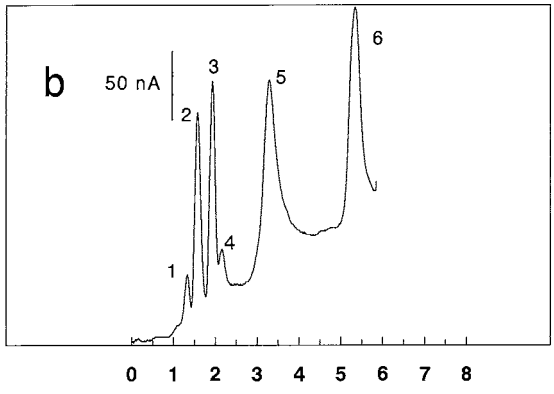

Fig. 4. HPLC showing the separation of six haloacetic acids on Econosphere C_{18} 3μ column. Detector: PG electrode coated with Nafion-DDAB film. Flow rate 0.8 ml/min. $E_{app} = -1.2$ V. (a) Injection 10 μL; sample composition: (1) MBA, 0.5 mM. (2) DCA, 10 mM. (3) DBA, 0.5 mM. (4) MCA, 20 mM. (5) TCA, 0.5 mM (6) TBA, 0.1 mM. (b) Injection 100 μl; sample composition: (1) MBA, 0.10 mM. (2) DCA, 4.0 mM. (3) DBA, 0.01 mM. (4) MCA, 4.0 mM. (5) TCA, 0.01 mM (6) TBA, 0.01 mM. Retention times are slightly different for the HAAs in the two chromatograms because two Econosphere C_{18} 3μ columns with different prior histories were used.

100 μl injection volume. Detection limits were generally lower than reported values for reversed-phase ion-pair HPLC with indirect UV detection [10], but higher than for ion exchange with conductivity detection [4] or ion exclusion with UV detection [4] and much higher than for GC-ECD [9] (Table 1). However, the HPLC-EC method is the only one which can determine all six acids simultaneously.

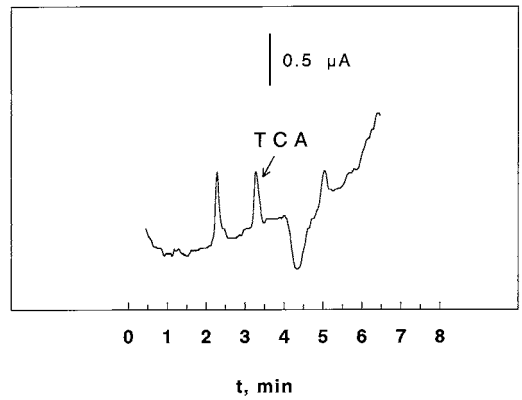

Fig. 5. HPLC showing detection of TCA in drinking water; preconcentration by direct evaporation. Column: Econosphere C_{18} 3μm 80×4.6 mm. Mobile phase: pH $5.5 + 50$ mM of NaBr. Detector: PG electrode coated with Nafion-DDAB film. Injection 100 μl; flow rate 0.8 ml/min; $E_{app} = -1.2$ V.

2.3. Comparative analysis of water samples

Drinking water samples from Windham Water Works, Windham, CT were analyzed with the HPLC-EC method using Nafion-DDAB coated detector electrodes, and by the EPA's GC-ECD method. Two sample pretreatments, direct evaporation and SPE, were also compared (see experimental).

A typical HPLC chromatogram after sample preparation by direct evaporation (Fig. 5) shows that the HPLC-EC method detected TCA. Other unknown peaks were observed, including a large

Table 2
Determination of haloacetic acids in drinking water[a]

Method	Acid	Found, μg/l	
		SPE	Evaporation
HPLC-EC	TCA	155 ± 17	168 ± 13
GC-EDC	TCA	145 ± 14	125 ± 20
GC-EDC	DCA	163 ± 21	132 ± 15
GC-EDC	MCA	5.9 ± 2.2	6.0 ± 3.0

[a] Source was Windham Water Works, Windham, CT. Three replicate samples were analyzed for each determination.

peak at a retention time of about 2.4 min present in all samples. Water samples spiked with HAAs gave similar retention times as standards, but no co-elution of the unknowns with added HAA standards was observed. Bromoacetic acids were not detected. The HPLC-EC analyses (Table 2) found average concentrations of 168 ± 13 μg/l of TCA in samples treated by the evaporation method and 155 ± 17 in samples treated by the SPE method.

The standard EPA GC-EDC method detected all three chloroacetic acids in the water samples. Values obtained for TCA by this method were within two standard deviations of that found by HPLC-EC using the Nafion-DDAB film detector. No other halogenated acetic acids were found by GC-EDC.

3. Discussion.

The direct reduction of haloacetic acids at the EC detector involves a stepwise removal of halide ions in a series of reductive dehalogenations [21,22]. With a mobile phase pH of 5.5, all the acids studied are ionized, and the haloacetic acid anions are presumably attracted by the cationic surfactants present in excess in the Nafion-surfactant coating to provide preconcentration, as previously documented for TCA in DDAB films [17], and facilitate the reduction. The surfactant excess arises because while one layer of cationic DDAB head groups bind to sulfonic acid sites in hydrophilic regions of the porous Nafion film, each DDAB layer is hydrophobically associated with an adjacent layer in a characteristic bilayer arrangement [13]. DDAB may also bind to hydrophobic Nafion regions. Voltammetric studies demonstrated that the Nafion-DDAB films shifted the reduction potential of the chloroacetic acids to more positive values (Fig. 1), decreasing interferences with background current.

The Econosphere 3 μm C_{18} column efficiently separated the six chloro- and bromo-acetic acids (Fig. 4). This column seems to be more effective than other reversed-phase and ion-exchange columns in separating HAAs. The separation of haloacetic acids using a Varian micropak SP-C18-5, 150 mm, column with a mobile phase of 80% 0.01 N of *n*-octylamine, pH 6.2 and 20% acetonitrile partially separated the HAAs [8]. MCA and MBA were apparently not separated. An ion pair method [10] using Spherisorb C_{18} columns and a mobile phase containing benzyltrimethylammonium and hexanesulfonate ions, potassium hydrogen phosphate and acetonitrile separated four of the acids. Aqueous octylamine at pH 6.0 was used to separate MCA, DCA, and TCA on a Partisil-10 ODS column [11], but TCA took 19 min to elute. Determination of HAAs by ion chromatography [4] required the complementary use of ion exchange and ion exclusion methods because of analyte co-elution.

Detection in drinking water samples by HPLC-EC was confined to TCA (Table 2, Fig. 5), but values found were comparable to those found by GC-ECD. GC-ECD is more sensitive than HPLC-EC for the analysis of HAAs in water, and also detected other chlorinated acids. However, the HPLC-EC method using the Nafion-DDAB-coated detector electrode is faster and avoids the chemical derivatization step in sample preparation. Another advantage of the HPLC-EC method is that it separates and determines all six bromo- and chloro-acetic acids simultaneously, provided their concentrations are sufficiently large. The existing EPA GC-EDC method is not applicable to TBA [9].

Acknowledgements

This work was supported by PHS Grant no. ES03154 from National Institute of Environmental Health Sciences, NIH. Contents are the responsibility of the authors and do not necessarily represent official views of NIH. The authors are grateful to Drs Shili Liu and Jianping Chen of the Environmental Research Institute, University of Connecticut, for GC-ECD analyses.

References

[1] K. Ramanand, M.T. Balba, J. Duffy, J. Appl. Environ. Sci. 59 (1993) 3266.

[2] N.K. Kristiansen, M. Froshaug, K.T. Aune, G. Becher, Environ. Sci. Technol. 28 (1994) 1669.
[3] E.A. Bryant, G.P. Fulton, G.C. Budd, Disinfection Alternatives for Safe Drinking Water, Van Nostrand Reinhold, New York, 1992.
[4] L.M. Nair, R. Saari-Nordhaus, J. Anderson, J. Chromatogr. A 617 (1994) 309.
[5] S. Reimann, K. Grob, H. Frank, Environ. Sci. Technol. 30 (1996) 2340.
[6] R. Kühn, M. Pattard, Water Res. 24 (1990) 31.
[7] G.A. Cowman, P.C. Singer, Environ. Sci. Technol. 30 (1996) 16.
[8] L. Heller-Grossman, J. Manka, B. Limoni-Relis, M. Rebhun, Water Res. 27 (1993) 1323.
[9] J.W. Hodgeson, D. Becker, Determination of Haloacetic Acids and Dalapon in Drinking Water by Ion-Exchange, Lipid-Solid Extraction and Gas Chromatography with an Electron Capture Detector. EPA Method 552.1, Revision 1.0 U.S. Environmental Protection Agency, Cincinnati, OH, 1992.
[10] R. Vichot, K.G. Furton, J. Liq. Chromatogr. 17 (1994) 4405.
[11] N.E. Skelly, Anal. Chem. 54 (1982) 712.
[12] R.P. Baldwin, K.N. Thomsen, Talanta 38 (1991) 1.
[13] Q. Huang, Z. Lu, J.F. Rusling, Langmuir 12 (1996) 5472.
[14] K. Abe, R.E. Schmukler, J.F. Rusling, Electroanalysis (in press).
[15] J.F. Rusling, H. Zhang, Langmuir 7 (1991) 1791.
[16] N. Hu, D.J. Howe, M.F. Ahmadi, J.F. Rusling, Anal. Chem. 64 (1992) 3180.
[17] H. Zhang, J.F. Rusling, Talanta 40 (1993) 741.
[18] A.-E. Nassar, J.M. Bobbitt, J.D. Stuart, J.F. Rusling, J. Am. Chem. Soc. 117 (1995) 10986.
[19] G.N. Kamau, W.S. Willis, J.F. Rusling, Anal. Chem. 57 (1985) 545.
[20] H. Carrero, Ph. D. Thesis, University of Connecticut, Storrs, CT. 1997.
[21] P.G. Elving, C.S. Tang, J. Am. Chem. Soc. 72 (1950) 3244.
[22] P.G. Elving, I. Rosenthal, M.K. Kramer, J. Am. Chem. Soc. 73 (1951) 1717.

ELSEVIER

Talanta 48 (1999) 719–728

Talanta

Simultaneous spectrofluorimetric determination of the rare earths with calcein

Iñaki Berregi [a,*], J. Senén Durand [b], J. Alfonso Casado [a]

[a] *Unity of Analytical Chemistry, Faculty of Chemistry, University of the Basque Country, 20009 Donostia/San Sebastián, Spain*
[b] *Department of Analytical Chemistry, Faculty of Sciences, U.N.E.D., 28040 Madrid, Spain*

Received 10 April 1998; received in revised form 8 September 1998; accepted 16 September 1998

Abstract

The reactivity of the fluorescent reagent calcein with the trivalent cations of the rare earths has been spectrofluorimetrically studied in aqueous solution. Optimum excitation and emission wavelengths were 492–497 and 519–522 nm, respectively. Optimum pH was in the range 6.0–9.2. The stoichiometry of the complexes was 1:1. A direct, rapid and sensitive method for the determination of rare earth mixtures has been proposed with a detection limit of 4.49×10^{-8} M and a coefficient of variation of 0.82%. © 1999 Elsevier Science B.V. All rights reserved.

Keywords: Calcein; Fluorexon; Rare earths; Spectrofluorimetry

1. Introduction

Calcein and its use were first described by Diehl and Ellingboe in 1956 [1]. It is prepared by a reaction between fluorescein, formaldehyde and iminodiacetic acid and its structure is shown in Fig. 1.

The molecule possesses both fluorescence and acid–base properties of fluorescein and chelating properties of ethylendiaminetetraacetic acid. The fluorescence of calcein rises from zero at a pH below 3 to a maximum at pH 6.5–8.5 and falls off again at a higher pH, being zero at pH 12 and above.

Calcein shows two different reactions toward metal ions. In solutions of pH 6.5–8.5, in which calcein shows a maximum in fluorescence, this is quenched by the addition of copper, cobalt, ferric ion, nickel and many other metal ions. In solutions of high pH, in which calcein exhibits no fluorescence, this is produced by the addition of calcium, strontium, barium, and of magnesium if the pH is not so high as to precipitate this cation as the hydroxide [2].

The original application of calcein was as metallochromic indicator in the EDTA titration of calcium in the presence of magnesium at pH 12 [1,3,4]. It has been used in the direct fluorimetric determination of calcium [5–7]. Other metals different from calcium have been also determined using calcein, either by fluorimetric or spec-

* Corresponding author. Tel.: 34-943-448000; Fax: 34-943-212236; e-mail: qapbeabi@sq.ehu.es.

PII: S0039-9140(98)00296-3

trophotometric methods [8–13], as well as other non-metallic species like cyanide [14] and sulphate [15]. The fluorescence and chelating properties of calcein have been also reported in many articles in the medical and biological fields, too numerous to be mentioned here.

The present work studies the reactivity of calcein with the rare earths, including yttrium, and the possibility of using this reactivity for screening of these metals. There are almost no references about this subject, as only one article has been found, which proposes a polarographic determination of total rare earths based on their complex with calcein [16].

2. Experimental

2.1. Apparatus

Fluorescence intensities were measured on a Shimadzu RF-540 spectrofluorimeter, using 1×1 cm quartz cells. The pH measurements were made using a Radiometer PHM 82 pH meter, provided with a combined electrode.

2.2. Reagents

All of the reagents used were obtained from Merck and were of analytical grade. Solutions were stored in polyethylene bottle.

Calcein. 1.29×10^{-3} M stock solution was prepared by dissolving 0.0803 g of dried calcein (at 80°C for 2 h) in 0.1 M KOH with the help of an ultrasounds bath, transferring the solution to a 100 ml flask and diluting to the mark with KOH 0.1 M. 1.29×10^{-4} M working solution was prepared by diluting the stock solution with doubly distilled water. Both solutions were stored in a refrigerator and protected from light.

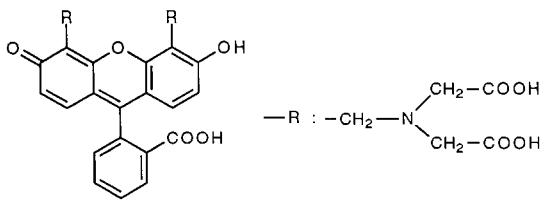

Fig. 1. Structure of calcein

Rare earths. 1.29×10^{-2} M stock solution was prepared by weighing the appropriate amount of dried oxide (at 110°C for 2 h), treating it with 2 ml of concentrated HCl and ~ 10 ml of water at 80°C with stirring, transferring the solution to a 50 ml flask and diluting to the mark with doubly distilled water. 1.29×10^{-4} M working solution was prepared by diluting the stock solution with doubly distilled water, previously adding four drops of concentrated HCl to avoid hydrolysis.

The oxides used included: La_2O_3, Pr_6O_{11}, Nd_2O_3, Sm_2O_3, Eu_2O_3, Gd_2O_3, Tb_4O_7, Dy_2O_3, Ho_2O_3, Er_2O_3, Tm_2O_3, Yb_2O_3, Lu_2O_3 and Y_2O_3. For Ce(III), $CeCl_3 \cdot 7H_2O$ was used dried at 80°C. The dissolution method given is general, however, it has some exceptions. $CeCl_3 \cdot 7H_2O$ is dissolved in pure water, without heating, and four drops of concentrate HCl are added to avoid hydrolysis. Tb_4O_7, Er_2O_3, Tm_2O_3 and Yb_2O_3 need 5 or 6 ml of HCl (2 ml for the last one) and 2 h or more to be dissolved. Lu_2O_3 needs 25 ml of concentrated HCl and 3 h for its dissolution, being the most difficult to dissolve.

Working solution for a global calibration curve. This is a solution which contains equimolar quantities of all of the rare earths except lanthanum, the sum concentration (total rare earth) being 1.29×10^{-4} M. This is obtained by diluting 179 μl of the stock solution of each rare earth in 250 ml, previously adding 10 drops of concentrated HCl to avoid hydrolysis.

Synthetic samples. These are obtained by the same method of the previous case, but taking different volumes from each stock solution (no equimolar quantities):

Sample A: Ce 663, Pr 83.9, Nd 351, Sm 147, Eu 15.3, Gd 84.6, Tb 13.3, Dy 292, Ho 15.4, Er 30.3, Tm 26.3, Yb 31.7, Lu 8.45, Y 736 μl.

Sample B: Ce 1183, Pr 118, Nd 345, Sm 53.9, Eu 8.32, Gd 49.7, Tb 8.42, Dy54.0, Ho 13.3, Er 30.2, Tm 5.11, Yb 26.6, Lu 3.36, Y 601 μl.

Sample C: Ce 887, Nd 318, Sm 66.9, Eu 1.47, Gd 56.7, Tb 12.0, Dy 66.6, Tm7.54, Yb 52.3, Lu 7.28, Y 1025 μl.

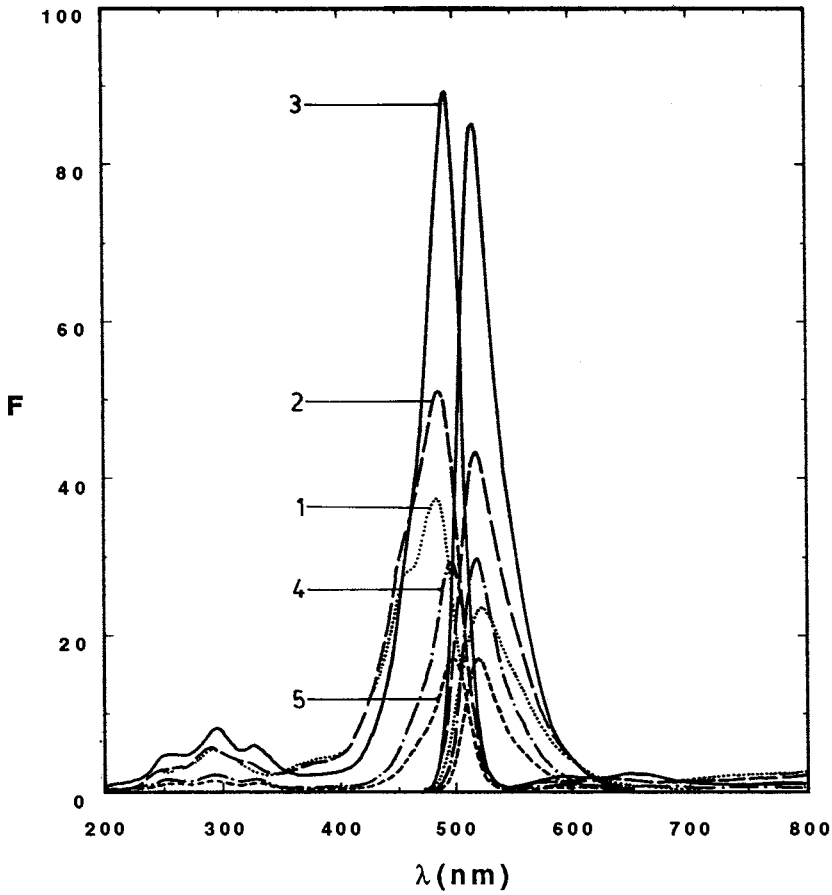

Fig. 2. Excitation and emission spectra of the complex calcein–Gd(III) [calcein] = $[Gd^{3+}] = 5.16 \times 10^{-6}$ M, $\mu = 0.1$, pH. (1) 1.03; (2) 3.05; (3) 6.13; (4) 9.12; (5) 12.08.

Table 1
Excitation/emission wavelength and pH selected

Metal	λ_{exc} (nm)	λ_{em} (nm)	pH	Metal	λ_{exc} (nm)	λ_{em} (nm)	pH
La	492	519	8.6	Dy	495	522	7.1–9.0
Ce	495	520	7.0–8.9	Ho	494	521	6.1–9.1
Pr	495	521	6.4–9.1	Er	495	522	6.3–9.2
Nd	495	522	6.2–9.1	Tm	496	522	6.1–9.2
Sm	495	522	6.0–9.1	Yb	497	521	6.9–9.1
Eu	495	522	6.3–9.1	Lu	497	521	7.2–9.2
Gd	494	522	7.0–9.0	Y	497	521	7.3–9.2
Tb	494	521	6.1–9.1	–	–	–	–

Auxiliary solutions. The following solutions were prepared by dissolving or diluting the appropriate amounts of the product with doubly distilled water: 5 M NH_4Cl/NH_3 buffer of pH 8.6, 2.5 M KCl, 0.1 M HCl and 0.1 M KOH.

2.3. Procedures

Excitation and emission spectra. Solutions containing 5.16×10^{-6} M of both calcein and trivalent rare earth and 0.1 M of KCl (to maintain a constant ionic strength) were prepared. The pH was ranged from 1 to 13 by adding HCl, KOH or NH_4Cl/NH_3. Excitation spectra of the solutions were recorded in a range 200–800 nm at an emission wavelength of 516 nm. For emission spectra, the range was from 400 to 800 nm and the excitation wavelength equalled 494 nm.

Difference emission spectra. Solutions containing 5.16×10^{-6} M of both calcein and trivalent rare earth and 0.1 M of KCl were prepared, together with the corresponding blanks (equivalent solutions without metal). The pH was ranged from 1 to 13 by adding HCl, KOH or NH_4Cl/NH_3. Emission spectra of the solutions were recorded in a range 400–800 nm at the excitation wavelength chosen for each metal ($\sim$495 nm), and so were the difference spectra, i.e. the spectrum of each solution minus that of the corresponding blank.

Variation of fluorescence with pH. Solutions were prepared the same way as before. The fluorescence was measured at the excitation/emission wavelength chosen for each metal ($\sim$495/521 nm), and also the difference ΔF was calculated,

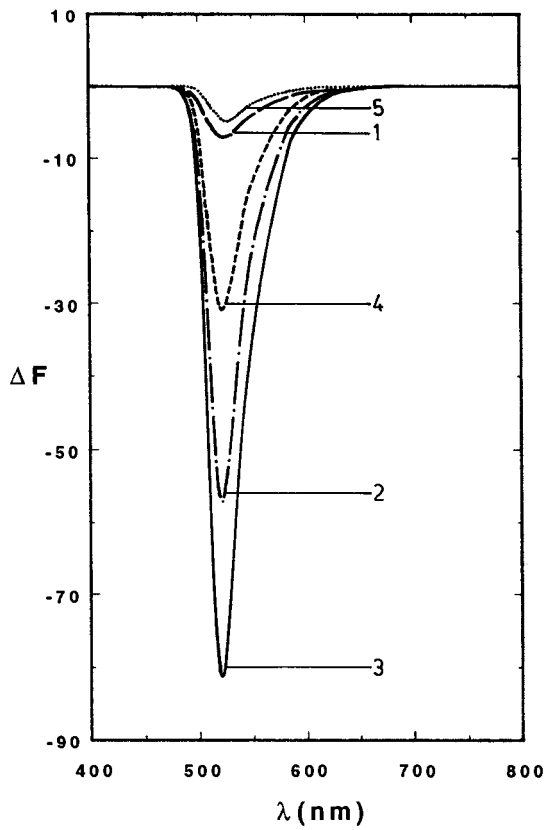

Fig. 3. Difference emission spectra of the complex calcein–Ho(III) [calcein] = $[Ho^{3+}] = 5.16 \times 10^{-6}$ M, λ_{exc}, 494 nm; $\mu = 0.1$, pH. (1) 3.30; (2) 5.33; (3) 7.88; (4) 10.95; (5) 12.01.

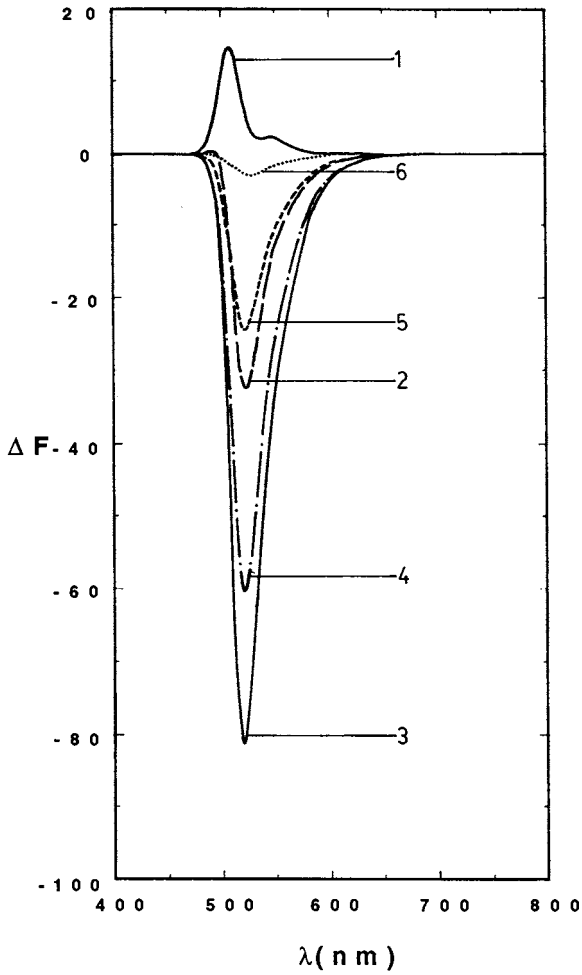

Fig. 4. Difference emission spectra of the complex calcein–Lu(III) [calcein] = $[Lu^{3+}] = 5.16 \times 10^{-6}$ M, λ_{exc}, 497 nm; $\mu = 0.1$, pH. (1) 4.29; (2) 5.29; (3) 8.12; (4) 10.21; (5) 11.11; (6) 12.25.

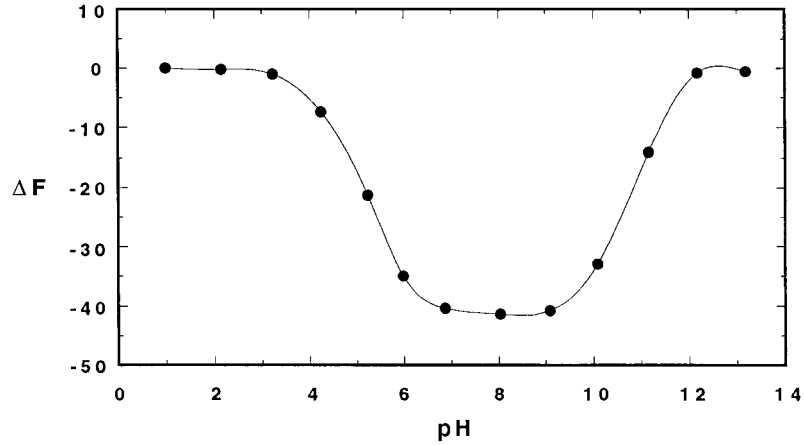

Fig. 5. Variation of fluorescence with pH [calcein] = $[Yb^{3+}] = 5.16 \times 10^{-6}$ M; $\mu = 0.1$; λ_{exc}, 497 nm; λ_{em}, 521 nm.

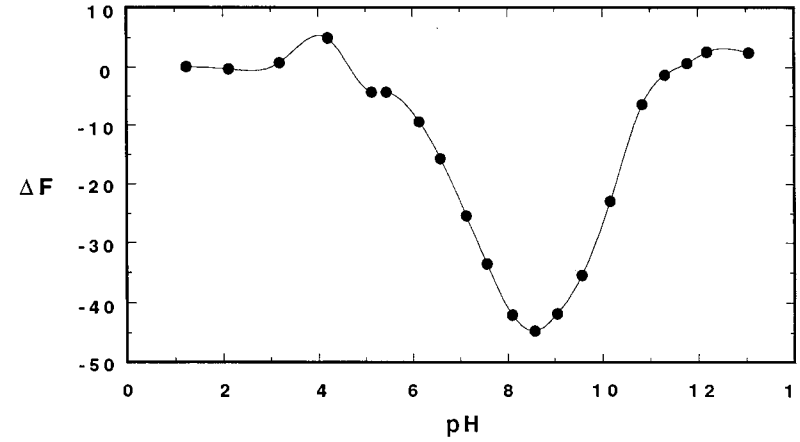

Fig. 6. Variation of fluorescence with pH [calcein] = $[La^{3+}] = 5.16 \times 10^{-6}$ M, $\mu = 0.1$; λ_{exc}, 492 nm; λ_{em}, 519 nm.

i.e. the fluorescence of each solution minus that of the corresponding blank.

Stoichiometry of the complex. Mole-ratio method. Solutions containing 5.16×10^{-6} M of calcein, a concentration of trivalent rare earth ranging from zero to three times that of the calcein and 0.1 M of KCl were prepared. The pH was fixed at 8.0 with NH_4Cl/NH_3 and HCl. Fluorescence was measured at the excitation/emission wavelength chosen for each metal ($\sim$495/521 nm).

Stoichiometry of the complex. Continuous-variations method. The same procedure as before except that solutions contained concentrations of calcein and trivalent rare earth ranging from 0 to 5.16×10^{-6} M and from 5.16×10^{-6} to 0 M, respectively.

Calibration curve. Solutions containing 5.16×10^{-6} M of calcein and a concentration of trivalent rare earth ranging from 0 to 5.16×10^{-6} M were prepared. A pH was fixed at 8.6 with 1 M NH_4Cl/NH_3 (ionic strength equalling 0.8) and fluorescence was measured at an excitation/emission wavelength of 495/521 nm. The global calibration curve was obtained in the same way, using the aforementioned total rare earth.

Sample analysis. Three synthetic samples were prepared containing 5.16×10^{-6} M of calcein and a concentration of total rare earth equal to 1.55×10^{-6} M for sample 1, 2.58×10^{-6} M for

sample 2 and 3.61×10^{-6} M for sample 3, obtained by the dilution of synthetic samples A, B and C, respectively. A pH was fixed at 8.6 with 1 M NH_4Cl/NH_3 (ionic strength equalling 0.8) and fluorescence was measured at an excitation/emission wavelength of 495/521 nm.

3. Results and discussion

3.1. Excitation and emission spectra

Many excitation bands were observed but the most important one was situated at 494 nm, which was chosen as the excitation working wavelength, see Fig. 2 for Gd(III). In the emission spectra, a single band placed at 520 nm was observed. The other rare earths gave similar spectra. The excitation wavelength selected for each metal is given in Table 1.

3.2. Difference emission spectra

This gives an idea of the reactivity between calcein and metal ion, so that the greater the difference, the greater the reactivity. See Fig. 3 for Ho(III).

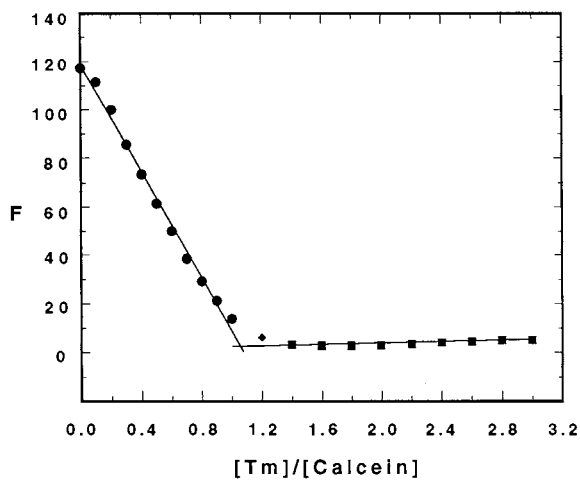

Fig. 7. Stoichiometry: mole-ratio method [calcein] = 5.16×10^{-6} M; pH 8.0; $\mu = 0.1$; λ_{exc}, 496 nm; λ_{em}, 522 nm.

A single attenuation band was obtained with a minimum at 521 nm, indicating that holmium quenches the fluorescence of calcein. This minimum was selected as the emission working wavelength. The other rare earths gave similar results. The emission wavelength selected for each metal is given in Table 1.

With lanthanum, lutetium and yttrium, an exaltation band was also observed at an acid pH with a maximum at 505 nm (516 nm with lanthanum), as it can be seen in Fig. 4 for Lu(III), but its intensity was much lower. Hence, the attenuation band was taken into account only to choose the emission working wavelengths.

3.3. Variation of fluorescence with pH

The plot of ΔF as a function of pH is shown in Fig. 5 for Yb(III). The quenching of the fluorescence of calcein by this metal was given here as negative values of ΔF. Greater absolute values of ΔF indicate greater reactivity between calcein and ytterbium. The greatest reactivity was achieved at pH 6.9–9.1, which was chosen as the working pH in the following steps. Similar results were obtained with the other rare earths. The pH selected for each of them is given in Table 1. Lanthanum is the only one whose greatest reactivity is not a pH interval but a punctual pH of 8.6, as it can be seen in the ΔF–pH plot for this metal (Fig. 6).

3.4. Influence of ionic strength and buffer concentration

When ionic strength was ranged from 0.4 to 1.2 by modifying the NH_4Cl/NH_3 buffer concentration from 0.5 to 1.5 M, ΔF increased slightly. A 1 M buffer concentration was used later in the calibration curves, guaranteeing a good fixing of pH.

3.5. Influence of time

The ΔF value of calcein–metal solutions protected from light remained constant for at least 7 h. When the solutions were exposed to light,

Table 2
Calibration curves—equations and parameters[a]

Metal	Equation	R	s[b]	CV(%)	LD(M)	LQ(M)
La	$F=67.601-5.1788\times10^{6}\ c-8.4627\times10^{11}\ c^{2}$	0.99741	1.33	2.86	6.90×10^{-7}	1.94×10^{-6}
	$F=66.152-7.2880\times10^{5}\ c-3.1071\times10^{12}\ c^{2}+2.9210\times10^{17}\ c^{3}$	0.99925	0.766	1.65	7.76×10^{-7}	1.57×10^{-6}
Ce	$F=66.565-1.7925\times10^{7}\ c+1.0235\times10^{12}\ c^{2}$	0.99915	1.00	3.37	1.70×10^{-7}	5.80×10^{-7}
Pr	$F=66.814-1.2796\times10^{7}\ c+3.2862\times10^{11}\ c^{2}$	0.99964	0.571	1.55	1.34×10^{-7}	4.51×10^{-7}
Nd	$F=66.404-1.2271\times10^{7}\ c+3.7280\times10^{11}\ c^{2}$	0.99977	0.423	1.11	$1.04\times10-7$	3.48×10^{-7}
Sm	$F=66.818-1.4308\times10^{7}\ c+5.5472\times10^{11}\ c^{2}$	0.99967	0.563	1.60	1.18×10^{-7}	3.99×10^{-7}
Eu	$F=66.464-1.5539\times10^{7}\ c+8.1550\times10^{11}\ c^{2}$	0.99987	0.348	1.03	6.75×10^{-8}	2.27×10^{-7}
Gd	$F=65.206-1.4684\times10^{7}\ c+7.3835\times10^{11}\ c^{2}$	0.99950	0.660	1.93	1.36×10^{-7}	4.60×10^{-7}
Tb	$F=66.365-1.9830\times10^{7}\ c+1.5892\times10^{12}\ c^{2}$	0.99985	0.397	1.32	6.04×10^{-8}	2.04×10^{-7}
Dy	$F=67.230-2.1281\times10^{7}\ c+1.8228\times10^{12}\ c^{2}$	0.99987	0.379	1.29	5.37×10^{-8}	1.81×10^{-7}
Ho	$F=65.635-2.1481\times10^{7}\ c+1.8934\times10^{12}\ c^{2}$	0.99962	0.637	2.29	8.97×10^{-8}	3.05×10^{-7}
Er	$F=66.266-2.2629\times10^{7}\ c+2.0479\times10^{12}\ c^{2}$	0.99970	0.584	2.17	7.80×10^{-8}	2.64×10^{-7}
Tm	$F=65.906-2.2408\times10^{7}\ c+2.0488\times10^{12}\ c^{2}$	0.99966	0.608	2.24	8.20×10^{-8}	2.78×10^{-7}
Yb	$F=66.633-2.2607\times10^{7}\ c+2.0647\times10^{12}\ c^{2}$	0.99975	0.529	1.92	7.06×10^{-8}	2.39×10^{-7}
Lu	$F=66.070-2.2777\times10^{7}\ c+2.0874\times10^{12}\ c^{2}$	0.99986	0.392	1.47	5.19×10^{-8}	1.75×10^{-7}
Y	$F=64.165-2.0324\times10^{7}\ c+1.7689\times10^{12}\ c2$	0.99970	0.536	1.90	7.97×10^{-8}	2.70×10^{-7}
Ln[c]	$F=64.465-1.7717\times10^{7}\ c+1.1487\times10^{12}\ c^{2}$	0.99993	0.264	0.82	4.49×10^{-8}	1.51×10^{-7}

[a] F, fluorescence; c, molar concentration of metal.
[b] Fluorescence unities.
[c] Ln, total rare earths.

Table 3
Fluorescence values obtained for different percents of metal

Metal	Metal/calcein relation (%)[a]										
	0	10	20	30	40	50	60	70	80	90	100
La	67.6	64.7	61.4	57.5	53.3	48.6	43.4	37.9	31.8	25.4	18.3
Ce	66.6	57.5	49.2	41.2	34.0	27.1	20.8	15.2	10.0	5.4	1.3
Pr	66.8	60.2	54.0	47.8	41.9	36.0	30.3	25.0	19.6	14.5	9.5
Nd	66.4	60.1	54.2	48.3	42.7	37.2	31.9	27.0	22.1	17.5	13.0
Sm	66.8	59.5	52.7	46.0	39.7	33.6	27.8	22.4	17.2	12.4	7.8
Eu	66.5	58.6	51.3	44.3	37.9	31.8	26.1	21.0	16.2	11.9	8.0
Gd	65.2	57.8	50.9	44.2	38.1	32.2	26.8	21.8	17.2	13.0	9.1
Tb	66.4	56.5	47.6	39.4	32.3	25.8	20.2	15.5	11.6	8.6	6.4
Dy	67.2	56.7	47.2	38.6	31.1	24.5	18.8	14.2	10.4	7.7	6.0
Ho	65.6	55.0	45.5	36.9	29.4	22.8	17.2	12.8	9.2	6.7	5.2
Er	66.3	55.1	45.1	36.1	28.3	21.5	15.8	11.3	7.7	5.4	4.0
Tm	65.9	54.8	45.0	36.1	28.4	21.7	16.1	11.7	8.3	6.0	4.8
Yb	66.6	55.4	45.5	36.6	28.8	22.1	16.4	11.9	8.5	6.2	5.0
Lu	66.1	54.8	44.8	35.8	28.0	21.2	15.5	11.0	7.6	5.3	4.1
Y	64.2	54.1	45.1	36.9	29.8	23.5	18.2	13.8	10.4	7.9	6.4

[a] [calcein] $=5.16\times10^{-6}$ M in all of the solutions.

ΔF increased gradually with time. Consequently, solutions were always protected from light before measuring the fluorescence.

The solutions were not stable by exposing them to the light source of the apparatus, and an increasing of ΔF was observed. Therefore, the fluorescence measurements were carried out quickly.

Table 4
Summary of several methods for the fluorimetric determination of rare earths

Reagent	LD (nM)	Metal	Reference
1,2,4,5-Tetracarboxylic acid/benzene	200	Tb	[21]
6-Hydroxysalicylic acid/EDTA	532	Sm	[22]
7-Iodo-8-hydroxyquinoline-5-sulfonic acid	50	Lu	[23]
6-Hydroxysalicylic acid/EDTA	308	Dy	[24]
1,10-Phenanthroline/EDTA	10	Ln[a]	[25]
Paracetamol	10	Ce	[26]
1,10-Phenanthroline/benzoylacetone	200	Sm	[27]
1,4-Bis(1-phenyl-3-methyl-5-oxopyrazole-4) butanedione	500	Tb	[28]
Calcein	45	Ln	Present method

[a] Total rare earths.

Table 5
Analysis of synthetic samples

Sample number	F^a	[Ln], M real	[Ln], M found	Recovery (%)	s^b	CV (%)
1	40.0	1.55×10^{-6}	1.54×10^{-6}	99.4	1.08×10^{-8}	0.701
2	26.8	2.58×10^{-6}	2.55×10^{-6}	98.8	8.43×10^{-9}	0.331
3	14.8	3.61×10^{-6}	3.69×10^{-6}	102.2	1.65×10^{-8}	0.448

[a] Mean of three values.
[b] Calculated in M unities for three determinations.

3.6. Stoichiometry of the complexes

Mole-ratio method. Results are presented in Fig. 7 for Tm(III). The points obtained fitted two straight lines, being the cut point at [Tm]/[Calcein] near 1, which corresponds to a 1:1 stoichiometry. The other rare earths gave similar results.

Continuous-variations method. The experimental points obtained fitted two straight lines, being the cut point at x near 0.5, which corresponds to a 1:1 stoichiometry. All of the rare earths gave similar results, except lanthanum, lutetium and yttrium. With these metals, points were fitted by three straight lines, and therefore, two cut points were obtained at x near 0.5 and $x = 0.24$, the first one corresponding to the metal:calcein 1:1 stoichiometry seen before, and the other one to a 3:1 stoichiometry.

As the 1:1 stoichiometry was common to all of the rare earths, the same concentration of calcein and metal ions were used in most of the measurements.

3.7. Calibration curves

In the previous sections, it has been observed that the reactivity of calcein with rare earths is very similar. In fact, only lanthanum shows significant differences. The determination of total rare earths requires the selection of common measure conditions, taking into account those chosen for each metal. The conditions selected were an excitation/emission wavelength of 495/521 nm and pH 8.6.

Individual calibration curves were made for each metal at the common measure conditions in order to compare them afterwards. Similar curves were obtained with all of the rare earths. The model which fitted the experimental points best was the second degree polynomial. The corresponding equations as well as different parameters obtained from them are given in Table 2 [17,18], i.e. multiple correlation coefficient (R), standard deviation of residuals (s), coefficient of variation (CV), limit of detection (LD) and limit of quantitation (LQ).

The calibration curve of lanthanum is significantly different from the others as it has inverse concavity. Moreover, it is the only case where the third degree polynomial model fits better the experimental points than the second degree one, as shown by comparing the parameters in Table 2.

To detect the possible interference of one rare earth toward the others, different solutions were prepared containing calcein 5.16×10^{-6} M and different proportions of metal/calcein, from 0 to 100%, and their fluorescence were measured at the optimum conditions selected previously. Results are presented in Table 3.

To decide on the existence of an interference, two statistical criteria were applied to each column of the table, i.e. Dixon's Q [19] and the Box and Whisker Plot [20]. Both of them gave results stating that lanthanum is the only element that gives fluorescence values significantly different from the other rare earths. The different behaviour is the reason why lanthanum was considered as an interference and was not included in the global calibration curve, which was carried out with equimolar quantities of the other rare earths (= total rare earth) in the same conditions as the individual curves. This calibration curve is also given in Table 2 under the symbol Ln. The curve is similar to that obtained with terbium, which shows that rare earths mixture does not have any special effect towards calcein because it behaves as if it were a single rare earth with concentration equal to the sum of all of them.

Table 4 lists the results of several methods used previously for the spectrofluorimetric determination of rare earths. It can be seen that the method proposed in this paper is one of the most sensitive.

3.8. Analysis of synthetic samples

The determination of total rare earths was made in three synthetic samples, free from lanthanum. The composition of these samples was carried out according to rare earth contents of some rocks of the earth's crust [29]. Results are presented in Table 5.

Using the global calibration curve, the concentration corresponding to each fluorescence was calculated and compared with the real one. Recoveries and coefficients of variation obtained show that both accuracy and precision are quite satisfactory.

It is important to remark that the samples did not have equimolar mixtures of rare earths, like in the global calibration curve, and the relative proportion of the metals differed in the three samples. In spite of this, good results were obtained, which indicates that the calibration curve can be used for rare earth mixtures of different compositions. The method is, therefore, valid to determine total rare earths and can be used for rapid screening of these metals with a limit of detection of 4.49×10^{-8} M.

From the results presented, it can be concluded that calcein is a very suitable reagent and that the fluorimetric screening of rare earths with calcein is a direct, rapid and sensitive method.

References

[1] H. Diehl, J.L. Ellingboe, Anal. Chem. 28 (1956) 882.
[2] H. Diehl, Calcein, Calmagite and o,o′-Dihydroxyazobenzene. Titrimetric, Colorimetric, and Fluorometric Reagents for Calcium and Magnesium, The G. Frederick Smith Chemical Company, Columbus, OH, 1964, pp. 62–86.
[3] D.F.H. Wallach, T.L. Steck, Anal. Biochem. 6 (1963) 176.
[4] M.D. Alvarez, M.I. Serrano, M.A. Palacios, L.M. Polo, Analyst 113 (4) (1988) 633.
[5] D.A. Mavrondis, Anal. Chim. Acta 209 (1988) 303.
[6] N. Chimpalee, D. Chimpalee, R. Jarungpattananon, S. Lawratchavee, D.T. Burns, Anal. Chim. Acta 271 (2) (1993) 247.
[7] D.T. Thuy, D. Decnop, W.T. Kok, P. Luan, T.V. Nghi, Anal. Chim. Acta 295 (1–2) (1994) 151.
[8] J. Aznárez, J. Galbán, C. Díaz, J.M. Rabadán, Anal. Chim. Acta 198 (1987) 281.
[9] J. Galbán, S. De Marcos, J.C. Vidal, C. Díaz, J. Aznárez, Anal. Sci. 6 (2) (1990) 187.
[10] M.F. Grigor'eva, Vestn. S.-Peterb. Univ., Ser. 4: Fiz., Khim (1) (1994) 102–107.
[11] A.J. Hefley, B. Jaselskis, Anal. Chem. 46 (1974) 2036.
[12] J. Tovar, C.L. Graham, M.H.B. Hayes, Anal. Proc. 20 (3) (1983) 125.
[13] S. Epsztejn, O. Kakhlon, H. Glickstein, W. Breuer, Z. Cabantchik, Anal. Biochem. 248 (1) (1997) 31–40.
[14] Z. Zhang, Y. Zhang, Fenxi Huaxue 14 (6) (1986) 415.

[15] N. Chimpalee, D. Chimpalee, S. Suparuknari, B. Boonyanitchayakul, D. Burns, Anal. Chim. Acta 298 (3) (1994) 401–404.
[16] R. Jianmin, G. Xiaoxia, Fenxi Huaxue 14 (12) (1986) 895.
[17] J.C. Miller, J.N. Miller, Statistics for Analytical Chemistry, 3rd ed., Ellis Horwood, Chichester, UK, 1993.
[18] L. Ott, An Introduction to Statistical Methods and Data Analysis, 3rd ed., PWS-Kent, 1988.
[19] D.B Rorabacher, Anal. Chem. 63 (1991) 139.
[20] M. Frigge, D.C. Hoagland, B. Iglewicz, Am. Stat. 43 (1989) 50.
[21] G.Y. Zhu, Z.K. Si, H.Z. Yin, W. Jiang, Guangpuxue Yu Guangpu Fenxi 15 (5) (1995) 115.
[22] Y. Xu, H.G. Huang, Lihua Jianyan, Huaxue Fence 31 (2) (1995) 80.
[23] L.M. He, Y. Ren, Fenxi Huaxue 21 (10) (1993) 1165.
[24] J. Gao, H.G. Huang, Fenxi Huaxue 20 (7) (1992) 761.
[25] M. Ishii, Y. Anazawa, T. Akai, Nippon Kagaku Kaishi 11 (1992) 1332.
[26] N. Jie, J. Yang, T. Liv, Talanta 41 (1994) 415.
[27] J. Yang, H. Zou, X. Ren, Y. Huang, Lihua Jianyan, Huaxue Fence 27 (3) (1991) 170.
[28] L. Yan, R. Yang, X. Ji, H. Liu, X. Zou, Fenxi Huaxue 20 (1) (1992) 100.
[29] G.Y. Zhu, Z.K. Si, P. Liu, Anal. Chim. Acta 245 (1991) 109.

ELSEVIER

Talanta 48 (1999) 729–736

Talanta

Short communication

Intra-laboratory testing of method accuracy from recovery assays

A. Gustavo González *, M. Angeles Herrador, Agustín G. Asuero

Department of Analytical Chemistry, University of Seville, 41012, Seville, Spain

Received 27 April 1998; received in revised form 6 August 1998; accepted 7 August 1998

Abstract

A revision on intra-laboratory testing of accuracy of analytical methods from recovery assays is given. Procedures based on spiked matrices and spiked samples are presented and discussed.

Keywords: Accuracy; Recovery assays; Spiked samples; Spiked matrices

1. Introduction

The accuracy of an analytical method is a key feature for validation purposes [1,2]. Four principal methods have been proposed to the study of accuracy of analytical methods [3–5]. They are based on: (i) the use of certified reference materials (CRM); (ii) the comparison of the proposed method with a reference one, (iii) the use of recovery assays on matrices or samples and, (iv) the round robin studies (collaborative tests).

CRMs, when available, are the preferred control materials because they are directly traceable to international standards or units. The procedure consists in analyzing a sufficient number of CRMs and comparing the results against the certified values [4,6,7]. The Community Bureau of Reference of the Commission of the European Community (BCR, Bureau Communautaire de Référence), the Laboratory of the Government Chemist of Middlesex (LGC), the National Institute of Standards and Technology of USA (NIST) and the National Institute for Environmental Studies of Japan, provide a general coverage of certified reference materials [8–10]. Nevertheless a series of shortcomings and limitations for CRMs have been pinpointed [11], specially: Their cost, the small amounts that may be purchased and the narrow range covered of matrices and analytes.

The performance of a newly developed method can be assessed by comparing the results obtained by it with those found with a reference or comparison method of known accuracy and precision [12–16].

* Corresponding author. Tel.: +34 5 4557173; fax: +34 5 4557168; e-mail: agonzale@cica.es

0039-9140/99/$ - see front matter
PII S0039-9140(98)00271-9

The use of Collaborative studies to control methodological bias is a very important topic [17,18]. However proficiency testing and round robin studies will not be considered here, this paper dealing with the internal (intra-laboratory) control of accuracy.

Unfortunately, within the realm of environmental, toxicological and pharmaceutical analysis, neither CRMs nor alternate methods are available for new contaminant, toxic and drug-related analytes. Accordingly, the remaining methods to check method accuracy, that is, the recovery assays are the tools of the trade for the study of accuracy in pharmaceutical analysis.

The aim of the present paper is to revise, outline and discuss the suitable procedures for testing accuracy in pharmaceutical analysis from recovery assays. For the sake of illustration some examples taken from literature are discussed.

2. General overview on recovery assays

Before embarking us in the body of the subject, some terminology should be established. According to the IUPAC paper (1990) on nomenclature for sampling in analytical chemistry [19,20] we will use the term test portion as the quantity of material removed from the test sample which is suitable in size to measure the concentration of the determinant by using the selected analytical method. The test portion may be dissolved with or without reaction to give the test solution. An aliquot (fractional part) of the test solution is then measured by following the analytical operating procedure. The test portion consists of analyte plus matrix [21].

Accordingly, if a test portion of weight m is dissolved into a total volume V, the test solution will have a concentration $c = m/V$ which is the sum of the analyte concentration (x) plus the matrix concentration (z).

Consider now the newly proposed analytical method which is applied to dissolved test portions of a given sample within the linear dynamic range of the analytical response (Y). This response may be expressed by the following relationship involving both analyte and matrix amounts [22]:

$$Y = A + Bx + Cz + Dxz \quad (1)$$

where A, B, C and D are constants

A is a constant that does not change when the concentrations of the matrix, z, and/or the analyte, x, change. It is called the true sample blank [23] and may be evaluated by using the Youden sample plot [24–26], which is defined as the 'sample response curve' [23]. By using our terminology, the application of the selected analytical operating procedure to different test portions, m, (different mass taken from the test sample) produces different analytical responses Y as outputs. The plot of Y versus m is the Youden sample plot and the intercept of the corresponding regression line is the so called Total Youden Blank (TYB) which is the true sample blank [23–30]. As will be discussed below, when a 'matrix without analyte' is available the term A can be more easily determined.

Bx is the fundamental term that justifies the analytical method and it is directly related to the analytical sensitivity [31].

Cz is the contribution from the matrix, depending only on its amount, z. When this term occurs, the matrix is called interferent. In general this kind of interference is very infrequent, because a validated analytical method should be selective enough with respect to the potential interferences appearing in the samples where the analyte is determined [32]. The USP monograph [33] defines the selectivity of an analytical method as its ability to measure accurately an analyte in presence of interference, such as synthetic precursors, excipients, enantiomers and known or likely degradation products that may be present in the sample matrix. Accordingly, the majority of validated methods do not suffer from such a direct matrix interference. Anyway, as it will be discussed below, the method accuracy may be tested even when faced with interferent matrices.

Dxz is an interaction analyte/matrix term. This matrix effect occurs when the sensitivity of

the instrument to the analyte is dependent on the presence of the other species (the matrix) in the sample [31]. For the sake of determining analytes, this effect may be overcome by using the method of standard additions (MOSA) [23–30].

Certain types of samples, of which pharmaceutical dosage forms are just an example, enables the sample matrix to be simulated by a laboratory preparation procedure with all the excipients present in their corresponding amounts except the analyte of interest. In other cases, the sample matrix may be a synthetic mixture of naturally complex substances such as an analyte-free body fluids from unmedicated patients. In both cases, it is said that the placebo is available and recoveries are obtained from spiked placebos. The term placebo was used by Cardone [28] to refer to free-analyte materials. However in order to avoid confusion and unify the jargon, the word matrix (or blank matrix) will be used throughout the text. Sometimes, however, it is not possible to prepare a matrix without the presence of analyte. This may occur, for instance with lyophilized materials, in which the speciation is significantly different when the analyte is absent [3]. In these cases, the matrix is not available and the MOSA must be applied [23–30] the recoveries being obtained from spiked samples. In spiked matrices or spiked samples, the analyte addition cannot be blindly performed. Addition should be accomplished over the suitable analyte range.

Some analytes when incorporated naturally into the matrix are chemically bound to the constituents of the matrix. In such cases, the mere addition to the sample or matrix will not mirror what happens in practice. It is recommended that the analyte is added to the matrix and then left in contact for several hours, preferably overnight, before applying the analytical method to allow analyte/matrix interactions to occur [34]. Spiked samples or matrices are also called fortified ones, the concentration of analyte added being the corresponding 'fortification level'. In the following the two procedures for demonstrating accuracy from recovery tests, namely, spiked matrices and spiked samples will be outlined. For the sake of generality, in all cases the coefficient C of Eq. (1) will be considered significant.

3. Recovery tests from spiked matrices

The recovery test is carried out from spiked matrices over the analyte range of interest, generally 75–125% of the expected assay value (label claim or theory), holding the matrix at the nominal constant level $z = z_0$. The analytical response when analyte is added follows the equation

$$Y = A + Bx + Cz_0 + Dxz_0$$
$$= (A + Cz_0) + (B + Dz_0)x = A' + B'x \quad (2)$$

where A' and B' are the intercept and the slope of the calibration line in the matrix environment which are constant because B, C, D and z_0 are also fixed.

By using this calibration function, several amounts of analyte are added to the matrix. From the analytical signal at each addition i, Y_i, the amount of analyte found is estimated as $\hat{x}_i = (Y_i - A')/B'$. The recovery (Rec) may be estimated as the average of the individual recoveries obtained at each spike i ($\mathrm{Rec}_i = \hat{x}_i/x_i$). Alternatively, a regression analysis of found versus added analyte concentrations may be performed, and the slope may be taken as the average recovery as it will be discussed in Section 5.

4. Recovery tests from spiked samples

In a way similar to the preceding section, the application of the MOSA on the test portions (matrix plus analyte) is performed. An important requirement for this technique is that all solutions, unspiked and spiked test portions be diluted to the same final volume. If we carry out analyte additions, x, on the final solution of a given test portion of concentration $c_0 = x_0 + z_0$ (x_0 is the concentration of analyte coming from the sample, present in the final solution), then the analytical response will be:

$$Y = A + B(x_0 + x) + Cz_0 + D(x_0 + x)z_0 =$$
$$(A + Cz_0) + (B + Dz_0)(x_0 + x) =$$
$$A' + B'(x_0 + x) =$$
$$A' + B'x_0 + B'x = A'' + B'x \quad (3)$$

Note that both A'' and B' are constant because A, B, C, D, x_0 and z_0 are also constants. By using this calibration function, from the analytical signal at each addition i, Y_i, the amount of analyte found is estimated as $\hat{x}_i = (Y_i - A'')/B'$. This is an estimation of the added analyte concentration (x_i) instead of the total analyte concentration ($x_0 + x_i$). A crucial requirement is that, the total final analyte concentration obtained for the maximum amount of analyte spiked should remain within the linear range obtained at the method development step. The remainder is the same as it was discussed above.

5. Evaluation of the recovery from spiked matrices or samples and significance tests for assessing accuracy

The calculation of recoveries from spiked matrices or samples may be performed (i) by computing the individual recoveries for each spiked amount (fortification level) of analyte, and evaluating the recovery as average; and (ii) from linear regression analysis of added versus found data.

5.1. Method of the averaged recovery

In this case, for each fortification level or analyte spike i, we have the concentration added of analyte x_i. From the calibration graph, the estimated concentration of analyte $\hat{x}_i$ is obtained. An individual recovery is then calculated as $\mathrm{Rec}_i = \hat{x}_i / x_i$. The mean recovery, Rec, is calculated as average of the individual ones

$$\mathrm{Rec} = \frac{1}{n} \sum_{i=1}^{i=n} \mathrm{Rec}_i \tag{4}$$

The average recovery may be tested for significance by using the Student t-test, the null hypothesis being that the recovery is unity (or 100 in percentage) and the method is accurate.

$$t = \frac{\mathrm{Rec} - 1}{s_{\mathrm{Rec}}/\sqrt{n}} \tag{5}$$

with

$$s_{\mathrm{Rec}} = \sqrt{\frac{\sum_{i=1}^{i=n} (\mathrm{Rec} - \mathrm{Rec}_i)^2}{n-1}} \tag{6}$$

n being the number of spike levels.

If the t value obtained from Eq. (5) is less than the tabulated value for $n-1$ degrees of freedom at a given significance level, then the null hypothesis is accepted and the method is accurate.

5.2. Regression analysis of added versus found data

Both in spiked matrices or samples, a regression analysis of estimated (found) against spiked (added) analyte concentration is performed. These studies are not new, indeed. In a landmark paper [35], Mandel and Linnig studied the accuracy in chemical analysis using linear calibration curves, by applying regression analysis to the linear relationships

$$x_{\mathrm{found}} = a + b x_{\mathrm{added}} \tag{7}$$

here x_{found} and x_{added} refer to the above concentrations of analyte estimated ($\hat{x}$) and spiked (x). The theory predicts a value of 1 for the slope, b, and a value of 0 for the intercept. However, the occurrence of systematic and random errors in the analytical procedure may produce deviations of the ideal situation [36]. Thus, it may occur that the straight line has a slope of 1 but a non-zero intercept, coming from a wrongly estimated background signal, and reflecting the need for a blank correction in the calibration graph. Another possibility is that the slope is significantly different from unity, indicating a source of proportional error in the proposed analytical method. The plot may present curvature or even may exhibit peculiar behaviour in case of analyte speciation.

Once the parameters a and b were calculated from the linear fit x_{found} versus x_{added}, and before to evaluate the recovery, diagnostic checking of the residuals (responses–model predictions), that is, $x_{\mathrm{found}} - a - b x_{\mathrm{added}}$ at each spike level, should be applied to assess model fit validity [37]. Certain underlying assumption have been outlined for the regression analysis such as the independence of the random error, homoscedasticity and Gaussian

distribution of the random error [38]. If the model represents the data suitably, the residuals should be randomly distributed about the value predicted by the model equation with normal distribution. A plot of the residuals on a normal probability paper is a useful technique [39]. If the error distribution is normal, then the plot will be linear. On the other hand, examinations of plots of residuals against the independent variable (here x_{added}) may be of great help in the diagnosis of the regression models [40]. Some systematic patterns indicated that the model is incorrect in some way. A sector pattern indicates heteroscedasticity in the data [41,42]. A non linear pattern indicates that the present model is incorrect [43]. Residuals also may be used to detect outliers. A very straightforward way is to consider as outlier any calibration point whose residual is greater than twice the value of the standard deviation of the regression line, although the use of jackknife residuals or the Cook distance method are more accurate tools for detecting outliers [44].

The heteroscedasticity revealed by residual analysis of the added versus found data comes from the heteroscedasticity in the responses (Y) of the calibration curve which is propagated to the estimates x_{found}. In such a case, instead of using ordinary least squares methods to fit the calibration straight line, the use of weighted least squares is advised. The weights w_i are given by $w_i = 1/s_i^2$, where s_i is the standard deviation of the responses, replicated at the concentration of analyte x_i [41,42,45].

Non-linear patterns detected by residual analysis of the added versus found plots arise because the calibration graph used for estimating the analyte concentration is by far non-linear. Curved patterns suggest the inclusion of a quadratic term in x^2 in the calibration function. In these situations, suitable non-linear calibration curves should be established in order to obtain unbiased estimates of x_{found}. Three methods are available for this purpose, namely the method of the linear segments, the method of the three-parameter function and the method based on polynomial functions [46,47].

After the validity of the fit has been appraised, then statistical comparison of a and b with their idealistic values, 0 and 1, must be performed. Conventional individual confidence intervals for the slope and the intercept once their standard deviations s_b and s_a are calculated, based on the t-test ($t_a = |a|/s_a$; $t_b = |b-1|/s_b$), although frequently used by the workers [48–50], can lead to erroneous conclusions because these tests, when carried out independently of each other ignore the strong correlation between slope and intercept [51]. Instead of these individual tests, the elliptic joint confidence region (EJCR) for the true slope (β) and intercept (α) derived by Working and Hotelling [52] and adopted by Mandel and Linnig [35] is recommended, whose equation is

$$n(a-\alpha)^2 + 2\left(\sum x_i\right)(a-\alpha)(b-\beta) + \left(\sum x_i^2\right)(b-\beta)^2 = 2s^2F_{2,\nu} \quad (8)$$

where n is the number of points, s^2 the regression variance and $F_{2,\nu}$ the critical value of the Snedecor–Fisher's statistic with 2 and $\nu = n-2$ degrees of freedom at a given P% confidence level, usually 95% [53,54].

The centre of ellipse is (a, b). Any point (α, β) which lies inside the EJCR is compatible with the data at the chosen confidence level P. In order to check constant (translational) or proportional (rotational) bias, the values $\alpha = 0$ and $\beta = 1$ are compared with the estimates a and b using the EJCR. If the point (0, 1) lies inside the EJCR, then bias are absent [13] and consequently, the recovery may be taken as unity (or 100% in percentile scale). This can be done from easy calculations as described in Appendix A.

Once the recovery is computed (from one or another procedure), it should be checked for fulfilling the accuracy criteria according to the AOAC guidelines [55] as indicated in Table 1. Note that for trace analysis, e.g. drug residues in tissues, recoveries about 50% is often the best that can be achieved.

6. Worked example

For the sake of illustration, a case study was selected. It deals with the recovery of trigonelline in coffee extracts from ion chromatography.

Trigonelline is determined in green and roasted coffee extracts by an ion chromatography procedure using as stationary phase polybutadiene–maleic acid (PBDMA) coated on silica, 2 mmol l^{-1} aqueous hydrochloric acid (pH 3) as eluent and UV detection at 254 nm. Test solutions were prepared by refluxing test portions of 3 g of dried coffee (green or roasted) with hot water (80°C) for 1 h. The extract was filtered and diluted to 250 ml. For trigonelline analysis, the test solution is diluted 1:5 (V/V) and 3 ml of the resulting solution is passed through a C_{18} SPE cartridge and then, the eluent is also passed to collect a total volume of 10 ml. An aliquot of this later solution was filtered through a 0.45 μm filter unit and subsequently injected on the HPLC system [56].

Owing to the lack of suitable certified reference materials, the validation methodology was based on recovery assays from spiked extracts of green and roasted coffees. Roasted coffees have trigonelline contents within 0.50–0.85% (w/w, dry basis). The corresponding extracts will present trigonelline concentrations in the range 60–102 mg l^{-1}, which corresponds to 15–25.5 mg trigonelline. Six spikes, additions or fortification levels were selected. Spiked extracts were allowed overnight and then analyzed. The added and found amounts of trigonelline are shown in Table 2.

The individual recoveries are also indicated in Table 2 at each fortification level. The averaged recovery is 0.9997 and its standard deviation, 0.0094. By applying Eq. (5), the observed t value is 0.078. The critical value for 5 degrees of freedom at a 95% confidence level is 2.015,

Table 1
Analyte recovery depending on the concentration range

Analyte concentration (%)	Recovery range (%)
≥10	98–102
≥1	97–103
≥0.1	95–105
≥0.01	90–107
≥0.001--≥0.00001	80–110
≥0.000001	60–115
≥0.0000001	40–120

Table 2
Recovery study of trigonelline on coffee extracts

x_{added}	x_{found}	Rec	Estimated x_{found}	Residual
5	5.02	1.004	4.88	0.14
10	9.89	0.989	9.94	−0.05
15	14.94	0.996	15.00	−0.06
20	19.81	0.990	20.06	−0.25
25	25.30	1.012	25.12	0.18
30	30.22	1.007	30.18	0.04

x_{added} and x_{found} refer to the amounts (in mg) of trigonelline added and found by analysis in the different extracts.

and therefore, the null hypothesis is accepted and the recovery do not differ statistically from 100%. The same conclusion could be drawn from comparison of the averaged recovery in percentile scale, 99.97, with the ranges provided by Table 1. Considering that trigonelline contents in coffee are of 0.5–0.85%, the third row of the table ($>0.1\%$) is selected and the corresponding recovery range is 95–105%. The averaged recovery 99.97 lies within this interval and consequently, meets with the requirements of the AOAC guidelines.

On the other hand, the regression approach can be carried out. The plot of x_{added} versus x_{found} was linear with an intercept of -0.18 and a slope of 1.012. The correlation coefficient was about 0.9999 and the regression variance $s^2 = 0.0355$. In Table 2 the estimated values of x_{found} and the corresponding residuals are presented. Residual analysis did not show any pathology with the exception of a large value (-0.25) for the point corresponding to the addition of 20 mg. However, the absolute value of this residual is lesser than twice the standard deviation of the regression line ($s = 0.1884$) and hence cannot be considered as outlier. A plot of the residuals on a normal probability paper was fairly linear, which ratifies the model validity.

In order to test if simultaneously the slope and intercept are not different from the idealistic values $\alpha = 0$ and $\beta = 1$, the procedure base on the EJCR was considered as it is explained

in Appendix A. Thus, by taking the critical value for the Snedecor–Fisher statistic at a 95% confidence level $F_{2,4} = 6.94$, we obtain $\beta_1 = 0.2304 < 1$, and $\beta_2 = 1.7770 > 1$. This indicates that the point (0, 1) lies inside the EJCR and then, the intercept may be considered to be zero and the slope to be unity, which leads to that the recovery can be considered as 100%.

Appendix A

The equation of the isoprobability ellipse is given by (8). One very easy way to determine if the point (0, 1), corresponding to the joint null hypothesis $\alpha = 0$ and $\beta = 1$, lies inside the ellipse (and therefore the null hypothesis is accepted) is to consider the intersections of the straight line $\alpha = 0$ and the ellipse: Only when the point (0, 1) lies inside the ellipse, the straight line $\alpha = 0$ and the ellipse intersect at two points $(0, \beta_1)$ and $(0, \beta_2)$ fulfilling that (for $\beta_2 > \beta_1$): $\beta_2 > 1$ and $\beta_1 < 1$ simultaneously. Otherwise, the point (0, 1) is outside the ellipse.

If in Eq. (8) we set $\alpha = 0$ and $z = b - \beta$, the following expression is obtained:

$$\left[\sum x_i^2\right] z^2 + \left[2\alpha \sum x_i\right] z + [na^2 - 2s^2 F_{2,v}] = 0 \tag{9}$$

after the following changes

$$L = \sum x_i^2$$

$$M = 2a \sum x_i$$

$$N = na^2 - 2s^2 F_{2,v} \tag{10}$$

the roots for z will be

$$z_1 = \frac{-M + \sqrt{M^2 - 4LN}}{2L}$$

$$z_2 = \frac{-M - \sqrt{M^2 - 4LN}}{2L} \tag{11}$$

and consequently, $\beta_1 = b - z_1$ and $\beta_2 = b - z_2$, which are the parameters needed to check if the point (0, 1) lies inside or outside the EJCR.

References

[1] ICH, International Conference on Harmonization, Validation of Analytical Procedures, Note for Guidance, Commission of European Community, Brussels, 1995.
[2] M. Thompson, Analyst 121 (1996) 285–288.
[3] J.M. Green, Anal. Chem. News Features May 1 (1996) 305A–309A.
[4] M. Thompson, Anal. Proc. 27 (1990) 142–144.
[5] J.K. Taylor, Anal. Chem. 55 (1983) 600A–608A.
[6] R. Sutarno, H.F. Steger, Talanta 32 (1985) 439–445.
[7] M. Valcárcel, A. Ríos, Analyst 120 (1995) 2291–2297.
[8] E. Prichard, Quality in the Analytical Chemistry Laboratory, ACOL series, Appendix 3: Some Sources of Reference Materials, Wiley, Chichester, UK, 1995, pp. 255–256.
[9] M. Valcárcel, A. Ríos, Materiales de referencia, in: M. Valcárcel, A. Ríos (Eds.), La calidad en los laboratorios analíticos, Editorial Reverté, Barcelona, 1992, Ch. 6, pp. 177–222.
[10] K. Lamble, S.J. Hill, Analyst 120 (1995) 413–417.
[11] Analytical Methods Committee, Analyst 120 (1995) 29–34.
[12] A.C. Metha, Analyst 122 (1997) 83R–88R.
[13] A.G. González, A.G. Asuero, Fresenius J. Anal. Chem. 346 (1993) 885–887.
[14] A.G. González, A. Márquez, J. Fernández-Sanz, Comput. Chem. 16 (1992) 25–27.
[15] M. Thompson, Anal. Chem. 61 (1989) 1942–1945.
[16] B.D. Ripley, M. Thompson, Analyst 112 (1987) 377–383.
[17] J.K. Taylor, J. Assoc. Off. Anal. Chem. 69 (1986) 398–400.
[18] G.T. Vernimont, Interlaboratory evaluation of an analytical process, in: W. Spendley (Ed.), Use of Statistics to Develop and Evaluate Analytical Methods, ch. 4, AOAC, Arlington, VA, 1990, pp. 87–143.
[19] W. Horwitz, Pure Appl. Chem. 62 (1990) 1193–1208.
[20] R.E. Majors, LC-GC Int. 5 (1992) 8–14.
[21] U.R. Kunze, Probenahme und Probenvorbereitung, in: Grundlagen der quantitativen Analyse, ch. 2, 3rd ed., Georg Thieme Verlag, Stutgart, 1990. pp. 2–4.
[22] R. Ferrús, Analytical function, calibration, interference, and modellization in quantitative chemical analysis, in: Miscel-lània Enric Cassasas, Bellaterra, Universitat Autònoma de Barcelona, 1991, pp. 147–150.
[23] M.J. Cardone, Anal. Chem. 58 (1986) 438–445.
[24] W.J. Youden, Anal. Chem. 19 (1947) 946–950.
[25] W.J. Youden, Biometrics 3 (1947) 61.
[26] W.J. Youden, Mater. Res. Stand. 1 (1961) 268–271.
[27] M.J. Cardone, J. Assoc. Off. Anal. Chem. 66 (1983) 1257–1282.
[28] M.J. Cardone, J. Assoc. Off. Anal. Chem. 66 (1983) 1283–1294.
[29] M.J. Cardone, J.G. Lehman, J. Assoc. Off. Anal. Chem. 68 (1985) 199–202.
[30] L. Cuadros Rodríguez, A.M. García Campaña, F. Alés Barrero, C. Jiménez Linares, M. Román Ceba, J. AOAC Int. 78 (1995) 471–476.

[31] K.S. Booksh, B.R. Kowalski, Anal. Chem. 66 (1994) 782A–791A.
[32] L. Huber, LC-GC Int. 11 (1998) 96–105.
[33] United States Pharmacopeia XXIII, National Formulary XVIII, Rockville, MD, The United States Pharmacopeial Convention, 1995, pp. 1610–1612.
[34] E. Prichard, Selecting the method, in: Quality in the Analytical Chemistry Laboratory, ACOL series, ch. 3, Wiley, Chichester, UK, 1995, pp 67–101.
[35] J. Mandel, F.J. Linnig, Anal. Chem. 29 (1957) 743–749.
[36] J.C. Miller, J.N. Miller, Errors in instrumental analysis; regression and correlation, in: Statistics for Analytical Chemistry, 3rd ed., ch. 5, Prentice Hall, Chichester, UK, 1993, pp. 101–139.
[37] W.P. Gardiner, Statistical Analysis Methods for Chemists, The Royal Society of Chemistry, Cambridge, 1997, pp. 182–185.
[38] A.G. González, Anal. Chim. Acta 360 (1998) 227–241.
[39] E. Morgan, Chemometrics: Experimental Design, ACOL Series, Wiley, Chichester, UK, 1991, pp. 126–128.
[40] M. Meloun, J. Militky, M. Forina, Chemometrics for Analytical Chemistry, vol. 2, Ellis Horwood, London, 1994, pp. 64–69.
[41] J.S. Garden, D.G. Mitchell, W.N. Mills, Anal. Chem. 52 (1980) 2310–2315.
[42] M. Davidian, P.D. Haaland, Chem. Int. Lab. Sys. 9 (1990) 231–248.
[43] P.C. Meier, R.E. Zünd, Statistical Methods in Analytical Chemistry, Wiley, New York, 1993, pp. 92–94.
[44] J.N. Miller, Analyst 118 (1993) 455–461.
[45] Analytical Methods Committee, Analyst 119 (1994) 2363–2366.
[46] L.M. Schwartz, Anal. Chem. 49 (1977) 2062–2068.
[47] L.M. Schwartz, Anal. Chem. 51 (1979) 723–727.
[48] Y. Lacroix, Analyse chimie, interprétation des résultats par le calcul statistique, Masson et Cie, Paris, 1962, pp. 31–33.
[49] K. Doerfel, Statistik in der analytische Chemie, 4th ed, VCH, Weinheim, 1987, pp 137–155.
[50] R.J. Tallarida, R.B. Murray, Manual of Pharmacologic Calculations with Computer Programs, 2nd ed., Springer, New York, 1987, p. 16.
[51] P.D. Lark, Anal. Chem. 26 (1954) 1712–1725.
[52] H. Working, H. Hotelling, Proc. J. Am. Stat. Assoc. 24 (1929) 73–85.
[53] J.S. Hunter, J. Assoc. Off. Anal. Chem. 64 (1981) 574–583.
[54] K.A. Brownlee, Statistical Theory and Methodology in Science and Engineering, Wiley, New York, 1965, pp. 362–366.
[55] AOAC, Peer Verified Method Program, Manual on Policies and Procedures, Arlington, VA, November 1993.
[56] M.J. Martín, F. Pablos, M.A. Bello, A.G. González, Fresenius J. Anal. Chem. 357 (1997) 357–358.

ELSEVIER

Talanta 48 (1999) 737

Talanta

Book Review

Instrumental Methods in Food Analysis, J.R.J. Pare and J.M.R. Belanger (editors), Elsevier, Amsterdam, 1997, xvii + 487 pp. US $287.50. ISBN 0-444-81868-5.

The preface to this book makes the valid point that, despite dramatic developments in tools to access information, there are serious deficiencies in terms of communication between various fields. Food chemistry is one such area and this book attempts to solve the problem by inviting contributions from food scientists and from analytical chemists. The book is aimed at the laboratory based technician and the graduate student, but will also be of interest to analytical chemists who wish to stay informed about new applications of modern instrumental techniques.

The book has 11 chapters, covering: chromatography (general aspects, HPLC and GC), FTIR, AA, AES, AFS, NMR, MS, electroanalytical techniques, capillary electrophoresis, microwave assisted processes and supercritical fluid extraction. All chapters have extensive and up-to-date bibliographies and are illustrated with plenty of useful tables, figures and diagrams. One feature that I like about the book is that it assumes only basic knowledge of each technique and will therefore be accessible to food scientists with different backgrounds. The result is a rather long book, but one that is a mine of information and a useful source of reference.

Although this book is about instrumental methods I feel it would have been useful to have included a chapter on sampling. This subject is of great importance in the analysis of foods and is an area that (unfortunately) receives only scant attention in most analytical texts. Although the book does give some excellent advice on sample preparation there is insufficient attention given to methods of sampling and sources of error created by improper sampling techniques.

B.A. McGaw
The Robert Gordon University,
School of Applied Sciences,
St. Andrews Street,
Aberdeen, Scotland AB24 1HG,
UK.
Tel.: +44-1224-262819
Fax: +44-1224-262828

PII: S0039-9140(98)00282-3

ELSEVIER

Talanta 48 (1999) 739–740

Talanta

Book Review

Self-assembling Complexes for Gene Delivery, A.V. Kabanov, P.L. Felgner and L.W. Seymour (editors), Wiley, Chichester, 1998, xvii + 442 pp., £70.00. ISBN 0-471-97269X (paperback).

This is an excellent book dealing with a field of study which is the topic of much research activity in recent times. There are 56 contributors to the contents of this book working in scientific institutions and universities in Europe and the USA. This work provides an in-depth study of current developments in the field of gene therapy which has captured the imagination of both researchers and the general public throughout the world because of its enormous potential therapeutic value. Gene therapy represents a departure from traditional medicine, which has in the past been directed towards treating metabolic diseases by correcting biochemical imbalances or overcoming symptoms. Gene delivery, on the other hand, tries to correct genetic diseases by providing replacement copies of the defective genes and hence to produce a true cure by removing the root cause. However the search for effective gene delivery systems has not been very successful up to the present time. Little, if any, therapeutic success has been achieved in spite of many clinical trials having been performed throughout the world. Finding a suitable synthetic vector for gene delivery has been a major problem in recent years, although there are several others associated with the nature of the vector itself. This book provides a focus on nonviral self-assembling systems. Workers in the field have directed their attention to developing new and novel synthetic vectors for gene therapy. Biologists and chemists working in pursuit of gene therapy strategies will find this book interesting and informative.

This book has been written for scientists and researchers in this field. There are eight parts to the book each of which is comprehensively referenced. Part 1 deals extensively with the principles of self-assembly covering topics of the polymorphism of nucleic acids, structure of polycation-DNA complexes and self-assembly of bacteriophage. Part 2 explains the natural mechanisms for gene delivery to cells. Part 3 describes novel systems using cationic liposomes, such as novel supramolecular assemblies for gene therapy, taking lipospermines and polyethylenimine from in vitro to in vivo, and a terplex system for delivery of DNA and oligonucleotides. The longest part is part 4 dealing with polyelectrolyte DNA complexes. Topics covered include the characterization of polycation complexes with DNA, cationic block copolymers as self-assembling vectors for gene delivery, gene transfer using Stardust™ dendrimers, as well as other interesting innovations. Systemic biodistribution of drug delivery systems is the title of part 5 investigating in vitro and in vivo availability of liposomes and the pharmacokinetics of macromolecules and synthetic gene delivery systems. Part 6 has four sections providing in depth coverage of the targeting of conjugates for gene delivery. New approaches to gene delivery are provided in part 7. This part deals with semi-synthetic systems for gene delivery as well as sustained-release gene delivery systems which is a particular topic of interest of this reviewer. The use of microspheres and nanospheres for DNA delivery using biodegradable polymers are described. The final part (part 8) is a review of the clinical evaluation involving gene therapy. It provides results to date of the clinical trials applying gene therapy in cystic fibrosis, and

0039-9140/99/$ - see front matter
PII: S0039-9140(98)00283-5

also clinical observations of cancer treatment using nonviral gene therapy.

The topics are neatly illustrated throughout the book and all 442 pages are packed with detailed information. Each part is extensively referenced with some of the references even as recent as 1997. The editors have done a fine job in arranging the topics in this excellent book in a systemic fashion.

D.L. Munday
The Robert Gordon University,
School of Pharmacy,
Schoolhill,
Aberdeen, Scotland AB10 1FR,
UK.
Tel.: +44-1224-262500
Fax: +44-1224-262555

ELSEVIER

Talanta 48 (1999) 741

Talanta

Book Review

Equilibria and Dynamics of Gas Adsorption on Heterogeneous Solid Surfaces, W. Rudzinski, W.A. Steele, and G. Zgrablich (editors), in Studies in Surface Science and Catalysis, Vol. 104, 1997, xvii + 890 pp., Elsevier, Amsterdam, ISBN 0-444-82243-7

Our present atomic model of gas adsorption on solid surfaces, heavily obscured for over a century, has been revealed by the great pioneering scientists, Langmuir, Freundlich, Roginski, Zettlemeyer, etc. as they stripped veil after veil from this mysterious subject. The denouement has been tantalizing and fitful, as theories and observations have not always been in accord. The final veil will no doubt be lowered with the aid of computer simulations if the proper choice of gas–solid interaction potentials and their parameters can be found.

Volume 104 in the series of Studies in Surface Science and Catalysis is a mighty work encompassing a wide field of gas adsorption on heterogeneous surfaces. The preface gives the reader a wonderful and historical glimpse of the whole field. Each of the seventeen chapters is both informative and authoritative, having been written by 35 leading exponents on gas adsorption. Though each chapter focuses on a particular area, the threads of equilibria (thermodynamics), kinetics (dynamics, statistical rate theories) and surface heterogeneities (geometric, energetic, structural) are interwoven throughout the book.

Almost every significant theory, model, principle, and technique is described, and almost every significant reference quoted, however, this work is not an encyclopaedia but a logical, well-balanced and well-written collection of detailed and critical essays on the complex nature of gas adsorption on various types of heterogeneous surfaces. Some sections can be read easily, even by the faint-hearted, but the conceptual and highly-mathematical portions would be appreciated by only the professional and dedicated surface scientist.

Volume 104 is a very worthy successor to the other volumes in the series, and I cannot imagine any reputable university, research institute, or commercial company with an interest in surface science not having a copy in their library. The book is expensive, but it is well worth it.

J.B. Craig
University of Aberdeen,
Department of Aberdeen,
Meston Walk,
Aberdeen,
Scotland AB24 3UE,
UK.

0039-9140/99/$ - see front matter
PII: S0039-9140(98)00284-7

ELSEVIER

Talanta 48 (1999) 747–753

Talanta

Cryo-trapping/SPME/GC analysis of cheese aroma

B. Jaillais, V. Bertrand, J. Auger *

IRBI, UPRES A CNRS 6035, and SAVIT, University F. Rabelais, Parc de Grandmont, 37200 Tours, France

Received 05 June 1997; received in revised form 07 October 1997; accepted 27 October 1997

Abstract

The advantages of combined cold-trapping of cheese volatiles and solid-phase microextraction-GC are demonstrated. This method is simple, cheap, compatible with classic identification equipment, and allows in-situ sampling.

Keywords: SPME; Cryo-trapping; Food volatiles; Headspace sampling

1. Introduction

For food and particularly for cheese, aroma perception is one of the foremost criteria of a consumer for its preference. To analyse a product's flavour by gas chromatography (GC), it is necessary to extract the compounds from their matrix. Many of the flavour compounds are present only at very low concentrations and hitherto several methods for collection, enrichment, and injection of volatile compounds from a solid matrix have been developed. Different methods of distillation have been investigated, including high-vacuum distillation with a cryo-trap [1] and steam distillation under reduced pressure [2]. However these methods can produce artefact from thermolabile substances and a loss of some volatile compounds. At the end of the 1970's, several headspace techniques (static and dynamic) appeared to study food aroma [3,4]. They are based on the equilibrium between sample phase and headspace around. The static method allows direct injection into a GC column, whereas the dynamic method includes a concentration step by purging sample and trapping volatiles. Cold or adsorbent traps can be used independently or integrated in the GC.

Solid-phase microextraction (SPME) is a new technique developed by Arthur and Pawliszyn [5]. SPME allows extraction and concentration of volatiles or semi-volatiles from the sample matrix (usually a water sample also used in headspace), and a good transfer to gas chromatograph using a splitless universal injector without modification (except the eventual use of a specific liner). This system is cheap and solvent-free and was used recently in food aroma analysis including a study of free fatty acids [6], truffle [7], beverages [8,9], fruit juices and drinks [10], and cheese [11].

In this work, the volatile fraction of camembert cheese is used to evaluate our method. Camem-

* Corresponding author. Tel.: + 33 0247 366970; fax: + 33 0247 366566.

0039-9140/99/$ - see front matter
PII S0039-9140(98)00091-5

bert cheese aroma has been studied by several authors and >100 compounds were identified [14] including ketones, esters, aldehydes, alcohols, sulfur compounds, fatty acids, aliphatic and aromatic compounds [15,16] (Table 1). Suggestions that 1-octen-3-ol was responsible for the mushroom odour note [15], 2-phenylethanol and β-phenyl-ethyl acetate for the floral note [15,17] and some sulfur compounds for the garlic note [15,16] were confirmed by aroma extract dilution analysis (AEDA) [18]. Our preliminary experiments and the work of Chin et al. [11] showed that direct headspace SPME analysis of cheese gives a limited abundance of significant compounds for its flavour. It was thus important to concentrate the sample.

We studied a new method based on SPME following a first step of concentration using cryo-trapping. Cryo-trapping leads to an intermediate water sample, easy to handle and to conserve [12].

This cryo-trapping-SPME method presents two steps of concentration. Cryo-trapping allows the extraction of volatiles from the solid matrix by changing the equilibrium between sample and head-space above, to be increased. A good concentration effect is also obtained because the coatings used in SPME have strong affinities for organic compounds (important values of partition coefficient) [13].

2. Experimental

2.1. Sample preparation

Camembert cheese (45% fat in dry matter) was purchased at a local market and stored at −18°C before use. Ten grams of frozen cheese was cut and placed in a 250 ml flask which was held at 60°C in a water bath. This flask was fitted to another flask immersed in liquid nitrogen and connected to a vacuum pump. Volatiles and water were simultaneously trapped during a 45 min period. This frozen sample can be immediately transferred to GC or conserved for future analysis.

2.2. SPME and transfer to GC

The frozen sample was allowed to warm at room temperature, the SPME fibre (100 mm poly(dimethylsiloxane) coating, non-bonded or 85 μm polyacrylate, partially crosslinked) was introduced into the septum closed vial containing trapping sample and remained for 4 min in the aqueous phase (cryo-trapping SPME) or above the aqueous phase (cryo-trapping headspace SPME).

During this time, the solution was stirred to homogenise and to increase volatile extraction. Indeed, the equilibration time is determined by diffusion through a thin static aqueous layer adjacent to the fibre. It is very difficult to remove this thin layer of water even when water is stirred rapidly to enhance the mass transfer of analytes. After trapping, the fibre is immediately inserted in the GC injector for desorption.

2.3. GC and GC-MS

2.3.1. GC conditions

For the trapping transferred by SPME syringe, the chromatographic separations were performed using a Varian 3300 instrument (Walnut Creek, CA), with a split-splitless injector with a special SPME liner (80 μl), and equipped with an FID (300°C). This chromatograph was interfaced to a Spectra-Physics (San Jose, CA) SP 4400 integrator for data processing and recording.

A 30 m × 0.32 mm id × 0.25 μm film thickness (cross-linked surface bonded methyl silicone), fused-silica DB-1 J & W Scientific (Folsom, CA) was used for separation of aroma components.

The conditions were as follows: carrier gas, helium; column flow rate, 1.0 ml min^{-1}; SPME fibre desorption during 3 min at 200°C; oven temperature program, 40°C increased at 2°C min^{-1} to 200°C.

2.3.2. GC-MS conditions

A Hewlett-Packard (Palo Alto, CA) HP 5890 II instrument was used for chromatographic separations with the same GC conditions as above.

Total ion chromatogram (TIC) and mass spectra were recorded using a Hewlett-Packard HP

Table 1
Identification of compounds found in Camembert cheese

Peak	Compounds	Retention time (min.)	Identification means[a]	Abundance
1	Methanethiol	01.94	MS	4712
2	Propanal	02.09	Rt, MS	11520
3	2-Propanol	02.17	Rt, MS	1485
4	2,3-Butanedione	02.39	Rt, MS	3448
5	Ethyl acetate	02.60	Rt	1430
6	2-Pentanone	03.54	Rt, MS	341
7	3-Methyl-1-butanol	04.04	Rt, MS	295
8	Dimethyl disulfide	04.18	Rt, MS	38729
9	Hexanal	05.33	Rt, MS	701
10	Butyl acetate	05.59	Rt, MS	187
11	Isoamyl acetate	07.99	Rt, MS	1134
12	2,4-Dithiapentane	08.24	Rt, MS	7890
13	2-Heptanone	08.56	Rt, MS	13167
14	Heptanal	08.99	Rt, MS	1509
15	2-Heptanol	09.39	Rt, MS	7658
16	Dimethyl trisulfide	11.96	Rt, MS	960
17	1-Ethyl-3-methyl benzene	13.08	Rt, MS	604
18	1-Octen-3-ol	13.60	Rt, MS	3245
19	2-Octanone1	3.82	Rt, MS	1872
20	Octanal	14.49	Rt, MS	4843
21	Ethyl caproate	14.72	Rt, MS	5593
22	Decane	15.79	Rt	273
23	D-Limonene	16.74	Rt, MS	1559
24	8-Nonen-2-one	19.55	Rt, MS	21694
25	2-Nonanone	20.48	Rt, MS	436654
26	2-Phenyl ethanol	21.21	Rt, MS	40911
27	2-Nonanol	21.63	Rt, MS	98574
28	Undecane	22.25	Rt	1085
29	Naphthalene	25.76	Rt, MS	12386
30	Tris(methylthio) methane	27.50	Rt	7836
31	Ethyl caprylate	28.35	Rt, MS	54989
32	Phenyl ethyl acetate	31.00	Rt, MS	17655
33	1-Methyl naphthalene	32.75	Rt, MS	4085
34	2-Methyl naphthalene	33.52	Rt, MS	8187
35	Damascenone	34.12	Rt	3976
36	2-Undecanone	34.60	Rt, MS	170563

[a] Rt, retention time; MS, mass spectrometry.
Volatiles of camembert cheese obtained by cryo-trapping followed by SPME non-polar fibre (100 mm) for 4 min.

5989 A 'Mass Engine' with an HP UX workstation in electron ionisation mode (EI) at 70 eV.

3. Results and discussion

Comparison of the chromatograms of cryo-trapping SPME (Fig. 1A) with cryo-trapping headspace SPME (Fig. 1B) points out a weak loss of sensitivity for cryo-trapping headspace SPME, which is in agreement with the theory [13].

The chromatogram shows the presence of many compounds, 31 have been identified by mass spectrometry (MS). We can notice high levels of a few medium molecular weight compounds. As a representative sample of cheese aroma can be obtained with a reduced number of compounds [19], our identifications are in agreement with the work of other authors. Particularly these results are comparable to those of Dumont et al. [15,16] and of Moinas et al. [20,21] who used different methods of sample preparation and transfer.

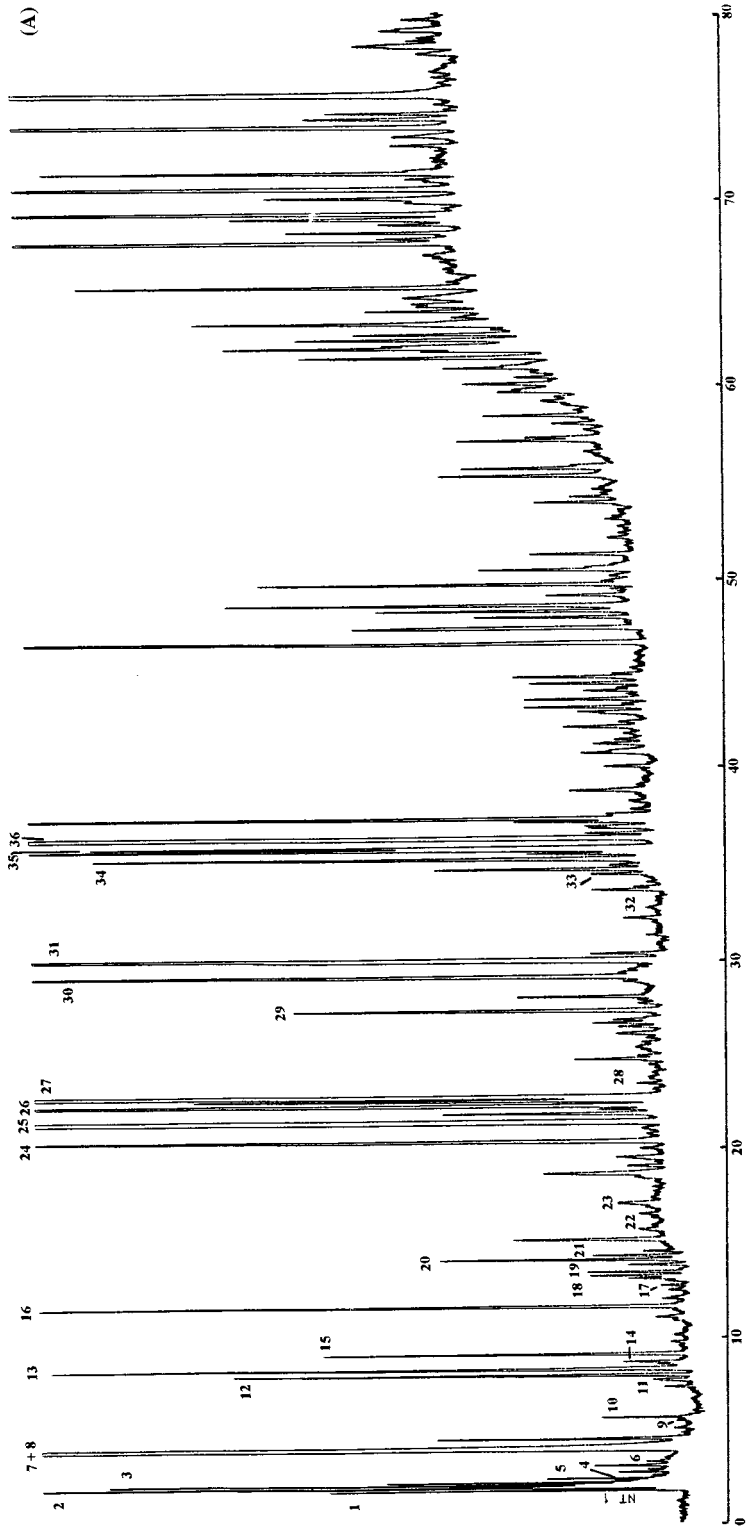

Fig. 1. Gas chromatograms (FID) of Camembert cheese aroma obtained by (A) cryo-trapping/SPME and (B) cryo-trapping headspace/SPME.

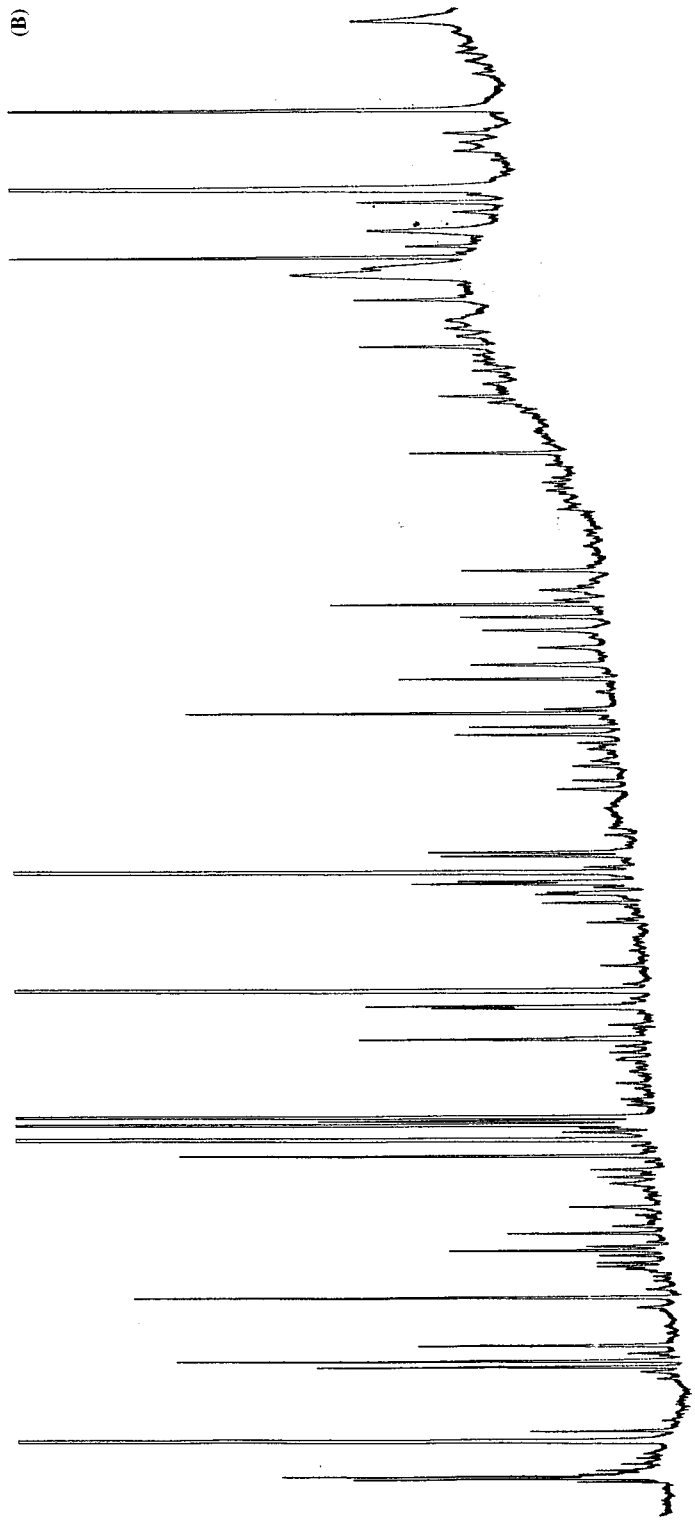

Fig. 1. (*Continued*)

The reproducibility of the method was determined by six replicate samples of the same cheese. Table 2[a] shows the coefficient of variation (% CV) for 14 compounds chosen for their regular peak shape. An acceptable variation of the value of % CV (6,39–24,07) for the peaks is observed [22].

To estimate the sampling time necessary to extract volatiles of cheese, sampling time of 4 and 10 min were tested (Table 2[b]). Similar results with quantitative differences were obtained. A sampling time of 10 min allowed the level of characteristic compounds of aroma already present at 4 min (especially the less volatile ones) to be increased. It is thus not necessary to wait the equilibration time of 10 min.

Moreover, to characterise acidic components, non-polar (poly(dimethylsiloxane)) and polar (polyacrylate) fibres were compared (Table 2[c]). With the polyacrylate fibre, a loss of abundance of most of the compounds was observed. It could introduce qualitative differences for minors components. The choice of the poly(dimethylsiloxane) coating is hence preferable.

Table 2
Reproducibility of the method [a], comparison of sampling time [a,b], and comparison of fibre coatings [a,c] on a selected list of relevant compounds for cheese aroma

Peak RT (min.)	Non polar fibre			Polar fibre
	4 min[a]		10 min[b]	4 min[c]
	Mean	% CV	Abundance	Abundance
1.94	5031	10.48	3093	2336
2.60	1678	18.56	1445	1496
5.33	617	14.30	518	209
9.39	10329	15.46	11387	10143
14.72	5122	13.80	3366	—
19.55	24142	13.93	26025	14217
20.48	475488	11.45	712569	206754
21.21	46082	20.49	90400	39275
21.63	111922	14.92	136029	85298
25.76	11070	21.89	26155	12995
27.50	10226	24.07	15721	4769
28.35	58445	13.92	130024	55141
32.75	541	18.39	1383	915
33.52	8057	06.39	16114	9886

This extraction method using cryo-trapping allowed the characterisation of the important compounds already described as potent odourants of camembert cheese [18], like methanethiol and sulfur compounds (garlic note), 2,3-butanedione, 1-octen-3-ol (mushroom odour), β-phenyl ethyl acetate (floral note) and 2-undecanone. This method is thus suitable for the characterisation of the aroma of cheese.

As SPME does not require any particular equipment, it may be possible to use general purpose hyphenated systems like gas chromatograph-mass spectrometry (GC-MS) or gas chromatograph-fourier transform infrared (GC-FTIR). SPME is especially convenient to GC-FTIR because there is no solvent and no water injection.

Besides, last year we showed that cryo-trapping/high-performances-liquid-chromatography (HPLC) was shown to be a good analytical method for thermolabile compounds [23]. Then the recent apparition of a SPME-HPLC interface should increase the sensitivity of this method.

4. Conclusion

In comparison with other methods, the first step of our method allows samples in-situ to be easily prepared. Moreover the frozen extracts are preserved and can be carried with simple and inexpensive equipment.

SPME analysis of these samples can be fully automated, and thus rapidly done. The method is cheap and compatible with any gas chromatograph or hyphenated technique (GC-MS, GC-FTIR) without modification [23], and can be used for many natural materials such as plants, insects and foods.

Acknowledgements

We thank RP-Texel company for their financial support of one of us (B. Jaillais) and for permission to publish this paper.

References

[1] J.P. Dumont, J. Adda, Le Lait 515–526 (1972) 311.
[2] J.C.C. Lin, I.J. Jeon, J. Food Sci. 50 (1985) 843.
[3] R. Imhof, J. Bosset, J. High Resol. Chromatogr. 14 (1991) 621.
[4] G. Arora, F. Cormier, B. Lee, J. Agric. Food Chem. 43 (1995) 748.
[5] C.L. Arthur, J. Pawliszyn, Anal. Chem. 62 (1990) 2145.
[6] L. Pan, M. Adams, J. Pawliszyn, Anal. Chem. 67 (1995) 4396.
[7] F. Pelusio, T. Nilsson, L. Montanarella, R. Tilio, B. Larsen, S. Facchetti, J.O. Madsen, J. Agric. Food Chem. 43 (1995) 2138.
[8] X. Yang, T. Peppard, J. Agric. Food Chem. 42 (1994) 1925.
[9] S. Hawthorne, D. Miller, J. Pawliszyn, C. Arthur, J. Chromatogr. 603 (1992) 185.
[10] B. Page, G. Lacroix, J. Chromatogr. 648 (1993) 199.
[11] H.W. Chin, R.A. Bernhard, M. Rosenberg, J. Food Sci. 61 (6) (1996) 1118.
[12] S. Ferary, J. Auger, J. Chromatogr. A 750 (1996) 63.
[13] Z. Zhang, J. Pawliszyn, Anal. Chem. 65 (1993) 1843.
[14] H. Maarse, C.A. Visscher, L.C. Willemsens, L.M. Nijssen, M.H. Boelens, Volatile Compounds in Food. Qualitative and Quantitative Data. TNO Nutrition and Food Research, Zeist, The Netherlands, 6 (5) 52
[15] J.P. Dumont, S. Roger, P. Cerf, J. Adda, Le Lait 538 (1974) 501.
[16] J.P. Dumont, S. Roger, J. Adda, Le Lait 559–560 (1976) 595.
[17] S. Roger, C. Degas, J.C. Gripon, Food Chem. 28 (1988) 129.
[18] J. Kubickova, W. Grosch, Int. Dairy J. 7 (1997) 65.
[19] G. Arora, F. Cormier, B. Lee, J. Agric. Food Chem. 43 (1995) 748.
[20] M. Moinas, M. Groux, I. Horman, Le Lait 529–530 (1973) 601.
[21] M. Moinas, M. Groux, I. Horman, Le Lait 547 (1975) 414.
[22] A. F. Wood, J.W. Aston, G.K. Douglas, Aust. J. Dairy Technol. 49 (1994) 42.
[23] S. Ferary, J. Auger, A. Touché, Talanta 43 (1996) 349.

ELSEVIER

Talanta 48 (1999) 755–762

Talanta

Sample preparation of atmospheric aerosol for the determination of carbonyl compounds

Gy. Kiss [a,*], B. Varga [b], Z. Varga Puchony [a], A. Gelencsér [a], Z. Krivácsy [a], J. Hlavay [b]

[a] *Air Chemistry Group of the Hungarian Academy of Sciences at University of Veszprém, 8201 Veszprém, P.O. Box 158, Hungary*
[b] *Department of Earth and Environmental Sciences, University of Veszprém, 8201 Veszprém, P.O. Box 158, Hungary*

Received 5 June 1997; received in revised form 29 December 1997; accepted 9 January 1998

Abstract

Sample preparation including sonication and solid phase extraction has been developed for the determination of carbonyl compounds in atmospheric aerosol. Aerosol samples were sonicated in acidified acetonitrile containing 2,4-dinitrophenylhydrazine (DNPH) to form hydrazone derivatives of aldehydes and ketones. Water was added to the extract to increase its polarity. Then the solution was passed through an octadecyl or phenyl solid phase extraction cartridge. The concentrated hydrazone derivatives were eluted with tetrahydrofuran, the eluate was evaporated to dryness then dissolved in acetonitrile/water mixture and finally analysed by RP-HPLC with UV detection at 360 nm. The absolute detection limits of the individual carbonyl compounds range from 0.4 to 5.8 ng.

Keywords: Aldehydes; Ketones; Atmospheric aerosol; Solid phase extraction

1. Introduction

Knowledge on the chemical composition of the atmosphere can help to understand atmospheric processes. Interest in the role of organic compounds in these processes has been increased rapidly. Aldehydes and ketones represent a reactive class of organic compounds. These compounds are emitted into the atmosphere by both anthropogenic (combustion of organic matter) [1–4] and natural (emission of plants) [5] primary sources and are also produced by the photochemical oxidation of alkanes, alkenes and aromatic hydrocarbons [2]. The carbonyl compounds play a role in the formation of photochemical ozone [6], N- and S-containing compounds [2,7,8].

In the past decade several methods have been developed for the determination of aldehydes and ketones in the gas phase [9–11] and the liquid phase [4,8] of the atmosphere. However, hardly any data can be found in the literature on the concentration of carbonyl compounds in atmospheric aerosol [3]. In our work a sample preparation method for the determination of carbonyl compounds in atmospheric aerosol samples was developed.

* Corresponding author.

0039-9140/99/$ - see front matter
PII S0039-9140(98)00092-7

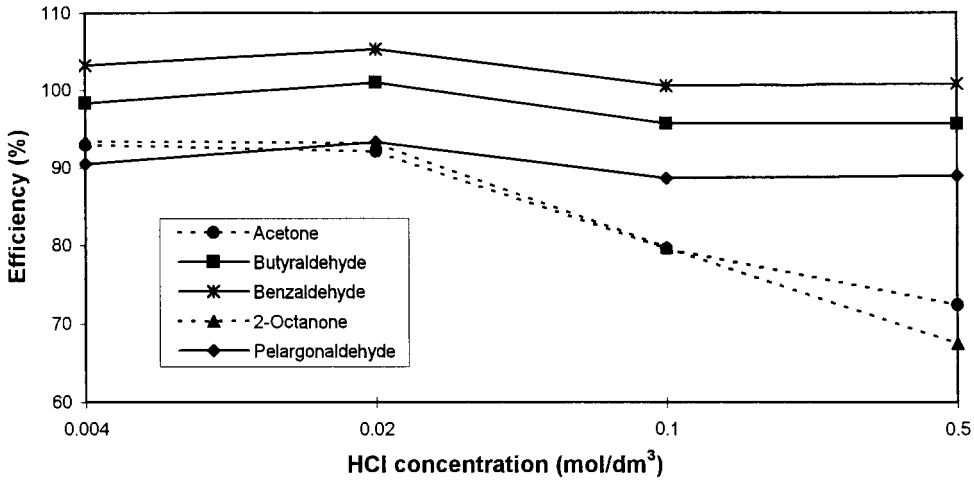

Fig. 1. Effect of HCl concentration on derivatisation.

2. Experimental

2.1. Solvents and standards

Acetone, acetonitrile and tetrahydrofuran (super purity solvents) were purchased from Romil, England, benzaldehyde (puriss p.a.), butyraldehyde (puriss), 2-octanone (purum) and pelargonaldehyde (purum) from Fluka, Switzerland. Concentrated HCl and 2,4-dinitrophenylhydrazine (puriss) were obtained from Reanal, Hungary. A carbonyl-DNPH mix (TO11/IP6A, Supelco, USA) containing 15 hydrazone derivatives were used for the identification of the carbonyl compounds in aerosol samples. HPLC grade water was supplied by a Milli-Q water purifier system (Millipore, USA).

2.2. Instruments

Analysis of the hydrazone derivatives was performed by HPLC. The solvent delivery system

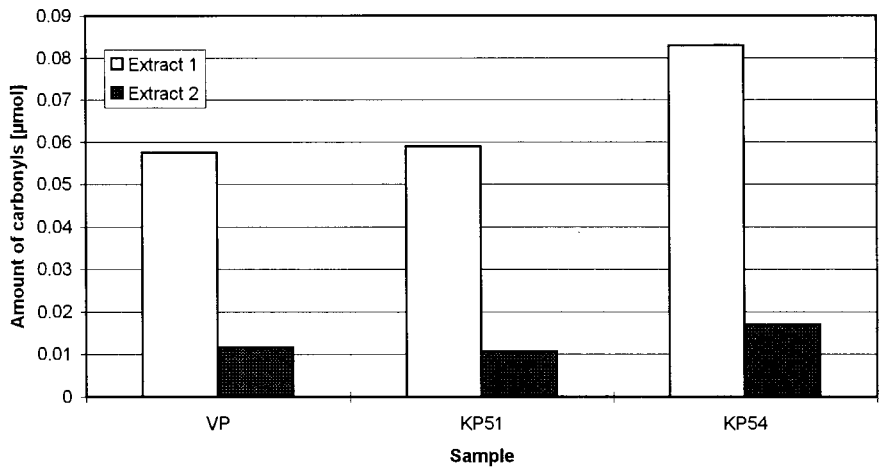

Fig. 2. Total amount of carbonyls in the extracts.

Table 1
Data of calibration lines

Component	Molecular weight	Equation of the calibration lines $[R] = Au*s$, $[C] =$ μmol ml^{-1}	r^2
Acetaldehyde	44	$R = -1.53\times10^{-4}+17.7*C$	0.9993
Acrolein	56	$R = -1.06\times10^{-4}+19.2*C$	0.9990
Acetone	58	$R = 4.62\times10^{-4}+17.3*C$	0.9995
Propionaldehyde	58	$R = -5.52\times10^{-5}+17.8*C$	0.9993
Crotonaldehyde	70	$R = -7.45\times10^{-5}+18.5*C$	0.9988
Butyraldehyde	72	$R = -1.09\times10^{-5}+18.5*C$	0.9988
Isovaleraldehyde	86	$R = 5.03\times10^{-5}+19.3*C$	0.9984
Valeraldehyde	86	$R = -7.22\times10^{-5}+17.5*C$	0.9983
Hexaldehyde	100	$R = -1.68\times10^{-4}+17.5*C$	0.9985
Benzaldehyde	106	$R = -2.27\times10^{-4}+19.6*C$	0.9976
o-Tolualdehyde	120	$R = -3.26\times10^{-4}+18.2*C$	0.9981
m,p-Tolualdehyde	120	$R = -6.45\times10^{-4}+18.9*C$	0.9992
2-Octanone	128	$R = 1.58\times10^{-4}+18.2*C$	0.9955
2,5-Dimethylbenzaldehyde	134	$R = -3.04\times10^{-4}+18.3*C$	0.9986
Pelargonaldehyde	142	$R = 1.93\times10^{-4}+16.9*C$	0.9987
AVERAGE slope of the calibration lines [Au∗s (μmol ml^{-1})$^{-1}$]		18.2	
RSD of the slopes		4.36%	

consisted of a Jasco PU-980 HPLC pump with a Jasco LG-980-02 ternary gradient unit maintaining a flow rate of 1.5 ml min^{-1}. For the separation of the hydrazone derivatives a gradient elution was applied: 100% A from 0 to 3 min then linear gradient to 100% B from 3 to 13 min, then linear gradient to 100% C from 13 to 21 min then 100% C from 21 to 28 min, where eluent A = water/acetonitrile/tetrahydrofuran 60/35/5 v/v, eluent B = water/acetonitrile 40/60 v/v and eluent C = 100% acetonitrile. 20 μl of sample was injected onto a Waters nova-pak C18 column ($l = 150$ mm, I.D. = 3.9 mm, $d_p = 4$ μm) by using a Rheodyne 7010 injector valve. The hydrazone derivatives were detected at 360 nm with a Waters 490E programmable multiwavelength detector. Data acquisition and processing were accomplished by a Waters maxima 820 chromatography software.

2.3. Sampling

Samples were collected at two locations in Hungary: in Veszprém and in K-puszta. Veszprém, with about 60000 inhabitants, is situated in western Hungary. Both the town and the region are free from major industrial sources. Samples were collected on the top of the student hostel of University of Veszprém on glass fibre filters (Whatman GF/F) at a flow rate of 1 m^3 h^{-1} for 60 h. K-puszta is a background air monitoring station in the Great Hungarian Plain. Samples were collected on quartz filters with a high volume sampler (60 m^3 h^{-1}) for 22 h.

The samples were protected from light and air and were stored in a refrigerator until analysis.

2.4. Sample preparation

Aerosol samples were sonicated in acetonitrile containing 2,4-dinitrophenyl–hydrazine (DNPH), water and hydrochloric acid. The extracting solution was composed as follows: 19 ml acetonitrile, 1 ml acetonitrile saturated with DNPH, 1 ml water and 0.9 ml 0.5 M HCl (resulting in a HCl concentration of 0.02 M).

The hydrazone derivatives were concentrated by solid phase extraction (SPE) on octadecyl (C18) and phenyl cartridges (Bakerbond, 3ml, 500 mg). Cartridges were activated with 4 ml acetonitrile, then conditioned with acetonitrile/water mixture. Thirty millilitres of the aerosol extracts were diluted with water and passed through the

Table 2
Absolute detection limits with and without solid phase extraction on C18 cartridge

Component	Without SPE (ng)	Enrichment factor	With SPE (ng)
Formaldehyde	18	39	0.46
Acetaldehyde	36	81	0.44
Acrolein	42	89	0.47
Acetone	36	88	0.41
Propionaldehyde	48	83	0.58
Crotonaldehyde	66	90	0.73
Butyraldehyde	66	82	0.8
Benzaldehyde	132	91	1.5
Isovaleraldehyde	132	94	1.4
Valeraldehyde	132	81	1.6
o-Tolualdehyde	144	92	1.6
m,*p*-Tolualdehyde	168	93	1.8
2-Hexanone	168	87	1.9
Hexaldehyde	168	84	2.0
2,5-Dimethylbenzaldehyde	168	93	1.8
2-Heptanone	168	90	1.9
2-Octanone	132	86	1.5
C8-Aldehyde	168	86	2.0
C9-Aldehyde	168	80	2.1
C10-Aldehyde	198	73	2.7
C11-Ketone	234	60	3.9
C12-Aldehyde	234	40	5.8

SPE cartridge. After sample loading the cartridge was dried, then the concentrated hydrazones were eluted with 3 ml tetrahydrofuran. The eluate was evaporated to dryness, dissolved in 300 μl acetonitrile/water = 1/1 and injected into the HPLC system. Factors affecting the efficiency of SPE are detailed later.

3. Results and discussion

It must be emphasised that sampling of atmospheric aerosol by using a single filter may introduce both positive and negative errors. Positive error may arise from the adsorption of gas phase compounds on the filter while negative error may result from the loss of volatile compounds during sampling. Nevertheless, the aerosol samples collected on a single filter can be used for studying extraction efficiency.

3.1. Investigations on the composition of the extracting solution

The usual way to form the hydrazone derivatives of carbonyl compounds is the reaction of carbonyls with DNPH in acidic aqueous solution. In our case, however, extraction and derivatisation were combined. Aldehydes and ketones are more soluble in organic solvents than in water therefore extraction was performed in acetonitrile. Since the efficiency of derivatisation depends on the acidity of the medium [12], the HCl concentration of the extracting solution was changed from 0.004 to 0.5 M. The efficiency of derivatisation at different HCl concentrations was tested with five compounds representing a shorter chain aldehyde (butyraldehyde) and ketone (acetone), a longer chain aldehyde (pelargonaldehyde (= nonanal)) and ketone (2-octanone) and an aromatic aldehyde (benzaldehyde). A standard solution of the five test compounds was prepared, then derivati-

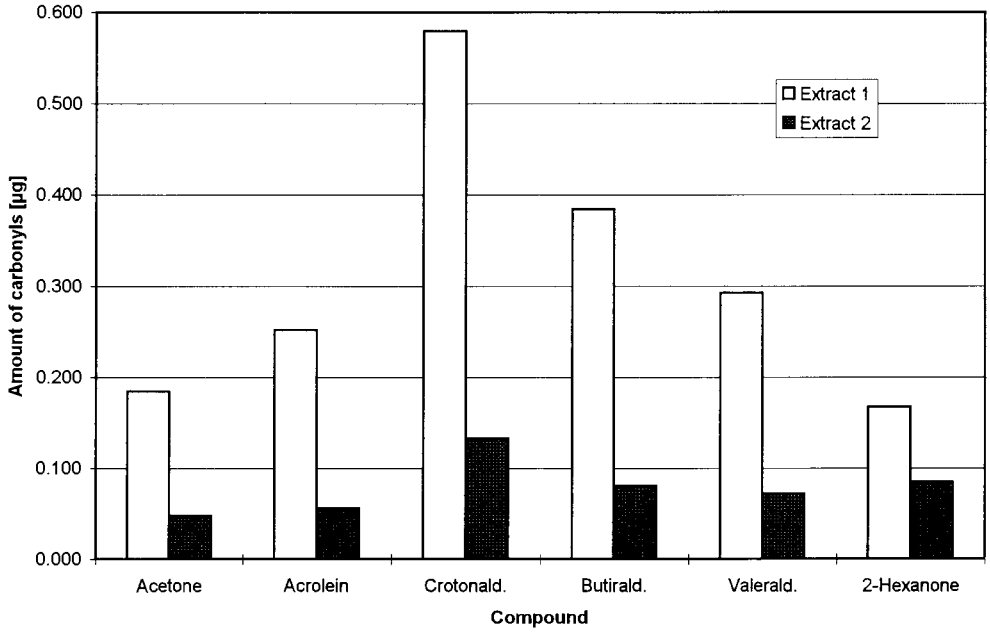

Fig. 3. Amount of individual carbonyls in the extracts of the sample KP51.

sation was performed and the hydrazone derivatives were quantified by HPLC. Results are summarised in Fig. 1. It can be seen that with increasing HCl concentration the conversions of the aldehydes were not influenced significantly but decreasing conversions for the two ketones were obtained. Efficiencies of $>90\%$ were obtained for all compounds when the HCl concentration was <0.02 M. Based on these results the following extraction and derivatisation solution was suggested: 19 ml acetonitrile, 1 ml acetonitrile saturated with DNPH, 1 ml water and 0.9 ml 0.5 M HCl (resulting in a HCl concentration of 0.02 M).

3.2. Study on the efficiency of extraction

Samples collected in Veszprém (VP) and K-puszta (KP51 and KP54) were extracted in an ultrasonic bath with 2×15 ml extracting solution (as described above) for 2×20 min. Concentrations of the hydrazone derivatives in the first and the second extract were compared. After analysing the first sample set it became evident that there were numerous carbonyl compounds in the aerosol extract and only some of them could be identified and quantified. Therefore, a better solution was to quantify all the carbonyl groups instead of the individual compounds. Since one carbonyl group reacts with one DNPH molecule, the total concentration of carbonyl groups can be determined if the total concentration of the hydrazones is known. The total concentration of the hydrazones can be determined from their UV absorption at 360 nm assuming that the absorption coefficient of the hydrazones is independent from the remaining part of the molecule. It means that the slope of the calibration lines of the different hydrazone derivatives is independent from the molecular weight. The validity of this assumption was examined for 15 carbonyl compounds with molecular weight from 44 to 142 amu. Results are summarised in Table 1.

It was found that the slopes of the calibration lines were around 18.2 AU∗s $(\mu\text{mol ml}^{-1})^{-1}$ independently from the molecular weight. Since the intercepts were close to zero it could be stated that the calibration lines for these compounds were almost identical. It means that the total concentration (in $\mu\text{mol ml}^{-1}$) of the hydrazones can be well estimated from the total area (AU∗s) of all the peaks in the chromatogram. Thus, the total amount of the carbonyl groups can be determined in the first and the second extract. This calculation was

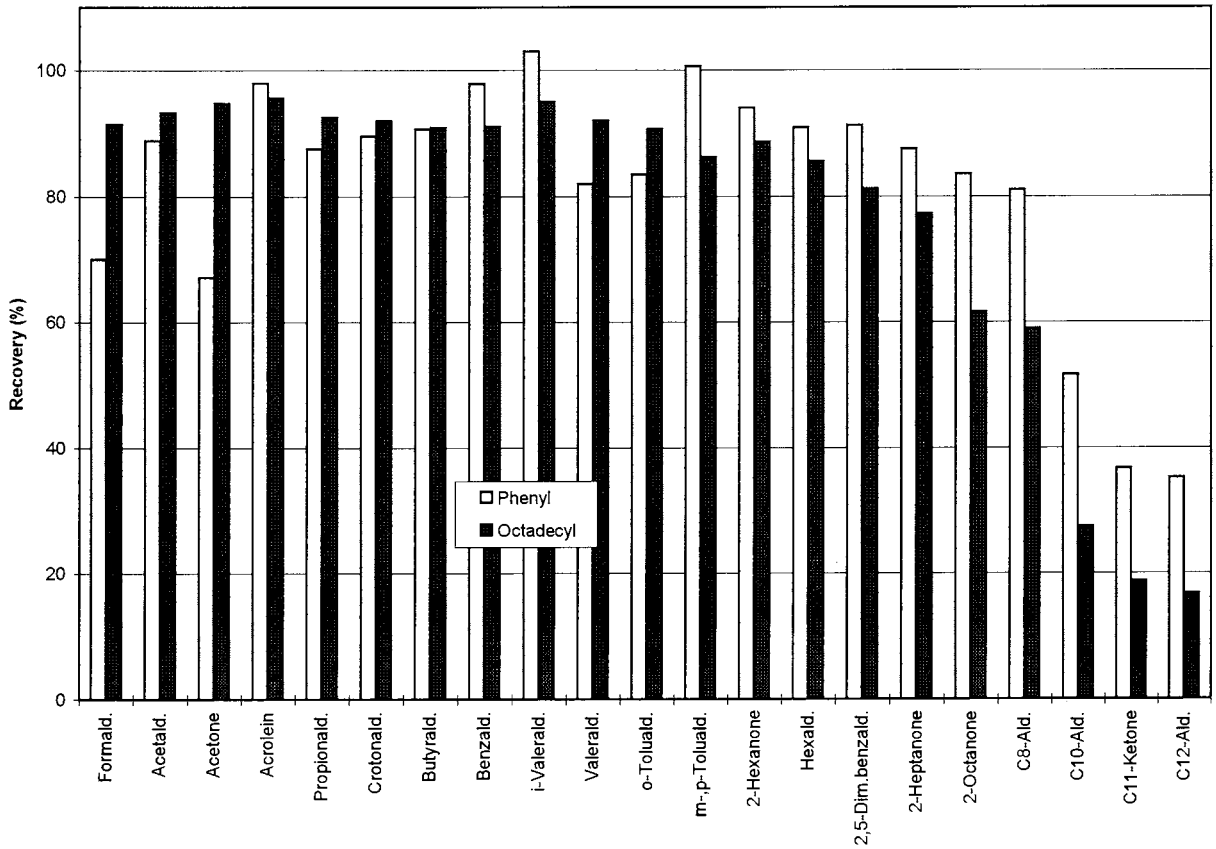

Fig. 4. Recovery of carbonyl-DNPH derivatives from test solution (V, 150 ml; 10% acetonitrile; n, 6).

performed for our samples and the results are depicted in Fig. 2.

It can be seen that only about one fifth of the carbonyls are detected in the second extract. This ratio was confirmed by the results obtained for the identified compounds (Fig. 3). On the basis of this observation it can be concluded that sonication with 2×15 ml solution for 2×20 min is sufficient for quantitative extraction.

3.3. Enrichment of the hydrazone-derivatives

The carbonyl compounds can be extracted from the atmospheric aerosol samples as described previously. However, the concentrations of the hydrazone-derivatives in the extract are to low for reliable quantitative analysis. So, the enrichment of the derivatives has to be performed. Reduction of the volume of the extract by evaporation cannot be suggested for two reasons: The concentration of HCl is increasing as acetonitrile evaporates from the extract and the strongly acidic solution cannot be injected onto the octadecyl-silica stationary phase. Furthermore, degradation of some derivatives in acidic medium was observed in our experiments and by other researchers as well [12].

Instead of evaporation of the extract solid phase extraction can be used for sample concentration. SPE cartridges with octadecyl and phenyl stationary phases have been tested. These cartridges can be used to concentrate less polar compounds from polar medium. Therefore, the polarity of the extract should be increased by dilution with water before applying SPE. In order to reach high recoveries of the hydrazones the acetonitrile content should be optimised. First, a standard solution of carbonyl derivatives was prepared with 10 (v/v)% acetonitrile content and SPE was performed both on C18 and

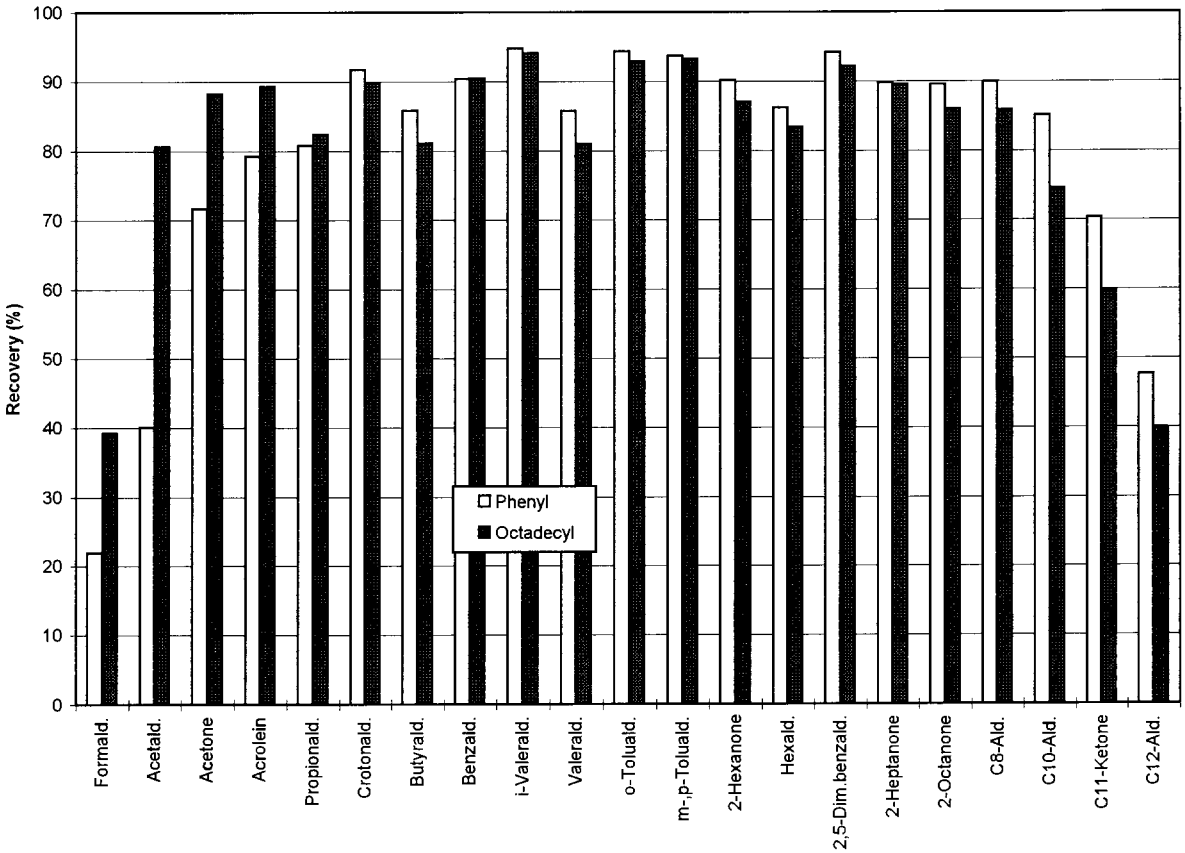

Fig. 5. Recovery of carbonyl-DNPH derivatives from test solution (V, 150 ml; 20% acetonitrile; n, 6).

phenyl stationary phases. Recoveries of the individual derivatives are shown in Fig. 4.

The recoveries on C18 stationary phase exceeded 80% up to carbon number 7 and decreased dramatically for the higher molecular weight carbonyls. This can be explained with the loss of activity of the C18 stationary phase. Similar results were obtained on the phenyl cartridge but the recovery of the longer chain carbonyls decreased to a lesser extent. The loss of activity of the stationary phase can be avoided by increasing the acetonitrile content. Therefore, the experiment was repeated with 20 (v/v)% acetonitrile content. Recoveries can be seen in Fig. 5. Higher recoveries were obtained on both stationary phases for the C8–C12 carbonyls but the recovery of formaldehyde and acetaldehyde decreased significantly (especially in case of the phenyl cartridge). This was caused by the increased eluent strength of the solution as a consequence of the higher acetonitrile content. Further increase of the acetonitrile content results in decreasing recovery of the lower molecular weight carbonyls and increasing recovery of the higher molecular weight carbonyls. So, 20 (v/v)% acetonitrile content can be a good compromise when enrichment of carbonyl derivatives from formaldehyde to C12-aldehyde is to be performed.

In Table 2 the absolute detection limits of the method with and without SPE are summarised. It can be seen that the detection limits without SPE range from 18 to 234 ng for formaldehyde and C12-aldehyde, respectively. With SPE these values (corrected for recovery) can be reduced to 0.46 and 5.8 ng, respectively.

4. Conclusion

A sample preparation method has been developed for the determination of carbonyl compounds in atmospheric aerosol. Extraction and derivatisation were performed simultaneously in the following solution: 38 ml acetonitrile, 2 ml acetonitrile saturated with DNPH, 2 ml water and 1.8 ml 0.5 M HCl. Quantitative extraction of the carbonyl compounds was achieved by sonication with 2×15 ml of this solution for 2×20 min. The hydrazone derivatives could be concentrated on octadecyl or phenyl solid phase extraction cartridges with 20 (v/v)% acetonitrile as organic modifier. Enrichment factors of 40–90 could easily be reached and absolute detection limits from 0.4 to 5.8 ng were achieved.

Acknowledgements

The financial supports of the National Scientific Research Fund of Hungary (OTKA F016262, F016272, F015684, T016315) and the World Bank (W 015165) are gratefully acknowledged.

References

[1] L. Johnson, Intern. J. Environ. Anal. Chem. 9 (1) (1981) 7.
[2] D. Daniel, J. Waste Manage. Assoc. 40 (11) (1990) 1522.
[3] J.B. de Andrade, J. Braz. Chem. Soc, 6 No. 3 (1995) 287.
[4] G. Chiavari, M.C. Facchini, J. Chromatogr. 333 (1) (1985) 262.
[5] L. Nondek, D.R. Rodier, Environ. Sci. Technol. 26 (6) (1992) 1174.
[6] S.B. Tejada, Intern. J. Environ. Anal. Chem. 26 (1986) 167.
[7] X. Zhou, J. Geophys. Res. [Oceans] 98 (C2) (1993) 2385.
[8] M.P. Keuken, Int. J. Environ. Anal. Chem. 35 (4) (1989) 227.
[9] Waters Sep-Pak DNPH-Silica Cartridge Care and Use Manual, Waters, (1994)
[10] D.W. Lempuhl, J. Chromatogr. A 740 (1) (1994) 71.
[11] R.L. Tanner, Z. Meng, Environ. Sci. Technol. 18 (9) (1984) 723.
[12] E. Cotsaris, B.C. Nicholson, Analyst 118 (1993) 265.

ELSEVIER

Talanta 48 (1999) 763–772

Talanta

Speciation of arsenic in mussels by the coupled system liquid chromatography—UV irradiation—hydride generation-inductively coupled plasma mass spectrometry

T. Dagnac [a], A. Padró [b], R. Rubio [a,*], G. Rauret [a]

[a] *Departament de Química Analítica, Universitat de Barcelona, Avda Diagonal 647, 08028 Barcelona, Spain*
[b] *Serveis Científico-Tècnics, Universitat de Barcelona, C/Lluís Solé y Sabarís 1-3, 08028 Barcelona, Spain*

Received 5 June 1997; received in revised form 9 September 1997; accepted 9 September 1997

Abstract

A method has been developed for the determination of seven arsenic species in mussel tissues by liquid chromatography—hydride generation—UV photo-oxidation and detection by inductively coupled plasma mass spectrometry. In order to determine the different species, two ion-exchange columns (anionic and cationic) were used with phosphate and nitric acid/ammonium nitrate as mobile phases, respectively. The optimisation of the conditions for separation, photo-oxidation and hydride generation is described. For each of these species, the limits of detection and repeatability are reported with the entire system coupling. This system was applied to the analysis of certified reference material (CRM 278) and mussels collected from Barcelona harbour. Extractions were achieved in methanol/water (1:1) using low-power focused microwaves as leaching process. As expected, arsenobetaine was the main compound extracted from both materials; the typical concentrations found were between 1 and 7 mg kg^{-1}. Other organoarsenical compounds, probably arsenosugars, were extracted in a concentration range of 0.3–1.5 mg kg^{-1} in both cases. Amounts of dimethylarsinate (DMA) were found to be significant in the CRM 278, but very low in mussels from Barcelona harbour. The low limits of detection of the coupled system allow us to quantify low contents of other species (As(V), arsenocholine and monomethylarsonate (MMA)).

Keywords: Arsenic speciation; Liquid chromatography; Inductively coupled plasma mass spectrometry; Focused-microwaves

1. Introduction

The determination of arsenic species in marine biological samples is an important research topic because of their different toxicity levels [1,2]. Arsenic may occur in the environment in inorganic forms such as arsenite and arsenate, which are the most toxic compounds [3,4]. High concentrations of organic forms, in a typical range of 1–100 mg kg^{-1}, have been reported in algae and marine animals due to accumulation and biotransforma-

* Corresponding author. Tel: +343 4021283; fax: +343 4021233; e-mail: rubio@zeus.qui.ub.es

0039-9140/99/$ - see front matter
PII S0039-9140(98)00093-9

tion processes [5]. The less toxic compounds such as monomethylarsonate (MMA) and dimethylarsinate (DMA) are sometimes detected in trace amounts in seafood products. The non-toxic organic forms are generally arsenocholine, arsenobetaine and dimethylarsinylribosides (arsenosugars). These two latter compounds are the major biosynthesis products in marine animals with arsenobetaine as final by-product [6,7]. In order to achieve separation of arsenic species, liquid chromatography (LC) by reversed phase and ion-exchange processes is commonly used [8–10]. Detection by inductively coupled plasma mass spectrometry (ICP/MS) offers many advantages, especially low limits of detection and large dynamic range [11–13]. Furthermore, the high selectivity of ICP/MS is well suited to the analysis of biological samples. A hydride generation (HG) derivatization process may be involved to improve the sensitivity for these natural sample analysis and to minimize matrix and interference effects in the ICP/MS [14–18]. Some inorganic and organic compounds can be reduced directly to their corresponding volatile arsines. However, reduction of arsenobetaine, arsenocholine and arsenosugars cannot be achieved directly by a typical hydride generation reaction. Thus, these species must be quantitatively transformed into hydride-forming compounds before reduction. Several efficient coupled systems with on-line microwave decomposition before hydride generation have been reported [19,20]. Our previous studies demonstrate on-line UV photolysis of organoarsenical compounds to be a successful method allowing hydride generation [21]. This paper deals with the application of the coupled system LC-UV-HG-ICP/MS to the speciation of arsenic compounds extracted from mussel tissues (*mytilus edulis*). Some of these bivalves were collected from Barcelona harbour (BHM), whereas the certified reference material (CRM 278) was studied to compare and validate our results with respect to previous results [22,23]. Extractions were performed in methanol/water (1:1) by using low-power focused microwaves as leaching process [24].

2. Experimental

2.1. Apparatus

A Perkin–Elmer 250 LC binary pump with a Rheodyne model 7125 injector and a 20 μl injection loop was used. An anion-exchange Hamilton PRP X-100, spherical poly(styrene-divinylbenzene) trimethylammonium exchanger and a cation-exchange Hamilton PRP X 200, spherical poly(styrene-divinylbenzene) sulfonate exchanger, both 10 μm particle size (250 mm × 4.1 mm i.d.), were used with guard columns packed with the same stationary phases.

The photoreactor system combines a Heraeus TNN 15/32 low-pressure mercury vapour lamp (254 nm, o.d. 2.5 cm, length 17 cm, 15 W) and a PTFE tubing (length 12 m i.d. 0.5 mm). More details are described elsewhere [14]. A computer controlled microburette (Microbur 2031, Crison) was used to introduce the peroxodisulfate solution onto the photoreactor.

The hydride generation was performed with a Perkin–Elmer FIAS 400 and a gas–liquid separator equipped with a PTFE membrane. The sample channel was connected to the outlet of the LC/UV system.

A Perkin–Elmer Elan 6000 ICP-MS instrument was used. Peak heights and areas were calculated from a custom developed software running with Matlab language. The operating conditions are given in Table 1.

A Prolabo microwave digester, (model A301, 2.45 GHz), equipped with a TX32 programmer

Table 1
ICP/MS operating conditions

Perkin–Elmer ICP/MS Model Elan 6000	
Measured mass (amu)	75
Resolution (amu)	0.7
Gas	Argon
Lens voltage (V)	6.5
ICP RF power (W)	1000
Sample cone	Nickel
Skimmer cone	Nickel
Dwell time (ms)	1000
Total acquisition time (s)	1000

Table 2
Digestion program for total arsenic determination by focused microwaves

No. Step	HNO_3 volume (ml)	H_2O_2 volume (ml)	Time (min)	Power (W)
1	10	—	5	40
—	—	—	10	70
2	—	5	10	60
3	3	—	15	40

was used. Powers of 20–200 W can be applied in steps of 10 W. This system works under atmospheric pressure with microwave energy focused into the vessel.

A Hettich centrifuge was used for the extraction procedure.

2.2. Reagents and standards

All the solutions were prepared using doubly deionized water (Culligan Ultrapure GS) of 18.3 MΩ cm resistivity.

Standard solutions (1000 mg l^{-1} [As]) of arsenic compounds were prepared and standardized with respect to As(III) by ICP-MS measurements. Arsenite, As_2O_3 (Merck) primary standard was dissolved in NaOH (4g l^{-1}); arsenate, $Na_2HAsO_4.7H_2O$ (Carlo Erba), monomethylarsonate, $(CH_3)As(ONa)_2.6H_2O$ (Carlo Erba), dimethylarsinate, $(CH_3)_2AsNaO_2.3H_2O$ (Fluka) and trimethylarsine oxide (TMAO, Hot Chemical) were dissolved in water. Solutions of arsenocholine (AsChol), $(CH_3)_3As + CH_2CH_2OHBr^-$ and arsenobetaine (AsBet), $(CH_3)_3As + CH_2COO^-$, were supplied by the 'Service Central d'Analyse', CNRS (Vernaison, France).

Phosphate buffers prepared from NaH_2PO_4 (Suprapur, Merck) and Na_2HPO_4 (Suprapur, Merck) were used with the anion-exchange column. Solutions of nitric acid 65% (Suprapur, Merck) and ammonium nitrate (Merck, pro analysis) were used for mobile phases with the cation-exchange column. Mobile phases were filtered through a 0.22 μm nylon membrane.

Acetonitrile (gradient grade, Merck) and dimethylsulfoxide (DMSO) were used for column washing.

Peroxodisulfate solutions ($K_2S_2O_8$, Fluka, purity > 99.5%) were prepared in sodium hydroxide (NaOH, Suprapur, Merck). Sulfuric acid at 10% (H_2SO_4, Suprapur 96%, Merck) and sodium borohydride ($NaBH_4$, Fluka, tablets, purity > 97%) in NaOH (Suprapur, Merck), used for reduction were prepared daily. The $NaBH_4$ solution was filtered through a 0.45 μm cellulose acetate membrane.

Methanol (gradient grade for HPLC, Merck) was used for extraction processes. Nitric acid 65% (Suprapur, Merck) and hydrogen peroxide 32% (Suprapur, Merck) were used to perform total arsenic determinations.

C_{18} snap-cap cartridges (300 or 600 mg of sorbent, Lida) were used for clean-up.

2.3. Procedure for determination of total As

Five hundred milligrams of lyophilized mussel tissue are placed in an open reflux vessel and focused microwaves are applied. For each material, three independent digestions are carried out. The appropriate digestion program is adjusted by addition of concentrated nitric acid and hydrogen peroxide (see Table 2). The final digested solution (a few ml) is diluted in water to 50 ml and filtered before analysis by direct ICP/MS.

2.4. Procedure for extraction processes

Five hundred milligrams of lyophilized mussel tissue and 20 ml of methanol/water (1:1) are placed in an open reflux vessel. Focused microwaves are applied at 50 W for 5 min. After decantation, the sample extract is centrifuged at 2500 rpm for 10 min to achieve the liquid–solid separation. The resulting liquid extract is evapo-

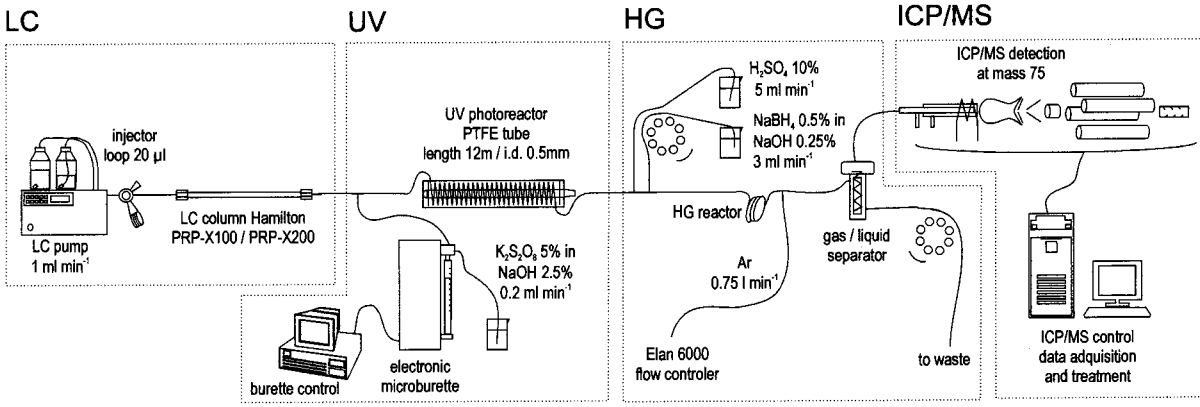

Fig. 1. LC-UV-HG-ICP/MS coupled system.

rated to complete dryness (12 h) at room temperature (all methanol must be removed before ion-exchange LC separation) and dissolved in 10 ml of water. This dense solution is filtered through a polysulfonic membrane with 0.2 µm of porosity and a sample of filtered fraction is defatted by clean-up. The C_{18} cartridge is conditioned by passing (1 ml min^{-1}) 5 ml of methanol and 5 ml of water through the sorbent successively. Then, 5 ml of sample are passed through the clean-up cartridge (1 ml min^{-1}) and the resulting extract is analysed with the LC-UV-HG-ICP/MS system.

2.5. Procedures for speciation analysis

A 20 µl volume of extract is injected onto the ion-exchange column with the optimal gradient and a flow-rate of 1 ml min^{-1}. When the anion-exchange column is used, the separation is achieved at pH 6 with a gradient of two phosphate mobile phases, NaH_2PO_4/Na_2HPO_4, 5 mmol l^{-1} (sol A) and NaH_2PO_4/Na_2HPO_4: 100 mmol l^{-1} (sol B). The gradient programme is then, 100% A for 2 min, decreasing to 50% in 0.1 min and maintained for 3 min, then increasing to 100% A in 0.1 min and maintained for 7 min. The two mobile phases chosen to operate with the cation-exchange column were HNO_3 4 mmol l^{-1} (sol A) and HNO_3 4 mmol l^{-1}/NH_4NO_3 20 mmol l^{-1} (sol B). The corresponding gradient is 100% A for 2 min, decreasing to 20% in 0.1 min and maintained for 4 min, then increasing to 100% A in 0.1 min and maintained for 8 min. Columns are equilibrated with the corresponding mobile phase (sol A) for at least 60 min before analysis.

Then, the eluate is carried onto the photoreactor with addition of peroxodisulfate solution and then introduced into the hydride generation system with addition of $NaBH_4$ and H_2SO_4 solutions. The final eluate reaches the gas–liquid separator and is then transferred to ICP/MS detector with the optimal argon flow. A scheme of the coupled system is shown in Fig. 1.

3. Results and discussion

3.1. Photo-oxidation and hydride generation conditions

The combination of the photoreactor volume and the total flow of peroxodisulfate solution and mobile phase (1.2 ml min^{-1}), meant that the sample was in contact with UV irradiation for 2 min. In these conditions, all arsenic species were successfully transformed in As(V) before the hydride generation step [25]. For this, the FIAS system operated in continuous mode. When only inorganic arsenic and methylated forms are present in the sample, the photo-oxidation reaction is not necessary because these species form hydrides directly. However, excepted for As(III), the signal obtained for methylarsines (in our conditions) is worse than with photo-oxidation.

To optimize hydride generation, we established $NaBH_4$ and H_2SO_4 flows to 3 and 5 ml min^{-1}, respectively. The AsBet responses without column suggested the system sensitivity was proportional to the $NaBH_4$ concentration. But values above 0.5%, or higher flows affect gas–liquid separation and cause plasma extinction. Sensitivity was not improved by decreasing three times the reactor volume in which reduction occurred. The reaction rate of arsine formation is then very high. Taking into account the total flow of reducing agent, acid, peroxodisulfate and mobile phase, the residence time of arsines in the reactor was about 4 s. The argon flow in the gas–liquid separator also influenced the residence time and the dilution of arsines in the reactor, transfer line and plasma. The optimal argon flow was determined daily by ICP/MS measurements of background levels of arsenic. Thus, the hydride system consisted of both reagents $NaBH_4$ 0.5% (in NaOH 0.25%) and H_2SO_4 10%, with a PTFE reactor (900 × 1 mm i.d) and the argon flow ranges between 0.70 and 0.80 ml min^{-1}.

3.2. Quality parameters

Preliminary studies have been carried out with the PRP X-100 column to test the repeatability of the chromatographic responses (peak areas) of the arsenic species. Responses of MMA, DMA, As(III) and As(V) did not change after the analysis of 50 biological extracts, whereas arsenocholine and arsenobetaine responses were affected. Furthermore, the excellent linearity of these two compound responses without LC column ($R^2 = 0.9991$ and $R^2 = 0.9999$, as a function of concentration), guaranteed the rest of coupled system to be perfect. Repeated injections of not defatted biological samples markedly changed the column behaviour (Fig. 2). By considering the discrepancies between AsChol and AsBet peak areas obtained with and without column, curves derived from Langmuir isotherms are adjusted (Fig. 3). The response linearity suggested that adsorption processes were probably involved. Hereby, the limits of detection (LOD) were dramatically increased and quantification by the method of standard additions gave erroneous results. As a result, the column was treated in an attempt to restore performance. The possible contaminants from sample matrix, such as fats and oils, were removed by washing the column with an acetonitrile /water solution (1/1) and several 20 μl injections of DMSO [26]. The perfect linearity of AsChol and AsBet responses between 1 and 100 μg l^{-1} ($R^2 = 0.9989$ and $R^2 = 0.9995$), indicated the column performance has been retrieved after this cleaning. Performance was then monitored before running extract analysis by injecting an AsBet 0.5 ppb solution. The absence of the AsBet peak on the corresponding chromatogram indicated the need to clean the column as described.

Quality parameters were determined for six species with the entire coupled system. LOD were calculated from concentrations corresponding to the background level plus three times its standard deviation (Table 3). The repeatability was calculated from five replicate injections of a sample (Table 3). The LOD and repeatability for As(III) were calculated by using the entire coupled system but switching off the UV lamp. The quality parameters for AsBet, MMA, DMA and As(V) were obtained by using the gradient separation.

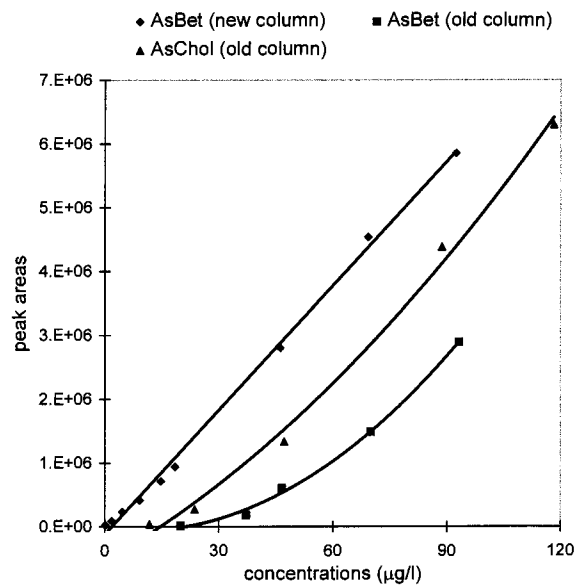

Fig. 2. Organoarsenical responses with the anion-exchange PRP X-100 column.

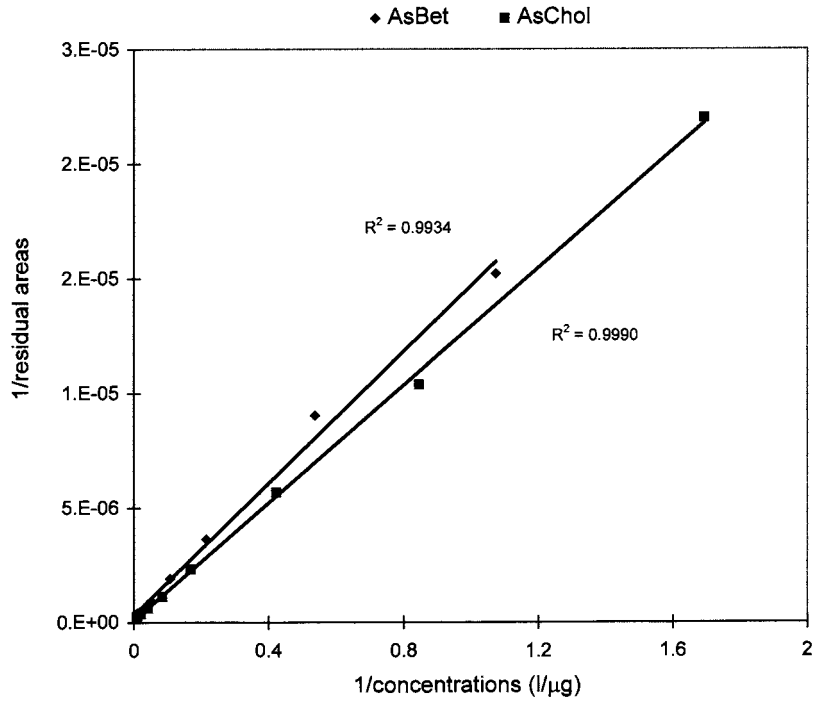

Fig. 3. Organoarsenical residual responses with the anion-exchange PRP X-100 column.

The LODs are much lower than those commonly encountered without the derivatization process and ICP/MS detection [11,13,27,28]. The highest values for the six compounds correspond to AsChol and As(V) with 2.6 and 2.4 pg of As, respectively. But during the As(V) elution, the arsenic present in phosphate solutions causes the background level to increase with the mobile phase gradient. Moreover, the AsChol peak shape can also explain its relatively high LOD. An extremely low value of 0.5 pg is obtained for As(III), due to its higher yield in arsine generation than in As(V).

The repeatability, expressed as the % RSD values of peak areas, was calculated for each compound with arsenic containing solutions of 4–7 μg l^{-1}, included of 50 and 100 times the LOD of each species. The values obtained ranged from 1 to 3% and can be considered satisfactory, especially owing to the great number of parameters governing the LC-UV-HG-ICP/MS system performances.

3.3. Analysis with anion-exchange separation

The chromatograms corresponding to CRM 278 and BHM extracts are given in Fig. 4. The separation between species is well performed with our operating conditions. On the CRM 278 corresponding chromatogram, six peaks can be numbered, whereas on BHM one, only five peaks are observed. In both cases, arsenobetaine is the major compound extracted, as expected, but the presence of other cationic species cannot be excluded. An unknown compound (U1), with a retention time very close to that of MMA, seems to reach great proportions in both materials. According to Gailer and Larsen [6,7,29], an arsenic-containing ribofuranoside such as a dimethylarsinylriboside is the most likely structure for the compound U1. Traces of MMA and of a cationic species are observed in CRM 278. Traces of As(V) and another unknown (U2) compound with a retention time close to DMA one are present in both materials. In an attempt to complete the speciation of inorganic arsenic, an analy-

Table 3
Quality parameters obtained with the LC-UV-HG-ICP/MS coupled system and a with 20 μl injection loop

Species	LOD (μg As l^{-1})	R^2 (1–100 μg As l^{-1})	Repeatability RSD (%) with peak areas ($n=5$)	Concentrations (μg As l^{-1})
AsBet	0.065	0.99945	3.12	4.7
AsChol	0.13	0.99967	1.77	5.9
DMA	0.10	0.99959	0.67	4.8
MMA	0.061	0.99961	2.51	7.1
As(V)	0.12	0.99966	1.13	7.4
As(III)[a]	0.025	0.99994	0.96	1.0

[a] Values acquired with the UV lamp switch off.

sis was carried out without photo-oxidation (Fig. 5). The absence of As(III) (coeluted with AsBet) was demonstrated and only As(V), DMA, and MMA could have been detected.

3.4. Analysis with cation-exchange separation

On the CRM 278 and BHM chromatograms (Fig. 6), seven peaks can be observed but with distinct relative proportions in terms of material. In order to identify the corresponding compounds, the retention times of seven arsenic species were determined (the same previous six species plus the TMAO). Moreover, the CRM 278 and BHM extracts were spiked with these same substances. As suggested from the anion-exchange

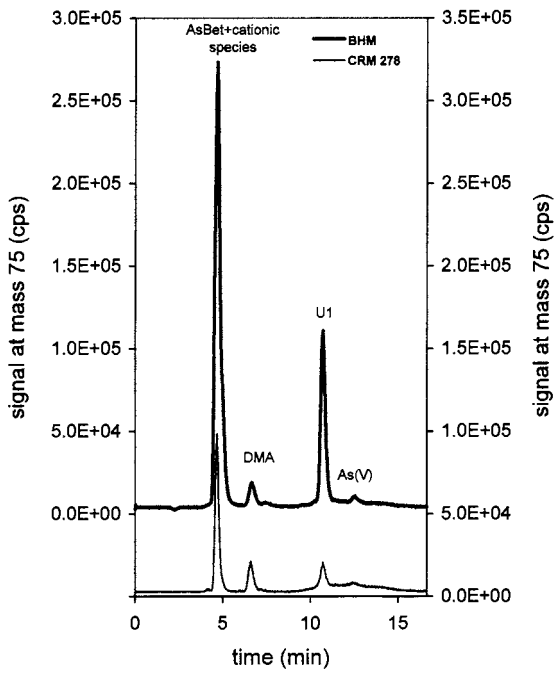

Fig. 4. Chromatograms corresponding to CRM 278 and BHM extracts with anion-exchange separation. Injection loop of 20 μl and gradient of two phosphate mobile phases at pH 6.

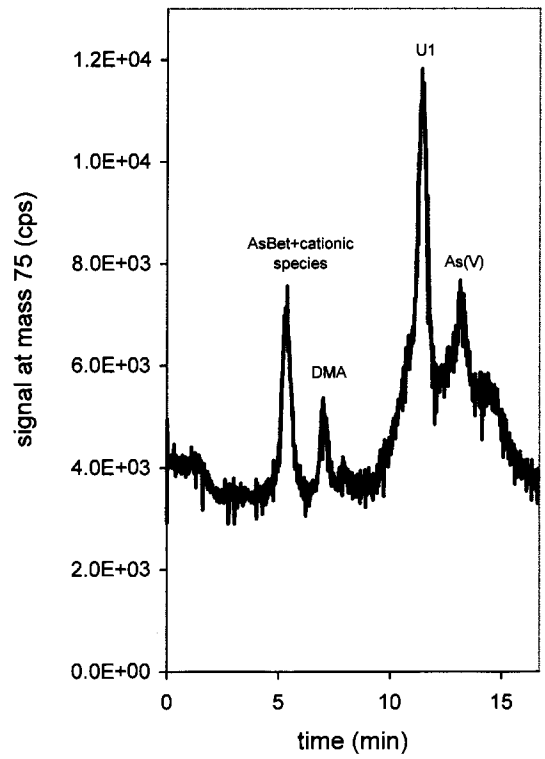

Fig. 5. Chromatogram corresponding to BHM extract with anion-exchange separation and without photo-oxidation. Injection loop of 20 μl and gradient of two phosphate mobile phases at pH 6.

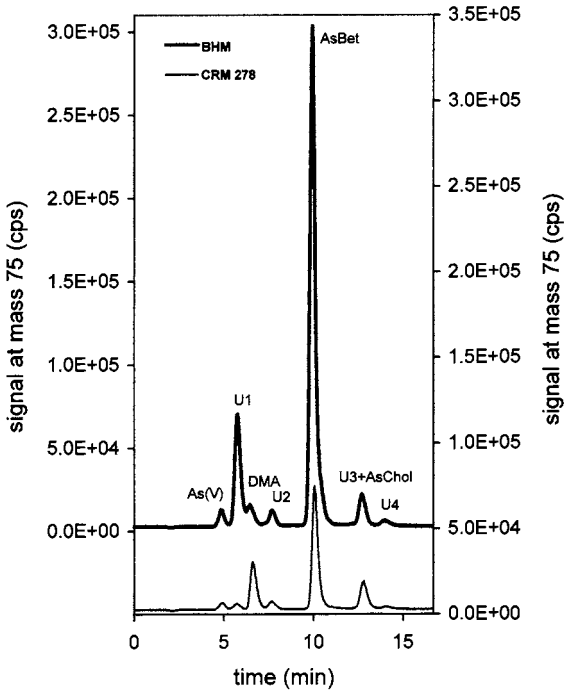

Fig. 6. Chromatograms corresponding to CRM 278 and BHM extracts with cation-exchange separation. Injection loop of 20 μl and gradient of two nitric acid mobile phases.

separation, As(V), DMA and AsBet were clearly identified. The relative areas of the arsenosugar U1 obtained with the PRP X-100 column indicated it was here eluted between the two methylated compounds. As described in recent studies with cation-exchange separation on bivalve extracts [7,29], U1 is probably a phosphorous-containing arsenosugar. Additionally, an isocratic elution (with sol A) of the BHM extract was performed to optimize the separation of cationic compounds. Without the mobile phase gradient, the run time was then extended to 25 min, but two retained coeluted cationic compounds were separated (Fig. 7). The unknown species U3 might be another dimethylarsinylriboside of low molecular weight and with hydrolyzed structure. The next compound eluted showed the same retention time as AsChol and the presence of this compound has been reported in mussels [12] but with a very low concentration (30 ng g^{-1}). Finally, none cationic unknown compound is eluted with the TMAO retention time.

3.5. Quantitative results

All the quantifications were obtained by the method of standard additions on the extract fraction previously defatted by clean-up. Quantitative results are summarized in Table 4, which contains the total arsenic values and the mass of each arsenic species per gram of dry material. The accuracy in total arsenic determinations for initial mussel tissues is checked by analysing the CRM 278. The value obtained is very close to the certified one. Total extraction yields are calculated by summing the mass of each extracted compound and not by considering the total arsenic in the residuals of extraction.

Concentrations of AsBet and coeluted cationic compounds were calculated with AsBet additions and U1 arsenosugar contents were calculated with MMA additions. For CRM 278 and BHM materials, the yield of extracted arsenic were 41.1 and

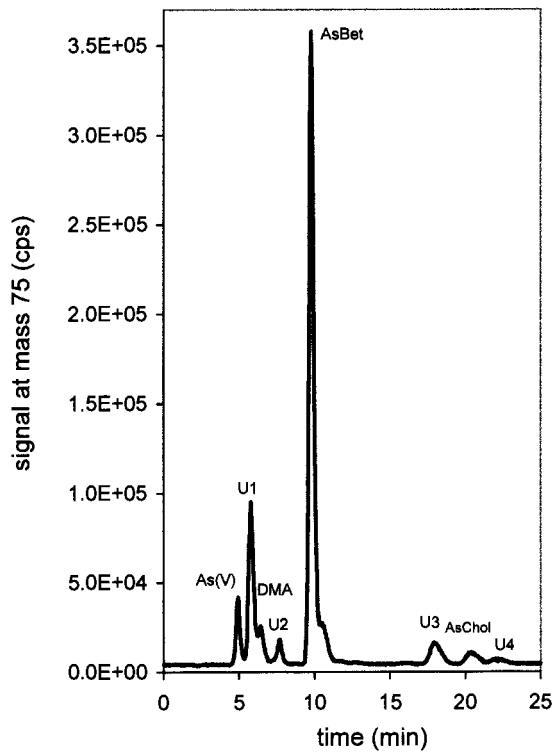

Fig. 7. Chromatogram corresponding to BHM extract with isocratic cation-exchange separation. Injection loop of 20 μl and nitric acid mobile phase.

Table 4
Quantitative results for arsenic extraction in mussel tissues

Mussel material	AsBet + cationic species (μg g^{-1})	DMA (μg g^{-1})	U1 (μg g^{-1})	As(V) (μg g^{-1})	Extraction yield (%)[b]	Total As (μg g^{-1})
CRM 278	1.40 ± 0.24	0.529 ± 0.078	0.374 ± 0.028	0.120 ± 0.031	41.1 ± 4.3	$5.85^{a} \pm 0.02$
BHM	7.45 ± 0.37	0.247 ± 0.037	1.38 ± 0.10	0.080 ± 0.012	87.1 ± 3.7	10.51 ± 0.08

[a] CRM 278 certified value: 5.9 ± 0.2 μg g^{-1}.
[b] Resulting from the sum of species mass.

87.1%, respectively. The value for CRM 278 is close to other results obtained with this material (46.4%) with successive ultrasonication and centrifugation steps as extraction process [22]. However in the present study, the time of sample preparation by using focused microwaves is extremely reduced.

In an attempt to explain the wide difference between the arsenic extracted in the two materials, each step of material preparation could be discussed. For instance, BHM were not subjected to high temperatures whereas the CRM 278 mussels were cooked under pressure at 120°C [30]. Thus, none rigorous comparison of extractable arsenic is possible in these mussel tissues. However, the number and the nature of species appear to be similar irrespective of the both mussel materials. In addition, a first approach of the species recuperation on BHM after clean-up showed 15% of arsenic compounds was lost. A more complete study will be presented elsewhere for each species.

These results confirm that AsBet (and minor cationic products) is the main species, especially in BHM. In this case, a quantitative approach was performed by using the cation-exchange column and the cationic species ratio (AsChol + U3) reaches 7% of the previous estimated AsBet amount (with anion-exchange column). The proportion of arsenosugar (U1) is significant in both materials (15%) and analogous to DMA ratio in CRM 278 mussels; but DMA appears with low concentration in BHM.

4. Conclusions

The LC-UV-HG-ICP/MS coupled system has been here demonstrated to be very powerful for arsenic speciation in mussel tissues. The limits of detection are much lower than those commonly encountered without derivatization process before ICP/MS detection. The use of both anion-exchange and cation-exchange separations is recommended for better identification of the species. However, the study emphasized that the PRP X-100 column performance was altered by repetitive analysis of raw biological extracts. We suggest an alternative method based upon the systematic clean-up of the extract previous to analysis to avoid column alteration.

The two main species extracted from both mussel materials are AsBet and an unknown organoarsenical compound, likely a phosphorous-containing arsenosugar. Quantitative extractions were performed by focused microwave-assisted leaching which dramatically reduced the time of sample preparation. The extractable arsenic in the CRM 278 was found to be close to the results previously obtained for this material. The optimisation of arsenic extraction in mussels is in progress by investigating the influence of microwave power and residence time in the microwave field.

Acknowledgements

The authors thank the DGICYT under pro-

ject PB95-0844 for the financial support. The authors also thank Dr J.M Bayona (Departament de Química Ambiental, CSIC, Barcelona) for the facilities in the use of the lyophilization system.

References

[1] Y. Shibata, M. Morita, K. Fuwa, Adv. Biophys. 28 (1992) 31–80.
[2] A. Amran, F. Lagarde, M.J.F. Leroy, A. Lamotte, C. Demesmay, M. Olle, A. Albert, G. Rauret, J.F. López-Sánchez, in: Ph. Quevauviller, E. Meier, B. Griepink (Eds.), Quality Assurance for Environmental Analysis, Elsevier, Amsterdam, 1995, pp. 285–304.
[3] T. Kaise, K. Hanaoka, S. Tagawa, T. Hirayama, S. Fukui, Appl. Organomet. Chem. 2 (1988) 539–546.
[4] T. Kaise, S. Fukui, Appl. Organomet. Chem. 6 (1992) 155–160.
[5] W.R. Cullen, J.C. Nelson, Appl. Organomet. Chem. 7 (1993) 319–327.
[6] J. Gailer, K.A. Francesconi, J.S. Edmonds, K.J. Irgolic, Appl. Organomet. Chem. 9 (1995) 341–355.
[7] E.H. Larsen, Fresenius J. Anal. Chem. 352 (1995) 582–588.
[8] J. Gailer, K.J. Irgolic, Appl. Organomet. Chem. 8 (1994) 129–140.
[9] E.H. Larsen, S.H. Hansen, Mikrochim. Acta 109 (1992) 47–51.
[10] J. Gailer, K.J. Irgolic, J. Chromatogr. A 730 (1996) 219–229.
[11] K. Kawabata, Y. Inoue, H. Takahashi, G. Endo, Appl. Organomet. Chem. 8 (1994) 245–248.
[12] E.H. Larsen, G. Pritzl, S.H. Hansen, J. Anal. Atom. Spectrom. 8 (1993) 1075–1084.
[13] H. Ding, J. Wang, J.G. Dorsey, J.A. Caruso, J. Chromatogr. A 694 (1995) 425–431.
[14] R. Rubio, A. Padró, J. Albertí, G. Rauret, Anal. Chim. Acta 283 (1993) 160–166.
[15] W.C. Story, J.A. Caruso, D.T. Heitkemper, L. Perkins, J. Chromatogr. Sci. 30 (1992) 427–431.
[16] X.C. Le, M. Ma, N.A. Wong, Anal. Chem. 68 (1996) 4501–4506.
[17] I. Martín, M.A. López-Gonzálvez, M. Gómez, C. Cámara, M.A. Palacios, J. Chromatogr. B 666 (1995) 101–109.
[18] J. Stummeyer, B. Harazim, T. Wippermann, Fresenius J. Anal. Chem. 354 (1996) 344–351.
[19] X.C. Le, W.R Cullen, K.J. Reimer, Talanta 41 (1994) 495–502.
[20] K.J. Lamble, S.J. Hill, Anal. Chim. Acta 334 (1996) 261–270.
[21] R. Rubio, J. Albertí, A. Padró, G. Rauret, Trends Anal. Chem. 14 (1995) 274–279.
[22] J. Albertí, R. Rubio, G. Rauret, Fresenius J. Anal. Chem. 351 (1995) 415–419.
[23] J. Albertí, R. Rubio, G. Rauret, Fresenius J. Anal. Chem. 351 (1995) 420–425.
[24] J. Szpunar, V.O. Schmitt, O.F.X. Donard, R. Lobinski, Trends Anal. Chem. 15 (1996) 181–187.
[25] R. Rubio, J. Albertí, G. Rauret, Int. J. Environ. An. Ch. 52 (1993) 203–213.
[26] J.W. Dolan, L.R. Snyder, Troubleshooting LC Systems, Humana Press (Eds), New Jersey, 1989, pp. 447–448.
[27] P. Thomas, K. Sniatecki, Fresenius J. Anal. Chem. 351 (1995) 410–414.
[28] P. Teräsahde, M.P. Pantsar-Kallio, K.G. Manninen, J. Chromatogr. A 750 (1996) 83–88.
[29] J.J. Corr, E.H. Larsen, J. Anal. Atom. Spectrom. 11 (1996) 1215–1224.
[30] The certification of the contents (mass fractions) of As, Cd, Cu, Fe, Hg, Mn, Pb, Se and Zn in mussel tissue (Mytilus edulis). CRM 278. BCR, Report, EU 11838 EN

ELSEVIER

Talanta 48 (1999) 773–780

Talanta

Raman spectroscopic determination of inosine nucleoside in nucleotides

R. Escobar [a], P. Carmona [b,*], A. Rodríguez-Casado [b], M. Molina [c]

[a] *Departamento de Química Analítica, Facultad de Química, Universidad de Sevilla, E-41012 Sevilla, Spain*
[b] *Instituto de Estructura de la Materia (CSIC), Serrano 121, E-28006 Madrid, Spain*
[c] *Departamento de Química Orgánica I, Escuela Universitaria de Optica, Universidad Complutense, E-28037 Madrid, Spain*

Received 05 June 1997; received in revised form 01 December 1997; accepted 02 December 1997

Abstract

Raman spectroscopy has been applied to the analytical determination of inosine nucleoside in nucleotides. Spectral characteristics of aqueous solutions of lithium, potassium and magnesium salts of inosine 5′-monophosphoric acid are described. Two characteristic bands located at 1553 and 1593 cm^{-1} whose frequencies are not sensitive either to the nucleotide concentration or to alkaline cations present in the medium, have been used for this purpose. The concentration ranges over which the method was applicable were 2.5–80 and 11.5–80 mg ml^{-1} of inosine using the 1553 and 1593 cm^{-1} bands, respectively, with relative standard deviations of 2.5 and 4.0% and detection limits of 0.25 and 1.16% (w/w). As the above bands are not generated by the standard nucleobases, this method can be applied to the quantitative determination of inosine in transfer ribonucleic acids.

Keywords: Inosine; Raman spectroscopy; Organic analysis; Nucleotides

1. Introduction

Inosine is a guanine derivative without the $N(2)H_2$ amino group and is also a constituent of some transfer nucleic acids in which it is thought to occupy the 5′-terminal position in a number of anticodon triplets [1].

The Raman analytical characterisation of this nucleoside rests, hence, on the fact that the physiological role of these nucleic acids is dependent on the chemical composition of the polynucleotide chains and their local structures. The use of Raman spectroscopy for the above analytical purpose requires a detailed understanding of the vibrational modes and the influence of the ionic medium on their frequencies and intensities. As metal ions such as alkali and alkaline earth metal ions are present in the body, nucleic acids and nucleotides may occur as complexes coordinate with the above ions. In a previous work dealing with crystalline metal salts of inosine 5′-monophosphoric acid [2], some Raman bands were found to be influenced by the binding of

* Corresponding author. Tel.: +34 1 5616800; fax: +34 1 5645557; e-mail: pcarmona@pinar1.csic.es

0039-9140/99/$ - see front matter
PII S0039-9140(98)00094-0

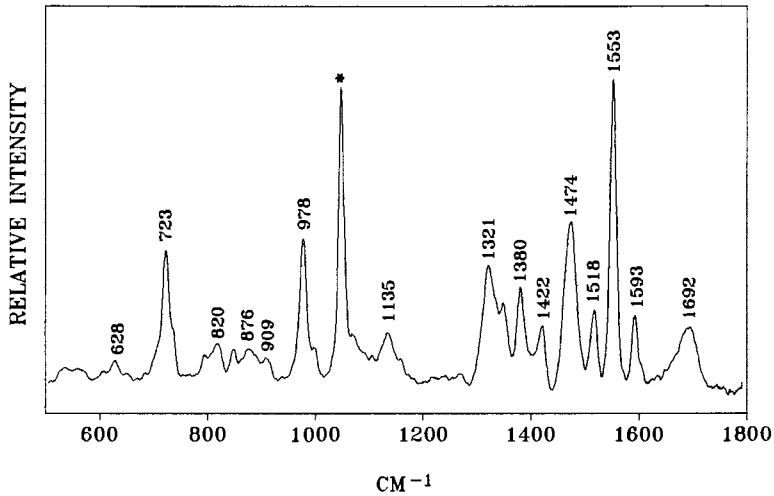

Fig. 1. Raman spectrum of $K_2(IMP).5H_2O$ in aqueous solution, 30% (w/w). The asterisked band corresponds to KNO_3 used as internal standard.

some alkaline and alkaline earth metal ions. This is particularly true for the imidazolic band located near 1480 cm^{-1} and the $\nu_s PO_3^{2-}$ band appearing in the 1000–900 cm^{-1} range. Generally speaking, metal cation-nucleic acid interactions and their effects on nucleic acid structure have been investigated by a variety of techniques including circular dichroism, UV-visible, NMR and vibrational spectroscopy [3–10].

Raman spectroscopy has the capability of showing many nucleoside bands and revealing metal binding sites. In addition, an advantage of Raman spectroscopy, besides of being a non-destructive technique, is that water (the biological medium) is a good solvent because of its weak Raman scattering. This technique, hence, is employed here for the determination of inosine in nucleotides in aqueous solution, which requires the previous knowledge of Raman bands non-perturbed by metal cation-nucleotide interactions. In this connection, aqueous solutions of Li(I), Na(I), K(I) and Mg(II) salts of inosine 5′-monophosphoric acid have been used to assess also binding sites and to use an appropriate characteristic Raman bands for the quantitative estimation of inosine. Apart from the fact that these nucleotide salts are soluble in water, their cations are used to be the counter ions with charge opposite to that of nucleic acid phosphate groups, which justifies the study of aqueous solutions of these compounds. To our knowledge, no previous work dealing with the determination of inosine in nucleotides or nucleic acids using Raman spectroscopy has been carried out.

2. Experimental

2.1. Sample preparations

All chemicals were analytical-reagent grade or equivalent and were used without further purification. Inosine 5′-monophosphoric acid, $H_2(IMP)$, was purchased from Sigma Chemical and was used as supplied.

The Li(I), Na(I) and K(I) salts of $H_2(IMP)$ were prepared by the addition of the respective hydroxide solutions to hot solutions (45°C) of the free $H_2(IMP)$ acid to obtain a 1:1 acid to hydroxide mole ratio. Ethanol was, then, added drop by drop in order to induce the precipitation of $Li_2(IMP).3H_2O$, $Na_2(IMP).8H_2O$ and $K_2(IMP).5H_2O$. The magnesium salt, $Mg(IMP).3H_2O$, was prepared by the same procedure as mentioned above, but without addition of ethanol. All of these compounds are soluble in water and were characterised by means of elemental analysis.

Table 1
Raman bands observed for metal salts of inosine 5′-monophosphoric acid in aqueous solution

Compound				Assignment
Li_2(IMP)	Na_2(IMP)	K_2(IMP)	Mg(IMP)	
1692 m	1692 m	1692 m	1689 m	νC═O
1593 m	1593 m	1593 m	1593 m	ν Six-membered ring
1553 vs	1553 vs	1553 vs	1553 vs	ν Six-membered ring
1518 m	1518 m	1518 m	1518 m	ν Purine ring
1473 m	1474 m	1474 m	1470 m	νN(7)—C(8)+δC(8)—H
1421 m	1422 m	1422 m	1420 m	ν Purine ring
1381 m	1380 m	1380 m	1380 m	ν Purine ring
1350 m	1350 m	1350 m	1350 m	ν Purine ring
1322 m	1321 m	1321 m	1322 m	ν Purine ring
1136 w	1135 w	1135 w	1135 w	νC—O+νC—C ribose
1072 w	1073 w	1073 w	1076 w	νC—O+νC—C ribose
978 s	978 s	978 s	985 vw	$\nu_s PO_3^{2-}$
			930 sh	νPO_3^{2-}
910 w	909 w	909 w	916 w	νC—O+νC—C ribose
882 w	876 w	876 w	880 w	νC—O+νC—C ribose
850 w	850 w	850 w	850 w	νC—O+νC—C ribose
820 w	820 w	820 w	822w	νP—O
735 sh	735 sh	735 sh	735 sh	Purine ring+ribose
723 s	723 s	723 s	724 s	Purine ring+ribose
628 w	628 w	628 w	628 w	Ribose

s, Strong; vs, very strong; m, medium; w, weak; sh, shoulder.

2.2. Raman spectroscopy

Raman spectra were measured on a Jobin–Yvon Ramanor U-1000 spectrometer with the 514.5 nm excitation line from a Spectra-Physics model 164 argon ion laser. Signals from a photomultiplier tube obtained through photon-counting electronics were fed to a Tandon personal computer for storage, display, plotting and processing. The acquisition time per spectral element was 1 s and each spectrum, measured in the 1800–500 cm^{-1} range, consisted of 1300 data points. The spectrometer resolution was generally set to 3 cm^{-1} and the band frequencies, calibrated with plasma lines from the laser, were accurate to within ± 1 cm^{-1}. Samples were transferred into glass capillary tubes and their spectra were obtained from the average of at least five scans. The excitation power was controlled at about 200 mw for each aqueous solution. Spectral data were generated in binary code and converted in ASCII for processing in standard graphics software.

Quantitative analysis was carried out to evaluate inosine nucleoside. For calibration, standard aqueous solutions containing K_2(IMP).5H_2O were prepared, and the concentration range used was between 5 and 30% (w/w). In order to apply this method to evaluation of inosine nucleobase in polynucleotides, the calibration graphs are given in function of nucleobase weight percentage. The intensity of the bands characteristic of inosine residue was measured relative to the 1048 cm^{-1} band of KNO_3 which was used as internal standard at 1 M concentration.

3. Results and discussion

3.1. Spectral analysis of the solutions

The observed Raman bands of an aqueous solution of the potassium salt of H_2(IMP) (Fig. 1) are listed in Table 1. Due to the nature of vibrational modes we present the results in three distinct spectral regions.

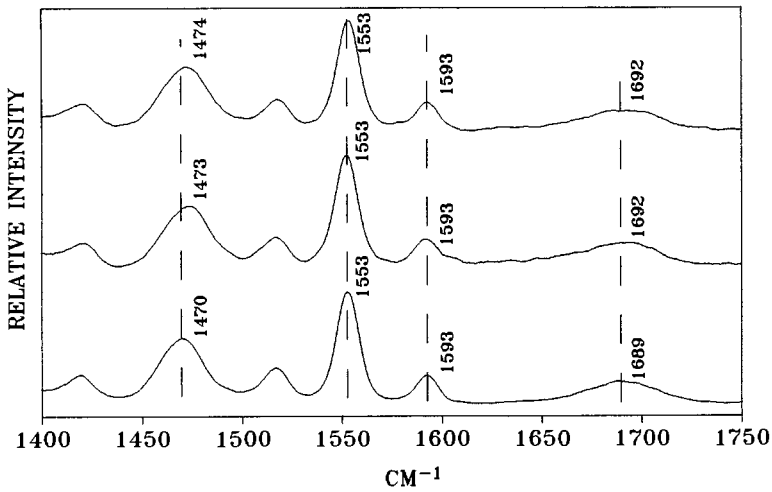

Fig. 2. Raman spectra in the 1750–1400 cm^{-1} region of (from top to bottom) $Li_2(IMP).3H_2O$, $K_2(IMP).5H_2O$ and $Mg(IMP).3H_2O$ in aqueous solution, 30% (w/w).

Most of the observed bands in the 1800–1200 cm^{-1} region are due to the in-plane vibration modes of inosine base. The band near 1692 cm^{-1} is usually assigned to the $\nu C(6)=O$ motion. This frequency can be considered as due to this nucleobase vibration itself in the absence of any interaction with metal cations, as previously shown [2] for the sodium and potassium salts of $H_2(IMP)$. This and the other visible bands of sodium and potassium salts in aqueous solution appear practically at the same frequencies (Table 1). The $\nu C=O$ band of these two salts, however, shifts to 1689 cm^{-1} for aqueous solutions of the magnesium salt (Fig. 2). The 1593, 1553 and 1518 cm^{-1} bands do not exhibit any significant intensity change and frequency shifting as a function of the cation present in solution and have been assigned to hexagonal ring stretching vibrations [11,12]. Therefore, these bands seem to be good candidates to be used for the quantitative estimation of inosine. Unlike these bands, the one with medium intensity appearing near 1472 cm^{-1} shifts to lower frequencies in the presence of magnesium ions (Fig. 2). Since this band was assigned to the purine ring N(7)—N(8) stretching and C(8)—H bending vibrations, cation binding throughout the N(7) site perturbs this band. The N(7)-binding of the Mg(II) ion was also demonstrated by proton NMR results obtained in DMSO solution [13]. The medium intensity bands centred at about 1420, 1380 and 1322 cm^{-1} were assigned to the purine ring vibrational frequencies [12], the latter remaining practically with the same frequency and relative intensity in the presence of different alkaline cations (Figs. 1, 3 and 4). However, this band is considerably overlapped with another one located near 1350 cm^{-1} and is not characteristic of this nucleoside. Thus, guanosine spectra show a vibrational mode very near this frequency [12] and consequently the Raman line at 1322 cm^{-1} can not be used for quantitative determination of inosine.

The Raman spectra in the 1200–800 cm^{-1} range are dominated by phosphate and ribose vibrations, one of the most prominent bands being that generated by the $\nu_s PO_3^{2-}$ motion. This is located near 980 cm^{-1} (Figs. 1 and 3) in the spectra of aqueous solutions of the alkaline salts. In contrast, this $\nu_s PO_3^{2-}$ medium intensity band commonly observed in these compounds decreases drastically in the solution of the magnesium salt (Fig. 4, Table 1). This results from the removal of the PO_3^{2-} symmetry, probably caused by direct metal–phosphate binding. This structural detail is in agreement with a previous study of this salt in the solid state [2].

The conformational structure of the ribofuranose ring is not affected by the different cations.

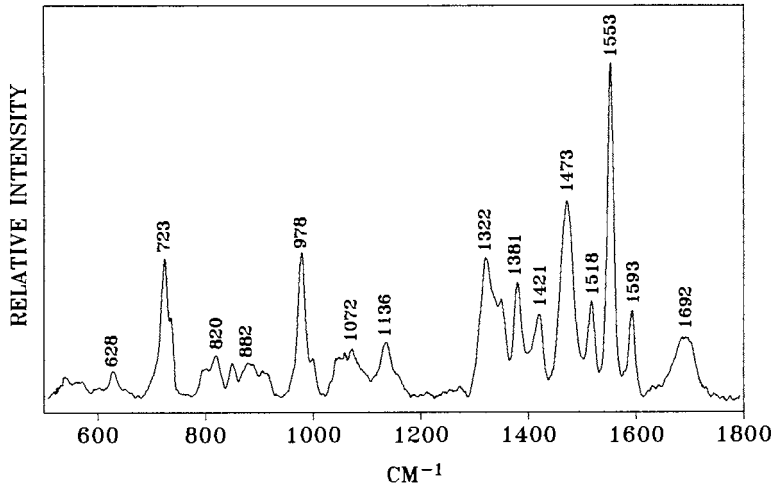

Fig. 3. Raman spectrum of $Li_2(IMP).3H_2O$ in aqueous solution, 30% (w/w).

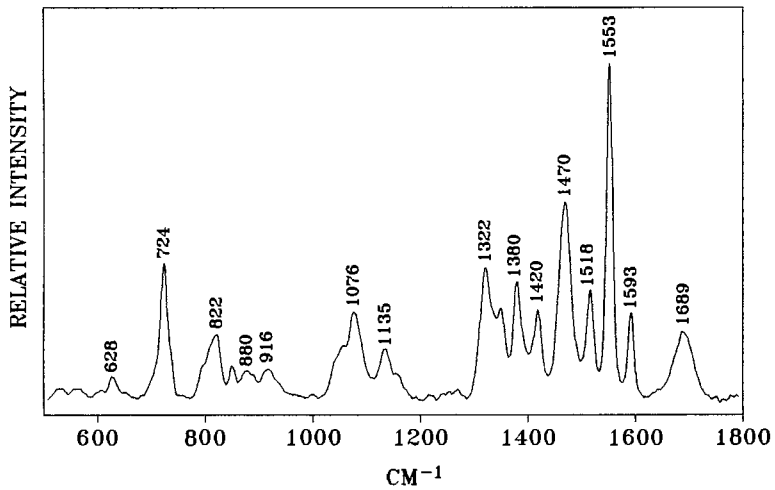

Fig. 4. Raman spectrum of $Mg(IMP).3H_2O$ in aqueous solution, 30% (w/w).

The Raman spectra of these compounds show a *v*P-O phosphoester band of medium intensity near 820 cm^{-1}, this frequency value falling in the range which is characteristic of the C(2′)-endo ribofuranose ring conformation [14]. Previous studies of aqueous solutions of nucleotides [1] also revealed that this ribofuranose ring conformation is favoured for purine nucleotides. The shoulder at 735 cm^{-1} is generated by the C(2′)-endo-anti conformation of inosine [2]. However, this band overlaps with the adenine ring-breathing band appearing near 730 cm^{-1} and is not appropriate for quantitative determination of this inosine structure.

3.2. Quantitative study

Although curve-fitting of the spectral profiles in the 800–700 cm^{-1} range provides relative intensities of the 735 cm^{-1} band for quantitative estimation of the C(2′)-endo-anti conformation, this would not be feasible for polynucleotides containing adenine, due to the band overlapping described above. Therefore, the 1553 and 1593 cm^{-1} bands are more appropriate from the point of view of the quantitative determination of inosine nucleoside. Moreover, the relative intensities of these bands per mol of solute are not affected by the nucleoside concentrations used

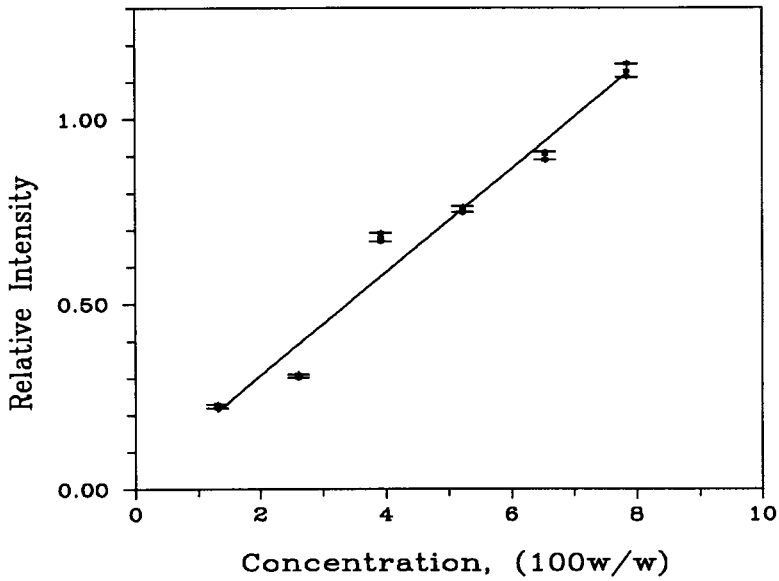

Fig. 5. Calibration graph of inosine nucleoside using the 1553 cm^{-1} Raman band. Data also present *s* values at each point.

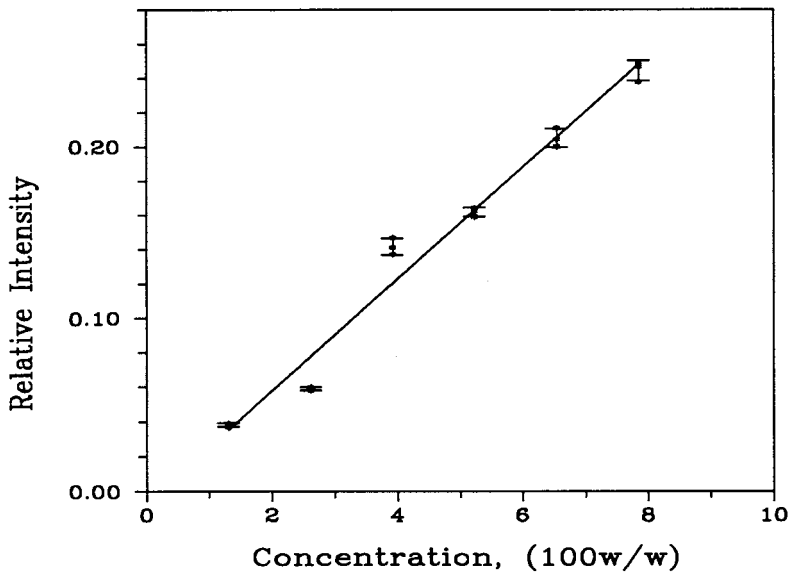

Fig. 6. Calibration graph of inosine nucleoside using the 1593 cm^{-1} Raman band. Data also present *s* values at each point.

here. This can be said because normalisation of solution spectra of different concentrations leads to spectral profiles having the same relative intensities. As these two bands are common to different ribofuranoside conformational structures, the method described here is intended for quantitative estimation of total inosine in aqueous solutions of nucleotides.

The calibration graphs (Figs. 5 and 6Table 2) fit the least squares equations: $I_{1553} = 0.142c + 0.018$ and $I_{1593} = 0.033c - 0.009$, where c is inosine concentration expressed as weight percentage of nucleobase, and I_{1553} and I_{1593} are the intensities of the 1553 and 1593 cm^{-1} bands relative to the intensity of the band at 1048 cm^{-1} due to potassium nitrate used as an internal standard. The

Table 2
Analytical parameters

Parameter	1553 cm^{-1} band	1593 cm^{-1} band
Slope	0.142	0.033
Intercept	0.018	−0.009
Correlation coefficient	0.982	0.989
Detection limit (% w/w)	0.25	1.16
s_r (%)	2.5	4.0

detection limit, defined as the concentration that produces a peak height two times that of the background noise, was 0.25 and 1.16% (w/w) for the 1553 and 1593 cm^{-1} bands respectively. The precision (repeatability) of the Raman spectral measurements (noise) was determined as the standard deviation (s) for four independent determinations of each standard solution at the concentration levels of 1.30, 2.61, 3.92, 5.23, 6.54 and 7.84% (w/w). The values of this parameter are represented as error bars on the intensities in Figs. 5 and 6, and the mean values of the relative standard deviations (s_r) were found to be about 2.5 and 4.0%.

3.3. Applications to nucleotide mixtures

As inosine nucleoside is present in ribonucleic acids, a detailed study of interference effects was carried out with respect to nucleosides constituting these nucleic acids. As Fig. 7 shows, the inosine nucleotide Raman band at 1553 cm^{-1} is well separated from the adenosine and cytidine nucleotide bands near 1578 and 1529 cm^{-1}, respectively. There can be, however, a very small overlapping between the 1553 cm^{-1} inosine nucleotide Raman band and the 1575 cm^{-1} one originated by guanosine nucleotides. Therefore,

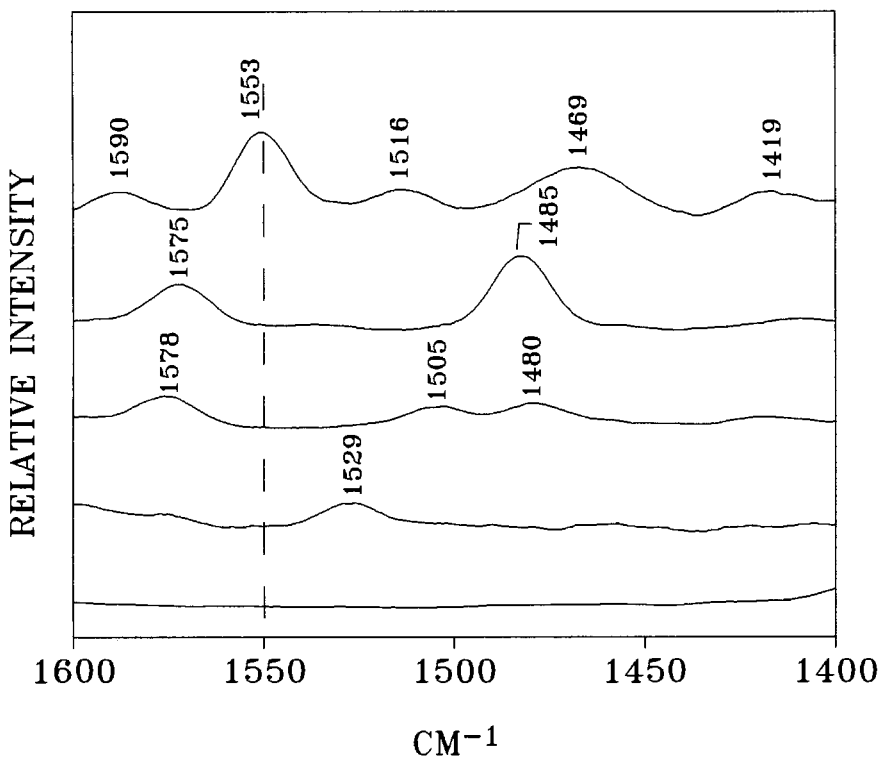

Fig. 7. Raman spectra of aqueous solutions (30% w/w) of mononucleotides: (From top to bottom) inosine 5′-monophosphate, potassium salt; guanosine 5′-monophosphate, sodium salt; adenosine 5′-monophosphate, sodium salt; cytidine 5′-monophosphate, sodium salt; and uridine 5′-monophosphate, sodium salt.

we have studied the influence of guanosine 5′-monophoshate (GMP) by preparing aqueous solutions of 0.01 M inosine 5′-monophoshate (IMP) and by increasing the concentration of the GMP potential interferent to give an error of $\pm 3\%$ in the analytical Raman inosine signal at 1553 cm^{-1}. The maximum tolerance ratio, expressed as the maximum GMP/IMP molar ratio tested, was found to be 25. Therefore, the selectivity of the method is good and permits the sensitive determination of inosine nucleoside, either in real samples of mononucleotide mixtures resulting from a previous hydrolysis of transfer ribonucleic acids or in these ribonucleic acids themselves, where the GMP/IMP molar ratio is not as high as 25. A preconcentration of biological samples is needed, for sensitivity reasons of this Raman technique, so that the inosine nucleotide concentrations fall in the above range. The sensitivity, however, can be significantly improved with multichannel detectors.

In conclusion, on the basis of measurements from the Raman spectra for aqueous solutions of alkaline and alkaline-earth metal salts of inosine 5′-monophosphoric acid, the 1553 and 1593 cm^{-1} Raman bands appear to be characteristic of inosine nucleoside and well separated from those of standard nucleobases. As these bands are generated by six-membered ring vibrations and cation binding occurs at the imidazolic N(7) position, these bands are not influenced by cations in biological medium where alkaline and alkaline-earth ions are present in proportions higher than 98%. Determinations of inosine were performed in standard solutions of the above mononucleotide. It was found that inosine concentrations can be calculated from the Raman spectra with an average relative error of about 3%, and such determinations were also found to be feasible for solutions in which the concentrations are in the range 2.5–80 mg ml^{-1} and 11.5–80 mg ml^{-1} using the 1553 and 1593 cm^{-1} bands, respectively. As these bands are not present in the spectra of the standard nucleobases, the above method can be applied for the quantitative determination of inosine in transfer ribonucleic acids.

Acknowledgements

We are grateful to the Dirección General de Investigación Científica y Técnica (DGICYT) for financial support (Project PB93-0131).

References

[1] W. Saenger, Principles of Nucleic Acid Structure, Springer, New York, 1984, p. 178.
[2] P. Carmona, R. Escobar, M. Molina, A. Rodríguez-Casado, J. Raman Spectrosc. 27 (1996) 817.
[3] J. Duguid, V.A. Bloomfield, J. Benevides, G.J. Thomas Jr., Biophys. J. 65 (1993) 1916.
[4] C. Zimmer, G. Luck, H. Triebel, Biopolymers 13 (1974) 425.
[5] D.E. Dix, D.B. Strauss, Arch. Biochem. Biophys. 152 (1972) 299.
[6] T.M. Jovin, D.M. Soumpasis, L.P. McIntosh, Annu. Rev. Phys. Chem. 38 (1987) 521.
[7] A. Woisard, G.V. Fazakerley, W. Guschlbauer, J. Biomol. Struct. Dyn. 2 (1985) 1205.
[8] M. Langlais, H.A. Tajmir-Riahi, R. Savoie, Biopolymers 30 (1990) 743.
[9] H.A. Tajmir-Riahi, M. Langlais, R. Savoie, Nucleic Acids Res. 16 (1988) 751.
[10] S.D. Kennedy, R.G. Bryant, Biophys. J. 50 (1986) 669.
[11] R.C. Lord, G.J. Thomas, Spectrochim. Acta 23A (1967) 2551.
[12] J.M. Delabar, W. Guschlbauer, Biopolymers 18 (1979) 2073.
[13] H.A. Tajmir-Riahi, T. Theophanides, Can. J. Chem. 63 (1985) 2065.
[14] H.A. Tajmir-Riahi, Biochim. Biophys. Acta 1009 (1989) 168.

ELSEVIER

Talanta 48 (1999) 781–794

Talanta

Chemometric analysis of skeletal data from non-fused and non-π-complexed pentafulvenes[1]

Xavier Tomas [a], José Manuel Andrade [b,*], Angel Alvarez-Larena [c]

[a] *Department of Chemometrics, Institut Químic de Sarriá, Universitat Ramón Llull, Vía Augusta 390, E-08017 Barcelona, Spain*
[b] *Department Analytical Chemistry, University of La Coruña, A Zapateira s/n, E-15071 La Coruña, Spain*
[c] *Unidad de Cristalografía, Universidad Autónoma de Barcelona, E-08193, Bellaterra, Barcelona, Spain*

Received 5 June 1997; received in revised form 8 August 1997; accepted 11 August 1997

Abstract

A broad chemometric study was made on structural data from non-fused and non-π-complexed pentafulvenes obtained both from the Cambridge structural database (CSD) and from several studies to synthesise new fulvene compounds. Three main differentiated pentafulvene groups can be established considering bond distances extracted from the CSD database. Structural data for the new 1-mono and 1,4-disubstituted 2,3,6-trioxypentafulvenes and 1,4-disubstituted-6-amino-2, 3-dioxypentafulvenes reveal different structural behaviours due to their high functionality. The chemometric techniques employed comprise principal component analysis, cluster analysis, selection of essential variables (Procrustes rotation) and isoprobability curves, all of them giving essentially the same general chemical conclusions.

Keywords: Pentafulvenes; Principal component analysis; Isoprobability curves; Selection of variables

1. Introduction

Pentafulvene is an isomer of benzene but with a very different electronic structure. In particular, its ground state presents a strong polyolefinic character as compared to the aromaticity associated to the benzene ring. The π-conjugation degree in substituted pentafulvenes is markedly dependent on the chemical nature of the substituents. For example, 6-alkyl or 6-arylsubstituted pentafulvenes are polyolefinic whereas 6-aminosubstituted pentafulvenes have a partial cyclic electronic delocalisation. Because of this, pentafulvenes have been studied from a theoretical point of view. On the other hand, these compounds have been widely used in the synthesis of unsaturated polyciclic systems and organometallics. Recently, the non-linear optical properties of some of them have been analysed.

Besides the importance of the study of the fulvenic skeleton to gain knowledge on its electronic distribution and, so, on its chemical reactivity and some other properties, there are not

* Corresponding author. Tel.: +34 81167000; fax: +34 81167065; e-mail: andrade@udc.es

[1] Part of this work was previously presented as an Invited Lecture (JMA) at the 5th. Symposium on Analytical Sciences, Nice, June 2–4, 1997.

0039-9140/99/$ - see front matter
PII S0039-9140(98)00095-2

many works covering the fulvene structural (geometrical) data [1]. This situation is, indeed, in contradiction with the important works related with either its synthesis and reactivity data [2–7].

Consequently, in the present paper we made use of one previous, exhaustive bibliographical compilation [8] to get data for non-fused pentafulvene structures providing they were obtained using diffraction techniques. The Cambridge structural database (CSD database)—version 5.09, April 1995—was considered with great detail [8].

A first search was made considering connectivity, i.e. searching for structures containing the core pentafulvene structure as it is plotted with alternated single and double bonds. Several restrictions had to be taken in order to avoid fused fulvenes (e.g. benzofulvenes or pentalenes). Fulvenes belonging to π-complexes were also discarded. A second additional search was to look for one ring formed by five atoms of carbon showing sp^2 hybridisation and which is linked to another sp^2 atom of carbon. Several substituted cyclopentadiene molecules containing fulvenic structures were found.

Unfortunately, not all the structures we have found were described with enough quality to include them in a statistical study of their geometric parameters. Here, only those structures attaining several prerequisites: the (average) intensities should have been measured using a difractometric analysis and with a good fitting index, $R(F) \leq 0.075$, as well as showing good precision on the bond distances ($\sigma_{C-C} < 0.01$ Å). The 35 structures finally considered in this work are summarised in Table 1. Also shown in Table 1 is the pentafulvene skeleton, from which the six bond distances considered through the present work are C1=C2, C3=C4, C5=C6, C2–C3, C1–C5 and C4–C5.

Additionally to the fulvenes obtained in the CSD-database, an additional set of 13 substituted molecules based on the fulvene structure has been considered. All of them where synthesised from 1972 up to now by one working group at the Institut Quimic de Sarria (IQS) facilities [9–14]. They are 1-mono and 1,4-disubstituted 2,3,6-trioxypentafulvenes and 1,4-disubstituted-6-amino-2,3-dioxypentafulvenes (the last 13 structures in Table 1, labelled as IQS). All the detailed structures, raw data and some chemical ideas have been presented in the paper mentioned above [8] and, so, it was decided not to repeat them here.

Without doubt, to relate the electronic properties to the structural data is an important point for establishing (maybe, predict) chemical and physical behaviours. Accordingly, and with the aim of getting a deep insight onto the underlying groups of compounds (different skeletal characteristics), several chemometric techniques were applied. The first stages involved the CSD dataset whereas the last ones where made considering the new substituted pentafulvenes, also. First, a principal component analysis (PCA) was made to determine variable relationships and differences as well as to visualise sample groups (if any). Then, cluster analysis is applied to sharply define the sample subsets and to confirm the PCA conclusions.

After these two studies and once the existing groups have been defined, a natural step forward could be to select the minimum set of original variables which best account for sample differences. Finally, a simplified algorithm to classify new samples into pre-existing groups (namely, isoprobability curves) was used considering the structural data of newly-synthesised substituted pentafulvenes in order to see if their behaviour correspond to some pre-defined type of fulvenes.

2. Multivariate analyses of the Cambridge structural database (CSD)

2.1. Principal component analysis

The CSD data set formed from the searching strategies consisted of 35 samples. Regarding the original variables, two groups of structural characteristics were analysed: bond angles and bond distances, being the results presented here those considering the six bond distances. Previous studies made using the angles data set did not conduct to satisfactory conclusions [8].

Autoscaling was selected as data pretreatment in order to avoid that bond distances with larger variances would obscure the general trends.

Table 1
Summary of the fulvenic structures used in the present studies

Sample #	Origin	Ref. code[a]	Comments
1	CSD	BIFTOZ	Polyolefinic
2	CSD	BPYCPY10	Polyolefinic with some cyclic delocalisation
3	CSD	CBCYIQ10	Polyolefinic with some cyclic delocalisation
4	CSD	CBPYHP	Polyolefinic with some cyclic delocalisation
5	CSD	CLFULV01	Polyolefinic
6	CSD	CPPCPD10	Not clearly defined, polyolefinic
7	CSD	DACNCP	Extended delocalisation
8	CSD	DBNCPD10	Extended delocalisation
9	CSD	DMAFUL	Cyclic delocalisation (π-donors in C6)
10	CSD	FMAFUL10	Extended delocalisation
11	CSD	FULHPF	Polyolefinic
12	CSD	GEZKOL	Polyolefinic with some cyclic delocalisation
13	CSD	HFULCA	Extended delocalisation
14	CSD	JEDAIC	Polyolefinic
15	CSD	JEHHEJ	Polyolefinic with some cyclic delocalisation
16	CSD	JEJDAD	Polyolefinic
17	CSD	JENNIZ	Polyolefinic
18	CSD	KAPBOS	Polyolefinic with some cyclic delocalisation
19	CSD	KEMPAT	Polyolefinic with some cyclic delocalisation
20	CSD	KICYOK	Polyolefinic
21	CSD	KUMRIT	Polyolefinic
22	CSD	LAGLAG	Cyclic delocalisation
23	CSD	MOXCPA	Extended delocalisation
Outlier	CSD	MPYBRA	It has a great electronic delocalisation
24	CSD	NMEFUL	Cyclic delocalisation (π-donors in C6)
25	CSD	PALDIM	Extended delocalisation
26	CSD	QQQACM01	Cyclic delocalisation (π-donors in C6)
27	CSD	SATNIK	Polyolefinic
28	CSD	SENDUK	Polyolefinic with some cyclic delocalisation
29	CSD	VAFREZ	Not clear, cyclic delocalisation
30	CSD	VARYUI	Polyolefinic with some cyclic delocalisation
31	CSD	VARZOD	Polyolefinic with some cyclic delocalisation
32	CSD	VAVHIJ	Polyolefinic
33	CSD	VAXWUM	Polyolefinic
34	CSD	VERSIU	Polyolefinic
35	IQS	FEC-MAN	Cyclic delocalisation
36	IQS	FEE-AN	Cyclic delocalisation
37	IQS	FEE-COA	Cyclic delocalisation
38	IQS	FEE-MA	Cyclic delocalisation
39	IQS	FEE-SBA	Cyclic delocalisation
40	IQS	MMFEE-MAN	Cyclic delocalisation
41	IQS	MMFEE-DAN	Cyclic delocalisation
42	IQS	MMFEE-MA	Cyclic delocalisation
43	IQS	FEE	Polyolefinic
44	IQS	MFEE	Polyolefinic
45	IQS	MACF-M	Polyolefinic
46	IQS	MAFE	Polyolefinic
47	IQS	MMFC-M	Polyolefinic

Codification of the bond distances for the fulvene structures

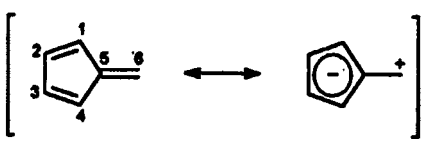

The column labelled 'Comments' summarises the main chemical behaviour.
(+) Synthesised at the IQS-facilities.
[a] CSD reference code.

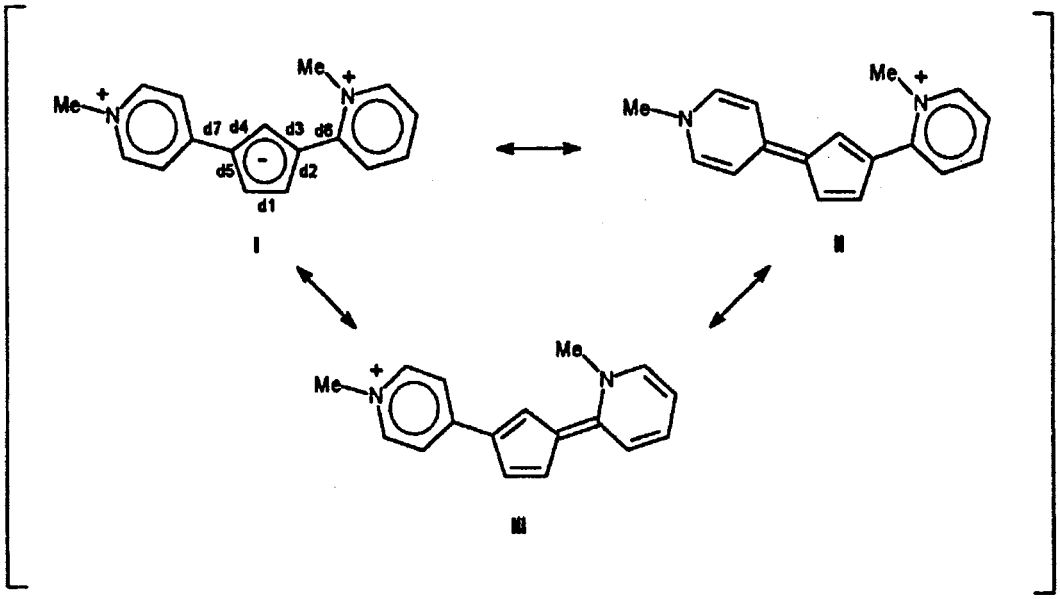

Fig. 1. Distinctive electronic delocalisation proposed for MPYBRA (the outlying sample for the CSD dataset).

After one previous study, sample # 24-named MPYBRA-presented quite high score figures when plotted against all the remaining samples and, so, it was considered to be an outlier; it was discarded and the PCA was repeated. MPYBRA's outlying behaviour reveals that its structure must be quite different from the other ones. Therefore, a distinctive ring electronic delocalisation has to be proposed given rise to three canonical forms that can be considered for understanding this structure and its behaviour (Fig. 1).

Table 2 presents the unrotated loadings derived from the final PCA. It can be observed that PC1 is strongly related to the overall six variables though an interesting pattern should be noted.

Table 2
Unrotated loading factors for the CSD database (after excluding MPYBRA)

Variable (code)	PC1	PC2	PC3
C1=C2 (B4)	0.866	0.329	−0.170
C3=C4 (B6)	0.895	0.247	−0.249
C5=C6 (B3)	0.921	0.015	−0.088
C2—C3 (B5)	−0.835	0.133	−0.503
C1—C5 (B1)	−0.577	0.778	0.229
C4—C5 (B2)	−0.927	−0.043	−0.176
Explained variance (%)	71.49	13.25	7.25

Double bonds (vars. B3, B4 and B6) load positive weights, whereas single bonds (vars. B1, B2 and B5) load negative values. Clearly, there is an opposition between single versus double bonds (Fig. 2).

The second PC is mainly related to B1 (C1–C5 bond) which revealed that this bond had a different particular variation as it was confirmed when the original data was studied.

PC3 is related to the C5=C6 bond, revealing that it has a special variability we should account for (Fig. 2) and that it can represent the molecules with extended delocalisation.

Fig. 3 shows a very interesting pattern when scores are plotted. There is a distinct group (marked with cube icons) grouping all the samples whose chemical behaviour can be defined as most similar to the non-substituted fulvene, i.e. like polyolefinic structures. Sample # 6, namely CP-PCPD10, is a bit far from the main group. This compound shows a clear bond alternation but with smaller single- double bond length differences. This fact implies a greater contribution of the polar canonical forms in the structure description (Fig. 4) although it has to be maintained in the 'polyolefinic' group.

The 'polyolefinic group' is formed also by BIFTOZ, CLFULV01, FULHPF, GEZKOL,

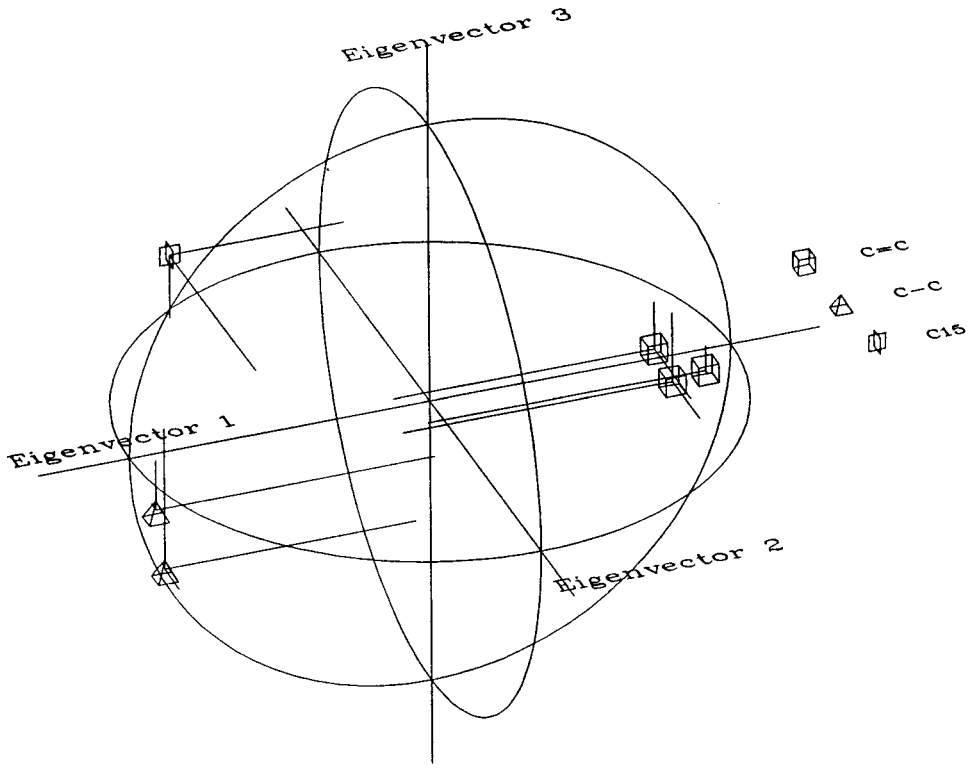

Fig. 2. Loading distribution in the PC1–PC2–PC3 subspace for the six original variables.

JEDAIC, JEHHEJ, JEJDAD, JENNIZ, KAPBOS, KEMPAT, KICYOK, KUMRIT, SATNIC, SENDUÑ, VARYUI, VARZOD, VAVHIJ, VAXWUM and VERSIU. Some score ranges can be imposed for this group: PC1 ranges from 0 to -2; PC2, from -1.5 to 1.25 and PC3 from -1 to 1.5.

The second group (cone icons, Fig. 3) is formed by BPYCPY10, CBCYIQ10, CBPYHP, DMAFUL, LAGLAG, NMEFUL, QQQACM01, VAFREZ and, eventually, FMAFUL10. They have slightly different structural characteristics although the main point in common is that all of them exhibit some cyclic delocalisation. Therefore, we might call this group 'cyclic conjugation'.

Sample # 10, FMAFUL10, seems to be rather different from its 'partners' and further comments can be presented. It possesses geometric characteristics close to the samples forming the third group (explained below) except that the two substituents in C1 and C6 imply a certain degree of molecular asymmetry and, consequently, resulting in larger bond distances (getting close similarity to the second group). This sample is not definitely assigned to one group into the PCA subspace lying between cyclic delocalisation and extended delocalisation. We think it would be better classified into the former group.

The score values for the cyclic group are: PC1 ranges from 0.75 to 2; PC2, from 0.4 to 1.5 and PC3, from 0 to 1.5.

The third group of the CSD samples comprises DACNCP, DBNCPD10, HFULCA, MOXCPA and PALDIM. All of them have characteristics of π-delocalisation in the carbon atom C6. In these compounds, an extended conjugation is also present but it is not cyclic. All five present hydrogen bonds, either symmetrical (DACNCP and DBNCPD10) or asymmetrical (PALDIM, MOXCPA, HFULCA). The scores intervals are: PC1, from 1.25 to 2.5; PC2, from 0 to -2.5 and PC3, from 0 to -0.5.

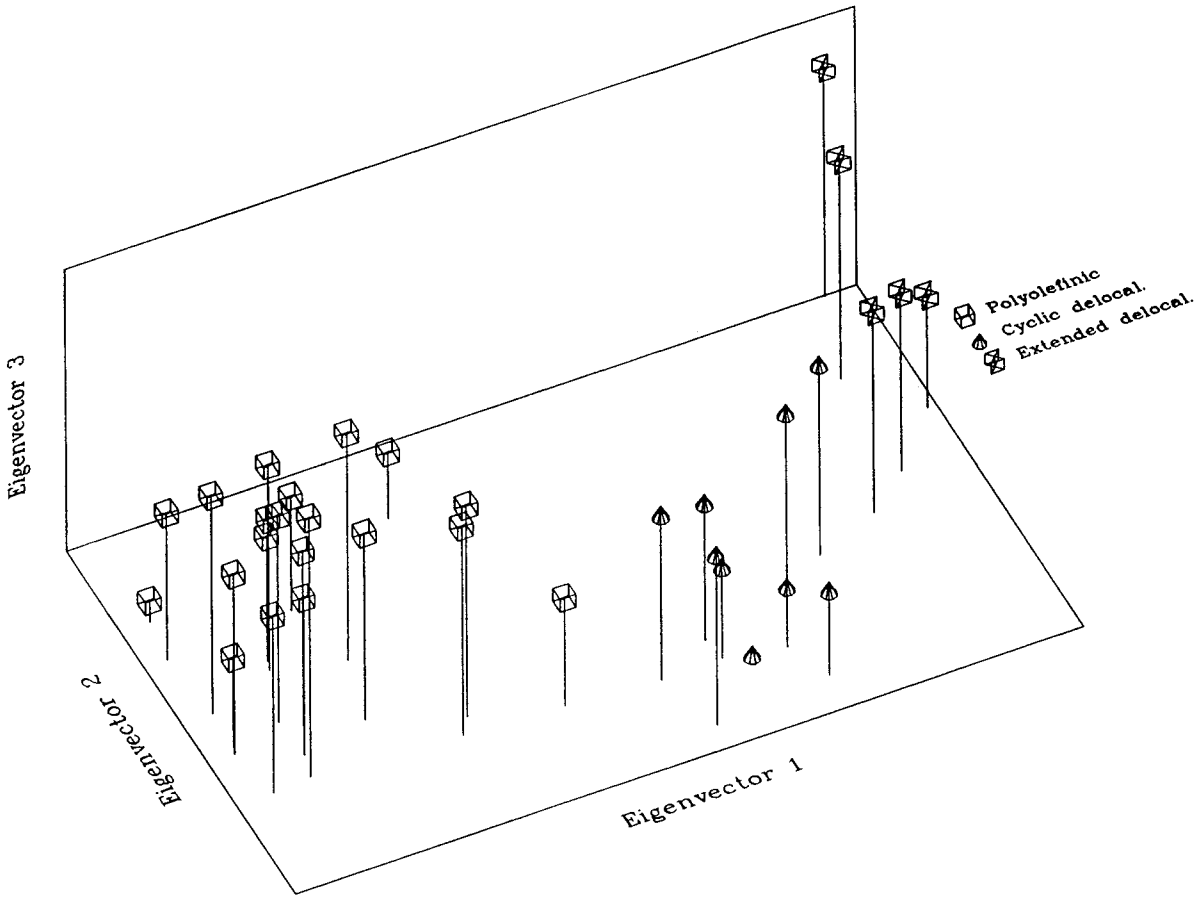

Fig. 3. Scoreplot for the CSD dataset where the three main groups of fulvenes are fairly well characterised.

The main difficulty when studying the three groups is that samples # 10 (FMAFUL10) and # 26 (QQQACM01) are too close to the expanded delocalisation group. This is not so strange as discussed above for FMAFUL10 and because QQQACM01 presents a rather important wringing (34°) and an exocyclic bond enlargement. Therefore, samples # 10 and # 26 are hard to classify following a single chemometric criterion. According to the chemical structures and taking into account all the considerations we have presented, we decided to include both of them in the cyclic delocalisation group since it comprises several slightly different types of molecules.

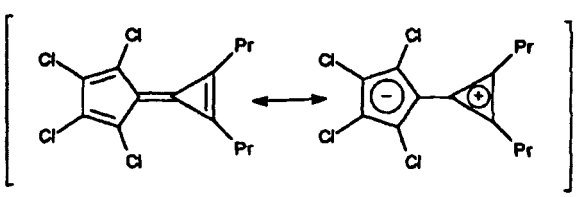

Fig. 4. Proposed structure for CPPCPD10 (CSD sample # 6) which has an intermediate behaviour from the polyolefins and the cyclic delocalisation.

2.2. Cluster analysis

Cluster analysis was used as a way to confirm the three groups of the CSD data. Fig. 5 depicts the dendrogram obtained using the Euclidean distance as a measure of similarity (autoscaling the original data matrix) and the average linkage method as the clustering method. Essentially identical results were obtained using the first score

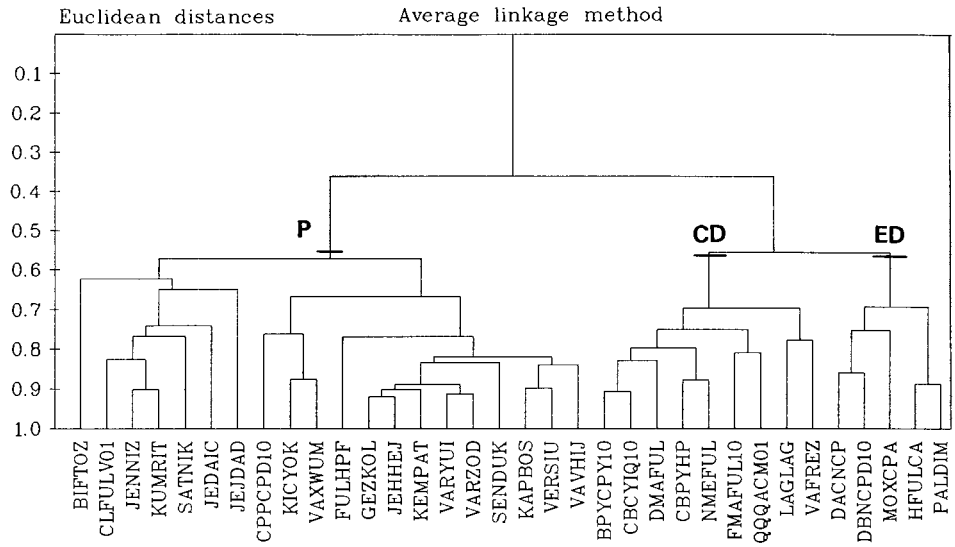

Fig. 5. Cluster analysis for the CSD dataset: P, polyolefinic; CD, cyclic delocalisation; ED, extended delocalisation.

coordinates as variables or when using the k-means algorithm (dendrograms not presented here).

The dendrogram depicts a clear differentiation between the polyolefinic samples (cluster P) and all the remaining samples suffering from electronic delocalisation. Cluster P reveals that some samples showing a 'typical polyolefinic behaviour' (from BIFTOZ to JEJDAD) are slightly different from the other ones where some cyclic delocalisation can be observed (from CPPCPD10 to VAVHIJ). Unfortunately, such differentiation is not sharp since VAXWUM, VAVHIJ and VERSIU (a priori typical of the polyolefinic behaviour) have been inserted onto the subgroup on the right side. Clearly, sample #6 (CPPCPD10) belongs to the polyolefinic cluster, as the score plot suggested.

Cluster CD (cyclic delocalisation) confirms that QQQACM01 and FMAFUL10 were correctly evaluated when explaining the PCA-scores and it comprises all the samples belonging to this class.

Cluster ED (extended delocalisation) groups all the samples with a clear extended delocalisation behaviour.

2.3. Selection of the most significant variables

After identifying several groups of samples, a 'natural' step forward could be to concentrate only on those variables which better differentiate such groups. Without doubt, as chemists, we are more interested in working with original variables rather than with abstract variables as, e.g. principal components. One of the most powerful techniques to carry out this task is Procrustes rotation, which was already used to deal with industrial [15] and environmental data [16]. It could be briefly summarised as a technique that excludes original variables on the grounds of redundancy. Each variable is deleted in turn, a new principal component subspace is recalculated and compared with the original one by means of translation, rotation and stretching and residuals are summed up. The variable giving the less amount of residuals is the less influential one and can be discarded. The process is repeated until q variables are kept (q equals the optimum number of PCs). In this work no spectacular results should be expected since there are only six initial variables to deal with, better benefits would be obtained if more variables were to be considered in other works.

Three components were considered for descriptive purposes in the previous studies (Table 2) and, moreover, it was also found that this same

Table 3
Prediction of the IQS-fulvenes behaviour using isoprobability curves after modelling with the CSD structural database, % of probability for each sample and type

IQS-Sample	'a priori' type	Class prediction		
		Extended delocalisation	Cyclic delocalisation	Polyolefinic
1	Cyclic delocalisation	0.00	14.72	0.38
2	Cyclic delocalisation	0.00	0.00	0.38
3	Cyclic delocalisation	0.00	0.30	0.01
4	Cyclic delocalisation	0.00	0.99	0.00
5	Cyclic delocalisation	0.00	1.31	0.00
6	Cyclic delocalisation	0.00	23.77	0.02
7	Cyclic delocalisation	2.06	11.64	0.00
8	Cyclic delocalisation	0.91	20.29	0.00
9	Polyolefinic	0.00	0.07	0.96
10	Polyolefinic	0.00	0.00	3.84
11	Polyolefinic	0.00	0.00	38.16
12	Polyolefinic	0.00	0.00	16.15
13	Polyolefinic	0.00	0.00	16.15

number should be chosen as the optimal number of factors to search for the minimum subset of 'essential variables' characterising this particular data set. This fact could be fairly well anticipated because three components are just good enough to describe our system. One note of caution has to be drawn here since descriptive purposes (e.g. see groups) are significantly different from 'predictive' objectives we will consider in next sections (e.g. discriminate and differentiate groups). Both points of view constitute two rather different objectives [17].

Accordingly, taking three principal components and applying the algorithms depicted above for Procrustes rotation, three variables were retained, namely B6 (C3=C4), B5 (C2–C3) and B1 (C1–C5). Each variable represents one of the three groups of variables described above for the PCA (see Fig. 2, loading plot). Nevertheless, using either Fig. 2 or Table 3 to select the 'best subset' of original variables is not a simple task, indeed. These three variables clearly characterise the fulvene structure: B6 characterises the C=C bonds; B5, the single ones and B3, the exocyclic delocalisation. It seems logical that variable B1 needs to be retained in spite of being B5 (C2–C3 bond) representative of the single bonds due to the particular C1–C5 behaviour, which do not follows the same structural pattern as the other single bonds.

Fig. 6 shows the sample subspace before and after variable selection. Clearly, the three selected variables account for the most important information since, again, three well-defined groups are seen, being totally coincident with the beforehand discussed ones. All groups are rather well defined and even sample #6 (mentioned when discussing PCA) was correctly grouped according with our criterion. Only sample #10 (FMAFUL10) and #26 (QQQACM01) seem to be misclassified because they are included in group 3 (extended delocalisation). Nevertheless, remember that FMAFUL10 and QQQACM01 (to a lesser extent) have an intermediate chemical behaviour and can not be definitely included in any of the two classes.

3. Multivariate classification of the pentasubstituted IQS-synthesised fulvenes using all the variables

3.1. Principal component analysis

One of the simplest ways to elucidate if the IQS-fulvenes have similar characteristics than the

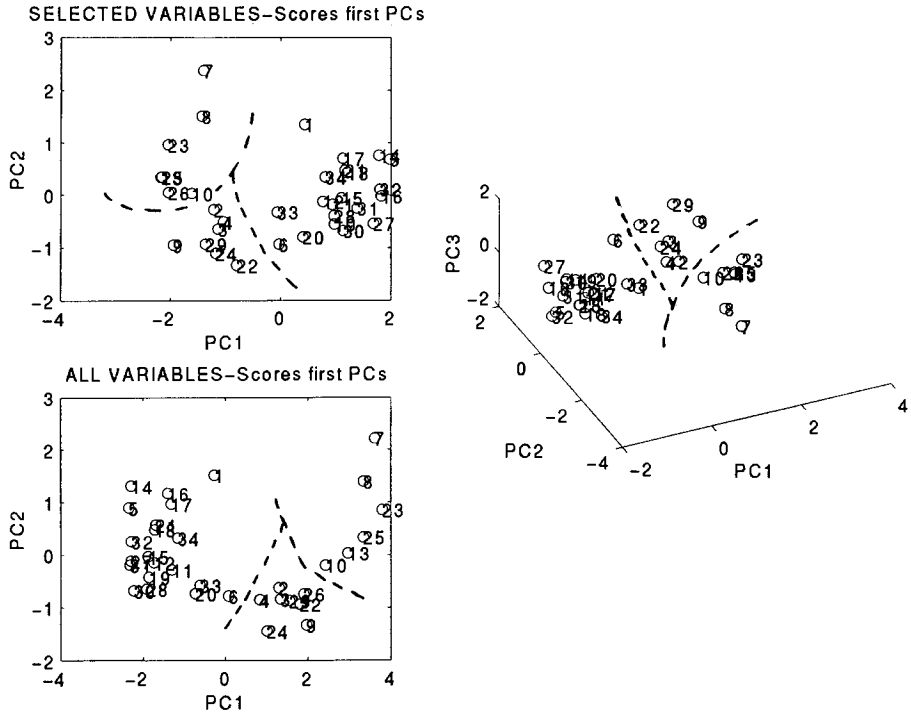

Fig. 6. Plot of the PC1-PC2 score subspace before and after variable selection. The 3-dimensional drawing corresponds to the PCA of the reduced dataset (compare with Fig. 3).

CSD-database ones is to repeat the PCA study and project the IQS-samples onto the CSD factorial space. Therefore, Fig. 7 depicts how the IQS-samples become distributed in the original CSD PC1-PC2 subspace. None of them gets included in the extended delocalisation group of the CSD-samples, which is consistent with their structures.

IQS-samples # 1–8 are 1,4-disubstituted-6-amino-2,3-dioxypentafulvenes, all of them having a significant cyclic electronic delocalisation and, thus, they are correctly classified. IQS-samples # 9 and 10 (FEE and MFEE) are chemically very similar though they are assigned to two different groups. In principle, they should be considered as polyolefinics, which is obtained for MFEE but not for FEE which, in turns, is placed close to the cyclic delocalisation group. The rest of the samples (# 11–13, tetrasubstituted fulvenes) are considered as of the polyolefinic type. Note how the IQS-samples occupy an intermediate zone between the polyolefinic and the cyclic delocalisation behaviours which was not present in the CSD dataset. This sounds reasonable because the IQS-samples are much more branched that the CSD ones, some of them exhibiting a push-pull system which brakes the cyclic delocalisation towards a no-cyclic delocalisation.

3.2. Cluster analysis

One straightforward method to classify new samples consists on merging data from both the CSD database and from the new synthesised samples and repeating the cluster analysis. Fig. 8 gives the following results (autoscaled data, euclidean distance, average linkage):

(1) no IQS-pentasubstituted fulvene was included into the extended delocalisation group (cluster ED), as expected since the presence of a donor group at C6 generates some cyclic delocali-

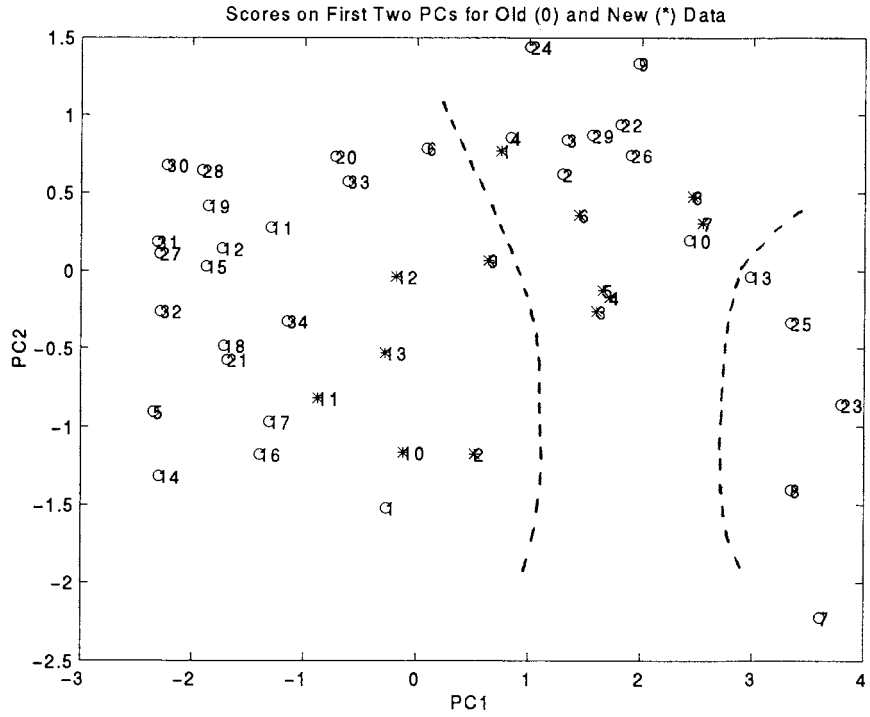

Fig. 7. IQS samples (*) projected onto the CSD sample score subspace (○).

sation, mainly when the donor groups directly linked to the ring concentrate the electronic charge in it.

(2) FEE-AN, FEE-COA, FEE-MA, FEE-SBA, MMFEE-MAN, MMFEE-DAN, MMFEE-MA (all of them 1,4-disubstituted-6-amino-2,3-dioxypentafulvene) are correctly enclosed in cluster CD (cyclic delocalisation) which is consistent with their bond distances.

(3) FEE and MFEE (1,4-disubstituted 2,3,6-trioxypentafulvenes), MAFC-M, MAFE and MMFC-M (all three 1-monosubstituted 2-3-6-trioxypentafulvenes) are considered as having a polyolefinic behaviour (cluster P). This classification is correct for all these molecules, particularly for the three last ones thanks to their exocyclic bond lenght (typically olefinic) and to the C1–C5 bond length. Also the C1=C2 distance is quite similar to the polyolefinic-type fulvenes considered from the CSD database.

The polyolefinic characteristics are not clear for FEC-MAN which, a priori, should be considered into the cyclic delocalisation group. The main reason for this wrong classification might be that when a PCA is made this sample lies rather close to the polyolefinic group; nevertheless, a clear reason was not found and it was simply considered as a misclassification of the clustering method.

3.3. Classification using isoprobability curves

The main idea behind the mathematical treatment involved into the isoprobability curves could be exemplified using the following analogy. Let us suppose one working area (e.g. a plane) where several groups of objects are distributed according with their cartesian coordinates, namely X, Y. Then, a new object whose coordinates are X', Y' will be assigned to the group to which most closely relais. Class-modelling techniques make a mathematical description of each class, independently from other classes.

The discriminant frontiers from class-modelling models have been assigned to different probability (density) functions like the triangular, rectangular

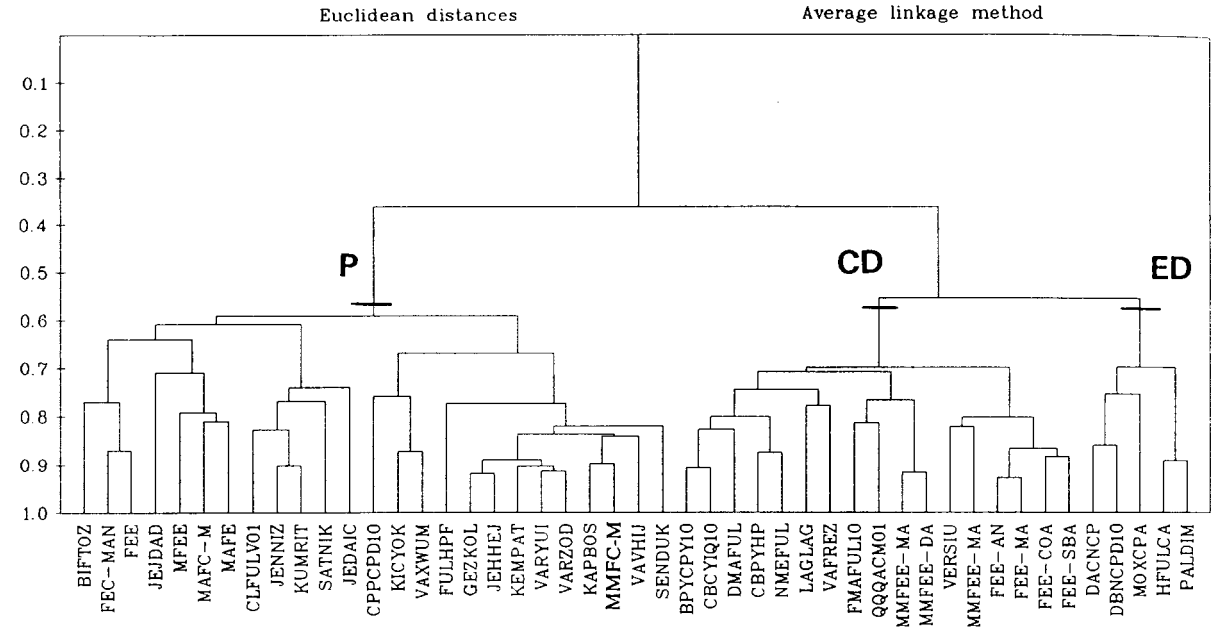

Fig. 8. Cluster analysis made after merging the CSD and IQS samples: P, polyolefinic; CD, cyclic delocalisation; ED, extended delocalisation.

or Gaussian distributions. Generally, the probability function (density function or potential curve) for any given group of samples has been obtained as the sum of each of the density functions associated to each sample from the group. This fact would imply that each sample has to be measured several times to estimate its mean and standard deviation. For obvious reasons, this is not always practical. An alternative could be to grossly estimate the probability function for each sample group.

The main hypothesis assumed by our simplified model is that samples from each group are homogeneously distributed into the PC1–PC2 space and that they can be separated by potential functions (isoprobability functions). In this work, isoprobability functions will follow a bivariate Gaussian distribution. If new samples are to be classified, they have to be projected onto the initial PC1–PC2 space; several constants recalculated and, after that, the samples will be assigned to the groups based upon each of the calculated probabilities. This approach is a natural simplification of the equivalent determinant method from Forina et al. [18,19] and it is quite similar to the conceptual ideas of the well known SIMCA class-modelling technique [20].

Therefore, the first two PCs are used to calculate isoprobability curves for each of the three CSD-groups and, then, to assign each IQS-sample to any of them according with the probability of belongingness. The results are summarised in Table 3 and show an excellent global prediction excepting, again, for sample #2 (FEE-AN). Without doubt, the usage of this simplified mode of potential curves allows an objective classification for the IQS-samples resulting in better performance than the rather subjective PCA-score visualisation or the cluster analysis, which is generally more difficult to interpret.

The unique mismatch arose just in the sample where several comments were made both in the PCA and cluster analysis, i.e. for the IQS-sample #2 (FEE-AN) which lies in a half way between the polyolefinic and the cyclic delocalisation groups. Overall, the probability assigned to this sample to belong to the polyolefinic group is rather low and it can be suspected that this

unique sample could be considered as a new group (i.e. a new intermediate chemical behaviour). Something similar can be viewed for sample #9 although in this case, a positive classification was achieved.

4. Multivariate classification of the pentasubstituted IQS-fulvenes using only the three selected variables

All the studies presented thereafter were made after B6 (C3=C4), B5 (C2–C3) and B1 (C1–C5) were found to be the three essential variables to characterise our system.

4.1. Principal components

Only the three mentioned variables were considered to perform a new PCA study on the CSD-dataset and, then, to project the IQS-data onto the PC1–PC2 subspace. It can be seen in Fig. 9 that the differentiation between the expanded and cyclic delocalisation is not so obvious as before (Fig. 3). The main reason is that each retained original variable is associated to one unique PC (which of course is coherent with their significance, as explained in the PCA study considering all the variables). So, any further reduction of dimensionality will worsen the discrimination between all the groups. Hence, the best frontiers are to be seen on the PC1-PC2-PC3 space (and using the reduce dataset Fig. 6). Despite this, the three groups can already be distinguished without great difficulties.

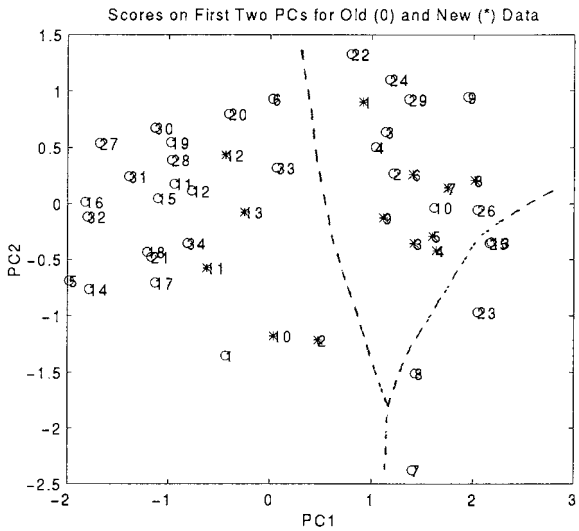

Fig. 9. IQS samples (*) projected onto the CSD-sample score subspace (○) after variable selection.

Table 4
Prediction of the IQS-fulvenes behaviour using isoprobability curves after modelling the CSD structural database with only three original variables (see text), % of probability for each sample and type

IQS-sample	'a priori' type	Class prediction		
		Extended delocalisation	Cyclic delocalisation	Polyolefinic
1	Cyclic delocalisation	0.00	55.77	0.27
2	Cyclic delocalisation	0.00	0.00	0.03
3	Cyclic delocalisation	0.00	8.19	0.00
4	Cyclic delocalisation	0.28	9.38	0.00
5	Cyclic delocalisation	0.02	16.19	0.00
6	Cyclic delocalisation	0.00	72.04	0.00
7	Cyclic delocalisation	0.00	55.00	0.00
8	Cyclic delocalisation	1.02	30.23	0.00
9	Polyolefinic	0.00	8.88	0.03
10	Polyolefinic	0.00	0.00	0.46
11	Polyolefinic	0.00	0.00	33.86
12	Polyolefinic	0.00	0.00	50.77
13	Polyolefinic	0.00	0.00	31.31

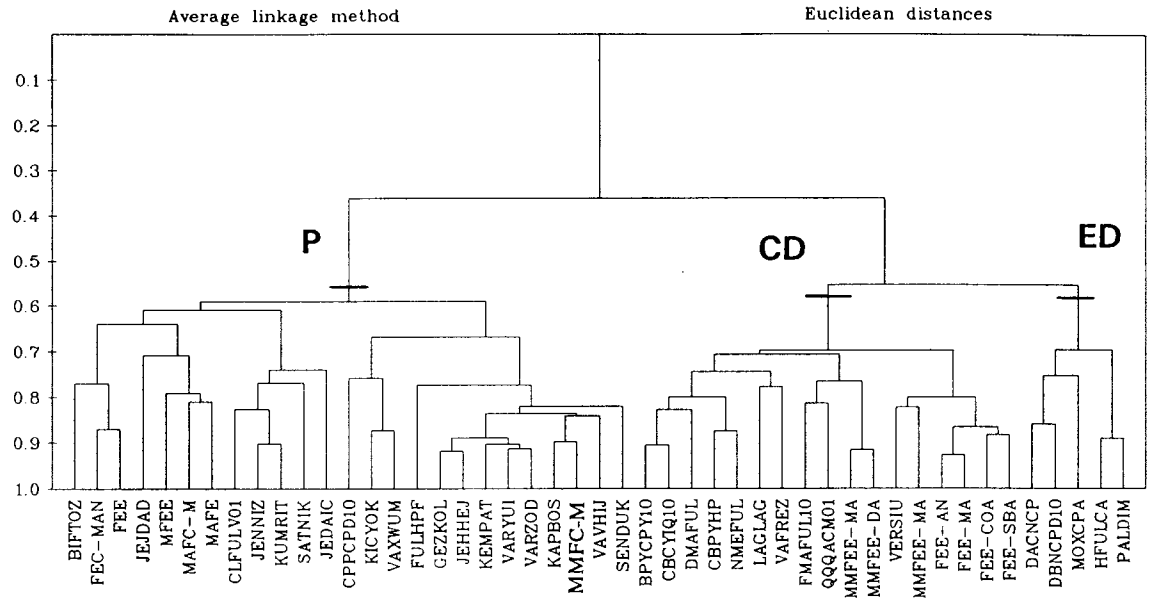

Fig. 10. Cluster analysis made after variable selection and combining the CSD and IQS samples: P, polyolefinic; CD, cyclic delocalisation; ED, extended delocalisation.

4.2. Cluster analysis

Fig. 10 reveals that applying the Euclidean distance and the average linkage over the reduced dataset exactly the same dendrogram as in Fig. 8 is obtained. This result is definitely more positive that the PCA-scores projection where the expanded and cyclic delocalisation became rather close each other.

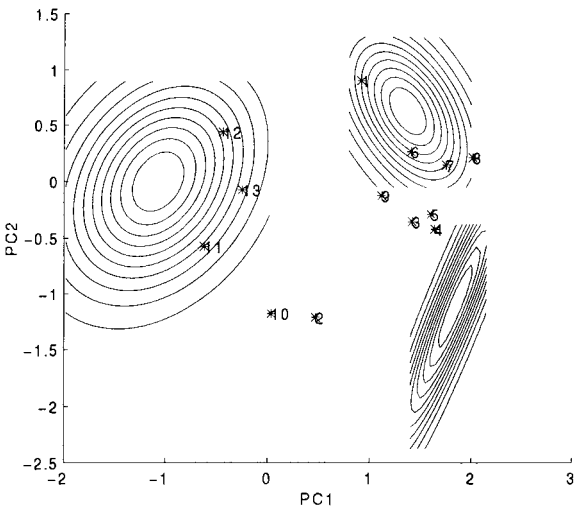

Fig. 11. Isoprobability ellipses found after variable selection for the CSD dataset. Also projected on them are the IQS samples.

4.3. Isoprobability curves

Using the same three variables as above and our simplified mode of isoprobability curves, a satisfactory classification rate was obtained. The predictions are shown on Table 4. The two 'conflicting' samples # 2 and 9, namely, FEE-AN and FEE were wrongly predicted which seems to be a constant behaviour for sample # 2. On the contrary, sample # 9 is misclassified when only three variables are considered. Nevertheless, its percentage of probability of belongliness to the cyclic delocalisation (8.88 considering the three variables) is not much bigger as its counterpart for pertaining to the olefinic group (0.96 considering all the variables). As it was suggested before, the IQS-sample # 9 seems to be a very particular one, maybe defining its own class.

All the remaining samples are correctly classified and Fig. 11 represents the isoprobability ellipses found for the reduced dataset projected onto the PC1-PC2 space where they are defined as well as the predicted IQS-samples.

5. Conclusions

Three main classes of fulvenes were found after consideration of the skeletal data of 35 samples (bibliographical searches) and 13 newly synthesised ones (testing group). Different chemometric techniques were used and it was verified that when Procrustes rotation is applied to select the minimum subset of original variables to deal with, a good classification rate is maintained. Therefore, the bond distances B6 (C3=C4), B5 (C2–C3) and B1 (C1–C5) appear to be the three essential variables to characterise the fulvene structures. Also, our simplified method of isoprobability curves is very effective in assigning new fulvene structures to each of the three main groups: parafinic, extended delocalisation and cyclic delocalisation. When the reduced data set is used to repeat the PCA, cluster and isoprobability studies, there are some misclassifications which might be attributed to the intermediate chemical behaviour of some substituted pentafulvenes.

Acknowledgements

JMA acknowledges a grant from the Vicerrectorado de Investigación, University of A Coruña partially supporting this work.

References

[1] H.L. Ammon, G.L. Wheeler, J. Am. Chem. Soc. 97 (1975) 2326–2336.
[2] T. Asao, G. Becker, H. Blaschke, H. Kolshom, H.J. Lidler, M. Oda, M. Saverbier, G. Use, K.P. Zeller, Carbocyclische π-elektronen-systeme, in: Houben-Weyl (Eds.), Methoden der Organischen Chemie, Vol 5/2c, G.T. Verlag, Germany, 1985, pp. 494–793.
[3] K. Hafner, K.H. Häfner, C. König, M. Kreuder, G. Ploss, G. Schultz, E. Sturm, K.H. Vöpel, Angwe. Chem. Int. Ed. Engl. 2 (1963) 123–134.
[4] P. Yates, Adv. Alicyclic Chem. 2 (1968) 59–68.
[5] E.D. Bergmann, Chem. Rev. 68 (1968) 41–76.
[6] D. Lloyd, Non-Benzenoid Conjugated Carbocyclic Compounds, Elsevier, Amsterdam, 1984, pp. 43–48.
[7] A.P. Scott, I. Agranat, P.U. Biedermann, N.V. Riggs, L. Radom, J. Org. Chem. 62 (7) (1997) 2026–2038.
[8] A. Alvarez–Larena, G. Andreu, J.F. Piniella, X. Tomás, Afinidad 52 (1995) 297–312.
[9] E. Barberá. Doctoral Thesis, Institut Quimic de Sarria, Barcelona, Spain, 1978.
[10] P. Victory, A. Alvarez-Larena, E. Barberá, X. Batllori, J.L. Borrell, C. Córdoba, J. Chem. Res. S (1989) 88; J. Chem. Res. M (1989) 631–674.
[11] P. Victory, A. Alvarez-Larena, C. Beti, X. Batllori, J.L. Borrell, C. Córdoba, Chem. Ber. 124 (1991) 207–212.
[12] R. Gompper, T. Gessner, Angew. Chem. Int. Ed. Engl. 24 (1985) 982–984.
[13] P. Victory, A. Alvarez-Larena, J.F. Piniella, G. Germain, E. Soler, M. Muñoz, An. Quim. 91 (1995) 32–41.
[14] P. Victory, A. Alvarez-Larena, X. Batllori, J.L. Borrell, A. Vidal-Ferran, J.F. Piniella, An. Quim. 88 (1992) 499–507.
[15] J.M. Andrade, D. Prada, S. Muniategui, B. Gómez, M. Pan, J. Chemometrics 7 (1993) 427–438.
[16] A. Carlosena, J.M. Andrade, M. Kubista, D. Prada, Anal. Chem. 67 (1995) 2373–2378.
[17] J.M. Andrade, D. Prada, S. Muniategui, B. Gomez, M. Pan, J. Chemometrics 7 (1993) 427–438.
[18] M. Forina, C. Armanino, R. Leardi, G. Drava, J. Chemometrics 5 (1991) 433–453.
[19] X. Tomás, J.M. Andrade, Afinidad 54 (1997) 103–108.
[20] S. Wold, M. Sjöström, SIMCA: A Method for Analysing Chemical Data in Terms of Similarity and Analogy, Chap. 12, in: B.R. Kowalski (Ed.), Chemometrics: Theory and Application ACS Symposium Series No. 52, Washington, 1977, pp. 243–282.

ELSEVIER

Talanta 48 (1999) 795–802

Talanta

Classification of edible vegetables affected by different traffic intensities using potential curves

A. Carlosena [a,*], J.M. Andrade [a], X. Tomas [b], E. Fernandez [a], D. Prada [a]

[a] *Department of Analytical Chemistry, University of La Coruña, Campus da Zapateira s/n, E-15071 La Coruña, Spain*
[b] *Deptartment of Chemometrics, Institut Químic de Sarriá, E-08017 Barcelona, Spain*

Received 05 June 1997; received in revised form 05 August 1997; accepted 07 August 1997

Abstract

Heavy metals in soils have largely been used to evaluate the impact of motorised traffic in the vicinity of motorways. Also in this field of work it is of paramount importance to analyse the vegetables grown in these areas since their consumption is one of the main sources of metal intake by people; not in vain human food is directly or indirectly derived from plants. Accordingly, a set of edible vegetable samples were first analysed and, then, classified employing different multivariate chemometric techniques; among them, SIMCA and a simplified mode of potential curves. The analytical variables were selected after a comprehensive study of roadside soil pollution where Pb, Cd and Cu were found to be the main metallic pollution tracers. Different groups of vegetables were obtained which were explained as a function of both the agricultural conditions (private versus commercial) and the different traffic intensities supported by the cultivated areas.

Keywords: Edible vegetables; Heavy metals; Roadside pollution; Potential curves

1. Introduction

The determination of heavy metals in soils as a way of measuring and monitoring the impact of vehicular traffic in the vicinity of highways, highroads, streets, etc. has largely been satisfactorily used [1–4]. Most of such works focused on measuring heavy metal contents in soils surrounding roadways since they are greatly increased by automobile fuel exhaust, tyres, mechanical friction, wear and tear, etc. [5–7]. Overall, another important focus in this environmental work area should be to establish the quality of the roadside vegetables in terms of heavy metals in the light of recent dietary guidelines which recommend the increasing consumption of vegetables [8]. There are a number of reasons for metal assessment, namely toxicological and nutritional effects related to the concentrations present. Accordingly, it seems that the most complete environmental perspective would be achieved conducting both types of works and, even, modelling the behaviour of metals in the soil-plant system [9–11].

Therefore, we first performed a comprehensive study of roadside soils considering heavy metals

* *Corresponding author. Tel.: +34 981 167000; fax: +34 981 167065; e-mail: alatzne@udc.es

0039-9140/99/$ - see front matter
PII S0039-9140(98)00096-4

(Cd, Co, Cr, Cu, Fe, Mn, Ni, Pb and Zn) as well as humidity, pH and LOI, in order to evaluate the influence of motor vehicle emissions over the surrounding areas. Four different sampling seasons were carried out and several multivariate statistical tools were applied [12]. Two main factors were found using principal component analysis (PCA); the first one was clearly linked to the natural soils' variability (including Fe, Co and Zn) whereas the second one showed a definite relation with the anthropogenic pollution sources (characterised by Pb, Cd, Cu, Ni and Cr). Another tool, which focused on selecting variables (Procrustes rotation) to describe the sample patterns, revealed that Pb, Cd and Co were the best subset of variables that described the sample grouping very well. Additionally, it was observed that Pb, Cd, Cu and Zn were the variables for which the sample scatter was more stable along the different seasons.

Following this broad study, it was decided to determine heavy metal contents in roadside vegetables taken close to the same areas considered in the previous study and grown either in domestic gardens and under commercial horticultural/agricultural conditions. Three metals were selected as the main pollution tracers: Pb, Cd and Cu, which are a direct consequence of the above discussion. Ash content was determined as well, which reflects the degree of mineral nutrient enrichment.

The final objective was to classify all the vegetable samples in groups, employing different chemometric multivariate techniques: PCA [13], cluster analysis [14], SIMCA (soft independent modelling of class analogy) [15] and a simplified mode of potential curves [16]. Presumably, the classification should be a function of the different traffic intensities supported by the cultivated areas under investigation.

2. Experimental

2.1. Sampling and sample treatment

A total set of 27 samples were taken in three differentiated areas. One subset of eight samples corresponds to one highway with huge traffic intensity. A second set of 13 samples was obtained from lands and private allotments supporting low and medium traffic densities. A third group (six samples) was specially collected on commercial agricultural land where *Lactuca sativa* constituted the unique crop with a negligible motor vehicle presence. Table 1 summarises the samples' characteristics. Only one sampling season was considered.

When possible, vegetables from domestic allotments were sampled because they can make a significant contribution to the metals intake of individuals and families. Moreover, gardens and domestic allotments may be exposed to a higher degree of environmental contamination than most agricultural land. This is particularly supported by the fact that a significant number of domestic garden allotments are located alongside busy roadways [17].

Two species of vegetables were taken, namely, lettuces (*L. sativa*) and cabbages (*Brassica oleracea*). There are two main reasons: (a) they are broadly cultivated either for commercial and domestic purposes in our geographical region (Galicia, NW Spain), and (b) they have been found to accumulate relatively high concentrations of cadmium and other metals [17,18]. In all cases, and for each species, random collection of edible portions of material was undertaken from plants located within a 1 m^2 grid area and placed into a clean polypropylene self-sealing bag. Samples were scrubbled and washed in order to better simulate the human intake conditions and, then, cut and oven-dried at 60°C during 48 h and milled. All these operations must be completed as expeditiously as possible to avoid degradation and/or sample contamination. Samples were dry-ashed overnight at 450°C, dissolved with 2M HCl, filtered and diluted to a known volume. Metal concentrations in the final aliquots were determined using a Perkin–Elmer atomic absorption spectrometer model 2380, an air-acetylene flame, single element hollow cathode lamps and running under the operational conditions summarised in Table 2.

All reagents were analytical-grade and high-purity water (Milli-Q water system, Millipore, Spain) was employed throughout. Working stan-

Table 1
Description of the samples under study

Sample number	Vegetable species	Traffic density (vehicles/day)	Cultivation
1	*B. olerácea*	80 000	Private
2	*B. olerácea*	80 000	Private
3	*B. olerácea*	80 000	Private
4	*B. olerácea*	80 000	Private
5	*B. olerácea*	80 000	Private
6	*B. olerácea*	80 000	Private
7	*B. olerácea*	80 000	Private
8	*B. olerácea*	80 000	Private
9	*L. sativa*	10 000–15 000	Private
10	*L. sativa*	10 000–15 000	Private
11	*L. sativa*	10 000–15 000	Private
12	*L. sativa*	5 000	Private
13	*L. sativa*	5 000	Private
14	*L. sativa*	5 000	Private
15	*B. olerácea*	5 000	Private
16	*B. olerácea*	5 000	Private
17	*B. olerácea*	Neglible	Private
18	*B. olerácea*	Neglible	Private
19	*B. olerácea*	Neglible	Private
20	*B. olerácea*	Neglible	Private
21	*B. olerácea*	Neglible	Private
22	*L. sativa*	Neglible	Commercial
23	*L. sativa*	Neglible	Commercial
24	*L. sativa*	Neglible	Commercial
25	*L. sativa*	Neglible	Commercial
26	*L. sativa*	Neglible	Commercial
27	*L. sativa*	Neglible	Commercial

dard solutions were prepared by diluting appropriate aliquots from stock metal solutions (Panreac, Spain) with 2M HCl.

The ash content was determined by total sample combustion in a mufle-furnace at 550°C. In this way, ash content can be considered as a measure of the sample total mineral content (TMC) [19].

Table 2
Operational set-up for flame AAS metal measurements

	Cd	Cu	Pb
Wavelenght, nm	228.8	324.8	217.0
Lamp current, mA	4	15	10
Spectral bandwith, nm	0.7	0.7	0.7
Air/acetylene flow-rate	5:1	5:1	5:1
Burner height, arbitrary scale	11	12	11

The aspiration nebulizer flow was 4.5 ml min^{-1}.

3. Results and discussion

3.1. Principal component analysis (PCA)

In order to study variable patterns as well as sample grouping, a PCA was made using autoscaled data (no rotation was applied). Two PCs were chosen as the most significant ones since they explain up to 84% of the total initial variance. Table 3 presents the loading vectors for each factor.

The first PC accounts for 52% of the initial information and it is mainly defined by Cd and TMC. This PC reveals its relation with the elemental composition of the soil where the vegetables are produced and with the agricultural practices. Therefore, this factor became revealed as the most significant pattern to take into account. The second PC (32% of the variance),

Table 3
Loading coefficients (only two significant figures are displayed)

	Factor 1	Factor 2
Cd	0.88	0.39
TMC	0.86	0.39
Cu	−0.38	0.81
Pb	−0.65	0.57

associated to Cu and Pb, shows the clear effects of the motor vehicle influence over the cultivated areas.

In spite of cadmium being a metal generally associated to oil or fossil fuel combustion, the first PC reveals that the use of phosphatic fertilisers was the more relevant source of this metal in our vegetables because the highest figures we have found corresponded to samples collected on commercial farmland with a negligible motor vehicle presence. In Fig. 1 it can be observed that this PC distinguishes two essential blocks of samples: vegetables grown at private domestic gardens (left side) and vegetables grown under commercial agricultural conditions (group A). Using sample scores, those samples on the right side showing values higher than 1 on the 1st PC characterise commercial lettuce samples. They have the maximum values for Cd and TMC (average values up to 0.93 μg g^{-1} and 28%, respectively), and medium for Cu and low for Pb (7.56 and 3.78 μg g^{-1}, respectively).

The remaining samples with PC1-scores $< +0.5$ correspond to private cultivations. There, several groups can be observed. The first group is characterised by PC1-scores < -1 being associated to high traffic intensity (group D), showing the highest values for Pb (average, 17.45 μg g^{-1}) and for Cu (12.53 μg g^{-1}).The second, shows PC1-scores from $+0.5$ to -1 and it groups samples affected by low, medium, and high traffic densities.

The second PC is defined mostly by Cu and to a lesser extent Pb. Considering the areas covered by our study, both metals essentially come from the exhausts of those vehicles running leaded petrol (Pb) and from mechanical abrasion and normal wear and tear of essential components of many alloys, pipes and wires in motor vehicles (Cu). This PC allows further discrimination within the above bulk of samples. As can be seen in Fig. 1, PC2-scores < -0.5 discriminate one set of samples (group C, only cabbages) arising from domestic gardens which support low and/or negligible traffic flow. They have low Pb and Cu contents (averages of 4.10 μg g^{-1} and 5.21 μg g^{-1}, respectively). Samples # 3 and 16 need some further comments; both of them became included in group C despite the fact that they were collected on sites supporting medium (5000–15000 vehicles/day) and high (80000 vehicles/day) traffic densities. Presumably, their inclusion here might be explained by natural washing, local topography, climatological conditions, etc.

Group B can be seen when PC1 scores range from -1 to $+0.5$ and PC2-scores are > -0.5. This group is formed by lettuces and cabbages grown at domestic gardens supporting medium and high traffic intensities. This group have samples showing medium–high values for Cu and Pb (ranging between 7.38 and 19.42 μg g^{-1}; 6.52 and 22.08 μg g^{-1}, respectively) along with low values in Cd (average, 0.48 μg g^{-1}) and TMC (16%).

Two further comments will be of interest:

(a) Attention has to be drawn on sample # 2 since it has the minimum cadmium content (0.20 μg g^{-1}) though high concentrations for Pb and Cu (15.29 and 12.38 μg g^{-1}, respectively). Moreover, this sample was taken close to the highway with huge traffic flow (see sampling section) thus it should clearly represent the samples influenced by road traffic. In contrast, group A (with almost no traffic influence but supporting commercial agricultural practices) showed the maximum values for cadmium. This fact justifies fairly well the link established between PC1 and the agricultural conditions (commercial versus private).

(b) When the species of the vegetables are considered, an interesting trend can be seen within group B. That is, all the private lettuces (excepting sample # 9) are grouped altogether. This suggests that the different vegetable species could led to a further discrimination between samples.

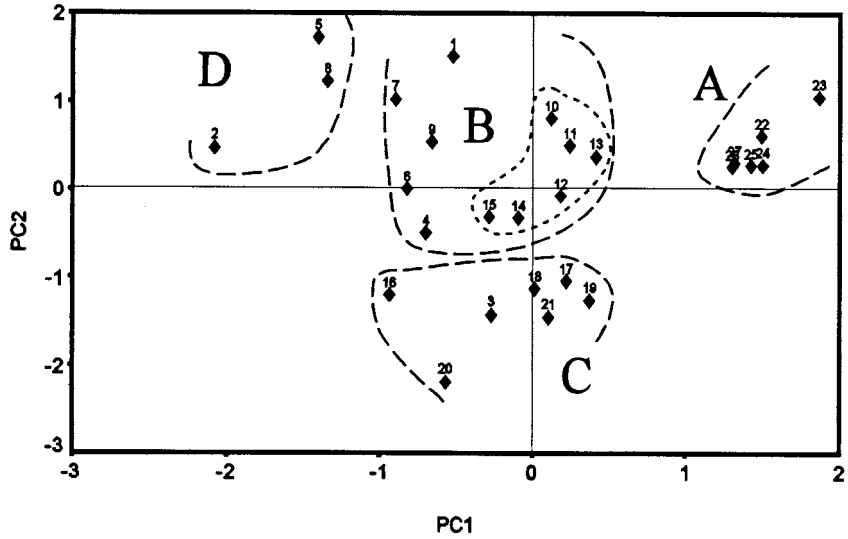

Fig. 1. PC1-PC2 sample score subspaces, unrotated components, autoscaled data.

3.2. Cluster analysis

A cluster analysis was made as an attempt to derive groups from the raw data set and to compare them with the previous ones from PCA. Autoscaled data was employed to avoid the influence of the different range levels of the variables; the Euclidean distance was chosen as the measure of similarity and the Ward method was the clustering algorithm. The Ward method considers all the possible associations between every two clusters and calculates the variances associated to their combination. Then, it groups those two clusters which conduct to the lesser increase in the variance of the joint group (see [14] for more mathematical details and a rigorously derivation considering 'heterogeneity' instead of variance).

Fig. 2 presents the dendrogram obtained using the beforehand conditions. Four main clusters, essentially corresponding to the ones described into the PCA study can be described.

Cluster A: it corresponds to the PCA-group A, formed by the commercial lettuce samples grown without significant motor vehicle influence.

Cluster C: equal to the PCA-group C, and constituted by domestic cabbage samples and supporting low-negligible traffic intensity.

Cluster D: the D group in the PCA score plot (Fig. 1). It corresponds to the three extreme values of Pb and Cu; also they have low Cd concentrations. These samples coincide with domestic cabbage allotments and high traffic flow.

Cluster B: in good agreement with group B in the PCA scatter plot. A little subgroup can be viewed at the upper part for samples # 10, 11, 12, 13, and 14, all of them considered in group B of the PCA-scores (private lettuces). This cluster combines samples from roads with high traffic intensities (# 1, 4, 6, 7) which should be present on the D group (high traffic), with samples from sites with medium traffic influence. This is caused because the concentration ranges for all of these samples became quite similar, which may be a consequence of the different factors affecting the pollutants dispersion and the vegetables uptake of heavy metals; namely, local topography, soil type and chemistry, plant species, wind directions and general atmospheric conditions (including precipitation), automobile speeds, etc.

3.3. Potential curves

The main idea behind the mathematical treatment involved onto the potential curves could be exemplified using the following analogy. Let us

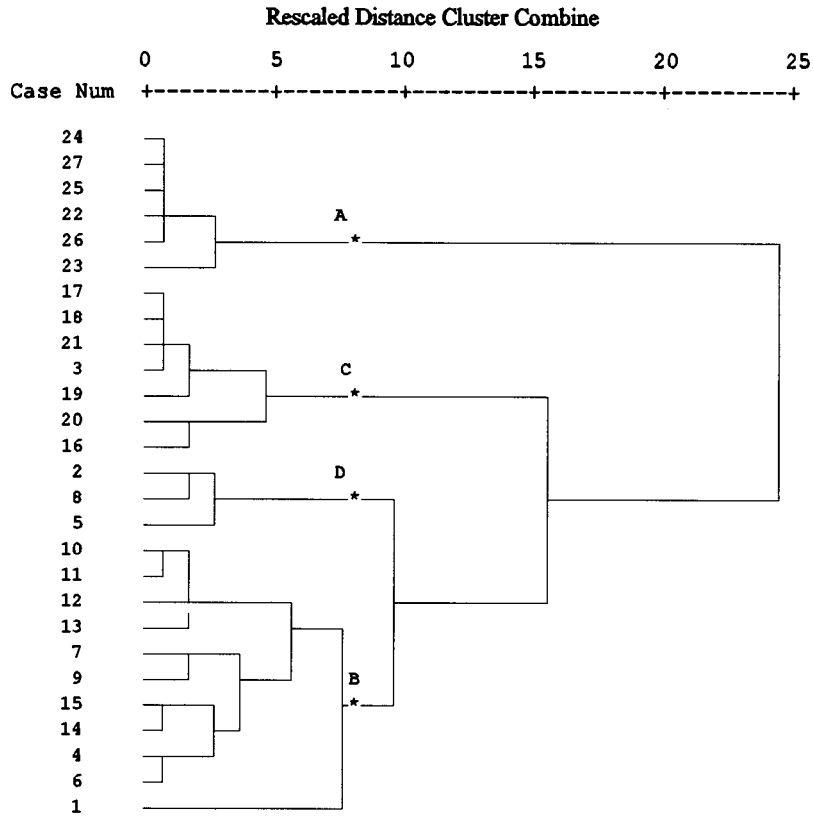

Fig. 2. Dendrogram showing the vegetables grouping. A, commercial samples with negligible motor vehicle influence; C, domestic samples supporting low–negligible traffic intensity; D, domestic allotments and high traffic flow; B, combined group, medium/medium–high traffic intensity.

suppose one working area (e.g. a plane) where groups of objects are distributed according to their Cartesian co-ordinates, namely X, Y. For simplicity, assume each group is homogeneously distributed and does not overlap with any other. Then, a new object—whose coordinates are X′ and Y′—will be assigned to the group to which it most closely relies. Class-modelling methods make a mathematical description for each class, independently from other classes. The discriminant frontiers have been assigned to different probability (density) functions like the triangular, rectangular or Gaussian distributions [20,21].

Generally, the probability function (density function or potential curve) for any given group of samples has been obtained as the sum of each of the density functions associated to each sample from the group. This fact would imply that each sample has to be measured several times to estimate its mean and standard deviation. An alternative could be to grossly estimate the probability function for each sample taking into account the precision figures of each analytical method.

We are aiming to look for a simplified mode of discriminant function. The main hypothesis assumed by the simplified model is that samples from each group are homogeneously distributed into the PC1-PC2 space and following a Gaussian distribution. Then, simplified potential curves are defined which describe the probability of each new sample to belongs to one pre-existing group. This reduced method is a simplification of the determinant method from Forina et al. [21]. A more exhaustive treatment can be found on [16]. Briefly, the main objective of using PCs instead of original variables is to avoid unuseful information

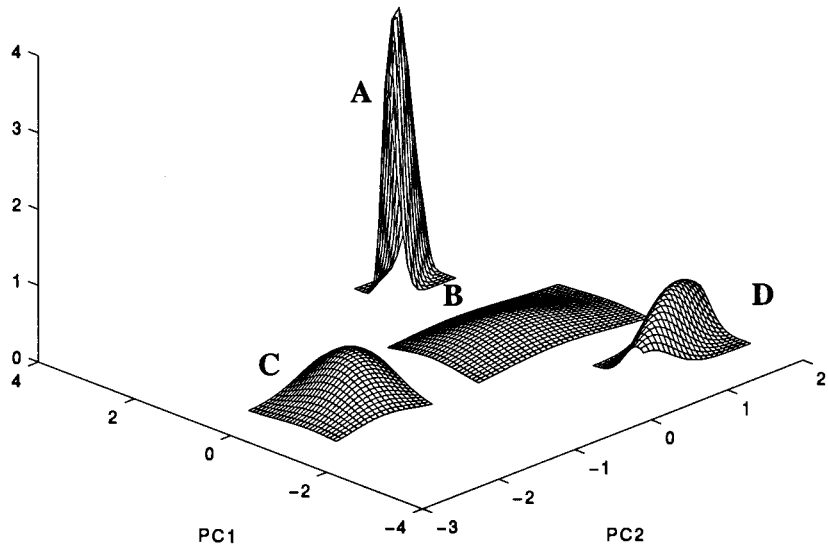

Fig. 3. Potential curves calculated for each kind of sample.

(noise) and take advantage of the natural sample grouping occurring in the reduced PC-subspace (which, of course, greatly simplify the following chemical interpretations).

Accordingly, the PCA scores for each of our group of samples were taken and included onto the multivariate equations and each isoprobability curve was created. Fig. 3 represents the four density functions plotted on the same scaled axis. All the four previously described groups are observed and, more importantly, they do not overlap. Once the isoprobability curves are calculated for each group, any new sample will be classified according to the calculated probability of pertainance to each group.

To exemplify and to test the effectiveness of such classification, a validation scheme was prepared where a small set of samples were excluded (samples # 4, 7, 18 and 25); selected because each of them represent different agricultural and traffic conditions and each one has a borderline position (see Fig. 1) and, therefore, they would allow us to estimate the power of the simplified potential curves. No sample was taken from group D since it is formed by only three samples. The remaining samples were used to prepare the density curves (and isoprobability equations). After that, the small set of excluded data was tested and the classification success ratio was studied. The density curves obtained in this validation stage totally agree with those in Fig. 3. The output of the classification step is summarised in Table 4 where highly successful results are seen.

As a conclusion, it seems reasonable to accept that the simplified potential curves can aid in the classification of new vegetables according to the traffic and agricultural conditions they support, providing they are taken in the geographical areas covered by this work.

3.4. SIMCA classification

To verify and compare the behaviour of the potential curves, the well known SIMCA tech-

Table 4
Potential curves behaviour; % of probability for each sample and class

Sample #	Actual class	Class prediction			
		A	B	C	D
4	B	0.0	14.3	0.8	0.0
7	B	0.0	14.6	0.0	0.0
18	C	0.0	3.9	74.8	0.0
25	A	63.5	0.2	0.0	0.0

Table 5
Classification of the testing set using SIMCA

Sample #	Actual class	Decisions
4	B	Belongs to class B
7	B	Belongs to class D
18	C	Belongs to class C
25	A	Belongs to class A

nique was applied also in the same way as previously discussed. Here, the algorithms from Wise [22] were applied. The classification decisions can be seen in Table 5 and, positive enough, they coincide with the ones from the potential curves, hence confirming their powerful use.

Regarding sample # 7, it has to be taken into account that its exclusion from the training step greatly influences the probability areas derived from the SIMCA model. This is better understood whether its position in Fig. 1 is seen. Clearly, its inclusion (or not) in the training set will modify the zone assigned to group B. On the contrary, its effect over the potential curves is not so drastic thanks to the smoothing effect inherent to the potential curves.

4. Conclusions

Three main classes of edible vegetables were encountered which respond to the two main discrimination factors derived for the sites considered in this work using several chemometric tools: (a) the commercial agricultural usage of the farmlands and (b) the road traffic intensity. It was verified that new vegetables would be classified in any of the three predefined classes of samples (or none of them) according to their closeness (probability of belongingness) either using SIMCA or potential curves.

References

[1] J.V. Lagerwerff, A.W. Specht, Environ. Sci. Technol. 4 (1970) 583.
[2] N.I. Ward, R.R. Brooks, E. Roberts, Environ. Sci. Technol. 11 (1977) 917.
[3] C.N. Hewitt, G.B.B. Candy, Environ. Pollut. 63 (1990) 129.
[4] R. García, E. Millán, Sci. Total Environ. 146/147 (1994) 157.
[5] N.I. Ward, Sci. Total Environ. 93 (1990) 393.
[6] P. Misaelides, C. Samara, M. Georgopoulos, T. Kouimtzis, S. Synetos, Toxicol. Environ. Chem. 24 (1989) 191.
[7] D. Münch, Sci. Total Environ. 138 (1993) 47.
[8] R. Tahvonen, J. Kumpulainen, Fresenius J. Anal. Chem. 340 (1991) 242.
[9] Y.B. Ho, K.M. Tai, Environ. Pollut. 49 (1988) 37.
[10] A. Alegría, R. Barberá, R. Boluda, F. Errecalde, R. Farré, M.J. Lagarda, Fresenius J. Anal. Chem. 339 (1991) 654.
[11] N.I. Ward, J.M. Savage, Sci. Total Environ. 146/147 (1994) 309.
[12] A. Carlosena, J.M. Andrade, M. Kubista, D. Prada, Anal. Chem. 67 (1995) 2373.
[13] M. Meloun, J. Militky, M. Forina, Chemometrics for Analytical Chemistry, vol. 1, Ellis Horwood, New York, 1992, pp. 226–244.
[14] D.L. Massart, L. Kaufman, The interpretation of Analytical Chemical Data by the use of Cluster Analysis, R.E. Krieger, Florida, 1989, pp. 81–94.
[15] S. Wold, M. Sjöström, SIMCA: A Method for Analysing Chemical Data in Terms of Similarity and Analogy ch.12, in: B.R. Kowalski (Ed.), Chemometrics: Theory and application, ACS Symposium Series, No.52, Washington, 1977, pp. 243–282.
[16] X. Tomás, J.M. Andrade, Afinidad 54 (1997) 103.
[17] B.J. Alloway, A.P. Jackson, H. Morgan, Sci. Total Environ. 91 (1990) 223.
[18] A. Kabata-Pendias, H. Pendias, Trace Elements in Soils and Plants, 2nd edn, CRC Press, Florida, 1992, pp. 113–116.
[19] S.E. Allen, Analysis of Vegetation and other Organic Materials, in: S.E. Allen (Ed.), Chemical Analysis of Ecological Materials, Oxford, 1989, pp. 54.
[20] D. Coomans, D.L. Massart, I. Broeckaert, A. Tassin, Anal. Chim. Acta 133 (1981) 215.
[21] M. Forina, C. Armanino, R. Leardi, G. Drava, J. Chemom. 5 (1991) 433.
[22] B. Wise, N.B. Gallagher, Manual for the use of the PLS_Toolbox for Matlab, Washington, 1995.

ELSEVIER

Talanta 48 (1999) 803–819

Talanta

New developments in immunochemical water analysis down to 30 μl sample volume

Ursula Pfeifer-Fukumura *, Iris Hartmann, Heike Holthues, Wolfram Baumann

Department of Chemistry and Pharmacy, University of Mainz, 55099 Mainz, Germany

Received 11 June 1997; received in revised form 26 September 1997; accepted 02 October 1997

Abstract

The determination of trace levels of pesticides like atrazine in water samples of small, restricted volumes is one of the future demands of environmental analysis. In a brief review existing chromatographic and immunochemical methods for atrazine are critically discussed. Then a simple rapid enzyme-linked immunosorbent assay (ELISA) using the tip of an inoculation needle as a solid surface is presented. The sample volume could be reduced to 30 μl. The assay had a centre of the test IC_{50} of 0.12 μg l^{-1} and permitted the characterisation of atrazine at levels of 0.022–2.90 μg l^{-1}. A first outlook for automatisation is given. The new method was compared with an ELISA using 96 well microtiter plates as a solid phase. Surface water samples with low atrazine contents were analysed to check the new method.

Keywords: Triazine; ELISA; Inoculation needle as solid phase; 30 μl sample volume

1. Introduction

Herbicides are widely used in agriculture for pre- and post-emergence control of crops and other plants. Due to their wide spread application the question arises about their dissemination in the environment. One of the most prominent herbicide classes used in Europe and the United States within the last 30 years are the s-triazines, in particular atrazine. Owing to its persistence and solubility in water atrazine is considered as a common pollutant in Germany even after its ban in April 1991. Recent studies show that in Germany atrazine is still found in soil [1] as well as in surface water and rain fall [2].

During and after direct application of atrazine to soil or plants only a part of the pesticide is incorporated into the target plant. Besides a major part being bound to soil and then leaking to surface water or ground water, atrazine is found in the atmosphere. This is due to its drift as small droplets from spray application, evaporation from plant and soil and its binding to small soil particles [3–5]. Surface water [2,6–10] and ground water or well water [8,9,11–13] are the subject of intensive monitoring because of their relevance for drinking water (allowed levels below 0.1 μg l^{-1} for a single pesticide in Germany [14]). However, so far only little research is performed to

* Corresponding author. Tel.: +49 6131 395365; fax: +49 6131 395380.

0039-9140/99/$ - see front matter
PII S0039-9140(98)00097-6

understand the transport processes of atrazine or other herbicides through the atmosphere. The determination of atrazine in rain water is generally considered to be an indicator of atrazine in the atmosphere, because a contamination of rain water is preceded by a contamination of the atmosphere [15]. Several groups are engaged in research on atrazine in rainfall [2,15,16] and liquid water of low-lying clouds [17]. In investigations performed before April 1991 typically up to 3.3 μg l^{-1} of this herbicide was found in rain fall, after its ban up to 0.3 μg l^{-1} [2] was found in 1992.

Rain water, itself, is only a rough estimation for the amount of a substance in the atmosphere, because it has to be considered as a summing up from the cloud till the sampler at the ground. To our knowledge no detailed study on the distribution of triazines in the atmosphere is available, though it should be noted that research on DDT indicates a restriction of the discussion to the troposphere, in particular to the planetary mixing layer of $\sim 1-2$ km thickness [5]. Therefore the amount of atrazine and its degradation product bound to hydro meteorites will be of particular interest. Such investigations, however, request for analytical methods which first of all can handle small sample volumes, preferably < 50 μl, and which can detect the analyte in such small samples in a concentration range below 0.3 μg l^{-1} since this level is found in rain water after the atrazine ban.

In the present communication a short critical overview of methods to determine atrazine in water samples will be given in regard to their suitability for analysing water of clouds. Then we will present a simple, rapid immunochemical method which needs as little as a 30 μl sample volume having a determination range for atrazine between 22 and 2900 ng l^{-1}. The principle of the method itself can be used for other herbicides and environmentally important substances, if suitable antibodies are available. The method is compared to an ELISA on a 96-well microtiter plate, and a first outlook for automatisation is given. Natural water samples with low atrazine contents are analysed to check the new method.

1.1. Chromatographic methods

Atrazine in a water matrix is frequently analysed by chromatographic methods like gas chromatography (GC) or liquid chromatography (LC). In the case of GC the detection is performed with an electron capture detector (ECD) or with a nitrogen-phosphorous selective detector (NPD). In many cases GC is coupled to mass spectroscopy (MS). Using LC techniques atrazine is in most cases determined by its absorbance using UV/VIS-detection.

However, in natural water samples atrazine is usually present at concentration levels that fall below the limits of detection of the above described methods. Hence, a preconcentration step is required. Liquid–liquid extraction (LLE) with organic solvents like dichloromethane has been applied first, but is continuously replaced by solid phase extraction (SPE) using for instance C_{18}-SPE cartridges or disks. Table 1 summarises preconcentration, chromatography and detection methods for the determination of atrazine in water as matrix. Only a representative selection of methods which use the whole procedure of preconcentration and then chromatographic analysis with real water samples or spiked water samples is presented; for far-reaching reviews see [50–52].

Evaluating the methods of Table 1 from the point of view as how to develop an analytical method for the determination of atrazine in water samples of small volumes, the chromatographic methods combined with a preconcentration step can yield the required concentration range, however, they need in general sample volumes of at least 100 ml, typically 500 or 1000 ml. In a few cases volumes < 10 ml are reported [23,25,31], however, no method could reach volumes below 100 μl. Present chromatographic methods are therefore applicable for surface water or ground water samples, but may not be suitable for natural water samples of restricted volume.

1.2. Methods based on enzyme-linked immunosorbent assays (ELISA)

Recently, immunoassay techniques are of increasing interest for the determination of environ-

Table 1
Preconcentration and chromatographic methods for the determination of atrazine in water as matrix

Preconcentration method	Chromatographic method	Required sample volume (ml)	Concentration range[a] [μg l^{-5}]	Ref.
LLE(CH_2Cl_2)	GC-NPD or GC-MS	1000–4000	0.001–1	[7]
LLE(CH_2Cl_2)	GC-NPD	100–500	>0.026	[18]
LLE(CH_2Cl_2)	GC-NPD	20	>0.1	[19]
LLE(CH_2Cl_2)	GC-MS	1000	recovery studies	[20]
LLE(CH_2Cl_2)	LC-DAD	1000–4000	0.05–1	[7]
LLE(CH_2Cl_2) or SPE	GC-MSD	250	>0.01	[17]
LLE (diethylether)	GC-PID	400	recovery studies	[21]
LLE ($CHCl_3$)	capillary isotachophoresis	1000	soil, >10 μg kg^{-1}	[24]
SPE	GC-ECD	500	>0.05	[15]
SPE	GC-ECD or GC-NPD	1–100	1–10	[23]
SPE	GC-NPD	1000	>0.001	[24]
SPME	GC-NPD	3	>0.03	[25]
SPE	GC-NPD or GC-MS	5000	0.002–0.140	[26]
SPE	GC-NPD or LC-UV	50	Recovery studies	[27]
SPE	GC-MS	1000	up to 0.46	[6]
SPE	GC-MS	800	>0.02	[28]
SPE	GC-MS	100	>0.05	[29]
SPE	GC-MS	10	>0.01	[30]
	or LC-DAD	100	>0.02	
	or LC-MS	100	>0.50	
SPE	GC-MS	1	Recovery studies	[31]
SPE	GC-MS or LC-DAD	100	0.01–0.135	[16]
SPE	LC-UV/VIS	1000	>0.01	[32]
SPE	LC-UV/VIS	250	Recovery studies	[33]
SPE	LC-UV/VIS	200	>0.01	[34]
SPE	LC-UV/VIS	100	>0.1	[35]
SPE	LC-UV/VIS	100	>0.015	[36]
SPE	LC-DAD	1000	0.05–0.25	[37]
SPE	LC-DAD	500	0.05–1.0	[38]
SPE	LC-DAD	400	0.5–15.6	[39]
SPE	LC-DAD	150	0.1–1.5	[40]
SPE	LC-DAD	100	>0.05	[41,42]
SPE	LC-DAD	25–100	>0.05	[43]
SPE	LC-thermospray MS	100	>0.02	[44]
SPE	LC-thermospray MS	50	>0.005	[45]
SPE	HPTLC-UV scanning densitometry	250	>0.03	[46]
SPE + sample stacking	MEKC-UV/VIS	125	>0.014	[47]
Immunosorbent	LC-DAD	25–100	0.1–1.5	[48]
Immunosorbent	LC-UV/VIS	10	Recovery studies	[49]

LLE, liquid–liquid-extraction; SPE, solid phase extraction; SPME, solid phase micro extraction; GC, gas chromatography; LC, liquid chromatography; HPTLC, high performance thin layer chromatography; MEKC, micellar electrokinetic capillary chromatography; ECD, electron capture detector; NPD, nitrogen phosphorous selective detector; MSD, mass selective detector; PID, photon ionisation detector; MS, mass spectroscopy; DAD, diode array detector.

[a] For detail and definition the references should be consulted.

Table 2
Enzyme-linked immunosorbent assay (ELISA) methods for the determination of atrazine in water as matrix.

Solid phase	ELISA-format[a]	Antibody[b]	Sample volume	IC_{50} value [μg l^{-1}]	Concentration range[c] [μg l^{-1}]	Ref.
Microtiter plate	1	Sheep S84	200 μl	0.25	0.02–2.5	[2]
		Sheep S2	200 μl	0.17	0.02–2.0	
Microtiter plate	1	Sheep	200 μl	0.18	0.03–1	[10]
Microtiter plate	1	Sheep	200 μl	0.2	0.02–2	[1]
Microtiter plate	1	Rabbit	100 μl	0.16	>0.01	[12]
Microtiter plate	1	Rabbit	200 μl	0.03	>0.001	[53]
Microtiter plate	1	Rabbit	200 μl	0.02	0.001–10	[54]
Microtiter plate	1	Rabbit	200 μl	—	0.011–33	[55]
Microtiter plate	1	Mo. mouse	100 μl	1	>0.01	[12]
Microtiter plate	1,2a, 2b,3b	Mo. mouse	50 μl	best 2a 0.25	best 2a >0.03	[56]
Microtiter plate	2a	Mo. mouse	150 μl	0.1	0.03–1	[57]
Microtiter plate	2a	Mo. mouse	40 μl	13	1–100[d]	[13]
Microtiter plate	3a	Mo. mouse	120 μl	2[d]	0.3–10[d]	[13]
Microtiter plate	4a	Rabbit	100 μl	—	—	[58]
Microtiter plate	4a	Rabbit	100 μl	—	>0.1	[59]
Microtiter plate	4b	Mo. mouse	850 μl	0.45	>0.05	[60]
Magnetic bead	1	Comm. Kit	200 μl	0.3 or 0.4	—	[61]
Magnetic bead	1	Comm. Kit	100 μl	1 ppb[c]	>0.05	[62]
Membran	FIIA,2b	Rabbit	—	0.1	0.03–1	[56]
PS test tube	1	Comm. Kit	160 μl	0.4	0.2–2	[63]
PS test tube	1-AP	Rabbit AK20	400 μl	6–8	>0.5	[8]
	1-HRP	Rabbit AK20	200 μl	1	>0.1	
	1-HRP	Rabbit C193	200 μl	0.1	>0.02	
PS sphere	1	Rabbit	20 ml	—	550[d]	[55]

PS, polystyrene; FIIA, flow injection immuno assay; AP, alkaline phosphatase tracer; HRP, peroxidase tracer.
[a] ELISA-format description see text and Fig. 1.
[b] If not specified polyclonal antibody; mo., monoclonal; comm. kit, commercial kit; numbers represent code used in Ref.
[c] For details and definition the references should be consulted.
[d] As estimated from plot.

mental pollutants. Enzyme immunoassays (EIA) combine the enormous discriminatory characteristics of antibodies having high affinity for a specific antigen or hapten with the high catalytic power of enzymes using them as amplification system. EIA techniques can be divided into two main groups: enzyme multiplied immunoassay techniques (EMIT) and ELISA. For the determination of atrazine the latter one is used, meaning parts of the reactions occur on a solid phase which also facilitates the separation of the immuno complex and unbound reactants.

In the following, formats used to determine atrazine according to Table 2 will be characterised briefly (see also Fig. 1).

ELISA-format 1 (direct coating of a solid phase): The solid phase is coated by anti-atrazine antibodies (Atr-Ab). After competition of the enzyme-hapten conjugate (tracer) and unlabelled analytes (standard or sample) for the antibody binding sites, the amount of bound tracer is quantified by the enzymatic reaction. The amount of tracer is inversely proportional to the amount of atrazine.

ELISA-format 2 (precoating of a solid phase): The solid phase is precoated with a secondary

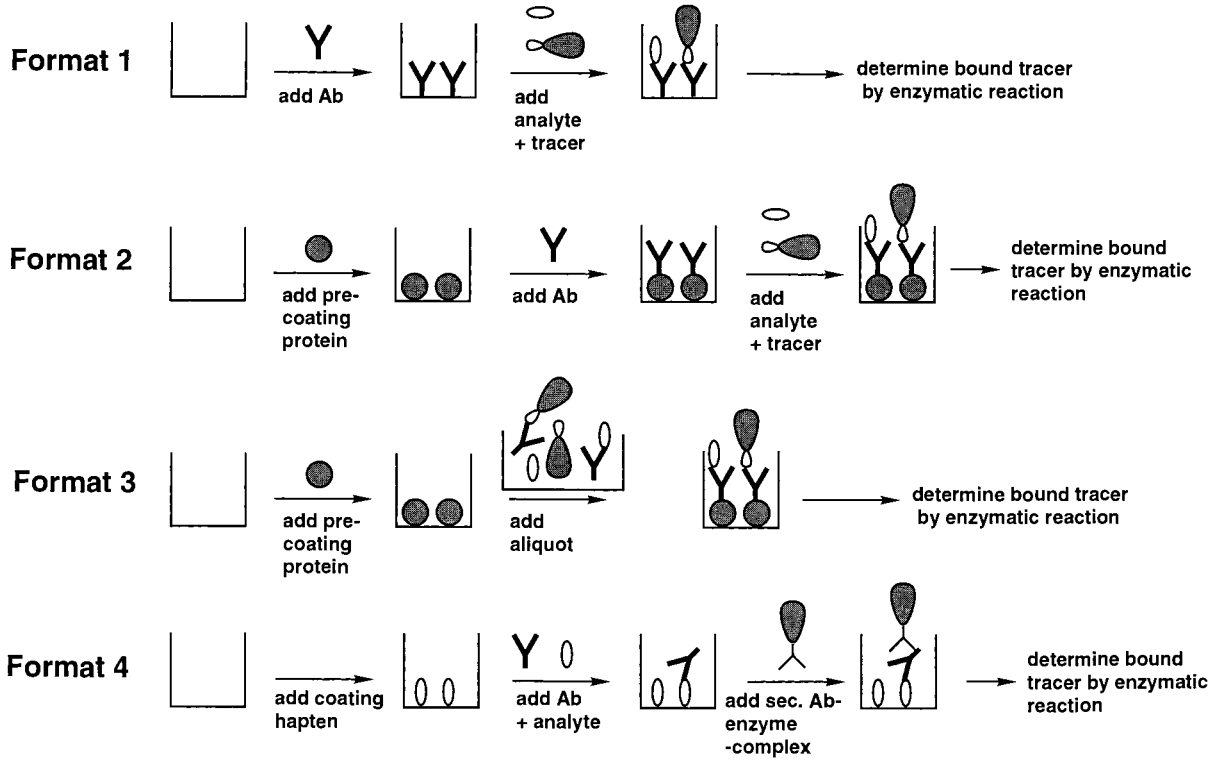

Fig. 1. Scheme of typical ELISA-formats. For details refer to the text.

antibody (Format 2a), or protein A (Format 2b). Then Atr-Ab are added for the coating step and bound to the protein of the precoating procedure. The following steps are identical to Format 1.

ELISA-format 3 (separated competition step): The competition reaction between unlabelled analyte, tracer and Atr-Ab is performed in a separate vessel. A part of the mixture is then added to a solid phase which is precoated with a secondary antibody (Format 3a) or with Protein A (Format 3b). The enzymatic activity of the bound tracer is measured meaning the amount of Atr-Ab-tracer complex. Here the amount of tracer is inversely proportional to the amount of analyte in the sample, too.

ELISA-format 4 (coating with an analyte derivative). To the solid phase which is coated with an analyte derivative or with an analyte derivative bound to a protein (e.g. albumin), the analyte and Atr-Ab are added in the competition step. Then an enzyme-labelled secondary antibody is added. The amount of enzyme-labelled anti-antibody and hence the amount of Atr-Ab is determined by enzymatic activity giving a result which is inversely proportional to the amount of analyte in the competition step.

In Table 2 the ELISAs used for the determination of atrazine are summarised according to the solid phase and assay format. The used sample volume, the centre of the test (IC_{50}, the 50% value of the ratio of tracer bound to the solid phase in the presence and absence of analyte), and the concentration range is given for comprehension. For details regarding the definition of the range of determination the references should be consulted.

Compared to chromatographic techniques one remarkable feature of immunoassays is their low detection limit with no need of a preconcentration step. Because of the high specificity of the antibody, analytes like atrazine can usually be detected in water samples without sample pretreatment. The general use of immunoassays in environmental analysis is critically reviewed by Sherry [64]. For atrazine polyclonal and mono-

clonal antibodies are available, even as commercial test kits [65,66]. All assay formats reach a low IC_{50}-value, some as low as 0.1 μg l^{-1} and there-fore will be up to the demands. The IC_{50}-value and the concentration range of the assay are determined by the assay format [56], the affinity of the antibody, which is itself subject of the immunogen and the cell clone [57], and the used tracer with respect to the enzyme [8] or the hapten [56]. The immunogen also determines the specificity of the antibody and therefore its cross-reactivity (the binding of structurally related substances besides the analyte to be checked). The detection limit is in generally not a question of using monoclonal or polyclonal antibodies, as was discussed in [67].

The solid phases used in the assays are mainly 96-well microtiter plates besides magnetic beads, polystyrene tubes, membranes or polystyrene spheres. All solid phases except the larger polystyrene spheres permit sample volumes of typically 100–200 μl. In two cases [13,56] as less as 50 or 40 μl were sufficient to run the assay, however, the IC_{50}-values are rather high. Both assays were performed by US research groups, and it should be noticed that the United States have different drinking water ordinances, which request different IC_{50}-value for the tests.

As a summary the ELISA technique is promising with respect to the concentration range expected for atrazine in cloud water, but the required sample volume must be reduced.

1.3. Other immunochemical and non immunochemical techniques

Besides chromatographic analysis with preconcentration and ELISA type immunoassays a few other methods to determine atrazine are described in literature.

A time-resolved fluorescence immunoassay using europium(III)-chelates has a detection limit of 0.1 μg l^{-1} and requires a sample volume of 100 μl [68].

Some methods are based on biosensors which have been recently reviewed for their potential in pesticide detection [69,70]. For atrazine several sensors using the concept of 'direct' immunological procedure have been developed to detect directly the binding of the analyte to the antibody without employing tracers and a competitive step. A direct potentiometric immunoelectrode with antibody immobilised on graphite could detect atrazine in a range of 20–250 ng l^{-1} [71], however, the required sample volume is still 9 ml and a further reduction is needed. A piezo sensor with immobilised antibodies has a detection limit of ~ 2 mg l^{-1} [72] which is not sufficient for the analysis of atmospheric water samples.

Another biosensor is based on reflectometric interference spectroscopy [73]. Here an atrazine derivative is covalently bound to the measuring chip, then anti atrazine antibodies and the analyte were added in a competition step. The sample loop is described to be 500 μl with 30 μl min^{-1} flow. Unfortunately the concentration range and the IC_{50}-value are given in terms of antibody concentrations.

A biosensor employing surface plasmon resonance method was developed for atrazine [74]. An atrazine derivative was immobilised on the sensor chip followed by the competition step (addition of Atr-Ab and analyte). To enhance the primary response a second antibody binding to Atr-Ab was added in a third step. The sample volume was 100 μl with a detection limit of 0.05 ppb.

An enzyme-based biosensor for atrazine is described, that is based on the inhibition of the enzymatic reaction of tyrosinase by the herbicide [75]. The system was tested for atrazine in the range of 5×10^{-6} mol l^{-1} (ca. 1 mg l^{-1}).

Besides methods to analyse atrazine, recently an interesting immuno system for alpha-fetoprotein and other clinical relevant proteins is described using the inner part of a pipette tip as solid phase [76]. The required sample volume is as small as 35 μl, however, the handling of the system which is combined with a pH sensitive field effect transition sensor seems to be rather complicated. The detection limit for the proteins was in the range of 0.09–0.35 μg l^{-1}.

As a summary, chromatographic methods require normally too large sample volumes of >100 ml at the beginning of the preconcentration step. ELISA methods are promising with regard to no need of preconcentration, no sample pretreatment and the available concentration range. However, assays on 96-well microtiter plates require sample

volumes of typically 100 μl. Biosensors still lack the use of small volumes or have high detection limits. Hence the most promising method for analysing atrazine in samples of restricted volume will be an ELISA performed on a solid phase in a specially designed reaction vessel. An approach will be given in this communication.

2. Experimental

2.1. Reagents and buffers

The following chemicals were used: atrazine (Riedel de Haen AG, Seeize), horse radish peroxidase (HRP; enzyme immunoassay grade, Boehringer, Mannheim), goat anti-mouse IgG (whole molecule, 3.8 mg antibody ml^{-1} antiserum, product number M-5899, Sigma), sephadex column G25 (Boehringer, Mannheim). All other chemicals were of analytical grade.

The antibody was obtained from Prof B. Hock and Dr T. Giersch, Technical University of Munich. It is named K4E7 and is a monoclonal antibody prepared by conventional immunisation of mouse and hybridoma technology (details see [57,77]). 2 mg of the lyophilised protein was reconstituted with 400 μl of sterilised PBS-buffer pH 7.6.

The atrazine derivative 6-((4-chloro-6-(isopropyl amino)-1,3,5-triazin-2yl) amino)-hexanoic acid was synthesised according to the literature [78].

For the synthesis of the enzyme tracer (Tr1) the atrazine derivative was coupled to HRP following closely the procedure described in [54]. For removing atrazine derivative a sephadex column G25 was used. Fractions containing the tracer were unified and stored after sterile filtration at 4°C. In parallel a similar tracer (Tr2) was obtained from Dr T. Giersch, Technical University of Munich. Both tracers showed comparable results when applying comparable dilutions. The stock solution of Tr1 was less concentrated by a factor of 5 than the one of Tr2.

The micro well plates were 96-well microtiter plates Nunc Maxisorb No. 442404 (Nunc). The polystyrene needles were inoculating needles (No. 253988, Nunc).

The following buffers were used within the experiments:

- carbonate buffer pH 9.5 (1.70 g Na_2CO_3, 2.68 g $NaHCO_3$ in 1 litre distilled water)
- PBS-buffer pH 7.6 (1.265 g $NaH_2PO_4 \times H_2O$, 13.450 g $Na_2HPO_4 \times 2H_2O$, 8.50 g NaCl in 1 litre distilled water)
- washing buffer pH 7.6 (100 ml PBS-buffer, 0.5 ml Tween 20, 900 ml distilled water)
- citrate buffer pH 5.0 (13.13 g citric acid hydrate, the pH adjusted with NaOH, in 0.5 l distilled water)
- H_2O_2-solution (50 μl 30% H_2O_2, 50 ml citrate buffer pH 5.0)
- OPD-solution (81 mg *o*-phenylene diamine, 50 ml citrate buffer pH 5.0)
- chromogen solution (H_2O_2-solution and OPD-solution were mixed in a ratio 1:2).

Standards of atrazine were prepared using a stock solution of 2 mg atrazine in 20 ml absolute ethanol and diluting it with PBS-buffer pH 7.6. When natural water samples were checked, standards for the calibration curve were obtained by diluting the stock solution with distilled water or PBS-buffer pH 7.6, however, no differences were observed between the two solvents.

2.2. Apparatus

Adjustable pipettes, Finnpette 40-200 μl (Labsystems), Finnpette 200–1000 μl (Labsystems), Eppendorf pipette 0.5–10 μl (Eppendorf, Hamburg) and Eppendorf Multipette (Eppendorf, Hamburg) were used to dispense the liquids.

All spectro photometric measurements when using the microtiter plates were carried out in an EIA Reader Dynatech MR5000 (Dynatech Laboratories). The software Biolinx2.21 (Dynatech Laboratories) was used to control the reader and to analyse the obtained data. The data were additionally analysed using the software Fig.P for Windows (Biosoft).

When performing the assay on the needles the precoating step and coating step were done in 50 ml glass vessels, the immunoreaction and the enzymatic reaction in small self-made glass vessels (2 cm length, 2 mm diameter). Alternatively for the enzymatic reaction a reactor was used which was

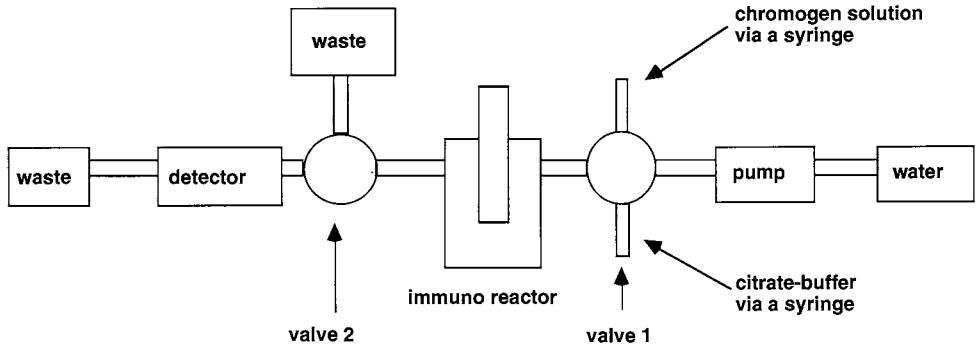

Fig. 2. Schematic diagram of the flow through apparatus used to determine the enzymatic activity of the tracer within the ELISA performed on inoculation needles.

coupled to a UV-detector and could be filled using syringes or operated in a flow through mode as schematically shown in Fig. 2. The equipment comprised two Rheodyne valves (Rheodyne), an HPLC-pump (2200, Bischoff), a self-made syringe holder, a UV-photometer with a flow-through cell (UV-VIS detector Lambda 1000, Bischoff). A cross-sectional view of the reactor is shown in Fig. 3.

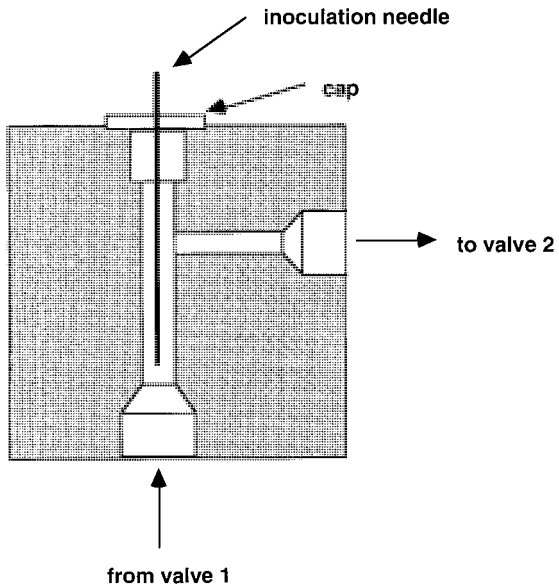

Fig. 3. Schematic cross-section of the flow through immuno reactor with built in inoculation needle.

2.3. ELISA procedure using micotiter plates

The assay was performed as a competitive assay following the ELISA format 2a as described in Section 1.2. The following steps were carried out.

Precoating step: 96 well microtiter plate was precoated with 200 µl of goat anti-mouse antibody solution (stock solution diluted 1:700 with carbonate buffer pH 9.5) overnight at 4°C. Unbound components were removed by washing three times with washing buffer.

Coating step: The plate was coated with 200 µl K4E7 stock solution diluted with PBS-buffer pH 7.6 for 3 h at room temperature. Unbound components were removed by washing three times with washing buffer.

Competition reaction step: 100 µl tracer and 100 µl standard or sample diluted with PBS-buffer pH 7.6 were added, and the competitive immuno reaction was performed for 2 h at room temperature. Unbound components were removed by washing three times with washing buffer.

Enzymatic reaction step: 200 µl chromogen solution was added for 15 min at room temperature, then the enzymatic reaction was stopped by the addition of 50 µl 4N HCl. The absorbance of the solution in the wells was determined in the EIA reader using the dual scan mode at 490 nm and 630 nm.

The standard curve was prepared from calibrates containing known levels of atrazine at 0, 0.01, 0.1, 1 and 1000 µg l^{-1} or 0, 0.01, 0.03, 0.1, 0.3, 1 and 1000 µg l^{-1}. The dilution of the stock solutions of the tracer and the K4E7 antibody

were optimised. All standards were measured as quadruplicates unless stated otherwise.

2.4. ELISA procedure using the inoculation needles

The assay was performed following the ELISA format 2a as described in Section 1.2 and is in principle similar to the procedure using the microtiter plates. Precoating and coating were performed in one vessel for all needles used for a calibration curve and the water samples belonging to it. For the competition step and the enzymatic reaction the needles were treated individually.

Precoating step: all needles needed for one assay were precoated with 21 ml of a goat anti-mouse antibody solution (stock solution diluted 1:700 with carbonate buffer pH 9.5) over night at 4°C. Unbound components were removed by washing three times with washing buffer.

Coating step: the needles were coated with 20 ml K4E7-antibody stock solution diluted with PBS-buffer pH 7.6 for 3 h at room temperature. Unbound components were removed by washing three times with washing buffer.

Competition step: each needle was transferred to a small glass vessel containing 30 μl tracer and 30 μl sample or standard solution. The competitive immuno reaction was performed for 2 h at room temperature. Unbound components were removed by washing three times with washing buffer.

Enzymatic reaction: procedure A: the reaction was carried out in the small glass vessels containing 60 μl of the chromogen solution for 20 min at room temperature. Then 50 μl of the resulting solution and 50 μl of 4N HCI were pipetted into a well of a microtiter plate, and the absorbance was measured in the dual scan mode at 490 nm and 630 nm using the EIA-reader. Procedure B (see Fig. 2 and Fig. 3): the reactor was filled with citrate buffer, and the needle was mounted into it. After rinsing the system with citrate buffer, the chromogen solution was injected by a syringe into the system. Valve 2 was set to pump the excess solution to waste, in order not to contaminate the UV-detector with citrate buffer or chromogen solution. After filling the reactor with the chromogen solution the feeding was stopped for 15 min to let the enzymatic reaction proceed. Then the solution was pumped through the detector cell of the UV-meter using the HPLC-pump, and the absorbance was read at 405 nm. Finally distilled water was pumped through to clean the whole system using the HPLC-pump.

The standard curve was prepared from calibrates containing known levels of atrazine at 0, 0.01, 0.1, 1 and 1000 μg l^{-1} or 0, 0.01, 0.1, 0.3, 1 and 1000 μg l^{-1} The dilution of the stock solutions of the tracer and the K4E7 antibody were optimised. All standards were measured as triplicates unless stated otherwise.

2.5. Analysis of natural water samples

Two water samples were provided by the ESWE Institut fur Wasserforschung, Wiesbaden, Germany. Both samples consisted of surface water and are to be considered as cumulated mixed samples. Sample I was collected between April 1–9, 1996, sample II between June 24 and July 1, 1996. Both samples have been independently analysed using a GC/MS-method by the ESWE Institute.

The water samples were used without pretreatment. For checking for matrix effects the samples were additionally diluted by a ratio 1:2, with PBS-buffer pH 7.6. The samples were analysed using the ELISA with microtiter plates or the needles as solid phase.

2.6. Analysis of the data

The absorbance data for all calibrates of one assay run were normalised by transformation to % B/B_0 according to Eq. (1),

$$\% B/B_0 = 100 \times (A - A_{ex})/(A_0 - A_{ex}) \quad (1)$$

with A = absorbance of the sample or standard A_0 = absorbance of the standard containing 0 μg l^{-1} of atrazine A_{ex} = absorbance of the standard with excess atrazine (1000 μg l^{-1})

% B/B_0 thus represents the absorbance for an arbitrary dose relative to that for the zero dose corrected for nonspecific absorbance. The 50% B/B_0-value is called the centre of the test or IC_{50}.

The determination range of the calibration curve is limited by the upper and lower determination limit which are not identical to the detection limits [79–81]. As operation limits of the assay presented here 10% B/B_0 and 80% B/B_0 were chosen as they mark the boundary of the part of the curve with highest sensitivity [82]. According to the Union of Pure and Applied Chemistry [79] curve fitting of the standard calibration curve should be performed with the 4-parameter-logistic equation of Rodbard [82].

$$y = d + (a - d)/(1 + (x/c)^b) \quad (2)$$

with a = upper asymptote of the curve, d = lower asymptote of the curve, c = analyte concentration at IC_{50}, b = slope of the curve at IC_{50}, y = test signal x = analyte concentration.

The obtained not normalised data were analysed using the software Biolinx 2.21. The software involves an iteration procedure based on Eq. (2) using directly the not normalised absorbances. In a parallel calculation the normalised data % B/B_0 were analysed according to Eq. (2) with the help of the software Fig. P.

For comparison of mean values (IC_{50} or the atrazine content of the sample obtained by different methods) the t-test was applied, variances were compared using the F-test [83,84].

3. Results and discussion

3.1. General outline of the assay

The developed immunoassay for atrazine is an enzyme-linked immunosorbent assay using immobilised antibodies, free tracer and analyte in the competition step, following the ELISA-format 2a as discussed in Section 1.2 (see Fig. 1). The solid phase was precoated by goat anti-mouse antibody, then the monoclonal anti-atrazine antibody K4E7 was bound in the coating step by the antibody of the precoating step. In the following competition step analyte and tracer competed for the binding sites of K4E7. The amount of bound tracer is then determined by its enzymatic reaction.

Schneider and Hammock [56] compared various test formats employing direct binding of antibody to the solid phase or precoating techniques and could show that best IC_{50}-values and detection limits are obtained using precoating. Precoating itself results in relatively high concentration of goat anti-mouse antibody on the solid phase. Hence there is no need of a blocking step. Precoating also allows the use of lower concentration of the anti-atrazine antibody and as a consequence lower tracer concentrations giving a lower IC_{50} value for the assay than an assay without precoating [56,85].

The antibody K4E7 is a monoclonal antibody produced by using hybridoma technique and characterised by Giersch et al. [57,77]. For the immunisation of mouse a conjugate of key hole limpet haemocyanine and the hapten 6-((4 chloro-6-(ethyl amino)-1,3,5-triazin-2yl)amino)-hexanoic acid was used. The spacer may mimic alkyl groups such as isopropyl when stimulating B-lymphocytes giving high affinity antibodies against atrazine and propazine as shown by the cross reactivity pattern of K4E7 [57]. The hapten used to synthesise the HRP-tracer had an isopropyl group instead of an ethyl group in 6-position and is recognised by the antibody, too.

The sensitivity of the assay and its IC_{50}-value is mainly determined by the affinity and specificity of the antibody, however, the choice of an appropriate tracer can enhance the IC_{50}-value markedly as was shown by [8]. HRP as the enzyme resulted in nearly a 10-fold improved assay compared to alkaline phosphatase as the enzyme. Hence in the work presented here an HRp tracer was chosen.

3.2. Microtiter plates as solid phase

In a first approach microtiter plates were used as solid phase and a sensitive assay was build up. Calibration curves were performed in quadruplicates for each standard. The dilution of the stock solution of the tracer and K4E7-antibody were varied to get a low IC_{50}-value preferably 0.1 μg l^{-1}. Table 3 shows the IC_{50} value as a function of the tracer dilution for a fixed K4E7 dilution, 1:50000 or 1:75000, respectively. All data points are mean values of four independent calibration curves.

Table 3
Centre of the test IC_{50}, 10% B/B_0 and 80% B/B_0 in dependence of the K4E7-antibody dilution and the HRP-tracer dilution

K4E7-dilution	Tracer dilution	n	IC_{50}-value[a] [μg l^{-1}]	80% B/B_0^a [μg l^{-1}]	10% B/B_0^a [μg l^{-1}]	$\Delta B/B_0^b$ [μg l^{-1}]
1:50 000	1:50 000	4	0.205 ± 0.012	0.053 ± 0.008	1.77 ± 0.08	1.72
1:50 000	1:75 000	5	0.161 ± 0.011	0.047 ± 0.006	1.41 ± 0.11	1.36
1:50 000	1:100 000	5	0.143 ± 0.013	0.038 ± 0.006	1.25 ± 0.05	1.21
1:50 000	1:150 000	5	0.120 ± 0.013	0.034 ± 0.003	0.90 ± 0.15	0.87
1:75 000	1:50 000	4	0.210 ± 0.013	0.053 ± 0.010	1.86 ± 0.20	1.81
1:75 000	1:75 000	4	0.172 ± 0.011	0.052 ± 0.006	1.36 ± 0.10	1.31
1:75 000	1:100 000	4	0.138 ± 0.015	0.037 ± 0.009	1.22 ± 0.10	1.18
1:75 000	1:150 000	4	0.129 ± 0.015	0.041 ± 0.006	1.02 ± 0.12	0.98

Tracer: Tr2.
[a] Mean values $\pm$ standard deviation of n independent calibration curves.
[b] 80% $B/B_0 - 10\%$ B/B_0.

As the suitable concentration range 80% B/B_0 was chosen as the lower limit, 10% B/B_0 as the upper limit. In literature the concentration range is not defined along the same lines. Sometimes detection limits are chosen, some use determination limits. When choosing the 10 and 80% B/B_0-values as limits the most sensitive almost linear part of the calibration curve is used being within the determination limits and in accordance with the suggestion of the Union of Pure and Applied Chemistry that the lower or upper limit of quantification should not exceed a variation coefficient of $\pm 25\%$ [79]. 80% B/B_0 is also favoured as a limit by Rodbard [82].

The applied concentration of antibody and enzyme tracer determine the detection limit, the IC_{50}-value and the sensitivity of the assay. The sensitivity is usually defined as slope of the curve at its inflection point. As discussed by Hock [85] the lower the antibody concentration and the total amount of hapten (analyte plus tracer) the better the detection limit and IC_{50}-value, but the sensitivity itself decreases. The sensitivity is defined as the slope at the IC_{50}-value; it can be approximated by the difference between the 80 and 10% B/B_0-value. For the purpose of detecting a low amount of the analyte (e.g. atrazine) the IC_{50}-value should be low, best about 0.1 μg l^{-1} as pointed out in the introduction. The assay presented here fulfils that requirement best for dilutions to be 1:50000 for K4E7 and 1:150000 for the tracer Tr2; tracer Tr1 was best when diluted by 1:30000. A further dilution of K4E7 down to 1:75000 gives same results for the IC_{50}-value, the 80 and 10% B/B_0-value within the experimental error showing that the affinity limit of the antibody was approached.

Fig. 4 presents a typical calibration curve using the optimised conditions. The IC_{50}-value as a mean value of eight independent calibration curves is 0.129 μg l^{-1} (see Table 4). The range between 80 and 10% B/B_0 is 32–1000 ng l^{-1}.

The K4E7-antibody is used in literature for determining atrazine [57,77]. The assays were performed in precoated microtiter plates using an HRP-tracer. The results of IC_{50}-value to be 0.1 μg l^{-1} and 80% B/B_0 to be 30 ng l^{-1} are comparable with those presented in this paper. The solid phase used in [57,77], however, was from a different manufacturer than those used in this communication. It should be noticed that microtiter plates from different companies may influence the IC_{50}-value and the variation coefficients as shown by [65].

Since the assay was designed for a serial screening test, it had to be robust and reliable. The reproducibility of the calibration curves was checked using the IC_{50}-value as indicator. Table 4 shows the results for measurements within different days. Within one day an IC_{50}-value of (0.128 ± 0.008) μg l^{-1} $(n = 2)$ was obtained, between days the IC_{50}-value was (0.129 ± 0.009) μg l^{-1} $(n = 8)$. The variances (F-test) and the IC_{50}-values (t-test) for measurements within or between

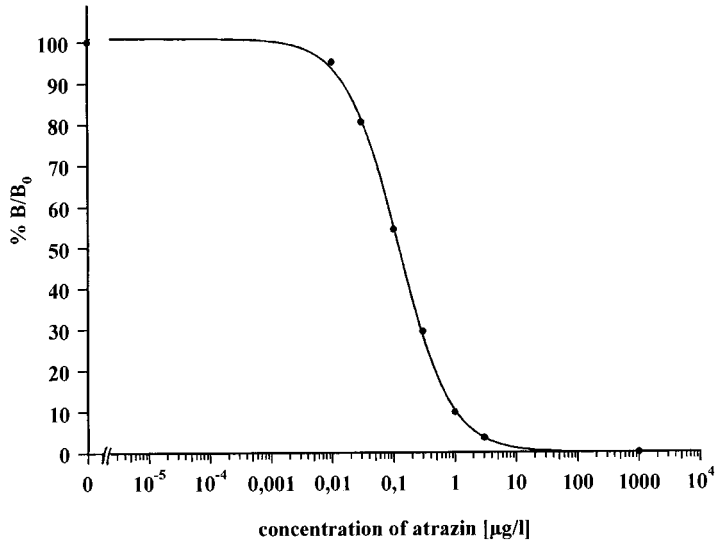

Fig. 4. Representative calibration curve for the determination of atrazine by a competitive ELISA using a microtiter plate as solid phase. Each data point is the mean value of 3 determinations. Results were obtained under optimised conditions using tracer Tr2 (see text).

days are similar on a 95% confidence level. Hence the IC_{50}-value as well as the 80 and 10% B/B_0 showed good reproducibility.

3.3. ELISA on inoculation needles as a solid phase

A second assay was developed to reduce the required sample volume below 50 µl, but without loss in its determination characteristics. As solid phase inoculation needles were used, in the following referred as needles. The assay format follows closely the one performed in microtiter plates as described in Section 3.1 using the same antibodies for precoating, the anti-atrazine antibody K4E7 and the HRP-tracer. All needles necessary to run one test, including calibration and sample analysis, were treated together in the precoating and coating step. As from the competition step each needle was treated individually. The competition was carried out in small special glasses which allow to reduce the sample volume to 30 µl compared to 100 µl when using microtiter plates. The enzyme reaction step was performed in two different ways.

In procedure A the enzymatic reaction was performed in the small glass vessels. Then a part of the solution was stopped after transferring it to a well of microtiter plate. This allows the convenient use of the EIA-reader and direct calculation of the calibration curve. Hence this procedure was applied to determine the best tracer dilution and K4E7 dilutions as well as for checking the reproducibility of the assay.

A K4E7-antibody dilution of 1:50000 was compared with one of 1:25000. A dilution of tracer Tr2 of 1:50000 was best, because lower tracer dilutions gave too low absorbance values. Both combinations gave comparable results (K4E7 1:50000: $IC_{50} = (0.124 \pm 0.025)$ µg l^{-1}, $n = 5$; K4E7 1:25000: $IC_{50} = (0.120 \pm 0.046)$ µg l^{-1}, $n = 3$). Hence the dilution consuming less antibody was chosen for further measurements. A more diluted antibody stock solution resulted in less reproducible assays.

Fig. 5 shows a typical calibration curve. The optimised assay conditions were K4E7 diluted 1:50000 and Tr1 diluted 1:12000 or Tr2 diluted 1:50000. Day to day reproducibility is demonstrated in Table 4. The IC_{50}-value obtained from five independent calibration curves was (0.124 ± 0.025) µg l^{-1} with a concentration range between 80 and 10% B/B_0 of 22–2900 ng l^{-1}. The IC_{50}-value of the ELISA on needles as solid phase and

Table 4
Between day reproducibility of calibration curve using ELISA with microtiter plate (plate) or inoculation needle (needle) as solid phase

Solid phase	No. of calibration curve	IC_{50}-value [μg l^{-1}]	80% B/B_0 [μg l^{-1}]	10% B/B_0 [μg l^{-1}]
plate	1	0.122	0.025	1.000
	2	0.137	0.035	0.990
	3	0.114	0.028	1.002
	4	0.130	0.030	1.070
	5	0.133	0.035	1.119
	6	0.135	0.035	1.129
	7	0.122	0.034	0.939
	8	0 138	0 037	0.981
	Means ± SD	0.129 ± 0.010	0.032 ± 0.004	1.029 ± 0.069
Needle[a]	1	0.101	0.012	3.18
	2	0.146	0.035	1.41
	3	0.122	0.014	3.68
	4	0.151	0.013	4.96
	5	0.098	0.036	1.71
	Means ± SD	0.124 ± 0.025	0.022 ± 0.012	2.99 ± 1.46

Each standard of a calibration curve was measured as quadruplicate (plate) or triplicate (needle). Tracer: Tr2, dilutions as optimised (see text).
SD, standard deviation.
[a] According to procedure A.

on microtiter plates are similar with respect to mean value and variance, at a significance level of $\alpha = 0.01$. The concentration range between 80 and 10% B/B_0 is larger for needles as solid phase than for microtiter plates, due to a smaller slope. Therefore the variances of 10 and 80% B/B_0 are higher than those obtained on microtiter plates.

The new assay using inoculation needles fulfils the requirements of a sample volume below 50 μl and of an IC_{50}-value about 0.1 μg l^{-1} to detect atrazine in concentrations < 0.3 μg l^{-1}. Although the day to day variation is higher than in the assay on microtiter plates, if sample having concentrations far from the IC_{50}-value are measured, it will be suitable as a generally applicable analysing method for research on samples only available in small quantities.

In procedure B all steps except the enzymatic reaction were performed as described. For the enzymatic reaction a special reactor was used as a first approach towards automatisation. The optimised conditions with regard to K4E7 and tracer concentrations were applied as defined with procedure A. It should be noticed that in procedure B due to the flow through mode the enzymatic reaction was not stopped by HCI, but directly pumped through the detector. Normally the addition of HCI gives a shift of the absorbance maximum of the product from 445 to 492 nm accompanied by an increase of the absorption coefficient [86]. Here the unstopped solution had to be measured at 405 nm resulting in lower absorbance values compared to a solution stopped with HCI.

A typical calibration curve is shown in Fig. 6. For two independent calibration curves the IC_{50}-value is (0.093 ± 0.018) μg l^{-1}, 80% B/B_0 is (0.028 ± 0.019) μg l^{-1} and 10% B/B_0 (0.682 ± 0.052) μg l^{-1}. For the IC_{50}-value and 80% B/B_0 procedure A and B give similar results with regard to variance (F-test) and mean values (t-test) at a significance level of $a = 0.05$.

The 10% B/B_0-value of procedure B is lower than for procedure A. If the fitting of the curve for both procedures is compared, the fitting for procedure A is better. This may be due to a loss of sensitivity using the unstopped solutions and their lower absorbances in procedure B.

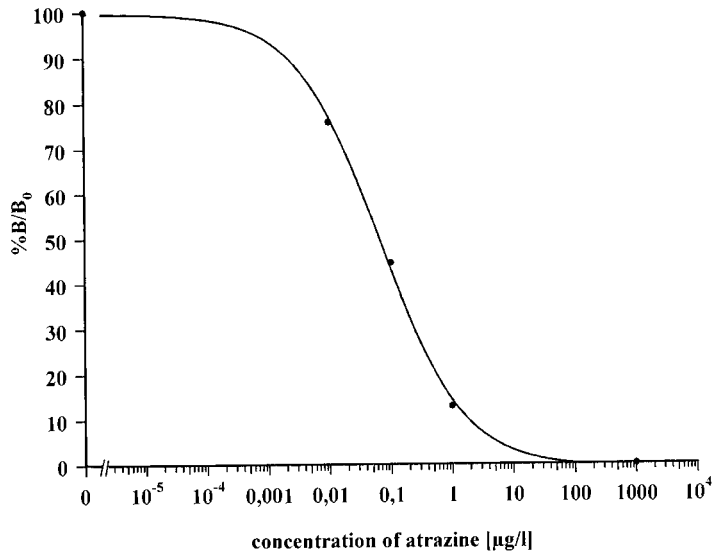

Fig. 5. Representative calibration curve for the determination of atrazine by a competitive ELISA using inoculation needles as solid phase. The enzymatic step was performed according to procedure A: the absorbance of the product was measured by the EIA-reader after transferring an aliquot to a microtiter plate. Each data point is the mean value of 4 determinations. Results were obtained under optimised conditions using tracer Tr2 (see text).

It is also of interest that-as compared to the assay on microtiter plates -the slope of the assay on needles is smaller, hence a greater concentration range can be checked but at a comparable IC_{50}-value.

3.4. Analysis of water samples

Two different natural water samples were analysed using the developed ELISA with microtiter plates or inoculation needles as solid phase. The probes were surface water samples collected in early April or at the end of June of 1996, five years after the atrazine ban in Germany. To check matrix effects the samples were analysed without dilution or after a 1:2 dilution with PBS-buffer. No matrix effects were observed.

Table 5 summarises the results obtained with microtiter plates or needles as a solid phase using procedure A between day to day measurements. Both methods gave similar results with regard to variance (F-test) and mean value (t-test) at a significance level of 0.01. The variation coefficient of sample I was larger than for sample II. This is due to the fact that the concentration of sample II is close to the IC_{50}-value of the test. At IC_{50} the sensitivity of the assay is highest and therefore the variation coefficient small [80]. In contrary sample I has an atrazine concentration which is near to the 80% B/B_0-value meaning near the lower determination limit and which is therefore attended with a large variation coefficient.

The results were then compared with the concentrations determined by a GC/MS analysis. According to this control method sample I contains 0.04 µg l^{-1} atrazine and 0.05 µg l^{-1} desethylatrazine. Sample II gave results of 0.06 µg l^{-1} atrazine, 0.09 µg l^{-1} desethylatrazine and 0.07 µg l^{-1} terbutylazine. For the immunoassays the calibration curves were obtained using atrazine standards and then the samples analysed as if they only contained that herbicide. However, antibodies normally show cross-reactivities to molecules which are structurally related to the analyte. The cross-reactivities of the K4E7-antibody was determined by Giersch [57] to be 18% for desethylatrazine and 26% for terbutylazine. Because both assays presented in this paper use an assay format with precoating using goat-anti mouse anti-

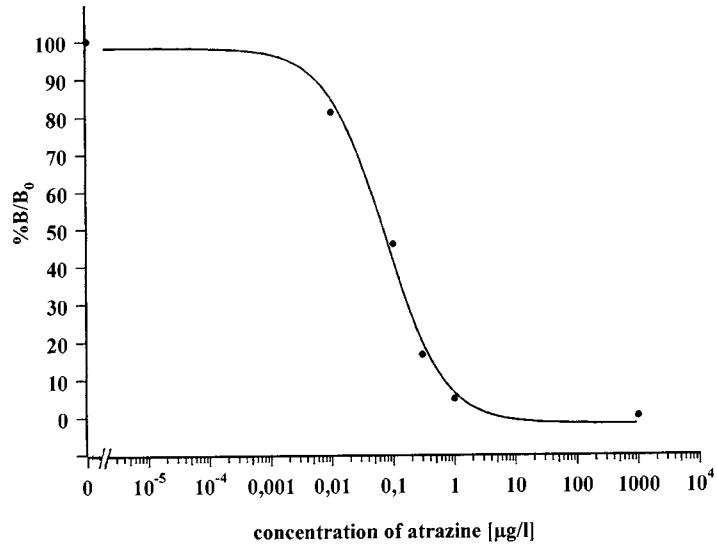

Fig. 6. Representative calibration curve for the determination of atrazine by a competitive ELISA using inoculation needles as solid phase. The enzymatic step was performed according to procedure B using the flow through system. Each data point is the mean value of 3 determinations. Results were obtained under optimised conditions using tracer Tr1 (see text).

bodies and HRP-tracer based on the same hapten as in [57], in the competition step the same cross-reactivity can be assumed. If then for the GC/MS data the cross-reactivities are taken into account, sample I would pretend 0.049 µg l^{-1} and sample II, 0.094 µg l^{-1} of atrazine. The results for sample I and II are in good agreement with the results obtained by the ELISA on microtiter plate and needle (procedure A).

4. Conclusion

The determination of pesticides like atrazine in water samples of restricted volume at trace levels is a future challenge of environmental analysis. Reviewing existing methods for atrazine immunochemical methods are the most promising ones, because they require almost no preconcentration and pretreatment of the sample.

Table 5
Comparison and reproducibility of the ELISA on microtiter plates (plate) and the ELISA on inoculation needles (needle)

ELISA-type	Analysis no.[a]	Sample I conc. [µg l^{-1}][b]	Sample II conc. [µg l^{-1}][b]
Plate	1	0.044 ± 0.0045	0.094 ± 0.0031
	2	0.051 ± 0.0015	0.097 ± 0.0024
	3	0.038 ± 0.0016	0.105 ± 0.011
	4	0.035 ± 0.0046	0.099 ± 0.0058
	Means $\pm$ SD	0.042 ± 0.0035	0.099 ± 0.0024
Needles[c]	1	0.034 ± 0.0051	0.121 ± 0.024
	2	0.043 ± 0.0042	0.096 ± 0.019
	3	0.038 ± 0.0057	0.116 ± 0.022
	Means $\pm$ SD	0.038 ± 0.0026	0.114 ± 0.013

Samples I and II are surface water samples. Tracer: Tr2, dilutions as optimised (see text).
SD, standard deviation.
[a] Analysis of different numbers were performed on different days.
[b] Mean value of 4 measurements (plate) or 3 measurements (needle).
[c] According to procedure A.

Based on the discussed necessities an ELISA has been developed using the surface of inoculation needles as a solid phase. The needles allowed the performance of the assay in small glass vessels reducing the sample volume to 30 μl compared to the 100 μl required by a parallel developed ELISA in microtiter plates. The centre of the test $IC_{50}$was 0.12 μg l^{-1} (needles) and 0.13 μg l^{-1} (microtiter plates), the concentration range between 80 and 10% B/B_0 was 0.022–2.90 μg l^{-1} (needle) and 0.03–1.00 μg l^{-1} (microtiter plate). A first approach towards automatisation for the enzymatic step was successful, but the use of the EIA-reader for measuring is more convenient when handling a large number of samples even if an additional pipetting step is necessary.

The developed assays were successfully employed in the analysis of two surface water samples having low atrazine contents. Both ELISA methods showed a good reproducibility.

The assay using inoculation needles as a solid phase has the smallest sample volume reported for ELISAs for atrazine, up to our knowledge. This fact and the low IC_{50}-value will make the assay suitable for the analysis of atrazine in water samples of restricted volumes, e.g. cloud water. The methodology, itself, will not only be restricted to atrazine, it can also be applied to virtually any pesticide when suitable antibodies are available. This opens the possibility of utilising ELISA technique for samples only available in small volumes at low concentrations.

Acknowledgements

We thank Prof Dr B. Hock and Dr T. Giersch of the Technical University of Munich for providing the K4E7 anti-atrazine antibody and the tracer Tr2. The financial support of the Deutsche Forschungsgemeinschaft (Ba 588/6-1) is greatly acknowledged.

References

[1] A. Dankwardt, S. Pullen, S. Rauchalles, K. Kramer, F. Just, B. Hock, R. Hofmann, R. Schewes, F.X. Maidl, Anal. Lett. 28 (1995) 621–634.
[2] A. Dankwardt, S. Wust, W. Wiling, E.M. Thurman, B. Hock, Environ. Sci. Pollut. Res. 1 (1994) 196–204.
[3] A. Boehncke, J. Siebers, H.G. Nolting, Chemosphere 21 (1990) 1109–1124.
[4] H. Neururer, R. Womastek, Die Bodenkultur (1991) 57–70.
[5] C. E. Junge, Pure Appl. Chem. 42 (1975) 95–104.
[6] H.R. Buser, Environ. Sci. Technol. 24 (1990) 1049–1058.
[7] G. Durand, V. Bouvot, D. Barcelo, J. Chromatogr. 607 (1992) 319–327.
[8] S. Wust, U. Doht, T. Giersch, C. Wittmann, B. Hock, GIT Fachz. Lab. 2 (1990) 99–106.
[9] C. Wittmann, B. Hock, Food Agric. Immunol. 2 (1990) 65–74.
[10] S. Wust, B. Hock, Anal. Lett. 25 (1992) 1025–1037.
[11] M. Klein, W. Kein, Nachr. Chem. Tech. Lab. 38 (1990) 594–600.
[12] M. Franek, V. Kolar, S.A. Eremin, Anal. Chim. Acta 311 (1995) 349–356.
[13] A.D. Lucas, P. Schneider, R.O. Harrison, J.N. Seiber, B.D. Hammock, J.W. Biggar, D.E. Rolston, Food Agric. Immunol. 3 (1991) 155–167.
[14] EEC Drinking Water Guidelines, 80/779/EEC, EEC No. L229/11-29, EEC, Brussels1980.
[15] Ch. Oberwalder, H. Gieβl, L. Irion, J. Kirchhoff, K. Hurle, Nachrichenbl. Deut. Pflanzenschutzd 43 (1991) 185–191.
[16] J. Scharf, R. Wiesiollek, K. Bachmann, Fresenius J. Anal. Chem. 342 (1992) 813–816.
[17] R. Herterich, Z. Umweltchem. Ökotox 3 (1991) 196–200.
[18] M. Grandet, L. Weil, K.E. Quentin, Z. Wasser Abwasser Forsch. 21 (1988) 21–24.
[19] T. Suzuki, K. Yaguchi, K. Ohnishi, T. Yamagishi, J. Chromatogr. A 662 (1994) 139–146.
[20] W.E. Pereira, C.E. Rostad, T.J. Leiker, Anal. Chim. Acta 228 (1990) 69–75.
[21] V. Janda, K. Marha, J. Chromatogr. 329 (1985) 186–188.
[22] Z. Stransky, J. Chromatogr. 320 (1985) 219–231.
[23] G.A. Junk, J.J. Richard, Anal. Chem. 60 (1988) 451–454.
[24] M. Ahel, K.M. Evans, T.W. Fileman, R.F.C. Mantoura, Anal. Chim. Acta 268 (1992) 195–204.
[25] R. Eisert, K. Levsen, Fresenius J. Anal. Chem. 351 (1995) 555–562.
[26] G. Durand, D. Barcelo, Talanta 40 (1993) 1665–1670.
[27] M. Popl, Z. Voznakova, V. Tatar, J. Strnadova, J. Chromatogr. Sci. 21 (1983) 39–42.
[28] D.A. Cassada, R.F. Spalding, Z. Cai, M.L. Gross, Anal. Chim. Acta 287 (1994) 7–15.
[29] M.T. Meyer, M.S. Mills, E.M. Thurman, J. Chromatogr. 629 (1993) 55–59.
[30] J. Slobodnik, A.C. Hogenboom, A.J.H. Louter, U.A.T. Brinkman, J. Chromatogr. A 730 (1996) 353–371.
[31] J.J. Vreuls, A.J. Bulterman, R.T. Ghijsen, U.A.T. Brinkman, Analyst 117 (1992) 1701–1705.

[32] M. Stahl, M. Luhrmann, H.G. Kicinski, A. Kettrup, Z. Wasser Abwasser Forsch. 22 (1989) 124–127.
[33] A. di Corcia, M. Marchetti, R. Samperi, J. Chromatogr. 405 (1987) 357–363.
[34] J.M. Huen, R. Gillard, A.G. Mayer, B. Baltensperger, H. Kern, Fresenius J. Anal. Chem. 348 (1994) 606–614.
[35] G. Sacchero, C. Sarzanini, E. Mentasti, J. Chromatogr. A 671 (1994) 151–157.
[36] J. Lintelmann, C. Mengel, A. Kettrup, Fresenius J. Anal. Chem. 346 (1993) 752–756.
[37] J. Schulein, D. Martens, P. Spitzauer, A. Kettrup, Fresenius J. Anal. Chem. 352 (1995) 565–571.
[38] B. Nouri, G. Toussaint, P. Chambon, R. Chambon, Analyst 120 (1995) 2683–2687.
[39] P. Parrilla, J.L. Martinez Vidal, M. Martinez Galera, A.G. Frenich, Fresenius J. Anal. Chem. 350 (1994) 633–637.
[40] S. Lacorte, D. Barcelo, Anal. Chim. Acta 296 (1994) 223–234.
[41] E. Papadopoulou-Mourkidou, J. Patsias, J. Chromatogr. A 726 (1996) 99–113.
[42] J. Slobodnik, M.G.M. Gronewegen, E.R. Brouwer, H. Lingeman, U.A.T. Brinkman, J. Chromatogr. 642 (1993) 359–370.
[43] H. Sabik, S. Cooper, P. Lafrance, J. Fournier, Talanta 42 (1995) 717–724.
[44] S. Chiron, S. Dupas, P. Scribe, D. Barcelo, J. Chromatogr. A 665 (1994) 295–305.
[45] H. Bagheri, E.R. Brouwer, R.T. Ghijsen, U.A.T. Brinkman, J. Chromatogr. 647 (1993) 121–129.
[46] H. Zahradnickova, P. Simek, P. Horicova, J. Triska, J. Chromatogr. A 688 (1994) 383–389.
[47] H. Susse, H. Muller, J. Chromatogr. A 730 (1996) 337–343.
[48] V. Pichon, L. Chen, N. Durand, F. Le Goffic, M.C. Hennion, J. Chromatogr. A 725 (1996) 107–119.
[49] A. Marx, T. Giersch, B. Hock, Anal. Lett. 28 (1995) 267–278.
[50] V. Pacakova, K. Stulik, J. Jiskra, J. Chromatogr. A 754 (1996) 17–31.
[51] M. Biziuk, A. Przyjazny, J. Czerwinski, M. Wiergowski, J. Chromatogr. A 754 (1996) 103–123.
[52] A. Balinova, J. Chromatogr. A 754 (1996) 125–135.
[53] C. Wittmann, R.D. Schmid, Sensors and Actuators B 15–16 (1993) 119–126.
[54] C. Wittmann, B. Hock, Food Agric. Immunol. 1 (1989) 211–224.
[55] S.J. Huber, B. Hock, Methods of Enzymatic Analysis, vol. XII, 1986, pp. 438–450.
[56] P. Schneider, B.D. Hammock, J. Agric. Food Chem. 40 (1992) 525–530.
[57] T. Giersch, J. Agric. Food Chem. 41 (1993) 1006–1011.
[58] M. Wortberg, M.H. Goodrow, S.J. Gee, B.D. Hammock, J. Agric. Food Chem. 44 (1996) 2210–2219.
[59] B. Dunbar, B. Riggle, G. Niswender, J. Agric. Food Chem. 38 (1990) 433–437.
[60] J.M. Schlaeppi, W. Fory, K. Ramsteiner, J. Agric. Food Chem. 37 (1989) 1532–1538.
[61] J. Gascon, E. Martinez, D. Barcelo, Anal. Chim. Acta 311 (1995) 357–364.
[62] F.M. Rubio, J.A. Itak, A.M. Scutellaro, M.Y. Selisker, D.P. Herzog, Food Agric. Immunol. 3 (1991) 113–125.
[63] E.M. Thurman, M. Mayer, M. Pomes, C.A. Perry, A.P. Schwab, Anal. Chem. 62 (1990) 2043–2048.
[64] J.P. Sherry, Crit. Rev. Anal. Chem. 23 (1992) 217–300.
[65] C. Mouvet, S. Broussard, R. Jeannot, C. Maciag, R. Abuknesha, G. Ismail, Anal. Chim. Acta 311 (1995) 331–339.
[66] R. Bushway, B. Perkins, S.A. Savage, B.S. Ferguson, Bull. Environ. Contam. Toxicol. 40 (1988) 647–654.
[67] B.D. Hammock, S.J. Gee, R.O. Harrison, F. Jung, M.H. Goodrow, Q.X. Li, A.D. Lucas, A. Szekacs, K.M.S. Sundaram, ACS Symp. Ser. 442 (1990) 112–139.
[68] M. Wortberg, K. Cammann, Fresenius J. Anal. Chem. 346 (1993) 757–760.
[69] J.L. Marty, D. Garcia, R. Rouillon, Trends Anal. Chem. 14 (1995) 329–333.
[70] M.P. Marco, S. Gee, B.D. Hammock, Trends Anal. Chem. 14 (1995) 341–350.
[71] L. Engel, W. Baumann, Fresenius J. Anal. Chem. 349 (1994) 447–450.
[72] R.D. Schmid, A. Gebbert, R. Kindervater, P. Kramer, Z. Wasser Abwasser Forsch. 24 (1991) 15–20.
[73] A. Brecht, J. Piehler, G. Lang, G. Gauglitz, Anal. Chim. Acta 311 (1995) 289–299.
[74] M. Minunni, M. Mascini, Anal. Lett. 26 (1993) 1441–1460.
[75] F.A. McArdle, K.C. Persaud, Analyst 118 (1993) 419–423.
[76] H. Tsuruta, H. Yamada, Y. Motoyashiki, K. Ota, C. Okada, M. Nakamura, J. Immunol. Methods 183 (1995) 221–229.
[77] T. Giersch, K. Kramer, DFG-Report (1995).
[78] M.H. Goodrow, R.O. Harrison, B.D. Hammock, J. Agric. Food Chem. 38 (1990) 990–996.
[79] A.J. Krotzky, B. Zeeh, Pure Appl. Chem. 67 (1995) 2065–2088.
[80] R.A. Dudley, P. Edwards, R.P. Ekins, D.J. Finney, I.G.M. McKenzie, G.M. Raab, D. Rodbard, R.P.C. Rodgers, Clin. Chem. 31 (1985) 1264–1271.
[81] S. Ebel, K. Kamm, Fresenius Z. Anal. Chem. 316 (1983) 382–385.
[82] D. Rodbard, Clin. Chem. 20 (1974) 1255–1270.
[83] J.C. Miller, J.N. Miller, Statistics for Analytical Chemistry, Ellis Horwood, Chichester, 1984.
[84] R.E. Walpole, R.H. Myers, Probability and Statistics for Engineers and Scientists, Prentice–Hall, Englewood Cliffs NJ, 1993.
[85] B. Hock, Z. Wasser Abwasser Forsch. 22 (1989) 78–84.
[86] P. Tjissen, Practice and Theory of Enzyme Immunoassays, Elsevier, Amsterdam, 1985.

ELSEVIER

Talanta 48 (1999) 821–825

Talanta

Radioanalytical determination of actinides and fission products in Belarus soils

H. Michel [a,*], J. Gasparro [a], G. Barci-Funel [a], J. Dalmasso [a], G. Ardisson [a], G. Sharovarov [b]

[a] *Laboratoire de Radiochimie, Faculté des Sciences, Université de Nice-Sophia Antipolis, 06108 Nice Cédex 2, France*
[b] *Institute of Radioecological Problems, Minsk, Belarus*

Received 18 June 1997; received in revised form 10 October 1997; accepted 10 October 1997

Abstract

Alpha emitting actinides such as plutonium, americium or curium were measured by α-spectrometry after radiochemical separation. The short range of α-particles within matter requires, after a pre-concentration process, a succession of isolation and purification steps based on the valence states modification of the researched elements. For counting, actinides were electrodeposited in view to obtain the mass-less source necessary to avoid self-absorption of the emitted radiations. Activity concentrations of gamma-emitting fission products were calculated after measurement with high purity germanium detectors (HPGe). These different methods were used to analyse soils sampled in the Republic of Belarus, not far from the Chernobyl nuclear plant.

Keywords: Radiochemistry; Actinide; Fission products; Chernobyl

1. Introduction

During the last 40 years, a great attention has been given to the development of methods in view to determine actinides (plutonium, americium, curium, other transuranium elements) and also fission products in the environment [1–8].

The main origin for these radionuclides is the nuclear weapons fallout and the Chernobyl fallout. The ratios between elements are different according to the origin of the fallout.

Plutonium has been produced in greater quantity than any other transuranic elements and has been the major subject of ecological research as atmospheric weapon tests, routing waste disposals and various nuclear accidents made it more prevalent than the other transuranic elements. Pu is present in the environment at very low concentrations and more than 95% of environmental Pu is found in soils. The determination of Pu in soils is therefore very important for radioecological studies of the elements [9].

^{137}Cs is one of the most important γ -emitting radionuclides found in the environment. The determination of its activity concentration can be used to estimate the activities of other radionuclides using the established radionuclide ratios.

* Corresponding author. Tel.: + 33 4 92076365; fax: + 33 4 92076364; e-mail: barci@unice.fr

0039-9140/99/$ - see front matter
PII S0039-9140(98)00098-8

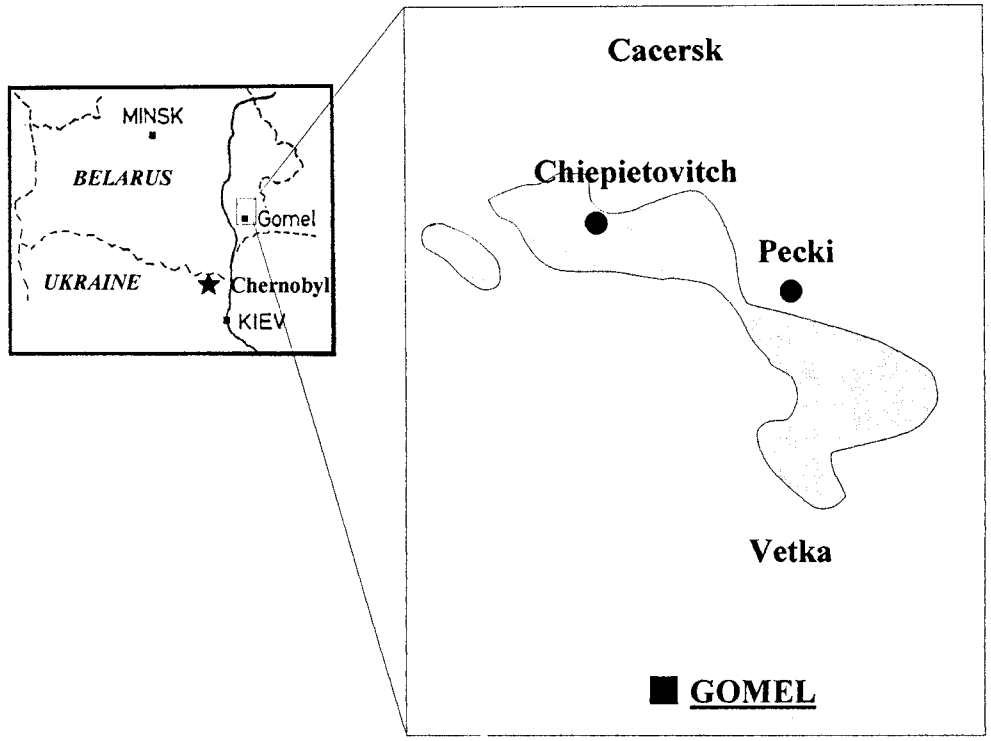

Fig. 1. Sampling: sites on the map are presented—the places where soils were sampled in the Republic of Belarus. The shaded area shows the highest radioactive contaminated zone in the studied region.

In this study, we present results concerning the alpha-radioanalytical determination of ^{238}Pu, $^{239+240}$Pu, ^{241}Am, $^{243+244}$Cm and the gamma-determination of ^{134}Cs, ^{137}Cs, ^{125}Sb, ^{40}K, ^{226}Ra and ^{232}Th in Belarus soils. The sampling was made in different sites, not far from the Chernobyl nuclear plant: Chiepietovitch (Cacersk) and Pecki (Vetka) in the region of Gomel, and at different depths (0–5, 5–10, and 10–15 cm).

2. Experimental

All reagents used were of analytical grade and solutions were prepared in unionised water.

Anionic columns were: Bio Rad AGMP1 and Dowex 1 × 4, 100–200 mesh in chloride form and cationic columns: Aldrich Dowex 50W × 8, 100–200 mesh in chloride form.

2.1. Sampling

Analysed samples were Belarus soils sampled at the end of 1996.

Belarus is near Ukraine and the region of Gomel, where the sampling was made, is ~140 km from Chernobyl. Sampling was made at three different depths: 0–5, 5–10 and 10–15 cm. Sampling sites are shown in Fig. 1. The studied soils were podzol with clay base over moraine in the Chiepietovitch site, and clay on alluvium in the Pecki site.

Pecki and Chiepietovitch, respectively situated in the district of Vetka and Cacersk, region of Gomel, are located in the south east of Minsk. As it can be seen on the map, one of them is situated in the highest Chernobyl contaminated zone, Chiepetovitch (Cacersk). The other one is near this zone, Pecki (Vetka).

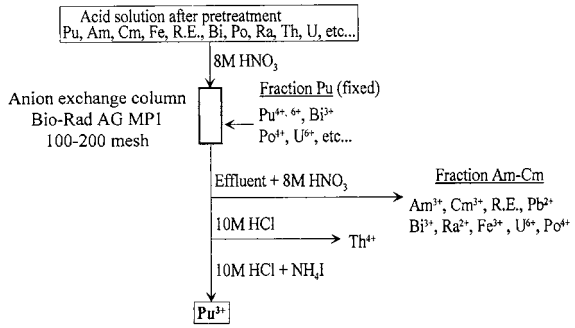

Fig. 2. Radiochemical separation of the different fractions, americium, thorium and plutonium after the pretreatment step.

2.2. Alpha spectrometry measurements

Analysis of Pu, Am, and Cm in soils is complex. The radiochemical separation involves a preconcentration step and two extraction procedures [10]. The first one in order to separate the plutonium isotopes, the second one in order to separate the fraction containing both americium and curium, before electrodeposition and the counting by α-spectrometry.

After destruction of the organic matter by calcination and addition of the yield determinants, ^{242}Pu and ^{243}Am, the soil is leached with 8 M HNO_3. Transuranium elements are then co-precipitated with ferric hydroxide in ammonia middle.

The purification procedure of plutonium by elution with different acid solutions on an anionic exchange column is shown on Fig. 2. After evaporation and addition of H_2O_2 in order to eliminate iodide, Pu isotopes are then electrodeposited in sulfuric acid-ammonia media at pH 2.4, on a stainless-steel disk, with a current of 1 A applied for 1 h.

The americium-curium fraction is purified by co-precipitation with calcium oxalate. After elution through a two-layer exchange column (cationic and anionic), in order to separate remaining traces of Th and Pu, and extraction into DDCP (dibutyl-*N*,*N*-diethyl carbamyl phosphate), another anion-exchange process is used to eliminate rare earth as described in Fig. 3. The eluate is evaporated and a few drops of concentrated HNO_3 are added in order to eliminate thiocyanates. Americium and curium isotopes are then electrodeposited for 2 h with the same procedure as for plutonium.

The α spectra were measured with Dual Alpha Spectrometers EG & G Ortec 576A equipped with boron implanted silicon detectors and the pulses were analysed with a multichannel buffer analyser (spectrum master ORTEC 919).

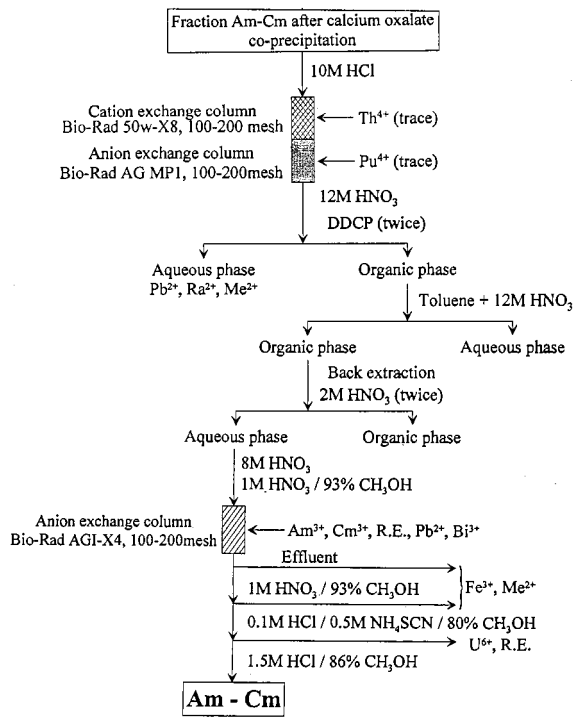

Fig. 3. Radiochemical separation of americium and curium from the fraction obtained after the radiochemical separation of plutonium.

2.3. Gamma-spectrometry measurements

The measurement of the X-γ emitting fission product is performed without radiochemical separation. Soil samples are oven-dried at 100°C and homogenised. All the samples are packed into plastic containers and counted in the same geometrical conditions as standard samples by γ-spectrometry [11]. Two types of germanium detectors were used for comparative measurements. The first one was a coaxial HPGe detector (EG & G Ortec) having 17% relative efficiency

Table 1
Activity concentrations measured in soils sampled in Belarus (1996) for γ emitting radionuclides

Radionuclide	Activity concentration (Bq. kg^{-1} dry)					
	Surface sample 0–5 cm		Middle depth sample 5–10 cm		Bigger depth sample 10–15 cm	
	Chiepietovitch	Pecki	Chiepietovitch	Pecki	Chiepietovitch	Pecki
^{137}Cs	33274 ± 600	11700 ± 200	239 ± 6	490 ± 9	72 ± 4	800 ± 15
^{134}Cs	630 ± 12	217 ± 6	5.4 ± 0.5	9.4 ± 0.4	1.3 ± 0.1	14.5 ± 0.4
^{125}Sb	83 ± 12	39 ± 2	8.5 ± 0.4	5.6 ± 0.5	1.3 ± 0.4	3.8 ± 0.5
^{40}K*	290 ± 32	247 ± 26	265 ± 27	268 ± 28	252 ± 26	261 ± 27
^{226}Ra + daugthers*	9 ± 3	7 ± 3	8 ± 2	10 ± 2	8 ± 1	9 ± 2
^{232}Th + daugthers*	11 ± 3	10 ± 2	10 ± 2	10 ± 2	7 ± 2	10 ± 2

* Natural radionuclides.

Table 2
Activity concentrations measured in the four most contaminated sampled soils from Belarus (1996) for α emitting radionuclides.

Radionuclide	Activity concentration (Bq. kg^{-1} dry)			
	Surface sample 0–5 cm		Middle depth sample 5–10 cm	Bigger depth sample 10–15 cm
	Chiepietovitch	Pecki	Pecki	Pecki
$^{239–240}$Pu	3.7 ± 0.5	0.8 ± 0.1	0.52 ± 0.06	0.45 ± 0.06
^{238}Pu	2.2 ± 0.3	0.39 ± 0.07	0.04 ± 0.01	0.06 ± 0.01
^{241}Am	1.3 ± 0.2	0.29 ± 0.04	0.11 ± 0.02	0.09 ± 0.02
$^{243–244}$Cm	10 ± 2	1.8 ± 0.3	0.61 ± 0.03	0.9 ± 0.2

and an energy resolution FWHM (full width at half maximum) of 1.9 keV on the 1.33 MeV photopeak of ^{60}Co. The second was a 2 cm^3 planar HPGe detector with a 130 μm beryllium window; the resolution (FWHM) of this counter was 190 eV on the Fe K_α X line. The pulses from these detectors were analysed with a multichannel buffer analyser (spectrum master ORTEC 919).

The background contribution was reduced by surrounding the detector with 2 mm thickness copper and 5 cm thickness lead castle. For the HPGe planar detector, a 1 cm thickness steel castle was sufficient to shield from background. For spectra measured with the coaxial HPGe detector, a one day counting time was generally sufficient to have reasonable statistic deviation on the main photopeaks. All fission products observed in the samples were identified by at least 2 γ-rays whose energies agreed within 0.2 keV with literature values.

3. Results and discussion

Results obtained for fission products ^{137C}Cs, ^{134}Cs and ^{125}Sb are presented, for the two studied sites on Table 1. For comparison activity concentrations of the natural radionuclides ^{40}K, ^{226}Ra and daughters, ^{232}Th and daughters are also given. In Table 2, results obtained after α-spectrometry measurements for the transuranium elements ^{238}Pu, $^{239+240}$Pu, ^{241}Am and $^{243+244}$Cm are shown. For each sample two alpha spectra were obtained, one with the plutonium isotopes and the other for the americium-curium fraction. Spectra obtained for a soil sample are shown in Fig. 4.

Results are in accordance with the existence of a more contaminated place as shown on Fig. 1, activity concentrations measured in the surface sample from Chiepietovitch are higher than those of Pecki. Activity concentrations vary with the depth of sampling (0–5, 5–10 or 10–15 cm). For

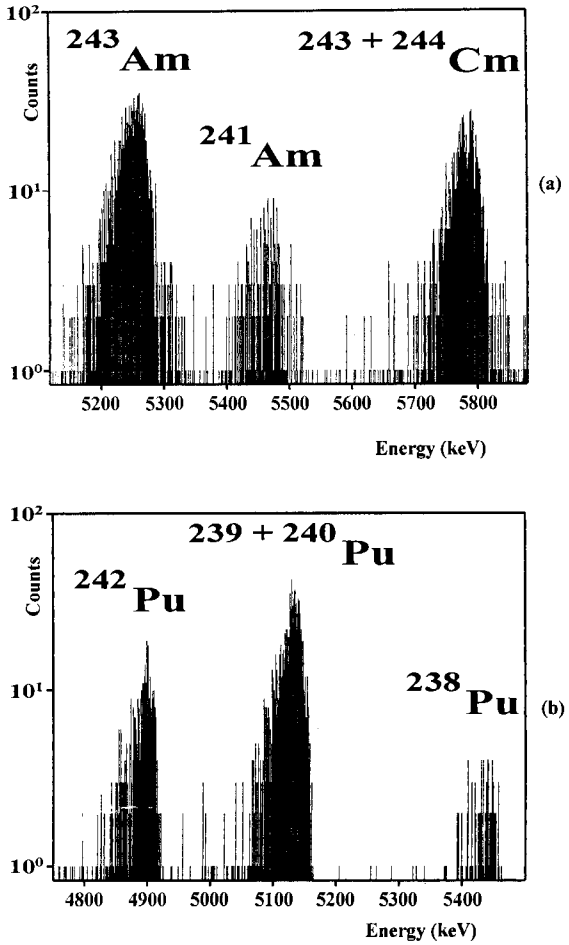

Fig. 4. α spectrum measured, for a Belarus soil sample, after radiochemical separation (a) americium-curium fraction, (b) plutonium isotopes.

Chiepietovitch soil the vertical migration of the radionuclides is less important than for the Pecki soil. This discrepancy observed in the comportment of the studied radionuclides can be explained by the different characteristics of the soils.

For all samples, the activity concentrations for the natural radionuclides are identical. Such a result was expected

The study of the activity concentration ratios (isotopic ratios), like $^{137}Cs/^{134}Cs$ and $^{238}Pu/^{239+}$ 240Pu, or activity ratio between different radionuclides, allows the determination of the radionuclides origin. In the Chernobyl fallout, the isotope ratio $^{137}Cs/^{134}Cs$ was about 2.1 due to the short half-life of ^{134}Cs ($T_{1/2} = 2.06$ years) compared to that of ^{137}Cs ($T_{1/2} = 30$ years) the isotopic ratio should be about 55 at the end of December 1996. The measured ratio, in the range 45–55, allowed the attribution of the main contamination of these Belarus samples to the Chernobyl fallout. The isotopic ratio $^{238}Pu/^{239+240}Pu$ was about 0.5 for Chernobyl fallout and in the range 0.04–0.13 for the global fallout [12]. The experimentally obtained ratio for the Belarus samples are 0.6 ± 0.1 and 0.5 ± 0.1 for the two surface samples and 0.08 ± 0.02 and 0.13 ± 0.03 for the deeper soils. This shows that, contrary to the cesium isotopes, the transuranium elements from the Chernobyl fallout are always in the first 5 cm of soil. This is confirmed by the activity ratio $^{241}Am/^{239+240}Pu$ which was found higher in surface soils: 0.35 (Chiepietovitch) and 0.36 (Pecki), than in deeper soils: 0.21 (Pecki: 5–10 cm) and 0.20 (Pecki: 10–15 cm). Alpha energies of the two curium isotopes ^{243}Cm and ^{244}Cm are almost the same, so we can only measure the sum of both isotopes activity. This activity of $^{243}Cm + ^{244}Cm$ was particularly high in the Belarus samples, which could show a more refractive comportment of curium isotopes comparatively to the other transuranium elements.

References

[1] N.A. Talvitie, Anal. Chem. 43 (1971) 13.
[2] M.K. Wong, Anal. Chim. Acta 56 (1971) 355.
[3] H.D. Livingston, D.L. Schneider, Earth Planet Sci. Lett. 25 (1975) 361.
[4] M. Sakanoue, M. Yamamoto, K. Kamura, J. Radioanal. Nucl. Chem. 115 (1987) 71.
[5] G. Barci, J. Dalmasso, G. Ardisson, Radioanal. Nucl. Chem. 156 (1992) 83.
[6] G. Barci-Funel, J. Dalmasso, G. Ardisson, J. Radioanal. Nucl. Chem. Lett. 164 (1992) 157.
[7] E. Holm, S. Ballestra, J.J. Lopez, A. Bulos, N.E. Whitehead, G. Barci, G. Ardisson, Radioanal. Nucl. Chem. 177 (1994) 51.
[8] W.C. Burnette, D.R. Corbett, M. Schlutz, J. Radioanal. Nucl. Chem., 1997, (in press).
[9] A. Yamato, J. Radioanal. Nucl. Chem. 75 (1982) 265.
[10] Technical reports no. 295, Measurement of Radionuclides in food and the environment, IAEA, Vienna, 1989.
[11] G. Barci, J. Dalmasso, G. Ardisson, Sci. Total Environ. 70 (1988) 373.
[12] R. Suutarinen, T. Jaakkola, J. Paatero, Sci. Total Environ. 130–131 (1993) 65–72.

ELSEVIER

Talanta 48 (1999) 827–837

Talanta

Analytical characterisation of a capacitively coupled plasma torch with a central tube electrode

Emil A. Cordos [a,*], Tiberiu Frentiu [a], Ana-Maria Rusu [a], Sorin D. Angel [b], Alpar Fodor [a], Michaela Ponta [a]

[a] *University of Cluj, Department of Chemistry, 3400 Cluj-Napoca, Romania*
[b] *University of Cluj, Department of Physics, 3400 Cluj-Napoca, Romania*

Received 18 July 1997; received in revised form 22 October 1997; accepted 24 October 1997

Abstract

A new type of radiofrequency capacitively coupled plasma torch is presented. The torch electrode geometry is coaxial with a tubular central electrode and one or two outer ring electrodes. The argon plasma is generated at 275 W radiofrequency power and 27.12 MHz and it has a very good stability and a low gas consumption of 0.4 l min^{-1}. The nebulized sample is introduced through the tubular electrode into the core of the annular shaped plasma thus achieving a better atomisation and a lower background. The limits of detection for 20 elements are in the range of ng ml^{-1} and the dynamic range between 2.5 and 3.5. The best results are obtained with the torch with two outer ring electrodes.

Keywords: Atomic spectroscopy; Plasma sources; Capacitively coupled plasma.

1. Introduction

The analytical performance in plasma atomic spectrometry is strongly dependent on the form and on the procedure by which the sample is introduced into the plasma discharge. The process involves two steps. The first is the dispersion of the sample by an appropriate method: ablation or sputtering for the solids, nebulization for the liquids, etc. The second step consists in the conditioning of the dispersed particles or droplets which are then carried further into the plasma discharge by a flow of gas. Most of the work in the sample introduction was devoted to the first step of the process. However, the second step has its critical points, one of which is the region of the plasma where the dispersed sample is introduced. It implies that the plasma torch has to be designed accordingly. A good example is the radio frequency inductively couple plasma (ICP). The exceptional analytical qualities of this plasma are the results of a o combination of two factors: plasma higher temperature and the plasma annular shape which allows the sample to be introduced right into the core of the discharge. Consequently the atomic and ionic excitation is very efficient; the spectral background is relatively

* Corresponding author. Fax: +40 64 420667; e-mail: cordos@re.ro

0039-9140/99/$ - see front matter
PII S0039-9140(98)00099-X

low, the detection limits are very good, the dynamic range is large and the matrix effect is not important [1–8]. The torches developed later for microwave capacitively coupled plasma (CMP) and microwave induced plasma (MIP) were designed such that the plasmas have an annular shape so that a better interaction between sample and plasma could be achieved. Winefordner et al. [9–11] were the first to build CMP torches of medium power (up to 500 W) with tantalum tube electrodes and of high power (1 kW) with graphite electrode, that allows for the sample aerosol to be introduced in the centre of the plasma. The detection limits obtained with these torches were 1–2 order of magnitude better that those obtained with torches with platinum wolfram tip electrode and side introduction of the sample aerosol. Okamoto et al. [12], by introducing the sample in the core of an annular shape, high power (1.3 kW), argon MIP have achieved in atomic emission, detection limits similar with those in Ar-ICP-AES. The same authors [13,14] using detection by mass spectrometry (MS) have obtained detection limits for nitrogen microwave plasma (N_2-MIP-MS) similar with those from Ar-ICP-MS. Jin et al. [15,16] have built a new microwave argon plasma torch, similar with an ICP torch but operated at less than 100 W. This plasma has also an annular shape which in combination with an ultrasonic nebulization system yields good detection limits for refractory elements in spite of its low power.

In the last years a number of radio frequency coupled plasma torches (r.f.-CCP) of low and medium power, were developed [17]. Cordos et al. [18–23] have built an atomic emission spectrometer based on a r.f.-CCP torch with coaxial electrodes in tip-ring geometry. The torch was low power (85–275 W at 27.12 MHz), adapted for pneumatic nebulized liquid samples. The sample aerosol was introduced at a distance of 5 mm from the plasma base using a teflon piece with 12 holes. For this type of torch a part of the sample remains in the plasma mantle and does not reach in the hot plasma core where the dissipated power is at maximum [20]. Obviously the plasma capabilities are not fully used. Therefore the authors of the present paper have designed a new type of Ar-r.f. CCP torch with a tubular central electrode and one or two ring counter electrodes. This new torch could be an alternative to low power CMP and MIP torches. A single argon gas flow is used both for sample nebulization and as support gas. By introducing the sample directly in the plasma core a more efficient atomisation and excitation is expected. In the present paper some figures of merit of this type of torch are compared with those of torch with electrodes in tip to ring geometry. The optimisation of torch parameters and the detection limits are presented.

2. Experimental

2.1. Instrumentation

The schematic diagram of the plasma torch is given in Fig. 1. The torch main body is made of brass and it is water-cooled. In the central channel of the torch is placed a PTFE tube with an inner

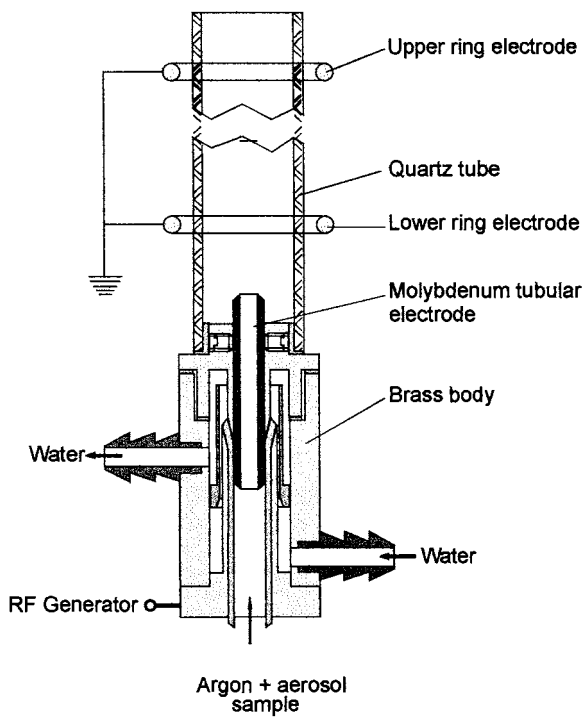

Fig. 1. Schematic diagram of the r.f. CCP torch with central tubular electrode and two outer ring electrodes.

Table 1
Instrumentation and operating conditions for plasma torch and spectrometer

Rf. Generator	EOP model, 27.12 MHz free running oscillator, 275 W (Research Institute for Analytical Instrumentation, Cluj-Napoca, Romania).
Plasma torch	Laboratory constructed. Watercooled torch body. Capacitively coupled, coaxial geometry with molybdenum tubular electrode, 2–4 mm i.d., 5 mm o.d. One or two outer ring electrodes, 25 mm diameter, made of 11 gauges copper wire. Support gas: argon spectral grade (Azo Mures, Tg. Mures, Romania), 0.4 l min^{-1} gas flow at atmospheric pressure.
Sample introduction system	Pneumatic nebulizer and 4 rollers peristaltic pump, 0.8 ml min^{-1} solution intake, 120 ml glass nebulization chamber, 10% nebulization efficiency (Research Institute for Analytical Instrumentation, Cluj-Napoca, Romania). Aerosol introduction into the plasma core via central tube electrode.
Optics	Monochromator Heath EU 700, 0.35 m focal length, 1200 grooves per mm grating.
Photomultiplier	R14 14 (Hamamatsu, Japan) operated at 700 V. Photomultiplier power supply Heath EU 701 (Heath Co. Benton Harbour, MI, USA)
Recorder	K 201 (Zeiss-Jena, Jena Germany)

diameter of 5 mm. Further, into this tube is introduced a molybdenum tubular electrode with the inner diameter of 2–4 mm. The electrode is centred and secured in position by 6 screws and connected to the r.f. generator. Over the whole torch assembly is placed a quartz tube, 15 mm inner diameter and 200 mm length. One or two rings, 25 mm diameter, made out of copper wire, are placed outside of the quartz tube and connected to the common of the r.f. generator. The rings position is adjustable. The plasma was generated using an r.f. generator of free running type, operated at 275 W and 27.12 MHz. The support gas was spectral grade argon at atmospheric pressure. This single gas flow is used both for sample nebulization and as support gas for the discharge.

The plasma develops between the tubular electrode and the outer ring electrodes. The samples were nebulized using a pneumatic nebulizer and a 4 rollers peristaltic pump and introduced into plasma core via the tubular electrode. The optical signal was measured by a Heath EU 700 monochromator, equipped with a Hamamatsu R1414 photomultiplier. The photocurrent was recorded on a Zeiss Jena K201 recorder. Details of the equipment were given in Table 1.

3. Reagents

Stock solutions of 1000 mg ml^{-1} of Al, Ba, Ca, Cd, Cr, Cu, Fe, Eu, Bi, Mg, Mn, Ni, Co, Pb, Zn, Hg, Yb, Li, Na, Ag were prepared by dissolution of high-purity metals, salts or oxides in HCl or HNO_3. Single element working standards were obtaining by diluting the stock solutions with 2% v/v HNO_3. For the blank measurements a 2% v/v HNO_3 solution was used.

4. Results and discussion

4.1. Optimisation of plasma torch working parameters

The discharge obtained with tubular electrode torch looks like a long and slim flame with an inner cone at the base. The cone is shorter than the plasma core obtained with a tip-ring torch [18]. Like in a regular chemical flame the emission is at maximum above the inner cone. The stability of the discharge and its analytical performance are dependent of the material and the dimensions of the tubular electrode, the placement of ring electrodes, plasma power and support gas flow. Since the intensity of the electric field is at maximum in the centre of the plasma the quartz tube is protected against excessive heating, in contrast with the torches having outer parallel plane electrodes, where the electric field is at maximum close to the tube walls. The role of the ring electrodes are different. The first electrode (lower ring electrode) influences the uniformity and density of electrical field lines in the lower part of the

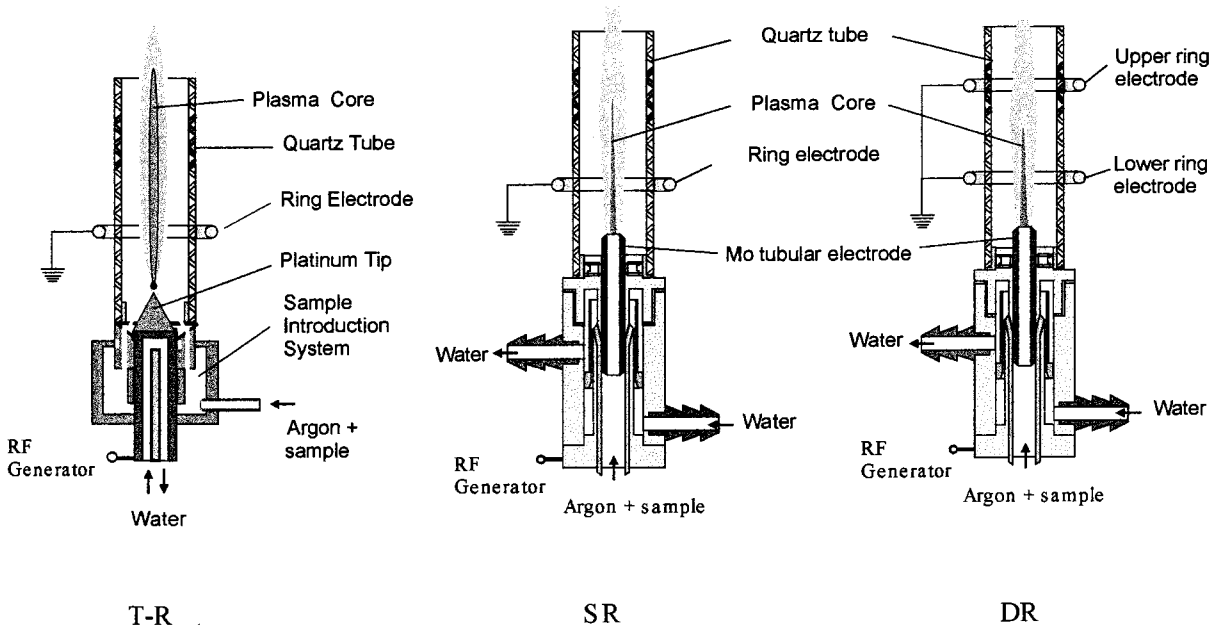

Fig. 2. The geometry of the r.f. CCP torches compared in the present paper. T-R. Torch with electrodes in tip-ring geometry SR. Torch with central tubular electrode and single ring outer electrode DR. Torch with central tubular electrode and double ring outer electrode.

plasma. A proper diameter and position of this electrode insures the discharge stability and its adherence to the electrode. The second (upper) ring electrode concentrates the electric field lines in the centre of the plasma, with the improvement of power transfer from the r.f. field to the plasma. This increases the atomic and ionic excitation. When using the second ring electrode the inner cone of the plasma discharge gets shorter and brighter. A schematic of the three torches compared in the present paper is given in Fig. 2.

In the first stage, the optimisation of plasma torch parameters was accomplished for the tubular central electrode torch with a single outer ring electrode. The optimisation implies the position of the ring electrode, maximum plasma power, argon gas flow and diameter of the tubular electrode. The influence of the second electrode upon the plasma properties was determined only as function of its relative position to the first one and it will be discussed later.

The optimum position of the ring electrode, in single ring configuration, is one close to the tubular electrode and it was established empirically. It was found that a distance of 5 mm between the top of the tubular electrode and the first ring electrode yields a stable discharge. At this distance between electrodes the divergence of the electric field lines provides an uniform heating of the top circumference of the tubular electrode and a good plasma adherence to the electrode. It was established by trials that the maximum power of the discharge that do not damage the electrodes is 275 W.

The optimum values for argon gas flow and for the diameter of the tubular electrode were established by monitoring the intensity of Na I 588.9 nm line. The influence of argon gas flow on Na I 588.9 nm line intensity, for two tube diameters, is presented in Fig. 3. The emission increases abruptly when gas flow changes from 0.3 to 0.4 l min^{-1}, but further, when the gas flow increases from 0.4 to 0.8 l min^{-1}, the signal growth do not exceed 25% in spite of the fact that nebulization efficiency increases two times. The relative signal plateau in this gas flow range, is due both to the decrease of analyte residence time in the zone of maximum excitation and to the cooling of the

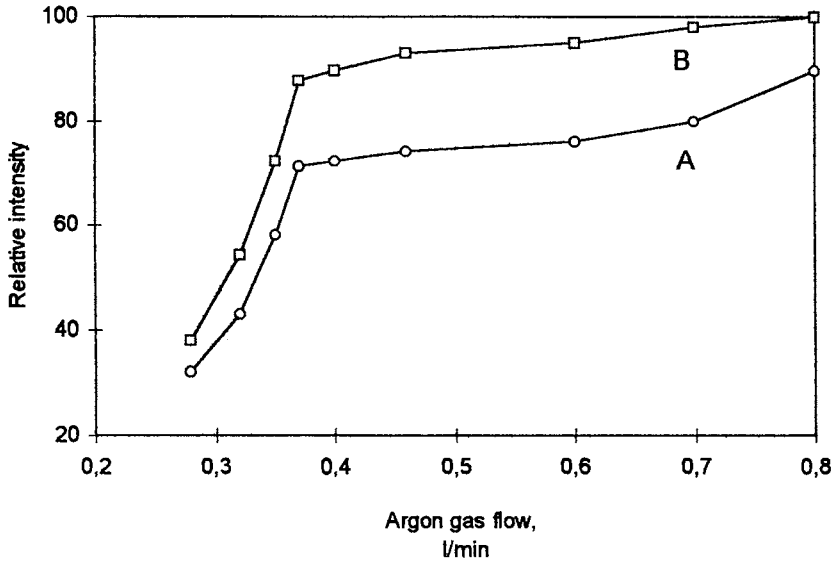

Fig. 3. Emission signal for Na I 588.9 nm line (solution concentration: 50 μg ml^{-1} Na) as function of argon gas flow. Inner diameter of the central molybdenum tubular electrode 3.0 mm (A) and 3.5 mm (B)

plasma. A more detailed picture is given in Table 2 where some figures of merit are presented for the above mentioned sodium line, as function of tubular electrode diameter and argon gas flow. The relative standard deviation of the background (RSDB) is an indicator of plasma mechanical stability. A very stable plasma is obtained at 0.4 l min^{-1} argon gas flow and 3.5 mm tube diameter where RSDB has a minimum values of 1.2.

The gas flow and the tube diameter affect the signal to background ratio (SBR) by influencing both the signal and the background but in different ways and proportions. For example, as shown before, an increase of gas flow from 0.4 to 0.8 l min^{-1} produces a moderate increase of the signal (10–25%) but, in exchange, the background increases two times for tubes having 3 or 3.5 mm diameter. If the tube diameter increases over 3.5 mm the background increases dramatically. The overall effect is a decrease of the SBR. For a given gas flow the decrease is a moderate one as long the tube diameters changes from 3 to 3.5 mm (546–450 for 0.4 l min^{-1} and 341–206 for 0.8 l min^{-1}). For a given diameter the doubling of the gas flow produces a more important decrease of the SBR (546–341 for 3 mm diameter and 450–206 for 3.5 mm diameter). Increasing the tube diameter to 4 mm decreases the SBR with almost an order of magnitude.

The limits of detection (LOD) follow the same pattern as the SBR. The best LOD's are obtained for argon gas flow of 0.4 l min^{-1}. Therefore the increase of gas flow much over 0.4 l min^{-1} and the use of tube diameters larger than 3.5 mm are not recommended. The optimum constructive and operating condition for the plasma torch are: 275 W r.f. power, 0.4 l min^{-1} argon gas flow, 3.5 mm inner diameter for the tubular electrode and a 5 mm distance between this electrode and the lower ring electrode. These conditions were also valid for other elements.

The figures of merit for the torch with a single ring electrode, in the above mentioned conditions are listed in Table 3. As expected, the LOD's improved for all elements as compared with the plasma torch in tip-ring electrode geometry, where the sample is not introduced in the centre of the discharge. Since the improvement is more notable for the elements with a lower dissociation energy of the oxides, Ag, Cd, Mn, Cd, Zn, Co, one may assume that the improvement is in the atomisation process.

Table 2
Analytical characteristics of sodium emission (Na I 588.9 nm) used for torch optimisation

Tubular electrode inner diameter, mm	Argon gas flow, l min^{-1}	SBR[a]	RSDB[b]	LOD[c]
3	0.4	546	1.5	4.0
3	0.8	341	1.8	8.0
3.5	0.4	450	1.2	4.0
3.5	0.8	206	1.4	10.0
4	0.8	42	1.5	54.0

[a] SBR, signal to background ratio for 50 μg ml^{-1} Na.
[b] RSDB, relative standard deviation of the background (determined on ten successive measurements).
[c] LOD, limit of detection (3 σ criteria), ng μl^{-1}.

4.2. Influence of the second ring electrode

The presence of the second ring electrode changes the shape of the plasma and the optimum observation height for the analytical signal. This changes are function of the distance between the lower and the higher electrode. As an example, in Fig. 4, the emission intensity for the Al I 396.15 nm line is represented as function of distance between electrodes and observation height. It could be seen that the optimum emission intensity could be obtained in a spot that covers about 4 mm in the observation height and 10 mm in the ring distance.

The optimum distance between ring electrodes, the optimum observation height and the detection limits are listed in Table 4, for the same elements as in Table 3. The elements were divided into 3 groups as function of distance between electrodes.

The first group includes elements for which the upper electrode is relatively close to the lower electrode, 60 mm, and the optimum observation height is generally higher, 12–20 mm. All ionic lines are in this group. The oxides dissociation energy is above 4 eV. For this group the improvement in LOD's are generally higher than those obtained for the other two groups. The most notable increase in emission signal is for Ba and Yb.

The elements from the second group exhibit the best emission when the electrodes are farther, 70 mm, but the optimum observation height is lower, 6–12 mm. The dissociation energy for the oxides is <4.3 eV. The decrease of LOD is generally smaller than for the first group, with an increasing factor of 1.4–1.8.

The third group includes elements with lower excitation energy so that they exhibit a good LOD even in plasma with a single ring electrode or in plasma of the tip-ring torch.

The emission signal improvement is illustrated in Fig. 5 where the actual experimental traces are given for Cd and Ba. For both these elements the reduction in the background level and background noise could be noticed, when changing from tip-ring torch to a torch with tubular central electrode. The increase in the signal level could also be seen when using two outer ring electrodes as compared with single outer electrode torch. At the element concentration of 250 and 500 ng ml^{-1} Ba yields an appreciable signal only for the tubular central electrode torch with two outer ring electrode.

Increasing plasma temperature or electron number density does not increase significantly the atomisation for this elements but rather increases the excitation efficiency or slightly decreases the background. As a matter of fact, the LOD's improvement, when switching from tip-ring torch to single ring tubular torch and further to double ring tubular torch, is the results of two effects: increase of the emission and decrease of the background. The contribution of these two effects is not the same for all elements. As an example, the changes in emission and background intensities are given in Table 5, for a number of selected elements. The intensities are relative, the column with higher values being equal with 100 units. One of the first things to be noticed is the lower background intensity of the tubular torches as compared with tip-ring torch. As for the listed

Table 3
Figures of merit for a CCP torch with central tubular electrode and single ring outer electrode

Element	λ nm	$E_{ex.}$, EV	$E_{ox.dis.}$, eV	Torch tubular electrode single ring (SR)			Torch tip-ring (T-R)	LOD's ratio
				Optimum observation height mm	SBR (for a 50 μg ml^{-1} solution)	LOD (SR) ng ml^{-1}	LOD[a] (T-R) ng ml^{-1}	(T-R) (SR)
Ca(I)	422.67	2.93	5.0	24	200	9	15	1,6
Na(I)	588.99	2.11	—	10	450	4	13	3,2
Li(I)	670.79	1.85	—	10	300	5	9	1,8
Mg(I)	285.21	4.34	4.4	20	225	6	9	1,5
Ag(I)	328.07	3.78	1.4	18	128	13	430	33
Ca(II)	393.36	3.15	—	25	46	32	—	—
Cu(I)	324.74	3.82	4.9	18	60	25	28	1,1
Mg(II)	279.55	4.43	—	22	38	35	—	—
Cd(I)	228.81	5.41	3.8	16	24	65	770	11,9
Cr(I)	425.43	2.91	4.2	24	15.5	100	120	1,2
Pb(I)	405.78	4.38	4.1	14	13.5	110	450	4,1
Mn(I)	403.08	3.08	4.0	18	12.2	125	750	6
Mn(II)	257.61	4.81	—	20	10.0	155	—	—
Ni(I)	352.45	3.54	4.3	18	9.1	170	1700	10
Zn(I)	213.85	5.80	4.0	12	26	60	700	11,7
Fe(I)	371.99	3.33	4.0	14	7.6	200	240	1,2
Al(I)	396.15	3.14	5.0	26	5.4	290	—	—
Co(I)	345.35	3.54	3.7	16	4.0	390	2500	6,4
Eu(I)	459.40	2.70	—	28	5.0	300	440	1,5
Hg(I)	253.65	4.88	—	12	2.0	750	750	1
Bi(I)	223.06	5.55	4.0	18	2.0	800	—	—
Yb(I)	346.44	3.58	—	26	1.4	1000	—	—
Cd(II)	214.44	5.78	—	24	1.4	1100	—	—
Ba(I)	493.41	2.51	6.0	28	0.8	1900	5700	3

[a] Data from [21].

Table 4
Figures of merit for a CCP torch with central tubular electrode and double ring outer electrode.

Element	λ nm	Torch					LOD's ratio
		tubular electrode double ring (DR)				Single ring (SR)	
		Optim. Obs. height mm	Distance between ring electrodes mm	SBR(for a 50 μg ml^{-1} solution)	LOD (DR) ng ml^{-1}	LOD (SR) ng ml^{-1}	SR/DR
Ca(I)	422.67	14	60	530	3	9	3
Ca(II)	393.36	16	60	300	5	32	6.4
Mg(I)	285.21	12	60	450	3	6	2
Mg(II)	279.55	14	60	150	9	35	3.9
Cu(I)	324.74	14	60	90	16	25	1.6
Ba(I)	493.41	20	60	44	40	1900	47.5
Cr(I)	425.43	18	60	28	50	100	2
Al(I)	396.15	16	60	21	70	290	4.1
Mn(I)	403.08	12	60	21	75	125	1.7
Mn(II)	257.61	16	60	17	90	155	1.7
Yb(I)	346.44	20	60	14	100	1000	10
Fe(I)	371.99	10	60	15	105	200	1.9
Eu(I)	459.40	16	60	25	60	300	5
Bi(I)	223.06	14	60	4	400	800	2
Cd(II)	214.44	18	60	3.6	400	1100	2.7
Cd(I)	228.81	12	70	40	40	65	1.6
Pb(I)	405.78	10	70	20	80	110	1.4
Ni(I)	352.45	8	70	13	120	170	1.4
Zn(I)	213.85	6	70	38	40	60	1.5
Co(I)	345.35	10	70	7	210	390	1.8
Hg(I)	253.65	6	70	3	500	750	1.5
Na(I)	588.99	6	80	540	3	4	1.3
Li(I)	670.79	6	80	360	4	5	1.3
Ag(I)	328.07	12	80	161	50	13	1.3

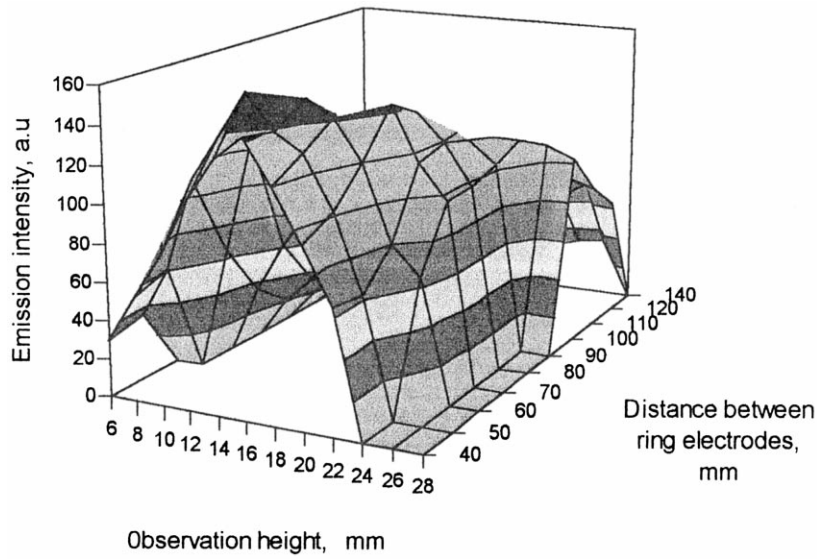

Fig. 4. Emission intensity of Al I 396.15 nm line as function of distance between outer ring electrodes and observation height.

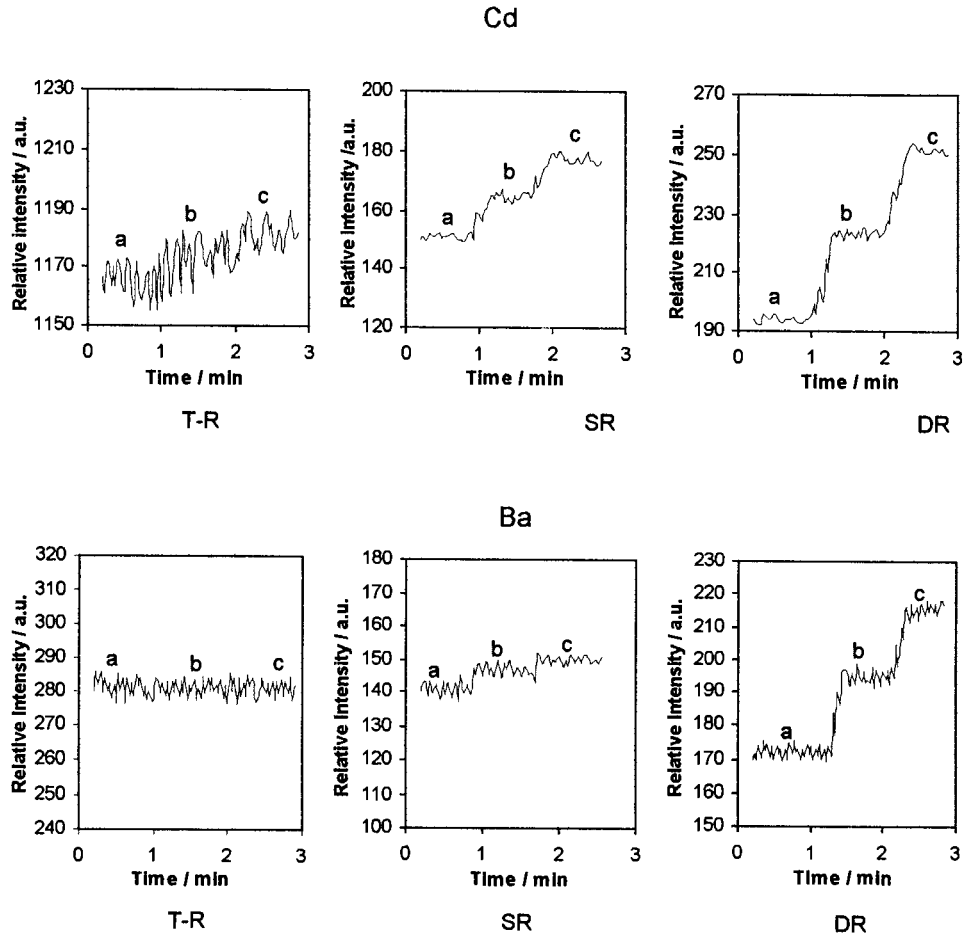

Fig. 5. The recorded emission signal for Cd and Ba. a, background; b, 250 ng ml^{-1}; c, 500 ng ml^{-1}; T-R., Torch with electrodes in tip-ring geometry; SR., Torch with central tubular electrode and single ring outer electrode; DR., Torch with central tubular electrode and double ring outer electrode.

Table 5
Line and background intensities for r.f. CCP torches with different electrode geometry

Element	Relative line intensity			Relative background intensity		
	T-R[a]	SR[b]	DR[c]	T-R[a]	SR[b]	DR[c]
Ba	1	1.4	100	100	45	60
Mn	15	32	100	100	36	63
Cd	32	48	100	100	13	17
Ni	36	50	100	100	14	18
Co	39	53	100	100	18	23
Pb	44	65	100	100	35	41
Ag	35	71	100	100	5.4	6

[a] T-R, CCP torch with tip ring electrode geometry (data according to [21]).
[b] SR, CCP torch, central tubular electrode single outer ring electrode.
[c] DR, CCP torch, central tubular electrode, double outer ring electrode.

elements, two extremes could be mentioned. In the case of Ba, the LOD improvement is due to the increase of the emission signal, especially when the double ring tubular torch is used. At the other end is Ag for which the decrease of background intensity is responsible for LOD decrease.

In comparing the tip-ring torch with the single ring tubular torch, the improvement of the analytical performance is due rather to the background decrease and in the lesser degree to the increase of the emission. Adding a second ring electrode to the tubular torch does not further reduce the

Table 6
Calibration curves parameters

Element	*a*	Standard deviation of '*a*'	*n*	Standard deviation of '*n*'	Correlation coefficient	Dynamic range
Ag	1.88	0.034	0.98	0.035	0.993	2.5
Al	1.31	0.016	0.82	0.014	0.997	3
Ba	2.14	0.026	0.96	0.020	0.995	3
Bi	2.48	0.017	1.03	0.020	0.996	3
Ca	2.63	0.013	0.87	0.022	0.996	3
Cd	1.88	0.014	0.89	0.016	0.998	2.5
Co	1.87	0.033	0.95	0.023	0.995	3.5
Cr	1.43	0.013	0.97	0.010	0.999	3
Cu	1.70	0.014	0.88	0.013	0.996	2.5
Eu	1.80	0.025	1.03	0.020	0.997	3
Fe	1.71	0.024	0.86	0.013	0.998	3
Hg	1.10	0.011	0.96	0.005	0.999	3.5
Li	1.97	0.026	0.91	0.018	0.997	3.5
Mg	1.87	0.030	1.01	0.034	0.994	2.5
Mn	2.48	0.017	0.88	0.016	0.997	2.5
Na	2.49	0.021	1.03	0.025	0.995	3
Ni	1.85	0.021	0.98	0.015	0.998	3
Pb	1.83	0.028	0.88	0.016	0.997	3.5
Yb	1.82	0.020	1.04	0.016	0.997	2.5
Zn	2.33	0.011	0.85	0.011	0.999	2.5

background but significantly increases the emission.

The dynamic range was established using the calibration curve:

$$\log y = a + n \log C$$

where y is the emission intensity in arbitrary units, a is the log (signal /concentration unit), C represents the concentration in μg $ml^{-1}$and n is the calibration curve slope.

The values of the above mentioned coefficients are listed in Table 6. The calibration curves were recorded starting from a minimum concentration five times LOD. The dynamic ranges are between 2.5 and 3.5 for all studied elements.

5. Conclusions

The analytical performance of a capacitively coupled plasma spectral source could be substantially improved by using a torch with a tubular central electrode instead of a tip electrode. To the enhancement of the analytical signal contribute both the increase of the emission, due to sample introduction into the plasma core, and the lowering of the background. The capacitively coupled plasma could be an attractive source for atomic spectrometry since it characterised by low power, good stability and a low gas consumption. The best figures of merit are obtained for the torch with tubular central electrode and two outer ring electrodes, properly positioned. The detection limits are in the range of ng ml^{-1} with a dynamic range from 2.5 to 3.5 orders of magnitude.

References

[1] G.A. Meyer, Anal. Chem. 59 (1987) 1345A.
[2] M.W. Blades, P. Banks, C. Gill, D. Huang, C. Le Blanc, D. Liang, IEEE Trans. Plasma Sci. 19 (1991) 1090.
[3] S. Greenfield, I.L.I. Jones, C.T. Berry, Analyst (London) 89 (1964) 713.
[4] R.H. Wendt, V.A. Fassel, Anal. Chem. 37 (1965) 920.
[5] V.A. Fassel, R.N. Kniselley, Anal. Chem. 46 (1974) 1110A.
[6] V.A. Fassel, R.N. Kniselley, Anal. Chem. 46 (1974) 1155A.
[7] S. Greenfield, Spex. Industries, 1977, XXII, 1
[8] S. Greenfield, H. McD. Mc Geachin, Chem. Br. 16 (1980) 653.
[9] B.M. Patel, E. Heithmar, J.D. Winefordner, Anal. Chem 59 (1987) 2374.
[10] J.D. Huang, W. Masamba, B.W. Smith, J.D. Winefordner, Can. J. Spectrosc. 33 (1988) 156.
[11] B.M. Patel, J.P. Deavor, J.D. Winefordner, Talanta 35 (1988) 641.
[12] Y. Okamoto, M. Yasuda, S. Murayama, Jpn. J. Appl. Phys. 20 (1990) 670.
[13] Y. Okamoto, Anal. Sci. 7 (1991) 273.
[14] Y. Okamoto, J. Anal. At. Spectrom. 9 (1994) 745.
[15] Q. Jin, C. Zhu, M.W. Boer, G.M. Hieftje, Spectrochim. Acta 46B (1991) 417.
[16] Q. Jin, H. Zhang, Y. Wang, X. Yuan, W. Yang, J. Anal. At. Spectrom. 9 (1994) 851.
[17] M.W. Blades, Spectrochim. Acta 49B (1994) 47.
[18] E.A. Cordos, S.D. Anghel, T. Frentiu, A. Popescu, J. Anal. At. Spectrom. 9 (1994) 635.
[19] E.A. Cordos, T. Frentiu, Ana Maria Rusu, G. Vatca, Analyst (London) 120 (1995) 725.
[20] E.A. Cordos, T. Frentiu, A. Fodor, Michaela Ponta, Ana Maria Rusu, S. Negoescu, ACH-Models in Chem.(Budapest) 132 (1995) 313.
[21] T. Frentiu, Ana Maria Rusu, Michaela Ponta, S.D. Anghel, E.A. Cordos, Fresenius J. Anal. Chem. 354 (1996) 254–255.
[22] S.D. Anghel, T. Frentiu, Ana Maria Rusu, A. Simon, E.A. Cordos, Fresenius J. Anal. Chem. 354 (1996) 252–253.
[23] S.D. Anghel, T. Frentiu, E. Darvasi, Ana Maria Rusu, E.A. Cordos, Fresenius J. Anal. Chem. 354 (1996) 250–251.

ELSEVIER

Talanta 48 (1999) 839–846

Talanta

Preconcentration of platinum group metals on modified silicagel and their determination by inductively coupled plasma atomic emission spectrometry and inductively coupled plasma mass spectrometry in airborne particulates

R. Vlašánkova [a], V. Otruba [a], J. Bendl [b], M. Fišera [c], V. Kanický [a,*]

[a] *Department of Analytical Chemistry, Masaryk University, CZ 611 37 Brno, Czech Republic*
[b] *ANALYTIKA, Ltd., CZ 198 00 Prague, Czech Republic*
[c] *Institute of Food Chemistry, Technical University, CZ 637 00 Brno, Czech Republic*

Received 18 July 1997; received in revised form 29 September 1997; accepted 02 October 1997

Abstract

Modified silicagel (C18) was studied for separation and preconcentration of platinum group metals (Ru, Rh, Pd, Os, Ir and Pt) as ion associates of their chlorocomplexes with cation of onium salt N(1–carbaethoxypentadecyl)-trimethyl ammonium bromide. Sample containing HCl and the onium salt was pumped through the column. After elution with ethanol the eluate was evaporated in the presence of HCl. Resulting aqueous solutions were analysed with inductively coupled plasma atomic emission spectrometry (ICP-AES) and inductively coupled plasma mass spectrometry (ICP-MS). Recovery values of 1–20 μg Pt and Pd from 50 ml of synthetic pure solution were 100 ± 3 and $100 \pm 1\%$, respectively, however, they diminished with increasing sample volume and in the presence of the real sample matrix or nitrate ions. Samples of engine soot (NIES No. 8), decomposed by low pressure oxygen high-frequency plasma, and airborne particulates from dust filters of meteorological stations, leached with HNO_3 and H_2O_2, were analysed. A reasonable agreement was found between ICP-MS and ICP-AES results for airborne dust samples and the values comparable with those in literature were determined in NIES No. 8.

Keywords: Platinum group metals; Ion associates; Inductively coupled plasma; Airborne particulates

1. Introduction

The determination of trace concentrations of platinum and palladium in environmental and biological samples has gained a considerable importance because of their toxicity and increasing occurrence, which is mainly due to industrial and automobile catalysts. Fresh air before the introduction of automobile catalysts contained 0.05 pg Pt m^{-3} and concentrations between 0.6 and 1.8 pg Pt m^{-3} were recently found in rural areas

* Corresponding author. Tel.: +420 5 41129283; fax: +420 5 41211214; e-mail: viktork@chemi.muni.cz

0039-9140/99/$ - see front matter
PII S0039-9140(98)00100-3

while in the neighbourhood of highways in Germany values between 1–13 pg Pt m^{-3} were determined in the ambient air [1]. Airborne dust collected at the area of Dortmund (FRG) during nearly a one-year period contained between 0.6 and 130 ng Pt g^{-1}, which corresponded to the concentration from 0.02 to 5.1 pg Pt m^{-3} in the air [2]. Pt-based catalytic converters cause the increase of concentration of platinum group metals (PGM) in soils next to highways and in the street or tunnel dust [3].

For the determination of these ultratrace concentrations the inductively coupled plasma mass spectrometry (ICP-MS) is sufficiently sensitive. The study of contamination of ambient air was performed using the ICP-MS instrumentation with electrothermal vaporisation (ETV-ICP-MS) which was applied to the analysis of particulates in automotive catalyst exhaust fractionated by inertial separation using a cascade impactor [4]. Detection limits were 0.2 pg of Ir, 0.3 pg of Pt, 0.4 pg of Rh, 0.7 pg of Pd, and laboratory measurements of catalysed car exhaust gave concentrations:150 ng Pt m^{-3}, 26 ng Rh m^{-3}, 2.5 ng Pd m^{-3}, 0.12 ng Ir m^{-3}, while field measurements in the highway tunnel yielded: 35 pg Pt m^{-3}, 285 pg Rh m^{-3}, 16 pg Pd m^{-3} and less than the detection limit for Ir [4]. For the determination of PGM in geological materials and also in the certified reference material NIES No. 8 (Vehicle Exhaust Particulates, Japan) these metals were preconcentrated using fire assay fusion and the collection into a NiS button prior to analysis with ETAAS [5]. Due to toxic properties of platinum, uptake of its compounds by plants and speciation to elucidate the metabolism of Pt in grass cultures were studied with size-exclusion chromatography coupled to ICP-MS [6].

Recently, modified silicagel Separon SGX C18 (particle size 7 mm) was found to be suitable for the preconcentration of 2–20 μg of Pt from 0.1 M HCl in the presence of cationic surfactants, especially dimethyllaurylbenzyl ammonium bromide, with subsequent elution with 96% ethanol. The recovery was 86–110% for 2 μg of Pt. The final emission spectrometry of Pt in plant ash matrix was carried out in 15 A dc-arc [7]. The preconcentration of ionic pairs is efficient also for some other elements, e.g. thallium (0.02–20 μg) which was successfully preconcentrated on silicagel C18 from 0.1 M HCl in the presence of various cationic surfactants as ion pairs with tetrachlorothallate(III) and subsequently eluted with 96% ethanol. Atomic emission spectrometry in a nitrous oxide-acetylene flame is suitable for the analysis of plants [8].

In this paper the simple selective preconcentration of Pt and Pd in the form of ion pairs of platinum(IV) and palladium(II) chlorocomplexes with cationic surfactant Septonex® on Separon™ SGX C18 column is used in combination with ICP-AES and ICP-MS for the determination of these elements in airborne particulates and the engine soot NIES No. 8. Besides Pt and Pd, the sorption of Au, Ru, Rh, Os and Ir was studied.

2. Experimental

2.1. Instruments

For analyses of environmental samples the ICP-MS instrument UltraMass (Varian, Australia) was used, which is installed at the laboratory of the ANALYTIKA Co. Ltd., Prague. Parameters of this instrument and operating conditions are presented below.

The ICP source was a generator with frequency 40.68 MHz operated at a power input of 1.2 kW and a reflected power of 7 W. A quartz plasma torch was provided with a corundum injector. Gas flows (Ar) were adjusted to the following values: plasma 14.5 l min^{-1}, auxiliary 1.2 l min^{-1}, carrier 0.94 l min^{-1}. A sampling depth was 6.5 mm. The V-groove nebulizer was fed by a peristaltic pump (1.5 ml min^{-1}). Internal standard (0.1 μg ml^{-1} of In) was on-line added to sample (1:2). Fast flush time was 10 s and stabilisation time when aspirating a sample was 15 s.

The mass spectrometer was a quadrupole mass filter. Ion optics voltages were optimised to the following values: extraction lens −416 V, 1st lens −234 V, 2nd lens −13.2 V, 3rd lens 0 V, 4th lens −72 V, photon stop −18 V, both entrance and exit plates 0 V. Measurement mode was peak-hopping with three points per peak and the sepa-

ration of points was $\Delta m = 0.025$ AMU. Intensity was integrated within 100 scans and three blocks of scans were measured. The dwell time was 20 ms for m/z from 3 to 114, 5 ms for m/z from 115 to 188, 20 ms for m/z from 189 to 256. Isotopes: 197 Au, 101 Ru, 103 Rh, 105 Pd, 106 Pd, 108 Pd, 110 Pd, 189 Os, 193 Ir, 194 Pt, 195 Pt, 196 Pt; 115 In.

The ICP-AES instrument IRIS-AP (Thermo Jarrel-Ash, USA) at the laboratory of the Faculty of Chemistry of the Technical University Brno was used for measurements to optimise the sorption and for comparative measurements of selected real samples. Parameters of this instrument and operating conditions are presented below.

The ICP source was a generator with frequency 27.12 MHz operated at a power input of 1.15 kW. Gas flows (Ar) were: plasma 12 l min^{-1}, auxiliary 0.5 l min^{-1} and carrier 1.0 l min^{-1}. The Meinhard nebulizer was fed by a peristaltic pump (1.9 ml min^{-1}).

The spectral apparatus was an echelle-based spectrometer with a prism predisperser. The observation mode was the axial view. The detector was a CID type, integration time was 30 s and each result was the average of three measurements. The spectral lines (nm) in high spectral orders (values in parentheses) were used: Au I 242.795 (107); Ru II 240.272 (108); Rh II 233.477 (111); Pd I 340.458 (76); Os II 225.585 (115); Ir II 224.268 (116); Pt II 214.423 (121). Background-corrected intensities were evaluated for the analysis of samples.

A peristaltic pump ID-100 (Skala Brno, Medical Technology) was used for preconcentration.

A mineralisation device Plasma 1101 (IPC, CA), installed at the Department of Analytical Chemistry, Masaryk University Brno, produces high-frequency (13.5 MHz, 1500 W) low-pressure (10–500 Pa) oxygen plasma that facilitates the combustion of samples. The apparatus has six combustion chambers for parallel samples.

A microwave mineralisation device MDS 2000 (CEM, USA) installed at the laboratory of the ANALYTIKA Co. Ltd., Prague, is a closed system using vessels with PTFE inserts.

2.2. Chemicals

The multielement standard stock solution containing 100 mg ml^{-1} of Au, Ru, Rh, Pd, Os, Ir, Pt in 20% HCl (Astasol, ANALYTIKA, Prague, Czech Republic) was used for the preparation of working and calibration samples. The 0.1 M aqueous stock solution of the cationic surfactant Septonex, N(1-carbaethoxypentadecyl)-trimethylammonium bromide, $C_{21}H_{44}ONBr$ (Farmakon, Olomouc, CR) was used. For elution, ethanol 96% denaturated with 5% (v/v) methanol, was ultrasonically deaerated. Other chemicals used include: HNO_3, HCl, H_2O_2, NaCl, $NaNO_3$, $Mg(NO_3)_2.6H_2O$ (Lachema, Brno, CR) and surfactant BRIJ 35 (Merck, Darmstadt). All the chemicals were of analytical grade quality. SilicaCart™ (Tessek, Prague) cartridges 9×20 mm with modified silicagel Separon™ SGX, 60 μm were used for preconcentration.

2.3. Characteristics of samples

Airborne particulate matter was collected on glass filters at five meteorological stations of the Czech Hydrometeorological Institute in the Czech. Rep.: Kočkov, Všechlapy, Souš, Sokolov and Měděnec. The filters were exposed for 24 h with a flow rate of 720 m^3 day^{-1}.

The reference material NIES No. 8 (Vehicle Exhaust Particulates, National Institute for Environmental Studies, Japan) is certified only for Al, As, Ca, Cd, Co, Cr, Cu, K, Mg, Na, Ni, Pb, Sb, Sr, V, Zn. The only results of PGM in NIES No.8 were published after fire assay fusion and the collection into an NiS button followed by analysis with ETAAS [5].

3. Results and discussion

3.1. Sorption and elution procedures

The cartridge SilicaCart TM with sorbent was initially washed with 20 ml of 96% ethanol and 5 ml of 10–2 M aqueous solution of Septonex. Solutions containing PGM, Septonex and HCl were then pumped through the cartridge. For the

desorption of ion associates of chlorocomplexes with quarternary base (Septonex), the 96% ethanol was pumped through the column and the first 4 ml of the eluate were collected to a calibrated test-tube containing 2 ml of 0.1 M HCl [7,8]. Owing to the known influence of volatile solvents on the ICP discharge stability the ethanol was evaporated in a Teflon® dish under an infrared lamp, the residue was transferred into a volumetric flask and filled up to the mark with 0.1 M HCl.

3.2. Selection of sorption conditions

To achieve maximum efficiency of the sorption, the concentrations of reagents were varied in these intervals: from 10^{-4} to 10^{-2} M of Septonex, from 0.02 to 0.3 M of HCl and from 0 to 0.5 M NaCl. Optimisation was performed with ICP-AES using the relaxation method.

Solutions for optimisation contained 20 μg of Au, Ru, Rh, Pd, Os Ir, and Pt in 50 ml, (0.1M HCl), i.e. their concentrations were 0.4 μg ml^{-1}. The behaviour of Au was studied as well, taking the advantage of its presence in the multielement standard solution. The sorption and desorption were performed as described in Section 3.1. The optimum concentration of Septonex was considered as the value at which maximum signals of all analytes in the solutions were achieved by desorption. This was found to be 0.006 M for Pt and Pd.

Test solutions containing 0.4 μg ml^{-1} of PGM and Au in 0.1 M HCl and 0.006 M Septonex were prepared for the evaluation of the sorption efficiency and the recovery of the preconcentration procedure. The set of calibration solutions containing 0, 0.1, 0.5, 1.0, 3.0 and 5.0 μg ml^{-1} of PGM and Au in 0.1 M HCl and 0.006 M Septonex was then prepared. The calibration lines with following values of coefficients of correlation, r, were obtained: Au 0.99989, Ru 0.99941, Rh 0.99964, Pd 0.99939, Os 0.99152, Ir 0.99988 and Pt 0.99987. Using these calibrations, the residual concentrations of PGM and Au were determined in the test solution outflowing at sorption procedure.

The efficiency of sorption was calculated based on a difference between the absolute amount of analyte brought onto the column in the test solution and the absolute amount of analyte determined in the test solution outflowing from the column, i.e. residual, not sorbed.

The recovery was determined based on the amount of analyte brought onto the column and the amount of analyte eluted with ethanol. It was found that the efficiency of sorption was practically the same as the recovery within the terms of experimental errors. In other words, the elution was considered quantitative.

The dependence of recovery on the concentration of Septonex is given in Fig. 1. The best recovery was achieved for Pd (100 ± 1)%, Pt (100 ± 3)%, and Au (100 ± 2)%. Slightly lower values were observed for Os (90 ± 9)% which reached recovery of 100% only at 0.01 M of Septonex, and for Ir (85 ± 5)%. Very poor sorption was observed for Ru (4%) and Rh (8%), thus, this system is not suitable for preconcentration of Ru and Rh. This may be due to the oxidation numbers of Ru and Rh and, consequently, due to the charge of corresponding complex anions, their distribution coefficients and formation of ion associates.

The influence of concentration of HCl on the recovery was not significant within the studied interval 0.02–0.3 M, as well as the influence of the concentration of NaCl in the range 0–0.5 M at the constant concentration 0.1M HCl.

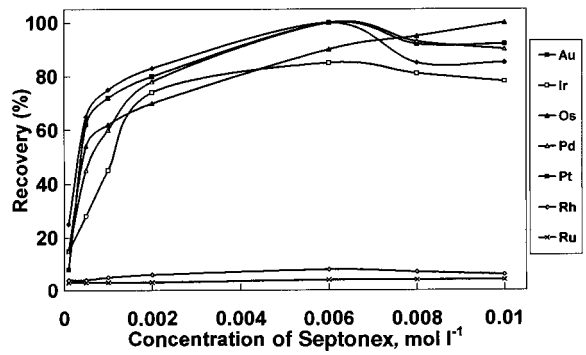

Fig. 1. Dependency of the efficiency of sorption of PGM on silicagel Separon™ SGX C18 on the concentration of Septonex. Conditions of sorption: 0.1 M HCl, 20 μg ml^{-1} of PGM and Au, sorption and elution flow rates: 0.6 and 1.5 ml min^{-1}, respectively.

Table 1
Recovery of PGM from pure solution, from leachate of airborne particulate matter and from model solutions spiked with hydrogen peroxide or sodium nitrate, and the relative standard deviation of repeatability for the pure solution

Analyte	Recovery of PGM (%)				RSD (%)[a]
	Pure solution[b]	Airborne dust[c]	H_2O_2 [d]	0.5 M NO_3^- [e]	Pure solution[b]
Au	100	82	90	74	2
Ru	5	7	1	5	13
Rh	10	0	2	2	26
Pd	100	22	100	54	1
Os	85	47	56	43	10
Ir	90	78	88	39	6
Pt	100	73	92	73	3

[a] Relative standard deviation of sorption obtained on 6 repetitions.
[b] Pure solution 50 ml) contained 0.4 mg ml^{-1} of PGM and Au, 0.006 M Septonex, 0.1 M HCl.
[c] Matrix of airborne dust leachate obtained from the procedure in Section 3.4.1
[d] 2 ml of H_2O_2 in 50 ml of solution with 0.4 mg ml^{-1} of each analyte, 0.006 M Septonex, 0.1 M HCl.
[e] 0.5 M $NaNO_3$ in 50 ml of solution with 0.4 mg ml^{-1} of each analyte, 0.006 M Septonex, 0.1 M HCl.

The recovery of PGM did not depend on the flow rate of sorption from 0.3 to at least 1.5 ml min^{-1}. Values >1.5 ml min^{-1} were not studied due to the lack of suitable peristaltic tubings and pump speeds. Desorption was performed with the flow rate of 1.5 ml min^{-1} and the first 2 ml of ethanolic eluate contained the whole desorbed amount of analytes.

For further experiments, the 0.006 M Septonex, 0.1 M HCl, 0.6 and 1.5 ml min^{-1} sorption and desorption flow rates, respectively, were employed.

The influence of the sample volume on the sorption was studied due to large volumes of solutions prepared from airborne particulate matter. With increasing volume of the sorbed solution the recovery decreased so that above 1000 ml it approached 65%. This might be caused by washing out of the sorbed ion associate by a large volume of solution. Therefore, the application of the standard addition method was necessary for quantitative determination.

The recovery did not exhibit the dependence on the concentration of PGM and Au in the range from 20 ng ml^{-1} to at least 400 ng ml^{-1} at a sorption from 50 ml volume.

3.3. Repeatibility of preconcentration

Six parallel preconcentrations were performed under the above optimum conditions from 50 ml of solution containing 20 μg of PGM and Au. Ethanolic eluates (4 ml) were treated as described in Section 3.1 and the resulting analysed solution was filled up to 10 ml volume. Samples were measured using ICP-AES. Relative standard deviations of repeatibility and recovery values for pure solution in Table 1 show that the highest recovery and the lowest relative standard deviation (% RSD) of repeatibility yielded Pd, Pt and Au.

3.4. Determination of Pd, Pt and Au in samples of airborne particulate matter

3.4.1. Decomposition procedure

Each glass filter was leached in a microwave device with 20 ml of HNO_3 and 4 ml of H_2O_2. The blank solutions characterising the whole procedure were prepared in the same way using unexposed filters. The leachate was transferred into a 250 ml volumetric flask, filled up to the mark and a portion of 100 ml was used for the determination of selected trace and matrix elements while 150 ml of the solution was used for the determination of PGM. To obtain a sufficient sample amount for preconcentration, the total volume of 26 one-day samples (each 150 ml) was taken as one sample. The corresponding volume of the air sample was thus 18720 m^3 for each site. The matrix contained

(average):3 mg kg^{-1} Na, 10 mg kg^{-1} K, 20 mg kg^{-1} Ca, 1 mg kg^{-1} Mg, 10 mg kg^{-1} Al, 2 mg kg^{-1} Fe, 10 mg kg^{-1} B, 3–15 mg kg^{-1} Zn.

3.4.2. Influence of sample matrix on sorption

One of the solutions of airborne particulate matter was spiked with 0.4 mg ml^{-1} of PGM and Au. Original concentrations of PGM were very low, e.g. 5.7 ng ml^{-1} of Pd, 2.6 ng ml^{-1} of Pt and 7.3 ng ml^{-1} of Au. After the addition of Septonex (0.006 M) and hydrochloric acid (0.1 M), a 50 ml volume of this spiked solution was sorbed on the Separon™ SGX. Recovery values of the added PGM concentrations in Table 1 show a significant decrease in comparison to pure solution, especially in the case of palladium. To recognise the component responsible for the sorption suppression, two sets of model solutions containing either H_2O_2 (0–2 ml/50 ml) or NO_3^- (0–0.5 M) were prepared and their sorption (50 ml) examined. While the hydrogen peroxide caused the significant diminuition of the sorption recovery only in the case of osmium, the presence of NO_3^- influenced the sorption of all analytes (Table 1). The explanation probably may be in the competitive formation and/or sorption of ionic associates of Septonex with nitrate anions.

The airborne dust was primarily sampled for the determination of elements other than PGM. Hence, the use of HCl had to be avoided due to known polyatomic interferences in the ICP-MS and the samples were thus decomposed using HNO_3. When special sampling would be for PGM determination, one could avoid the concurrent sorption problems by evaporating the aqua regia after leaching, followed by dissolution of a residue in HCl.

3.4.3. Analysis of leachates of airborne particulate matter

To the volume of 2500–3000 ml of a sample the stock solution of Septonex and HCl were added to obtain the final concentrations of 0.006 M Septonex and 0.1 M HCl. After sorption, elution and evaporation of ethanol the solution was filled up to 25 ml in the volumetric flask with 0.1 M HCl. Hence, the preconcentration by two orders of magnitude was performed.

Samples were analysed using both ICP-MS and ICP-AES. Limits of detection of ICP-MS, defined as concentrations corresponding to threefold of the standard deviation of the signal of the synthetic calibration blank solution, were 0.09 ng ml^{-1} of Pd, 0.05 ng ml^{-1} of Pt and 0.1 ng ml^{-1} of Au, limits of detection of axial ICP-AES, defined in the same way, were $\sim$5 ng ml^{-1} of Pd, Pt or Au.The synthetic calibration blank solution contained 0.006 M Septonex and 0.1 M HCl.

Blank values corresponding to dummy filters were 4 ng ml^{-1} for Pd, 0.5 ng ml^{-1} for Pt and 2 ng ml^{-1} for Au. The standard deviation of repeatibility of measurement of the dummy filter blank solution using ICP-MS was 0.24 ng ml^{-1} for Pd, 0.16 ng ml^{-1} for Pt and 0.2 ng ml^{-1} for Au. The enriched sample solutions exhibited concentrations in ranges: 6–35 ng ml^{-1} of Pd, 3–16 ng ml^{-1} of Pt and 7–20 ng ml^{-1} of Au (except for 590 ng ml^{-1} of Au in the site Sokolov).

The precision of measurement with ICP-MS was characterised with RSD between 7% and 3% within above concentration range for airborne dust samples. After the dummy filter blank values were subtracted from found concentration values, the RSD of the blank-corrected concentrations increased to 24–5%. Limits of quantitatively determinable concentrations (LQDC) defined for 10% RSD of the concentration in pre-concentrated sample solution were 10 ng ml^{-1} of Pd, 5 ng ml^{-1} of Pt and 8 ng ml^{-1} of Au when taking into consideration the dummy filter blank value subtraction. The LQDC values of ICP-AES were 20 ng ml^{-1} of Pd, Pt, Au.

Obtained concentration values were recalculated using volumes of filtered air to content per cubic meter (Table 2). In some cases, a reasonable agreement was found between ICP-AES and ICP-MS results obtained on the same solution. However, the ICP-AES results have only a limited information meaning owing to the lower detection power. The reliability of ICP-MS results was supported with close values obtained on 2 isotopes of both Pt and Pd. Surprisingly high values of palladium and gold were found in the region of Sokolov, however, this city is in the centre of an

Table 2
Determination of Pt, Pd and Au in airborne dust by ICP-MS and ICP-AES (pg m^{-3})

Sampling station	Analyte Pt		Pd		Au	
	ICP-AES	ICP-MS	ICP-AES	ICP-MS	ICP-AES	ICP-MS
Kočkov	21	25[a]; 36[b]	nd	81[c]; 27[d]	nd	13
Všechlapy	62	19[a]; 27[b]	30	42[c]; 45[d]	13	16
Souš	16	15[a]; 21[b]	nd	nd[c]; 23[d]	nd	15
Sokolov	43	42[a]; 41[b]	280	253[c]; 283[d]	1410	1620
Měděnec	9	13[a]; 24[b]	31	67[c]; 78[d]	19	11

nd, not detected.
Isotopes, [a]195 Pt; [b]196 Pt; [c]105 Pd; [d]108 Pd.

industrial area (brown coal mines, thermal power plant). Nevertheless, all the other sites also exhibit concentrations of Pt and Pd that are two or three times higher in comparison to values reported for highway areas with heavy traffic [1–4]. This would be further examined.

3.5. Determination of platinum group metals in reference material NIES No. 8

3.5.1. Decomposition procedure

Reference material NIES No. 8 (0.5 g) was placed on the glass dish, wetted with BRIJ 35 and then several drops of the solution of $Mg(NO_3)_2$ were added to obtain a bulk residue after combustion [9]. The dish was dried under an infrared lamp and inserted into the combustion chamber of the PLASMA 1101 mineralisation apparatus. After the combustion (4 h) the ash was leached for 1.5 h with aqua regia (2 ml) at 60°C, the solution was diluted with distilled water (10 ml) and filtered through a sintered glass crucible, the filtrate was transferred into a 50 ml volumetric flask, the stock solution of Septonex was added to obtain its final concentration of 0.006 M and the sample filled up to the mark. This solution was then pumped through the SilicaCart™ with Separon™ SGX and the elution followed as described earlier. The sample was transferred to a 25 ml volumetric flask because of the need to preserve some solution for possible comparison measurement, however, the final volume can be reduced to 5–2 ml which could result in a preconcentration factor of 10–25.

3.5.2. Analysis of engine soot

Six parallel samples were prepared by procedure described in the Section 3.5.1 and they were analysed using ICP-MS. Results presented in Table 3 show large differences between individual determinations. One of the reasons may be the inhomogeneity of this standard reference material in respect to the PGM, already reported in Ref. [5]. This inhomogeneity may be due to the metallic character of PGM particulates and, hence, different distribution in the engine soot in comparison to other elements. However, excluding the extreme result for Pt in the sample no. 2 we obtain an average value of 160 ng g^{-1} of Pt with the standard deviation of 90 ng g^{-1} of Pt which is close to 185 ng g^{-1} of Pt found by Paukert and Rubeška [5] (Table 3). Similarly, six parallel determinations yielded 230 ng g^{-1} of Pd (the standard deviation is 94 ng g^{-1} of Pd), which is compara-

Table 3
Determination of Pt, Pd, Ir and Au in reference material NIES No. 8 vehicle exhaust particulates ng g^{-1})

Sample no.	Analyte Pt	Pd	Ir	Au
1	66	189	5	182
2	1259	332	35	601
3	193	365	87	163
4	90	147	5	38
5	296	158	20	111
6	155	188	3	94
x^a_{ref}	185 ± 14	180 ± 28	39 ± 21.1	—

[a] average value $\pm$ standard deviation, taken from Ref. [5].

ble with 180 ng g^{-1} of Pd reported in [5] (Table 3). The larger standard deviations of our results in comparison with those obtained by Paukert and Rubeška [5] (Table 3), may be influenced also by the amount of sample taken for decomposition (2 g reported in [5]). However, there is a reasonable agreement between our results and ETAAS values after preconcentration to NiS button [5].

4. Conclusion

Preconcentration technique based on the sorption of ion associates of chlorocomplexes of platinum group metals with the surfactant N1-carbaethoxypentadecyl)-trimethylammonium bromide on the modified silicagel C18 was developed and applied to the determination of the platinum group metals in airborne dust collected on the air filters, and in certified reference material NIES no. 8 Vehicle Exhaust Particulates). Inductively coupled plasma mass spectrometry was suitable for the analysis of enriched samples. Concentrations of Pt and Pd on the level of tens of pg m^{-3} were found in air filtered through the filters installed in six Czech meteorological stations. Reasonable agreement was found with results obtained on NIES no. 8 by ETAAS values after preconcentration to NiS button [5].

Acknowledgements

Thanks are due to Professor Lumír Sommer for his deep interest and valuable comments. Authors wish to thank to the Czech Hydrometeorological Institute for providing the samples of airborne dust collected at meteorological stations of the Czech Republic. V.K. thanks to Dr Ivan Rubeška for providing the certified reference material NIES No. 8. This work has been supported by the Grant Agency of the Czech Republic (project no. 203/96/0478).

References

[1] Platinum, Environmental Health Criteria 125, World Health Organization, Geneva, 1991.
[2] F. Alt, A. Bambauer, K. Hoppstock, B. Mergler, G. Tölg, Fresenius J. Anal. Chem. 346 (1993) 693.
[3] M. Parent, H. Vanhoe, L. Moens, R. Dams, Fresenius J. Anal. Chem. 354 (1996) 664.
[4] C. Luedke, E. Hoffmann, European Winter Conference on Plasma Spectrochemistry, 12–17 January 1997, University of Gent, Gent, Belgium, 1997.
[5] T. Paukert, I. Rubeska, Anal. Chim. Acta 278 (1993) 125.
[6] D. Klueppel, N. Jakubowski, J. Messerschmidt, D. Stuewer, D. Klockow, European Winter Conference on Plasma Spectrochemistry, 12–17 January 1997, University of Gent, Gent, Belgium, 1997.
[7] V. Otruba, M. Strnadová, B. Skalníková, Talanta 40 (1993) 221.
[8] V. Otruba, J. Stepánková, L. Sommer, Talanta 41 (1994) 1185.
[9] V. Otruba, J. Kaláček, Chem. Listy 87 (1993) 64.

ELSEVIER

Talanta 48 (1999) 847–857

Talanta

Analytical monitoring of photocatalytic treatments. Degradation of 2,3,6-trichlorobenzoic acid in aqueous TiO_2 dispersions[1]

Alessandra Bianco Prevot, Edmondo Pramauro *

Dipartimento di Chimica Analitica, Università di Torino, 10125 Torino, Italy

Received 28 July 1997; received in revised form 16 December 1997; accepted 22 December 1997

Abstract

The photocatalytic degradation of 2,3,6-trichlorobenzoic acid (2,3,6-TBA) in aqueous TiO_2 dispersions irradiated with simulated solar light was investigated. Fast primary degradation of the herbicide, which obeys a pseudo-first order law, was observed. Complete mineralisation of the organic carbon to CO_2 was obtained after long term irradiation, with corresponding stoichiometric transformation of organic chlorine into chloride ion. Various aromatic intermediates, originating from 2,3,6-TBA, were detected during the treatment and identified using GC-MS. From the analytical data, a possible multi-step degradation scheme was proposed. The photocatalytic treatment of the pesticide was also performed in the presence of Brij 35 micellar solutions, although strong inhibition of the process was observed. When surfactant aggregates are present the photocatalytic destruction of 2,3,6-TBA is still possible at reasonable rates only after a proper dilution of the waste and by increasing significantly the semiconductor/pollutant ratio.

Keywords: Photocatalysis; Pesticide degradation; Analysis

1. Introduction

Photocatalysis over irradiated semiconductor dispersions is a decontamination method suitable for the treatment of water and waste water containing inorganic or organic pollutants present at low concentration levels. It is based on a sequence of light-induced redox transformation, occurring at the semiconductor/water interface upon irradiation with light of proper energy, and involves either the generated electron/hole pairs and oxidising radical species coming from water and from adsorbed oxygen. Suspended TiO_2 particles (anatase form) were largely used as efficient catalysts for the decomposition of a variety of organic compounds present in water [1–5]. Carbon dioxide has been reported to be the end product of transformation of the organic carbon in most studies.

Due to the complex nature of the process, a careful analytical monitoring using different tech-

* Corresponding author.

[1] Work presented at the 5th Symposium on Analytical Sciences, Nice, France, June 1997.

0039-9140/99/$ - see front matter
PII S0039-9140(98)00101-5

niques is essential in order to control all the transformation steps, to identify any harmful intermediate and to give insight into the reaction mechanism. The simple assessment of the pollutant disappearance is, in fact, not enough since heterogeneous photocatalysis may generate a variety of organic intermediates (in some cases more toxic than the starting substrate) if the treatment is not pursued until complete mineralisation.

Among the compounds of environmental concern, benzoic acid derivatives constitute an important class of herbicides which are especially useful for the control of deep rooted perennial weeds. Within this family, the widely used 2,3,6-TBA shows the highest persistence in soils (up to about 1 year) [6] and a great diffusion in this environmental phase, being included in the mobility class V of the Helling classification [7]. If the pesticide concentration in surface or ground water supplies exceeds the admitted concentration limits, removal of this compound from contaminated streams becomes a necessary treatment of practical interest.

In this work, the use of photocatalysis to decompose 2,3,6-TBA present at the ppm concentration level was investigated in aqueous media containing suspended TiO_2 particles, under simulated solar light irradiation. Attention has been paid to the mass balance of the degradation process, to the kinetic aspects of the primary process and to the identification of transient aromatic intermediates formed. The conditions necessary for a possible coupling of this destruction treatment with surfactant-based removal steps were also examined and defined.

2. Experimental

2.1. Reagents and materials

High-purity 2,3,6-TBA purchased from Ehrenstorfer–Schaefers (Germany) was used. TiO_2 P25 from Degussa with a surface area of $\approx 55\ m^2\ g^{-1}$ was used throughout the work. This oxide was previously washed with water and irradiated with simulated solar light for ~ 12 h, in order to remove any organic impurity. The washed semiconductor was then dried in the oven at 80°C.

Acetonitrile (Lichrosolv, Merck) and tetrabutylammonium hydrogensulphate (Fluka) were used to prepare the LC eluents, NaOH and phosphate buffer pH 7 (Merck) were used to adjust the pH. Dichloromethane (Merck) and Bis(trimethylsylil)trifluoroacetamide (Aldrich) were used in GC-MS analysis. Na_2CO_3 and $NaHCO_3$ (Merck) were used to prepare the eluents for the ionic chromatography. Doubly distilled water, filtered through 0.45 μm HA cellulose acetate membranes (Millipore), was used throughout the work. Stock solutions of 2,3,6-TBA (100 mg l^{-1}) were prepared in water, protected from light and stored at 5°C.

2.2. Procedure

2.2.1. Ultrafiltrations with micellar solutions

Experiments were performed on aqueous solutions containing a constant concentration of pesticide (1.5×10^{-4} M) to which an excess of surfactant (2.0×10^{-2} M) was added. Removal of 2,3,6-TBA from these micellar solutions was performed by ultrafiltration in stirred cells (S 43-70, Spectrum) through hydrophilic cellulose membranes (Spectra-Por C, Spectrum) having a molecular weight cut-off of 10000 dalton. Typically 35 ml of micellar solution were filtered under a nitrogen pressure of ca. 3 atm and 25 ml of permeate were collected and successively analysed by HPLC, as described in the next section.

2.2.2. Irradiation experiments

A cylindrical photochemical reactor (diameter: 80 mm; height: 230 mm) from Helios-Italquartz was used (see Fig. 1). The total capacity of the reactor when the lamp is placed is about 550 ml. Degradations were performed on 500 ml of aqueous solutions containing the desired concentration of 2,3,6-TBA (34 mg l^{-1}) and the proper amount of TiO_2 (340 mg l^{-1}), having an initial pH of 3. NaOH was added to increase the solution pH when necessary. The temperature within the reactor was kept at 25°C. After irradiation for a given time with simulated solar light emitted from a 125 W medium pressure Hg lamp, 2.0 ml of the dispersion were taken and filtered through a cellulose acetate membrane (HA 0.45 mm, Millipore). 20 μl of the filtered sample were injected in the chromatograph and analysed by HPLC, working at the following

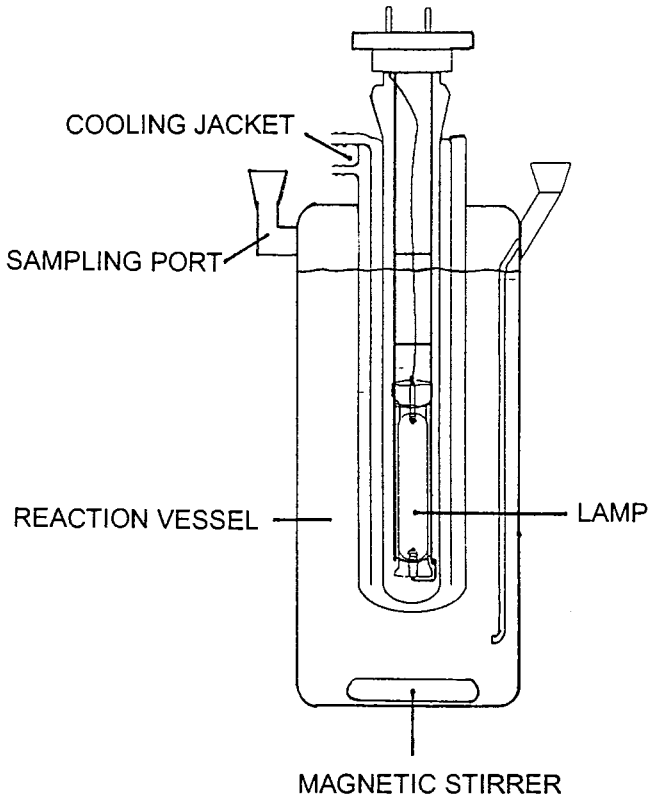

Fig. 1. Schematic representation of the photochemical reactor equipped with a medium pressure Hg lamp.

conditions: column Lichrospher RP-C_{18} 5 μm, 4.0 mm i.d. × 125 mm long, from Merck; eluent: acetonitrile/phosphate buffer pH 7 (40:60 v/v); flow rate: 1 ml min^{-1}; detector wavelength: 223 nm. The buffer also contained tetrabutylammonium hydrogensulfate 15 mM added as ion-pairing reagent.

2.2.3. Evolution of CO_2 and TOC measurements

Complete mineralisation of organic samples to CO_2 is very often obtained by using the photocatalytic method. According to a previously reported procedure [8], the formation of this end product was followed in a closed cylindrical Pyrex glass cells (4 cm i.d. × 2.5 cm height) on 5 ml of stirred aqueous suspensions. The experiments were carried out in a solarbox (from CO.FO.ME.GRA, dimensions: 28 cm large, 20 cm depth, 20 cm height), equipped with a 1500-W Xe lamp and a 340 nm cut-off filter, using the headspace gas chromatography to analyse the gas phase of the cell after acidification of the solution with 5 ml of H_2SO_4, 5.0 M. Typically, 200 μl of such gaseous phase were injected on a Carlo Erba 4600 gas chromatograph equipped with a Hayesep 80/100 mesh column (2 m long, 6 mm i.d.). Helium was used as carrier gas (flow rate: 30 ml min^{-1}). The column and injector temperatures were 110 and 130°C, respectively. A TCD detector was used (block temperature: 150°C, filament temperature: 250°C). Calibration curves were obtained by analysing standard solutions of Na_2CO_3, placed in closed vials and treated as described above. Blanks obtained after long-term irradiation experiments indicated a very low contribution from the reagents (< 0.3 mM), which was taken into account to correct the data.

When working in the open reactor, the evolution of the organic carbon was followed using a Shimadzu 5000 total organic carbon (TOC) analyser, on 5.0 ml of the filtered irradiated suspension.

2.2.4. Chloride ion determination

The formation of chloride was followed by suppressed ion chromatography, using a Biotronik IC 5000 apparatus equipped with a 200 mm long $\times 4$ mm i.d. AS4A-SC column (Dionex) and a conductometric detector BT0330 (Biotronik). The eluent was a mixture (1:1, v/v) of Na_2CO_3 (1.5 mM) and $NaHCO_3$ (1.5 mM); flow rate: 1.5 ml min^{-1}.

2.2.5. Identification of aromatic intermediates

After extraction in dichloromethane, most unknown aromatic intermediates were identified by GC-MS using a Finnigan-MAT 95Q double-focusing reverse geometry mass spectrometer interfaced to a Varian 3400 gas chromatograph, equipped with a J&W DB-MS capillary silica column (30 m long, 0.25 mm i.d.), coated with methylphenylsiloxane. Qualitative analyses were performed in the electron impact (EI) mode, at 70 eV potential. The ion-source temperature was 220°C. The mass range was 150–250 amu. GC conditions were the following: injection volume: 1 μl (splitless injection), injector temperature: 300°C, carrier: helium. The oven temperature was programmed as follows: isothermal at 50°C for 3 min, from 50–300°C at 20°C min^{-1}, isothermal at 300°C for 10 min.

3. Results and discussion

3.1. Primary degradation

Most organic pollutants undergo photocatalytic degradation when irradiated in the presence of suitable semiconductors. This occurs through a multistep process involving the attack of the substrate by radical species among which the $^{\bullet}OH$ radical was recognised to be the most powerful oxidant [5,9–15]. The detailed mechanism of such transformations has been abundantly discussed in the literature [1–5] and will be only summarised here. Basically, the semiconductor irradiation with light of energy higher than the band-gap induces the formation of electron-hole pairs:

$$TiO_2 + h\nu_{(E > Ebg)} \rightarrow e^-_{CB} + h^+_{VB} \quad (1)$$

Electrons and holes can recombine, can be trapped by active sites present at the semiconductor surface or sub-surface or can react with adsorbed electron donors or acceptors. In aqueous solutions containing hydrated and hydroxylated TiO_2, hole trapping can lead to the formation of surface-bound $^{\bullet}OH$ radicals, solvated $^{\bullet}OH$ radicals and other oxidant species (including H_2O_2) from reactions with adsorbed oxygen and water molecules. These species are very reactive agents, able to attack and transform the organic molecule.

Under the experimental conditions reported in the reactor, complete disappearance of 2,3,6-TBA was observed after ≈ 60 min (see Fig. 2). The reaction follows a pseudo-first order kinetic law, according to the equation:

$$-dC_{subs}/dt = k_{obs}C_{subs} \quad (2)$$

where C_{subs} is the pesticide concentration and k_{obs} is the observed first-order rate constant. According to Eq. (2), linear plots of $\ln C/C_o$ versus time are expected (see inset in Fig. 2) from which slopes k_{obs} can be evaluated.

Irradiation of 2,3,6-TBA solutions at pH 3 and in the absence of TiO_2 shows a negligible decomposition of the pesticide, indicating that photochemical processes are scarcely responsible for the observed fast transformations under these conditions.

The effect of initial pH on photocatalytic degradation kinetics was also investigated. No significant changes of the measured substrate half-lives (around 17 ± 1 min) were observed in the pH range 3–9. Taking into account the low pK_a of the acid (≈ 2, as determined by spectrophotometry), a favourable electrostatic contribution to the substrate adsorption on the TiO_2 particles is expected at pH 3, below the isoelectric point of the oxide. In fact, the point of zero charge for TiO_2 (anatase form) is at pH ≈ 5 and below this point the surface of the particles becomes positively charged. On the contrary, electrostatic repulsion is expected at pH 9. Since it is known that the concentration of the active $^{\bullet}OH$ species increases with increasing pH [3], the electrostatic effects can be compensated and this explains the nearly constant reaction rate measured in the reported pH range.

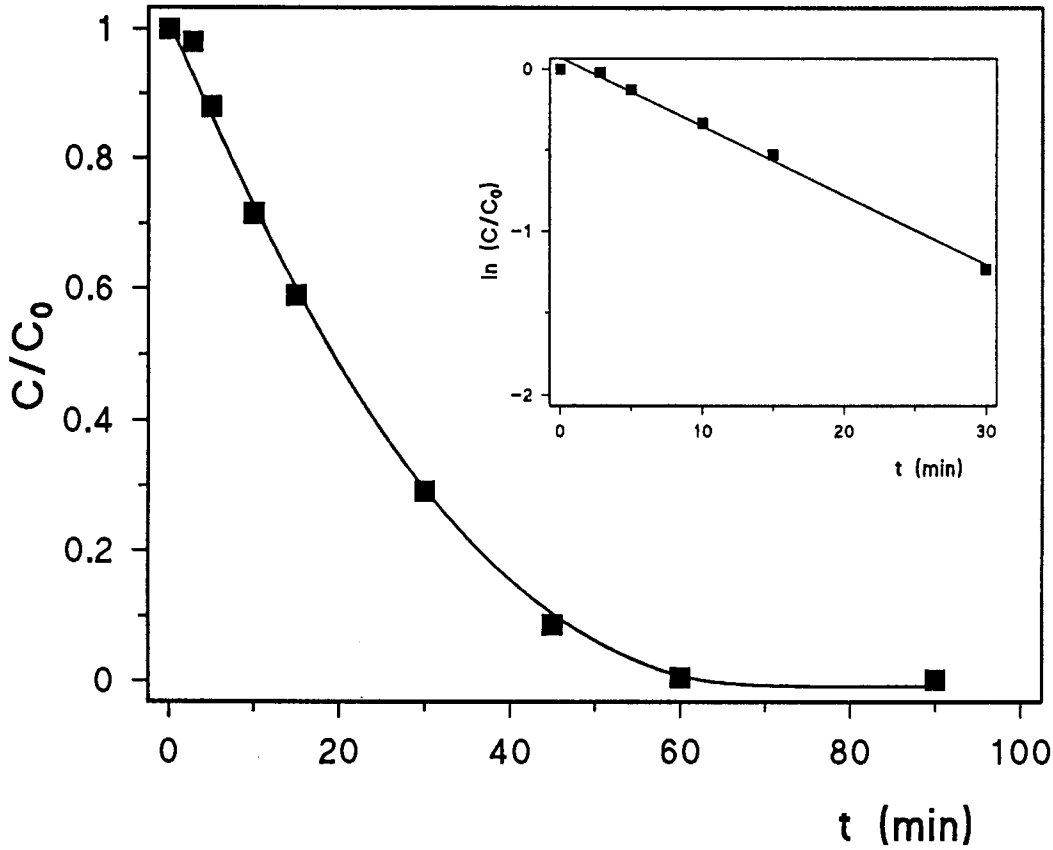

Fig. 2. Kinetics of 2,3,6-TBA degradation under light irradiation (primary process). Starting conditions: 2,3,6-TBA 34 mg l^{-1}; TiO_2 340 mg l^{-1}; pH, 3.

3.2. Analysis of the end products:

The evolution of TOC and chloride ion were monitored in all the experiments performed with the laboratory reactor. Taking into account that the complete disappearance of the pesticide in the reactor occurs after about 60 min and that the reduction of TOC up to negligible levels is observed after ≈ 90 min (see Fig. 3), this provides an indirect evidence of the presence of transient organic intermediates in the reaction system. The evolution of chloride ions, which becomes quantitative after ≈ 90 min irradiation, also supports the above hypothesis.

Since experiments performed in the reactor could allow the formation of volatile intermediates which can be lost from the open vessel, degradations were also monitored in closed cells irradiated in the solarbox. Stoichiometric formation of CO_2 was observed under these conditions, after ≈ 90 min irradiation (see Fig. 4). These results confirmed that complete mineralisation of 2,3,6-TBA occurs via photocatalysis over TiO_2, in agreement with the previously observed behaviour of most benzene derivatives.

3.3. Monitoring of aromatic intermediates

The observed evolution of the UV solution spectra of 2,3,6-TBA under irradiation is shown in Fig. 5, together with the HPLC profiles of the filtered samples. These profiles show the presence of UV-absorbing species formed in the solution after low irradiation times (15 min), at which the concentrations of transient aromatic intermediates are high enough, whereas at longer times the

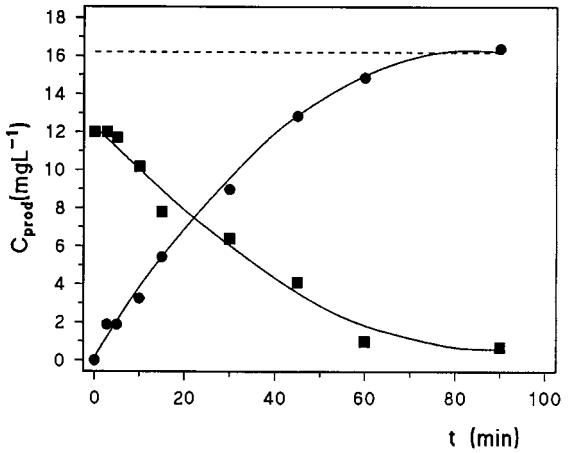

Fig. 3. Kinetics of the pesticide mineralisation. TOC (■) and chloride (●) evolution; the dotted line corresponds to the stoichiometric chloride amount. Experimental conditions as in Fig. 2.

peaks of these compounds are less evident. It appears clearly that simple spectrophotometric monitoring cannot be used to follow the primary process since different species absorb in the same UV region.

It must be noted that only few peaks corresponding to reaction intermediates, very close to the column void volume, are observed in the HPLC experiments. Moreover, due to the nature of the radical attack, a great number of compounds potentially originated from 2,3,6-TBA could be possibly identified as intermediates. For the above reasons, the use of HPLC analysis appeared to be a difficult task and our attention was focused on the GC-MS approach.

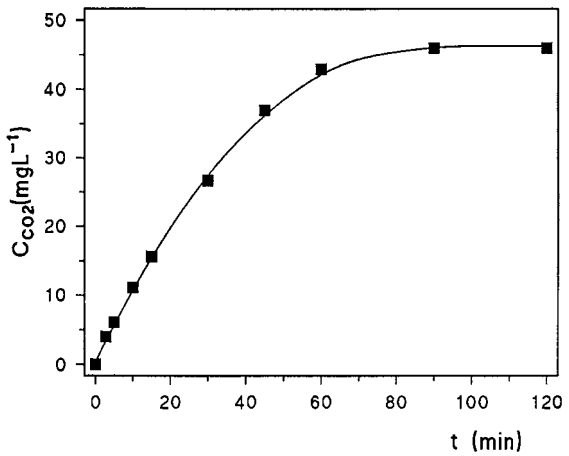

Fig. 4. Kinetics of CO_2 formation in experiments performed in closed cells. Conditions as in Fig. 2.

In order to identify the aromatic compounds formed during the treatment, 15.0 ml samples of homogenised irradiated suspensions were extracted with 10.0 ml of methylene chloride. After concentration under nitrogen stream to ≈ 200 μl into conic vials, the extracts were analysed by GC-MS. The GC pattern of extracts of samples obtained after 15 min irradiation are shown in Fig. 6. The observed neat peaks corresponding to degradation products were analysed by the MS detector.

A group of compounds, which produced clear, distinguishable and easy-to-interpret mass spectra, were identified by EI mass spectra through $>90\%$ match with the Wiley MS library. The recognised intermediates are the following (the roman number within parenthesis corresponds to that assigned in the reaction Scheme 1): (I) 2,3,6-TBA; (XIII) dichlorobenzene isomers; (VI) 1,2,5-t richlorobenzene; (XI) 2,3,5-trichlorophenol; (X) 2,3,6-trichlorophenol; (XII) trichlorohydroquinone; (XIV) 2,5-dichlorophenol; traces of 2,4,5-trichlorophenol and monochlorophenol isomers were also detected.

The more abundant compounds, which have in common the presence of at least two chlorine atoms and only one or two hydroxyl groups, are quite hydrophobic and can be easily extracted in dichloromethane. Taking into account that more hydrophilic species could be formed in the system, in particular through extended dechlorination and hydroxylation of the initial molecule, their extraction in CH_2Cl_2 would become more difficult.

A second GC-MS analysis was thus performed after derivatisation of the organic extracts using Bis(trimethylsilyl)trifluoroacetamide as reagent. The CH_2Cl_2 extract was evaporated to dryness under an N_2 stream and 50 μl of derivatising agent were added; the samples were then kept in closed vials at 80°C for 20 min. The corresponding derivatives of the intermediate products, injected in the GC and analysed by the MS detector, indicated the presence of other compounds (previously not found). From the corre-

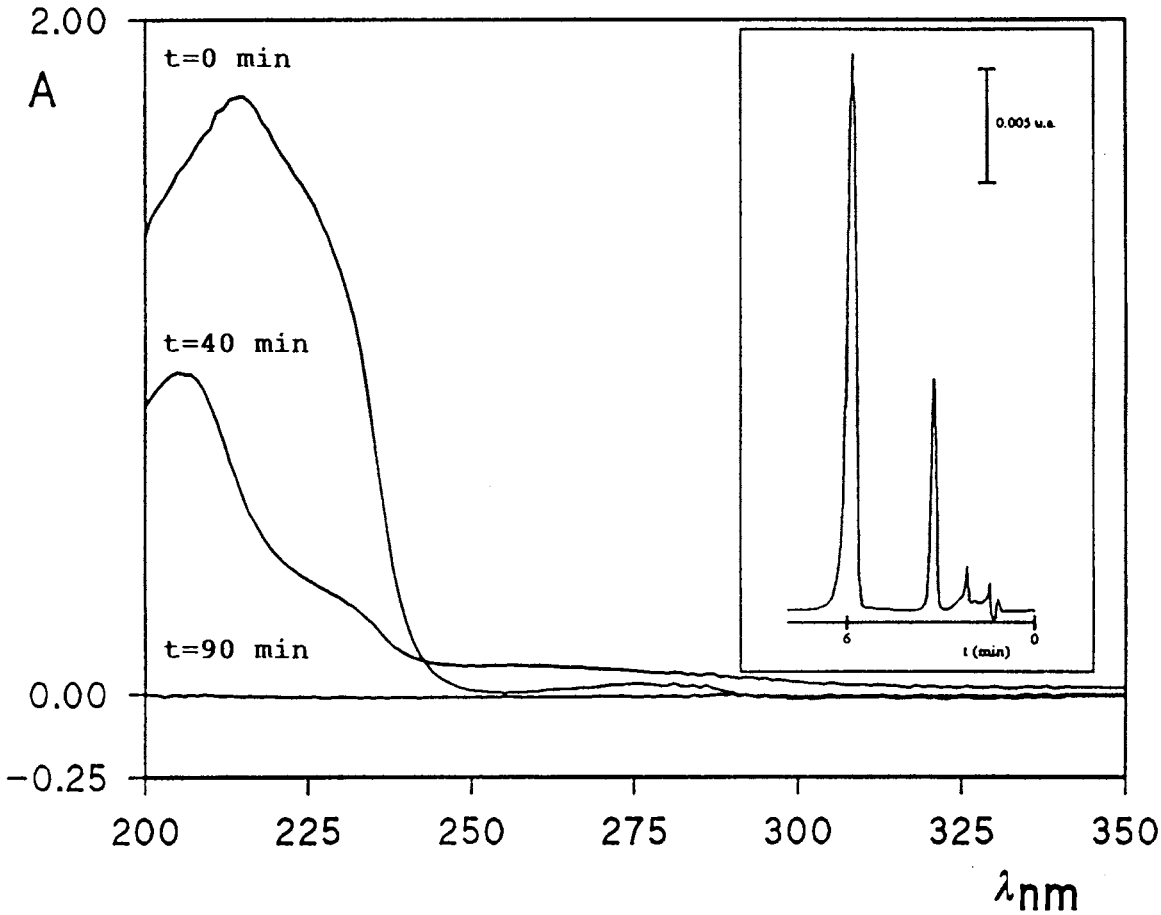

Fig. 5. Change of UV spectra of irradiated pesticide as a function of time. Inset: HPLC profile of 2,3,6-TBA solutions after 15 min irradiation. Initial conditions as in Fig. 2.

sponding mass spectra and taking into account the reagent contribution and the possible ways of derivatives fragmentation, the following assignments were made: (II, III) 2,3,6-TBA monohydroxylated; (IV) 2,3,6-TBA dihydroxylated; (V) trichlorotrihydroxybenzene, (XII) trichlorohydroquinone (confirmed), (X) 2,3,6-trichlorophenol (confirmed); (XI) 2,3,5-trichlorophenol (confirmed); (VIII) dichloro dihydroxybenzene (structure hypothesised); (XV) dichlorotrihydroxybenzene (structure hypothesised); (VII) hydroxydichlorobenzoic acid (structure hypothesised).

The symbol * in Scheme 1 indicates one of the possible isomers, consistent with the observed m/z fragments, which could be originated from identified precursors. Due to the lack of the corresponding authentic standards, these structures were simply hypothesised. The symbol ** indicates compounds present at very low abundance level and/or determined with a low match with the MS library.

GC-MS analysis of extracts from solutions subjected to longer time irradiation (for e.g. 30 min) showed a drastic reduction of the intermediates concentration, indicating that the identified aromatics undergo fast transformation in the reaction media.

3.4. Degradation paths

On the basis of the GC-MS data, taking into account the identified structures of the more abundant intermediates, a tentative degradation scheme can be proposed which accounts for the main processes originated from the attack of generated radical species on the substrate (see Scheme 1). Although it is difficult to depict the complete sequence of reactions linking all the observed products without the use of authentic standards (most of them were not available), some considerations about the observed transformations may be done: hydroxylation of aromatic ring with corresponding H abstraction is confirmed as a major reaction step (a); decarboxylation could be invoked to justify the formation of compounds such as VI, IX and XIV (paths b); substitution of the carboxylic group with OH is indicated under path (c), although the sequence (b) + (a) could give the same result; substitution of the chlorine atoms by OH groups is another typical process occurring in the reaction system (paths d); dechlorination without hydroxylation may justify the formation of compounds (XIII) from trichlorobenzenes (path e).

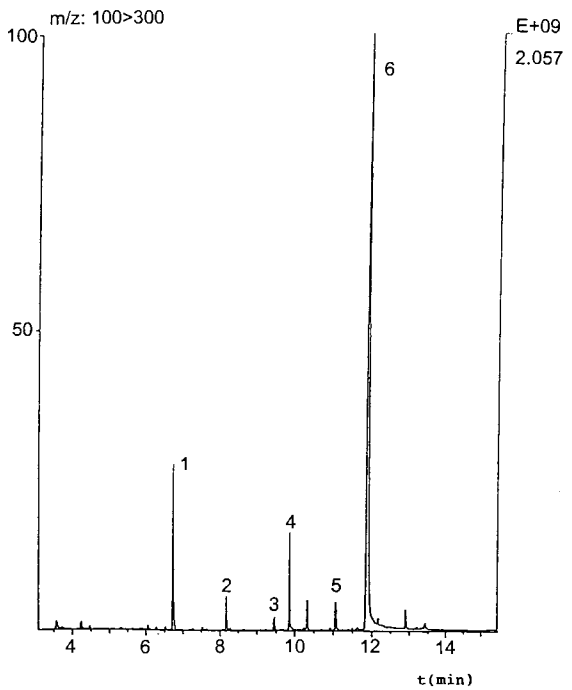

Fig. 6. GC analysis of dichlorometane extracts after 15 min irradiation. Peaks (1): dichlorobenzene isomers; (2) 1,2,5-trichlorobenzene; (3) 2,3,5-trichlorophenol; (4) 2,3,6-trichlorophenol; (5) 2,3,6 trichlorohydroquinone; (6) 2,3,6-TBA.

Moreover, the presence in the HPLC profile (see inset in Fig. 5) of peaks with retention time in the range 1.5–2.5 min, allows the hypothesis of formation of dihydroxybenzene isomers (retention time 1.8–2.6 min). The identification of these intermediates only on HPLC analysis basis is difficult, in particular taking into account that they are hydrophilic compounds having retention times near to the column dead time ($t_m = 1.2$ min). However, traces of compounds of this type (e.g. 1,2- and 1,4-dihydroxybenzene) have been previously identified [16] during the GC-MS analysis of irradiated solutions of other aromatics showing similar HPLC patterns, indicating that the formation of polyhydroxybenzenes could be one of the reaction steps.

The opening of the benzene ring after oxidation-hydroxylation giving rise to the formation of aliphatic products [17–20] which are successively transformed into CO_2, is known from previous studies on photocatalytic degradation of other aromatic products and was not investigated in the present study.

It is known that coupling reactions between intermediate radicals can give rise to the formation of transient biphenyl derivatives (found during the treatment of other aromatic and heteroaromatic pollutants) [21–23]. The presence of such compounds was not detected in the present system.

3.5. Effect of surfactants on the degradation of 2,3,6-TBA

The presence of surfactants in the aqueous waste streams prior to treatment must be carefully considered when pesticides are used since these components are usually added to facilitate the active product dispersion. Moreover, surfactants have been also recently introduced as mild cleaning agents in remediation treatments of contaminated environmental phases [24–26].

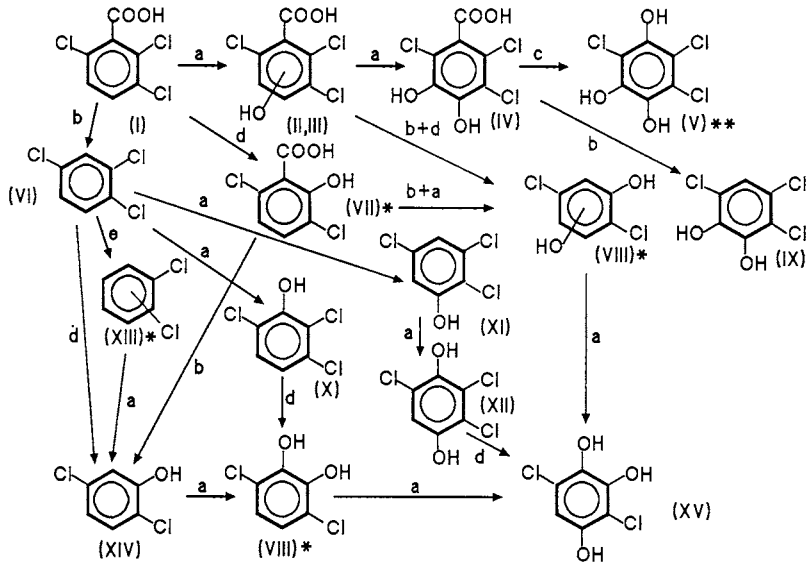

Scheme 1.

We have considered this expected condition by examining in particular the possible removal of 2,3,6-TBA from water using micellar-enhanced ultrafiltration (MEUF) [27]. The solubilisation ability of Brij 35 (polyoxyethylene(23)dodecyl ether), HTAB (hexadecyltrimethylammonium bromide) and SDS (sodium dodecyl sulfate) towards the substrate was preliminarily evaluated by measuring the ultrafiltration rejection coefficient, defined as:

$$R = 1 - C_p/C_o \quad (3)$$

where C_p and C_o are the concentrations of 2,3,6-TBA in the permeate and in the feed solution, respectively. The results obtained using 2.0×10^{-2} M surfactant solutions in the pH range 3–9 suggest a strong binding between the pesticide and the micelles of Brij 35 and HTAB ($R \approx 1$), whereas electrostatic repulsion limits the use of SDS ($R \approx 0.3$). Among the two more efficient surfactants, Brij 35 was selected because it has a lower critical micellar concentration (cmc) and the amount of surfactant released in the permeate is much lower.

Several UF runs were performed starting from 35 ml of surfactant-containing solution. Surfactant-rich retentates, containing the total amount of removed pollutant, were then subjected to degradation in the reactor after dilution with water to 500 ml. Under these conditions, the initial concentrations of surfactant and 2,3,6-TBA in the vessel were 1.4×10^{-3} M (1.68 g l^{-1}) and 8.0×10^{-6} M (1.8 mg l^{-1}), respectively. The TiO_2/pesticide ratio (10:1) was kept constant in the experiments.

Comparison of the corresponding degradation kinetics with that observed in the same conditions in water clearly indicates that a strong inhibition effect is exerted by the amphiphile (see Fig. 7). This result is not surprising since photocatalytic degradation of surfactants was already proven [28,29] and competition for the active sites of the catalyst occurs between the surfactant (present in large excess) and 2,3,6-TBA. Moreover, the micelles could exert a protective role towards the incorporated solutes by reducing their adsorbed fraction onto the semiconductor particles. Only increasing significantly the semiconductor/pesticide ratio (up to 500:1), the degradation process becomes fast enough for practical purposes (see curve c in Fig. 7).

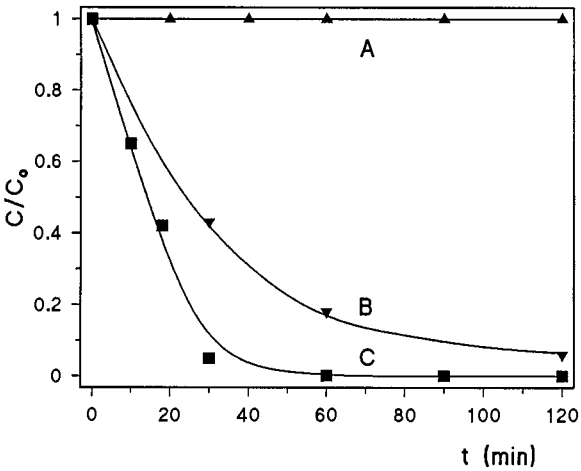

Fig. 7. Surfactant effect on the primary degradation of 2,3,6-TBA. Pesticide concentration: 1.8 mg l^{-1}; initial pH, 3. (A) Brij 35: 1.68 g l^{-1}; TiO_2 18 mg l^{-1}. (B) Brij 35 1.68 g l^{-1}; TiO_2 900 mg l^{-1}. C) TiO_2 18 mg l^{-1}; surfactant absent.

4. Conclusions

The photocatalytic destruction of 2,3,6-TBA over illuminated TiO_2 suspensions is a feasible and fast treatment which can be applied to clean contaminated water supplies. The complete mineralisation of the pesticide is observed with the corresponding formation of CO_2 and Cl^- as end products. The analysis of aromatic intermediates reveals the presence of hydroxylation, dechlorination, decarboxylation and oxidation-reduction steps leading to the complete transformation of the starting molecule. Harmful biphenyl intermediates were not detected during the treatment.

The presence of amphiphiles and, in particular, of micellar aggregates in the waste largely affects the pesticide degradation rate. The effect of the investigated Brij 35 micelles, formed at low surfactant concentrations, is so relevant that the fast destruction of 2,3,6-TBA can be performed only after dilution of the contaminated stream and by drastically increasing the semiconductor concentration.

Due to the complex sequence of reactions involving reactive radicals, the nature of potentially toxic transient intermediates must be always assessed, even when they are present at trace level in the reaction vessel. The role played by a strict analytical control of the process is, thus, fundamental.

Acknowledgements

The authors thank Dr Marco Vincenti for the MS measurements. Financial support from Ministero Università e Ricerca Scientifica e Tecnologica (MURST), Consiglio Nazionale delle Ricerche (CNR) and Project: Sistema Lagunare Veneziano is gratefully acknowledged.

References

[1] N. Serpone, E. Pelizzetti (Eds.), Photocatalysis: Fundamentals and Applications, Wiley, New York, 1989, p. 650.
[2] D.F. Ollis, H. Al-Ekabi (Eds.), Photocatalytic Purification and Treatment of Water and Air, Elsevier, Amsterdam, 1993, p. 820.
[3] D. Bahnemann, J. Cunningham, M.A. Fox, E. Pelizzetti, P. Pichat, N. Serpone, in: G.R. Helz, R.G. Zepp, D.G. Crosby (Eds.), Aquatic and Surface Photochemistry, Ch. 21, Lewis, Boca Raton (FL), 1994, pp. 261–316.
[4] M.R. Hoffmann, S.T. Martin, W. Choi, D.W. Bahnemann, Chem. Rev. 95 (1995) 69.
[5] N. Serpone, R.F. Khairutdinov, Semiconductor nanoclusters. Physical, chemical and catalytic aspects, in: P.V. Kamat, D. Meisel (Eds.), Studies in Surface Science and Catalysis, vol. 103, Elsevier, Amsterdam, 1996, pp. 417–444.
[6] S.U. Khan, Pesticides in the Soil Environment, Ch. 5, Elsevier, Amsterdam, 1980, p. 169.
[7] C.S. Helling, Soil Sci. Soc. Am. Proc. 35 (1971) 732.
[8] E. Pelizzetti, V. Maurino, C. Minero, V. Carlin, E. Pramauro, O. Zerbinati, M.L. Tosato, Environ. Sci. Technol. 24 (1990) 1559.
[9] R.W. Matthews, J. Chem. Soc. Faraday Trans.1. 80 (1984) 457.
[10] C.S. Turchi, D.F. Ollis, J. Catal. 122 (1990) 178.
[11] J. Cunningham, G. Al-Sayyed, J. Chem. Soc. Faraday Trans. 1 86 (1990) 3985.
[12] C. Kohrmann, D.W. Bahnemann, M.R. Hoffmann, Environ. Sci. Technol. 25 (1991) 494.
[13] G.K.C. Low, S.R. McEvoy, R.W. Matthews, Environ. Sci. Technol. 25 (1991) 460.
[14] M.W. Peterson, J.A. Turner, A.J. Nozik, J. Phys. Chem. 95 (1991) 221.
[15] C. Minero, F. Catozzo, E. Pelizzetti, Langmuir. 8 (1992) 481.
[16] E. Pramauro, A. Bianco Prevot, M. Vincenti, G. Brizzolesi, Environ. Sci. Technol. 31 (1997) 3126.

[17] K. Hashimoto, T. Kawai, T. Sakata, J. Phys. Chem. 88 (1984) 4083.
[18] J.C. D'Oliveira, G. Al-Sayyed, P. Pichat, Environ. Sci. Technol. 24 (1990) 990.
[19] L. Amalric, C. Guillard, P. Pichat, Res. Chem. Intermediates 21 (1995) 33.
[20] C. Guillard, P. Pichat, G. Huber, C. Hoang-Van, J. Adv. Oxid. Technol. 1 (1996) 53.
[21] C. Maillard-Dupuy, C. Guillard, H. Courbon, P. Pichat, Environ. Sci. Technol. 28 (1994) 2176.
[22] C. Minero, E. Pelizzetti, P. Pichat, M. Sega, M. Vincenti, Environ. Sci. Technol. 29 (1995) 2226.
[23] J. Theurich, M. Lindner, D.W. Bahnemann, Langmuir. 12 (1996) 6368.
[24] S. Sun, W.P. Inskeep, S.A. Boyd, Environ. Sci. Technol. 29 (1995) 903.
[25] I.T. Yeom, M.M. Ghosh, C.D. Cox, K.G. Robinson, Environ. Sci. Technol. 29 (1995) 3021.
[26] D. Roy, R.R. Kommalapati, S.S. Mandava, K.T. Valsaraj, W.D. Constant, Environ. Sci. Technol. 31 (1997) 670.
[27] S.D. Christian, J.F. Scamehorn, in: J.F. Scamehorn, J.H. Harwell (Eds.), Surfactant based separation processes, Ch. 1, vol. 33, Marcel Dekker, New York, 1989, pp. 3–28.
[28] E. Pelizzetti, C. Minero, V. Maurino, A. Sclafani, H. Hidaka, N. Serpone, Environ. Sci. Technol. 23 (1989) 1380.
[29] E. Pelizzetti, C. Minero, H. Hidaka, N. Serpone, in: D.F. Ollis, H. Al-Ekabi (Eds.), Photocatalytic Purification and Treatment of Water and Air, Elsevier, Amsterdam, 1993, pp. 261–273.

ELSEVIER

Talanta 48 (1999) 859–866

Talanta

Comparison of some analytical performance characteristics in inductively coupled plasma spectrometry of platinum group metals and gold

V. Kanický [a,*], V. Otruba [a], J.-M. Mermet [b]

[a] *Department of Analytical Chemistry, Masaryk University, CZ 611 37 Brno, Czech Republic*
[b] *Laboratoire des Sciences Analytiques (UMR 5619), Université Claude Bernard-Lyon I, F 696 22 Villeurbanne Cedex, France*

Received 14 October 1997; received in revised form 20 February 1998; accepted 26 February 1998

Abstract

The limits of detection, precision and matrix effects in the inductively coupled plasma spectrometry of platinum group metals (PGMs) and gold were measured and evaluated for four ICP-AES and one ICP-MS instrument. The sample matrix was a cationic surfactant used for the PGMs and gold preconcentration on a modified silica gel (C18). A sorption of ion associates of PGMs and gold chlorocomplexes with the cation of onium salt N(1-carbaethoxypentadecyl)-trimethyl ammonium bromide was considered. The calibration curves, limits of detection and matrix effects were evaluated in the presence of 0.003 mol dm^{-3} of onium salt (1.3 mg cm^{-3}) and 0.1 mol dm^{-3} HCl. The values of limits of detection (3 σ_{bl}) of PGMs for all axial ICP instruments were mostly below 10 ng cm^{-3}. Lateral observation on dual view ICP instrument yielded only 3 times higher detection limits in comparison to the axial mode of the same spectrometer and the detection limits for ICP-MS instrument were on the levels of units or tens of pg cm^{-3}. These limits of detection did not significantly differ from values obtained with pure solutions. Matrix effects in the presence of onium salt did not exceed 12% depression in the analytical signals. Besides the coefficients of correlation, the uncertainties on centroids of concentrations were calculated for calibration graphs obtained by linear regression.

Keywords: Platinum group metals; Inductively coupled plasma spectrometry; Ion associates; Surfactants

1. Introduction

Platinum group metals (PGM) and gold exhibit very low natural concentrations on the Earth. The Clark values are reported to be $X \cdot 10^{-2}$ ng g^{-1} for Ru and Rh, $X \cdot 10^{-1}$ ng g^{-1} for Os, 1 ng g^{-1} for Ir, 5 ng g^{-1} for Pt, 13 ng g^{-1} for Pd, and 4 ng g^{-1} for Au [1]. Special attention is given to Pt because of its increasing occurrence in the biosphere. The average concentration of Pt in the rocky crust ranges from 1–5 ng g^{-1}, while substantially higher concentrations (1–500 μg g^{-1} Pt) exist in PGM deposits. In environmental samples, the following concentrations of Pt were found: 21.9 ng g^{-1} in ocean sediments, 0.03–0.3

* Corresponding author. Tel.: +42 5 41129283; fax: +42 5 41211214; e-mail: viktork@chemi.muni.cz

0039-9140/99/$ - see front matter
PII S0039-9140(98)00102-7

ng dm^{-3} in a sea-water, 0.08–0.32 ng g^{-1} in marine algae, 56 ng g^{-1} in limber pines, and 100–830 ng g^{-1} in plants on ultrabasic soils [2]. Because of anthropogenic activities, an increase of platinum concentration is observed in the environment. An ambient air near the roads was reported to contain < 50 fg m^{-3} of Pt before the introduction of automobile catalysts, while along the highways the values between 1–13 pg m^{-3} of Pt were found due to the widespread use of cars with Pt-catalysts. Platinum and its compounds are toxic, and some compounds have also carcinogenic effects [2].

For the trace determination of Pt and other PGMs in geological, biological and environmental matrices, spectrophotometry [3], neutron activation analysis [4], total-reflection X-ray fluorescence spectrometry [5], electron spectroscopy for chemical analysis [6], electrochemical analysis [7], liquid chromatography [8,9], atomic absorption spectrometry with electrothermal atomisation [10], and inductively coupled plasma mass spectrometry (ICP-MS) [11] have been used.

Nowadays, ICP-MS technique is frequently used for the determination of ppb and sub-ppb levels of PGM in environmental samples, such as in airborne particulate matter [12], dust [13], particulate matter of automotive catalyst exhaust [14], and in plants [15]. Advanced electroanalytical methods are also largely employed, such as differential pulse polarography [16], adsorption voltammetry for the analysis of human body fluids [17], capillary zone electrophoresis for detection of platinum species in plant material [18] or for the determination of Pt, Pd, Os, Ir, Rh and Au [19], and adsorptive cathodic stripping voltammetry for the determination of Pt in sea water [7].

Atomic emission spectrometry methods do not meet entirely the requirements concerning the de-

Table 1
Characteristics of ICP emission spectrometers

Instrument	Spectrometer	Nebulizer/Chamber	View	Detector
OPTIMA 3000 Dual view	Simultaneous AES echelle cross dispersion	Cross-flow/Scott	Axial lateral	SCD-Segmented charge coupled device
Jobin-Yvon 138 Ultrace	Sequential AES Czerny Turner	Conespray[a]/Cyclonic	Axial	Photomultiplier tube
Jobin-Yvon model 166	Sequantial AES Czerny Turner HR 1000	Meinhard/Scott	Axial	Photomultiplier tube
IRIS AP Thermo Jarrel-Ash	Simultaneous AES echelle cross dispersion	Meinhard/Cyclonic	Axial	CID-Charge injection device

[a] The Perkin–Elmer nebulizer.

Table 2
Operating conditions of studied ICP spectrometers

Instrument	P (kW)	F_p (dm^{-3} min^{-1})	F_a (dm^{-3} min^{-1})	F_c (dm^{-3} min^{-1})	Q_l (cm^{-3} min^{-1})
OPTIMA 3000	1.20	15	0	0.8	1.50
JY-138	1.05	12	0	0.7	1.00
JY-166	1.00	12	0	1.0	1.00
IRIS AP	1.15	12	0.5	1.0	1.85
POEMS	1.35	15	0.5	0.7	1.67

P, the power input; flow rates: F_p, the outer gas; F_a, the intermediate gas; F_c, the carrier gas; Q_l, the solution uptake rate. The optimum observation height for the lateral viewing (OPTIMA 3000) was 8 mm.

Table 3
Coefficients of correlation of linear regressions in the presence of 0.003 mol dm^{-3} Septonex (in 0.1 M HCl) obtained with ICP-AES instruments

Analytical line, λ (nm)	Coefficients of correlation						
	Au I 242.795	Ru II 240.272	Rh II 233.477	Pd I 340.458	Os II 225.585	Ir II 224.268	Pt II 214.423
OPTIMA-L[a]	0.99985	0.99923	0.99958	0.99996	0.99941	0.99911	0.99992
OPTIMA-A[b]	0.99994	0.99989	0.99981	0.99993	0.99961	0.99954	0.99994
JY-138-A[b]	0.99991	0.99966	0.99945	0.99997	0.99917	0.99946	0.99989
JY-166-A[b]	0.99996	0.99999	0.99992	1.00000	0.99980	0.99997	0.99994
IRIS-AP[b]	0.99989	0.99941	0.99964	0.99939	0.99152	0.99988	0.99987

[a] Lateral.
[b] Axial.

Table 4
Coefficients of correlation of linear regressions in the presence of 0.003 mol dm^{-3} Septonex (in 0.1 M HCl) obtained with ICP-MS instrument

	Coefficient of correlation									
Isotope	Au 197	Ru 101	Rh 103	Pd 105	Pd 108	Os 188	Os 189	Ir 193	Pt 194	Pt 195
POEMS	0.99825	0.99951	0.99905	0.99961	0.99949	0.99958	0.99900	0.99848	0.99929	0.99915

termination of the PGMs in environmental samples. However, their limits of detection can approach expected concentration levels by combining with a preconcentration step. A modified silica gel sorbent (C18) was suitable for the preconcentration of 2–20 μg of Pt from 0.1 M HCl in the presence of cationic sufactants, especially dimethyllaurylbenzylammonium bromide, with subsequent elution with 96% ethanol. The recovery was 86–110% for 2 μg of Pt. The final emission spectrometry of Pt in plant ash matrix was carried out using a 15 A dc-arc [20]. The preconcentration of ion pairs based on cationic surfactants was also efficient for some other elements. Thallium, e.g. was efficiently preconcentrated on the silica gel C18 from 0.1 M HCl in the presence of various cationic surfactants as ion pairs with tetrachlorothallate(III) and subsequently eluted with 96% ethanol. Emission spectrometry using a nitrous oxide- acetylene flame was suitable for the determination of preconcentrated Tl in plants [21], and in water or aqueous extracts of wastes and soils [22].

Recently the preconcentration of PGMs and Au on silica gel C18 in the form of ion associates of their chlorocomplexes with a quaternary base *N*-(1-ethoxycarbonyl pentadecyl)-trimethylammonium bromide was described [23]. Ion associate was eluted with ethanol which was then evaporated in the presence of HCl. Solutions were analysed with ICP-AES, ICP-MS.

In this paper some analytical performance characteristics of four ICP emission spectrometers and one ICP mass spectrometer are given in the presence of a cationic surfactant which is used for a formation of ion associates with the chlorocomplexes of PGMs. The presence of significant concentration of an organic matrix in solution may bring an excessive plasma load. Therefore, surfactants may influence both the excitation conditions and the efficiency of aerosol formation [24].

2. Experimental

2.1. Instruments and operating conditions

The following ICP instruments were tested.

2.1.1. Optical spectrometers

The Optima 3000 dual view system (Perkin Elmer), the JY 138 axial ICP system (Jobin-Yvon), installed at Laboratoire des Sciences Analytiques, Université Claude Bernard-Lyon I, Villeurbanne, France; the JY 166 system (Jobin-Yvon), installed at the laboratory of Laboratoire Wolff, Clichy, France; the IRIS AP system (Thermo Jarrel Ash), installed at the Faculty of Chemistry, Technical University Brno, Czech Republic.

2.1.2. Mass spectrometer

The POEMS system (Thermo Jarrel Ash), installed at Laboratoire des Sciences Analytiques, Université Claude Bernard-Lyon I, Villeurbanne, France.

The basic features of the ICP spectrometers are given in Table 1. Operating conditions of the ICP sources are listed in Table 2. Optimisations of the carrier gas flow rates were performed to minimise the signal-to-background ratio values and matrix effects. In case of the ICP-MS, the voltages of the ion optics lenses were adjusted to obtain a maximum sensitivity for the employed isotopes. The spectral lines and isotopes are given in corresponding tables. The isotope of indium, In 115, was used as the internal standard for the ICP-MS.

2.2. Chemicals

The multielement standard stock solution containing 100 μg ml^{-1} of Au, Ru, Rh, Pd, Os, Ir, Pt in 20% HCl (Astasol, Analytika, Prague, Czech Republic) was used for preparation of working solutions. The cationic surfactant Septonex, *N*(1-ethoxycarbonylpentadecyl)-trimethyl ammonium bromide ($C_{21}H_{44}O_2NBr$, m.w. 422.5) was used as quarternary base. A commercial preparation Septonex (Farmakon, Olomouc, Czech Republic, pu-

Table 5
Relative uncertainities on centroids of linear regressions expressed for 95% confidence level, obtained with ICP-AES instruments; 0.003 mol dm^{-3} Septonex and 0.1 M HCl

Analytical line, λ (nm)	Relative uncertainity on centroid of concentration, (%)						
	Au I 242.795	Ru II 240.272	Rh II 233.477	Pd I 340.458	Os II 225.585	Ir II 224.268	Pt II 214.423
OPTIMA-L[a]	2.1	3.7	3.2	1.5	4.1	3.2	17
OPTIMA-A[b]	1.8	1.5	1.9	1.1	4.8	2.3	0.98
JY-138-A[b]	1.7	0.54	2.1	0.42	3.2	1.9	1.9
JY-166-A[b]	1.9	0.65	2.6	0.35	4.1	1.7	2.3
IRIS-AP[b]	2.4	5.4	4.3	5.5	4.2	2.5	2.5

[a] Lateral.
[b] Axial.

Table 6
Relative uncertainties on centroids of linear regressions expressed for 95% confidence level, obtained with ICP-AES instruments

	Relative uncertainty on centroid of concentration (%)								
Isotope	Au 197	Rh 103	Pd 105	Pd 108	Os 188	Os 189	Ir 193	Pt 194	Pt 195
POEMS	5.5	3.7	2.6	3.4	6.8	5.9	4.3	2.5	2.8

Matrix: 0.003 mol dm^{-3} Septonex and 0.1 M HCl.

Table 7
Matrix effects, I_L^M/I_L, in the presence of 0.003 mol dm^{-3} Septonex obtained with ICP-AES

Analytical line, λ (nm)	Matrix effect, I_L^M/I_L						
	Au I 242.795	Ru II 240.272	Rh II 233.477	Pd I 340.458	Os II 225.585	Ir II 224.268	Pt II 214.423
OPTIMA-L[a]	0.94 ± 0.02	0.93 ± 0.02	0.93 ± 0.03	0.96 ± 0.02	0.90 ± 0.04	0.90 ± 0.03	0.97 ± 0.02
OPTIMA-A[b]	0.95 ± 0.02	0.91 ± 0.03	0.91 ± 0.03	0.97 ± 0.03	0.93 ± 0.04	0.92 ± 0.03	0.95 ± 0.01
JY-138-A[b]	0.97 ± 0.02	0.89 ± 0.03	0.94 ± 0.03	0.93 ± 0.03	0.92 ± 0.03	0.97 ± 0.02	0.94 ± 0.03
JY-166-A[b]	0.99 ± 0.02	0.99 ± 0.01	1.00 ± 0.02	0.97 ± 0.02	0.94 ± 0.03	0.91 ± 0.03	0.99 ± 0.01

[a] Lateral.
[b] Axial.
Concentration of PGM in test solutions was 1000 ng cm^{-1}, in 0.1 M HCl.

rity according to the Czechoslovak Pharmacopoeia no. (3) was further purified by dissolving in hot ethanol and the solution was added dropwise into ethyl ether (Merck, FRG).The precipitated plates of pure surfactant were collected on a sintered glass filter and dried. Using this purified preparation, the 0.01M aqueous stock solution was prepared. A 0.1 mol dm^{-3} concentration of chlorides was maintained in solutions using HCl of analytical grade purity (Merck, FRG).

2.3. Measurements

Calibration curves for ICP-AES and ICP-MS were measured using different sets of standard solutions. The set for the ICP-AES consisted of standards containing 0, 50, 100, 200, 500 and 1000 ng cm^{-3} of PGM and Au, the set for the ICP-MS included standards 0, 1, 5, 10, 20 and 50 ng cm^{-3} of PGM and Au. Calibration solutions were prepared both with and without Septonex, and all of them contained HCl. Employed concentrations of Septonex and HCl were 0.003 and 0.1 mol dm^{-3}, respectively. The highest calibration points, 1000 ng ml^{-1} of PGM for the ICP-AES and 50 ng ml^{-1} of PGM for the ICP-MS, with and without Septonex, were used for estimation of the magnitude of the matrix effect. Three replicates were measured with each solution both for the calibration and the evaluation of the matrix effect. Blank solutions containing 0.1 M HCl, both with and without Septonex, were used for the measurement of limits of detection. The standard deviation of the background signal was obtained for the estimation of limits of detection, based on ten consecutive measurements during the continuous nebulisation of the blank solution.

2.4. Evaluation

The linear regression by the method of least squares was used for the construction of calibration graphs. Besides the coefficient of correlation, the uncertainty interval on the centroid of concentrations was calculated for the calibrations on the 95% probability level [25].

The matrix effect, **X**, was characterised with the ratio of the net analyte signal in the presence of 0.003 mol dm^{-3} Septonex to the net analyte signal obtained with the Septonex-free solution.

$$\mathbf{X} = I_L^M/I_L$$

Confidence intervals were calculated on 95% probability level, based on three replicates. Limit of detection was calculated as the concentration that produces a net line signal equivalent to three times the standard deviation of the background signal, σ_{bl}, [26–30]. The resulting instrumental limit of detection (IDL), or c_L, is expressed as

$$c_L = 3 \times \sigma_{bl}/S$$

where S stands for the slope of the calibration line. Limits of detection were calculated both with and without Septonex.

Table 8
Matrix effects, I_L^M/I_L, in the presence of 0.003 mol dm^{-3} Septonex obtained with the ICP-MS

	Matrix effect, I_L^M/I_L									
Isotope	Au 197	Ru 101	Rh 103	Pd 105	Pd 108	Os 188	Os 189	Ir 193	Pt 194	Pt 195
POEMS	0.99 ± 0.01	0.98 ± 0.02	0.92 ± 0.02	0.99 ± 0.01	0.94 ± 0.02	0.94 ± 0.02	0.93 ± 0.02	0.91 ± 0.03	0.93 ± 0.02	0.97 ± 0.02

Concentration of PGM in test solutions was 50 ng cm^{-1}, in 0.1 M HCl.

Table 9
Limits of detection in the presence of 0.003 mol dm^{-3} Septonex (in 0.1M HCl) obtained with emission spectrometers

Analytical line, λ (nm)	Limit of detection, 3 σ_{bl} (ng cm^{-3})						
	Au I 242.795	Ru II 240.272	Rh II 233.477	Pd I 340.458	Os II 225.585	Ir II 224.268	Pt II 214.423
OPTIMA-L[a]	9	15	43	25	8	15	21
OPTIMA-Ab	3	5	16	8	4	5	7
JY-138-A[b]	3	4	4	12	1	5	4
JY-166-A[b]	4	4	7	2	8	3	1
IRIS-AP[b]	7	6	7	5	2	8	7

[a] Lateral.
[b] Axial.

Table 10
Limits of detection in the presence of 0.003 mol dm^{-3} Septonex (in 0.1 M HCL) obtained with a mass spectrometer

	Limit of detection, 3 σ_{bl} (ng cm^{-3})									
Isotope	Au 197	Ru 101	Rh 103	Pd 105	Pd 108	Os 188	Os 189	Ir 193	Pt 194	Pt 195
POEMS	0.12	0.013	0.004	0.036	0.011	0.010	0.010	0.005	0.018	0.040

3. Results

Calibration curves for ICP-AES and ICP-MS both with and without Septonex are described with coefficients of correlation better than 0.99, cf. Tables 3 and 4. Relative values of confidence intervals characterising the uncertainties on centroids of concentrations do not exceed 6 and 7% for emission and mass spectrometry, respectively (Tables 5 and 6).

Matrix effects, **X**, mostly do not exceed the 10% depression, and their confidence intervals on 95% level show that the differences both between elements and individual instruments are not significant (Tables 7 and 8). This applies even between laterally- and axially-viewed plasmas or between atomic emission and mass spectrometry.

Limits of detection in ICP-AES are mostly better than 10 ng cm^{-3} of PGM and Au for axial plasma configurations. The lateral viewing mode of Optima 3000 DV instrument yields limits of detection about three times higher than the axial observation (Table 9). Limits of detection of ICP mass spectrometer are in the range of units and tens of pg cm^{-3} for PGMs and $\sim$0.1 ng cm^{-3} for gold (Table 10). It was also found that limits of detection in the presence of Septonex did not significantly differ from those obtained for pure solutions containing HCl.

4. Conclusion

Preconcentration of PGM and gold in the form of ion associates of their chlorocomplexes with the quaternary ammonium base using modified silicagel C18 can be followed by elemental determination with various ICP-AES systems and ICP-MS without significant matrix interferences or deterioration of limits of detection.

Acknowledgements

V.K. and J.M.M. wish to thank Perkin–Elmer for the loan of the Optima 3000 DV ICP system, Jobin-Yvon for the loan of the JY-138 axial ICP system and Thermo Jarrel-Ash for the loan of the POEMS ICP system. V.K. wishes to thank Jobin-Yvon and Laboratoire Wolff (Clichy, France) for the occasion to work with JY-166 ICP system. V.K. and V.O. wish to thank the Faculty of Chemistry

of the Technical University Brno, Czech Republic, for the possibility to obtain data with the IRIS AP Thermo Jarrel-Ash ICP system. V.K. and V.O. gratefully acknowledge the Grant Agency of the Czech Republic (projects 203/94/0511 and 203/96/0478).

References

[1] V. Bouska, P. Jakes, T. Paces, J. Pokorný (Eds.), Geochemie (Geochemistry), Academia, Prague, 1980, pp. 457–458.
[2] V. Bencko, R.E. Biagini, C.W. Bradford, I. Farkas, U. Heinrich, R. Hertel, G. Kazantzis, A. Massoud, R. Merget, G. Rosner, A.E. Soyombo, Environmental Health Criteria for Platinum (125), World Health Organisation, Geneva, 1991, pp. 16–17.
[3] K. Brajter, U. Kozicka, Talanta 26 (1979) 417.
[4] H.W. Stockman, J. Radioanal. Chem. 78 (1983) 307.
[5] A. von Bohlen, R. Eller, R. Klockenkämper, G. Tölg, Anal. Chem. 59 (1987) 2551.
[6] R. Schlögl, G. Indlekofer, P. Ölhafen, Angew. Chem. 99 (1987) 312.
[7] C.M.G. van den Berg, G.S. Jacinto, Anal. Chim. Acta 211 (1988) 129.
[8] R.D. Rocklin, Anal. Chem. 56 (1984) 1959.
[9] J. Doležal, L. Sommer, Collect. Czech. Chem. Commun. 62 (1997) 1029.
[10] T. Paukert, I. Rubeska, Anal. Chim. Acta 278 (1993) 125.
[11] D.C. Gregoire, J. Anal. At. Spectrom. 3 (1988) 309.
[12] F. Alt, A. Bambauer, K. Hoppstock, B. Mergler, G. Tölg, Fresenius J. Anal. Chem. 346 (1993) 693.
[13] M. Parent, H. Vanhoe, L. Moens, R. Dams, Fresenius J. Anal. Chem. 354 (1996) 664.
[14] C. Lüdke, E. Hoffmann, 1997 European Winter Conference on Plasma Spectrochemistry, 12–17 January 1997, University of Gent, Gent, Belgium.
[15] D. Klueppel, N. Jakubowski, J. Messerschmidt, D. Stuewer, D. Klockow, 1997 European Winter Conference on Plasma Spectrochemistry, 2–17 January 1997, University of Gent, Gent, Belgium.
[16] Z. Zhao, H. Freiser, Anal. Chem. 58 (1986) 1498.
[17] F. Alt, G. Tölg, J. Angerer, K.H. Schaller, Fresenius J. Anal. Chem. 343 (1992) 391.
[18] J. Messerschmidt, F. Alt, G. Tölg, Electrophoresis 16 (1995) 800.
[19] A.V. Pirogov, J. Havel, J. Chromatogr. A 772 (1997) 347.
[20] V. Otruba, M. Strnadová, B. Skalníková, Talanta 40 (1993) 221.
[21] V. Otruba, J. Stepánková, L. Sommer, Talanta 41 (1994) 1185.
[22] V. Otruba, D. Adamová, XIIIth Seminar on Atomic Spectrochemistry, 23–27 September 1996, Podbanské, Slovakia, Proceedings, pp. 302–306.
[23] R. Vlasánkova, V. Otruba, J. Bendl, M. Fisera, V. Kanický, Talanta, (accepted).
[24] A.G.T. Gustavsson, Liquid sample introduction into plasmas, in: A. Montaser, D.W. Golightly (Eds.), Inductively Coupled Plasmas in Analytical Atomic Spectrometry, VCH, New York, 1987, pp. 415–416.
[25] J.-M. Mermet, Spectrochim. Acta 49B (1976) 1313.
[26] I.U.P.A.C., Pure Appl. Chem., 45 (1976) 99.
[27] I.U.P.A.C., Pure Appl. Chem., 51 (1979) 1195.
[28] P.W.J.M. Boumans, Basic concepts and characteristics, in: P.W.J.M. Boumans (Ed.), Inductively Coupled Plasma Emission Spectroscopy, Part 1, Methodology, Instrumentation and Performance, John Wiley, New York, 1987, pp. 102–170.
[29] M. Thompson, Analytical performance of inductively coupled plasma-atomic emission spectrometry, in: A. Montaser, D.W. Golightly (Eds.), Inductively Coupled Plasmas in Analytical Atomic Spectrometry, VCH, New York, 1987, pp. 163–1987.
[30] P.W.J.M. Boumans, Spectrochim. Acta 31B (1976) 147.

ELSEVIER

Talanta 48 (1999) 867–875

Talanta

Short communication

Measurement of sugar content by multidimensional analysis and mid-infrared spectroscopy

Frédéric Cadet *

Laboratoire de Biochimie, Faculté des Sciences, Université de la Réunion, 15 avenue René Cassin, BP 7151, 97715 Saint-Denis Messag Cedex 9, La Réunion, France

Received 7 July 1997; received in revised form 9 March 1998; accepted 10 March 1998

Abstract

The advent of more and more powerful micro-computers has allowed the introduction of multidimensional analysis in research laboratories. Complex mathematical treatments are now possible within a few seconds. Prediction equations that linked sucrose, fructose, glucose, total sugars and reducing sugars concentrations to the spectral data, were established by regression on the principal components. Very high correlation coefficient values between the first ten axes and the chemical values were obtained. The bias and standard deviation (S.D.) values obtained between reference and predicted values were good. From such aqueous biological samples containing a ternary mixture of sucrose, fructose and glucose it was possible to (i) identify the characteristic IR bands of these different sugars (and their combination: reducing sugars, total sugars)—using spectral pattern; and (ii) to specifically measure their concentrations with good accuracy.

Keywords: Fourier transform infrared; Principal component analysis; Principal component regression; Sugars

1. Introduction

The use of computers has revolutionised studies in many aspects of biological sciences. The advent of more and more powerful micro-computers has allowed the introduction of multidimensional analysis in research laboratories.

After recalling the principles underlying the principal component analysis (PCA) we will see an application example: measurement of multi-sugars contents by multidimensional analysis and mid-infrared spectroscopy (MIR).

MIR spectroscopy has been used since 1950 for the analysis of sugars. Besides starch, sugars that present the best interest for the food industry are sucrose, glucose and fructose [1,2]. The aim of this communication is to evaluate the interest of using PCA for the processing and description of MIR spectral data of complex biological samples (raw sugar cane juices) that contained a ternary mixture of sucrose, glucose and fructose (and subse-

* Tel.: +33 262938202; fax: +33 262938166; e-mail: cadet@univ-reunion.fr

0039-9140/99/$ - see front matter
PII S0039-9140(98)00103-9

	VARIABLES Wavenumbers					
INDIVIDUALS		800	801	802	------	1250 cm-1
	spectrum 1	0.2	0.21	0.25	-	0.07
	spectrum 2	0.3	0.27	0.42	-	0.09
	-	-	-	-	-	-
	-	-	-	-	-	-
	-	-	ABSORBANCE VALUES			-
	-	-	-	-	-	-
	-	-	-	-	-	-
	spectrum n	0.5	0.23	0.21	0.35	0.23

Fig. 1. The matrix (n, p): n, spectra; p, wavenumbers.

quently reducing sugars and total sugars) and other ingredients.

1.1. Principles underlying the principal component analysis

Multidimensional analyses are statistical methods for processing data. They are usually used when numerous variables and samples are involved and give a synthetic representation of the whole set of data. Multidimensional statistical analysis processes tables of data by taking into account all variables and all samples at the same time.

PCA is purely a descriptive method. There are no hypotheses that is made a priori on the set of data. PCA is concerned with tables containing quantitative data. PCA is applied on rectangular tables containing n lines and p columns. Each line constitutes an individual or an 'observation,' and each column represents a variable (Fig. 1).

As shown in Fig. 1, the table is concerned with the measurement of p variables on a sample of n individuals: Each spectrum is an individual and each wavelength is a variable. The content of the matrix (n, p) are absorbance values. Since multidimensional analysis of data is performed on a matrix constituted of absorbance values, it is obvious that the principal components represented by axes in the factorial maps are absorbance values (in fact linear combination of absorbance values). It is therefore possible to give a spectroscopic interpretation, hence a biochemical interpretation of an axis. This spectroscopic representation is called a 'spectral pattern'. This notion of spectral pattern is relatively recent and original [3,4].

1.2. Raw sugar cane juices

Sampling of sugar by coring is used. The average of core is about 7000 g. After pulverisation, a subsample of approximately 1000 g is removed. A hydraulic press is used to extract juice from the samples obtained from the coring and from the disintegrator. The sample is pressed for 2.5 min at 250 bars.

1.3. Mid-infrared attenuated total reflectance spectra

Mid-fourier transform infrared (mid-FTIR) spectra were collected on a Michelson-100 fourier transform spectrophotometer. Attenuated total reflectance spectra were obtained with a Specac overhead ATR system. Experimental temperature

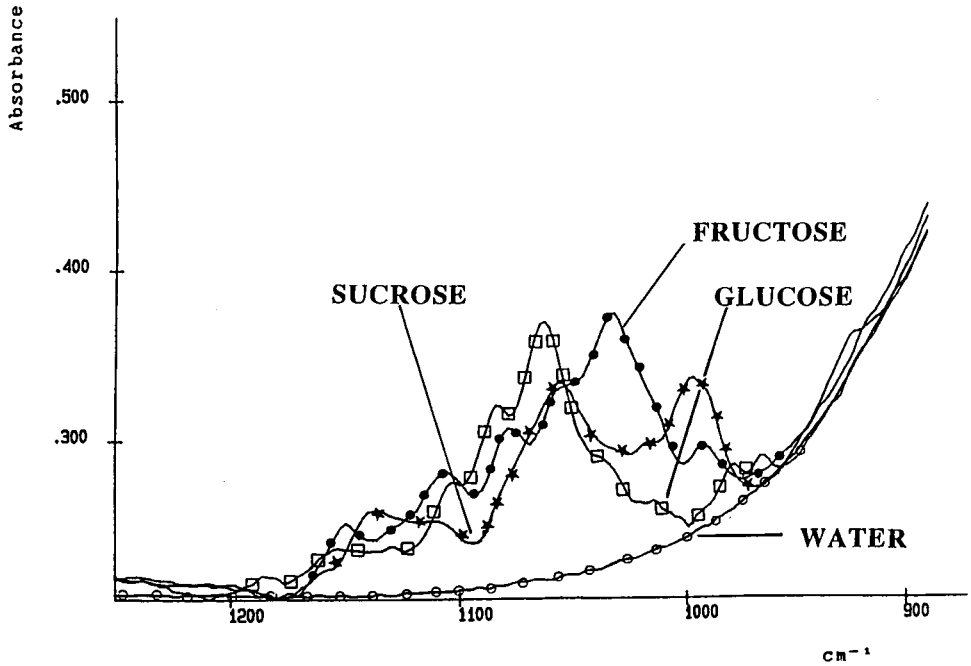

Fig. 2. Mid-FTIR spectra of sucrose, glucose, fructose and water. The concentration of each sugar is 10% (m/v).

was 25°C. The crystal of the reflectance element is made from zinc selenide, a material that is quite inert to water; it is quite rapidly cleaned between samples by being sprayed with water and then dried with filter paper.

The data were recorded from 800 to 1250 cm^{-1} in 4 cm^{-1} increments as $\log(I/R)$, in which R is the ratio of the reflected intensity for the background to that of the sample. Although the ATR experiment does involve the reflection of the radiation within a crystal, the interaction of the radiation with the sample is the transmittance of radiation through the sample; this depth of penetration is wavelength dependent, but it is passing through a finite layer of the sample. For this reason, plots can read according to absorbance (or transmittance). The combination of four scans resulted in an average spectrum.

2. Results and discussion

Before any prediction of quatitative values, a calibration of the apparatus and method with references values is needed: the calibration set was constituted of a collection of 20 spectra of raw sugar cane juices while the verification set was composed of 19 spectra.

The mid-FTIR spectra of glucose, fructose and sucrose are given in Fig. 2. The spectra were recorded between 800 and 1250 cm^{-1}. It has been shown that this spectral region featured the characteristic absorption bands of saccharides [5,6]. The spectra obtained with the complex biological samples are the result of the different absorption bands of the three major constituents: sucrose, fructose and glucose (Fig. 3).

2.1. Principal component analysis and spectral patterns

In order to extract the spectral information corresponding to each of the three sugars (sucrose, fructose and glucose), the collected spectra of all the sugar cane juices from the calibration set were entered into a PCA. Table 1 gives the correlation patterns between the axes and the variables, sucrose, glucose, total sugars, fructose and reduc-

Table 1
Priority of the axes and their corresponding correlation coefficient values associated with each variable

Sucrose		Glucose		Total sugars		Fructose		Reducing sugars	
Latest introduced PCA axis	Cumulated correlation coefficient	Latest introduced PCA axis	Cumulated correlation coefficient	Latest introduced PCA axis	Cumulated correlation coefficient	Latest introduced PCA axis	Cumulated correlation coefficient	Latest introduced PCA axis	Cumulated correlation coefficient
1	0.948	5	0.354	1	0.959	4	0.332	5	0.342
3	0.969	1	0.612	3	0.982	5	0.608	4	0.632
5	0.981	4	0.841	5	0.986	1	0.803	1	0.878
4	0.987	8	0.883	16	0.988	13	0.835	8	0.915

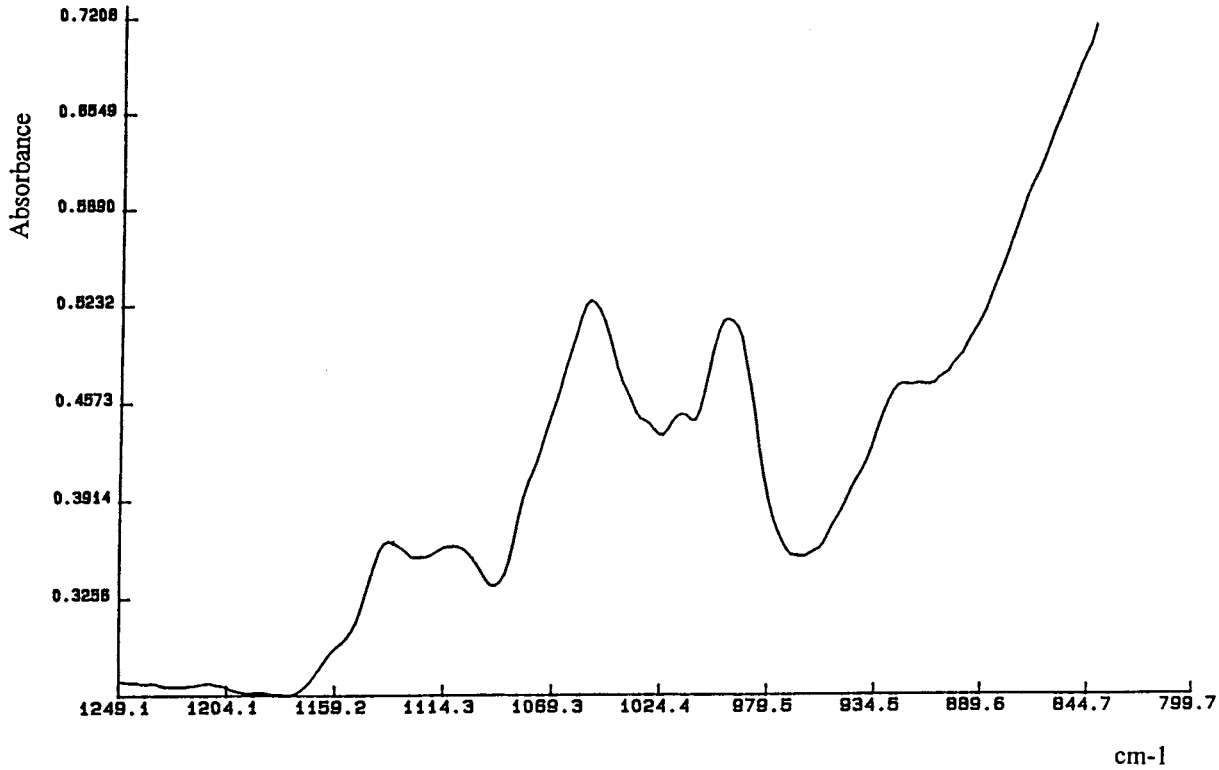

Fig. 3. Mid-FTIR spectra of a biological sample (raw sugarcane juice).

ing sugars concentrations. The correlation coefficients indicated here the correlation between the axes and the chemical values (concentrations) of each variable. They also indicated the order of priority of these axes in the description of each variable: it can be noticed that the priority of the first axes is not the same for each and every variable. Cumulated correlation coefficients are given: the first coefficient corresponds only to one axis; the following coefficients are obtained by successive introduction of additional axes. For example, the correlation coefficient between the sucrose concentration and axis 1 is 0.948 but is 0.021 (0.969 − 0.948) with axis 3. Axes 1 and 3 are mostly correlated to the concentration values of sucrose and total sugars. Fructose is associated with axes 4 and 5 while glucose is mostly correlated with axes 5 and 1. The reducing sugars are best described by axes 5 and 4.

An example of factorial map as assessed by PCA on a spectral collection is shown in Fig. 4. The projection plan formed between the first axis and the second axis shows that the samples are distributed according to their sucrose (or total sugars) content along a concentration gradient. However, glucose, fructose and reducing sugars are not clearly classified according to their concentrations on this factorial map. If the spectral pattern of the principal component (axis 1) can be generally explained, this is more difficult for the axes that follow. However, in the light of the correlation coefficient values, the spectroscopic interpretation of the absorption bands of these axes is facilitated. Axes 1 and 3 have, respectively, correlation coefficient values of 0.948 and 0.021 with respect to the sucrose variable. The spectral pattern that describes the principal component, as shown in Fig. 5, features absorption peaks at 925, 997, 1053, 1112 and 1136 cm^{-1} that are characteristic of sucrose. The band at 997 cm^{-1} has been shown to be characteristic of the dissacharide link of the sucrose molecule [7].

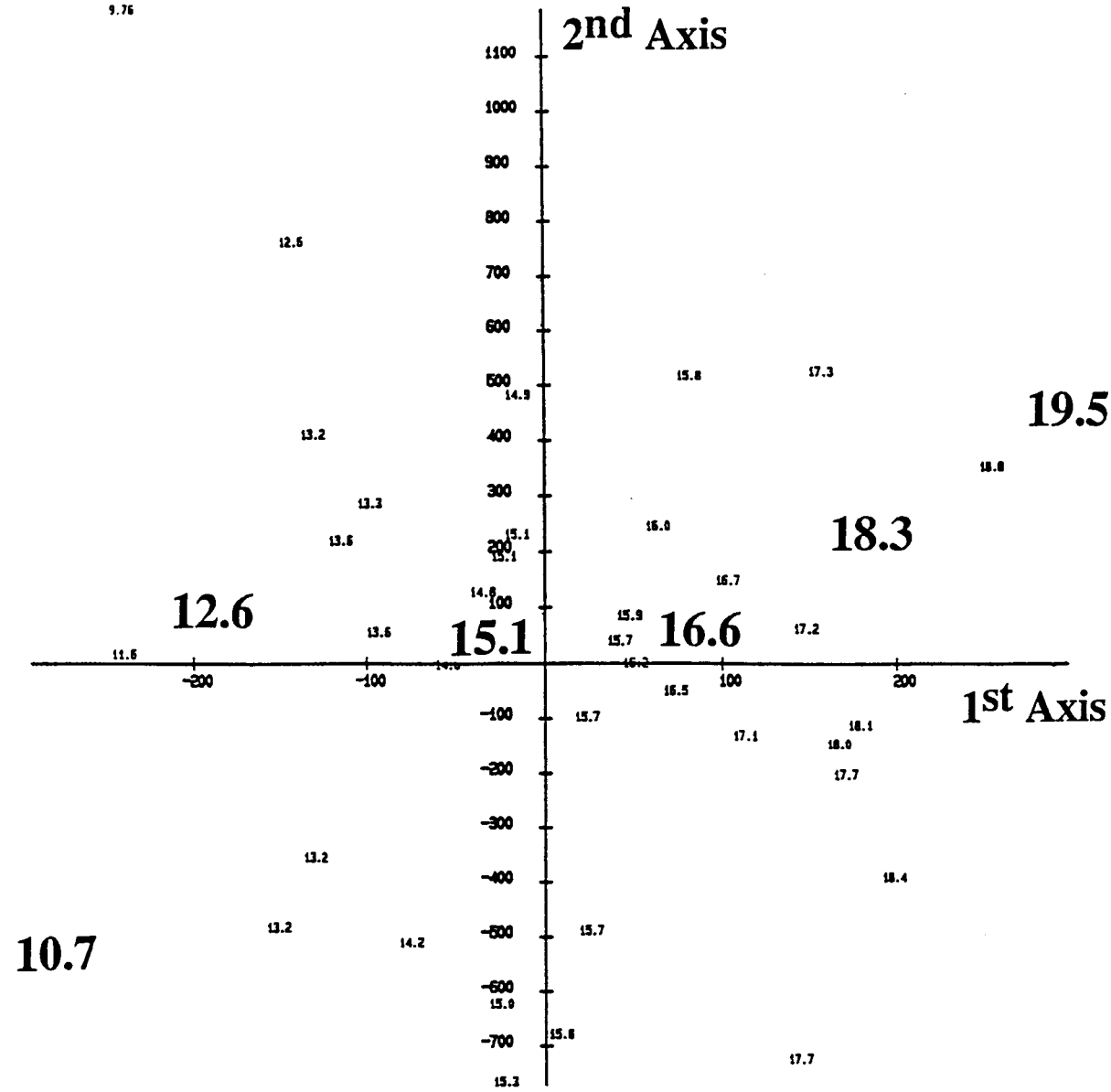

Fig. 4. An example of factorial map: distribution of the sucrose content according to the first and the second axis.

2.2. Predictions of the concentrations

Principal component regression (PCR) on the calibration set scores as assessed by PCA were carried out in order to establish prediction equations that linked spectral data to sucrose, total sugars, fructose, glucose and reducing sugars concentrations.

The influence of the number of axes on the prediction equations established for each variable is shown in Table 1. The regression and correlation coefficients for each of the first four axes are given. The correlation coefficient values are very high and range between 0.987 and 0.835. It can be noticed that the priority of the first axes are not the same for each and every variable. However

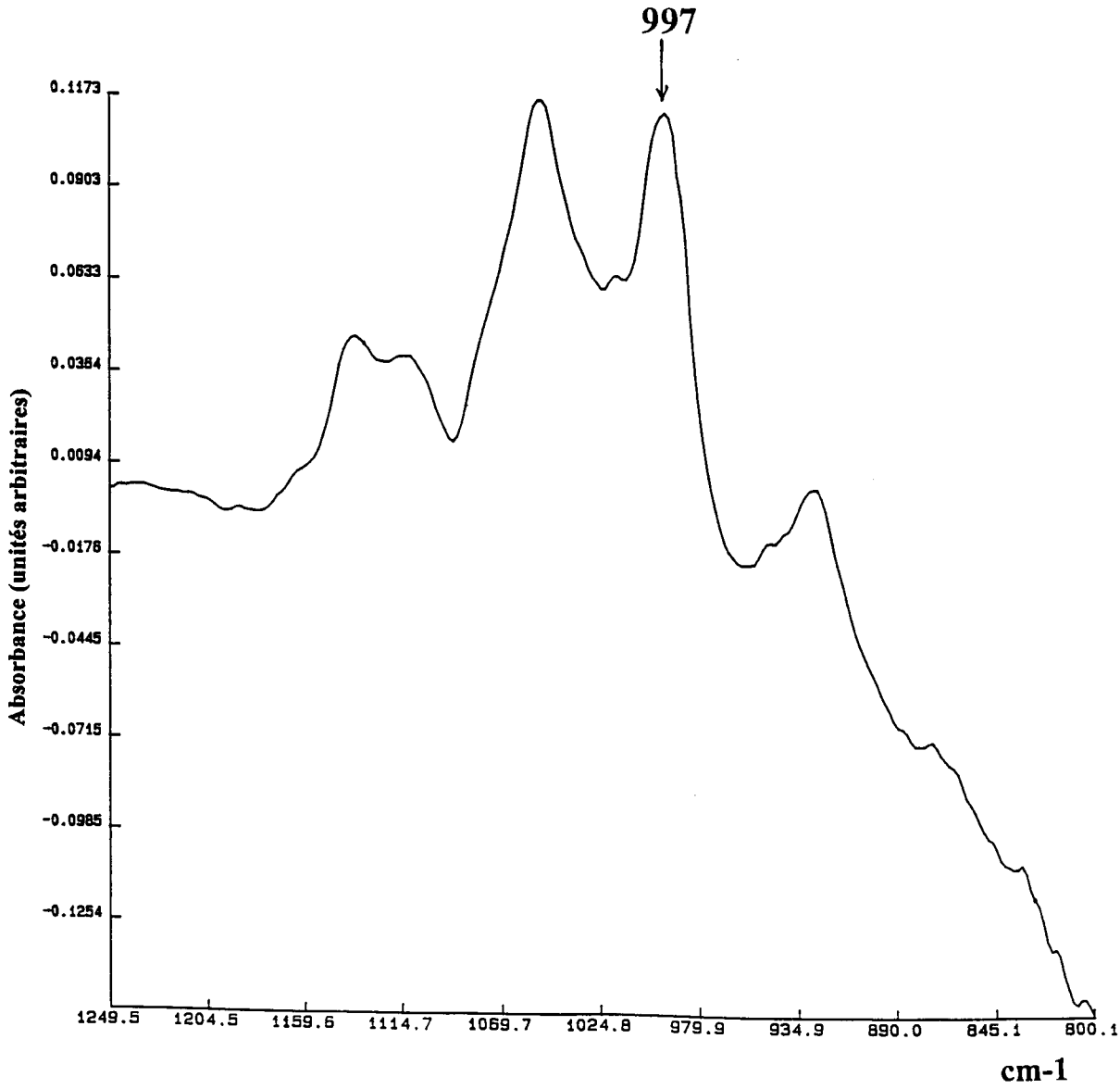

Fig. 5. The spectral pattern of the first axis.

the axes 1, 3, 4 and 5 have the highest correlation coefficient values whatever the sugar. Specific prediction equations were subsequently established for each variable (with ten axes).

Table 2 gives an example of predicted concentrations for sucrose, fructose, glucose, total sugars and for the reducing sugars for the verification set (19 samples); goods results are obtained.

3. Conclusion

The use of such mathematical treatments was unimaginable some 10 years ago. With the use of powerful micro-computers, these are now possible within a few seconds. Prediction equations that linked sucrose, fructose, glucose, total sugars and reducing sugars concentrations to the spectral data, were established by regression on the princi-

Table 2

Spectra number	Sucrose (g 100 ml^{-1})			Glucose (g 100 ml^{-1})			Reducing sugars RS (g 100 ml^{-1})			Fructose (g 100 ml^{-1})			Total sugars (g 100 ml^{-1})		
	Ref. (a)	Pred.	Dev.	Ref. (b)	Pred.	Dev.	Ref. (c)	Pred.	Dev.	RS-Glucose (d)	Pred. (e)	(e-d)	Ref. (a+c)	Pred. (g)	g-(a+c)
1	20.808	21.15	0.342	0.08	0.114	0.034	0.24	0.284	0.044	0.16	0.17	0.01	21.048	21.436	0.388
2	19.288	19.264	−0.024	0.16	0.181	0.021	0.38	0.441	0.061	0.22	0.26	0.04	19.668	19.703	0.035
—	—	—	—	—	—	—	—	—	—	—	—	—	—	—	—
—	—	—	—	—	—	—	—	—	—	—	—	—	—	—	—
—	—	—	—	—	—	—	—	—	—	—	—	—	—	—	—
—	—	—	—	—	—	—	—	—	—	—	—	—	—	—	—
17	17.25	17.158	−0.092	0.18	0.25	0.07	0.42	0.537	0.117	0.24	0.287	0.047	17.67	17.693	0.023
18	18.048	18.172	0.124	0.24	0.185	−0.055	0.52	0.404	−0.116	0.28	0.219	−0.061	18.568	18.574	0.006
19	16.899	16.827	−0.072	0.19	0.196	0.006	0.37	0.435	0.065	0.238	0.058	17.269	17.259	17.259	−0.01
Bias	—	—	0.076	—	—	0.015	—	—	0.034	—	—	0.019	—	—	0.088
Standard dev.	—	—	0.203	—	—	0.046	—	—	0.088	—	—	0.048	—	—	0.168

pal component. Very high correlation coefficients values between the first ten axes and the chemical values were obtained. The bias and standard deviation (S.D.) values obtained between reference and predicted values were good. From such natural aqueous biological samples containing a ternary mixture of sucrose, fructose and glucose (and other ingredients) it was possible to (i) identify the characteristic IR bands of these different sugars (and their combination: reducing sugars, total sugars)—using spectral pattern and (ii) to specifically measure their concentrations with a good accuracy.

Owing to these results, a more accurate, less time consuming and non polluting direct spectroscopic method than the currently used HPLC or polarimetric methods was proposed for the routine quantitative determination of sucrose on raw sugar cane juices. The method was validated on a panel of 1267 samples representative of a sugar cane harvest: the values of the predicted sucrose concentration were more accurate (bias = 0.041 g 100 ml^{-1}) than those obtained by direct polarimetry (bias = -0.163 g 100 ml^{-1}) [8,9].

We have, at the laboratory of biochemistry at the University of La Réunion, already proposed a few applications which implied 'mid-FTIR/multidimensional analysis' combination for biochemical investigations: method for classification of biological samples [10], extraction of characteristic bands of molecules [11], investigation of interactions between biomolecules [12], enzyme kinetics [7], etc.

References

[1] D. Baker, Cereal Foods World 6 (30) (1985) 389.
[2] BG. Osborne, T. Fearn, Near Infrared Spectroscopy in Food Analysis, Longman Scientific and Technical, Wiley, New York, 1986, p. 200.
[3] I.A. Cowe, J. McNicol, Appl. Spectrosc. 39 (1985) 257.
[4] M.F. Devaux, D. Bertrand, P. Robert, V Qannari, Appl. Spectrosc. 42 (6) (1988) 1015.
[5] S.A. Barker, E.J. Bourne, R. Stephens, D.A. Whiffen, J. Chem. Soc. (1954) 3468.
[6] V. Tul'chinsky, S. Zurabian, K. Asankozhoev, G. Kogan, A. Khorlin, Carbohydr. Res. 51 (1976) 133.
[7] F. Cadet, F. WongPin, C. Rouch, C. Robert, P. Baret, Biochim. Biophys. Acta 1246 (1995) 142.
[8] F. Cadet, C. Robert, B. Offmann, Appl. Spectrosc. 3 (51) (1997) 369.
[9] F. Cadet, B. Offmann, J. Agric. Food Chem. 1 (45) (1997) 166.
[10] F. Cadet, Appl. Spectrosc. 12 (50) (1996) 1590.
[11] F. Cadet, B. Offmann, Spectrosc. Lett. 3 (29) (1996) 523.
[12] F. Cadet, B. Offmann, Spectrosc. Lett. 7 (29) (1996) 1353.

ELSEVIER

Talanta 48 (1999) 879–883

Talanta

Use of the triiodide–hexadecylpyridinium chloride micellar system for the kinetic determination of tungsten (VI)

Farzaneh Shemirani *, Ali Reza Asghari, Mohammad Ali Hajimoosa

Department of Chemistry, Faculty of Sciences, University of Tehran, Tehran, Iran

Received 13 October 1997; received in revised form 28 February 1998; accepted 5 March 1998

Abstract

The associate formed by triiodide ion and hexadecylpyridinium chloride (cetylpyridinium chloride (CPC)) micelles was used to enhance the kinetic spectrophotometric determination of W^{VI} by its catalytic action on the oxidation of iodide with hydrogen peroxide in an acidic medium. The reaction was monitored spectrophotometrically by measuring the increase in absorbance of I_3^-–CPC associate at 525 nm by the fixed-time method of 3 min from initiation of the reaction. The micellar medium allowed the determination of W^{VI} at concentrations between 4 and 90 ng ml^{-1} with a detection limit of 2.4 ng ml^{-1} (i.e. about 12–13 times lower than those of methods implemented in aqueous media). The relative standard deviation for nine replicate analyses was 0.03% for 76.6 ng ml^{-1} of W^{VI}. The proposed method was applied to the determination of W^{VI} in aqueous extracts of soil sample with no prior separation.

Keywords: Cetylpyridinium chloride; Micellar media; Triiodide; Tungsten (VI)

1. Introduction

A few methods for the catalytic determination of tungsten have been reported. Pavlova et al. [1] used the reduction of triarylmethane dyes by titanium (III) as an indicator reaction, but the determinable range, 0.18–3.7 ng ml^{-1}, is not very wide and the sensitivity is not sufficient for determining tungsten in water samples. Voevutskaya et al. [2] reported a kinetic method for the determination of tungsten by its catalytic effect on the iodide–hydrogen peroxide reaction involving the Landold effect; the detection limit was 30 μg l^{-1} and μg amounts of tungsten had to be concentrated from 1 l of water sample by coprecipitation with MnO_2. Thus, it needs tedious preconcentration and separation procedures which require large volumes of sample.

As spectrophotometric detection of triiodide is highly sensitive, development of improved methods for monitoring this species is essential.

Micellar systems have been successfully used to enhance existing analytical methods [3]. The selec-

* Corresponding author. Tel.: +98 21 6113301; fax: +98 21 6113301.

0039-9140/99/$ - see front matter
PII S0039-9140(98)00124-6

tivity of analytical kinetic methods can be improved by including micelles in the reaction medium. This can be accomplished by altering the reaction pH or its mechanism [4], and by inducing spectral shifts [5] and excluding interfering species from micelle surfaces [6], among others.

In this context, the interaction between triiodide ion and hexadecylpyridinium chloride (cetylpyridinium chloride (CPC)) micelles [7] is of special interest. At surfactant concentrations slightly above its critical micellization concentration (c.m.c), triiodide ion undergoes a bathochromic shift from 350 to 500–530 nm, depending on the experimental conditions used, in addition to a substantial increase in its stability constant ($(5.4 \pm 0.2) \times 10^4$ mol l^{-1}, i.e. approximately 50 times that in water) and absorptivity ($\epsilon = (3.89 \pm 0.008) \times 10^3$ m^2 mol^{-1}, i.e. approximately 1.6 times that in water).

These effects can be used to overcome completely, or at least minimize, selectivity and sensitivity problems that confront many of the original spectrophotometric procedures for monitoring iodine, involving aqueous media. The interaction between triiodide ion and CPC has been studied in depth [7]. In this work, it was exploited to enhance the spectrophotometric determination of W^{VI} by its catalytic effect on the oxidation of iodide with hydrogen peroxide. The method thereby developed was successfully applied to the determination of W^{VI} in soils.

2. Experimental

2.1. Apparatus

Kinetic measurements were performed on a Shimadzu UV-265 FW spectrophotometer fitted with a 1-cm path-length cell spectrophotometer. The cell compartment was thermostatically controlled by circulating water from a thermostated tank.

2.2. Reagents

All reagents used were of analytical reagent grade and were used as received. W^{VI} stock solution (5.21×10^{-3} mol l^{-1}) was prepared by dissolving 0.1719 g of $Na_2WO_4 \cdot 2H_2O$ (Merck) in 100 ml of doubly distilled water. More dilute solutions (2.08×10^{-5} mol l^{-1}) were prepared from this stock solution, before each set of experiment, by dilution with doubly distilled water. A hydrogen peroxide solution (2.43×10^{-2} mol l^{-1}) was prepared daily. A 6.6×10^{-2} mol l^{-1} aqueous iodide solution was prepared and stored in a dark bottle. Aqueous solutions of the surfactant CPC (1.4×10^{-3} mol l^{-1}; Merck) and hydrochloric acid (3.16×10^{-2} mol l^{-1}) were also prepared. All working standards and reagent solutions were kept in a water-bath at 24 ± 0.1°C when used.

2.3. Recommended procedure for the determination of W

In a 10-ml calibrated flask, place in sequence the volume of hydrochloric acid (3.16×10^{-2} mol l^{-1}) required to obtain a final pH of 2.5 (approximately 1 ml for standard samples), appropriate volumes of the W^{VI} stock solution (2.08×10^{-5} mol l^{-1}) to provide a final concentration of between 4 and 90 ng ml^{-1}, 0.3 ml of hydrogen peroxide (2.43×10^{-2} mol l^{-1}), 0.4 ml of CPC (1.4×10^{-3} mol l^{-1}) and 0.8 ml of 6.6×10^{-2} mol l^{-1} iodide. Start the stopclock immediately after the iodide is added and then dilute the solution to the mark with doubly distilled water.

Transfer an aliquot of the reaction mixture into a cell kept at 24 ± 0.1°C and measure the increase in absorbance ($\lambda = 525$ nm) during the 0.5–3 min from initiation of the reaction. Measurements are to be started exactly 0.5 min after the iodide is added. Blank solutions were prepared in the same way as the samples but with no tungsten (VI), and their signals were subtracted from those obtained for the samples.

3. Results and discussion

Both the bathochromic shift in the maximum absorbance of the triiodide ion from 350 to 525 nm and the increased absorptivity provided by the CPC micellar medium can be used to enhance the

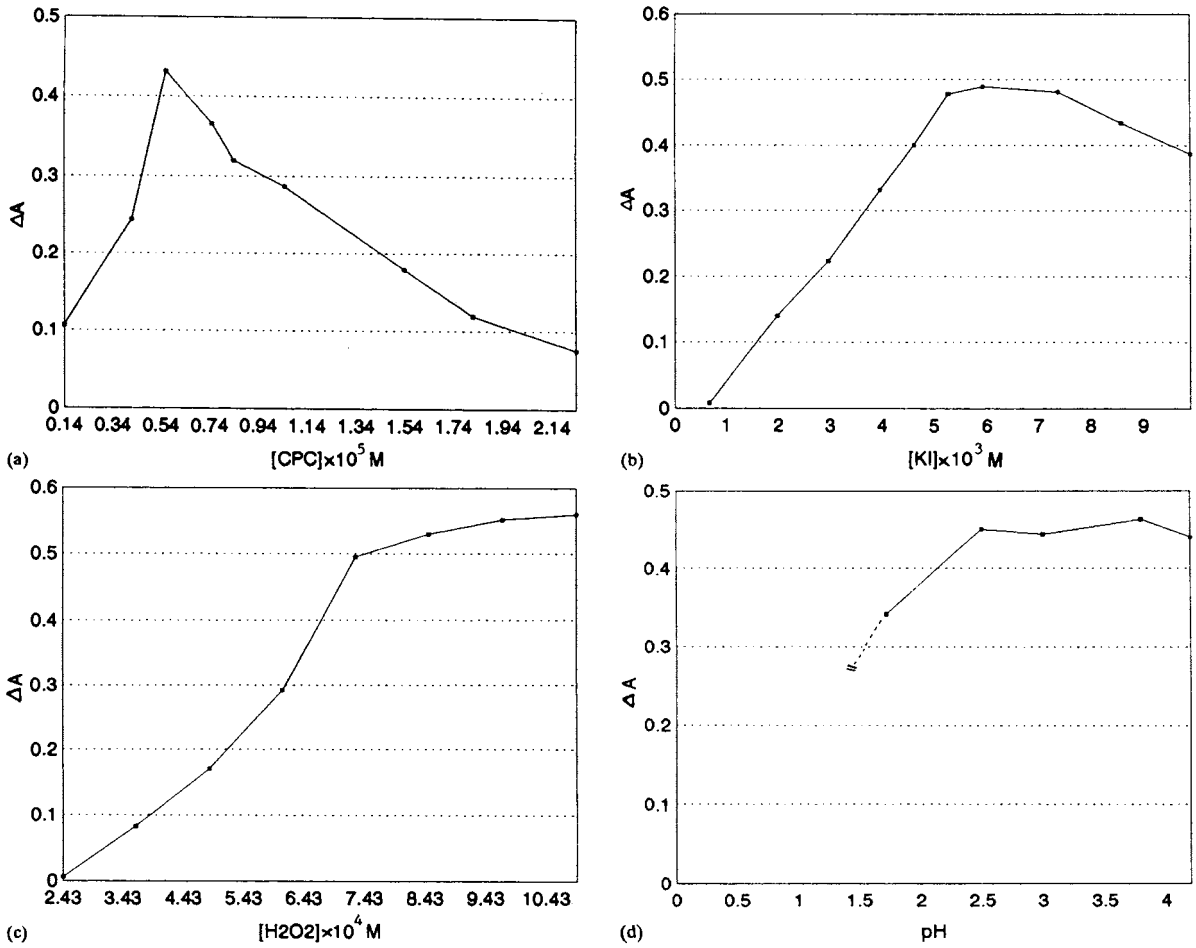

Fig. 1. Influence of the concentration of (a) CPC, (b) iodide, (c) hydrogen peroxide, and (d) hydrogen ion on the change of absorbance of the W^{VI}-catalysed reaction between iodide and hydrogen peroxide. $[W^{VI}] = 80\ \mu g\ l^{-1}$, $[CPC] = 5.65 \times 10^{-5}$ M (b,c,d); $[KI] = 5.28 \times 10^{-3}$ M (a,c,d); $[H_2O_2] = 7.29 \times 10^{-4}$ M (a,b,d); pH 2.5 (a,b,c).

selectivity and sensitivity of analytical methods involving the I_2–I^- system. Hence, it can be exploited for the determination of catalysts that accelerate the conversion of excess iodide into I_3^- by hydrogen peroxide, as is the case with the determination of W^{VI}.

3.1. Study of the experimental conditions

As the signal intensity and temporal stability of the I_3^-–CPC associate depend on parameters [7] such as the temperature, iodide concentration and pH, some parameter values affecting the catalytic determination of W^{VI} were found to behave differently from previously performed studies. Deviant variables were changed individually in turn to study their effects. Because the uncatalysed oxidation of iodide by hydrogen peroxide also proceeds in an acidic medium, the ratio of the catalysed to the uncatalysed reaction also required a selection of the experimental conditions of reaction.

Fig. 1a shows the dependence of the change in absorbance of the W^{VI}-catalysed iodide–hydrogen peroxide system on the CPC concentration. The absorbances yielded by the blanks (containing no W^{VI}) were subtracted before constructing the graph. The surfactant concentration affected the final absorbance obtained. Concentrations of

CPC below 0.14×10^{-5} mol l^{-1} could not be used as the absorbance increments obtained as a function of time were very small; hence, they provided irreproducible absorbance measurements.

On the other hand, surfactant concentrations above 5.65×10^{-5} mol l^{-1} caused the absorbance to decrease gradually, probably owing to dilution of reagents on the micellar surface. The spectral feature of the I_3^-–CPC associate did not change over the surfactant concentration range assayed.

A concentration of 5.65×10^{-5} mol l^{-1} was, therefore, chosen for subsequent experiments. The c.m.c of CPC in the reaction medium was calculated from surface tension measurements performed with a stalagmometer (Brand, Germany). A value of 4×10^{-5} mol l^{-1} CPC was found. The concentration is lower than the c.m.c calculated for distilled water (1.2×10^{-4} mol l^{-1}) and the analytical concentration used (5.65×10^{-5} mol l^{-1}), which suggests that micelles are indeed formed under the experimental concentration.

The dependence of the change in absorbance of the W^{VI}-catalysed reaction on the iodide concentration is illustrated in Fig. 1b. As can be seen, the change in absorbance increases with iodide concentrations up to 5.16×10^{-3} mol l^{-1}, above which it remains virtually constant.

Because iodide ion yields an insoluble salt with CPC, excess of this ion should be avoided in order to prevent precipitation. A 5.28×10^{-3} mol l^{-1} iodide concentration was selected in order to ensure maximum sensitivity.

The effect of hydrogen peroxide concentrations $1.2–12.2 \times 10^{-4}$ mol l^{-1} on the uncatalysed and catalysed reaction was similarly studied. Up to about 7.2×10^{-4} mol l^{-1}, the change in absorbance of both reactions increased with hydrogen peroxide concentration, but no significant increase was observed above 7.29×10^{-4} mol l^{-1} (Fig. 1c; W^{VI}-catalysed reaction). Fig. 1d shows the variation of the change in absorbance of the W^{VI}-catalysed reaction with hydrogen ion concentration. The effect of this parameter was studied over the range 0.7–5, by adjusting it with hydrochloric acid. The catalytic effect of W^{VI} was only observed at pH values between approximately 1.7 and 5. Because the reaction was rather too rapid below pH 1.5, absorbance measurements performed by using conventional techniques were highly irreproducible.

Even though higher acidities results in slightly enhanced sensitivities (Fig. 1d), the rate of blank reaction was also higher; hence, no real advantage in terms of the detection limit was gained. A pH of 2.5 was selected as a compromise between adequate sensitivity and reproducibility in the measurements. on the other hand, the formation of the I_3^-–CPC associate was independent of pH over the range 2–10 [7].

Increased temperatures had an adverse effect on the absorbance of the I_3^-–CPC associate, at 525 nm [7] which, however, remained virtually constant between 10 and 25°C. On the other hand, as the W^{VI}-catalysed reaction between iodide and hydrogen peroxide had a relatively small temperature coefficient [8], and the blank signal increased as the temperature increased, 25°C was chosen as the optimum. The change in absorbance obtained for the reaction in the CPC micellar medium at temperatures above 25°C were irreproducible.

A change in ionic strength of the solution had no considerable effect on the rate of reaction up to 0.1 mol l^{-1} potassium nitrate. The order in which the reactants were mixed also influenced the reaction rate.

Hence, the greater sensitivity was obtained when CPC was added before iodide, which was added last in order to control the start of the reaction.

Under the optimum conditions described above, a linear calibration graph was obtained for the W^{VI} concentration range of 4–90 ng ml^{-1} with a regression equation of $\Delta A = 0.0058X + 0.1098$ ($r = 0.9998$) where ΔA is the change in absorbance for 3 min from initiation of the reaction and X is the ng ml^{-1} of W^{VI}, respectively.

The detection limit (3 s) was 2.4 ng ml^{-1}, i.e. approximately 12–13 times lower than those of typical spectrophotometric methods based on the detection of triiodide ion [2]. The precision, expressed as relative standard deviation was 0.03% ($n = 9$) for 76.6 ng ml^{-1} of W^{VI}. The effect of foreign ions on the catalytic determination of W^{VI} was examined. The results are summarized in Table 1. The tolerance limit is that giving not more that $\pm 3\%$ error.

Table 1
Tolerated foreign ion concentrations in the determination of 0.050 μg ml^{-1} of W^{VI}

Foreign ion	Tolerated concentration[a] (μg ml^{-1})
Cl^-, Br^-	900
Zn^{II}	360
Mg^{II}	140
Mn^{II}	100
Ca^{II}	11
PO_4^{3-}	0.96
V^V	0.3
Cr^{VI}	0.1
Ti^{IV}	0.1
MO^{VI}	0.05

[a] Concentration yielding a variation of more than ±3% in the measurment.

3.2. Analytical features of the method

No significant selectivity enhancement for ions that catalyse the oxidation of iodide by hydrogen peroxide was achieved in the presence of micelles. The enhanced selectivity provided by the CPC micellar medium relative to the aqueous medium essentially arose from the bathochromic shift in the maximum absorbance of the triiodide ion in the micellar system.

4. Determination of W^{VI} in soil extracts

The applicability of the proposed method was tested by determining the W^{VI} content of soil. The results obtained in the determination of W^{VI} in the soil sample are summarized in Table 2 and compared with those obtained by using the thiocyanate method [9]. As the W^{VI} content in most of the samples studied was somewhat low, it could not be quantified by the thiocyanate method. Several spiked samples were therefore prepared by adding aliquots (a few microlitres) of a W^{VI} solution to homogenized soil samples that were subsequently extracted.

Table 2
Determination of W^{VI} in soil sample

Sample	W^{VI} content (μg g^{-1})	
	Proposed method[a]	Thiocyanate method[a]
1	142.69 ± 4.48	143.02 ± 5.29
2	140.77 ± 4.20	140.00 ± 5.40

[a] Average and standard deviation of three determinations.

References

[1] V.K. Pavlova, A.T. Pilipenko, R.N. Voevutskaya, Zh. Anal. Kim. 30 (1975) 2190.
[2] R.N. Voevutskaya, V.K. Pavlova, A.T. Pilipenko, Zh. Anal. Kim. 34 (1979) 1299.
[3] G.L. McIntire, CRC Crit. Rev. Anal. Chem. 21 (1990) 257.
[4] D. Sicilia, S. Rubio, D. Perez-Bendito, Talanta 38 (1991) 1147.
[5] D. Sicilia, S. Rubio, D. Perez-Bendito, Fresenius' J. Anal. Chem. 342 (1992) 327.
[6] M.L. Lunar, S. Rubio, D. Perez-Bendito, Talanta 39 (1992) 1163.
[7] M.L. Lunar, S. Rubio, D. Perez-Bendito, Anal. Chim. Acta 268 (1992) 145.
[8] T.P. Hadjiioanou, Anal. Chim. Acta 35 (1966) 360.
[9] Marczenko, in: Separation and Spectrophotometric Determination of Elements, ch. 57, Wiley, New York, 1986, p. 603.

ELSEVIER

Talanta 48 (1999) 885–893

Talanta

Determination of bismuth in biological samples using on-line flow-injection microwave-assisted mineralization and precipitation/dissolution for electrothermal atomic absorption spectrometry

J.L. Burguera *, M. Burguera, C. Rivas, C. Rondon, P. Carrero, M. Gallignani

IVAIQUIM (Venezuelan Andean Institute of Chemistry), Faculty of Science, University of Los Andes, P.O. Box 542, Mérida 5101-A, Venezuela

Received 27 June 1998; received in revised form 15 September 1998; accepted 16 September 1998

Abstract

An on-line automated flow injection system with microwave-assisted sample digestion for the electrothermal atomic absorption spectrometric determination of bismuth in biological materials is described. After the exposure of the sample to microwave radiation, the analyte was subject to a precipitation/dissolution process. Bismuth was precipitated with the stannite ion in basic medium and collected on the walls of a knotted coil, while the other matrix components flowed downstream to waste. The precipitate was dissolved with nitric acid and a sub-sample was collected in a capillary of a sampling arm assembly, to introduce 20 μl volumes into the graphite tube by means of positive displacement with air through a time-based injector. The analytical figures of merit were first evaluated by filling the sampling arm with a standard solution of bismuth and thereafter injecting aliquots of this solution into the atomizer. The calibration graph was linear from the detection limit (8 pg) to 1.2 ng of bismuth. The sensitivity was of 26.8 μg l^{-1} for 0.2 A-s and the characteristic mass (m_o) was of 11.8 pg/0.0044 A-s. The precision of the method, evaluated by replicate analyses of solutions containing 20 and 200 pg of bismuth, were 5.5 and 3.0% ($n = 10$), respectively. When solutions were introduced in the flow system here described, the calibration graph was linear in the range 0.04–6.0 μg l^{-1}, which means that a preconcentration factor of 10 was obtained for bismuth. The precision slightly deteriorated, e.g. the replicate analysis of solutions containing 1 and 10 pg of bismuth were 7.1 and 5.3% ($n = 10$), respectively. However, the recoveries values obtained with urine and whole blood bismuth spiked samples were over 96.5% and the agreement between observed and certified values was good.

Keywords: Bismuth; Biological samples; Flow injection; Electrothermal atomic absorption spectrometry

* Corresponding author. Fax: + 58-74-401286; e-mail: burguera@ciens.vla.ve.

0039-9140/99/$ - see front matter
PII S0039-9140(98)00298-7

1. Introduction

Bismuth is not considered an essential element for plants and animals [1]. Because of its low abundance, accumulation of bismuth in plant and animal tissues is slight. Although intestinal absorption is limited in man by the poor solubility of bismuth and its propensity to form insoluble oxy-chloride salts, some absorption from food and water must occur to produce measurable concentrations in body fluids and tissues [1,2]. Clinical/medical interest in bismuth dates back about 70 years, when the element was first introduced in a pharmaceutical used in the treatment of syphilis [3]. Since then, its pharmaceutical uses have expanded to antiacids, peptic ulcer treatments, and topical dermatological creams. However, there have been several reported cases of nephrotoxic, neurotoxic, and kidney damage symptoms attributable to the use of bismuth-containing pharmaceuticals [1,2]. These cases underscore the necessity for methods to determine bismuth concentrations at ultra-trace levels in biological fluids such as serum, whole blood or urine, and body tissues.

A variety of techniques has been described for the determination of bismuth with adequate detection limits ($\leq 1 \mu g\ l^{-1}$) and specificity for clinical studies. Recent methods such as inductively-coupled plasma atomic-emission spectrometry (ICP-AES) [4], hydride generation (HG)-ICP-AES [5], ICP-mass spectrometry (MS) [6,7], X-ray fluorescence spectrometry [8], electrothermal atomic absorption spectrometry (ETAAS) [9], HG-(ETAAS) with in-situ preconcentration [10], are now widely used for the determination of bismuth in biological materials. However, most of these methods suffer from either widespread availability of instrumentation, prohibitive cost, or technical. Because of these considerations, ETAAS seems attractive for determinations of bismuth in most biological samples.

In this work, an attempt is made to develop a flow injection (FI) system coupled with ETAAS for the determination of bismuth in urine and blood serum of human receiving low doses of colloidal bismuth citrate. The FI system allows the on-line sample digestion with the aid of microwave (MW) radiation, the bismuth preconcentration by precipitation/dissolution processes and the separation of the analyte from the matrix components. In this way, manipulation of samples is greatly reduced and the use of chemical modification [11] or tedious extraction procedures [9] for the determination of bismuth by ETAAS are not necessary. Also, this may be the first report on the successful collection of trace amounts of precipitate using a knotted reactor without a carrier.

2. Experimental

2.1. Apparatus

The FI-MO-ETAAS system is shown schematically in Fig. 1. It consisted of an Ismatec IPC eight-channel peristaltic pump, two 4-ways Latek TMW injectors (V_1 and V_2), a home made time-solenoid injector ($TBSI_1$) [12], two two-ways normally closed Cole-Parmer electronically controlled solenoid valves ($TBSI_2$ and $TBSI_3$) and a Prolabo MW oven microdigest (model 301). PTFE tubing (0.8 mm i.d.) was used throughout. A Perkin Elmer 4100 model atomic absorption spectrometer equipped with a bismuth hollow-cathode lamp, operated at 10 mA and a wavelength of 223.1 nm with a spectral bandpass of 0.5 nm was used. Zeeman-effect background correction was used for all measurements. Pyrolytic graphite coated graphite tubes were used with pyrolytic graphyte coated graphite platforms. Time-resolved absorbance signals were recorded on an IBM printer and integrated absorbance values were computerized using the Perkin-Elmer software version 9.1 for evaluating results. A Prolabo microwave microdigest 301 oven was used. A Branson (model 2210) ultrasonic bath (Branson Ultrasonic Corporation Danbury, CT, USA) was used to improve the bismuth dissolution step. Argon was used as the puge gas, the flow of which was interrupted during atomization. A sampling arm assembly allowed a quartz tube to be moved horizontally in an out of the waste vessel, graphite furnace, and washing solution [13]. A TDK model 286 computer was interfaced with the three TBSI, both rotary injection valves, the MW oven, and

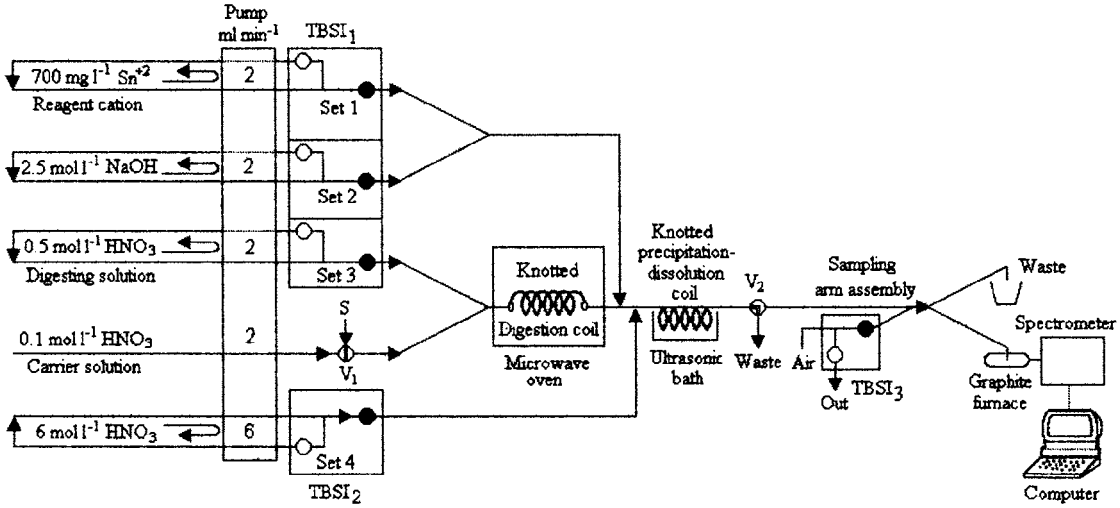

Fig. 1. Flow injection-microwave oven-ETTAS manifold. Numbers in the pump indicate the flow rate in ml min^{-1}. The system is shown in the sequence 1 (sample loading and rising operation).

the sampling arm assembly (SAA) (Fig. 1). The knotted digestion coil was vertically wound along a PTFE tube located inside the MW oven with the stream entering at the lower end. The knotted precipitation/dissolution coil was located inside the ultrasonic bath.

2.2. Reagents

All regents were of analytical grade, unless otherwise stated. Distilled deionized water was used for the aqueous solutions. Nitric acid was suprapur grade from Merck.

Bismuth stock solution (100 mg l^{-1}) was prepared by dissolving 0.100 g of specpure bismuth in 20 ml of concentrated nitric acid and diluting to 1000 ml with water. All working solutions were prepared by serial dilution of the stock solutions with 0.1 mol l^{-1} nitric acid immediately before use.

A 1 g Sn l^{-1} solution was prepared by dissolving 0.5 g of metallic Sn (mossy 99.9%, ACS reagent from J.B. Baker) in 50 ml of nitric acid and diluting to 500 ml with 1 mol l^{-1} nitric acid.

The argon used in this study was from AGA which certifies a purity of 99.99%. All glassware was cleaned as previously described [14].

2.3. Samples

Whole blood and urine samples were obtained from healthy male laboratory employees. They were selected at random without knowledge of origin or pathology and were not known to be taking any bismuth containing drugs.

Five ml of each whole blood sample was added to a heparinized clean polypropylene tube in order to prevent its coagulation and kept under refrigeration until its analysis. On the other hand, 50 ml urine samples were obtained on several occasions from healthy male laboratory employees, before its analysis.

2.4. Procedure

For the present work, $TBSI_1$ [12,15] has three sets of tubing: set 1, to regulate the reagent cation introduction; set 2, to regulate the sodium hydroxide introduction; and set 3, to regulate the nitric acid digesting solution introduction. The $TBSI_2$ has a set of tubing: set 4, to regulate nitric acid introduction, which was used to dissolve the analyte in the precipitation/dissolution coil. The solenoid of the $TBSI_1$ was in the normally closed position to avoid unnecessary reagent consumption during the different operations. The different

Table 1
Graphite tube atomizer programme for the determination of bismuth in urine and whole blood

	Step				
	1	2	3	4	5
Parameter	Dry	Pyrolyis	Atomize	Clean	Cool
Temperature (°C)	120	600	1800	2600	20
Ramp time (s)	30	20	0	1	1
Hold time (s)	40	30	5	5	20
Internal gas flow (ml min^{-1})	300	300	0	300	300

tubing sets were in its closed position. When a set was in the closed position, its solution flowed at will in a closed-flow circuit; however, in the open position the solution was introduced downstream in the FI system. The procedure consisted on various steps. The duration and function of each sequence of the FI-MW oven program are described as follows.

In sequence 1 (sample loading and rising operation), the sample valve (V_1) and the $TBSI_1$ injectors were in the loading and its normally closed position, respectively. In this way, only the carrier solution flowed at will through V_1, the digestion and precipitation/dissolution coils, V_2 and finally to waste through the SAA. This eliminated completely any residual sample matrix in the lines before sequence 2.

In sequence 2 (sample injection and analyte precipitation operations), V_1, V_2, and $TBSI_1$ were concomitantly activated to the alternate position for a period of 40 s and the MW oven turned on to allow: (i) the introduction and mixing of the reagent cation (through set 1) and NaOH solutions (through set 2); (ii) to introduce the sample plug in the carrier stream; and (iii) to introduce the digesting solution (through set 3).

In sequence 3 (analyte dissolution operation), V_1, V_2, and $TBSI_1$ were concomitantly activated to its initial position, the $TBSI_2$ was activated to its open position to introduce the analyte dissolving solution (through set 4), which flowed through the precipitation/dissolution coil and the activated V_2 to fill the SAA. The duration of this sequence was 18 s.

In sequence 4 (analyte determination), all injectors were set to sequence 1 and the activation of TBS_3 allowed the sequential deposition of aliquots of sample on the graphite tube platform by means of the SAA operated in the injection mode. This sequence was timed to synchronize with the spectrometer computer to run the furnace temperature program (Table 1). The duration of this sequence was 120 s.

3. Results and discussion

3.1. Preliminary experiments

In preliminary experiments the basic setting used for the graphite tube atomizer were optimized and are given in Table 1. A 30 s ramp from ambient to a final drying temperature of 120 °C avoided spattering of the of liquids and resulted in a uniform solid deposit on the surface of the atomizer platform. A complete dryness of aqueous standards and samples was observed with a holding time of 40 s. The best results were obtained when the temperature difference between pyrolysis and atomization steps was kept to a minimum (600 and 1800 °C, respectively). The addition of hydrochloric acid to the nitric acidic solution used for the dissolution of the precipitated bismuth greatly reduced the reproducibility of the results. This effect could be due to the appearance of two absorption peaks in the atomization of bismuth in the presence of chloride similar those previously reported by Ohta and Suzuki [16]. The first absorption resulted from the atomization of bismuth metal and the second absorption may result from atomization of some volatile bismuth compound [3], such as trichloride

[16]. Therefore, in this study the use of hydrochloric acid was avoided.

3.2. Effect of the bismuth precipitation process

The mixing of a solution of stannous nitrate with an excess of sodium hydroxide solution forms the stannite ion (reagent ion) [17], which is the precipitating species, according to the reaction:

$$Sn(NO_3)_2 + 2NaOH$$

$$= Sn(OH)_2 + 2NaNO_3$$

$$Sn(OH)_2 + 2NaOH$$

$$= Na_2(SnO_2) + 2H_2O$$

The amount of bismuth precipitated is determined by the concentration of the reagent ion. The effect of Sn^{2+} and NaOH concentrations on the determination of bismuth is very important and were therefore thoroughly studied (Figs. 2 and 3). Equal flow rates of an acidified $SnCl_2$ and NaOH solutions were introduced by means of the $TBSI_1$ (sets 1 and 2) and mixed downstream. As seen in Fig. 3, the absorbance signals and the

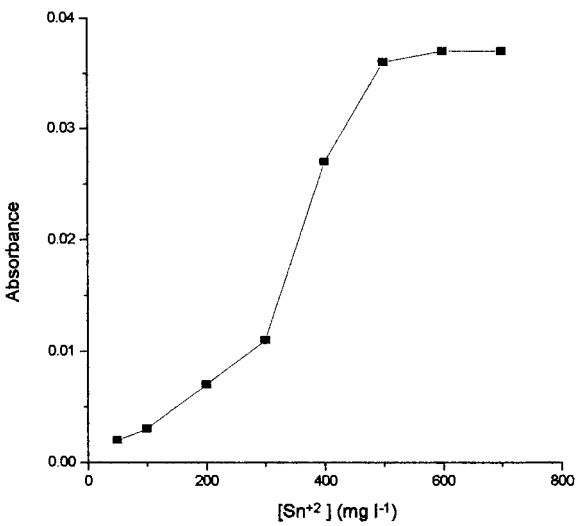

Fig. 2. Effect of the reagent ion concentration on the integrated absorbance of 0.5 μg Bi l^{-1}. All other conditions as in Tables 1 and 2.

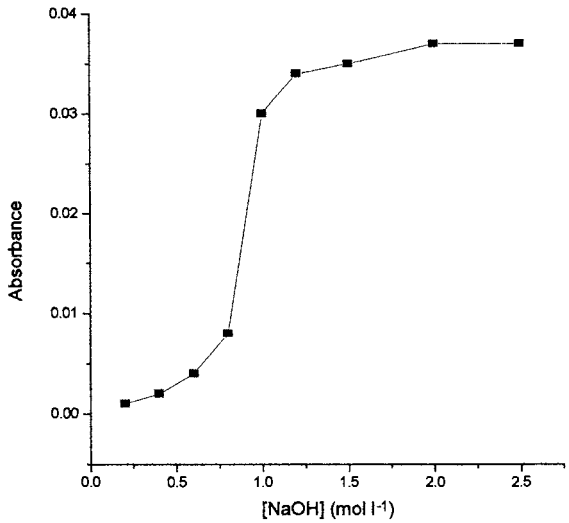

Fig. 3. Effect of the sodium hydroxide concentration for the production of reagent ion on the integrated absorbance of 0.5 μg Bi l^{-1}. All other conditions as in Tables 1 and 2.

reproducibility increased gradually (from 7.8 to 1.2% RDS) as the stannous ion concentration increased from 50 up to 400 mg l^{-1}. The absorbance signal was virtually unchanged at stannous ion concentrations above 500 mg l^{-1}. The poor reproducibility at lower Sn^{2+} concentrations could be due to an incomplete and varying conversion of Bi^{2+} to Bi. It also indicates that an excess of stannous ion (700 mg l^{-1}) is required for a complete precipitation of bismuth. Changes in the NaOH concentration from 0.2 to 0.6 mol l^{-1} did not greatly affects the absorbance values, possibly because at low pH values a white precipitate of stannous hydroxide is formed. Above 0.6 mol l^{-1} the analytical signal increased rapidly, reaching a constant value at concentrations above 1.0 mol $^{-1}$. It was notice that the reproducibility signals increased (RSD of ca. 1.1%) if an excess of NaOH (above 1.0 mol l^{-1}) was used. This indicates that an excess of alkali (2.5 mol l^{-1}) should be added to form the sodium stannite species necessary for a complete bismuth precipitation.

Some tests were performed in order to establish whether the stannous hydroxide (which is formed during the insufficient mixing of the stannous ion and base) acts as a carrier during the collection. These were performed by introducing a 700 mg

l^{-1} solution of $Na_2(SnO_2)$ kept under continuos stirring through the reagent channel following the sequence 2 of the procedure. In this case, no traceable amounts of analyte were detected in the solution flowing to waste through V_2, which confirms that the collection of the analyte in the knotted reactor is quantitative and that the stannous hydroxide stream does not act carrier.

3.3. Optimization of sample mineralization conditions

In a previous study of our research team, nitric acid behaved ideally for the MW-assisted digestion of whole blood samples in a FI-ETAAS system [15]. Besides, this acid is one of the few acids that can be obtained in ultrahigh purity for very low-level analytical analyses. Therefore, this acid was selected for this study. As previously found [15], in this study the use of 0.5 mol l^{-1} of nitric acid also proved to be an optimum decomposition agent for both whole blood and urine samples. Higher concentrations of nitric acid were avoided because they interfere with the reaction of $Sn(NO_3)_2$ with NaOH to form the SnO_2^{2-} ion. Some vapours formed in the digested sample zone did not influenced the precision of the results because they were sent to waste with the other flowing components through V_2 (Fig. 1). However, the gaseous by-products formed in the digestion coil were more smoothly eliminated if an ice bath was placed after the digestion coil, probably because the build-up of high pressures is in this way minimized.

The irradiation power contributed significantly to improve the precision and accuracy of the measurements. The absorbance signals and the precision of the measurements decreased as the MW oven power setting was lowered below 30 W, indicating incomplete mineralization of both urine and whole blood samples, whereas power setting above 80 W resulted in pronounced bubble formation generated by high temperature, which greatly deteriorated the precision of the measurements. Therefore, a power setting of 50 W was found adequate for the on-line digestion of the samples under evaluation.

The carrier solution flow rate and the digestion coil length determined the residence time of the sample–nitric acid mixture inside the oven. This residence time of the sample–nitric acid mixture in the oven must be optimal to achieve satisfactory results. As the total flow rate should not higher than 4 ml min^{-1} (see below), an adequate flow rate of 1 ml min^{-1} of the carrier stream was found to be adequate. Either too long or too short digestion coils tended to provide less precise and accurate results, respectively [15]. If the residence time was kept in the 30–75 s range good results were obtained. However, a residence time of ca. 7 s (using a 2 m long coil) was found to be adequate for good sampling rate, accuracy, and precision.

3.4. Effect of the bismuth dissolution process

The black precipitate of finely divided bismuth collected on the walls of the knotted precipitation coil was dissolved by the introduction of nitric acid. The effect of this acid concentration on the dissolution of the precipitate is shown in Fig. 4a. The dissolution of bismuth was not affected when the nitric acid concentration was in the range of 2–3 mol l^{-1}. The dissolution process greatly in-

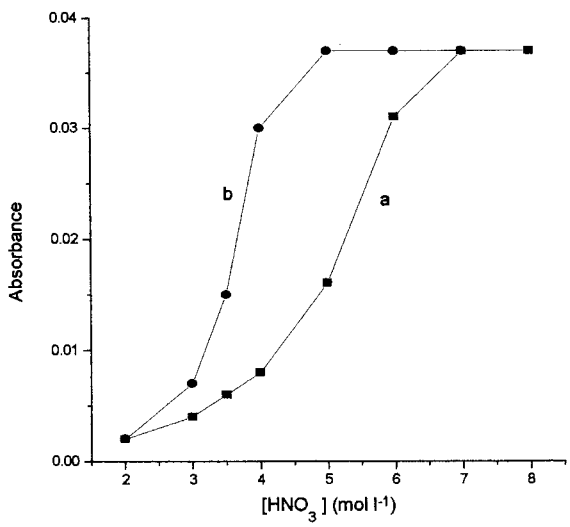

Fig. 4. Influence of nitric acid concentration for the analyte dissolution process on the integrated absorbance of 0.5 μg Bi l^{-1}. The KR was without (a) and under (b) ultrasonic treatment. All other conditions as in Tables 1 and 2.

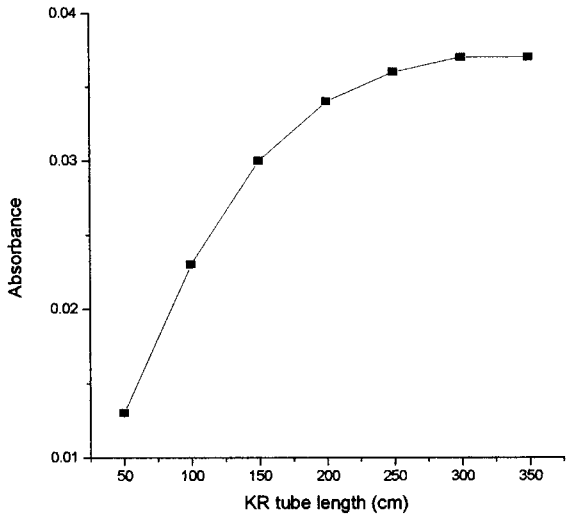

Fig. 5. Influence of KR tube length on the integrated absorbance of 0.5 μg Bi l^{-1}. All other conditions as in Tables 1 and 2.

creased at higher acid concentrations until a concentration of 7 mol l^{-1}, above which the dissolution of the precipitate is virtually complete, so a constant absorbance value was obtained. If the precipitation coil was subject to ultrasonic agitation it has the added benefit of aiding the dissolution process by improving the mixing of the acid with the precipitate particles (Fig. 4b). Therefore, the dissolution process was favoured and the precipitate dissolution occurs at lower acid concentration (above 5 mol l^{-1}).

3.5. Optimization of flow injection conditions

The efficiency of the MW digestion and precipitation/dissolution processes are directly influenced by the sample injected volume, digestion and precipitation/dissolution coil lengths, flow rates, and tubing lengths.

The essential requirements of an FI on-line coprecipitation preconcentration system for ETAAS have been discussed by Fang and Dong [18]. The knotted precipitation/dissolution coil length significantly influenced the precipitation/dissolution efficiency. With shorter coils (< 200 cm) the absorbance decreased (Fig. 5) as the reaction is incomplete due to a very short contact time between the Bi^{2+} and the reagent ion. The peak absorbance increased up to a length of 300 cm, beyond which the signals remained almost constant, implying complete collection of precipitate at this tubing length (residence time of ca. 4 s).

The amount of bismuth precipitated is determined by the concentration of the element and volume of sample injected. The amount of precipitate to be collected within a cycle is limited by the flow resistance and the collection capacity of the reactor. Our experiments showed that bismuth concentrations above 100 μg Bi l^{-1} created considerable back-pressure and flow-rate fluctuation even at low total flow rates (4 ml min^{-1}), particularly when the precipitate had been accumulated. Therefore, if a maximum amount of 80 μg Bi l^{-1} of bismuth were introduced a constant flow-rate could be guaranteed in such a system for a total flow rate of 4 ml min^{-1}. Higher sample volumes decreased the sample throughput and the waste of sample, which is highly important in any study of clinical interest. Too low samples volumes could not contain measurable amounts of analyte. Therefore, a sample volume of 500 μl was found to be appropriate when analysing urine and whole blood samples.

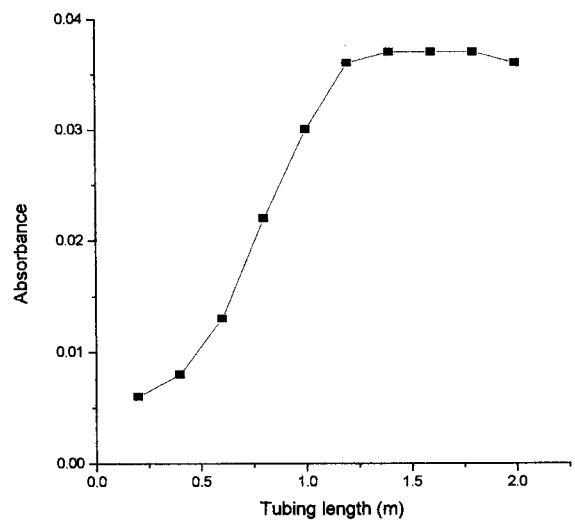

Fig. 6. Influence of the tubing length used for the merging of the reagent ion/hydroxide solutions on the integrated absorbance of 0.5 μg Bi l^{-1}. All other conditions as in Tables 1 and 2.

The length of the merging zones tube of the mixed reagent ion/hydroxide solutions greatly influenced the precipitation process. The results, which are depicted in Fig. 6 show that for tubing lengths below 0.5 m the absorbance values slowly increased, probably due to local inhomogeneity in the reaction mixture immediately after merging of the sample and reagent, which was found to produce a white solution of stannous hydroxide. For reactor tube lengths between 0.5 and 1.2 m the absorbance of bismuth increased rapidly and remained almost constant for higher tubing lengths, implying that sufficient time is allowed for the on-line solubilization of the stanouss hydroxide compound in the presence of an excess of alkali.

The flow rates of the different channels are an important factor which influence the response and therefore were fixed to allow an appropriate residence time of the solutions within the FI system. Too slow flow rates: (i) lower the sampling frequency; (ii) dilution/diffusion effects due to a slow dissolution processes may occur. However, with too high flow rates: (i) incomplete precipitate collection; (ii) increases the impedance to the flow (back pressure) and dislodged some collected precipitate; (iii) it did not provided a reasonably wide safety merging for the digestion of samples induced by MW radiation and the precipitate collection capacity of the reactor; (iv) there could be a failure to achieve complete dissolution of larger precipitate particles; (v) a very fast collection time makes difficult the selection of the appropriate segment to be introduced for ETAAS evaluation. Moderate total flow-rates of 4.0 (for sequences 1 and 2) and 3 (for sequence 3) ml min^{-1} were therefore used. This implies 1 ml min^{-1} flow rates for the sets 1–3 and for the carrier stream, and 3 ml min^{-1} for set 4.

3.6. Analytical performance

The analytical figure of merits were first evaluated by filling the SAA with a standard solution of bismuth and thereafter injecting 20 μl aliquots of this solution into the atomizer using the furnace programme given in Table 1. The precision of the method, evaluated by replicate analyses of solutions containing 20 and 200 pg of bismuth, were 5.5 and 3.0% (n = 10), respectively. The calibration graph was linear from the detection limit (8 pg) to 1.2 ng of bismuth (solutions of 0.4–60 μg Bi l^{-1}, respectively), corresponding to a linear range of nearly 3 orders of magnitude. The sensitivity was of 26.8 μg l^{-1} for 0.2 A-s and the characteristic mass (m_o) was of 11.8 pg/0.0044 A-s.

When standard solutions were introduced following the procedure previously described and the optimal experimental conditions given in Tables 1 and 2, the calibration graph was linear in the range 0.04–6.0 μg Bi l^{-1} solutions, which means that a preconcentration factor of 10 was obtained for bismuth. The precision slightly deteriorated, e.g. the replicate analysis of solutions containing 1 and 10 pg of bismuth were 7.1 and 5.3% ($n = 10$), respectively. This could be attributed to the on-line operation of MW sample treatment and to the precipitation/dissolution processes that could con-

Table 2
Optimum operating MW oven-FI conditions

Component	Parameter	Value
MW sample digestion	Microwave oven power	50 W
	KR digestion tubing length	2 m
	Nitric acid concentration	0.5 mol l^{-1}
	Sample volume	500 μl
Sample precipitation	Concentration of the stannous reagent ion	700 mg l^{-1}
	Effect of sodium hydroxide concentration	2.5 mol l^{-1}
	KR precipitation/dissolution coil length	400 cm
	Reagent ion/hydroxide solution merging tubing length	1.5 m
Sample dissolution	Nitric acid concentration (with ultrasonic agitation)	5.5 mol l^{-1}
	Carrier stream flow rate	2 ml min^{-1}
	Reagent cation stream flow rate	2 ml min^{-1}
	Sodium hydroxide stream flow rate	2 ml min^{-1}
	Digesting nitric acid solution stream flow rate	2 ml min^{-1}
	Dissolving nitric acid solution stream flow rate	6 ml min^{-1}
	Total flow rate	8 ml min^{-2}

tribute to some non-homogenous analyte distribution in the FI system.

Recovery studies were performed on pools of whole blood and urine samples of subjects without any treatment with bismuth compounds. There was no loss of metal during the procedure, and the average recovery for the addition of 0.1 and 1.0 μg Bi l^{-1} in both samples were of 98.5% (range 97.0–102%) and 98.0% (range 96.5–101%), respectively. The accuracy of the procedure was further investigated by determining bismuth content in Seronorm CRM whole blood (Oslo, Norway) and high-purity standards (HPS, Charleston, USA) drinking water. The results obtained were: 4.9 μg Bi $l^{-1} \pm 1.5\%$ (whole blood, batch no. 905), 9.8 μg Bi $l^{-1} \pm 1.2\%$ (whole blood, batch no. 906) and 9.9 μg Bi $l^{-1} \pm 0.9\%$ (lot no. 590321), which were in good agreement with the certified values 5, 10, and $10 \pm 1.5\%$ μg Bi l^{-1}, respectively.

3.7. Analysis of samples

In the urine and whole blood of the 25 subjects under study concentrations from 0.2 to 1.4 μg Bi l^{-1} (mean 0.8 ± 0.3 μg Bi l^{-1}) and from 0.5 to 1.9 μg Bi l^{-1} (1.2 ± 0.4 μg Bi l^{-1}) were respectively detected. The results obtained are in a general good agreement with those previously published by other authors and obtained from healthy individuals [10,19].

4. Conclusions

The proposed on-line automated method for the determination of bismuth at very low levels in urine and whole blood has proven to be sensitive, simple, reliable, and reproducible. Since bismuth is present at very low concentrations in biological samples, specially in unexposed individuals, the use of ETAAS with direct injection of urine or blood in the atomizer could lead to not detectable levels of the analyte or to irreproducible results. The detection limit obtained in this study was better or was comparable to the literature values [3–5,9,10,20]

Acknowledgements

The authors appreciate financial support from CDCHT (Consejo de Desarrollo Científico y Humanístico) of Los Andes University.

References

[1] D.W. Thomas, T.F. Hartley, P. Coyle, S. Sobecki, Bismuth, in: H.G. Seiler, H. Sigel (Eds.), Handbook on Toxicity of Inorganic Compounds, Marcel Dekker, New York, 1987, pp. 115–127.
[2] D.W. Thomas, Bismuth, in: E. Merian (Ed.), Metals and their Compounds in the Environment, VCR, Weinhem, 1991, pp. 789–801.
[3] R.L. Bertholf, B.W. Renoe, Anal. Chim. Acta 139 (1982) 287.
[4] P. Schramel, Y. Wendler, L. Angerer, Int. Arch. Occup. Environ. Health 69 (1997) 219.
[5] P. Schramel, L.Q. Xu, Fresenius J. Anal. Chem. 340 (1991) 41.
[6] Y. Mauras, A. Premelcabic, S. Berre, P. Allain, Clin. Chim. Acta 218 (1993) 201.
[7] H.Y. Li, B.M. Keohane, H.Z. Sun, P.J. Sadler, J. Anal. At. Spectrom. 12 (1997) 1111.
[8] J. Messerschmidt, a von Bohlen, F. Alt, R. Klockenkamper, J. Anal. At. Spectrom. 12 (1997) 1251.
[9] Z.M. Ni, X.Q. Shan, L.Z. Jin, S. Luan, L. Zhan, K.S. Subramanian, ACS Symp. Ser. 445 (1991) 206.
[10] H. Matusiewicz, M. Kopras, A. Suszka, Microchem. J. 52 (1995) 282.
[11] K. Matsusaki, Anal. Chim. Acta 248 (1991) 251.
[12] P. Carrero, J.L. Burguera, M. Burguera, C. Rivas, Talanta 40 (1993) 1967.
[13] J.L. Burguera, M. Burguera, J. Anal. At. Spectrom. 8 (1993) 235.
[14] M. Burguera, J.L. Burguera, C. Rivas, P. Carrero, R. Brunetto, M. Gallignani, Anal. Chim. Acta 308 (1995) 339.
[15] M. Burguera, J.L. Burguera, C. Rondon, et al., J. Anal. At. Spectrom. 10 (1995) 343.
[17] A.I. Vogel, Macro and Semimicro Qualitative Inorganic Analysis, 4th ed., Longman, London, 1953, pp. 252–253.
[16] K. Ohta, M. Suzuki, Anal. Chim. Acta 96 (1978) 77.
[18] Z.L. Fang, L.P. Dong, J. Anal. At. Spectrom. 7 (1992) 439.
[19] S. Caroli, A. Alimonti, E. Coni, F. Petrucci, O. Senofonte, N. Violante, Crit. Rev. Anal. Chem. 24 (1994) 363.
[20] A.T. Wan, P. Froomes, At. Spectrosc. 12 (1991) 77.

ELSEVIER

Talanta 48 (1999) 895–903

Talanta

Simultaneous spectrophotometric determination of tartrazine, patent blue V, and indigo carmine in commercial products by partial least squares and principal component regression methods.

J.J. Berzas Nevado *, J. Rodríguez Flores, M.J. Villaseñor Llerena, N. Rodríguez Fariñas

Department of Analytical Chemistry and Food Technology, University of Castilla-La Mancha. 13071 Ciudad Real, Spain

Received 11 May 1998; received in revised form 24 July 1998; accepted 16 September 1998

Abstract

Two multivariate calibration methods, partial least squares (PLS-1) and principal component regression (PCR) were proposed and successfully applied to the simultaneous determination of three dyes, tartrazine (T) (E-102), patent blue V (P) (E-131), and indigo carmine (I) (E-132) in mixtures by ultraviolet-visible absorption spectrophotometry. Calibration models were evaluated by internal validation (prediction of dyes concentration in its own designed training set of calibration), by cross-validation (obtaining statistical parameters that show the efficiency for a calibration fit model), and by external validation over 19 synthetic mixtures of the three dyes in different ratios containing 2.4–17.6 mg l^{-1} of T, 1.6–5.6 mg l^{-1} of P, and 3.2–17.5 mg/l^{-1} of I, with recoveries between 93.5 and 103.1% and over three commercial products, in which the proposed calibration models were satisfactorily applied without separation step. Repeatability and reproducibility studies (with the Students's and *F* tests) were achieved over two series of nine standards for each dye, showing no significant differences at 95% confidence level.

Keywords: Dyes; Spectrophotometry; Partial least squares; Principal component regression

1. Introduction

The term color additive (artificial colorant) can be applied to any dye, pigment, or other substance made or obtained from a vegetable, mineral, or another natural source that are capable of coloring food, drugs, or cosmetic [1].

Tartrazine (T), patent blue V (P), and indigo carmine (I) are three synthetic dyes available as yellow and blue powder that can be present in common food (drinks, yogurts, ice cream, sweets...). The toxicological evidence for synthetic colors are considerably greater than for natural

* Corresponding author. Tel: + 34-26-295300; fax: + 34-26-295318; e-mail: jrflores@qata.uclm.es.

0039-9140/99/$ - see front matter
PII S0039-9140(98)00301-4

colors since the chemical complexity and the difficulty in defining specifications for them make the toxicological evaluation of natural colors virtually impossible. The present and/or contact of some of these dyes (e.g. tartrazine) with drugs like aspirin, benzoic acid, and other analgesics in the human body can induce allergic and asthmatic illness in sensitive people. An extensive review of the genotoxicity of food, drugs, and cosmetic colors and other azo, triphenylmethane, and xanthene dyes has been completed by Combes and Haveland-Smith [2].

Chromatographic methods have been used for colorant analysis in food and they are recommended when the mixture contains many different colorants [3,4].

Adsorptive stripping voltammetry has been also applied by the authors in order to quantify separately several dyes [5] in different commercial products.

Under computer-controlled instrumentation, derivative techniques and multivariate calibration methods are playing a very important role in the multicomponent analysis of mixtures by ultraviolet-visible molecular absorption spectrophotometry [6]. Both of them are useful in the resolution of band overlapping in quantitative analysis. Derivative techniques have proved to be very useful in the resolution of sample binary mixtures of dyes [7] whereas multivariate calibration has been found to be the method of choice for more complex mixtures [8,9]. The advantages of multicomponent analysis using multivariate calibration is the speed in the determination of components in a mixture, avoiding preliminary separation step.

The application of quantitative chemometric methods, particularly principal component regression (PCR) and partial least squares (PLS) to multivariate chemical data is becoming more widespread owing to the availability of digitized spectroscopic data and commercial software for laboratory computers. Each method needs a calibration step where the relationship between the spectra and the component concentration is deduced from a set of reference samples, followed by a prediction step in which the results of the calibration are used to determine the component concentrations from the sample spectrum.

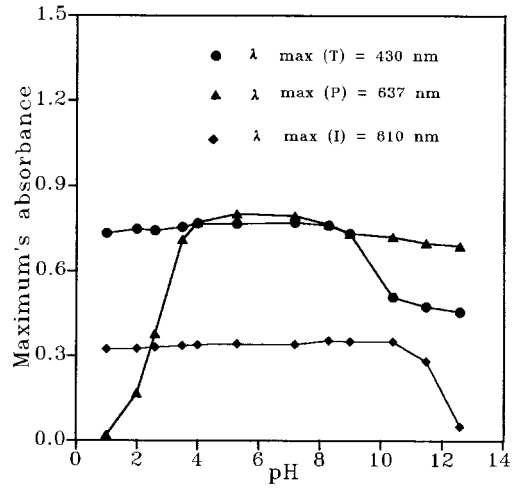

Fig. 1. Influence of pH over the maximum of absorption spectra for solutions of 16 mg l^{-1} of T, 4 mg l^{-1} of P, and 8 mg l^{-1} of I.

The basic concept of PLS regression was originally developed by Wold [10,11] and the use of the PLS method for chemical applications was also pioneered by Wold and co-workers [12].

The aim of this work is to propose two multivariate calibration methods to resolve ternary

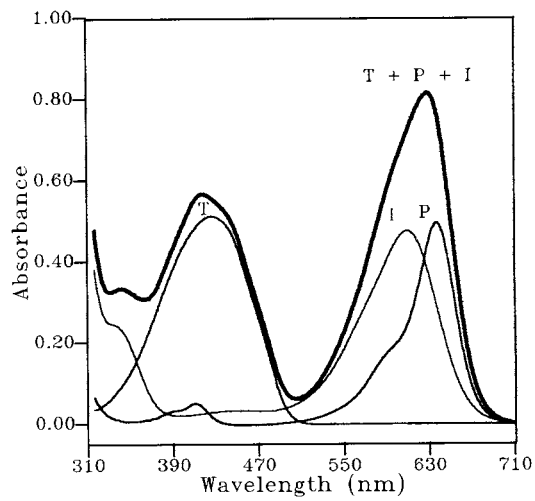

Fig. 2. Absorption spectra for solutions of 10.4 mg l^{-1} of T, 2.4 mg l^{-1} of P, 10.4 mg l^{-1} of I, and their mixture (T + P + I), prepared in acetate buffer medium (pH 4.8) and recorded against a blank of Milli Q water with a scan speed of 600 nm min^{-1}.

Table 1
Composition of calibration training set

Standard	T[a]	P[a]	I[a]
M1	4.0	0.0	0.0
M2	20.0	0.0	0.0
M3	0.0	0.8	0.0
M4	0.0	6.0	0.0
M5	0.0	0.0	4.0
M6	0.0	0.0	17.6
M7	3.2	6.0	0.8
M8	3.2	5.2	3.2
M9	3.2	4.0	6.4
M10	3.2	3.2	10.4
M11	3.2	2.0	14.4
M12	3.2	0.4	17.6
M13	0.8	1.6	17.6
M14	3.2	1.6	14.4
M15	6.4	1.6	10.4
M16	16.0	1.6	3.2
M17	20.0	1.6	0.8
M18	20.0	0.4	3.2
M19	16.0	2.0	3.2
M20	12.8	3.2	3.2
M21	6.4	4.0	3.2
M22	3.2	5.2	3.2
M23	0.8	6.0	3.2
M24	6.4	2.0	14.4
M25	12.8	3.2	6.4
M26	16.0	2.0	10.4
M27	6.4	4.0	6.4
M28	10.4	4.0	8.0
M29	4.8	2.0	4.0
M30	5.6	1.2	8.0
M31	10.4	2.0	12.0
M32	4.8	2.0	8.0

[a] Units concentration: mg/l.

mixtures of T, P, and I in commercial products without prior separation. In the same way, these methods yield accurate and reproducible results in three different commercial products with regard to the contents provided by their respective manufacturer enterprises.

2. Experimental

2.1. Apparatus

A Beckman Instruments DU-70 spectrophotometer equipped with 1.0 cm cells and connected to an IBM-PS2 model 30 computer provided with a Beckman data leader software [13].

The Grams-386 Level 1 version 3.01 software package with the PLS plus version 2.1 G application software [14] connected to an EGA computer and a Hewlett Packard LaserJet IIIP, which were used for the statistical treatment of the data and for the application of PLS and PCR methods.

2.2. Reagents

All solvents and reagents were of analytical reagent-grade unless indicated otherwise. T was supplied by Sigma (St Louis, MO; T0388); P and I were provided by Sancolor S.A. T, P, and I stock aqueous solutions with a concentration of 200 mg l^{-1} were prepared. Acetic acid–sodium acetate (0.1 M and pH 4.8) was used as buffer solution.The two chemometric approaches were applied to following food commercial applications:

- Confectionery dye vahiné: with water and authorized artificial dyes: E-102, E-131. From the enterprise Ducros S.A. (Spain).
- Cherries in syrup: with cherries, sugar, glucose, acidulant (citric acid), and dye:E-102, E-131. From the enterprise DYC Helios S.A. (Spain).

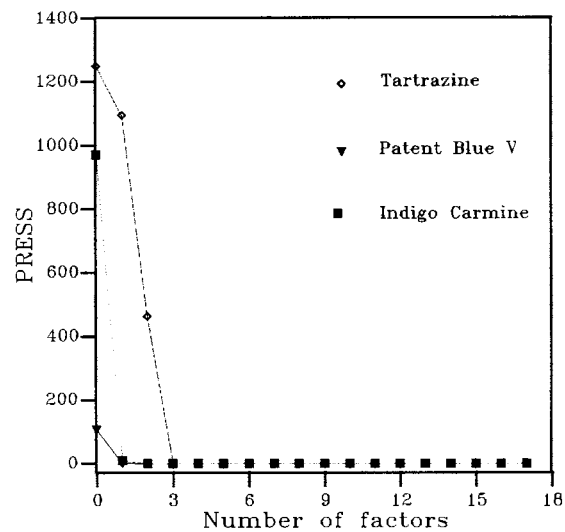

Fig. 3. Representation of PRESS values generated by cross-validation of PLS-1 calibration model for the resolution of the ternary mixture: T, P, and I.

Table 2
Statistical parameters of cross-validation process for PLS-1 and PCR[a]

Dye	Factor	PRESS	RMSD	SEC/SEP	R^2	REP (%)
PLS-1						
T	3	0.0622	0.0441	0.0448	0.99995	0.6234
P	3	0.0334	0.0323	0.0328	0.99968	1.3125
I	2	0.3270	0.1011	0.1027	0.99967	1.4866
PCR						
T	3	0.0622	0.0441	0.0448	0.99995	0.6234
P		0.0334	0.0323	0.0328	0.99968	1. 3125
I		0.3271	0.1011	0.1027	0.99966	1.4868

[a] RMSD = (PRESS/n) $^{1/2}$; SEC/SEP = (PRESS/n-1)$^{1/2}$; REP (%) = RMSD·100/μ

- Gelatin, flavor lemon: with sugar, dextrose, gelatin, acidulant (citric acid, sodium citrate), flavorings, ascorbic acid, salt, and dyes: E-102, E-132. From the enterprise Nabisco Iberia S.L. (Spain).

The ingredients are in all products in decreasing order of concentrations.

2.3. Procedure

In 25 ml calibrated flasks, aliquots of the stock solutions were added to obtain concentrations between 0.8 and 20.0 mg l^{-1} of T, between 0.4 and 6.0 mg l^{-1} of P, and between 0.8 and 17.6 mg l^{-1} of I; 5 ml of acetate buffer solution (pH 4.8) and deionized water (milli Q quality) to the mark were also introduced. The absorption spectra were recorded between 315 and 710 nm with a scan rate of 600 nm min^{-1} against a blank of deionized water. The optimized calibration matrix, obtained by the use of recorded absorption spectra of standards (in the spectral ranges: 420–480 nm and 550–660 nm) was applied to analyze the spectra and to calculate the concentrations of T, P, and I in synthetic and commercial mixtures. In order to do this, a number of 3, 3, and 2 factors were selected for T, P, and I, respectively by PLS-1 chemometric approach and a number of 3 factors was chosen for the three dyes resolution by PCR method.

Absorption spectra of standards were employed in order to optimize the calibration matrix by internal validation procedure using PLS and PCR multivariate calibration. The external validation of calibration model was achieved over the spectra of 19 synthetic mixtures of dyes in different ratios and over the spectra of three food commercial preparations by the application of PLS and PCR methods to determine T, P, and I content in them.

The procedure for the preparation of the commercial food samples was as follows:

- for the first product, once homogenized the commercial mixture, different known aliquots (40–80 μl) were placed in 25 ml calibrated flasks, adding also 5 ml of HOAc–NaOAc 0.1 M, 8 mg l^{-1} of dye I (not contained in this commercial product) and deionized water to the mark
- for the second product, in order to analyze the content of dyes in the syrup, once removed the cherries it was necessary to clarify the syrup by decanting, from this moment the followed procedure was the same as above described adding in this case 12 mg l^{-1} of I (absent too in this commercial product)
- in the third case, a stock solution of gelatin was preparing by dissolving 10 g in hot water with strong stirring conditions, transferring the clarified solution to 100 ml calibrated flask, adding a known content of P standard (dye not contained in this gelatin) and deionized water to the mark. After that, different diluted solutions were obtained by adding in

25 ml calibrated flasks different known volumes of stock solution, 5 ml of selected buffer and deionized water to the mark

The spectra of the commercial samples thus prepared were recorded against a blank of milli Q water with a scan speed of 600 nm min^{-1} between 315 and 710 nm wavelength range. The contents of T, P, and I in commercial samples were calculated by analyzing the recorded spectra with PLS-1 and PCR chemometric approaches.

3. Results and discussion

3.1. Influence of chemical variables

The influence of pH on the absorption spectra for solutions of T (16 mg l^{-1}), P (4 mg l^{-1}), and I (8 mg l^{-1}) is studied (Fig. 1). In order to establish a suitable pH for this study a range between 1.5 and 12 pH values is examined obtaining the following results: the spectra of T shows a

Table 3
Recoveries found in synthetic mixtures by PLS-1 and PCR

Content (mg/l)			PLS-1 (rec %)			PCR (rec %)		
T	P	I	T	P	I	T	P	I
17.6	1.6	3.2	100.4	95.9	96.4	100.4	95.9	97.4
15.2	2.4	3.2	99.8	98.7	96.0	99.8	98.7	96.7
12.0	3.2	3.2	100.1	98.1	96.6	100.1	98.1	97.1
8.8	4.0	3.2	98.9	98.4	95.8	98.9	98.4	96.0
6.4	4.8	3.2	98.3	98.0	96.4	98.3	98.0	96.7
3.2	5.6	3.2	93.5	98.0	95.3	93.5	98.0	95.1
15.2	1.6	6.4	100.3	97.6	99.5	100.3	97.6	99.9
12.0	1.6	9.6	100.4	96.9	98.9	100.4	96.9	99.1
8.8	1.6	12.0	100.6	99.1	98.6	100.6	99.1	98.7
6.4	1.6	15.2	102.1	98.1	98.1	102.1	98.1	98.2
3.2	1.6	17.5	99.7	97.7	97.6	99.7	97.7	97.6
3.2	2.4	15.2	98.3	98.5	98.0	98.3	98.5	98.0
3.2	3.2	12.0	96.9	97.4	98.1	96.9	97.4	98.1
3.2	4.0	9.6	96.1	99.4	98.5	96.1	99.4	98.4
3.2	4.8	6.4	94.3	98.3	98.7	94.3	98.3	98.6
12.0	2.4	6.4	100.4	99.3	99.5	100.4	99.3	99.8
6.4	2.4	12.0	101.0	99.6	98.0	101.0	99.6	98.1
4.0	5.6	6.4	95.0	98.3	98.3	95.0	98.3	98.3
2.4	5.6	8.0	89.0	97.7	97.9	89.0	97.7	97.9

Table 4
Found contents of T, P, and I in commercial preparations food

Products	Nominal contents			Found contents					
				PLS-1			PCR		
	T (ppm)	P (ppm)	I (ppm)	T (ppm)	P (ppm)	I (ppm)	T (ppm)	P (ppm)	I (ppm)
Confectionery dye	[a]	[a]	8.00[b]	5.07 10^3	1.97 10^3	7.92	5.07 10^3	1.97 10^3	7.96
Syrup	20.00	4.00	12.00[b]	18.04	3.84	11.0	18.04	3.84	10.99
Gelatin	260.0	8.00[b]	0.15	246.5	7.53	[c]	246.8	7.54	[c]

[a] Unknown nominal values.
[b] Added dye.
[c] Lower than detection limits.

Table 5
Statistical parameters for precision studies at different days ($n = 9$)[a]

M	Series	T					P					I				
		μ	SD	RSD	F_{exp}	t_{exp}	μ	SD	RSD	$F_{exp.}$	t_{exp}	μ	SD	RSD	F_{exp}	t_{exp}
PLS-1	1	10.44	0.037	0.36	1.479	2.059	4.05	0.040	0.99	1.778	0.601	12.05	0.065	0.54	2.926	0.399
	2	10.40	0.045	0.43			4.04	0.030	0.75			12.04	0.038	0.31		
PCR	1	10.44	0.037	0.36	1.479	2.059	4.05	0.040	0.99	1.778	0.601	12.02	0.065	0.54	2.966	0.797
	2	10.40	0.045	0.43			4.04	0.030	0.75			12.00	0.038	0.31		

[a] $F_{8,8}$ (theoretic) = 3.44; t_{18} (theoretic) = 2.12

maximum at 430 nm between 1.0 and 9.0 pH values whereas for higher pH values this maximum decreases; P shows a maximum at 637 nm whose absorbance rises between 1.0 and 3.5 pH units, remaining constant from 3.5 to 8.0 pH values and undergoing a batocromic shift for higher pH values than 8; with regard to I, its absorbance spectrum displays a maximum at 610 nm whose absorbance stays constant between 1.0 and 10.6 pH units decreasing from this last value. We have chosen a pH value of 4.8 as optimum.

In Fig. 2 the zero order spectra of T, P, and I recorded in the 310–710 nm wavelength range are shown. As it can be seen the absorption spectra of the three dyes are overlapped obstructing the resolution of this ternary mixture from direct absorbance measurements, reason why we have proposed two multivariate calibration methods in order to resolve this ternary mixture.

3.2. Partial least squares and principal component regression multivariate calibration

PLS and PCR methods were evaluated for the resolution of the mixtures and a comparative study of the prediction capabilities of the two chemometric approaches in our particular work was undertaken.

3.2.1. Experimental design of the calibration matrix and selection of the spectral zone for the analysis

A training set of 32 standards samples was taken. T concentration was varied between 0.8 and 20.0 mg l^{-1}, P concentration between 0.4 and 6.0 mg l^{-1}, and I content between 0.8 and 17.6 mg l^{-1}. In Table 1 there are summarized the composition of the standard mixtures used in the calibration matrix.

The spectral regions placed between 420 and 480 nm, and 550–660 nm were selected as optima for the analysis, which implies to work with 241 experimental points for each spectrum. The two selected wavelength zones were chosen because these ones contained the main spectral information for the three components of the samples, rejecting the range between 480 and 550 nm since did not contribute any interesting spectral information for the analysis as it can be seen in Fig. 2.

3.2.2. Selection of the optimum number of factors

To select the number of factors in the PLS and PCR algorithms in order to model the system without overfitting the concentration data, a cross validation method leaving out one sample at a time was used. The process was repeated 32 times for each tested number of factors until each calibration standard has been left out once ($n = 32$, number of calibration samples). The predicted concentrations ($\hat{x}$) of the compounds in each sample were compared with the already known concentrations (x) and the prediction error sum of squares (PRESS) was calculated by each number of factors:$\mathrm{PRESS} = \Sigma_{i=1}^{n} (x_i - \hat{x}_i)^2$

In our particular case, a number of 3, 3, and 2 factors were obtained as optima for T, P, and I components, respectively by PLS-1 method using the Haaland and Thomas's criterion [8], who empirically determined than an F ratio probability of 0.75 is a good choice. Also the PCR model was optimized by using the same set of standard samples and finding as optimum a number of 3 factors for this model. In Fig. 3 is shown the obtained PRESS for each dye when the different number of factors were tested in order to optimize this parameter in the PLS-1 chemometric approach using the designed calibration matrix of the absorption spectra of the samples.

The proposed PLS and PCR calibration models were evaluated by internal validation (prediction of dyes concentration in its own designed training set of calibration) obtaining, in general terms, recoveries between 97.5 and 106.2%.

3.2.3. Statistical parameters of cross-validation method

Using the cross-validation method the following statistical parameters have been obtained: the values of root mean squares difference (RMSD), the standard error of calibration (SEC/SEP), the square of the correlation coefficient (R^2) and the relative error of prediction (REP).

In Table 2 the obtained results for these parameters by the two proposed chemometric approaches are shown. We can see that R^2 val-

ues are in all cases very nearly to 1, which is an indication of similitude between predicted and known values. On the other hand, in this table is shown how the obtained values of the statistical parameters are the same by both multivariate calibration method, resulting higher those reached in I determination than those obtained in T and P determination.

3.2.4. External validation of partial least squares and principal component regression calibration models

3.2.4.1. Determination of tartrazine, patent blue V, and indigo carmine in synthetic mixtures. One set of 17 synthetic mixtures containing from 2.4 to 17.6 mg l^{-1} of T, from 1.6 to 5.6 mg l^{-1} of P, and from 3.2 to 17.5 mg l^{-1} of I in different ratios were predicted by means of PLS-1 and PCR chemometric calibration methods.

The composition of these mixtures and the recoveries obtained by each method are summarized in Table 3, where it can be seen the results obtained by the two chemometric approaches are not significantly different from each other in agreement with findings of other workers [15,16], even in this case, these results are the same for T and P determination and lightly different for I determination and reaching recoveries between 93.5 and 102.1 for all mixtures, showing thus the efficiency for concentrations prediction of the two methods.

3.2.4.2. Food commercial preparation applications. The contents of T, P, and I in commercial samples were calculated by analyzing the recorded spectra with PLS-1 and PCR chemometric approaches. The predicted concentrations, expressed as mass:volume ratio (mg of dye:l of commercial products) in the two first applications and as mass:mass ratio (mg of dye:kg of commercial product) for the third one are summarized in Table 4, where there are also shown the contents supplied by the manufacturer enterprise.

In this table, we can see the results obtained by PLS-1 and PCR methods are very similar between them and they are also very nearly to provided values by the manufacturer (nominal contents), reaching relative errors lower than 10% for the cases where these amounts are known, except for I determination in the third product, in which, because of the very small levels of this dye (lower than detection limit), and of containing a very unfavorable ratio of T:P:I (see Table 4), this determination could not be successfully realized.

3.3. Repeatability and reproducibility studies

In order to achieve these studies, two series of nine samples of 10.40 mg l^{-1} of T, 4.00 mg l^{-1} of P, and 12.00 mg l^{-1} of I respective and separately were recorded in consecutive days.

The results are shown in Table 5, obtaining satisfactory results for the repeatability at day for each dye in terms of RSD; with regard to reproducibility studies, the comparison of standard deviations between the two sets of data to detect random errors was made with the *F*-test, whereas the comparison of averages concentrations to check determinate errors was made with the Student's test ($n = 18$) and did not show significant differences in any case at a confidence level of 95%. Consequently, successfully results were obtained for the three dyes when the precision of the chemometric approaches was tested.

4. Conclusions

Ultraviolet-visible data usually contain nonspecific data, which can be converted into useful information by multivariate calibration method; in order to achieve this, chemometry has generated much interest in analytical molecular spectroscopy. Clear explanations of the different chemometric approaches and properly designed software use, should provide a bridge between chemometric, mathematicians, and spectroscopic technicians, enabling them to make successful use of these powerful tools.

A comparative study of the use of PLS-1 and PCR methods for the resolution of ternary mixtures of T, P, and I has been accomplished showing that these methods provide, with ade-

quate software support, a clear example of the high resolving power of these techniques. In general terms, there have not been noticeable differences between the two proposed calibration methods neither in cross-validation parameters (PRESS, RMSD...) nor in the external validation of calibration method, obtaining similar results for the three dyes in both synthetic and commercial applications by PLS-1 and PCR methods and also, reaching agreement between chemometric data and nominal contents in commercial preparations.

On the other hand, successfully results were obtained when the precision of chemometric approaches was checked at a confidence level of 95% for the three dyes.

According to these studies, we conclude the two multivariate calibration methods are suitable choices to resolve overlapped absorption spectra of mixtures of the dyes T, P, and I with satisfactory results and an easy treatment for the preparation of commercial samples.

Acknowledgements

The authors thank to the DGICYT of the Ministerio de Educación y Ciencia (Spain) for supporting this study (Project PB 94-0743).

References

[1] A. Branen, P. Davidson, S. Salminen, Food additives, Marcel Dekker, New York, 1989.
[2] R. Combes, R. Haveland-Smith, Mutat. Res. 98 (1982) 101.
[3] M. Puttemans, L. Dryon, D. Massart, J. Assoc. Anal. Chem. 65 (1982) 737.
[4] M. Puttemans, L. Dryon, D. Massart, J. Assoc. Anal. Chem. 66 (1983) 1039.
[5] J.J. Berzas Nevado, J. Rodríguez Flores, M.J. Villaseñor Llerena, Talanta 44 (1997) 467.
[6] J.J. Berzas Nevado, J. Rodríguez Flores, G. Castañeda Peñalvo, Anal. Chim. Acta 340 (1997) 257.
[7] J.J Berzas Nevado, C. Guiberteau Cabanillas, A. Contento Salcedo, Analusis 22 (1994) 5.
[8] D. Haaland, E. Thomas, Anal. Chem. 60 (1988) 1193.
[9] D. Haaland, E. Thomas, Anal. Chem. 62 (1990) 1091.
[10] H. Wold, Research Papers in Statistics, Wiley, New York, 1966, pp. 411–444.
[11] H. Jores-Kong, H. Wold (Eds.),Systems Under Indirect Observation vol. 2, North-Holland, Amsterdam, 1982, pp. 1–54.
[12] H. Wold, H. Martens, S. Wold, Multivariate Calibration Problems in Chemistry Solved by PLS; A. Ruhe, B. Kagstrom (Eds.), Heidelberg, 1983, pp. 286–293.
[13] Data Leader Software Package, Beckman Instruments, Fullerton CA, 1989.
[14] Lab. Calc. Software Package, Galactic Industries, Salem, NH, 1989.
[15] P. Maclaurin, P. Worsfold, M. Crane, P. Norman, Anal. Proc. 29 (1992) 65.
[16] R. Jones, T. Coomber, J. McCormick, A. Fell, B. Clark, Anal. Proc. 25 (1988) 381.

ELSEVIER

Talanta 48 (1999) 905–912

Talanta

Determination of molybdenum, chromium and aluminium in human urine by electrothermal atomic absorption spectrometry using fast-programme methodology

N. Campillo, P. Viñas, I. López-García, M. Hernández-Córdoba *

Department of Analytical Chemistry, Faculty of Chemistry, University of Murcia, E-30071 Murcia, Spain

Received 7 July 1998; received in revised form 16 September 1998; accepted 16 September 1998

Abstract

Rapid and direct procedures for the determination of molybdenum, chromium and aluminium in human urine samples are developed. Fast-programme methodology is used to simplify the heating cycles. Hydrogen peroxide, nitric acid and Triton X-100 are added to the urine samples which are directly introduced into the furnace. For molybdenum, two successive injection steps are required due to the low level of this element in the samples analyzed. Calibration is carried out using aqueous standards for aluminium and the standard additions method for both molybdenum and chromium. The reliability of the procedures is checked by analyzing two certified reference materials. © 1999 Elsevier Science B.V. All rights reserved.

Keywords: Electrothermal atomization; Molybdenum; Chromium; Aluminium; Urine

1. Introduction

Electrothermal atomic absorption spectrometry (ETAAS) is commonly used for trace and ultra-trace metal analyses in biological fluids because it offers excellent detection limits with minimum sample consumption [1]. Since urine is the principal route by which aluminium, chromium and molybdenum are excreted and taking into account the clinical relevance of these metals, rapid ETAAS procedures for their determination are of interest for the biological monitoring in the general population or in occupationally exposed persons. Most of the absorbed aluminium is eliminated with urine at a rate of less than 14 μg day^{-1} in normal persons. Although absorbed chromium is principally excreted in the urine, a small amount is also eliminated in hair, sweat and bile. Urine levels appear to be a useful indicator of chromium intake when dietary intake is >40 μg day^{-1} although levels remain almost constant when the intake is <40 μg day^{-1}. Molybdenum is readily and rapidly absorbed from most diets, with urine again being the principal excretion route. The average amount of Mo excreted by humans is about 50–70 μg per day [1]. These levels can be determined by means of ETAAS and

* Corresponding author. Tel.: +34-968-307100; fax: +34-968-364148; e-mail: hcordoba@fcu.um.es.

PII S0039-9140(98)00300-2

a number of procedures have been proposed [2–20].

When dealing with clinical samples, a problem can appear due to high background levels. This problem is less severe for the case of urine samples than for other physiological fluids, the appropriate dilution of the sample before its injection into the electrothermal atomizer being a simple solution, although at the expense of a decrease in sensitivity. The background can also be reduced by including an air-ashing step in the heating cycle [21], but this way has the disadvantage of decreasing the useful lifetime of the expensive pyrolytic material. Recently, it has been demonstrated that the same purpose can be served by incorporating hydrogen peroxide and nitric acid in the samples, with the additional advantage that no deterioration of the graphite atomizers is involved [22–24]. The combination of these chemicals has proved so effective that the conventional calcination stage can also be avoided and fast-programme methodology can be used [25].

In this study, procedures for the direct determination of molybdenum, chromium and aluminium in human urine with no previous treatment of the sample are discussed. The urine samples are diluted in a medium containing hydrogen peroxide, nitric acid and Triton X-100 and then directly introduced into the electrothermal atomizer. Our data indicate that although a Zeeman-effect background corrector is highly recommended for trace determinations in clinical samples [1], the widely available deuterium-based corrector is sufficient for the applications here reported.

2. Experimental

2.1. Instrumentation

A Perkin-Elmer Model 1100B atomic absorption spectrometer equipped with deuterium-arc background correction and a HGA-400 (Perkin-Elmer) graphite furnace atomizer were used. Pyrolytic graphite coated tubes (part number B013-5653) and pyrolytic graphite platforms (part number B012-1092) inserted into pyrolytic graphite coated tubes were obtained from Perkin-Elmer. Wall atomization was used for molybdenum and chromium, while aluminium was atomized using platform. Measurements were performed, using a bandwidth of 0.7 nm, at 313.3, 309.3 and 357.9 nm using hollow cathode lamps operated at 12, 10 and 15 mA for molybdenum, aluminium and chromium, respectively. Argon was used as the inert gas, the flow rate being 300 ml min^{-1} during all the stages except atomization, when the flow was stopped.

For comparison purposes, some measurements were made with an ATI-Unicam (Unicam Atomic Absorption, Cambridge, UK) 939QZ spectrometer equipped with a GF90 graphite furnace and a FS90 Plus autosampler. Zeeman correction was used for these comparison experiments. Pyrolytic tubes were obtained from Unicam.

2.2. Reagents

The ubiquitous abundance of aluminium made it necessary to intensify precautions to avoid the contamination. A clean-room was not used but, if available, is recommended. All the chemicals used were of the highest purity available and all the glassware and plasticware was nitric acid-washed and rinsed with ultrapure water. High quality water, obtained using a Milli-Q system (Millipore), was used exclusively. Aluminium and chromium standard solutions (1000 μg ml^{-1}) were obtained from Panreac (Spain) and the molybdenum standard solution (1000 μg ml^{-1}) from Sigma; these solutions were diluted as necessary to obtain working standards. High quality concentrated (65% w/v) nitric acid (Merck), 30% w/v hydrogen peroxide (Fluka) and Triton X-100 (Merck) were also used. Urine samples (24 h specimens) from volunteers were directly collected into acid-washed plastic containers and analyzed as soon as possible after collection.

2.3. Reference materials

Freeze-dried urine reference samples, SRM 2670 (normal level and elevated level) were supplied by NIST (USA). Samples were supplied in freeze-dried form and were reconstituted by adding 20 ml of distilled water to each bottle.

2.4. Procedures

The samples were prepared by adding 0.5 ml of concentrated hydrogen peroxide, 100 μl of concentrated nitric acid and 100 μl of a 10% (w/v) Triton X-100 solution to a 10 ml urine aliquot. In this way, the final concentrations were 1.5, 0.65 and 0.1% w/v for hydrogen peroxide, nitric acid and Triton X-100, respectively. Aliquots of 25 μl of urine for chromium detection and 20 μl for aluminium were injected into the furnace. For molybdenum, it was necessary to inject 50 μl of urine, which was done by injecting two succesive aliquots of 25 μl separated by a drying step. The heating programmes given in Table 1 (where the quoted temperatures are values set on the HGA-400 power supply) were run and the background-corrected peak areas due to the analytes obtained. Calibration for aluminium was performed with aqueous standards and for both molybdenum and chromium by using the standard additions method.

Table 1
Heating furnace programmes

Step	Parameter	Mo[b]	Cr	Al
Dry	Temperature (°C)	120	120	250
	Ramp (s)	1	1	1
	Hold (s)	45	45	45
Atomization[a]	Temperature (°C)	2650	2500	2500
	Ramp (s)	0	0	0
	Hold (s)	5	2	4
Cleaning	Temperature (°C)	2650	2650	2650
	Ramp (s)	1	1	1
	Hold (s)	3	3	3

[a] The flow of argon was stopped during the atomization step.

[b] Molybdenum required a double injection and, consequently, two successive drying steps separated by a cooling step at 20°C hold for 35 s.

3. Results and discussion

3.1. Optimization of the heating furnace programmes

Preliminary experiments for molybdenum determination revealed no significant differences in the atomization profiles when nitric acid plus hydrogen peroxide were added to the samples and when a conventional or a fast-heating programme was used, the background levels being similar. All subsequent experiments for this analyte were carried out using fast-programme methodology and wall atomization. The optimal drying temperature and the holding time to be used in the modified drying step were studied so that the samples were completely dry before atomization and to avoid sputtering. The optimal values were 120°C with a 45 s holding time. It was verified that the sensitivity of molybdenum was insufficient to permit the analysis of urine from healthy subjects and, consequently, two successive injections were carried out. An aliquot of 25 μl was injected and submitted to the drying step and the heating programme was stopped. Then, a second aliquot was injected and the total programme was run. Both drying stages were separated by a cooling step at 20°C with a ramp of 1 s and a holding time of 35 s. The atomization stage was carried out at the maximum temperature permitted by the spectrometer (2650°C). A cleaning stage was also necessary to remove molybdenum from the tube, thus avoiding memory effects or cross-contamination problems due to the reaction of the analyte with the pyrolytic coating of the graphite atomizer to form thermally stable molybdenum carbides [20,24].

For chromium, platform atomization resulted in delayed peaks with pronounced tails and so fast-programme methodology using wall atomization was again selected. The optimal atomization temperature was studied in the 1900–2600°C range. Very broad peaks appeared below 2000°C and the atomization curves did not level off. Good results were obtained at 2500°C, which was selected as optimal because higher temperatures decreased the life of the coated tubes after successive firings.

For aluminium, both wall and platform atomization modes using both conventional and fast-heating methodologies were tried. The experiments using wall atomization produced very narrow profiles leading to an excessively restricted linear response range. In addition, the peak appeared before 1 s, when isothermal conditions are still far from being reached. Taking this into account, and the fact that the use of platform atomization [5] allows spectral and matrix interferences to be decreased or minimized, this atomization mode was finally selected. The temperature and holding time to be used in fast-programme methodology were studied, 250°C and 45 s, respectively, being found as optimal. The atomization temperature was varied between 2400 and 2600°C. At 2400°C the peak was not totally resolved after 5 s, while at 2600°C, the height of the peak was twice its area. A temperature of 2500°C was selected because both area and height values were similar and the maximum of the peak appeared at 2.5 s.

3.2. Optimization of the chemical agents concentrations

The reproducibility attained in the sampling of urine was not good because small drops remained in the tip of the micropipette. A marked improvement in sampling reproducibility was found when Triton X-100 was added to the samples. A 0.1% w/v concentration was selected because this did not increase the background values.

Fig. 1A shows the profile obtained for molybdenum atomization in an urine sample. The background was not very high but appeared in the form of two peaks at the start of atomization. It also distorted the atomic peak by giving a false prepeak. When both hydrogen peroxide and nitric acid were added to the urine sample, the first background peak was considerable decreased and no distortion of the atomic signal was observed (Fig. 1B). Similar results were obtained for aluminium, for which the profile showed negative area at the start of atomization in the absence of the oxidants (Fig. 1C); this effect disappeared in the presence of both hydrogen peroxide and nitric acid (Fig. 1D). The optimal concentrations of both chemicals were studied in order to ascertain the minimum amount which could be used in order to avoid unnecessary dilution of the urine samples and a subsequent loss of sensitivity. Fig. 2 shows the variation of both the analytical and the background signals for the atomization of aluminium when different oxidant (graph A) and nitric acid (graph B) concentrations were assayed. Concentrations of 1.5% w/v hydrogen peroxide and 0.65% w/v nitric acid were chosen because the background was minimal. Higher oxidant and acid concentrations led to higher blank values, the samples being unnecessarily diluted. Similar results were observed for both molybdenum and chromium. When using the recommended concen-

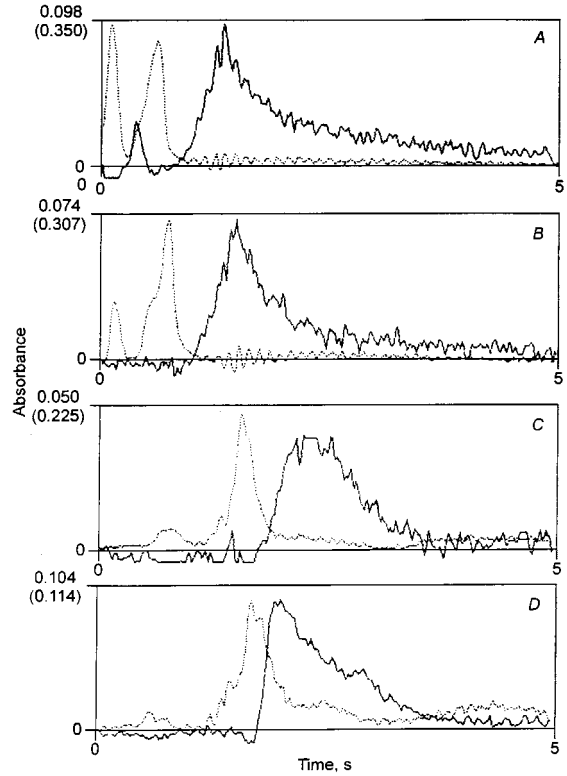

Fig. 1. Comparison of the profiles obtained for the atomization of molybdenum in the absence of both hydrogen peroxide and nitric acid (A) and in the presence of both chemicals (B). Idem for atomization of aluminium without (C) and with the oxidants (D). For all cases, the urine sample was prepared in the presence of 0.1% w/v Triton X-100, 1.5% w/v hydrogen peroxide and 0.65% w/v nitric acid. The broken lines show the background signals.

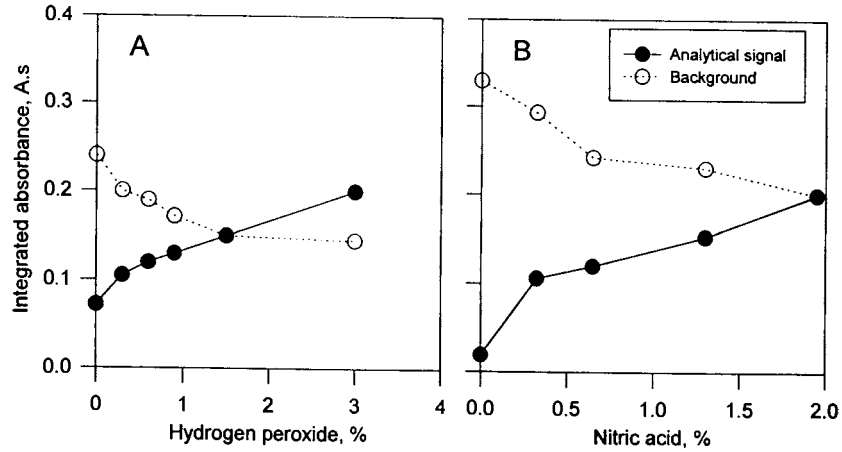

Fig. 2. Effect of hydrogen peroxide (A) and nitric acid (B) concentrations on both the analytical and the background signals for the atomization of aluminium from an urine sample. (A) Sample containing 0.65% w/v nitric acid and 0.1% w/v Triton X-100. (B) Sample containing 0.1% Triton X-100 and 1.5% w/v hydrogen peroxide.

trations, no apparent damage to the atomizer was observed and neither did the weight of the tube suffer appreciable changes even after fifty successive firings in the conditions used for molybdenum determination.

3.3. Study of matrix effect

To establish possible interferences due to the urine matrix, the slopes of aqueous calibration and standard additions calibration graphs were compared. Fig. 3 shows the results obtained for molybdenum in different experimental conditions. As can be seen, the slopes for aqueous standards and standard additions were quite different. In the absence of hydrogen peroxide and nitric acid, the slopes also differed. The addition of barium fluoride (0.003% w/v) or sodium fluoride (0.004% w/v) did not eliminate the matrix effect. Other possible modifiers such as palladium [20] (300 μg ml^{-1}) or palladium (300 μg ml^{-1}) plus magnesium (0.05%) [20], increased the slopes of the standard additions graphs although a difference of about 30% with respect to aqueous standards still remained. This mixture (Pd + Mg) was assayed with both the fast programme and a conventional programme involving a drying step at 120°C, charring at 600°C, calcination at 1400°C, atomization and cleaning, and no differences were observed. Calibration with aqueous standards in the presence of 2.5% w/v urea (concentration usually added to synthetic urine samples [26]), led to a slope value similar to that found in the absence of urea. This study was repeated using the Zeeman corrector and identical results were obtained. Because the matrix effect could not be

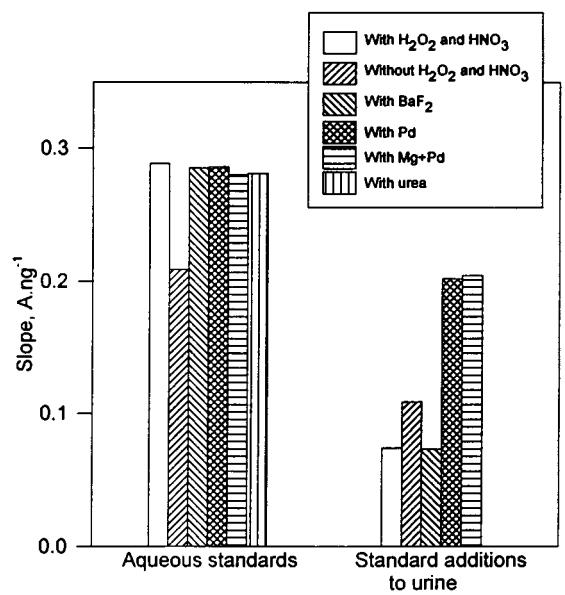

Fig. 3. Slopes of aqueous calibration and standard additions calibration graphs for atomization of molybdenum.

removed, the standard additions method was used for molybdenum determination.

A similar study was performed for chromium determination. Previous reports have produced contradictory results concerning the usefulness of the conventional deuterium arc background correction system [8,9] the need to use a Zeeman-based device [3,7,10], the use of a quartz halogen light source for background correction [2,4] and even the determination of chromium without background correction [19]. Consequently, a comparative study was carried out. Using the deuterium system, the slope was 0.5167 A ng^{-1} for aqueous calibration and 0.2665 A ng^{-1} for standard additions to the normal level SRM urine; the addition of different chemicals did not remove this discrepancy. The introduction of the Zeeman corrector led to slopes of 0.7065 and 0.3739 A ng^{-1} being obtained for aqueous calibration and standard additions, respectively. The high level present in the SRM urine required a 20-fold dilution and, after this, similar slopes were found. However, in the case of urine from healthy subjects, this high level of dilution could not be performed due to the low concentrations of chromium it contained. The results indicated that the use of Zeeman correction did not affect the difference in the slopes. Halls [9] reported elimination of the matrix effect for chromium in a $1+1$ diluted urine sample by the addition of Triton X-100; thus, several amounts in the 0.01–0.5% w/v range were assayed. However, for the no-diluted urine samples, differences in the slope values, even at the higher Triton X-100 concentration, remained. Consequently, the standard additions method is recommended for this determination. Our results agree with other studies on urinary chromium determination, which also recommend the standard additions method to minimize errors due to both matrix interference and graphite tube deterioration [4]. The atomization of aluminium, however, gave similar slopes for aqueous and standard additions calibration (0.2442 ± 0.0146 and 0.2338 ± 0.0126 A ng^{-1}, respectively) and calibration using aqueous standards could be performed.

Table 2
Results for the analysis of urine samples

Urine	Content[a], μg l^{-1}		
	Mo	Al	Cr
1	12 ± 1	14 ± 0.3	20 ± 1
2	2.4 ± 0.1	2.3 ± 0.2	0.61 ± 0.05
3	6.5 ± 0.1	11 ± 0.6	0.87 ± 0.04
4	14 ± 1	ND[b]	7.0 ± 0.4

[a] Mean $\pm$ SD ($n = 9$).
[b] Non detected.

3.4. Repeatability and calibration graphs

For molybdenum, the repeatability obtained for ten successive simple and double injections was compared and similar RSD values were found. The RSD values were $\pm 5.9\%$ for the urine containing 6.5 ng ml^{-1} of Mo, $\pm 4.37\%$ for an urine sample containing 0.87 ng ml^{-1} of Cr and $\pm 7.15\%$ for the urine with 2.3 ng ml^{-1} of Al. The detection limits calculated for ten successive injections of the blank and using the 3σ criterium were 40.5 pg (0.81 ng ml^{-1}) for Mo, 10.5 pg (0.42 ng ml^{-1}) for Cr and 23.4 pg (1.1 ng ml^{-1}) for Al. Calibration graphs were linear up to 40, 25 and 70 ng ml^{-1} for molybdenum, chromium and aluminium, respectively.

3.5. Results and recovery study

The proposed methods were applied to determining the metals in urine samples of several healthy subjects. Table 2 shows the results obtained. The reliability of the methods was checked by using two certified reference freeze-dried urine samples. As can be seen, a good agreement between the reference values and the results was obtained (Table 3). The molybdenum contents were not certified and a recovery study was carried out to validate the method. Table 4 shows that for four different urine matrices spiked with 10 and 20 ng ml^{-1} of molybdenum, a good recovery was obtained. The average recovery was 98.9% (range 95–103%).

There has been growing interest in recent years in the determination of aluminium and numerous

Table 3
Results for the standard reference materials[a]

Sample	Content, mg l^{-1} Al		Cr	
	Found	Certified	Found	Certified
SRM 2670 Normal level	0.18 ± 0.01	(0.18)	0.014 ± 0.002	(0.013)
SRM 2670 Elevated level	0.15 ± 0.01	(0.18)	0.086 ± 0.005	0.085 ± 0.006

[a] Values into brackets are not certified, they are given for information.

studies on interferences have been published. Consequently, the influence of possible interferent species on variations in both the analytical signal and the background for the blank, aqueous aluminium and urine sample was studied. The slopes obtained for aqueous standards and standard additions graphs were also compared. The species assayed were chloride, phosphate, calcium, magnesium, iron, glucose, uric acid and urea, species which are commonly present in urine samples. Chloride (2000 μg ml^{-1}) introduced a background signal at the same position as the urine background and its presence produced a broadening of the peak. Phosphate (2000 μg ml^{-1}) did not affect the signal of aluminium in the urine, but increased the slope for aqueous standards. The presence of calcium (1250 μg ml^{-1}) produced an increase in the slopes for both aqueous standards and standard additions graphs. Magnesium did not affect the aluminium signals in the urine in either aqueous solutions, the only effect observed being a delay in the atomization time due to its stabilizing effect. No interference was found for the other species studied.

Table 4
Recovery study of added molybdenum (μg l^{-1})

Matrix	Mo in sample	Mo added	Mo found	Recovery (%)
Urine 1	11.8	10	21.7	99.5
		20	30.3	95.3
Urine 2	2.4	10	12.5	100.6
		20	22.1	98.5
Urine 3	6.5	10	16.3	98.7
		20	25.9	97.7
Urine 4	14.1	10	24.8	103.0
		20	33.5	98.2

In addition, a pharmacokinetic study on the recovery of aluminium from urine after the oral administration to a volunteer of a tablet containing aluminium (Almax, Almiral Lab.) was carried out. Serial samples of urine were collected from 0 to 6 h after administration of the drug and these were analyzed using the proposed method. Fig. 4 shows a plot of the urinary excretion of the metal.

4. Conclusion

The addition of both hydrogen peroxide and nitric acid to the urine samples reduces background signal. No sample pre-treatment is necessary, and so the risk of contamination is also reduced. Molybdenum, aluminium and chromium can be determined using fast-programme method-

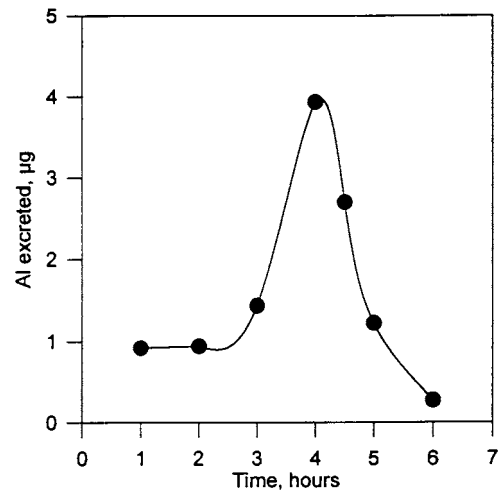

Fig. 4. Plot of the excretion of aluminium in urine after an oral dose.

ology and Zeeman-based correction is not mandatory. As urine samples are not previously diluted, there is no unnecessary loss in sensitivity. Since they are fast and reliable, the procedures here reported may be of interest for the routine determination of urinary molybdenum, aluminium and chromium in the general population and in those exposed to high levels of contamination.

Acknowledgements

The authors are grateful to the Spanish DGICYT (Project PB96-1100) and Comunidad Autónoma de la Región de Murcia (Fundación Séneca, Project PB/7FS/97) for financial support.

References

[1] H.G. Seiler, A. Sigel, H. Sigel, Handbook on Metals in Clinical and Analytical Chemistry, Marcel Dekker, New York, 1994.
[2] F.J. Kayne, G. Komar, H. Laboda, R.E. Vanderlinde, Clin. Chem. 24 (1978) 2151.
[3] B.E. Guthrie, W.R. Wolf, C. Veillon, Anal. Chem. 50 (1978) 1900.
[4] C. Veillon, K.Y. Patterson, N.A. Bryden, Anal. Chim. Acta 136 (1982) 233.
[5] F.Y. Leung, A.R. Henderson, Clin. Chem. 28 (1982) 2139.
[6] J. Bauslaugh, B. Radziuk, K. Saeed, Y. Thomassen, Anal. Chim. Acta 165 (1984) 149.
[7] J.N. Egila, D. Littlejohn, J.M. Ottaway, S. Xiao-quan, Anal. Proc. 23 (1986) 426.
[8] D.J. Halls, G.S. Fell, J. Anal. Atom. Spectrom. 1 (1986) 135.
[9] D.J. Halls, G.S. Fell, J. Anal. Atom. Spectrom. 3 (1988) 105.
[10] P. Dube, Analyst 113 (1988) 917.
[11] M.B. Knowles, J. Anal. Atom. Spectrom. 4 (1989) 257.
[12] W. Slavin, D.C. Manning, G.R. Carnrick, Spectrochim. Acta 44B (1989) 1237.
[13] M.J. Lagarda, V. Alonso de Armino, R. Farre, J. Pharm. Biomed. Anal. 9 (1991) 191.
[14] D.C. Paschal, G.G. Bailey, At. Spectrosc. 12 (1991) 151.
[15] O.O. Ajayi, T.M. Ansari, D. Littlejohn, J. Anal. Atom. Spectrom. 7 (1992) 689.
[16] E. Bulska, K. Wróbel, A. Hulanicki, Fresenius J. Anal. Chem. 342 (1992) 740.
[17] J.M. Marchante Gayón, J. Pérez Pajarón, A. Sanz-Medel, J. Anal. Atom. Spectrom. 7 (1992) 743.
[18] R. Rubio, A. Sahuquillo, G. Rauret, L. García Beltrán, Ph. Quevauviller, Anal. Chim. Acta 283 (1993) 207.
[19] V.A. Granadillo, Ll. Parra de Machado, R.A. Romero, Anal. Chem. 66 (1994) 3624.
[20] C. Pita Calvo, P. Bermejo Barrera, A. Bermejo Barrera, Anal. Chim. Acta 310 (1995) 189.
[21] S.C. Stephen, D. Littlejohn, J.M. Ottaway, Analyst 110 (1985) 1147.
[22] P. Viñas, N. Campillo, I. López-García, M. Hernández-Córdoba, Talanta 42 (1995) 527.
[23] I. López-García, P. Viñas, N. Campillo, M. Hernández-Córdoba, J. Agric. Food Chem. 44 (1996) 836.
[24] P. Viñas, N. Campillo, I. López-García, M. Hernández-Córdoba, Anal. Chim. Acta 356 (1997) 267.
[25] D.J. Halls, Analyst 109 (1984) 1081.
[26] M. Márquez, M. Silva, M.D. Pérez-Bendito, Analyst 113 (1988) 1373.

ELSEVIER

Talanta 48 (1999) 913–921

Talanta

Equilibrium studies of the binary and ternary complexes involving tetracycline and amino acid or DNA constituents

W.M. Hosny, S.M. El-Medani, M.M. Shoukry *

Department of Chemistry, Faculty of Science, Cairo University, Giza, Egypt

Received 24 September 1997; received in revised form 16 September 1998; accepted 16 September 1998

Abstract

The acid–base equilibria of tetracycline and its copper(II) complex formation equilibria are investigated in dioxane–water mixtures. The ternary complexes of copper(II) with tetracycline as primary ligand and amino acid or DNA constituent as secondary ligand are studied in 50% dioxane–water solution. The formation constants of the ternary and binary complexes with amino acids or DNA constituents are determined. The concentration distribution of the various complex species are evaluated. Probable mode of chelation with tetracycline and DNA constituents is discussed. © 1999 Elsevier Science B.V. All rights reserved.

Keywords: Tetracycline complexes; Amino acid complexes; DNA complexes; Stability constants

1. Introduction

Most pharmaceuticals contain electron-donor groups likely to bind metal ions occurring in vivo [1]. Among these, tetracycline antibiotics (TC) have long been known to behave as relatively efficient chelating agents [2]. Essential trace metal ions like zinc and copper are present in too low concentration in blood plasma to significantly influence the bioavailability of these drugs [3,4]. Following the recent evidence of the important roles of calcium and magnesium in the transport of these drugs in blood plasma, it is now suggested that copper can act as a cofactor of their antibiotic activity. The structural flexibility of copper binary complexes within the three distinct donor sites of bioactive tetracyclines is expected to favor mixed-ligand coordination with bacterial nucleic acids, then, through the formation of such ternary complexes, copper may induce the attack of free radicals known to damage these nucleic acids [5,6].

It is now well established that the 'effective' or 'equivalent solution' dielectric constants in proteins [7,8] or active site cavities of enzymes [9] are low compared to that in bulk water. Estimates of the dielectric constants in such locations range from ~ 30 to 70 [7–9]. Hence, by employing

* Corresponding author.

PII S0039-9140(98)00297-5

aqueous solutions that contain ~10–50% 1,4-dioxane [10], one may expect to simulate to some degree the situation in active site cavities [11] and extrapolate the data to physiological conditions. With this in mind and in conjunction to our research project on metal complexes of antibiotics [12–14], the present investigation deals with the solution equilibria of the binary and ternary copper(II) complexes involving tetracycline, amino acids and DNA constituents. The structural formulae of tetracycline and DNA constituents used are given in Fig. 1.

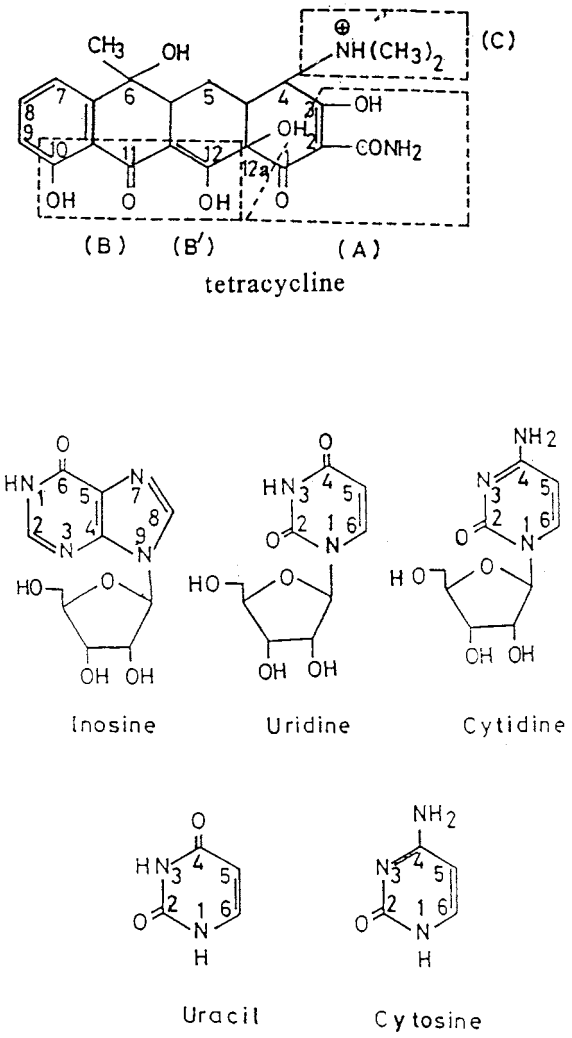

Fig. 1. Structural formulae of the investigated ligands.

2. Experimental

Materials: Tetracycline HCl (TC) was kindly supplied by El-Nile Chem., Egypt. Chemical analysis for acid contents, shows that it is sufficiently reliable to be used without further purification. On account of the well-documented instability of tetracycline in aqueous media [15], fresh solutions were systematically prepared every day. The amino acids and DNA constituents used were provided by Sigma (St. Louis, MO). Cytosine and cytidine solutions were prepared in aqueous equimolar nitric acid solution. Copper nitrate was provided by BDH. The Cu-content of solutions was estimated complexometrically [16].

2.1. Procedure and measuring techniques:

The potentiometric measurements were performed by a Metrohm 686 Titroprocessor equipped with a 665 Dosimat (Switzerland). The electrode couple is calibrated in standard buffer solutions prepared according to NBS specifications [17], and the pH meter in dioxane–water solutions were used in the calculation of equilibrium constants, i.e. these constants are so-called practical, 'mixed' or Bronsted constants [18].

The protonation constants of the ligands were determined by titrating 40 ml of ligand solution (2.5×10^{-3} M) and $NaNO_3$ (0.1 M). The conditions of measurements for the determination of stability constants of the binary complexes were the same as for the protonation constants, but a part of $NaNO_3$ was replaced by $Cu(NO_3)_2$ with the ratio $[Cu^{2+}]:[L] = 1:1$ for tetracycline and 1:2 for amino acids and DNA complexes. The conditions of measurements for the titration of the ternary complexes were the same as for the binary ones, but the solutions contained equivalent amounts of tetracycline, Cu^{2+} and the other ligand (D). The stability constants of $K^{Cu(TC)}_{Cu(TC)D}$ for the ternary complexes were determined using the data obtained within the pH range corresponding to the complete formation of the Cu–TC complex. Hence, in the calculation only complex formation between [Cu–TC] and ligand (D) is considered and each of these systems could be

Table 1
Effect of dioxane on the dissociation constants of tetracycline and formation constants of copper–tetracycline complex

System	%Dioxane V/V	pK_1^{Ha}	pK_2^H	pK_3^H	pH-range	S^b
Tetracycline	0.00	3.36(0.04)	7.77(0,02)	9.27(0.02)	3.15–10.18	2.3×10^{-7}
	25.0	3.84(0.02)	7.94(0.01)	9.39(0.01)	3.38–10.41	5.6×10^{-8}
	37.5	4.10(0.02)	8.00(0.01)	9.41(0.01)	3.52–10.53	2.7×10^{-8}
	50.0	4.32(0.02)	8.02(0.01)	9.36(0.01)	3.63–10.62	5.5×10^{-8}
	62.5	4.52(0.02)	8.00(0.01)	9.32(0.01)	3.68–10:15	3.7×10^{-8}
		$\log\beta_{CuL}$	$\log\beta_{CuHL}$			
Cu–Tetracycline	0.00	12.31(0.03)	18.19(0 01)	–	2.65–5.68	2.4×10^{-7}
	25.0	12.38(0.17)	18.01(0.17)	–	2.65–4.51	8.7×10^{-8}
	37.5	12.48(0.07)	19.09(0.01)	–	2.70–5.86	2.4×10^{-7}
	50.0	12.89(0.19)	19.50(0 01)	–	2.65–5.21	2.1×10^{-7}
	62.5	14.52(0.19)	20.06(0.02)	–	2.57–4.71	3.0×10^{-7}

[a] Standard deviations are given in parentheses.
[b] Sum of squares of residuals.

treated as a binary one. All pH-metric titrations were carried out at 25°C in a purified N_2 atmosphere. The calculations were carried out with the aid of the MINIQUAD-75 computer program [19] on a IBM-486 computer. The model selected was that which gave the best statistical fit to, and proved chemically consistent with the titration data, without showing any systematic bias in residuals, as described in [19].

3. Results and discussion

3.1. Protonation equilibria

A maximum number of three protons can be released from tetracycline in the fully protonated form (H_3L^+) on titration with strong base in the pH range 2–11. The titration data indicates the presence solely of simple HL^-, H_2L and H_3L^+ complexes. The acid dissociation constants of the tetracycline were given in Table 1. The protonation sites of tetracycline are shown in Fig. 1, as the amide system (A), the phenolic β-diketone moieties (B) and (B′) and the dimethyl–ammonium cation (C). The first dissociation constant pK_1^H, is generally attributed to site (A). The second dissociation constant pK_2^H is due to the combined (B) and (B′) system. The third dissociation constant pK_3^H is assigned to site (C). The order of the protonation sites attributed to the stepwise protonation steps determined in aqueous medium is subjected to change in less polar media.

3.2. Effect of solvent

The protonation constants of tetracycline and the formation constants of copper(II) complex in dioxane–water mixtures of various compositions are given in Table 1. The variation of pK_1^H as a function of solvent composition is shown in Fig. 2. Careful examination of the results reveals the following features:

(1) The first dissociation constant (pK_1^H) value increases linearly with increasing concentration of the organic solvent. This results from the ability of a solvent of low dielectric constant, as dioxane, to increase the electrostatic forces between the ions and to facilitate the formation of molecular species [12]. The second and third dissociation constants values expressed as pK_2^H and pK_3^H increase with increasing dioxane content up to 50%, as explained previously, then tend to become constant. This behaviour may be interpreted by non-electrostatic forces which could include hydrogen bonding and solvent–solute interaction. This finding is in agreement with the conclusion that the non-electrostatic phenomena become increasingly important in solutions containing greater than 50% organic solvent [20].

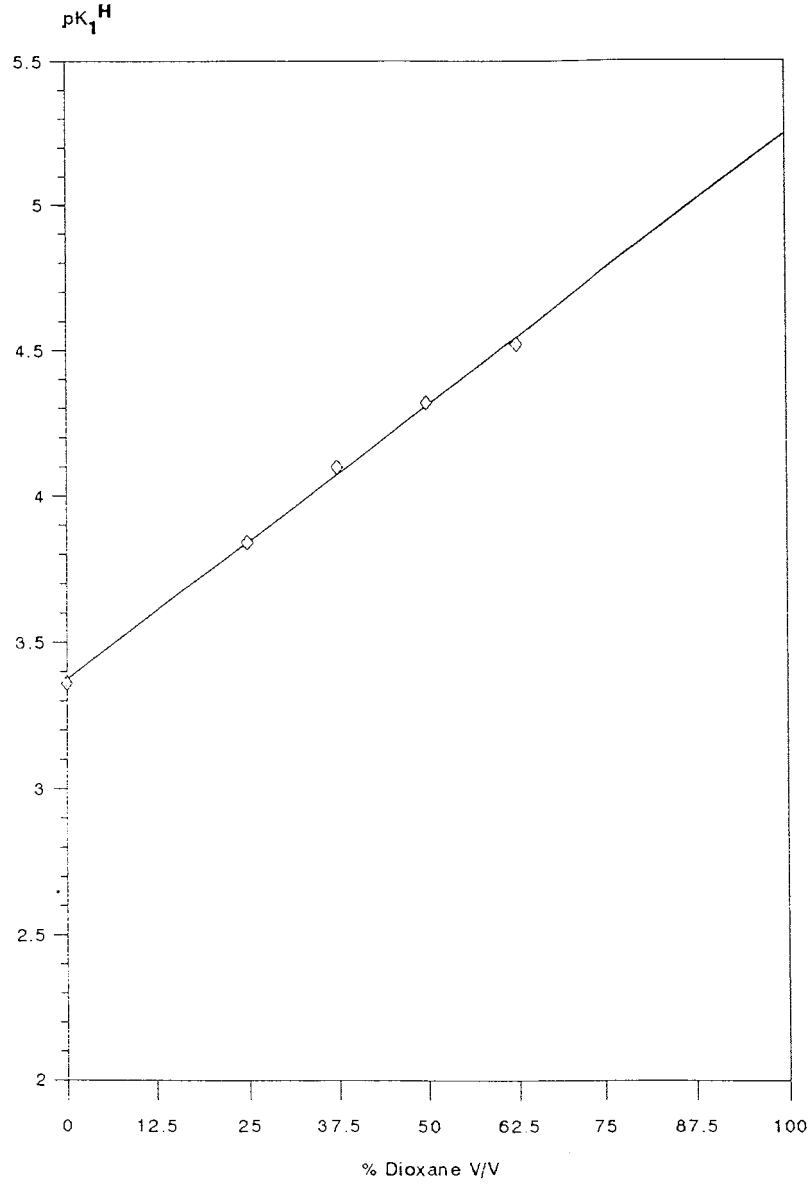

Fig. 2. Variation of pK_1^H of tetracycline as a function of solvent composition.

(2) The formation constant of copper(II)–tetracycline complex shows a more or less increase with increasing the organic solvent content. This behaviour can be explained by the variation of the protonation ability of the amide group (site A), which is one of the binding site in the complex formation, as the organic solvent content increases.

3.3. Binary complexes

The copper(II)-complexes of amino acids and DNA constituents have been extensively investigated in aqueous media [21]. The acid–base and binary complex formation equilibria involving the amino acid and DNA constituents are investigated in a medium, 50% dioxane–water solutions,

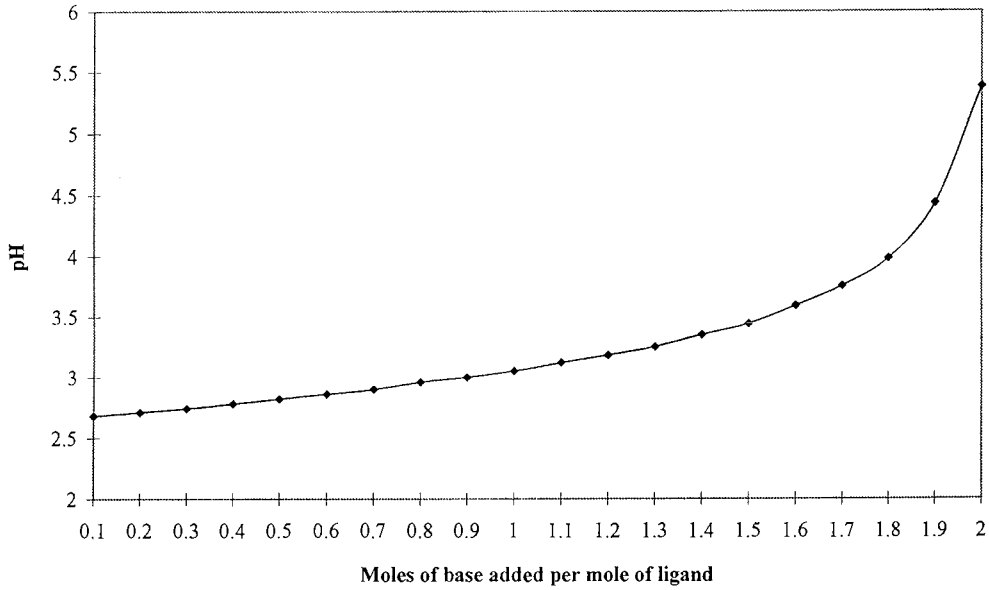

Fig. 3. Potentiometric titration curve of Cu–Tetracycline system in 50% dioxane–water mixture. The solid curve through the experimental points is the theoretical curve.

considered as a model of the biological system. Tetracycline is capable of assuming several conformations in solution [22,23] as well as in the solid state [24,25]. The relative flexibility of this molecule largely conditions its capacity to accommodate diverse metal bonding modes. The composition and structure of tetracycline complexes are depending on the nature of metal ion and solvent. Copper(II)–tetracycline complexes were previously investigated in aqueous media [2]. Under this condition $CuLH_2$ and CuLH complexes are formed. CuL complex was not detected, possibly due to its insolubility in water. The accepted model for Cu–tetracycline in 50% dioxane involving the formation of CuL and CuLH species only is tested by comparing the theoretical titration curve with the experimental data points, Fig. 3. The good fit is indicative of the validity of the complex formation model. The noncharacterization of $CuLH_2$ species may explained on the premise that $CuLH_2$ is formed only in strongly acidic medium which is not the case in the present investigation. The complex equilibria leading to the formation of the species CuL, CuLH and Cu(HL) were described by Eqs. (1)–(3).

$$Cu + L \rightleftharpoons CuL; \quad \beta_{CuL} \frac{[CuL]}{[Cu][L]} \tag{1}$$

$$Cu + L + H \rightleftharpoons CuLH; \quad \beta_{CuLH} \frac{[CuLH]}{[Cu][H][L]} \tag{2}$$

$$Cu + HL \rightleftharpoons Cu(HL); \quad \beta_{Cu(LH)} \frac{[Cu(HL)]}{[Cu][HL]} \tag{3}$$

(charges are omitted for simplicity)

Examination of the species CuLH and CuL stability constants (Table 2), may provide preliminary information on the bonding modes of copper. Supposing that ligand–proton interactions remain unaffected in the presence of copper, stability of the metal–ligand bond formed in the protonated complex species Cu(HL) can be estimated by subtracting step protonation increment from parent overall formation constant. According to this, the formation constant $\beta_{Cu(HL)}$, obtained in 50% dioxane–water solutions, is calculated using Eq. (4) [2].

$$\log \beta_{Cu(HL)} = \log \beta_{CuHL} - \log \beta_{HL} \tag{4}$$

The values of $\log \beta_{CuHL}$ (Table 2) and $\log \beta_{HL}$(expressed as pK_3^H in Table 1) are 19.50 and 9.36, respectively. The calculated $\log \beta_{Cu(HL)}$ value, i.e. 10.14 is much smaller than $\log \beta_{CuL}$

Table 2
Formation constants of binary and ternary complexes involving Cu(II), tetracycline and amino acids or DNA in 50% dioxane.

Binary complexes						
System	l	p	q[a]	log β[b]	S[c]	$\Delta \log K$
Glycine	0	1	1	9.82(0.00)	4.2×10^{-8}	–
	1	1	0	8.64(0.03)	2.1×10^{-7}	–
	1	2	0	16.60(0.03)	–	–
Methionine	0	1	1	9 39(0.01)	9.9×10^{-8}	–
	1	1	0	8.32(0.04)	3.5×10^{-7}	–
	1	2	0	16.37(0.02)	–	–
Valine	0	1	1	9.66(0.01)	6.5×10^{-7}	–
	1	1	0	8.30(0.05)	2.2×10^{-7}	–
	1	2	0	16.59(0.02)	–	–
Serine	0	1	1	9.34(0.00)	4.3×10^{-8}	–
	1	1	0	8.40(0.03)	5.3×10^{-7}	–
	1	2	0	16.30(0.02)	–	–
Alanine	0	1	1	9.78(0.01)	1.6×10^{-7}	–
	1	1	0	8.52{0.03)	3.1×10^{-7}	–
	1	2	0	16.36(0.03)	–	–
Uridine	0	1	1	10.33(0.01)	8.7×10^{-8}	–
	1	1	0	7.02(0.09)	3.7×10^{-7}	–
Uracil	0	1	1	10.18(0.01)	4.3×10^{-8}	–
	1	1	0	6.21(0.04)	4.2×10^{-7}	–
Inosine	0	1	1	9.16(0.01)	9.4×10^{-8}	–
	1	1	0	6.47(0.09)	8.5×10^{-7}	–
	1	2	0	11.74(0.06)	–	–
Cytosine	0	1	1	4.67(0.00)	7.4×10^{-9}	–
	1	1	0	3.35(0.04)	6.7×10^{-7}	
Inosine–5–mono–phosphate	0	1	1	9.78(0.03)	9.7×10^{-7}	–
	1	1	0	Precipitated	–	–
Guanosine–5–mono–phosphate	0	1	1	10.77(0.04)	2.1×10^{-6}	–
	1	1	0	Precipitated	–	–
Ternary complexes						
Cu–TC–glycine	1	1	0	4.13(0.02)	2.9×10^{-7}	−4.51
Cu–TC–methionine	1	1	0	2.86(0.07)	1.6×10^{-6}	−5.46
Cu–TC–valine	1	1	0	3.28(0.08)	3.3×10^{-6}	−5.02
Cu–TC–serine	1	1	0	3.90(0.03)	5.3×10^{-7}	−4.50
Cu–TC–alanine	1	1	0	3 99(0.02)	3.5×10^{-7}	−4.53
Cu–TC–uridine	1	1	0	3.81(0.02)	9.1×10^{-7}	−3.21
Cu–TC–uracil	1	1	0	3.89(0.02)	3.6×10^{-7}	−2.32
Cu–TC–inosine	1	1	0	2.81(0.05)	6.4×10^{-7}	−3.66
Cu–TC–inosine–5–monophosphate	1	1	0	3.14(0.04)	5.6×10^{-7}	–
Cu–TC–guanosine–5–monophosphate	1	1	0	4.20(0.03)	6.3×10^{-7}	–

[a] l, p and q are the stoichiometric coefficients corresponding to the Cu(II)–TC complex, amino acid or DNA units and H^+, respectively,
[b] Standard deviations are given in parentheses.
[c] Sum of squares of residuals.

value, i.e. 12.89 (Table 2). This reveals that important changes take place in the copper coordination mode along the pH range investigated. It is suggested that in CuLH complex, chelation is taking place at O(10)–O(12) system. In the CuL complex, the dianionic form of tetracycline binds to copper(II) through the N(4)–O(12_a) centres. This is in agreement with the data of the cop-

per(II) complex of 6–desoxy–6–demethyltetracycline [2], which has a structure similar to tetracycline. In Table 1, the value of log β_{CuL} is 14.52 in 62.5% dioxane. This value is considerably higher than those for the other solvent mixtures. This may be explained on the premise that the mode of chelation is changed in less polar solvents (62.5% dioxane).

3.4. Ternary complexes

The potentiometric titration curve of the ternary system Cu(II)–tetracycline–glycine, taken as a representative, nearly coincides with the 1:1 Cu(II)–tetracycline curve in the region $0 < a < 3$ (a = the number of moles of base added per mole of ligand) (Fig. 4). In this region, the Cu(II)–tetracycline complex was formed first, presumably due to its high stability compared to that of Cu(II)–amino acid or DNA constituent (D), (Table 2). The formation of ternary complex was ascertained by comparison of the mixed ligand titration curve with the composite curve obtained by graphical addition of the secondary ligand (D) titration data to the Cu(II)–tetracycline titration curve. The mixed ligand curve was found to deviate considerably from the resultant composite curve indicating the formation of a ternary complex. A further evidence for the formation of ternary complex by a stepwise mechanism is confirmed by comparing the theoretical curve, constructed based on the formation of ternary complex by a stepwise mechanism, and the experimental titration data points Fig. 5. The good fit is indicative of the validity of the complex formation model. Thus, formation of ternary complexes can be described by the following equilibria (5,6):

$$Cu + TC \rightleftharpoons Cu–TC \quad (5)$$

$$(Cu–TC) + D \rightleftharpoons (Cu–TC)–D \quad (6)$$

Serine has β-alcoholato group and may participate as an extra binding centre as reported previously [26]. The stability constant of the mixed-ligand complex of serine is in fair agreement with those of other amino acids studied. This indicates that serine binds in mixed-ligand complex formation as substituted glycinate. The lower stability of methionine and valine complexes may be due to steric interaction caused by the bulky alkyl group attached to the mentioned amino acids.

Inosine has two donor sites, N_1 and N_7. In the acidic pH range, N_1 remains protonated, while the metal ion is attached to N_7. The gradual change from N_7-binding to N_1 binding in the complex formation with increasing pH has been rather extensively documented by NMR and EPR [27,28] spectroscopic measurements. The proposed structure for the mixed ligand complex with

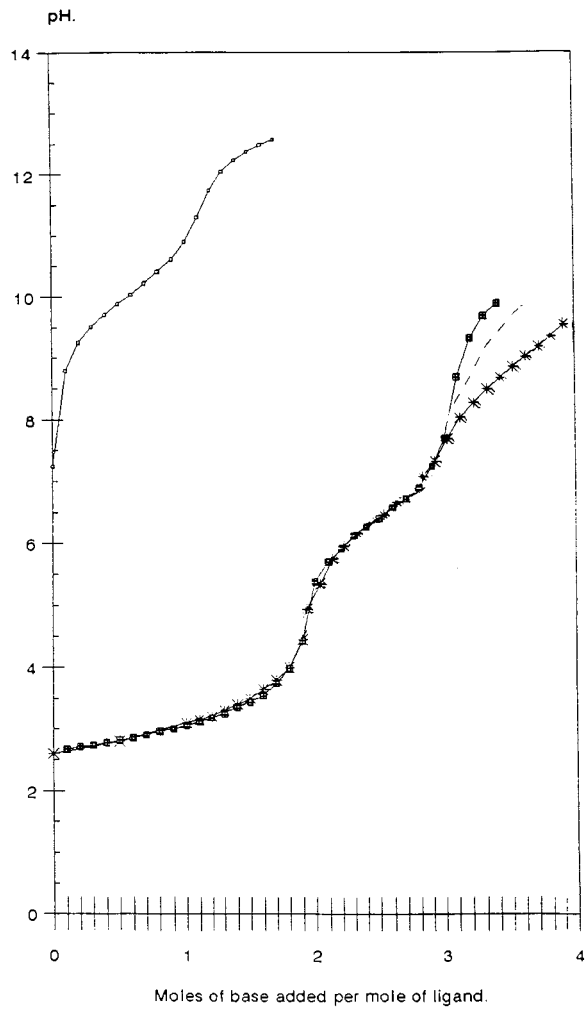

Fig. 4. Potentiometric titration curves of Cu(II)–Tetracycline–glycine system.

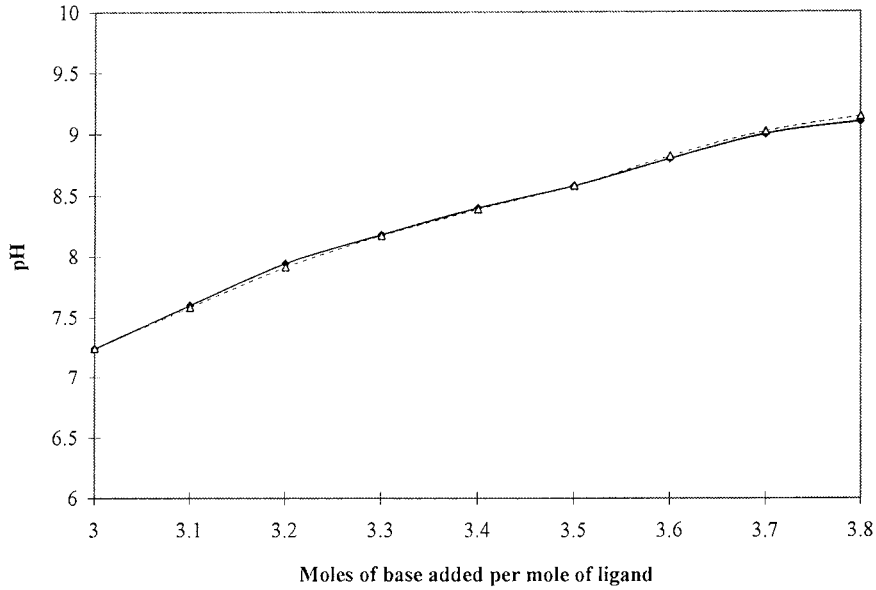

Fig. 5. Potentiometric titration curve of Cu–Tetracycline–glycine system in 50% dioxane–water mixture.

inosine, studied in the pH range 7–9, involves N_1 binding.

The protonation constant of uracil and uridine is corresponding to the [N(3)–C(4)O] group. The pK^H values have been compared with those of the protonation of the analogous [N(1)–C(6)O] grouping in inosine. The purinic derivative (inosine) is slightly more acidic than the pyrimidinic ones (uracil and uridine), a property which can be related to the existence in the anion of the purinic derivatives of a higher number of resonance forms in equilibrium as a result of the presence of two condensed rings in this ligand. Based on the existing data, uracil and uridine are ligating in the deprotonated form, through N_3 atom.

The potentiometric data of Cu–TC–cytosine or cytidine, showed the absence of any significant interaction between Cu–TC complex and cytosine or cytidine. Similar behaviour was found for the system M-EDTA-cytosine or cytidine [29].

Further investigations to provide convincing evidence for the structure of the mixed-ligand complexes need to be carried out, including, for example X-ray diffraction studies of the solid complexes. However, such studies are not available now and will be considered in the future.

The difference in stability between the ternary and binary complexes ($\Delta \log K$) given by Eq. (7) is a way to characterize the tendency for ternary complex formation.

$$\Delta \log K = \log K^{Cu(TC)}_{Cu(TC)D} - \log K^{Cu}_{Cu(D)} \quad (7)$$

Statistically, $\Delta \log K$ for distorted octahedral complexes has been calculated to be negative and equal to -0.9. The $\Delta \log K$ values, given in Table 2, are invariably negative. This means that the amino acid or DNA unit forms more stable complex with free copper(II) ion than with Cu–TC complex. This is expected statistically since more coordination positions are available for binding the secondary ligand by copper(II) ion than copper–tetracycline complex. The values of $\Delta \log K$ for all of the amino acids are ranging from -4.50 to -5.46 and compared with those found (from -2.32 to -3.66) for the DNA constituents. The substantial difference originates in the bidentate coordination of the amino acids and on the other hand DNA constituents are behaving as monodentate ligands, as reported previously [21].

3.5. Speciation distribution plots

Estimation of equilibrium concentrations of copper(II) complexes as a function of pH provides a useful picture of metal ion binding in biological systems. In all of the species distributions, the concentration of the ternary complexes increases with increasing pH, thus making the complex formation more favoured in physiological pH range. The species distribution pattern for the Cu–TC–amino acids system indicates that the mixed-ligand complex starts to form at a pH ~ 8 and reaches the maximum concentration ($\sim 40\%$) at a pH ~ 10. The ternary complexes formed with DNA constituents reach the maximum concentration ($\sim 10\%$) at a pH ~ 9. Thus the ternary complexes of DNA are less favoured than those of amino acids, i.e. the amino acid will compete with the DNA for the reaction with Cu–tetracycline complex.

4. Conclusion

The present results may have important biological implications. The structural flexibility of bioactive tetracycline as well as its capacity to coordinate copper via three different donor sites may favour the formation of ternary complexes of this metal with various ligands occurring in vivo. In particular, such mixed-ligand coordination is likely to occur with bacterial nucleic acids.

References

[1] A. Albert, Nature 172 (1953) 201.
[2] M. Jezowska-Bojczuk, L. Lambs, H. Kozlowski, G. Berthon, Inorg. Chem. 32 (1993) 428.
[3] M. Brion, L. Lambs, G. Berthon, Agents Actions 17 (1985) 229.
[4] M. Brion, L. Lambs, G. Berthon, Inorg. Chim. Acta 123 (1986) 61.
[5] G.L. Quinlan, J.M.C. Gutteridge, Free Rad. Biol. Med. 5 (1988) 341.
[6] P. Mikclens, W. Levinson, Bioinorg. Chem. 9 (1978) 421.
[7] D.O. Rees, J. Mol. Biol. 141 (1980) 323.
[8] N.K. Rogers, G.R. Moore, M.J.E. Sternberg, J. Mol. Biol. 182 (1985) 613.
[9] H. Sigel, R.B. Martin, R. Tribolet, U.K. Haring, R. Malini-Balakrishnan, Eur. J. Biochem. 152 (1985) 187.
[10] G. Akerlof, O.A. Short, J. Am. Chem. Soc. 75 (1953) 6357.
[11] H. Sigel, Pure Appl. Chem. 61 (1989) 923.
[12] M.M. Shoukry, E.M. Shoukry, S.M. El-Medani, Monatsh Fur Chem. 126 (1995) 909.
[13] M.M. Shoukry, Ann. Chim. (Rome) 83 (1993) 147.
[14] M.M. Shoukry, Talanta 39 (1992) 1625.
[15] S.T. Day, W.G. Crou, L.C. Martinelli, J.K.H. Ma, J. Am. Chem. Soc. 67 (1978) 1518.
[16] F.J. Welcher, The Analytical Uses of Ethelenediaminetetraactic Acid, Van Nostrand Reinhold, New York, 1965.
[17] R.G. Bates, Determination of pH, Wiley-Interscience, New York, 1973, p. 71.
[18] H. Sigel, A.D. Zuberbuhler, O. Yamauchi, Anal. Chem. Acta 255 (1991) 63.
[19] P. Gans, A. Sabatini, A. Vacca, Inorg. Chim. Acta 18 (1976) 237.
[20] N. Kole, A.K. Chandhury, J. Inorg. Nucl. Chem. 43 (1981) 2471.
[21] D.D. Perrin, Stability Constants of Metal Ion Complexes, Part B, Organic Ligands, Pergamon, Oxford, 1979.
[22] G.W. Everett Jr., J. Gulbis, J. Shaw, J. Am. Chem. Soc. 104 (1982) 445.
[23] J. Shaw, G.W. Everett Jr., J. Inorg. Biochem. 17 (1982) 305.
[24] R. Prewo, J.J. Stezowski, J. Am. Chem. Soc. 99 (1977) 1117.
[25] R. Prewo, J.J. Stezowski, J. Am. Chem. Soc. 101 (1979) 7657.
[26] L.D. Pettit, Z.L.M. Swash, J. Chem. Soc., Dalton Trans. 2416 (1976).
[27] K. Maskos, Acta Biochem. Po. 28 (1981) 317.
[28] K. Maskos, J. Inorg. Biochem. 25 (1985) 1.
[29] K. Ramalingam, C.R. Krishnamoorthy, Inorg. Chim. Acta 67 (1982) 167.

ELSEVIER

Talanta 48 (1999) 923–931

Talanta

Simple and specific method for flow injection analysis determination of cationic surfactants in environmental and commodity samples

Rajmani Patel, Khageshwar Singh Patel *

School of Studies in Chemistry, Pt. Ravishankar Shukla University, Raipur 492010, MP, India

Received 9 March 1998; received in revised form 14 September 1998; accepted 17 September 1998

Abstract

A new, simple, rapid and specific flow injection analysis (FIA) procedure for the determination of cationic surfactants (CS) i.e. dodecyltrimethylammonium bromide (DTAB), tetradecyltrimethyl-ammonium bromide (TTAB), cetyltrimethylammonium bromide (CTAB), cetylpyridinium chloride (CPC) in the environmental and commodity samples is proposed. Their determinations are based on the enhancement of colour intensity of the Fe(III)–SCN^- complex. The value of apparent molar absorptivity of the Fe(III)–SCN^-–CS^+ complexes in the terms of CS lie in the range of $(2.10–4.30) \times 10^3$ l mol^{-1} cm^{-1} at absorption maximum 475 nm. The most sensitive surfactant, cetylpyridinium chloride (CPC) imparted detection limit (absorbance >3 s) of 250 ppb CPC has been selected for the detailed studies. The working range is linear over 0.5–30.0 ppm CPC with slope, intercept, correlation coefficient and sample throughput of 0.67, 0.02, +0.99 and 100 samples h^{-1}, respectively. The effect of analytical and FIA variables on the determination of the surfactant and the composition of the complex are discussed. The method is free from interferences of almost all ions which commonly associated with the surfactant in the environmental samples. The analytical potentiality i.e. sensitivity, linearity, precision and optimal analytical conditions of FIA to the manual system for the determination of the surfactant are compared. It is reproducibly applicable for the analysis of CS to the various environmental i.e. ground, surface, municipal waste water, and commodity i.e. detergent, soap, shampoo samples.

Keywords: Cationic surfactants; Flow injection analysis; Spectrophotometry; Fe(III)–SCN^-; Water and detergent samples

1. Introduction

Cationic surfactants (CS) are widely used in the manufacture of commodity samples, i.e. detergents, soaps, shampoo, etc. as surface cleaning agents but they have also been reported as pollutants [1]. The concentration of the surfactants in water bodies, i.e. ground water aquifers, surface and municipal waste water reservoirs of the highly populated Asian countries like India is increasing rapidly due to high anthropogenic stress gener-

* Corresponding author. Tel.: +91-771-223075; fax: +91-771-254819.

0039-9140/99/$ - see front matter
PII S0039-9140(98)00306-3

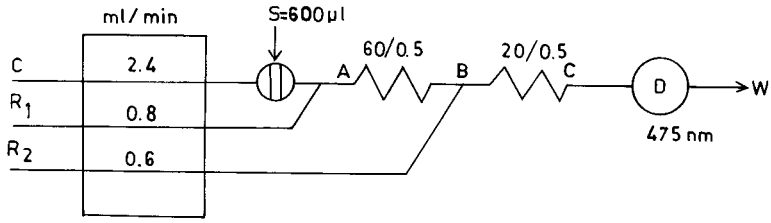

Fig. 1. Schematic diagram of FIA configuration. C = carrier, deionized double distilled water; $R_1 = 1.5 \times 10^{-4}$ M iron solution in 0.005 M nitric acid; $R_2 = 0.7$ M ammonium thiocyanate solution.

ated by change in life style in the fashion similar to western countries. The flow injection analysis (FIA) method based on the extraction of the CS with anionic dyes, i.e. Orange II, tetrabromophenolphthalein ethyl ester, bromochlorophenol blue + quinidine into organic solvents were reported for their determination [2–10]. The selectivity and sensitivity of these methods are very poor with low sample throughput and precision. A new, simple and specific FIA method for the determination of CS in the term of cetylpyridinium chloride (CPC) based on the enhancement of colour intensity of the Fe(III)–SCN^- complex in the nitric acid medium is described. The simplicity, sensitivity, rapidity and reproducibility of the proposed method are better than the Orange II and other FIA methods reported for the analysis of the CS. The method is found to be precisely applicable for the analysis of CS to a variety of environmental and commodity samples.

2. Experimental

2.1. Reagents

All chemicals used were of analytical grade reagents (E. Merck). The standard solution (1000 ppm) of CPC was prepared by dissolving 1.00 g CPC in deionized double distilled water and diluted to 1 l. Fresh solution of ammonium thiocyanate (5.0%, w/v or 0.7 M), and iron (8.0 ppm or 1.5×10^{-4} M) in 0.005 M nitric acid were employed. All solutions used were prior filtered and degassed.

2.2. Apparatus

Tecator flow injection analyzer type-5012 equipped with ALPKEM UV–VIS spectrophotometer type-510 matched with 5.5 mm flow cell and Systronics VIS spectrophotometer type-106 matched with 1-cm quartz cell were employed. The schematic FIA configuration used in the present method is shown in Fig. 1.

2.3. Sampling

The surface, ground, and municipal waste water samples of Raipur city were collected in 100-ml polyethylene bottles during November 1997 as prescribed in the literature [11]. For the commodity samples, weighed amounts of detergents, soaps and shampoo were dissolved in 100 ml double distilled water. All sample solutions were filtered with Whatman filter paper no. 42.

2.4. Procedure

Three solutions: deionized double distilled water (C), iron solution in the nitric acid (R_1) and ammonium thiocyanate (R_2) solutions were propelled through appropriate silicon tubes, Fig. 1. The base line having practically negligible absorption at wavelength 475 nm was recorded at gain factor 1. A 600 µl aliquot of the surfactant solution (containing upto 30.0 ppm CPC) was injected into the flowing stream by keeping injection (the span elapsed in delivery of the sample solution from the injection loop into the flowing stream) and residence time (the span elapsed after injec-

tion of the sample solution until the complete recording of the peak signal) to be 15 and 20 s, respectively. The signal peak height was recorded

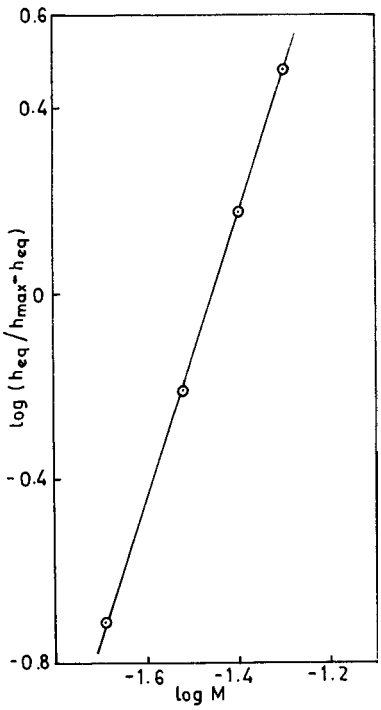

Fig. 2. Curve-fitting method for the determination of mole ratio of the Fe(III) to SCN^- in the Fe(III)–SCN^-–CS^+ complex.

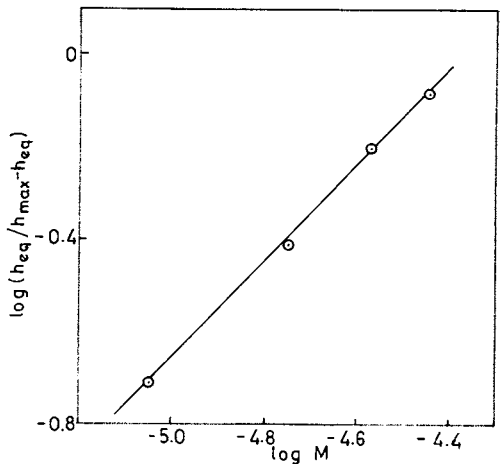

Fig. 3. Curve-fitting method for the determination of mole ratio of the Fe(III) to CS^+ in the Fe(III)–SCN^-–CS^+ complex.

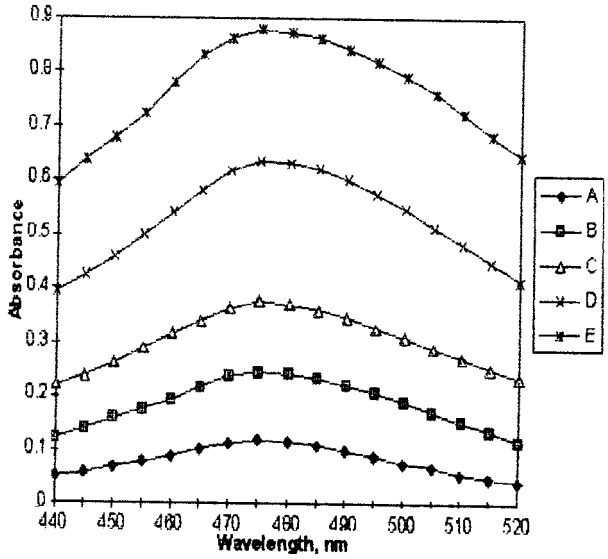

Fig. 4. Absorption spectra of the Fe(III)–SCN^-–CP^+ complex. Iron = 1.5×10^{-4} M. Thiocyanate = 0.7 M. Concentration of CPC: A = 0 (blank); B = 5.0 ppm; C = 10.0 ppm; D = 20.0 ppm; E = 30.0 ppm CPC.

at 475 nm. A calibration curve for the determination of CS in the term of CPC was prepared by plotting signal peak height versus concentration of the surfactant injected. The filtered sample solutions were injected in the similar way. The concentration of surfactant in the sample solutions was computed by using the calibration curve prepared under similar condition.

3. Results and discussion

3.1. Reaction mechanism and composition of the complex

Ferric ions react with SCN^- ions to give a variety of red–orange complexes but the presence of CS activates the formation of a higher thiocyanato species with enhanced kinetics [12].

$$Fe^{3+} + nSCN^- + mCS^+ \Leftrightarrow [Fe(SCN)_n]^{3-n}\, mCS^+$$

where the value of n may vary from 2 to 6.

This reaction has been used for the determina-

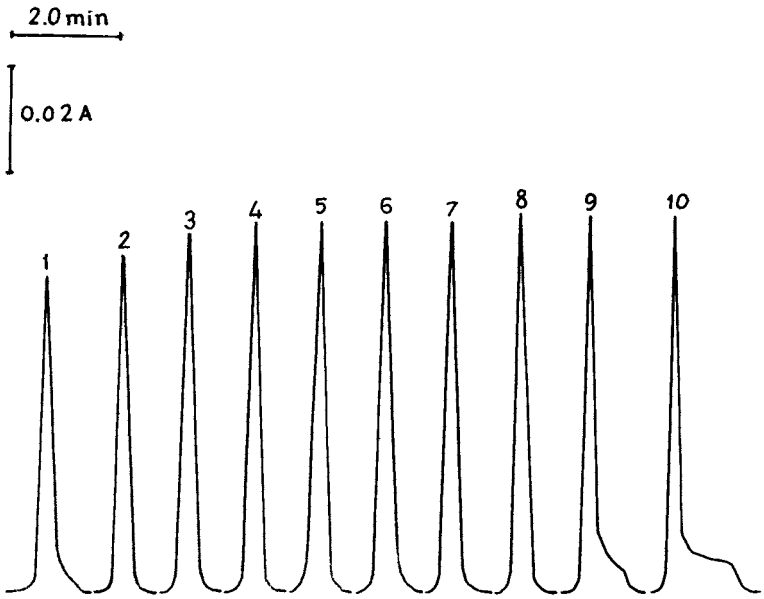

Fig. 5. Effect of concentration of nitric acid on the signal peak height and absorptivity. 1 = 0.0005 M, 2 = 0.001 M, 3 = 0.003 M, 4 = 0.005 M, 5 = 0.05 M, 6 = 0.2 M, 7 = 0.4 M, 8 = 0.6 M, 9 = 0.8 M, 10 = 1.0 M HNO_3.

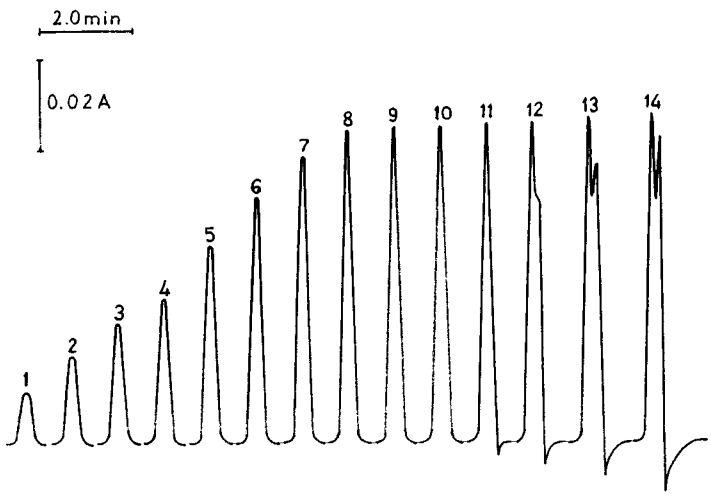

Fig. 6. Effect of concentration of iron on the signal peak height and absorptivity. $1 = 9.0 \times 10^{-6}$ M, $2 = 1.8 \times 10^{-5}$ M, $3 = 2.7 \times 10^{-5}$ M, $4 = 3.6 \times 10^{-5}$ M, $5 = 5.4 \times 10^{-5}$ M, $6 = 7.2 \times 10^{-5}$ M, $7 = 9.0 \times 10^{-5}$ M, $8 = 1.0 \times 10^{-4}$ M, $9 = 1.5 \times 10^{-4}$ M, $10 = 2.0 \times 10^{-4}$ M, $11 = 4.0 \times 10^{-4}$ M, $12 = 4.5 \times 10^{-4}$ M, $13 = 5.0 \times 10^{-4}$ M, $14 = 5.5 \times 10^{-4}$ M Fe.

tion of the cationic surfactants in the present work. The mole ratio of Fe^{3+} to SCN^- and CS^+ ions involved in the formation of the complex in the flowing stream were determined using the curve-fitting method by plotting $\log(h_{eq}/h_{max} - h_{eq})$ (h_{eq} = peak height of the signal at gain factor 1 when the reagent was in equilibrium and h_{max} = peak height of the signal when the reagent was in constant excess) versus log molar concentration of SCN^- propelled into channel R_2, and log molar concentration of CP^+ injected. The values of slope were found to be 3.1 and 1.1, close to

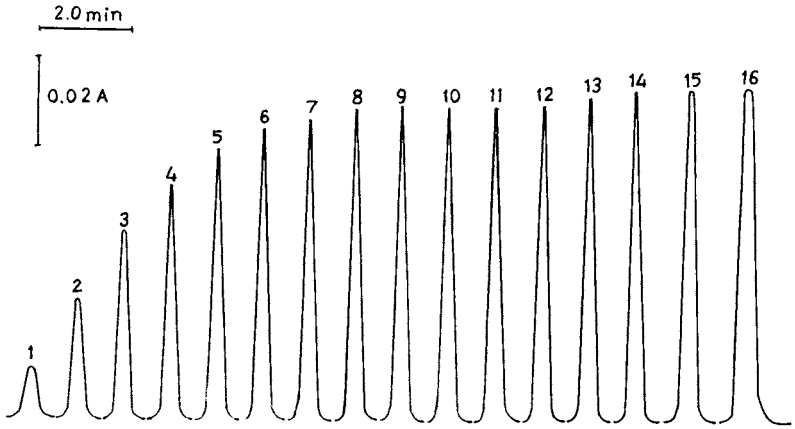

Fig. 7. Effect of concentration of thiocyanate on the signal peak height and absorptivity. 1 = 0.02 M, 2 = 0.03 M, 3 = 0.04 M, 4 = 0.05 M, 5 = 0.2 M, 6 = 0.3 M, 7 = 0.4 M, 8 = 0.6 M, 9 = 0.7 M, 10 = 0.8 M, 11 = 0.9 M, 12 = 1.0 M, 13 = 1.2 M, 14 = 1.3 M 15 = 1.4 M, 16 = 1.5 M SCN^-.

integer 3 and 1, respectively, Figs. 2 and 3. The probable reaction occurred in the flowing stream in the HNO_3 medium is expressed as

$$Fe^{3+} + 3SCN^- + nNO_3^- + CP^+ \Leftrightarrow \{[Fe(SCN)_3(NO_3)n]CP\}^{n-1}$$

where n may vary from 1 to 3.

3.2. Absorption spectra of the complexes

The Fe(III)–SCN^-–CS^+ (CS^+ = cationic surfactant) complexes exhibit the sharp absorption maximum around 475 nm. The position of λ_{max} did not change when different CS was used but absorptivity was affected. In the presence of the surfactant, a hyperchromic shift of the complex was observed due to formation of a higher thiocyanato complex, Fig. 4.

3.3. Optimization of analytical and FIA variables

The effect of acids, i.e. HCl, H_2SO_4, HNO_3 on the signal peak height of the complex was examined in the determination of CPC and all of them were found to be adequate for the analysis of the surfactant. Of these, HNO_3 acid was selected for the detailed investigation as several reductants, i.e. CN^-, Mn^{2+}, Sn^{2+}, S^{2-}, $S_2O_3^{2-}$, oxalic acid, ascorbic acid did not interfere. At least 0.003 M HNO_3 ($\approx$ pH 3.0) was required to attain a maximum and constant peak height of signal and no adverse effect up to 0.6 M HNO_3 was seen, Fig. 5. Similarly, at least 1.0×10^{-4} M Fe and 0.4 M NH_4SCN were required to attain maximum and constant peak height of signal and their further addition up to 4.0×10^{-4} M and 1.3 M, respectively have no adverse effects, Figs. 6 and 7. The acidity range of the sample solution injected was very wide and lie in the range of pH 2.0–7.0. The optimum bore size of silicon tubes used to propel the carrier, iron and thiocyanate solutions were 1.52, 0.51 and 0.38 mm with flow rates of 2.4, 0.8 and 0.6 ml min^{-1}, respectively, Fig. 1. A teflon tube of bore size 0.5 mm was used throughout the work. The adequate length of teflon coils used between merging zones AB and BC were 60 and 20 cm, respectively. Increase in volume size of sample solutions enhanced the signal peak height from 100 to 600 μl and thereafter, no adverse effect was observed. The optimal injection, and residence time observed were 15 and 20 s, respectively. The sample throughput of the method was determined and found to be 100 samples h^{-1} at flow rate, and pump speed of 3.5 ml min^{-1} and 48 cycles min^{-1}, respectively.

3.4. Effect of type of surfactants

The effect of various types of surfactants on the

Table 1
Values of molar absorptivity with various surfactants

Surfactant	λ_{max} (mm)	Value of ε ($\times 10^3$ l mol^{-1} cm^{-1})	
		FIA (apparent)	Manual (real)
Cetylpyridinium chloride	475	4.30	9.20
Cetyltrimethylammonium bromide	475	3.00	7.10
Tetradecyltrimethylammonium bromide	475	2.40	5.80
Dodecyltrimethylammonium bromide	475	2.10	5.10

colour intensity of the Fe(III)–SCN$^-$ complex was examined by the present FIA and the manual methods. The nature of CS, i.e. dodecyltrimethylammonium bromide (DTAB), tetradecyltrimethylammonium bromide (TTAB), cetyltrimethylammonium bromide (CTAB) and CPC were found to remarkably affect the colour intensity of the complex in the both systems. The value of molar absorptivity of the complexes in terms of CS with above four surfactants with the FIA and manual methods lie in the range of $(2.10–4.30) \times 10^3$ and $(5.10–9.20) \times 10^3$ l mol^{-1} cm^{-1} at λ_{max} 475 nm, Table 1. The highest sensitivity was recorded with the cationic surfactant, i.e. CPC in the both systems may be due to higher basic character and lower steric hinderence Fig. 8. In this work, CPC was selected for the detailed studies.

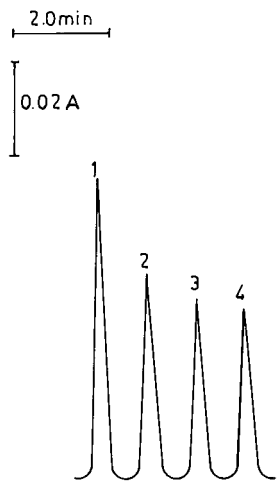

Fig. 8. Signals of various cationic surfactants. 1 = cetylpyridinium chloride (CPC), 10 ppm; 2 = cetyltrimethylammonium bromide (CTAB), 10 ppm; 3 = tetradecyltrimethylammonium bromide (TTAB), 10 ppm; 4 = dodecyltrimethylammonium bromide (DTAB), 10 ppm.

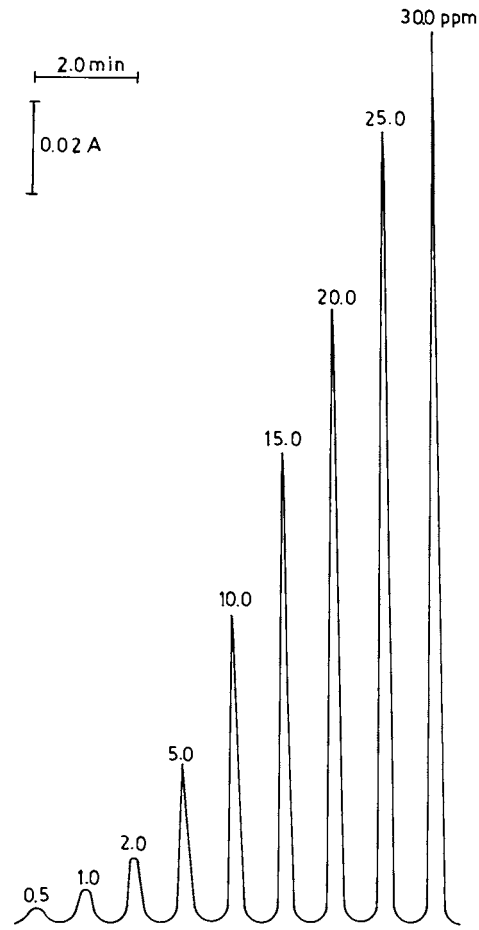

Fig. 9. FIA Signal peak height recorded for the standard solutions of CPC, 0.5–30.0 ppm.

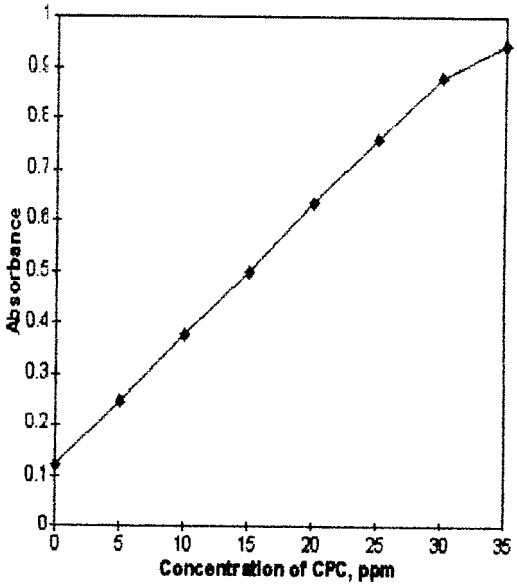

Fig. 10. Calibration graph for spectrophotometric determination of CPC.

3.5. Optimum concentration range, detection limit, sensitivity and statistics

The signal peak height and the absorbance for the different concentration of CPC in the FIA and manual systems are shown in Figs. 9 and 10. The methods followed linearity upto 30.0 ppm of CPC with slope, intercept and correlation coefficient of 0.67, 0.02 and 0.99; and 0.024, 0.13 and 0.99, respectively. The value of apparent molar absorptivity (calculated by taking the concentration of the surfactant injected in molarity and path length of the flow cell to be 0.55 cm) and real molar absorptivity (concentration of CPC in molarity and path length of the cell to be 1.0 cm) with CPC in term of the surfactant are $(4.30)\times10^3$ and $(9.20)\times10^3$ l mol^{-1} cm^{-1} at absorption maximum 475 nm in the FIA and in the manual systems, respectively. The detection limit (absorbance/peak height >3 SD) was found to be 250 ppb in the both systems. The relative standard deviation for the analysis of six different solutions of the surfactants containing 5.0 ppm CPC in the FIA and the manual systems were found to be ±0.9 and $\pm1.5\%$, respectively.

Table 2
Effect of various diverse ions in the determination of 2.0 ppm CS

Ions added	Tolerance limit (ppm)[a]
Na(I), K(I)	500
Cl^-, NO_3^-, SO_4^{2-}	400
SLS,	250
Ca(II), Mg(II), S^{2-}, citrate, tartrate TX-100, TX-300, Brij-35	200
Al(III), Cr(VI), PO_4^{3-}, SO_3^{2-}, Br^-	50
Thiourea, I^-	40
Ni(II)	25
Cu(II), Zn(II), Mn(II), Co(II), Bi(III), oxalic acid, ascorbic acid	20
V(V), F^-, CN^-	10

[a] $<\pm2\%$ error. SLS, sodium laurylsulphate; TX-100, Triton X-100; TX-300, Triton X-300.

3.6. Effect of diverse ions

The effect of various diverse ions in the determination of 2.0 ppm CPC at gain factor 1 was examined separately. None of the tested diverse ions including neutral and anionic surfactants were found to interfere in the determination of CPC. However, the ions i.e. V(V), F^-, CN^- are tolerated at moderate levels as V(V) reacts with SCN^- to give a deep coloured thiocyanato complex causing a positive interference whereas anions i.e. F^-, CN^- react with Fe^{3+} to give a colourless or less coloured complex by causing negative interference. Their tolerance limits (in ppm) in the determination of CPC are summarized in Table 2.

4. Comparison of FIA and manual systems

In the both systems, the complex shows a sharp absorption maximum at 475 nm. The value of molar absorptivity in the FIA system is approximately two times less than the manual method due to dispersion of the surfactant in the flowing stream. In the both systems, the calibration curve was found to be linear up to 30.0

Table 3
Analysis of CS in water and detergent samples in terms of CPC

Sample	By the Orange II method		By the present method	
	CPC found (pm)	RSD[a] (±%)	CPC found (pm)	RSD[a] (±%)
Ponds, Raipur				
Kankali	NA[b]	–	2.6	0.9
Raja	NA	–	1.6	0.8
Bendri	NA	–	2.0	0.9
Katora	NA	–	2.5	0.8
Budha	NA	–	3.2	1.0
Handi	NA	–	3.5	0.9
Ground water aquifers (tubewells), Raipur				
Kankalipara	NA	–	0.8	0.9
Raja talab	NA	–	0.5	1.0
Katora talab	NA	–	1.0	0.8
Budha para	NA	–	1.2	0.9
Handi para	NA	–	1.3	1.0
Municipal waste water, Raipur				
Raja talab	NA	–	4.2	1.0
Katora talab	NA	–	5.0	0.9
Kota	NA	–	3.0	0.8
Dagania	NA	–	3.7	0.9
Household commodities				
Vim (Mfd. by Hindustan Lever, India)	NA	–	5.0	0.7
Ghari detergent (Mfd. by Rahul Detergents, India)	21.2	1.9	20.0	1.0
Surf detergent (Mfd. by Hindustan Lever, India)	30.4	1.8	31.0	1.1
Lifebuoy soap (Mfd. by Hindustan Lever, India)	70.2	1.7	72.0	1.0
Nirma soap (Nirma Chemicals, India)	54.1	1.7	53.0	0.9
Clinic Plus shampoo (Mfd. by Hindustan Lever, India)	132	1.6	135	0.8
Pantene shampoo (Procter & Gamble, India)	150	1.7	148	1.0
Organics shampoo (Mfd. by Hindustan Lever, India)	165	1.5	168	1.1

[a] Six samples were analyzed.
[b] NA, not applicable.

ppm CPC and thereafter a negative deviation was observed. The minimum concentration of HNO_3, NH_4SCN and Fe^{3+} required in the both systems were found to be almost same: ≥ 0.001 M HNO_3, ≥ 0.4 M NH_4SCN and $\geq 1.0 \times 10^{-4}$ M Fe^{3+}. The absorbance of the complex was found stable for atleast 30 min in the room temperature (20 ± 2°C) in the manual system. The method is not found to be simple and easy to work with the manual system for the analysis of the surfactant as the reagent blank has an absorbance value of 0.12.

5. Application of the method

The precision of the present method was compared with well established Orange II–FIA method [2]. They were applied for the analysis of CS in the term of CPC to the various environmental and commodity samples, i.e. surface waters, ground waters, municipal waste waters, detergents, soaps, and shampoo, Table 3. The filtered water samples were directly injected whereas the commodity sample solutions were injected after appropriate dilution. The peak

height of signal was recorded at 475 nm and concentration of CS in terms of CPC was evaluated using the calibration curve. The Orange II method was not found to be applicable to the samples containing CPC down to 5.0 ppm due to poor sensitivity. The precision of the proposed method was found to be better than the Orange II method. The concentration level of the CS in the eight commodity, five ground water, six surface water and four municipal waste water samples were in the range 5.0–168, 0.5–1.3, 1.6–3.5 and 3.0–5.0 ppm, respectively. The main expected sources of the cationic surfactants in water bodies of Raipur area are household commodities, i.e. detergents, soaps, shampoo, liberated from human activities.

6. Conclusion

The proposed method is very simple, rapid and specific for the FIA determination of the CS, i.e. DTAB, TTAB, CTAB, CPC in the various water and commodity samples. It is reproducibly applicable for the analysis of CS down to 0.5 ppm in the water samples. The selectivity, sensitivity and reproducibility of the proposed method is better than the Orange II–FIA method. All the stationary surface water bodies (ponds), municipal waste water reservoirs and ground water aquifers lie nearer to the sources i.e. ponds, municipal waste water reservoirs, etc. were found to be contaminated with CS in the range of 0.5–5.0 ppm CPC.

Acknowledgements

Authors are thankful to Pt. Ravishankar Shukla University, Raipur, Ministry of Environment and Forests, New Delhi and Alexander von Humboldt Foundation, Bonn, for providing financial support, for this work.

References

[1] H.P. Drobeck, Surfactant Sci. Ser. 53 (1994) 61.
[2] J. Kawase, Anal. Chem. 52 (1980) 2124.
[3] J. Ruzicka, E.H. Hansen, Anal. Chim. Acta 99 (1978) 37.
[4] D. Betteridge, Anal. Chem. 50 (1979) 832.
[5] J. Kawase, M. Yamanaka, Analyst (Lond.) 104 (1979) 750.
[6] T. Masadome, T. Imato, J. Flow Inject. Anal. 13 (1996) 120.
[7] M. Bos, J.H.H.G. van Willigen, W.E. van der Linden, Anal. Chim. Acta 156 (1984) 307.
[8] T. Sakai, N. Ohno, Anal. Sci. 7 (1991) 297.
[9] T. Sakai, Analyst (Lond.) 117 (1992) 211.
[10] T. Sakai, H. Ohto, N. Ohno, H. Sasaki, Fresenius J. Anal. Chem. 369 (1994) 475.
[11] S.P. Pandey, V.S. Narayanswamy, M.Z. Hasan, Indian J. Environ. Health 21 (1979) 35.
[12] A.N. Tripathi, S. Chikhalikar, K.S. Patel, J. Autom. Chem. 19 (1997) 45.

ELSEVIER

Talanta 48 (1999) 933–942

Talanta

Effects of organic and aqueous solvents on the electronic absorption and fluorescence of chloroaluminum (III) tetrasulphonated naphthalocyanine

Lawrence Evans III, Gabor Patonay *

Georgia State University, Department of Chemistry, Atlanta, GA 30303, USA

Received 2 September 1998; received in revised form 16 September 1998; accepted 17 September 1998

Abstract

The effects of various solvents on the ground and excited states of chloroaluminum (III) tetrasulphonated naphthalocyanine ($AlNcS_4$) were studied. Both the absorbance and fluorescence spectra were found to be influenced by the hydrogen bond donating ability of various solvents. As the hydrogen bond donating ability of the solvent increased, hypsochromic and bathochromic shifts in the absorbance and fluorescence spectra were observed in protic and aprotic solvents respectively. Plots of the absorbance and fluorescence maxima versus the $E_T(30)$ solvent parameter showed linear relationships in binary mixtures of protic–protic (methanol–H_2O) and aprotic–protic (DMSO–H_2O) solvents. Aggregation was indicated by a broad band in the ground state absorption spectra and a low quantum efficiency 0.04 relative to the efficiency observed in organic solvents. A face-to-face conformation of the monomeric subunits of the dimer is suggested due to the red-shifted absorbance band. The acid-base properties of the dye were studied and were indicative of a multi-step process. In acidic conditions (pH 1), protonation of the bridging nitrogen atoms was identified by a broad band appearing red-shifted to those obtained at higher pH values. Under slightly acidic conditions a p*K*a value of 6.7 was determined for one of the *meso*-nitrogen. In alkaline conditions a p*K*a of 11.5 was determined for another *meso*-nitrogen and a second fluorescence band emerged at 804 nm, red-shifted to the emission maxima.

Keywords: Chloroaluminum (III) tetrasulphonated naphthalocyanine; Absorbance; Fluorescence; Solvents

1. Introduction

The unique structure and chemical properties of phthalocyanines and naphthalocyanines allow them to be biologically and chemically useful macrocyclic compounds. Several derivatives of these compounds have been used as sensitizing agents for photodynamic therapy due to their ability to absorb light in the near-infrared spectral region [1–5]. Naphthalocyanines also exhibit interesting optical and electrical properties [6–8]. A limited number of studies have been devoted to the photochemical and photophysical properties

* Corresponding author. Tel.: +1-404-651-3856; fax: +1-404-651-1416.

0039-9140/99/$ - see front matter
PII S0039-9140(98)00299-9

of phthalocyanines and naphthalocyanines [9,10]. The effects of various metal substituents on the electronic absorption spectra have been described as well [11–13]. The spectral properties in acidic conditions have also been investigated to elucidate the reason for the broad, red-shifted absorbance peak [14,15].

Naphthalocyanines (Nc) are azaporphyrin derivatives with properties similar to the naturally occurring porphyrins. A cyclic tetrapyrrole unit makes up the central macrocycle that is linked by nitrogen atoms rather than methine bridges. The fusion of naphthalene rings with each of the four pyrrole subunits extends the conjugation of the macrocycle resulting in a strong absorption band between 700 and 900 nm. Metal chelation with the four pyrrole nitrogen atoms of the macrocycle help stabilize the complex. These complexes are insoluble in water, however solubility is achieved by incorporating sulphonate groups in the outer benzo rings. The photophysical properties of metal-naphthalocyanines (MNc) closely resemble that of their counterpart, the metal-phthalocyanines (MPc). The characteristic Soret (≈ 350 nm) and Q (≈ 670 nm) bands of the MPc are blue-shifted relative to those of the MNc.

In the present studies we report the effect of the hydrogen bond donating ability of various solvents on the electronic absorption and fluorescence spectra of chloroaluminum (III) tetrasulphonated naphthalocyanine ($AlNcS_4$) (Fig. 1). Investigations were also conducted to evaluate the effect of pH on the photophysical properties of $AlNcS_4$.

2. Experimental

The chloroaluminum (III) tetrasulphonated naphthalocyanine was synthesized in house and its synthesis was previously reported [16]. Lesser sulfonated fractions of the naphthalocyanine derivative are assumed to be present in the sample, however because of the nature of the sulphonate group to increase water solubility, a subtle if any effect will be observed in the dyes aggregation properties. The solvents were of spectral grade quality and used as received from the supplier (Aldrich or Fischer Scientific). Buffers (0.1 M) were prepared using H_3PO_4 (pH 1–3), NaH_2PO_4 (pH 4–7), $NaHCO_3$ (pH 8–11), and NaOH (pH 12–13) with the pH being adjusted using concentrated HCl or NaOH. For the solvent studies a stock solution of the dye was prepared in DMSO and then diluted in the appropriate solvent yielding a final dye concentration of 2.5 μM (DMSO < 2% V/V). The absorption spectra were acquired between 600 and 850 nm on a Lambda 20 UV/vis spectrometer (Perkin-Elmer, Norwalk, CT). The extinction coefficients were determined from the slope of the Beer–Lambert plot. Steady-state fluorescence measurements were acquired using a multifrequency cross-correlation phase-modulation spectrofluorometer (K2, ISS, Champaign, IL). Data acquisition was controlled by a 50 MHz 486 computer (Gateway, Bozeman, SD). Excitation at 690 nm was provided by a continuous wave 27 mW laser diode (LAS-200-690-30, LaserMax, Rochester, NY) with a collimated output beam of ≈ 3.3 mm in diameter. Steady-state spectra were collected at 90° to the excitation, dispersed by a monochromator equipped with a 1200 groove mm^{-1} grating and 2 mm entrance and exit slits (DH10, Instruments SA, Edison NJ) then detected by a photomultiplier tube (R928, Hamamatsu, Bridgewater, NJ).

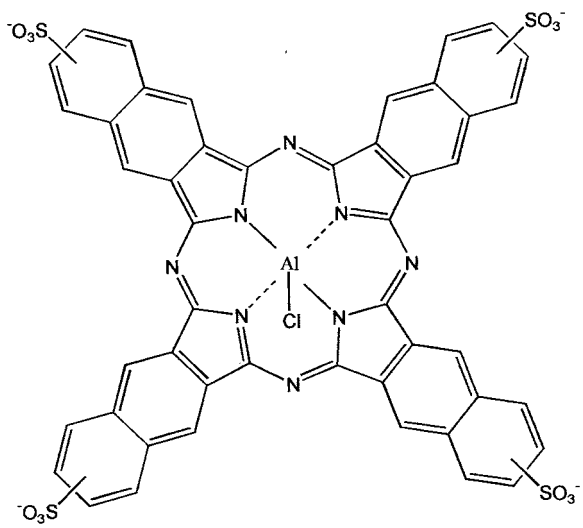

Fig. 1. Structure of chloroaluminum(III) tetrasulphonated naphthalocyanine ($AlNcS_4$).

Table 1
Absorption and duorescence properties in protic and aprotic solvents

Solvent	λ_{ex} (nm)	ν_{ex} (cm^{-1})	ε (mol l^{-1} cm^{-1})	λ_{em} (nm)	ν_{em} (cm^{-1})	Φ	$\Delta\nu$ (cm^{-1})
Water	781	12 804	43 000	791	12 642	0.04	162
Methanol	782	12 788	59 000	792	12 626	0.45	162
Ethanol	783	12 771	45 000	792	12 626	0.19	145
1-Propanol	784	12, 755	40 000	793	12 610	0.18	145
1-Butanol	785	12 739	44 000	793	12 610	0.13	129
DMF	783	12 771	48 000	794	12 594	0.31	177
DMSO	791	12 642	44 000	800	12 500	0 36	142
Nitromethane	794	12 594	44 000	799	12 516	0.09	78

The fluorescence quantum yields (Φ) were determined using a dilute solution of 1H-Benz-[e]indolium,2 - [7 - [1,3 - dihydro - 1,1 - dimethyl - 3-(4 - sulfobutyl) - 2H - benz[e]indol - 2 - ylidene] - 1,3,5-heptatrienyl]-1,1-dimethyl-3-(4-sulfobutyl)-, inner salt, sodium salt (IR-125, Ex = 795 nm, Em = 833 nm) in DMSO at 20°C as the reference (Φ° = 0.13) [17]. Solutions were measured at room temperature and were not deoxygenated.

3. Results

3.1. Solvent dependence on the absorption and fluorescence of $AlNcS_4$.

The photophysical properties of the naphthalocyanine dye in various protic and aprotic solvents as well as binary mixtures are listed in Tables 1 and 2. The absorption maximum for $AlNcS_4$ in methanol is 782 nm. The absorbance maximum of the dye in a series of alcohol's (methanol, ethanol, 1-propanol, and 1-butanol) displays a hypsochromic shift with increasing hydrogen bond donating ability. The electronic spectra in water (781 nm) is blue shifted and broad relative to the spectra obtained in methanol. Emission is observed at the longest wavelengths in the aprotic solvents along with relatively high quantum yields (0.31 and 0.36). A linear relationship was identified between the wavenumber of the absorption and fluorescence maxima in several protic (alcohol's) and aprotic solvents with the corresponding solvent parameter $E_T(30)$. To further investigate the influence of the hydrogen bond donating ability of various solvents on the ground and excited states of $AlNcS_4$, absorbance and fluorescence spectra were obtained in binary mixtures of protic–protic (water–methanol) and protic–aprotic (water–DMSO) solvents. The overall spectral features of the dye in the protic–protic binary mixtures are consistent with a progressive blue-shift in the emission maxima along with a decrease in quantum yield with the addition of water. A hypsochromic shift of the absorbance maxima is also observed with increasing amounts of water to the protic–aprotic binary mixture. The protic–aprotic binary solvent system exhibited a decrease in quantum yield with increasing amounts of water along with a blue-shift in the emission maximum.

3.2. Effect of aggregation on the absorption and fluorescence of $AlNcS_4$.

Spectra obtained in 100% water, resulted in broad blue-shifted spectra, due to the tendency of these molecules to aggregate in water. The absorbance spectra obtained in water when using DMSO as a co-solvent resulted in a narrow absorbance band indicative of the monomeric form of the molecule. The excited state photophysical properties were effected as well. A dramatic decrease in the quantum yield (4.1%) along with a blue shift in the fluorescence spectra is observed compared to the spectra obtained in organic media. These results along with the ground state

Table 2
Absorption and fluorescence properties in binary solvent mixtures

Solvent (% H_2O)	λ_{ex} (nm)	ν_{ex} (cm^{-1})	λ_{em} (nm)	ν_{em} (cm^{-1})	Φ	$\Delta\nu$ (cm^{-1})
25[a]	783	12 771	789	12 674	0.29	97
50[a]	782	12 788	788	12 690	0.24	98
75[a]	780	12 821	785	12 739	0.16	82
25[b]	791	12 642	800	12 500	0.28	142
50[b]	788	12 690	798	12 531	0.25	159
75[b]	786	12 723	795	12 579	O.19	144

[a] Represents a binary mixture consisting of water and methanol.
[b] Represents a binary mixture consisting of water and DMSO.

spectral features corresponds well with results obtained by others [2,3].

3.3. Influence of pH on the absorption and fluorescence of $AlNcS_4$.

The ground state absorbance maxima ranged from 726 to 785 nm with the most red-shifted absorbance maxima appearing in a buffered solution at pH 1. The spectra obtained at pH 1 is broader, featureless, and red-shifted relative to those obtained at higher pH values (Fig. 2). From pH 1 to 6 the observed absorbance maxima are between 785 and 779 nm. Two absorbance bands (738 and 772 nm) of equal intensity are observed at pH 7. With further titration, the absorbance maxima shifts to 728 nm in solutions buffered between pH 8 and 10. At pH 11, two absorbance bands are present at 726 and 757 nm. Beyond pH 11, the absorbance maxima evolves at 758 nm with two blue-shifted side bands at 679 and 728 nm. An isosbestic point at 742 nm is seen in spectra obtained in solutions buffered between pH 10 and 13 (Fig. 3), indicative of two species present.

In very acidic conditions (pH 1–4), the fluorescence intensity of the molecule increased with increasing pH accompanied by a hypsochromic shift (791–783 nm) in the emission profile. As the pH was increased from 5 to 9 the fluorescence intensity decreased with a hypsochromic shift in the emission maxima. The excited state spectra obtained at pH 10 supported the absorbance data indicating the presence of two species under these conditions. A closer look at Fig. 4 shows a band near 764 nm and the formation of a new less intense band near 804 nm. The smaller band was absent in all fluorescence spectra obtained at pH > 10.

4. Discussion

The hypsochromic shift with increasing hydrogen bond donating ability associated with the protic solvents is indicative of negative solvatochromism. This can be attributed to the ability of the protic solvents to form hydrogen bonds with lone pairs of the nitrogen in the macrocycle, thus lowering the energy of the π-state without modifying the π^*-state (stabilization of the ground state energy). The inability of the aprotic solvents to form hydrogen bonds and influence the π-state was identified by the bathochromic shifts observed in DMSO and nitromethane (791 and 794 nm).

The hydrogen bond donating ability was further investigated by plotting the $E_T(30)$ solvent parameter as a function of the absorbance and fluorescence maxima. The $E_T(30)$ scale is based on the solvatochromic band of pyridinium-*N*-phenolbetaine. This value gives the transition energy (kcal mol^{-1}) of the intramolecular charge transfer of pyridinium-*N*-phenolbetaine. The slope of the lines demonstrate hydrogen bonding to the macrocyclic compound (Fig. 5). The plot of the data obtained in aprotic solvents has a negative slope, which corresponds to a bathochromic shift

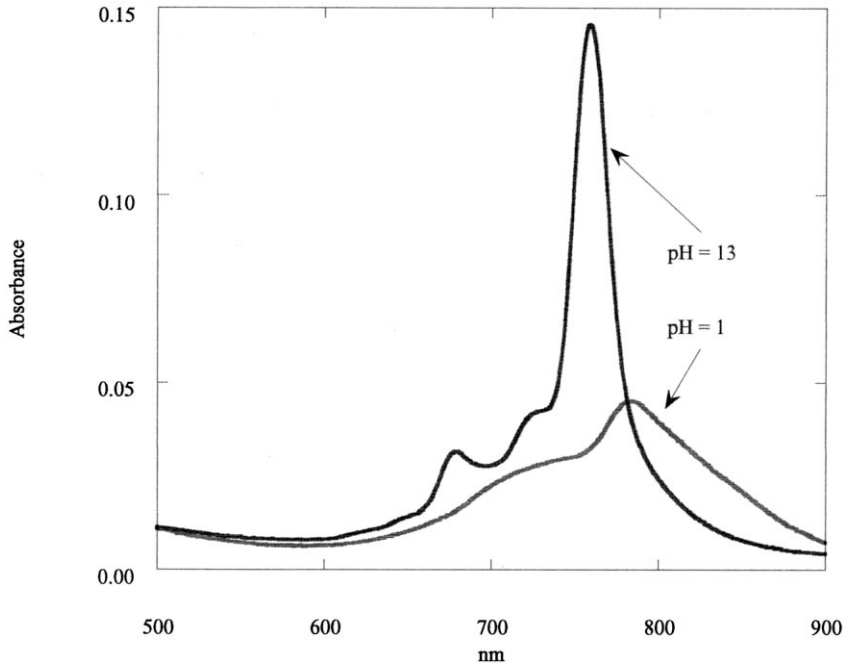

Fig. 2. Absorption spectra of $AlNcS_4$ at pH values 1 and 13.

with increasing hydrogen bond donating ability. The data obtained in the protic solvents produced a linear plot with a positive slope. In Fig. 6, the plots of the protic–aprotic and protic–protic solvents featured positive slopes suggesting that with the addition of water, their electronic spectra undergo hypsochromic shifts in polar protic solvents. The slope of the line produced by data obtained in the protic–aprotic binary mixture was less than that collected in the protic–protic binary mixture. This indicates that the 18π system of the naphthalocyanine is more influenced by protic solvents implying stabilization via hydrogen bond formation.

Phthalocyanines and naphthalocyanines aggregate regularly in water, due to electronic interactions between the rings of two or more Nc molecules [18–21]. This effect leads to blue shifts, broadening or splitting of the Q band in the absorbance spectra and changes in the excited state as well [21]. The tendency to aggregate is primarily dependent on the degree of substitution on the outer rings. It can also be associated with the proximity of the approaching rings, their overlap position, the adopted tilt angle by the rings, the size of the peripheral groups, and the solvent type [21]. As expected, aggregation of the dye (in water) was observed in the absorbance and emission spectra. The phenomena was very obvious in the emission profile. The low quantum yield was the result of self-quenching. In the absorbance spectra, aggregation occurred red-shifted relative to the monomer peak coinciding well with similar studies on chloroaluminum (III) tetrasulphonated phthalocyanine [20]. This is in contrast to the face-to-face stacking conformation associated with the blue-shift of dimer absorption bands of other metal phthalocyanines [22]. However, in the case of $AlPcS_4$ and Th-2, 3, 7, 8, 12, 13, 17, 18-octaethylporphin dimers, a face-to-face stacking conformation is suggested when a red-shift is observed in the dimer's absorption bands [20,23]. Yoon and co-workers explained their observations using a one electron molecular orbital (MO) interpretation. In their interpretation, the dimer's highest occupied molecular orbital (HOMO) is the result of the two monomer antibonding HOMOs. The dimer's lowest unoccupied molecular

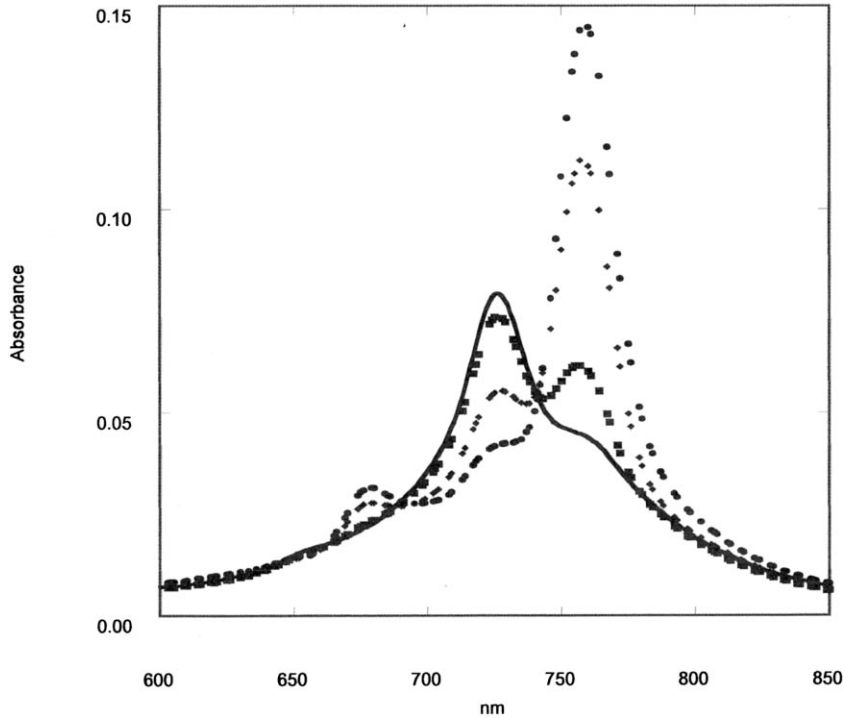

Fig. 3. Influence of pH on the absorption spectra of $AlNcS_4$: pH 13 (●); pH 12 (◆); pH 11 (■); pH 10 (– –). Isobestic point at 742 nm.

orbital (LUMO) is the result of the monomers' LUMO. The energy gap between the LUMO and HOMO of the dimer is therefore less than that of the monomer. The result of which is the red-shifted absorption of the dimer relative to the monomer. The red-shifted absorption of $AlNcS_4$ can also be attributed to the dimer maintaining a face-to-face conformation.

The photophysical properties of $AlNcS_4$ are pH dependent. However, this dependence is not influenced by the acid–base properties of the sulphonic groups (SO_3H) of the naphthalocyanine due to their high acidity. Using proton nmr and raman spectrometry, the p*K*a of several sulfonic acids has been found to exist from -1.06 to -1.86 [24–27]. Lower values of -6.65 and -6.0 for benzenesulfonic acid and methylsulphonic acid, respectively have also been reported [28,29]. Lastly, this can be supported by the fact that the chromophoric region of the Nc extends into the outer benzo rings near the sulphonic groups yet no significant influence by the sulphonic group is observed.

At pH 1, the absorbance band was very broad and the most red-shifted. Different explanations have been given for the featureless shape of the Q-band in very acidic conditions. Ferraudi [14] attributed changes to the protonation of axial ligands co-ordinated to the metal centre and ruled out the possibility of protonation of the macrocycle. Mikhalenko [15] and co-workers believed that protonation of the macrocycle caused the bathochromic shift. A similar shift in the electronic absorbance spectra of tetraazaphorphyrin in solutions of acetonitrile and perchloric acid was observed by Malkova[30]. In this case the spectral shift was also attributed to the protonation of a nitrogen atom in the chromophoric macrocycle of the molecule. Analysis of our data suggest protonation of nitrogen atoms within the central macrocycle as well. This is based on the two key structural features of the molecule: (1) lack of

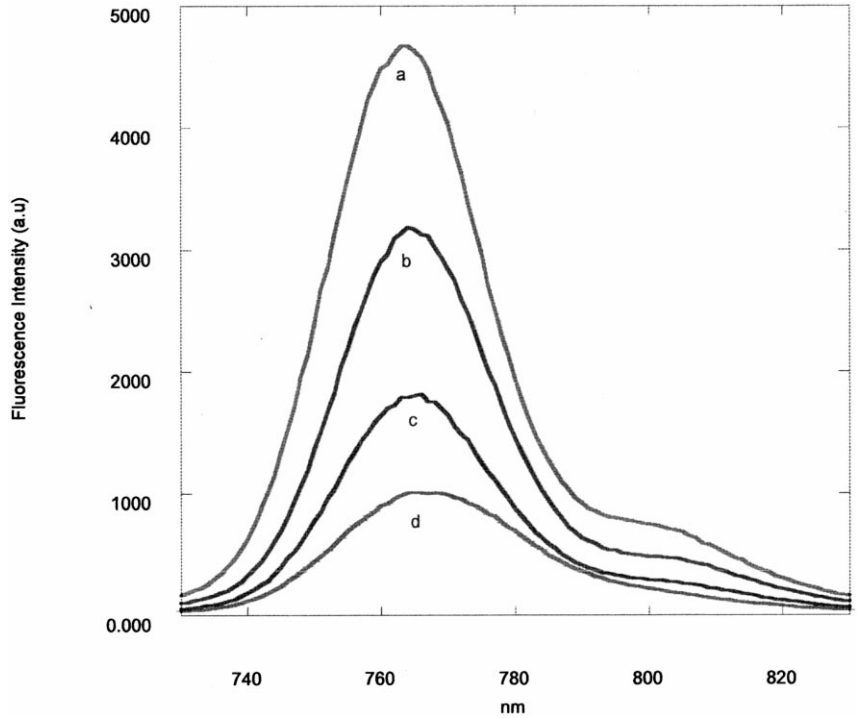

Fig. 4. Influence of pH on the fluorescence spectra of $AlNcS_4$: (a) pH 12; (b) pH 11.5; (c) pH 11; (d) pH 10. A new emission band at 804 nm appears in solutions buffered at pH > 9.

axial ligands co-ordinated to the central metal that are capable of protonation; and (2) the availability of lone pair electrons on the nitrogen linking the adjacent pyrrole units. The Nc studied contained aluminium chloride. Having this in mind, the chloride ligand is not influenced by solvent pH, leaving the nitrogen atoms as the most likely site of protonation. The MNc has six nitrogen atoms which makeup part of it's chromophoric region. Two of the chromophoric nitrogen atoms are involved in co-ordination with the metal ligand, thus making their lone pairs unavailable. This leaves the four bridging nitrogen as likely sites of protonation. The p*K*a of bridging or *meso*-nitrogen in mono-, di-, and tetraazaporphyrins were determined by Malkova to be 10.80, 8.18, and 6.60, respectively. Similar values can be assumed to exist for Nc dyes. If so this help establish the existence of the protonated species in acidic conditions.

The protonation of the nitrogen atoms can be viewed as a multi-step equilibrium reaction. This is indicated by the shifts in the ground and excited state spectra as a function of pH. We believe the equilibrium processes are overlapping and most are not completely resolvable by absorbance and fluorescence spectroscopy. The p*K*a values of two of the nitrogen were determined to be approximately 6.7 and 11.5. The p*K*a values of diphthalocyanine complexes of gadolinium, yttrium, and lutetium were determined spectroscopically by Moslalev and Kirin to be 8.7, 8.6, and 10.2 [31]. Although not stated it is assumed that the p*K*a values of the other ionizable nitrogen were unable to be elucidated. These values support the assumption made earlier regarding the protonation of the *meso*-nitrogen in acidic conditions.

The emission spectra of the dye at pH values > 10 are indicative of the presence of a second fluorescing species by the emergence of a new band at 804 nm red-shifted to the primary emission band at 764 nm. The ratio of the fluorescence intensities I_1 at 764 nm and I_2 at 804 nm are given in Table 3. The maximum ratio 6.83 is observed

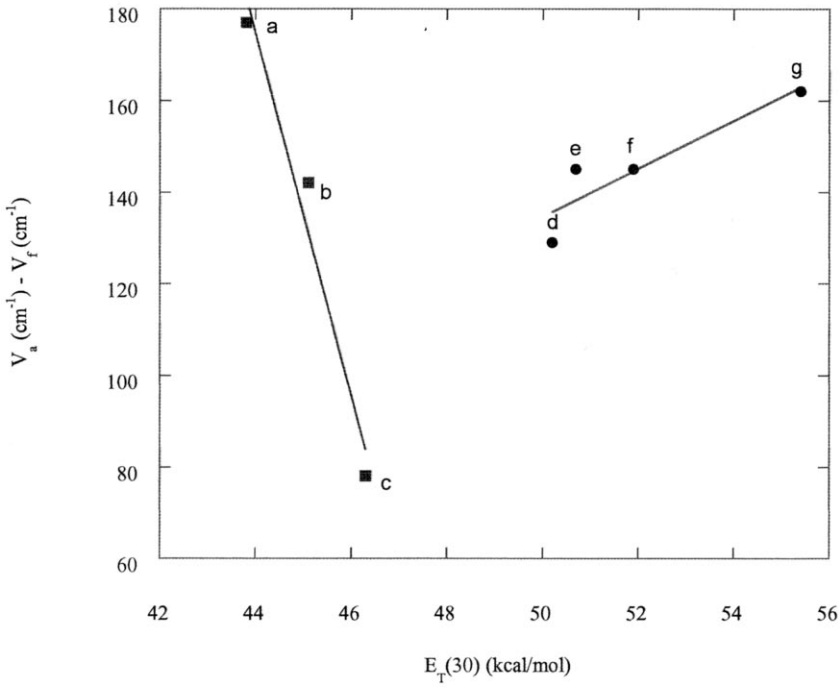

Fig. 5. Plots of the stokes' shift (cm^{-1}) versus $E_T(30)$ solvent parameter of aprotic (■) and protic (●) solvents. (a) DMSO; (b) DMF; (c) nitromethane; (d) 1-butanol; (e) 1-propanol; (f) ethanol; (g) methanol.

at pH 11.5. This also corresponds well with one of the ground state p*K*a values determined from the absorbance data.

5. Conclusions

Both the ground and excited states of $AlNcS_4$ are effected by the hydrogen bond donating ability of solvents. Protic solvents lower the energy of the π-state without modifiying the π^*-state by hydrogen bonding with the bridging nitrogen of the macrocycle thus producing the observed hypsochromic shifts with solvents of greater $E_T(30)$ values. Aprotic solvents lack the hydrogen atom necessary for hydrogen bonding. As expected the $AlNcS_4$ molecules aggregated in water causing a broad red-shifted absorbance peak along with a dramatic decrease in the quantum yield. The red-shift of the absorbance band indicated that the two monomeric subunits of the dimer exist in a face to face conformation. Absorbance and fluorescence pH titration data suggested the protonation of the *meso*-nitrogens in the macrocycle to be a multi-step process. Our results also support the work by Mikhalenko and Malkova [15,31], attributing the large red-shifted absorbance band observed in acidic conditions to the protonation of *meso*-nitro-

Table 3
Ratio of fluorescence intensities at various pH*

pH	I_1	I_2	I_1:I_2
10.0	1006	187	5.38
11.0	1789	273	6.55
11.5	3184	466	6.83
12.0	4671	696	6.71
13.0	4704	760	6.19

* I_1 and I_2 are the fluorescence intensities (a.u.) at 764 and 804 nm, respectively.

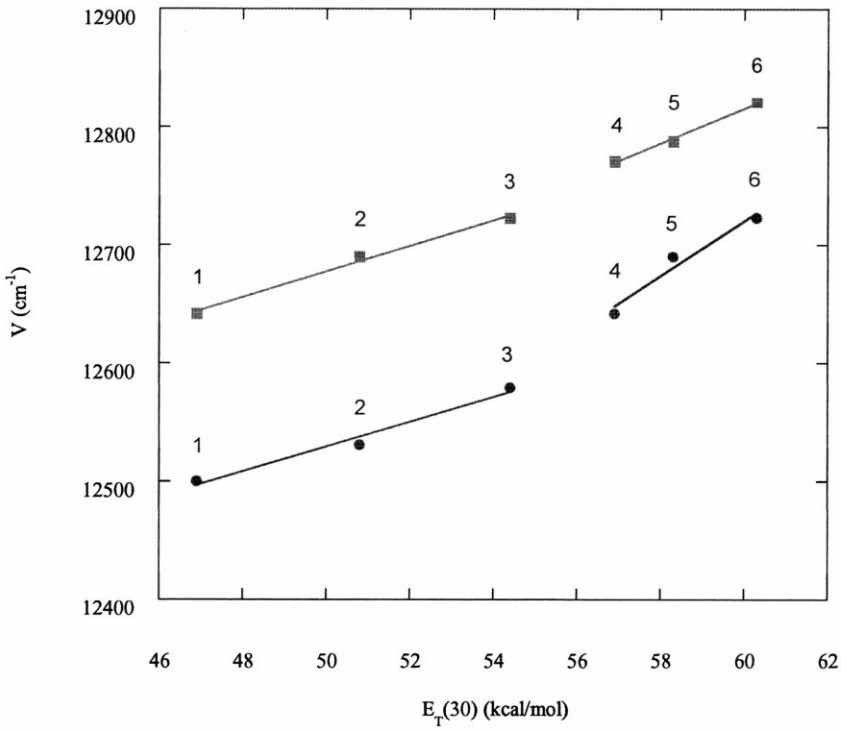

Fig. 6. Linear plots of absorbance (■) and fluorescence (●) maxima (cm^{-1}) versus $E_T(30)$ solvent parameter of binary solvent mixtures. (1–3) DMSO–H_2O ratio: (1) 75:25; (2) 50:50; (3) 25:75. (4–6) methanol–H_2O ratio: (4) 75:25; (5) 50:50; (6) 25:75.

gens in the macrocycle. Lastly, more plans are being discussed to examine the properties of the fluorophore using fluorescence lifetime. This information will help substantiate the conclusions made regarding the relationships between solvents and both the π and π^* states. Questions have also been raised concerning whether or not the trends observed were valid for naphthalocyanines containing metals other than aluminum, such as gallium and zinc. McCubbin and Phillips found that the absorption and emission properties for aluminum naphthalocyanine and zinc naphthalocyanine were very comparable with a Q-band at 769 and 754 nm respectively and identical molar absorptivities [12]. Later Ford and co-workers found similar properties to exist between aluminum and gallium naphthalocyanines [11]. Although this is not definitive information, is does suggest the presence of a few general trends that are influenced by the central metal.

References

[1] J.R. Wagner, H. Ali, R. Langlois, N. Brasseur, J.E. van Lier, Photochem. Photobiol. 45 (1987) 587.
[2] N. Brasseur, H. Ali, R. Langlois, J.R. Wagner, J. Rousseau, J.E. van Lier, Photochem. Photobiol. 45 (1987) 581.
[3] E. Ben-Hur, I. Rosenthal, Photochem. Photobiol. 42 (1985) 129.
[4] J.D. Spikes, Photochem. Photobiol. 43 (1986) 691.
[5] R.C. Straight, J.D. Spikes, Photochem. Photobiol. 43 (1986) 63S.
[6] L.B. Wheeler, A.J.B. Nagaasubramanian, L.A. Schechtman, D.R. Dininny, M.E. Kenney, J. Am. Chem. Soc. 106 (1984) 7404.
[7] R.S. Nohr, P.M. Kuznesof, K.J. Wynne, M.E. Kenney, P.G.J. Siebenman, J. Am. Chem. Soc. 103 (1981) 4371.
[8] A.B.P. Lever, S. Licoccia, B.S. Ramaswamy, A. Kandil, D.V. Stynes, Inorg. Chem. Acta. 51 (1980) 169.
[9] T. Harazono, I. Takagishi, Bull. Chem. Soc. Jpn. 66 (1993) 1016.
[10] L.D. Rollman, R.T.J. Iwamoto, J. Am. Chem. Soc. 90 (1968) 1455.
[11] W.E. Ford, M.A.J. Rodgers, L.A. Schechtman, J.R. Sounik, B.D. Rihter, M.E. Kenney, Inorg. Chem 31 (1992) 3371.

[12] I. McCubbin, D.J. Phillips, J. Photochem. 34 (1986) 187.
[13] M.J. Cook, A.J. Dunn, S.D. Howe, A..J. Thomson, K.J. Harrison, J. Chem. Soc. Perkin Trans. 1 (1988) 2453.
[14] G. Ferraudi, G.A. Arguello, H. Ali, J.E. van Lier, Photochem. Photobiol. 47 (1988) 657.
[15] S.A. Mikhalenko, L.I.J. Solov'eva, Gen. Chem. USSR (Engl. Transl.) 61 (1991) 905.
[16] G.A. Casay, N. Narayanan, L. Evans III, T. Czuppon, G. Patonay, Tala. 43 (1996) 1997.
[17] S.A. Soper, Q.L. Mattingly, J. Am. Chem. Soc. 116 (1994) 3744.
[18] E.W. Abel, J.M. Pratt, R.J. Whelan, J. Chem. Soc. Dalton Trans. 6 (1976) 509.
[19] Y. Yang, J.R. Ward, R.P. Seiders, Inorg. Chem. 24 (1985) 1765.
[20] M. Yoon, Y. Cheon, D. Kim, Photochem. Photobiol. 58 (1993) 31.
[21] O. Ohno, N. Ishikawa, H. Matsuzawa, Y. Kaizu, H. Kobayashi, J. Phys. Chem. 93 (1989) 1713.
[22] O. Bilsel, J. Rodriguez, D. Holten, G.S. Girolami, S.M. Milam, K.S. Suslick, J. Am. Chem. Soc. 112 (1990) 4075.
[23] M.J. Stillman, T. Nyokong, Absorption and magnetic circular dichroism spectral properties of phthalocyanines part 1: complexes of the dianion Pc (-2), in: C.C. Leznoff, A.B.P. Lever (Eds.), Phthalocyanines: Properties and Applications, VCH Publishers, New York, 1989, pp. 133–290.
[24] A.K. Covington, T.H. Lilley, Trans. Farad. Soc. 63 (1967) 1749.
[25] J.H.R. Clarke, L.A. Woodward, Trans. Farad. Soc. 62 (1966) 2226.
[26] R.H. Dinius, G.R. Choppin, J. Phys. Chem. 66 (1962) 268.
[27] O.D. Bonner, A.L. Torres, J. Phys. Chem. 69 (1965) 4109.
[28] H. Cerfontain, A. Koeberg-Telder, C. Kruk, Tetra. Lett. 42 (1975) 3639.
[29] J. March, Advanced Organic Chemistry: Reactions, Mechanism, and Structure, 4th ed., Wiley-Intersciences, New York, 1992, p. 250.
[30] O.V. Malkova, I.Y. Bazlova, V.G. Andrianov, A.S. Semekin, B.D. Berezin, Russ. J. Phys. Chem. (Engl. Transl.) 71 (1997) 889.
[31] P.N. Moskalev, I.S. Kirlin, Russ. J. Inorg. Chem. (Engl. Transl.) 16 (1971) 57.

ELSEVIER

Talanta 48 (1999) 943–949

Talanta

Sequential metal vapor elution analysis for the determination of Cu and Mn in biological materials and waters

Kiyohisa Ohta *, Hiroya Uegomori, Satoshi Kaneco, Takayuki Mizuno

Department of Chemistry for Materials, Faculty of Engineering, Mie University, Mie, Tsu, 514-8507, Japan

Received 18 June 1998; received in revised form 14 September 1998; accepted 18 September 1998

Abstract

The determination of copper and manganese in biological materials and river waters by sequential metal vapor elution analysis (SMVEA) using an atomic absorption detector (AA) is reported. An improved molybdenum column (open column, i.d. 1.22 mm) with three ring supporters was developed for SMVEA. An optimum flow rate of carrier gas (pure argon) for separation of metal vapors was 4.0 ml min^{-1}. Copper and manganese peaks separated from Al, Ca, Cd, Fe, K, Mg, Na, Pb, and Zn peaks at a vaporization temperature of 1950°C and a column temperature of 1900°C. The appearing order of these metals was Cd, Zn, Pb, Cu, Na and Mn. It was understood by considering the boiling points of these metals or chlorides. The delay of appearing time is due to an interaction between the metal vapors and inside surface of the column. Under the experimental conditions, the number of theoretical plates was 11.3 for Cd, 89.6 for Cu, 160 for Na, and 258 for Mn in the improved column. Under the optimal experimental conditions, NIST biological standards and river waters were analyzed for copper and manganese. The analytical results agreed well with the certified values and the recoveries were in the range of 94 to 109%. By SMVEA, it was found that copper and manganese in biological materials and waters were determined without interference of matrix elements, after only acid digestion for biological materials and no chemical treatment for river water samples.

Keywords: Sequential metal vapor elution analysis (SMVEA); Cu and Mn; Biological materials; River water; Atomic absorption detection

1. Introduction

pn1In recent times, a separation system with a high temperature column (700–2000°C), sequential metal vapor elution analysis (SMVEA) has been demonstrated for separation and analysis of trace metal elements [1–10]. The advantages of SMVEA are: (a) direct separation of metal vapors; (b) rapid analysis without a prior chemical treatment; (c) simplicity; (d) elimination of spectral and chemical interferences occurring in conventional atomic absorption spectrometry (AAS) and inductively coupled plasma-atomic emission

* Corresponding author. +81-59-2319426; fax: +81-59-2319426/9427/9478/9442; e-mail: ohta@chem.mie-u.ac.jp.

0039-9140/99/$ - see front matter
PII S0039-9140(98)00307-5

spectrometry (ICP-AES); and (e) possibility as a powerful accessory of analytical instruments like mass spectrometer. However, in spite of the attraction, since there is the technical difficulty of instrumentation, little information has been reported.

Manganese and copper are essential elements for mammals, but the excess causes serious problems for the mammal body [11–13]. Recently, Mn has been suspected as one of the source substances for blackfoot and Parkinsonian diseases etc. [11,12]. Therefore, many researchers have reported the determination of copper and manganese in biological materials and waters by AAS, ICP-AES or ICP-mass spectrometry (MS) [11–29]. However, there are some problems such as optical and chemical interference for the determination in biological and water samples [16,27,30]. To eliminate the interference from matrix elements, adsorption [20], flotation [21,24,28,29], ion exchange [28,29], liquid–liquid extraction [22,28,29], matrix modifier [14,16,28,29], and standard addition [28,29] methods have been used. In the previous studies of SMVEA [1–10], it was found that SMVEA was useful for the elimination of the interferences on the determination of trace metal having relatively low melting point such as cadmium.

In this study, a separation of copper and manganese, having relatively high melting point, from Al, Ca, Cd, Fe, K, Mg, Na, Pb, and Zn by SMVEA-AA using an improved high temperature column (>1900°C) with argon carrier gas is investigated. The method is applied to the determination of Cu and Mn in biological and water samples.

2. Experimental

2.1. Apparatus and experimental conditions

An improved column used in the SMVEA system is shown in Fig. 1 (open column). The column consists of a molybdenum capillary tube (99.95% purity, Goodfellow) and three alumina tubes (2.5 mm i.d., 8 mm long). The molybdenum column is set in a Pyrex glass dome. Argon and hydrogen purge gas was flowed into the dome to prevent oxidation of the column. The column consists of vaporization part (60 mm) and separative part (190 mm). The vaporization part is connected to a transformer (YAMABISHI S-130-30, Cap.3 k VA) for heating to atomize sample. The separative part is heated with a power supply (dc generator, KIKUSUI PAD 35-60L). The alumina tubes were combined with three tungsten rods in a Pyrex glass dome and supported the molybdenum open column to prevent bending of the column during heating. A 0.5 mm diameter hole was drilled at the midpoint of the vaporization portion, in which sample was heated to vaporize, in

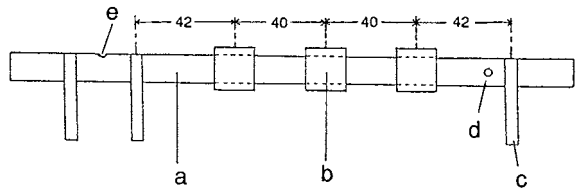

Fig. 1. An improved column for SMVEA. (a) Molybdenum column (250 mm long, 1.22 mm i.d.); (b) alumina tube (8 mm long, 2.8 mm i.d., 5.0 mm o.d.); (c) column supporter; (d) hole for detection; (e) hole for injection of sample.

Table 1
Apparatus and experimental conditions

SMVEA column: molybdenum column (250 mm long, 1.22 mm i.d.) with alumina tubes
Transformer: YAMABISHI S-130-30, Cap.3 k VA
Power supply: KIKUSUI PAD 35-60L
Column temperature: 1900°C, 2020°C
Dry temperature: 80°C for 10 s
Pyrolysis temperature: 210°C for 10 s
Vaporization temperature: 1950°C
Purge gas: Ar 3 l min^{-1} + H_2 0.2 l min^{-1}
Carrier gas: Ar 1.0, 2.0, 3.0, 4.0, 5.0 ml min^{-1}
Detector: atomic absorption spectrometer
Monochromator: Nippon Jarrell-Ash 0.5 m Ebert-type
Lock-in amplifier: NF LI-575
Storage oscilloscope: Kikusui 5516ST
Computer: EPSON PC-286VG
Light source: hollow cathode lamp, Hamamatsu photonics Co.
Al 309.3 nm, Ca 422.7 nm, Cu 324.8 nm, Cd 228.8 nm, Fe 248.3 nm, K 766.5 nm, Mg 285.2 nm, Mn 279.5 nm, Na 589.0 nm, Pb 217.0 nm, Zn 213.9 nm

Table 2
Retention times of SMVE peaks obtained with an improved column at 2020°C of column temperature, 1950°C of vaporization temperature and 1.0 ml Ar min^{-1} carrier gas[a]

Retention time	Element					
	Cd	Zn	Pb	Cu	Na	Mn
t_r, s	5.0	5.4	6.1	24.6	29.5	–
RSD of t_r,%	4.0	3.9	2.9	6.2	8.9	–

[a] $n = 3$–4, The signals of Mn, Al, Ca, Fe, K, and Mg did not appear.

Table 4
Retention times of SMVE peaks obtained with an improved column at 2020°C of column temperature, 1950°C of vaporization temperature and 3.0 ml Ar min^{-1} carrier gas[a]

Retention time	Element					
	Cd	Zn	Pb	Cu	Na	Mn
t_r, *s*	1.7	1.9	2.0	10.7	16.8	–
RSD of t_r, %	3.4	3.0	3.5	4.9	2.9	–

[a] $n = 3$–4, The signals of Mn, Al, Ca, Fe, K, and Mg did not appear.

the column to inject a sample solution. The detection portion has an 0.8 mm hole, perpendicular to the hole in the vaporization portion, for atomic absorption measurement. The apparatus and the experimental conditions for the measurements are shown in Table 1. The absorption signal from the amplifier was fed into the microcomputer. The temperature of column was measured with an optical pyrometer (Chino Works). Two pinhole apertures were placed in front of and in the rear of the detection hole to provide a narrow beam of light and to remove background emission from the column surface.

2.1.1. Reagents

All chemicals used were of analytical grade purity or spectroscopic purity. Stock solutions (10 mg ml^{-1}) of Al, Cu and Zn were prepared from the high purity metal as chlorides in 0.1 mol l^{-1} HCl, and Fe in 1 mol l^{-1} HCl. Stock solutions (10 mg ml^{-1}) of Ca, Cd, K, Mg and Na were prepared by solving the high purity chloride into water. Standard stock solutions (1 mg ml^{-1}, 1 mol l^{-1} HCl solution) of Pb and Mn (spectroscopic purity) were obtained from Nacalai Tesque Inc, Kyoto, Japan. A working solution for the separation study in SMVEA was made by mixing these stock solutions. The concentrations of Al, Ca, Cd, Cu, Fe, K, Mg, Mn, Na, Pb, and Zn in the working solution were 10, 1000, 1, 10, 1000, 1000, 1000, 50, 1000, 1, and 1 mg ml^{-1}, respectively.

Table 3
Retention times of SMVE peaks obtained with an improved column at 2020°C of column temperature, 1950°C of vaporization temperature and 2.0 ml Ar min^{-1} carrier gas[a]

Retention time	Element					
	Cd	Zn	Pb	Cu	Na	Mn
t_r, *s*	2.3	2.5	3.1	15.4	21.7	–
RSD of t_r, %	3.4	3.6	3.1	7.1	7.7	–

[a] $n = 3$–4, The signals of Mn, Al, Ca, Fe, K, and Mg did not appear.

2.1.2. Procedure

Biological samples (NIST standards), weighed accurately about 0.5 g, in a Uni-seal decomposition vessel were added 3 ml of nitric acid (14 M) and 1 ml of hydrogen peroxide (30%). Then the solution was put into an electric oven maintained at 120°C for 3 h to digest. The solution cooled was transferred into a Teflon beaker in a polyethylene glycol bath (110°C) to evaporate. Then the residue was dissolved in 5 ml of 6-M hydrochloric acid on the bath. The evaporation

Table 5
Retention times of SMVE peaks obtained with an improved column at 2020°C of column temperature, 1950°C of vaporization temperature and 5.0 ml Ar min^{-1} carrier gas[a]

Retention time	Element					
	Cd	Zn	Pb	Cu	Na	Mn
t_r, *s*	1.1	1.1	1.2	3.5	5.5	29.1
RSD of t_r, %	1.9	2.0	2.5	3.9	2.8	3.1

[a] $n = 3$–4, The signals of Al, Ca, Fe, K, and Mg did not appear.

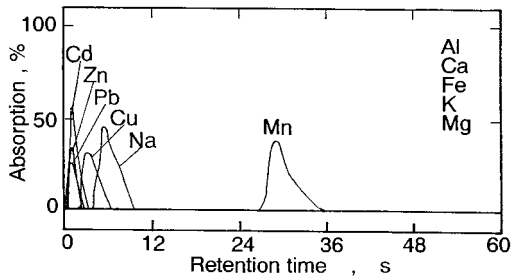

Fig. 2. SMVE peaks with an improved column at 2020°C of column temperature, 1950°C of vaporization temperature and 5.0 ml Ar min^{-1} carrier gas. Purge gas: Ar 3 l min^{-1} + H_2 0.2 l min^{-1}.

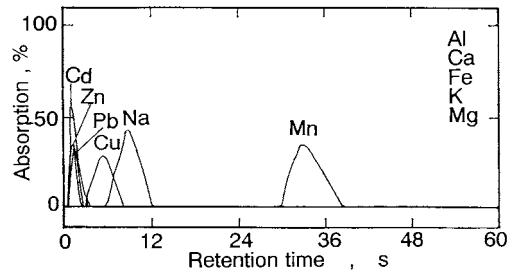

Fig. 3. SMVE peaks with an improved column at 1900°C of column temperature, 1950°C of vaporization temperature and 5.0 ml Ar min^{-1} carrier gas. Purge gas: Ar 3 l min^{-1} + H_2 0.2 l min^{-1}.

was repeated twice more with addition of hydrochloric acid in between. The residue was dissolved in 5 ml of 1-M hydrochloric acid. The solution was diluted to adequate volume (10–20 ml) with high purity water for SMVE measurements. Water samples spiked Cu and Mn were directly injected into a vaporization portion in the improved column without pretreatment.

For SMVEA measurements, after stopping the carrier gas, a 1 ml of the sample solution was pipetted into a vaporization portion in the molybdenum column. The sample solution was dried at 80°C for 10 s and pyrolyzed 210°C for 10 S. After flowing argon carrier gas again, the column was heated at 1900 or 2020°C and then the sample in the vaporization portion was vaporized at 1950°C for >60 s. The metal vapors were detected at a detection hole in the column by AAS. The temperatures of vaporization part and separation part in the column were measured with an optical pyrometer (Chino Works, Tokyo, Japan). During the pyrolyzing step at 210°C volatile organic compounds were removed.

3. Results and discussion

It was difficult for a formerly developed-column of SMVEA to be heated at more than 1700°C for a long time (>2 min) and a short life time because of bending of the column, so that it was difficult to separate metals having relatively high melting point like copper and manganese. To overcome the difficulties, three alumina tubes were used as a sheath of a molybdenum open column to prevent heat-bending. The tubes were bound to three bars with tantalum wire in a column chamber.

First, the effect of flow rate of carrier gas on the separation and retention time of Al, Ca, Cd, Cu, Fe, K, Mg, Mn, Na, Pb, and Zn was evaluated at 2020°C of column temperature and

Table 6
Retention times of SMVE peaks obtained with an improved column at 1900°C of column temperature, 1950°C of vaporization temperature and 5.0 ml Ar min^{-1} carrier gas[a]

Retention time	Element					
	Cd	Zn	Pb	Cu	Na	Mn
t_r, s	1.1	1.2	1.2	5.2	8.4	33.3
RSD of t_r,%	3.9	2.5	2.0	7.4	7.9	4.1

[a] $n=3$–4, The signals of Al, Ca, Fe, K, and Mg did not appear.

Table 7
SMVE peaks with an improved column at 1900°C of column temperature, 1950°C of vaporization temperature and 4.0 ml Ar min^{-1} carrier gas[a]

Retention time	Element					
	Cd	Zn	Pb	Cu	Na	Mn
t_r, s	1.8	1.9	1.9	7.6	13.1	44.8
RSD of t_r,%	5.2	3.6	4.0	6.0	3.7	5.0

[a] $n=3$–4, The signals of Al, Ca, Fe, K, and Mg did not appear.

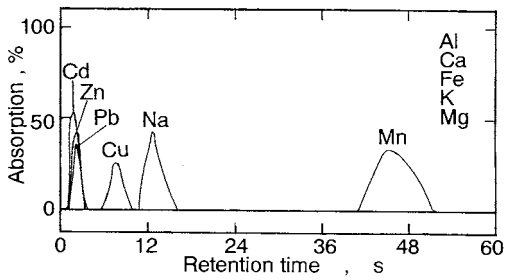

Fig. 4. SMVE peaks with an improved column at 1900°C of column temperature, 1950°C of vaporization temperature and 4.0 ml Ar min^{-1} carrier gas. Purge gas: Ar 3 l min^{-1} + H_2 0.2 l min^{-1}.

1950°C of vaporization temperature. Tables 2–5 show the retention times of Cd, Zn, Pb, Cu, Na, and Mn at 1.0, 2.0, 3.0 and 5.0 ml min^{-1} of argon carrier gas. At this column temperature, the SMVE peaks of Cd, Zn, Pb, Cu, and Na appeared at 1.0, 2.0 and 3.0 ml min^{-1} of argon, but the signals of Mn, Al, Ca, Fe, K, and Mg did not be observed. The SMVE peaks of Cd, Zn, Pb, Cu, and Na overlapped each other and did not separate. Mn vapor eluted in argon carrier gas of 5.0 ml min^{-1}, as shown in Fig. 2. At this carrier flow rate, therefore, the separation of Cu and Mn from others was investigated at lower column temperature (1900°C). The results are shown in Table 6 and Fig. 3. Even at the low temperature, the Cu peak did not separate from Cd, Zn, Pb and Na signals though Mn signal separated. Cu, Na and Mn SMVE signals did not appear at less than 1900°C of column temperature. Next, Cu and Mn separation was investigated at 4.0 ml min^{-1} argon carrier. Consequently Cu and Mn could be completely separated at 1900°C of column temperature and 1950°C of vaporization temperature, as shown in Table 7 and Fig. 4.

The order of appearance of these metals was Cd, Zn, Pb, Cu, Na, and Mn. It is reasonable by considering boiling points of these metals or chlorides (Cd 765°C, Zn 907°C, $PbCl_2$ 950°C, $CuCl_2$ 993°C decomposition to CuCl, NaCl 1413°C and Mn 1960°C) [31]. The chlorides of Pb, Cu, alkaline-earth metals and alkali metals are relatively stable <1900°C [32,33]. However, it could not be understood from boiling points of Mg, Ca, and K chlorides (1412°C, >1600°C, 1500°C subl) [31] that Mg, Ca, and K signals did not appear $>$ 2020°C of column temperature. These chloride vapors probably go through the improved column without decomposition at the column temperature. If it is assumed that the elution phenomena are caused only by boiling point of metal, first SMVE peak (Cd) must appear within 0.328 s ($0.174 \times 273 \times 60/(4 \times 2173)$, 0.174 ml; void volume of the column) at 1900°C of column temperature and 4.0 ml min^{-1} carrier gas, but in fact the signal appeared >1.8 s. This delay means an interaction between the metal vapors and inside surface of the column (Mo). However, there was no information concerning metal–Mo bond strengths. Therefore, we could not discuss the sequential elution on the basis of the interaction.

The retention volume for the separation by SMVEA, $V(t, T)$, is defined as follows;

$$V(t, T) = V_g(t, T_c) + V_h(t, T_v)$$

where $V_g(t, T_c)$ is related to a gas chromatographic separation at a column temperature of T_c in kelvin. Vaporized gaseous metals is governed by gas chromatographic principle in an open SMVE column. $V_h(t, T_v)$ is the term concerning a thermal separative principle at a vaporization temperature of T_v, which refers to physical properties (bond energy, melting point, boiling point and vapor pressure) of compounds and metals. t, conventionally called as retention time (t_r), is the time required for the metal vapor to reach an AA detector.

The number of theoretical plates N is given by

$$N = L/H = L^2/\sigma^2 = 5.54(t_r/W_{1/2})^2$$

where L is the length of the column in centimeters, H is the plate height, σ is the standard deviation of a measurement, and $W_{1/2}$ is the width of SMVE peak at half its maximum height. Under optimum experimental conditions (1900°C column temperature, 1950°C vaporization temperature, and 4.0 ml Ar min^{-1} carrier), the number of theoretical plates was 11.3 for Cd, 89.6 for Cu, 160 for Na, and 258 for Mn in the improved column.

3.1. Determination of Cu and Mn

SMVEA with an improved column was applied to the determination of copper and manganese in

Table 8
Determination of Cu and Mn in biological materials and water by SMVEA at 1900°C of column temperature and 1950°C of vaporization temperature[a,b]

Sample	Analyte amount, mg g^{-1} (mg ml^{-1} for water)				Recovery (%)
		Spiked	Found	Certified value	
Apple leaves	Cu	–	5.4 ± 0.8	5.64 ± 0.24	
(NIST SRM1515)	Zn	–	51 ± 5	54 ± 3	
Bovine liver	Cu	–	160 ± 10	158 ± 7	
(NIST SRM1577a)	Mn	–	9.5 ± 1.6	9.9 ± 0.8	
Oyster tissue	Cu	–	65 ± 5	63.0 ± 3.5	
(NIST SRM1566)	Mn	–	17 ± 1	17.5 ± 1.2	
Iwata	Cu	–	ND	–	
River		5	4.7 ± 0.3		94
		10	9.7 ± 1.7		97
	Mn	–	ND	–	
		10	9.9 ± 2.5		99
		20	21 ± 1		107
Shitomo	Cu	–	ND	–	
River		5	5.0 ± 0.9		100
		10	9.6 ± 0.9		96
	Mn	–	ND	–	
		10	11 ± 1		109
		20	21 ± 2		107

[a] $n = 5$–6.
[b] ND; not detected.

biological materials (NIST standard) and river waters. The calibration curves were prepared from copper and manganese standard solutions. The peak area of absorbance was measured for the analysis. The linear ranges of the calibration curves were up to 50 ng for manganese and up to 20 ng for copper. The analytical results obtained under optimal experimental conditions were in good agreement with the certified values, as shown in Table 8. The recoveries of spiked-manganese and copper in river waters were in the range of 94 to 107%. The results by the SMVEA-AA were also in good agreement with the spiked values. The RSDs for copper and manganese determinations in these samples were in a range of 4.8 to 25%. The relatively good precisions were obtained.

As described above, the improvement for a molybdenum column made the column long life and gave a direct separation of copper and manganese, which could not be separated until now, and manganese and copper vapors were separated from Al, Ca, Cd, Fe, K, Mg, Na, Pb, and Zn metals at a vaporization temperature of 1950°C and a column temperature of 1900°C, so that the interference of some elements observed by ETAAS could be eliminated. Consequently, under the experimental conditions, accurate determinations of manganese and copper in biological materials and river waters were possible after just only acidic digestion of the samples.

Acknowledgements

This work was supported financially by the Ministry of Education of Japan.

References

[1] K. Ohta, B.W. Smith, M. Suzuki, J.D. Winefordner, Spectrochim. Acta Part B 37 (1982) 343–347.
[2] K. Ohta, B.W. Smith, J.D. Winefordner, Anal. Chem. 54 (1982) 320–321.

[3] K. Ohta, B.W. Smith, J.D. Winefordner, Microchem. J. 32 (1985) 50–54.
[4] K. Ohta, N. Nakajima, S. Inui, J.D. Winefordner, T. Mizuno, Talanta 39 (1992) 1643–1645.
[5] K. Ohta, T. Sugiyama, S. Inui, T. Suzuki, T. Mizuno, J. Anal. At. Spectrom. 8 (1993) 595–597.
[6] K. Ohta, N. Yamanaka, S. Inui, J.D. Winefordner, T. Mizuno, Analyst 118 (1993) 1031–1033.
[7] K. Ohta, S. Inui, M. Yokoyama, T. Mizuno, Anal. Chim. Acta 285 (1994) 53–56.
[8] K. Ohta, H. Kawai, M. Yokoyama, T. Mizuno, Chem. Lett. 1996, 409–410.
[9] K. Ohta, Y. Koike, T. Mizuno, Anal. Chim. Acta 329 (1996) 191–195.
[10] K. Ohta, H. Taniguti, S. Itoh, T. Mizuno, Mikrochim. Acta 127 (1997) 51–54.
[11] B.S. Iversen, A. Panayi, J.P. Camblor, E. Sabbioni, J. Anal. At. Spectrom. 11 (1996) 591–594.
[12] T.-C. Pan, Y.-L. Chen, W.-J. Wa, C.-W. Huang, Jpn. J. Toxicol. Environ. Health 42 (1996) 437–442.
[13] J. Szpunar, J. Bettmer, M. Robert, H. Chassaigne, K. Cammann, R. Lobinski, O.F.X. Donard, Talanta 44 (1997) 1389–1396.
[14] P. Bermejo-Barrera, A. Moreda-Pineiro, J. Moreda-Pineiro, A. Bermejo-Barrera, Talanta 43 (1996) 1783–1792.
[15] U. Tinggi, C. Reilly, C. Patterson, Food Chem. 60 (1997) 123–128.
[16] H. InceTekgul, S. Akman, Spectrochim. Acta Part B 57B (1997) 621–631.
[17] F. Deutsch, P. Hoffmann, H.M. Ortner, Fresenius J. Anal. Chem. 357 (1997) 105–111.
[18] N.D. Kareva, Zavod. Lab. B 62 (1996) 28–29.
[19] P. Bermejo-Barrera, A. Moreda-Pineiro, J. Moreda-Pineiro, A. Bermejo-Barrera, J. Anal. At. Spectrom. 12 (1997) 301–306.
[20] M. Yaman, Chem. Anal.(Warsaw) 42 (1997) 79–86.
[21] T. Stafilov, S. Atanasov, Analusis 24 (1996) 371–374.
[22] C.A. de Abreu, M.F. de Abbreu, L.H. Soares, J.C. de Andrade, Commun. Soil Sci. Plant Anal. 28 (1997) 1–11.
[23] D.T. Takuwa, G. Sawula, G. Wibetoe, J. Anal. At. Spectrom. 12 (1997) 849–854.
[24] K. Cundeva, T. Stafilov, Anal. Lett. 30 (1997) 833–845.
[25] J.G. Williams, B.C.H. Gibson, E. Temmerman, C. De-Cuyper, Analyst 121 (1996) 1928–1933.
[26] L. Racz, L. Papp, B. Prokai, Z. Kovacs, Microchem. J. 54 (1996) 444–451.
[27] W. Frech, E. Lundberg, A. Cedergren, Prog. Anal. At. Spectrosc. 8 (1985) 308–312, 316–320.
[28] K.S. Subramanian, Prog. Anal. At. Spectrosc. 9 (1986) 246–251, 286–291.
[29] K.S. Subramanian, Prog. Anal. At. Spectrosc. 11 (1988) 553–555, 576.
[30] J.W. Robinson, In Atomic Spectroscopy, 2nd ed., Marcel Dekker, New York, 1996, pp. 320–322.
[31] D.R. Lide, (Ed.), Handbook of Chemistry and Physics, 72nd ed., CRC Press, Boston, 1991, pp. 4–46, 47, 56, 67, 71, 73, 85, 98, 111.
[32] M. Suzuki, K. Ohta, Prog. Anal. At. Spectrosc. 6 (1983) 49–162.
[33] M. Suzuki, K. Ohta, Anal. Chim. Acta 151 (1983) 401–407.

ELSEVIER

Talanta 48 (1999) 951–957

Talanta

Solubilities of some recently synthesized 1,8-dihydroxy-9,10-anthraquinone derivatives in supercritical carbon dioxide

Mohammad Reza Fat'hi [a], Yadollah Yamini [a], Hashem Sharghi [b], Mojtaba Shamsipur [c,*]

[a] *Department of Chemistry, Tarbiat Modarres University, Tehran, Iran*
[b] *Department of Chemistry, Shiraz University, Shiraz, Iran*
[c] *Department of Chemistry, Razi University, Kermanshah, Iran*

Received 15 May 1998; received in revised form 2 September 1998; accepted 25 September 1998

Abstract

The solubility of four recently synthesized 1,8-dihydroxy-9,10-anthraquinone derivatives, as potential complexing agents in some extraction and membrane transport experiments, have been measured in supercritical carbon dioxide. The measurements were carried out in the pressure range 120–400 atm at temperatures 35, 45, 55, 65, and 75 °C. The measured solubilities were correlated using the model proposed by Chrastil. The calculated results show good agreement with the experimental data. © 1999 Elsevier Science B.V. All rights reserved.

Keywords: 1,8-Dihydroxy-9,10-anthraquinones; Solubility data; Supercritical CO_2

1. Introduction

In the past 2 decades increasing attention has been focused on the supercritical fluid extraction (SFE) as an interesting alternative to conventional extraction methods [1,2]. The most widely used supercritical fluid is carbon dioxide because it is nontoxic, nonflammable, and relatively inexpensive and possesses reasonable critical properties as well as high solvent power for a wide range of nonpolar and intermediately polar organic compounds [2]. The use of SFE method has provided both analytical and large-scale techniques for organic waste extraction from contaminated matrices [3,4]. In recent years, the supercritical fluids modified by the addition of complexing agents have been used in the development of analytical methods for the extraction of metal ions from various solid and liquid matrices [5]. Information on solubilities in supercritical fluids is perhaps the most important thermophysical property that must be determined and modelled in order to efficiently design the extraction procedures based on supercritical solvents.

* Corresponding author. Tel.: +98-831-94066; fax: +98-831-831618.

0039-9140/99/$ - see front matter
PII S0039-9140(98)00302-6

9,10-Anthraquinones are the largest groups of natural quinones and historically the most important. In addition to a wide variety of chemical and industrial applications [6–8], recently synthetic derivatives of anthraquinones, as well as naturally occurring derivatives, have been used for medical purposes [7,9]. While there are numerous reports available on the solubility of low-volatility organic compounds such as alkanes, aromatic hydrocarbons, alcohols, phenols, acids, etc. [1], limited studies on the solubility of solid aromatic carbons (e.g. quinones, anthrones and anthraquinones) are reported in the literature [10–12].

Due to the special importance of 1,8-dihydroxy-9,10-anthraquinones as metal ion complexing agents in analytical chemistry [7,8,13], in recent years we have been involved in the synthesis [14–16], acid–base studies [17–19] and some applications in extraction and membrane transport [20,21] of new derivatives of these quinone compounds. Due to the key role of the solubility data of chelating agents in supercritical CO_2 in the design of analytical SFE methods, in this paper we determined the solubilities of four 1,8-dihydroxy-9,10-anthraquinone derivatives, recently synthesized by this research group [14], in supercritical carbon dioxide over a wide range of temperatures and pressures. The measured solubilities were nicely correlated using the model proposed by Chrastil [22].

2. Experimental

HPLC grade methanol (Aldrich) was used as received. Pure carbon dioxide (Sabalan Tehran, 99.99%) was used for all SFEs. Reagent grade 1,8-dihydroxy-9,10-anthraquinone (A1, Merck) was of the highest purity available and used as received. 1-Hydroxy-4-(prop-2′-enyloxy)-9,10-anthraquinone (A2), 1,8-bis(prop-2′-enyloxy)-9,10-anthraquinone (A3) and 1,8-dihydroxy-2,7-bis (prop-1′-enyl)-9-10-anthraquinone (A4) were synthesized [14] and used after recrystallization from pure benzene and vacuum drying. Structures of the anthraquinone derivatives used are given in Fig. 1.

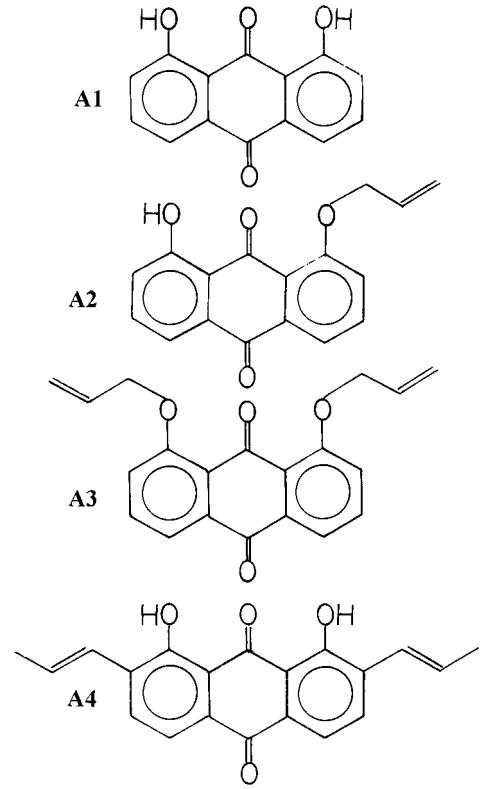

Fig. 1. Structures of anthraquinones.

A Suprex MPS/225 integrated SFE–SFC system modified for the solubility determination in SFE mode was used. A schematic diagram of the modified static system used is shown in Fig. 2. Solubility measurements were accomplished with

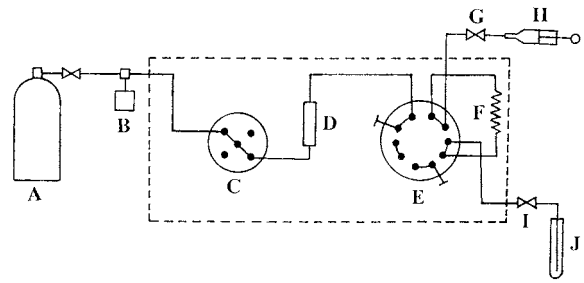

Fig. 2. Schematic diagram of experimental apparatus for measuring solubilities: (A) CO_2 gas tank; (B) supercritical fulid pump; (C) 5-port, 4-position valve; (D) 1 ml equilibrium cell; (E) 10-port, 2-postition valve; (F) injection loop; (G) on/off valve; (H) syringe; (I) microadjust valve; (J) collection vial.

Table 1
Solubility of naphthalene in supercritical carbon dioxide at 35°C

P (atm)	10^3y				
	This work	Ref. [23]	Ref. [24]	Ref. [25]	Ref. [26]
105.6	11.6	–	11.7	–	–
136.2	14.2	14.1	–	13.9	–
165.8	16.2	16.5	–	–	–
201.3	17.4	17.6	–	–	17.59

a 1 ml extraction vessel in the pressure range from 120 to 400 atm at temperatures 35, 45, 55, 65, and 75 °C for a duration of 15 min. The solid solutes (100–200 mg) were mixed well with some 1 g of glass beads and packed into the extraction vessel. This procedure prevents channelling, increases the contact surface between the sample and the supercritical fluid and, consequently, reduces the equilibration time. Sintered stainless steel filters (5 μm) were used to prevent any carryover of the solutes. Supercritical CO_2 was pressurized and passed into the vessel D through the 5-port, 4-position valve C. After reaching equilibrium at the desired temperature and pressure (for about 15 min), a 122 μl portion of the saturated supercritical CO_2 was loaded into injection loop F by means of a 10-port, 2-position valve E. Then the loop was depressurized into the collection vial J containing a known volume of methanol by switching the injection valve E. In order to prevent solvent dispersal, the depressurizing rate of the sample loop was adjusted by the valve I. Finally, the G and I valves were opened completely and the sample loop was washed with some methanol and collected into the collection vial J.

The solubilities were calculated by absorbance measurements at λ_{max} of each compound using a Model 2100 Shimadzu UV–Vis spectrophotometer. The stock solutions of the compounds Al–A3 (100 ppm) were prepared by dissolving appropriate amounts of the solid samples in methanol. A set of standard solutions was then prepared by appropriate dilution of the stock solutions. The calibration curves obtained (with regression coefficients better than 0.999) were used to establish the concentration of the anthraquinone derivatives in the collection vial.

3. Results and discussion

In recent years, the use of supercritical fluids modified by the addition of complexing agents in the extraction of metal ions from various solid and liquid matrices has grown rapidly [5,23–26]. The need for charge neutralization of metal ions is the most important aspect in their SFE. The addition of a proper complexing agent to the supercritical fluid phase can not only neutralize the charge on the metal ion, but also will introduce some tipophilic groups to the metal–ligand system, so that the solubilization of the metal complex into the supercritical fluid will be facilitated. Obviously, a search for promising complexing agents would be of vital importance. We have recently used some 1,8-dihydroxy-9,10-anthraquine derivatives such as A4 as suitable ligands in construction of lead ion-selective electrodes [21] and in solid phase extraction of Pb^{2+} ions [27]. In this work, the solubility of the anthraquinone derivatives were determined, as a first step in investigating the possibility of their use in the SFE of metal ions with carbon dioxide.

The reliability of the apparatus and the experimental method was checked by measuring the solubilities (mole fraction, y) of naphthalene in supercritical carbon dioxide at 35°C and different pressures and the results are summarized in Table 1. The values given in Table 1 are obtained from an arithmetic average of three replicate measurements with relative standard deviations $< 3\%$. These solubility data are in good agreement with those reported previously [28–31] (Table 1). The largest relative deviation is about 2%.

Table 2 represents the solubilities of anthraquinones A1–A4 at temperatures 35, 45, 55,

65, and 75°C over a pressure range from 120 to 400 atm. The resulting solubilities are reported in terms of equilibrium mole fraction, y, of the solute and in g l^{-1}, s, of the solute in supercritical carbon dioxide. Each reported datum is the average of at least three replicate samples. The mole fractions of the solutes were reproducible within $\pm 2\%$.

The data given in Table 2 revealed that the solubilities of the solutes increase with pressure at

Table 2
Solubilities of anthraquinones A1–A4 in supercritical carbon dioxide

T (°C)	P (atm)	ρ (g l^{-1})	A1		A2		A3		A4	
			$10^4 y$	s (g m^{-3})	$10^4 y$	s (g m^{-3})	$10^4 y$	s (g m^{-3})	$10^4 y$	s (g m^{-3})
35	120	770	0.22	9	2.5	121	–	–	0.8	29
	160	833	0.30	12	3.7	199	–	–	1.2	47
	200	871	0.41	20	4.7	264	–	–	2.9	132
	240	898	0.49	24	5.5	314	–	–	–	–
	280	922	0.54	27	6.4	377	–	–	4.2	243
	320	942	0.56	29	7.0	426	–	–	7.0	381
	360	960	0.62	32	7.8	478	–	–	9.3	547
	400	975	–	–	8.5	531	–	–	10.3	676
45	120	665	0.20	8	1.9	82	0.36	18	–	–
	160	763	0.31	13	3.8	187	0.43	24	0.6	26
	200	815	0.47	21	5.6	290	0.45	27	2.4	122
	240	852	0.55	26	7.4	399	0.55	36	4.8	266
	280	880	0.64	31	9.0	504	0.63	42	7.6	426
	320	905	0.75	37	0.2	590	0.68	46	9.5	554
	360	924	0.83	42	11.5	677	0.71	49	11.0	700
	400	945	–	–	12.4	745	–	–	–	–
55	120	524	0.21	6	1.5	50	–	–	–	–
	160	685	0.39	15	4.1	178	0.80	40	1.8	90
	200	757	0.56	23	6.8	328	0.88	49	3.8	207
	240	805	0.63	28	9.0	463	0.91	53	7.1	410
	280	838	0.88	40	11.3	604	0.94	57	8.1	492
	320	867	1.03	49	13.7	754	1.01	63	9.4	609
	360	889	1.12	54	16.0	907	1.19	77	11.0	752
	400	909	–	–	–	–	1.25	83	11.4	779
65	120	397	0.19	4	1.0	26	0.43	12	1.9	90
	160	601	0.54	18	4.1	155	0.92	40	3.5	194
	200	695	0.83	31	7.7	340	1.52	77	5.1	303
	240	754	1.08	45	11.6	556	–	–	7.2	448
	280	796	1.18	50	15.4	778	1.67	96	8.9	570
	320	828	1.26	57	19.3	1017	2.03	22	10.3	681
	360	854	1.54	71	22.7	1238	2.39	48	11.2	761
	400	876	–	–	25.9	1446	2.53	161	11.6	785
75	120	328	0.14	2	–	–	0.50	12	5.4	300
	160	519	0.54	15	–	–	0.85	32	4.3	440
	200	631	0.93	32	–	–	2.04	94	8.8	558
	240	702	1.28	49	–	–	2.90	148	–	–
	280	750	1.40	57	–	–	3.63	199	11.4	766
	320	788	1.65	71	–	–	4.64	266	12.3	862
	360	818	2.02	90	–	–	4.83	287	13.9	967
	400	843	–	–	–	–	5.34	328	15.6	1109

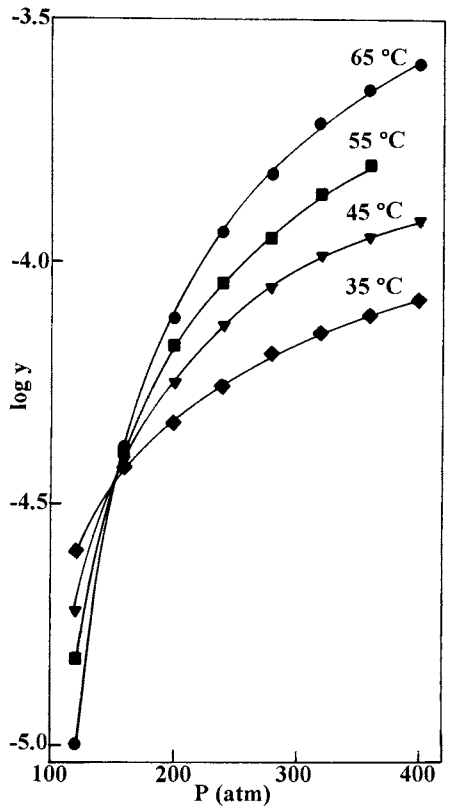

Fig. 3. Solubility isotherms for anthraquinone A2.

any constant temperature; the effect of pressure on the solubilities being more pronounced at higher temperatures. However, this considerable increase in solubility with temperature occurs despite the decreased density of supercritical CO_2 at elevating temperatures. This observation is in contrast to the conventional wisdom stating that the density of a supercritical fluid increase in order to increase both the solubility and the extraction efficiency [32]. While increasing supercritical fluid density at a constant temperature generally does increase solubility, increasing density at a constant pressure (by lowering temperature) results in diminished anthraquinone solubility.

Sample solubility isotherms for anthraquinone A2 are shown in Fig. 3. As it is seen from Fig. 3, the curves of solubility increase very steeply with pressure. The pressures above the region of steep increase are suitable for the supercritical extraction. Moreover, it is interesting to note that there is a clear crossover point in the resulting solubility–pressure curves, which is the cross point of two or more isotherms. Beyond the crossover point, solubility increases with increasing both pressure and temperature, while below this point, solubility increases with the increased pressure but decreases with increased temperature. A similar retrograde solubility (crossover/pressure effect) behavior for the solubility of different organic compounds in supercritical CO_2 has been reported in the literature [12,33,34]. It is interesting to note that in all cases, for a given pressure above the crossover points, the highest solubility values were observed at the lowest density for the anthraquinones (i.e. highest temperatures).

The observed different effects of temperature on solubility of compounds A1–A4 could be due to the influences of temperature on such diverse properties of the system as the solute vapor pressure, the solvent density and the intermolecular interactions in the supercritical fluid phase. At lower pressures, the fluid density is lowered by small increases in temperature. Since the density effect predominates at this region, the solubility will decrease with increasing temperature. While, at higher pressures, the fluid density is less dependent on temperature so that the observed increase in solubility with temperature could be primarily due to other factors, especially the higher vapor pressure of the solid samples.

The results obtained in this study indicate that, among different 1,8-dihydroxy-9,10-anthraquinone derivatives used, compound A2 and A1 show the highest and lowest solubility in supercritical CO_2, respectively. The diminished solubility of A1 can be related to the self-association and possible intermolecular interactions, mainly via H-bonding, in the solid state [35]. However, substitution of the enyl groups on the mother compound A1 will result in enhanced solubility in supercritical CO_2, mainly due to the reduced chance of solute–solute interactions in the system. On the other hand, compound A2 with only one substituted enyl group and smaller molecular size than A3 and A4 (both bearing two substituted enyl groups) is expected to show the highest solubility in the series [34,36].

The experimental solubility data for the anthraquinones A1–A4 were correlated using the model proposed by Chrastil [22]. This model is based on the hypothesis that each molecule of a solute (S) associates with k molecules of supercritical solvent (C) to from a solvato complex (SC_k) in equilibrium with the system. The model proposes a linear relationship between the logarithm of the solubility, s, and the logarithm of fluid density, ρ, as follows

$$\ln(s) = k \ln(\rho) + a/T + b \quad (1)$$

where

$$a = \Delta H/R$$

and

$$b = -\ln[M_C^k/(M_S + kM_C)] + q$$

s is solubility, ρ is the fluid density, T is absolute temperature, k is the dissociation number, ΔH is the total heat of reaction (i.e. heat of solvation plus heat of vaporization of the solute), q is a constant, and M_S and M_C are the molecular weights of the solute and solvent, respectively. The $\ln s$ is a linear function of $1/T$ at constant density and has a slope given by a. The value of b can be chosen to minimize the deviation of the model from experimental data.

The solubility data obtained in this study show the expected linear relationship predicted by the Chrastil model. Sample plots of $\ln s$ versus $\ln \rho$ for compound A2 at various temperatures are shown in Fig. 4. The straight lines reported in Fig. 4 are the best fit of Eq. (1) to the solubility data. The slopes of the solubility isotherms are with a good approximation equal. The optimum calculated values of k, a, and b for solutes A1–A4 are given in Table 3.

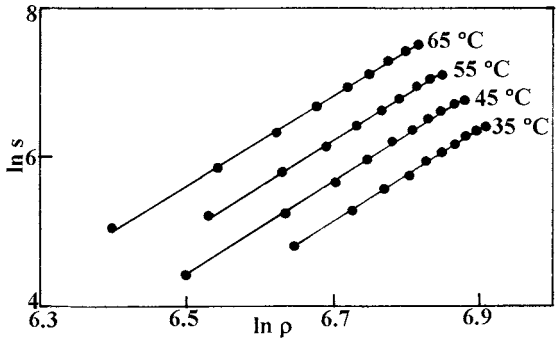

Fig. 4. Plots of solubility against density of supercritical CO_2 for anthraquinone A2.

Table 3
Solubility constants of Chrastil model for anthraquinones A1–A4 in supercritical CO_2

Anthraquinone	k	a	b
A1	4.65	–5800	3.1
A2	6.16	–5632	23.7
A3	4.34	–7897	28.3
A4	6.06	–932	9.2

It is noteworthy that the comparison of the solubility data given in Table 2 with those reported for some ionizable crown ethers (which were used for selective extraction of mercury by supercritical CO_2) [26] revealed a more or less similar behavior. Thus, ionizable anthraquinones bearing some lipophilic groups (e.g. compounds A2 and A4) [18] could be considered as potential candidates for the SFE of metal cations such as Pb^{2+} ion. Of course, the extraction efficiency of the resulting metal complexes is expected to influence by several parameters, including pressure and temperature of supercritical CO_2, the nature of modifier, the identity of the metal and its oxidation state and the complexant functional groups [37].

References

[1] K.D. Bartle, A.A. Clifford, S.A. Jafar, G.F. Shilstone, J. Phys. Chem. Ref. Data 20 (1991) 713.
[2] M. McHugh, V. Krukonis, Supercritical Fluid Extraction, 2nd ed., Butterworth-Heinemann, MA, 1994.
[3] K.M. Dooley, C.C. Koa, R.P. Gambrell, R.C. Knopf, Ind. Eng. Chem. Res. 26 (1987) 2058.
[4] S.J. MacNaughton, N.R. Foster, Ind. Eng. Chem. Res. 33 (1994) 2757.
[5] N.G. Smart, T. Carleson, T. Kast, A.A. Clifford, M.D. Burford, C.M. Wai, Talanta 44 (1997) 137 (and references therein).
[6] R.H. Thomson, Naturally Occurring Quinones, Academic Press, New York, 1971.
[7] M. Luckner, Secondary Metabolism in Microorganisms, Plants and Animals, Springer-Verlag, Berlin, 1984.

[8] G.A. Qureshi, G. Svehla, M.A. Leonard, Analyst 104 (1979) 705.
[9] F. Arcamone, Med. Res. Rev. 14 (1984) 153.
[10] W.J. Schmitt, R.C. Reid, J. Chem. Eng. Data 31 (1986) 204.
[11] P. Coutsikos, K. Magoulas, D. Tassios, J. Chem. Eng. Data 42 (1997) 463.
[12] M.R. Fat'hi, Y. Yamini, H. Sharghi, M. Shamsipur, J. Chem. Eng. Data 43 (1998) 400.
[13] P.L. Gutierrez, B. Nguyen, in: G. Dryhurst, K. Niki (Eds.), Redox Chemistry and Interfacial Behavior of Biological Molecules, Plenum, New York, 1988.
[14] F. Tamaddon, MS Thesis, Shiraz University, Shiraz, Iran, 1991.
[15] H. Sharghi, A. Forghaniha, Iran. J. Chem. Chem. Eng. 14 (1995) 16.
[16] H. Sharghi, A. Forghaniha, J. Sci. I. R. Iran 7 (1996) 89.
[17] M. Shamsipur, J. Ghasemi, F. Tamaddon, H. Sharghi, Talanta 40 (1993) 697.
[18] S. Rouhani, R. Rezaei, H. Sharghi, M. Shamsipur, G. Rounaghi, Microchem. J. 52 (1995) 22.
[19] D. Almasifar, A. Forghaniha, Z. Khojasteh, J. Ghasemi, H. Sharghi, M. Shamsipur, J. Chem. Eng. Data 42 (1997) 1212.
[20] S. Dadfarnia, M. Shamsipur, F. Tamaddon, H. Sharghi, J. Membr. Sci. 78 (1993) 115.
[21] N. Tavakkoli, Z. Khojasteh, H. Sharghi, M. Shamsipur, Anal. Chim. Acta 360 (1998) 203.
[22] J. Chrastil, J. Phys. Chem. 86 (1982) 3016.
[23] K.E. Laintz, J.J. Yu, C.M. Wai, Anal. Chem. 64 (1992) 311.
[24] K.E. Laintz, C.M. Wai, C.R. Yonker, R.D. Smith, Anal. Chem. 64 (1992) 2875.
[25] Y. Lin, N.G. Smart, C.M. Wai, Trends Anal. Chem. 14 (1995) 123.
[26] S. Wang, S. Elshami, C.M. Wai, Anal. Chem. 67 (1995) 919.
[27] F. Raoufi, Y. Yamini, H. Sharghi, M. Shamsipur (1998) (submitted for publication).
[28] Y. Iwai, T. Fukuda, Y. Koga, Y. Aral, J. Chem. Eng. Data 36 (1991) 430.
[29] Y.V. Tsckhaskaya, M.B. Iomtev, E.V. Muskina, Rus. J. Phys. Chem. (Engl. Transl.) 38 (1964) 1173.
[30] E. Reverchon, P. Russo, A. Stassi, J. Chem. Eng. Data 38 (1993) 458.
[31] S. Mitra, J.W. Chen, D.S. Viswanath, J. Chem. Eng. Data 33 (1988) 35.
[32] D.J. Miller, S.B. Hawthorne, Anal. Chem. 67 (1995) 273.
[33] Z. Kenz, M. Skerget, P. Sencar-Bozic, A. Rizner, J. Chem. Eng. Data 40 (1995) 216.
[34] K.L. Tsai, F.N. Tsai, J. Chem. Eng. Data 40 (1995) 264.
[35] W.J. Schmitt, R.C. Reid, J. Chem. Eng. Data 31 (1986) 204.
[36] T. Nakatani, T. Tohdo, K. Ohgaki, T. Katayama, J. Chem. Eng. Data 36 (1991) 314.
[37] N.G. Smart, Y. Lin, C.M. Wai, Environ. Lab. Chem. (February 1996) 26.

ELSEVIER

Talanta 48 (1999) 959–966

Talanta

Determination of trace metals in waters and compost by on-line precipitation coupled to flame atomic absorption spectrophotometry or ion chromatography

A. Martín-Esteban [a,1], R.M. Garcinuño [a], S. Angelino [b], P. Fernández [a], C. Cámara [a,*]

[a] *Departamento de Química Analítica. Facultad de Ciencias Químicas. Universidad Complutense de Madrid. 28040 Madrid, Spain*
[b] *Dipartimento di Chimica Analitica. Universita' di Torino. Via Pietro Giuria, 5. 10125 Torino, Italy*

Received 6 May 1998; received in revised form 18 September 1998; accepted 25 September 1998

Abstract

A general rapid on-line preconcentration method for the determination of trace metals coupled to flame atomic absorption spectrophotometry (FAAS) or ion chromatography (IC) with spectrophotometric detection is described. The method is based on the on-line precipitation of metal hydroxides with sodium hydroxide and their dissolution in a small volume of nitric acid solution. All the chemical and physical variables that affect the efficiency of metal precipitation and elution in the flow injection system have been studied. The detection limits obtained by FAAS are 0.1, 0.3, 0.5 and 0.5 μg l^{-1} for Zn, Cu, Ni and Pb, respectively. When the on-line precipitation is coupled to IC with post-column derivatization with the spectrophotometric reagent 4-(2-pyridylazo) resorcinol (PAR), the detection limits are 3, 1, 5, 3, and 3 μg l^{-1} for Cu, Zn, Ni, Co and Mn, respectively. The proposed general method was successfully applied to determine independently the above mentioned metals in compost and tap and river water samples.

Keywords: Trace metals; On-line precipitation; Flame atomic absorption spectrophotometry; Ion chromatography

1. Introduction

Industrial activities have produced an increase in the concentration of several heavy metals present in environmental waters. Heavy metals are usually determined by flame atomic absorption spectrophotometry (FAAS) due to its rapidity and simplicity, but this technique is not sensitive enough to allow the determination of metals at very low concentration levels. The simultaneous determination of trace metals can be also carried out by ion chromatography coupled to different detectors, but this technique also lacks sensitivity. Therefore, it is usually necessary to

* Corresponding author. Tel.: +34-91-3944318; fax: +34-91-3944329; e-mail: ccamara@eucmax.sim.ucm.es.

[1] Present address: Departamento de Química, Facultad de Ciencias, Universidad Europea de Madrid-CEES, Villaviciosa de Odón, E-28670 Madrid, Spain.

0039-9140/99/$ - see front matter
PII S0039-9140(98)00303-8

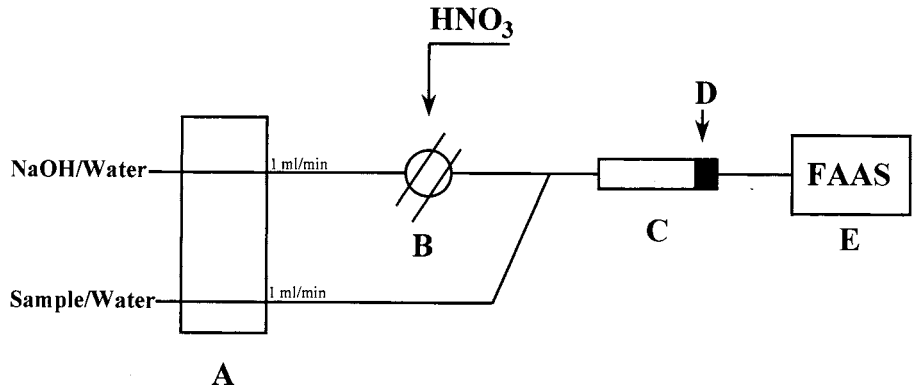

Fig. 1. FIA system for metal preconcentration by FAAS. (A) Peristaltic pump; (B) injection valve; (C) PTFE microcolumn filled with zirconia spheres; (D) PTFE filter; (E) detector.

include a previous trace enrichment step which allows not only metal preconcentration but also the separation of the analyte from the matrix components. Since flow injection analysis (FIA) first appeared in the literature [1], the development of on-line preconcentration methods, such as ion-exchange, liquid–liquid extraction, etc. coupled to different detection techniques has grown considerably.

Precipitation is a common separation and/or preconcentration technique in classical analytical chemistry, although it is less frequently used in FIA. Only there was a certain activity in this field at the end of the eighties, when several methods using on-line precipitation systems were developed. In every case, the flow injection system was coupled to FAAS allowing the direct determination of several metals, such as lead [2], copper [3] and calcium [4], and the indirect determination of anions such as sulphide [5] and halides (chloride and iodide) [6]. However, since then there has not been any attempt to continue in this direction. This is perhaps due to the opinion that precipitation and filtration are not well defined processes under flow conditions and to the tendency of precipitates to be adsorbed on the inner walls of manifold tubing and the need to periodically clean the whole system, as well as the risk of backpressures in the flow system. The latter was sorted out by using knotted reactors, however the amount of precipitate handled is limited by the length of the reactor and so the sample volumes typically used are lower than 5 ml [7,8]. We consider that the on-line precipitation technique can be a useful tool if the analyte readily forms a filterable precipitate which is rapidly dissolved by a small volume of a suitable reagent in order to obtain sharp FIA peaks.

Accordingly, the aim of this work is to develop an analytical method for the determination of several metals (Zn, Cu, Ni, Co, Pb, Hg, and Mn) in compost and tap and river water by on-line precipitation of their corresponding hydroxides which are easily dissolved in nitric acid and subsequent determination of the metals either by FAAS or by ion chromatography with postcolumn derivatization with the spectrophotometric reagent 4-(2-pyridylazo) resorcinol (PAR) [9].

2. Experimental

2.1. Apparatus

A Perkin Elmer 2380 atomic absorption spectrophotometer optimised for the determination of each metal equipped with its corresponding hollow cathode lamp with an air–acetylene flame was used. The instrument settings were: absorption line 217 nm and width 0.7 nm for Pb, 232 and 0.2 nm for Ni, 213.9 and 0.7 nm for Zn and 324.8 and 0.7 nm for Cu. The analytical signal was monitored on a XT-chart recorder (Perkin Elmer).

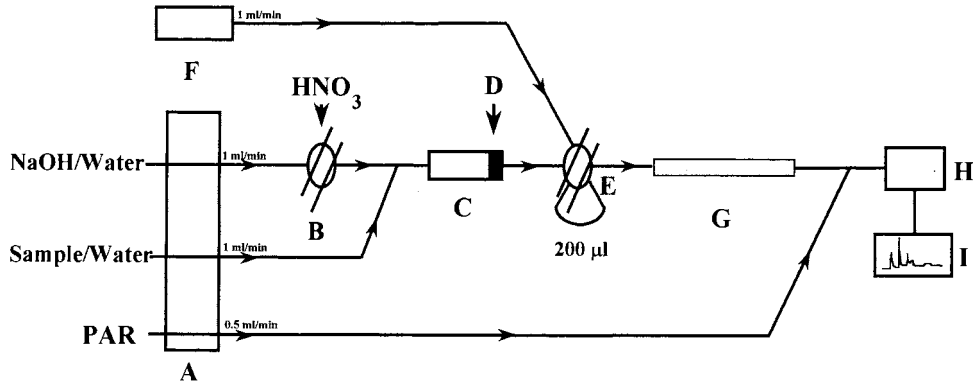

Fig. 2. FIA system for metal preconcentration by ion chromatography. (A) Peristaltic pump; (B) injection valve; (C) PTFE microcolumn filled with zirconia spheres; (D) PTFE filter; (E) injection valve; (F) high pressure pump; (G) analytical column; (H) detector; (I) chart recorder.

A Perkin Elmer 1100B atomic absorption spectrophotometer equiped with a Perkin Elmer HGA 400 graphite furnance was used for method validation purposes.

A Gilson HP4 peristaltic pump, an Omnifit six-way injection valve, polytetrafluoroethylene (PTFE) tubes and Omnifit connectors were used in the flow injection system (Fig. 1). The filtration unit, inserted in the manifold, consisted of a microcolumn made of PTFE tube (2.5 cm × 5 mm i.d.) filled with zirconia spheres (1.5 mm diameter) (Glen Creston). A PTFE filter (J.T. Baker) with a pore size of 0.45 μm, 5 mm diameter and 1 mm thickness was fitted at the end of the PTFE tube.

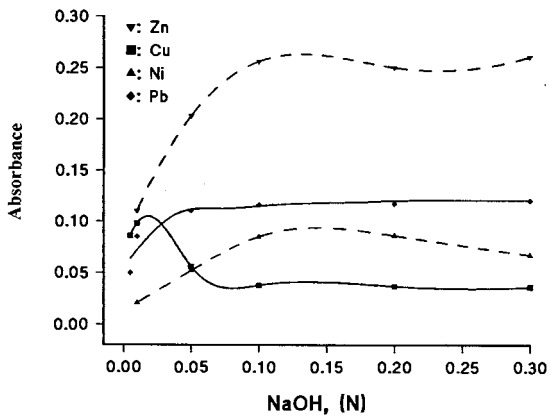

Fig. 3. Effect of NaOH concentration on analyte response. Metal concentrations: 50 μg^{-1}; Sample volume: 10 ml.

The ion chromatography system consisted of a PU-980 high pressure pump (Jasco) coupled with a spectroMonitor 3100 (Milton Roy) and a chart recorder (Hitachi). The analytical column was a 25 cm × 4.6 mm i.d. packed Spherisorb SCX 5 μm purchased from Symta.

A Microwave Sample Preparation System MSP 1000 (CEM) was used in the mineralization of compost samples.

2.2. Reagents

Standard working metal solutions were prepared daily by appropriate dilution of 1000 mg l^{-1} stock metal solutions (Spectrosol) obtained from BDH. Sodium hydroxide (Merck), nitric acid (Carlo Erba), tartaric acid (Merck) and PAR (Fluka) were also used. All the reagents employed were analytical-reagent grade.

PAR solution (0.2 mM) was prepared in 1 M acetic acid and 3 M ammonium hydroxide medium.

Final solutions were prepared in high purity water from a Milli-Q water system (Millipore).

2.3. Procedure

2.3.1. On-line precipitation coupled to FAAS

A schematic diagram of the flow injection system is shown in Fig. 1. Standard solutions, aqueous samples and solutions of compost (at the

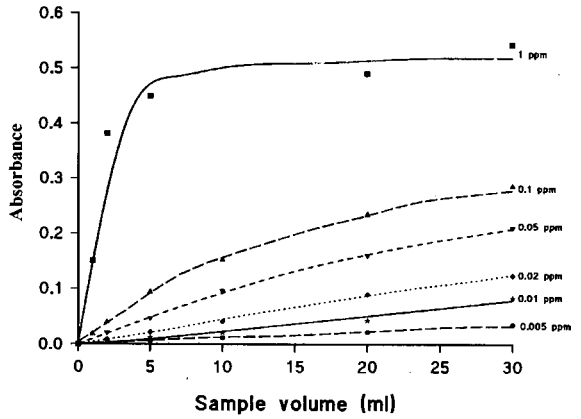

Fig. 4. Effect of sample volume on PB on-line precipitation.

pH obtained after microwave treatment) were pumped into the system and mixed with 0.1 M NaOH (0.025 M when Cu was analysed) at 1 ml min^{-1} in both cases, and the precipitate formed was retained on the PTFE filter. Then, after a washing step with 2 ml Milli-Q water, a 70 μl volume of 1.5 M nitric acid was injected into the system at 1 ml min^{-1}. The nitric acid dissolved the collected hydroxides and the metals passed directly to the nebulizer.

2.3.2. On-line precipitation coupled to ion chromatography

A schematic diagram of the system precipitation–ion chromatography is shown in Fig. 2. Once the precipitation process has been carried out according to the procedure described above, the redissolved metals passed directly to the loop (200 μl) of a Rheodyne valve. The valve was switched to introduce the metals into the chromatographic system, where they were separated in the analytical column with 0.1 M tartaric acid (pH 2.95) as mobile phase at 1 ml min^{-1}. The eluent was mixed with a 0.2 mM PAR solution with the aid of a Y piece. The metal complexes formed were detected spectrophotometrically at 500 nm.

2.3.3. Sample pretreatment

Water samples were filtered through a 0.47 μm nylon filter (Whatman) before analysis.

Compost samples were prepared for analysis by microwave digestion. A known amount of accurately weighed compost sample (0.3 g) was dissolved in 2.5 ml of nitric acid and after 30 min the sample was placed in the microwave oven and heated at 650 W and 40 psi for 5 min, followed by a second step at 650 W and 85 psi for 30 min. The sample was cooled and, after addition of 1 ml of H_2O_2, treated by microwaving at 650 W and 85 psi for 15 min. After cooling, the solution was transferred to a volumetric flask and diluted to 100 ml with Milli-Q water.

3. Results and discussion

In this work, all the physical and chemical variables affecting analyte precipitation and elution were optimised for each metal by FAAS. During the study, it was kept in mind of developing a general on-line precipitation method for the determination of all metals under study by FAAS and by ion chromatography.

3.1. Effect of precipitation parameters

Different kinds of filters of different dimensions and pore sizes were tested in order to allow quantitative retention of the precipitates formed as well as to avoid overpressure in the on-line system. Paper, nylon and PTFE filters with pore sizes ranging from 0.2 to 0.8 μm were tested. Paper and nylon filters successful retained the precipitates, but they were easily destroyed by the eluting reagent (nitric acid) after only two analysis. However, PTFE filters could be used for more than 20 analysis without losing their retention properties. The best performance of the filtration unit was obtained using a PTFE filter (0.45 μm pore size and 1 mm thickness) inserted in a PTFE microcolumn.

When real samples were analysed (see below), a high amount of precipitate was obtained, which produced a strong matrix effect in the determination of the selected metals as well as overpressure in the system. These drawbacks were remedied by filling the microcolumn with small zirconia spheres, since the high surface area available for

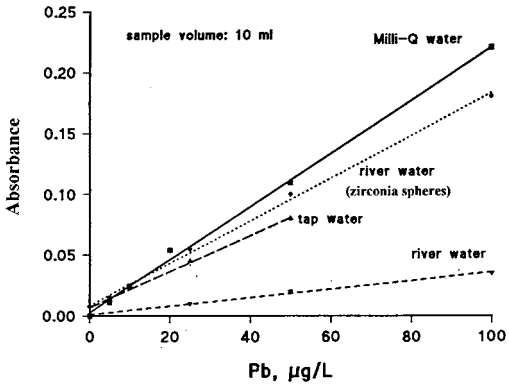

Fig. 5. Calibration graphs obtained in the determination of Pb in different water samples by the proposed on-line precipitation method.

precipitate retention prevented overpressure and facilitated the redissolution of the precipitates formed. Microcolumns of different lengths (0.5, 1.5, and 2.5 cm) were tested and the best performance was obtained using the longer microcolumn due to the reasons mentioned above.

The effect of sample and precipitation agent (sodium hydroxide) flow-rates was evaluated within the range 0.5–1.2 ml min^{-1}. For flow-rates higher than 1 ml min^{-1} the signals obtained were not reproducible due to random overpressure in the system. Flow-rates lower than 1 ml min^{-1} allowed quantitative precipitation of all metals tested so, in order to increase the sampling frequency, a flow-rate of 1 ml min^{-1} was chosen as appropriate.

The effect of NaOH concentration from 1 mM to 0.3 M on precipitation efficiency was evaluated. Fig. 3 shows that for Pb, Ni and Zn the best sensitivity is reached for NaOH concentrations higher than 0.1 M as well as for Co and Mn (curves not shown). However, the Cu calibration slope decreases at NaOH concentrations higher than 0.01 M due to redissolution of the precipitate by the excess NaOH [10]. Mercuric hydroxide was not formed in the system described and thus Hg was excluded from the study.

Fig. 4 shows the curves obtained after on-line precipitation of different standard solution volumes at different Pb concentrations. At concentrations below 0.02 mg l^{-1} it is possible to preconcentrate up to at least 30 ml of sample volume without losses of metal, which means that precipitation efficiency is constant whichever sample volume is used. At higher concentrations, a short linear range is observed suggesting that it may only be possible to preconcentrate up to ≈ 0.8 µg of Pb because at this point preconcentration may become non-proportional. Similar results were obtained for the other metals tested. Thus, it can be concluded that high enrichment factors are obtainable since no washing effect was observed for any metal.

3.2. Effect of elution parameters

Nitric acid was chosen as eluting agent due to its ability to quantitatively dissolve the precipi-

Table 1
Calibration graphs obtained in the metal determination by on-line precipitation of 10 ml of enriched water samples coupled to FAAS

	Milli-Q water		Tap water		River water[a]		River water[b]	
	Calibration equation[c]	R^2	Calibration equation[c]	R^2	Calibration equation[c]	R^2	Calibration equation[c]	R^2
Zn	$y=0.012+0.0049x$	0.9978	$y=0.12+0.0048x$	0.9979	$y=0.037+0.0046x$	0.9975	–	–
Ni	$y=0.001+0.0017x$	0.9998	$y=0.003+0008x$	0.9981	$y=0.002+0.0004x$	0.9894	$y=0.008+0.0014x$	0.9971
Cu	$y=0.003+0.0020x$	0.9971	$y=0.008+0.0013x$	0.9979	$y=0.002+0.0016x$	0.9928	–	–
Pb	$y=0.003+0.0022x$	0.9978	$y=0.007+0.0014x$	0.9979	$y=0.000+0.0003x$	0.9936	$y=0.008+0.0017x$	0.9978

[a] Filtration unit without zirconia spheres.
[b] Filtration unit with zirconia spheres.
[c] y, Absorbance; x, concentration (µg l^{-1}).

Table 2
Determination of metals in real samples by on-line precipitation coupled to FAAS[a] and GF AAS

Sample	Metal concentration ($\mu g\ l^{-1}$) $\pm$ SD[b]							
	Pb		Zn		Cu		Ni	
	FAAS	GF AAS	FAAS	GF AAS	FAAS	GF AAS	FAAS	GF AAS
Tap water	5.1 ± 0.4	5.0 ± 0.3	25 ± 1	26 ± 1	5.8 ± 0.5	5.6 ± 0.2	4.0 ± 0.3	3.8 ± 0.3
River water	4.7 ± 0.4	5.0 ± 0.5	8.0 ± 0.7	7.0 ± 0.4	1.2 ± 0.3	1.0 ± 0.4	5.7 ± 0.6	5.9 ± 0.5

[a] Sample volume: 10 ml.
[b] Average of three independent determinations.

tates studied. The nitric acid concentration range evaluated was 0.1–4 M. At concentrations above 1.5 M it was possible to dissolve quantitatively the precipitates evaluated. In order to protect the filter from high acidity, a 1.5 M nitric acid solution was used for further experiments.

The injection volume of nitric acid was studied over the 20 μl–1 ml range. Low elution volumes did not dissolve completely the precipitate formed, producing memory effects in the determination of the different metals. Optimum results were obtained using 70 μl nitric acid, which produced very sharp FIA peaks.

The acid flow-rate had a strong effect on the speed of precipitate dissolution. Acid flow-rates below 1 ml min^{-1} dissolved the precipitates slowly, so the analytical peaks obtained were too broad. A flow-rate of 1 ml min^{-1} provided sharp peaks and avoided any risk of overpressure in the flow system. Thus, 1 ml min^{-1} was chosen as appropriate.

As the preconcentration efficiency remained constant with increasing sample volume up to 30 ml (lack of washing effect), the enrichment factor found was 140 for a 10 ml sample volume, although it could have been raised by using larger sample volumes.

3.3. Analytical performance and applications

3.3.1. On-line precipitation coupled to FAAS

Linear calibration graphs were obtained up to 100 $\mu g\ l^{-1}$ of each metal by preconcentrating 10 ml calibrants with regression coefficients better than 0.993 in every case. The relative SD for ten independent determinations of each of the four metals tested, using a 10 ml sample volume, averaged 4% at the 50 $\mu g\ l^{-1}$ concentration level. The detection limits, calculated as three times the SD of the blank, and preconcentrating a 10 ml sample volume were 0.1, 0.3, 0.5 and 0.5 $\mu g\ l^{-1}$ for Zn, Cu, Ni and Pb, respectively, although they could be lower by using a higher sample volume.

The influence of several foreign ions (Al^{3+}, Cr^{3+}, Cd^{2+}, Sn^{2+}, Fe^{3+}, NO_3^-, Cl^-, CO_3^{2-} and EDTA) at several concentration levels, on the determination of the above mentioned metals by the proposed method was investigated. Only EDTA and Fe (III) seriously interfered in the determination of Pb, the former due to the formation of a stable complex and the latter due to competition for the hydroxide ions between both metals, respectively.

The proposed method was applied to determine Pb, Zn, Cu and Ni in tap and river water samples. Quantification was carried out by the standard additions method. As an example, Fig. 5 shows the calibration graphs obtained for Pb in Milli-Q, tap and river water samples, where a strong matrix effect can be observed in river water. However, when the filtration unit microcolumn is filled with small zirconia spheres, the matrix effect is almost completely eliminated, allowing the determination of Pb in this kind of sample by the proposed method. Similar results were obtained for Ni (see Table 1) by comparing the slopes of the calibration graphs obtained in the different samples. However, the matrix effect is smaller for Zn and Cu, so the use of zirconia spheres should not be necessary in the determination of these metals in river water.

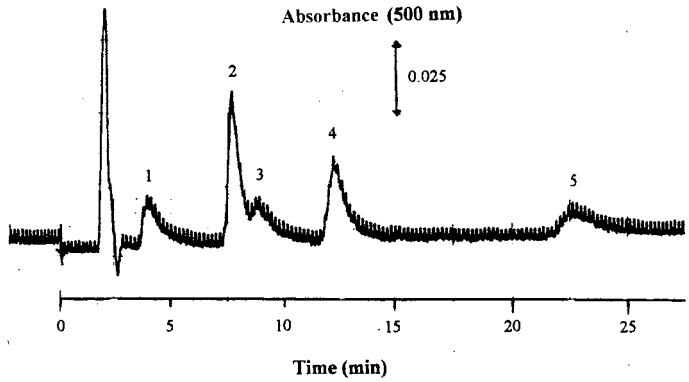

Fig. 6. Chromatogram obtained at 500 nm after on-line precipitation coupled to ion chromatography of 10 ml of Milli-Q water spiked with 10 μg l^{-1} of each metal. Peak numbers: (1) Cu; (2) Zn; (3) Ni; (4) Co; (5) Mn. Chromatographic conditions: See Section 2.

Table 2 shows the metal concentrations found in tap and river water samples by the proposed on-line precipitation method. The results were compared with those obtained by graphite furnace atomic absorption spectrophotometry (GF AAS) and it was found that there were no significant differences at the 95% confidence level.

3.3.2. On-line preconcentration coupled to ion chromatography

The metals evaluated in this study were Cu, Zn, Co, Ni, Mn and Cd, as they can form a filterable precipitate by reaction with NaOH and a coloured complex with PAR. The ion chromatography method used was adapted from that proposed by Weiss [11]. In the conditions described in Section 2, Cd did not form an appropriate precipitate and it was excluded from the study. In addition, although Pb was easily determined by FAAS, it could not be determined by ion chromatography due to lack of sensitivity. Therefore, the metals Cu, Zn, Ni, Co and Mn were determined in one run by the proposed on-line precipitation-ion chromatography method. Fig. 6 shows the chromatogram obtained after on-line preconcentration of Milli-Q water spiked with 10 μg l^{-1} of each metal.

In these conditions, the calibration graphs obtained were linear up to at least 20 μg l^{-1} of each metal by preconcentrating 10 ml of sample with regression coefficients better than 0.988 in every case. The relative SD for five independent determinations, using 10 ml of sample, averaged 8% at the 10 μg l^{-1} concentration level. The detection limits, calculated by using a signal-to-noise ratio of 3, were 3, 1, 5, 3, and 3 μg l^{-1} for Cu, Zn, Ni, Co and Mn, respectively.

The proposed method was successfully applied to the determination of the above mentioned metals in river water (reference material SLRS-3 from National Research Council of Canada) and compost samples. Table 3 shows the results obtained for Zn, Ni and Mn in the analysis of river water compared with the certified values, as well as those obtained for Cu, Zn and Ni in compost by the proposed method compared with those obtained by direct FAAS. In both cases, there are no significant differences at the 95% confidence level (at the 99% level for Zn and Ni in the compost analysis).

4. Conclusions

The proposed on-line precipitation of several metals with sodium hydroxide allows their independent determination at trace concentration levels by FAAS without changing the operating FIA conditions. The proposed method is simple and rapid, easily carried out in any laboratory and allows metal determination in environmental samples at low concentration levels.

Table 3
Mean value ± SD[a] obtained in the determination of trace metals by on-line precipitation coupled to ion chromatography

	River water (μg l^{-1})		Compost (μg g^{-1})	
	Ion chromatography[b]	Certified value	Ion chromatography[c]	Direct FAAS
Zn	0.93 ± 0.06	1.04 ± 0.09	489 ± 25	432 ± 16
Ni	1.0 ± 0.1	0.83 ± 0.08	66 ± 4	75 ± 3
Mn	4.5 ± 0.5	3.9 ± 0.3	–	–
Cu	–	–	273 ± 45	301 ± 28

[a] Average of three independent determinations.
[b] Sample volume: 20 ml.
[c] Sample volume: 1 ml.

As Cu, Zn, Ni, Co and Mn are precipitated simultaneously, they can be separated after redissolution by using ion chromatography and individually determined by UV-vis detector after postcolumn derivatization with PAR.

Both methods were successfully applied and validated for the determination of the above mentioned metals in environmental samples.

Acknowledgements

The authors wish to thank CICYT (Project no PB-95-0366-C01-C02) for financial support and Max Gorman for the revision of the manuscript. S. Angelino is recipient of an EERO (European Environmental Research Organisation) fellowship.

References

[1] J. Ruzicka, E.H. Hansen, Flow Injection Analysis, John Wiley, New York, 1981.
[2] P. Martínez-Jiménez, M. Gallego, M. Valcárcel, Analyst 112 (1987) 1233.
[3] E. Debrah, C.E. Adeeyinwo, S.R. Bysouth, J.F. Tyson, Analyst 115 (1990) 1543.
[4] C.E. Adeeyinwo, J.F. Tyson, Anal. Proc. 26 (1989) 375.
[5] B.A. Petersson, Z. Fang, J. Ruzicka, E.H. Hansen, Anal. Chim. Acta 184 (1986) 165.
[6] P. Martínez-Jiménez, M. Gallego, M. Valcárcel, Anal. Chim. Acta 193 (1987) 127.
[7] Z. Fang, M. Sperling, B. Welz, J. Anal. At. Spectrom. 6 (1991) 301.
[8] E. Ivanova, X.-P. Yan, W. Van Mol, F. Adams, Analyst 122 (1997) 667.
[9] D. Roston, Anal. Chem. 56 (1984) 241.
[10] F. Burriel, F. Lucena, J. Arribas, J. Hernández, in: S.A. Paraninfo (Eds.), Química Analítica Cualitativa, Madrid, 1988.
[11] J. Weiss, Ion Chromatography, VCH, Weinheim, 1995.

ELSEVIER

Talanta 48 (1999) 967–978

Talanta

Simultaneous detection of monovalent anions and cations using all solid-state contact PVC membrane anion and cation-selective electrodes as detectors in single column ion chromatography☆

Ibrahim Isildak *, Adem Asan

Ondokuzmayis University, Faculty of Science, Department of Chemistry, 55300 Samsun, Turkey

Received 14 July 1998; received in revised form 21 September 1998; accepted 25 September 1998

Abstract

The overall efficiency of ion chromatographic procedures allows the possibility of routine separation and detection of common inorganic and organic anions and cations at low levels in a simultaneous system. A simple and rapid independent separation, and sensitive simultaneous detection of monovalent common anions and cations were achieved using 2 mM copper sulfate, (at pH: 5.40), as eluent with low cell-volume potentiometric detectors. This was established using all-solid state contact, tubular, PVC-matrix membrane anion and cation-selective electrodes in series as detectors with mixed-bed ion-exchange column in ion chromatography. The developed method is reproducible and highly selective to monovalent anions and cations, and takes less than 8 min. Under all operation conditions, the detection limits of the developed method, for potassium, rubidium, cesium, thallium(I), nitrite, nitrate, benzoate and bromide, were of the order of tens of ppb, for sodium, ammonium, chloroacetate, cyanate and chloride ions, values were of the order of hundreds of ppb for an injected volume of 20 μl. The method was flexible since most of anions do not interfere the detection of cations and most of cations do not affect the detection of anions, so that the method can be applied to many sample types e.g. environmental. The application of the method for river, sea and tap water samples were illustrated.

Keywords: Simultaneous determination of anions and cations; Single column ion chromatography; All solid-state contact tubular membrane ion-selective electrodes; Potentiometric detection

1. Introduction

Ion chromatography developed by Small et al. [1] has become a routine tool for the sensitive determination of ion content in many sample matrices in industry, analytical laboratories, the clinical environment, etc. Originally, ion chro-

☆ The methods described in this paper are the subject of pending patents.

* Corresponding author. Tel.: +90-362-4576020, Fax: +90-362-2330853; e-mail: oandac@ihlas.net.tr.

0039-9140/99/$ - see front matter
PII S0039-9140(98)00304-X

matography was applied to determine either anions or cations using suppressed conductivity detection. The applicability of only a limited number of eluents and the expense of suppressor columns and a limited detection capability have created interest in other means of detection.

One area of ion chromatography that holds particular promise for further improvements in ion determination is the development of alternative detection methods. The technology of ion selective electrode (ISE) fabrication at low cost, design of miniaturized flow-cells to minimize dead space and carry over sample solutions, low detection limits and cost, and less selectivity of some of ISEs have led to increase the use of ISEs as detectors in ion chromatography [2–4]. Liquid membrane electrodes are less selective compared to other counter parts and hence could be more suited for more general potentiometric detection of ions in ion chromatography. Schultz and Mathis [5] first described the use of a commercial liquid membrane nitrate-selective electrode to determine nitrite, nitrate, and various phthalate isomers by ion chromatography. A platinum wire electrode coated with PVC, employing a mixture of neutral carrier ligands, has been used for potentiometric detection of alkali cations and ammonium [6]. With this type of arrangement, detection limits varied with the selectivity of each neutral carrier ligand toward the individual ions, possibly due to the response of the electrode to the components present in the eluent exhibiting poor sensitivity. A PVC tubular membrane electrode has been successfully used for the determination of Cl^-, Br^-, NO_2^-, and NO_3^- in environmental samples by ion chromatography [7]. An interesting application of a highly selective liquid membrane electrode is described by Trojanowicz and Meyerhoff [8] who used a wall-jet, valinomycin, potassium-selective electrode for detection of anions and cations in replacement ion chromatography. The same authors [9] also determined anions and cations using flow-through, wall-jet, polymeric pH electrodes in suppressed ion chromatography. Isildak and Covington [10] have demonstrated the use off all solid-state-contact tubular PVC-matrix membrane electrodes as detectors for the determination of monovalent

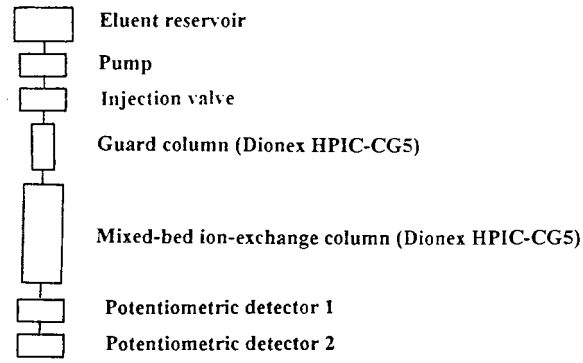

Fig. 1. Schematic diagram of the single column ion chromatographic system for the simultaneous determination of monovalent anions and cations.

inorganic and organic ions in ion chromatography. Recently, Hong et al. [11] have used a neutral carrier-based potentiometric detector in ion chromatography for simultaneous monitoring of mono- and divalent cations.

There was a recognition that the routine separation and detection of common anions and cations at low ppb levels in a simultaneous system is a useful goal for maximizing the overall efficiency of ion chromatographic procedures. Therefore, another area of ion chromatography that holds a particular promise for further improve-

Table 1
Single column ion chromatographic parameters of the simultaneous determination system

Eluent	0.5×10^{-3} mol dm^{-3} copper sulfate, pH:5.62 and 2×10^{-3} mol dm^{-3} copper sulfate, pH:5.40
Flow-rate	0.5 ml min^{-1} and 0.8 ml min^{-1}
Separator column	2.0×250 mm Dionex HPIC-CS5 (mixed-bed)
Guard column	4.0×50 mm Dionex HPIC-CG5 (mixed-bed)
Injection volume	20 μl
Detectors	
Detection for monovalent anions	All solid-state contact tubular PVC-membrane monovalent anion-selective electrode
Detection for monovalent cations	All-solid-state contact tubular PVC-membrane monovalent cation-selective electrode

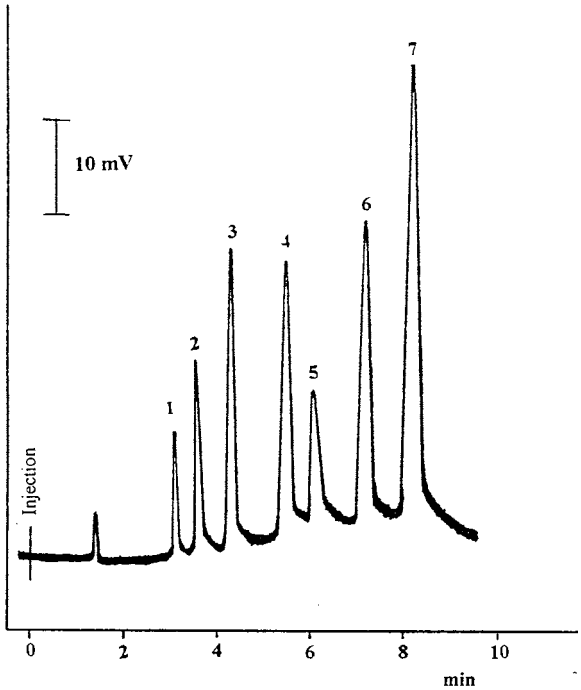

Fig. 2. Ion chromatographic separation and potentiometric detection of monovalent anions using the mixed-bed column with the all solid-state contact PVC-membrane anion-selective electrode as detector. Eluent: 0.5×10^{-3} mol dm^{-3} copper sulfate, pH: 5.62, flow-rate: 0.5 ml min^{-1}. Injection: 20 μl of 10^{-4} mol dm^{-3} standard solution of each anion. (1) Chloroacetate (2) Chloride (3) Nitrite (4) Benzoate (5) Cyanate (6) Bromide (7) Nitrate.

ments in ion determination is the achievement of simultaneous analysis of common anions and cations. The main drawback to simultaneous detection of a large variety of anions and cations is non-specificity of most detection methods used in simultaneous determination. Therefore, several approaches have been envisaged for simultaneous determination of anions and cations. Potentially, the most straightforward approach is a single channel system in which an anion- and a cation-exchange column are connected in series with an eluent that is compatible with both [12,13]. The ion exchange capacities of the two columns can be manipulated to give appropriate retention time for both species, and a suitable detection mode can be used to perform simultaneous determination by conductometric, spectrophotometric, and potentiometric detection methods. An outstanding method developed by present author, in which the simultaneous determination of fourteen inorganic and organic anions and cations at sub-ppb levels was demonstrated by using anion- and cation-exchange columns in series with two all solid-state contact tubular liquid membrane electrodes as detectors in ion chromatography [10]. It is believed that the efficiency would be improved if the anion- and cation-exchange columns could subsequently be modified into a single column by using a mixed-bed ion-exchange column.

We now describe, a simple and economic, single column ion chromatographic method which permits a full independent separation and simultaneous detection to determine of a group of 13 inorganic and organic common monovalent anions and cations in about 8 min at sub-ppb levels.

This was achieved by using Dionex-HPIC-CS5 mixed-bed ion-exchange column with a simple eluent system, and two all solid-state contact, tubular, PVC-matrix membrane monovalent anion and cation-selective electrodes as detectors in series in ion chromatographic system. The method was successfully applied to river, sea and tap water samples.

2. Experimental

2.1. Preparation of all solid-state contact tubular membrane electrodes and flow cells

The construction of all solid-state contact tubular PVC matrix membrane anion and cation-selective electrodes without an inner reference solution was carried out, as described by Alegret et al. [14]. Two identical potentiometric cells were designed to use for the simultaneous detection of anions and cations. Each consisted of two perspex holders into which 3 mm diameter channels were drilled and a perspex cylinder body containing a cast graphite-epoxy conductive support into which a central 1.5 mm diameter channel was drilled. The PVC-tetrahydrofuran (THF) solution comprised the electroactive material and the plasticizer was applied dropwise to the inside surface, the inner-diameter of which was thereby reduced to ca. 1.2 mm.

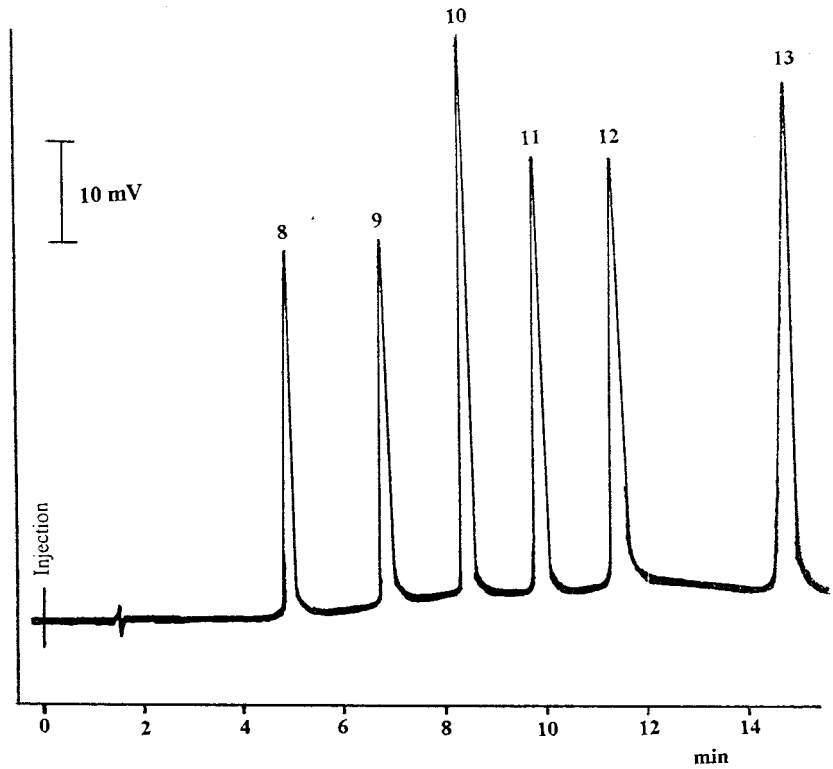

Fig. 3. Ion chromatographic separation and potentiometric detection of monovalent cations using the mixed-bed column with the all solid-state contact PVC-membrane cation-selective electrode as detector.. Eluent: 0.5×10^{-3} mol dm^{-3} copper sulfate, pH: 5.62, flow-rate: 0.5 ml min^{-1}. Injection: 20 μl of 10^{-4} mol dm^{-3} standard solution of each cation. (8) Sodium (9) Ammonium (10) Potassium (11) Rubidium (12) Cesium (13) Thallium(I).

The sensing membrane consisted of 25 wt.% PVC, 4 wt.% tetradodecylammonium bromide (TDAB) for anion selective electrode and dibenzo-(18-crown-6) (DBC) or dicyclo-(18-crown-6) (DCC) for cation selective electrode as active ligands, 67 wt.% dibutylphalate (DBP) for anion selective electrode and dioctylsebacate (DOS) for cation selective electrode as plasticizers after evaporation of THF at room temperature open to air for 4 h. To reduce the membrane resistivity and anionic selectivity, in the case of neutral carrier electroactive materials, the membrane contained 1 wt.% potassium tetraphenylborate (KTPB). The epoxy resin mixture used to bind the graphite in preparing the internal conducting support of the electrode was made from epoxy and hardener in THF solvent in the proportions of $1 + 0.5$. The powdered graphite was mixed with epoxy resin in the proportions of $1 + 1$. Electrical connection was made by a copper rod inserted into a hole in the epoxy-graphite conductive support. When not in use for a long time the all solid-state contact tubular PVC-matrix electrodes were stored dry after washing with deionized water. They were reconditioned by using primary ion solutions before use. The detector cell consisted of an all solid-state tubular PVC-matrix anion selective or cation-selective electrode and a double junction calomel reference electrode (Russell pH, Auchtermuchty, Fife, Scotland) with tetramethylammonium chloride in the outer compartment. In case of simultaneous detection, two ISEs associated with a double junction calomel reference electrode.

2.2. Chemicals and procedures

All standard sample solutions of anions and cations, and eluent were prepared from their analytical reagent grade chemicals in deionized water, then diluted to the desired concentrations. Suitable compositions of eluents were prepared freshly before use.

Chemicals for preparation of sensing membranes were from Fluka except DBP which was from Aldrich.

Calibration plots of the detectors for anions and cations were obtained by the constant volume dilution method [15,16]. Speed of response and selectivity were obtained by testing in a flow-injection mode.

The normal procedure for the use of ion chromatograph was followed with the exception of the use of a mixed-bed column with two detectors in series. The solutions were injected, and the detectors and recorder were adjusted appropriately to provide peaks of useful height for anions and cations.

Samples of river, sea and tap water collected from local areas of Samsun district were filtered over a 0.45 μm membrane filter (Millipore SA 67120 Molshem, France) before use.

During the experiments, 20 μl of samples or of standard sample solutions were injected into the chromatographic system by a Rhodyne injection valve provided with a loop. Identification of species of interest was performed by comparing retention times of peaks with those of peaks in standards. Chloride solutions of cations and sodium solutions of anions were used in the identification studies.

2.3. Apparatus

Chromatography was performed using the dual channel pump and injection valve with 20 μl sample loop of a Perkin Elmer (Series 3) high performance liquid chromatography (HPLC).

Separations were made on Dionex-HPIC-CS5 analytical and -CG5 guard mixed-bed columns. Other components of the system used for the recording of chromatogram and for the reading of the potential were as previously described [10]. The instrumental scheme, and the full operating parameters of the simultaneous determination system is given in Fig. 1 and Table 1, respectively.

3. Result and discussion

The selection of an eluent is important to the success of simultaneous determination of anions and cations using mixed-bed column and potentiometric detection in ion chromatography.

In ion chromatography employing potentiometric detector, strength of detector response is based upon the selectivity of the electrode membrane between the eluent ion and analyte ion. The strength of detector response toward an analyte ion will be much higher if the electrode membrane selective to analyte ion than that of eluent ion. If the vice versa is true, there will be no detector response for analyte ion.

We tested polyvalent anions and cations as eluent components to separate and detect monovalent ions as the all solid-state contact PVC-matrix membrane electrodes as detectors are highly selective to monovalent anions and cations. Only, the detection of anions in the simultaneous system was achieved with Na_2SO_4, or Na_3PO_4/Na_2HPO_4 buffer solutions as eluents. The reason of this might be the high selectivity of the cation-selective electrode detector toward the Na^+ cation present in the eluent. Chloride solutions of Cu^{2+}, Mg^{2+} and Ca^{2+} were used as eluents and only monovalent cations were detected in the simultaneous system. This can also be attributed to the high selectivity of the anion-selective electrode detector toward chloride ion present in the eluent.

It is obviously believed that, for simultaneous determination, one of each of Cu^{2+}, Mg^{2+} and Ca^{2+} components present in the eluent system is responsible for the elution of monovalent cations while the sulfate counterpart has responsibility for the elution of monovalent anions. Consequently, by using sulfate solutions of Cu^{2+}, Mg^{2+} and Ca^{2+} as eluents, efficient and rapid separations with the mixed-bed column, and sensitive detection with all solid-state contact tubular PVC-matrix anion and cation selective membrane electrodes for both monovalent anions and

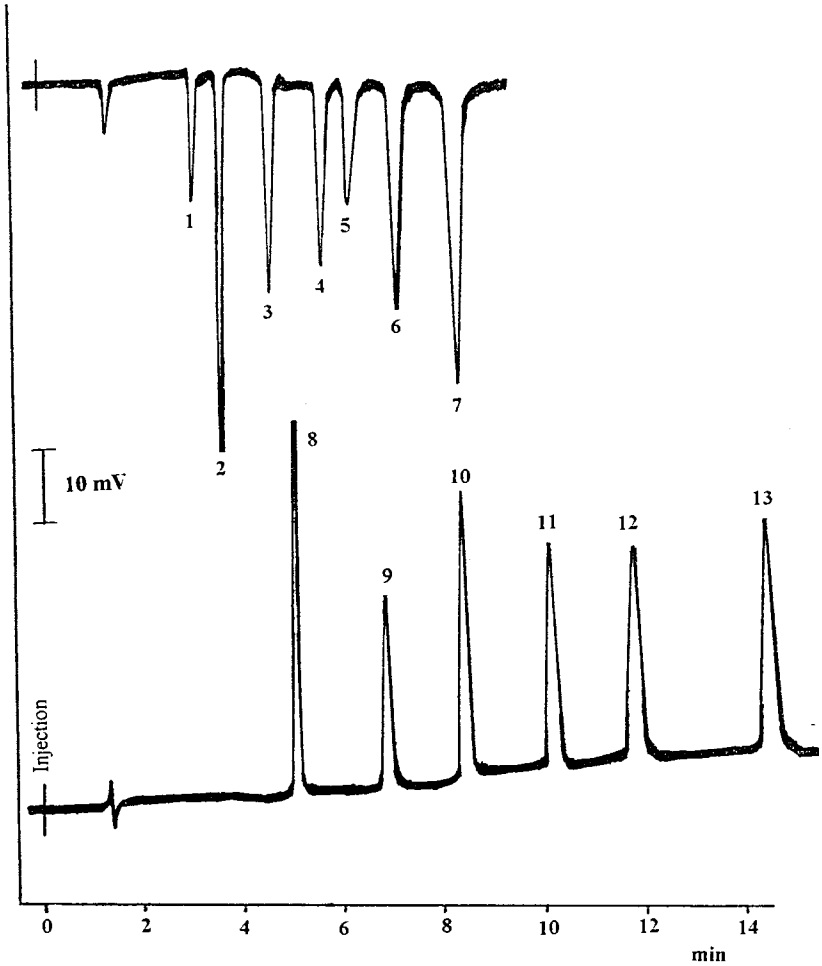

Fig. 4. Simultaneous detection of anions and cations using the mixed-bed column followed by all solid-state contact PVC-matrix monovalent anion and cation selective electrodes as detectors in series. Eluent: 0.5×10^{-3} mol dm^{-3} copper sulfate, pH: 5.62, flow-rate: 0.5 ml min^{-1}. Injection: 20 μl of 10^{-4} mol dm^{-3} standard solution of each ion. (1) Chloroacetate (2) Chloride (3) Nitrite (4) Benzoate (5) Cyanate (6) Bromide (7) Nitrate (8) Sodium (9) Ammonium (10) Potassium (11) Rubidium (12) Cesium (13) Thallium (I).

cations were achieved. It was seen that, Cu^{2+} ion present in the eluent was about two times stronger than of either Mg^{2+} or Ca^{2+} ions in the eluent for the elution of cation when compared, hence, $CuSO_4$ eluent was chosen throughout the study. The high selectivity of each of all solid-state contact tubular PVC-matrix membrane electrodes towards monovalent ions over $CuSO_4$ eluent ions has also created responses for both anions and cations at ppb concentrations in the standard sample solution injected into the chromatographic system.

Single detection, of monovalent anions by using the anion-selective electrode detector at the end of the mixed-bed column, and of monovalent cations by using the cation-selective electrode detector at the end of the mixed-bed column with 0.5 mM $CuSO_4$ (pH: 5.62) as eluent are shown in Figs. 2 and 3 respectively.

The time required, for the determination of anions is about 8 min, and for the determination of cations is about 14 min. In present authors previous study, it was found that anion-exchange

resin in the Dionex HPIC-AS4A anion-exchange column exhibited some degree of cation-exchange capacity. The same anion-exchange resin has been packed into the mixed-bed column to separate anions according to Dionex HPIC-CS5 mixed-bed column instruction notes. Therefore, the long retention time of cations can be attributed to both; relativly high cation-exchange capacity of the cation-exchange resin, or the cation-exchange charecteristics of the anion-exchange resin in the mixed-bed column. Fig. 4 shows independent separation and simultaneous detection of 13 inorganic and organic monovalent anions and cations by using the same eluent with two all solid-state contact tubular anion and cation-selective membrane electrodes as detectors in series and the mixed-bed column in a single injection volume ion chromatography. Anion and cation concentrations in the standard sample solution injected were adjusted by mixing different anion solutions of metals of interest at required concentrations.

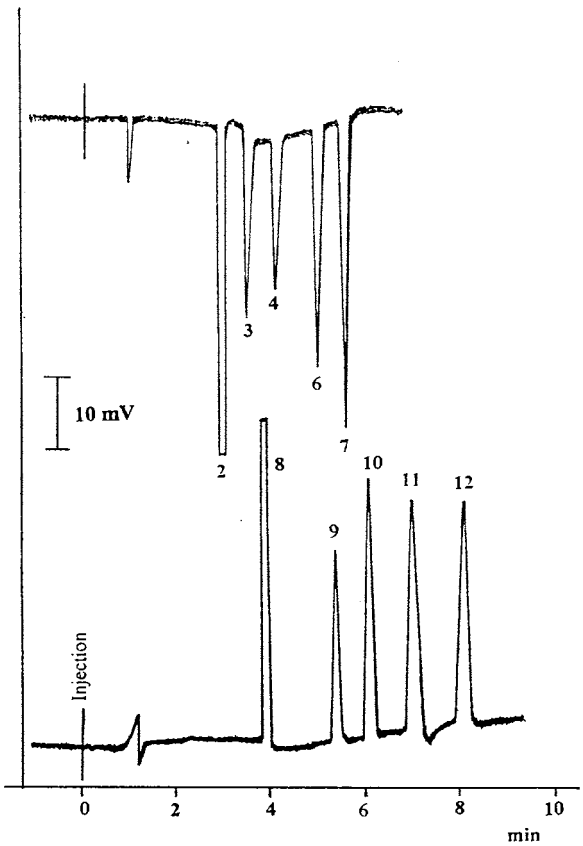

Fig. 5. Simultaneous detection of anions and cations at relativly high sodium and chloride levels, using the mixed-bed column followed by all solid-state contact PVC-matrix monovalent anion and cation selective electrodes as detectors in series. Eluent: 2×10^{-3} mol dm^{-3} copper sulfate, pH: 5.40, flow – rate: 0.8 ml min^{-1}. Injection: 20 μl of 10^{-4} mol dm^{-3} standard solution of each ion except sodium and chloride which were 0.5×10^{-3} mol dm^{-3} and 0.6×10^{-3} mol dm^{-3} respectively. (2) Chloride (3) Nitrite (4) Benzoate (5) Cyanate (6) Bromide (7) Nitrate (8) Sodium (9) Ammonium (10) Potassium (11) Rubidium (12) Cesium.

Shortening of the analysis time is possible by increasing the eluent ionic strength while maintaining good resolution in the chromatogram. In Fig. 5, simultaneous determination of ten common monovalent anions and cations in about 8 min was achieved by using 2 mM $CuSO_4$ (pH: 5.40) as eluent. The standard sample solution injected was prepared by mixing required volumes of sodium solutions of anions of interest and chloride solutions of cations of interest. Increasing the ionic strength of the eluent, shortens the retention times of all ions, but does not change the elution sequence of anions and cations studied.

The chromatograms demonstrate selectivity, simplicity, flexibility, the high capability and sensitivity of the method.

3.1. Detection limits and retention times

Table 2 shows the detection limits and retention times for anions and cations measured in the simultaneous system. Some organic acids such as acetate and propionate have resulted almost the same retention times with Cl-acetate. Although the detector showed some degree of selectivity for Cl-acetate over acetate and propionate. However, in the detection of 10^{-5} mol dm^{-3} of Cl-acetate, interference occurred only by the concentration level of 1×10^{-4} mol dm^{-3} acetate and propionate. Two configurations of all solid-state contact tubular membrane anion and cation-selective electrode detectors placed immediately after the end of the mixed-bed column are possible. Either the anion-selective electrode detector or the cation-selective detector can be placed first in line. For any given ion the detection limits and reten-

Table 2
Retention times and simultaneous detection limits of monovalent anions and cations using Dionex HPIC-CS5 mixed-bed column with the all solid state-contact PVC membrane anion and cation-selective electrodes as detectors in series

Ion	Eluent: 0.5×10^{-3} mol dm^{-3} $CuSO_4$, (pH: 5.62) Flow-rate: 0.5 ml min^{-1}	Eluent: 2×10^{-3} mol dm^{-3} $CuSO_4$, (pH: 5.40) Flow-rate: 0.8 ml min^{-1}		
	Retention time (min)	Detection limits (ppb)	Retention time (min)	Detection limits (ppb)
Cl-acetate	3.1	500	–	–
Chloride	3.4	120	2.8	130
Nitrite	4.1	20	3.2	20
Benzoate	5.3	50	3.8	70
Cyanate	5.9	200	–	–
Bromide	6.8	20	4.6	15
Nitrate	7.8	10	5.2	8
Sodium	4.8	100	3.8	100
Ammonium	6.6	100	5.4	100
Potassium	8.0	20	6.6	20
Rubidium	9.4	30	7.4	25
TMA[a]	9.7	120	–	–
Cesium	11.2	30	8.4	25
Thallium(I)	14.4	50	–	–

[a] Tetramethylammonium.

tion times obtained with the two configurations were essentially the same owing to the short distance between the detectors in line as 2 cm.

The detection limits for the anions and cations determined in the simultaneous system using two all solid-state contact tubular membrane electrode detectors were estimated from calibration plots obtained from chromatograms. Under all operations conditions, the detection limits for nitrite, benzoate, bromide, nitrate, potassium, rubidium, cesium and thallium(I), defined as the amount for a signal to noise ratio of 2 and 20 μl sample volume, are of the order of tens ppb, for other ions values are of the order of hundreds of ppb. In addition these detection limits were obtained

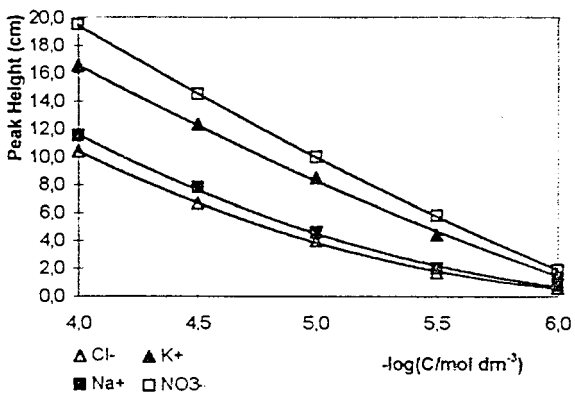

Fig. 6. Response behaviour of the single column ion chromatographic system with all solid state-contact PVC membrane anion and cation-selective electrodes as detectors in series. (100 mV scale is equal to 20 cm)

Table 3
Calibration response equation for chloride, nitrate, sodium, and potassium in the simultaneous detection system[a]

Ion	Equation[b]	r
Chloride	$E = 146.4 + 27.2\ \log[C]$ $h = 29.28 + 4.92\ \log[C]$	0.9817
Sodium	$E = 162.7 + 27.2\ \log[C]$ $h = 32.54 + 5.44\ \log[C]$	0.9846
Potassium	$E = 230.7 + 37.5\ \log[C]$ $h = 46.36 + 7.75\ \log[C]$	0.9980
Nitrate	$E = 271.2 + 43.9\ \log[C]$ $h = 54.24 + 8.78\ \log[C]$	0.9988

[a] $n = 5$ and range: 10^{-4}–10^{-6} mol dm^{-3} for all ions.
[b] E, potential (mV); h, peak height (cm); C, concentration of ion (mol dm^{-3}).

Table 4
Reproducibility for simultaneous anion and cation determination system[a]

Ion	Retention time per minute			Peak height per centimeter		
	$\overline{X}$	Range	RSD%	$\overline{X}$	Range	RSD%
Nitrate	5.2	5.1–5.3	1.7	8.4	8.1–8.8	1.8
Potassium	6.6	6.6–6.7	1.0	6.2	6.0–6.5	1.4

[a] $n = 10$, eluent: 2×10^{-3} mol dm^{-3} $CuSO_4$ (pH: 5.40), injection: 10^{-5} mol dm^{-3} solution of each ion, flow-rate: 0.8 ml min^{-1}.

under normal operation conditions and not any special care to improve the quality of the numbers.

The effect of the concentration of $CuSO_4$ eluent on the retention time of anions and cations was examined. The relative retention times of the anions and cations in respect to the first eluted anion and cation were essentially the same. In general, when the eluent concentration was decreased, a corresponding increase in the retention times of anions and cations was observed. The increase in the retention times was greater for the cations than the anions. The retention of anions and cations is controlled by ratios of anion- and cation-exchange capacity in the column. Therefore, the reason that might be higher ratio of cation-exchange capacity in the mixed-bed column.

3.2. Reproducibility and calibration

Standard solutions of Cl^-, Na^+, K^+ and NO_3^- prepared in the concentration range of 10^{-4}–10^{-6} were injected into the simultaneous system and calibration curves, shown in Fig. 6, were obtained by measuring the peak height (in cm) versus the logarithmic concentration of each anion and cation (in molarity). Calibration response equations are also given in Table 3. From the calibration curves and calibration response equations the response of the electrode detectors for the anions and cations are logarithmic in the concentration range studied.

The reproducibility of peak heights for repeated injections of all anions and cations was generally better than 2%. As examples the reproducibility of the simultaneous system obtained after 10 repeated injections of nitrate and potassium ion solutions at concentration level of 10^{-5} mol dm^{-3} is given in Table 4.

In two years time, the sensitivity of most detectors constructed remained almost constant for at least 7 weeks. Such a constant response obtained may be due to continuous washing of the electrode membrane by the eluent. When the sample included species, such as amino acids or long-chain organic ions which may coat the surface of the membranes of the electrodes and influence their sensitivity.

3.3. Applications

The method developed in this study was easily applied for the simultaneous determination of monovalent anions and cations in environmental water samples without any pre-treatment. Samples were diluted and filtered prior to injection. As examples the chromatograms of river, sea and tap water are shown in Fig. 7(a), (b) and (c) respectively.

The analytical results of river, sea and tap water samples are listed in Table 5. The peak height calibration graphs were used for quantitative determinations. In chromatograms in Fig. 7(a) and (b), the peak numbered as 1 can be a peak of Cl-acetate in the samples. It was not quantified, because of interference from the organic acid anions which may be present in the samples. The three species chloroacetate, acetate and propionate might be determined together, as the acetate and propionate peaks overlap with chloroacetate peak. Using the mixed-bed column and the potentiometric detectors, the determination of the all anions and cations except chloroacetate was not influenced by any other anion and cation.

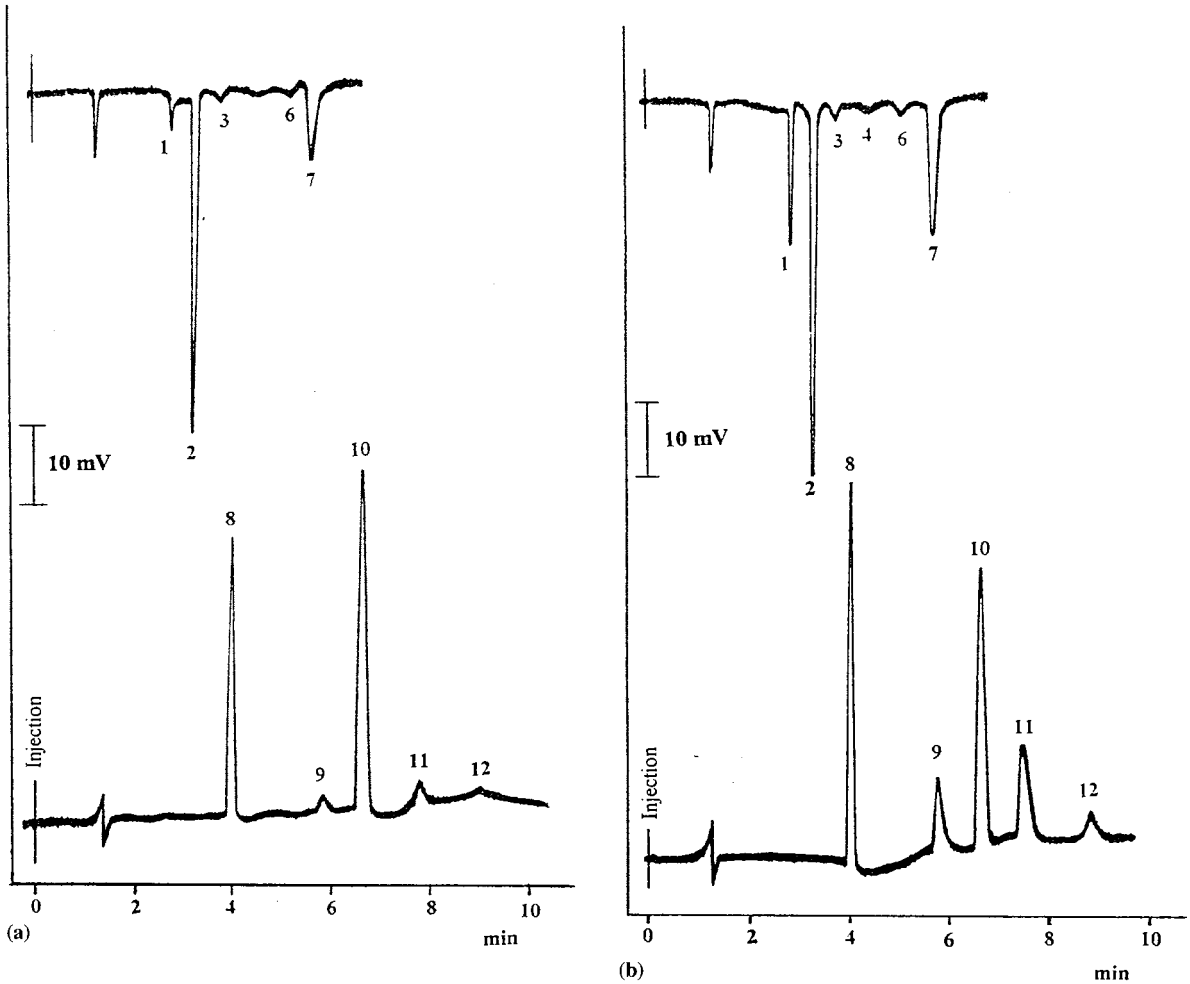

Fig. 7. Simultaneous determination of anions and cations in (a) river; (b) sea; (c) tap water samples by single column ion chromatography with all solid-state contact PVC-membrane electrodes as detectors in series. Eluent: 2×10^{-3} mol dm^{-3} copper sulfate, pH: 5.40, flow – rate: 0.8 ml min^{-1}, injection: 20 μl of sample solution. The analytical results as in Table 5.

4. Conclusions

The use of all solid-state contact tubular PVC-matrix anion and cation-selective electrodes as detectors offers so far the best simultaneous sensitivity toward all monovalent anions and cations studied when compared with other simultaneous detection methods.

It is interesting that the method, requires separations of anions and cations independently as there is no interference in the detection for anions from cations or for cations from anions in the ranges studied, and is unlike to most of other simultaneous determination methods in which anions and cations must be separated from each other during the run makes separation difficult and time consuming. In the determination no overlap problem arises when the retention time of a cation is equal to that of anion, namely no need to provide better resolution between the cations

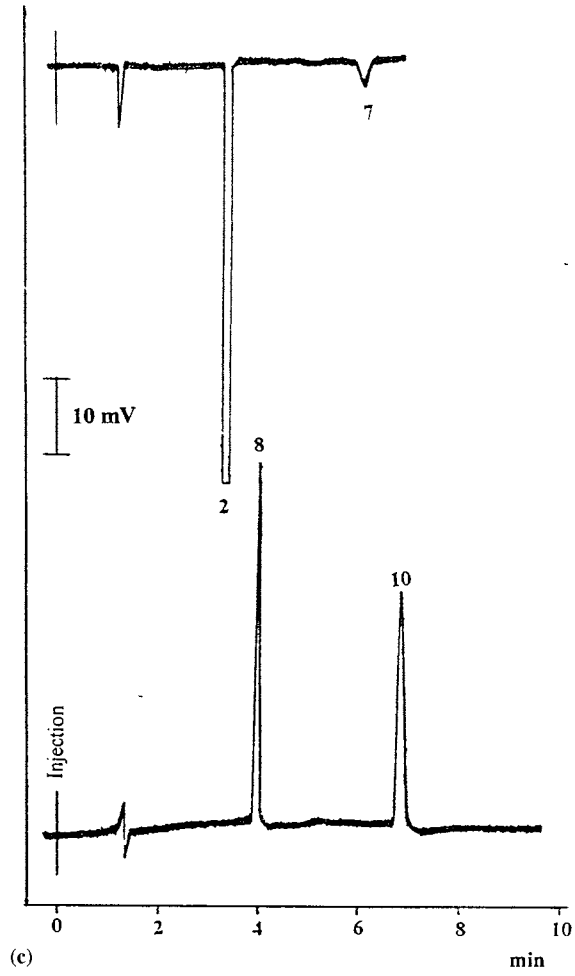

Fig. 7. (*Continued*)

and anions makes separation easy and less time consuming.

The selection of an eluent-column-detector combination is critical to the success of simultaneous determination of anions and cations in ion chromatography. The system developed here can be generalized as the best suitable combination for the simultaneous determination of monovalent anions and cations when compared to other combinations developed up to now. The system is simple and cheap, and allows rapid and sensitive determination of common monovalent anions and cations in the minute sample volume injected into the chromatographic system.

Acknowledgements

The authors would like to acknowledge the financial support of the Science and Technology Research Council of Turkey (TUBITAK).

Table 5
Analytical results of monovalent anions and cations in sea, river and tap water samples by the simultaneous determination system[a]

Ion	Sea water		River water		Tap water	
	$\overline{X}$	*ts*	$\overline{X}$	*ts*	$\overline{X}$	*ts*
(2) Chloride	19.5	2.4	6.2	2.9	14.5	2.3
(3) Nitrite	0.02	2.3	>0.01	2.5	–	–
(4) Benzoate	>0.01	2.6	>0.005	2.7	–	–
(6) Bromide	0.02	2.3	>0.01	2.0	–	–
(7) Nitrate	8.2	2.2	2.5	2.6	0.04	2.0
(8) Sodium	13.4	1.8	4.5	2.1	3.4	2.0
(9) Ammonium	0.3	2.1	0.3	2.8	–	–
(10) Potassium	8.4	1.6	1.2	1.6	0.8	1.5
(11) Rubidium	0.8	2.3	0.6	2.4	–	–
(12) Cesium	<0.005	2.4	0.08	2.4	–	–

[a] Values represent, the average ($\overline{X}$ = mg l^{-1}), standard deviation (ts = %), for $n = 5$ in confidence level of 95%.

References

[1] H. Small, T.S. Stevens, W.C. Bauman, Anal.Chem. 47 (1975) 1801.
[2] K. Watanabe, K. Tohda, H. Sugimoto, et al., J. Chromatogr. 566 (1991) 109.
[3] S.H. Han, K.S. Lee, G.S. Cha, J. Chromatogr. 648 (1993) 283.
[4] B.L. Baker, L.J. Nagels, Anal. Chim. Acta 290 (1994) 259.
[5] F.A. Schultz, D.E. Mathis, Anal. Chem. 46 (1974) 2253.
[6] K. Suzuki, H. Aruga, T. Shirai, Anal. Chem. 55 (1983) 2011.
[7] Z. Lizhu, C. Jinglan, Y. Jinyao, Fenxi Huaxue 16 (8) (1988) 735.
[8] M. Trojanowicz, M.E. Meyerhoff, Anal. Chim. Acta 222 (1989) 95.
[9] M. Trojanowicz, M.E. Meyerhoff, Anal. Chem. 61 (1989) 787.
[10] I. Isildak, A.K. Covington, Electroanalysis 5 (1993) 815.
[11] U.S. Hong, H.K. Kwon, H. Nam, G.S. Cha, K.H. Kwon, K.J. Peang, Anal. Chim. Acta 315 (1995) 303.
[12] J.G. Tarter, J. Chromatogr. Sci. 27 (1989) 462.
[13] W. Frenzel, D. Schepers, G. Schulze, Anal. Chim. Acta 277 (1993) 103.
[14] S. Alegret, J. Alonso, J. Batroli, E. Martinez-Fabregas, Analyst 114 (1989) 1443.
[15] A.K. Covington, P.D. Whalley, J. Chem. Soc. Faraday I 82 (1986) 1209.
[16] R. Kataky, P.E. Nicholson, D. Parker, A.K. Covington, Analyst 116 (1991) 135.

ELSEVIER

Talanta 48 (1999) 979–983

Talanta

Short Communication

Quantitative determination of the non-entrapped chlorothiazide in the presence of liposomes using differential pulse polarography

Christos G. Kontoyannis [a,b,*], Sophia G. Antimisiaris [b], Dionisis Douroumis [a,b]

[a] *Institute of Chemical Engineering and High Temperature Chemical Processes, University Campus, PO Box 1414, GR-26500 Patras, Greece*

[b] *Department of Pharmacy, University of Patras, PO Box 1414, GR-26500 Patras, Greece*

Received 29 June 1998; received in revised form 22 September 1998; accepted 25 September 1998

Abstract

Differential Pulse Polarography (DPP) was used for the quantitative determination of the free and adsorbed (non-entrapped) chlorothiazide (CHT) in the presence of liposomes. It was found that CHT polarographic signal depends both on the concentration of multilamelar (MLV) liposomes, due to its adsorption on the liposomal surface, and on their size. Calibration plots of CHT concentration versus current density, at pH 7.4, in the presence of different liposomes concentrations were constructed. Based on these curves the non-entrapped chlorothiazide was determined. Results were compared to those obtained from the application of conventional procedure i.e. chromatographic separation of CHT from liposomes followed by UV spectrophotometric determination. Both techniques were found to be comparable with respect to their accuracy, with a relative error of 0.47%. Determination of the drug using DPP was faster.

Keywords: Differential pulse polarography; Chlorothiazide; Liposomes

1. Introduction

When evaluating retention of drugs in liposomes in most cases size exclusion or dialysis separation of the entrapped liposomal drug is required followed by spectrophotometric determination of the non-entrapped portion [1]. An additional more perplexing reason for applying such procedure is that a direct spectrophotometric analysis applicable to two-component mixtures is usually ruled out since a number of drugs possess overlapping UV spectra with the lipids commonly used. Unfortunately, this process is time consum-

* Corresponding author. Tel.: +30-61-997582; Fax: +30-61-993255; e-mail: cgk@iceht.forth.gr.

0039-9140/99/$ - see front matter
PII S0039-9140(98)00305-1

ing and its application is prohibiting for an in-situ evaluation of drug release kinetics where monitoring of the non-entrapped concentration is needed. It is apparent that a less cumbersome, fast, reliable and accurate technique for measuring the non-entrapped drug in the presence of liposomes is needed.

Classical, dropping mercury polarography, has been used in the past for determining some thiazides in tablets at different pH values [2] but the influence of liposomes and their characteristics, i.e. concentration and size, on the performance of the polarographic techniques has not been studied.

In the present work, differential pulse polarography (DPP) was applied for the determination of the non-entrapped chlorothiazide (CHT), a derivative of benzothiadiazine used as a diuretic and/or mild antihypertensive, in the presence of known concentrations of multilamelar liposomes (MLV). A new methodology was developed and it was compared to the conventional procedure. [1].

2. Methods and materials

Chlorothiazide was obtained from Aldrich, Germany while phosphadicholine PC lipid was acquired from Lipid Products, Nutfield, UK. Both chemicals were used as received. All solutions were buffered with Tris buffered saline (TBS) at pH = 7.4. TBS was prepared by dissolving 8.2 g NaCl (Merck, pro-analysis), 1.21 g Tris[hydroxymethyl]-aminomethane (Sigma, 99.5%) and 0.2 g NaN_3 (Serva) in 1 l triply distilled water.

Multilammelar liposomes (MLV) were prepared from 5 μmol phospholipid. The lipid (supplied as a solution in CH_3Cl:MeOH [2:1]) was dried by rotary evaporation of the organic solvent to a thin film on the walls of a 50-ml round-bottomed flask, and any traces of solvent was removed under a stream of nitrogen and by overnight connection to a vacuum pump. Lipids were dispersed by vortexing with TBS (pH 7.4). The liposome preparations were sonicated for 15 min in a Branson bath type sonicator, and allowed to stand at room temperature for 1 h.

The DPP system used consisted of: (a) An EG & G 303A Static Mercury Electrode with a Ag/AgCl reference electrode and a Pt counter electrode, (b) An EG & G 264A Polarographic Analyzer, (c) a personal computer interfaced with the polarographic analyzer through an SMM PCL-818-H data acquisition card, (d) A Julabo MV-F-25 thermostat which was set at 37°C and (e) A 99.999% Ar gas for solution deaeration. Before each experiment a 3 min gentle deaeration was applied.

Liposome size was measured by PCS, using the Mastersizer of the Malvern Instruments.

Pharmacia gel chromatographic system was used for the separation of the liposomal from the non-entrapped drug.

A Shimadzu single beam UV-Vis spectrophotometer was used for the quantitative analysis of the separated non-liposomal chlorothiazide.

3. Results and discussion

3.1. DPP calibration curve for CHT

Chlorothiazide is hydrolyzed to yield 4-amino-6 chloro-m-benzene disulfonamide to a small extent ($-\log k = 3.7$ for 87.5°C at pH 7.4 [3]), and thus the possibility of hydrolysis affecting the DPP peak was examined. A solution of CHT buffered at 7.4 at 37°C was prepared and the peak current intensity was measured at -1.6 V versus external Ag/AgCl at 1 h intervals for 10 h; no change was observed.

The calibration curve for the concentration of CHT versus the current density was constructed. As it was expected a linear relation between the peak height of the DPP peak and its concentration was observed. The linear fit equation, forced through 0, was:

$$j = 0.157\ X_{\mathrm{CHT}} \quad (1)$$

where j is the current density in μA cm^{-2} and X_{CHT} is the CHT concentration in ppm (mg l^{-1}). Correlation coefficient was 0.9998, data points were 8, while the standard deviation for the slope was 6.6×10^{-4}. The detection limit defined as $6\ s\ b^{-1}$ [4],where b is the slope and s the standard

Table 1
Cumulative results for the calibration curves of the current densities against the CHT concentration in ppm in the presence of 3.5 μm MLV liposomes

Calibration line[a]	Liposomal Concentration/mg ml^{-1}	n	r	SD slope
$j = 0.143\ X_{CHT}$	(2) 4	5	0.9995	1.5×10^{-3}
$j = 0.149\ X_{CHT}$	(3) 2	5	0.9999	6.2×10^{-4}
$j = 0.154\ X_{CHT}$	(4) 1	5	0.9998	7.6×10^{-4}
$j = 0.155\ X_{CHT}$	(5) 0.5	4	0.9996	9.4×10^{-4}

[a] j, current density/μA cm^{-2}; X_{CHT}, CHT concentration/ppm; r, correlation co-efficient; SD, standard deviation; n, data points.

deviation of n blank measurements, was calculated to be 0.04 ppm.

3.2. Effect of liposomal concentration

When liposomes were added to chrolothiazide solutions a DPP signal reduction was observed. This phenomenon was attributed to adsorbed drug on the external surface of the liposomes. Specific adsorption of liposomes on the mercury electrode surface could have been also the cause for the observed signal reduction but this possibility was ruled out since it was found that current intensity depends also on: (a) on liposome size (Section 3.3) and (b) drug lipophility. For example in the case of diazepam, $\log P = 2.86$, an almost 50% signal depression was recorded for 3.5 μm diameter 1 mg ml^{-1} liposomes [5] as opposed to $\sim 2\%$ reduction for identical CHT solution, $\log P = -0.27$, which was calculated using Eq. (1) and Eq. (4) (Table 1). P is defined as the partition co-efficient of a compound between n-octanol and the aqueous phase i.e. $P = C_{n\text{-octanol}}/C_{aq}$, where $C_{n\text{-octanol}}$ is the concentration in n-octanol and C_{aq} is the concentration in the aqueous phase.

To obviate this drawback a set of calibration plots were constructed. TBS buffered solutions with 4, 2, 1 and 0.5 mg ml^{-1} empty MLV liposomes, 3.5 μm diameter, and 35, 70, 150, 200, 250 ppm CHT were prepared. The current densities of the DPP peaks were recorded and by plotting them against the CHT concentration, in ppm, linear relations were observed. The respected equations and their statistics can be seen in Table 1. It is also interesting to note that by re-plotting the current densities versus the liposomal concentration, in mg ml^{-1}, linear equations, tabulated in Table 2, were also obtained.

Usage of information in Tables 1 and 2 permits non-entrapped chlorothiazide determination of solutions, consisting of the free and the adsorbed drug, with 3.5 μm diameter liposomes as follows: The lipid concentration, in mg ml^{-1}, which was used in the liposome preparation, is entered into the equations of Table 2 and the expected current intensities are calculated. The determined current intensities are then plotted against the chlorothiazide concentration, in ppm, and a linear equation resembling those of Table 1 is obtained. The DPP current density due to CHT is then introduced to the new equation and the unknown CHT concentration is determined. An example of this procedure is described in Section 3.4.

3.3. Effect of liposome size

A dependence of the DPP current intensities on the liposome size was observed. Solutions having empty liposomes with mean diameters of 3.5 μm, $w = 0.96$; 5.6 μm, $w = 2$; 7.1 μm, $w = 2.2$; 9.2 μm, $w = 2.3$; 10.2 μm, $w = 2.5$; were prepared from identical lipid films by varying the sonication

Table 2
Linear equations reflecting the influence of the concentration of 3.5 μm liposomes on the current density of the CHT DPP peak

Calibration line[a]	CHT Concentration/ppm	*n*	*r*	SD slope	SD intercept
$j = 39.1 - 0.68\ X_{lip}$	(6) 250	4	0.999	2.2×10^{-3}	5.2×10^{-3}
$j = 31.3 - 0.84\ X_{lip}$	(7) 200	4	0.999	3.8×10^{-3}	1.6×10^{-3}
$j = 23.6 - 0.73\ X_{lip}$	(8) 150	4	0.990	1.3×10^{-2}	3.0×10^{-2}
$j = 11.1 - 0.40\ X_{lip}$	(9) 70	4	0.991	3.9×10^{-3}	9.0×10^{-3}

[a] j, current density/μA cm^{-2}; X_{lip}, Lipid concentration/mg ml^{-1}; r, correlation co-efficient; SD, standard deviation; n, data points.

time. The w is the span of the size distribution and is define as $w = \{d(90) - d(10)\}/d(50)$ where $d(90)$, $d(10)$, $d(50)$, represent the size of the particles below of which are the 90, 10 and 50% of all liposomes, respectively. The liposome concentration in all cases was 1 mg ml^{-1} while the amount of the chlorothiazide added was 150 ppm. A linear relationship appears to exist between the DPP current density and the liposome size:

$$j = 23.4 - 0.29\ S \quad (10)$$

where j is the current density in μA cm^{-2} and S is the size of the liposomes in μm. Correlation co-efficient was 0.986, data points were 5, while the standard deviations for the slope and the intercept were 4.6×10^{-2} and 3.5×10^{-1} respectively. The rather poor correlation co-efficient and the large standard deviations reflect the liposomes size distribution, w. Nevertheless, Eq. (10) appears to be valid since for no liposomes ($S = 0$) j equals 23.4 μA cm^{-2} which in turn, by using Eq. (1), yields a CHT concentration of 150.9 ppm, a relative error of 0.6%. Larger liposomal size yields lower current densities which translates to higher chlorothiazide adsorption percentages.

3.4. DPP versus classical method

The analytical methodology which was described in Section 3.2 was compared with the technique currently used [1]. A TBS buffered solution with 3 mg ml^{-1} MLV PC liposomes with 3.5 μm in diameter was prepared and 212 ppm chlorothiazide was added. Using DPP the current density of the solution was determined as the average of five measurements and found to be 31.1 ± 0.15 μAcm^{-2}. According to the methodology described in Section 3.2 the liposome concentration, 3 mg ml^{-1}, was entered into the equations of Table 2 and the j values for 250, 200, 150 and 70 ppm CHT were determined. By plotting the current densities against the respected CHT concentrations in the presence of 3 mg ml^{-1} 3.5 μm liposomes the following linear relationship was obtained:

$$j = 0.146\ X_{CHT} \quad (11)$$

Correlation co-efficient was 0.9995, data points were 4, while the standard deviation for the slope was 1.5×10^{-3}. Entering into Eq. (11) the current density of the under consideration solution the concentration of the added CHT was determined to be 213 ± 2 ppm, a relative error of 0.47%.

A 1 ml sample of the same solution was then introduced to a size exclusion chromatography column, Sephadex G-50 (35×1 cm) equilibrated with TBS, where liposomes were separated from free drug. Liposomes were eluted in the column void volume and chlorothiazde in the bed volume. Please note that the adsorption problem was effectively eliminated through the large dilution taking place during the separation processes thus the concentration of free CHT coincides with the concentration of the non-entrapped drug. All the

non-liposomic segments with the chlorothiazide were added and the CHT concentration, taking into account the dilution factor and using a UV calibration line based on the Beer's law, was found to be 211 ± 0.5 ppm, a relative error of 0.47%.

The two methodologies were equally accurate but the precision of the classical procedure was better. The proposed method was less time consuming since no separation of the drug was needed and eventually can be used for in-situ measurements of drug release rates from liposomes. With respect to the classical methodology, the disadvantage was the need for more calibrations lines instead of the one required for the spectrophotometric determination.

4. Conclusions

DPP was used successfully for the fast and accurate and non-destructive determination of chlorothiazide in the presence of known concentration of PC MLV liposomes. Calibration curves, incorporating DPP peak current density, liposomal concentration, and CHT concentration, were constructed using liposomes with a diameter of 3.5 μm. On the basis of these plots the non-entrapped CHT concentration, at pH 7.4, was determined. The proposed procedure was found to be equally reliable as the conventional analytical method currently in use and exhibits the following advantages: (a) it is faster (b) requires only one system i.e. polarograph as opposed to the two techniques needed for the conventional method i.e. chromatograph and UV spectrometer (c) is less cumbersome and (d) can be used for monitoring of drug release from liposomes.

Acknowledgements

The authors acknowledge the help of D. Fatouros in preparing some liposomal films.

References

[1] R.R.C. New, Liposomes: A Practical Approach, IRL Press, Oxford University Press, 1990, pp. 91–95.
[2] E. Kkolos, J. Walker, Anal. Chim. Acta 80 (1975) 17.
[3] K. Connors, G. Amidon, B. Stella, Chemical Stability of Pharmaceuticals. A Handbook for Pharmacists, Wiley Intersciences, New York, 1986, pp. 345–350.
[4] K. Danzer, Accreditation and Quality Assurance in Analytical Chemistry, Gunzler, H. (Ed.), Springer-Verlag, Heidelberg, Berlin, 1996, p. 130.
[5] C. Kontoyannis, D. Douroumis, unpublished results.

ELSEVIER

Talanta 48 (1999) 985

Talanta

Book review

Handbook of Chemometrics and Qualimetrics: *Part A*. D.L. Massart, B.G.M. Vandeginste, L.M.C. Buydens, S. De Jong, P.J. Lewi and J. Smeyers-Verbeke, Elsevier, Amsterdam, 1997. xvii + 867 pp. US$ 293.25. ISBN 0-444-89724-0.

A handbook needs to be as comprehensive and all embracing as possible to warrant such a description. It also needs to be as self-contained as possible with lots of examples and extensive and relevant reference lists. Above all, it has to be biased towards practical applications. Thus a handbook of chemometrics and qualimetrics is a tall order since it needs a full background in statistical theory and the relevant mathematics as well as covering an extensive variety of applications in the world of design and analysis of chemical experiments.

At 848 pages plus index, this book is undoubtedly comprehensive, covering basic statistics, hypothesis testing, the analysis of variance, quality control, regression (both linear and non-linear), non-parametric (robust) statistics, principal component analysis, information theory, and experimental designs. In addition there are chapters that introduce and explain some necessary mathematics that may not always be familiar to chemists including vector analysis and optimisation theory. Indeed there is so much material covered, that a second volume is necessary that promises a more advanced treatment with emphasis on multivariate systems.

How useful is it? A single experimenter cannot fully judge because of the scope of the book, but at the time of this review I was involved in the use of non-parametric statistics for matching X-ray powder diffraction patterns. Chapters 5 and 12 discussed much of what was needed: the Spearman rank correlation coefficient, the Mann–Whitney test and the Kolgomorov–Smirnov test, but no Kendal τ (perhaps that is in Part B). The examples of how these methods are used were clear. This is true of the whole book: the references are extensive and useful, the diagrams and text are always clear, and every technique has at least one example of chemical relevance that is explained in detail. At the end of each section the experimenter should be able to carry out the test or procedure for themselves and hopefully adapt it to their needs.

It is up to date as well. For example, the section on optimisation theory has a comprehensive description of genetic algorithms as efficient search mechanisms in multi-dimensional, non-linear spaces with an example involving the sums of exponentials in which the arguments are polynomials. Occasionally I felt that there was an insufficient description of when a given test could be used and when it may break down. Does it, for example, assume that the variables are normally distributed? What happens if the sample is very small? A feature that I would also like to see added is a critical list of web sites. There is a lot of good (and poor) statistical software available free on the Internet and it is useful to say where this can be found. Statistics computer packages too could be mentioned. It all adds to the practical value of a handbook.

However, it is altogether very well done, and is indeed a handbook that will useful in any industrial or academic laboratory where quantitative procedures are involved. But the price: get your library to buy it!

C.J. Gilmore

PII S0039-9140(98)00199-4

ELSEVIER

Talanta 48 (1999) 987

Talanta

Book review

Preparative Chromatography Techniques—Applications in Natural Product Isolation. K. Hostettmann, A. Marston and M. Hostettmann, Springer, Berlin, 1998. xi + 244 pp. US$ 129.00. ISBN 3-540-62459-7.

Due to the importance of bioactive compounds from natural sources, there have been tremendous advances in the different chromatographic instruments and numerous new applications since the first edition of this book in 1986. The objective of this book (second edition), is, on the same bases as the first edition, to provide an update for techniques and protocols in the preparative separation of natural products. The book is successful in achieving this goal. With the emphasis on applications, the authors not only present concrete examples of preparative separations but also provide readers with the means of selecting an approach for their separation problem. Overall, this book will be of significant interest to natural product chemists, biochemists and newcomers to the field.

The book is organized into 11 chapters that cover a set of topics from sample preparation to separation strategy and combination of methods. Chapter 1 is a very brief introduction which describes the link between chromatography and natural products, and the history of method development. Chapter 2 describes the important area of sample preparation, and gives practical methods for pre-treatment of a sample prior to chromatography. Chapters 3 to 7 cover the liquid–solid and all-liquid chromatographic procedures with emphasis on techniques which involve the application of pressure, separation of problematic labile compounds and the advantages of the various methodologies. Subsequently, chapters 8 and 9 illustrate the isolation of macromolecules and chiral molecules which are, in most cases, difficult to separate. Chapter 10 discusses the strategy when designing separation protocols for complex mixtures. The final chapter provides a useful subject index for readers.

While a vast amount of literature is available about natural products isolation and identification due to the increasing interests in this field, books that deal practically with preparative separation of natural products are very few. This book obviously makes a significant effort to fill this gap. Most readers will find this book very useful in their bench work.

L.X. Liu

PII S0039-9140(98)00200-8

ELSEVIER

Talanta 48 (1999) 989

Talanta

Book review

Basic Gas Chromatography. H.M. McNair and J.M. Miller, Wiley, Chichester, 1997. xii + 200 pp. Softback, £24.95. ISBN 0-471-17261-8.

This is a book in the Techniques in Analytical Chemistry Series. This series of books addresses current techniques widely used in analytical laboratories. Few would deny that gas chromatography (GC) is one such technique.

This is an excellent, concise, easily understandable, well-written, well-presented and well-illustrated, small text-book (200 pages long) which covers the basic principles and techniques of modern GC. It provides a rapid, easily assimilated, not too theoretical, basic textbook for undergraduate students or those wishing to rapidly acquire the basics of the technique to understand or do some practical GC work. Wherever appropriate theory and practice are intermeshed—this aids the learning process. The book, as one would expect, covers basic theory, instrumentation, columns (packed and capillary), detectors and the principles of qualitative and quantitative analysis. Except for the chapter which gives an overview of the instrumentation, every chapter is adequately referenced to allow further reading for those who wish to expand their knowledge on particular aspects. Particular mention is made of specialities such as GC–MS, chiral separation, sample preparation and derivatives. At the end there is an excellent chapter (seven pages) on trouble-shooting—this could be a big time saver for a beginner and experienced analyst alike! Another important source of information is the nine appendices which cover a variety of useful facts such as a list of symbols and acronyms, guidelines for selecting capillary columns, how to avoid problems in GC, a short list of recent books (latest published in 1996) and recent, general literature.

A unique little book which presents the basics of GC and much more.

R.R. Moody

PII S0039-9140(98)00201-X

ELSEVIER

Talanta 48 (1999) 991

Talanta

Book review

Capillary Electrophoresis in the Life Sciences. A.M. Krstulovic (editor), Elsevier, Amsterdam, 1997. 293 pp. D*f* 216.25. ISBN 0-444-82868-0.

This book represents a collection of review articles (5), research papers (12) and short communications (7) reprinted from the Journal of Chromatography B, Volume 697. There can be little doubt that capillary electrophoresis (CE) is being used increasingly as a means of analysis for biological molecules and smaller molecules, including drugs, in complex matrices because of its speed, efficiency and the small sample volume. The rapidity of the expansion of CE applications in this field is epitomised by the contents of this book which include substantive contributions from some of the world's leading experts from Japan, USA, Canada and Europe.

The reviews cover analytical applications in clinical chemistry, pharmacokinetics, recombinant protein purity, gene defects and the quality of dairy products. The papers and short communications give more specific illustrative examples of the applications of CE in the life sciences. In particular, they collectively highlight the current methods employed to overcome sensitivity-detection problems.

As expected from peer reviewed work the quality of the contents is of a uniformly high standard throughout and as an aid to the reader an author and compound index is included at the end of the book.

For those with limited library facilities this hard-backed edition is well worth having as a quality reference source to current methodology, problems and the future potential of CE in the biological and medical fields.

R.R. Moody

PII S0039-9140(98)00202-1

ELSEVIER

Talanta 48 (1999) 997–1004

Talanta

Continuous monitoring for cyanide in waste water with a galvanic hydrogen cyanide sensor using a purge system

Hiromitsu Hachiya [a], Satoshi Ito [a], Yoshito Fushinuki [b], Takashi Masadome [c], Yasukazu Asano [c,*], Toshihiko Imato [d]

[a] *R & D division, DKK Corporation, 4-13-14 Kichijoji, Kitamachi, Musashino-shi, Tokyo 180-0001, Japan*
[b] *Scientific Investigation Research Laboratory, Kagoshima Pref. Police HQ, 10-1 Kamoikeshinmachi, Kagoshima-shi, Kagoshima 890-0064, Japan*
[c] *Ariake National College of Technology, 150 Higashihagiomachi, Omuta-shi, Fukuoka 836-8585, Japan*
[d] *Faculty of Engineering, Kyushu University, 6-10-1 Hakozaki, Higashi-ku, Fukuoka-shi, Fukuoka 812-0053, Japan*

Received 17 August 1998; received in revised form 2 September 1998; accepted 2 September 1998

Abstract

A continuous monitoring system for cyanide with a galvanic hydrogen cyanide sensor and an aeration pump for purging was developed. Hydrogen cyanide evolved from cyanide solution using a purging pump was measured with the hydrogen cyanide sensor. The system showed good performance in terms of stability and selectivity. A linear calibration curve was obtained in the concentrating range from 0 to 15 mg dm^3 of cyanide ion with a slope of -0.24 μA mg^{-1} dm^{-3}. The lower detection limit was 0.1 mg dm^{-3}. The 90% response time of the sensor system was within 3.5 min for a 0.5 mg dm^{-3} cyanide solution, when the flow rate of the purging air was 1 dm^3 min^{-1}. The system maintained the initial performance for 6 months in the field test. The developed galvanic sensor system was not subject to interference from sulfide and residual chlorine, compared with a potentiometric sensor system developed previously. The analytical results obtained by the present system were in good agreement with those obtained by the pyridine pyrazolone method. The correlation factor and regression line between both methods were 0.979 and $Y = 2.30 \times 10^{-4} + 1.12X$, respectively. This system was successfully applied for a continuous monitoring of cyanide ion in waste water.

Keywords: Galvanic cell; Chemical sensor; Cyanide; Continuous monitoring; Gas phase; Industrial waste water

1. Introduction

Cyanide is one of the most toxic compounds but it has been used widely in industrial fields such as hydrometalogy and metal plating due to its excellent chemical properties. Cyanide concen-

* Corresponding author. Tel.: +81-944-53-8876; e-mail: asano@ariake-nct.ac.jp.

0039-9140/99/$ - see front matter
PII: S0039-9140(98)00314-2

tration in industrial waste water had been regulated strictly to be 1 mg dm^{-3} in Japan [1,2] because the leakage of cyanide causes serious damage to the ecosystem. A potentiometric cyanide ion selective electrode has been widely used as a continuous cyanide-monitor to control cyanide in industrial waste water. However, the method needs several procedures such as sampling, adjustments of pH and ionic strength of the samples prior to determine. Therefore a simple and more inexpensive monitoring system for cyanide is needed to replace the system with the conventional ion selective electrode [3–5]. Absorption spectrometry based on the Knöig reaction such as the pyridine pyrazolone method has also been used to determine cyanide. However this method needs several procedures and is time-consuming [6–8].

Recently, rapid and simple analytical methods for cyanide using ion chromatography [9,10] and flow injection analysis [11,12] have been reported. However, both methods may have some difficulty in application as a continuous, maintenance-free monitor because a sampling pump, a separation column and pretreatment of the samples are needed and the running costs seem to be high for continuous monitoring. Leakage of cyanide into the environment is accidental, therefore a continuous cyanide-monitoring system with the characteristics of simplicity, selectivity, reliability, low cost and long-stability in the field is desirable presently.

We have developed a system for monitoring cyanide by combining a potentiometric gas sensor for hydrogen cyanide with an air-bubbling flow system [13,14]. Though the developed system is simple and of low-cost and is of commercial use, it is subject to interference from concentrated residual chlorine and traces of sulfide which coexist in the sample solution. These interferences may be due to the fact that the sensing element of the system consists of Ag_2S which shows a response to residual chlorine and sulfide [14].

In this work we have developed a galvanic hydrogen cyanide sensor system in order to improve the interference from residual chlorine and sulfide. The monitoring system consists of an air pump, a purge tube, a galvanic hydrogen cyanide sensor and an ammeter. The performance of the sensor system and its application to waste water monitoring are described.

2. Experimental

2.1. Apparatus

The output-current of the galvanic hydrogen cyanide sensor was measured by an electrometer (model 612, Keithley Instruments). The signals from the electrometer were fed to a recorder (model LR4110, Yokogawa Denki). An aeration pump (model NS-SUN, Nissei) was used for air-purging. A silver ion-selective electrode (model 7084L, DKK) and a double junction type reference electrode (model 4083, DKK) were used to standardize the cyanide stock solution by argentometry.

2.2. Reagents

All reagents used were of analytical grade. Deionized water (Milli-Q water) was used throughout the experiment. A stock solution of 1000 mg dm^{-3} cyanide solution was prepared by dissolving 1.252 g potassium cyanide in 0.5 dm^3 of a 0.1 mg dm^{-3} NaOH solution. This solution was standardized by argentometry before use. A 0.25 mol dm^{-3} phosphate buffer solution was prepared by dissolving 34.0 g KH_2PO_4 and 35.5 g Na_2HPO_4 in 1 dm deionized water.

2.3. Galvanic hydrogen cyanide sensor

The structure of the galvanic hydrogen cyanide sensor is shown in Fig. 1. An inner electrode, which consists of a silver working electrode and a silver counter electrode, was fabricated. The silver working electrode (2mm diameter, plate) was fixed at the end of the inner body and a silver wire (0.4 mm diameter, 350 mm long) was reeled around the inner body. The inner electrode was inserted into a sensor body (26 mm outer diameter, 65 mm long). The sensor body has a compartment for an internal filling solution. A gas-permeable polytetrafuluoroethylene (PTFE)

membrane was fixed at the end of the sensor body by an O-ring. The pore size and porosity of the membrane were 0.22 μm and 65%, respectively. An internal filling solution (4 cm^3), which was a mixture of 4.6 mg dm^{-3} silver nitrate and 0.02 mg dm^{-3} nitric acid in 70% ethylene glycol to prevent evaporation of the inner solution, was filled into the inner compartment of the sensor body. The thickness of the internal filling solution layer between the working electrode and the PTFE membrane was less than 0.1 mm.

Because the sensor was a galvanic cell, any potential between the working and the counter electrode was not applied.

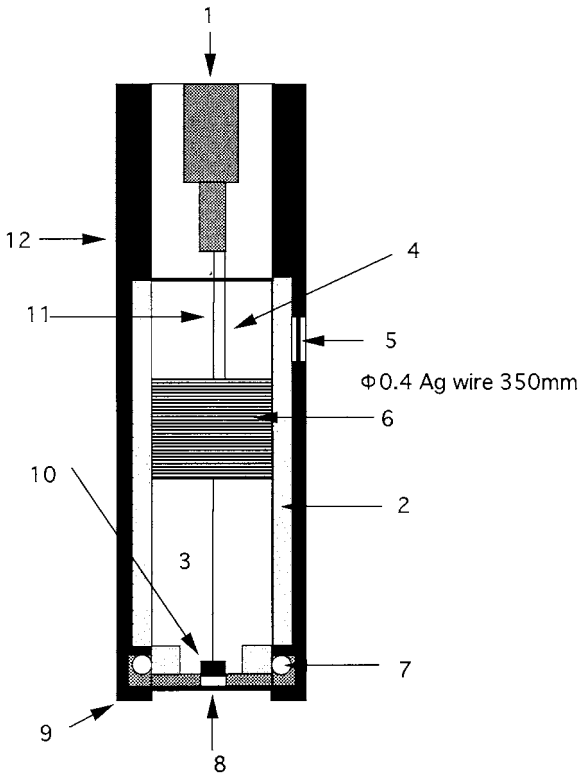

Fig. 1. Structure of the galvanic hydrogen cyanide sensor. 1, Terminal; 2, inner solution (4.6×10^{-1} M Ag^+/0.2 M HNO_3 in70% ethylene glycol); 3, inner body; 4, lead wire from counter electrode; 5, membrane for pressure balance; 6, counter electrode (ϕ 4 Ag wire 350 mm); 7, O-ring; 8, gas permeable membrane; 9, membrane support; 10, working electrode (ϕ 2 Ag plate); 11, lead wire from working electrode; 12, sensor body.

2.4. Principle of determination of cyanide concentration by the hydrogen cyanide sensor

In an aqueous sample solution containing cyanide, the following equilibrium is established between the hydrogen ion, cyanide ion and hydrogen cyanide;

$$H^+ + CN^- = HCN \quad (1)$$

The formation constant of hydrogen cyanide is expressed as follows:

$$[HCN]/[H+]\,[CN^-] = 1/K_a \quad (2)$$

where K_a is the acid dissociation constant and is reported as $10^{-9.24}$. From Eq. (2), using the pH of the solution, the concentration ratio of HCN and CN^- is expressed as follows:

$$[HCN]/[CN^-] = 10^{9.24-pH} \quad (3)$$

In the neutral pH region (pH 6.86), most of cyanide exists in the form of hydrogen cyanide judging from Eq. (3). When air is bubbled into the sample solution at the flow rate of more than 1 dm^3 min^{-1}, hydrogen cyanide is evolved into a gaseous phase immediately. When the gas phase is transported to the hydrogen cyanide sensor, the hydrogen cyanide permeates through the PTFE membrane of the sensor and is dissolved in the internal filling solution. The hydrogen cyanide is oxidized according to Eq. (4) at the surface of the working electrode spontaneously, while the silver ion internal filling is reduced to silver according to the Eq. (5) [15] at the counter electrode. Thus the current generated is measured by the ammeter.

$$Ag + 2HCN \rightarrow Ag(CN)^{2-} + 2H^+ + e^- \quad (4)$$

$$Ag^+ + e^- \rightarrow Ag \quad (5)$$

Since the current changes are proportional to the hydrogen cyanide concentration in aqueous phase, and the hydrogen concentration is related to the cyanide in aqueous solution by Henry's law, the cyanide concentration in the sample solution can be determined by measuring the current from the hydrogen cyanide sensor.

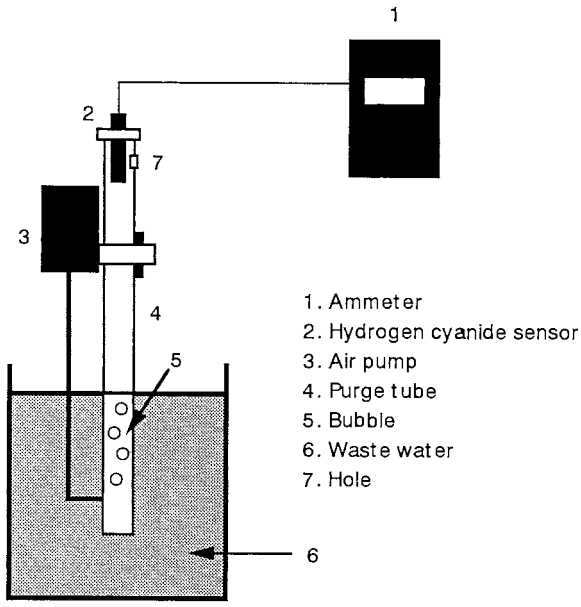

Fig. 2. Continuous monitoring system for cyanide with a galvanic hydrogen cyanide sensor.

2.5. Evaluation of the performance of the galvanic hydrogen cyanide sensor

The performance of the sensor in the gaseous phase was evaluated in a 1 dm^3 brown colored closed vessel containing 0.1 dm^3 cyanide solutions of different concentrations at pH 6.86 adjusted by phosphate buffer. The sensor was suspended in the aqueous phase of the vessel containing the cyanide solution (pH 6.86) and then the sensor was inserted into the gas phase of the closed sample solution. The temperature of the solution was kept constant. The current from the sensor was measured after gas–liquid equilibrium was attained. The accuracy of the results from the sensor was evaluated by measuring the hydrogen cyanide gas in the gas phase after absorbing hydrogen cyanide gas in a 0.1 mol dm^{-3} NaOH solution and by argentometric titration of the absorbed solution.

2.6. Construction of the continuous monitoring system for cyanide

The schematic diagram of the continuous cyanide-monitor is shown in Fig. 2. Air was bubbled through the Teflon tube (3 mm i.d.) at 70 mm from the surface of the sample solution by the aeration pump. The hydrogen cyanide evolved from the solution was transported to the sensor by air through the polypropylene tube (27 mm i.d., 1.0 m long) immersed in the sample solution at depth of 15 cm. The evolved hydrogen cyanide was detected by the sensor located at the top of the polypropylene tube. Therefore, the sensor signals was reproducible since the surface of the sensor was always kept clean. The current from the sensor was measured by the ammeter and its signals were fed to a recorder. The hydrogen cyanide and air were evacuated through a hole which was bored at 80 mm from the top of the polypropylene tube.

3. Results and discussion

3.1. Performance of the hydrogen cyanide sensor

3.1.1. Calibration curve

The calibration curve of the hydrogen cyanide sensor, which was obtained for the cyanide solutions (pH 6.86) at 25°C in the closed vessel is shown in Fig. 3. The linear calibration curve was obtained in the range 0–15 mg dm^{-3} cyanide concentration. The slope of the calibration curve was -0.24 μA mg^{-1} dm^{-3}. The lower detection limit of the sensor was 0.1 mg dm^{-3} cyanide.

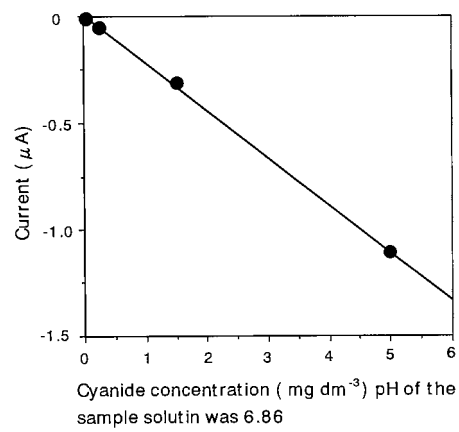

Fig. 3. Typical calibration curve for cyanide.

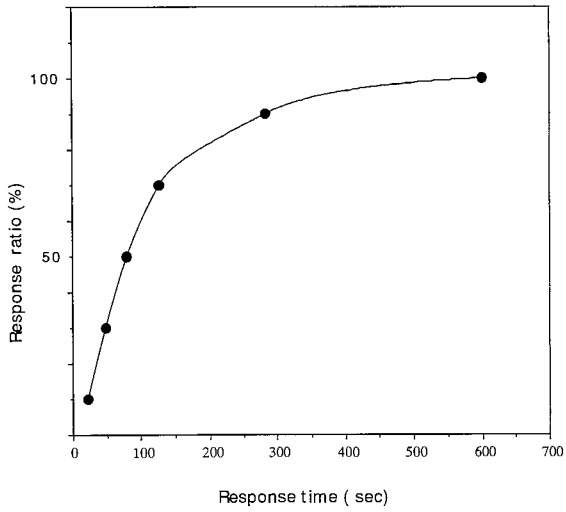

Fig. 4. Response time of the galvanic hydrogen cyanide sensor (0.1 mg dm^{-3} cyanide, pH 6.68).

3.1.2. Response time

Fig. 4 shows the typical response curve of the 0.1 mg dm^{-3} cyanide solution. The 90% response times for 0.1, 0.5, 3 and 10 mg dm^{-3} cyanide solutions were 282, 208, 91 and 47 s, respectively. The 50% response times for 0.1, 0.5, 3 and 10 mg dm^{-3} cyanide solutions were 80, 98, 24 and 13 s, respectively. The fast response time is characteristic of the present sensor even for a sample solution of low cyanide concentration.

3.1.3. Reproducibility and stability

The reproducibility and the long-term stability of the sensor are important for continuous monitoring in the field. The reproducibilities for 0.1, 1, 3 and 10 mg dm^{-3} cyanide solutions were 1.0, 4.3, 8.4 and 7.8%, respectively. The variation of the current from the sensor for the 0.5 mg dm^{-3} cyanide solution over a period for 6 months was within $\pm 20\%$ reproducibility. These results indicate that the good reproducibility and long-term stability of the present sensor meet the requirement continuous monitoring.

3.1.4. Effect of interferences

Because the waste water containing cyanide is generally treated with hypochlorite for decomposition of cyanide, the waste water after treatment usually contains residual chlorine. Therefore the cyanide monitor should have good selectivity for cyanide against residual chlorine. Although the present hydrogen cyanide sensor was immersed in the brown colored closed vessel containing 100 dm^3 of 500 mg dm^{-3} hypochlorite solution for 30 min to examine the interference from residual chlorine, the current from the sensor was not changed. Even after immersing the sensor for 30 min. in the hypochlorite solution, the sensitivity to cyanide remained at the same level as the initial sensitivity of -0.24 μA mg^{-1} dm^{-3}.

In addition, when the sensor was exposed to 1 ppm Cl_2 gas for 5 min it did not show any response to the Cl_2 gas. However, the potentiometric hydrogen cyanide sensor showed 65% errors for measurement of 1 and 10 mg dm^{-3} cyanide when exposed to the same Cl_2 gas. From these experiments the present galvanic sensor was confirmed to be applicable to the aqueous phase containing residual chlorine and the gaseous phase containing chlorine.

On the other hand, the sensor was subjected to interference from sulfide as shown in Fig. 5. The current from the sensor for 0.1, 1 and 10 mg dm^3 sulfide solutions corresponded to the one for 1.41, 15.8 and 65.6 mg dm^{-3} cyanide solution, respectively. Sulfide exists as dissolved hydrogen sulfide

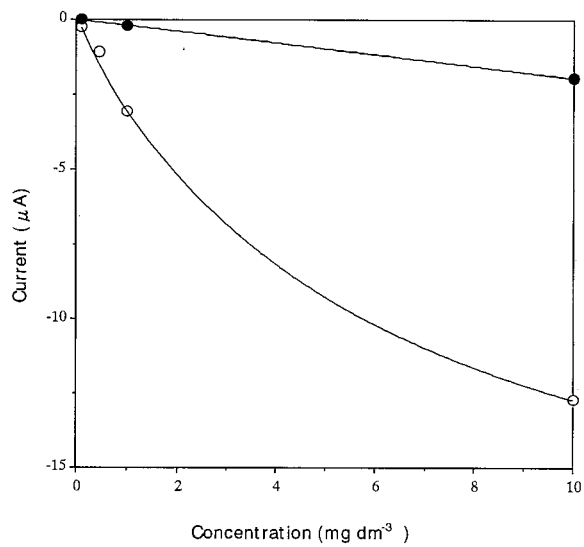

Fig. 5. Effect of hydrosulfide: ●, cyanide; ○, hydrosulfide.

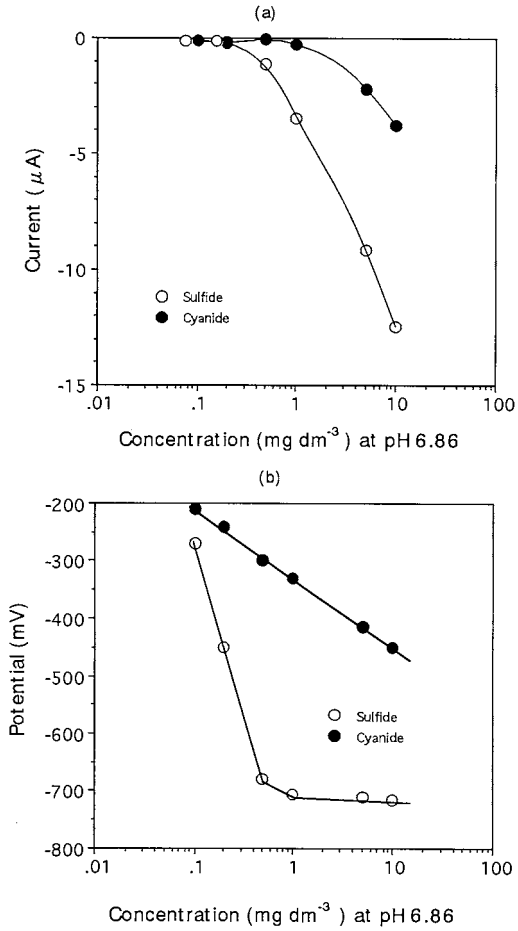

Fig. 6. Comparison of the effect of sulfide between the galvanic and the potentiometric sensors.

in the solution at near neutral pH. The sensor signals to a 1 mg dm^{-3} cyanide solution and a 1 mg dm^{-3} sulfide solution correspond to 2 ppm HCN and 8 ppm H_2S, respectively. However, the effect of sulfide on the signal of the present sensor was not so large compared with that of the potentiometric hydrogen cyanide sensor, as shown in Fig. 6 which indicates that sulfide is insoluble in the inner solution because the inner solution of the present sensor is acidic while that of the potentiometric sensor is alkaline. Accordingly, the reactivity of the present sensor to sulfide is very low and, as a result, the present galvanic hydrogen cyanide sensor is more selective for sulfide compared to the potentiometric hydrogen cyanide sensor reported previously.

3.1.5. Effect of temperature

The effect of temperature on the sensor response is shown in Fig. 7. The sensitivity and the slope of the calibration curve increased with increasing temperature. The increasing sensitivity of the sensor with temperature may be due to the fact that the concentration of hydrogen cyanide in the gas phase increases with increasing temperature of the aqueous phase. This indicates that the sensor response is subject to temperature variation of the sample solution. In order to reduce the effect of temperature a temperature compensation circuit was combined in the system..

3.2. Performance of the continuous monitoring system for cyanide

3.2.1. Response time

The performance of the continuous monitoring system for cyanide as shown in Fig. 2 was evaluated with respect to response time by aeration through the cyanide standard solutions instead of the sample solutions. The 90% response times of the system to 0.5 mg dm^{-3} was 3.5 min. The longer response time of the system compared to the hydrogen sensor itself may be due to the fact

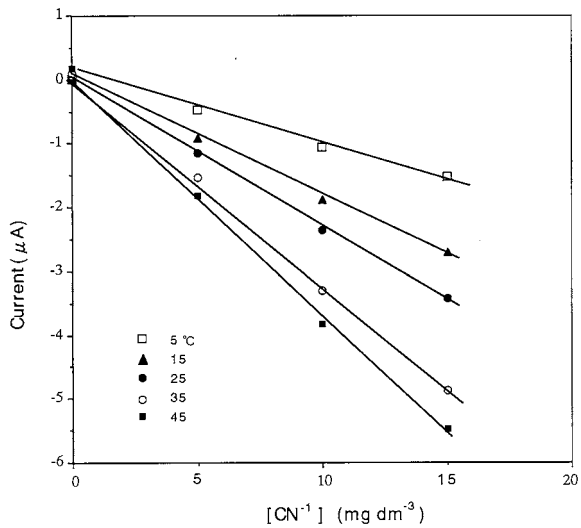

Fig. 7. Effect of temperature on the sensor signals.

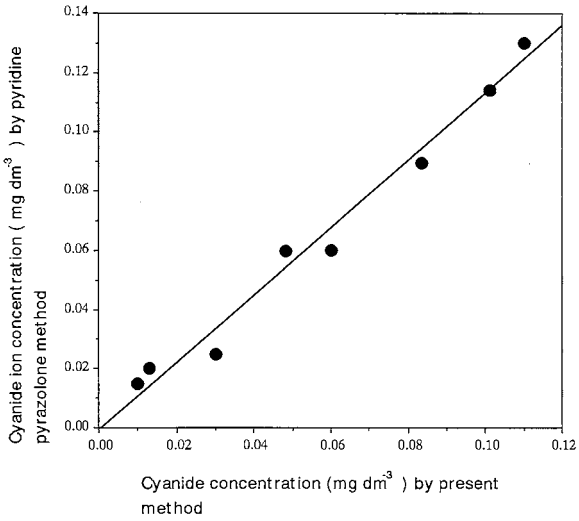

Fig. 8. Correlation between the present method and the conventional method. The samples are waste water from a plating factory.

that there is a time-lag to attain the phase equilibrium and transportation of the evolved hydrogen cyanide to the sensor by air. Shortening the length of the gas purge tube and more powerful aeration may reduced the response time.

3.2.2. Correlation between the present amperometric method and a conventional pyridine pyrazolone method

The present continuous monitoring system for cyanide was applied to the determination of cyanide in waste water. Several waste water samples containing cyanide from a plating factory were used. The analytical results obtained by the present sensor system method were compared with those from the conventional pyridine pyrazolone method. The correlation between two methods was fairly good as shown in Fig. 8. From these data the regression line expressed by $Y = 2.30 \times 10^{-4} + 1.12X$ and a correlation factor of 0.979 were obtained. This good correlation indicates that the present sensor system can be applied for the continuous monitoring of cyanide directly in nearly neutral pH solutions such as waste water.

3.2.3. Stability of the sensor system in the field

The long term stability of the present system was tested by setting the system in the waste water from a plating factory and the results are shown in Fig. 9. The system was periodically checked with a standard solution of 0.5 mg dm^{-3} cyanide during the period of the test. The variation for 6 months was within $\pm 20\%$. The initial performance of the cyanide monitor remained constant for 6 months.

4. Conclusion

We have developed a galvanic hydrogen cyanide sensor, in which selectivity to cyanide against sulfide and residual chlorine was improved and used it in a continuous monitoring system with a purge unit for the detection of cyanide. A linear response curve was obtained in the range from 0 to 15 mg dm^{-3} cyanide concentration. The lower detection limit was 0.1 mg dm^{-3}, and the 90% response time of the system was shorter than 3.5 min for 0.5 mg dm^{-3} cyanide solution. The system maintained a good

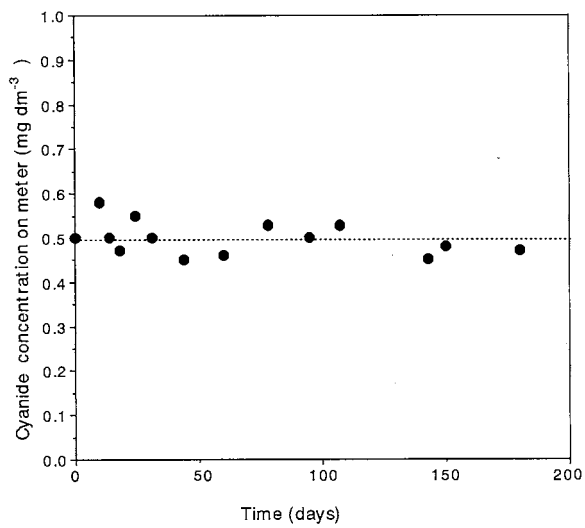

Fig. 9. Long-term stability test of the continuous monitoring system for cyanide with a galvanic hydrogen cyanide sensor. Field, a plating factory. The system was checked with a standard solution of 0.5 mg dm^{-3} cyanide periodically.

performance for 6 months. This long-term stability was due to the gas phase measurement in which the surface of the sensor was kept clean. Residual chlorine and chlorine gas did not interfere with the present system. Although there was an error for the measurement of a cyanide sample in the presence of sulfide greater than 0.1 mg dm^{-3}, selectivity of the sensor system against sulfide was improved greatly compared to that of the potentiometric hydrogen cyanide sensor system. This improved selectivity against sulfide and residual chlorine was due to the low reactivity with the sensing element and the low solubility of those gases in the inner solution. A linear regression line with a correlation factor of 0.979 was obtained between the present amperometric method and the conventional pyridine pyrazolone method. It can be concluded that the present system is applicable as a continuous monitor for cyanide in industrial waste water.

References

[1] Regulations by The Prime Minister's Office on Waste Water Standards: Basic Six Environmental Laws, Chuohoki Publisher, Japan, 1995.
[2] Testing Methods for Industrial Waste Water, Japanese Industrial Standard JIS K 0102-1991, pp. 122–123.
[3] Y. Asano, Chem. Eng. 17 (1972) 90–97.
[4] M.S. Frant, J.W. Ross Jr., J.H. Riseman, Anal. Chem. 44 (1972) 2227–2232.
[5] R.J. O'Herron, EPA-670/4-75-005, April 1975, p. 7.
[6] J. Estein, Anal. Chem. 19 (1947) 272.
[7] Testing Methods for Industrial Waste Water, Japanese Industrial Standard JIS K 0102-1991, pp. 119–121.
[8] E. Tanaka, S. Ohara, S. Adachi, M. Nunoura, J. Jpn. Water Works Assoc. 61 (1992) 21.
[9] J.E. Girad, Anal. Chem. 51 (1979) 836–839.
[10] Y. Liu, R.D. Rocklin, R.J. Joyce, M. Doyle, Anal. Chem. 62 (1990) 766.
[11] O. Elshoz, W. Frenzel, C.-Y. Liu, J. Moller, Fresenius' Z. Anal. Chem. 338 (1990) 159.
[12] V. Kuban, Anal. Chem. 64 (1992) 1106.
[13] Y. Asano and S. Ito, Japanese Patent, 1416967 (1987).
[14] Y. Asano, S. Ito, Bunseki Kagaku 39 (1990) 785–787.
[15] W.M. Latimer, Oxidation Potentials, 2nd edn, Prentice-Hall, Englewood Cliffs, 1952, p. 191.

ELSEVIER

Talanta 48 (1999) 1005–1011

Talanta

Determination of nitric oxide with ultramicrosensors based on electropolymerized films of metal tetraaminophthalocyanines

Jiye Jin [a], Tomoo Miwa [a], Lanqun Mao [b], Huiping Tu [b], Litong Jin [b,*]

[a] *Department of Chemistry, Faculty of Engineering, Gifu University, Yanagido1-1, Gifu 501-1193, Japan*
[b] *Department of Chemistry, East China Normal University, Shanghai 200062, People's Republic of China*

Received 19 May 1998; received in revised form 11 September 1998; accepted 17 September 1998

Abstract

Preparation and electrochemical responses to nitric oxide (NO) of the electropolymerized films of metal tetraaminophthalocyanines (MTAPc, M = Co, Ni, Cu) are studied to test them as molecular devices for design and construction of amperometric ultramicrosensors for selective and sensitive determination of NO. The ultramicrosensors based on electropolymerized films of MTAPc and Nafion, are found to show a low detection limit, high selectivity and sensitivity to NO determination. The potential interference from some endogenous electroactive substances in biological tissues, such as catecholamines and their metabolites, ascorbic acid (AA), uric acid (UA), and nitrite (NO_2^-), the metabolite of NO at the concentrations higher than those in biological systems could be eliminated by using a technique of DPV or DPA and further coating the modified ultramicrosensors with a layer of Nafion.

Keywords: Nitric oxide; Ultramicrosensor; Metal tetraaminophthalocyanines

1. Introduction

NO has been proved out to be an extremely important and mysterious bioregulator molecule of great physiological and pathophysiological importance since its recognition as an endothelium-derived relaxing factor (EDRF) in the vascular systems [1] in the latter half of 1980's. For example, it has been identified as a neurotransmitter with a crucial role in neural communication in central and peripheral nervous systems, [2], a cytotoxic factor in the immune systems [3]. Moreover, it is related to some tissue damage such as ischemia/reperfusion damage [4] and excitatory neuronal death [5]. Several pathophysiological processes are associated with abnormalities of EDRF [6–11].

It is well known that electrochemical technique is very promising for NO determination due to its in vivo and real time performance. Consequently, there is an explosive interest in the design and

* Corresponding author. Fax: +86-21-62451876; e-mail: ltjin@ch.ecnu.edu.cn.

0039-9140/99/$ - see front matter
PII: S0039-9140(98)00308-7

construction of amperometric ultramicrosensors because they are now contributing very actively to the promotion of the utilization of electrochemical technique for in vivo performance [12–21]. Synthetic metal porphyrin, phthalocyanine and shiff-base complexes have been promoted to serve as biomimetric oxidation catalysts and oxygen carriers [22–24]. Very recently, we have developed for the first time new ultramicrosensors based on electropolymerized film of metal shiff-bases [25–27]. And also metalloporphyrins have been reported as the best candidate for the construction of NO sensors [15–18]. Metallophthalocyanines, as macrocyclic complexes, have been exploited extensively in electrocatalysis [28–33]. However, up to now, to our best knowledge there is no report concerning its application in NO determination. In this work, we develop ultramicrosensors based on electropolymerized films of cobalt, nickel and copper tetraaminophthalocyanines(denoted as CoTAPc, NiTAPc, and CuTAPc, respectively) and Nafion. The ultramicrosensors are found to display a low detection limit, high selectivity and sensitivity to NO determination.

2. Experimental

2.1. Chemicals

A NO saturated solution was obtained by bubbling NO gas through deoxygenated distilled water for 30 min, using a value of 1.9 mmol l^{-1} for its concentration at saturation [34]. A series of standard NO solutions were prepared by diluting aliquots of NO saturated solution. NO standard solutions could also be obtained by NO Producing System developed in our laboratory [35]. The prepared NO solutions were kept in a glass flask with a rubber septum, and stored in the dark to ensure stability for 3 h.

Metal tetraaminophthalocyanines were synthesized and purified according to the procedure described by Achar et al. [36]. Their structures were characterized by FT-IR, FT-IR spectra data (KBr, cm^{-1}): 3281, 3183 (γ_{-NH2}), 1345, 1258, 1060, 1090 (γ_{C-N}), 826, 868 (δ_{Ar}), 735, 752, 950, 1607(δ_{N-H}). Tetra-*n*-butylammonium perchlorate(TBAP) was prepared by the reaction of tetra-*n*-butylammonium bromide with sodium perchlorate. Nafion (5% solution in ethanol) was purchased from Aldrich. Dopamine,5-hydroxytryptamine,5-hydroxyindole-3-acetic acid, 3,4-dihydroxyphenyl- acetic acid and epinephrine were purchased from Sigma Chem. Co. Phosphate-buffered saline (PBS) containing 137 mmol l^{-1} NaCl, 2.7 mmol l^{-1} KCl, 8.0 mmol l^{-1} Na_2HPO_4 and 1.5 mmol l^{-1} KH_2PO_4 was prepared and adjusted to pH 7.4. Other chemicals were of at least reagent grade quality and used as received. The aqueous solutions were prepared with doubly distilled water.

2.2. Apparatus

Electrochemical experiments were carried out with Biosensing Unit (BS-1) (Bioanalytical Systems Co., Japan) equipped with X–Y Recorder 4032 or CHI832 Electrochemical Analyzer from USA in conjunction with a IBM compatible pentium-133 computer. An electrochemical cell with three electrodes system was used. A platinum disc ultramicroelectrode prepared by sealing a platinum wire (ϕ15 μm) into a capillary served as a working electrode. Prior to experiment, it was polished with diamond paste (ϕ0.05 μm) and rinsed thoroughly with water and acetone. Its electrochemical pretreatment was performed by scanning the potential from -0.30 V to $+1.30$ V at a scan rate of 100 mV s^{-1} for ten cycles in a 0.50 mol l^{-1} sulfuric acid solution. A Ag–AgCl electrode (saturated with KCl solution) was used as a reference electrode and platinum electrode as an auxiliary electrode. During NO determination, a hermetic electrochemical cell with the provision for gas addition was employed. All joints were closely sealed to prevent NO leakage and avoid O_2 permeation because NO is very active and could be oxidized in presence of O_2.

2.3. Preparation of the ultramicrosensors

The pretreated ultramicroelectrodes were thoroughly ultrasonicated in distilled water before used. Then the electrodes were allowed to air-dry and placed into dimethyl sulfoxide(DMSO) solu-

tion containing 5.0×10^{-3} mol l^{-1} monomer of MTAPc and 0.1 mol l^{-1} TBAP as supporting electrolyte. MTAPc were deposited onto the ultramicroelectrode surface by a means of scanning potential between -0.20 and $+0.90$ V at a scan rate of 100 mV s^{-1}. After consecutively cycling for 40 cycles, the electrodes were taken out from the electroploymerization solution, rinsed with acetone and distilled water and allowed to air-dry. Prior to the determination of NO, the modified ultramicroelectrodes were further coated with Nafion twice by depositing 1 μl 1% (w/v) Nafion solution on the surface of the electrode and then placing the electrode under an infrared lamp to allow the ethanol to evaporate.

2.4. Electrochemical determination of NO

Prior to NO determination, the ultramicrosensors were placed in PBS solution and cyclic voltammetry was performed in the potential range between 0.00 to $+1.00$ V until steady cyclic voltammetric and differential pulse voltammetric (DPV) responses were obtained (Typically for about ten cycles). Electrochemical responses of the ultramicrosensors to NO and selectivity tests were evaluated by employing the method of DPV. DPV was performed at a sweep rate of 5 mV s^{-1} and 5 pulses s^{-1} (pulse height 50 mV, pulse width 60 ms). Calibration of the ultramicrosensor was performed using the technique of DPA. The electrode was cleaned at 0.00 V for 1 s, pulsed to $+0.70$ V for 50 ms and then pulsed to $+0.80$ V for 50 ms from $+0.70$ V. The current was measured as the current change between the values at $+0.70$ V and $+0.80$ V. Aliquots of NO solution was subsequently added with a gas-tight syringe, and the current response due to NO oxidation was recorded after each addition.

3. Results and discussion

3.1. The sensitivity of the ultramicrosensor to NO

The sensitivity of the developed ultramicrosensors were studied by comparing the responses of NO with the same concentration at an unmodified and modified ultramicroelectrode in the fashion mentioned above. Fig. 1 depicts, using polyNiTAPc/Nafion modified ultramicrosensor as an example, the DPV responses of NO at different electrodes. As can be seen that the DPV response of NO at the unmodified ultramicroelectrode exhibits a small and broad peak. However, a sharp peak could be observed at the polyNiTAPc/Nafion modified ultramicrosensor. The responses of NO at other two ultramicrosensors based on polyCoTAPc/Nafion and polyCuTAPc/Nafion, respectively, are similar to that based on polyNiTAPc/Nafion, indicating that the ultramicrosensors based on polyMTAPc film show a higher sensitivity to NO determination.

NO, like other simple diatomic molecules, such as O_2 and CO, has been reported not only to react with hemoproteins and metalloenzymes, but also to interact with nonheme metal complexes to form its adducts [37–39]. This confers to us a fact that there exists some interaction between NO and certain metal complexes which is similar to

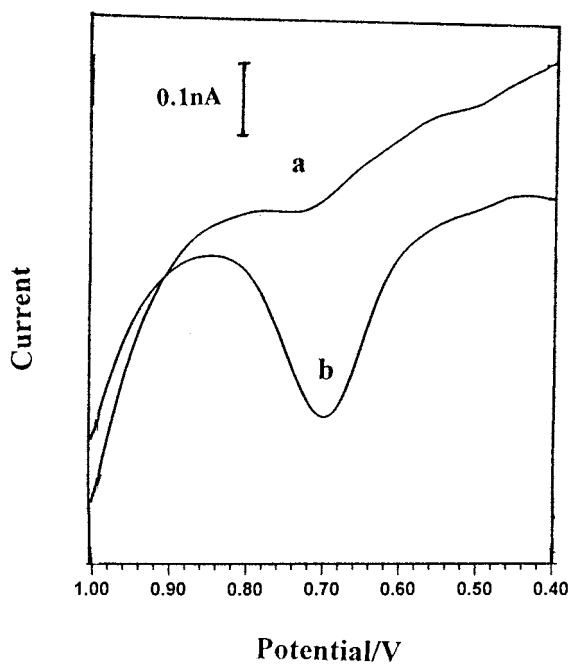

Fig. 1. Differential pluse voltammograms of: (a) bare platium ultramicroelctrode; and (b) polyNiTAPc/Nafion modified ultramicroelectrode in a deoxygenated PBS solution containing NO with a concentration of 2.0×10^{-6} mol l^{-1}.

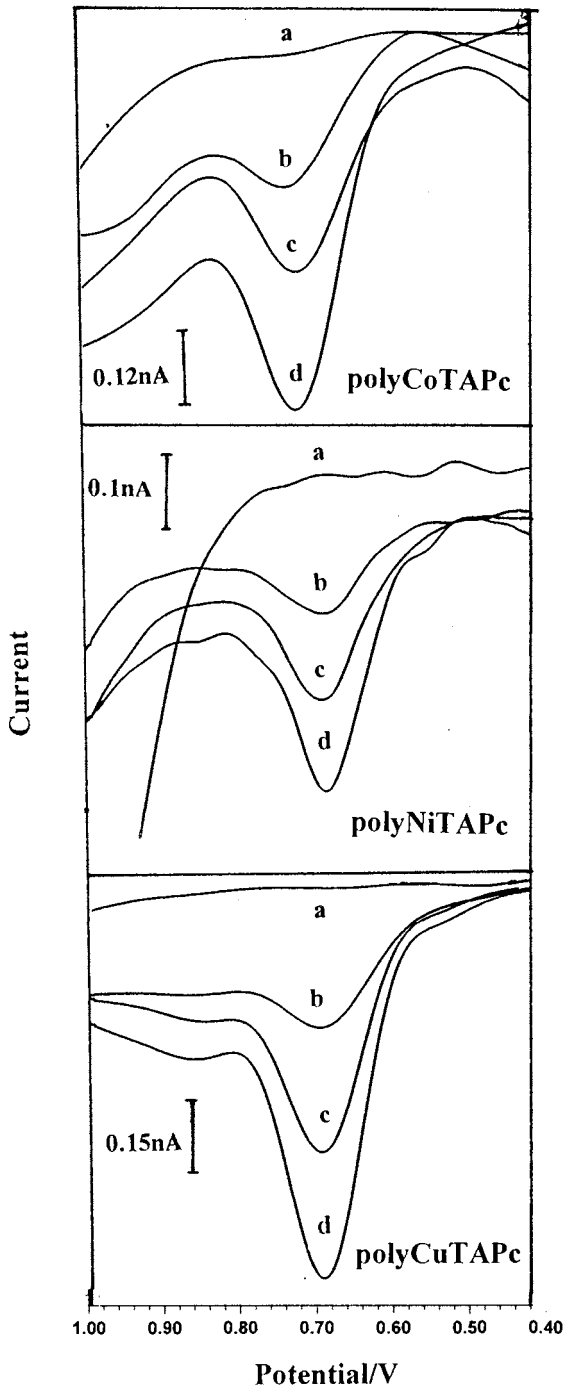

Fig. 2. Differential pulse voltammograms of ultramicrosensors based on Nafion and electropolymerizaed film of CoTAPc, NiTAPc, or CuTAPc(denoted polyCoTAPc, polyNiTAPc, and polyCuTAPc,respectively) in a deoxygenated PBS solution containing 1.0×10^{-5} mol l^{-1} NO_2^- and NO with concentrations of: (a) 0.0; (b) 1.0×10^{-6}; (c) 2.0×10^{-6}; and (d) 3.0×10^{-6} mol l^{-1}, respectively.

that between simple diatomic molecular such as O_2, CO and certain metal complexes to form their adducts [40,41]. Moreover, NO is an extremely powerful ligand, giving binding constants to metal ions free or in complex form often greatly in excess of those of CO and almost always much high than those of O_2. We are now carrying out the performance regarding the complexation of NO with MTAPc using the techniques of quantum chemistry, and the preliminary results concerning this issue give us an index that NO can also react with MTAPc as mentioned above. Consequently, in this work the mechanism of NO responses at the developed ultramicrosensors could be described as follows in terms of our experimental facts and preliminary results of quantum chemistry:

$$\text{PolyM(TAPc)}_{\text{film}} \rightarrow \text{Poly[(NO)M(TAPc)]}_{\text{film}}$$

$$\text{Poly[(NO)M(TAPc)]}_{\text{film}} - \text{e}$$

$$\rightarrow \text{PolyM(TAPc)}_{\text{film}} + \text{NO}^+$$

NO, a highly active gas, could penetrate through Nafion film and form its adduct with MTAPc. The formed adduct, poly[MTAPc(NO)] could be oxidized easily resulting in a high current responses in a negative-shifted potential at the ultramicrosensors. The product of the electrochemical reaction, NO^+ can be fixed in Nafion film and not be further oxidized to produce NO_2^-, which will interfere with NO determination in turn while at a high concentration.

3.2. The selectivity of the ultramicrosensors for NO

The purpose of the design for NO ultramicrosensors was carrying out the performance of in vivo measurements of NO, therefore, the constructed ultramicrosensors should be free from interference from other electroactive substances coexisting in biological fluid, such as ascorbate, uric acid, nitrite, some neurotransmitters and their metabolites. Fig. 2 demonstrates the typical differential pulse voltammograms of the ultramicrosensors based on electropolymerized film of MTAPc and Nafion in

the presence of NO at various concentrations and 1.0×10^{-5} mol l^{-1} of nitrite. As shown in Fig. 2 the ultramicrosensors could effectively eliminate the interference from nitrite. We also found other coexisting substances, such as ascorbate and uric acid at a concentration of 1.0×10^{-4} mol l^{-1}, 5-hydroxyindole-3-acetic acid and 3,4-dihydroxyphenylacetic acid at a concentration of 1.0×10^{-5}mol l^{-1} show no responses at the ultramicrosensors, suggesting these coexisting substances do not interfere with NO determination with the concentrations of 1–2 orders of magnitude higher than expected in biological systems using a technique of DPV or DPA method. However, a voltammetric peak at a typical potential of about +0.30 V is observed in presence of dopamine or epinephrine or 5-hydroxytryptamine while concentration is high that 1.0×10^{-6}mol l^{-1}, suggesting that the ultramicrosensors also show responses to these substances. Bearing this fact in mind, DPA technique can be employed as an in vivo method on the condition that the level of catecholamines is independent of some physiological conditions, which is believe to be related to NO. Otherwise, DPV technique can be served for in vivo determinations due to its good discrimination.

3.3. The linear range, detection limit and life time of the ultramicrosensors

The NO concentration varies between 10^{-6} and 10^{-9} mol l^{-1} in biological tissues. We found that it is difficult to calibrate the ultramicrosensor when NO concentration was below 0.1 μmol l^{-1} using a DPV method. Furthermore, it is more important to measure the relative change of the chemical substances while studying their physiological roles. Therefore, when NO concentration ranges from 1 nmol l^{-1} to 0.1 μmol l^{-1}, the ultramicrosensors should be calibrated using a technique of DPA, an active method. In this work, the ultramicrosensors were calibrated using DPA. Fig. 3 shows, using polyNiTAPc/Nafion modified ultramicrosensor as an example, the differential pulse amperogram of the poly[Ni(TAPc)]/Nafion modified electrode in deoxygenated PBS solution with successive addition of 3.0×10^{-8} mol l^{-1} NO. The ultramicrosensor clearly shows a remarkable increase in the oxidation current upon the successive addition of NO, and the steady-state oxidation currents of the ultramicrosensor are proportional to NO concentration. The other two ultramicrosensors based

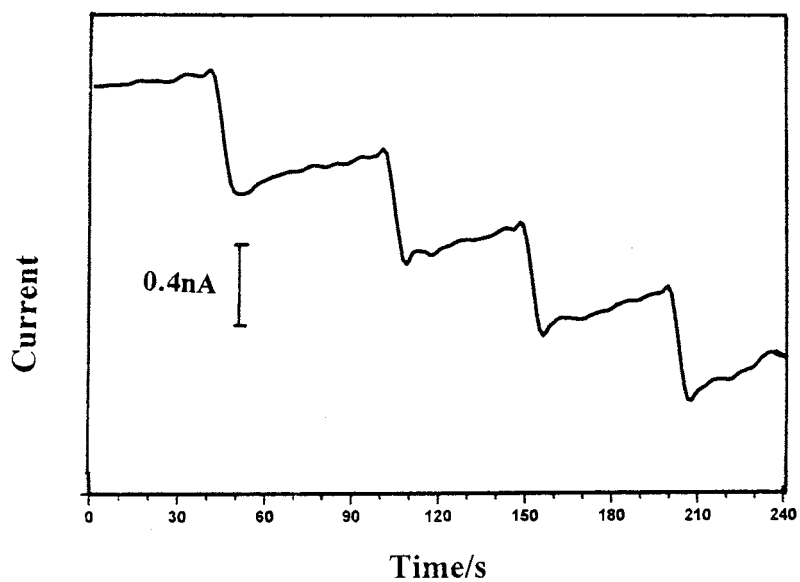

Fig. 3. Differential pulse amperograms of ultramicrosensor based on polyNiTAPc and Nafion in a deoxygenated PBS solution with successive addition of NO at a final concentration of 3.0×10^{-8} mol l^{-1}.

Table 1
Calibrations of NO at the ultramicrosensors based on electropolymerized film of MTAPc and Nafion[a,b,c]

Electroplymerized films	Linear range(mol l^{-1})	LC	DL (mol l^{-1})
Co(TAPc)	2.00×10^{-8}–1.20×10^{-7}	0.999	1×10^{-8}
	2.00×10^{-7}–4.00×10^{-6}	0.994	
Ni(TAPc)	1.98×10^{-8}–1.59×10^{-5}	0.995	1.00×10^{-8}
Cu(TAPc)	2.50×10^{-8}–1.20×10^{-6}	0.999	1.20×10^{-8}

[a] DL, Determination limit.
[b] LC, Linear coefficient.
[c] DL was measured based on $S/N=3$.

on electroplymerized film of CoTAPc and CuTAPc, respectively, were studied in the same fashion as mentioned above. The calibrations of the ultramicrosensors based on electropolymerized film of MTAPc and Nafion were illustrated in Table 1. As can be seen from Table 1, the ultramicrosensors have a good responses to NO with a calculated detection limit of about 1.00×10^{-8} mol l^{-1} (based on a signal-to-noise ratio of three). The RSD for ten measurements of 1 μM NO is 1.5%. The sensitivity of the ultramicrosensors shows no observable change after one month storage in PBS solution, or successive potential cycling from 0.00 to 1.00 V for 5 h. The ultramicrosensors can be used without degradation of performance for at least 20 days. These indicate that the electropolymerized film of MTAPc and Nafion were stable and that the ultramicrosensors developed in this work could have a long lifetime.

4. Conclusion

We developed NO ultramicrosensors based on metal macrocyclic complexes, metal tetraaminophthalocyanines and demonstrated that the ultramicrosensors display a high sensitivity and selectivity for NO determination. Therefore, the ultramicrosensors are promising in application for in vivo determination of NO. We also found that, through our preliminary results of quantum chemical calculation, NO could interact with metallophthalocyanines to form its adducts. These findings not only offer us a new approach to prepare ultramirosensors for selective and sensitive determination of NO but also provided a new precision and insight to the mechanism of NO ultramicrosensors based on chemically modified electrode which has been drawn intensive attention. We will explore this work an good extension for the determination of NO in biological models. These results will be reported in the future.

Acknowledgements

This work is supported by The Natural Science Foundation of China and The Natural Science Foundation of Shanghai.

References

[1] P.M.J. Palmer, A.G. Ferrige, S. Moncada, Nature 327 (1987) 524.
[2] C. Nathan, J. FASEB 6 (1992) 3051.
[3] H. Ischiropoulos, L. Zhu, J.S. Beckman, Arch. Biochem. Biophys. 298 (1992) 451.
[4] S. Moncada, D. Lekieffre, B. Arvin, B. Meddrum, Neuroreports 343 (1992) 530.
[5] S.A. Lipton, Y-B. Choi, Z-H. Pan, et al., Nature 364 (1993) 626.
[6] L. Linder, W. Kiowski, F. Buhler, T.F. Lusher, Circulation 81 (1990) 1762.
[7] H.H.H.W. Schmidt, T.D. Warner, K. Ishii, F. Murand, Science 255 (1992) 676.
[8] P.M. Vanhoute, J. Cardiovas. Pharmacol. 16 (1990) 15.
[9] R.C. Freiman, G.G. Mitchell, D.D. Halsted, M.L. Armatrong, A.G. Harrison, Cir. Res. 58 (1986) 783.
[10] D.D. Rees, S. Celleck, R.M.J. Palmer, S. Moncada, Biochem. Biophys. Res. Commun. 197 (1990) 541.
[11] S. Moncada, R.M.J. Palmer, E.A. Higgs, Biochem. Pharmacol. 38 (1989) 1709.
[12] S. Archer, J. FASEB 7 (1993) 349.
[13] K. Ichimori, H. Ishida, M. Fukahori, H. Nakazawa, E. Murakami, Rev. Sci. Instrum. 65 (1994) 2714.

[14] F. Parient, J.L. Alonso, H.D. Abruna, J. Electroanal. Chem. 379 (1994) 191.
[15] M.N. Friedemann, S.W. Robinson, G.A. Gerhardt, Anal. Chem. 68 (1996) 2612.
[16] T. Malinski, Z. Taha, Nature 358 (1992) 676.
[17] T. Malinski, S. Grunfeld, A. Burewicz, P. Tomboulian, Anal. Chim. Acta 279 (1993) 135.
[18] S. Trevin, F. Bedioui, J. Devynck, Talanta 43 (1996) 303.
[19] S. Trevin, F. Bedioui, J. Devynck, J. Electroanal. Chem. 408 (1996) 261.
[20] M. Maskus, F. Pariente, Q. Wu, A. Toffanin, J.P. Shapleigh, D. Abruna, Anal. Chem. 68 (1996) 3128.
[21] A. Yu, H. Zhang, H. Chen, Anal. Lett. 30 (1997) 1013.
[22] R.E. White, M.J. Coon, Ann. Rev. Biochem. 49 (1980) 315.
[23] I.C. Gunsalus, S.C. Sligar, Adv. Enzymol. 47 (1978) 1.
[24] D. Mansay, P. Battioni, in: J. Reedijk (Eds.), Bioinorganic Catalysis, Marcel Dekker, New York, 1993, p. 395.
[25] L. Mao, T. Yu, H. Lian, L. Jin, Chin. J. Anal. Sci. (In press).
[26] L. Mao, T. Yu, H. Lian, L. Jin, Chin. J. Anal. Chem. 26 (1998) 6.
[27] L. Mao, Y. Tian, G. Shi, H. Liu, L. Jin, K. Yamamot, S. Tao, J. Jin, Anal. Lett. 31 (1998) 6.
[28] F. Xu, H. Li, S.J. Cross, T.F. Guarr, J. Electroanal. Chem. 368 (1994) 221.
[29] H. Li, T.F. Guarr, J. Electroanal. Chem. 317 (1991) 189.
[30] C.M. Lieber, N.S. Lewis, J. Am. Chem. Soc. 106 (1984) 5033.
[31] H. Li, T.F. Guarr, Synth. Met. 23 (1990) 243.
[32] X. Qi, R.P. Baldwin, H. Li, T.F. Guarr, Electroanalysis 3 (1991) 119.
[33] F. Bedioui, S. Trevin, J. Devynck, F. Lantoine, A. Brunet, M-A. Devynck, Biosens. Bioelec. 12 (1997) 205.
[34] W. Gerrard, Gas Solubilities Widespread Applications, Pergamon, Oxford, 1980.
[35] L. Mao, Y. Tian, Y. Xian, L. Jin, NO Producing Systems, Chinese Patent No. 97206334.
[36] B.N. Achar, G.M. Fohlen, J.A. Parker, J. Keshavayya, Polyhedron 6 (1987) 1463.
[37] H. Sugimori, H. Uchida, T. Akiyama, M. Mukaida, K. Shimizu, Chem. Lett. 8 (1982) 1135.
[38] M. Kubota, M.K. Chen, C.D. Boyd, K.R. Mann, Inorg. Chem. 26 (1987) 3261.
[39] H. Ikezawa, E. Miki, K. Mizumachi, T. Ishimori, T. Nagai, M. Tanaka, Bull. Chem. Jpn. 66 (1993) 89.
[40] D.C. Detschman, S.G. Utterback, J. Am. Chem. Soc. 103 (1981) 2847.
[41] W.S. Bringar, C.K. Chang, J. Am. Chem. Soc. 96 (1974) 5595.

ELSEVIER

Talanta 48 (1999) 1013–1022

Talanta

A new resin containing benzimidazolylazo group and its use in the separation of heavy metals

Debasis Das, Arabinda K. Das, Chittaranjan Sinha *

Department of Chemistry, The University of Burdwan, Burdwan 713 104, India

Received 12 June 1998; received in revised form 11 September 1998; accepted 17 September 1998

Abstract

A new resin incorporating benzimidazolylazo group into a matrix of polystyrene divinylbenzene has been prepared. The exchange capacity of the resin for the ions mercury(II), silver(I) and palladium(II) as a function of pH has been determined. The resin exhibits no affinity for alkali or alkaline earth metals. It is highly selective for Hg(II), Ag(I) and Pd(II). In column operation, it has been observed that Hg(II), Ag(I) and Pd(II) in trace quantities can be selectively separated from geological, medicinal and environmental samples. © 1999 Elsevier Science B.V. All rights reserved.

Keywords: Resin; Earth metals; Alkali

1. Introduction

Metal ions are non-biodegradable in nature, their intake at a certain level are toxic [1]. Detoxification can be achieved by membrane extraction process using suitable exchangers [2–7].The idea of hard soft acid base (HSAB) concept [8,9] and stability of the metal complexes are the valuable guidelines for the active site selection. Bulk and other liquid membrane systems have a major disadvantage [10] because the carrier ligand is slowly removed into the aqueous phase. Anchoring the active site to a solid support in a polymer matrix removes this disadvantage and provides an immobilised active surface capable of selective and quantitative separation of cations from aqueous solutions. These solid-phase extraction systems can be operated indefinitely without loss of the expensive ligating group [10,11].The developed procedure has been used to selectively remove and concentrate specific cations from the synthetic mixture of metal ions and environmental wastes, recovery and purification of precious metals, separation of components from nuclear wastes [10,11].The process has gaining popularity and in some cases they have been commercialised by multinational agencies [12]

Solid surfaces having heterocyclic donor centres have specific activity towards transition metal ions [13–16]. We have reported earlier the design of a resin incorporating imidazolylazo function in a polystyrene bed and is used for the separation of Hg(II) [16]. Polymeric matrices containing benz-

* Corresponding author. Fax: +91-342-64452; e-mail: bdnuvlib@giascl01.vsnl.net.in.

PII: S0039-9140(98)00310-5

imidazole with bare N–H are scarce [17]. The pyrrolic-N, has a high affinity to class 'b' metal ions viz. Cu(I), Ag(I) and Hg(I)/(II), Pd(II). Besides benzimidazole has biological importance [18] and has the ability to form complexes with a number of metal ions [19]. Recent literature survey suggests that the transition metal complexes of benzimidazole derivatives are extensively used as low molecular weight mimics/model of the active sites in many metalloproteins [18,19].They serve as basic unit to conjugated redox polymer and initiate electronic communication between redox centres [20]. This has encouraged us to design polymeric bed incorporating benzimidazole active site. Herein, we report the preparation and characterisation of benzimidazolylazo resin incorporating benzimidazole on a polystyrene divinylbenzene matrix. The resin is used for the separation of Hg(II), Pd(II) and Ag(I) from the synthetic mixture, environmental, geological and medicinal samples. Separated Hg(II) and Ag(I) are estimated radiometrically using radioisotopes ^{203}Hg and ^{110m}Ag, respectively. Palladium(II) is estimated spectrophotometrically using 1-(2-pyridylazo)-2-naphthol (PAN) as a spectrophotometric reagent. Inspite of difficulties of handling, availability and stability of radioisotopes, the method is popular [21] over the other standard methods because of low cost of the instrument used, high sensitivity, rapidity, operational simplicity as well as the least operational cost of measurements.

2. Experimental

2.1. Apparatus and reagents

A Shimadzu UV-VIS spectrophotometer (Model UV190) was used for absorbance measurements. The adjustment of pH was done with a Systronics digital pH meter (Model 362). IR spectra was recorded on a Shimadzu (IR-408) spectrophotometer and thermogravimetric analysis was done on Shimadzu TG 50/DT 50. The radioactivity was measured by a scintillation counter equipped with a well type NaI (Tl) crystal detector. Benzimidazole (Loba-Chemie Indo-Austranal, India), polystyrene resin (Bird and Company, India), $PdCl_2$ (Arrora Mathey, India), $AgNO_3$ (Glaxo Lab, Bombay), 1-(2-pyridylazo)-2-naphthol (Fluka) were reagent grade and used as provided. All other chemicals were reagent grade and used as received. The metal ion solutions were prepared from analytical grade reagents. The radioisotopes ^{110m}Ag and ^{203}Hg were supplied by Bhaba Atomic Research Centre, Trombay and were used as tracers.

2.2. Preparation of the resin

Air dried polystyrene divinylbenzene copolymer containing 8% divinylbenzene was used as starting material. The polystyrene beads (5 g, 30–60 mesh) were swollen in chloroform and separated by suction. These beads were first nitrated followed by reduction to the amino compound. This product was diazotised according to the procedure described by Davies et al. [22]. The diazotised product was rapidly filtered off, washed with cold distilled water until free from acid and then coupled at 0–5°C with a solution of benzimidazole (1.6 g) in 20% aqueous sodium carbonate solution over a period of 5–6 days. The dark brown coloured resin was then filtered off and thoroughly washed with distilled water until free from base. The resulting compound was then extracted in a Soxhlet extractor with alcohol for 3 days. Finally, it was washed with dilute (1:4) hydrochloric acid, then with de-ionised distilled water until free from acid. The resin was air dried and sieved, the particles of 30–60 mesh being retained for use.

2.3. Stability of the resin

A 0.5 g portion of the resin was shaken with 100 ml of acid or alkaline solutions of various concentrations for 7 days, then filtered off and washed with water. After drying, the nitrogen content and exchange capacity for Ag(I) were determined with the basic form of the resin. To study the effect of γ-radiation on the resin matrix, the resin was exposed to γ-radiation for 48 h. The stability of the resin towards temperature was studied thermogravimetrically.

2.4. Water regain

Dry resin in basic form was stirred in doubly distilled water for 48 h, then filtered off by suction, weighed, dried at 100°C for 48 h and reweighed.

Table 1
Composition of the benzimidazolylazo resin

Nitrogen content of the nitro resin	7.84 mmol g^{-1} nitro-resin (10.98%)
Nitrogen content of the amino resin	11.38%
Amino group in the amino resin	3.56 mmol g^{-1} amino resin
Nitrogen content of the benzimidazolylazo resin	10.2 mmol g^{-1} benzimidazolylazo resin (14.28%)
Composition of the final resin	
a. Amount of benzimidazolylazoresin	1.48 mmol g^{-1}
b. Amount of unconverted nitroresin	4.28 mmol g^{-1}
c. Amount of resin containing phenolic OH	2.08 mmol g^{-1}

Table 2
Physical and chemical characteristics of the benzimidazolylazo resin[a]

Bead size	30–60 mesh
Water regain	11.35 mmol g^{-1}
Thermal stability	300°C
Hydrogen capacity	
(benzimidazolylazo group)	1.42 mmol g^{-1}
Total hydrogen ion capacity	2.90 mmol g^{-1}
Equilibration rate ($t_{1/2}$)	
for Ag(I)	55 min
for Pd(II)	60 min
for Hg(II)	50 min
IR data	3424 cm^{-1}, 1730 cm^{-1} for N–H stretching 1600 cm^{-1} for >C=N stretching 1516 cm^{-1} for –N=N– stretching 860, 830, 800, 750 w, 700 s, 660 m for the benzimidazole content

[a] w, weak, s, strong, m, medium.

Table 3
Maximum exchange capacities for the metal ions

Metal ion	Maximum capacity (mmol g^{-1})	pH
Ag(I)	1.00	4.0–6.0
Pd(II)	0.62	5.0–6.0
Hg(II)	0.83	4.0–6.0

2.5. Estimation of nitrogen and amino groups

The nitrogen content of the dried samples of the nitrated polystyrene, amino polystyrene and the final resin was determined using a Perkin Elmer 240 C elemental analyser. The amino group content of the amino polystyrene was determined by non-aqueous titrimetry [23].

2.6. Hydrogen ion capacity

A 0.5 g portion of the resin was first converted into its acid chloride form by treating with 6 mol l^{-1} HCl. The resin was filtered off, washed with water and then dried at 100°C for 6 h to remove free HCl. The acidic hydrogen content of the acidic form of the resin was determined by back titration with a standard alkali solution. The acidic form of the resin was equilibrated with 20 ml of 0.1 mol l^{-1} sodium hydroxide solution for 6 h at room temperature with stirring to determine the total acidic hydrogen content of the resin. Similarly, another portion of the resin in acidic form was equilibrated with sodium bicarbonate solution instead of sodium hydroxide for the determination of the hydrogen ion content of the resin from the benzimidazolium group. In both cases, the solution was filtered under suction and the excess of alkali was titrated with 0.1 mol l^{-1} hydrochloric acid.

2.7. Metal ion capacity as a function of pH

A batch technique was used, taking metal ions in excess to the resin. Capacities were determined in the pH range 1.0–6.0. To note, the pK_a of the resin is not accurately obtained. It may be < 5.6

Table 4
Desorption of Ag(I), Pd(II) and Hg(II) by different eluents

Eluent	Recovery of Ag(I) (%)	Recovery of Pd(II) (%)	Recovery of Hg(II) (%)
4 mol l^{-1} HCl		40	45
8 mol l^{-1} HCl		85	80
1 mol l^{-1} $HClO_4$			
6 mol l^{-1} $HClO_4$	60		55
5% thiourea in 0.1 mol l^{-1} $HClO_4$	100	60	100
12 mol l^{-1} HCl followed by dilute acidic thiourea solution (pH 3)	45	100	65

(pK_a of benzimidazole 5.6) due to the presence of electron withdrawing azo group at C-2 position of benzimidazole. To a glass stoppered centrifuge tube (diameter 2.0 cm) containing 100 mg of the dry resin in basic form, 9 ml of the perchloric acid of desired pH (between 1.0 and 6.0) was added. After equilibration of this mixture 1 ml of 0.2 mol l^{-1} metal ion solution was added to the tube; then the mixture was shaken for a period of 24 h. The pH of the equilibrating solution was adjusted either by the addition of sodium hydroxide or perchloric acid throughout the equilibrating period until it remained constant at the desired level. Mercury(II) and silver(I) capacities were obtained by using the tracer technique. The amount of each metal ion adsorbed on the resin was determined by the measurement of the γ-activity of equal portions of the solutions, before and after the adsorption of metal ions. Palladium(II) capacity was determined by the spectrophotometric method using 1-(2-pyridylazo)-2-naphthol (PAN) [24].

2.8. Desorption of metal ions

The resin (0.1 g) containing maximum adsorbed metal ions were shaken with 10 ml of various desorbents for 1 h. After filtration, the amount of metal ions in the filtrate were determined.

2.9. Equilibration rates

Equilibration rates for the metal ions mercury(II), silver(I) and palladium(II) were studied at pH 6.0, 5.5 and 6.0, respectively. The time required for 50% uptake of the metal ions was determined.

2.10. Column operations

A 130×10 mm glass column was used. Air dried resin (2 g) was immersed in de-ionised distilled water and allowed to swell for 24 h. The column was then packed with fully swollen beads. The bed volume was 2.5 ml. The resin bed was thoroughly washed with 10 bed volumes of perchloric acid at appropriate pH.

The sorption and recovery characteristics for mercury(II), silver(I) and palladium(II) in the presence of various metal ions were thoroughly studied. A 100 ml portion of the mixture of the test metal ion, spiked with appropriate tracer [for Hg(II) and Ag(I)] and the foreign metal ions was allowed to flow through the resin column at a flow rate 0.5 ml min^{-1}. The metal ions not sorbed by the resin were completely washed out using

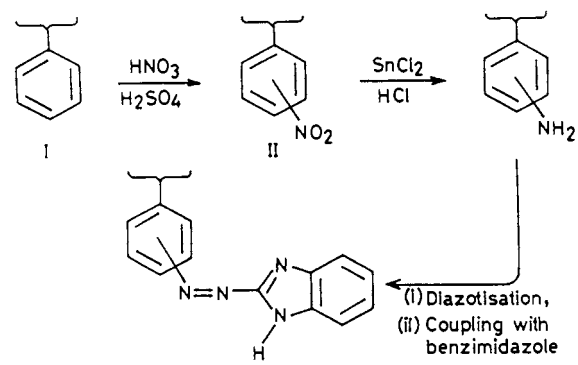

Scheme 1.

Table 5
Separation of 2 μg ml^{-1} Ag(I), Pd(II) and Hg(II) from several binary mixture with other metal ions in a sample volume of 50 ml at pH 5, 6, and 6, respectively

Foreign ion[a]	Ag(I) found (μg), % recovery in parenthesis	Pd(II) found (μg), % recovery in parenthesis	Hg(II) found (μg), % recovery in parenthesis
Cu(II)	92 (92)	94 (94)	91 (91)
Zn(II)	96 (96)	97 (97)	94 (94)
Cr(III)	100 (100)	100 (100)	100 (100)
Co(II)	100 (100)	100 (100)	100 (100)
Ni(II)	100 (100)	100 (100)	100 (100)
Fe(III)	100 (100)	98 (98)	97 (97)
Mn(II)	100 (100)	100 (100)	100 (100)
Ca(II)	100 (100)	100 (100)	100 (100)
Ba(II)	100 (100)	100 (100)	100 (100)
Mg(II)	100 (100)	100 (100)	100 (100)
Na(I)	100 (100)	100 (100)	100 (100)

[a] In each case, the amount of ion added was 2000 μg.

Table 6
Separation of Pd(II) from synthetic mixture of other platinum group metals, Pd(II) present as 2 μg ml^{-1}, the total volume of the solution is 50 ml

Platinum group metal ion	Amount in binary mixture, (μg)	Pd(II) found (μg), % of recovery in parenthesis
Pt(II)	1000	100 (100)
Ru(III)	1000	100 (100)
Ir(III)	1000	100 (100)
Rh(III)	1000	100 (100)
Os(III)	1000	100 (100)

perchloric acid having pH at which the metal ions have maximum exchange capacity. The sorbed mercury(II) and silver(I) were completely eluted with about 50 bed volumes of 5% thiourea in 0.5 mol l^{-1} $HClO_4$ solution and sorbed palladium(II) was completely eluted with 12 mol l^{-1} HCl followed by dilute solution of thiourea in hydrochloric acid (pH 3.0). Desorption of palladium(II) from resin by using only thiourea solution was avoided because of technical difficulty regarding decomposition of Pd(II)-thiourea complex which burns with explosion in air. The metal ions thus eluted were measured as described earlier.

2.11. Removal of mercury(II) from river water

Natural river water (pH 5.6) was spiked with mercury(II) and ^{203}Hg, so that the concentration of mercury became 2.0 μg ml^{-1} in the river water [25]. The above mixture was passed through the 130×10 mm glass column containing 2.0 g of the resin at a flow rate of 0.5 ml min^{-1}. The break-through of mercury(II) was observed after 175 ml of the mixture has been allowed to pass through. The concentration of mercury(II) in the effluent before the break-through point was determined by the tracer technique.

2.12. Studies with resin blanks

To confirm that benzimidazolylazo group is involved in the metal ion sorption, the diazotised amino polystyrene in sodium carbonate solution was boiled for several hours to replace the diazo group by the hydroxyl group. The palladium(II) exchange capacity of the resin thus formed was examined at pH 6.2. The exchange capacity was found to be almost zero.

3. Applications

3.1. Separation of palladium(II) from synthetic mixtures

Five binary mixtures, each having a volume 50 ml, consisting of palladium(II) with other platinum group metals platinum(II), ruthenium(III), osmium(IV), rhodium(III) and iridium(III) were prepared. Sorption and desorption processes were performed as described earlier. The results are collected in Table 6.

3.2. Separation of palladium from geological sample

A 6.29 g rock sample (obtained from Geological Survey of India, Calcutta) was digested [26] in a Teflon beaker with 1:1:1 mixture of 15 mol l^{-1} nitric acid, hydrofluoric acid (40%) and perchloric acid (70%), on a hot plate, until all the fumes of perchloric acid had disappeared. Next, 5 ml of aqua-regia were added and heated until the volume reduced to ≈ 1 ml. Then 10 ml of 6 mol l^{-1} hydrochloric acid were added and digested until the solution became almost clear. Finally, it was filtered through Whatman 41 filter paper, washed with doubly distilled water and made up to volume 100 ml. Then 50 ml of this solution were passed through the resin column. Sorption and desorption processes of palladium was carried out by the proposed method. The concentration of Pd(II) was measured spectrophotometrically using PAN as spectrophotometric reagent. The result is shown in Table 7.

3.3. Separation of palladium from metallic platinum

A 0.1675 g Pt-wire (Johnson Mathey) was brought into solution [26] by treatment with aqua-regia followed by 12 mol l^{-1} hydrochloric acid. After dissolution, the proposed method of separation was applied. Results are collected in Table 7.

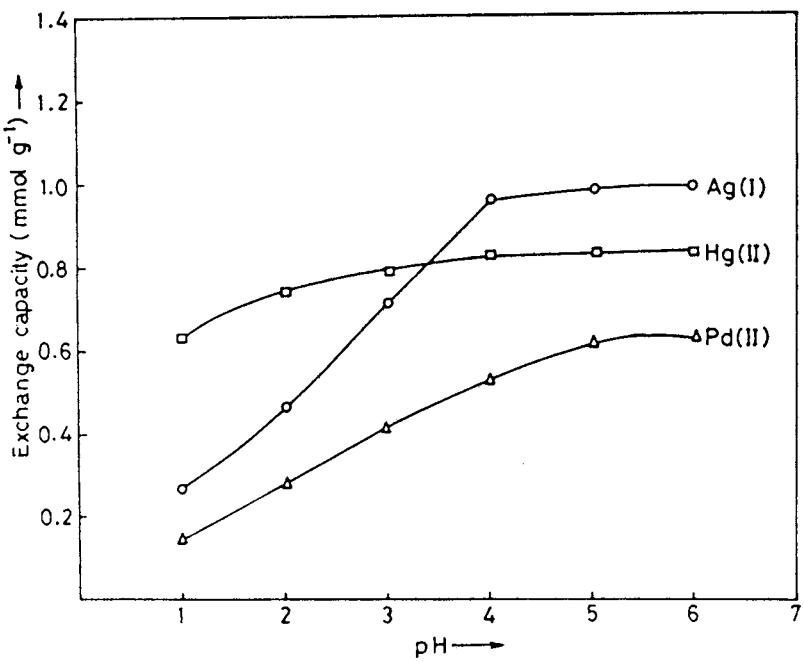

Fig. 1. Exchange capacity (mmol g^{-1}) of the resin for different metal ions vs. pH.

Table 7
Separation of Pd(II) from geological and Pt-wire samples

Sample source	Recommended[a]/direct value[b] (μg g^{-1})	Obtained value (μg g^{-1})	% recovery
Rock sample (G.S.I., Calcutta)	1.26[a]	1.0	79
Pt-wire sample (Johnson Mathey)	161.2[b]	155.0	96

[a] Recommended value from G.S.I., Calcutta.
[b] Direct measurement.

Table 8
Separation and radiometric estimation of Ag(I) from geological, medicinal and photographic washing samples

Sample	Recommended value[a]/other method[b] (μg g^{-1})	Obtained value (μg g^{-1})	% Recovery
Rock sample (G.S.I., Calcutta)	600[a]	580	97
Rock sample (G.S.I., Calcutta)	2700[a]	2670	99
Chawanprash (DABUR)	66[b]	63	96
Sulfadiazine (Silverex)	1.5[b]	1.3	87
Photographic washing	52.81[b]	48	91

[a] Recommended value from G.S.I., Calcutta.
[b] Gravimetry.

3.4. Separation of silver(I) from geological samples

Two geological samples, obtained from Geological Survey of India, Calcutta, containing silver were brought into solution by usual method [27]. Separation and estimation of silver(I) was done radiometrically using isotope dilution technique. For this purpose a labelled silver solution [tracer Ag(I) solution] containing 2.15 mg $AgNO_3$ in 100 ml with appropriate amount of ^{110m}Ag tracer was prepared. For the estimation of silver content in unknown sample, 1 ml sample solution was mixed with 0.5 ml of tracer silver solution and then fed into the column. When adsorption was complete, the column was washed with 25 ml $HClO_4$ acid of pH 5, then silver was eluted with 5% thio-urea in 0.5 mol l^{-1} $HClO_4$ acid (30 ml). After elution, the activity of the solution measured in a γ-ray spectrometer coupled with NaI (Tl) detector. The experiment was repeated with 0.5 ml tracer silver solution with 1 ml doubly distilled water. The amount of silver present in unknown solution was computed from the Eq. (1):

$$W_{\text{inactive}} = \frac{C_0 - C}{C} \times W_{\text{active}} \quad (1)$$

where C_0 and C are the activities in absence and presence of unknown sample. W_{inactive} is the amount of silver present in labelled solution.

Similarly separation and estimation of silver(I) present in other samples were done and the results are collected in Table 8.

3.5. Separation and estimation of mercury in industrial waste water and sludge sample

A total of 50 ml waste water or 2.0 g dried sludge sample (of Durgapur Industrial Area) was taken in a 500 ml round bottom flask. A total of 10 ml 15 N HNO_3 and 2.5 ml 36 N H_2SO_4 were added. The mixture was refluxed for 2 h on a heating mantle in a Bethge's[28] apparatus at $\approx$200°C. The mixture was cooled, filtered and made up to 100 ml in a volumetric flask. Then separation and estimation of mercury was performed by the method already described and similar to the separation and estimation of silver. The results are compared to the values obtained by direct atomic absorption spectroscopy (AAS, Table 9).

Table 9
Determination of Hg(II) in waste water and sludge samples

Sample	Waste water (μg ml^{-1})		Sludge (μg mg^{-1})	
	Present method	Direct analysis	Present method	Direct analysis
1	1.90 ± 0.04	1.02 ± 0.12	108 ± 0.08	107.08 ± 0.31
2	1.49 ± 0.03	0.92 ± 0.10	61.21 ± 0.15	59.16 ± 0.27

4. Results and discussion

4.1. Synthesis and characterisation of the resin

The resin was synthesised from 30–60 mesh macroreticular styrene divinylbenzene copolymer beads through the steps shown in Scheme 1. The nitrogen content of the compound II was 10.98% (7.84 mmol of nitro resin g^{-1}). After reduction, the total nitrogen content in compound III was found to be 11.38%. The estimation of the amino group in the amino resin was 3.56 mmol g^{-1} which accounts for about 45.4% conversion from step II to step III. The nitrogen content of the final benzimidazolylazo resin (compound IV) was found to be 14.28% or 10.2 mmol g^{-1} of the resin. A rough estimate of the composition of the final product may be obtained by considering that diazotisation is complete but the subsequent coupling reaction is not. The unreacted diazonium ion will ultimately decompose, leaving the corresponding phenolic compound. It is also assumed that the phenol thus formed may not form any azo phenol by binding with another diazonium ion, only because the phenolic –OH is firmly attached to the resin matrix and may not find another fixed diazonium ion nearby. Calculations based on this considerations show that conversion efficiency from step III to step IV is about 42%. The final product may therefore contain 1.48, 4.28 and 2.08 mmol g^{-1} of benzimidazolylazo, unconverted nitro and phenolic –OH resin, respectively. Different parameters related to the composition of the final product are shown in Table 1.

The hydrogen ion capacity of the resin was found to be 1.42 mmol g^{-1} which further confirmed the composition of the final product. The maximum exchange capacity of the resin for silver(I) was found to be 1.0 mmol g^{-1} If the resin-metal complex is 1:1 (most likely), the maximum exchange capacity should be 1.42 mmol g^{-1}. Steric factors are probably responsible for lower exchange capacities.

The infrared spectrum of the resin showed bands at ca 1600 cm^{-1} for ν(C=N), at ≈1516 cm^{-1} for ν(N=N) and at ≈3424 cm^{-1} for ν(N–H) stretchings. Other vibrations due to benzimidazole skeleton are shown in Table 2 and are the indication of benzimidazole incorporation into the polymeric matrix.

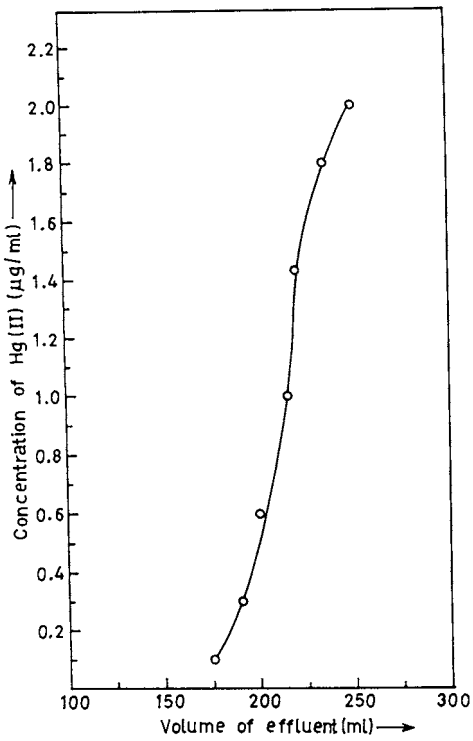

Fig. 2. Break-through curve for Hg(II) in water spiked with Hg(II). Concentration of Hg(II) in the sample solution 2.0 μg ml^{-1}, resin 2g, flow rate 0.5 ml min^{-1}.

The chemical stability of the resin in 1–12 mol l^{-1} hydrochloric acid, 1–6 mol l^{-1} perchloric acid and 1–6 N sodium hydroxide solutions was examined. No significant changes in nitrogen content was observed and the exchange capacities for the above mentioned metal ions remain the same. Thus the resin is fairly stable in both acidic and alkaline medium. Thermogravimetric analysis showed that the resin is stable up to 300°C. The resin was exposed to γ- radiation for 48 h and no appreciable change in metal ion exchange capacity was observed.

The time required for 50% uptake of the maximum capacity for palladium(II), silver(I) and mercury(II) was found to be 50, 45 and 50 min, respectively. Thus the resin is suitable for column operation under a low flow rate. The water regain value for the resin is 11.25, which is satisfactory for column operation.

4.2. Sorption and desorption of metal ions

The sorption behaviour of palladium(II), silver(I) and mercury(II) on the resin by the batch method is shown in Fig. 1. and the maximum exchange capacity for the metal ions is given in Table 3.

The effect of different eluents on the desorption of the metal ions is given in Table 4. Complete desorption of palladium(II) took place with 12 mol l^{-1} hydrochloric acid followed by elution with dilute acidic solution (pH 3.0) of thiourea.

In column operation (Table 5), the presence of macro amounts of diverse metal ions like alkali and alkaline earth metal ions and metal ions of the first transition series did not interfere in the sorption of palladium(II), silver(I) and mercury(II). Cu(II), however, interferes to some extent (5%, Table 5). Other platinum metal ions like Ru(III), Rh(III), Ir(III), Os(III) and Pt(II) did not interfere (Table 6). Desorption of each of palladium(II) and silver(I) was done with 100% recovery using suitable eluent as already described. Hence, attempts were made to separate palladium(II) from platinum group metals present in geological samples, metallic platinum and synthetic mixtures (Table 7). Similarly, silver(I) was separated from medicinal sample viz, Chawanprash (Indian herbal medicine, Dabur), photographic washings and geological samples (Table 8). Mercury(II) was separated from mercury contaminated water. The break-through curve for the removal of mercury(II) from river water [25] spiked with mercury(II) is shown in Fig. 2. No mercury(II) was detected in the effluent from the column until the break-through point is reached. Separation and estimation of mercury in industrial waste water and sludge samples of Durgapur Industrial Area was carried out. As is evident from Table 9, direct analysis of waste water and sludge samples by AAS gives lower results than the proposed method. This is due to the interference of the matrix elements.

The results show that the resin is highly selective for palladium(II), mercury(II) and silver(I). This high selectivity may be due to soft basic pyrrolic N–H of the benzimidazolylazo moiety. The bare N–H plays the key role in binding and may be followed by chelation via azo-N. This resin can be very effectively used for separation and pre-concentration of palladium(II), silver(I) and mercury(II) from geological, medicinal, industrial effluents, sludge samples and polluted water samples.

Acknowledgements

The authors wish to thank Professor H.R. Das, Presidency College, Calcutta, Dr. S. Basu, Deptartment of Chemistry, Burdwan University and Dr. D.K. Das, G.S.I., Calcutta for their help. Financial help from CSIR and UGC, New Delhi is gratefully acknowledged.

References

[1] H. Sigel (Ed.), Metal ions in biological systems, 1973, 2; 1976, 5; 1976, 6; 1980, 10; 1983, 15; 1983, 16; 1984, 17; 1986, 20; 1988, 23; 1988, 24 Dekker, New York.
[2] A. Syamal, M.M. Singh, Ind. J. Chem. 33A (1994) 58.
[3] B. Konar, S. Basu, Fresenius J. Anal. Chem. 384 (1994) 281.
[4] B. Sengupta, S. Laskar, J. Das, Ind. J. Technol. 26 (1988) 139.

[5] K.S. Suresh, J. Reedijk, Coord. Chem. Rev. 59 (1984) 1 and references there in.
[6] J.P. Ghosh, H.R. Das, Talanta 28 (1981) 274.
[7] A. Sugii, N. Ogawa, H. Tamamura, Talanta 28 (1981) 551.
[8] R.G. Pearson, J. Am. Chem. Soc. 85 (1963) 3533.
[9] R.T. Myers, Inorg. Chem. 17 (1978) 952.
[10] J.S. Bradshaw, R.M. Izatt, Acc. Chem. Res. 30 (1997) 338; J.S. Bradshaw, R.L. Bruening, K.E. Krakownik, B.J. Tarbet, M.L. Bruening, R.M. Izatt, J.J. Christenson, J. Chem. Soc. Chem. Commun. (1988) 812.
[11] R.M. Izatt, K. Pawlak, J.S. Bradshaw, R.L. Bruening, Chem. Rev. 95 (1995) 2529; G. Wu, W. Jiang, J.D. Lamb, J.S. Bradshaw, R.M. Izatt, J. Am. Chem. Soc. 113 (1991) 6538; R.L. Bruening, B.J. Tarbet, K. Krakowni, M.L. Bruening, R.M. Izatt, J.S. Bradshaw, Anal. Chem. 63 (1991) 104 and references therein; J.D. Lamb, R.M. Izatt, D.G. Ganick, J.S. Bradshaw, J.J. Christenson, J. Membren. Sci. 9 (1981) 83.
[12] I.B.C. Advanced Technologies, Inc. (IBC) American Fork, UT.
[13] R.S. Drago, J.H. Gout, Inorg. Chem. 18 (1979) 2019.
[14] J.P. Coolman, R.R. Gogne, J. Kouba, H. Lansberg-Wahren, J. Am. Chem. Soc. 96 (1974) 6800.
[15] D.H. Gold, H.P. Gregar, J. Phys. Chem. 64 (1960) 1464.
[16] P. Chattopadhyay, C. Sinha, D.K. Pal, Fresenius J. Anal. Chem. 357 (1997) 368; K. Hanabusa, H. Shiral, J. Chem. Soc. Chem. Commun. (1997) 2061.
[17] C. Mathews, T.A. Leese, D. Thorp, J.C. Lockhart, J. Chem. Soc. Dalton Trans. (1998) 79.
[18] J.B. Wright, Chem. Rev. 48 (1951) 397.
[19] M. Gullotti, L. Casella, G. Pallanza, Polyhedron 9 (1990) 1469; C.J. Matthews, W. Clegg, S.L Heath, N.C. Martin, M.N. Stuart Hill, J.C. Lockhart, Inorg. Chem. 37 (1998) 199; R. Rajan, R. Rajaram, B.U. Nair, T. Ramsami, S.K. Mondal, J. Chem. Soc. Dalton Trans. (1996) 2019; C.J. Matthews, W. Clegg, M.R. J. Lsegood, T.A. Leese, D. Thorp, P. Thoruton, J.C. Lockhart, J. Chem. Soc. Dalton Trans. (1996) 1531.
[20] C.G. Cameron, P.G. Pickup, J. Chem. Soc. Chem. comm. (1997) 303; M. Suzuki, M. Kimura, H. Shiral, J. Chem. Soc. Chem. comm. (1997) 2061.
[21] A. Chatterjee, S.Basu, J. Radioanal. Nucl.Chem. 162 (1992) 259; J. Dutta, S. Basu, J. Radioanal. Nucl. Chem. Lett. 200 (1995) 491.
[22] R.V. Davies, J. Kennedy, E.S. Lane, J.L. Willians, J. Appl. Chem. 9 (1959) 368.
[23] G.E. Ficken, E.S. Lane, Anal. Chim. Acta. 16 (1957) 207.
[24] A.I. Busev, L.U. Kiseleva, Vestnik Maskov. Univ. Ser. Mat. Mekhan Astion Fiz. I. Khim. 13 (1958) 179; A.R. Casal, N.P. De Laiseea, Bol. Soc. Quim. Peru 53 (1987) 213.
[25] S.S. Bhattacharyya, A.K. Das, At. Spectrosc. 9 (1988) 68.
[26] R.R. Brooks, B.-S. Lee, Anal. Chim. Acta. 204 (1988) 333.
[27] A.I.Vogel, in: A Text Book of Quantitative Inorganic Analysis, 3rd ed., Longmans, p. 638.

ELSEVIER

Talanta 48 (1999) 1023–1029

Talanta

Analysis of ephedrine in ephedra callus by acetonitrile modified capillary zone electrophoresis

Guanbin Li [a], Ziping Zhang [a], Xingguo Chen [a], Zhide Hu [a,*], Zhengfeng Zhao [b], Martin Hooper [b]

[a] *Department of Chemistry, Lanzhou University, Lanzhou 730000, People's Republic of China*
[b] *School of Applied Sciences, Monash University, Churchill, Vic., 3842, Australia*

Received 1 April 1998; received in revised form 8 September 1998; accepted 21 September 1998

Abstract

A simple method has been developed for the quantitative determination of ephedrine in ephedra callus. The dependence of effective mobility of ephedrine on pH was investigated, and a simulated equation was obtained. The separation was performed in an uncoated capillary and detected at 185 nm. A new Tris–NaOH–H_3PO_4 run buffer was used and the pH was adjusted to 3.20. To increase the solubility of hydrophobic analytes and improve the separation efficiency, 15% acetonitrile was used in the buffer as a modifier. The content of ephedrine in an ephedra callus sample and an ephedra herba sample were determined with this method, and the result was satisfactory.

Keywords: Electrophoresis; Ephedra; Ephedrine

1. Introduction

Medicinal plants are an important resource for obtaining many pharmaceuticals. In recent years, with the increased requirement of medicinal plants, there has been an excessive gathering of them, and therefore the natural resource of these plants has been destroyed. Ephedrine, which is generally derived from ephedra plant, is used as a pharmaceutical for exciting central nervous system, the systole of blood vessel, and the lysis of spasm of bronchial smooth muscle. It produces a good curative effect on bronchial asthma [1]. The natural resource of ephedrae herba has decreased in the last few years because of gathering. A new biological technique for artificially cultivating ephedra callus was developed for obtaining this important pharmaceutical [2]. The general chromatography method for analysis of the ephedrine in callus was not satisfactory because of the long separation time and weak separation efficiency [3]. A capillary electrophoresis (CE) method, which contained

* Corresponding author. Fax: +86 931 8912540; e-mail: huzd@lzu.edu.cn.

0039-9140/99/$ - see front matter
PII: S0039-9140(98)00311-7

0.005 M barium hydroxide and 0.02 M isoleucine as buffer solution, was established for determining alkaloids in ephedrae herba [4]. However, this method was not suitable for the analysis of ephedrine in ephedra callus, for we find in the experiment that the capillary will be blocked by precipitate in the run buffer at high pH. Therefore it is necessary to develop a new CE method to solve this problem.

In this work, a new CE method for the analysis of ephedrine in ephedra callus has been established. A Tris–NaOH–H_3PO_4 buffer system was used at pH 3.20 and acetonitrile was introduced into this buffer as modifier for improving the solubility of the sample. The migration behaviour of ephedrine was investigated, and a simulated equation was obtained. A sample of ephedra callus was cultivated for 1 week and the content of ephedrine in it was determined by this CE method. A sample of ephedra herba was also analysed with this CE system for comparing with the callus sample.

2. Experimental

2.1. Instruments

HPCE has been carried out using a Waters Quanta 4000 system (Waters Chromatography Division of Milford, MA, USA) with a positive power supply at a detection wavelength of 254 nm and a temperature of 20 ± 1°C. Separation were performed in uncoated fused silica capillaries manufactured by Waters Accasep. Capillaries of 75 μm i.d., 42.4 cm effective length (50 cm total length) were used. Direct UV detection was performed with a D Lamp and 185 nm optical filter. Samples were introduced from the anodic end of the capillary by hydrodynamic injection where the sample vial was raised by 10.0 cm for 5 s. Data acquisition was carried out with a Maxima820 chromatography workstation. A 3 min wash cycle with 0.5 M NaOH solution followed by 3 min distilled water, and 3 min separation buffer was necessary to condition the capillary.

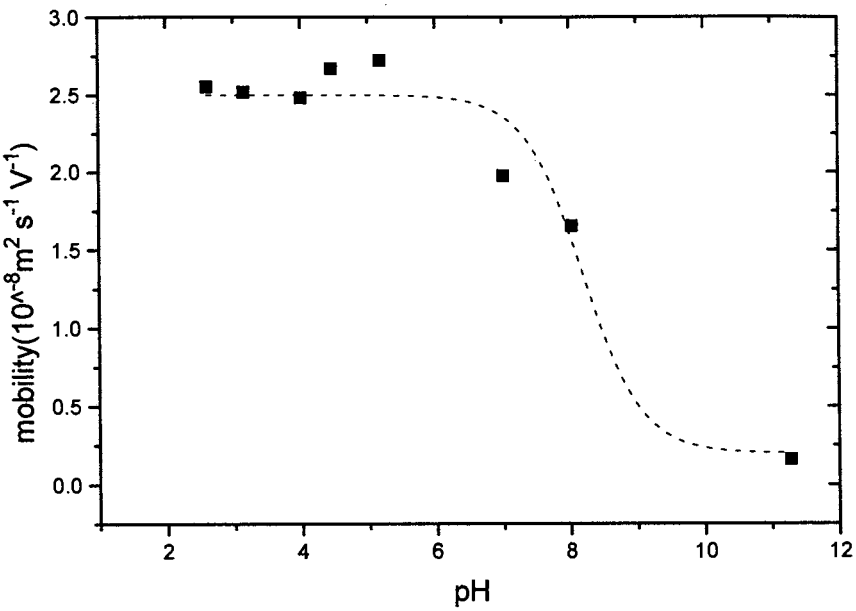

Fig. 1. Influence of pH on the effective mobility of ephedrine. Concentration of Na^+ 0.0010 M, Tris 0.010 M; pH was adjusted with H_3PO_4.

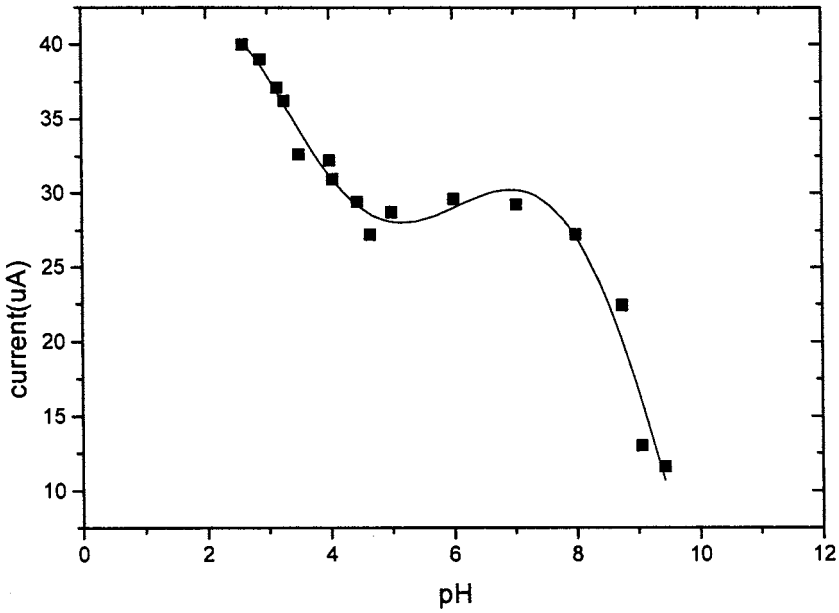

Fig. 2. Influence of pH on the current. Concentration of Na^+ 0.0010 M, Tris 0.010 M; pH was adjusted with H_3PO_4.

2.2. Reagent

Authentic ephedrine was obtained from the National Institute for the Control of Pharmaceutical and Biological Products, Beijing, People's Republic of China. A sample of ephedrae herba was obtained from the hospital of Lanzhou University. Ephedra callus was cultivated for 1 week in the Department of Biology of Lanzhou University.

2.3. Sample extraction

A total of 0.3000 g of powder of ephedra callus or ephedrae herba was refluxed with 30 ml ethanol for 1 h. After being filtered, the residue was refluxed with 30 ml ethanol for 20 min again. After being filtered, the ethanol extracting solution was collected together and distilled to dry. The extract of callus was then dissolved with 5 ml ethanol and that of ephedrae herba with 100 ml ethanol. This ethanol solution of extract was injected directly into the HPCE system.

2.4. Preparation of electrolyte

Tris–NaOH–H_3PO_4 buffer was prepared by mixing 0.10 M NaOH with 0.10 M Tris solution and it was diluted with distilled water. The concentration of NaOH was 0.0010 M, and the Tris concentration was 0.010M. pH of this buffer was adjusted to appropriate value by H_3PO_4. Unless otherwise specified, all chemicals were of analytical reagent grade.

3. Results and discussion

3.1. Calculations

The effective mobility was calculated by the following equation [5]:

$$\mu_{\text{eff}} = \left(\frac{1}{t_R} - \frac{1}{t_0}\right)\frac{lL}{V} \quad (1)$$

where μ_{eff} is the effective mobility of analyte, t_R is the migration time of analyte, and t_0 is the

migration time of electroosmotic flow, which was marked with ethanol.

The separation efficiency was calculated by:

$$N = 5.54\left(\frac{t_R}{t_{wh}}\right)^2 \quad (2)$$

where N is the theoretical plate number, and t_{wh} is the peak width at half height.

3.2. Separation conditions

There was a large effect of pH on the effective mobility of ephedrine. The dependence of ephedrine effective mobility on pH was shown in Fig. 1 and was simulated as follows:

$$\mu_{eff} = \frac{(\mu_1 - \mu_2)}{1 + e^{\frac{pH - pK_a}{c}}} + \mu_2 \quad (3)$$

where μ_{eff} is the effective mobility, and μ_1 and μ_2 are the effective mobilities at high and low pH values, respectively. It was known from simulation that $\mu_1 = 2.201 \times 10^{-6}$ cm^2 s^{-1} V^{-1}, $\mu_2 = 2.609 \times 10^{-4}$ cm^2 s^{-1} V^{-1}, and $pK_a = 8.19$ is the apparent dissociation constant when ion strength is ignored, and $c = 0.9953$ is a constant. The difference of dissociation constant between values from literature and experiment was probably due to the temperature in capillary being higher than that of the literature [6].

At low pH, there were positive charges on the ephedrine molecule, and a markable positive mobility could be observed. The electropherogram was simple for samples and the separation was sufficient. Although the current will increase when pH is decreased, since the ion strengths of Tris–NaOH–H_3PO_4 buffer was very low, the current could be still acceptable, as was shown in Fig. 2. In fact, the Tris–NaOH–H_3PO_4 buffer system is a mixed buffer system which consists of sodium phosphate and Tris–phosphate. From pH 6.0 to 8.0, the ionic strength of buffer changed little when pH is changed, because in this pH range the buffer solution has a sufficient buffer capacity, so the current changed little. The pH of buffer was kept at 3.20 in the analysis of sample.

There were reports on separation and determination of ephedrine by CE [4], however, those methods could not be used in the analysis of ephedrine in ephedra callus. It was found that

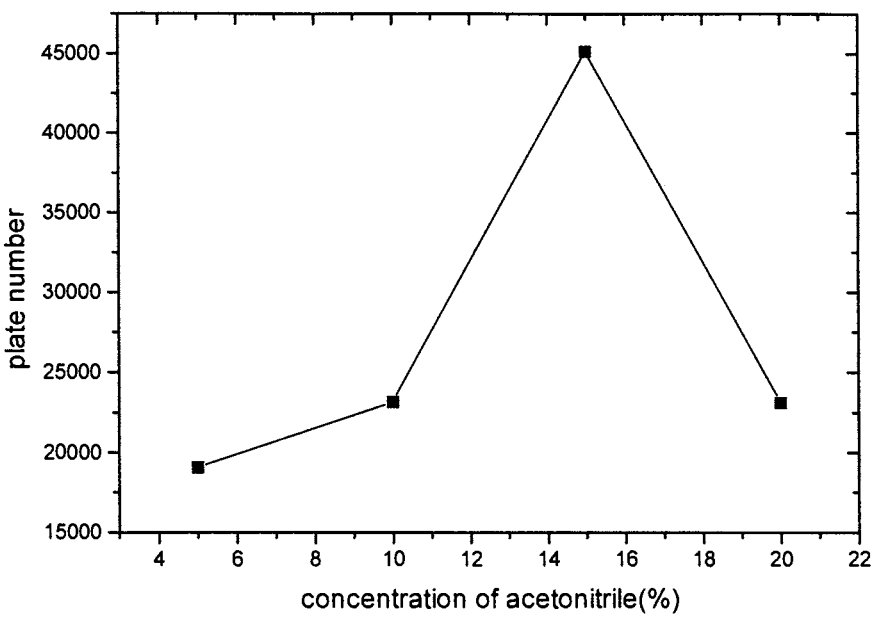

Fig. 3. Influence of concentration of acetonitrile (%) on the theoretical plate number. Concentration of Na^+ 0.0010 M, Tris 0.010 M; pH was adjusted with H_3PO_4 to 3.20.

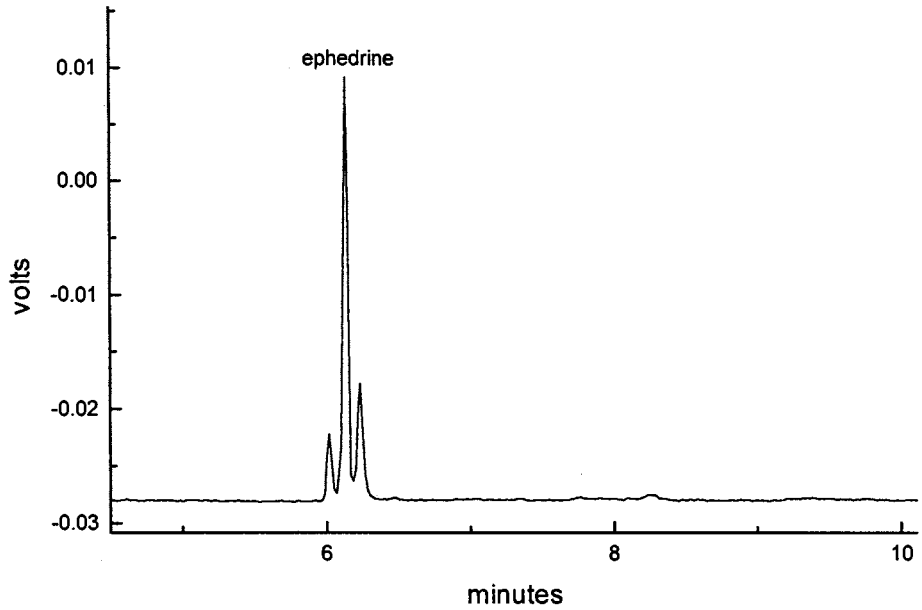

Fig. 4. Electropherogram of ethanol extract of ephedrae herba. Concentration of Na^+ 0.0010 M, Tris 0.010 M; pH was adjusted with H_3PO_4 to 3.20; concentration of acetonitrile, 15%. Applied voltage, 22 kV.

when the sample was directly introduced into the capillary, some hydrophobic components and additional chemicals in the extract of this callus will precipitate in the aqueous buffer and block the capillary, resulting in failure of analysis. Modification of run buffer was widely used in CE; methanol, ethanol and acetonitrile are effective modifiers on improving separation efficiency and reducing the adsorption of analyte [7–10]. In this work, acetonitrile was introduced to change the characteristic of buffer and keep the electrophoresis proceeding smoothly. The current and migration time of analyte changed little when concentration of acetonitrile was increased, however, the solubility of analyte was increased markably and therefore the separation efficiency increased. The dependence of theoretical plate number of ephedrine on content of acetonitrile was shown in Fig. 3. It was known from this figure that with the increase of the concentration of acetonitrile, the adsorption and diffusion of analyte are decreased because the dissociation of silanol in the inner wall of the capillary and the current are decreased; these lead to the increase of plate number. When the concentration of acetonitrile is higher, the dissociation of analyte is decreased. This leads to the decrease of the concentration of charged molecules and broadens the peak width, so the plate number is decreased too. The concentration of 15.0% acetonitrile was selected in the analysis of samples.

The typical electropherograms of samples were shown in Figs. 4 and 5. It was known from these electropherograms that component in callus was different from that in ephedrae herba, and this proposed method was suitable for the analysis of the ephedra callus sample for its high selectivity at low pH.

3.3. Peak identification

Peaks were identified by addition of standard substances of ephedrine in sample solution. It was demonstrated in Figs. 4 and 5 that the electropherogram of extract of callus and ephedrae herba was simple, peak of ephedrine could be easily identified by the increasing of peak area after adding the standard substance in sample solution.

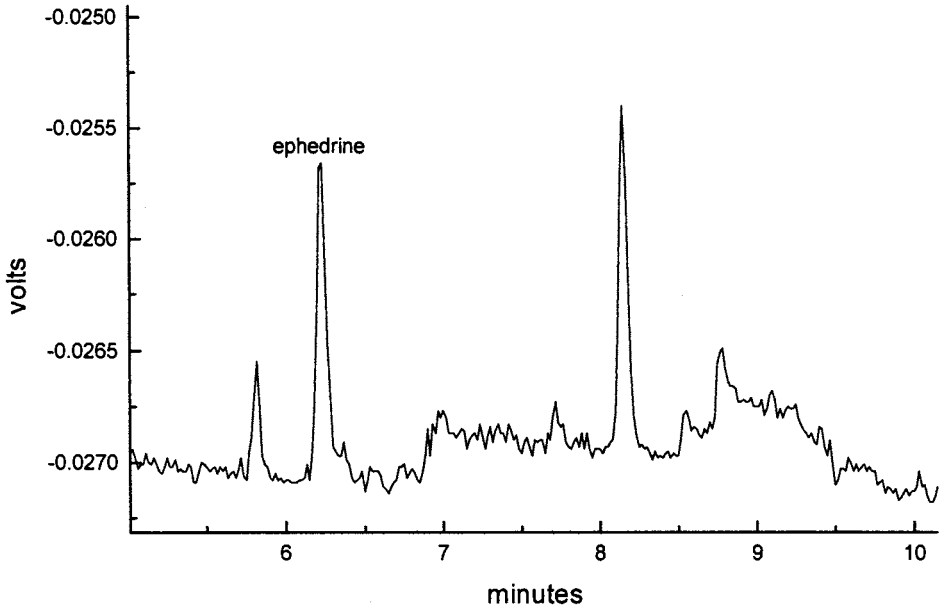

Fig. 5. Electropherogram of ethanol extract of ephedra callus. Concentration of Na^+ 0.0010 M, Tris 0.010 M; pH was adjusted with H_3PO_4 to 3.20; concentration of acetonitrile, 15%. Applied voltage, 22 kV.

3.4. Stability

The stability of ephedrine in ethanol and aqueous solution was demonstrated by leaving solution of standard ephedrine for 2 days at room temperature. The electropherogram of analytes in ethanol was not changed.

3.5. Linearity and reproducibility

A linear relationship between the concentration of ephedrine and the corresponding peak area was found in the 10.0–50.0 μg ml^{-1} concentration range. An ephedrine concentration of 1.74 μg ml^{-1} approaches the limit of detection.

The calibration curve is as follows:

$$S = 3084.12C - 1549.8;\ r = 0.9997$$

where S is peak area (mV·s), and C is the concentration of analytes. The unit is μg ml^{-1}.

The reproducibility of migration time and peak area were investigated. It was known from experiments that the average migration time at

Table 1
Analysis result of ephedrine in real samples

Sample	Ephedrine content (%)	Concentration (μg ml^{-1})	Added (μg ml^{-1})	Detected (μg ml^{-1})	Recovery (%)
Ephedrae herba	0.81 ($n = 5$)	24.72	10.0	35.55	108.3
			20.0	43.80	95.4
Ephedra callus	0.003 ($n = 5$)	10.94	10.0	21.38	104.4
			20.0	30.25	96.6
			30.0	41.74	102.7

the optimum condition is 6.23 min, and its relative standard deviation (RSD) equals 0.32% ($n = 5$). The RSD of peak area is 2.05% ($n = 5$).

4. Applications

This method was applied to the separation and determination of ephedrine in ephedrae herba and its callus. The result was shown in Table 1. It was known from this table that the content of ephedrine in ephedra callus was lower than that in ephedrae herba.

5. Conclusions

A capillary zone electrophoresis (CZE) method for determination of ephedrine in ephedra callus was established using Tris–NaOH–H_3PO_4 buffer system containing 15% acetonitrile as modifier. This method could also be used in the determination of ephedrine in ephedrae herba. The addition of acetonitrile increased the plate number and improved the migration behaviour of hydrophobic analytes. It was proved that the co-operating effect of buffer system was important in obtaining satisfactory separation.

Acknowledgements

This project is financially supported by the National Natural Science Foundation (No. 29475194), Natural Science Foundation of Gansu Province, and the Doctoral Point Foundation of the State Education Commission of the People's Republic of China.

References

[1] Dictionary of Traditional Chinese Medicine, New Medical College of Jiangsu, People's Publisher of Shanghai, 1977, pp. 2222.
[2] K.G. Ramawat, H.C. Arya, Phytomorphology 26 (4) (1976) 395.
[3] J. Hu, Yaowu Fenxi Zazhi 14 (5) (1994) 33.
[4] Y.M. Liu, S.J. Sheu, J. Chromatogr. A 600 (1992) 370.
[5] J. Lukaces, Anal. Chem. 53 (1981) 1298.
[6] D.R. Lide (Ed.), CRC Handbook of Chemistry and Physics, 73rd ed., CRC Press, Boca Raton Inc., 1992–1993, pp. 8–38.
[7] C.L. Ng, C.P. Ong, H.K. Lee, S.F.Y. Li, J. Chromatogr. A 680 (1994) 579.
[8] C.X. Zhang, F. von Heeren, W. Thormann, Anal. Chem. 67 (1995) 2070.
[9] Z. Hu, L. Jia, Z. Zhang, Anal. Lett. 29 (14) (1996) 2573.
[10] Y.M. Liu, S.J. Sheu, J. Chromatogr. A 623 (1992) 196.

ELSEVIER

Talanta 48 (1999) 1031–1038

Talanta

Optimal conditions and sample storage for the determination of H_2O_2 in marine waters by the scopoletin–horseradish peroxidase fluorometric method

Ling-Su Zhang [1], George T.F. Wong *

Department of Ocean, Earth and Atmospheric Sciences, Old Dominion University, Norfolk, VA 23529-0276, USA

Received 21 July 1998; received in revised form 14 September 1998; accepted 21 September 1998

Abstract

The conditions presently in use for the fluorometric determination of H_2O_2 in marine waters, by reacting H_2O_2 with scopoletin in the presence of horseradish peroxidase (HRP) and measuring the quenching of the fluorescence intensity of scopoletin, are not the optimal conditions. Under the optimized conditions of a pH of 8.5–9.5, an excitation wavelength of 390 nm and an emission wavelength of 460, the sensitivity of the method can be increased significantly, by up to more than a factor of 3 and the variations in the sensitivity from sample to sample can be significantly reduced. Furthermore, the samples need not be analyzed immediately after sample collection as presently prescribed. After scopoletin and HRP have been added to a sample immediately after sample collection, the sample may be stored at room temperature in the dark for up to four days before the quenched fluorescence intensity of scopoletin is read.

Keywords: Fluorescence; H_2O_2; Marine waters

1. Introduction

H_2O_2 has been found rather ubiquitously in the surface marine waters in concentrations ranging from undetectable to 10^2 nM [1–3]. It can affect the marine ecosystem by its direct interactions with the biota [4,5] or indirectly by causing changes in the speciation of a number of biologically important trace elements, such as Fe [6–8], Cu [9–12] and Cr [13,14], as H_2O_2 acts as an oxidizing and/or reducing agent [15]. H_2O_2 is formed primarily by the interactions between dissolved organic matter and sunlight and is decomposed primarily through biological processes [3]. The effects of these processes can become discernible within a time scale of hours. Thus, the concentration of H_2O_2 in marine waters is highly variable temporally and spatially. The fluorometric scopoletin–horseradish peroxidase (HRP) method is one of the most widely used methods

* Corresponding author. Fax: +1-757-6835303; e-mail: gwong@odu.edu.

[1] Present address: Soil and Plant Analysis Laboratory, Department of Soil Science, University of Wisconsin–Madison, 5711 Mineral Point Rd., Madison, WI 53705-4453, USA.

0039-9140/99/$ - see front matter
PII: S0039-9140(98)00312-9

for the determination of H_2O_2 in marine waters [1,16–19]. In this method, the reaction between H_2O_2 and scopoletin is catalyzed by the enzyme HRP. The concentration of H_2O_2 is estimated from the decrease in the fluorescence intensity of scopoletin as it is consumed in the reaction. This method has an excellent detection limit which has been reported to be about 2–10 nM [20,21]. However, it also suffers from a serious limitation: the need to analyze the sample immediately after sample collection. It has been stated that serious errors may result if the sample is stored for more than an hour [17,21]. This tight schedule creates severe logistic restrictions in coordinating the programs for sample collection and analysis. The availability of a scheme for even a short term storage of a day or two can greatly ease the inconvenience. The necessity for immediate sample analysis follows from the instability of H_2O_2 in marine waters. However, if this is the case and if scopoletin is stable, the sample may be stored once the reaction between H_2O_2 and scopoletin is allowed to go to completion. The quenched fluorescence intensity of scopoletin may then be measured at a later time. Indeed, in an aqueous solution, scopoletin has been reported to be stable in diffuse light, and is not oxidized by either peroxidase or hydrogen peroxide alone [22]. Furthermore, without providing explicit reasons, a range of slightly different experimental conditions has been adopted in different studies. Thus, earlier investigators [22,23] allowed the reaction between H_2O_2 and scopoletin to proceed at a pH of 4.5 and the quenched fluorescence intensity of the remaining scopoletin was measured at pH 10. More recently, the need for using a different pH for each step, which would have required an additional pH adjustment, has apparently been circumvented. However, while some used a pH of 8 [24], others used a pH of 7 [17,20] for both steps. Although the importance of pH-buffering has been noted [17], the selection of a particular pH for these steps was not substantiated by experimental data. In this study, the possibility for storing the samples for later analyses and the optimal combination of pH, the excitation wavelength and the emission wavelength for the determination of H_2O_2 in marine waters by the scopoletin-HRP method were re-evaluated.

2. Experimental

2.1. Reagents and apparatus

All chemicals used were of reagent grade whenever available.

Standard 2.5 μM H_2O_2 solutions: a 1-ml portion of a 30% (w/w) solution of H_2O_2 was diluted to 1000 ml to make an approximately 0.01 M stock solution. The exact concentration of H_2O_2 in the stock solution was standardized by an iodometric titration of the tri-iodide, formed by the reaction between H_2O_2 and excess iodide under acidic conditions, with thiosulfate [25]. A standard 2.5 μM solution was prepared by serial dilutions of the standardized 0.01 M stock solution with distilled deionized water.

Scopoletin (15 μM): a 15 mg portion of scopoletin (SIGMA, S-2500, 7-hydroxy-6-methoxy-2H-1-benzopyran-2-one, $C_{10}H_8O_4$, $M_w = 192.2$) was dissolved in 500 ml of distilled deionized water to make a 150 μM stock solution. This stock solution was further diluted in a 1:10 (v/v) ratio to make a 15 μM solution. This reagent was stored in the dark at room temperature, and was stable for at least 1 year.

Horseradish peroxidase (HRP) (20 purpurogallin units (p.u.) ml^{-1}): a 10 mg portion of HRP (SIGMA, P-8250, 200 p.u. mg^{-1}) was dissolved in 10 ml of dissolved deionized water to make a 200 p.u. ml^{-1} stock solution. This stock solution was further diluted in a 1:10 (v/v) ratio to make a 20 p.u. ml^{-1} solution. These solutions were stored at 4°C in a refrigerator. The catalytic effect of this reagent on the reaction between H_2O_2 and scopoletin could be maintained for at least 2 months.

Saturated solution of $Na_2B_4O_7$: a sufficient amount of $Na_2B_4O_7$ was added to about 100 ml of distilled deionized water so that a small amount of solid remained undissolved.

Artificial seawater: artificial seawater was prepared from inorganic salts according to the method of Lyman and Fleming [26]. In the ex-

periments where the pH of the solution was adjusted to 10 or above, the salts of calcium, magnesium, and strontium, which were required in the method for the preparation of artificial seawater, were substituted with an equimolar amount of the sodium salt in order to avoid the precipitation of the hydroxides of the alkaline earth elements at high pH.

Fluorescence intensity and excitation and emission spectra were recorded with a Perkin-Elmer model 650-10S fluorescence spectrophotometer.

The pH was measured with an Orion model 701A digital ionalyzer.

2.2. Procedures

A 10-ml aliquot of the sample was transferred into each of three glass bottles marked A, B and C. Next, 0.5 ml of distilled deionized water was added to bottles A and B while 0.5 ml of the standard 2.5 μM H_2O_2 solution was added to bottle C. Then, 0.5 ml of the 15 μM scopoletin solution was added to each bottle. Finally, 0.025 ml of the 20 p.u. ml^{-1} HRP solution was added to bottles B and C. The bottles were then stored in the dark at room temperature until their fluorescence intensities were measured.

Within 4 days, for each bottle, 3 ml of the solution together with 0.1 ml of the saturated $Na_2B_4O_7$ solution were transferred to a 1-cm fluorescence cell. After mixing the mixture on a vortex mixer for 1 min, the fluorescence intensity was measured at the following settings: excitation wavelength, 390 nm; excitation slit width, 6 nm; emission wavelength, 460 nm; emission slit width, 5 nm; sensitivity, 0.1.

The concentration of H_2O_2 in the sample was calculated by using the following formula:

$$C_{sam} = [(F_A - F_B)/(F_B - F_C)]\cdot[(V_{std}\cdot C_{std})/V_{sam}]$$

where F_A, F_B and F_C were the fluorescence intensities of the solutions in bottles A, B and C, V_{std} and C_{std} were the volume and the concentration of the standard H_2O_2 solution added to bottle C and C_{sam} and V_{sam} were the concentration of the sample and the volume of the sample used in the analysis.

3. Results and discussion

3.1. Optimization of experimental conditions

The excitation and emission spectra of a 0.1 μM scopoletin solution in natural seawater, between pH 4 and 9, and artificial seawater, between pH 4 and 10, were recorded between 250 and 750 nm. (The spectra of the solution in natural seawater above pH 9 were not recorded since the precipitation of the hydroxides of the alkaline earth elements in natural seawater occurs at high pH. In the artificial seawater, at high pH, the alkaline earth elements were substituted with an equimolar concentration of sodium so that no precipitation would occur.) The excitation spectra were recorded at an emission wavelength of 490 nm while the emission spectra were recorded at excitation wavelengths of 365 and 390 nm. Natural seawater and artificial seawater behaved identically. In all cases, there was a single excitation and a single emission maximum. The wavelength of the excitation maximum was pH-dependent (Fig. 1). Below pH 5, the wavelength of the excitation maximum was located at 345 nm. Between pH 5 and 7.8, it increased rapidly with increasing pH to 390 nm. No further change in the wavelength of the excitation maximum was

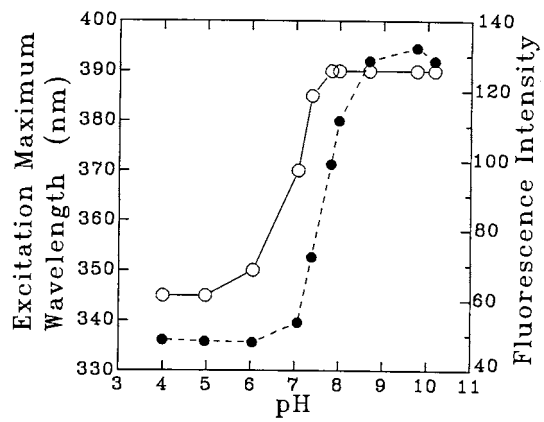

Fig. 1. The effect of pH on the wavelength of the excitation maximum of scopoletin at an emission wavelength of 460 nm (○) and on the fluorescence intensity of scopoletin at the excitation and emission maxima at each pH value (●) in artificial seawater. Fluorescence intensity is given in arbitrary relative fluorescence unit.

observed above pH 7.8. In previous studies, an excitation wavelength of 365 nm was invariably used and the fluorescence was measured at pH 7 [17,20], 8 [24] or 10 [22,23]. At pH 8 and 10, the fluorescence intensity was not measured at the wavelength of the excitation maximum. Thus, the method was not utilized at its highest sensitivity. At pH 7, the excitation wavelength used was still off but not as far off as in the other two schemes from the wavelength of the excitation maximum. However, around this pH, the wavelength of the excitation maximum was most sensitive to small pH changes. Thus, the sensitivity of the method could vary significantly if the pH of the sample was not strictly controlled to the same value from one sample to the other. In contrast to the excitation maximum, the wavelength of the emission maximum was independent of pH. It stayed at 460 nm between pH 4 and 10.2 at the excitation wavelengths of 365 and 390 nm in both natural and artificial seawater. An emission wavelength of 490 nm has been used by several investigators [17,27]. This is again not the optimal condition for this method.

The relationship between the fluorescence intensity of a 0.1 μM scopoletin solution and pH, when both the wavelengths of the excitation and the emission maxima at each pH were used, between pH 4 and 10 in artificial seawater is also shown in Fig. 1. (Again, similar behavior was found in natural seawater between pH 4 and 9.) Between pH 4 and 6, the fluorescence intensity was almost invariant with pH. It increased abruptly by more than a factor of 2 between pH 7 and 8.5. Above pH 9, the fluorescence intensity stayed relatively constant. Thus, measuring the fluorescence intensity at a pH of 8 or below, as preferred by previous investigators [17,18,24], is not the optimal condition for this method even if the excitation and emission maxima at these values of pH are used. However, at a pH of about 10 or above, the precipitation of the hydroxides of the alkaline earth elements occurs in marine waters. Thus, as a compromise, in the proposed procedure, a borate buffer was used so that the pH of the sample was maintained between 8.5 and 9. (Similar results were obtained by using a buffer of 0.6 M sodium bicarbonate adjusted to pH 9 by the addition of sodium carbonate.) The fluorescence intensity was measured at an excitation wavelength of 390 nm and an emission wavelength of 460 nm. The concentration of H_2O_2 was determined by an internal addition to each sample in order to accommodate any variations in pH and/or the bulk composition of the samples. For seawater, whose pH is about 8, the fluorescence intensity may be determined at its natural pH without adding a buffer. The addition of the other reagents does not alter the pH of the sample significantly.

3.2. Comparison with an un-optimized method

A sample of estuarine water collected from the lower Chesapeake Bay was stored in the dark for at least three days before it was used in subsequent experiments. During this period of time, most, if not all, of the H_2O_2 present initially in the sample would have decomposed [2,21,28]. H_2O_2 was added to one sub-sample to a concentration of added H_2O_2 of 0.30 μM. Another sub-sample was exposed to sunlight for three hours to induce the in situ formation of H_2O_2. Then, the concentration of H_2O_2 in the sample before and after the addition of H_2O_2 and after the exposure to sunlight were measured repeatedly by the scopoletin–HRP fluorometric method under the optimized experimental conditions reported here (i.e. a pH of 8.5 to 9, an excitation wavelength of 390 nm and emission wavelength of 460) and under the un-optimized experimental conditions that are presently in use [17] (i.e. a pH of 7, an excitation wavelength of 365 nm and an emission wavelength of 490 nm). The results are shown in Table 1. Both methods were similarly precise, ranging between $\pm 18\%$ at 0.017 μM to $\pm 1.5\%$ at 0.337 μM under the optimized conditions and between $\pm 14\%$ at 0.037 μM to $\pm 1.2\%$ at 0.331 μM under the un-optimized conditions. Both schemes detected about the same amount of added H_2O_2 and the same amount of H_2O_2 formed upon the irradiation of the sample with sunlight. Both recovered the added H_2O_2 approximately quantitatively. The concentrations obtained by using the optimized method were slightly lower systematically, by 0.02 μM, than those obtained by using the un-optimized method. The difference is small and

Table 1
Determination of H_2O_2 in marine waters by the scopoletin-HRP fluorimetric method under the optimized and previously adopted conditions

Sample	Optimized[a]		Un-optimized[b]		H_2O_2
	H_2O_2 (μM)	Sp. fl.[c] (fu μM^{-1})	H_2O_2 (μM)	Sp. fl. (fu μM^{-1})	Added μM
Estuarine water	0.015	97	0.042	29	0
Lower Chesapeake Bay	0.019		0.038		
Salinity = 23 g kg^{-1}			0.032		
Average (μM)	0.017 ± 0.003		0.037 ± 0.005		
Estuarine water with added H_2O_2	0.337	88	0.374	67	0.30
	0.332		0.356		
	0.341		0.339		
Average (μM)	0.337 ± 0.005		0.356 ± 0.018		
Recover (μM) (%)	0.320		0.319		
	107		106		
Estuarine water	0.304	77	0.336	77	0
Irradiated with sunlight	0.298		0.331		
	0.313		0.326		
			0.329		
Average (μM)	0.305 ± 0.008		0.331 ± 0.004		
H_2O_2 formed (μM)	0.288		0.294		

[a] pH, 8.5–9.5; excitation wavelength, 390 nm; emission wavelength, 460 nm—this work.
[b] pH, 7; excitation wavelength, 365 nm; emission wavelength, 490 nm—Holm et al. [17].
[c] Sp. fl., specific fluorescence in fluorescence unit (fu, relative arbitrary values) per μM of added H_2O_2.

is not considered significant when the combined analytical uncertainties of these analytical schemes are taken into account.

While both sets of analytical conditions yielded similar results, their sensitivities, which were given by their specific fluorescences (i.e. the decrease in fluorescence intensity per unit concentration of added H_2O_2) varied. The specific fluorescences of the optimized method were 97, 88 and 77 fu μM^{-1}, where fu is fluorescence intensity in arbitrary relative fluorescence unit, while the corresponding values of the un-optimized method were 29, 67 and 77 (Table 1). Thus, the optimized method yielded sensitivities that were up to more than three times higher than those of the un-optimized method. Furthermore, the variations in the specific fluorescences were much smaller in the optimized method. In the samples that were analyzed with the optimized method after various periods of storage time (Tables 2 and 3), the variations in the specific fluorescence in each sample over time were $< \pm 7\%$. The higher variability of the sensitivity of the un-optimized method probably results from its strong dependence on even small changes in pH. The specific fluorescence and thus the sensitivity of the method apparently decrease with increasing salinity. The specific fluorescences in a sample of marine water, distilled deionized water and a 1:1 mixture of the two were 88, 152 and 99 fu μM^{-1} respectively (Table 2).

3.3. Sample storage

H_2O_2 was added to two samples of coastal seawater collected from the Cobb Island Bay and the Lynnhaven Inlet, to distilled deionized water and to a 1:1 mixture of the Lynnhaven Inlet water and distilled deionized water. These solutions containing added H_2O_2 were then treated as samples. Scopoletin, distilled deionized water, standard H_2O_2 and/or HRP were added to sub-sets of each

Table 2
Effect of storage on the determination of H_2O_2 in marine waters by the scopoletin–HRP fluorometric method

Sample A[a]			Sample B[b]			Sample C[c]			Sample D[d]		
Storage time (h)	H_2O_2 (μM)	Sp. fl.[e] (fu μM^{-1})	Storage time (h)	H_2O_2 (μM)	Sp. fl. (fu μM^{-1})	Storage time (h)	H_2O_2 (μM)	Sp., fl. (fu μM^{-1})	Storage time (h)	H_2O_2 (μM)	Sp. fl. (fu μM^{-1})
0	0.253	75	0	0.136	89	0	0.172	153	0	0.138	110
2	0.245	76	23.8	0.135	90	23.8	0.158	169	23.8	0.158	98
8.5	0.259	75	48.8	0.143	92	48.8	0.176	153	74.5	0.168	99
18.3	0.259	76	74.5	0.148	81	74.5	0.184	144	74.5	0.156	97
26.3	0.256	75	74.5	0.150	80	74.5	0.183	142	75.3	0.165	99
50.3	0.249	74	75.3	0.128	89	75.3	0.185	147	75.3	0.163	97
73.3	0.272	73	75.3	0.134	87	75.3	0.180	147	76	0.157	105
99	0.272	73	76	0.144	92	76	0.178	151	76	0.155	105
			76	0.115	92	76	0.182	146	90.8	0.134	83
			90.8	0.134	83	90.8	0.153	171			
Avg.	0.258	75		0.136	88		0.175	152		0.155	99
SD[f]	0.009	1		0.010	5		0.010	10		0.011	7

[a] Sample A, Cobb Island Bay water; salinity = 31 g kg^{-1}.
[b] Sample B, Lynnhaven Inlet water; salinity ≈ 25 g kg^{-1}.
[c] Sample C, distilled deionized water.
[d] Sample D, 1:1 mixture of sample B and distilled deionized water.
[e] Sp. fl., specific fluorescence in fluorescence unit (fu, relative arbitrary values) per μM of added H_2O_2.
[f] SD, one standard deviation.

Table 3
Effect of storage and direct internal addition to the sample on the determination of H_2O_2 in marine waters by the scopoletin–HRP fluorometric method[a]

Time of storage (h)	With additional HRP		Without additional HRP	
	H_2O_2 (μM)	Sp. fl.[b] (fu μM^{-1})	H_2O_2 (μM)	Sp. fl. (fu μM^{-1})
0	0.169	92	0.184	84
12	0.163	94	0.178	86
23	0.163	90	0.177	83

[a] Lower Chesapeake Bay water; salinity = 23 g kg^{-1}.
[b] Sp. fl., specific fluorescence in fluorescence unit (fu, relative arbitrary values) per μM of added H_2O_2.

of these samples as described in the proposed method for sample storage. Then, these sub-sets of these samples were stored in the dark at room temperature for various periods of time before they were retrieved, one sub-set at a time, for the determination of the concentration of H_2O_2. The results are summarized in Table 2. In all cases, there was no significant change in the concentration of H_2O_2 with storage time, even for the longest storage time of 99 h. The average concentrations of H_2O_2 in these samples of water over all the periods of storage were 0.258 ± 0.009, 0.136 ± 0.010, 0.175 ± 0.010 and 0.155 ± 0.011 μM. Samples B, C and D were determined repeatedly over a period of 1.5 h after a storage time of 74.5–76 h. Their average concentrations over this period of time were 0.137 ± 0.012, 0.182 ± 0.002 and 0.161 ± 0.005 μM. These uncertainties were a good indication of the analytical uncertainty inherent in the method and their magnitudes were similar to those reported by previous workers [17]. Since the variations in the concentrations of H_2O_2 in the samples during the storage periods were similar to these analytical uncertainties, by using the proposed scheme, the storage of samples of marine water for up to 99 h, or about 4 days, does not affect the determination of their concentrations of H_2O_2.

In another experiment, a sub-sample with added standard H_2O_2 which served as an internal standard was not included for storage. Instead, after the fluorescence intensity of the sample was read, a known amount of H_2O_2 (0.05 ml of a 10 μM solution) was added directly to the fluorescence cell containing the sample (3 ml) with or without the further addition of HRP (0.01 ml of a 200 p.u. ml^{-1} solution) and the fluorescence intensity of the sample was read again. The scheme without a further addition of HRP has been the standard scheme for the determination of H_2O_2 [17] if a sample can be analyzed immediately after sample collection [17]. In either of these schemes, only two, the blank and the sample, rather than three sub-samples need to be stored. The scheme without the further addition of HRP will work, if, during sample storage, the ability of the HRP, which is added prior to sample storage, to catalyze the reaction between H_2O_2 and scopoletin is not altered. If there is a further addition of HRP, the scheme should work unless compounds, which can interfere with the reaction between H_2O_2 and scopoletin in the presence of the freshly added HRP, are formed during storage. The results (Table 3) indicate that there was no significant change in the concentration of H_2O_2 for up to 23 h, the length of the experiment. The variations around the mean during storage was within the analytical uncertainty of about 0.010 μM. Slightly lower results were found when there was a further addition of HRP. The difference, about 0.014 μM, was small. The cause could be traced to a slight decrease in the specific fluorescence, from 92 to 84 fu μM^{-1} of added H_2O_2, without the further addition of HRP. This may indicate a slight deactivation of the enzyme HRP during storage. Thus, for shorter periods of storage of up to a day, only the sample may need to be stored after H_2O_2 in the sample has been allowed to react with scopoletin in the presence of HRP. The concentration of H_2O_2 in the sample may be quantified later on

by a direct internal addition of a standard H_2O_2 solution to the sample together with an additional amount of HRP.

Acknowledgements

This work was supported in part by the National Science Foundation under grant numbers OCE-9301298 and INT-9515521 to Wong and by the National Science Council of Taiwan when this manuscript was prepared while Wong occupied a research chair at the National Center for Ocean Research (NCOR) of Taiwan. It also constitutes part of the doctoral dissertation research of L.-S. Zhang. This is contribution no. 6 of NCOR.

References

[1] R.G. Zika, J.W. Moffett, R.G. Petasne, W.J. Cooper, E.S. Saltzman, Geochem. Cosmochim. Acta 49 (1985) 1173.
[2] K.S. Johnson, S.W. Willason, D.A. Wiesenburg, S.E. Lohrenz, R.A. Arnone, Deep-Sea Res. 36 (1989) 241.
[3] W.J. Cooper, C. Shao, D.R.S. Lean, A.S. Gordon, F.E. Scully, Environmental Chemistry of Lakes and Reservoirs, ACS Adv. Chem. Ser, vol. 237, American Chemical Society, Washington, DC, 1994, pp. 391–422.
[4] B. Palenik, O.C. Zafiriou, F.M.M. Morel, Limnol. Oceanogr. 32 (1987) 1365.
[5] B. Palenik, F.M.M. Morel, Limnol. Oceanogr. 33 (1988) 1606.
[6] T.D. Waite, F.M.M. Morel, Environ. Sci. Technol. 18 (1984) 860.
[7] J.W. Moffett, R.G. Zika, Environ. Sci. Technol. 21 (1987) 804.
[8] F.J. Millero, S. Sotolongo, Geochim. Cosmochim. Acta 53 (1989) 1867.
[9] J.W. Moffett, R.G. Zika, Mar. Chem. 13 (1983) 235.
[10] J.W. Moffett, R.G. Zika, Photochemistry of Environmental Aquatic Systems, ACS Symposium Series, vol. 327, American Chemical Society, Washington, DC, 1987, pp. 116–130.
[11] V.K. Sharma, F.J. Millero, Geochim. Cosmochim. Acta 53 (1989) 2269.
[12] F.J. Millero, V.K. Sharma, B. Karn, Mar. Chem. 36 (1991) 71.
[13] M. Pettine, F.J. Millero, Limnol. Oceanogr. 35 (1990) 730.
[14] M. Pettine, F.J. Millero, T. La Noce, Mar. Chem. 34 (1991) 29.
[15] J.W. Moffett, O.C. Zafiriou, Limnol. Oceanogr. 35 (1990) 1221.
[16] R.J. Kieber, G.R. Helz, Anal. Chem. 58 (1986) 2312.
[17] T.R. Holm, G.K. George, M. Barcelona, Anal. Chem. 59 (1987) 582.
[18] W.J. Cooper, E.S. Saltzman, R.G. Zika, J. Geophys. Res. 92 (1987) 2970.
[19] R. Szymczak, T.D. Waite, Aust. J. Mar. Freshwater Res. 39 (1988) 289.
[20] R.G. Zika, E.S. Saltzman, W.L. Chameides, D.D. Davis, J. Geophys. Res. 87 (1982) 5015.
[21] W.J. Cooper, D.R. Lean, Environ. Sci. Technol. 23 (1989) 1425.
[22] W.A. Andreae, Nature 175 (1955) 859.
[23] H. Perschke, E. Broda, Nature 190 (1961) 257.
[24] C. Van Baalen, J.E. Marler, Nature 211 (1966) 951.
[25] I.M. Kolthoff, R. Belcher, Volumetric Analysis, vol. 3, Interscience, New York, 1957, pp. 282–283.
[26] J. Lyman, R.H. Fleming, J. Mar. Res. 3 (1940) 134.
[27] R.G. Zika, E.S. Saltzman, Geophys. Res. Lett. 9 (1982) 231.
[28] R.G. Zika, E.S. Saltzman, W.J. Cooper, Mar. Chem. 17 (1985) 265.

ELSEVIER

Talanta 48 (1999) 1039–1044

Talanta

Selective spectrophotometric determination of palladium(II) with 2(5-nitro-2-pyridylazo)-5-(*N*-propyl-*N*-3-sulfopropylamino) phenol(5-NO_2.PAPS) and tartaric acid with 5-NO_2.PAPS-niobium(V) complex

Itsuo Mori *, Tatsuya Kawakatsu, Yoshikazu Fujita, Takako Matsuo

Osaka University of pharmaceutical Sciences, 4-20-1 Nasahara, Takatsuki, Osaka 569-1094, Japan

Received 27 June 1998; received in revised form 16 September 1998; accepted 21 September 1998

Abstract

Spectrophotometric determinations of palladium(II) and tartaric acid were respectively investigated by using the color reactions between 2(5-nitro-2-pyridylazo)-5-(*N*-propyl-*N*-3-sulfopropylamino)phenol(5-NO_2.PAPS) and palladium(II) in strong acidic media, and between 5-NO_2.PAPS, niobium(V) tartaric acid in weak acidic media. The calibration graphs were linear in the range of 0–25 μg/10 ml palladium(II), with an apparent molecular coefficient (ε) of 6.2×10^4 l mol^{-1} cm^{-1} at 612 nm, and 0–23 μg/10 ml tartaric acid with $\varepsilon = 1.08 \times 10^6$ l mol^{-1} cm^{-1} at 612 nm, respectively. The proposed methods were selective and sensitive in comparison with other chelating pyridylazo dyes–palladium(II) or metavanadic acid–tartaric acid method, and the effect of foreign ions such as copper(II) was negligible for the assay of palladium(II) with 5-NO_2.PAPS. © 1998 Elsevier Science B.V. All rights reserved.

Keywords: Spectrophotometric determination; Palladium(II); Tartaric acid

1. Introduction

Generally, palladium(II) has been used as a catalytic metal, an alloy of precious metal goods, etc. However, tartaric acid has been used as starting material for pharmaceutical preparations, refrigerant, lemonade, etc. Various spectrophotometric methods for the assay of palladium(II), have been reported, such as coloring agents for palladium(II), dithizone, *p*-nitrodiphenylamine, Chromazurol *S*, 2(pyridylazo)resorcinol (PAR), etc. [1–11] were used. In addition, the volumetry or colorimetry [12,13] were used for the assay of tartaric acid. However, these analytical methods for the assay of palladium(II) or tartaric acid lack sensitivity and selectivity. In this paper,

* Corresponding author.

0039-9140/99/$ - see front matter
PII: S0039-9140(98)00309-9

with a view to obtaining a more selective and sensitive spectrophotometric method for palladium(II) or tartaric acid with chelating azo dye, we first investigated the systematic color reaction between various chelating azo dyes and palladium(II), and also among various chelating azo dyes, metal ions and tartaric acid. Second, new sensitive and selective spectrophotometric determinations for palladium(II) with 5-NO_2.PAPS as a chelating azo dye in strong acidic media, and for tartaric acid with 5-NO_2.PAPS-niobium(V) complex in weak acidic media were proposed.

2. Experimental

2.1. Apparatus and reagents

The absorption spectra were recorded on a Shimadzu UV 260 spectrophotometer with 1.0-cm quartz cells. Hitachi-Horiba Models F-8 and F-11 pH meters were used for pH measurement.

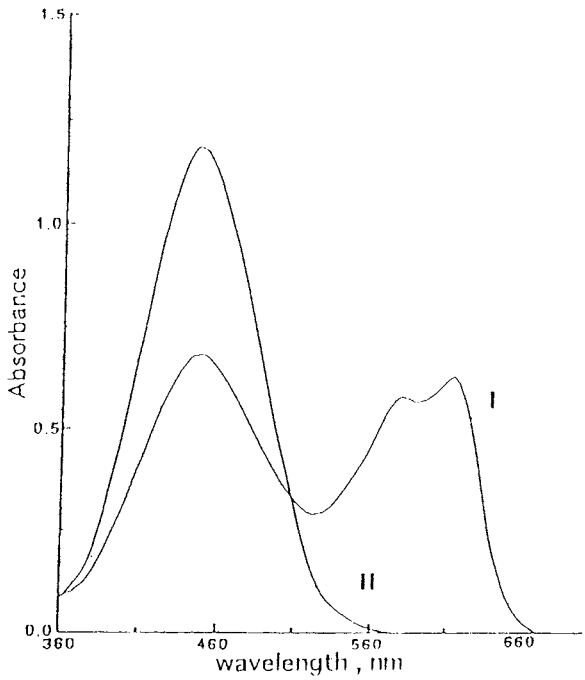

Fig. 1. Absorption spectra of 5-NO_2.PAPS and 5-NO_2.PAPS-palladium(II) solutions. Palladium(II), 1.0×10^{-5} mol l^{-1}; 5-NO_2.PAPS, 5.0×10^{-5} mol l^{-1}; HNO_3, 4*N*; curve I, 5.0-NO_2.PAPS-palladium(II) solution; curve II, 5-NO_2.PAPS solution; reference, water.

Table 1
Effect of foreign ions[a]

Foreign ions	Added as	Permissible molar ratio[b]
Ca(II)	Nitrate	400
Al(III)	Nitrate	150
Co(II)	Nitrate	400
Ni(II)	Nitrate	400
Cu(II)	Sulphate	400
Fe(III)	Sulphate	300
Fe(II)	Sulphate	80
Mn(II)	Chloride	60
VO^{3-}	Ammmonium	60
Ce(III)	Chloride	80
Th(IV)	Nitrate	300
Pt(IV)	Chloride	1
F^-	Potassium	400
I^-	Potassium	1/20
NO_2^-	Sodium	200
Tartarate	Sodium	400
Oxalate	Sodium	400
Citrate	Sodium	400
Ascorbic acid	Acid	200

[a] Palladium(II) used, 1.0×10^{-5} mol l^{-1};5-NO_2.PAPS, 5.0×10^{-5} mol l^{-1}; HNO_3, 4*N*.

[b] Difference of absorbance between 5-NO_2.PAPS-palladium(II) and 5-NO_2.PAPS-palladium(II)-foreign ions solution; absorbance error = ± 0.01.

A solution of 1.0×10^{-3} mol l^{-1} 5-NO_2.PAPS was prepared by dissolving 5-NO_2.PAPS (Dojindo Chemical, Japan) in methanol. A 1.0×10^{-3} mol l^{-1} palladium(II) solution was prepared by dissolving palladium chloride in

Table 2
Recovery test of palladium(II) in various water[a]

Sample	Added (μg)	Calculated	Recovery (%)
Waste water			
A	10.6	10.4	99.0
	10.6	10.5	99.5
B	10.6	10.7	101.0
	10.6	10.65	100.5

[a] 5-NO_2.PAPS, 5.0×10^{-4} mol l^{-1}; HNO_3, 4*N*; reference, reagent blank; waste water A, Cu(II):Co(II):Hg(II):Pd(II) = 20:20:10:1 (palladium used 5.3 μg); waste water B, Cu(II):Fe(II):Ni(II):Pd(II) = 20:20:20:1 (palladium used 5.3 μg).

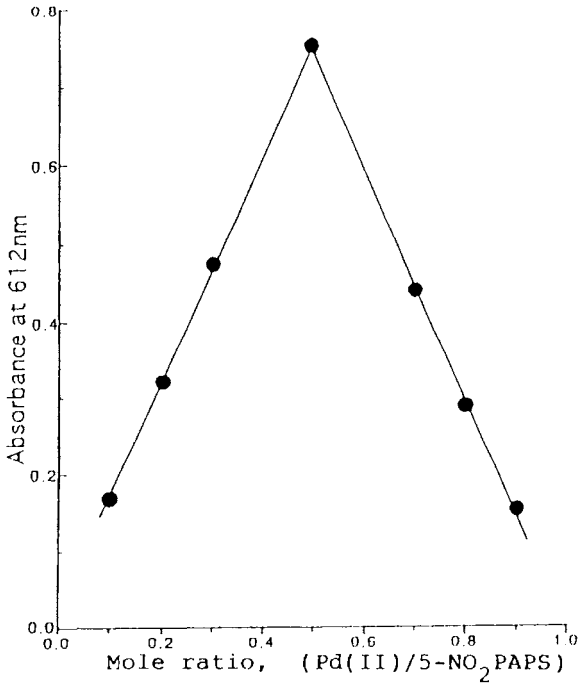

Fig. 2. Composition of 5-NO_2.PAPS-palladium(II) complex by continuous variation method. 5-NO_2.PAPS + palladium(II) = 2.5×10^{-5} mol l^{-1}; HNO_3, 4*N*.

water, as described by a previous report [1], and corrected by ethylenediamine tetraacetic acid (EDTA) titration. A 1.0×10^{-3} mol l^{-1} niobium(V) solution was prepared by dissolving niobium in water by adding of hydrofluoric acid, and a tartaric acid solution was prepared by dissolving tartaric acid in water. A 1.0% hexadecyltrimethylammmoniumchloride (HTAC) solution was prepared by dissolving HTAC in water. All materials and reagents were of analytical grade and were used with further purification. Deionized water was used throughout.

2.2. Standard procedure

2.2.1. Determination of palladium(II)

To a sample solution containing 0–25 μg palladium(II) in a 10-ml calibrated flask, 4.0 ml of a 10 *N* nitric acid and 0.5 ml of 1.0×10^{-3} mol l^{-1} 5-NO_2.PAPS solution were added. The mixture was diluted to the mark with water and kept at room temperature for 20 min together with a reference solution. The amount of palladium (II) was calculated by measuring the absorbance of 5-NO_2.PAPS-palladium(II) solution at 612 nm against a blank (5-NO_2.PAPS solution) prepared without palladium(II).

2.2.2. Determination of tartaric acid

To a sample solution containing 0–23 μg tartaric acid in a 10-ml calibrated flask, 2.5 ml of sodium acetate–acetic acid buffer solution (pH 4.0), 1.0 ml of 1.0% HTAC solution, 1.0 ml of a 5.0×10^{-4} mol l^{-1} niobium(V) solution and 0.75 ml of a 1.0×10^{-3} mol l^{-1} 5-NO_2.PAPS solution were added. The mixture was diluted to the mark with water, kept at 60°C for 15 min. After cooling the solution to room temperature (10–25°C) for 10 min, the absorbance at 612 nm of the 5-NO_2.PAPS-niobium(V)-tartaric acid solution was measured against a blank (5-NO_2.PAPS-niobium(V)) solution that was treated in the same manner, with the exception that tartaric acid was not added.

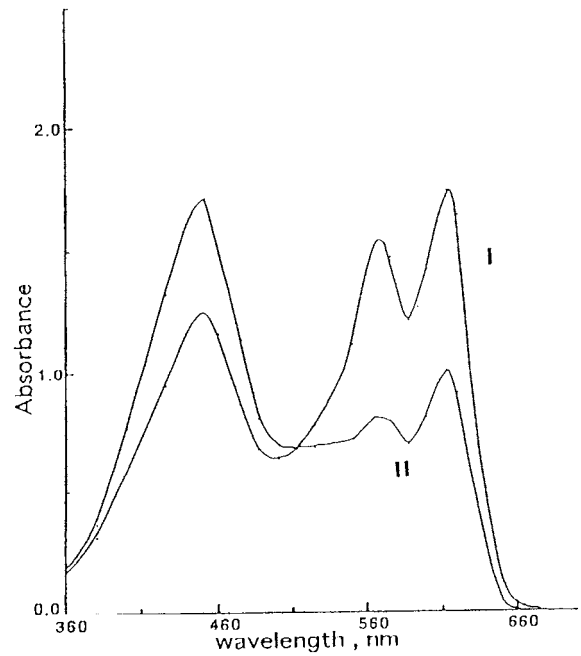

Fig. 3. Absorption spectra of 5-NO_2.PAPS-niobium(V) and 5-NO_2.PAPS-niobium(V)-tartaric acid solutions. Tartaric acid, 1.0×10^{-5} mol l^{-1}; niobium(V), 5.0×10^{-5}; mol l^{-1}; 5-NO_2.PAPS, 7.5×10^{-5} mol l^{-1}; pH, 4.0; curve I, 5-NO_2.PAPS-niobium(V)-tartaric acid solution; curve II, 5-NO_2.PAPS-niobium(V) solution; reference, water.

Table 3
Effect of various surfactants in the coloring reaction among 5-NO_2.PAPS, niobium(V) and tartaric acid[a]

Surfactant	Absorbance (maximum)
—	0.278 (606)
HTAC	0.684 (612)
Hexadecylpyridinium Cl	0.609 (612)
Tetradecyltrimethylammmonium Cl	0.208 (631)
Dodecyltrimethylammmonium Cl	0.120 (608)
Benzalkonium Cl	0.375 (612)
Sodium dodecylbenzene sulphate	0.313 (608)
Sodium decylsulphate	0.264 (608)
Polyvinylalcohol (n = 500)	0.246 (608)
Triton X100	0.291 (608)
Brij 35	0.272 (608)
Tween 20	0.275 (608)

[a] Tartaric acid, 5.0×10^{-6} mol l^{-1}; niobium(V), 5.0×10^{-5} mol l^{-1}; 5-NO_2.PAPS, 5.0×10^{-5} mol l^{-1}; pH 4.0; reference, 5-NO_2.PAPS-niobium(V) solution.

3. Results and discussion

3.1. Determination of palladium(II)

3.1.1. Coloring reactions and absorption spectra

The coloring reactions between various azo-chelating agents such as 5-NO_2.PAPS and palladium(II) in strong acidic media were systematically investigated. Although the coloring reactions between palladium(II) and the majority of PAR derivatives—PAR, 1-(2-pyridylazo)-2-naphthol (PAN), 4-(2-thiazolylazo)resorcinol(TAR), 1-(2-thiazolylazo)-2-naphthol(TAN)—in strong acidic media were scarcely recognized, 5-NO_2.PAPS was found to be the most appropriate agent for the assay of palladium(II) in tested azo-chelating agents. Fig. 1 shows the absorption spectra of 5-NO_2.PAPS and 5-NO_2.PAPS-palladium(II) solutions in strong acidic media.

3.1.2. Effect of acid

The coloring reactions in strong acidic media using hydrochloric acid, sulfuric acid, nitric acid, etc. were stable and reproducible in comparison with the coloring reaction in weak acidic media using acetate buffer solution; in particular, coloring in the presence of nitric acid was stable, and its optium final concentration was 3–5 *N* nitric acid.

3.1.3. Effects of temperature and reaction time

The coloring reactions at various temperatures (25, 40, 50 and 60°C for 0–30 min) and times were discussed. As a result, the coloring reaction at room temperature was immediately carried, and its absorbance was stable for 48 h after initiation of the color reaction. In this case, the coexisting effects of surfactant (cationic-, anionic-, nonionic-) was not entirely recognized.

3.1.4. Effect of concentration of 5-NO_2.PAPS

The recommended optimum concentration of 5-NO_2.PAPS was final 5.0×10^{-5} mol l^{-1}, and the subsequent procedure was investigated at final 5.0×10^{-5} mol l^{-1} 5-NO_2.PAPS.

3.1.5. Calibration graph and reproducibility

The calibration graph was linear for concentrations lower than 30 μg palladium(II) per 10 ml.

Table 4
Effect of foreign ions[a]

Foreign ions	Added as	Permissible molar ratio (ion/tartaric acid)[b]
Ca(II)	Nitrate	200
Al(III)	Nitrate	1
Co(II)	Nitrate	5
Ni(II)	Nitrate	20
Cu(II)	Sulphate	10
Sm(III)	Chloride	1
Zn(II)	Chloride	1
Pt(IV)	Chloride	1/10
Fe(II)	Sulphate	10
Ti(IV)	Sulphate	1/50
Hg(II)	Nitrate	10
I^-	Potassium	1/20
CN^-	Sodium	10
$S_2O_3^{2-}$	Sodium	10
Citric acid	Sodium	40
Ascorbic acid	Acid	10

[a] Tartaric acid used, 5.0×10^{-6} mol l^{-1}; niobium(V), 5.0×10^{-5} mol l^{-1}; 5-NO_2.PAPS, 7.5×10^{-5} mol l^{-1}; HTAC, 0.1%; pH 4.0; reference, 5-NO_2.PAPS-niobium(V) solution.

[b] Difference of absorbance at 612 nm between 5-NO_2.PAPS-niobium(V)-tartaric acid and 5-NO_2.PAPS-niobium(V) solution; absorbance error = ±0.01.

The apparent molar absorption coefficient (ε) was estimated to be 6.2×10^4 l mol^{-1} cm^{-1} with a Sandell sensitivity of 0.0017 μg cm^{-2} palladium(II) at 612 nm. The proposed method is about 2-fold more sensitive than the PAR-extraction method [4]. The reproducibility for 10.6 μg palladium(II) per 10 ml (ten experiments) was 0.41% relative standard deviation (R.S.D.).

3.1.6. Effect of foreign ions

The effect of foreign ions and substances was investigated. As shown in Table 1, the presence of many metal ions was permitted in a 50–300-fold excess over palladium(II), but the coexsitence of platinum(IV) gave a positive error, and thiocyanate, iodide ions gave a negative error for the assay of palladium(II).

3.1.7. Application

The proposed method was applied to the assay of palladium(II) in waste water containing of copper(II), cobalt(II), mercury(II), iron(III), etc. with satisfactory results, as shown in Table 2.

3.1.8. Composition of complex

The molar ratio of palladium(II) to 5-NO_2.PAPS in the complex was determined by the continuous variation and molar ratio methods to be 1:1 (Fig. 2).

3.2. Determination of tartaric acid

3.2.1. Coloring reaction and absorption spectra

The coloring reaction between niobium(V), 5-NO_2.PAPS and/or tartaric acid in the presence or absence of surfactant were systematically investigated in acidic media. Although the coloring between 5-NO_2.PAPS and niobium(V) in the absence of surfactant and tartaric acid was unstable in weak acidic media, 5-NO_2.PAPS-niobium(V) coloring reaction with the coexistence of tartaric acid and a cationic surfactant such as HTAC was stable, strong and reproducible.

Fig. 3 shows the absorption spectra of 5-NO_2.PAPS-niobium(V)–tartaric acid and 5-NO_2.PAPS-niobium(V) solutions at pH 4.0 in the presence of HTAC as a cationic surfactant.

3.2.2. Effect of pH and fluoride ion

A maximum and almost constant absorbance was obtained at 610 nm (maximum absorption wavelength) within the limited range of pH 3.7–4.3, by using 1.5–3.0 ml of Walpole acetate buffer solution for 10 ml. The coexistence of fluoride ions was effective in the coloring reaction between 5-NO_2.PAPS and niobium(V), and its recommended optimum concentration was final concentration 1.5×10^{-3} mol l^{-1} fluoride ions for the assay of tartaric acid.

3.2.3. Effect of surfactant

The effect of single or mixed surfactants was systematically examined in the coloring reactions among 5-NO_2.PAPS, niobium(V), tartaric acid and fluoride ion. The coexistence of cationic surfactant, such as HTAC alone, was generally effective. HTAC in the tested cationic surfactants was most effective, and the optimum concentration was final concentration 0.05–0.12 % HTAC (Table 3).

3.2.4. Effect of 5-NO_2.PAPS–niobium(V) concentration

The recommended optimum concentrations of 5-NO_2.PAPS and niobium(V) were final concentration 5.0×10^{-5} mol l^{-1} niobium(V) and 7.5×10^{-5} mol l^{-1} 5-NO_2.PAPS, respectively; the molar ratio of 5-NO_2.PAPS to niobium(V) was 1.5:1.

3.2.5. Effects of temperature and stability

The coloring reaction between 5-NO_2.PAPS, niobium(V), fluoride ions and tartaric acid was rapid at elevated temperatures (30–60°C) for 10 min in comparison with that at room temperature (15–25°C). The absorbance of the system remained stable and constant for at least 90 min after initiation of the color reaction.

3.2.6. Calibration graph and reproducibility

The calibration graph was linear for the concentration lower than 23 μg tartaric acid per 10 ml. The apparent molar absorption coefficient (ε) was estimated to be 1.05×10^6 l mol^{-1} cm^{-1}. The proposed method is much more sensitive than potentiometry. The reproducibility for 7.1 μg tar-

taric acid per 10 ml (five experiments) was 0.79% (R.S.D.).

3.2.7. Effect of interferences

The effect of foreign ions and substances was investigated. The coexistence of platinum(IV), rare earth elements, titanium(IV) and manganese(II) gave a positive error, but these interference ions could be masked by addition of EDTA or nitrilotriacetic acid (NTA). As shown in Table 4, the coexistence of metal ions such as cobalt(II), zinc(II) and iron(III) was permitted in a 10–20-fold excess over tartaric acid. However, the coexsistence of citrate, oxalate ions and L-ascorbic acid was permissible in a 10–40-fold excess over tartaric acid.

4. Conclusion

The coloring reactions among 5-NO_2.PAPS, palladium(II) or niobium(V) and/or tartaric acid were systematically investigated, as were the procedures for the assay of palladium(II) and tartaric acid, by using 5-NO_2.PAPS-palladium(II) and 5-NO_2.PAPS-niobium(V) coloring reactions. The proposed methods were relatively simple, selective and sensitive in comparison with other spectrophotometric methods [1–12].

References

[1] I. Mori, Y. Fujita, T. Enoki, Bunseki Kagaku 28 (1979) 685.
[2] E.B. Sandell, Colorimetric Determination of Trace Metals, 3rd ed., Interscience, New York, 1959, pp. 711.
[3] Z. Marczenko, S. Ku's, Analyst 110 (1985) 1005.
[4] A.K. Chakkar, L.R. Kakker, Fresenius J. Anal. Chem. 19 (1991) 340.
[5] R. Ishida, Bull. Chem. Soc. Jpn. 36 (1963) 889.
[6] E.R. Marcenko, E.B. Sandell, Anal. Chim. Acta 28 (1969) 259.
[7] T. Yotsuyanagi, H. Hoshino, K. Aomura, Anal. Chim. Acta 71 (1974) 349.
[8] W.F. Davis, Talanta 16 (1969) 1330.
[9] Y. Horiuchi, H. Nishida, Bunseki Kagaku 16 (1967) 1018.
[10] K. Mizuno, G. Miyatani, Bull. Chem. Soc. Jpn. 19 (1976) 2479.
[11] Z. Marczenki, Separation and Spectrophotometric Determination of Elements, Wiley, New York, 1986, pp. 437.
[12] F.D. Snell, Colorimetric Methods of Analysis, 3rd edn, Van Nostrand Reinhold, New York, 1953, p. 382.
[13] AOAC, Methods of Analysis, 13th ed., 1980, pp. 144.

ELSEVIER

Talanta 48 (1999) 1045–1050

Talanta

Chloromethylstyrene encapsulated and quaternized silica anion exchanger in high performance liquid chromatography

Ruiqin Yang, Shengxiang Jiang, Xia Liu, Liren Chen *

Analytical Chemistry Division, Lanzhou Institute of Chemical Physics, Chinese Academy of Sciences, Lanzhou 730000, People's Republic of China

Received 17 March 1998; received in revised form 2 September 1998; accepted 29 September 1998

Abstract

A kind of strong anion exchanger (SAX) was prepared with chloromethylstyrene encapsulated silica. This strong anion silica column has superior ability for the separation of anions, organic acids and also the mixture of them. Using this strong anion exchanger, the sulfonic acids can be separated. With gradient elution, the separation of petroleum mono- and di- sulfonates in Yumen sample can be also well obtained. This anion exchanger's stability has been studied. After continuous use for three months the carbon and nitrogen contents and the chromatographic behavior of the exchanger were unchanged. © 1999 Elsevier Science B.V. All rights reserved.

Keywords: Chloromethylstyrene; Encapsulated; Anion exchanger; HPLC

1. Introduction

Anion-exchange phases containing differently substituted amines as the effective groups have always been of interest for the selective separation of ionizable species. Such phases are obtained either by chemical modification of polymeric organic support materials [1–4] or by chemical bonding of molecules with ion-exchange capability to the surface of silica by silanization [5,6] using the corresponding type of reagent. Contrary to silica based materials, stationary phases on the basis of organic polymers are stable against mobile phase of pH value beyond 8. However, the disadvantages of organic polymer packing materials (swelling in certain organic solvents and poor pressure stability) should not be overlooked. Silica based ion-exchange phases obtained by silanization have a limited chemical stability and can not be used with mobile phases at a pH value higher than 8. Such phases exhibit a poor long-term stability even at low pH value when aqueous mobile phases containing buffer salts were used [7].

It has previously been proven [8] that effective polar spacer groups in the common modified silica are not stable against protic attack by aqueous

* Corresponding author. Fax: +86-931-8417088; e-mail: wincaqt@ns.lzb.ac.cn.

0039-9140/99/$ - see front matter
PII: S0039-9140(98)00313-0

media as mentioned above. Therefore, stationary phases which combine the good properties of organic polymers (high pH stability) and of silica gel (optimal porosity for fast mass transfer, as well as good mechanical strength at high pressures) could be of practical interest as a new type of HPLC-packing.

Regnier [8] was the first to immobilize organic polymers by cross-linking on inorganic support materials without covalent chemical bonding to the surface. But for this synthesis one has to rely on the properties of the prepolymer, which has to be photolytically immobilized. In 1996, Engelhardt [9] reported a newly synthesized weak cation-exchanger with acrylic acid coated vinyl silica, which combined the advantages of both the chemical bonding and coating silica.

In this paper, the silica was modified with methylvinyldiethoxysilane, the vinyl silica was encapsulated with chloromethylstyrene and then quaternized with *N*,*N*-dimethylbenzylamine. The resulting phases exhibit superior chromatographic properties in anion-exchange process. The use of these phases for the separation of some groups of anions and organic acids is well accepted in HPLC.

2. Experimental

2.1. Reagents

Micro silica beads, 6 μm, specific surface area 100 $m^2\ g^{-1}$ (BET method), mean pore size 6.7 nm (Hg intrusion method), were prepared in this laboratory. Chloromethylstyrene was obtained from Acros Organic Reagent (USA). Other reagents used in experiment were analytical pure. The mobile phases were prepared with deionized water.

2.2. Chromatography and equipment

HPLC was performed with a Waters High Performance Liquid Chromatograph fitted with a 150 × 4.6 mm i.d. stainless steel column of which the stationary phase was slurried in CCl_4: dioxane (3:2) and packed at 37 MPa with *n*-C_6 as eluent. The detection of the anions and organic acids was performed with a Sichuan SY-221 DDJ-01 conductivity detector. The separation of sulfonic acids and the petroleum sulfonates were performed on a HP 1090 High Performance Liquid Chromatograph with UV detection at 280 nm. 10 μl volume loop was used for sample injection.

2.3. Preparation of the SAX

In order to increase the bonding strength of chloromethylstyrene on the silica surface and thus to enhance the stability of the stationary phase, the synthesis of the SAX includes the modification of the support with an unsaturated reagent (methylvinyldiethoxysilane) as a first step, and subsequent polymerization of the monomer on the modified surface. Firstly, this pretreatment can make the surface of silica more favorable for the adsorption of monomers. Secondly, unsaturated groups on the surface can also take part in the polymerization and thus be introduced into the polymer chains. In such a way, the polymer layer is chemically bound to the surface of silica. Thus these SAX have superior stability. Table 1 shows the carbon and nitrogen contents of two SAX prepared under different conditions.

2.3.1. Modification of the silica beads [10,11]

The pretreated silica beads were heated under reflux in a toluene solution of methylvinyldiethoxysilane for 10 h. The mixture was centrifugalized, and the beads were washed consecutively with toluene and acetone to remove unreacted silane and then dried. The carbon content of bonded silica (MVDS) was 1.9–2.2%

Table 1
The results of carbon and nitrogen contents of different SAX[a,b,c]

	C (%)	N (%)	Q_0 (mmol g^{-1})
SAX-I	3.42	0.16	0.11
SAX-II	4.20	0.22	0.22

[a] Q_0, Theoretical specific capacity (mmol g^{-1}).
[b] $Q_0 = 10N/14$ (mmol g^{-1}).
[c] N, Nitrogen content of SAX (%).

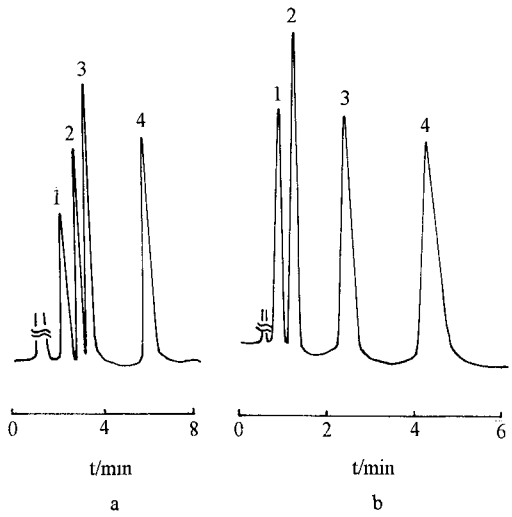

Fig. 1. Separation of some anions. Chromatographic conditions: stationary phase, SAX-I; conductivity detection; flow-rate, 2.0 ml min^{-1}. (a) Mobile phase, 0.75 mmol l^{-1} potassium hydrogen phthalate. 1. NO_2^-; 2. NO_3^-; 3. I^-; 4. SO_4^{2-}. (b) Mobile phase, 0.3 mmol l^{-1} sodium benzoate: 1. Cl^-; 2. Br^-; 3. NO_3^-; 4. I^-.

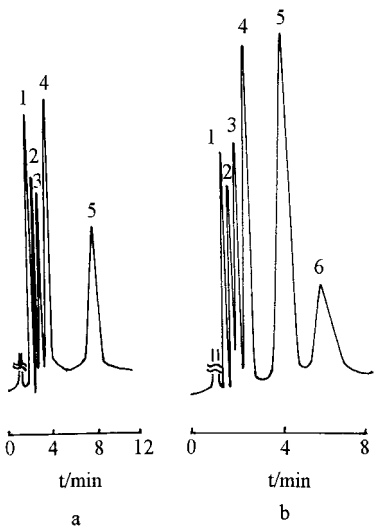

Fig. 2. Separation of some anions. Chromatographic conditions: stationary phase, SAX-II; conductivity detection; flow-rate, 2.0 ml min^{-1}. (a) Mobile phase, 0.5 mmol l^{-1} potassium hydrogen phthalate—0.5 mmol l^{-1} sodium citrate. 1. Cl^-; 2. NO_2^-; 3. Br^-; 4. NO_3^-; 5. SO_4^{2-}. (b) Mobile phase, 1.0 mmol l^{-1} potassium hydrogen phthalate—0.5 mmol l^{-1} sodium citrate. 1. Cl^-; 2. NO_2^-; 3. Br^-; 4. NO_3^-; 5. SO_4^{2-}; 6. I^-.

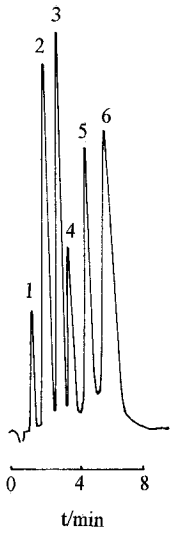

Fig. 3. Separation of organic acids. Chromatographic conditions: stationary phase, SAX-II; conductivity detection; flow-rate, 2.0 ml min^{-1}; mobile phase: 0.5 mmol l^{-1} potassium hydrogen phthalate (pH, 5.4). 1. Formic acid; 2. acetic acid; 3. propanoic acid; 4. butyric acid; 5. pentanoic acid; 6. hexanoic acid.

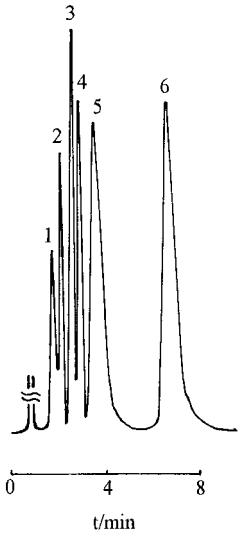

Fig. 4. Separation of a mixture of organic acids and anions. Mobile phase: 2.0 mmol l^{-1} potassium hydrogen phthalate, other chromatographic conditions are the same as that in Fig. 3. 1. Formic acid; 2. acetic acid; 3. Cl^-; 4. NO_2^-; 5. Br^-; 6. NO_3^-.

2.3.2. Encapsulation of the chloromethylstyrene

The MVDS were heated for 8 h under reflux in a toluene solution which consisted of chloromethylstyrene (distilled under vacuum condition) and 5% benzyl peroxide (relative to the volume of chloromethylstyrene). The encapsulation products were formed by copolymerization of the ethylene groups on the silica surface with chloromethylstyrene. This product was washed with toluene. The encapsulations with different carbon contents were obtained by varying the ratio of the amounts of modified beads and chloromethylstyrene. This reaction is shown below.

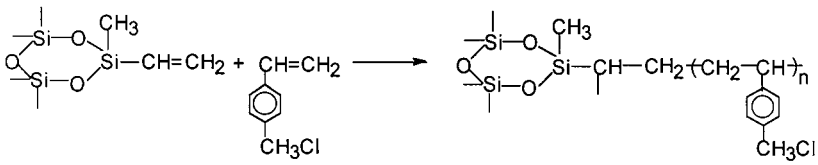

2.3.3. Quaternization of the N,N-dimethylbenzylamine

5 g encapsulation products were heated for 6 h under reflux in a toluene solution which contained 2.5 ml *N*,*N*-dimethylbenzylamine. Thus the quaternary ammonium chloride products were obtained. These products were washed with toluene and dioxane to remove unreacted reactants. Strong anion exchangers (SAX) with different ion-exchange capacity were thus obtained (see Table 1). This reaction process is shown:

Table 2
Elemental analysis results of the exchanger SAX-II

	C (%)	N (%)
Before use	4.20	0.22
After 3 months service	4.12	0.21

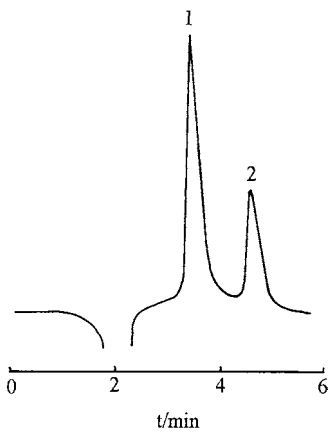

Fig. 5. Separation of sulfonic acids mobile phase, 0.125 mol l^{-1} sodium phosphate monobasic-methanol (60/40%,v/v); flow-rate, 1.0 ml min^{-1}; ultraviolet detection at 254 nm; other chromatographic conditions are the same as that in Fig. 3. 1. *p*-toluene sulfonic acid; 2. naphthalene-1,5-disulfonic acid.

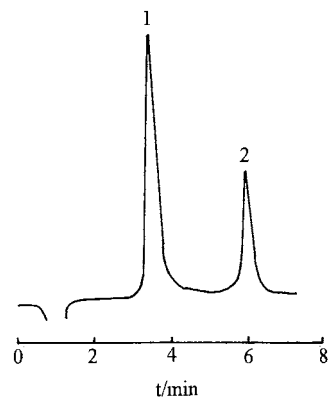

Fig. 6. Separation of petroleum mono- and di- sulfonates in Yumen sample. Mobile phase, A: methanol-water 60/40%, v/v; B: 0.125 mol l^{-1} sodium phosphate monobasic-methanol (60/40%, v/v). The sample is first eluted with 100% A for 1 min, then the eluent linearly changes to 100% B within 1 min, then the sample is continuously eluted with 100%B for 6 min); flow-rate, 1.0 ml min^{-1}; ultraviolet detection at 254 nm; flow-rate, 1.0 ml min^{-1}; other chromatographic conditions are the same as that in Fig. 3. 1. Petroleum mono-sulfonate; 2. petroleum di- sulfonate).

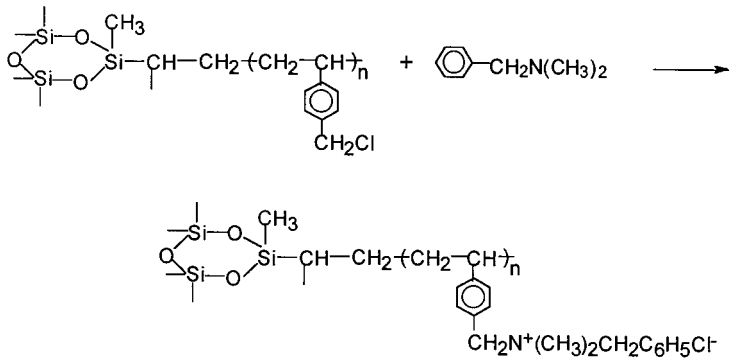

3. Results and discussion

3.1. Chromatography

3.1.1. Separation of anions

Using strong anion exchanger SAX-I, the baseline separation of anions such as NO_2^-, NO_3^-, I^-, SO_4^{2-} can be obtained with 0.75 mmol l^{-1} potassium hydrogen phthalate as mobile phase (see Fig. 1a, N m^{-1} of $SO_4^{2-} = 9970$). The retention time of solutes is decreased with the increase in the concentration of potassium hydrogen phthalate. Fig. 1b shows the separation of Cl^-, Br^-, NO_3^-, I^- with 0.3 mmol l^{-1} sodium benzoate as mobile phase. If the coating thickness of quaternary ammonium chloride is enhanced, the ion-exchange capacity would be increased, and anion exchanger SAX-II was obtained, with which the separation of six anions was presented in Fig. 2a. If the concentration of potassium hydrogen phthalate in mobile phase is increased, the iodine ion can also be separated under the same condition (see Fig. 2b).

3.1.2. Separation of some organic acids

Using strong anion-exchanger SAX-II, the separation of some organic acids can be obtained in 8 minutes with 0.5 mmol l^{-1} potassium hydrogen phthalate as mobile phase (see Fig. 3).

3.1.3. Separation of the mixture of inorganic anions and organic acids

Using strong anion-exchanger SAX-II, the separation of formic acid, acetic acid, Cl^-, NO_2^-, Br^-, NO_3^- was obtained in 8 min with 2.0 mmol l^- potassium hydrogen phthalate as mobile phase (Fig. 4).

3.2. Application

As a kind of surface active agent, petroleum sulfonates are widely used as oil-displacing agent. The oil-displacing effect and the wastage during adsorption process are relative to the kind of sulfonates. So the separation of petroleum sulfonates is important. An ion chromatographic method for fast separation and analysis of petroleum sulfonates has been established by Chen et al. [12]. Chloromethylstyrene encapsulated silica

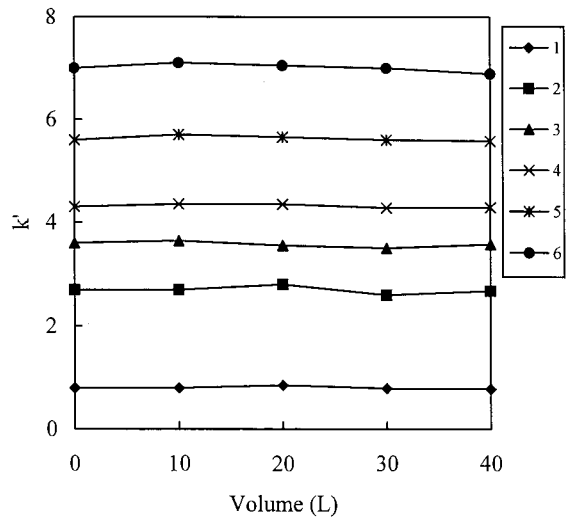

Fig. 7. Stability test. Conditions are the same as that in Fig. 4. 1. Formic acid; 2. acetic acid; 3. Cl^-; 4. NO_2^-; 5. Br^-; 6. NO_3^-.

(SAX) has good ability for the separation of sulfonates. Fig. 5 shows the separation of p-toluene sulfonic acid and naphthalene-1,5-disulfonic acid. The application, the separation of the petroleum sulfonates sample from Yumen oil field, was dipicted in Fig. 6.

3.3. Stability

Elemental analysis of the encapsulated phase was performed with a vario EL Elemental Analyzer (Germany) before and after 3 months use (passage of 40 l of 2 mmol l^{-1} potassium hydrogen phthalate). The results are shown in Table 2, the standard deviation was 0.3%. It is clear that there was no fundamental difference between C and N contents before and after three months service. As is apparent from Fig. 7 the retention of solutes remained constant during operation, demonstrating the high stability of the exchanger.

References

[1] A. Sugii, K. Harada, N. Ogawa, J. Chromatogr. 354 (1986) 211.
[2] A. Sugii, N. Ogawa, K. Harada, J. Chromatogr. 294 (1984) 185.
[3] D.T. Gjerde, J.S. Fritz, G. Schmuckler, J. Chromatogr. 186 (1979) 509.
[4] J.S. Fritz, D.T. Gjerde, B.M. Becker, Anal. Chem. 52 (1980) 1519.
[5] W. Jost, K.K. Unger, R. Lipecky, H.G. Gassen, J. Chromatogr. 185 (1979) 403.
[6] X.J. Zuo, L.R. Chen, W.L. Yu, Chin. J. Chromatogr. 10 (1992) 297.
[7] M. Gimpel, K.K. Unger, Chromatographia 16 (1982) 117.
[8] J. Alpert, F.E. Regnier, J. Chromatogr. 185 (1980) 375.
[9] F. Steiner, C. Niederländer, H. Engelhardt, Chromatographia 43 (1996) 117.
[10] S.X. Jiang, R.Q. Yang, L.R. Chen, Chromatographia 44 (1997) 263.
[11] R.Q. Yang, S.X. Jiang, L.R. Chen, J. Liq. Chromatogr. (1998) (In press).
[12] S.X. Jiang, L.R. Chen, M.F. Zhao, F.Y. Sun, Chin. J. Anal. Chem. 20 (1992) 677.

ELSEVIER

Talanta 48 (1999) 1051–1060

Talanta

Determination of nickel, chromium and cobalt in wheat flour using slurry sampling electrothermal atomic absorption spectrometry

Mar González, Mercedes Gallego, Miguel Valcárcel *

Department of Analytical Chemistry, Faculty of Sciences, University of Córdoba, E-14004 Córdoba, Spain

Received 3 June 1998; received in revised form 29 September 1998; accepted 2 October 1998

Abstract

The slurry technique was applied to the determination of Ni, Cr and Co in wheat flour by electrothermal atomic absorption spectrometry (ETAAS). The influence of the graphite furnace temperature programme was optimized. Optimum sensitivity was obtained by using a mixture of 15% HNO_3–10% H_2O_2 as suspended medium for a 3% w/v slurry in the determination of Ni; lower concentrations of HNO_3 were necessary for the determination of Co and Cr (viz. 5 and 10%). The precision of direct analyses of the slurries was improved by using mechanical agitation between measurements; thus, the RSD of the measurements was ca. 5% for repeatability. The direct slurry sampling (SS) technique is suitable for the determination of Ni and Cr in wheat flour samples at levels of 150–450 and 30–72 ng g^{-1}, respectively, as it provides results similar to those obtained by ashing the sample. However, the typically low level of Co in these samples precluded its determination by the proposed method (the study was made in an SRM spiked wholemeal flour), at least in those samples that were contaminated with elevated concentrations of the metal (viz. more than 90 ng of Co per g of flour). The method provides a relative standard deviation of 6, 8, and 4% for Ni, Cr, and Co, respectively.

Keywords: Electrothermal atomic absorption spectrometry; Slurry sampling; Wheat flour; Nickel; Chromium; Cobalt

1. Introduction

Cereal flours are staple foods in most countries. Thus, wheat flour is consumed every day in bread, cake, sauces, etc. Analyses for trace element in flours are therefore important from both a nutritional and a toxicological point of view. Soil is the main vehicle by which heavy metals enter plants; in response, a European Union directive (86/278/CEE) has been issued to control the maximum allowable contents of some metals in agricultural sewage sludge [1]. The average daily intake in food for metals is well documented; for example Ni, Cr, and Co occur at very low concentrations in cereals (viz. 100–400, 20–50 and 10–20 ng g^{-1}, for Ni, Cr, and Co, respectively) [2]. While Cr, Co, and Ni have been shown to be essential

* Corresponding author. Tel.: +34-57-218614; fax: +34-57-218606; e-mail: qa1meobj@uco.es.

0039-9140/99/$ - see front matter
PII: S0039-9140(98)00317-8

for humans, the necessary levels of Ni have not been quantified.

Trace metals can be determined by using various techniques. In recent times, the ICP-MS [3] technique has gained momentum for this purpose. However, ETAAS has for some time been at most laboratories and used in many determinations of Ni, Cr, and Co. The low concentrations of Co normally found in cereals usually require preconcentration prior to the determination proper. Co in feed grains has been determined in this way following digestion [4], as has in cereals after decomposition of organic matter and extraction into a 2-nitroso-1-naphthol solution in xylene [5], or in heptan-2-one [6]. Ni in various matrices including rice flours has also been determined by ETAAS, following microwave-assisted digestion [7]; Cr in grain and cereal products require prior wet digestion [8]. Cr and Ni, in addition to other metals, were determined in wheat flour by using a graphite boat with direct Zeeman-AAS [9]. Co and Ni were determined in cereals after digestion with the $HNO_3/HClO_4$ mixture with recoveries from 87 to 104% [10]. The contents of Ni, Cr, and Co in foods including cereals on the Swedish market between 1983 and 1990 were studied by the Nordic Committee on Food Analysis; the official methodology selected for determination of different elements was dry ashing followed by ETAAS [11].

Slurry sampling (SS) ETAAS methodology, originally developed by Brady et al. [12] is by now well established and widely used in the determination of trace elements in food samples. The most attractive advantages of SS over dry or wet ashing can be summarized as follows: (i) it reduces sample pretreatment and analysis times; (ii) it minimizes contamination/loss risks; (iii) it uses a conventional sample introduction system; (iv) it ensures appropriate calibration with aqueous standards; and (v) it provides acceptable accuracy and precision. However, this technique has some disadvantages that arise essentially from non-homogeneous distribution of the trace elements in the slurry as well as differences in the chemical species under which they are present [13]. The benefits of SS were demonstrated in an international collaborative study involving 25 laboratories that was intended to assess the state of the art in the technique. Preliminary results [14] suggested that SS is mature enough for routine analyses; at a later stage, the usefulness of ultrasonic SS was evaluated [15]. The results showed that extracting analyte into the liquid phase of the slurry is not a prerequisite for accurate slurry analyses.

Slurry sampling for electrothermal atomization is a very active, widely documented area applications of which were reviewed [16]. A comprehensive review of SS for foods in atomic spectrometry has also been published [17]. Reported applications involving cereals are scant relative to other foods. Also, Co and Ni have been determined less frequently than Cr in this way. Viñas et al. used their experience in the use of slurry procedures to determine Co and Ni in vegetables and legumes [18], and Cr in vegetables [19], following treatment of dried samples with the ethanol–H_2O_2–HNO_3 mixture; in all instances, calibration was against aqueous standards. Direct slurry sampling was used to determine Ni and Co in rice by ICP-MS [20], and Cr and Ni in spinach leaves by simultaneous multi-element atomic absorption spectrometer with continuum source (SIMAAC) [21]. In the latter application, the slurry solution (5–10 mg of sample in 5 ml of 5% HNO_3) was homogenized by immersing an ultrasonic probe in the autosampler cup, which avoided settling of particles.

In this work, the potential of slurry sampling for the determination of Ni, Cr, and Co in wheat flour by ETAAS was explored. The influence of various parameters such as the drying and pyrolysis time, pyrolysis and atomization temperature, and presence of modifier on the atomic signal was studied. Efforts were aimed at using the advantages of the HNO_3–H_2O_2 mixture as the medium for sample preparation in order to transfer the analytes to the aqueous phase. The proposed method was applied to various samples with acceptable recoveries for Ni and Cr.

Table 1
Instrumental parameters and optimized furnace conditions for the determinations of Ni, Cr and Co in wheat flour[a]

	Ni			Cr			Co		
Lamp current/mA	25			10			30		
Wavelength/nm	232.0			357.9			240.7		
Bandpass/nm	0.2			0.7			0.2		
	Temperature (°C)	Ramp (s)	Hold (s)	Temperature	Ramp	Hold	Temperature	Ramp	Hold
Step									
Dry 1	100	5	15	100	5	15	100	5	15
Dry 2	300	10	30	300	10	30	300	10	30
Pyrolysis	1400	20	30	1700	20	30	1400	20	30
Atomize	2600	0	0	2600	0	6	2600	0	6
Clean	2650	1	1	2650	1	3	2650	1	3

[a] A stream of argon at 300 ml min^{-1} was used (the flow was stopped during the atomization step); injected volume, 20 μl

2. Experimental

2.1. Apparatus

Slurry samples were analysed by using a model 1100-B atomic absorption spectrometer from Perkin-Elmer (Überlingen, Germany) equipped with a deuterium-lamp background corrector, an HGA-700 graphite furnace, and an AS-70 autosampler, and interfaced to an Epson FX-850 printer. Analyses were carried out by using platforms inserted into pyrolytically coated graphite tubes (Perkin-Elmer) and measurements (integrated absorbance peak areas) were made by using single-element hollow cathode lamps (Perkin-Elmer). Argon was used as sheeting gas for the furnace in all cases. The operational parameters recommended by the manufacturer for Ni, Cr, and Co are listed in Table 1. Slurries were homogenized in an ultrasonic bath (Bandelin, Tk52, Berlin, Germany) or a vortex mixer (Heidolph, Kelheim, Germany).

2.2. Reagents

Working metal standards were prepared daily from a 1000 mg l^{-1} stock metal solution (Panreac, Barcelona, Spain) by diluting appropriate aliquots with 0.2% HNO_3. A 10.0 g l^{-1} solution of magnesium nitrate (Merck, Darmstadt, Germany) was used as matrix modifier. Triton X-100 (Serva Feinbiochemica, Heidelberg, Germany) was tested as stabilizing agent.

2.3. Certified reference material

SRM wholemeal flour no. 189, with reference contents (non-certified values) for Ni and Cr obtained from the European Commission (Belgium) was dried to constant mass in an oven at 103°C as per the supplier's recommendations, and used for method validation. Because the Co concentration in this reference material was too low for its determination by the slurry sampling technique, the material was spiked with this metal from an aqueous salt solution. For this purpose, 40 ml of a solution containing 250 ng ml^{-1} Co was added to 20.0 g of the SRM. The slurry thus obtained was dried at room temperature for 2 weeks in a closed fume hood to avoid contamination and then to constant mass in an oven at 103°C. The wholemeal flour spiked with 500 ng of cobalt per g of sample was employed to optimize the cobalt determination in this matrix.

2.4. Sample preparation

Flour samples were prepared at a pilot plant from wheat produce in different Spanish locations. An amount of 0.5–1 kg of wheat contain-

ing ca. 15% w/w of water was ground in a metal rolling mill to obtain 60% of white flour and 40% of byproducts. The flour was screened with a 130 μm sieve. All other samples were purchased at a local supermarket.

2.5. Procedures

In order to avoid contamination, all polytetrafluoroethylene (PTFE) materials, pipettes, and calibrated flasks were immersed in freshly made 10% HNO_3 for 24 h and then rinsed thoroughly with high purity water (Milli-Q Water System, Millipore, Madrid, Spain) before use.

For slurry analyses, reference and sample materials were accurately weighed (ca. 150 mg) into PTFE tubes and supplied with 5 ml of 15% HNO_3 containing 10% v/v H_2O_2. Slurries (3% w/v, i.e. 3 g into 100 ml) were homogenized by agitating for 15 min in an ultrasonic immediately before each analysis. Aliquots of 2 ml were placed in the 2 ml polyethylene vials of the autosampler; between measurements, samples were mixed in a vortex shaker for 5 s in order to ensure reproducible results using autosampler cups provided with covers. Five sample replicates were analysed in each case. The sample blanks contained the same concentration of nitric acid and hydrogen peroxide as the slurry samples. Calibration graphs (spanning the range 0–20 $\mu g\ l^{-1}$ for Cr, 0–40 $\mu g\ l^{-1}$ for Co, and 0–50 $\mu g\ l^{-1}$ for Ni) were obtained from variable volumes of standard solutions containing 30, 40, and 50 $\mu g\ l^{-1}$ Cr, Co, and Ni, respectively, that were mixed in the graphite tube with appropriate amounts of 0.2% HNO_3 to a volume of 20 μl; 20 μl of 0.2% HNO_3 was used as blank.

For mineralization of the flours, 3.0 g of material was accurately weighed into a platinum crucible and carbonized in a burner at a low temperature for about 3 h; then, the black residue was supplied with several drops of concentrated H_2O_2 and ashed in a muffle furnace at 600–650 °C for 2 h. The completely ashed sample obtained was dissolved in 10 ml of 0.5% HNO_3; three sample replicates and four injections per replicate were analysed. Cr and Co were measured directly, whereas Ni required ten-fold dilution in 0.2% HNO_3.

3. Results and discussion

The different factors that influence the performance of slurry ETAAS have been comprehensively examined by several authors [14–17,22–25]. Slurry introduction has been found to pose some problems related to concentration and particle size, which influence stability, deposition and atomization efficiency; these in turn may affect the accuracy and precision of analyses. Ensuring accurate results and good reproducibility in this context entails using homogeneous slurries; mechanical mixing devices, gas bubbling, and ultrasonic agitation has proved useful for this purpose [23]. Thus, Miller-Ihli [26] designed an ultrasonic, pneumatically movable slurry sampler and, more recently, López-García et al. [27] based on previous experiments of other authors [23], developed an efficient slurry sampling device that uses argon bubbles to homogenize slurries in the autosampler cups without the need to alter the instrument operation.

3.1. Furnace temperature programs and chemical modifiers

The temperature programs and the effect of using magnesium nitrate as modifier on both standards and slurries were carefully examined. The SRM whole meal flour spiked with 0.5 μg of cobalt per g was the sample used in this study. In all instances, slurries of 3% w/v were prepared in 15% HNO_3 containing 10% H_2O_2. A 15 μl volume of standard/slurry and 5 μl of chemical modifier (10 g l^{-1} magnesium nitrate) were injected into the pyrolytic graphite tube with platform. Two drying steps were required to ensure mild, totally dry conditions for the sample, and no splattering; the slurry sample required higher temperatures (100 and 300°C) than the standard (100 and 140°C).

3.1.1. Nickel

The pyrolysis and atomization temperatures were tested, in the absence of chemical modifier, over the ranges 500–1900°C, and 1900–2650°C, respectively. At a constant atomization temperature of 2600°C, the pyrolysis temperature did not

affect the signal for the standard (10 μg l^{-1} Ni) up to 1500°C; on the other hand, the optimum pyrolysis temperature for the slurry sample was 1400°C. A similar behavior was observed with magnesium nitrate as modifier. Peak areas increased with increasing atomization temperature up to 2600°C, both for the standard and for the sample. As can be seen in Fig. 1A, the background signal for the slurry sample decreased at high atomization temperatures. On the other hand, the use of magnesium nitrate at the optimum atomization temperature (2600°C) increased of background signal for the slurry sample (see Fig. 1A). Although this modifier is recommended for the determination of nickel in different matrices, its use in this case stabilized a higher proportion to the concomitants. Based on these considerations, the pyrolysis and atomization temperature were fixed at 1400°C and 2600°C, respectively, and no chemical modifier was employed for this element.

3.1.2. Cobalt

The pyrolysis temperature had no effect on the determination of the standard (10 μg l^{-1} Co) neither on the spiked slurry whole meal over the range 800–1400°C. As no cobalt was lost up to 1400°C, this temperature was fixed while the atomization temperature was changed. The best results were obtained at an atomization temperature of 2600°C. The use of magnesium nitrate as modifier provided no advantages for the whole meal slurry sample (the background signal was ca. 0.050 A s with and without modifier); on the other hand, the modifier increased the background signal for the standard solution two-fold (which was 0.060 and 0.120 A s in its absence and presence, respectively). In order to facilitate reliable deuterium background correction, use of the modifier was discarded.

3.1.3. Chromium

The maximum pyrolysis temperature was the same with and without modifier, 1700°C, for both the standard solution (5 μg l^{-1} Cr) and the slurry (3% whole meal in the HNO_3–H_2O_2 mixture). Moreover, the addition of 50 μg of magnesium nitrate increased slightly both the atomic absorption and background signals, so its presence it provided no advantage. As can be seen from Fig. 1B, better separation of atomic and background signals was obtained in the absence of this modifier.

On the other hand the addition of 5 μl of palladium nitrate (1.0 g l^{-1}) to the slurry sample provided results similar to those obtained with magnesium nitrate for the three elements studied. Therefore, the temperature programs listed in Table 1 were employed for standards and slurries (prepared in the HNO_3–H_2O_2 mixture), with no chemical modifier.

3.2. Optimization of the slurry preparation

The factors potentially influencing the accuracy and precision of the analytical results were studied, namely suspension medium, the homogenization and stability of the slurry, and slurry concentration (% w/v) were examined in order to optimize preparation of the slurries. The effect of the slurry particle size was not studied as all flours were finely powdered (less than 130 μm), which is similar to the SRM whole meal flour (less than 125 μm).

The slurries of SRM whole meal flour spiked with cobalt, at 3% w/v, were prepared at variable HNO_3 concentrations (0–20% v/v) and contained 10% H_2O_2. Agitation for 5 min in a vortex mixer was needed to homogenize the slurry before it was transferred into the autosampler cup and 20 μl was injected into the graphite furnace. As can be seen in Fig. 2, the nitric acid concentration had a marked effect on the Ni signal, and somewhat lesser effects on the Cr and Co signals. A concentration of nitric acid of 5%, 10%, and 20% for Co, Cr, and Ni, respectively, was needed to favor the extraction of the analytes into solution. The determination of Cr and Co required no addition of H_2O_2 to the slurry sample when prepared in 10% HNO_3; however, that of Ni required 10% H_2O_2 and high nitric acid concentration (20%). The higher nitric acid concentration required for the determination of Ni can be explained probably because Co and Cr are extracted more efficiently into the liquid phase than is Ni or because these elements are more efficiently determined in the

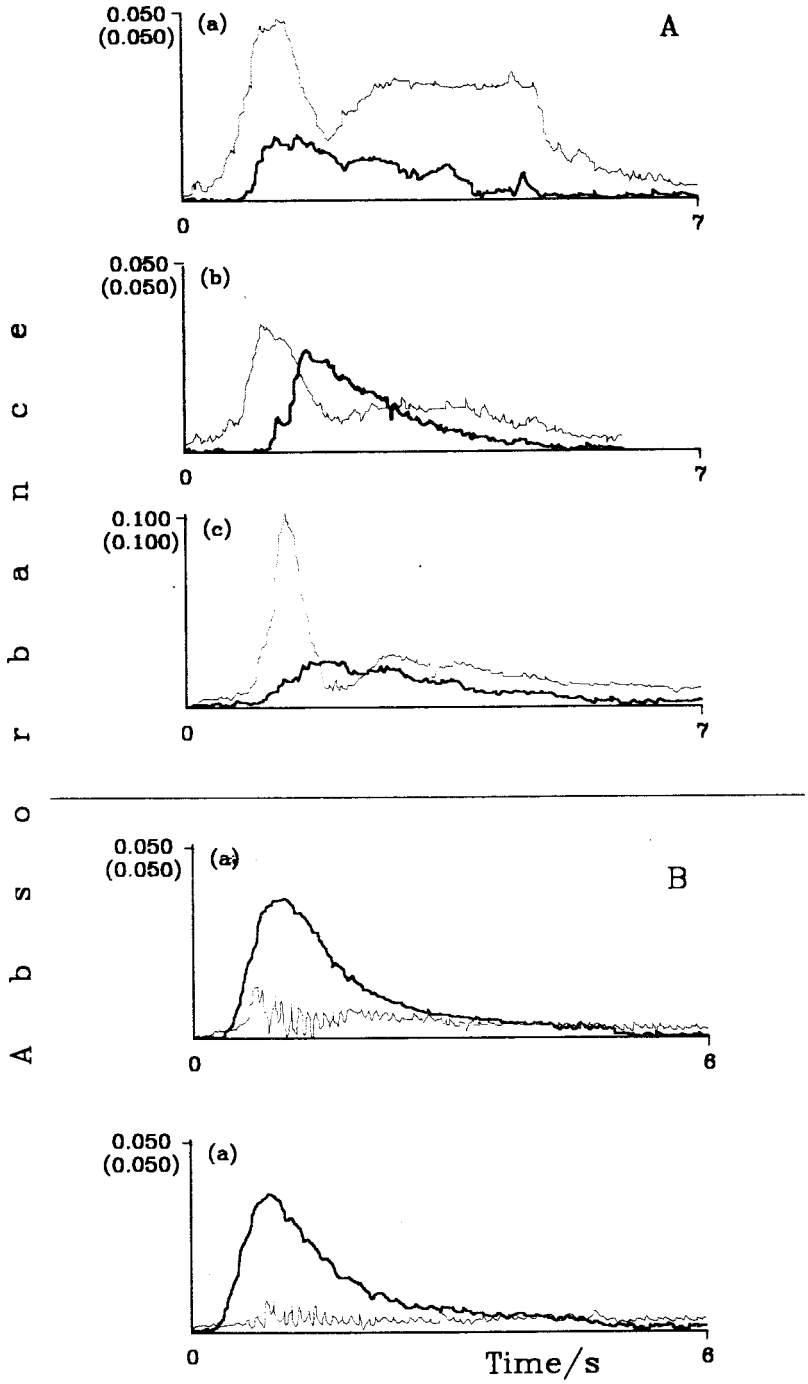

Fig. 1. Atomic absorption profile and background lines for Ni (A) and Cr (B) in SRM wholemeal slurry samples (3% w/v in 15% HNO_3 containing 10% H_2O_2). A, Ni determination (pyrolysis temperature, 1400°C): (a) and (b) in the absence of chemical modifier, at an atomization temperature of 2250°C and 2600°C (background signals, 0.154 and 0.071 A s, respectively); and (c) in the presence of 50 μg of $Mg(NO_3)_2$, at a atomization temperature of 2600°C (background signal, 0.122 A s). B, Cr determination with $Mg(NO_3)_2$ (a) and without chemical modifier (b) (pyrolysis and atomization temperature, 1700°C and 2600°C, respectively). Solid and dashed lines represent atomic and background signals, respectively. Injected slurry volume, 15 and 20 μl for Ni and Cr, respectively.

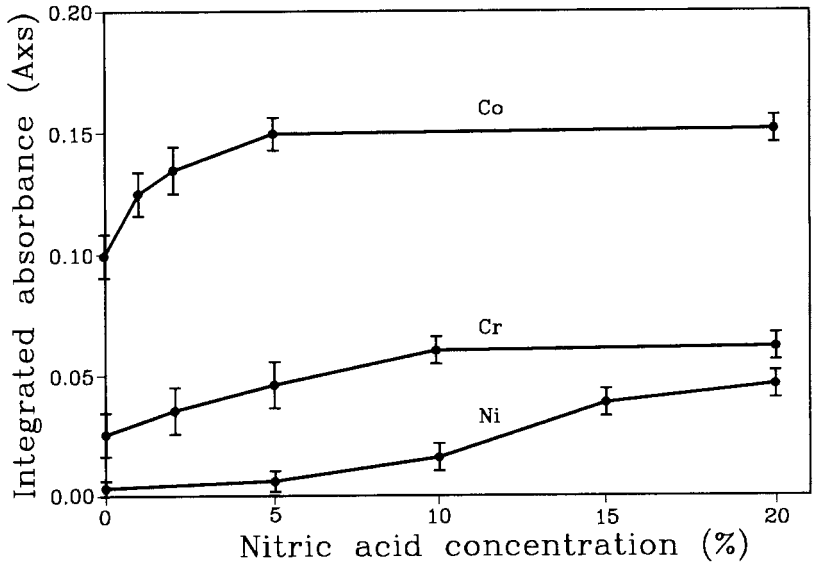

Fig. 2. Effect of the concentration of the nitric acid as the medium used to prepare the slurry of SRM wholemeal flour spiked with cobalt. All slurries also contained 10% H_2O_2.

solid phase than is Ni. In order to decrease the high nitric acid concentration (20% v/v) required by the Ni determination, the effectiveness of ultrasonic and mechanical (vortex) agitation for slurry homogenization was studied. For this purpose, various samples of 3% w/v SRM whole meal spiked flour slurry were prepared in a medium containing 15% HNO_3 plus 10% H_2O_2 for all of the elements. The slurries were shaken in a vortex mixer or an ultrasonic bath for 1–30 min. Both homogenization devices required at least 15 min to ensure stabilization of integrated absorbance average values ($n=3$ at each time). However, ultrasonic mixing provided higher precision (RSD 6.0, 3.5, and 12.6% for Ni, Co, and Cr, respectively) than mechanical stirring (RSD 7.5, 6.5, and 19.0%, respectively). As Cr detection was scarcely precise, Triton X-100 was tested as a stabilizing agent.

Thus, several samples of 3% w/v whole meal flour slurry (in 15% HNO_3 containing 10% H_2O_2) were spiked with different amounts of surfactant from 0 to 0.5% v/v and homogenized by ultrasonication for 15 min before analysis. In the presence of Triton X-100, the sensitivity for Cr decreased gradually as the concentration of the surfactant was increased (e.g. the signal decreased by about 35% in the presence of 0.1% Triton X-100). On the other hand, the surfactant made no difference to the Ni and Co determinations. The precision, as repeatability, of Cr measurements (after homogenization in an ultrasonic bath for 15 min) was similar with and without Triton X-100 (RSD 9.8 and 12.8%, respectively). Such low precision can be ascribed to rapid deposition of the slurry in the bottom of the autosampler cup; probably, a portion of the Cr present remained in the solid phase and required introducing the solid particles into the platform and hence homogenizing slurry. The repeatability can be raised to 7.5% with mechanical mixing of the autosampler cup contents between measurements.

The slurry concentration is a critical variable in the proposed method owing to the differential concentration levels of these elements in flour samples and their sensitivities (e.g. Ni is present in these matrices at the $\mu g\ g^{-1}$ level, whereas Co and Cr occur at the $ng\ g^{-1}$ level). The effect of variable slurry concentrations on sensitivity and precision was investigated by using the spiked SRM sample. Based on reported facts [29], concentrations above 5% may result in inefficient

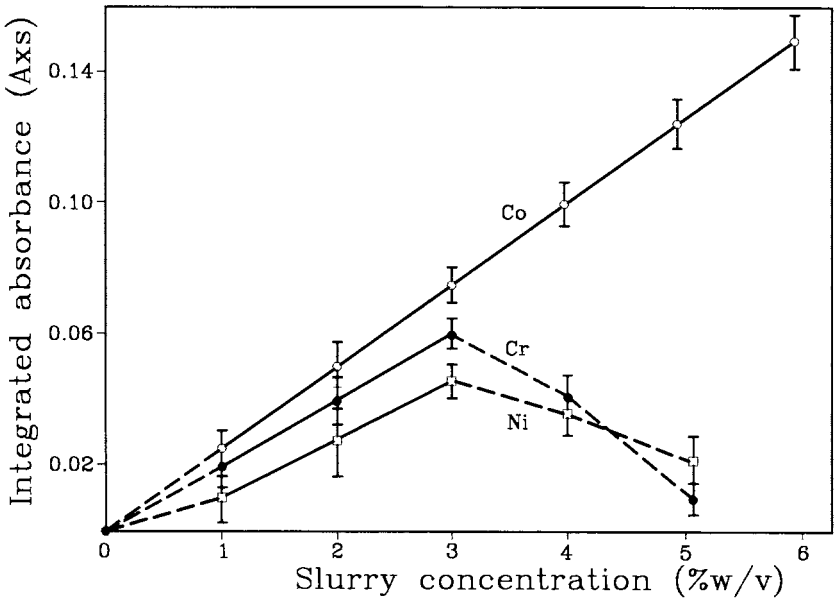

Fig. 3. Effect of slurry concentration (% w/v) for a SRM wholemeal flour spiked with cobalt on the integrated absorbance signal in the determination of Co, Cr, and Ni by slurry sampling. Solid line, working range. Injected slurry volume, 20 μl (10 μl for cobalt).

pipetting of the slurry aliquot; the problem worsens with several matrices as a result of particles settling too early, which affects both the accuracy and the precision. Fig. 3 shows the influence of the slurry concentration in the whole meal flour sample spiked with cobalt on the integrated absorbance for Co, Cr, and Ni. A linear response was obtained for Co throughout the range studied (1–6%); on the other hand, this variable was critical for Ni and Cr. The wide range for Co can be ascribed to the fact that it was spiked to the whole meal flour, so it was more readily extracted from the liquid phase than were Ni and Cr. However, the results obtained for the three elements in slurries of vegetables and SRM materials to which no Co was added were similar [28]. As expected, the precision suffered when using highly diluted slurries because only a small number of particles was sampled. Increased slurry concentrations led to more marked matrix effects and to more pronounced deterioration of sensitivity for Ni and Cr.

From the experiments described above it can be concluded that the determination of Ni in this matrix requires a higher HNO_3 concentration (as medium composition) than do Co and Cr, probably because the determination of the former is more favorable in the liquid phase than in the solid phase. The determination of Cr is more markedly affected by the slurry homogeneity than by the HNO_3 concentration, probably because Cr can be determined in the solid particle and is easily released with no occlusion of the solid matrix. In order to sequentially determine the three elements in the same sample, the optimum conditions for Ni were selected. It should be noted that the main problem encountered in the atomization of biological slurries is that carbonaceous residues build up inside the platform owing to incomplete ashing of the organic matrix. In this respect, the HNO_3–H_2O_2 mixture acts as an oxidant modifier [19,28] that allows one to dispense with conventional chemical modifiers (e.g. Mg and Pd). Therefore, sample slurries were prepared at concentrations between 1 and 3% w/v in a 15% HNO_3–10% H_2O_2 medium, and homogenized by ultrasonication for 15 min; in this medium the slurry samples remained undigested, which was visually observed by the white color of the suspension. Cr require mechanical mixing of the cup

contents between measurements. Under these conditions, the precision, as RSD, was ca. 5% for the three elements. The blank signal (15% HNO_3–10% H_2O_2 solution) was 0.006 A s.

3.3. Analytical features

The analytical figures of merit of the proposed method were established by using aqueous standards (0.2% HNO_3) and the furnace program shown in Table 1. The sensitivities (expressed as average slopes, $n=3$, of the calibration graphs) were 0.24 ± 0.02, 0.51 ± 0.03, and 1.35 ± 0.05 A s ng^{-1} for Ni, Co, and Cr, respectively. In order to compare the slopes of the calibration and standard addition graphs for slurries of SRM whole meal flour spiked with Co, the *t*-test was applied. No significant differences at a confidence level of 95% between the slopes of the additions and calibration graphs for the three elements were found, which suggests that both calibrations were statistically similar. The absence of significant matrix effects affords direct calibration with aqueous standards when using sample blank.

The detection limits (calculated as three times the standard deviation of the signals obtained from 15 sample blanks) were 44, 30, and 23 ng g^{-1} (for a 3% slurry sample) for Ni, Co, and Cr, respectively. The characteristic masses, based on integrated absorbances (amounts, in picograms, providing a signal of 0.0044 A s), were 21, 9, and 4 for Ni, Co, and Cr, respectively.

3.4. Analysis of slurried flour samples

Only the concentrations of Ni and Cr in the SRM whole meal flour were stated by the supplier. In addition, the rather low cobalt concentration in this sample (ca. 8 ng g^{-1}) entailed preparing highly concentrated slurries (ca. 25% w/v) that gave high background signals and poor analytical results, and made pipetting cumbersome. Consequently, as stated under Section 2, the reference material was spiked with Co at an elevated level (viz. 500 ng g^{-1}). The reliability of the proposed slurry method was checked by analyzing five individual SRM whole meal flour samples in triplicate, as well as a wheat flour 1 sample, and comparing the results with those for samples digested by dry ashing. As can be seen in Table 2, the results obtained for Ni and Cr with the slurry procedure and by dry ashing in both samples were quite consistent; also the Co recovery from the spiked SRM sample was near 100%. Therefore, the proposed slurry method is fairly accurate and can be used to determine these elements in similar samples. Table 2 summarizes the results for Ni and Cr in slurried flours (3% w/v); the concentration of Co in all samples was below the detection limit. Aqueous standards for calibration graphs and sample blanks were employed. The metal levels found in all samples were lower than their tolerated limits in foods. It should be noted that the highest Ni and Cr levels were obtained in the chick-pea flour. Flours containing Ni and Cr at concentrations below 200 and 40 ng g^{-1}, respectively, were also determined, using the

Table 2
Analysis of wheat and legume flours by direct slurry sampling[a]

Sample	Element	Dry ashing ($n=3$)	Direct slurry ($n=5$)
Whole meal flour (SRM No. 189)	Ni	347 ± 15 (380)[b]	355 ± 15
	Cr	62 ± 4 (57–76)[b]	65 ± 4
	Co	8 ± 1	—
	Co[c]	—	500 ± 20
Wheat flour 1	Ni	200 ± 10	205 ± 15
	Cr	70 ± 4	62 ± 5
	Co	20 ± 1	—
	Ni	Cr	
Wheat flour 2	160 ± 10	30 ± 2	
Wheat flour 3	280 ± 20	46 ± 2	
Wheat flour 4	230 ± 15	36 ± 2	
Wheat flour 5	255 ± 20	43 ± 5	
Wheat flour 6	208 ± 15	35 ± 3	
Wheat flour 7	210 ± 15	40 ± 2	
Corn flour	150 ± 10	34 ± 4	
Chick-pea flour	450 ± 30	72 ± 6	

[a] Concentrations expressed in ng $g^{-1} \pm$ S.
[b] Non-certified value.
[c] SRM No. 189 spiked with 500 ng of Co per g

standard additions method, which provided concentrations similar to those of the direct method.

References

[1] Council Directive of June 12, On the protection of the environment, and in particular of the soil, when sewage sludge is used in agriculture, Official J. EC L 181/6–12, Brussels, 1986.
[2] A. Kabata-Pendias, H. Pendias, Trace Elements in Soils and Plants, 2nd ed., CRC Press, Boca Raton, FL, 1992.
[3] C.J. Park, J.K. Suh, J. Anal. At. Spectrom. 12 (1997) 573.
[4] Z. Wu, Z. Wu, Fenxi-Huaxue 16 (1988) 710.
[5] O.K. Borggaard, H.E.M. Christensen, S.P. Lund, Analyst 109 (1984) 1179.
[6] W.J. Blanchflower, A. Cannavan, D.G. Kennedy, Analyst 115 (1990) 1323.
[7] R. Chakraborty, A.K. Das, Anal. Lett. 30 (1997) 283.
[8] M. Plessi, A. Monzani, J. Assoc. Off. Anal. Chem. 73 (1990) 798.
[9] A. Rosopulo, K.H. Grobecker, U. Kurfuerst, Fresenius J. Anal. Chem. 319 (1984) 540.
[10] Y. Zhang, J.H. Pan, Guangpuxue Yu Guangpu Fenxi 17 (1997) 94.
[11] L. Jorhem, B. Sundstrom, J. Food Compos. Anal. 6 (1993) 223.
[12] D.V. Brady, J.G. Montalvo, J. Jung, R.A. Curran, At. Absorpt. Newsl. 13 (1974) 118.
[13] V.I. Slaveykova, M. Hoenig, Analyst 122 (1997) 337.
[14] N.J. Miller-Ihli, Spectrochim. Acta 50 (Part B) (1995) 477.
[15] N.J. Miller-Ihli, J. Anal. At. Spectrom. 12 (1997) 205.
[16] Atomic Spectrometry Update, J. Anal. At. Spectrom. 12 (1997) 119R and 327R.
[17] M.A.Z. Arruda, M. Gallego, M. Valcárcel, Quím. Anal. 14 (1995) 17.
[18] P. Viñas, N. Campillo, I. López-García, M. Hernández-Córdoba, At. Spectrosc. 16 (1995) 86.
[19] P. Viñas, N. Campillo, I. López-García, M. Hernández-Córdoba, Talanta 42 (1995) 527.
[20] T. Mochizuki, A. Sakashita, H. Iwata, Y. Ishibashi, N. Gunji, Fresenius J. Anal. Chem. 339 (1991) 889.
[21] N.J. Miller-Ihli, J. Anal. At. Spectrom. 3 (1988) 73.
[22] J.A. Holcombe, V. Majidi, J. Anal. At. Spectrom. 4 (1989) 423.
[23] C. Bendicho, M.T.C. de Loos-Vollebregt, J. Anal. At. Spectrom. 6 (1991) 353.
[24] N.J. Miller-Ihli, Fresenius J. Anal. Chem. 345 (1993) 482.
[25] N.J. Miller-Ihli, J. Anal. At. Spectrom. 9 (1994) 1129.
[26] N.J. Miller-Ihli, At. Spectrosc. 13 (1992) 1.
[27] I. López-García, M. Sánchez-Merlos, M. Hernández-Córdoba, J. Anal. At. Spectrom. 12 (1997) 777.
[28] A. Carlosena, M. Gallego, M. Valcárcel, J. Anal. At. Spectrom. 12 (1997) 479.
[29] S. Lynch, D. Littlejohn, Talanta 37 (1990) 825.

ELSEVIER

Talanta 48 (1999) 1061–1073

Talanta

Stopped-flow determination of dipyridamole in pharmaceutical preparations by micellar-stabilized room temperature phosphorescence

A. Muñoz de la Peña [a,*], A. Espinosa Mansilla [a], J.A. Murillo Pulgarín [b], A. Alañón Molina [b], P. Fernández López [b]

[a] *Department of Analytical Chemistry, University of Extremadura, 06071, Badajoz, Spain*
[b] *Department of Analytical Chemistry and Foods Technology, University of Castilla La Mancha, 13071, Ciudad Real, Spain*

Received 17 July 1998; received in revised form 29 September 1998; accepted 2 October 1998

Abstract

The stopped flow mixing technique has been used to study the kinetic determination of dipyridamole by means of micellar-stabilized room temperature phosphorescence (RTP). This mixing system diminishes the time required for the deoxygenation of the micellar medium by sodium sulfite. The phosphorescence enhancers thallium (I) nitrate, sodium dodecyl sulfate (SDS), and sodium sulfite were optimized to obtain maximum sensitivity and selectivity. A pH value of 10.6 was selected as adequate for phosphorescence development. The kinetic curve of dipyridamole phosphorescence was scanned at $\lambda_{ex} = 303$ nm and $\lambda_{em} = 616$ nm. Then, the intensity at 10 s, and the maximum slope of phosphorescence development, for an interval time of 1 s, were measured. Two determination approaches: intensity and rate methods, were proposed. The calibration graphs were linear for the concentration range from 50 to 400 ng ml^{-1}. The detection limits, according to Clayton et al., Anal. Chem. 59 (1987) 2506, were 21.5 and 37.5 ng ml^{-1}, for intensity and initial rate measurements, respectively. By applying the error propagation theory, the detection limits were 19.0 and 33.0 ng ml^{-1}, for intensity and initial rate measurements, respectively. Two commercial formulations (persantin and asasantin) were analyzed by both proposed methodologies. Adequate recovery values were obtained in both cases.

Keywords: Dipyridamole; Stopped flow; Room temperature phosphorescence; Micellar medium

1. Introduction

Usually, in fluid solution, room-temperature phosphorescence (RTP) emission is too weak to be used for analytical purposes. The use of microscopically organized media allows triplet state stabilization and RTP emission. Observation of RTP in a micellar medium usually requires the presence of a heavy atom, which is placed as a counter ion outside the micelle, thus being in proximity to the hydrophobic molecules associated with the mi-

* Corresponding author. Tel.: +34-24-289378; fax: +34-24-289375; e-mail: arsenio@unex.es.

0039-9140/99/$ - see front matter
PII: S0039-9140(98)00315-4

celles. Normal micelles, mainly sodium dodecyl sulfate (SDS) [1–3] and cetyltrimethylammonium bromide (CTB) micelles [4,5] have been used in RTP analysis. Microemulsions, formed in heptane-SDS-1-pentanol have also been reported as an alternative for RTP analysis [6]. On the other hand, phosphorescence can only be observed in oxygen-free solutions, as oxygen is an effective quencher that easily penetrates into the micelles.

Several classes of polycyclic aromatic hydrocarbons (PAHs), and drug-related compounds, such as propranolol, diflunisal, naphalozine, and selected quinoline derivatives, were found to give micelle-stabilized RTP in deoxygenated solutions, by use of thallium or silver as 'external' heavy atoms [7,8].

Deoxygenation of aqueous solutions is usually performed by bubbling nitrogen through, but this procedure applied to micellar solutions is problematic owing to foam formation. Sodium sulfite was proposed for deoxygenation instead of bubbling nitrogen through the solution [9]. The technique was applied to niobium [4], and aluminium [5] determination, and was also implemented in a FIA system [10].

Several authors discussed the factors affecting micellar-stabilized RTP [11,12], and methods for the determination of several PAHs by the technique have been reported [13].

More recently, the simultaneous determination of phenanthrene and fluoranthene [14], the determination of barbital, codeine, morphine,and practalol [15], acenaphthene [16], naproxen and propranolol [17], carbaryl [18,19], 2-naphthoxyacetic acid [20], and 1-naphthalenacetamide [21] have been reported.

One of the present trends in analytical chemistry is the development of very fast automatic methods. Kinetic methodology, in combination with the stopped-flow mixing technique, is highly suitable for this purpose as it allows sample and reagent solutions to be mixed automatically and rapidly, as well as measurements to be made shortly after mixing.

The stopped-flow mixing technique and micellar stabilized RTP were recently used in combination. This approach can be used to develop kinetic determination methods by measuring the slope, or equilibrium methods by measuring the amplitude of the kinetic curves obtained. To date, only two analytical applications of the stopped-flow mixing technique in combination with RTP have been reported. Panadero et al. [22] reported for the first time on the determination of carbaryl. Later on, the same authors applied the technique to the analytical determination of naproxen [23].

The RTP determination of dipyridamol based on equilibrium measurements has been proposed, and is rather slow (the reaction involved take 15 min to reach equilibrium) [24]. In this work, the use of kinetic methodology by the stopped-flow mixing technique has been investigated to improve the dipyridamole determination method by fluid solution RTP.

Dipyridamole, a vasodilator agent, is a yellow crystalline powder, practically insoluble in water. Its solutions give a yellowish-blue fluorescence. Owing to the increase of energy production that this vasodilator can produce, it is classified in doping terms as an stimulant. Dipyridamole is widely used in medicine, but it has unfortunately a fraudulent consumption in certain sports, with the purpose of increasing efficiency and decreasing tiredness. Nevertheless, the uncontrolled used of this drug could cause the loss of mental power, and serious secondary effects which could cause grave danger for health.

2. Experimental

2.1. Apparatus

The phosphorimetric measurements were performed on an Aminco Bowman series 2 luminescence spectrometer, connected to a PC microcomputer with the AB2 software which runs on the OS2 operating system. The instrument utilizes a 7 W integral pulsed xenon lamp for phosphorescence measurements. To measure the kinetic luminescence reactions, the instrument incorporates the MilliFlow stopped flow reactor, allowing the study of changes in luminescence reactions when two reactants are vigorously forced through the mixing chamber and suddenly stopped into the observation cell.

The MilliFlow stopped flow reactor consists of two fill syringes, two drive syringes, an observation cell (path length of 2 mm), a stop syringe, a stop block and an exhaust, and a fill valve levers. Hamilton Gasting Syringes of 2.5 ml (drive syringes) were used to contain the two reactant solutions. The syringes are made from controlled, inner-diameter, borosilicate glass with precision machined teflon plunger tips (these pistons are simultaneously driven by air-operated plunger) (Scheme 1). Thermostatic equipment permits to maintain a constant temperature of 20°C into the MilliFlow stopped flow reactor. A Crison model 2001 pH meter with a glass-saturated calomel combination electrode was used to measure pH of solutions.

2.2. Software

The AB2 program allows file management, define parameters of the instrument for the acquisition, and set up the acquisition parameters to obtain excitation and emission spectra and kinetic curves. The kinetic curve processing was performed by means of the SLOPES program developed by us, which allows the linear region optimization in the kinetic curve, and fit by means of least squares regression to obtain the maximum rate of the reaction. The statistical analysis was performed by means of the LSWR program developed by us, which includes the following options: least squares regression with replicates, limits of detection assuming the error propagation theory [25,26] and by the Clayton criterium [27], linearity test of ANOVA, precision of the method by means of the confidence bands of the calibration line, homocedasticity and heterocedasticity criteria, and the true region for the slope and intercept estimates from least squares regression of the calibration line.

2.3. Reagents

All experiments were performed with analytical reagent grade chemicals, pure solvents and Milli-Q-purified water. SDS was obtained from Sigma

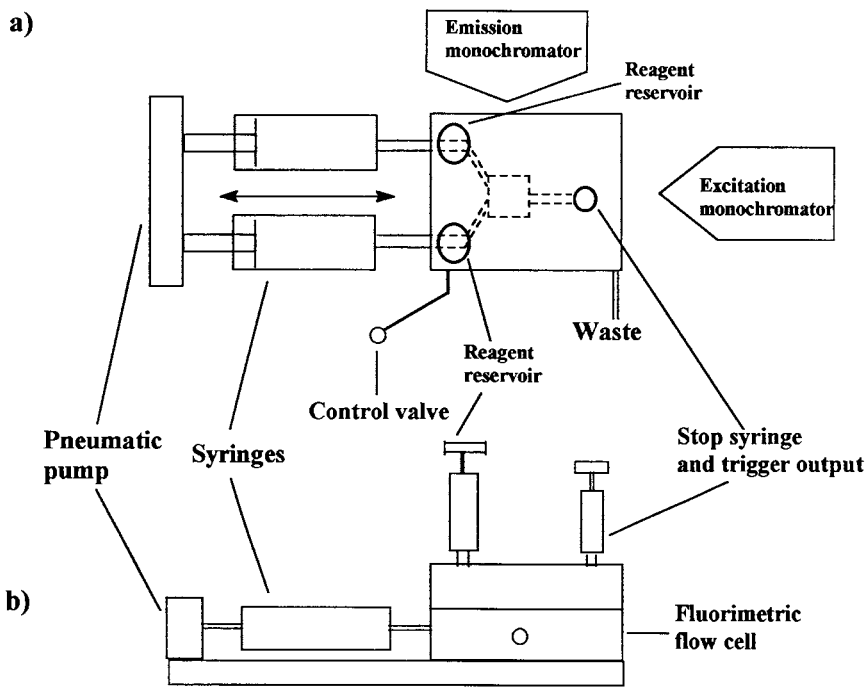

Scheme 1. (a) Top and (b) side views.

(St Louis, MO), and thallium (I) nitrate and sodium sulfite from Merck (Darmstadt, Germany). The standard dipyridamole was obtained from Aldrich (Milwaukee, WI). A stock solution of dipyridamole (100.0 mg dissolved in 100 m of 0.1 M SDS) was diluted to prepare working standard solutions. The stock standard solution of dipyridamole was stored, protected from the light, and maintained below 5°C. Under these conditions, it was stable for at least 2 weeks. The working standard solutions of dipyridamole were stable for at least 2 days at room temperature.

Stock standard solutions of 0.1 M SDS and 0.15 M thallium (I) nitrate were used. A 0.25 M sodium sulfite solution was prepared daily, and kept in tightly stoppered containers.

2.4. Procedure

For the preparation of the calibration graph (all concentrations given are initial concentrations in the syringes) fill one of the drive syringes with a solution containing SDS 9.0×10^{-3} M, sodium hydroxide 1.0×10^{-3} M, a volume of dipyridamole standard solution to give a final concentration between 50–400 ng $ml^{-1,}$ and sodium sulfite 1.5×10^{-2} M. The other syringe was filled with a solution containing sodium hydroxide 1.0×10^{-3} M, sodium sulfite 1.5×10^{-2} M and thallium nitrate 6.0×10^{-2} M. The stopped flow reactor was prepared for the acquisition of the kinetic curve. The instrument was setting up as follow: $\lambda_{ex} = 303$ nm, $\lambda_{em} = 616$ nm (bandpass 16 nm), detector voltage 1200 V, select flash lamp in phosphorescence > 200 μs (PMT masked) mode with delay after flash 70 μs, gate width 3000 μs and minimum flash period 5 ms. The kinetic curve was scanned up to 10 s, with a resolution of 50 ms and wait for trigger activated. Therefore, record three replicates of the time trace scan, calculate its average and smooth it to obtain the kinetic curve. In order to obtain the maximum rate, export the file in ASCII mode and run the SLOPES program after selecting 1 s as interval of time, that corresponds to 21 experimental data. Besides, get the phosphorescence intensity at 10 s, and finally, determine the dipyridamole content, by using the appropriate calibration graphs.

For the analysis of asasantin 75 mg (Boehringer Ingelheim, Barcelona, Spain) whose capsules contain dipyridamole inside as minute tablets, and for the analysis of persantin 100 mg (Boehringer Ingelheim), three tablets of each other were dissolved in 100 ml of SDS 0.1 M by using an ultrasonic bath during 15 min. Suitable dilutions were made with SDS 0.1 M and the samples were measured as described above.

3. Results and discussion

3.1. Spectral characteristics

Fig. 1 shows the total phosphorescence spectrum (solid line) and the total fluorescence spectrum (broken line) of dipyridamole in micellar medium under the optimal conditions previously established [24]. In order to study the room temperature phosphorescence kinetic curve, the maximum at $\lambda_{ex} = 303$ nm and $\lambda_{em} = 616$ nm in the total luminescence spectrum of dipyridamole was chosen to scan the phosphorescence evolution.

3.2. Factors affecting phosphorescence

According to a previous paper [24], the development of fluid solution RTP of dipyridamole requires the presence of SDS, thallium (I) nitrate, sodium sulfite, and a pH value of 11.5, and at least 15 min are necessary for the total phosphorescence development. In preliminary studies, we have observed that a sharp increase in phosphorescence is obtained in a short interval of time, by applying the stopped flow mixing technique, because the fast through mixing of the streams from the syringes in the flow cell, resulting from the pressure exerted by the instrumental system, favors the interaction of oxygen molecules with sulfite ions and their removal. The equilibrium conditions are obtained in only 5 s and, in consequence, the analytical time needed is vastly reduced. In this work, a kinetic study has been carried out, with the object of investigating the influence of instrumental and chemical variables, to obtain the maximum rate of the luminescence reaction and an adequate selectivity.

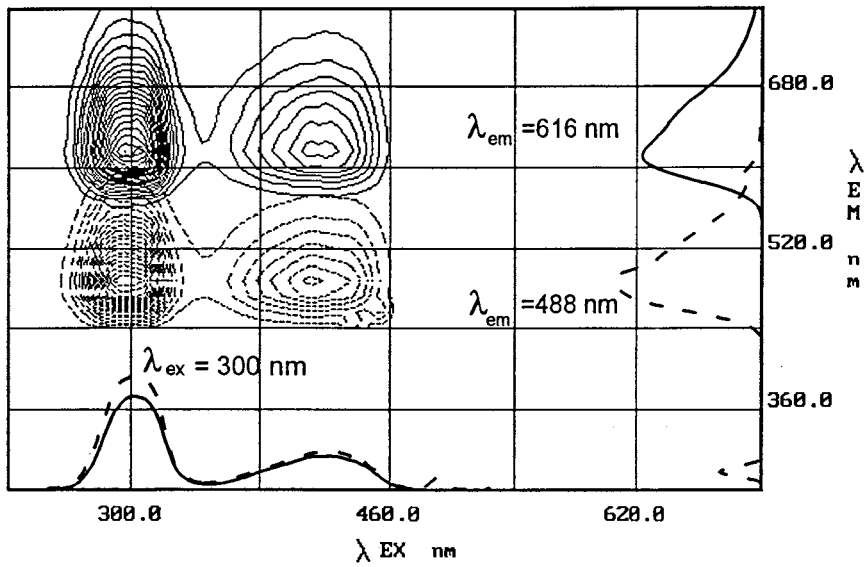

Fig. 1. Total phosphorescence spectrum (solid line) and total fluorescence spectrum (broken line) of dipyridamole. The projections of the axis correspond to the bidimensional emission and excitation spectra of fluorescence and phosphorescence.

Fig. 2 shows the changes on the phosphorescence intensity, and deviation owing to noise, with variations in gate time and delay after acquisition. As can be observed, the analytical signal diminishes, whereas the deviation owing to noise remains constant, as delay after acquisition increases. A delay after flash of 70 μs was selected, having the best sensitivity conditions. Although intensity diminishes as gate time increases, a sharp diminution occurs in the deviation owing to noise. Therefore, a gate time of 3000 μs was used as adequate. Other parameters selected for the instrumental setup were excitation and emission bandpass of 16 nm, and a photomultiplier tube voltage of 1200 V.

The influence of pH in the phosphorescence development was studied by adding different amounts of H_2SO_4 and NaOH to the syringes solution. Fig. 3a shows the influence of pH in the intensity and rate of phosphorescence. It is important to emphasize that, owing to the luminescent characteristics of dipyridamole, the phosphorescence is not significant at pH values up to 9.0. A maximum of reaction rate and intensity of phosphorescence can also be observed, being the interval of pH interesting to this determination about 10.6. In Fig. 3b, various kinetic curves at different pH values between 9.7 and 11.1 are represented. As can readily be observed, the phosphorescence development is strongly affected by the basicity of the medium. The kinetic curves are due to several coupled processes: deoxygenation, phosphorescence development, and equilibrium steps. In the interval between pH values from 9.7 to 10.6, the slope of the kinetic curve slightly increases, whereas its period of induction time drastically diminishes. In the range of pH values from 10.6 to 11.1, the slope of the kinetic curve decreases, whereas its period of induction time increases. The variation in the period of induction appears due to optimization in the deoxygenation process. It can also be observed that the phosphorescence intensity in equilibrium conditions remains practically constant between pH values from 10.2 to 11.1. A pH of 10.6 was selected as adequate to the determination. This pH was proportioned by the addition of 1.0×10^{-3} M NaOH.

Sodium sulfite [20] was used to eliminate the oxygen in the micellar solution, avoiding the quenching that oxygen produces in the phosphorescence emission by the triplet state of excited luminescent analytes. Any significant variation in

the rate of RTP development was noticed, whereas the period of induction time was greatly shortened, as sodium sulfite concentration was increased from 7.5×10^{-3} up to 3.0×10^{-2} M (Fig. 4). It was also observed that an excess of sodium concentration produces an RTP intensity decreases. This decreases in phosphorescence intensity has been interpreted as the displacement of thallium (I) by sodium from the micelle surface. A concentration of sodium sulfite 1.5×10^{-2} M was enough to complete the deoxygenation process in the solutions, producing a minimum period of induction time, and an adequate curve of phosphorescence development for the corresponding kinetic study.

Fig. 5a illustrates the influence of SDS concentration in the rate and intensity of phosphorescence. For concentration values of the surfactant higher than about 3×10^{-3} M, a drastic increasing in the analytical signals (intensity and rate) was observed. However, at concentration greater than this, both signals remain constant. Insolubility phenomena in the dissolution were observed at SDS concentrations higher than 8.5×10^{-3} M. The experimental result allows to conclude that a 4.5×10^{-3} M concentration of SDS is adequate to produce the semirigid structure necessary for phosphorescence development.

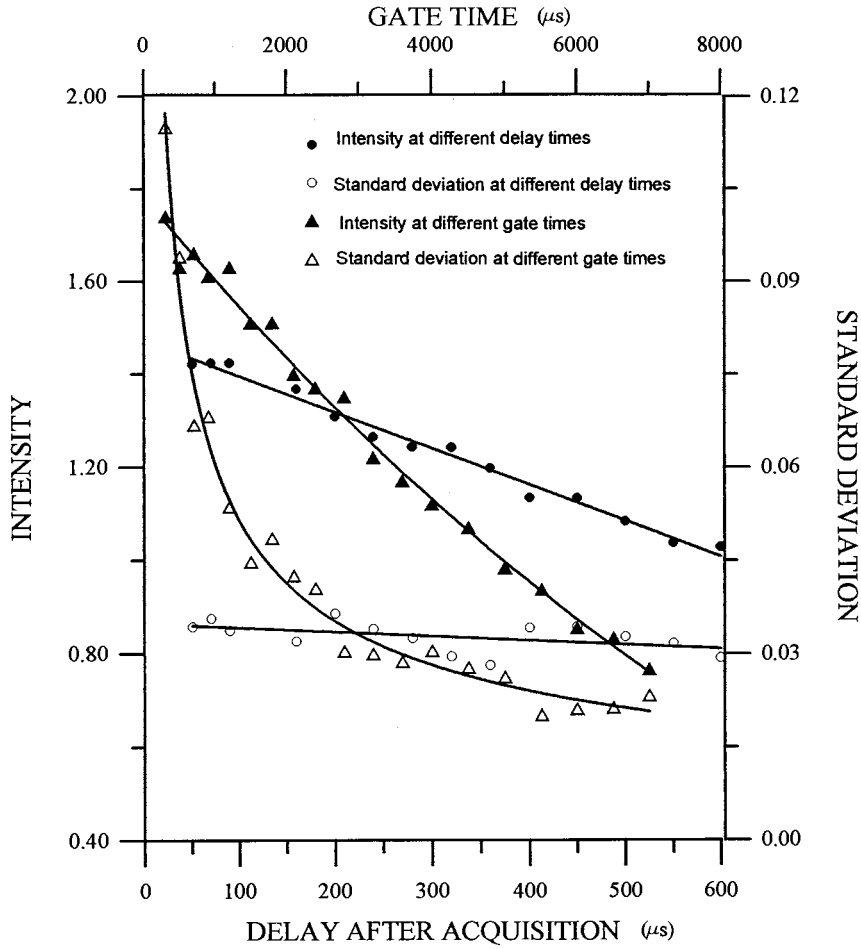

Fig. 2. Influence of delay time after flash and gate time, in the intensity and the rate of phosphorescence. $\lambda_{ex} = 303$ nm, $\lambda_{em} = 616$ nm

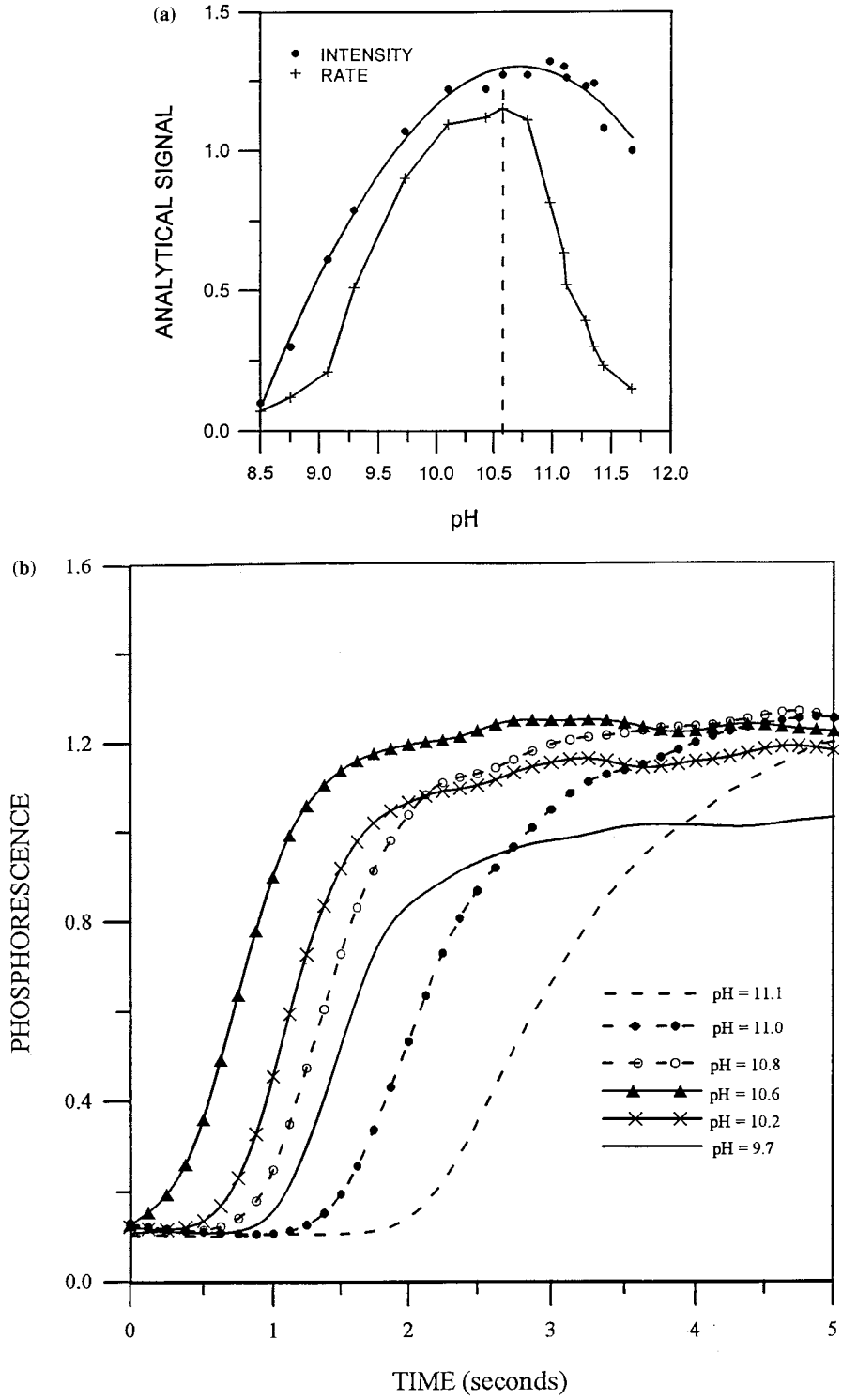

Fig. 3. (a) Variation of pH in the intensity and rate of phosphorescence; and (b) kinetic curves of dipyridamole phosphorescence at different pH values between 9.5 and 11.2.

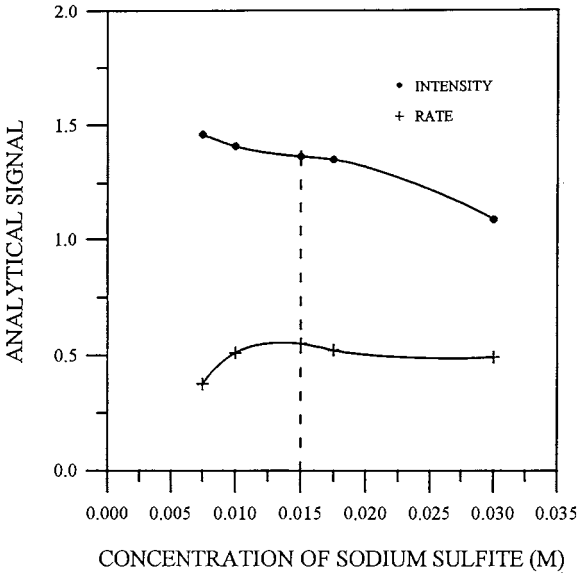

Fig. 4. Behaviour of intensity of phosphorescence and rate of phosphorescence development with sodium sulfite concentration.

Thallium (I) produces an effective spin-orbital coupling that reduces the triplet character of excited state, facilitating the phosphorescence development. In this Fig. 5b, a sharp increases in the reaction rate is observed for concentrations of thallium salt up to 2.0×10^{-2} M. At concentrations between 2.0×10^{-2} and 4.5×10^{-2} M, the rate of phosphorescence development was practically constant. A similar behavior occurs with the phosphorescence intensity but the latter slightly diminishing in the concentration range from 2.0×10^{-2} M to 4.5×10^{-2} M. Insolubility phenomena in the dissolution were observed again at thallium (I) nitrate concentrations higher than 4.5×10^{-2} M. It can be also observed that, when the thallium salt is not present, phosphorescence intensity disappears. A concentration of thallium 3.0×10^{-2} M was selected as optimum.

According to the above experiences, the optimal thallium nitrate to SDS ratio is 6.7. Fig. 5c illustrates the rate and intensity of phosphorescence versus SDS and thallium concentrations, maintaining the thallium and SDS in that ratio. As can be observed, the rate of phosphorescence development increases as SDS and thallium concentrations do, reaching a constant value at thallium 3.0×10^{-2} M (SDS $= 4.5 \times 10^{-3}$ M). The phosphorescence intensity shows a constant value for concentrations higher than 2.0×10^{-2} M of thallium (SDS $= 3.0 \times 10^{-3}$ M). Insolubility phenomena in the dissolution were also observed at concentrations greater than 3.6×10^{-2} M of thallium (SDS $= 5.2 \times 10^{-3}$ M). This experience confirms the concentration chosen before for the species studied.

Temperature affects reaction rate and intensity of phosphorescence. In the experimental range of temperature, i.e. from 10 up to 40°C, phosphorescence intensity shows a linear decrease, whereas the rate of phosphorescence is practically constant. Although temperature increases the rate of deoxygenation, also increments the collision frequency, producing a collisional relaxation increase which diminishes the luminescence yield. Both factors compensate the rate of phosphorescence development maintaining this rate at a constant value. The decrease of phosphorescence intensity is measured by plotting the relative signal increment versus temperature, scaled at 100%, i.e. the intensity at each temperature divided by the intensity of the higher temperature, and multiplied by 100, versus each temperature minus the lowest temperature, divided by the increment of experimental temperatures, and multiplying by 100. By fitting this relationship to a linear equation, the following parameters were obtained: slope (temperature coefficient) 0.42%°C^{-1}, intercept on the ordinate 103% and coefficient of the determination (r^2) 0.98.

By using the stopped flow system, the range for the proportional relation phosphorescence intensity or rate, versus concentration, was found for dipyridamole concentration up to 400 ng ml^{-1}. Consequently, the calibration was performed for dipyridamole concentration up to 400 ng ml^{-1}, with three replicates per point, with three injections each.

3.3. Calibration graphs

Under the instrumental and chemical operating conditions outlined above, we propose a method to determine dipyridamole by scanning the phos-

phorescence curve development, at 616 nm of emission wavelength, and 303 nm of excitation wavelength, in the concentration range of 50–400 ng ml^{-1}. The calibration graph was constructed, with three replicates per point, by measuring the reaction rate and intensity of the phosphorescence scan. The intensity was measured at 10 s, where phosphorescence was totally developed. The reaction rate of phosphorescence development was the slope obtained, by means of the straight line having maximum slope, after fitting the experimental data for an interval time of 1 s. This mathematical operation was performed by means of the SLOPES program.

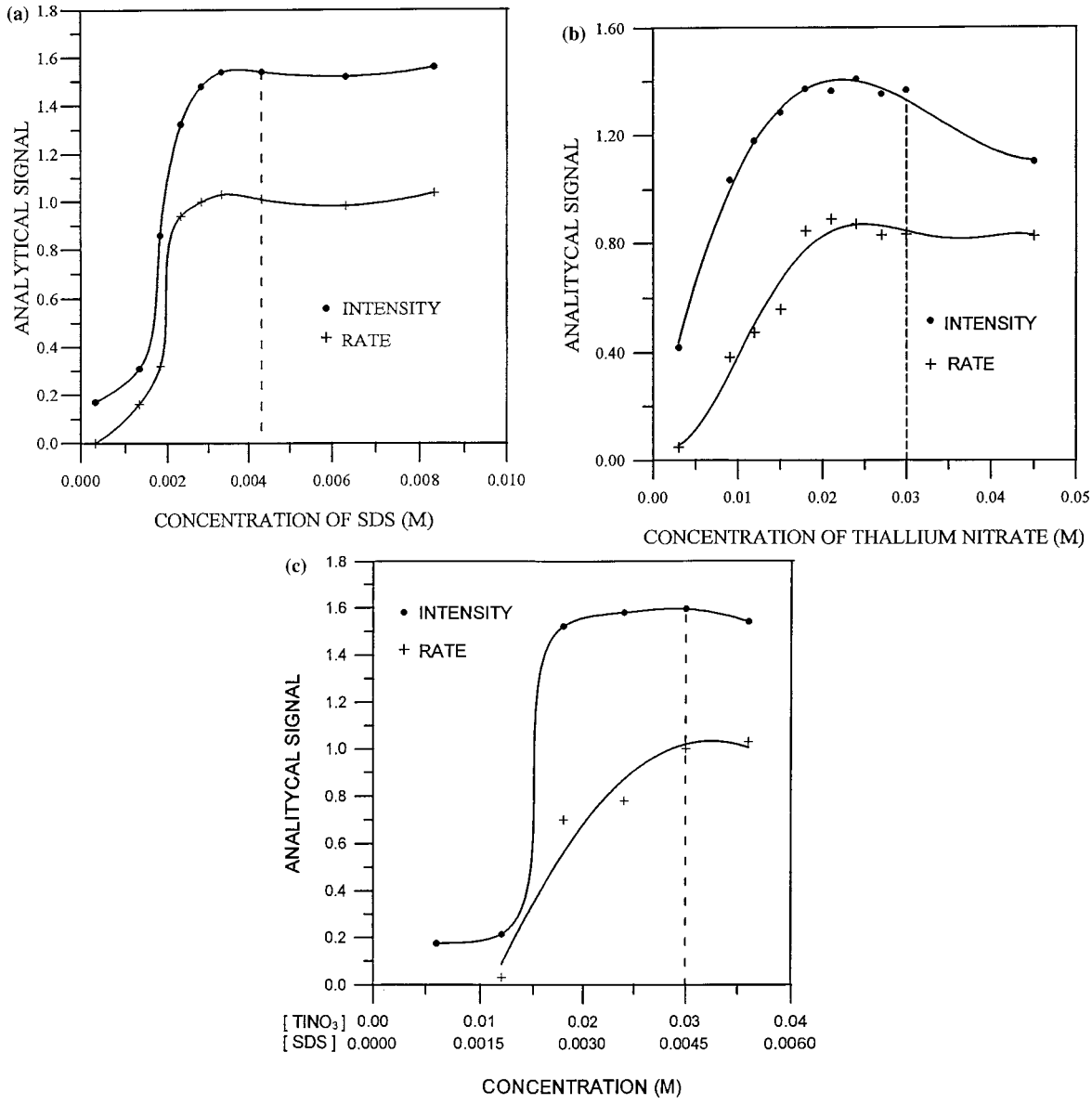

Fig. 5. (a) Effect of SDS concentration in phosphorescence intensity and rate; and (b) effect of thallium (I) concentration in phosphorescence intensity and rate; and (c) effect of SDS and thallium (I) concentration in phosphorescence intensity and rate at a thallium (I) SDS ratio of 6.7.

Table 1
Outstanding results from statistical analysis of data; least squares regression with replicates

	Intensity method	Initial-rate method
Intercept on ordinate (a)	1.963×10^{-1}	3.656×10^{-2}
SD of intercept on ordinate (Sa)	6.5×10^{-3}	6.9×10^{-3}
Slope (b)	1.743×10^{-3}	9.987×10^{-4}
SD of slope (Sb)	2.6×10^{-5}	2.7×10^{-5}
SD of regression ($S_{y.x}$)	1.4×10^{-2}	1.5×10^{-2}
Determination coefficient (r^2)	0.9950	0.9831
CI[a] of intercept on ordinate	2.098×10^{-1}, 1.828×10^{-1}	5.086×10^{-2}, 2.225×10^{-2}
CI of slope	1.796×10^{-3}, 1.689×10^{-3}	1.055×10^{-3}, 9.421×10^{-4}

[a] CI = confidence interval.

The proposed methods, intensity and initial rate measurements versus concentration, were evaluated by an statistical analysis of the experimental data, by fitting the overall least-squares line according to $y = a + bx$. Table 1 shows the outstanding results from the statistical analysis.

According to the residual distribution obtained, it can be assumed that both calibration lines observe homocedasticity criteria. In order to test the linearity of the overall least squares regression the ANOVA test was performed [28]. The results are given in Table 2, concluding that the model chosen in each case is an adequate description of the true relationship between intensity or rate of phosphorescence and dipyridamole concentration. By plotting the 95% confidence region for true slope and intercept [29] estimated, the intercept due to blank signals falls within the joint confidence region. This means that the intercept on the ordinate is not significantly different from the blank signals, therefore, it can be interpreted as the absence of proportional error.

If the theory of error propagation is considered, the detection limit is consistent with the reliability of the blank measurements and the signal measurements of the standards [25,30]. In this case, the detection limit were 19.0 and 33.0 ng ml^{-1} for intensity and rate measurements, respectively. The detection limit according to Clayton [27], considering the probability of false positive and false negative being 21.5 and 37.5 ng $ml^{-1,}$ for intensity and rate measurements, respectively ($\alpha = \beta = 0.05$; $n = 24$).

The precision of the method was established by testing the analytical signal corresponding to the concentrations of the calibration line. As can be seen from the RSDs in Table 3, these deviations diminishes as concentration increases, i.e. from 11.5 to 1.43% for intensity measurements and from 20.1 to 2.7% for rate measurements. In the

Table 2
ANOVA test: linearity test[a]

Source of variation	SS	DF	MS	F_{exp}	F_{theor}
Intensity method					
Due to regression	9.569×10^{-1}	1	9.569×10^{-1}		
Set means about the line (lack of fit)	1.508×10^{-3}	6	2.514×10^{-4}		
				1.29	2.74
Within line (pure error)	3.115×10^{-3}	16	1.947×10^{-4}		
Total	9.6159×10^{-1}	23	4.180×10^{-2}		
Initial rate method					
Due to regression	3.142×10^{-1}	1	3.142×10^{-1}		
Set means about the line (lack of fit)	2.181×10^{-3}	6	3.635×10^{-4}		
				1.94	2.74
Within line (pure error)	2.991×10^{-3}	16	1.870×10^{-4}		
Total	3.193×10^{-1}	23	1.389×10^{-2}		

[a] SS = Sum of squares of deviations; DF = degrees of freedom; MS = mean squares (SS/DF).

Table 3
RSDs obtained by applying error propagation theory

Dipyridamole (ng ml^{-1})	RSD (%)	
	Intensity method	Initial rate method
50	11.5	21.0
100	5.4	10.0
150	3.5	6.4
200	2.6	4.7
250	2.0	3.8
300	1.7	3.2
350	1.5	2.8
400	1.4	2.7

distribution obtained of the RSDs, two major factors can be considered: the first one is that if the standard deviation is constant with concentration, lower levels of dipyridamole produce great values of relative standard deviation, whereas higher levels produce low values of relative standard deviation. The second is a consequence of the mathematical model used, since the confidence and dispersion bands of the true line have hyperbolae shape closest at the concentration mean. Then, it can be interpreted that the repeatability, expressed as the RSDs, presents two behaviors, the first one is for concentrations up to the concentration mean, where a sharp decrease is produced in RSD as concentration increases. The second one is for concentrations from the concentration mean where a slight decrease is observed in RSD as concentration increases. Therefore, when the concentration of dipyridamole of a sample must be calculated, it is suitable to calculate the corresponding interval of confidence.

3.4. Applications and interference study

The specificity of this determination was studied by adding related drugs to the pharmaceutical preparation of dipyridamole (saccharose, lactose, and glucose) and other drugs with intrinsic luminescence, and testing to see if the added drugs cause interference in the kinetic behaviour of dipyridamole (200 ng ml^{-1}). The assay results, expressed as a percentage of recuperation of dipyridamole, are given in Table 4. It can be deduced that saccharose, lactose, and glucose do not interfere in the dipyridamole quantification. In the case of the substances with intrinsic luminescence, only a small number of them (amiloride, triamterene, and quinine) produce interferences.

Table 4
Recovery values in the determination of dipyridamole in the presence of several foreign species

Foreign specie	Interference/dipyridamol tolerance ratio (w/w)	Recovery (%)	
		Intensity method	Initial rate method
Lactose	50	96.8	95.1
Glucose	50	96.7	102.0
Saccharose	50	103.1	101.8
Nadolol	10	103.6	93.7
Hydrochlorithiazide	5	101.7	94.2
Aspirin	2.5	93.5	106.9
Quinine	2.5	94.1	<80
Ibuprofen	2.5	100.0	92.1
Metoprolol	2.5	103.6	104.5
Atenolol	2.5	100.3	99.6
Propanolol	1.25	105.0	106.1
Amiloride	1	<80	<80
Triamterene	1	<80	<80
Methotrexate	1	95.3	90.8
Neopterin	1	96.1	93.2
6-Biopterin	1	97.1	95.1
Xanthopterin	1	100.7	98.4

Table 5
Results obtained by the application of the proposed methods: intensity and rate of phosphorescence measurements

Pharmaceutical preparation	Dipyridamol nominal content (mg per tablet)	Dipyridamol found (mg per tablet) ± SD	
		Intensity method	Rate method
Asasantin	75	72.0/0.3	79.7/2.0
Persantin	100	99.4/2.5	105.6/4.3

The recommended procedure has been satisfactorily applied to the determination of dipyridamole in the Spanish pharmaceutical products that contain this vasodilator agent in different proportions (persantin 100 mg and asasantin 75 mg). The assay results, expressed as a percentage of the nominal contents, resulting from the average of three determinations of three different tablets, are summarized in Table 5. The recoveries agree well enough with the nominal content and the precision is quite satisfactory.

4. Conclusions

The coupling of stopped flow and room temperature phosphorescence supposes a rapid technique for the determination of phosphorescent substances as dipyridamole. Besides, the stopped flow reactor provides kinetic studies. In this work, a new method for direct phosphorimetric determination of dipyridamole in pharmaceutical preparations is described. The determination of this vasodilator agent was done by scanning the phosphorescence development, at 616 nm of emission wavelength and at 313 of excitation wavelength, with excellent repeatability and sensitivity.

By applying this technique, the dipyridamole phosphorescence was totally developed in only seconds, whereas the phosphorescence method without the use of the mixing system develops the phosphorescence in 15 min at least.

An exhaustive statistical analysis of the calibration graph has been performed, including the least squares regression with replicates and ANOVA test. The calibration graphs present homocedasticity. The validity of the overall least squares regression was proved by the ANOVA test, the variation of group mean about the line, which means the lack of fit, not being significantly different from the variation within groups (pure error). Therefore, the model chosen is an adequate description of the true relationship between phosphorescence intensity and reaction rate with dipyridamole concentration. The detection limits, assuming the error propagation theory were 19.0 and 33.0 ng ml^{-1} for intensity and rate, respectively. The detection limit, according to Clayton, were 21.5 and 37.5 ng ml^{-1} for intensity and rate measurements, respectively. The proposed method shows high selectivity and it was satisfactorily applied to the determination of dipyridamole in persantin 100 mg and asasantin 75 mg.

Acknowledgements

The authors gratefully acknowledge financial support from DGES (project no. PB 95-1141) and from DGICYT (project no. PB 94-0743)

References

[1] K. Kalyanasundaram, F. Grieser, J.K. Thomas, Chem. Phys. Lett. 51 (1977) 501.
[2] L.J. Cline Love, M. Skrilec, J.G. Habarta, Anal. Chem. 52 (1980) 754.
[3] M. Skrilec, L.J. Cline Love, J. Phys. Chem. 85 (1981) 2047.
[4] A. Sanz-Medel, P.L. Martínez García, M.E. Díaz García, Anal. Chem. 59 (1987) 774.
[5] M.R. Fernández de la Campa, M.E. Díaz García, A. Sanz-Medel, Anal. Chim. Acta 212 (1988) 235.
[6] G. Ramis Ramos, I.M. Khasawneh, M.C. García-Alvarez Coque, J.D. Winefordner, Talanta 35 (1988) 41.
[7] R.A. Femia, L.J. Cline Love, Anal. Chem. 56 (1984) 327.

[8] L.J. Cline Love, M.L. Grayeski, J. Noroski, R. Weinberger, Anal. Chim. Acta 170 (1985) 3.
[9] M.E. Díaz García, A. Sanz Medel, Anal. Chem. 58 (1986) 1436.
[10] Y.M. Liu, M.R. Fernández de la Campa, M.E. Díaz García, A. Sanz Medel, Anal. Chim. Acta 234 (1990) 233.
[11] N.E. Nugara, A.D. King Jr., Anal. Chem. 61 (1989) 1431.
[12] H. Kim, S.R. Crouch, M.J. Zabik, S.A. Selim, Anal. Chem. 62 (1990) 2365.
[13] J. Weijun, L. Changsong, Microchem. J. 48 (1993) 94.
[14] W.J. Jin, C.S. Liu, Fenxi Huaxue 21 (1993) 509.
[15] A.J. Tong, Y.G. Wu, L.D. Li, Talanta 43 (1996) 1429.
[16] C. Cruces-Blanco, A. Segura-Carretero, A. Fernández-Gutiérrez, Anal. Chim. Acta 318 (1996) 357.
[17] I. Rapado Martínez, R.M. Villanueva Camañas, M.C. García-Alvarez Coque, Analyst 119 (1994) 1093.
[18] W. Yansheng, J. Weijun, Z. Rohua, L. Changsong, L.Z. Sushe, Talanta 41 (1994) 1617.
[19] A. Segura Carretero, C. Cruces Blanco, A. Fernández Gutiérrez, Anal. Sci. 12 (1996) 653.
[20] A. Segura-Carretero, C. Cruces-Blanco, A. Fernández-Gutiérrez, Talanta 43 (1996) 1001.
[21] A. Segura-Carretero, C. Cruces Blanco, A. Fernández-Gutiérrez, Analyst 122 (1997) 925.
[22] S. Panadero, A. Gómez-Hens, D. Pérez-Bendito, Anal. Chem. 66 (1995) 919.
[23] S. Panadero, A. Gómez-Hens, D. Pérez-Bendito, Anal. Letters 28 (1995) 1405.
[24] J.A. Murillo, A. Alañon Molina, A. Fernández López, Analyst 122 (1997) 253.
[25] L. Long, J.D. Winefordner, Anal. Chem. 55 (1983) 712.
[26] L. Cuadros Rodríguez, A.M. García Lampaña, C. Jiménez Linares, M. Román Ceba, Anal. Letters 26 (1993) 1243.
[27] C.A. Clayton, J.W. Hines, P.D. Elkins, Anal. Chem. 59 (1987) 2506.
[28] D.L. Massart, B.G.M. Vandeginste, S.N. Deming, L. Kaufman, Chemometrics: a Textbook, Oxford, London, 1988.
[29] P.D. Lark, B.R. Craven, R.C.L. Bosworth, The Handling of Chemical Data, Pergamon, Exeter, 1968, Chap 4.
[30] J.N. Miller, Analyst 116 (1991) 3.

ELSEVIER

Talanta 48 (1999) 1075–1084

Talanta

Sensitive spectrofluorimetric determination of ruthenium at nanotrace levels using 2-(α-pyridyl) thioquinaldinamide [PTQA]

B.K. Pal [a,*], M. Sahedur Rahman [b]

[a] *Analytical Chemistry Division, Department of Chemistry, Jadavpur University, P.O. Box 17030, Calcutta-700 032, India*
[b] *Department of Applied Chemistry and Chemical Technology, Rajshahi University, Rajshahi, Bangladesh*

Received 3 December 1997; accepted 7 October 1998

Abstract

A new spectrofluorimetric method for the determination of ruthenium with nonfluorescent 2-(α-pyridyl) thioquinaldinamide (PTQA) is described. The oxidative reaction of Ru(III) upon PTQA gives oxidised fluorescent product ($\lambda_{ex(max)} = 347$ nm; $\lambda_{em(max)} = 486$ nm). The sensitivity of the fluorescence reaction between ruthenium and PTQA is greatly increased in the presence of Fe (III). The reaction is carried out in the acidity range 0.01–0.075 M H_2SO_4. The influence of reaction variables is discussed. The range of linearity is 1–400 μg l^{-1} Ru(III). The standard deviation and relative standard deviation of the developed method are ± 1.210 μg l^{-1} Ru (III) and 2.4%, respectively (for 11 replicate determinations of 50 μg l^{-1} Ru (III)). The effect of interferences from other metal ions, anions and complexing agents was studied; the masking action is discussed. The developed method has been successfully tested over synthetic mixtures of various base metals and platinum group metals, synthetic mixtures corresponding to osmiridium, certified reference materials in spiked conditions and rock samples.

Keywords: Ruthenium; Spectrofluorometric; Nanotrace levels

1. Introduction

Ruthenium is an industrially important [1–3] and highly precious metal in the Platinum Group (PG). Anti-tumor activities of ruthenium compounds are also well known [4,5]. Very few data exist on ruthenium concentrations in common igneous and sedimentary rocks because of its very low abundance in most terrestrial materials. The estimation of the element in ores and man made sources can be only studied with sensitive and selective analytical methods.

Fluorimetry is a well known ultra-trace analytical technique, but only few methods have been reported for the fluorimetric determination of ruthenium. Literature survey reveals that there are only two fluorimetric methods. [6,7] based on fluoresecent chelate formation with ruthenium (II)

* Corresponding author. E-mail: bkpal@hotmail.com.

0039-9140/99/$ - see front matter
PII: S0039-9140(98)00318-X

and only one indirect method [8] based on nonfluorescent ternary complex formation with ruthenium (III) using Rhodamine 6G and thiocyanate. The lowest detection limits of these existing methods are inadequate for the determination of ruthenium, at ultratrace levels moreover, they subject to many interferences. An ultrasensitive method is proposed where the nonfluorescent 2-(α-pyridyl) thioquinaldinamide is converted into a intensely fluorescent species by ruthenium (III) in the presence of iron (III).

2. Experimental

2.1. Instrumentation

A Shimadzu Spectrofluorophotometer (Model RF-5000), computer controlled and equipped with a 150 W continuous wave xenon lamp, 12 in colour video display, parallel line thermosensitive printer recorder, 1×1 cm^2 quartz cells and a Shimadzu ASC-5 auto sample changer, was used to record the uncorrected spectra, to scan the fluorescence intensity-time curves and to measure the fluoresence intensities. Performance of the instrument were checked by running Raman Spectrum of distilled water and wavelength error was below ± 0.2 nm.

A Hanovia Fluoresence lamp (Model 11A, 240 V, 50 Hz, Arc tube, Hanovia, England) was employed for visual qualitative study of fluoresence intensity changes. A digital pH-meter (Model pH 5651, Electronics Corporation of India) was used for the measurement of pH.

2.2. Reagents and solutions

2.2.1. 2-(α-pyridyl) thioquinaldinamide (PTQA) solution

2-(α-pyridyl) thioquinaldinamide (PTQA, $C_{15}H_{11}N_3S$), (Molecular wt. = 265.18) was synthesized according to the method of Porter [9]. A 1×10^{-3} M PTQA solution was prepared by dissolving the requisite amount of PTQA in distilled ethanol. The reagent solution, if kept in refrigerator, is stable for one week; however, a freshly prepared reagent solution was used whenever required. More dilute solutions were prepared from this stock solution with ethanol.

2.2.2. Ruthenium (III) standard solution

An accurately weighed 1.132 g of ruthenium trichloride nomohydrate (43% Ru Johnson Matthey) was dissolved in a small volume of 2 M HCl and diluted to 100 ml in a volumetric flask with hydrochloric acid in order to make the final solution 1 M in HCl. The solution was standardized gravimetrically as metallic ruthenium [10]. Working solutions were obtained by diluting the stock solution with 0.1 M H_2SO_4 immediately before use.

2.2.3. Other platinum group metal solutions (1000 mg l^{-1} each)

Solutions of Rh(III), Pd(II), Ir(III) and Pt(IV) were prepared from their highest available purity grade salts in 0.1 M hydrochloric acid and Os (VIII) solution was prepared from p.a. grade OsO_4 in 0.1 M H_2SO_4.

2.2.4. Iron (III) solution

Fe(III), 0.0179 M (1000 mg l^{-1}) solution was prepared from $NH_4Fe(SO_4)_2 \cdot 12H_2O$ (Merck, Germany) in 0.1 M H_2SO_4 and standardized volumetrically by $KMnO_4$ method [11]. More dilute solution was prepared form the stock solution.

2.2.5. Sodium oxalate solution

A 1% (w/v) sodium oxalate ($Na_2C_2O_4$) (AnalaR BDH) was prepared in 100 ml volumetric flask with deionized water.

A large number of solutions of inorganic ions and complexing agents were prepared from their AnalaR Grade or equivalent grade water soluble salts (or oxides and carbonates in hydrochloric acid). In the case of insoluble substances special methods were adopted [12]. Double distilled deionized water nonfluorescent under ultraviolet radiation was used throughout.

2.3. General procedure

To a 10-ml volumetric flask containing 0.01–0.1 μg or 0.1–1.0 μg or 1.0–4.0 μg of ruthenium (III) were added 1.0 ml of 0.5 M H_2SO_4, 0.5 ml of

1.79×10^{-3} M (100 mg l^{-1}) Fe (III) and 0.2–0.3 ml of 1×10^{-3} M PTQA solution respectively. The resultant solution was mixed well and allowed to stand for 30 min. Sodium oxalate, 0.2 ml of 1% (w/v) solution and 1 ml of distilled ethanol were added and the volume was made up with deionized water. The fluorescence intensity of the solution was measured against a reagent blank at 486 nm keeping excitation wavelength at 347 nm at room temperature (25 ± 5°C). In the case of multicomponent systems (synthetic and real samples) 0.2 ml of 1% (w/v) potassium-sodium tartrate was added as masking agent.

2.3.1. Procedure and sample mineralisation

Alloys. An accurately weighed 0.1 g portion of the sample was dissolved in 4 ml of mixture (1:1) of concentrated HCl–HNO_3 with heating and diluted to 100 ml with deionized water. Suitable aliquots of this sample solution with and without ruthenium (III) spiking were analysed fluorimetrically according to general procedure described before.

2.3.2. Rock sample treatment

1.0 g of each pulverized rock (250–300 mesh) was placed in a Teflon bomb and 2.0 ml conc. HNO_3 and 1.0 ml hydrogen peroxide (30 wt%) were added [13]. The Teflon bomb was closed and kept around 120°C on a hot plate around for ca. 10 min. Heating was then discontinued and the sample was kept overnight at room temperature. This was followed by heating in an oven for 6 h at about 120–130°C then allowed to cool to room temperature and the lid was opened and the extract was evaporated to almost dryness on a steam bath. To this 5 ml of 1 M HCl was added and filtered. The filtrate was then diluted to 25 ml with deionized water in a volumetric flask.

2.3.3. Ion exchange separation

Ruthenium was separated form base metals by ion exchange method before application of the fluorimetric method to the determination of ruthenium in rock samples. The procedure of Zachariasen and Beamish [14] for the separation of base metals from ruthenium using cation exchanger was modified slightly owing to the micro-sized sample.

Strong cationic (AG 50 W X 8 (H form) 100–200 mesh) exchange resin was used for the preparation of resin bed of uniform dimension (9.0×0.7 cm^2) in all glass column after its conditioning and washing with deionized water to completely free it from soluble chloride ions. A solution containing known amounts of ruthenium (III) and other interfering ions was placed in a 25-ml beaker and 1 ml 1% NaCl and 2 ml concentrated HCl were added respectively. The solution was evaporated to near dryness on a steam bath. 1 ml conc. HCl was added and the salts were dissolved by slow addition of distilled water with stirring. The solution was diluted with water to 10 ml and the pH was adjusted with HCl to within pH 0.9–1.1. The solution was then passed through the prepared cation exchange column at a rate of about 1 ml per minute. The resin was washed with 20 ml of water which was previously adjusted with HCl to pH 1.0. Then effluent, collected in a 50-ml beaker, was evaporated to expel all the HCl. The resultant solution was diluted with deionized water to 25 ml. From suitable aliquots, the ruthenium content was then determined fluorimetrically with PTQA as described earlier with calibration graph being prepared from standard Ru(III) solution also treated with HCl and NaCl and passed through the resin bed identically.

3. Results and discussion

3.1. Spectral characteristics

The excitation and emission spectra of the fluorescence system [Ru(III)-PTQA] in 0.05 M H_2SO_4 were recorded, the wavelength maxima of excitation and emission were found to occur at 347 and 486 nm respectively. The reagent blank was found to exhibit a fluorescent maxima in the same wavelength region but its intensity was very low. The uncorrected spectra are shown in Fig. 1.

3.2. Effect of catalyst, Fe(III)

By means of catalytic analytical methods, extremely low levels can be determined with a high

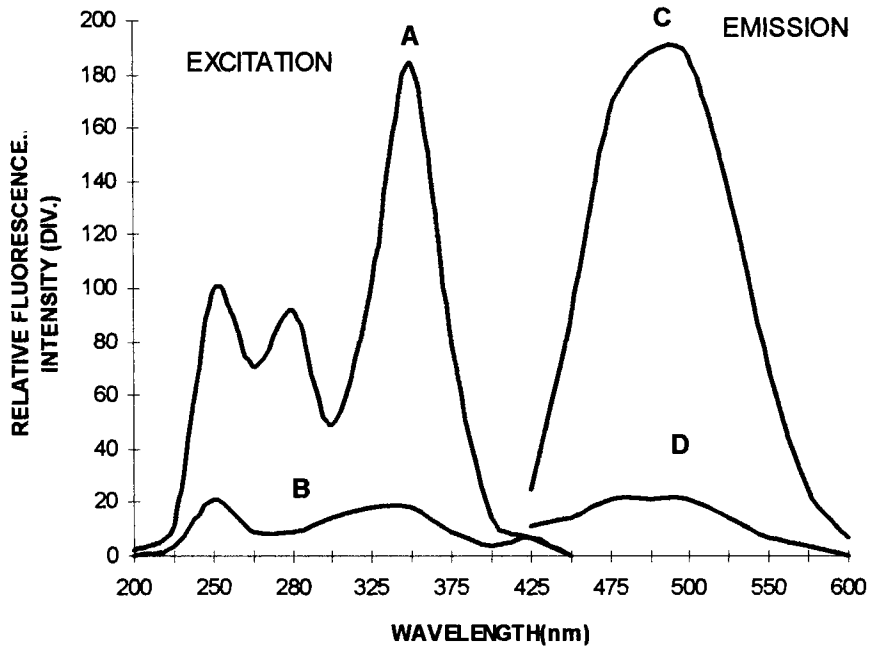

Fig. 1. Uncorrected spectra A and B, excitation spectra of Ru(III)-PTQA system and the reagent blank respectively (emission wavelength = 486 nm); C and D corresponding emission spectra (excitation wavelength = 347 nm). [Ru (III)] = 100 μg l^{-1}.

sensitivity. From the preliminary study it was found that the reaction between ruthenium(III) and PTQA in acidic media is slow and takes several hours to reach the equilibrium florescence intensity. To increase the optimum sensitivity of the proposed method for determination of ruthenium(III), an attempt was made of the catalysing action of certain substance (Mn(II), Co(II), V(V), Fe(II) and Fe(III)) [15,16]. It was found that the reaction could be made rapid by addition of microgram amounts of Fe(III). Fe(III) in absence of Ru(III) does not give any fluorescent product with PTQA in the reaction conditions mention before. The fluorescence intensity-time curves were obtained separately for Fe(III)-PTQA system and Ru(III)-PTQA system both in the absence and presence of Fe(III) under identical conditions are shown in Fig. 2. It is revealed that when both Fe(III) and Ru(III) are present in the medium, the slope of the curve increases and the time require to reach the maximum constant fluorescence intensity decreases.

The Fe(III) concentration was optimised by measuring the fluorescence intensity at different Fe(III) concentration ratios the data obtained which is shown in Fig. 3, shows that the relative fluorescence intensity increases sharply with Fe(III) mass fold up to 20 remaining constant

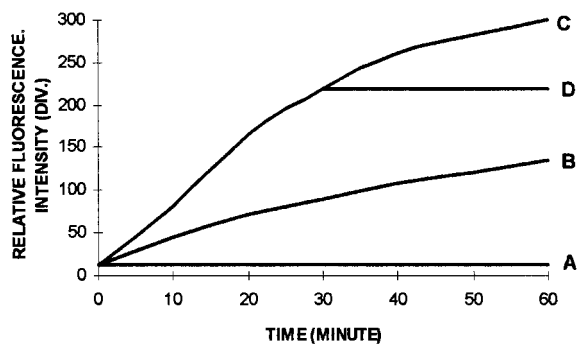

Fig. 2. Fluorescence intensity versus time curves. (A) PTQA + Fe(III). (B) PTQA + Ru (III) (100 μg l^{-1}). (C) PTQA + Ru(III) (100 μg l^{-1}) + Fe(III). (D) PTQA + Ru(III) (100 μg l^{-1}) + Fe(III) + sodium oxalate (after 30 min of Ru(III)-PTQA mixing).

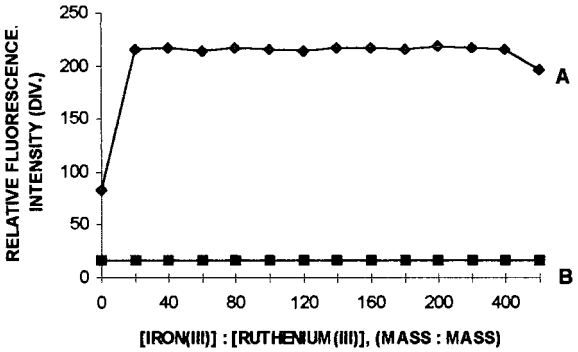

Fig. 3. Effect of Fe(III) concentration on the fluorescence intensity of Ru(III)-PTQA system. (A) Ru(III) (100 μg l^{-1}) + PTQA + Fe(III). (B) Fe(III) + PTQA.

within the range of 20–400 mass fold of Fe(III) (to Ru(III)) then decreases gradually with the increase of Fe(III) concentration.

3.3. Effect of time

Ruthenium(III) forms complex compound [17] with oxalate. Sodium oxalate solution was added after predetermined lapse of time from metal-reagent mixing, to halt the progress of the reaction (i.e. formation of fluorescence product) and measurements were made before reaching equilibrium. Fluorescence intensity of Ru(III)-PTQA-Fe(III)-sodium oxalate remained unaltered event after 6 h. Longer periods were not studied.

3.4. Effect of acidity

Effects of different common acids such as H_2SO_4, HNO_3, HCl, H_3PO_4, $HClO_4$ and CH_3COOH were studied. In H_2SO_4 medium, fluorescence intensities were relatively greater than those in other acids. The constant maximum fluorescence intensities were corrected against corresponding reagent blanks were found in the presence of 0.2–1.5 ml of 0.5 M H_2SO_4 per 10 ml.

3.5. Effect of sodium oxalate

The fluorescence intensity remained constant up to 10 000 mass fold of sodium oxalate (to ruthenium(III)).

3.6. Effect of reagent concentration

To study the influence of reagent concentration on fluorescence intensity of PTQA-ruthenium(III) system, different molar fold excess of PTQA was added to fixed metal ion concentration and fluorescence intensities were measured according to the general procedure. The effect of reagent concentration is represented in Fig. 4. The Figure shows that at the 100 μg l^{-1} Ru(III), the reagent metal molar ratios between 15 and 260 produce constant fluorescence intensity. The reagent metal molar ratios greater than 260 was not studied because the solution became coloured and turbid at higher reagent concentrations.

3.7. Effect of metal concentration

The effect of Ru concentration was studied over a wide overall range of 1.0–1000 μg l^{-1} Ru(III), distributed in three different sets (1.0–10 μg l^{-1}, 10–100 μg l^{-1} and 100–1000 μg l^{-1}) of ruthenium(III) for convenience of measurement (Fig. 5). The fluorescence intensities maintained a linear relationship in the range of 1.0–400 μg l^{-1} of ruthenium(III). The standard deviation and relative standard deviation of the method on 50 μg l^{-1} Ru(III) (11 replicate determinations) were found to be $\pm$1.210 μg l^{-1} Ru(III) and 2.4%

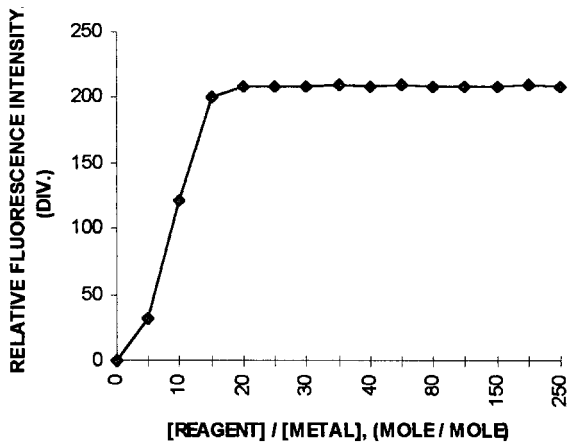

Fig. 4. Effect of PTQA (reagent) concentration on the fluorescence intensity of Ru(III)-PTQA system [Ru(III)] = 100 μg l^{-1}, [Fe(III)] = 5000 μg l^{-1}.

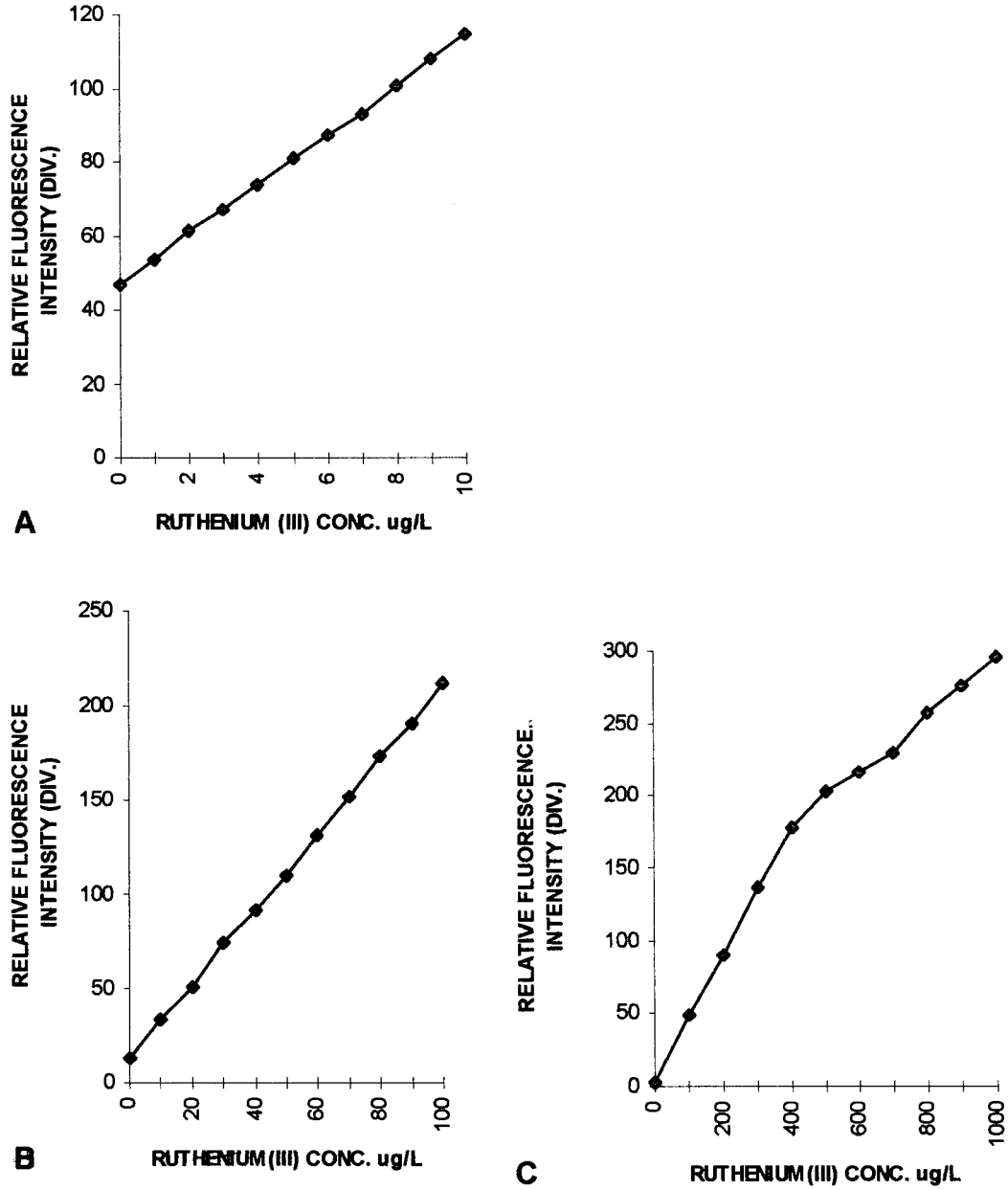

Fig. 5. Calibration graphs: (A) 1–10 μg l^{-1} Ru(III); Bandwidth: Ex = 10nm, Em = 10 nm; (B) 10–100 μg l^{-1} Ru(III); Bandwidth: Ex = 5 nm, Em = 10 nm; (C) 100–1000 μg l^{-1} Ru(III); Bandwidth: Ex = 5 nm, Em = 5 nm; Response(s): Auto; Sensitivity: High; Degree: 1; Con, output Factor: 1.000.

respectively. For concentration lower than 1 μg l^{-1} Ru(III), if the reaction time was increased from 30 minute to 60 minute before the addition of sodium oxalate still lower concentration range can well be established.

3.8. Effect of foreign ions

The effects of foreign ions on the proposed method have been evaluated. Different amounts of the ionic species were added to 50 μg l^{-1} of

Table 1
Tolerance limits in the determination of 50 μg l^{-1} of ruthenium(III)

Mass fold tolerated (species/Ru(III))	Species tested
5000	Tartrate, ClO_4^-, HPO_4^{2-}, Na(I), K(I), Ca(II), HSO_4^-
1000	Cl^-, NO_3^-, NaN_3, acetate, citrate, borate
500	F^-, I^-, $S_2O_8^{2-}$, HF_2^-, Mg(II), Zn(II), Cd(II)
200	As(V), Cr(III), Ni(II), Al(III), Mn(II), La(III), Se(VI), Tl(I), Th(IV), U(VI), Bi(III)
100	Co(II), Pb(II), Ba(II), Sb(III), W(VI)
50	Sb(V), Mo(VI), Ga(III), V(V), As(III)
20	Fe(II), Ag(I)[a], Hg(II)[a]
10	Ce(IV)[b], Tl(III)[b], Rh(III), Pd(II), Ir(III), Os(VIII)[b]
5	Pt(IV), Cr(VI)[c]
2	Cu(II)[c]

[a] In the presence of 500-fold iodide.
[b] In the presence of 1000-fold NaN_3.
[c] In the presence of 1000-fold tartrate.

ruthenium(III), first testing a 10 000 fold mass ratio of potential interferent to ruthenium and if interference occurred, progressively reducing the ratio until interference ceased. The criterion for interference was a fluorescence intensity value varying by more than ± 5% from expected value for ruthenium alone and results are given in Table 1. During the interference studies, if any precipitate was formed, it was removed by centrifugation.

EDTA, NTA and oxalate cause the highest negative interference. Se(IV) produces fluorescence with the reagent but Se(VI) does not. So when Se(IV) and Ru(III) are treated with HNO_3, Se(IV) is oxidised to Se(VI) which has no interference at all.

3.9. Applications

The proposed method for the determination of Ru(III) was applied to synthetic mixtures containing base metals and platinum group metals, synthetic mixtures corresponding to osmiridium ore, certified reference materials in spiked condition and to some platinum group metal bearing rock samples.

3.9.1. Analysis of synthetic mixtures

Various synthetic mixtures of common metals and platinum group metals (PGM) were prepared. During preparing synthetic mixtures the compositions were made in such a way that the components do not interact with Ru(III) and PTQA in the condition described in general procedure. From suitable aliquots, the ruthenium(III) con-

Table 2
Analysis of synthetic mixtures (recovery studies of ruthenium(III))

Sample	Composition of synthetic mixture/mg l^{-1}	Ru(III) taken/mg l^{-1}	Ru(III) found[a]/mg l^{-1}	Per cent recovery[a] ± standard deviation
A	$Ru^{3+}(0.05)+Al^{3+}(1.0)+As^{5+}(1.0)+Ca^{2+}(2.0)+Cr^{3+}(1.0)+Tl^{+}(1.0)$+tartrate (100)	0.0500	0.0502	100.4 ± 0.0030
B	As in sample A+$Mg^{2+}(2.0)+Th^{4+}(1.0)+U^{6+}(1.0)+Cd^{2+}(1.0)+Mn^{2+}(1.0)$	0.0500	0.0495	99.0 ± 0.0032
C	As in sample B+$Li^{+}(2.0)+Pb^{2+}(1.0)+Se^{6+}(1.0)+B^{3+}(1.0)+Ba^{2+}(1.0)$	0.0500	0.0503	100.6 ± 0.0041
D	As in sample C+$Ni^{2+}(1.0)+Co^{2+}(1.0)+Zn^{2+}(1.0)+V^{5+}(1.0)+W^{6+}(0.5)$	0.0500	0.0505	101.0 ± 0.0037
E	As in sample D+$Bi^{5+}(1.0)+La^{3+}(1.0)$+azide (50)	0.0500	0.0486	97.2 ± 0.0042
F	as in sample E+$Os^{8+}(0.25)+Ir^{3+}(0.25)+Pt^{4+}(0.25)+Rh^{3+}(0.25)+Pd^{2+}(0.25)$	0.0500	0.0494	98.8 ± 0.0045

[a] Average of five replicate determinations.

Table 3
Analysis of synthetic ores (osmiridium)

Name of sample and composition[18]/%	Composition of synthetic mixture/μg l^{-1}	Ru taken/μg l^{-1}	Ru found[a]/μg l^{-1}	Per cent recovery[a] ± standard deviation
South Africa Ru(8.9), Os(69.9), Ir(17), Pt(0.2)	Ru (1000)	40	40.3	100.8 ± 2.8
	Os (7690) Ir (1925) Pt (25)	80	80.1	100.1 ± 2.5
Colombia Ru(6.37), Os(35.1), Ir(57.8), Pd(0.63)	Ru (1000)	40	40.5	101.3 ± 3.0
	Os (5560) Ir (9160) Pd (110)	80	80.7	100.9 ± 2.7
Australia Ru(5.22), Os(33.46), Ir(58.13), Pd(3.04)	Ru (1000)	40	39.8	99.5 ± 2.8
	Os (6410) Ir (11140) Pd (580)	80	81.2	101.5 ± 2.9

[a] Average of three determinations.

tent, was then determined fluorimetrically by the procedure described earlier. The mixture composition and results are shown in Table 2. The Table shows the excellent recoveries of ruthenium(III) in synthetic matrices containing Os(VIII), Pd(II), Ir(III), Pt(IV), Rh(III), Co(II), Ni(II) etc.

3.9.2. Determination of ruthenium in synthetic ores

As no Ru-bearing standard samples were available for testing the validity of the method for the analysis of real samples, the method was applied to synthetic mixtures corresponding to osmiridium samples [18]. Synthetic mixtures containing platinum metals corresponding to osmiridium were prepared and ruthenium content was then determined. The results are shown in Table 3. The results in Table 3 show that the recoveries were satisfactory.

Table 4
Determination of ruthenium in certified reference materials

Reference sample and composition% (w/w)	Ru(III) spiked		
	Added/μg l^{-1}	Found[a]/μg l^{-1}	Per cent[a] recovery ± standard deviation
NBS 33 b (cast iron) Mn = 0.64, Si = 2.74, Mo = 0.04, Cr = 0.61, Ni = 2.24, P = 0.11	0.0	0.0	–
	40	40.2	100.5 ± 3.6
	80	80.1	100.1 ± 3.2
MS le (mild steel) Mn = 0.65, C = 0.20, Si = 0.06, S = 0.052, *P* = 0.041	0.0	0.0	–
	40	40.4	101.0 ± 3.0
	80	79.6	99.5 ± 3.5

[a] Average of five determinations.

Table 5
Analysis of ruthenium in rock samples

Sample	Ruthenium/μg g^{-1}	
	I.C.P. AES method	Proposed method[a]
Rock 1 (sulphide ore of copper and nickel)	3.52	3.67 ± 0.04
Rock 2 (chromite ore)	10.15	10.32 ± 0.03
Rock 3 (chromite ore)	7.50	7.79 ± 0.03

[a] Average of three determinations ± standard deviation.

3.9.3. Ruthenium determination in certified reference materials

The possibility of using the method for analysis of alloys and catalysts was tested by determining the recovery of known amounts of ruthenium (III) added to the samples of ferrous alloy, (NBS (33 b) and MS le). The standard addition technique was followed to evaluate the reproducibility and effectiveness of the method. The results showed high reproducibility of the method in its application to the alloy analysis (Table 4).

3.9.4. Determination of ruthenium in rock samples

The method was extended to the determination of ruthenium in PGM-bearing rock-samples (sulphide ore of copper and nickel and chromite ore).

The digestion procedure is very important for ruthenium. Depending on the power of oxidizing agents and the temperature, a considerable amount of ruthenium may be lost [19,20]. The loss of ruthenium during digestion can be reduced using PTFE vessel under pressure. The ratio of base metals to ruthenium in rock samples was very high. Thus ruthenium was separated from large amount of base metals by ion exchange [14].

A 5 ml rock sample solution was digested according to the method described earlier, was treated and subjected to the ion exchange separation, as described earlier. After chloride removal by evaporation with H_2SO_4 the solution was diluted with water to 25 ml. Aliquots of the ion exchanged solution were taken for ruthenium analysis fluorimetrically according to the general procedure. The results of rock analyses by the fluorimetric method were found to be in excellent agreement with those obtained by inductively coupled plasma atomic emission spectrometry. The results are shown in Table 5.

4. Conclusion

The PTQA [2-(α-pyridyl) thioquinaldinamide] method has the requisite sensitivity to determine ruthenium at the low part per billion in rock (ore) or in solution. The method is approximately ten times more sensitive and selective that existing fluorimetric procedure. The method is accurate and rapid. It can serve as a routine method particularly valuable for Geochemical investigations.

Acknowledgements

One of the authors (M.S.R.) gratefully acknowledges the laboratory facilities provided by Jadavpur University, Calcutta and also expresses his gratitude to Rajshahi University (Bangladesh) Authority for granting study leave. The free service of COSIST equipment, Shimadzu (RF-5000) of the Department of Chemistry of Jadavpur University sanctioned by the University Grants Commission is also gratefully acknowledged.

References

[1] G.G. Robson, Platinum 1987, Johnson Matthey, London, 1987.
[2] F.J. Smith, Platinum 1989, Johnson Matthey, London, 1989.
[3] J.C. Chaston, Platinum Metals Rev. 26 (1982) 3.
[4] G. Mestroni, G. Zassinovich, E. Allesio, A. Bontempi, Inorg. Chim. Acta 137 (1987) 63.
[5] G. Sava, S. Zorzet, T. Giraldi, G. Mestroni, G. Zassinovich, Eur. J. Cancer Clin. Oncol. 20 (1984) 841.
[6] H. Veening, W.W. Brandt, Anal. Chem. 32 (11) (1960) 1426.
[7] D.P. Shcherbov, G.P. Gladysheva, A.I. Ivankova, Zavod. Lab. 37 (11) (1971) 1300.
[8] S. Jingxuan, S. Yuming, P. Yucheng, Z. ran Kexueban 2 (1986) 40.
[9] H.D. Proter, J. Am. Chem. Soc. 76 (1954) 127.

[10] F.E. Beamish, The Analytical Chemistry of the Noble metals, Pergamon, Oxford, 1966.
[11] A.I. Vogel, A Text Book of Quantitative Inorganic Analysis, 3rd edition, ELBS and Longman, London, 1969, p. 293.
[12] B.K. Pal, B. Chowdhury, Mikrochim. Acta, (Wien) II (1984) 121.
[13] A. Chatterjee, D. Das, D. Chakraborty, Environ. Pollution 80 (1993) 57.
[14] H. Zachariasen, F.E. Beamish, Anal. Chem. 34 (8) (1962) 964.
[15] M. Valcarcel, F. Grases, Talanta 30 (3) (1983) 139.
[16] M. Otto, H. Mueller, G. Werner, Talanta 25 (1978) 123.
[17] S.E. Livingstone, The Chemistry of Ruthenium, Rhodium, Palladium, Osmium, Iridium and Platinum, Pergamon Press, Oxford, 1973, p. 1205.
[18] J.W. Mellor, A Comprehensive Treatise on Inorganic and Theoretical Chemistry, vol. XVI, Longmans, London, 1957, p. 6.
[19] S.B. Shirey, R.J. Walker, Anal. Chem. 67 (13) (1995) 2136.
[20] Y. Vin Yi, A. Masuda, Anal. Chem. 68 (1996) 1444.

ELSEVIER

Talanta 48 (1999) 1085–1094

Talanta

Spectrophotometric method for determination of vanadium and its application to industrial, environmental, biological and soil samples

M. Jamaluddin Ahmed *, Saera Banoo

Laboratory of Analytical Chemistry, Department of Chemistry, University of Chittagong, Chittagong 4331, Bangladesh

Received 28 May 1998; received in revised form 6 October 1998; accepted 7 October 1998

Abstract

The very sensitive, fairly selective direct spectrophotometric method for the determination of trace amount of vanadium (V) with 1,5-diphenylcarbohydrazide (1,5-diphenylcarbazide) has been developed. 1,5-diphenylcarbohydrazide (DPCH) reacts in slightly acidic (0.0001–0.001 M H_2SO_4 or pH 4.0–5.5) 50% acetonic media with vanadium (V) to give a red–violet chelate which has an absorption maximum at 531 nm. The average molar absorption coefficient and Sandell's sensitivity were found to be 4.23×10^4 l mol^{-1} cm^{-1} and 10 ng cm^{-2} of V^v, respectively. Linear calibration graph were obtained for 0.1–30 μg ml^{-1} of V^v: the stoichiometric composition of the chelate is 1:3 (V: DPCH). The reaction is instantaneous and absorbance remain stable for 48 h. The interference from over 50 cations, anions and complexing agents has been studied at 1 μg ml^{-1} of V^v. The method was successfully used in the determination of vanadium in several standard reference materials (alloys and steels), environmental waters (potable and polluted), biological samples (human blood and urine), soil samples, solution containing both vanadium (V) and vanadium (IV) and complex synthetic mixtures. The method has high precision and accuracy ($s = \pm 0.01$ for 0.5 μg ml^{-1}).

Keywords: Spectrophotometry; Vanadium determination; 1,5-diphenylcarbohydrazide; Alloy; Steel; Environmental; Biological samples; Soil samples

1. Introduction

Vanadium poisoning is an industrial hazard [1]. Environmental scientists have declared vanadium as a potentially dangerous chemical pollutant that can play havoc with the productivity of plants, crops and the entire agricultural system. High amounts of vanadium are said to be present in fossil fuels such as crude petroleum, fuel, oils, some coals, and lignite. Burning these fuels releases vanadium into the air that then settles on the soil. There are cases of vanadium poisoning, the symptoms of which are nervous depression, coughing, vomiting, diarrhoea, anaemia and increased risk of lung cancer, that are sometimes

* Corresponding author. Fax: +880-31-610938/726310; e-mail: vc-cu@spnetctg.com.

0039-9140/99/$ - see front matter
PII: S0039-9140(98)00329-4

fatal [2]. Recently, vanadium has been noticed as the index element in urban environmental pollution, especially air pollution [3]. Laboratory and epidemiological evidence suggests that vanadium may also play a beneficial role in the prevention of heart-disease [4]. Shamberger [5] has pointed out that human heart-disease death rates are lower in countries where more vanadium occurs in the environment. Vanadium in environmental samples has been determined by NAA [6], ICP-atomic emission spectrometry [7], AAS [8] and spectrophotometry [10–22]. The first two methods are disadvantageous in terms of cost and instruments used in routine analysis. AAS is often lacking in sensitivity and affected by matrix conditions of samples such as salinity. Catalytic solvent extractive methods are highly sensitive but are generally lacking in simplicity. Hence its accurate determination at trace levels using simple and rapid methods is of paramount importance.

The aim of this study is to develop a simpler direct spectrophotometric method for the trace determination of vanadium. 1,5-Diphenylcarbohydrazide (DPCH) has been reported as a spectrophotometric reagent for chromium [9] and has previously been used for spectrophotometric determination of vanadium [10] but this method is solvent extractive, lengthy and time consuming and lack selectivity due to much interference. Pyridine and chloroform had been used as solvents for this extraction which can be classified as toxic and as environmental pollutants [3] and have been listed as carcinogens by the Environmental Protection Agency (EPA) [9a]. This paper reports its use in a very sensitive, highly specific non-extractive spectrophometric method for trace determination of vanadium. The method possesses distinct advantages over existing methods with respect to sensitivity [10–15], selectivity [10–15,18–22], range of determination [10–15], simplicity [10–13,17], speed [10,12,18], pH/acidity range [10,17–22], thermal stability [10–22], accuracy [10–15,22], precision [10–22] and ease of operation [10–22]. The method is based on the reaction of non-absorbent DPCH in slightly acidic solution (0.0001–0.001 M sulfuric acid or pH 4.0–5.5) with vanadium (V) to produce a highly absorbent red–violet chelate product followed by direct measurement of the absorbance in aqueous solution. With suitable masking, the reaction can be made highly selective and the reagent blank solutions do not show any absorbance.

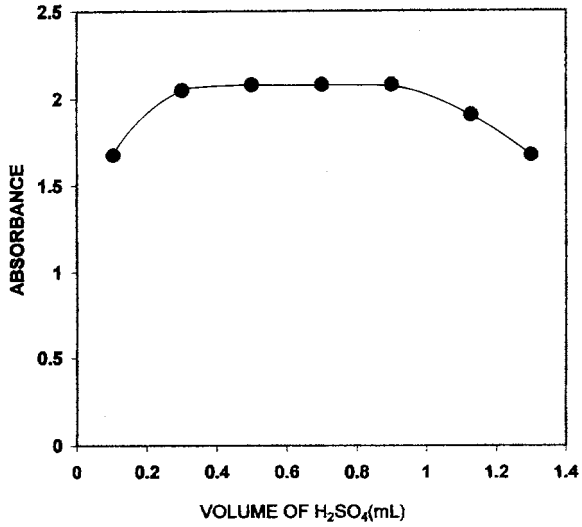

Fig. 1. Effect of the acidity on the absorbance V(V) DPCH-system.

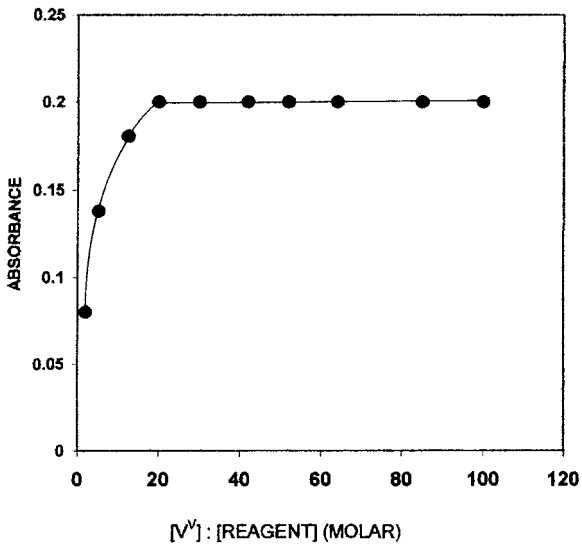

Fig. 2. Effect of reagent (DPCH:V(V) molar concentration ratio) on the absorbance of V(V)-DPCH system.

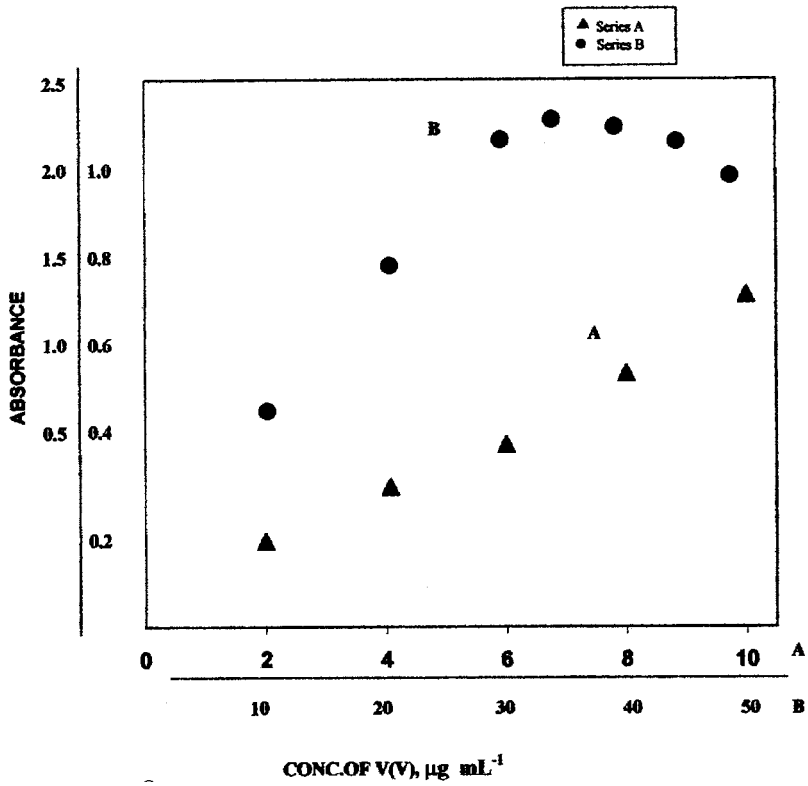

Fig. 3. Calibration graphs: A, 1–10 μg ml^{-1} of vanadium (V) and B, 10–30 μg ml^{-1} of vanadium (V).

2. Experimental

2.1. Apparatus

A Shimadzu (Kyoto, Japan) (model-160) double-beam UV/VIS spectrophotometer and Jenway (England, UK) (Model 3010) pH meter with a combination of electrodes were used for the measurements of absorbance and pH, respectively. A Shimadzu (Model 5000) atomic absorption spectrometer equipped with a microcomputer-controlled graphite furnace was used for comparison of the results.

2.2. Reagents

All chemicals used were of analytical-reagent grade or the highest purity available.

Doubly distilled de-ionized water and HPLC-grade acetone, which is non-absorbent under ultraviolet radiation, were used throughout.

2.2.1. DPCH solution, $4.12 \times 10^{-4}M$

Prepared by dissolving the requisite amount of DPCH (Merck Darmastadt, Germany) in a known volume of distilled acetone. More dilute solutions of the reagent were prepared as required.

2.2.2. Vanadium (V) standard solutions

A 100-ml amount of stock solution (1 mg ml^{-1}) of pentavalent vanadium was prepared by dissolving 0.2269 mg of ammonium metavanadate (Merck) in doubly distilled de-ionized water containing 1–2 ml of nitric acid (1 + 1). More dilute standard solutions were prepared from this stock solution as and when required.

2.2.3. Vanadium (IV) stock solution

A 100-ml amount of stock solution (1 mg ml^{-1}) was prepared by dissolving 390.7 mg of purified grade vanadyl sulfate (Fisher Scientific) in

doubly distilled de-ionized water. The working standard of vanadium (IV) was prepared by appropriate dilution of this solution.

2.2.4. Other solutions

Solutions of a large number of inorganic ions and complexing agents were prepared from their AnalaR grade or equivalent grade water soluble salts. In the case of insoluble substances, special dissolution methods were adopted [23].

All glassware was kept in nitric acid (1 + 1) for at least a day and then was rinsed with de-ionized water before use. Stock solutions and environmental water samples were kept in poly (propylene) bottles containing 1 ml of concentrated nitric acid.

3. Procedure

To 0.1–1 ml of slightly acidic solutions containing 1–300 μg of vanadium (V) in a 10-ml calibrated flask was mixed with a 0.1–1.0 (preferably 0.5 ml) of 0.001 M H_2SO_4 (or pH 4.0–5.5) followed by the addition of 20–100-fold molar excess of DPCH solution (preferably 1 ml of 4.12×10^{-4} M). After 1 min, 5 ml of acetone were added and the mixture was diluted to the mark with de-ionized water. The absorbance was measured at 531 nm against a corresponding reagent blank. The vanadium content in an unkown samples was determined using a concurrently prepared calibration graph.

4. Results and discussion

4.1. Factors affecting the absorbance

4.1.1. Absorption spectra

The absorption spectra of the vanadium (V)-DPCH system in 0.001 M sulfuric acid medium was recorded using the spectrophotometer. The absorption spectra of the vanadium (V)-DPCH is a symmetric curve with maximum absorbance at 531 nm and average molar absorption of 4.23×10^4 l mol^{-1} cm^{-1}. DPCH did not show any absorbance. In all instances measurements were made at 531 nm against a reagent blank. The reaction mechanism of the present method is as reported earlier [24].

4.1.2. Effect of solvent

Of the various solvents (benzene, chloroform, carbon tetrachloride, nitrobenzene, isobutyl alcohol, *n*-butanol, isobutyl methyl ketone, ethanol, acetone and 1,4-dioxane) studied, acetone was found to be the best solvent for the system. No absorbance was observed in the organic phase with the exception of *n*-butanol. In 50 ± 2% (v/v)

Table 1
Determination of vanadium in some synthetic mixtures

Sample	Composition of mixture (μg ml^{-1})	Vanadium (V) (μg ml^{-1})		
		Added	Found[a]	Recovery ± SD[b] (%)
A	V(V)	0.50	0.50	100 ± 0.0
		1.00	0.99	99 ± 0.5
B	As in A + Zn(25) + Cd(25) + Ca(25) + tartrate	0.50	0.49	98 ± 0.5
		1.00	1.01	101 ± 0.7
C	As in B + Mn^{2+}(25) + NO_3^-(25)	0.50	0.52	104 ± 1.0
		1.00	1.02	102 ± 0.8
D	As in C + Cr^{VI} (25) + NH_4^+(25)	0.05	0.05	100 ± 0.0
		1.00	1.02	102 ± 0.6
E	As in D + Co^{2+}(25) + K(25)	0.50	0.54	108 ± 1.5
		1.00	1.06	106 ± 1.3

[a] Average of five analyses of each sample.
[b] The measure of precision is the SD.

Table 2
Analysis of high-speed steel and alloys

Certified reference material (composition)	Vanadium(%) Certified value	Found[a]	SD
BAS-CRM 64b High-speed steel (Cr,Mo,Vand Tc)	1.99	1.98	±0.05
BCS-CRM 241/1 High-speed steel (Cr,V,W,Co, Mn, C, Si, Pand S)	1.57	1.58	±0.07
BCS-CRM 220/1 High-speed steel (C,Si,S,P,Mn, Mo,V,Ni,Cr,Co, W and Cu)	2.09	2.10	±0.06
BAS-CRM 10g High tensil (Cu,Sn,Zn,Pb,Ni,Fe,Al,Mn, and V)	0.52	0.58	±0.08

[a] Average of five determinations.

acetonic medium, however, maximum absorbance was observed; hence a 50% acetonic solution was used in the determination procedure.

4.1.3. Effect of acidity

Of the various acids (nitric, sulfuric, hydrochloric and phosphoric) studied, sulfuric acid was found to be the best acid for the system. The absorbance was at a maximum and constant when the 10 ml of solution (1 μg ml^{-1}) contained 0.1–1.0 ml of 0.001 M sulfuric acid (or pH 4.0–5.5) at room temperature (25 ± 5°C). Outside this range of acidity, the absorbance decreased (Fig. 1). For all subsequent measurements 0.5 ml of 0.001 M sulfuric acid (or pH 4.75) was added.

4.1.4. Effect of time

The reaction is very fast constant maximum absorbance was obtained just after the dilution to volume and remained strictly unaltered for 48 h.

4.1.5. Effect of reagent concentration

Different molar excesses of DPCH were added to fixed metal ion concentration and absorbance were measured according to the standard procedure. It was observed that at 1 μg ml^{-1} V-chelate metal, the reagent molar ratio 1:20 and 1:100 produce a constant absorbance of the V-chelate (Fig. 2). Greater excesses of reagent were not studied.

4.1.6. Calibration graph (Beer's law and sensitivity)

The effect of metal concentration was studied over 0.1–30 μg ml^{-1} distributed in three different sets (0.1–1.0, 1–10, and 10–30 μg ml^{-1}) for convenience of measurement. The absorbance was linear for 0.1–30 μg ml^{-1} of vanadium at 531 nm (Fig. 3). The molar absorption coefficient and the Sandell's sensitivity [25] were 4.23×10^4 l mol^{-1} cm^{-1} and 10 ng cm^{-2} of V^v, respectively.

4.1.7. Effect of foreign ions

The effect of over 50 ions and complexing agents on the determination of only 1 μg ml^{-1} of V^v was studied. The criterion for an interference [26] was an absorbance value varying by more than 5% from the expected value for vanadium alone. There was no interference from the following: 1000-fold amount of sulfate, sulfite, nitrate, perchloride, bromide, chloride, iodide, thiocyanide, Na, Mg, Ba,K, Mn^{II}, Zn, NH_4^+, Ca or Cd; 100-fold amounts of tartrate, fluoride, Co^{III}, Ni^{II} or Hg^{II}; 10-fold amounts of EDTA, oxalate, citrate, Cr^{III}, Pb^{II} azide, persulphate, phosphate, W^{VI}, As^{III}, As^V, Cs, Mn^{VII},Cr^{VI}, Fe^{II}, Fe^{III}, CN^-, or U^{VI}. EDTA prevented the interference of a 10-fold amounts of Ag, Al, Cu^{II} or Mo^{VI}. The quantities of these diverse ions mentioned were the actual amounts added and not the tolerance limits. A 50-fold excess of iron Fe^{II} and Fe^{III} or Cu^{II} could be masked with ammonium thiocyanate or fluoride. During the interference studies, if a precipitate was formed, it was removed by centrifugation.

4.1.8. Composition of the absorbance

Job's method [27] of continuous variation and the molar-ratio [28] method were applied to ascertain the stoichiometric composition of the complex. A V-DPCH (1:3) complex was indecated by both methods.

4.1.9. Precision and accuracy

The relative SD ($n = 5$) was 1.5–0.0% for 1–300 μg of vanadium in 10.0 ml, indicating that this method is highly precise and reproducible. The detection limit (3 SD of the blank) and Sandell's sensitivity (concentration for 0.001 ab-

Table 3
Determination of vanadium in some environmental water samples

Sample	Vanadium, μg l^{-1} Added	Found[a]	Recovery ± SD (%)	SD_r (%)[b]
Tap water	0	1.6	±0.1	0.31
	100	101.05	99.9 ± 0.2	0.35
	500	502.0	100 ± 0.1	0.42
Well water	0	8.0		
	100	107.0	99 ± 0.3	0.19
	500	509.0	100.2 ± 0.4	0.39
Rain water	0	1.4		
	100	102.0	100.5 ± 0.1	0.14
	500	501.5	100 ± 0.0	0.00
River water				
Karnaphuli (upper)	0	11.2		
	100	112.0	100.7 ± 0.3	0.18
	500	511.0	100 ± 0.0	0.00
Karnaphuli (lower)	0	14.4		
	100	115.0	100.4 ± 0.2	0.3
	500	513.0	99.7 ± 0.4	0.37
Sea-water				
Bay of Bengal (upper)	0	5.0		
	100	104.0	99 ± 0.01	0.08
	500	505.0	100 ± 0.0	0.00
Bay of Bengal (lower)	0	6.0		
	100	106.0	100 ± 0.0	0.00
	500	507.0	100.2 ± 0.05	0.08
Lake water				
Kaptai (upper)	0	18.5		
	100	119.0	100.4 ± 0.4	0.29
	500	520.0	100.3 ± 0.5	0.34
Kaptai (lower)	0	20.0		
	100	119.0	99 ± 0.3	0.41
	500	5021.0	100.2 ± 0.2	0.32
Drain water				
Karnaphuli Paper Mill[c]	0	35.00		
	100	136.0	100.7 ± 0.5	0.45
	500	536.0	102.0 ± 0.6	0.35
Steel Mill[d]	0	75.0		
	100	176.0	100.6 ± 0.3	0.08
	500	580.0	100.9 ± 0.5	0.15
Eastern refinery[e]	0	145.0		
	100	250.0	102.0 ± 0.6	0.49
	500	640.0	99.2 ± 0.5	0.55

[a] Average of five replicate determinations.
[b] The measure precision is the relative SD.
[c] Karnaphuli Paper Mill, Chandraghona, Chittagong
[d] Chittagong Steel Mill, Patenga, Chittagong.
[e] Eastern Refinery, North Patenga, Chittagong.

Table 4
Concentration of vanadium in blood and urine samples

Serial No.	Sample	Vanadium, μg l^{-1}		Sample source[b]
		AAS	Proposed method[a]	
1	Blood	9.0	10.0 ± 1.5	Heart-diseases
	Urine	2.5	2.8 ± 1.2	Patient (male)
2	Blood	370.0	381.0 ± 1.0	Lung cancer
	Urine	75.0	85.0 ± 1.5	Patient (male)
3	Blood	10.0	12.0 ± 1.4	Normal
	Urine	3.0	3.2 ± 1.3	Adult (male)

[a] Average of five determinations ± SD.
[b] Samples were from Dhaka Medical College Hospital.

sorbance unit) for vanadium (V) were found to be 20 ng ml^{-1} and 10ng cm^{-2}, respectively. The result for total vanadium were in good agreement with certified values (Table 2). The reliability of our V-chelate procedure was tested by recovery studies. The average percentage recovery obtained for addition of a vanadium (V) spike to some environmental water samples was quantitative as shown in Table 3. The method was also tested by analysing several synthetic mixtures containing vanadium (V) and diverse ions. The results of biological analyses by the spectrophotometric method were excellent agreement with those obtained by AAS (Table 4). The precision and accuracy of the method were excellent.

4.2. Applications

4.2.1. Determination of vanadium in synthetic mixtures

Several synthetic mixtures of varying compositions containing vanadium (V) and divers ions of known concentrations were determined by the present method using sodium tartrate as masking agent. The results are shown in Table 1.

4.2.2. Determination of vanadium in alloys and steels

A 0.1 g amount of an alloy or steel samples containing 0.52–2.09% of vanadium was weighed accurately and placed in a 50 ml Erlenmeyer flask. To it, 10 ml of 20% (v/v) sulfuric acid was added, carefully covering with a watch-glass untill the brisk reaction subsided. The solution was heated and simmered gently after addition of 5 ml of concentrated HNO_3 untill all carbides were decomposed. Then 2 ml of 1:1 (v/v) H_2SO_4 was added and solution was evaporated carefully to dense white fumes to drive off the oxides of nitrogen and then cooled to room temperature (25–30°C). After suitable dilution with de-ionized

Table 5
Determination of vanadium in some surface soil samples[a,b]

Sl. No.	Vanadium (μg g^{-1})	Sample source
S_1[c]	0.0295	Clevedon Tea Estate (Sylhet)
S_2	0.0401	Esturine soil (Karnaphuli)
S_3	0.0215	Chittagong University Campus
S_4	0.0265	Karnaphuli Paper Mill
S_5	0.0198	Marine Soil (Bay of Bangle)
S_6	0.0310	Steel Mill
S_7	0.0295	Clevedon Tea Estate (Sylhet)
S_8	0.0229	Bangladesh Oxygen Company (BOC)
S_9	0.0225	T.S.P. Complex
S_{10}	0.0570	Eastern Refinery

[a] Mean = 0.03 (μg g^{-1})
[b] SD = ±0.01
[c] Composition of the soil samples: C, N, P, K, Na, Ca, Mg, Fe, NO_3, NO_2, Zn, SO_4, Mn, Mo, Co etc.

Table 6
Determination of vanadium (IV) and vanadium (V) speciation in mixtures

Sl. No.	V (V):V(IV)	V, taken (μg ml^{-1})		V,found (μg ml^{-1})		Error (μg ml^{-1})	
		V(V)	V(IV)	V(V)	V(IV)	V(V)	V(IV)
1	1:1	1.00	1.00	0.99	0.98	0.01	0.02
2	1:1	1.00	1.00	1.00	1.00	0.00	0.00
3	1:1	1.00	1.00	0.99	0.98	0.01	0.02
Mean error: V(V) = ±0.0067; V(IV) = ±0.013							
SD: V(V) = ±0.0058; V(IV) = ±0.011							
1	1:5	1.00	5.00	0.99	4.98	0.01	0.02
2	1:5	1.00	5.00	0.98	4.98	0.02	0.02
3	1:5	1.00	5.00	0.99	4.99	0.01	0.01
Mean error: V(V) = ±0.013; V(IV) = ±0.016							
SD: V(V) = ±0.0058; V(IV) = ±0.0058							
1	1:10	1.00	10.00	0.98	10.99	0.02	0.01
2	1:10	1.00	10.00	0.99	10.98	0.01	0.02
3	1:10	1.00	10.00	0.98	10.98	0.02	0.02
Mean error: V(V) = ±0.016; V(IV) = ±0.016							
SD: V(V) = ±0.0058; V(IV) = ±0.0058							

water, the contents of the Erlenmeyer flask were warmed to dissolve the soluble salts. The solution was then cooled and neutralized with dilute NH_4OH in the presence of 1–2 ml 0.01% (w/v) tartrate solution. The resulting solution was filtered, if necessary, through a Whatman No. 40 filter paper into a 50-ml calibrated flask. The residue (silica and tungstic acid) was washed with a small volume of hot (1 + 99) H_2SO_4 followed by water and the volume was made up to the mark with de-ionized water.

A suitable aliquot of the above solution was taken into a 10-ml calibrated flask and the vanadium content was determined as described under procedure using thiocyanide or fluoride as masking agent. The results are shown in Table 2.

4.2.3. Determination of vanadium in environmental water samples

Each filtered environmental water sample (1000 ml) was evaporated nearly to dryness with a mixture of 1 ml of concentrated H_2SO_4 and 5 ml of concentration HNO_3 in a fume cupboard and was then heated with 10 ml of de-ionized water in order to dissolve the salts. The solution was then cooled and neutralized with dilute NH_4OH in the presence of 1–2 ml of 0.01% w/v tartrate solution. The resulting solution was then quantitatively transferred into a 25-ml calibrated flask and made upto the mark with de-ionized water.

An aliquot 1 ml of this preconcentrated water sample was pipetted into a 10-ml calibrated flask and the vanadium content was determined as described under procedure using thiocyanide or fluoride as a masking agent. The results are shown in Table 3.

Most spectrophotometric methods for the determination of vanadium in natural and sea-water require preconcentration of vanadium [29]. The concentration of vanadium in nutral and sea-water is a few ng ml^{-1} in Japan [17]. The mean concentration of vanadium found in US drinking waters is 6 ng ml^{-1} [29].

4.2.4. Determination of vanadium in biological samples

Human blood (20–50 ml) or urine (30–50 ml) was taken into a 100-ml micro-Kjeldahl flask. A glass bead and 5 ml of concentrated nitric acid were added and the flask was placed on the digester under gentle heating. When the initial brisk reaction was over, the solution was removed and cooled. Sulfuric acid (1 ml of concentrated) was added carefully followed by the addition of 1

ml of 70% perchloric acid and heating was continued to dense white fumes, repeating nitric acid addition if necessary. Heating was continued for at least 1/2 h. and then cooled. The content of the flask was filtered and neutralized with dilute NH_4OH in presence of 1–2 ml of 0.01% (w/v) tartrate solution, transferred quantitatively into a 10-ml calibrated flask and made upto the mark with de-ionized water.

A suitable aliquot of this preconcentrated solution was pipetted out into a 10-ml calibrated flask and the vanadium content was determined as described under procedure using thiocyanide or fluoride as masking agent. The results of biological analyses by the spectrophotometric method were found to be in excellent agreement with those obtained by AAS. The results are shown in Table 4.

The abnormally high value for the lung cancer patient is probably due to the involvement of high vanadium concentrations with As and Zn. Occurrence of such high vanadium contents are also reported in cancer patients from some developed countries [2]. The low value for the heart-disease patient is probably due to a low vanadium concentration in the environment. There is an inverse correlation between human heart-disease and vanadium concentration in the environment [29].

4.2.5. Determination of vanadium in soil samples

An air-dried homogenized soil sample (100 g) was weighed accurately and placed in a 100-ml Kjeldahl flask. The sample was digested in the presence of an oxidizing agent following the method recommended by Jackson [30]. The content of flask was filtered through a Whatman No. 40 filter paper into a 25-ml calibrated flask and neutratized with dilute ammonia in the presence of 1–2 ml of 0.01% (w/v) tartrate solution. It was then diluted up to the mark with de-ionized water.

Suitable aliquots 1–2 ml was transferred into a 10-ml calibrated flask and a calculated amount of 0.001 M sulfuric acid needed to give a final acidity of 0.0001–0.001 M H_2SO_4 (or pH 4.0–5.5) was added followed by 1–2 ml of 0.01% (w/v) thiocyanide or fluoride solution as masking agent. Vanadium was then determined by the above procedure and quantified from calibration graph prepared concurrently. The results are shown in Table 5.

4.2.6. Determination of vanadium (IV) and vanadium (V) speciation in mixtures

Suitable aliquots (1–2 ml) of vanadium (IV + V) mixtures (preferably 1:1, 1:5, 1:10) were taken in a 25 ml conical flask. A few drops of 0.001 M sulfuric acid and 1–3 ml of 1% (w/v) potassium permanganate solution was added to oxidize the tetravalent vanadium. 5 ml of water was added to the mixtures and heated on the steam bath for 10–15 min. with occasional gentle shaking and then cooled to room temperature. Then 3–4 drops of freshly prepared sodium azide solution (2.5% w/v) was added and heated gently with further addition of 2–3 ml of water, if necessary, for 5 min. to drive off the azide cooled to room temperature. The reaction mixture was transferred quantitatively into a 10-ml volumetric flask, 1 ml of 4.12×10^{-4}M DPCH reagent solution was added followed by addition of 0.5 ml of 0.001 M H_2SO_4, it was made up to the mark with de-ionized water. The absorbance was measured after 1 min. at 531 nm against a reagent blank. The total vanadium content was calculated with help of the calibration graph.

An equal aliquot of the above vanadium (IV + V) mixture was taken in a 25 ml beaker, 1 ml of 0.01% (w/v) tartrate was added to mask vanadium (IV) and neutralize with dilute NH_4OH. The content of the beaker was transferred in to a 10-ml volumetric flask, then 0.5 ml of 0.001 M sulfuric acid solution was added followed by addition of 1 ml of 4.12×10^{-4} M DPCH and made up to a volume with de-ionized water. After 1 min the absorbance was measured against a reagent blank, as before. The vanadium concentration was calculated in $\mu g\ l^{-1}$ or $\mu g\ ml^{-1}$ with the aid of a calibration graph. This gives a measure of vanadium (V) originally present in the mixture. This value was substracted from that of the total vanadium to get vanadium (IV) present in the mixture. The results were found to be highly reproducible. Occurrence of such reproducible results are also reported for different oxidation states of vanadium [31]. The results of a set of determination are given in Table 6.

5. Conclusion

The proposed method using DPCH not only is one of the most sensitive methods for the determination of vanadium but also is excellent in terms of selectivity and simplicity. Therefore this method will be successfully applied to the monitoring of small amounts of vanadium in environmental, biological and soil samples. No extraction step is required and hence the use of organic solvents, which are generally toxic pollutants, is avoided.

References

[1] G.D. Clayton, F.E. Clayton (Eds.), Patty's Industrial Hygiene and Toxicology, vol. 2A, 3rd ed., Wiley, New York, 1981 p. 2013.
[2] B. Venugopal, T.D. Luckey, Metal Toxicity in Mammals, vol. 2, Plenum Press, New York, 1979, p. 220.
[3] S. Langard, T. Norseth, in: L. Friberg, G.F. Nordberg, V.B. Vouk (Eds.), Handbook on the Toxicology of Metals, Elsevier, Amsterdam, 1986.
[4] M. Mracova, D. Jirova, H. Janci, J. Lener, Sci. Total Environ., part 1, 1993 E 16/633.
[5] R.J. Shamberger, M.S. Gunsch, C.F. Willis, I.J. McCormack, in: D.D. Hemphil (Eds.), Trace Substances in Environmental Health XII, University of Missouri, Columbia, 1978.
[6] R.R. Greenberg, H.M. Kingston, Anal. Chem. 55 (1983) 1160.
[7] C.F. Wang, T.T. Miau, J.Y. Perng, S. J. Yeh, P.C. Chiang, H.T. Tsai, M.H. Yang, Analyst 114 (1989) 1067.
[8] T. Yamashige, M. Yamamoto, H. Sunahara, Analyst 114 (1989) 1071.
[9] M. Jamaluddin Ahmed, M. Salim, J. Bangladesh Acad. Sci. 16 (1992) 223. (a) Second Annual Report on Carcinogens, Environmental Protection Agency, NTP 81-43, Dec, 1981, pp. 73–80.
[10] S.P Arya, J.L. Malla, J. Indian Chem. Soc. 64 (4) (1987) 238.
[11] M. Jamaluddin Ahmed, Arpan Kanti Banerjee, Analyst 120 (1995) 2019.
[12] A.R.S. Chauhan, L.R. Kakkar, Chem. Anal 39 (5) (1994) 585.
[13] Rezaie Behrooz, A.K. Goswami, D.N. Purohit, Acta Cienc. Indica Chem. 19 (3) (1993) 101–102.
[14] A.E. Arifien, J. Chem. 4 (4) (1992) 804.
[15] M.J.C. Taylor, J.F. Van Staden, Analyst 119 (6) (1994) 1263.
[16] G. Chakrapani, D.S.R. Murty, B.K. Balaji, R. Rangaswamy, Talanta 40 (4) (1993) 541.
[17] J. Miura, Anal. Chem. 62 (1990) 1424.
[18] Y. Anjaneyulu, C.S. Kavipurapu, R.R. Manda, C.M. Pillutla, Anal. Chem. 58 (1986) 1451.
[19] Zotou C. Anastasia, C.G. Papadopoulos, Analyst 115 (1990) 323.
[20] E. Kavlentis, Anal. Lett. 22 (9) (1989) 2083.
[21] I. Mori, Y. Fujita, K. Fujita, T. Tanaka, Y. Nakahashi, A. Yoshu, Anal. Lett. 20 (5) (1987) 747.
[22] S.P. Bag, A.B. Chatterjee, A.K. Chakrabarti, P.R. Chakaraborty, Talanta 29 (1982) 526.
[23] B.K. Pal, B. Chowdhury, Mikrochim. Acta 2 (1984) 121.
[24] Analytical Chemistry of Rare Elements, A.I. Busev, V.G. Tiptsova, V. M. Ivanov (Eds.), Mir Publishers, Moscow, 1981, p. 385
[25] E.B. Sandell, Colorimetric Determination of Traces of Metals, 3rd ed., Interscience, New York, 1965, p. 269.
[26] C. Bosch Ojeda, A. Garcia de Torres, F. Sanchez Rojas, J.M. Cano Pavon, Analyst 112 (1987) 1499.
[27] P. Job, Ann. Chim. (Paris) 9 (1928) 113.
[28] J.A. Yoe, A.L. Jones, Ind. Eng. Chem. Anal. Ed. 16 (1944) 11.
[29] E. Arnold, Greenberg, S. Lenore, Clesceri, D. Andrew, Eaton (Eds.), Standard Methods for the Examination of Water and Wastewater, 18th ed., American Public Health Association, Washington DC, 1992, p. 3–98.
[30] M.L. Jackson, Soil Chemical Analysis, Prentice-Hall, Englewood Cliffs, 1965, p. 326.
[31] R.W. Wanty, M.B. Goldhaber, Talanta 32 (1985) 395.

ELSEVIER

Talanta 48 (1999) 1095–1101

Talanta

Investigation on the binding site in heparin by spectrophotometry

Q.C. Jiao [a], Q. Liu [a,*], C. Sun [b], H. He [c]

[a] *Department of Biological Science and Technology, Nanjing University, Nanjing 210093, People's Republic of China*
[b] *Department of Environmental Sciences and Engineering, Nanjing University, Nanjing 210093, People's Republic of China*
[c] *Division of Analytical Chemistry, China Pharmaceutical University, Nanjing 210093, People's Republic of China*

Received 8 July 1998; received in revised form 5 October 1998; accepted 7 October 1998

Abstract

Heparin has a variety of biological activities, most of them due to heparin's high sulfate groups. To gain insight into the mechanism of activation of the spectroscopic probe with sulfate groups of heparin *in vitro*, we have used a cationic dye by a spectrophotometric method. It is considered that the combination of heparin with methylene blue is due to noncovalent binding forces. Dye binding requires an organic chain structure form with sulfate groups. The solution equilibria of the reaction system are discussed. A new linear regression equation has been proposed, in which the maximum binding number N expresses the binding ability of methylene blue (MB) with sulfate groups of heparin. The linear regression equation can estimate this parameter.

Keywords: Spectroscopic probe; Heparin; Total binding number N

1. Introduction

Therapeutic emphasis on heparin traditionally has focused on its anticoagulant, antithrombotic, and antilipemic activities. However, recent evidence highlights the functional versatility of this molecule and its therapeutic potential outside these traditional areas [1], for example, its effect on angiogenesis to the regulation of the immune response [2]. It is known to interact with a wide variety of biological proteins, including proinflammatory chemokines, growth factors, extracellular matrix proteins, and leukocyte proteases [3–6], and to bind to platelets [7]. The efficacy of the heparin correlates with the gross sulfate content of the compound, reflecting a requirement for a level of sulfation not directly dependent upon the molecular weight or the anticoagulant activity [8,9].

In order to deeply understand heparin's physiological function *in vivo*, a spectroscopic probe is used for investigation the sulfate groups of heparin *in vitro*. The cationic dye methylene blue (MB) [10] is used here as a spectroscopic probe. Owing to the presence of the sulfate and carboxyl groups, the whole heparin molecule is negatively charged [1,11,12]. However, the MB species has a

* Corresponding author. Fax: +86-25-3592684; e-mail: zh@netra.nju.edu.cn.

0039-9140/99/$ - see front matter
PII: S0039-9140(98)00330-0

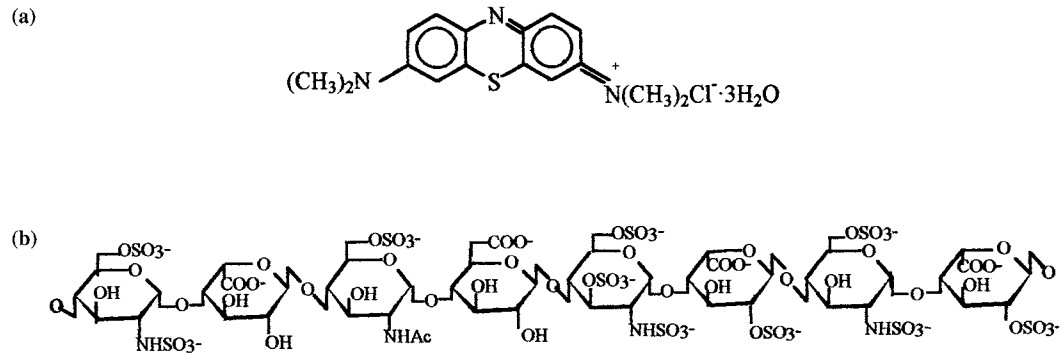

Fig. 1. (a) Structure of MB dye; (b) structure of heparin octasaccharide sequence.

positive charges. Therefore, the heparin and MB species should be bound together by electrostatic forces.

A study of this kind of reaction should be beneficial not only with regard to the mechanism of dye response but also to a deep understanding of the interaction between heparin and small ions or molecules.

2. Experimental

2.1. Apparatus

A Kontron Uvikon 860 spectrophotometer (Kontron Co., Switzerland) is used for recording absorption spectra, or measuring the absorbance at a given wavelength, using a 1 cm path length. A pH-HJ90B model portable acidity meter (Beijing Hangtian Computer Co, China) is used for the pH measurements.

2.2. Reagents

Heparin, sodium salt, ≥ 160 IU mg^{-1}, is obtained from Shanghai reagent factory and used without further purification. The average molecular mass of commercial heparin preparations is 12 000 Da [13]. The aqueous heparin solution (5.21×10^{-5} mol l^{-1}) is prepared by dissolving 50 mg heparin reagent in 80 ml deionized water. This stock solution of heparin is pipetted 2 ml into 100 ml volumetric flask, and then diluted to the mark with water. Low molecular weight heparin (LMWH) is kindly supplied by NanDa pharmaceutical Co., with an average molecular weight of 4000 Da. The aqueous LMWH solution (8.98×10^{-5} mol l^{-1}) is prepared by dissolving 17.95 mg LMWH reagent in 50 ml deionized water. This stock solution of LMWH is pipetted 8 ml into 100 ml volumetric flask, and then diluted to the mark with water. These stock solutions are stable for several weeks when kept in the dark at 4°C.

The MB is purchased from Shanghai (the third reagent factory). The MB stock solution (1.34×10^{-3} mol l^{-1}) is prepared by dissolving 500 mg dye in 1000 ml deionized water. The operating solution of MB is prepared by diluting 5 ml stock solution with water into 30 ml. Dye operating solution should be used soon after preparation, although little difficulty is encountered with dye solutions up to several h old. Due to light sensitivity of the dye, the MB stock solution must be stored in the dark Fig. 1.

All other reagents are of analytical or guaranteed reagent grade.

2.3. Methods

MB operating solution is transferred into a series of 12×100mm test tubes, then heparin solution, aliquots of NaCl and other components are added in different amounts to each test tube. The mixtures are diluted to a certain volume with water and mixed either by inversion or vortexing. After 4 min and before 2 h, spectra or absorbances of these solutions are measured with

reference to water. After 24 h a precipitate is not observed. Since the heparin–MB complex has a tendency to bind to cuvettes, there is a decrease in absorbance after long standing in cuvettes. As a precaution of the absorbance of samples should be read 1–5 min after the MB–heparin mixtures are pipetted into cuvettes. This still gives ample time to read samples. The binding of the heparin–MB complex has been observed only with quartz cuvettes and may be eliminated by using plastic cuvettes.

All runs are thermostated at room temperature and are performed in triplicate.

3. Results and discussion

3.1. Dye-heparin spectra

Fig. 2 shows the absorption spectra of MB dye and MB–heparin complexes from 400 to 800 nm. They are obtained by keeping the pH and MB concentrations constant and changing the heparin concentration. With an increase in heparin concentration, the absorption peaks at 664 and 614 nm decrease, while a new absorption peak at 566 nm appears. This peak, attributable to the heparin–dye complex, is apparently different from the absorption peak of the dye because the wavelengths corresponding to both absorbance maxima are different. The decrease in absorbance at 664 nm is in proportion to heparin concentration (these results also show that the assay at 664 nm is about twice as sensitive as that at 566 nm). Two isobestic points are found at 590 nm and 703 nm. Fig. 2 indicates that there are interactions between MB and heparin [14–16].

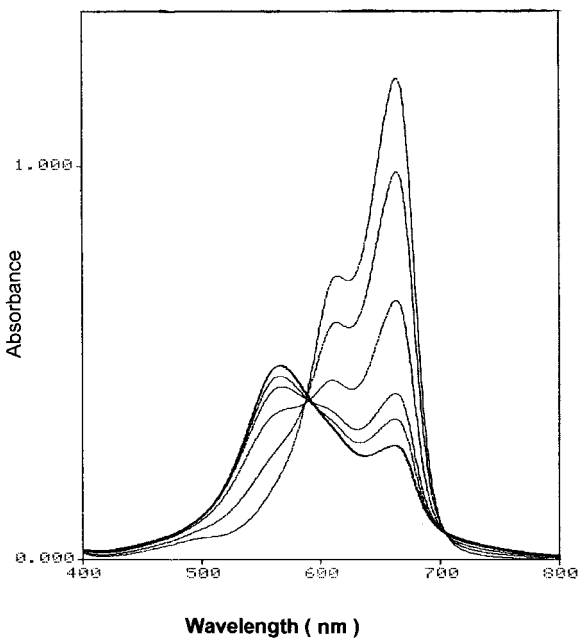

Fig. 2. Absorption spectra of MB–heparin mixtures. MB operating solution constants at 1.86×10^{-5} mol l^{-1}, pH 8.05. In order of decreasing peak absorbances at 664 nm, heparin concentrations are: 0.0, 8.68, 17.36, 26.03, 34.72, and 43.4×10^{-8} mol l^{-1} in total assay volume.

3.2. Structural requirements of heparin for dye binding

In view of the molecular structure of MB and heparin, it is not possible to reach a conclusion that MB combines preferentially with a particular group on heparin to form a complex. A reasonable explanation of these molecular events is that MB interacts with the anionic groups of heparin by non-specific, electrostatic forces.

To identify the heparin functional groups responsible for dye binding, we also test the response of the MB to a variety of inorganic salts (Table 1). None of these compounds gives a significant color response. The greatest color response is given by sodium dodecyl sulfate (SDS) (see Table 1). When SDS is added to heparin–dye complex, the inhibition on dye becomes slightly larger than that of heparin alone but is less than the expected extent. This indicates that SDS and heparin interact with the same site on the dye and compete against each other. Yutaka et al. [17] reported the metachromasia: For the first stage of metachromasia, a certain minimum surface density of negative charge was a primary requirement. The positively charged dye molecules were then attracted by the negative charge, and came close enough to aggregate. Under such conditions, π-electrons (including chromophore and auxochrome) of the dye interact with each other, so that a hypochromism and then a hypsochromism occurred.

Table 1
Effect of various reagents on MB–heparin complex and MB dye[a]

Substance	Concentration	Ionic strength	Absorbance at 664 nm	
			Blank (MB)	Hep–MB complex
1. Distilled water			1.20	0.48
2. Na_2SO_4	0.2 M	0.600	1.20	1.20
3. $(NH_4)_2SO_4$	0.2 M	0.600	1.20	1.20
4. Na_2SO_3	0.2 M	0.600	1.20	1.15
5. NaAC	0.2 M	0.200	1.20	1.00
6. PBS	0.2 M	0.578	1.20	1.20
7. NaCl	0.2 M	0.200	1.20	0.95
8. SDS	0.05%		0.47	0.49
9. PTA	0.10%		1.20	0.88

[a] The above values are obtained when 1ml of each substance is pipetted in the standard assay. NaAc, sodium acetate; PBS, sodium phosphate buffer. MB concentration is: 1.86×10^{-5} mol l^{-1}; heparin concentration is: 2.60×10^{-7} mol l^{-1}.

Na_2SO_4, like $(NH_4)_2SO_4$, has only one sulfate group. The dye activates these compounds by forming '1:1' binding complex, dye molecules could not come close enough to aggregate. Furthermore, it is demonstrated by lack of dye response to a wide range of inorganic anions and P-Toluenesulfonic acid (PTA) that nonelectrostatic interactions must play an important role in the metachromasia mechanism.

According to the model of Powell et al. [18], carboxyl groups will also bind cationic dye. We find, however, that treatment of protein in conditions negative modification of carboxyl groups residues is present [19] has no significant effect on dye response (treated with NaOH, pH 8.5, 1 h, 20°C).

From Table 2 and Table 3 we can conclude that the dye is most responsive to macromolecular compounds with sulfate groups. The carboxyl group alone compound gives no responses.

3.3. Determination of maximum binding number

The simplest mechanism able to describe the reversible interaction between heparin and dye is (in the text ion charges will be omitted for simplicity):

$$D_F + \text{Heparin} \overset{K}{\rightleftharpoons} D_B \quad (1)$$

where D_F represents the MB species. D_B refers to heparin bound dye. D_T as the total analytical concentration of MB. With an increase in heparin concentration will shift equilibrium Eq. (1) from the left to the right, causing spectral changes as can be seen in Fig. 2.

$$D_T = D_F + D_B \quad (2)$$

The absorbance at 664 nm is attributed to the fact that both the dye and the dye–heparin complex absorb appreciably at 664 nm. This situation can be analyzed according to Beer's law, as follows:

$$A = \epsilon_F D_F + \epsilon_B D_B = \epsilon_F D_T + (\epsilon_B - \epsilon_F) D_B \quad (3)$$

Table 2
Data from MB–heparin assay used for linear regressions[a]

C_P(mol/l)	ΔA	n	$(D_T\ \Delta\epsilon/\Delta A-1)C_P$
1.74×10^{-8}	0.047	49.10	3.61×10^{-7}
5.21×10^{-8}	0.141	49.20	3.26×10^{-7}
8.68×10^{-8}	0.236	49.43	2.89×10^{-7}
12.15×10^{-8}	0.328	49.07	2.57×10^{-7}
15.62×10^{-8}	0.425	49.46	2.19×10^{-7}
19.09×10^{-8}	0.515	49.04	1.88×10^{-7}
22.56×10^{-8}	0.608	48.99	1.48×10^{-7}
26.03×10^{-8}	0.697	48.68	1.21×10^{-7}
29.50×10^{-8}	0.728	44.86	1.19×10^{-7}
32.97×10^{-8}	0.779	42.95	1.03×10^{-7}
36.44×10^{-8}	0.799	39.86	1.02×10^{-7}
39.91×10^{-8}	0.817	37.21	1.00×10^{-7}

[a] pH 8.05, $D_T = 1.86\times10^{-5}$ mol l^{-1}, $\Delta\epsilon = 5.501\times10^{4}$ mol l^{-1} at 664 nm, $\Delta A_{max} = 1.022$.

Table 3
Data from MB–LMWH assay used for linear regressions[a]

C_P(mol l^{-1})	ΔA	n	$(D_T \Delta\epsilon/\Delta A - 1)C_P$
2.39×10^{-7}	0.108	11.42	13.88×10^{-7}
4.78×10^{-7}	0.220	11.65	11.19×10^{-7}
7.18×10^{-7}	0.330	11.63	8.81×10^{-7}
9.57×10^{-7}	0.445	11.78	6.24×10^{-7}
11.96×10^{-7}	0.506	10.71	5.41×10^{-7}
14.36×10^{-7}	0.569	10.03	4.19×10^{-7}
16.75×10^{-7}	0.590	8.92	4.12×10^{-7}
19.14×10^{-7}	0.608	8.04	4.00×10^{-7}
21.54×10^{-7}	0.623	7.32	3.87×10^{-7}

[a] pH 6.85, $D_T = 1.861\times10^{-5}$ mol l^{-1}, $\Delta\epsilon = 3.95\times10^{4}$ mol l^{-1}, at 664 nm, $\Delta A_{max} = 0.735$

where ϵ_F, is the molar absorptivity of free dye, ϵ_B is that of the bound dye. They are constants when measuring wavelength is given.

Define the average binding number of dye molecules per heparin molecule as:

$$n = D_B/C_P \tag{4}$$

where C_P represents the analytical concentration of heparin.

Rearranging Eq. (3) yields:

$$D_B = (A - \epsilon_F D_T)/(\epsilon_B - \epsilon_F) \tag{5}$$

where A is the absorbance of dye–heparin mixtures, and $\epsilon_F D_T$ the absorbance of a zero-heparin solution. Both A and $\epsilon_F D_T$ can be measured.

Let

$$\Delta A = A - \epsilon_F D_T \tag{6}$$

$$\Delta\epsilon = \epsilon_B - \epsilon_F \tag{7}$$

then Eq. (5) may be simplified as:

$$D_B = \Delta A/\Delta\epsilon \tag{8}$$

If ϵ_B and ϵ_F are determined previously from the absorbance of solutions with an excess of heparin and without herparin, then $\Delta\epsilon$ is a known quantity.

According to Eq. (1), the conditional binding equilibrium constant of the total binding reaction should be:

$$K = D_B/[\text{Hep}]D_F \tag{9}$$

where [Hep] represents the concentration of unoccupied binding sites on heparin:

$$[\text{Hep}] = NC_P - D_B = (N - n)C_P \tag{10}$$

where C_P is the analytical concentration of heparin, N the total number of binding sites per heparin molecule, n the average binding number of dye molecules per heparin molecules.

Substituting Eq. (4) and Eq. (10) into Eq. (9) gives:

$$K = nC_P/D_F(N - n)C_P \tag{11}$$

then

$$n = KND_F/(1 + KD_F) \tag{12}$$

Substituting Eq. (12) into Eq. (8) gives:

$$\Delta A/\Delta\epsilon = C_P KN(D_T - D_B)/(1 + K(D_T - D_B)) \tag{13}$$

Rearranging this equation yields:

$$\Delta A = \Delta\epsilon(1 + KD_T)/K - \Delta\epsilon N(D_T\ \Delta\epsilon/\Delta A - 1)C_P \tag{14}$$

where $\Delta\epsilon N$ is a constant, and $\Delta\epsilon(1 + KD_T)/K$ has a fixed value at given MB concentration D_T. $\Delta A \sim (D_T\ \Delta\epsilon/\Delta A - 1)C_P$ is a linear equation. In fact, $D_T\ \Delta\epsilon$ is the maximum value of ΔA, which can be measured directly at high heparin–dye concentration ratios.

Calculating Eqs. (2)–(14) yields Table 2 and Table 3. Table 2 gives a group of data taken from MB–heparin assay. Using these data, a $\Delta A \sim (D_T\ \Delta\epsilon/\Delta A - 1)C_P$ regression equation is obtained:

$$\Delta A = 1.07 - 2.88\times10^{6}(D_T\ \Delta\epsilon/\Delta A - 1)C_P$$

$$R = -0.998$$

From the slopes and intercepts of this equation, $K = 1.15\times10^{6}$, $N = 52.35$ are obtained.

Table 3 gives a group of data taken from MB–LMWH assay. Using these data, a $\Delta A \sim (D_T\ \Delta\epsilon/\Delta A - 1)C_P$ regression equation is obtained:

$$\Delta A = 0.79 - 5.07\times10^{5}(D_T\ \Delta\epsilon/\Delta A - 1)C_P$$

$$R = -0.995$$

From the slopes and intercepts of this equation, $K = 6.89 \times 10^5$, $N = 12.84$ are obtained.

Heparin has five sulfate groups per tetrasaccharide unit [20]. The two N suggest that the heparin used here contains 42 monosaccharide units, LMWH has 10 monosaccharide units. These results agree with the data reported [21,22]. The N has a significant physical meaning for heparin.

With the increase in heparin concentration, the average binding number of dye molecules per heparin molecule (n) decreases (see Table 2 and Table 3). This indicates noncovalent binding forces involve in the binding energy in dye binding assay.

3.4. Influence of anion on dye binding reaction

Discrepancies may arise from nonheparin interference that produce heparin overestimation, underestimation (see Table 1). The potential interference problems may generally be avoided by using the proper control.

A set of experiments were done, keeping the MB concentration constant and increasing the NaCl and heparin concentrations. The results are shown in Table 4 that an increase in salt concentration causes a significant decrease in K and $\Delta\epsilon$ values, thus decreasing the sensitivity of the MB–heparin binding assay [23]. This effect may be explained as a competition between anion and heparin for the same binding sites on dye species. In this case the concentrations of the anions are 100–1000 fold higher than that of the MB species [23], so the cationic dye species are actually surrounded by anions which prevent the MB species from binding to heparin, thus decreasing assay response to heparin. MB species have positive charges. Therefore, heparin, MB species and NaCl should be bound together by electrostatic forces. The N is elevated with the salt's ionic strength increase, and this is most likely due to NaCl bound to dye [16].

Table 4
Effect of NaCl ionic strength on the binding of MB on heparin[a]

I_{naCl}(mol l^{-1})	$\Delta\epsilon$	N	K	R
0	55.01×10^3	52.35	1.15×10^6	−0.998
3.57×10^{-3}	42.96×10^3	56.11	8.67×10^5	−0.998
7.13×10^{-3}	34.72×10^3	60.80	6.67×10^5	−0.998
10.70×10^{-3}	30.28×10^3	73.89	4.54×10^5	−0.996
14.26×10^{-3}	27.18×10^3	91.66	3.57×10^5	−0.995

[a] pH 8.05, $D_T = 1.86 \times 10^{-5}$ mol l^{-1}, at 664 nm.

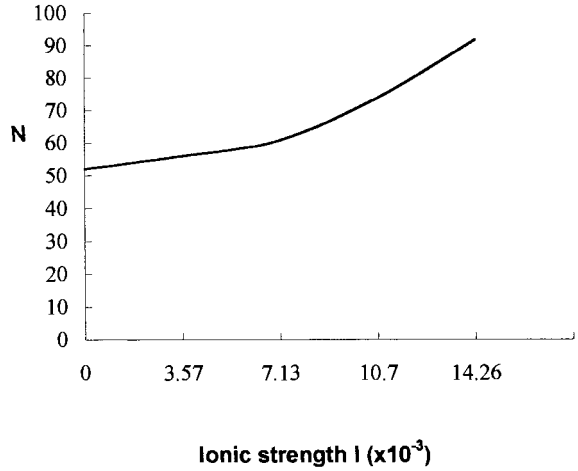

Fig. 3. Effect of the NaCl ionic strength on N.

From Fig. 3 we can see, with an increasing NaCl ionic strength at pH 8.05, the N gradually increase. Only low concentration of NaCl (about 100 fold lower than that of MB, data not shown) can be used for spectrophotometric determinations. While many workers consider the choice of dye–heparin assay method advantageous due to its sensitivity, speed, and economy, its limitations must also be considered. Reagents affecting the dye equilibria can cause interference. We hope that this more mechanistic understanding of the dye reagent system will allow anticipation of other possible interference and promote a more effective use of the assay.

4. Conclusions

We conclude that the MB dye will be most responsive to organic chain compound with sulfate group. The longer the organic chain of

compound is, the higher the sensitivity of the dye binding assay is.

It seems that this method is useful and convenient for the investigation of sulfate groups of heparin. N is the total number of binding sites per heparin molecule, this number reflecting the density of sulfate groups of heparin, N can be determined easily from Eq. (14).

Experimental conditions such as ionic strength have effects on the maximum binding number, the equilibrium constant and the molar absorptivities of free and bound dye, thereby influencing the sensitivity of a heparin assay.

References

[1] D.J. Tyrrell, S. Kilfeather, C.P. Page, Trends Pharmacol. Sci. 16 (1995) 198.
[2] J. Shute, Clin. Exp. Allergy 24 (1994) 203.
[3] L. Kjellen, U. Lindahl, Annu. Rev. Biochem. 60 (1991) 443.
[4] A. Bobik, J.H. Campbell, Pharmacol. Rev. 45 (1993) 1.
[5] I.V.S. Tersariol, C.P. Dietrich, H.B. Nader, Eur. J. Biochem. 245 (1997) 40.
[6] S. Ecke, M. Geiger, B.R. Binder, Eur. J. Biochem. 248 (1997) 475.
[7] L. Silvestro, L. Viano, M. Macario, D. Colangelo, G. Montrucchio, S. Panico, R. Fantozzir, Semin. Thromb. Haeostasis. 20 (1994) 254.
[8] U. Lindahl, K. Lidholt, D. Spillmann, L. Kjellen, Thromb. Res. 75 (1994) 1.
[9] I. Masayuki, K. Yutaka, K. Hiroshi, M. Tosikazu, Y. Keiichi, J. Biochem. 121 (1997) 345.
[10] Y.E. Zheng, H.S. Zhang, Z.H. Chen, Handbook of Modern Chemical Reagent Part IV, Chemical Industry Press, Beijing PRC, 1989, p. 421.
[11] M.W. Jeanine, P.J. Walter, B. Lucienne, M.S. Meyer, F. Jawed, Thromb. Res. 86 (1997) 1.
[12] Z. Liu, A.S. Perlin, Carbohydrate Res. 22 (1992) 29.
[13] R. Malsch, G. Guerrini, G. Torri, G. Lohr, B. Casu, J. Harenberg, Anal. Biochem. 217 (1994) 255.
[14] R.W. Congdom, G.W. Muth, A.G. Splittgerber, Anal. Biochem. 213 (1993) 407.
[15] Y.J. Wei, K.A. Li, S.Y. Tong, Talanta 43 (1996) 1.
[16] Q.C. Jiao, Q. Liu, Spectroscopy Letters 317 (1998) 353.
[17] T. Yutaka, A. Hatsuo, O. Naomichi, Thromb. Res. 55 (1989) 329.
[18] R.K. Powell, J.D. Hendley, K.E. Pohl, A. Freidberg, W.A. Volk, Anal. Biochem. 19 (1982) 31.
[19] M.L. Guo, Y.M. Jiang, Prog. Biochem. Biophys. PRC 23 (1996) 558.
[20] T. Katayama, E.I. Takai, R. Kariyama, Y. Kanemasa, Anal. Biochem. 88 (1978) 382.
[21] J. Fareed, Med. J. Aust. 144 (1986) HS 23.
[22] Y. Cao, Y. Tao, C. Yang, Chinese J. Biochem. Pharma. 17 (1996) 1.
[23] Q.C. Jiao, Q. Liu, Anal. Letters 31 (1998) 1311.

ELSEVIER

Talanta 48 (1999) 1103–1110

Talanta

Examination of dodecylpyridinium chloride as a potentially selective fluorescence quenching agent for discriminating between alternant versus nonalternant polycyclic aromatic hydrocarbons

Siddharth Pandey [a], Lindsay E. Roy [a], William E. Acree Jr. [a,*], John C. Fetzer [b]

[a] *Department of Chemistry, University of North Texas, Denton, Texas 76203-5070, USA*
[b] *Chevron Research and Technology Center, Richmond, California 794802-0627, USA*

Received 10 August 1997; received in revised form 8 October 1998; accepted 12 October 1998

Abstract

Fluorescence behavior is reported for 13 alternant and 12 nonalternant polycyclic aromatic hydrocarbons (PAHs) dissolved in aqueous micellar cetyltrimethylammonium chloride (CTAC) + dodecylpyridinium chloride (DDPC) and sodium dodecylsulfate (SDS) + DDPC mixed surfactant solvent media. Experimental measurements indicate that the dodecylpyridinium cation selectively quenches fluorescence emission of alternant PAHs. Emission intensities of nonalternant PAHs, with a few noted exceptions, essentially remain constant, irrespective of both DDPC concentration and cosurfactant headgroup charge. © 1999 Elsevier Science B.V. All rights reserved.

Keywords: Fluorescence quenching; Selective quenching agents; Surfactants; Mixed micelles; Polycyclic aromatic hydrocarbons

1. Introduction

Reverse-phase liquid chromatographic methods using micellar eluents are becoming increasingly popular in the separation and/or analysis of polycyclic aromatic hydrocarbon (PAH) mixtures [1–5], partly due to the lower cost and reduced toxicity associated with aqueous–surfactant solutions. Published applications include the separation of benzene derivatives and PAHs on an octylsilica column using micellar sodium dodecylsulfate (SDS) and cetyltri-methylammonium bromide (CTAB) mobile phases in both the absence and presence of organic modifiers (methanol, 1-propanol and 1-butanol), PAH separations using a micellar SDS mobile phase and short C_1- and C_4-chain columns, and the separation of 11 PAHs in particulate air samples via acetonitrile–aqueous 0.20 molar SDS gradient elution. Resolution of structurally similar PAHs results largely from differences in the solutes' partitioning behavior be-

* Corresponding author. Fax: +1-940-5654318; e-mail: acree@unt.edu..

0039-9140/99/$ - see front matter
PII: S0039-9140(98)00332-4

tween the stationary phase and mobile phase micellar aggregates. Greater sensitivity and lower detection limits in spectrofluorometric determinations are achieved through increased quantum yields and larger linearity ranges in plots of relative emission intensity versus PAH fluorophore concentration.

Environmentally important PAHs are inherently fluorescent, and sample preconcentration or derivatization is not necessary in many spectrofluorometric determinations. Detection limits at the parts-per-billion level have been reported. [6,7] Spectrofluorometry is more selective than other spectroscopic methods in that the excitation and emission wavelength can be varied independently. An excitation spectrum is obtained by measuring the fluorescence intensity at a fixed emission wavelength as the excitation wavelength is varied, whereas an emission spectrum is recorded by irradiating the solution at a single wavelength and then measuring the intensity as a function of emission wavelengths. While several polycyclic aromatic compounds may absorb at the same excitation wavelength, not all will emit at the wavelength(s) monitored by the detector. Fluorescence determinations do have their limitations, particularly if spectrally interfering substances are present. Unbiased quantification is possible, however, all interferants must be included in the calibration curves.

The utilization of selective fluorescence quenching agents further simplify observed fluorescence spectra by eliminating signals from undesired chemical interferences having only slightly different molecular structures. Sawicki et al. [8,9] introduced selective fluorescence quenching agents to thin-layer chromatographic analysis. Blümer and Zander [10] later extended the ideas to liquid chromatography. The authors noted that both nitromethane and nitrobenzene selectively quenched the fluorescence emission of perylene, dibenzo[*h*,*rst*]pentaphene and dibenzo[*b*,*k*]chrysene dissolved in aqueous–acetonitrile (20:80% by volume) mixture. Emission intensities of the three nonalternant PAHs (e.g. naphtho[1,2*b*]fluoranthene, indeno[1,2,3*cd*]pyrene and acenaphthyleno[1,2*k*]fluoranthene) were unaffected by nitromethane addition. Nitromethane (and nitrobenzene to a much lesser extent [11]) is a selective quenching agent for discriminating between alternant versus nonalternant PAHs. Polycyclic aromatic hydrocarbons are classified as alternant PAHs if every alternant carbon atom in the aromatic ring system can be 'starred'. Nonalternant PAHs, on the other hand, would have at least one pair of adjacent starred atoms. [12,13]

As part of a 7-year continuing spectroscopic investigation, we [14–33] have reported the fluorescence properties and quenching behavior of numerous PAH6 benzenoids, fluoranthenoids and fluorenoids, methylene-bridged cyclopenta-PAHs, acenaphthylene and acephenanthrylene derivatives, bi-PAHs, and polycyclic aromatic nitrogen heterocycles (PANHs) in organic nonelectrolyte and in aqueous micellar solvent media. In later studies, we observed that nitromethane selectivity was lost in the case of the four anionic micellar solvent media studied. Nitromethane quenched the fluorescence emission of both alternant and nonalternant PAHs, which is contrary to the 'nitromethane selective quenching rule'. Unexpected fluorescence was found when we extended [34,35] our studies to include mixed cetyltrimethylammonium chloride + cetylpyridinium chloride (CPC) micelles in that we expected to observe a significant increase in the fluorescence emission intensity due to the fact that the PAH fluorophores were solubilized in a rigid micellar microenvironment. Instead, a reduction in the emission intensities was observed in the case of the alternant polycyclic aromatic hydrocarbons. The cetylpyridinium cation was found to be a selective fluorescence quenching agent for alternant PAHs. Of the 41 PAH solutes examined, the only exceptions noted were four nonalternant PAHs (e.g. naphtho[2,3*b*]fluoranthene, benzo[*k*]fluoranthene, naphtho[1,2*b*]fluoranthene and benzo[*b*]fluoranthene). It should be noted that Ayala et al. [36–38] concurrently reported that the cetylpyridinium cation selectively quenches fluorescence emission of alternant polycyclic aromatic hydrocarbons. The authors' conclusions were based upon a study of the fluorescence behavior of only 14 PAH solutes.

The discovery of the cetylpyridinium cation as a selective fluorescence quenching agent is impor-

tant from a chemical analysis standpoint in that its solutions are optically transparent in the excitation spectral region of many of the PAHs. Primary inner-filtering corrections are minimized, and in many cases even eliminated. Inner-filtering corrections are much larger for nitromethane solutions as a few drops of quenching agent results in appreciable absorbances. Accurate quantification of PAH concentrations requires both absorbance and fluorescence emission measurements when using the quenching agent nitromethane. To provide additional experimental data for micellar alkylpyridinium chloride solutions, we report in this communication the fluorescence behavior of 13 alternant and 12 nonalternant PAHs in aqueous micellar dodecylpyridinium chloride (DDPC) + cetyltrimethylammonium chloride (CTAC) and DDPC + SDS. These particular systems were judiciously selected so as to enable us to determine if quenching selectivity extends to the smaller alkylpyridinium cations, which could be exploited to overcome immiscibility problems encountered in mixed surfactant systems. Mixed micelles are currently being used in analytical chemistry as mobile phases in chromatographic separations because of their increased solubilizing capacity and ability to form micelles at much lower surfactant concentrations. In mixtures containing both cationic and anionic surfactants, the concentration region over which the two surfactants are miscible is governed to a large extent by the relative sizes of the two alkyl chains. In general, miscibility is favored by a large hydrophobic mismatch caused by very dissimilar alkyl chain lengths. However, this may lead to vesicle formation rather than to mixed micelles. Comparable alkyl chain lengths, on the other hand, often result in precipitation of the catanionic surfactant at relative mole fraction compositions near the equimolar concentration, i.e. anionic/cationic mole fraction ratio of unity. [39–47] Moreover, our solvent media selection enables us to examine what role the cosurfactant headgroup charge has on the quenching processes. Our earlier study [34] considered just mixed cationic micelles of CTAC + CPC. In the case of the nitromethane selective quenching agent, we have shown that quenching selectivity was lost in aqueous micellar anionic surfactant solvent media. Nitromethane quenched the fluorescence emission of both alternant and nonalternant PAHs in aqueous micellar SDS, sodium octanoate (SO), sodium dodecylbenzenesulfonate (SDBS) and sodium dodecanoate (SDD) solvent media, which is contrary to the nitromethane selective quenching rule.

2. Materials and experimental methods

The different aqueous micellar CTAC (Aldrich) + DDPC (Aldrich, 98%) and SDS (Aldrich) + DDPC mixed surfactant solvent media were prepared by dissolving the commercial surfactants in doubly deionized water. Synthetic references and/or commercial suppliers for the PAH solutes contained in Tables 1–4 are listed in our earlier papers (for a single source listing, see Tucker [28]). Stock solutions were prepared by dissolving the solutes in dichloromethane, and were stored in closed amber glass bottles in the dark to retard any photochemical reactions between the PAH solutes and dichloromethane solvent. Small 25-μl aliquots of each stock solutions were transferred by Eppendorf pipette into test tubes, allowed to evaporate, and diluted with 10 ml (graduate cylinder) of the micellar solvent media of interest. Solute concentrations were sufficiently dilute (10^{-6} M) so as to prevent excimer formation. All solutions were ultrasonicated, vortexed and allowed to equilibrate for a minimum of 24 h before any spectrofluorometric measurements were made. Experimental results were unaffected by longer equilibration times.

Absorption spectra were recorded on a Milton Roy Spectronic 1001 Plus and a Hewlett-Packard 8450A photodiode-array spectrophotometer in the usual manner. The fluorescence spectra were measured on a Shimadzu RF-5000U spectrofluorimeter with the detector set at high sensitivity. Solutions were excited at the wavelengths listed in Table 1. Fluorescence data were accumulated in a 1 cm^2 quartz cuvette at 21°C (ambient room temperature) with excitation and emission slit width settings of 15 and 3 nm, respectively. The fluorescence spectra represent a single scan which was then solvent blank corrected and verified by repetitive measurements.

Table 1
List of polycyclic aromatic hydrocarbons examined along with the excitation and emission wavelengths used

Alternant polycyclic ar	Naphtho[1,2*k*]benzo[*ghi*]fluoranthene	3388	33888
Letter	Polycyclic aromatic hydrocarbon	λ_{ex} (nm)	λ_{em} (nm)
Alternant polycyclic aromatic hydrocarbons			
A	Benzo[*ghi*]perylene	380	419
B	Benzo[*e*]pyrene	335	409
C	Pyrene	338	373
D	Naphtho[2,3*g*]chrysene	350	425
E	Chrysene	320	381
F	Benzo[*g*]chrysene	320	380
G	Perylene	403	441
H	Benzo[*rst*]pentaphene	307	434
I	Naphtho[1,2,3,4*ghi*]perylene	316	420
J	Anthracene	340	425
K	Coronene	334	445
L	Benzo[*a*]pyrene	350	404
M	Dibenzo[*a*,*e*]pyrene	360	396
Nonalternant fluoranthenoids and fluorenoids			
N	Naphtho[1,2*b*]fluoranthene	350	439
O	Benzo[*ghi*]fluoranthene	340	422
P	Benz[*def*]indeno[1,2,3*hi*]chrysene	406	473
Q	Benzo[*a*]fluoranthene	406	490
R	Naphtho[2,1*k*]benzo[*ghi*]fluoranthene	368	425
S	Naphtho[1,2*k*]benzo[*ghi*]fluoranthene	366	435
T	Benz[*def*]indeno[1,2,3*qr*]chrysene	408	488
U	Dibenzo[*a*,*e*]fluoranthene	390	504
V	Benzo[*j*]fluoranthene	315	509
W	Dibenzo[*ghi*,*mno*]fluoranthene	290	436
X	Naphtho[2,1*a*]fluoranthene	400	491
Y	Benzo[*b*]fluoranthene	346	449

Emission intensities associated with the quenching measurements were corrected for primary inner-filtering artifacts and self-absorption arising from the absorption of excitation radiation by dodecylpyridinium chloride and the PAH solute, respectively, according to the following expression [49–51]:

$$f_{prim} = F^{corr}/F^{obs} = 2.303\ A\ (y-x)/[10^{-Ax} - 10^{-Ay}] \quad (1)$$

which differs slightly from the approximate form [52]

$$f_{prim} \approx 10^{0.5\,A} \quad (2)$$

In the above equations, F^{corr} and F^{obs} refer to the corrected and observed fluorescence emission signal, respectively, A is the absorbance per centimeter of pathlength at the excitation wavelength, and x and y denote distances from the boundaries of the interrogation zone to the excitation plane. For many of the fluorescence measurements primary inner-filtering correlations were relatively minor as the observed absorbance was often $A\ cm^{-1} \leq 0.05$, even in the 300–320 nm spectral region. Secondary inner-filtering corrections were not necessary. Aqueous micellar CTAC + DDPC and SDS + DDPC mixed surfactant solutions were 'optically transparent' in the PAH emission ranges. Computational procedures and interrogation zone dimensions are discussed in greater detail elsewhere. [17–19,53,54].

3. Results and discussion

Tables 2 and 3 summarize the fluorescence emission intensities of 25 representative polycyclic aromatic hydrocarbons dissolved in aqueous micellar CTAC + DDPC and SDS + DDPC mixed surfactant solvent media. The emission wavelengths used are listed in Table 1. Three different DDPC concentrations were studied for each mixed surfactant system. The aqueous micellar cosurfactant solvent media served as the point of reference for the quenching studies. Careful examination of the numerical entries reveals that addition of DDPC surfactant led to a significant

Table 2
Relative emission intensities of alternant and nonalternant PAHs dissolved in aqueous micellar (CTAC+DDPC) solvent media

Letter[a]	I[b]	II[c]	III[d]	IV[e]
Alternant polycyclic aromatic hydrocarbons				
A	840	760	290	16
B	610	500	230	11
C	860	680	150	8.3
D	560	560	290	45
E	900	810	380	24
F	400	330	180	16
G	720	270	120	46
H	280	190	80	2.5
I	390	250	130	31
J	330	210	130	38
K	840	750	430	120
L	530	480	230	8.5
M	940	520	180	22
Nonalternant fluoranthenoids and fluorenoids				
N	630	360	240	290
O	960	940	940	890
P	570	560	500	490
Q	540	530	530	490
R	180	160	180	180
S	390	350	330	350
T	170	190	150	150
U	500	490	530	490
V	400	350	340	360
W	460	470	450	430
X	560	560	490	470
Y	490	460	460	330

[a] Letters refer to the compounds listed in Table 1.
[b] Solvent media was $\sim 3.78 \times 10^{-2}$ Molar in cetyltrimethylammonium chloride.
[c] Solvent media was $\sim 3.78 \times 10^{-2}$ Molar in cetyltrimethylammonium chloride + $\sim 2.0 \times 10^{-4}$ M in dodecylpyridinium chloride.
[d] Solvent media was $\sim 3.78 \times 10^{-2}$ Molar in cetyltrimethylammonium chloride + $\sim 2.0 \times 10^{-3}$ M in dodecylpyridinium chloride.
[e] Solvent media was $\sim 3.78 \times 10^{-2}$ Molar in cetyltrimethylammonium chloride + $\sim 2.0 \times 10^{-2}$ Molar in dodecylpyridinium chloride.

Table 3
Relative emission intensities of alternant and nonalternant PAHs dissolved in aqueous micellar (SDS+DDPC) solvent media

Letter[a]	I[b]	II[c]	III[d]	IV[e]
Alternant polycyclic aromatic hydrocarbons				
A	740	480	40	13
B	910	610	67	12
C	850	480	23	20
D	280	150	35	12
E	810	530	69	8.0
F	360	290	47	7.1
G	840	680	210	44
H	140	66	8.3	4.6
I	170	56	19	11
J	790	650	250	35
K	230	140	29	12
L	530	340	50	14
M	370	230	24	8.9
Nonalternant fluoranthenoids and fluorenoids				
N	370	330	320	360
O	880	890	900	910
P	340	280	270	320
Q	230	230	250	260
R	90	99	120	140
S	210	200	180	180
T	130	130	140	180
U	320	380	340	390
V	400	370	410	380
W	460	440	430	470
X	410	420	390	410
Y	440	380	370	400

[a] Letters refer to the compounds listed in Table 1.
[b] Solvent media was $\sim 3.71 \times 10^{-2}$ Molar in sodium dodecylsulfate.
[c] Solvent media was $\sim 3.71 \times 10^{-3}$ Molar in sodium dodecylsulfate + $\sim 2.0 \times 10^{-4}$ Molar in dodecylpyridinium chloride.
[d] Solvent media was $\sim 3.71 \times 10^{-2}$ Molar in sodium dodecylsulfate + $\sim 2.0 \times 10^{-3}$ Molar in dodecylpyridinium chloride.
[e] Solvent media was $\sim 3.71 \times 10^{-3}$ Molar in sodium dodecylsulfate + $\sim 1.0 \times 10^{-2}$ Molar in dodecylpyridinium chloride.

decrease in the emission signals of all 13 alternant PAHs considered at DDPC concentrations of 2.0×10^{-3} M or larger. Emission intensities of the 12 nonalternant PAHs were for the most part unaffected by DDPC. No special significance is given to slight variations in emission intensities, which in all likelihood partly result from the fact that the solutions were prepared using a graduate cylinder. Differences in partitioning behavior of PAHs between bulk aqueous phase and different binary micelles, as well as differences in oxygen solubilities in the various solvent media, may also contribute to part of the observed variation in emission intensities. It should be noted that our experimental methodology allows us to study a wide range of PAH solutes. By comparing experimental PAH intensities for the cosurfactant + DDPC mixed surfactant systems back to emission intensities observed in the neat cosurfactant micelles in the absence of DDPC, we are able to investigate even those larger PAHs which are not very soluble in water. Ayala and coworkers [36,37], on the other hand, used as their point of reference the measured PAH intensities in water. As a result, the authors were able to study only the smaller, commercially available PAHs.

The numerical entries in Tables 2 and 3 further reveal that the dodecylpyridinium cation's quenching selectively is not affected by the headgroup charge on the cosurfactant. This initially came as a surprise because we expected that quenching selectivity would be lost in the case of the anionic SDS cosurfactant. The cetylpyridinium ion (CPy^+) is known to be a good electron acceptor [48,55–58], and it is not unreasonable to expect the dodecylpyridinium cation ($DDPy^+$) to behave in similar fashion. The two alkylpyridinium cations differ only in the size of the alkyl chain, 16 carbon atoms versus 12 carbon atoms. From simple coulombic considerations, the negatively charged SDS headgroup was expected to stabilize the developing positive charge (or partial charge) on the PAH ring system, thereby facilitating electron transfer from the excited PAH fluorophore to $DDPy^+$, which acts as an electron acceptor. This would have been in line with our published [30,32,33,59,60] nitromethane quenching studies. At sodium dodecylsulfate, sodium octanoate, sodium dodecanoate and sodium dodecylbenzenesulfonate surfactant concentrations above the critical micelle concentration (cmc), nitromethane quenched the fluorescence emission of both alternant and nonalternant polycyclic aromatic hydrocarbons.

The inability of the negatively-charged SDS anionic headgroup to facilitate electron transfer in the case of nonalternant PAHs is perhaps best explained in terms of the properties of mixed surfactant solutions and the effective micellar surface charge density. Mixed surfactant solutions do form a wide range of microstructures depending upon the surfactant headgroup charges and alkylchain lengths, concentrations and mole fraction ratios. Microstructures formed include spherical or rodlike micelles, lamellae, precipitate or vesicles. Largest structural micellar changes are expected for systems which display strong intra-micellar interactions, such as zwitterionic + anionic and anionic + cationic surfactant systems. In the case of SDS + DDPC solvent media, both surfactants would have to be in fairly close proximity to the dissolved PAH molecule in order to affect its fluorescence behavior. This would also place the oppositely charged surfactants in close proximity to each other. Attractive interactions between oppositely charged headgroups would reduce the negative electron surface density in the vicinity of the solubilized PAH molecule, perhaps to the point where the SDS headgroup is no longer able to stabilize any developing charge on the PAH ring system.

Readers are reminded that it is entirely possible that the relative concentrations of the SDS and DDPC surfactants in the micelle may be significantly different than the bulk stoichiometric molar concentration ratios used in preparing the various solvent media. Support for a different micellar concentration ratio can be found in the published theoretical computations of Graciaa et al. [61]. The authors calculated compositions of mixed micelles based upon the regular solution thermodynamic model. Binary interaction parameters that best described the experimental cmc data were used in the theoretical computations. Computations indicated that micelles formed from cationic + anionic surfactants should

have large ranges of nearly equimolar concentrations as already found at the air/anionic + cationic surfactant solution interfaces [62,63]. Formation of amphiphilic anion-amphiphilic cation salts/ion-pairs lead to equimolar surfactant concentrations. Kato et al. [64] used light scattering and NMR methods to deduce micelle sizes and compositions in aqueous sodium dodecylsulfate + octyltrimethylammonium bromide (OTAB) mixtures. Measurements revealed that in SDS-rich solutions, the micellar OTAB mole fraction increased with decreasing total surfactant concentration.

Observation that the dodecylpyridinium cation is a selective fluorescence quenching agent for discriminating between alternant versus nonalternant PAHs has important analytical consequences. First, it increases the number of mixed surfactant mobile phases that can be used in chromatographic separations that employ fluorescence detection. As noted in the Introduction, the miscibility region of mixtures containing both cationic and anionic surfactants is governed to a large extent by the relative sizes of the two alkyl chains. There will be occasions whenever phase miscibility can be achieved simply by substituting dodecylpyridinium chloride for cetylpyridinium chloride and vice versa. Secondly, our observations regarding the fluorescence quenching behavior of $DDPy^+$ suggest that quenching selectivity may extend to even smaller alkylpyridinium cations, perhaps even down to the methylpyridinium cation. This raises the possibility that one might be able to replace the nitromethane selective quenching agent with perhaps a small alkylpyridinium chloride for use with neat acetonitrile or binary aqueous–acetonitrile mixtures. Large inner-filtering corrections are often required in the case of nitromethane, and it would be advantageous to find a selective fluorescence quenching agent that is more optically transparent in the PAHs' excitation spectral regions.

Acknowledgements

This work was supported in part by the University of North Texas Research Council.

References

[1] E. Pramauro, E. Pelezetti, Surfactants in Analytical Chemistry: Applications of Organized Amphiphilic Media; Elsevier, Amsterdam, 1996, Chap. 6 and references therein.
[2] M.R. Hadjmohammadi, M.H. Fatemi, J. Liq. Chromatogr. 18 (1995) 2569.
[3] M.N. Kayali, S. Rubio-Barroso, L.M. Polo-Diez, J. Liq. Chromatogr. Rel. Technol. 19 (1996) 759.
[4] M. Angeles Garcia, M. Luisa Mariana, J. Liq. Chromatogr. Rel. Technol. 19 (1996) 1757.
[5] M.N. Kayali, S. Rubio-Barroso, L.M. Polo-Diez, J. Liq. Chromatog. 17 (1994) 3623.
[6] L.A. Files, J.A. Winefordner, J. Agric. Food Chem. 35 (1987) 471.
[7] J.J.S. Rodriquez, J.H. Garcia, M.M.B. Suarez, A.B. Martin-Lazaro, Analyst 118 (1993) 917.
[8] E. Sawicki, T.W. Stanley, W.C. Elbert, Talanta 11 (1964) 1435.
[9] E. Sawicki, W.C. Elbert, T.W. Stanley, J. Chromatogr. 17 (1965) 120.
[10] G.P. Blümer, M. Zander, Fresenius Z. Anal. Chem. 296 (1979) 409.
[11] F.K. Ogasawara, Y. Wang, V.L. McGuffin, Appl. Spectrosc. 49 (1995) 1.
[12] E. Zimmerman, Quantum Mechanics for Organic Chemists, Academic Press, New York, 1975, pp. 141–146.
[13] J. March, Advanced Organic Chemistry: Reactions, Mechanisms and Structure, McGraw-Hill, New York, 1968, pp. 46–48.
[14] S.A. Tucker, H. Darmodjo, W.E. Acree Jr., M. Zander, E.C. Meister, M.J. Tanga, S. Tokita, Appl. Spectrosc. 46 (1992) 1630.
[15] S.A. Tucker, W.E. Acree Jr., C. Upton, Appl. Spectrosc. 47 (1993) 201.
[16] S.A. Tucker, W.E. Acree Jr., C. Upton, Polycycl. Aromat. Compd. 3 (1993) 221.
[17] S.A. Tucker, W.E. Acree Jr., B.P. Cho, R.G. Harvey, J.C. Fetzer, Appl. Spectrosc. 45 (1991) 1699.
[18] V.L. Amszi, Y. Cordero, B. Smith, S.A. Tucker, W.E. Acree Jr., C. Yang, E. Abu-Shaqara, R.G. Harvey, Appl. Spectrosc. 46 (1992) 1156.
[19] S.A. Tucker, H. Darmodjo, W.E. Acree Jr., J.C. Fetzer, M. Zander, Appl. Spectrosc. 46 (1992) 1260.
[20] S.A. Tucker, W.E. Acree Jr., Appl. Spectrosc. 46 (1992) 1388.
[21] S.A. Tucker, W.E. Acree Jr., J.C. Fetzer, R.G. Harvey, M.J. Tanga, P.-C. Cheng, L.T. Scott, Appl. Spectrosc. 47 (1993) 715.
[22] S.A. Tucker, H.C. Bates, V.L. Amszi, W.E. Acree Jr., H. Lee, P. Di Raddo, R.G. Harvey, J.C. Fetzer, G. Dyker, Anal. Chim. Acta 278 (1993) 269.
[23] S.A. Tucker, H.C. Bates, W.E. Acree Jr., J.C. Fetzer, Appl. Spectrosc. 47 (1993) 1775.

[24] S.A. Tucker, J.M. Griffin, W.E. Acree Jr., M. Zander, R.H. Mitchell, Appl. Spectrosc. 48 (1994) 458.
[25] S.A. Tucker, J.M. Griffin, W.E. Acree Jr., P.P.J. Mulder, J. Lugtenburg, J. Cornelisse, Analyst 119 (1994) 2129.
[26] S.A. Tucker, J.M. Griffin, W.E. Acree Jr., J.C. Fetzer, M. Zander, O. Reiser, A. De Meijere, I. Murata, Polycycl. Aromat. Compd. 4 (1994) 141.
[27] S.A. Tucker, J.M. Griffin, W.E. Acree Jr., M.J. Tanga, J.E. Bupp, T.K. Tochimoto, J. Lugtenburg, K. Van Haeringen, J. Cornelisse, P.-C. Cheng, L.T. Scott, Polycycl. Aromat. Compd. 4 (1994) 161.
[28] S.A. Tucker, Ph.D. Dissertation, University of North Texas, Denton, Texas, 1994.
[29] J.R. Powell, S. Pandey, B.J. Miller, W.E. Acree Jr., P.E. Hansen, J.C. Fetzer, J. Lumin. 69 (1996) 27.
[30] S. Pandey, W.E. Acree Jr., J.C. Fetzer, Anal. Chim. Acta 324 (1996) 175.
[31] S. Pandey, J.R. Powell, W.E. Acree Jr., B.P. Cho, J. Kum, C. Yang, R.G. Harvey, Polycycl. Aromat. Compd. 12 (1997) 1.
[32] S. Pandey, K.A. Fletcher, J.R. Powell, M.E.R. McHale, A.-S.M. Kauppila, W.E. Acree Jr., J.C. Fetzer, W. Dei, R.G. Harvey, Spectrochim. Acta 57A (1997) 165.
[33] S. Pandey, W.E. Acree Jr., B.P. Cho, J.C. Fetzer, Talanta 44 (1997) 413.
[34] S. Pandey, W.E. Acree Jr., J.C. Fetzer, Talanta 45 (1997) 39.
[35] S. Pandey, Ph.D. Dissertation, University of North Texas, Denton, Texas, 1998.
[36] J.H. Ayala, A.M. Afonso, V. Gonzalez, Talanta 44 (1997) 257.
[37] J.H. Ayala, A.M. Afonso, V. Gonzalez, Appl. Spectrosc. 51 (1997) 380.
[38] J.H. Ayala, A.M. Afonso, V.G. Diaz, J. Fluoresc. 7 (1997) 147.
[39] R. Talhout, J.B.F.N. Engberts, Langmuir 13 (1997) 5001.
[40] A. Malliaris, W. Binana-Limbele, R. Zana, J. Colloid Interface Sci. 110 (1986) 114.
[41] G.-Z. Li, F. Li, L.-Q. Zheng, H.-L. Wang, Colloid Surf. A: Phys.–Chem. Eng. Asp. 76 (1993) 257.
[42] E. Rivara-Minten, P. Baglioni, L. Kevan, J. Phys. Chem. 92 (1988) 2613.
[43] T. Kato, H. Takeuchi, T. Seimiya, J. Colloid Interface Sci. 140 (1990) 253.
[44] K.L. Herrington, E.W. Kaler, D.D. Miller, J.A. Zasadzinski, S. Chiruvolu, J. Phys. Chem. 97 (1993) 13792.
[45] K.K. Karukstis, S.W. Suljak, P.J. Waller, J.A. Whiles, E.H.Z. Thompson, J. Phys. Chem. 100 (1996) 11125.
[46] L.L. Brasher, E.W. Kaler, Langmuir 12 (1996) 6270.
[47] M.T. Yatcilla, K.L. Herrington, L.L. Brasher, E.W. Kaler, S. Chiruvolu, J.A. Zasadzinski, J. Phys. Chem. 100 (1996) 5874.
[48] G. Persson, B. Lindstrom, Progr. Colloid Polym. Sci. 105 (1997) 317.
[49] C.A. Parker, W.J. Barnes, Analyst 82 (1957) 606.
[50] J.F. Holland, R.E. Teets, P.M. Kelly, A. Timnick, Anal. Chem. 49 (1977) 706.
[51] M.C. Yappert, J.D. Ingle, Appl. Spectrosc. 43 (1989) 759.
[52] J.R. Lakowicz, Principles of Fluorescence Spectroscopy, Plenum, New York, 1983.
[53] S.A. Tucker, W.E. Acree Jr., J.C. Fetzer, J. Jacob, Polycycl. Aromat. Compd. 3 (1992) 1.
[54] S.A. Tucker, V.L. Amszi, W.E. Acree Jr., J. Chem. Educ. 69 (1992) 8.
[55] S. Hashimoto, J.K. Thomas, J. Am. Chem. Soc. 105 (1983) 5230.
[56] A. Malliaris, J. Lang, R. Zana, J. Chem. Soc., Faraday Trans. 1 (82) (1986) 109.
[57] A.S. Varela, M.I.S. Macho, A.G. Gonzalez, Colloid Polym. Sci. 273 (1995) 876.
[58] M.M. Velazquez, S.M.B. Costa, J. Chem. Soc., Faraday Trans. 86 (1990) 4043.
[59] S. Pandey, W.E. Acree Jr., J.C. Fetzer, Mikrochim. Acta 129 (1998) 41.
[60] S. Pandey, W.E. Acree Jr., J.C. Fetzer, J. Lumin. 71 (1997) 189.
[61] M. Graciaa, M.B. Ghoulam, G. Marion, J. Lachaise, J. Phys. Chem. 93 (1989) 4167.
[62] E.H. Lucassen-Reynders, J. Lucassen, D.J. Gilles, J. Colloid Interface Sci. 81 (1980) 150.
[63] J. Rodakiewica-Novak, J. Colloid Interface Sci. 85 (1982) 856.
[64] T. Kato, H. Takeuchi, T. Seimiya, J. Colloid Interface Sci. 140 (1990) 253.

ELSEVIER

Talanta 48 (1999) 1111–1120

Talanta

Reaction of aluminium chloride with poly(divinyl benzene) particles—a reaction kinetic study using infrared spectroscopy

Alfred A. Christy [a,*], Anne K. Nyhus [b], O.M. Kvalheim [a], Steinar Hagen [c], Jon S. Schanche [c]

[a] *Department of Chemistry, University of Bergen, N-5007 Bergen, Norway*
[b] *Department of Industrial Chemistry, Norwegian University of Science and Technology, N-7034 Trondheim, Norway*
[c] *Amersham Pharmacia Biotech AS, P.O.Box 213, N-2001 Lillestrøm, Norway*

Received 18 May 1998; received in revised form 24 September 1998; accepted 13 October 1998

Abstract

Porous poly(para-divinylbenzene) and poly(meta-divinylbenzene) particles were synthesised from para-divinylbenzene and meta-divinylbenzene monomers with toluene and 2-ethylhexanoic acid as porogens. The residual vinyl groups in the particles were thereafter reacted using aluminium chloride with dichlorobenzene as a catalyst. The conversion of vinyl groups was followed by analysing polymer particles taken from the reaction mixture at different time intervals. Infrared spectroscopy both in the mid and near infrared region was used as the analytical technique. The intensity changes in the overtone absorption at 1628 nm due to the vinyl bonds were used as the basis for the quantification of the vinyl group consumption. Infrared spectra of the particles in the mid IR were also measured to understand changes taking place in the polymer matrix during the reaction. The results indicated that residual vinyl groups in these polymer particles were consumed during the reaction with aluminium chloride. The reaction of aluminium chloride with the polymer matrix was explained by proposing mechanisms for the formation of different products during the reaction. The complex formed between aluminium chloride and the residual vinyl groups seemed to induce addition of HCl to the vinyl group or leads to crosslinking and/or cyclisation in the case poly(para-DVB) particles. The reaction of aluminium chloride with poly(meta-DVB) takes place to a lesser extent.

Keywords: Aluminium chloride; Poly(divinylbenzene); Infrared spectroscopy; Reaction kinetics; Reaction mechanism

1. Introduction

Porous polymer particles play a very important role in separation chemistry. Styrene–divinylbenzene copolymers have been widely used as precursors for such porous particles. Relationships

* Corresponding author. Present address: Department of Chemistry, Agder College, Tordenskjoldsgt-65, N-4604 Kristiansand, Norway. Tel.: +47-38-141502; fax: +47-38-141011; e-mail: alfred.christy @hia.no.

0039-9140/99/$ - see front matter
PII: S0039-9140(98)00333-6

between the method of preparation, morphology and properties have been dealt with in many papers[1–5]. The porous particles contain channels of pores within their matrix and the functional groups attached to them will have different accessibility to bypassing molecules. The efficiency of these porous particles in separating biomolecules depends both on the pore size distribution and the polarity of the surface which again depends on the functional groups attached to the end groups.

The importance of separation science has made synthesis of new polymer materials a challenge. Synthesis of porous polymer particles involves several steps. First of all, basis polymer matrices containing modifiable sites should be synthesised. Then suitable functional groups have to be introduced. Their efficiency in separation of molecules have then to be evaluated.

Two of such materials synthesised in our laboratory were monodisperse poly(para-DVB) and poly(meta-DVB) particles. These particles were prepared from pure para-DVB and pure meta-DVB monomers. Two sets of these materials were prepared with toluene; and 2-ethylhexanoic acid as porogens. Different types of porogens (solvent and non-solvent) give rise to various pore-size distributions and can in turn affect the way the functional groups involve in chemical reactions. The residual vinyl groups in these particles were targeted for introduction of new functional groups [6]. One of such attempts involved the possibility of linking the residual vinyl groups in these systems.

Addition of alkenes to alkenes using catalysts have been discussed in several articles. Jones and Symes [7] have studied dimerisation of 1-olefins using nickel β-diketonate and aluminium alkyl complexes. Alderson et al. [8] have also studied olefin-to-olefin addition reactions using rhodium chloride, rhodium and ruthenium derivatives. Wilke et al. [9] have reported stereospecific oligomerisation of butadiene using acetylacetonate-aluminium alkyl mixture catalysts. All these studies indicate the possibility of linking vinyl groups using a suitable catalyst.

We report in this paper an attempt to link the residual vinyl groups in the polymer systems mentioned above with aluminium chloride catalyst and the study of the progress of reaction by infrared spectroscopy.

2. Experimental

2.1. Materials

Meta-divinylbenzene (meta-DVB) of 99% purity was synthesised by reaction between isophtalaldehyde and methyltriphenylphosphonium bromide. Para-divinylbenzene (para-DVB) of 99% purity was synthesised by reacting terepthalaldehyde with methyltriphenyl-phosphonium bromide. Both reactions were carried out in the presence of a strong base by Wittig reaction according to the literature [10]. Isophtalaldehyde (98%), terephtalaldehyde (98%), methyltriphenylphosphonium bromide (98%) and potassium tert-butoxide (97%) were purchased from Fluka Chemica (Chemie AG, CH-9470 Buchs). Toluene (99%), 2-ethylhexanoic acid (98%), bromine (99.5%), tetrachloromethane (99%), acetone (99%), 1,2 dichlorobenzene (99%), tetrahydrofurane (99.5%) and 0.1 M hydrochloric acid were purchased from Merck (Darmstadt). Aluminium chloride $AlCl_3$ (98.5%) was purchased from Acros Chimica (Belgium).

2.2. Preparation of monodisperse porous basis polymer particles

Four types of porous, monosized polymer particles of diameter 15 μm were prepared by the two-step activated swelling method [11,12]. The particle matrices were homopolymers either from pure meta-divinylbenzene or pure para-divinylbenzene. The porosity was obtained using toluene and 2-ethylhexanoic acid, respectively, as porogens. The polymer particles prepared from para and meta-divinylbenzene with toluene as porogen will be referred to as A and B; and the particles prepared with 2 ethyl hexanoic acid as porogen will be referred to as C and D respectively in this article.

2.3. Reaction with aluminium chloride catalyst

The Friedel–Crafts type reaction was carried out by adding aluminium chloride dispersed in 1,2 dichlorobenzene to a suspension of monosized polymer particles in 1,2 dichlorobenzene. The amount of aluminium chloride added was 2:1 mmole $AlCl_3$ $mmole^{-1}$ vinyl. The reaction was run in a round-bottomed bottle with stirring at a temperature of 22°C. Samples were withdrawn after several reaction times for characterisation. The samples (0.1 g) were washed by filtration with 15 ml tetrahydrofurane, 15 ml tetrahydrofurane/0.1 M HCl (1:1 by volume), 15 ml tetrahydrofurane/water (1:1 by volume) and 15 ml acetone. The worked-up samples were dried for 5 min at 120°C.

2.4. Near Infrared spectroscopic analysis

The samples removed during the experiments were analysed using a Perstrop Analytical NIR systems instrument equipped with a fibre cable. The sampling accessory used in the analysis of the polymer particles using near infrared spectroscopy is given by Christy et al. [6]. Each sample was placed in the sample cup and the surface was levelled by a spatula. NIR measurements were made using 16 scans in the range 1100–2500 nm with the spectrum of a quartz disc placed in the cable probe as the background. The spectra were then converted into ASCII format and imported into SIRIUS [13] multivariate data analysis program and MATLAB for further analysis.

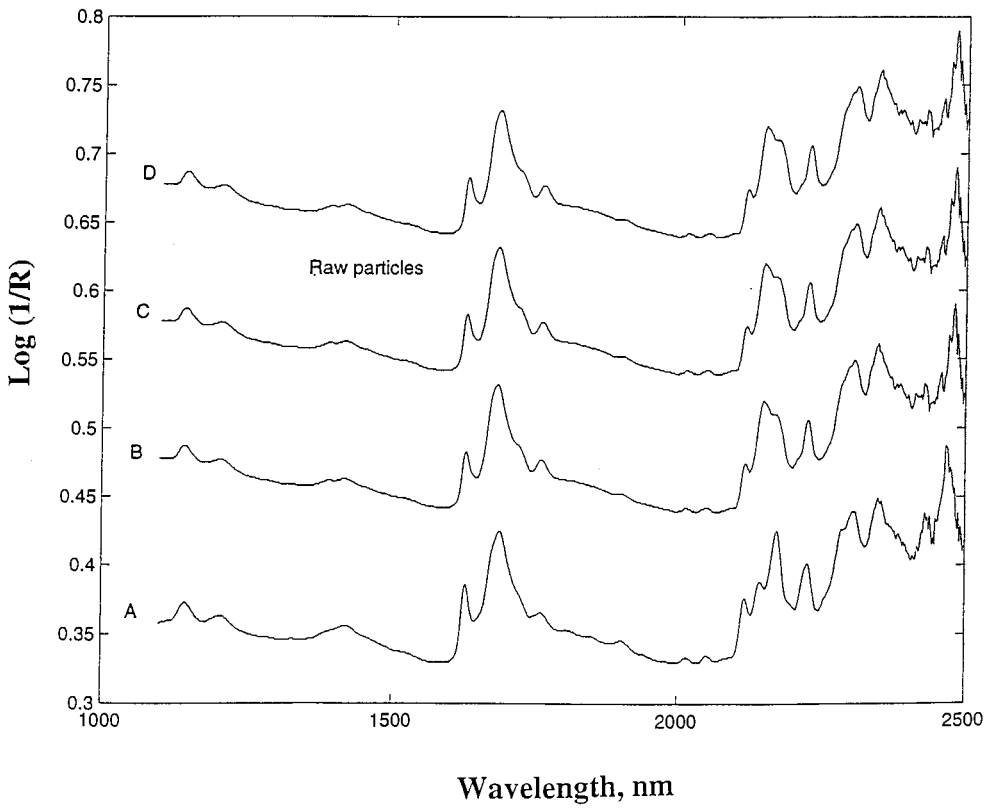

Fig. 1. NIR spectra of the basis particles of types A, B, C and D. The capital letter on the spectrum indicates the type belonging of the particles. The spectra are offset for the sake of clarity.

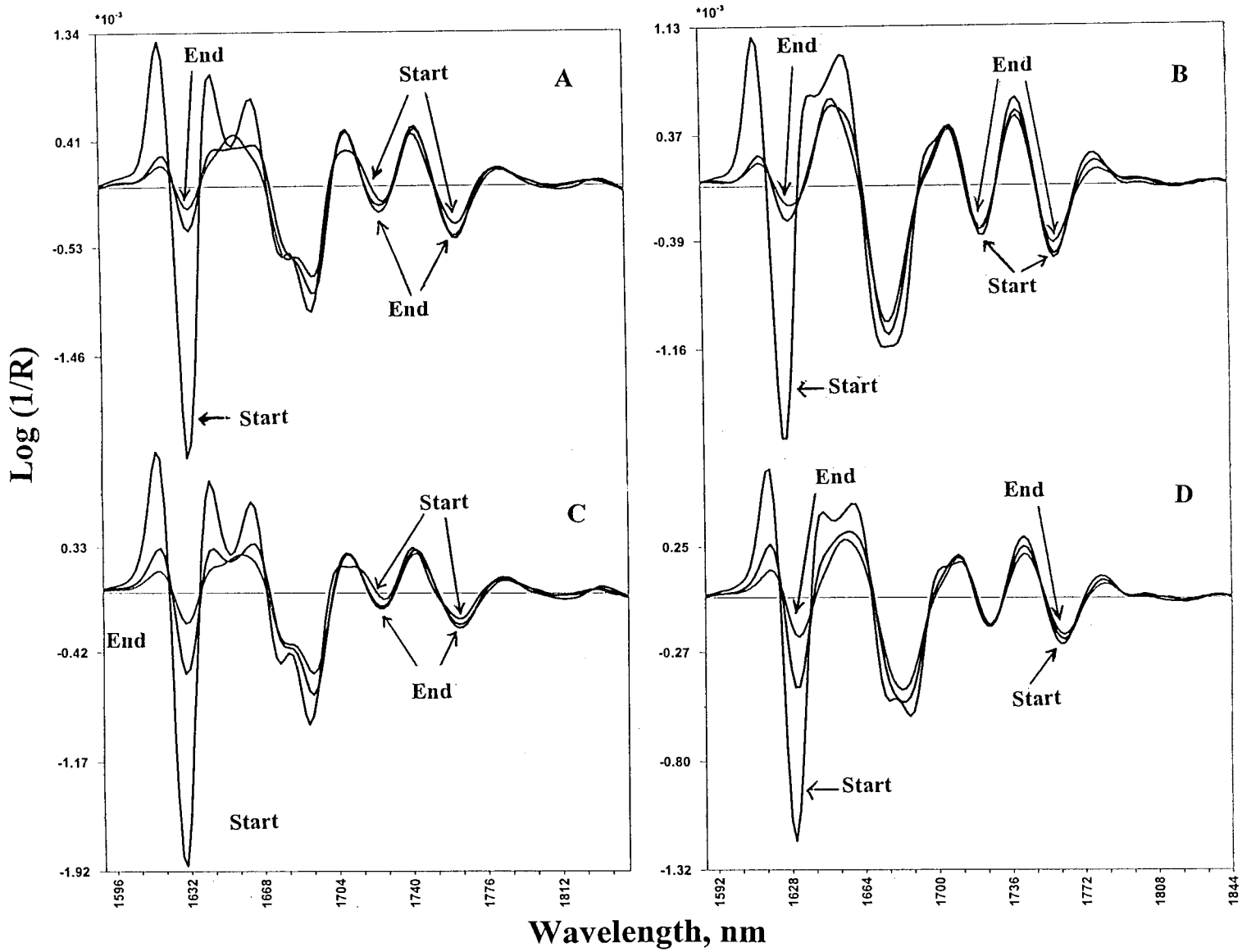

Fig. 2. Second derivative NIR spectra (in the region 1590–1845 nm) of the particles of types A, B, C and D taken during the reaction at times 0, 120 and 1440 min.

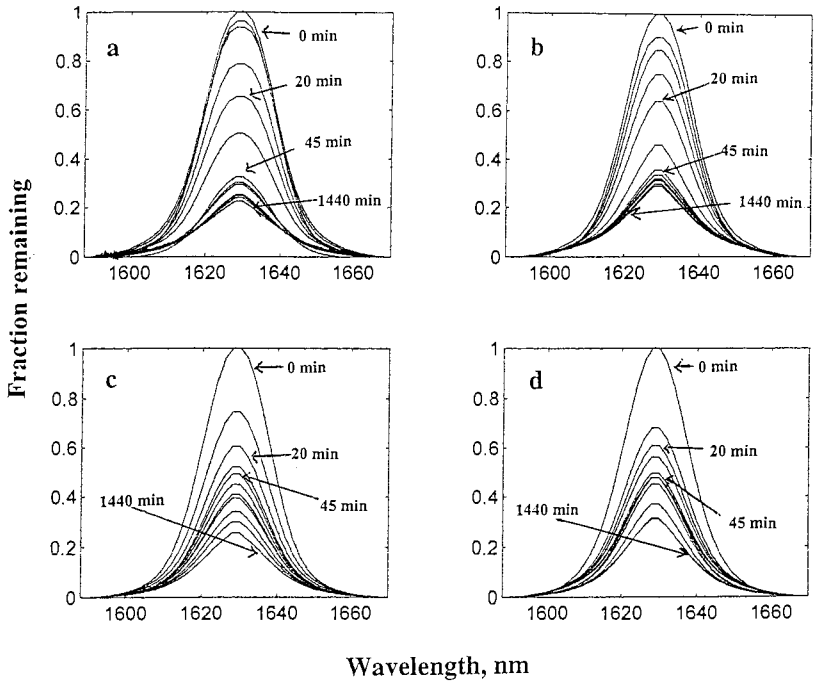

Fig. 3. (a, b, c, d) Integrated spectra representing the peaks at 1628 nm for particles of types A, B, C and D, respectively. The peaks are normalised and given as fraction remaining.

2.5. Mid infrared spectroscopic analysis

Mid infrared spectroscopic analysis was carried out using a PE 1720 FT-IR spectrometer equipped with a Spectra-Tech diffuse reflectance accessory. The polymer particle samples from all the four experiments were mixed with KBr to give approximately 4% w/w mixtures. These were then packed in sample cups (6 mm diameter and 12 mm deep) [14]. A total of 20 scans using a resolution of 4 cm^{-1} were made on the samples with the spectrum of ground pure KBr powder as the background. The resulting reflectance spectra were used for comparison.

3. Results and discussion

NIR spectroscopy is based on the anharmonicity of the fundamental vibrations. The anharmonicity results in the overtones and combination frequencies absorbing in the near infrared region. These absorptions are relatively weak compared to fundamental absorptions. This is a blessing in disguise because it allows raw samples of several fold thickness be analysed using near infrared spectroscopy. Furthermore, modern sampling techniques involving fibre cables allow easy sampling with solid particles.

The NIR spectra of the basis polymer particles used in the reaction show similarities in the spectral profiles. NIR spectra of the particles of types A, B, C and D are shown in Fig. 1. The CH stretchings of the vinyl groups absorb at 1628 nm. Combination band arising from CH and C=C stretchings absorb at 2118 nm and; combination band arising from methylenic CH stretchings and alkenic C=C stretchings absorb at 2228 nm. The NIR spectra show some differences in the 2100–2250 nm region. These arise because of the combination of aromatic CH and C=C stretchings. Poly(meta-DVB) particles have a strong absorption at 1600 cm^{-1} and poly(para-DVB) at 1510 cm^{-1} due to the aromatic C=C stretchings. These are reflected in the combination bands at 2146 and 2174 nm. The NIR spectra of the polymer

particles taken during the reaction with aluminium chloride were accompanied by base line shift. The spectra were also noisy in the longer wavelength region compared to shorter wavelength region. The second derivative of the spectra were taken to remove the base line shift in the NIR spectra and to identify whether the absorption peaks related to vinyl absorptions are overlapped with neighbouring peaks. The second derivative spectra of all the four types of particles analysed during their reaction with aluminium chloride are shown for the region 1590–1845 nm in Fig. 2. These spectra clearly show that the base line shift is removed and the first half part of the 1628 nm peak is free from overlap. The second derivative spectra also enhances and amplifies the changes in the spectra which are difficult to visualise from their absorption spectra.

The qualitative and quantitative evaluation of the reaction progress of residual vinyl groups with aluminium chloride catalyst was based on the second derivative spectral profiles of the NIR spectra. Second derivative NIR spectra of the particles taken during the kinetic experiments with particles of types A, B, C and D are shown in Fig. 2 in the region 1590–1845 nm. This spectral region contains the first overtones of the alkenic CH, aromatic CH and methylenic stretchings and will be useful in understanding the changes in the systems under investigation here.

The peaks at 1628, 2118 and 2228 nm which are related to the absorption of vinyl groups decreased prominently during the reaction. After studying the second derivative spectra of the particles taken during the reaction, we decided to use the peak at 1628 nm for semi quantitative purposes. The first half part of the absorption peak equivalent at 1628 nm was reconstructed from the second derivative spectral profiles [6].

The reconstruction of the half peak that represents the absorption of each of the sample was carried out in two steps: (i) first derivative equivalent of half the top was constructed. Here, every reconstructed variable (intensity) at a particular wavelength in the first derivative equivalent was obtained by summing up the intensities (y co-ordinates) in the second derivative curve from 1590 nm to the wavelength position that represents the new variable. (ii) the integration was repeated in the same manner to obtain intensities of absorptions from wavelength 1590 nm to 1628. These intensities represent the absorption profiles of the half top having maximum at 1628 nm. This half top was then mirror reflected to obtain a symmetrical top.

Table 1
Area under the reconstructed peak at 1628 nm and fraction of the vinyl groups remaining in the polymer particles from series A and B with time

Time (min)	Particles			
	Type A area vinyl absorption	Type A fraction remaining	Type B area vinyl absorption	Type B fraction remaining
0	236	1.00	153	1.00
5	238	1.01	156	1.02
10	201	0.85	142	0.93
15	169	0.71	126	0.83
20	130	0.55	107	0.70
30	71	0.30	76	0.50
45	74	0.31	62	0.41
60	74	0.31	60	0.39
120	63	0.27	58	0.38
180	62	0.26	57	0.37
360	62	0.26	54	0.35
1440	62	0.26	52	0.34

Table 2
Area under the reconstructed peak at 1628 nm and fraction of the vinyl groups remaining in the polymer particles from series C and D with time

Time (min)	Particles			
	Type C area vinyl absorption	Type C fraction remaining	Type D area vinyl absorption	Type D fraction remaining
0	233	1.00	136	1.00
10	172	0.74	94	0.69
20	138	0.59	84	0.62
30	118	0.51	78	0.57
45	112	0.48	70	0.51
60	103	0.44	67	0.49
90	94	0.41	64	0.47
120	92	0.40	61	0.44
180	80	0.34	50	0.37
360	71	0.30	43	0.32
1440	61	0.26	43	0.32

The integrated peak areas of the reconstructed peaks at 1628 nm of the particles were used to calculate the relative amount of vinyl groups remaining in the particles during the reaction. By assuming a linear relationship between the concentration of the residual vinyl groups and area of the reconstructed peak at 1628 nm, the relative amount of the vinyl groups remaining in the particles can be calculated. Here, the integrated area of the 1628 nm peak of the starting material was assumed to represent 100% of the vinyl groups and the amount of vinyl groups in the other particles taken during the reaction with aluminium chloride were calculated accordingly. The normalised reconstructed peaks at 1628 nm for all the samples analysed during the reaction with aluminium chloride are shown as fractions remaining in Fig. 3a,b,c,d. The fraction of vinyl groups remaining in the polymer particles of types A, B and C, D during the reaction are shown in Tables 1 and 2 respectively. The integrated peak areas and the peaks shown in Fig. 3a,b,c,d indicate that the reaction is faster at the initial stages in systems C and D compared to A and B. The reactions in systems A and B become faster during the middle part of the reaction. After 60 min of reaction time the particles of types A and B have 31 and 39% of the residual vinyl bonds left compared to particles of types C and D which have 44 and 49% of unreacted vinyl groups. However, after 24 h of reaction time the particles of types A and C have both 26% unreacted vinyl groups left. The particles of types B and D have

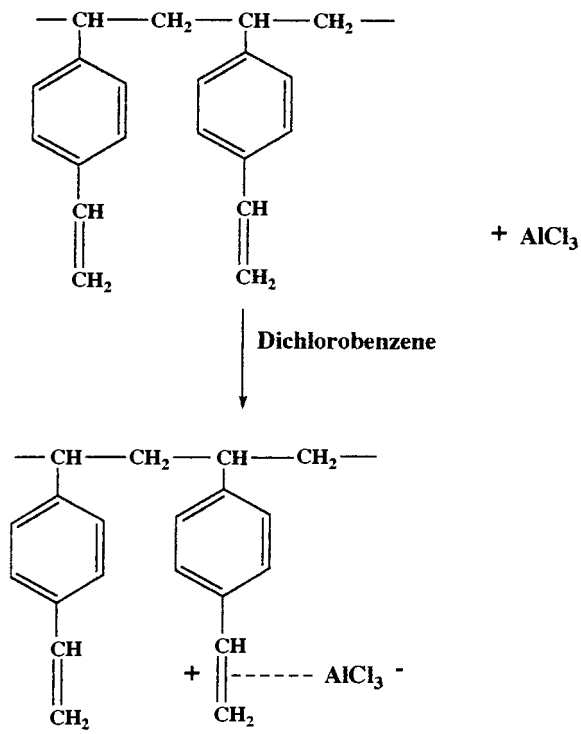

Scheme 1.

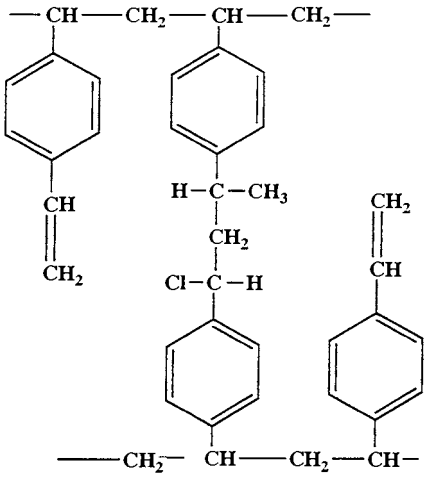

Scheme 2.

34 and 32% unreacted vinyl groups left, respectively. The absolute values of the peak areas of the unmodified particles indicate the proportionality of the residual vinyl groups among these particles. It means that at the start of reaction, the polymer particles prepared from para-DVB monomer had a higher amount of residual vinyl groups than the polymer particles made from meta-DVB monomer.

3.1. Reaction mechanisms

Some of the residual vinyl groups will form a complex with the Lewis acid, aluminium chloride, as shown in Scheme 1. The intermediate in Scheme 1 can form two different products as shown in Schemes 2 and 3.(i) the reaction is believed to proceed via electrophilic attack on neighbouring residual carbon–carbon double bonds in the polymer matrix as given in Scheme 2. This type of reaction will result in additional intermolecular crosslinking or cyclisation depending on whether the residual vinyl groups are attached to another chain or the same chain. (ii) a nucleophilic attack from a chloride ion on the activated complex (shown in Scheme 1) during the work-up procedure may occur, resulting in the product given in Scheme 3.

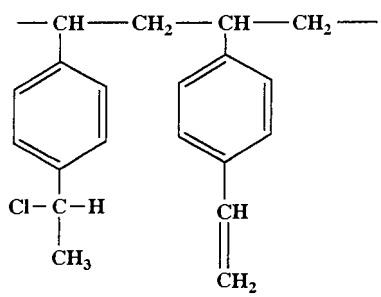

Scheme 3.

The NIR spectra of the polymer particles in the range 1590–1845 nm can give us leads regarding the changes in the vinyl group structures and methylenic structures. Second derivative spectra of the particles taken during the kinetic experiments with particles of types A, B, C and D are given (in the range 1590–1845 nm) in Fig. 2. The peaks at 1726 and 1762 nm are due to first overtones of methylenic stretchings arising from $-CH_2-$ and $-CH_3$ groups. The spectra show that there is an increase in the intensity of the 1762 nm overtone in the end products of particles of types A and C; and a decrease in the end products of particles of types B and D. There is a relative intensity decrease in the first overtone (1688 nm) of the aromatic CH stretching. This decrease is due to the transformation of a vinyl bond in conjugation with a benzene ring into a saturated methylenic CH bond.

The mid-IR spectra of the same polymer particles taken from the experiments are shown in reflectance format in Fig. 4a,b,c,d for particles of types A, B, C and D respectively. The peak at 700 cm^{-1} in the spectra of particles of types A and C, and at 750 cm^{-1} in the spectra of particles of type B are due to the C–Cl stretching vibration of mono aliphatic chlorides. There is no corresponding absorption for particles of type D.

The increase in the absorptions of the C–Cl stretchings with time indicates the formation of C–Cl bonds during the reaction. The intensities of the C–Cl stretchings in the spectra of particles of types A and C are high compared to that of particles of types B and D. These high intensities of the C–Cl stretchings are due to the crosslinking and /or cyclisation within the polymer matrix of particles of types A and C (Scheme 2) and partially due to the reaction occurring during the

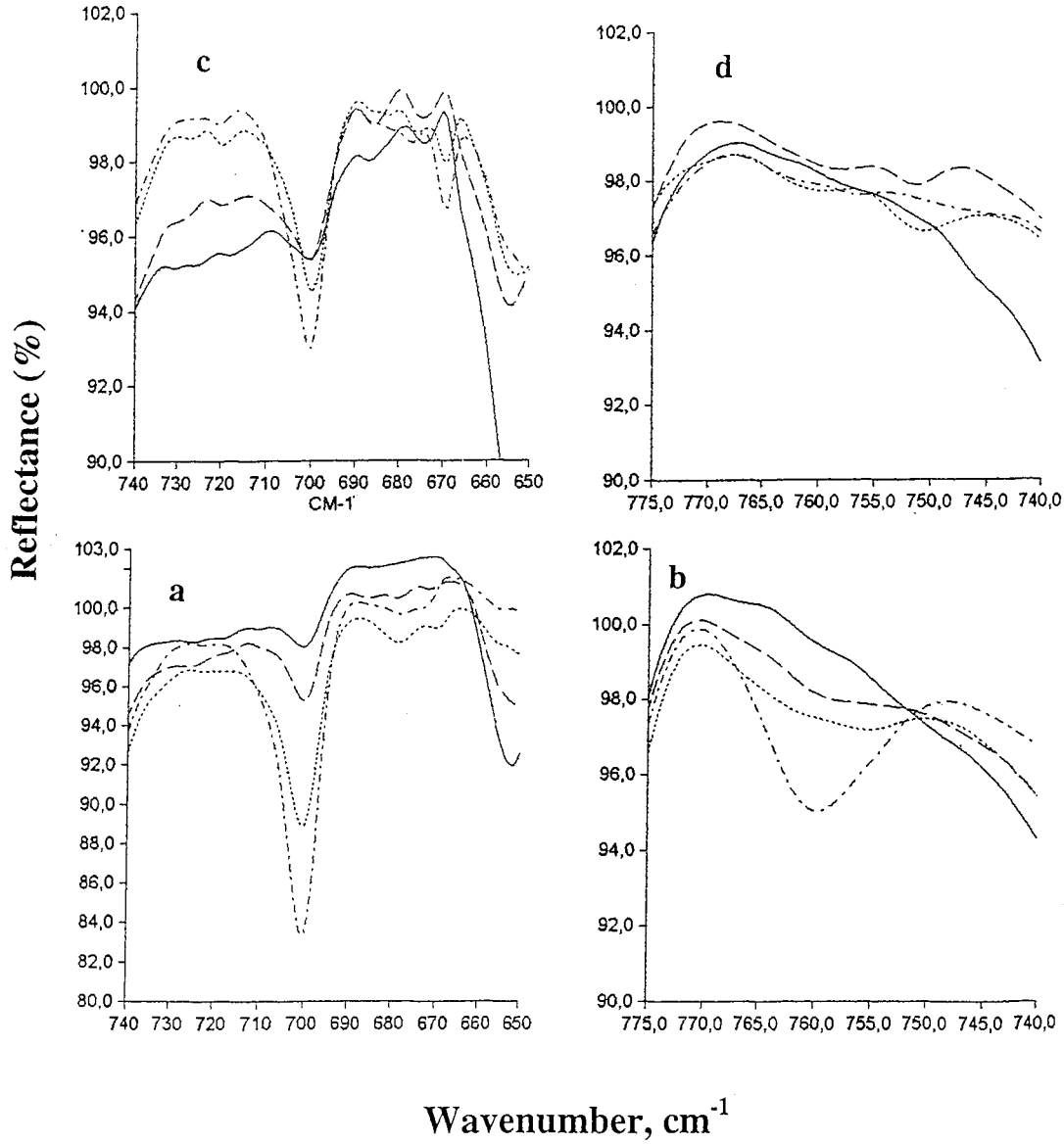

Fig. 4. Mid-IR spectra of the particles of types A, B, C and D taken during the reaction in reflectance format. (a) particles of type A taken at time intervals 5 min (–), 15min (– –), 30 min (…) and 120 min (– · –). (b) particles of type B taken at time intervals 5 min (–), 15 min (– –), 30 min (…) and 120 min (– · –). (c) particles of type C taken at time intervals 10 min (–), 30min (– –), 60 min (…) and 120 min (– · –). (d)particles of type D taken at time intervals 10 min (–), 30min (– –), 60 min (…) and 120 min (– · –).

work up procedure (Scheme 3). The crosslinking between the polymer units through the mechanism shown in Scheme 2 is supported by the increase in the overtones at 1726 nm (–CH_2–) and 1762 nm (–CH_3) in the near infrared spectra.

A weaker absorption of C–Cl stretching absorptions in the mid-infrared spectra and an increase in the first overtone of the –CH_3 absorptrions in the near infrared spectra of the particles of types B and D suggests that the

crosslinking takes place to a lesser extent in these particles. However, the relatively weak absorption of C–Cl stretchings in particles of type B and absent C–Cl stretchings in particles of type D may also suggest that the product formed as shown in Scheme 2 in these particles react with the neighbouring vinyl group and leads to cyclisation within the polymer molecule.

These results indicate that the residual vinyl groups in poly (para-DVB) particles are oriented in space of the bulk and at the surface of the pores in the polymer matrix that makes crosslinking possible. It also appears that the crosslinking in these particles is unaffected by the pore sizes obtained by using different porogens.

3.2. Kinetic parameters

The experimental evidences indicate that there are three different reactions taking place in the systems. The reactions are complex and we chose not to derive kinetic parameters for these reactions.

4. Conclusion

We have shown in this paper that aluminium chloride reacts with residual vinyl groups in poly(-para-DVB) particles and leads to partial crosslinking, cyclisation and addition of the HCl to the vinyl groups. We have also shown that this type of crosslinking is not favoured with poly (meta-DVB) particles.

We have also shown how infrared spectroscopy can be used in studying the progress of the consumption of residual vinyl groups in these particles. These studies have also helped us to understand possible reaction mechanisms for the reactions taking place in the systems.

The reactivity of the polymer particles under investigation show that the consumption of the residual vinyl groups in the particles of types C and D is faster at the initial stages. However, at the end of 24 h reaction time particles of types A and C have 26%; and B and D have around 33% unreacted residual vinyl groups.

Acknowledgements

Mr Steinar Vatne is thanked for manufacturing the sampling unit for NIR analysis. Amersham Pharmacia Biotech AS and the Norwegian Reserach Council are thanked for financial support.

References

[1] J.M. Millar, D.D. Smith, W.E. Marr, T.R.E. Kressmann, J. Chem. Soc. (1963) 218.
[2] J. Seidl, J. Malinksy, K. Dusek, W. Heitz, Adv. Polym. Sci. 5 (1967) 113.
[3] K.A. Kun, R. Kunin, J. Polym. Sci. Part A1 6 (1968) 2689.
[4] J. Hilgen, G.L. DeJong, W.E. Sederel, J. Appl. Pol. Sci. 19 (1975) 2647.
[5] H. Jacobelli, M. Bartholin, A. Guyot, Angew. Macromol. Chem. 80 (1979) 31.
[6] A.A. Christy, O.M. Kvalheim, A.K. Nyhus, S. Hagen, J.S. Schanche, Appl. Spectrosc. 52 (1998) 1230.
[7] J.R. Jones, T.J. Symes, J. Chem. Soc. C, (1971) 1124.
[8] T. Alderson, E.L. Jenner, R.V. Lindsey Jr., J. Am. Chem. Soc. 87 (24) (1965) 5638.
[9] G. Wilke, Angew. Chem. Internat. Edn. 2 (1963) 105.
[10] Y. Le Bigot, M. Delmas, A. Gaset, Synth. Comm. 13 (1983) 177.
[11] J. Ugelstad, P.C. Mørk, K. Herder Kaggerud, T. Ellingsen, A. Berge, Adv. Colloid Interface Sci. 13 (1980) 101.
[12] J. Ugelstad, A. Berge, T. Ellingsen, R. Schmid, T.N. Nilsen, P. C. Mørk, P. Stenstad, E. Hornes, Ø. Olsvik, Prog. Pol. Sci. 17 (1992) 87.
[13] Pattern Recognition Systems, High Technology Centre in Bergen, N-5007 Bergen, Norway.
[14] A.A. Christy, R.A. Velapoldi, J.E. Tvedt, Rev. Sci. Inst. 59 (1988) 423.

ELSEVIER

Talanta 48 (1999) 1121–1132

Talanta

Chromium speciation in natural waters using serially connected supported liquid membranes

Nii-Kotey Djane, Kuria Ndung'u, Carin Johnsson, Helen Sartz, Tina Tornstrom, Lennart Mathiasson *

Department of Analytical Chemistry, University of Lund, P.O. Box 124, S-221 00, Lund, Sweden

Received 19 June 1998; received in revised form 6 October 1998; accepted 13 October 1998

Abstract

A supported liquid membrane (SLM) method for the speciation of chromium has been developed. The method is based on selective extraction and enrichment of anionic Cr(VI) and cationic Cr(III) species in two serially connected SLM units. Methyltricaprylammonium chloride (Aliquat) and di-(2-ethylhexyl) phosphoric acid (DEHPA), respectively were used as the selective extractants in the membrane liquid. Graphite furnace atomic absorption spectrometry (GFAAS) was utilised for final determination. Optimised conditions for the DEHPA membrane were, sample solution at pH 3, acceptor solution 0.1 M HNO_3 and 10% w/w carrier in kerosene. The corresponding values for the Aliquat membrane were pH 7, 0.75 M HNO_3 and 6% w/w carrier in di-*n*-hexylether. This gave extraction efficiencies for Cr(III) and Cr(VI) of 90 and 40%, respectively. The method was used to measure the concentration of Cr III and Cr VI in surface water from an abandoned tannery site. Storage experiments at different pH showed that preservation at neutral pH gave almost constant values over a period of one month. At acidic pH (pH = 3.0) the concentration of Cr(VI) decreased rapidly while the concentration of Cr(III) increased. The detection limit, expressed as three times the standard deviation of enriched blank samples was 0.01 μg l^{-1}.

Keywords: Speciation; Chromium supported liquid membrane (SLM); Preconcentration

1. Introduction

The extensive use of chromium in leather tanning, metallurgy, electroplating and other industries has resulted in the release of aqueous chromium to the subsurface at numerous sites. While chromium oxidation states range from -2 to $+6$ [1], the $+3$ and $+6$ states are most prevalent in the environment. The hexavalent chromium anions chromate (CrO_4^{2-}), bichromate ($HCrO_4^-$) and dichromate ($Cr_2O_7^{2-}$) are not strongly sorbed in many soils under alkaline to slightly acidic conditions [2]. Thus they can be very mobile in subsurface environment. In contrast, Cr(III) readily precipitates as $Cr(OH)_3$ or as the solid solution $Fe_xCr_{1-x}(OH)_3$ under alkaline to slightly acidic conditions [3,4]. Since both the mobility and toxicity of Cr depend on its oxida-

* Corresponding author. Tel.: +46-46-2228165; fax: +46-46-2224544; e-mail: lennart.mathiasson@analykem.lu.se.

0039-9140/99/$ - see front matter
PII: S0039-9140(98)00334-8

tion state speciation of Cr is important in determining its fate in the environment and its risk to human health.

Speciation analysis is particularly demanding when applied to trace elements. Here, the analytical difficulties are not only related to the choice of relevant analytical techniques for measuring the individual species, but also to the fact that even the total concentration is extremely difficult to determine. A further fractionation is then rarely possible, unless preconcentration techniques which will not disturb the distribution of the species are used [5].

In the last decade, various analytical methods have been developed in order to separate and determine Cr(III) and Cr(VI) species in different biological as well as environmental samples. These include ion-exchange methods [6,7], spectrophotometric methods [8] and capillary electrophoresis [9]. Direct flow injection systems combined with atomic absorption spectrometry (AAS) [10] or inductively coupled plasma mass spectrometry (ICP-MS) [11] have also been utilised.

Supported liquid membranes have been used for the removal of chromium VI from ground water [12] and tannery effluent [13]. However, the use of SLM technology for analytical trace metal analysis has been limited. Recently we presented a flow system for on-line analysis of some metal ions in river water by combining SLM and graphite furnace atomic absorption spectroscopy (GFAAS) [14]. In this paper we report the use of SLM for selective enrichment and speciation of chromium species in natural waters using two serially connected membrane units of different configurations.

2. Experimental

2.1. Equipment

2.1.1. Supported liquid membrane device

The SLM device was similar to the one described previously [15]. It consists of two circular poly(vinylidene)-difluoride (PVDF) blocks (with a diameter of 120 mm and a thickness of 30 mm) with machined grooves like Archimedes spiral (depth 0.25 mm, width 1.5 mm and length 250 cm giving a total volume of ca. 0.95 ml). A porous PTFE membrane with polyethylene backing, (pore size 0.2 μm, total thickness 175 μm, of which 115 μm is polyethylene backing, porosity 0.70, FG Millipore Bedford, MA, USA) was impregnated with the appropriate membrane liquid by soaking for at least 15 min. The membrane was then placed between the two PVDF blocks and clamped with a stainless screw in the middle. The stainless steel screws were covered with PTFE to prevent any contact with the solution in the membrane channels.

2.1.2. Atomic absorption spectrometry

The electrothermal atomic absorption spectroscopic (GFAAS) system was a Varian AA-1475, connected to a GTA-95 graphite tube atomizer and a programmable sample dispenser (Varian, Springvale, Australia). Background correction was made with a deuterium lamp. Parameter settings, such as lamp current and wavelength were those recommended by the manufacturer. Pyrolytic graphite tubes were used.

2.2. Reagents

All solutions were prepared either from suprapur or analytical reagent grade chemicals and high purity water was obtained from a MilliQ-RO4 unit (Millipore, Bedford, MA, USA). Polyethene bottles were used throughout. These were cleaned with 4 M HNO_3 for at least 4 days and rinsed with high purity water before use. Nitric acid 65% was Suprapur (Merck). Metal standard solutions were made by dilution of 1000 mg l^{-1} chromium stock solutions prepared from chromic chloride and potassium dichromate (BDH Chemicals, UK). Di-(2-ethylhexyl) phosphoric acid (DEHPA) 95%, and di-*n*-hexyl ether were obtained from Sigma Chemicals (St. Louis MO, USA). Methyltricapryl ammoniumchloride (Aliquat®) was purchased from Janssen Chimica (Beerse, Belgium) and kerosene from Kebo Lab (Spånga, Sweden).

2.3. Experimental procedures

2.3.1. Experimental set-up

Fig. 1 shows the automated experimental set-up for the analysis of the samples in the laboratory with two serially connected membrane devices. Peristaltic pumps (Minipuls, Gilson, Villiers-le-Bel, France) were used for pumping sample solutions through the donor side of the membrane devices and eluent solutions through the acceptor side into the vials in the fraction collector. The set-up is similar to the one described previously [14].

The sample solution, containing both Cr(III) and Cr(VI) species is pumped using pump P1 to the first membrane, M1, containing DEHPA in kerosene which selectively extracts Cr(III) and further through M2, containing Aliquat in di-*n*-hexyl ether which extracts anionic Cr(VI) species ($HCrO_4^-$, CrO_4^{2-} or $Cr_2O_7^{2-}$). After the enrichment, pump P2 is used to pump the selectively enriched analytes in the stagnant acceptor solutions from the two membranes devices into two different vials in the fraction collector.

Usually, 2 ml of solution is used to ensure a complete transfer of the enriched sample from the acceptor channel (volume 1 ml) to the vials. Carry-over effects are minimized by washing the acceptor channels with fresh acceptor solution before starting a new enrichment. Pump P3 is used to empty the tubings that elute the enriched samples to the vials in the autosampler.

2.3.2. Blank determination

Blank determinations were done by enriching reagent water solutions adjusted to pH 3 or 7. The metal concentration in the sample was calculated by subtracting the blank value from the calculated chromium concentration. This value was obtained from the enrichment factor which was based on the extraction efficiency value determined from a standard solution. Chromium cali-

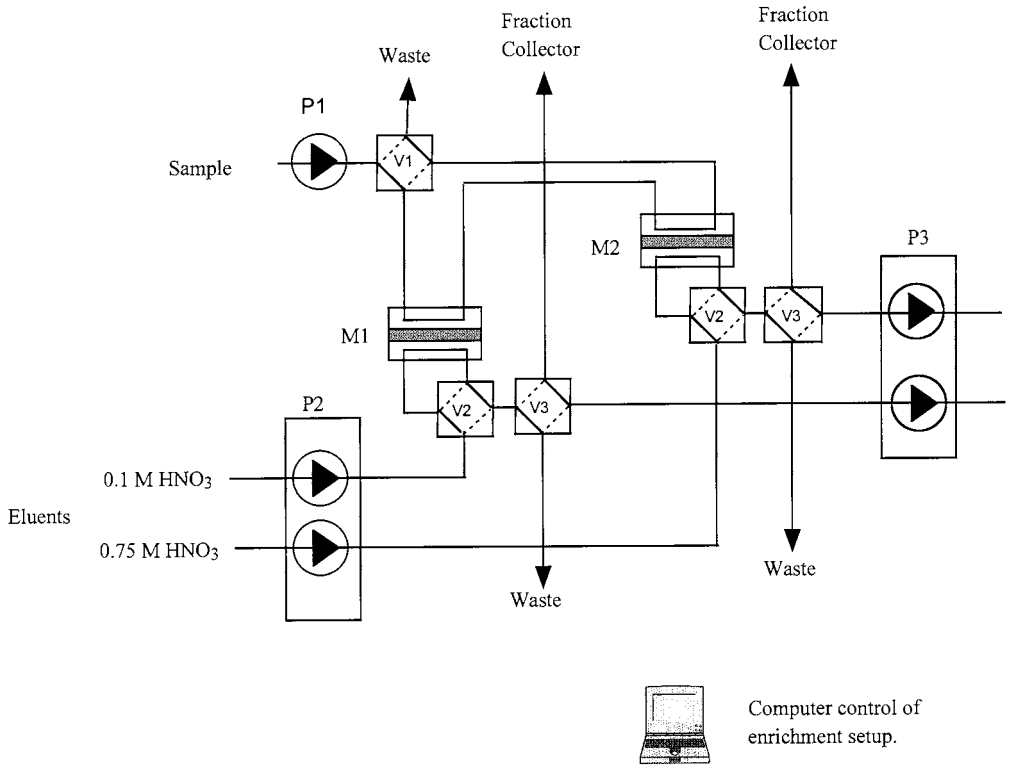

Fig. 1. Set-up for the serially connected membrane enrichment system.

bration standard solutions were prepared in 0.1 or 0.75 M HNO_3 solutions for Cr(III) and Cr(VI), respectively.

2.3.3. Sampling and sample handling

The samples were collected from surface water flowing from a tannery site into a small brook about 300 m down the valley. Although the factory has been closed since 1989 and nearly 5 million Swedish kronor has been spent on site decontamination, the tannery building and surrounding sediment are heavily contaminated with chromium which drains into the river during precipitation. In order to reduce the amount of Cr flowing into the river, two dams have been constructed to sediment chromium. The first is an underground concrete dam next to the tannery building, while the second one is an open dam adjacent to the river bank. Water samples were collected at several points along the drainage path. The first sample was collected from the pipe draining water from the underground concrete dam and at several other points along the flow path including the open sedimentation dam, and from the river, seven samples were collected in total.

The sampling bottles (polyethylene) had previously been soaked in 2 M HNO_3 for a few days and were thoroughly rinsed with high purity water before sampling. Two samples were collected from each sampling point and their pH measured, one was immediately adjusted to pH 3.0 with a few drops of nitric acid and the total Cr concentration determined by direct injection on the GFAAS. All of them were kept in the fridge at 4°C. Filtration of the water samples was not necessary as clogging is not a problem with the SLM flow-through preconcentration system.

3. Results and discussion

3.1. Extractant concentration

Fig. 2 shows the effect of extractant concentration on extraction efficiency using standard solutions of Cr(III) and Cr(VI) in reagent water.

There is an increase in extraction efficiency with extractant concentration up to 5–10% after which it starts to drop for both ions. The decrease in extraction efficiency can be attributed to an increase in viscosity of the organic phase at higher extractant concentrations in the SLM and/or increased formation of aggregate complexes with low diffusion constants especially for Cr(VI) [16]. Similar results were previously obtained in the extraction of lead, copper and cadmium with DEHPA [14] and of cobalt with Aliquat [15].

3.1.1. Effect of nitric acid concentration on chromium trapping in the acceptor

An efficient stripping of chromium from the membrane liquid to the acceptor solution is essential for quantitative transport. Fig. 3 shows the effect of the concentration of the stripping agent (HNO_3) in the acceptor solution on the extraction efficiency of the analytes. For Cr(III) the stripping is accomplished by substituting Cr(III) in the Cr(III)–DEHPA complex with protons and substitution of Cr(VI) with NO_3^- in the Cr(VI)–Aliquat ion-pair.

As expected there is no noticeable chromium transport in pure reagent water (distilled and deionised) since the driving force is the proton gradient across the membrane. The optimum nitric acid concentration for Cr(III) is 0.10 M. The decrease in extraction efficiency with increasing nitric acid concentration might depend on the interaction of nitric acid with the alkyl phosphate extractant (HA), to form complexes of the type HA m HNO_3,which has been observed in the metal extraction from nitric acid media using tributyl phosphate [17] which may compete with the formation of neutral chromium species Cr-phosphate species, necessary for the mass transfer across the membrane. However, the exact explanation for the decrease in extraction efficiency is not clear.

The extraction efficiency for Cr(VI) follows the same pattern but the optimum is at 0.75 M.

3.1.2. Effect of initial donor analyte concentration on the recovery

The concentration dependence of the extraction efficiency E (%) was investigated by varying the

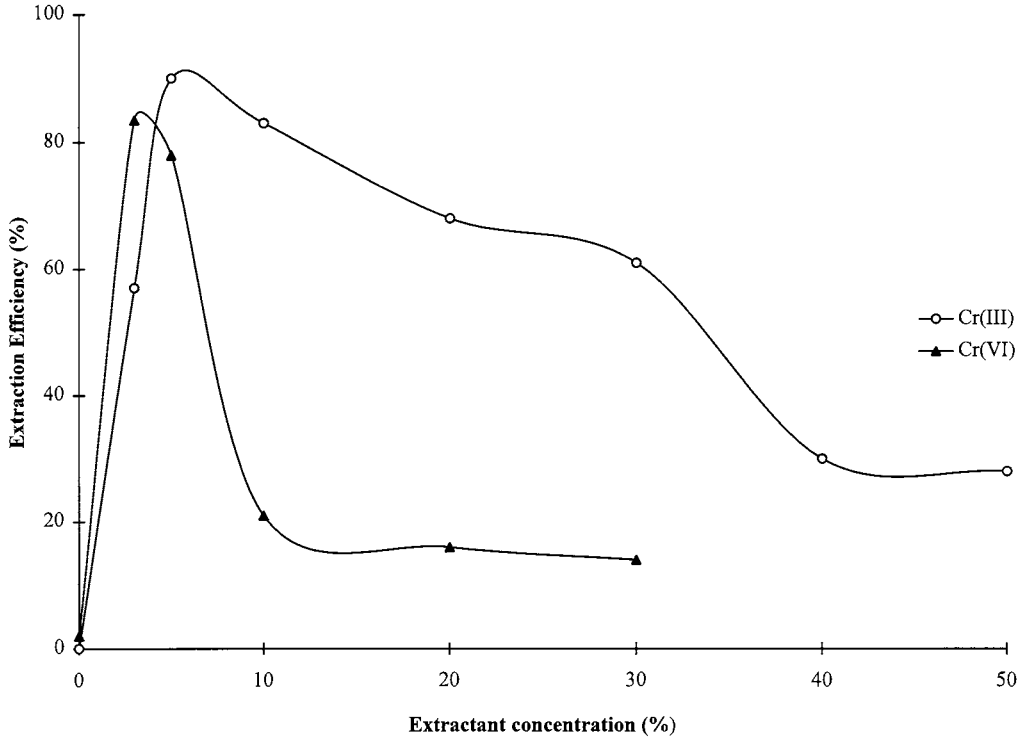

Fig. 2. Extraction efficiency E (%) vs. carrier concentration (% m/m) in kerosene (DEHPA) or di-*n*-hexyl ether (Aliquat). Donor: 5 and 2 μg l^{-1} Cr(III) and Cr(VI), respectively. Acceptor: 0.1 and 0.75 M HNO_3, respectively. Donor flow rate 1 ml min^{-1}. Enrichment time, 30 min.

donor concentration of Cr(III) and Cr(VI) in the range 0–40 μg l^{-1} and performing a 30 min enrichment at optimum operational conditions. The results are shown in Fig. 4.

The extraction efficiency E (%) of both species was independent of the initial donor concentration over the concentration range tested. The extraction efficiency values for Cr(VI) are lower than those in Figs. 2 and 3 because different membrane devices were used. This problem is further discussed below.

3.1.3. Effect of sample pH on chromium recovery

The extraction efficiency of Cr(III) at pH 3.0 in reagent water solutions was 90% at pH 3 but only around 10% at pH 7 while that of Cr(VI) was constant at around 40% at both pH 3 and 7. This can be understood from the solution chemistry of Cr. The pH of the donor sample solution is critical for Cr(III) owing to its hydrolysis reactions. Below pH 6.5, the dominant species is $CrOH^{2+}$ while the insoluble $Cr(OH)_3^0$ species dominates between pH 6.5 and 10.5 [3]. Although Cr(VI) is reduced to Cr(III) in acidic conditions and the rate of reduction increases with decreasing pH, very little $HCrO_4^-$ will be reduced at $pH > 3$ [18] and hence the constant extraction efficiency over the pH range 3–7 obtained for Cr(VI) is not surprising.

3.1.4. Optimization of the serial connection

With the Aliquat membrane used to extract Cr(VI) connected before the DEHPA membrane (opposite of the set-up in Fig. 1), the extraction efficiency for Cr(III) was noted to decrease with every subsequent enrichment replicate where as that of Cr(VI) remained constant. We found that this could be attributed to the decrease in pH on the stagnant donor side of the DEHPA membrane during the 10 min washing procedure of the ac-

ceptor solution between enrichments. When enrichment commences, it will take some time before enough donor solution is pumped to raise the pH to the optimal value. This was confirmed by maintaining the arrangement but replacing the 0.75 M HNO_3 acceptor solution in the Aliquat membrane with 0.75 M $NaNO_3$, since the driving force for the extraction is the NO_3 anion concentration. The extraction efficiencies were constant but the blank Cr value in the $NaNO_3$ solution was unacceptably high. The problem was solved by changing the order of the membrane devices with the DEHPA membrane, with an acceptor solution of only 0.1 M HNO_3 before the Aliquat membrane. This set-up was maintained in all further experiments and gave constant extraction efficiencies for both Cr species.

3.1.5. Investigation of carry-over effects in the membrane

To increase the accuracy and precision of the SLM method, carry-over effects in the membrane should be kept to a minimum. Previously, for other metal ions a washing time of 10 min was included in the programme to ensure that the background contribution from the previous sample was negligible [14,19]. To confirm that this procedure was also reliable in these measurements, the acceptor channel was flushed with the stripping solution at a flow-rate of 1 ml min^{-1} for 10 min and each second minute a 2 ml fraction was collected. It was found that the first 2 ml fraction contained the major fraction of the enriched analytes. Using the above routine washing procedure at a flow rate of 1 ml min^{-1} for 10 min, carry-over effects were reduced to $< 2\%$.

3.1.6. Detection limit

The concentration of Cr(III) in acidified reagent water (pH 3.0) was 0.12 μg l^{-1} (in 0.1 M HNO_3.) with a SD of 0.004. The concentration of Cr(VI)

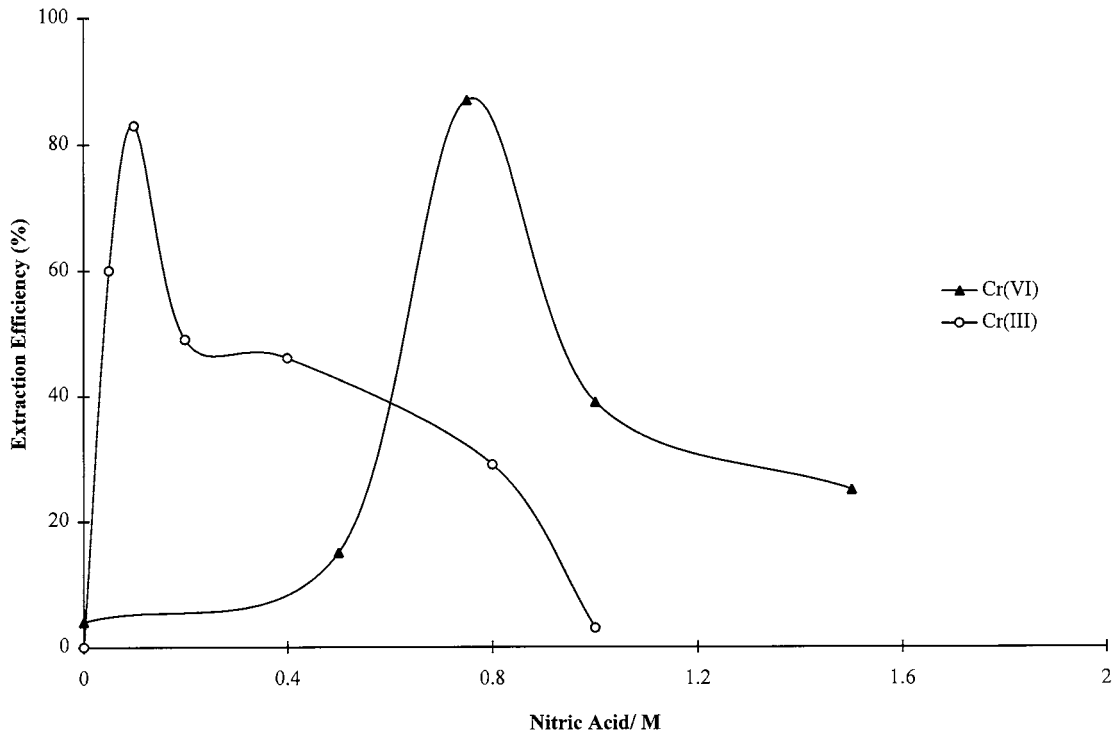

Fig. 3. Extraction efficiency E (%) vs. nitric acid concentration. SLM 10% m/m DEHPA in kerosene and 6% Aliquat 336 (m/m) in di-n-hexylether. Donor: 5 and 2 μg l^{-1} Cr(III) and Cr(VI), respectively at pH 3. Enrichment time, 30 min.

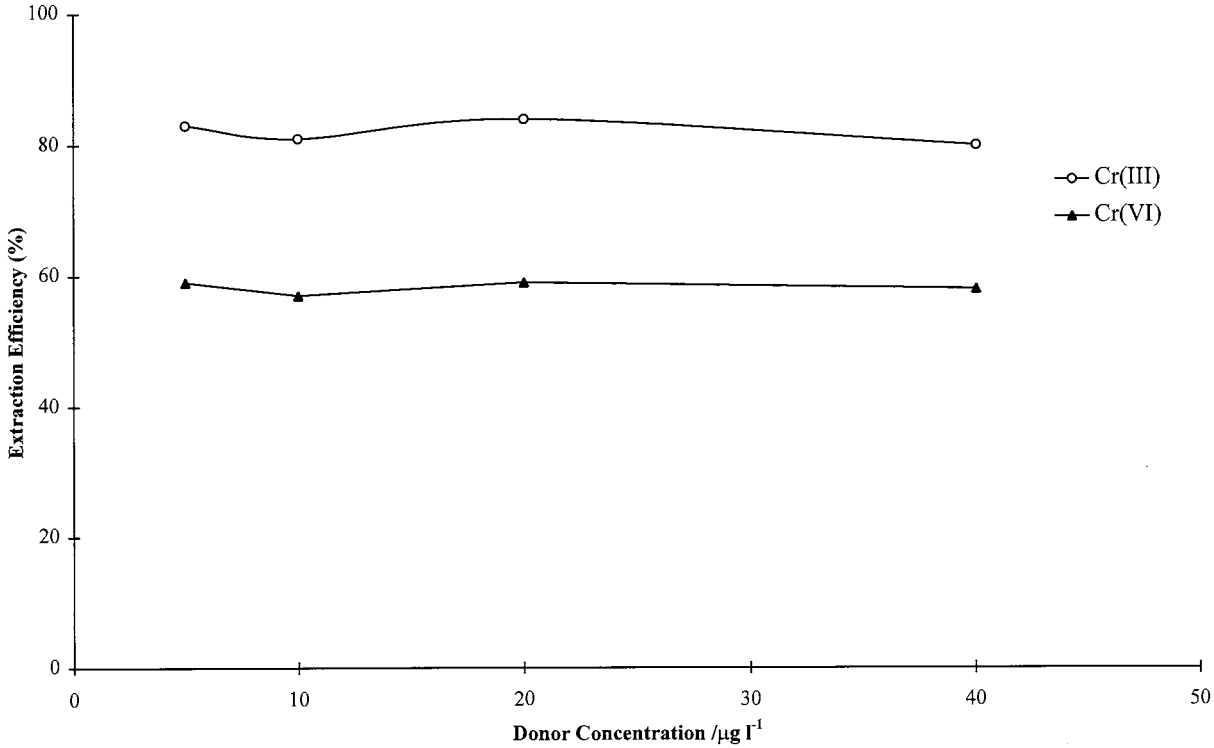

Fig. 4. Extraction efficiency E (%) vs. donor concentration. Membrane 10% m/m DEHPA and 6% m/m Aliquat in kerosene and di-*n*-hexyl ether, respectively. Donor: 5 and 2 μg l^{-1} Cr(III) and Cr(VI), respectively. Acceptor: 0.1 and 0.75 M HNO_3, respectively.

in reagent water at both pH 3 and 7 was 0.01 μg l^{-1} with a SD of 0.003.

The figures are based on a 2 h enrichment period and 2 ml acceptor volume. This corresponds to enrichment factors of 54 and 24 for Cr(III) and Cr(VI) respectively. The limit of detection, expressed as three times the SD, will then be 0.012 and 0.01 μg l^{-1} for Cr(III) and Cr(VI),respectively.

3.2. Surface water samples

3.2.1. Extraction efficiency

Experiments were carried out to investigate the extraction efficiency of Cr(III) and Cr(VI) species in spiked natural water samples, low in chromium concentration by performing enrichments at pH 3 and 7, which was close to the natural pH of the collected water samples. In spiked unpolluted river water samples adjusted to pH 3.0, the extraction efficiency for Cr(III) and Cr(VI) were 86 and 35%, respectively which are slightly lower than in reagent water (90 and 40%, respectively). While the extraction efficiency for Cr(VI) at pH 7 remains constant in both natural and reagent water samples, that of Cr(III) drops to 10%. This could be due to the formation of the insoluble $Cr(OH)_3^0$ species at this pH [3].

The extraction efficiency at different donor concentrations at the natural pH of the collected spiked surface water samples was also investigated for Cr(VI). The samples were spiked with Cr(VI) at concentrations between 5 and 40 μg l^{-1}. As shown in Fig. 5 the extraction efficiency for Cr(VI)was constant over the entire concentration range investigated.

In this experimental work, different membrane devices, manufactured at our workshop have been used. We know that the manufacturing process may lead to differences in channel depths. This will lead to differences in absolute extraction efficiencies and is the probable explanation for the

differences obtained e.g. in absolute recoveries for Cr(VI) in Figs. 4 and 5. Interactions between Cr(VI) and species in the natural water matrix resulting in lower efficiency should lead to a concentration dependence, which was not observed.

3.3. Chromium speciation in surface water samples

Total Cr concentrations in the collected water samples were determined by direct injection of the acidified samples on the GFAAS before any SLM preconcentration. The level of Cr in some of the samples was high which necessitated dilution before the GFAAS determination. However SLM extraction was still necessary as a sample clean-up step rather than an as an enrichment step in order to selectively extract each Cr species. Table 1 shows the concentrations of each chromium species including the total Cr of the seven water samples collected.

The sum of Cr(III) and Cr(VI) does not add up to the total chromium concentration determined by GFAAS as expected. With the SLM, one only determines free Cr(III) and Cr(VI) species or such species loosely bound to organic or anthropogenic ligands or adsorbed on soil particles, while the GFAAS technique gives the total chromium concentration. Fig. 6 shows Cr(VI) concentration profile along the drainage path.

The concentration of all the Cr species including the total decreases exponentially from first sampling point to the last. This was expected since sample 1 was collected from a point about 80 m from the source (tannery building) and more Cr adsorbs on the sediment along the drainage path. Sample 4 and 5 were collected from the sedimentation dam (about 200 m)adjacent the river bank especially constructed to sediment the Cr in the water before it drains into the river. At this point, $\approx 90\%$ of Cr(VI) has adsorbed in the sediment

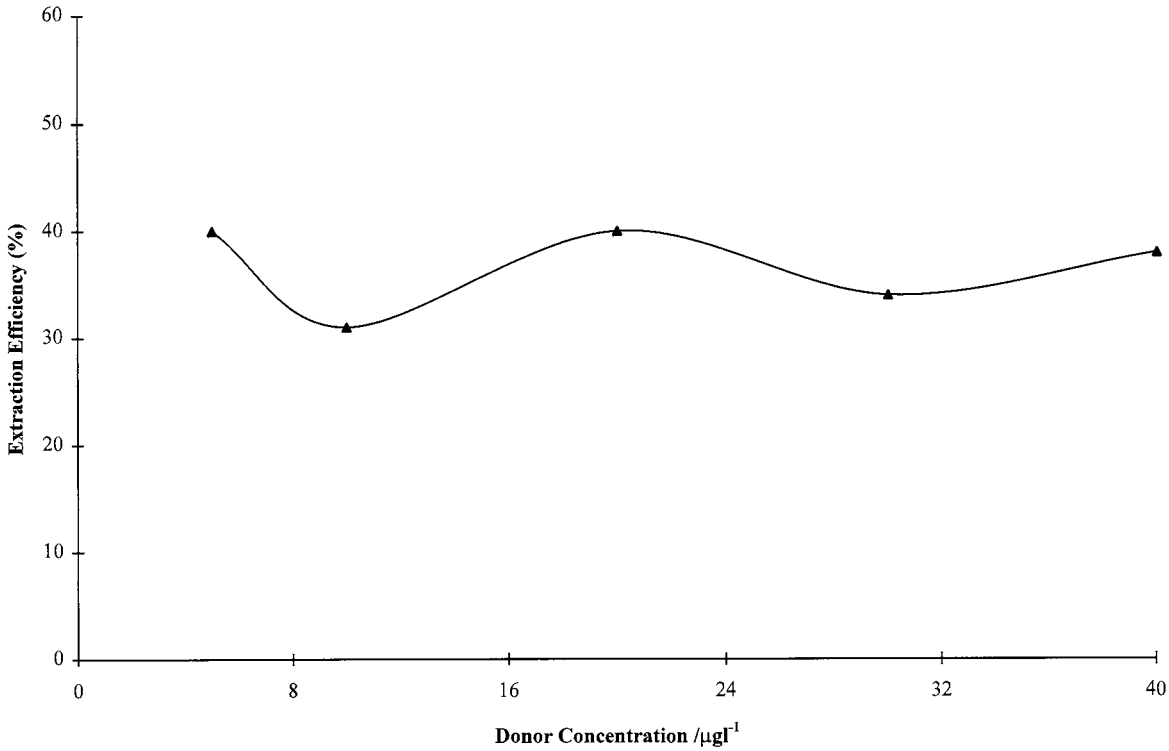

Fig. 5. Extraction efficiency E (%) vs. donor concentration. Donor unpolluted river water pH 7 spiked with Cr(VI). Enrichment time, 30 min.

Table 1
Cr(III) and Cr(VI) concentration in surface water samples

Sample no.	Sample pH	Distance from tannery (m)	Enrichment time (min)	Cr concentration (μg l^{-1})			
				Total Cr, pH 3.0	Cr(III), pH 3.0	Cr(VI), pH 3.0	Cr(VI), pH 7.0
1	7.6	80	15	225 (2)[a]	1.1 (4)	63 (9)	63 (1)
2	7.7	120	15	56 (1)	0.9 (8)	18 (5)	17.2 (4)
3	7.1	160	15	35 (1)	0.1 (6)	1.1 (1)	4.2 (6)
4	7.5	200	20	12.5 (3)	0.3 (2)	1.3 (2)	2.1 (2)
5	8.1	250	20	13 (4)	0.3 (4)	1.6 (6)	2.5 (2)
6	7.6		80	<0.05	<0.05	<0.05	<0.05
7	7.5	300	80	<0.05	<0.05	<0.05	<0.05

[a] Bracketed values represent RSD values of at least three replicate determinations.

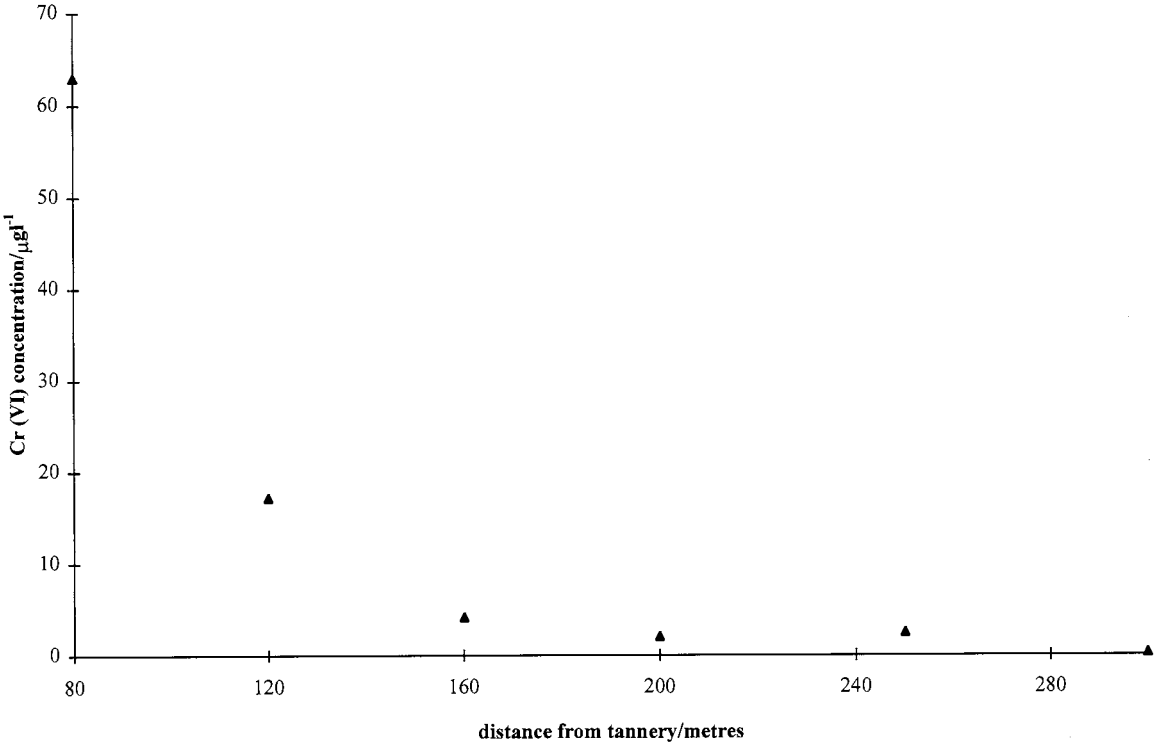

Fig. 6. Cr(VI) concentration profile along the drainage path from the tannery building. For details see text.

along the flow path. Sample 7 was taken from the river, a few metres downstream of the drainage point from the dam. Sample 6 in Table 1 was taken a few metres upstream of the drainage point from the surface water flowing from the tannery site and should represent the background level. The concentration of Cr(VI) in samples 6 and 7 are very low and about the same implying that most of the Cr(VI) is deposited on the sediment along the drainage path and the sedimentation dam.

3.4. Chromium (VI) stability

When an available source of electrons, such as organic matter or reduced forms of various inorganic species such as Fe(II) are present, chromium(VI) will be reduced to Cr(III). The rate of Cr(VI) reduction increases with decreasing pH and can be summarized by:

$$HCrO_4^- + 7H^+ + 3e^- \Leftrightarrow Cr^{3+} + 4H_2O$$

Several other factors affect the rate of Cr(VI) reduction including temperature, ionic strength, microbial activity and adsorption on container surfaces [18].

To investigate the rate of Cr(VI) reduction the concentrations of Cr(III) and Cr(VI) in sample number 2 (adjusted to pH 3 and at pH 7.7) were determined soon after collection and stored in the fridge at 4°C. The concentration of Cr(III) and VI was measured every 10 days for the next 30 days. Fig. 7 shows the concentrations of Cr(III) and (VI) in the water samples preserved at pH 3 and 7.7 for 1 month.

The concentration of Cr(VI) in the acidified samples gradually reduces while that of Cr(III) increases gradually. The rate of reduction of Cr(VI) is more pronounced in the first 10 days, where about 20% of the total Cr disappears and then the relative amount of Cr(VI) stabilises to about 12% of total Cr. There is a similar trend in the increase in Cr(III) concentration. However the rate of reduction of Cr(VI) is larger than the

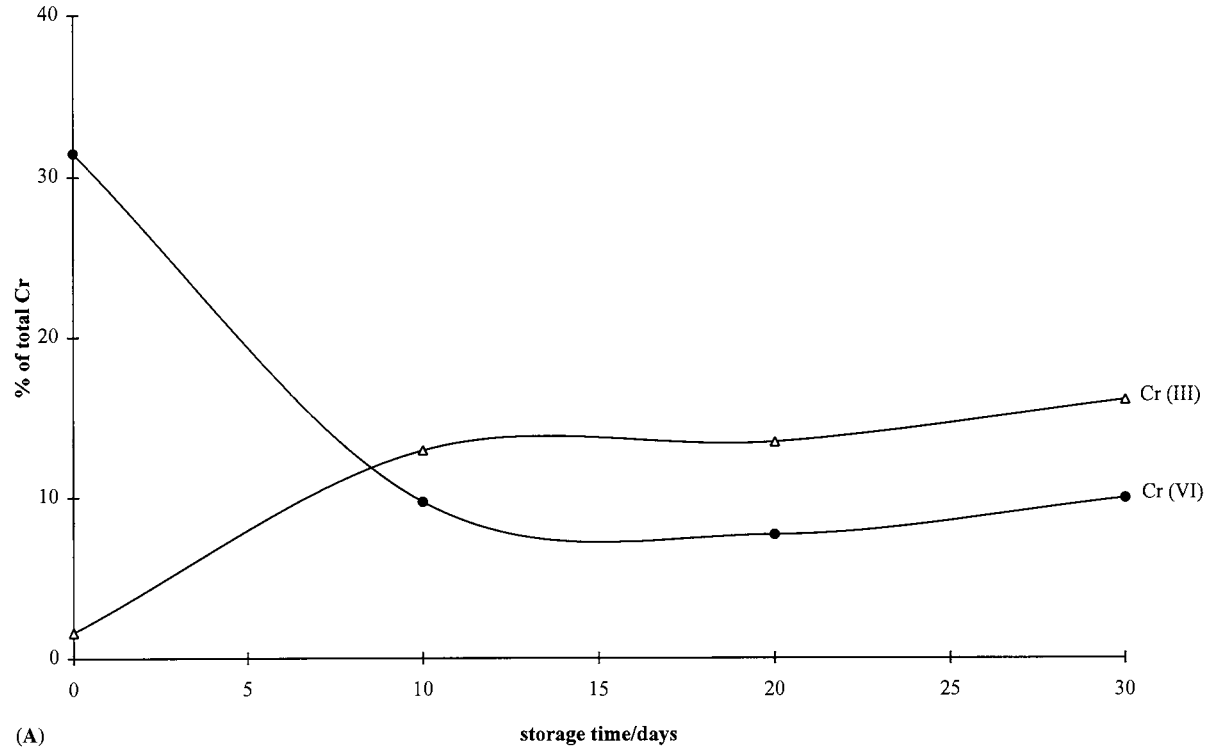

(A)

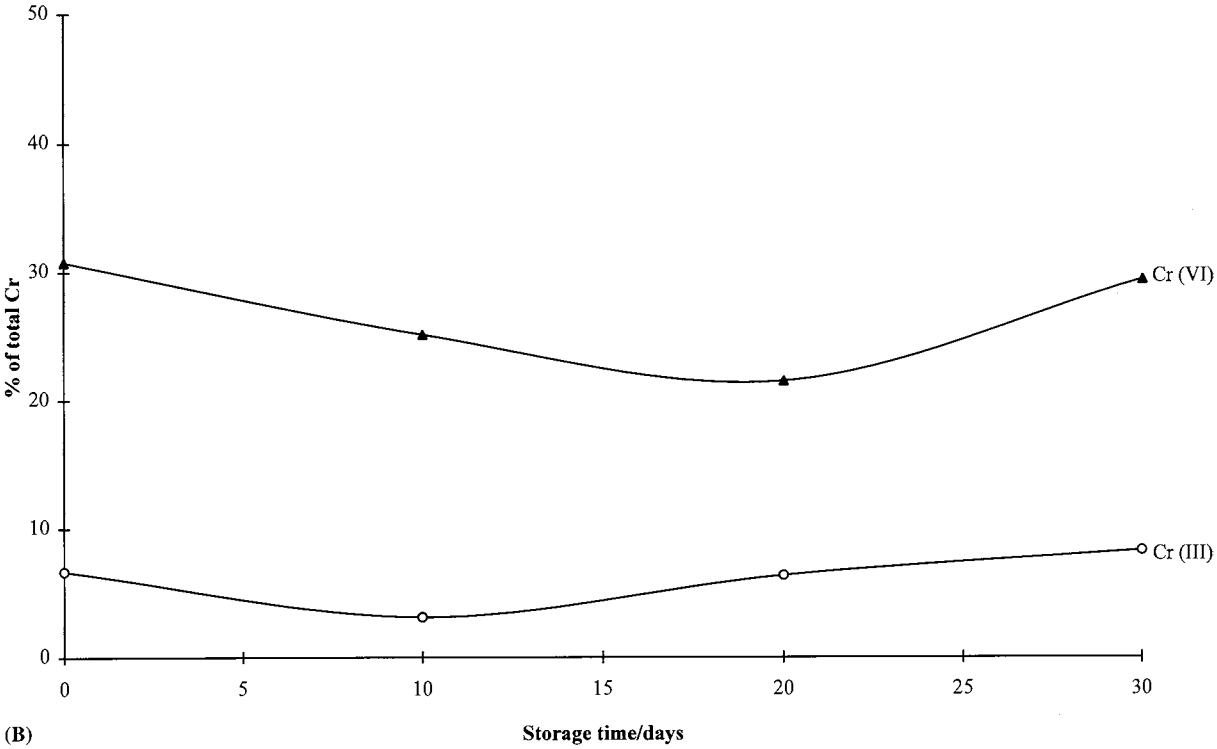

(B)

Fig. 7. Percentage of Cr(III) or Cr(VI) of the total Cr in water samples stored at 4°C at pH 3 (A) and at pH 7 (B).

increase in Cr(III) concentration. This could imply that not all Cr(VI) is reduced to Cr(III). This could be due to some of the Cr forming complexes with the ligands in the water and hence not available for extraction by the SLM.

The concentration of both Cr species preserved at the natural pH remains constant as expected.

4. Conclusion

This work has demonstrated that supported liquid membranes can be used for chromium speciation studies of complex matrices such as natural waters. By using different membrane liquids, soluble Cr(III) and Cr(VI) species and those complexes loosely bound to colloidal particles which can be broken down during the residence time of the sample plug in the donor channels of the SLM unit can be selectively enriched avoiding the need for any chromatographic separation prior to final determination. This combined with the unique capability of the SLM technique to process complex-matrix samples such as river water without any filtration, helps in preserving the prevailing redox conditions where the species of interest remain intact and lowers the limit of detection.

Acknowledgements

The authors wish to thank Fredrik Malcus for technical assistance and Birgitta Johansson Sternerup for her assistance with the sampling. Financial assistance from The Swedish Natural Research Council (NFR) and the Swedish Environmental Protection Fund (SNV) is also kindly acknowledged.

References

[1] A.F. Cotton, G. Wilkinson, in: Advanced Inorganic Chemistry, 5th edn., John Wiley and Sons, New York, 1988, p. 680.
[2] J.M. Zachara, C.C. Ainsworth, C.E. Cowan, C.T. Resch, Soil Sci. Soc. Am. J. 53 (1989) 418.
[3] D. Rai, B.M. Sass, D.A. Moore, Inorg. Chem. 26 (1987) 345.
[4] B.M. Sass, D. Rai, Inorg. Chem. 26 (1987) 2228.
[5] W. Lund, Fresenius J. Anal. Chem. 337 (1990) 557.
[6] R.M. Crespon-Romero, M.C. Yebra-Biurrun, M.P. Bermejo-Barrera, Anal. Chim. Acta. 327 (1996) 37.
[7] P.A. Sule, J.D. Ingle, Anal. Chim. Acta. 326 (1996) 85.
[8] A. Padarauskas, G. Schwed, Talanta 42 (1995) 693.
[9] A.R. Timerbaev, O.P. Semenova, W. Buchberger, G.K. Bonn, Fresenius J. Anal. Chem. 354 (1996) 414.
[10] S. Sperling, S. Xu, B. Welz, Anal. Chem. 64 (1992) 3101.
[11] G. Zoorob, M. Tomlinson, J.S. Wang, J. Caruso, J. Anal. Atom. Spectrom. 10 (1995) 853.
[12] R. Chiarizia, E.P. Horwitz, K.M. Hodgson, Acs Symposium Series 509 (1992) 22.
[13] M.A. Chaudry, S. Ahmad, M.T. Malik, Waste Manage. 17 (1997) 211.
[14] N.-K. Djane, K. Ndung'u, F. Malcus, G. Johansson, L. Mathiasson, Fresenius J. Anal. Chem. 358 (1997) 822.
[15] M. Papantoni, N.-K. Djane, K. Ndung'u, J.Å. Jönsson, L. Mathiasson, Analyst Lond. 120 (1995) 1471.
[16] J. Babcock, J. Memb. Sci. 7 (1980) 71.
[17] J. Korkisch, in: Modern Methods for the Separation of Rarer Metal Ions, Pergamon Press, London, 1969, p. 235.
[18] K.G. Stollenwerk, D.B. Grove, J. Environ. Qual. 14 (1985) 396.
[19] N.-K. Djane, I.A. Bergdahl, K. Ndung'u, A. Schutz, G. Johannsson, L. Mathiasson, Analyst 122 (1997) 1073.

ELSEVIER

Talanta 48 (1999) 1133–1137

Talanta

The study of the partitioning mechanism of methyl orange in an aqueous two-phase system

Yoshifumi Akama [a,*], Aijun Tong [b], Maria Ito [a], Shigeyuki Tanaka [a]

[a] *Department of Chemistry, Faculty of Science and Engineering, Meisei University, Hino, Tokyo 191, Japan*
[b] *Department of Chemistry, Tsinghua University, Beijing 100084, China*

Received 29 December 1997; received in revised form 12 October 1998; accepted 14 October 1998

Abstract

An aqueous two-phase system of dodecyl triethylammonium bromide (C_{12}NE, cationic surfactant) and sodium dodecyl sulfate (SDS, anionic surfactant) mixture is proposed for the extraction of some dyes and porphyrin compounds. Transparent two phase-systems are formed when the surfactant concentrations and C_{12}NE/SDS ratios are in certain regions. In this study, the aqueous two phase-systems were prepared by mixing 0.1 mol l^{-1} C_{12}NE and SDS with a molar ratio of 1.7:1.0. The results showed that negatively charged chlorophyll (sodium copper chlorophyllin) and positively charged dye (methyl violet) were efficiently extracted into the upper phase. The negatively charged methyl orange (pH > 7) was moved into the upper phase mostly while amphoteric methyl orange (pH < 3) was distributed in the two phases uniformly. Except for hydrophobic force, charge interaction between solute and surfactant also play an important role in the extraction process.

Keywords: Aqueous two phase-system; Chlorophyll; Dodecyl triethylammonium bromide (C_{12}NE); Methyl orange; Sodium dodecyl sulfate (SDS)

1. Introduction

Solvent extraction is an effective technique for the selective separation and concentration of a certain substance from others coexisting in matrices by adding an organic solvent to a liquid or a solid sample. It is widely used in the purification of industrial samples and concentration of trace materials from large amounts of samples prior to instrumental analysis. The most commonly used solvents for the solvent extraction technique are benzene, chloroform and/or other organic solvents. However, the use of chloride containing solvents such as chloroform, tetrachloromethane may cause environmental pollution and thus are not appreciated. On the other hand, separation and purification of enzyme, nucleic acid and other biomaterials are very important in biological tech-

* Corresponding author. Tel.: +81-42-5915111; fax: +81-42-5918181; e-mail: akama@chem.meisei-u.ac.jp.

0039-9140/99/$ - see front matter
PII: S0039-9140(98)00331-2

niques. Aqueous two-phase extraction was thus developed to avoid treatment of large amounts of organic solvents and to provide a mild medium similar to their biophysical environment. Aqueous polymer two-phase extraction is a well known effective technique and there are many reports [1–3] on such systems. This paper deals with an aqueous two-phase system consisting of differently charged surfactant. Mixed surfactant solution usually has a higher surface activity than that of a solution composed of a single surfactant; the systems of equally charged surfactants of a cationic or anionic surfactant with nonionic surfactant have been well studied. Regarding the system of a mixed cationic and anionic surfactant solution, precipitation may occur and thus their surface activity may be lost. It is also found that surface activity may rise and that homogeneous or even aqueous two-phase system can be obtained when cationic and anionic surfactants are mixed under certain conditions [4,5]. The aqueous two-phase system of cationic and anionic surfactant mixture proposed by Zhao et al. [5] is one of the examples.

When anionic surfactant sodium dodecyl sulfate (SDS) and cationic surfactant dodecyltriethylammonium bromide (C_{12}NE) are mixed in certain surfactant concentrations region, aqueous two-phase is formed. For example, when each 0.1mol l^{-1} C_{12}NE and SDS is mixed in the ratio range of 1.7:1.0 to 1.8:1.0, an aqueous two-phase can easily be obtained. The two phases are both transparent. This paper reports the results of partitioning of porphyrin and related compounds as well as some organic dyes in an aqueous two-phase system, their partitioning behaviors in this system are also discussed in view of the molecular structure of the solutes.

2. Experimental

2.1. Apparatus

Concentration of a substance partitioned in the aqueous two-phase system is determined using a Hitachi 170-30 atomic absorption spectrometer (AAS) or a Simadzu digital double beam spectrometer UV-210.

2.2. Reagents

C_{12}NE is synthesized according to the improved method of Zhao et al. [6]. Lauryl bromide and triethylamine are dissolved in methanol with a molar ratio of 1:2 and refluxed for 48 h at 70 C under agitation. The product is recrystallized four times with a mixed solvent of acetone and ethyl ether, the final C_{12}NE obtained is in the form of white crystals. The biochemical reagent of SDS was purchased and used without further purifiations. These surfactants are dissolved in water to a molarity of 0.1 mol l^{-1}, respectively.

Copper chlorophyllin sodium salt, hematoporphyrin dihydrochrolic acid, vitamin B_{12}, methyl violet and methyl orange are used as received without further purification.

2.3. Procedure

Aqueous two-phase is formed by mixing 1.7 ml of 0.1 mol l^{-1} C_{12}NE and 1.0 ml of 0.1 mol l^{-1} SDS, the two-phase system thus obtained is of 0.9 ml upper phase and 1.8 ml lower phase. It can be seen that most surfactants are concentrated in the upper phase. The powders of porphyrin and related compounds as well as methyl violet and methyl orange are correctly weighed and dissolved in the two-phase system, respectively. The mixture is agitated and allowed to stand for a while, then the two phases are separated and certain volumes of the upper and lower phases are taken. Such solutions of the upper and lower phases are diluted, and then the materials extracted in corresponding solution are determined with AAS or visible spectrometry. When copper chlorophyllin sodium salt is used, the upper phase is diluted with water and copper is determined by AAS; as to hematoporphyrin or methyl violet, the upper phase are diluted with ethanol and determination is performed with visible spectrometry. The matrices of standard and sample solution are made in the same conditions.

3. Results and discussion

Aqueous two-phase separation method is a new kind of liquid–liquid extraction that different from the traditional solvent extraction. It received increasing attention because the method is non-volatile, nonflammable, having safety and cost benefits. Although several aqueous two-phase extraction techniques have been proposed, studies on the two-phase systems composed of cationic and anionic surfactant mixture are few [4–8]. We have reported the extractions of porphyrin chelating agents [7] with the C_{12}NE–SDS cationic two-phase system, the reults showed that besides the hydrophobic force, the sorts of substituted groups outside the porphyrin ring play an important role in the extraction. In this study, other porphyrin compounds that exist in living things or plants, as well as some dyes are extracted with the C_{12}NE–SDS two-phase system, their partitioning behaviors are studied.

When copper chlorophyllin sodium salt, hematoporphyrin and vitamin B_{12} are partitioned in the two phases respectively, it is clearly seen from the difference in color that these compounds mostly moved into the upper phase while vitamin B_{12} partitioned in the two phases almost uniformly. The extraction efficiency is calculated from the results of determinations of copper chlorophyllin sodium salt with AAS and others based on the visible detection. The results are summarized in Table 1.

It could be seen that copper chlorophyllin sodium salt and hematoporphyrin are concentrated into the upper phase with an extraction efficiency higher than 99 and 95%, respectively, while vitamin B_{12} moved into the upper phase about 40%. Copper chlorophyllin sodium salt is well known as an aqueous chlorophyll and thus it dissolves well in water, its chemical structure is listed in Fig. 1. When the compound is dissolved in water, sodium ion is dissociated and thus negatively charged porphyrin is obtained. Such negatively charged porphyrin is extracted into the upper phase in which the surfactant concentration is much more higher than the bottom phase and the cationic surfactant C_{12}NE is in excess. A similar result has been obtained when tetraphenyl

Table 1
Extraction results with the aqueous two-phase system

Sample	Taken (mg)	Extraction in the upper phase Efficiency (%)
Copper chlorophyllin sodium salt	5.0	99.1
	3.2	99.3
	2.8	99.9
	2.7	99.1
Hematoporphyrin	1.3	95.4
	1.0	96.9
	0.9	96.8
Vitamin B_{12}	1.0	41.3
	4.0×10^{-5}	40.6
Methyl violet	0.8	91.3
	0.6	92.1

porphine sulfonic acid was extracted. The extraction efficiency of hematoporpyrin is also high, the reason may be due to its hydrophobicity and the possibility of negatively charged hematoporphyrin existing when the carbonyl groups dissociated. However, in the case of vitamin B_{12}, positively and negatively charged parts both existed in the molecule. It is considered that when such differently charged parts both existed in a same molecule it distributed in the two-phase system uniformly as have been observed in the case of methylene blue [8].

In order to conform these results, organic dyes methyl violet and methyl red were added to the two-phase system, respectively. The results are that the two dyes were moved into the upper phase perfectly. Methyl violet is in its positively charged form while methyl red is in its negatively

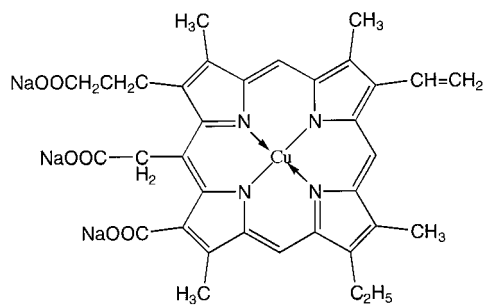

Fig. 1. Structure of copper chlorophyllin sodium.

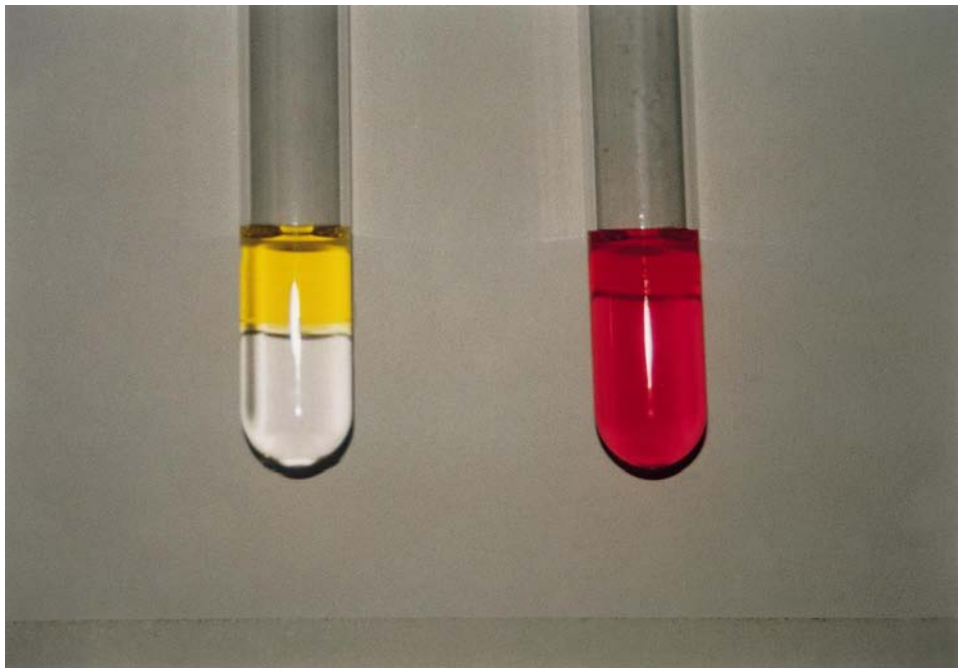

Fig. 2. Partitioning behavior of methyl orange in aqueous two-phase systems. Methyl orange is yellow in the anionic form and is red in amphoteric form.

charged form when dissolved in water, respectively. In other words, positively or negatively charged species could be effectively extracted into the upper phase from aqueous solution with our two-phase extraction system.

Methyl orange is a well known indicator in acid–base titration and it is selected as our another test compound. The extraction result is interesting and it reveals the relation between the partitioning behavior of a substance and its chemical structure. The indicator was dissolved in the two-phase system and then the extraction procedure performed, it could be seen that the methyl orange mostly moved into the upper phase with the phase color being yellow. The pH of the system was about 7. When little amount of acid solution was added to the system, the color of methyl orange changed from yellow to red and the indicator became to distribute in the two-phase system uniformly. The partitioning behavior of methyl orange is shown in Fig. 2. The change of partitioning behavior of methyl orange when acid solution was added could be explained as follows. The methyl orange molecule existed in its negatively charged form when dissolved in water at pH 7, namely, sodium ion dissociated at

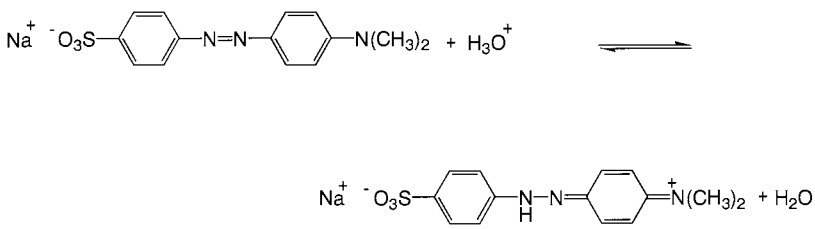

Fig. 3. Structure of methyl orange.

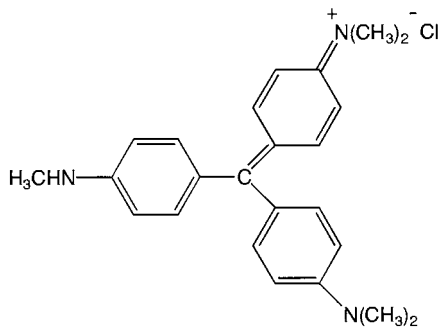

Fig. 4. Structure of methyl violet.

this condition and thus distributed in the upper phase. When acid solution is added, hydrogen ion would be attached to the nitrogen atom of azo group and the molecule became being both positively and negatively charged species as shown in Fig. 3. As is observed in the case of vitamin B_{12}, zwitter ion has less charge interaction with large amounts of differently charged surfactants in the upper phase compared to the negatively charged species and thus distributed in the two phases uniformly.

Extraction of methyl violet (Fig. 4) and methyl red were also performed. At pH 7, methyl red may be negatively charged due to the dissociation of proton ion in carboxyl group, while methyl violet exists in its positively charged form. The extraction efficiencies of methyl red and methyl violet are 100 and 90%, respectively, indicating strong charge interaction of positively or negatively charged species being extracted with the top phase in which the surfactant concentration is much higher than the lower phase and both positive and negative charge exist in the mixed micelles.

The factors that govern the partitioning behavior of a substance in the two-phase system of differently charged surfactant mixture would be various and complex: hydrophobic property, bulk and charge of a molecule being partitioned would be the main factors to influence extraction. The results of this study suggest that positively or negatively charged molecules with relatively large structure could effectively be extracted from the aqueous solution with the proposed aqueous two-phase extraction system, but this system could not be applied to the extraction of zwitter ions. In the present C_{12}NE–SDS two-phase extraction system, the main factors that influence the extraction of a substance are considered to be the charge and the hydrophobicity of a substance being partitioned.

Acknowledgements

This work was partially supported by the Frontier Research Center for the Global Environment Protection.

References

[1] H. Watanabe, H. Tanaka, Talanta 25 (1978) 585.
[2] J. Miura, H. Ishii, H. Watanabe, Bunseki Kagaku 25 (1976) 252.
[3] S. Igarashi, T. Yotsuyanagi, Mikrochim. Acta 106 (1992) 37.
[4] M. Abe, T. Arai, T. Kawakami, Sekiyu Kagakukaishi 36 (1993) 326.
[5] G.X. Zhao, J.X. Xiao, Colloid Polym. Sci. 273 (1995) 1088.
[6] G.X. Zhao, J.X. Xiao, Colloid Polym. Sci. 177 (1996) 513.
[7] A.J. Tong, Y. Wu, L. Li, Y. Akama, S. Tanaka, Anal. Sci.(suppl) 13 (1997) 111.
[8] A.J. Tong, Y. Wu, S. Tan, L. Li, Y. Akama, S. Tanaka, Anal. Chim. Acta 369 (1998) 11.

ELSEVIER

Talanta 48 (1999) 1139–1143

Talanta

A new construction for a potentiometric, enantioselective membrane electrode—its utilization to the *S*-captopril assay

Raluca-Ioana Stefan [a], Jacobus (Koos) F. van Staden [a,*], Hassan Y. Aboul-Enein [b]

[a] *Department of Chemistry, University of Pretoria, Pretoria 0002, South Africa*
[b] *Bioanalytical and Drug Development Laboratory, Biological and Medical Research Department (MBC-03), King Faisal Specialist Hospital and Research Centre, P.O. Box 3354, Riyadh 11211, Saudi Arabia*

Received 30 April 1998; received in revised form 19 October 1998; accepted 20 October 1998

Abstract

A novel potentiometric, enantioselective membrane electrode based on graphite paste (graphite powder and paraffin oil) has been constructed. The graphite paste is impregnated with 2-hydroxy-3-trimethylammoniopropyl-β-cyclodextrin (as chloride salt) solution, 10^{-3} mol l^{-1}. The potentiometric, enantioselective membrane electrode can be used reliable for *S*-captopril assay as raw material and from Novocaptopril tablets, using a chronopotentiometry (zero current) technique, in the 10^{-6}–10^{-2} mol l^{-1} concentration range (detection limit 2×10^{-7} mol l^{-1}), with an average recovery of 99.99% (RSD = 0.05%). The enantioselectivity was determined over *R*-captopril and D-proline. The response characteristics of the enantioselective, potentiometric membrane electrode were determined also for *R*-captopril. It was shown that only L-proline is the main interfering compound. The surface of the electrode can be regenerated by simply polishing, obtaining fresh surface ready to be used in a new assay.

Keywords: Potentiometric; Enantioselective membrane electrode; Enantioselective analysis; 2-hydroxy-3-trimethylammoniopropyl-β-cyclodextrin; Captopril

1. Introduction

Enantioselective analysis has become increasingly important in the analysis of pharmaceutical products, because many of the drugs marketed today are administered as racemic mixture despite the significant differences in pharmacological, pharmacodynamics, and pharmacokinetics of the individual enantiomers. It must take into account that one of the enantiomers can be more active, toxic, or totally inactive than its antipode [1]. Accordingly, enantioselective analysis to evaluate the enantiomeric purity is becoming increasingly important in pharmaceutical analysis.

* Corresponding author. Tel.: +27-12-4202515; Fax: +27-12-3625297; e-mail: koos.vanstaden@chem.up.ac.za.

0039-9140/99/$ - see front matter
PII: S0039-9140(98)00335-X

Several separation techniques were applied for the enantioselective analysis of enantiomers, e.g. liquid chromatography [2], thin-layer chromatography [3], gas chromatography [4], and capillary zone electrophoresis [5], using as chiral selectors β-cyclodextrin derivatives. These separation methods are very laborious, and there are many problems concerning the selective retention of one of the enantiomers on the column. The quality of enantiomers discrimination was improved recently by using the potentiometric, enantioselective membrane electrodes based on crown ethers [6] and β-cyclodextrines [7]. Accordingly it is possible to determine direct, and without any separation the activity of the enantiomers in the solutions. By using β-cyclodextrin derivatives a double selectivity is achieved: an internal selectivity (due to the cavity size) and an external selectivity (due to the functional groups).

Because the PVC membrane electrodes are not reproducible as to their construction [8], it is necessary to improve the construction of the potentiometric, enantioselective membrane electrodes by using carbon paste electrodes impregnated with a β-cyclodextrin derivative solution.

This paper describes a new type of potentiometric, enantioselective membrane electrode based on 2-hydroxy-3-trimethylammoniopropyl-β-cyclodextrin. The β-cyclodextrin derivative is impregnated in a carbon paste. The potentiometric, enantioselective membrane electrode is used for enantioselective assay of *S*-captopril.

The *S*-captopril (1-[3-mercapto-2-(*S*)-methyl-1-oxopropyl]-*S*(L)proline is an angiotensin-converting enzyme (ACE) inhibitor which is extensively used for the treatment of hypertention and congestive heart failure [9]. The compound contains two asymmetric centers, one associated with the proline moeity and the other associated with the 3-mercapto-2-methylpropionic acid side chain. Accordingly there are three other possible stereoisomers. One of these stereoisomers is *R*-captopril, 1-[3-mercapto-2(*S*)-methyl-1-oxopropyl]-*R*(D)-proline. It has been reported that the biological acivity resides mainly in *S*-captopril while *R*-captopril possesses non-ACE inhibiting activity [10].

2. Experimental

2.1. Electrode design

The paraffin oil and graphite powder were mixed in a ratio of 1:4 (w/w) followed by the addition of the solution of 2-hydroxy-3-trimethylammoniopropyl-β-cyclodextrin (10^{-3} mol l^{-1}) (100 μl chiral selector solution to 100 mg carbon paste). The graphite-paraffin oil paste was filled into a plastic pipette peak leaving 3–4 mm empty in the top to be filled with the carbon paste that contains the chiral selector. The diameter of the potentiometric, enantioselective membrane sensor was 3 mm. Electric contact was made by inserting a silver wire in the carbon paste.

Before each use, the surface of the electrode was wetted with deionised water and then polished with an alumina paper (polishing strips 30144-001, Orion). When is not in use, the electrode was immersed in a 10^{-3} mol l^{-1} *S*-captopril solution.

2.2. Apparatus

A 663 VA Stand (Metrohm, Herisau, Switzerland) in connection with a PGSTAT 20 and a software version 4.4 were used for all chronopotentiometrical (zero current) measurements. A glassy carbon electrode and a Ag/AgCl (0.1 mol l^{-1} KCl) served as the counter and reference electrodes in the cell.

2.3. Reagents and materials

S-captopril (SCpt) (SQ-014534) and *R*-captopril (RCpt) (SQ-034459) were supplied by Bristol–Myers Squibb Pharmaceutical Research Institute (Princeton, NJ). Novocaptopril tablets (25 mg *S*-captopril/tablet) were supplied by Novopharma, Toronto, Canada. The 2-hydroxy-3-trimethylammoniopropyl-β-cyclodextrin was supplied by Wacker-Chemie GmbH (Germany). Graphite powder, 1–2 micron, synthetic was supplied by Aldrich. Paraffin oil was supplied by Fluka.

Deionised water from a Modulab system (Continental Water Systems, San Antonio, TX) was

used for all solutions. The *S* and *R*-captopril solutions were prepared from standard *S* and *R*-captopril solutions (10^{-2} mol l^{-1}), respectively, by serial dilutions.

2.4. Recommended procedures

2.4.1. Direct potentiometry

The chronopotentiometric (zero current) technique was used for potential determination of each standard solution (10^{-8}–10^{-2} mol l^{-1}). The electrodes were placed in the stirred standard solutions and graphs of E (mV) versus pSCpt and pRCpt, respectively were plotted. The unknown concentrations were determined from the calibration graphs.

2.4.2. Content uniformity assay of novocaptopril tablets

A total of ten tablets were placed in ten separate calibrated flasks (25 ml), shaking with 10 ml deionised water and 12.5 ml citrate buffer (pH = 4.0); after tablet dissolution the solution was diluted up to the mark with deionised water. The *E* (mV) was determined for each solution through the chronopotentiometry (zero current) technique. The unknown concentration was determined from the calibration graph, as described above.

3. Results and discussion

3.1. Electrode response

The electrode response was determined for both enantiomers: *S*-captopril and *R*-captopril. The equations of calibration obtained are:

S-Captopril: $E = -150.40 + 57.70$ pSCpt

R-Captopril: $E = 30.79 + 27.30$ pRCpt

where *E* (mV) is the cell potential, pSCpt = $-\log$[SCpt], pRCpt = $-\log$[RCpt]. For both calibration equations, the correlation coefficient is 0.9999.

The response characteristics of the electrode for both enantiomers are shown in the Table 1.

The limits of detection are low: 2.7×10^{-7} mol l^{-1} and 1.5×10^{-6} mol l^{-1} for *S*-captopril and *R*-captopril, respectively. As it can be seen from the Table 1 and from the equations of calibration, the membrane electrode has a linear response for both enantiomers, but only for *S* enantiomer the response is near-Nernstian.

The electrode response displayed good stability and reproducibility over the tests, as shown by the relative standard deviation values.

The response time is lower for *S* enantiomer than for *R* enantiomer; *S*-Captopril: <1 min. for 10^{-3}–10^{-2} mol l^{-1} concentration range, and >1 min. for 10^{-8}–10^{-4} mol l^{-1} concentration range; *R*-Captopril: 3 min. 10^{-3}–10^{-2} mol l^{-1} concentration range, and >3 min. for 10^{-6}–10^{-4} mol l^{-1} concentration range.

3.2. Effect of pH on the response of the electrode

The effect of pH on the response of the potential readings of the *S*-captopril was checked by recording the emf of the cell, through chronopotentiometric (zero current) technique, which contained 10^{-4} mol l^{-1} *S*-captopril solution at various pH values, which were obtained by the addition of very small volumes of HCl and/or NaOH solution (10^{-1} mol l^{-1} or 1 mol l^{-1} of each).

The E (mV) versus pH graph presented in Fig. 1.a. shows the pH independence in the range

Table 1
Response characteristics of potentiometric, enantioselective membrane electrode for *S*-captopril and *R*-captopril (all measurements were made at room temperature; all values are the average of ten determinations)

Parameter Enantiomer	Slope (mV/pS(R)Cpt)	Intercept, E° (mV)	Linear range (mol l^{-1})	Detection limit (mol l^{-1})
S-captopril	57.70 ± 0.30	-150.40 ± 2.00	10^{-6}–10^{-2}	2×10^{-7}
R-captopril	27.30 ± 0.50	30.79 ± 5.00	2.9×10^{-6}–2.7×10^{-2}	1.5×10^{-6}

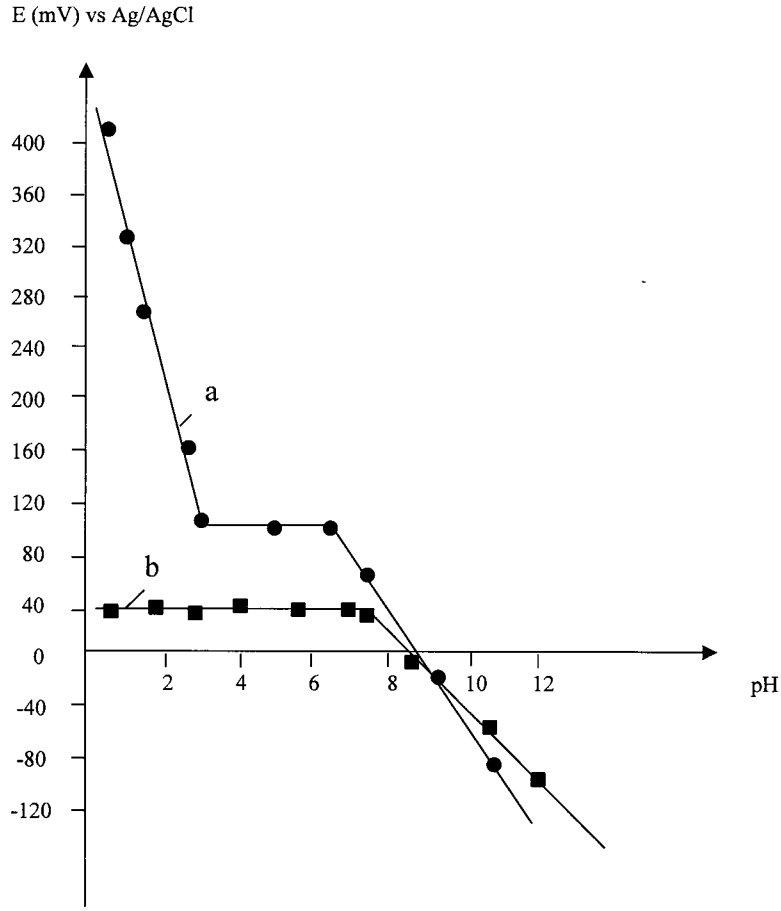

Fig. 1. (a) Effect of pH on the response of the potentiometric, enantioselective membrane electrode for *S*-captopril (10^{-4} mol l^{-1} *S*-captopril solution). (b) Effect of citrate buffer pH on the response of the potentiometric, enantioselective membrane electrode.

3.0–6.5. It is also proved the basic behavior of *S*-captopril at the pH < 3, and its acidic behavior at pH > 6.5.

To prove the electrode behavior in this pH range, there were making measurements of citrate buffer solutions of various pH values. Fig. 1b shows the independence of E (mV) versus pH on the acidic medium, up to 7.5 pH value. After this value, the potential decreases fast.

3.3. Selectivity of the electrode

The selectivity of the potentiometric membrane electrode was checked through the mixed solutions method. The concentrations of interfering ions and *S*-captopril were 10^{-3} and 10^{-4} mol l^{-1}, respectively. The enantioselectivity was checked against *R*-captopril and D-proline. As it is shown in Table 2, *R*-captopril and D-proline do not interfere thus demonstrating the enantioselec-

Table 2
Selectivity coefficients for the potentiometric, enantioselective membrane electrode for *S*-captopril (all measurements were made at room temperature; all values are the average of ten determinations)

Interfering species (J)	K_{sel}
R-captopril	3.8×10^{-4}
D-proline	1.4×10^{-4}
Polyvinylpyrolidone	1.2×10^{-4}
L-proline	2.9×10^{-2}

Table 3
The results obtained for *S*-captopril assay from Novocaptopril tablets (25 mg *S*-captopril/tablet) using the new potentiometric, enantioselective membrane electrode in comparison with those obtained by standard method [11][a]

Sample	Recovery, mg *S*-Captopril, by proposed method	Recovery, mg *S*-Captopril, by standard method [11]
1	24.6 ± 0.3	24.4 ± 0.60
2	24.8 ± 0.2	25 ± 1
3	25.0 ± 0.2	24.9 ± 0.6
4	25.0 ± 0.09	26.0 ± 0.7
5	24.8 ± 0.2	24.9 ± 0.6
6	25.0 ± 0.1	25.0 ± 0.6
7	24.9 ± 0.1	25 ± 0.8
8	24.7 ± 0.3	24.9 ± 0.5
9	24.9 ± 0.1	24.8 ± 0.6
10	25.0 ± 0.2	25 ± 0.2

[a] All values represent average of ten determinations.

tivity property of the constructed potentiometric membrane electrode. Furthermore, the selectivity of the electrode was also tested for polyvinylpyrolidone (PVP) a commonly used compound for tablet compression;the results in Table 2 shows that PVP do not. Also inorganic cations like Na^+, K^+, Ca^{2+} do not interfere in the analysis of *S*-captopril.

3.4. Analytical applications

The electrode proved to be useful for the determination of the enantiopurity of *S*-captopril-raw material as well as for the content uniformity test of Novocaptopril tablets, by chronopotentiometry (zero current) technique. The recovery test demonstrated the suitability of this potentiometric, enantioselective membrane electrode for enantiopurity of *S*-captopril assay: 99.99%—average recovery and RSD of 0.05%.

The results obtained for the uniformity content test are presented in the Table 3. The *S*-captopril can be reliable assayed from the tablets with an average recovery of 99.69%, and a RSD of 0.39%. The results are in good concordance with those obtained using standard method [11].

4. Conclusions

The potentiometric, enantioselective membrane electrode presented in this paper provides the electrodes with excellent features to develop enantioselective analysis. The construction of electrode is simple, faster and reproducible. The reliability of the analytical information is assured by the RSD values obtained in the recovery test and in the uniformity content test.

The electrode enantioselectivity made it suitable for enantiopurity assay of *S*-captopril-raw material and pharmaceutical tablet formulations.

References

[1] H.Y. Aboul-Enein, I.W. Wainer, The Impact of Stereochemistry on Drug Development and Use, Wiley, New York, 1997.
[2] M.S. Han, Biomed.Chromatogr. 11 (1997) 259.
[3] C.P. Granville, B. Gehrcke, W.A. Konig, I.W. Wainer, J. Chromatogr. 452 (1988) 323.
[4] R. Uruta, H. Nakazawa, Chromatographia 35 (1993) 555.
[5] H. Wang, J.L. Gu, H.F. Hu, R.J. Dai, T.H. Ding, R.N. Fu, Anal. Chim. Acta 359 (1998) 39.
[6] V. Horváth, T. Takács, G. Horvai, P. Huszthy, J.S. Bradshaw, R.M. Izatt, Anal. Lett. 30 (1997) 1591.
[7] R. Kataky, D. Parker, P.M. Kelly, Scand. J. Clin. Lab. Invest. 55 (1994) 409.
[8] R.I. Stefan, H.Y. Aboul-Enein, Accred. Qual. Assur. 3 (1998) 194.
[9] D.W. Cushman, H.S. Cheung, E.F. Sabo, M.A. Ondetti, in: Z.P. Horowitz (Ed.), Angiotensine-Converting Enzyme Inhibitors, Urban and Schwarzenberg, München, 1981, p. 3.
[10] A. Gringauz, Drugs and the Cardiovascular Disears, in Introduction to Medicinal Chemistry. How Drugs Act and Why, Wiley-VCH, New York, 1997, p. 454.
[11] The United States Pharmacopoeia XXII, US Pharmacopoeia Convention Inc., Rockville, MD, (1990).

ELSEVIER

Talanta 48 (1999) 1145–1157

Talanta

The spectrophotometric multicomponent analysis of a ternary mixture of ascorbic acid, acetylsalicylic acid and paracetamol by the double divisor-ratio spectra derivative and ratio spectra-zero crossing methods

Erdal Dinç *

Department of Analytical Chemistry, Faculty of Pharmacy, University of Ankara, 06100 Ankara, Turkey

Received 8 May 1998; received in revised form 16 September 1998; accepted 20 October 1998

Abstract

The double divisor–ratio spectra derivative and ratio spectra–zero crossing methods were applied to the analysis of an effervescent tablet containing the title compounds without using a chemical separation procedure. In the use of both methods, the calibration graphs were linear in the range of 8–28 μg ml^{-1} for three compounds. Comparison of the results obtained by the two methods indicates that both methods gives the best results.

Keywords: Double divisor-ratio spectra derivative and ratio spectra-zero crossing methods; Ascorbic acid; Acetylsalicylic acid; Paracetamol

1. Introduction

For the simultaneous determination of two or more active compounds in the same mixtures without a separation step, several spectrophotometric methods, such as classical derivative spectrophotometry [1–4], Vierordt's method [5] and its modified version [6], orthogonal function method [7], dual wavelength spectrophotometry [8–10], pH-induced differential spectrophotometry [11], and least square method [12], the multicomponent analysis program [13,14] and a method; multi-wavelength linear regression analysis (MLRA) which was referred to by Blanco and co-workers [15] have been utilized.

Salinas et al. [16] proposed a new spectrophotometric method for the simultaneous determination of two compounds in binary mixtures. Two new methods were developed from this theory for resolving ternary mixtures, as explained below.

Berzas Nevado et al. [17], developed a new method for the resolution of ternary mixtures of compounds by the derivative ratio spectra-zero crossing method. In the method, the simultaneous determination of three compounds in ternary mix-

* Tel.: +90-0312-212-6805; fax: +90-0312-213-1081; e-mail: dinc@pharmacy.ankara.edu.tr.

0039-9140/99/$ - see front matter
PII: S0039-9140(98)00337-3

tures are realized by the measurements of the amplitude at the zero-crossing points in the derivative spectrum of the ratio spectra.

However, recently for the simultaneous determination of the three compounds in ternary mixtures, another new spectrophotometric method has been developed by us, which is very easy to apply, very sensitive and very useful and yet very cheap [18]. This method was called 'the double divisor-ratio spectra derivative method'. The method is based on the use of the coincident spectra of the derivative of the ratio spectra obtained by using a 'double divisor' (sum of two spectra) and the measurements at either the maximum or minimum wavelengths.

The quantitative determination of ingredients in pharmaceutical formulations containing acetylsalicylic acid (ASA), ascorbic acid (ASCA) and paracetamol (PAR), and their mixtures with different active compounds using various methods including spectrophotometry (ASA [19,20], ASCA [23–28]and PAR [30–34]), HPLC (ASA [21,22], ASCA [29]) and TLC (PAR [35]), have been demonstrated for several mixtures and pharmaceutical preparations.

In this paper, two new spectrophotometric methods have been applied successfully to the analysis of the synthetic ternary mixtures and an effervescent tablet containing ASA, ASCA and PAR, which have closely overlapped the spectra. The results obtained by the double divisor-ratio spectra derivative method were compared with those obtained by ratio spectra derivative-zero crossing method.

2. Experimental

2.1. Apparatus

A Shimadzu 1601PC double beam spectrophotometer with a fixed slit width (2 nm) connected to an IBM computer loaded with Shımadzu UVPC software which was equipped with an HP 1150C printer was used for all the absorbance measurements and treatment of data.

2.2. Pharmaceutical formulation

A commercial product AFEBRYL® effervescent tablet (produced by Laboratoires SBM Farmaceutica N.V., Belgium, Batch no.B01, containing 300 mg ASA, 300 mg ASCA and 200 mg PAR per tablet) were studied.

2.3. Standard solutions

Stock solutions of 100 mg/100 ml of ASCA, ASA and PAR (Bayer and Nobel, Turkey) were prepared in methanol and 0.2 M HCl (1:3). All the solutions were prepared freshly and protected from light. Working standard solutions were prepared in 25-ml volumetric flasks containing 8–28 μg ml^{-1} ASCA, ASA and PAR and their different synthetic mixtures by using the stocks solutions. They were diluted with ethanol–0.2 M HCl (3:1) to the mark.

2.4. Procedures

Twenty effervescent tablets, were weighed and powdered in a mortar. An amount equivalent to one tablet was transferred to a 100-ml calibrated flask and dissolved in 50 ml of methanol and 0.2 M HCl (1:3), swirled until effervescence ceases, and diluted with same solvent to the volume. After, these solutions were filtered through a filter paper into a 100-ml calibrated flask and the residue was washed three times with 10 ml of solvent, then the volume was completed to the mark with the same solvent as was used above. The resulting solution was diluted to 1:167 in a 25-ml calibrated flask with methanol and 0.2 M HCl (1:3). The methods were applied to the prepared solutions.

3. Application of methods

3.1. Double divisor-ratio spectra derivative method

In this method, to determine ASA, the stored spectra of the mixture of ASA, ASCA and PAR were divided by the sum of the spectra of ASCA

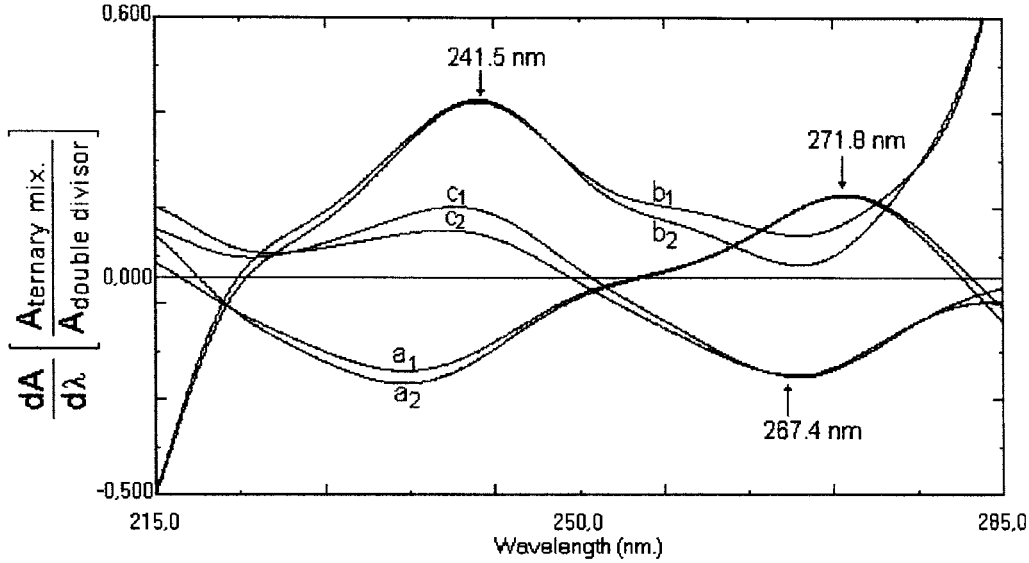

Fig. 1. The coincident spectra of the first derivative of the ratio spectra of: (a_1) 16 μg ml^{-1} pure ASA and (a_2) ternary mixture (16 μg ml^{-1} ASA, 16 μg ml^{-1} ascorbic acid (ASCA) and 12 μg ml^{-1} paracetamol (PAR)), 28 μg ml^{-1} PAR + 28 μg ml^{-1} ASCA as a double divisor; (b_1) 16 μg ml^{-1} pure PAR and (b_2) ternary mixture (16 μg ml^{-1} PAR, 16 μg ml^{-1} ASA and 16 μg ml^{-1} ASCA), 12 μg ml^{-1} ASCA + 12 μg ml^{-1} ACA as a double divisor; and (c_1) 12 μg ml^{-1} pure ASCA and (c_2) ternary mixture (12 μg ml^{-1} pure ASCA, 16 μg ml^{-1} ACA and 12 μg ml^{-1} PAR), 20 μg ml^{-1} ACA + 20 μg ml^{-1} PAR as a double divisor in methanol and 0.2 M HCl (1:3) (to save space three curves are shown in the same figure).

and PAR as 'double divisor' and their ratio spectra were obtained. First derivatives of the ratio spectra are plotted. At the results of the above mentioned procedure, the amplitudes measured of the maximum at 271.8 nm are dependent only to the concentrations values C_{ASA} and C^0_{PAR} (C^0 is standard concentration), but are independent of the concentration values C_{ASCA} and C_{PAR} in the ternary mixture. The mathematical expression of this procedure is shown in the following equation:

$$\lambda_i = 271.8 \text{ nm}$$

$$\frac{d}{d\lambda}\left[\frac{A_{\text{ternary mix.},\lambda_i}}{[\alpha_{ASCA,\lambda_i}+\beta_{PAR,\lambda_i}]C^0_{PAR}}\right] = \frac{d}{d\lambda}\left[\frac{\gamma_{ASA,\lambda_i}}{[\alpha_{ASCA,\lambda_i}+\beta_{PAR,\lambda_i}]}\right]\frac{C_{ASA}}{C^0_{PAR}}$$

were the amplutides measured, $d/d\lambda$ ($A_{\text{ternary mix.}}/[\alpha_{ASCA,\lambda_i}+\beta_{PAR,\lambda_I}]C^0_{PAR}$), were drawn as a graph, versus concentrations of ASA and a straight line was obtained. By using the calibration graph, ASA was determined in the mixture of ASA, ASCA and PAR.

On the other hand, to determine ASCA, the absorption spectra of the mixture containing ASCA, ASA and PAR were divided by the sum of the spectra of ASA and PAR as 'double divisor' and the ratio spectra were obtained. First derivatives of the ratio spectra were calculated. The amplitude of the minimum at 267.4 nm are dependent only to the concentrations values C_{ASCA} and C^0_{ASA}, but are independent of the concentration values C_{ASA} and C_{PAR} in the ternary mixture, as shown below:

$$(\lambda_i = 267.4 \text{ nm})$$

$$\frac{d}{d\lambda} = \left[\frac{A_{\text{ternary mix.},\lambda_i}}{[\alpha_{ASA,\lambda_i}+\beta_{PAR,\lambda_i}]C^0_{ASA}}\right] = \frac{d}{d\lambda}\left[\frac{\gamma_{ASCA,\lambda_i}}{[\alpha_{ASA,\lambda_i}+\beta_{PAR,\lambda_i}]}\right]\frac{C_{ASCA}}{C^0_{ASA}}$$

In this case, also a straight line was obtained by using the amplitudes measured for ASCA. By means of the calibration graph, the content of ASCA was determined in the sample.

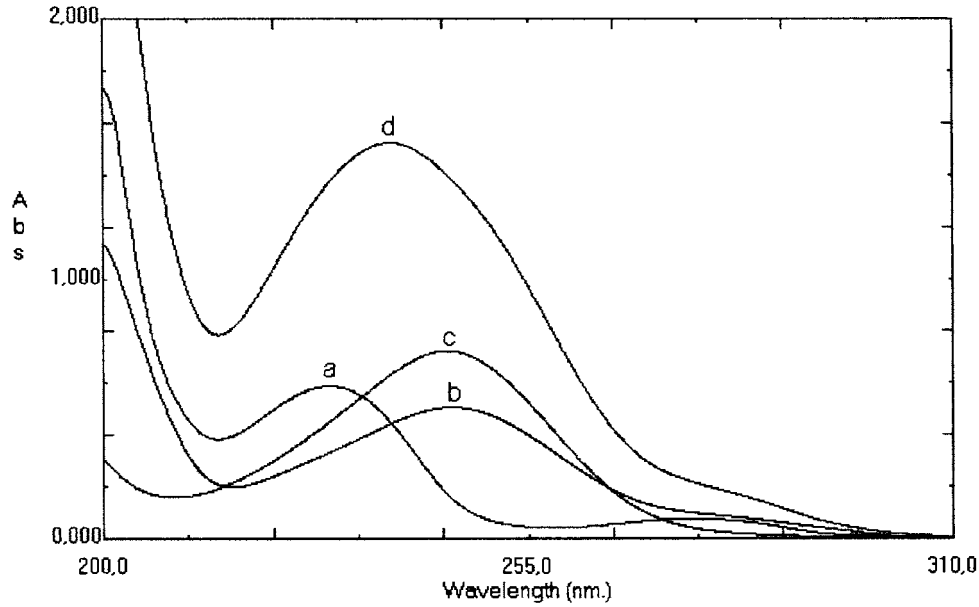

Fig. 2. Zero-order spectra of: (a) 12 μg ml^{-1} acetylsalicylic acid (ACA); (b) 8 μg ml^{-1} paracetamol (PAR); (c) 12 μg ml^{-1} ascorbic acid (ASCA); (d) their ternary mixture in methanol and 0.2 M HCl (1:3).

In the same way, to determine PAR, the stored spectra of the mixture containing PAR, ASCA and ASA were divided by the sum of the spectra of ASA and ASCA as 'double divisor'. From the resulting ratio spectra, the first derivative of the ratio spectra were traced. the concentration of PAR in the ternary mixture was proportional to the amplitude of the maximum at 241.5 nm with respect to the following equation:

$(\lambda_i = 241.5 \text{ nm})$

$$\frac{d}{d\lambda}=\left[\frac{A_{\text{ternary mix.},\lambda_i}}{[\alpha_{ASA,\lambda_i}+\beta_{ASCA,\lambda_i}]C^0_{ASCA}}\right]$$

$$=\frac{d}{d\lambda}\left[\frac{\gamma_{PAR,\lambda_i}}{[\alpha_{ASA,\lambda_i}+\beta_{ASCA,\lambda_i}]}\right]\frac{C_{PAR}}{C^0_{ASCA}}$$

As explained above, a straight line was obtained and the amount of PAR is determined in the sample containing the above mentioned ternary mixture.

3.1.1. Selection of the working wavelength

In the application of this method, the first derivative of the ratio spectra of pure compound and its ternary mixture would be coincided in the spectral region corresponding to a maximum point or a minimum point of the wavelength as shown in Fig. 1. These coinciding points of the derivative of the ratio spectra can be selected as working wavelengths for the determinations of the subject compounds in the ternary mixture.

3.1.2. Establishment of double divisor

The double divisor was obtained either by the sum of the absorption spectra of the same concentration of the two compounds in the same ternary mixture, as is carried out in this paper or it was obtained by preparing the mixed solution of two compounds of the same concentration in the ternary mixture [18]. If the double divisor will be used as the sum of the spectra of the two compounds, this can be performed with the help of Shımadzu UVPC software.

3.2. Derivative ratio spectrum-zero crossing method

The absorption spectra of ASA, ASCA and their ternary mixture with PAR, were divided by a standard spectrum of PAR and the first derivative

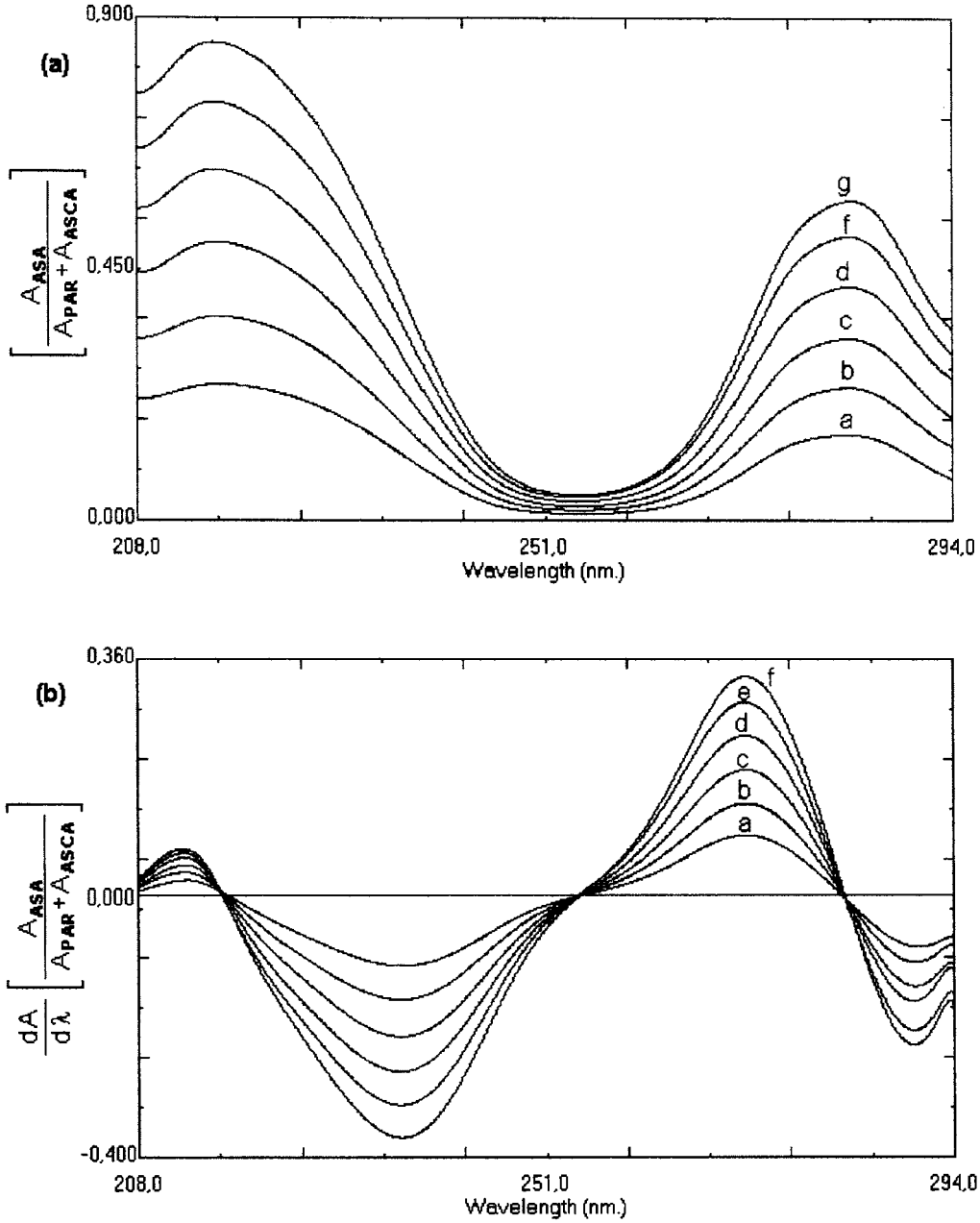

Fig. 3. Ratio spectra (a) and first derivative of the ratio spectra (b) of acetylsalicylic acid (ACA): (a) 8 μg ml^{-1}; (b) 12 μg ml^{-1}; (c) 16 μg ml^{-1}; (d) 20 μg ml^{-1}; (e) 24 μg ml^{-1}; (f) 28 μg ml^{-1} (28 μg ml^{-1} ascorbic acid (ASCA) + 28 μg ml^{-1} paracetamol (PAR) as a double divisor) in methanol and 0.2 M HCl (1:3) ($\Delta\lambda = 8$ nm).

of the ratio spectra was calculated. In the ternary mixture, the concentrations of ASCA and ASA were proportional to the first derivative signals at 255.1 and 281.1 nm (zero-crossing point for ASA) and 241.2 nm (zero-crossing point for ASCA), respectively, in the first derivative of the ratio

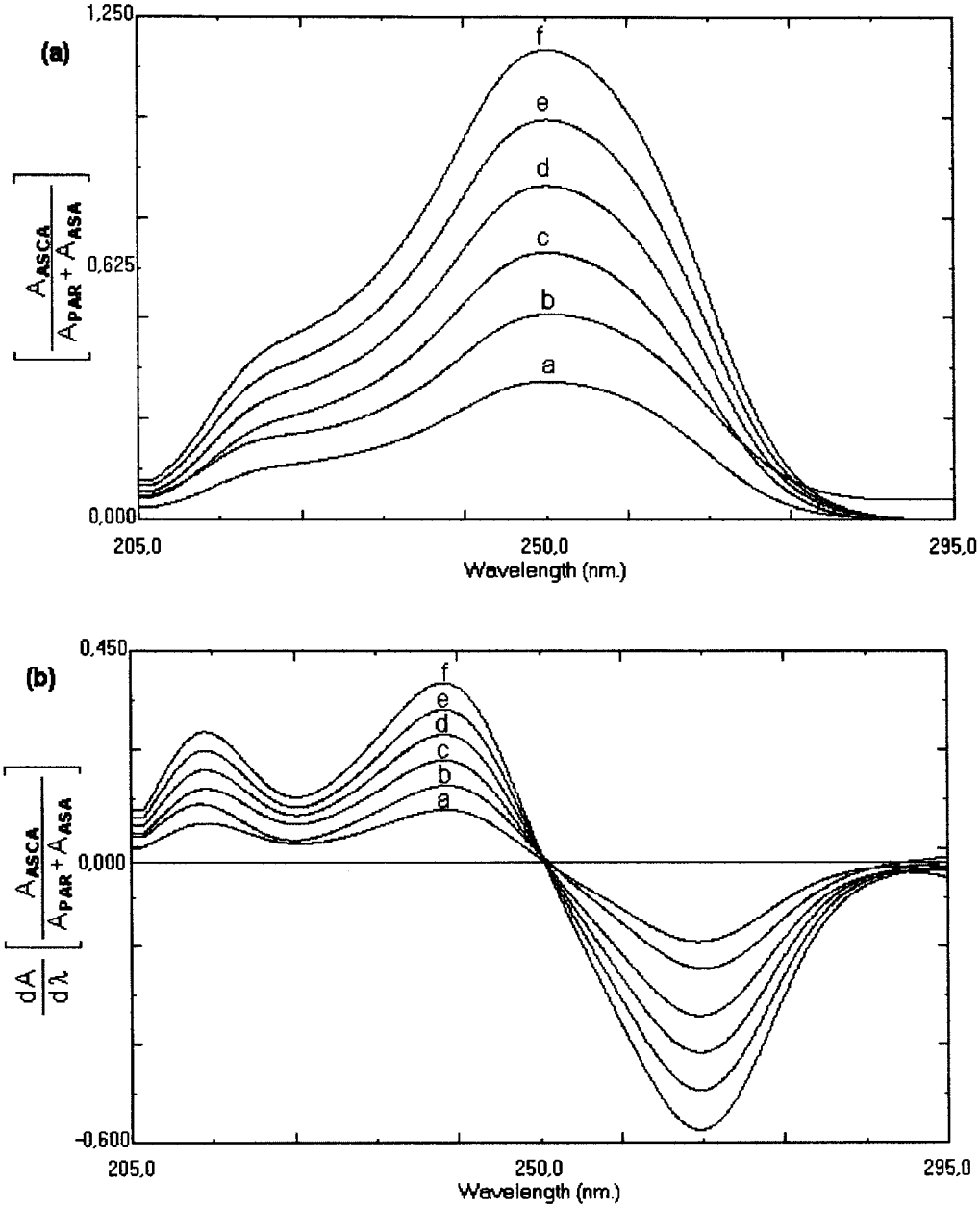

Fig. 4. Ratio spectra (a) and first derivative of the ratio spectra (b) of ascorbic acid (ASCA): (a) 8 μg ml^{-1}; (b) 12 μg ml^{-1}; (c) 16 μg ml^{-1}; (d) 20 μg ml^{-1}; (e) 24 μg ml^{-1}; (f) 28 μg ml^{-1} (20 μg ml^{-1} ASCA + 20 μg ml^{-1} paracetamol (PAR) as a double divisor) in methanol and 0.2 M HCl (1:3) ($\Delta\lambda = 8$ nm).

spectra. Two calibration graphs were obtained by measuring the derivative amplitudes against the increasing concentrations of pure ASA and pure ASCA and by using pure PAR as a divisor. The contents of ASA and ASCA can be determined by use of the above mentioned calibration graphs.

By using the same procedure, the stored spectra of ASA, PAR and their ternary mixture with

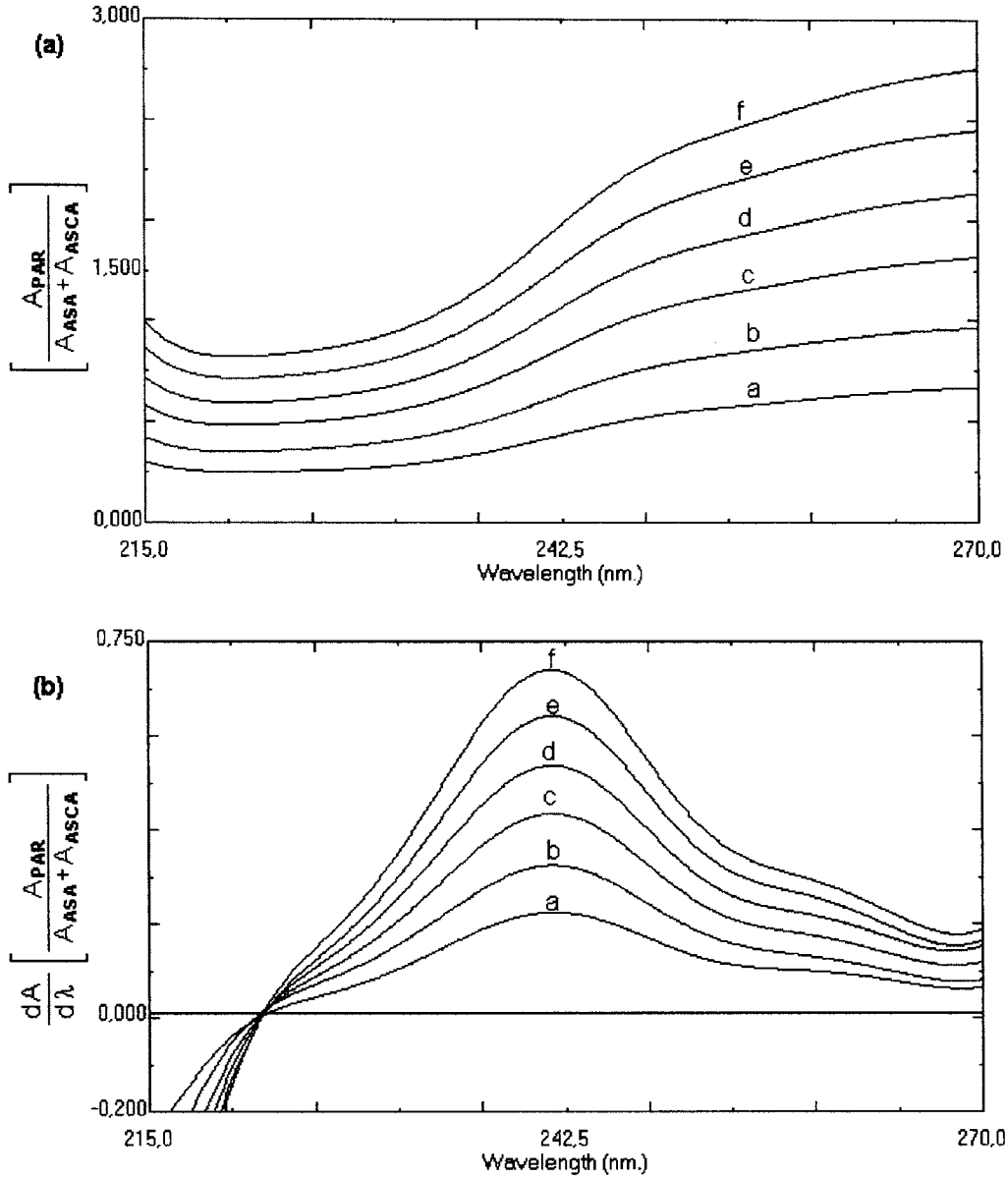

Fig. 5. Ratio spectra (a) and first derivative of the ratio spectra (b) of paracetamol (PAR): (a) 8 μg ml^{-1}; (b) 12 μg ml^{-1}; (c) 16 μg ml^{-1}; (d) 20 μg ml^{-1}; (e) 24 μg ml^{-1}; (f) 28 μg ml^{-1} (28 μg ml^{-1} ascorbic acid (ASCA) + 28 μg ml^{-1} paracetamol (PAR) as a double divisor) in methanol and 0.2 M HCl (1:3) ($\Delta\lambda = 8$ nm).

ASCA, were divided by a standard spectrum of ASCA and the first derivative of the result was plotted. ASA and PAR were proportional to derivative signals at 239.3 and 292.4 nm (zero-crossing point for PAR) and 286.1 nm (zero-crossing point for ASA), respectively, in the first derivative of the ratio spectra. For the determination of ASA and PAR, the calibration graphs were obtained by measuring the first derivative values, versus the increasing concentrations of pure ASA and pure PAR, and by using pure ASCA as a divisor. With this procedure, ASA and PAR can be determined.

Table 1
Recovery data obtained for the synthetic ternary mixtures by using the double divisor-ratio spectra derivative method[a]

Composition mixture: ASCA	PAR	ASA	ASA	ASCA and PAR (double divisor)
	Added (μg ml^{-1})		Found (μg ml^{-1})	Recovery (%)
18.00	12.00	8.00	7.90	98.8
18.00	12.00	12.00	11.80	98.3
18.00	12.00	16.00	15.05	100.3
18.00	12.00	20.00	19.56	97.8
18.00	12.00	24.00	24.05	100.2
18.00	12.00	28.00	27.60	98.6
				$\bar{X} = 99.0$
				RSD = 1.04%
Composition mixture: ASA	PAR	ASCA	ASCA	ASA and PAR (double divisor)
	Added (μg ml^{-1})		Found (μg ml^{-1})	Recovery (%)
18.00	12.00	8.00	8.04	100.5
18.00	12.00	12.00	12.09	100.8
18.00	12.00	16.00	15.90	99.4
18.00	12.00	20.00	20.06	100.3
18.00	12.00	24.00	23.88	99.5
18.00	12.00	28.00	28.59	102.1
				$\bar{X} = 100.4$
				RSD = 0.98%
Composition mixture: ASA	ASCA	PAR	PAR	ASA and ASCA (double divisor)
	Added (μg ml^{-1})		Found (μg ml^{-1})	Recovery (%)
18.00	18.00	8.00	8.00	100.0
18.00	18.00	12.00	11.82	98.5
18.00	18.00	16.00	16.02	100.1
18.00	18.00	20.00	19.75	98.8
18.00	18.00	24.00	24.00	100.0
18.00	18.00	28.00	27.70	99.9
				$\bar{X} = 99.6$
				RSD = 0.71%

[a] RSD, relative standard deviation.

In this case, the amount of ASA in ternary mixture has been determined by both procedures.

4. Results and discussion

The absorption spectra of the three compounds, ASA, ASCA and PAR overlapped closely in the region 200–310 nm in Fig. 2. For this reason, the determination of the above compounds was not possible from direct measurements of absorbances in the zero-order spectra. On the other hand, also the classical derivative spectrophotometric method was tested (from first to fourth) for simultaneous determination of compounds (ASA, ASCA and PAR) in the same mixture. By these methods, in the same order of derivative spectra and method of direct absorbance measurement could not be realized for the ASA, ASCA and PAR determinations within same mixture.

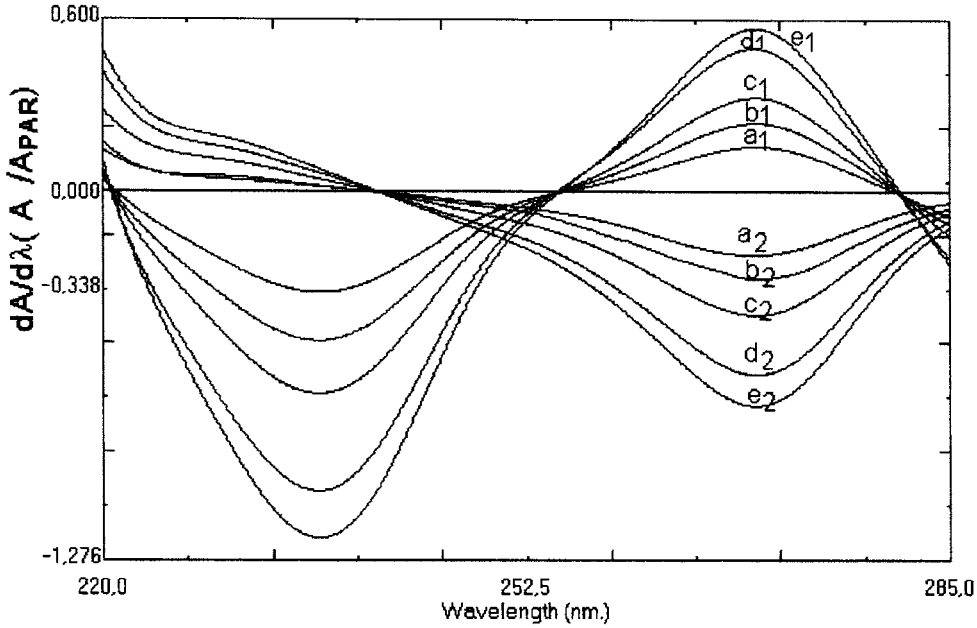

Fig. 6. First derivative of the ratio spectra of acetylsalicylic acid (ACA): (a_1) 8 μg ml^{-1}; (b_1) 12 μg ml^{-1}; (c_1) 16 μg ml^{-1}; (d_1) 20 μg ml^{-1}; (e_1) 24 μg ml^{-1}; (f_1) 28 μg ml^{-1} and of ascorbic acid (ASCA) (a_2) 8 μg ml^{-1}; (b_2) 12 μg ml^{-1}; (c_2) 16 μg ml^{-1}; (d_2) 20 μg ml^{-1}; (e_2) 24 μg ml^{-1}; (f_2) 28 μg ml^{-1} (16 μg ml^{-1} paracetamol (PAR) as a divisor) in methanol and 0.2 M HCl (1:3) ($\Delta\lambda = 8$ nm).

4.1. Double divisor-ratio spectra derivative method

The absorption spectra of the solutions of ASA in methanol and 0.2 M HCl (1:3) were recorded in the range 208–294 nm and divided by the double divisor (28 μg ml^{-1} ASCA and 28 μg ml^{-1} PAR)and their ratio spectra was obtained. They were smoothened at $\Delta\lambda = 8$ nm (Fig. 3(a)). Fig. 3(b) indicates the first derivatives which were calculated with interval of $\Delta\lambda = 8$ nm and scaling factor of 10 from the ratio spectra. The concentration of ASA was determined by measuring the amplitude at 271.8 nm corresponding to a maximum point.

Then, the absorption spectra of the solutions of ASCA in methanol and 0.2 M HCl (1:3) were recorded in between 205 and 295 nm and divided by the 'double divisor' (20 μg ml^{-1} ASA and 20 μg ml^{-1} PAR). The ratio spectra of the result were smoothened at $\Delta\lambda = 8$ nm (Fig. 4(a)) and their first derivatives were traced with intervals of $\Delta\lambda = 8$ nm and scaling factor of 10 (Fig. 4(b)). The amount of ASCA was determined by measuring the signals at 267.4 nm corresponding to a minimum point of wavelength.

In the same way, the absorption spectra of the solutions of PAR were stored in the spectral range 215–270 nm and divided the 'double divisor' (12 μg ml^{-1} ASA and 12 μg ml^{-1} ASCA). The resulting ratio spectra were smoothened with intervals of $\Delta\lambda = 8$ nm (Fig. 5(a)). And their first derivatives were traced with $\Delta\lambda = 8$ nm intervals and scaling factor of 10 (Fig. 5(b)).The content of PAR was determined by measuring the amplitudes at 241.5 nm corresponding to a maximum wavelength.

In this method, various mixtures of PAR, ASA and ASCA were prepared and tested between 8 and 28 μg ml^{-1} for ASA, ASCA and PAR in their ternary mixtures. Mean recoveries and the relative standard deviations of the method were found as 99 and 1.04% for ASA, 100.4 and 0.98% for ASCA and 99.6 and 0.71% for PAR, in the synthetic mixtures prepared by adding known amounts of ASA, ASCA, and PAR (Table 1).

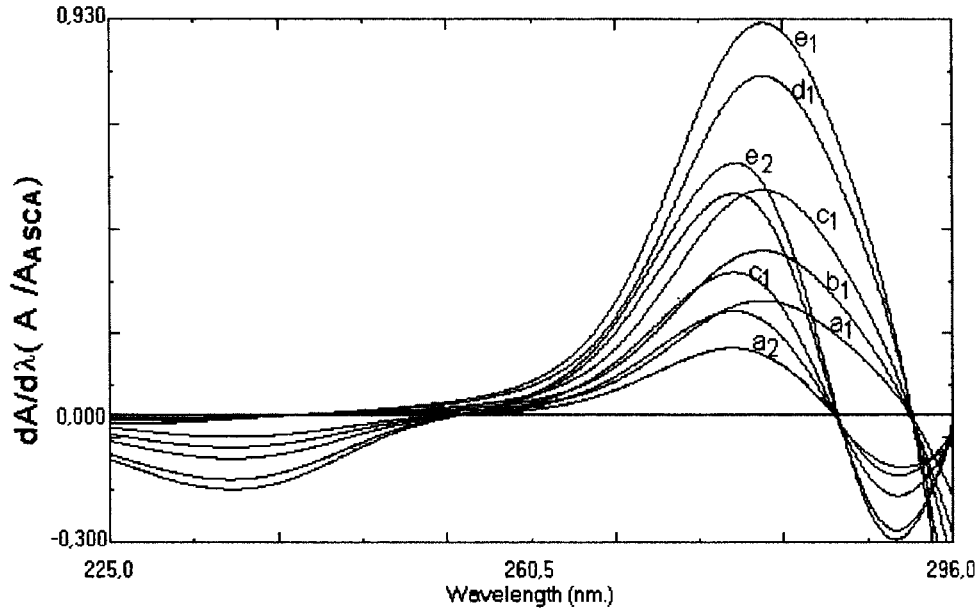

Fig. 7. First derivative of the ratio spectra of paracetamol (PAR): (a_1) 8 μg ml^{-1}; (b_1) 12 μg ml^{-1}; (c_1) 16 μg ml^{-1}; (d_1) 20 μg ml^{-1}; (e_1) 24 μg ml^{-1}; (f_1) 28 μg ml^{-1} and of acetylsalicylic acid (ACA) (a_2) 8 μg ml^{-1}; (b_2) 12 μg ml^{-1}; (c_2) 16 μg ml^{-1}; (d_2) 20 μg ml^{-1}; (e_2) 24 μg ml^{-1}; (f_2) 28 μg ml^{-1} (12 μg ml^{-1} ascorbic acid (ASCA) as a divisor) in methanol and 0.2 M HCl (1:3) ($\Delta\lambda = 8$ nm).

The main instrumental parameter conditions were optimized for a reliable determination of the subject matter compounds. For selecting the sum of the spectra as 'double divisor' at an appropriate concentrations, which is a very important factor in practice, some double divisor concentrations were tested in the determinations. The sum of the spectra of 28 μg ml^{-1} ASCA and 28 μg ml^{-1} PAR as a 'double divisor' for determining ASA; of 20 μg ml^{-1} ASA and 20 μg ml^{-1} PAR as a 'double divisor' for determining ASCA and of 12 μg ml^{-1} ASA and 12 μg ml^{-1} ASCA as a 'double divisor' for determining PAR in their ternary mixtures were found suitable. The smoothing function for the ratio spectra and the influence of the $\Delta\lambda$ for the first derivative of the ratio spectra were tested and found very appropriate to use the values of $\Delta\lambda = 8$, for both cases, in the determination of the compounds. Furthermore, the scaling factor of 10 was tested and found suitable as for all the determinations.

4.2. Ratio spectra derivative-zero crossing method

In this method, the stored spectra of the solutions of ASA and ASCA in methanol and 0.2 M HCl (1:3) were divided by the spectrum of the standard solution of 16 μg ml^{-1} PAR and the ratio spectra was obtained in the region 220–285 nm. Fig. 6 indicates the first derivative of the ratio spectra which was plotted with intervals of $\Delta\lambda = 8$ nm. The concentrations of ASA and ASCA in the ternary mixture were determined by measuring the analytical signals at 241.2 nm for ASA and 255.1 or 281.1 nm for ASCA.

In the same way, the absorption spectra of the solutions of ASA and PAR in methanol and 0.2 M HCl (1:3) were divided by the spectrum of the standard solution of 12 μg ml^{-1} ASCA and their ratio spectra were obtained in the spectral region 225–296. Fig. 7 indicates the first derivative of the ratio spectra which was calculated with intervals of $\Delta\lambda = 8$ nm. The concentrations of ASA and PAR in the ternary mixture were determined by measuring the signals at

Table 2
Recovery data obtained for the synthetic ternary mixtures by using the ratio spectra derivative-zero crossing method[a]

Composition mixture ASCA	PAR	ASA	ASA	(PAR as divisor)
	Added (μg ml^{-1})		Found (μg ml^{-1})	Recovery (%)
18.00	12.00	8.00	8.05	100.6
18.00	12.00	12.00	12.30	102.2
18.00	12.00	16.00	15.75	98.4
18.00	12.00	20.00	20.65	103.3
18.00	12.00	24.00	23.80	99.2
18.00	12.00	28.00	28.70	102.5
				$\bar{X}$ = 101.0
				RSD = 1.94%
Composition mixture ASA	PAR	ASCA	ASCA	(PAR as divisor)
	Added (μg ml^{-1})		Found (μg ml^{-1})	Recovery (%)
18.00	12.00	8.00	8.09	101.1
18.00	12.00	12.00	12.20	101.7
18.00	12.00	16.00	16.00	100.0
18.00	12.00	20.00	20.50	102.5
18.00	12.00	24.00	24.10	100.4
18.00	12.00	28.00	28.45	101.6
				$\bar{X}$ = 101.2
				RSD = 0.90%
Composition mixture ASA	ASCA	PAR	PAR	(ASA as divisor)
	Added (μg ml^{-1})		Found (μg ml^{-1})	Recovery (%)
18.00	18.00	8.00	8.05	100.6
18.00	18.00	12.00	12.10	100.8
18.00	18.00	16.00	16.20	101.3
18.00	18.00	20.00	19.80	99.0
18.00	18.00	24.00	24.40	101.6
18.00	18.00	28.00	28.30	101.1
				$\bar{X}$ = 100.7
				RSD = 0.91%

[a] RSD, relative standard deviation.

286.1 nm for PAR and 239.3 or 292.4 nm for ASA.

In the method, various mixtures of ASA, ASCA and PAR were prepared and tested between 8 and 28 μg ml^{-1} for ASA, ASCA and PAR in the ternary mixture. Mean recoveries and the relative standard deviations were found to be 101 and 1.94% for ASA, 101.2 and 0.90% for ASCA and 100.7 and 0.91% for PAR, in the synthetic mixtures prepared by adding known amounts of ASA, ASCA, and PAR (Table 2).

The main instrumental parameter conditions were optimized to obtain the most distinct curve of first derivative of the ratio spectra. For selecting a divisor of the appropriate concentration, some divisor concentrations were tested in the determination. The standard solutions of 16 μg ml^{-1} of PAR for determining ASA and ASCA and of 12 μg ml^{-1} of ASCA for the determination of ASA and PAR in their ternary mixtures were found suitable. The influence of the $\Delta\lambda$ for obtaining the first derivative of the ratio spectra

Table 3
Calibration data in the determination of ASA, ASCA and PAR by two methods

Methods	λ (nm)	Linearity range (μg ml^{-1})	Equation	Regression coefficient (r)
Double divisor-ratio spectra deviation	271.8	8–28	$Y^a = 1.2\times10^{-2}C_{ASA} - 2.5\times10^{-3}$	0.9999
	267.4	8–28	$Y^a = 3.0\times10^{-2}C_{ASCA} - 2.7\times10^{-3}$	0.9991
	241.5	8–28	$Y^a = 2.5\times10^{-2}C_{PAR} + 5.9\times10^{-3}$	0.9998
Ratio spectra derivative-zero crossing	286.1	8–28	$Y^a = 2.4\times10^{-2}C_{PAR} + 7.2\times10^{-3}$	0.9995
	239.3	8–28	$Y = 5.6\times10^{-3}C_{ASA} + 9.1\times10^{-4}$	0.9998
	292.4	8–28	$Y = 4.7\times10^{-3}C_{ASA} + 8.0\times10^{-3}$	0.9980
	241.2	8–28	$Y^a = 3.6\times10^{-2}C_{ASA} + 6.9\times10^{-3}$	0.9999
	255.1	8–28	$Y^a = 9.1\times10^{-3}C_{ASCA} + 1.9\times10^{-4}$	0.9998
	281.1	8–28	$Y = 1.9\times10^{-3}C_{ASCA} + 2.0\times10^{-4}$	0.9994

[a] The calibration graphs were used in the determinations: C_{ASA} = μg ml^{-1} of acetylsalicylic acid; C_{ASCA} = μg ml^{-1} of ascorbic acid; C_{PAR} = μg ml^{-1} of paracetamol.

was tested and a value of $\Delta\lambda = 8$ nm was considered as suitable for both determinations.

For application of these methods, Table 3 shows the regression coefficients and linearity ranges of the calibration curves for the determinations of ASA, ASCA and PAR in their ternary mixture.

A good coincidence was observed for the assay results of the commercial preparations by application of the two methods in this work (Table 4).

5. Conclusion

By applying these methods for the analysis of synthetic ternary mixtures and pharmaceutical effervescent tablets containing the three compounds, successful results were obtained. In spite of the three compounds which produce a perfect overlapping spectrum in the zero-order spectra, without requiring a separation procedure, it was observed that the methods proposed in this paper were more simple and precise than the methods described in the literature. For example, compared to alternative methods, such as HPLC or GC, these spectrophotometric methods were simple and less expensive, and require neither sophisticated instrumentation nor any prior separation step.

In the first method, for each compound in the ternary mixture, without searching the critical point at the separated peaks, the maximum amplitude of the separated peaks can be measured where this can be considered to be superior to the new method over to alternative spectrophotometric method for the resolution of the ternary mixture. In the case of Berzas Nevado's method, together with the utilization of the derivative of the ratio spectra, at the same time a zero-crossing point is necessary for the determination of compounds in a ternary mixture.

These methods have a very promising field in the

Table 4
Results obtained for the pharmaceutical samples (mg tablet^{-1}) by using the two spectrophotometric methods[a]

Methods	ASA Mean ± S.D.	ASCA Mean ± S.D.	PAR Mean ± S.D.
Double divisor ratio spectra derivative	299 ± 1	301.3 ± 0.7	199.8 ± 0.6
Derivative ratio spectra zero-crossing	300 ± 1	302.3 ± 0.8	200.8 ± 0.9

[a] Results obtained are average of ten experiments for each method.

routine analysis of compounds for the multi-mixtures and for the pharmaceutical preparations containing these mixtures.

References

[1] A.T. Giese, C.S. French, Appl. Spectrosc. 9 (1955) 78.
[2] T.C. O'Haver, G.L. Green, Anal. Chem. 48 (1976) 312.
[3] T.C O'Haver, Anal. Chem. 51 (1979) 91A.
[4] P. Levillain, D. Fompeydie, Analysis 14 (1986) 1.
[5] Spectrophotometry in Medicine, Heilmeyer, Adam Hilger, London, 1943, p. 7.
[6] A.L. Glenn, J. Pharm. Pharmacol. 12 (1960) 595.
[7] A.L. Glenn, J. Pharm. Pharmacol, Suppl. 15 (1963) 123T.
[8] S. Shibata, M. Furukawa, K. Goto, Anal.Chim.Acta 46 (1969) 27.
[9] S. Shibata, M. Furukawa, K. Goto, Anal.Chim.Acta 53 (1971) 369.
[10] S. Shibata, K. Gote, Y. Ishiguro, Anal. Chim. Acta 62 (1972) 305.
[11] A.M. Wahbi, A.M. Faraghaly, J. Pharm. Pharmacol. 22 (1970) 848.
[12] A.M. Wahbi, H. Abdine, M.A. Korany, F.A. El Yazbi, J. Pharm. Sci. 67 (1978) 140.
[13] Y.R. Tahboud, H.L. Pardue, Anal. Chem. 57 (1985) 38.
[14] D.T. Rossi, H.L. Pardue, Anal. Chim. Acta 175 (1995) 153.
[15] M. Blanco, J. Gene, H. Iturriaga, S. Maspoch, J. Riba, Talanta 34 (1987) 987.
[16] F. Salinas, J.J. Berzas Nevado, M.A. Espinosa, Talanta 37 (1990) 347.
[17] J.J. Nevado Berzas, C.C. Guiberteau, F. Salinas, Talanta 39 (1992) 547.
[18] E. Dinç, F. Onur, Anal. Chim. Acta. 359 (1998) 93.
[19] H. Fang, L. Lei, C. Sun, Zhongguo Yiyuan Yaoxue Zazhi 16 (1996) 304.
[20] K. Kitamura, M. Tagaki, K. Hozumi, Chem. Pharm. Bull. 32 (1984) 1489.
[21] M.A. Abuirjeice, M.E. Abdel-Hamid, E.A. İbrahim, Anal. Lett. 22 (1989) 365.
[22] R.J. O'Kurk, M.A. Adams, R.B. Philip, J. Chromatogr. Biomed. Appl. 25 (1984) 343.
[23] I.I. Hewala, Anal. Lett. 26 (1993) 2217.
[24] M. Tabata, H. Morita, Talanta 44 (1997) 151.
[25] C.M. Ashraf, Y. Ghaffar, A. Rahman, Sci. Int. (Lahore) 7 (1995) 483.
[26] M.E. Abdel-Hamid, M.H. Barary, E.M. Hassan, M.A. Elsayed, Analyst 110 (1985) 831.
[27] J.A. Nobrega, G.S. Lopes, Talanta 43 (1986) 971.
[28] P.B. Issopoulos, S.E. Salta, J. Anal. Chem. 357 (1997) 317.
[29] M.W. Dong, J.L. Parce, LC-GC 14 (1996) 794.
[30] J. Smeyers-Verbeke, M.R. Detaevernier, D.L. Massart, Anal. Chim. Acta 191 (1986) 181.
[31] D.Y. Tobias, J. Assoc. Off. Anal. Chem. 66 (1993) 1450.
[32] M.A. Korany, M. Bedair, H. Mahgoub, M.A. Elsayd, J. Assoc. Off. Anal. Chem. 69 (1986) 608.
[33] A. Bozdoğan, A.M. Acar, G.K. Kunt, Talanta 39 (1992) 977.
[34] Z. Bouhsain, S. Garriguesand, Miguel de la Guardia, Analyst 121 (1996) 636.
[35] M.A. Sheikh, H.N. Alkaysi, A.M. Gharaibeh, Anal. Lett. 22 (1989) 585.

ELSEVIER

Talanta 48 (1999) 1159–1166

Talanta

Potentiometric study of Cd(II) and Pb(II) complexation with two high molecular weight poly(acrylic acids); comparison with Cu(II) and Ni(II)

Catherine Morlay *, Monique Cromer, Yolande Mouginot, Olivier Vittori

Laboratoire d'Electrochimie Analytique-LICAS, Université Claude Bernard Lyon 1, CPE, 43 Bvd du 11 novembre 1918, 69622 Villeurbanne Cedex, France

Received 6 July 1998; received in revised form 19 October 1998; accepted 20 October 1998

Abstract

The cadmium (II) or lead (II) complex formation with two poly(acrylic acids) of high molecular weight ($Mw = 2.5 \times 10^5$ and 3×10^6) was investigated in dilute aqueous solution ($NaNO_3$ 0.1 mol l^{-1}; 25°C). Potentiometric titrations were carried out to determine the stability constants of the MA and MA_2 complex species formed. Bjerrum's method, modified by Gregor et al. (J. Phys. Chem. 59 (1955) 34–39), for the study of polymeric acids was used. The results were compared to those previously obtained in the same conditions with copper (II) and nickel (II) [1]. It appeared that the two polymers under study present similar binding properties and that the stability constants of the complex species formed increased in the following order, depending on the metal ion: Ni(II) < Cd(II) < Cu(II) < Pb(II). Lead (II) ions seemed to be particularly well bound to PAAs (the global stability constant log β_{102} was found to be close to 7.0) and allowed the formation of the predominant PbA_2 species in a quite large pH domain. Finally, the greater stability of PAA complexes compared to those of their monomeric analogs, glutaric and acetic acids, was confirmed.

Keywords: High molecular weight poly(acrylic acids); Cadmium (II); Lead (II); Complexation

1. Introduction

Linear hydrosoluble poly(acrylic acids) (PAAs) of high molecular weight are used as flocculants in the water treatment field. They also constitute relatively simple models in the study of the binding properties of particular organic macromolecules such as humic substances for example [2–6]. Natural waters that are treated to produce drinking water or wastewaters that are treated before their release in the environment may contain both natural organic molecules as part of the bulk organic matter and flocculants introduced during the physicochemical treatment step. The fate and elimination of low concentrations of metal ions present as pollutants in such complex aqueous media depend on the interactions with

* Corresponding author. Tel.: + 33-4-72448263 fax: + 33-4-72448479; e-mail: morlay@univ-lyon1.fr.

0039-9140/99/$ - see front matter
PII: S0039-9140(98)00336-1

the organic or inorganic substances present in the bulk water and in particular with the organic molecules of a polymeric nature.

The aim of this work was to assess the metal binding properties of two high molecular weight hydrosoluble PAAs towards cadmium (II) and lead (II) ions. The experiments were carried out in dilute aqueous solution using protometry as an investigation mean.

In a previous work, we studied the complexation of copper (II) and nickel (II) ions by the same PAAs [1]. As the examined PAAs were not fully described [7–11] in several papers, we chose to study commercial PAAs having a well defined average molecular weight: $Mw = 2.5 \times 10^5$ and 3×10^6. The first value of Mw is comparable to those previously considered by several authors [7–11] whereas the second one typically corresponds to those of cationic flocculants used in the water treatment field. Several studies have dealt with the metal binding properties of hydrosoluble PAAs in aqueous solution using potentiometric titrations [7–11]. However, almost all of these studies only considered copper (II) complexation. In our previous work, we also studied copper (II) in order to be able to compare our results with the largest literature data available in that field of research but also to validate our experimental procedure and data treatment. This now allows us to go forward with cadmium (II) and lead (II) which are heavy metal cations and which constitute as such highly pollutant substances.

The European Community, the USA-EPA (Environmental Protection Agency) and the World Health Organization (WHO) have mentioned either maximal concentrations or guideline values for cadmium and lead in drinking water and that limits are generally lower than those cited for copper or nickel we previously studied.

2. Theoretical considerations

The metal complexation by PAA 2.5×10^5 or PAA 3×10^6 was studied during the alkali titration of the protonated polyacid (HA) in the presence of metal ions (M). The Bjerrum approach [12], modified by Gregor et al. [7] for the analysis of complexes formed with macromolecules, was used. All of the definitions and assumptions needed for this study as well as the characteristics of the weak acidity of both PAAs under study have been described in a previous paper [1].

In our precedent work, we considered the global stability constant β_{102} for the formation of the MA_2 species determined using the logarithms of the complexation constants, log b_r, which were the values of $p([HA]/h)$ at the successive half integral values of r, provided that these constants were sufficiently separated [1]. Another way to solve this problem is as follows. According to Gregor et al. [7], who studied a PAA-copper (II) system, when the formation curve $\bar{r}$ versus $p([HA]/h)$ can be represented by a straight line around $\bar{r} = 1$ and when the slope of this straight line is quite large indicating a small spreading factor (b_1/b_2), it may be assumed that $b_2 \neq b_1$. In other words, it means that the chance for a second ligand group to attach itself to the metal ion after one has already attached itself is great. In this case, according to Gregor et al. [7], the significant constant is the over-all complexation constant $B_2 = b_1 \cdot b_2 = B_{av}^2$ corresponding to the over-all process:

$$M + 2\,HA \leftrightarrows MA_2 + 2\,H \quad (1)$$

$$B_2 = ([MA_2] \cdot h^2)/(m \cdot [HA]^2) \quad (2)$$

In any case, regardless of the separation between the constants, the value of $p([HA]/h)$ at integral values of $\bar{r}$ gives an average constant, e.g. at $\bar{r} = 1.0$ the average constant $B_{av} = (b_1 \cdot b_2)^{1/2}$ for a two-step process. The 'classical' global complexation constant $B_{102} = [MA_2]/(m \cdot a^2)$ is then calculated using the following relation:

$$B_{102} = B_2/(K_A^H)^2 \quad (3)$$

3. Experimental

The preparation of all the solutions was described previously [1]. Metal ion stock solutions (2×10^{-2} mol l^{-1}) were prepared from cadmium nitrate and lead nitrate (Fluka Chemika, Switzerland) and standardized using an EDTA disodium salt solution (Merck, Germany).

The whole apparatus description and use to perform the potentiometric analyses (protometric titrations) were presented earlier [1]. Samples containing known constant volumes of one of the two stock solutions of the studied PAAs were titrated with the carbonate-free 0.1 mol l^{-1} NaOH solution either in the absence or in the presence of metal ions cadmium (II) or lead (II). All the samples were evaluated in rigorously the same way and according to the previously described operative conditions. All the solutions to be analyzed contained $NaNO_3$ as supporting electrolyte at a 0.1 mol l^{-1} final concentration. The measurements were performed at 25.0 ± 0.1°C under a nitrogen atmosphere.

Two different concentration ratios $R = C_A/C_M$ were examined for each PAA with each metal ion. C_A represents the total content of titratable acid functions (carboxylic groups) of the dilute solution of PAA in the analysis cell, expressed in eq l^{-1}.

4. Results and discussion

4.1. Qualitative study

Calculations were made, using the formula proposed by Baes and Mesmer [13] to assess the possible existence of metal hydroxides. Taking into account the value of C_M, we checked that neither soluble nor insoluble metal hydroxides were significantly formed during the alkali titration, even in the higher pH region.

Fig. 1 shows the evolution of pH versus α_A or α_M for PAA 3×10^6 in the absence or in presence of cadmium (II) or lead (II), respectively and for the same ratio C_A/C_M examined. For any pH located in the pH range where complexation takes place, the dissociation coefficient of the PAA 3×10^6 in the presence of metal ions, α_M, is higher than the corresponding α_A obtained in the absence of metal ions. By comparison with the curve obtained with the ligand alone, the 'ligand + metal ion' titration curves show a supplementary release of protons which is attributed to the formation of metal complexes. For $R = C_A/C_M$ around 12.5, the complexation occurs significantly in the 4.0–7.5 pH range for cadmium (II) and in the 3.0–7.0 pH range for lead (II). Similar results were obtained with PAA 2.5×10^5. These pH ranges are quite similar to that previously reported for copper (II) and nickel (II) [1].

4.2. Quantitative study

Two different ligand to metal ratios, $R = C_A/C_M$, were studied for each PAA with each of the metal ions. R values were ~ 6.4 and 12.8 for cadmium (II). Because of the shape of the formation curves obtained, we had to use a higher value of R for lead (II): the R values were ~ 12.7 and 25.4. C_A was 5.3 and 5.0 meq l^{-1} for PAA 2.5×10^5 and PAA 3×10^6, respectively. C_M was in the 2×10^{-4}–8×10^{-4} mol l^{-1} concentration range.

Fig. 2 shows the formation curves obtained with PAA 3×10^6 in the presence of cadmium (II) or lead (II), respectively, and for the different C_A/C_M ratios investigated. The formation curves obtained with PAA 2.5×10^5 presented a very similar shape to that obtained with PAA 3×10^6. The values of log b_r were obtained by a graphical interpolation of the formation curves. The values of the complexation constants K_1, K_2 and β_{102}, as well as the pH and pK_A^H values for which K_1 and K_2 were determined are presented in Table 1 for PAA 2.5×10^5. The apparent dissociation con-

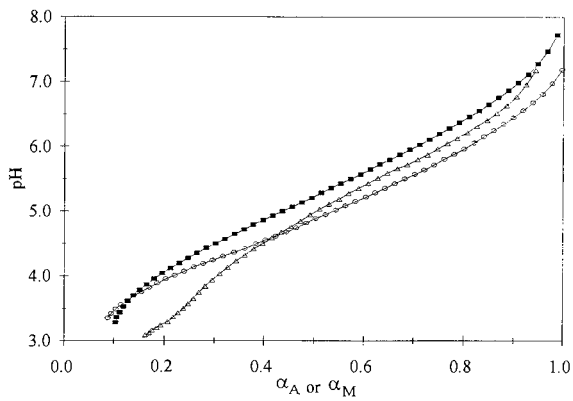

Fig. 1. Plot of pH versus the dissociation coefficient of PAA 3×10^6 in the absence (α_A; ■) or in the presence (α_M) of metal ion (○, Cd(II) with $R = 12.6$; △, Pb(II) with $R = 12.3$; $C_A = 5.0$ meq l^{-1}).

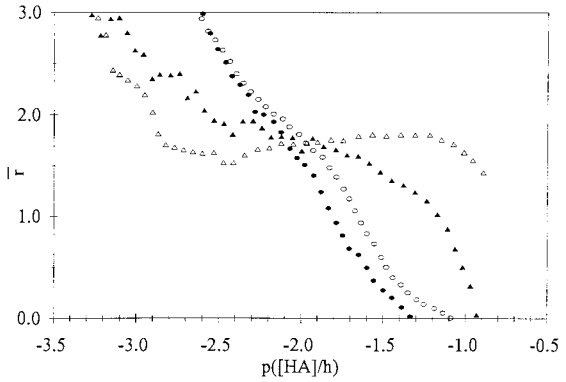

Fig. 2. Formation curves obtained for the Cd(II)/PAA 3×10^6 and Pb(II)/PAA 3×10^6 systems with different values of R (Cd(II): ○, $R = 6.3$; ●, $R = 12.6$; Pb(II): △, $R = 12.3$; ▲, $R = 24.6$; $C_A = 5.0$ meq l^{-1}).

stant of the ligand, K_A^H, in the presence of metal ions and at a given pH was determined from the curve $pK_A^H = f(pH)$ previously established [1]. Not significantly different results were obtained with PAA 3×10^6.

The reproducibility of both cadmium (II) and lead (II) complexation was examined by making two determinations in each case. The experimental error on the values of log K (log K_1 or log K_2) was estimated to be ± 0.1. The experimental error on the values of log β_{102} or log B_{102} was estimated to be ± 0.2.

Table 1
Stability constants log K_1 and log K_2 and corresponding pH and pK_A^H values obtained for the Cd(II)/PAA 2.5×10^5 and Pb(II)/PAA 2.5×10^5 systems with different values of $R = C_A/C_M$ ($C_A = 5.3$ meq l^{-1}).

R	Cd(II)		Pb(II)	
	6.4	12.9	13.1	26.1
log K_1 ($\bar{r} = 0.5$)[a]	3.1	3.0	3.7	3.7
pH	4.04	4.15	3.32	3.30
pK_A^{Hb}	4.80	4.84	4.68	4.68
log K_2 ($\bar{r} = 1.5$)[a]	3.0	2.9	3.4	3.3
pH	4.57	4.69	3.69	3.82
pK_A^{Hb}	5.00	5.06	4.69	4.72
log β_{102}[c]	6.1	5.9	7.1	7.0

[a] The error on log K_1 and log K_2 was estimated to be ± 0.1.
[b] The error on pK_A^H was estimated to be ± 0.01.
[c] The error on log β_{102} was estimated to be ± 0.2.

From these results, it appears that several remarks previously formulated in the case of copper (II) and nickel (II) complexation [1] may also apply in the present case with cadmium (II) and lead (II):

1. When three parameters are selected: molecular weight of the PAA, nature of the metal ion and concentration ratio C_A/C_M, the values of log K_1 and log K_2 for MA and MA_2 species, respectively, are very close, log K_2 being hardly lower than log K_1; log K_2 is systematically estimated at a higher pH than log K_1
2. When two parameters are selected: molecular weight of the PAA and nature of the metal ion, a decrease in the concentration ratio C_A/C_M leads to a slight increase of log K_1 and log K_2 values
3. Complexes formed with PAA 2.5×10^5 or PAA 3×10^6 exhibit very similar stabilities and are also formed at very close pH values
4. Moreover, whatever the PAA considered and whatever the concentration ratio examined, MA or MA_2 complexes formed with lead (II) present a higher stability and are formed at a lower pH than the corresponding complexes formed with cadmium (II).

The formation curves obtained for lead (II)-PAA systems present a marked decrease of their slope for the average coordination number $\bar{r}$ in the 1.5–2.0 range and approaching 2.0 ($3.3 < pH < 5.7$ and $0.22 < \alpha_M < 0.68$ for $R = 12.3$ and $4.0 < pH < 5.2$ and $0.25 < \alpha_M < 0.53$ for $R = 24.6$; Fig. 2). This plateau means that the corresponding PbA_2 complex species is thus the predominant species formed in that region compared to the PbA species. Remembering the definition of $\bar{r}$, it means that two reactive sites (carboxylate groups) of the ligand are involved in the complexation of one metal ion Pb(II). It is strongly believed that these two carboxylate groups are vicinal on the polymer chain which implies the formation of eight membered rings [1].

Elsewhere, the formation curves $\bar{r}$ versus $p([HA]/h)$ for lead (II)-PAA systems present an important slope for $\bar{r}$ about 1 ($pH = 3.5$ and $\alpha_M = 0.15$ for $R = 24.6$; Fig. 2). One may conclude that the stability constants of the PbA and PbA_2 species are quite close and that, as a consequence,

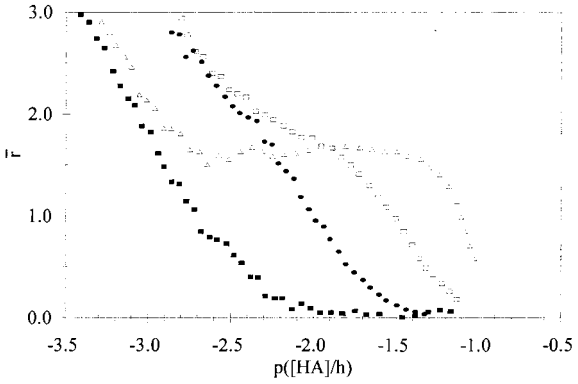

Fig. 3. Formation curves obtained for the different Metal (II)/PAA 2.5×10^5 systems with the intermediate value of R ($R \neq 13$): Cu(II), □; Ni(II), ■; Cd(II), ●; Pb(II), △ ($C_A = 5.3$ meq l^{-1}).

both species exist with comparable concentrations in that domain.

Finally, the value of $\bar{r}$ increases in a very important manner above $\bar{r} = 2$ (pH > 5.7 and $\alpha_M > 0.68$ for $R = 12.3$ and pH > 5.2 and $\alpha_M > 0.53$ for $R = 24.6$; Fig. 2). This suggests that in that region some other complexes may possibly be formed besides the PbA_2 complex species but their precise nature cannot be found from the formation curves [8–10].

Concerning the cadmium (II)-PAA systems, the formation curves do not present any plateau for $\bar{r}$ in the 0–2 range ($3.4 < pH < 4.9$ and $0.11 < \alpha_M < 0.61$ for $R = 6.3$ and $3.7 < pH < 4.8$ and $0.15 < \alpha_M < 0.48$ for $R = 12.6$; Fig. 2), which means that none of the two complex species MA and MA_2 becomes predominant in that domain of $\bar{r}$.

In order to compare the results obtained in this study with cadmium (II) and lead (II) to those previously obtained with copper (II) and nickel (II) for the same PAAs [1], we considered, for each of the four metal ions studied, the shape of the corresponding formation curve and the values of the global stability constants. Fig. 3 shows the formation curves computed for each of the four metal ions with PAA 2.5×10^5 for the intermediate concentration ratio ($R = C_A/C_M \neq 13$). Table 2 presents, for PAA 2.5×10^5 in the presence of each of the four metal ions studied, the values of log β_{102}, log B_{102} as well as the values of B_2; these last values correspond to an intermediate step in the calculation of B_{102} (Eq. (3)), but allow for a comparison with most of the data found in literature.

From Fig. 3, one can see that the formation curves obtained for nickel (II) and cadmium (II) have a very similar shape, presenting no decrease of their slope above $\bar{r} = 0.5$. On the other hand, the curves obtained for copper (II) and lead (II) can also be compared because they present a decrease of their slope for $\bar{r}$ in the 1.5–2.0 range. However, for lead (II) ions, a large plateau is obtained which means that the PbA_2 complex species remains predominant in a much larger pH domain than the CuA_2 complex species (3.5–5.6 and 4.1–4.6 pH ranges, respectively, for $R \neq 13$).

Table 2
Values of B_2, log B_{102} and log β_{102} obtained for the different metal (II)/PAA 2.5×10^5 systems with different values of $R = C_A/C_M$ ($C_A = 5.3$ meq l^{-1})

	Cu(II)		Ni(II)		Cd(II)		Pb(II)	
R	6.3	12.6	6.6	13.2	6.4	12.9	13.1	26.1
B_2	1.7×10^{-3}	9.1×10^{-4}	5.5×10^{-6}	3.8×10^{-6}	1.8×10^{-4}	9.6×10^{-5}	6.0×10^{-3}	4.6×10^{-3}
pH	3.80	3.89	5.27	5.31	4.32	4.43	3.45	3.50
pK_A^{Ha}	4.71	4.74	5.33	5.35	4.90	4.94	4.68	4.68
log β_{102}[b]	6.6	6.4	5.4	5.3	6.1	5.9	7.1	7.0
log β_{102}[b]	6.6[c]	6.3[c]	5.5[c]	5.3[c]	6.1	5.9	7.1	7.0

[a] The error on pK_A^H was estimated to be ±0.01.
[b] The error on log B_{102} and log β_{102} was estimated to be ±0.2.
[c] Values from previous work [1].

Table 3
Values of B_2 found in the literature for copper (II)-PAA complexes and obtained by potentiometric measurements

Average molecular weight	$NaNO_3$ or KNO_3 concentration (mol l^{-1})	C_A (eq l^{-1})	C_M (mol l^{-1})	$R=C_A/C_M$	B_2	Reference
2.5×10^5	$NaNO_3$ 0.1	5.2×10^{-3}	8.4×10^{-4}	6.3	1.7×10^{-3}	[1]
			4.2×10^{-4}	12.6	9.1×10^{-4}	
3×10^6	$NaNO_3$ 0.1	5.1×10^{-3}	1.6×10^{-3}	3.1	1.5×10^{-2}	[1]
			8.1×10^{-4}	6.1	7.2×10^{-3}	
			4.0×10^{-4}	12.2	2.2×10^{-3}	
3×10^4–10^5	$NaNO_3$ 0.2	10^{-2}	2.46×10^{-3}	4.1		[7]
			9.85×10^{-3}	1.0	4.6×10^{-3}	
1.92×10^6	$NaNO_3$ 0.25	1.5×10^{-4}	1.5×10^{-5}–4.2×10^{-5}	3.6–10.0	7.95×10^{-5}	[8]
1.92×10^6	$NaNO_3$ 0.25	2.5×10^{-3}	2.00×10^{-4}–9.47×10^{-4}	2.6–12.5	1.45×10^{-5}	[8]
[a]	$NaNO_3$ 0.1	1.6×10^{-3}–1.9×10^{-3}	2×10^{-4}	8.0–9.5	4×10^{-2}	[9]
[a]	KNO_3 0.1	9.9×10^{-3}	10^{-3}	9.9	10^{-3}[b]	[10]

[a] Value not mentioned.
[b] According to the authors, only the order of magnitude should be considered.

It was also noticed for one metal ion that the shape of the formation curves obtained with both PAAs was identical, indicating that the difference in the average molecular weights considered here does not seem to have any influence on the complexation phenomenon.

From Table 2, showing the results obtained with PAA 2.5×10^5, we can see that whatever the parameter considered (B_2, log B_{102} or log β_{102}), the following order can be established for the metal ions studied to form increasingly stable complexes with PAAs:

$$Ni(II) < Cd(II) < Cu(II) < Pb(II).$$

The same order was obtained with PAA 3×10^6 (data not shown).

We did not find any stability constant relative to lead (II)-PAA complexes obtained by potentiometric measurements in the literature. With this technique, only one work relative to cadmium (II)-PAA complexes was found. Miyajima et al. [14] studied the complexation of cadmium (II) ions (from $Cd(NO_3)_2$ at 10^{-4} mol l^{-1}) with a 2.5×10^3 average molecular weight PAA (3.3×10^{-3} eq l^{-1}) from the titration of the mixture with a standard sodium hydroxide solution (0.01 mol l^{-1}) in the presence of sodium nitrate (0.1 mol l^{-1}) at 25°C and under a nitrogen atmosphere. They estimated the stability constants of the CdA and CdA_2 complexes to be $\sim3.2\times10$ (log $K_1=1.5$) and 1.6×10^2 (log $K_2=2.2$), respectively.

In order to compare our results with those reported in the literature and obtained by potentiometric measurements, we chose to consider the B_2 value as it is the parameter most often mentioned by authors to describe the binding properties of PAAs. However, as most of the authors do not give the corresponding K_A^H value (the K_A^H value corresponding to the pH for which $\bar{r}=1.0$), it is not possible to deduce the log B_{102} value (Eq. (3)). Unfortunately, no value of B_2 was found which was relative to cadmium (II) or lead (II)-PAA systems.

Tables 3 and 4 present the values of B_2 obtained for Cu(II)-PAA 2.5×10^5 and Ni(II)-PAA 2.5×10^5 systems and the values cited in the literature. As mentioned earlier [1], the stability 'constants' vary with many factors, e.g. the composition of the solution [7,8,10,11]. It is gener-

Table 4
Values of B_2 found in the literature for nickel (II)-PAA complexes and obtained by potentiometric measurements

Average molecular weight	$NaNO_3$ concentration (mol l^{-1})	C_A (eq l^{-1})	C_M (mol l^{-1})	$R = C_A/C_M$	B_2	Reference
2.5×10^5	0.1	5.2×10^{-3}	8.0×10^{-4}	6.6	5.5×10^{-6}	[1]
			4.0×10^{-4}	13.2	3.8×10^{-6}	
3×10^6	0.1	5.1×10^{-3}	1.60×10^{-3}	3.2	2.8×10^{-5}	[1]
			7.9×10^{-4}	6.4	3.3×10^{-5}	
			4.0×10^{-4}	12.7	1.5×10^{-5}	
1.92×10^6	0.25	1.5×10^{-4}	1.5×10^{-5}	10.0		[8]
			3.0×10^{-5}	5.0	1.9×10^{-4}	
1.92×10^6	0.25	2.5×10^{-3}	2.5×10^{-4}–9.5×10^{-4}	2.6–10.0	2.4×10^{-7}	[8]

Table 5
Values of log K_1 and log β_{102} found in the literature [15] for the complex species formed with the analogous monomers acetic acid and glutaric acid (25°C, ionic strength = 0.1 mol l^{-1})

	Cu(II)	Ni(II)	Cd(II)	Pb(II)
Acetic acid	log $K_1 = 1.83 \pm 0.06$	log $K_1 = 0.74$[a]	log $K_1 = 1.56 \pm 0.06$	log $K_1 = 2.15 \pm 0.05$
	log $\beta_{102} = 3.09$	–	log $\beta_{102} = 2.68$	log $\beta_{102} = 3.5$
Glutaric acid	log $K_1 = 2.4$	log $K_1 = 1.6$	log $K_1 = 2.0$	log $K_1 = 2.8$

[a] Ionic strength = 0.5 mol l^{-1}.

ally assumed that only orders of magnitude of these constants could be given and compared [10]. We thus selected the few works performed with PAAs in similar operative conditions [7–10]. These conditions are reported in Tables 3 and 4.

The comparison of the different B_2 values obtained for copper (II) or nickel (II)-PAA systems is not easy. However, we can notice that the B_2 values for the copper (II)-PAA systems are in good agreement with those mentioned by several authors [7,9,10]. For the nickel (II)-PAA systems, our values are in the range of those reported by McLaren et al. [8] (B_2 in the 10^{-6}–10^{-5} range for nickel (II) from our study).

Moreover, the comparison of our results with those obtained for metal complexes of simple carboxylic acids, i.e. the analogous monomers glutaric acid or acetic acid, reveals an increased stability for the complexes of polymeric acids ([15]; Table 5). It should also be noticed that the same order can be established for the different metal ions to form increasingly stable complexes with both simple carboxylic acids or PAAs.

5. Conclusion

The aim of this study was to assess the binding properties of two poly(acrylic acids) of 2.5×10^5 and 3×10^6 average molecular weight towards cadmium (II) and lead (II) ions in dilute aqueous solution and to compare these results to those previously obtained in the same conditions with copper (II) and nickel (II) ions [1].

From our results, it was possible to establish the following order for the different metal ions to form increasingly stable complex species with both PAAs studied:

$$Ni(II) < Cd(II) < Cu(II) < Pb(II).$$

The difference in the average molecular weight of the two PAAs did not seem to have any influence on the complexation phenomenon.

Compared to the monomer analogs, i.e. glutaric acid and acetic acid, it appears that PAAs are better complexing agents. Finally, the values of the stability constants obtained (log $\beta_{102} \geq 5.3$)

suggest that the PAAs of high molecular weight studied here could contribute to the elimination of the different metal ions during the flocculation step of contaminated water treatment.

References

[1] C. Morlay, M. Cromer, Y. Mouginot, O. Vittori, Talanta 45 (1998) 1177–1188.
[2] J. Buffle, Complexation reactions in aquatic systems: an analytical approach, Horwood, Chichester, 1988.
[3] M. Vasconcelos, A. Machado, F. Rey, An. Quim. Int. Ed. 92 (4) (1996) 243–248.
[4] H. Powell, E. Fenton, Anal. Chim. Acta 334 (1–2) (1996) 27–28.
[5] M. Ricart, I. Villaescusa, F. de la Torre, React. Funct. Polym. 28 (2) (1996) 159–165.
[6] E. Tipping, Binding Models Concern. Nat. Org. Subst. Perform. Assess, Proc. NEA Workshop 1994 (1995) 163–168.
[7] H.P. Gregor, L.B. Luttinger, E.M. Loebl, J. Phys. Chem. 59 (1955) 34–39.
[8] J.V. McLaren, J.D. Watts, A. Gilbert, J. Polym. Sci. C 16 (1967) 1900–1915.
[9] P. Monjol, Bull. Soc. Chim. 4 (1972) 1319–1323.
[10] F. Yamashita, T. Komatsu, T. Nakagawa, Bull. Chem. Soc. Jpn. 52 (1) (1979) 30–33.
[11] J.A. Marinsky, N. Imai, M.C. Lim, Isr. J. Chem. 11 (5) (1973) 601–622.
[12] J. Bjerrum, Metal ammine formation in aqueous solution, Haase, Copenhagen, 1941.
[13] C.F. Baes, R.E. Mesmer, The hydrolysis of cations, Wiley, New York, 1976.
[14] T. Miyajima, M. Mori, S. Ishiguro, K. Ho Chung, C. Hichung Moon, J. Colloid Interface Sci. 184 (1996) 279–288.
[15] A.E. Martell, R.M. Smith, Critical stability constants, Volume 3: Other organic ligands, Plenum, New York, 1977.

ELSEVIER

Talanta 48 (1999) 1167–1172

Talanta

Selective transport of silver ions through bulk liquid membrane using Victoria blue as carrier

Afsaneh Safavi *, Esmaeil Shams

Department of Chemistry, College of Sciences, Shiraz University, Shiraz, Iran

Received 14 July 1998; received in revised form 20 October 1998; accepted 21 October 1998

Abstract

Transport of Ag^+ as $Ag(CN)_2^-$ ions through a bulk liquid membrane is reported. The bulk liquid membrane used is a solution of Victoria blue (VB) in chloroform. The effects of pH of the source phase, cyanide concentration in the source phase, sodium hydroxide in the receiving phase, and VB concentration in the organic phase on the efficiency of the transport system were studied. The above system has a high selectivity for Ag^+ and can selectively and efficiently transport $Ag(CN)_2^-$ ion from aqueous solutions containing other cations such as alkali and alkaline earths, Zn^{2+}, Pd^{2+}, Cu^{2+}, Cd^{2+},Hg^{2+}, Co^{2+}, Fe^{2+}, Pb^{2+}, Ni^{2+}, and Al^{3+}.

Keywords: Silver cyanide; Transport; Victoria blue

1. Introduction

In many analytical procedures usually a separation step is needed before the final analysis can be performed. Often various interfering compounds must be removed and/or the compounds of interest must be enriched before determination is possible. Liquid membranes, i.e. organic liquids in contact with two separated aqueous phases, have many applications in the separation sciences. This technique has been widely used for carrier facilitated metal ion separations [1–8], and to a lesser degree separation of organic substances [9–12]. In comparison with liquid–liquid extraction (which is a common method in separation), liquid membrane transport in which the extraction and stripping operations are combined in a single process reduces the solvent inventory requirement and also allows the use of expensive and highly selective extractants, which otherwise would be uneconomic in solvent extractions. Means have been developed whereby cation transport of this type can be coupled to free-energy gradients which derive the flux of cations against the cation concentration gradient. One of the interesting possibilities for the transport of a given metal ion involves its incorporation into a complex anion in the source phase. In such a case, due to its low hydration energy, the resulting complex anion will

* Corresponding author. Tel.: +98-71-678-742; fax: +98-71-678-742; e-mail: safavi@chem.susc.ac.ir.

0039-9140/99/$ - see front matter
PII: S0039-9140(98)00344-0

accompany a positively charged ion across the organic membrane. Recently, the transport of metal ions such as zinc, mercury, silver, palladium, and gold in the anionic form of the complexes has been reported [13–18].

Precious metal and metal impurities such as copper, nickel, and iron are usually present in anionic form after hydrometallurgical extraction of precious metal ores [19] which can be extracted via an ion pair extraction process. The corresponding co-cation can be of various types such as quaternary amines, protonated amines, solvated cations, and cationic metal complexes [17].

Cationic dyes tend to form an extractable ion-pair with anionic metal complexes of halide, cyanide, thiocyanate, and other inorganic or organic anionic ligands. The extraction of anionic complex with various cationic dyes has been extensively studied [20]. However, the study of the permeation of anionic complexes through liquid membranes has drawn less attention.

Victoria blue (VB) is a cationic dye which tends to form an ion pair with bulky anions. To the best of our knowledge no work on the use of VB as a carrier in transport systems has been reported previously. In this paper we describe the transport of silver as $Ag(CN)_2^-$ in bulk liquid membranes with VB as the carrier.

2. Experimental

2.1. Reagents

VB was purchased from BDH and used as received. Stock solutions of silver were prepared by dissolving silver nitrate (Merck). Reagent grade chloroform (Fluka) was used as the organic membrane solvent. All other chemicals used in this study were of the highest purity available from either Merck or Fluka and used without further purification. Doubly distilled deionized water was used throughout.

2.2. Apparatus

The atomic absorption spectrophotometer used for the measurement of metal ion concentrations was a Philips Pye Unicam SP9 instrument. pH measurements were made with a Metrohm 691 pH-meter using a combined glass electrode.

2.3. Procedure

All transport experiments were carried out at ambient temperature. A cylindrical glass cell (4.0 cm i.d.) holding a glass tube (2.0 cm i.d.), for separating the two aqueous phases was used (Fig. 1). The aqueous source phase (5 ml) contained Ag^+ (5.0×10^{-4} M) and 0.005 M KCN buffered at pH 5.5 with acetate buffer. The receiving phase (10 ml) contained 0.05 M sodium hydroxide. The chloroform solution (25 ml) containing 4.0×10^{-4} M VB lay below these aqueous phases, and bridged them. The organic layer was stirred by a Teflon-coated magnetic bar. In the course of the transport experiment, samples of both aqueous phases were analyzed for metal content by atomic absorption spectroscopy.

3. Results and discussion

VB is a cationic dye with a hydrophobic moiety which can form an ion pair with bulky anions. Thus, it is a desirable carrier for transport of bulky anions such as silver cyanide. The process of the formation of an ion pair at the aqueous source phase–organic layer membrane interface

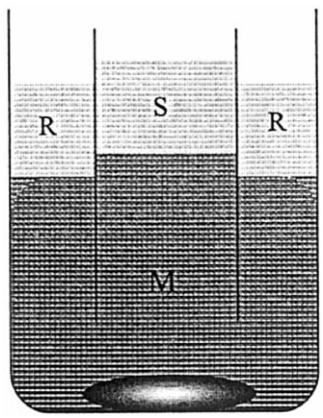

Fig. 1. Liquid membrane apparatus (S: source phase; R: receiving phase; M: liquid membrane).

Table 1
Effect of pH of the source phase on the transport of $Ag(CN)_2^-$ ion[a]

pH	Remained (%)	Transported (%)
2.0	83	9
3.0	79	14
4.0	67	18
5.0	62	25
5.5	58	35
6.0	64	28
6.5	72	22
7.0	78	18
8.0	85	12
9.0	90	0

[a] Experimental conditions: source phase, 5 ml 4.5×10^{-4}M Ag^+ ion and 0.01 M KCN; liquid membrane phase, 25 ml 8.0×10^{-5} M VB; receiving phase, 10 ml 0.015 M NaOH; rate of stirring, 250 rpm; time of transport, 60 min.

and the dissociation process of the ion pair at the membrane–receiving phase interface are sufficiently fast.

In preliminary experiments, it was found that the VB mediated transport of $Ag(CN)_2^-$ to a neutral aqueous receiving phase is quiet low. This is probably because of the stability of the ion pair in the membrane. However, in the presence of sodium hydroxide in the receiving phase $Ag(CN)_2^-$ is replaced by OH^- in the receiving phase, and the efficiency of the transport process is increased. In the next step, the experimental variables such as the pH of the source phase, the concentration of potassium cyanide in the source phase, the concentration of sodium hydroxide in the receiving phase, and the concentration of the carrier in the organic layer were optimized in order to achieve the highest efficiency in the transport of $Ag(CN)_2^-$ across the membrane.

3.1. Effect of pH of the source phase

Table 1 shows the effect of pH of the source phase on the efficiency of silver transport. The results revealed that the maximum silver transport occurs at pH 5.5. At lower pH values there was a decrease in the percentage of transport of silver probably due to decomposition of $Ag(CN)_2^-$.The efficiency of transport decreases at higher pH values probably due to the competition of OH^- with $Ag(CN)_2^-$. From the results a pH of 5.5 was selected for further studies.

3.2. Effect of cyanide concentration in the source phase

The effect of cyanide concentration in the source phase on the efficiency of $Ag(CN)_2^-$ transport was studied (Table 2), and it was found that the efficiency of silver transport increases with an increase in cyanide concentration up to 0.005 M potassium cyanide. At lower cyanide concentrations, there was a decrease in the percentage of transport of silver probably due to uncompleted formation of $Ag(CN)_2^-$. Thus, 0.005 M potassium cyanide concentration was adopted for further studies.

3.3. Effect of sodium hydroxide concentration in the receiving phase

The effect of sodium hydroxide in the receiving phase was also investigated (Table 3). The results show that an increase in hydroxide concentration up to 0.05 M increases the efficiency of silver transport. Further increases in hydroxide concentrations did not improve the efficiency of transport. For this reason 0.05 M sodium hydroxide concentration was selected for the receiving phase.

Table 2
Effect of potassium cyanide concentration in the source phase on the transport of $Ag(CN)_2^-$ ion[a]

Concentration of KCN (M)	Remained (%)	Transported (%)
0	90	4
0.002	54	26
0.005	62	32
0.010	65	29
0.015	68	25
0.020	75	20
0.025	79	18

[a] Experimental conditions: source phase, 5 ml 4.5×10^{-4}M Ag^+ ion at pH 5.5; liquid membrane phase, 25 ml 8.0×10^{-5} M VB; receiving phase, 10 ml 0.015 M NaOH; rate of stirring, 250 rpm; time of transport, 60 min.

Table 3
Effect of NaOH concentration in the receiving phase on the transport of $Ag(CN)_2^-$ ion[a]

Concentration of NaOH (M)	Remained (%)	Transported (%)
0	89	0
0.01	71	18
0.02	65	28
0.03	57	34
0.04	55	42
0.05	52	45
0.06	50	44

[a] Experimental conditions: source phase, 5 ml 4.5×10^{-4}M Ag^+ ion and 0.005 M KCN at pH 5.5; liquid membrane phase, 25 ml 8.01×0^{-5} M VB; rate of stirring, 250 rpm; time of transport, 60 min.

3.4. Effect of VB concentration in the organic phase

The influence of the concentration of VB in the organic phase on the transport efficiency of silver was also studied. The results are shown in Table 4. As is seen the percentage transport of silver increases with an increase in VB concentration in the organic phase. Maximum transport occurs at a concentration of about 4.0×10^{-4} M VB. Further excess of the carrier had no considerable effect on the transport efficiency. Thus, a concentration of 4.0×10^{-4} M VB was adopted for further studies.

Table 4
Effect of VB concentration in the organic phase on the transport of $Ag(CN)_2^-$ ion[a]

Concentration of VB ($\times10^{-4}$ M)	Remained (%)	Transported (%)
0	96	2
0.40	72	22
0.80	46	42
1.20	20	61
1.60	8	75
2.40	3	79
3.20	2	94
4.00	0	95
4.80	0	94

[a] Experimental conditions: source phase, 5 ml 4.5×10^{-4}M Ag^+ ion and 0.005 M KCN at pH 5.5; receiving phase, 10 ml 0.05 M NaOH; rate of stirring, 250 rpm; time of transport, 60 min.

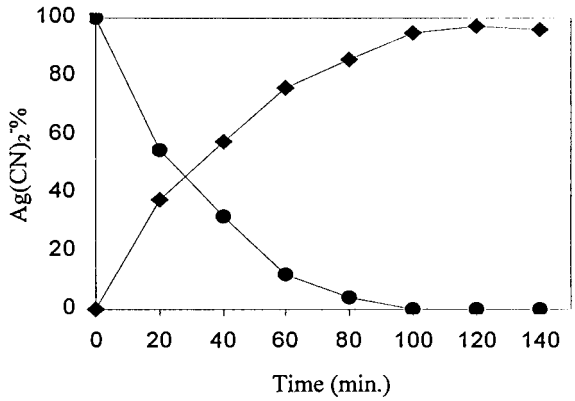

Fig. 2. Percent of $Ag(CN)_2^-$ vs. time in source (●) and receiving phases (■). Experimental conditions: source phase, 5 ml 5.0×10^{-4} M $Ag(CN)_2^-$ ion and 0.005 M KCN at pH 5.5; liquid membrane phase, 25 ml 4.0×10^{-4} M VB; receiving phase, 10 ml 0.05 M NaOH; rate of stirring, 250 rpm.

As an additional experiment the above optimization processes were performed on two other concentrations of silver ion. The optimum conditions with respect to OH^- concentration in the receiving phase and VB concentration in the membrane obtained for the transport of 1×10^{-3} and 1×10^{-4} M silver were similar to the optimum concentrations for the transport of 5×10^{-4} M silver (i.e. 0.05 M OH^- and 4.0×10^{-4} M VB). Thus, excess concentrations of OH^- and VB do not affect the efficiency of transport experiments. The optimum concentration of cyanide in the source phase was different for different ranges of silver concentration, however, a cyanide:silver ratio of about 10 was found to be suitable.

3.5. Effect of time

Additionally, the concentration–time profile of silver cyanide transport was studied. Fig. 2 shows a rapid rise in metal concentration in the receiving phase as well as a sharp decrease in silver concentration in the source phase during the first 100 min of transport. After this time concentrations of silver in the aqueous phases are independent of time.

3.6. Reproducibility of bulk liquid membrane technique

The reproducibility of the above system was studied by performing eight replicate transport experiments. The R.S.D. was found to be 1.9%.

3.7. Selectivity of bulk liquid membrane technique

The selectivity of the above system for transport of silver over other cations in equimolar mixtures is illustrated in Table 5. In addition to the above cations, the interference effects of alkali and alkaline earth cations were also studied. All of these cations remained completely in the source phase. As is seen the system is very selective, and none of the cations studied interferes with this system.

Table 5
Transport of Ag^+ for a competitive experiment with an equimolar mixture of foreign ions[a]

Mixture of cations	Cation	Remained (%)	Transported (%)
Ag^+, Hg^{2+}, Ni^{2+}, Co^{2+}	Ag^+	0	92
	Hg^{2+}	100	0
	Ni^{2+}	100	0
	Co^{2+}	100	0
Ag^+, Pd^{2+}, Cd^{2+}, Fe^{2+}	Ag^+	0	94
	Pd^{2+}	100	0
	Cd^{2+}	94	0
	Fe^{2+}	90	0
Ag^+, Zn^{2+}, Cu^{2+}	Ag^+	0	95
	Zn^{2+}	90	4
	Cu^{2+}	87	8
Ag^+, Pb^{2+}, Al^{3+}	Ag^+	0	97
	Pb^{2+}	100	0
	Al^{3+}	95	0

[a] Experimental conditions: source phase, 5 ml 4.01×0^{-4}M Ag^+ ion and 0.005 M KCN at pH 5.5; liquid membrane phase, 25 ml 4.01×0^{-4} M VB; receiving phase, 10 ml 0.05 M NaOH; rate of stirring, 250 rpm; time of transport, 100 min.

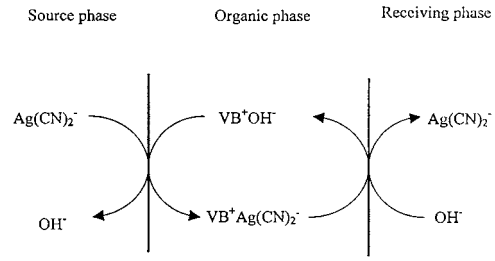

Fig. 3. Simplified representation of the transport mechanism of $Ag(CN)_2^-$ by VB.

3.8. Suggested mechanism

From the results obtained, the following mechanism is suggested for the transport of silver across a liquid membrane containing VB (Fig. 3). In the source phase silver forms an anionic complex ($Ag(CN)_2^-$). VB is a cationic dye with a single positive charge. In the source phase–organic phase interface VB forms an ion pair with silver cyanide and extracts it into the organic phase. At the receiving phase–organic phase interface, silver cyanide is abstracted from the organic phase while OH^- is given back to the carrier. A similar mechanism has been reported previously for the transport of a metal ion complex with thiocyanate [21].

4. Conclusion

A transport system for silver as a silver cyanide ion through a bulk liquid membrane system containing VB as the carrier was studied and it was found that VB is an excellent carrier for selective and efficient transport of silver. This study demonstrates the usefulness of the liquid membrane technique for making it possible to combine extraction and stripping operations in a single process and reducing the solvent inventory requirements. In conclusion, therefore, the above system, which is specific for silver is a potential candidate for practical use in silver separation, especially as it has the advantage of low solvent requirement, high precision, efficiency, selectivity, simplicity, and speed.

Acknowledgements

The authors wish to express their gratitude to Shiraz University Research Council for the supporting this work.

References

[1] T. Saito, Sep. Sci. Technol. 28 (1993) 1629.
[2] J.A. Jonsson, L. Mathiasson, Trac 11 (1992) 106.
[3] K. Hiratani, T. Takahashi, H. Sugihara, K. Kasuga, K. Fujiwara, T. Hayashita, R.A. Bartsch, Anal. Chem. 69 (1997) 3002.
[4] A. Safavi, S. Rastegarzadeh, Talanta 42 (1995) 2039.
[5] A. Safavi, E. Shams, J. Membr. Sci. 144 (1998) 37.
[6] M.A. Chaudry, S. Amin, M.T. Malik, Sep. Sci Technol. 31 (1996) 1309.
[7] N. Parthasarathy, J. Buffle, Anal. Chim. Acta 254 (1991) 9.
[8] C. Sirlin, M. Burgard, M.J.F. Leroy, J. Membr. Sci. 54 (1990) 299.
[9] G. Audunsson, Anal Chem. 58 (1986) 2714.
[10] Y. Kuo, H.P. Gregor, Sep. Sci. Technol. 18 (1983) 421.
[11] R.G. Stehle, W.I. Higuchi, J. Pharm. Sci. 56 (1967) 1367.
[12] J. Behr, J. Lehn, J. Am. Chem. Soc. 95 (1973) 6108.
[13] R.M. Izatt, G.A. Clark, J.J. Christensen, J. Membr. Sci. 24 (1985) 1.
[14] H. Parham, M. Shamsipur, J. Membr. Sci. 86 (1994) 29.
[15] M. Akhoond, M. Shamsipur, J. Chin. Chem. Soc. 43 (1996) 225.
[16] R. Chiarizia, A. Castagnola, Proc. Int. Solvent Extraction Conf., ISEC'83, Denever, CO, 26 August–2 September 1983, p. 393.
[17] M. Tromp, M. Burgard, M.J.F. Leroy, M. Prevost, J. Membr. Sci. 38 (1988) 295.
[18] R.M. Izatt, G.A. Clark, J.J. Christensen, Sep. Sci. Technol. 22 (1987) 691.
[19] E.J. Stevenson, Chem. Technol. Rev. 93 (1977) 275–304.
[20] K.L. Cheng, K. Ueno, T. Imamura, Handbook of Organic Analytical Reagent, CRC Press, Boca Raton, FL, 1982, pp. 459–470.
[21] M. Papantoni, N.K. Djane, K. Ndung'u, J.A. Jonsson, L. Mathiasson, Analyst 120 (1995) 1471.

ELSEVIER

Talanta 48 (1999) 1173–1177

Talanta

Nickel determination in saline matrices by ICP-AES after sorption on Amberlite XAD-2 loaded with PAN

Sérgio L.C. Ferreira *, Cristiane F. de Brito, Alailson F. Dantas, Neyla M. Lopo de Araújo, A.C. Spinola Costa

Instituto de Química, Universidade Federal da Bahia, Campus Universitário da Federação, Salvador, Bahia 40170-290, Brazil

Received 25 April 1998; received in revised form 21 October 1998; accepted 22 October 1998

Abstract

In the present paper, a solid phase extraction system for separation and preconcentration of nickel (ng g^{-1}) in saline matrices is proposed. It is based on the adsorption of nickel(II) ions onto an Amberlite XAD-2 resin loaded with 1-(2-pyridylazo)-2-naphthol (PAN) reagent. Parameters such as the pH effect on the nickel extraction, the effect of flow rate and sample volume on the extraction, the sorption capacity of the loaded resin, the nickel desorption from the resin and the analytical characteristics of the procedure were studied. The results demonstrate that nickel(II) ions, in the concentration range 0.10–275 μg l^{-1}, and pH 6.0–11.5, contained in a sample volume of 25–250 ml, can be extracted by using 1 g Amberlite XAD-2 resin loaded with PAN reagent. The adsorbed nickel was eluted from the resin by using 5 ml 1 M hydrochloric acid solution. The extractor system has a sorption capacity of 1.87 μmol nickel per g of Amberlite XAD-2 resin loaded with PAN. The precision of the method, evaluated as the R.S.D. obtained after analyzing a series of seven replicates, was 3.9% for nickel in a concentration of 0.20 μg ml^{-1}. The proposed procedure was used for nickel determination in alkaline salts of analytical grade and table salt, using an inductively coupled plasma atomic emission spectroscopy technique (ICP-AES). The standard addition technique was used and the recoveries obtained revealed that the proposed procedure shows good accuracy.

Keywords: Nickel preconcentration; Solid phase extraction; Inductively coupled plasma atomic emission spectroscopy; Alkaline salts

1. Introduction

The determination of nickel traces in saline matrices by inductively coupled plasma atomic emission spectrometry (ICP-AES) is difficult, because the aspiration of solutions with high salt concentrations in the plasma can cause problems such as blockage of the nebulizer, considerable background emission, and transport and chemical interferences with a consequent drop in sensitivity and precision [1–4]. Thus, trace determination in saline solutions always needs a prior separation.

* Corresponding author. Tel: +55-71-2375784/2375785; fax: +55-71-2355166/2374117; e-mail: slcf@ufba.br.

0039-9140/99/$ - see front matter
PII: S0039-9140(98)00339-7

Several papers on this subject have appeared in the literature [5–9]. The process involving extraction in the solid phase has received more acceptance due to a number of possible advantages including availability of the solid phase, getting large preconcentration factors, and the facility for enrichment using systems with continuos flow, besides this they dispense with the need of organic solvents which are usually toxic [10].

A chelating sorbent loaded with dithizone [5] was obtained by chemical reaction with styrene-DVB (5%) copolymer as matrix. It was used for the preconcentration of nickel and other metals. A column containing silica loaded with 8-hydroxyquinoline [6] was used for preconcentration and determination of nickel, iron, zinc and copper by GFAAS. A procedure [7] for preconcentration of nickel, cadmium, cobalt, copper, manganese, lead and zinc was developed. In it, the metal cations were complexed with diethyldithiocarbamate, adsorbed on a C_{18} column and eluted with methanol. Amberlite XAD-2 chemically modified with alizarin red-S [8] and pyrocatechol violet [9] was recommended for the preconcentration and determination of nickel and other metals by spectrometric techniques.

This paper proposes an analytical procedure for the preconcentration and determination of nickel in alkaline salts, using atomic emission spectrometry with inductively coupled plasma, after chelation onto a column containing Amberlite XAD-2 resin loaded with 1-(2-pyridylazo)-2-naphthol (PAN).

Amberlite XAD-2 (polystyrene-divinylbenzene polymer) is a resin very used in preconcentration procedures. In our laboratory, it has been used in the preconcentration and simultaneous determination of zinc and copper in natural waters [11].

PAN is a chromogenic reagent proposed several times for spectrophotometric determinations of metal cations [12]. It reacts with the nickel (II) cation, forming a stable complex of composition 1:2 nickel(II)–PAN. The complex formed has a red color.

2. Experimental

2.1. Apparatus

An Applied Research Laboratories model 3410 minitorch sequential inductively coupled plasma spectrometer with an IBM PC-AT computer was used. The emission measurements were made using the conditions given in Table 1. A nickel calibration graph (0–2.0 μg ml^{-1}) was obtained using solutions prepared from 1 mg ml^{-1} stock solution. The limit of detection and the background equivalent concentration (BEC) were 16

Table 1
Operating parameters for the inductively coupled plasma spectrometer

Spectrometer	1 m, Czerny-Turner, vacuum
Grating	2400 grooves mm^{-1}, holographic
Bandwidth	13 pm, 1st order 7 pm, 2nd order
Slit widths	20 μm
PMT	R955 Hamamatsu
RF generator	Crystal controlled solid state exciter, class AB2 amplifier, 27.12 MHz
Forward power	650 W
Reflected power	<5 W
Torch	3-Tube minitorch (ARL)
Observation height	9 mm Above load coil
Nebulizer	Meinhard concentric glass
Spray chamber	Conical glass 45 ml volume, impact sphere
Pump	Peristaltic, Gilson Minipuls2
Sample uptake	2.5 ml min^{-1}
Outer argon flow	7.5 l min^{-1}
Intermediate argon flow	0.8 l min^{-1}
Carrier argon flow	0.8 l min^{-1}
Wavelength	221.646 nm
Signal integration time	5 s
Integration for determination	3

and 98 μg l^{-1}, respectively. The correlation coefficient was 0.9994.

An Ismatec peristaltic pump model Reglo furnished with tygon tubes were employed to propel the sample solutions. A 300 ANALYSER pH meter was used to measure the pH values.

2.2. Reagents

All reagents were of analytical reagent grade unless otherwise stated. Double distilled water was used for the preparation of solutions. The nitric acid and hydrochloric acid were of suprapur quality (Merck). The laboratory glassware was kept overnight in a 5% nitric acid solution. Before use, the glassware was washed with deionized water and dried in a dust-free environment.

The nickel solution (10.00 μg ml^{-1}) was prepared by diluting a 1000 μg ml^{-1} nickel solution (atomic absorption, Aldrich) using a 5% hydrochloric acid solution. The PAN solution (0.10%) was prepared by dissolving 0.25 g PAN (Aldrich) in 250 ml ethanol. The hexamine buffer solution (pH 6.5) was prepared by dissolving 56.0 g hexametilenetetramine in 1000 ml deionized water and the pH adjusted with 5% hydrochloric acid solution.

2.3. Preparation of the Amberlite XAD-2 column loaded with PAN

XAD-2 was treated with an ethanol–hydrochloric acid–water (2:1:1) solution over night. Later, the resin was rinsed with deionized water until it was pH neutral, being dried in an oven at a temperature of 110°C for 3 h.

The packing of the column must be done using ethanol as eluent because with water the grains of resin float. The resin is saturated with the reagent by elution of 10 ml of a 0.10% PAN solution in ethanol at a flow rate of 0.50 ml min^{-1}. Later it is rinsed with water until the complete elimination of excess reagent occurs. All experiments were done in glass columns with a 0.80 cm i.d. and length of 15 cm, containing 1g XAD-2. Before the sample elution the column must be preconditioned by passing a buffer solution.

2.4. Procedure for the sorption of nickel(II) on the Amberlite XAD-2

Transfer 25–200 ml of the sample solution containing nickel in the concentration range 0.10–275 μg l^{-1} to a 250 ml beaker, add 10 ml of buffer solution pH 6.5. This solution must be passed through the column at a flow rate of 0.60 ml min^{-1}. After passing this solution, the column was rinsed with 10 ml of deionized water. The adsorbed nickel(II) on the column was eluted with 5 ml 1 M hydrochloric acid solution, at a flow rate of 0.60 ml min^{-1}. The eluent was collected in a 10-ml volumetric flask with dilution using 1 M hydrochloric acid solution and the nickel determinate by the ICP-AES technique.

3. Results and discussion

3.1. pH effect on the nickel sorption onto Amberlite XAD-2 resin

The effect of pH on the sorption of nickel(II) ions was studied and the results demonstrated that it is maximum and quantitative ($>95\%$) in the pH range 6.0–11.5, as can be seen in Fig. 1. pH control was done using an acetate buffer with pH 4.0–6.0, a hexamine buffer with pH 6.5, a borate buffer pH 8.0 and an ammonium buffer with pH 10.0. For pH 11.5 a solution of sodium hydroxide was used. In the proposed procedure, a hexamine buffer with pH 6.5–7.0 is recommended because at alkaline pH the PAN reagent reacts with other metallic ions.

3.2. Effect of flow rate and sample volume

The effect of flow rate on nickel retention was examined by varying the flow rate from 0.30 to 2.50 ml min^{-1} under optimum conditions. The results demonstrated that the retention of nickel on the resin is quantitative ($>95\%$) only for a flow rate lower than 0.60 ml min^{-1}. The effect of the sample volume on the nickel extraction was investigated by passing 25, 50, 100, 200 and

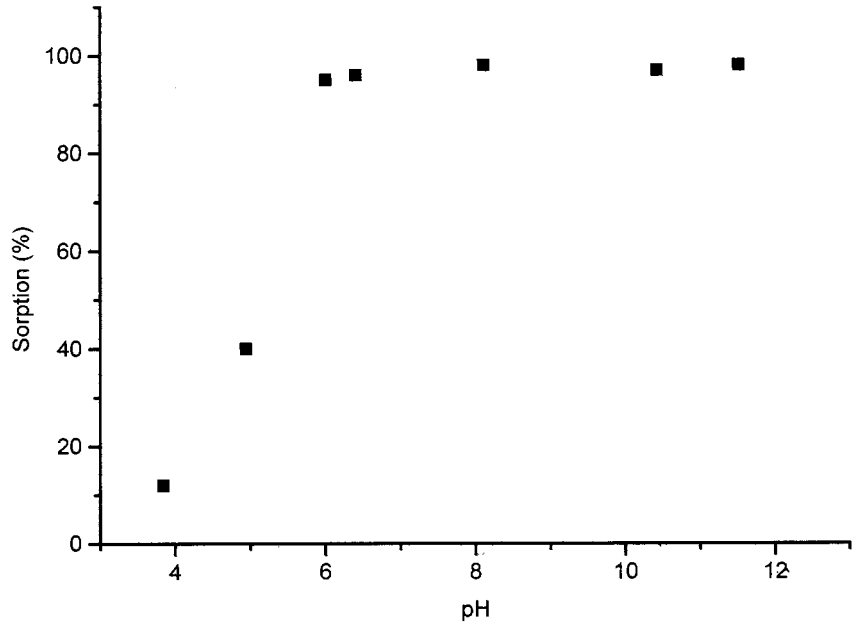

Fig. 1. Effect of pH on the nickel sorption on the XAD-2 column.

250 ml through the column at a constant flow-rate of 0.60 ml min^{-1}. In all cases the recovery obtained was higher than 95%.

3.3. Effect of electrolytes on the sorption of the nickel

The influence of electrolytes on the sorption of nickel(II) ions in the proposed system was also studied. The results demonstrated that the extraction is quantitative ($>95\%$) even in the presence of 200 ml 30% sodium chloride solution or 200 ml 30% potassium nitrate. The salts used in this experiment were of suprapur quality (Merck).

3.4. Sorption capacity

The sorption capacity of the Amberlite XAD-2 resin loaded with PAN for the extraction of nickel was also determined. Increasing amounts of nickel were added to a column containing 1.0 g of loaded resin. The results demonstrated that the resin has a sorption capacity of 1.87 μmol nickel per g XAD-2 resin. Under conditions of maximum adsorption the distribution coefficient was higher than 1.0×10^4 l kg^{-1}.

3.5. Nickel desorption from XAD-2 resin

In order to determine the nickel desorption from resin 5.0 ml solutions of hydrochloric acid with concentrations of 0.10, 0.50, 1.0 and 2.0 M were tested. The results demonstrated that the desorption is acceptable ($>95\%$) for solutions with concentrations ≥ 1 M. In this procedure a concentration of 1 M is recommended.

3.6. Application

The proposed procedure can be applied to the preconcentration and separation of nickel, in the concentration range 0.10–275 μg l^{-1}, contained in a solution volume of 25–250 ml, by using of 1 g Amberlite XAD-2 resin loaded with PAN reagent.

The precision of the method, evaluated as the R.S.D. obtained after analyzing a series of seven replicates, was 3.9% for nickel in a concentration of 0.20 μg ml^{-1}.

The method proposed was applied for nickel determination in alkaline salts and table salt. A volume of 200 ml of the sample solution at a

Table 2
Determination and recovery of nickel in alkaline salt samples

Sample	Concentration added (ng g^{-1} salt)	Nickel found * (ng g^{-1} salt)	Recovery (%)
NaCl	0	34 ± 2	–
	500	504 ± 16	94
$NaNO_3$	0	49 ± 8	–
	500	526 ± 10	95
KNO_3	0	38 ± 3	–
	500	523 ± 14	97
KCl	0	39 ± 4	–
	500	554 ± 14	103
Table salt	0	78 ± 8	–
	500	548 ± 16	94

* At 95% confidence level.

concentration of 30% was used during the analyses. The standard addition technique was applied and the recoveries obtained revealed that the proposed procedure has good accuracy. The results are described in Table 2.

4. Conclusions

The present paper is opportune considering the analytical problem of trace determination in saline matrices by ICP-AES, and the fact that nickel is frequently present at trace levels in these substances.

The great advantages of this procedure are: (i) preparation of the extractor system is simple and fast; (ii) the elution step does not involve the use of organic solvents as in other procedures; (iii) during the nickel desorption the PAN reagent remains in the resin, allowing use of the column several times; (iv) the proposed procedure can be adapted easily for preconcentration and determination of nickel by the flow injection analysis technique.

The recovery obtained, measured by the standards addition technique, revealed that the proposed procedure shows good accuracy.

The procedure proposed was applied for nickel determination in alkaline salts by using ICP-AES, however it can be used for other samples and using other analytical methods such as AAS and GFAAS.

Acknowledgements

The authors acknowledge the financial support of the CNPq, FINEP and CAPES.

References

[1] G. Bekjarov, V. Kmetov, Fresenius Z. Anal. Chem. 335 (1989) 971.
[2] A. Montaser, D.W. Golightly, Inductively Coupled Plasma in Analytical Atomic Spectrometry, Wiley-VCH, New York, 1992.
[3] B. Budic, V. Hudnik, J. Anal. At. Spectrom. 9 (1994) 53.
[4] K. Nakagawa, K. Haraguchi, T. Ogata, T. Kato, Y. Nakata, K. Akatsuta, Anal. Sci. 14 (1998) 317.
[5] J. Chwastowska, E. Kosiarska, Talanta 35 (1988) 439.
[6] L.C. Azeredo, R.E. Sturgeon, A.J. Curtius, Spectrochim. Acta 48 (1993) 91.
[7] A. Bortolli, M. Gerotto, M. Marchiori, F. Mariconti, M. Palonta, A. Troncon, Microchem. J. 54 (1996) 402.
[8] R. Saxena, A.K. Singh, S.S. Sambi, Anal. Chim. Acta 295 (1994) 199.
[9] R. Saxena, A.K. Singh, Anal. Chim. Acta 340 (1997) 285.
[10] G.D. Christian, Analytical Chemistry, Wiley, New York, 1994.
[11] S.L.C. Ferreira, H.C. Santos, D.S. Jesus, J. Ferreira, A. C.S. Costa, J. Braz. Chem. Soc. (1998) (in press).
[12] K.L. Cheng, K. Ueno, I. Imamura, Handook of Organic Reagents, CRC Press, Boca Raton, FL, 1992.

ELSEVIER

Talanta 48 (1999) 1179–1189

Talanta

Application of packed column supercritical fluid chromatography to the simultaneous determination of seven anticonvulsant drugs

Indravadan C. Bhoir, Suvarna T. Patil, M. Sundaresan *

Shri C.B. Patel Research Centre for Chemistry and Biological Sciences, 3rd Floor, Bhaidas Hall, Vile Parle (West), Mumbai 400 056, India

Received 6 July 1998; received in revised form 20 October 1998; accepted 26 October 1998

Abstract

Studies of speed, resolution, and selectivity have shown that packed column supercritical fluid chromatography (PCSFC) is a viable technique for the isocratic, isothermal and isobaric separation of seven anticonvulsants, viz., phenobarbitone, phenytoin sodium, phethenylate sodium, nitrazepam, clonazepam, carbamazepine, and primidone, and their simultaneous estimation. The drugs were eluted from a JASCO, RP-C_{18} (250 × 4.6 mm) 10 μ packed column with a binary mobile phase of carbon dioxide and methanol, using ibuprofen as the internal standard. The effect of pressure, temperature, modifier concentration, and the rate of flow of CO_2 on retention and selectivity of all the analytes were studied and the parameters optimised. Without methanol in the mobile phase none of the solutes eluted. Changing modifier concentration was the most effective physical parameter for changing retention and selectivity. The analytes were detected using a UV detector at 215 nm. An arbitrary mixture of eight components was baseline resolved in ~7 min. The study includes a successful attempt at quantification of the drugs. Chromatographic and analytical figures of merit have been listed. The present work holds promise for a possible replacement of HPLC with SFC for the separation and assay of drugs of different families.

Keywords: PCSFC; Phenobarbitone; Phenytoin sodium; Phethenylate sodium; Nitrazepam; Clonazepam; Carbamazepine; Primidone; Separation; Estimation

1. Introduction

Interest in the applicability of packed column supercritical fluid chromatography (SFC) in pharmaceutical and drug analysis in the last few years has increased. Recent publications [1–5] have highlighted the ability of packed column SFC to separate basic drugs of the same 'family'. However little interest has been shown on the general applicability of the method to an arbitrary group of drugs which are basically of different chemical structures and polarities but are comparable in their pharmacological effects. Nor has much interest been shown in the methods of quantifica-

* Corresponding author. Fax: +91-22-6133400.

0039-9140/99/$ - see front matter
PII: S0039-9140(98)00341-5

tion of drugs and pharmaceuticals using SFC. Bhoir [6,9], Bari [7] and Patel [8] have attempted the simultaneous isocratic separation and estimation of several drugs in bulk and dosage forms. The present group of drugs, viz., phenobarbitone, phenytoin sodium, phethenylate sodium, nitrazepam, clonazepam, carbamazepine, and primidone form a group of anticonvulsant drugs which are used for the treatment and prophylaxis of epileptic seizures. The present paper reports a successful, isocratic, simultaneous separation and full validation of the determination of the seven drugs using PCSFC employing carbon dioxide doped with methanol. Ibuprofen was used as the internal standard for quantitation. The structures of these eight drugs are listed in Fig. 1. The present work involves method development for the separation of the above-mentioned seven anticonvulsants and forms part of an on-going programme to explore the possibilities of the replacement of HPLC with PCSFC for the analysis of drugs.

2. Experimental

The apparatus used was a JASCO supercritical fluid chromatograph-900 series configured for dynamic mixing with a 2-pump system of JASCO-PU 980. The instrument incorporated an on-line organic modifier addition facility to the supercritical fluid mobile phase. The rate of flow of CO_2 and the modifier could be changed from 0.01 to 10.0 ml min^{-1}. The apparatus was capable of giving pressures in the range 6.86–44.88 MPa and temperatures in the range 30–80°C. Furthermore, the use of a variable restrictor allowed for a constant flow rate of the fluid, thus producing stability in system pressure. These system improvements have made SFC more accurate and precise. The temperature of the column could be kept at any desired point between 30–80°C using a JASCO-CO-965 oven. A Rheodyne injector, model-7125 with a 20 μl external loop was used to introduce the sample into the column. The analytes were separated on

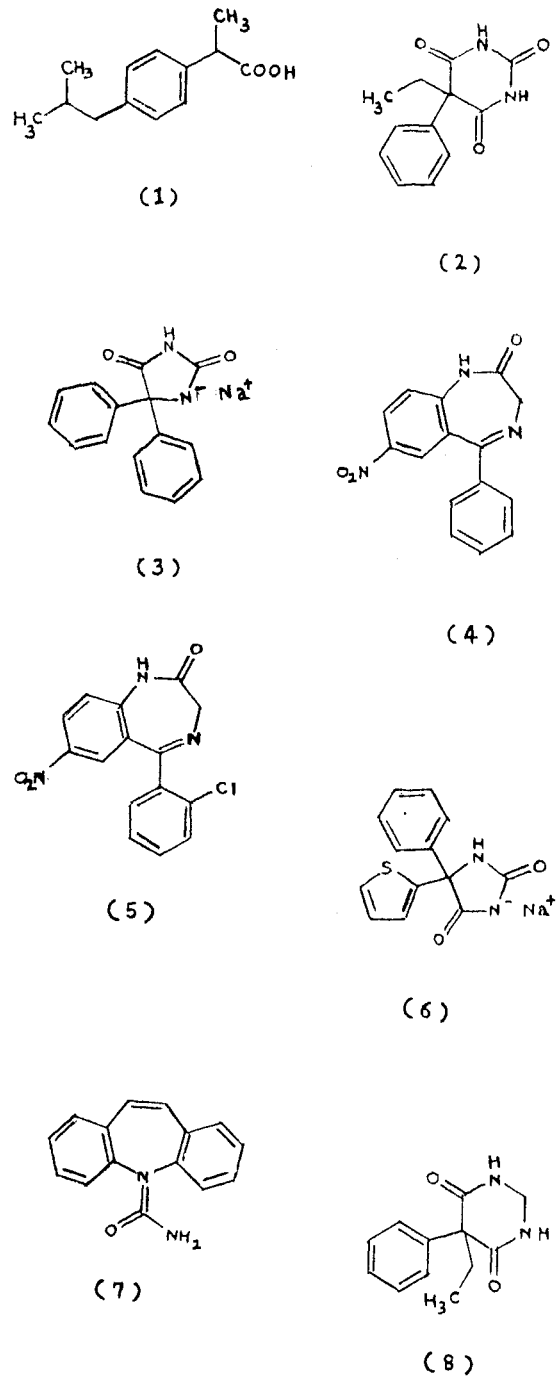

Fig. 1. Structure of the drugs: (1) ibuprofen (2), phenobarbitone, (3) phenytoin sodium, (4) nitrazepam, (5) clonazepam, (6) phethenylate sodium, (7) carbamazepine, and (8) primidone.

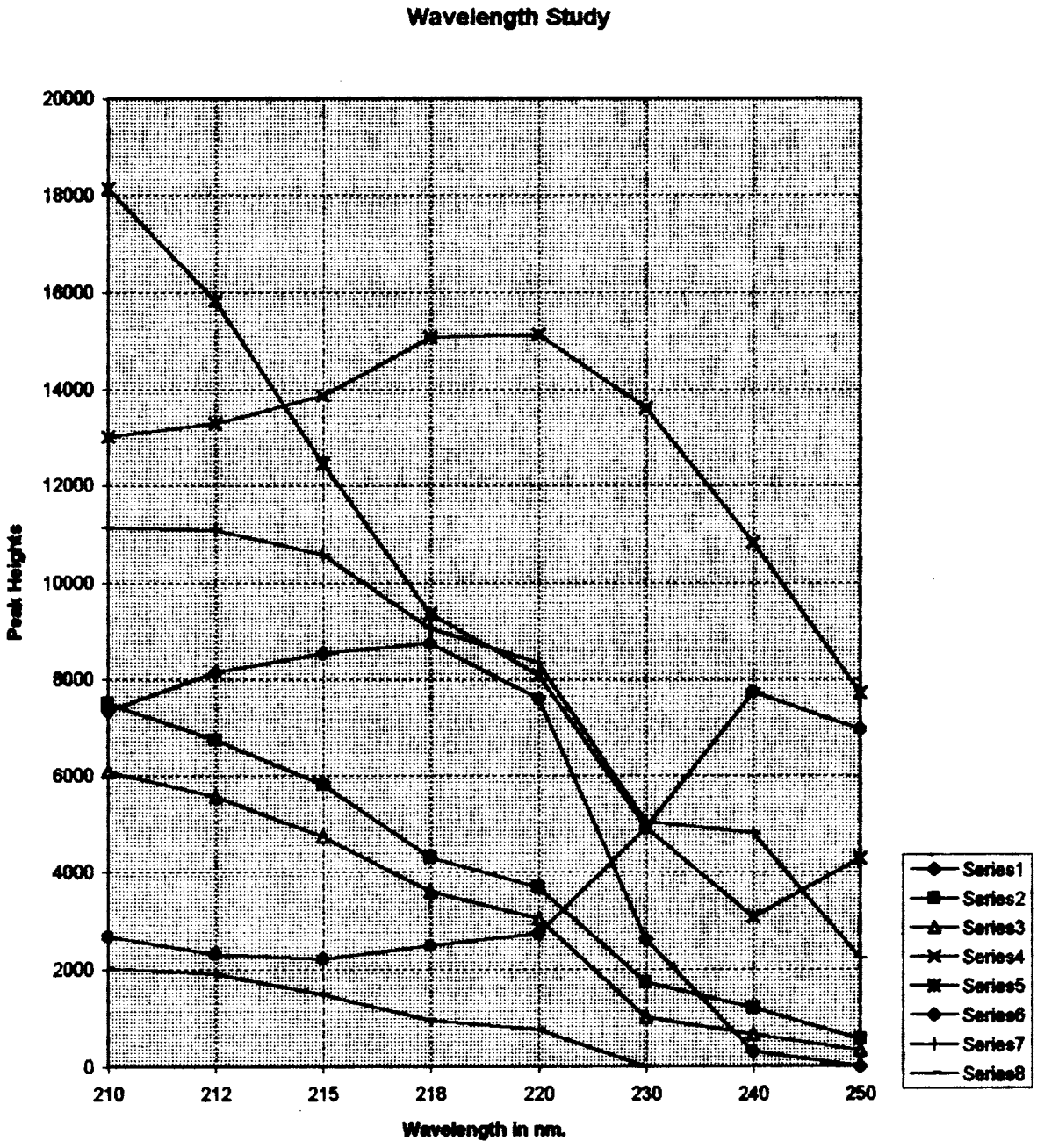

Fig. 2. Wavelength study. The conditions were as follows: 16.67% (0.6 ml min^{-1}) methanol in CO_2 at 3.0 ml min^{-1}, 45°C, 9.81 MPa, and 20 μl injected. (1) Series 1, ibuprofen; (2) series 2, phenobarbitone; (3) series 3, phenytoin sodium; (4) series 4, nitrazepam; (5) series 5, clonazepam; (6) series 6, phethenylate sodium; (7) series 7, carbamazepine; and (8) series 8, primidone.

a JASCO, RP-C_{18} (250 × 4.6 mm) 10 μ packed column. The detection was done using a JASCO-UV–vis detector, equipped with a 4 μl high pressure flow cell of 5 mm path length. Borwin chromatographic software was used for data integration.

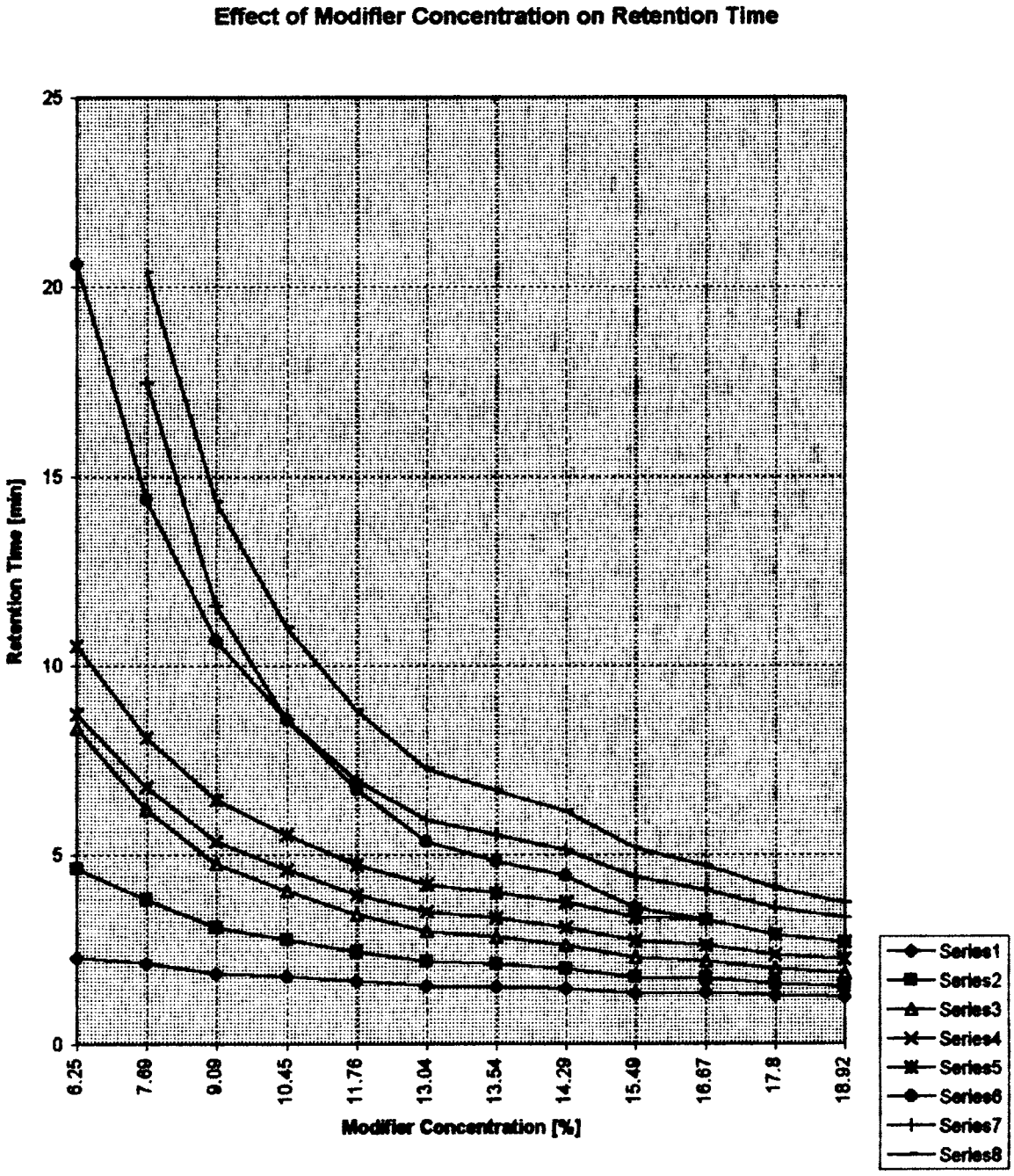

Fig. 3. Effect of modifier concentration on retention time. The conditions were as follows: 6.25–18.92% methanol in CO_2 at 3.0 ml min^{-1}, 50°C; 9.81 MPa, and 20 μl injected. UV Detection at 215 nm. The retention order was as follows: (1) series 1, ibuprofen; (2) series 2, phenobarbitone; (3) series 3, phenytoin sodium; (4) series 4, nitrazepam; (5) series 5, clonazepam; (6) series 6, phethenylate sodium; (7) series 7, carbamazepine; and (8) series 8, primidone.

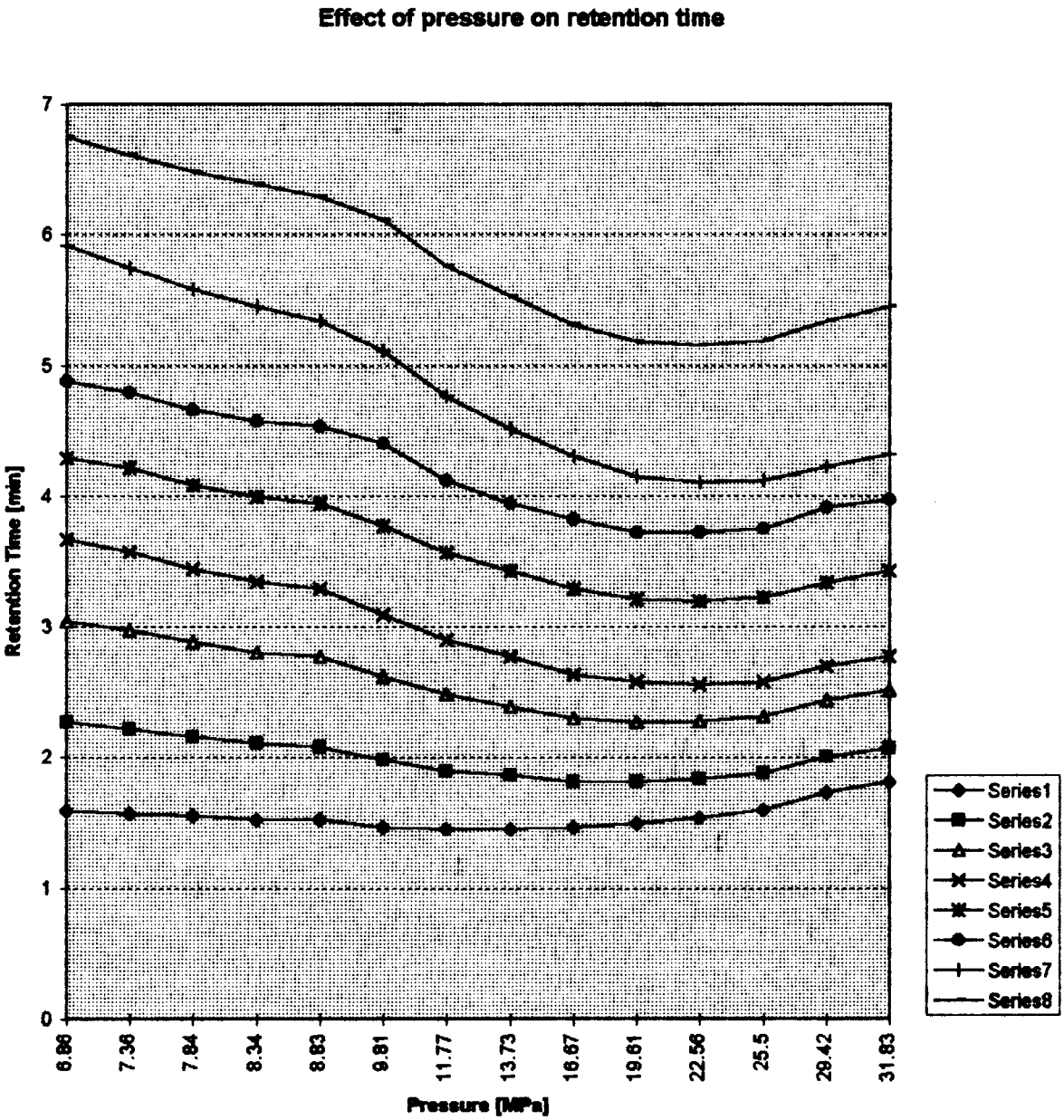

Fig. 4. Effect of pressure on retention time. The conditions were as follows: 14.29% (0.5 ml min^{-1}) methanol in CO_2 at 3.0 ml min^{-1}, 50°C, 7.18–31.83 MPa, and 20 μl injected. Detection at 215 nm. The retention order was as follows: (1) series 1, ibuprofen; (2) series 2, phenobarbitone; (3) series 3, phenytoin sodium; (4) series 4, nitrazepam; (5) series 5, clonazepam; (6) series 6, phethenylate sodium; (7) series 7, carbamazepine; and (8) series 8, primidone.

3. Materials and reagents

The methanol used was of E. Merck, HPLC grade. The drug samples and the internal standard were received in solid state from different U.K. companies with certified copies of analysis. The carbon dioxide used was 99.9% pure obtained from the Bombay Carbon Dioxide Company, Mumbai.

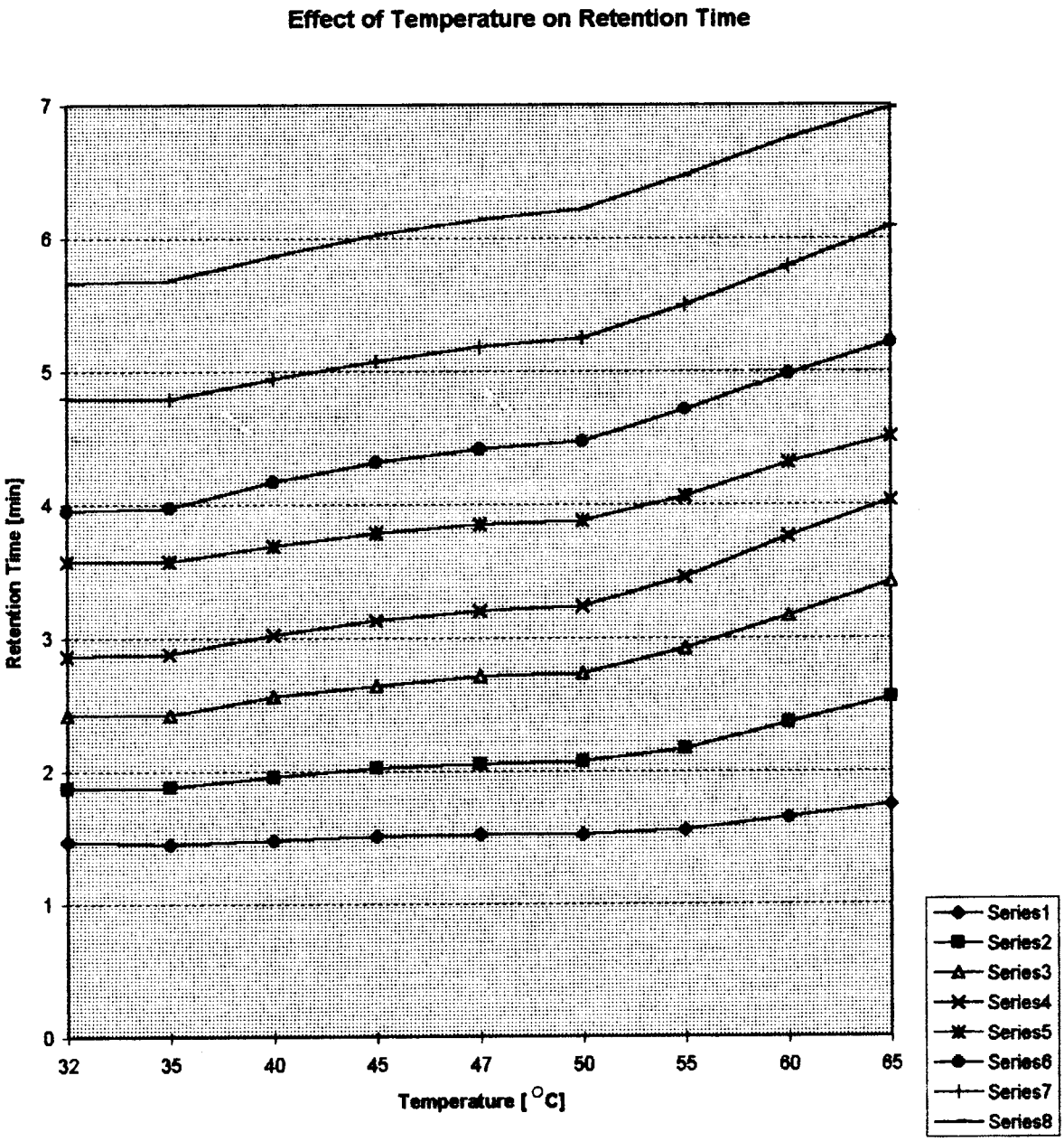

Fig. 5. Effect of temperature on retention time. The conditions were as follows: 14.29% (0.5 ml min^{-1}) methanol in CO_2 at 3.0 ml min^{-1}, 32.5–65°C, 9.81 MPa, and 20 μl injected. Detection at 215 nm. The retention order was as follows: (1) series 1, ibuprofen; (2) series 2, phenobarbitone; (3) series 3, phenytoin sodium; (4) series 4, nitrazepam; (5) series 5, clonazepam; (6) series 6, phethenylate sodium; (7) series 7, carbamazepine; and (8) series 8, primidone.

4. Preparation of solutions

Separate stock solutions of all the seven drugs and the internal standard (ibuprofen) were made by dissolving 100 mg of the analyte in 100 ml methanol. Stock solution containing 100 μg ml^{-1}

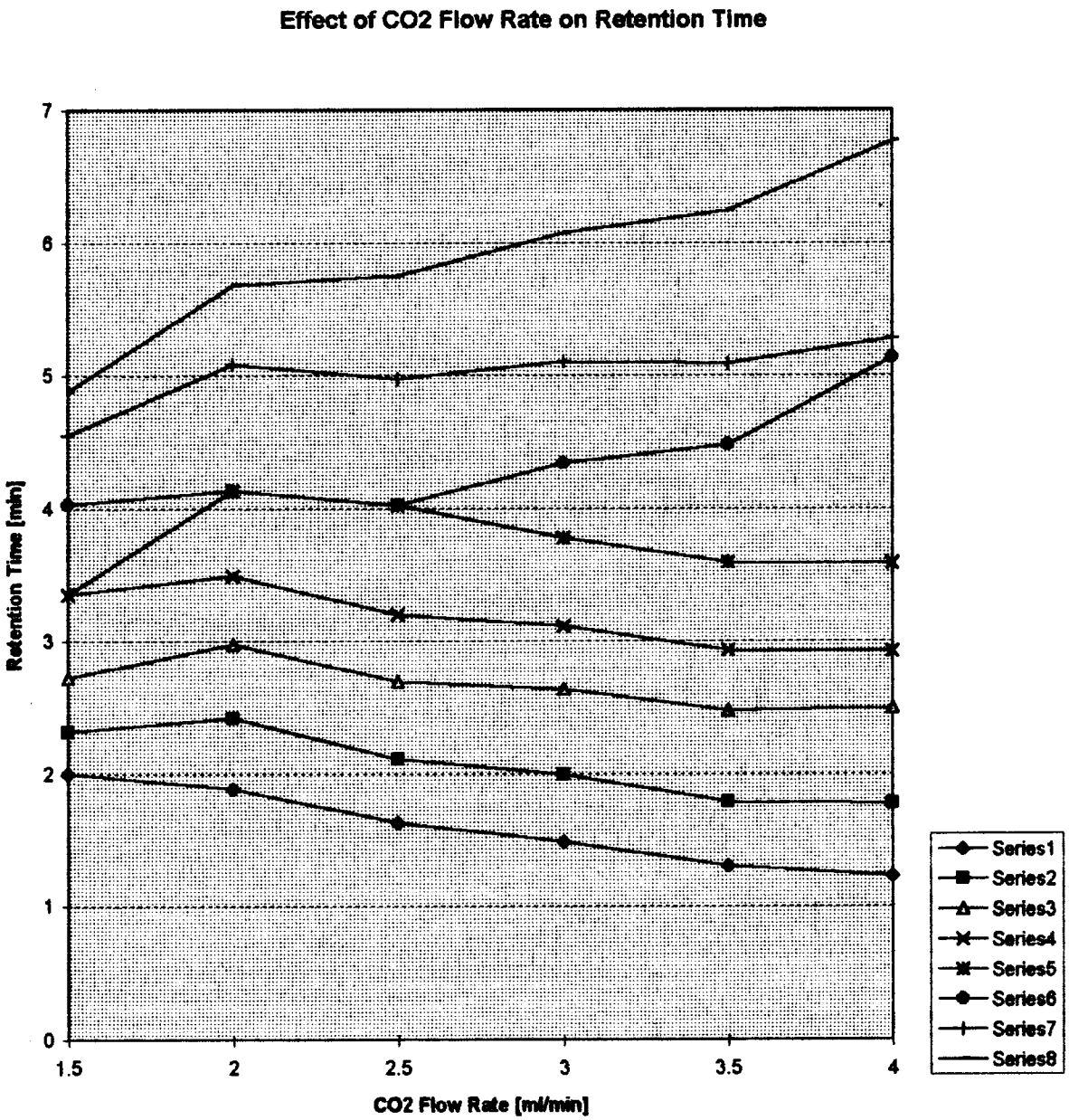

Fig. 6. Effect of CO_2 flow rate on retention time. The conditions were as follows: 0.5 ml min^{-1} methanol in CO_2 at a flow rate of 1.5–4.0 ml min^{-1}, 50°C; 9.81 MPa, and 20 μl injected. UV Detection at 215 nm. The retention order was as follows: (1) series 1, ibuprofen; (2) series 2, phenobarbitone; (3) series 3; phenytoin sodium; (4) series 4, nitrazepam; (5) series 5, clonazepam; (6) series 6, phethenylate sodium; (7) series 7, carbamazepine; and (8) series 8, primidone.

of all the five solutes was prepared by diluting in a 10-fold stage the initial solutions of 1 mg ml^{-1}. Mixtures of the drug solutions were prepared by pipetting out appropriate quantities of individual stock solutions and then mixing them.

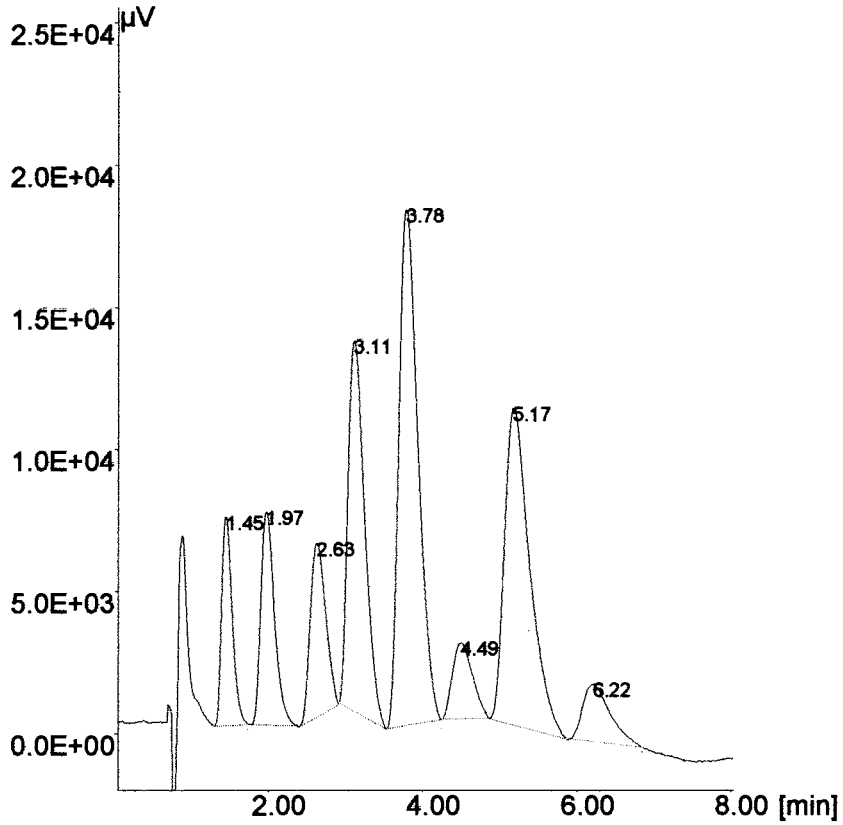

Fig. 7. Typical SFC separation of seven anticonvulsants eluted from a JASCO-RP-C_{18} (250 × 4.6 mm) 10 μ column. The conditions were as follows: 14.29% (0.5 ml min^{-1}) methanol in CO_2 at 3.0 ml min^{-1}, 50°C, and 9.81 MPa outlet pressure. The retention order was as follows: (1) ibuprofen ~1.45 (I.S.), (2) phenobarbitone ~1.97, (3) phenytoin sodium ~2.63, (4) nitrazepam ~3.11, (5) clonazepam ~3.78, (6) phethenylate sodium ~4.49, (7) carbamazepine ~5.17, and (8) primidone ~6.22.

5. SFC of anticonvulsants

The immediate problem of separation of a group of compounds by SFC is the choice of pressure, temperature and modifier concentration. The effect of each of these factors on retention times of these drugs was first measured individually. Retention time curves were found to intersect at some values of the parameters studied. Optimised parameters were found from the curves by choosing those parameters whose retention times could be separated as much as possible and where satisfactory chromatographic figures of merit like resolution (R), capacity factor (k'), symmetry factor (T), and no. of plates (N) are obtained.

As all the analytes are soluble in methanol, methanol could be considered as a modifier. Method development was done by trial and error, changing pressure, temperature and modifier concentration.

6. Results and discussions

6.1. Wavelength study

Fig. 2 depicts the effect of wavelength on the peak responses (peak heights) of the seven anticonvulsants and the internal standard. For this study 20 μl of the individual drug solutions containing 10 μg ml^{-1} of each drug were injected at an arbitrary pressure of 9.81 MPa, 45°C temperature and with a modifier concentration of 16.67% (0.6 ml min^{-1}) methanol in carbon dioxide at 3.0

Table 1
Chromatographic figures of merit for the drugs

Drug	RRT	Symmetry factor (T)	Capacity factor (k')	No. of plates (N)	Resolution (R)	Selectivity (α)
Ibuprofen	1.00	1.00	1.07	580	–	–
Phenobarbitone	1.36	1.03	1.81	637	1.16	1.69
Phenytoin sodium	1.81	1.13	2.83	758	1.32	1.56
Nitrazepam	2.14	1.00	3.57	1057	1.02	1.26
Clonazepam	2.61	1.05	4.57	1188	1.28	1.28
Phethenylate sodium	3.10	1.00	5.64	1392	1.26	1.23
Carbamazepine	3.57	1.07	6.69	1400	1.11	1.19
Primidone	4.29	1.12	8.29	1667	1.56	1.24

ml min^{-1}. The range of wavelength studied was from 210 to 250 nm. It can be seen from Fig. 1 that an optimised compromise wavelength can be chosen at 215 nm for the simultaneous estimation of all the seven drugs.

6.2. Effect of modifier concentration on retention time

Modifier concentrations were changed from 6.25 to 18.92% methanol (v/v) at an arbitrary pressure of 9.81 MPa and a temperature of 45.0°C, with flow rates of CO_2 constant at 3.0 ml min^{-1} and varying the methanol flow rate from 0.2 to 0.7 ml min^{-1}. For these experiments 20 μl of individual drug solutions containing 10 μg ml^{-1} of the analytes were injected. Detection was at 215 nm. Fig. 3 shows the relationship between the modifier concentrations and retention times of the eight analytes at 45°C and 9.81 MPa. As can be seen from the figure the retention times decrease with increased modifier concentration and nearly merged above 16% concentration. At 14.29% (0.5 ml min^{-1}) modifier, optimum retention times are obtained, with baseline resolved peaks for all the eight analytes. The run time was nearly 7 min.

6.3. Effect of pressure on retention time

The range of pressures studied was from 6.86 to 31.83 MPa. Fig. 4 shows the relationship between pressures and retention times of the eight analytes. The modifier concentration was kept constant at 14.29% methanol and the temperature was kept at 50°C. The effect of pressure was found to be minimal and followed the same pattern for all the compounds through the range studied. Favourable separation conditions were obtained at a pressure of 9.81 MPa. For a given column and temperature the retention generally decreased as the operating pressure was increased because the fluid density increases at higher pressures.

6.4. Effect of temperature on retention time

Fig. 5 depicts the effect of temperature on the retention times, keeping the other parameters as before. The temperature of the column was varied from 32.5 to 65°C. Fig. 5 shows that 50°C is the optimum temperature as there is enough separation at this temperature. The choice of this temperature strikes a balance between selectivity and run time. Actual experimentation showed that no discernible pattern was obtained at 55°C and above.

6.5. Effect of CO_2 flow rate on retention time

Fig. 6 shows the relationship between the CO_2 flow rate and retention times of the eight analytes at 0.5 ml min^{-1} methanol, 9.81 MPa pressure and

Table 2
Linear regression (least-squares fit) data for the calibration curves

Drug	Concentration range (μg ml^{-1})	Slope ($m \pm S_m$)	Intercept ($b \pm S_b$)	r^2	S_{yx}
Phenobarbitone	0.50–10.00	0.51 ± 0.02	-0.06 ± 0.12	0.999	0.20
Phenytoin sodium	0.50–10.00	0.41 ± 0.01	0.02 ± 0.03	0.999	0.05
Nitrazepam	0.25–10.00	0.88 ± 0.01	0.02 ± 0.01	0.999	0.02
Clonazepam	0.25–10.00	1.23 ± 0.01	0.05 ± 0.03	0.999	0.05
Phethenylate–sodium	1.00–10.00	0.18 ± 0.01	0.03 ± 0.04	0.999	0.05
Carbamazepine	0.25–10.00	0.76 ± 0.01	0.01 ± 0.06	0.999	0.12
Primidone	1.00–10.00	0.13 ± 0.01	0.03 ± 0.01	0.999	0.02

50°C temperature. The CO_2 flow rate was varied from 1.5 to 4.0 ml min^{-1} and thus the modifier concentrations also changed from 25.0 to 11.1%. The rule that doubling the rate of flow results in a halving of the retention time does not seem to be applicable here as the concentration of the modifier was also changing simultaneously. The reversal of the trend in retention times in Fig. 6 could be attributed to the same cause. It is discernible from Fig. 6 that the optimised CO_2 flow rate can be selected as 3.0 ml min^{-1} for isocratic separation of all the eight drugs; with symmetrical baseline resolved peaks.

7. Optimization of parameters

Experimentation revealed that a pressure of 9.81 MPa, a temperature of 50°C and 14.29% (0.5 ml min^{-1}) methanol, in CO_2 at a flow rate of 3.0

Table 3
Accuracy and precision of the method

Drug	Spiked concentration (μg ml^{-1})	Found concentration (μg ml^{-1})	C.V. ($n = 5$)
Phenobarbitone	1.00	1.08	1.81
	5.00	5.11	1.60
	10.00	10.09	1.20
Phenytoin sodium	1.00	1.01	3.12
	5.00	5.18	2.04
	10.00	10.04	0.35
Nitrazepam	1.00	1.05	2.54
	5.00	5.03	1.18
	10.00	10.10	0.25
Clonazepam	1.00	1.03	1.46
	5.00	5.09	0.53
	10.00	10.13	0.54
Phethenylate sodium	1.00	1.07	3.30
	5.00	5.12	0.34
	10.00	10.14	0.62
Carbamazepine	1.00	0.99	3.71
	5.00	5.07	0.56
	10.00	10.21	0.59
Primidone	1.00	1.14	2.98
	5.00	5.06	0.98
	10.00	10.25	1.15

ml min^{-1} provided the maximum selectivity and most efficient separation of the seven anticonvulsants and the internal standard as evidenced from the typical chromatogram (Fig. 7) of the eight drugs at 200 ng ml^{-1} of each analyte in the mixture and from the chromatographic figures of merit listed in Table 1.

8. Estimation of the seven anticonvulsants

For linearity studies seven different concentrations of the individual drug (concentration ranges given in Table 2) with the internal standard constant at 2 μg ml^{-1} were assayed ($n = 5$) under the optimized SFC conditions. After ascertaining the linearity of the peak responses (peak height ratios of drug:i.s.), 20 μl of a mixture of all the seven drugs was injected. The concentration ranges of the different drugs are listed in Table 2.

For convenience only the peak height ratios are mentioned here, even though the peak area ratios were also found to be linear. Linear regression least squares fit data obtained from the measurements are given in Table 2. The respective slopes $m \pm S_m$, and the intercepts $b \pm S_b$, the regression factors and the S.D. of the residuals from the linear least squares regression are all quoted in Table 2.

The minimum quantifiable concentration (MQC) listed in Table 2 is a compromise due to the selection of one wavelength for all the compounds. It could be improved by a more selective choice of UV-wavelength if only one or two of the drugs are to be determined.

9. Accuracy and precision of the method

A study of precision and accuracy was performed by assaying three composite solutions of low, medium and high concentrations. The peak height ratios of drug:i.s. obtained were then related to the slopes and intercepts mentioned in Table 2 to obtain the analytical recoveries. Table 3 lists the recoveries of the drugs from a series of spiked concentrations and shows that the R.S.D. does not exceed 4% for all the compounds.

10. Conclusions

Packed column SFC has been shown to be suitable for the separation and quantitative estimation of seven anticonvulsants, widely varying in their chemical structures, but with similar pharmacological properties. As the total run time is only 8 min the technique is fast. The paper presents in a condensed manner the methods of determination of seven different anticonvulsants.

Acknowledgements

The authors thank Shri Kelkar C.P., Director (Admn.), Dr A.M. Bhagwat, Director (Research), C.B. Patel Research Centre, Mumbai-56, and coworkers Yagnesh Patel, Viddesh Bari and Nehal Shah, for encouragement in carrying out this work.

References

[1] T.A. Berger, W.H. Wilson, J. Pharm. Sci. 83 (3) (1994) 281–286.
[2] T.A. Berger, W.H. Wilson, J. Pharm. Sci. 83 (3) (1994) 287–290.
[3] C.J. Bailey, R.J. Ruane, I.D. Wilson, J. Chromatogr. Sci. 32 (1994) 426–429.
[4] J.T.B. Strode, L.T. Taylor, A.L. Howard, D. Ip, M.A. Brookes, J. Pharm. Biomed. Anal. 12 (1994) 1003–1014.
[5] M.B. Evans, M.S. Smith, Chromatographia 39 (1994) 569–576.
[6] I. C. Bhoir, M. Sundaresan, B. Raman, A.M. Bhagwat, Anal. Chim. Acta, 354(1–3) 123.
[7] V.R. Bari, M. Sundaresan, U.J. Dhorda, Talanta 45 (1997) 297.
[8] Y.P. Patel, M. Sundaresan, U.J. Dhorda, Ind. J. Pharm. Sci. 59 (3) (1997) 132–134.
[9] I. C. Bhoir, M. Sundaresan, A.M.Bhagwat Bhanu Raman, J. Pharm. Biomed. Anal. 17 (1998) 539.

ELSEVIER

Talanta 48 (1999) 1191–1197

Talanta

Determination of stability constants of complexes of $M_iK_jH_kL$ type in concentrated solutions of mixed salts

Dariusz Janecki [a], Katarzyna Doktór [a], Tadeusz Michałowski [b,*]

[a] *Faculty of Chemistry, Jagiellonian University, ul. R. Ingardena 3, 30-060 Cracow, Poland*
[b] *Department of Analytical Chemistry, Faculty of Engineering and Chemical Technology, Technical University of Cracow, ul. Warszawska 24, 31-155 Cracow, Poland*

Received 17 July 1998; received in revised form 27 October 1998; accepted 30 October 1998

Abstract

This paper suggests a non-conventional approach towards the correct determination of stability constants K_{ijk} of mixed complexes from the results of potentiometric titrations. The method is based on inaccurate (in principle) results of titrations made in isomolar titrand–titrant systems. The data thus obtained are validated on the basis of relationships between $\log K_{ijk}$ and relative error (‰e) of the determination of an analyte concentration. Accurate values for K_{ijk} are calculated for the set (ijk) of possible complexes. The accuracy depends on the degree of linearity between the variables considered. The model obtained was thoroughly tested on the system containing malonic acid together with sodium and potassium nitrates.

Keywords: Potentiometric titration; Stability constants of complexes; Curve fitting

1. Introduction

Potentiometry is a widely accepted method providing accurate, reliable results as well as a convenient investigative tool applied to electrolytic systems. It possesses a number of attributes that make it a useful and sensitive tool allowing accurate equilibrium data to be obtained for complexes formed within the system; these data can be provided efficiently [1]. Moreover, it withstands the contemporary demands put on the information gained from analytical procedures: speed, simplicity of operation, reliability, analytical performance and automation. A great informative potential inherent in it should be particularly stressed. Potentiometric (pH-metric) titration provides the data (V_j, Y_j), where V_j is the volume of titrant added at j-th point of titration, Y_j is the experimental value (i.e. pH_j or potential E_j) found at this point.

* Corresponding author. Tel.: +48-12-33-03-00; fax: +48-12-33-33-74.

0039-9140/99/$ - see front matter
PII: S0039-9140(98)00345-2

The stringent requirement concerned with validation of physicochemical data is (or rather should be) an important part of research procedures made in this area of activity. Taking into account the obvious fact that measurements of Y_j are loaded in principle by systematic errors, the matter in question is an approach that enables the erroneous data to be applied for the evaluation of true values for the parameters considered. This approach, in comparison with the procedures applied previously, provides a distinct step towards better evaluation of the data. An example of some procedures of this kind is provided in Fortuin's paper [2].

Another approach to these systems was suggested by Michalowski [3–6] who drew attention to the linear relationships between relative error (%e) of an analyte concentration and related $pK = -\log K$ or standard potential (E_o) values. Expressions for $K = K_{so}$ (solubility product) and E_o, originated there from sophisticated formulae, were derived for diluted titrand + titrant systems [5]. The linearity between $\log K$ (or pK) and %e enables us to evaluate $K = (K)_{\%e=0}$ by perpendicular projection of the point referred to %e = 0 on the ordinate axis.

A similar approach was subsequently applied to more complex systems with polybasic organic acid involved in concentrated titrand + titrant isomolar systems of high ionic strength values [7]. Conditional equilibrium constants (x_i) of the kind defined in the literature [7–9] were evaluated there. Values for coefficients of linear correlation between the variables assumed were usually close to +1 or −1.

High ionic strength values of electrolytic solutions yield incorrect values of the activity coefficient (f) for hydrogen ions based on empirical extensions of the Debye–Hückel and Davies equations [10] reliant solely on the ionic strength. A widely accepted opinion is that some basic assumptions (e.g. constant dielectric permeability of the ionic medium) in the Debye–Hückel theory are doubtful and cannot be recognised, even for diluted solutions. On the other hand, an indubitable effect of a basal form of a weak acid on the activity coefficient (f) of hydrogen ions is not considered there. The problems encountered provide arguments for the application of an aligning approach, similar to the one used for evaluation of other physicochemical data, e.g. equilibrium constants of complexes. In the present paper, the f-value is one of the parameters evaluated in the optimisation procedure, while the value of pH measured is defined as $-\log h$, where h is the activity of hydrogen ions.

The possible complexes formed between cations of alkali metals and basal forms of (particularly) organic acids are usually omitted in calculations. Though this assumption enables us to maintain a simple form of the related regression equations, it provides inaccurate physicochemical data. The discrepancies resulting from omission of complexes with alkali metals are, for example, due to H_3PO_4, with pK_2 values 6.9 [11] and 7.21 [12], obtained in different media. These considerations have prompted systematic studies by different authors.

Few papers written hitherto, e.g. [13,14], deal with the determination of stability constants of alkali metals with dicarboxylic acids at high ionic strengths (I). Most of the studies apply to diluted solutions with ionic strength rarely exceeding 1.0 M. The aim of our paper is to find the stability constants of complexes formed in the system with malonic acid together in a mixture with potassium and sodium nitrates at much higher ionic strengths, ca. 1.5 and 1.9 M.

The stability constants K_{ijk} of weak complexes of $M_iK_jH_kL$ type [8,15,16] are defined by the relation:

$$[M_iK_jH_kL] = K_{ijk}[M]^i[K]^j[H]^k[L] \quad (1)$$

where $0 < i + j + k \leq 2$, $K_{000} \equiv 1$. The complexes are assumed to be formed in isomolar titrand + titrant systems containing malonic acid (H_2L) together with sodium and potassium nitrates. The measurements were made at high ionic strengths of the electrolytic system prepared in compliance with an unconventional procedure described elsewhere [8]. Although the resulting algorithms appear to have some similarities with the ones described, the calculation procedure applied here is quite different.

2. Theoretical part

The substances present in the titrand (D) + titrant (T) system are specified in Table 1 together with primary concentrations (M) and volumes (cm^3) of the solutions added. D and T were prepared in an unconventional manner [6–9] in flasks of equal volumes (V_f) and filled up to the mark with distilled water. V_0 ml of D ($V_0 \leq V_f$) was titrated with V ml of T and the points (V_j, pH_j) were recorded.

Assuming the conceivable complexes of $M_iK_jH_kL$ type and the isomolarity condition expressed by the formula:

$$C_1V^*_{MB} = CV_M + C_2V^*_{KB} \quad (2)$$

where: $V^*_{MB} = V_{MB} - V'_{MB}$, $V^*_{KB} = V_{KB} - V'_{KB}$, we get the following relationship [8]:

$$\sum k[M_iK_jH_kL] + [H] - [OH] = n \cdot d \cdot C_0 - b_M/V_0 + b_M/W \quad (3)$$

where $W = V_0 + V$, $d = V_t/V_f$, $b_M = CV_MV_0/V_f$. For $n = 2$ (diprotic acid, H_2L), within a pH interval where $[H] \gg [OH]$, the Eq. (3) can be rewritten as:

$$h^3 + 3ah^2 + bh + c = 0 \quad (4)$$

where:

$$a = f \cdot (x_1 + b_M/V_0 - b_M/W)/3 \quad (5a)$$

$$b = f^2 \cdot (x_0 - (d \cdot C_0 - b_M/V_0 + b_M/W) \cdot x_1) \quad (5b)$$

$$c = f^3 \cdot x^{\bullet}_0 (b_M/V_0 - b_M/W - 2d \cdot C_0) \quad (5c)$$

and h and f stand for activity and activity coefficient of hydrogen ions $f = h/[H]$, $pH = -\log h$ and [8]:

Table 1
Composition of titrand (D) and titrant (T)

Substance	D (V_0)	T (V)
H_nL (C_0)	V_t	V_t
MOH (C)	–	V_M
MB (C_1)	V_{MB}	V'_{MB}
KB (C_2)	V'_{KB}	V_{KB}

$$x_1 = a_0 + a_1 \cdot [M] + a_2 \cdot [K] \quad (6a)$$

$$x_0 = b_0 + b_1 \cdot [M] + b_2 \cdot [K] + b_3 \cdot [M]2 + b_4 \cdot [K]2 + b_5 \cdot [M] \cdot [K] \quad (6b)$$

$$a_0 = K_{001}/K_{002}, \quad a_1 = K_{101}/K_{002}, \quad a_2 = K_{011}/K_{002} \quad (7a)$$

$$b_0 = 1/K_{002}, \quad b_1 = K_{100}/K_{002}, \quad b_2 = K_{010}/K_{002} \quad (7b)$$

$$b_3 = K_{200}/K_{002}, \quad b_4 = K_{020}/K_{002} \quad b_5 = K_{110}/K_{002} \quad (7c)$$

With a great excess of M and K, namely for:

$$[M] \geqq \sum i[M_iK_jH_kL], \qquad [K] \geqq \sum j[M_iK_jH_kL] \quad (8)$$

one can assume that:

$$[M] = z_1 + y/W, \qquad [K] = z_2 - y/W$$

where:

$$z_1 = (C_1V_{MB}) - C_2V^*_{KB})/V_f, \quad z_2 = C_2V^*_{KB}/V_f,$$

$$y = C_2V^*_{KB}V_0/V_f.$$

From Eq. (4) we get:

$$pH = -\log \{2 \cdot p^{1/2} \cdot \cos(\Phi/3) - a\} \quad (9)$$

where:

$$\Phi = \arccos\{(-q/2) \cdot p^{-3/2}\} \quad (10a)$$

$$p = a^2 - b/3 \quad (10b)$$

$$q = 2 \cdot a^3 - a \cdot b + c \quad (10c)$$

Eq. (9) together with the related defining expressions (Eqs. (5a), (5b), (5c), (6a), (6b), (7a), (7b), (7c), (10a), (10b) and (10c)) for the parameters and variables involved is the basis for calculations made according to an iterative computer program. The sum of unweighted squares

$$SS = \sum_{j=1}^{N} (pH_j - pH(V_j))^2 \quad (11)$$

was chosen as the criterion of optimisation, where $pH(V_j)$ is the pH-value calculated for the j-th experimental point (V_j, pH_j), $j = 1,\ldots, N$, at a defined stage of the optimisation procedure; $W_j =$

Table 2
Preparation of D and T in series 1, 2 and 3

Solution	Series 1		Series 2		Series 3	
	D	T	D	T	D	T
H_2L ($C_0 = 0.10034$)	5	5	5	5	5	5
NaOH ($C = 0.1583$)		25		25		25
$NaNO_3$ ($C_1 = 2.5$)	120	30	100	30	80	40
KNO_3 ($C_2 = 2\ 5$)	31.56	120	31.56	100	41.56	80

$V_0 + V_j$ is the total volume of the system at this point.

The set of parameters under optimisation consisting of C_0, f and nine stability constants of complexes (K_{ijk}) was found according to an iterative computer program MINUIT 96.03 (Function Minimization and Error Analysis) from CERN Program Library (entry D506). In order to fulfil the requirement of positive values for optimised K_{ijk} and avoid deleterious application of the constraints put on them, K_{ijk} were expressed by $\log K_{ijk}$, taken as the quantities optimised, $K_{ijk} \equiv 10^{\log K_{ijk}}$.

3. Experimental

3.1. Materials and equipment

Solutions of $NaNO_3$ and KNO_3 were prepared by dissolving the corresponding salts (POCh Gliwice, anal. grade) in water. Malonic acid (H_2L) solution was obtained by dissolving the preparation (Merck, purity > 99%) in water and standardisation against NaOH solution, standardised previously against potassium hydrogen phthalate (POCh Gliwice, anal. grade). Doubly distilled water, boiled to remove CO_2, was used for preparation of stock solutions, titrand (D) and titrant (T).

pH-metric titrations were performed with an automatic titrator Mettler-Toledo DL 25 equipped with electrode DG 11-SC (Mettler-Toledo) and interfaced with a computer Pentium 90 where the results were stored and then handled according to the iterative computer program. The titrations were made at 20°C. The electrode was calibrated against standard buffer solutions with pH 4.00 and 7.00 (POCh Gliwice).

3.2. Procedure

Three series of mixtures (D and T), were prepared in $V_f = 200$ cm^3 flasks in accordance with Table 1. The composition (concentrations (M) and volumes (cm^3) of stock solutions) of D and T is shown in Table 2. The number of titrations made for the series 1, 2 and 3 was 13, 16 and 15, respectively; $V_0 = 50$ cm^3 of titrand (D) taken for titration was titrated up to ca. pH 6.0. The number (N) of the titration points (V_j, pH_j) taken for evaluation was equal to 85. The overdetermined set of experimental points covers the pH-interval where relatively high levels of concentrations of particular forms is available.

4. Results and discussion

A good degree of fit, within the range 10^{-3}–10^{-4} attained for SS (Eq. (11)), was achieved at the number of titration points assumed; the convergence was generally accomplished after about 500 calls to the function. The optimised values were then used to plot the linear relationship between $\log K_{ijk}$ and $\%e$, where

$$\%e = 100 \cdot (C_0 - C_{00})/C_{00} \quad (\%) \tag{12}$$

and C_{00} is the C_0 value found from independent, preliminary titrations of malonic acid with the standardised NaOH solution.

The values of $\log K_{ijk}$ evaluated from the corresponding plots of $\log K_{ijk}$ versus $\%e$ dependencies (Fig. 1a and b) at $\%e = 0$ are specified in Table 3. The values $K_{ijk} = (K_{ijk})_{\%e=0}$ thus obtained are considered as unbiased ones.

The values for dissociation constants of malonic acid ($pK_1 = 3.41$, 3.34 and 3.18; $pK_2 = 5.80$, 5.74 and 5.72) differ from the ones found in literature [17–19]: $pK_1 = 2.76$ and $= 5$ 54 (at $I =$ 0.76 M and $T = 25$°C) but they follow the general tendency: the higher ionic strength, the higher value of dissociation constants [13,20]. In our titrations, ionic strength (I) ranged from ca. 1.5 to 1.9 M and this tendency proved correct.

The complexes NaHL and KHL are of similar

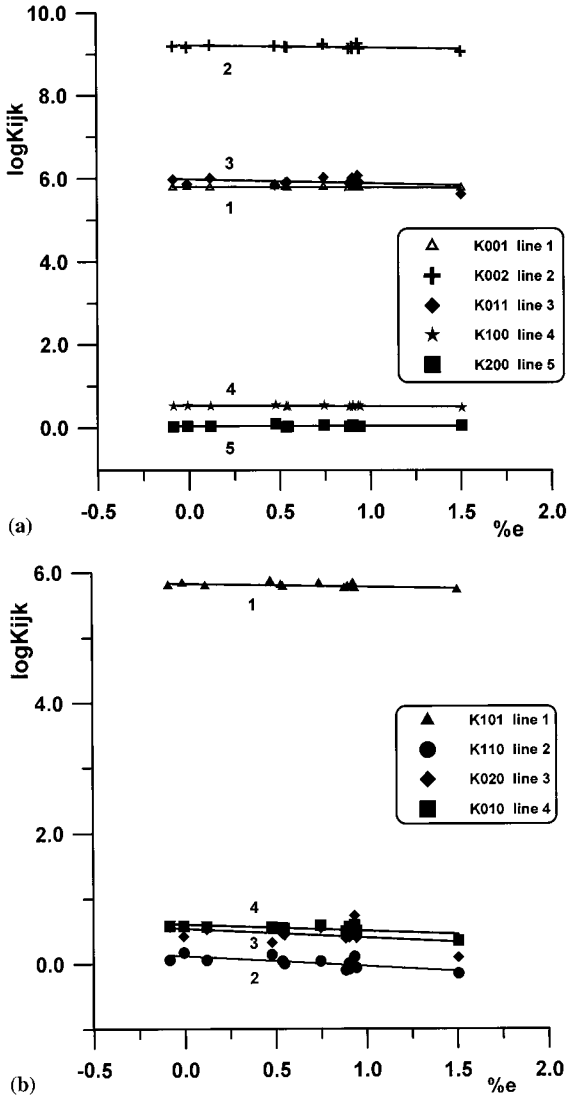

Fig. 1. (a, b) The points (%e, log K_{ijk}) related to different sets (ijk) of series 1.

stability. Better immediate inspection on the strength of complexes of MHL type provide the values K_M^{HL}, $[MHL] = K_M^{HL}[M][HL]$, there are: $\log K_{Na}^{HL} = 0.02$, -0.07 and 0.1 for NaHL ($K_{Na}^{HL} = K_{101}/K_{001}$), $\log K_K^{HL} = 0.18$, 0.2 and -0.24 for KHL ($K_K^{HL} = K_{011}/K_{001}$). The $\log K_M^{HL}$ values recalculated from the data given in [17] are -0.05 and -0.21, respectively. It should be noted that the iterative program did not even started when the respective parameters taken from [18] were applied as initial estimates; it provides a scale of the discrepancies observed. The plots of the $\log K_{ijk}$ versus %e relationships are nearly parallel to the %e-axis.

The presumable complexes Na_2L and K_2L were considered in our studies as well. However, the related values of their stability constants (K_{200} and K_{020}) obtained from the calculations were too low. Also, if the constraints were put on the K_{ijk} values expressed immediately, the K_{200} and K_{020} values, referred to Na_2L and K_2L, 'glues', to a lower limit of the related interval. This regularity was observed for all concentrations of $NaNO_3$ applied.

Refering to the mixed complex NaKL, the small decrement of the values was stated between series 1, 2 and 3, but still stayed in the range of their S.D.s. Omission of Na_2L, K_2L and NaKL complexes in the model applied leads to substantial growth of S.D.s of the remaining complexes.

The $f = (f)_{\%e=0}$ values found for the series 1, 2 and 3 were 2.16, 2.42 and 1.45, respectively (Fig. 2). It should be stressed that the activity constant was considered as one of the equilibrium constants of the system in question; the related calculations were not aided by the doubtful empirical formulae for the f-value.

5. Final remarks

With emphasis on the detailed nature of chemical interactions, the new methodology provided in this paper is applicable for solving different problems involved with handling the results obtained from potentiometric (pH-metric) titration, particularly the ones carried out in solutions with high ionic strength values (I) [20]. High and constant ionic strength is needed to firstly maintain a con-

Table 3
Values of log K_{ijk} and f found at $\%e = 0$ for series 1, 2 and 3 (together with the related S.D.s)[a]

Parameter	Series 1 ($I = 1.89$ M)	Series 2 ($I = 1.64$ M)	Series 3 ($I = 1.52$ M)
Log K_{002} (H_2L)	9.21 ± 0.02	9.08 ± 0.03	8.90 ± 0.06
Log K_{001} (HL)	5.80 ± 0.01	5.74 ± 0.03	5.72 ± 0.04
Log K_{100} (NaL)	0.54 ± 0.01	0.55 ± 0.02	$0.44 \pm 0\ 08$
Log K_{010} (KL)	0.60 ± 0.02	0.45 ± 0.04	0.49 ± 0.14
Log K_{101} (NaHL)	5.82 ± 0.02	5.67 ± 0.04	5.84 ± 0.04
Log K_{011} (KHL)	5.98 ± 0.05	5.94 ± 0.09	5.48 ± 0.12
Log K_{200} (Na_2L)	$0.04 \pm 0\ 01$	0.11 ± 0.03	0.38 ± 0.31
Log K_{020} (K_2L)	0.54 ± 0.07	0.18 ± 0.07	0.80 ± 0.21
Log K_{110} (NaKL)	0.12 ± 0.03	-0.02 ± 0.02	-0.06 ± 0.53
f	2.16 ± 0.04	2.42 ± 0.08	1.45 ± 0.09

[a] I-ionic strength.

stancy of physicochemical parameters and secondly fulfil the simplifying assumption (Eq. (8)) concerning an admissible level of a weak acid concentration in the system. Note, for example, that the concentration of malonic acid in the system considered above equals $0.10034 \cdot 5/200 = 2.5 \cdot 10^{-3}$ M only. For low $C_0 V_t / V_f$ values (see Table 1), an inadmissible growth of the relative error of C_0 determination occurs. Constancy of ionic strength and total concentration of the acid in the system is possible if the D + T system is prepared according to the unconventional procedure described in [8] which is a very substantial improvement compared to the conventional one. In addition, the similarity between D and T makes the value of the dielectric permeability constant [10] during titration and additivity of volumes of the solution is fulfilled to a high degree.

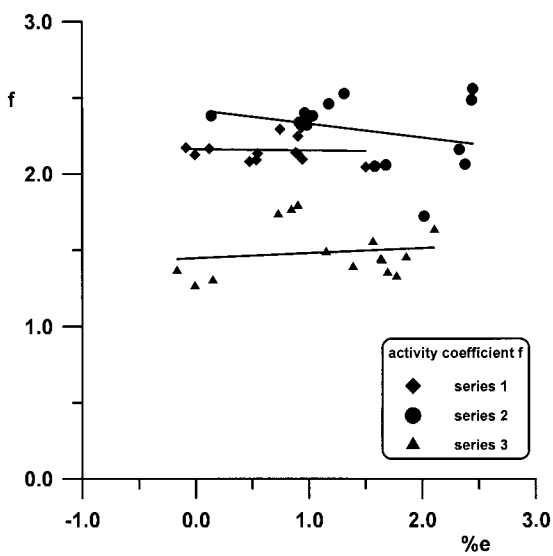

Fig. 2. The points $(\%e, f)$ related to series 1, 2 and 3.

The simplifying assumption that a basal electrolyte does not affect the complexation equilibria in the system is not required there; both Na^+ and K^+ complexes are admitted in the model applied. Different compositions of these two species (Na^+, K^+) in D and T provides the possibility to distinguish between the related complexes; such a possibility does not exist if the concentrations of Na^+ and K^+ remain (nearly) unchanged during the titration. At the same time the concentration of $B^- = NO_3^-$ ions becomes constant and the possibility of considering more general complexes of $M_j K_j H_k B_b L$ type is not possible there; such a model seems to be rather artificial.

References

[1] J.-F. Chen, Y.-X. Xia, G.R. Choppin, Anal. Chem. 68 (1996) 3973.
[2] J.M.H. Fortuin, Anal. Chim. Acta 24 (1961) 175.
[3] T. Michałowski, Chem. Anal. 26 (1981) 799.
[4] T. Michałowski, Zesz. Nauk. UJ, Pr. Chem. 32 (1989) 15.
[5] T. Michałowski, R. Stępak, Anal. Chim. Acta 172 (1985) 207.
[6] T. Michałowski, A. Rokosz, P. Kościelniak, M. Łagan, J. Mrozek, Analyst 114 (1989) 1689.

[7] T. Michałowski, A. Rokosz, A. Tomsia, Analyst 112 (1987) 1739.
[8] T. Michałowski, Talanta 39 (1992) 1127.
[9] T. Michałowski, E. Gibas, Talanta 41 (1994) 1311.
[10] C.W. Davies, Electrochemistry, George Newnes, London, 1961.
[11] J. Inczédy, Analitycal Applications of Complex Equilibria, Horwood, Chichester, 1976.
[12] P.G. Daniele, A. De Robertis, C. De Stefano, A. Gianguzza, S. Sammartano, J. Solut. Chem. 20 (1991) 495.
[13] R. Castano, N. Etxebarria, J.M. Madariaga, J. Chem. Soc. Dalton Trans. (1994) 2729.
[14] A.A.E.H. Zaghloul, G.A. Elnaggar, M.F. Amira, Gaz. Cim. Ital. 126 (1996) 735.
[15] T. Michałowski, D. Janecki, Proc. Sci. Conf. of PTCh and SITPChem, No. S-11, G-2, Poznań, 1996.
[16] D. Janecki, K. Doktór, T. Michałowski, Proc. of XL Sci. Conf. of PTCh and SITPChem, No. S-1, K-5, Gdańsk 1997.
[17] S. Capone, A. De Robertis, C. De Stefano, S. Sammartano, R. Scarcella, C. Rigano, Thermochim. Acta 86 (1985) 273.
[18] P.G. Daniele, A. De Robertis, C. De Stefano, S. Sammartano, C. Rigano, J. Chem. Soc. Dalton Trans. (1985) 2353.
[19] C. De Stefano, P. Princi, C. Rigano, S. Sammartano, Ann. Chim. 78 (1988) 55.
[20] M.D.M. Marcosarroyo, Khoshkbarchi, J.H. Vera, J. Solut. Chem. 25 (1996) 983.

ELSEVIER

Talanta 48 (1999) 1199–1202

Talanta

Short communication

Determination of paracetamol in dosage forms by non-suppressed ion chromatography

Juan Luis Pérez, Miguel Angel Bello *

Department of Analytical Chemistry, Faculty of Chemistry, University of Seville, 41012 Seville, Spain

Received 22 June 1998; received in revised form 29 September 1998; accepted 2 October 1998

Abstract

An ion-chromatography procedure for the simultaneous determination of paracetamol and salicylic acid without suppression using UV detection is proposed. The method is applied to the determination of paracetamol in pharmaceuticals and also permits the quantitation of the total acetylsalicylic acid as salicylic acid. © 1999 Elsevier Science B.V. All rights reserved.

Keywords: Paracetamol; Salicylic acid; Ion chromatography; Pharmaceuticals

1. Introduction

Non narcotic analgesics are a kind of substances of great pharmacological significance. Paracetamol (acetaminophen, *N*-acetyl-*p*-aminophenol) is one of the most important non narcotic analgesics without the secondary effects of the salicylates on the gastric mucose, although it may causes liver damage in some instances [1,2].

A plethora of analytical methods for determining paracetamol are available: Spectrophotometric and spectrofluorimetric methods [3–5], reversed-phase HPLC [6–9], ion-pairing HPLC [10], MEKC [11,12], and FIA [13–15] among others. However, we have not found any reference about the use of ion chromatography (IC).

The use of anionic non-suppressed IC permits the separation of very weak acids like paracetamol, that the suppressed IC is unable to carry out. The eluent used must have a suitable pH for the deprotonation of the acid species. In our case, the eluent used was LiOH due to its ability to ionize weak acids [16].

This study reports a new, simple, rapid and highly sensitive non-suppressed IC method for the separation and quantitation of paracetamol using photometric detection. The fact that salicylic derivatives are hydrolized at the high pH value of the eluent enables the direct determination of paracetamol in analgesic pharmaceuticals, in which the presence of both active substances is

* Corresponding author. Tel.: +34-9-54-557172; fax: +34-9-54-557168; e-mail: mabello@cica.es.

PII: S0039-9140(98)00316-6

Table 1
Calibration data

Analyte	Regression parameters	LCR[a]	r[b]	LOD[c]
Paracetamol	$y = (0.05 \pm 0.05) + (2.42 \pm 0.01)x$	0.5–7	0.9998	0.06
Salicylic acid	$y = (0.03 \pm 0.04) + (1.00 \pm 0.02)x$	0.5–12	0.9995	0.12

[a] Linear concentration range ($mg \cdot l^{-1}$).
[b] Correlation coefficient.
[c] Detection limit ($mg \cdot l^{-1}$).

frequent. Likewise, it is possible the simultaneous determination of the total content of acetylsalicylic acid as salicylic acid.

2. Experimental

2.1. Apparatus

A Waters (Milford, MA, USA) Model 501 pump was used together with a Waters IC-Pak™ A HR 10 cm column packed with polymetacrylate resin with a quaternary ammonium functional group (6 μm particle size and exchange capacity of 30 ± 3 μeq ml^{-1}). Samples were injected using a Rheodyne (Cotati, CA, USA) injector with a 100 μl sample loop. Detection was done from a Waters 486 Tunable Absorbance Detector at 300 nm and AUFS 0.2. Peak evaluations were made with an Hewlett Packard (Palo Alto, CA, USA) Model HP3395 Integrator with an attenuation of 8. The mobile phase consists of 5 mM LiOH dissolved in an aqueous solution of 5% (v/v) acetonitrile, and the flow rate was 1 ml min^{-1}.

2.2. Reagents and chemicals

Salicylic acid and paracetamol were supplied by Sigma (St. Louis, MO, USA). Lithium hydroxide and acetonitrile were obtained from Merck (Darmstadt, Germany). Milli-Q treated water was used throughout.

2.3. Samples

Paracetamol were determined in five pharmaceuticals: actron® (Bayer); fiorinal codeina® (Sandoz); veganin® (Parke-Davis); melabon® (Lacer); and analgilasa® (Laboratorios Lasa). The composition of each formulation is given in Appendix A. If salicylic derivatives are present, its total content, as salicylic acid, were also determined.

2.4. Sample treatments

Pharmaceuticals were treated with aqueous LiOH 5 mM to ionize the acid groups, diluted and passed through a Waters C18 SEP-Pak™ Plus cartridge (short body) before injection, with the aim to eliminate possible neutral interferences.

2.5. Calibration features

The chromatographic signal used in calibrations was the height peak ratio according their reliability, better than peak area ratio.

A series ($n = 10$) of standard solutions (four replicates) of paracetamol and salicylic acid were prepared and measured. Data about the calibrations are collected in Table 1.

The application of Student's t-test shows that, in both cases, the intercepts are insignificant and accordingly, the straight lines pass through the origin.

2.6. Chromatographic parameters

A series of chromatographic parameters were determined for paracetamol and salicylic acid according to the chromatograms obtained. The number of theorical plates for the column used are 94 and 576 for paracetamol and salicylic acid, respectively. Peak-asymmetry factors are 1.85 for paracetamol and 1.40 for salicylic acid, and the

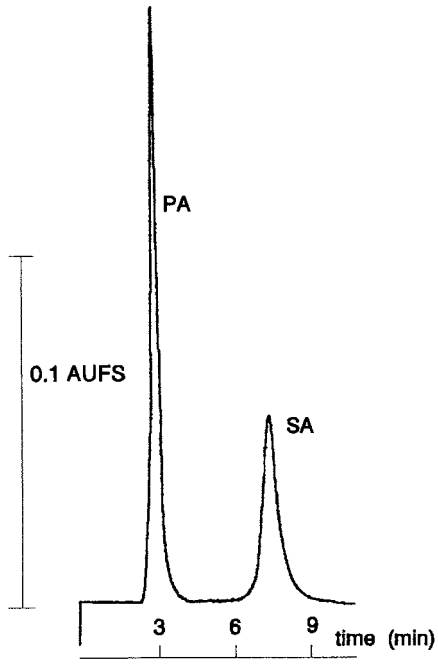

Fig. 1. Separation of paracetamol (PA) and salicylic acid (SA) by the described procedure. Concentrations: PA 6 mg·l^{-1} and SA 4 mg·l^{-1}.

resolution (R_s) between both peaks shows a value of 1.96.

3. Results and discussion

Separation of paracetamol and salicylic acid according to the proposed procedure shows good resolution as can be observed in Fig. 1. Sensitivity is remarkable and the detection limits of about 0.06–0.12 mg·l^{-1}. Recoveries within 97–101% were found for both analytes.

Concerning the pharmaceuticals analysed, it is noticeable that only anions actually present in the treated sample are separated and detected, the remaining components being eliminated in the previous clean up through C18 SEP-Pak.

The proposed procedure was applied to the determination of paracetamol in pharmaceuticals; if acetylsalicylic acid is present in the formulation, its total content as salicylic acid can also be determined. The samples were also analyzed by an HPLC standard method [17]. The results obtained are collected in Table 2. As can be seen, good agreement were found between the standard and the proposed method (statiscally proved according to the paired t-test [18]) and respect to the label claimed for analyzed samples, within the confidence ranges accepted by the pharmacopoeias.

This fact shows the applicability of the proposed method in the pharmaceutical analysis, without interference problems derived from other substances which frequently attend paracetamol in analgesic formulations.

4. Conclusions

The proposed method for the simultaneous de-

Table 2
Results for the analyzed samples

Sample	Paracetamol			Acetylsalicylic acid		
	Claimed (mg)	Standard method[a] (mg)	Proposed method[a] (mg)	Claimed (mg)	Standard method[a] (mg)	Proposed method[a,b] (mg)
Actron®	133	123 ± 1	121 ± 2	267	250 ± 2	249 ± 3
Fiorinal Codeina®	300	302 ± 3	299 ± 2	200	209 ± 4	209 ± 5
Veganin®	250	260 ± 3	265 ± 4	250	262 ± 3	264 ± 4
Melabon®	350	354 ± 4	355 ± 3			
Analgilasa®	400	427 ± 5	432 ± 5			

[a] Average of three determinations ± standard deviation.
[b] Determined as salicylic acid.

termination of paracetamol is sensitive, useful, fast and unlike HPLC methods, practically does not require the use of organic solvents, with only a small quantity of acetonitrile necessary.

The methodology was successfully applied to the determination of paracetamol in analgesic formulations and also permits the determination of acetylsalicylic acid as salicylic acid if it is present.

Acknowledgements

Authors thank to Waters Associates for providing the IC-Pak™ A HR column for this work.

Appendix A. Composition of the analyzed samples

Actron® (contents for one effervescent tablet)	
Paracetamol	133 mg
Acetylsalicylic acid	267 mg
Caffeine	40 mg
Citric acid	954 mg
Sodium bicarbonate	1.60 g
Excipient	
Fiorinal codeina® (contents for one capsule)	
Paracetamol	300 mg
Acetylsalicylic acid	200 mg
Caffeine	40 mg
Codeine phosphate	14.67 mg
Excipient	
Veganin® (contents for one tablet)	
Paracetamol	250 mg
Acetylsalicylic acid	250 mg
Codeine phosphate	10 mg
Excipient	
Melabon® (contents for one tablet)	
Paracetamol	350 mg
Propiphenazone	200 mg
Caffeine	8 mg
Excipient	
Analgilasa® (contents for one tablet)	
Paracetamol	400 mg
Caffeine	30 mg
Codeine phosphate	10 mg
Excipient	

References

[1] R.M. Walker, W.J. Racz, T.F. McElligott, Lab. Invest. 42 (1980) 181.
[2] D.J. Miller, R. Hickman, R. Fratter, J. Terblanche, S.J. Saunders, Gastroenterology 71 (1976) 109.
[3] J.A. Murillo, L.F. Garcia, Anal. Lett. 29 (3) (1996) 423.
[4] M.I. Toral, P. Richtery, O. Martinez, Bol. Soc. Chil. Quim. 41 (3) (1996) 283.
[5] P. Nagaraja, J. Pharm. Biomed. Anal. 17 (3) (1998) 501.
[6] K. Yuen, K. Peh, Y. Quah, K. Chan, Drug Dev. Ind. Pharm. 23 (2) (1997) 225.
[7] D. Prochazkova, P. Drasar, J. Vacha, Chem. Listy 91 (5) (1997) 373.
[8] A. Maisch, Labor Praxis 21 (3) (1997) 56.
[9] A.I. Gascó-López, R. Izquierdo-Hornillos, A. Jiménez, J. Chromatogr. A 775 (1997) 179.
[10] S. Yamato, M. Sakai, K. Shimada, Yakugaku Zasshi 116 (4) (1996) 329.
[11] L. Steinmann, W. Thormann, Electrophoresis 17 (8) (1996) 1348.
[12] D. Zou, X. Wu, G. Nan, Yaowu Fenxi Zazhi 17 (3) (1997) 160.
[13] Z. Bouhsain, S. Garrigues, A. Morales-Rubio, M. de la Guardia, Anal. Chim. Acta 330 (1) (1996) 59.
[14] D. Wang, J. Xu, X. Guo, Y. Zhao, Xiamen Daxue Xuebao 34 (6) (1995) 965.
[15] Z. Bouhsain, S. Garrigues, A. Morales-Rubio, M. de la Guardia, Analyst 121 (5) (1996) 635.
[16] Water Ion Chromatography Cookbook, Millipore Corporation, Water Chromato-graphy Division, Manual number 20195, Mildford, 1989.
[17] USP-NF (USP-23, NF-18), United States Pharmacopoeial Convention, Rockville, MD, 1994.
[18] J.C. Miller, J.N. Miller, Statistics for Analytical Chemistry, 3rd edition, Ellis Horwood-Prentice Hall, Chichester, 1993.

ELSEVIER

Talanta 48 (1999) 1203–1206

Talanta

Short communication

Microwave-assisted extraction of C_{60} and C_{70} from fullerene soot

Matthew J. Youngman, David B. Green *

Natural Science Division, Pepperdine University, Malibu, CA 90263, USA

Received 4 June 1998; received in revised form 20 October 1998; accepted 28 October 1998

Abstract

Microwave-assisted extraction (MAE) was examined as an alternative to the traditional Soxhlet method of extracting C_{60} and C_{70} from fullerene soot. MAE of 0.20 g of fullerene soot with 95:5 toluene–acetonitrile yielded greater than 7.8 mg of C_{60} and greater than 0.54 mg of C_{70} in 4 min with no further increase in yield after 30 min of irradiation. By comparison, exhaustive Soxhlet extraction of the same size sample with the same solvent yielded 7.1 mg of C_{60} and 0.58 mg of C_{70} in 340 min. Reextraction by MAE of soot initially extracted by Soxhlet increased the yield of Soxhlet alone. Although MAE was limited to less than 0.5-g sample per extraction vessel, multiple samples were extracted with minimal increased extraction time and no reduction in the amount of material recovered.

Keywords: Microwave-assisted extraction; C60; C70; Fullerene soot

1. Introduction

Microwave-assisted extraction (MAE) techniques are used to extract organic and inorganic compounds from a wide variety of solid matrices [1–10]. In many applications, MAE accelerates the extraction process and requires less solvent, making MAE a competitive option to processes such as Soxhlet extraction [2,3,7,9–12]. One drawback of MAE is the inability to heat nonpolar solvents since they lack the dipole moment necessary to interact with microwave radiation. This limitation can be overcome by the use of a mixed solvent system in which one component of the solvent mixture is polar. Common solvent modifiers include acetone, acetonitrile, or water [8,10].

Exhaustive Soxhlet extraction has been the preferred method for the extraction of C_{60} and C_{70} from fullerene-containing carbon soot [13–16]. The time necessary for exhaustive Soxhlet extraction of fullerenes from 6 g carbon soot is 10 h in toluene [14]. Others report extractions of C_{60} and

* Corresponding author. Fax: +1-310-456-4785; e-mail: dgreen@pepperdine.edu.

0039-9140/99/$ - see front matter
PII: S0039-9140(98)00340-3

C_{70} in benzene that require 24 h [13,15]. Sonication and simple reflux methods have been employed as alternatives for extracting C_{60} and C_{70} from fullerene-containing carbon soot, however neither technique gives the maximum yield [13,17]. We present here a practical method for liquid-phase MAE of C_{60} and C_{70} from fullerene-containing carbon soot, using readily available instrumentation with reliable safety features.

This study compares MAE and Soxhlet extraction of C_{60} and C_{70} from fullerene soot by using a toluene–acetonitrile solvent mixture. For certain matrices MAE has been shown to reduce the amount of solvent required to extract some classes of compounds [6,7]. In this application, however, our results indicate that when using the same amount of solvent MAE of carbon soot is over 10 times faster than Soxhlet extraction of C_{60} and $C_{70.}$

2. Experimental

2.1. Reagents

All solvents were of analytical grade or better. Standard solutions of the fullerenes C_{60} and C_{70} were prepared in toluene from the pure (99 + %) compounds purchased from Fluka Chemika (Switzerland). Fullerene-containing (2–20%) carbon soot was purchased from Strem Chemicals (Newburyport, MA).

2.2. MAE procedure

All MAEs were conducted using a 1000-W MSP-1000 microwave sample preparation system (CEM, Matthews, NC). Lined extraction vessels (LEVs) consisting of an Ultem poly(etherimide) outer-body and a Teflon PFA inner liner (110 ml in volume), liner cover, and safety rupture membrane were used for all extractions. The rupture membrane was replaced prior to each extraction. One LEV, the control vessel, was equipped with a special cap which permitted the insertion of a Fluoroptic temperature probe and provided a connection to the instrument's inboard pressure control system. In each MAE performed both the temperature and pressure were monitored, however only the temperature was regulated by programmable set points. Inside the microwave cavity, the LEVs were positioned around a central vapor-containment vessel on the turntable carousel. Teflon tubes (1/8 in.) in the vent system connected all LEVs to the vapor-containment vessel while a Teflon tube (1/4 in.) in the center of that vessel led to the cavity exhaust duct to provide expedient removal of solvent vapor from the oven cavity in the event of a rupture membrane failure. Use of a microwave transparent valve on the pressure control system allowed the LEV to be removed from the cavity immediately after irradiation was completed.

Fullerene-containing carbon soot (0.1–0.5 g) was weighed into an aluminum dish and quantitatively transferred to the LEV. A 95:5 toluene–acetonitrile solvent mixture (65 ml) was added to the LEV and the vessel capped. The volume of solvent was selected as a compromise of those reported in the literature by others [14,17]. Each MAE of fullerene soot was carried out by irradiating the sample at 750 W (75% of full microwave power). The extractions were conducted at the setpoint temperature for a programmed amount of time. Following irradiation, the LEV was removed from the microwave cavity, cooled in an ice-bath, and ≤ 100 μl of the extract solution removed for HPLC analysis. In studies investigating the extraction efficiency over time, the LEV was then re-capped and the sample irradiated for the next time period.

2.3. Soxhlet extraction procedure

Fullerene-containing carbon soot (0.1–0.5 g) was directly weighed into a cellulose extraction thimble. The extractions were performed using 65 ml of a 95:5 mixture of toluene–acetonitrile for more than 340 min. Samples of ≤ 100 μl were taken at regular intervals throughout the extraction for HPLC analysis.

2.4. HPLC procedure

The chromatographic system consisted of a ternary gradient pump (Spectra-Physics 8800) at-

tached to a variable-wavelength UV–visible absorption detector (Spectra-Physics 8450) set at 330 nm. A manual injector (Rheodyne 7125) was equipped with a 20-μl sample loop. The samples were filtered through a 0.45-μm Acrodisc-3 (Gelman Sciences, Ann Arbor, MI) syringe filter prior to injection onto the HPLC column. The HPLC separations were executed on a 250-mm length × 4.6-mm i.d. column packed with 5-μm d_p Spherisorb ODS-2 (Phenomenex, Torrance, CA) and isocratically eluted with hexanes at a flow rate of 1.0 ml min^{-1}. Quantitation of C_{60} and C_{70} was determined from the straight-line calibration obtained from authentic C_{60} and C_{70} external standards. The minimum detectable quantities of the fullerenes were measured to be <20 ng ml^{-1} (2 S.D.). Confirmation of peak identities was by comparison of the retention times with external standards and by UV–visible spectroscopic analysis of the peak fractions.

3. Results and discussion

Toluene has become the most widely used solvent for extracting C_{60} and C_{70} from fullerene soot [18–20]. Although toluene does not absorb microwave radiation, indirect heating of a nonpolar extraction solvent by the addition of a miscible polar solvent is well-established [10]. We found that with the addition of as little as 5% acetonitrile the setpoint temperature (typically 130°C) could be achieved in less than 4 min. The ratio of acetonitrile was varied from 1 to 20%, and except for an increased heating rate, we found little change in the extraction efficiency.

A difficulty often encountered in microwave sample preparation is electrical arcing when extracting or digesting electrically conductive solids [21]. The largest sample which could be treated in any single extraction vessel without arcing was 0.5 g or less of fullerene soot. In the interest of safety and economics we chose to limit extractions to a maximum of 0.2 g.

The recovered mass of C_{60} by MAE at 130°C and by Soxhlet extraction at 110°C of separate 0.20-g samples of fullerene soot observed over time is shown in Fig. 1A. Fig. 1B shows the recovery data of C_{70} under the same conditions. After 4 min at the setpoint temperature, the MAE recovery of C_{60} was >7.8 mg and increases to 8.0 mg after 30 min of irradiation. The recovery of C_{70} was >0.54 mg in 4 min increasing to 0.64 mg after 30 min of irradiation. No further increase in recovery was observed after 30 min for C_{60} or C_{70}. In contrast, the recovery by Soxhlet extraction of C_{60} was 7.1 mg while the recovery of C_{70} was 0.58 mg at 340 min. When the soot remaining after 340 min of Soxhlet extraction was reextracted by MAE with 65 ml of fresh solvent for 20 min at 130°C, another 1.3 mg of C_{60} and 0.30 mg more

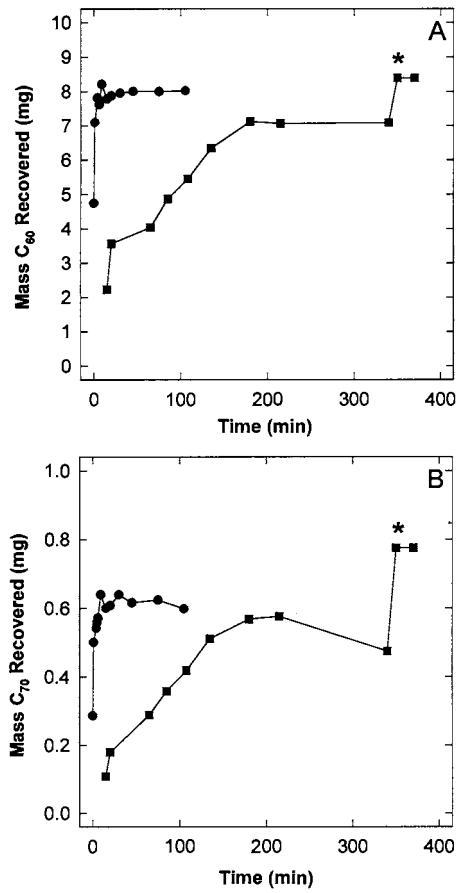

Fig. 1. Recovered mass of C_{60} (A) and C_{70} (B) from fullerene soot measured temporally during Soxhlet extraction (■) or MAE (●). Each data point is a single determination of mass and each plot is representative of replicate extractions. The asterisk shows added recovery of C_{60}/C_{70} when Soxhlet-extracted soot was reextracted by MAE.

of C_{70} was recovered (starred point in Fig. 1). The increased extraction rate and slightly improved recovery of the fullerenes by MAE is attributed to the higher temperatures attainable in the pressure-tight LEVs.

The efficiency of recovery of the fullerenes is demonstrated by the results of three successive microwave-assisted extractions of 0.10 g of fullerene soot. Each extraction was performed for 20 min at 130°C with 65 ml toluene–acetonitrile solvent. Following irradiation, the soot was recovered and returned to the LEV with 65 ml of fresh solvent. The second extraction yielded $<$ 3% more C_{60} and 5% more C_{70} than the first extraction. The third extraction yields $<0.2\%$ additional C_{60} and $<0.9\%$ more C_{70} over the first extraction. Consequently, near quantitative recovery of C_{60} is attainable by MAE in less than 20 min of irradiation.

An advantage of the microwave oven system used in this study is the ability to accommodate up to 12 extraction vessels simultaneously in the oven cavity. Since small samples absorb only a modest fraction of the total microwave energy in the oven cavity, simultaneous extractions in general require little extra time to reach the setpoint temperature. For example, the heating time of four identical 0.1-g samples to 130°C was only 1 min longer than when heating a single sample and the extent of recovery was comparable with extractions of only one sample.

4. Conclusions

Microwave-assisted extraction (MAE) of the fullerenes C_{60} and C_{70} is a viable alternative to the traditional Soxhlet method. Extraction efficiencies by MAE are comparable to those achieved by Soxhlet extraction. The smaller throughput of <0.5 g per extraction vessel is ameliorated by the larger number of extractions which can be performed simultaneously without sacrificing time or compromising the completeness of extraction. Even with the necessary additional step of filtering the soot from the extraction solvent, the time savings remains significant.

Acknowledgements

The authors are grateful to the Parson's Foundation and to the University Research Council of Pepperdine University for their generous financial support.

References

[1] Y. Aoki, M. Takeda, M. Uchiyama, J. AOAC 58 (1975) 1286.
[2] K. Ganzler, J. Bati, K. Valko, J. Chromatogr. 371 (1986) 299.
[3] C.S.E. Papp, L.B. Fischer, Analyst 112 (1987) 337.
[4] F.I. Onsuka, K.A. Terry, Chromatographia 36 (1993) 191.
[5] T.R. Steinheimer, J. Agric. Food Chem. 41 (1993) 488.
[6] V. Lopez-Avila, R. Young, W.F. Beckert, Anal. Chem. 66 (1994) 1097.
[7] V. Lopez-Avila, R. Young, J. Benedicto, P. Ho, R. Kim, W.F. Beckert, Anal. Chem. 67 (1995) 2096.
[8] F.I. Onuska, K.A. Terry, J. High. Resolut. Chromatogr. 18 (1995) 417.
[9] Y. Daghbouche, S. Garrigues, M. de la Guardia, Analyst 121 (1996) 1031.
[10] V. Lopez-Avila, R. Young, N. Teplitsky, J. AOAC Int. 79 (1996) 142.
[11] J. Nieuwenhuize, C.H. Poley-Vos, A.H. van den Akker, W. van Delft, Analyst 116 (1991) 347.
[12] J.C. Young, J. Agric. Food Chem. 43 (1995) 2904.
[13] D.H. Parker, P. Wurz, K. Chatterjee, et al., J. Am. Chem. Soc. 113 (1991) 7499.
[14] N. Coustel, P. Bernier, R. Aznar, A. Zahab, J. Lambert, P. Lyard, J. Chem. Soc. Chem. Commun. (1992) 1402.
[15] F. Diederich, R.L. Whetten, Acc. Chem. Res. 25 (1992) 119.
[16] K. Chatterjee, D.H. Parker, P. Wurz, K.R. Lykke, D.M. Gruen, L.M. Stock, J. Org. Chem. 57 (1992) 3253.
[17] K. Tohji, A. Paul, L. Moro, R. Malhotra, D.C. Lorents, R.S. Ruoff, J. Phys. Chem. 99 (1995) 17785.
[18] R.E. Haufler, J. Conceicao, L.P.F. Chibante, et al., J. Phys. Chem. 94 (1990) 8634.
[19] D.M. Cox, S. Behal, M. Disko, et al., J. Am. Chem. Soc. 113 (1991) 2940.
[20] G. Zhennan, Q. Jiuxin, Z. Xihuang, et al., J. Phys. Chem. 95 (1991) 9615.
[21] H.M. Kingston, L.B. Jassie (Eds.), Introduction to Microwave Sample Preparation, American Chemical Society, Washington, DC, 1988.

ELSEVIER

Talanta 48 (1999) 1207

Talanta

Book Review

Trace Determination of Pesticides and their Degradation Products in Water by D. Barcelo and M.-C. Hennion, Elsevier, Amsterdam, 1997. xiii + 542 pp., US $273.00. ISBN 0-444-818142-1.

The title of this book may suggest a text dedicated to the methodologies used to identify and quantify pesticides in water. However, while providing detailed discussion on a wide number of analytical approaches, this excellent volume also presents in depth background information on the use and behaviour of pesticides in the environment, and issues such as quality assurance. Six well structured chapters make up this book beginning with a substantial section clearly describing the nature of pesticides, how they enter the aquatic environment and the degradation they undergo. This chapter is very easily read and gives a good introduction to the field supported by high quality diagrams. The second chapter which covers sampling, storage and interlaboratory performance studies provides a valuable overview of the aspects which should be considered prior to committing resources to expensive analytical procedures. The contents of this chapter will be equally of interest to those considering water monitoring for any number of trace contaminants, not just pesticides.

Chapter 3 provides an excellent review of chromatographic methods for pesticide analysis covering all the main groups in detail, supported by example chromatograms. It contains useful method summaries of approved EPA techniques for both gas and liquid chromatography. It also discusses the more advanced techniques such as LC–MS and CE–MS which are of increasing importance in environmental analysis. In chapters 4 and 5 the authors explore sample handling techniques, chapter 4 focusing on extraction and clean-up methods including liquid–liquid, solid–phase and supercritical phase extraction and chapter 5 giving a detailed account of on-line methods for sample handling. Both chapters include all the most recent developments in this field and provide detailed outlines of suitable methodologies. The book concludes with a chapter covering an area which has gained increasing interest amongst analysts, that is, the use of immunochemical methods and biosensors. Again the subject area is introduced very clearly with the chapter logically progressing through a description of antibody production, cross-reactivity and the formats of immunoassay kits. Biosensors are dealt with relatively briefly, maybe a reflection that their use is currently an emerging area.

This is a book which I have thoroughly enjoyed reading and have particularly appreciated its logical layout. It gently guides the reader through the topic making it easily accessible to those less familiar with the subject while at the same time providing an excellent current review of the field which will be of interest to those active in this area.

L.A. Lawton
Robert Gordon University,
School of Applied Sciences,
Saint Andrew Street,
Aberdeen AB25 1HG,
UK.
Tel.: +44 1224 262823
Fax: +44 1224 262828

PII: S0039-9140(98)00281-1

ELSEVIER

Talanta 48 (1999) 1209

Talanta

Book Review

GC/MS: *A Practical User's Guide* by M. McMaster and C. McMaster, Wiley-VCH, Weinheim, 1998. xii+167 pp., £38.95. ISBN 0-471-24826-6.

The authors present a hardcover laboratory handbook to guide postgraduate students, as well as experienced technicians, from the basics of GC/MS in theory and instrumentation to method development, optimization, calibration, cleaning and troubleshooting of instruments, and their applications in environmental chemistry.

The text comprises short descriptive sections accompanied by very helpful and easily interpreted diagrams. Each of the short sections is well indexed with clear headings and numerical reference points, making the text very useful for quick reference. There is also a troubleshooting section that is handy as a checklist when problems are experienced. However, I would appreciate an expansion of the appendix on troubleshooting and source of contamination. This book is written for use with a quadrupole instrument. Extra information on other types of mass spectrometer such as ion trap and TOF, and other introduction systems such as liquid chromatography, is compressed into 20 pages out of 167. For the user in the lab I think that these pages would have been better spent on discussion of interpretation of fragmentation patterns. The most important fragmentations and transformations should have been included in this user's guide. On the other hand, the short descriptions of e.g. iron traps, TOF–MS, and electrospray are valuable information for the GC-quadrupole-MS user.

Nevertheless, this is a very well written book; it is always clear and to the point without missing any important details. There is minimal use of jargon and where it is unavoidable there is a glossary section to provide an explanation. The use of excellent illustrations is helpful in demonstrating instrumental device and explaining method schematics which might otherwise be difficult to appreciate. Overall, it is an easy read for researchers who would like to learn the methods, and for anyone who encounters a problem with an GC–MS instrument. I will use this book as the reference text for a postgraduate course on GC/MS.

J. Feldmann,
Chemistry Department,
Aberdeen University,
Meston Walk,
Aberdeen,
AB24 3UE,
Scotland.

PII: S0039-9140(98)00319-1

ELSEVIER

Talanta 48 (1999) 1211

Talanta

Book Review

150 and More Basic NMR Experiments—A Practical Course by S.H. Braun, H.-O. Kalinowski and S. Berger. Wiley-VCH, Weinheim, 1998, xiii & 596 pp, £29.95. Softback. ISBN 3-527-29512-7.

The first edition of this book was released in 1996, and has proved very useful, so useful in fact, that the authors have updated the book and added more experiments, making the total up to 162 experiments. This new edition takes account of recent developments in the field, and improvements in spectrometer design. The main emphasis of the book is to guide the chemist through setting up NMR pulse sequences, and it includes detailed parameters for each experiment. The parameter abbreviations used are for Bruker spectrometers, but these are readily translated to instruments made by other manufacturers (a translation table is provided). The book is divided into 14 chapters and the first four chapters are concerned with calibrations and the instruments itself. The first chapter contains a description of the NMR spectrometer, tuning and shimming details, including gradient shimming, a relatively recent development.

Chapters 2–4 indicate how the pulse durations can be determined and also standard tests and routine experiments, followed by decoupling techniques. Chapter 5 covers mainly variable temperature NMR. Chapter 6 introduces the concept of multipulse NMR and gives details for different types of water suppression. The next two chapters will prove very useful as these contain up-to-date methods. In chapter 7 we get the use of shaped pulses in 1D experiments, such as selective 1D TOCSY, and chapter 8 gives details of quantitative NMR and the use of auxiliary reagents such as shift reagents and relaxation agents as well as agents for the determination of enantiomeric purity.

Chapter 9 gives a brief description of NMR spectroscopy of nuclei other than ^{1}H or ^{13}C, including those with $I > 1/2$, those with quadrupoles and those with negative magnetogyric ratios. After this follows the longest chapter, covering all the indirect and inverse detected experiments, from COLOC to HMBC. A recent development in NMR has been the ready availability of pulsed field gradients, and chapter 11 covers the calibration of gradients and the application of these to 1D experiments. This is followed in chapter 12 by the use of gradients in 2D experiments, and surely all these experiments described will soon be routinely available on all spectrometers sold. There is a short chapter on 3D NMR, but I fear that this will not be routine for most of us, and will remain the territory of protein NMR spectroscopists. The last short chapter gives scant details on how to perform solid state NMR experiments. I think the authors have justly chosen to keep the experiments in the last two chapters to a minimum, as these are huge fields in their own rights. Appendices are included on product operator formalism rules, and a translator between the different instrument dialects. The book gives pulse sequence diagrams throughout, phases to be used, spectra to be expected, operator products, and each experiment is well referenced. This book is destined to become a standard reference work that will see regular usage by experimental NMR spectroscopists.

M. Jaspars,
Chemistry Department,
Aberdeen University,
Meston Walk,
Aberdeen,
AB24 3UE,
Scotland.

PII: S0039-9140(98)00320-8

ELSEVIER

Talanta 48 (1999) 1213

Talanta

Book Review

High Performance Liquid Chromatography, *Second Edition* by S. Lindsay, Wiley, Chichester, 1998. Single user: £150.00, 2–10 networked users: £450.00, 10–20 networked users: £750.00. Computer diskette. ISBN 0-471-97964-3.

This is a computer HPLC teaching aid in the Analytical Chemistry by Open Learning (ACOL) series. It is made up of an introduction to the subject followed by three lessons. Notes for the tutor and student are included, as is a very comprehensive library on HPLC. The suggested duration of the lessons is roughly 8 h, but there are convenient break points throughout, and you may stop anytime if you wish, and continue at a later time. The objectives for the whole package and each lesson are clear and stated in point form at the beginning of each. The program begins with a rather trivial reminder of the components of an HPLC system, and a curious animation of a separation in progress. The first lesson is an excellent example of how the structure of a molecule affects the choice of chromatographic conditions, and I found myself forced to think carefully and justifying choices I make routinely in the chromatography laboratory. When I erred more than once the program gave me another chance, and on more than one occasion admonished me for not trying hard enough! The program gives a clear rationale for optimising conditions, including mobile and stationary phase choices as well as types of detector. The second lesson concerns quantitative analysis and covers internal normalisation and the use of internal and external standards. This lesson carries through from lesson 1, and we learn how to quantify caffeine and aspirin by all three methods, as well as covering ion chromatography of tap water. The calculations are followed through and results are compared between all three methods and their advantages and disadvantages are discussed. Lesson 3 is all about the treatment of complex samples, in this case the quantitative determination of a plant hormone from raw plant material. It covers the difficult area of developing a sample cleanup method, and the inherent problems. Method development is discussed with reference to mobile phase, columns, and detection, which leads to the description of sample derivatisation to remove unwanted interferences in the spectrum. As a final point the method developed is scrutinised and the user is asked where it may be improved. As a whole I think that this program may be useful in getting students to understand why particular conditions are used in a separation method. Its most useful part is to get students to come to grips with calculations involving internal and external standards and response factors, as these always seem to be a stumbling block. One topic I would like to see more extensively discussed is the use of gradient elution and when/where to use it and how to develop a gradient method.

M. Jaspars,
Chemistry Department,
Aberdeen University,
Meston Walk,
Aberdeen,
AB24 3UE,
Scotland.

PII: S0039-9140(98)00321-X

ELSEVIER

Talanta 48 (1999) 1215–1216

Talanta

Book Review

Solid Sample Analysis by U. Kurfürst (editor). Springer, Berlin, 1988. xix + 423 pp. US$159.00 ISBN 3-540-62470-8.

'Direct GF-AAS analysis of solids has also been developed…this method has been progressively abandoned.' So commented the writer in a very recent (1998) large textbook on Analytical Chemistry. What the problems are, and how they may be overcome, is discussed in this excellent monograph, while the 'proof of the pudding' can be found, for example, by trying out the new model 'AAS 5 solid' instrument manufactured by Analytik Jena.

Chapter 1 provides all the reasons why one should use direct GF-AAS—simplicity, speed of operation, sensitivity, small sample size, and so on. Preparing the sample and choosing the calibration method are dealt with in Chapter 2, stressing the importance of finding, for use as a standard, a CRM similar in nature to the samples to be analysed. Grinding, particle size and sample inhomogeneity are key points here, but the importance, for confidence in the quality of the results, of having 'on-line' statistical data handling is made clear. Chapter 3 discusses the direct introduction of solid samples into the graphite furnace—with sample sizes varying from 50 μg to 3 mg and limits of detection in the sub-ppm range. Some specific details are then given for 12 different elements, and a lengthy bibliography includes references on over 30 elements in a wide range of matrices.

Chapter 4 presents the combination of electrothermal vaporisation as a means of sample introduction into the ICP, again with a substantial bibliography. Chapter 5 returns to the use of the graphite furnace, but this time with slurry nebulisation—a well proven approach to the analysis of refractory materials and other substances which are difficult to bring into solution. Handling the slurry is always the problem—How long should one shake? Is ultra-sonic agitation necessary? Can the slurry be stabilised? These and many more questions are debated here. The bibliography in this chapter is particularly extensive. Finally, we are brought to Chapter 6 dealing with applications, optimistically called 'Advantageous fields of application'.

We are left, after reading this book, with a good idea of the power of the technique—how easily sub-ppm levels can be quantified in tiny amounts of sparingly soluble materials in a short time with minimum sample preparation and therefore with minimum possibility of introducing contamination. It is clear that the percision is poorer than has been traditionally aimed at—10% rsd is quite acceptable here—but, as the main author, Dr Kurfürst, says in his introduction—we are up against a psychological rather than a chemical barrier. And this book will help the reader to make the decision—when is the performance of SS-GF-AAS adequate for the task in hand, and when will its clear advantages outweigh the disadvantages. I think this book gives a clear and balanced account, presented neverthe-

0039-9140/99/$ - see front matter
PII: S0039-9140(98)00322-1

less with an enthusiasm without which much of the earlier development work would never have been finished. There is no good reason for abandoning this powerful and simple technique, but every good reason for reading first, thinking carefully and finally, arriving at an informed opinion as to when it will be the method of choice.

I. Marr,
Chemistry Department,
Aberdeen University,
Meston Walk,
Aberdeen,
AB24 3UE,
Scotland.

ELSEVIER

Talanta 48 (1999) 1229–1231

Talanta

Author Index

Volume 48 (1999)

PII: S0039-9140(99)00063-6

ELSEVIER

Talanta 48 (1999) 1233–1237

Talanta

Subject Index

Volume 48 (1999)

PII S0039-9140(99)00064-8